QUANTUM TUTORIALS



Frank Rioux
College of Saint Benedict/Saint John's University

LibreTexts™

College of Saint Benedict/Saint John's University

Quantum Tutorials

Frank Rioux

This text is disseminated via the Open Education Resource (OER) LibreTexts Project (https://LibreTexts.org) and like the thousands of other texts available within this powerful platform, it is freely available for reading, printing, and "consuming."

The LibreTexts mission is to bring together students, faculty, and scholars in a collaborative effort to provide an accessible, and comprehensive platform that empowers our community to develop, curate, adapt, and adopt openly licensed resources and technologies; through these efforts we can reduce the financial burden born from traditional educational resource costs, ensuring education is more accessible for students and communities worldwide.

Most, but not all, pages in the library have licenses that may allow individuals to make changes, save, and print this book. Carefully consult the applicable license(s) before pursuing such effects. Instructors can adopt existing LibreTexts texts or Remix them to quickly build course-specific resources to meet the needs of their students. Unlike traditional textbooks, LibreTexts' web based origins allow powerful integration of advanced features and new technologies to support learning.



LibreTexts is the adaptable, user-friendly non-profit open education resource platform that educators trust for creating, customizing, and sharing accessible, interactive textbooks, adaptive homework, and ancillary materials. We collaborate with individuals and organizations to champion open education initiatives, support institutional publishing programs, drive curriculum development projects, and more.

The LibreTexts libraries are Powered by NICE CXone Expert and was supported by the Department of Education Open Textbook Pilot Project, the California Education Learning Lab, the UC Davis Office of the Provost, the UC Davis Library, the California State University Affordable Learning Solutions Program, and Merlot. This material is based upon work supported by the National Science Foundation under Grant No. 1246120, 1525057, and 1413739.

Any opinions, findings, and conclusions or recommendations expressed in this material are those of the author(s) and do not necessarily reflect the views of the National Science Foundation nor the US Department of Education.

Have questions or comments? For information about adoptions or adaptions contact info@LibreTexts.org or visit our main website at https://LibreTexts.org.

This text was compiled on 05/10/2026

TABLE OF CONTENTS

Licensing

1: Quantum Fundamentals

- 1.1: An Approach to Quantum Mechanics
- 1.2: Atomic and Molecular Stability
- 1.3: Atomic and Molecular Stability
- 1.4: Atomic and Molecular Stability
- 1.5: Quantum Computation - A Short Course
- 1.6: Quantum Computation- A Short Course
- 1.7: Quantum Computation- A Short Course
- 1.8: Quantum Computation- A Short Course
- 1.9: Quantum Computation- A Short Course
- 1.100: Analysis of the Stern-Gerlach Experiment
- 1.101: Related Analysis of the Stern-Gerlach Experiment
- 1.103: Bloch Sphere
- 1.104: 88. Related Analysis of the Stern-Gerlach Experiment
- 1.105: Bill the Cat and the Superposition Principle
- 1.106: Schroedinger's Dog
- 1.107: The Bloch Sphere
- 1.108: Density Matrix, Bloch Vector and Entropy
- 1.109: State Vectors and State Operators- Superpositions, Mixed States, and Entanglement
- 1.10: Quantum Computation- A Short Course
- 1.110: The Gram-Schmidt Procedure
- 1.11: Quantum Computation- A Short Course
- 1.12: Quantum Computation- A Short Course
- 1.13: Quantum Mechanics and the Fourier Transform
- 1.14: Quantum Mechanics and the Fourier Transform
- 1.15: Quantum Mechanics and the Fourier Transform
- 1.16: Quantum Mechanics and the Fourier Transform
- 1.17: Quantum Mechanics and the Fourier Transform
- 1.18: Exploring the Origin of Schrödinger’s Equations
- 1.19: Basic Quantum Mechanics in Coordinate, Momentum and Phase Space
- 1.20: The Repackaging of Quantum Weirdness
- 1.21: Quantum Principles Illuminated with Polarized Light
- 1.22: Relationship Between the Coordinate and Momentum Representations
- 1.23: Very Brief Relationship Between the Coordinate and Momentum Representations
- 1.24: Getting Accustomed to the Superposition Principle
- 1.25: The Dirac Delta Function
- 1.26: Elements of Dirac Notation
- 1.27: The Dirac Notation Applied to Variational Calculations
- 1.28: Raising and Lowering; Creating and Annihilating
- 1.29: Single Slit Diffraction and the Fourier Transform
- 1.30: From Coordinate Space to Momentum Space and Back
- 1.31: The Position and Momentum Commutation Relation in Coordinate and Momentum Space
- 1.32: Simulating the Aharonov-Bohm Effect

- 1.33: Basic Matrix Mechanics
- 1.34: Rudimentary Matrix Mechanics
- 1.35: Matrix Mechanics
- 1.36: Aspects of Dirac's Relativistic Matrix Mechanics
- 1.37: The Double-Slit Experiment
- 1.38: Double-Slit Experiment with Polarized Light
- 1.39: The Consequences of Path Information in a Mach-Zehnder Interferometer
- 1.40: Another look at the Consequences of Path Information in a Mach-Zehnder Interferometer
- 1.41: The Double-Slit Experiment with Polarized Light
- 1.42: The Quantum Eraser
- 1.43: Which Way Did It Go? - The Quantum Eraser
- 1.44: Which Path Information and the Quantum Eraser
- 1.45: Terse Analysis of Triple-slit Diffraction with a Quantum Eraser
- 1.46: Which Path Information and the Quantum Eraser (Brief)
- 1.47: Terse Analysis of Triple-slit Diffraction with a Quantum Eraser
- 1.48: Which-way Markers and Post-selection in the Double-slit Experiment
- 1.49: A Stern-Gerlach Quantum "Eraser"
- 1.50: Using the Mach-Zehnder Interferometer to Illustrate the Impact of Which-way Information
- 1.51: Quantum Theory, Wave-Particle Duality and the Mach-Zehnder Interferometer
- 1.52: Analysis of a Temporal Double-slit Experiment
- 1.53: An Analysis of Three-Path Interference
- 1.54: An Analysis of Three-Slit Interference
- 1.55: Using a Mach-Zehnder Interferometer to Illustrate Feynman's Sum Over Histories Approach to Quantum Mechanics
- 1.56: The Paradox of Recombined Beams
- 1.57: Evidence for Quantized Gravitational States of the Neutron
- 1.58: Quantized Gravitational States A Variational Approach
- 1.59: The Quantum Bouncer Doesn't Bounce, Unless...
- 1.60: Kinetic Energy Is Important in the Nanoscale World
- 1.61: Energy Expectation Values and the Origin of the Variation Principle
- 1.62: Examining the Wigner Distribution Using Dirac Notation
- 1.63: The Wigner Function for the Single Slit Diffraction Problem
- 1.64: Wigner Distribution for the Double Slit Experiment
- 1.65: Wigner Distribution for the Triple Slit Experiment
- 1.66: Wigner Distribution for the Quadruple Slit Experiment
- 1.67: Quantum Tunneling in Coordinate, Momentum and Phase Space
- 1.68: Another Look at the Wigner Function
- 1.69: The Wigner Distribution Function for the Harmonic Oscillator
- 1.70: Wigner Distribution for the Particle in a Box
- 1.71: The Wigner Distribution for a Particle in a One-dimensional Box
- 1.72: Superposition vs. Mixture
- 1.73: Time-dependent Wigner Function for Harmonic Oscillator Transitions
- 1.74: Momentum Operator in Coordinate Space
- 1.75: Momentum Wave Functions for the Particle in a Box
- 1.76: A Graphical Illustration of the Heisenberg Uncertainty Relationship
- 1.77: The Quantum Harmonic Oscillator
- 1.78: Coherent Superpositions for the Harmonic Oscillator
- 1.79: The Harmonic Oscillator and the Uncertainty Principle
- 1.80: Another view of the Harmonic Oscillator and the Uncertainty Principle
- 1.81: Hydrogen Atom and Helium Ion Spatial and Momentum Distribution Functions Illustrate the Uncertainty Principle

- 1.82: The Position-Momentum Uncertainty Relation in the Hydrogen Atom
- 1.83: Demonstrating the Uncertainty Priniciple for Angular Momentum and Angular Position
- 1.84: A Brief Tutorial on Wavepackets
- 1.85: The Difference Between Fermions and Bosons
- 1.86: Quantum Corrals - Electrons within a Ring
- 1.87: Planck's Radiation Equation Fit to Experimental Data
- 1.88: Planck's Radiation Equation Fit to Experimental Data - Another Algorithm
- 1.89: Fitting Einstein's Heat Capacity Equation to Experimental Data for Silver
- 1.90: Einstein's Heat Capacity Equation Fit to Experimental Data - Another Algorithm
- 1.91: Fitting Debye's Heat Capacity Equation to Experimental Data for Silver
- 1.92: Debye's Heat Capacity Equation Fit to Experimental Data - Another Algorithm
- 1.93: Wave-particle Duality and the Uncertainty Principle
- 1.94: Wave-Particle Duality for Matter and Light
- 1.95: What Part of the Quantum Theory Don't You Understand?
- 1.96: Quantum Potpourri - An Attempt to Demonstrate Two Fundamental Quantum Concepts- Wave-particle Duality and The Superposition Principle
- 1.97: Quantum Dynamics- One Step at a Time
- 1.98: Quantum Mechanical Pressure
- 1.99: Visualizing the Difference Between a Superposition and a Mixture

2: Atomic Structure

- 2.1: The de Broglie-Bohr Model for the Hydrogen Atom
- 2.2: The de Broglie-Bohr Model for the Hydrogen Atom - Version 3
- 2.3: The de Broglie-Bohr Model for the Hydrogen Atom - Version 3
- 2.4: A de Broglie-Bohr Model for Positronium
- 2.5: The de Broglie-Bohr Model for the Hydrogen Atom - Version 4
- 2.6: The de Broglie-Bohr Model for a Hydrogen Atom Held Together by a Gravitational Interaction
- 2.7: The de Broglie-Bohr Model for Positronium
- 2.8: The Bohr Model for the Earth-Sun System
- 2.9: Extracting Atomic and Molecular Parameters from the deBroglie-Bohn Model for the Atom
- 2.10: Electronic Structure and the Superposition Principle
- 2.11: Atomic Spectroscopy and the Correspondence Principle
- 2.12: Hydrogen-Like Calculations with Variable Lepton Mass
- 2.13: Atomic Stability
- 2.14: Quantum Mechanical Calculations for the One-Dimensional Hydrogen Atom
- 2.15: Quantum Mechanical Calculations for the Hydrogen Atom
- 2.16: Atomic Stability
- 2.17: Atomic Stability - Mathcad Version
- 2.18: 110. Critique of the Centrifugal Effect in the Hydrogen Atom
- 2.19: A Shorter Critique of the Centrifugal Effect in the Hydrogen Atom
- 2.20: Exploring the Role of Lepton Mass in the Hydrogen Atom
- 2.21: The Effect of Lepton Mass on the Energy and Bond Length of the Hydrogen Molecule Ion
- 2.22: The Hydrogen Atom with Finite Sized Nucleus
- 2.23: The Hyperfine Interaction in the Hydrogen Atom
- 2.24: Positronium Annihilation
- 2.25: Positronium Annihilation- Another View
- 2.26: Positronium Annihilation- Yet Another View
- 2.27: The Hyperfine Interaction in the Deutrium Atom
- 2.28: A Tensor Algebra Approach to Spin-Orbit Coupling

- 2.29: A Bohr Model for Multi-electron Atoms and Ions
- 2.30: Atomic Variational Calculations- Hydrogen to Boron
- 2.31: Some Calculations on the Lithium Atom Ground State
- 2.32: E. B. Wilson's Calculation on the Lithium Atom Ground State
- 2.33: The Importance of the Pauli Principle
- 2.34: Splitting the 2s-2p Degeneracy in the Lithium Atom
- 2.35: Addition of Spin Angular Momentum- A Tensor Algebra Approach
- 2.36: Hund's Rule
- 2.37: Hund's Rule - Singlet-Triplet Calculations with Mathcad
- 2.38: Electron Correlation in Two-electron Systems
- 2.39: First Trial Wave Function
- 2.40: Second Trial Wavefunction
- 2.41: Third Trial Wavefunction
- 2.42: 129.4 Fourth Trial Wavefunction
- 2.43: Fifth Trial Wavefunction and Summary
- 2.44: The Crucial Role of Kinetic Energy in Interpreting Ionization Energies
- 2.45: Quantum Dots Are Artificial Atoms
- 2.46: Calculating the Atomic Radius of Polonium
- 2.47: Calculating the Atomic Radius of Gold
- 2.48: How Many Bibles Can Fit on the Head of a Pin
- 2.49: Momentum Wavefunctions and Distributions for the Hydrogen Atom
- 2.50: The SCF Method for Two Electrons
- 2.51: Outline of the SCF Method for Two Electrons
- 2.52: The SCF Method for Two Electrons Using a Gaussian Wave Function
- 2.53: An Interactive SCF Calculation for the Helium Atom
- 2.54: Quantum Calculations on the Hydrogen Atom in Coordinate, Momentum and Phase Space
- 2.55: The Wigner Distribution for the 1s State of the 1D Hydrogen Atom
- 2.56: The Wigner Distribution for the 2s State of the 1D Hydrogen Atom
- 2.57: The Wigner Distribution for the 2p State of the 1D Hydrogen Atom
- 2.58: The Wigner Distribution for the 3s State of the 1D Hydrogen Atom
- 2.59: The Wigner Distribution for the 3p State of the 1D Hydrogen Atom
- 2.60: The Wigner Distribution for the 4s State of the 1D Hydrogen Atom
- 2.61: One-dimensional H-atom with Delta Function Potential
- 2.62: The Atomic Structure Factor in Coordinate and Momentum Space

3: Chemical Bonding

- 3.1: The Covalent Bond and Quantum Mechanics
- 3.2: The Covalent Bond in the Hydrogen Molecule
- 3.3: The Covalent Bond Clarified Through the Use of the Virial Theorem
- 3.4: Brief Version of the Covalent Bond Clarified Through the Use of the Virial Theorem
- 3.5: The H2 Covalent Bond and the Virial Theorem
- 3.6: The Covalent Bond According to Slater and Ruedenberg
- 3.7: Slater's Analysis of the Covalent Bond using the Virial Theorem
- 3.8: Two Analyses of the Covalent Bond using the Virial Theorem
- 3.9: A Simple Charge Cloud Model for Molecular Hydrogen- Or, Is It a DFT Model?
- 3.10: Three Mechanisms for Bond Formation in the Hydrogen Molecule Ion
- 3.11: A Mechanistic Approach to Bond Formation in the Hydrogen Molecule Ion
- 3.12: A Lite Version of Ruedenberg's Analysis of the Covalent Bond in the Hydrogen Molecule Ion
- 3.13: Molecular Orbital Analysis for the Hydrogen Molecule Ion Bond

- 3.14: A One-dimensional Model for the Covalent Bond in the Hydrogen Molecule Ion
- 3.15: Localized and Delocalized Molecular Orbitals
- 3.16: Two Perspectives on the Bonding in Water
- 3.17: Covalent Bonding in Ammonia from Several Perspectives
- 3.18: A Molecular Orbital Approach to Bonding in Methane
- 3.19: A Simple Calculation of the Lattice Energy of LiH
- 3.20: An Even Simpler LiH Lattice Energy Calculation
- 3.21: Charge Cloud Models for Some Simple Atomic, Molecular and Solid Systems
- 3.22: A Critique of the Valence Shell Electron Pair Repulsion Model
- 3.23: A Simple Electrostatic Critique of VSEPR
- 3.24: Another Critique of VSEPR
- 3.25: Why Nonbonding Electrons Occupy the Equatorial Position in Trigonal Bipyramidal Geometry
- 3.26: A Modified Tangent Spheres Model Analysis of Trigonal Bipyramidal Geometry
- 3.27: A Symbolic Huckel MO Calculation Using Mathcad
- 3.28: A Numeric Huckel MO Calculation Using Mathcad
- 3.29: A Numerical Huckel MO Calculation on C60
- 3.30: Chemical Bonding and Electronic Structure of Buckminsterfullerene
- 3.31: Quantum Mechanics, Group Theory and C60
- 3.32: A Numerical Huckel Calculation on Anthracene and Phenanthrene
- 3.33: A Numerical Huckel Calculation on C10H8 Isomers
- 3.34: Semi-empirical Molecular Orbital Calculation on HF
- 3.35: Semi-empirical Molecular Orbital Calculation on XeF2
- 3.36: Posch-Teller Potential Model for Metals

4: Spectroscopy

- 4.1: Rudiments of Atomic Spectroscopy Using Mathcad
- 4.2: A Particle-in-a-Box Model for Color Centers
- 4.3: Cyanine Dyes as Two-State Electronic Systems
- 4.4: The Ammonia Inversion and the Maser
- 4.5: A Symmetric Double Well Potential Illustrating Tunneling
- 4.6: Analyses of the Pure Rotational Spectrum of HCl
- 4.7: A Rudimentary Analysis of the Vibrational-Rotational HCl Spectrum
- 4.8: Visualizing the Formally Forbidden Overtone Vibrational Transitions in HCl
- 4.9: The Quantum Jump
- 4.10: Another Look at the Quantum Jump
- 4.11: Quantum Beats
- 4.12: The 1s-2s Electronic Transition in the 1D Hydrogen Atom
- 4.13: The Quantum Jump in Momentum Space
- 4.14: The Harmonic Oscillator Quantum Jump
- 4.15: Coherent States of the Harmonic Oscillator
- 4.16: Analysis of the Electronic Spectrum of Ti(H2O)3+
- 4.17: Quantum Jumps for an Electron on a Ring
- 4.18: Analysis of the Vibrational and Electronic Spectrum of Benzene
- 4.19: NMR - Quantum Mechanics of a Three Proton System
- 4.20: AB Proton NMR Using Tensor Algebra
- 4.21: Calculating the AB Proton NMR Using Tensor Algebra
- 4.22: AB Proton NMR Analysis for 2,3-dibromothiophene
- 4.23: ABC Proton NMR Using Tensor Algebra
- 4.24: AB2 Proton NMR Using Tensor Algebra

- 4.25: AB3 Proton NMR Using Tensor Algebra
- 4.26: HD-Like NMR Spectrum Calculated Using Tensor Algebra
- 4.27: The Michelson Interferometer and Fourier Transform Spectroscopy
- 4.28: A Sum Over Histories Approach to Fourier Transform Infrared Spectroscopy
- 4.29: Modeling the Pi-electrons of Benzene as Particles on a Ring
- 4.30: Modeling the Pi-electrons of Benzene as Particles on a Ring - Version 2
- 4.31: Calculating the Pi-electron HOMO-LUMO Electronic Transition for Benzene
- 4.32: Modeling the Pi-electrons of Benzene as Particles in a Ring
- 4.33: Modeling the Pi-electrons of Corannulene as Particles in a Ring
- 4.34: The Vibrational and Electronic States of C60

5: Diffraction Phenomena

- 5.1: Using Optical Transforms to Teach Quantum Mechanics
- 5.2: Single-slit Diffraction and the Uncertainty Principle
- 5.3: Single-slit Diffraction and the Uncertainty Principle (Mathcad Version)
- 5.4: Simulating DNA's Diffraction Pattern
- 5.5: Simulating DNA's Diffraction Pattern with a More Realistic Model
- 5.6: Simulating DNA's Diffraction Pattern - Short Version
- 5.7: A Model Graphene Diffraction Pattern
- 5.8: Is a Two-dimensional Fibonacci Array a Quasilattice?
- 5.9: Calculating Diffraction Patterns
- 5.10: Modeling the C60 Diffraction Pattern
- 5.11: Diffraction Pattern for Pentagonal Point Scatterers
- 5.12: Diffraction Pattern for Pentagonal Finite Point Scatterers
- 5.13: Pentagram Diffraction Pattern
- 5.14: Model Diffraction Pattern for Napthalene
- 5.15: Calculating the Airy Diffraction Pattern
- 5.16: Diffraction Pattern for Two Concentric Rings
- 5.17: Density Operator Approach to the Double-Slit Experiment
- 5.18: Another Look at the Double-Slit Experiment
- 5.19: A Quantum Mechanical Interpretation of Diffraction
- 5.20: Electron Diffraction at Multiple Slits
- 5.21: Multiple Slit Diffraction and the Fourier Transform
- 5.22: The Double-Slit Experiment with C60 Molecules
- 5.23: Crystal Structure, Rotational Symmetry, and Quasicrystals
- 5.24: X-ray Crystallography from a Quantum Mechanical Perspective
- 5.25: Holography Involves Single Photon Interference
- 5.26: X-ray Diffraction
- 5.27: Holography Involves Single Photon Interference

6: Group Theory with Mathcad

- 6.1: Group Theory Principles Applied to H2O
- 6.2: Dodecahedrane
- 6.3: Xenon Tetrafluoride
- 6.4: Diborane
- 6.5: Cubane
  - 6.5.1: Buckminsterfulerene
- 6.6: BCl3

- 6.7: Ti(H2O)6 3+
- 6.8: CH_4
- 6.9: P_4
- 6.10: Tetrahedrane
- 6.11: PH3
- 6.12: Cyclopropane
- 6.13: An Extensive Set of Group Theory Problems for Chemists
- Index

7: Quantum Optics

- 7.1: Single-Photon Interference - First Version
- 7.2: Single-Photon Interference - Second Version
- 7.3: Single-photon Interference - Third Version
- 7.4: Single Photon Interference - Fourth Version
- 7.5: Single Photon Interference - Mathcad version
- 7.6: The Polarizing Beam Splitter and the Superposition Principle
- 7.7: Mach-Zehner Polarization Interferometer Analyzed Using Tensor Algebra
- 7.8: Illustrating the Superposition Principle with Single Photon Interference
- 7.9: Pure States, Mixtures and the Density Operator
- 7.10: Using the Trace Function to Calculate Expectation Values
- 7.11: Polarized Light and Quantum Superposition
- 7.12: Polarized Light and Quantum Mechanics
- 7.13: The Three-Polarizer Paradox
- 7.14: Matrix Mechanics Approach to Polarized Light
- 7.15: Matrix Mechanics Approach to Polarized Light - Version 2
- 7.16: Matrix Mechanics Exercises Using Polarized Light
- 7.17: Polarized Light and Quantum Mechanics
- 7.18: Neutron Interferometry with Polarized Spin States
- 7.19: Interaction Free Measurement - Seeing in the Dark
- 7.20: Quantum Seeing in the Dark - A Matrix-Tensor Analysis
- 7.21: Two Analyses of the Michelson Interferometer
- 7.22: A Quantum Circuit for a Michelson Interferometer
- 7.23: The Ramsey Atomic Interferometer
- 7.24: Optical Activity - A Quantum Perspective
- 7.25: A Quantum Optical Cheshire Cat
- 7.26: Two Photon Interference - The Creation of an Entangled Superposition
- 7.27: Two-particle Interference for Bosons and Fermions
- 7.28: Analysis of a Two-photon Interferometer
- 7.29: Two-photon Interferometry
  - 7.29.1: Another Two Photon Interference Experiment
- 7.30: Another Two Photon Interference Experiment
- 7.31: Quantum Correlations Illuminated with Tensor Algebra
- 7.32: Two Photon Entanglement - A Tensor Algebra Analysis
- 7.33: Two Photon Interference - Matrix Mechanics Approach
- 7.34: Two-electron Interference
- 7.35: Bosonic and Fermionic Photon Behavior at Beam Splitters
- 7.36: Bosonic and Fermionic Photon Behavior at Beam Splitters- A Tensor Algebra Analysis
- 7.37: Entangled Photons Can Behave Like Fermions
- 7.38: Analyzing Two-photon Interferometry Using Mathcad and Tensor Algebra

- 7.39: Analysis of a Two-photon Quantum Eraser
- 7.40: Another Example of a Two-photon Quantum Eraser
- 7.41: A Quantum Delayed-Choice Experiment
- 7.42: A Quantum Delayed-Choice Experiment
- Index

8: Quantum Teleportation

- 8.1: A Single Page Summary of Quantum Teleportation
- 8.2: Quantum Teleportation - A Brief Introduction
- 8.3: Quantum Teleportation at a Glance
- 8.4: Another Look at Quantum Teleportation
- 8.5: Teleportation Using Quantum Gates
- 8.6: Another Example of Teleportation Using Quantum Gates
- 8.7: Yet Another Quantum Teleportation Circuit
- 8.8: Quantum Teleportation - Another Look
- 8.9: A Quantum Teleportation Experiment for Undergraduates
- 8.10: A Simple Teleportation Exercise
- 8.11: Teleportation as a Quantum Computation
- 8.12: Quantum Teleportation - Four Perspectives
- 8.13: Teleportation of Two Qubits
- 8.14: Greenaberger-Hrne-Zeilinger (GHZ) Entanglement and Local Realism
- 8.15: GHZ Math Appendix
- 8.16: GHZ Entanglement - A Tensor Algebra Analysis
- 8.17: Simulation of a GHZ Gedanken Experiment
- 8.18: Another Simulation of a GHZ Gedanken Experiment
- 8.19: A Surgical Refutation of the Local Realism Heresy
- 8.20: GHZ Four-Photon Entanglement Analyzed Using Tensor Algebra
- 8.21: Quantum v. Realism
- 8.22: Elements of Reality- Another GHZ Gedanken Experiment Analyzed
- 8.23: Brief Elements of Reality
- 8.24: A Brief Analysis of Mermin's GHZ Thought Experiment
- 8.25: Lucien Hardy's Paradox as Presented by N. David Mermin
- 8.26: Hardy's Paradox - An Algebraic Analysis
- 8.27: Quantum Entanglement Leads to Nonclassical Correlations
- 8.28: Nonclassial Correlations Revealed with Mermin's Pentagram
- 8.29: Spooky Action at a Distance- The EPR Experiment with Photons
- 8.30: David Bohm's EPR Gedanken Experiment
- 8.31: An Extension of Bohm's EPR Experiment
- 8.32: A Surgical Adjudication of the Conflict Between Quantum Theory and Local Realism
- 8.33: A Thought Experiment Reveals the Conflict Between Quantum Theory and Local Realism
- 8.34: Positronium Annihilation
- 8.35: Mermin's Version of Bohm's EPR Gedanken Experiment
- 8.36: A Concise Version of Mermin's EPR Gedanken Experiment
- 8.37: Another Look at Mermin's EPR Gedanken Experiment
- 8.38: Mermin's Version of Bohm's EPR Gedanken Experiment Using Tensor Algebra
- 8.39: A GHZ Gedanken Experiment Using Spatial Degrees of Freedom and Tensor Algebra
- 8.40: Another GHZ Example Using Spin-1/2 Particles
- 8.41: Entanglement Reveals a Conflict Between Local Realism and Quantum Theory
- 8.42: A Summary of Feynman's "Simulating Physics with Computers"

- 8.43: Another Summary of Fenyman's "Stimulating Physics with Computers"
- 8.44: Yet Another Assault on Local Realism
- 8.45: Yet Another Assault on Local Realism - A Matrix/Tensor Algebra Approach
- 8.46: Jim Baggott's Bell Theorem Analysis
- 8.47: Another Bell Theorem Analysis
- 8.48: Another Bell Theorem Analysis - Shorter Version
- 8.49: EPR Analysis for a Composite Singlet Spin System
- 8.50: EPR Analysis for a Composite Singlet Spin System - Short Version
- 8.51: Analysis of the Stern-Gerlach Experiment
- 8.52: Hardy's Paradox
- 8.53: Bell State Exercises
- 8.54: Expressing Bell and GHZ States in Vector Format Using Mathcad
- 8.55: Quantum Circuit for the Generation of GHZ States
- 8.56: A Brief Description of Aspect's Experiment
- 8.57: The Kochen-Specker Theorem Illustrated Using a Three-Qubit GHZ System
- 8.58: A Brief Introduction to Entanglement Swapping
- 8.59: An Entanglement Swapping Protocol
- 8.60: Quantum Correlations Simplified
- 8.61: Simulating Quantum Correlations with a Quantum Computer
- 8.62: Quantum Computer Simulation of Photon Correlations
- 8.63: Quantum Correlations Illustrated with Photons
- 8.64: Examining the Local States of an Entangled Bipartate Superposition
- 8.65: A Brief Introduction to the Quantum Computer
- 8.66: A Very Simple Example of Parallel Quantum Computation
- 8.67: Another Simple Example of Parallel Quantum Computation
- 8.68: A Simple Solution to Deutsch's Problem
- 8.69: Another Example of Deutsch's Algorithm
- 8.70: Evaluating a Function Using a Quantum Circuit and a Demonstration of Parallel Computation
- 8.71: A Simple Quantum Circuit for Parallel Computation
- 8.72: An Illustration of the Deutsch-Jozsa Algorithm
- 8.73: Another Illustration of the Deutsch-Jozsa Algorithm
- 8.74: Aspects of Simon's Algorithm
- 8.75: Qubit Quantum Mechanics
- 8.76: Implementation of Deutsch's Algorithm Using Mathcad
- 8.77: Using Quantum Gates to Create Superpositions and Entangled States
- 8.78: A Simple Quantum Computer
- 8.79: Solving Equations Using a Quantum Circuit
- 8.80: Introduction to Superdense Coding
- 8.81: A Brief Introduction to Quantum Dense Coding
- 8.82: The Discrete or Quantum Fourier Transform
- 8.83: Factoring Using Shor's Quantum Algorithm
- 8.84: Shor's Quantum Algorithm - A Summary
- 8.85: Simulating the Deutsch-Jozsa Algorithm with a Double-Slit Apparatus
- 8.86: Simulating a Quantum Computer with a Mach-Zehnder Interferometer
- 8.87: Quantum Restrictions on Cloning
- 8.88: Quantum Error Correction
- 8.89: Matrix Mechanics Analysis of the BB84 Key Distribution
- 8.90: 388. The Quantum Math Behind Ekert's Key Distribution Scheme
- 8.91: A Shorter Version of the Quantum Math Behind Ekert's Key Distribution Scheme
- 8.92: Quantum Key Distribution Using a Mach-Zehnder Interferometer

- 8.93: Coding and Decoding Venus
- 8.94: Grover's Quantum Search Algorithm
- 8.95: Grover's Search Algorithm- Implementation for Two Items
- 8.96: Grover's Search Algorithm- Four-Card Monte

9: Numerical Solutions for Schrödinger's Equation

- 9.1: Introduction to Numerical Solutions of Schödinger's Equation
- 9.2: Particle in an Infinite Potential Well
- 9.3: Particle in a Gravitational Field
- 9.4: Particle in a One-dimensional Egg Carton
- 9.5: Particle in a Finite Potential Well
- 9.6: Particle in a Semi-infinite Potential Well
- 9.7: Particle in a Slanted Well Potential
- 9.8: Numerical Solutions for a Particle in a V-Shaped Potential Well
- 9.9: Numerical Solutions for the Harmonic Oscillator
- 9.10: Numerical Solutions for a Double-Minimum Potential Well
- 9.11: Numerical Solutions for the Quartic Oscillator
- 9.12: Numerical Solutions for Morse Oscillator
- 9.13: Numerical Solutions for the Lennard-Jones Potential
- 9.14: Numerical Solutions for the Double Morse Potential
- 9.15: Particle in a Box with an Internal Barrier
- 9.16: Another Look at the in a Box with an Internal Barrier
- 9.17: Particle in a Box with Multiple Internal Barriers
- 9.18: Particle in an Infinite Spherical Potential Well
- 9.19: Numerical Solutions for the Two-Dimensional Harmonic Oscillator
- 9.20: Numerical Solutions for the Three-Dimensional Harmonic Oscillator
- 9.21: Numerical Solutions for the Hydrogen Atom Radial Equation
- 9.22: Numerical Solutions for a Modified Harmonic Potential

10: Approximate Quantum Mechanical Methods

- 10.1: Trial Wavefunctions for Various Potentials
- 10.2: Energy Minimization - Four Methods Using Mathcad
- 10.3: The Variation Theorem in Dirac Notation
- 10.4: A Rudimentary Model for Alpha Particle Decay
- 10.5: Variational Method for a Particle in a Finite Potential Well
- 10.6: Variation Method for a Particle in a Symmetric 1D Potential Well
- 10.7: Variation Method for the Rydberg Potential
- 10.8: Variation Method for the Quartic Oscillator
- 10.9: Momentum-Space Variation Method for the Quartic Oscillator
- 10.10: Variation Method for a Particle in a Gravitational Field
- 10.11: Linear Variational Method for a Particle in a Slanted 1D Box
- 10.12: Variation Method for a Particle in a Semi-Infinite Potential Well
- 10.13: Variation Method for a Particle in a Box with an Internal Barrier
- 10.14: Variation Method for a Particle in a 1D Ice Cream Cone
- 10.15: Variation Method for a Particle in an Ice Cream Cone
- 10.16: Variation Method for a Particle in a Finite 3D Spherical Potential Well
- 10.17: Variation Method for the Harmonic Oscillator
- 10.18: Trigonometric Trial Wave Function for the Harmonic Potential Well
- 10.19: Trigonometric Trial Wave Function for the 3D Harmonic Potential Well

- 10.20: Gaussian Trial Wavefunction for the Hydrogen Atom
- 10.21: Variation Calculation on the 1D Hydrogen Atom Using a Trigonometric Trial Wave Function
- 10.22: Variation Calculation on the 1D Hydrogen Atom Using a Gaussian Trial Wavefunction
- 10.23: Variational Calculation on the Two-dimensional Hydrogen Atom
- 10.24: Variational Calculation on Helium Using a Hydrogenic Wavefunction
- 10.25: Gaussian Trial Wave Function for the Helium Atom
- 10.26: Trigonometric Trial Wavefunction for the Helium Atom
- 10.27: Trigonometric Trial Wavefunction for the Hydrogen Atom
- 10.28: Hydrogen Atom Calculation Assuming the Electron is a Particle in a Sphere of Radius R
- 10.29: Electronic Structure - Variational Calculations on the Lithium Atom
- 10.30: The Variation Method in Momentum Space
- 10.31: Momentum-Space Variation Method for Particle in a Gravitational Field
- 10.32: Momentum-Space Variation Method for the Abs(x) Potential
- 10.33: Variational Method for the Feshbach Potential
- 10.34: Numerical Solution for the Feshbach Potential
- 10.35: First Order Degenerate Perturbation Theory - the Stark Effect of the Hydrogen Atom
- 10.36: Variational Calculation for the Polarizability of the Hydrogen Atom
- 10.37: Hybrid Variational Calculation for the 1D Hydrogen Atom with Delta Function Potential
- 10.38: Variation Method Using the Wigner Function- Finite Potential Well
- 10.39: 455. Variation Method Using the Wigner Function- V(x) = |x|
- 10.40: Variation Method Using the Wigner Function- The Harmonic Oscillator
- 10.41: Variation Method Using the Wigner Function - The Quartic Oscillator
- 10.42: Variation Method Using the Wigner Function - The Feshbach Potential

11: Miscellaneous

- 11.1: The Art of Science
- 11.2: Mass-Energy Equivalence
- 11.3: Commentary on “Probing the Orbital Energy of an Electron in an Atom”
- 11.4: The Use of Models in Introductory Chemistry
- 11.5: Reaction to Gillespie's Six Great Ideas in Chemistry - Another Great Idea
- 11.6: An Alternative Derivation of Gas Pressure Using the Kinetic Theory
- 11.7: Examining Fourier Synthesis with Dirac Notation
- 11.8: Finding Roots of Transcendental Equations
- 11.9: Calculation of the Composition of a Weak Polyprotic Acid Using Mathcad
- 11.10: Solving Linear Equations Using Mathcad
- 11.11: Let's Teach High School Students Computer Algebra Methods
- 11.12: Thermodynamics and Kinetics
- 11.13: Simple Kinetic Derivations of Thermodynamic Relations
- 11.14: The Global Approach to Thermodynamics
- 11.15: Global Thermodynamic Analyses of Heat Engines
- 11.16: Using Charles' Law to Determine Absolute Zero
- 11.17: The Origin of KE = 3/2 RT
- 11.18: Cosmic Background Radiation
- 11.19: Age of the Elements

Index

Glossary

Detailed Licensing

Licensing

*A detailed breakdown of this resource's licensing can be found in **Back Matter/Detailed Licensing**.*

CHAPTER OVERVIEW

1: Quantum Fundamentals

1.1: An Approach to Quantum Mechanics
1.2: Atomic and Molecular Stability
1.3: Atomic and Molecular Stability
1.4: Atomic and Molecular Stability
1.5: Quantum Computation - A Short Course
1.6: Quantum Computation- A Short Course
1.7: Quantum Computation- A Short Course
1.8: Quantum Computation- A Short Course
1.9: Quantum Computation- A Short Course
1.10: Quantum Computation- A Short Course
1.100: Analysis of the Stern-Gerlach Experiment
1.101: Related Analysis of the Stern-Gerlach Experiment
1.103: Bloch Sphere
1.104: 88. Related Analysis of the Stern-Gerlach Experiment
1.105: Bill the Cat and the Superposition Principle
1.106: Schroedinger's Dog
1.107: The Bloch Sphere
1.108: Density Matrix, Bloch Vector and Entropy
1.109: State Vectors and State Operators- Superpositions, Mixed States, and Entanglement
1.11: Quantum Computation- A Short Course
1.110: The Gram-Schmidt Procedure
1.12: Quantum Computation- A Short Course
1.13: Quantum Mechanics and the Fourier Transform
1.14: Quantum Mechanics and the Fourier Transform
1.15: Quantum Mechanics and the Fourier Transform
1.16: Quantum Mechanics and the Fourier Transform
1.17: Quantum Mechanics and the Fourier Transform
1.18: Exploring the Origin of Schrödinger’s Equations
1.19: Basic Quantum Mechanics in Coordinate, Momentum and Phase Space
1.20: The Repackaging of Quantum Weirdness
1.21: Quantum Principles Illuminated with Polarized Light
1.22: Relationship Between the Coordinate and Momentum Representations
1.23: Very Brief Relationship Between the Coordinate and Momentum Representations
1.24: Getting Accustomed to the Superposition Principle
1.25: The Dirac Delta Function
1.26: Elements of Dirac Notation
1.27: The Dirac Notation Applied to Variational Calculations
1.28: Raising and Lowering; Creating and Annihilating
1.29: Single Slit Diffraction and the Fourier Transform
1.30: From Coordinate Space to Momentum Space and Back

1.31: The Position and Momentum Commutation Relation in Coordinate and Momentum Space
1.32: Simulating the Aharonov-Bohm Effect
1.33: Basic Matrix Mechanics
1.34: Rudimentary Matrix Mechanics
1.35: Matrix Mechanics
1.36: Aspects of Dirac′s Relativistic Matrix Mechanics
1.37: The Double-Slit Experiment
1.38: Double-Slit Experiment with Polarized Light
1.39: The Consequences of Path Information in a Mach-Zehnder Interferometer
1.40: Another look at the Consequences of Path Information in a Mach-Zehnder Interferometer
1.41: The Double-Slit Experiment with Polarized Light
1.42: The Quantum Eraser
1.43: Which Way Did It Go? - The Quantum Eraser
1.44: Which Path Information and the Quantum Eraser
1.45: Terse Analysis of Triple-slit Diffraction with a Quantum Eraser
1.46: Which Path Information and the Quantum Eraser (Brief)
1.47: Terse Analysis of Triple-slit Diffraction with a Quantum Eraser
1.48: Which-way Markers and Post-selection in the Double-slit Experiment
1.49: A Stern-Gerlach Quantum ″Eraser″
1.50: Using the Mach-Zehnder Interferometer to Illustrate the Impact of Which-way Information
1.51: Quantum Theory, Wave-Particle Duality and the Mach-Zehnder Interferometer
1.52: Analysis of a Temporal Double-slit Experiment
1.53: An Analysis of Three-Path Interference
1.54: An Analysis of Three-Slit Interference
1.55: Using a Mach-Zehnder Interferometer to Illustrate Feynman's Sum Over Histories Approach to Quantum Mechanics
1.56: The Paradox of Recombined Beams
1.57: Evidence for Quantized Gravitational States of the Neutron
1.58: Quantized Gravitational States A Variational Approach
1.59: The Quantum Bouncer Doesn′t Bounce, Unless...
1.60: Kinetic Energy Is Important in the Nanoscale World
1.61: Energy Expectation Values and the Origin of the Variation Principle
1.62: Examining the Wigner Distribution Using Dirac Notation
1.63: The Wigner Function for the Single Slit Diffraction Problem
1.64: Wigner Distribution for the Double Slit Experiment
1.65: Wigner Distribution for the Triple Slit Experiment
1.66: Wigner Distribution for the Quadruple Slit Experiment
1.67: Quantum Tunneling in Coordinate, Momentum and Phase Space
1.68: Another Look at the Wigner Function
1.69: The Wigner Distribution Function for the Harmonic Oscillator
1.70: Wigner Distribution for the Particle in a Box
1.71: The Wigner Distribution for a Particle in a One-dimensional Box
1.72: Superposition vs. Mixture
1.73: Time-dependent Wigner Function for Harmonic Oscillator Transitions
1.74: Momentum Operator in Coordinate Space
1.75: Momentum Wave Functions for the Particle in a Box

1.76: A Graphical Illustration of the Heisenberg Uncertainty Relationship
1.77: The Quantum Harmonic Oscillator
1.78: Coherent Superpositions for the Harmonic Oscillator
1.79: The Harmonic Oscillator and the Uncertainty Principle
1.80: Another view of the Harmonic Oscillator and the Uncertainty Principle
1.81: Hydrogen Atom and Helium Ion Spatial and Momentum Distribution Functions Illustrate the Uncertainty Principle
1.82: The Position-Momentum Uncertainty Relation in the Hydrogen Atom
1.83: Demonstrating the Uncertainty Priniciple for Angular Momentum and Angular Position
1.84: A Brief Tutorial on Wavepackets
1.85: The Difference Between Fermions and Bosons
1.86: Quantum Corrals - Electrons within a Ring
1.87: Planck's Radiation Equation Fit to Experimental Data
1.88: Planck's Radiation Equation Fit to Experimental Data - Another Algorithm
1.89: Fitting Einstein's Heat Capacity Equation to Experimental Data for Silver
1.90: Einstein's Heat Capacity Equation Fit to Experimental Data - Another Algorithm
1.91: Fitting Debye's Heat Capacity Equation to Experimental Data for Silver
1.92: Debye's Heat Capacity Equation Fit to Experimental Data - Another Algorithm
1.93: Wave-particle Duality and the Uncertainty Principle
1.94: Wave-Particle Duality for Matter and Light
1.95: What Part of the Quantum Theory Don’t You Understand?
1.96: Quantum Potpourri - An Attempt to Demonstrate Two Fundamental Quantum Concepts- Wave-particle Duality and The Superposition Principle
1.97: Quantum Dynamics- One Step at a Time
1.98: Quantum Mechanical Pressure
1.99: Visualizing the Difference Between a Superposition and a Mixture

---

This page titled 1: Quantum Fundamentals is shared under a CC BY 4.0 license and was authored, remixed, and/or curated by Frank Rioux via source content that was edited to the style and standards of the LibreTexts platform.

1.1: An Approach to Quantum Mechanics

The purpose of this tutorial is to introduce the basics of quantum mechanics using Dirac bracket notation while working in one dimension. Dirac notation is a succinct and powerful language for expressing quantum mechanical principles; restricting attention to one-dimensional examples reduces the possibility that mathematical complexity will stand in the way of understanding. A number of texts make extensive use of Dirac notation (1-5).

Wave-particle duality is the essential concept of quantum mechanics. DeBroglie expressed this idea mathematically as $\lambda = h/m\nu = h/p$. On the left is the wave property λ, and on the right the particle property mν, momentum. The most general coordinate space wavefunction for a free particle with wavelength λ is the complex Euler function shown below.

$$\langle x|\lambda\rangle = \exp\left(i2\pi\frac{x}{\lambda}\right) = \cos\left(2\pi\frac{x}{\lambda}\right) + i\sin\left(2\pi\frac{x}{\lambda}\right) \tag{1.1.1}$$

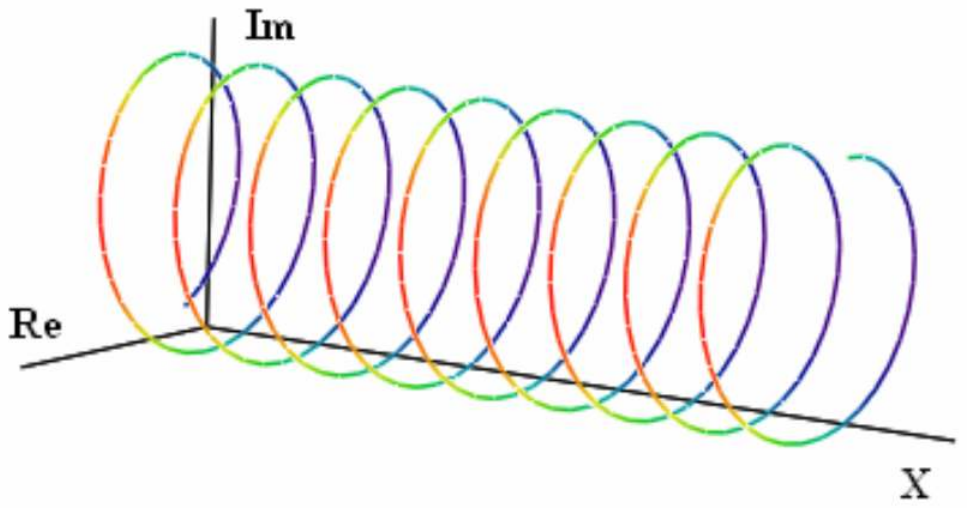
Feynman called this equation “the most remarkable formula in mathematics.” He referred to it as “our jewel.” A nd indeed it is, because when it is enriched with de Broglie’s relation it serves as the foundation of quantum mechanics.

According to de Broglie=s hypothesis, a particle with a well-defined wavelength also has a well-defined momentum. Therefore, we can obtain the momentum wavefunction (unnormalized) of the particle in coordinate space by substituting the deBroglie relation into Equation 1.1.1.

$$\langle x|p\rangle = \exp\left(\frac{ipx}{\hbar}\right) \tag{1.1.2}$$

When Equation 1.1.2 is graphed it creates a helix about the axis of propagation (X-axis). Z is the imaginary axis and Y is the real axis. It is the simplest example of a fourier transform, translating momentum into coordinate language. It also has in it the heart of the uncertainty principle.

Everyday examples of this important mathematical formula include telephone cords, spiral notebooks and slinkies.



Quantum mechanics teaches that the wavefunction contains all the physical information about a system that can be known, and that one extracts information from the wavefunction using quantum mechanical operators. There is, therefore, an operator for each observable property.

For example, in momentum space if a particle has a well-defined momentum we write its state as $|p\rangle$. If we operate on this state with the momentum operator $\hat{p}$, the following eigenvalue equation is satisfied.

$$\hat{p}|p\rangle = p|p\rangle \tag{1.1.3}$$

We say the system is in a state which is an eigenfunction of the momentum operator with eigenvalue p. In other words, operating on the momentum eigenfunction with the momentum operator, in momentum space, returns the momentum eigenvalue times the original momentum eigenfunction. From

$$\langle p|\hat{p}|p\rangle = p\langle p|p\rangle \tag{1.1.4}$$

it follows that,

$$\langle p|\hat{p} = p\langle p| \tag{1.1.5}$$

Equations (3) and (5) show that in its own space the momentum operator is a multiplicative operator, and can operate either to the right on a ket, or to the left on a bra. The same is true of the position operator in coordinate space.

To obtain the momentum operator in coordinate space, equation (3) is projected onto coordinate space by operating on the left with $\langle x|$. After inserting equation (2) we have,

$$\langle x|\hat{p}|p\rangle = p\langle x|p\rangle = p\exp\left(\frac{ipx}{h}\right) = \frac{\hbar}{i}\frac{d}{dx}\exp\left(\frac{ipx}{\hbar}\right) = \frac{\hbar}{i}\frac{d}{dx}\langle x|p\rangle \tag{1.1.6}$$

Comparing the first and last terms reveals that

$$\langle x|\hat{p} = \frac{\hbar}{i}\frac{d}{dx}\langle x| \tag{1.1.7}$$

and that $\frac{\hbar}{i}\frac{d}{dx}\langle x|$ is the momentum operator in coordinate space.

The position wavefunction in momentum space is the complex conjugate of the momentum wavefunction coordinate space.

$$\langle p|x\rangle = \langle x|p\rangle^* = \exp\left(\frac{-ipx}{\hbar}\right) \tag{1.1.8}$$

Starting with the coordinate-space eigenvalue equation

$$\hat{x}|x\rangle = x|x\rangle \tag{1.1.9}$$

and using the same approach as with momentum, it is easy to show that

$$\langle x|\hat{x} = x\langle x| \tag{1.1.10}$$

$$\langle p|\hat{x} = -\frac{\hbar}{i}\frac{d}{dp}\langle p| \tag{1.1.11}$$

In summary, the two fundamental dynamical operators are position and momentum, and the two primary representations are coordinate space and momentum space. The results achieved thus far are shown in the following table.

	Coordinate Space	Momentum Space
position operator: $\hat{x}$	$x\langle x\|$	$-\frac{\hbar}{i}\frac{d}{dp}\langle p\|$
momentum operator: $\hat{p}$	$\frac{\hbar}{i}\frac{d}{dx}\langle x\|$	$p\langle p\|$

Other quantum mechanical operators can be constructed from $\hat{x}$ and $\hat{p}$ in the appropriate representation, position or momentum. To illustrate this, Schrödinger's equation for the one-dimensional harmonic oscillator will be set up in both coordinate and momentum space using the information in the table. Schrödinger's equation is the quantum mechanical energy eigenvalue equation, and for the harmonic oscillator it looks like this initially,

the information in the table. Schrödinger's equation is the quantum mechanical energy eigenvalue equation, and for the harmonic oscillator it looks like this initially,

$$\left[\frac{\hat{p}^2}{2m} + \frac{1}{2}k\hat{x}\right]|\Psi\rangle = E|\Psi\rangle \tag{1.1.12}$$

The term in brackets on the left is the classical energy written as an operator without a commitment to a representation (position or momentum) for the calculation.

Most often, chemists solve Schrödinger's equation in coordinate space. Therefore, to prepare Schrödinger's equation for solving, equation (12) is projected onto coordinate space by operating on the left with $\langle x|$.

$$\langle x|\left[\frac{\hat{p}^2}{2m}+\frac{1}{2}k\hat{x}\right]|\Psi\rangle=\langle x|E|\Psi\rangle \tag{1.1.13}$$

Using the information in the table this yields,

$$\left[-\frac{\hbar^2}{2m}\frac{d^2}{dx^2}+\frac{1}{2}kx^2\right]\langle x|\Psi\rangle=E\langle x|\Psi\rangle \tag{1.1.14}$$

The square bracket on the left contains the quantum mechanical energy operator in coordinate space. Before proceeding we illustrate how the kinetic energy operator emerges as a differential operator in coordinate space using equation (7).

$$\frac{1}{2m}\langle x|\hat{p}\hat{p}|\Psi\rangle=\frac{1}{2m}\frac{\hbar}{i}\frac{d}{dx}\langle x|\hat{p}|\Psi\rangle=\frac{1}{2m}\frac{\hbar}{i}\frac{d}{dx}\frac{\hbar}{i}\frac{d}{dx}\langle x|\Psi\rangle=-\frac{hbar^2}{2m}\frac{d^2}{dx^2}\langle x|\Psi\rangle \tag{1.1.15}$$

Equation (10) is used in a similar fashion to show that potential energy is a multiplicative operator in coordinate space.

$$\frac{1}{2}k\langle x|\hat{x}\hat{x}|\Psi\rangle=\frac{1}{2}kx\langle x|\hat{x}|\Psi\rangle=\frac{1}{2}kx^2\langle x|\Psi\rangle \tag{1.1.16}$$

Obviously the calculation could also have been set up in momentum space. It is easy to show that in the momentum representation Schrödinger=s equation is

$$\left[\frac{p^2}{2m}-\frac{\hbar^2k}{2}\frac{d^2}{dp^2}\right]\langle p|\Psi\rangle=E\langle p|\Psi\rangle \tag{1.1.17}$$

In momentum space the kinetic energy operator is multiplicative and the potential energy operator is differential. The one-dimensional simple harmonic oscillator problem is exactly soluble in both coordinate and momentum space. The solution can be found in any chemistry and physics text dealing with quantum mechanics, and will not be dealt with further here, other than to say that equations (14) and (17) reveal an appealing symmetry.

Unfortunately, for most applications the potential energy term in momentum space presents more of a mathematical challenge than it does for the harmonic oscillator problem. A general expression for the potential energy in the momentum representation when its form in the coordinate representation is specified is given below.

$$\langle p|\hat{V}|Psi\rangle=\int\int\exp\left[\frac{i(p'-p)x}{\hbar}\right]V(x)\langle p'|\Psi\rangle dp'dx \tag{1.1.18}$$

To see how this integral is handled for a specific case see reference (10).

If a system is in a state which is an eigenfunction of an operator, we say the system has a well-defined value for the observable associated with the operator, for example, position, momentum, energy, etc. Every time we measure we get the same result. However, if the system is in a state that is not an eigenfunction of the operator, for example, if $\hat{o}|\Psi\rangle=|\Phi\rangle$, the system does not have a well-defined value for the observable. Then the measurement results have a statistical character and each measurement gives an unpredictable result in spite of the fact that the system is in a well-defined state $|\Psi\rangle$. Under these circumstances, all we can do is calculate a mean value for the observable. This is unheard of in classical physics where, if a system is in a well-defined state, all its physical properties are precisely determined. In quantum mechanics a system can be in a state which has a well-defined energy, but its position and momentum are un-determined.

The quantum mechanical recipe for calculating the mean value of an observable is now derived. Consider a system in the state $|\Psi\rangle$, which is not an eigenfunction of the energy operator, $\hat{H}$. A statistically meaningful number of such states are available for the purpose of measuring the energy. Quantum mechanical principles require that an energy measurement must yield one of the energy eigenvalues, ϵ_i, of the energy operator. Therefore, the average value of the energy measurements is calculated as,

$$\langle E\rangle=\frac{\sum_i n_i\epsilon_i}{N} \tag{1.1.19}$$

where n_i is the number of times ϵ_i is observed, and N is the total number of measurements. Therefore, $p_i = n_i/N$, is the probability that ϵ_i is observed. Equation (19) becomes

$$\langle E\rangle=\sum_i p_i\epsilon_i \tag{1.1.20}$$

According to quantum mechanics, for a system in the state $|\Psi\rangle, p_i = \langle\Psi|i\rangle\langle i|\Psi\rangle$, where the $|i\rangle$ are the eigenfunctions of the energy operator. Equation (20) can now be re-written as,

$$\langle E\rangle = \sum_i \langle\Psi|i\rangle\langle i|\Psi\rangle\epsilon_i = \sum_i \langle\Psi|i\rangle\epsilon_i\langle i|\Psi\rangle \tag{1.1.21}$$

However, it is also true that

$$\hat{H}|i\rangle = \epsilon_i|i\rangle = |i\rangle\epsilon_i \tag{1.1.22}$$

Substitution of equation (22) into (21) yields

$$\langle E\rangle = \sum_i \langle\Psi|\hat{H}|i\rangle\langle i|\Psi\rangle \tag{1.1.23}$$

As eigenfunctions of the energy operator, the $|i\rangle$ form a complete basis set, making available the discrete completeness condition, $\sum_i |i\rangle\langle i| = 1$, the use of which in equation (23) yields

$$\langle E\rangle = \langle\Psi|\hat{H}|\Psi\rangle \tag{1.1.24}$$

This formalism is general and applies to any operator-observable pair. The average value for the observed property may always be calculated as,

$$\langle o\rangle = \langle\Psi|\hat{o}|\Psi\rangle \tag{1.1.25}$$

These principles are now applied to a very simple problem B the particle in a box. Schrödinger's equation in coordinate space,

$$-\frac{\hbar^2}{2m}\frac{d^2}{dx^2}\langle x|\Psi\rangle = E\langle x|\Psi\rangle \tag{1.1.26}$$

can be solved exactly, yielding the following eigenvalues and eigenfunctions,

$$E_n = \frac{n^2h^2}{8ma^2} \tag{1.1.27}$$

$$\langle x|\Psi_n\rangle = \sqrt{\frac{2}{a}}\sin\left(\frac{n\pi x}{a}\right) \tag{1.1.28}$$

where a is the box dimension, m is the particle mass, and n is a quantum number restricted to integer values starting with 1.

Substitution of equation (28) into (26) confirms that it is an eigenfunction with the manifold of allowed eigenvalues given by equation (27). However, equation (28) is not an eigenfunction of either the position or momentum operators, as is shown below.

$$\langle x|\hat{x}|\Psi_n\rangle = x\langle x|\Psi_n\rangle = x\sqrt{2}a\sin\left(\frac{n\pi x}{a}\right) \tag{1.1.29}$$

$$\langle x|\hat{p}|\Psi_n\rangle = \frac{\hbar}{i}\frac{d}{dx}\langle x|\Psi_n\rangle = \frac{n\pi}{a}\sqrt{2}a\cos\left(\frac{n\pi x}{a}\right) \tag{1.1.30}$$

To summarize, the particle in a box has a well-defined energy, but the same is not true for its position or momentum. In other words, it is not buzzing around the box executing a classical trajectory. The outcome of an energy measurement is certain, but position and momentum measurements are uncertain. All we can do is calculate the expectation value for these observables and compare the calculations to the mean values found through a statistically meaningful number of measurements.

Next we set up the calculation for the expectation value for position utilizing the recipe expressed in equation (25).

$$\langle x\rangle_n = \langle\Psi_n|\hat{x}|\Psi_n\rangle \tag{1.1.31}$$

Evaluation of (31) in coordinate space requires the continuous completeness condition.

$$\int_0^a |x\rangle\langle x|dx = 1 \tag{1.1.32}$$

Substitution of (32) into (31) gives

$$\langle x\rangle_n = \int_0^a \langle \Psi_n|x\rangle\langle x|\hat{x}|\Psi_n\rangle dx = \int_0^a \langle \Psi_n|x\rangle x\langle x|\Psi_n\rangle dx = \frac{a}{2} \tag{1.1.33}$$

The expectation value for momentum is calculated in a similar fashion,

$$\langle p\rangle_n = \int_0^a \langle \Psi_n|x\rangle\langle x|\hat{p}|\Psi_n\rangle dx = \int_0^a \langle \Psi_n|x\rangle \frac{\hbar}{i}\frac{d}{dx}\langle x|\Psi_n\rangle dx = 0 \tag{1.1.34}$$

In other words, the expectation values for position and momentum are the same for all the allowed quantum states of the particle in a box.

It is now necessary to explore the meaning of $\langle x|\Psi\rangle$. It is the probability amplitude that a system in the state $|\Psi\rangle$, will be found at position x. $|\langle x|\Psi\rangle|^2$ or $\langle\Psi|x\rangle\langle x|\Psi\rangle$, is the probability density that a system in the state $|\Psi\rangle$ will be found at position x. Thus equation (28) is an algorithm for calculating probability amplitudes and probability densities for the position of the particle in a one-dimensional box. This, of course, is true only if $|\Psi\rangle$ is normalized.

$$\langle\Psi|\Psi\rangle = \int_0^a \langle\Psi|x\rangle\langle x|\Psi\rangle dx = 1 \tag{1.1.35}$$

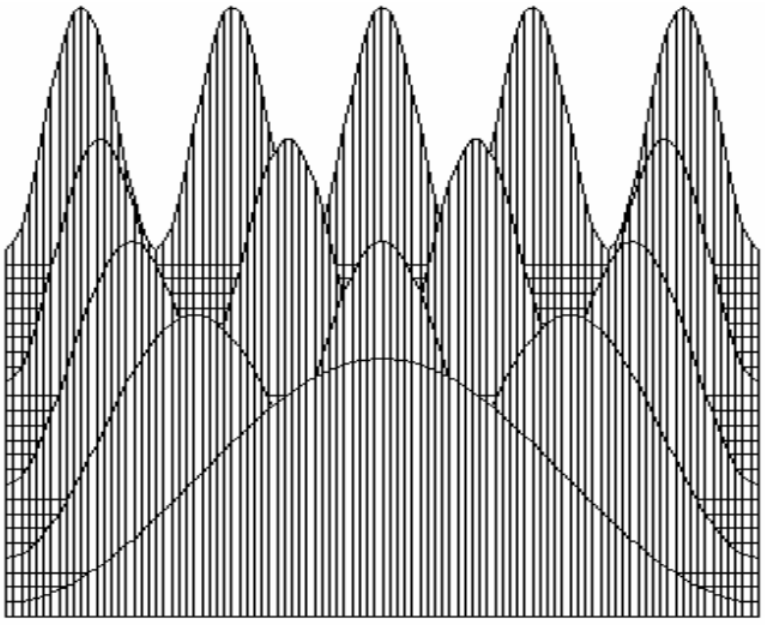
There are two ways to arrive at the integral in equation (34). One can insert the continuous completeness relation (32) at the | on the left side, or, equivalently one can express $|\Psi\rangle$, as a linear superposition in the continuous basis set x,

$$|\Psi\rangle = \int_0^a |x\rangle\langle x|\Psi\rangle dx \tag{1.1.36}$$

and projecting this expression onto $\langle\Psi|$.

A quantum particle is described by its wavefunction rather than by its instantaneous position and velocity; a confined quantum particle, such as a particle in a box, is not moving in any classical sense, and must be considered to be present at all points in space, properly weighted by $|\langle x|\Psi\rangle|^2$.

Thus, $\langle x|\Psi\rangle$ allows us to examine the coordinate space probability distribution and to calculate expectation values for observables such as was done in equations (33) and (34). Plots of $|\langle x|\Psi_n\rangle|^2$ show that the particle is distributed symmetrically in the box, and $\langle x|\Psi_n\rangle$, allows us to calculate the probability of finding the particle anywhere inside the box.



Position_Distribution

The coordinate-space wavefunction does not say much about momentum, other than its average value is zero (see equation 34). However, a momentum-space wavefunction, $\langle p|\Psi\rangle$, can be generated by a Fourier transform of $\langle x|\Psi\rangle$. This is accomplished by

projecting equation (36) onto momentum space by multiplication on the left by $\langle p|$.

$$\langle p|\Psi_n\rangle = \int_0^a \langle p|x\rangle\langle x|\Psi_n\rangle dx = \frac{1}{\sqrt{2\pi\hbar}}\int_0^a \exp\left(-\frac{ipx}{\hbar}\right)\sqrt{\frac{2}{a}}\sin\left(\frac{n\pi x}{a}\right)dx \tag{1.1.37}$$

The term preceding the integral is the normalization constant (previously ignored) for the momentum wavefunction. Evaluation of the integral on the right side yields,

$$\langle p|\Psi_n\rangle = n\sqrt{a\pi\hbar^3}\left[\frac{1-\cos(n\pi)\exp(-\frac{ipa}{\hbar})}{n^2\pi^2\hbar^2 - a^2p^2}\right] \tag{1.1.38}$$

Now with the continuous completeness relationship for momentum,

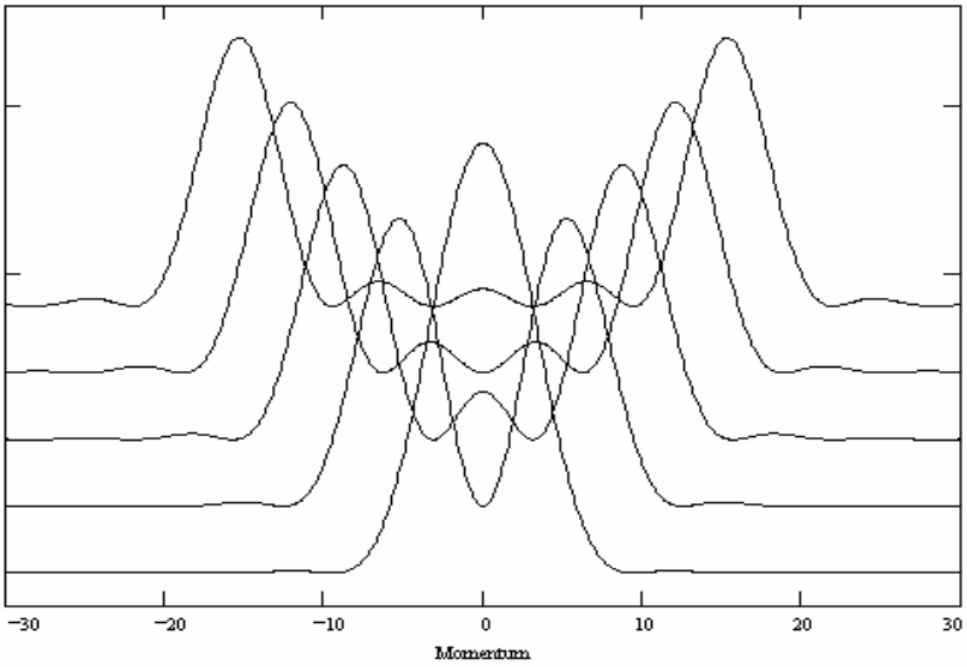
$$\int_{-\infty}^{\infty} |p\rangle\langle p|dp = 1 \tag{1.1.39}$$

one can re-calculate $\langle x\rangle_n$ and $\langle p\rangle_n$ in momentum space.

$$\langle x\rangle_n = \int_{-\infty}^{\infty}\langle\Psi_n|p\rangle\langle p|\hat{x}|\Psi_n\rangle dp = \int_{-\infty}^{\infty}\langle\Psi_n|p\rangle\frac{-\hbar}{i}\frac{d}{dp}\langle p|\Psi_n\rangle dp = \frac{a}{2} \tag{1.1.40}$$

$$\langle p\rangle_n = \int_{-\infty}^{\infty}\langle\Psi_n|\hat{p}|p\rangle\langle p|\Psi_n\rangle dp = \int_{-\infty}^{\infty}\langle\Psi_n|p\rangle p\langle p|\Psi_n\rangle dp = 0 \tag{1.1.41}$$

It is clear that $\langle x|\Psi_n\rangle$ and $\langle p|\Psi_n\rangle$ contain the same information; they just present it in different languages (representations). The coordinate space distribution functions for the particle in a box shown above are familiar to anyone who has studied quantum theory, however, because chemists work mainly in coordinate space, the momentum distributions are not so well known. A graphical representation of $|\langle p|\Psi_n\rangle|^2$ for the first five momentum states is shown below. The distribution functions are offset by small increments for clarity of presentation.



As just shown, the particle in a box can be used to illustrate many fundamental quantum mechanical concepts. To demonstrate that some systems can be analyzed without solving Schrödinger's equation we will briefly consider the particle on a ring. This model has been used to study the behavior of the π-electrons of benzene.

In order to satisfy the requirement of being single-valued, the momentum wavefunction in coordinate space for a particle on a ring of radius R must satisfy the following condition,

$$\langle x + 2\pi R|p\rangle = \langle x|p\rangle \tag{1.1.42}$$

This leads to,

$$\exp\left(\frac{i2\pi Rp}{\hbar}\right)\exp\left(\frac{ipx}{\hbar}\right)=\exp\left(\frac{ipx}{\hbar}\right) \tag{1.1.43}$$

This equation can be written as,

$$\exp\left(\frac{i2piRp}{\hbar}\right)=1=\exp(i2\pi m)\quad where\ m=0,\pm1,\pm2,... \tag{1.1.44}$$

Comparison of the left with the far right of this equation reveals that,

$$\frac{Rp}{\hbar}=m \tag{1.1.45}$$

It is easy to show that the energy manifold associated with this quantum restriction is,

$$E_m=m^2\left(\frac{\hbar^2}{2m_eR^2}\right) \tag{1.1.46}$$

The corresponding wavefunctions can be found in the widely used textbook authored by Atkins and de Paula (11).

There are, of course, many formulations of quantum mechanics, and all of them develop quantum mechanical principles in different ways from diverse starting points, but they are all formally equivalent. In the present approach the key concepts are de Broglie's hypothesis as stated in equation (2), and the eigenvalue equations (3) and (9) expressed in the momentum and coordinate representations, respectively.

Another formulation (Heisenberg's approach) identifies the commutation relation of equation (47) as the basis of quantum theory, and adopts operators for position and momentum that satisfy the equation.

$$[\hat{p},\hat{x}]=\hat{p}\hat{x}-\hat{x}\hat{p}=\frac{\hbar}{i} \tag{1.1.47}$$

Equation (47) can be confirmed in both coordinate and momentum space for any state function $|\Psi\rangle$ using the operators in the table above.

$$\langle x|(\hat{p}\hat{x}-\hat{x}\hat{p})|\Psi\rangle=\frac{\hbar}{i}\left(\frac{d}{dx}x-x\frac{d}{dx}\right)\langle x|\Psi\rangle=\frac{\hbar}{i}\langle x|\Psi\rangle \tag{1.1.48}$$

$$\langle p|(\hat{p}\hat{x}-\hat{x}\hat{p})|\Psi\rangle=i\hbar\left(p\frac{d}{dd}-\frac{d}{dp}p\right)\langle p|\Psi\rangle=\frac{\hbar}{i}\langle p|\Psi\rangle \tag{1.1.49}$$

The meaning associated with equations (48) and (49) is that the observables associated with non-commuting operators cannot simultaneously have well-defined values. This, of course, is just another statement of the uncertainty principle.

The famous double-slit experiment illustrates the uncertainty principle in a striking way. To illustrate this it is mathematically expedient to begin with infinitesimally thin slits. Later this restriction will be relaxed.

A screen with infinitesimally thin slits (6) at x_1 and x_2 projects the incident beam into a linear superposition of position eigenstates.

$$|\Psi\rangle=\frac{1}{\sqrt{2}}[|x_1\rangle+|x_2\rangle] \tag{1.1.50}$$

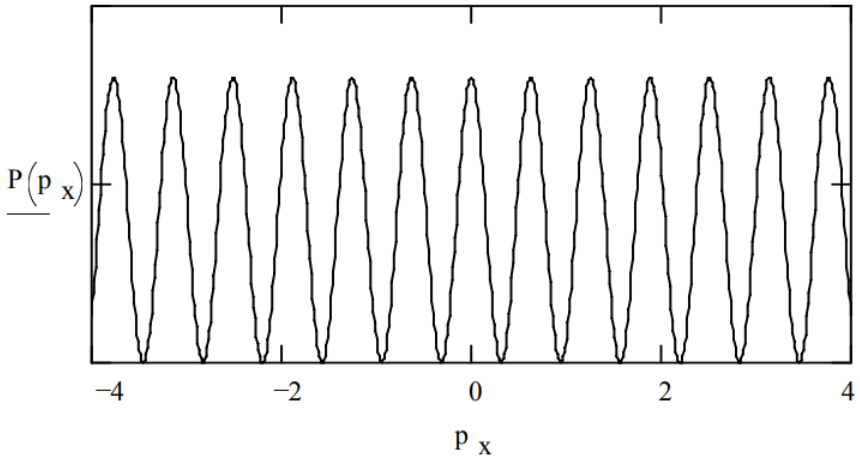
Expressing this state in the coordinate representation yields the following superposition of Dirac delta functions.

$$\langle x|\Psi\rangle=\frac{1}{\sqrt{2}}[\langle x|x_1\rangle+\langle x|x_2\rangle]=\frac{1}{\sqrt{2}}[\delta(x-x_1)+\delta(x-x_2)] \tag{1.1.51}$$

According to the uncertainty principle this localization of the incident beam in coordinate space is accompanied by a delocalization of the x-component of the momentum, p_x. This can be seen by projecting $|\Psi\rangle$ onto momentum space.

$$\langle p_x|\Psi\rangle=\frac{1}{\sqrt{2}}[\langle p_x|x_1\rangle+\langle p_x|x_2\rangle]=\frac{1}{2\sqrt{\pi\hbar}}\left[\exp\left(-\frac{ip_xx_1}{\hbar}\right)+\exp\left(-\frac{ip_xx_2}{\hbar}\right)\right] \tag{1.1.52}$$

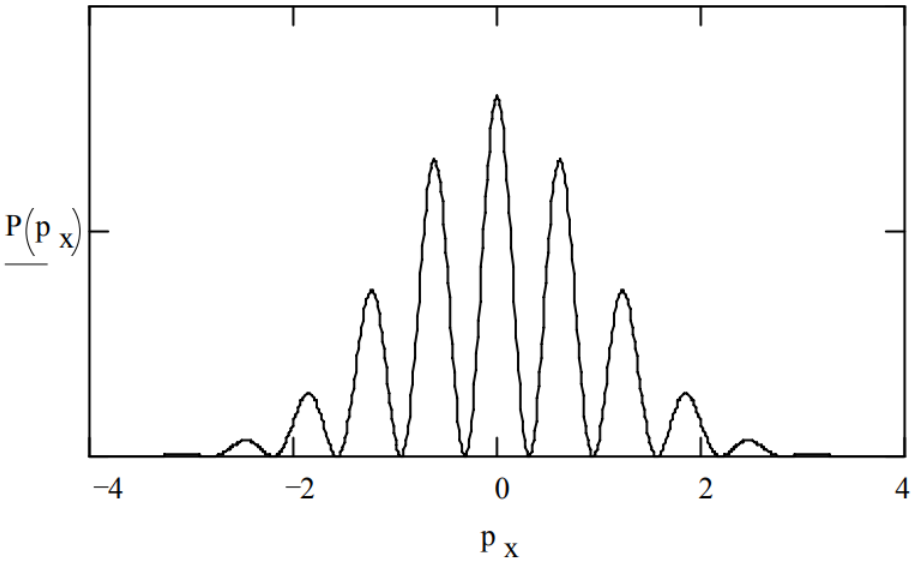
The momentum probability distribution in the x-direction, $P(p_x) = |\langle p_x|\Psi\rangle|^2$, reveals the required spread in momentum, plus the interesting interference pattern in the momentum distribution that will ultimately be projected onto the detection screen. As Marcella (6) points out the detection screen is actually measuring the x-component of the momentum.



Of course, in the actual experiment the slits are not infinitesimally thin and the diffraction pattern takes on the more familiar appearance reported in the literature (7) and textbooks (8). For example, a linear superposition of Gaussian functions can be used to represent the coordinate-space wavefunction at a screen with two slits of finite width.

$$\langle x|\Psi\rangle = \exp[-(x-x_1)^2] + \exp[-(x-x_2)^2] \tag{1.1.53}$$

The Fourier transform of this state into momentum space leads to the momentum distribution shown in the figure below (9).



The double-slit experiment reveals the three essential steps in a quantum mechanical experiment:

1. state preparation (interaction of incident beam with the slit-screen)
2. measurement of observable (arrival of scattered beam at the detection screen)
3. calculation of expected results of the measurement step

The Dirac delta function appeared in equation (51). It expresses the fact that the position eigenstates form a continuous orthogonal basis. The same, of course, is true for the momentum eigenstates.

The bracket $\langle x|x'\rangle$ is zero unless x = x′. This expresses the condition that an object at x′ is not at x. It is instructive to expand this bracket in the momentum representation.

$$\langle x|x'\rangle = \int_{-\infty}^{\infty} \langle x|p\rangle\langle p|x'\rangle dp = \frac{1}{2\pi\hbar}\int_{-\infty}^{\infty} \exp\left(\frac{ip(x-x')}{\hbar}\right) dp = \delta(x-x') \tag{1.1.54}$$

The same approach for momentum yields,

$$\langle p|p'\rangle = \int_{-\infty}^{\infty} \langle p|x\rangle\langle x|p'\rangle dx = \frac{1}{2\pi\hbar}\int_{-\infty}^{\infty} \exp\left(\frac{-i(p-p')x}{\hbar}\right) dx = \delta(p-p') \tag{1.1.55}$$

The Dirac delta function has great utility in quantum mechanics, so it is important to be able to recognize it in its several guises.

The time-dependent energy operator can be obtained by adding time dependence to equation (1) so that it represents a classical one-dimensional plane wave moving in the positive x-direction.

$$\langle x|\lambda\rangle\langle t|\nu\rangle = \exp\left(i2\pi\frac{x}{\lambda}\right)\exp(-i2\pi\nu t) \tag{1.1.56}$$

This classical wave equation is transformed into a quantum mechanical wavefunction by using (as earlier) the de Broglie relation and E = hν.

$$\langle x|p\rangle\langle t|E\rangle = \exp\left(\frac{ipx}{\hbar}\right)\exp\left(-\frac{iEt}{\hbar}\right) \tag{1.1.57}$$

From this equation we obtain the important Dirac bracket relating energy and time.

$$\langle t|E\rangle = \exp\left(-\frac{iEt}{\hbar}\right) \tag{1.1.58}$$

The time-dependent energy operator is found by projecting the energy eigenvalue equation,

$$\hat{H}|E\rangle = E|E\rangle \tag{1.1.59}$$

into the time domain.

$$\langle t|\hat{H}|E\rangle = E\langle t|E\rangle = E\exp\left(-\frac{iEt}{\hbar}\right) = i\hbar\frac{d\langle t|E\rangle}{dt} \tag{1.1.60}$$

Comparison of the first and last terms reveals that the time-dependent energy operator is

$$\langle t|\hat{H} = i\hbar\frac{d}{dt}\langle t| \tag{1.1.61}$$

We see also from equation (60) that

$$i\hbar\frac{d}{dt}\langle t| = E\langle t| \tag{1.1.62}$$

So that in general,

$$i\hbar\frac{d}{dt}\langle t|\Psi\rangle = E\langle t|\Psi\rangle \tag{1.1.63}$$

Integration of equation (63) yields a general expression for the time-dependence of the wavefunction.

$$\langle t|\Psi\rangle = \exp\left(-\frac{iE(t-t_0)}{\hbar}\right)\langle t_0|\Psi\rangle \tag{1.1.64}$$

References

1. Chester, M. *Primer of Quantum Mechanics*; Krieger Publishing Co.:Malabar, FL, 1992.
2. Das, A.; Melissinos, A. C. *Quantum Mechanics: A Modern Introduction*; Gordon and Breach Science Publishers: New York, 1986.
3. Feynman, R. P.; Leighton, R. B.; Sands, M. *The Feynman Lectures on Physics, Vol.3*; Addison-Wesley: Reading, 1965.
4. Martin, J. L. *Basic Quantum Mechanics*; Claredon Press, Oxford, 1981.
5. Townsend, J. S. *A Modern Approach to Quantum Mechanics*; University Science Books, Sausalito, 2000.
6. Marcella, T. V. "Quantum interference with slits," *European Journal of Physics* **23**, 615-621 (2002).

7. Tonomura A.; Endo, J.; Matsuda, T.; Kawasaki, T.; Ezawa, H. “Demonstration of single-electron buildup of an interference pattern,” *American Journal of Physics* **57**,117-120 (1989).
8. French, A. P.; Taylor, E. F. An Introduction to Quantum Physics; W. W. Norton & Co., Inc. New York, 1978.
9. For further detail visit: www.users.csbsju.edu/~frioux/...t/new-slit.htm. For different approach see: www.users.csbsju.edu/~frioux/...other2slit.pdf. A description of a recent example of a temporal double-slit is available at www.users.csbsju.edu/~frioux/...poral2slit.pdf.
10. Lieber, M. “Quantum mechanics in momentum space: An illustration,” *American Journal of Physics* **43**, 486-487 (1975).
11. Atkins, P.; de Paulo, J. Physical Chemistry; 7th ed. W. H. Freeman & Co., New York, 2002, p. 347.

Contributors and Attributions

- Prof. Emeritus Frank Rioux (St. John's University and College of St. Benedict)

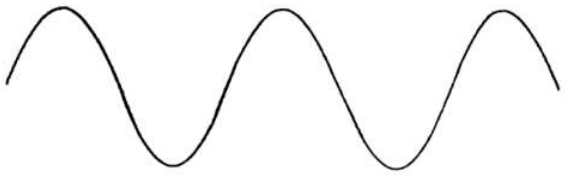
This page titled 1.1: An Approach to Quantum Mechanics is shared under a CC BY 4.0 license and was authored, remixed, and/or curated by Frank Rioux via source content that was edited to the style and standards of the LibreTexts platform.

1.2: Atomic and Molecular Stability

Klaus Ruedenberg once wrote that there are no ground states in classical mechanics. In other words, quantum principles are required to understand the stability of atoms and molecules, and the nature of the chemical bond. Quantum mechanics is not mathematically more difficult than classical physics, the real challenge it offers is of a conceptual nature. That's because it says that understanding the stability of matter requires that it possess both particle and wave properties. The conceptual challenge is that particle and wave are contradictory concepts.

Wave-Particle Duality for Matter and Light

A wave is spatially delocalized



A particle is spatially localized

•

These incompatible concepts are united by the deBroglie wave equation with the wave property (wavelength) on the left and the particle property (momentum) on the right in a reciprocal relationship mediated by the ubiquitous Planck's constant.

$$\lambda = \frac{h}{m\nu}$$

Investing matter with wave behavior subjects it to interference effects and leads immediately to a redefinition of kinetic energy. In quantum mechanics the concept kinetic energy should be replaced with confinement energy, because the former implies classical motion. According to quantum mechanical principles a confined particle, a **quon**, because of its wave-like character is described by a wave function which is a weighted superposition of all possible positions. Quons do not execute trajectories in the classical sense. They are not here and later there; they are here and there simultaneously. As Werner Heisenberg said, "There is no space-time inside the atom." In other words there is also no space-time for confined quons.

"A quon is any entity (electron, proton, neutron, atom, molecule, C60 etc.), no matter how immense, that exhibits both wave and particle aspects in the peculiar quantum manner." Nick Herbert, Quantum Reality, page 64. The following tutorial outlines the origin of de Broglie's wave hypothesis for matter and how it transforms classical kinetic energy into quantum mechanical confinement energy.

Wave-Particle Duality

Wave-particle duality as expressed in the de Broglie equation is the foundational concept of quantum theory. The mathematical form of de Broglie's equation is derived for the photon. It is subsequently assumed that it applies also to matter.

The momentum of a photon is inversely proportional to its wavelength. The derivation begins with Einstein's mass-energy equation which applies in general.

$$E = mc^2 \xrightarrow[E=h\nu]{p=mc} pc = h\nu \xrightarrow{c=\nu\lambda} p = \frac{h}{\lambda}$$

De Broglie postulated that this expression involving the particle property momentum and the wave property wavelength also applies to matter. Therefore the wavelength of a particle is inversely proportional to its momentum. This is the origin of wave-particle duality.

$$\lambda = \frac{h}{m\nu} = \frac{h}{p}$$

A wave is spatially delocalized. A particle is spatially localized. These incompatible concepts are united by the de Broglie equation with the wave property (wavelength) on the left and the particle property (momentum) on the right in a reciprocal relationship mediated by the ubiquitous Planck's constant.

The de Broglie equation is a dictionary for translating classical kinetic energy into quantum language. The quantum equivalent of kinetic energy should be called confinement energy because there is no motion; a particle confined to a circular orbit, as in the Bohr model of the hydrogen atom, is in a stationary state. Restrictions are placed on the particle's wavelength ($n\lambda = 2\pi R$) in order to avoid self-interference.

$$T = \frac{p^2}{2m} \xrightarrow{p=\frac{h}{\lambda}} \frac{h^2}{2m\lambda^2} \xrightarrow[n\lambda=2\pi R^2]{confinement} \frac{n^2h^2}{8\pi^2mR^2}$$

We always measure particles (detectors click, photographic film is darkened, etc.), but we interpret what happened or predict what will happen by assuming wavelike behavior. In other words, quantum particles exhibit both wave and particle properties in every experiment. To paraphrase Nick Herbert (Quantum Reality), particles are always detected, but the experimental results observed are the result of wavelike behavior.

In *The Character of Physical Law* Feynman described wave-particle duality as follows, "I will summarize, then, by saying that electrons arrive in lumps, like particles, but the probability of arrival of these lumps is determined as the intensity of waves would be. It is in this sense that the electron behaves sometimes like a particle and sometimes like a wave. It behaves in two different ways at the same time." Lawrence Bragg summarized wave-particle behavior saying, "Everything in the future is a wave, everything in the past is a particle."

In his 1951 treatise *Quantum Theory*, David Bohm described wave-particle duality as follows: "One of the characteristic features of quantum theory is wave-particle duality, i.e. the ability of matter or light quanta to demonstrate the wave-like property of interference, and yet to appear subsequently in the form of localizable particles, even after such interference has taken place." In other words, to explain interference phenomena wave properties must be assigned to matter and light quanta prior to detection as particles.

Whenever it is measured the world seems particle-like, but the pattern formed by these particles leads to the conclusion that between measurements the world acts like a wave.

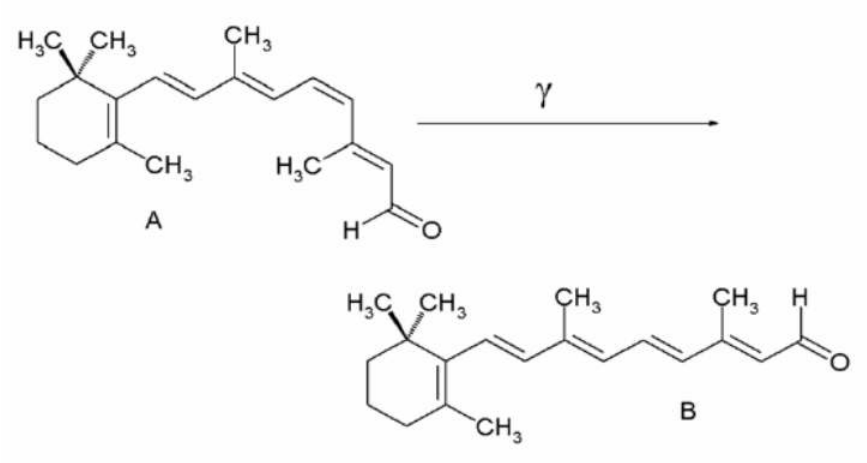
Nothing but particles are ever detected, but the pattern of these (detected) particles must have been caused by some sort of wave - the form light seems to take when it is not being measured.

The following three-slide power-point presentation attempts to provide a concrete illustration of the ideas presented above by Feynman, Bohm, Bragg and Herbert by examining single-slit diffraction through the lense of wave-particle duality.

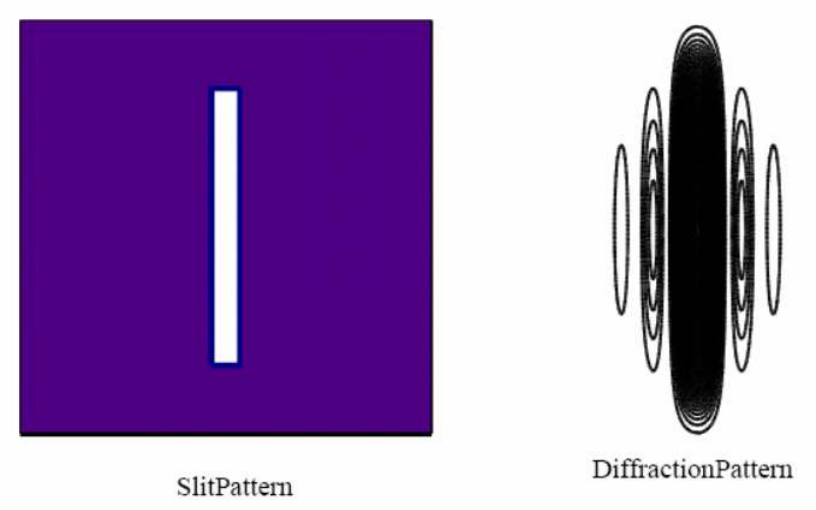
Wave-particle Duality Illustrated

- Source emits light
- When viewed through a narrow slit interference fringes are observed, the signature of wave-like behavior.
- However, the detector (eye) registers particles (retinal absorbs a photon and changes shape ultimately causing a signal to be sent to the brain via the optic nerve)
- We detect particles, but we predict what will happen, or interpret what happened, by assuming wave-like behavior
- “Everything in the future is a wave, everything in the past is a particle.” Lawrence Bragg

Retinal Absorbs a Photon



Single-slit Diffraction



The double-slit diffraction experiment provides an even more dramatic illustration of wave-particle duality in action. Richard Feynman once said that if anyone asks you a question about quantum mechanics, you can always reply "You remember the experiment with the two slits? It's the same thing."

Regarding the double-slit experiment, Feynman also wrote "We choose to examine a phenomenon which is impossible, *absolutely* impossible, to explain in any classical way, and which has in it the heart of quantum mechanics. In reality, it contains the *only* mystery. We cannot make the mystery go away by 'explaining' how it works. We will just *tell* you how it works. In telling you how it works we will have told you about the basic peculiarities of all quantum mechanics.

The stabilities of hydrogen and helium, the most abundant elements in the universe, are now explained using rudimentary quantum principles.

Atomic Stability

Neils Bohr once observed that from the perspective of classical physics the stability of matter was a pure miracle. The problem, of course, is that two of the basic building blocks of matter are oppositely charged - the electron and the proton.Given Coulomb's Law the troubling question is what keeps them from coalescing?

Quantum mechanics is considered by many to be an abstract and esoteric science that doesn't have much to do with everyday life. Yet it provides an explanation for atomic and molecular stability, and classical physics fails at that task. Thus, to achieve some understanding of one of the basic facts about the macro-world requires quantum mechanical concepts and tools.

The issue of atomic stability will be explored with a quantum mechanical analysis of the two simplest elements in the periodic table - hydrogen and helium. They are also the two most abundant elements in the universe. Schrödinger's equation can be solved exactly for the hydrogen atom, but approximate methods are required for the helium atom. In this study, the variational method will be used for both hydrogen and helium.

Variational Method for the Hydrogen Atom

Normalized trial wave function:

$$\Psi(\alpha, r) := \sqrt{\frac{\alpha^3}{\pi}} \cdot \exp(-\alpha \cdot r)$$

where α is a scale-factor that controls the size of the wave function.

Integral:

$$\int_0^\infty \square \cdot 4\pi r^2 \, dr$$

Kinetic energy operator:

$$-\frac{1}{2r}\frac{d^2}{dr^2}(r \cdot \square)$$

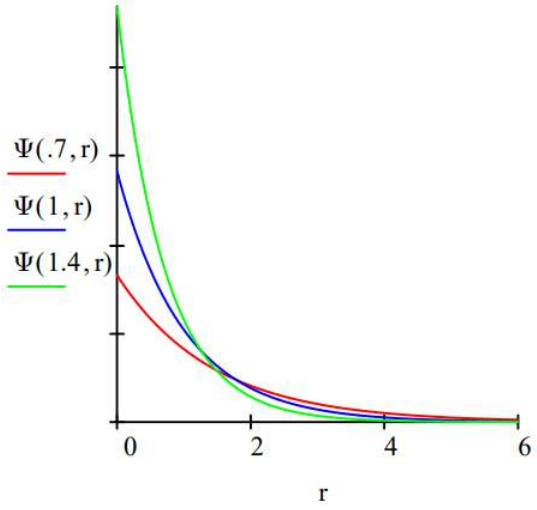
Potential energy operator:

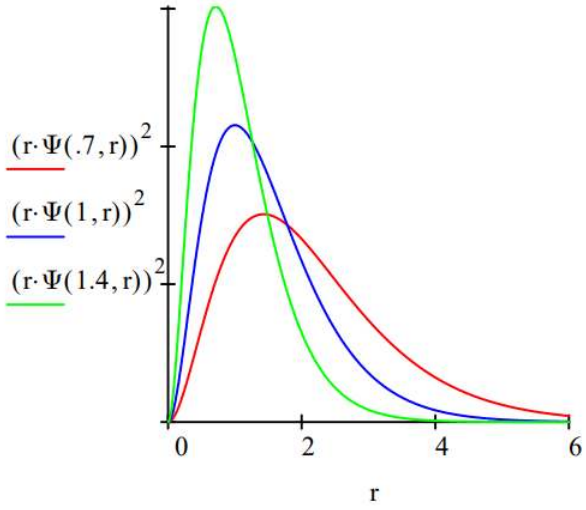
$$\frac{-Z}{r} \cdot \square$$

Demonstrate that the trial function is normalized:

$$\int_0^\infty \Psi(\alpha, r)^2 \cdot 4\pi r^2 \, dr \text{ assume, } \alpha > 0 \rightarrow 1$$

Plot trial wave function for several values of α, the variational parameter:





Calculate the average value of the kinetic energy of the electron:

$$T(\alpha) := \int_0^\infty \Psi(\alpha, r) \cdot -\frac{1}{2r}\frac{d^2}{dr^2}(r \cdot \Psi(\alpha, r)) \cdot 4\pi r^2 \, dr \text{ assume, } \alpha > 0 \rightarrow \frac{\alpha^2}{2}$$

Calculate the average value of the potential energy of the electron:

$$V(\alpha, Z) := \int_0^\infty \Psi(\alpha, r) \cdot -\frac{Z}{r} \cdot \Psi(\alpha, r) \cdot 4\pi r^2 \, dr \text{ assume, } \alpha > 0 \rightarrow -Z \cdot \alpha$$

Calculate R, the average distance of the electron from the nucleus:

$$R(\alpha) := \int_0^\infty \Psi(\alpha, r) \cdot r \cdot \Psi(\alpha, r) \cdot 4\pi r^2 \, dr \text{ assume, } \alpha > 0 \rightarrow \frac{3}{2\alpha}$$

From this we find that:

$$E(\alpha) = T(\alpha) + V(\alpha, Z) = \frac{\alpha^2}{2} - \alpha \cdot Z$$

But from above we know:

$$\alpha = \frac{3}{2R}$$

This allows us to express the total energy and its components in terms of R the average distance of the electron from the nucleus.

Total energy:

$$E(R, Z) := \frac{\alpha^2}{2} - \alpha \cdot Z \Big|_{\text{expand}}^{\text{substitute, } \alpha = \frac{3}{2R}} \rightarrow \frac{9}{8R^2} - \frac{3Z}{2R}$$

Electron kinetic energy:

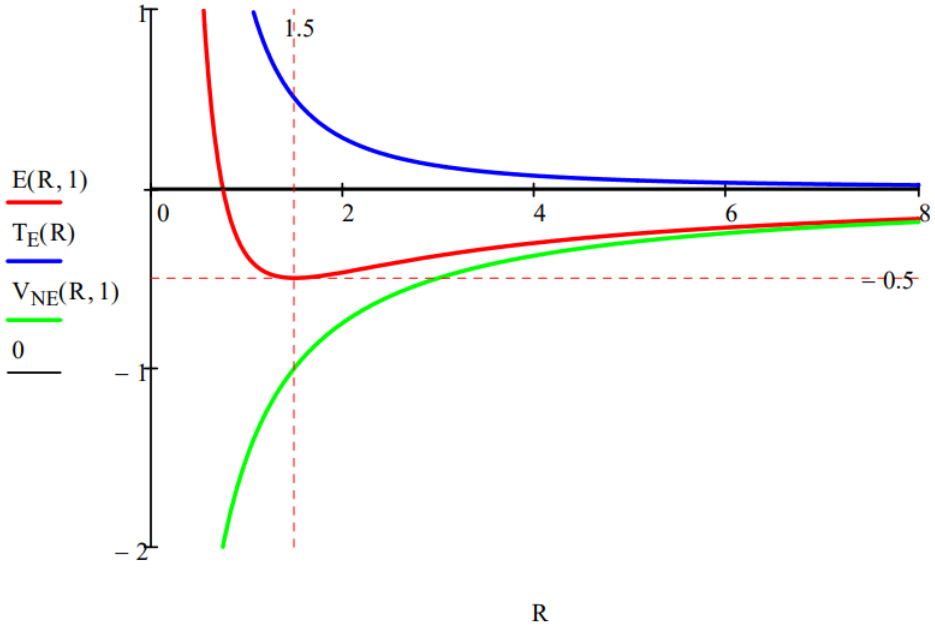
$$T_E(R) := \frac{9}{8R^2}$$

Electron-nucleus potential energy:

$$V_{NE}(R, Z) := \frac{-3Z}{2R}$$

E, T_E and V_{NE} are graphed versus R for the hydrogen atom (Z=1):

$$R := 0, 0.01, \ldots 8$$



The hydrogen atom ground-state energy is determined by minimizing its energy with respect to R:

$$R := R \qquad R := \frac{d}{dR} E(R, 1) = 0 \text{ solve, } R \rightarrow \frac{3}{2} \qquad E(R, 1) = -0.5$$

Imagine a hydrogen atom forming as an electron approaches a proton from a great distance. The electron is drawn toward the proton by the Coulombic attractive interaction between the two opposite charges and the potential energy decreases like -1/R. The

attractive potential energy interaction confines the electron to a smaller volume and the kinetic energy increases as $1/R^2$. Thus the kinetic energy goes to positive infinity faster than the potential energy goes to negative infinity and a total energy minimum (ground state) is achieved at **R = 1.5**, as shown in the figure above.

The electron does not collapse into (coalesce with) the proton under the influence of the attractive Coulombic interaction because of the repulsive effect of the confinement energy - that is, kinetic energy. Kinetic energy, therefore, is at the heart of understanding atomic stability.

Variational Method for the Helium Atom

Now we will proceed to the He atom. There are five contributions to the total electronic energy: kinetic energy of each electron, the interaction of each electron with the nucleus, and the electron-electron interaction.The only new term is the last, electron-electron potential energy. It is evaluated as follows for two electrons in 1s orbitals.

The electrostatic potential at r due to electron 1 is:

$$\Phi(\alpha, r) := \frac{1}{r}\int_0^r \Psi(\alpha, x)^2 4\pi x^2\, dx + \int_r^\infty \frac{\Psi(\alpha, x)^2 4\pi x^2}{x} dx \Big|_{\text{simplify}}^{\text{assume, } \alpha>0} \rightarrow \frac{e^{-2\alpha r} + \alpha r e^{-2\alpha r} - 1}{r}$$

The electrostatic interaction between the two electrons is:

$$V_{EE} := \int_0^\infty \Phi(\alpha, r)\Psi(\alpha, r)^2 4\pi r^2\, dr \Big|_{\text{simplify}}^{\text{assume, } \alpha>0} \rightarrow \frac{5\alpha}{8}$$

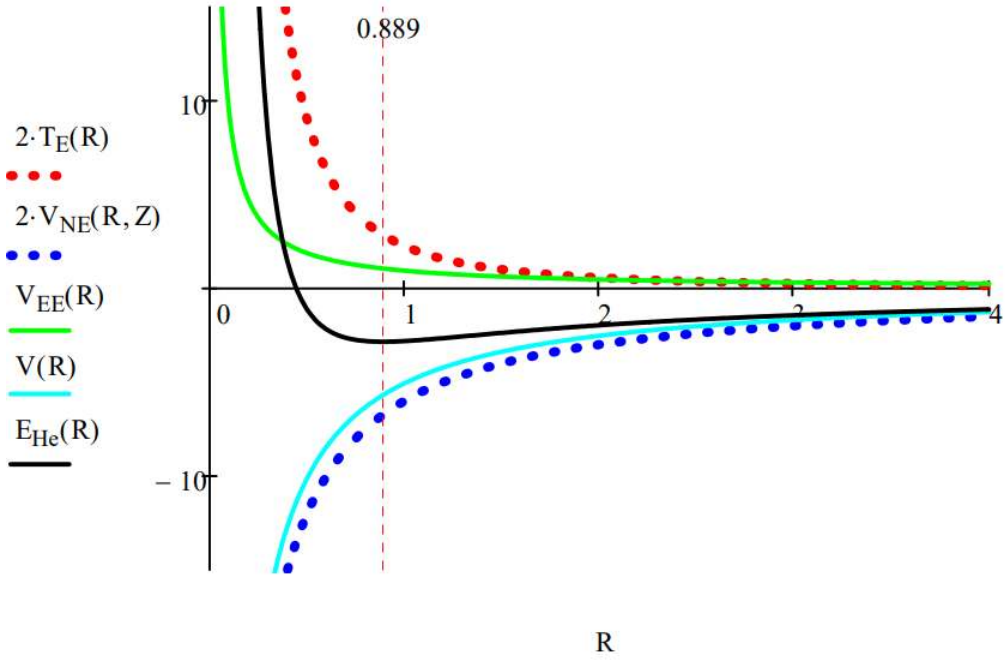
In terms of R, the electron-electron potential energy is:

$$V_{EE}(R) := \frac{15}{16R}$$

$$Z := 2 \qquad E_{He}(R) := (R)2T_E(R) + 2V_{NE}(R, Z) + V_{EE}(R) \qquad V(R) := 2V_{NE}(R, Z) + V_{EE}(R)$$

The various contributions to the total electronic energy of the helium atom are plotted below.

$$R := 0, 0.01 \ldots 4$$



The helium atom ground-state energy is determined by minimizing its energy with respect to R:

$$R := R \qquad R := \frac{d}{dR}E_{He}(R) = 0 \text{ solve, } R \rightarrow \frac{8}{9} \qquad R = 0.889 \qquad E_{He}(R) = -2.848$$

Graphing E_{He} vs. <R> reveals again that kinetic energy (confinement energy) is the key to atomic stability. Several things should be noted in the graph shown above. First, that when the total energy minimum is achieved V_{NE} and V (V_{NE} + V_{EE}) are still in a steep decline. This is a strong indication that V_{EE} is really a rather feeble contribution to the total energy, increasing significantly only long after the energy minimum has been attained. Thus electron-electron repulsion cannot be used to explain atomic stability. The graph above clearly shows that on the basis of classical electrostatic interactions, the electron should collapse into the nucleus. This is prevented by the kinetic energy term for the same reasons as were given for the hydrogen atom.

Unfortunately chemists give too much significance to electron-electron repulsion (VSEPR for example) when it is really the least important term in the Hamiltonian energy operator. And to make matters worse they completely ignore kinetic energy as an important factor in atomic and molecular phenomena. It is becoming increasing clear in the current literature that many traditional explanations for chemical phenomena based exclusively on electrostatic arguments are in need of critical re-examination.

Scientists work almost exclusively in coordinate space when they do quantum calculations. There are two other options, momentum space and phase space, as the following tutorial shows. Calculations on the hydrogen atom are provided for all three computational venues in the following box.

Quantum Calculations on the Hydrogen Atom in Coordinate, Momentum and Phase Space

Coordinate Space Operators

Position operator	$x \cdot \square$
Momentum operator	$p = \frac{1}{i}\frac{d}{dx}\square$
Integral	$\int_0^\infty \square \, dx$
Kinetic energy operator	$KE = -\frac{1}{2}\frac{d^2}{dx^2}\square$
Potential energy operator	$PE = \frac{-1}{x} \cdot \square$

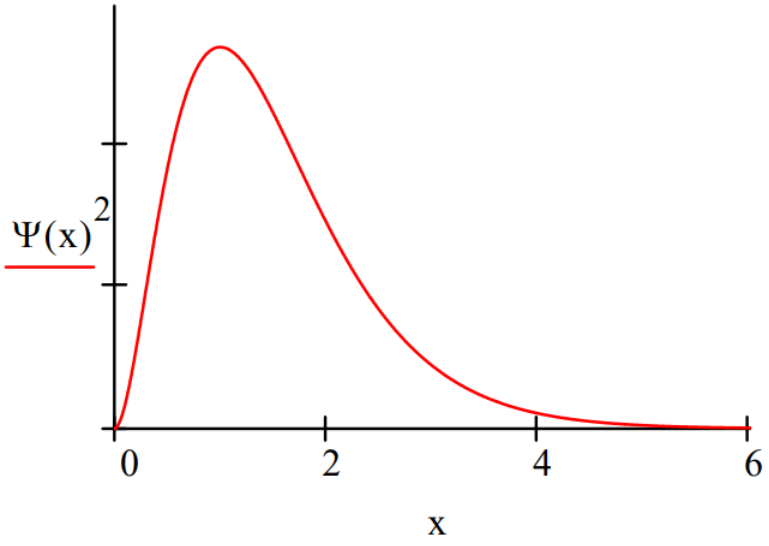
The energy operator for the one-dimensional hydrogen atom in atomic units is:

$$\frac{-1}{2}\frac{d^2}{dx^2}\square - \frac{1}{x}\square$$

The ground state wave function in coordinate space is:

$$\Psi(x) := 2 \cdot x \cdot \exp(-x)$$

Display the coordinate-space distribution function:



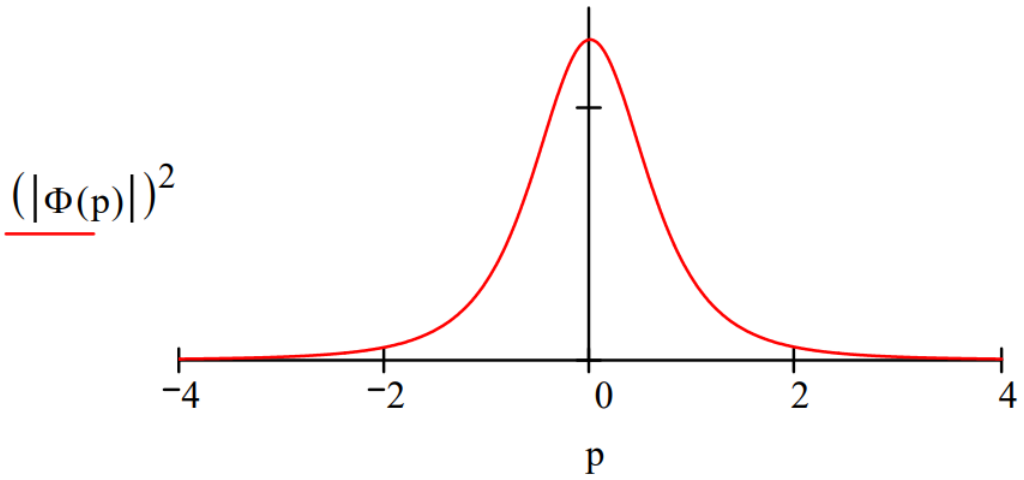
The ground state energy is -0.5 E_h.

$$\frac{-1}{2}\frac{d^2}{dx^2}\Psi(x) - \frac{1}{x}\Psi(x) = E\cdot\Psi(x) \text{ solve, } E \to \frac{-1}{2}$$

The coordinate wave function is normalized	$\int_0^\infty \Psi(x)^2\ dx = 1$
The expectation value for position	$\int_0^\infty x\cdot\Psi(x)^2\ dx = 1.5$
The expectation value for momentum	$\int_0^\infty \Psi(x)\cdot\frac{1}{i}\frac{d}{dx}\Psi(x)\ dx = 0$
The expectation value for kinetic energy	$\int_0^\infty \Psi(x)\cdot\frac{-1}{2}\frac{d^2}{dx^2}\Psi(x)\ dx = 0.5$
The expectation value for potential energy	$\int_0^\infty \frac{-1}{x}\cdot\Psi(x)^2\ dx = -1$

The momentum wave function is generated by the following Fourier transform of the coordinate space wave function.

$$\Phi(p) := \frac{1}{\sqrt{2\pi}}\int_0^\infty \exp(-ipx)\cdot\Psi(x)\ dx \to \frac{2^{1/2}}{\pi^{1/2}\cdot(ip+1)^2}$$



Momentum Space Operators

Momentum space integral	$\int_{-\infty}^\infty \square\ dp$
Momentum operator	$p\cdot\square$
Kinetic energy operator	$\frac{p^2}{2}$
Position operator	$i\cdot\frac{d}{dp}\square$

The same calculations made with the momentum space wave function:

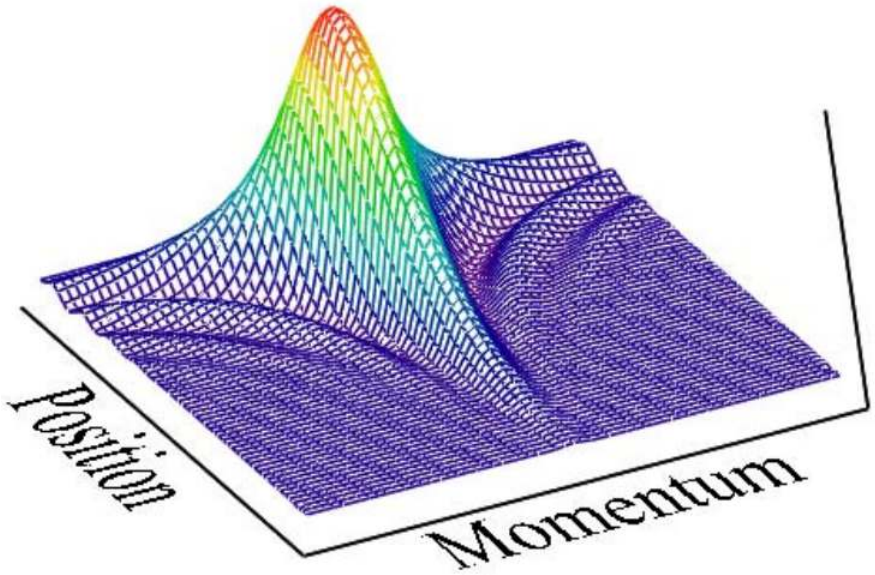
The coordinate wave function is normalized	$\int_{-\infty}^\infty (\lvert\Phi(p)\rvert)^2\ dp = 1$
The expectation value for position	$\int_{-\infty}^\infty \overline{\Phi(p)}\cdot i\cdot\frac{d}{dp}\Phi(p)\ dp = 1.5$
The expectation value for momentum	$\int_{-\infty}^\infty p\cdot(\lvert\Phi(p)\rvert)^2\ dp = 0$
The expectation value for kinetic energy	$\int_{-\infty}^\infty \frac{p^2}{2}\cdot(\lvert\Phi(p)\rvert)^2\ dp = 0.5$
The expectation value for potential energy	

The Wigner function for the hydrogen atom ground state is generated using the momentum wave function.

$$W(x,p) := \frac{1}{2\pi}\int_{-\infty}^{\infty} \overline{\Phi(p+\frac{s}{2})}\cdot \exp(-isx)\cdot \Phi(p-\frac{s}{2})\, ds$$

The Wigner distribution is displayed graphically.

$$N := 60 \quad i := 0 \ldots N \quad x_i := \frac{6i}{N} \quad j := 0 \ldots N \quad p_j := -5 + \frac{10\cdot j}{N} \quad Wigner_{i,j} := W(x_i, p_j)$$



One of the interesting features of doing quantum mechanics with the Wigner distribution is that the position and momentum operators retain their classical forms; they are both multiplicative operators. By comparison in the coordinate representation position is multiplicative and momentum is differential. In the momentum representation it's the reverse. This is illustrated below with the following calculations.

Phase space integral	$\int_{-\infty}^{\infty}\int_{0}^{\infty} \square\, dx\, dp$
Position operator	$x\cdot\square$
Momentum operator	$p\cdot\square$
Kinetic energy operator	$KE = \frac{p^2}{2}\cdot\square$
Potential energy operator	$PE = \frac{-1}{x}\cdot\square$

Phase space calculations using the Wigner distribution:

The Wigner distribution is normalized	$\int_{-\infty}^{\infty}\int_{0}^{\infty} W(x,p)\, dx\, dp = 1$
The expectation value for position	$\int_{-\infty}^{\infty}\int_{0}^{\infty} x\cdot W(x,p)\, dx\, dp = 1.5$
The expectation value for momentum	$\int_{-\infty}^{\infty}\int_{0}^{\infty} p\cdot W(x,p)\, dx\, dp = 0$
The expectation value for kinetic energy	$\int_{-\infty}^{\infty}\int_{0}^{\infty} \frac{p^2}{2}\cdot W(x,p)\, dx\, dp = 0.5$
The expectation value for potential energy	$\int_{-\infty}^{\infty}\int_{0}^{\infty} \frac{-1}{x}\cdot W(x,p)\, dx\, dp = -1$

The phase space calculations require the Wigner distribution function. This link provides further information about the Wigner distribution and how it repackages quantum weirdness.

Contributors and Attributions

- Prof. Emeritus Frank Rioux (St. John's University and College of St. Benedict)

This page titled 1.2: Atomic and Molecular Stability is shared under a CC BY 4.0 license and was authored, remixed, and/or curated by Frank Rioux via source content that was edited to the style and standards of the LibreTexts platform.

1.3: Atomic and Molecular Stability

Sometimes practitioners of quantum mechanics misinterpret energy contributions when studying the details of atomic behavior. This can happen when classical concepts are allowed to intrude on the quantum realm where they are not valid.

Another Critique of the Centrifugal Effect in the Hydrogen Atom

On page 174 of *Quantum Chemistry & Spectroscopy, 3rd ed.* Thomas Engel derives equation 9.5 which is presented in equivalent form in atomic units ($e = m_e = \frac{h}{2\pi} = 4\pi\epsilon_0 = 1$) here.

$$-\frac{1}{2r^2}\frac{d}{dr}(r^2\frac{d}{dr}R(r)) + \left[\frac{L(L+1)}{2r^2} - \frac{1}{r}\right] \cdot R(r) = E \cdot R(r) \tag{1.3.1}$$

At the bottom of the page he writes,

> *Note that the second term (in brackets) on the left-hand side of Equation 9.5 can be viewed as a effective potential, $V_{eff}(r)$. It is made up of the **centrifugal potential**, which varies as +1/r^2, and the **Coulomb potential**, which varies as -1/r.*
>
> $$V_{eff}(r) = \frac{L(L+1)}{2r^2} - \frac{1}{r}$$

Engel notes that because of its positive mathematical sign, the **centrifugal potential** is repulsive, and goes on to say,

> *The net result of this repulsive **centrifugal potential** is to force the electrons in orbitals with **L** > 0 (p, d, and f electrons) on average farther from the nucleus than s electrons for which **L** = 0.*

This statement is contradicted by the radial distribution functions shown in Figure 9.10 on page 187, which clearly show the opposite effect. As **L** increases the electron is on average closer to the nucleus. It is further refuted by calculations of the average value of the electron position from the nucleus as a function of the **n** and **L** quantum numbers. For a given **n** the larger **L** is the closer on average the electron is to the nucleus. In other words, these calculations support the graphical representation in Figure 9.10.

$$r(n,L) := \frac{3n^2 - L(L+1)}{2} \qquad \begin{pmatrix} L & 0 & 1 & 2 & 3 \\ n=1 & 1.5 & ' & ' & ' \\ n=2 & 6 & 5 & ' & ' \\ n=3 & 13.5 & 12.5 & 10.5 & ' \\ n=4 & 24 & 23 & 21 & 18 \end{pmatrix}$$

On page 180 in Example Problem 9.2, Engel introduces the virial theorem. For systems with a Coulombic potential energy, such as the hydrogen atom, it is

$$\langle V \rangle = 2\langle E \rangle = \text{-}2\langle T \rangle.$$

We will work with the version

$$\frac{\langle E \rangle}{\langle V \rangle} = 0.5.$$

The values of the energy, the so called **centrifugal potential energy** and the **Coulombic potential energy** are as shown below as a function of the appropriate quantum numbers.

$$E(n) := \frac{-1}{2n^2} \qquad V_{centrifugal}(n,L) := \frac{L(L+1)}{2n^3(L+\frac{1}{2})} \qquad V_{coulomb}(n) := -\frac{1}{n^2}$$

The calculations below show that the virial theorem is violated for any state for which L > 0.

$$1s \quad n:=1 \quad L:=0 \quad \frac{E(n)}{V_{centrifugal}(n,L)+V_{coulomb}(n)}=0.5$$

$$2s \quad n:=2 \quad L:=0 \quad \frac{E(n)}{V_{centrifugal}(n,L)+V_{coulomb}(n)}=0.5$$

$$2p \quad n:=2 \quad L:=1 \quad \frac{E(n)}{V_{centrifugal}(n,L)+V_{coulomb}(n)}=0.75$$

$$3s \quad n:=3 \quad L:=0 \quad \frac{E(n)}{V_{centrifugal}(n,L)+V_{coulomb}(n)}=0.5$$

$$3p \quad n:=3 \quad L:=1 \quad \frac{E(n)}{V_{centrifugal}(n,L)+V_{coulomb}(n)}=0.643$$

$$3d \quad n:=3 \quad L:=2 \quad \frac{E(n)}{V_{centrifugal}(n,L)+V_{coulomb}(n)}=0.833$$

These calculations are now repeated eliminating the centrifugal term, showing that the virial theorem is satisfied and supporting the claim that the "centrifugal potential" is actually a kinetic energy term.

$$1s \quad n:=1 \quad L:=0 \quad \frac{E(n)}{V_{coulomb}(n)}=0.5$$

$$2s \quad n:=2 \quad L:=0 \quad \frac{E(n)}{V_{coulomb}(n)}=0.5$$

$$2p \quad n:=2 \quad L:=1 \quad \frac{E(n)}{V_{coulomb}(n)}=0.5$$

$$3s \quad n:=3 \quad L:=0 \quad \frac{E(n)}{V_{coulomb}(n)}=0.5$$

$$3p \quad n:=3 \quad L:=1 \quad \frac{E(n)}{V_{coulomb}(n)}=0.5$$

$$3d \quad n:=3 \quad L:=2 \quad \frac{E(n)}{V_{coulomb}(n)}=0.5$$

We finish by rewriting Equation 1.3.1 with brackets showing that the first two terms are quantum kinetic energy and that the Coulombic term is the only potential energy term.

$$\left[-\frac{1}{2r^2}\frac{d}{dr}(r^2\frac{d}{dr}R(r))+\frac{L(L+1)}{2r^2}\cdot R(r)\right]-\frac{1}{r}\cdot R(r)=E\cdot R(r)$$

In summary, the "centrifugal potential" and the concept of "effective potential energy" are good examples of the danger in thinking classically about a quantum mechanical system. Furthermore, it's bad pedagogy to create fictitious forces and to mislabel energy contributions in a misguided effort to provide conceptual simplicity.

Further evidence that confinement energy is not kinetic energy is seen in the following analysis of the effect of lepton mass in the hydrogen atom. In what follows the electron is replaced by the muon and the tauon in the hydrogen atom. Positronium, in which the proton is replaced by the positron, is also examined. These analyses also provide a graphical illustration of the uncertainty principle.

Exploring the Role of Lepton Mass in the Hydrogen Atom

Under normal circumstances the the hydrogen atom consists of a proton and an electron. However, electrons are leptons and there are two other leptons which could temporarily replace the electron in the hydrogen atom. The other leptons are the muon and tauon, and their fundamental properties, along with those of the electron, are given in the following table.

Property	e	μ	τ
$\frac{Mass}{m_e}$	1	206.8	3491
$\frac{Effective\ Mass}{m_e}$	1	185.86	1203
$\frac{Life\ Time}{s}$	$Stable$	2.2×10^{-6}	3.0×10^{-13}

The purpose of this exercise is to demonstrate the importance of mass in atomic systems, and therefore also kinetic energy. Substitution of the deBroglie relation ($\lambda = \frac{h}{m\nu}$) into the classical expression for kinetic energy yields a quantum mechanical expression for kinetic energy. It is of utmost importance that in quantum mechanics, kinetic energy is inversely proportional to mass.

$$T = \frac{1}{2}mv^2 = \frac{h^2}{2m\lambda^2}$$

A more general and versatile quantum mechanical expression for kinetic energy is the differential operator shown below, where again mass appears in the denominator. *An Approach to Quantum Mechanics* outlines the origin of kinetic energy operator.

Atomic units ($e = m_e = \frac{h}{2\pi} = 4\pi\epsilon_0 = 1$) will be used in the calculations that follow. Please note that μ in the equations below is the effective mass and not a symbol for the muon.

Kinetic energy operator:

$$T = -\frac{1}{2\mu r}\frac{d^2}{dr^2}(\cdot\square) \tag{1.3.2}$$

Potential energy operator:

$$V = -\frac{1}{r}\cdot\square \tag{1.3.3}$$

Variational trial wave function with variational parameter β:

$$\Psi(r,\beta) := \left(\frac{\beta^3}{\pi}\right)^{1/2} \cdot \exp(-\beta \cdot r)$$

Evaluation of the variational energy integral:

$$E(\beta,\mu) := \int_0^\infty \Psi(r,\beta)\left[-\frac{1}{2\mu r}\frac{d^2}{dr^2}(r\cdot\Psi(r,\beta)\right] 4\pi r^2\, dr \ldots$$

$$\Big|_{\text{simplify}}^{\text{assume, }\beta>0} \rightarrow \frac{\beta^2}{2\mu} - \beta + \int_0^\infty \Psi(r,\beta)\cdot -\frac{1}{r}\cdot\Psi(r,\beta)\cdot 4\pi r^2\, dr$$

Minimize the energy with respect to the variational parameter β.

$$\frac{d}{d\beta}E(\beta,\mu) = 0 \text{ solve, } \beta \rightarrow \mu$$

Express energy in terms of reduced mass:

$$E(\beta,\mu) \text{ substitute, } \beta = \mu \rightarrow -\frac{\mu}{2}$$

Using the virial theorem the kinetic and potential energy contributions are:

$$T = \frac{\mu}{2} \qquad V = -\mu$$

Express the trial wave function in terms of reduced mass.

$$\Psi(r,\beta) \text{ substitute, } \beta = \mu \rightarrow \frac{e^{-\mu r}\sqrt{\mu^3}}{\sqrt{\pi}}$$

Demonstrate the effect of mass on the radial distribution function with plots of mass equal to 0.5, 1 and 2.

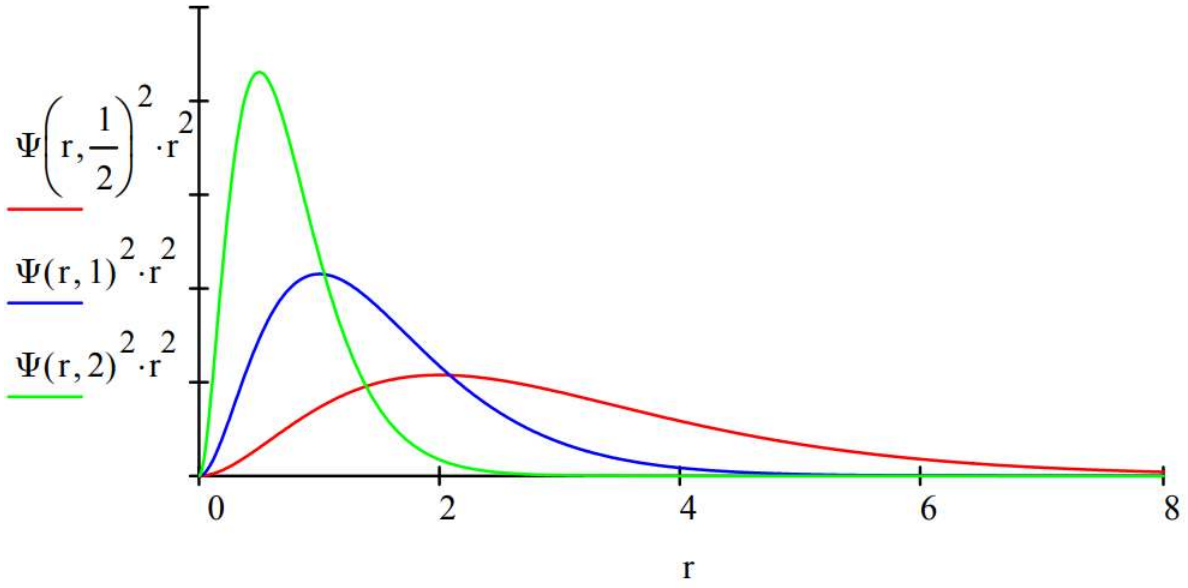


Figure 1

Calculate the expectation value for position to show that it is consistent with the graphical representation above. The more massive the lepton the closer it is on average to the proton.

$$\int_0^\infty \Psi(r,\mu)\cdot r\cdot \Psi(r,\mu)\cdot 4\pi r^2\, dr \text{ assume, } \mu > 0 \rightarrow \frac{3}{2\mu}$$

Summarize the calculated values for the physical properties of H_e, H_μ and H_τ.

Species	$\frac{E}{E_h}$	$\frac{T}{E_h}$	$\frac{V}{E_h}$	$\frac{r_{avg}}{a_0}$
H_e	$\frac{-1}{2}$	$\frac{1}{2}$	-1	$\frac{3}{2}$
H_μ	-92.93	92.93	-185.86	8.07×10^{-3}
H_τ	-601.5	601.5	-1203	1.25×10^{-3}

Now imagine that you have a regular hydrogen atom in its ground state and the electron is suddenly by some mechanism replaced by a muon. Nothing has changed from an electrostatic perspective, but the change in energy and average distance of the lepton from the proton are very large. The ground state energy and the average distance from the nucleus decrease by a factor of 185.6, the ratio of the effective masses of the electron and the muon.

This mass effect provides a challenge for those who think all atomic physical phenomena can be explained in terms of electrostatic potential energy effects. Of course, there is an even bigger problem for the potential energy aficionados, and that is the fundamental issue of atomic and molecular stability. Quantum mechanical kinetic energy effects are required to explain the stability of matter.

A Fourier transform of the coordinate wave function yields the corresponding momentum distribution and the opportunity to create a visualization of the uncertainty principle.

$$\Phi(p,\mu) := \frac{1}{4\sqrt{\pi^3}}\int_0^\infty \exp(-ipr)\cdot\Psi(r,\mu)\cdot 4\pi r^2\, dr\Big|_{\text{simplify}}^{\text{assume, }\mu>0} \rightarrow \frac{2\mu^{3/2}}{\pi(\mu+p\cdot i)^3}$$

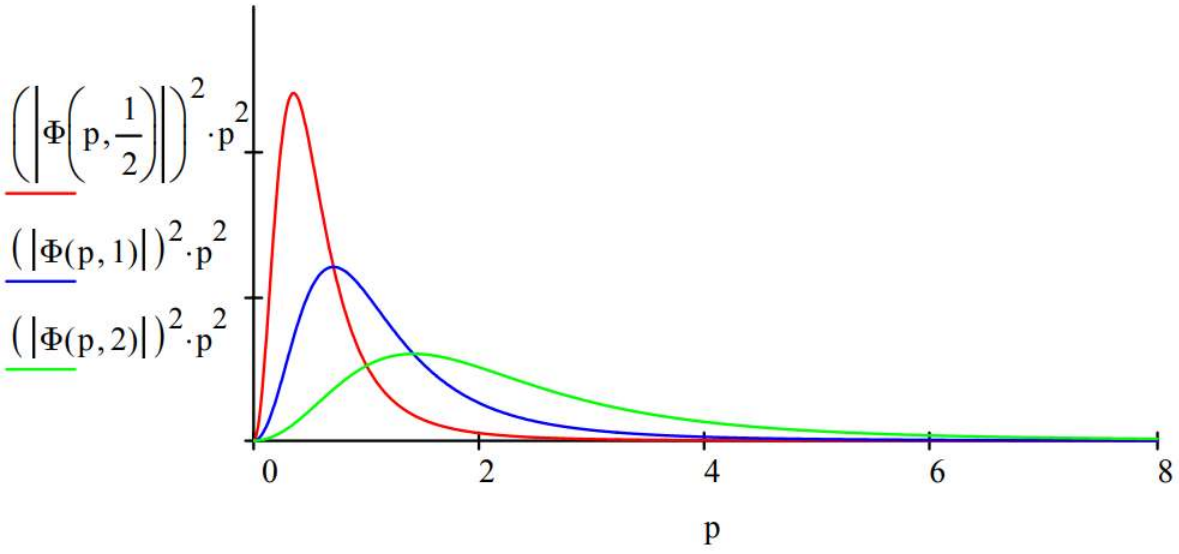


Figure 2

Figure 2 shows that the most massive particle has the most delocalized momentum distribution. This is consistent with the uncertainty principle which states less spatial uncertainty is accompanied by greater uncertainty in the momentum distribution.

Replacing the proton with a positron, the electron's anti-particle, creates another exotic atom, positronium (Ps). In its singlet ground state electron-positron annihilation occurs in 125 ps creating two γ rays. Positronium's (μ = 1/2) spatial and momentum distributions are shown in Figures 1 and 2. A revised table including positronium is provided below.

Species	$\frac{E}{E_h}$	$\frac{T}{E_h}$	$\frac{V}{E_h}$	$\frac{r_{avg}}{a_0}$
H_e	$-\frac{1}{2}$	$\frac{1}{2}$	-1	$\frac{3}{2}$
H_μ	-92.93	92.93	-185.86	8.07×10^{-3}
H_τ	-601.5	601.5	-1203	1.25×10^{-3}
Ps	$-\frac{1}{4}$	$\frac{1}{4}$	$-\frac{1}{2}$	3

Many in the chemical education community teach chemical bonding as simply an electrostatic phenomenon. I and many others have argued against this incorrect, simplistic view on many occasions. In an effort to get a better understanding let’s look at an overview of the nature of the chemical bond written by Frank E. Harris many years ago.

The Chemical Bond and Quantum Mechanics*

The behavior of electrons in molecules and atoms is described by quantum mechanics; classical (Newtonian) mechanics cannot be used because the de Broglie wavelengths ($\lambda = \frac{h}{mv}$) of the electrons are comparable with molecular (and atomic) dimensions. The relevant quantum-mechanical ideas are as follows:

- Electrons are characterized by their entire distributions (called wave functions or orbitals) rather than by instantaneous positions and velocities: an electron may be considered always to be (with appropriate probability) at all points of its distribution (which does not vary with time).
- The kinetic energy of an electron decreases as the volume occupied by the bulk of its distribution increases, so delocalization lowers its kinetic energy.

$$KE = \frac{p^2}{2m} = \frac{h^2}{2m\lambda^2} \approx \frac{A}{D^2} \approx \frac{A}{V^{2/3}} \tag{1.3.4}$$

- The potential energy of interaction between an electron and other charges is as calculated by classical physics, using the appropriate distribution (wave function) for the electron: an electron distribution is therefore attracted by nuclei and its potential energy decreases as the average electron-nuclear distance decreases.

$$PE \approx -\frac{B}{D} \approx -\frac{B}{V^{1/3}} \tag{1.3.5}$$

- A minimum-energy electron distribution represents the best compromise between concentration near the nuclei (to reduce potential energy) and delocalization (to reduce kinetic energy).

$$E = KE + PE \approx \frac{A}{V^{2/3}} - \frac{B}{V^{1/3}} \tag{1.3.6}$$

A bond will form between two atoms when the electron distribution of the combined atoms (molecular orbital) yields a significantly lower energy than the separate-atom distributions (atomic orbitals). An example is a covalent bond, in which two electrons, one originally on each atom, change their distributions so that each extends over both atoms.

---

* Taken from "Molecules" in The Encyclopedia of Physics by Frank E. Harris (with some additions and modifications by Frank Rioux)

We go deeper with the following treatment of the covalent bond in the hydrogen molecule ion using the virial theorem (John C. Slater) and **ab initio** quantum mechanics (Klaus Ruedenberg). In my opinion, Slater and Ruedenberg are the true pioneers in understanding the covalent chemical bond. Many books have been written about the chemical bond, but few are as insightful as the papers published by Slater and Ruedenberg.

Two Analyses of the Covalent Bond Using the Virial Theorem

Atomic and molecular stability and spectroscopy, and the nature of the chemical bond cannot be explained using classical physics: quantum mechanical principles are required. Bohr was a pioneer in an effort to apply an early version of quantum theory to these important issues with his models of the hydrogen atom and hydrogen molecule. Of course, Bohr's approach became "old" quantum mechanics and was abandoned in the 1920s with the creation of a "new" quantum mechanics by Heisenberg and Schrödinger and their collaborators. This tutorial deals exclusively with the chemical bond and summarizes Slater's contribution to our current understanding of the energetics of its formation using the virial theorem. Since the acceptance of the "new" quantum mechanics many others have contributed to the interpretation of chemical bond formation, but like Bohr, Slater was an insightful pioneer.

In a seminal paper, *J.Chem. Phys.* **1933**, **1**, 687-691, John C. Slater used the virial theorem to analyze chemical bond formation and was the first (in my opinion) to recognize the importance of kinetic energy in covalent bond formation. Regarding the universally valid virial theorem he wrote,

> *...this theorem gives a means of finding kinetic and potential energy separately for all configurations of the nuclei, as soon as the total energy is known, from **experiment** or **theory**.*

The purpose of this tutorial is to demonstrate the validity of this assertion. The experimental method employs a **Morse** function for the energy of the **hydrogen molecule** ion parametrized using spectroscopic data. The theoretical approach is based on an ab initio **LCAO-MO** calculation of the energy based on a molecular orbital consisting a superposition of scaled hydrogen atomic orbitals.

Experimental Method

The kinetic energy, potential energy and total energy of the **hydrogen molecule** ion are calculated as a function of **R** using the virial theorem and a Morse function for the total energy based on experimental parameters.

Total energy:	$E(R) = T(R) + V(R)$	(1)
Virial theorem:	$2 \cdot T(R) + V(R) = -R\frac{d}{dR}E(R)$	(2)
Morse parameters:	$D_e := 0.103 \cdot E_h \qquad R_e := 2.003 \cdot a_0$ $\beta := 0.708 a_0^{-1}$	(1.3.7)

These parameters are from Levine, I. N. **Quantum Chemistry**, 6th ed., p. 400.

Morse Function:	\[E(R) : = D_{e} (1- \exp [- \beta (R - R_{e})])^{2} - D_{e} \tag{3}$$

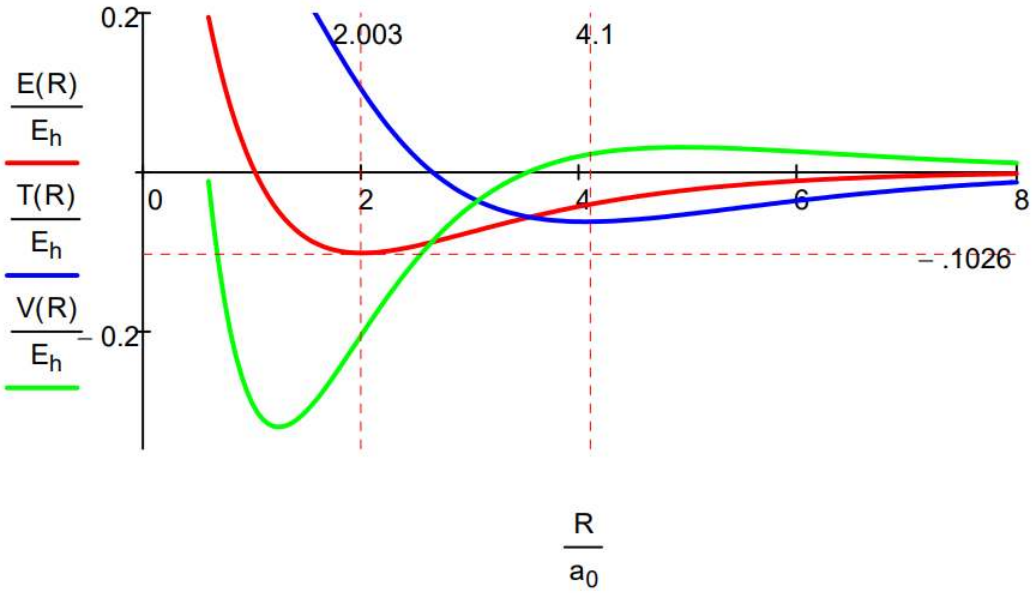
Using equation (1) to eliminate V(R) in equation (2) yields an equation for kinetic energy as a function of the internuclear separation. Using equation (1) to eliminate T(R) in equation (2) yields an equation for potential energy as a function of the internuclear separation.

$$T(R) := -E(R) - R\frac{d}{dR}E(R) \tag{4}$$

$$V(R) := 2E(R) + R\frac{d}{dR}E(R) \tag{5}$$

These important equations determine the mean kinetic and potential energies as functions of R, one might almost say experimentally, directly from the curves of E as a function of R which can be found from band spectra. The theory is so simple and direct that one can accept the results without question....

$$R := 0.6a_0, 0.65a_0 \ldots 8a_0$$



While the Morse calculation has an empirical flavor to it, its results are interpreted in terms of rudimentary quantum theory concepts. This energy profile shows that as the protons approach, the potential energy rises because molecular orbital formation (constructive interference) draws electron density away from the nuclei into the internuclear region. The kinetic energy decreases because molecular orbital formation brings about electron delocalization.

At about $4.1a_0$ this trend reverses as atomic orbital contraction begins. The kinetic energy rises because the volume occupied by the electron decreases and the potential energy decreases for the same reason: a smaller electronic volume brings the electron closer to the nuclei on average. Only at R ~ $1a_0$ does nuclear repulsion cause the total potential energy to increase and contribute to the repulsion energy of the molecule. In other words, the kinetic energy increase is the immediate cause of the energy minimum or ground state.

Theoretical Method

The following LCAO-MO calculation uses a superposition of scaled 1s atomic orbitals and yields the following result for the energy of the hydrogen molecule ion as a function of the internuclear distance and the orbital scale factor.

$$1s_a = \sqrt{\frac{\alpha^3}{\pi}}\exp(-\alpha r_a)$$

$$1s_b = \sqrt{\frac{\alpha^3}{\pi}}\exp(-\alpha r_b)$$

$$S_{ab} = \int 1s_a \cdot 1s_b d\tau$$

$$\Psi_{mo} = \frac{1s_a + 1s_b}{\sqrt{2 + 2S_{ab}}}$$

$$E(\alpha, R) := \frac{-\alpha^2}{2} + \frac{[\alpha^2 - \alpha - \frac{1}{R} + \frac{1+\alpha R}{R}\exp(-2\alpha R) + \alpha(\alpha - 2)\cdot(1 + \alpha R)\exp(-\alpha R)]}{[1 + \exp(-\alpha R)\cdot(1 + \alpha R + \frac{\alpha^2 R^2}{3})]} + \frac{1}{R}$$

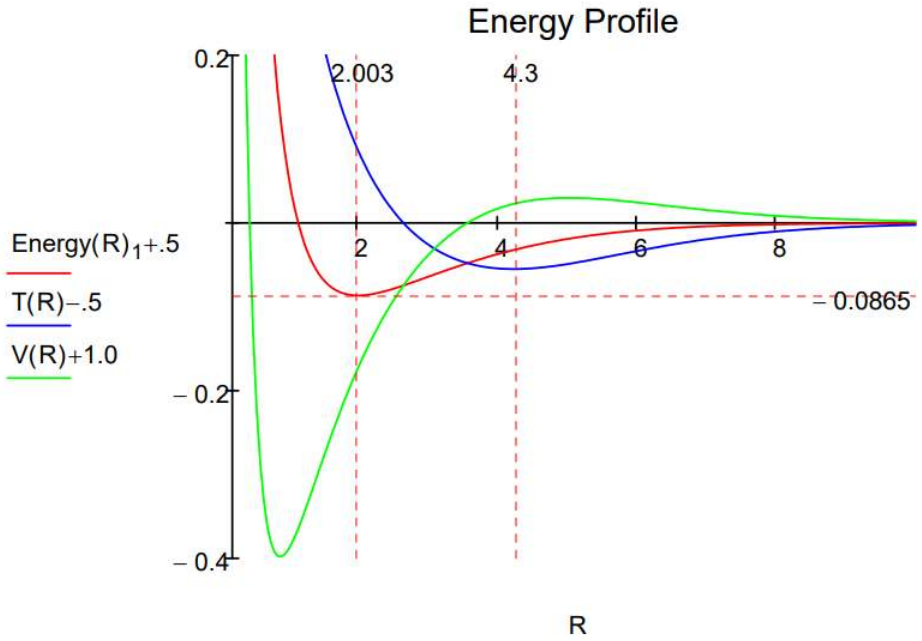
$\alpha := 1$	Energy := 2

Given $Energy = E(\alpha, R)$ $\quad \frac{d}{d\alpha}E(\alpha, R) = 0$ $\quad Energy(R) := Find(\alpha, Energy)$

As noted above, using $E = T + V$ with the virial theorem $2T + V = -R\frac{d}{dR}E$ leads to the following expressions for T and V.

$$T(R) := -Energy(R)_1 - R\frac{d}{dR}Energy(R)_1$$

$$V(R) := 2\cdot Energy(R)_1 + R\frac{d}{dR}Energy(R)_1 \qquad R := 0.2, 0.25 \ldots 10$$



It is clear that both methods lead to very similar energy profiles. The only significant difference is that the Morse calculation leads to a lower energy minimum, -0.1026 E_h versus -0.0865 E_h for the molecular orbital calculation. Therefore, the interpretation provided for the Morse energy profile is valid for the LCAO-MO profile.

Conversion factors: $a_0 = 5.29177\cdot 10^{-11}\ m$ $\qquad E_h = 4.359748\cdot 10^{-18}\ joule$

The following link provides graphical displays of the electron density in the hydrogen molecule ion.

The following calculation shows that the lepton mass effect in molecules is the same as it is atoms. This mass effect provides a challenge for those who think atomic and molecular stability can be explained solely in terms of electrostatic potential energy

effects. The mass effect is important because quantum mechanical kinetic energy (confinement energy) is inversely proportional to mass, but classical kinetic energy is directly proportional to mass.

A Molecular Orbital Calculation for H_2^+

An *ab initio* molecular orbital calculation yields the following result for the energy of the hydrogen molecule ion as a function of the internuclear separation, lepton mass (highlighted below) and the orbital decay constant.

$$1s_a = \sqrt{\frac{\alpha^3}{\pi}} \cdot \exp(-\alpha \cdot r_a) \qquad 1s_b = \sqrt{\frac{\alpha^3}{\pi}} \cdot \exp(-\alpha \cdot r_b)$$

$$S_{ab} = \int 1s_a \cdot 1s_b d\tau \qquad \Psi_{mo} = \frac{1s_a + 1s_b}{\sqrt{2 + 2 \cdot s_{ab}}}$$

$$m := 0.5 \quad E(\alpha, R) := \frac{-\alpha^2}{2 \cdot m} + \frac{\frac{\alpha^2}{m} - \alpha - \frac{1}{R} + \frac{1}{R} \cdot (1 + \alpha \cdot R) \cdot \exp(-2 \cdot \alpha \cdot R) + \alpha \cdot \left(\frac{\alpha}{m} - 2\right) \cdot (1 + \alpha \cdot R) \cdot \exp(-\alpha \cdot R)}{1 + \exp(-\alpha \cdot R) \cdot \left(1 + \alpha \cdot R + \frac{\alpha^2 \cdot R^2}{3}\right)} + \frac{1}{R}$$

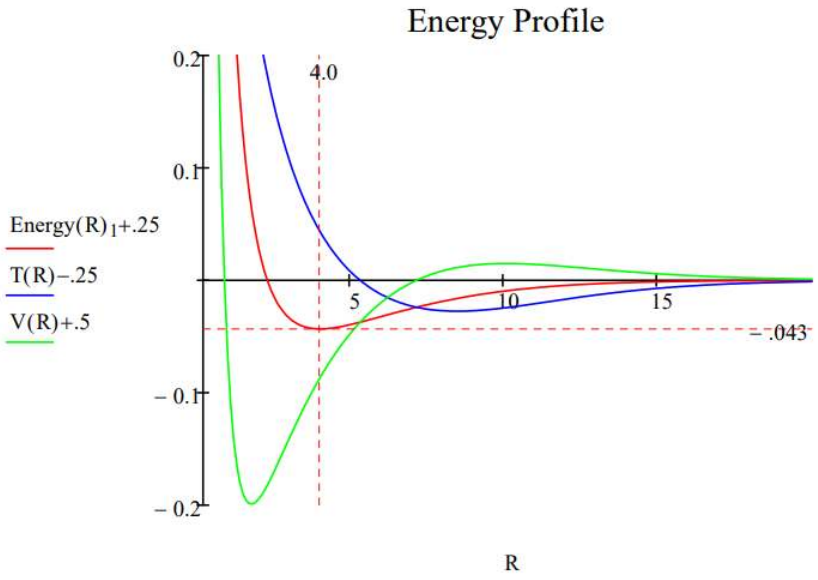
$$\alpha := 1 \quad Energy := -2 \qquad Given \quad Energy = E(\alpha, R)$$

$$\frac{d}{d\alpha} E(\alpha, R) = 0 \quad Energy(R) := Find(\alpha, Energy)$$

Using $E = T + V$ in the virial theorem $2T + V = -R \cdot \frac{d}{dR} E$ yields expressions for T and V.

$$R := 0.2, 0.3 \ldots 20 \quad T(R) := -Energy(R)_1 - R \cdot \frac{d}{dR} Energy(R)_1$$

$$V(R) := 2 \cdot Energy(R)_1 + R \cdot \frac{d}{dR} Energy(R)_1$$



Note that halving the lepton mass reduces the ground state energy by half and doubles the bond length. The same mass effect was found earlier for the hydrogen atom.

Some might feel uncomfortable relying on a one-electron molecule to gain an understanding of the chemical bond. After all don't chemical bonds consist of electron pairs? So we move to the hydrogen molecule for a quantum analysis of the more traditional two-electron bond. The only new contribution to the total energy is electron-electron potential energy, and the significance of confinement energy in understanding molecular stability survives.

This page titled 1.3: Atomic and Molecular Stability is shared under a CC BY 4.0 license and was authored, remixed, and/or curated by Frank Rioux via source content that was edited to the style and standards of the LibreTexts platform.

1.4: Atomic and Molecular Stability

I apologize for the considerable overlap in the following, but it does provide some additional interpretive graphics. It also contains references to the publications of Slater and Ruedenberg.

The Chemical Bond According to Slater and Ruedenberg

John Slater pioneered the use of the virial theorem in interpreting the chemical bond in a benchmark paper published in the inaugural volume of the *Journal of Chemical Physics* (1). This early study indicated that electron kinetic energy played an important role in bond formation. Thirty years later Klaus Ruedenberg and his collaborators published a series of papers (2,3,4) detailing the crucial role that kinetic energy plays in chemical bonding, thereby completing the project that Slater started. This Mathcad worksheet recapitulates Slater's use of the virial theorem in studying chemical bond formation and summarizes Ruedenberg final analysis.

Equation [1] gives the virial theorem for a diatomic molecule as a function of internuclear separation, while Equation 1.4.2 is valid at the energy minimum.

$$1 \cdot T(R) + V(R) = -R\frac{d}{dR}E(R) \tag{1.4.1}$$

$$E(R_e) = \frac{v(R_e)}{2} = -T(R_e) \tag{1.4.2}$$

At non-equilibrium values for the internuclear separation the virial equation can be used, with $E = T + V$, to obtain equations for the kinetic and potential energy as a function of the inter-nuclear separation.

$$T(R) := -E(R) - R\frac{d}{dR}E(R) \tag{1.4.3}$$

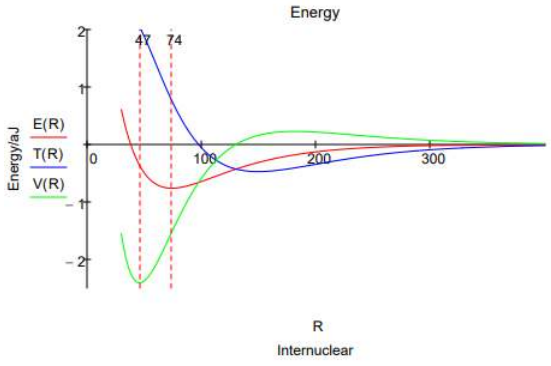
$$V(R) := 2E(R) + R\frac{d}{dR}E(R) \tag{1.4.4}$$

Thus, if $E(R)$ is known one can calculate $T(R)$ and $V(R)$ and provide a detailed energy profile for the formation of a chemical bond. $E(R)$ can be provided from spectroscopic data or from *ab initio* quantum mechanics. In this examination of the chemical bond we employ the empirical approach and use spectroscopic data for the hydrogen molecule to obtain the parameters (highlighted below) for a model of the chemical bond based on the Morse function (5). However, it should be noted that quantum mechanics tells the same story and yields an energy profile just like that shown in the following figure.

$$R \equiv 30, 30.2 \ldots 400 \quad D_e \equiv 0.761 \quad \beta = 0.0193 \quad R_e \equiv 74.1$$

$$E(R) \equiv [D_e(1 - \exp[-\beta(R - R_e)])^2 - D_e]$$

The dissociation energy, D_e, is given in atta (10^{-18}) joules, the internuclear separation in picometers, and the constant β in inverse picometers.



This energy profile shows that as the internuclear separation decreases, the potential energy rises, falls, and then rises again. The kinetic energy first decreases and then increases at about the same internuclear distance that the potential energy begins to decrease.

As the molecular orbital is formed at large R constructive interference between the two overlaping atomic orbitals draws electron density away from the nuclear centers into the internuclear region. The potential energy rises as electron density is drawn away from the nuclei, but the total energy decreases because of a larger decrease in kinetic energy due to charge delocalization. Thus a decrease in kinetic energy funds the initial build up of charge between the nuclei that we normally associate with chemical bond formation.

Following this initial phase, at an internuclear separation of about 180 pm the potential energy begins to decrease and the kinetic energy increases, both sharply (eventually), while the total energy continues to decrease gradually. This is an atomic effect, not a molecular one as Ruedenberg so clearly showed. The initial transfer of charge away from the nuclei and into the bond region allows the atomic orbitals to contract significantly (α increases) causing a large decrease in potential energy because the electron density has moved, on average, closer to the nuclei. The kinetic energy increases because the orbitals are smaller and kinetic energy increases inversely with the square of the orbital radius.

An energy minimum is reached while the potential energy is still in a significant decline (6), indicating that kinetic energy is the immediate cause of a stable bond and the molecular ground state in H_2. The final increase in potential energy which is due mainly to nuclear-nuclear repulsion, and not electron-electron repulsion, doesn't begin until the internuclear separation is less than 50 pm, while the equilibrium bond length is 74 pm . Thus the common explanation that an energy minimum is reached because of nuclear-nuclear repulsion does not have merit.

The H_2 ground state, E = -0.761 aJ, is reached at an internuclear separation of 74 pm (1.384 a0). In light of the previous arguments it is instructive to partition the total H2 electron density into atomic and molecular contributions. Each electron is in a molecular orbital which is a linear combination of hydrogenic 1s orbitals, as is shown below.

$$\Psi_{mo} = \frac{\Psi_{1sa} + \Psi_{1sb}}{\sqrt{2 + 2S_{ab}}} \quad where \quad \Psi_{1sa} = \sqrt{\frac{\alpha^3}{\pi}} \exp(-\alpha r_a) \quad \Psi_{1sb} = \sqrt{\frac{\alpha^3}{\pi}} \exp(-\alpha r_b)$$

The total electron density is therefore $2\Psi_{MO}^2$. The atomic, or non-bonding, electron density is given by the following equation, which represents the electron density associated with two non-interacting atomic orbitals.

$$\rho_n = 2\left(\left|\frac{\Psi_{1sa} + i\Psi_{1sb}}{\sqrt{2}}\right|\right)^2 = \Psi_{1sa}^2 + \Psi_{1sb}^2$$

Clearly, the bonding electron density must be the difference between the total electron density and the non-bonding, or atomic, electron density.

$$\rho_b = \Psi_{MO}^2 - \rho_n = \rho_t - \rho_n$$

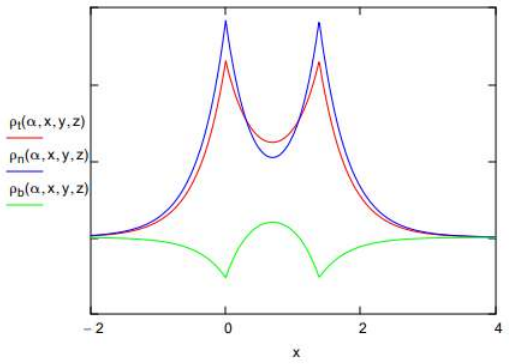
These three terms are plotted along the bond axis in the figure below. Alpha is the optimum orbital scale factor, S_{ab} is the overlap integral, and R is the equilibrium internuclear distance in atomic units.

$$\alpha := 1.197 \quad S_{ab} := 0.681 \quad R := 1.384 \quad y := 0 \quad z := 0 \quad x := -3, -2.99 \ldots 5$$

$$\rho_t(\alpha, x, y, z) := \frac{\frac{\alpha^3}{\pi}\left[\exp(-\alpha\sqrt{x^2 + y^2 + z^2}) + \exp(-\alpha\sqrt{(x-R)^2 + y^2 + z^2})\right]^2}{1 + S_{ab}}$$

$$\rho_n(\alpha, x, y, z) := \frac{\alpha^3}{\pi}\left[\exp(-2\alpha\sqrt{x^2 + y^2 + z^2}) + \exp(-2\alpha\sqrt{(x-R)^2 + y^2 + z^2})\right]$$

$$\rho_b(\alpha, x, y, z) := \rho_t(\alpha, x, y, z) - \rho_n(\alpha, x, y, z)$$



The bonding electron density illustrates that constructive interference accompanying atomic orbital overlap transfers charge from the nuclei into the internuclear region, while the non-bonding density clearly shows the subsequent atomic orbital contraction which draws some electron density back toward the nuclei.

Literature cited:

1. Slater, J. C. *J. Chem. Phys.* 1933, **1**, 687-691.
2. Ruedenberg, K. *Rev. Mod. Phys.* 1962, **34**, 326-352.
3. Feinberg, M. J.; Ruedenberg, K. *J. Chem. Phys.* 1971, **54**, 1495-1511; 1971, **55**, 5804-5818.
4. Feinberg, M. J.; Ruedenberg, K.; Mehler, E. L. *Adv. Quantum Chem.* 1970, **5**, 27-98.
5. McQuarrie, D. A.; Simon, J. D. *Physical Chemistry: A Molecular Approach*, University Science Books, Sausalito, CA, 1997, p. 165.
6. Slater, J. C. *Quantum Theory of Matter*, Krieger Publishing, Huntington, N.Y., 1977, pp. 405-408.
7. Rioux, F. *The Chemical Educator*, 1997, **2**, No. 6.

I close with a rather mystical description of the chemical bond by Charles A. Coulson, the author of Valence, an influential monograph on the chemical bond published in 1952.

> *Sometimes it seems to me that a bond between two atoms has become so real, so tangible, so friendly, that I can almost see it. Then I awake with a little shock, for a chemical bond is not a real thing. It does not exist. No one has ever seen one. No one ever will. It is a figment of our own imagination.... Here is a strange situation. The tangible, the real, the solid, is explained by the intangible, the unreal, the purely mental.*

Addendum: The Bohr Model of Atomic and Molecular Stability

The purpose of this study was to outline the success of quantum mechanics in explaining the stability and structure of matter. But quantum mechanics didn't emerge out of a vacuum; it had a precursor – the Bohr model. So I thought it appropriate to take a brief look at that precursor and present its explanation of atomic and molecular stability.

> *My starting point (for the development of the Bohr model) was not at all the idea that an atom is a small-scale planetary system and as such governed by the laws of astronomy. I never took things as literally as that.* ***My starting point was rather the stability of matter, a pure miracle when considered from the standpoint of classical physics.*** *-Niels Bohr*

All matter consists of elements that are made up of electrons, protons and neutrons. Given that the electron and the proton have opposite charges and therefore are attracted to one another provides the problem that classical physics has in explaining the stability of matter. What keeps these oppositely charged building blocks apart? There is no more fundamental question in science and Bohr was the first to attempt an explanation of atomic stability by creating, by fiat, the necessary rudimentary quantum mechanical concepts.

We begin with the Bohr model for the simplest element, the hydrogen atom. In the following tutorial the Bohr model is enriched with de Broglie's hypothesis of wave properties for the electron. This allows the reinterpretation of some of the apparently arbitrary features of Bohr's initial atomic model.

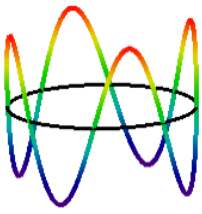
A deBroglie-Bohr Model for the Hydrogen Atom

The 1913 Bohr model of the hydrogen atom was replaced by Schrödinger′s wave mechanical model in 1926. However, Bohr′s model is still profitably taught today because of its conceptual and mathematical simplicity, and because it introduced a number of key quantum mechanical ideas such as the quantum number, quantization of observable properties, quantum jump and stationary state.

Bohr calculated the manifold of allowed electron energies by balancing the mechanical forces (centripetal and electron-nucleus) on an electron executing a circular orbit of radius R about the nucleus, and then arbitarily quantizing its angular momentum. Finally by fiat he declared that the electron was in a non-radiating stationary state because an orbiting (accelerating) charge radiates energy and will collapse into the oppositely charge nucleus. In 1924 de Broglie postulated wave-particle duality for the electron and other massive particles, thereby providing the opportunity to remove some of the arbitariness from Bohr′s model. For example, an electron possessing wave properties is subject to constructive and destructive interference. As will be shown this leads naturally to quantization of electron momentum and kinetic energy, and consequently a manifold of allowed energy states for the electron relative to the nucleus.

The de Broglie-Bohr model of the hydrogen atom presented here treats the electron as a particle on a ring with wave-like properties.

$\lambda = \frac{h}{m_e \nu}$	(1.4.5)	de Broglie′s hypothesis that matter has wave-like properties
$n\lambda = 2\pi r$	(1.4.6)	The consequence of de Broglie′s hypothesis; an integral number of wavelengths must fit within the circumference of the orbit. This introduces the quantum number which can have values 1,2,3,... The n = 4 electron state is shown below.



$m_e \nu = \frac{n \cdot h}{2\pi r}$	(1.4.7)	Substitution of the first equation into the second equation reveals that momentum is quantized.
$T = \frac{1}{2} m_e \nu^2 = \frac{n^2 h^2}{8\pi^2 m_e r^2}$	(1.4.8)	If momentum is quantized, so is kinetic energy.
$E = T + V = \frac{n^2 h^2}{8\pi^2 m_e r^2} - \frac{e^2}{4\pi\epsilon_0 r}$	(1.4.9)	Which means that total energy is quantized. The second term is the electron-proton electrostatic potential energy.

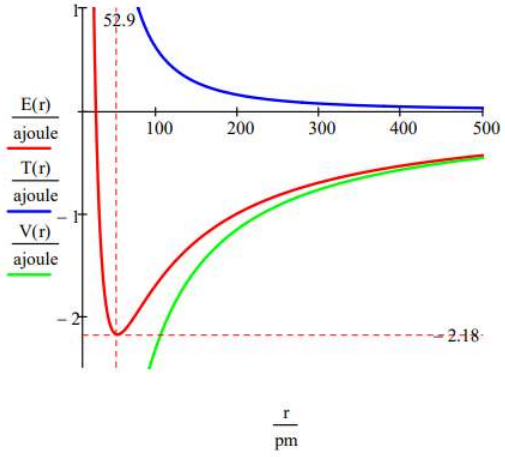
The quantum mechanical interpretation of these ″Bohr orbits″ is that they are stationary states. In spite of the fact that we use the expression kinetic energy, which implies electron motion, there is no motion. The electron **occupies** the orbit as a particle-wave, it is **not orbiting** the nucleus. If it was orbiting in a classical sense it would radiate energy and quickly collapse into the nucleus. Clearly the stability of matter requires the quantum mechanical version of kinetic energy.

The ground state energy and orbit radius of the electron in the hydrogen atom is found by plotting the energy as a function of the orbital radius. The ground state is the minimum in the total energy curve. Naturally calculus can be used to obtain the same information by minimizing the energy with respect to the orbit radius. However, the graphical method has the virtue of illuminating the issue of atomic stability.

Fundamental constants: electron charge, electron mass, Planck's constant, vacuum permitivity.	$e := 1.6021777 \times 10^{-19}\ coul$	$m_e := 9.10939 \times 10^{-31}\ kg$
	$h := 6.62608 \times 10^{-34}\ joule \cdot sec$	$\epsilon_0 := 8.85419 \times 10^{-12}\ \frac{coul^2}{joule \cdot m}$

Quantum number and conversion factor between meters and picometers and joules and attojoules.	$n := 1 \qquad pm := 10^{-12}\ m \qquad ajoule := 10^{-18}\ joule$

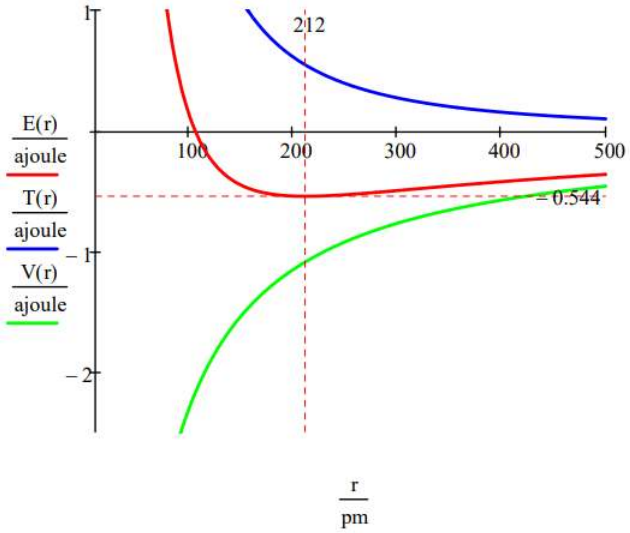
$$r := 20, 20.5 \ldots 500\ pm \quad T(r) := \frac{n^2 h^2}{8\pi^2 m_e r^2} \quad V(r) := \frac{e^2}{4\pi\epsilon_0 r} \quad E(r) := T(r) + V(r)$$



This figure shows that atomic stability involves a balance between potential and kinetic energy. The electron is drawn toward the nucleus by the attractive potential energy interaction (~ -1/R), but is prevented from collapsing into the nucleus by the extremely large kinetic energy (~$1/R^2$) associated with small orbits.

As shown below, the graphical approach can also be used to find the electronic excited states.

$$n := 2 \quad T(r) := \frac{n^2 h^2}{8\pi^2 m_e r^2} \quad V(r) := -\frac{e^2}{4\pi\epsilon_0 r} \quad E(r) := T(r) + V(r)$$



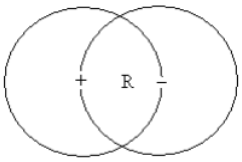
As mentioned earlier the manifold of allowed electron energies can also be obtained by minimizing the energy with respect to the orbit radius. This procedure yields,

$$E_n = -\frac{m_e e^4}{2(4\pi\epsilon_0)^2\hbar^2}\frac{1}{n^2} \quad and \quad r_n = \frac{4\pi\epsilon_0\hbar^2}{m_e e^2}n^2$$

The Bohr model gives correct results for any one-electron atomic atom or ion. The following tutorial shows that it is also accurate when applied to the rather esoteric and short-lived hydrogen atom analog positronium, in which the proton is replaced the positron, the electron's antiparticle.

A deBroglie-Bohr Model for Positronium

Positronium is a metastable bound state consisting of an electron and its positron antiparticle. In other words it might be thought of as a hydrogen atom in which the proton is replaced by a positron. Naturally it decays quickly after formation due to electron-positron annihilation. However, it exists long enough for its ground state energy, -0.25 E_h, to be determined. The purpose of this tutorial is to calculate this value using the Bohr model for positronium shown below.



The electron **occupies** a circular orbit of radius R which has a positron at its center. Likewise the positron **occupies** a circular orbit of radius R which has an electron at its center. Occupies has been emphasized to stress that there is no motion, no orbiting. Both particles are behaving as waves (this is the meaning of wave-particle duality) occupying the orbit. As waves they are subject to interference, and to avoid destructive interference the wavelength for the ground state is one orbit circumference.

$$\lambda = 2\pi R$$

Introducing the de Broglie relationship between wavelength and momentum, $\lambda = \frac{h}{p}$, yields the following expression for momentum in atomic units (h = 2π).

$$p = \frac{h}{2\pi R} = \frac{1}{R}$$

In atomic units $m_e = m_p = 1$. Therefore, the kinetic energy of each particle is,

$$T = \frac{p^2}{2m} = \frac{1}{2R^2}$$

The total energy of positronium is the sum of electron and positron kinetic energies and their coulombic potential energy.

$$E = T_e + T_p + V_{ep} = \frac{1}{2R^2} + \frac{1}{2R^2} - \frac{1}{R} = \frac{1}{R^2} - \frac{1}{R}$$

Energy minimization with respect to the electron-positron distance R yields the following result.

$$\frac{d}{dR}\left(\frac{1}{R^2} - \frac{1}{R}\right) = 0 \quad \text{solve, } R \to 2$$

The optimum R value yields a ground state energy of -0.25 Eh, in agreement with experiment.

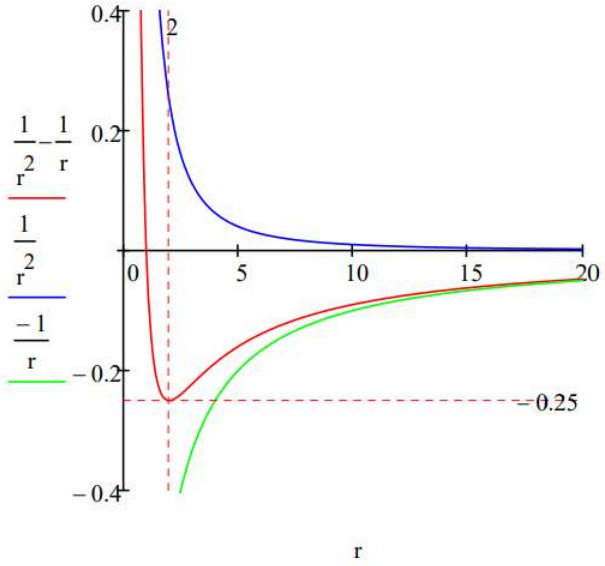
$$E = \frac{1}{R^2} - \frac{1}{R} \quad \text{substitute, } R = 2 \to E = -\frac{1}{4}$$

Including the symbols for mass in the kinetic energy contributions facilitates the introduction of the concept of effective mass of the composite system.

$$T = \frac{1}{2m_eR^2} + \frac{1}{2m_pR^2} = \frac{1}{2R^2}\left(\frac{1}{m_e} + \frac{1}{m_p}\right) = \frac{1}{2R^2}\left(\frac{m_e + m_p}{m_e \cdot m_p}\right) = \frac{1}{2\mu_{ep}R^2}$$

$$\mu_{ep} = \frac{m_e \cdot m_p}{m_e + m_p} = \frac{1 \cdot 1}{1 + 1} = \frac{1}{2}$$

The positronium energy minimum can also be located graphically.



Plotting kinetic and potential energy along with total energy reveals that a ground state is achieved because beginning at R = 2, the kinetic energy is approaching positive infinity more quickly than the potential energy is approaching negative infinity.

After reviewing the Bohr model for the hydrogen atom, the following tutorial outlines Bohr's model for the hydrogen molecule. It shows that it yields plausible values for bond energy and bond length.

Extracting Atomic and Molecular Parameters From the de Broglie-Bohr Model of the Atom

The 1913 Bohr model of the hydrogen atom was replaced by Schrödinger′s wave mechanical model in 1926. However, Bohr′s model is still profitably taught today because of its conceptual and mathematical simplicity, and because it introduced a number of key quantum mechanical ideas such as the quantum number, quantization of observable properties, quantum jump and stationary state. In addition it provided realistic values for such parameters as atomic and molecular size, electron ionization energy, and molecular bond energy.

In his ″planetary″ model of the hydrogen atom Bohr began with a Newtonian analysis of the electron executing a circular orbit of radius R about a stationary nucleus, and then arbitrarily quantized the electron′s angular momentum. Finally, by fiat he declared

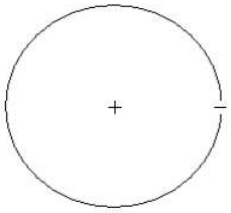
that the electron was in a non-radiating stationary state because an orbiting (accelerating) charge radiates energy and will collapse into the oppositely charge nucleus.

In 1924 de Broglie postulated wave-particle duality for the electron and other massive particles, thereby providing the opportunity to remove some of the arbitrariness from Bohr′s model. For example, an electron possessing wave properties is subject to constructive and destructive interference. As will be shown this leads naturally to quantization of electron momentum and kinetic energy, and consequently to a stable ground state for the hydrogen atom.

The de Broglie-Bohr model of the hydrogen atom presented here treats the electron as a particle on a ring with wave-like properties. The key equation is wave-particle duality as expressed by the de Broglie equation. The particle concept momentum and the wave concept λ are joined in a reciprocal relationship mediated by the ubiquitous Planck′s constant.

$$p = \frac{h}{\lambda}$$

This equation will be used with the Bohr model of the hydrogen atom to explain atomic stability and to generate estimates of atomic size and electron binding energy in the atom.



In the de Broglie version of the Bohr hydrogen atom we say that the electron **occupies** a ring of radius R. It is not orbiting the nucleus, it is behaving as a stationary wave. In order to avoid self-interference the following wavelength restriction must be obeyed for the ground state of the hydrogen atom.

$$\lambda = 2\pi R$$

When combined with the de Broglie equation it reveals the following restriction on the electron′s particle property, linear momentum.

$$p = \frac{h}{2\pi R}$$

This means there is also a restriction on the electron′s kinetic energy. Use of this equation in the classical expression for kinetic energy yields the quantum mechanical kinetic energy or more accurately electron confinement energy

$$T = \frac{p^2}{2m} = \frac{h^2}{8\pi^2 m R^2} = \frac{1}{2R^2}$$

In this equation we have moved from the classical definition of kinetic energy to the quantum mechanical version expressed on the right in atomic units.

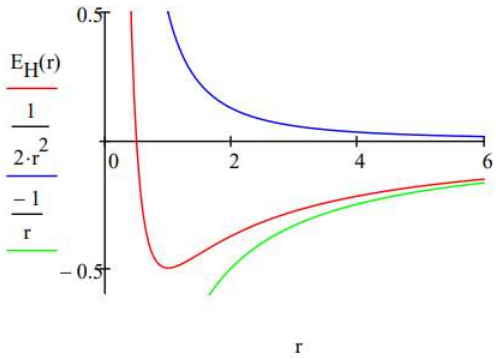
$$\frac{h}{2\pi} = m = e = 4\pi\epsilon_0 = 1$$

The electrostatic potential energy retains its classical definition in quantum mechanics.

$$V = \frac{-e^2}{4\pi\epsilon_0 R} = \frac{-1}{R}$$

The total electron energy, $E_H(R) = T(R) + V(R)$, is now minimized with respect to the ring or orbit radius, the only variational parameter in the model. The total energy, and kinetic and potential energy are also displayed as a function of ring radius.

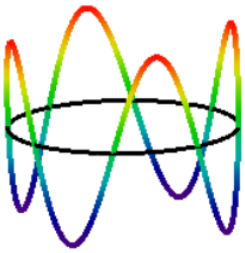
$$R := 0.5 \quad E_H(R) := \frac{1}{2R^2} - \frac{1}{R} \quad R := \text{Minimize}(E_H, R) \quad R = 1.000 \quad E_H(R) = -0.500$$



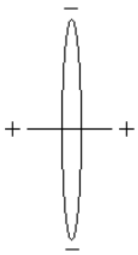
From this simple model we learn that it is the wave nature of the electron that explains atomic stability. The electron′s ring does not collapse into the nucleus because kinetic (confinement) energy goes to positive infinity ($\sim R^{-2}$) faster than potential energy goes to negative infinity ($\sim -R^{-1}$). This is seen very clearly in the graph. The ground state is due to the sharp increase in kinetic energy as the ring radius decreases. This is a quantum effect, a consequence of de Broglie′s hypothesis that electrons have wave-like properties. As Klaus Ruedenberg has written, ″There are no ground states in classical mechanics.″

The minimization process above the figure provides the ground state ring radius and electron energy in atomic units, a_0 and Eh, respectively. R = 1 a_0 = 52.9 pm gives us the benchmark for atomic size. Tables of atomic and ionic radii carry entries ranging from approximately half this value to roughly five or six times it. The ground state (binding) energy, E = -0.5 Eh = -13.6 eV = -1312 kJ/mol, is the negative of the ionization energy. This value serves as a benchmark for how tightly electrons are held in atoms and molecules.

A more comprehensive treatment of the Bohr atom utilizing the restriction that an integral number of wavelengths must fit within the ring, $n\lambda = 2\pi R$, where n = 1, 2, 3, ... reveals a manifold of allowed energy states ($-0.5\ E_h/n^2$) and the basis for Bohr′s concept of the quantum jump which ″explained″ the hydrogen atom emission spectrum. Here for example is the n = 4 Bohr atom excited state.



Rudimentary estimates of some molecular parameters, the most important being bond energy and bond length, can be obtained using the following Bohr model for H_2. The distance between the protons is D, the electron ring radius is R, and the bond axis is perpendicular to the plane of the ring



There are eight contributions to the total molecular energy based on this model: electron kinetic energy (2), electron-proton potential energy (4), proton-proton potential energy (1) and electron-electron potential energy (1).

$$E_{H2}(R,D) := \frac{1}{R^2} - \frac{4}{\sqrt{R^2 + (\frac{D}{2})^2}} + \frac{1}{D} + \frac{1}{2R}$$

Minimization of the energy with respect to ring radius and proton-proton distance yields the following results.

$$D := 2 \quad \begin{pmatrix} R \\ D \end{pmatrix} := \text{Minimize}(E_{H2}, R, D) \quad \begin{pmatrix} R \\ D \end{pmatrix} = \begin{pmatrix} 0.953 \\ 1.101 \end{pmatrix} \quad E_{H2}(R,D) = -1.100$$

The H-H bond energy is the key parameter provided by this analysis. We see that it predicts a stable molecule and that the energy released on the formation of H_2 is 0.1 E_h or 263 kJ/mol, compared with the experimental value of 458 kJ/mol. The model predicts a H-H bond length of 58 pm (D.52.9 pm), compared to the literature value of 74 pm. These results are acceptable given the primitive character of the model.

$$H + H = H_2$$

$$\Delta E_{bond} := E_{H2}(R,D) = -2E_H(1) \quad \Delta E_{bond} = -0.100$$

In addition to these estimates of molecular parameters, the model clearly shows that molecular stability depends on a balancing act between electron-proton attraction and the "repulsive" character of electron kinetic energy. Just as in the atomic case, it is the $1/R^2$ dependence of kinetic (confinement) energy on ring radius that prevents molecular collapse under electron-proton attraction. As the energy profile provided in the Appendix shows, the immediate cause of the molecular ground state is a rise in kinetic energy. Potential energy is still declining at this point and does not begin to rise until 0.55 a_0, well after the ground state is reached at 1.10 a_0.

Although the model is a relic from the early days of quantum theory it still has pedagogical value. Its mathematical simplicity clearly reveals the importance of the wave nature of matter, the foundational concept of quantum theory.

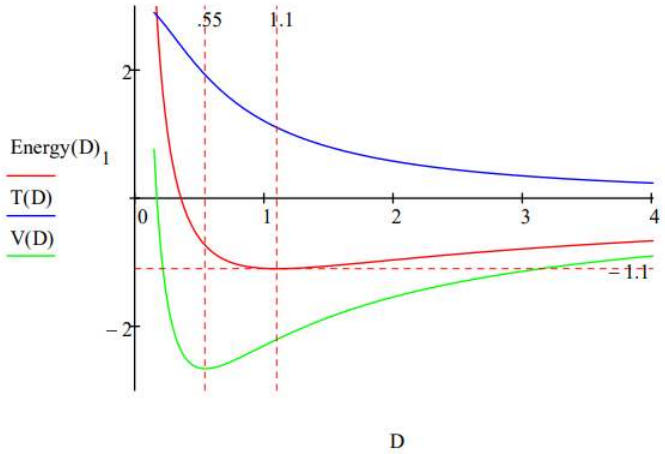
Two relatively recent appraisals of Bohr's models of atomic and molecular structure have been appeared in Physics Today:

- "Niels Bohr between physics and chemistry," by Helge Kragh, May 2013, 36-41.
- "Bohr's molecular model, a century later," by Anatoly Svidzinsky, Marlan Scully, and Dudley Herschbach, January 2014, 33-39.

Appendix:

$$R := 0.1 \quad \text{Energy} := -1 \quad \textit{Given}\ \text{Energy} = E_{H2}(R,D) \quad \frac{d}{dR}E_{H2}(R,D) = 0 \quad \text{Energy(D)} := \text{Find(R, Energy)}$$

$$D := 0.15, 0.16 \ldots 4 \quad T(D) := \frac{1}{[Energy(D)_0]^2} \quad V(D) := -\frac{4}{\sqrt{[Energy(D)_0]^2 + (\frac{D}{2})^2}} + \frac{1}{D} + \frac{1}{2 \cdot \text{Energy}(D)_0}$$



The examples presented in this addendum are based on classical pictures of the hydrogen atom, positronium, and the hydrogen molecule that have been moved in the quantum direction with de Broglie's hypothesis of wave-particle duality for matter. Bohr and

de Broglie are the early quantum theorists who cut a path for those who created modern quantum theory.

This page titled 1.4: Atomic and Molecular Stability is shared under a CC BY 4.0 license and was authored, remixed, and/or curated by Frank Rioux via source content that was edited to the style and standards of the LibreTexts platform.

1.5: Quantum Computation - A Short Course

The reason I was keen to include at least some mathematical descriptions was simply that in my own study of quantum computation the only time I **really** felt that I understood what was happening in a quantum program was when I examined some typical quantum circuits and followed through the equations. Julian Brown, *The Quest for the Quantum Computer*, page 6.

My reason for beginning with Julian Brown's statement is that I accept it wholeheartedly. I learn the same way. So in what follows I will present mathematical analyses of some relatively simple and representative quantum circuits that are designed to carry out important contemporary processes such as parallel computation, teleportation, data-base searches, prime factorization, quantum encryption and quantum simulation. I will conclude with a foray into the related area of Bell's theorem and the battle between local realism and quantum mechanics.

Quantum computers use superpositions, entanglement and interference to carry out calculations that are impossible with a classical computer. Click here for insightful descriptions of the non-classical character of superpositions and entangled superpositions.

To illuminate the difference between classical and quantum computation we begin with a review of the fundamental principles of quantum theory using the computational methods of matrix mechanics.

Rudimentary Matrix Mechanics

A quon (an entity that exhibits both wave and particle aspects in the peculiar quantum manner - Nick Herbert, *Quantum Reality*, page 64) has a variety of properties each of which can take on two values. For example, it has the property of hardness and can be either *hard* or *soft*. It also has the property of color and can be either black or white, and the property of taste and be *sweet* or *sour*. The treatment that follows draws on material from Chapter 3 of David Z Albert's book, *Quantum Mechanics and Experience*.

The basic principles of matrix and vector math are provided in Appendix A. An examination of this material will demonstrate that most of the calculations presented in this tutorial can easily be performed without the aid of Mathcad or any other computer algebra program. In other words, they can be done by hand.

In the matrix formulation of quantum mechanics the hardness and color states are represented by the following vectors.

$$Hard := \begin{pmatrix} 1 \\ 0 \end{pmatrix} \quad Soft := \begin{pmatrix} 0 \\ 1 \end{pmatrix} \quad Black := \begin{pmatrix} \frac{1}{\sqrt{2}} \\ \frac{1}{\sqrt{2}} \end{pmatrix} \quad White := \begin{pmatrix} \frac{1}{\sqrt{2}} \\ \frac{-1}{\sqrt{2}} \end{pmatrix}$$

Hard and *Soft* represent an **orthonormal basis** in the two-dimensional *Hardness* vector space.

Illegal pream-token (h)

Likewise *Black* and *White* are an **orthonormal basis** in the two-dimensional *Color* vector space.

Missing argument for b column declaration

The relationship between the two bases is reflected in the following projection calculations. Note: $\frac{1}{\sqrt{2}} = 0.707$

Illegal pream-token (h)

The values calculated above are probability amplitudes. The absolute square of those values is the probability. In other words, the probability that a black quon will be found to be hard is 0.5. The probability that a white quon will be found to be soft is also 0.5.

Illegal pream-token (a)

Clearly *Black* and *White* can be written as **superpositions** of *Hard* and *Soft*, and vice versa.

Illegal pream-token (a)

Hard, *Soft*, *Black* and *White* are measurable properties and the vectors representing them are eigenstates of the *Hardness* and *Color* operators with **eigenvalues** ± 1. The Identity operator is also given and will be discussed later. Of course, the *Hardness*

and *Color* operators are just the Pauli spin operators in the z- and x-directions. Later the *Taste* operator will be introduced; it is the y-direction Pauli spin operator.

Operators

$$Hardness := \begin{pmatrix} 1 & 0 \\ 0 & -1 \end{pmatrix} \qquad Color := \begin{pmatrix} 0 & 1 \\ 1 & 0 \end{pmatrix} \qquad I := \begin{pmatrix} 1 & 0 \\ 0 & 1 \end{pmatrix}$$

Eigenvalue +1	Eigenvalue -1
$Hardness \cdot Hard = \begin{pmatrix} 1 \\ 0 \end{pmatrix}$ (1.5.1) $\begin{pmatrix} 1 & 0 \\ 0 & -1 \end{pmatrix} \begin{pmatrix} 1 \\ 0 \end{pmatrix} = \begin{pmatrix} 1 \\ 0 \end{pmatrix}$	$Hardness \cdot Soft = \begin{pmatrix} 0 \\ -1 \end{pmatrix}$ (1.5.2) $\begin{pmatrix} 1 & 0 \\ 0 & -1 \end{pmatrix} \begin{pmatrix} 0 \\ 1 \end{pmatrix} = \begin{pmatrix} 0 \\ -1 \end{pmatrix}$
$Color \cdot Black = \begin{pmatrix} 0.707 \\ 0.707 \end{pmatrix}$ (1.5.3) $\begin{pmatrix} 0 & 1 \\ 1 & 0 \end{pmatrix} \begin{pmatrix} \frac{1}{\sqrt{2}} \\ \frac{1}{\sqrt{2}} \end{pmatrix} = \begin{pmatrix} 0.707 \\ 0.707 \end{pmatrix}$	$Color \cdot White = \begin{pmatrix} -0.707 \\ 0.707 \end{pmatrix}$ (1.5.4) $\begin{pmatrix} 0 & 1 \\ 1 & 0 \end{pmatrix} \begin{pmatrix} \frac{1}{\sqrt{2}} \\ \frac{-1}{\sqrt{2}} \end{pmatrix} = \begin{pmatrix} -0.707 \\ 0.707 \end{pmatrix}$

Another way of showing this is by calculating the **expectation (or average) value**. Every time the hardness of a hard quon is measured the result is +1. Every time the hardness of a soft quon is measured the result is -1.

The characteristic feature of a quantum computer is its ability to calculate in parallel. How this is accomplished is illustrated in the following one-page tutorial.

The Quantum Computer

A quantum computer exploits quantum mechanical effects such as superpositions, entanglement and interference to perform new types of calculations that are impossible on a classical computer. Quantum computation is therefore nothing less than a distinctly new way of harnessing nature. (Adapted from David Deutsch, The Fabric of Reality, page 195.)

Whereas classical computers perform operations on classical bits, which can be in one of two discrete states, 0 or 1, quantum computers perform operations on quantum bits, or qubits, which can be put into any superposition of two quantum states, |0> and |1>. Peter Pfeifer, McGraw-Hill Encyclopedia of Science and Industry.

The following example demonstrates how a quantum circuit can function as an algorithm for the evaluation of a mathematical function f(x), and how the same algorithm is capable of parallel evaluations of that function.

$$\begin{pmatrix} x & f(x) \\ 0 & 1 \\ 1 & 0 \end{pmatrix} \quad \left| \begin{array}{ccccccc} x\rangle & \cdots & \bullet & \ldots & \ldots & |x\rangle \\ & & | & & & \\ |0\rangle & \cdots & \oplus & \text{NOT} & \cdots & |f(x)\rangle \end{array} \right| \quad \hat{U}_f|x\rangle|0\rangle = |x\rangle|f(x)\rangle$$

As shown below, when |x> is |0> or |1> the circuit behaves like a classical computer yielding the value of f(x). When |x> is a superposition of |0> and |1> the circuit is a quantum computer, operating on both input values simultaneously in a single pass through the circuit, yielding both values of f(x). Note that in the latter case, the intermediate and final states are entangled Bell superpositions. The Bell states are an essential resource in many quantum information applications.

Illegal pream-token (a)

Haroche and Raimond (pages 94-95 of *Exploring the Quantum*) describe the latter process as follows: "By superposing the inputs of a computation, one operates the machine 'in parallel', making it compute simultaneously all the values of a function and keeping its state, before any final bit detection is performed, suspended in a coherent superposition of all the possible outcomes." However, as Haroche and Raimond note, on a practical level only one result can be realized for each operation of the circuit because on measurement the superposition created by the circuit collapses to one of the states forming the

superposition. Therefore, the exploitation of quantum parallelism for practical purposes such as searches and factorization requires more elaborate quantum circuits than the one presented here.

Truth tables for the quantum circuit:

Illegal pream-token (a)

The following tutorial adds a matrix analysis to the previous example of parallel calculation.

A Very Simple Example of Parallel Quantum Computation

This tutorial deals with quantum function evaluation and parallel computation. The example is taken from pages 94-95 of *Exploring the Quantum* by Haroche and Raimond. A certain function of x yields the following table of results.

$$\begin{pmatrix} x & 0 & 1 \\ f(x) & 1 & 0 \end{pmatrix}$$

First we establish that the circuit shown below yields the results given in the table, and then demonstrate that it also carries out a parallel calculation in one step using both input values of x.

$$\begin{vmatrix} |x\rangle & \cdots & \bullet & \ldots & \ldots & |x\rangle \\ & & | & & & \\ |0\rangle & \cdots & \oplus & \text{NOT} & \cdots & |f(x)\rangle \end{vmatrix} \quad \text{where, for example } |0\rangle = \begin{pmatrix} 1 \\ 0 \end{pmatrix} \quad |1\rangle = \begin{pmatrix} 0 \\ 1 \end{pmatrix}$$

The top wire carries the value of x and the bottom wire is initially set to |0 >. After operation of the controlled-NOT and NOT gates, x remains on the top wire while the bottom wire carries the value of the function, f(x). In other words,

$$\hat{U}_f|x\rangle|0\rangle = |x\rangle|f(x)\rangle$$

The quantum gates in matrix form are:

$$\text{I} := \begin{pmatrix} 1 & 0 \\ 0 & 1 \end{pmatrix} \quad \text{NOT} := \begin{pmatrix} 0 & 1 \\ 1 & 0 \end{pmatrix} \quad \text{CNOT} := \begin{pmatrix} 1 & 0 & 0 & 0 \\ 0 & 1 & 0 & 0 \\ 0 & 0 & 0 & 1 \\ 0 & 0 & 1 & 0 \end{pmatrix}$$

U_f (controlled-NOT, followed by a NOT operation on the lower wire) is a reversible operator. Doing it twice in succession on the initial two-qubit state is equivalent to the identity operation.

Kronecker is Mathcad's command for carrying out matrix tensor multiplication. Note that the identity operator is required when a wire is not involved in an operation. In what follows the quantum circuit is constructed, displayed and its reversibility demonstrated. In other words, repeating the circuit is equivalent to the identity operation. Reversibility is a crucial property in quantum computer circuitry.

$$\text{QuantumCircuit} := \text{kronecker (I, NOT)} \cdot \text{CNOT}$$

$$\text{QuantumCircuit} = \begin{pmatrix} 0 & 1 & 0 & 0 \\ 1 & 0 & 0 & 0 \\ 0 & 0 & 1 & 0 \\ 0 & 0 & 0 & 1 \end{pmatrix} \qquad \text{QuantumCircuit}^2 = \begin{pmatrix} 1 & 0 & 0 & 0 \\ 0 & 1 & 0 & 0 \\ 0 & 0 & 1 & 0 \\ 0 & 0 & 0 & 1 \end{pmatrix}$$

Given the simplicity of the matrix representing the circuit, the following calculations can easily be done by hand.

	Input	Calculation	Output
f(0) = 1	$\begin{pmatrix}1\\0\end{pmatrix} \otimes \begin{pmatrix}1\\0\end{pmatrix} = \begin{pmatrix}1\\0\\0\\0\end{pmatrix}$ (1.5.5)	$\text{QuantumCircuit} \cdot \begin{pmatrix}1\\0\\0\\0\end{pmatrix} = \begin{pmatrix}0\\1\\0\\0\end{pmatrix}$ (1.5.6)	$\begin{pmatrix}0\\1\\0\\0\end{pmatrix} = \begin{pmatrix}1\\0\end{pmatrix} \otimes \begin{pmatrix}0\\1\end{pmatrix}$ (1.5.7)
f(1) = 0	$\begin{pmatrix}0\\1\end{pmatrix} \otimes \begin{pmatrix}1\\0\end{pmatrix} = \begin{pmatrix}0\\0\\1\\0\end{pmatrix}$ (1.5.8)	$\text{QuantumCircuit} \cdot \begin{pmatrix}0\\0\\1\\0\end{pmatrix} = \begin{pmatrix}0\\0\\1\\0\end{pmatrix}$ (1.5.9)	$\begin{pmatrix}0\\0\\1\\0\end{pmatrix} = \begin{pmatrix}0\\1\end{pmatrix} \otimes \begin{pmatrix}1\\0\end{pmatrix}$ (1.5.10)

These calculations demonstrate that the quantum circuit is a valid algoritm for the calculation of f(x). We now demonstrate parallel computation by putting |x> in a balanced superposition of |0> and |1>. As shown below, the operation of the circuit yields a superposition of the previous results. The function has been evaluated for both values of x in a single pass through the circuit.

$$\frac{1}{\sqrt{2}}\begin{pmatrix}1\\1\end{pmatrix} \otimes \begin{pmatrix}1\\0\end{pmatrix} = \frac{1}{\sqrt{2}}\begin{pmatrix}1\\0\\1\\0\end{pmatrix}$$

$$\text{QuantumCircuit} \cdot \frac{1}{\sqrt{2}} \cdot \begin{pmatrix}1\\0\\1\\0\end{pmatrix} = \begin{pmatrix}0\\0.707\\0.707\\0\end{pmatrix}$$

$$\frac{1}{\sqrt{2}} \cdot \begin{pmatrix}0\\1\\1\\0\end{pmatrix} = \frac{1}{\sqrt{2}} \cdot \left[\begin{pmatrix}0\\1\\0\\0\end{pmatrix} + \begin{pmatrix}0\\0\\1\\0\end{pmatrix}\right] = \frac{1}{\sqrt{2}} \cdot \left[\begin{pmatrix}1\\0\end{pmatrix} \cdot \begin{pmatrix}0\\1\end{pmatrix} + \begin{pmatrix}0\\1\end{pmatrix} \cdot \begin{pmatrix}1\\0\end{pmatrix}\right]$$

Haroche and Raimond describe this process as follows: "By superposing the inputs of a computation, one operates the machine 'in parallel', making it compute simultaneously all the values of a function and keeping its state, before any final bit detection is performed, suspended in a coherent superposition of all the possible outcomes."

In summary, simple calculations have demonstrated how a quantum circuit can function as an algorithm for the evaluation of a mathematical function, and how the same circuit is capable of parallel evaluations of that function.

Illegal pream-token (a)

However, as Haroche and Raimond note, on a practical level only one result can be realized for each operation of the circuit because on measurement the superposition created by the circuit collapses to one of the states forming the superposition. This

is simulated with projection operators (|0><0| and |1><1|) on both registers for the four possible measurement outcomes for each value of x.

$$f(0) = 0$$

$$\left[\left|\text{kronecker}\left[\begin{pmatrix}1\\0\end{pmatrix}\cdot\begin{pmatrix}1\\0\end{pmatrix}^{\mathrm{T}},\begin{pmatrix}1\\0\end{pmatrix}\cdot\begin{pmatrix}1\\0\end{pmatrix}^{\mathrm{T}}\right]\cdot\text{QuantumCircuit}\cdot\frac{1}{\sqrt{2}}\begin{pmatrix}1\\0\\1\\0\end{pmatrix}\right|\right]^2 = 0$$

$$f(0) = 1$$

$$\left[\left|\text{kronecker}\left[\begin{pmatrix}1\\0\end{pmatrix}\cdot\begin{pmatrix}1\\0\end{pmatrix}^{\mathrm{T}},\begin{pmatrix}0\\1\end{pmatrix}\cdot\begin{pmatrix}0\\1\end{pmatrix}^{\mathrm{T}}\right]\cdot\text{QuantumCircuit}\cdot\frac{1}{\sqrt{2}}\begin{pmatrix}1\\0\\1\\0\end{pmatrix}\right|\right]^2 = 0.5$$

$$f(1) = 0$$

$$\left[\left|\text{kronecker}\left[\begin{pmatrix}0\\1\end{pmatrix}\cdot\begin{pmatrix}0\\1\end{pmatrix}^{\mathrm{T}},\begin{pmatrix}1\\0\end{pmatrix}\cdot\begin{pmatrix}1\\0\end{pmatrix}^{\mathrm{T}}\right]\cdot\text{QuantumCircuit}\cdot\frac{1}{\sqrt{2}}\begin{pmatrix}1\\0\\1\\0\end{pmatrix}\right|\right]^2 = 0.5$$

$$f(1) = 1$$

$$\left[\left|\text{kronecker}\left[\begin{pmatrix}0\\1\end{pmatrix}\cdot\begin{pmatrix}0\\1\end{pmatrix}^{\mathrm{T}},\begin{pmatrix}0\\1\end{pmatrix}\cdot\begin{pmatrix}0\\1\end{pmatrix}^{\mathrm{T}}\right]\cdot\text{QuantumCircuit}\cdot\frac{1}{\sqrt{2}}\begin{pmatrix}1\\0\\1\\0\end{pmatrix}\right|\right]^2 = 0$$

As Haroche and Raimond write, "It is, however, one thing to compute potentially at once all the values of f(x) and quite another to be able to exploit this quantum parallelism and extract from it more information than from a mundane classical computation. The final stage of information acquisition must always be a measurement." Therefore, the exploitation of quantum parallelism for practical purposes such as searches and factorization requires more elaborate quantum circuits than the one presented here.

Truth tables for quantum circuit elements:

Illegal pream-token (a)

Solving systems of equations is a relatively routine task for a quantum circuit.

Solving Equations Using a Quantum Circuit

This tutorial demonstrates the solution of two linear simultaneous equation using a quantum circuit. The circuit is taken from **arXiv:1302.1210**. See this reference for details on the experimental implementation of the circuit and also for a discussion of the potential of quantum solutions for systems of equations. Two other sources (**arXiv:1302.1946** and **1302.4310**) provide alternative quantum circuits and methods of implementation.

First we consider the conventional method of solving systems of linear equation for a particular matrix A and three different |b> vectors.

$$A|x\rangle = |b\rangle \qquad |x\rangle = A^{-1}|b\rangle$$

$$A := \begin{pmatrix}1.5 & 0.5\\0.5 & 1.5\end{pmatrix} \qquad b_1 := \frac{1}{\sqrt{2}}\begin{pmatrix}1\\1\end{pmatrix} \qquad b_2 := \frac{1}{\sqrt{2}}\begin{pmatrix}1\\-1\end{pmatrix} \qquad b_3 := \begin{pmatrix}1\\0\end{pmatrix}$$

$$A^{-1} \cdot b_1 = \begin{pmatrix} 0.354 \\ 0.354 \end{pmatrix} \quad A^{-1} \cdot b_2 = \begin{pmatrix} 0.707 \\ -0.707 \end{pmatrix} \quad A^{-1} \cdot B_3 = \begin{pmatrix} 0.75 \\ -0.25 \end{pmatrix}$$

The following quantum circuit (see arXiv:1302.1210) generates the same solutions.

Illegal pream-token (a)

In this circuit, R is the matrix of eigenvectors of matrix **A** and $\mathbf{R^T}$ its transpose. The last step on the bottom wire is the measurement of |1>, which is represented by the projection operator $\mathbf{M_1}$. The identity operator is required for cases in which a quantum gate operation is occurring on one wire and no operation is occurring on the other wire.

$$R := \text{eigenvecs(A)} \quad \text{R} = \begin{pmatrix} 0.707 & -0.707 \\ 0.707 & 0.707 \end{pmatrix} \quad \text{R}^{\text{T}} = \begin{pmatrix} 0.707 & 0.707 \\ -0.707 & 0.707 \end{pmatrix}$$

$$\text{M}_1 := \begin{pmatrix} 0 & 0 \\ 0 & 1 \end{pmatrix} \longleftarrow \begin{pmatrix} 0 \\ 1 \end{pmatrix} \cdot \begin{pmatrix} 0 & 1 \end{pmatrix} \quad \text{I} = \begin{pmatrix} 1 & 0 \\ 0 & 1 \end{pmatrix}$$

The controlled rotation, CR(θ), is the only two-qubit gate in the circuit. The rotation angle required is determined by the ratio of the eigenvalues of **A** as shown below.

$$\text{CR}(\theta) := \begin{pmatrix} 1 & 0 & 0 & 0 \\ 0 & 1 & 0 & 0 \\ 0 & 0 & \cos\left(\frac{\theta}{2}\right) & -\sin\left(\frac{\theta}{2}\right) \\ 0 & 0 & \sin\left(\frac{\theta}{2}\right) & \cos\left(\frac{\theta}{2}\right) \end{pmatrix} \qquad \text{eigenvals(A)} = \begin{pmatrix} 2 \\ 1 \end{pmatrix} \qquad \theta := -2 \cdot \text{acos}\left(\frac{1}{2}\right)$$

The input (|b>|1>) and output (|x>|1>) states are expressed in tensor format. **Kronecker** is Mathcad's command for the tensor product of matrices.

Input |b>|1>	Quantum Circuit	Output |x>|1>
|1>" class="lt-chem-135493">	Illegal pream-token (a)	

This page titled 1.5: Quantum Computation - A Short Course is shared under a CC BY 4.0 license and was authored, remixed, and/or curated by Frank Rioux via source content that was edited to the style and standards of the LibreTexts platform.

1.6: Quantum Computation- A Short Course

One of the most intriguing applications of entanglement is quantum teleportation, which uses entanglement and a classical communication channel to transfer a quantum state from one location to another. However, to truly understand teleportation it is necessary to distinguish it from cloning. So first we look at the quantum no-cloning principle followed by a one-page snapshot of teleportation.

Quantum Restrictions on Cloning

Suppose a quantum copier exists which is able to carry out the following cloning operation.

$$\begin{pmatrix} 0 \\ 1 \end{pmatrix} \overset{\text{Clone}}{\longrightarrow} \begin{pmatrix} 0 \\ 1 \end{pmatrix} \otimes \begin{pmatrix} 0 \\ 1 \end{pmatrix} = \begin{pmatrix} 0 \\ 0 \\ 0 \\ 1 \end{pmatrix}$$

Next the cloning operation (using the same copier) is carried out on the general qubit shown below.

$$\begin{pmatrix} \cos(\theta) \\ \sin(\theta) \end{pmatrix} \overset{\text{Clone}}{\longrightarrow} \begin{pmatrix} \cos(\theta) \\ \sin(\theta) \end{pmatrix} \otimes \begin{pmatrix} \cos(\theta) \\ \sin(\theta) \end{pmatrix} = \begin{pmatrix} \cos^2(\theta) \\ \cos(\theta)\sin(\theta) \\ \cos(\theta)\sin(\theta) \\ \sin^2(\theta) \end{pmatrix}$$

Quantum transformations are unitary, meaning probability is preserved. This requires that the scalar products of the initial and final states must be the same.

Initial state:

$$\begin{pmatrix} \cos(\theta) & \sin(\theta) \end{pmatrix} \begin{pmatrix} 0 \\ 1 \end{pmatrix} = \sin(\theta)$$

Final state:

$$\begin{pmatrix} \cos^2(\theta) & \cos(\theta)\sin(\theta) & \sin(\theta)\cos(\theta) & \sin^2(\theta) \end{pmatrix} \begin{pmatrix} 0 \\ 0 \\ 0 \\ 1 \end{pmatrix} = \sin^2(\theta)$$

It is clear from this analysis that quantum theory puts a significant restriction on copying. Only states for which sin(θ) = 0 or 1 (0 and 90 degrees) can be copied by the original cloner.

In conclusion, two quotes from Wootters and Zurek, *Physics Today*, February 2009, page 76.

> *Perfect copying can be achieved only when the two states are orthogonal, and even then one can copy those two states (...) only with a copier specifically built for that set of states.*
>
> *In sum, one cannot make a perfect copy of an unknown quantum state, since, without prior knowledge, it is impossible to select the right copier for the job. That formulation is one common way of stating the no-cloning theorem.*

An equivalent way to look at this (see arXiv:1701.00989v1) is to assume that a cloner exists for the V-H polarization states.

$$\hat{C}|V\rangle|X\rangle = |V\rangle|V\rangle \quad \hat{C}|H\rangle|X\rangle = |H\rangle|H\rangle$$

A diagonally polarized photon is a superposition of the V-H polarization states.

$$|D\rangle = \frac{1}{\sqrt{2}}(|V\rangle + |H\rangle)$$

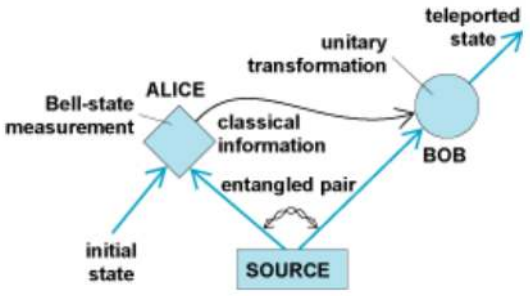
However, due to the linearity of quantum mechanics the V-H cloner cannot clone a diagonally polarized photon.

$$\hat{C}|D\rangle|X\rangle = \hat{C}\frac{1}{\sqrt{2}}(|V\rangle + |H\rangle)|X\rangle = \frac{1}{\sqrt{2}}\hat{C}(|V\rangle|X\rangle + |H\rangle|X\rangle) = \frac{1}{\sqrt{2}}(|V\rangle|V\rangle + |H\rangle|H\rangle)$$

$$\hat{C}|D\rangle|X\rangle \neq |D\rangle|D\rangle = \frac{1}{2}(|V\rangle|V\rangle + |V\rangle|H\rangle + |H\rangle|V\rangle + |H\rangle|H\rangle)$$

Quantum Teleportation

As shown in the graphic below (Nature, December 11, 1997, page 576), quantum teleportation is a form of information transfer that requires pre-existing entanglement and a classical communication channel to send information from one location to another. Alice has the photon to be teleported and a photon of an entangled pair (β_{00}) that she shares with Bob. She performs a measurement on her photons that projects them into one of the four Bell states and Bob's photon, via the entangled quantum channel, into a state that has a unique relationship to the state of the teleportee. Bob carries out one of four unitary operations on his photon depending on the results of Alice's measurement, which she sends him through a classical communication channel.



The teleportee and the Bell states indexed in binary notation:

$$\text{Teleportee:} \begin{pmatrix} \sqrt{\frac{1}{3}} \\ \sqrt{\frac{2}{3}} \end{pmatrix} \quad \text{Bell states}$$

$$: \beta_{00} = \frac{1}{\sqrt{2}} \cdot \begin{pmatrix} 1 \\ 0 \\ 0 \\ 1 \end{pmatrix} \quad \beta_{01} := \frac{1}{\sqrt{2}} \cdot \begin{pmatrix} 0 \\ 1 \\ 1 \\ 0 \end{pmatrix} \quad \beta_{10} := \frac{1}{\sqrt{2}} \cdot \begin{pmatrix} 1 \\ 0 \\ 0 \\ -1 \end{pmatrix} \quad 3_{11} = \frac{1}{\sqrt{2}} \begin{pmatrix} 0 \\ 1 \\ -1 \\ 0 \end{pmatrix}$$

The three-cubit initial state is rewritten as a linear superposition of the four possible Bell states that Alice can find on measurement.

$$|\Psi\rangle = \begin{pmatrix} \sqrt{\frac{1}{3}} \\ \sqrt{\frac{2}{3}} \end{pmatrix} \otimes \beta_{00} = \frac{1}{2} \left[\beta_{00} \otimes \begin{pmatrix} \sqrt{\frac{1}{3}} \\ \sqrt{\frac{2}{3}} \end{pmatrix} + \beta_{01} \otimes \begin{pmatrix} \sqrt{\frac{2}{3}} \\ \sqrt{\frac{1}{3}} \end{pmatrix} + \beta_{10} \otimes \begin{pmatrix} \sqrt{\frac{1}{3}} \\ -\sqrt{\frac{2}{3}} \end{pmatrix} + \beta_{11} \otimes \begin{pmatrix} -\sqrt{\frac{2}{3}} \\ \sqrt{\frac{1}{3}} \end{pmatrix} \right]$$

Alice's Bell state measurement result ($\beta_{00}, \beta_{01}, \beta_{10}$ *or* β_{11}) determines the operation (I, X, Z or ZX) that Bob performs on his photon. The matrices for these operations are as follows.

$$\mathrm{I} := \begin{pmatrix} 1 & 0 \\ 0 & 1 \end{pmatrix} \quad \mathrm{X} := \begin{pmatrix} 0 & 1 \\ 1 & 0 \end{pmatrix} \quad \mathrm{Z} := \begin{pmatrix} 1 & 0 \\ 0 & -1 \end{pmatrix} \quad \mathrm{Z} \cdot \mathrm{X} = \begin{pmatrix} 0 & 1 \\ -1 & 0 \end{pmatrix}$$

Tabular summary of teleportation experiment:

$$\begin{pmatrix} \text{Alice Measurement Result} & \beta_{00} & \beta_{01} & \beta_{10} & \beta_{11} \\ \text{Bob's Action} & I & X & Z & Z \cdot X \end{pmatrix}$$

Summary of the quantum teleportation protocol:

"Quantum teleportation provides a 'disembodied' way to transfer quantum states from one object to another at a distant location, assisted by previously shared entangled states and a classical communication channel." Nature **518**, 516 (2015)

The following tutorial provides four in-depth perspectives on teleportation.

Quantum Teleportation: Four Perspectives

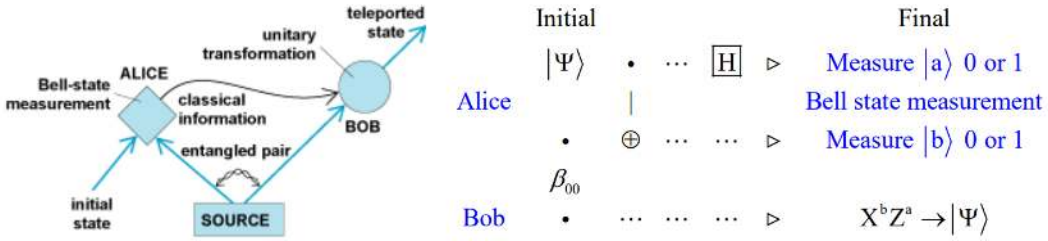
The science fiction dream of "beaming" objects from place to place is now a reality - at least for particles of light. Anton Zeilinger, Scientific American, April 2000, page 50.

Quantum teleportation is a way of transferring the state of one particle to a second, effectively teleporting the initial particle. (Tony Sudbery, Nature, December 11, 1997, page 551.)

As shown in the graphic below, quantum teleportation is a form of information transfer that requires pre-existing entanglement and a classical communication channel to send information from one location to another.

Alice has the photon to be teleported and a photon of an entangled pair that she shares with Bob. She performs a measurement on her photons that projects them into one of the four Bell states and Bob's photon, via the entangled quantum channel, into a state that has a unique relationship to the state of the teleportee. Bob carries out one of four unitary operations on his photon depending on the results of Alice's measurement, which she sends him through a classical communication channel.

The figure (Nature, December 11, 1997, page 576) on the left provides a graphic summary of the first successful teleportation experiment. The quantum circuit on the right shows a method of implementation.



The teleportee and the Bell states indexed in binary notation:

$$\text{Teleportee:} \begin{pmatrix} \sqrt{\frac{1}{3}} \\ \sqrt{\frac{2}{3}} \end{pmatrix} \quad \text{Bell states}$$

$$: \beta_{00} = \frac{1}{\sqrt{2}} \cdot \begin{pmatrix} 1 \\ 0 \\ 0 \\ 1 \end{pmatrix} \quad \beta_{01} := \frac{1}{\sqrt{2}} \cdot \begin{pmatrix} 0 \\ 1 \\ 1 \\ 0 \end{pmatrix} \quad \beta_{10} := \frac{1}{\sqrt{2}} \cdot \begin{pmatrix} 1 \\ 0 \\ 0 \\ -1 \end{pmatrix} \quad 3_{11} = \frac{1}{\sqrt{2}} \begin{pmatrix} 0 \\ 1 \\ -1 \\ 0 \end{pmatrix}$$

The three-cubit initial state is rewritten as a linear superposition of the four possible Bell states that Alice can find on measurement.

$$|0\rangle = \begin{pmatrix} 1 \\ 0 \end{pmatrix} \quad |1\rangle = \begin{pmatrix} 0 \\ 1 \end{pmatrix} \quad \mathrm{X} = \begin{pmatrix} 0 & \text{to} & 1 \\ 1 & \text{to} & 0 \end{pmatrix} \quad \mathrm{Z} = \begin{pmatrix} 0 & \text{to} & 0 \\ 1 & \text{to} & -1 \end{pmatrix}$$

$$H = \begin{bmatrix} 0 & \text{to} & \frac{(0+1)}{\sqrt{2}} \\ 1 & \text{to} & \frac{(0-1)}{\sqrt{2}} \end{bmatrix} \quad \text{CNOT} = \begin{pmatrix} 00 & \text{to} & 00 \\ 01 & \text{to} & 01 \\ 10 & \text{to} & 11 \\ 11 & \text{to} & 10 \end{pmatrix}$$

$$\mathrm{I} := \begin{pmatrix} 1 & 0 \\ 0 & 1 \end{pmatrix} \quad \mathrm{X} := \begin{pmatrix} 0 & 1 \\ 1 & 0 \end{pmatrix} \quad \mathrm{Z} := \begin{pmatrix} 1 & 0 \\ 0 & -1 \end{pmatrix} \quad H := \frac{1}{\sqrt{2}} \cdot \begin{pmatrix} 1 & 1 \\ 1 & -1 \end{pmatrix}$$

$$\mathrm{H} := \frac{1}{\sqrt{2}} \cdot \begin{pmatrix} 1 & 1 \\ 1 & -1 \end{pmatrix} \quad \text{CNOT} := \begin{pmatrix} 1 & 0 & 0 & 0 \\ 0 & 1 & 0 & 0 \\ 0 & 0 & 0 & 1 \\ 0 & 0 & 1 & 0 \end{pmatrix}$$

Perspective I.

Using the truth tables, the operation of the teleportation circuit is expressed in Dirac notation.

$$\left(\sqrt{\frac{1}{3}}|0\rangle+\sqrt{\frac{2}{3}}|1\rangle\right)\frac{1}{\sqrt{2}}(|00\rangle+|11\rangle)=\frac{1}{\sqrt{2}}\left[\sqrt{\frac{1}{3}}(|00\rangle|0\rangle+|01\rangle|1\rangle)+\sqrt{\frac{2}{3}}(|10\rangle|0\rangle+|11\rangle|1\rangle)\right]$$

$$\mathrm{CNOT}\otimes\mathrm{I}$$

$$\frac{1}{\sqrt{2}}\left[\sqrt{\frac{1}{3}}(|00\rangle|0\rangle+|01\rangle|1\rangle)+\sqrt{\frac{2}{3}}(11\rangle|0\rangle+|10\rangle|1\rangle)\right]=\frac{1}{\sqrt{2}}\left[\sqrt{\frac{1}{3}}|0\rangle(|00\rangle+|11\rangle)+\sqrt{\frac{2}{3}}|1\rangle(|10\rangle+|01\rangle)\right]$$

$$\mathrm{H}\otimes\mathrm{I}\otimes\mathrm{I}$$

$$\frac{1}{2}\left[\sqrt{\frac{1}{3}}(|0\rangle+|1\rangle)(|00\rangle+|11\rangle)+\sqrt{\frac{2}{3}}(|0\rangle-|1\rangle)(|10\rangle+|01\rangle)\right]$$

$$\downarrow$$

$$\frac{1}{2}\left[|00\rangle\begin{pmatrix}\sqrt{\frac{1}{3}}\\\sqrt{\frac{2}{3}}\end{pmatrix}+|01\rangle\begin{pmatrix}\sqrt{\frac{2}{3}}\\\sqrt{\frac{1}{3}}\end{pmatrix}+|10\rangle\begin{pmatrix}\sqrt{\frac{1}{3}}\\-\sqrt{\frac{2}{3}}\end{pmatrix}+|11\rangle\begin{pmatrix}-\sqrt{\frac{2}{3}}\\\sqrt{\frac{1}{3}}\end{pmatrix}\right]$$

$$\xrightarrow{Action}\frac{1}{2}\left[\mathrm{I}\cdot\begin{pmatrix}\sqrt{\frac{1}{3}}\\\sqrt{\frac{2}{3}}\end{pmatrix}+\mathrm{X}\cdot\begin{pmatrix}\sqrt{\frac{2}{3}}\\\sqrt{\frac{1}{3}}\end{pmatrix}+\mathrm{Z}\cdot\begin{pmatrix}\sqrt{\frac{1}{3}}\\-\sqrt{\frac{2}{3}}\end{pmatrix}+\mathrm{Z}\cdot\mathrm{X}\cdot\begin{pmatrix}-\sqrt{\frac{2}{3}}\\\sqrt{\frac{1}{3}}\end{pmatrix}\right]$$

Alice's Bell state measurement result (|00>, |01>. |10> or |11>, see indexed Bell states above) determines the operation (I, X, Z or ZX) that Bob performs on his photon.

Perspective II.

The three-cubit initial state is re-written as a linear superposition of the four possible Bell states that Alice can find on measurement. Note that this is a equivalent to the expression on the left side of the equation immediately above if the Bell states are replaced by their binary indices, as they would be after the Bell state measurement.

$$|\Psi\rangle=\begin{pmatrix}\sqrt{\frac{1}{3}}\\\sqrt{\frac{2}{3}}\end{pmatrix}\otimes\sqrt{\frac{1}{2}}\begin{pmatrix}1\\0\\0\\1\end{pmatrix}=\sqrt{\frac{1}{2}}\begin{pmatrix}\sqrt{\frac{1}{3}}\\0\\0\\\sqrt{\frac{1}{3}}\\\sqrt{\frac{2}{3}}\\0\\0\\\sqrt{\frac{2}{3}}\end{pmatrix}$$

$$=\frac{1}{2}\left[\sqrt{\frac{1}{2}}\begin{pmatrix}1\\0\\0\\1\end{pmatrix}\otimes\begin{pmatrix}\sqrt{\frac{1}{3}}\\\sqrt{\frac{2}{3}}\end{pmatrix}+\sqrt{\frac{1}{2}}\begin{pmatrix}0\\1\\1\\0\end{pmatrix}\otimes\begin{pmatrix}\sqrt{\frac{2}{3}}\\\sqrt{\frac{1}{3}}\end{pmatrix}+\sqrt{\frac{1}{2}}\begin{pmatrix}1\\0\\0\\-1\end{pmatrix}\otimes\begin{pmatrix}\sqrt{\frac{1}{3}}\\-\sqrt{\frac{2}{3}}\end{pmatrix}+\sqrt{\frac{1}{2}}\begin{pmatrix}0\\1\\-1\\0\end{pmatrix}\otimes\begin{pmatrix}-\sqrt{\frac{2}{3}}\\\sqrt{\frac{1}{3}}\end{pmatrix}\right]$$

Condensed version of the equation:

$$|\Psi\rangle=\begin{pmatrix}\sqrt{\frac{1}{3}}\\\sqrt{\frac{2}{3}}\end{pmatrix}\otimes\beta_{00}$$

$$=\frac{1}{2}\left[\beta_{00}\otimes\begin{pmatrix}\sqrt{\frac{1}{3}}\\\sqrt{\frac{2}{3}}\end{pmatrix}+\beta_{01}\otimes\begin{pmatrix}\sqrt{\frac{1}{3}}\\\sqrt{\frac{1}{3}}\end{pmatrix}+\beta_{0}\otimes\begin{pmatrix}\sqrt{\frac{1}{3}}\\-\sqrt{\frac{2}{3}}\end{pmatrix}+\beta_{11}\otimes\begin{pmatrix}-\sqrt{\frac{2}{3}}\\\sqrt{\frac{1}{3}}\end{pmatrix}\right]$$

Another way to write this equation:

$$|\Psi\rangle=\begin{pmatrix}\sqrt{\frac{1}{3}}\\\sqrt{\frac{2}{3}}\end{pmatrix}\otimes\beta_{00}$$

$$=\frac{1}{2}\left[\beta_{00}\otimes I\begin{pmatrix}\sqrt{\frac{1}{3}}\\\sqrt{\frac{2}{3}}\end{pmatrix}+\beta_{01}\otimes X\begin{pmatrix}\sqrt{\frac{1}{3}}\\\sqrt{\frac{2}{3}}\end{pmatrix}+\beta_{0}\otimes Z\begin{pmatrix}\sqrt{\frac{1}{3}}\\\sqrt{\frac{2}{3}}\end{pmatrix}+\beta_{11}\otimes X\cdot Z\begin{pmatrix}\sqrt{\frac{1}{3}}\\\sqrt{\frac{2}{3}}\end{pmatrix}\right]$$

Perspective III.

The teleportation circuit (TC) is written as a composite matrix operator which then operates on the initial three-qubit state.

$$\Psi:=\frac{1}{\sqrt{2}}\cdot\begin{pmatrix}\sqrt{\frac{1}{3}}&0&0&\sqrt{\frac{1}{3}}&\sqrt{\frac{2}{3}}&0&0&\sqrt{\frac{2}{3}}\end{pmatrix}^{\mathrm{T}}$$

$$\mathrm{TC}:=\ \mathrm{kronecker}\ (\mathrm{H},\ \mathrm{kronecker}\ (\mathrm{I},\mathrm{I}))\cdot\ \mathrm{kronecker}\ (\mathrm{CNOT},\mathrm{I})$$

After operation of the circuit the system is in a superposition state involving the **Bell state indices** on the top two registers. The third register contains a state that can easily be transformed into the teleportee once Alice tells Bob which Bell state she observed.

$$
\begin{aligned}
\underset{\cdot \Psi}{\mathrm{TC}} &= \begin{pmatrix} 0.289 \\ 0.408 \\ 0.408 \\ 0.289 \\ 0.289 \\ -0.408 \\ -0.408 \\ 0.289 \end{pmatrix} \\
&= \frac{1}{2}\left[\begin{pmatrix} 1 \\ 0 \end{pmatrix} \otimes \begin{pmatrix} 1 \\ 0 \end{pmatrix} \otimes \begin{pmatrix} \sqrt{\frac{1}{3}} \\ \sqrt{\frac{2}{3}} \end{pmatrix} + \begin{pmatrix} 1 \\ 0 \end{pmatrix} \otimes \begin{pmatrix} 0 \\ 1 \end{pmatrix} \otimes \begin{pmatrix} \sqrt{\frac{2}{3}} \\ \sqrt{\frac{1}{3}} \end{pmatrix}\right. \\
&\quad \left. + \begin{pmatrix} 0 \\ 1 \end{pmatrix} \otimes \begin{pmatrix} 1 \\ 0 \end{pmatrix} \otimes \begin{pmatrix} \sqrt{\frac{1}{3}} \\ -\sqrt{\frac{2}{3}} \end{pmatrix} + \begin{pmatrix} 0 \\ 1 \end{pmatrix} \otimes \begin{pmatrix} 0 \\ 1 \end{pmatrix} \otimes \begin{pmatrix} -\sqrt{\frac{2}{3}} \\ \sqrt{\frac{1}{3}} \end{pmatrix}\right] \\
&= \frac{1}{2}\left[\begin{pmatrix} 1 \\ 0 \\ 0 \\ 0 \end{pmatrix} \otimes \begin{pmatrix} \sqrt{\frac{1}{3}} \\ \sqrt{\frac{2}{3}} \end{pmatrix} + \begin{pmatrix} 0 \\ 1 \\ 0 \\ 0 \end{pmatrix} \otimes \begin{pmatrix} \sqrt{\frac{2}{3}} \\ \sqrt{\frac{1}{3}} \end{pmatrix} \begin{pmatrix} 0 \\ 0 \\ 1 \\ 0 \end{pmatrix} \otimes \begin{pmatrix} \sqrt{\frac{1}{3}} \\ -\sqrt{\frac{2}{3}} \end{pmatrix}\right. \\
&\quad \left. + \begin{pmatrix} 0 \\ 0 \\ 0 \\ 1 \end{pmatrix} \otimes \begin{pmatrix} -\sqrt{\frac{2}{3}} \\ \sqrt{\frac{1}{3}} \end{pmatrix}\right]
\end{aligned}
$$

Tabular summary of teleportation experiment:

$$
\begin{pmatrix} \text{Alice Measurement Result} & \beta_{00} & \beta_{01} & \beta_{10} & \beta_{11} \\ \text{Bob's Action} & I & X & Z & Z \cdot X \end{pmatrix}
$$

Bell state indices:

$$
\text{kronecker}(\mathrm{H}, \mathrm{I}) \cdot \mathrm{CNOT} \cdot \beta_{00} = \begin{pmatrix} 1 \\ 0 \\ 0 \\ 0 \end{pmatrix} \tag{1.6.1}
$$

$$
\text{kronecker}(\mathrm{H}, \mathrm{I}) \cdot \mathrm{CNOT} \cdot \beta_{01} = \begin{pmatrix} 0 \\ 1 \\ 0 \\ 0 \end{pmatrix} \tag{1.6.2}
$$

$$
\text{kronecker}(\mathrm{H}, \mathrm{I}) \cdot \mathrm{CNOT} \cdot \beta_{10} = \begin{pmatrix} 0 \\ 0 \\ 1 \\ 0 \end{pmatrix} \tag{1.6.3}
$$

$$
\text{kronecker}(\mathrm{H}, \mathrm{I}) \cdot \mathrm{CNOT} \cdot \beta_{11} = \begin{pmatrix} 0 \\ 0 \\ 0 \\ 1 \end{pmatrix} \tag{1.6.4}
$$

A similar approach is to use projection operators on the top two qubits to simulate the four measurement outcomes. See the **Appendix** for more on this method.

Bob's action

Measure $|00\rangle$ $2 \cdot \text{kronecker}\left[\begin{pmatrix}1\\0\end{pmatrix} \cdot \begin{pmatrix}1\\0\end{pmatrix}^{\mathrm{T}}\right]$, No action required.

$$\text{kronecker}\left[\begin{pmatrix}1\\0\end{pmatrix} \cdot \begin{pmatrix}1\\0\end{pmatrix}^{\mathrm{T}}, \mathrm{I}\right] \cdot \mathrm{TC} \cdot \Psi = \begin{pmatrix}0.577\\0.816\\0\\0\\0\\0\\0\\0\end{pmatrix}$$

Measure $|01\rangle$ $2 \cdot \text{kronecker}\left[\begin{pmatrix}1\\0\end{pmatrix} \cdot \begin{pmatrix}1\\0\end{pmatrix}^{\mathrm{T}}\right]$, Operate with X

$$\text{kronecker}\left[\begin{pmatrix}0\\1\end{pmatrix} \cdot \begin{pmatrix}0\\1\end{pmatrix}^{\mathrm{T}}, \mathrm{I}\right] \cdot \mathrm{TC} \cdot \Psi = \begin{pmatrix}0\\0\\0.816\\0.577\\0\\0\\0\\0\end{pmatrix}$$

Measure $|10\rangle$ $2 \cdot \text{kronecker}\left[\begin{pmatrix}0\\1\end{pmatrix} \cdot \begin{pmatrix}0\\1\end{pmatrix}^{\mathrm{T}}\right]$, Operate with Z

$$\text{kronecker}\left[\begin{pmatrix}1\\0\end{pmatrix} \cdot \begin{pmatrix}1\\0\end{pmatrix}^{\mathrm{T}}, \mathrm{I}\right] \cdot \mathrm{TC} \cdot \Psi = \begin{pmatrix}0\\0\\0\\0\\0.577\\-0.816\\0\\0\end{pmatrix}$$

Measure $|11\rangle$ $2 \cdot \text{kronecker}\left[\begin{pmatrix}0\\1\end{pmatrix} \cdot \begin{pmatrix}0\\1\end{pmatrix}^{\mathrm{T}}\right]$, Operate with ZX

$$\text{kronecker}\left[\begin{pmatrix}0\\1\end{pmatrix} \cdot \begin{pmatrix}0\\1\end{pmatrix}^{\mathrm{T}}, \mathrm{I}\right] \cdot \mathrm{TC} \cdot \Psi = \begin{pmatrix}0\\0\\0\\0\\0\\0\\-0.816\\0.577\end{pmatrix}$$

Perspective IV.

Projecting the teleportee photon 1 (green) onto the result of Alice's Bell state measurement (blue) yields the state of photon 2 which was initially entangled with Bob's photon 3. Projection of this state onto the original 2-3 entangled state (red) transforms Bob's photon to the teleportee state 25% of the time. As is now shown this happens when Alice's Bell state measurment yields β_{00}.

$$\begin{aligned}{}_{12}\langle\beta_{00}|\Psi\rangle_1\,|\beta_{00}\rangle_{23} = \frac{1}{\sqrt{2}}&\left[\begin{pmatrix}1\\0\end{pmatrix}_1^{\mathrm{T}} \otimes \begin{pmatrix}1\\0\end{pmatrix}_2^{\mathrm{T}} + \begin{pmatrix}0\\1\end{pmatrix}_1^{\mathrm{T}} \otimes \begin{pmatrix}0\\1\end{pmatrix}_2^{\mathrm{T}}\right]\begin{pmatrix}\sqrt{\frac{1}{3}}\\\sqrt{\frac{2}{3}}\end{pmatrix}_1 \frac{1}{\sqrt{2}}\\ &\left[\begin{pmatrix}1\\0\end{pmatrix}_2 \otimes \begin{pmatrix}1\\0\end{pmatrix}_3 + \begin{pmatrix}0\\1\end{pmatrix}_2 \otimes \begin{pmatrix}0\\1\end{pmatrix}_3\right]\\ = \frac{1}{2}&\begin{pmatrix}\sqrt{\frac{1}{3}}\\\sqrt{\frac{2}{3}}\end{pmatrix}_3\end{aligned}$$

An algebraic analysis of this example is as follows.

$$\begin{gathered}\text{Teleportee}\\ \frac{1}{\sqrt{2}}[{}_1\langle 0|_2\,\langle 0| + {}_1\langle 1|_2\,\langle 1|][\alpha|0\rangle_1 + \beta|1\rangle_1]\frac{1}{\sqrt{2}}[|0\rangle_2|0\rangle_3 + |1\rangle_2|1\rangle_3]\\ \downarrow\\ \frac{1}{\sqrt{2}}[\alpha_2\langle 0| + \beta_2\langle 1|]\frac{1}{\sqrt{2}}[|0\rangle_2|0\rangle_3 + |1\rangle_2|1\rangle_3]\\ \downarrow\\ \frac{1}{2}[\alpha|0\rangle_3 + \beta|1\rangle_3]\end{gathered}$$

Naturally this approach yields the same results as the previous perspectives when Alice's Bell state measurement is β_{01}, β_{10} and β_{11}. As demonstrated previously for these results Bob's action is X, Z and ZX, respectively.

$$
\begin{aligned}
{}_{12}\langle\beta_{01}|\Psi_1\rangle\,|\beta_{00}\rangle_{23} &= \frac{1}{\sqrt{2}}\left[\begin{pmatrix}1\\0\end{pmatrix}_1^{\mathrm{T}}\otimes\begin{pmatrix}0\\1\end{pmatrix}_2^{\mathrm{T}}+\begin{pmatrix}0\\1\end{pmatrix}_1^{\mathrm{T}}\otimes\begin{pmatrix}1\\0\end{pmatrix}_2^{\mathrm{T}}\right]\begin{pmatrix}\sqrt{\frac{1}{3}}\\\sqrt{\frac{2}{3}}\end{pmatrix}_1\frac{1}{\sqrt{2}}\\
&\quad\left[\begin{pmatrix}1\\0\end{pmatrix}_2\otimes\begin{pmatrix}1\\0\end{pmatrix}_3+\begin{pmatrix}0\\1\end{pmatrix}_2\otimes\begin{pmatrix}0\\1\end{pmatrix}_3\right]\\
&= \frac{1}{2}\begin{pmatrix}\sqrt{\frac{2}{3}}\\\sqrt{\frac{1}{3}}\end{pmatrix}_3
\end{aligned}
$$

$$
\begin{aligned}
{}_{12}\langle\beta_{10}|\Psi_1\rangle\,|\beta_{00}\rangle_{23} &= \frac{1}{\sqrt{2}}\left[\begin{pmatrix}1\\0\end{pmatrix}_1^{\mathrm{T}}\otimes\begin{pmatrix}0\\1\end{pmatrix}_2^{\mathrm{T}}-\begin{pmatrix}0\\1\end{pmatrix}_1^{\mathrm{T}}\otimes\begin{pmatrix}1\\0\end{pmatrix}_2^{\mathrm{T}}\right]\begin{pmatrix}\sqrt{\frac{1}{3}}\\\sqrt{\frac{2}{3}}\end{pmatrix}_1\frac{1}{\sqrt{2}}\\
&\quad\left[\begin{pmatrix}1\\0\end{pmatrix}_2\otimes\begin{pmatrix}1\\0\end{pmatrix}_3+\begin{pmatrix}0\\1\end{pmatrix}_2\otimes\begin{pmatrix}0\\1\end{pmatrix}_3\right]\\
&= \frac{1}{2}\begin{pmatrix}\sqrt{\frac{1}{3}}\\-\sqrt{\frac{2}{3}}\end{pmatrix}_3
\end{aligned}
$$

$$
\begin{aligned}
{}_{12}\langle\beta_{11}|\Psi_1\rangle\,|\beta_{00}\rangle_{23} &= \frac{1}{\sqrt{2}}\left[\begin{pmatrix}1\\0\end{pmatrix}_1^{\mathrm{T}}\otimes\begin{pmatrix}0\\1\end{pmatrix}_2^{\mathrm{T}}-\begin{pmatrix}0\\1\end{pmatrix}_1^{\mathrm{T}}\otimes\begin{pmatrix}1\\0\end{pmatrix}_2^{\mathrm{T}}\right]\begin{pmatrix}\sqrt{\frac{1}{3}}\\\sqrt{\frac{2}{3}}\end{pmatrix}_1\frac{1}{\sqrt{2}}\\
&\quad\left[\begin{pmatrix}1\\0\end{pmatrix}_2\otimes\begin{pmatrix}1\\0\end{pmatrix}_3+\begin{pmatrix}0\\1\end{pmatrix}_2\otimes\begin{pmatrix}0\\1\end{pmatrix}_3\right]\\
&= \frac{1}{2}\begin{pmatrix}-\sqrt{\frac{2}{3}}\\\sqrt{\frac{1}{3}}\end{pmatrix}_3
\end{aligned}
$$

Summary of the quantum teleportation protocol:

> *"Quantum teleportation provides a 'disembodied' way to tranfer quantum states from one object to another at a distant location, assisted by previously shared entangled states and a classical communication channel." Nature* ***518****, 516 (2015)*

The paper cited above reported the first successful teleportation of two degrees of freedom of a single photon. The analysis is somewhat more complicated than that provided in this tutorial, but the general principle is the same. The quantum channel is a hyper-entangled state shared by Alice and Bob, rather than one of the simple entangled Bell states.

Appendix:

Addendum to Perspective III.

In these calculations the required operations by Bob are actually carried out on the third qubit.

Measure |00> do nothing.	$\text{kronecker}(1,\ \text{kronecker}\ (\text{I},\text{I}))\cdot 2\cdot\ \text{kronecker}\left[\begin{pmatrix}1\\0\end{pmatrix}\cdot\begin{pmatrix}1\\0\end{pmatrix}^{\mathrm{T}},\ \text{kronecker}\left[\begin{pmatrix}1\\0\end{pmatrix}\cdot\begin{pmatrix}1\\0\end{pmatrix}^{\mathrm{T}},\text{I}\right]\cdot\text{TC}\cdot\Psi = \begin{pmatrix}0.577\\0.816\\0\\0\\0\\0\\0\\0\end{pmatrix}$
Measure |01> operate with X.	$\text{kronecker}(1,\ \text{kronecker}\ (\text{I},\text{X}))\cdot 2\cdot\ \text{kronecker}\left[\begin{pmatrix}1\\0\end{pmatrix}\cdot\begin{pmatrix}1\\0\end{pmatrix}^{\mathrm{T}},\ \text{kronecker}\left[\begin{pmatrix}0\\1\end{pmatrix}\cdot\begin{pmatrix}0\\1\end{pmatrix}^{\mathrm{T}},\text{I}\right]\cdot\text{TC}\cdot\Psi = \begin{pmatrix}0\\0\\0.577\\0.816\\0\\0\\0\\0\end{pmatrix}$
Measure |10> operate with Z.	$\text{kronecker}(1,\ \text{kronecker}\ (\text{I},\text{Z}))\cdot 2\cdot\ \text{kronecker}\left[\begin{pmatrix}0\\1\end{pmatrix}\cdot\begin{pmatrix}0\\1\end{pmatrix}^{\mathrm{T}},\ \text{kronecker}\left[\begin{pmatrix}1\\0\end{pmatrix}\cdot\begin{pmatrix}1\\0\end{pmatrix}^{\mathrm{T}},\text{I}\right]\cdot\text{TC}\cdot\Psi = \begin{pmatrix}0\\0\\0\\0\\0.577\\0.816\\0\\0\end{pmatrix}$
Measure |11> operate with ZX.	$\text{kronecker}(1,\ \text{kronecker}\ (\text{I},\text{Z}\cdot\text{X}))\cdot 2\cdot\ \text{kronecker}\left[\begin{pmatrix}0\\1\end{pmatrix}\cdot\begin{pmatrix}0\\1\end{pmatrix}^{\mathrm{T}},\ \text{kronecker}\left[\begin{pmatrix}0\\1\end{pmatrix}\cdot\begin{pmatrix}0\\1\end{pmatrix}^{\mathrm{T}},\text{I}\right]\cdot\text{TC}\cdot\Psi = \begin{pmatrix}0\\0\\0\\0\\0\\0\\0.577\\0.816\end{pmatrix}$

This page titled 1.6: Quantum Computation- A Short Course is shared under a CC BY 4.0 license and was authored, remixed, and/or curated by Frank Rioux via source content that was edited to the style and standards of the LibreTexts platform.

1.7: Quantum Computation- A Short Course

As can be seen in the previous tutorials, teleportation involves entanglement transfer. Alice projects her photons onto one of the entangled Bell states and Bob receives a photon state which using information provided via the classical communication channel can be transformed into the teleportee state. Given the importance of entanglement in quantum computing a more elaborate example of entanglement transfer is provided in the following tutorial.

An Entanglement Swapping Protocol

In the field of quantum information interference, superpositions and entangled states are essential resources. Entanglement, a non-factorable superposition, is routinely achieved when two photons are emitted from the same source, say a parametric down converter (PDC). Entanglement swapping involves the transfer of entanglement to two photons that were produced independently and never previously interacted. The Bell states are the four maximally entangled two-qubit entangled basis for a four-dimensional Hilbert space and play an essential role in quantum information theory and technology, including teleportation and entanglement swapping. The Bell states are shown below.

Illegal pream-token (a)

A four-qubit state is prepared in which photons 1 and 2 are entangled in Bell state Φ_p, and photons 3 and 4 are entangled in Bell state Ψ_m. The state multiplication below is understood to be tensor vector multiplication.

$$\Psi = \Phi_p \cdot \Psi_m = \frac{1}{\sqrt{2}} \cdot \begin{pmatrix} 1 \\ 0 \\ 0 \\ 1 \end{pmatrix} \cdot \frac{1}{\sqrt{2}} \cdot \begin{pmatrix} 0 \\ 1 \\ -1 \\ 0 \end{pmatrix}$$

$$\Psi := \frac{1}{2} \cdot \begin{pmatrix} 0 & 1 & -1 & 0 & 0 & 0 & 0 & 0 & 0 & 0 & 0 & 0 & 0 & 1 & -1 & 0 \end{pmatrix}^{\mathrm{T}} \quad \mathrm{I} := \begin{pmatrix} 1 & 0 \\ 0 & 1 \end{pmatrix}$$

Four Bell state measurements are now made on photons 2 and 3 which entangles photons 1 and 4. Projection of photons 2 and 3 onto Φ_p projects photons 1 and 4 onto Ψ_m.

$$\left(\text{kronecker} \left(\mathrm{I}, \text{kronecker} \left(\Phi_p \cdot \Phi_p^{\mathrm{T}}, \mathrm{I} \right) \right) \cdot \Psi \right)^{\mathrm{T}}$$

$$= \begin{pmatrix} 0 & 0.25 & 0 & 0 & 0 & 0 & 0 & 0.25 & -0.25 & 0 & 0 & 0 & 0 & 0 & -0.25 & 0 \end{pmatrix}$$

$$\frac{1}{2\sqrt{2}} \cdot \left[\begin{pmatrix} 1 \\ 0 \end{pmatrix} \cdot \frac{1}{\sqrt{2}} \cdot \begin{pmatrix} 1 \\ 0 \\ 0 \\ 1 \end{pmatrix} \cdot \begin{pmatrix} 0 \\ 1 \end{pmatrix} - \begin{pmatrix} 0 \\ 1 \end{pmatrix} \cdot \frac{1}{\sqrt{2}} \cdot \begin{pmatrix} 1 \\ 0 \\ 0 \\ 1 \end{pmatrix} \cdot \begin{pmatrix} 1 \\ 0 \end{pmatrix} \right]^{T}$$

$$= \frac{1}{4} \cdot \begin{pmatrix} 0 & 1 & 0 & 0 & 0 & 0 & 0 & 1 & -1 & 0 & 0 & 0 & 0 & 0 & -1 & 0 \end{pmatrix}$$

Projection of photons 2 and 3 onto Φ_m projects photons 1 and 4 onto Ψ_p.

$$\left(\text{kronecker} \left(\mathrm{I}, \text{kronecker} \left(\Phi_m \cdot \Phi_m^{\mathrm{T}}, \mathrm{I} \right) \right) \cdot \Psi \right)^{\mathrm{T}}$$

$$= \begin{pmatrix} 0 & 0.25 & 0 & 0 & 0 & 0 & 0 & -0.25 & 0.25 & 0 & 0 & 0 & 0 & 0 & -0.25 & 0 \end{pmatrix}$$

$$\frac{1}{2\sqrt{2}} \cdot \left[\begin{pmatrix} 1 \\ 0 \end{pmatrix} \cdot \frac{1}{\sqrt{2}} \cdot \begin{pmatrix} 1 \\ 0 \\ 0 \\ -1 \end{pmatrix} \cdot \begin{pmatrix} 0 \\ 1 \end{pmatrix} + \begin{pmatrix} 0 \\ 1 \end{pmatrix} \cdot \frac{1}{\sqrt{2}} \cdot \begin{pmatrix} 1 \\ 0 \\ 0 \\ -1 \end{pmatrix} \cdot \begin{pmatrix} 1 \\ 0 \end{pmatrix} \right]^{T}$$

$$= \frac{1}{4} \cdot \begin{pmatrix} 0 & 1 & 0 & 0 & 0 & 0 & 0 & -1 & 1 & 0 & 0 & 0 & 0 & 0 & -1 & 0 \end{pmatrix}$$

Projection of photons 2 and 3 onto Ψ_p projects photons 1 and 4 onto Φ_m.

$$\left(\text{kronecker} \left(\mathrm{I}, \text{kronecker} \left(\Phi_p \cdot \Phi_p^{\mathrm{T}}, \mathrm{I} \right) \right) \cdot \Psi \right)^{\mathrm{T}}$$

$$= \begin{pmatrix} 0 & 0 & -0.25 & 0 & -0.25 & 0 & 0 & 0 & 0 & 0 & 0.25 & 0 & 0.25 & 0 & 0 & 0 \end{pmatrix}$$

$$\frac{1}{2\sqrt{2}} \cdot \left[\begin{pmatrix} 0 \\ 1 \end{pmatrix} \cdot \frac{1}{\sqrt{2}} \cdot \begin{pmatrix} 0 \\ 1 \\ 1 \\ 0 \end{pmatrix} \cdot \begin{pmatrix} 0 \\ 1 \end{pmatrix} - \begin{pmatrix} 1 \\ 0 \end{pmatrix} \cdot \frac{1}{\sqrt{2}} \cdot \begin{pmatrix} 0 \\ 1 \\ 1 \\ 0 \end{pmatrix} \cdot \begin{pmatrix} 1 \\ 0 \end{pmatrix} \right]^{T}$$

$$= \frac{1}{4} \cdot \begin{pmatrix} 0 & 0 & -1 & 0 & -1 & 0 & 0 & 0 & 0 & 0 & 1 & 0 & 1 & 0 & 0 & 0 \end{pmatrix}$$

Finally, projection of photons 2 and 3 onto Φ_m projects photons 1 and 4 onto Ψ_p.

$$\left(\text{kronecker} \left(\mathrm{I}, \text{kronecker} \left(\Phi_m \cdot \Phi_m^{\mathrm{T}}, \mathrm{I} \right) \right) \cdot \Psi \right)^{\mathrm{T}}$$

$$= \begin{pmatrix} 0 & 0 & -0.25 & 0 & 0.25 & 0 & 0 & 0 & 0 & 0 & -0.25 & 0 & 0.25 & 0 & 0 & 0 \end{pmatrix}$$

$$\frac{-1}{2\sqrt{2}} \cdot \left[\begin{pmatrix} 1 \\ 0 \end{pmatrix} \cdot \frac{1}{\sqrt{2}} \cdot \begin{pmatrix} 0 \\ 1 \\ -1 \\ 0 \end{pmatrix} \cdot \begin{pmatrix} 1 \\ 0 \end{pmatrix} + \begin{pmatrix} 0 \\ 1 \end{pmatrix} \cdot \frac{1}{\sqrt{2}} \cdot \begin{pmatrix} 0 \\ 1 \\ -1 \\ 0 \end{pmatrix} \cdot \begin{pmatrix} 0 \\ 1 \end{pmatrix} \right]^{T}$$

$$= \frac{1}{4} \cdot \begin{pmatrix} 0 & 0 & -1 & 0 & 1 & 0 & 0 & 0 & 0 & 0 & -1 & 0 & 1 & 0 & 0 & 0 \end{pmatrix}$$

In our earlier examination of the quantum computer we saw that a quantum circuit can calculate all the values of f(x) simultaneously, but we can only retrieve one value due to the collapse of the superposition of answers on observation. To achieve a quantum advantage in computation requires more subtle programming techniques which exploit the effects of quantum interference. The following tutorials reveal how the quantum advantage can be achieved in several areas of practical importance.

> *While quantum mechanics could spell disaster for public-key cryptography, it may also offer salvation. This is because the resources of the quantum world appear to offer the ultimate form of secret code, one that is guaranteed by the laws of physics to be unbreakable. Julian Brown, The Quest for the Quantum Computer, page 189.*

In other words, “The quantum taketh away and the quantum giveth back!” Asher Peres

We begin with Shor’s algorithm which demonstrates how quantum entanglement and interference effects can facilitate the factorization of large integers into their prime factors. The inability of conventional computers to do this is essential to the integrity of public-key cryptography.

Factoring Using Shor's Quantum Algorithm

This tutorial presents a toy calculation dealing with quantum factorization using Shor's algorithm. Before beginning that task, traditional classical factorization is reviewed with the example of finding the prime factors of 15. As shown below the key is to find the period of **a^x modulo 15**, where **a** is chosen randomly.

$$a := 4 \qquad N := 15 \qquad f(x) := \mathrm{mod}\,(a^x, N) \qquad Q := 8 \qquad x := 0 \ldots Q - 1$$

x	f(x)
0	1
1	4
2	1
3	4
4	1
5	4
6	1
7	4

Seeing that the period of f(x) is two, the next step is to use the Euclidian algorithm by calculating the greatest common denominator of two functions involving the period and **a**, and the number to be factored, **N**.

$$\mathrm{period} := 2 \qquad \gcd\left(a^{\frac{\mathrm{period}}{2}} - 1, N\right) = 3 \qquad \gcd\left(a^{\frac{\mathrm{period}}{2}} + 1, N\right) = 5$$

We proceed by ignoring the fact that we already know that the period of f(x) is 2 and demonstrate how it is determined using a quantum (discrete) Fourier transform. After the registers are loaded with x and f(x) using a **quantum** computer, they exist in the following **superposition**.

$$\frac{1}{\sqrt{Q}} \sum_{x=0}^{Q-1} |x\rangle |f(x)\rangle = \frac{1}{2}[|0\rangle|1\rangle + |1\rangle|4\rangle + |2\rangle|1\rangle + |3\rangle|4\rangle + \cdots]$$

The next step is to find the period of f(x) by performing a quantum Fourier transform (QFT) on the input register |x>.

$$Q := 4 \qquad m := 0 \ldots Q - 1 \qquad n := 0 . Q - 1 \qquad \mathrm{QFT}_{m,n} := \frac{1}{\sqrt{Q}} \cdot \exp\left(i \cdot \frac{2 \cdot \pi \cdot m \cdot n}{Q}\right)$$

$$\mathrm{QFT} = \frac{1}{2} \cdot \begin{pmatrix} 1 & 1 & 1 & 1 \\ 1 & i & -1 & -i \\ 1 & -1 & 1 & -1 \\ 1 & -i & -1 & i \end{pmatrix}$$

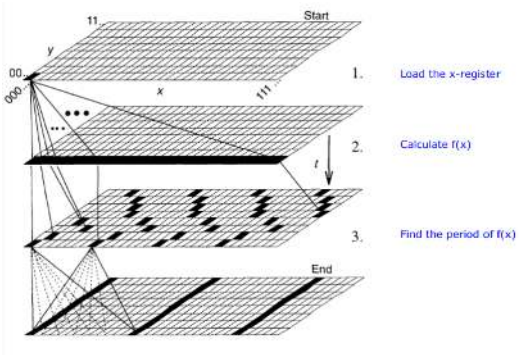
$$x = 0 \quad \mathrm{QFT} \cdot \begin{pmatrix} 1 \\ 0 \\ 0 \\ 0 \end{pmatrix} = \begin{pmatrix} 0.5 \\ 0.5 \\ 0.5 \\ 0.5 \end{pmatrix} \qquad x = 1 \quad \mathrm{QFT} \cdot \begin{pmatrix} 0 \\ 1 \\ 0 \\ 0 \end{pmatrix} = \begin{pmatrix} 0.5 \\ 0.5i \\ -0.5 \\ -0.5i \end{pmatrix}$$

$$x = 2 \quad \mathrm{QFT} \cdot \begin{pmatrix} 0 \\ 0 \\ 1 \\ 0 \end{pmatrix} = \begin{pmatrix} 0.5 \\ -0.5 \\ 0.5 \\ -0.5 \end{pmatrix} \qquad x = 3 \quad \mathrm{QFT} \cdot \begin{pmatrix} 0 \\ 0 \\ 0 \\ 1 \end{pmatrix} = \begin{pmatrix} 0.5 \\ -0.5i \\ -0.5 \\ 0.5i \end{pmatrix}$$

The operation of the QFT on the x-register is expressed algebraically in the middle term below. Quantum interference in this term yields the result on the right which shows a period of 2 on the x-register.

Illegal pream-token (a)

Figure 5 in "Quantum Computation," by David P. DiVincenzo, *Science* **270**, 258 (1995) provides a graphical illustration of the steps of Shor's factorization algorithm.



How quantum theory gives back is demonstrated by an examination of Ekert's quantum secret key proposal.

The Quantum Math Behind Ekert's Key Distribution Scheme

Alice and Bob share an entangled photon (EPR) pair in the following state.

$$|\Psi\rangle = \frac{1}{\sqrt{2}}[|\mathrm{R}\rangle_A|\mathrm{R}\rangle_B + |\mathrm{L}\rangle_A|\mathrm{L}\rangle_B] = \frac{1}{2\sqrt{2}}\left[\begin{pmatrix}1\\i\end{pmatrix}_A \otimes \begin{pmatrix}1\\i\end{pmatrix}_B + \begin{pmatrix}1\\-i\end{pmatrix}_A \otimes \begin{pmatrix}1\\-i\end{pmatrix}_B\right]$$
$$= \frac{1}{\sqrt{2}}\begin{pmatrix}1\\0\\0\\-1\end{pmatrix} = \frac{1}{\sqrt{2}}[|\mathrm{V}\rangle_A|\mathrm{V}\rangle_B - |\mathrm{H}\rangle_A|\mathrm{H}\rangle_B]$$

They agree to make random polarization measurements in the rectilinear and circular polarization bases. When a measurement is made on a quantum system the result is always an eigenstate of the measurement operator. The eigenstates in the circular and rectilinear bases are:

$$\mathrm{R} := \frac{1}{\sqrt{2}} \cdot \begin{pmatrix}1\\\mathrm{i}\end{pmatrix} \quad \mathrm{L} := \frac{1}{\sqrt{2}} \cdot \begin{pmatrix}1\\-\mathrm{i}\end{pmatrix} \quad \mathrm{V} := \begin{pmatrix}1\\0\end{pmatrix} \quad \mathrm{H} := \begin{pmatrix}0\\1\end{pmatrix}$$

Pertinent superpositions:

$$\mathrm{V} = \frac{1}{\sqrt{2}} \cdot (\mathrm{R} + \mathrm{L}) \quad \mathrm{H} = \frac{\mathrm{i}}{\sqrt{2}} \cdot (\mathrm{L} - \mathrm{R}) \quad \mathrm{R} = \frac{1}{\sqrt{2}} \cdot (\mathrm{V} + \mathrm{i} \cdot \mathrm{H}) \quad \mathrm{L} = \frac{1}{\sqrt{2}} \cdot (\mathrm{V} - \mathrm{i} \cdot \mathrm{H})$$

Alice's random measurement effectively sends a random photon to Bob due to the correlations built into the entangled state of their shared photon pair. Alice's four measurement possibilities and their consequences for Bob are now examined.

Alice's photon is found to be right circularly polarized, |R>. If Bob measures circular polarization he is certain to find his photon to be |R>. But if he chooses to measure in the rectilinear basis the probability he will observe |V> is 0.5 and the probability he will observe |H> is 0.5.

$$\frac{1}{\sqrt{2}} \cdot \mathrm{R} \cdot \mathrm{R} = \frac{1}{\sqrt{2}} \cdot \mathrm{R} \cdot \left[\frac{1}{\sqrt{2}} \cdot (\mathrm{V} + \mathrm{i} \cdot \mathrm{H})\right]$$

If Alice observes |L>, Bob will also if he measures circular polarization. But if he measures in the rectilinear basis the probability he will observe |V> is 0.5 and the probability he will observe |H> is 0.5.

$$\frac{1}{\sqrt{2}} \cdot \mathrm{L} \cdot \mathrm{L} = \frac{1}{\sqrt{2}} \cdot \mathrm{L} \cdot \left[\frac{1}{\sqrt{2}} \cdot (\mathrm{V} - \mathrm{i} \cdot \mathrm{H})\right]$$

The same kind of reasoning applies to measurements Alice makes in the rectilinear basis.

$$\frac{1}{\sqrt{2}} \cdot \mathrm{V} \cdot \mathrm{V} = \frac{1}{\sqrt{2}} \cdot \mathrm{V} \cdot \left[\frac{1}{\sqrt{2}} \cdot (\mathrm{R} + \mathrm{L})\right] \qquad \frac{1}{\sqrt{2}} \cdot \mathrm{H} \cdot \mathrm{H} = -\frac{1}{\sqrt{2}} \cdot \mathrm{H} \cdot \left[\frac{\mathrm{i}}{\sqrt{2}} \cdot (\mathrm{L} - \mathrm{R})\right]$$

Alice and Bob keep the results for the experiments for which they measured in the same basis (blue in the table below), and make the following bit value assignments: |V> = |R> = 0 and |H> = |L> = 1. This leads to the secret key on the bottom line.

Alice	R	V	V	L	H	L	H	R	V	L	H
Bob	R	L	V	L	R	H	H	R	V	V	H
Key	0		0	1			1	0	0		1

The following demonstrates how a binary message is coded and subsequently decoded using a shared binary secret key and modulo 2 arithmetic.

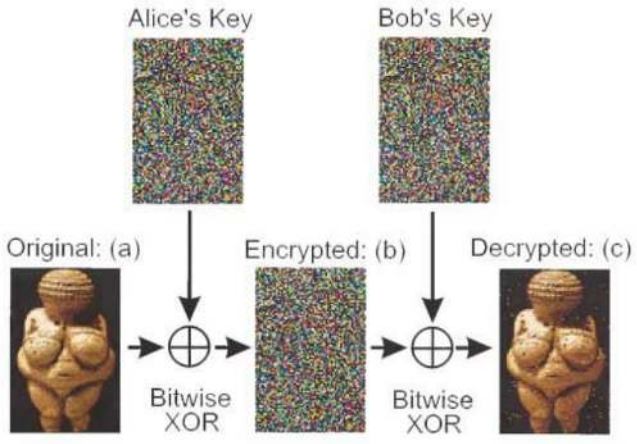
Message	Key	Coded Message	Decoded
$\mathrm{Mes} := \begin{pmatrix}0\\1\\0\\0\\0\\1\\1\\0\\0\\1\\0\\1\\0\\1\end{pmatrix}$ (1.7.1)	$\mathrm{Key} := \begin{pmatrix}0\\0\\1\\1\\0\\0\\1\\0\\0\\1\\1\\0\\0\\1\end{pmatrix}$ (1.7.2)	$\mathrm{CMes} := \mathrm{mod}(\mathrm{Mes} + \mathrm{Key}, 2) \begin{pmatrix}0\\1\\1\\1\\0\\1\\0\\0\\0\\0\\1\\1\\0\\1\end{pmatrix}$ (1.7.3)	DM := mod (CMes

It is clear by inspection that the message has been accurately decoded. This is confirmed by calculating the difference between the message and the decoded message.

$$(\mathrm{Mes} - \mathrm{DMes})^{\mathrm{T}} = \begin{pmatrix}0&0&0&0&0&0&0&0&0&0&0&0&0&0\end{pmatrix}$$

Coding and Decoding Venus

In 2000 Anton Zeilinger and his research team sent an encrypted photo of the fertility goddess Venus of Willendorf from Alice to Bob, two computers in two buildings about 400 meters apart. The figure summarizing this achievement first appeared in *Physical Review Letters* and later in a review article in *Nature*.



It is easy to produce a rudimentary simulation of the experiment. Bitwise XOR is nothing more than addition modulo 2. The original Venus and the shared key are represented by the following matrices, where the matrix elements are pixels that are either off (0) or on (1).

$$i = 1..7 \qquad j := 1..6 \qquad \mathrm{Key}_{i,j} := \mathrm{trunc}(\mathrm{md}(2))$$

$$\mathrm{Key} = \begin{pmatrix} 0 & 0 & 1 & 0 & 1 & 0 \\ 1 & 0 & 0 & 0 & 1 & 0 \\ 0 & 1 & 1 & 0 & 0 & 0 \\ 1 & 1 & 1 & 1 & 1 & 0 \\ 1 & 1 & 1 & 1 & 0 & 1 \\ 0 & 1 & 0 & 0 & 1 & 1 \\ 0 & 1 & 0 & 1 & 1 & 1 \end{pmatrix}$$

$$\mathrm{Venus} := \begin{pmatrix} 1 & 1 & 1 & 1 & 1 & 1 \\ 0 & 1 & 1 & 1 & 1 & 0 \\ 0 & 0 & 1 & 1 & 0 & 0 \\ 0 & 0 & 1 & 1 & 0 & 0 \\ 0 & 0 & 1 & 1 & 0 & 0 \\ 0 & 1 & 1 & 1 & 1 & 0 \\ 1 & 1 & 1 & 1 & 1 & 1 \end{pmatrix}$$

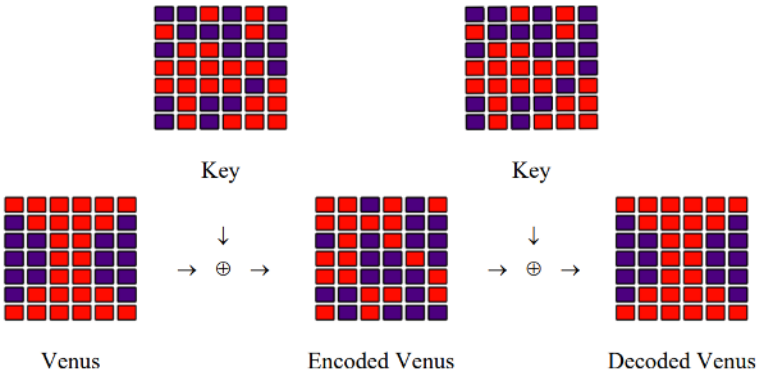
A coded version of Venus is prepared by adding Venus and the Key modulo 2 and sent to Bob.

$$C_{i,j} := \mathrm{Venus}_{i,j} \oplus Key_{i,j} \qquad \mathrm{CVenus} = \begin{pmatrix} 1 & 1 & 0 & 1 & 0 & 1 \\ 1 & 1 & 1 & 1 & 0 & 0 \\ 0 & 1 & 0 & 1 & 0 & 0 \\ 1 & 1 & 0 & 0 & 1 & 0 \\ 1 & 1 & 0 & 0 & 0 & 1 \\ 0 & 0 & 1 & 1 & 0 & 1 \\ 1 & 0 & 1 & 0 & 0 & 0 \end{pmatrix}$$

Bob adds the key to CVenus modulo 2 and sends the result to his printer.

$$\mathrm{DVenus}_{i,j} := \mathrm{CVenus}_{i,j} \oplus \mathrm{Key}_{i,j} \qquad \mathrm{DVenus} = \begin{pmatrix} 1 & 1 & 1 & 1 & 1 & 1 \\ 0 & 1 & 1 & 1 & 1 & 0 \\ 0 & 0 & 1 & 1 & 0 & 0 \\ 0 & 0 & 1 & 1 & 0 & 0 \\ 0 & 0 & 1 & 1 & 0 & 0 \\ 0 & 1 & 1 & 1 & 1 & 0 \\ 1 & 1 & 1 & 1 & 1 & 1 \end{pmatrix}$$

A graphic summary of the simulation:



This page titled 1.7: Quantum Computation- A Short Course is shared under a CC BY 4.0 license and was authored, remixed, and/or curated by Frank Rioux via source content that was edited to the style and standards of the LibreTexts platform.

1.8: Quantum Computation- A Short Course

If you are asked if two pieces of glass have the same thickness, the conventional thing to do is to measure the thickness of each piece – two measurements. As shown in the first two tutorials a double-slit apparatus and a Mach-Zehnder interferometer can answer the question with a single measurement. The third tutorial is a version of the first which shows how path information destroys interference and how the interference can be restored. The fourth tutorial summarizes David Deutsch's solution to an equivalent mathematical problem using a function introduced earlier. The double-slit apparatus, the Mach-Zehnder interferometer and Deutsch's circuit are quantum computers which use superpositions and interference effects to cut the effort of answering the question by a factor of two.

Simulating the Deutsch-Jozsa Algorithm with a Double-Slit Apparatus

The Deutsch-Jozsa algorithm determines if either **[1]** 2N numbers are either all 0 or all 1 (a constant function), or **[2]** half are 0 and half are 1 (a balanced function) in one step instead of up to 2N-1 + 1 steps. For N = 1, the Deutsch-Jozsa algorithm can be visualized as putting two pieces of glass, which may be thin (0) or thick (1), behind the apertures of a double-slit apparatus and measuring the interference pattern of a light source illuminating the slits. If the pattern is unchanged compared to the empty apparatus, the glass pieces have the same thickness (constant function); otherwise they have different thickness (balanced function). Peter Pfeifer, "Quantum Computation," Access Science, Vol. 17, p. 678, slightly modified by F.R.

This is demonstrated by calculating the diffraction pattern without glass present, and with glass present of the same thickness and different thickness. The diffraction pattern is the momentum distribution, which is the Fourier transform of the slit geometry.

Slit positions:

$$x_L = 1 \quad x_R = 2$$

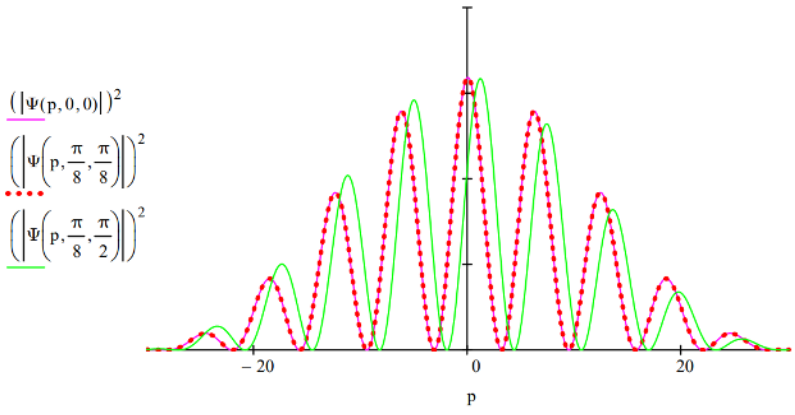
Slit width:

$$\delta := 0.2$$

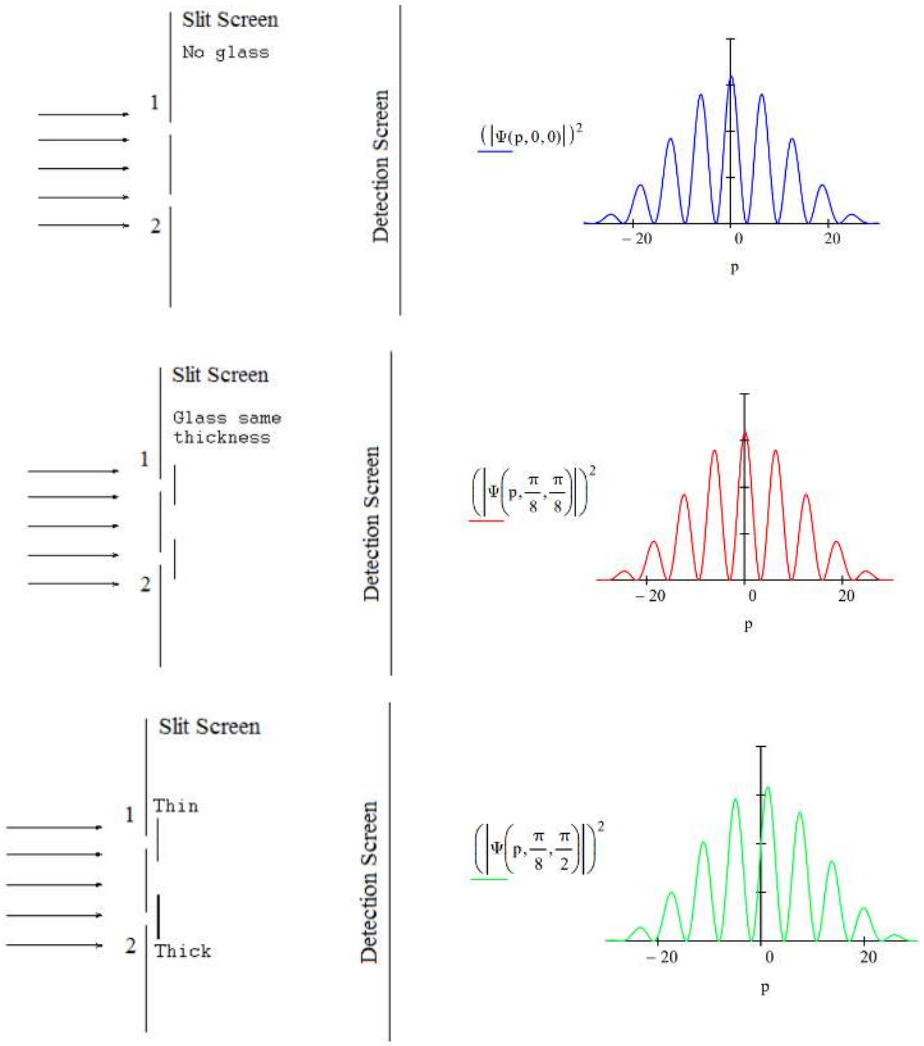
The momentum wave function with possible phase shifts θ and ϕ at the two slits is represented by the following superposition. The phase shifts are directly proportional to the thickness of the glass.

$$\Psi(p,\theta,\varphi) = \frac{\int_{x_L-\frac{\delta}{2}}^{x_L+\frac{\delta}{2}} \frac{1}{\sqrt{2\cdot\pi}} \cdot \exp(-i\cdot p\cdot x)\cdot\frac{1}{\sqrt{\delta}}dx \cdot \exp(i\cdot\theta) + \int_{x_R-\frac{\delta}{2}}^{x_R+\frac{\delta}{2}} \frac{1}{\sqrt{2\cdot\pi}} \cdot \exp(-i\cdot p\cdot x)\cdot\frac{1}{\sqrt{\delta}}dx \cdot \exp(i-\varphi)}{\sqrt{2}}$$

The diffraction patterns (momentum distributions) for the empty apparatus ($\theta = \phi = 0$), for an apparatus with glass pieces of the same thickness ($\theta = \phi = \frac{\pi}{8}$) and for one that has glass of different thickness ($\theta = \frac{\pi}{8}$ $\phi = \frac{\pi}{2}$) behind the slits are displayed below.



Another look at the calculations with graphical support on the left is provided below.



Simulating a Quantum Computer with a Mach-Zehnder Interferometer

Suppose you are asked if two pieces of glass are the same thickness. The convential thing to do is to measure the thickness of each piece of glass and then compare the results. As David Deutsch pointed out this is overkill. You were asked only if they were the same thickness, but you made two measurements to answer that question, when in fact it can be done with one.

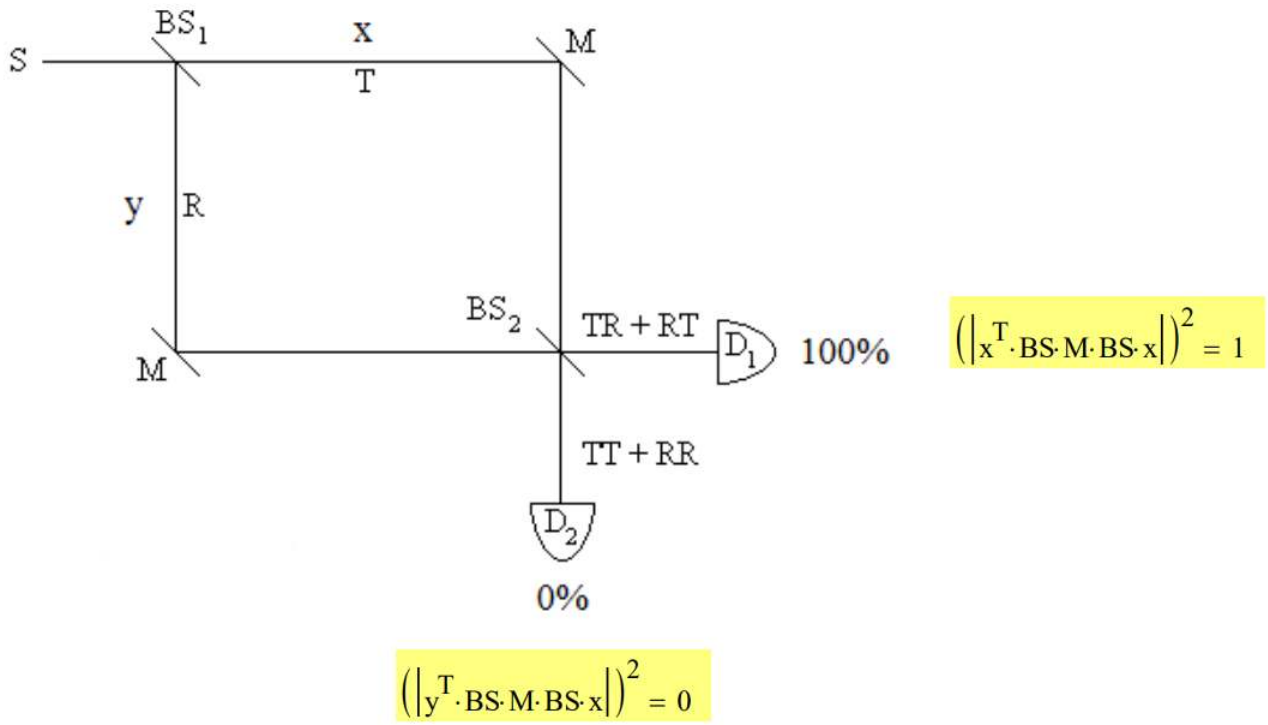
Quantum mechanics provides two ways to answer the question; using a double-slit apparatus or a Mach-Zehnder interferometer. They both operate on the same quantum principles. Using the double-slit apparatus you put a piece of glass behind each of the slits and shine light on the slits. If the resulting diffraction pattern is symmetrical about the center of the slits, the glasses are the same thickness. See the previous tutorial: Simulating the Deutsch-Jozsa Algorithm with a Double-Slit Apparatus.

Alternatively you could put a piece of glass in each arm of an equal-arm Mach-Zehnder interferometer (MZI). How this approach works is the subject of this tutorial. First we need to get acquainted with a MZI.

As shown in the following figure a MZI consists of a photon source, two 50-50 beam splitters, two mirrors and two detectors. The Appendix contains the mathematical information necessary to carry out a matrix mechanics analysis of the operation of the interferometer. The motional states of the photon are represented by vectors, while the beam splitters and mirrors are represented by matrices and operate on the vectors.

Yogi Berra has famously said "When you come to a fork in the road, take it." This is exactly what the photon does at a beam splitter. After the first beam splitter the photon, which was moving in the x-direction being emitted by the source, is now in a

superposition of moving in both the x- and y-directions. It has been transmitted and reflected at the beam splitter. By convention a 90 degree ($\frac{\pi}{2}, i$) phase shift is assigned to reflection.



$$\left(\left|x^{T}\cdot BS\cdot M\cdot BS\cdot x\right|\right)^{2}=1$$

$$\left(\left|y^{T}\cdot BS\cdot M\cdot BS\cdot x\right|\right)^{2}=0$$

The following calculations illustrate the formation of the superposition state created by the photon's interaction with the first beam splitter.

$$BS\cdot x\rightarrow\begin{pmatrix}\frac{\sqrt{2}}{2}\\ \frac{\sqrt{2}\cdot i}{2}\end{pmatrix}\qquad S=\frac{1}{\sqrt{2}}\cdot(T+iR)\qquad \frac{1}{\sqrt{2}}\cdot x+\frac{i}{\sqrt{2}}\cdot y\rightarrow\begin{pmatrix}\frac{\sqrt{2}}{2}\\ \frac{\sqrt{2}\cdot i}{2}\end{pmatrix}$$

After the initial beam splitter, the mirrors direct the transmitted and reflected photon states to a second beam splitter where they are recombined. The consequence of this in an equal arm MZI is that the photon is alway registered at D_1. There are two paths (histories) to each detector and the amplitudes for these paths interfere. To reach D_1 both paths experience one reflection and so arrive in phase with each other with their phases shifted by 90 degrees. The paths to D_2, however, are 180 degrees out of phase and destructively interfere. The photon is never detected at D_2.

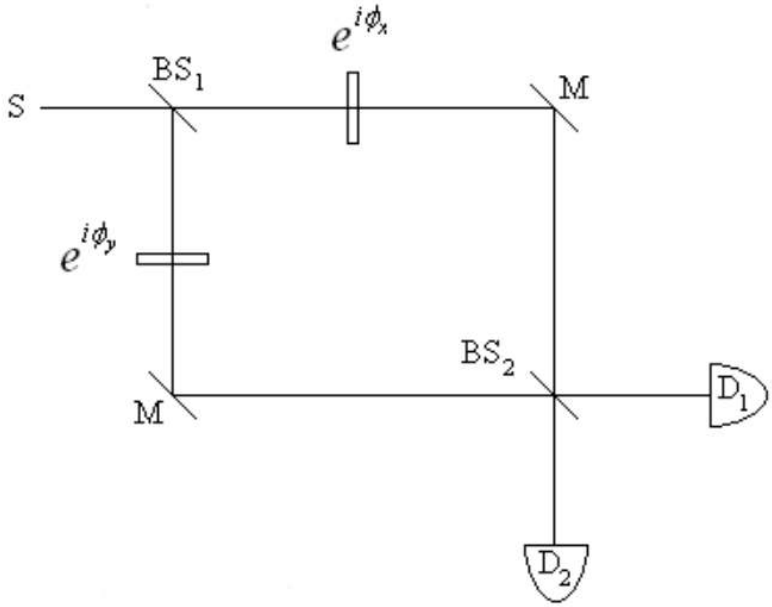
A photon entering the MZI in the x-direction exits in the x-direction phase-shifted by 90 degrees:

$$BS\cdot M\cdot BS\cdot x\rightarrow\begin{pmatrix}i\\ 0\end{pmatrix}\qquad i\cdot x\rightarrow\begin{pmatrix}i\\ 0\end{pmatrix}$$

The highlighted areas above next to the detectors show the matrix mechanics calculations for the probability of the photon being registered at D_1 and D_2. The equations are read from the right. A photon moving in the x-direction interacts with a beam splitter, a mirror and another beam splitter. This state is then projected onto x- and y-direction motion to calculate which detector will register the photon. The absolute square of this calculation (the probability amplitude) is the probability.

Now we place the pieces of glass in the arms of the interferometer as shown below. The speed of light in glass is different from that in air. Therefore glass causes a phase shift depending on its thickness as is shown below. If the pieces of glass are the same thickness, δ, they will cause the same phase shift and the photon will be detected at D_1. However, if they have different thicknesses, the phase shifts will be different in the two arms of the interferometer. For example, if ϕx is $\frac{\pi}{2}$ and ϕy is $\frac{\pi}{4}$ then D_2 will fire almost 15% of the time indicating that the glasses are not the same thickness.

$$\phi_x=2\cdot\pi\cdot\frac{\delta_x}{\lambda}\qquad \phi_x=\frac{\pi}{2}\qquad \phi_y=2\cdot\pi\cdot\frac{\delta_y}{\lambda}\qquad \phi_y=\frac{\pi}{4}$$



$$\left(\left|x^T \cdot BS \cdot M \cdot A(\phi_x, \phi_y) \cdot BS \cdot x\right|\right)^2 = 0.854$$

$$\left(\left|y^T \cdot BS \cdot M \cdot A(\phi_x, \phi_y) \cdot BS \cdot x\right|\right)^2 = 0.146$$

Appendix:

State Vectors

Photon moving horizontally:

$$x \equiv \begin{pmatrix} 1 \\ 0 \end{pmatrix}$$

Photon moving vertically:

$$y \equiv \begin{pmatrix} 0 \\ 1 \end{pmatrix}$$

Operators

Operator representing a beam splitter:

$$BS \equiv \frac{1}{\sqrt{2}} \cdot \begin{pmatrix} 1 & i \\ i & 1 \end{pmatrix}$$

Operator representing interaction with glass:

$$A(\phi_x, \phi_y) \equiv \begin{pmatrix} e^{i \cdot \phi_x} & 0 \\ 0 & e^{i \cdot \phi_y} \end{pmatrix}$$

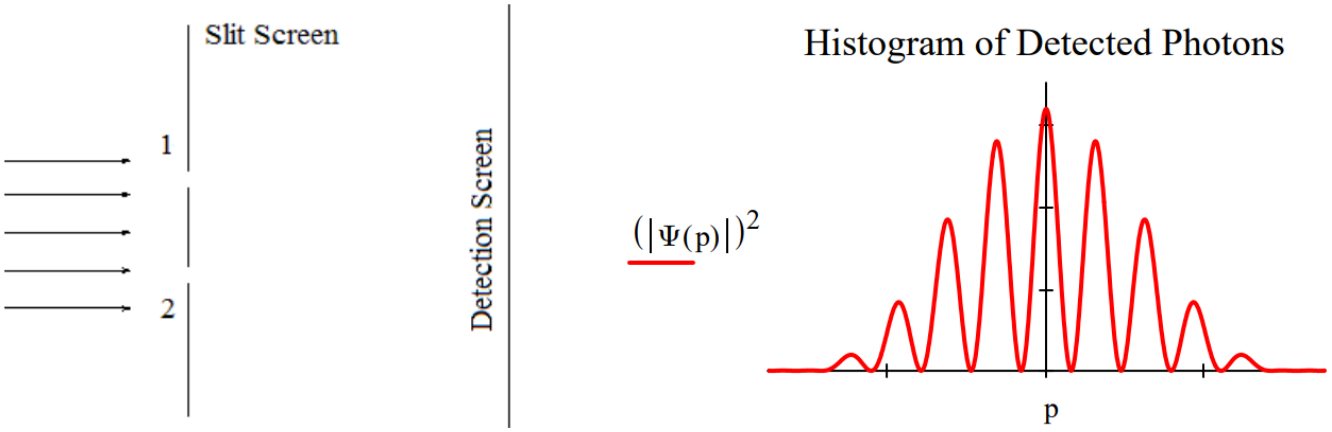
Operator representing a mirror:

$$M \equiv \begin{pmatrix} 0 & 1 \\ 1 & 0 \end{pmatrix}$$

Which Path Information and the Quantum Eraser

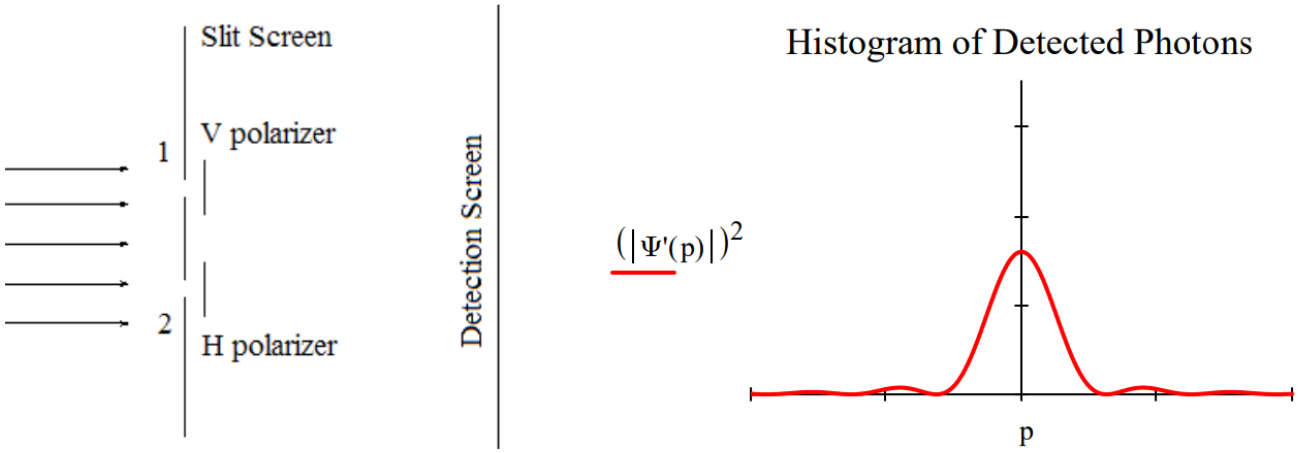
This tutorial examines the real reason which-path information destroys the double-slit diffraction pattern and how the so-called "quantum eraser" restores it. The wave function for a photon illuminating the slit screen is written as a superposition of the photon being present at both slits simultaneously. The double-slit diffraction pattern is calculated by projecting this superposition into momentum space. This is a Fourier transform for which the mathematical details can be found in the Appendix.

$$|\Psi\rangle = \frac{1}{\sqrt{2}}[|x_1\rangle + |x_2\rangle] \qquad \Psi(p) = \langle p|\Psi\rangle = \frac{1}{\sqrt{2}}[\langle p|x_1\rangle + \langle p|x_2\rangle]$$



Attaching polarizers to the slits creates an entangled superposition of the photon being at slit 1 with vertical polarization and at slit 2 with horizontal polarization. This leads to the following momentum distribution at the detection screen. The interference fringes have disappeared leaving a single-slit diffraction pattern.

$$|\Psi'\rangle = \frac{1}{\sqrt{2}}[|x_1\rangle|V\rangle + |x_2\rangle|H\rangle] \qquad \Psi'(p) = \langle p|\Psi'\rangle = \frac{1}{\sqrt{2}}[\langle p|x_1\rangle|V\rangle + \langle p|x_2\rangle|H\rangle]$$

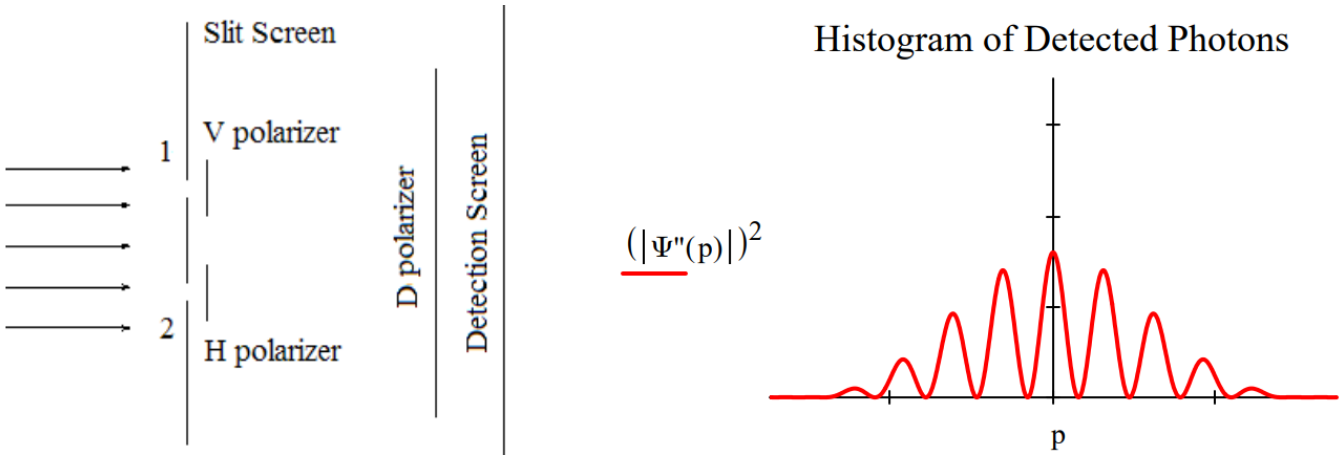


The usual explanation for this effect is that it is now possible to know which slit the photons went through, and that such knowledge destroys the interference fringes because the photons are no longer in a superposition of passing through both slits, but rather a mixture of passing through one slit or the other.

However, a better explanation is that the superposition persists with orthogonal polarization tags, and because of this the interference (cross) terms in the momentum distribution, $|\Psi'(p)|^2$, vanish leaving a pattern at the detection screen which is the sum of two single-slit diffraction patterns, one from the upper slit and the other from the lower slit.

That this is a reasonable interpretation is confirmed when a so-called quantum eraser, a polarizer (D) rotated clockwise by 45 degrees relative to the vertical, is placed before the detection screen.

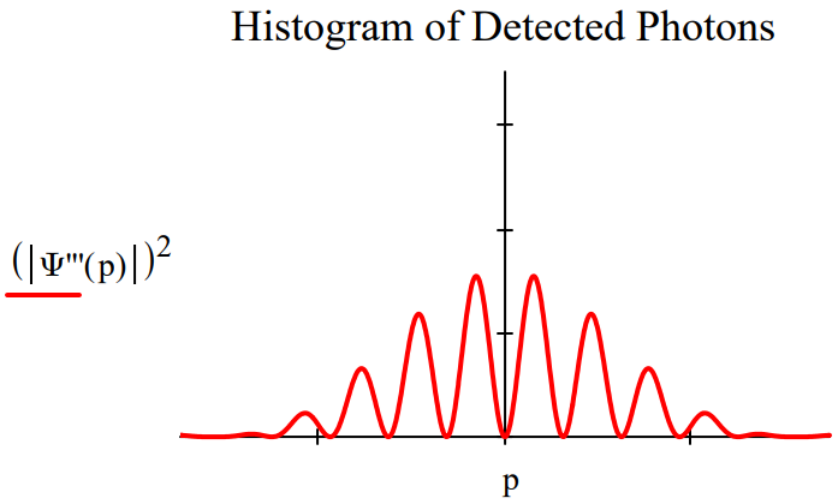
$$\Psi''(p) = \langle D|\Psi'(p)\rangle = \frac{1}{\sqrt{2}}[\langle p|x_1\rangle\langle D|V\rangle + \langle p|x_2\rangle\langle D|H\rangle] = \frac{1}{2}[\langle p|x_1\rangle + \langle p|x_2\rangle]$$



The diagonal polarizer is called a quantum eraser because it appears to restore the interference pattern lost because of the which-path information provided by the V/H polarizers. However, it is clear from this analysis that the diagonal polarizer doesn′t actually erase, it simply passes the diagonal component of $|\Psi'\rangle$ which then shows an attenuated (by half) version of the original interference pattern produced by $|\Psi\rangle$.

Placing an anti-diagonal polarizer (rotated counterclockwise by 45 degrees relative to the vertical) before the detection screen causes a 180 degree phase shift in the restored interference pattern.

$$\Psi''(p) = \langle A|\Psi'(p)\rangle = \frac{1}{\sqrt{2}}[\langle p|x_1\rangle\langle A|V\rangle + \langle p|x_2\rangle\langle A|H\rangle] = \frac{1}{2}[\langle p|x_1\rangle - \langle p|x_2\rangle]$$



This phase shift is inconsistent with any straightforward explanation based on the concept of erasure of which-path information. Erasure implies removal of which-path information. If which-path information has been removed shouldn′t the original interference pattern be restored without a phase shift?

Appendix:

The V/H polarization which-path tags and the D/A polarization ″erasers″ in vector format:

$$|\mathrm{V}\rangle = \begin{pmatrix} 1 \\ 0 \end{pmatrix} |\mathrm{H}\rangle = \begin{pmatrix} 0 \\ 1 \end{pmatrix} \qquad |\mathrm{D}\rangle = \frac{1}{\sqrt{2}}\begin{pmatrix} 1 \\ 1 \end{pmatrix} |\mathrm{A}\rangle = \frac{1}{\sqrt{2}}\begin{pmatrix} 1 \\ -1 \end{pmatrix}$$

$$\langle \mathrm{D}|\mathrm{H}\rangle = \langle \mathrm{A}|\mathrm{V}\rangle = \langle \mathrm{A}|\mathrm{v}\rangle = \frac{1}{\sqrt{2}}\langle \mathrm{A}|\mathrm{H}\rangle = -\frac{1}{\sqrt{2}}$$

For infinitesimally thin slits the momentum-space wave function is

$$\Psi(p) = \langle p|\Psi\rangle = \frac{1}{\sqrt{2}}[\langle p|x_1\rangle + \langle p|x_2\rangle] = \frac{1}{\sqrt{2}}\left[\frac{1}{\sqrt{2\pi}}\exp(-ipx_1) + \frac{1}{\sqrt{2\pi}}\exp(-ipx_2)\right]$$

Assuming a slit width δ the calculations of Ψ(p), Ψ'(p), Ψ''(p) and Ψ'''(p) are carried out as follows:

Position of first slit: $x_1 \equiv 0$

Position of second slit: $x_2 \equiv 1$

Slit width: $\delta \equiv 0.2$

$$\Psi(\mathrm{p}) \equiv \frac{1}{\sqrt{2}}\left[\int_{x_1-\frac{\delta}{2}}^{x_1+\frac{\delta}{2}} \frac{1}{\sqrt{2\cdot\pi}}\cdot\exp(-i\cdot p\cdot x)\cdot\frac{1}{\sqrt{\delta}}dx + \int_{x_2-\frac{\delta}{2}}^{x_2+\frac{\delta}{2}} \frac{1}{\sqrt{2\cdot\pi}}\cdot\exp(-i\cdot p\cdot x)\cdot\frac{1}{\sqrt{\delta}}dx\right]$$

For Ψ'(p) the V/H polarization which-path tags are added to the two terms of Ψ(p)

$$\Psi'(\mathrm{p}) \equiv \frac{1}{\sqrt{2}}\left[\int_{x_1-\frac{\delta}{2}}^{x_1+\frac{\delta}{2}} \frac{1}{\sqrt{2\cdot\pi}}\cdot\exp(-i\cdot p\cdot x)\cdot\frac{1}{\sqrt{\delta}}dx\cdot\begin{pmatrix}1\\0\end{pmatrix} + \int_{x_2-\frac{\delta}{2}}^{x_2+\frac{\delta}{2}} \frac{1}{\sqrt{2\cdot\pi}}\cdot\exp(-i\cdot p\cdot x)\cdot\frac{1}{\sqrt{\delta}}dx\cdot\begin{pmatrix}0\\1\end{pmatrix}\right]$$

$\Psi''(p) is the projection of \(\Psi'$(p) onto a diagonal polarizer <D|.

$$\Psi''(p) \equiv \frac{1}{\sqrt{2}}\cdot\begin{pmatrix}1\\1\end{pmatrix}^{\mathrm{T}}\cdot\Psi'(\mathrm{p})$$

Ψ''(p) is the projection of Ψ'(p) onto an anti-diagonal polarizer <A|.

$$\Psi^{m}(\mathrm{p}) \equiv \frac{1}{\sqrt{2}}\cdot\begin{pmatrix}1\\-1\end{pmatrix}^{\mathrm{T}}\cdot\Psi'(\mathrm{p})$$

Rewriting Ψ'(p) in terms of |D> and |A> clearly shows the origin of the phase difference between the $(|\Psi''(p)|)^2$ and $(|\Psi'''(p)|)^2$ interference patterns.

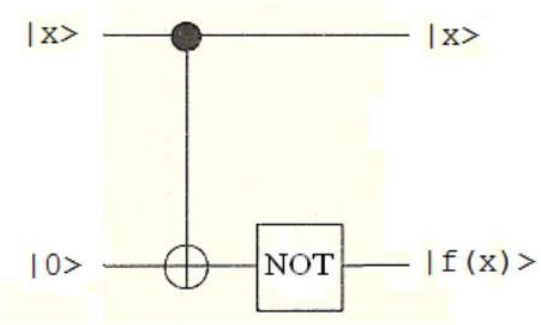
$$\Psi'(p) = \langle p|\Psi'\rangle = \frac{1}{2}[(\langle p|x_1\rangle + \langle p|x_2\rangle)|D\rangle + (\langle p|x_1\rangle - \langle p|x_2\rangle)|A\rangle]$$

A Brief Analysis of Deutsch's Problem

A certain function of x maps {0,1} to {0,1}. The four possible outcomes of the evaluation of f(x) are given in tabular form.

$$\begin{pmatrix} x & ' & 0 & 1 & ' & 0 & 1 & ' & 0 & 1 & ' & 0 & 1 \\ f(x) & ' & 0 & 0 & ' & 1 & 1 & ' & 0 & 1 & ' & 1 & 0 \end{pmatrix}$$

The circuit shown below yields the result given in the right most section of the table. In other words, f(x) is a **balanced** function, because $f(0) \neq f(1)$, as is the result immediately to its left. The results in the first two sections are labelled **constant** because $f(0) = f(1)$.



where

$$|0\rangle = \begin{pmatrix} 1 \\ 0 \end{pmatrix} \qquad |1\rangle = \begin{pmatrix} 0 \\ 1 \end{pmatrix}$$

From the classical perspective, if the question (as asked by Deutsch) is whether f(x) is **constant** or **balanced** then one must calculate both f(0) and f(1) to answer the question. Deutsch pointed out that quantum superpositions and the interference effects between them allow the answer to be given with one pass through the following modified version of the circuit.

Illegal pream-token (a)

An algebraic analysis of the operation of Deutsch's algorithm is now provided. Truth tables for H, CNOT, NOT and the identity are provided in the Appendix.

$$|0\rangle|1\rangle = |01\rangle$$
$$\text{H} \otimes \text{H}$$
$$\frac{1}{\sqrt{2}}[|0\rangle+|1\rangle]\frac{1}{\sqrt{2}}[|0\rangle - |1\rangle] = \frac{1}{2}[|00\rangle-|01\rangle + |10\rangle-|11\rangle]$$
$$\text{CNOT}$$
$$\frac{1}{2}[|00\rangle - |01\rangle+|11\rangle - |10\rangle] = \frac{1}{2}(|0\rangle-|1\rangle)(|0\rangle - |1\rangle)$$
$$\text{I} \otimes \text{NOT}$$
$$\frac{1}{2}[(|0\rangle-|1\rangle)(|1\rangle-|0\rangle)]$$
$$\text{H} \otimes \text{I}$$
$$|1\rangle\frac{1}{\sqrt{2}}(|1\rangle-|0\rangle)$$

The top wire contains |1 > indicating the function is balanced.

Appendix:

Identity

$$\begin{pmatrix} 0 & \text{to} & 0 \\ 1 & \text{to} & 1 \end{pmatrix}$$

NOT

$$\begin{pmatrix} 0 & \text{to} & 1 \\ 1 & \text{to} & 0 \end{pmatrix}$$

CNOT

$$\begin{pmatrix} 00 & \text{to} & 00 \\ 01 & \text{to} & 01 \\ 10 & \text{to} & 11 \\ 11 & \text{to} & 10 \end{pmatrix}$$

Hadamard operation

$$\begin{bmatrix} 0 & ' & H & ' & \frac{1}{\sqrt{2}} \cdot (0+1) & ' & H & ' & 0 \\ 1 & ' & H & ' & \frac{1}{\sqrt{2}} \cdot (0-1) & ' & H & ' & 1 \end{bmatrix}$$

The Hadamard operation is a simple example of a discrete Fourier transform. In other words, the final step of Deutsch's algorithm is to carry out a Fourier transform on the input wire. This also occurs on the input wires in Grover's search algorithm, Simon's query algorithm and Shor's factorization algorithm. These are other types of calculations in which quantum superpositions and interference effects enable a quantum computer to outperform a classical computer.

This page titled 1.8: Quantum Computation- A Short Course is shared under a CC BY 4.0 license and was authored, remixed, and/or curated by Frank Rioux via source content that was edited to the style and standards of the LibreTexts platform.

1.9: Quantum Computation- A Short Course

The Mach-Zehnder interferometer introduced above can be used to illuminate several contentious issues in quantum mechanics. The sub-microscopic building blocks of the natural world (electrons, protons, neutrons and photons) do not behave like the macroscopic objects we encounter in daily life because they have both wave and particle characteristics. Nick Herbert (Quantum Reality, p. 64) called them quons. “A quon is any entity … that exhibits both wave and particle aspects in the peculiar quantum manner.” The ‘peculiar quantum manner’ is that while we always observe particles, prior to measurement or observation quons behave like waves. This peculiar behavior is illustrated in the following tutorial.

Using a Mach-Zehnder Interferometer to Illustrate Feynman's Sum Over Histories Approach to Quantum Mechanics

> *Thirty-one years ago Dick Feynman told me about his 'sum over histories' version of quantum mechanics. "The electron does anything it likes," he said. "It just goes in any direction, at any speed, forward and backward in time, however it likes, and then you add up the amplitudes and it gives you the wave function." I said to him "You're crazy." But he isn't.* ***Freeman Dyson, 1980.***

In Volume 3 of the celebrated **Feynman Lectures on Physics**, Feynman uses the double-slit experiment as the paradigm for his 'sum over histories' approach to quantum mechanics. He said that any question in quantum mechanics could be answered by responding, "You remember the experiment with the two holes? It's the same thing." And, of course, he's right.

A 'sum over histories' is a superposition of probability amplitudes for the possible experimental outcomes which in quantum mechanics carry phase and therefore interfer constructively and destructively with one another. The square of the magnitude of the superposition of histories yields the probabilities that the various experimental possibilities will be observed.

Obviously it takes a minum of two 'histories' to demonstrate the interference inherent in the quantum mechanical superposition. And, that's why Feynman chose the double-slit experiment as the paradigm for quantum mechanical behavior. The two slits provide two paths, or 'histories' to any destination on the detection screen. In this tutorial a close cousin of the double-slit experiment, single particle interference in a Mach-Zehnder interferometer, will be used to illustrate Feynman's 'sum over histories' approach to quantum mechanics.

A Beam Splitter Creates a Quantum Mechanical Superposition

Single photons emitted by a source (S) illuminate a 50-50 beam splitter (BS). Mirrors (M) direct the photons to detectors D_1 and D_2. The probability amplitudes for transmission and reflection are given below. By convention a 90 degree phase shift (i) is assigned to reflection.

Probability amplitude for photon transmission at a 50-50 beam splitter:

$$\langle T|S\rangle = \frac{1}{\sqrt{2}}$$

Probability amplitude for photon reflection at a 50-50 beam splitter:

$$\langle R|S\rangle = \frac{i}{\sqrt{2}}$$

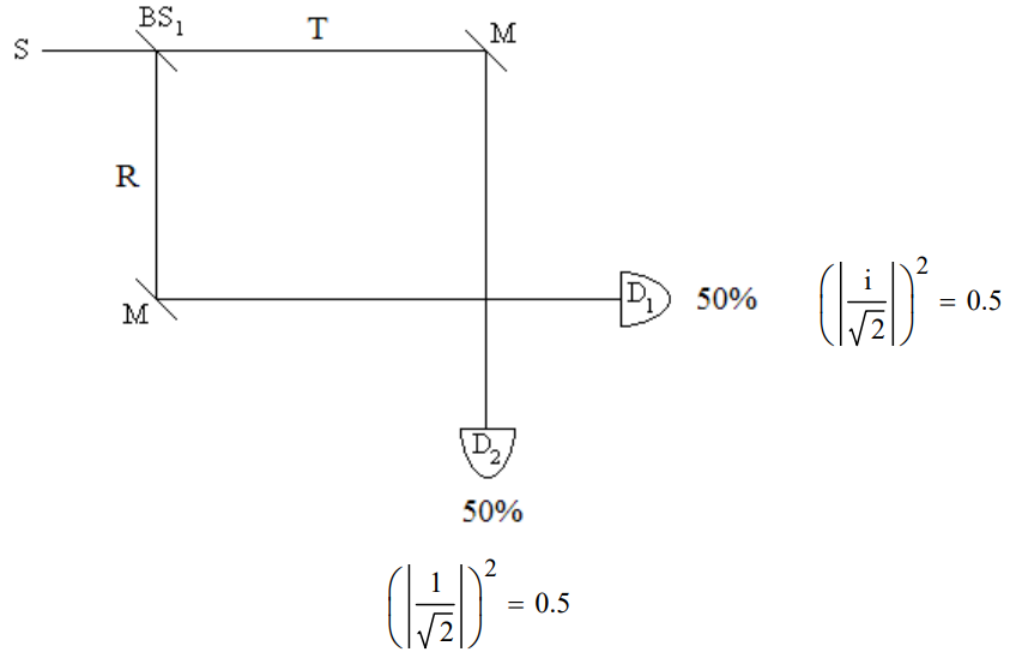
After the beam splitter the photon is in a superposition state of being transmitted and reflected.

$$|S\rangle \rightarrow \frac{1}{\sqrt{2}}\left[|T\rangle + i|R\rangle\right]$$

As shown in the diagram below, mirrors reflect the transmitted photon path to D_2 and the reflected path to D_1. The source photon is expressed in the basis of the detectors as follows.

$$|S\rangle \rightarrow \frac{1}{\sqrt{2}}[|T\rangle + i|R\rangle] \underset{R\rightarrow D_1}{\overset{T\rightarrow D_2}{>>}} \frac{1}{\sqrt{2}}[|D_2\rangle + i|D_1\rangle]$$

The square of the magnitude of the coefficients of D_1 and D_2 give the probabilities that the photon will be detected at D_1 or D_2. Each detector registers photons 50% of the time. In other words, in the quantum view the superposition collapses randomly to one of the two possible measurement outcomes it represents.



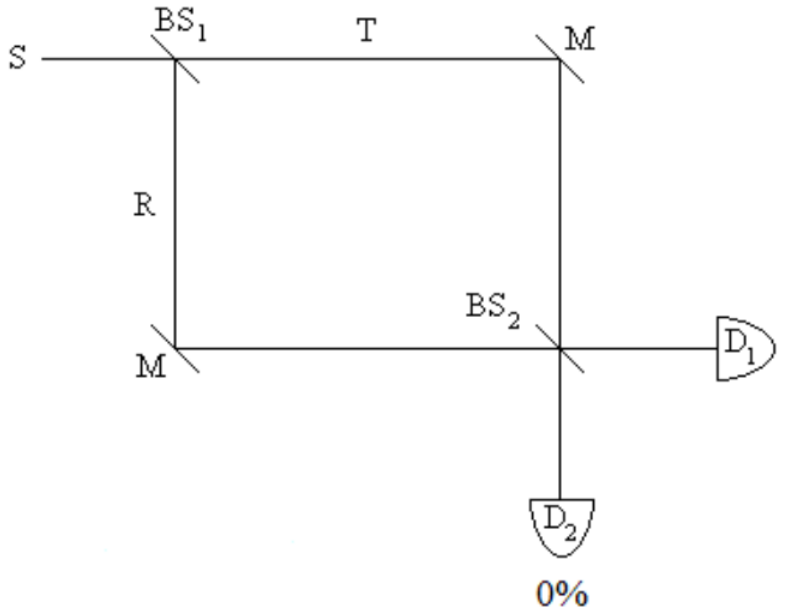
$$\left(\left|\frac{i}{\sqrt{2}}\right|\right)^2 = 0.5$$

$$\left(\left|\frac{1}{\sqrt{2}}\right|\right)^2 = 0.5$$

The classical view that detection at D_1 means the photon was reflected at BS_1 and that detection at D_2 means it was transmitted at BS_1 is not tenable as will be shown using a Mach-Zehnder interferometer which has a second beam splitter at the path intersection before the detectors.

A Second Beam Splitter Provides Two Paths to Each Detector

If a second beam splitter is inserted before the detectors the photons always arrive at D_1. In the first experiment there was only one path to each detector. The construction of a Mach-Zehnder interferometer by the insertion of a second beam splitter creates a second path to each detector and the opportunity for constructive and destructive interference on the paths to the detectors.



$$\left(\left|\frac{1}{\sqrt{2}}\cdot\frac{i}{\sqrt{2}} + \frac{i}{\sqrt{2}}\cdot\frac{1}{\sqrt{2}}\right|\right)^2 = 1$$

$$\left(\left|\frac{1}{\sqrt{2}}\cdot\frac{1}{\sqrt{2}} + \frac{i}{\sqrt{2}}\cdot\frac{i}{\sqrt{2}}\right|\right)^2 = 0$$

Given the superposition state after BS_1, the probability amplitudes after BS_2 interfere constructively at D_1 and destructively at D_2.

$$\begin{array}{ccccc} \text{After BS}_1 & & \text{After BS}_2 & & \text{Final State} \\ & & |T\rangle \rightarrow \frac{1}{\sqrt{2}}[i|D_1\rangle + |D_2\rangle] & & \\ |S\rangle \rightarrow \frac{1}{\sqrt{2}}[|T\rangle + i|R\rangle] \rightarrow & & + & \rightarrow & i|D_1\rangle \\ & & i|R\rangle \rightarrow \frac{i}{\sqrt{2}}[|D_1\rangle + i|D_2\rangle] & & \end{array}$$

Adopting the classical view that the photon is either transmitted or reflected at BS_1 does not produce this result. If the photon was transmitted at BS_1 it would have equal probability of arriving at either detector after BS_2. If the photon was reflected at BS_1 it would also have equal probability of arriving at either detector after BS_2. The predicted experimental results would be the same as those of the single beam splitter experiment. In summary, the quantum view that the photon is in a superposition of being transmitted and reflected after BS_1 is consistent with both experimental results described above; the classical view that it is either transmitted or reflected is not.

Some disagree with this analysis saying the two experiments demonstrate the dual, complementary, behavior of photons. In the first experiment particle-like behavior is observed because both detectors register photons indicating the individual photons took one path or the other. The second experiment reveals wave-like behavior because interference occurs - only D_1 registers photons. According to this view the experimental design determines whether wave or particle behavior will occur and somehow the photon is aware of how it should behave. Suppose in the second experiment that immediately after the photon has interacted with BS_1, BS_2 is removed. Does what happens at the detectors require the phenomenon of retrocausality or delayed choice? Only if you reason classically about quantum experiments.

We always measure particles (detectors click, photographic film is darkened, etc.) but we interpret what happened or predict what will happen by assuming wavelike behavior, in this case the superposition created by the initial beam splitter that delocalizes the position of the photon. Quantum particles (quons) exhibit both wave and particle properties in every experiment. To paraphrase Nick Herbert (**Quantum Reality**), particles are always detected, but the experimental results observed are the result of wavelike behavior. Richard Feynman put it this way (**The Character of Physical Law**), "I will summarize, then, by saying that electrons arrive in lumps, like particles, but the probability of arrival of these lumps is determined as the intensity of waves would be. It is in this sense that the electron behaves sometimes like a particle and sometimes like a wave. It behaves in two different ways at the same time (in the same experiment)." Bragg said, "Everything in the future is a wave, everything in the past is a particle."

In 1951 in his treatise **Quantum Theory**, David Bohm described wave-particle duality as follows: "One of the most characteristic features of the quantum theory is the wave-particle duality, i.e. the ability of matter or light quanta to demonstrate the wave-like property of interference, and yet to appear subsequently in the form of localizable particles, even after such interference has taken place." In other words, to explain interference phenomena wave properties must be assigned to matter and light quanta prior to detection as particles.

Matrix Mechanics Approach

As a companion analysis, the matrix mechanics approach to single-photon interference in a Mach-Zehnder interferometer is outlined next.

State Vectors

Photon moving horizontally:

$$\mathrm{x} := \begin{pmatrix} 1 \\ 0 \end{pmatrix}$$

Photon moving vertically:

$$\mathrm{y} := \begin{pmatrix} 0 \\ 1 \end{pmatrix}$$

Operators

Operator representing a beam splitter:

$$\mathrm{BS} := \frac{1}{\sqrt{2}} \cdot \begin{pmatrix} 1 & \mathrm{i} \\ \mathrm{i} & 1 \end{pmatrix}$$

Operator representing a mirror:

$$\mathrm{M} := \begin{pmatrix} 0 & 1 \\ 1 & 0 \end{pmatrix}$$

Single beam splitter example:

Reading from right to left.

The probability that a photon leaving the source moving in the (horizontal) x-direction, encountering a beam splitter and a mirror will be detected at D_1.	$\left(\left\|x^{\mathrm{T}} \cdot \mathrm{M} \cdot \mathrm{BS} \cdot \mathrm{x}\right\|\right)^2 = 0.5$	(1.9.1)
The probability that a photon leaving the source moving in the (horizontal) x-direction, encountering a beam splitter and a mirror will be detected at D_2.	$\left(\left\|y^{\mathrm{T}} \cdot \mathrm{M} \cdot \mathrm{BS} \cdot \mathrm{x}\right\|\right)^2 = 0.5$	(1.9.2)

Two beam splitter example (MZI):

The probability that a photon leaving the source moving in the (horizontal) x-direction, encountering a beam splitter, a mirror and another beam splitter will be detected at D_1.	$\left(\left\|\mathrm{x}^{\mathrm{T}} \cdot \mathrm{BS} \cdot \mathrm{M} \cdot \mathrm{BS} \cdot \mathrm{x}\right\|\right)^2 = 1$	(1.9.3)
The probability that a photon leaving the source moving in the (horizontal) x-direction, encountering a beam splitter, a mirror and another beam splitter will be detected at D_2.	$\left(\left\|y^{\mathrm{T}} \cdot \mathrm{BS} \cdot \mathrm{M} \cdot \mathrm{BS} \cdot \mathrm{x}\right\|\right)^2 = 0$	(1.9.4)

Some quantum physicists believe they can isolate wave and particle behavior in a properly designed experiment. They also invoke the concept of delayed choice. I disagree with both in the next tutorial, but first some remarks by John Wheeler.

John Wheeler, designer of several delayed-choice experiments (both terrestrial and cosmological), had the following to say about the interpretation of such experiments.

> *... in a loose way of speaking, we decide what the photon shall have done after it has already done it. In actuality it is wrong to talk of the 'route' of the photon. For a proper way of speaking we recall once more that it makes no sense to talk of a phenomenon until it has been brought to a close by an irreversible act of amplification. 'No elementary phenomenon is a phenomenon until it is a registered (observed) phenomenon.'*

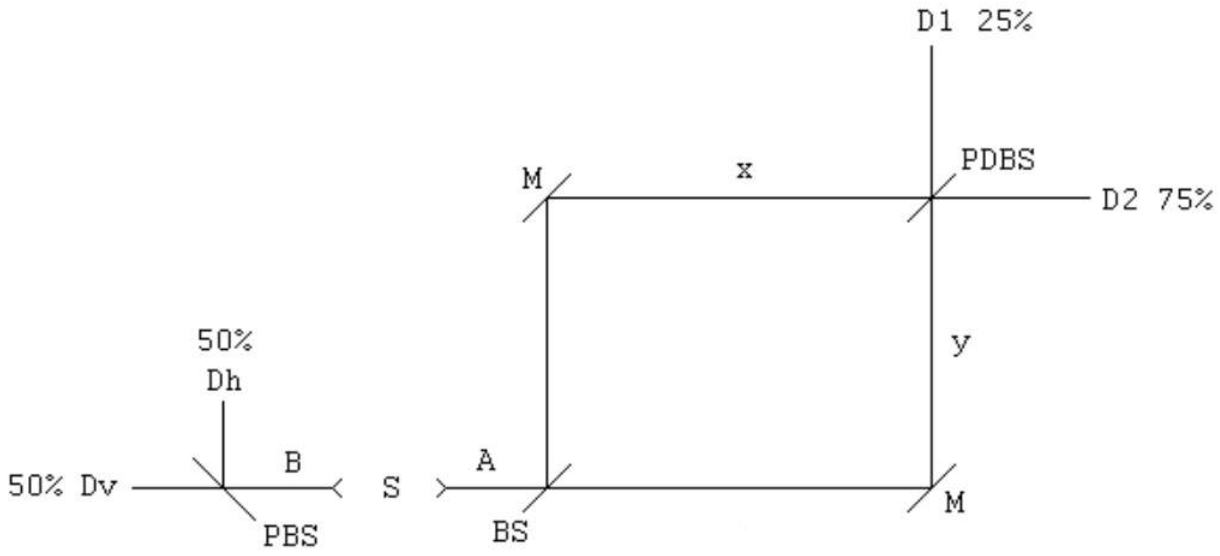
A Quantum Delayed-Choice Experiment?

This note presents a critique of "Entanglement-Enabled Delayed-Choice Experiment," F. Kaiser, et al. Science 338, 637 (2012). This experiment was also summarized in section 6.3 of **Quantum Weirdness**, by William Mullin, Oxford University Press, 2017.

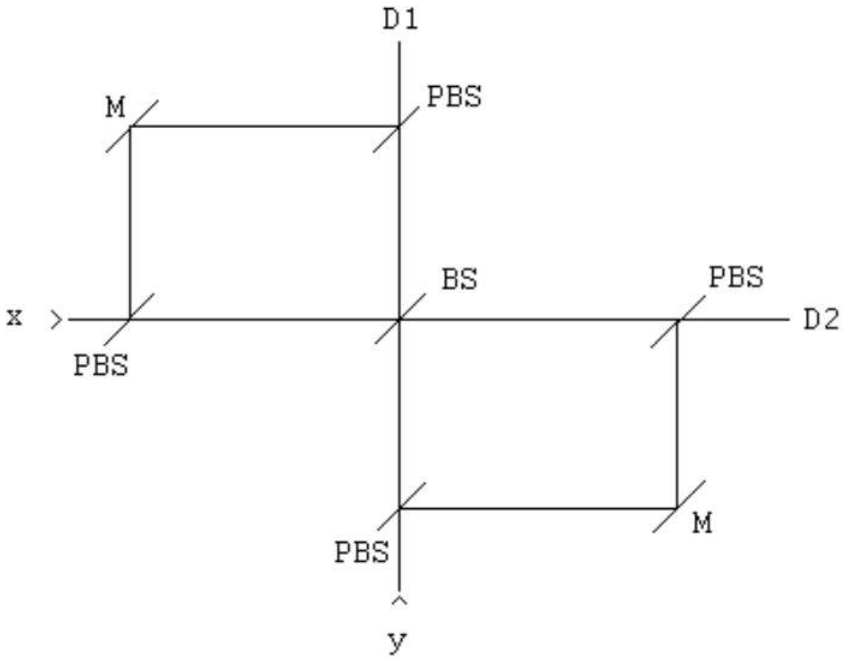
A source, S, emits two photons in opposite directions on the x-axis in the following polarization state, where v and h represent vertical and horizontal polarization, respectively.

$$|\Psi\rangle_{AB} = \frac{1}{\sqrt{2}}[|x\nu\rangle_A|x\nu\rangle_B + |xh\rangle_A|xh\rangle_B]$$

Photon B travels to the left to a polarizing beam splitter, PBS. Photon A travels to the right entering an interferometer whose elements are a beam splitter (BS), two mirrors (M), and a polarization-dependent beam splitter (PDBS).



The implementation of the PDBS is shown here.



The operation of the optical elements are as follows. A mirror simply reflects the photon's direction of motion.

$$M = |y\rangle\langle x| + |x\rangle\langle y|$$

A 50-50 BS splits the photon beam into a superposition of motion in the x- and y-directions. By convention the reflected beam collects a pi/2 (i) phase shift relative to the transmitted beam.

$$BS = \frac{|x\rangle + i|y\rangle}{\sqrt{2}}\langle x| + \frac{i|x\rangle + |y\rangle}{\sqrt{2}}\langle y| = \frac{1}{\sqrt{2}}(|x\rangle\langle x| + i|y\rangle\langle x| + i|x\rangle\langle y| + |y\rangle\langle y|)$$

A PBS transmits vertically polarized photons and reflects horizontally polarized photons.

$$PBS = |xv\rangle\langle xv| + |yh\rangle\langle xh| + |yv\rangle\langle yv| + |xh\rangle\langle yh|$$

The PDBS uses an initial PBS to reflect horizontally polarized photons to a second PBS which reflects them to the detectors. Vertically polarized photons are transmitted by the first PBS to a BS which has the action shown above, after which they are

transmitted to the detectors by the second PBS. PBS/PDBS blue/red color coding highlights the action of the central BS.

$$PDPS = \frac{|xv\rangle + i|yv\rangle}{\sqrt{2}}\langle xv| + |yh\rangle\langle xh| + \frac{i|xv\rangle + |yv\rangle}{\sqrt{2}}\langle yv| + |xh\rangle\langle yh|$$

Given the state produced by the source, half the time a horizontal photon will enter the interferometer and half the time a vertical photon will enter. The following algebraic analysis shows the progress of the h- and v-polarized photons entering the interferometer. It is clear from this analysis that D1 will fire 25% of the time and D2 75% of the time.

$$\begin{array}{cc} |xh\rangle & |x\nu\rangle \\ BS & BS \\ \frac{|xh\rangle+i|yh\rangle}{\sqrt{2}} & \frac{|xv\rangle+i|yv\rangle}{\sqrt{2}} \\ M & M \\ \frac{|yh\rangle+i|xh\rangle}{\sqrt{2}} & \frac{|yv\rangle+i|xv\rangle}{\sqrt{2}} \\ PDBS & PDBS \\ \frac{|D2\rangle|h\rangle+i|D1\rangle|h\rangle}{\sqrt{2}} & \frac{1}{\sqrt{2}}\left[\frac{|D1\rangle|v\rangle+i|D2\rangle|v\rangle}{\sqrt{2}} + \frac{i(i|D1\rangle|v\rangle+|D2\rangle|v\rangle)}{\sqrt{2}}\right] \\ & \downarrow \\ & i|D2\rangle|v\rangle \end{array}$$

This analysis suggests to some that inside the interferometer h-photons behave like particles and v-photons behave like waves. The argument for this view is that interference occurs at the PDBS for v-photons, but not for h-photons. However, in both cases the state illuminating the PDBS, highlighted in blue, is a superposition of the photon being in both arms of the interferometer. In my opinion this superposition implies delocalization which implies wavelike behavior. At the PDBS the h-photon superposition is reflected away from the central BS to D1 and D2, leading to the final superposition in the left-hand column above, which collapses on observation to either D1 or D2. The v-photon superposition is transmitted at the PDBS to the central BS allowing for destructive interference at D1 and constructive interference at D2 as is shown at the bottom of the right-hand column.

Those who interpret this experiment in terms of particle or wave behavior also invoke the concept of delayed-choice, claiming that if D2 fires we don't know for sure which behavior has occurred because both h and v photons can arrive there. They argue that until photon B has been observed at Dv or Dh, which by design can be long after photon A has exited the interferometer, the polarization of the photon detected at D2 is unknown and therefore so is whether particle or wave behavior has occurred. These analysts write the final two photon wavefunction as the following entangled superposition, where particle behavior is highlighted in red and wave behavior in blue.

$$\begin{aligned} |\Psi\rangle_{\text{final}} &= \frac{1}{\sqrt{2}}\left(\left(\frac{|D2,h\rangle + i|D1,h\rangle}{\sqrt{2}}\right)_A |Dh\rangle_B + i|D2,\nu\rangle_A |D\nu\rangle_B\right) \\ &= \frac{1}{\sqrt{2}}(|Particle\rangle_A|Dh\rangle_B + |Wave\rangle_A|Dv\rangle_B) \end{aligned}$$

For the reasons expressed above I do not find this interpretation convincing. We always observe particles (detectors click, photographic film is darkened, etc.), but we interpret what happened or predict what will happen by assuming wavelike behavior. In other words, objects governed by quantum mechanical principles (quons) exhibit both wave and particle properties in every experiment. To paraphrase Nick Herbert (**Quantum Reality**), particles are always detected, but the experimental results observed are the result of wavelike behavior. Bragg summarized wave-particle duality saying, "Everything in the future is a wave, everything in the past is a particle."

In summary, I accept the Copenhagen interpretation of quantum mechanics for the reasons so cogently stated by David Lindley on page 164 of *Where Does The Weirdness Go?*

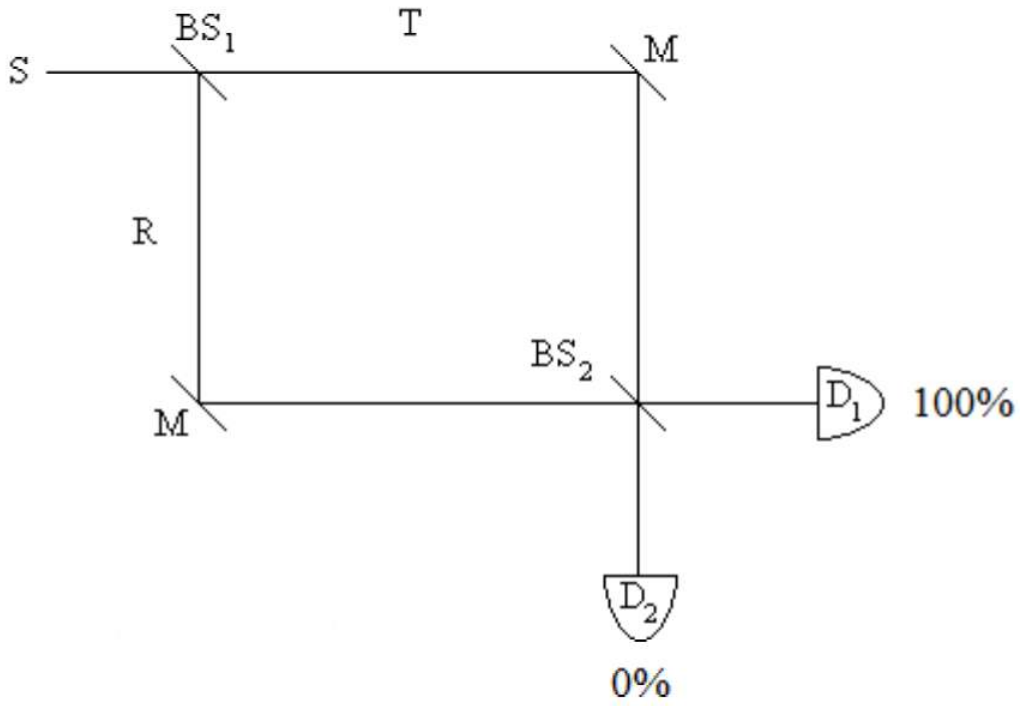
> *And since none of the other "interpretations" of quantum mechanics that we have looked at has brought us any real peace of mind, they simply push the weirdness around, from one place to another, but cannot make it go away – let us stick with the Copenhagen interpretation, which has the virtues of simplicity and necessity. It takes quantum*

> *mechanics seriously, takes its weird aspects at face value, and provides an economical, austere, perhaps even antiseptic, account of them.*

We now turn to some true quantum weirdness. The following tutorial uses a Mach-Zehnder interferometer (MZI) and Feynman's sum over histories approach to demonstrate interaction-free measurement, or how to see in the dark.

Interaction Free Measurement: Seeing in the Dark

The illustration of the concept of interaction-free measurement requires the use of an interferometer. A simple illustration employs a Mach-Zehnder interferometer (MZI) like the one shown here.



This equal-arm MZI consists of two 50-50 beam splitters (BS_1, BS_2), two mirrors (M) and two detectors (D_1, D_2). A source emits a photon which interacts with BS_1 producing the following superposition. (By convention a 90 degree (i) phase shift is assigned to reflection.)

$$S = \frac{1}{\sqrt{2}} \cdot (T + i \cdot R)$$

The transmitted and reflected branches are united at BS_2 by the mirrors, where they evolve into the following superpositions in the basis of the detectors.

$$T = \frac{1}{\sqrt{2}} \cdot (i \cdot D_1 + D_2)$$

$$R = \frac{1}{\sqrt{2}} \cdot (D_1 + i \cdot D_2)$$

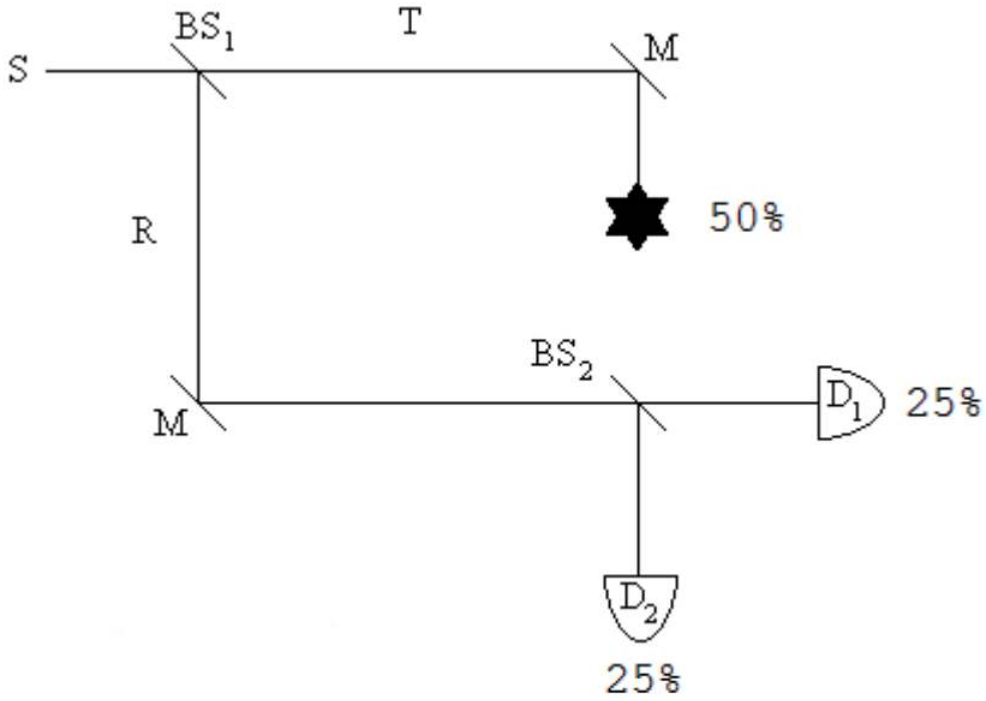
Substitution of 2 and 3 into 1 reveals that the output photon is always registered at D_1. There are two paths to each detector and constructive interference occurs at D_1 and destructive interference at D_2.

$$S = \frac{1}{\sqrt{2}} \cdot (T + i \cdot R) \Big|_{\substack{\text{substitute, } T=\frac{1}{\sqrt{2}}\cdot(i\cdot D_1+D_2) \\ \text{substitute, } R=\frac{1}{\sqrt{2}}\cdot(D_1+i\cdot D_2)}} \rightarrow S = D_1 \cdot i$$

Probability at D_1:

$$(|i|)^2 = 1$$

The MZI provides a rudimentary method of determining whether an obstruction is present in its upper arm without actually interacting with it. As we shall see, it is not an efficient method, but it does clearly illustrate the principle involved which then can be used in a more elaborate and sophisticated interferometer to yield better results.



In the presence of the obstruction equation 2 becomes $T = \gamma_{Absorbed}$. This leads to the following result at the detectors.

$$s = \frac{1}{\sqrt{2}} \cdot (T + i \cdot R)\Big|_{\substack{\text{substitute, } T=\gamma_{Absorbed} \\ \text{substitute, } R=\frac{1}{\sqrt{2}}\cdot(D_1+i\cdot D_2)}} \rightarrow S = \frac{\sqrt{2}\cdot\gamma_{Absorbed}}{2} - \frac{D_2}{2} + \frac{D_1 i}{2}$$

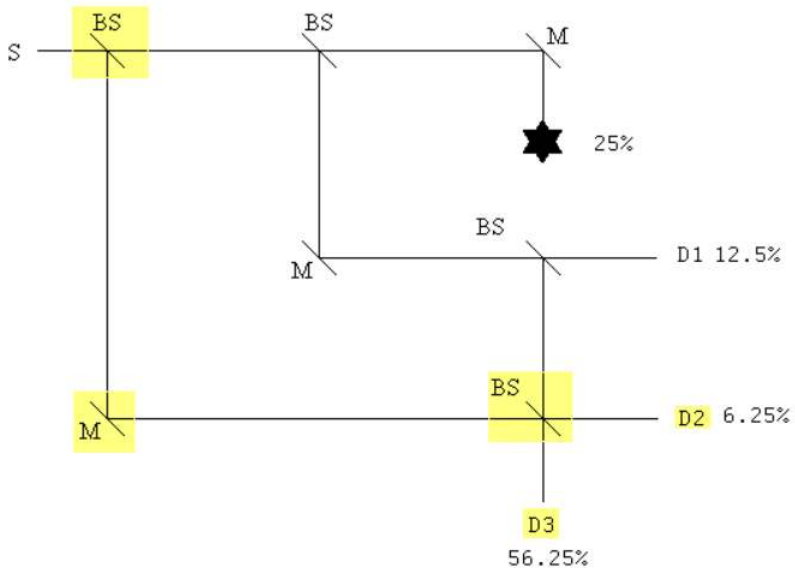
Quantum mechanics predicts that for a large number of experiments 50% of the photons will be absorbed by the obstruction, 25% will be detected at D_1 and 25% will be detect at D_2. This later result is the signature of interaction-free measurement. Even if the photon is not absorbed, the mere presence of the obstruction causes the probability of detection at D_2 to go from zero to 25%. The photon's arrival at D_2 signals the presence of an obstruction in the upper arm of the MZI, and the obstruction is detected without an interaction.

Of course, 25% is not great efficiency, so this is "a proof of principle" example. However, with a little ingenuity the probability of interaction-free detection can be increased dramatically. To see how this can be accomplished read "Quantum Seeing in the Dark" by Kwiat, Weinfurter and Zeilinger in the November 1996 issue of *Scientific American*.

However, it is possible to improve performance significantly by using a system of nested MZIs which is only slightly more complicated than the simple MZI used earlier. To simplify analysis Feynman's "sum over histories" approach to quantum mechanics will be used. The probability amplitudes for transmission and reflection at the beam splitters are required.

$$T := \frac{1}{\sqrt{2}} \qquad R := \frac{i}{\sqrt{2}}$$

Placing an additional BS before the original MZI and another BS before D_2 and renaming it D_3, plus an additional mirror and new detector D_2, yields a nested interferometer configuration that significantly increases the probability of interaction-free detection of the obstruction.



To interact with the obstruction a photon must be transmitted at the first and second beam splitters. In this case there is only one history and the probability of the interaction occuring is the square of its absolute magnitude.

$$(|\mathrm{T}\cdot\mathrm{T}|)^2 \rightarrow \frac{1}{4} = 25\%$$

The probabilities of detectors 1, 2 and 3 firing are calculated using the same methodology.

The probability D_1 registers a photon:

$$(|\mathrm{T}\cdot\mathrm{R}\cdot\mathrm{T}|)^2 \rightarrow \frac{1}{8} = 12.5\%$$

The probability D_2 registers a photon:

$$(|\mathrm{T}\cdot\mathrm{R}\cdot\mathrm{R}\cdot\mathrm{R}+\mathrm{R}\cdot\mathrm{T}|)^2 \rightarrow \frac{1}{16} = 6.25\%$$

The probability D_3 registers a photon:

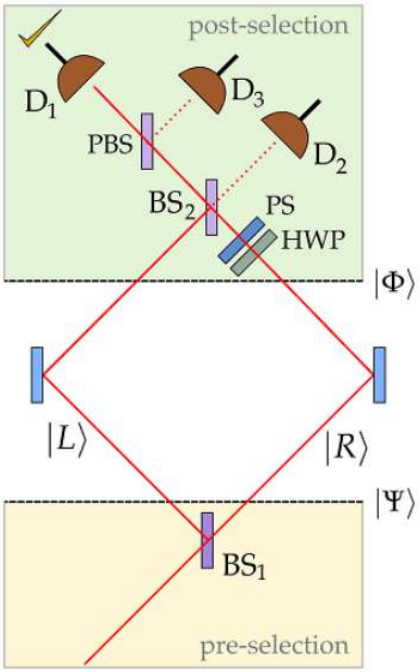
$$(|\mathrm{T}\cdot\mathrm{R}\cdot\mathrm{R}\cdot\mathrm{T}+\mathrm{R}\cdot\mathrm{R}|)^2 \rightarrow \frac{9}{16} = 56.25\%$$

With the modified interferometer detecting the presence of the obstruction without interacting with it increases from 25% to 56.25%.

Perhaps weirder is the quantum Cheshire cat. The following tutorial shows how a MZI can be engineered to create a situation in which a photon is separated from a property, in this case its angular momentum.

A Quantum Optical Cheshire Cat

The following is a summary of "Quantum Cheshire Cats" by Aharonov, Popescu, Rohrlich and Skrzypczyk which was published in the *New Journal of Physics* **15**, 113015 (2013) and can also be accessed at: arXiv:1202.0631v2.



In the absence of the half-wave plate (HWP) and the phase shifter (PS) a horizontally polarized photon entering the interferometer from the lower left (propagating to the upper right) arrives at D_2 with a 90 degree ($\frac{\pi}{2}, i$) phase shift. (By convention reflection at a beam splitter introduces a 90 degree phase shift.)

$$|R\rangle|H\rangle \xrightarrow{BS_i} \frac{1}{\sqrt{2}}[i|L\rangle + |R\rangle]|H\rangle \xrightarrow{Bs_2} i|D_2\rangle|H\rangle$$

The state immediately after the first beam splitter is the pre-selected state.

$$|\Psi\rangle = \frac{1}{\sqrt{2}}[i|L\rangle + |R\rangle]|H\rangle$$

The post-selected state is,

$$|\Phi\rangle = \frac{1}{\sqrt{2}}[|L\rangle|H\rangle + |R\rangle|V\rangle]$$

The HWP (converts |V> to |H> in the R-branch) and PS transform this state to,

$$|\Phi\rangle \xrightarrow[PS]{HWP} \frac{1}{\sqrt{2}}[|L\rangle + i|R\rangle]|H\rangle$$

which exits the second beam splitter through the left port to encounter a polarizing beam splitter which transmits horizontal polarization and reflects vertical polarization. Thus, the post-selected state is detected at D_1. The evolution of the post-selected state is summarized as follows:

$$|\Phi\rangle = \frac{1}{\sqrt{2}}[|L\rangle|H\rangle + |R\rangle|V\rangle] \xrightarrow[PS]{HWP} [|L\rangle + i|R\rangle]|H\rangle \xrightarrow{BS_2} i|L\rangle|H\rangle \xrightarrow{PBS} i|D_1\rangle|H\rangle$$

The last term on the right side below is the weak value of **A** multiplied by the probability of its occurrence for the preselected state Ψ and the post-selected state Φ.

$$\langle\Psi|\widehat{\mathrm{A}}|\Psi\rangle = \sum_j \langle\Psi|\Phi_j\rangle \left\langle\Phi_j|\hat{\mathrm{A}}|\Psi\right\rangle = \sum_j \langle\Psi|\Phi_j\rangle \langle\Phi_j|\Psi\rangle \frac{\left\langle\Phi_j|\hat{\mathbf{A}}|\Psi\right\rangle}{\langle\Phi_j|\Psi\rangle} = \sum_j p_j \frac{\left\langle\Phi_j|\hat{\mathbf{A}}|\Psi\right\rangle}{\langle\Phi_j|\Psi\rangle}$$

The weak value calculations are carried out in a 4-dimensional Hilbert space created by the tensor product of the photon's direction of propagation and polarization vectors.

Direction of propagation vectors:

$$L := \begin{pmatrix} 1 \\ 0 \end{pmatrix} \qquad R := \begin{pmatrix} 0 \\ 1 \end{pmatrix}$$

Polarization state vectors:

$$H := \begin{pmatrix} 1 \\ 0 \end{pmatrix} \qquad V := \begin{pmatrix} 0 \\ 1 \end{pmatrix}$$

Pre-selected state:

$$\Psi = \frac{1}{\sqrt{2}} \cdot (i \cdot L + R) \cdot H = \frac{1}{\sqrt{2}} \cdot \left[i \cdot \begin{pmatrix} 1 \\ 0 \end{pmatrix} + \begin{pmatrix} 0 \\ 1 \end{pmatrix} \right] \cdot \begin{pmatrix} 1 \\ 0 \end{pmatrix} = \frac{1}{\sqrt{2}} \cdot \begin{pmatrix} i \\ 1 \end{pmatrix} \cdot \begin{pmatrix} i \\ 0 \end{pmatrix}$$

$$\Psi := \frac{1}{\sqrt{2}} \cdot \begin{pmatrix} i \\ 0 \\ 1 \\ 0 \end{pmatrix}$$

Post-selected state:

$$\Phi := \frac{1}{\sqrt{2}} \cdot (L \cdot H + R \cdot V) = \frac{1}{\sqrt{2}} \cdot \left[\begin{pmatrix} 1 \\ 0 \end{pmatrix} \cdot \begin{pmatrix} 1 \\ 0 \end{pmatrix} + \begin{pmatrix} 0 \\ 1 \end{pmatrix} \cdot \begin{pmatrix} 0 \\ 1 \end{pmatrix} \right] \qquad \Phi := \frac{1}{\sqrt{2}} \cdot \begin{pmatrix} 1 \\ 0 \\ 0 \\ 1 \end{pmatrix}$$

Direction of propagation operators:

$$Left := \begin{pmatrix} 1 \\ 0 \end{pmatrix} \cdot \begin{pmatrix} 1 & 0 \end{pmatrix} \rightarrow \begin{pmatrix} 1 & 0 \\ 0 & 0 \end{pmatrix} \qquad Right := \begin{pmatrix} 0 \\ 1 \end{pmatrix} \cdot \begin{pmatrix} 0 & 1 \end{pmatrix} \rightarrow \begin{pmatrix} 0 & 0 \\ 0 & 1 \end{pmatrix}$$

Photon angular momentum operator:

$$Pang := \begin{pmatrix} 0 & -i \\ i & 0 \end{pmatrix}$$

Identity operator:

$$I := \begin{pmatrix} 1 & 0 \\ 0 & 1 \end{pmatrix}$$

The following weak value calculations show that for the pre- and post-selection ensemble of observations the photon is in the left arm of the interferometer while its angular momentum is in the right arm. Like the case of the Cheshire cat, a photon property has been separated from the photon.

$$\begin{pmatrix} & \text{“Left Arm”} & \text{“Right Arm”} \\ \text{“Arm”} & \frac{\Phi^T \cdot \text{kronecker (Left,1)} \cdot \Psi}{\Phi^T \cdot \Psi} & \frac{\Phi^T \cdot \text{kronecker (Right,I)} \cdot \Psi}{\Phi^T \cdot \Psi} \\ \text{“Pang”} & \frac{\Phi^T \cdot \text{kronecker (Left, Pang)} \cdot \Psi}{\Phi^T \cdot \Psi} & \frac{\Phi^T \cdot \text{kronecker (Right , Pang)} \cdot \Psi}{\Phi^T \cdot \Psi} \end{pmatrix}$$

$$= \begin{pmatrix} & \text{“Left Arm”} & \text{“Right Arm”} \\ \text{“Arm”} & 1 & 0 \\ \text{“Pang”} & 0 & 1 \end{pmatrix}$$

The following shows the evolution of the pre-selected state to the final state at the detectors. The intermediate is the state illuminating BS_2. The polarization state at the detectors is ignored.

$$|\Psi\rangle \rightarrow \frac{i}{\sqrt{2}}[|L\rangle|H\rangle + |R\rangle|V\rangle] \rightarrow -\frac{1}{2}|D_1\rangle + \frac{i}{2}|D_3\rangle + \frac{(i-1)}{2}|D_2\rangle$$

Squaring the magnitude of the probability amplitudes shows that the probabilities that D_1, D_3 and D_2 will fire are 1/4, 1/4 and 1/2, respectively. The probability at D_1 is consistent with the probability that the post-selected state is contained in the pre-selected

state. A photon in the post-selected state has a probability of 1 of reaching D_1 and it represents a 25% contribution to the pre-selected state.

$$\left(\left|\Phi^{T} \cdot \Psi\right|\right)^{2} \rightarrow \frac{1}{4}$$

Note that the expectation values for the pre-selected state show no path-polarization separation.

$$\begin{bmatrix} & \text{“Left Arm”} & \text{“Right Arm”} \\ \text{“Arm”} & \left(\overline{\Psi}\right)^{T} \cdot \text{ kronecker (Left, I)} \cdot \Psi & \left(\overline{\Psi}\right)^{T} \cdot \text{ kronecker (Right, I)} \cdot \Psi \\ \text{“Pang”} & \left(\overline{\Psi}\right)^{T} \cdot \text{ kronecker (Left, Pang)} \cdot \Psi & \left(\overline{\Psi}\right)^{T} \cdot \text{ kronecker (Right, Pang)} \cdot \Psi \\ \text{“Hop”} & \left(\overline{\Psi}\right)^{T} \cdot \text{ kronecker } \left(\text{ Left }, H \cdot H^{T}\right) \cdot \Psi & \left(\overline{\Psi}\right)^{T} \cdot \text{ kronecker } \left(\text{ Right }, H \cdot H^{T}\right) \cdot \Psi \\ \text{“Vop”} & \left(\overline{\Psi}\right)^{T} \cdot \text{ kronecker } \left(\text{ Left }, V \cdot V^{T}\right) \cdot \Psi & \left(\overline{\Psi}\right)^{T} \cdot \text{ kronecker } \left(\text{ Right }, V \cdot V^{T}\right) \cdot \Psi \end{bmatrix}$$

$$= \begin{pmatrix} & \text{“Left Arm”} & \text{“Right Arm”} \\ \text{“Arm”} & 0.5 & 0.5 \\ \text{“Pang”} & 0 & 0 \\ \text{“Hop”} & 0.5 & 0.5 \\ \text{“Vop”} & 0 & 0 \end{pmatrix}$$

In addition the following table shows that linear polarization (HV) is not separated from the photon's path.

$$HV := \begin{pmatrix} 1 & 0 \\ 0 & -1 \end{pmatrix}$$

$$\begin{pmatrix} & \text{“Left Arm”} & \text{“Right Arm”} \\ \text{“Arm”} & \frac{\Phi^{T} \cdot \text{ kronecker (Left,1)} \cdot \Psi}{\Phi^{T} \cdot \Psi} & \frac{\Phi^{T} \cdot \text{ kronecker (Right,I)} \cdot \Psi}{\Phi^{T} \cdot \Psi} \\ \text{“HIV”} & \frac{\Phi^{T} \cdot \text{ kronecker (Left, Pang)} \cdot \Psi}{\Phi^{T} \cdot \Psi} & \frac{\Phi^{T} \cdot \text{ kronecker (Right , Pang)} \cdot \Psi}{\Phi^{T} \cdot \Psi} \end{pmatrix}$$

$$= \begin{pmatrix} & \text{“Left Arm”} & \text{“Right Arm”} \\ \text{“Arm”} & 1 & 0 \\ \text{“HIV”} & 1 & 0 \end{pmatrix}$$

The "Complete Quantum Cheshire Cat" by Guryanova, Brunner and Popescu (arXiv 1203.4215) provides an optical set-up which achieves complete path-polarization separation for the photon.

This page titled 1.9: Quantum Computation- A Short Course is shared under a CC BY 4.0 license and was authored, remixed, and/or curated by Frank Rioux via source content that was edited to the style and standards of the LibreTexts platform.

1.10: Quantum Computation- A Short Course

The last several tutorials were a bit off the theme of quantum computation. We get back on track with a look at data base searching the quantum way, or the best way to find a needle in a hay stack. This is followed by a demonstration of Simon's algorithm, an illustration of quantum dense coding and an example of quantum error correction.

Grover Search Algorithm Implementation for Two Items

Chris Monroe's research group recently published an experimental implementation of the Grover search algorithm in Nature Communications 8, 1918 (2017). In this report the Grover search is implemented for N = 3 using the three qubit quantum circuit shown below. In this particular example it is demonstrated that the search algorithm successfully searches for two items in one operation of the circuit. The lead sentence in the paper states "The Grover search algorithm has four stages: initialization (red), oracle (green), amplification (blue) and measurement (black)."

$$
\begin{array}{lllllllllll}
|0\rangle & \triangleright & \mathrm{H} & \lceil & & \rceil & \mathrm{H} & \mathrm{X} & \cdot & \mathrm{X} & \mathrm{H} & \triangleright & \text{Measure} \\
 & & & | & & | & & & | & & & & \\
|0\rangle & \triangleright & \mathrm{H} & | & \text{Oracle} & | & \mathrm{H} & \mathrm{X} & | & \mathrm{X} & \mathrm{H} & \triangleright & \text{Measure} \\
 & & & | & & | & & & | & & & & \\
|0\rangle & \triangleright & \mathrm{H} & \lfloor & & \rfloor & \mathrm{H} & \mathrm{X} & \mathrm{Z} & \mathrm{X} & \mathrm{H} & \triangleright & \text{Measure}
\end{array}
$$

The oracle, highlighted below, contains 3 (|011>) and 5 (|101>).

$$
\mathrm{H} := \frac{1}{\sqrt{2}} \begin{pmatrix} 1 & 1 \\ 1 & -1 \end{pmatrix} \qquad \mathrm{X} := \begin{pmatrix} 0 & 1 \\ 1 & 0 \end{pmatrix}
$$

$$
\mathrm{Oracle} = \begin{pmatrix}
1 & 0 & 0 & 0 & 0 & 0 & 0 & 0 \\
0 & 1 & 0 & 0 & 0 & 0 & 0 & 0 \\
0 & 0 & 1 & 0 & 0 & 0 & 0 & 0 \\
0 & 0 & 0 & -1 & 0 & 0 & 0 & 0 \\
0 & 0 & 0 & 0 & 1 & 0 & 0 & 0 \\
0 & 0 & 0 & 0 & 0 & -1 & 0 & 0 \\
0 & 0 & 0 & 0 & 0 & 0 & 1 & 0 \\
0 & 0 & 0 & 0 & 0 & 0 & 0 & 1
\end{pmatrix}
$$

$$
\mathrm{CCZ} := \begin{pmatrix}
1 & 0 & 0 & 0 & 0 & 0 & 0 & 0 \\
0 & 1 & 0 & 0 & 0 & 0 & 0 & 0 \\
0 & 0 & 1 & 0 & 0 & 0 & 0 & 0 \\
0 & 0 & 0 & 1 & 0 & 0 & 0 & 0 \\
0 & 0 & 0 & 0 & 1 & 0 & 0 & 0 \\
0 & 0 & 0 & 0 & 0 & 1 & 0 & 0 \\
0 & 0 & 0 & 0 & 0 & 0 & 1 & 0 \\
0 & 0 & 0 & 0 & 0 & 0 & 0 & -1
\end{pmatrix}
$$

$$
\mathrm{HHH} := \mathrm{kronecker}(\mathrm{H}, \mathrm{kronecker}(\mathrm{H}, \mathrm{H})) \qquad \mathrm{XXX} := \mathrm{kronccker}\ (\mathrm{X},\ \mathrm{kronecker}\ (\mathrm{X}, \mathrm{X}))
$$

The initial Hadamard gates on the three circuit wires feed the Grover search algorithm (in blue) a superposition of all possible queries yielding a superposition of the correct answers.

$$\text{GroverSearch} := \text{HHH} \cdot \text{XXX} \cdot \text{CCZ} \cdot \text{XXX} \cdot \text{HHH} \cdot \text{Oracle} \cdot \text{HHH}$$

$$\text{GroverSearch} \cdot \begin{pmatrix} 1 \\ 0 \\ 0 \\ 0 \\ 0 \\ 0 \\ 0 \\ 0 \end{pmatrix} = \begin{pmatrix} 0 \\ 0 \\ 0 \\ -0.707 \\ 0 \\ -0.707 \\ 0 \\ 0 \end{pmatrix} = -\frac{1}{\sqrt{2}}[|011\rangle + |101\rangle]$$

Aspects of Simon's Algorithm

A concealed quantum algorithm calculates f(x) from an input register containing a superposition of all x-values. Pairs of x-values (x,x') generate the same output. Simon's algorithm is an efficient method for finding the relationship between the pairs: $f(x) = f(x') = f(x \oplus s)$, where **s** is a secret string and the addition on the right is bitwise modulo 2 . In a classical calculation one could compute f(x) until some pattern emerged and find the pairs by inspection. This approach is illustrated below.

Decimal	Binary		Binary	Decimal
$\|0\rangle$	$\|000\rangle$	$\xrightarrow{f(0)}$	$\|011\rangle$	$\|3\rangle$
$\|1\rangle$	$\|001\rangle$	$\xrightarrow{f(1)}$	$\|001\rangle$	$\|1\rangle$
$\|2\rangle$	$\|010\rangle$	$\xrightarrow{f(2)}$	$\|010\rangle$	$\|2\rangle$
$\|3\rangle$	$\|011\rangle$	$\xrightarrow{f(3)}$	$\|000\rangle$	$\|0\rangle$
$\|4\rangle$	$\|100\rangle$	$\xrightarrow{f(4)}$	$\|001\rangle$	$\|1\rangle$
$\|5\rangle$	$\|101\rangle$	$\xrightarrow{f(5)}$	$\|011\rangle$	$\|3\rangle$
$\|5\rangle$	$\|101\rangle$	$\xrightarrow{f(5)}$	$\|011\rangle$	$\|3\rangle$
$\|6\rangle$	$\|110\rangle$	$\xrightarrow{f(6)}$	$\|000\rangle$	$\|0\rangle$
$\|7\rangle$	$\|111\rangle$	$\xrightarrow{f(7)}$	$\|010\rangle$	$\|2\rangle$

The table of results reveals the pairs {(0,5), (1,4), (2,7), (3,6)} and that |s> = |101>. Adding |s> bitwise modulo 2 to any |x> reveals its partner |x'>.

The following quantum circuit is a rudimentary implementation of Simon's algorithm. The section in blue is the concealed algorithm. It has been discussed in two other tutorials: **Quantum Parallel Calculation** and **An Illustration of the Deutsch-Jozsa Algorithm**. Its operation yields the results shown in the following table.

$$\begin{pmatrix} x & 0 & 1 & 2 & 3 \\ f(x) & 1 & 0 & 0 & 1 \end{pmatrix}$$

Initial		1		2		3		4		5		Final
$\|0\rangle$	$\triangleright$	H	$\cdots$	$\cdot$	$\cdots$	$\cdots$	$\cdots$	$\cdots$	$\cdots$	H	$\triangleright$	
				$\vert$								
$\|0\rangle$	$\triangleright$	H	$\cdots$	$\vert$	$\cdots$	$\cdot$	$\cdots$	$\cdots$	$\cdots$	H	$\triangleright$	
				$\vert$		$\vert$						
$\|0\rangle$	$\triangleright$	$\cdots$	$\cdots$	$\oplus$	$\cdots$	$\oplus$	$\cdots$	NOT	$\cdots$	$\cdots$	$\triangleright$	Measure, 0 or 1

Next we prepare a table showing the results of a classical calculation. It is clear that the pairs are (0,3) and (1,2), and that |s> = |11>.

Decimal	Binary		Binary	Decimal
$\|0\rangle$	$\|000\rangle$	$\xrightarrow{f(0)}$	$\|011\rangle$	$\|3\rangle$
$\|1\rangle$	$\|001\rangle$	$\xrightarrow{f(1)}$	$\|001\rangle$	$\|1\rangle$
$\|2\rangle$	$\|010\rangle$	$\xrightarrow{f(2)}$	$\|010\rangle$	$\|2\rangle$
$\|3\rangle$	$\|011\rangle$	$\xrightarrow{f(3)}$	$\|000\rangle$	$\|0\rangle$

Now we examine the operation of the quantum circuit that implements Simon's algoritm by two different, but equivalent methods. The matrices representing the quantum gates in the circuit are:

$$\mathrm{I} := \begin{pmatrix} 1 & 0 \\ 0 & 1 \end{pmatrix} \qquad \mathrm{NOT} := \begin{pmatrix} 0 & 1 \\ 1 & 0 \end{pmatrix} \qquad \mathrm{H} := \frac{1}{\sqrt{2}} \cdot \begin{pmatrix} 1 & 1 \\ 1 & -1 \end{pmatrix}$$

$$\mathrm{CNOT} := \begin{pmatrix} 1 & 0 & 0 & 0 \\ 0 & 1 & 0 & 0 \\ 0 & 0 & 0 & 1 \\ 0 & 0 & 1 & 0 \end{pmatrix}$$

$$\mathrm{CnNOT} := \begin{pmatrix} 1 & 0 & 0 & 0 & 0 & 0 & 0 & 0 \\ 0 & 1 & 0 & 0 & 0 & 0 & 0 & 0 \\ 0 & 0 & 1 & 0 & 0 & 0 & 0 & 0 \\ 0 & 0 & 0 & 1 & 0 & 0 & 0 & 0 \\ 0 & 0 & 0 & 0 & 0 & 1 & 0 & 0 \\ 0 & 0 & 0 & 0 & 1 & 0 & 0 & 0 \\ 0 & 0 & 0 & 0 & 0 & 0 & 0 & 1 \\ 0 & 0 & 0 & 0 & 0 & 0 & 1 & 0 \end{pmatrix}$$

The three qubit input state is:

$$\Psi_{\mathrm{in}} := \begin{pmatrix} 1 & 0 & 0 & 0 & 0 & 0 & 0 & 0 \end{pmatrix}^{\mathrm{T}}$$

The concealed algorithm:

$$U_f := \mathrm{kronecker}(\mathrm{I},\ \mathrm{kronecker}(\mathrm{I},\ \mathrm{NOT})) \cdot \mathrm{kronecker}(\mathrm{I},\ \mathrm{CNOT}) \cdot \mathrm{CnNOT}$$

The complete quantum circuit:

$$\mathrm{QuantumCircuit} := \mathrm{kronecker}(\mathrm{H},\ \mathrm{kronecker}(\mathrm{H},\ \mathrm{I})) \cdot U_f \cdot \mathrm{kronecker}(\mathrm{H},\ \mathrm{kronecker}(\mathrm{H},\ \mathrm{I}))$$

The operation of the quantum circuit on the input state yields the following result:

$$\mathrm{QuantumCircuit} \cdot \Psi_{\mathrm{in}} = \begin{pmatrix} 0.5 \\ 0.5 \\ 0 \\ 0 \\ 0 \\ 0 \\ -0.5 \\ 0.5 \end{pmatrix}$$

$$= \frac{1}{2}\left[\begin{pmatrix} 1 \\ 0 \end{pmatrix} \otimes \begin{pmatrix} 1 \\ 0 \end{pmatrix} - \begin{pmatrix} 0 \\ 1 \end{pmatrix} \otimes \begin{pmatrix} 0 \\ 1 \end{pmatrix}\right] \begin{pmatrix} 1 \\ 0 \end{pmatrix} + \frac{1}{2}\left[\begin{pmatrix} 1 \\ 0 \end{pmatrix} \otimes \begin{pmatrix} 1 \\ 0 \end{pmatrix} + \begin{pmatrix} 0 \\ 1 \end{pmatrix} \otimes \begin{pmatrix} 0 \\ 1 \end{pmatrix}\right] \begin{pmatrix} 0 \\ 1 \end{pmatrix}$$

$$= \frac{1}{2}[|00\rangle - |11\rangle]|0\rangle + \frac{1}{2}[|00\rangle + |11\rangle]|1\rangle$$

The terms in brackets are superpositions of the x-values which are related by $x' = x \oplus s$. Thus we see by inspection that |s> = |11>. The actual implementation of Simon's algorithm involves multiple measurements in order to determine the secret string. The **Appendix** modifies the quantum circuit to include the effect of measurement on the bottom wire.

The second method of analysis uses the following truth tables for the quantum gates and the operation of the Hadamard gate to trace the evolution of the input quibits through the quantum circuit.

$$\text{NOT} \quad \begin{pmatrix} 0 & \prime & 1 \\ 1 & \prime & 0 \end{pmatrix}$$

$$\text{CNOT} \quad \begin{pmatrix} \text{Decimal} & \text{Binary} & \prime & \text{Binary} & \text{Decimal} \\ 0 & 00 & \prime & 00 & 0 \\ 1 & 01 & \prime & 01 & 1 \\ 2 & 10 & \prime & 11 & 3 \\ 3 & 11 & \prime & 10 & 2 \end{pmatrix}$$

$$\text{CnNOT} \quad \begin{pmatrix} \text{Decimal} & \text{Binary} & \prime & \text{Binary} & \text{Decimal} \\ 0 & 000 & \prime & 000 & 0 \\ 1 & 001 & \prime & 001 & 1 \\ 2 & 010 & \prime & 010 & 3 \\ 3 & 011 & \prime & 011 & 3 \\ 4 & 100 & \prime & 101 & 5 \\ 5 & 101 & \prime & 100 & 4 \\ 6 & 110 & \prime & 111 & 7 \\ 7 & 111 & \prime & 110 & 6 \end{pmatrix}$$

$$\text{Hadamard operation:} \quad \begin{bmatrix} 0 & \prime & H & \prime & \frac{1}{\sqrt{2}} \cdot (0+1) & \prime & H & \prime & 0 \\ 1 & \prime & H & \prime & \frac{1}{\sqrt{2}} \cdot (0-1) & \prime & H & \prime & 1 \end{bmatrix}$$

$$|000\rangle$$

$$\text{H} \otimes \text{H} \otimes \text{I}$$

$$\tfrac{1}{\sqrt{2}}[|0\rangle + |1\rangle]\tfrac{1}{\sqrt{2}}[|0\rangle + |1\rangle]|0\rangle = \tfrac{1}{2}[|000\rangle + |010\rangle + |100\rangle + |110\rangle]$$

$$\text{CnNOT}$$

$$\tfrac{1}{2}[|000\rangle + |010\rangle + |101\rangle + |111\rangle]$$

$$\text{I} \otimes \text{CNOT}$$

$$\tfrac{1}{2}[|000\rangle + |011\rangle + |101\rangle + |110\rangle]$$

$$\text{I} \otimes \text{I} \otimes \text{NOT}$$

$$\tfrac{1}{2}[|001\rangle + |010\rangle + |100\rangle + |111\rangle]$$

$$\text{H} \otimes \text{H} \otimes \text{I}$$

$$\tfrac{1}{2}[(|00\rangle - |11\rangle)|0\rangle + (|00\rangle + |11\rangle)|1\rangle]$$

Appendix:

The circuit modification shown below includes the effect of measurement on the bottom wire.

Measure |0> on the bottom wire:

$$\text{QuantumCircuit} := \text{kronecker}\left(\text{H},\ \text{kronecker}\left[\text{H},\ \begin{pmatrix}1\\0\end{pmatrix}\cdot\begin{pmatrix}1\\0\end{pmatrix}^{T}\right]\right)\cdot U_f\cdot\text{kronecker}(\text{H},\ \text{kronecker}(\text{H},\ \text{I}))$$

$$\text{QuantumCircuit}\cdot\Psi_{\text{in}} = \begin{pmatrix}0.5\\0\\0\\0\\0\\0\\-0.5\\0\end{pmatrix}$$

$$\begin{pmatrix}0.5\\0\\0\\0\\0\\0\\-0.5\\0\end{pmatrix} = \frac{1}{2}\cdot\left[\begin{pmatrix}1\\0\end{pmatrix}\cdot\begin{pmatrix}1\\0\end{pmatrix}-\begin{pmatrix}0\\1\end{pmatrix}\cdot\begin{pmatrix}0\\1\end{pmatrix}\right]\cdot\begin{pmatrix}1\\0\end{pmatrix}$$

Measure |1> on the bottom wire:

$$\text{QuantumCircuit} := \text{kronecker}\left(\text{H},\ \text{kronecker}\left[\text{H},\ \begin{pmatrix}0\\1\end{pmatrix}\cdot\begin{pmatrix}0\\1\end{pmatrix}^{T}\right]\right)\cdot U_f\cdot\text{kronecker}(\text{H},\ \text{kronecker}(\text{H},\ \text{I}))$$

$$\text{QuantumCircuit}\cdot\Psi_{\text{in}} = \begin{pmatrix}0\\0.5\\0\\0\\0\\0\\0\\0.5\end{pmatrix}$$

$$\begin{pmatrix}0\\0.5\\0\\0\\0\\0\\0\\0.5\end{pmatrix} = \frac{1}{2}\cdot\left[\begin{pmatrix}1\\0\end{pmatrix}\cdot\begin{pmatrix}1\\0\end{pmatrix}-\begin{pmatrix}0\\1\end{pmatrix}\cdot\begin{pmatrix}0\\1\end{pmatrix}\right]\cdot\begin{pmatrix}0\\1\end{pmatrix}$$

Quantum Dense Coding

> *Quantum superdense coding reliably transmits two classical bits through an entangled pair of particles, even though only one member of the pair is handled by the sender. Charles Bennett, Physics Today, October 1995, p. 27*

This tutorial is based on Brad Rubin's "Superdense Coding" at the Wolfram Demonstration Project: http:demonstrations.wolfram.com/SuperdenseCoding/. The quantum circuit shown below impliments quantum dense coding. Alice and Bob share the entangled pair of photons in the Bell basis shown at the left. Alice encodes two classical bits of information (four possible messages) on her photon, and Bob subsequently reads her message by performing a Bell state measurement on the modified entangled photon pair. In other words, although Alice encodes two bits on her photon Bob's readout requires a measurement involving both photons. In this example Alice sends |11> to Bob.

$$\begin{array}{cccccccc} \cdot & & \mathrm{X}^1 & \cdot & \mathrm{Z}^1 & \cdot & \cdot & H \\ \begin{pmatrix} 1/\sqrt{2} \\ 0 \\ 0 \\ 1/\sqrt{2} \end{pmatrix} & & \begin{pmatrix} 0 \\ 1/\sqrt{2} \\ 1/\sqrt{2} \\ 0 \end{pmatrix} & & \begin{pmatrix} 0 \\ 1/\sqrt{2} \\ -1/\sqrt{2} \\ 0 \end{pmatrix} & | & & \begin{pmatrix} 0 \\ 0 \\ 0 \\ 1 \end{pmatrix} = \begin{pmatrix} 0 \\ 1 \end{pmatrix} \begin{pmatrix} 0 \\ 1 \end{pmatrix} \\ \cdot & & \mathrm{I} & \cdot & \mathrm{I} & \cdot & \oplus & \mathrm{I} \end{array}$$

The operation of the circuit is outlined in both matrix and algebraic format. The necessary truth tables and matrix operators are provided in the Appendix.

Matrix Method

$$\mathrm{H} \otimes \mathrm{I} \cdot \mathrm{CNOT} \cdot \mathrm{Z} \otimes \mathrm{I} \cdot \mathrm{X} \otimes \mathrm{I} \cdot \frac{1}{\sqrt{2}} \begin{pmatrix} 1 \\ 0 \\ 0 \\ 1 \end{pmatrix} = \begin{pmatrix} 0 \\ 0 \\ 0 \\ 1 \end{pmatrix} = \begin{pmatrix} 0 \\ 1 \end{pmatrix} \otimes \begin{pmatrix} 0 \\ 1 \end{pmatrix} = |11\rangle$$

Algebraic Method

$$\frac{|00\rangle+|11\rangle}{\sqrt{2}} \xrightarrow{\mathrm{X}^1 \otimes \mathrm{I}} \frac{|10\rangle+|01\rangle}{\sqrt{2}} \xrightarrow{\mathrm{Z}^1 \otimes \mathrm{I}} \frac{-|10\rangle+|01\rangle}{\sqrt{2}} \xrightarrow{CNOT} \frac{-|11\rangle+|01\rangle}{\sqrt{2}}$$

$$\xrightarrow{\mathrm{H} \otimes \mathrm{I}} \frac{-(|0\rangle-|1\rangle)|1\rangle+(|0\rangle+|1\rangle)|1\rangle}{2} = |11\rangle = \begin{pmatrix} 0 \\ 1 \end{pmatrix} \otimes \begin{pmatrix} 0 \\ 1 \end{pmatrix} = \begin{pmatrix} 0 \\ 0 \\ 0 \\ 1 \end{pmatrix}$$

Appendix:

Truth tables for the quantum circuit:

$$\mathrm{X} = \mathrm{NOT} \begin{pmatrix} 0 & \text{to} & 1 \\ 1 & \text{to} & 0 \end{pmatrix} \quad Z \begin{pmatrix} 0 & \text{to} & 0 \\ 1 & \text{to} & -1 \end{pmatrix} \quad \mathrm{H} = \mathrm{Hadamard} \begin{bmatrix} 0 & \text{to} & \frac{1}{\sqrt{2}} \cdot (0+1) \\ 1 & \text{to} & \frac{1}{\sqrt{2}} \cdot (0-1) \end{bmatrix} \quad \mathrm{CNOT} \begin{pmatrix} 00 & \text{to} & 00 \\ 01 & \text{to} & 01 \\ 10 & \text{to} & 11 \\ 11 & \text{to} & 10 \end{pmatrix}$$

Circuit elements in matrix format:

$$\mathrm{I} \equiv \begin{pmatrix} 1 & 0 \\ 0 & 1 \end{pmatrix} \quad \mathrm{X} \equiv \begin{pmatrix} 0 & 1 \\ 1 & 0 \end{pmatrix} \quad \mathrm{Z} \equiv \begin{pmatrix} 1 & 0 \\ 0 & -1 \end{pmatrix} \quad H \equiv \frac{1}{\sqrt{2}} \cdot \begin{pmatrix} 1 & 1 \\ 1 & -1 \end{pmatrix} \quad \mathrm{CNOT} \equiv \begin{pmatrix} 1 & 0 & 0 & 0 \\ 0 & 1 & 0 & 0 \\ 0 & 0 & 0 & 1 \\ 0 & 0 & 1 & 0 \end{pmatrix}$$

Quantum Error Correction

This tutorial deals with quantum error correction as presented by Julian Brown on pages 274-278 in *The Quest for the Quantum Computer.* Brown's three-qubit example includes an input qubit and two ancillary qubits in the initial state $|\Psi 00\rangle$. This state is encoded and subsequently decoded, with the possibility that in between it acquires an error. The quantum circuit demonstrates how correction occurs if a qubit is flipped due to decoherence at the intermediate state.

The quantum gates required for the error correction algorithm are:

$$\mathrm{I} := \begin{pmatrix} 1 & 0 \\ 0 & 1 \end{pmatrix} \qquad \mathrm{CNOT} := \begin{pmatrix} 1 & 0 & 0 & 0 \\ 0 & 1 & 0 & 0 \\ 0 & 0 & 0 & 1 \\ 0 & 0 & 1 & 0 \end{pmatrix}$$

$$\mathrm{CNOT} := \begin{pmatrix} 1 & 0 & 0 & 0 & 0 & 0 & 0 & 0 \\ 0 & 1 & 0 & 0 & 0 & 0 & 0 & 0 \\ 0 & 0 & 1 & 0 & 0 & 0 & 0 & 0 \\ 0 & 0 & 0 & 1 & 0 & 0 & 0 & 0 \\ 0 & 0 & 0 & 0 & 0 & 1 & 0 & 0 \\ 0 & 0 & 0 & 0 & 1 & 0 & 0 & 0 \\ 0 & 0 & 0 & 0 & 0 & 0 & 0 & 1 \\ 0 & 0 & 0 & 0 & 0 & 0 & 1 & 0 \end{pmatrix}$$

$$\mathrm{IToffoli} := \begin{pmatrix} 1 & 0 & 0 & 0 & 0 & 0 & 0 \\ 0 & 1 & 0 & 0 & 0 & 0 & 0 \\ 0 & 0 & 1 & 0 & 0 & 0 & 0 \\ 0 & 0 & 0 & 0 & 0 & 0 & 1 \\ 0 & 0 & 0 & 1 & 0 & 0 & 0 \\ 0 & 0 & 0 & 0 & 1 & 0 & 0 \\ 0 & 0 & 0 & 0 & 0 & 1 & 0 \\ 0 & 0 & 0 & 1 & 0 & 0 & 0 \end{pmatrix}$$

The encoding and decoding elements of the circuit in terms of these gates are shown in the appropriate place above the circuit diagram.

$$\mathrm{Encode} := \mathrm{CnNOT} \cdot \mathrm{kronecker}(\mathrm{CNOT}, \mathrm{I}) \qquad \mathrm{Decode} := \mathrm{IToffoli} \cdot \mathrm{Encode}$$

$$\begin{array}{lccccccccccccc} \sqrt{\frac{1}{3}}|0\rangle + \sqrt{\frac{2}{3}}|1\rangle & \cdots & \cdot & \cdots & \cdot & \cdots & \mathrm{E} & \cdots & \cdot & \cdots & \cdot & \cdots & \oplus & \triangleright & \sqrt{\frac{1}{3}}|0\rangle + \sqrt{\frac{2}{3}}|1\rangle \\ & & | & & | & & \mathrm{R} & & | & & | & & | & & \\ |0\rangle & \cdots & \oplus & \cdots & | & \cdots & \mathrm{R} & \cdots & \oplus & \cdots & | & \cdots & \cdot & \triangleright & |0\rangle \text{ or } |1\rangle \\ & & & & | & & \mathrm{O} & & & & | & & | & & \\ |0\rangle & \cdots & \cdots & \cdots & \oplus & \cdots & \mathrm{R} & \cdots & \cdots & \cdots & | & \cdots & \cdot & \triangleright & |0\rangle \text{ or } |1\rangle \end{array}$$

Given an initial state, the encoding step creates and entangled Bell state as demonstrated below.

Initial State

$$\left(\sqrt{\frac{1}{3}}\right) \cdot \begin{pmatrix} 1 \\ 0 \end{pmatrix} \cdot \begin{pmatrix} 1 \\ 0 \end{pmatrix} \cdot \begin{pmatrix} 1 \\ 0 \end{pmatrix} = \begin{pmatrix} \sqrt{\frac{1}{3}} \\ 0 \\ 0 \\ 0 \\ \sqrt{\frac{2}{3}} \\ 0 \\ 0 \\ 0 \end{pmatrix}$$

Encode

$$\mathrm{Encode} = \begin{pmatrix} \sqrt{\frac{1}{3}} \\ 0 \\ 0 \\ 0 \\ \sqrt{\frac{2}{3}} \\ 0 \\ 0 \\ 0 \end{pmatrix} = \begin{pmatrix} 0.577 \\ 0 \\ 0 \\ 0 \\ 0 \\ 0 \\ 0 \\ 0.816 \end{pmatrix}$$

Encoded state

$$\left(\sqrt{\frac{1}{3}}\right)\cdot\begin{pmatrix}1\\0\end{pmatrix}\cdot\begin{pmatrix}1\\0\end{pmatrix}+\begin{pmatrix}0\\\sqrt{\frac{2}{3}}\end{pmatrix}\begin{pmatrix}0\\1\end{pmatrix}\cdot\begin{pmatrix}0\\1\end{pmatrix}=\begin{pmatrix}\sqrt{\frac{1}{3}}\\0\\0\\0\\0\\0\\0\\0\\\sqrt{\frac{2}{3}}\end{pmatrix}$$

As an initial example, it is assumed that between encoding and decoding no errors are introduced to the encoded state. This case demonstrates that decoding simply returns the initial state. Susbsequent to this the operation of the circuit when errors occur on each of the wires are examined. These cases demonstrate that the original state appears on the top wire at the completion of the error correction circuit.

No errors:

$$\begin{pmatrix}\sqrt{\frac{1}{3}}\\0\end{pmatrix}\cdot\begin{pmatrix}1\\0\end{pmatrix}\cdot\begin{pmatrix}1\\0\end{pmatrix}+\left(\sqrt{\frac{2}{3}}\right)\cdot\begin{pmatrix}0\\1\end{pmatrix}\cdot\begin{pmatrix}0\\1\end{pmatrix}=\begin{pmatrix}\sqrt{\frac{1}{3}}\\0\\0\\0\\0\\0\\0\\0\\\sqrt{\frac{2}{3}}\end{pmatrix}$$

$$\text{Decode}\cdot\begin{pmatrix}0.577\\0\\0\\0\\0\\0\\0\\0.816\end{pmatrix}=\begin{pmatrix}0.577\\0\\0\\0\\0.816\\0\\0\\0\end{pmatrix}\qquad\left(\sqrt{\frac{1}{3}}\right)\cdot\begin{pmatrix}1\\0\end{pmatrix}\cdot\begin{pmatrix}1\\0\end{pmatrix}=\begin{pmatrix}\sqrt{\frac{1}{3}}\\0\\0\\0\\\sqrt{\frac{2}{3}}\\0\\0\\0\end{pmatrix}=\begin{pmatrix}\sqrt{\frac{1}{3}}\\0\\0\\0\\\sqrt{\frac{2}{3}}\\0\\0\end{pmatrix}$$

Next it is shown that if the input state, $|\Psi\rangle$, is corrupted that the decoder corrects the error and returns the original $|\Psi\rangle$ to the top wire of the circuit. In the example shown below the top qubit is flipped.

Top qubit flipped:

$$\begin{pmatrix} 0 \\ \sqrt{\frac{1}{3}} \end{pmatrix} \cdot \begin{pmatrix} 1 \\ 0 \end{pmatrix} \cdot \begin{pmatrix} 1 \\ 0 \end{pmatrix} + \begin{pmatrix} \sqrt{\frac{2}{3}} \\ 0 \end{pmatrix} \cdot \begin{pmatrix} 0 \\ 1 \end{pmatrix} \cdot \begin{pmatrix} 0 \\ 1 \end{pmatrix} = \begin{pmatrix} 0 \\ 0 \\ 0 \\ \sqrt{\frac{2}{3}} \\ \sqrt{\frac{1}{3}} \\ 0 \\ 0 \end{pmatrix}$$

$$\text{Decode} \cdot \begin{pmatrix} 0 \\ 0 \\ 0 \\ \sqrt{\frac{2}{3}} \\ \sqrt{\frac{1}{3}} \\ 0 \\ 0 \end{pmatrix} = \begin{pmatrix} 0 \\ 0 \\ 0 \\ 0.577 \\ 0 \\ 0 \\ 0 \\ 0.816 \end{pmatrix} \quad \begin{pmatrix} \sqrt{\frac{1}{3}} \\ \sqrt{\frac{2}{3}} \end{pmatrix} \cdot \begin{pmatrix} 0 \\ 1 \end{pmatrix} \cdot \begin{pmatrix} 0 \\ 1 \end{pmatrix} = \begin{pmatrix} 0 \\ 0 \\ 0 \\ \sqrt{\frac{1}{3}} \\ 0 \\ 0 \\ 0 \\ 0 \\ \sqrt{\frac{2}{3}} \end{pmatrix}$$

The circuit can also be expressed using Dirac notation. Truth tables for the gates are provided in the Appendix.

$$\left(\sqrt{\frac{1}{3}}|0\rangle + \sqrt{\frac{2}{3}}|1\rangle\right)|00\rangle \xrightarrow{\text{encode}} \sqrt{\frac{1}{3}}|000\rangle + \sqrt{\frac{2}{3}}|111\rangle \xrightarrow[\text{qubit}]{\text{flip top}} \sqrt{\frac{1}{3}}|100\rangle + \sqrt{\frac{2}{3}}|011\rangle \xrightarrow{\text{CNOT,I}} \sqrt{\frac{1}{3}}|$$

$$110\rangle + \sqrt{\frac{2}{3}}|011\rangle \xrightarrow{\text{CnNOT}} \sqrt{\frac{1}{3}}|111\rangle + \sqrt{\frac{2}{3}}|011\rangle \xrightarrow{\text{InToffoli}} \sqrt{\frac{1}{3}}|011\rangle$$

$$+ \sqrt{\frac{2}{3}}|111\rangle = \left(\sqrt{\frac{1}{3}}|0\rangle + \sqrt{\frac{2}{3}}|1\rangle\right)|11\rangle$$

Naturally the ancillary qubits are also susceptible to errors. The following examples show that if a qubit flip occurs on the middle or bottom wire, the circuit still functions properly.

Middle qubit flipped:

$$\begin{pmatrix} \sqrt{\frac{1}{3}} \\ 0 \end{pmatrix} \cdot \begin{pmatrix} 0 \\ 1 \end{pmatrix} \cdot \begin{pmatrix} 1 \\ 0 \end{pmatrix} + \begin{pmatrix} 0 \\ \sqrt{\frac{2}{3}} \end{pmatrix} \cdot \begin{pmatrix} 1 \\ 0 \end{pmatrix} \cdot \begin{pmatrix} 0 \\ 1 \end{pmatrix} = \begin{pmatrix} 0 \\ 0 \\ \sqrt{\frac{1}{3}} \\ 0 \\ 0 \\ \sqrt{\frac{2}{3}} \\ 0 \\ 0 \end{pmatrix}$$

$$\text{Decode} \cdot \begin{pmatrix} 0 \\ 0 \\ \sqrt{\frac{1}{3}} \\ 0 \\ 0 \\ \sqrt{\frac{2}{3}} \\ 0 \\ 0 \end{pmatrix} = \begin{pmatrix} 0 \\ 0 \\ 0.577 \\ 0 \\ 0 \\ 0 \\ 0.816 \\ 0 \end{pmatrix} \quad \begin{pmatrix} \sqrt{\frac{1}{3}} \\ \sqrt{\frac{2}{3}} \end{pmatrix} \cdot \begin{pmatrix} 0 \\ 1 \end{pmatrix} \cdot \begin{pmatrix} 1 \\ 0 \end{pmatrix} = \begin{pmatrix} 0 \\ 0 \\ \sqrt{\frac{1}{3}} \\ 0 \\ 0 \\ 0 \\ \sqrt{\frac{2}{3}} \\ 0 \end{pmatrix}$$

https://chem.libretexts.org/@go/page/137734

$$\left(\sqrt{\frac{1}{3}}|0\rangle+\sqrt{\frac{2}{3}}|1\rangle\right)|00\rangle \xrightarrow{\text{encode}} \sqrt{\frac{1}{3}}|000\rangle+\sqrt{\frac{2}{3}}|111\rangle \xrightarrow[\text{qubit}]{\text{flip middle}} \sqrt{\frac{1}{3}}|010\rangle$$
$$+\sqrt{\frac{2}{3}}|101\rangle \xrightarrow{\text{CNOT,I}} \sqrt{\frac{1}{3}}|010\rangle \xrightarrow{\text{CnNOT}} \sqrt{\frac{1}{3}}|010\rangle+\sqrt{\frac{2}{3}}|110\rangle \xrightarrow{\text{InToffoli}} \sqrt{\frac{1}{3}}|010\rangle+\sqrt{\frac{2}{3}}|110\rangle$$
$$=\left(\sqrt{\frac{1}{3}}|0\rangle+\sqrt{\frac{2}{3}}|1\rangle\right)|10\rangle$$

Bottom qubit flipped:

$$\left(\sqrt{\frac{1}{3}}\right)\cdot\begin{pmatrix}1\\0\end{pmatrix}\cdot\begin{pmatrix}0\\1\end{pmatrix}+\begin{pmatrix}0\\\sqrt{\frac{2}{3}}\end{pmatrix}\cdot\begin{pmatrix}0\\1\end{pmatrix}\cdot\begin{pmatrix}1\\0\end{pmatrix}=\begin{pmatrix}0\\\sqrt{\frac{1}{3}}\\0\\0\\0\\0\\\sqrt{\frac{2}{3}}\\0\end{pmatrix}$$

$$\text{Decode}\cdot\begin{pmatrix}0\\\sqrt{\frac{1}{3}}\\0\\0\\0\\0\\\sqrt{\frac{2}{3}}\\0\end{pmatrix}=\begin{pmatrix}0\\0.577\\0\\0\\0\\0.816\\0\\0\end{pmatrix}\quad\begin{pmatrix}\sqrt{\frac{1}{3}}\\\sqrt{\frac{2}{3}}\end{pmatrix}\cdot\begin{pmatrix}1\\0\end{pmatrix}\cdot\begin{pmatrix}0\\1\end{pmatrix}=\begin{pmatrix}0\\\sqrt{\frac{1}{3}}\\0\\0\\0\\\sqrt{\frac{2}{3}}\\0\\0\end{pmatrix}$$

$$\left(\sqrt{\frac{1}{3}}|0\rangle+\sqrt{\frac{2}{3}}|1\rangle\right)|00\rangle \xrightarrow{\text{encode}} \sqrt{\frac{1}{3}}|000\rangle+\sqrt{\frac{2}{3}}|111\rangle \xrightarrow[\text{quibt}]{\text{flip bottom}} \sqrt{\frac{1}{3}}|001\rangle$$
$$+\sqrt{\frac{2}{3}}|110\rangle \xrightarrow{\text{CNOT, I}} \sqrt{\frac{1}{3}}|001\rangle+\sqrt{\frac{2}{3}}|100\rangle \xrightarrow{\text{CnNOT}} \sqrt{\frac{1}{3}}|001\rangle+\sqrt{\frac{2}{3}}|101\rangle \xrightarrow{\text{InToffoli}} \sqrt{\frac{1}{3}}|001\rangle$$
$$+\sqrt{\frac{2}{3}}|101\rangle=\left(\sqrt{\frac{1}{3}}|0\rangle+\sqrt{\frac{2}{3}}|1\rangle\right)|01\rangle$$

Appendix:

CNOT

Decimal	Binary	to	Binary	Decimal
0	00	to	00	0
1	01	to	01	1
2	10	to	11	3
3	11	to	10	2

CnNOT

Decimal	Binary	to	Binary	Decimal
0	000	to	000	0
1	001	to	001	1
2	010	to	010	2
3	011	to	011	3
4	100	to	101	5
5	101	to	100	4
6	110	to	111	7
7	111	to	110	6

IToffoli

Decimal	Binary	to	Binary	Decimal
0	000	to	000	0
1	001	to	001	1
2	010	to	010	2
3	011	to	111	7
4	100	to	100	4
5	101	to	101	5
6	110	to	110	6
7	111	to	011	3

And now we move to Bell's theorem and the battle between local realism and quantum mechanics.

> *Quantum theory is both stupendously successful as an account of the small-scale structure of the world and it is also the subject of unresolved debate and dispute about its interpretation. J. C. Polkinghorne, The Quantum World.*

So we end this short course with the conflict between quantum mechanics and the classical view of reality held by Einstein and others known as local realism. Until the work of John Bell this battle was regarded by most scientists as a distracting philosophical debate. According to David Mermin quantum physicists were admonished to ignore the debate and "Shut up and calculate!"

In 1964 Bell demonstrated that experiments were possible for which quantum theory and local realism gave conflicting predictions, thus moving the disagreement from the realm of philosophical debate to the jurisdiction of the laboratory. In *Where Does the Weirdness Go?* David Lindley summarized Bell's achievement.

> *The hallmark of Bell's work was his success in locating precisely the point at which classical views of reality ran into trouble with quantum mechanics, and in devising a means by which the two viewpoints could be empirically compared. Bell's sympathies seem often to have lain with Bohm and the effort to establish a hidden variables version of quantum mechanics. His greatest achievement, though, was to demonstrate incontrovertibly the price that must be paid to make such a theory work.*

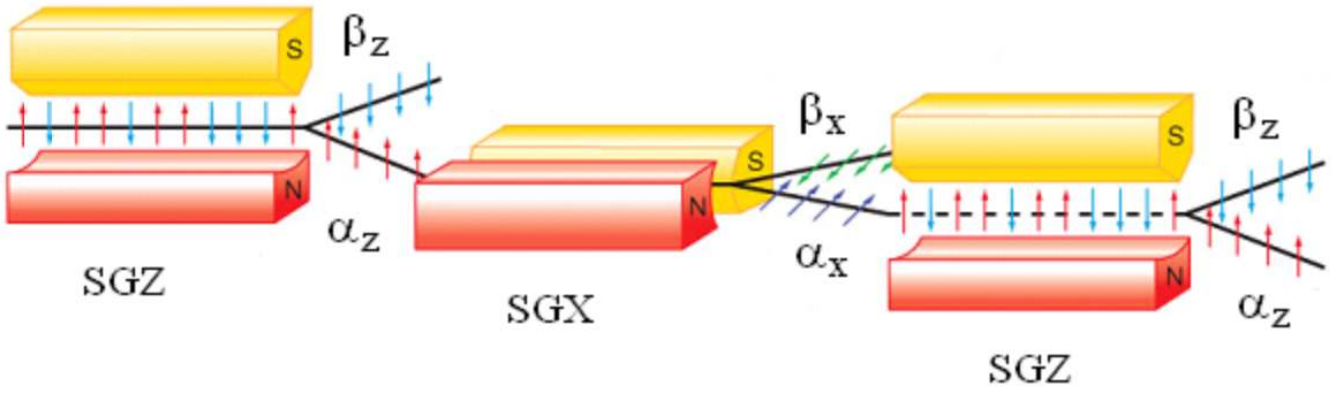
Bell said that if a theory of reality was local it would not agree with quantum mechanics, and if it agreed with quantum mechanics it would contain non-local interactions, in other words "spooky interactions at a distance" to use Einstein's phrase. Here's the best description of this spookiness that I have read: "A non-local interaction links up one location with another without crossing space, without decay, and without delay. A non-local event is, in short, unmediated, unmitigated and immediate." Nick Herbert, *Quantum Reality*, page 214.

In 1981 Richard Feynman gave a lecture titled "Simulating Nature with Computers." His thesis was that the simulation of nature at the nanoscopic level required a quantum computer. "I'm not happy with all the analyses that go with just the classical theory, because nature isn't classical, dammit. And if you want to make a simulation of nature, you'd better make it quantum mechanical …"

This page titled 1.10: Quantum Computation- A Short Course is shared under a CC BY 4.0 license and was authored, remixed, and/or curated by Frank Rioux via source content that was edited to the style and standards of the LibreTexts platform.

1.100: Analysis of the Stern-Gerlach Experiment

The purpose of this tutorial is to analyze the Stern-Gerlach experiment using matrix mechanics. The figure below is taken (and modified) from Thomas Engel's text, *Quantum Chemistry & Spectroscopy*.



Silver atoms are deflected by an inhomogeneous magnetic field because of the two-valued magnetic moment associated with their unpaired 5s electron ([Kr]$5s^1 4d^{10}$). The beam of silver atoms entering the Stern-Gerlach magnet oriented in the z-direction (SGZ) on the left is unpolarized. This means it is a mixture of randomly spin-polarized Ag atoms. As such, it is impossible to write a quantum mechanical wavefunction for this initial state.

This situation is exactly analogous to the three-polarizer demonstration described in a previous tutorial. Light emerging from an incadescent light bulb is unpolarized, a mixture of all possible polarization angles, so we can't write a wave function for it. The first Stern-Gerlach magnet plays the same role as the first polarizer, it forces the Ag atoms into one of measurement eigenstates - spin-up or spin-down in the z-direction. The only difference is that in the three-polarizer demonstration only one state was created - vertical polarization. Both demonstrations illustrate an important quantum mechanical postulate - the only values that are observed in a measurement are the eigenvalues of the measurement operator.

To continue with the analysis of the Stern-Gerlach demonstration we need vectors to represent the various spin states of the Ag atoms. We will restrict our attention to the x- and z- spin directions, although the spin states for the y-direction are also available.

Spin Eigenfunctions

Spin-up in the z-direction:	$\alpha_Z := \begin{pmatrix} 1 \\ 0 \end{pmatrix}$
Spin-down in the z-direction:	$\beta_z := \begin{pmatrix} 0 \\ 1 \end{pmatrix}$
Spin-up in the x-direction:	$\alpha_x := \frac{1}{\sqrt{2}} \cdot \begin{pmatrix} 1 \\ 1 \end{pmatrix}$
Spin-down in the x-direction:	$\beta_x := \frac{1}{\sqrt{2}} \cdot \begin{pmatrix} 1 \\ -1 \end{pmatrix}$

After the SGZ magnet, the spin-up beam (deflected toward the magnet's north pole) enters a magnet oriented in the x-direction, SGX. The α_z beam splits into α_x and β_x beams of equal intensity. This is because it is a superposition of the x-direction spin eigenstates as shown below.

$$\frac{1}{\sqrt{2}} \cdot \left[\frac{1}{\sqrt{2}} \cdot \begin{pmatrix} 1 \\ 1 \end{pmatrix} + \frac{1}{\sqrt{2}} \cdot \begin{pmatrix} 1 \\ -1 \end{pmatrix} \right] \rightarrow \begin{pmatrix} 1 \\ 0 \end{pmatrix} \qquad \frac{1}{\sqrt{2}} \cdot (\alpha_x + \beta_x) \rightarrow \begin{pmatrix} 1 \\ 0 \end{pmatrix}$$

Next the α_x beam is directed toward a second SGZ magnet and splits into two equal α_z and β_z beams. This happens because α_x is a superposition of the α_z and β_z spin states.

$$\frac{1}{\sqrt{2}} \cdot \left[\begin{pmatrix} 1 \\ 0 \end{pmatrix} + \begin{pmatrix} 0 \\ 1 \end{pmatrix} \right] = \begin{pmatrix} 0.707 \\ 0.707 \end{pmatrix} \qquad \frac{1}{\sqrt{2}} \cdot (\alpha_z + \beta_z) = \begin{pmatrix} 0.707 \\ 0.707 \end{pmatrix}$$

Operators

We can also use the Pauli operators (in units of h/4pi) to analyze this experiment. The matrix operators associated with the two Stern-Gelach magnets are shown below.

SGZ operator:

$$\mathrm{SGZ} := \begin{pmatrix} 1 & 0 \\ 0 & -1 \end{pmatrix}$$

SGX operator:

$$\mathrm{SGX} := \begin{pmatrix} 0 & 1 \\ 1 & 0 \end{pmatrix}$$

The spin states α_z and β_z are eigenfunctions of the SGZ operator with eigenvalues +1 and -1, respectively:

$$SGZ \cdot \alpha_z = \alpha_z \qquad \mathrm{SGZ} \cdot \alpha_z = \begin{pmatrix} 1 \\ 0 \end{pmatrix}$$

$$SGZ \cdot \beta_z = -\beta_z \qquad \mathrm{SGZ} \cdot \beta_z = \begin{pmatrix} 0 \\ -1 \end{pmatrix}$$

The spin states α_x and β_x are eigenfunctions of the SGX operator with eigenvalues +1 and -1, respectively:

$$SGX \cdot \alpha_x = \alpha_x \qquad \mathrm{SGX} \cdot \alpha_x = \begin{pmatrix} 0.707 \\ 0.707 \end{pmatrix}$$

$$SGX \cdot \beta_x = -\beta_x \qquad \mathrm{SGX} \cdot \beta_x = \begin{pmatrix} -0.707 \\ 0.707 \end{pmatrix}$$

The spin states α_x and β_x are not eigenfunctions of the SGZ operator as is shown below.

$$SGZ \cdot \alpha_x = \beta_x \qquad \mathrm{SGZ} \cdot \alpha_x = \begin{pmatrix} 0.707 \\ -0.707 \end{pmatrix}$$

$$SGZ \cdot \beta_x = \alpha_x \qquad \mathrm{SGZ} \cdot \beta_x = \begin{pmatrix} 0.707 \\ 0.707 \end{pmatrix}$$

And, of course, the spin states α_z and β_z are not eigenfunctions of the SGX operator as is shown below.

$$SGX \cdot \alpha_z = \beta_z \qquad \mathrm{SGX} \cdot \alpha_z = \begin{pmatrix} 0 \\ 1 \end{pmatrix}$$

$$SGX \cdot \beta_z = \alpha_z \qquad \mathrm{SGX} \cdot \beta_2 = \begin{pmatrix} 1 \\ 0 \end{pmatrix}$$

The Predicted Results After the SGX Magnet

The probability that an α_z Ag atom will emerge spin-up after passing through a SGX magnet:

$$|\langle \alpha_x | SGX | \alpha_z \rangle|^2 = 1/2 \qquad \left(|\alpha_x^{\mathrm{T}} \cdot \mathrm{SGX} \cdot \alpha_2| \right)^2 \rightarrow \frac{1}{2}$$

The probability that an α_z Ag atom will emerge spin-down after passing through a SGX magnet:

$$|\langle \beta_x | \, \mathrm{SGX} \, | \alpha_z \rangle|^2 = 1/2 \qquad \left(|\beta_{\mathrm{x}}^{\mathrm{T}} \cdot \mathrm{SGX} \cdot \alpha_2| \right)^2 \rightarrow \frac{1}{2}$$

The Predicted Results After the Final SGZ Magnet

The probability that an α_x Ag atom will emerge spin-up after passing through a SGZ magnet:

$$|\langle\alpha_z|\,\mathrm{SGZ}\,|\alpha_x\rangle|^2 = 1/2 \qquad \left(|\alpha_2^{\mathrm{T}}\cdot\mathrm{SGZ}\cdot\alpha_{\mathrm{x}}|\right)^2 \rightarrow \frac{1}{2}$$

The probability that an α_x Ag atom will emerge spin-down after passing through a SGZ magnet:

$$|\langle\beta_z|\,\mathrm{SGZ}\,|\alpha_x\rangle|^2 = 1/2 \qquad \left(|\beta_2^{\mathrm{T}}\cdot\mathrm{SGZ}\cdot\alpha_{\mathrm{x}}|\right)^2 \rightarrow \frac{1}{2}$$

The Predicted Results for the First SGZ Magnet

Now we deal with the most difficult part of the analysis. How does quantum mechanics predict what will happen when an unpolarized spin beam encounters the initial SGZ magnet. As mention earlier, an unpolarized spin beam is a **mixture** of all possible spin polarizations. We proceed by introducing the density operator, which is a more general quantum mechanical construct that can be used to represent both pure states and mixtures, as shown below.

$$\hat{\rho}_{\mathrm{pure}} = |\Psi\rangle\langle\Psi| \qquad \hat{\rho}_{mixed} = \sum p_i\,|\Psi_i\rangle\,\langle\Psi_i|$$

In the equation on the right, p_i is the fraction of the mixture in the state Ψ_i. It is not difficult to elucidate the origin of the density operator and its utility in quantum mechanical calculations. The expectation value for a pure state Ψ for the measurement operator **A** is traditionally written as follows.

$$\langle A\rangle = \langle\Psi|\hat{A}|\Psi\rangle$$

Expansion of Ψ in the eigenfunctions of the measurement operator, followed by rearrangement of the brackets yields the calculation of the expectation value of **A** in terms of the product of density operator and the measurement operator, **A**.

$$\langle A\rangle = \langle\Psi|\hat{A}|\Psi\rangle = \sum\langle\Psi|\hat{A}|a\rangle\langle a|\Psi\rangle = \sum_d\langle a|\Psi\rangle\langle\Psi|\hat{A}|a\rangle = \sum\langle a|\hat{\rho}\hat{A}|a\rangle = \mathrm{Trace}(\hat{\rho}\hat{A})$$

We now show that the traditional method and the method using the trace function give the same result for the z-direction spin eigenfunctions.

$$\begin{array}{ll}\alpha_z^{\mathrm{T}}\cdot\mathrm{SGZ}\cdot\alpha_z = 1 & \mathrm{tr}\left(\alpha_z\cdot\alpha_z^{\mathrm{T}}\cdot\mathrm{SGZ}\right) = 1\\ \beta_{\mathrm{Z}}^{\mathrm{T}}\cdot\mathrm{SGZ}\cdot\beta_z = -1 & \mathrm{tr}\left(\beta_{\mathrm{Z}}\cdot\beta_{\mathrm{Z}}^{\mathrm{T}}\cdot\mathrm{SGZ}\right) = -1\end{array}$$

An unpolarized beam can be written as a 50-50 mixture of any of the orthogonal spin eigenfunctions - α_z and β_z, or α_x and β_x, or α_y and β_y. Thus, according to the previous definition the density operator for an unpolarized spin beam is as follows.

$$\hat{\rho}_{\mathrm{mix}} = \frac{1}{2}|\alpha_z\rangle\langle\alpha_z| + \frac{1}{2}|\beta_z\rangle\langle\beta_z| = \frac{1}{2}|\alpha_x\rangle\langle\alpha_x| + \frac{1}{2}|\beta_x\rangle\langle\beta_x| = \frac{1}{2}|\alpha_y\rangle\langle\alpha_y| + \frac{1}{2}|\beta_y\rangle\langle\beta_y|$$

Fifty percent of the silver atoms are deflected toward the north pole (α_z, eigenvalue +1) and fifty percent toward the south pole (β_z, eigenvalue -1). Therefore, the expectation value should be zero as is calculated below using both z- and x- spin directions.

$$\mathrm{tr}\left[\left(\frac{1}{2}\cdot\alpha_2\cdot\alpha_2^T + \frac{1}{2}\cdot\beta_z\cdot\beta_z^T\right)\cdot\mathrm{SGZ}\right] = 0 \qquad \mathrm{tr}\left[\left(\frac{1}{2}\cdot\alpha_x\cdot\alpha_x^T + \frac{1}{2}\cdot\beta_x\cdot\beta_x^T\right)\cdot\mathrm{SGZ}\right] = 0$$

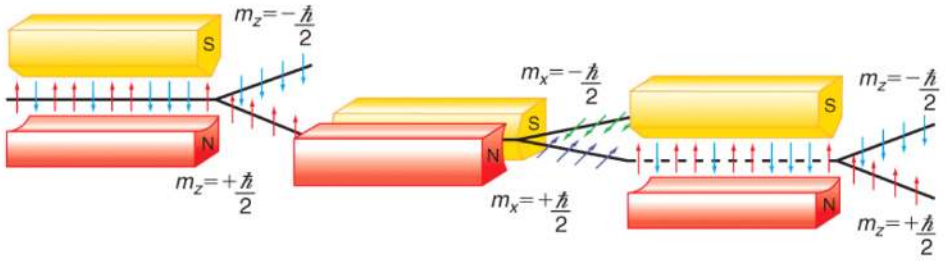
An equivalent method of obtaining the same result is shown below.

$$\frac{1}{2}\cdot\alpha_z^T\cdot\mathrm{SGZ}\cdot\alpha_z + \frac{1}{2}\cdot\beta_z^T\cdot\mathrm{SGZ}\cdot\beta_z = 0 \qquad \frac{1}{2}\cdot\alpha_z^T\cdot\mathrm{SGZ}\cdot\alpha_z + \frac{1}{2}\cdot\beta_z^T\cdot\mathrm{SGZ}\cdot\beta_z = 0$$

This page titled 1.100: Analysis of the Stern-Gerlach Experiment is shared under a CC BY 4.0 license and was authored, remixed, and/or curated by Frank Rioux via source content that was edited to the style and standards of the LibreTexts platform.

1.101: Related Analysis of the Stern-Gerlach Experiment

Silver atoms are deflected by an inhomogeneous magnetic field because of the two-valued magnetic moment associated with their unpaired 5s electron ($[Kr]5s^1 4d^{10}$). The beam of silver atoms entering the Stern-Gerlach magnet oriented in the z-direction (SGZ) on the left is unpolarized. This means it is a mixture of randomly polarized Ag atoms. A mixture cannot be represented by a wave function, it requires a density matrix, as will be shown later.



This situation is exactly analogous to the three-polarizer demonstration. Light emerging from an incadescent light bulb is unpolarized, a mixture of all possible polarization angles, so we can't write a wave function for it. The first Stern-Gerlach magnet plays the same role as the first polarizer, it forces the Ag atoms into one of measurement eigenstates - spin-up or spin-down in the z-direction. The only difference is that in the three-polarizer demonstration only one state was created - vertical polarization. Both demonstrations illustrate that the only values that are observed in an experiment are the eigenvalues of the measurement operator.

To continue with the analysis of the Stern-Gerlach demonstration we need vectors to represent the various spin states of the Ag atoms.

Spin Eigenfunctions

Spin-up in the z-direction:	$\alpha_Z := \begin{pmatrix} 1 \\ 0 \end{pmatrix}$
Spin-down in the z-direction:	$\beta_z := \begin{pmatrix} 0 \\ 1 \end{pmatrix}$
Spin-up in the x-direction:	$\alpha_x := \frac{1}{\sqrt{2}} \cdot \begin{pmatrix} 1 \\ 1 \end{pmatrix}$
Spin-down in the x-direction:	$\beta_x := \frac{1}{\sqrt{2}} \cdot \begin{pmatrix} 1 \\ -1 \end{pmatrix}$

In the next step, the spin-up beam (deflected toward by the magnet's north pole) enters a magnet oriented in the x-direction, SGX. The α_z beam splits into α_x and β_x beams of equal intensity. This is because it is a superposition of the x-direction spin eigenstates as shown below.

$$\frac{1}{\sqrt{2}} \cdot \left[\frac{1}{\sqrt{2}} \cdot \begin{pmatrix} 1 \\ 1 \end{pmatrix} + \frac{1}{\sqrt{2}} \cdot \begin{pmatrix} 1 \\ -1 \end{pmatrix} \right] \rightarrow \begin{pmatrix} 1 \\ 0 \end{pmatrix} \qquad \frac{1}{\sqrt{2}} \cdot (\alpha_x + \beta_x) \rightarrow \begin{pmatrix} 1 \\ 0 \end{pmatrix}$$

Next the α_x beam is directed toward a second SGZ magnet and splits into two equal α_z and β_z beams. This happens because α_x is a superposition of the α_z and β_z spin states.

$$\frac{1}{\sqrt{2}} \cdot \left[\begin{pmatrix} 1 \\ 0 \end{pmatrix} + \begin{pmatrix} 0 \\ 1 \end{pmatrix} \right] = \begin{pmatrix} 0.707 \\ 0.707 \end{pmatrix} \qquad \frac{1}{\sqrt{2}} \cdot (\alpha_z + \beta_z) = \begin{pmatrix} 0.707 \\ 0.707 \end{pmatrix}$$

Operators

We can also use the Pauli operators (in units of h/4π) to analyze this experiment.

SGZ operator:

$$SGZ := \begin{pmatrix} 1 & 0 \\ 0 & -1 \end{pmatrix}$$

SGX operator:

$$\mathrm{SGX} := \begin{pmatrix} 0 & 1 \\ 1 & 0 \end{pmatrix}$$

The probability that an α_z Ag atom will emerge spin-up after passing through a SGX magnet:

Probability amplitude:

$$\alpha_{\mathrm{x}}^{\mathrm{T}} \cdot \mathrm{SGX} \cdot \alpha_{\mathrm{Z}} = 0.707$$

Probability:

$$\left(\alpha_x^T \cdot \mathrm{SGX} \cdot \alpha_z\right)^2 = 0.5$$

The probability that an α_z Ag atom will emerge spin-down after passing through a SGX magnet:

Probability amplitude:

$$\beta_{\mathrm{x}}^{\mathrm{T}} \cdot \mathrm{SGX} \cdot \alpha_z = -0.707$$

Probability:

$$\left(\beta_{\mathrm{x}}^{\mathrm{T}} \cdot \mathrm{SGX} \cdot \alpha_z\right)^2 = 0.5$$

The probability that an α_x Ag atom will emerge spin-up after passing through a SGZ magnet:

Probability amplitude:

$$\alpha_z^T \cdot \mathrm{SGX} \cdot \alpha_x = 0.707$$

Probability:

$$\left(\alpha_z^T \cdot \mathrm{SGX} \cdot \alpha_x\right)^2 = 0.5$$

The probability that an α_x Ag atom will emerge spin-down after passing through a SGZ magnet:

Probability amplitude:

$$\beta_{\mathrm{z}}^{\mathrm{T}} \cdot \mathrm{SGX} \cdot \alpha_{\mathrm{x}} = 0.707$$

Probability:

$$\left(\beta_{\mathrm{z}}^{\mathrm{T}} \cdot \mathrm{SGX} \cdot \alpha_{\mathrm{x}}\right)^2 = 0.5$$

In examining the figure above we note that the SGX magnet distroys the entering α_z state, creating a superposition of spin-up and spin-down in the x-direction. Again measurement forces the system into one of the eigenstates of the measurement operator.

Density Operator (Matrix) Approach

A more general analysis is based on the concept of the density operator (matrix), in general given by the following outer product $|\Psi >< \Psi|$. It is especially important because it can be used to represent mixtures, which cannot be represented by wave functions as noted above.

For example, the probability that an α_z spin system will emerge in the α_x channel of a SGX magnet is equal to the trace of the product of the density matrices representing the α_z and α_x states as shown below.

$$\begin{aligned} |\langle\alpha_x|\alpha_z\rangle|^2 &= \langle\alpha_z|\alpha_x\rangle \langle\alpha_x|\alpha_z\rangle \\ &= \sum_i \langle\alpha_z|i\rangle \langle i|\alpha_x\rangle \langle\alpha_x|\alpha_z\rangle \\ &= \sum_i \langle i|\alpha_x\rangle \langle\alpha_x|\alpha_z\rangle \langle\alpha_z|i\rangle \\ &= \mathrm{Tr}\left(|\alpha_x\rangle \langle\alpha_x|\alpha_z\rangle \langle\alpha_z|\right) = \mathrm{Tr}\left(\widehat{\rho_{\alpha_x}\rho_{\alpha_z}}\right) \end{aligned}$$

where the completeness relation $\sum_i |i\rangle\langle i| = 1$ has been employed.

Density matrices for spin-up and spin-down in the z-direction:

$$\rho_{\alpha z} := \alpha_z \cdot \alpha_z^T \qquad \rho_{\beta z} := \beta_z \cdot \beta_z^T$$

Density matrices for spin-up and spin-down in the x-direction:

$$\rho_{\mathrm{Qx}} := \alpha_{\mathrm{x}} \cdot \alpha_{\mathrm{x}}^{\mathrm{T}} \qquad \rho_{\beta \mathrm{x}} := \beta_{\mathrm{x}} \cdot \beta_{\mathrm{x}}^{\mathrm{T}}$$

An unpolarized spin system can be represented by a 50-50 mixture of any two orthogonal spin density matrices. Below it is shown that using the z-direction and the x-direction give the same answer.

$$\rho_{\mathrm{mix}} := \frac{1}{2} \cdot \rho_{\alpha z} + \frac{1}{2} \cdot \rho_{\beta z} = \begin{pmatrix} 0.5 & 0 \\ 0 & 0.5 \end{pmatrix}$$

Now we re-analyze the Stern-Gerlach experiment using the density operator (matrix) approach.

The probability that an unpolarized spin system will emerge in the α_z channel of a SGZ magnet is 0.5:

$$\mathrm{tr}\left(\rho_{\alpha z} \cdot \rho_{\mathrm{mix}}\right) = 0.5$$

The probability that the α_z beam will emerge in the α_x channel of a SGX magnet is 0.5:

$$\mathrm{tr}\left(\rho_{\alpha \mathrm{x}} \cdot \rho_{\alpha \mathrm{z}}\right) = 0.5$$

The probability that the α_x beam will emerge in the α_z channel of the final SGZ magnet is 0.5:

$$\mathrm{tr}\left(\rho_{\alpha z} \cdot \rho_{\alpha x}\right) = 0.5$$

The probability that the α_x beam will emerge in the β_z channel of the final SGZ magnet is 0.5:

$$\mathrm{tr}\left(\rho_{\beta z} \cdot \rho_{\alpha \mathrm{x}}\right) = 0.5$$

After the final SGZ magnet, 1/8 of the original Ag atoms emerge in the α_z channel and 1/8 in the β_z channel.

$$\mathrm{tr}\left(\rho_{\alpha z} \cdot \rho_{\alpha x}\right) \cdot \mathrm{tr}\left(\rho_{\alpha x} \cdot \rho_{\alpha z}\right) \cdot \mathrm{tr}\left(\rho_{\alpha z} \cdot \rho_{\mathrm{mix}}\right) = 0.125$$
$$\mathrm{tr}\left(\rho_{\beta z} \cdot \rho_{\alpha x}\right) \cdot \mathrm{tr}\left(\rho_{\alpha x} \cdot \rho_{\alpha z}\right) \cdot \mathrm{tr}\left(\rho_{\alpha z} \cdot \rho_{\mathrm{mix}}\right) = 0.125$$

This page titled 1.101: Related Analysis of the Stern-Gerlach Experiment is shared under a CC BY 4.0 license and was authored, remixed, and/or curated by Frank Rioux via source content that was edited to the style and standards of the LibreTexts platform.

1.103: Bloch Sphere

The eigenfunctions of the Pauli spin matrices

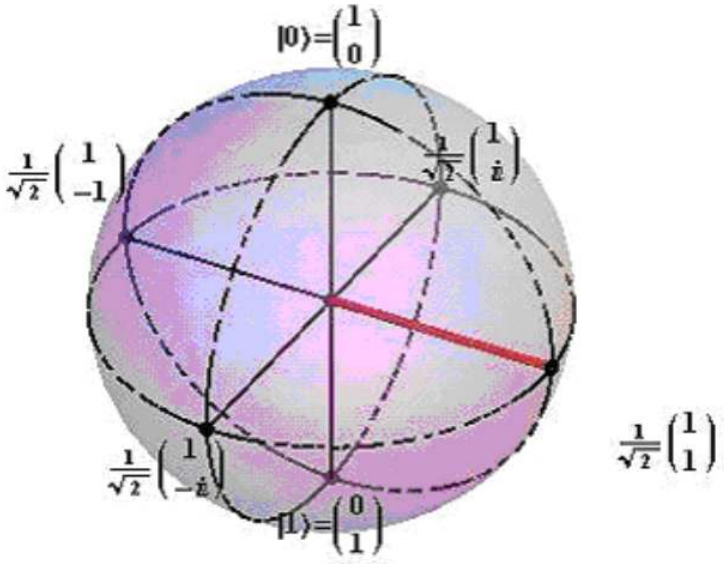
$$\sigma_Z := \begin{pmatrix} 1 & 0 \\ 0 & -1 \end{pmatrix} \qquad \sigma_x := \begin{pmatrix} 0 & 1 \\ 1 & 0 \end{pmatrix} \qquad \sigma_y := \begin{pmatrix} 0 & -i \\ i & 0 \end{pmatrix}$$

are presented mathematically and shown on the Bloch sphere below. The X_u state is highlighted.

$$Z_u := \begin{pmatrix} 1 \\ 0 \end{pmatrix} \qquad Z_d := \begin{pmatrix} 0 \\ 1 \end{pmatrix}$$

$$X_u := \frac{1}{\sqrt{2}} \cdot \begin{pmatrix} 1 \\ 1 \end{pmatrix} \qquad X_d := \frac{1}{\sqrt{2}} \cdot \begin{pmatrix} 1 \\ -1 \end{pmatrix}$$

$$Y_u := \frac{1}{\sqrt{2}} \cdot \begin{pmatrix} 1 \\ i \end{pmatrix} \qquad Y_d := \frac{1}{\sqrt{2}} \cdot \begin{pmatrix} 1 \\ -i \end{pmatrix}$$



This figure was taken from demonstrations.wolfram.com/QubitsOnThePoincareBlochSphere/ a contribution by Rudolf Muradian.

The Bloch sphere is prepared in Cartesian coordinates using Mathcad graphics.

$$numpts := 100 \qquad i := 0 \ldots numpts \qquad j := 0 \ldots numpts$$

$$\theta_i := \frac{\pi \cdot i}{numpts} \qquad \phi_j := \frac{2 \cdot \pi \cdot j}{numpts}$$

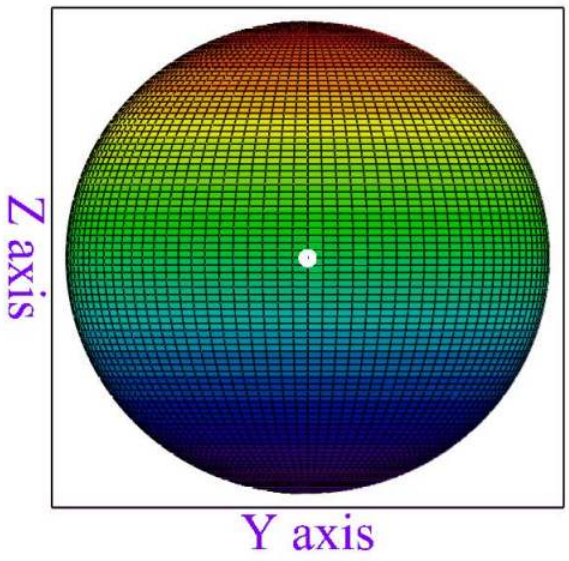
$$X_{i,j} = \sin(\theta_i) \cdot \cos(\phi_j) \qquad Y_{i,j} := \sin(\theta_i) \cdot \sin(\phi_j) \qquad z_{i,j} := \cos(\theta_i)$$

Next, the coordinates of a quantum qubit are calculated and displayed on the Bloch sphere as a white dot. As the polar and azmuthal angles are changed, you will need to rotate the figure to see where the white dot is on the surface of the Bloch sphere.

$$\theta 1 := \frac{\pi}{2} \qquad \phi 1 := 0$$

$$\Psi(\theta 1, \phi 1) := \cos\left(\frac{\theta 1}{2}\right) \cdot \begin{pmatrix} 1 \\ 0 \end{pmatrix} + \exp(i \cdot \phi 1) \cdot \sin\left(\frac{\theta 1}{2}\right) \cdot \begin{pmatrix} 0 \\ 1 \end{pmatrix} \qquad \Psi(\theta 1, \phi 1) = \begin{pmatrix} 0.707 \\ 0.707 \end{pmatrix}$$

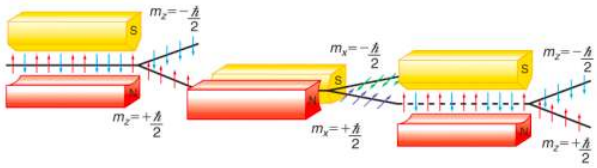
$$XX_{i,j} = \sin(\theta 1) \cdot \cos(\phi 1) \qquad YY_{i,j} := \sin(\theta 1) \cdot \sin(\phi 1) \qquad ZZ_{i,j} := \cos(\theta 1)$$



$(X, Y, Z), (XX, YY, ZZ)$

This page titled 1.103: Bloch Sphere is shared under a CC BY 4.0 license and was authored, remixed, and/or curated by Frank Rioux via source content that was edited to the style and standards of the LibreTexts platform.

1.104: 88. Related Analysis of the Stern-Gerlach Experiment



Silver atoms are deflected by an inhomogeneous magnetic field because of the two-valued magnetic moment associated with their unpaired 5s electron ([Kr]$5s^1 4d^{10}$). The beam of silver atoms entering the Stern-Gerlach magnet oriented in the z-direction (SGZ) on the left is unpolarized. This means it is a mixture of randomly polarized Ag atoms. A mixture cannot be represented by a wave function, it requires a density matrix, as will be shown later.

This situation is exactly analogous to the three-polarizer demonstration. Light emerging from an incadescent light bulb is unpolarized, a mixture of all possible polarization angles, so we can't write a wave function for it. The first Stern-Gerlach magnet plays the same role as the first polarizer, it forces the Ag atoms into one of measurement eigenstates - spin-up or spin-down in the z-direction. The only difference is that in the three-polarizer demonstration only one state was created - vertical polarization. Both demonstrations illustrate that the only values that are observed in an experiment are the eigenvalues of the measurement operator.

To continue with the analysis of the Stern-Gerlach demonstration we need vectors to represent the various spin states of the Ag atoms.

Spin Eigenfunctions

Spin-up in the z-direction:

$$\alpha_z = \begin{pmatrix} 1 \\ 0 \end{pmatrix}$$

Spin-down in the z-direction:

$$\beta_z = \begin{pmatrix} 0 \\ 1 \end{pmatrix}$$

Spin-up in the x-direction:

$$\alpha_x = \frac{1}{\sqrt{2}} \begin{pmatrix} 1 \\ 1 \end{pmatrix}$$

Spin-down in the x-direction:

$$\beta_x = \frac{1}{\sqrt{2}} \begin{pmatrix} 1 \\ -1 \end{pmatrix}$$

In the next step, the spin-up beam (deflected toward by the magnet's north pole) enters a magnet oriented in the x-direction, SGX. The α_z beam splits into α_x and β_x beams of equal intensity. This is because it is a superposition of the x-direction spin eigenstates as shown below.

$$\tfrac{1}{\sqrt{2}} \left[\tfrac{1}{\sqrt{2}} \begin{pmatrix} 1 \\ 1 \end{pmatrix} + \tfrac{1}{\sqrt{2}} \begin{pmatrix} 1 \\ -1 \end{pmatrix} \right] \rightarrow \begin{pmatrix} 1 \\ 0 \end{pmatrix} \quad \tfrac{1}{\sqrt{2}} (\alpha_x + \beta_x) \rightarrow \begin{pmatrix} 1 \\ 0 \end{pmatrix}$$

Next the α_x beam is directed toward a second SGZ magnet and splits into two equal α_z and β_z beams. This happens because α_x is a superposition of the α_z and β_z spin states.

$$\tfrac{1}{\sqrt{2}} \left[\begin{pmatrix} 1 \\ 0 \end{pmatrix} + \begin{pmatrix} 0 \\ 1 \end{pmatrix} \right] = \begin{pmatrix} 0.707 \\ 0.707 \end{pmatrix} \quad \tfrac{1}{\sqrt{2}} (\alpha_z + \beta_z) = \begin{pmatrix} 0.707 \\ 0.707 \end{pmatrix}$$

Operators

We can also use the Pauli operators (in units of h/4π) to analyze this experiment.

SGZ operator:

$$\mathrm{SGZ} = \begin{pmatrix} 1 & 0 \\ 0 & -1 \end{pmatrix}$$

SGX operator:

$$\mathrm{SGX} = \begin{pmatrix} 0 & 1 \\ 1 & 0 \end{pmatrix}$$

The probability that an α_z Ag atom will emerge spin-up after passing through a SGX magnet:

Probability amplitude:

$$\alpha_x^T \mathrm{SGX} \alpha_z = 0.707$$

Probability:

$$\left(\alpha_x^T \mathrm{SGX} \alpha_z\right)^2 = 0.5$$

The probability that an α_z Ag atom will emerge spin-down after passing through a SGX magnet:

Probability amplitude:

$$\beta_x^T \mathrm{SGX} \alpha_z = -0.707$$

Probability:

$$\left(\beta_x^T \mathrm{SGX} \alpha_z\right)^2 = 0.5$$

The probability that an α_x Ag atom will emerge spin-up after passing through a SGZ magnet:

Probability amplitude:

$$\alpha_z^T \mathrm{SGX} \alpha_x = 0.707$$

Probability:

$$\left(\alpha_z^T \mathrm{SGX} \alpha_x\right)^2 = 0.5$$

The probability that an α_x Ag atom will emerge spin-down after passing through a SGZ magnet:

Probability amplitude:

$$\beta_z^T \mathrm{SGX} \alpha_x = 0.707$$

Probability:

$$\left(\beta_z^T \mathrm{SGX} \alpha_x\right)^2 = 0.5$$

In examining the figure above we note that the SGX magnet distroys the entering α_z state, creating a superposition of spin-up and spin-down in the x-direction. Again measurement forces the system into one of the eigenstates of the measurement operator.

Density Operator (Matrix) Approach

A more general analysis is based on the concept of the density operator (matrix), in general given by the following outer product |Ψ >< Ψ|. It is especially important because it can be used to represent mixtures, which cannot be represented by wave functions as noted above.

For example, the probability that an α_z spin system will emerge in the α_x channel of a SGX magnet is equal to the trace of the product of the density matrices representing the α_z and α_x states as shown below.

$$|\langle\alpha_x|\alpha_z\rangle|^2 = \langle\alpha_z|\alpha_x\rangle\langle\alpha_x|\alpha_z\rangle = \sum_i \langle\alpha_z|i\rangle\langle i|\alpha_x\rangle\langle\alpha_x|\alpha_z\rangle = \sum_i \langle i|\alpha_z\rangle\langle\alpha_x|\alpha_z\rangle\langle\alpha_z|i\rangle$$
$$= Tr\left(|\alpha_x\rangle\langle\alpha_x|\alpha_z\rangle\langle\alpha_z|\right) = Tr\left(\widetilde{\rho_{\alpha x}\rho_{\alpha z}}\right)$$

where the completeness relation $\sum_i |i\rangle\langle i| = 1$ has been employed.

Density matrices for spin-up and spin-down in the z-direction:

$$\rho_{\alpha z} = \alpha_z\alpha_z^T \quad \rho_{\beta z} = \beta_z\beta_z^T$$

Density matrices for spin-up and spin-down in the x-direction:

$$\rho_{\alpha x} = \alpha_x\alpha_x^T \quad \rho_{\beta x} = \beta_x\beta_x^T$$

An unpolarized spin system can be represented by a 50-50 mixture of any two orthogonal spin density matrices. Below it is shown that using the z-direction and the x-direction give the same answer.

$$\rho_{mix} = \frac{1}{2}\rho_{\alpha z} + \frac{1}{2}\rho_{\beta z} = \begin{pmatrix} 0.5 & 0 \\ 0 & 0.5 \end{pmatrix}$$

Now we re-analyze the Stern-Gerlach experiment using the density operator (matrix) approach.

The probability that an unpolarized spin system will emerge in the α_z channel of a SGZ magnet is 0.5:

$$\mathrm{tr}\left(\rho_{\alpha z}\rho_{\mathrm{mix}}\right) = 0.5$$

The probability that the α_z beam will emerge in the α_x channel of a SGX magnet is 0.5:

$$\mathrm{tr}\left(\rho_{\alpha x}\rho_{\alpha z}\right) = 0.5$$

The probability that the α_x beam will emerge in the α_z channel of the final SGZ magnet is 0.5:

$$\mathrm{tr}\left(\rho_{\alpha z}\rho_{\alpha x}\right) = 0.5$$

The probability that the α_x beam will emerge in the β_z channel of the final SGZ magnet is 0.5:

$$\mathrm{tr}\left(\rho_{\beta x}\rho_{\alpha z}\right) = 0.5$$

After the final SGZ magnet, 1/8 of the original Ag atoms emerge in the α_z channel and 1/8 in the β_z channel.

$$\mathrm{tr}\left(\rho_{\alpha z}\rho_{\alpha x}\right)\mathrm{tr}\left(\rho_{\alpha x}\rho_{\alpha z}\right)\mathrm{tr}\left(\rho_{\alpha z}\rho_{\mathrm{mix}}\right) = 0.125 \quad \mathrm{tr}\left(\rho_{\beta z}\rho_{\alpha x}\right)\mathrm{tr}\left(\rho_{\alpha x}\rho_{\alpha z}\right)\mathrm{tr}\left(\rho_{\alpha z}\rho_{\mathrm{mix}}\right) = 0.125$$

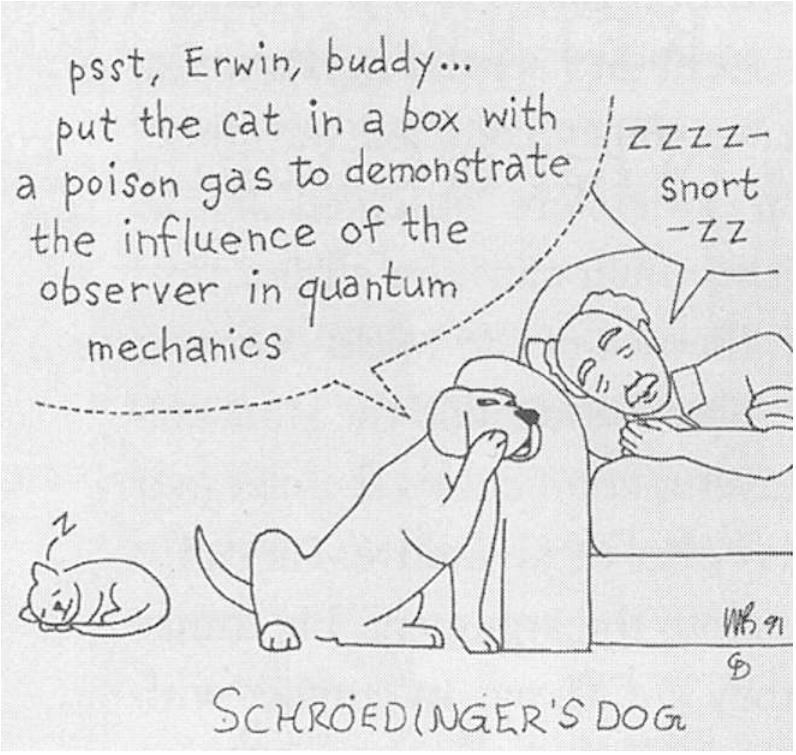
1.104: 88. Related Analysis of the Stern-Gerlach Experiment is shared under a not declared license and was authored, remixed, and/or curated by LibreTexts.

1.105: Bill the Cat and the Superposition Principle

$$|\Psi\rangle = \frac{|\ \rangle + |\ \rangle}{\sqrt{2}}$$

1.105: Bill the Cat and the Superposition Principle is shared under a not declared license and was authored, remixed, and/or curated by LibreTexts.

1.106: Schroedinger's Dog



1.106: Schroedinger's Dog is shared under a not declared license and was authored, remixed, and/or curated by LibreTexts.

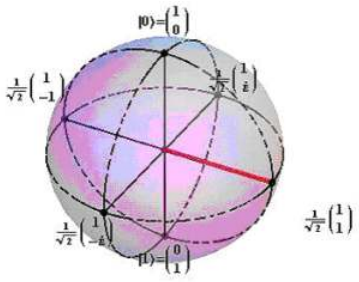
1.107: The Bloch Sphere

The eigenfunctions of the Pauli spin matrices.

$$\sigma_z = \begin{pmatrix} 1 & 0 \\ 0 & -1 \end{pmatrix} \quad \sigma_x = \begin{pmatrix} 0 & 1 \\ 1 & 0 \end{pmatrix} \quad \sigma_y = \begin{pmatrix} 0 & -i \\ i & 0 \end{pmatrix}$$

are presented mathematically and shown on the Bloch sphere below. The Xu state is highlighted.

$$Z_u = \begin{pmatrix} 1 \\ 0 \end{pmatrix} \quad Z_d = \begin{pmatrix} 0 \\ 1 \end{pmatrix} \quad X_u = \frac{1}{\sqrt{2}} \begin{pmatrix} 1 \\ 1 \end{pmatrix} \quad X_d = \frac{1}{\sqrt{2}} \begin{pmatrix} 1 \\ -1 \end{pmatrix} \quad Y - u = \frac{1}{\sqrt{2}} \begin{pmatrix} 1 \\ i \end{pmatrix} \quad Y_d = \frac{1}{\sqrt{2}} \begin{pmatrix} 1 \\ -i \end{pmatrix}$$



This figure was taken from demonstrations.wolfram.com/QubitsOnThePoincareBlochSphere/ a contribution by Rudolf Muradian. The Bloch sphere is prepared in Cartesian coordinates using Mathcad graphics.

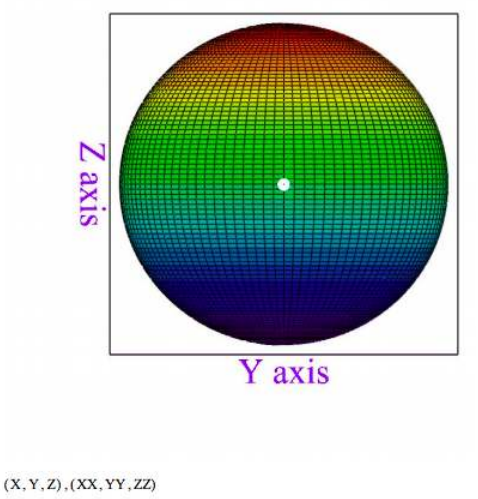
$$\text{numpts} = 100 \quad i = 0..\text{numpts} \quad j = 0..\text{numpts} \quad \theta_i = \frac{\pi i}{\text{numpts}} \quad \phi_j = \frac{2\pi j}{\text{numpts}}$$

$$X_{i,\,j} = \sin(\theta_i)\cos(\phi_j) \quad Y_{i,\,j} = \sin(\theta_i)\sin(\phi_j) \quad Z_{i,\,j} = \cos(\theta_i)$$

Next, the coordinates of a quantum qubit are calculated and displayed on the Bloch sphere as a white dot. As the polar and azmuthal angles are changed, you will need to rotate the figure to see where the white dot is on the surface of the Bloch sphere.

$$\theta 1 = \frac{\pi}{2} \quad \phi 1 = 0 \quad \Psi(\theta 1,\ \phi 1) = \cos\left(\frac{\theta 1}{2}\right)\begin{pmatrix} 1 \\ 0 \end{pmatrix} + \exp(i\phi 1)\sin\left(\frac{\theta 1}{2}\right)\begin{pmatrix} 0 \\ 1 \end{pmatrix} \quad \Psi(\theta 1,\ \phi 1) = \begin{pmatrix} 0.707 \\ 0.707 \end{pmatrix}$$

$$XX_{i,\,j} = \sin(\theta 1)\cos(\phi 1) \quad YY_{i,\,j} = \sin(\theta 1)\sin(\phi 1) \quad ZZ_{i,\,j} = \cos(\theta 1)$$



1.107: The Bloch Sphere is shared under a not declared license and was authored, remixed, and/or curated by LibreTexts.

1.108: Density Matrix, Bloch Vector and Entropy

A spin-1/2 state is represented by the following density matrix.

$$\rho = \begin{pmatrix} \frac{2}{3} & \frac{1}{6} - \frac{i}{3} \\ \frac{1}{6} + \frac{i}{3} & \frac{1}{3} \end{pmatrix}$$

Show that this is a mixed state.

$$\mathrm{tr}(\rho) \to 1 \quad \mathrm{tr}\left(\rho^2\right) \to \frac{5}{6}$$

A value of less than unity for the trace of the square of the density matrix indicates a mixed state.

Given the Pauli matrices,

$$\sigma_x = \begin{pmatrix} 0 & 1 \\ 1 & 0 \end{pmatrix} \quad \sigma_y = \begin{pmatrix} 0 & -i \\ i & 0 \end{pmatrix} \quad \sigma_z = \begin{pmatrix} 1 & 0 \\ 0 & -1 \end{pmatrix}$$

calculate the Bloch vector and its magnitude.

$$R_x = \mathrm{tr}\left(\rho\sigma_x\right) \to \frac{1}{3} \quad R_y = \mathrm{tr}\left(\rho\sigma_y\right) \to \frac{2}{3} \quad R_z = \mathrm{tr}\left(\rho\sigma_z\right) \to \frac{1}{3} \quad R = \sqrt{R_x^2 + R_y^2 + R_z^2} = 0.816$$

A value of less than unity for the magnitude of the Bloch vector also indicates a mixed state.

Calculate the eigenvalues, λ, of ρ and use them to calculate the entropy of the state represented by ρ.

$$\lambda = \mathrm{eigenvals}(\rho) = \begin{pmatrix} 0.908 \\ 0.092 \end{pmatrix} \quad -\sum_{i=1}^{2}\left(\lambda_i \log\left(\lambda_i,\ 2\right)\right) = 0.422$$

Use the magnitude of the Bloch vector to calculate the entropy (Haroche and Raimond, p. 168).

$$-\frac{1+R}{2}\log\left(\frac{1+R}{2},\ 2\right) - \frac{1-R}{2}\log\left(\frac{1-R}{2},\ 2\right) = 0.442$$

Calculate the expectation values for the measurements of spin in the x- and z-directions.

$$\mathrm{tr}\left(\rho\sigma_x\right) \to \frac{1}{3} \quad \mathrm{tr}\left(\rho\sigma_z\right) \to \frac{1}{3}$$

$$\mathrm{Sxu} = \frac{1}{\sqrt{2}}\begin{pmatrix} 1 \\ 1 \end{pmatrix} \quad \mathrm{Sxd} = \frac{1}{\sqrt{2}}\begin{pmatrix} 1 \\ -1 \end{pmatrix} \quad \mathrm{Szu} = \begin{pmatrix} 1 \\ 0 \end{pmatrix} \quad \mathrm{Szd} = \begin{pmatrix} 0 \\ 1 \end{pmatrix}$$

Form projection operators for spin-up and spin-down in the x- and z-directions using the spin states provided above, and calculate the probabilities for spin-up and spin-down measurements in each direction. The eigenvalue for Sxu and Szu is +1 and the eigenvalue for Sxd and Szd is -1. It is easy to see that the results below are consistent with the expectation value calculations.

$$\mathrm{Sxu}\ \mathrm{Sxu}^T \to \begin{pmatrix} \frac{1}{2} & \frac{1}{2} \\ \frac{1}{2} & \frac{1}{2} \end{pmatrix} \quad \mathrm{Sxd}\ \mathrm{Sxd}^T \to \begin{pmatrix} \frac{1}{2} & -\frac{1}{2} \\ -\frac{1}{2} & \frac{1}{2} \end{pmatrix} \quad \mathrm{Szu}\ \mathrm{Szu}^T \to \begin{pmatrix} 1 & 0 \\ 0 & 0 \end{pmatrix} \quad \mathrm{Szd}\ \mathrm{Szd}^T \to \begin{pmatrix} 0 & 0 \\ 0 & 1 \end{pmatrix}$$

$$\mathrm{tr}\left(\mathrm{Sxd}\ \mathrm{Sxd}^T\rho\right) \to \frac{1}{3} \quad \mathrm{tr}\left(\mathrm{Sxu}\ \mathrm{Sxu}^T\rho\right) \to \frac{2}{3} \quad \mathrm{tr}\left(\mathrm{Szd}\ \mathrm{Szd}^T\rho\right) \to \frac{1}{3} \quad \mathrm{tr}\left(\mathrm{Szu}\ \mathrm{Szu}^T\rho\right) \to \frac{2}{3}$$

$$\mathrm{Sxd}^T\rho\mathrm{Sxd} \to \frac{1}{3} \quad \mathrm{Sxu}^T\rho\mathrm{Sxu} \to \frac{2}{3} \quad \mathrm{Szd}^T\rho\mathrm{Szd} \to \frac{1}{3} \quad \mathrm{Szu}^T\rho\mathrm{Szu} \to \frac{2}{3}$$

Calculate the eigenvectors of the density matrix and use them to diagonalize it, showing that the diagonal elements are the eigenvalues as calculated above.

$$\mathrm{Vecs} = \mathrm{eigenvecs}(\rho) \quad \mathrm{Vecs} = \begin{pmatrix} 0.839 & -0.243 + 0.478i \\ 0.243 + 0.487i & 0.839 \end{pmatrix}$$

$$\left(\overline{\mathrm{Vecs}}\right)^T \rho\mathrm{Vecs} = \begin{pmatrix} 0.908 & 0 \\ 0 & 0.092 \end{pmatrix} \quad \mathrm{Vecs}^{-1}\rho\mathrm{Vecs} = \begin{pmatrix} 0.908 & 0 \\ 0 & 0.092 \end{pmatrix}$$

Using the density matrix the pure state Sxu show that its entropy is 0.

$$\rho = \frac{1}{2}\begin{pmatrix}1 & 1\\ 1 & 1\end{pmatrix}$$

Show that this is a pure state.

$$\mathrm{tr}(\rho) \to 1 \quad \mathrm{tr}\left(\rho^2\right) \to 1$$

Calculate the Bloch vector and its magnitude.

$$R_x = \mathrm{tr}\left(\rho\sigma_x\right) \quad R_y = \mathrm{tr}\left(\rho\sigma_y\right) \to 0 \quad R_z = \mathrm{tr}\left(\rho\sigma_z\right) \to 0 \quad R = \sqrt{R_x^2 + R_y^2 + R_z^2} = 1$$

A value of unity for the magnitude of the Bloch vector indicates a pure state.

Calculate the eigenvalues of ρ and use them to calculate the entropy of the state represented by ρ.

$$\lambda = \mathrm{eigenvals}(\rho) = \begin{pmatrix}1\\ 0\end{pmatrix} \quad \sum_{i=1}^{2}\left(\lambda_i \log\left(\lambda_i,\ 2\right)\right) = 0$$

Two-particle, entangled Bell states are also pure states. This is demonstrated for the anti-symmetric singlet state, Ψ_m.

$$|\Psi_m\rangle = \frac{1}{\sqrt{2}}\left[|\uparrow_1\rangle|\downarrow_2\rangle - |\downarrow_1\rangle|\uparrow_1\rangle\right] = \frac{1}{\sqrt{2}}\left[\begin{pmatrix}1\\ 0\end{pmatrix}\otimes\begin{pmatrix}0\\ 1\end{pmatrix} - \begin{pmatrix}0\\ 1\end{pmatrix}\otimes\begin{pmatrix}1\\ 0\end{pmatrix}\right] = \frac{1}{\sqrt{2}}\begin{pmatrix}0\\ 1\\ -1\\ 0\end{pmatrix}$$

$$\Psi_m = \frac{1}{\sqrt{2}}\begin{pmatrix}0\\ 1\\ -1\\ 0\end{pmatrix} \quad \rho = \Psi_m \Psi_m^T \quad \rho = \begin{pmatrix}0 & 0 & 0 & 0\\ 0 & 0.5 & -0.5 & 0\\ 0 & -0.5 & 0.5 & 0\\ 0 & 0 & 0 & 0\end{pmatrix} \quad \mathrm{tr}(\rho) = 1 \quad \mathrm{tr}\left(\rho^2\right) = 1$$

One of the eigenvalues of ρ is 1 and the rest are 0, so the entropy is 0.

$$\lambda = \mathrm{eigenvals}(\rho) \quad \lambda = \begin{pmatrix}1\\ 0\\ 0\\ 0\end{pmatrix}$$

When a two-spin system is in an entangled superposition such as Ψ_m, the individual spins states are not definite. Tracing (see below) the composite density matrix over spin 2 yields the following spin density matrix for spin 1 showing that it is a mixed state with one unit of entropy.

$$\rho_1 = \frac{1}{2}\begin{pmatrix}1\\ 0\end{pmatrix}\begin{pmatrix}1\\ 0\end{pmatrix}^T + \frac{1}{2}\begin{pmatrix}0\\ 1\end{pmatrix}\begin{pmatrix}0\\ 1\end{pmatrix}^T \to \begin{pmatrix}\frac{1}{2} & 0\\ 0 & \frac{1}{2}\end{pmatrix} \qquad \mathrm{tr}\left(\rho_1\right) \to 1 \qquad \mathrm{tr}\left(\rho_1^2\right) \to \frac{1}{2}$$

$$\lambda = \mathrm{eigenvals}\left(\rho_1\right) = \begin{pmatrix}0.5\\ 0.5\end{pmatrix} \qquad -\sum_{i=1}^{2}\left(\lambda_i \log\left(\lambda_i,\ 2\right)\right) = 1$$

The same holds for spin 2.

In this entangled state we know the state of the composite system (zero entropy), but do not know the states of the individual spins (two units of entropy).

The trace operation is outlined below:

$$|\Psi\rangle = \frac{1}{\sqrt{2}}\left[|\uparrow_1\rangle|\downarrow_2\rangle - |\downarrow_1\rangle|\uparrow_2\rangle\right]$$

$$\widehat{\rho_{12}} = |\Psi\rangle\langle\Psi| = \frac{1}{2}\left[|\uparrow_1\rangle|\downarrow_2\rangle - |\downarrow_1\rangle|\uparrow_2\rangle\right] = \frac{1}{2}\begin{pmatrix}0 & 0 & 0 & 0\\ 0 & 1 & -1 & 0\\ 0 & -1 & 1 & 0\\ 0 & 0 & 0 & 0\end{pmatrix}$$

$$\widehat{\rho_1} = \frac{1}{2}\left[\langle\uparrow_2|\Psi\rangle\langle\Psi|\uparrow_2\rangle + \langle\downarrow_2|\Psi\rangle\langle\Psi|\downarrow_2\rangle\right] = \frac{1}{2}\left[|\downarrow_1\rangle\langle\downarrow_1| + |\uparrow_1\rangle\langle\uparrow_1|\right] = \frac{1}{2}\begin{pmatrix}1 & 0\\ 0 & 1\end{pmatrix}$$

$$\widehat{\rho_2} = \frac{1}{2}\left[\langle\uparrow_1|\Psi\rangle\langle\Psi|\uparrow_1\rangle + \langle\downarrow_1|\Psi\rangle\langle\Psi|\downarrow_1\rangle\right] = \frac{1}{2}\left[|\downarrow_2\rangle\langle\downarrow_2| + |\uparrow_2\rangle\langle\uparrow_2|\right] = \frac{1}{2}\begin{pmatrix}1 & 0\\ 0 & 1\end{pmatrix}$$

1.108: Density Matrix, Bloch Vector and Entropy is shared under a not declared license and was authored, remixed, and/or curated by LibreTexts.

1.109: State Vectors and State Operators- Superpositions, Mixed States, and Entanglement

This tutorial will use the concepts of state vector and state operator to examine superpositions and mixed states using the matrix formulation of quantum mechanics. The state vectors required are given immediately below. An unsubscripted spin arrow refers to spin in the z-direction.

$$|\Psi\rangle = \begin{pmatrix}1\\0\end{pmatrix} \quad \langle\uparrow| = (1 \quad 0) \quad |\downarrow\rangle = \begin{pmatrix}0\\1\end{pmatrix} \quad \langle\downarrow| = (0 \quad 1) \qquad \begin{matrix}|\uparrow_x\rangle \\ = \frac{1}{\sqrt{2}}\begin{pmatrix}1\\1\end{pmatrix}\end{matrix} \qquad \begin{matrix}|\downarrow_x\rangle \\ = \frac{1}{\sqrt{2}}\begin{pmatrix}1\\-1\end{pmatrix}\end{matrix} \qquad \begin{matrix}\langle\downarrow_x| = \frac{1}{\sqrt{2}} \\ (1 \quad -1)\end{matrix}$$

These same states are now defined using Mathcad syntax.

$$\begin{pmatrix} \mathrm{Szu} = \begin{pmatrix}1\\0\end{pmatrix} & \mathrm{Szd} = \begin{pmatrix}0\\1\end{pmatrix} & \mathrm{Sxu} = \frac{1}{\sqrt{2}}\begin{pmatrix}1\\1\end{pmatrix} & \mathrm{Sxd} = \frac{1}{\sqrt{2}}\begin{pmatrix}1\\-1\end{pmatrix} \\ \mathrm{Szu}^T = (1 \quad 0) & \mathrm{Szd}^T = (0 \quad 1) & \mathrm{Sxu}^T = (0.707 \quad 0.707) & \mathrm{Sxd}^T = (0.707 \quad -0.707) \end{pmatrix}$$

The identity and z- and x-direction spin operators (in units of h/4π) will be used.

$$I = \begin{pmatrix}1 & 0\\0 & 1\end{pmatrix} \quad \sigma_z = \begin{pmatrix}1 & 0\\0 & -1\end{pmatrix} \quad \sigma_x = \begin{pmatrix}0 & 1\\1 & 0\end{pmatrix}$$

Dirac has said that the superposition principle is at the heart of quantum mechanics. He elaborated in *The Physical Principles of Quantum Mechanics*.

> The nature of the relationships which the superposition principle requires to exist between states of any system is of a kind that cannot be explained in terms of familiar physical concepts. One cannot in the classical sense picture a system being partly in each of two states and see the equivalence of this to the system being completely in some other state. There is an entirely new idea involved, to which one must get accustomed and in terms of which one must proceed to build up an exact mathematical theory, without having any detailed classical picture.

N. David Mermin [*American Journal of Physics* 71, 29, (2003)] succinctly summarized Dirac′s statement when he wrote, ″Superpositions have no classical interpretation. They are sui generis, an intrinsically quantum-mechanical construct...″

We now illustrate the properties of a superposition with a specific example. A spin system with spin up in the x-direction is prepared using a Stern-Gerlach apparatus. We see from the mathematics below that this system can also be considered to be an even superposition of spin up and spin down in the z-direction.

$$|\uparrow_x\rangle = \frac{1}{\sqrt{2}}\begin{pmatrix}1\\1\end{pmatrix} = \frac{1}{\sqrt{2}}\left[\begin{pmatrix}1\\0\end{pmatrix} + \begin{pmatrix}0\\1\end{pmatrix}\right] = \frac{1}{\sqrt{2}}[|\uparrow\rangle + |\downarrow\rangle] = |\Psi\rangle \quad \Psi = \frac{1}{\sqrt{2}}\begin{pmatrix}1\\1\end{pmatrix}$$

Subsequent spin measurements confirm what is expressed mathematically above. If the spin system is passed through a Stern-Gerlach magnet oriented in the x-direction, the beam bends in one direction, the direction associated with spin up in the x-direction. However, if the system is passed through a Stern-Gerlach magnet oriented in the z-direction, it is split into two beams, one associated with spin up in the z-direction and one associated with spin down in the z-direction. The expectation values calculated below are consistent with these experimental results.

$$\Psi^T\sigma_x\Psi = 1 \quad \Psi^T\sigma_z\Psi = 0$$

The state operator is a more versatile quantum construct than the mathematically simpler state vector. It is the outer product of the state vector.

$$\hat{\rho} = |\uparrow_x\rangle\langle\uparrow_x| = \frac{1}{2}\begin{pmatrix}1\\1\end{pmatrix}(1 \quad 1) = \frac{1}{2}\begin{pmatrix}1 & 1\\1 & 1\end{pmatrix} = |\Psi\rangle\langle\Psi| \quad \rho = \frac{1}{2}\begin{pmatrix}1 & 1\\1 & 1\end{pmatrix}$$

Expectation values can also be calculate using the state operator.

$$\langle\Psi|\hat{A}|\Psi\rangle = \sum_i \langle\Psi|\hat{A}|i\rangle\langle i|\Psi\rangle = \sum_i \langle i|\Psi\rangle\langle\Psi|\hat{A}|i\rangle = Tr\left(\hat{\rho}_\Psi\hat{A}\right) \text{ where } \sum_i |i\rangle\langle i| = Identity$$

$$\mathrm{tr}\left(\rho\sigma_x\right)=1 \quad \mathrm{tr}\left(\rho\sigma_z\right)=0$$

It is not uncommon for people to look at the superposition

$$|\Psi\rangle=\frac{1}{\sqrt{2}}\left[|\Psi\rangle+|\Psi\rangle\right]$$

we are considering and think of it as a 50-50 mixture of spin up and spin down in the z-direction.

However, a mixture cannot be represented by a state vector. A mixture must be represented by a state operator which is a weighted sum of the outer products of the vectors contributing to the mixture, as shown below.

$$\hat{\rho}_{Mix}=\tfrac{1}{2}|\uparrow\rangle\langle\uparrow|+\tfrac{1}{2}|\downarrow\rangle\langle\downarrow|=\tfrac{1}{2}\left[\begin{pmatrix}1\\0\end{pmatrix}\begin{pmatrix}1 & 0\end{pmatrix}+\begin{pmatrix}0 & 1\end{pmatrix}\begin{pmatrix}0 & 1\end{pmatrix}\right]=\tfrac{1}{2}\begin{pmatrix}1 & 0\\0 & 1\end{pmatrix} \quad \rho_{\mathrm{mix}}=\tfrac{1}{2}\begin{pmatrix}1 & 0\\0 & 1\end{pmatrix}$$

Measurement of the z-direction spin gives the same results as above and might lead one to conclude that a superposition and a mixture cannot be distinguished experimentally. However, the x-direction calculation shows that a superposition is not a classical mixture of spin states, because it is in disagreement with the experimental results presented above.

$$\mathrm{tr}\left(\rho_{\mathrm{mix}}\sigma_z\right)=0 \quad \mathrm{tr}\left(\rho_{\mathrm{mix}}\sigma_x\right)=0$$

Before moving on to composite systems and entanglement, a few additional features of the state operators for superpositions (pure states) and mixtures are illustrated.

$$\rho_{\mathrm{sup}}=\tfrac{1}{2}\begin{pmatrix}1 & 1\\1 & 1\end{pmatrix} \quad \rho_{\mathrm{mix}}=\tfrac{1}{2}\begin{pmatrix}1 & 0\\0 & 1\end{pmatrix}$$

One rather obvious difference between these state operators is that the one representing a classical mixture is diagonal, while the one representing the superposition has off-diagonal elements. The presence of off-diagonal elements in a state operator is the signature of a quantum mechanical system.

All valid state operators have unit traces; the sum of the diagonal elements equals unity.

$$\mathrm{tr}\left(\rho_{\mathrm{sup}}\right)=1 \quad \mathrm{tr}\left(\rho_{\mathrm{mix}}\right)=1$$

However, the trace of the square of the state operator distinguishes between a pure state and a mixture as shown below.

$$\mathrm{tr}\left(\rho_{\mathrm{sup}}^2\right)=1 \quad \mathrm{tr}\left(\rho_{\mathrm{mix}}^2\right)=1$$

Finally we show that ρ_{mix} cannot represent a superposition.

$$\frac{1}{2}\begin{pmatrix}1 & 0\\0 & 1\end{pmatrix}\neq\begin{pmatrix}a\\b\end{pmatrix}\begin{pmatrix}a & b\end{pmatrix}=\begin{pmatrix}a^2 & ab\\ab & b^2\end{pmatrix}$$

Comparing the left and right sides we conclude that: $a^2 = b^2 = 1/2$ and $ab = 0$. These constraints are contradictory.

Composite two-particle entangled states are also superpositions. Below one of the Bell states is constructed. Bell states are maximally entangled superpositions of two-particle states.

$$|\Psi\rangle=\frac{1}{\sqrt{2}}\left[|\uparrow_1\rangle\otimes|\uparrow_2\rangle+|\downarrow_1\rangle\otimes|\downarrow_2\rangle\right]=\frac{1}{\sqrt{2}}[]=\frac{1}{\sqrt{2}}\left[\begin{pmatrix}1\\0\end{pmatrix}\otimes\begin{pmatrix}1\\0\end{pmatrix}+\begin{pmatrix}0\\1\end{pmatrix}\otimes\begin{pmatrix}0\\1\end{pmatrix}\right]=\frac{1}{\sqrt{2}}\begin{pmatrix}1\\0\\0\\1\end{pmatrix}$$

This is an entangled state because it cannot be factored as is shown below.

$$\frac{1}{\sqrt{2}}\begin{pmatrix}1\\0\\0\\1\end{pmatrix}\neq\begin{pmatrix}a_1\\a_2\end{pmatrix}\otimes\begin{pmatrix}b_1\\b_2\end{pmatrix}=\begin{pmatrix}a_1b_1\\a_1b_2\\a_2b_1\\a_2b_2\end{pmatrix}$$

Comparing the left and right sides we conclude that: $a_1b_1 = a_2b_2 = 1/\mathrm{sqrt}(2)$ and $a_1b_2 = a_2b_1 = 0$. There are no values of a_1, a_2, b_1 and b_2 that satisfy these constraints.

Because entangled wave functions are not separable the entangled particles represented by such wave functions do not have separate identities or individual properties. However, if the spin orientation of particle 1 is learned through measurement, the spin orientation of particle 2 is also immediately known no matter how far away it may be. Entanglement suggests nonlocal phenomena which in the words of Nick Herbert are "unmediated, unmitigated and immediate."

Next we form the state operator of the two-particle entangled state.

$$|\Psi\rangle\langle\Psi| = \frac{1}{2}\left[|\uparrow_1\rangle \otimes |\uparrow_2\rangle + |\downarrow_1\rangle \otimes |\downarrow_2\rangle\right]\left[\langle\uparrow_2| \otimes \langle\uparrow_1| + \langle\downarrow_2| \otimes \langle\downarrow_1|\right]$$

$$|\Psi\rangle\langle\Psi| = \frac{1}{\sqrt{2}}\begin{pmatrix}1\\0\\0\\1\end{pmatrix}\frac{1}{\sqrt{2}}\begin{pmatrix}1 & 0 & 0 & 1\end{pmatrix} = \frac{1}{2}\begin{pmatrix}1 & 0 & 0 & 1\\0 & 0 & 0 & 0\\1 & 0 & 0 & 1\end{pmatrix} \quad \rho_{ent} = \frac{1}{2}\begin{pmatrix}1 & 0 & 0 & 1\\0 & 0 & 0 & 0\\1 & 0 & 0 & 1\end{pmatrix}$$

The two-spin entangled state is a pure state:

$$\mathrm{tr}\left(\rho_{ent}\right) = 1 \quad \mathrm{tr}\left(\rho_{ent}^2\right) = 1$$

Next we demonstrate the correlation inherent in this entangled state. Spin measurements in the z- and x-directions on the spins always yields the same result (highlighted below). Kronecker is Mathcad's command for tensor multiplication of matrices.

$$\mathrm{SzSz} = \mathrm{kronecker}\left(\sigma_z,\ \sigma_z\right) \quad \mathrm{tr}\left(\rho_{ent}\mathrm{SzSz}\right) = 1 \quad \mathrm{SxSx} = \mathrm{kronecker}\left(\sigma_x,\ \sigma_x\right) \quad \mathrm{tr}\left(\rho_{ent}\mathrm{SxSx}\right) = 1$$

Initially the x-direction measurement result may seem strange. However, it is easy to show that writing the entangled wave function in the x-basis is identical to the z-basis version.

$$|\uparrow_x\rangle = \frac{1}{\sqrt{2}}\begin{pmatrix}1\\1\end{pmatrix} \quad \langle\uparrow_x| = \frac{1}{\sqrt{2}}\begin{pmatrix}1 & 1\end{pmatrix} \quad |\downarrow_x\rangle = \frac{1}{\sqrt{2}}\begin{pmatrix}1\\-1\end{pmatrix} \quad \langle\downarrow_x| = \frac{1}{\sqrt{2}}\begin{pmatrix}1 & -1\end{pmatrix}$$

$$|\Psi\rangle = \frac{1}{\sqrt{2}}\left[|\uparrow_{x1}\rangle \otimes |\uparrow_{x2}\rangle + |\downarrow_{x1}\rangle \otimes |\downarrow_{x2}\rangle\right] = \frac{1}{2\sqrt{2}}\left[\right]$$

$$= \frac{1}{2\sqrt{2}}\left[\begin{pmatrix}1\\1\end{pmatrix} \otimes \begin{pmatrix}1\\1\end{pmatrix} + \begin{pmatrix}1\\-1\end{pmatrix} \otimes \begin{pmatrix}1\\-1\end{pmatrix}\right] = \frac{1}{\sqrt{2}}\begin{pmatrix}1\\0\\0\\1\end{pmatrix}$$

In spite of the strong correlation observed when the spins of both particles are measured in the same direction, spin measurements on the individual particles are completely random.

$$\mathrm{SzI} = \mathrm{kronecker}\left(\sigma_z,\ I\right) \quad \mathrm{SxI} = \mathrm{kronecker}\left(\sigma_x,\ I\right) \quad \mathrm{ISz} = \mathrm{kronecker}\left(I,\ \sigma_z\right) \quad \mathrm{ISx} = \mathrm{kronecker}\left(I,\ \sigma_x\right)$$

$$\mathrm{tr}\left(\rho_{ent}\mathrm{SzI}\right) = 0 \quad \mathrm{tr}\left(\rho_{ent}\mathrm{SxI}\right) = 0 \quad \mathrm{tr}\left(\rho_{ent}\mathrm{ISx}\right) = 0 \quad \mathrm{tr}\left(\rho_{ent}\mathrm{ISx}\right) = 0$$

This can be confirmed by expanding the state operator in the fashion shown below, and then "tracing" over the spin states of particle 1. The terms highlighted in blue survive the trace operation.

$$|\Psi\rangle\langle\Psi| = \frac{1}{2}\left[|\uparrow_1\rangle|\uparrow_2\rangle\langle\uparrow_2|\langle\uparrow_1| + |\uparrow_1\rangle|\uparrow_2\rangle\langle\downarrow_2|\langle\downarrow_1| + |\downarrow_1\rangle|\downarrow_2\rangle\langle\downarrow_2|\langle\uparrow_1| + |\downarrow_1\rangle|\downarrow_2\rangle\langle\downarrow_2|\langle\downarrow_1|\right]$$

$$\rho_2 = \frac{1}{2}\left[\langle\uparrow_1|\Psi\rangle\langle\Psi|\uparrow_1\rangle + \downarrow_1|\Psi\rangle\langle\Psi|\downarrow_1\rangle\right] = \frac{1}{2}\left[|\uparrow_2\rangle\langle\uparrow_2| + |\downarrow_2\rangle\langle\downarrow_2|\right]$$

This yields the partial state operator of particle 2 and shows that it behaves like a classical mixture, consistent with the previous results.

Now the calculations on the entangled state using the state operator will be repeated using the state vector.

$$\Psi_{ent} = \frac{1}{\sqrt{2}}\begin{pmatrix}1 & 0 & 0 & 1\end{pmatrix}^T$$

$$\Psi_{ent}^T\mathrm{SzSz}\Psi_{ent} = 1 \quad \Psi_{ent}^T\mathrm{SxSx}\Psi_{ent} = 1$$

$$\Psi_{ent}^T\mathrm{SzI}\Psi_{ent} = 0 \quad \Psi_{ent}^T\mathrm{ISz}\Psi_{ent} = 0 \quad \Psi_{ent}^T\mathrm{SxI}\Psi_{ent} = 0 \quad \Psi_{ent}^T\mathrm{ISx}\Psi_{ent} = 0$$

Finally we calculate the expectation values when the spins are measured in different direction using both computational methods.

$$\begin{array}{ll} \mathrm{SzSx} = \mathrm{kronecker}\left(\sigma_z,\ \sigma_x\right) & \mathrm{SxSz} = \mathrm{kronecker}\left(\sigma_x,\ \sigma_z\right) \\ \mathrm{tr}\left(\rho_{\mathrm{ent}}\mathrm{SzSx}\right) = 0 & \mathrm{tr}\left(\rho_{\mathrm{ent}}\mathrm{SxSz}\right) = 0 \\ \Psi_{\mathrm{ent}}^{T}\mathrm{SzSx}\Psi_{\mathrm{ent}} = 0 & \Psi_{\mathrm{ent}}^{T}\mathrm{SxSz}\Psi_{\mathrm{ent}} = 0 \end{array}$$

Say the first spin is measured in the z-direction and found to be spin-up. This means the second spin is also spin-up in the z-direction, which is an even superposition of spin-up and spin-down in the x-direction, giving an over all expectation value of zero.

Ψ_{ent} is one of the Bell states. For extensive calculations on it and the other three Bell states see ″Bell State Exercises.

1.109: State Vectors and State Operators- Superpositions, Mixed States, and Entanglement is shared under a not declared license and was authored, remixed, and/or curated by LibreTexts.

1.11: Quantum Computation- A Short Course

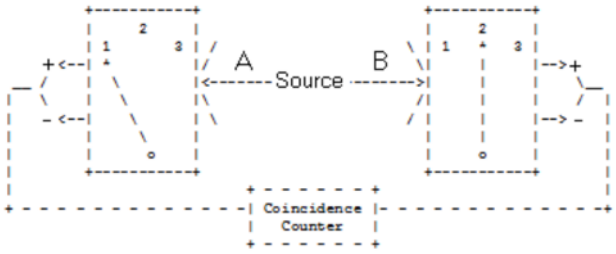
The four remaining tutorials deal with this clash between quantum mechanics and local realism, and the simulation of physical phenomena. The first two examine entangled spin systems and the third entangled photon systems. The fourth provides a terse mathematical summary for both spin and photon systems. They all clearly show the disagreement between the predictions of quantum theory and those of local hidden-variable models.

Another Look at Mermin's EPR Gedanken Experiment

> *Quantum theory is both stupendously successful as an account of the small-scale structure of the world and it is also the subject of an unresolved debate and dispute about its interpretation. J. C. Polkinghorne, The Quantum World, p. 1.*

In Bohm's EPR thought experiment (*Quantum Theory*, 1951, pp. 611-623), both local realism and quantum mechanics were shown to be consistent with the experimental data. However, the local realistic explanation used composite spin states that were invalid according to quantum theory. The local realists countered that this was an indication that quantum mechanics was incomplete because it couldn't assign well-defined values to all observable properties prior to or independent of observation. In the 1980s N. David Mermin presented a related thought experiment [*American Journal of Physics* (October 1981, pp 941-943) and *Physics Today* (April 1985, pp 38-47)] in which the predictions of local realism and quantum mechanics disagree. As such Mermin's thought experiment represents a specific illustration of Bell's theorem.

A spin-1/2 pair is prepared in a singlet state and the individual particles travel in opposite directions to detectors which are set up to measure spin in three directions in x-z plane: along the z-axis, and angles of 120 and 240 degrees with respect to the z-axis. The detector settings are labeled 1, 2 and 3, respectively.



The switches on the detectors are set randomly so that all nine possible settings of the two detectors occur with equal frequency.

Local realism holds that objects have properties independent of measurement and that measurements at one location on a particle cannot influence measurements of another particle at a distant location even if the particles were created in the same event. Local realism maintains that the spin-1/2 particles carry instruction sets (hidden variables) which dictate the results of subsequent measurements. Prior to measurement the particles are in an unknown but well-defined state.

The following table presents the experimental results expected on the basis of local realism. Singlet spin states have opposite spin values for each of the three measurement directions. If A's spin state is (+-+), then B's spin state is (-+-). A '+' indicates spin-up and a measurement eigenvalue of +1. A '-' indicates spin-down and a measurement eigenvalue of -1. If A's detector is set to spin direction "1" and B's detector is set to spin direction "3" the measured result will be recorded as +-,with an eigenvalue of -1.

There are eight spin states and nine possible detector settings, giving 72 possible measurement outcomes all of which are equally probable. The next to bottom line of the table shows the average (expectation) value for the nine possible detector settings given the local realist spin states. When the detector settings are the same there is perfect anti-correlation between the detectors at A and B. When the detectors are set at different spin directions there is no correlation.

Spin States	Detector Settings								
	12	13	21	23	31	32	11	22	33
+++/---	+-	+-	+-	+-	+-	+-	+-	+-	+-
++-/--+	+-	++	+-	++	--	--	+-	+-	-+
+-+/-+-	++	+-	--	--	+-	++	+-	-+	+-
-++/+--	--	--	++	+-	++	+-	-+	+-	+-
+--/-++	++	++	--	-+	--	-+	+-	-+	-+
-+-/+-+	--	-+	++	++	-+	--	-+	+-	-+
--+/++-	-+	--	-+	--	++	++	-+	-+	+-
---/+++	-+	-+	-+	-+	-+	-+	-+	-+	-+
Average Value	0	0	0	0	0	0	-1	-1	-1
Quantum Value	.5	.5	.5	.5	.5	.5	-1	-1	-1

As will now be shown quantum mechanics (bottom line of the table) disagrees with this local realistic analysis. The singlet state produced by the source is the following entangled superposition, where the arrows indicate the spin orientation for any direction in the x-z plane. As noted above the directions used are 0, 120 and 240 degrees, relative to the z-axis.

$$|\Psi\rangle = \frac{1}{\sqrt{2}}[|\uparrow\rangle_1|\downarrow\rangle_2 - |\downarrow\rangle_1|\uparrow\rangle_2]$$

$$= \frac{1}{\sqrt{2}}\left[\begin{pmatrix}\cos\left(\frac{\varphi}{2}\right)\\ \sin\left(\frac{\varphi}{2}\right)\end{pmatrix}\otimes\begin{pmatrix}-\sin\left(\frac{\varphi}{2}\right)\\ \cos\left(\frac{\varphi}{2}\right)\end{pmatrix} - \begin{pmatrix}-\sin\left(\frac{\varphi}{2}\right)\\ \cos\left(\frac{\varphi}{2}\right)\end{pmatrix}\otimes\begin{pmatrix}\cos\left(\frac{\varphi}{2}\right)\\ \sin\left(\frac{\varphi}{2}\right)\end{pmatrix}\right] = \frac{1}{\sqrt{2}}\begin{pmatrix}0\\1\\-1\\0\end{pmatrix}$$

$$\Psi := \frac{1}{\sqrt{2}}\cdot\begin{pmatrix}0\\1\\-1\\0\end{pmatrix}$$

The single particle spin operator in the x-z plane is constructed from the Pauli spin operators in the xand z-directions. ϕ is the angle of orientation of the measurement magnet with the z-axis. Note that the Pauli operators measure spin in units of \frac{h}{4 \pi}\). This provides for some mathematical clarity in the forthcoming analysis.

$$\sigma_Z := \begin{pmatrix} 1 & 0 \\ 0 & -1 \end{pmatrix} \qquad \sigma_x := \begin{pmatrix} 0 & 1 \\ 1 & 0 \end{pmatrix}$$

$$S(\varphi) := \cos(\varphi) \cdot \sigma_Z + \sin(\varphi) \cdot \sigma_x \rightarrow \begin{pmatrix} \cos(\varphi) & \sin(\varphi) \\ \sin(\varphi) & -\cos(\varphi) \end{pmatrix}$$

The joint spin operator for the two-spin system in tensor format is,

$$\begin{pmatrix} \cos\varphi_A & \sin\varphi_A \\ \sin\varphi_A & -\cos\varphi_A \end{pmatrix} \otimes \begin{pmatrix} \cos\varphi_B & \sin\varphi_B \\ \sin\varphi_B & -\cos\varphi_B \end{pmatrix}$$
$$= \begin{pmatrix} \cos\varphi_A \begin{pmatrix} \cos\varphi_B & \sin\varphi_B \\ \sin\varphi_B & -\cos\varphi_B \end{pmatrix} & \sin\varphi_A \begin{pmatrix} \cos\varphi_B & \sin\varphi_B \\ \sin\varphi_B & -\cos\varphi_B \end{pmatrix} \\ \sin\varphi_A \begin{pmatrix} \cos\varphi_B & \sin\varphi_B \\ \sin\varphi_B & -\cos\varphi_B \end{pmatrix} & -\cos\varphi_A \begin{pmatrix} \cos\varphi_B & \sin\varphi_B \\ \sin\varphi_B & -\cos\varphi_B \end{pmatrix} \end{pmatrix}$$

In Mathcad syntax this operator is:

$$\text{kronecker}\left(S\left(\varphi_A\right), S\left(\varphi_B\right)\right)$$

When the detector settings are the same quantum theory predicts an expectation value of -1, in agreement with the analysis based on local realism.

$$\Psi^T \cdot \text{ kronecker } (S(0 \cdot \text{deg}), S(0 \cdot \text{deg}))\Psi = -1 \quad \Psi^T \cdot \text{ kronecker } (S(120 \cdot \text{deg}), S(120 \cdot \text{deg}))\Psi = -1$$
$$\Psi^T \cdot \text{ kronecker } (S(240 \cdot \text{ deg }), S(240 \cdot \text{deg}))\Psi = -1$$

However, when the detector settings are different quantum theory predicts an expectation value of 0.5, in disagreement with the local realistic value of 0.

$$\Psi^T \cdot \text{ kronecker } (S(0 \cdot \text{deg}), S(120 \cdot \text{deg}))\Psi = 0.5 \quad \Psi^T \cdot \text{ kronecker } (S(0 \cdot \text{deg}), S(240 \cdot \text{deg}))\Psi = 0.5$$
$$\Psi^T \cdot \text{ kronecker } (S(120 \cdot \text{deg}), S(240 \cdot \text{deg}))\Psi = 0.5$$

Considering all detector settings local realism predicts an expectation value of **-1/3** [2/3(0) + 1/3(-1)], while quantum theory predicts an expectation value of **0** [2/3(1/2) + 1/3(-1)]. (See the two bottom rows in the table above.)

Furthermore, the following calculations demonstrate that the various spin operators do not commute and therefore represent incompatible observables. In other words, they are observables that cannot simultaneously be in well-defined states. Thus, quantum theory also rejects the realist's spin states used in the table.

$$S(0 \cdot \text{deg}) \cdot S(120 \cdot \text{deg}) - S(120 \cdot \text{deg}) \cdot S(0 \cdot \text{deg}) = \begin{pmatrix} 0 & 1.732 \\ -1.732 & 0 \end{pmatrix}$$

$$S(0 \cdot \text{deg}) \cdot S(240 \cdot \text{deg}) - S(240 \cdot \text{deg}) \cdot S(0 \cdot \text{deg}) = \begin{pmatrix} 0 & -1.732 \\ 1.732 & 0 \end{pmatrix}$$

$$S(120 \cdot \text{deg}) \cdot S(240 \cdot \text{deg}) - S(240 \cdot \text{deg}) \cdot S(120 \cdot \text{deg}) = \begin{pmatrix} 0 & 1.732 \\ -1.732 & 0 \end{pmatrix}$$

The local realist is undeterred by this argument and the disagreement with the quantum mechanical predictions, asserting that the fact that quantum theory cannot assign well-defined states to all elements of reality independent of observation is an indication that it provides an incomplete description of reality.

However, results available for experiments of this type with photons support the quantum mechanical predictions and contradict the local realists analysis shown in the table above. Thus, there appears to be a non-local interaction between the two spins at their measurement sites. Nick Herbert provides a memorable and succinct description of such non-local influences on page 214 of *Quantum Reality*.

> *A non-local interaction links up one location with another without crossing space, without decay, and without delay. A non-local interaction is, in short,* ***unmediated***, ***unmitigated***, *and* ***immediate***.

Jim Baggott puts it this way (*The Meaning of Quantum Theory*, page 135):

> *The predictions of quantum theory (in this experiment) are based on the properties of a two-particle state vector which ... is 'delocalized' over the whole experimental arrangement. The two particles are, in effect, always in 'contact' prior to measurement and can therefore exhibit a degree of correlation that is impossible for two Einstein separable particles.*

> *"...if [a hidden-variable theory] is local it will not agree with quantum mechanics, and if it agrees with quantum mechanics it will not be local. This is what the theorem says." -John S. Bell*

Further Information

The eigenvectors of the single particle spin operator, S(*phi*), in the x-z plane are given below along with their eigenvalues.

$$\varphi_u(\varphi) := \begin{pmatrix} \cos\left(\frac{\varphi}{2}\right) \\ \sin\left(\frac{\varphi}{2}\right) \end{pmatrix} \qquad \varphi_d(\varphi) := \begin{pmatrix} -\sin\left(\frac{\varphi}{2}\right) \\ \cos\left(\frac{\varphi}{2}\right) \end{pmatrix}$$

$$\varphi_u(\varphi)^T \cdot \varphi_u(\varphi) \text{ simplify } \rightarrow 1 \quad \varphi_d(\varphi)^T \cdot \varphi_d(\varphi) \text{ simplify } \rightarrow 1 \quad \varphi_d(\varphi)^T \cdot \varphi_u(\varphi) \text{ simplify } \rightarrow 0$$

Eigenvalue +1	Eigenvalue -1
$S(\varphi) \cdot \varphi_u(\varphi) \text{ simplify } \rightarrow \begin{pmatrix} \cos\left(\frac{\varphi}{2}\right) \\ \sin\left(\frac{\varphi}{2}\right) \end{pmatrix}$ (1.11.1)	$S(\varphi) \cdot \varphi_d(\varphi) \text{ simplify } \rightarrow \begin{pmatrix} \sin\left(\frac{\varphi}{2}\right) \\ -\cos\left(\frac{1}{2} \cdot \varphi\right) \end{pmatrix}$ (1.11.2)

A summary of the quantum mechanical calculations:

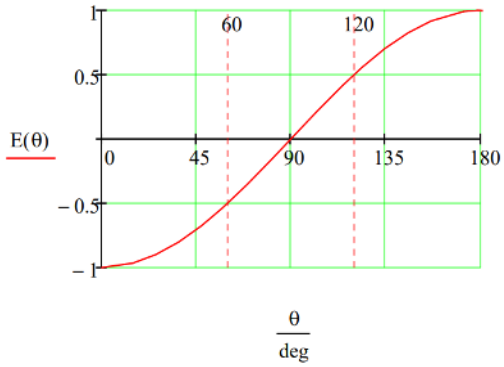
$$\begin{pmatrix} \Psi^T \cdot \text{ kronecker } (S(0\cdot\text{deg}), S(120\cdot\text{deg}))\Psi \\ \Psi^T \cdot \text{ kronecker } (S(0\cdot\text{deg}), S(240\cdot\text{deg}))\Psi \\ \Psi^T \cdot \text{ kronecker } (S(120\cdot\text{deg}), S(0\cdot\text{deg}))\Psi \\ \Psi^T \cdot \text{ kronecker } (S(120\cdot\text{deg}), S(240\cdot\text{deg}))\Psi \\ \Psi^T \cdot \text{ kronecker } (S(240\cdot\text{deg}), S(0\cdot\text{deg}))\Psi \\ \Psi^T \cdot \text{ kronecker } (S(240\cdot\text{deg}), S(120\cdot\text{deg}))\Psi \\ \Psi^T \cdot \text{ kronecker } (S(0\cdot\text{deg}), S(0\cdot\text{deg}))\Psi \\ \Psi^T \cdot \text{ kronecker } (S(120\cdot\text{deg}), S(120\cdot\text{deg}))\Psi \\ \Psi^T \cdot \text{ kronecker } (S(240\cdot\text{deg}), S(240\cdot\text{deg}))\Psi \end{pmatrix}^T$$
$$= \begin{pmatrix} 0.5 & 0.5 & 0.5 & 0.5 & 0.5 & 0.5 & -1 & -1 & -1 \end{pmatrix}$$

Calculation of the overall spin expectation value:

$$\sum_{i=0}^{2}\sum_{j=0}^{2}\left[\Psi^T \cdot \text{ kronecker } [S[i\cdot(120\cdot\text{deg})], S[j\cdot(120\cdot\text{deg})]]\Psi\right] = 0$$

The expectation value as a function of the relative orientation of the detectors reveals the level of correlation between the two spin measurements. For θ = 0° there is perfect anti-correlation; for θ = 180° perfect correlation; for θ = 90° no correlation; for θ = 60° intermediate anti-correlation (-0.5) and for θ = 120° intermediate correlation (0.5).

$$E(\theta) := \Psi^T \cdot \text{kronecker}(S(0), S(\theta))\,\Psi$$



A Quantum Simulation

This thought experiment is simulated using the following quantum circuit. As shown below the results are in agreement with the previous theoretical quantum calculations. The initial Hadamard and CNOT gates create the singlet state from the |11> input. $R_Z(\theta)$ rotates spin B. The final Hadamard gates prepare the system for measurement. See arXiv:1712.05642v2 for further detail.

Spin A $|1\rangle$ ▷ H · ··· H ▷ Measure 0 or 1: Eigenvalue 1 or -1
Spin B $|1\rangle$ ▷ ··· ⊕ $R_Z(\theta)$ H ▷ Measure 0 or 1: Eigenvalue 1 or -1

The quantum gates required to execute this circuit:

Identity	Hadamard gate	R_z rotation	Controlled NOT
$I := \begin{pmatrix} 1 & 0 \\ 0 & 1 \end{pmatrix}$ (1.11.3)	$H := \frac{1}{\sqrt{2}} \cdot \begin{pmatrix} 1 & 1 \\ 1 & -1 \end{pmatrix}$ (1.11.4)	$R_Z(\theta) := \begin{pmatrix} 1 & 0 \\ 0 & e^{i\cdot\theta} \end{pmatrix}$ (1.11.5)	$CNOT := \begin{pmatrix} 1 & 0 & 0 & 0 \\ 0 & 1 & 0 & 0 \\ 0 & 0 & 0 & 1 \\ 0 & 0 & 1 & 0 \end{pmatrix}$ (1.11.6)

The operator representing the circuit is constructed from the matrix operators provided above.

$$Op(\theta) := \text{ kronecker } (H, H) \cdot \text{ kronecker } (I, R_Z(\theta)) \text{ CNOT kronecker } (H, I)$$

There are four equally likely measurement outcomes with the eigenvalues and overall expectation values shown below for relative measurement angles 0 and 120 deg ($\frac{2\pi}{3}$).

|00> eigenvalue +1	$\left[\left[\begin{pmatrix} 1 \\ 0 \\ 0 \\ 0 \end{pmatrix}^T \cdot Op(0\cdot\text{deg}) \cdot \begin{pmatrix} 0 \\ 0 \\ 0 \\ 1 \end{pmatrix}\right]\right]^2 = 0$ (1.11.7)	|01> eigenvalue -1	$\left[\left[\begin{pmatrix} 0 \\ 1 \\ 0 \\ 0 \end{pmatrix}^T \cdot Op(0\cdot\text{deg}\right.\right.$ $= 0.5$
|10> eigenvalue -1	$\left[\left[\begin{pmatrix} 0 \\ 0 \\ 1 \\ 0 \end{pmatrix}^T \cdot Op(0\cdot\text{deg}) \cdot \begin{pmatrix} 0 \\ 0 \\ 0 \\ 1 \end{pmatrix}\right]\right]^2 = 0.5$ (1.11.9)	|11> eigenvalue +1	$\left[\left[\begin{pmatrix} 0 \\ 0 \\ 0 \\ 1 \end{pmatrix}^T \cdot Op(0\cdot\text{deg}\right.\right.$ $= 0$

Expectation value: 0 - 0.5 - 0.5 + 0 = -1

|00> eigenvalue +1	$\left[\left[\begin{pmatrix}1\\0\\0\\0\end{pmatrix}^{\mathrm{T}}\cdot \mathrm{Op}(\frac{2\pi}{3})\cdot\begin{pmatrix}0\\0\\0\\1\end{pmatrix}\right]\right]^2 = 0.375$ (1.11.11)	|01> eigenvalue -1	$\left[\left[\begin{pmatrix}0\\1\\0\\0\end{pmatrix}^{\mathrm{T}}\cdot \mathrm{Op}(\frac{2\pi}{3}),\right.\right. = 0.125$
|10> eigenvalue -1	$\left[\left[\begin{pmatrix}0\\0\\1\\0\end{pmatrix}^{\mathrm{T}}\cdot \mathrm{Op}(\frac{2\pi}{3})\cdot\begin{pmatrix}0\\0\\0\\1\end{pmatrix}\right]\right]^2 = 0.125$ (1.11.13)	|11> eigenvalue +1	$\left[\left[\begin{pmatrix}0\\0\\0\\1\end{pmatrix}^{\mathrm{T}}\cdot \mathrm{Op}(\frac{2\pi}{3}),\right.\right. = 0.375$

Expectation value: 0.375 - 0.125 + 0.375 - 0.125 = 0.5

Another Simulation of a GHZ Gedanken Experiment

Many years ago N. David Mermin published two articles (*Physics Today*, June 1990; *American Journal of Physics*, August 1990) in the general physics literature on a Greenberger-Horne-Zeilinger (*American Journal of Physics*, December 1990; *Nature*, 3 February 2000) thought experiment involving spins that sharply revealed the clash between local realism and the quantum view of reality.

Three spin-1/2 particles are created in a single event and move apart in the horizontal y-z plane. Subsequent spin measurements will be carried out in units of $\frac{h}{4\pi}$ with spin operators in the x- and y-directions.

The z-basis eigenfunctions are:

$$\mathrm{Sz}_{\mathrm{up}} := \begin{pmatrix}1\\0\end{pmatrix} \qquad \mathrm{Sz}_{\mathrm{down}} := \begin{pmatrix}0\\1\end{pmatrix}$$

The x- and y-direction spin operators:

$$\sigma_{\mathrm{x}} := \begin{pmatrix}0 & 1\\1 & 0\end{pmatrix} \quad \mathrm{eigenvals}\ (\sigma_{\mathrm{x}}) = \begin{pmatrix}1\\-1\end{pmatrix} \quad \sigma_{\mathrm{y}} := \begin{pmatrix}0 & -\mathrm{i}\\\mathrm{i} & 0\end{pmatrix} \quad \mathrm{eigenvals}\ (\sigma_{\mathrm{y}}) = \begin{pmatrix}1\\-1\end{pmatrix}$$

The initial entangled spin state for the three spin-1/2 particles in tensor notation is:

$$|\Psi\rangle = \frac{1}{\sqrt{2}}\left[\begin{pmatrix}1\\0\end{pmatrix}\otimes\begin{pmatrix}1\\0\end{pmatrix}\otimes\begin{pmatrix}1\\0\end{pmatrix} - \begin{pmatrix}0\\1\end{pmatrix}\otimes\begin{pmatrix}0\\1\end{pmatrix}\otimes\begin{pmatrix}0\\1\end{pmatrix}\otimes\begin{pmatrix}0\\1\end{pmatrix}\otimes\begin{pmatrix}0\\1\end{pmatrix}\right]$$

$$= \frac{1}{\sqrt{2}}\begin{pmatrix}1\\0\\0\\0\\0\\0\\0\\-1\end{pmatrix} \qquad \Psi := \frac{1}{\sqrt{2}}\cdot\begin{pmatrix}1\\0\\0\\0\\0\\0\\0\\-1\end{pmatrix}$$

The following operators represent the measurements to be carried out on spins 1, 2 and 3, in that order.

$$\sigma_x^1\otimes\sigma_y^2\otimes\sigma_y^3 \quad \sigma_y^1\otimes\sigma_x^2\otimes\sigma_y^3 \quad \sigma_y^1\otimes\sigma_y^2\otimes\sigma_x^3 \quad \sigma_x^1\otimes\sigma_x^2\otimes\sigma_x^3$$

The matrix tensor product is also known as the Kronecker product, which is available in Mathcad. The four operators in tensor format are formed as follows.

$\sigma_{\mathrm{xyy}} := \mathrm{kronecker}\ (\sigma_{\mathrm{x}},\ \mathrm{kronecker}\ (\sigma_{\mathrm{y}},\sigma_{\mathrm{y}}))$ (1.11.15)	$\sigma_{\mathrm{yxy}} := \mathrm{kronecker}\ (\sigma_{\mathrm{y}},\ \mathrm{kronecker}\ (\sigma_{\mathrm{x}},\sigma_{\mathrm{y}}))$ (1.11.16)
$\sigma_{\mathrm{yyx}} := \mathrm{kronecker}\,(\sigma_{\mathrm{y}},\mathrm{kronecker}\,(\sigma_{\mathrm{y}},\sigma_{\mathrm{x}}))$ (1.11.17)	$\sigma_{\mathrm{xxx}} := \mathrm{kronecker}\ (\sigma_{\mathrm{x}},\ \mathrm{kronecker}\ (\sigma_{\mathrm{x}},\sigma_{\mathrm{x}}))$ (1.11.18)

These composite operators are Hermitian and mutually commute which means they can have simultaneous eigenvalues.

$\sigma_{\mathrm{xyy}}\cdot\sigma_{\mathrm{yxy}} - \sigma_{\mathrm{yxy}}\cdot\sigma_{\mathrm{xyy}} \to 0$ (1.11.19)	$\sigma_{\mathrm{xyy}}\cdot\sigma_{\mathrm{yyx}} - \sigma_{\mathrm{yyx}}\cdot\sigma_{\mathrm{xyy}} \to 0$ (1.11.20)	$\sigma_{\mathrm{xyy}}\cdot\sigma_{\mathrm{xxx}} - \sigma_{\mathrm{xxx}}\cdot\sigma_{\mathrm{xyy}} \to 0$ (1.11.21)
$\sigma_{\mathrm{yxy}}\cdot\sigma_{\mathrm{yyx}} - \sigma_{\mathrm{yyx}}\cdot\sigma_{\mathrm{yxy}} \to 0$ (1.11.22)	$\sigma_{\mathrm{yxy}}\cdot\sigma_{\mathrm{xxx}} - \sigma_{\mathrm{xxx}}\cdot\sigma_{\mathrm{yxy}} \to 0$ (1.11.23)	$\sigma_{\mathrm{yyx}}\cdot\sigma_{\mathrm{xxx}} - \sigma_{\mathrm{xxx}}\cdot\sigma_{\mathrm{yyx}} \to 0$ (1.11.24)

The expectation values of the operators are now calculated.

$$\Psi^{\mathrm{T}}\cdot\sigma_{\mathrm{xyy}}\cdot\Psi = 1 \qquad \Psi^{\mathrm{T}}\cdot\sigma_{\mathrm{yxy}}\cdot\Psi = 1 \qquad \Psi^{\mathrm{T}}\cdot\sigma_{\mathrm{yyx}}\cdot\Psi = 1 \qquad \Psi^{\mathrm{T}}\cdot\sigma_{\mathrm{xxx}}\cdot\Psi = -1$$

Consequently the product of the four operators has the expectation value of -1.

$$\Psi^{\mathrm{T}}\cdot\sigma_{\mathrm{xyy}}\cdot\sigma_{\mathrm{yxy}}\cdot\sigma_{\mathrm{yyx}}\cdot\sigma_{\mathrm{Xxx}}\cdot\Psi = -1$$

Local realism assumes that objects have definite properties independent of measurement. In this example it assumes that the x- and y-components of the spin have definite values prior to measurement. This position leads to a contradiction with the above result as demonstrated by Mermin (*Physics Today*, June 1990). Looking again at the measurement operators, notice that there is a σx measurement on the first spin in the first and fourth experiment. If the spin state is well-defined before measurement those results have to be the same, either both +1 or both -1, so that the product of the two measurements is +1.

$$\left(\sigma_x^1\otimes\sigma_y^2\otimes\sigma_y^3\right)\left(\sigma_y^1\otimes\sigma_x^2\otimes\sigma_y^3\right)\left(\sigma_y^1\otimes\sigma_y^2\otimes\sigma_x^3\right)\left(\sigma_x^1\otimes\sigma_x^2\otimes\sigma_x^3\right))$$

Likewise there is a y measurement on the second spin in experiments one and three. By similar arguments those results will lead to a product of +1 also. Continuing with all pairs in the total operator using local realistic reasoning unambiguously shows that its expectation value should be +1, in sharp disagreement with the quantum mechanical result of -1. **This result should cause all mathematically literate local realists to renounce and recant their heresy**. However, they may resist saying this is just a thought experiment. It hasn't actually been performed. However, if you believe in quantum simulation it has been performed.

Quantum Simulation

"Quantum simulation is a process in which a quantum computer simulates another quantum system. Because of the various types of quantum weirdness, classical computers can simulate quantum systems only in a clunky, inefficient way. But because a quantum computer is itself a quantum system, capable of exhibiting the full repertoire of quantum weirdness, it can efficiently simulate other quantum systems. **The resulting simulation can be so accurate that the behavior the computer will be indistinguishable from the behavior of the simulated system itself."** (Seth Lloyd, Programming the Universe, page 149.) The thought experiment can be simulated using the quantum circuit shown below which is an adaptation of one that can be found at: arXiv:1712.06542v2.

$$
\begin{array}{lccccccccc}
|1\rangle & \triangleright & H & \cdot & \cdots & \cdots & H & \triangleright & \text{Measure, 0 or 1} \\
 & & & | & & & & & \\
|0\rangle & \triangleright & \cdots & \oplus & \cdot & S & H & \triangleright & \text{Measure, 0 or 1} \\
 & & & & | & & & & \\
|0\rangle & \triangleright & \cdots & \cdots & \oplus & S & H & \triangleright & \text{Measure, 0 or 1} \\
 & & & & | & & & &
\end{array}
$$

The matrix operators required for the implementation of the quantum circuit:

$$
\mathrm{I} := \begin{pmatrix} 1 & 0 \\ 0 & 1 \end{pmatrix} \quad \mathrm{H} := \frac{1}{\sqrt{2}} \cdot \begin{pmatrix} 1 & 1 \\ 1 & -1 \end{pmatrix} \quad \mathrm{S} := \begin{pmatrix} 1 & 0 \\ 0 & -\mathrm{i} \end{pmatrix} \quad \mathrm{CNOT} := \begin{pmatrix} 1 & 0 & 0 & 0 \\ 0 & 1 & 0 & 0 \\ 0 & 0 & 0 & 1 \\ 0 & 0 & 1 & 0 \end{pmatrix}
$$

$\mathrm{HII} := \mathrm{kronecker}(\mathrm{H}, \mathrm{kronecker}(\mathrm{I}, \mathrm{I}))$	$\mathrm{CNOTI} := \mathrm{kronecker}(\mathrm{CNOT}, \mathrm{I})$	$\mathrm{ICNOT} := \mathrm{kronecker}(\mathrm{I}, \mathrm{CNOT})$
$\mathrm{ISS} := \mathrm{kronecker}(\mathrm{I}, \mathrm{kronecker}(\mathrm{S}, \mathrm{S}))$	$\mathrm{SIS} := \mathrm{kronecker}(\mathrm{S}, \mathrm{kronecker}(\mathrm{I}, \mathrm{S}))$	$\mathrm{SSI} := \mathrm{kronecker}(\mathrm{S}, \mathrm{kronecker}(\mathrm{S}, \mathrm{I}))$
$\mathrm{HHH} := \mathrm{kronecker}(\mathrm{H}, \mathrm{kronecker}(\mathrm{H}, \mathrm{H}))$		

First it is demonstrated that the first three steps of the circuit create the initial state.

$$
\begin{gathered}
[\mathrm{ICNOT} \cdot \mathrm{CNOTI} \cdot \mathrm{HII} \cdot \begin{pmatrix} 0 & 0 & 0 & 0 & 1 & 0 & 0 & 0 \end{pmatrix}^{\mathrm{T}}]^{T} \\
= \begin{pmatrix} 0.707 & 0 & 0 & 0 & 0 & 0 & 0 & -0.707 \end{pmatrix}
\end{gathered}
$$

The complete circuit shown above simulates the expectation value of the $\sigma_x\sigma_y\sigma_y$ operator. The presence of S on a line before the final H gates indicates the measurement of the σ_y, its absence a measurement of σ_x. The subsequent simulations show the absence of S on the middle and last line, and finally on all three lines for the simulation of the expectation value for $\sigma_x\sigma_x\sigma_x$.

Eigenvalue |0> = +1; eigenvalue |1> = -1

$$
\begin{gathered}
[\mathrm{HHH} \cdot \mathrm{ISS} \cdot \mathrm{ICNOT} \cdot \mathrm{CNOTI} \cdot \mathrm{HII} \cdot \begin{pmatrix} 0 & 0 & 0 & 0 & 1 & 0 & 0 & 0 \end{pmatrix}^{\mathrm{T}}]^{T} \\
= \begin{pmatrix} 0.5 & 0 & 0 & 0.5 & 0 & 0.5 & 0.5 & 0 \end{pmatrix}
\end{gathered}
$$

$$
\frac{1}{2}(|000\rangle + |011\rangle + |101\rangle + |110\rangle) \Rightarrow \langle\sigma_x\sigma_y\sigma_y\rangle = 1
$$

Given the eigenvalue assignments above the expectation value associated with this measurement outcome is 1/4[(1)(1)(1)+(1)(-1)(-1)+(-1)(1)(-1)+(-1)(-1)(1)] = 1. Note that 1/2 is the probability amplitude for the product state. Therefore the probability of each member of the superposition being observed is 1/4. The same reasoning is used for the remaining simulations.

$$
\begin{gathered}
[\mathrm{HHH} \cdot \mathrm{SIS} \cdot \mathrm{ICNOT} \cdot \mathrm{CNOTI} \cdot \mathrm{HII} \cdot \begin{pmatrix} 0 & 0 & 0 & 0 & 1 & 0 & 0 & 0 \end{pmatrix}^{\mathrm{T}}]^{T} \\
= \begin{pmatrix} 0.5 & 0 & 0 & 0.5 & 0 & 0.5 & 0.5 & 0 \end{pmatrix}
\end{gathered}
$$

$$
\frac{1}{2}(|000\rangle + |011\rangle + |101\rangle + |110\rangle) \Rightarrow \langle\sigma_y\sigma_x\sigma_y\rangle = 1
$$

$$
\begin{gathered}
[\mathrm{HHH} \cdot \mathrm{SSI} \cdot \mathrm{ICNOT} \cdot \mathrm{CNOTI} \cdot \mathrm{HII} \cdot \begin{pmatrix} 0 & 0 & 0 & 0 & 1 & 0 & 0 & 0 \end{pmatrix}^{\mathrm{T}}]^{T} \\
= \begin{pmatrix} 0.5 & 0 & 0 & 0.5 & 0 & 0.5 & 0.5 & 0 \end{pmatrix}
\end{gathered}
$$

$$
\frac{1}{2}(|000\rangle + |011\rangle + |101\rangle + |110\rangle) \Rightarrow \langle\sigma_y\sigma_y\sigma_x\rangle = 1
$$

$$
\begin{gathered}
[\mathrm{HHH} \cdot \mathrm{ICNOT} \cdot \mathrm{CNOTI} \cdot \mathrm{HII} \cdot \begin{pmatrix} 0 & 0 & 0 & 0 & 1 & 0 & 0 & 0 \end{pmatrix}^{\mathrm{T}}]^{T} \\
= \begin{pmatrix} 0 & 0.5 & 0.5 & 0 & 0.5 & 0 & 0 & 0.5 \end{pmatrix}
\end{gathered}
$$

$$
\frac{1}{2}(|001\rangle + |010\rangle + |100\rangle + |111\rangle) \Rightarrow \langle\sigma_x\sigma_x\sigma_x\rangle = -1
$$

Individually and in product form the simulated results are in agreement with the previous quantum mechanical calculations.

$$
\langle\sigma_x\sigma_x\sigma_x\rangle \langle\sigma_x\sigma_y\sigma_y\rangle \langle\sigma_y\sigma_x\sigma_y\rangle \langle\sigma_y\sigma_y\sigma_x\rangle = -1
$$

The appendix provides algebraic calculations of $< \sigma_x\sigma_y\sigma_y >$ and $< \sigma_x\sigma_x\sigma_x >$.

Appendix:

Truth tables for the operation of the circuit elements:

$$\mathrm{I} = \begin{pmatrix} 0 & \text{to} & 0 \\ 1 & \text{to} & 1 \end{pmatrix} \quad H = \begin{bmatrix} 0 & \text{to} & \frac{(0+1)}{\sqrt{2}} \\ 1 & \text{to} & \frac{(0-1)}{\sqrt{2}} \end{bmatrix} \quad \mathrm{CNOT} = \begin{pmatrix} 00 & \text{to} & 00 \\ 01 & \text{to} & 01 \\ 10 & \text{to} & 11 \\ 11 & \text{to} & 10 \end{pmatrix} \quad \mathrm{S} = \begin{pmatrix} 0 & \text{to} & 0 \\ 1 & \text{to} & -\mathrm{i} \end{pmatrix}$$

$$\begin{array}{c} |100\rangle \\ H \otimes I \otimes I \\ \frac{1}{\sqrt{2}}[|000\rangle - |100\rangle] \\ CNOT \otimes I \\ \frac{1}{\sqrt{2}}[|000\rangle - |110\rangle] \\ I \otimes CNOT \\ \frac{1}{\sqrt{2}}[|000\rangle - |111\rangle] \\ I \otimes S \otimes S \\ \frac{1}{\sqrt{2}}[|000\rangle - |1 - i - i\rangle] \\ H \otimes H \otimes H \\ \frac{1}{2}[|000\rangle + |011\rangle + |101\rangle + |110\rangle] \\ \langle \sigma_x \sigma_y \sigma_y \rangle = 1 \end{array} \tag{1.11.25}$$

$$\begin{array}{c} |100\rangle \\ H \otimes I \otimes I \\ \frac{1}{\sqrt{2}}[|000\rangle - |100\rangle] \\ CNOT \otimes I \\ c\frac{1}{\sqrt{2}}[|000\rangle - |110\rangle] \\ I \otimes CNOT \\ \frac{1}{\sqrt{2}}[|000\rangle - |111\rangle] \\ H \otimes H \otimes H \\ \frac{1}{2}[|001\rangle + |010\rangle + |100\rangle + |111\rangle] \\ \langle \sigma_x \sigma_x \sigma_x \sigma_x \rangle = -1 \end{array} \tag{1.11.26}$$

Quantum Correlations Illustrated With Photons

A two-stage atomic cascade emits entangled photons (A and B) in opposite directions with the same circular polarization according to observers in their path. The experiment involves the measurement of photon polarization states in the vertical/horizontal measurement basis, and allows for the rotation of the right-hand detector through an angle θ, in order to explore the consequences of quantum mechanical entanglement. PA stands for polarization analyzer and could simply be a calcite crystal.

$$\begin{array}{ccccccccc} V & \lhd & \lceil & & \rceil & & & & \lceil & & \rceil & \rhd & V \\ & & | & 0 & | & \xleftarrow{A} & \backslash\text{xleftrightarrow}Source & \xrightarrow{B} & | & \theta & | & & \\ H & \lhd & \lfloor & & \rfloor & & & & \lfloor & & \rfloor & \rhd & H \\ & & PA_A & & & & PA_B & & & & & & \end{array}$$

The entangled two-photon polarization state is written in the circular and linear polarization bases,

$$|\Psi\rangle = \frac{1}{\sqrt{2}}[|L\rangle_A|L\rangle_B + |R\rangle_A|R\rangle_B] = \frac{1}{\sqrt{2}}[|V\rangle_A|V\rangle_B - |H\rangle_A|H\rangle_B] \text{using} \quad |L\rangle = \frac{1}{\sqrt{2}}[|V\rangle + i|H\rangle] \quad |R\rangle$$
$$= \frac{1}{\sqrt{2}}[|V\rangle - i|H\rangle]$$

The vertical (eigenvalue +1) and horizontal (eigenvalue -1) polarization states for the photons in the measurement plane are given below. Θ is the angle of the measuring PA.

$$\mathrm{V}(\theta) := \begin{pmatrix} \cos(\theta) \\ \sin(\theta) \end{pmatrix} \quad \mathrm{H}(\theta) := \begin{pmatrix} -\sin(\theta) \\ \cos(\theta) \end{pmatrix} \quad \mathrm{V}(0) = \begin{pmatrix} 1 \\ 0 \end{pmatrix} \quad \mathrm{H}(0) = \begin{pmatrix} 0 \\ 1 \end{pmatrix}$$

If photon A has vertical polarization photon B also has vertical polarization, the probability that photon B has vertical polarization when measured at an angle θ giving a composite eigenvalue of +1 is,

$$\left(\mathrm{V}(\theta)^{\mathrm{T}} \cdot \mathrm{V}(0)\right)^2 \to \cos(\theta)^2$$

If photon A has vertical polarization photon B also has vertical polarization, the probability that photon B has horizontal polarization when measured at an angle θ giving a composite eigenvalue of -1 is,

$$\left(\mathrm{H}(\theta)^{\mathrm{T}} \cdot \mathrm{V}(0)\right)^2 \to \sin(\theta)^2$$

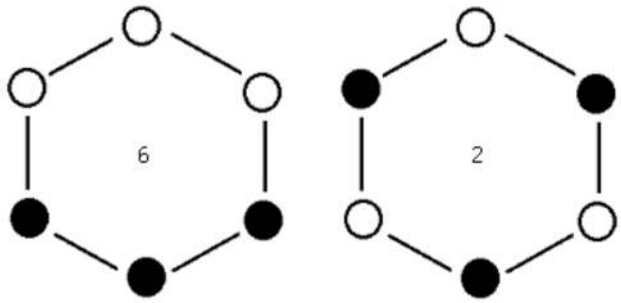
Therefore the overall quantum correlation coefficient or expectation value is:

$$\mathrm{E}(\theta) := \left(\mathrm{V}(\theta)^{\mathrm{T}} \cdot \mathrm{V}(0)\right)^2 - \left(\mathrm{H}(\theta)^{\mathrm{T}} \cdot \mathrm{V}(0)\right)^2 \text{ simplify } \to \cos(2 \cdot \theta) \quad \mathrm{E}(0 \cdot \deg) = 1$$
$$\mathrm{E}(30 \cdot \deg) = 0.5 \quad \mathrm{E}(90 \cdot \deg) = -1$$

Now it will be shown that a local-realistic, hidden-variable model can be constructed which is in agreement with the quantum calculations for 0 and 90 degrees, but not for 30 degrees (highlighted).

If objects have well-defined properties independent of measurement, the results for θ = 0 degrees and θ = 90 degrees require that the photons carry the following instruction sets, where the hexagonal vertices refer to θ values of 0, 30, 60, 90, 120, and 150 degrees.

There are eight possible instruction sets, six of the type on the left and two of the type on the right. The white circles represent vertical polarization with eigenvalue +1 and the black circles represent horizontal polarization with eigenvalue -1. In any given measurement, according to local realism, both photons (A and B) carry identical instruction sets, in other words the same one of the eight possible sets.



The problem is that while these instruction sets are in agreement with the 0 and 90 degree quantum calculations, with expectation values of +1 and -1 respectively, they can't explain the 30 degree predictions of quantum mechanics. The figure on the left shows that the same result should be obtained 4 times with joint eigenvalue +1, and the opposite result twice with joint eigenvalue of -1. For the figure on the right the opposite polarization is always observed giving a joint eigenvalue of -1. Thus, local realism predicts an expectation value of 0 in disagreement with the quantum result of 0.5.

$$\frac{6 \cdot (1 - 1 + 1 + 1 - 1 + 1) + 2 \cdot (-1 - 1 - 1 - 1 - 1 - 1)}{8} = 0$$

This analysis is based on "Simulating Physics with Computers" by Richard Feynman, published in the *International Journal of Theoretical Physics* (volume 21, pages 481-485), and Julian Brown's *Quest for the Quantum Computer* (pages 91-100). Feynman used the experiment outlined above to establish that a local classical computer could not simulate quantum physics.

A local classical computer manipulates bits which are in well-defined states, 0s and 1s, shown above graphically in white and black. However, these classical states are incompatible with the quantum mechanical analysis which **is** consistent with experimental results. This two-photon experiment demonstrates that simulation of quantum physics requires a computer that can manipulate 0s and 1s, superpositions of 0 and 1, and entangled superpositions of 0s and 1s.

Simulation of quantum physics requires a quantum computer. The following quantum circuit simulates this experiment exactly. The Hadamard and CNOT gates transform the input, |10>, into the required entangled Bell state. R(θ) rotates the polarization of photon B clockwise through an angle θ. Finally measurement yields one of the four possible output states: |00>, |01>, |10> or |11>.

$$\begin{array}{lllll} |1\rangle & \triangleright & H & \cdots & \triangleright \text{ Measure 0 or 1} \\ & & | & & \\ |0\rangle & \triangleright & \cdots \oplus & R(\theta) & \triangleright \text{ Measure 0 or 1} \end{array}$$

The following algebraic analysis of the quantum circuit shows that it yields the correct expectation value for all values of θ. This analysis requires the truth tables for the matrix operators. Recall from above that |0> = |V> with eigenvalue +1, and |1> = |H> with eigenvalue -1.

$$H = \begin{bmatrix} 0 & \text{to} & \frac{1}{\sqrt{2}} \cdot (0+1) \\ 1 & \text{to} & \frac{1}{\sqrt{2}} \cdot (0-1) \end{bmatrix} \quad \text{CNOT} = \begin{pmatrix} 00 & \text{to} & 00 \\ 01 & \text{to} & 01 \\ 10 & \text{to} & 11 \\ 11 & \text{to} & 10 \end{pmatrix} \quad \begin{pmatrix} 1 \\ 0 \end{pmatrix} \xrightarrow{R(\theta)} \begin{pmatrix} \cos\theta \\ \sin\theta \end{pmatrix} \quad \begin{pmatrix} 0 \\ 1 \end{pmatrix} \xrightarrow{R(\theta)} \begin{pmatrix} -\sin\theta \\ \cos\theta \end{pmatrix}$$

$$|1\rangle|0\rangle = |10\rangle$$

$$\text{H} \otimes \text{I} \frac{1}{\sqrt{2}}[|0\rangle - |1\rangle]|0\rangle = \frac{1}{\sqrt{2}}[|00\rangle - |10\rangle$$

$$\text{CNOT} \quad \begin{matrix} \frac{1}{\sqrt{2}}[|00\rangle - |11 \\ \text{I} \otimes \text{R}(\theta) \end{matrix} \quad \frac{1}{\sqrt{2}}[|0\rangle(\cos\theta|0\rangle + \sin\theta|1\rangle) - |1\rangle(-\sin\theta|0\rangle + \cos\theta|1\rangle)]$$

$$\Downarrow$$

$$\frac{1}{\sqrt{2}}[\cos\theta|00\rangle + \sin\theta|01\rangle + \sin\theta|10\rangle - \cos\theta|11\rangle]$$

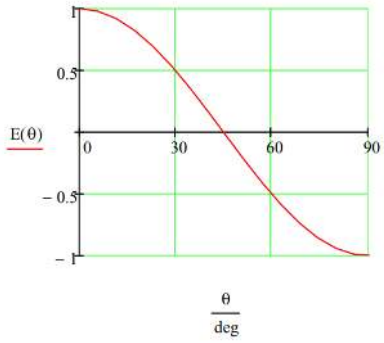
Probabilities

$$\Downarrow$$

$$\frac{\cos^2\theta}{2}|00\rangle + \frac{\sin^2\theta}{2}|01\rangle + \frac{\sin^2\theta}{2}|10\rangle + \frac{\cos^2\theta}{2}|11\rangle$$

|00> = |VV> and |11> = |HH> have a composite eigenvalue of +1. |01> = |VH> and |10> = |HV> have a composite eigenvalue of -1. Therefore,

$$E(\theta) := \cos(\theta)^2 - \sin(\theta)^2 \text{ simplify } \rightarrow \cos(2\cdot\theta)$$



This page titled 1.11: Quantum Computation- A Short Course is shared under a CC BY 4.0 license and was authored, remixed, and/or curated by Frank Rioux via source content that was edited to the style and standards of the LibreTexts platform.

1.110: The Gram-Schmidt Procedure

In this exercise the Gram-Schmidt method will be used to create an orthonormal basis set from the following vectors which are neither normalized nor orthogonal.

$$u1 = \begin{pmatrix} 1+i \\ 1 \\ i \end{pmatrix} \quad u2 = \begin{pmatrix} i \\ 3 \\ 1 \end{pmatrix} \quad u3 = \begin{pmatrix} 0 \\ 28 \\ 0 \end{pmatrix}$$

Demonstrate that the vectors are not normalized and are not orthogonal.

$$\left(\overline{u1}\right)^T u1 = 4 \quad \left(\overline{u2}\right)^T u2 = 11 \quad \left(\overline{u3}\right)^T u3 = 784$$
$$\left(\overline{u1}\right)^T u2 = 4 \quad \left(\overline{u1}\right)^T u3 = 28 \quad \left(\overline{u2}\right)^T u3 = 84$$

Using the first vector make u2 orthogonal to it by subtracting its projection on u1.

$$u2 = u2 - \frac{\left(\overline{u1}\right)^T u2}{\left(\overline{u1}\right)^T u1} u1$$

Make u3 orthogonal to u1 and u2 by subtracting its projection on u1 and u2.

$$u3 = u3 - \frac{\left(\overline{u1}\right)^T u3}{\left(\overline{u1}\right)^T u1} u1 - \frac{\left(\overline{u2}\right)^T u3}{\left(\overline{u2}\right)^T u2} u2$$

Finally, normalize the new orthogonal vectors.

$$u1 = \frac{u1}{\sqrt{\left(\overline{u1}\right)^T u1}} \quad u2 = \frac{u2}{\sqrt{\left(\overline{u2}\right)^T u2}} \quad u3 = \frac{u3}{\sqrt{\left(\overline{u3}\right)^T u3}}$$

Demonstrate that an orthonormal basis set has been created.

$$\left(\overline{u1}\right)^T u1 = 1 \quad \left(\overline{u2}\right)^T u2 = 1 \quad \left(\overline{u3}\right)^T u3 = 1$$
$$\left(\overline{u1}\right)^T u2 = 0 \quad \left(\overline{u1}\right)^T u3 = 0 \quad \left(\overline{u2}\right)^T u3 = 0$$

Display the orthonormal basis set.

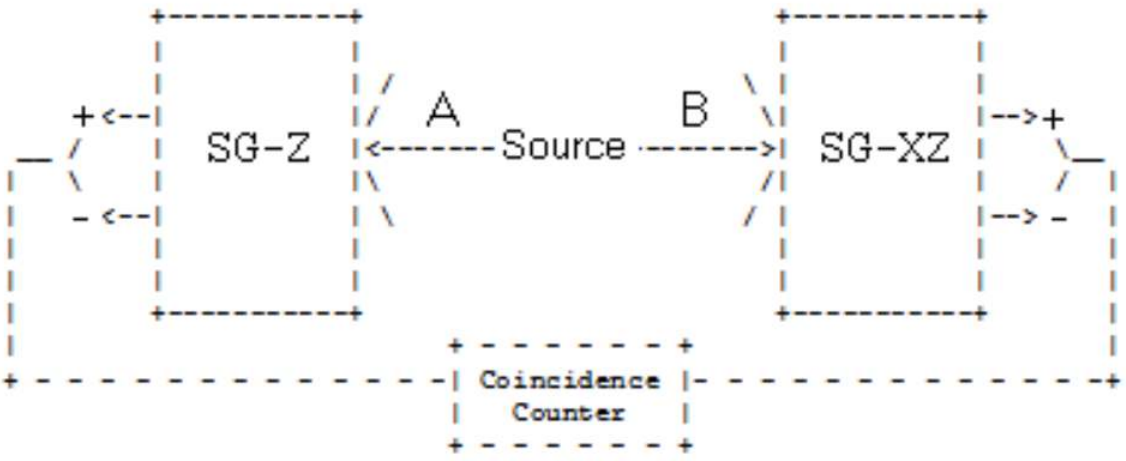
$$u1 = \begin{pmatrix} 0.5+0.5i \\ 0.5 \\ 0.5i \end{pmatrix} \quad u2 = \begin{pmatrix} -0.378 \\ 0.756 \\ 0.378-0.378i \end{pmatrix} \quad u3 = \begin{pmatrix} 0.085-0.592i \\ 0.423 \\ -0.676+0.085i \end{pmatrix}$$

1.110: The Gram-Schmidt Procedure is shared under a not declared license and was authored, remixed, and/or curated by LibreTexts.

1.12: Quantum Computation- A Short Course

Quantum Correlations Illustrated With Spin-1/2 Particles

A spin-1/2 pair is prepared in an entangled singlet state and the individual particles travel in opposite directions on the y-axis to a pair of Stern-Gerlach detectors which are set up to measure spin in the x-z plane. Particle A's spin is measured along the z-axis, and particle B's spin is measured at an angle θ with respect to the z-axis.



Spin-up eigenstate Eigenvalue +1	Spin-down eigenstate Eigenvalue -1
$\varphi_{\mathrm{u}}(\theta) = \begin{pmatrix} \cos\left(\frac{\theta}{2}\right) \\ \sin\left(\frac{\theta}{2}\right) \end{pmatrix}$	$\varphi_{\mathrm{d}}(\theta) := \begin{pmatrix} -\sin\left(\frac{\theta}{2}\right) \\ \cos\left(\frac{\theta}{2}\right) \end{pmatrix}$

The singlet state wave function in the xz-plane:

$$|\Psi\rangle = \frac{1}{\sqrt{2}}[|\uparrow\rangle_{\mathrm{A}}|\downarrow\rangle_{\mathrm{B}} - |\downarrow\rangle_{\mathrm{A}}|\uparrow\rangle_{\mathrm{B}}]$$

$$= \frac{1}{\sqrt{2}}\left[\begin{pmatrix} \cos\left(\frac{\theta}{2}\right) \\ \sin\left(\frac{\theta}{2}\right) \end{pmatrix}_A \otimes \begin{pmatrix} -\sin\left(\frac{\theta}{2}\right) \\ \cos\left(\frac{\theta}{2}\right) \end{pmatrix}_B - \begin{pmatrix} -\sin\left(\frac{\theta}{2}\right) \\ \cos\left(\frac{\theta}{2}\right) \end{pmatrix}_A \otimes \begin{pmatrix} \cos\left(\frac{\theta}{2}\right) \\ \sin\left(\frac{\theta}{2}\right) \end{pmatrix}_B\right]$$

$$= \frac{1}{\sqrt{2}}\begin{pmatrix} 0 \\ 1 \\ -1 \\ 0 \end{pmatrix}$$

The spin operator in the θ direction:

$$\mathrm{S}(\theta) := \varphi_{\mathrm{u}}(\theta)\cdot\varphi_{\mathrm{u}}(\theta)^{\mathrm{T}} - \varphi_{\mathrm{d}}(\theta)\cdot\varphi_{\mathrm{d}}(\theta)^{\mathrm{T}} \text{ simplify } \rightarrow \begin{pmatrix} \cos(\theta) & \sin(\theta) \\ \sin(\theta) & -\cos(\theta) \end{pmatrix}$$

$$\sigma_{\mathrm{Z}} := \begin{pmatrix} 1 & 0 \\ 0 & -1 \end{pmatrix} \quad \sigma_{\mathrm{X}} = \begin{pmatrix} 0 & 1 \\ 1 & 0 \end{pmatrix} \quad \mathrm{S}(\theta) := \cos(\theta)\cdot\sigma_{\mathrm{Z}} + \sin(\theta)\cdot\sigma_{\mathrm{x}} \rightarrow \begin{pmatrix} \cos(\theta) & \sin(\theta) \\ \sin(\theta) & -\cos(\theta) \end{pmatrix}$$

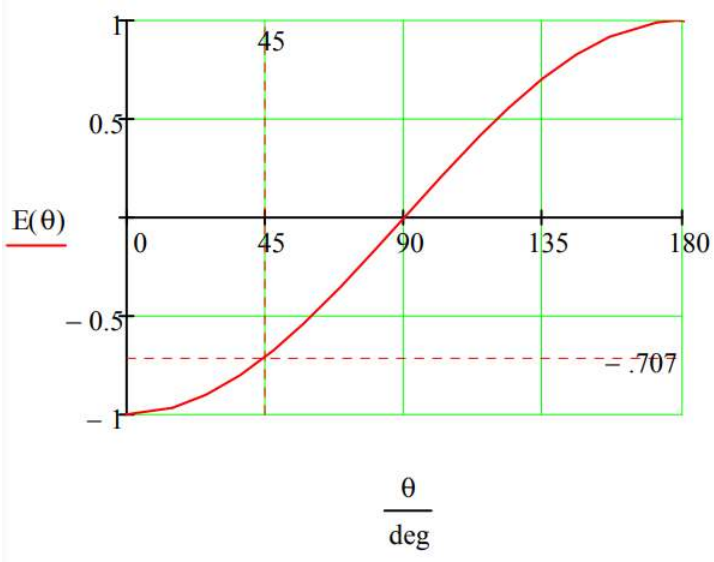
The composite spin operator in the z-direction for A and at an angle θ in the xz-plane for B.

$$S(0)\otimes S(\theta) = \begin{pmatrix} 1 & 0 \\ 0 & -1 \end{pmatrix} \otimes \begin{pmatrix} \cos\theta & \sin\theta \\ \sin\theta & -\cos\theta \end{pmatrix} = \begin{pmatrix} \cos\theta & \sin\theta & 0 & 0 \\ \sin\theta & -\cos\theta & 0 & 0 \\ 0 & 0 & -\cos\theta & -\sin\theta \\ 0 & 0 & -\sin\theta & \cos\theta \end{pmatrix}$$

Calculate and display the expectation value or correlation coefficient.

$$\Psi_m := \frac{1}{\sqrt{2}} \begin{pmatrix} 0 \\ 1 \\ -1 \\ 0 \end{pmatrix}$$

$$E(\theta) := \Psi_m^T \begin{pmatrix} \cos(\theta) & \sin(\theta) & 0 & 0 \\ \sin(\theta) & -\cos(\theta) & 0 & 0 \\ 0 & 0 & -\cos(\theta) & -\sin(\theta) \\ 0 & 0 & -\sin(\theta) & \cos(\theta) \end{pmatrix} \cdot \Psi_m \rightarrow -\cos(\theta)$$



Demonstrate that a hidden-value model that assigns spin orientations in non-orthogonal directions to A and B disagrees with the quantum calculation at 45 degrees.

Particle A	Particle B	$\hat{S}_0(\mathrm{A}) \cdot \hat{S}_0(\mathrm{B})$	$\hat{S}_{45}(\mathrm{A}) \cdot \hat{S}_{45}(\mathrm{B})$	$\hat{S}_0(\mathrm{A}) \cdot \hat{S}_{45}(\mathrm{B})$
$\lvert\uparrow\rangle \lvert\nearrow\rangle$	$\lvert\downarrow\rangle \lvert\swarrow\rangle$	−1	−1	−1
$\lvert\uparrow\rangle \lvert\swarrow\rangle$	$\lvert\downarrow\rangle \lvert\nearrow\rangle$	−1	−1	1
$\lvert\downarrow\rangle \lvert\nearrow\rangle$	$\lvert\uparrow\rangle \lvert\swarrow\rangle$	−1	−1	1
$\lvert\downarrow\rangle \lvert\swarrow\rangle$	$\lvert\uparrow\rangle \lvert\nearrow\rangle$	−1	−1	−1
Realist	Value	−1	−1	0
Quantum	Value	−1	−1	−0.707

Quantum Correlations Illustrated With Photons

A two-stage atomic cascade emits entangled photons (A and B) in opposite directions with the same circular polarization according to observers in their path. The experiment involves the measurement of photon polarization states in the vertical/horizontal measurement basis, and allows for the rotation of the right-hand detector through an angle of θ, in order to explore the consequences of quantum mechanical entanglement. PA stands for polarization analyzer and could simply be a calcite crystal.

$$\begin{array}{ccccccc} V & \triangleleft & \lceil & & & & \rceil \\ & & | & 0 & | & \xleftarrow{A} \text{\xleftrightarrowSource} \xrightarrow{B} & | & \theta & | \\ H & \triangleleft & \lfloor & & \rfloor & & \lfloor & & \rfloor \\ & & & PA_A & & & & PA_B & \end{array} \quad \begin{array}{c} \rceil \\ | \\ \rfloor \end{array} \triangleright \begin{array}{c} V \\ \\ H \end{array}$$

$$|\Psi\rangle = \frac{1}{\sqrt{2}}[|L\rangle_A|L\rangle_B + |R\rangle_A|R\rangle_B] = \frac{1}{\sqrt{2}}[|V\rangle_A|V\rangle_B - |H\rangle_A|H\rangle_B] = \frac{1}{\sqrt{2}} \begin{pmatrix} 1 \\ 0 \\ 0 \\ -1 \end{pmatrix}$$

using

$$|L\rangle = \frac{1}{\sqrt{2}}[|V\rangle + i|H\rangle] \quad |R\rangle = \frac{1}{\sqrt{2}}[|V\rangle - i|H\rangle]$$

Calculate the composite polarization measurement operator for 0 degrees (A) and θ degrees (B):

$$V(\theta) := \begin{pmatrix} \cos(\theta) \\ \sin(\theta) \end{pmatrix} \quad H(\theta) := \begin{pmatrix} -\sin(\theta) \\ \cos(\theta) \end{pmatrix}$$

$$V(\theta) \cdot V(\theta)^{T} - H(\theta) \cdot H(\theta)^{T} \text{ simplify } \rightarrow \begin{pmatrix} \cos(2 \cdot \theta) & \sin(2 \cdot \theta) \\ \sin(2 \cdot \theta) & 2 \cdot \sin(\theta)^2 - 1 \end{pmatrix}$$

$$1 - 2 \cdot \sin(\theta)^2 \text{ simplify } \rightarrow \cos(2 \cdot \theta)$$

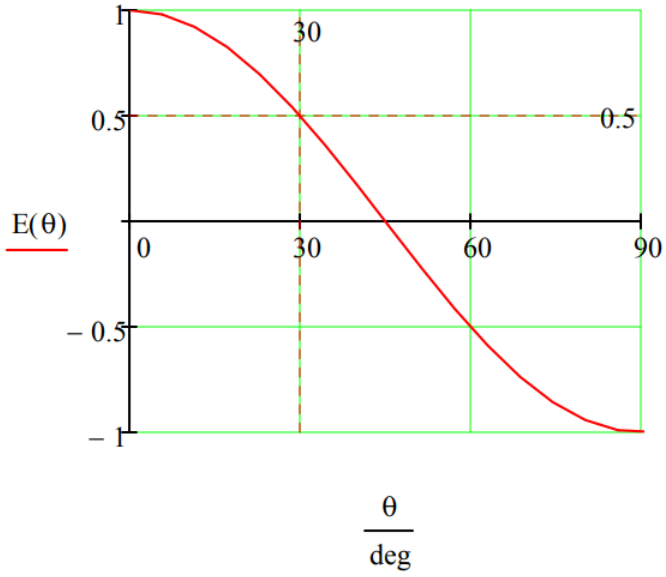
$$\begin{pmatrix} 1 & 0 \\ 0 & -1 \end{pmatrix} \otimes \begin{pmatrix} \cos(2\theta) & \sin(2\theta) \\ \sin(2\theta) & -\cos(2\theta) \end{pmatrix} = \begin{pmatrix} \cos(2\theta) & \sin(2\theta) & 0 & 0 \\ \sin(2\theta) & -\cos(2\theta) & 0 & 0 \\ 0 & 0 & -\cos(2\theta) & -\sin(2\theta) \\ 0 & 0 & -\sin(2\theta) & \cos(2\theta) \end{pmatrix}$$

Calculate and display the expectation value or correlation coefficient.

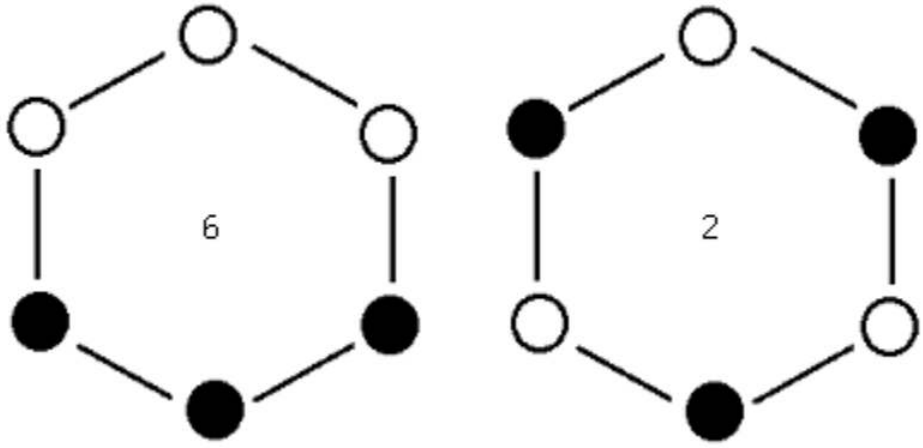
$$\Psi := \frac{1}{\sqrt{2}} \cdot \begin{pmatrix} 1 \\ 0 \\ 0 \\ -1 \end{pmatrix}$$

$$E(\theta) = \Psi^{T} \cdot \begin{pmatrix} \cos(2 \cdot \theta) & \sin(2 \cdot \theta) & 0 & 0 \\ \sin(2 \cdot \theta) & -\cos(2 \cdot \theta) & 0 & 0 \\ 0 & 0 & -\cos(2 \cdot \theta) & -\sin(2 \cdot \theta) \\ 0 & 0 & -\sin(2 \cdot \theta) & \cos(2 \cdot \theta) \end{pmatrix} \cdot \Psi \text{ simplify } \rightarrow \cos(2 \cdot \theta)$$

Quantum expectation value for 30 degrees:



Demonstrate that a hidden-value model that agrees with the 0 and 90 degree quantum expectation values, disagrees with the 30 degree result.



Hidden variable expectation value for 30 degrees:

$$\frac{6\cdot(1-1+1+1-1+1)+2\cdot(-1-1-1-1-1-1)}{8}=0$$

I turn to David Lindley again (*Where Does the Weirdness Go?* page 15) for a concluding comment on the issues dealt with in this section.

We are, through long familiarity, grounded in the assumption of an external, objective, and definite reality, regardless of how much or how little we actually know about it. It is hard to find the language or the concepts to deal with a "reality" that only becomes real when it is measured. There is no easy way to grasp this change of perspective, but persistence and patience allow a certain new familiarity to supplant the old.

Bibliography

- *The Quest for the Quantum Computer*, Julian Brown
- *The Meaning of Quantum Theory*, Jim Baggott
- *Quantum Reality*, Nick Herbert
- *Where Does the Weirdness Go?*, David Lindley
- *The Cosmic Code*, Heinz Pagels
- *Quantum Mechanics and Experience*, David Z Albert
- *Quantum Mechanics*, Alastair Rae
- *Quantum Physics: Illusion or Reality*, Alastair Rae
- *The Quantum Divide*, Gerry and Bruno
- *Quantum Weirdness*, William J. Mullin
- *Through Two Doors at Once*, Anil Ananthaswamy
- *Beyond Weird*, Philip Ball
- *Quantum Physics: What Everyone Needs to Know*, Michael G. Raymer
- *Quantum Theory: A Very Short Introduction*, John Polkinhorne
- *The Quantum Challenge*, Greenstein and Zajonc
- *Quantum Enigma*, Rosenblum and Kuttner
- *Programming the Universe*, Seth Lloyd

This page titled 1.12: Quantum Computation- A Short Course is shared under a CC BY 4.0 license and was authored, remixed, and/or curated by Frank Rioux via source content that was edited to the style and standards of the LibreTexts platform.

1.13: Quantum Mechanics and the Fourier Transform

Wave-particle duality as expressed by the de Broglie wave equation

$$\lambda = \frac{h}{mv} = \frac{h}{p}$$

is the seminal concept of quantum mechanics. On the left side we have the wave property, wavelength, and on the right in a reciprocal relationship mediated by the ubiquitous Planck's constant, we have the particle property, momentum.

Wave and particle are physically incompatible concepts because waves are spatially delocalized, while particles are spatially localized. In spite of this incongruity we find in quantum theory that they are necessary companions in the analysis of atomic and molecular phenomena. Both concepts are required for a complete examination of experiments at the nanoscale level.

This view can be summarized by saying that in quantum-level experiments we always detect particles, but we predict or interpret the experimental outcome by assuming wavelike behavior prior to particle detection. As Bragg once said, "Everything in the future is a wave; everything in the past is a particle." It has also been said that between release and detection particles behave like waves.

Wave-particle duality, a strange dichotomous co-dependency, was first recognized as a permanent feature of modern nanoscience when Niels Bohr proclaimed the complementarity principle as the corner stone of the Copenhagen interpretation of quantum theory. This scientific dogma states, among other things, that there will be no future resolution of the cognitive dissonance that results from analyses that require, at root level, the use of irreconcilable concepts such as wave and particle.

In what follows it will be shown that wave-particle duality leads naturally to other conjugate relationships between traditional physical variables such as position and momentum, and energy and time. The vehicle for this extension will turn out to be the Fourier transform.

To reason mathematically about wave behavior requires a wave function. The one-dimensional, time-independent plane wave expression for a free particle is suitable for this purpose.

$$\exp\left(i2\pi\frac{x}{\lambda}\right)$$

We see that this expression contains the basics of wave-particle duality; x represents position, a particle characteristic, and λ represents wave behavior. Substitution of the de Broglie equation for λ yields one of the most important mathematical functions in quantum mechanics.

$$\exp\left(\frac{ipx}{h}\right)$$

By convention this function is called the momentum eigenfunction in the coordinate representation. We express this in Dirac notation as follows (the normalization constant is ignored for the time being).

$$\langle x|p\rangle = \exp\left(\frac{ipx}{\hbar}\right)$$

Its complex conjugate is the position eigenfunction in the momentum representation.

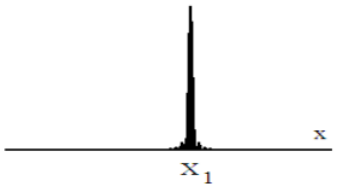
$$\langle p|x\rangle = \langle x|p\rangle^* = \exp\left(\frac{-ipx}{\hbar}\right)$$

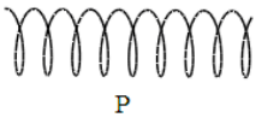
Both expressions are also simple examples of Fourier transforms. They are dictionaries for translating between two different languages or representations. A rudimentary graphical illustration of this ability to translate also provides a concise illustration of the uncertainty principle. (See *The Emperor's New Mind*, by Roger Penrrose, page 246.)

A quon ("A quon is any entity, no matter how immense, that exhibits both wave and particle aspects in the peculiar quantum manner." *Quantum Reality* by Nick Herbert page 64.) with a precise position is represented by a Dirac delta function in coordinate space and a helix in momentum space. If the position is known exactly, the momentum is completely unknown because $|\langle p|x_1\rangle|^2$ is a constant for all values of the momentum. All momentum values have the same probability of being observed.

A quon has position $x_1 : |x_1\rangle$

Coordinate space	$\Leftrightarrow$	Momentum space
$\langle x\|x_1\rangle = \delta(x - x_1)$		$\langle p\|x_1\rangle = \exp\left(-\frac{ipx_1}{\hbar}\right)$



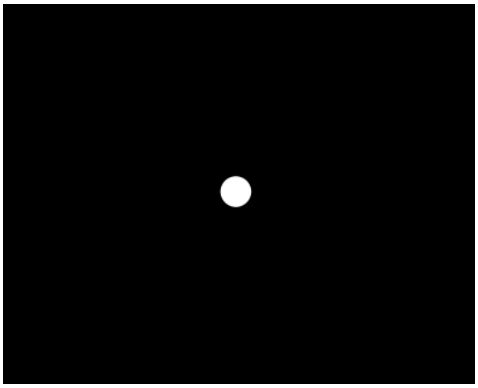


These rudimentary examples of the use of the Fourier transform in quantum mechanics involve infinitesimal points in coordinate and momentum space. To employ the Fourier transform for objects of finite dimensions requires integration over the spatial or momentum dimensions.

For example, suppose we ask what the pattern of diffracted light on a distant screen would look like if a light source illuminated a mask with a single small circular aperture. This, of course, yields the well-known Airy diffraction pattern, which is nothing more than the Fourier transform of the coordinate wave function (the circular aperture) into momentum space. The Airy pattern calculation is given in the following tutorial, along with illustrations of how the radius of the hole illustrates the uncertainty principle.

Calculating the Airy Diffraction Pattern

The Airy diffraction pattern is created by illuminating a screen containing a circular hole with photons. The experiment can be performed with weak sources such that there is only one photon interacting with the screen at a time. This photon-screen interaction constitutes a position measurement.



The position wave function has a constant amplitude within the area of the hole and is shown to be normalized.

$$\Psi(x,y) := \frac{1}{\sqrt{\pi \cdot R^2}} \quad \mathrm{R}^2 = x^2 + y^2 \quad \int_{-R}^{\mathrm{R}} \int_{-\sqrt{\mathrm{R}^2-\mathrm{x}^2}}^{\sqrt{\mathrm{R}^2-\mathrm{x}^2}} \Psi(\mathrm{x},\mathrm{y})^2 \mathrm{dydx} = 1$$

The Airy diffraction pattern is the Fourier transform of the position wave function into the momentum representation. In other words, the interference pattern at the detection screen actually represents a momentum measurement. The following calculations are carried out in atomic units using a hole radius of 0.2.

Hole radius: $R := 0.2$

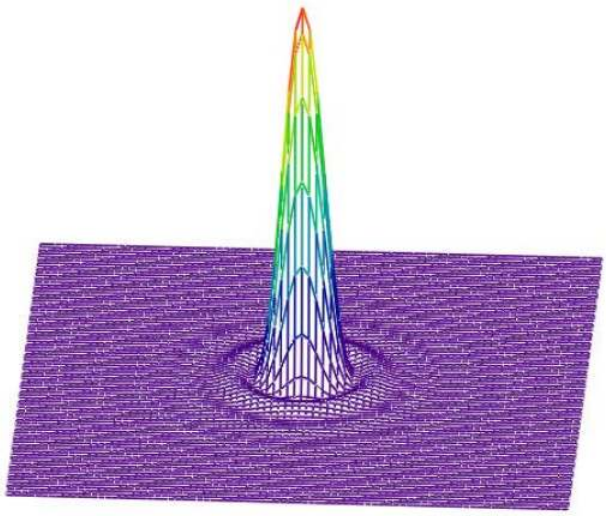
Calculate the Airy diffraction pattern:

$$\Delta := 100 \quad \mathrm{N} := 80 \quad \mathrm{j} := 0 \ldots \mathrm{N} \quad \mathrm{p_{x_j}} = -\Delta + \frac{2 \cdot \Delta \cdot \mathrm{j}}{\mathrm{N}} \quad \mathrm{k} := 0 \ldots \mathrm{N} \quad \mathrm{p_{y_k}} := -\Delta + \frac{2 \cdot \Delta \cdot \mathrm{k}}{\mathrm{N}}$$

$$\Phi(\mathrm{p_x}, \mathrm{p_y}) := \frac{1}{\pi} \cdot \int_{-\mathrm{R}}^{\mathrm{R}} \int_{-\sqrt{\mathrm{R}^2-\mathrm{x}^2}^2}^{\sqrt{\mathrm{R}^2-\mathrm{x}^2}^2} \frac{1}{\sqrt{\pi \cdot \mathrm{R}^2}} \cdot \exp(-\mathrm{i} \cdot \mathrm{p_x} \cdot \mathrm{x}) \cdot \exp(-\mathrm{i} \cdot \mathrm{p_y} \cdot \mathrm{y})\, dy\, dx$$

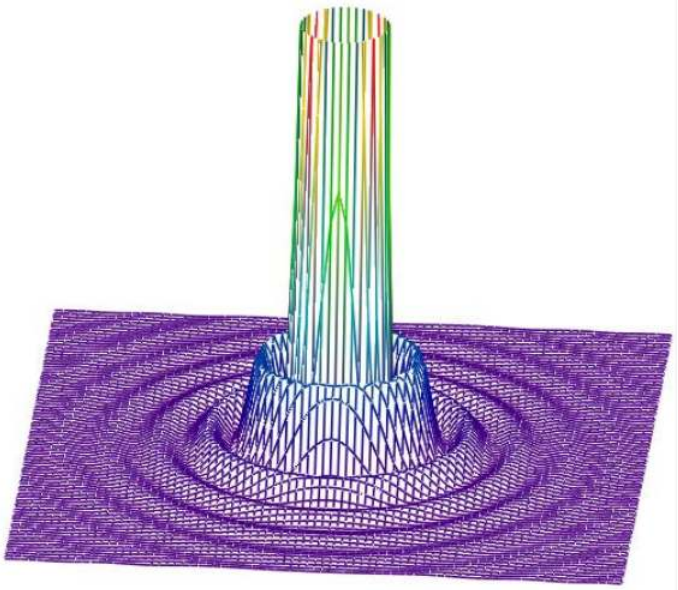
$$\mathrm{P_{j,k}} := \left(|\Phi \mathrm{p_{x_j}}, \mathrm{p_{y_k}})|\right)^2$$

Display the Airy diffraction pattern.



P

Truncating the high intensity central disk provides a better picture of the outer maxima and minima.

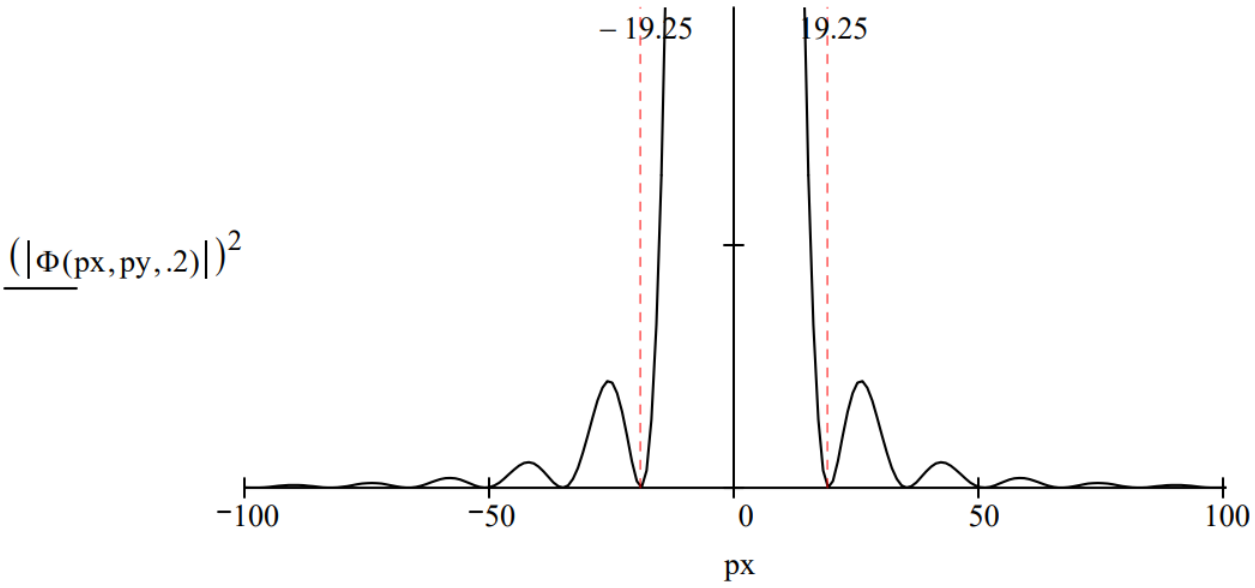


P

Examining a radial slice of the Airy diffraction pattern provides a simple illustration of the uncertainty principle. Assume that the position uncertainty is given by the diameter of the hole and that the momentum uncertainty is given by the momentum range of the central disk.

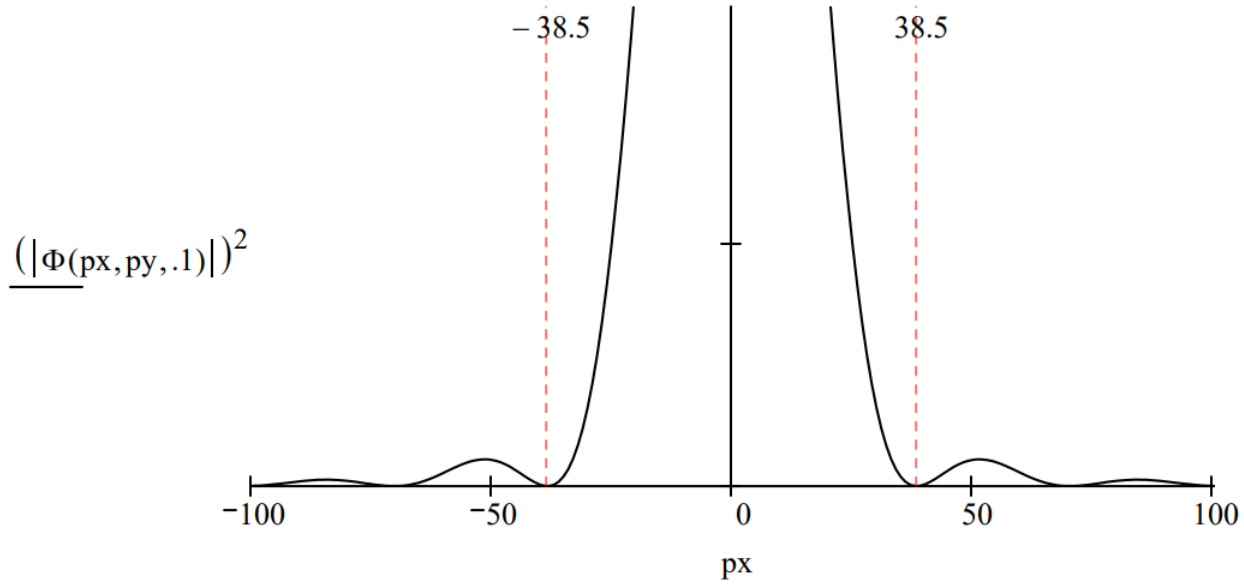
$$\text{py} := 0 \quad \text{px} := -100, -99$$

$$\ldots 100 \quad \Phi(\text{px}, \text{py}, \text{R}) := \frac{1}{\pi} \cdot \int_{-\text{R}}^{\text{R}} \int_{-\sqrt{\text{R}^2-\text{x}^2}}^{\sqrt{\text{R}^2-\text{x}^2}} \frac{1}{\sqrt{\pi \cdot \text{R}^2}} \cdot \exp(-\text{i} \cdot \text{px} \cdot \text{x}) \cdot \exp(-\text{i} \cdot \text{py} \cdot \text{y}) dy\, dx$$



For a diameter of 0.4 the position-momentum uncertainty product is:

$$0.4 \cdot 38.5 = 15.4$$



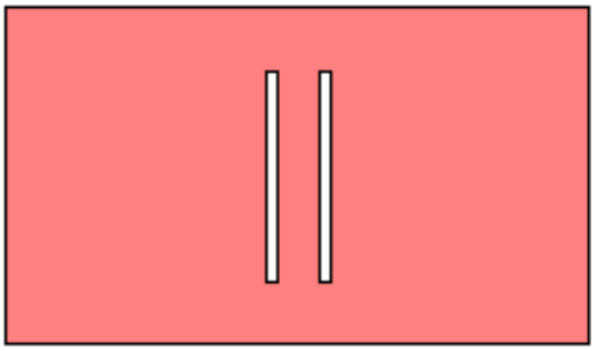
For a diameter of 0.2 the position-momentum uncertainty product is:

$$0.2 \cdot 77.0 = 15.4$$

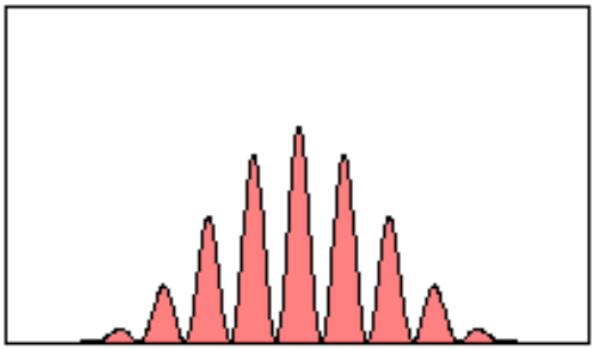
The reciprocal relationship between the uncertainty in position and momentum is clearly revealed in this example.

The Double-Slit Experiment

Slit Screen



Diffraction Pattern



Coordinate wave function:

$$|\Psi\rangle = \frac{1}{\sqrt{2}}[|x_1\rangle + |x_2\rangle]$$

Momentum wave function for infinitesimally thin slits:

$$\langle p|\Psi\rangle = \frac{1}{\sqrt{2}}[\langle p|x_1\rangle + \langle p|x_2\rangle] = \frac{1}{2\sqrt{\pi}}\left[\exp\left(-\frac{ipx_1}{\hbar}\right) + \exp\left(-\frac{ipx_2}{\hbar}\right)\right]$$

Position of first slit:

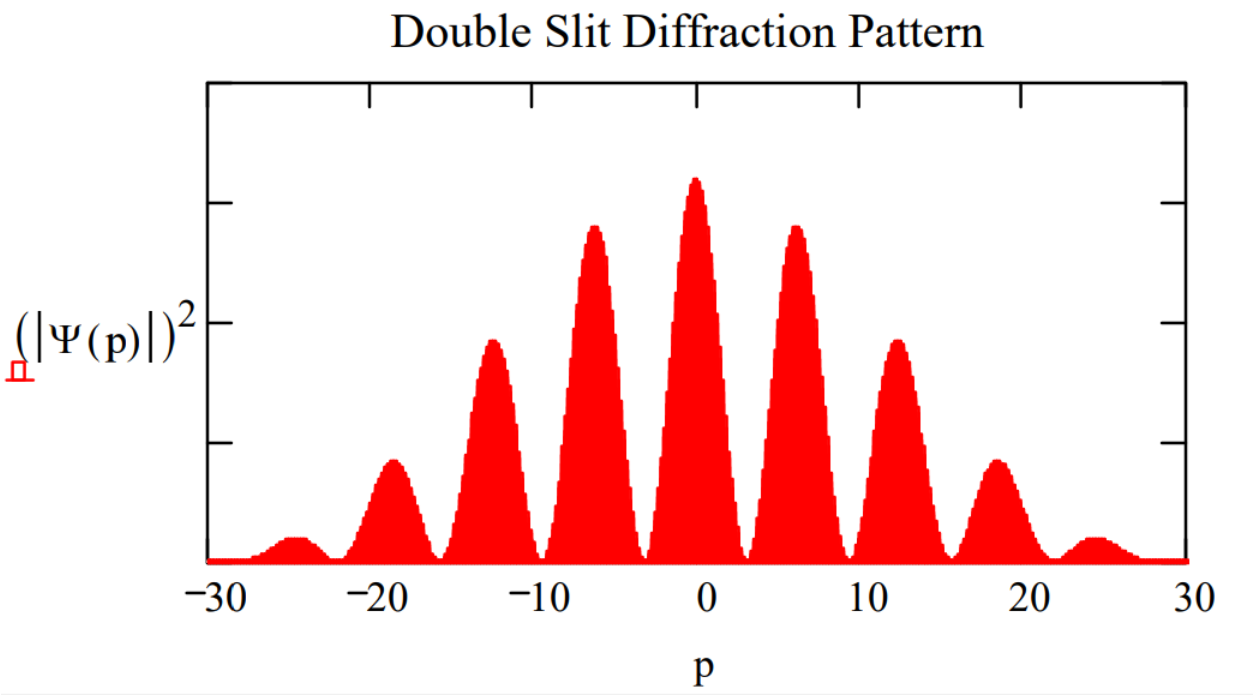
$$x_1 := 0$$

Position of second slit:

$$x_2 := 1$$

Momentum wave function for finite slits:

$$\Psi(p) := \frac{\int_{x_1-\frac{\delta}{2}}^{x_1+\frac{\delta}{2}} \frac{1}{\sqrt{2\cdot\pi}} \cdot \exp(-i \cdot p \cdot x) \cdot \frac{1}{\sqrt{\delta}} dx + \int_{x_2-\frac{\delta}{2}}^{x_2+\frac{\delta}{2}} \frac{1}{\sqrt{2\cdot\pi}} \cdot \exp(-i \cdot p \cdot x) \cdot \frac{1}{\sqrt{\delta}} dx}{\sqrt{2}}$$

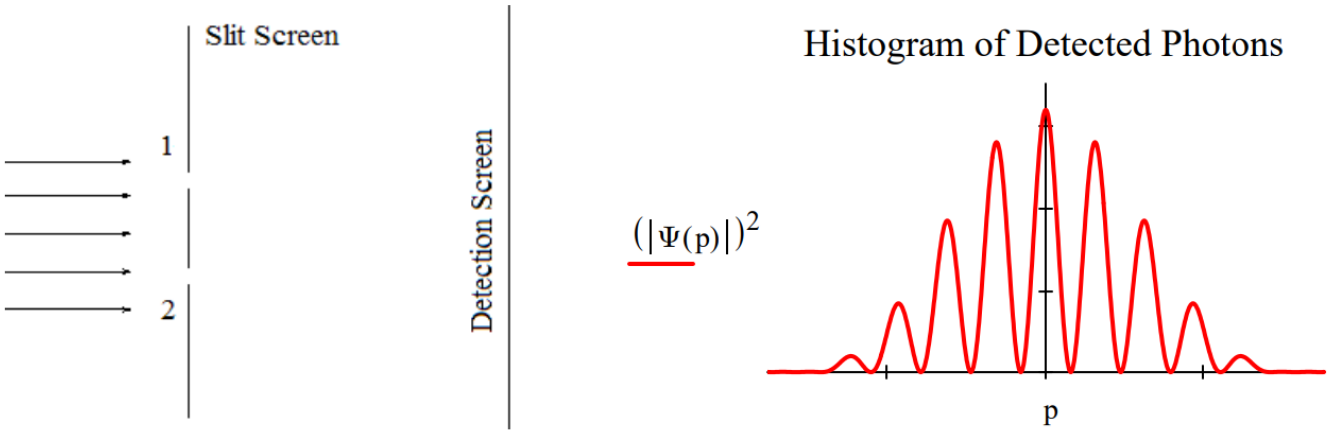


According to the *Encyclopedia Britannica*, Fresnel and Arago "using an apparatus based on Young's experiment" observed that "two beams polarized in mutually parallel planes never yield fringes." In the following tutorial this phenomenon is examined from the quantum mechanical perspective and a critique of the concept of the quantum eraser is provided.

Which Path Information and the Quantum Eraser

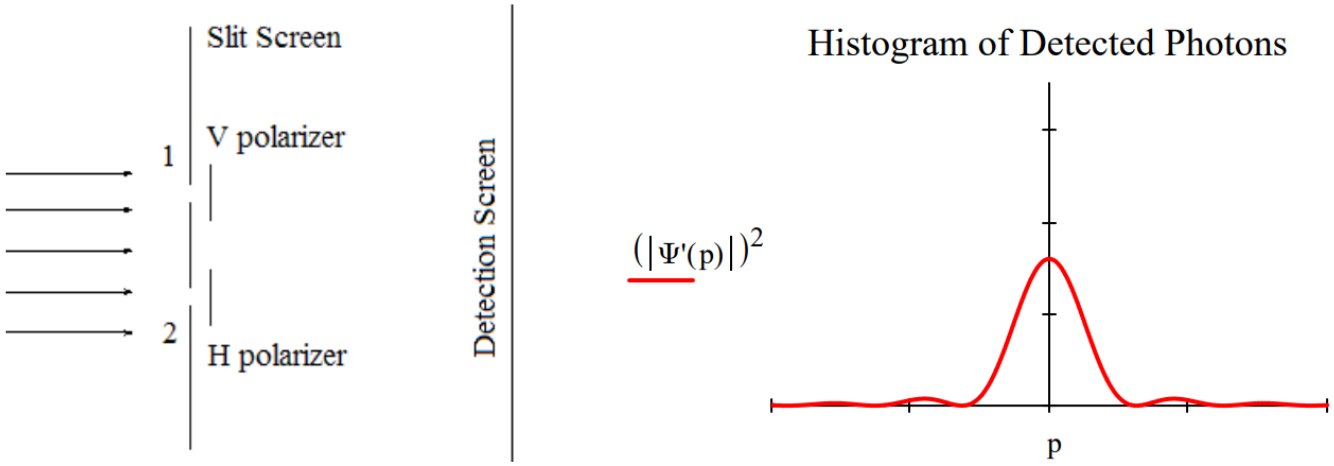
This tutorial examines the **real** reason which-path information destroys the double-slit diffraction pattern and how the so-called "quantum eraser" restores it. The wave function for a photon illuminating the slit screen is written as a superposition of the photon being present at both slits simultaneously. The double-slit diffraction pattern is calculated by projecting this superposition into momentum space. This is a Fourier transform for which the mathematical details can be found in the Appendix.

$$|\Psi\rangle = \frac{1}{\sqrt{2}}[|x_1\rangle + |x_2\rangle] \qquad \Psi(p) = \langle p|\Psi\rangle = \frac{1}{\sqrt{2}}[\langle p|x_1\rangle + \langle p|x_2\rangle]$$



Attaching polarizers to the slits creates an entangled superposition of the photon being at slit 1 with vertical polarization and at slit 2 with horizontal polarization. This leads to the following momentum distribution at the detection screen. The interference fringes have disappeared leaving a single-slit diffraction pattern.

$$|\Psi'\rangle = \frac{1}{\sqrt{2}}[|x_1\rangle|V\rangle + |x_2\rangle|H\rangle] \qquad \Psi'(p) = \langle p|\Psi'\rangle = \frac{1}{\sqrt{2}}[\langle p|x_1\rangle|V\rangle + \langle p|x_2\rangle|H\rangle]$$

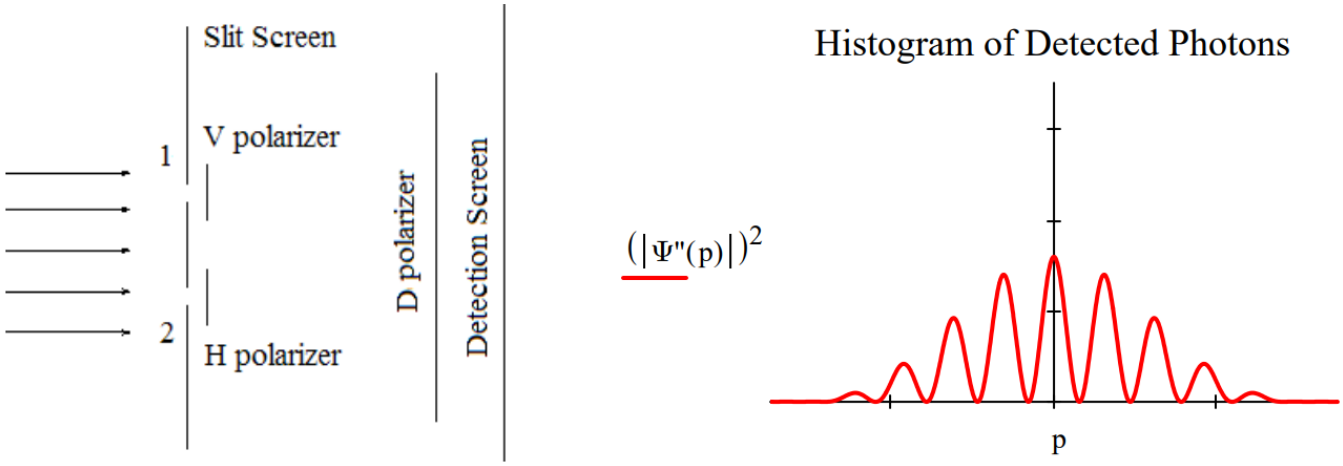


The usual explanation for this effect is that it is now possible to know which slit the photons went through, and that such knowledge destroys the interference fringes because the photons are no longer in a superposition of passing through both slits, but rather a mixture of passing through one slit or the other.

However, a better explanation is that the superposition persists with orthogonal polarization tags, and because of this the interference (cross) terms in the momentum distribution, $|\Psi'(p)|^2$, vanish leaving a pattern at the detection screen which is the sum of two single-slit diffraction patterns, one from the upper slit and the other from the lower slit.

That this is a reasonable interpretation is confirmed when a so-called quantum eraser, a polarizer (D) rotated clockwise by 45 degrees relative to the vertical, is placed before the detection screen.

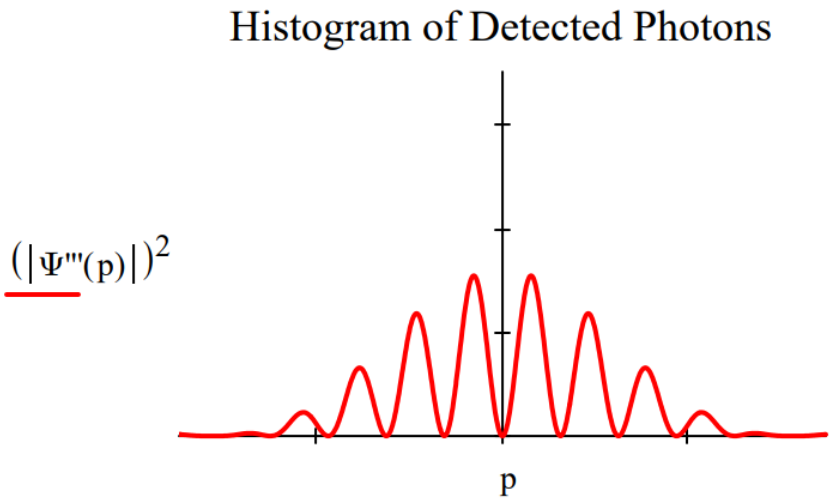
$$\Psi''(p) = \langle D|\Psi'(p)\rangle = \frac{1}{\sqrt{2}}[\langle p|x_1\rangle\langle D|V\rangle + \langle p|x_2\rangle\langle D|H\rangle] = \frac{1}{2}[\langle p|x_1\rangle + \langle p|x_2\rangle]$$



The diagonal polarizer is called a quantum eraser because it appears to restore the interference pattern lost because of the which-path information provided by the V/H polarizers. However, it is clear from this analysis that the diagonal polarizer doesn't actually erase, it simply passes the diagonal component of $|\Psi'\rangle$ which then shows an attenuated (by half) version of the original interference pattern produced by $|\Psi\rangle$.

Placing an anti-diagonal polarizer (rotated counterclockwise by 45 degrees relative to the vertical) before the detection screen causes a 180 degree phase shift in the restored interference pattern.

$$\Psi''(p) = \langle A|\Psi'(p)\rangle = \frac{1}{\sqrt{2}}[\langle p|x_1\rangle\langle A|V\rangle + \langle p|x_2\rangle\langle A|H\rangle] = \frac{1}{2}[\langle p|x_1\rangle - \langle p|x_2\rangle]$$



This phase shift is inconsistent with any straightforward explanation based on the concept of erasure of which-path information. Erasure implies removal of which-path information. If which-path information has been removed shouldn't the original interference pattern be restored without a phase shift?

Appendix:

The V/H polarization which-path tags and the D/A polarization "erasers" in vector format:

$$|\mathrm{V}\rangle = \begin{pmatrix} 1 \\ 0 \end{pmatrix} \quad |\mathrm{H}\rangle = \begin{pmatrix} 0 \\ 1 \end{pmatrix} \quad |\mathrm{D}\rangle = \frac{1}{\sqrt{2}}\begin{pmatrix} 1 \\ 1 \end{pmatrix} \quad |\mathrm{A}\rangle = \frac{1}{\sqrt{2}}\begin{pmatrix} 1 \\ -1 \end{pmatrix}$$

$$\langle \mathrm{D}|\mathrm{V}\rangle = \langle \mathrm{D}|\mathrm{H}\rangle = \langle \mathrm{A}|\mathrm{V}\rangle = \frac{1}{\sqrt{2}} \quad \langle \mathrm{A}|\mathrm{H}\rangle = -\frac{1}{\sqrt{2}}$$

For infinitesimally thin slits the momentum-space wave function is,

$$\Psi(p) = \langle p|\Psi\rangle = \frac{1}{\sqrt{2}}[\langle p|x_1\rangle + \langle p|x_2\rangle] = \frac{1}{\sqrt{2}}\left[\frac{1}{\sqrt{2\pi}}\exp(-ipx_1) + \frac{1}{\sqrt{2\pi}}\exp(-ipx_2)\right]$$

Assuming a slit width δ the calculations of $\Psi(p), \Psi'(p), \Psi''(p)$ and $\Psi'''(p)$ are carried out as follows:

Position of first slit: $x_1 \equiv 0$	Position of second slit: $x_2 \equiv 1$	Slit width: $\delta \equiv 0.2$

$$\Psi(p) \equiv \frac{1}{\sqrt{2}} \cdot \left(\int_{x_1-\frac{\delta}{2}}^{x_1+\frac{\delta}{2}} \frac{1}{\sqrt{2\cdot\pi}} \cdot \exp(-i\cdot p\cdot x)\cdot\frac{1}{\sqrt{\delta}}dx + \int_{x_2-\frac{\delta}{2}}^{x_2+\frac{\delta}{2}} \frac{1}{\sqrt{2\cdot\pi}} \cdot \exp(-i\cdot p\cdot x)\cdot\frac{1}{\sqrt{\delta}}dx\right]$$

For $\Psi'(p)$ the V/H polarization which-path tags are added to the two terms of $\Psi(p)$

$$\Psi'(\mathrm{p}) \equiv \frac{1}{\sqrt{2}} \cdot \left[\int_{\mathrm{x}_1-\frac{\delta}{2}}^{\mathrm{x}_1+\frac{\delta}{2}} \frac{1}{\sqrt{2\cdot\pi}} \cdot \exp(-\mathrm{i}\cdot\mathrm{p}\cdot\mathrm{x})\cdot\frac{1}{\sqrt{\delta}}\mathrm{dx}\cdot\begin{pmatrix}1\\0\end{pmatrix} + \int_{x_2-\frac{\delta}{2}}^{x_2+\frac{\delta}{2}} \frac{1}{\sqrt{2\cdot\pi}} \cdot \exp(-\mathrm{i}\cdot\mathrm{p}\cdot\mathrm{x})\cdot\frac{1}{\sqrt{\delta}}\mathrm{dx}\cdot\begin{pmatrix}0\\1\end{pmatrix}\right]$$

$\Psi''(p)$ is the projection of $\Psi'(p)$ onto a diagonal polarizer $\langle D|$.

$$\Psi''(\mathrm{p}) \equiv \frac{1}{\sqrt{2}} \cdot \begin{pmatrix}1\\1\end{pmatrix}^{\mathrm{T}} \cdot \Psi'(\mathrm{p})$$

$\Psi'''(p)$ is the projection of $\Psi'(p)$ onto an anti-diagonal polarizer $\langle A|$.

$$\Psi'''(\mathrm{p}) \equiv \frac{1}{\sqrt{2}} \cdot \begin{pmatrix}1\\-1\end{pmatrix}^{\mathrm{T}} \cdot \Psi'(\mathrm{p})$$

Rewriting $\Psi'(p)$ in terms of $|D\rangle$ and $|A\rangle$ clearly shows the origin of the phase difference between the $(|\Psi''(\mathrm{p})|)^2$ and $(|\Psi'''(\mathrm{p})|)^2$ interference patterns.

$$\Psi'(p) = \langle p|\Psi'\rangle = \frac{1}{2}[\langle p|x_1\rangle + \langle p|x_2\rangle)|D\rangle + (\langle p|x_1\rangle - \langle p|x_2\rangle)|A\rangle]$$

This page titled 1.13: Quantum Mechanics and the Fourier Transform is shared under a CC BY 4.0 license and was authored, remixed, and/or curated by Frank Rioux via source content that was edited to the style and standards of the LibreTexts platform.

1.14: Quantum Mechanics and the Fourier Transform

However, just as with the circular aperture (Airy pattern) a single slit also yields a diffraction pattern when illuminated. Both are examples of the superposition principle because the photons that arrive at the detection screen can get there from any points within the aperture or slit. So, in general, we calculate the diffraction pattern by a Fourier transform of the coordinate space geometry, slit or circle or something more complicated. The following tutorial explores single-slit diffraction and the uncertainty principle.

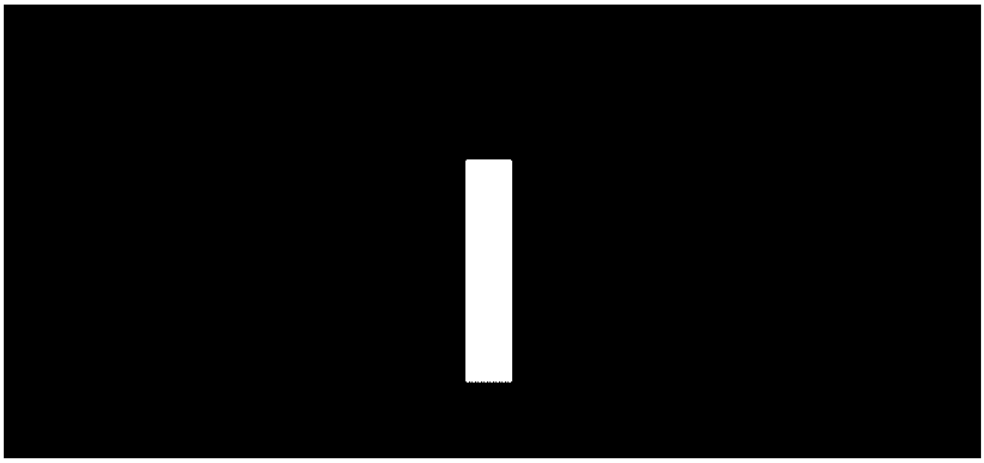
A Quantum Mechanical Interpretation of Single-slit Diffraction

Diffraction has a simple quantum mechanical interpretation based on the uncertainty principle. Or we could say diffraction is an excellent way to illustrate the uncertainty principle.

A screen with a single slit of width, w, is illuminated with a coherent photon or particle beam. The normalized coordinate-space wave function at the slit screen is,

$$\mathrm{w} := 1 \qquad \Psi(\mathrm{x},\mathrm{w}) := \mathrm{if}\left[\left(\mathrm{x} \geq -\frac{\mathrm{w}}{2}\right)\cdot\left(\mathrm{x} \leq \frac{\mathrm{w}}{2}\right), \frac{1}{\sqrt{\mathrm{w}}}, 0\right] \qquad \mathrm{x} := \frac{-\mathrm{w}}{2}, \frac{-\mathrm{w}}{2} + 0.005 \ldots \frac{\mathrm{w}}{2}$$

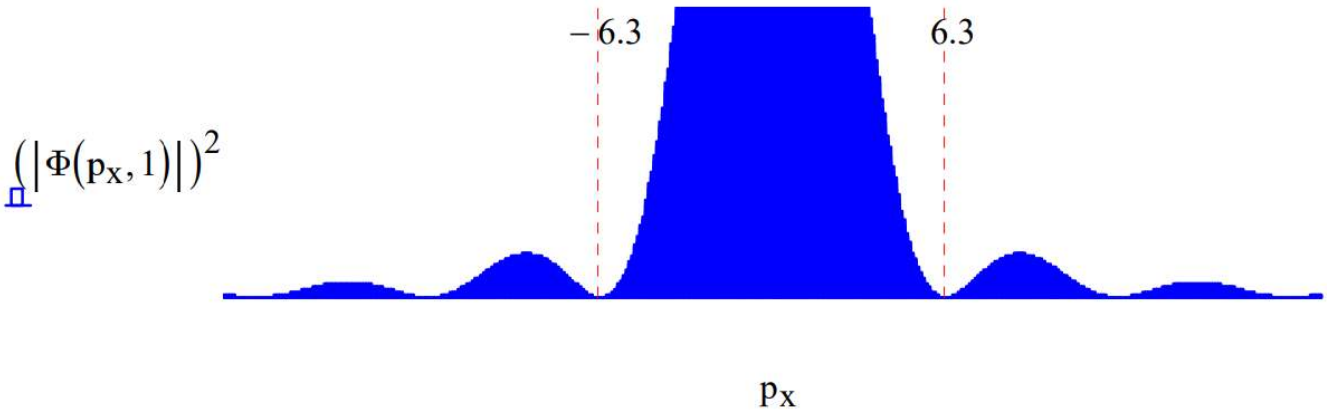
The coordinate-space probability density, $|\Psi(x,w)|^2$, is displayed for a slit of unit width below



The slit-screen measures position, it localizes the incident beam in the x-direction. According to the uncertainty principle, because position and momentum are complementary, or conjugate, observables, this measurement must be accompanied by a delocalization of the x-component of the momentum. This can be seen by a Fourier transform of $\Psi(x,w)$ into momentum space to obtain the momentum wave function, $\Phi(p_x,w)$.

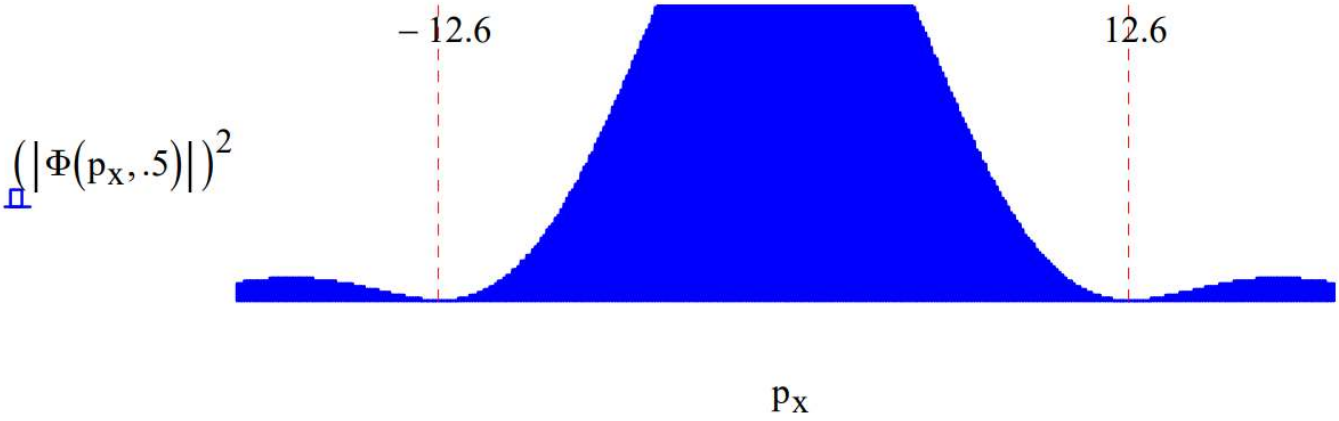
$$\Phi\left(\mathrm{p_x},\mathrm{w}\right) := \frac{1}{\sqrt{2\cdot\pi}}\cdot\int_{-\frac{\mathrm{w}}{2}}^{\frac{\mathrm{w}}{2}} \exp\left(-\mathrm{i}\cdot\mathrm{p_x}\cdot\mathrm{x}\right)\cdot\frac{1}{\sqrt{\mathrm{w}}}\mathrm{dx}\ \mathrm{simplify}\ \rightarrow \frac{\sqrt{2}\cdot\sin\left(\frac{\mathrm{p_x}\cdot\mathrm{w}}{2}\right)}{\sqrt{\pi}\cdot\mathrm{p_x}\cdot\sqrt{\mathrm{w}}}$$

It is the momentum distribution, $|\Phi(p_x,w)|^2$, shown histographically below that is projected onto the detection screen. Thus, a position measurement at the detection screen is also effectively a measure of the x-component of the particle momentum.

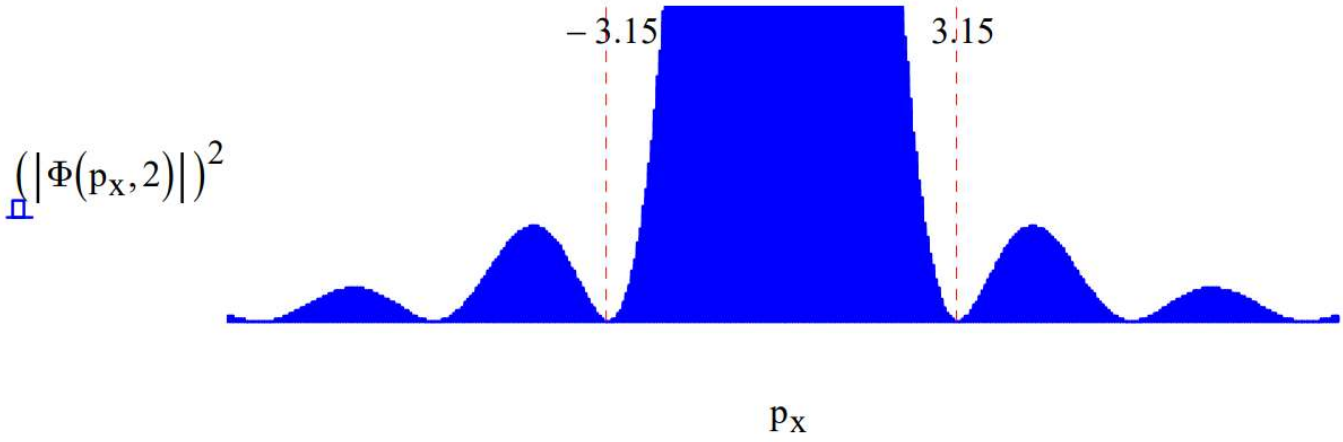


In this figure we see the spread in momentum required by the uncertainty principle, plus interference fringes due to the fact that the incident beam can imerge from any where within the slit, allowing for constructive and destructive interference at the detection screen. If the slit width is decreased the position is more precisely known and the uncertainty principle demands a broadening in the momentum distribution as shown below.

Equating uncertainty in position with slit width and uncertainty in momentum with the width of the intense center of the diffraction pattern, we have in atomic units: $\Delta x \Delta p_x = 12.6$. If the slit width is decreased the position is more precisely known and the uncertainty principle demands a broadening in the momentum distribution as shown below. For slit width 0.5 we again find the product of the uncertainties is 12.6.



Naturally if the slit width is increased to 2.0 the position uncertainty increases and the uncertainty in momentum decreases yielding again $\Delta x \Delta p_x = 12.6$.

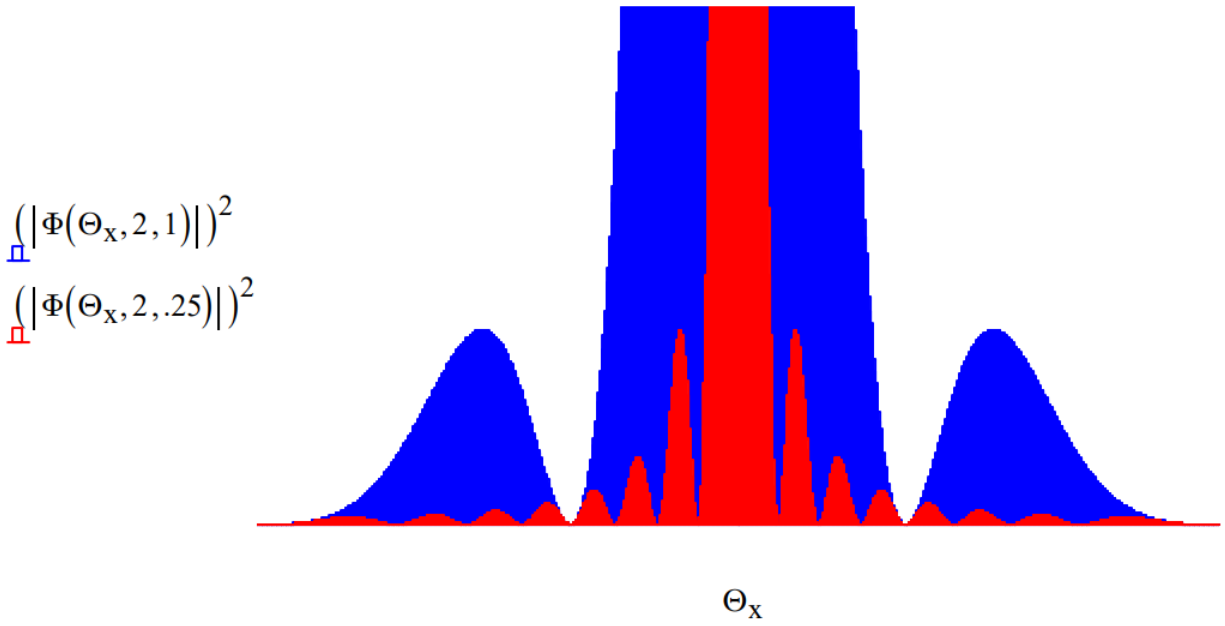


The x-direction momentum can be expressed in terms of the wavelength of the illuminating beam and the diffraction angle using the following sequence of equations of which the second is the de Broglie relation in atomic units (h = 2π).

$$p_x = p \cdot \sin(\Theta) \qquad p = \frac{2 \cdot \pi}{\lambda} \qquad p_x = \frac{2 \cdot \pi}{\lambda} \cdot \sin(\Theta)$$

$$\Phi(\Theta_x, w, \lambda) := \sqrt{\frac{2}{\pi \cdot w}} \cdot \cdot \frac{\sin\left(\frac{\pi \cdot w}{\lambda} \cdot \sin(\Theta_x)\right)}{\frac{2 \cdot \pi}{\lambda} \cdot \sin(\Theta_x)}$$

This allows one to explore the effect of the wavelength of the illuminating beam on the diffraction pattern. The figure below shows that a short wavelength (high momentum) illuminating beam gives rise to a narrower diffraction pattern.



The method used here to calculate single-slit diffraction patterns (momentum-space distribution functions) is easily extended to multiple slits, and also to diffraction at two-dimensional masks with a variety of hole geometries.

Relevant Literature:

Primary source: "Quantum interference with slits," Thomas Marcella which appeared in *European Journal of Physics* **23**, 615-621 (2002).

See also: "Calculating diffraction patterns," F. Rioux in *European Journal of Physics*, **24**, N1-N3 (2003). "Using Optical Transforms to Teach Quantum Mechanics," F. Rioux; B. J. Johnson, *The Chemical Educator*, **9**, 12-16 (2004). "Single-slit Diffraction and the Uncertainty Prinicple," F. Rioux in Journal *of Chemical Education*, **82**, 1210 (2005).

"Experimental verification of the Heisenberg uncertainty principle for hot fullerene molecules", O. Nairz, M. Arndt, and A. Zeilinger, *Phys. Rev. A*, **65**, 032109 (2002).

"Introducing the Uncertainty Principle Using Diffraction of Light Waves," Pedro L. Muino, *Journal of Chemical Education*, **77**, 1025-1027 (2000).

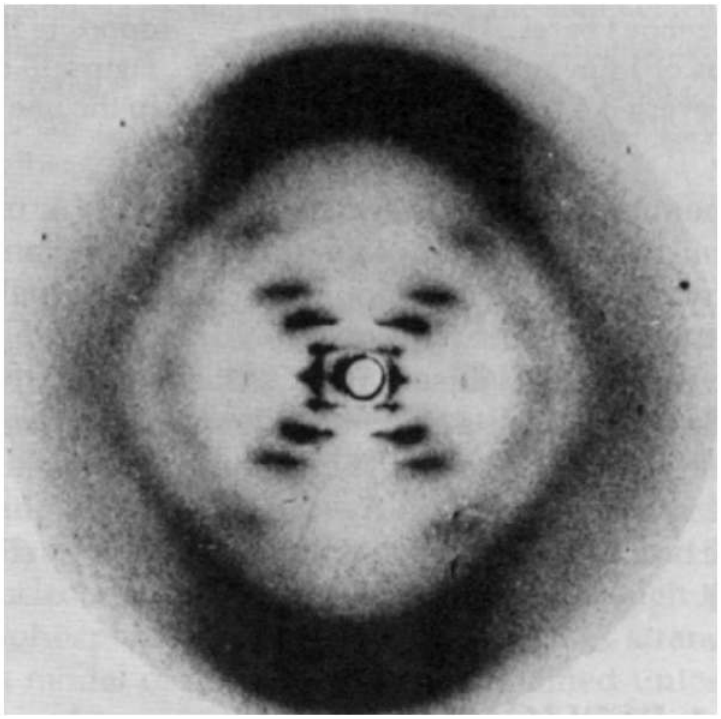
The next link shows how the methods used to examine these relatively simple cases can be expanded to more interesting geometries, including the DNA double helix. The following tutorial provides details regarding a simple simulation of the DNA diffraction pattern.

Simulating the DNA Diffraction Pattern

The publication of the DNA double-helix structure by x-ray diffraction in 1953 is one the most significant scientific events of the 20th century (1). Therefore, it is important that science students and their teachers have some understanding of how this great

achievement was accomplished. X-ray diffraction is conceptually simple: a source of X-rays illuminates a sample which scatters the x-rays, and a detector records the arrival of the scattered x-rays (diffraction pattern). However, the mathematical analysis required to extract from diffraction pattern the molecular geometry of the sample that caused the diffraction pattern is quite formidable. Therefore, the purpose of this tutorial is to illustrate some of the elements of the mathematical analysis required to solve a structure.

The famous X-ray diffraction pattern obtained by Rosalind Franklin is shown below (2).



This X-ray picture stimulated Watson and Crick to propose the now famous double-helix sturcture for DNA. It was surely fortuitous that Crick had recently completed an unrelated study of the diffraction patterns of helical molecules (3).

To gain some understanding of how the experimental pattern led to the hypothesis of a double-helical structure we will work in reverse. We will assume the double-helix structure, calculate the diffraction pattern, and compare it with the experimental result. This, therefore, is a deductive exercise as opposed to the brilliant inductive accomplishment of Watson and Crick in determining the DNA structure from Franklin's experimental X-ray pattern.

The experimental pattern will be simulated by modeling DNA solely as a planar double strand of sugar-phosphate backbone groups shown below. Reference 4 provides the justification and the limitations in using two-dimensional models for three-dimensional structures when simulating X-ray diffraction experiments.

The double-strand geometry shown below was created using the following mathematics. Calculations are carried out in atomic units.

Sugar-phosphate groups per strand: $A := 20$	Strand radius: $R := 1$	Phase difference between strands: $0.8 \cdot \pi$

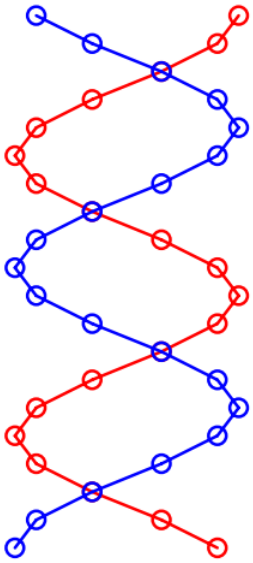
First strand:

$$m := 1 \ldots A \quad \Theta_m := \frac{4 \cdot \pi \cdot m}{A} \quad y_m := m \quad x_m := R \cdot \cos(\Theta_m)$$

Second strand:

$$m := 21 \ldots 40 \quad \Theta_m := \frac{4 \cdot \pi \cdot (m - A)}{A} \quad y_m := (m - A) \quad x_m := R \cdot \cos(\Theta_m + 0.8 \cdot \pi)$$

$$m := 1 \ldots 20 \quad n := 21 \ldots 40$$



According to quantum mechanical principles, the photons illuminating this geometrical arrangement interact with all its members simultaneously thus being cast into the spatial superposition, Ψ, given below.

$$|\Psi\rangle = \frac{1}{\sqrt{N}} \sum_{i=1}^{N} |x_i, y_i\rangle$$

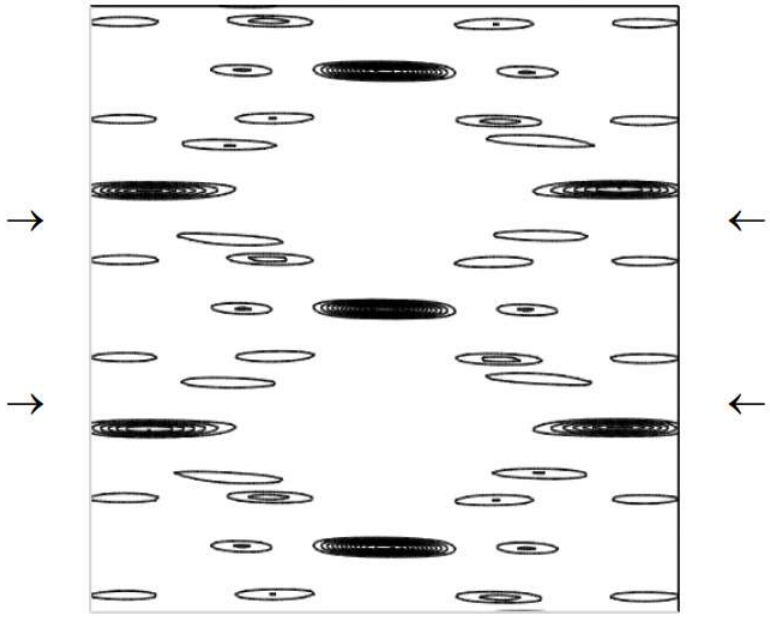
This spatial wave function is then projected into momentum space by a Fourier transform to yield the theoretical diffraction pattern. What is measured at the detector according to quantum mechanics is the two-dimensional momentum distribution created by the spatial localization that occurs during illumination of the structure. If the sugar-phosphate groups are treated as point scatterers the momentum wave function is given by the following Fourier transform.

$$\Phi\left(p_x, p_y\right) := \frac{1}{2 \cdot \pi} \cdot \sum_{m=1}^{40} \exp\left(-i \cdot p_x \cdot x_m\right) \cdot \exp\left(-i \cdot p_y \cdot y_m\right)$$

The theoretical diffraction pattern can now be displayed as the absolute magnitude squared of the momentum wave function.

$$\Delta := 8 \quad N := 200 \quad j := 0 \ldots N \quad p_x := -\Delta + \frac{2 \cdot \Delta \cdot j}{N} \quad k := 0 \ldots N \qquad p_y := -\Delta + \frac{2 \cdot \Delta \cdot k}{N}$$

$$\text{DiffractionPattern}_{j,k} := \left(\left|\Phi\left(p_{x_j}, p_{y_k}\right)\right|\right)^2$$



DiffractionPattern

Clearly the naive model diffraction pattern presented here captures several important features of the experimental diffraction pattern. Among those are the characteristic X-shaped cross of the diffraction pattern and the missing fourth horizontal layer (indicated by arrows).

Lucas, Lisensky, and co-workers (4, 5) have simulated the DNA diffraction pattern using the optical transform method. This tutorial might therefore be considered to be a theoretical companion to their more empirical approach to the subject.

References:

1. Watson, J. D.; Crick, F. H. C. *Nature* **1953**, 171, 737.
2. Franklin, R. E.; Gosling, R. G. *Nature* **1953**, 171, 740.
3. Cochran, W.; Crick, F. H. C.; Vand, V. *Acta Crystallogr*. **1952**, 5, 581.
4. Lucas, A. A.; Lambin, Ph.; Mairesse, R.; Mathot, M. *J. Chem. Educ*. **1999**, 76, 378.
5. Lisensky, G. C.; Lucas, A. A.; Nordell, K. J.; Jackelen, A. L.; Condren, S. M.; Tobe, R. H.; Ellis, A. B. DNA Optical Transform Kit; Institute for Chemical Education: University of Wisconsin, WI, 1999.

A brief discussion of the impact of rotational symmetry in determining diffraction patterns and the concept of the quasi-crystal can be found at the following tutorial.

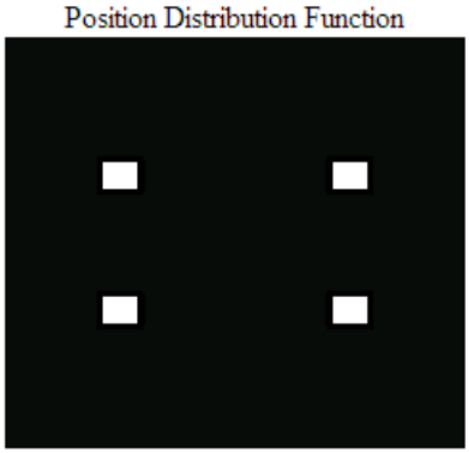
Crystal Structure, Rotational Symmetry and Quasicrystals

Prior to 1991 crystals were defined to be solids having only 2-, 3-, 4- and 6-fold rotational symmetry because only these rotational symmetries have the required translational periodicity to build the long-range order of a crystalline solid. Long-range order is synonymous with periodicity, requiring some unit structure which repeats itself by translation in all directions infinitely. It is easy to demonstrate that a pentagon, with 5-fold rotational symmetry cannot be used as a unit cell to create long-range order in a plane or in three-dimensions.

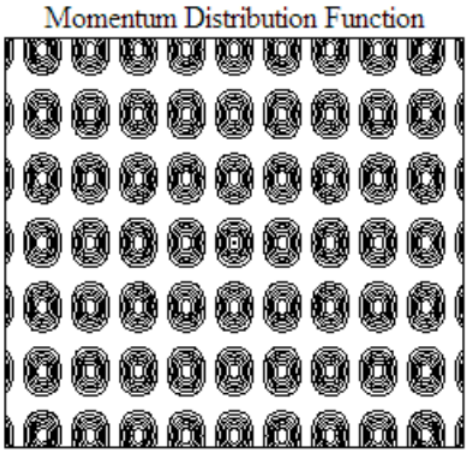
The justification for this definition was that solid structures with 2-, 3-, 4- and 6-fold rotational symmetry yield discrete diffraction patterns that also have translational periodicity. Another way to put this is to say that solid structures with 2-, 3-, 4- and 6-fold rotational symmetry have reciprocal lattices that also have translational periodicity. Yet, another way to put this, of course, is that the Fourier transforms of geometries with 2-, 3-, 4- and 6-fold rotational symmetry yield lattice-like momentum distributions with translational periodicity. This latter statement is preferred by the author because it emphasizes that diffraction patterns are actually the momentum distributions of the diffracted particles.

The key in this latter interpretation is that diffraction experiments involve an initial spatial localization of the radiation through interaction with the crystal lattice, followed as required by the uncertainty principle, a delocalization of the momentum distribution in the detection plane.

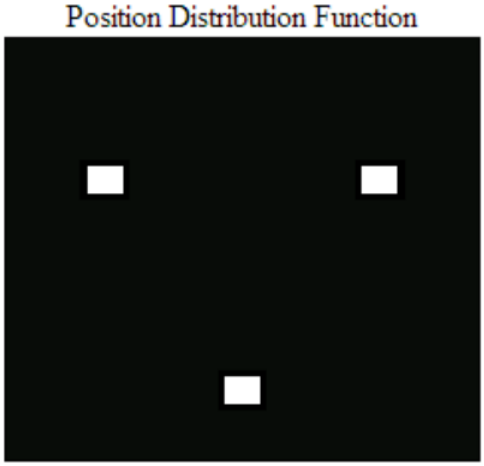
Let's look at some examples. First we examine the Fourier transforms of two mini-lattices with two- and three-fold rotational symmetry.



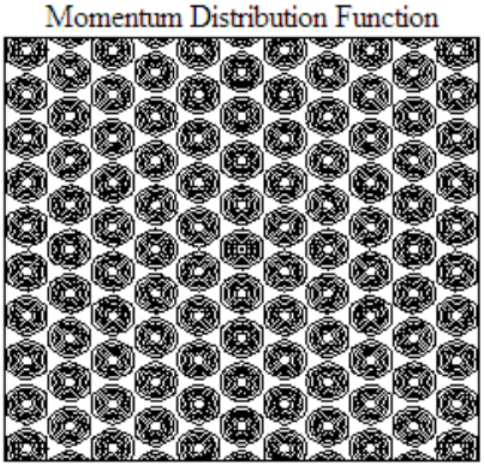
MaskPattern



DiffractionPattern



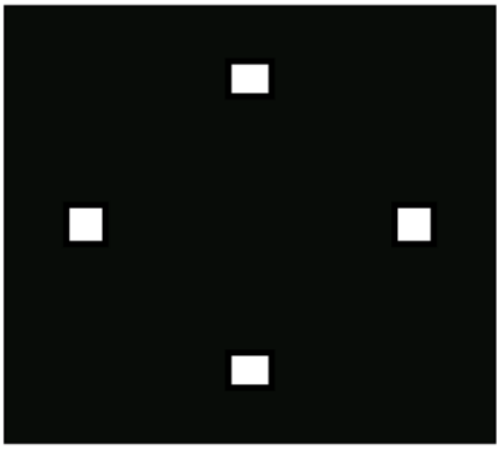
MaskPattern



DiffractionPattern

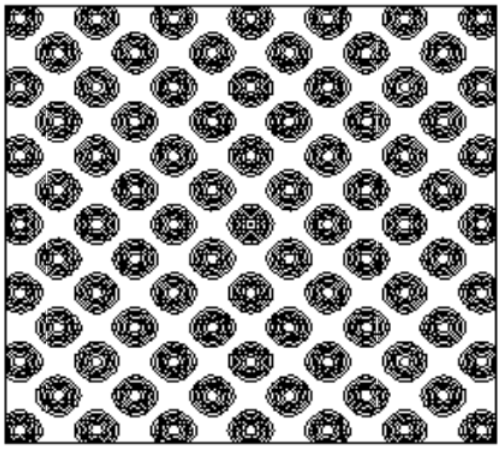
Clearly both diffraction patterns exhibit translational periodicity, their repeating units being a 90 degree rotation of the spatial structure. Next we look at four-fold rotational symmetry and see that the unit cell is obvious.

Position Distribution Function



MaskPattern

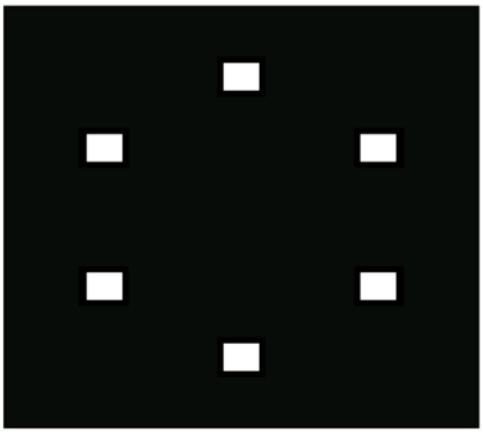
Momentum Distribution Function



DiffractionPattern

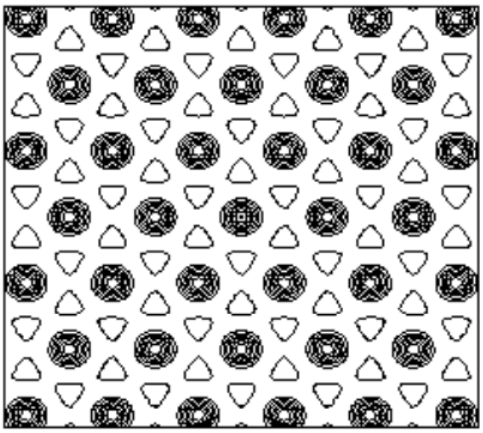
Six-fold rotational symmetry is more interesting than the previous three examples, but again the unit cell is easy to find.

Position Distribution Function



MaskPattern

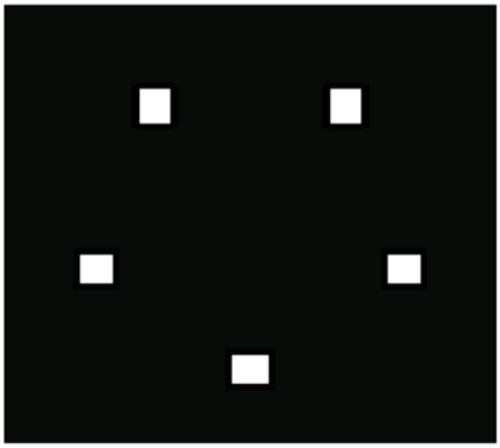
Momentum Distribution Function



DiffractionPattern

Now look at what happens when we consider 5-fold symmetry – the diffraction pattern generated by a pentagon.

Position Distribution Function



MaskPattern

Momentum Distribution Function



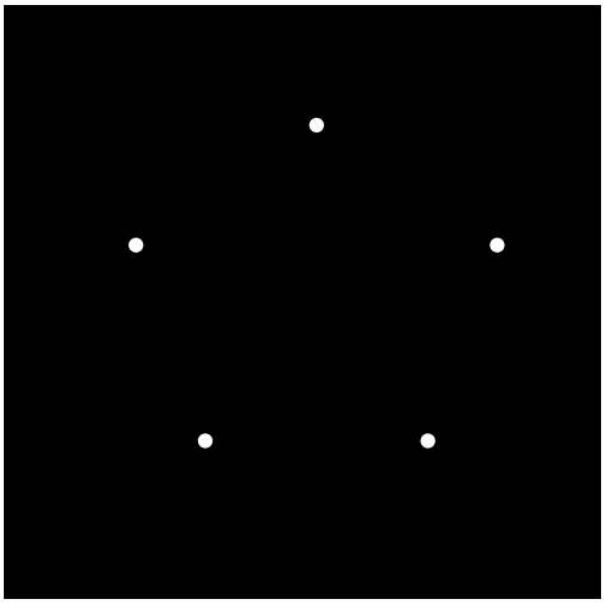
DiffractionPattern

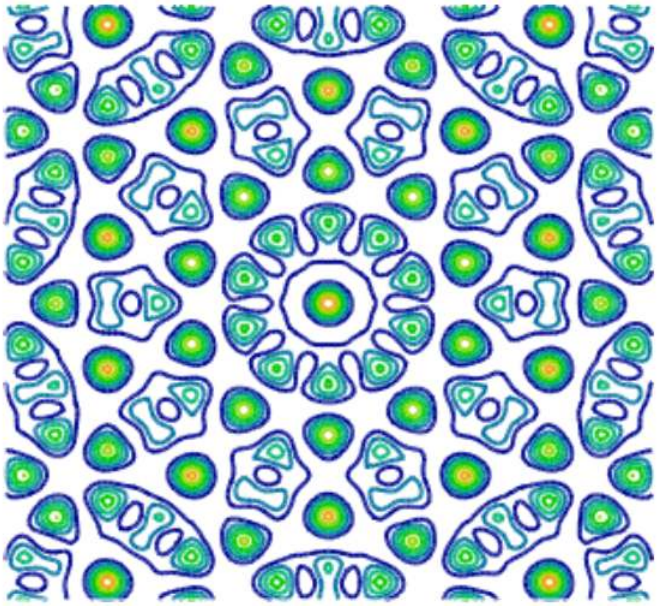
The unit cell, the universal repeating unit, is gone. The diffraction pattern is well-defined, it has rotational symmetry and it is appealing, but it does not satisfy the criterion for translational periodicity. That's why 5-fold rotational symmetry is excluded from the list of symmetries that can generate diffraction patterns that have translational periodicity, and why by definition crystalline solids are not supposed to have 5-fold axes, or rotational axes greater than order six.

However, in 1984 an international research team consisting of D. Shechtman, I. Blech, D. Gratias and J. W. Cahn, published "Metallic phase with long-range orientational order and no translational symmetry" in *Physical Review Letters* **53**, 1951-1953 (1984). The crystalline metallic phases they studied produced discrete diffraction patterns that were characteristic of the 5- and 10-fold rotational symmetry axes that were prohibited by the accepted definition of a crystalline solid.

In the face of this contradictory evidence, 5-fold rotational symmetry and a well-defined diffraction pattern, the International Union of Crystallography in 1991 redefined **crystal** to mean any solid having a discrete diffraction pattern. However, the solid phases discovered by Shechtman and his co-workers go by the name quasicrystals, indicating that they don't quite have the same stature as those that don't violate the rotational symmetry rule.

The striking diffraction pattern created by a pentagon of point scatterers is shown below.



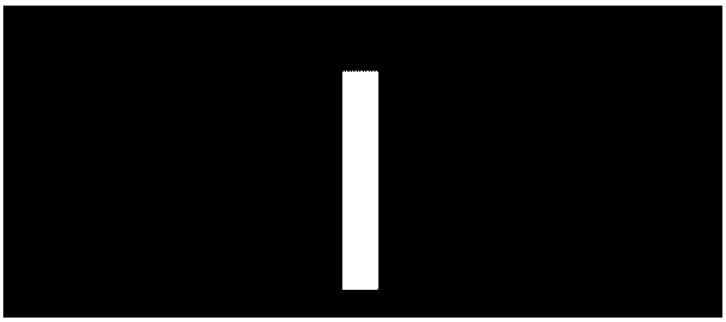


In these recent examples we have been Fourier transforming from coordinate space to momentum space because the momentum distribution function is the diffraction pattern, and our experiments are set up in coordinate space. In quantum mechanics an experiment requires two steps: state preparation followed by a measurement. State preparation occurs at the slit screen and measurement at the detection screen. The following link shows how to go from the coordinate representation to the momentum representation and back again.

Single Slit Diffraction and the Fourier Transform

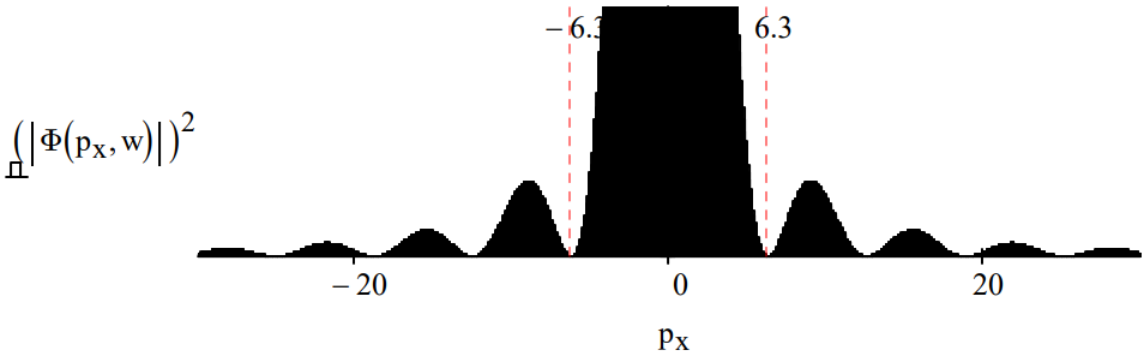
Slit width: $w := 1$	Coordinate-space wave function: $\Psi(x, w)$ $:=$ if $[(x \geq -\frac{w}{2}) \cdot (x \leq \frac{w}{2}), 1, 0]$

$$x := \frac{-w}{2}, \frac{-w}{2} + 0.005 \ldots \frac{w}{2}$$



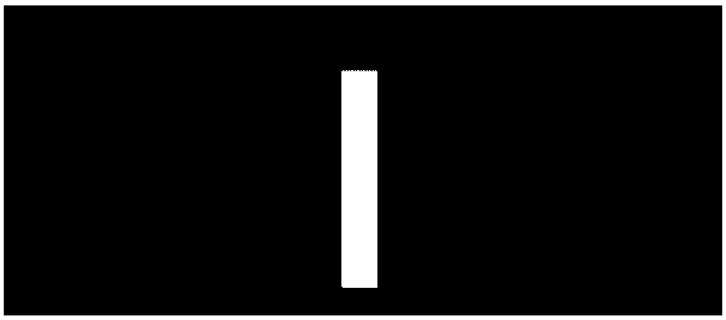
A Fourier transform of the coordinate-space wave function yields the momentum wave function and the momentum distribution function, which is the diffraction pattern.

$$\Phi(p_x, w) := \frac{1}{\sqrt{2 \cdot \pi \cdot w}} \cdot \int_{-\frac{w}{2}}^{\frac{w}{2}} \exp(-i \cdot p_x \cdot x)\, dx \text{ simplify } \rightarrow \frac{\sqrt{2} \cdot \sin\left(\frac{p_x \cdot w}{2}\right)}{\sqrt{\pi} \cdot p_x \cdot \sqrt{w}}$$



Now Fourier transform the momentum wave function back to coordinate space and display result. This is done numerically using large limits of integration for momentum.

$$\Psi(x, w) := \int_{-5000}^{5000} \frac{\frac{1}{2}\sin\left(\frac{1}{2} \cdot w \cdot p_x\right)}{\pi^{\frac{1}{2}} \cdot w^{\frac{1}{2}} \cdot p_x} \cdot \frac{\exp(i \cdot p_x \cdot x)}{\sqrt{2 \cdot \pi}} dp_x$$



This page titled 1.14: Quantum Mechanics and the Fourier Transform is shared under a CC BY 4.0 license and was authored, remixed, and/or curated by Frank Rioux via source content that was edited to the style and standards of the LibreTexts platform.

1.15: Quantum Mechanics and the Fourier Transform

Quantum chemists work almost exclusively in coordinate space because they need wave functions that will help them understand molecular structure and chemical reactivity. They need the location of the nuclear centers and electron density maps. Consequently undergraduate physical chemistry texts examine all the traditional model problems (particle in a box, rigid rotor, harmonic oscillator, hydrogen atom, hydrogen molecule ion, hydrogen molecule, etc.) using spatial wave functions. Students learn how to interpret graphical representations of the various wave functions. If knowledge is required about electron momentum, for example, expectation values are calculated using the coordinate wave function.

For the model systems listed above, it is a simple matter to carry out a Fourier transform into momentum space. This allows the same kind of visualization in momentum space that is available in the coordinate representation. The value of this capability in presenting a graphical illustration of the uncertainty principle for the particle-in-the-box (PIB) problem is illustrated in the following tutorial.

A Graphical Illustration of the Heisenberg Uncertainty Relationship

According to quantum mechanics position and momentum are conjugate variables; they cannot be simultaneously known with high precision. The uncertainty principle requires that if the position of an object is precisely known, its momentum is uncertain, and vice versa. This reciprocal relationship is captured by the well-known uncertainty relation, which says that the product of the uncertainties in position and momentum must be greater than or equal to Planck's constant divided by 4π.

$$\Delta x \cdot \Delta p \geq \frac{h}{4 \cdot \pi}$$

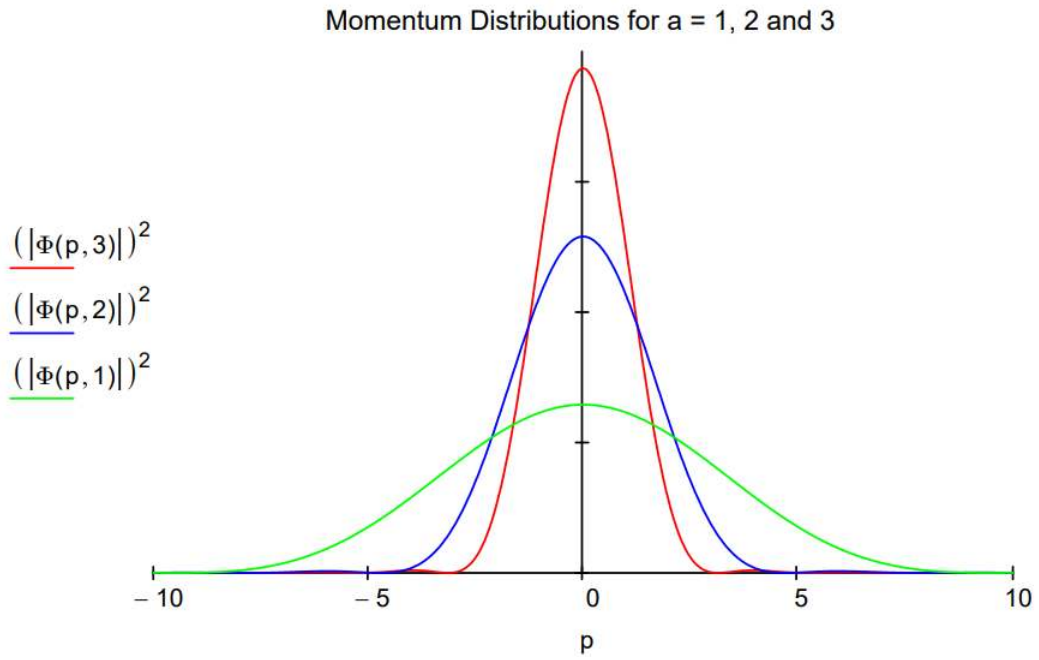
This simple mathematical relation can be visualized using the traditional work horse - the quantum mechanical particle in a box (infinite one-dimensional potential well). The particle's ground-state wave function in coordinate space for a box of width a is shown below.

$$\Psi(\mathrm{x}, \mathrm{a}) := \sqrt{\frac{2}{\mathrm{a}}} \cdot \sin\left(\frac{\pi \cdot \mathrm{x}}{\mathrm{a}}\right)$$

To illustrate the uncertainty principle and the reciprocal relationship between position and momentum, Ψ(x,a) is Fourier transformed into momentum space yielding the particle's ground-atate wave function in the momentum representation.

$$\Phi(p, a) := \sqrt{\frac{1}{2 \cdot \pi}} \cdot \int_0^a \exp(-i \cdot p \cdot x) \cdot \sqrt{\frac{2}{a}} \cdot \sin\left(\frac{\pi \cdot x}{a}\right) dx \text{simplify} \rightarrow \frac{\pi \cdot a \cdot \left(e^{-a \cdot p \cdot 1} + 1\right) \cdot \sqrt{\frac{1}{a}}}{\pi^{\frac{5}{2}} - \sqrt{\pi} \cdot a^2 \cdot p^2}$$

In the figure below, the momentum distribution, $|\Phi(p, a)|^2$, is shown for three sizes, a = 1,2 and 3. The uncertainty principle is illustrated as follows: as the box size increases the position uncertainty increases and momentum uncertainty decreases because the momentum distribution narrows.



We use the particle-in-the-box example to introduce students to almost all the fundamental quantum mechanical concepts. When we come to spectroscopy and the chemical bond, we initially model the chemical bond as a harmonic oscillator. Here there are two physical parameters, force constant and effective mass. The following tutorial shows how the coordinate and momentum wave functions can be used to illustrate the uncertainty principle for various values of k and μ.

The Harmonic Oscillator and the Uncertainty Principle

Schrödinger's equation in atomic units (h = 2π) for the harmonic oscillator has an exact analytical solution.

$$V(x,k) := \frac{1}{2}\cdot k\cdot x^2 \qquad \frac{-1}{2\cdot\mu}\cdot\frac{d^2}{dx^2}\Psi(x) + V(x)\cdot\Psi(x) = E\cdot\Psi(x)$$

The ground-state wave function (coordinate space) and energy for an oscillator with reduced mass μ and force constant k are as follows.

$$\Psi(x,k,\mu) := \left(\frac{\sqrt{k\cdot\mu}}{\pi}\right)^{\frac{1}{4}}\cdot\exp\left(-\sqrt{k\cdot\mu}\cdot\frac{x^2}{2}\right) \qquad E(k,\mu) := \frac{1}{2}\cdot\sqrt{\frac{k}{\mu}}$$

The first thing we want to illustrate is that tunneling occurs in the simple harmonic oscillator. The classical turning point is that position at which the total energy is equal to the potential energy. In other words, classically the kinetic energy is zero and the oscillator's direction is going to reverse. For the ground state the classical turning point is,

$$\frac{1}{2}\cdot\sqrt{\frac{k}{\mu}} = \frac{1}{2}\cdot k\cdot x^2 \text{ has solution } (s)\begin{pmatrix}\frac{-1}{k^{\frac{1}{4}}\cdot\mu^{\frac{1}{4}}}\\ \frac{1}{k^{\frac{1}{4}}\cdot\mu^{\frac{1}{4}}}\end{pmatrix}$$

From the quantum mechanical perspective the oscillator is not vibrating; it is in a stationary state. To the extent that the oscillator's wave function extends beyond the classical turning point, tunneling is occurring. The calculation below shows that the probability that tunneling occurs is independent of the values of k and μ for the ground state.

$$2\cdot\left[\int_{\frac{1}{(k\cdot\mu)^{\frac{1}{4}}}}^{\infty}\left[\left(\frac{\sqrt{k\cdot\mu}}{\pi}\right)^{\frac{1}{4}}\cdot\exp\left(-\sqrt{k\cdot\mu}\cdot\frac{x^2}{2}\right)\right]^2 dx\right]\Bigg|_{\text{simplify}}^{\text{assume, } k>0,\mu>0} \rightarrow 1-\text{erf}(1) = 0.157$$

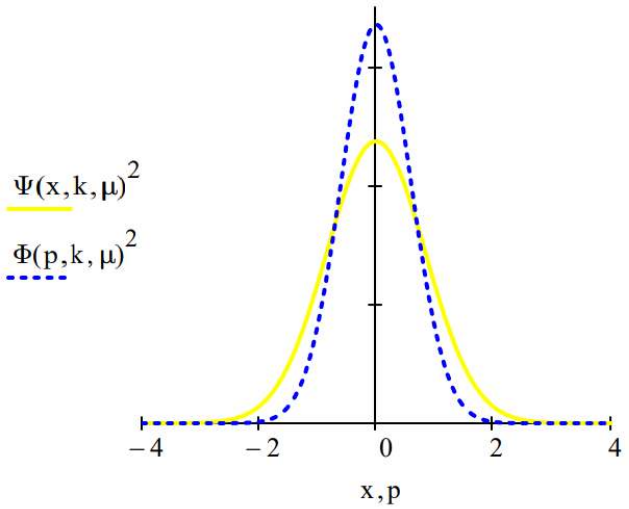
A Fourier transform of the coordinate wave function provides its counter part in momentum space.

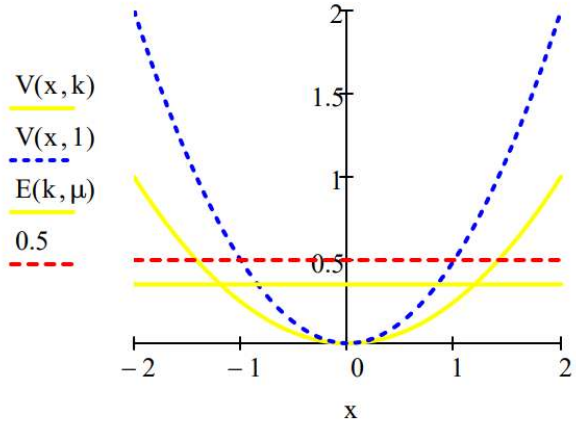
$$\Phi(\mathbf{p},\mathbf{k},\boldsymbol{\mu}) := \frac{1}{\sqrt{2\cdot\pi}}\cdot\int_{-\infty}^{\infty}\exp(-\mathbf{i}\cdot\mathbf{p}\cdot\mathbf{x})\cdot\Psi(\mathbf{x},\mathbf{k},\boldsymbol{\mu})\mathrm{d}\mathbf{x}\Big|\begin{array}{l}\text{assume, } \mathrm{k}>0\\ \text{assume, } \mu>0\\ \text{simplify}\end{array}\rightarrow\frac{e^{-\frac{p^2}{2\cdot\sqrt{\mu}\cdot\sqrt{k}}}}{\pi^{\frac{1}{4}}\cdot\mu^{\frac{1}{8}}\cdot k^{\frac{1}{8}}}$$

The uncertainty principle can now be illustrated by comparing the coordinate and momentum wave functions for a variety values of k and μ. For the benchmark case, k = μ = 1, we see that the coordinate and momentum wave functions are identical and the classical turning point (CTP) is 1. The classical turning point will be taken as a measure of the spatial domain of the oscillator.

- For k = 2 and μ =1, the force constant has doubled reducing the amplitude of vibration (CTP =0.841) and therefore the uncertainty in position. Consequently there is an increase in the uncertainty in momentum which is manifested by a broader momentum distribution function.
- For k = 1 and μ = 2, the increase in effective mass drops the oscillator in the potential well decreasing the vibrational amplitude (CTP = 0.841) causing a decrease in Δx and an increase in Δp.
- For k = 0.5 and μ = 1, the lower force constant causes a larger vibrational amplitude (CTP = 1.189) and an accompanying increase in Δx. Consequently Δp decreases.

Force constant: $k := 0.5$	Effective mass: $\mu := 1$	Energy: $\mathrm{E}(\mathrm{k},\mu) = 0.354$	CTP: $\frac{1}{\mathrm{k}^{\frac{1}{4}}\cdot\mu^{\frac{1}{4}}} = 1.189$





The uncertainties in position and momentum are calculated as shown below because for the harmonic oscillator \(<x>= =0\).

$$\Delta x := \sqrt{\int_{-\infty}^{\infty} x^2\cdot\Psi(x,k,\mu)^2 dx} = 0.841 \quad \Delta\mathrm{p} := \sqrt{\int_{-\infty}^{\infty}\mathrm{p}^2\cdot\Phi(\mathrm{p},\mathrm{k},\mu)^2\mathrm{dp}} = 0.595 \quad \Delta x\cdot\Delta p = 0.5$$

A summary of the four cases considered is provided in the table below.

$$\begin{pmatrix} \mu & k & CTP & \Delta x & \Delta p & \Delta x\Delta p \\ 1 & 1 & 1.00 & 0.707 & 0.707 & 0.5 \\ 1 & 2 & 0.841 & 0.595 & 0.841 & 0.5 \\ 2 & 1 & 0.841 & 0.595 & 0.841 & 0.5 \\ 1 & 0.5 & 1.189 & 0.841 & 0.594 & 0.5 \end{pmatrix}$$

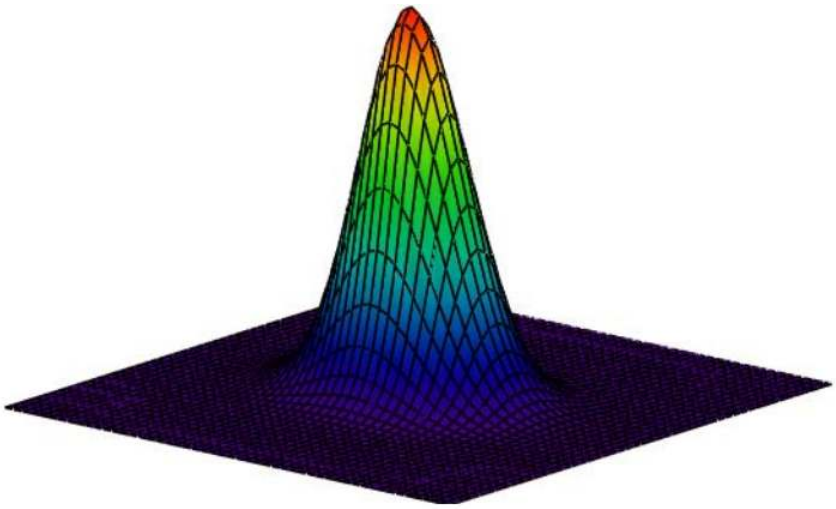
The Wigner function, W(x,p), is a phase-space distribution that can be used to provide an alternative graphical representation of the results calculated above. As shown below it can be generated using either the coordinate or momentum wave function.

Calculate Wigner distribution:

$$\mathrm{W}(\mathrm{x},\mathrm{p}) := \frac{1}{\pi^{\frac{3}{2}}}\cdot\int_{-\infty}^{\infty}\Psi\left(\mathrm{x}+\frac{\mathrm{s}}{2},\mathrm{k},\mu\right)\cdot\exp(\mathrm{i}\cdot\mathrm{s}\cdot\mathrm{p})\cdot\Psi\left(\mathrm{x}-\frac{\mathrm{s}}{2},\mathrm{k},\mu\right)\mathrm{ds}$$

Display Wigner distribution:

$$N := 50 \quad i := 0 \dots N \quad x_i := -4 + \frac{8 \cdot i}{N} \quad j := 0 \dots N \quad p_j := -4 + \frac{8 \cdot j}{N} \quad \text{Wigner}_{i,j} = W(x_i, p_j)$$

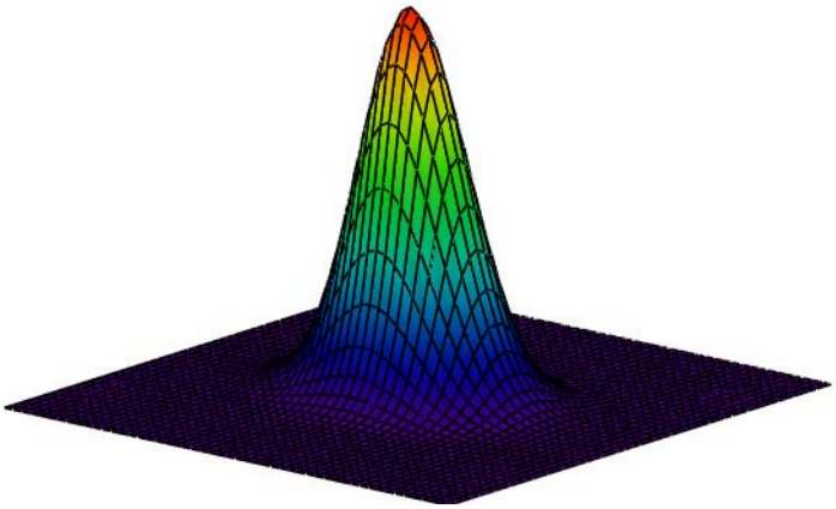


Calculate Wigner distribution:

$$W(x, p) := \frac{1}{\pi^{\frac{3}{2}}} \cdot \int_{-\infty}^{\infty} \Phi\left(p + \frac{s}{2}, k, \mu\right) \cdot \exp(i \cdot s \cdot x) \cdot \Phi\left(p - \frac{s}{2}, k, \mu\right) ds$$

Display Wigner distribution:

$$N := 50 \quad i := 0 \dots N \quad x_i := -4 + \frac{8 \cdot i}{N} \quad j := 0 \dots N \quad p_j := -4 + \frac{8 \cdot j}{N} \quad \text{Wigner}_{i,j} := W(x_i, p_j)$$



It is easy to derive the angular position, angular momentum uncertainty relationship for a particle on a ring using the position-momentum uncertainty equation and the classical definition of angular momentum. Visualization is provided by the next tutorial.

Demonstrating the Uncertainty Principle for Angular Momentum and Angular Position

The uncertainty relation between angular momentum and angular position can be derived from the more familiar uncertainty relation between linear momentum and position

$$\Delta p \cdot \Delta x \geq \frac{h}{4 \cdot \pi}$$

Consider a particle with linear momentum p moving on a circle of radius r. The particle′s angular momentum is given by equation (2).

$$L = m \cdot v \cdot r = p \cdot r$$

In moving a distance x on the circle the particle sweeps out an angle ϕ in radians.

$$\phi = \frac{x}{r}$$

Equations (2) and (3) suggest,

$$\Delta p = \frac{\Delta L}{r} \qquad \Delta x = \Delta \phi \cdot r$$

Substitution of equations (4) into equation (1) yields the angular momentum, angular position uncertainty relation.

$$\Delta L \cdot \Delta \phi \geq \frac{h}{4 \cdot \pi}$$

In addition to the Heisenberg restrictions represented by equations (1) and (5), conjugate observables are related by Fourier transforms. For example, for position and momentum it is given by equation (6) in atomic units (h = 2π).

$$\langle p|x\rangle = \frac{1}{\sqrt{2\pi}}\exp(-ipx)$$

Equations (2) and (3) can be used with (6) to obtain the Fourier transform between angular momentum and angular position.

$$\langle L|\phi\rangle = \frac{1}{\sqrt{2\pi}}\exp(-iL\phi)$$

Equations (6) and (7) are mathematical dictionaries telling us how to translate from x language to p language, or ϕ language to L language. The complex conjugates of (6) and (7) translate in the reverse direction, from p to x and from L to ϕ.

The work-horse particle-in-a-box (PIB) problem can be used to provide a compelling graphical illustration of the position-momentum uncertainty relation. The position wave function for the ground state of a PIB in a box of length a is given below.

$$\langle x|\Psi\rangle = \sqrt{\frac{2}{a}}\sin\left(\frac{\pi x}{a}\right)$$

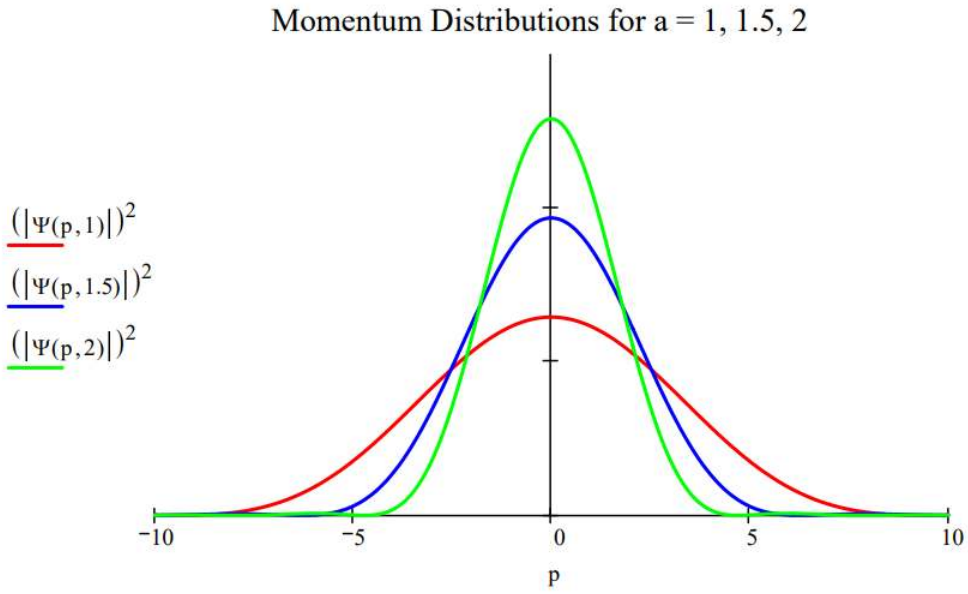
The conjugate momentum-space wave function is obtained by the following Fourier transform.

$$\langle p|\Psi\rangle = \int_0^a \langle p|x\rangle\langle x|\Psi\rangle dx = \frac{1}{\sqrt{\pi a}}\int_0^a \exp(-ipx)\sin\left(\frac{\pi x}{a}\right)$$

Evaluation of the integral in equation (9) yields

$$\Psi(p, a) := \sqrt{a \cdot \pi} \cdot \frac{\exp(-i \cdot p \cdot a) + 1}{\pi^2 - p^2 \cdot a^2}$$

Plotting the momentum distribution function for several box lengths, as is done in the figure below, clearly reveals the position-momentum uncertainty relation. The greater the box length the greater the uncertainty in position. However, as the figure shows, the greater the box length the narrower the momentum distribution, and, consequently, the smaller the uncertainty in momentum.



A similar visualization of the angular-momentum/angular-position uncertainty relation is also possible. Suppose a particle on a ring is prepared in such a way that its angular wave function is represented by the following gaussian function,

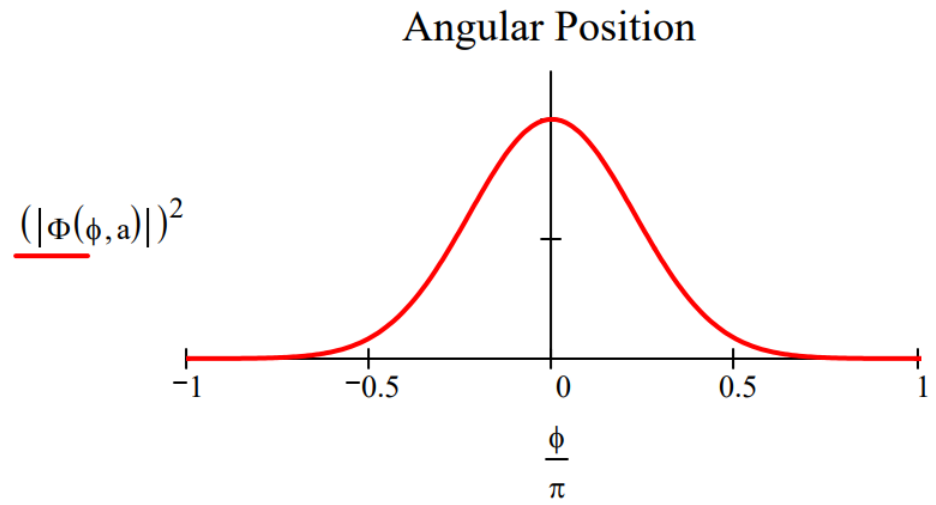
$$\langle \phi | \Psi \rangle = \exp\left(-a\phi^2\right)$$

where the parameter a controls the width of the angular distribution. The conjugate angular momentum wave function is obtained by the following Fourier transform.

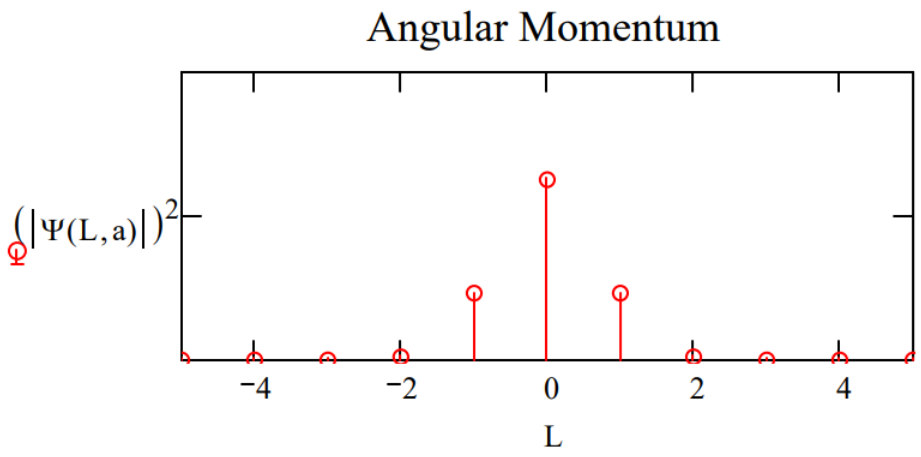
$$\langle L | \Psi \rangle = \int_{-\pi}^{\pi} \langle L | \phi \rangle \langle \phi | \Psi \rangle d\phi = \frac{1}{\sqrt{2\pi}} \int_{-\pi}^{\pi} \exp(-iL\phi) \exp\left(-a\phi^2\right) d\phi$$

Plots of $| < \phi | \Psi > |^2$ and $| < L | \Psi > |^2$ shown below for two values of the parameter a illustrate the angular momentum/angular position uncertainty relation. The larger the value of a, the smaller the angular positional uncertainty and the greater the angular momentum uncertainty. In other words, the greater the value of a the greater the number of angular momentum eigenstates observed.

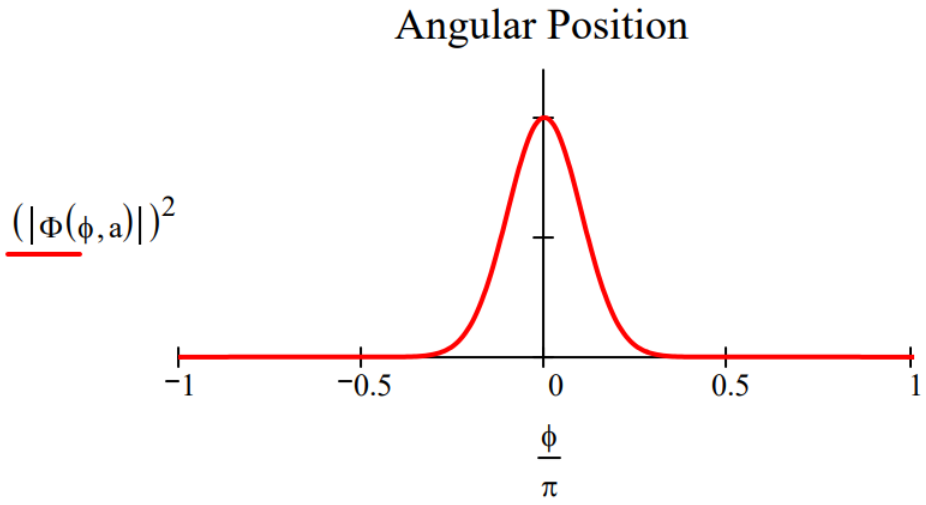
$$a := 0.5 \qquad \Phi(\phi, a) := \exp\left(-a \cdot \phi^2\right)$$



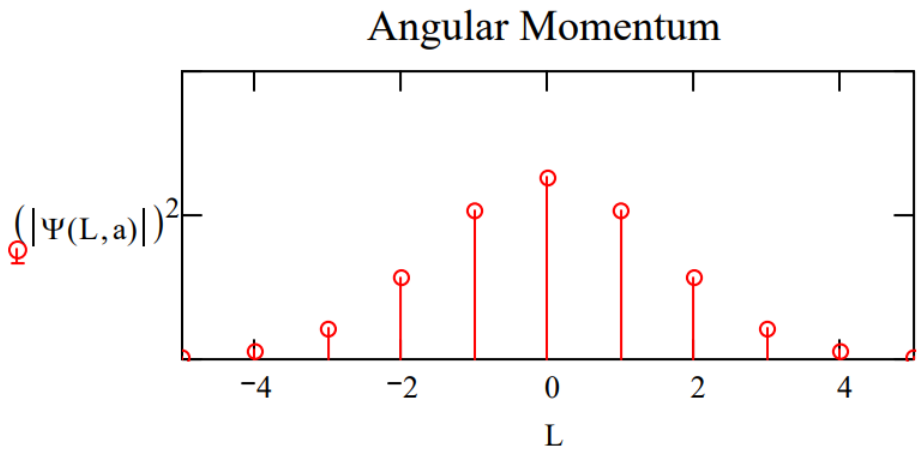
$$L := -5 \ldots 5 \qquad \Psi(L, a) := \int_{-\pi}^{\pi} \exp(-i \cdot L \cdot \phi) \Phi(\phi, a) d\phi$$



Make the angular position distribution narrower: $a := 2.5$



Observe a broader distribution in angular momentum.



The uncertainty relation between angular position and angular momentum as outlined above is a simplified version of that presented by S. Franke-Arnold et al. in *New Journal of Physics* **6**, 103 (2004).

This page titled 1.15: Quantum Mechanics and the Fourier Transform is shared under a CC BY 4.0 license and was authored, remixed, and/or curated by Frank Rioux via source content that was edited to the style and standards of the LibreTexts platform.

1.16: Quantum Mechanics and the Fourier Transform

Moving on to the hydrogen atom, we can use the spatial and momentum wave functions for the 1s, 2s and 3s energy states to again illustrate visually the uncertainty principle.

The Position-Momentum Uncertainty Relation in the Hydrogen Atom

The hydrogen atom coordinate and momentum wave functions can be used to illustrate the uncertainty relation involving position and momentum.

The 1s wave function is used to calculate the average distance of the electron from the nucleus.

$$\Psi_{1s}(r) := \frac{1}{\sqrt{\pi}} \cdot \exp(-r) \quad r_{1s} := \int_0^{\infty} r \cdot \Psi_{1s}(r)^2 \cdot 4 \cdot \pi \cdot r^2 dr \quad r_{1s} = 1.500$$

The Fourier transform of the 1s wave function yields the momentum wave function. The momentum wave function is used to calculate the average magnitude of the electron momentum.

$$\Phi_{1s}(p) := \frac{1}{\sqrt{8 \cdot \pi^3}} \cdot \int_0^{\infty} \int_0^{\pi} \int_0^{2 \cdot \pi} \Psi_{1s}(r) \cdot \exp(-i \cdot p \cdot r \cdot \cos(\theta)) \cdot r^2 \cdot \sin(\theta) d\phi d\theta dr$$

$$\rightarrow 2 \cdot \frac{2^{\frac{1}{2}}}{\pi \cdot [(-1) + i \cdot p]^2 \cdot (1 + i \cdot p)^2}$$

$$p_{1s} := \int_0^{\infty} p \cdot (|\Phi_{1s}(p)|)^2 \cdot 4 \cdot \pi \cdot p^2 dp \qquad p_{1s} = 0.849$$

The 2s wave function is used to calculate the average distance of the electron from the nucleus.

$$\Psi_{2s}(r) := \frac{1}{\sqrt{32 \cdot \pi}} \cdot (2 - r) \cdot \exp\left(-\frac{r}{2}\right) \quad r_{2s} := \int_0^{\infty} r \cdot \Psi_{2s}(r)^2 \cdot 4 \cdot \pi \cdot r^2 dr \quad r_{2s} = 6.000$$

The Fourier transform of the 2s wave function yields the momentum wave function. The momentum wave function is used to calculate the average magnitude of the electron momentum.

$$\Phi_{2s}(p) := \frac{1}{\sqrt{8 \cdot \pi^3}} \cdot \int_0^{\infty} \int_0^{\pi} \int_0^{2 \cdot \pi} \Psi_{2s}(r) \cdot \exp(-i \cdot p \cdot r \cdot \cos(\theta)) \cdot r^2 \cdot \sin(\theta) d\phi d\theta dr \text{ simplify}$$

$$\rightarrow \frac{-16}{\pi} \cdot \frac{(-1) + 4 \cdot p^2}{[(-1) + 2 \cdot i \cdot p]^3 \cdot (1 + 2 \cdot i \cdot p)^3}$$

$$p_{2s} := \int_0^{\infty} p \cdot (|\Phi_{2s}(p)|)^2 \cdot 4 \cdot \pi \cdot p^2 dp \qquad p_{2s} = 0.340$$

The 3s wave function is used to calculate the average distance of the electron from the nucleus.

$$\Psi_{3s}(r) := \frac{1}{81 \cdot \sqrt{3 \cdot \pi}} \cdot (27 - 18 \cdot r + 2 \cdot r^2) \exp\left(\frac{-r}{3}\right)$$

$$r_{3s} := \int_0^{\infty} r \cdot \Psi_{3s}(r)^2 \cdot 4 \cdot \pi \cdot r^2 dr \quad r_{3s} = 13.500$$

The Fourier transform of the 3s wave function yields the momentum wave function. The momentum wave function is used to calculate the average magnitude of the electron momentum.

$$\Phi_{3s}(p) := \frac{1}{\sqrt{8 \cdot \pi^3}} \cdot \int_0^{\infty} \int_0^{\pi} \int_0^{2 \cdot \pi} \Psi_{3s}(r) \cdot \exp(-i \cdot p \cdot r \cdot \cos(\theta)) \cdot r^2 \cdot \sin(\theta) d\phi d\theta dr \text{ simplify}$$

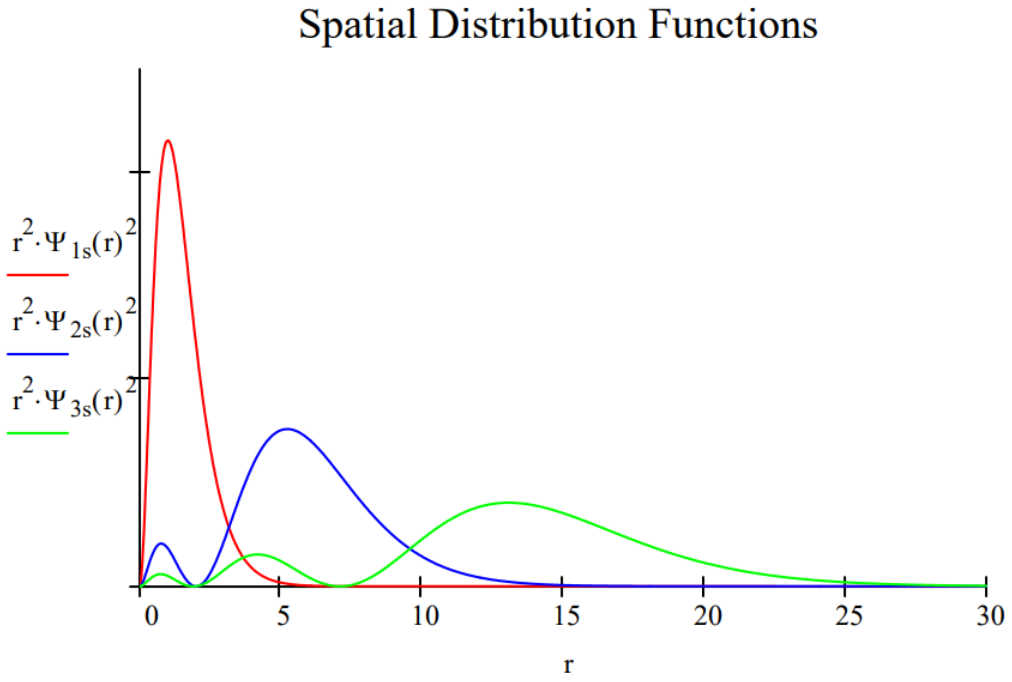
$$\rightarrow 18 \cdot \frac{2^{\frac{1}{2}}}{\pi} \cdot 3^{\frac{1}{2}} \cdot \frac{1 - 30 \cdot p^2 + 81 \cdot p^4}{[(-1) + 3 \cdot i \cdot p]^4 \cdot (1 + 3 \cdot i \cdot p)^4}$$

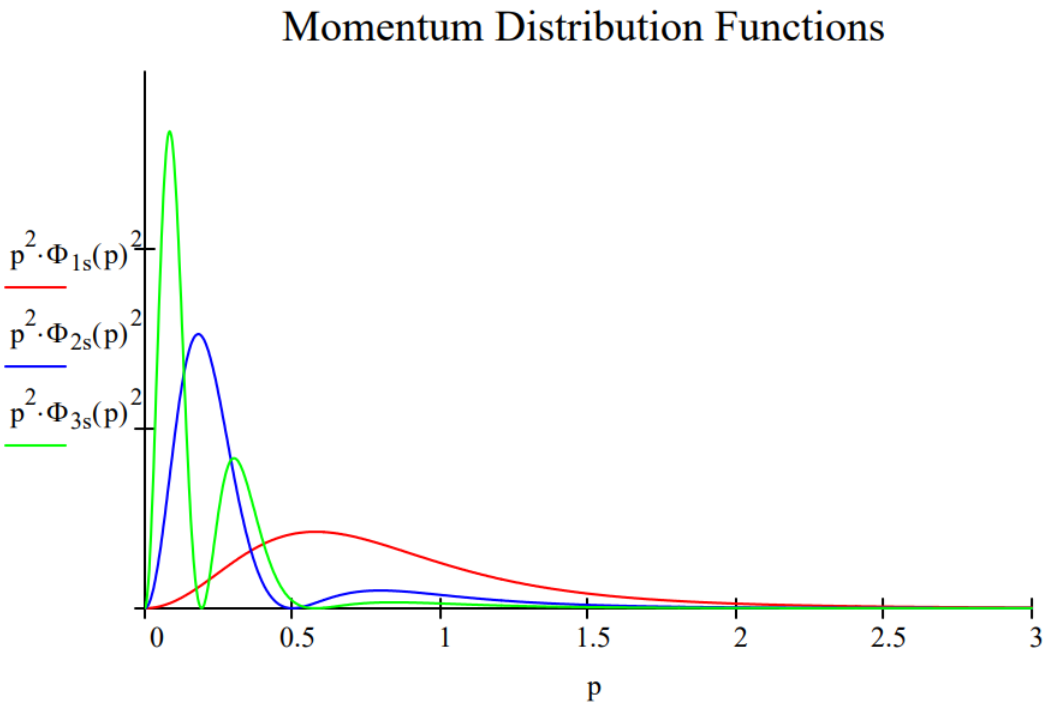
$$p_{3s} := \int_0^{\infty} p \cdot (|\Phi_{3s}(p)|)^2 \cdot 4 \cdot \pi \cdot p^2 dp \qquad p_{3s} = 0.218$$

These results can be summarize in both tabular and graphical form.

Orbital	AveragePosition	AverageMomentum
1s	1.5	0.849
2s	6.0	0.340
3s	13.5	0.218

The table shows that the average distance of the electron from the nucleus increases from 1s to 3s, indicating an increase in the uncertainty in the location of the electron. At the same time the average magnitude of electron momentum decreases from 1s to 3s, indicating a decrease in momentum uncertainty. The spatial and momentum distribution functions shown below illustrate this effect graphically.





In addition to the coordinate and momentum representation, there is also the phase space approach to quantum mechanics, which physicist in particular find useful. It combines the coordinate and momentum approaches and requires a phase-space distribution function such as the Wigner function. The following tutorial illustrates the computational consistency of the three approaches to quantum mechanics. Two related tutorials dealing with quantum mechanical tunneling and the repackaging of quantum weirdness are also available.

Quantum Tunneling in Coordinate, Momentum and Phase Space

A study of quantum mechanical tunneling brings together the classical and quantum mechanical points of view. In this tutorial the harmonic oscillator will be used to analyze tunneling in coordinate-, momentum- and phase-space. The Appendix provides the position and momentum operators appropriate for these three representations.

The classical equation for the energy of a harmonic oscillator is,

$$E = \frac{p^2}{2 \cdot \mu} + \frac{1}{2} \cdot k \cdot x^2$$

The quantum mechanical counter part is Schrödinger's equation (in atomic units, h = 2 π),

$$\frac{-1}{2 \cdot \mu} \cdot \frac{d^2}{dx^2} \Psi(x) + \frac{1}{2} \cdot k \cdot x^2 \cdot \Psi(x) = E \cdot \Psi(x)$$

In atomic units the quantum mechanical wave function in coordinate space for the harmonic oscillator ground state with reduced mass μ and force constant k is given by,

$$\Psi(x, k, \mu) := \left(\frac{\sqrt{k \cdot \mu}}{\pi} \right)^{\frac{1}{4}} \cdot \exp\left(-\sqrt{k \cdot \mu} \cdot \frac{x^2}{2} \right)$$

In the interest of mathematical simplicity and expediency we will use k = μ =1. The normalized ground state wave function under these conditions is,

$$\Psi(x) := \left(\frac{1}{\pi} \right)^{\frac{1}{4}} \cdot \exp\left(\frac{-x^2}{2} \right) \qquad \int_{-\infty}^{\infty} \Psi(x)^2 dx = 1$$

Solving Schrödinger's equation for this wave function yields a ground state energy of 0.5 in atomic units.

$$\frac{-1}{2} \cdot \frac{d^2}{dx^2} \Psi(x) + \frac{1}{2} \cdot x^2 \cdot \Psi(x) = E \cdot \Psi(x) \text{ solve, } E \rightarrow \frac{1}{2}$$

Classically a harmonic oscillator, like a pendulum, has a turning point when kinetic energy is zero and the pendulum bob changes direction. The turning point is calculated as follows using the classical expression for the energy.

$$\frac{1}{2} = \frac{1}{2} \cdot x^2 \text{ solve, } x \rightarrow \begin{pmatrix} 1 \\ -1 \end{pmatrix}$$

Thus, the permissible range of position values is between -1 and +1. Position values outside this range are classically forbidden. However, quantum theory permits position values for which the total energy is less than the potential energy. This is referred to as quantum tunneling. The probability that tunneling is occurring is calculated below.

$$2 \cdot \int_{1}^{\infty} \Psi(x)^2 dx = 0.157$$

Next we move to a similar calculation in momentum space. First the coordinate wave function is Fourier transformed into momentum space and normalization is demonstrated.

$$\Phi(p) := \frac{1}{\sqrt{2 \cdot \pi}} \cdot \int_{-\infty}^{\infty} \exp(-i \cdot p \cdot x) \cdot \Psi(x) dx \rightarrow \frac{1}{\pi^{\frac{1}{4}}} \cdot e^{\frac{-1}{2} \cdot p^2} \qquad \int_{-\infty}^{\infty} (|\Phi(p)|)^2 dp = 1$$

Solving Schrödinger's equation in momentum space naturally gives the same energy eigenvalue.

$$\frac{p^2}{2}\cdot\Phi(p)-\frac{1}{2}\cdot\frac{d^2}{dp^2}\Phi(p)=E\cdot\Phi(p)\ \text{solve, E}\rightarrow\frac{1}{2}$$

And we find that the classically permissible range of momentum values is the same given the reduced mass and force constant values used in these calculations.

$$\frac{1}{2}=\frac{p^2}{2}\ \text{solve, p}\rightarrow\begin{pmatrix}1\\-1\end{pmatrix}$$

Next we see that the tunneling probability in momentum space is the same as it is in coordinate space.

$$2\cdot\int_1^\infty\Phi(p)^2dp=0.157$$

Moving to phase space requires a distribution function that depends on both position and momentum. The Wigner function fits these requirements and is generated here using both the coordinate and momentum wave functions. Please see “Examining the Wigner Distribution Using Dirac Notation,” arXiv: 0912.2333 (**2009**) for further detail.

$$W(x,p):=\frac{1}{2\cdot\pi}\cdot\int_{-\infty}^{\infty}\Psi\left(x+\frac{s}{2}\right)\cdot\exp(i\cdot s\cdot p)\cdot\Psi\left(x-\frac{s}{2}\right)ds\rightarrow\frac{1}{\pi}\cdot e^{(-x^2)-p^2}$$

$$W(x,p):=\frac{1}{2\cdot\pi}\cdot\int_{-\infty}^{\infty}\Phi\left(p+\frac{s}{2}\right)\cdot\exp(i\cdot s\cdot x)\cdot\Phi\left(p-\frac{s}{2}\right)ds\rightarrow\frac{1}{\pi}\cdot e^{(-x^2)-p^2}$$

The Wigner function is normalized over position and momentum, and yields the appropriate energy expectation value for the ground state of the harmonic oscillator.

$$\int_{-\infty}^{\infty}\int_{-\infty}^{\infty}W(x,p)dxdp=1\qquad\int_{-\infty}^{\infty}\int_{-\infty}^{\infty}\left(\frac{p^2}{2}+\frac{x^2}{2}\right)\cdot W(x,p)dxdp=0.5$$

Tunneling probability in phase space is calculated as follows:

$$4\int_1^\infty\int_1^\infty W(x,p)dxdp=0.025$$

This is in agreement with the separate coordinate and momentum space calculations which gave values of 0.157.

$$0.157\cdot0.157=0.025$$

Appendix

The table lists the forms of the position and momentum operators in the coordinate, momentum and phase space representations. Clearly the multiplicative character of the phase space operators appeals to our classical prejudices and intuition. However, we must remind ourselves that the phase space distribution function on which they "operate" is generated from either the coordinate or momentum wave function. In the coordinate representation the momentum operator is differential; in the momentum representation the coordinate operator is differential. As is shown in other tutorials in this series, the apparent "classical character" of the phase space representation only temporarily hides the underlying quantum weirdness.

Operator	CoordinateSpace	MomentumSpace	PhaseSpace
position	$x\cdot\square$	$i\cdot\frac{d}{dp}\square$	$x\cdot\square$
momentum	$\frac{1}{i}\cdot\frac{d}{dx}\square$	$p\cdot\square$	$p\cdot\square$

This page titled 1.16: Quantum Mechanics and the Fourier Transform is shared under a CC BY 4.0 license and was authored, remixed, and/or curated by Frank Rioux via source content that was edited to the style and standards of the LibreTexts platform.

1.17: Quantum Mechanics and the Fourier Transform

Finally, I would like to point out that the elementary Fourier transforms that we started with, $< x|p >$ and $< p|x >$, can also be used to derive the mathematical form of quantum mechanical operators. This is shown in some detail in *An Approach to Quantum Mechanics*.

An Approach to Quantum Mechanics

The purpose of this tutorial is to introduce the basics of quantum mechanics using Dirac bracket notation while working in one dimension. Dirac notation is a succinct and powerful language for expressing quantum mechanical principles; restricting attention to one-dimensional examples reduces the possibility that mathematical complexity will stand in the way of understanding. A number of texts make extensive use of Dirac notation (1-5).

Wave-particle duality is the essential concept of quantum mechanics. DeBroglie expressed this idea mathematically as $\lambda = \frac{h}{mv} = \frac{h}{p}$. On the left is the wave property λ, and on the right the particle property mv, momentum. The most general coordinate space wavefunction for a free particle with wavelength λ is the complex Euler function shown below.

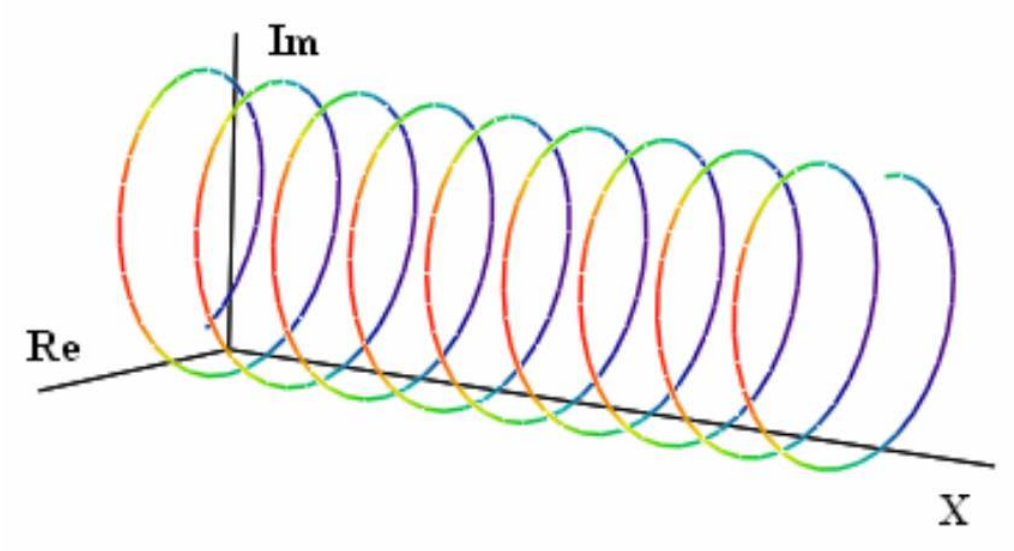
$$\langle x|\lambda\rangle = \exp\left(i2\pi\frac{x}{\lambda}\right) = \cos\left(2\pi\frac{x}{\lambda}\right) + i\sin\left(2\pi\frac{x}{\lambda}\right)$$

Feynman called this equation “the most remarkable formula in mathematics.” He referred to it as “our jewel.” And indeed it is, because when it is enriched with de Broglie’s relation it serves as the foundation of quantum mechanics.

According to de Broglie=s hypothesis, a particle with a well-defined wavelength also has a well-defined momentum. Therefore, we can obtain the momentum wavefunction (unnormalized) of the particle in coordinate space by substituting the deBroglie relation into Equation .

$$\langle x|p\rangle = \exp\left(\frac{ipx}{\hbar}\right)$$

When Equation is graphed it creates a helix about the axis of propagation (X-axis). Z is the imaginary axis and Y is the real axis. It is the simplest example of a fourier transform, translating momentum into coordinate language. It also has in it the heart of the uncertainty principle. Everyday examples of this important mathematical formula include telephone cords, spiral notebooks and slinkies.



Quantum mechanics teaches that the wavefunction contains all the physical information about a system that can be known, and that one extracts information from the wavefunction using quantum mechanical operators. There is, therefore, an operator for each observable property.

For example, in momentum space if a particle has a well-defined momentum we write its state as $|p>$. If we operate on this state with the momentum operator $\hat{p}$, the following eigenvalue equation is satisfied.

$$\hat{p}|p\rangle = p|p\rangle$$

We say the system is in a state which is an eigenfunction of the momentum operator with eigenvalue p. In other words, operating on the momentum eigenfunction with the momentum operator, in momentum space, returns the momentum eigenvalue times the original momentum eigenfunction. From

$$\langle p|\hat{p}|p\rangle = p\langle p|p\rangle$$

it follows that,

$$\langle p|\hat{p} = p\langle p|$$

Equations and show that in its own space the momentum operator is a multiplicative operator, and can operate either to the right on a ket, or to the left on a bra. The same is true of the position operator in coordinate space.

To obtain the momentum operator in coordinate space, Equation is projected onto coordinate space by operating on the left with < x |. After inserting Equation we have,

$$\langle x|\hat{p}|p\rangle = p\langle x|p\rangle = p\exp\left(\frac{ipx}{\hbar}\right) = \frac{\hbar}{i}\frac{d}{dx}\exp\left(\frac{ipx}{\hbar}\right) = \frac{\hbar}{i}\frac{d}{dx}\langle x|p\rangle$$

Comparing the first and last terms reveals that

$$\langle x|\hat{p} = \frac{\hbar}{i}\frac{d}{dx}\langle x|$$

and that $\frac{\hbar}{i}\frac{d}{dx}\langle x|$ is the momentum operator in coordinate space.

The position wavefunction in momentum space is the complex conjugate of the momentum wavefunction coordinate space.

$$\langle p|x\rangle = \langle x|p\rangle^* = \exp\left(\frac{-ipx}{\hbar}\right)$$

Starting with the coordinate-space eigenvalue equation

$$\hat{x}|x\rangle = x|x\rangle$$

and using the same approach as with momentum, it is easy to show that

$$\langle x|\hat{x} = x\langle x|$$

$$\langle p|\hat{x} = -\frac{\hbar}{i}\frac{d}{dp}\langle p|$$

In summary, the two fundamental dynamical operators are position and momentum, and the two primary representations are coordinate space and momentum space. The results achieved thus far are shown in the following table.

	Coordinate Space	Momentum Space
position operator: $\hat{x}$	$x\langle x\|$	$-\frac{\hbar}{i}\frac{d}{dp}\langle p\|$
momentum operator: $\hat{p}$	$\frac{\hbar}{i}\frac{d}{dx}\langle x\|$	$p\langle p\|$

Other quantum mechanical operators can be constructed from $\hat{x}$ and $\hat{p}$ in the appropriate representation, position or momentum. To illustrate this, Schrödinger=s equation for the one-dimensional harmonic oscillator will be set up in both coordinate and momentum space using the information in the table. Schrödinger=s equation is the quantum mechanical energy eigenvalue equation, and for the harmonic oscillator it looks like this initially,

$$\left[\frac{\hat{p}^2}{2m} + \frac{1}{2}k\hat{x}^2\right]|\Psi\rangle = E|\Psi\rangle$$

The term in brackets on the left is the classical energy written as an operator without a commitment to a representation (position or momentum) for the calculation.

Most often, chemists solve Schrödinger=s equation in coordinate space. Therefore, to prepare Schrödinger=s equation for solving, Equation is projected onto coordinate space by operating on the left with < x |.

$$\left\langle x \left| \left[\frac{\hat{p}^2}{2m} + \frac{1}{2} k \hat{x}^2 \right] \right| \Psi \right\rangle = \langle x|E|\Psi\rangle$$

Using the information in the table this yields,

$$\left[-\frac{\hbar^2}{2m} \frac{d^2}{dx^2} + \frac{1}{2} k x^2 \right] \langle x|\Psi\rangle = E\langle x|\Psi\rangle$$

The square bracket on the left contains the quantum mechanical energy operator in coordinate space. Before proceeding we illustrate how the kinetic energy operator emerges as a differential operator in coordinate space using Equation .

$$\frac{1}{2m}\langle x|\hat{p}\hat{p}|\Psi\rangle = \frac{1}{2m}\frac{\hbar}{i}\frac{d}{dx}\langle x|\hat{p}|\Psi\rangle = \frac{1}{2m}\frac{\hbar}{i}\frac{d}{dx}\frac{\hbar d}{dx}\langle x|\Psi\rangle = -\frac{\hbar^2}{2m}\frac{d^2}{dx^2}\langle x|\Psi\rangle$$

Equation is used in a similar fashion to show that potential energy is a multiplicative operator in coordinate space.

$$\frac{1}{2}k\langle x|\hat{x}\hat{x}|\Psi\rangle = \frac{1}{2}kx\langle x|\hat{x}|\Psi\rangle = \frac{1}{2}kx^2\langle x|\Psi\rangle$$

Obviously the calculation could also have been set up in momentum space. It is easy to show that in the momentum representation Schrödinger=s equation is

$$\left[\frac{p^2}{2m} - \frac{\hbar^2 k}{2} \frac{d^2}{dp^2} \right] \langle p|\Psi\rangle = E\langle p|\Psi\rangle$$

In momentum space the kinetic energy operator is multiplicative and the potential energy operator is differential. The one-dimensional simple harmonic oscillator problem is exactly soluble in both coordinate and momentum space. The solution can be found in any chemistry and physics text dealing with quantum mechanics, and will not be dealt with further here, other than to say that equations (14) and (17) reveal an appealing symmetry.

Unfortunately, for most applications the potential energy term in momentum space presents more of a mathematical challenge than it does for the harmonic oscillator problem. A general expression for the potential energy in the momentum representation when its form in the coordinate representation is specified is given below.

$$\langle p|\hat{V}|\Psi\rangle = \iint \exp\left(\frac{i\,(p'-p)\,x}{\hbar} \right) V(x)\,\langle p'|\Psi\rangle\,dp'dx$$

To see how this integral is handled for a specific case see reference (10).

If a system is in a state which is an eigenfunction of an operator, we say the system has a well-defined value for the observable associated with the operator, for example, position, momentum, energy, etc. Every time we measure we get the same result. However, if the system is in a state that is not an eigenfunction of the operator, for example, if $\hat{o}|\Psi\rangle = |\Phi\rangle$, the system does not have a well-defined value for the observable. Then the measurement results have a statistical character and each measurement gives an unpredictable result in spite of the fact that the system is in a well-defined state $|\Psi\rangle$. Under these circumstances, all we can do is calculate a mean value for the observable. This is unheard of in classical physics where, if a system is in a well-defined state, all its physical properties are precisely determined. In quantum mechanics a system can be in a state which has a well-defined energy, but its position and momentum are un-determined.

The quantum mechanical recipe for calculating the mean value of an observable is now derived. Consider a system in the state $|\Psi\rangle$, which is not an eigenfunction of the energy operator, $\hat{H}$. A statistically meaningful number of such states are available for the purpose of measuring the energy. Quantum mechanical principles require that an energy measurement must yield one of the energy eigenvalues, ϵ_i, of the energy operator. Therefore, the average value of the energy measurements is calculated as,

$$\langle E\rangle = \frac{\sum_i n_i \varepsilon_i}{N}$$

where n_i is the number of times ϵ_i is observed, and N is the total number of measurements. Therefore, $p_i = n_i/N$, is the probability that ϵ_i is observed. Equation becomes

$$\langle E \rangle = \sum_i p_i \varepsilon_i$$

According to quantum mechanics, for a system in the state $|\Psi\rangle, p_i = \langle\Psi|i\rangle\langle i|\Psi\rangle$, where the | i > are the eigenfunctions of the energy operator. Equation can now be re-written as,

$$\langle E \rangle = \sum_i \langle\Psi|i\rangle\langle i|\Psi\rangle\varepsilon_i = \sum_i \langle\Psi|i\rangle\varepsilon_i\langle i|\Psi\rangle$$

However, it is also true that

$$\hat{H}|i\rangle = \varepsilon_i|i\rangle = |i\rangle\varepsilon_i$$

Substitution of Equation) into Equation yields

$$\langle E \rangle = \sum_i \langle\Psi|\hat{H}|i\rangle\langle i|\Psi\rangle$$

As eigenfunctions of the energy operator, the | i > form a complete basis set, making available the discrete completeness condition, $\sum_i |i\rangle\langle i| = 1$, the use of which in Equation yields

$$\langle E \rangle = \langle\Psi|\hat{H}|\Psi\rangle$$

This formalism is general and applies to any operator-observable pair. The average value for the observed property may always be calculated as,

$$\langle o \rangle = \langle\Psi|\hat{o}|\Psi\rangle$$

These principles are now applied to a very simple problem B the particle in a box. Schrödinger=s equation in coordinate space,

$$-\frac{\hbar^2}{2m}\frac{d^2}{dx^2}\langle x|\Psi\rangle = E\langle x|\Psi\rangle$$

can be solved exactly, yielding the following eigenvalues and eigenfunctions,

$$E_n = \frac{n^2h^2}{8ma^2}$$

$$\langle x|\Psi_n\rangle = \sqrt{\frac{2}{a}}\sin\left(\frac{n\pi x}{a}\right)$$

where a is the box dimension, m is the particle mass, and n is a quantum number restricted to integer values starting with 1.

Substitution of Equation into Equation confirms that it is an eigenfunction with the manifold of allowed eigenvalues given by Equation . However, Equation is not an eigenfunction of either the position or momentum operators, as is shown below.

$$\langle x|\hat{x}|\Psi_n\rangle = x\langle x|\Psi_n\rangle = x\sqrt{\frac{2}{a}}\sin\left(\frac{n\pi x}{a}\right)$$

$$\langle x|\hat{p}|\Psi_n\rangle = \frac{\hbar}{i}\frac{d}{dx}\langle x|\Psi_n\rangle = \frac{n\pi}{a}\sqrt{\frac{2}{a}}\cos\left(\frac{n\pi x}{a}\right)$$

To summarize, the particle in a box has a well-defined energy, but the same is not true for its position or momentum. In other words, it is not buzzing around the box executing a classical trajectory. The outcome of an energy measurement is certain, but position and momentum measurements are uncertain. All we can do is calculate the expectation value for these observables and compare the calculations to the mean values found through a statistically meaningful number of measurements.

Next we set up the calculation for the expectation value for position utilizing the recipe expressed in Equation .

$$\langle x \rangle_n = \langle\Psi_n|\hat{x}|\Psi_n\rangle$$

Evaluation of Equation in coordinate space requires the continuous completeness condition.

$$\int_0^a |x\rangle\langle x| dx = 1$$

Substitution of (32) into (31) gives

$$\langle x\rangle_n = \int_0^a \langle \Psi_n|x\rangle \, \langle x|\hat{x}|\Psi_n\rangle \, dx = \int_0^a \langle \Psi_n|x\rangle \, x\langle x|\Psi_n\rangle dx = \frac{a}{2}$$

The expectation value for momentum is calculated in a similar fashion,

$$\langle p\rangle_n = \int_0^a \langle \Psi_n|x\rangle \, \langle x|\hat{p}|\Psi_n\rangle \, dx = \int_0^a \langle \Psi_n|x\rangle \, \frac{\hbar}{i}\frac{d}{dx}\langle x|\Psi_n\rangle dx = 0$$

In other words, the expectation values for position and momentum are the same for all the allowed quantum states of the particle in a box.

It is now necessary to explore the meaning of $\langle x|\Psi\rangle$. It is the probability amplitude that a system in the state $|\Psi\rangle$, will be found at position x. $|\langle x|\Psi\rangle|^2$ or $\langle \Psi|x\rangle\langle x|\Psi\rangle$ is the probability density that a system in the state $|\Psi\rangle$, will be found at position x. Thus Equation is an algorithm for calculating probability amplitudes and probability densities for the position of the particle in a one-dimensional box. This, of course, is true only if $|\Psi\rangle$ is normalized.

$$\langle \Psi|\Psi\rangle = \int_0^a \langle \Psi|x\rangle\langle x|\Psi\rangle dx = 1$$

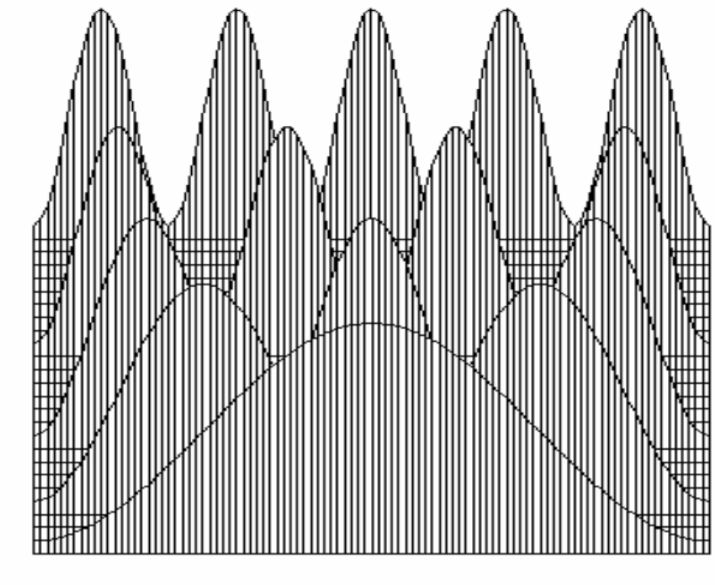
There are two ways to arrive at the integral in Equation . One can insert the continuous completeness relation (32) at the * on the left side, or, equivalently one can express $|\Psi\rangle$ as a linear superposition in the continuous basis set x,

$$|\Psi\rangle = \int_0^a |x\rangle\langle x|\Psi\rangle dx$$

and projecting this expression onto $\langle \Psi|$.

A quantum particle is described by its wavefunction rather than by its instantaneous position and velocity; a confined quantum particle, such as a particle in a box, is not moving in any classical sense, and must be considered to be present at all points in space, properly weighted by $|\langle x|\Psi\rangle|^2$.

Thus, $\langle x|\Psi\rangle$ allows us to examine the coordinate space probability distribution and to calculate expectation values for observables such as was done in equations (33) and (34). Plots of $|\langle x|\Psi_n\rangle|^2$ show that the particle is distributed symmetrically in the box, and $\langle x|\Psi_n\rangle$, allows us to calculate the probability of finding the particle anywhere inside the box.



Position_Distribution

The coordinate-space wavefunction does not say much about momentum, other than its average value is zero (see equation 34). However, a momentum-space wave function, $\langle p|\Psi\rangle$, can be generated by a Fourier transform of $\langle x|\Psi\rangle$. This is accomplished by projecting Equation \ref{36) onto momentum space by multiplication on the left by$\langle p|$.

$$\langle p|\Psi_n\rangle = \int_0^a \langle p|x\rangle\langle x|\Psi_n\rangle dx = \frac{1}{\sqrt{2\pi\hbar}}\int_0^a \exp\left(-\frac{ipx}{\hbar}\right)\sqrt{\frac{2}{a}}\sin\left(\frac{n\pi x}{a}\right)dx$$

The term preceding the integral is the normalization constant (previously ignored) for the momentum wave function. Evaluation of the integral on the right side yields,

$$\langle p|\Psi_n\rangle = n\sqrt{a\pi h^3}\left[\frac{1-\cos(n\pi)\exp\left(-\frac{ipa}{\hbar}\right)}{n^2\pi^2\hbar^2 - a^2p^2}\right]$$

Now with the continuous completeness relationship for momentum,

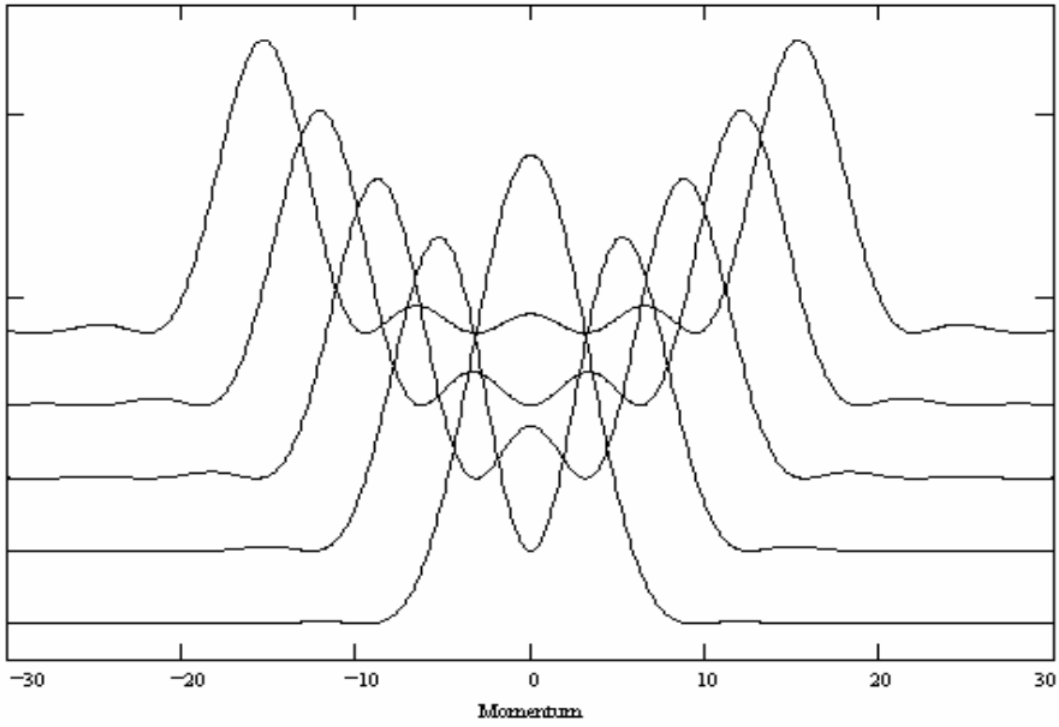
$$\int_{-\infty}^{\infty}|p\rangle\langle p|dp = 1$$

one can re-calculate $\langle x\rangle_n$ and $\langle p\rangle_n$ in momentum space.

$$\langle x\rangle_n = \int_{-\infty}^{\infty}\langle\Psi_n|p\rangle\,\langle p|\hat{x}|\Psi_n\rangle\,dp = \int_{-\infty}^{\infty}\langle\Psi_n|p\rangle\,\frac{-\hbar}{i}\frac{d}{dp}\langle p|\Psi_n\rangle dp = \frac{a}{2}$$

$$\langle p\rangle_n = \int_{-\infty}^{\infty}\langle\Psi_n|\hat{p}|p\rangle\,\langle p|\Psi_n\rangle dp = \int_{-\infty}^{\infty}\langle\Psi_n|p\rangle\,p\langle p|\Psi_n\rangle dp = 0$$

It is clear that $\langle x|\Psi_n\rangle$ and $\langle p|\Psi_n\rangle$ contain the same information; they just present it in different languages (representations). The coordinate space distribution functions for the particle in a box shown above are familiar to anyone who has studied quantum theory, however, because chemists work mainly in coordinate space, the momentum distributions are not so well known. A graphical representation of $|\langle p|\Psi_n\rangle|^2$ for the first five momentum states is shown below. The distribution functions are offset by small increments for clarity of presentation.



As just shown, the particle in a box can be used to illustrate many fundamental quantum mechanical concepts. To demonstrate that some systems can be analyzed without solving Schrödinger's equation we will briefly consider the particle on a ring. This model has been used to study the behavior of the π-electrons of benzene.

In order to satisfy the requirement of being single-valued, the momentum wavefunction in coordinate space for a particle on a ring of radius R must satisfy the following condition,

$$\langle x + 2\pi R|p\rangle = \langle x|p\rangle$$

This leads to,

$$\exp\left(\frac{i2\pi Rp}{\hbar}\right)\exp\left(\frac{ipx}{\hbar}\right) = \exp\left(\frac{ipx}{\hbar}\right)$$

This equation can be written as,

$$\exp\left(\frac{i2\pi Rp}{\hbar}\right) = 1 = \exp(i2\pi m) \quad \text{where} \quad \mathrm{m} = 0, \pm 1, \pm 2, ...$$

Comparison of the left with the far right of this equation reveals that,

$$\frac{Rp}{\hbar} = m$$

It is easy to show that the energy manifold associated with this quantum restriction is,

$$E_m = m^2\left(\frac{\hbar^2}{2m_eR^2}\right)$$

The corresponding wave functions can be found in the widely used textbook authored by Atkins and de Paula (11).

There are, of course, many formulations of quantum mechanics, and all of them develop quantum mechanical principles in different ways from diverse starting points, but they are all formally equivalent. In the present approach the key concepts are de Broglie's hypothesis as stated in Equation , and the eigenvalue equations (3) and (9) expressed in the momentum and coordinate representations, respectively.

Another formulation (Heisenberg's approach) identifies the commutation relation of Equation as the basis of quantum theory, and adopts operators for position and momentum that satisfy the equation.

$$[\hat{p}, \hat{x}] = \hat{p}\hat{x} - \hat{x}\hat{p} = \frac{\hbar}{i}$$

Equation can be confirmed in both coordinate and momentum space for any state function *Ψ, using the operators in the table above.

$$\langle x|(\hat{p}\hat{x} - \hat{x}\hat{p})|\Psi\rangle = \frac{\hbar}{i}\left(\frac{d}{dx}x - x\frac{d}{dx}\right)\langle x|\Psi\rangle = \frac{\hbar}{i}\langle x|\Psi\rangle$$

$$\langle p|(\hat{p}\hat{x} - \hat{x}\hat{p})|\Psi\rangle = i\hbar\left(p\frac{d}{dp} - \frac{d}{dp}p\right)\langle p|\Psi\rangle = \frac{\hbar}{i}\langle p|\Psi\rangle$$

The meaning associated with equations (48) and (49) is that the observables associated with non-commuting operators cannot simultaneously have well-defined values. This, of course, is just another statement of the uncertainty principle.

The famous double-slit experiment illustrates the uncertainty principle in a striking way. To illustrate this it is mathematically expedient to begin with infinitesimally thin slits. Later this restriction will be relaxed.

A screen with infinitesimally thin slits (6) at x_1 and x_2 projects the incident beam into a linear superposition of position eigenstates.

$$|\Psi\rangle = \frac{1}{\sqrt{2}}[|x_1\rangle + |x_2\rangle]$$

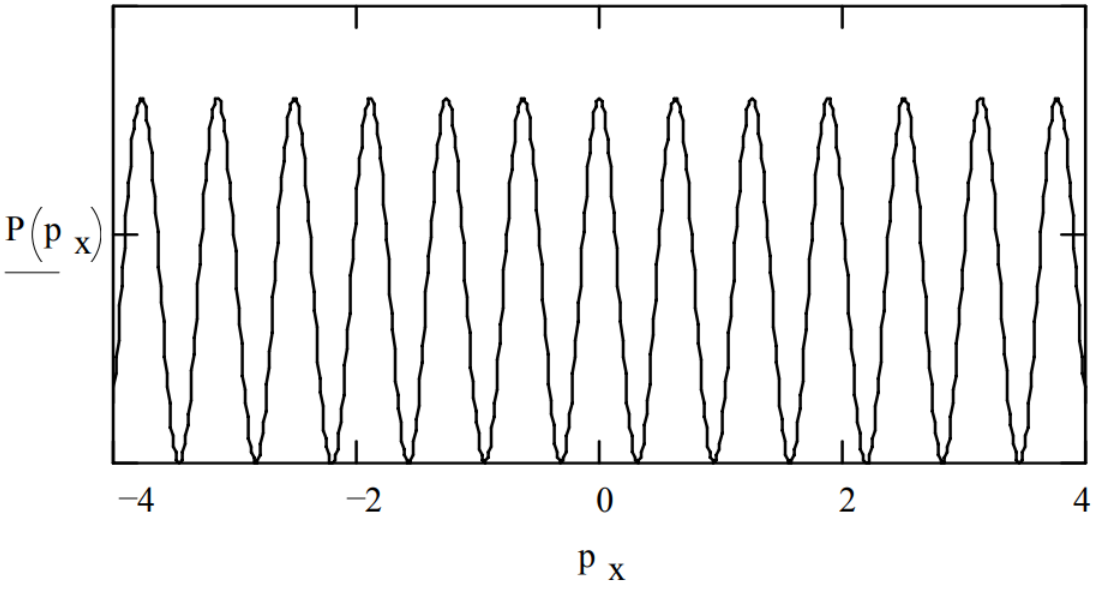
Expressing this state in the coordinate representation yields the following superposition of Dirac delta functions.

$$\langle x|\Psi\rangle = \frac{1}{\sqrt{2}}[\langle x|x_1\rangle + \langle x|x_2\rangle] = \frac{1}{\sqrt{2}}\left[\delta\left(x - x_1\right) + \delta\left(x - x_2\right)\right]$$

According to the uncertainty principle this localization of the incident beam in coordinate space is accompanied by a delocalization of the x-component of the momentum, p_x. This can be seen by projecting $|\Psi\rangle$ onto momentum space.

$$\langle p_x|\Psi\rangle = \frac{1}{\sqrt{2}}\left[\langle p_x|x_1\rangle + \langle p_x|x_2\rangle\right] = \frac{1}{2\sqrt{\pi\hbar}}\left[\exp\left(-\frac{ip_x x_1}{\hbar}\right) + \exp\left(-\frac{ip_x x_2}{\hbar}\right)\right]$$

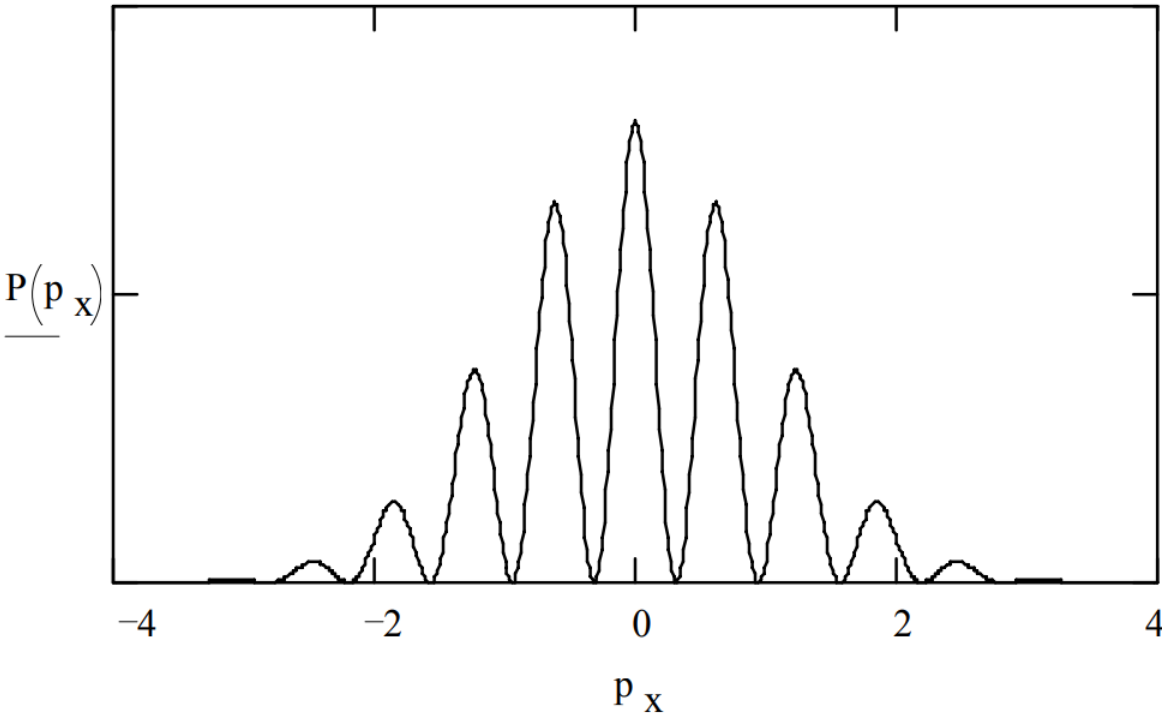
The momentum probability distribution in the x-direction, $P(p_x) = |\langle p_x|\Psi\rangle|^2$, reveals the required spread in momentum, plus the interesting interference pattern in the momentum distribution that will ultimately be projected onto the detection screen. As Marcella (6) points out the detection screen is actually measuring the x-component of the momentum.



Of course, in the actual experiment the slits are not infinitesimally thin and the diffraction pattern takes on the more familiar appearance reported in the literature (7) and textbooks (8). For example, a linear superposition of Gaussian functions can be used to represent the coordinate-space wavefunction at a screen with two slits of finite width.

$$\langle x|\Psi\rangle = \exp\left(-(x-x_1)^2\right) + \exp\left(-(x-x_2)^2\right)$$

The Fourier transform of this state into momentum space leads to the momentum distribution shown in the figure below (9).



The double-slit experiment reveals the three essential steps in a quantum mechanical experiment:

1. state preparation (interaction of incident beam with the slit-screen)
2. measurement of observable (arrival of scattered beam at the detection screen)
3. calculation of expected results of the measurement step

The Dirac delta function appeared in Equation . It expresses the fact that the position eigenstates form a continuous orthogonal basis. The same, of course, is true for the momentum eigenstates.

The bracket $\langle x|x'\rangle$ is zero unless x = x′. This expresses the condition that an object at x′ is not at x. It is instructive to expand this bracket in the momentum representation.

$$\langle x|x'\rangle = \int_{-\infty}^{\infty}\langle x|p\rangle\langle p|x'\rangle dp = \frac{1}{2\pi\hbar}\int_{-\infty}^{\infty}\exp\left(\frac{ip\,(x-x')}{\hbar}\right)dp = \delta\,(x-x')$$

The same approach for momentum yields,

$$\langle p|p'\rangle = \int_{-\infty}^{\infty}\langle p|x\rangle\langle x|p'\rangle dx = \frac{1}{2\pi\hbar}\int_{-\infty}^{\infty}\exp\left(\frac{-i\,(p-p')\,x}{\hbar}\right)dx = \delta\,(p-p')$$

The Dirac delta function has great utility in quantum mechanics, so it is important to be able to recognize it in its several guises.

The time-dependent energy operator can be obtained by adding time dependence to Equation so that it represents a classical one-dimensional plane wave moving in the positive x-direction.

$$\langle x|\lambda\rangle\langle t|v\rangle = \exp\left(i2\pi\frac{x}{\lambda}\right)\exp(-i2\pi vt)$$

This classical wave equation is transformed into a quantum mechanical wavefunction by using (as earlier) the de Broglie relation and E = hν.

$$\langle x|p\rangle\langle t|E\rangle = \exp\left(\frac{ipx}{\hbar}\right)\exp\left(-\frac{iEt}{\hbar}\right)$$

From this equation we obtain the important Dirac bracket relating energy and time.

$$\langle t|E\rangle = \exp\left(-\frac{iEt}{\hbar}\right)$$

The time-dependent energy operator is found by projecting the energy eigenvalue equation,

$$\hat{H}|E\rangle = E|E\rangle$$

into the time domain.

$$\langle t|\hat{H}|E\rangle = E\langle t|E\rangle = E\exp\left(-\frac{iEt}{\hbar}\right) = i\hbar\frac{d\langle t|E\rangle}{dt}$$

Comparison of the first and last terms reveals that the time-dependent energy operator is

$$\langle t|\hat{H} = i\hbar\frac{d}{dt}\langle t|$$

We see also from Equation that

$$i\hbar\frac{d}{dt}\langle t| = E\langle t|$$

So that in general,

$$i\hbar\frac{d}{dt}\langle t|\Psi\rangle = E\langle t|\Psi\rangle$$

Integration of Equation \ref{63) yields a general expression for the time-dependence of the wave function.

$$\langle t|\Psi\rangle = \exp\left(-\frac{iE\,(t-t_0)}{\hbar}\right)\langle t_0|\Psi\rangle$$

References

1. Chester, M. *Primer of Quantum Mechanics*; Krieger Publishing Co.:Malabar, FL, 1992.
2. Das, A.; Melissinos, A. C. *Quantum Mechanics: A Modern Introduction*; Gordon and Breach Science Publishers: New York, 1986.
3. Feynman, R. P.; Leighton, R. B.; Sands, M. *The Feynman Lectures on Physics, Vol.3*; Addison-Wesley: Reading, 1965.
4. Martin, J. L. *Basic Quantum Mechanics*; Claredon Press, Oxford, 1981.
5. Townsend, J. S. *A Modern Approach to Quantum Mechanics*; University Science Books, Sausalito, 2000.
6. Marcella, T. V. "Quantum interference with slits," *European Journal of Physics* **23**, 615-621 (2002).
7. Tonomura A.; Endo, J.; Matsuda, T.; Kawasaki, T.; Ezawa, H. "Demonstration of single-electron buildup of an interference pattern," *American Journal of Physics* **57**, 117-120 (1989).
8. French, A. P.; Taylor, E. F. An Introduction to Quantum Physics; W. W. Norton & Co., Inc. New York, 1978.
9. For further detail visit: www.users.csbsju.edu/~frioux/...t/new-slit.htm. For different approach see: www.users.csbsju.edu/~frioux/...other2slit.pdf. A description of a recent example of a temporal double-slit is available at www.users.csbsju.edu/~frioux/...poral2slit.pdf.
10. Lieber, M. "Quantum mechanics in momentum space: An illustration," *American Journal of Physics* **43**, 486-487 (1975).
11. Atkins, P.; de Paulo, J. Physical Chemistry; 7th ed. W. H. Freeman & Co., New York, 2002, p. 347.

This page titled 1.17: Quantum Mechanics and the Fourier Transform is shared under a CC BY 4.0 license and was authored, remixed, and/or curated by Frank Rioux via source content that was edited to the style and standards of the LibreTexts platform.

1.18: Exploring the Origin of Schrödinger's Equations

The purpose of this tutorial is to explore the connections between Schrödinger's equations (time-dependent and time-independent) and prior concepts in classical mechanics and quantum mechanics. For the sake of mathematical simplicity we will work in one spatial dimension.

The foundation of quantum mechanics is de Broglie's hypothesis of wave-particle duality for matter and electromagnetic radiation. Therefore, our starting point is the equation for a classical plane wave moving in the positive x direction,

$$F(x,t) = A\exp\left(i2\pi\frac{x}{\lambda}\right)\exp(-i2\pi\nu t)$$

where λ is wavelength, ν is wave frequency, and A is wave amplitude.

$F(x,t)$ can be converted to a quantum mechanical particle wave function using the relations shown below, which are succinct mathematical expressions of de Broglie's wave-particle hypothesis.

$$\lambda = \frac{h}{p} \quad \text{and} \quad E = h\nu$$

Substitution of these equations into F(x,t) yields,

$$\Psi(x,t) = A\exp\left(\frac{ipx}{\hbar}\right)\exp\left(-\frac{iEt}{\hbar}\right)$$

where $\hbar = \frac{h}{2\pi}$.

The next step is to write the classical expression for the energy of a free particle,

$$E = \frac{p^2}{2m}$$

and ask what operations must be performed on $\Psi(x,t)$ to obtain this equation.

Clearly, with appropriate pre-multipliers, the first derivative with respect to time will yield E, and the second derivative with respect to x will give kinetic energy.

$$i\hbar\frac{\partial\Psi(x,t)}{\partial t} = E\Psi(x,t)$$

$$-\frac{\hbar^2}{2m}\frac{\partial^2\Psi(x,t)}{\partial x^2} = \frac{p^2}{2m}\Psi(x,t)$$

We therefore assert that the quantum mechanical equivalent free-particle energy equation is,

$$i\hbar\frac{\partial\Psi(x,t)}{\partial t} = -\frac{\hbar^2}{2m}\frac{\partial^2\Psi(x,t)}{\partial x^2}$$

and name it the time-dependent Schrödinger equation. For a particle subject to a time-independent potential, V(x), we generalize this equation as follows,

$$i\hbar\frac{\partial\Psi(x,t)}{\partial t} = -\frac{\hbar^2}{2m}\frac{\partial^2\Psi(x,t)}{\partial x^2} + V(x)\Psi(x,t) = \hat{H}(x)\Psi(x,t)$$

An elegant expression of this equation, $i\hbar\dot{\psi} = H\psi$, can be found on Schrödinger's tombstone in Alpbach, Austria. Because V(x) is independent of time, we assume $\Psi(x,t)$ is still separable in space and time,

$$\Psi(x,t) = \Psi(x)\exp\left(-\frac{iEt}{\hbar}\right)$$

Substitution of this function into the time-dependent Schrödinger equation allows us to extract the time-independent Schrödinger equation,

$$-\frac{\hbar^2}{2m}\frac{\partial^2\Psi(x)}{\partial x^2} + V(x)\Psi(x) = E\Psi(x)$$

Solutions to this equation for various V(x) and the appropriate boundary conditions yield, in general, a manifold of allowed energy eigenvalues and associated eigenfunctions.

Sources

1. J. C. Polkinghorne, *The Quantum World*, Princeton University Press, 1984.
2. Edward Gerjuoy, “Quantum Mechanics”, in AccessScience@McGraw-Hill, http://www.accessscience.com, DOI 10.1036/1097-8542.562900, last modified: 9/11/2002

This page titled 1.18: Exploring the Origin of Schrödinger’s Equations is shared under a CC BY 4.0 license and was authored, remixed, and/or curated by Frank Rioux via source content that was edited to the style and standards of the LibreTexts platform.

1.19: Basic Quantum Mechanics in Coordinate, Momentum and Phase Space

The purpose of this paper is to use calculations on the harmonic oscillator to illustrate the relationship between the coordinate, momentum and phase space representations of quantum mechanics.

First, the ground-state coordinate space eigenfunction for the harmonic oscillator is used for several traditional quantum mechanical calculations. Then the coordinate wave function is Fourier transformed into the momentum representation, and the calculations repeated showing that the same results are obtained. Next, the coordinate (and subsequently the momentum) wave function is used to generate the Wigner phase-space distribution function. It is then used to repeat the quantum mechanical calculations done in the coordinate and momentum representations, yielding the same results. Finally, a variational calculation is carried out in all three representations for the V = |x| potential energy function using a Gaussian trial wave function. As might be expected the three calculations yield identical results.

All calculations are carried out in atomic units (h = 2π) with the effective mass and force constant set to unity (μ = k = 1) for the sake of computational convenience.

The first three harmonic oscillator eigenfunctions are given below. While the ground-state eigenfunction is used in the example calculations, it is easy for the interested reader to edit the companion Mathcad file to repeat the calculations for the other eigenfunctions.

$$\Psi_0(x) := \pi^{-\frac{1}{4}} \cdot \exp\left(-\frac{x^2}{2}\right) \qquad \Psi_1(x) := \left(\frac{4}{\pi}\right)^{\frac{1}{4}} \cdot x \cdot \exp\left(-\frac{x^2}{2}\right)$$

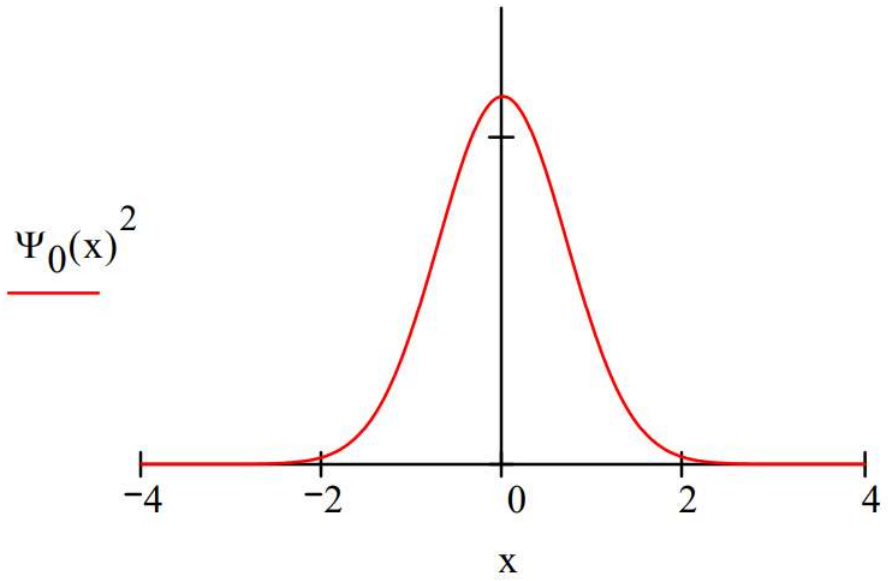
$$\Psi_2(x) := (4 \cdot \pi)^{-\frac{1}{4}} \cdot \left(2 \cdot x^2 - 1\right) \cdot \exp\left(-\frac{x^2}{2}\right)$$

As is well-known, in coordinate space the position operator is multiplicative and the momentum operator is differential. In momentum space it is the reverse, while in phase space, both position and momentum are multiplicative operators. In Appendix A Dirac notation is used to derive the position and momentum operators in coordinate and momentum space. Case (1) uses the Weyl transform to show that both the position and momentum operators are multiplicative in phase space. In Appendix B a deductive rationalization for the multiplicative character of the position operator in phase space is presented. The extension to the multiplicative character of the momentum operator is straightforward.

Coordinate Space Calculations

Coordinate space integral:	Position operator:	Potential energy operator:	Momentum operator:	Kinetic energy operator:
$\int_{-\infty}^{\infty} \square \, dx$	$x \cdot \square$	$\frac{x^2}{2} \cdot \square$	$\frac{1}{i} \cdot \frac{d}{dx} \square$	$-\frac{1}{2} \cdot \frac{d^2}{dx^2} \square$

Display the v = 0 coordinate distribution function.



Demonstrate that the wave function is normalized and calculate <x>, <x^2>,

, and <p^2>. Then use these results to demonstrate that the uncertainty principle is satisfied.

$$\int_{-\infty}^{\infty} \Psi_0(x)^2 dx = 1 \qquad x_{\text{ave}} = \int_{-\infty}^{\infty} x \cdot \Psi_0(x)^2 dx \to 0 \qquad \text{x2}_{\text{ave}} := \int_{-\infty}^{\infty} \text{x}^2 \cdot \Psi_0(\text{x})^2 \text{dx} \to \frac{1}{2}$$

$$\text{p}_{\text{ave}} := \int_{-\infty}^{\infty} \Psi_0(\text{x}) \cdot \frac{1}{\text{i}} \cdot \frac{\text{d}}{\text{dx}} \Psi_0(\text{x}) \text{dx} \to 0 \qquad \text{p2}_{\text{ave}} := \int_{-\infty}^{\infty} \Psi_0(\text{x}) \cdot \frac{\text{d}^2}{\text{dx}^2} \Psi_0(\text{x}) \text{dx} \to \frac{1}{2}$$

In the coordinate representation the expectation values involving position appear to be calculated classically. The average value is the sum over each value of x weighted by its probability of occurring, $\Psi(x)^2$. This is clearly not the case for the momentum expectation values in coordinate space. Quantum weirdness is manifest in the momentum calculations and hidden in the coordinate calculations. As mentioned above, Appendix A shows the origin of this computational difference between position and momentum expectation values in coordinate space. Basically it comes down to the fact that in its own (eigen) space an operator has special privileges, it appears to operate multiplicatively

The uncertainty principle requires that $\Delta x \cdot \Delta p \geq \frac{1}{2}$ (in atomic units). The expectation values from above show that the harmonic oscillator is in compliance.

$$\Delta x := \sqrt{x2_{\text{ave}} - x_{\text{ave}}^2} \to \frac{1}{2} \cdot 2^{\frac{1}{2}} \qquad \Delta \text{p} := \sqrt{\text{p2}_{\text{ave}} - \text{p}_{\text{ave}}^2} \to \frac{1}{2} \cdot 2^{\frac{1}{2}} \qquad \Delta \text{x} \cdot \Delta \text{p} \to \frac{1}{2}$$

Demonstrate that $\Psi_0(x)$ is an eigenfunction of the energy operator and use the expectation values from above to calculate the expectation value for energy.

$$\frac{-1}{2} \cdot \frac{\text{d}^2}{\text{dx}^2} \Psi_0(\text{x}) + \frac{1}{2} \cdot \text{x}^2 \cdot \Psi_0(\text{x}) = \text{E} \cdot \Psi_0(\text{x}) \text{ solve, E} \to \frac{1}{2} \qquad \frac{\text{p2}_{\text{ave}}}{2} + \frac{\text{x2}_{\text{ave}}}{2} \to \frac{1}{2}$$

Momentum Space Calculations

The energy operator for the harmonic oscillator is,

$$\hat{H} = \frac{\hat{p}^2}{2m} + \frac{1}{2} k \hat{x}^2$$

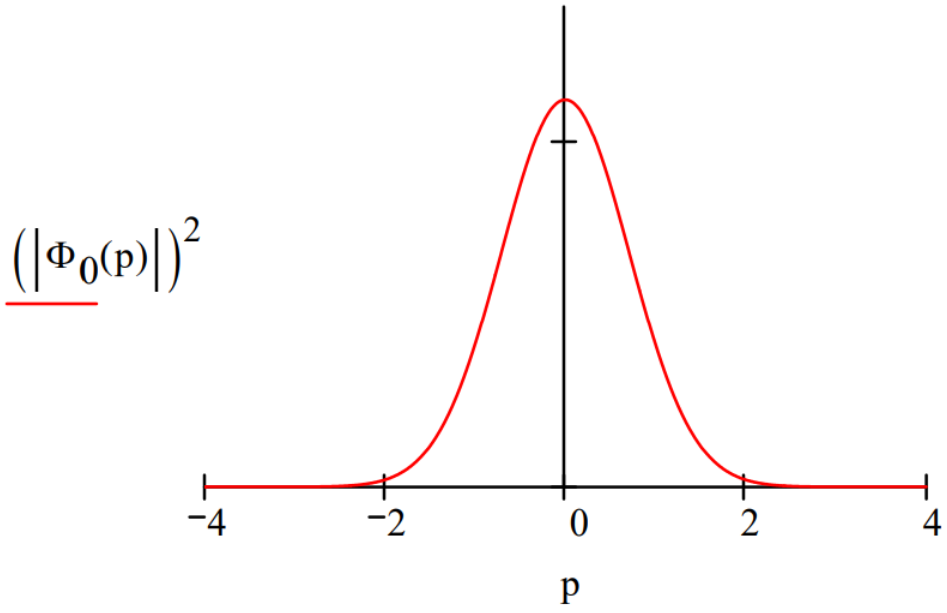
Most quantum mechanical problems are easier to solve in coordinate space. Because of its symmetry, the harmonic oscillator is as easy to solve in momentum space as it is in coordinate space. However, we generate the momentum wave function by Fourier transform of the coordinate-space wave function. It is then shown that it gives the same results as the wave function in the position basis.

$$\Phi_0(p) := \frac{1}{\sqrt{2\cdot\pi}} \cdot \int_{-\infty}^{\infty} \exp(-i\cdot p\cdot x)\Psi_0(x)dx \text{ simplify } \rightarrow \frac{\frac{e^2}{2}\cdot p^2}{\pi^{\frac{1}{4}}}$$

First, we demonstrate that the Fourier transform of this momentum wave function returns the coordinate space wave function.

$$\frac{1}{\sqrt{2\cdot\pi}} \cdot \int_{-\infty}^{\infty} \exp(i\cdot p\cdot x)\Phi_0(p)\ dp \text{ simplify } \rightarrow \frac{1}{\pi^{\frac{1}{4}}}\cdot e^{\frac{-1}{2}\cdot x^2}$$

Display the v = 0 momentum distribution function.



Notice that the coordinate and momentum distribution functions are identical given the parameterization of the calculation (μ = k = 1).

Momentum space integral: $\int_{-\infty}^{\infty} \square\, dp$	Momentum operator: $p\cdot\square$	Kinetic energy operator: $\frac{p^2}{2}\cdot\square$	Position operator: $i\cdot\frac{d}{dp}\square$	Potential energy operator: $\frac{-1}{2}\cdot\frac{d^2}{dp^2}\square$

Demonstrate that the wave function is normalized and calculate <x>, <x^2>,

, and <p^2>. Then use these results to demonstrate that the uncertainty principle is satisfied.

$$\int_{-\infty}^{\infty} (|\Phi_0(p)|)^2\, dp = 1 \quad p_{ave} := \int_{-\infty}^{\infty} p\cdot\Phi_0(p)^2 dp \rightarrow 0 \quad p2_{ave} := \int_{-\infty}^{\infty} p^2\cdot(|\Phi_0(p)|)^2\, dp \rightarrow \frac{1}{2}$$

$$x_{ave} := \int_{-\infty}^{\infty} \Phi_0(p)\cdot i\cdot\frac{d}{dp}\Phi_0(p)dp \rightarrow 0 \qquad x_{2ave} := \int_{-\infty}^{\infty} \overline{\Phi_0(p)}\cdot -\frac{d^2}{dp^2}\Phi_0(p)dp \rightarrow \frac{1}{2}$$

In momentum space, it is the momentum operator that appears to behave classically, and the position operator that manifests quantum weirdness.

These momentum space calculations are in compliance with the uncertainty principle.

$$\Delta x := \sqrt{x2_{ave} - x_{ave}^2} \rightarrow \frac{1}{2}\cdot 2^{\frac{1}{2}} \qquad \Delta p := \sqrt{p2_{ave} - p_{ave}^2} \rightarrow \frac{1}{2}\cdot 2^{\frac{1}{2}} \qquad \Delta x\cdot\Delta p \rightarrow \frac{1}{2}$$

Demonstrate that $\Phi_0(p)$ is an eigenfunction of the energy operator and use the expectation values from above to calculate the expectation value for energy.

$$\frac{p^2}{2}\cdot\Phi_0(p) - \frac{1}{2}\cdot\frac{d^2}{dp^2}\Phi_0(p) = E\cdot\Phi_0(p) \text{ solve, } E \rightarrow \frac{1}{2} \qquad \frac{p2_{ave}}{2} + \frac{x2_{ave}}{2} \rightarrow \frac{1}{2}$$

In summary, we see that coordinate and momentum space calculations give the same results. However, the coordinate wave function does not tell us anything about the distribution of momentum states, only the average value. Likewise, the momentum wave function does not provide detail on the spatial distribution of the particle it represents, only the average position.

Phase Space Calculations

Phase-space calculations require a phase-space distribution, such as the Wigner function. Because this approach to quantum mechanics is not as familiar as the Schrödinger formulation, several important equations will be deconstructed using Dirac notation. Expressed in Dirac notation, the Wigner function resembles a classical trajectory.

$$W(x,p) = \int_{-\infty}^{\infty} \left\langle \Psi | x + \frac{s}{2} \right\rangle \left\langle x + \frac{s}{2} | p \right\rangle \left\langle p | x - \frac{s}{2} \right\rangle \left\langle x - \frac{s}{2} | \Psi \right\rangle ds$$

The four Dirac brackets are read from right to left as follows: (1) is the amplitude that a particle in the state Ψ has position (x - s/2); (2) is the amplitude that a particle with position (x - s/2) has momentum p; (3) is the amplitude that a particle with momentum p has position (x + s/2); (4) is the amplitude that a particle with position (x + s/2) is (still) in the state Ψ. The Wigner function is the integral of the product of these probability amplitudes over all values of s.

We get the traditional form of the Wigner distribution function by recognizing that the middle brackets, which function as a propagator between the initial and final positional states, can be combined as follows,

$$\left\langle x + \frac{s}{2} | p \right\rangle \left\langle p | x - \frac{s}{2} \right\rangle = \frac{1}{\sqrt{2\pi}} e^{ip(x+\frac{\Delta}{2})} \frac{1}{\sqrt{2\pi}} e^{-ip(x-\frac{\delta}{2})} = \frac{1}{2\pi} e^{ips}$$

Now we can generate the Wigner function for the v = 0 harmonic oscillator state using the coordinate eigenfunction.

$$W_0(x,p) := \frac{1}{2\pi} \cdot \int_{-\infty}^{\infty} \Psi_0\left(x + \frac{s}{2}\right) \cdot \exp(i \cdot s \cdot p) \cdot \Psi_0\left(x - \frac{s}{2}\right) \text{ ds simplify } \rightarrow \frac{1}{\pi} \cdot e^{(-x^2)-p^2}$$

Now we can generate the Wigner function for the v = 0 harmonic oscillator state using the coordinate eigenfunction.

$$W_0(x,p) := \frac{1}{2\pi} \cdot \int_{-\infty}^{\infty} \Psi_0\left(x + \frac{s}{2}\right) \cdot \exp(i \cdot s \cdot p) \cdot \Psi_0\left(x - \frac{s}{2}\right) \text{ ds simplify } \rightarrow \frac{1}{\pi} \cdot e^{(-x^2)-p^2}$$

In coordinate space, momentum is represented by a differential operator, the first derivative with respect to position. In momentum space, position is represented by the first derivative with respect to momentum. Part of the appeal of the phase-space approach to quantum mechanics is that both position and momentum are represented by multiplicative operators (1). Thus phase-space quantum mechanics, at first glance, appears to more closely resemble classical mechanics than the traditional Schrödinger formulation with its differential operators.

Phase space integral:	Position operator:	Potential energy operator:	Momentum operator:	Kinetic energy operator:
$\int_{-\infty}^{\infty} \square \, dx \, dp$	$x \cdot \square$	$\frac{x^2}{2} \cdot \square$	$p \cdot \square$	$\frac{p^2}{2} \cdot \square$

Demonstrate that the Wigner function is normalized over phase space and calculate <x>, <x^2>,

, and <p^2>. Then use these results to demonstrate that the uncertainty principle is satisfied. In Appendix B Dirac notation is used to deconstruct (unpack) the first two phase-space calculations below and show that they are equivalent to the traditional quantum mechanical calculations carried out previously.

$$\int_{-\infty}^{\infty}\int_{-\infty}^{\infty} W_0(x,p)dx\ dp\ \text{simplify}\ \rightarrow 1$$

$$x_{\text{ave}} := \int_{-\infty}^{\infty}\int_{-\infty}^{\infty} W_0(x,p) \cdot x\ dx\ dp\ \text{simplify}\ \rightarrow 0 \tag{1.19.1}$$

$$x2_{\text{ave}} := \int_{-\infty}^{\infty}\int_{-\infty}^{\infty} W_0(x,p) \cdot x^2 dx\ dp\ \text{simplify}\ \rightarrow \frac{1}{2} \tag{1.19.2}$$

$$p_{\text{ave}} := \int_{-\infty}^{\infty}\int_{-\infty}^{\infty} W_0(x,p) \cdot p dx\ dp\ \text{simplify}\ \rightarrow 0 \tag{1.19.3}$$

$$p2_{\text{ave}} := \int_{-\infty}^{\infty}\int_{-\infty}^{\infty} W_0(x,p) \cdot p^2 dx\ dp\ \text{simplify}\ \rightarrow \frac{1}{2} \tag{1.19.4}$$

$$\Delta x := \sqrt{x2_{\text{ave}} - x_{\text{ave}}^2} \rightarrow \frac{1}{2}\cdot 2^{\frac{1}{2}} \quad \Delta p := \sqrt{p2_{\text{ave}} - p_{\text{ave}}^2} \rightarrow \frac{1}{2}\cdot 2^{\frac{1}{2}} \quad \Delta x \cdot \Delta p \rightarrow \frac{1}{2}$$

Calculate the expectation value for the total energy

$$\int_{-\infty}^{\infty}\int_{-\infty}^{\infty} W_0(x,p)\cdot\left(\frac{p^2}{2}+\frac{x^2}{2}\right) dx\ dp\ \text{simplify}\ \rightarrow \frac{1}{2}$$

In summary, the phase-space calculations based on the Wigner function give the same results as the calculations carried out in coordinate and momentum space.

Next, we demonstrate that integrating the Wigner function over momentum space yields the coordinate distribution function. (See the Appendix C for a deconstruction of this integral using Dirac notation.)

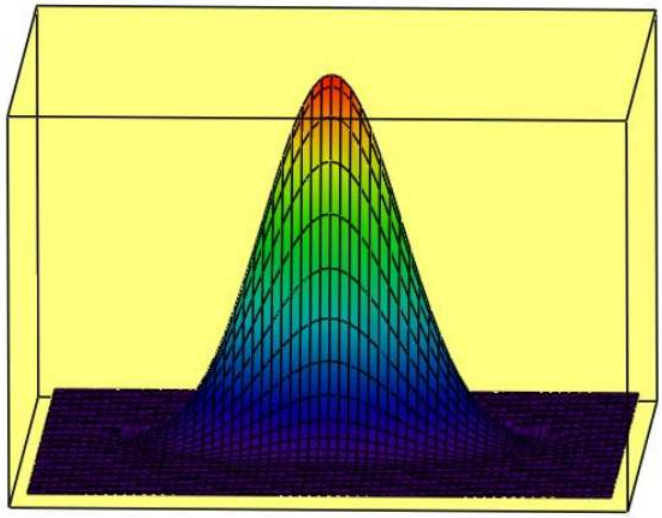
$$\int_{-\infty}^{\infty} W_0(x,p)dp\ \text{simplify}\ \rightarrow \frac{e^{-x^2}}{\pi^{\frac{1}{2}}} \qquad \Psi_0(x)^2\ \text{simplify}\ \rightarrow \frac{e^{-x^2}}{\pi^{\frac{1}{2}}}$$

Likewise, integrating the Wigner function over coordinate space yields the momentum distribution function. (See the Appendix C for a deconstruction of this integral using Dirac notation.)

$$\int_{-\infty}^{\infty} W_0(x,p)dx\ \text{simplify}\ \rightarrow \frac{e^{-p^2}}{\pi^{\frac{1}{2}}} \qquad \Phi_0(p)^2\ \text{simplify}\ \rightarrow \frac{e^{-p^2}}{\pi^{\frac{1}{2}}}$$

Just as we have previous graphed the coordinate and momentum distribution functions, we now display the Wigner distribution function.

$$N := 60 \qquad i := 0 \ldots N \qquad x_i := -3 + \frac{6\cdot i}{N} \qquad j := 0$$
$$\ldots N p_j := -5 + \frac{10\cdot j}{N} \qquad \text{Wigner}_{i,j} := W_0(x_i, p_j)$$



Wigner

In these phase-space calculations W(x,p) appears to behave like a classical probability function. By eliminating the need for differential operators, it seems to have removed some of the weirdness from quantum mechanics. However, we will now see that the Wigner function, phase-space approach only temporarily hides the weirdness. This shouldn′t come as a surprise because, after all, the Wigner function was generated using a Schrödinger wave function.

To see how the weirdness is hidden we generate the Wigner function for the v = 1 harmonic oscillator state.

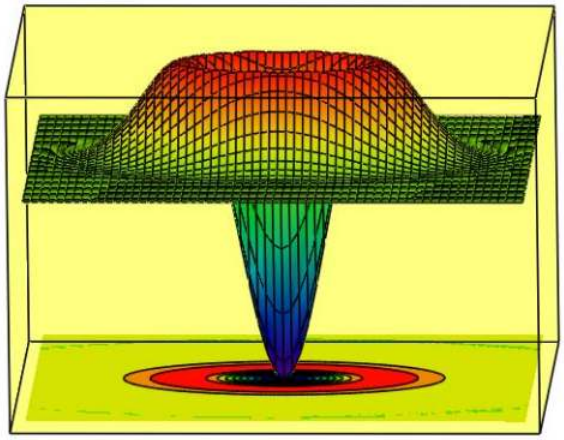
$$W_1(x,p) := \frac{1}{2\pi}\int_{-\infty}^{\infty} \Psi_1\left(x+\frac{s}{2}\right)\cdot\exp(i\cdot s\cdot p)\cdot\Psi_1\left(x-\frac{s}{2}\right)\,ds \text{ simplify}$$
$$\rightarrow e^{(-x^2)-p^2}\cdot\frac{2\cdot x^2+2\cdot p^2-1}{\pi}$$

Next, it is demonstrate that the Wigner functions for the ground and excited harmonic oscillator states are orthogonal over phase space.

$$\int_{-\infty}^{\infty}\int_{-\infty}^{\infty} W_0(x,p)\cdot W_1(x,p)dxdp \rightarrow 0$$

This result indicates that W_1(x,p) must be negative over some part of phase space, because the graph of W_0(x,p) shows that it is positive for all values of position and momentum. To explore further we display the Wigner distribution for the v = 1 harmonic oscillator state.

$$\text{Wigner}_{i,j} := W_1(x_i, p_j)$$



Wigner, Wigner

This graphic shows that the Wigner function is indeed negative for certain regions of phase space. This makes it impossible to interpret it as a probability distribution function. For this reason the Wigner function is frequently referred to as a quasiprobability distribution.

The Variation Method

As a final example of the equivalence of the three approaches to quantum mechanics presented, we look at a variation method calculation on a potential function that resembles (somewhat) the harmonic oscillator.

$$V(x) := |x|$$

A Gaussian trial wave function is chosen for the coordinate space calculation.

$$\Psi(x,\beta) := \left(\frac{2\cdot\beta}{\pi}\right)^{\frac{1}{4}} \cdot \exp\left(-\beta\cdot x^2\right)$$

The variational energy integral is evaluated.

$$E(\beta) := \int_{-\infty}^{\infty} \Psi(x,\beta)\cdot -\frac{1}{2}\cdot\frac{d^2}{dx^2}\Psi(x,\beta)dx \ldots \Bigg|_{\text{simplify}}^{\text{assume, }\beta>0}$$
$$\rightarrow \frac{1}{2}\cdot\frac{\beta^2\cdot\pi + 2^{\frac{1}{2}}\cdot(\beta\cdot\pi)^{\frac{1}{2}}}{\beta\cdot\pi} + \int_{-\infty}^{\infty} V(x)\cdot\Psi(x,\beta)^2 dx$$

The momentum wave function is obtained from the coordinate wave function by Fourier transform.

$$\Phi(p,\beta) := \frac{1}{\sqrt{2\cdot\pi}}\cdot\int_{-\infty}^{\infty}\exp(-i\cdot p\cdot x)\cdot\Psi(x,\beta)dx$$
$$\Bigg|_{\text{simplify}}^{\text{assume, }\beta>0} \rightarrow \frac{1}{2}\cdot\frac{\pi^{\frac{1}{2}}\cdot\beta^{\frac{3}{2}} + 2^{\frac{1}{2}}}{\pi^{\frac{1}{2}}\cdot\beta^{\frac{1}{2}}} + \int_{-\infty}^{\infty}\overline{\Phi(p,\beta)}\cdot\left|i\frac{d}{dp}\Phi(p,\beta)\right| dp$$

The Wigner function is calculated using the coordinate wave function (the momentum wave function will yield the same result).

$$W(x,p,\beta) := \frac{1}{2\pi}\int_{-\infty}^{\infty}\Psi\left(x+\frac{s}{2},\beta\right)\cdot\exp(i\cdot s\cdot p)\cdot\Psi\left(x-\frac{s}{2},\beta\right)ds\Bigg|_{\text{assume, }\beta>0}^{\text{simplify}} \rightarrow \frac{1}{\pi}\cdot e^{\frac{-1}{2}\cdot\frac{4\cdot\beta^2\cdot x^2+p^2}{\beta}}$$

The variational energy integral in phase space is evaluated.

$$E(\beta) := \int_{-\infty}^{\infty}\int_{-\infty}^{\infty} W(x,p,\beta)\cdot\left(\frac{p^2}{2}+V(x)\right)dxdp\Bigg|_{\text{simplify}}^{\text{assume, }\beta>0} \rightarrow \frac{1}{2}\cdot\frac{\pi^{\frac{1}{2}}\cdot\beta^{\frac{3}{2}}+2^{\frac{1}{2}}}{\pi^{\frac{1}{2}}\cdot\beta^{\frac{1}{2}}}$$

As is to be expected, the three methods yield the same expression for the variational energy. Minimization of the energy with respect to the variational parameter, β, yields β = 0.542 and E(β) = 0.813. This is in good agreement with the result obtained by numerical integration of Schrödinger′s equation for this potential, E = 0.809.

Appendix A

In coordinate space, the position eigenvalue equation can be written in two equivalent forms. In both cases the operator, in its home space, extracts the eigenvalue and returns the eigenfunction. It thus appears to be a multiplicative operator.

$$\hat{x}|x\rangle = x|x\rangle \quad \langle x|\hat{x} = x\langle x|$$

Using the form on the right we demonstrate that the position operator in the coordinate representation operates multiplicatively on an arbitrary state function.

$$\langle x|\hat{x}|\Psi\rangle = x\langle x|\Psi\rangle = x\Psi(x)$$

Making use of the coordinate space completeness relation,

$$\int |x\rangle\langle x|dx = 1$$

we can illuminate the position expectation value in the coordinate representation.

$$\langle x\rangle = \langle\Psi|\hat{x}|\Psi\rangle = \int\langle\Psi|x\rangle\langle x|\hat{x}|\Psi\rangle dx = \int\langle\Psi|x\rangle x\langle x|\Psi\rangle dx = \int x|\Psi(x)|^2 dx$$

In momentum space, the momentum eigenvalue equation can also be written in two equivalent forms. As in coordinate space, the home-space operator extracts the eigenvalue and returns the eigenfunction.

$$\hat{p}|p\rangle = p|p\rangle \quad \langle p|\hat{p} = p\langle p|$$

Using the form on the right we demonstrate that the momentum operator in momentum space operates multiplicatively on an arbitrary state function.

$$\langle p|\hat{p}|\Phi\rangle = p\langle p|\Phi\rangle = p\Phi(p)$$

To proceed to a justification of the differential form of the momentum operator in coordinate space and the differential form of the position operator in momentum space requires the following Dirac bracket between position and momentum.

$$\langle x|p\rangle = \langle p|x\rangle^* = \exp\left(\frac{ipx}{\hbar}\right)$$

This relation is obtained by substitution of the deBroglie wave equation into the Euler equation for a plane wave (2).

$$\lambda = \frac{h}{mv} = \frac{h}{p} \qquad \langle x|\lambda\rangle = \exp\left(i2\pi\frac{x}{\lambda}\right)$$

The Dirac brackets, <x|p> and <p|x> are ubiquitous in quantum mechanics and are, essentially, a dictionary for translating from momentum language to position language and vice versa. In other words, they are momentum-position Fourier transforms.

The momentum operator in coordinate space is obtained by projecting the momentum eigenvalue expression onto coordinate space.

$$\langle x|\hat{p}|p\rangle = p\langle x|p\rangle = p\exp\left(\frac{ipx}{\hbar}\right) = \frac{\hbar}{i}\frac{d}{dx}\langle x|p\rangle$$

Comparing the first and the last terms, gives the momentum operator in position space.

$$\langle x|\hat{p} = \frac{\hbar}{i}\frac{d}{dx}\langle x|$$

Using this form we demonstrate the momentum operator in coordinate space operating on an arbitrary state function.

$$\langle x|\hat{p}|\Psi\rangle = \frac{\hbar}{i}\frac{d}{dx}\langle x|\Psi\rangle = \frac{\hbar}{i}\frac{d}{dx}\Psi(x)$$

Using the coordinate completeness relation, we derive the mathematical structure of the calculation of the momentum expectation value in the coordinate representation.

$$\langle p\rangle = \langle\Psi|\hat{p}|\Psi\rangle = \int\langle\Psi|x\rangle\langle x|\hat{p}|\Psi\rangle dx = \int\langle\Psi|x\rangle\frac{\hbar}{i}\frac{d\langle x|\Psi\rangle}{dx}dx = \int\Psi^*(x)\frac{\hbar}{i}\frac{d\Psi(x)}{dx}dx$$

The position operator in momentum space is obtained by projecting the position eigenvalue expression onto momentum space.

$$\langle p|\hat{x}|x\rangle = x\langle p|x\rangle = x\exp\left(\frac{-ipx}{\hbar}\right) = -\frac{\hbar}{i}\frac{d}{dp}\langle p|x\rangle$$

Comparing the first and the last terms, gives the position operator in momentum space.

$$\langle p|\hat{x} = -\frac{\hbar}{i}\frac{d}{dp}\langle p|$$

Using this form we demonstrate the position operator in momentum space operating on an arbitrary state function.

$$\langle p|\hat{x}|\Phi\rangle = -\frac{\hbar}{i}\frac{d}{dp}\langle p|\Phi\rangle = -\frac{\hbar}{i}\frac{d}{dp}\Phi(p)$$

Illustrating the origin of the quantum mechanical calculations for the expectation values for momentum and position in momentum space are similar to the calculations in coordinate space, except that the completeness relation in momentum space is required.

$$\int|p\rangle\langle p|dp = 1$$

In the text it was noted that in phase space, both position and momentum are multiplicative operators (1). The following table summarizes the operator notation for the three spaces.

$$\begin{pmatrix} \text{Operator} & \text{CoordinateSpace} & \text{MomentumSpace} & \text{PhaseSpace} \\ \text{position} & x & \frac{-1}{\text{i}}\cdot\frac{\text{d}}{\text{dp}}\square & x \\ \text{momentum} & \frac{1}{\text{i}}\cdot\frac{\text{d}}{\text{dx}}\square & p & p \end{pmatrix}$$

Appendix B

In Dirac notation the phase-space normalization condition is,

$$\int_{-\infty}^{\infty}\int_{-\infty}^{\infty}W(x,p)dxdp = \int_{-\infty}^{\infty}\int_{-\infty}^{\infty}\int_{-\infty}^{\infty}\langle\Psi|x+\frac{s}{2}\rangle\left\langle x+\frac{s}{2}|p\right\rangle\langle p|x-\frac{s}{2}\rangle\left\langle x-\frac{s}{2}|\Psi\right\rangle dsdxdp$$

Utilizing the momentum completeness relation,

$$\int_{-\infty}^{\infty}|p\rangle\langle p|dp = 1$$

yields,

$$\int_{-\infty}^{\infty}\int_{-\infty}^{\infty}\left\langle\Psi|x+\frac{s}{2}\right\rangle\left\langle x+\frac{s}{2}|x-\frac{s}{2}\right\rangle\left\langle x-\frac{s}{2}|\Psi\right\rangle dsdx$$

However, the integral over s is zero unless s = 0. Thus, for a normalized coordinate wave function we arrive at,

$$\int_{-\infty}^{\infty}\langle\Psi|x\rangle\langle x|\Psi\rangle dx = 1$$

Using similar arguments it is easy to show that,

$$\int_{-\infty}^{\infty}\int_{-\infty}^{\infty}W(x,p)xdxdp = \int_{-\infty}^{\infty}\langle\Psi|x\rangle x\langle x|\Psi\rangle dx = \langle x\rangle$$

Appendix C

To show that integrating the Wigner function over momentum space yields the coordinate distribution function, we proceed as shown below.

$$\int_{-\infty}^{\infty} W(x,p)dp = \int_{-\infty}^{\infty}\int_{-\infty}^{\infty} \left\langle \Psi|x+\frac{s}{2}\right\rangle \left\langle x+\frac{s}{2}|p\right\rangle \left\langle p|x-\frac{s}{2}\right\rangle \left\langle x-\frac{s}{2}|\Psi\right\rangle dsdp$$

Using the momentum completeness relation (see above) on the right side gives,

$$\int_{-\infty}^{\infty} W(x,p)dp = \int_{-\infty}^{\infty} \left\langle \Psi|x+\frac{s}{2}\right\rangle \left\langle x+\frac{s}{2}|x-\frac{s}{2}\right\rangle \left\langle x-\frac{s}{2}|\Psi\right\rangle ds$$

However, the right side is zero unless s = 0, yielding

$$\int_{-\infty}^{\infty} W(x,p)dp = \langle\Psi|x\rangle\langle x|\Psi\rangle = \Psi^*(x)\Psi(x)$$

To facilitate the demonstration that integrating the Wigner function over coordinate space yields the momentum distribution function, we first show that the Wigner function can also be generated using the momentum wave function.

$$\mathrm{Wp_0(x,p)} := \frac{1}{2\cdot\pi}\cdot\int_{-\infty}^{\infty}\Phi_0\left(\mathrm{p}+\frac{\mathrm{s}}{2}\right)\cdot\exp(-\mathrm{i}\cdot\mathrm{s}\cdot\mathrm{x})\cdot\Phi_0\left(\mathrm{p}-\frac{\mathrm{s}}{2}\right)\mathrm{ds\ simplify}\rightarrow\frac{1}{\pi}\cdot\mathrm{e}^{(-\mathrm{x}^2)-\mathrm{p}^2}$$

$$\int_{-\infty}^{\infty} W(x,p)dx = \int_{-\infty}^{\infty}\int_{-\infty}^{\infty} \langle\Phi|p+\frac{s}{2}\rangle \left\langle p+\frac{s}{2}|x\right\rangle \langle x|p-\frac{s}{2}\rangle \left\langle p-\frac{s}{2}|\Phi\right\rangle dsdx$$

Employing the coordinate completeness relation

$$\int_{-\infty}^{\infty} |x\rangle\langle x|dx = 1$$

yields

$$\int_{-\infty}^{\infty} W(x,p)dx = \int_{-\infty}^{\infty} \left\langle \Phi|p+\frac{s}{2}\right\rangle \left\langle p+\frac{s}{2}|p-\frac{c}{2}\right\rangle \left\langle p-\frac{s}{2}|\Phi\right\rangle ds$$

However, the right side is zero unless s = 0, yielding

$$\int_{-\infty}^{\infty} W(x,p)dx = \langle\Phi|p\rangle\langle p|\Phi\rangle = \Phi^*(p)\Phi(p)$$

References

1. Case, W. B. Wigner functions and Weyl transforms for pedestrians. *Am. J. Phys.* **2008**, 76 937-946.
2. Rioux, F.; Johnson, B. J. Using Optical Transforms to Teach Quantum Mechanics. *Chem. Educator.* **2004**, 9, 12-16.

This page titled 1.19: Basic Quantum Mechanics in Coordinate, Momentum and Phase Space is shared under a CC BY 4.0 license and was authored, remixed, and/or curated by Frank Rioux via source content that was edited to the style and standards of the LibreTexts platform.

1.20: The Repackaging of Quantum Weirdness

Quantum mechanics offers its students and practitioners several significant conceptual challenges, among them differential operators, wave-particle duality, tunneling, uncertainty, superpositions, interference, entanglement, and non-local correlations. This tutorial deals with just one of these challenges - the concept of the quantum mechanical operator and how it extracts information from the wavefunction. Professor Chris Cramer (University of Minnesota) likens the wavefunction to an oracle - it knows all and tells some when properly addressed and questioned.

According to Daniel F. Styer (Oberlin College) there are at least nine formulations of quantum mechanics. In this tutorial the position and momentum operators will be examined in the coordinate, momentum and phase space formulations of quantum mechanics. The table below lists the forms of the operators in each of these representations. Clearly the multiplicative character of the phase space operators appeals to our classical prejudices and intuition. The differential form of the momentum operator in coordinate space and position operator in momentum space are signatures of the weird and deeply non-classical character of quantum theory. However, as we shall see the quantum weirdness in the phase-space formulation has simply been temporarily hidden.

According to Styer [*Amer. J. Phys.* **70**, 297 (2002)], "The various formulations package that weirdness in various ways, but none of them can eliminate it because the weirdness comes from the facts, not the formalism."

$$\begin{pmatrix} \text{Operator} & \text{CoordinateSpace} & \text{MomentumSpace} & \text{PhaseSpace} \\ \text{position} & x\cdot\square & i\cdot\frac{d}{dp}\square & x\cdot\square \\ \text{momentum} & \frac{1}{i}\cdot\frac{d}{dx}\square & p\cdot\square & p\cdot\square \end{pmatrix}$$

The first excited state of the harmonic oscillator will be used to illustrate the repackaging of quantum weirdness. All calculations are carried out in atomic units (h = 2π), and in the interest of mathematical clarity and expediency we add the following restriction, μ = k =1.

We begin in coordinate space by demonstrating that the $v = 1$ wavefunction is normalized and displaying its spatial distribution function. Next we calculate the expectation value for the energy and demonstrate that the wavefunction is an eigenfunction of the energy operator.

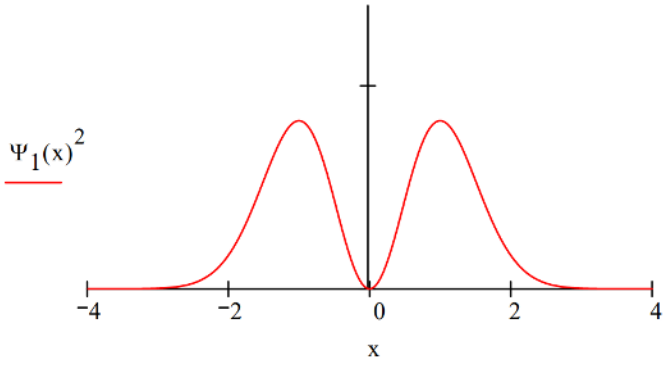
Next the v = 1 spatial wavefunction is Fourier transformed into the momentum representation and everything done for the coordinate wavefunction is repeated. We get the same result for the energy calculation, as expected. We also find, also as expected, that the momentum wavefunction is also an eigenfunction of the energy operator. To prove that this is a two-way street, we Fourier transform the momentum wavefunction back to the coordinate representation.

In the last section the Wigner function, a phase-space (coordinate-momentum space) distribution function is generated from both the coordinate and momentum wavefunctions. The calculation for the energy has a classical look to it (both position and momentum are multiplicative operators) and the result agrees with the coordinate and momentum space calculations. However, it will be easy to show that the quantum weirdness has just been hidden from direct view.

Coordinate Representation

$$\Psi_1(x) := \left(\frac{4}{\pi}\right)^{\frac{1}{4}} \cdot x \cdot \exp\left(-\frac{x^2}{2}\right) \qquad \int_{-\infty}^{\infty} \Psi_1(x)^2 dx = 1$$

Figure 1. Spatial Distribution Function



Energy expectation value:

$$\int_{-\infty}^{\infty} \Psi_1(x) \cdot \frac{-1}{2} \cdot \frac{d^2}{dx^2} \Psi_1(x) dx + \int_{-\infty}^{\infty} \Psi_1(x) \cdot \frac{1}{2} \cdot x^2 \cdot \Psi_1(x) dx = 1.5$$

The wavefunction is an eigenfunction of the energy operator:

$$\frac{-1}{2} \cdot \frac{d^2}{dx^2} \Psi_1(x) + \frac{1}{2} \cdot x^2 \cdot \Psi_1(x) = E \cdot \Psi_1(x) \text{ solve }, E \rightarrow \frac{3}{2}$$

Momentum Representation

A Fourier transform of the coordinate wavefunction yields the momentum space wavefunction.

$$\Phi_1(p) := \frac{1}{\sqrt{2 \cdot \pi}} \cdot \int_{-\infty}^{\infty} \exp(-i \cdot p \cdot x) \Psi_1(x) dx \text{ simplify } \rightarrow (-i) \cdot \frac{2^{\frac{1}{2}}}{\pi^{\frac{1}{4}}} \cdot e^{\frac{-1}{2} \cdot p^2} \cdot p$$

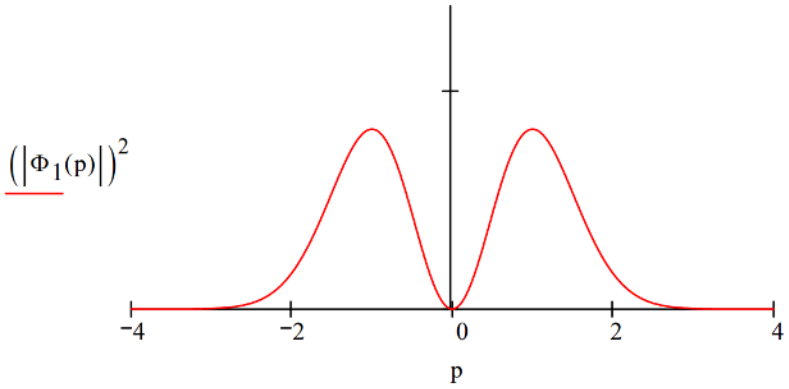
$$\int_{-\infty}^{\infty} (|\Phi_1(p)|)^2 dp = 1$$

Of course, a Fourier transform of the momentum wavefunction returns the coordinate wavefunction.

$$\frac{1}{\sqrt{2 \cdot \pi}} \cdot \int_{-\infty}^{\infty} \exp(i \cdot p \cdot x) \Phi_1(p) dp \text{ simplify } \rightarrow e^{\frac{-1}{2} \cdot x^2} \cdot \frac{2^{\frac{1}{2}}}{\pi^{\frac{1}{4}}} \cdot x$$

The momentum distribution is displayed and the energy calculations executed.

Figure 2. Momentum Distribution Function



$$\int_{-\infty}^{\infty} \overline{\Phi_1(p)} \cdot \frac{p^2}{2} \cdot \Phi_1(p) dp + \int_{-\infty}^{\infty} \overline{\Phi_1(p)} \cdot \frac{-1}{2} \cdot \frac{d^2}{dp^2} \Phi_1(p) dp = 1.5$$

$$\frac{p^2}{2} \cdot \Phi_1(p) + \frac{-1}{2} \cdot \frac{d^2}{dp^2} \Phi_1(p) = E \cdot \Phi_1(p) \text{ solve }, E \rightarrow \frac{3}{2}$$

Phase Space Representation

As shown below, the Wigner phase-space distribution function can be generated from either the coordinate or momentum wavefunctions. A deconstruction of the Wigner function can be found at: http://www.users.csbsju.edu/~frioux/wigner/wigner.pdf.

$$W_1(x,p) := \frac{1}{2\pi}\cdot\int_{-\infty}^{\infty}\exp(i\cdot s\cdot p)\cdot\Psi_1\left(x+\frac{s}{2}\right)\cdot\Psi_1\left(x-\frac{s}{2}\right)\,ds \text{ simplify}$$
$$\rightarrow e^{(-x^2)-p^2}\cdot\frac{2\cdot x^2+2\cdot p^2-1}{\pi}$$

$$\frac{1}{2\pi}\cdot\int_{-\infty}^{\infty}\exp(i\cdot s\cdot x)\cdot\Phi_1\left(p+\frac{s}{2}\right)\cdot\Phi_1\left(p-\frac{s}{2}\right)\,ds \text{ simplify}$$
$$\rightarrow -e^{(-x^2)-p^2}\cdot\frac{2\cdot x^2+2\cdot p^2-1}{\pi}$$

Integration over the spatial and momentum coordinates shows that the Wigner function is normalized.

$$\int_{-\infty}^{\infty}\int_{-\infty}^{\infty}W_1(x,p)dxdp = 1$$

Integration over the momentum coordinate yields the spatial distribution function, exactly the same as graphed in Figure 1.

$$\int_{-\infty}^{\infty}W_1(x,p)\ dp \text{ simplify } \rightarrow 2\cdot e^{-x^2}\cdot\frac{x^2}{\pi^{\frac{1}{2}}}$$

Integration over the spatial coordinate yields the momentum distribution function, exactly the same as graphed in Figure 2.

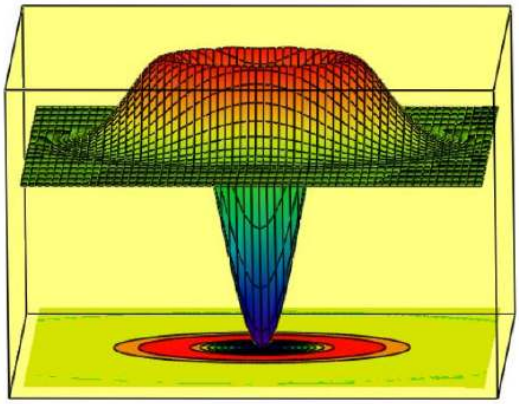
$$\int_{-\infty}^{\infty}W_1(x,p)dx \text{ simplify } \rightarrow 2\cdot e^{-p^2}\cdot\frac{p^2}{\pi^{\frac{1}{2}}}$$

The expectation value for the total energy using the Wigner distribution is the same as that obtained previously with the coordinate and momentum wavefunctions.

$$\int_{-\infty}^{\infty}\int_{-\infty}^{\infty}\left(\frac{p^2}{2}+\frac{x^2}{2}\right)\cdot W_1(x,p)dxdp = 1.5$$

This calculation has true classical flavor. The energy values, which are a function of x and p, are weighted by the phase-space (p-x) distribution function, followed by integration over all possible values of position and momentum. That quantum weirdness is being hidden is revealed when the Wigner distribution function is graphed. It can have negative values and therefore can't be a true probability distribution function. For this reason the Wigner function is referred to as a quasi-probability distribution function. In summary, in order to recover a classical-like energy calculation in quantum mechanics one has to be able to tolerate negative probabilities!

$$N := 60 \qquad i := 0\ldots N \qquad x_i := -3+\frac{6\cdot i}{N} \qquad j := 0\ldots N \qquad p_j := -5+\frac{10\cdot j}{N} \qquad \text{Wigner}_{i,j} := W_1(x_i,p_j)$$



Wigner, Wigner

This page titled 1.20: The Repackaging of Quantum Weirdness is shared under a CC BY 4.0 license and was authored, remixed, and/or curated by Frank Rioux via source content that was edited to the style and standards of the LibreTexts platform.

1.21: Quantum Principles Illuminated with Polarized Light

When unpolarized light illuminates a polarizing film oriented in the vertical direction 50% of the photons are transmitted. In quantum mechanics this event is called state preparation; the transmitted photons are now in a well-defined state – they are vertically polarized and may be represented by a Dirac ket, $|\updownarrow\rangle$. According to quantum mechanics only two subsequent experiments have certain outcomes.

1. The probability that the vertically polarized photons will pass a second vertical polarizer is 1, $(|\langle\updownarrow|\updownarrow\rangle|^2 = 1)$.
2. The probability that the vertically polarized photons will pass a second polarizer that is oriented horizontally is $(|\langle\leftrightarrow|\updownarrow\rangle|^2 = 0)$. In other words, the projection of $|\updownarrow\rangle$ onto $|\leftrightarrow\rangle$ is zero because $|\updownarrow\rangle$ and $|\leftrightarrow\rangle$ are orthogonal.

For all other experiments involving two polarizers only the probability of the outcome can be predicted, and this is $\cos^2(\theta)$, where θ is the relative angle of the polarizing films. See Figure 1 in the appendix for a graphical illustration of the trigonometry involved.

We now proceed to what is usually called the "three polarizer paradox." With two polarizers opposed in the vertical and horizontal orientations, a third polarizer is inserted between them at a 45° angle. Now some light is transmitted by the final horizontal polarizer. The quantum mechanical interpretation of this experiment is based on the superposition principle and is outlined below.

A vertically polarized photon can be represented as a linear superposition of any other set of orthogonal basis states, for example ± 45° relative to the vertical.

Note

$$|\swarrow\nearrow\rangle = |\nearrow\rangle$$

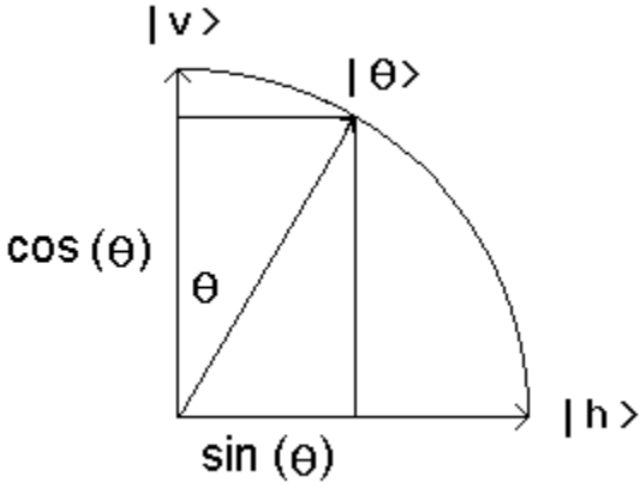
$$|\nwarrow\searrow\rangle = |\nwarrow\rangle$$

$$|\updownarrow\rangle = \frac{1}{\sqrt{2}}[|\nwarrow\searrow\rangle + |\swarrow\nearrow\rangle]$$

Thus, a vertically polarized photon has a probability of $\frac{1}{2}\left(|\langle\swarrow\nearrow|\updownarrow\rangle|^2 = \left|\frac{1}{\sqrt{2}}\right|^2 = \frac{1}{2}\right)$ of passing a polarizer oriented at a 45° angle. A photon that has passed a 45° polarizer is in the state $|\swarrow\nearrow\rangle =$. This state can be written as a linear superposition of a vertically and horizontally polarized photon.

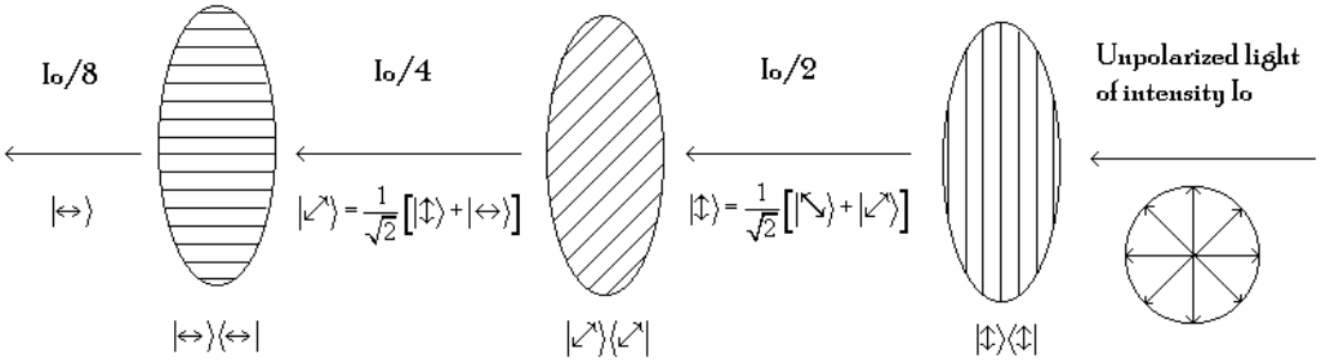
$$|\swarrow\nearrow\rangle = \frac{1}{\sqrt{2}}[|\updownarrow\rangle + |\leftrightarrow\rangle]$$

Photons that have passed the 45° polarizer have a probability of $\frac{1}{2}\left(|\langle\leftrightarrow|\swarrow\nearrow\rangle|^2 = \left|\frac{1}{\sqrt{2}}\right|^2 = \frac{1}{2}\right)$ of passing the final horizontal polarizer. To summarize, in the absence of the diagonally oriented polarizer none of the original unpolarized photons pass the final horizontal polarizer, but in its presence 12.5% of the photons are transmitted $(\frac{1}{2}\frac{1}{2}\frac{1}{2})$. See the second figure in the appendix for a graphical representation of the three-polarizer demonstration.



The probability amplitude that a θ-polarized photon will pass a vertical polarizer is $\langle v|\theta\rangle = \cos(\theta)$. The probability for this event, therefore, is $|\langle v|\theta\rangle|^2 = \cos^2(\theta)$

.



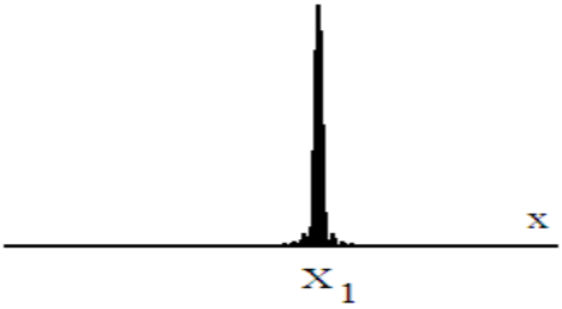
This page titled 1.21: Quantum Principles Illuminated with Polarized Light is shared under a CC BY 4.0 license and was authored, remixed, and/or curated by Frank Rioux via source content that was edited to the style and standards of the LibreTexts platform.

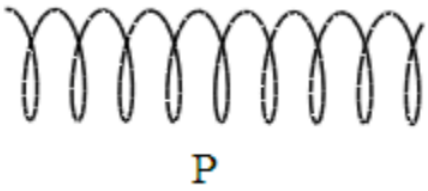
1.22: Relationship Between the Coordinate and Momentum Representations

A quon has position $x_1 : |x_1\rangle$

Coordinate space $\Leftrightarrow$ Fourier Transform $\Leftrightarrow$ Momentum space

$$\langle x|x_1\rangle = \delta(x - x_1) \underset{\int\langle x|p\rangle\langle p|x_1\rangle dp}{\overset{\int\langle p|x\rangle\langle x|x_1\rangle dx}{\rightleftharpoons}} \langle p|x_1\rangle = \exp\left(-\frac{ipx_1}{\hbar}\right)$$

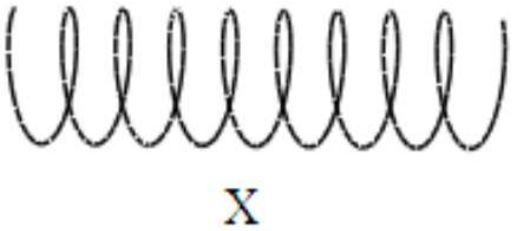


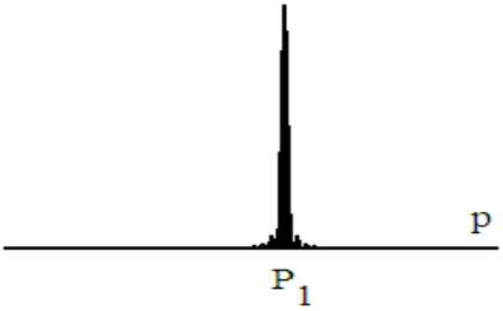


A quon has momentum $p_1 : |p_1\rangle$

Coordinate space $\Leftrightarrow$ Fourier Transform $\Leftrightarrow$ Momentum space

$$\langle x|p_1\rangle = \exp\left(\frac{ip_1x}{\hbar}\right) \underset{\int\langle x|p\rangle\langle p|p_1\rangle dp}{\overset{\int\langle p|x\rangle\langle x|p_1\rangle dx}{\rightleftharpoons}} \langle p|p_1\rangle = \delta(p - p_1)$$





Please note the important role that the coordinate and momentum completeness relations play in these transformations.

$$\int |x\rangle\langle x|dx = 1 \quad \text{and} \quad \int |p\rangle\langle p|dp = 1$$

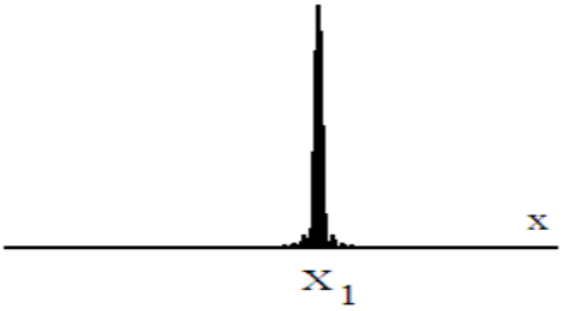
This page titled 1.22: Relationship Between the Coordinate and Momentum Representations is shared under a CC BY 4.0 license and was authored, remixed, and/or curated by Frank Rioux via source content that was edited to the style and standards of the LibreTexts platform.

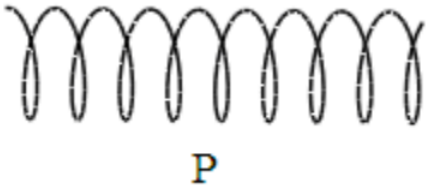
1.23: Very Brief Relationship Between the Coordinate and Momentum Representations

A quon has position $x_1 : |x_1\rangle$

Coordinate space $\Leftrightarrow$ Momentum space

$$\langle x|x_1\rangle = \delta(x - x_1) \qquad \langle p|x_1\rangle dp] \int \langle p|x\rangle\langle x|x_1\rangle dx\langle p|x_1\rangle = \exp\left(-\frac{ipx_1}{\hbar}\right)$$

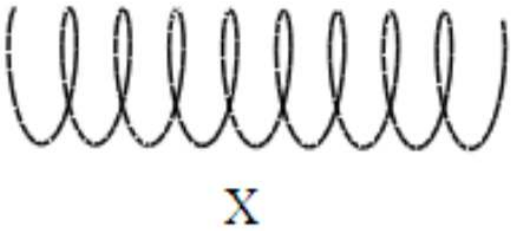


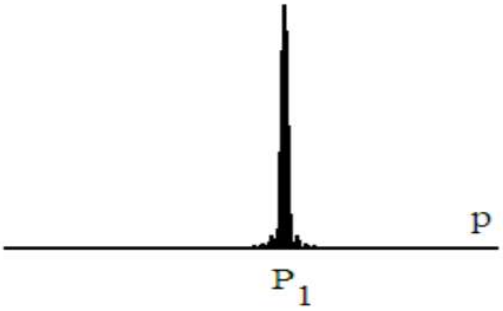


A quon has momentum $p_1 : |p_1\rangle$

Coordinate space $\Leftrightarrow$ Momentum space

$$\langle x|p_1\rangle = \exp\left(\frac{ip_1x}{\hbar}\right) \qquad \int \langle p|x\rangle\langle x|p_1\rangle dx\langle p|p_1\rangle = \delta(p - p_1)$$





This page titled 1.23: Very Brief Relationship Between the Coordinate and Momentum Representations is shared under a CC BY 4.0 license and was authored, remixed, and/or curated by Frank Rioux via source content that was edited to the style and standards of the LibreTexts platform.

1.24: Getting Accustomed to the Superposition Principle

It is impossible to simulate a quantum mechanical superposition with a mixture of M&M candies, or any other ensemble of macroscopic objects (*1*). Among the defining characteristics of a superposition is that ***it is not a mixture***. Miller acknowledges that while his demonstration is not "*strictly* accurate", it is "quite effective and achieves a variety of educational goals." In spite of Miller's claims it is my contention that the students have not been provided with a concrete or correct picture of the superposition principle with his exercise.

Here is what Dirac had to say about the linear superposition in his famous treatise on quantum mechanics:

> *The nature of the relationships which the superposition principle requires to exist between the states of any system is of a kind that cannot be explained in terms of familiar physical concepts. One cannot in the classical sense picture a system being partly in each of two states and see the equivalence of this to the system being completely in some other state. There is an entirely new idea involved, to which one must get accustomed and in terms of which one must proceed to build up an exact mathematical theory, without having any detailed classical picture. (2)*

With regard to the desire for classical pictures, Dirac said,

> *...the main object of physical science is not the provision of pictures, but is the formulation of laws governing phenomena and application of these laws to the discovery of new phenomena. If a picture exists, so much the better; but whether a picture exists or not is a matter of only secondary importance. In the case of atomic phenomena no picture can be expected to exist in the usual sense of the word 'picture' by which is meant a model functioning essentially on classical lines. (3)*

We do more harm than good by constructing facile, but false classical analogies for non-classical concepts. Therefore, the only reliable way to *get accustomed* to the non-classical nature of the quantum mechanical superposition is by direct appeal to experiment. One must study those cases in optics and spectroscopy, for example, where the superposition principle manifests itself most directly. The available examples are edifying, plentiful, and usually quite surprising.

Before reviewing some of these experimental examples I would like to comment on two errors in Miller's application of the superposition principle to the particle in a one-dimensional box. First, he incorrectly writes that the wave function is $\Psi(x) := N \cdot \sin(n \cdot k \cdot x)$, but clearly the argument of the sine function is either ($k_n x$) or $\frac{n\pi x}{a}$), where *a* is the box dimension. This initial error is compounded by the assertion that the coordinate-space wave function is an equal superposition of two momentum eigenstates with eigenvalues "proportional" (?) to $\frac{kh}{2\pi}$. Basically the same error is made by Atkins (*4*), Miller's primary reference.

The expectation value for momentum is indeed zero, but to describe in more detail the outcome of momentum measurements on a particle in a one-dimensional box a momentum-space wave function is required. Such a wave function can be obtained by a Fourier transform of the coordinate-space wave function into momentum space (*5*, *6*, *7*). For the particle in a one-bohr box, in atomic units, the Fourier transform is,

$$\Phi(\mathrm{p}) := \frac{1}{\sqrt{2 \cdot \pi}} \cdot \int_0^1 \exp(-\mathrm{i} \cdot \mathrm{p} \cdot \mathrm{x}) \cdot \sqrt{2} \cdot \sin(\mathrm{n} \cdot \pi \cdot \mathrm{x}) \mathrm{dx}$$

Evaluation of this integral yields,

$$\Phi(\mathrm{p}) := \frac{\mathrm{n} \cdot \pi - \mathrm{n} \cdot \exp(-\mathrm{i} \cdot \mathrm{p}) \cdot \cos(\mathrm{n} \cdot \mathrm{p}) - \mathrm{i} \cdot \mathrm{p} \cdot \exp(-\mathrm{i} \cdot \mathrm{p}) \cdot \sin(\mathrm{n} \cdot \pi)}{\sqrt{\pi} \cdot (\mathrm{n}^2 \cdot \pi^2 - \mathrm{p}^2)}$$

Graphical representations of the momentum-space distribution, $|\Phi(\mathrm{p})|^2$, as a function of the quantum number *n* demonstrate that the momentum distribution is never simply $\frac{kh}{2\pi}$ (*5*, *6*, *7*).

Turning now to empirical examples of the superposition principle, we consider first the double-slit experiment which Richard Feynman made so famous.

> *We choose to examine a phenomenon which is impossible, **absolutely** impossible, to explain in any classical way, and which has in it the heart of quantum mechanics. In reality, it contains the **only** mystery. We cannot make the mystery go away by "explaining" how it works. We will just **tell** you how it works. In telling you how it works we will have told you about the basic peculiarities of all quantum mechanics. (8)*

Amplifying the last sentence of this quotation Feynman said, at another time, the double-slit experiment is so fundamental that if asked a question about quantum mechanics one can always reply, "You remember the case of the experiment with the two holes? It's the same thing." (*9*)

The salient feature of all double-slit experiments is, as shown in Fig. 1, that between source (S) and detector (D) the particle is offered two paths (P_1, P_2).

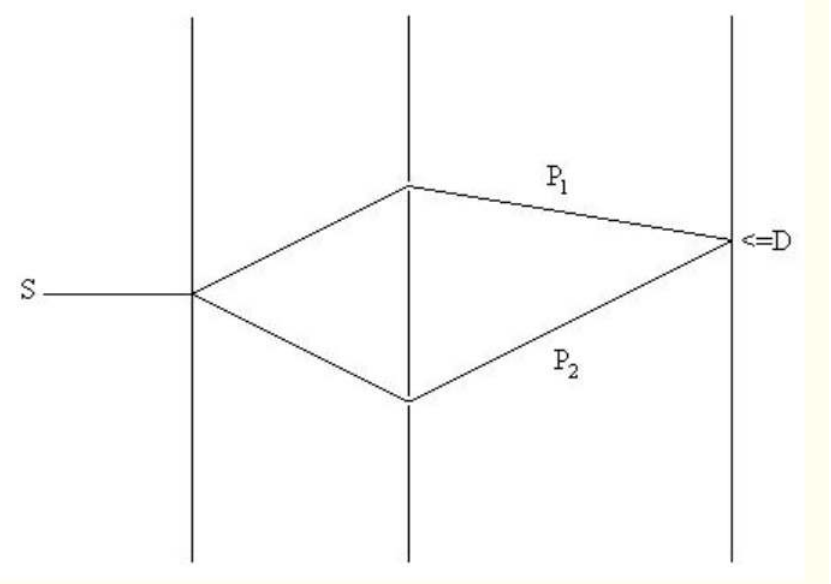


Fig. 1 - Schematic diagram of the double-slit experiment. S = source; D = detector; P_1 = path 1; P_2 = path 2.

If the path of the particle is not observed quantum mechanics requires its wave function to be a linear superposition of arriving at D by taking both paths. Under these circumstances, the probability that a particle leaving S will be detected at D is calculated as the absolute square of the sum of the probability amplitudes for arriving at D via $P_1$and P_2. (*10*)

$$P(S \rightarrow D) = |\langle D|S\rangle\ |^2 = |\langle D|P_1\rangle\langle P_1|S\rangle + |\langle D\,|P_2\rangle\langle P_2|\,S\rangle\ |^2$$

Calculation of the double-slit interference pattern is straightforward (*11*). The probability amplitude for reaching the detector via P_1, for example, is proportional to $\frac{\exp\left(\frac{2\pi i\delta_1}{\lambda}\right)}{\delta_1}$, where λ is the de Broglie wavelength of the particle and δ_1 is the distance between source and detector via P_1. Substitution of this expression and a similar one for P_2 into the previous equation yields,

$$P(S,D) := \left[\left|\frac{\exp\left(2\cdot\pi\cdot i\cdot\frac{\delta_1}{\lambda}\right)}{\delta_1} + \frac{\exp\left(2\cdot\pi\cdot i\cdot\frac{\delta_2}{\lambda}\right)}{\delta_2}\right|\right]^2$$

The addition of probability amplitudes before squaring (rather than squaring the individual probability amplitudes) leads to interference effects, a signature of the linear superposition, and one of its essential features that Miller's mixtures of M&Ms can't capture.

While Feynman presented the double-slit example pedagogically as a 'thought experiment' in his text, it has ample empirical verification for a variety of particles. For example, a demonstration of the double-slit experiment involving single electrons (only one electron in the apparatus at a time) has been reported in the pedagogical literature (*12*). Quite recently a striking interference pattern has been observed for C_{60} in a multi-slit apparatus using a diffraction grating. C_{60} is the most massive particle, so far, to demonstrate the wave-particle duality underlying the double-slit experiment (*13*). Very recently a temporal double-slit experiment with attosecond windows in the time domain has been reported. *13a*

The results reported above, and those that will follow, are stunning examples of quantum mechanical behavior with roots deep in the superposition principle. In these experiments the source produces particles and the detector registers particles, but between source and detector the behavior is wave-like with the *particle* apparently traversing both paths simultaneously. In light of this bizarre behavior Feynman said,

> *I think I can safely say that nobody understands quantum mechanics... Do not keep saying to yourself, if you can possibly avoid it, 'But how can it be like that?' because you will 'get down the drain', into a blind alley from which nobody has yet escaped. Nobody knows how it can be like that. (9)*

I think Feynman's comment, delivered in his well-known colloquial style, carries the same message as the more formal statements by Dirac quoted earlier. Dirac and Feynman are saying we must get accustomed to the fact that the nano-world is not simply a miniature of the macro-world. We must resist the expectation of being able to employ naive, visually-based, classical concepts in the nanoscopic realm. When we can't resist, we fail and then blame quantum theory for being abstract and remote from experience. However, our blame is misplaced as Marvin Chester points out in the following quotation.

> *The mathematical predictions of quantum mechanics yield results that are in agreement with experimental findings. That is the reason we use quantum theory. That quantum theory fits experiment is what validates the theory, but why experiment should give such peculiar results is a mystery." (14)*

We continue with manifestations of the superposition principle using an example from chemistry. Chemical reactions that occur by more than one mechanism create the possibility, under favorable circumstances, of a chemical double-slit phenomena with accompanying interference effects. This is how Dixon, et al. (*15*) have recently interpreted some unusual results in the photo-dissociation of water. The reaction $H_2O + h\nu$ ---> H + OH can occur through two linear intermediates I_1 (HOH), and I_2 (HHO). The OH moiety has a relative 180^o phase difference in the two intermediates, which leads to an observed even-odd intensity oscillation in the rotational states of the product OH. For the transition from reactants (R) to products (P) by a two-intermediate mechanism the previous equation becomes,

$$P(R \rightarrow P) = |\langle P|R\rangle|^2 = |\langle P|I_1\rangle\langle I_1|R\rangle + |\langle P|I_2\rangle\langle I_2|R\rangle|^2 = |\Psi(I_1) + (-1)^N \Psi(I_2)|^2$$

where N is the rotational quantum number and the term $(-1)^N$ takes into account that even rotational states are symmetric with respect to a 180^o rotation, while odd rotational states are anti-symmetric to such rotations. Clearly the interference term in this equation will be alternatively positive and negative, in agreement with the spectroscopic data.

Perhaps the most simple and striking version of the double-slit experiment is single-photon interference performed with a Mach-Zehnder interferometer (*16*). This apparatus, as Fig. 2 shows, consists of a photon source S, two 50-50 beam splitters BS, two mirrors M, and two detectors, D_1 and D_2.

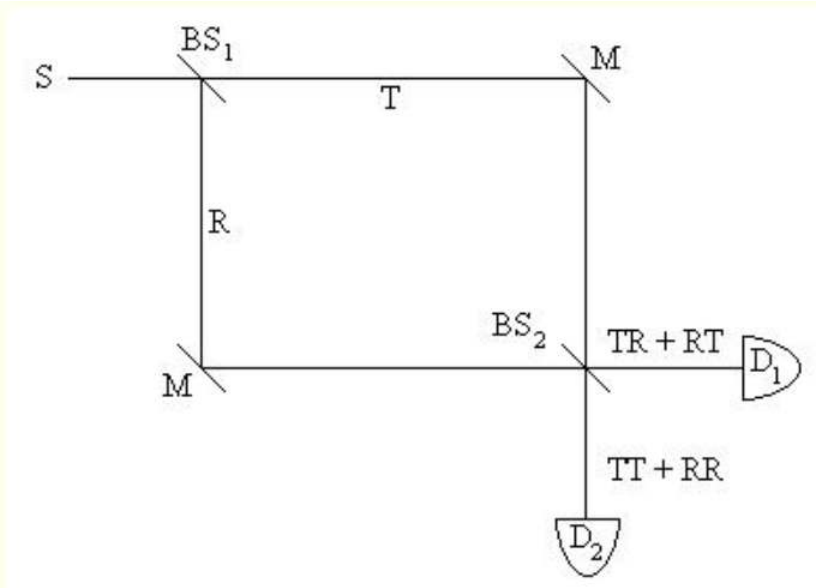


Fig. 2 - Schematic diagram of a Mach-Zehnder interferometer. S = source; BS = beam splitter; M = mirror; R = reflected; T = transmitted; D = detector; TT = transmitted at BS_1 and transmitted at BS_2; TR = transmitted at BS_1 and reflected at BS_2; etc.

The experiment can be performed with a low intensity source such that there is only one photon in the interferometer at any time. With equal path lengths to the detectors, the photon is always detected at D_1. Each detector can be reached by both paths and this requires the addition of probability amplitudes for each path, just as in the previous examples.

For D_1 the amplitudes are in phase and for D_2 they are 180 out of phase, so the photon is never detected at D_2. At the beam splitters the probability amplitude for transmission is $2^{-1/2}$ (= 0.707), while for reflection it is $i\ 2^{-1/2}$ (= 0.707 i). A 90° phase difference between transmission and reflection at the beam splitters (*17*, *18*) is assigned by convention to the reflected beam. The probability for the arrival of a photon at D_1 or $D_2$is calculated using the same formalism as in the previous examples.

$$|\langle D_1|\ S\rangle\ |^2 = |\langle D_1|\ I\rangle\langle T|S\rangle + |\langle D_1|R \times R|S\rangle\ |^2 = |(0.707i)(0.707) + (0.707)\ (0.707i)|^2 = 1$$

$$|\langle D_2|\ S\rangle\ |^2 = |\langle D_2|\ I\rangle\langle T|S\rangle + |\langle D_2|R \times R|S\rangle\ |^2 = |(0.707)(0.707) + (0.707i)\ (0.707i)|^2 = 0$$

If either path is blocked 50% of the photons get through, and 25% reach D_1 and 25% reach D_2. If the second beam splitter is removed 50% of the photons are detected at $D_1$and 50% at D_2. In both cases there is only one path to each detector, so there is no opportunity for interference of probability amplitudes.

In the examples presented so far particles have been described as being in a linear superposition of having taken both paths, not a mixture of some particles taking one path and some taking the other. The evidence in favor of the superposition has been interference effects, something which doesn't occur with mixtures of particles. However, it is possible to distinguish superpositions from mixtures without observing interference.

This example will treat Stern-Gerlach measurements in the x-z plane on spin-$\frac{1}{2}$ particles (*19*). Spin in the x- and z-directions are incompatible observables because their associated operators do not commute, which means that they cannot have simultaneous eigenstates. If a particle has a well-defined spin in the z-direction, its spin in the x-direction is uncertain, and vice versa. There are two eigenstates for each spin direction.

Let's say they are $|\uparrow\rangle$ and $|\downarrow\rangle$ in the z-direction, and $|\rightarrow\rangle$ and $|\leftarrow\rangle$ in the x-direction. The incompatibility of these observables is expressed by the following superpositions, which may also be expressed in vector form (*19*).

$$|\uparrow\rangle = \frac{1}{\sqrt{2}}[|\rightarrow\rangle + |\leftarrow\rangle] \qquad |\downarrow\rangle = \frac{1}{\sqrt{2}}[|\rightarrow\rangle - |\leftarrow\rangle]$$

$$|\rightarrow\rangle = \frac{1}{\sqrt{2}}[|\uparrow\rangle + |\downarrow\rangle] \qquad |\leftarrow\rangle = \frac{1}{\sqrt{2}}[|\uparrow\rangle - |\downarrow\rangle]$$

Now suppose that a beam of spin-$\frac{1}{2}$ particles is passed through a Stern-Gerlach apparatus oriented in the z-direction. A statistically meaningful number of measurements yields 50% $|\uparrow\rangle$ and 50% $|\downarrow\rangle$. Two hypotheses that are consistent with this outcome will be considered: the beam of particles could be completely un-polarized in the x-z plane, a random mixture of $|\uparrow\rangle$, $|\downarrow\rangle$, $|\rightarrow\rangle$, and $|\leftarrow\rangle$; or it could be a linear superposition, $|\uparrow\rangle \pm |\downarrow\rangle$. To distinguish between these alternatives it is only necessary to rotate the Stern-Gerlach magnet so that it is oriented along the x-direction. If the beam is an un-polarized mixture a large number of measurements will yield 50% $|\rightarrow\rangle$ and 50% $|\leftarrow\rangle$. However, if it is a linear superposition of $|\uparrow\rangle$ and $|\downarrow\rangle$, by the equations shown above, it will yield either 100% $|\rightarrow\rangle$ or 100% $|\leftarrow\rangle$. Experiments of this type have been reported in the primary literature (*20*) and summarized in the review literature (*21*).

Another example of the importance of the linear superposition is the ammonia maser which was first achieved experimentally in 1953. In an early paper on the maser in the popular scientific literature, J. P. Gordon (*22*) correctly described it as a "quantum-mechanical device." The maser is based on the ammonia molecule's umbrella inversion which in the classical view the nitrogen atom oscillates "back and forth" through the plane of the hydrogen atoms. This inversion vibration can be modeled quantum mechanically by a dominant harmonic potential supplemented with an internal Gaussian barrier which creates the required double potential well (*23*).

$$V = \frac{1}{2}kx^2 + b\exp\left(-cx^2\right)$$

The presence of the internal barrier causes a bunching of adjacent symmetric (+) and anti-symmetric (-) harmonic oscillator states. All states are raised in energy by the presence of the barrier, but the (-) states are elevated less than the (+) states because they have a node in the barrier and the (+) states do not. Thus v = 0 and v = 1, v = 2 and v = 3, etc. become paired with the effect declining in importance with increasing **v** quantum number as the magnitude of the energy barrier becomes less significant.

The ammonia maser is based on a microwave transition involving the first pair of symmetric and anti-symmetric states, v = 0 and v = 1. Numerical integration of Schrödinger's equation (*24*) for the first two states yields the wave equations shown in Fig. 3.

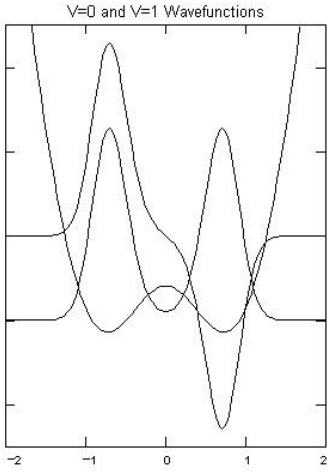


Fig. 3 - First two states (v = 0 and v = 1) for the harmonic oscillator with an internal Gaussian barrier. The wave functions are off-set on the vertical axis for clarity of presentation.

Clearly these states represent in-phase and out-of-phase superpositions of the nitrogen atom being on both sides of the plane of the hydrogen atoms. If $|NH_3\rangle$ represents the left-hand well and $|H_3N\rangle$ the right-hand well, we can write the wave functions for these states symbolically as shown below.

$$|\Psi\rangle_0 = 2^{-1/2}\left[|NH_3\rangle + |H_3N\rangle\right] \quad \text{and} \quad |\Psi\rangle_1 = 2^{-1/2}\left[|NH_3\rangle - |H_3N\rangle\right]$$

The energy difference between these states is only 0.79 cm^{-1} (*23*), so they are essentially equally populated at room temperature. However, $|\Psi\rangle_1$ can be separated from $|\Psi\rangle_0$ by electrostatic means and directed to a resonant cavity. Irradiation of the v = 1 state with a 24 GHz signal causes stimulated emission and coherent amplification of the original signal.

Up to this point we have been dealing with "one-particle" superpositions in which a single particle or system is assumed to occupy a linear superposition of two states. However, there is no limit to the number of particles or the number of states involved in the linear superposition. Einstein, in collaboration with Podolsky and Rosen (EPR), was first to explore bizarre implications of the two-particle superposition (*25*). Schrödinger called this an entangled state and identified it as a fundamental trait of quantum mechanical systems.

For example, suppose that an excited atom (calcium for example) emits two photons in a cascade in opposite directions (*26*). Conservation of angular momentum requires that the photons are either both right circularly polarized or left circularly polarized. According to the superposition principle the wave function of the composite system must be,

$$|\Psi\rangle = 2^{-1/2}\left[|\mathrm{R}\rangle_1|\,\mathrm{R}\rangle_2 + |\mathrm{L}\rangle_1|\,\mathrm{L}\rangle_2\right]$$

An EPR-like analysis demonstrated, and experiment confirmed, that such a quantum mechanically entangled state violated the realistic principle of locality and permitted in Einstein's words "spooky action at a distance." Once together, always together, or according to Lucien Hardy, "When two particles are in an entangled state they appear to continue to talk to each other even after they have finished interacting directly." (*27*) Einstein and his co-authors took this unusual prospect (at that time) as evidence that quantum mechanics was not complete and would ultimately have to be superseded by a more comprehensive theory that did not have its unpleasant non-local characteristics.

The EPR thought experiment, in the light of more recent suggestions by Bohm (*28*) and the penetrating analysis of Bell (*29*), has generated a remarkable experimental effort during the last 20 years that has confirmed Einstein's worst fear - "spooky action at a distance" is permitted, at least, in the nano-world (*30*, *31*). The experimental study of the Greenberger-Horne-Zeilinger three-particle entanglement by Pan, et al. (*32*) is among the latest confirmations of the non-locality inherent in entangled superpositions.

The empirical support for the superposition principle outlined above validates its use for theoretical interpretation. For example, we can use the superposition principle to understand the electronic ground state of the hydrogen atom, which in atomic units is, $\langle \mathrm{r}|\Psi\rangle = \Psi(\mathrm{r}) = \pi^{-1/2}exp(-r)$. This equation says that the hydrogen atom's electron is in a weighted superposition of all possible distances, r, from the nucleus. It is not orbiting the nucleus in a circular orbit or an elliptical orbit, it is not moving at all in any ordinary sense. The electron does not execute a classical trajectory within the atom. This is why in quantum mechanics we say the electron is in a stationary state, and why, un-like moving charges, it does not radiate or absorb energy unless it is making a transition from one allowed stationary state to another.

The superposition principle also provides a simple interpretation of the covalent chemical bond. In H_2^+, for example, at the most rudimentary level of theory, we write the molecular orbital as a linear superposition of the 1s orbitals of the two hydrogen atoms: $\Psi_{\mathrm{MO}} = 2^{-1/2}\left(\psi_{1\mathrm{sa}} + \psi_{1\mathrm{sb}}\right)$. Adding the probability amplitudes, ψ_{1sa} and ψ_{1sb}, is equivalent to saying the electron is delocalized over the molecule as a whole, and just as in the hydrogen atom case it is not correct to think of the electron as executing a trajectory or hopping back and forth between the two atoms. Squaring Ψ_{MO} (the sum of two probability amplitudes) to obtain the probability density yields an interference term, $2\psi_{1sa}\psi_{1sb}$, which leads to a build-up of charge in the internuclear region. Thus constructive interference associated with an in-phase linear superposition of atomic states provides an understanding of the mechanism of chemical bond formation.

Of course, a linear superposition in which the atomic orbitals are 180° (π radians)out of phase leads to destructive interference (charge depletion in the internuclear region) and an anti-bonding molecular orbital. If the atomic orbitals are 90° $\frac{\pi}{2}$ radians) out of phase, the interference term disappears yielding a non-bonding molecular orbital. In fact the superposition principle supports a continuum of atomic orbital combinations from in-phase bonding to out-of-phase anti-bonding interactions.

Moving from H_2^+ to larger molecules of more interest to chemists, we employ the same general procedure by writing a trial molecular orbital as a linear combination of all relevant atomic orbitals (LCAO-MO). Application of the variation method to solve Schrödinger's equation yields a set of optimized cannonical molecular orbitals in which the electron density is delocalized (DMO) over the molecule as a whole. While these DMOs have the most direct experimental support through photo-electron spectroscopy (and are, therefore, also called spectroscopic orbitals), they frequently are not the most useful to the chemist who has found localized electron pairs extremely helpful in understanding chemistry. The superposition principle comes to the rescue of the chemist as a number of excellent articles in this *Journal* have demonstrated over the years (*33*, *34*, *35*, *36*, *37*, *38*). Any linear combination of the cannonical orbitals is also a valid solution to Schrödinger's equation. This is the theoretical justification for

hybridizing atomic orbitals and forming localized molecular orbitals (LMOs) from DMOs. The superposition principle also provides a quantum mechanical justification for the use of the schematic, but also very useful, Lewis resonance structures (*39*).

When quantum mechanical principles are applied to atomic and molecular systems, the result is an explanation of atomic and molecular stability (the emergence of a ground state), and a manifold of quantized energy states for the internal degrees of freedom of the system being studied. Spectroscopy deals with the interaction of electromagnetic radiation with matter, and spectra are, therefore, usually interpreted as manifesting "quantum jumps" between the allowed energy levels. The superposition principle provides, as McMillen clearly showed some years ago in this *Journal* (*40*), a simple and serviceable model for the ubiquitous quantum jump.

To illustrate this model we consider an electron in the ground state of a one-dimensional box that is exposed to electromagnetic radiation. Under the influence of this perturbation the electron moves into a state that is a time-dependent linear superposition of the ground state and the manifold of excited states (in atomic units).

$$\Psi := c_1 \cdot \psi_1 \cdot \exp\left(-i \cdot E_1 \cdot t\right) + \sum_{n=2}^{\infty} c_n \cdot \psi_n \cdot \exp\left(-i \cdot E_n \cdot t\right)$$

For a transition to occur between the ground state and the first excited state, for example, two conditions must be met according to the model proposed by McMillin. First, the Bohr frequency condition must be satisfied, $\nu = \frac{E_2 - E_1}{h}$ Second, the electron density represented by the square of the absolute magnitude of the time-dependent linear superposition,

$$\left|\Psi_{1\to 2}\right|^2 = \left|c_1\psi_1 \exp\left(-i\mathrm{E}_1\mathrm{t}\right) + \mathrm{c}_2\psi_2 \exp\left(-i\mathrm{E}_2\mathrm{t}\right)\right|^2$$

must exhibit oscillating dipole character (*41*). This latter criterion is the selection rule and provides a mechanism for a coupling between the radiation field of frequency n and the electron density also oscillating with frequency ν. By comparison the n = 1 to n = 3 transition is forbidden, even if the Bohr frequency condition is satisfied, because the time-dependent superposition of these states does not exhibit oscillating dipole character; the electron density oscillates symmetrically about the center of the box and there is no coupling with the oscillating electromagnetic field (*41*).

These examples, and others not discussed here (*26*), show that the linear superposition is indeed a fundamental concept in the nanoscopic world of photons, atoms, and molecules. It has in it "the heart of quantum mechanics" to repeat Feynman's words, but what is its status in our macro-world? If quantum mechanics has universal validity, why don't we find macroscopic examples of the superposition principle? Einstein and Schrödinger answered by saying that quantum theory wasn't universally valid and that it did not present a complete physics for even the nano-world.

As noted previously, Einstein and his collaborators (*25*) demonstrated that quantum mechanics challenged certain scientific assumptions about the nature of physical reality, in particular calling into question traditional ideas regarding determinism, causality, and locality. Schrödinger formulated his famous 'cat paradox' (*42*) to demonstrate the absurdity of thinking that quantum mechanics and the superposition principle applied to the macro-world. In this ingenious thought experiment he created an entangled linear superposition which coupled the nano-world to the macro-world. Schrödinger postulated that a cat and a radioactive atom with a half-life of one hour were sealed in a box with a device (diabolical, in his words) that kills the cat if the atom decays. Therefore, after one hour the cat is presumably in an even superposition of being both alive and dead - clearly an absurd outcome from the macroscopic point of view. Furthermore, in order to reconcile quantum theory with macro-reality it is necessary to postulate that opening the box for the purpose of observing the actual state of the cat causes the wave function to "collapse" into one or the other of the equally likely contributions to the linear superposition.

$$|\Psi >= 2^{-1/2}[|\text{ cat alive }\rangle|\text{ atom not decayed }\rangle + |\text{ cat dead }\rangle|\text{ atom decayed }\rangle]$$

In this thought-experiment Schrödinger exposed a serious conflict between the formalism of quantum theory and our everyday experience, and a significant experimental and theoretical effort to resolve the conflict ensued. At the experimental level researchers have attempted to create mesocopic and macroscopic "cat" states (*43* - *45*). Theorists, for their part, have put considerable effort into creating a mechanism to explain the "collapse" of the wave function and to delineate the border between the quantum and classical worlds (*46*). For a recent survey of both experimental and theoretical work in this area the interested reader is directed to reference (*26*).

In summary, my premise has been that there are no classical analogs for the quantum mechanical superposition. To understand it one must study its experimental manifestations which, fortunately, are numerous at the nanoscopic level. To this end I have provided a brief survey of some of the more well-known empirical examples of the superposition principle. Areas of current research involving the quantum mechanical superposition that have been omitted from this presentation in the interest of brevity include quantum computing, quantum cryptography, and quantum teleportation.

Literature Cited

1. Miller, J. B. *J. Chem. Educ.* **2000**, *77*, 879.

   My critique of Miller's paper is not meant to imply that there are no pedagogically effective classical analogs for quantum mechanical principles. For successful attempts to simulate the superposition principle with macro objects see the following:

   - de Barros Neto, B. *J. Chem. Educ.* **1984**, *61*, 1044.
   - Fleming, P. E. *J. Chem. Educ.* **2001**, *78*, 57.
2. Dirac, P. A. M. *Principles of Quantum Mechanics*, 4th ed.; Oxford U. P.: London, 1958, p. 12.
3. Ibid., p. 10.
4. Atkins, P. W. *Physical Chemistry*, 6th ed.; Freeman: New York, 1998; p. 316.
5. Markley, F. L. *Am. J. Phys.* **1972**, *40*, 1545.
6. Liang, Y. Q.; Zhang, H; Dardenne, Y. X. *J. Chem. Educ.* **1995**, *72*, 148.
7. Rioux, F. *J. Chem. Educ.* **1999**, 726, 156. See also,http://www.users.csbsju.edu/~frioux/...b-momentum.htm.
8. Feynman, R. P.; Leighton, R. B.; Sands, M. *The Feynman Lectures on Physics, Vol. 3*; Addison-Wesley: Reading, 1965, p. 1-1.
9. Feynman, R. P. *The Character of Physical Law*; MIT Press: Cambridge, 1967; p. 130.
10. Dirac's bra-ket notation is used throughout this paper. Feynman's text, ref 8, is perhaps the most accessible introduction to bra-ket notation. In addition, the author has posted a Dirac notation tutorial at: http://www.users.csbsju.edu/~frioux/dirac/dirac.htm.
11. See reference 8 page 3 - 4 and www.users.csbsju. edu/~frioux/two-slit/2slit.htm for an example of how to do this calculation using Mathcad.
12. Tonomura, A.; Endo, T.; Matsuda, T.; Kawasaki, T.; Ezawa, H. *Am. J. Phys.* **1989**, *57*, 117.
13. Arndt. M.; Nairz, O.; Vos-Andreae, J.; Keller, C.; Van der Zouw, G.; Zeilinger, A. *Nature*, **1999**, *401*, 680.
    - For a description and analysis of the temporal double-slit experiment see http://www.users.csbsju.edu/~frioux/...oral-2slit.pdf and references therein.
    - For the short version see http://www.users.csbsju.edu/~frioux/...poral2slit.pdf.
14. Chester, M. *Primer of Quantum Mechanics*; Krieger Publishing Co.:Malabar, FL, 1992.
15. Dixon, R. N.; Hwang, D. W.; Yang, X. F.; Harich, S.; Lin, J. J.; Yang. X. *Science*, **1999**, *285*, 1249.
16. Scarani, V.; Suarez, A. *Am. J. Phys.* **1998**, 66, 718. For additional methods of analysis of single photon interference see:
    - http://www.users.csbsju.edu/~frioux/interfer.html
    - http://www.users.csbsju.edu/~frioux/1photon.html
    - http://www.users.csbsju.edu/~frioux/photon/photon.htm
    - http://www.users.csbsju.edu/~frioux/nu-photon.html
17. Degiorgio, V. *Am. J. Phys.* **1980**, *48*, 81.
18. Zeilinger, A. *Am. J. Phys.* **1981**, *49*, 882.
19. Rae, A. I. M. *Quantum Mechanics*, 3rd ed.; Institute of Physics Publishing, Ltd.: Bristol, 1992, pp 110-115.
20. Sumhammer, J.; Badurek, G.; Rauch, H.; Kisko, J.; Zeilinger, A. *Phys. Rev. A.* **1983**. *27*, 2523.
21. Leggett, A. J. *Contemp. Phys.* **1984**, *25*, 583.
22. Gordon, J. P. *Sci. Amer.* **1958**, *199(6)*, 42.
23. Swalen, J. D.; Ibers, J. A. *J. Chem. Phys.* **1962**, *36*, 1914.
24. The numerical integration was carried out using Mathcadwww.users.csbsju.edu/~...er/AMMONIA.pdf. with the integration algorithm described in, Hansen, J. C. *JCE: Software* **1996**, *8C(2)*.
25. Einstein, A.; Podolsky, B.; Rosen, N. *Phys. Rev.* **1935**, *45*, 777.
26. Greenstein, G.; Zajonc, A. G. *The Quantum Challenge*; Jones and Bartlett Pub.: Sudbury, 1997, and references cited therein.

27. Hardy, L. *Contemp. Phys.* **1998**, *39*, 419. For a simple example of two-photon entanglement see: http://www.users.csbsju.edu/~frioux/2photon.htm.
28. Bohm, D. *Quantum Theory*; Prentice-Hall: New York, 1951.
29. Bell, J. S. *Physics* **1964**, *1*, 195. Reprinted in: Bell, J. S. *Speakable and Unspeakable in Quantum Mechanics*, Cambridge, U. P.: Cambridge, 1987.
30. Aspect, A.; Grangier, P.; Roger, G. *Phys. Rev. Lett.* **1981**, *41*, 460.
31. Greenberger, D. M.; Horne, M. A.; Zeilinger, A. *Phys. Today*, **1993**, *44(8)*, 22.
32. Pan, J-W.; Bouwmeester, D.; Daniel, M.; Winfurter, H.; Zeilinger, A. *Nature***2000**, *403*, 515.
33. Cohen, I.; Del Bene, J. *J. Chem. Educ.* **1969,** *46*, 487.
34. Bernett, W. A. *J. Chem. Educ.* **1969**, *46*, 746.
35. Hoffman, D. K,; Ruedenberg, K. ; Verkade, J. G. *J. Chem. Educ.* **1977**, *54*, 590.
36. Liang, M. *J. Chem. Educ.* **1987**, *64*, 124.
37. Gallup, G. A. *J. Chem. Educ.* **1988**, *65*, 671.
38. Martin, R. B. *J. Chem. Educ.* **1988**, *65*, 668.
39. Feynman, R. P.; Leighton, R. B.; Sands, M., op. cit., chapter 15.
40. McMillin, D. R. *J. Chem. Educ.* **1978**, *55*, 7.
41. Rioux, F. *JCE: Software* **1993**, 1D(2). See also: http://www.users.csbsju.edu/~frioux/q-jump/njump.pdf.
42. Wheeler, J. A.; Zurek, W. H., Editors. *Quantum Theory and Measurement*; Princeton, U. P.: Princeton, 1983, pp 152-167.
43. Monroe, C.; Meekhof, D. M.; King, B. E.; Wineland, D. J. *Science* **1996**, *272*, 1131.
44. Friedman, J. R.; Patel, V.; Chen, W.; Tolpygo, S. K.; Lukens, J. E. *Nature* **2000**, *406*, 43.
45. van der Wal, C., *et al. Science* **2000**, *290*, 773. See also:www.sciencemag.org/cgi/conten...l/290/5492/720
46. Zurek, W. *Phys. Today*, **1991**, *44(10)*, 36.

This page titled 1.24: Getting Accustomed to the Superposition Principle is shared under a CC BY 4.0 license and was authored, remixed, and/or curated by Frank Rioux via source content that was edited to the style and standards of the LibreTexts platform.

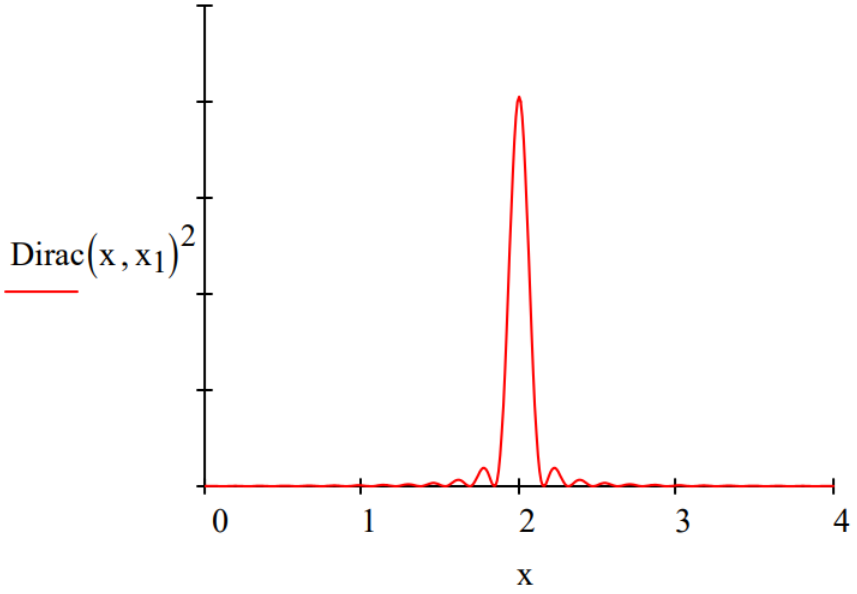
1.25: The Dirac Delta Function

The Dirac delta function expressed in Dirac notation is: $\Delta(x - x_1) = \langle x|x_1\rangle$. The $\langle x|x_1\rangle$ bracket is evaluated using the momentum completeness condition. See the Mathematical Appendix for definitions of the required Dirac brackets and other mathematical tools used in the analysis that follows.

$$\langle x|x_1\rangle = \int_{-\infty}^{\infty} \langle x|p\rangle\langle p|x_1\rangle dp = \frac{1}{2\pi}\int_{-\infty}^{\infty} \exp(ipx)\exp(-ipx_1)\,dp = \frac{1}{2\pi}\int_{-\infty}^{\infty} \exp[ip(x - x_1)]\,dp$$

Evaluation of this integral over a finite range of momentum values shows that the delta function is small except in the immediate neighborhood of x_1. Integrating from -20 to 20 to reduce computational time shows that < x | x_1 = 2> is small except in the area x = 2.

$$x_1 = 2 \quad x = 0, 0.01 \ldots 4 \quad \text{Dirac}(x, x_1) = \frac{1}{2\cdot\pi}\cdot\int_{-20}^{20} \exp[i\cdot p\cdot(x - x_1)]\,dp$$



The Fourier transform of the Dirac delta function into the momentum representation yields the following result.

$$\int_{-\infty}^{\infty} \langle p|x\rangle\langle x|x_1\rangle dx = \frac{1}{\sqrt{2\pi}}\exp(-ipx_1) = \langle p|x_1\rangle$$

The normalization constant is omitted for clarity of expression and the previous value of x_1 is cleared to allow symbolic calculation.

$$x_1 = x_1 \qquad \int_{-\infty}^{\infty} \exp(-i\cdot p\cdot x)\cdot\Delta(x - x_1)\,dx \text{ simplify } \rightarrow e^{-p\cdot x_1\cdot i}$$

Mathematical Appendix

The position and momentum completeness conditions:

$$\int |x\rangle\langle x|dx = 1 \qquad \int |p\rangle\langle p|dp = 1$$

The momentum eigenstate in the coordinate representation:

$$\langle x|p\rangle = \frac{1}{\sqrt{2\pi}}\exp(ipx)$$

The position eigenstate in the momentum representation:

$$\langle p|x\rangle = \frac{1}{\sqrt{2\pi}}\exp(-ipx)$$

This page titled 1.25: The Dirac Delta Function is shared under a CC BY 4.0 license and was authored, remixed, and/or curated by Frank Rioux via source content that was edited to the style and standards of the LibreTexts platform.

1.26: Elements of Dirac Notation

In the early days of quantum theory, P. A. M. (Paul Adrian Maurice) Dirac created a powerful and concise formalism for it which is now referred to as Dirac notation or bra-ket (bracket $\langle\,|\,\rangle$) notation.

Two major mathematical traditions emerged in quantum mechanics: **Heisenberg's matrix mechanics** and **Schrödinger's wave mechanics**. These distinctly different computational approaches to quantum theory are formally equivalent, each with its particular strengths in certain applications. Heisenberg's variation, as its name suggests, is based matrix and vector algebra, while Schrödinger's approach requires integral and differential calculus. Dirac's notation can be used in a first step in which the quantum mechanical calculation is described or set up. After this is done, one chooses either matrix or wave mechanics to complete the calculation, depending on which method is computationally the most expedient.

Kets

In Dirac's notation what is known is put in a ket, $|\,\rangle$. So, for example, $|p\rangle$ expresses the fact that a particle has momentum p. It could also be more explicit: $|p = 2\rangle$, the particle has momentum equal to 2; $|x = 1.23\rangle$, the particle has position 1.23. $|\psi\rangle$ represents a system in the state ψ and is therefore called the state vector. The ket can also be interpreted as the initial state in some transition or event.

Bras

The bra $\langle\,|$ represents the final state or the language in which you wish to express the content of the ket $|\,\rangle$. For example,$\langle 0.25|\psi\rangle$ is the probability amplitude that a particle in state ψ will be found at position $x = 0.25$. In conventional notation we write this as $\psi(x = 0.25)$, the value of the function ψ at x=0.25. The absolute square of the probability amplitude, $|\langle x = 0.25|\psi\rangle|^2$, is the probability density that a particle in state ψ will be found at x = 0.25. Thus, we see that a bra-ket pair can represent an event, the result of an experiment. In quantum mechanics an experiment consists of two sequential observations - one that establishes the initial state (ket) and one that establishes the final state (bra).

Bra-Ket Pairs

If we write $\langle x|\psi\rangle$, we are expressing ψ in coordinate space without being explicit about the actual value of x. $\langle 0.25|\psi\rangle$ is a **number**, but the more general expression $\rangle x|\psi\rangle$ is a mathematical function, a mathematical function of x, or we could say a mathematical algorithm for generating all possible values of $\langle x|\psi\rangle$, the probability amplitude that a system in state $|\psi\rangle$ has position x.

Example

For the ground state of the well-known particle-in-a-box of unit dimension.

$$\langle x|\psi\rangle = \psi(x)\ 2^{1/2}\sin(\pi x)$$

However, if we wish to express ψ in momentum space we would write

$$\langle p|\psi\rangle = \psi(p) = 2^{1/2}\frac{e^{-ip}+1}{\pi^2 - p^2}$$

How one finds this latter expression will be discussed later.

The major point here is that there is more than one language in which to express $|\psi\rangle$. The most common language for chemists is coordinate space (x, y, and z, or r, θ, and ϕ, etc.), but we shall see that momentum space offers an equally important view of the state function. It is important to recognize that $\langle x|\psi\rangle$ and $\langle p|\psi\rangle$ are formally equivalent and contain the same physical information about the state of the system. One of the tenets of quantum mechanics is that if you know $|\psi\rangle$, you know everything there is to know about the system, and if, in particular, you know $\langle x|\psi\rangle$, you can calculate all of the properties of the system and transform $\langle x|\psi\rangle$, if you wish, into any other appropriate language such as momentum space.

A bra-ket pair can also be thought of as a vector projection (i.e., a dot product) - the projection of the content of the ket onto the content of the bra, or the "shadow" the ket casts on the bra. For example, $\langle\Phi|\psi\rangle$ is the projection of state ψ onto state Φ. It is the

amplitude (probability amplitude) that a system in state $|\psi\rangle$ will be subsequently found in state $|\Phi\rangle$. It is also what we have come to call an **overlap integral**.

The $|\psi\rangle$ state vector can be a complex function (that is have the form, $a + ib$, or $exp(-ipx)$, for example, where $i = \sqrt{-1}$). Given the relation of amplitudes to probabilities mentioned above, it is necessary that $\langle\psi|\psi\rangle$, the projection of $|\psi\rangle$ onto itself is real. This requires that

$$\langle\psi| = |\psi\rangle^*$$

where $|\psi\rangle^*$ is the complex conjugate of $|\psi\rangle$. So if $|\psi\rangle = a + ib$ then $\langle\psi| = a - ib$, which yields $\langle\psi|\psi\rangle = a^2 + b^2$, a real number.

The Linear Superposition

The analysis above can be approached in a less direct, but still revealing way by writing $|\psi\rangle$ and $\langle\Phi|$ as linear superpositions in the eigenstates of the position operator as is shown below.

$$|\psi\rangle = \int |x\rangle\langle x|\psi\rangle \, dx$$

$$\langle\Phi| = \int \langle\Phi|x'\rangle\langle x'| \, dx'$$

Combining these as a bra-ket pair yields,

$$\langle\Phi|\psi\rangle = \iint \langle\Phi|x'\rangle\langle x'|x\rangle\langle x|\psi\rangle \, dx' \, dx = \int \langle\Phi|x\rangle\langle x|\psi\rangle \, dx$$

The x' disappears because the position eigenstates are an **orthogonal basis** set and $\langle x'|x\rangle = 0$ unless $x' = x$ in which case it equals 1.

$|\psi\rangle = \sum_n |n\rangle\langle n|\psi\rangle$ is a linear superposition in the discrete (rather than continuous) basis set $\{|n\rangle\}$. A specific example of this type of superposition is easy to demonstrate using matrix mechanics.

It cannot be stressed too strongly that a linear superposition is **not** a mixture. For example, when the system is in the state $|S_{su}\rangle$ every measurement of the x-direction spin yields the same result: *spin-up*. However, measurement of the z-direction spin yields spin-up 50% of the time and spin-down 50% of the time. The system has a well-defined value for the spin in the x-direction, but an indeterminate spin in the z-direction. It is easy to calculate the probabilities for the z-direction spin measurements:

$$|\langle S_{zu}|S_{xu}\rangle|^2 = \frac{1}{2}$$

and

$$|\langle S_{zd}|S_{xu}\rangle|^2 = \frac{1}{2}.$$

The reason $|S_{xu}\rangle$ cannot be interpreted as a 50-50 mixture of $|S_{zu}\rangle$ and $|S_{zu}\rangle$ is because $|S_{zu}\rangle$ and$|S_{zu}\rangle$ are linear superpositions of $|S_{xu}\rangle$ and $|S_{zxd}\rangle$:

$$|S_{zu}\rangle = \frac{|S_{xu}\rangle + |S_{xd}\rangle}{2^{1/2}}$$

and

$$|S_{zd}\rangle = \frac{|S_{xu}\rangle + |S_{xd}\rangle}{2^{1/2}}$$

Thus, if $|S_{xu}\rangle$ is a mixture of $|S_{zu}\rangle$ and $|S_{zd}\rangle$and it would yield an indefinite measurement of the spin in the x-direction in spite of the fact that it is an eigenfunction of the x-direction spin operator.

Example

Just one more example of the linear superposition. Consider a trial wave function for the particle in the one-dimensional, one-bohr box such as:

$$\Phi(x) = \sqrt{105}(x^2 - x^3)$$

Because the eigenfunctions for the particle-in-a-box problem form **a complete basis set**, $\Phi(x)$ can be written as a linear combination (i.e., a linear superposition) of these eigenfunctions.

$$|\Phi\rangle = \sum_n |n\rangle\langle n|\Phi\rangle = \sum_n |n\rangle \int \langle n|x\rangle\langle x|\Phi\rangle dx$$

In this notation $\langle n|\Phi\rangle$ is the projection of $|\Phi\rangle$ onto the eigenstate $|n\rangle$. This projection or shadow of Φ onto n can be written as c_n. It is a measure of the contribution $|n\rangle$) makes to the state $|\Phi\rangle$. It is also an overlap integral. Therefore we can write

$$|\Phi\rangle = \sum_n |n\rangle c_n$$

Using a numerical software like Matlab, it is easy to show that the first ten coefficients in this expansion are:

c_1	c_2	c_3	c_4	c_5	c_6	c_7	c_8	c_9	c_{10}
0.935	-0.351	0.035	-0.044	0.007	-0.013	0.003	-0.005	0.001	-0.003

These expansion coefficients argue that the trail wavefunction strongly resembles the lowest energy eigenstate ($|n\rangle$) of the particle in the box system.

Operators, Eigenvectors, Eigenvalues, and Expectation Values

In matrix mechanics operators are matrices and states are represented by vectors. The matrices operate on the vectors to obtain useful physical information about the state of the system. According to quantum theory there is an operator for every physical observable and a system is either in a state with a well-defined value for that observable or it is not. The operators associated with spin in the x- and z-direction are shown below in units of

When operates on the result is S is an eigenfunction or eigenvector of with eigenvalue 1 (in units of h/4). However, Sxu is not an eigenfunction of because where This means, as mentioned in the previous section, that S does not have a definite value for spin in the z- direction. Under these circumstances we can't predict with certainty the outcome of a z-direction spin measurement, but we can calculate the average value for a large number of measurements. This is called the **expectation value** and in Dirac notation it is represented as follows: In matrix mechanics it is calculated as follows.

This result is consistent with the previous discussion which showed that is a 50-50 linear superposition of and with eigenvalues of +1 and -1, respectively. In other words, half the time the result of the measurement is +1 and the other half -1, yielding an average value of zero. Now we will look at the calculation for the expectation value for a system in the state , which is set up as follows: To make this calculation computationally friendly we expand in the eigenstates of the position operator. Note the simplification that occurs because

The Variation Method

We have had a preliminary look at the variation method, an approximate method used when an exact solution to Schrödinger's equation is not available. Using

$$\Phi(x) = \sqrt{30}x(1-x)$$

as a trial wave function for the particle-in-the-box problem, we evaluate the expectation value for the energy as

$$\langle E\rangle = \langle\Phi|\hat{H}|\Phi\rangle$$

However, employing Dirac's formalism we can expand Φ as noted above, in terms of the eigenfunctions of H as follows.

$$\langle E\rangle = \langle\Phi|\hat{H}|\Phi\rangle = \sum_n \langle|\hat{H}|n\rangle\langle n|\Phi\rangle$$

However,

$$\hat{H}|n\rangle = E_n|n\rangle$$

because the states

$$|n\rangle = \sqrt{2}\sin(n\pi x)$$

are eigenfunctions of the energy operator $\hat{H}$, Thus, the energy expression becomes.

$$\langle E\rangle = \sum_n \langle|n\rangle E_n\langle n|\Phi\rangle = \sum_n |C_n|^2 E_n$$

with

$$E_n = \frac{n^2\pi^2}{2}$$

Because Φ is not an eigenfunction of $\hat{H}$, the energy operator, this system. does not have a well-defined energy and all we can do is calculate the average value for many experimental measurements of the energy. Each individual energy measurement will yield one of the eigenvalues of the energy operator, E_n, and the $|c_n|^2$ values tells us the probability of this result being achieved. Using Mathcad it is easy to show that

c_1^2	c_3^2	c_5^2	c_4^2
0.9987	0.0014,	0.00006	0.00001

All other coefficients are zero or vanishingly small. These results say that if we make an energy measurement on a system in the state represented by M there is a 99.87% chance we will get 4.935, a 0.14% chance we will get 19.739, and so on. We might say then that the state Φ is a linear combination of the first four odd eigenfunctions, with the first eigenfunction making by far the biggest contribution.

The variational theorem says that no matter how hard you try in constructing trial wave functions you cannot do better than the 'true' ground state value for the energy, and this equation captures that important principle. The only way M can give the correct result for the ground state of the particle in the box, for example, is if $c_1 = 1$, or if M is the eigenfunction itself. If this is not true, then c < 1 and the other values of c are non-zero and the energy has to be greater than E. Taking another look at the last two equations reveals that a measurement operator can always be written as a projection operator involving its eigenstates.

Momentum Operator in Coordinate Space

Wave-particle duality is at the heart of quantum mechanics. A particle with wavelength has wave function (un-normalized) . However, according to deBroglie's wave equation e the particle's momentum is . Therefore the momentum wave function of the particle in coordinate space is . In momentum space the following eigenvalue equation holds: . Operating on the momentum eigenfunction with the momentum operator in momentum space returns the momentum eigenvalue times the original momentum eigenfunction. In other words, in its own space the momentum operator is a multiplicative operator (the same is true of the position operator in coordinate space). To obtain the momentum operator in coordinate space this expression can be projected onto coordinate space by operating on the left by .

Comparing the first and last terms reveals that and that is the momentum operator in coordinate space. is the position wave function in momentum space. Using the method outlined above it is easy to show that the position operator in momentum space is

Fourier Transform

Quantum chemists work mainly in position (x,y,z) space because they are interested in electron densities, how the electrons are distributed in space in atoms and molecules. However, quantum mechanics has an equivalent formulation in momentum space. It answers the question of what does the distribution of electron velocities look like? The two formulations are equivalent, that is,

they contain the same information, and are connected formally through a Fourier transform. The Dirac notation shows this connection very clearly.

$$ppxxdx\psi = \psi$$

Starting from the left we have the amplitude that a system in state Q has position x. Then, if it has position x, the amplitude that it has momentum p. We then sum over all values of x to find all the ways a system in the stateQ can have momentum p. As a particular example we can chose the particle-in-a-box problem with eigenfunctions noted above. It is easy to show that the momentum eigenstates in position space in atomic units (see previous section) are . This, of course, means that the complex conjugate is. Therefore, the Fourier transform of Q(x) into momentum space

This integral can be evaluated analytically and yields the following momentum space wavefunctions for the particle-in-a-box. A graphical display of the momentum distribution function,(p), for several states is shown below.

Summary and References

J. L. Martin (see references below) has identified four virtues of Dirac notation.

1. It is concise. There are a small number of basic elements to Dirac's notation: bras, kets, bra-ket pairs, ket-bra products, and the completeness relation (continuous and discreet). With these few building blocks you can construct all of quantum theory.
2. It is flexible. You can use it to say the same thing in several ways; translate with ease from one language to another. Perhaps the insight that the Dirac notation offers to the Fourier transform is the best example of this virtue.
3. It is general. It is a syntax for describing what you want to do without committing yourself to a particular computational approach. In other words, you use it to set up a problem and then choose the most expeditious way to execute the calculation.
4. While it is not exactly the industry standard, it should be for the reasons listed in 1-3 above. It is widely used, so if you want to read the literature in quantum chemistry and physics, you need to learn Dirac notation. In addition most of the best quantum textbooks in chemistry and physics use it.
5. I would like to add a 5th virtue. Once you get the "hang of it" you will find that it is simple to use and very enlightening. It facilitates the understanding of all the fundamental quantum concepts.

References

1. Chester, M. Primer of Quantum Mechanics ; Krieger Publishing Co.:Malabar, FL, 1992.
2. Das, A.; Melissinos, A. C. Quantum Mechanics: A Modern Introduction; Gordon and Breach Science Publishers: New York, 1986.Feynman, R. P.; Leighton, R. B.; Sands, M. The Feynman Lectures on Physics, Vol.3 ;Addison-Wesley: Reading, 1965.
3. Martin, J. L. Basic Quantum Mechanics ; Claredon Press, Oxford, 1981.

Contributors and Attributions

- Prof. Emeritus Frank Rioux (St. John's University and College of St. Benedict)

This page titled 1.26: Elements of Dirac Notation is shared under a CC BY 4.0 license and was authored, remixed, and/or curated by Frank Rioux via source content that was edited to the style and standards of the LibreTexts platform.

1.27: The Dirac Notation Applied to Variational Calculations

The particle-in-a-box problem is exactly soluble and the solution is calculated below for the first 20 eigenstates. All calculations will be carried out in atomic units.

$$\psi(n,x) = \sqrt{2}\sin(n\pi x)$$

$$E_n = \frac{n^2\pi^2}{2}$$

with $n = 1, 2, ..., 20$

The First five EigenValues

The first five energy eigenvalues are:

$$E_1 = 4.935\ E_2 = 19.739\ E_3 = 44.413\ E_4 = 78.957\ E_5 = 123.37$$

The first three eigenfunctions are displayed below:

```
%matplotlib inline

import matplotlib.pyplot as plt
import numpy as np

t = np.linspace(0,1,100)
t1 = t*np.pi
t2 = t*np.pi*2
t3 = t*np.pi*3
a = np.sin(t1)
b = np.sin(t2)
c = np.sin(t3)
plt.xlim(0,1)
plt.plot(t,a,color = "red", label= "\u03C8 (1,x)")
plt.plot(t,b,color = "blue",label = "\u03c8 (2,x)")
plt.plot(t,c,color = "limegreen",label = "\u03c8 (3,x)")
plt.plot(t,(t*0), color ="black")

plt.xticks([0,0.5,1])
plt.yticks([-.5,0,.5],[])
plt.xlabel("x")
leg = plt.legend(loc = "center", bbox_to_anchor=[-.11,.5],frameon=False)
plt.tick_params(top=True,right=True,direction="in")

```

run | run all | restart | restart & run all

The set of eigenfunctions forms a complete basis set and any other functions can be written as a linear combinations in this basis set. For examples, Φ, χ, and Γ are three trial functions that satisfy the boundary conditions for the particle in a 1 bohr box.

$$\Phi(x) = \sqrt{30}(x - x^2)$$

$$\chi(x) = \sqrt{105}(x^2 - x^3)$$

$$\Gamma(x) = \sqrt{105}x(1 - x)^2$$

In Dirac bra-ket notation we can express and of these functions as a linear combination in the basis set as follows:

$$\langle x|\Phi\rangle = \sum_n^\infty \langle x|\psi_n\rangle\langle\psi_n|\Phi\rangle \tag{1.27.1}$$

$$= \sum_n^\infty \langle x|\psi_n\rangle \int_0^1 \langle\psi_n|x\rangle\langle x|\Phi\rangle dx \tag{1.27.2}$$

The various overlap integral for the three trial function are evaluated below.

$$a_n = \int_0^1 \psi(n,x)\Phi(x)dx$$

$$b_n = \int_0^1 \psi(n,x)\chi(x)dx$$

$$c_n = \int_0^1 \psi(n,x)\Gamma(x)dx$$

```
%matplotlib inline

import matplotlib.pyplot as plt
import numpy as np
import math

t = np.arange(0,1,.001)
plt.plot(t,math.sqrt(2)*np.sin(t*np.pi),color = "red", label = "\u03C8 (1,x)")
plt.plot(t,math.sqrt(30)*(t-t**2),color ="blue", linestyle = "--",label = "\u03A6(x)")
plt.plot(t,math.sqrt(105)*t*(1-t)**2,color = "lime", linestyle = "--", label = "\u0393 (x)")
plt.plot(t,math.sqrt(105)*(t**2 - t**3),color = "magenta", linestyle = "-.", label = "\u03A7 (x)")
plt.xticks([0.2,0.4,0.6,0.8])
plt.yticks([.5,1,1.5],[ ])
plt.tick_params(direction="in")
plt.xlabel("x")
leg = plt.legend(loc = "center",bbox_to_anchor=[-.11,.5], frameon=False)
plt.tick_params(top=True, right=True)
plt.xlim(0,1)
plt.ylim(0,2)
plt.show()
```

run | run all | restart | restart & run all

The figure shown below demonstrate that only Φ is a reasonable representative for the ground state wavefunction.

First Five Particle in a BOx EigenFunctions

If χ is written as a linear combination of the first 5 PIB eigenfunctions, one gets two functions that are essentially indistinguishable from one another.

The same, of course, is true for χ and Γ, as is demonstrated in the graphs shown below.

Traditionally we use energy as a criterion for the quality of a trial wavefunction by evaluating the variational integral in the following way.

$$\int_0^1 \Phi(x) - \frac{1}{2}\cdot\frac{d^2}{dx^2}\Phi(x)dx = 5 \quad \int_0^1 \chi(x) - \frac{1}{2}\cdot\frac{d^2}{dx^2}\chi(x)dx = 7 \quad \int_0^1 \Gamma(x)\cdot\frac{1}{2}\cdot\frac{d^2}{dx^2}\Gamma(x)dx = 7$$

In Dirac notation we write:

$$\langle E\rangle = \langle\Phi|\hat{H}|\Phi\rangle = \sum_n \langle\Phi|\hat{H}|\Psi_n\rangle\langle\Psi_n|\Phi\rangle = \sum \langle\Phi|\Psi_n\rangle E_n \langle\Psi_n|\Phi\rangle = \sum_n a_n^2 E_n$$

Thus we easily show the same result.

$$\sum_n \left[(a_n)^2\cdot E_n\right] = 5 \quad \sum_n \left[(b_n)^2\cdot E_n\right] = 6.999 \quad \sum_n \left[(c_n)^2\cdot E_n\right] = 6.999$$

We now show, belatedly, that the three trial functions are normalized by both methods.

$$\int_0^1 \Phi(x)^2 dx = 1 \quad \int_0^1 \chi(x)^2 dx = 1 \quad \int_0^1 \Gamma(x)^2 dx = 1$$

In Dirac notation this is formulated as:

$$\langle \Phi|\Phi\rangle = \sum_n \langle \Phi|\Psi_n\rangle \langle \Psi_n|\Phi\rangle = \sum_n a_n^2$$

$$\sum_{\mathrm{n}} (a_n)^2 = 1 \quad \sum_n (b_n)^2 = 1 \quad \sum_n (c_n)^2 = 1$$

We now calculate some over-lap integrals:

$$\int_0^1 \Phi(x)\cdot\chi(x)dx = 0.935 \qquad \int_0^1 \Phi(x)\cdot\Gamma(x)dx = 0.935 \qquad \int_0^1 \chi(x)\cdot\Gamma(x)dx = 0.75$$

In Dirac notation this is formulated as:

$$\langle \Phi|\Gamma\rangle = \sum_n \langle \Phi|\Psi_n\rangle \langle \Psi_n|\Gamma\rangle = \sum_n a_n c_n$$

$$\sum_{\mathrm{n}} (\mathrm{a_n}\cdot \mathrm{b_n}) = 0.935 \quad \sum_{\mathrm{n}} (\mathrm{a_n} - \mathrm{c_n}) = 0.935 \quad \sum_{\mathrm{n}} (\mathrm{b_n} - \mathrm{c_n}) = 0.75$$

This page titled 1.27: The Dirac Notation Applied to Variational Calculations is shared under a CC BY 4.0 license and was authored, remixed, and/or curated by Frank Rioux via source content that was edited to the style and standards of the LibreTexts platform.

1.28: Raising and Lowering; Creating and Annihilating

The purpose of this tutorial is to illustrate uses of the creation (raising) and annihilation (lowering) operators in the complementary coordinate and matrix representations. These operators have routine utility in quantum mechanics in general, and are especially useful in the areas of quantum optics and quantum information.

The harmonic oscillator eigenstates are regularly used to represent (in a rudimentary way) the vibrational states of diatomic molecules and also (more rigorously) the quantized states of the electromagnetic field. The creation operator adds a quantum of energy to the molecule or the electromagnetic field and the annihilation operator does the opposite.

The harmonic oscillator eigenfunctions in coordinate space are given below, where **v** is the quantum number and can have the values 0, 1, 2, ...

$$\Psi(v, x) := \frac{1}{\sqrt{2^v \cdot v! \cdot \sqrt{\pi}}} \cdot \mathrm{Her}(v, x) \cdot \exp\left(\frac{-x^2}{2}\right)$$

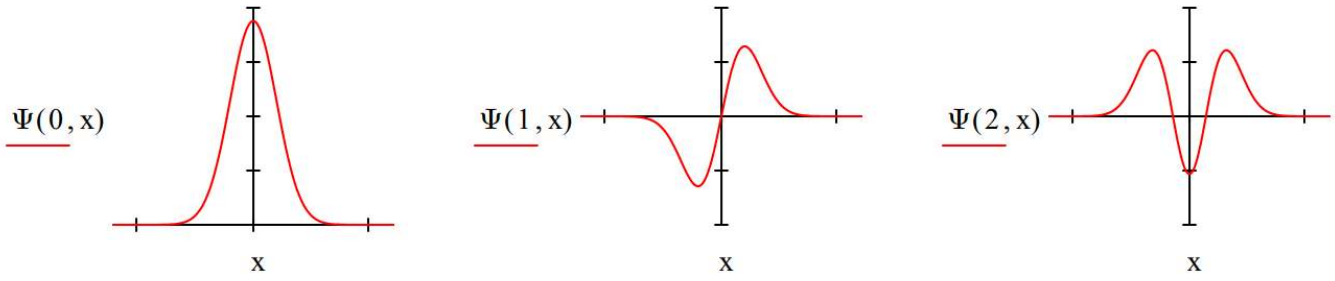
First we demonstrate that the harmonic oscillator eigenfunctions are normalized.

$$\int_{-\infty}^{\infty} \Psi(0, x)^2 dx = 1 \qquad \int_{-\infty}^{\infty} \Psi(1, x)^2 dx - 1 \qquad \int_{-\infty}^{\infty} \Psi(2, x)^2 dx = 1$$

Next we demonstrate that they are orthogonal:

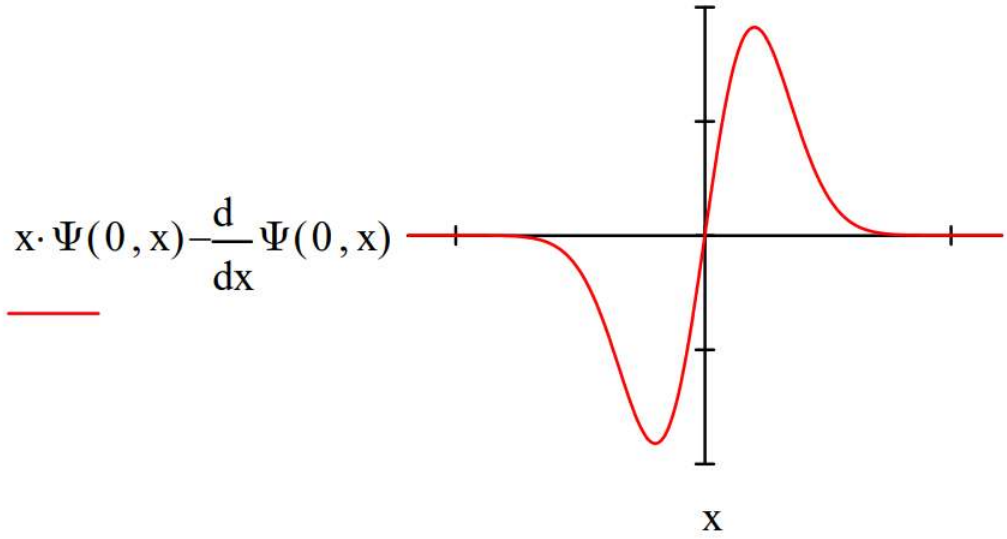
$$\int_{-\infty}^{\infty} \Psi(0, x) \cdot \Psi(1, x) dx = 0 \qquad \int_{-\infty}^{\infty} \Psi(0, x) \cdot \Psi(2, x) dx = 0 \qquad \int_{-\infty}^{\infty} \Psi(1, x) \cdot \Psi(2, x) dx = 0$$

The harmonic oscillator eigenfunctions form an orthonormal basis set. They are displayed below.



The raising or creation operator in the coordinate representation in reduced units is the position operator minus i times the coordinate space momentum operator:

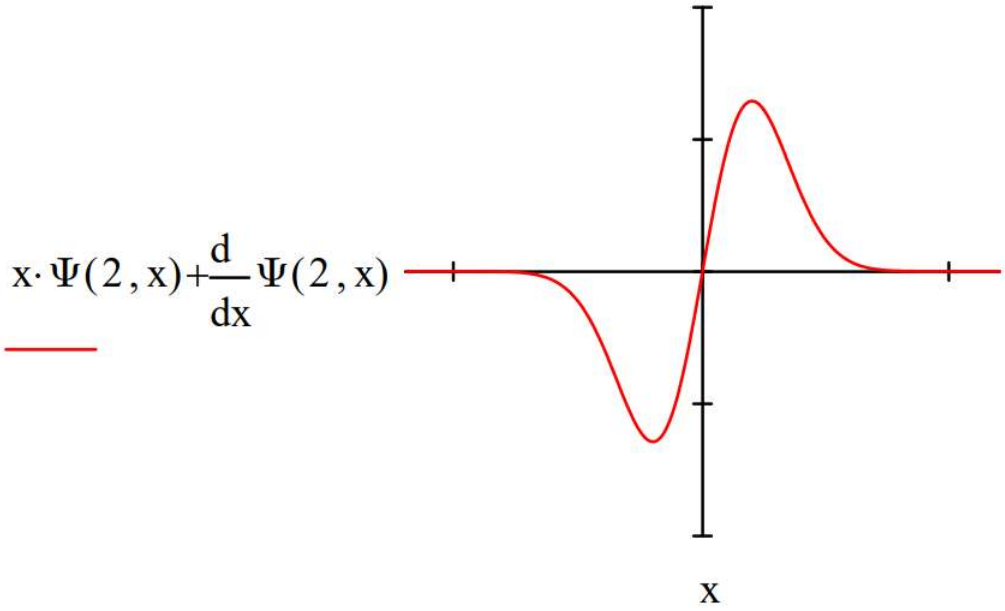
Operating on the v = 0 eigenfunction yields the v = 1 eigenfunction:



The lowering or annihilation operator in the coordinate representation in reduced units is the position operator plus i times the coordinate space momentum operator:

$$x\cdot\square + \frac{d}{dx}\square$$

Operating on the v = 2 eigenfunction yields the v = 1 eigenfunction:



The energy operator in coordinate space and the energy expectation value for the v = 2 state are given below. E_v = v + 1/2 in atomic units.

$$H = \frac{-1}{2}\cdot\frac{d^2}{dx^2}\square + \frac{1}{2}\cdot x^2\cdot\square \qquad \int_{-\infty}^{\infty}\Psi(2,x)\cdot\left[\frac{-1}{2}\cdot\frac{d^2}{dx^2}\Psi(2,x) + \frac{1}{2}\cdot x^2\cdot\Psi(2,x)\right]dx = 2.5$$

In the matrix formulation of quantum mechanics the harmonic oscillator eigenfunctions are vectors. The matrix representations for the first five eigenstates are given below. They are actually infinite vectors which for practical purposes are truncated at order 5.

$$v0 := \begin{pmatrix} 1 \\ 0 \\ 0 \\ 0 \\ 0 \end{pmatrix} \quad v1 := \begin{pmatrix} 0 \\ 1 \\ 0 \\ 0 \\ 0 \end{pmatrix} \quad v2 := \begin{pmatrix} 0 \\ 0 \\ 1 \\ 0 \\ 0 \end{pmatrix} \quad v3 := \begin{pmatrix} 0 \\ 0 \\ 0 \\ 1 \\ 0 \end{pmatrix}$$

They form an orthonormal basis set:

$$v0^{T} \cdot v0 = 1 \quad v1^{T} \cdot v1 = 1 \quad v2^{T} \cdot v2 = 1 \qquad v0^{T} \cdot v1 = 0 \quad v0^{T} \cdot v2 = 0 \quad v1^{T} \cdot v2 = 0$$

In this context the creation and annihilation operators are 5x5 matrices.

$$\text{Create} := \begin{pmatrix} 0 & 0 & 0 & 0 & 0 \\ \sqrt{1} & 0 & 0 & 0 & 0 \\ 0 & \sqrt{2} & 0 & 0 & 0 \\ 0 & 0 & \sqrt{3} & 0 & 0 \\ 0 & 0 & 0 & \sqrt{4} & 0 \end{pmatrix} \qquad \text{Annihilate} := \begin{pmatrix} 0 & \sqrt{1} & 0 & 0 & 0 \\ 0 & 0 & \sqrt{2} & 0 & 0 \\ 0 & 0 & 0 & \sqrt{3} & 0 \\ 0 & 0 & 0 & 0 & \sqrt{4} \\ 0 & 0 & 0 & 0 & 0 \end{pmatrix}$$

The annihilation operator on the v = 2 state:

$$\hat{a}|n\rangle = \sqrt{n}|n-1\rangle \qquad \text{Annihilate} \cdot \begin{pmatrix} 0 \\ 0 \\ 1 \\ 0 \\ 0 \end{pmatrix} = \begin{pmatrix} 0 \\ 1.414 \\ 0 \\ 0 \\ 0 \end{pmatrix}$$

The annihilation operator on the v = 0 state:

$$\text{Annihilate} \cdot \begin{pmatrix} 1 \\ 0 \\ 0 \\ 0 \\ 0 \end{pmatrix} = \begin{pmatrix} 0 \\ 0 \\ 0 \\ 0 \\ 0 \end{pmatrix}$$

The creation operator on the v = 2 state:

$$\hat{a}^{\dagger}|n\rangle = \sqrt{n+1}|n+1\rangle \qquad \text{Create} \cdot \begin{pmatrix} 0 \\ 0 \\ 1 \\ 0 \\ 0 \end{pmatrix} = \begin{pmatrix} 0 \\ 0 \\ 0 \\ 1.732 \\ 0 \end{pmatrix}$$

The number operator on the v = 2 state:

$$\hat{a}^{\dagger}\hat{a}|n\rangle = n|n\rangle$$

$$\text{Create} \cdot \text{Annihilate} = \begin{pmatrix} 0 & 0 & 0 & 0 & 0 \\ 0 & 1 & 0 & 0 & 0 \\ 0 & 0 & 2 & 0 & 0 \\ 0 & 0 & 0 & 3 & 0 \\ 0 & 0 & 0 & 0 & 4 \end{pmatrix} \qquad \text{Create} \cdot \text{Annihilate} \cdot \begin{pmatrix} 0 \\ 0 \\ 1 \\ 0 \\ 0 \end{pmatrix} = \begin{pmatrix} 0 \\ 0 \\ 2 \\ 0 \\ 0 \end{pmatrix}$$

Or do it this way:

$$v0^{T} \cdot \text{ Create } \cdot \text{ Annihilate } \cdot v0 = 0 \qquad v1^{T} \cdot \text{ Create } \cdot \text{ Annihilate } \cdot v1 = 1$$
$$v2^{T} \cdot \text{ Create } \cdot \text{ Annihilate } \cdot v2 = 2 \qquad v3^{T} \cdot \text{ Create } \cdot \text{ Annihilate } \cdot v3 = 3$$

The energy operator operating on the v = 2 and 5 states:

$$\left(\hat{a}^{\dagger}\hat{a} + \frac{1}{2}\right)|n\rangle = \left(n + \frac{1}{2}\right)|n\rangle$$

$$\text{Create} \cdot \text{Annihilate} \cdot \begin{pmatrix} 0 \\ 0 \\ 1 \\ 0 \\ 0 \end{pmatrix} + \frac{1}{2} \cdot \begin{pmatrix} 0 \\ 0 \\ 1 \\ 0 \\ 0 \end{pmatrix} = \begin{pmatrix} 0 \\ 0 \\ 2.5 \\ 0 \\ 0 \end{pmatrix}$$

$$\text{Create} \cdot \text{Annihilate} \cdot \begin{pmatrix} 0 \\ 0 \\ 0 \\ 0 \\ 1 \end{pmatrix} + \frac{1}{2} \cdot \begin{pmatrix} 0 \\ 0 \\ 0 \\ 0 \\ 1 \end{pmatrix} = \begin{pmatrix} 0 \\ 0 \\ 0 \\ 0 \\ 4.5 \end{pmatrix}$$

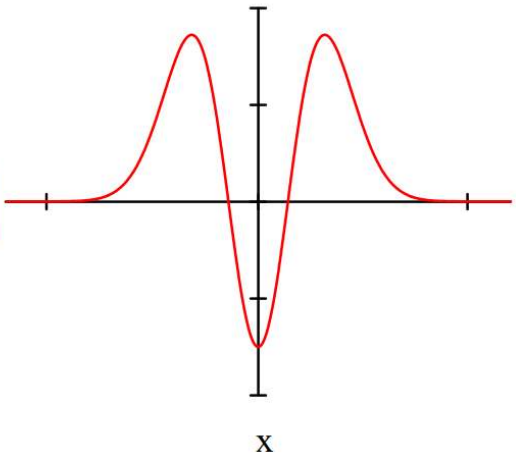
Creating the v = 2 eigenstate from the vacuum:

$$|n\rangle = \frac{1}{\sqrt{n!}} \left(\hat{a}^{\dagger}\right)^{n} |0\rangle \qquad \frac{1}{\sqrt{2!}} \cdot \text{Create}^{\,2} \cdot \begin{pmatrix} 1 \\ 0 \\ 0 \\ 0 \\ 0 \end{pmatrix} \rightarrow \begin{pmatrix} 0 \\ 0 \\ 1 \\ 0 \\ 0 \end{pmatrix}$$

$$\frac{1}{\sqrt{2!}} \cdot \text{Create}^{\,2} \cdot \text{v0} = \begin{pmatrix} 0 \\ 0 \\ 1 \\ 0 \\ 0 \end{pmatrix}$$

This operation is illustrated graphically in the coordinate representation as follows:

$$x \cdot \left(x \cdot \Psi(0, x) - \frac{d}{dx} \Psi(0, x) \right) - \frac{d}{dx} \left(x \cdot \Psi(0, x) - \frac{d}{dx} \Psi(0, x) \right)$$



Construct the matrix forms of the position and momentum operators using the annihilation and creation operators. See E. E. Anderson, *Modern Physics and Quantum Mechanics*, page 201.

$$\text{Position} := \frac{\text{Annihilate} + \text{Create}}{\sqrt{2}} \qquad \text{Momentum} := \frac{i}{\sqrt{2}} \cdot (\text{Create} - \text{Annihilate})$$

Calculate the position and momentum expectation values for several states:

$$\text{v0}^{\text{T}} \cdot \text{Position} \cdot \text{v0} = 0 \quad \text{v0}^{\text{T}} \cdot \text{Momentum}\ \text{v0} = 0$$
$$\text{v1}^{\text{T}} \cdot \text{Position} \cdot \text{v1} = 0 \quad \text{v1}^{\text{T}} \cdot \text{Momentum} \cdot \text{v1} = 0$$

Calculate the position-momentum uncertainty product $(\Delta x \Delta p)$ for several states:

$$\sqrt{\text{v0}^{\text{T}} \cdot \text{Position}^2 \cdot \text{v0} - \left(\text{v0}^{\text{T}} \cdot \text{Position} \cdot \text{v0}\right)^2} \cdot \sqrt{\text{v0}^{\text{T}} \cdot \text{Momentum}^{\,2} \cdot \text{v0} - \left(\text{v0}^{\text{T}} \cdot \text{Momentum} \cdot \text{v0}\right)^2} = 0.5$$

$$\sqrt{\mathrm{v1}^{\mathrm{T}} \cdot \mathrm{Position}^2 \cdot \mathrm{v1} - \left(\mathrm{v1}^{\mathrm{T}} \cdot \ \mathrm{Position}\ \cdot \mathrm{v1}\right)^2} \cdot \sqrt{\mathrm{v1}^{\mathrm{T}} \cdot \ \mathrm{Momentum}\ ^2 \cdot \mathrm{v1} - \left(\mathrm{v1}^{\mathrm{T}} \cdot \ \mathrm{Momentum}\ \cdot \mathrm{v1}\right)^2} = 1.5$$

Calculate the energy expectation value for the following superposition state.

$$\Psi := \frac{1}{\sqrt{2}} \cdot \mathrm{v0} + \frac{1}{\sqrt{3}} \cdot \mathrm{v1} + \frac{1}{\sqrt{6}} \cdot \mathrm{v2} \qquad \Psi^{\mathrm{T}} \cdot \left(\ \mathrm{Create} \cdot \ \mathrm{Annihilate} \cdot \Psi + \frac{1}{2} \cdot \Psi\right) \rightarrow \frac{7}{6}$$

$$\mathrm{P}_0 \cdot \mathrm{E}_0 + \mathrm{P}_1 \cdot \mathrm{E}_1 + \mathrm{P}_2 \cdot \mathrm{E}_2 = \frac{7}{6} \qquad \frac{1}{2} \cdot \frac{1}{2} + \frac{1}{3} \cdot \frac{3}{2} + \frac{1}{6} \cdot \frac{5}{2} \rightarrow \frac{7}{6}$$

Below it is demonstrated that there are two equivalent forms of the harmonic oscillator energy operator in the matrix formulation of quantum mechanics.

$$\left(\hat{a}^{\dagger}\hat{a} + \frac{1}{2}\right)|n\rangle = \left(n + \frac{1}{2}\right)|n\rangle \qquad \left(\hat{a}\hat{a}^{\dagger} - \frac{1}{2}\right)|n\rangle = \left(n + \frac{1}{2}\right)|n\rangle$$

$$\mathrm{Create} \cdot \mathrm{Annihilate} \cdot \begin{pmatrix} 0 \\ 0 \\ 0 \\ 1 \\ 0 \end{pmatrix} + \frac{1}{2} \cdot \begin{pmatrix} 0 \\ 0 \\ 0 \\ 1 \\ 0 \end{pmatrix} = \begin{pmatrix} 0 \\ 0 \\ 0 \\ 3.5 \\ 0 \end{pmatrix}$$

$$\mathrm{Annihilate} \cdot \mathrm{Create} \cdot \begin{pmatrix} 0 \\ 0 \\ 0 \\ 1 \\ 0 \end{pmatrix} - \frac{1}{2} \cdot \begin{pmatrix} 0 \\ 0 \\ 0 \\ 1 \\ 0 \end{pmatrix} = \begin{pmatrix} 0 \\ 0 \\ 0 \\ 3.5 \\ 0 \end{pmatrix}$$

Or, do it this way

$$\frac{\mathrm{Create} \cdot \ \mathrm{Annihilate} + \mathrm{Annihilate} \cdot \ \mathrm{Create}}{2} \cdot \begin{pmatrix} 0 \\ 0 \\ 0 \\ 1 \\ 0 \end{pmatrix} = \begin{pmatrix} 0 \\ 0 \\ 0 \\ 3.5 \\ 0 \end{pmatrix}$$

Or this way:

$$\left(\frac{\mathrm{Momentum}\ ^2}{2} + \frac{\mathrm{Position}\ ^2}{2}\right) \cdot \begin{pmatrix} 0 \\ 0 \\ 0 \\ 1 \\ 0 \end{pmatrix} = \begin{pmatrix} 0 \\ 0 \\ 0 \\ 3.5 \\ 0 \end{pmatrix}$$

Demonstrate that the position and momentum operators don't commute using the matrix form of the operators.

$$i \cdot (\mathrm{Momentum} \cdot \mathrm{Position} - \mathrm{Postion} \cdot \mathrm{Momentum}) = \begin{pmatrix} 1 & 0 & 0 & 0 & 0 \\ 0 & 1 & 0 & 0 & 0 \\ 0 & 0 & 1 & 0 & 0 \\ 0 & 0 & 0 & 1 & 0 \\ 0 & 0 & 0 & 0 & -4 \end{pmatrix}$$

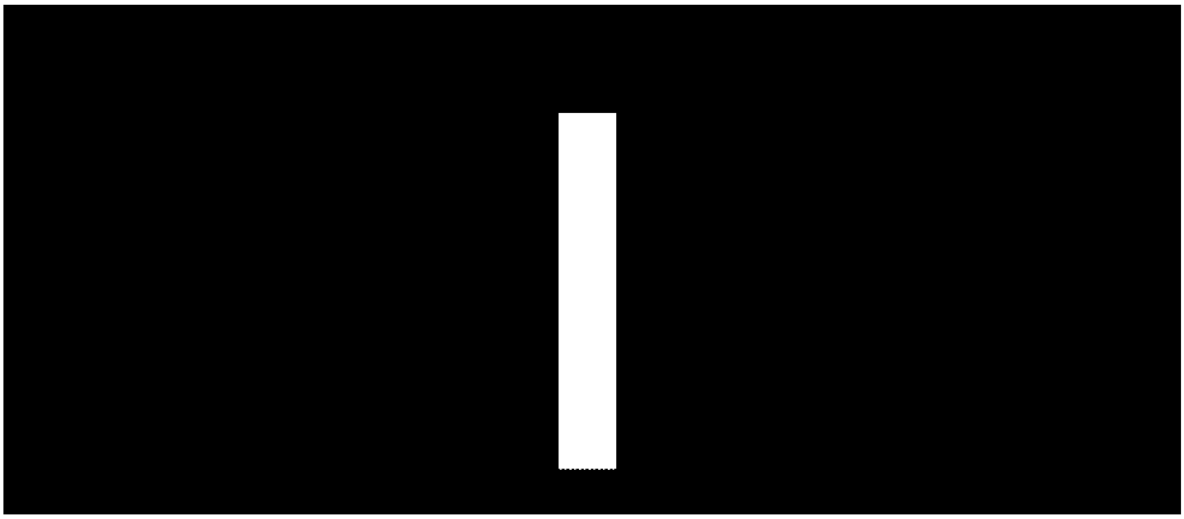
This calculation yields the identity matrix as expected, except for the value of the last diagonal element. The latter is a mathematical artifact of using truncated matrices for operators which are infinite.

This page titled 1.28: Raising and Lowering; Creating and Annihilating is shared under a CC BY 4.0 license and was authored, remixed, and/or curated by Frank Rioux via source content that was edited to the style and standards of the LibreTexts platform.

1.29: Single Slit Diffraction and the Fourier Transform

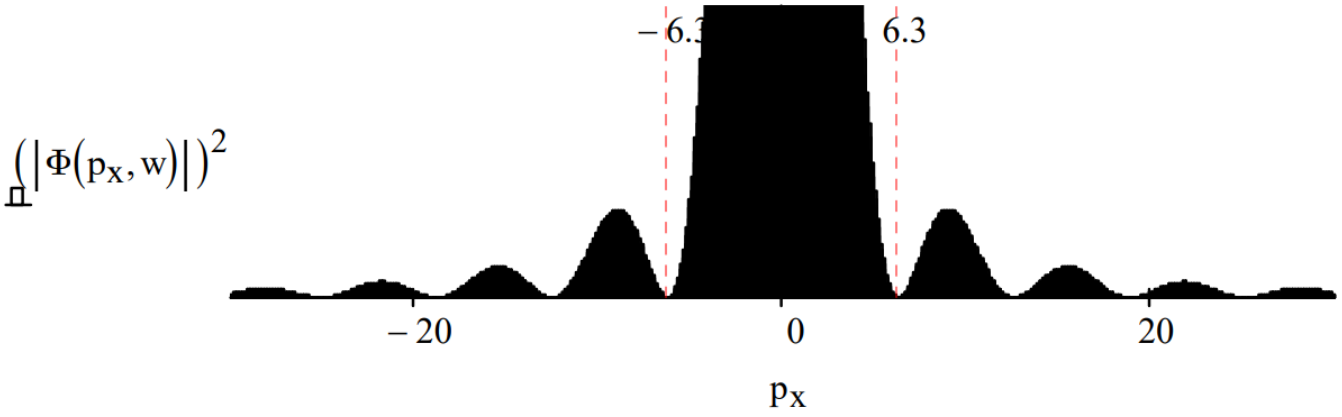
Slit width: $w := 1$	Coordinate-space wave function: $\Psi(x, w)$ $:=$ if $[(x \geq -\frac{w}{2}) \cdot (x \leq \frac{w}{2}), 1, 0]$

$$x := \frac{-w}{2}, \frac{-w}{2} + .005 \ldots \frac{w}{2}$$



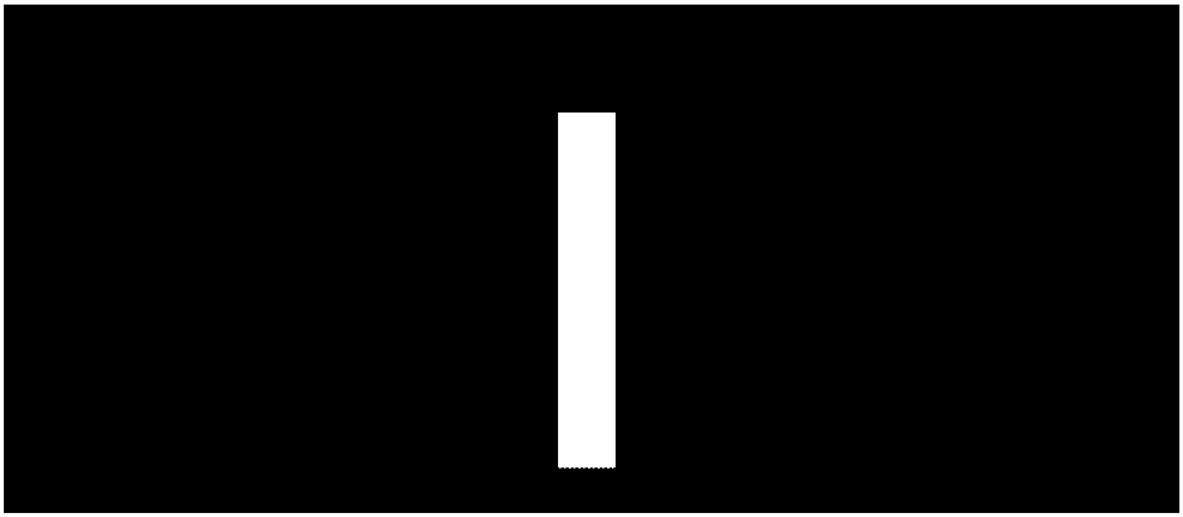
A Fourier transform of the coordinate-space wave function yields the momentum wave function and the momentum distribution function, which is the diffraction pattern.

$$\Phi\left(p_X, w\right) := \frac{1}{\sqrt{2 \cdot \pi \cdot w}} \cdot \int_{-\frac{w}{2}}^{\frac{w}{2}} \exp\left(-i \cdot p_x \cdot x\right) dx \text{ simplify } \rightarrow \frac{\sqrt{2} \cdot \sin\left(\frac{p_x \cdot w}{2}\right)}{\sqrt{\pi} \cdot p_x \cdot \sqrt{w}}$$



Now Fourier transform the momentum wave function back to coordinate space and display result. This is done numerically using large limits of integration for momentum.

$$\Psi(x, w) := \int_{-5000}^{5000} \frac{\frac{1}{2}\sin\left(\frac{1}{2} \cdot w \cdot p_x\right)}{\pi^{\frac{1}{2}} \cdot w^{\frac{1}{2}} \cdot p_x} \cdot \frac{\exp\left(i \cdot p_x \cdot x\right)}{\sqrt{2 \cdot \pi}} dp_x$$

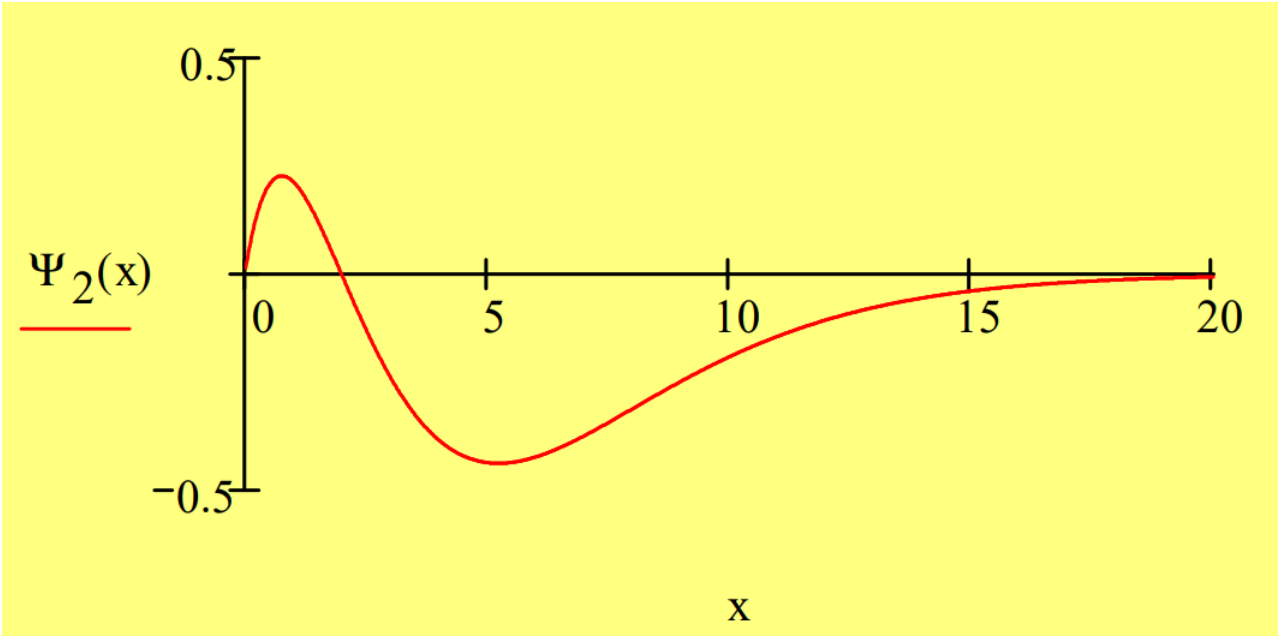


This page titled 1.29: Single Slit Diffraction and the Fourier Transform is shared under a CC BY 4.0 license and was authored, remixed, and/or curated by Frank Rioux via source content that was edited to the style and standards of the LibreTexts platform.

1.30: From Coordinate Space to Momentum Space and Back

The 2s state of the one-dimensional hydrogen atom is used to illustrate transformations back and forth between the coordinate and momentum representations.

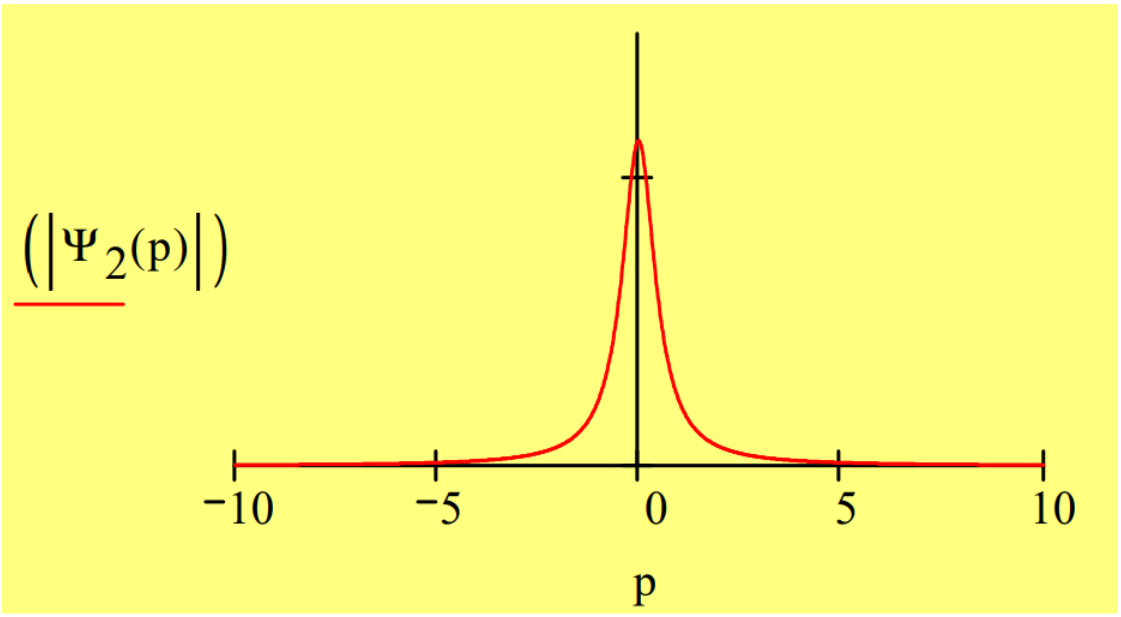
$$\Psi_2(x) := \frac{1}{\sqrt{8}} \cdot x \cdot (2 - x) \cdot \exp\left(-\frac{x}{2}\right)$$



The 2s state is Fourier transformed into momentum space (using atomic units) and the magnitude of the momentum wave function is displayed.

$$\langle p|\Psi_2\rangle = \int_0^\infty \langle p|x\rangle\langle x|\Psi_2\rangle dx \quad \text{where} \quad \langle p|x\rangle = \frac{1}{\sqrt{2\pi}}\exp\left(\frac{-ipx}{\hbar}\right)$$

$$\Psi_2(\mathrm{p}) := \frac{1}{\sqrt{2\cdot\pi}}\int_0^\infty \exp(-\mathrm{i}\cdot\mathrm{p}\cdot\mathrm{x})\cdot\Psi_2(\mathrm{x})\mathrm{d}x \text{ simplify } \rightarrow \frac{2}{\pi^{\frac{1}{2}}}\cdot\frac{2\cdot\mathrm{i}\cdot\mathrm{p}-1}{(2\cdot\mathrm{i}\cdot\mathrm{p}+1)^3}$$

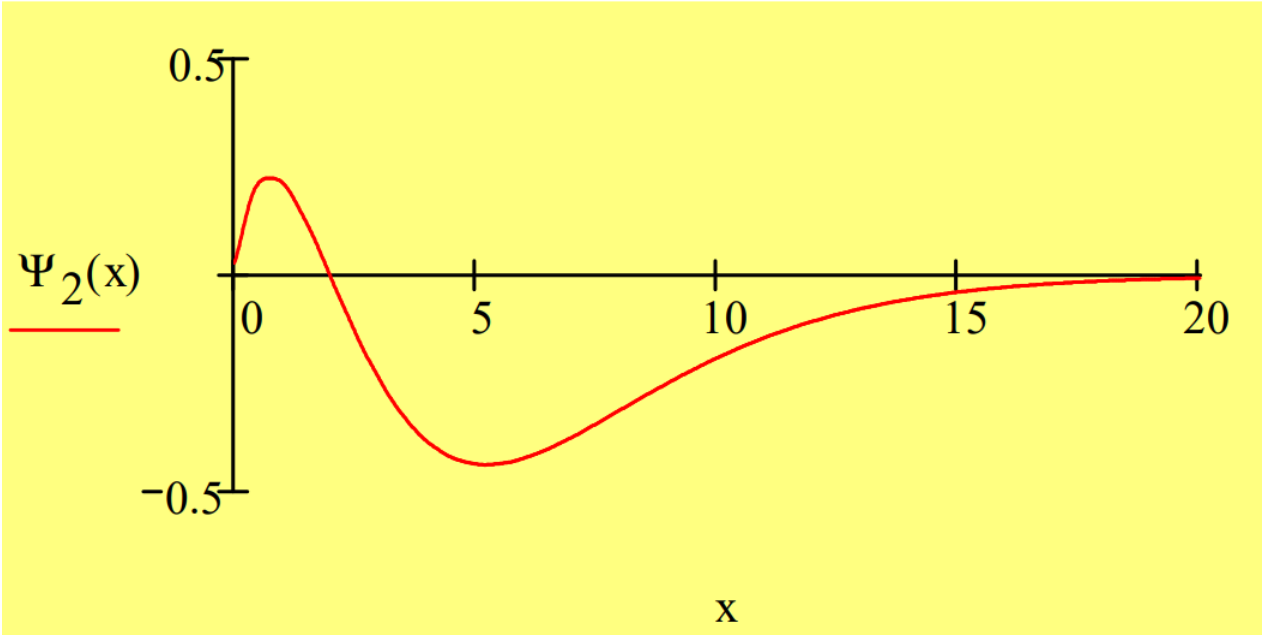


The return to coordinate space is carried out in the numeric mode, integrating over the range of momentum values shown above (± 10 is effectively ±∞).

$$\langle x|\Psi_2\rangle = \int_{-\infty}^{\infty} \langle x|p\rangle\langle p|\Psi_2\rangle dp \quad \text{where} \quad \langle x|p\rangle = \frac{1}{\sqrt{2\pi}}\exp\left(\frac{ipx}{\hbar}\right)$$

$$\Psi_2(x) := \int_{-10}^{10} \frac{1}{\sqrt{2\cdot\pi}} \cdot \exp(i\cdot p\cdot x)\cdot \Psi_2(p)dp$$

The graphical display below shows that we have successfully returned to coordinate space.



This page titled 1.30: From Coordinate Space to Momentum Space and Back is shared under a CC BY 4.0 license and was authored, remixed, and/or curated by Frank Rioux via source content that was edited to the style and standards of the LibreTexts platform.

1.31: The Position and Momentum Commutation Relation in Coordinate and Momentum Space

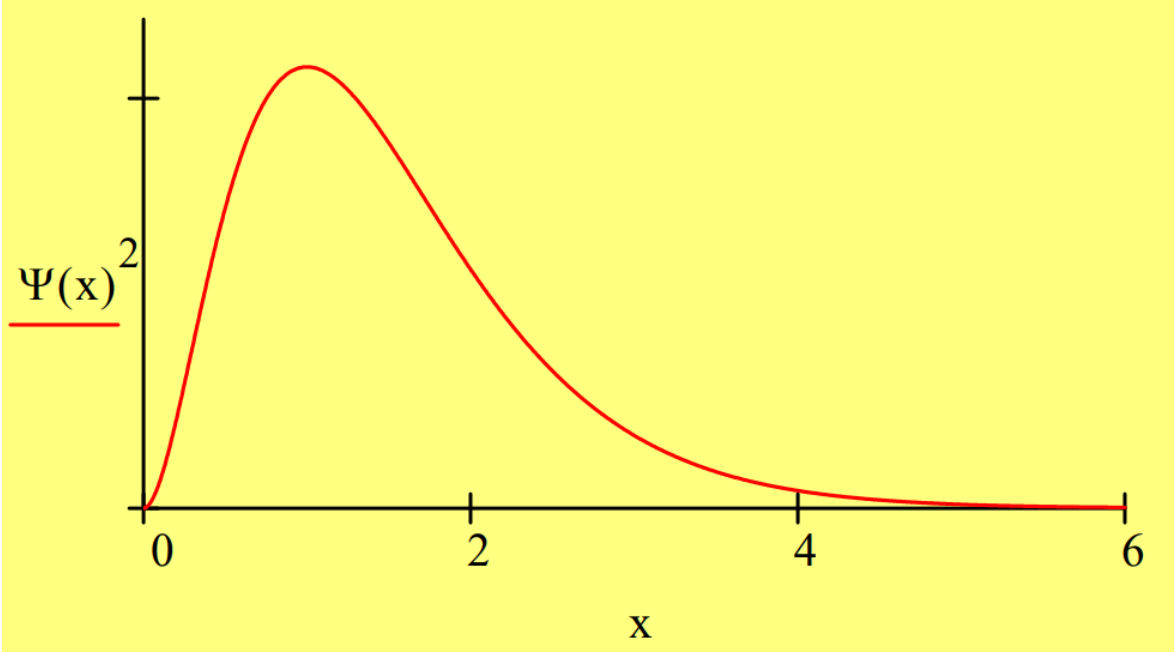
The purpose of this exercise is to illustrate the commutation relation between position and momentum in the coordinate and momentum representations using a one-dimensional representation of the hydrogen atom. The relevance of the uncertainty principle to these calculations will also be demonstrated. All calculations are done in atomic units: e = m_e = $4\pi\epsilon_o = \frac{h}{2\pi}$ = 1.

Coordinate Representation

Position operator: $x\cdot\square$	Momentum operator: $p = \frac{1}{i}\cdot\frac{d}{dx}\square$	Integral: $\int_0^\infty \square dx$	Kinetic energy operator: $KE = -\frac{1}{2}\cdot\frac{d^2}{dx^2}\square$	Potential energy operator: $PE = \frac{-1}{x}$

The 1s state of the hydrogen can be represented in one-dimension by the following wave function:

$$\Psi(x) = 2\cdot x\cdot\exp(-x) \qquad \int_0^\infty \Psi(x)^2 dx \rightarrow 1$$



First we demonstrate that Ψ(x) is an eigenfunction of the energy operator with eigenvalue -0.5 in atomic units.

$$\frac{-\frac{1}{2}\cdot\frac{d^2}{dx^2}\Psi(x) - \frac{1}{x}\cdot\Psi(x)}{\Psi(x)} \rightarrow \frac{-1}{2}$$

It is easy to show that $\Psi(x)$ is not an eigenfunction of the position or momentum operators. This means that while the electron in the hydrgogen atom ground state has a well-defined energy, it does not have a well-defined position or momentum. This fact is consistent with the commutator and uncertainty calculations shown below.

Next it is shown that the position and momentum operators do not commute.

$$\frac{x\cdot\left(\frac{1}{i}\cdot\frac{d}{dx}\Psi(x)\right) - \frac{1}{i}\cdot\frac{d}{dx}(x\cdot\Psi(x))}{\Psi(x)} \text{ simplify } \rightarrow i$$

This result indicates that $\Psi(x)$ is not an eigenstate of the position and momentum operators, and therefore the order of measurement is important. Gaining knowledge of one observable through measurement destroys information about the other. The commutation relation is closely related to the uncertainty principle, which states that the product of uncertainties in position and momentum must equal or exceed a certain minimum value, 0.5 in atomic units.

The uncertainties in position and momentum are now calculated to show that the uncertainty principle is satisfied.

$$\Delta x := \sqrt{\int_0^\infty \Psi(x) \cdot x^2 \cdot \Psi(x) dx - \left(\int_0^\infty \Psi(x) \cdot x \cdot \Psi(x) dx\right)^2} \rightarrow \frac{1}{2} \cdot 3^{\frac{1}{2}}$$

$$\Delta p := \sqrt{\int_0^\infty \Psi(x) \cdot \frac{d^2}{dx^2} \Psi(x) dx - \left(\int_0^\infty \Psi(x) \cdot \frac{1}{i} \cdot \frac{d}{dx} \Psi(x) dx\right)^2} \rightarrow 1$$

$$\Delta x \cdot \Delta p = 0.866$$

We now move to momentum space to show that the results are identical to those calculate in coordinate space.

Momentum Representation

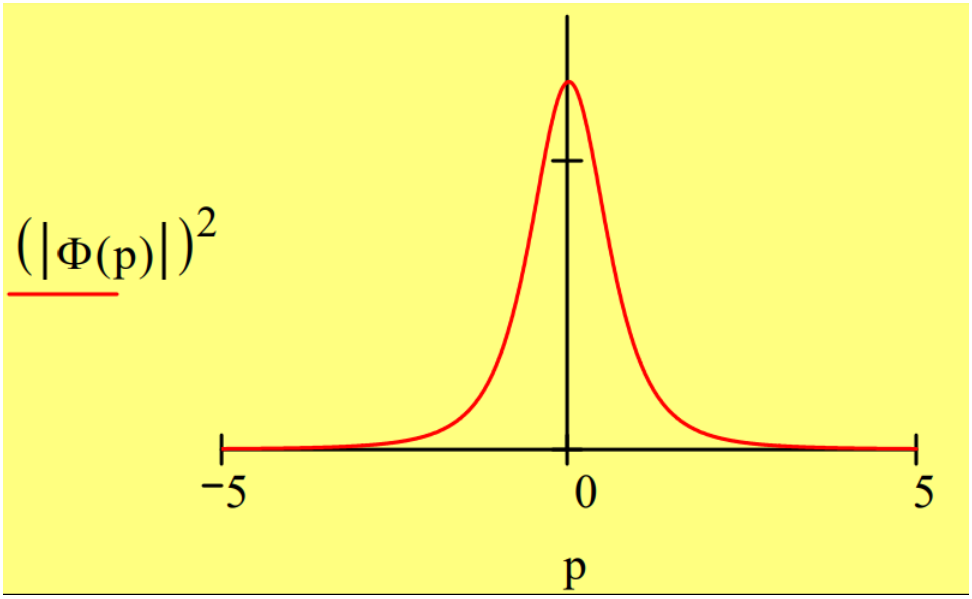
Position operator: $i \cdot \frac{d}{dp} \square$	Momentum operator: $p \cdot \square$	Momentum space integral: $\int_{-\infty}^{\infty} \square dp$

A momentum wave function is obtained by a Fourier transform of the coordinate wave function.

$$\Phi(\mathrm{p}) := \frac{1}{\sqrt{2 \cdot \pi}} \cdot \int_0^\infty \exp(-\mathrm{i} \cdot \mathrm{p} \cdot \mathrm{x}) \cdot \Psi(\mathrm{x}) \mathrm{dx} \text{ simplify } \rightarrow \frac{2^{\frac{1}{2}}}{\pi^{\frac{1}{2}} \cdot (\mathrm{i} \cdot \mathrm{p} + 1)^2}$$

$$\int_{-\infty}^{\infty} (|\Phi(p)|)^2 dp \rightarrow 1$$

The coordinate and momentum wave functions are equivalent representations of the hydrogen-atom ground state. That they contain the same information as is illustrated below.



The position and momentum operators do not commute in momentum space.

$$\frac{\mathrm{i} \cdot \frac{\mathrm{d}}{\mathrm{dp}} (\mathrm{p} \cdot \Phi(\mathrm{p})) - \mathrm{p} \cdot \mathrm{i} \cdot \frac{\mathrm{d}}{\mathrm{dp}} \Phi(\mathrm{p})}{\Phi(\mathrm{p})} \text{ simplify } \rightarrow \frac{-(\mathrm{p} - \mathrm{i})}{\mathrm{i} \cdot \mathrm{p} + 1}$$

It is easy to show that this result is equal to i.

The product of the position-momentum uncertainty is the same in momentum space as it is in coordinate space.

$$\Delta \mathrm{p} := \sqrt{\int_{-\infty}^{\infty} \mathrm{p}^2 \cdot (|\Phi(\mathrm{p})|)^2 \mathrm{dp} - \left[\int_{-\infty}^{\infty} \mathrm{p} \cdot (|\Phi(\mathrm{p})|)^2 \mathrm{dp}\right]^2} \rightarrow 1$$

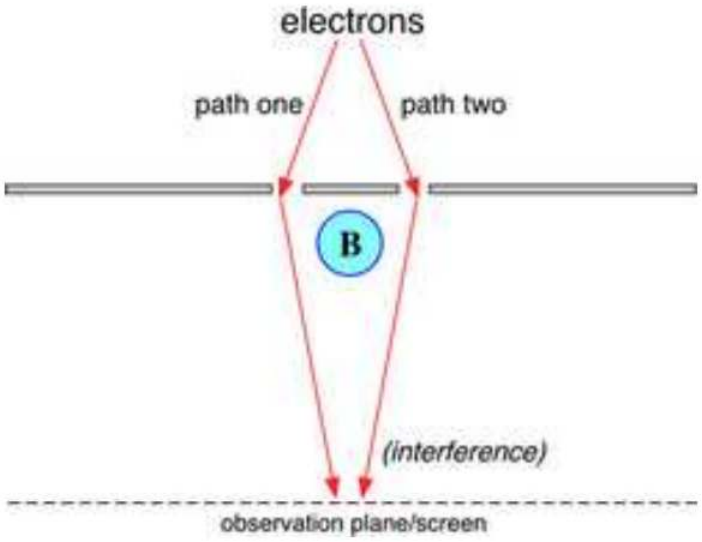
$$\Delta x := \sqrt{\int_{-\infty}^{\infty} \overline{\Phi(p)} \cdot -\frac{d^2}{dp^2}\Phi(p)dp - \left[\int_{-\infty}^{\infty} \overline{\Phi(p)} \cdot i \cdot \left(\frac{d}{dp}\Phi(p)\right) dp\right]^2} \rightarrow \frac{1}{2} \cdot 3^{\frac{1}{2}}$$

$$\Delta \mathrm{x} \cdot \Delta \mathrm{p} = 0.866$$

This page titled 1.31: The Position and Momentum Commutation Relation in Coordinate and Momentum Space is shared under a CC BY 4.0 license and was authored, remixed, and/or curated by Frank Rioux via source content that was edited to the style and standards of the LibreTexts platform.

1.32: Simulating the Aharonov-Bohm Effect

The Aharonov–Bohm effect is a phenomenon by which an electron is affected by the vector potential, **A**, in regions in which both the magnetic field **B**, and electric field **E** are zero. The most commonly described case occurs when the wave function of an electron passing around a long solenoid experiences a phase shift as a result of the enclosed magnetic field, despite the magnetic field being zero in the region through which the particle passes.



Schematic of double-slit experiment in which Aharonov–Bohm effect can be observed: electrons pass through two slits, interfering at an observation screen, with the interference pattern shifted when a magnetic field B is turned on in the cylindrical solenoid. (All of the above adapted from Wikipeida)

The effect on the interference fringes is calculated and displayed below. Please consult other tutorials on the double-slit interference effect on my page for background information.

Slit positions: $x_L := 1 \quad x_R := 2$	Slit width: $\delta := 0.2$	Relative phase shift: $\phi := \pi$

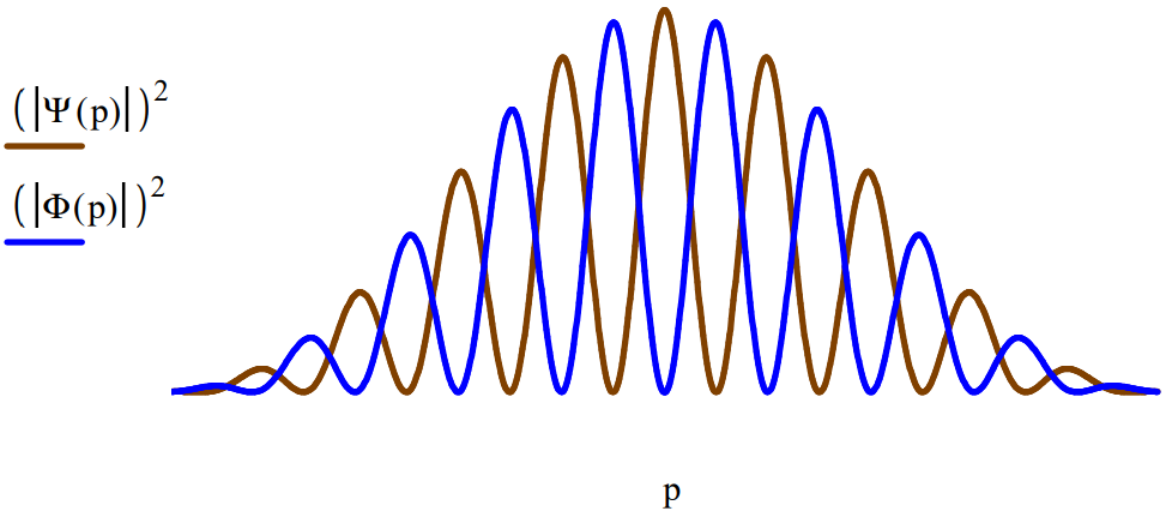
Momentum Distribution/Diffraction Pattern for **B** = 0:

$$\Psi(p) := \frac{1}{\sqrt{2}} \left(\int_{x_L-\frac{\delta}{2}}^{x_L+\frac{\delta}{2}} \frac{1}{\sqrt{2\cdot\pi}} \cdot \exp(-i\cdot p\cdot x)\cdot \frac{1}{\sqrt{\delta}} dx + \int_{x_R-\frac{\delta}{2}}^{x_R+\frac{\delta}{2}} \frac{1}{\sqrt{2\cdot\pi}} \cdot \exp(-i\cdot p\cdot x)\cdot \frac{1}{\sqrt{\delta}} dx \right)$$

Relative phase shift, ϕ, introduced at right-hand slit for **B** not equal to zero:

$$\Phi(\mathrm{p}) := \frac{1}{\sqrt{2}}$$
$$\left(\int_{\mathrm{x_L}-\frac{\delta}{2}}^{\mathrm{x_L}+\frac{\delta}{2}} \frac{1}{\sqrt{2\cdot\pi}} \cdot \exp(-\mathrm{i}\cdot \mathrm{p}\cdot \mathrm{x})\cdot \frac{1}{\sqrt{\delta}} \mathrm{dx} + \exp(\mathrm{i}\cdot\phi)\cdot \int_{\mathrm{x_R}-\frac{\delta}{2}}^{\mathrm{x_R}+\frac{\delta}{2}} \frac{1}{\sqrt{2\cdot\pi}} \cdot \exp(-\mathrm{i}\cdot \mathrm{p}\cdot \mathrm{x})\cdot \frac{1}{\sqrt{\delta}} \mathrm{dx} \right)$$

Display both diffraction patterns:



This page titled 1.32: Simulating the Aharonov-Bohm Effect is shared under a CC BY 4.0 license and was authored, remixed, and/or curated by Frank Rioux via source content that was edited to the style and standards of the LibreTexts platform.

1.33: Basic Matrix Mechanics

A quon (an entity that exhibits both wave and particle aspects in the peculiar quantum manner - Nick Herbert, *Quantum Reality*, page 64) has a variety of properties each of which can take on two values. For example, it has the property of **hardness** and can be either *hard* or *soft*. It also has the property of **color** and can be either *black* or *white*, and the property of **taste** and be *sweet* or *sour*. The treatment that follows draws on material from Chapter 3 of David Z Albert's book, *Quantum Mechanics and Experience*.

The basic principles of matrix and vector math are provided in Appendix A. An examination of this material will demonstrate that most of the calculations presented in this tutorial can easily be performed without the aid of Mathcad or any other computer algebra program. In other words, they can be done by hand.

In the matrix formulation of quantum mechanics the hardness and color states are represented by the following vectors.

$$\text{Hard} := \begin{pmatrix} 1 \\ 0 \end{pmatrix} \quad \text{Soft} := \begin{pmatrix} 0 \\ 1 \end{pmatrix} \quad \text{Black} := \begin{pmatrix} \frac{1}{\sqrt{2}} \\ \frac{1}{\sqrt{2}} \end{pmatrix} \quad \text{White} := \begin{pmatrix} \frac{1}{\sqrt{2}} \\ \frac{-1}{\sqrt{2}} \end{pmatrix}$$

Hard and *Soft* represent an orthonormal basis in the two-dimensional **Hardness** vector space.

Likewise *Black* and *White* are an orthonormal basis in the two-dimensional **Color** vector space.

$$\text{Black}^T \cdot \text{Black} = 1 \qquad \text{White}^T \cdot \text{White} = 1 \qquad \text{Black}^T \cdot \text{White} = 0$$

$$\begin{pmatrix} \frac{1}{\sqrt{2}} & \frac{1}{\sqrt{2}} \end{pmatrix} \cdot \begin{pmatrix} \frac{1}{\sqrt{2}} \\ \frac{1}{\sqrt{2}} \end{pmatrix} = 1 \qquad \begin{pmatrix} \frac{1}{\sqrt{2}} & \frac{-1}{\sqrt{2}} \end{pmatrix} \cdot \begin{pmatrix} \frac{1}{\sqrt{2}} \\ \frac{-1}{\sqrt{2}} \end{pmatrix} = 1 \qquad \begin{pmatrix} \frac{1}{\sqrt{2}} & \frac{1}{\sqrt{2}} \end{pmatrix} \cdot \begin{pmatrix} \frac{1}{\sqrt{2}} \\ \frac{-1}{\sqrt{2}} \end{pmatrix} = 0$$

The relationship between the two bases is reflected in the following projection calculations.

Note

$$\frac{1}{\sqrt{2}} = 0.707$$

$$\text{Hard}^T \cdot \text{Black} = 0.707 \qquad \text{Hard}^T \cdot \text{White} = 0.707 \qquad \text{Soft}^T \cdot \text{Black} = 0.707 \qquad \text{Soft}^T \cdot \text{White} = -0.707$$

$$\begin{pmatrix} 1 & 0 \end{pmatrix} \cdot \begin{pmatrix} \frac{1}{\sqrt{2}} \\ \frac{1}{\sqrt{2}} \end{pmatrix} = 0.707 \qquad \begin{pmatrix} 1 & 0 \end{pmatrix} \cdot \begin{pmatrix} \frac{1}{\sqrt{2}} \\ \frac{-1}{\sqrt{2}} \end{pmatrix} = 0.707 \qquad \begin{pmatrix} 0 & 0 \end{pmatrix} \cdot \begin{pmatrix} \frac{1}{\sqrt{2}} \\ \frac{1}{\sqrt{2}} \end{pmatrix} = 0.707 \qquad \begin{pmatrix} 0 & 1 \end{pmatrix} \cdot \begin{pmatrix} \frac{1}{\sqrt{2}} \\ \frac{-1}{\sqrt{2}} \end{pmatrix} = -0.707$$

The values calculated above are probability amplitudes. The absolute square of those values is the probability. In other words, the probability that a black quon will be found to be hard is 0.5. The probability that a white quon will be found to be soft is also 0.5.

$$\left(\left|\text{Hard}^T \cdot \text{Black}\right|\right)^2 = 0.5 \quad \left(\left|\text{Hard}^T \cdot \text{White}\right|\right)^2 = 0.5 \quad \left(\left|\text{Soft}^T \cdot \text{Black}\right|\right)^2 = 0.5 \quad \left(\left|\text{Soft}^T \cdot \text{White}\right|\right)^2 = 0.5$$

$$\left\|\begin{pmatrix} 1 & 0 \end{pmatrix} \cdot \begin{pmatrix} \frac{1}{\sqrt{2}} \\ \frac{1}{\sqrt{2}} \end{pmatrix}\right\|^2 = 0.5 \quad \left\|\begin{pmatrix} 1 & 0 \end{pmatrix} \cdot \begin{pmatrix} \frac{1}{\sqrt{2}} \\ \frac{-1}{\sqrt{2}} \end{pmatrix}\right\|^2 = 0.5 \quad \left\|\begin{pmatrix} 0 & 0 \end{pmatrix} \cdot \begin{pmatrix} \frac{1}{\sqrt{2}} \\ \frac{1}{\sqrt{2}} \end{pmatrix}\right\|^2 = 0.5 \quad \left\|\begin{pmatrix} 0 & 1 \end{pmatrix} \cdot \begin{pmatrix} \frac{1}{\sqrt{2}} \\ \frac{-1}{\sqrt{2}} \end{pmatrix}\right\|^2 = 0.5$$

Clearly *Black* and *White* can be written as superpositions of *Hard* and *Soft*, and vice versa. This means hard and soft quons do not have a well-defined color, and black and white quons do not have a well-defined hardness.

$\frac{1}{\sqrt{2}} \cdot (\text{Hard} + \text{Soft}) = \begin{pmatrix} 0.707 \\ 0.707 \end{pmatrix}$	$\frac{1}{\sqrt{2}} \cdot \left[\begin{pmatrix} 1 \\ 0 \end{pmatrix} + \begin{pmatrix} 0 \\ 1 \end{pmatrix}\right] = \begin{pmatrix} 0.707 \\ 0.707 \end{pmatrix}$
$\frac{1}{\sqrt{2}} \cdot (\text{Hard} - \text{Soft}) = \begin{pmatrix} 0.707 \\ -0.707 \end{pmatrix}$	$\frac{1}{\sqrt{2}} \left[\begin{pmatrix} 1 \\ 0 \end{pmatrix} - \begin{pmatrix} 0 \\ 1 \end{pmatrix}\right] = \begin{pmatrix} 0.707 \\ -0.707 \end{pmatrix}$
$\frac{1}{\sqrt{2}} \cdot (\ \text{Black} \ + \ \text{White}\ ) = \begin{pmatrix} 1 \\ 0 \end{pmatrix}$	$\frac{1}{\sqrt{2}} \left[\begin{pmatrix} \frac{1}{\sqrt{2}} \\ \frac{1}{\sqrt{2}} \end{pmatrix} + \begin{pmatrix} \frac{1}{\sqrt{2}} \\ \frac{-1}{\sqrt{2}} \end{pmatrix}\right] = \begin{pmatrix} 1 \\ 0 \end{pmatrix}$
$\frac{1}{\sqrt{2}} \cdot (\ \text{Black} \ - \ \text{White}\ ) = \begin{pmatrix} 0 \\ 1 \end{pmatrix}$	$\frac{1}{\sqrt{2}} \left[\begin{pmatrix} \frac{1}{\sqrt{2}} \\ \frac{1}{\sqrt{2}} \end{pmatrix} - \begin{pmatrix} \frac{1}{\sqrt{2}} \\ \frac{-1}{\sqrt{2}} \end{pmatrix}\right] = \begin{pmatrix} 0 \\ 1 \end{pmatrix}$

Hard, *Soft*, *Black* and *White* are measurable properties and the vectors representing them are eigenstates of the *Hardness* and *Color* operators with **eigenvalues** $\pm$ 1. The **Identity** operator is also given and will be discussed later. Of course, the *Hardness* and *Color* operators are just the Pauli spin operators in the z- and x-directions. Later the *Taste* operator will be introduced; it is the y-direction Pauli spin operator.

Operators

$\text{Hardness} := \begin{pmatrix} 1 & 0 \\ 0 & -1 \end{pmatrix}$	$\text{Color} := \begin{pmatrix} 0 & 1 \\ 1 & 0 \end{pmatrix}$	$\text{I} := \begin{pmatrix} 1 & 0 \\ 0 & 1 \end{pmatrix}$

Eigenvalue +1		Eigenvalue -1	
$\text{Hardness} \cdot \text{Hard} = \begin{pmatrix} 1 \\ 0 \end{pmatrix}$	$\begin{pmatrix} 1 & 0 \\ 0 & -1 \end{pmatrix} \cdot \begin{pmatrix} 1 \\ 0 \end{pmatrix} = \begin{pmatrix} 1 \\ 0 \end{pmatrix}$	$\text{Hardness} \cdot \text{Soft} = \begin{pmatrix} 0 \\ -1 \end{pmatrix}$	$\begin{pmatrix} 1 & 0 \\ 0 & -1 \end{pmatrix} \cdot \begin{pmatrix} 0 \\ 1 \end{pmatrix} = \begin{pmatrix} 0 \\ -1 \end{pmatrix}$
$\text{Color} \cdot \text{Black} = \begin{pmatrix} 0.707 \\ 0.707 \end{pmatrix}$	$\begin{pmatrix} 0 & 1 \\ 1 & 0 \end{pmatrix} \cdot \begin{pmatrix} \frac{1}{\sqrt{2}} \\ \frac{1}{\sqrt{2}} \end{pmatrix} = \begin{pmatrix} 0.707 \\ 0.707 \end{pmatrix}$	$\text{Color} \cdot \text{White} = \begin{pmatrix} -0.707 \\ 0.707 \end{pmatrix}$	$\begin{pmatrix} 0 & 1 \\ 1 & 0 \end{pmatrix} \cdot \begin{pmatrix} \frac{1}{\sqrt{2}} \\ \frac{-1}{\sqrt{2}} \end{pmatrix} = \begin{pmatrix} -0.707 \\ 0.707 \end{pmatrix}$

Another way of showing this is by calculating the **expectation (or average) value**. Every time the hardness of a hard quon is measured the result is +1. Every time the hardness of a soft quon is measured the result is -1.

$\text{Hard}^T \cdot \text{Hardness} \cdot \text{Hard} = 1$	$\begin{pmatrix} 1 & 0 \\ 0 & -1 \end{pmatrix} \cdot \begin{pmatrix} 1 \\ 0 \end{pmatrix} = 1$	$\text{Soft}^T \cdot \text{Hardness} \cdot \text{Soft} = -1$	$\begin{pmatrix} 0 & 1 \end{pmatrix} \cdot \begin{pmatrix} 1 & 0 \\ 0 & -1 \end{pmatrix} \cdot \begin{pmatrix} 0 \\ 1 \end{pmatrix} = -1$
$\text{Black}^T \cdot \text{Color} \cdot \text{Black} = 1$	$\begin{pmatrix} \frac{1}{\sqrt{2}} & \frac{1}{\sqrt{2}} \end{pmatrix} \cdot \begin{pmatrix} 0 & 1 \\ 1 & 0 \end{pmatrix} \cdot \begin{pmatrix} \frac{1}{\sqrt{2}} \\ \frac{1}{\sqrt{2}} \end{pmatrix} = 1$	$\text{White}^T \cdot \text{Color} \cdot \text{White} = 1$	$\begin{pmatrix} \frac{1}{\sqrt{2}} & \frac{-1}{\sqrt{2}} \end{pmatrix} \cdot \begin{pmatrix} 0 & 1 \\ 1 & 0 \end{pmatrix} \cdot \begin{pmatrix} \frac{1}{\sqrt{2}} \\ \frac{-1}{\sqrt{2}} \end{pmatrix} = -1$

If a quon is in a state which is an eigenfunction of an operator, it means it has a well-defined value for the observable represented by the operator. If the quon is in a state which is not an eigenfunction of the operator, it does not have a well-defined value for the observable.

Hard and *Soft* are not **eigenfunctions** of the *Color* operator, and *Black* and *White* are not eigenfunctions of the **Hardness** operator. Hard and soft quons do not have a well-defined color, and black and white quons do not have a well-defined hardness.

$\text{Hardness} \cdot \text{Black} = \begin{pmatrix} 0.707 \\ -0.707 \end{pmatrix}$	$\begin{pmatrix} 1 & 0 \\ 0 & -1 \end{pmatrix} \cdot \begin{pmatrix} \frac{1}{\sqrt{2}} \\ \frac{1}{\sqrt{2}} \end{pmatrix} = \begin{pmatrix} 0.707 \\ -0.707 \end{pmatrix}$	$\text{Hardness} \cdot \text{White} = \begin{pmatrix} 0.707 \\ 0.707 \end{pmatrix}$	$\begin{pmatrix} 1 & 0 \\ 0 & -1 \end{pmatrix} \cdot \begin{pmatrix} \frac{1}{\sqrt{2}} \\ \frac{-1}{\sqrt{2}} \end{pmatrix} = \begin{pmatrix} 0.707 \\ 0.707 \end{pmatrix}$
$\text{Color} \cdot \text{Hard} = \begin{pmatrix} 0 \\ 1 \end{pmatrix}$	$\begin{pmatrix} 0 & 1 \\ 1 & 0 \end{pmatrix} \cdot \begin{pmatrix} 1 \\ 0 \end{pmatrix} = \begin{pmatrix} 0 \\ 1 \end{pmatrix}$	$\text{Color} \cdot \text{Soft} = \begin{pmatrix} 1 \\ 0 \end{pmatrix}$	$\begin{pmatrix} 0 & 1 \\ 1 & 0 \end{pmatrix} \cdot \begin{pmatrix} 0 \\ 1 \end{pmatrix} = \begin{pmatrix} 1 \\ 0 \end{pmatrix}$

Therefore their **expectation values** are zero. In other words if the hardness of a black quon is measured, half the time it will register hard and half the time soft. If the color of a soft quon is measured, half the time it will register white and half the time black.

$\text{Black}^T \cdot \text{Hardness} \cdot \text{Black} = 0$	$\begin{pmatrix} \frac{1}{\sqrt{2}} & \frac{1}{\sqrt{2}} \end{pmatrix} \cdot \begin{pmatrix} 1 & 0 \\ 0 & -1 \end{pmatrix} \cdot \begin{pmatrix} \frac{1}{\sqrt{2}} \\ \frac{1}{\sqrt{2}} \end{pmatrix} = 0$	$\text{White}^T \cdot \text{Hardness} \cdot \text{White} = 0$	$\begin{pmatrix} \frac{1}{\sqrt{2}} & \frac{-1}{\sqrt{2}} \end{pmatrix} \cdot \begin{pmatrix} 1 & 0 \\ 0 & -1 \end{pmatrix} \cdot \begin{pmatrix} \frac{1}{\sqrt{2}} \\ \frac{-1}{\sqrt{2}} \end{pmatrix} = 0$
$\text{Hard}^T \cdot \text{Color} \cdot \text{Hard} = 0$	$\begin{pmatrix} 1 & 0 \end{pmatrix} \cdot \begin{pmatrix} 0 & 1 \\ 1 & 0 \end{pmatrix} \cdot \begin{pmatrix} 1 \\ 0 \end{pmatrix} = 0$	$\text{Soft}^T \cdot \text{Color} \cdot \text{Soft} = 0$	$\begin{pmatrix} 0 & 1 \end{pmatrix} \cdot \begin{pmatrix} 0 & 1 \\ 1 & 0 \end{pmatrix} \cdot \begin{pmatrix} 0 \\ 1 \end{pmatrix} = 0$

As the **Hardness-Color** commutator shows, the **Hardness** and **Color** operators do not commute. They represent incompatible observables; observables that cannot simultaneously have well-defined values.

$\text{Hardness} \cdot \text{Color} - \text{Color} \cdot \text{Hardness} = \begin{pmatrix} 0 & 2 \\ -2 & 0 \end{pmatrix}$	$\begin{pmatrix} 1 & 0 \\ 0 & -1 \end{pmatrix} \begin{pmatrix} 0 & 1 \\ 1 & 0 \end{pmatrix} - \begin{pmatrix} 0 & 1 \\ 1 & 0 \end{pmatrix} \cdot \begin{pmatrix} 1 & 0 \\ 0 & -1 \end{pmatrix} = \begin{pmatrix} 0 & 2 \\ -2 & 0 \end{pmatrix}$

This means that the measurement of the color and then the hardness of a hard quon gives a different result than the measurement of the hardness and then the color.

$\text{Hardness} \cdot \text{Color} \cdot \text{Hard} = \begin{pmatrix} 0 \\ -1 \end{pmatrix}$	$\begin{pmatrix} 1 & 0 \\ 0 & -1 \end{pmatrix} \cdot \begin{pmatrix} 0 & 1 \\ 1 & 0 \end{pmatrix} \cdot \begin{pmatrix} 1 \\ 0 \end{pmatrix} = \begin{pmatrix} 0 \\ -1 \end{pmatrix}$	$\text{Color} \cdot \text{Hardness} \cdot \text{Hard} = \begin{pmatrix} 0 \\ 1 \end{pmatrix}$	$\begin{pmatrix} 0 & 1 \\ 1 & 0 \end{pmatrix} \cdot \begin{pmatrix} 1 & 0 \\ 0 & -1 \end{pmatrix} \cdot \begin{pmatrix} 1 \\ 0 \end{pmatrix} = \begin{pmatrix} 0 \\ 1 \end{pmatrix}$

We can also look at this from the perspective of the uncertainty principle. The uncertainty in a measurement is the square root of the difference between *the mean of the square* and *the square of the mean*.

Suppose we measure the color of a Black or White quon. Because Black and White are eigenfunctions of the Color operator the uncertainty in the measurement results are zero.

$$\sqrt{\text{Black}^T \cdot \text{Color}^2 \cdot \text{Black} - (\text{Black}^T \cdot \text{Color} \cdot \text{Black})^2} = 0$$
$$\sqrt{\text{White}^T \cdot \text{Color}^2 \cdot \text{White} - (\text{White}^T \cdot \text{Color} \cdot \text{White})^2} = 0$$

However, the measurement of the color of a Soft or Hard quon is by the same criterion uncertain.

$$\sqrt{\text{Soft}^T \cdot \text{Color}^2 \cdot \text{Soft} - (\text{Soft}^T \cdot \text{Color} \cdot \text{Soft})^2} = 1$$
$$\sqrt{\text{Hard}^T \cdot \text{Color}^2 \cdot \text{Hard} - (\text{Hard}^T \cdot \text{Color} \cdot \text{Hard})^2} = 1$$

The calculations of **Hardness** and **Color** reveal the strange behavior of quons. In the macro world we frequently find objects that simultaneously have well-defined values for these physical attributes. But we see this is not possible in the quantum world.

Mathcad has high-level commands which find the eigenvalues and eigenvectors of matrices which in quantum mechanics are operators. Below it is shown that they give the same results as were demonstrated above. See the Appendix for additional computational methods.

$\text{eigenvals}(\text{Hardness}) = \begin{pmatrix} 1 \\ -1 \end{pmatrix}$	$\text{eigenvals}(\text{Hardness}, -1) = \begin{pmatrix} 0 \\ 1 \end{pmatrix}$	$\text{eigenvals}(\text{Hardness}, 1) = \begin{pmatrix} 1 \\ 0 \end{pmatrix}$
$\text{eigenvals}(\text{Color}) = \begin{pmatrix} 1 \\ -1 \end{pmatrix}$	$\text{eigenvals}(\text{Color}, -1) = \begin{pmatrix} -0.707 \\ 1 \end{pmatrix}$	$\text{eigenvals}(\text{Color}, 1) = \begin{pmatrix} 0.707 \\ 0.707 \end{pmatrix}$

Besides the properties of hardness and color, suppose the quon also has the property of taste, tasting either *Sweet* or *Sour*. The **Taste** operator is defined below and its eigenvalues and eigenvectors calculated.

Operator	Eigenvalues	Sweet/Sour Eigenvectors
$\text{Taste} := \begin{pmatrix} 0 & -\text{i} \\ \text{i} & 0 \end{pmatrix}$	$\text{eigenvals}(\text{Taste}) = \begin{pmatrix} 1 \\ -1 \end{pmatrix}$	$\text{eigenvals}(\text{Taste}) = \begin{pmatrix} -0.707\text{i} & 0.707 \\ 0.707 & -0.707\text{i} \end{pmatrix}$

Squaring the **Hardness**, **Color** and **Taste** operators gives the **Identity** operator, that is they are unitary matrices. The **Identity** operator leaves the vector it operates on unchanged.

$$\text{Hardness}^2 = \begin{pmatrix} 1 & 0 \\ 0 & 1 \end{pmatrix} \qquad \begin{pmatrix} 1 & 0 \\ 0 & -1 \end{pmatrix} \cdot \begin{pmatrix} 1 & 0 \\ 0 & -1 \end{pmatrix} = \begin{pmatrix} 1 & 0 \\ 0 & 1 \end{pmatrix}$$

$$\text{Color}^2 = \begin{pmatrix} 1 & 0 \\ 0 & 1 \end{pmatrix} \qquad \begin{pmatrix} 0 & 1 \\ 1 & 0 \end{pmatrix} \cdot \begin{pmatrix} 0 & 1 \\ 1 & 0 \end{pmatrix} = \begin{pmatrix} 1 & 0 \\ 0 & 1 \end{pmatrix}$$

$$\text{Taste}^2 = \begin{pmatrix} 1 & 0 \\ 0 & 1 \end{pmatrix} \qquad \begin{pmatrix} 0 & -\text{i} \\ \text{i} & 0 \end{pmatrix} \cdot \begin{pmatrix} 0 & \\ \text{i} & 0 \end{pmatrix} = \begin{pmatrix} 1 & 0 \\ 0 & 1 \end{pmatrix}$$

Another important property of these operators is that they are equal to their Hermitian conjugate as shown below. The physical significance of this is that they have real eigenvalues, something we know from earlier calculations.

$$\overline{\text{Hardness}}^T = \begin{pmatrix} 1 & 0 \\ 0 & -1 \end{pmatrix} \qquad \left[\overline{\begin{pmatrix} 1 & 0 \\ 0 & -1 \end{pmatrix}}\right]^T = \begin{pmatrix} 1 & 0 \\ 0 & -1 \end{pmatrix}$$

$$\overline{\text{Color}}^T = \begin{pmatrix} 0 & 1 \\ 1 & 0 \end{pmatrix} \qquad \left[\overline{\begin{pmatrix} 0 & 1 \\ 1 & 0 \end{pmatrix}}\right]^T = \begin{pmatrix} 0 & 1 \\ 1 & 0 \end{pmatrix}$$

$$\overline{\text{Taste}}^{T} = \begin{pmatrix} 0 & -i \\ i & 0 \end{pmatrix} \qquad \left[\overline{\begin{pmatrix} 0 & -\mathrm{i} \\ \mathrm{i} & 0 \end{pmatrix}}\right]^{T} = \begin{pmatrix} 0 & -i \\ i & 0 \end{pmatrix}$$

The Hadamard matrix is another operator which is important in quantum optics and quantum computing.

$$\text{Hadamard} := \frac{1}{\sqrt{2}} \begin{pmatrix} 1 & 1 \\ 1 & -1 \end{pmatrix}$$

The Hadamard matrix performs a Fourier transform between the **Hardness** and **Color** basis vectors.

$\text{Hadamard} \cdot \text{Hard} = \text{Black}$	$\text{Hadamard} \cdot \text{Hard} = \begin{pmatrix} 0.707 \\ 0.707 \end{pmatrix}$	$\text{Hadamard} \cdot \text{Black} = \text{Hard}$	$\text{Hadamard} \cdot \text{Black} = \begin{pmatrix} 1 \\ 0 \end{pmatrix}$
$\text{Hadamard} \cdot \text{Soft} = \text{White}$	$\text{Hadamard} \cdot \text{Soft} = \begin{pmatrix} 0.707 \\ -0.707 \end{pmatrix}$	$\text{Hadamard} \cdot \text{White} = \text{Soft}$	$\text{Hadamard} \cdot \text{White} = \begin{pmatrix} 0 \\ 1 \end{pmatrix}$

The eigenvalues and eigenvectors of the Hadamard matrix:

$\text{eigenvals}(\text{Hadamard}) = \begin{pmatrix} 1 \\ -1 \end{pmatrix}$	$\text{eigenvals}(\text{Hadamard}, 1) = \begin{pmatrix} 0.924 \\ 0.383 \end{pmatrix}$	$\text{eigenvals}(\text{Hadamard}, -1) = \begin{pmatrix} -0.383 \\ 0.924 \end{pmatrix}$

The Hadamard matrix is also unitary and its own Hermitian conjugate like the other matrices.

$$\text{Hadamard}^2 = \begin{pmatrix} 1 & 0 \\ 0 & 1 \end{pmatrix} \qquad \overline{\text{Hadamard}}^{T} = \begin{pmatrix} 0.707 & 0.707 \\ 0.707 & -0.707 \end{pmatrix}$$

In addition to performing a Fourier transform between the **Hardness** and **Color** basis vectors, it has been reported in the *Journal of Olfactory Science* that the Hadamard matrix is the operator representing the property of **Odor**. It's eigenstates, shown above, are **Pleasant** and **Foul**, with eigenvalues +1 and -1, respectively. It is left to the interested reader to return to the beginning of this tutorial to explore the quantum relationship of **Odor** to **Hardness**, **Color** and **Taste**.

Concluding Remarks

The reason for using the properties of hardness, color and taste in these exercises is to emphasize how different the quantum world is from the macro world that we occupy. It is not an uncommon experience (it has happened to me) to eat a piece of candy that is hard, white and sweet. But this is not possible for *quantum candy* because the matrix operators representing these observables do not commute. Therefore, the observables cannot simultaneously be well defined.

In quantum mechanics these operators,

$$\text{Hardness} := \begin{pmatrix} 1 & 0 \\ 0 & -1 \end{pmatrix} \quad \text{Color} := \begin{pmatrix} 0 & 1 \\ 1 & 0 \end{pmatrix} \quad \text{Taste} := \begin{pmatrix} 0 & -\mathrm{i} \\ \mathrm{i} & 0 \end{pmatrix}$$

are actually the Pauli spin matrices and represent the observables for spin in the z-, x- and y-directions as mentioned earlier.

$$\sigma_z = \begin{pmatrix} 1 & 0 \\ 0 & -1 \end{pmatrix} \quad \sigma_{\mathrm{x}} = \begin{pmatrix} 0 & 1 \\ 1 & 0 \end{pmatrix} \quad \sigma_{\mathrm{y}} := \begin{pmatrix} 0 & -\mathrm{i} \\ \mathrm{i} & 0 \end{pmatrix}$$

They are also the operators for the rectilinear, diagonal and circular polarization properties of photons. In this case the eigenvectors are vertical, horizontal, diagonal, anti-diagonal, and right and left circular polarization.

$$\begin{aligned} \mathrm{V} &:= \begin{pmatrix} 1 \\ 0 \end{pmatrix} & \mathrm{H} &:= \begin{pmatrix} 0 \\ 1 \end{pmatrix} \\ \mathrm{D} &:= \frac{1}{\sqrt{2}} \cdot \begin{pmatrix} 1 \\ 1 \end{pmatrix} & \mathrm{A} &:= \frac{1}{\sqrt{2}} \begin{pmatrix} 1 \\ -1 \end{pmatrix} \\ \mathrm{R} &:= \frac{1}{\sqrt{2}} \cdot \begin{pmatrix} 1 \\ \mathrm{i} \end{pmatrix} & \mathrm{L} &:= \frac{1}{\sqrt{2}} \begin{pmatrix} 1 \\ -\mathrm{i} \end{pmatrix} \end{aligned}$$

Appendix: Vector and Matrix Math

Vector inner product:

$$(ab) \cdot \begin{pmatrix} c \\ d \end{pmatrix} \to a \cdot c + b \cdot d$$

Vector outer product:

$$\begin{pmatrix} c \\ d \end{pmatrix} - (ab) \to \begin{pmatrix} a \cdot c & b \cdot c \\ a \cdot d & b \cdot d \end{pmatrix}$$

$$\operatorname{tr}\left[\begin{pmatrix} c \\ d \end{pmatrix} \cdot (ab)\right] \to a \cdot c + b \cdot d$$

Matrix-vector product:

$$\begin{pmatrix} a & b \\ c & d \end{pmatrix} \cdot \begin{pmatrix} x \\ y \end{pmatrix} \to \begin{pmatrix} a \cdot x + b \cdot y \\ c \cdot x + d \cdot y \end{pmatrix}$$

$$(x, y) \cdot \begin{pmatrix} a & b \\ c & d \end{pmatrix}^T \to (a \cdot x + b \cdot y \quad c \cdot x + d \cdot y)$$

Expectation value:

$$(x \quad y) \cdot \begin{pmatrix} a & b \\ c & d \end{pmatrix} \cdot \begin{pmatrix} x \\ y \end{pmatrix} \text{ simplify } \to a \cdot x^2 + d \cdot y^2 + b \cdot x \cdot y + c \cdot x \cdot y$$

$$(x, y) \cdot \begin{pmatrix} a & b \\ c & d \end{pmatrix}^T \cdot \begin{pmatrix} x \\ y \end{pmatrix} \text{ simplify } \to a \cdot x^2 + d \cdot y^2 + b \cdot x \cdot y + c \cdot x \cdot y$$

$$\operatorname{tr}\left[\begin{pmatrix} x \\ y \end{pmatrix} \cdot \begin{pmatrix} a & b \\ c & d \end{pmatrix}\right] \to a \cdot x^2 + d \cdot y^2 + b \cdot x \cdot y + c \cdot x \cdot y$$

$$\operatorname{tr}\left[\begin{pmatrix} a & b \\ c & d \end{pmatrix} \cdot \begin{pmatrix} x \\ y \end{pmatrix} \cdot \begin{pmatrix} x & y \end{pmatrix}\right] \text{ simplify } \to a \cdot x^2 + d \cdot y^2 + b \cdot x \cdot y + c \cdot x \cdot y$$

Matrix product:

$$\begin{pmatrix} a & b \\ c & d \end{pmatrix} \cdot \begin{pmatrix} w & x \\ y & z \end{pmatrix} \to \begin{pmatrix} a \cdot w + b \cdot y & a \cdot x + b \cdot z \\ c \cdot w + d \cdot y & c \cdot x + d \cdot z \end{pmatrix}$$

Vector tensor product:

$$\begin{pmatrix} a \\ b \end{pmatrix} \otimes \begin{pmatrix} c \\ d \end{pmatrix} = \begin{pmatrix} a \begin{pmatrix} c \\ d \end{pmatrix} \\ b \begin{pmatrix} c \\ d \end{pmatrix} \end{pmatrix} = \begin{pmatrix} ac \\ ad \\ bc \\ bd \end{pmatrix}$$

Matrix tensor product:

$$\begin{pmatrix} a & b \\ c & d \end{pmatrix} \otimes \begin{pmatrix} w & x \\ y & z \end{pmatrix} = \begin{pmatrix} a \begin{pmatrix} w & x \\ y & z \end{pmatrix} & b \begin{pmatrix} w & x \\ y & z \end{pmatrix} \\ c \begin{pmatrix} w & x \\ y & z \end{pmatrix} & d \begin{pmatrix} w & x \\ y & z \end{pmatrix} \end{pmatrix} = \begin{pmatrix} aw & ax & bw & bx \\ ay & az & by & bz \\ cw & cx & dw & dx \\ cy & cz & dy & dz \end{pmatrix}$$

Matrix eigenvalues and eigenvectors (unnormalized):

$$\operatorname{eigenvals}\left(\begin{pmatrix} a & b \\ b & a \end{pmatrix}\right) \to \begin{pmatrix} a - b \\ a + b \end{pmatrix}$$

or

$$\left|\begin{pmatrix} a-\lambda & b \\ b & a-\lambda \end{pmatrix}\right| = 0 \text{ solve }, \lambda \to \begin{pmatrix} a+b \\ a-b \end{pmatrix}$$

or

$$\begin{pmatrix} -1 & 1 \\ 1 & 1 \end{pmatrix}^{-1} \begin{pmatrix} a & b \\ b & a \end{pmatrix} \begin{pmatrix} -1 & 1 \\ 1 & 1 \end{pmatrix} \to \begin{pmatrix} a-b & 0 \\ 0 & a+b \end{pmatrix}$$

using

$$\text{eigenvecs}\left(\begin{pmatrix} a & b \\ b & a \end{pmatrix}\right) \to \begin{pmatrix} -1 & 1 \\ 1 & 1 \end{pmatrix}$$

$$\begin{pmatrix} a & b \\ b & a \end{pmatrix} \cdot \begin{pmatrix} x \\ y \end{pmatrix} = (a-b) \cdot \begin{pmatrix} x \\ y \end{pmatrix} \text{ solve,} y \to -x \qquad \begin{pmatrix} x \\ y \end{pmatrix} = \begin{pmatrix} -1 \\ 1 \end{pmatrix}$$

$$\begin{pmatrix} \mathrm{a} & \mathrm{b} \\ \mathrm{b} & \mathrm{a} \end{pmatrix} \cdot \begin{pmatrix} \mathrm{x} \\ \mathrm{y} \end{pmatrix} = (\mathrm{a}+\mathrm{b}) \cdot \begin{pmatrix} \mathrm{x} \\ \mathrm{y} \end{pmatrix} \text{ solve, } \mathrm{y} \to \mathrm{x} \qquad \begin{pmatrix} \mathrm{x} \\ \mathrm{y} \end{pmatrix} = \begin{pmatrix} 1 \\ 1 \end{pmatrix}$$

Completeness relations:

$$\text{Black} \cdot \text{Black}^T + \text{White} \cdot \text{White}^T = \begin{pmatrix} 1 & 0 \\ 0 & 1 \end{pmatrix}$$

$$\text{Hard} \cdot \text{Hard}^T + \text{Soft} \cdot \text{Soft}^T = \begin{pmatrix} 1 & 0 \\ 0 & 1 \end{pmatrix}$$

This page titled 1.33: Basic Matrix Mechanics is shared under a CC BY 4.0 license and was authored, remixed, and/or curated by Frank Rioux via source content that was edited to the style and standards of the LibreTexts platform.

1.34: Rudimentary Matrix Mechanics

A quon (an entity that exhibits both wave and particle aspects in the peculiar quantum manner - Nick Herbert, *Quantum Reality*, page 64) has a variety of properties each of which can take on two values. For example, it has the property of **hardness** and can be either *hard* or *soft*. It also has the property of **color** and can be either *black* or *white*, and the property of **taste** and be *sweet* or *sour*. The treatment that follows draws on material from Chapter 3 of David Z Albert's book, *Quantum Mechanics and Experience*.

The basic principles of matrix and vector math are provided in Appendix A. An examination of this material will demonstrate that most of the calculations presented in this tutorial can easily be performed without the aid of Mathcad or any other computer algebra program. In other words, they can be done by hand.

In the matrix formulation of quantum mechanics the hardness and color states are represented by the following vectors.

$$\text{Hard} := \begin{pmatrix} 1 \\ 0 \end{pmatrix} \quad \text{Soft} := \begin{pmatrix} 0 \\ 1 \end{pmatrix} \quad \text{Black} := \begin{pmatrix} \frac{1}{\sqrt{2}} \\ \frac{1}{\sqrt{2}} \end{pmatrix} \quad \text{White} := \begin{pmatrix} \frac{1}{\sqrt{2}} \\ \frac{-1}{\sqrt{2}} \end{pmatrix}$$

Hard and *Soft* represent an orthonormal basis in the two-dimensional **Hardness** vector space.

$$\text{Hard}^T \cdot \text{Hard} = 1 \qquad \text{Soft}^T \cdot \text{Soft} = 1 \qquad \text{Hard}^T \cdot \text{Soft} = 0$$

$$\begin{pmatrix} 1 & 0 \end{pmatrix} \cdot \begin{pmatrix} 1 \\ 0 \end{pmatrix} = 1 \quad \begin{pmatrix} 0 & 1 \end{pmatrix} \cdot \begin{pmatrix} 0 \\ 1 \end{pmatrix} = 1 \quad \begin{pmatrix} 1 & 0 \end{pmatrix} \cdot \begin{pmatrix} 0 \\ 1 \end{pmatrix} = 0$$

Likewise *Black* and *White* are an orthonormal basis in the two-dimensional **Color** vector space.

$$\text{Black}^T \cdot \text{Black} = 1 \qquad \text{White}^T \cdot \text{White} = 1 \qquad \text{Black}^T \cdot \text{White} = 0$$

$$\begin{pmatrix} \frac{1}{\sqrt{2}} & \frac{1}{\sqrt{2}} \end{pmatrix} \cdot \begin{pmatrix} \frac{1}{\sqrt{2}} \\ \frac{1}{\sqrt{2}} \end{pmatrix} = 1 \quad \begin{pmatrix} \frac{1}{\sqrt{2}} & \frac{-1}{\sqrt{2}} \end{pmatrix} \cdot \begin{pmatrix} \frac{1}{\sqrt{2}} \\ \frac{-1}{\sqrt{2}} \end{pmatrix} = 1 \quad \begin{pmatrix} \frac{1}{\sqrt{2}} & \frac{1}{\sqrt{2}} \end{pmatrix} \cdot \begin{pmatrix} \frac{1}{\sqrt{2}} \\ \frac{-1}{\sqrt{2}} \end{pmatrix} = 0$$

The relationship between the two bases is reflected in the following projection calculations.

Note

$$\frac{1}{\sqrt{2}} = 0.707$$

$$\begin{pmatrix} 1 & 0 \end{pmatrix} \cdot \begin{pmatrix} \frac{1}{\sqrt{2}} \\ \frac{1}{\sqrt{2}} \end{pmatrix} = 0.707 \quad \begin{pmatrix} 1 & 0 \end{pmatrix} \cdot \begin{pmatrix} \frac{1}{\sqrt{2}} \\ \frac{-1}{\sqrt{2}} \end{pmatrix} = 0.707 \quad \begin{pmatrix} 0 & 0 \end{pmatrix} \cdot \begin{pmatrix} \frac{1}{\sqrt{2}} \\ \frac{1}{\sqrt{2}} \end{pmatrix} = 0.707 \quad \begin{pmatrix} 0 & 1 \end{pmatrix} \cdot \begin{pmatrix} \frac{1}{\sqrt{2}} \\ \frac{-1}{\sqrt{2}} \end{pmatrix} = -0.707$$

$\text{Hard}^T \cdot \text{Black} = 0.707$ $\quad$ $\text{Hard}^T \cdot \text{White} = 0.707$ $\quad$ $\text{Soft}^T \cdot \text{Black} = 0.707$ $\quad$ $\text{Soft}^T \cdot \text{White} = -0.707$

The values calculated above are probability amplitudes. The absolute square of those values is the probability. In other words, the probability that a black quon will be found to be hard is 0.5. The probability that a white quon will be found to be soft is also 0.5.

$$\left(\left|\text{Hard}^T \cdot \text{Black}\right|\right)^2 = 0.5 \quad \left(\left|\text{Hard}^T \cdot \text{White}\right|\right)^2 = 0.5 \quad \left(\left|\text{Soft}^T \cdot \text{Black}\right|\right)^2 = 0.5 \quad \left(\left|\text{Soft}^T \cdot \text{White}\right|\right)^2 = 0.5$$

$$\left|\left|\begin{pmatrix} 1 & 0 \end{pmatrix} \cdot \begin{pmatrix} \frac{1}{\sqrt{2}} \\ \frac{1}{\sqrt{2}} \end{pmatrix}\right|\right|^2 = 0.5 \quad \left|\left|\begin{pmatrix} 1 & 0 \end{pmatrix} \cdot \begin{pmatrix} \frac{1}{\sqrt{2}} \\ \frac{-1}{\sqrt{2}} \end{pmatrix}\right|\right|^2 = 0.5 \quad \left|\left|\begin{pmatrix} 0 & 0 \end{pmatrix} \cdot \begin{pmatrix} \frac{1}{\sqrt{2}} \\ \frac{1}{\sqrt{2}} \end{pmatrix}\right|\right|^2 = 0.5 \quad \left|\left|\begin{pmatrix} 0 & 1 \end{pmatrix} \cdot \begin{pmatrix} \frac{1}{\sqrt{2}} \\ \frac{-1}{\sqrt{2}} \end{pmatrix}\right|\right|^2 = 0.5$$

Clearly *Black* and *White* can be written as superpositions of *Hard* and *Soft*, and vice versa. This means hard and soft quons do not have a well-defined color, and black and white quons do not have a well-defined hardness.

$\frac{1}{\sqrt{2}} \cdot (\text{Hard} + \text{Soft}) = \begin{pmatrix} 0.707 \\ 0.707 \end{pmatrix}$	$\frac{1}{\sqrt{2}} \cdot \left[\begin{pmatrix} 1 \\ 0 \end{pmatrix} + \begin{pmatrix} 0 \\ 1 \end{pmatrix} \right] = \begin{pmatrix} 0.707 \\ 0.707 \end{pmatrix}$
$\frac{1}{\sqrt{2}} \cdot (\text{Hard} - \text{Soft}) = \begin{pmatrix} 0.707 \\ -0.707 \end{pmatrix}$	$\frac{1}{\sqrt{2}} \left[\begin{pmatrix} 1 \\ 0 \end{pmatrix} - \begin{pmatrix} 0 \\ 1 \end{pmatrix} \right] = \begin{pmatrix} 0.707 \\ -0.707 \end{pmatrix}$
$\frac{1}{\sqrt{2}} \cdot (\ \text{Black} + \text{White}\ ) = \begin{pmatrix} 1 \\ 0 \end{pmatrix}$	$\frac{1}{\sqrt{2}} \left[\begin{pmatrix} \frac{1}{\sqrt{2}} \\ \frac{1}{\sqrt{2}} \end{pmatrix} + \begin{pmatrix} \frac{1}{\sqrt{2}} \\ \frac{-1}{\sqrt{2}} \end{pmatrix} \right] = \begin{pmatrix} 1 \\ 0 \end{pmatrix}$
$\frac{1}{\sqrt{2}} \cdot (\ \text{Black} - \text{White}\ ) = \begin{pmatrix} 0 \\ 1 \end{pmatrix}$	$\frac{1}{\sqrt{2}} \left[\begin{pmatrix} \frac{1}{\sqrt{2}} \\ \frac{1}{\sqrt{2}} \end{pmatrix} - \begin{pmatrix} \frac{1}{\sqrt{2}} \\ \frac{-1}{\sqrt{2}} \end{pmatrix} \right] = \begin{pmatrix} 0 \\ 1 \end{pmatrix}$

Hard, *Soft*, *Black* and *White* are measurable properties and the vectors representing them are eigenstates of the *Hardness* and *Color* operators with **eigenvalues** ± 1. The **Identity** operator is also given and will be discussed later. Of course, the *Hardness* and *Color* operators are just the Pauli spin operators in the z- and x-directions. Later the *Taste* operator will be introduced; it is the y-direction Pauli spin operator.

Operators

$\text{Hardness} := \begin{pmatrix} 1 & 0 \\ 0 & -1 \end{pmatrix}$	$\text{Color} := \begin{pmatrix} 0 & 1 \\ 1 & 0 \end{pmatrix}$	$\text{I} := \begin{pmatrix} 1 & 0 \\ 0 & 1 \end{pmatrix}$

Eigenvalue +1		Eigenvalue -1	
$\text{Hardness} \cdot \text{Hard} = \begin{pmatrix} 1 \\ 0 \end{pmatrix}$	$\begin{pmatrix} 1 & 0 \\ 0 & -1 \end{pmatrix} \cdot \begin{pmatrix} 1 \\ 0 \end{pmatrix} = \begin{pmatrix} 1 \\ 0 \end{pmatrix}$	$\text{Hardness} \cdot \text{Soft} = \begin{pmatrix} 0 \\ -1 \end{pmatrix}$	$\begin{pmatrix} 1 & 0 \\ 0 & -1 \end{pmatrix} \cdot \begin{pmatrix} 0 \\ 1 \end{pmatrix} = \begin{pmatrix} 0 \\ -1 \end{pmatrix}$
$\text{Color} \cdot \text{Black} = \begin{pmatrix} 0.707 \\ 0.707 \end{pmatrix}$	$\begin{pmatrix} 0 & 1 \\ 1 & 0 \end{pmatrix} \cdot \begin{pmatrix} \frac{1}{\sqrt{2}} \\ \frac{1}{\sqrt{2}} \end{pmatrix} = \begin{pmatrix} 0.707 \\ 0.707 \end{pmatrix}$	$\text{Color} \cdot \text{White} = \begin{pmatrix} -0.707 \\ 0.707 \end{pmatrix}$	$\begin{pmatrix} 0 & 1 \\ 1 & 0 \end{pmatrix} \cdot \begin{pmatrix} \frac{1}{\sqrt{2}} \\ \frac{-1}{\sqrt{2}} \end{pmatrix} = \begin{pmatrix} -0.707 \\ 0.707 \end{pmatrix}$

Another way of showing this is by calculating the **expectation (or average) value**. Every time the hardness of a hard quon is measured the result is +1. Every time the hardness of a soft quon is measured the result is -1.

$\text{Hard}^T \cdot \text{Hardness} \cdot \text{Hard} = 1$	$\begin{pmatrix} 1 & 0 \\ 0 & -1 \end{pmatrix} \cdot \begin{pmatrix} 1 \\ 0 \end{pmatrix} = 1$	$\text{Soft}^T \cdot \text{Hardness} \cdot \text{Soft} = -1$	$\begin{pmatrix} 0 & 1 \end{pmatrix} \cdot \begin{pmatrix} 1 & 0 \\ 0 & -1 \end{pmatrix} \cdot \begin{pmatrix} 0 \\ 1 \end{pmatrix} = -1$
$\text{Black}^T \cdot \text{Color} \cdot \text{Black} = 1$	$\begin{pmatrix} \frac{1}{\sqrt{2}} & \frac{1}{\sqrt{2}} \end{pmatrix} \cdot \begin{pmatrix} 0 & 1 \\ 1 & 0 \end{pmatrix} \cdot \begin{pmatrix} \frac{1}{\sqrt{2}} \\ \frac{1}{\sqrt{2}} \end{pmatrix} = 1$	$\text{White}^T \cdot \text{Color} \cdot \text{White} = 1$	$\begin{pmatrix} \frac{1}{\sqrt{2}} & \frac{-1}{\sqrt{2}} \end{pmatrix} \cdot \begin{pmatrix} 0 & 1 \\ 1 & 0 \end{pmatrix} \cdot \begin{pmatrix} \frac{1}{\sqrt{2}} \\ \frac{-1}{\sqrt{2}} \end{pmatrix} = -1$

If a quon is in a state which is an eigenfunction of an operator, it means it has a well-defined value for the observable represented by the operator. If the quon is in a state which is not an eigenfunction of the operator, it does not have a well-defined value for the observable.

Hard and *Soft* are not **eigenfunctions** of the *Color* operator, and *Black* and *White* are not eigenfunctions of the **Hardness** operator. Hard and soft quons do not have a well-defined color, and black and white quons do not have a well-defined hardness.

$\text{Hardness} \cdot \text{Black} = \begin{pmatrix} 0.707 \\ -0.707 \end{pmatrix}$	$\begin{pmatrix} 1 & 0 \\ 0 & -1 \end{pmatrix} \cdot \begin{pmatrix} \frac{1}{\sqrt{2}} \\ \frac{1}{\sqrt{2}} \end{pmatrix} = \begin{pmatrix} 0.707 \\ -0.707 \end{pmatrix}$	$\text{Hardness} \cdot \text{White} = \begin{pmatrix} 0.707 \\ 0.707 \end{pmatrix}$	$\begin{pmatrix} 1 & 0 \\ 0 & -1 \end{pmatrix} \cdot \begin{pmatrix} \frac{1}{\sqrt{2}} \\ \frac{-1}{\sqrt{2}} \end{pmatrix} = \begin{pmatrix} 0.707 \\ 0.707 \end{pmatrix}$
$\text{Color} \cdot \text{Hard} = \begin{pmatrix} 0 \\ 1 \end{pmatrix}$	$\begin{pmatrix} 0 & 1 \\ 1 & 0 \end{pmatrix} \cdot \begin{pmatrix} 1 \\ 0 \end{pmatrix} = \begin{pmatrix} 0 \\ 1 \end{pmatrix}$	$\text{Color} \cdot \text{Soft} = \begin{pmatrix} 1 \\ 0 \end{pmatrix}$	$\begin{pmatrix} 0 & 1 \\ 1 & 0 \end{pmatrix} \cdot \begin{pmatrix} 0 \\ 1 \end{pmatrix} = \begin{pmatrix} 1 \\ 0 \end{pmatrix}$

Therefore their **expectation values** are zero. In other words if the hardness of a black quon is measured, half the time it will register hard and half the time soft. If the color of a soft quon is measured, half the time it will register white and half the time black.

$\text{Black}^T \cdot \text{Hardness} \cdot \text{Black} = 0$	$\begin{pmatrix} \frac{1}{\sqrt{2}} & \frac{1}{\sqrt{2}} \end{pmatrix} \cdot \begin{pmatrix} 1 & 0 \\ 0 & -1 \end{pmatrix} \cdot \begin{pmatrix} \frac{1}{\sqrt{2}} \\ \frac{1}{\sqrt{2}} \end{pmatrix} = 0$	$\text{White}^T \cdot \text{Hardness} \cdot \text{White} = 0$	$\begin{pmatrix} \frac{1}{\sqrt{2}} & \frac{-1}{\sqrt{2}} \end{pmatrix} \cdot \begin{pmatrix} 1 & 0 \\ 0 & -1 \end{pmatrix} \cdot \begin{pmatrix} \frac{1}{\sqrt{2}} \\ \frac{-1}{\sqrt{2}} \end{pmatrix} = 0$
$\text{Hard}^T \cdot \text{Color} \cdot \text{Hard} = 0$	$\begin{pmatrix} 1 & 0 \end{pmatrix} \cdot \begin{pmatrix} 0 & 1 \\ 1 & 0 \end{pmatrix} \cdot \begin{pmatrix} 1 \\ 0 \end{pmatrix} = 0$	$\text{Soft}^T \cdot \text{Color} \cdot \text{Soft} = 0$	$\begin{pmatrix} 0 & 1 \end{pmatrix} \cdot \begin{pmatrix} 0 & 1 \\ 1 & 0 \end{pmatrix} \cdot \begin{pmatrix} 0 \\ 1 \end{pmatrix} = 0$

As the **Hardness-Color** commutator shows, the **Hardness** and **Color** operators do not commute. They represent incompatible observables; observables that cannot simultaneously have well-defined values.

$\text{Hardness} \cdot \text{Color} - \text{Color} \cdot \text{Hardness} = \begin{pmatrix} 0 & 2 \\ -2 & 0 \end{pmatrix}$	$\begin{pmatrix} 1 & 0 \\ 0 & -1 \end{pmatrix} \begin{pmatrix} 0 & 1 \\ 1 & 0 \end{pmatrix} - \begin{pmatrix} 0 & 1 \\ 1 & 0 \end{pmatrix} \cdot \begin{pmatrix} 1 & 0 \\ 0 & -1 \end{pmatrix} = \begin{pmatrix} 0 & 2 \\ -2 & 0 \end{pmatrix}$

This means that the measurement of the color and then the hardness of a hard quon gives a different result than the measurement of the hardness and then the color.

$\text{Hardness} \cdot \text{Color} \cdot \text{Hard} = \begin{pmatrix} 0 \\ -1 \end{pmatrix}$	$\begin{pmatrix} 1 & 0 \\ 0 & -1 \end{pmatrix} \cdot \begin{pmatrix} 0 & 1 \\ 1 & 0 \end{pmatrix} \cdot \begin{pmatrix} 1 \\ 0 \end{pmatrix} = \begin{pmatrix} 0 \\ -1 \end{pmatrix}$	$\text{Color} \cdot \text{Hardness} \cdot \text{Hard} = \begin{pmatrix} 0 \\ 1 \end{pmatrix}$	$\begin{pmatrix} 0 & 1 \\ 1 & 0 \end{pmatrix} \cdot \begin{pmatrix} 1 & 0 \\ 0 & -1 \end{pmatrix} \cdot \begin{pmatrix} 1 \\ 0 \end{pmatrix} = \begin{pmatrix} 0 \\ 1 \end{pmatrix}$

We can also look at this from the perspective of the uncertainty principle. The uncertainty in a measurement is the square root of the difference between *the mean of the square* and *the square of the mean*.

Suppose we measure the color of a Black or White quon. Because Black and White are eigenfunctions of the Color operator the uncertainty in the measurement results are zero.

$$\sqrt{\text{Black}^T \cdot \text{Color}^2 \cdot \text{Black} - (\text{Black}^T \cdot \text{Color} \cdot \text{Black})^2} = 0$$
$$\sqrt{\text{White}^T \cdot \text{Color}^2 \cdot \text{White} - (\text{White}^T \cdot \text{Color} \cdot \text{White})^2} = 0$$

However, the measurement of the color of a Soft or Hard quon is by the same criterion uncertain.

$$\sqrt{\text{Soft}^T \cdot \text{Color}^2 \cdot \text{Soft} - (\text{Soft}^T \cdot \text{Color} \cdot \text{Soft})^2} = 1$$
$$\sqrt{\text{Hard}^T \cdot \text{Color}^2 \cdot \text{Hard} - (\text{Hard}^T \cdot \text{Color} \cdot \text{Hard})^2} = 1$$

The calculations of **Hardness** and **Color** reveal the strange behavior of quons. In the macro world we frequently find objects that simultaneously have well-defined values for these physical attributes. But we see this is not possible in the quantum world.

Mathcad has high-level commands which find the eigenvalues and eigenvectors of matrices which in quantum mechanics are operators. Below it is shown that they give the same results as were demonstrated above. See the Appendix for additional

computational methods.

$\text{eigenvals}(\text{Hardness}) = \begin{pmatrix} 1 \\ -1 \end{pmatrix}$	$\text{eigenvals}(\text{Hardness}, -1) = \begin{pmatrix} 0 \\ 1 \end{pmatrix}$	$\text{eigenvals}(\text{Hardness}, 1) = \begin{pmatrix} 1 \\ 0 \end{pmatrix}$
$\text{eigenvals}(\text{Color}) = \begin{pmatrix} 1 \\ -1 \end{pmatrix}$	$\text{eigenvals}(\text{Color}, -1) = \begin{pmatrix} -0.707 \\ 1 \end{pmatrix}$	$\text{eigenvals}(\text{Color}, 1) = \begin{pmatrix} 0.707 \\ 0.707 \end{pmatrix}$

Besides the properties of hardness and color, suppose the quon also has the property of taste, tasting either *Sweet* or *Sour*. The **Taste** operator is defined below and its eigenvalues and eigenvectors calculated.

Operator	Eigenvalues	Sweet/Sour Eigenvectors
$\text{Taste} := \begin{pmatrix} 0 & -\text{i} \\ \text{i} & 0 \end{pmatrix}$	$\text{eigenvals}(\text{Taste}) = \begin{pmatrix} 1 \\ -1 \end{pmatrix}$	$\text{eigenvals}(\text{Taste}) = \begin{pmatrix} -0.707\text{i} & 0.707 \\ 0.707 & -0.707\text{i} \end{pmatrix}$

Squaring the **Hardness**, **Color** and **Taste** operators gives the **Identity** operator, that is they are unitary matrices. The **Identity** operator leaves the vector it operates on unchanged.

$$\text{Hardness}^2 = \begin{pmatrix} 1 & 0 \\ 0 & 1 \end{pmatrix} \qquad \begin{pmatrix} 1 & 0 \\ 0 & -1 \end{pmatrix} \cdot \begin{pmatrix} 1 & 0 \\ 0 & -1 \end{pmatrix} = \begin{pmatrix} 1 & 0 \\ 0 & 1 \end{pmatrix}$$

$$\text{Color}^2 = \begin{pmatrix} 1 & 0 \\ 0 & 1 \end{pmatrix} \qquad \begin{pmatrix} 0 & 1 \\ 1 & 0 \end{pmatrix} \cdot \begin{pmatrix} 0 & 1 \\ 1 & 0 \end{pmatrix} = \begin{pmatrix} 1 & 0 \\ 0 & 1 \end{pmatrix}$$

$$\text{Taste}^2 = \begin{pmatrix} 1 & 0 \\ 0 & 1 \end{pmatrix} \qquad \begin{pmatrix} 0 & -\text{i} \\ \text{i} & 0 \end{pmatrix} \cdot \begin{pmatrix} 0 & \\ \text{i} & 0 \end{pmatrix} = \begin{pmatrix} 1 & 0 \\ 0 & 1 \end{pmatrix}$$

Another important property of these operators is that they are equal to their Hermitian conjugate as shown below. The physical significance of this is that they have real eigenvalues, something we know from earlier calculations.

$$\overline{\text{Hardness}}^T = \begin{pmatrix} 1 & 0 \\ 0 & -1 \end{pmatrix} \qquad \left[\overline{\begin{pmatrix} 1 & 0 \\ 0 & -1 \end{pmatrix}}\right]^T = \begin{pmatrix} 1 & 0 \\ 0 & -1 \end{pmatrix}$$

$$\overline{\text{Color}}^T = \begin{pmatrix} 0 & 1 \\ 1 & 0 \end{pmatrix} \qquad \left[\overline{\begin{pmatrix} 0 & 1 \\ 1 & 0 \end{pmatrix}}\right]^T = \begin{pmatrix} 0 & 1 \\ 1 & 0 \end{pmatrix}$$

$$\overline{\text{Taste}}^T = \begin{pmatrix} 0 & -i \\ i & 0 \end{pmatrix} \qquad \left[\overline{\begin{pmatrix} 0 & -\text{i} \\ \text{i} & 0 \end{pmatrix}}\right]^T = \begin{pmatrix} 0 & -i \\ i & 0 \end{pmatrix}$$

The Hadamard matrix is another operator which is important in quantum optics and quantum computing.

$$\text{Hadamard} := \frac{1}{\sqrt{2}} \begin{pmatrix} 1 & 1 \\ 1 & -1 \end{pmatrix}$$

The Hadamard matrix performs a Fourier transform between the **Hardness** and **Color** basis vectors.

$\text{Hadamard} \cdot \text{Hard} = \text{Black}$	$\text{Hadamard} \cdot \text{Hard} = \begin{pmatrix} 0.707 \\ 0.707 \end{pmatrix}$	$\text{Hadamard} \cdot \text{Black} = \text{Hard}$	$\text{Hadamard} \cdot \text{Black} = \begin{pmatrix} 1 \\ 0 \end{pmatrix}$
$\text{Hadamard} \cdot \text{Soft} = \text{White}$	$\text{Hadamard} \cdot \text{Soft} = \begin{pmatrix} 0.707 \\ -0.707 \end{pmatrix}$	$\text{Hadamard} \cdot \text{White} = \text{Soft}$	$\text{Hadamard} \cdot \text{White} = \begin{pmatrix} 0 \\ 1 \end{pmatrix}$

The eigenvalues and eigenvectors of the Hadamard matrix:

$\text{eigenvals}(\text{Hadamard}) = \begin{pmatrix} 1 \\ -1 \end{pmatrix}$	$\text{eigenvals}(\text{Hadamard}, 1) = \begin{pmatrix} 0.924 \\ 0.383 \end{pmatrix}$	$\text{eigenvals}(\text{Hadamard}, -1) = \begin{pmatrix} -0.383 \\ 0.924 \end{pmatrix}$

The Hadamard matrix is also unitary and its own Hermitian conjugate like the other matrices.

$$\text{Hadamard}^2 = \begin{pmatrix} 1 & 0 \\ 0 & 1 \end{pmatrix} \qquad \overline{\text{Hadamard}}^T = \begin{pmatrix} 0.707 & 0.707 \\ 0.707 & -0.707 \end{pmatrix}$$

Composite Systems

$\text{Hardness} := \begin{pmatrix} 1 & 0 \\ 0 & -1 \end{pmatrix}$	$\text{Hard} := \text{eigenvec}(\text{Hardness}, 1) = \begin{pmatrix} 1 \\ 0 \end{pmatrix}$	$\text{Soft} := \text{eigenvec}(\text{Hardness}, -1) = \begin{pmatrix} 0 \\ 1 \end{pmatrix}$
$\text{Color} := \begin{pmatrix} 0 & 1 \\ 1 & 0 \end{pmatrix}$	$\text{Black} := \text{eigenvec}(\text{Color}, 1) = \begin{pmatrix} 0.707 \\ 0.707 \end{pmatrix}$	$\text{White} := \text{eigenvec}(\text{Color}, -1) = \begin{pmatrix} -0.707 \\ 0.707 \end{pmatrix}$
$\text{Taste} := \begin{pmatrix} 0 & -i \\ i & 0 \end{pmatrix}$	$\text{Sweet} := \text{eigenvec}(\text{Taste}, 1) = \begin{pmatrix} -0.707i \\ 0.707 \end{pmatrix}$	$\text{Sweet} := \text{eigenvec}(\text{Taste}, -1) = \begin{pmatrix} 0.707i \\ 0.707 \end{pmatrix}$
$\text{Odor} := \frac{1}{\sqrt{2}} \cdot \begin{pmatrix} 1 & 1 \\ 1 & -1 \end{pmatrix}$	$\text{P} := \text{eigenvec}(\text{Odor}, 1) = \begin{pmatrix} 0.924 \\ 0.383 \end{pmatrix}$	$\text{F} := \text{eigenvec}(\text{Odor}, -1) = \begin{pmatrix} -0.383 \\ 0.924 \end{pmatrix}$

Quantum mechanics gets even more interesting for composite systems - quantum systems consisting of two or more quons. Suppose two quons are created in the same event and one is hard (**H**) and the other is soft (**S**), but of course because of the indistinquishability principle we don't know which is which. Under this circumstance an appropriate state vector is the following **entangled superposition**. (See Appendix A for vector tensor multiplication),

$$\Psi = \frac{1}{\sqrt{2}}[|H\rangle_A|S\rangle_B - |S\rangle_A|H\rangle_B] = \frac{1}{\sqrt{2}}\left[\begin{pmatrix} 1 \\ 0 \end{pmatrix} \otimes \begin{pmatrix} 0 \\ 1 \end{pmatrix} - \begin{pmatrix} 0 \\ 1 \end{pmatrix} \otimes \begin{pmatrix} 1 \\ 0 \end{pmatrix}\right] = \frac{1}{\sqrt{2}} \begin{pmatrix} 0 \\ 1 \\ -1 \\ 0 \end{pmatrix}$$

$$\Psi := \frac{1}{\sqrt{2}} \cdot \begin{pmatrix} 0 \\ 1 \\ -1 \\ 0 \end{pmatrix}$$

If the hardness of A or the hardness of B is measured the expectation value is 0, because half the time the quon will be found to be hard (+1) and half the time soft (-1). However if the hardness of both quons is measured the joint expectation value is -1, because they are in opposite hardness states. This is perfect anti-correlation. The joint measurements show correlation in spite of the fact that the individual measurements are totally random. This is the "spooky action at a distance" that bothered Einstein. Kronecker is Mathcad's command for matrix tensor multiplication which is illustrated in Appendix A.

$$\Psi^{\mathrm{T}} \cdot \text{kronecker}(\text{ Hardness }, \mathrm{I}) \cdot \Psi = 0$$

$$\Psi^{\mathrm{T}} \cdot \text{ kronecker } (\mathrm{I}, \text{Hardness}) \ \Psi = 0$$

$$\Psi^{\mathrm{T}} \cdot \text{ kronecker}(\text{Hardness}, \text{Hardness}) \ \cdot \Psi = -1$$

Now suppose we do color measurements on the same pair of quons. Again we find perfect color anti-correlation between the two quons. Individually the color measurements are randomly black (**B**) or white (**W**), but when we measure the color of both quons we always get different colors.

$$\Psi^{\mathrm{T}} \cdot \text{ kronecker } (\text{Color}, \mathrm{I}) \cdot \Psi = 0$$

$$\Psi^{\mathrm{T}} \cdot \text{kronecker}(\mathrm{I}, \text{ Color}) \cdot \Psi = 0$$

$$\Psi^{\mathrm{T}} \cdot \text{ kronecker } (\text{Color}, \text{Color}) \ \cdot \Psi = -1$$

This result can be understood by recalling that black and white are superpositions of hard and soft. Substitution of the appropriate superpositions into the original composite state vector expresses it in the black/white basis and reveals the perfect anti-correlation.

$$\Psi = \frac{1}{\sqrt{2}}[|W\rangle_A|B\rangle_B - |B\rangle_A|W\rangle_B]$$

$$= \frac{1}{\sqrt{2}}\left[\frac{1}{\sqrt{2}}\begin{pmatrix}1\\-1\end{pmatrix}\otimes\frac{1}{\sqrt{2}}\begin{pmatrix}1\\1\end{pmatrix} - \frac{1}{\sqrt{2}}\begin{pmatrix}1\\1\end{pmatrix}\otimes\frac{1}{\sqrt{2}}\begin{pmatrix}1\\-1\end{pmatrix}\right] = \frac{1}{\sqrt{2}}\begin{pmatrix}0\\1\\-1\\0\end{pmatrix}$$

The same thing that is true for black and white is also true for sweet (**Sw**) and sour (**So**). The taste measurements are individually random, but collectively perfectly anti-correlated.

$$\Psi^{\mathrm{T}} \cdot \mathrm{kronecker}(\mathrm{Taste}\ , \mathrm{I}) \cdot \Psi = 0$$

$$\Psi^{\mathrm{T}} \cdot \mathrm{kronecker}(\mathrm{I},\ \mathrm{Taste}) \cdot \Psi = 0$$

$$\Psi^{\mathrm{T}} \cdot \mathrm{kronecker}(\mathrm{Taste},\ \mathrm{Taste}) \cdot \Psi = -1$$

Below the original state vector is written in the sweet/sour basis.

$$\Psi = \frac{1}{\sqrt{2}}[|So\rangle_A|Sw\rangle_B - |Sw\rangle_A|So\rangle_B]$$

$$= \frac{1}{\sqrt{2}}\left[\frac{1}{\sqrt{2}}\begin{pmatrix}1\\-i\end{pmatrix}\otimes\frac{1}{\sqrt{2}}\begin{pmatrix}-i\\1\end{pmatrix} - \frac{1}{\sqrt{2}}\begin{pmatrix}-i\\1\end{pmatrix}\otimes\frac{1}{\sqrt{2}}\begin{pmatrix}1\\-i\end{pmatrix}\right] = \frac{1}{\sqrt{2}}\begin{pmatrix}0\\1\\-1\\0\end{pmatrix}$$

If different properties of the quons are measured the expectation values are zero - there is no correlation.

$$\Psi^{\mathrm{T}} \cdot\ \mathrm{kronecker}\ (\mathrm{Hardness},\ \mathrm{Color})\ \cdot \Psi = 0$$

$$\Psi^{\mathrm{T}} \cdot\ \mathrm{kronecker}\ (\mathrm{Hardness},\ \mathrm{Taste})\ \cdot \Psi = 0$$

$$\Psi^{\mathrm{T}} \cdot\ \mathrm{kronecker}\ (\mathrm{Color},\ \mathrm{Taste})\ \cdot \Psi = 0$$

A realist believes that objects, macro, micro or nano, have well-defined properties prior to and independent of the nature of the observation performed on them. Experiment simply reveals the unknown state of the system under observation.

Objects with three properties (hardness, color and taste) which can be in either of two states (hard +1, soft -1, black +1, white -1, sweet +1 and sour -1) can be in any one of eight states according to a realist: HBSw, HBSo, HWSw, HWSo, SBSw, SBSo, SWSw and SWSo. Due to the correlation values when the same property is measured on both quons, the realist can explain all measurement results as shown in the table below.

Because the states were constructed on the basis of anti-correlation for hardness, color and taste, it is only necessary to show agreement between the quantum calculations and the realist's states for the cases in which different properties are measured. The three right-hand columns of the table show no correlation, in agreement with the quantum calculations.

QuonA	QuonB	Hardness-Color	Hardness-Taste	Color-Taste
HBSw	SWSo	$1 \times -1 = -1$	$1 \times -1 = -1$	$1 \times -1 = -1$
HBSo	SWSw	$1 \times -1 = -1$	$1 \times 1 = 1$	$1 \times 1 = 1$
HWSw	SBSo	$1 \times 1 = 1$	$1 \times -1 = -1$	$-1 \times -1 = 1$
HWSo	SBSw	$1 \times 1 = 1$	$1 \times 1 = 1$	$-1 \times 1 = -1$
Expectation	Value	0	0	0

In spite of this agreement, the quantum theorist objects. Earlier it was shown that the hardness and color operators do not commute, meaning that from the quantum perspective hardness and color cannot be simultaneously well-defined. The same is true for hardness and taste, and for color and taste. Therefore, the states in the table proposed by the realist are not legitimate.

$$\mathrm{Hardness} \cdot \mathrm{Taste} - \ \mathrm{Taste} \cdot \mathrm{Hardness} = \begin{pmatrix}0 & -2\mathrm{i}\\ -2\mathrm{i} & 0\end{pmatrix}$$

$$\text{Color} \cdot \text{Taste} - \text{Taste} \cdot \text{Color} = \begin{pmatrix} 2i & 0 \\ 0 & -2i \end{pmatrix}$$

The superpositions tell the same story. For example, if a quon is hard (H) its color and taste are indeterminate because hard is an even superposition of black and white, and sweet and sour.

$$H = \frac{1}{\sqrt{2}} \cdot (B + W) \qquad H = \frac{1}{\sqrt{2}} \cdot (i \cdot Sw + So)$$

While this line of reasoning is compelling, the realist is undeterred. The fact that quantum mechanics can't assign specific values to all properties of an object is evidence that it does not provide a complete theory of reality!

Thought experiments like this clarify the conflict between quantum theory and local realism, but they do not provide, as we have seen, a final adjudication of the disagreement. That changed in 1964 with a theoretical analysis by John Bell that showed that there are experimental situations where the predictions of quantum mechanics and local realism are in disagreement. We look at one of them now.

Odor is another physical property of objects. The Hadamard operator is renamed the Odor operator. It has two eigenstates Pleasant and Foul, with eigenvalues +1 and -1, respectively, as shown below.

$$\text{Odor} := \frac{1}{\sqrt{2}} \cdot \begin{pmatrix} 1 & 1 \\ 1 & -1 \end{pmatrix} \qquad (\text{Odor}) = \begin{pmatrix} 1 \\ -1 \end{pmatrix}$$

$$\text{Pleasant} := \text{eigenvec}\,(\text{Odor}, 1) = \begin{pmatrix} 0.924 \\ 0.383 \end{pmatrix}$$

$$\text{Foul} := \text{eigenvec}\,(\text{Odor}, -1) = \begin{pmatrix} -0.383 \\ 0.924 \end{pmatrix}$$

$$\Psi = \frac{1}{\sqrt{2}}[|P\rangle_A|F\rangle_B - |F\rangle_A|P\rangle_B]$$

$$= \frac{1}{\sqrt{2}}\left[\begin{pmatrix} 0.924 \\ 0.383 \end{pmatrix} \otimes \begin{pmatrix} -0.383 \\ 0.924 \end{pmatrix} - \begin{pmatrix} -0.383 \\ 0.924 \end{pmatrix} \otimes \begin{pmatrix} 0.924 \\ 0.383 \end{pmatrix}\right] = \frac{1}{\sqrt{2}} \begin{pmatrix} 0 \\ 1 \\ -1 \\ 0 \end{pmatrix}$$

Carrying out some of the same quantum mechanical calculations that we have done for the other observable properties, we see that the individual odor measurements are random, there is perfect anti-correlation in the joint odor measurements and intermediate anti-correlation in the joint hardness-odor measurements. This latter result is of utmost importance, because a local realist can't explain it.

$$\Psi^T \cdot \text{kronecker}\,(\text{Odor}, I) \cdot \Psi = 0$$

$$\Psi^T \cdot \text{kronecker}(\text{Odor}, \text{Odor}) \cdot \Psi = -1$$

$$\Psi^T \cdot \text{kronecker}(\text{Hardness}, \text{Odor}) \cdot \Psi = -0.707$$

Given that we are now dealing with four properties, each of which can have two values, there are 16 composite states. However, for now we only need to consider the four states involving the properites of hardness and odor to show that the local realist model cannot explain the anti-correlation predicted by quantum mechanics for the joint hardness-odor measurements. In the following table H =Hard, S = Soft, P = Pleasant, and F = Foul. Appendix B provides a complete analysis for all four observable properties.

Quon1	Quon2	HardnessHardness	OdorOdor	HardnessOdor
HP	SF	−1	−1	−1
HF	SP	−1	−1	1
SP	HF	−1	−1	1
SF	HP	−1	−1	−1
Expectation	Value	−1	−1	0
Quantum	Result	−1	−1	−0.707

The last column shows that a local realist model predicts no correlation between the joint hardness-odor measurements, while a quantum mechanical calculation predicts anti-correlation of -0.707. This example illustrates the significance of Bell's analysis: there are experiments for which a local realist model cannot reproduce all the quantum mechanical predictions. And to date the quantum mechanical predictions have been verified experimentally. Thus, a local realist model of nature is not tenable. As mentioned above Appendix B provides additional computational detail regarding this issue.

Concluding Remarks

The reason for using the properties of hardness, color and taste in these exercises is to emphasize how different the quantum world is from the macro world that we occupy. It is not an uncommon experience (it has happened to me) to eat a piece of candy that is hard, white and sweet. But this is not possible for *quantum candy* because the matrix operators representing these observables do not commute. Therefore, the observables cannot simultaneously be well defined.

In quantum mechanics these operators,

$$\text{Hardness} := \begin{pmatrix} 1 & 0 \\ 0 & -1 \end{pmatrix} \quad \text{Color} := \begin{pmatrix} 0 & 1 \\ 1 & 0 \end{pmatrix} \quad \text{Taste} := \begin{pmatrix} 0 & -\mathrm{i} \\ \mathrm{i} & 0 \end{pmatrix}$$

are actually the Pauli spin matrices and represent the observables for spin in the z-, x- and y-directions as mentioned earlier.

$$\sigma_z = \begin{pmatrix} 1 & 0 \\ 0 & -1 \end{pmatrix} \quad \sigma_{\mathrm{x}} = \begin{pmatrix} 0 & 1 \\ 1 & 0 \end{pmatrix} \quad \sigma_{\mathrm{y}} := \begin{pmatrix} 0 & -\mathrm{i} \\ \mathrm{i} & 0 \end{pmatrix}$$

They are also the operators for the rectilinear, diagonal and circular polarization properties of photons. In this case the eigenvectors are vertical, horizontal, diagonal, anti-diagonal, and right and left circular polarization.

$$\begin{aligned} \mathrm{V} &:= \begin{pmatrix} 1 \\ 0 \end{pmatrix} & \mathrm{H} &:= \begin{pmatrix} 0 \\ 1 \end{pmatrix} \\ \mathrm{D} &:= \frac{1}{\sqrt{2}} \cdot \begin{pmatrix} 1 \\ 1 \end{pmatrix} & \mathrm{A} &:= \frac{1}{\sqrt{2}} \begin{pmatrix} 1 \\ -1 \end{pmatrix} \\ \mathrm{R} &:= \frac{1}{\sqrt{2}} \cdot \begin{pmatrix} 1 \\ \mathrm{i} \end{pmatrix} & \mathrm{L} &:= \frac{1}{\sqrt{2}} \begin{pmatrix} 1 \\ -\mathrm{i} \end{pmatrix} \end{aligned}$$

Appendix A: Vector and Matrix Math

Vector inner product:

$$(ab) \cdot \begin{pmatrix} c \\ d \end{pmatrix} \rightarrow a \cdot c + b \cdot d$$

Vector outer product:

$$\begin{pmatrix} c \\ d \end{pmatrix} - (ab) \rightarrow \begin{pmatrix} a \cdot c & b \cdot c \\ a \cdot d & b \cdot d \end{pmatrix}$$

$$\mathrm{tr}\left[\begin{pmatrix} c \\ d \end{pmatrix} \cdot (ab) \right] \rightarrow a \cdot c + b \cdot d$$

Matrix-vector product:

$$\begin{pmatrix} a & b \\ c & d \end{pmatrix} \cdot \begin{pmatrix} x \\ y \end{pmatrix} \rightarrow \begin{pmatrix} a \cdot x + b \cdot y \\ c \cdot x + d \cdot y \end{pmatrix}$$

$$(x, y) \cdot \begin{pmatrix} a & b \\ c & d \end{pmatrix}^T \rightarrow (a \cdot x + b \cdot y \quad c \cdot x + d \cdot y)$$

Expectation value:

$$(x \quad y) \cdot \begin{pmatrix} a & b \\ c & d \end{pmatrix} \cdot \begin{pmatrix} x \\ y \end{pmatrix} \text{ simplify } \rightarrow a \cdot x^2 + d \cdot y^2 + b \cdot x \cdot y + c \cdot x \cdot y$$

$$(x, y) \cdot \begin{pmatrix} a & b \\ c & d \end{pmatrix}^T \cdot \begin{pmatrix} x \\ y \end{pmatrix} \text{ simplify } \rightarrow a \cdot x^2 + d \cdot y^2 + b \cdot x \cdot y + c \cdot x \cdot y$$

$$\text{tr}\left[\begin{pmatrix} x \\ y \end{pmatrix} \cdot \begin{pmatrix} a & b \\ c & d \end{pmatrix}\right] \rightarrow a \cdot x^2 + d \cdot y^2 + b \cdot x \cdot y + c \cdot x \cdot y$$

$$\text{tr}\left[\begin{pmatrix} a & b \\ c & d \end{pmatrix} \cdot \begin{pmatrix} x \\ y \end{pmatrix} \cdot \begin{pmatrix} x & y \end{pmatrix}\right] \text{ simplify } \rightarrow a \cdot x^2 + d \cdot y^2 + b \cdot x \cdot y + c \cdot x \cdot y$$

Matrix product:

$$\begin{pmatrix} a & b \\ c & d \end{pmatrix} \cdot \begin{pmatrix} w & x \\ y & z \end{pmatrix} \rightarrow \begin{pmatrix} a \cdot w + b \cdot y & a \cdot x + b \cdot z \\ c \cdot w + d \cdot y & c \cdot x + d \cdot z \end{pmatrix}$$

Vector tensor product:

$$\begin{pmatrix} a \\ b \end{pmatrix} \otimes \begin{pmatrix} c \\ d \end{pmatrix} = \begin{pmatrix} a \begin{pmatrix} c \\ d \end{pmatrix} \\ b \begin{pmatrix} c \\ d \end{pmatrix} \end{pmatrix} = \begin{pmatrix} ac \\ ad \\ bc \\ bd \end{pmatrix}$$

Matrix tensor product:

$$\begin{pmatrix} a & b \\ c & d \end{pmatrix} \otimes \begin{pmatrix} w & x \\ y & z \end{pmatrix} = \begin{pmatrix} a \begin{pmatrix} w & x \\ y & z \end{pmatrix} & b \begin{pmatrix} w & x \\ y & z \end{pmatrix} \\ c \begin{pmatrix} w & x \\ y & z \end{pmatrix} & d \begin{pmatrix} w & x \\ y & z \end{pmatrix} \end{pmatrix} = \begin{pmatrix} aw & ax & bw & bx \\ ay & az & by & bz \\ cw & cx & dw & dx \\ cy & cz & dy & dz \end{pmatrix}$$

Matrix eigenvalues and eigenvectors (unnormalized):

$$\text{eigenvals}\left(\begin{pmatrix} a & b \\ b & a \end{pmatrix}\right) \rightarrow \begin{pmatrix} a - b \\ a + b \end{pmatrix}$$

or

$$\left|\begin{pmatrix} a - \lambda & b \\ b & a - \lambda \end{pmatrix}\right| = 0 \text{ solve }, \lambda \rightarrow \begin{pmatrix} a + b \\ a - b \end{pmatrix}$$

or

$$\begin{pmatrix} -1 & 1 \\ 1 & 1 \end{pmatrix}^{-1} \begin{pmatrix} a & b \\ b & a \end{pmatrix} \begin{pmatrix} -1 & 1 \\ 1 & 1 \end{pmatrix} \rightarrow \begin{pmatrix} a - b & 0 \\ 0 & a + b \end{pmatrix}$$

using

$$\text{eigenvecs}\left(\begin{pmatrix} a & b \\ b & a \end{pmatrix}\right) \rightarrow \begin{pmatrix} -1 & 1 \\ 1 & 1 \end{pmatrix}$$

$$\begin{pmatrix} a & b \\ b & a \end{pmatrix} \cdot \begin{pmatrix} x \\ y \end{pmatrix} = (a - b) \cdot \begin{pmatrix} x \\ y \end{pmatrix} \text{ solve,} y \rightarrow -x \qquad \begin{pmatrix} x \\ y \end{pmatrix} = \begin{pmatrix} -1 \\ 1 \end{pmatrix}$$

$$\begin{pmatrix} \text{a} & \text{b} \\ \text{b} & \text{a} \end{pmatrix} \cdot \begin{pmatrix} \text{x} \\ \text{y} \end{pmatrix} = (\text{a} + \text{b}) \cdot \begin{pmatrix} \text{x} \\ \text{y} \end{pmatrix} \text{ solve, y} \rightarrow \text{x} \qquad \begin{pmatrix} \text{x} \\ \text{y} \end{pmatrix} = \begin{pmatrix} 1 \\ 1 \end{pmatrix}$$

Completeness relations:

$$\text{Black} \cdot \text{Black}^T + \text{White} \cdot \text{White}^T = \begin{pmatrix} 1 & 0 \\ 0 & 1 \end{pmatrix}$$

$$\text{Hard} \cdot \text{Hard}^T + \text{Soft} \cdot \text{Soft}^T = \begin{pmatrix} 1 & 0 \\ 0 & 1 \end{pmatrix}$$

Appendix B: Additional Computational Details

In order to explain the perfect anti-correlation predicted by quantum mechanics when the same type of measurement is made on both quons, the local realist makes the following state assignments. Remember that these states are not legitimate according to quantum theory because hardness, color, taste and odor are incompatible observables.

QuonA	QuonB
HBSwP	SWSoF
HBSwF	SWSoP
HBSoP	SWSwF
HBSoF	SWSwP
HWSwP	SBSoF
HWSwF	SBSoP
HWSoP	SBSwF
HWSoF	SBSwP

Property	Eigenvalue
H	1
S	−1
B	1
W	−1
Sw	1
So	−1
P	1
F	−1

It is easy to show that these state assignments are in agreement with the following quantum mechanical calculations.

$\Psi^{\mathrm{T}} \cdot \text{ kronecker (Hardness, Hardness) } \cdot \Psi = -1$	$\Psi^{\mathrm{T}} \cdot \text{ kronecker (Color, Color)} \cdot \Psi = -1$	$\Psi^{\mathrm{T}} \cdot \text{kronecker(Taste, Taste)} \cdot \Psi = -1$
$\Psi^{\mathrm{T}} \cdot \text{kronecker(Odor, Odor)} \cdot \Psi = -1$	$\Psi^{\mathrm{T}} \cdot \text{ kronecker (Hardness, Color) } \cdot \Psi = 0$	$\Psi^{\mathrm{T}} \cdot \text{kronecker(Hardness, Taste)} \cdot \Psi = 0$
$\Psi^{\mathrm{T}} \cdot \text{ kronecker (Color, Taste) } \cdot \Psi = 0$	$\Psi^{\mathrm{T}} \cdot \text{ kronecker (Taste, Odor) } \cdot \Psi = 0$	

However, the state assignments are not consistent with the following quantum calculations.

$$\Psi^{\mathrm{T}} \cdot \text{kronecker(Hardness , Odor)} \cdot \Psi = -0.707$$

$$\Psi^{\mathrm{T}} \cdot \text{kronecker(Color, Odor)} \cdot \Psi = -0.707$$

The last two rows of the following table compare the local realist and quantum mechanical predictions, showing the disagreement for the hardness/odor and color/odor joint measurements.

QuonA	QuonB	HH	CC	TT	OO	HC	HT	HO	CT	CO	TO
HBSwP	SWSoF	−1	−1	−1	−1	−1	−1	−1	−1	−1	−1
HBSwF	SWSoP	−1	−1	−1	−1	−1	−1	1	−1	1	1
HBSoP	SWSwF	−1	−1	−1	−1	−1	1	−1	1	−1	1
HBSoF	SWSwP	−1	−1	−1	−1	−1	1	1	1	1	−1
HWSwP	SBSoF	−1	−1	−1	−1	1	−1	−1	1	1	−1
HWSwF	SBSoP	−1	−1	−1	−1	1	−1	1	1	−1	1
HWSoP	SBSwF	−1	−1	−1	−1	1	1	−1	−1	1	1
HWSoF	SBSwP	−1	−1	−1	−1	1	1	1	−1	−1	−1
Expectation	Value	−1	−1	−1	−1	0	0	0	0	0	0
Quantum	Result	−1	−1	−1	−1	0	0	−0.707	0	−0.707	0

This page titled 1.34: Rudimentary Matrix Mechanics is shared under a CC BY 4.0 license and was authored, remixed, and/or curated by Frank Rioux via source content that was edited to the style and standards of the LibreTexts platform.

1.35: Matrix Mechanics

The basic principles of quantum theory can be demonstrated very simply by exploring the properties of electron spin using Heisenberg's formulation of quantum mechanics which is usually referred to as matrix mechanics. The matrix formulation provides clear illustrations of the following essential quantum mechanical concepts: eigenvector, operator, eigenvalue, expectation value, the linear superposition, and the commutation relations.

Four quantum numbers are required to describe the electron in quantum mechanics. The last of these is the spin quantum number, s. The electron has a spin component in the x-, y-, and z-directions and for each of these directions the electron can have a value of spin-up or spin-down, or +1 and -1 in units of $\frac{h}{4\pi}$. These spin states are represented by vectors as is shown below.

$S_{xu} := \frac{1}{\sqrt{2}} \cdot \begin{pmatrix} 1 \\ 1 \end{pmatrix}$	$S_{xd} := \frac{1}{\sqrt{2}} \cdot \begin{pmatrix} 1 \\ -1 \end{pmatrix}$	$\left(\overline{S_{xu}}\right)^T = (0.707 \quad 0.707)$	$\left(\overline{S_{xd}}\right)^T = (0.707 \quad -0.707)$
$S_{yu} := \frac{1}{\sqrt{2}} \cdot \begin{pmatrix} 1 \\ i \end{pmatrix}$	$S_{yd} := \frac{1}{\sqrt{2}} \cdot \begin{pmatrix} 1 \\ -i \end{pmatrix}$	$\left(\overline{S_{yu}}\right)^T = (0.707 \quad -0.707i)$	$\left(\overline{S_{yd}}\right)^T = (0.707 \quad 0.707i)$
$S_{zu} := \begin{pmatrix} 1 \\ 0 \end{pmatrix}$	$S_{zd} := \begin{pmatrix} 0 \\ 1 \end{pmatrix}$	$\left(\overline{S_{zu}}\right)^T = (1 \quad 0)$	$\left(\overline{S_{yd}}\right)^T = (0 \quad 1)$

Let's look at the the y-direction spin states because they are complex, and therefore are slightly more difficult to deal with. In Dirac notation these four vectors are written as $|S_{yu}>$, $|S_{yd}>$, $<S_{yu}|$, and $<S_{yd}|$. Note that the bra-vectors are the transpose of the complex conjugate of the ket-vectors. It is also easy to show that these spin vectors in the x-, y-, and z-directions form orthonormal basis sets. That means they are normalized and orthogonal to each other.

$\left(\overline{S_{xu}}\right)^T \cdot S_{xu} = 1$	$\left(\overline{S_{xd}}\right)^T \cdot S_{xd} = 1$	$\left(\overline{S_{xu}}\right)^T \cdot S_{xd} = 0$
$\left(\overline{S_{yu}}\right)^T \cdot S_{yu} = 1$	$\left(\overline{S_{yd}}\right)^T \cdot S_{yd} = 1$	$\left(\overline{S_{yu}}\right)^T \cdot S_{yd} = 0$
$\left(\overline{S_{zu}}\right)^T \cdot S_{zu} = 1$	$\left(\overline{S_{zd}}\right)^T \cdot S_{zd} = 1$	$\left(\overline{S_{zu}}\right)^T \cdot S_{zd} = 0$

In Dirac notation we would write the first row as: $<S_{xu}|S_{xu}> = <S_{xd}|S_{xd}> = 1$, $<S_{xu}|S_{xd}> = 0$. In other words the projection of the spin states onto themselves is 1 (normalized) and the projection onto the other state is zero (orthogonal).

The calculations above for the y-direction spin vectors are shown explicitly below. You should do hand calculations on all of the above for practice and to have some appreciation for what the computer is doing.

$$(0.707 - 0.707\mathrm{i}) \cdot \begin{pmatrix} 0.707 \\ 0.707\mathrm{i} \end{pmatrix} = 1$$

$$(0.707 \quad 0.707\mathrm{i}) \cdot \begin{pmatrix} 0.707 \\ -0.707\mathrm{i} \end{pmatrix} = 1$$

$$(0.707 - 0.707\mathrm{i}) \cdot \begin{pmatrix} 0.707 \\ -0.707\mathrm{i} \end{pmatrix} = 0$$

It is easy to show that x- and z-spin states are not orthogonal to one another. This is true of any two different spin directions. $<S_{xu}|S_{zu}> = 0.707$, for example.

$$\left(\overline{S_{xu}}\right)^T \cdot S_{zu} = 0.707 \quad \left(\overline{S_{xu}}\right)^T \cdot S_{zd} = 0.707 \quad \left(\overline{S_{xd}}\right)^T \cdot S_{zu} = 0.707 \quad \left(\overline{S_{xd}}\right)^T \cdot S_{zd} = -0.707$$

This of course means that $|S_{xu}>$ and $|S_{xd}>$ can be written as linear superpositions of $|S_{zu}>$ and $|S_{zd}>$, and $|S_{zu}>$ and $|S_{zd}>$ can be written as linear superpositions of $|S_{xu}>$ and $|S_{xd}>$.

$$S_{xu} = \begin{pmatrix} 0.707 \\ 0.707 \end{pmatrix} \quad \frac{1}{\sqrt{2}} \cdot S_{zu} + \frac{1}{\sqrt{2}} \cdot S_{zd} = \begin{pmatrix} 0.707 \\ 0.707 \end{pmatrix}$$

$$S_{xd} = \begin{pmatrix} 0.707 \\ -0.707 \end{pmatrix} \quad \frac{1}{\sqrt{2}} \cdot S_{zu} - \frac{1}{\sqrt{2}} \cdot S_{zd} = \begin{pmatrix} 0.707 \\ -0.707 \end{pmatrix}$$

$$S_{zu} = \begin{pmatrix} 1 \\ 0 \end{pmatrix} \quad \frac{1}{\sqrt{2}} \cdot S_{xu} + \frac{1}{\sqrt{2}} \cdot S_{xd} = \begin{pmatrix} 1 \\ 0 \end{pmatrix}$$

$$S_{zd} = \begin{pmatrix} 0 \\ 1 \end{pmatrix} \quad \frac{1}{\sqrt{2}} \cdot S_{xu} - \frac{1}{\sqrt{2}} \cdot S_{xd} = \begin{pmatrix} 0 \\ 1 \end{pmatrix}$$

The concept of the linear superposition is central in quantum theory and has no classical analog. For example, if by measurement an electron is found to have spin-up in the z-direction, this means that the electron does not have a definite spin in either the x- or the y-direction because $|S_{zu}>$ is a linear superposition of the x- and y-direction spin states.

$$S_{zu} = \begin{pmatrix} 1 \\ 0 \end{pmatrix} \quad \frac{1}{\sqrt{2}} \cdot S_{xu} + \frac{1}{\sqrt{2}} \cdot S_{xd} = \begin{pmatrix} 1 \\ 0 \end{pmatrix} \quad \frac{1}{\sqrt{2}} \cdot S_{yu} + \frac{1}{\sqrt{2}} \cdot S_{yd} = \begin{pmatrix} 1 \\ 0 \end{pmatrix}$$

In spite of its appearance, a linear superposition is not a mixture. In other words $|S_{zu}>$ is not 50% $|S_{xu}>$ and 50% $|S_{xd}>$, or 50% $|S_{yu}>$ and 50% $|S_{yd}>$.

Another central dogma of quantum theory is that the wavefunction or state vector contains all the physical information available for the system. Quantum mechanics therefore consists, in large part, of extracting physical information from the wavefunction or state vector. Quantum mechanics consists of a small set of rules for carrying this procedure out mathematically.

For every observable of the system there is an operator. Since electrons can spin in the x-, y-, or z-directions, there are spin operators in those directions, or for that matter in any other arbitrary direction you might think of. (See Appendix B for the construction of a general spin operator.) In quantum mechanics states are vectors and operators are matrices. The spin operators in units of $\frac{h}{4\pi}$ are shown below. Note that squaring these operators gives the identity operator.

$S_x = \begin{pmatrix} 0 & 1 \\ 1 & 0 \end{pmatrix}$	$S_y := \begin{pmatrix} 0 & -i \\ i & 0 \end{pmatrix}$	$S_z := \begin{pmatrix} 1 & 0 \\ 0 & -1 \end{pmatrix}$
$S_x^2 = \begin{pmatrix} 1 & 0 \\ 0 & 1 \end{pmatrix}$	$S_y^2 = \begin{pmatrix} 1 & 0 \\ 0 & 1 \end{pmatrix}$	$S_2^2 = \begin{pmatrix} 1 & 0 \\ 0 & 1 \end{pmatrix}$

The square of the total spin operator in units of $\frac{h}{4\pi}$ is

$$S2 := S_x^2 + S_y^2 + S_z^2 \quad S2 = \begin{pmatrix} 3 & 0 \\ 0 & 3 \end{pmatrix}$$

A measurement operator extracts information about the system by operating on the wavefunction or state vector. One possible outcome is that the operation returns the state vector multiplied by a numerical constant. For example,

$$S_x \cdot S_{xu} = \begin{pmatrix} 0.707 \\ 0.707 \end{pmatrix}$$

$$S_x \cdot S_{xd} = \begin{pmatrix} -0.707 \\ 0.707 \end{pmatrix}$$

$$S_y \cdot S_{yu} = \begin{pmatrix} 0.707 \\ 0.707i \end{pmatrix}$$

$$S_y \cdot S_{yd} = \begin{pmatrix} -0.707 \\ 0.707i \end{pmatrix}$$

$$S_z \cdot S_{zu} = \begin{pmatrix} 1 \\ 0 \end{pmatrix}$$

$$S_z \cdot S_{zd} = \begin{pmatrix} 0 \\ -1 \end{pmatrix}$$

or, for example:

$$\begin{pmatrix} 1 & 0 \\ 0 & -1 \end{pmatrix} \cdot \begin{pmatrix} 0 \\ 1 \end{pmatrix} = \begin{pmatrix} 0 \\ -1 \end{pmatrix}$$

In Dirac notation we would summarize these calculations as follows: $S_x|S_{xu}> = +1|S_{xu}>$, $S_x|S_{xd}> = -1|S_{xd}>$, $Sy|S_{yu}> = +1|S_{yu}>$, $S_y|S_{yd}> = -1|S_{yd}>$, $S_z|S_{zu}> = +1|S_{zu}>$, $S_z|S_{zd}> = -1|S_{zd}>$. In each of these cases, the state vector is an eigenfunction of the measurement operator with eigenvalue of either +1 or -1 (in units of $\frac{h}{4\pi}$). We say, for example, that $|S_{xu}>$ is an eigenfunction of $\mathbf{S_x}$ with eigenvalue +1. The electron has a well-defined value for spin in the x-direction (spin-up) and subsequent measurements of the x-direction spin will yield the value of +1 as long as no intervening measurements in another spin direction are made.

The other possible outcome of the measurement operation is that it yields another state vector.

$S_x \cdot S_{yu} = \begin{pmatrix} 0.707i \\ 0.707 \end{pmatrix}$	$S_x \cdot S_{yd} = \begin{pmatrix} -0.707i \\ 0.707 \end{pmatrix}$	$S_x \cdot S_{zu} = \begin{pmatrix} 0 \\ 1 \end{pmatrix}$	$S_x \cdot S_{zd} = \begin{pmatrix} 1 \\ 0 \end{pmatrix}$
$S_y \cdot S_{xu} = \begin{pmatrix} -0.707i \\ 0.707i \end{pmatrix}$	$S_y \cdot S_{xd} = \begin{pmatrix} 0.707i \\ 0.707i \end{pmatrix}$	$S_y \cdot S_{zu} = \begin{pmatrix} 0 \\ i \end{pmatrix}$	$S_y \cdot S_{zd} = \begin{pmatrix} -i \\ 0 \end{pmatrix}$
$S_z \cdot S_{xu} = \begin{pmatrix} 0.707 \\ -0.707 \end{pmatrix}$	$S_Z \cdot S_{xd} = \begin{pmatrix} 0.707 \\ 0.707 \end{pmatrix}$	$S_z \cdot s_{yu} = \begin{pmatrix} 0.707 \\ -0.707i \end{pmatrix}$	$S_z \cdot S_{yd} = \begin{pmatrix} 0.707 \\ 0.707i \end{pmatrix}$

In Dirac notation these operations appear as: $S_x|S_{yu}> = i|S_{yd}>$, $S_x|S_{yd}> = -i|S_{yu}>$, $S_x|S_{zu}> = |S_{zd}>$, $S_x|S_{zd}> = |S_{zu}>$, etc. In each case the resulting vector is different than the vector operated on. We say, for example, $|S_{yu}>$ is not an eigenfunction of $\mathbf{S_x}$, and therefore an electron in this state does not have a definite value for spin in the x-direction. X-direction spin measurements on a system known to be in state $|S_{yu}>$ will yield completely random results.

To put it another way, quantum mechanical principles state that a system can be in a well-defined state, $|S_{yu}>$, and yet the outcome of all experiments are not unikely determined. While a measurement of spin in the y-direction will yield a predictable result, +1, measurement of spin in the x- or z-direction is completely unpredictable and all we can calculate is the average value, or expectation value for a large number of measurements. This is completely different than classical physics where if you know the state of the system, you know the values of all physical observables.

As another example, consider the ground state of the hydrogen atom for which the electron's wave function is $\Psi = \pi^{-1/2}\exp(-r)$. When the electron is in this state it has a precise energy, but not a well-defined position or momentum. This, of course, makes the concept of an electron trajectory impossible and it is, therefore, meaningless to think of the electron as moving in any traditional sense.

The quantum mechanical algorithm for calculating the expectation value is to execute the following matrix multiplication: <State Vector | **Operator** | State Vector>. This formalism is quite general and can be used whether the state vector is an eigenfunction of the operator or not. This is demonstrated below for the spin states that we have been studying.

$\left(\overline{S_{xu}}\right)^T \cdot S_x \cdot S_{xu} = 1$	$\left(\overline{S_{xd}}\right)^T \cdot S_x \cdot S_{xd} = -1$	$\left(\overline{S_{zu}}\right)^T \cdot S_x \cdot S_{zu} = 0$
$\left(\overline{S_{zd}}\right)^T \cdot S_x \cdot S_{zd} = 0$	$\left(\overline{S_{yu}}\right)^T \cdot S_x \cdot S_{yu} = 0$	$\left(\overline{S_{yd}}\right)^T \cdot S_x \cdot S_{yd} = 0$
$\left(\overline{S_{xu}}\right)^T \cdot S_y \cdot S_{xu} = 0$	$\left(\overline{S_{xd}}\right)^T \cdot S_y \cdot S_{xd} = 0$	$\left(\overline{S_{zu}}\right)^T \cdot S_y \cdot S_{zu} = 0$
$\left(\overline{S_{zd}}\right)^T \cdot S_y \cdot S_{zd} = 0$	$\left(\overline{S_{yu}}\right)^T \cdot S_y \cdot S_{yu} = 1$	$\left(\overline{S_{yd}}\right)^T \cdot S_y \cdot S_{yd} = -1$
$\left(\overline{S_{xu}}\right)^T \cdot S_z \cdot S_{xu} = 0$	$\left(\overline{S_{xd}}\right)^T \cdot S_z \cdot S_{xd} = 0$	$\left(\overline{S_{zu}}\right)^T \cdot S_z \cdot S_{zu} = 1$
$\left(\overline{S_{zd}}\right)^T \cdot S_z \cdot S_{zd} = -1$	$\left(\overline{S_{yu}}\right)^T \cdot S_z \cdot S_{yu} = 0$	$\left(\overline{S_{yd}}\right)^T \cdot S_z \cdot S_{yd} = 0$

Let's look at the first six enteries because they are representative of the remaining results. If the electron is in the state $|S_{xu}>$ measurement of $\mathbf{S_x}$ will always yield the value of +1 (in units of $\frac{h}{4\pi}$)). If the electron is in the state $|S_{xd}>$ measurement of $\mathbf{S_x}$ will always yield the value of -1 (in units of $\frac{h}{4\pi}$)). If instead $\mathbf{S_y}$ or $\mathbf{S_z}$ are measured, the measurement results will be a statistically

random collection of +1 and -1, and the average value will, of course, be zero. Only when the system is in an eigenstate of the measurement operator is the outcome of the experiment certain.

This brings us to the concept of probability and how it is calculated in quantum mechanics. The projection of one state on to another, $<S_{zu} \mid S_{xd}> = 0.707$, is a **probability amplitude**. Its absolute square, $<S_{xd} \mid S_{zu}><S_{zu} \mid S_{xd}> = |<S_{zu} \mid S_{xd}>|^2 = 0.5$ (remember $<S_{xd} \mid S_{zu}> = <S_{zu} \mid S_{xd}>^*$), is the **probability** that an electron in state $|S_{xd}>$ will be found by measurement in the state $|S_{zu}>$. Representative calculations are shown below. (See the Appendix A for another computational method.)

$$\left[\left|\left(\overline{S_{zu}}\right)^{T} \cdot S_{xu}\right|\right]^2 = 0.5 \quad \left[\left|\left(\overline{S_{zd}}\right)^{T} \cdot S_{xu}\right|\right]^2 = 0.5 \quad \left[\left|\left(\overline{S_{xu}}\right)^{T} \cdot S_{yu}\right|\right]^2 = 0.5 \quad \left[\left|\left(\overline{S_{xu}}\right)^{T} \cdot S_{xd}\right|\right]^2 = 0.5$$

Let's review these concepts by taking a specific example. The electron is in the state $|S_{xu}>$ and we wish to measure $\mathbf{S_z}$. According to quantum mechanical procedures the average value for a statistically meaningful number of measurements is zero -$<S_{xu} \mid \mathbf{S_z} \mid S_{xu}> = 0$. The eigenstates (eigenfunctions) for $\mathbf{S_z}$ are $|S_{zu}>$ and $|S_{zd}>$ with eigenvalues +1 and -1, respectively. As the first two entries above show, the probability that an electron in state $|S_{xu}>$ will be found in $|S_{zu}>$ with eigenvalue +1 is 0.5, and the probaility that it will be found in state $|S_{zd}>$ with eigenvalue -1 is 0.5. Thus, the **average value is expected** to be zero, and the two ways of determining the average or expectation value of a measurement are consistent and equivalent.

There is yet another way to look at this issue. In quantum mechanics for most pairs of observables the order of measurement is important. Quantum mechanical operators don't generally commute. For example, as shown below, $\mathbf{S_xS_y}|S_{zu}>$ does not equal $\mathbf{S_yS_x}|S_{zu}>$. This means that if the electron is in the state $|S_{zu}>$ the combined operators $\mathbf{S_xS_y}$ and S_yS_x yield different measurement results.

$$S_x \cdot S_y \cdot S_{zu} = \begin{pmatrix} i \\ 0 \end{pmatrix} \quad S_y \cdot S_x \cdot S_{zu} = \begin{pmatrix} -i \\ 0 \end{pmatrix} \quad (S_x \cdot S_y - S_y \cdot S_x) \cdot S_{zu} = \begin{pmatrix} 2i \\ 0 \end{pmatrix}$$

Operators that do not commute have incompatible eigenstates. If a state vector is an eigenstate of one of the operators, it is not an eigenstate of the other. The fact that $\mathbf{S_x}$ and **Sy** do not commute means that an electron cannot simultaneously have well-defined values for $\mathbf{S_x}$ and $\mathbf{S_y}$. It is not surprising that there is a deep connection between these properties of operators and the Uncertainty Principle. The commutators for the spin operators are shown below.

$$S_x \cdot S_y - S_y \cdot S_x = \begin{pmatrix} 2i & 0 \\ 0 & -2i \end{pmatrix} \qquad 2 \cdot i \cdot S_z = \begin{pmatrix} 2i & 0 \\ 0 & -2i \end{pmatrix}$$

$$S_z \cdot S_x - S_x \cdot S_z = \begin{pmatrix} 0 & 2 \\ -2 & 0 \end{pmatrix} \qquad 2 \cdot i \cdot S_y = \begin{pmatrix} 0 & 2 \\ -2 & 0 \end{pmatrix}$$

$$S_y \cdot S_z - S_z \cdot S_y = \begin{pmatrix} 0 & 2i \\ 2i & 0 \end{pmatrix} \qquad 2 \cdot i \cdot S_x = \begin{pmatrix} 0 & 2i \\ 2i & 0 \end{pmatrix}$$

The Uncertainty Principle can also be illustrated by calculating ΔS_x and ΔS_y for an electron known to be in the S_{zu} state. Since we are working in units of $\frac{h}{4\pi}$, the uncertainty relation is: $\Delta S_x \cdot \Delta S_y \geq 1$.

$$\sqrt{S_{zu}^T \cdot S_x \cdot S_x \cdot S_{zu} - \left(S_{zu}^T \cdot S_x \cdot S_{zu}\right)^2} \cdot \sqrt{S_{zu}^T \cdot S_y \cdot S_y \cdot S_{zu} - \left(S_{zu}^T \cdot S_y \cdot S_{zu}\right)^2} = 1$$

We have been dealing with matrix operators and their associated eigenvectors and eigenvalues. The eigenvectors and eigenvalues can be obtained from the matrix operators with Mathcad's **eigenvecs** and **eigenvals** commands as is shown below.

$$\text{eignevals}\left(S_x\right) = \begin{pmatrix} 1 \\ -1 \end{pmatrix} \quad \text{eigenvec}\left(S_x, 1\right) = \begin{pmatrix} 0.707 \\ 0.707 \end{pmatrix} \quad \text{eigenvec}\left(S_x, -1\right) = \begin{pmatrix} -0.707 \\ 0.707 \end{pmatrix}$$

$$\text{eignevals}\left(S_y\right) = \begin{pmatrix} 1 \\ -1 \end{pmatrix} \qquad \text{eigenvec}\left(S_y\right) = \begin{pmatrix} -0.707i & 0.707 \\ 0.707 & -0.707i \end{pmatrix}$$

$$\text{eignevals}\left(S_z\right) = \begin{pmatrix} 1 \\ -1 \end{pmatrix} \quad \text{eigenvec}\left(S_z\right) = \begin{pmatrix} 1 & 0 \\ 0 & 1 \end{pmatrix}$$

One final thing we will do is to demonstrate the completeness relationship. For example, $|S_{zu}><S_{zu}| + |S_{zd}><S_{zd}| = \mathbf{I}$, the identity operator. This demonstrates that the spin eigenfunction for the various Cartesian directions span the two-dimensional space.

$$S_{zu} \cdot S_{zu}^{T} + S_{zd} \cdot S_{zd}^{T} = \begin{pmatrix} 1 & 0 \\ 0 & 1 \end{pmatrix}$$

$$S_{xu} \cdot S_{xu}^{T} + S_{xd} \cdot S_{xd}^{T} = \begin{pmatrix} 1 & 0 \\ 0 & 1 \end{pmatrix}$$

$$S_{yu} \cdot \left(\overline{S_{yu}}\right)^{T} + S_{yd} \cdot \left(\overline{S_{yd}}\right)^{T} = \begin{pmatrix} 1 & 0 \\ 0 & 1 \end{pmatrix}$$

Appendix A

By the method outlined above we can show that the probability that a S_{zu} electron will be found in the S_{xu} spin state is 0.5.

$$\left[\left|\left(\overline{S_{xu}}\right)^{T} \cdot S_{zu}\right|\right]^{2} = 0.5$$

This calculation can be rewritten in terms of the trace of the product of the $|S_{zu}\rangle \langle S_{zu}|$ and $|S_{xu}\rangle \langle S_{xu}|$ projection operators.

$$\left|\langle S_{xu}|S_{zu}\rangle\right|^{2} = \langle S_{zu}|S_{xu}\rangle \langle S_{xu}|S_{zu}\rangle = \sum_{i} \langle S_{zu}|i\rangle \langle i|S_{xu}\rangle \langle S_{xu}|S_{zu}\rangle$$

$$= \sum_{i} \langle i|S_{xu}\rangle \langle S_{xu}|S_{zu}\rangle \langle S_{zu}|i\rangle = \mathrm{Trace}(|S_{xu}\rangle \langle S_{xu}|S_{zu}\rangle \langle S_{zu}|)$$

where the completeness relation $\sum_i |i\rangle\langle i| = 1$ has been employed.

$$\mathrm{tr}\left[\left(S_{xu} \cdot S_{xu}^{T}\right) \cdot \left(S_{zu} \cdot S_{zu}^{T}\right)\right] = 0.5$$

Appendix B

A general spin operator can be constructed using the spherical coordinate system, where θ is the angle relative to z-axis and f is the angle relative to the x-axis.

$$S(\theta, \phi) := \cos(\phi) \cdot \sin(\theta) \cdot S_x + \sin(\phi) \cdot \sin(\theta) \cdot S_y + \cos(\theta) \cdot S_z$$

To confirm the validity of this general operator, we generate the traditional x-, y- and z-direction spin operators.

$$S\left(\frac{\pi}{2}, 0\right) = \begin{pmatrix} 0 & 1 \\ 1 & 0 \end{pmatrix} \quad S\left(\frac{\pi}{2}, \frac{\pi}{2}\right) = \begin{pmatrix} 0 & -i \\ i & 0 \end{pmatrix} \quad S(0,0) = \begin{pmatrix} 1 & 0 \\ 0 & -1 \end{pmatrix}$$

For the Hadamard gate (operator), which is important in quantum computing, $\theta = \frac{\pi}{4}$ and $\phi = 0$.

$$S\left(\frac{\pi}{4}, 0\right) = \begin{pmatrix} 0.707 & 0.707 \\ 0.707 & -0.707 \end{pmatrix}$$

As shown below it represents a Fourier transform between the x and z spin eigenstates.

$$S\left(\frac{\pi}{4}, 0\right) S_{zu} = \begin{pmatrix} 0.707 \\ 0.707 \end{pmatrix} \quad S\left(\frac{\pi}{4}, 0\right) S_{xu} = \begin{pmatrix} 1 \\ 0 \end{pmatrix}$$

$$S\left(\frac{\pi}{4}, 0\right) S_{zd} = \begin{pmatrix} 0.707 \\ -0.707 \end{pmatrix} \quad S\left(\frac{\pi}{4}, 0\right) S_{xd} = \begin{pmatrix} 0 \\ 1 \end{pmatrix}$$

This page titled 1.35: Matrix Mechanics is shared under a CC BY 4.0 license and was authored, remixed, and/or curated by Frank Rioux via source content that was edited to the style and standards of the LibreTexts platform.

1.36: Aspects of Dirac's Relativistic Matrix Mechanics

This tutorial provides a brief summary of the last chapter of C. W. Sherwin's excellent *Introduction to Quantum Mechanics* which deals with relativistic quantum mechanics.

The relativistic equation for the energy of a free particle has positive and negative roots, where the positive root signifies the energy of a particle and the negative root the energy of its antiparticle. This interpretation was confirmed experimentally with the discovery of the anti-electron (positron) in 1932 by Anderson.

$$E = \pm c\sqrt{p_x^2 + p_y^2 + p_z^2 + m^2c^2}$$

Dirac converted this to a soluble quantum mechanical operator by first writing the argument of the square root as a perfect square in order to get rid of the troubling radical operator which defied physical interpretation. In a second step he replaced energy and momentum with their differential operators, $E = -\left(\frac{h}{2\pi i}\right)\frac{d}{dt}$ and $p_q = \left(\frac{h}{2\pi i}\right)\frac{d}{dq}$, from non-relativistic quantum mechanics.

$$\mathrm{p_x^2 + p_y^2 + p_Z^2 + m^2 \cdot c^2 = (\alpha_x \cdot p_x + \alpha_y \cdot p_y + \alpha_z \cdot p_z + \beta \cdot m \cdot c)^2}$$

For this mathematical maneuver to be valid the following conditions must hold: $\alpha_x^2 = \alpha_y^2 = \alpha_Z^2 = \beta^2 = 1$

$\alpha_x \cdot \alpha_y + \alpha_y \cdot \alpha_x = 0$	$\alpha_x \cdot \alpha_Z + \alpha_z \cdot \alpha_x = 0$	$\alpha_X \cdot \beta + \beta \cdot \alpha_x = 0$
$\alpha_y \cdot \alpha_z + \alpha_z \cdot \alpha_y = 0$	$\alpha_y \cdot \beta + \beta \cdot \alpha_y = 0$	$\alpha_Z \cdot \beta + \beta \cdot \alpha_Z = 0$
$p_x \cdot p_y = p_y \cdot p_X$	$p_x \cdot p_Z = p_Z \cdot p_x$	$p_y \cdot p_Z = p_z \cdot p_y$

In other words, the αs and βs must anticommute while the momentum operators as used above must commute. From the non-relativistic formulation of quantum mechanics it was already clear that the momentum operator pairs above did commute. In formulating a relativistic quantum mechanics, Dirac assumed the validity of the various multiplicative and differential operators of non-relativistic quantum mechanics for observable properties like energy, position and momentum.

Being cognizant of Heisenberg's matrix approach to non-relativistic quantum mechanics, Dirac realized the restrictions above regarding the αs and β could be satisfied by the following 4x4 matrices.

$$\alpha_X = \begin{pmatrix} 0 & 0 & 0 & 1 \\ 0 & 0 & 1 & 0 \\ 0 & 1 & 0 & 0 \\ 1 & 0 & 0 & 0 \end{pmatrix}$$

$$\alpha_y = \begin{pmatrix} 0 & 0 & 0 & -i \\ 0 & 0 & i & 0 \\ 0 & -i & 0 & 0 \\ i & 0 & 0 & 0 \end{pmatrix}$$

$$\alpha_z = \begin{pmatrix} 0 & 0 & 1 & 0 \\ 0 & 0 & 0 & -1 \\ 1 & 0 & 0 & 0 \\ 0 & -1 & 0 & 0 \end{pmatrix}$$

$$\beta = \begin{pmatrix} 1 & 0 & 0 & 0 \\ 0 & 1 & 0 & 0 \\ 0 & 0 & -1 & 0 \\ 0 & 0 & 0 & -1 \end{pmatrix}$$

First we show that $\alpha_X^2 = \alpha_y^2 = \alpha_Z^2 = \beta^2 = \mathrm{I}$ where I is the identity operator.

$$\mathrm{I} = \begin{pmatrix} 1 & 0 & 0 & 0 \\ 0 & 1 & 0 & 0 \\ 0 & 0 & 1 & 0 \\ 0 & 0 & 0 & 1 \end{pmatrix}$$

$$\alpha_\mathrm{x} \cdot \alpha_\mathrm{x} = \begin{pmatrix} 1 & 0 & 0 & 0 \\ 0 & 1 & 0 & 0 \\ 0 & 0 & 1 & 0 \\ 0 & 0 & 0 & 1 \end{pmatrix}$$

$$\alpha_y \cdot \alpha_y = \begin{pmatrix} 1 & 0 & 0 & 0 \\ 0 & 1 & 0 & 0 \\ 0 & 0 & 1 & 0 \\ 0 & 0 & 0 & 1 \end{pmatrix}$$

$$\alpha_z \cdot \alpha_z = \begin{pmatrix} 1 & 0 & 0 & 0 \\ 0 & 1 & 0 & 0 \\ 0 & 0 & 1 & 0 \\ 0 & 0 & 0 & 1 \end{pmatrix}$$

$$\beta \cdot \beta = \begin{pmatrix} 1 & 0 & 0 & 0 \\ 0 & 1 & 0 & 0 \\ 0 & 0 & 1 & 0 \\ 0 & 0 & 0 & 1 \end{pmatrix}$$

Now we show that the αs and β anticommute:

$$\alpha_x \cdot \alpha_y + \alpha_y \cdot \alpha_x = \begin{pmatrix} 0 & 0 & 0 & 0 \\ 0 & 0 & 0 & 0 \\ 0 & 0 & 0 & 0 \\ 0 & 0 & 0 & 0 \end{pmatrix}$$

$$\alpha_\mathrm{x} \cdot \alpha_\mathrm{z} + \alpha_\mathrm{z} \cdot \alpha_\mathrm{x} = \begin{pmatrix} 0 & 0 & 0 & 0 \\ 0 & 0 & 0 & 0 \\ 0 & 0 & 0 & 0 \\ 0 & 0 & 0 & 0 \end{pmatrix}$$

$$\alpha_\mathrm{x} \cdot \beta + \beta \cdot \alpha_\mathrm{x} = \begin{pmatrix} 0 & 0 & 0 & 0 \\ 0 & 0 & 0 & 0 \\ 0 & 0 & 0 & 0 \\ 0 & 0 & 0 & 0 \end{pmatrix}$$

$$\alpha_y \cdot \alpha_z + \alpha_z \cdot \alpha_y = \begin{pmatrix} 0 & 0 & 0 & 0 \\ 0 & 0 & 0 & 0 \\ 0 & 0 & 0 & 0 \\ 0 & 0 & 0 & 0 \end{pmatrix}$$

$$\alpha_y \cdot \beta + \beta \cdot \alpha_y = \begin{pmatrix} 0 & 0 & 0 & 0 \\ 0 & 0 & 0 & 0 \\ 0 & 0 & 0 & 0 \\ 0 & 0 & 0 & 0 \end{pmatrix}$$

$$\alpha_z \cdot \beta + \beta \cdot \alpha_z = \begin{pmatrix} 0 & 0 & 0 & 0 \\ 0 & 0 & 0 & 0 \\ 0 & 0 & 0 & 0 \\ 0 & 0 & 0 & 0 \end{pmatrix}$$

It is now possible to write Dirac′s relativistic energy equation as follows:

$$E = \pm c\left(\alpha_x p_x + \alpha_y p_y + \alpha_z p_z + \beta mc\right)$$

Before proceeding to the next step, the substitution of the differential operators for energy and momentum, it is instructive to look at the right side of the above equation which is a 4x4 Dirac relativistic energy operator. Of course, the left side is a 4x4 matrix with E on the diagonal and zeros everywhere else.

$$\begin{matrix} & -c\cdot\left(\alpha_x\cdot p_x+\alpha_y\cdot p_y+\alpha_z\cdot p_z+\beta\cdot m\cdot c\right) & & & \\ \rightarrow & \begin{bmatrix} -c^2\cdot m & 0 & -ccdotp_z & -c\left(p_x-p_y\cdot i\right) \\ 0 & -c^2\cdot m & -c\left(p_x+p_y\cdot i\right) & c\cdot p_z \\ -c\cdot p_z & -c\left(p_x-p_y\cdot i\right) & c^2\cdot m & 0 \\ -c\left(p_x+p_y\cdot i\right) & c\cdot p_z & 0 & c^2\cdot m \end{bmatrix} & & & \end{matrix}$$

Substituting the traditional operators for energy and momentum yields,

$$-\frac{\hbar}{i}\frac{\partial\Psi}{\partial t} = -\left[\frac{c\hbar}{i}\left(\alpha_x\frac{\partial}{\partial x}+\alpha_y\frac{\partial}{\partial y}+\alpha_z\frac{\partial}{\partial z}\right)+\beta mc^2\right]\Psi$$

Assuming the separability of the space and time coordinates $[\Psi(x,y,z,t)=\psi(x,y,z)\phi(t)]$, this four dimensional differential equation is decoupled in to two differential equations. The time-dependent equation is easily solved and has the following solution.

$$\varphi(t) = e^{-i\frac{Et}{\hbar}}$$

The space part of the differential equation has the following form, with the relativistic Hamiltonian operating on the wavefunction.

$$-\left[\frac{c\hbar}{i}\left(\alpha_x\frac{\partial}{\partial x}+\alpha_y\frac{\partial}{\partial y}+\alpha_z\frac{\partial}{\partial z}\right)+\beta mc^2\right]\psi = E\psi$$

As demonstrated above (Equation) the relativistic energy operator is a 4x4 matrix. Therefore, the wavefunction must be a four-component vector.

At this point Sherwin turns to the example of the free particle in the x-direction (see pages 292-295). He assumes that the solution has the form of a plane wave. However, as shown below substitution of the deBroglie equation in the plane wave equation yields the momentum eigenfunction in coordinate space.

$$\exp\left(i\frac{2\pi}{\lambda}x\right)\overset{\lambda=h/p}{\longrightarrow}\exp\left(i\frac{px}{\hbar}\right)$$

This means that this problem is extremely easy to solve in momentum space where the momentum operator is multiplicative. The calculation of the energy eigenvalues is straight forward using Mathcad′s *eigenvals* command. We simply ask for the eigenvalues of the relativistic energy operator as shown below.

$$\text{eigenvals}\left[-\text{c}\cdot\left(\alpha_\text{x}\cdot\text{p}_\text{x}+\beta\cdot\text{m}\cdot\text{c}\right]\right]\rightarrow\begin{pmatrix} \text{c}\cdot\sqrt{\text{c}^2\cdot\text{m}^2+\text{p}_\text{x}^2} \\ \text{c}\cdot\sqrt{\text{c}^2\cdot\text{m}^2+\text{p}_\text{x}^2} \\ -\text{c}\cdot\sqrt{\text{c}^2\cdot\text{m}^2+\text{p}_\text{x}^2} \\ -\text{c}\cdot\sqrt{\text{c}^2\cdot\text{m}^2+\text{p}_\text{x}^2} \end{pmatrix}$$

Calculation of the (unnormalized) eigenvectors is equally easy.

$$\text{eigenvecs}\left[-\text{c}\cdot\left(\alpha_\text{x}\cdot\text{p}_\text{x}+\beta\cdot\text{m}\cdot\text{c}\right]\right]=\begin{pmatrix} \frac{\text{W}+\text{m}\cdot\text{c}^2}{\text{p}_\text{x}\cdot\text{c}} & 0 & 0 & \frac{-\text{W}+\text{m}\cdot\text{c}^2}{\text{p}_\text{x}\cdot\text{c}} \\ 0 & \frac{\text{W}+\text{m}\cdot\text{c}^2}{\text{p}_\text{x}\cdot\text{c}} & \frac{-\text{W}+\text{m}\cdot\text{c}^2}{\text{p}_\text{x}\cdot\text{c}} & 0 \\ 0 & 1 & 1 & 0 \\ 1 & 0 & 0 & 1 \end{pmatrix}$$

$$\text{W}=\sqrt{\text{p}_\text{x}^2\cdot\text{c}^2+\text{m}^2\cdot\text{c}^4}$$

This page titled 1.36: Aspects of Dirac′s Relativistic Matrix Mechanics is shared under a CC BY 4.0 license and was authored, remixed, and/or curated by Frank Rioux via source content that was edited to the style and standards of the LibreTexts platform.

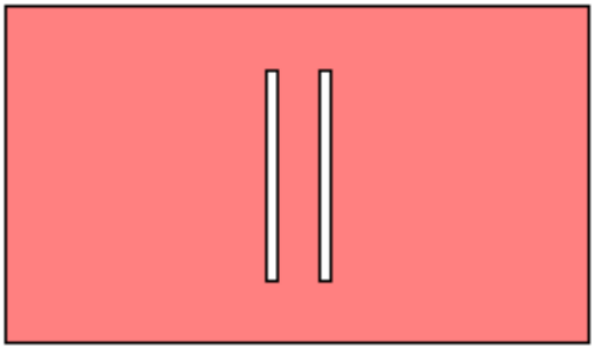
1.37: The Double-Slit Experiment

Thomas Young used the double-slit experiment to establish the wave nature of light. Richard Feynman used it to demonstrate the superposition principle as the paradigm of all quantum mechanical phenomena, illustrating wave-particle duality as stated above: between release and detection quons behave as waves.

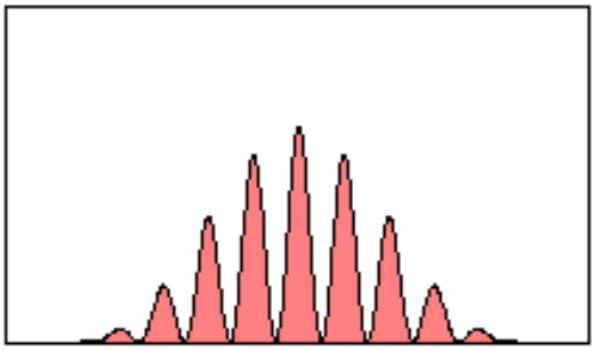
The Experiment

The slit screen on the left produces the diffraction pattern on the right when illuminated with a coherent radiation source.

Slit Screen



Diffraction Pattern



The Quantum Mechanical Explanation

Illumination of a double-slit screen with a coherent light source leads to a Schrödinger "cat state", in other words a superposition of the photon being localized at both slits simultaneously.

$$|\Psi\rangle = \frac{1}{\sqrt{2}}[|x_1\rangle + |x_2\rangle]$$

Here x_1 and x_2 are positions of the two slits. It is assumed initially, for the sake of mathematical simplicity, that the slits are infinitesimally thin in the x-direction and infinitely long in the y-direction.

Because the slits localize the photon in the x-direction the uncertainty principle $\left(\Delta x \Delta p_x > \frac{h}{4\pi}\right)$ demands a compensating delocalization in the x-component of the momentum. To see this delocalization in momentum requires a momentum wave function, which is obtained by a Fourier transform of the position wave function given above.

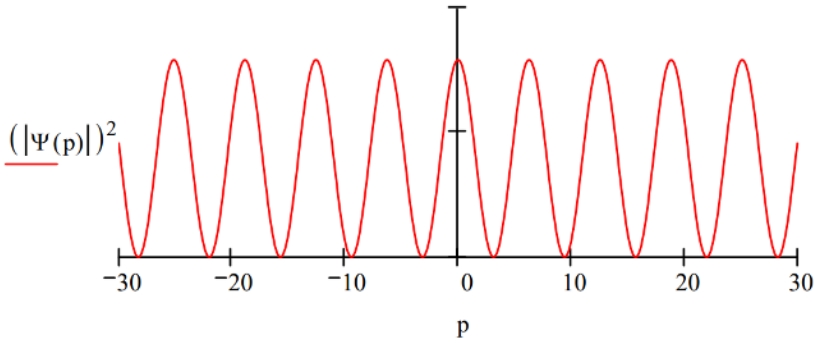
In this case the Fourier transform is simply the projection of the position wave function onto momentum space. See the Appendix for further information on the Fourier transform.

$$\langle p|\Psi\rangle = \frac{1}{\sqrt{2}}[\langle p|x_1\rangle + \langle p|x_2\rangle] = \frac{1}{2\sqrt{\pi}}\left[\exp\left(-\frac{ipx_1}{\hbar}\right) + \exp\left(-\frac{ipx_2}{\hbar}\right)\right]$$

The quantum mechanical interpretation of the double-slit experiment, or any diffraction experiment for that matter, is that the diffraction pattern is actually the momentum distribution function, $|<p|\Psi>|^2$. This is illustrated below. The following calculations are carried out in atomic units (h = 2 π).

Position of first slit: $x_1 := 0$	Position of second slit: $x_2 := 1$

$$p := -30, -29.9 \ldots 30 \quad \Psi(p) := \frac{\frac{1}{\sqrt{2\cdot\pi}} \cdot \exp(-i \cdot p \cdot x_1) + \frac{1}{\sqrt{2\cdot\pi}} \cdot \exp(-i \cdot p \cdot x_2)}{\sqrt{2}}$$

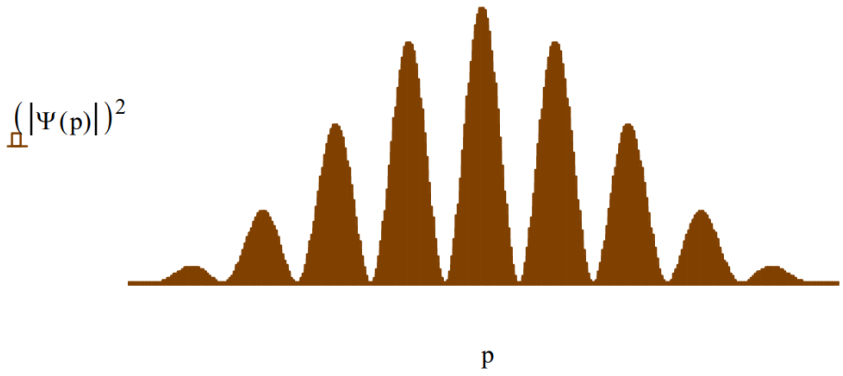


The momentum distribution shows interference fringes because the photons were localized in space at two positions: the maxima represent constructive interference and the minima destructive interference. Notice also that the momentum distribution in the x-direction is completely delocalized; it shows no sign of attenuating at large momentum values. This is due to the fact that under the present model the photons are precisely localized at x_1 and x_2 - in other words the slits are infinitesimally thin in the x-direction as specified above.

This of course is not an adequate representation of the actual double-slit diffraction pattern because any real slit has a finite size in both directions. It's really not a problem that the slit is infinite in the y-direction, because that means the photon is simply not localized in that direction. So all we need to do to get a more realistic double-slit diffraction pattern is make the slits finite (not infinitesimal) in the x-direction. This is accomplished by giving the slits a finite width, δ, in the x-direction, and recalculating the momentum wave function.

Slit width:

$$\delta := 0.2 \quad \Psi(p) := \frac{\int_{x_1-\frac{\delta}{2}}^{x_1+\frac{\delta}{2}} \frac{1}{\sqrt{2\cdot\pi}} \cdot \exp(-i \cdot p \cdot x) \cdot \frac{1}{\sqrt{\delta}} dx + \int_{x_2-\frac{\delta}{2}}^{x_2+\frac{\delta}{2}} \frac{1}{\sqrt{2\cdot\pi}} \cdot \exp(-i \cdot p \cdot x) \cdot \frac{1}{\sqrt{\delta}} dx}{\sqrt{2}}$$



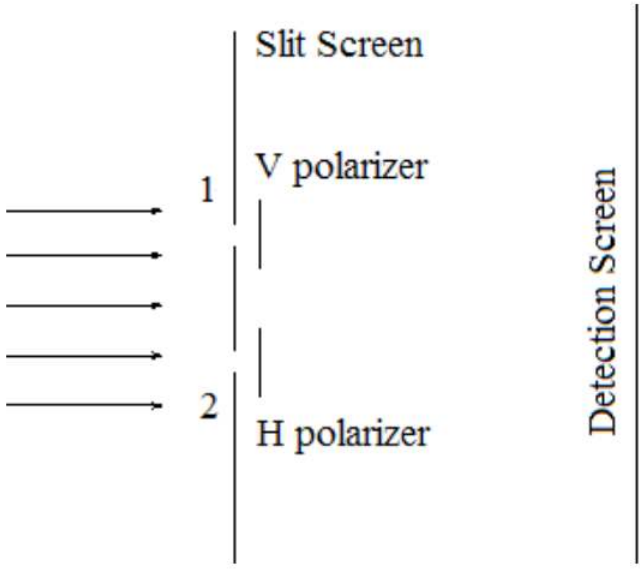
In summary, the quantum mechanical interpretation of the double-slit experiment is that position is measured at the slit screen and momentum is measured at the detection screen. Position and momentum are conjugate observables which are connected by a Fourier transform and governed by the uncertainty principle. Knowing the slit screen geometry makes it possible to calculate the momentum distribution at the detection screen. Varying the slit width, δ, gives a clear and simple demonstration of the uncertainty principle in action. Narrow slit widths give broad momentum distributions and wide slit widths give narrow momentum distributions.

This page titled 1.37: The Double-Slit Experiment is shared under a CC BY 4.0 license and was authored, remixed, and/or curated by Frank Rioux via source content that was edited to the style and standards of the LibreTexts platform.

1.38: Double-Slit Experiment with Polarized Light

According to the Encyclopedia Britannica, Fresnel and Arago “using an apparatus based on Young’s [double-slit] experiment” observed that “two beams polarized in mutually perpendicular planes never yield fringes.” The purpose of this tutorial is to examine this phenomenon from a quantum mechanical perspective.

A schematic diagram of the double-slit experiment with polarizers behind the slits is shown below. V and H stand for vertical and horizontal, respectively.



We begin with a review of the double-slit experiment in the absence of the polarizers shown in the figure above. Illumination of the double-slit screen with a coherent light source leads to a Schrödinger ″cat state″, in other words a superposition of the photon being localized at the both slits simultaneously. In effect, the slit screen performs a position measurement on the photons emanating from the light source.

$$|\Psi\rangle = \frac{1}{\sqrt{2}}[|x_1\rangle + |x_2\rangle]$$

Here x_1 and x_2 are the positions of the two slits. For the sake of mathematical simplicity it is assumed that the slits are infinitesimally thin in the x-direction and infinitely long in the y-direction.

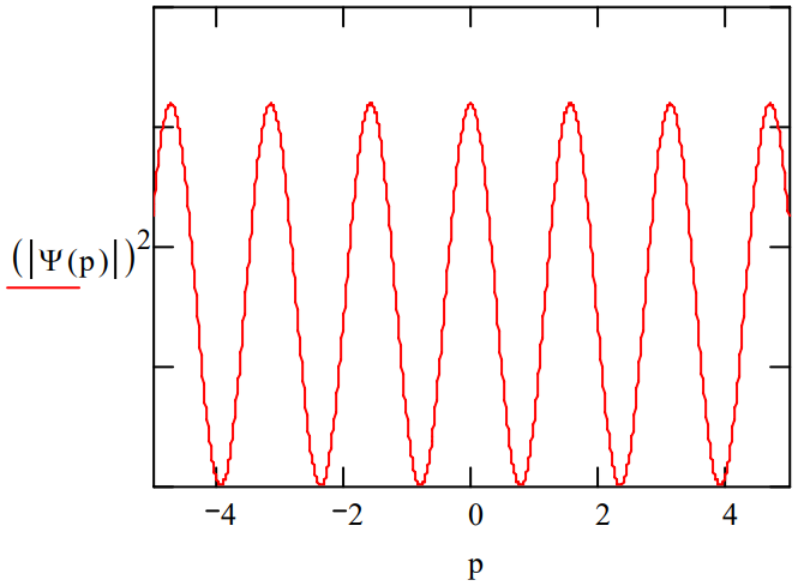
Because the slits localize the photon in the x-direction the uncertainty principle demands a compensating delocalization in the x-component of the momentum. To see this delocalization in momentum requires a momentum wave function, which is obtained by a Fourier transform of the position wave function given above. In this case the Fourier transform is simply the projection of the position wave function onto momentum space in atomic units (h = 2π).

$$\Psi(p) = \langle p|\Psi\rangle = \frac{1}{\sqrt{2}}[\langle p|x_1\rangle + \langle p|x_2\rangle] = \frac{1}{2\sqrt{\pi}}\left[\exp\left(-ipx_1\right) + \exp\left(-ipx_2\right)\right]$$

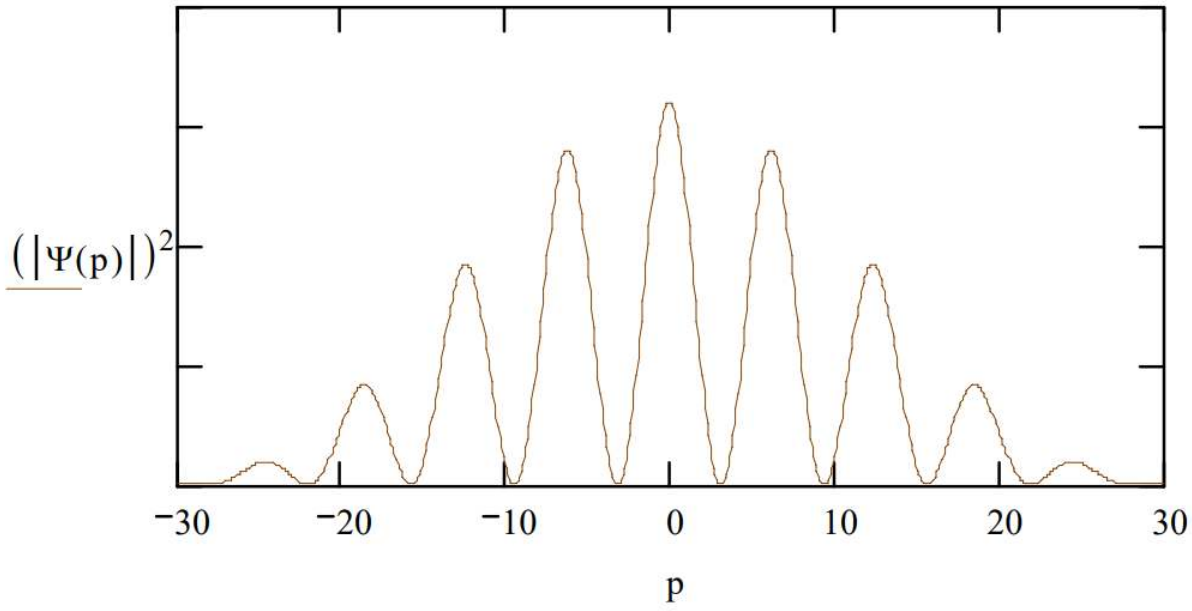
The diffraction pattern created by the double-slit configuration of the screen is the square of the absolute magnitude of the momentum wave function, $|\Psi(p)|^2$.

$$|\langle p|\Psi\rangle|^2 = \frac{1 + \cos\left(px_1\right)\cos\left(px_2\right) + \sin\left(px_1\right)\sin\left(px_2\right)}{2\pi}$$

The diffraction pattern below shows the required delocalization of momentum by the infinitesimally thin slits and interference fringes because the photon was localized at two spatial positions.



If slits of finite width were used the mathematics would be a little more complicated and lead to the following familiar diffraction pattern.



In the presence of the polarizing films, the spatial wave function becomes,

$$|\Psi\rangle = \frac{1}{\sqrt{2}}[|x_1\rangle|v\rangle + |x_2\rangle|h\rangle]$$

where v and h represent the vertical and horizontal polarization states. Projecting this wave function onto momentum space yields,

$$\Psi(p) = \langle p|\Psi\rangle = \frac{1}{\sqrt{2}}[\langle p|x_1\rangle|v\rangle + \langle p|x_2\rangle|h\rangle]$$

The square of the absolute magnitude of the momentum wave function is, again, the diffraction pattern,

$$|\langle p|\Psi\rangle|^2 = \frac{1}{\sqrt{2}}\left[|\langle p|x_1\rangle|^2 + |\langle p|x_2\rangle|^2\right] = \frac{1}{2\pi}$$

We see that due to the presence of the polarizing films the interference terms (fringes) disappear.

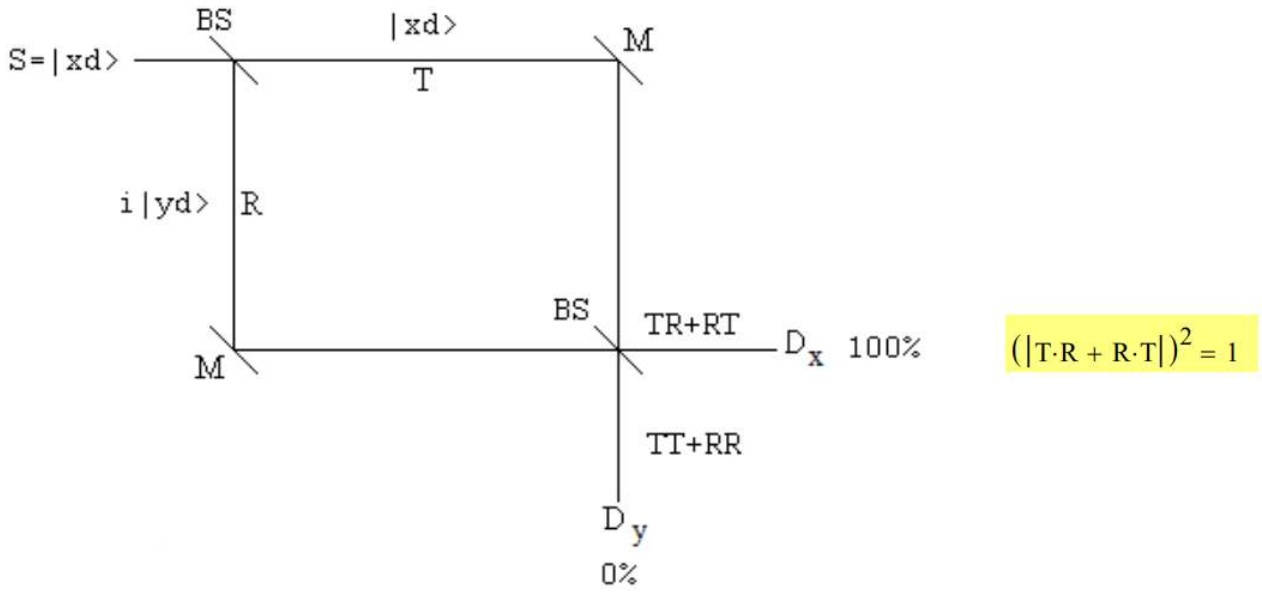
This page titled 1.38: Double-Slit Experiment with Polarized Light is shared under a CC BY 4.0 license and was authored, remixed, and/or curated by Frank Rioux via source content that was edited to the style and standards of the LibreTexts platform.

1.39: The Consequences of Path Information in a Mach-Zehnder Interferometer

This tutorial deals with the effect of path information in a Mach-Zehnder interferometer (MZI). A related analysis involving the double-slit experiment is available in the preceding tutorial. We begin with an analysis of the operation of an equal arm MZI illuminated with diagonally polarized light.

The source emits photons in the x-direction illuminating a 50/50 beam splitter (BS) which splits the beam into a superposition of propagation in the x- and y-directions. The reflected beam collects a 90 degree ($\frac{\pi}{2}$, i) phase shift relative to the transmitted beam. Mirrors redirect the two beams to a second 50/50 BS. For an equal arm interferometer the photons are always registered at D_x and never at D_y. One way to explain this is shown in the figure below. A photon has two paths to each detector. At D_x the probability amplitudes of the photon's paths add in phase each being shifted by 90 degrees, resulting in constructive interference. At D_y the probability amplitudes are 180 degrees out of phase causing destructive interference. The beam splitters do not operate on the polarization states of the photons.

Probability amplitude for photon transmission at a 50/50 beam splitter: $T := \frac{1}{\sqrt{2}}$	Probability amplitude for photon reflection at a 50/50 beam splitter: $R := \frac{i}{\sqrt{2}}$



$$(|T \cdot R + R \cdot T|)^2 = 1$$

$$(|T \cdot T + R \cdot R|)^2 = 0$$

An equivalent matrix mechanics analysis uses vectors to represent the photon's direction of propagation and polarization, and matrices to represent the objects that operate on the photon states, such as beam splitters and mirrors. In the analyses which follow a photon can be moving in the x- or y-direction with diagonal, horizontal or vertical polarization.

Propagation states:

$$x := \begin{pmatrix} 1 \\ 0 \end{pmatrix} \qquad y := \begin{pmatrix} 0 \\ 1 \end{pmatrix}$$

Polarization states:

$$d := \frac{1}{\sqrt{2}} \cdot \begin{pmatrix} 1 \\ 1 \end{pmatrix} \qquad h := \begin{pmatrix} 1 \\ 0 \end{pmatrix} \qquad v := \begin{pmatrix} 0 \\ 1 \end{pmatrix}$$

The Appendix shows how the propagation and polarization states are written as a composite state using tensor multiplication of vectors.

$$\mathrm{xd} := \frac{1}{\sqrt{2}} \cdot \begin{pmatrix} 1 \\ 1 \\ 0 \\ 0 \end{pmatrix} \qquad \mathrm{yd} := \frac{1}{\sqrt{2}} \cdot \begin{pmatrix} 0 \\ 0 \\ 1 \\ 1 \end{pmatrix}$$

$$\mathrm{xh} := \begin{pmatrix} 1 \\ 0 \\ 0 \\ 0 \end{pmatrix} \qquad \mathrm{yh} := \begin{pmatrix} 0 \\ 0 \\ 1 \\ 0 \end{pmatrix}$$

$$\mathrm{xv} := \begin{pmatrix} 0 \\ 1 \\ 0 \\ 0 \end{pmatrix} \qquad \mathrm{yv} := \begin{pmatrix} 0 \\ 0 \\ 0 \\ 1 \end{pmatrix}$$

The beam splitters and mirrors operate on the photon's direction of propagation but not on its polarization. The identity (do nothing) operates on the second degree of freedom, polarization.

Beam splitter:

$$\frac{1}{\sqrt{2}} \cdot \begin{pmatrix} 1 & \mathrm{i} \\ \mathrm{i} & 1 \end{pmatrix}$$

Mirror:

$$\begin{pmatrix} 0 & 1 \\ 1 & 0 \end{pmatrix}$$

Identity:

$$\begin{pmatrix} 1 & 0 \\ 0 & 1 \end{pmatrix}$$

Kronecker, Mathcad's command for tensor multiplication of matrices, insures that the beam splitters and mirrors operate on direction of motion, and that photon polarization evolves unchanged. See the Appendix for the details of the tensor product of two matrices.

$$\mathrm{BS} := \mathrm{kronecker}\left[\frac{1}{\sqrt{2}} \cdot \begin{pmatrix} 1 & \mathrm{i} \\ \mathrm{i} & 1 \end{pmatrix}, \begin{pmatrix} 1 & 0 \\ 0 & 1 \end{pmatrix}\right]$$

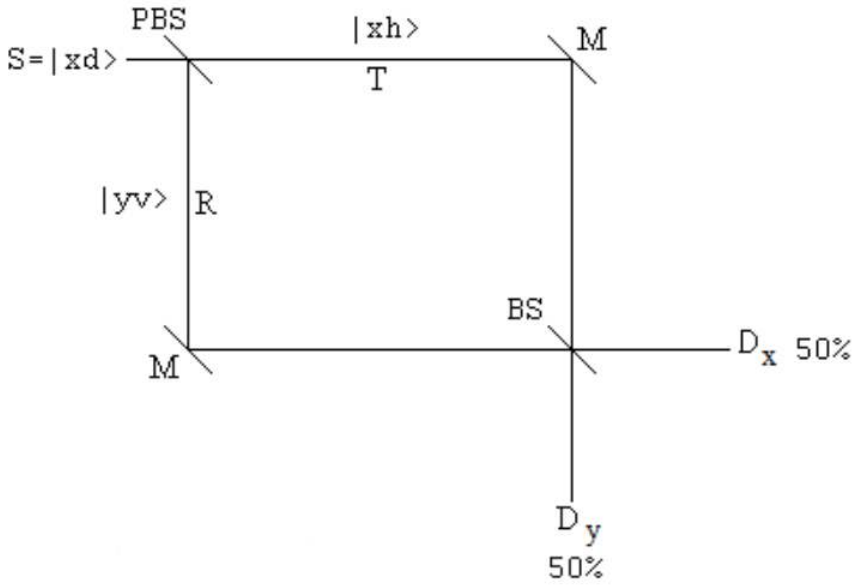
$$\mathrm{M} := \mathrm{kronecker}\left[\begin{pmatrix} 0 & 1 \\ 1 & 0 \end{pmatrix}, \begin{pmatrix} 1 & 0 \\ 0 & 1 \end{pmatrix}\right]$$

The probability that the photon will be moving in the x-direction after the second BS and detected at D_x is 1. The probability it will be registered at D_y is 0.

$$\left(\left|\mathrm{xd}^{\mathrm{T}} \cdot \mathrm{BS} \cdot \mathrm{M} \cdot \mathrm{BS} \cdot \mathrm{xd}\right|\right)^2 = 1$$

$$\left(\left|\mathrm{yd}^{\mathrm{T}} \cdot \mathrm{BS} \cdot \mathrm{M} \cdot \mathrm{BS} \cdot \mathrm{xd}\right|\right)^2 = 0$$

Photon path information can be added by replacing the first BS with a polarizing beam splitter (PBS), which transmits horizontal polarization and reflects vertical polarization. There is no phase shift between transmission and reflection in a PBS.



The matrix representing a PBS can be constructed by considering the fate of the individual photon states encountering a PBS. The individual terms are from right to left. For example, |yv> <yx| means xv --> yv.

$$\widehat{PBS} = |xh\rangle\langle xh| + |yv\rangle\langle xv| + |yh\rangle\langle yh| + |xv\rangle\langle yv|$$

$$\mathrm{PBS} := \mathrm{xh}\cdot\mathrm{xh}^{\mathrm{T}} + \mathrm{yv}\cdot\mathrm{xv}^{\mathrm{T}} + \mathrm{yh}\cdot\mathrm{yh}^{\mathrm{T}} + \mathrm{xv}\cdot\mathrm{yv}^{\mathrm{T}} = \begin{pmatrix} 1 & 0 & 0 & 0 \\ 0 & 0 & 0 & 1 \\ 0 & 0 & 1 & 0 \\ 0 & 1 & 0 & 0 \end{pmatrix}$$

After the PBS the diagonally polarized photon is in a superposition of being transmitted with horizontal polarization and reflected with vertical polarization. In other words the two photon paths have been labeled with orthogonal polarization states; path information is available.

$$\mathrm{PBS}\cdot\mathrm{xd} = \begin{pmatrix} 0.707 \\ 0 \\ 0 \\ 0.707 \end{pmatrix}$$

$$\frac{1}{\sqrt{2}}\cdot(\mathrm{xh}+\mathrm{yv}) = \begin{pmatrix} 0.707 \\ 0 \\ 0 \\ 0.707 \end{pmatrix}$$

The following calculations show that this path information destroys the interference observed in the original MZI. Now both detectors fire with equal probability as shown in the diagram above. Half the time the photon is detected at D_x with either horizontal or vertical polarization, and half the time the photon is detected at D_y with horizontal or vertical polarization. This occurs because the path tags are orthogonal polarization states.

$$\left(\left|\mathrm{xv}^{\mathrm{T}}\cdot\mathrm{BS}\cdot\mathrm{M}\cdot\mathrm{PBS}\cdot\mathrm{xd}\right|\right)^2 = 0.25 \qquad \left(\left|\mathrm{xh}^{\mathrm{T}}\cdot\mathrm{BS}\cdot\mathrm{M}\cdot\mathrm{PBS}\cdot\mathrm{xd}\right|\right)^2 = 0.25$$

$$\left(\left|\mathrm{yv}^{\mathrm{T}}\cdot\mathrm{BS}\cdot\mathrm{M}\cdot\mathrm{PBS}\cdot\mathrm{xd}\right|\right)^2 = 0.25 \qquad \left(\left|\mathrm{yh}^{\mathrm{T}}\cdot\mathrm{BS}\cdot\mathrm{M}\cdot\mathrm{PBS}\cdot\mathrm{xd}\right|\right)^2 = 0.25$$

An algebraic representation of the steps from source to detectors gives the same numbers when the magnitudes of the probability amplitudes are squared to give the probabilities for each possible measurement outcome at D_x and D_y.

$$|xd\rangle \xrightarrow{PBS} \frac{1}{\sqrt{2}}[|xh\rangle + |yv\rangle] \xrightarrow[BS]{M} \frac{1}{\sqrt{2}}[i|xh\rangle + |yh\rangle]$$

If the PBS is illuminated with horizontally or vertically polarized photons, there is only one path to the beam splitter in front of the detectors. Again both detectors fire with equal probability because there is no opportunity for path interference.

Horizontally polarized source:

$$\left(\left|\mathrm{xh}^{\mathrm{T}} \cdot \mathrm{BS} \cdot \mathrm{M} \cdot \mathrm{PBS} \cdot \mathrm{xh}\right|\right)^2 = 0.5 \qquad \left[\left|\mathrm{yh}^{\mathrm{T}} \cdot (\mathrm{BS} \cdot \mathrm{M} \cdot \mathrm{PBS}) \cdot \mathrm{xh}\right|\right]^2 = 0.5$$

$$|xh\rangle \xrightarrow{PBS} |xh\rangle \xrightarrow[BS]{M} \frac{1}{\sqrt{2}}[i|xh\rangle + |yh\rangle]$$

Vertically polarized source:

$$\left(\left|\mathrm{xv}^{\mathrm{T}} \cdot \mathrm{BS} \cdot \mathrm{M} \cdot \mathrm{PBS} \cdot \mathrm{xv}\right|\right)^2 = 0.5 \qquad \left[\left|\mathrm{yv}^{\mathrm{T}} \cdot (\mathrm{BS} \cdot \mathrm{M} \cdot \mathrm{PBS}) \cdot \mathrm{xv}\right|\right]^2 = 0.5$$

$$|xv\rangle \xrightarrow{PBS} |yv\rangle \xrightarrow[BS]{M} \frac{1}{\sqrt{2}}[i|xv\rangle + i|yh\rangle]$$

Appendix

Tensor products for the various propagation/polarization states are formed as follows:

$$|xd\rangle = \begin{pmatrix} 1 \\ 0 \end{pmatrix} \otimes \frac{1}{\sqrt{2}} \begin{pmatrix} 1 \\ 1 \end{pmatrix} = \frac{1}{\sqrt{2}} \begin{pmatrix} 1 \\ 1 \\ 0 \\ 0 \end{pmatrix} \qquad |yd\rangle = \begin{pmatrix} 0 \\ 1 \end{pmatrix} \otimes \frac{1}{\sqrt{2}} \begin{pmatrix} 1 \\ 1 \end{pmatrix} = \frac{1}{\sqrt{2}} \begin{pmatrix} 0 \\ 0 \\ 1 \\ 1 \end{pmatrix}$$

$$|xh\rangle = \begin{pmatrix} 1 \\ 0 \end{pmatrix} \otimes \begin{pmatrix} 1 \\ 0 \end{pmatrix} = \begin{pmatrix} 1 \\ 0 \\ 0 \\ 0 \end{pmatrix} \qquad |xv\rangle = \begin{pmatrix} 1 \\ 0 \end{pmatrix} \otimes \begin{pmatrix} 0 \\ 1 \end{pmatrix} = \begin{pmatrix} 0 \\ 1 \\ 0 \\ 0 \end{pmatrix}$$

$$|yh\rangle = \begin{pmatrix} 0 \\ 1 \end{pmatrix} \otimes \begin{pmatrix} 1 \\ 0 \end{pmatrix} = \begin{pmatrix} 0 \\ 0 \\ 1 \\ 0 \end{pmatrix} \qquad |yv\rangle = \begin{pmatrix} 0 \\ 1 \end{pmatrix} \otimes \begin{pmatrix} 0 \\ 1 \end{pmatrix} = \begin{pmatrix} 0 \\ 0 \\ 0 \\ 1 \end{pmatrix}$$

An example of the tensor product of two matrices:

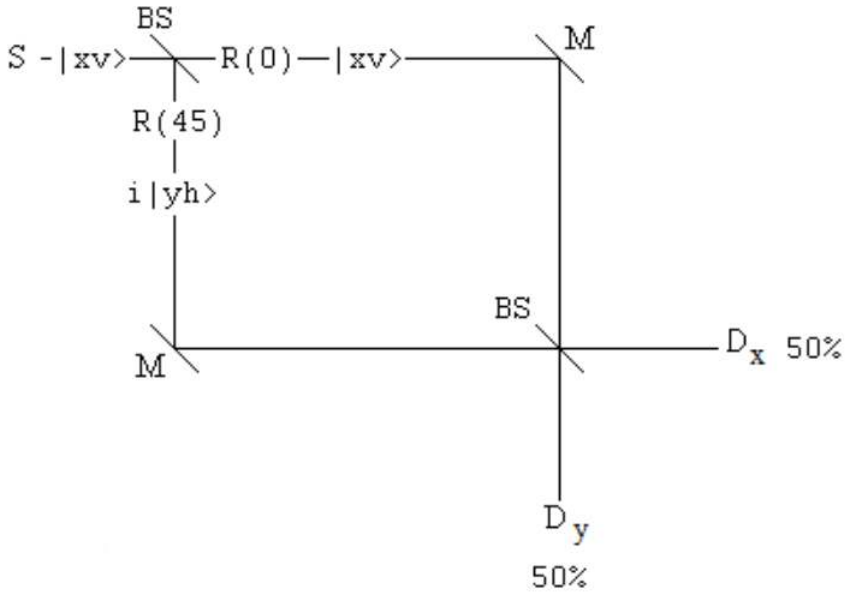
$$\begin{pmatrix} a & b \\ c & d \end{pmatrix} \otimes \begin{pmatrix} w & x \\ y & z \end{pmatrix} = \begin{pmatrix} a \begin{pmatrix} w & x \\ y & z \end{pmatrix} & b \begin{pmatrix} w & x \\ y & z \end{pmatrix} \\ c \begin{pmatrix} w & x \\ y & z \end{pmatrix} & d \begin{pmatrix} w & x \\ y & z \end{pmatrix} \end{pmatrix} = \begin{pmatrix} aw & ax & bw & bx \\ ay & az & by & bz \\ cw & cx & dw & dx \\ cy & cz & dy & dz \end{pmatrix}$$

This page titled 1.39: The Consequences of Path Information in a Mach-Zehnder Interferometer is shared under a CC BY 4.0 license and was authored, remixed, and/or curated by Frank Rioux via source content that was edited to the style and standards of the LibreTexts platform.

1.40: Another look at the Consequences of Path Information in a Mach-Zehnder Interferometer

This tutorial deals with the effect of path information and its so-called erasure in a Mach-Zehnder interferometer (MZI). A related analysis involving the double-slit experiment is available with the title "Which Path Information and the Quantum Eraser."

The source emits vertically polarized photons in the x-direction illuminating a 50/50 beam splitter (BS) which splits the beam into a superposition of propagation in the x- and y-directions. The reflected beam collects a 90 degree ($\frac{\pi}{2}$,i) phase shift relative to the transmitted beam. A polarization rotator rotates the polarization in the lower arm to horizontal. Mirrors redirect the two beams to a second 50/50 BS. In the absense of the polarization rotator the photons are always registered at Dx and never at Dy. In its presence the detectors both fire 50% of the time. The algebraic analyses below the figure show the evolution of the photons through the interferometer in the absence and presence of the polarization rotator. Note that the orthogonal **v/h** polarization tags have become orthogonal **d/a** tags. The significance of this will be come clear in the matrix mechanics analysis that is provided below.



Photon behavior in the absence of the polarization rotator in the lower arm of the interferometer.

$$|xv\rangle \xrightarrow{BS} \frac{1}{\sqrt{2}}(|xv\rangle + i|yv\rangle) \xrightarrow{BS} \frac{1}{2}(i|xv\rangle + |yv\rangle + i|xv\rangle - |yv\rangle) = i|xv\rangle$$

Photon behavior in the presence of the polarization rotator in the lower arm of the interferometer.

$$|xv\rangle \xrightarrow{BS} \frac{1}{\sqrt{2}}(|xv\rangle + i|yv\rangle) \xrightarrow[M]{y/h} \frac{1}{\sqrt{2}}(|yv\rangle + i|xh\rangle) \xrightarrow{BS} \frac{1}{2}(i|xv\rangle + |yv\rangle + i|xh\rangle - |yh\rangle)$$
$$= \frac{1}{\sqrt{2}}(i|xd\rangle + |ya\rangle)$$

The following equations were used to reach the final state:

$$|d\rangle = \frac{1}{\sqrt{2}}(|h\rangle + |v\rangle) \qquad |a\rangle = \frac{1}{\sqrt{2}}(|h\rangle - |v\rangle)$$

A **matrix mechanics** analysis uses vectors to represent states and matrices to represent the optical elements that they encounter in the MZI.

Photon moving horizontally: x	Photon moving vertically: y	Vertical polarization: v	Horizontal polarization: h
$:= \begin{pmatrix} 1 \\ 0 \end{pmatrix}$	$:= \begin{pmatrix} 0 \\ 1 \end{pmatrix}$	$:= \begin{pmatrix} 1 \\ 0 \end{pmatrix}$	$= \begin{pmatrix} 0 \\ 1 \end{pmatrix}$

Photon direction of propagation and polarization states:

$$\mathrm{xv} := \begin{pmatrix} 1 \\ 0 \\ 0 \\ 0 \end{pmatrix} \quad \mathrm{xh} := \begin{pmatrix} 0 \\ 1 \\ 0 \\ 0 \end{pmatrix} \quad \mathrm{yv} := \begin{pmatrix} 0 \\ 0 \\ 1 \\ 0 \end{pmatrix} \quad \mathrm{yh} := \begin{pmatrix} 0 \\ 0 \\ 0 \\ 1 \end{pmatrix}$$

Projection operators for the x- and y-detectors:

$$\mathrm{Dx} := \mathrm{x} \cdot \mathrm{x}^{\mathrm{T}} = \begin{pmatrix} 1 & 0 \\ 0 & 0 \end{pmatrix} \qquad \mathrm{Dy} := \mathrm{y} \cdot \mathrm{y}^{\mathrm{T}} = \begin{pmatrix} 0 & 0 \\ 0 & 1 \end{pmatrix}$$

Beam splitter:

$$\mathrm{BS} := \frac{1}{\sqrt{2}} \begin{pmatrix} 1 & \mathrm{i} \\ \mathrm{i} & 1 \end{pmatrix}$$

Mirror:

$$M := \begin{pmatrix} 0 & 1 \\ 1 & 0 \end{pmatrix}$$

Identity:

$$\mathrm{I} := \begin{pmatrix} 1 & 0 \\ 0 & 1 \end{pmatrix}$$

Polarization rotator for the lower arm of the interferometer:

$$\mathrm{R}(\varphi) := \begin{pmatrix} 1 & 0 & 0 & 0 \\ 0 & -1 & 0 & 0 \\ 0 & 0 & \cos(2 \cdot \varphi) & \sin(2 \cdot \varphi) \\ 0 & 0 & \sin(2 \cdot \varphi) & -\cos(2 \cdot \varphi) \end{pmatrix}$$

Diagonal and anti-diagonal projection operators:

$$\mathrm{Pd} := \frac{1}{2} \cdot \begin{pmatrix} 1 & 1 & 0 & 0 \\ 1 & 1 & 0 & 0 \\ 0 & 0 & 1 & 1 \\ 0 & 0 & 1 & 1 \end{pmatrix}$$

$$\mathrm{Pa} := \frac{1}{2} \cdot \begin{pmatrix} 1 & -1 & 0 & 0 \\ -1 & 1 & 0 & 0 \\ 0 & 0 & 1 & -1 \\ 0 & 0 & -1 & 1 \end{pmatrix}$$

Vertical and horizontal projection operators:

$$\mathrm{Pv} := \begin{pmatrix} 1 & 0 & 0 & 0 \\ 0 & 0 & 0 & 0 \\ 0 & 0 & 1 & 0 \\ 0 & 0 & 0 & 0 \end{pmatrix}$$

$$\mathrm{Ph} := \begin{pmatrix} 0 & 0 & 0 & 0 \\ 0 & 1 & 0 & 0 \\ 0 & 0 & 0 & 0 \\ 0 & 0 & 0 & 1 \end{pmatrix}$$

MZI with lower arm polarization rotator:

$$\mathrm{MZ}(\varphi) := \mathrm{kronecker}(\mathrm{BS},\ \mathrm{I}) \cdot \mathrm{R}(\varphi) \cdot \mathrm{kronecker}(\mathrm{M},\ \mathrm{I}) \cdot \mathrm{kronecker}(\mathrm{BS},\ \mathrm{I})$$

Without polarization rotation in the lower arm of the interferometer all photons are detected at Dx. See the algebraic analysis.

$$(|\text{kronecker}(\text{Dx}, \text{I}) \cdot \text{MZ}(0) \cdot \text{xv}|)^2 = 1 \qquad (|\text{kronecker}(\text{Dy}, \text{I}) \cdot \text{MZ}(0) \cdot \text{xv}|)^2 = 0$$

Adding orthogonal path information by rotating the polarization in the lower arm to horizontal destroys the interference effect at the second beam splitter causing both detectors to register photons. See the algebraic analysis.

$$\left(|\text{kronecker}(\text{Dx}, \text{I}) \cdot \text{MZ}\left(\frac{\pi}{4}\right) \cdot \text{xv}|\right)^2 = 0.5 \qquad \left(|\text{ kronecker }(\text{Dy}, \text{I}) \cdot \text{MZ}\left(\frac{\pi}{4}\right) \cdot \text{xv}|\right)^2 = 0.5$$

Placing vertical or horizontal polarizers in front of both detectors reduces the count rates by half. See the algebraic analysis.

$$\left(|\text{kronecker}(\text{Dx}, \text{I}) \cdot \text{Pv} \cdot \text{MZ}\left(\frac{\pi}{4}\right) \cdot \text{xv}|\right)^2 = 0.25$$
$$\left(|\text{kronecker}(\text{Dy}, \text{I}) \cdot \text{Pv} \cdot \text{MZ}\left(\frac{\pi}{4}\right) \cdot \text{xv}|\right)^2 = 0.25$$

$$\left(|\text{kronecker}(\text{Dx}, \text{I}) \cdot \text{Ph} \cdot \text{MZ}\left(\frac{\pi}{4}\right) \cdot \text{xv}|\right)^2 = 0.25$$
$$\left(|\text{ kronecker }(\text{Dy}, \text{I}) \cdot \text{Ph} \cdot \text{MZ}\left(\frac{\pi}{4}\right) \cdot \text{xv}|\right)^2 = 0.25$$

A diagonal polarizer placed in front of both detectors passes the x-direction photons and absorbs the y-direction photons. See the algebraic analysis.

$$\left(|\text{kronecker}(\text{Dx}, \text{I}) \cdot \text{Pd} \cdot \text{MZ}\left(\frac{\pi}{4}\right) \cdot \text{xv}|\right)^2 = 0.5 \qquad \left(|\text{kronecker}(\text{Dy}, \text{I}) \cdot \text{Pd} \cdot \text{MZ}\left(\frac{\pi}{4}\right) \cdot \text{xv}|\right)^2 = 0$$

An anti-diagonal polarizer placed in front of the detectors passes the y-direction photons and absorbs the x-direction photons. See the algebraic analysis.

$$\left(|\text{ kronecker }(\text{Dx}, \text{I}) \cdot \text{Pa} \cdot \text{MZ}\left(\frac{\pi}{4}\right) \cdot \text{xv}|\right)^2 = 0$$
$$\left(|\text{ kronecker }(\text{Dy}, \text{I}) \cdot \text{Pa} \cdot \text{MZ}\left(\frac{\pi}{4}\right) \cdot \text{xv}|\right)^2 = 0.5$$

These calculations demonstrate that the lower arm polarization rotator does its job.

$$\text{R}(0) \cdot \text{kronecker}(\text{BS}, \text{I}) \cdot \text{xv} = \begin{pmatrix} 0.707 \\ 0 \\ 0.707\text{i} \\ 0 \end{pmatrix} \frac{\text{xv} + \text{i} \cdot \text{yv}}{\sqrt{2}} = \begin{pmatrix} 0.707 \\ 0 \\ 0.707\text{i} \\ 0 \end{pmatrix}$$

$$\text{R}\left(\frac{\pi}{4}\right) \cdot \text{kronecker}(\text{BS}, \text{I}) \cdot \text{xv} = \begin{pmatrix} 0.707 \\ 0 \\ 0 \\ 0.707\text{i} \end{pmatrix} \frac{\text{xv} + \text{i} \cdot \text{yh}}{\sqrt{2}} = \begin{pmatrix} 0.707 \\ 0 \\ 0 \\ 0.707\text{i} \end{pmatrix}$$

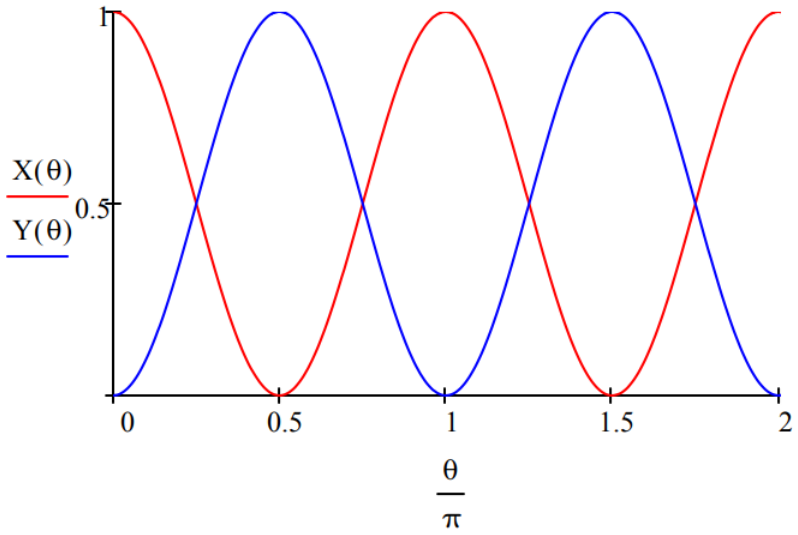
The following calculations show the behavior of the detectors as a function of the polarization rotator angle.

Detection at Dx:

$$\text{X}(\theta) := (|\text{kronecker}(\text{Dx}, \text{I}) \cdot \text{MZ}(\theta) \cdot \text{xv}|)^2$$

Detection at Dy:

$$\text{Y}(\theta) := (|\text{kronecker}(\text{Dy}, \text{I}) \cdot \text{MZ}(\theta) \cdot \text{xv}|)^2$$

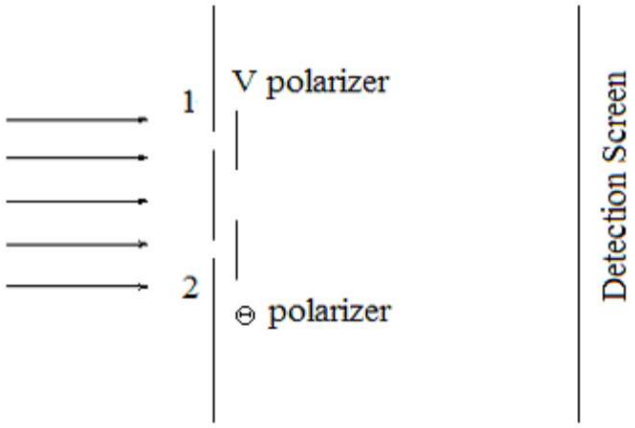


This page titled 1.40: Another look at the Consequences of Path Information in a Mach-Zehnder Interferometer is shared under a CC BY 4.0 license and was authored, remixed, and/or curated by Frank Rioux via source content that was edited to the style and standards of the LibreTexts platform.

1.41: The Double-Slit Experiment with Polarized Light

Fresnel and Arago "using an apparatus based on Young's [double-slit] experiment" observed that "two beams polarized in mutually perpendicular planes never yield fringes." The purpose of this tutorial is to examine this phenomenon from a quantum mechanical perspective.

A schematic diagram of the double-slit experiment with polarizers behind the slits is shown below.V and Θ stand for vertical and Θ polarizers, respectively.



Assuming infinitessimally thin slits, the photon wave function is a superposition of being at slit 1 with vertical polarization and slit 2 with polarization at an angle θ relative to the vertical.

$$|\Psi\rangle = \frac{1}{\sqrt{2}}\left[|x_1\rangle\,|\mathrm{V}\rangle + |x_2\rangle|\Theta\rangle\right]$$

The vertical and θ polarization states are represented by the following vectors.

$$|\mathrm{V}\rangle = \begin{pmatrix} 1 \\ 0 \end{pmatrix} \text{ and } |\Theta\rangle = \begin{pmatrix} \cos(\theta) \\ \sin(\theta) \end{pmatrix}$$

The diffraction pattern is the Fourier transform of the state above into the momentum representation.

$$\langle p|\Psi\rangle = \frac{1}{\sqrt{2}}\left[\langle p|x_1\rangle\,|\mathrm{V}\rangle + \langle p|x_2\rangle\,|\Theta\rangle\right]$$

This calculation is implemented in Mathcad for slits of finite width as follows.

Slit positions:

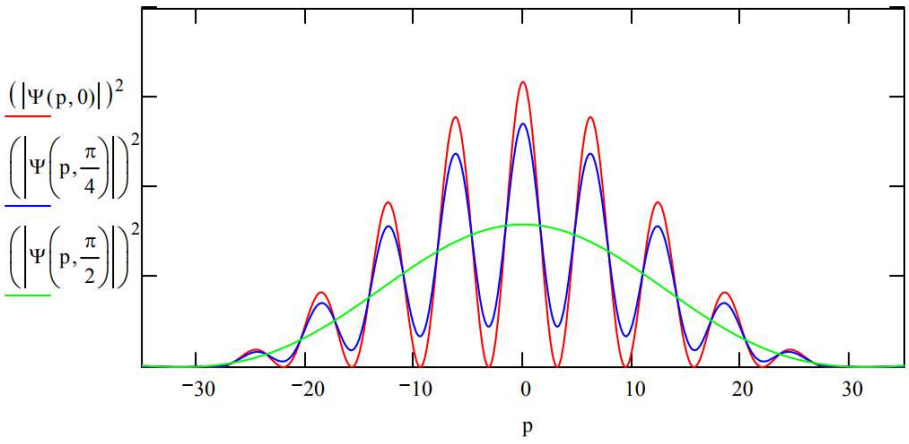
$$\mathrm{x}_1 := 1 \qquad \mathrm{x}_2 := 2$$

Slit width:

$$\delta := 0.2$$

$$\Psi(p,\theta) := \frac{\int_{\mathrm{x}_1-\frac{\delta}{2}}^{\mathrm{x}_1+\frac{\delta}{2}} \frac{1}{\sqrt{2\cdot\pi}}\cdot\exp(-\mathrm{i}\cdot\mathrm{p}\cdot\mathrm{x})\cdot\frac{1}{\sqrt{\delta}}\mathrm{dx}\cdot\begin{pmatrix}1\\0\end{pmatrix} + \int_{x_2-\frac{\delta}{2}}^{x_2+\frac{\delta}{2}} \frac{1}{\sqrt{2\cdot\pi}}\cdot\exp(-\mathrm{i}\cdot\mathrm{p}\cdot\mathrm{x})\cdot\frac{1}{\sqrt{\delta}}\mathrm{dx}\cdot\begin{pmatrix}\cos(\theta)\\\sin(\theta)\end{pmatrix}}{\sqrt{2}}$$

To confirm the assertion of Fresnel and Arago the momentum distributions for three angles of the polarizer at the right slit are calculated.



We see that when the polarizers are oriented at the same angle, the diffraction pattern is the usual one for the Young double-slit experiment. When the polarizers are crossed the fringes, as Fresnel and Arago assert, disappear. Finally, when the relative angle of the two polarizers is 45 degrees, we see a reduced interference pattern.

This page titled 1.41: The Double-Slit Experiment with Polarized Light is shared under a CC BY 4.0 license and was authored, remixed, and/or curated by Frank Rioux via source content that was edited to the style and standards of the LibreTexts platform.

1.42: The Quantum Eraser

Paul Kwiat and an undergraduate research assistant published "A Do-It-Yourself Quantum Eraser" in the May 2007 issue of *Scientific American*. The purpose of this tutorial is to show the quantum math behind the laser demonstrations illustrated in this article.

The quantum mechanics behind the quantum eraser is very similar to that previously used to analyze the double-slit experiment with polarized light. By way of review we recall that the interference pattern produced in the traditional double-slit experiment is actually the momentum distribution created by the double-slit geometry. In other words, the interference pattern is the Fourier transform of the spatial geometry of the slits.

$$|\Psi\rangle = \frac{1}{\sqrt{2}}\left[|x_1\rangle + |x_2\rangle\right]$$

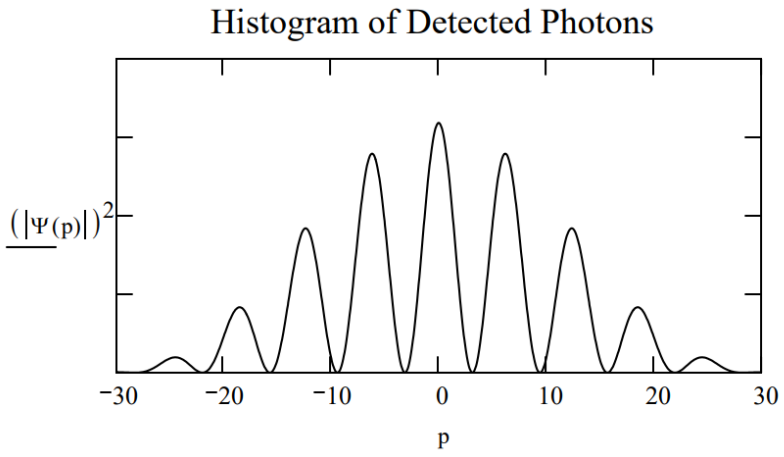
$$\langle p|\Psi\rangle = \frac{1}{\sqrt{2}}\left[\langle p|x_i\rangle + \langle p|x_2\rangle\right] = \frac{1}{\sqrt{2}}\left[\frac{1}{\sqrt{2\pi}}\exp\left(-ipx_1\right) + \frac{1}{\sqrt{2\pi}}\exp\left(-ipx_2\right)\right]$$

For slits of width δ positioned as indicated below we have,

Position of first slit: $x_1 := 0$	Position of second slit: $x_2 := 1$	Slit width: $\delta := 0.2$

$$\Psi(p) := \frac{\int_{x_1-\frac{\delta}{2}}^{x_1+\frac{\delta}{2}} \frac{1}{\sqrt{2\cdot\pi}}\cdot\exp(-i\cdot p\cdot x)\cdot\frac{1}{\sqrt{\delta}}dx + \int_{x_2-\frac{\delta}{2}}^{x_2+\frac{\delta}{2}} \frac{1}{\sqrt{2\cdot\pi}}\cdot\exp(-i\cdot p\cdot x)\cdot\frac{1}{\sqrt{\delta}}dx}{\sqrt{2}}$$

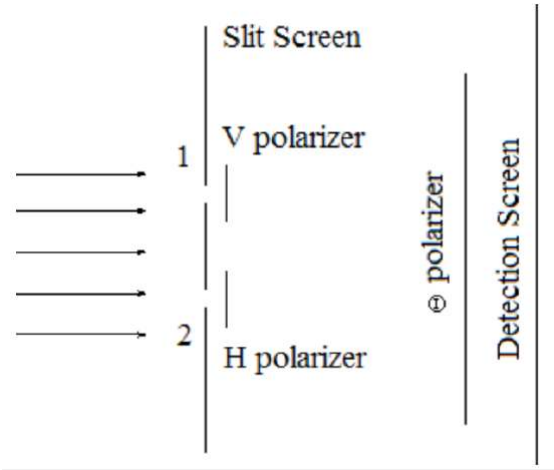
yielding the following diffraction pattern.



To gain "which-way" information a vertical polarizer is placed behind the first slit and a horizontal polarizer behind the second slit. Essentially two state preparation measurements have been made yielding the following entangled superposition state. (Path and polarization information have been entangled; the path part and polarizaton part cannot be factored into a product of terms.)

$$|\Psi\rangle = \frac{1}{\sqrt{2}}\left[|x_1\rangle\,|V\rangle + |x_2\rangle|H\rangle\right]$$

Next come the measurements - polarization state, followed by momentum distribution (the spatial distribution of photon arrivals at the detection screen). The state preparation and measurement apparatus is shown skematically below.

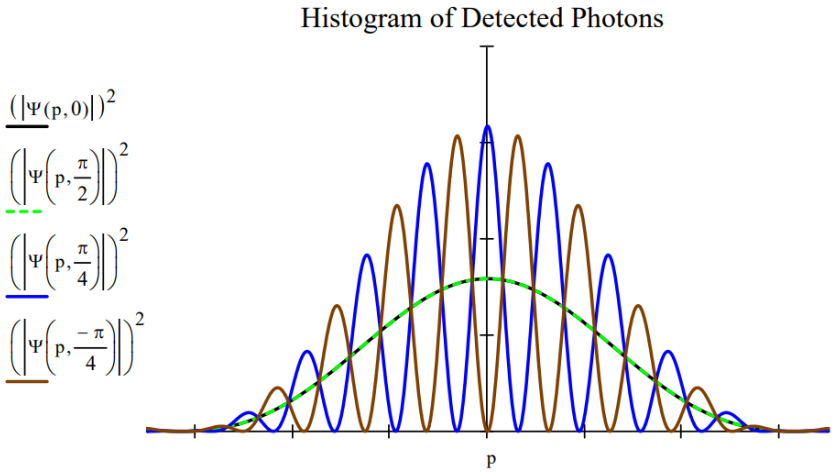


To calculate the results of these sequential measurements $|\Psi>$ is projected onto $<\theta, \mathrm{p}|$, yielding for slits of width δ the following measurement state.

$$\Psi(p,\theta) := \frac{\int_{x_1-\frac{\delta}{2}}^{x_1+\frac{\delta}{2}} \frac{1}{\sqrt{2\cdot\pi}} \cdot \exp(-\mathrm{i}\cdot \mathrm{p}\cdot \mathrm{x}) \cdot \frac{1}{\sqrt{\delta}} dx \cdot \cos(\theta) + \int_{x_2-\frac{\delta}{2}}^{x_2+\frac{\delta}{2}} \frac{1}{\sqrt{2\cdot\pi}} \cdot \exp(-\mathrm{i}\cdot \mathrm{p}\cdot \mathrm{x}) \cdot \frac{1}{\sqrt{\delta}} \mathrm{d}x \sin(\theta)}{\sqrt{2}}$$

Kwiat and Hillmer create a double-slit effect by illuminating a thin wire with a narrow laser beam which is displayed on a distant screen. A brief discussion of their demonstrations in light of the mathematics presented here follows.

- Observing the double-slit interference effect. The quantum mechanics is outlined at the beginning of this tutorial.
- Labeling the photon path with crossed polarizers (figure above without the third polarizer in front of the detection screen). The quantum math for this demonstration can be found in the previous tutorial, "The Double-Slit Experiment with Polarized Light." No interference fringes are predicted and none are observed. This effect was first observed by Fresnel and Arago in the first part of the 19th Century. It appears that this was the first example of the importance of path information in interference phenomena.
- Same as the previous demonstration, but with a third polarizer positioned in front of the detection screen. If the third polarizer is vertically (θ = 0) or horizontally ($\theta = \frac{\pi}{2}$) oriented no interference fringes are observed. The first two traces in the figure below show that no fringes are predicted.
- Same as the previous demonstration, except that the third polarizer is diagonally oriented ($\theta = \frac{\pi}{4}$) and anti-diagonally oriented ($\theta = -\frac{\pi}{4}$). Now fringes are observed and predicted, as can be seen in the third and fourth traces in the figure.



Regarding the last demonstration, the reason for the restoration of the interference fringes is that the "which-way" information provided by the crossed polarizers has been lost or erased. The vertically and horizontally polarized photons from slits 1 and 2 both

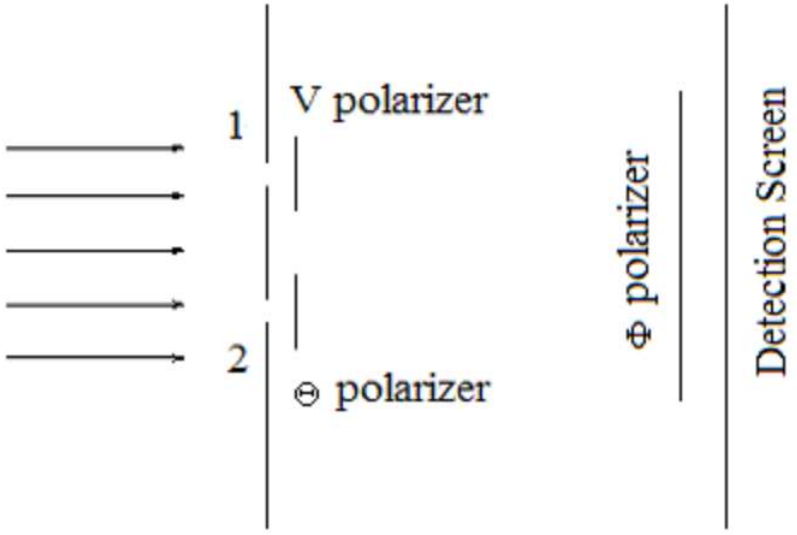
have a 50% chance of passing the diagonally or anti-diagonally oriented third polarizer. Thus, knowledge of the origin of a photon emerging from the third polarizer has been destroyed.

This page titled 1.42: The Quantum Eraser is shared under a CC BY 4.0 license and was authored, remixed, and/or curated by Frank Rioux via source content that was edited to the style and standards of the LibreTexts platform.

1.43: Which Way Did It Go? - The Quantum Eraser

Paul Kwiat and Rachel Hillmer, an undergraduate research assistant, published "A Do-It-Yourself Quantum Eraser" based on the double-slit experiment in the May 2007 issue of *Scientific American*. The purpose of this tutorial is to show the quantum math behind the laser demonstrations illustrated in this article.

Hillmer and Kwiat created the double-slit effect by illuminating a thin wire with a laser beam. They carried out a number of demonstrations with laser light and polarizing films using an experimental set up that effectively is as shown schematically below.



Assuming (initially) infinitesimally thin slits, the photon wave function at the slit screen is an entangled superposition of being at slit 1 with vertical polarization and slit 2 with polarization at an angle θ relative to the vertical. This entanglement provides which-way information if θ is not equal to 0 and, therefore, has an important effect on the diffraction pattern.

$$|\Psi\rangle = \frac{1}{\sqrt{2}}\left[|x_1\rangle\,|v\rangle + |x_2\rangle|\theta\rangle\right]$$

This state is projected onto ϕ and **p** because a ϕ-oriented polarizer (eraser) precedes the detection screen and because a diffraction pattern is actually the momentum distribution of the scattered photons. In other words, position is measured at the slit screen and momentum is measured at the detection screen.

$$\langle p\phi|\Psi\rangle = \frac{1}{\sqrt{2}}\left[\langle p|x_1\rangle\,\langle\phi|v\rangle + \langle p|x_2\rangle\,\langle\phi|\theta\rangle\right]$$

The polarization brackets (amplitudes) are easily shown to be the trigonometric functions shown below.

$$\langle p\phi|\Psi\rangle = \frac{1}{\sqrt{2}}\left[\langle p|x_1\rangle\cos(\phi) + \langle p|x_2\rangle\cos(\theta-\phi)\right]$$

The position-momentum brackets are the position eigenstates in the momentum representation and are given by,

$$\langle p|x\rangle = \frac{1}{\sqrt{2\pi\hbar}}\exp\left(-\frac{ipx}{\hbar}\right)$$

This allows us to write,

$$\langle p\phi|\Psi\rangle = \frac{1}{\sqrt{2}}\left[\frac{1}{\sqrt{2\pi\hbar}}\exp\left(-\frac{ipx_1}{\hbar}\right)\cos(\phi) + \frac{1}{\sqrt{2\pi\hbar}}\exp\left(-\frac{ipx_2}{\hbar}\right)\cos(\theta-\phi)\right]$$

Working in atomic units (h = 2π) and now assuming slits of finite width this expression becomes,

Slit positions:

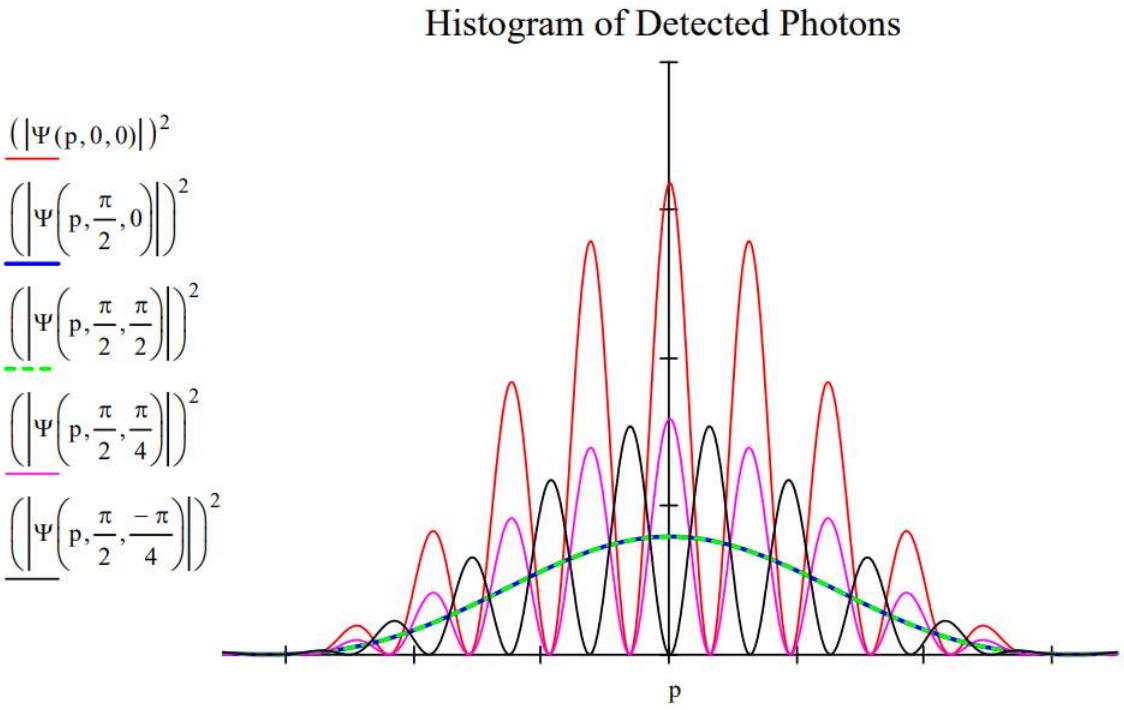
$$x_1 := 1 \qquad x_2 = 2$$

Slit width:

$$\delta := 0.2$$

$$\Psi(p,\theta,\phi) := \frac{\int_{x_1-\frac{\delta}{2}}^{x_1+\frac{\delta}{2}} \frac{1}{\sqrt{2\cdot\pi}} \cdot \exp(-i\cdot p\cdot x)\cdot\frac{1}{\sqrt{\delta}}dx\cdot\cos(\phi) + \int_{x_2-\frac{\delta}{2}}^{x_2+\frac{\delta}{2}} \frac{1}{\sqrt{2\cdot\pi}} \cdot \exp(-i\cdot p\cdot x)\cdot\frac{1}{\sqrt{\delta}}dx\cdot\cos(\theta-\phi)}{\sqrt{2}}$$

The square of the absolute magnitude of this function yields a representation of the diffraction pattern as a histogram of photon arrivals on the detection screen. The results shown in the figure will be discussed below.



Discussion of Results

The polarizer at slit 1 is always oriented vertically so only the orientations (θ and ϕ) of the other polarizers need to be specified.

[θ = 0; ϕ = 0]

The photons emerging from the slits are vertically polarized and encounter a vertical polarizer before the detection screen. This is the reference experiment and yields the traditional diffraction pattern, as shown by the plot of $(|\Psi(p,0,0)|)^2$. There is no which-way information in this experiment and 100% of the photons emerging from the vertically polarized slit screen reach the detection screen.

$$\int_{-\infty}^{\infty} (|\Psi(p,0,0)|)^2 dp \text{ float }, 3 \rightarrow 1.00$$

[$\theta = \frac{\pi}{2}$, ϕ = 0] and [$\theta = \frac{\pi}{2}, \phi = \frac{\pi}{2}$]

The crossed polarizers at the slit screen provide which-way information and the interference fringes disappear if the third polarizer is vertically or horizontally oriented. This is shown by the plots of $(|\Psi(p,\frac{\pi}{2},0)|)^2$ and $(|\Psi(p,\frac{\pi}{2},\frac{\pi}{2})|)^2$. Furthermore, relative to the reference experiment, 50% of the photons reach the detection screen.

$$\int_{-\infty}^{\infty} \left(|\Psi\left(p,\frac{\pi}{2},0\right)|\right)^2 dp \text{ float }, 3 \rightarrow 0.500$$

$$\int_{-\infty}^{\infty} \left(\left| \Psi\left(p, \frac{\pi}{2}, \frac{\pi}{2}\right) \right| \right)^2 dp \text{ float }, 3 \rightarrow 0.500$$

In the absence of the third polarizer, there is also no diffraction pattern but 100% of the photons reach the detection screen.

$[\theta = \frac{\pi}{2}, \phi = \frac{\pi}{4}]$ and $[\theta = \frac{\pi}{2}, \phi = -\frac{\pi}{4}]$

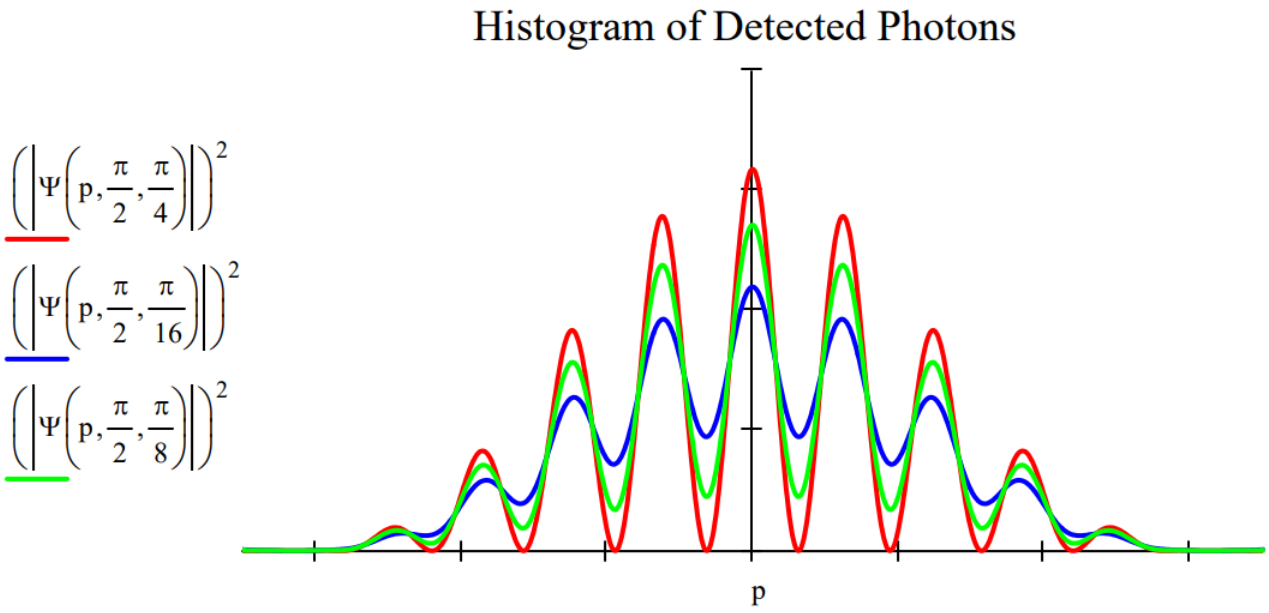
The which-way information provided by the crossed polarizers at the slit screen is erased by diagonally and anti-diagonally oriented polarizers in front of the detection screen. This is shown by the plots of $(|\Psi(p, \frac{\pi}{2}, \frac{\pi}{4})|)^2$ and $(|\Psi(p, \frac{\pi}{2}, -\frac{\pi}{4})|)^2$. The reason the which-way information has been erased is that vertically and horizontally polarized photons emerging from slits 1 and 2 both have a 50% chance of passing the diagonally or anti-diagonally oriented third polarizer. Thus, it is impossible to determine the origin of a photon that passes the third polarizer and the interference fringes are restored. Again, for this experiment 50% of the photons reach the detection screen.

$$\int_{-\infty}^{\infty} \left(\left| \Psi\left(p, \frac{\pi}{2}, \frac{\pi}{4}\right) \right| \right)^2 dp \text{ float }, 3 \rightarrow 0.500$$

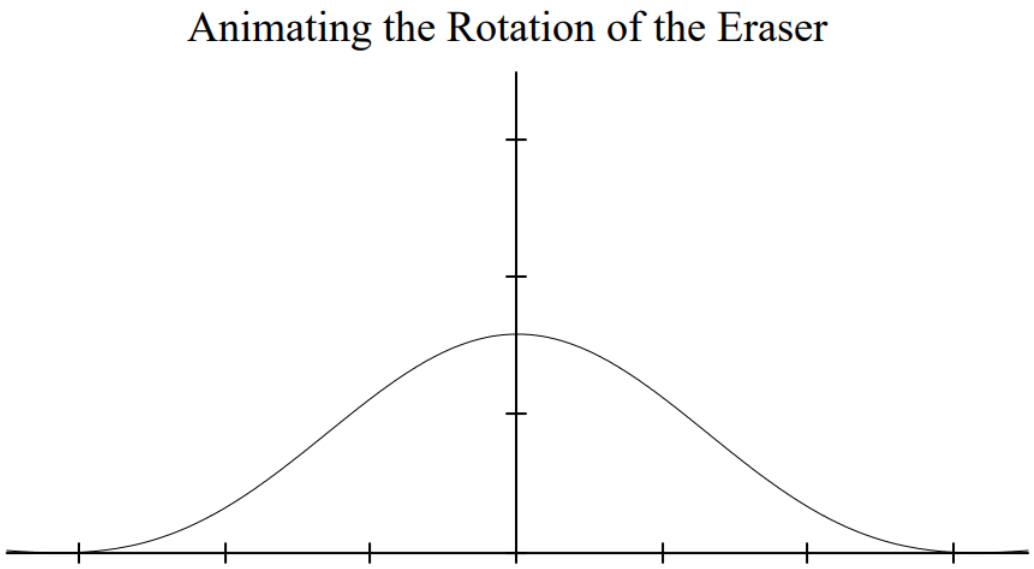
$$\int_{-\infty}^{\infty} \left(\left| \Psi\left(p, \frac{\pi}{2}, -\frac{\pi}{4}\right) \right| \right)^2 dp \text{ float }, 3 \rightarrow 0.500$$

The shift in the interference fringes calculated for $(|\Psi(p, \frac{\pi}{2}, \frac{\pi}{4})|)^2$ and $(|\Psi(p, \frac{\pi}{2}, -\frac{\pi}{4})|)^2$ is observed in the Kwiat/Hillmer experiment.

The visibility of the restored fringes is maximized for $\phi = \pm\frac{\pi}{4}$. As the figure belows shows the visibility is reduced for other values of ϕ.



It is possible to animate the rotation of the polarizer in front of the detection screen, the eraser. From Tools select Animation and use the following setting: **From: 0 To: 120 At: 5 Frames/Sec**.



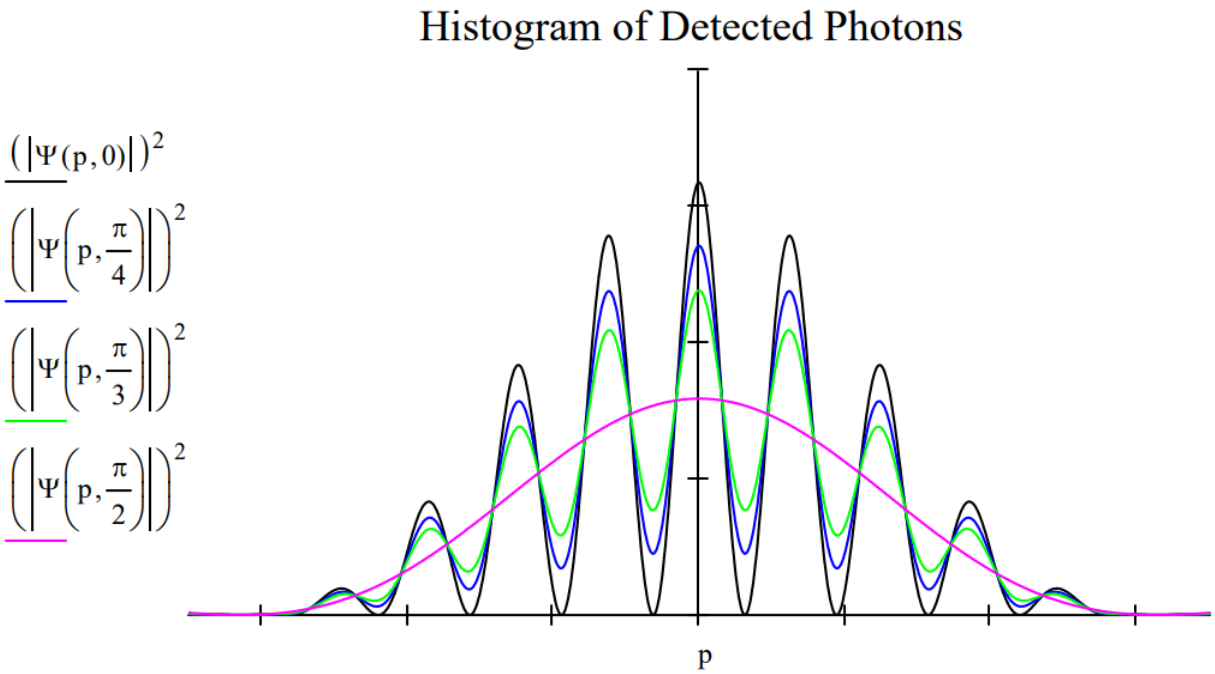
Explicit Vector Approach

In what follows an explicit vector approach to the analysis above is provided.

$$\frac{1}{\sqrt{2}}\left[|x_1\rangle\,|v\rangle+|x_2\rangle|\theta\rangle\right]=\frac{1}{\sqrt{2}}\left[|x_1\rangle\begin{pmatrix}1\\0\end{pmatrix}+|x_2\rangle\begin{pmatrix}\cos(\theta)\\\sin(\theta)\end{pmatrix}\right]\xrightarrow{\langle p|}\frac{1}{\sqrt{2}}\begin{pmatrix}\langle p|x_1\rangle+\cos(\theta)\,\langle p|x_2\rangle\\\sin(\theta)\,\langle p|x_2\rangle\end{pmatrix}$$

Assuming finite slit widths, the <p | x> amplitudes become integrals as outlined above. The appropriate Mathcad expression and its graphical display is shown below.

$$\Psi(\mathrm{p},\theta):=\frac{1}{2\cdot\sqrt{\pi}}\begin{pmatrix}\int_{x_1-\frac{\delta}{2}}^{x_1+\frac{\delta}{2}}\exp(-i\cdot p\cdot x)\cdot\frac{1}{\sqrt{\delta}}dx+\cos(\theta)\cdot\int_{x_2-\frac{\delta}{2}}^{x_2+\frac{\delta}{2}}\exp(-i\cdot p\cdot x)\cdot\frac{1}{\sqrt{\delta}}dx\\\sin(\theta)\cdot\int_{x_2-\frac{\delta}{2}}^{x_2+\frac{\delta}{2}}\exp(-i\cdot p\cdot x)\cdot\frac{1}{\sqrt{\delta}}dx\end{pmatrix}$$



Next $\Psi(\mathrm{p},\theta)$ is projected onto the eraser polarizer oriented at an angle ϕ and the probability distributions for several combinations of θ and ϕ are displayed.

$$\Psi(p,\theta,\phi) = (\cos(\phi) \quad \sin(\phi)) \frac{1}{\sqrt{2}} \begin{pmatrix} \langle p|x_1\rangle + \cos(\theta)\langle p|x_2\rangle \\ \sin(\theta)\langle p|x_2\rangle \end{pmatrix}$$

$$\Psi(\mathrm{p},\theta,\phi) := (\cos(\phi) \quad \sin(\phi)) \cdot \Psi(\mathrm{p},\theta)$$

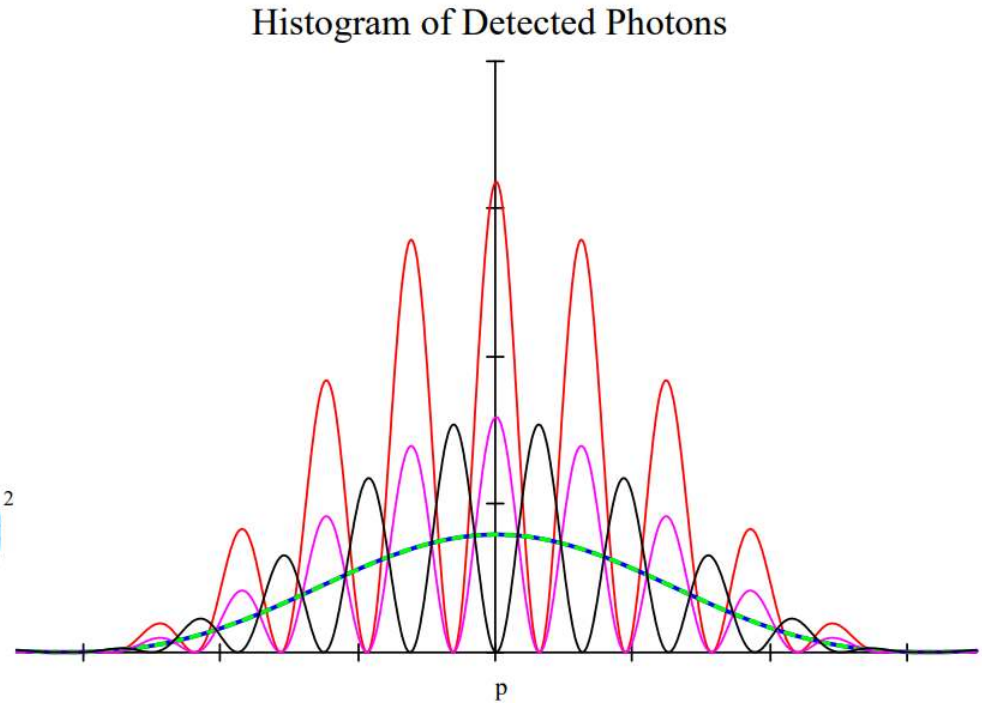
$$\left(\left|\Psi(\mathrm{p},0,0)\right|\right)^2$$

$$\left(\left|\Psi\left(\mathrm{p},\frac{\pi}{2},0\right)\right|\right)^2$$

$$\left(\left|\Psi\left(\mathrm{p},\frac{\pi}{2},\frac{\pi}{2}\right)\right|\right)^2$$

$$\left(\left|\Psi\left(\mathrm{p},\frac{\pi}{2},\frac{\pi}{4}\right)\right|\right)^2$$

$$\left(\left|\Psi\left(\mathrm{p},\frac{\pi}{2},\frac{-\pi}{4}\right)\right|\right)^2$$

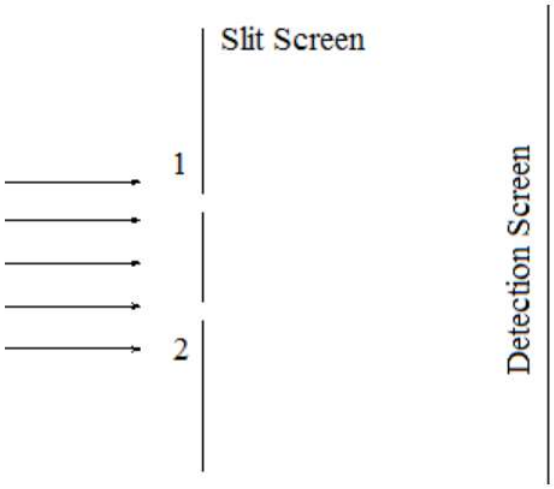


Play Animation for Rotating Eraser

This page titled 1.43: Which Way Did It Go? - The Quantum Eraser is shared under a CC BY 4.0 license and was authored, remixed, and/or curated by Frank Rioux via source content that was edited to the style and standards of the LibreTexts platform.

1.44: Which Path Information and the Quantum Eraser

This tutorial examines the **real** reason which-way information destroys the double-slit diffraction pattern and how the so-called "quantum eraser" restores it. The traditional double-slit experiment is presented schematically below.



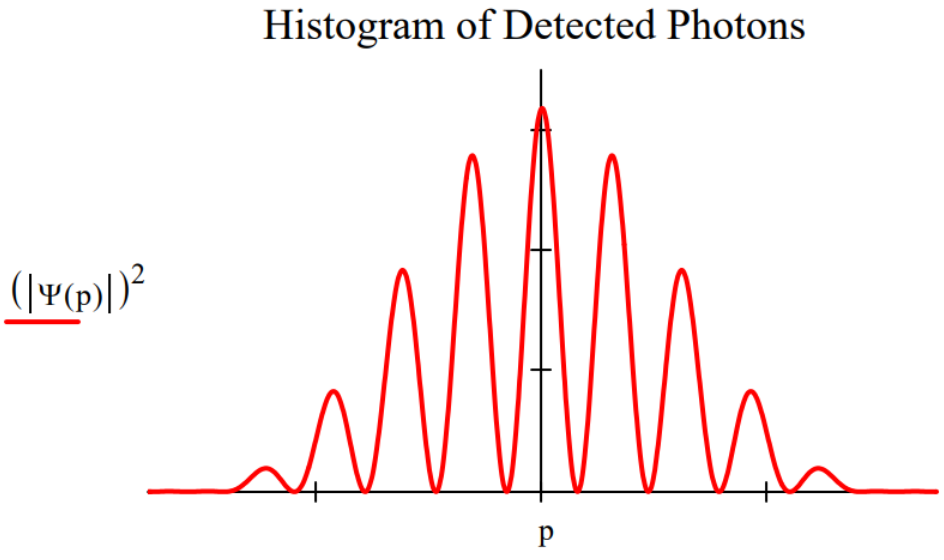
The wave function for a photon illuminating the slit screen is written as a superposition of the photon being present at both slits simultaneously.

$$|\Psi\rangle = \frac{1}{\sqrt{2}}\left[|x_1\rangle + |x_2\rangle\right]$$

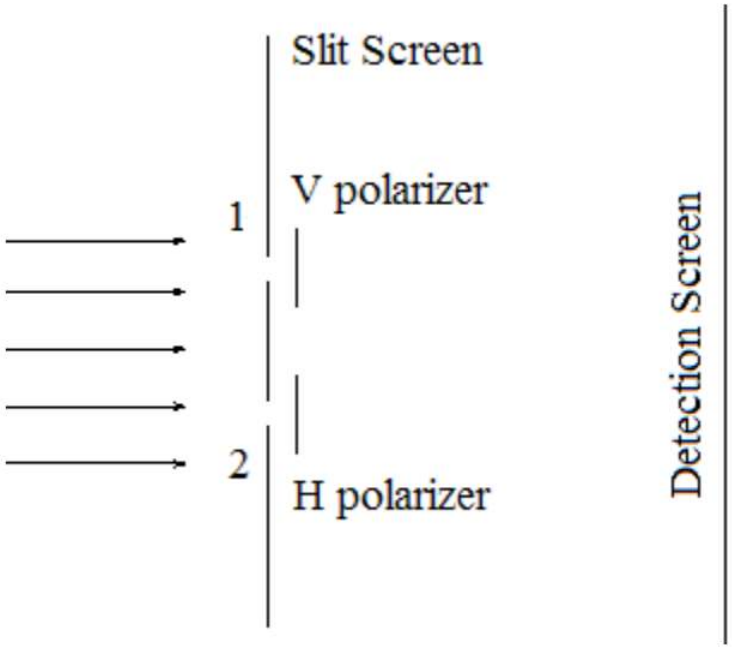
The diffraction pattern is calculated by projecting this superposition into momentum space. This is a Fourier transform for which the mathematical details can be found in the Appendix.

$$\Psi(p) = \langle p|\Psi\rangle = \frac{1}{\sqrt{2}}\left[\langle p|x_1\rangle + \langle p|x_2\rangle\right]$$

The well-known double-slit diffraction pattern is displayed below.



When polarization markers are attached to the slits we have the following schematic of the double-slit experiment with so-called which-way information.



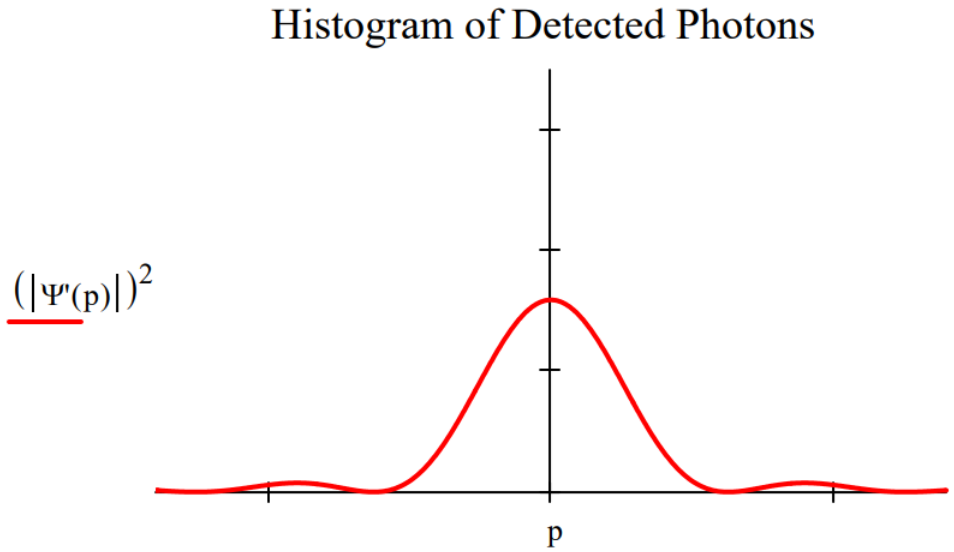
According to the Encyclopedia Britannica, Fresnel and Arago "using an apparatus based on Young's [double-slit] experiment" observed that "two beams polarized in mutually perpendicular planes never yield fringes." We now look at the quantum mechanical explanation of this phenomena. Fresnel and Arago, working during the 19th Century, provided a valid classical explanation.

The coordinate and momentum wave functions now become,

$$|\Psi'\rangle = \frac{1}{\sqrt{2}}\left[|x_1\rangle\,|V\rangle + |x_2\rangle|H\rangle\right] \quad \text{where} \quad |\mathrm{V}\rangle = \begin{pmatrix} 1 \\ 0 \end{pmatrix} \quad |\mathrm{H}\rangle = \begin{pmatrix} 0 \\ 1 \end{pmatrix}$$

$$\Psi'(p) = \langle p|\Psi'\rangle = \frac{1}{\sqrt{2}}\left[\langle p|x_1\rangle\,|V\rangle + \langle p|x_2\rangle\,|H\rangle\right]$$

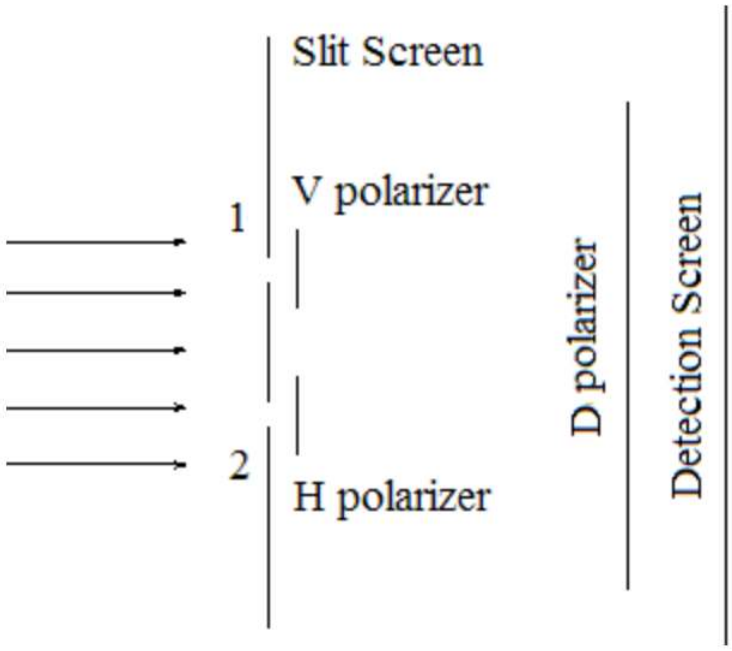
This leads to the following momentum distribution at the detection screen. The highly visible interference fringes have disappeared leaving a single-slit diffraction pattern, but the areas of the two histograms are the same. This is demonstrated later.



The usual explanation for this effect is that it is now possible to know which slit the photons went through, and that such knowledge destroys the interference fringes because the photons are no longer in a superposition of passing through both slits, but rather a mixture of passing through one slit or the other.

However, a more reasonable explanation is that the tags are orthogonal polarization states, and because of this the interference (cross) terms in the momentum distribution, $|\Psi'(\mathrm{p})|^2$, vanish leaving a pattern at the detection screen which is the sum of two single-slit diffraction patterns, one from the upper slit and the other from the lower slit.

That this is a reasonable analysis is confirmed when the so-called quantum eraser, a diagonal polarizer, is placed before the detection screen as diagramed below.



Projection of Ψ' (p) onto $\langle D|$ accounts for the action of the diagonal polarizer, yielding the following wave function after the diagonal polarizer.

$$|\Psi''\rangle = \langle D|\Psi'\rangle = \frac{1}{\sqrt{2}}\left[|x_1\rangle\langle D|V\rangle + |x_2\rangle\langle D|H\rangle\right] = \frac{1}{2}\left[|x_1\rangle + |x_2\rangle\right] \quad \text{where} \quad |D\rangle = \frac{1}{\sqrt{2}}\begin{pmatrix}1\\1\end{pmatrix}$$

The Fourier transform of $|\Psi''\rangle$ yields the momentum wave function and ultimately the momentum distribution function which is the diffraction pattern.

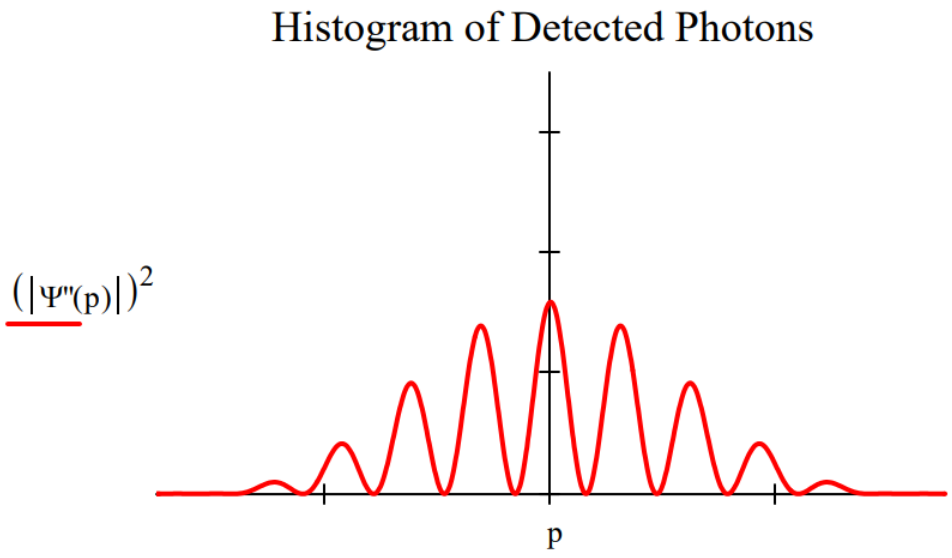
$$\Psi''(p) = \left\langle p|\Psi''\right\rangle = \frac{1}{2}\left[\langle p|x_1\rangle + \langle p|x_2\rangle\right]$$

The diagonal polarizer is called a quantum eraser because it appears to erase the which-path information provided by the H/V polarizers. However, it is clear from this analysis that the diagonal polarizer doesn't actually erase, it passes the diagonal component of $|\Psi''\rangle$ which then shows an attenuated (by half) version of the original diffraction pattern produced by $|\Psi\rangle$. If which-path erasure was occurring the integral on the right would equal 1.0.

$$\int_{-\infty}^{\infty}(|\Psi(\mathrm{p})|)^2 \mathrm{dp}\ \text{float}\ ,2 \rightarrow 1.0$$

$$\int_{-\infty}^{\infty}(|\Psi''(\mathrm{p})|)^2\, \mathrm{d}p\ \text{float}\ ,2 \rightarrow 1.0$$

$$\int_{-\infty}^{\infty}(|\Psi''(\mathrm{p})|)^2 \mathrm{dp}\ \text{float}\ ,2 \rightarrow 0.50$$



Appendix

For infinitesimally thin slits the momentum-space wave function is,

$$\Psi(p) = \langle p|\Psi\rangle = \frac{1}{\sqrt{2}}\left[\langle p|x_1\rangle + \langle p|x_2\rangle\right] = \frac{1}{\sqrt{2}}\left[\frac{1}{\sqrt{2\pi}}\exp\left(-ipx_1\right) + \frac{1}{\sqrt{2\pi}}\exp\left(-ipx_2\right)\right]$$

Assuming a slit width δ the calculations of Ψ(p), Ψ'(p) and Ψ''(p) are carried out as follows:

Position of first slit: $x_1 \equiv 0$	Position of second slit: $x_2 \equiv 1$	Slit width: $\delta \equiv 0.2$

$$\Psi(p) \equiv \frac{\int_{x_1-\frac{\delta}{2}}^{x_1+\frac{\delta}{2}} \frac{1}{\sqrt{2\cdot\pi}} \cdot \exp(-i\cdot p\cdot x)\cdot\frac{1}{\sqrt{\delta}}dx + \int_{x_2-\frac{\delta}{2}}^{x_2+\frac{\delta}{2}} \frac{1}{\sqrt{2\cdot\pi}} \cdot \exp(-i\cdot p\cdot x)\cdot\frac{1}{\sqrt{\delta}}dx}{\sqrt{2}}$$

$$\Psi'(p) \equiv \frac{\int_{x_1-\frac{\delta}{2}}^{x_1+\frac{\delta}{2}} \frac{1}{\sqrt{2\cdot\pi}} \cdot \exp(-i\cdot p\cdot x)\cdot\frac{1}{\sqrt{\delta}}dx\cdot\begin{pmatrix}1\\0\end{pmatrix} + \int_{x_2-\frac{\delta}{2}}^{x_2+\frac{\delta}{2}} \frac{1}{\sqrt{2\cdot\pi}} \cdot \exp(-i\cdot p\cdot x)\cdot\frac{1}{\sqrt{\delta}}dx\cdot\begin{pmatrix}0\\1\end{pmatrix}}{\sqrt{2}}$$

$$\equiv \frac{\Psi'(p)}{\frac{1}{\sqrt{2}}\cdot\begin{pmatrix}1\\1\end{pmatrix}^T\cdot\left[\int_{x_1-\frac{\delta}{2}}^{x_1+\frac{\delta}{2}} \frac{1}{\sqrt{2\cdot\pi}} \cdot \exp(-i\cdot p\cdot x)\cdot\frac{1}{\sqrt{\delta}}dx\cdot\begin{pmatrix}1\\0\end{pmatrix} + \int_{x_2-\frac{\delta}{2}}^{x_2+\frac{\delta}{2}} \frac{1}{\sqrt{2\cdot\pi}} \cdot \exp(-i\cdot p\cdot x)\cdot\frac{1}{\sqrt{\delta}}dx\cdot\begin{pmatrix}0\\1\end{pmatrix}\right]}{\sqrt{2}}$$

This page titled 1.44: Which Path Information and the Quantum Eraser is shared under a CC BY 4.0 license and was authored, remixed, and/or curated by Frank Rioux via source content that was edited to the style and standards of the LibreTexts platform.

1.45: Terse Analysis of Triple-slit Diffraction with a Quantum Eraser

Slit positions, slit width and the wavefunction at the slit screen which is a superposition of the photon being simultaneously present at all three slits.

$$x_1 := -\frac{1}{2} \quad x_2 := 0 \quad x_3 := \frac{1}{2} \quad \delta := 0.1$$

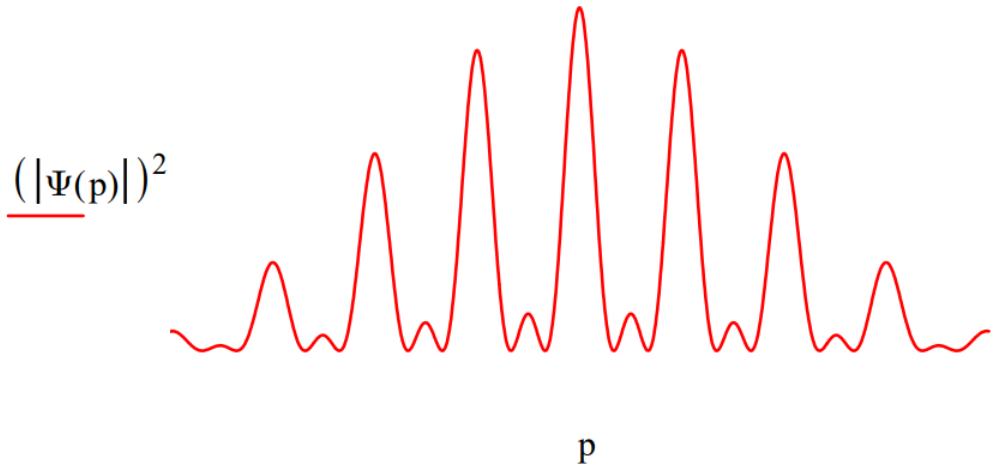
$$|\Psi\rangle = \frac{1}{\sqrt{3}}\left[|x_1\rangle + |x_2\rangle + |x_3\rangle\right]$$

Calculate the diffraction pattern by a Fourier transform of the spatial wavefunction into momentum space.

$$\langle p|\Psi\rangle = \frac{1}{\sqrt{3}}\left[\langle p|x_1\rangle + \langle p|x_2\rangle + \langle p|x_3\rangle\right]$$

$$\Psi(p) := \int_{x_1-\frac{\delta}{2}}^{x_1+\frac{\delta}{2}} \frac{1}{\sqrt{2\cdot\pi}} \cdot \exp(-i\cdot p\cdot x)\cdot\frac{1}{\sqrt{\delta}}dx + \int_{x_2-\frac{\delta}{2}}^{x_2+\frac{\delta}{2}} \frac{1}{\sqrt{2\cdot\pi}} \cdot \exp(-i\cdot p\cdot x)\cdot\frac{1}{\sqrt{\delta}}dx + \int_{x_3-\frac{\delta}{2}}^{x_3+\frac{\delta}{2}} \frac{1}{\sqrt{2\cdot\pi}} \cdot \exp(-i\cdot p\cdot x)\cdot\frac{1}{\sqrt{\delta}}dx$$

Display the momentum distribution function which is the diffraction pattern.



Tag the slits with orthogonal states.

$$\langle p|\Psi'\rangle = \frac{1}{\sqrt{3}}\left[\langle p|x_1\rangle\,|\uparrow\rangle + \langle p|x_2\rangle\,|\rightarrow\rangle + \langle p|x_3\rangle\,|\downarrow\rangle\right]$$

Recalculate the momentum distribution.

$$\Psi'(p) := \int_{x_1-\frac{\delta}{2}}^{x_1+\frac{\delta}{2}} \frac{1}{\sqrt{2\cdot\pi}} \cdot \exp(-i\cdot p\cdot x)\cdot\frac{1}{\sqrt{\delta}}dx \cdot \begin{pmatrix}1\\0\\0\end{pmatrix} + \int_{x_2-\frac{\delta}{2}}^{x_2+\frac{\delta}{2}} \frac{1}{\sqrt{2\cdot\pi}} \cdot \exp(-i\cdot p\cdot x)\cdot\frac{1}{\sqrt{\delta}}dx \cdot \begin{pmatrix}0\\1\\0\end{pmatrix} + \int_{x_3-\frac{\delta}{2}}^{x_3+\frac{\delta}{2}} \frac{1}{\sqrt{2\cdot\pi}} \cdot \exp(-i\cdot p\cdot x)\cdot\frac{1}{\sqrt{\delta}}dx \cdot \begin{pmatrix}0\\0\\1\end{pmatrix}$$

Display the momentum distribution at the detection screen showing that the diffraction pattern has disappeared. The orthogonallity of the tags destroys the cross-terms in the momentum distribution, \left|\Psi^{\prime}(\mathrm{p})\right|^{2}, which give rise to the interference effects shown in the original diffraction pattern.

$$\left(\left|\Psi'(p)\right|\right)^2$$



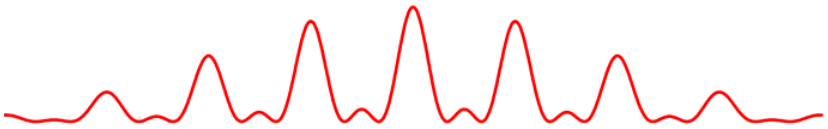
p

Insert an "eraser" after the slit screen and before the detection screen.

$$\Psi''(p) := \frac{1}{\sqrt{3}} \cdot \begin{pmatrix} 1 \\ 1 \\ 1 \end{pmatrix}^T \cdot \Psi'(p)$$

The diffraction pattern is restored but attenuated because the so-called "eraser" filters out the orthogonal tags restoring the interference terms.

$$\left(\left|\Psi''(p)\right|\right)^2$$



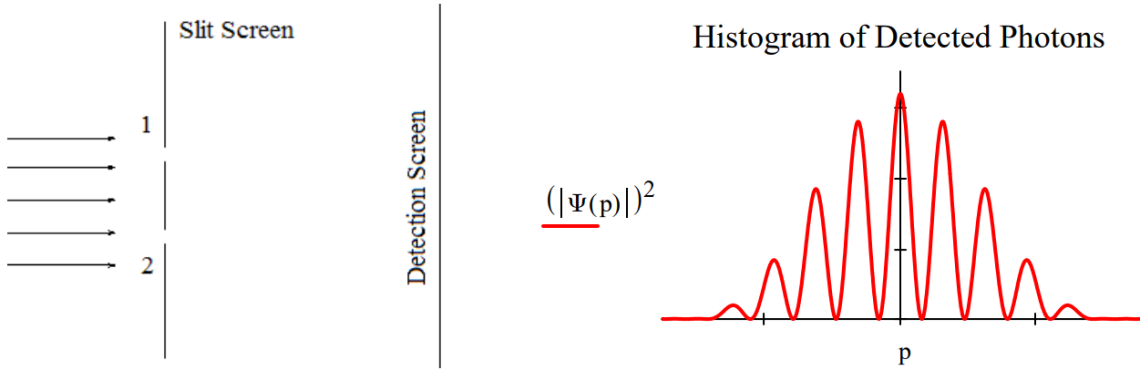
p

This page titled 1.45: Terse Analysis of Triple-slit Diffraction with a Quantum Eraser is shared under a CC BY 4.0 license and was authored, remixed, and/or curated by Frank Rioux via source content that was edited to the style and standards of the LibreTexts platform.

1.46: Which Path Information and the Quantum Eraser (Brief)

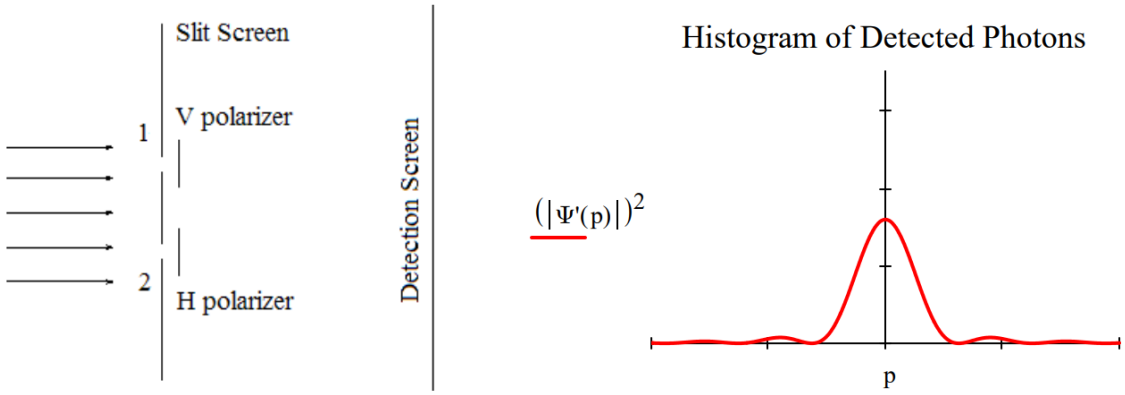
This tutorial examines the **real** reason which-path information destroys the double-slit diffraction pattern and how the so-called "quantum eraser" restores it. The wave function for a photon illuminating the slit screen is written as a superposition of the photon being present at both slits simultaneously. The double-slit diffraction pattern is calculated by projecting this superposition into momentum space. This is a Fourier transform for which the mathematical details can be found in the Appendix.

$$|\Psi\rangle = \frac{1}{\sqrt{2}}\left[|x_1\rangle + |x_2\rangle\right] \qquad \Psi(p) = \langle p|\Psi\rangle = \frac{1}{\sqrt{2}}\left[\langle p|x_1\rangle + \langle p|x_2\rangle\right]$$



Attaching polarizers to the slits creates an entangled superposition of the photon being at slit 1 with vertical polarization and at slit 2 with horizontal polarization. This leads to the following momentum distribution at the detection screen. The interference fringes have disappeared leaving a single-slit diffraction pattern.

$$|\Psi'\rangle = \frac{1}{\sqrt{2}}\left[|x_1\rangle\,|V\rangle + |x_2\rangle|H\rangle\right] \qquad \Psi'(p) = \langle p|\Psi'\rangle = \frac{1}{\sqrt{2}}\left[\langle p|x_1\rangle\,|V\rangle + \langle p|x_2\rangle\,|H\rangle\right]$$

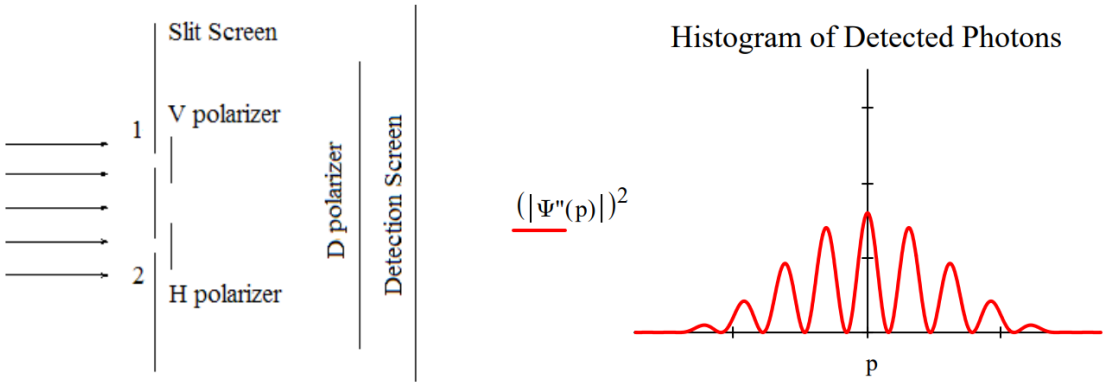


The usual explanation for this effect is that it is now possible to know which slit the photons went through, and that such knowledge destroys the interference fringes because the photons are no longer in a superposition of passing through both slits, but rather a mixture of passing through one slit or the other.

However, a better explanation is that the superposition persists with orthogonal polarization tags, and because of this the interference (cross) terms in the momentum distribution, $|\Psi'(p)|^2$, vanish leaving a pattern at the detection screen which is the sum of two single-slit diffraction patterns, one from the upper slit and the other from the lower slit.

That this is a reasonable interpretation is confirmed when a so-called quantum eraser, a polarizer (D) rotated clockwise by 45 degrees relative to the vertical, is placed before the detection screen.

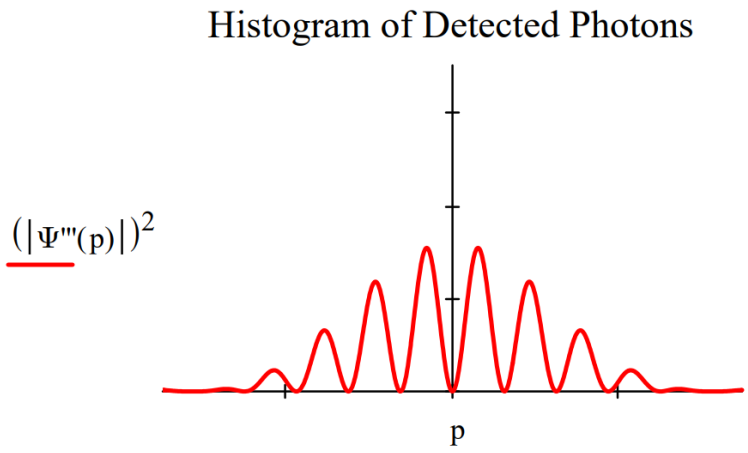
$$\Psi''(p) = \langle D|\Psi'(p)\rangle = \frac{1}{\sqrt{2}}\left[\langle p|x_1\rangle\,\langle D|V\rangle + \langle p|x_2\rangle\,\langle D|H\rangle\right] = \frac{1}{2}\left[\langle p|x_1\rangle + \langle p|x_2\rangle\right]$$



The diagonal polarizer is called a quantum eraser because it appears to restore the interference pattern lost because of the which-path information provided by the V/H polarizers. However, it is clear from this analysis that the diagonal polarizer doesn't actually erase, it simply passes the diagonal component of $|\Psi'\rangle$ which then shows an attenuated (by half) version of the original interference pattern produced by $|\Psi\rangle$.

Placing an anti-diagonal polarizer (rotated counterclockwise by 45 degrees relative to the vertical) before the detection screen causes a 180 degree phase shift in the restored interference pattern.

$$\Psi''(p) = \langle A|\Psi'(p)\rangle = \frac{1}{\sqrt{2}}\left[\langle p|x_1\rangle\langle A|V\rangle + \langle p|x_2\rangle\langle A|H\rangle\right] = \frac{1}{2}\left[\langle p|x_1\rangle - \langle p|x_2\rangle\right]$$



This phase shift is inconsistent with any straightforward explanation based on the concept of erasure of which-path information. Erasure implies removal of which-path information. If which-path information has been removed shouldn't the original interference pattern be restored without a phase shift?

Appendix

The V/H polarization which-path tags and the D/A polarization "erasers" in vector format:

$$|\mathrm{V}\rangle = \begin{pmatrix} 1 \\ 0 \end{pmatrix} |\mathrm{H}\rangle = \begin{pmatrix} 0 \\ 1 \end{pmatrix} \quad |\mathrm{D}\rangle = \frac{1}{\sqrt{2}}\begin{pmatrix} 1 \\ 1 \end{pmatrix} \quad |\mathrm{A}\rangle$$
$$= \frac{1}{\sqrt{2}}\begin{pmatrix} 1 \\ -1 \end{pmatrix} \langle \mathrm{D}|\mathrm{V}\rangle = \langle \mathrm{D}|\mathrm{H}\rangle = \langle \mathrm{A}|\mathrm{V}\rangle = \frac{1}{\sqrt{2}} \qquad \langle \mathrm{A}|\mathrm{H}\rangle = -\frac{1}{\sqrt{2}}$$

For infinitesimally thin slits the momentum-space wave function is,

$$\Psi(p) = \langle p|\Psi\rangle = \frac{1}{\sqrt{2}}\left[\langle p|x_1\rangle + \langle p|x_2\rangle\right] = \frac{1}{\sqrt{2}}\left[\frac{1}{\sqrt{2\pi}}\exp\left(-ipx_1\right) + \frac{1}{\sqrt{2\pi}}\exp\left(-ipx_2\right)\right]$$

Assuming a slit width δ the calculations of $\Psi(p)$, $\Psi'(p)$, $\Psi''(p)$ and $\Psi'''(p)$ are carried out as follows:

Position of first slit: $x_1 \equiv 0$	Position of second slit: $x_2 \equiv 1$	Slit width: $\delta \equiv 0.2$

$$\Psi(p) \equiv \frac{1}{\sqrt{2}} \cdot \left(\int_{x_1-\frac{\delta}{2}}^{x_1+\frac{\delta}{2}} \frac{1}{\sqrt{2 \cdot \pi}} \cdot \exp(-i \cdot p \cdot x) \cdot \frac{1}{\sqrt{\delta}} dx + \int_{x_2-\frac{\delta}{2}}^{x_2+\frac{\delta}{2}} \frac{1}{\sqrt{2 \cdot \pi}} \cdot \exp(-i \cdot p \cdot x) \cdot \frac{1}{\sqrt{\delta}} dx \right)$$

For $\Psi'(p)$ the V/H polarization which-path tags are added to the two terms of $\Psi(p)$

$$\Psi'(p) \equiv \frac{1}{\sqrt{2}} \cdot \left[\int_{x_1-\frac{\delta}{2}}^{x_1+\frac{\delta}{2}} \frac{1}{\sqrt{2 \cdot \pi}} \cdot \exp(-i \cdot p \cdot x) \cdot \frac{1}{\sqrt{\delta}} dx \cdot \begin{pmatrix} 1 \\ 0 \end{pmatrix} + \int_{x_2-\frac{\delta}{2}}^{x_2+\frac{\delta}{2}} \frac{1}{\sqrt{2 \cdot \pi}} \cdot \exp(-i \cdot p \cdot x) \cdot \frac{1}{\sqrt{\delta}} dx \cdot \begin{pmatrix} 0 \\ 1 \end{pmatrix} \right]$$

$\Psi''(p)$ is the projection of $\Psi'(p)$ onto a diagonal polarizer $\langle D|$.

$$\Psi''(p) \equiv \frac{1}{\sqrt{2}} \cdot \begin{pmatrix} 1 \\ 1 \end{pmatrix}^T \cdot \Psi'(p)$$

$\Psi'''(p)$ is the projection of $\Psi'(p)$ onto a diagonal polarizer $\langle A|$.

$$\Psi'''(p) \equiv \frac{1}{\sqrt{2}} \cdot \begin{pmatrix} 1 \\ -1 \end{pmatrix}^T \cdot \Psi'(p)$$

Rewriting $\Psi'(p)$ in terms of $|D\rangle$ and $|A\rangle$ clearly shows the origin of the phase difference between the $(|\Psi''(p)|)^2$ and $(|\Psi'''(p)|)^2$ interference patterns.

$$\Psi'(p) = \langle p|\Psi'\rangle = \frac{1}{2} \left[\left(\langle p|x_1\rangle + \langle p|x_2\rangle \right) |D\rangle + \left(\langle p|x_1\rangle - \langle p|x_2\rangle \right) |A\rangle \right]$$

This page titled 1.46: Which Path Information and the Quantum Eraser (Brief) is shared under a CC BY 4.0 license and was authored, remixed, and/or curated by Frank Rioux via source content that was edited to the style and standards of the LibreTexts platform.

1.47: Terse Analysis of Triple-slit Diffraction with a Quantum Eraser

Slit positions, slit width and the wavefunction at the slit screen which is a superposition of the photon being simultaneously present at all three slits.

$$x_1 := -\frac{1}{2} \quad x_2 := 0 \quad x_3 := \frac{1}{2} \qquad \delta := 0.1$$

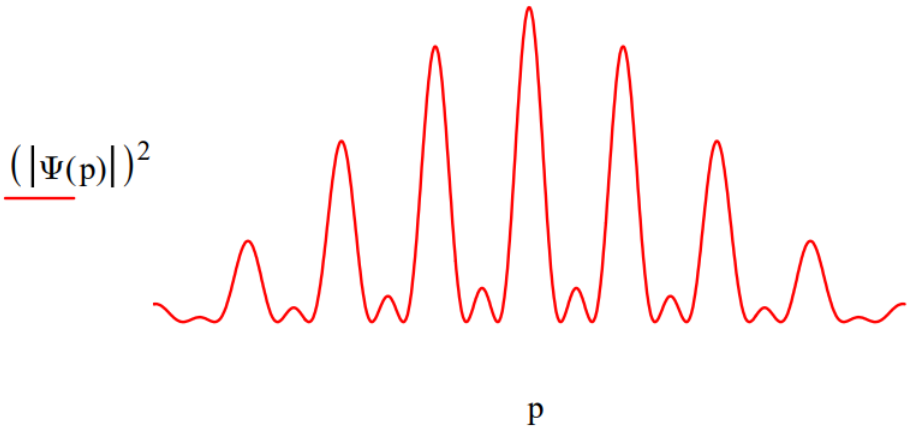
$$|\Psi\rangle = \frac{1}{\sqrt{3}}\left[|x_1\rangle + |x_2\rangle + |x_3\rangle\right]$$

Calculate the diffraction pattern by a Fourier transform of the spatial wavefunction into momentum space.

$$\langle p|\Psi\rangle = \frac{1}{\sqrt{3}}\left[\langle p|x_1\rangle + \langle p|x_2\rangle + \langle p|x_3\rangle\right]$$

$$\Psi(p) = \int_{x_1-\frac{\delta}{2}}^{x_1+\frac{\delta}{2}} \frac{1}{\sqrt{2\cdot\pi}}\cdot\exp(-i\cdot p\cdot x)\cdot\frac{1}{\sqrt{\delta}}dx + \int_{x_2-\frac{\delta}{2}}^{x_2+\frac{\delta}{2}} \frac{1}{\sqrt{2\cdot\pi}}\cdot\exp(-i\cdot p\cdot x)\cdot\frac{1}{\sqrt{\delta}}dx + \int_{x_3-\frac{\delta}{2}}^{x_3+\frac{\delta}{2}} \frac{1}{\sqrt{2\cdot\pi}}\cdot\exp(-i\cdot p\cdot x)\cdot\frac{1}{\sqrt{\delta}}dx$$

Display the momentum distribution function which is the diffraction pattern.



Tag the slits with orthogonal states.

$$\langle p|\Psi'\rangle = \frac{1}{\sqrt{3}}\left[\langle p|x_1\rangle\,|\uparrow\rangle + \langle p|x_2\rangle\,|\rightarrow\rangle + \langle p|x_3\rangle\,|\downarrow\rangle\right]$$

Recalculate the momentum distribution.

$$\Psi'(p) = \int_{x_1-\frac{\delta}{2}}^{x_1+\frac{\delta}{2}} \frac{1}{\sqrt{2\cdot\pi}}\cdot\exp(-i\cdot p\cdot x)\cdot\frac{1}{\sqrt{\delta}}dx\cdot\begin{pmatrix}1\\0\\0\end{pmatrix} + \int_{x_2-\frac{\delta}{2}}^{x_2+\frac{\delta}{2}} \frac{1}{\sqrt{2\cdot\pi}}\cdot\exp(-i\cdot p\cdot x)\cdot\frac{1}{\sqrt{\delta}}dx \cdot\begin{pmatrix}0\\1\\0\end{pmatrix} + \int_{x_3-\frac{\delta}{2}}^{x_3+\frac{\delta}{2}} \frac{1}{\sqrt{2\cdot\pi}}\cdot\exp(-i\cdot p\cdot x)\cdot\frac{1}{\sqrt{\delta}}dx\cdot\begin{pmatrix}0\\0\\1\end{pmatrix}$$

Display the momentum distribution at the detection screen showing that the diffraction pattern has disappeared. The orthogonallity of the tags destroys the cross-terms in the momentum distribution, $|\Psi'(p)|^2$, which give rise to the interference effects shown in the original diffraction pattern.

$$\left(\left|\Psi'(p)\right|\right)^2$$



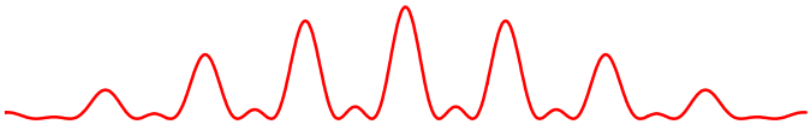
p

Insert an "eraser" after the slit screen and before the detection screen.

$$\Psi''(p) := \frac{1}{\sqrt{3}} \cdot \begin{pmatrix} 1 \\ 1 \\ 1 \end{pmatrix}^T \cdot \Psi'(p)$$

The diffraction pattern is restored but attenuated because the so-called "eraser" filters out the orthogonal tags restoring the interference terms.

$$\left(\left|\Psi''(p)\right|\right)^2$$

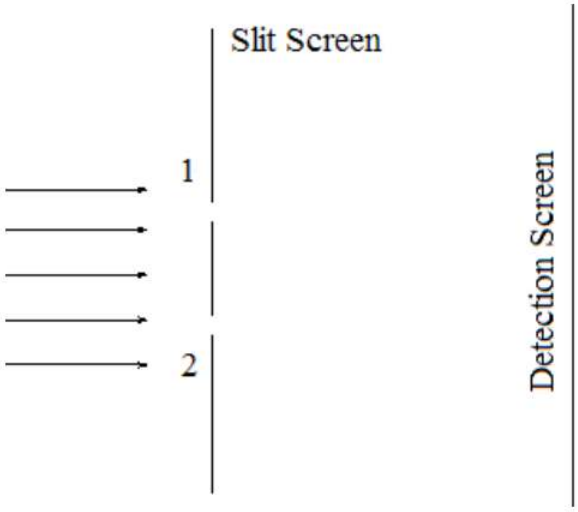


p

This page titled 1.47: Terse Analysis of Triple-slit Diffraction with a Quantum Eraser is shared under a CC BY 4.0 license and was authored, remixed, and/or curated by Frank Rioux via source content that was edited to the style and standards of the LibreTexts platform.

1.48: Which-way Markers and Post-selection in the Double-slit Experiment

This tutorial examines the **real** reason which-way information destroys the double-slit diffraction pattern and how the so-called "quantum eraser" restores it. The double-slit experiment is presented schematically below.



The wave function for a photon illuminating the slit screen is written as a superposition of the photon being present at both slits simultaneously.

$$|\Psi\rangle = \frac{1}{\sqrt{2}}\left[|x_1\rangle + |x_2\rangle\right]$$

Assuming initially infinitesimally thin slits, the diffraction pattern is calculated by projecting this superposition into momentum space.

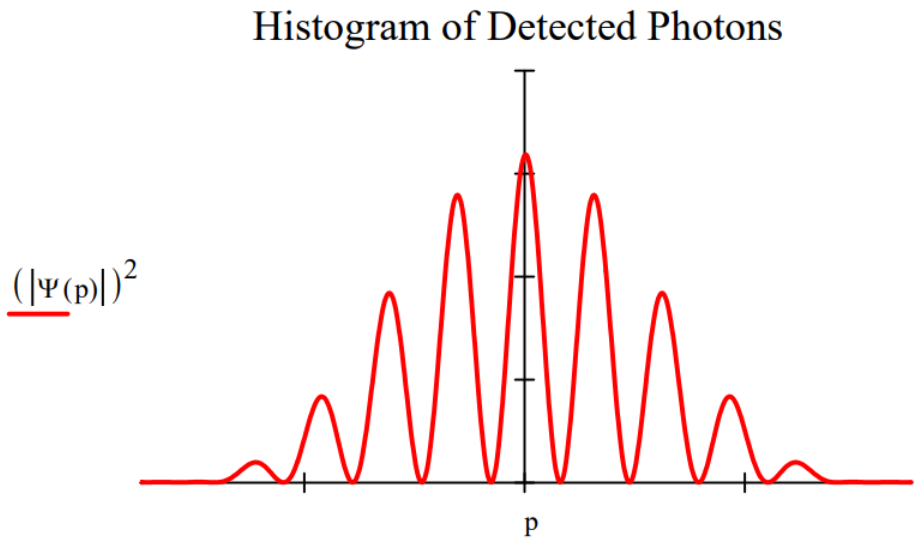
$$\langle p|\Psi\rangle = \frac{1}{\sqrt{2}}\left[\langle p|x_1\rangle + \langle p|x_2\rangle\right] = \frac{1}{\sqrt{2}}\left[\frac{1}{\sqrt{2\pi}}\exp\left(-ipx_1\right) + \frac{1}{\sqrt{2\pi}}\exp\left(-ipx_2\right)\right]$$

Assuming slits of finite width, δ, positioned as indicated below, the momentum wave function becomes,

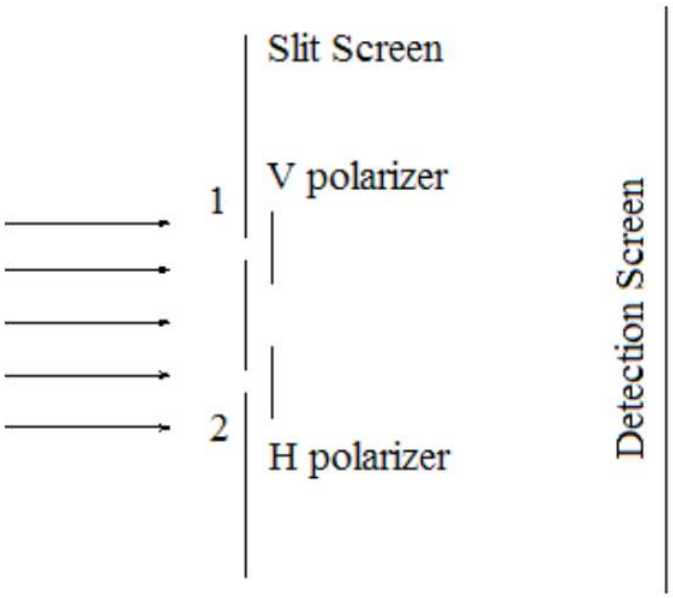
Position of first slit: $x_1 := 0$	Position of second slit: $x_2 := 1$	Slit width: $\delta := 0.2$

$$\Psi(p) := \frac{\int_{x_1-\frac{\delta}{2}}^{x_1+\frac{\delta}{2}} \frac{1}{\sqrt{2\cdot\pi}}\cdot\exp(-i\cdot p\cdot x)\cdot\frac{1}{\sqrt{\delta}}dx + \int_{x_2-\frac{\delta}{2}}^{x_2+\frac{\delta}{2}} \frac{1}{\sqrt{2\cdot\pi}}\cdot\exp(-i\cdot p\cdot x)\cdot\frac{1}{\sqrt{\delta}}dx}{\sqrt{2}}$$

The double-slit diffraction pattern is the momentum distribution function.



When polarization markers are attached to the slits we have the following schematic of the double-slit experiment with which-way information.



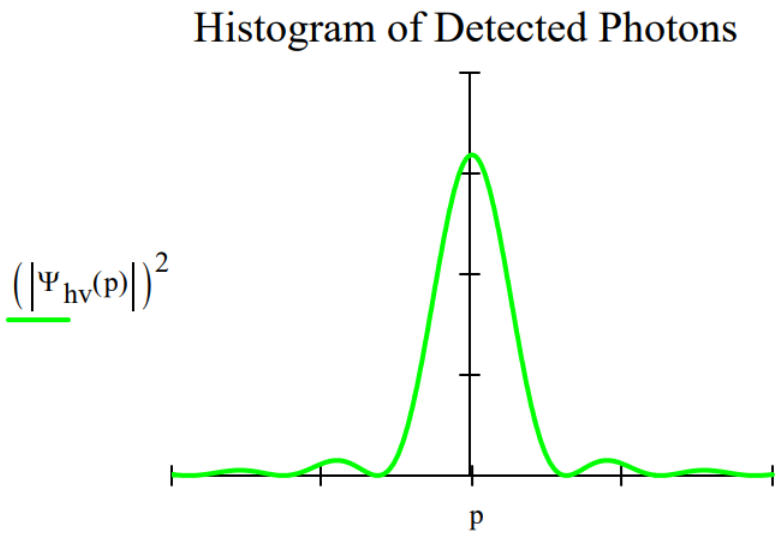
According to the Encyclopedia Britannica, Fresnel and Arago "using an apparatus based on Young's [double-slit] experiment" observed that "two beams polarized in mutually perpendicular planes never yield fringes." We now look at the quantum mechanical explanation of this phenomena. Fresnel and Arago, working during the 19th Century, provided a valid classical explanation.

The coordinate and momentum wave functions now become,

$$|\Psi\rangle = \frac{1}{\sqrt{2}}\left[|x_1\rangle|\mathrm{V}\rangle + |x_2\rangle|H\rangle\right] \quad \text{where } |\mathrm{V}\rangle = \begin{pmatrix} 1 \\ 0 \end{pmatrix} \qquad |\mathrm{H}\rangle = \begin{pmatrix} 0 \\ 1 \end{pmatrix}$$

$$\Psi_{\mathrm{hv}}(\mathrm{p}) := \frac{1}{\sqrt{2}} \int_{\mathrm{x}_1-\frac{\delta}{2}}^{\mathrm{x}_1+\frac{\delta}{2}} \frac{1}{\sqrt{2\cdot\pi}} \exp(-\mathrm{i}\cdot\mathrm{p}\cdot\mathrm{x}) \cdot \frac{1}{\sqrt{\delta}} \mathrm{dx} \cdot \begin{pmatrix} 1 \\ 0 \end{pmatrix}$$
$$+ \frac{1}{\sqrt{2}} \cdot \int_{x_2\frac{\delta}{2}}^{x_2+\frac{\delta}{2}} \frac{1}{\sqrt{2\cdot\pi}} \cdot \exp(-i\cdot p\cdot x) \cdot \frac{1}{\sqrt{\delta}} dx \cdot \begin{pmatrix} 0 \\ 1 \end{pmatrix}$$

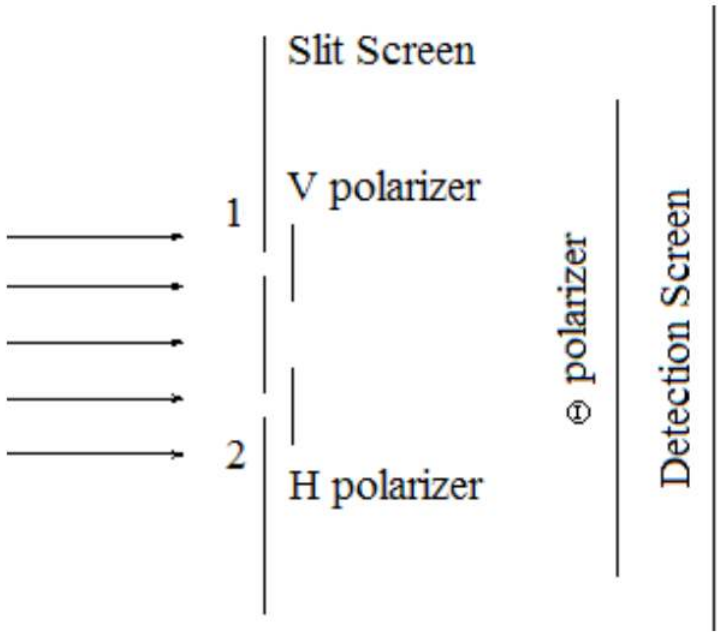
This leads to the following momentum distributions at the detection screen.



The usual explanation for this effect is that it is now possible to know which slit the photons went through, and that such knowledge destroys the interference fringes because the photons are no longer in a superposition of passing through both slits, but rather a mixture of passing through each slit half the time.

However, a more reasonable explanation is that the tags are orthogonal polarization states, and because of this the interference (cross) terms in the momentum distribution, $|\Psi_{hy}(p)|^2$, vanish leaving a pattern at the detection screen which is the sum of two single-slit diffraction patterns, one from the upper slit and the other from the lower slit.

That this is a reasonable analysis is confirmed when the so-called quantum eraser, a θ polarizer, is placed before the detection screen as diagramed below.

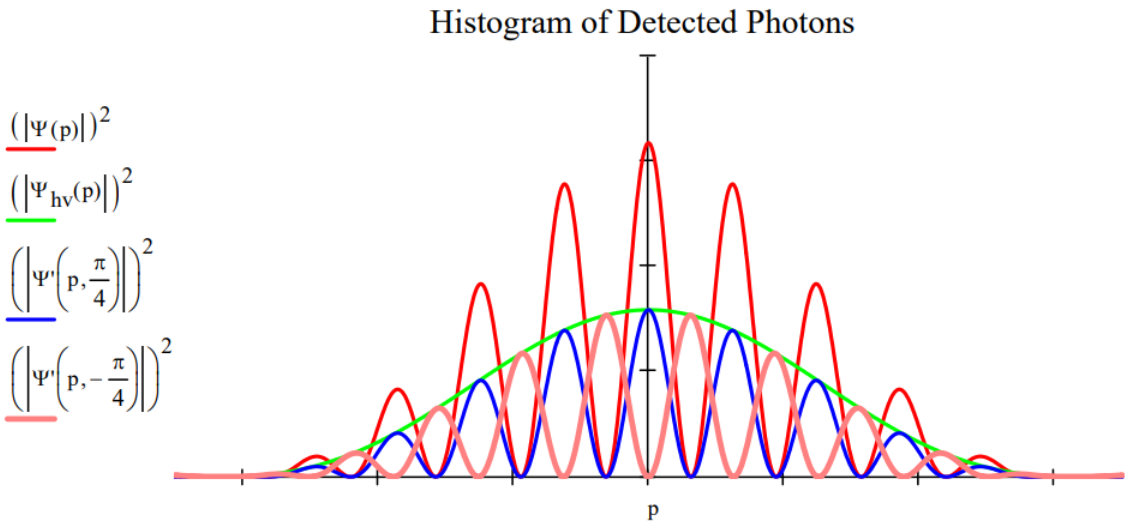


The presence of the θ polarizer is represented mathematically by: $\langle\theta| = (\cos(\theta) \quad \sin(\theta))$

Projection of $\Psi_{hv}(p)$ onto $\langle\theta|$ accounts for the action of the θ polarizer, yielding the momentum wave function after the polarizer.

$$\Psi'(p,\theta) = \begin{pmatrix} \cos(\theta) \\ \sin(\theta) \end{pmatrix}^{T} \cdot \Psi_{hv}(p)$$

If the θ polarizer is oriented at any angle other than 0 or multiples of $\frac{\pi}{2}$, the interference fringes reappear to some degree. As an example the diffraction pattern observed for a angles of $\pm\frac{\pi}{4}$ are shown along with the results from the previous graphs.



A common explanation for the reappearance of the interference fringes is that the $\frac{\pi}{4}$ polarizers have erased the which-way information. A less esoteric explanation is achieved by recognizing that |H > and |V > are even superpositions of |D > (D = diagonal = $\frac{\pi}{4}$) and |A > (A = anti-diagonal = $-\frac{\pi}{4}$), and that the probability that |H > and |V > photons will pass a diagonal polarizer is 0.5. It also easily explains the phase shift that is observed with the anti-diagonal ($-\frac{\pi}{4}$) "eraser."

$$|\mathrm{V}\rangle = \frac{1}{\sqrt{2}}[|\mathrm{D}\rangle + |\mathrm{A}\rangle] = \frac{1}{\sqrt{2}}\left[\frac{1}{\sqrt{2}}\begin{pmatrix}1\\1\end{pmatrix} + \frac{1}{\sqrt{2}}\begin{pmatrix}1\\-1\end{pmatrix}\right]$$

$$|\mathrm{H}\rangle = \frac{1}{\sqrt{2}}[|\mathrm{D}\rangle - |\mathrm{A}\rangle] = \frac{1}{\sqrt{2}}\left[\frac{1}{\sqrt{2}}\begin{pmatrix}1\\1\end{pmatrix} - \frac{1}{\sqrt{2}}\begin{pmatrix}1\\-1\end{pmatrix}\right]$$

This is an example of **post-selection**. After passing the slit screen with its polarization markers (state preparation), but before the detection screen (measurement), a **subset** of photon states is selected by the orientation of the θ polarizer, say |D> or |A>. After these polarizers the photons are in one of the following polarized superpositions.

$$|\Psi\rangle = \frac{1}{2}\left[|x_1\rangle\,|\mathrm{D}\rangle + |x_2\rangle\,|\mathrm{D}\rangle\right] \text{ or } |\Psi\rangle = \frac{1}{2}\left[|x_1\rangle\,|\mathrm{A}\rangle - |x_2\rangle\,|\mathrm{A}\rangle\right]$$

Projecting these states into momentum space assuming finite slit widths yields the reduced diffraction patterns shown in the figure above. The following probability calculations support the arguments presented here.

$$\int_{-\infty}^{\infty} (|\Psi(p)|)^2 dp \text{ float, } 2 \rightarrow 1.0$$

$$\int_{-\infty}^{\infty} (|\Psi_{hv}(p)|)^2 dp \text{ float, } 2 \rightarrow 1.0$$

$$\int_{-\infty}^{\infty} \left(\left|\Psi^n\left(p,\frac{\pi}{4}\right)\right|\right)^2 dp \text{ float, } 2 \rightarrow 0.50$$

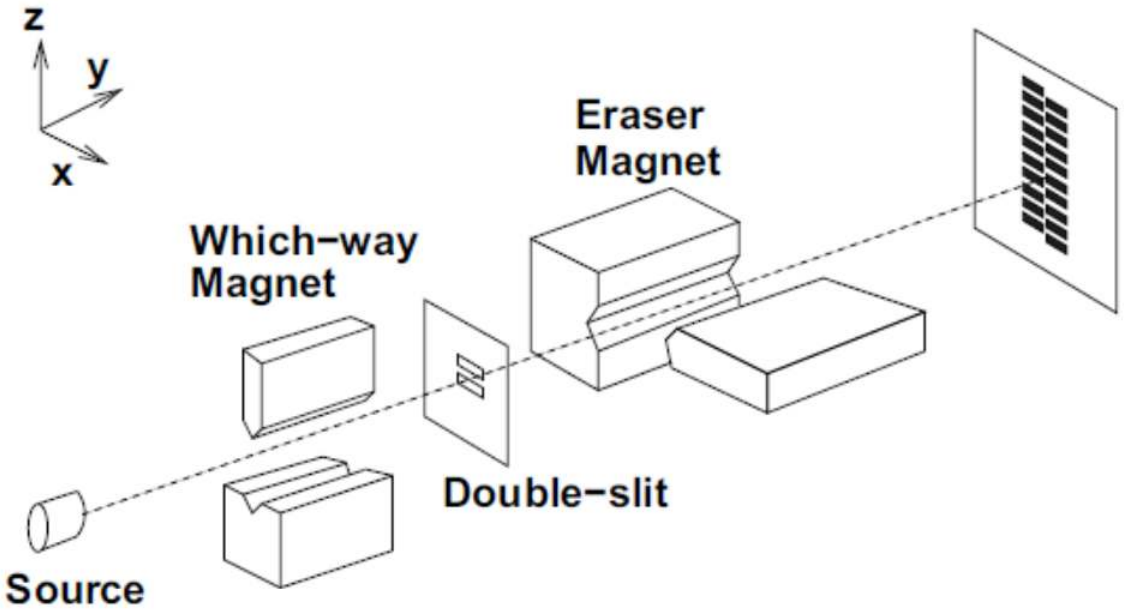
$$\int_{-\infty}^{\infty} \left(\left|\Psi^r\left(p,-\frac{\pi}{4}\right)\right|\right)^2 dp \text{ float, } 2 \rightarrow 0.50$$

If which-path erasure was really occurring the last two integrals would equal 1.0

This page titled 1.48: Which-way Markers and Post-selection in the Double-slit Experiment is shared under a CC BY 4.0 license and was authored, remixed, and/or curated by Frank Rioux via source content that was edited to the style and standards of the LibreTexts platform.

1.49: A Stern-Gerlach Quantum "Eraser"

This tutorial provides a brief mathematical analysis of a proposed quantum eraser experiment involving spin-1/2 particles which is available at arXiv:quant-ph/0501010v2. Please see the two immediately preceding tutorials for another example of the quantum eraser and additional mathematical detail.



The first magnet attaches which-way information such that the spin-1/2 particles leaving the double-slit screen are described by the following entangled wave function,

$$|\Psi\rangle = \frac{1}{\sqrt{2}}\left[|\uparrow_z\rangle\,|z_1\rangle + |\downarrow_z\rangle\,|z_2\rangle\right]$$

where z_1 and z_2 represent the positions of the horizontal slits on the z-axis and the spin eigenstates in the z-direction are given below.

$$\Psi_{\text{zup}} := \begin{pmatrix} 1 \\ 0 \end{pmatrix} \qquad \Psi_{\text{zdown}} = \begin{pmatrix} 0 \\ 1 \end{pmatrix}$$

Recognizing that a diffraction pattern is actually a momentum distribution function, we project Ψ onto momentum space as follows (in atomic units, h = 2π).

$$\langle p|\Psi\rangle = \frac{1}{\sqrt{2}}\left[|\uparrow_z\rangle\,\langle p|z_1\rangle + |\downarrow_z\rangle\,\langle p|z_2\rangle\right] = \frac{1}{\sqrt{2}}\left[|\uparrow_z\rangle\,\frac{\exp\left(-ipz_1\right)}{\sqrt{2\pi}} + |\downarrow_z\rangle\,\frac{\exp\left(-ipz_2\right)}{\sqrt{2\pi}}\right]$$

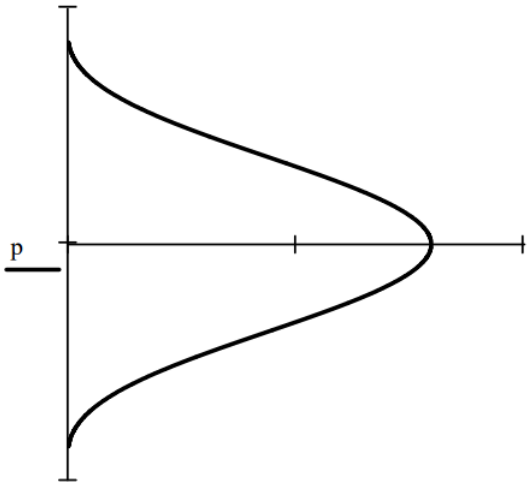
Here the exponential terms are the position eigenfunctions in momentum space for infinetesimally thin slits located at z_1 and z_2. For slits of finite width $< p|\Psi >$ is written as shown below. Again see the previous tutorials in this series for further mathematical detail. The slit positions and slit width chosen are arbitrary.

Slit positions: $z_1 := 1 \qquad z_2 := 2$	Slit width: $\delta := 0.2$

$$\Psi(\mathrm{p}) := \frac{1}{\sqrt{2}} \cdot \left(\Psi_{\text{zup}} \cdot \int_{z_1-\frac{\delta}{2}}^{z_1+\frac{\delta}{2}} \frac{1}{\sqrt{2\cdot\pi}} \cdot \exp(-\mathrm{i}\cdot \mathrm{p}\cdot \mathrm{z}) \cdot \frac{1}{\sqrt{\delta}}\mathrm{dz} + \Psi_{\text{zdown}} \cdot \int_{z_2-\frac{\delta}{2}}^{z_2+\frac{\delta}{2}} \frac{1}{\sqrt{2\cdot\pi}} \cdot \exp(-\mathrm{i}\cdot p\cdot z) \cdot \frac{1}{\sqrt{\delta}}\mathrm{dz}\right)$$

Because of the addition of path information there are no interference fringes associated with this two-slit wave function; the encoded orthogonal z-direction eigenstates destroy the interference cross terms as shown graphically below.

$$p := -30, -29.98 .. 30$$

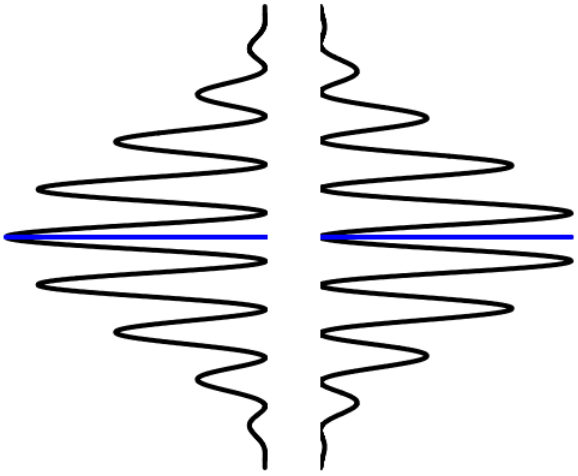


$$\left(\left|\Psi(p)\right|\right)^2$$

The second Stern-Gerlach magnet oriented in the x-direction, according to the conventional interpretation, "erases" the which-way information. This is shown by projecting the state after the first magnet and the slit screen, $\Psi(p)$, onto the x-direction spin eigenstates.

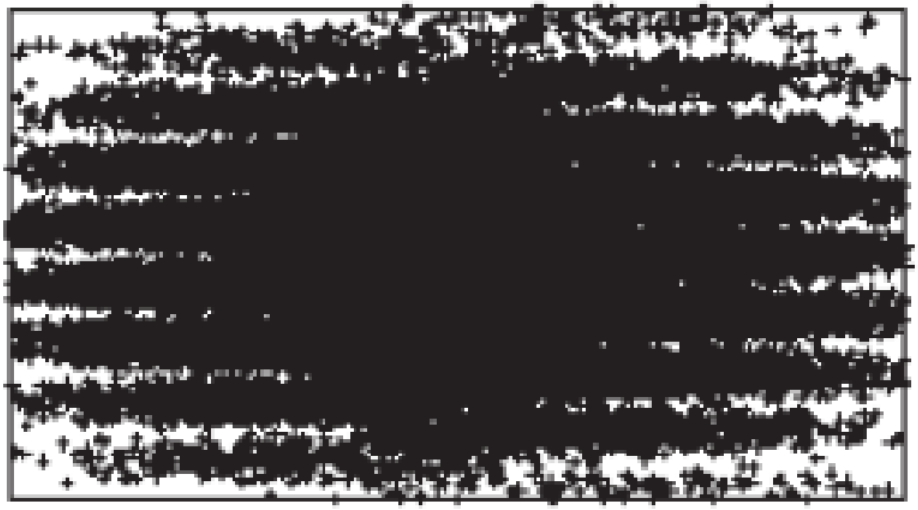
$$\Psi_{xup} = \frac{1}{\sqrt{2}} \cdot (1 \quad 1) \qquad \Psi_{xdown} = \frac{1}{\sqrt{2}} \cdot (1 \quad -1)$$

$$\Psi_{left}(p) := \Psi_{xup} \cdot \Psi(p) \qquad \Psi_{right}(p) := \Psi_{xdown} \cdot \Psi(p)$$



$$\left(\left|\Psi_{left}(p)\right|\right)^2 \qquad \left(\left|\Psi_{right}(p)\right|\right)^2$$

Figure 2b in the reference cited and shown below.

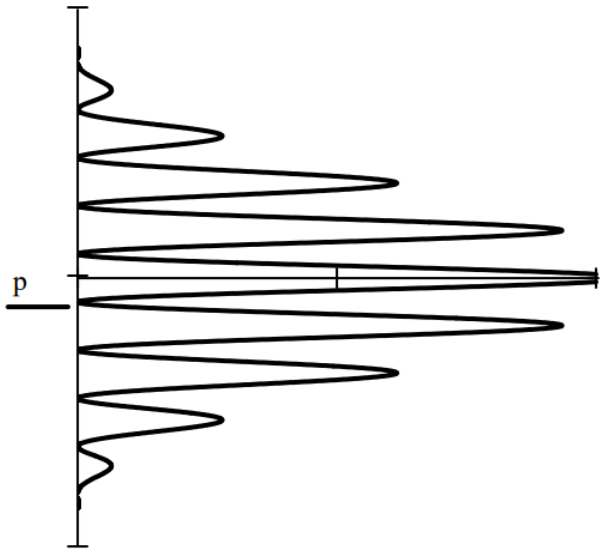


The horizontal blue line marks p = 0 on the z-axis. On the left is the interference pattern of the part of the beam emerging from the x-up magnet direction with spin state Ψ_{xup}, and on the right is the interference pattern of the part of the beam emerging from the x-down magnet direction with spin state Ψ_{xdown}. As shown in the Summary, Ψ(p) can be rewritten in terms of the x-direction spin states clearly show in the superpositions responsible for the interference fringes on the left and right.

$$\langle p|\Psi\rangle = \frac{1}{2}\left[|\uparrow_x\rangle\left(\langle p|z_1\rangle + \langle p|z_2\rangle\right) + |\downarrow_x\rangle\left(\langle p|z_1\rangle - \langle p|z_2\rangle\right)\right]$$

In the absence of both Stern-Gerlach magnets the usual double-slit interference pattern is observed.

$$\Psi(p) = \frac{1}{\sqrt{2}} \cdot \left(\int_{z_1-\frac{\delta}{2}}^{z_1+\frac{\delta}{2}} \frac{1}{\sqrt{2\cdot\pi}} \cdot \exp(-\mathrm{i}\cdot \mathrm{p}\cdot \mathrm{z}) \cdot \frac{1}{\sqrt{\delta}} \mathrm{dz} + \int_{z_2-\frac{\delta}{2}}^{z_2+\frac{\delta}{2}} \frac{1}{\sqrt{2\cdot\pi}} \cdot \exp(-i\cdot p\cdot z) \cdot \frac{1}{\sqrt{\delta}} dz \right)$$



$$\left(\left|\Psi(\mathrm{p})\right|\right)^2$$

Alternative Analysis

It is possible to express the mathematics in an alternative but equivalent form. The first wave function,

$$\frac{1}{\sqrt{2}}\left[|\uparrow_z\rangle\,|z_1\rangle + |\downarrow_z\rangle\,|z_2\rangle\right]$$

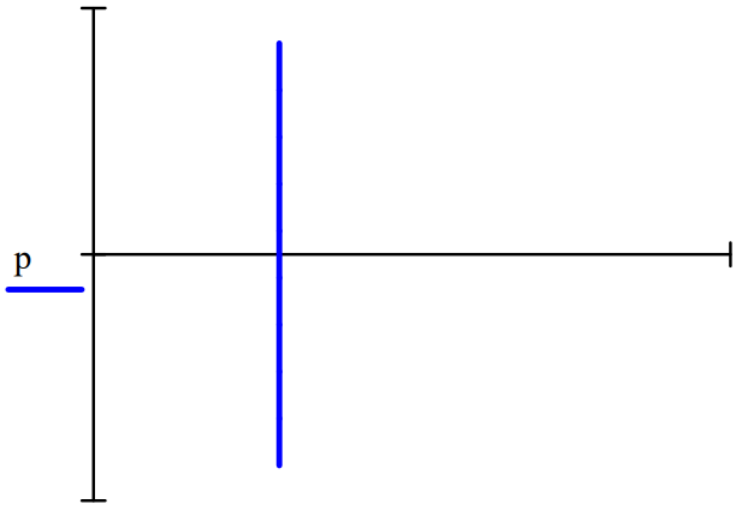
can be expressed explicitly in vector format in the momentum representation. This analysis will be based on infinitesimally thin slits as introduced earlier.

$$\frac{1}{\sqrt{2}}\left[\begin{pmatrix}1\\0\end{pmatrix}|z_1\rangle+\begin{pmatrix}0\\1\end{pmatrix}|z_2\rangle\right]=\frac{1}{\sqrt{2}}\begin{pmatrix}|z_1\rangle\\|z_2\rangle\end{pmatrix}\xrightarrow{\langle p|}\frac{1}{\sqrt{2}}\begin{pmatrix}\langle p|z_1\rangle\\\langle p|z_2\rangle\end{pmatrix}$$

It is easily shown that this wave function does not lead to interference fringes at the detection screen by calculating the square of its absolute magnitude.

$$\frac{1}{2}\begin{pmatrix}\langle z_1|p\rangle & \langle z_2|p\rangle\end{pmatrix}\begin{pmatrix}\langle p|z_1\rangle\\\langle p|z_2\rangle\end{pmatrix}=\frac{1}{2}\left[|\langle p|z_1\rangle|^2+|\langle p|z_2\rangle|^2\right]$$

$$\Psi(\mathrm{p}):=\frac{1}{2\cdot\sqrt{\pi}}\cdot\begin{pmatrix}\exp(-\mathrm{i}\cdot\mathrm{p}\cdot z_1)\\\exp(-\mathrm{i}\cdot\mathrm{p}\cdot z_2)\end{pmatrix}$$



$$\left(|\Psi(\mathrm{p})|\right)^2$$

However, in the presence of the second Stern-Gerlach magnet vector B is projected onto the two output channels of the magnet.

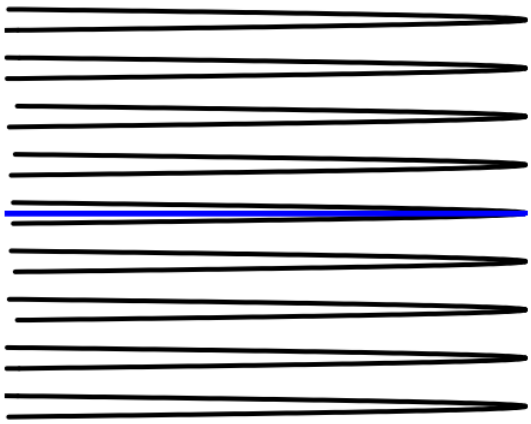
$$\frac{1}{2}\begin{pmatrix}1 & 1\end{pmatrix}\begin{pmatrix}\langle p|z_1\rangle\\\langle p|z_2\rangle\end{pmatrix}=\frac{1}{2}\left[\langle p|z_1\rangle+\langle p|z_2\rangle\right]$$

$$\frac{1}{2}\begin{pmatrix}1 & -1\end{pmatrix}\begin{pmatrix}\langle p|z_1\rangle\\\langle p|z_2\rangle\end{pmatrix}=\frac{1}{2}\left[\langle p|z_1\rangle-\langle p|z_2\rangle\right]$$

The probability distributions of these states show interference fringes.

$$\Psi_{\text{left}}(p) := \frac{1}{\sqrt{2}} \cdot (1 \quad 1) \cdot \frac{1}{2 \cdot \sqrt{\pi}} \cdot \begin{pmatrix} \exp(-i \cdot p \cdot z_1) \\ \exp(-i \cdot p \cdot z_2) \end{pmatrix}$$

$$\Psi_{\text{right}}(p) := \frac{1}{\sqrt{2}} \cdot (1 \quad -1) \cdot \frac{1}{2 \cdot \sqrt{\pi}} \cdot \begin{pmatrix} \exp(-i \cdot p \cdot z_1) \\ \exp(-i \cdot p \cdot z_2) \end{pmatrix}$$



$$\left(\left|\Psi_{\text{right}}(p)\right|\right)^2$$

Summary

The z-direction Stern-Gerlach magnet and the slit screen create the following entangled superposition which does not produce interference fringes due to the orthogonality of the spin states marking the slits.

$$\langle p|\Psi\rangle = \frac{1}{\sqrt{2}}\left[|\uparrow_z\rangle \langle p|z_1\rangle + |\downarrow_z\rangle \langle p|z_2\rangle\right]$$

To understand what happens at the x-direction magnet this state is rewritten in the x-direction spin basis.

$$\langle p|\Psi\rangle = \frac{1}{\sqrt{2}}\left[\frac{1}{\sqrt{2}}\left(|\uparrow_x\rangle + |\downarrow_x\rangle\right)\langle p|z_1\rangle + \frac{1}{\sqrt{2}}\left(|\uparrow_x\rangle - |\downarrow_x\rangle\right)\langle p|z_2\rangle\right]$$

Collecting terms on the x-direction spin eigenstates yields,

$$\langle p|\Psi\rangle = \frac{1}{2}\left[|\uparrow_x\rangle\left(\langle p|z_1\rangle + \langle p|z_2\rangle\right) + |\downarrow_x\rangle\left(\langle p|z_1\rangle - \langle p|z_2\rangle\right)\right]$$

The in-phase and out-of-phase superpositions, highlighted in blue and red, exit the magnet in opposite directions. Because of this the superpositions become spatially separated which leads to two sets of interference fringes with a one-fringe relative phase shift at the detection screen.

It′s clear to me that erasure is not a satisfactory explanation for this process. Because fringes appear after the x-direction magnet it might seem plausible, at first glance, to assume that the which-way markers have been erased. But actually the x-direction magnet sorts < p|Ψ> into two components in terms of the x-direction spin eigenstates. Nothing has been erased.

This page titled 1.49: A Stern-Gerlach Quantum "Eraser" is shared under a CC BY 4.0 license and was authored, remixed, and/or curated by Frank Rioux via source content that was edited to the style and standards of the LibreTexts platform.

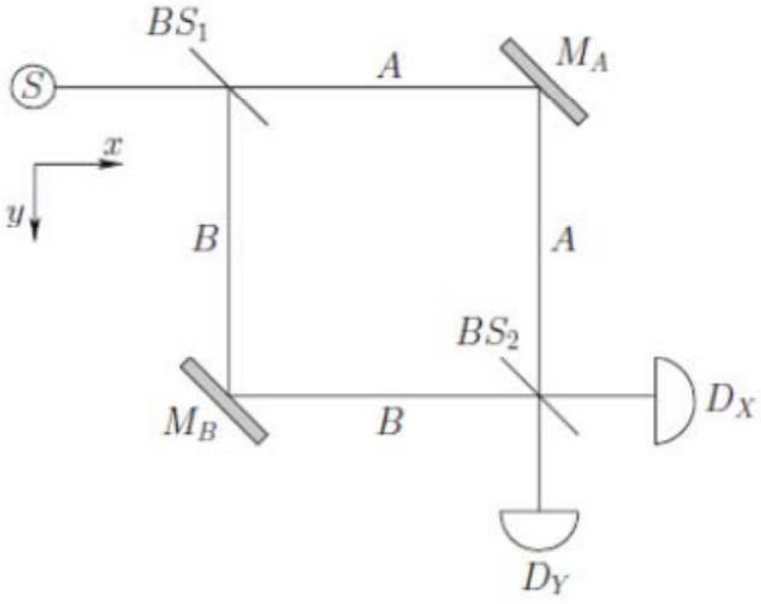
1.50: Using the Mach-Zehnder Interferometer to Illustrate the Impact of Which-way Information

Richard Feynman raised Young's double-slit experiment to canonical status by presenting it as the paradigm for all quantum mechanical behavior. In *The Character of Physical Law* he wrote, "Any other situation in quantum mechanics, it turns out, can always be explained by saying, 'You remember the case of the experiment with the two holes? It's the same thing.'"

Following Feynman, teachers of quantum theory use the double-slit experiment to illustrate the superposition principle and its signature effect, quantum interference. A single particle (photon, electron, etc.) arrives at any point on the detection screen by two paths, whose probability amplitudes interfere yielding the characteristic diffraction pattern. This is called single-particle interference.

Single-particle interference in a Mach-Zehnder (MZ) interferometer is a close cousin of the traditional double-slit experiment. Using routine complex number algebra, it can be used to illustrate the same fundamentals as the two-slit experiment and also to introduce students to the field of quantum optics.

This tutorial draws heavily on a recent article in the American Journal of Physics and papers quoted therein [*Am. J. Phys.* 78(8), 792-795 (2010)]. An equal-arm MZ interferometer is shown below. In this configuration the photon is always detected at Dx. The analysis below provides an explanation why this happens.



A key convention in the analysis of MZ interferometers is that reflection at a beam splitter (BS) is accompanied by a 90 degree phase shift ($\frac{\pi}{2}$, i). The behavior of a photon traveling in the x- or y-direction at the beam splitters and mirrors is as follows.

At the 50-50 beam splitters the following photon superpositions are formed:

$$|x\rangle \rightarrow \frac{1}{\sqrt{2}}[|x\rangle + i|y\rangle] \qquad |y\rangle \rightarrow \frac{1}{\sqrt{2}}[|y\rangle + i|x\rangle]$$

At the mirrors the behavior of the photon is as follows:

$$|x\rangle \rightarrow |y\rangle \quad |y\rangle \rightarrow |x\rangle$$

Using the information provided above and complex number algebra, the history of a photon leaving the source (moving in the x-direction) is:

$$|S\rangle \xrightarrow{BS_1} \frac{1}{\sqrt{2}}[|x\rangle + i|y\rangle] \xrightarrow{Mirrors} \frac{1}{\sqrt{2}}[|y\rangle + i|x\rangle] \xrightarrow{BS_2} i|x\rangle$$

Thus we see that, indeed, the photon always arrives at D_x in the equal-arm MZ interferometer shown above. The paths to D_x (TR+RT) are in phase and constructively interfere. The paths to D_y (TT+RR) are 180 degrees (i^2) out of phase and therefore destructively interfere. (T stands for transmitted and R stands for reflected.)

$$\text{Probability}\,(D_x) = |\langle x|S\rangle|^2 = 1 \quad \text{Probability}\ \ (D_y) = |\langle y|S\rangle|^2 = 0$$

The detection of the photon exclusively at D_x is the equivalent of the appearance of the interference fringes in the double-slit experiment.

Another quantum mechanical point that Feynman made with the double-slit experiment is that if path information (which slit the photon went through) is available (even in principle) the interference fringes disappear. This is also the case with the MZ interferometer.

If after the first beam splitter the photon is observed in path A, we have the following history,

$$|S\rangle \xrightarrow{PathA} |x\rangle \xrightarrow{MirrorA} |y\rangle \xrightarrow{BS_2} \frac{1}{\sqrt{2}}(i|x\rangle + |y\rangle)$$

which leads to equal probabilities of detecting the photon at D_x and D_y.

$$P\,(D_x) = |\langle x|S\rangle|^2 = \left|\frac{i}{\sqrt{2}}\right|^2 = \frac{1}{2} \quad P\,(D_y) = |\langle y|S\rangle|^2 = \left|\frac{1}{\sqrt{2}}\right|^2 = \frac{1}{2}$$

Alternatively, if after the first beam splitter the photon is observed in path B, we have the following history,

$$|S\rangle \xrightarrow{PathB} |y\rangle \xrightarrow{MirrorB} |x\rangle \xrightarrow{BS_2} \frac{1}{\sqrt{2}}(|x\rangle + i|y\rangle)$$

which also leads to equal probabilities of detecting the photon at D_x and D_y.

$$P\,(D_x) = |\langle x|S\rangle|^2 = \left|\frac{1}{\sqrt{2}}\right|^2 = \frac{1}{2} \quad P\,(D_y) = |\langle y|S\rangle|^2 = \left|\frac{i}{\sqrt{2}}\right|^2 = \frac{1}{2}$$

In these cases, where path information is available the detection of the photon at both detectors in equal percentages is the equivalent of the disappearance of the interference fringes in the double-slit experiment when knowledge of which slit the particle went through is available.

This page titled 1.50: Using the Mach-Zehnder Interferometer to Illustrate the Impact of Which-way Information is shared under a CC BY 4.0 license and was authored, remixed, and/or curated by Frank Rioux via source content that was edited to the style and standards of the LibreTexts platform.

1.51: Quantum Theory, Wave-Particle Duality and the Mach-Zehnder Interferometer

A Beam Splitter Creates a Quantum Mechanical Superposition

Single photons emitted by a source (S) illuminate a 50-50 beam splitter (BS). Mirrors (M) direct the photons to detectors D_1 and D_2. The probability amplitudes for transmission and reflection are given below. By convention a 90 degree phase shift (i) is assigned to reflection.

Probability amplitude for photon transmission at a 50-50 beam splitter:

$$\langle T|S\rangle = \frac{1}{\sqrt{2}}$$

Probability amplitude for photon reflection at a 50-50 beam splitter:

$$\langle R|S\rangle = \frac{i}{\sqrt{2}}$$

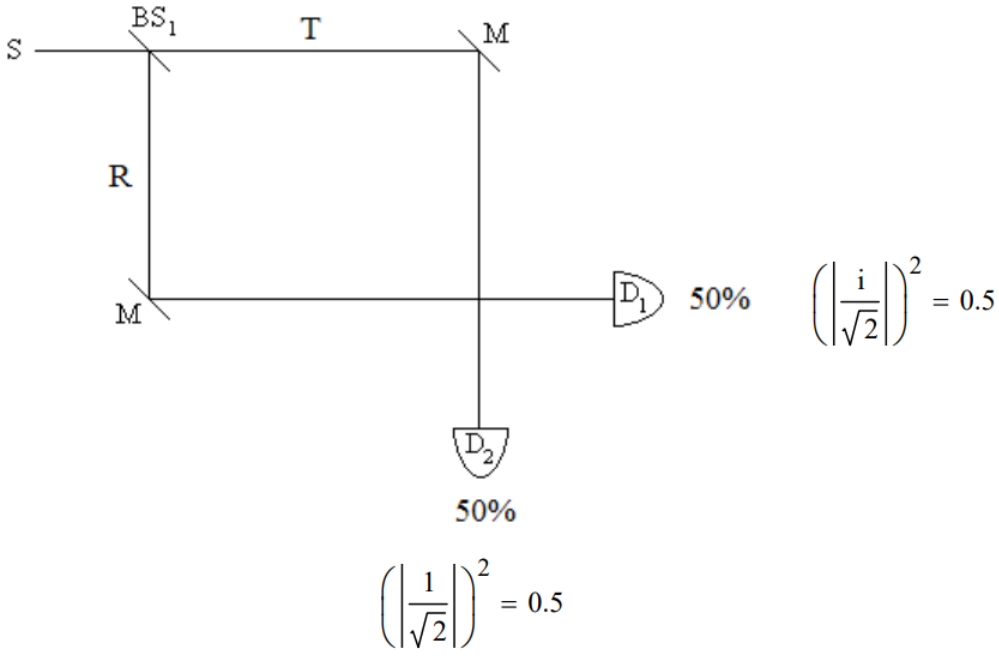
After the beam splitter the photon is in a superposition state of being transmitted and reflected.

$$|S\rangle \rightarrow \frac{1}{\sqrt{2}}[|T\rangle + i|R\rangle]$$

As shown in the diagram below, mirrors reflect the transmitted photon path to D_2 and the reflected path to D_1. The source photon is expressed in the basis of the detectors as follows.

$$|S\rangle \rightarrow \frac{1}{\sqrt{2}}[|T\rangle + i|R\rangle] \xrightarrow[R\rightarrow D_1]{T\rightarrow D_2} \rightarrow \frac{1}{\sqrt{2}}[|D_2\rangle + i\,|D_1\rangle]$$

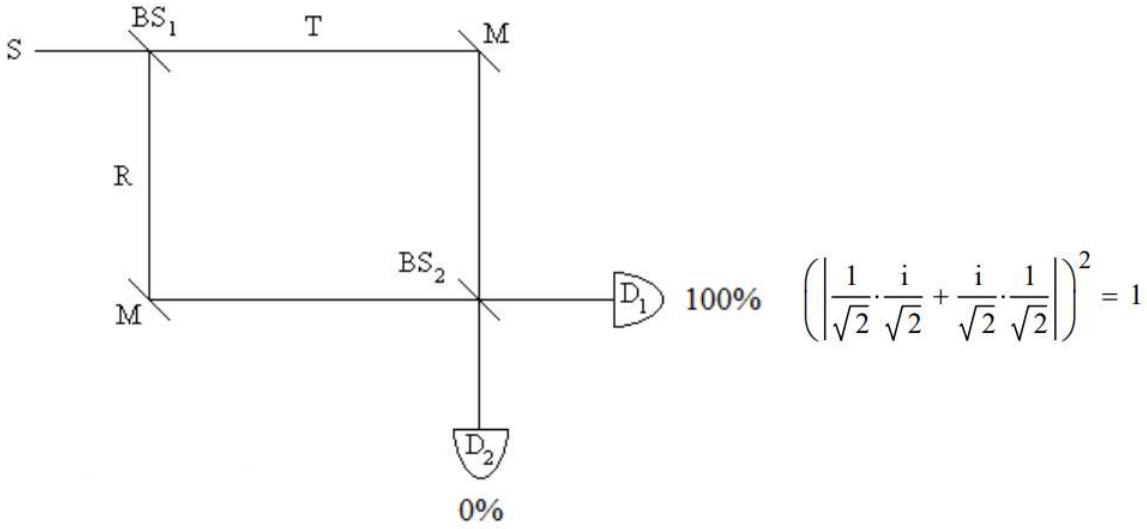
The square of the magnitude of the coefficients of D_1 and D_2 give the probabilities that the photon will be detected at D_1 or D_2. Each detector registers photons 50% of the time. In other words, in the quantum view the superposition collapses randomly to one of the two possible measurement outcomes it represents.



The classical view that detection at D_1 means the photon was reflected at BS_1 and that detection at D_2 means it was transmitted at BS_1 is not tenable as will be shown using a Mach-Zehnder interferometer which has a second beam splitter at the path intersection before the detectors.

A Second Beam Splitter Provides Two Paths to Each Detector

If a second beam splitter is inserted before the detectors the photons always arrive at D_1. In the first experiment there was only one path to each detector. The construction of a Mach-Zehnder interferometer by the insertion of a second beam splitter creates a second path to each detector and the opportunity for constructive and destructive interference on the paths to the detectors.



$$\left(\left|\frac{1}{\sqrt{2}}\cdot\frac{i}{\sqrt{2}}+\frac{i}{\sqrt{2}}\cdot\frac{1}{\sqrt{2}}\right|\right)^2=1$$

$$\left(\left|\frac{1}{\sqrt{2}}\cdot\frac{1}{\sqrt{2}}+\frac{i}{\sqrt{2}}\cdot\frac{i}{\sqrt{2}}\right|\right)^2=0$$

Given the superposition state after BS_1, the probability amplitudes after BS_2 interfere constructively at D_1 and destructively at D_2.

$$\begin{array}{ccccc} \text{After } BS_1 & & \text{After } BS_2 & & \text{Final State} \\ & & |T\rangle \rightarrow \frac{1}{\sqrt{2}}\left[i\,|D_1\rangle + |D_2\rangle\right] & & \\ |S\rangle \rightarrow \frac{1}{\sqrt{2}}[|T\rangle + i|R\rangle] & \rightarrow & + & \rightarrow & i\,|D_1\rangle \\ & & i|R\rangle \rightarrow \frac{i}{\sqrt{2}}\left[|D_1\rangle + i\,|D_2\rangle\right] & & \end{array}$$

Adopting the classical view that the photon is either transmitted or reflected at BS_1 does not produce this result. If the photon was transmitted at BS_1 it would have equal probability of arriving at either detector after BS_2. If the photon was reflected at BS_1 it would also have equal probability of arriving at either detector after BS_2. The predicted experimental results would be the same as those of the single beam splitter experiment. In summary, the quantum view that the photon is in a superposition of being transmitted and reflected after BS_1 is consistent with both experimental results described above; the classical view that it is either transmitted or reflected is not.

Some disagree with this analysis saying the two experiments demonstrate the dual, complementary, behavior of photons. In the first experiment particle-like behavior is observed because both detectors register photons indicating the individual photons took one path or the other. The second experiment reveals wave-like behavior because interference occurs - only D_1 registers photons. According to this view the experimental design determines whether wave or particle behavior will occur and somehow the photon is aware of how it should behave. Suppose in the second experiment that immediately after the photon has interacted with BS_1, BS_2 is removed. Does what happens at the detectors require the phenomenon of retrocausality or delayed choice? Only if you reason classically about quantum experiments.

We always measure particles (detectors click, photographic film is darkened, etc.) but we interpret what happened or predict what will happen by assuming wavelike behavior, in this case the superposition created by the initial beam splitter that delocalizes the position of the photon. Quantum particles (quons) exhibit both wave and particle properties in every experiment. To paraphrase Nick Herbert (*Quantum Reality*), particles are always detected, but the experimental results observed are the result of wavelike behavior. Richard Feynman put it this way (*The Character of Physical Law*), "I will summarize, then, by saying that electrons arrive in lumps, like particles, but the probability of arrival of these lumps is determined as the intensity of waves would be. It is in

this sense that the electron behaves sometimes like a particle and sometimes like a wave. It behaves in two different ways at the same time (in the same experiment)." Bragg said, "Everything in the future is a wave, everything in the past is a particle."

In 1951 in his treatise *Quantum Theory*, David Bohm described wave-particle duality as follows: "One of the most characteristic features of the quantum theory is the wave-particle duality, i.e. the ability of matter or light quanta to demonstrate the wave-like property of interference, and yet to appear subsequently in the form of localizable particles, even after such interference has taken place." In other words, to explain interference phenomena wave properties must be assigned to matter and light quanta prior to detection as particles.

This page titled 1.51: Quantum Theory, Wave-Particle Duality and the Mach-Zehnder Interferometer is shared under a CC BY 4.0 license and was authored, remixed, and/or curated by Frank Rioux via source content that was edited to the style and standards of the LibreTexts platform.

1.52: Analysis of a Temporal Double-slit Experiment

Contemporary chemistry is built on a quantum mechanical foundation, and prominent among the fundamental concepts of quantum theory is the superposition principle. Previously the author and others have illustrated the importance of the superposition principle in understanding chemical and physical phenomena [1-5]. Furthermore, the primary literature is replete with manifestations of the quantum superposition in current research [6-8]. Very recently, for example, Hawking and Hertog [9] have published a theory of the origin of the universe based squarely on the superposition princple.

As Richard Feynman demonstrated, the spatial double-slit experiment is a simple and compelling example of the quantum superposition in action [10-11]. All fundamental quantum mechanical phenomena, according to Feynman, can be illuminated by comparison to the double-slit experiment [11].

Now this paradigmatic experiment has a companion in the temporal domain. A temporal doubleslit experiment with attosecond windows was recently reported by an international team led by Gehard Paulus [12]. This note demonstrates that the quantum mechanics behind this remarkable experiment is analogous to that for the spatial double-slit experiment for photons or massive particles.

The spatial and temporal experiments for electrons, juxtaposed in Figure 1A [13], are analyzed in terms of conjugate observables united by a Fourier transform. For the spatial experiment the observables are position and momentum, while for the temporal version they are time and energy.

In the spatial double-slit experiment illumination of the slit screen with an electron beam places each electron in a superposition of being simultaneously at slits located at x_1 and x_2.

$$|\Psi\rangle = \frac{1}{\sqrt{2}}\left[|x_1\rangle + |x_2\rangle\right]$$

According to quantum mechanical principles spatial localization at two positions leads to delocalization and interference fringes in the electron's momentum distribution. This can be seen by a Fourier transform of equation (1) into momentum space, initially assuming infinitesimally thin slits.

$$\langle p|\Psi\rangle = \frac{1}{\sqrt{2}}\left[\langle p|x_1\rangle + \langle p|x_2\rangle\right] = \frac{1}{2\sqrt{\pi\hbar}}\left[\exp\left(-\frac{ipx_1}{\hbar}\right) + \exp\left(-\frac{ipx_2}{\hbar}\right)\right]$$

Clearly the two exponential terms will oscillate in and out of phase for various values of the momentum. (See the Appendix for mathematical background on the Dirac brackets used in this paper.) For finite spatial slits of width δ the momentum wave function is given by equation (3)

$$\langle p|\Psi\rangle = \frac{1}{2\sqrt{\pi\hbar\delta}}\left[\int_{x_1-\frac{\delta}{2}}^{x_1+\frac{\delta}{2}} \exp\left(-\frac{ipx}{\hbar}\right)dx + \int_{x_2-\frac{\delta}{2}}^{x_2+\frac{\delta}{2}} \exp\left(-\frac{ipx}{\hbar}\right)dx\right]$$

The observed diffraction pattern is actually the electron's momentum distribution projected onto the detection screen, as is revealed by a graphical representation of $|\langle p|\Psi\rangle|^2$ [14].

In the temporal double-slit experiment a very short laser pulse (~5 fs), which consists of two maxima (temporal double-slit) and one minimum (temporal single-slit) in the electric field, is used to ionize individual argon atoms.



Figure 1B. The minor fringes associated with single-slit ionization are discussed in reference [12].

$$|\Psi\rangle = \frac{1}{\sqrt{2}}\left[|t_1\rangle + |t_2\rangle\right]$$

The kinetic energy of the ionized electron is measured at the detector, and as Figure 1B shows interference fringes are observed in the kinetic energy distribution. A Fourier transform of equation (4) into the energy domain reveals the origin of the fringes; the probability amplitudes for being ionized with kinetic energy E at the two different times interfere constructively and destructively.

$$\langle E|\Psi\rangle = \frac{1}{\sqrt{2}}\left[\langle E|t_1\rangle + \langle E|t_2\rangle\right] = \frac{1}{2\sqrt{\pi\hbar}}\left[\exp\left(\frac{iEt_1}{\hbar}\right) + \exp\left(\frac{iEt_2}{\hbar}\right)\right]$$

For finite windows of time duration δ equation (5) becomes,

$$\langle E|\Psi\rangle = \frac{1}{2\sqrt{\pi\hbar\delta}}\left[\int_{t_1-\frac{\delta}{2}}^{t_1+\frac{\delta}{2}} \exp\left(-\frac{iEt}{\hbar}\right) dt + \int_{x_2-\frac{\delta}{2}}^{x_2+\frac{\delta}{2}} \exp\left(-\frac{iEt}{\hbar}\right) dt\right]$$

Figure 2 shows that a plot of $|\langle E|\Psi\rangle|^2$ vs E using equation (6) with estimates for t_1, t_2 (Δt) and \detla from reference [12] generates a 15 eV envelope with 11 prominent interference fringes. This calculated result is in reasonable quantitative agreement with the experimental data displayed in Figure 1B.

The temporal double-slit diffraction pattern reported in reference [12] is a single-electron effect – only one ionized electron is being observed at a time. Likewise the spatial analog has been performed at low source intensity such that there is only one electron in the apparatus at a time [15,16]. The fact that an interference pattern is observed under single-particle conditions leads to terms such as single-particle interference or self-interference. Glauber [17] has argued against such language because it is physically misleading.

> *The things that interfere in quantum mechanics are not particles. They are probability amplitudes for certain events. It is the fact that probability amplitudes add up like complex numbers that is responsible for all quantum mechanical interferences.*

The interference of probability amplitudes that Glauber identifies as the source of all quantum mechanical interference phenomena is clearly revealed in the mathematical analysis provided in this note; it is especially clear in equations (2) and (5).

Appendix

A one-dimensional plane wave traveling in the positive x-direction has the following mathematical form.

$$F(x,t) = \exp\left(i\frac{2\pi x}{\lambda}\right)\exp(-i2\pi\upsilon t)$$

Substitution of h/p for λ (de Broglie) and E/h for ν (Planck/Einstein) transforms F(x,t) into a quantum mechanical free-particle wave function.

$$\Psi(x,t) = \exp\left(\frac{ipx}{\hbar}\right)\exp\left(-\frac{iEt}{\hbar}\right)$$

Assigning Dirac brackets containing the complementary observable pairs to this equation yields,

$$\langle x|p\rangle = \exp\left(\frac{ipx}{\hbar}\right) \quad \text{and} \quad \langle t|E\rangle = \exp\left(-\frac{iEt}{\hbar}\right)$$

Dirac notation reveals that these equations are Fourier transforms between complementary variables. The complex conjugates of these relations are used in the analysis presented in this paper.

$$\langle p|x\rangle = \langle x|p\rangle^* = \exp\left(-\frac{ipx}{\hbar}\right) \text{ and } \quad \langle E|t\rangle = \langle t|E\rangle^* = \exp\left(\frac{iEt}{\hbar}\right)$$

Additional information on Dirac notation is available online [18].

Acknowledgment

I wish to acknowledge helpful comments by Professor Gerhard Paulus of Max-Planck-Institut für Quantenoptik, Ludvig-Maximilians-Universität München, and Texas A&M University.

References

1. McMillin, D. R. “Fluctuating Electric Dipoles and the Absorption of Light,” *J. Chem. Educ.* **1978**, *55*, 7-11.
2. Weinhold, F. A. “Chemical Bonding as a Superposition Phenomenon,” *J. Chem. Educ.* **1999**, *76*, 1141-1146.

3. Baskin, J. S.; Zewail, A. H. “Freezing Atoms in Motion: Principles of Femtochemistry and Demonstration by Laser Stroboscopy,” *J. Chem. Educ.* **2001**, *78*, 737-751.
4. Rioux, F.; Johnson, B. J. “Using Optical Transforms to Teach Quantum Mechanics,” *Chem. Educator* **2004**, *9*, 12-16.
5. Rioux, F. “Illustrating the Superposition Principle with Single-Photon Interference,” *Chem. Educator* **2005**, *10*, 424-426.
6. Dixon, R. N.; Hwang, D. W.; Yang, X. F.; Harich, S.; Lin, J. J.; Yang. X. “Chemical ‘Double Slits’: Dynamical Interference of Photodissociation Pathways in Water,” *Science*, **1999**, *285*, 1249-1253.
7. van der Wal, C. H.; ter Haar, A. C. J.; Wilhelm, F. K.; Schouten, R. N.; Harmans, C. J. P. M.; Orlando, T. P.; Lloyd, S.; Mooij, J. E. “Quantum Superposition of Macroscopic Persistent-Current States,” *Science*, **2000**, *290*, 773-777.
8. Weinhold, F. “A new twist on molecular shape,” *Nature* **2001**, *411*, 539-541 (and references quoted therein).
9. Hawking, S. W.; Hertog, T. “Populating the landscape: A top-down approach,” *Phys. Rev.* D **2006**, *73* 123527.
10. Feynman, R. P.; Leighton, R. B.; Sands, M. *The Feynman Lectures on Physics, Vol. 3*; Addison-Wesley: Reading, 1965, p. 1-1.
11. Feynman, R. P. *The Character of Physical Law*; MIT Press: Cambridge, 1967; p. 130.
12. Lindner, F.; Schätzel, M. G.; Walther, H.; Baltuška, A.; Goulielmakis, E.; Krausz, F.; Milošević, D. B.; Bauer, D.; Becker, W.; Gaulus, G. G. “Attosecond Double-Slit Experiment,” *Phys. Rev. Lett.* **2005**, 95, 040401.
13. Physics World and PhysicsWeb (www.physicsweb.org/articles/news/9/3/1/1)
14. Marcella, T. V. “Quantum interference with slits,” *Eur. J. Phys.* **2002**, *23*, 615-621.
15. Merli P. G.; Missiroli G. F.; Pozzi G. “On the statistical aspects of electron interference phenomena,” *Am. J. Phys.* **1976**, *44*, 306-307.
16. Tonomura A.; Endo, T.; Matsuda, T.; Kawasaki, T.; Ezawa, H. “Demonstration of singleelectron buildup of an interference pattern,” *Am. J. Phys.* **1989**, *57*, 117-120.
17. Glauber, R. “Dirac’s Famous Dictum on Interference: One Photon or Two?” *Am. J. Phys.* **1995**, *63*, 12.
18. Tutorial on Dirac notation

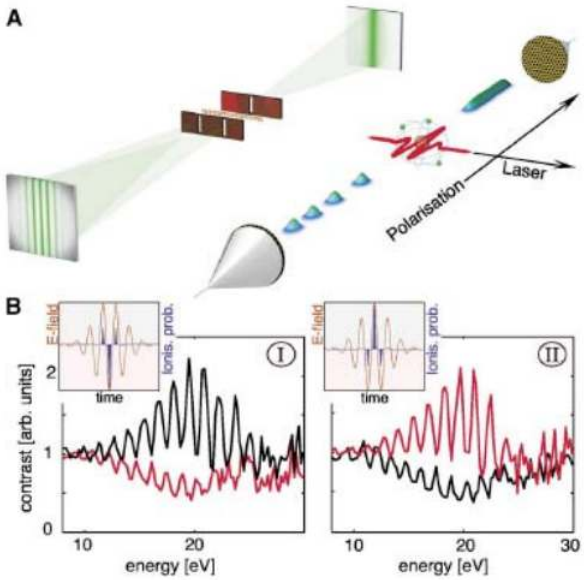


Figure 1. (A) Comparison of the spatial single/double-slit experiment (left) and the temporal version (right). (B) The results for the time domain experiment. The major interference fringes are due to the double-slit ionization, while the minor fringes are due to the single-slit effect (see reference [12] for an explanation as to why they are observed). The difference between panels I and II is a 180° phase shift in the electric field of the ionizing laser, as indicated in the figure insets. (Permission to reproduce this figure is pending.)

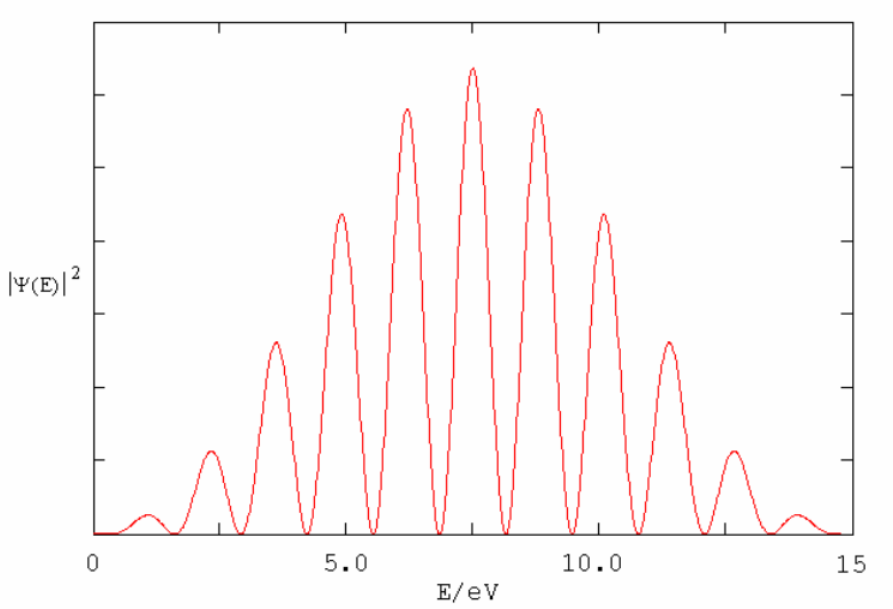


Figure 2. Relative electron kinetic energy distribution in eV. Estimating from reference [1] that)t = t_2 - t_1 = 2.9 fs and * = 500 as yields a 15 eV envelope showing 11 interference fringes.

This page titled 1.52: Analysis of a Temporal Double-slit Experiment is shared under a CC BY 4.0 license and was authored, remixed, and/or curated by Frank Rioux via source content that was edited to the style and standards of the LibreTexts platform.

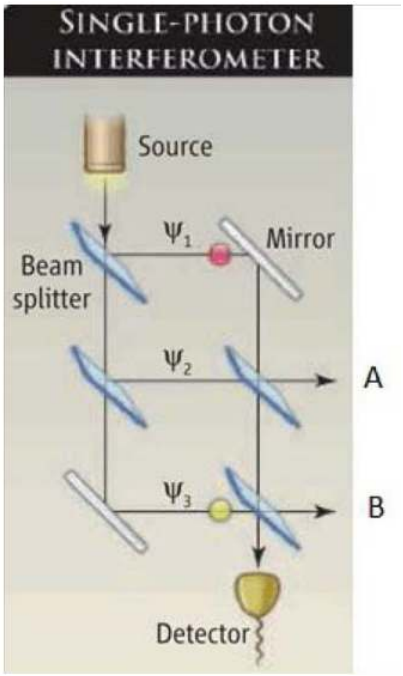
1.53: An Analysis of Three-Path Interference

Quantum mechanics teaches that if there is more than one path to a particular destination interference effects are likely. Using Feynman's sum over histories' approach to quantum mechanics the probability of arrival at a location is the square of the magnitude of the sum of the probability amplitudes for each path to that location. For example, in a triple-slit diffraction experiment the probability of arriving at x on the detection screen in Dirac notation is,

$$P_{123} = |\langle x|S\rangle|^2 = |\langle x|3\rangle\langle 3|S\rangle + \langle x|2\rangle\langle 2|s\rangle + \langle x|1\rangle\langle (1|s)|^2$$

The single-photon interferometer shown below [Franson, *Science* **329**, 396 (2010)] is a close cousin of the triple-slit experiment because it provides three paths to the detector. Initially we will ignore the other two output channels **A** and **B**.

Three Path Interference



Probability Amplitudes

In this analysis the probability amplitudes are calculated using the following conventions.

Assume 50-50 beam splitters and assign $\frac{\pi}{2}$ (i) phase shift to reflection (usual convention).

Transmission at a beam splitter: $\mathrm{T} := \frac{1}{\sqrt{2}}$	Reflection at a beam splitter: $\mathrm{R} := \frac{i}{\sqrt{2}}$	Reflection at a mirror: $M := 1$

First, using Feynman's 'sum over histories' method we calculate the probability that the photon will arrive at the **Detector** (3 paths):

$$(|\mathrm{R}\cdot\mathrm{M}\cdot\mathrm{T}\cdot\mathrm{T} + \mathrm{T}\cdot\mathrm{R}\cdot\mathrm{R}\cdot\mathrm{T} + \mathrm{T}\cdot\mathrm{T}\cdot\mathrm{M}\cdot\mathrm{R}|)^2 = 0.5625$$

To establish that probability is conserved the probabilities for arrival at **A** and **B** are calculated.

Calculate the probability that the photon will arrive at **A** (2 paths):

$$(|\mathrm{T}\cdot\mathrm{R}\cdot\mathrm{T} + \mathrm{R}\cdot\mathrm{M}\cdot\mathrm{R}|)^2 = 0.375$$

Calculate the probability that the photon will arrive at **B** (3 paths):

$$(|\mathrm{R}\cdot\mathrm{M}\cdot\mathrm{T}\cdot\mathrm{R} + \mathrm{T}\cdot\mathrm{R}\cdot\mathrm{R}\cdot\mathrm{R} + \mathrm{T}\cdot\mathrm{T}\cdot\mathrm{M}\cdot\mathrm{T}|)^2 = 0.0625$$

Demonstrate that probability is conserved:

$$0.5625 + 0.375 + 0.0625 = 1$$

While this traditional analysis postulates three-path interference for the arrival probability at the detector, Sinha et al. [*Science* **329**, 418 (2010)] argue that true interference only occurs between pairs of paths. In this case between paths 1 & 2, 1 & 3, and 2 & 3. Franson summarized this view as follows: "Quantum interference between many different pathways is simply the sum of the effects from all pairs of pathways."

The probability expression for an event involving two equivalent paths is

$$P_{ij} = |\Psi_i + \Psi_j|^2 = |\Psi_i|^2 + |\Psi_j|^2 + \Psi_i^* \Psi_j + \Psi_j^* \Psi_i = P_i + P_j + I_{ij}$$

where I_{ij} is the interference term and P_i is defined as the probability when only the i^{th} path is open. It is my opinion that this latter designation is not strictly valid. However, accepting it for the time being leads to the following definition for two-path interference.

$$I_{ij} = P_{ij} - P_i - P_j$$

Therefore, the probability for an event involving three equivalent paths to a destination using only two-path interference is,

$$P_{123} = P_1 + P_2 + P_3 + I_{12} + I_{13} + I_{23} = P_{12} + P_{13} + P_{23} - P_1 - P_2 - P_3$$

The probabilities in this equation are now calculated.

$\mathrm{P}_1 \quad (\lvert \mathrm{R}\cdot\mathrm{M}\cdot\mathrm{T}\cdot\mathrm{T}\rvert)^2 = 0.125$	$\mathrm{P}_2 \quad (\lvert \mathrm{T}\cdot\mathrm{R}\cdot\mathrm{R}\cdot\mathrm{T}\rvert)^2 = 0.0625$	$\mathrm{P}_3 \quad (\lvert \mathrm{T}\cdot\mathrm{T}\cdot\mathrm{M}\cdot\mathrm{R}\rvert)^2 = 0.125$
$\mathrm{P}_{12} \quad (\lvert \mathrm{R}\cdot\mathrm{M}\cdot\mathrm{T}\cdot\mathrm{T} + \mathrm{T}\cdot\mathrm{R}\cdot\mathrm{R}\cdot\mathrm{T}\rvert)^2 = 0.1875$	$\mathrm{P}_{13} \quad (\lvert \mathrm{R}\cdot\mathrm{M}\cdot\mathrm{T}\cdot\mathrm{T} + \mathrm{T}\cdot\mathrm{T}\cdot\mathrm{M}\cdot\mathrm{R}\rvert)^2 = 0.5$	
$\mathrm{P}_{23} \quad (\lvert \mathrm{T}\cdot\mathrm{R}\cdot\mathrm{R}\cdot\mathrm{T} + \mathrm{T}\cdot\mathrm{T}\cdot\mathrm{M}\cdot\mathrm{R}\rvert)^2 = 0.1875$		

The probability of arriving at a detector which can be reached by three paths, but using only two-path interference is,

$$\mathrm{P}_{12} + \mathrm{P}_{13} + \mathrm{P}_{23} - \mathrm{P}_1 - \mathrm{P}_2 - \mathrm{P}_3 = 0.5625$$

Clearly this result does not prove that "Quantum interference between many different pathways is simply the sum of the effects from all pairs of pathways." Why is it necessary to subtract P_1, P_2 and P_3 from the two-path interference terms if they are what it's all about?

The previous Feynman calculation produces the same result using a more transparent method; add the probability amplitudes for the three paths to the detector and square the absolute magnitude.

$$(|A_1 + A_2 + A_3|)^2 = 0.5625$$

$$(|\mathrm{R}\cdot\mathrm{M}\cdot\mathrm{T}\cdot\mathrm{T} + \mathrm{T}\cdot\mathrm{R}\cdot\mathrm{R}\cdot\mathrm{T} + \mathrm{T}\cdot\mathrm{T}\cdot\mathrm{M}\cdot\mathrm{R}|)^2 = 0.5625$$

Objection to the Definitions

Sinha et al. write the double-slit wave function (unnormalized) as a linear superposition of the photon taking two paths (A and B) to the detector. The square modulus of the wave function gives the probability expression.

$$|\Psi|^2 = |\psi_A|^2 + |\psi_B|^2 + \psi_A^* \psi_B + \psi_B^* \psi_A$$

Obviously this is just traditional quantum mechanical mathematical procedure. The problem I have is with the interpretation or partition of this equation that comes next. The authors write the probability expression as

$$|\Psi|^2 = P_A + P_B + I_{AB}$$

where P_A(P_B) is the probability that only slit A(B) is open and the remaining terms represent the actual interference. I do not believe this sort of partitioning of the terms of $|\Psi|^2$ is quantum mechanically legitimate. If only slit A is open then the wave

function is $\Psi = \Psi_A$ and not $\Psi = \Psi_A + \Psi_B$. It is incorrect to say, in the double-slit experiment, that $|\Psi_A|^2$ is the probability that the photon goes through slit A.

As Roy Glauber has written [AJP **63**, 12 (1995)], "The things that interfere in quantum mechanics ... are the probability amplitudes for certain events." The triple-slit experiment involves the interference of three probability amplitudes because there are three paths from the source (S) to each position (x) on the detection screen. According to quantum fundamentals, each photon takes all three paths simultaneously.

$$\Psi_{123} = \langle x|S\rangle = \langle x|3\rangle\langle 3|S\rangle + \langle x|2\rangle\langle 2|S\rangle + \langle x|1\rangle\langle 1|S\rangle$$

In Chapter 3 of Volume III of *The Feynman Lectures* on Physics, Feynman discusses a diffraction experiment in which a two-slit screen followed by a three-slit screen are placed before the detection screen providing six paths to any point on the detection screen. Feynman's analysis leads to the following probability amplitude for the particle to be detected at x.

$$\begin{aligned}\langle x|S\rangle = {} & \langle x|a\rangle\langle a|1\rangle\langle 1|S\rangle + \langle x|b\rangle\langle b|1\rangle\langle 1|S\rangle + \langle x|c\rangle\langle c|1\rangle\langle 1|S\rangle + \langle x|a\rangle\langle a|2\rangle\langle 2|S\rangle \\ & + \langle x|b\rangle\langle b|2\rangle\langle 2|S\rangle + \langle x|c\rangle\langle c|2\rangle\langle 2|S\rangle\end{aligned}$$

Or more succinctly (Feynman's equation 3.6 on page 3-4 of Volume III)

$$\langle x|S\rangle = \sum_{\substack{i=1,2 \\ \alpha=a,b,c}} \langle x|\alpha\rangle\langle\alpha|i\rangle\langle i|S\rangle$$

In summary, these superpositions of probability amplitudes are simple examples of Feynman's sum-over-histories approach to quantum mechanics, of which the double-slit experiment is the simplest example. It is clear that pair wise interference is not suggested in this approach, except for the double-slit experiment and then only because in that case there are only two paths. Feynman's rule is, sum the amplitudes for all paths to allow for interference before squaring the absolute magnitude of the sum to obtain the probability.

Freeman Dyson had the following reaction when he first heard of Feynman's novel approach to quantum mechanics. "Thirty-one years ago, Dick Feynman told me about his 'sum over histories' version of quantum mechanics. 'The electron does anything it likes,' he said. 'It just goes in any direction, at any speed, forward or backward in time, however it likes, and then you add up the amplitudes and it gives you the wave function.' I said to him 'You're crazy.' But he isn't."

This page titled 1.53: An Analysis of Three-Path Interference is shared under a CC BY 4.0 license and was authored, remixed, and/or curated by Frank Rioux via source content that was edited to the style and standards of the LibreTexts platform.

1.54: An Analysis of Three-Slit Interference

Quantum mechanics teaches that if there is more than one path to a particular destination interference effects are likely. Using Feynman's 'sum over histories' approach to quantum mechanics the probability of arrival at a location is the square of the magnitude of the sum of the probability amplitudes for each path to that location. For example, in the triple-slit diffraction experiment the probability of a photon leaving a source and arriving at x on the detection screen shows three-path interference.

$$P_{123} = |\langle x \mid 1\rangle\langle 1 \mid S\rangle + \langle x \mid 2\rangle\langle 2 \mid S\rangle + \langle x \mid 3\rangle\langle 3 \mid S\rangle|^2 \tag{1.54.1}$$

However, Sinha et al. [Science 329, 418 (2010)] argue that true interference only occurs between pairs of paths. In this case between paths 1 & 2, 1 & 3, and 2 & 3. Sinha's interpretation of triple-slit diffraction leads to an expression that is complex when compared to the lean equation above.

$$\begin{aligned} P_{123} = {} & |\langle x \mid 1\rangle\langle 1 \mid S\rangle + \langle x \mid 2\rangle\langle 2 \mid S\rangle|^2 + |\langle x \mid 1\rangle\langle 1 \mid S\rangle + \langle x \mid 3\rangle\langle 3 \mid S\rangle|^2 \\ & + |\langle x \mid 2\rangle\langle 2 \mid S\rangle + \langle x \mid 3\rangle\langle 3 \mid S\rangle|^2 - |\langle x \mid 1\rangle\langle 1 \mid S\rangle|^2 \\ & - |\langle x \mid 2\rangle\langle 2 \mid S\rangle|^2 - |\langle x \mid 3\rangle\langle 3 \mid S\rangle|^2 \end{aligned} \tag{1.54.2}$$

It will now be shown that the two expressions, as they must, lead to the same calculated diffraction pattern. My question is whether there is any real physical significance to Sinha's reinterpretation of multi-path interference in terms of two-path interference effects.

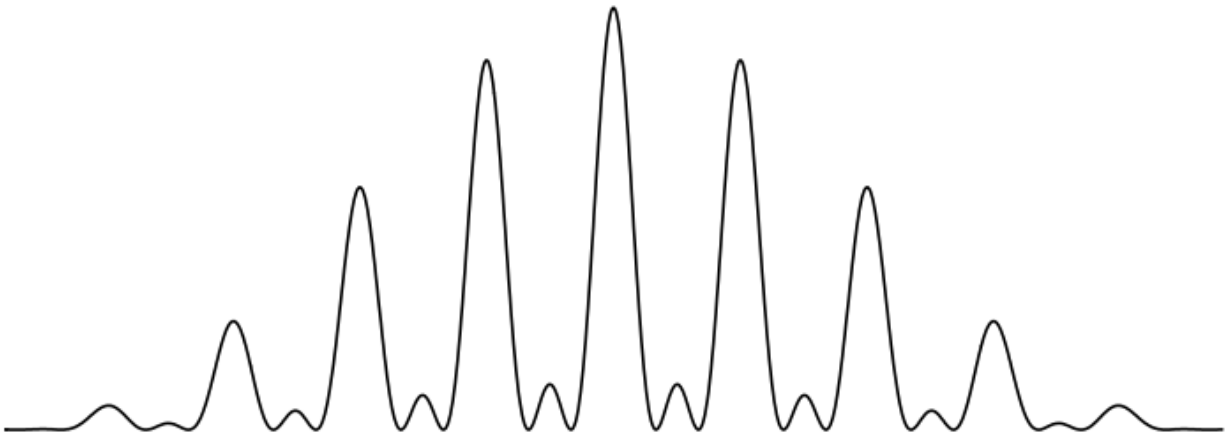
We begin with the traditional approach of writing the photon wave function as a superposition of being at all three slits and then Fourier transforming it into momentum space to give the diffraction pattern.

number of slit: $\mathrm{n} := 3$

Slit position: $\mathrm{j} := 1..\mathrm{n} \quad \mathrm{x_j} := \mathrm{j}$

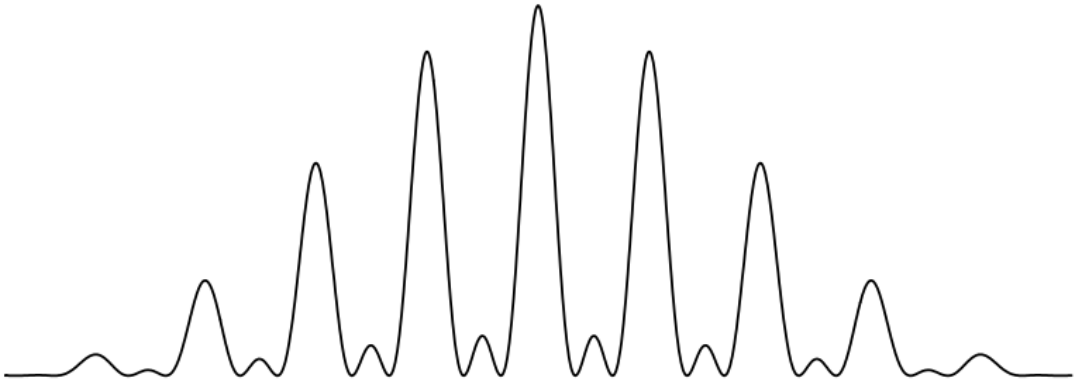
Slit width: $\delta := .2$

Calculate diffraction pattern: $\Psi(\mathrm{p}) := \left(\left| \sum_{j=1}^{\mathrm{n}} \int_{\mathrm{x_j}-\frac{\delta}{2}}^{x_j+\frac{\delta}{2}} \frac{1}{\sqrt{2\cdot\pi}} \cdot \exp(-\mathrm{i}\cdot \mathrm{p}\cdot \mathrm{x}) \cdot \frac{1}{\sqrt{\delta}} \mathrm{dx} \right| \right)^2$



Next, following Sinha, the diffraction pattern is recalculated using equation (1.54.2). This equation is a generalization of the double-slit probability expression as shown in the Appendix.

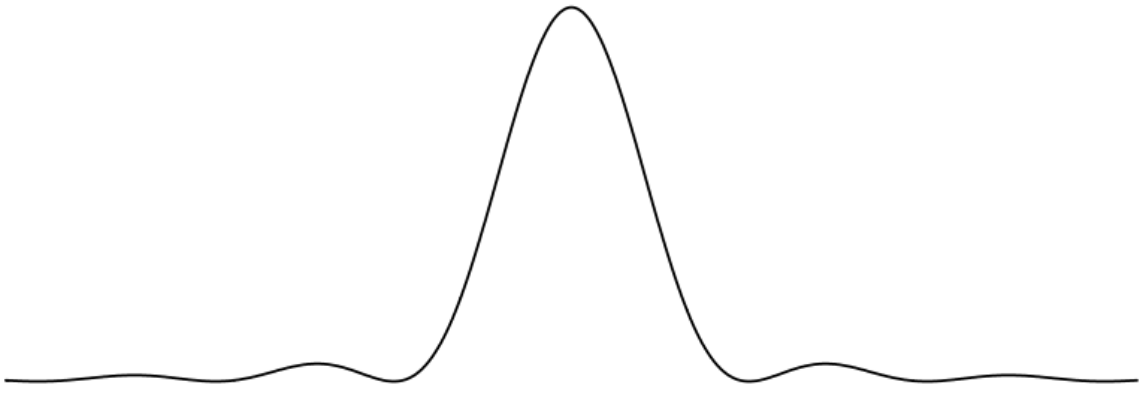
$$P_{123} = P_1 + P_2 + P_3 + I_{12} + I_{13} + I_{23} = P_{12} + P_{13} + P_{23} - P_1 - P_2 - P_3$$



Franson [Science 329, 396 (2010)] summarized this view as follows: "Quantum interference between many different pathways is simply the sum of the effects from all pairs of pathways." If that is so why is it necessary to subtract the single-slit diffraction patterns?

$$P_{1\text{ slit}}(p) := \left(\left|\int_{-\frac{\delta}{2}}^{\frac{\delta}{2}} \frac{1}{\sqrt{2\cdot\pi}} \cdot \exp(-i\cdot p\cdot x)\cdot\frac{1}{\sqrt{\delta}}dx\right|\right)^2$$

$$\begin{aligned}\Psi(\mathrm{p}) = &\left(\left|\int_{1-\frac{\delta}{2}}^{1+\frac{\delta}{2}} \frac{1}{\sqrt{2\cdot\pi}}\cdot\exp(-\mathrm{i}\cdot\mathrm{p}\cdot\mathrm{x})\cdot\frac{1}{\sqrt{\delta}}\mathrm{dx} + \int_{2-\frac{\delta}{2}}^{2+\frac{\delta}{2}} \frac{1}{\sqrt{2\cdot\pi}}\cdot\exp(-\mathrm{i}\cdot\mathrm{p}\cdot\mathrm{x})\cdot\frac{1}{\sqrt{\delta}}\mathrm{dx}\right|\right)^2 \\ &+ \left(\left|\int_{1-\frac{\delta}{2}}^{1+\frac{\delta}{2}} \frac{1}{\sqrt{2\cdot\pi}}\cdot\exp(-\mathrm{i}\cdot\mathrm{p}\cdot\mathrm{x})\cdot\frac{1}{\sqrt{\delta}}\mathrm{dx} + \int_{3-\frac{\delta}{2}}^{3+\frac{\delta}{2}} \frac{1}{\sqrt{2\cdot\pi}}\cdot\exp(-\mathrm{i}\cdot\mathrm{p}\cdot\mathrm{x})\cdot\frac{1}{\sqrt{\delta}}\mathrm{dx}\right|\right)^2 \\ &+ \left(\left|\int_{2-\frac{\delta}{2}}^{2+\frac{\delta}{2}} \frac{1}{\sqrt{2\cdot\pi}}\cdot\exp(-\mathrm{i}\cdot\mathrm{p}\cdot\mathrm{x})\cdot\frac{1}{\sqrt{\delta}}\mathrm{dx} + \int_{3-\frac{\delta}{2}}^{3+\frac{\delta}{2}} \frac{1}{\sqrt{2\cdot\pi}}\cdot\exp(-\mathrm{i}\cdot\mathrm{p}\cdot\mathrm{x})\cdot\frac{1}{\sqrt{\delta}}\mathrm{dx}\right|\right)^2 \\ &+ -3\left(\left|\int_{-\frac{\delta}{2}}^{\frac{\delta}{2}} \frac{1}{\sqrt{2\cdot\pi}}\cdot\exp(-\mathrm{i}\cdot\mathrm{p}\cdot\mathrm{x})\cdot\frac{1}{\sqrt{\delta}}\mathrm{dx}\right|\right)^2\end{aligned}$$



A 1980 reminiscence by Freeman Dyson is relevant to my critque.

> Thirty-one years ago Dick Feynman told me about his ′sum over histories′ version of quantum mechanics. "The electron does anything it likes," he said. "It just goes in any direction, at any speed, forward and backward in time, however it likes, and then you add up the amplitudes and it gives you the wave function." I said to him "You′re crazy." But he isn′t.

It is obvious from Feynman′s description of his ′sum over histories′ approach to quantum interference that it puts no restriction on the number of interfering probability amplitudes.

The conceptual and mathematical clarity of Equation (1.54.1) is lost in the transition to Equation (1.54.2), which consists of three two-path interferences and three single-slit diffraction terms. Consequently Equation (1.54.2) does not actually show that the triple-slit experiment involves only the interference of pairs of paths.

Appendix

The probability expression for an event involving two equivalent paths is

$$P_{ij} = |\Psi_i + \Psi_j|^2 = |\Psi_i|^2 + |\Psi_j|^2 + \Psi_i^* \Psi_j + \Psi_j^* \Psi_i = P_i + P_j + I_{ij}$$

where I_{ij} is the interference term and Pi is defined as the probability when only the i_{th} path is open. It is my opinion that this latter designation is not strictly valid. However, accepting it for the time being leads to the following definition for two-path interference.

$$I_{ij} = P_{ij} - P_i - P_j$$

Therefore, the probability for an event involving three equivalent paths to a destination using only two-path interference is,

$$P_{123} = P_1 + P_2 + P_3 + I_{12} + I_{13} + I_{23} = P_{12} + P_{13} + P_{23} - P_1 - P_2 - P_3$$

This page titled 1.54: An Analysis of Three-Slit Interference is shared under a not declared license and was authored, remixed, and/or curated by Frank Rioux via source content that was edited to the style and standards of the LibreTexts platform.

1.55: Using a Mach-Zehnder Interferometer to Illustrate Feynman's Sum Over Histories Approach to Quantum Mechanics

> *Thirty-one years ago Dick Feynman told me about his 'sum over histories' version of quantum mechanics. "The electron does anything it likes," he said. "It just goes in any direction, at any speed, forward and backward in time, however it likes, and then you add up the amplitudes and it gives you the wave function." I said to him "You're crazy." But he isn't.* ***Freeman Dyson, 1980.***

In Volume 3 of the celebrated *Feynman Lectures on Physics*, Feynman uses the double-slit experiment as the paradigm for his 'sum over histories' approach to quantum mechanics. He said that any question in quantum mechanics could be answered by responding, "You remember the experiment with the two holes? It's the same thing." And, of course, he's right.

A 'sum over histories' is a superposition of probability amplitudes for the possible experimental outcomes which in quantum mechanics carry phase and therefore interfer constructively and destructively with one another. The square of the magnitude of the superposition of histories yields the probabilities that the various experimental possibilities will be observed.

Obviously it takes a minum of two 'histories' to demonstrate the interference inherent in the quantum mechanical superposition. And, that's why Feynman chose the double-slit experiment as the paradigm for quantum mechanical behavior. The two slits provide two paths, or 'histories' to any destination on the detection screen. In this tutorial a close cousin of the double-slit experiment, single particle interference in a Mach-Zehnder interferometer, will be used to illustrate Feynman's 'sum over histories' approach to quantum mechanics.

A Beam Splitter Creates a Quantum Mechanical Superposition

Single photons emitted by a source (S) illuminate a 50-50 beam splitter (BS). Mirrors (M) direct the photons to detectors D_1 and D_2. The probability amplitudes for transmission and reflection are given below. By convention a 90 degree phase shift (i) is assigned to reflection.

Probability amplitude for photon transmission at a 50-50 beam splitter:

$$\langle T|S\rangle = \frac{1}{\sqrt{2}}$$

Probability amplitude for photon reflection at a 50-50 beam splitter:

$$\langle R|S\rangle = \frac{i}{\sqrt{2}}$$

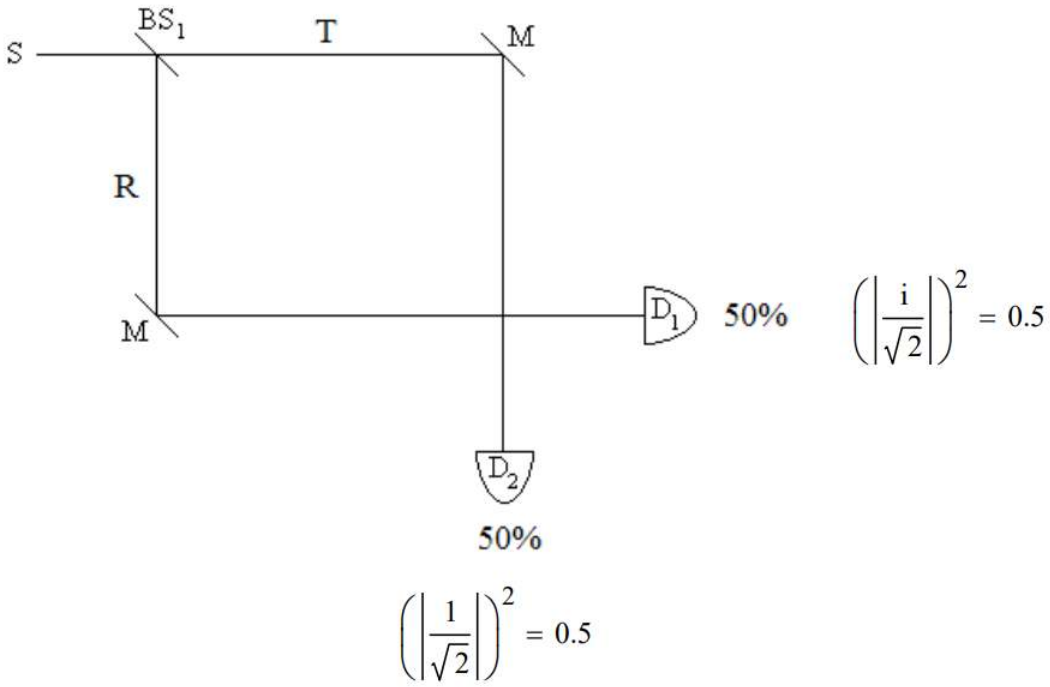
After the beam splitter the photon is in a superposition state of being transmitted and reflected.

$$|S\rangle \rightarrow \frac{1}{\sqrt{2}}[|T\rangle + i|R\rangle]$$

As shown in the diagram below, mirrors reflect the transmitted photon path to D_2 and the reflected path to D_1. The source photon is expressed in the basis of the detectors as follows.

$$|S\rangle \rightarrow \frac{1}{\sqrt{2}}[|T\rangle + i|R\rangle] \xrightarrow[R\rightarrow D_1]{T\rightarrow D_2} \frac{1}{\sqrt{2}}[|D_2\rangle + i\,|D_1\rangle]$$

The square of the magnitude of the coefficients of D_1 and D_2 give the probabilities that the photon will be detected at D_1 or D_2. Each detector registers photons 50% of the time. In other words, in the quantum view the superposition collapses randomly to one of the two possible measurement outcomes it represents.



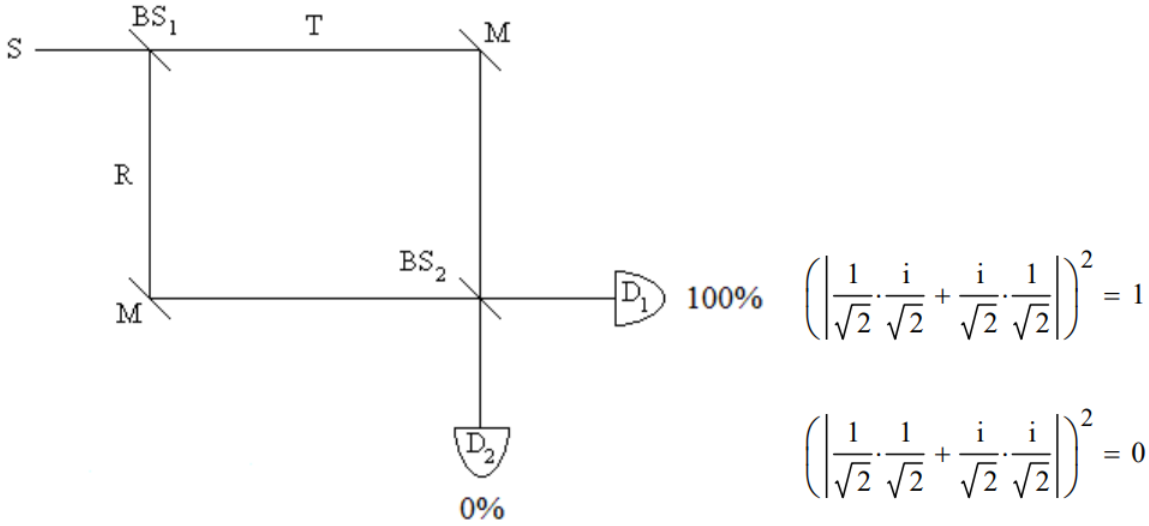
$$\left(\left|\frac{i}{\sqrt{2}}\right|\right)^2 = 0.5$$

$$\left(\left|\frac{1}{\sqrt{2}}\right|\right)^2 = 0.5$$

The classical view that detection at D_1 means the photon was reflected at BS_1 and that detection at D_2 means it was transmitted at BS_1 is not tenable as will be shown using a Mach-Zehnder interferometer which has a second beam splitter at the path intersection before the detectors.

A Second Beam Splitter Provides Two Paths to Each Detector

If a second beam splitter is inserted before the detectors the photons always arrive at D_1. In the first experiment there was only one path to each detector. The construction of a Mach-Zehnder interferometer by the insertion of a second beam splitter creates a second path to each detector and the opportunity for constructive and destructive interference on the paths to the detectors.



$$\left(\left|\frac{1}{\sqrt{2}}\cdot\frac{i}{\sqrt{2}} + \frac{i}{\sqrt{2}}\cdot\frac{1}{\sqrt{2}}\right|\right)^2 = 1$$

$$\left(\left|\frac{1}{\sqrt{2}}\cdot\frac{1}{\sqrt{2}} + \frac{i}{\sqrt{2}}\cdot\frac{i}{\sqrt{2}}\right|\right)^2 = 0$$

Given the superposition state after BS_1, the probability amplitudes after BS_2 interfere constructively at D_1 and destructively at D_2.

$$\begin{array}{ccccc} \text{After } BS_1 & & \text{After } BS_2 & & \text{Final State} \\ & & |T\rangle \rightarrow \frac{1}{\sqrt{2}}\left[i\,|D_1\rangle + |D_2\rangle\right] & & \\ |S\rangle \rightarrow \frac{1}{\sqrt{2}}[|T\rangle + i|R\rangle] & \rightarrow & + & \rightarrow & i\,|D_1\rangle \\ & & i|R\rangle \rightarrow \frac{i}{\sqrt{2}}\left[|D_1\rangle + i\,|D_2\rangle\right] & & \end{array}$$

Adopting the classical view that the photon is either transmitted or reflected at BS_1 does not produce this result. If the photon was transmitted at BS_1 it would have equal probability of arriving at either detector after BS_2. If the photon was reflected at BS_1 it would also have equal probability of arriving at either detector after BS_2. The predicted experimental results would be the same as those of the single beam splitter experiment. In summary, the quantum view that the photon is in a superposition of being transmitted and reflected after BS_1 is consistent with both experimental results described above; the classical view that it is either transmitted or reflected is not.

Some disagree with this analysis saying the two experiments demonstrate the dual, complementary, behavior of photons. In the first experiment particle-like behavior is observed because both detectors register photons indicating the individual photons took one path or the other. The second experiment reveals wave-like behavior because interference occurs - only D_1 registers photons. According to this view the experimental design determines whether wave or particle behavior will occur and somehow the photon is aware of how it should behave. Suppose in the second experiment that immediately after the photon has interacted with BS_1, BS_2 is removed. Does what happens at the detectors require the phenomenon of retrocausality or delayed choice? Only if you reason classically about quantum experiments.

We always measure particles (detectors click, photographic film is darkened, etc.) but we interpret what happened or predict what will happen by assuming wavelike behavior, in this case the superposition created by the initial beam splitter that delocalizes the position of the photon. Quantum particles (quons) exhibit both wave and particle properties in every experiment. To paraphrase Nick Herbert (*Quantum Reality*), particles are always detected, but the experimental results observed are the result of wavelike behavior. Richard Feynman put it this way (*The Character of Physical Law*), "I will summarize, then, by saying that electrons arrive in lumps, like particles, but the probability of arrival of these lumps is determined as the intensity of waves would be. It is in this sense that the electron behaves sometimes like a particle and sometimes like a wave. It behaves in two different ways at the same time (in the same experiment)." Bragg said, "Everything in the future is a wave, everything in the past is a particle."

In 1951 in his treatise *Quantum Theory*, David Bohm described wave-particle duality as follows: "One of the most characteristic features of the quantum theory is the wave-particle duality, i.e. the ability of matter or light quanta to demonstrate the wave-like property of interference, and yet to appear subsequently in the form of localizable particles, even after such interference has taken place." In other words, to explain interference phenomena wave properties must be assigned to matter and light quanta prior to detection as particles.

Matrix Mechanics Approach

As a companion analysis, the matrix mechanics approach to single-photon interference in a Mach-Zehnder interferometer is outlined next.

State Vectors

Photon moving horizontally:

$$\mathrm{x} := \begin{pmatrix} 1 \\ 0 \end{pmatrix}$$

Photon moving vertically:

$$\mathrm{y} := \begin{pmatrix} 0 \\ 1 \end{pmatrix}$$

Operators

Operator representing a beam splitter:

$$BS := \frac{1}{\sqrt{2}} \cdot \begin{pmatrix} 1 & i \\ i & 1 \end{pmatrix}$$

Operator representing a mirror:

$$M := \begin{pmatrix} 0 & 1 \\ 1 & 0 \end{pmatrix}$$

Single beam splitter example:

Reading from right to left.

The probability that a photon leaving the source moving in the (horizontal) x-direction, encountering a beam splitter and a mirror will be detected at D_1.

$$\left(\left|x^T \cdot M \cdot BS \cdot x\right|\right)^2 = 0.5$$

The probability that a photon leaving the source moving in the (horizontal) x-direction, encountering a beam splitter and a mirror will be detected at D_2.

$$\left(\left|y^T \cdot M \cdot BS \cdot x\right|\right)^2 = 0.5$$

Two beam splitter example (MZI):

The probability that a photon leaving the source moving in the (horizontal) x-direction, encountering a beam splitter, a mirror and another beam splitter will be detected at D_1.

$$\left(\left|x^T \cdot BS \cdot M \cdot BS \cdot x\right|\right)^2 = 1$$

The probability that a photon leaving the source moving in the (horizontal) x-direction, encountering a beam splitter, a mirror and another beam splitter will be detected at D_2.

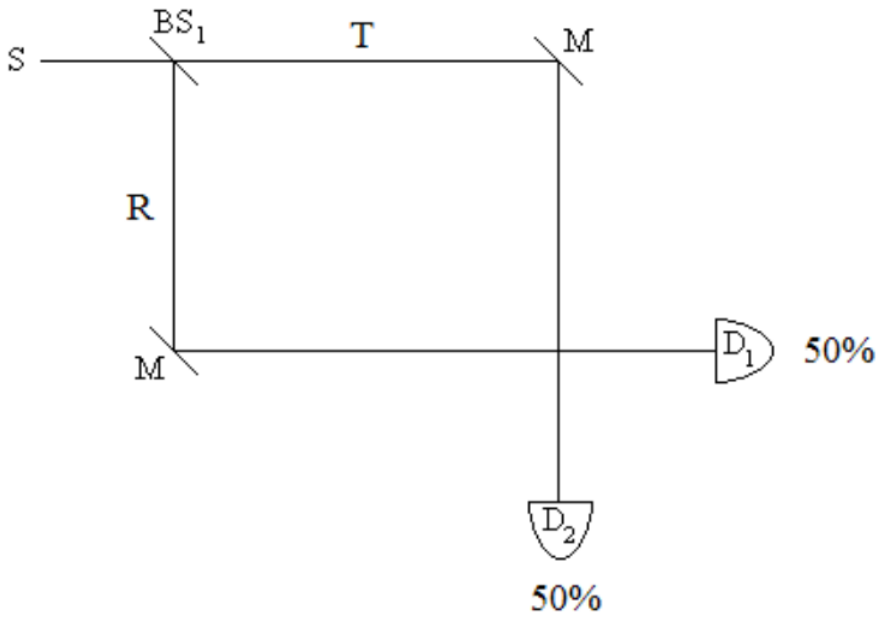
$$\left(\left|y^T \cdot BS \cdot M \cdot BS \cdot x\right|\right)^2 = 0$$

This page titled 1.55: Using a Mach-Zehnder Interferometer to Illustrate Feynman's Sum Over Histories Approach to Quantum Mechanics is shared under a CC BY 4.0 license and was authored, remixed, and/or curated by Frank Rioux via source content that was edited to the style and standards of the LibreTexts platform.

1.56: The Paradox of Recombined Beams

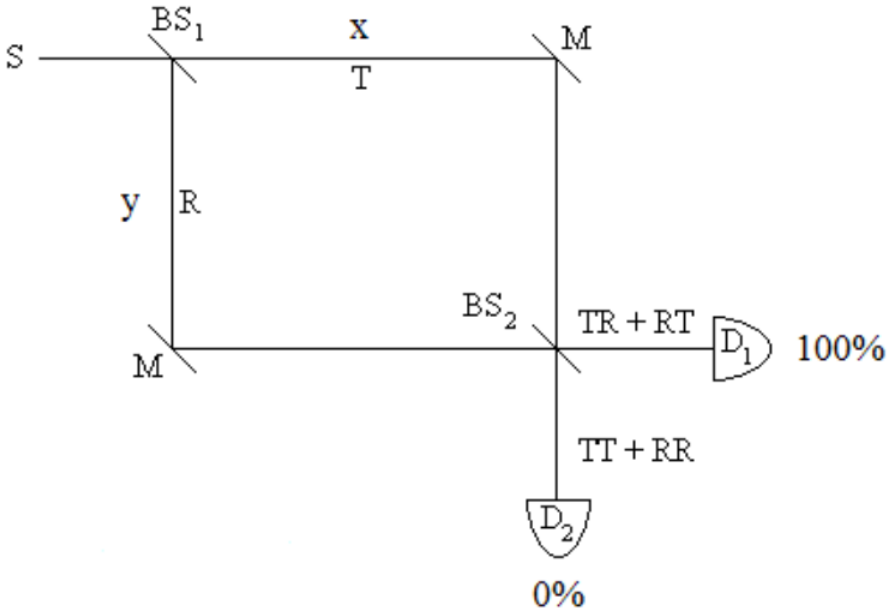
French and Taylor illustrate the paradox of the recombined beams with a series of experiments using polarized photons in section 7-3 in *An Introduction to Quantum Physics*. It is my opinion that it is easier to demonstrate this so-called paradox using photons, beam splitters and mirrors. Of course, the paradox is only apparent, being created by thinking classically about a quantum phenomenon.

Single photons illuminate a 50-50 beam splitter and mirrors direct the photons to detectors D1 and D2. For a statistically meaningful number of observations, it is found that 50% of the photons are detected at D_1 and 50% at D_2. One might, therefore, conclude that each photon is either transmitted or reflected at the beam splitter.



Recombining the paths with a second beam splitter creates a Mach-Zehnder interferometer (MZI). On the basis of the previous reasoning one might expect again that each detector would fire 50% of the time. Half of the photons are in the T branch of the interferometer and they have a 50% chance of being transmitted to D_2 and a 50% chance of being reflected to D_1 at the second beam splitter. The same reasoning applies to the photons in the R branch. However what is observed in an equal arm MZI is that all the photons arrive at D_1.

The reasoning used to explain the first result is plausible, but we see that the attempt to extend it to the MZI shown below leads to a contradiction with actual experimental results. It is clear that some new concepts are required. As will be shown *probability amplitude* and the quantum *superposition* are the required concepts. They will yield predictions that are consistent with all experimental results, but they will require a non-classical, quantum way of thinking that most people find bizarre and a bit unsettling.



A Beam Splitter Creates a Quantum Superposition

The probability amplitudes for transmission and reflection at a beam splitter are given below. By convention a 90 degree phase shift (i) is assigned to reflection to conserve probability.

Probability amplitude for transmission at a 50-50 beam splitter:

$$\langle T|S\rangle = \frac{1}{\sqrt{2}}$$

Probability amplitude for reflection at a 50-50 beam splitter:

$$\langle R|S\rangle = \frac{i}{\sqrt{2}}$$

After the beam splitter the photon is in a superposition of being transmitted and reflected. In other words according to quantum theory prior to observations the photon state is not |T> or |R>, but |T> and |R>. Observation causes the superposition to collapse with equal probability to either |T> (|D_2>) or |R> (|D_1>) according to the Born rule and the Copenhagen interpretation.

$$\mathrm{S} = \frac{1}{\sqrt{2}} \cdot (\mathrm{T} + \mathrm{iR})$$

As shown in the first diagram, mirrors direct the transmitted photon to D_2 and the reflected photon to D_1. This can be expressed quantum mechanically as shown below.

$$\mathrm{T} = \mathrm{D}_2 \qquad \mathrm{R} = \mathrm{D}_1$$

Expressing the source photon in the basis of the detectors we have,

$$\mathrm{S} = \frac{1}{\sqrt{2}} \cdot (\mathrm{T} + \mathrm{iR}) \Big|_{\substack{\text{substitute, R=D}_1 \\ \text{substitute, T=D}_2}} \rightarrow \mathrm{S} = \sqrt{2} \cdot \left(\frac{\mathrm{D}_2}{2} + \frac{\mathrm{D}_1 \cdot \mathrm{i}}{2} \right)$$

The magnitude squared of the coefficients of D_1 and D_2 gives the probabilities that the photon will be detected at D_1 and D_2. As shown below, each detector registers photons 50% of the time in agreement with experiment.

$$\text{Probability } \mathrm{D}_1 = \left(\left| \frac{\mathrm{i} \cdot \sqrt{2}}{2} \right| \right)^2 \rightarrow \text{ Probability } \mathrm{D}_1 = \frac{1}{2}$$

$$\text{Probability } D_2 = \left(\left|\frac{\sqrt{2}}{2}\right|\right)^2 \rightarrow \text{ Probability } D_2 = \frac{1}{2}$$

A Second Beam Splitter Allows Probability Amplitudes to Interfere

The presence of the second beam splitter provides two paths to each detector and the opportunity for the interference of the probability amplitudes. The probability amplitudes for the paths to D_1 interfere constructively, while the probability amplitudes for the paths to D_2 interfere destructively. Thus, the evolution of |T> and |R> at the second beam splitter result in the photon always arriving at D_1.

$$T = \frac{1}{\sqrt{2}} \cdot (i \cdot D_1 + D_2) \qquad R = \frac{1}{\sqrt{2}} \cdot (D_1 + i \cdot D_2)$$

$$S = \frac{1}{\sqrt{2}} \cdot (T + iR) \left| \begin{array}{l} \text{substitute }, T = \frac{1}{\sqrt{2}} \cdot (i \cdot D_1 + D_2) \\ \text{substitute, } R = \frac{1}{\sqrt{2}} \cdot (D_1 + i \cdot D_2) \\ \text{simplify} \end{array} \right. \rightarrow S = D_1 \cdot i$$

$$\text{Probability } D_1 = (|i|)^2 \rightarrow \text{ Probability } D_1 = 1$$

"The things that interfere in quantum mechanics are are the probability amplitudes for certain events. It is the fact that probability amplitudes add up like complex numbers that accounts for all quantum mechanical interferences." [Roy Glauber, *American Journal of Physics* **63**, 12 (1995)]

This page titled 1.56: The Paradox of Recombined Beams is shared under a CC BY 4.0 license and was authored, remixed, and/or curated by Frank Rioux via source content that was edited to the style and standards of the LibreTexts platform.

1.57: Evidence for Quantized Gravitational States of the Neutron

Particle confinement and the wave-like properties of matter lead, according to quantum mechanical principles, to self-interference which is the origin of energy quantization. The particle-in-a-box problem is used in introductory quantum mechanics courses to illustrate this fundamental quantum effect.

Terrestrial objects are confined by the Earth's gravitational field, but the quantum effects of gravity are not observed in the macro-world because the gravitational interaction is weak. Thus, the gravitational energy levels are very closely spaced and for all practical purposes form a continuum.

In spite of the lack of evidence for quantized gravitational energy levels, the "quantum bouncer" has been a favorite example in the repertoire of solvable one-dimensional problems for those who teach quantum chemistry and quantum physics. Schrödinger's equation for the quantum bouncer near the surface of the Earth is,

$$-\frac{\hbar^2}{2m}\frac{d^2\Psi(z)}{dz^2} + mgz\Psi(z) = E\Psi(z)$$

where the particle is confined by the impenetrable potential barrier of the Earth's surface (V = ∞) and the attractive gravitational interaction (V = mgz for z > 0).

The energy eigenvalues for the quantum bouncer are (*1*,*2*,*3*),

$$E_i = \left(\frac{\hbar^2 g^2 m}{2}\right)^{\frac{1}{3}} a_i$$

where a_i are the roots of the Airy function. The first five roots are 2.33810, 4.08794, 5.52055, 6.78670, and 7.94413.

The associated eigenfunctions are,

$$\Psi_i(z) = N_i Ai\left[\left(\frac{2m^2 g}{\hbar^2}\right)^{1/3} z - a_i\right]$$

where

$$N_i = \left(\int_0^\infty \Psi_i(z)^2 dz\right)^{-1/2}$$

Because there is no analytical expression for the eigenfunctions each one must be normalized using a numeric algorithm.

Very recently an international team at the Institute Laue-Langevin in Grenoble France lead by V. Nesvizhevsky (*4*) published evidence for the quantized gravitational states of the neutron. To read a short summary of this experiment in *Nature Magazine* by Thomas Bowles (*5*) click here. Another summary has just been published in *Physics Today*. (*6*)

To appreciate the significance of this accomplishment we calculate the neutron's ground state energy and wave function in the Earth's gravitational field using the equations above. The mass of the neutron is 1.675×10^{-27} kg which yields a ground-state energy of $E_1 = 2.254 \times 10^{-31}$ J. This corresponds to a classical vertical velocity of 1.6 cm/s. Thus gravitational confinement requires a source of ultra-cold neutrons (UCNs).

Furthermore, the energy of the first excited state is 3.941×10^{-31} J, so the energy difference between the ground state and the first excited state is equivalent to photon with a wavelength of 1.2×10^{6} m. Clearly traditional spectroscopic methods cannot be used to establish the existence of quantized gravitational states for the neutron.

The probability distributions, $\Psi(z)^2$, for the ground and first excited states are shown in Figures 1 and 4. They hold the key to the experimental design that Nesvizhevsky's and his group used to establish that the neutron's gravitational states are quantized. To down-load a Mathcad file that will generate the neutron eigenstates numerically click here.

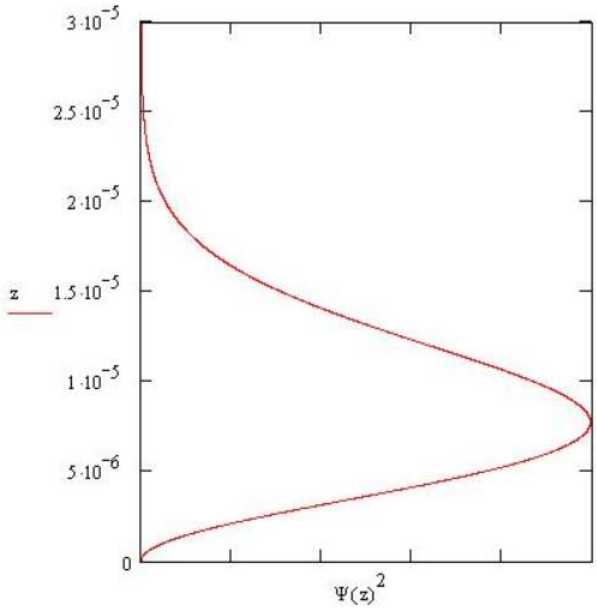


Figure 1

Figure 2. The neutron is confined by the attractive gravitational field and the repulsive reflecting mirror surface. Ultra-cold neutrons (UCNs) with total velocities less than 8 m/s are "lobbed" into the apparatus. In the vertical direction the neutrons are subject to the gravitational interaction with the Earth, but there are no forces in the horizontal direction. The vertical and horizontal degrees of freedom are independent of one another in the design of this experiment, because care has been taken to eliminate vibrations, and extraneous electric and magnetic fields.

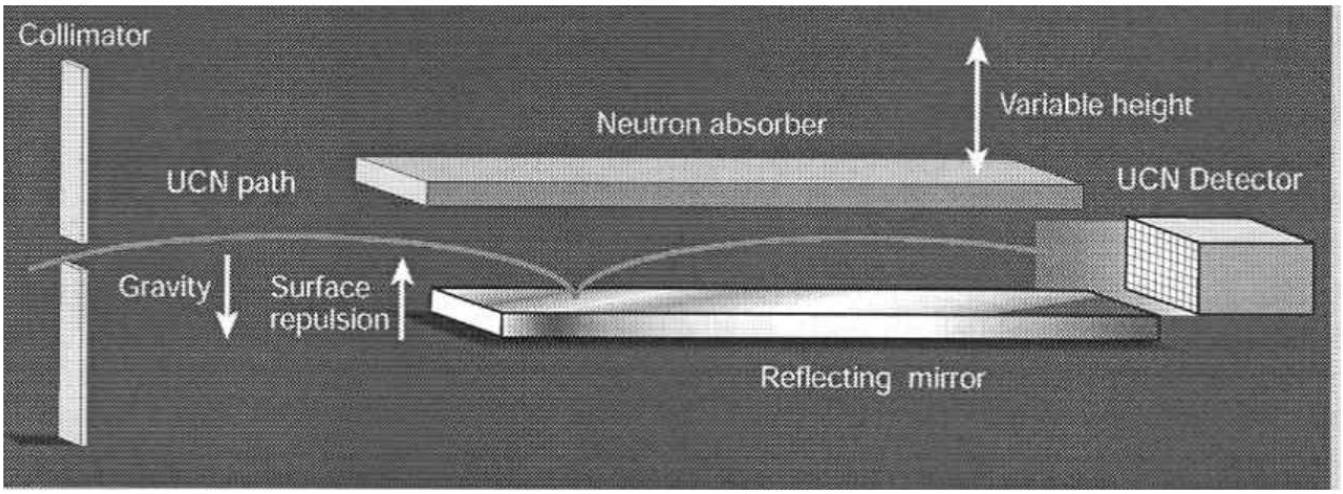


Figure 2 [Reprinted by permission from Nature (Volume **415** page 267) copyright 2002 Macmillan Publishers Ltd.]

The apparatus shown in Figure 2 records neutron throughput as a function of absorber height. The data collected are shown in Figure 3. The shaded circles are the actual data points. We will not be concerned with the solid, dashed, or dotted lines in the figure. The most important feature of the data for this analysis is the sharp increase in neutron throughput at about 20 μm.

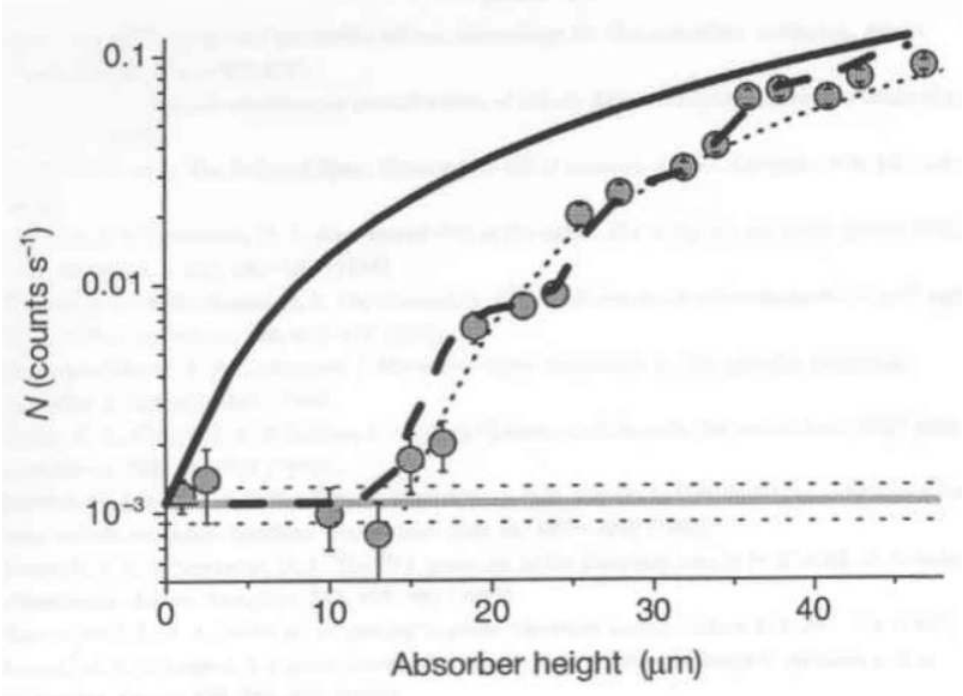


Figure 3 [Reprinted by permission from Nature (Volume **415** page 299) copyright 2002 Macmillan Publishers Ltd.]

The argument will be made that the neutron wave function shown in Figure 1 is consistent with the data presented in Figure 3. To demonstrate this we calculate the probability that the ground-state neutron will be found in the absorber for a variety of absorber heights. This requires numerical evaluation of

$$\int_{a_z}^{\infty} \Psi_1(z)^2 dz$$

where a_z is the absorber height. These calculations are presented in the table given below.

Absorber height/mm	Probability in Absorber
10	0.380
15	0.089
20	0.012
25	0.001

It is clear from these calculations and Figure 1 that the probability of finding the neutron in the absorber falls off sharply at about 20 μm. This analysis, therefore, is consistent with the sharp increase in neutron throughput at this absorber height.

Many neutron gravitational states besides the ground state are occupied and it is therefore necessary to explore the experimental implications of this fact. The first excited state is, as mentioned previously, shown in Figure 4. This wave function extends further in the z-direction than the ground state function, going to zero around 35 μm. The experimental significance of this is that the neutron throughput should show another abrupt increase in the neighborhood of 30 μm, an absorber height for which, the first excited state neutrons have a low probability of being absorbed. This phenomena should be repeated for all other occupied excited states as the absorber reaches the spatial extent of each excited state wave function.

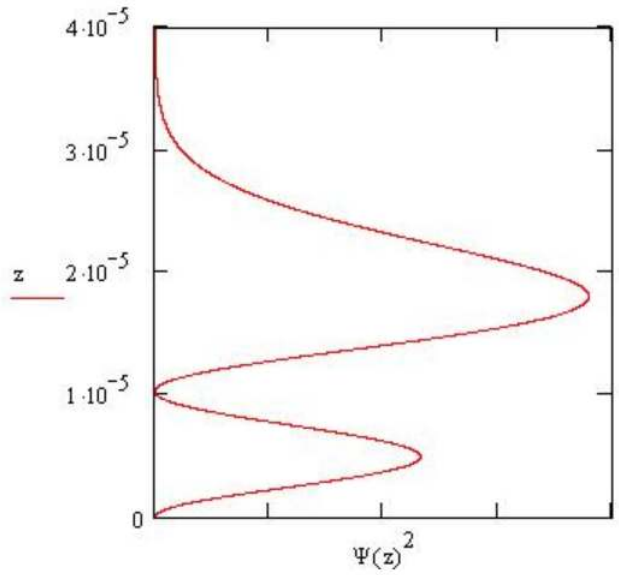


Figure 4

With regard to this expected effect Bowles has commented (5)

> *The data show some hint of stepped increases at the values corresponding to higher energy states, consistent with the existence of these states, but they are not yet conclusive. Nonetheless, the evidence for the existence of the first energy state is convincing and confirms that a quantum effect occurs in the gravitational trap. The difficulty of this measurement should not be underestimated. The researchers are measuring a quantum effect caused by gravity that requires a resolution of 10^{-15} eV. Interactions of the neutrons with other fields would normally obscure such a tiny effect, but the neutron's lack of electric charge and the low kinetic energy of the UCNs make such observations possible.*

In summary, thanks to Nesvizhevsky and his team, we now have some direct evidence for quantized gravitational states. The "quantum bouncer", previously a purely academic exercise, can now be applied to a real-life example.

Literature cited:

1. P. W. Langhoff, "Schrödinger particle in a gravitational well," *Am. J. Phys.* **39**, 954-957 (1971).
2. R. L. Gibbs, "The quantum bouncer," *Am. J. Phys.* **43**, 25-28 (1975).
3. J. Gea-Banacloche, "A quantum bouncing ball," *Am. J. Phys.* **67**, 776-782 (1999).
4. V. Nesvizhevsky, *et al.*, "Quantum states of neutrons in the Earth's gravitational field," *Nature* **415** 297-299 (2002).
5. T. J. Bowles, "Quantum effects of gravity," *Nature* **415** 267-268 (2002).
6. B. Schwartzchild, "Ultracold Neutrons Exhibit Quantu States in the Earth's Gravitational Field," *Physics Today* **55** (3) 20-23 (2002).

This page titled 1.57: Evidence for Quantized Gravitational States of the Neutron is shared under a CC BY 4.0 license and was authored, remixed, and/or curated by Frank Rioux via source content that was edited to the style and standards of the LibreTexts platform.

1.58: Quantized Gravitational States A Variational Approach

Recently an international team of researchers at the Institute Laue-Langevin in Grenoble France published evidence for the quantized gravitational states of the neutron (1,2,3). The purpose of this paper is to analyze this phenomenon using the variational theorem.

Schrödinger's equation for an object subject to a gravitational field near the surface of the earth is

$$-\frac{h^2}{2m}\frac{d^2\Psi(z)}{dz^2}+mgz\Psi(z)=E\Psi(z)$$

Equation (1) has an exact solution and the ground state energy for the neutron is given by

$$E=2.3381\left(\frac{mg^2h^2}{2}\right)^{\frac{1}{3}}=2.254\times10^{-31}\text{J}$$

where 2.3381 is the first root of the Airy function.

The performance of two trial wave functions for the "quantum bouncer" will be evaluated. The functions given in equations (3) and (4) were previously suggested for this purpose by J. L. Martin (4).

$$\Psi(z)=2\alpha^{\frac{3}{2}}z\exp(-\alpha z)$$

$$\Phi(z)=\left(\frac{128\beta^3}{\pi}\right)^{\frac{1}{4}}z\exp\left(-\beta z^2\right)$$

First Trial Wave Function

Evaluation of the variational integral for Ψ(z) yields

$$\langle E\rangle=\int_0^\infty\Psi(z)\hat{H}\Psi(z)dz=\frac{h^2\alpha^2}{2m}+\frac{3mg}{2\alpha}$$

Minimization of the energy provides the optimum value of α

$$\alpha=\left(\frac{3m^2g}{2h^2}\right)^{\frac{1}{3}}$$

and the ground-state energy.

$$\langle E\rangle=1.9656\left(mg^2h^2\right)^{\frac{1}{3}}=2.387\times10^{-31}\text{J}$$

This result is in error by 6% indicating that Ψ(z) is a reasonable trial wave function for an object subjected to a confining gravitational interaction.

Second Trial Wave Function

It will be seen, however, that Φ(z) is a much better trial wave function. Evaluation of the variational integral yields

$$\langle E\rangle=\int_0^\infty\Phi(z)\hat{H}\Phi(z)dz=\frac{3\hbar^2\beta}{2m}+mg\left(\frac{2}{\pi\beta}\right)^{\frac{1}{2}}$$

Minimization of the energy provides the optimum value of β

$$\beta=\left(\sqrt{\frac{2}{\pi}}\frac{m^2g}{3h^2}\right)^{\frac{2}{3}}$$

and the ground-state energy.

$$\langle E\rangle=\frac{3}{2}\left(\frac{6mg^2h^2}{\pi}\right)^{\frac{1}{3}}=2.260\times10^{-31}\text{J}$$

The error for this trial function is less 0.3%, so it is a very good approximation to the exact wave function.

The trial wave functions are compared with the exact solution in Figure 1 (exact solution, solid blue; Ψ(z) green dots; Φ(z) red dashes.

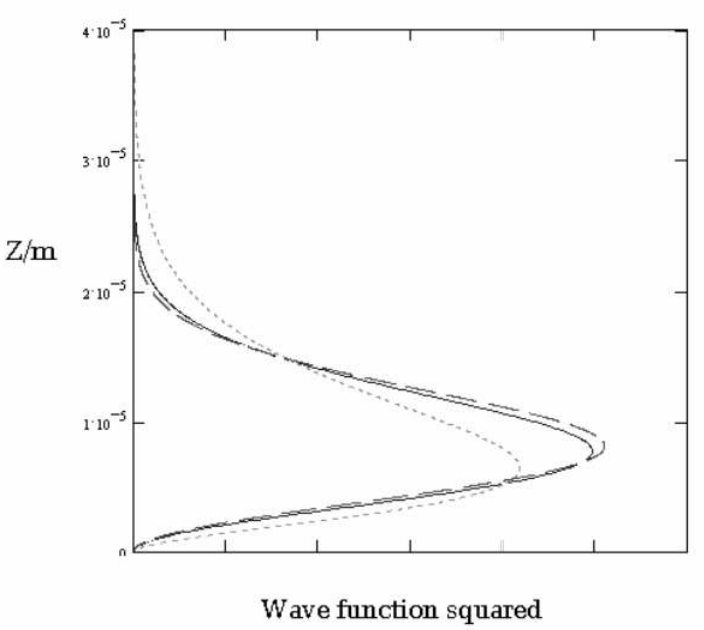


Figure 1

The Experiment

Thus far we have used the exact theoretical ground-state energy as a criterion to evaluate two trial wave functions. However, Nesvizhevsky and co-workers did not use energy or spectroscopy to gather evidence for the quantized gravitational states of the neutron.

This is impractical given how closely spaced the neutron gravitational states are. For example, the first excited state for the neutron is E_2 = 3.941 x 10^{-31} J. Therefore, the energy difference between the ground state and first excited state is equivalent to a photon with a wavelength of 1.2 million meters. Clearly traditional spectroscopic methods cannot be used to establish the existence of quantized gravitational states for the neutron.

A schematic of the experiment Nesvizhevsky's team used to gather evidence for quantized neutron gravitational states is shown in Figure 2. The neutron is confined by the attractive gravitational field and the repulsive reflecting mirror surface. Ultra-cold neutrons (UCNs) with total velocities less than 8 m/s are "lobbed" into the apparatus. In the vertical direction the neutrons are subject to the gravitational interaction with the Earth, but there are no forces in the horizontal direction. The vertical and horizontal degrees of freedom are independent of one another in the design of this experiment, because care has been taken to eliminate vibrations, and extraneous electric and magnetic fields.

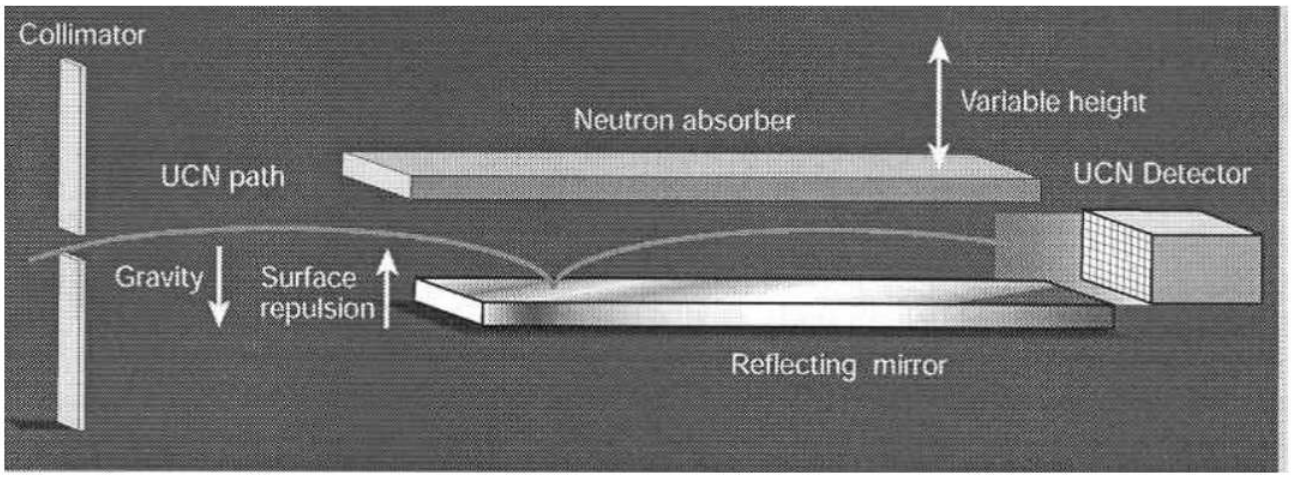


Figure 2 [Reprinted by permission from *Nature* (Volume **415** page 267) copyright 2002 Macmillan Publishers Ltd.]

This apparatus records neutron throughput as a function of absorber height. The data collected are shown in Figure 3. The shaded circles are the actual data points. We will not be concerned with the solid, dashed, or dotted lines in the figure. The most important feature of the data for this analysis is the sharp increase in neutron throughput at about 20 μm.

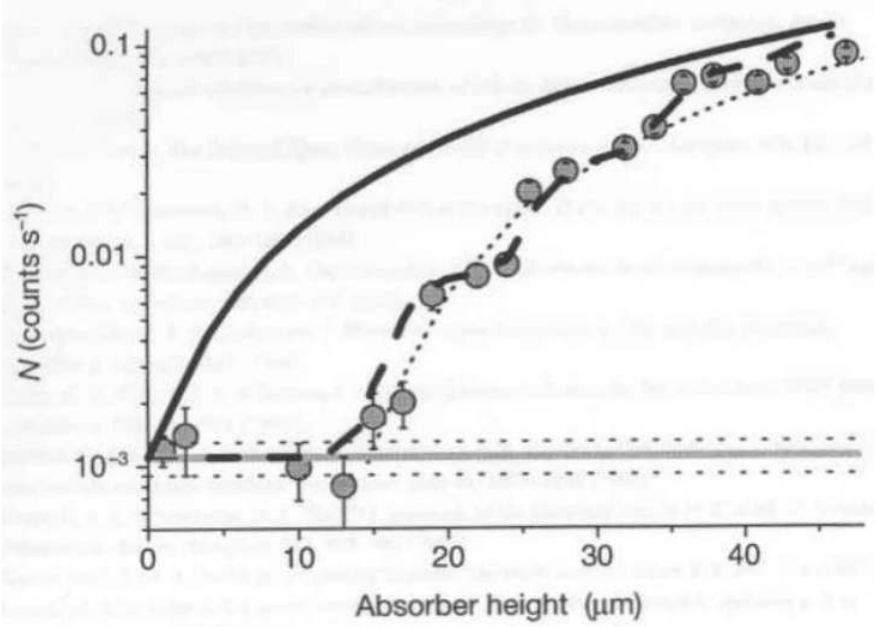


Figure 3 [Reprinted by permission from *Nature* (Volume **415** page 299) copyright 2002 Macmillan Publishers Ltd.]

Interpretation

The probability that a neutron will be found in the absorber, or the probability it will be absorbed is given by

$$\int_{a_z}^{\infty} |\Phi(z)|^2 dz$$

where a_z is the absorber height. Using the second trial wave function the probability is calculated for several absorber heights and displayed in the table below.

Absorber height (μm)	Probability in Absorber
10	0.388
15	0.078
20	0.007
25	3×10^{-4}

It is clear from these calculations that the probability of finding the neutron in the absorber has declined significantly by 20 μm. This analysis, therefore, is consistent with the sharp increase in neutron throughput at this absorber height.

Literature cited:

1. Nesvizhevsky, V.; et al. Quantum States of Neutrons in the Earth's Gravitationsl Field. *Nature* **2002**, *415*, 297-299.
2. Bowles, T. J. Quantum Effects of Gravity. *Nature* **2002**, *415*, 267-268.
3. Rioux, F. Nature: Evidence for Quantized Gravitational States of the Neutron. *J. Chem. Educ.* **2002**, *79*, 1404-1406.
4. Martin, J. L. *Basic Quantum Mechanics;* Clarendon Press, Oxford, 1981, p. 207.

This page titled 1.58: Quantized Gravitational States A Variational Approach is shared under a CC BY 4.0 license and was authored, remixed, and/or curated by Frank Rioux via source content that was edited to the style and standards of the LibreTexts platform.

1.59: The Quantum Bouncer Doesn't Bounce, Unless...

The Earth's gravitational field is a confining potential and according to quantum mechanical principles, confinement gives rise to quantized energy levels. The one-dimensional, time-independent Schrödinger equation for a quantum object (**quon**, to use Nick Herbert's term) in the Earth's gravitational field near the surface is,

$$\frac{-h^2}{8\cdot\pi^2\cdot m}\cdot\frac{d^2}{dz^2}\Psi(z)+m\cdot g\cdot z\cdot\Psi(z)=E\cdot\Psi(z)$$

Here **m** is the mass of the quon, **z** its vertical distance from the Earth's surface, and **g** the acceleration due to gravity.

The solution to Schrödinger's equation for the **mgz** potential energy operator is well-known. The energy eigenvalues and eigenfunctions are expressed in terms of the roots of the Airy function.

$$\mathrm{E_i}=\left(\frac{\mathrm{h^2\cdot g^2\cdot m}}{8\cdot\pi^2}\right)^{\frac{1}{3}}\cdot\mathrm{a_i}\qquad\Psi_\mathrm{i}(\mathrm{z})=\mathrm{N_i}\cdot\mathrm{Ai_i}\cdot\left[\left(\frac{8\cdot\pi^2\cdot\mathrm{m^2\cdot g}}{\mathrm{h^2}}\right)^{\frac{1}{3}}\cdot\mathrm{z}-\mathrm{a_i}\right]$$

The first five roots of the Airy function are presented below.

$$a_1:=2.33810\quad a_2:=4.08794\quad a_3:=5.52055\quad a_4:=6.78670\qquad a_5:=7.94413$$

Time dependence is introduced by multiplying the spatial wave function by $\exp\left(-i\cdot\frac{2\cdot\pi\cdot E_i\cdot t}{h}\right)$. The calculations that follow will be carried out in atomic units. In addition, the acceleration due to gravity and the quon mass will be set to unity for the sake of computational simplicity.

$$\mathrm{h}:=2\cdot\pi\quad\mathrm{g}:=1\quad\mathrm{m}:=1\quad\mathrm{i}:=1\ldots5$$

$$\mathrm{E_i}:=\left(\frac{\mathrm{h^2\cdot g^2\cdot m}}{8\cdot\pi^2}\right)^{\frac{1}{3}}\cdot\mathrm{a_i}$$

The wave functions for the ground state and first excited state are shown below.

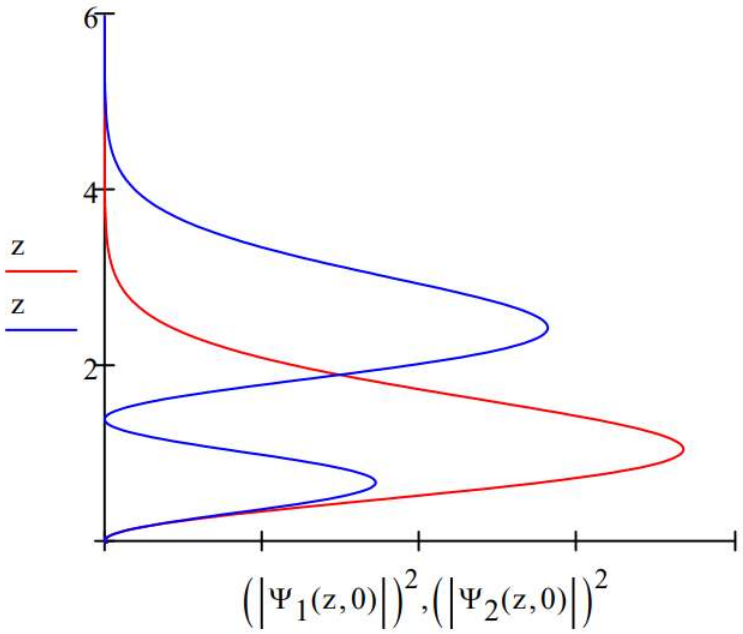
$$\Psi_1(z,t):=1.6\cdot\mathrm{Ai}\left[\left(\frac{8\cdot\pi^2\cdot m^2\cdot g}{h^2}\right)^{\frac{1}{3}}\cdot z-a_1\right]\cdot e^{-i\cdot E_1\cdot t}$$

$$\Psi_2(\mathrm{z,t}):=1.4\cdot\mathrm{Ai}\left[\left(\frac{8\cdot\pi^2\cdot\mathrm{m^2\cdot g}}{\mathrm{h^2}}\right)^{\frac{1}{3}}\cdot\mathrm{z}-\mathrm{a_2}\right]\cdot\mathrm{e}^{-\mathrm{i\cdot E_2\cdot t}}$$

This excercise is usually called the **quantum bouncer**, but the first thing to stress is that these energy eigenfunctions are stationary states. In other words a quon in the Earth's gravitational field is in a state which is a weighted superposition of all possible positions above the surface of the earth which does not vary with time. It is not moving, it is not bouncing in any classical sense.

In other words the behavior of a quon is described by its time-independent distribution function, $|\Psi(z)|^2$, rather than by a trajectory - a sequence of instantaneous positions and velocities. Quantum mechanics predicts the probability of finding the quon at any position above the Earth's surface, but the fact that it can be found at many different locations does not mean it is moving from one position to another. Quantum mechanics predicts the probability of observations, not what happens between two observations.

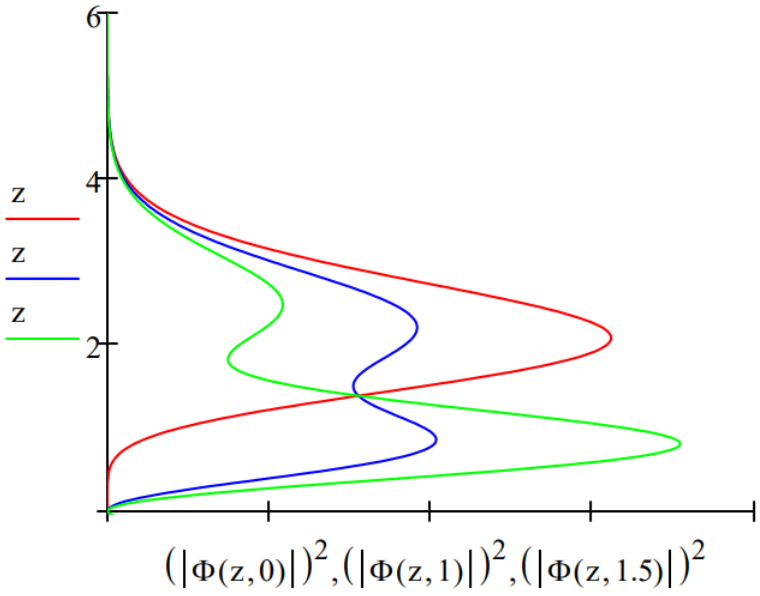
The position distribution functions, $|\Psi(z)|^2$, for the ground- and first-excited state are shown below.



The quantum bouncer doesn't "bounce" until it perturbed and forced into a superposition of eigenstates, for example, the ground- and first-excited states

$$\Phi(z,t) := \frac{\Psi_1(z,t) + \Psi_2(z,t)}{\sqrt{2}}$$

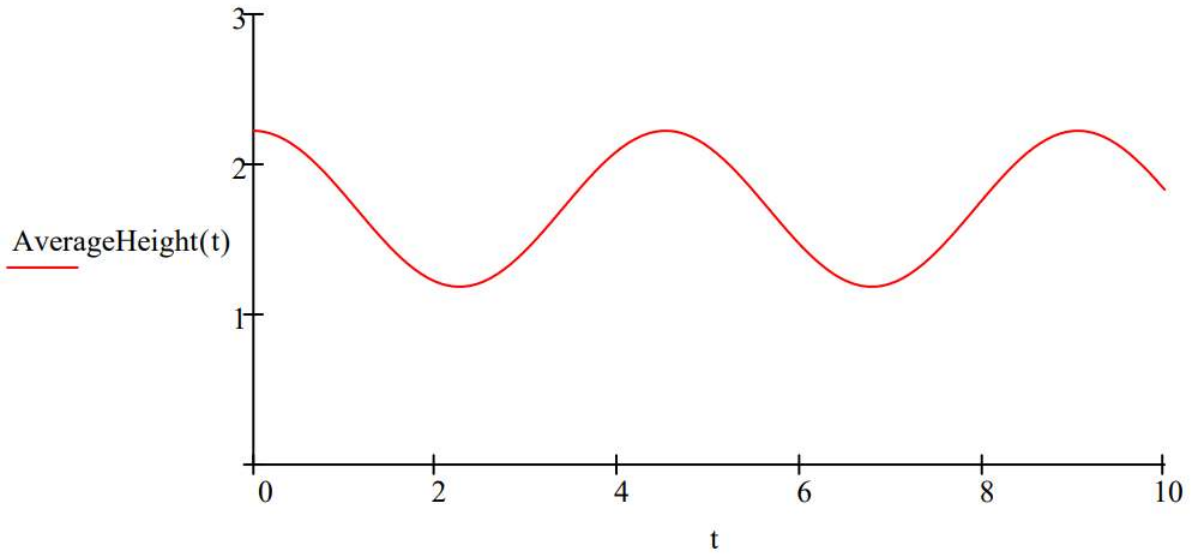
Below the quon distribution function is shown for three different times.



As the figure shows, now there is motion in the gravitational field. The quon is moving up and down, bouncing, because it is in a time-dependent superposition of eigenstates.

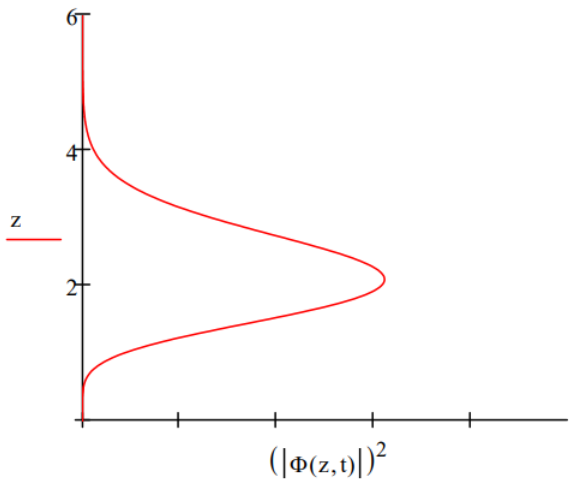
Another way this quantum mechanical "bouncing motion" can be illustrated is by displaying the time-dependence of the average value of the position of the quon in the gravitational field.

$$\text{AverageHeight(t)} := \int_0^\infty z \cdot (|\Phi(z,t)|)^2 dz$$



It is also possible to animate the time-dependent superposition. Click on **Tools, Animation, Record** and follow the instructions in the dialog box. Choose **From: 0, To: 100, At: 6 Frames/Sec.**

t := FRAME



This page titled 1.59: The Quantum Bouncer Doesn't Bounce, Unless... is shared under a CC BY 4.0 license and was authored, remixed, and/or curated by Frank Rioux via source content that was edited to the style and standards of the LibreTexts platform.

1.60: Kinetic Energy Is Important in the Nanoscale World

Most explanations of atomic and molecular phenomena found in textbooks are expressed in terms of potential-energy-only (PEO) models. Inclusion of kinetic energy in the analysis is generally considered to be unnecessary or irrelevant. This view is of questionable validity, and it is becoming increasing clear that ignoring kinetic energy at the nanoscopic level can lead to facile but incorrect explanations of atomic and molecular behavior. (1-4)

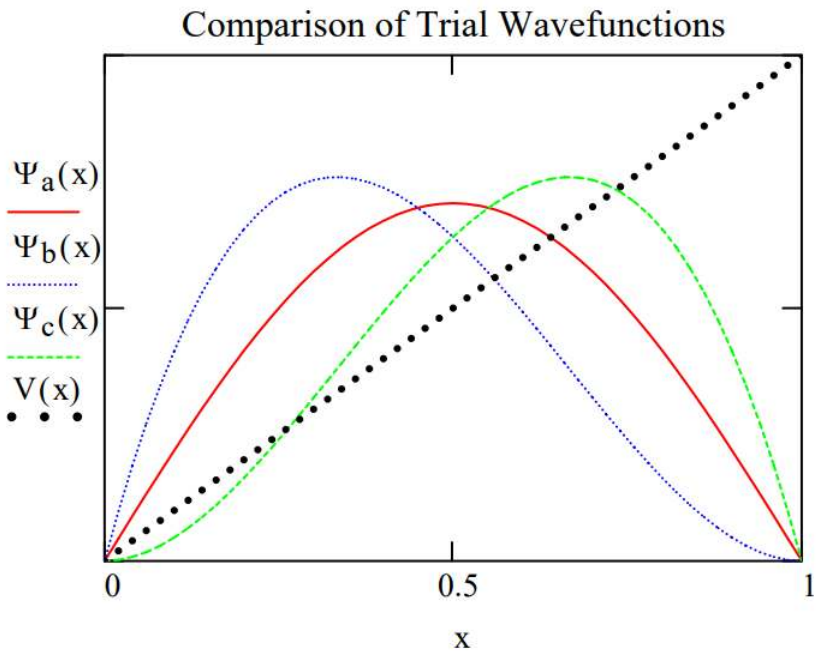
The idea that kinetic energy should not be ignored is not too surprising since quantum mechanical calculations involve minimization of the total energy, which includes both kinetic and potential energy contributions. In other words, kinetic energy plays an important role at the computational level, and therefore should not be excluded at the level of analysis and interpretation. For example, the fundamental questions regarding the stability of matter, the nature of the covalent bond, and the interaction of electromagnetic radiation with matter cannot be answered without a consideration of kinetic energy in the quantum mechanical context. (5)

The following simple variational calculation on a particle in a one-dimensional box with a linear internal potential clearly illustrates the importance of kinetic energy. For a particle of unit mass in a one-dimensional box of length one bohr ($1a_o$ =52.9 pm = 0.0529 nm) with internal potential energy V = 2x the Schrödinger equation in atomic units (h = 2π) is,

$$\frac{-1}{2}\cdot\frac{d^2}{dx^2}\Psi(x)+V(x)\cdot\Psi(x)=E\cdot\Psi(x)\quad\text{where}\quad V(x):=2\cdot x$$

Three normalized trial wave functions are considered in this analysis, and are shown below both mathematically and graphically. The potential energy function is superimposed on the graphical representation of the trial wave functions.

$$\Psi_a(x):=\sqrt{2}\cdot\sin(\pi\cdot x)$$
$$\Psi_b(x):=\sqrt{105}\cdot x\cdot(1-x)^2$$
$$\Psi_c(x):=\sqrt{105}\cdot x^2\cdot(1-x)$$
$$x:=0,0.02\ldots1$$



If asked to choose the best trial wave function by inspection, one would undoubtedly be inclined to select Ψ_b because it is skewed to the left side of the box where the potential energy is lowest. Ψ_a would be next best because it is symmetric, and Ψ_c would be last because it is skewed to the right side of the box where the potential energy is highest. However, the quantum mechanical calculations reveal that Ψ_a is the best trial function of the three because it gives the lowest total energy, the primary criterion of the variational principle.

For each trial wave function the expectation values for kinetic energy (T), potential energy (V), total energy (E = T + V), and position are calculated. Atomic units are used all calculations: $1E_h$ = 4.36 aJ and $1a_o$ = 52.9 pm)

Calculations for trial wave function Ψ_a

Kinetic energy:	$T_a := \int_0^1 \Psi_a(x) \cdot -\frac{1}{2} \cdot \frac{d^2}{dx^2} \Psi_a(x) dx$	$T_a = 4.935$
Potential energy:	$V_a := \int_0^1 \Psi_a(x) \cdot 2 \cdot x \cdot \Psi_a(x) dx$	$V_a = 1.000$
Total energy:	$E_a := T_a + V_a$	$E_a = 5.935$
Average position:	$X_a := \int_0^1 \Psi_a(x) \cdot x \cdot \Psi_a(x) dx$	$X_a = 0.500$

Calculations for trial wave function Ψ_b

Kinetic energy:	$T_b := \int_0^1 \Psi_b(x) \cdot -\frac{1}{2} \cdot \frac{d^2}{dx^2} \Psi_b(x) dx$	$T_b = 7.000$
Potential energy:	$V_b := \int_0^1 \Psi_b(x) \cdot 2 \cdot x \cdot \Psi_b(x) dx$	$V_b = 0.750$
Total energy:	$E_b := T_b + V_b$	$E_b = 7.750$
Average position:	$X_b := \int_0^1 \Psi_b(x) \cdot x \cdot \Psi_b(x) dx$	$X_b = 0.375$

Calculations for trial wave function Ψ_c

Kinetic energy:	$T_c := \int_0^1 \Psi_c(x) \cdot -\frac{1}{2} \cdot \frac{d^2}{dx^2} \Psi_c(x) dx$	$T_c = 7.000$
Potential energy:	$V_c := \int_0^1 \Psi_c(x) \cdot 2 \cdot x \cdot \Psi_c(x) dx$	$V_c = 1.250$
Total energy:	$E_c := T_c + V_c$	$E_c = 8.250$
Average position:	$X_c := \int_0^1 \Psi_c(x) \cdot x \cdot \Psi_c(x) dx$	$X_c = 0.625$

These calculations are summarized in following table.

Property\Wave function	Qa	Qb	Qc
Kinetic Energy/E_h	4.935	7.000	7.000
Potential Energy/E_h	1.000	0.750	1.250
Total Energy/E_h	5.935	7.750	8.250
Average Position/a_o	0.500	0.375	0.625

Ψ_a is a symmetric function which favors neither the low potential energy region nor the high potential energy region, but has the lowest total energy because it has a significantly lower kinetic energy than the other trial wave functions. The reason it has a lower kinetic energy is because it has a lower curvature than the other wave functions (curvature is the second derivative of the function). Ψ_b has a somewhat lower potential energy than Ψ_a because it favors the left side of the box, but consequentially a much higher kinetic energy because of its greater curvature. Total energy, as noted above, is what counts in a variational calculation. Ψ_c is the worst trial function because it has both high kinetic energy and high potential energy.

Of course, Ψ_a is not the best possible wave function for this problem; it is only the best of the three considered here. The best wave function can be found by a more elaborate variational calculation or by numerical integration of Schrödinger's equation. A Mathcad (6) program for numerical integration of Schrödinger's equation for a particle in a box with linear internal potential is given in the appendix.

This latter method yields a wave function with the following physical properties: = 4.942 E_h; = 0.983 E_h; = 5.925 E_h; = 0.491 a_o. Note that this optimum wave function is skewed a little to the left of center, increasing kinetic energy slightly (+.007 Eh) and

reducing potential energy slightly more (-.017 E_h), and overall yielding an energy reduction of -.01 E_h. The details of these calculations can be found in the appendix.

However, it is also important to note that Ψ_a, the eigenfunction for the particle in a box problem [V(x)=0], is a very good trial wave function for this particular problem. It is in error by only 0.17% when compared with the more accurate, and essentially exact, numerical solution. Ψ_a is displayed along with the numerical wave function in the appendix to show how little it differs from the numerical solution.

Another point that should be noted is that Ψ_b does not become the preferred trial function until V(x) = 16.6x. In other words it requires a rather steeply rising internal potential energy to offset the kinetic energy advantage that Ψ_a has. The energy calculations for both wave functions are given below.

$$V_a := \int_0^1 \Psi_a(x) \cdot 16.6 \cdot x \cdot \Psi_a(x) dx$$
$$V_a = 8.300 \qquad E_a := T_a + V_a \qquad E_a = 13.235$$

$$V_b := \int_0^1 \Psi_b(x) \cdot 16.6 \cdot x \cdot \Psi_b(x) dx$$
$$V_b = 6.255 \qquad E_b := T_b + V_b \qquad E_b = 13.235$$

In conclusion, this simple example reveals that our intuition about the importance of potential energy in the analysis of physical phenomena at the nanoscale level should be tempered by a realization that the quantum mechanical nature of kinetic energy cannot be safely ignored.

Literature cited:

1. Tokiwa, H.; Ichikawa, H. Int. *J. Quantum Chem.* **1994**, *50*, 109-112.
2. Rioux, F.; DeKock, R. L. *J. Chem. Educ.* **1998**, *75*, 537-539.
3. Weinhold, F. *Nature* **2001**, *411*, 539-541.
4. Rioux, F. *Chem. Educator* **2003**, *8*, S1430-4171(03)01650-9; DOI 10.1333/s00897030650a..
5. In the context of quantum mechanics, confinement energy is probably a better descriptor than kinetic energy, because the latter implies classical motion. According to quantum mechanical principles, confined particles, because of their wave-like charcter, are described by a weighted superposition of the allowed position eignestates. They are not executing a trajectory in the classical sense. In other words, they are not here and later there; they are here and there, simultaneously
6. Mathcad 11 is a product of Mathsoft, Cambridge, MA 02142; www.mathsoft.com/.

Appendix

Numerical Solution for the Particle in a Slanted Box

Parameters:

$$x_{max} := 1 \qquad m := 1 \qquad V_0 := 2$$

Potential energy:

$$V(x) := V_0 \cdot x$$

Solve Schrödinger's equation numerically:

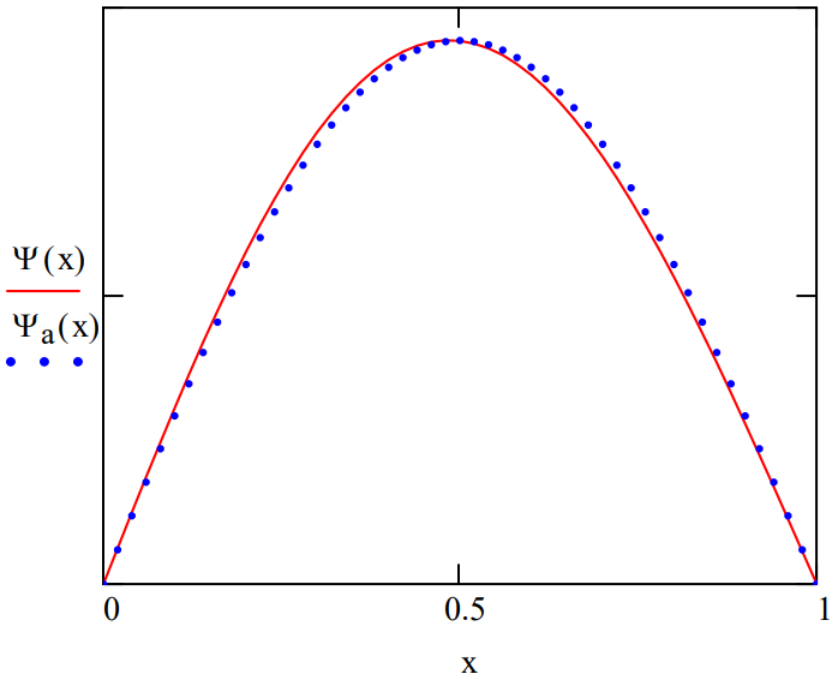
Given

$$\frac{-1}{2 \cdot m} \cdot \frac{d^2}{dx^2} \Psi(x) + V(x) \cdot \Psi(x) = E \cdot \Psi(x)$$
$$\Psi(0) = 0 \qquad \Psi'(0) = 0.1$$
$$\Psi := \text{Odesolve}\ (x, x_{max})$$

Normalize wavefunction:

$$\Psi(x) := \frac{\Psi(x)}{\sqrt{\int_0^{x_{max}} \Psi(x)^2 dx}}$$

Enter energy guess: E = 5.925



Calculate most probable position:

$$x := .5 \text{ Given} \qquad \frac{d}{dx}\Psi(x) = 0 \qquad \text{Find } (x) = 0.485$$

Calculate average position:

$$X_{avg} := \int_0^1 \Psi(x) \cdot x \cdot \Psi(x)dx \qquad X_{avg} = 0.491$$

Calculate potential and kinetic energy:

$$V_{avg} := V_0 \cdot X_{avg} \qquad V_{avg} = 0.983$$

$$T_{avg} := E - V_{avg} \qquad T_{avg} = 4.942$$

This page titled 1.60: Kinetic Energy Is Important in the Nanoscale World is shared under a CC BY 4.0 license and was authored, remixed, and/or curated by Frank Rioux via source content that was edited to the style and standards of the LibreTexts platform.

1.61: Energy Expectation Values and the Origin of the Variation Principle

A system is in the state $|\Psi\rangle$, which is not an eigenfunction of the energy operator, $\hat{H}$. A statistically meaningful number of such states are available for the purpose of measuring the energy. Quantum mechanical principles state that an energy measurement must yield one of the energy eigenvalues, ϵ_i, of the energy operator. Therefore, the average value of the energy measurements is calculated as,

$$\langle E\rangle = \frac{\sum_i n_i \varepsilon_i}{N}$$

where n_i is the number of times ϵ_i is measured, and N is the total number of measurements. Therefore, $p_i = n_i/N$, is the probability that ϵ_i will be observed. Equation (1) becomes

$$\langle E\rangle = \sum_i p_i \varepsilon_i \geq \varepsilon_1 = \varepsilon_{gs}$$

where gs stands for ground state. As shown above, it is clear that the average energy has to be greater than ($p_1 < 1$) or equal to ($p_1 = 1$) the lowest energy. This is the origin of the quantum mechanical variational theorem.

According to quantum mechanics, for a system in the state $|\Psi\rangle, p_i = \langle\Psi|i\rangle\langle i|\Psi\rangle$, where the $|i\rangle$ are the eigenfunctions of the energy operator. Equation (2) can now be re-written as,

$$\langle E\rangle = \sum_i \langle\Psi|i\rangle\langle i|\Psi\rangle\varepsilon_i = \sum_i \langle\Psi|i\rangle\varepsilon_i\langle i|\Psi\rangle$$

However, it is also true that

$$\hat{H}|i\rangle = \varepsilon_i|i\rangle = |i\rangle\varepsilon_i$$

Substitution of equation (4) into (3) yields

$$\langle E\rangle = \sum_i \langle\Psi|\hat{H}|i\rangle\langle i|\Psi\rangle$$

As eigenfunctions of the energy operator, the $|i\rangle$ form a complete basis set, making available the discrete completeness relation, $\sum_i |i\rangle\langle i| = 1$, the use of which in equation (5) yields

$$\langle E\rangle = \langle\Psi|\hat{H}|\Psi\rangle \geq \varepsilon_{gs}$$

Chemists generally evaluate expectation values in coordinate space, so we now insert the continuous completeness relationship of coordinate space, $\int |x\rangle\langle x|dx = 1$, in equation (6) which gives us,

$$\langle E\rangle = \int \langle\Psi|x\rangle\langle x|\hat{H}|\Psi\rangle dx = \int \langle\Psi|x\rangle\hat{H}(x)\langle x|\Psi\rangle dx$$

where

$$\hat{H}(x) = -\frac{\hbar^2}{2m}\frac{d}{dx^2} + V(x)$$

This page titled 1.61: Energy Expectation Values and the Origin of the Variation Principle is shared under a CC BY 4.0 license and was authored, remixed, and/or curated by Frank Rioux via source content that was edited to the style and standards of the LibreTexts platform.

1.62: Examining the Wigner Distribution Using Dirac Notation

abstract

Expressing the Wigner distribution function in Dirac notation reveals its resemblance to a classical trajectory in phase space.

References to the Wigner distribution function [1-3] and the phase-space formulation of quantum mechanics are becoming more frequent in the pedagogical and review literature [4-26]. There have also been several important applications reported in the recent research literature [27, 28]. Other applications of the Wigner distribution are cited in Ref. 25.

The purpose of this note is to demonstrate that when expressed in Dirac notation the Wigner distribution resembles a classical phase-space trajectory. The Wigner distribution can be generated from either the coordinate- or momentum-space wave function. The coordinate-space wave function will be employed here and the Wigner transform using it is given in equation (1) for a one-dimensional example in atomic units.

$$W(p,x) = \frac{1}{2\pi}\int_{-\infty}^{\infty} \Psi^*\left(x+\frac{s}{2}\right)\Psi\left(x-\frac{s}{2}\right)e^{ips}ds$$

In Dirac notation the first two terms of the integrand are written as follows,

$$\Psi^*\left(x+\frac{s}{2}\right) = \left\langle \Psi | x+\frac{s}{2}\right\rangle \qquad \Psi\left(x-\frac{s}{2}\right) = \left\langle x-\frac{s}{2}|\Psi\right\rangle$$

Assigning $1/2\pi$ to the third term and utilizing the momentum eigenfunction in coordinate space and its complex conjugate we have,

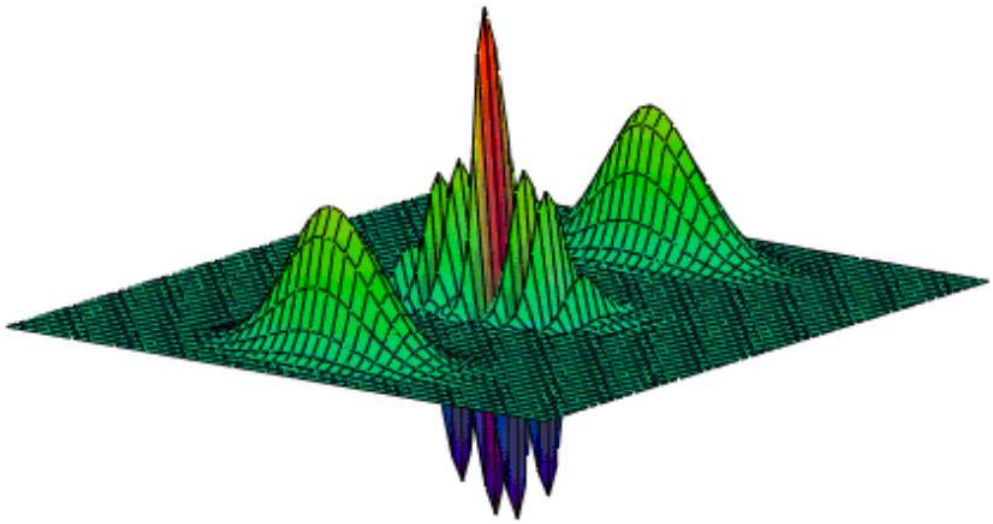
$$\frac{1}{2\pi}\mathrm{e}^{ips} = \frac{1}{\sqrt{2\pi}}\mathrm{e}^{ip(x+\frac{s}{2})}\frac{1}{\sqrt{2\pi}}\mathrm{e}^{-ip(x-\frac{s}{2})} = \left\langle x+\frac{s}{2}|p\right\rangle\left\langle p|x-\frac{s}{2}\right\rangle$$

Substituting equations (2) and (3) into equation (1) yields after arrangement

$$W(x,p) = \int_{-\infty}^{+\infty}\left\langle \Psi|x+\frac{s}{2}\right\rangle\left\langle x+\frac{s}{2}|p\right\rangle\left\langle p|x-\frac{s}{2}\right\rangle\left\langle x-\frac{s}{2}|\Psi\right\rangle ds$$

The four Dirac brackets are read from right to left as follows: (1) is the amplitude that a particle in the state Ψ has position (x - s/2); (2) is the amplitude that a particle with position (x - s/2) has momentum p; (3) is the amplitude that a particle with momentum p has position (x + s/2); (4) is the amplitude that a particle with position (x + s/2) is (still) in the state Ψ. Thus, in Dirac notation the integrand is the quantum equivalent of a classical phase-space trajectory for a quantum system in the state Ψ.

Integration over s creates a superposition of all possible quantum trajectories of the state Ψ, which interfere constructively and destructively, providing a quasi-probability distribution in phase space. As an example, the Wigner probability distribution for a double-slit experiment is shown in the figure below [14, 27]. The oscillating positive and negative values in the middle of the Wigner distribution signify the interference associated with a quantum superposition, distinguishing it from a classical phase-space probability distribution. In the words of Leibfried et al. [14], the Wigner function is a “mathematical construct for visualizing quantum trajectories in phase space.”



Wigner distribution function for the double-slit experiment.

The Wigner double- and triple-slit distribution functions are calculated in the following tutorials.

Wigner Distribution for the Double Slit Experiment

Wigner Distribution for the Triple Slit Experiment

Examples of the generation and use of the Wigner distribution are available in the following tutorials.

Wigner Distribution for the Particle in a Box

Quantum Calculations on the Hydrogen Atom in Coordinate, Momentum and Phase Space

Variation Method Using the Wigner Function: The Feshbach Potential

The Wigner Distribution Function for the Harmonic Oscillator

Given the quantum number this Mathcad file calculates the Wigner distribution function for the specified harmonic oscillator eigen state.

Quantum number: $\mathrm{n} := 2$

Harmonic oscillator eigenstate:

$$\Psi(x) := \frac{1}{\sqrt{2^n \cdot n! \sqrt{\pi}}} \cdot \mathrm{Her}(n, x) \cdot \exp\left(-\frac{x^2}{2}\right)$$

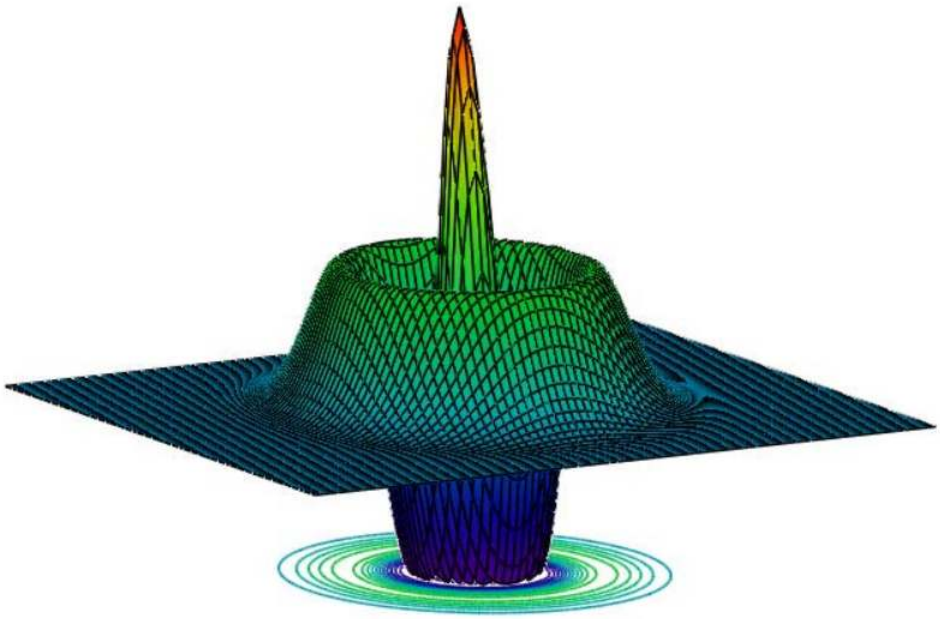
Calculate the Wigner distribution:

$$\mathrm{W}(\mathrm{x}, \mathrm{p}) := \frac{1}{\pi^{\frac{3}{2}}} \cdot \int_{-\infty}^{\infty} \Psi\left(\mathrm{x} + \frac{\mathrm{s}}{2}\right) \cdot \exp(\mathrm{i} \cdot \mathrm{s} \cdot \mathrm{p}) \cdot \Psi\left(\mathrm{x} - \frac{\mathrm{s}}{2}\right) \mathrm{ds}$$

Display the Wigner distribution:

$$\mathrm{N} := 80 \qquad \mathrm{i} := 0 \ldots \mathrm{N} \qquad x_i := -4 + \frac{8 \cdot i}{N}$$

$$\mathrm{j} := 0 \ldots \mathrm{N} \qquad \mathrm{p_j} := -5 + \frac{10 \cdot \mathrm{j}}{\mathrm{N}} \qquad \mathrm{Wigner}_{i,j} := W\left(x_i, p_j\right)$$



Wigner, Wigner

Phase-space quantum mechanical calculations using the Wigner distribution are compared with coordinate- and momentum-space calculations in the following tutorial.

The Cliff Notes version of the above can be accessed in the following tutorial.

Literature cited:

[1] E. P. Wigner, "On the quantum correction for thermodynamic equilibrium," *Phys. Rev.* **40**, 749 – 759 (1932).

[2] M. Hillery, R. F. O'Connell, M. O. Scully, and E. P. Wigner, "Distribution functions in physics: Fundamentals," *Phys. Rep.* **106**, 121 – 167 (1984).

[3] Y. S. Kim and E. P. Wigner, "Canonical transformations in quantum mechanics," *Am. J. Phys.* **58**, 439 – 448 (1990).

[4] J. Snygg, "Wave functions rotated in phase space," *Am. J. Phys.* **45**, 58 – 60 (1977).

[5] N. Mukunda, "Wigner distribution for angle coordinates in quantum mechanics," *Am. J. Phys.* **47**, 192 – 187 (1979).

[6] S. Stenholm, "The Wigner function: I. The physical interpretation," *Eur. J. Phys.* **1**, 244 – 248 (1980).

[7] G. Mourgues, J. C. Andrieux, and M. R. Feix, "Solutions of the Schrödinger equation for a system excited by a time Dirac pulse of pulse of potential. An example of the connection with the classical limit through a particular smoothing of the Wigner function," *Eur. J. Phys.* **5**, 112 – 118 (1984).

[8] M. Casas, H. Krivine, and J. Martorell, "On the Wigner transforms of some simple systems and their semiclassical interpretations," *Eur. J. Phys.* **12**, 105 – 111 (1991).

[9] R. A. Campos, "Correlation coefficient for incompatible observables of the quantum mechanical harmonic oscillator," *Am. J. Phys.* **66**, 712 – 718 (1998).

[10] H-W Lee, "Spreading of a free wave packet," *Am. J. Phys.* **50**, 438 – 440 (1982).

[11] D. Home and S. Sengupta, "Classical limit of quantum mechanics," *Am. J. Phys.* **51**, 265 – 267 (1983).

[12] W. H. Zurek, "Decoherence and the transition from quantum to classical," *Phys. Today* **44**, 36 – 44 (October 1991).

[13] M. C. Teich and B. E. A. Saleh, "Squeezed and antibunched light," *Phys. Today* **43**, 26 – 34 (June 1990).

[14] D. Leibfried, T. Pfau, and C. Monroe, “Shadows and mirrors: Reconstructing quantum states of motion,” *Phys. Today* **51**, 22 – 28 (April 1998).

[15] W. P. Schleich and G. Süssmann, “A jump shot at the Wigner distribution,” *Phys. Today* **44**, 146 – 147 (October 1991).

[16] R. A. Campos, “Correlation coefficient for incompatible observables of the quantum harmonic oscillator,” *Am. J. Phys.* **66**, 712 – 718 (1998).

[17] R. A. Campos, “Wigner quasiprobability distribution for quantum superpositions of coherent states, a Comment on ‘Correlation coefficient for incompatible observables of the quantum harmonic oscillator,’” *Am. J. Phys.* **67**, 641 – 642 (1999).

[18] C. C. Gerry and P. L. Knight, “Quantum superpositions and Schrödinger cat states in quantum optics,” *Am. J. Phys.* **65**, 964 – 974 (1997).

[19] K. Ekert and P. L. Knight, “Correlations and squeezing of two-mode oscillations,” *Am. J. Phys.* **57**, 692 – 697 (1989).

[20] P. J. Price, “Quantum hydrodynamics and virial theorems,” *Am. J. Phys.* **64**, 446 – 448 (1995).

[21] M. G. Raymer, “Measuring the quantum mechanical wave function,” *Contemp. Phys.* **38**, 343 – 355 (1997).

[22] H-W Lee, A. Zysnarski, and P. Kerr, “One-dimensional scattering by a locally periodic potential,” *Am. J. Phys.* **57**, 729 – 734 (1989).

[23] A. Royer, “Why are the energy levels of the quantum harmonic oscillator equally spaced?” *Am. J. Phys.* **64**, 1393 – 1399 (1996).

[24] D. F. Styer, et al., “Nine formulations of quantum mechanics,” *Am. J. Phys.* **70**, 288 – 297 (2002).

[25] M. Belloni, M. A. Doncheski, and R. W. Robinett, “Wigner quasi-probability distribution for the infinite square well: Energy eigenstates and time-dependent wave packets,” *Am. J. Phys.* **72**, 1183 – 1192 (2004).

[26] W. B. Case, “Wigner functions and Weyl transforms for pedestrians,” *Am. J. Phys.* **76**, 937 – 946 (2008).

[27] Ch. Kurtsiefer, T. Pfau, and J. Mlynek, “Measurement of the Wigner function of an ensemble of helium atoms,” *Nature* **386**, 150 – 153 (1997).

[28] W. H. Zurek, “Sub-Planck structure in phase space and its relevance for quantum decoherence,” *Nature* **412**, 712 – 717 (2001).

This page titled 1.62: Examining the Wigner Distribution Using Dirac Notation is shared under a CC BY 4.0 license and was authored, remixed, and/or curated by Frank Rioux via source content that was edited to the style and standards of the LibreTexts platform.

1.63: The Wigner Function for the Single Slit Diffraction Problem

The quantum mechanical interpretation of the single-slit experiment is that position is measured at the slit screen and momentum is measured at the detection screen. Position and momentum are conjugate observables connected by a Fourier transform and governed by the uncertainty principle. Knowing the slit screen geometry makes it possible to calculate the momentum distribution at the detection screen.

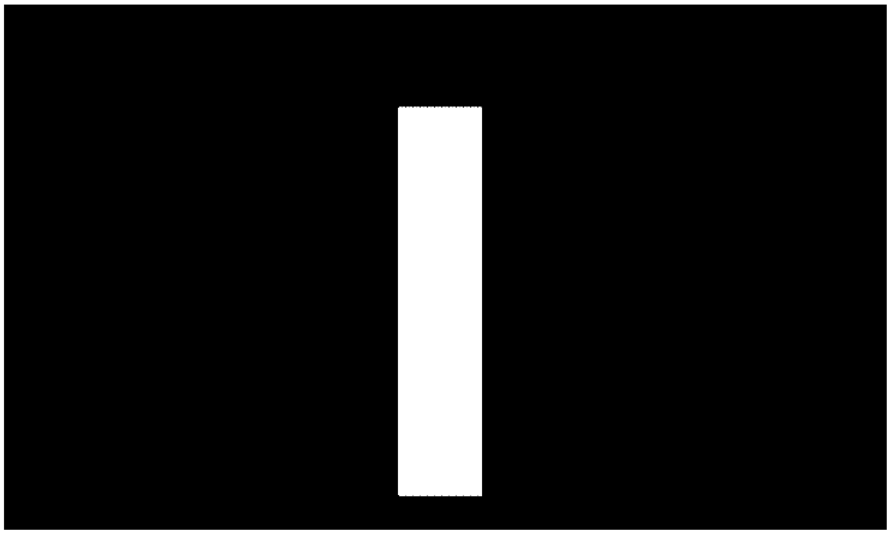
The slit-screen geometry and therefore the coordinate wavefunction is calculate as follows.

Slit width: $w := 2$

Coordinate-space wave function:

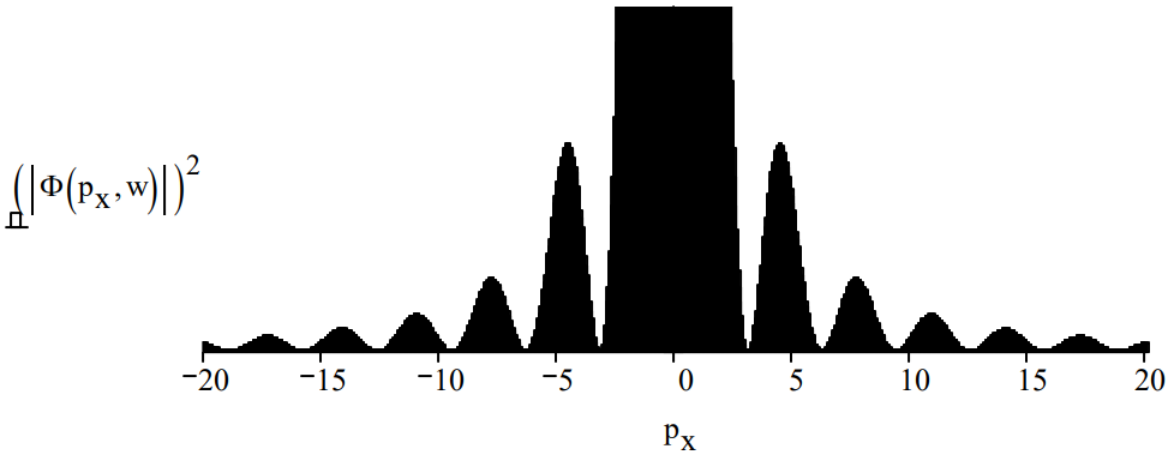
$$\Psi(x, w) := \text{ if } \left[\left(x \geq -\frac{w}{2}\right) \cdot \left(x \leq \frac{w}{2}\right), 1, 0\right]$$

$$x := \frac{-w}{2}, \frac{-w}{2} + .005 \ldots \frac{w}{2}$$



A Fourier transform of the coordinate-space wave function yields the momentum wave function and the momentum distribution function, which is the diffraction pattern.

$$\Phi\left(\mathrm{p_X}, \mathrm{w}\right) := \frac{1}{\sqrt{2 \cdot \pi \cdot \mathrm{w}}} \cdot \int_{-\frac{\mathrm{w}}{2}}^{\frac{\mathrm{w}}{2}} \exp\left(-\mathrm{i} \cdot \mathrm{p_X} \cdot \mathrm{x}\right) \mathrm{dx} \text{ simplify } \rightarrow 2^{\frac{1}{2}} \cdot \frac{\sin\left(\frac{1}{2} \cdot w \cdot p_x\right)}{\pi^{\frac{1}{2}} \cdot w^{\frac{1}{2}} \cdot p_x}$$



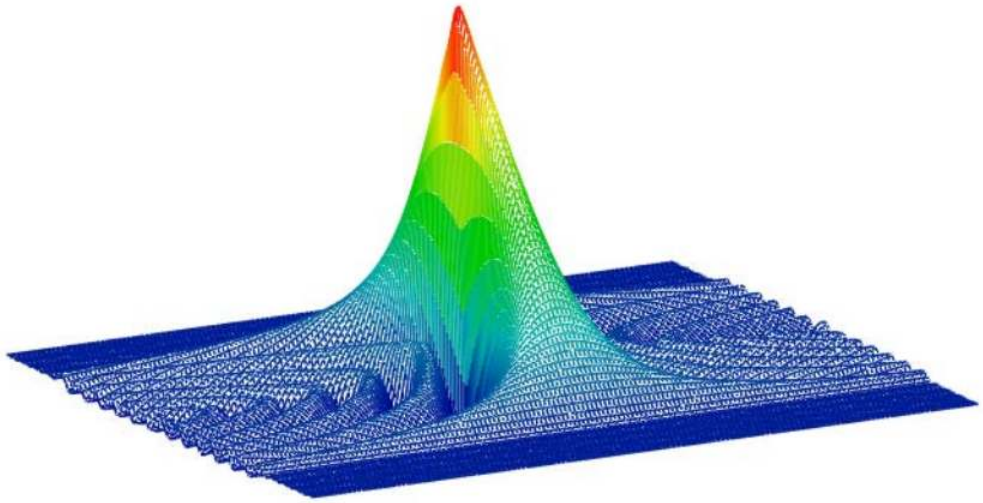
The Wigner function for the single-slit screen geometry is generated using the momentum wave function. (Fifty is effectively infinity and is therefore as the limits of integration.)

$$W(x,p) := \frac{1}{2\cdot\pi}\cdot\int_{-50}^{50}\overline{\Phi\left(p+\frac{s}{2},w\right)}\cdot\exp(-i\cdot s\cdot x)\cdot\Phi\left(p-\frac{s}{2},w\right)ds$$

The single-slit Wigner function is displayed graphically.

$$N := 150 \quad i := 0\ldots N \qquad x_i := -1.5+\frac{3\cdot i}{N}$$

$$j := 0\ldots N \qquad p_j := -20+\frac{40\cdot j}{N} \qquad \text{Wigner}_{i,j} := W\left(x_i,p_j\right)$$



Wigner

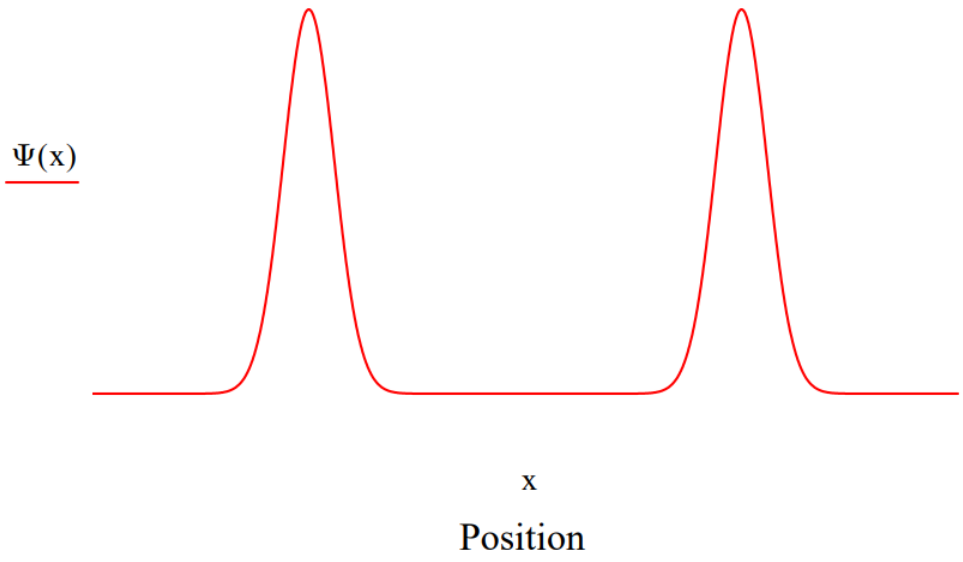
This page titled 1.63: The Wigner Function for the Single Slit Diffraction Problem is shared under a CC BY 4.0 license and was authored, remixed, and/or curated by Frank Rioux via source content that was edited to the style and standards of the LibreTexts platform.

1.64: Wigner Distribution for the Double Slit Experiment

The quantum mechanical interpretation of the double-slit experiment is that position is measured at the slit screen and momentum is measured at the detection screen. Position and momentum are conjugate observables connected by a Fourier transform and governed by the uncertainty principle. Knowing the slit screen geometry makes it possible to calculate the momentum distribution at the detection screen.

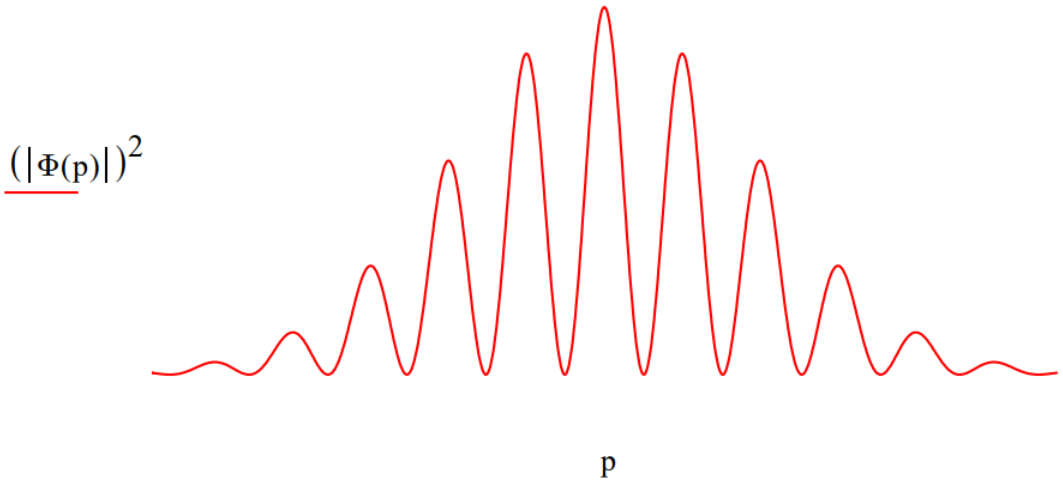
The slit-screen geometry and therefore the coordinate wavefunction is modeled as a superposition of two Gaussian functions.

$$\Psi(x) := \exp\left[-4 \cdot (x-3)^2\right] + \exp\left[-4 \cdot (x+3)^2\right]$$



The coordinate wavefunction is Fourier transformed into momentum space to yield the diffraction pattern. Note that this calculation is in agreement with the well-known double slit diffraction pattern.

$$\Phi(p) := \frac{1}{\sqrt{2 \cdot \pi}} \int_{-6}^{6} \exp(-\mathrm{i} \cdot p \cdot x) \cdot \Psi(x) dx$$

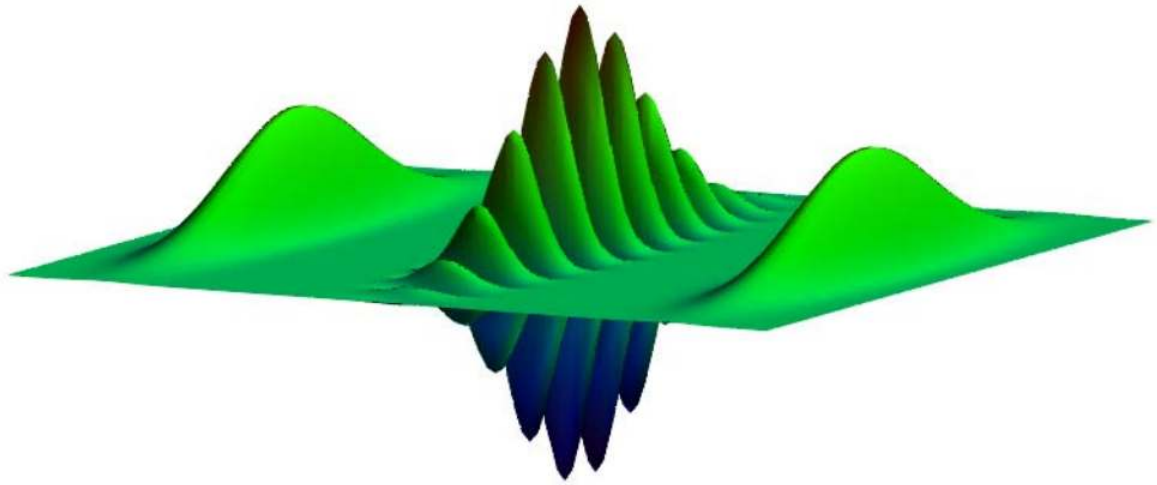


The Wigner function is a phase-space distribution that is obtained by the Fourier transform of either the coordinate or momentum wavefunction. We use the coordinate wavefunction.

$$W(x,p) := \frac{1}{\pi^{\frac{3}{2}}} \cdot \int_{-\infty}^{\infty} \Psi\left(x + \frac{s}{2}\right) \cdot \exp(i \cdot s \cdot p) \cdot \Psi\left(x - \frac{s}{2}\right) ds$$

$$N := 100 \qquad i := 0 \ldots N \qquad x_i = -4 + \frac{8 \cdot i}{N}$$

$$j := 0 \ldots N \qquad p_j = -6 + \frac{12 \cdot j}{N} \qquad Wigner_{i,j} := W\left(x_i, p_j\right)$$

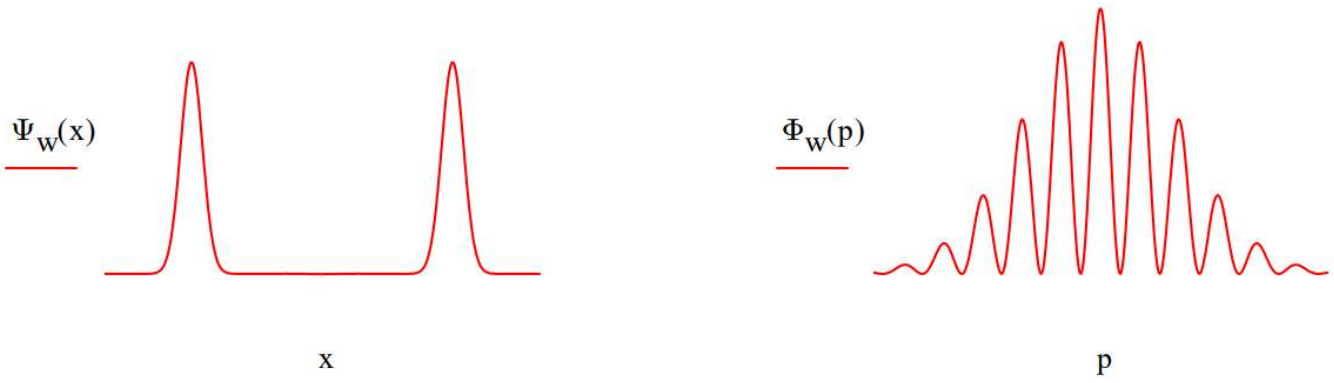


Wigner

The Wigner distribution is frequently called a quasi-probability distribution because, as can be seen in the display above, it can have negative values. Integration of the Wigner function with respect to momentum recovers the coordinate wavefunction and integration with respect to position yields the momentum wavefunction.

$$\Psi_w(x) := \int_{-6}^{6} W(x,p)\ dp \qquad x := -5, -4.98 \ldots 5$$

$$\Phi_w(p) := \int_{-5}^{5} W(x,p) dx \qquad p := -6, -5.98 \ldots 6$$



The Wigner distribution can be reconstructed from experimental measurements using quantum state tomography. Reconstructive tomography is a widely used technique in medicine, for example, for obtaining the shape of an inaccessible two-dimensional object from a set of different one-dimensional "shadows" cast by that object.

Quantum state reconstruction is possible if a system can be prepared repeatedly in the same state. Subsequent measurements on such a system are then effectively mutltiple measurements on the same quantum state. The theoretical Wigner distribution shown above for the double-slit experiment has been reconstructed for the helium atom. [See, *Nature*, **386**, 150 (1997).

See Figure 1 of "Shadows and Mirrors:Reconstructing Quantum States of Atom Motion," Physics Today, April 1998, by Leibfried, Pfau, and Monroe.

Reference: Decoherence and the Transition form Quantum to Classical, Wojciech Jurek, Physics Today, October 1991, pages 36-44.

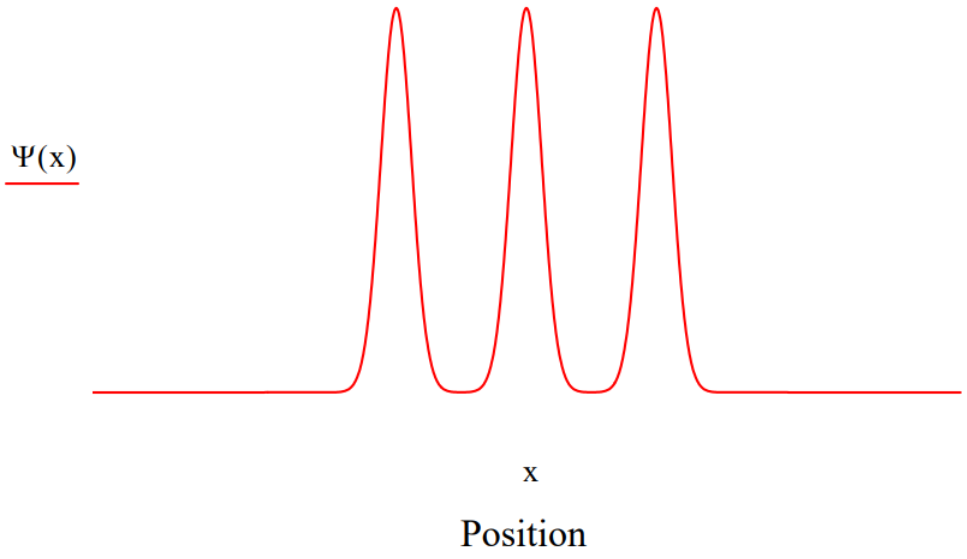
This page titled 1.64: Wigner Distribution for the Double Slit Experiment is shared under a CC BY 4.0 license and was authored, remixed, and/or curated by Frank Rioux via source content that was edited to the style and standards of the LibreTexts platform.

1.65: Wigner Distribution for the Triple Slit Experiment

The quantum mechanical interpretation of the triple-slit experiment is that position is measured at the slit screen and momentum is measured at the detection screen. Position and momentum are conjugate observables connected by a Fourier transform and governed by the uncertainty principle. Knowing the slit screen geometry makes it possible to calculate the momentum distribution at the detection screen.

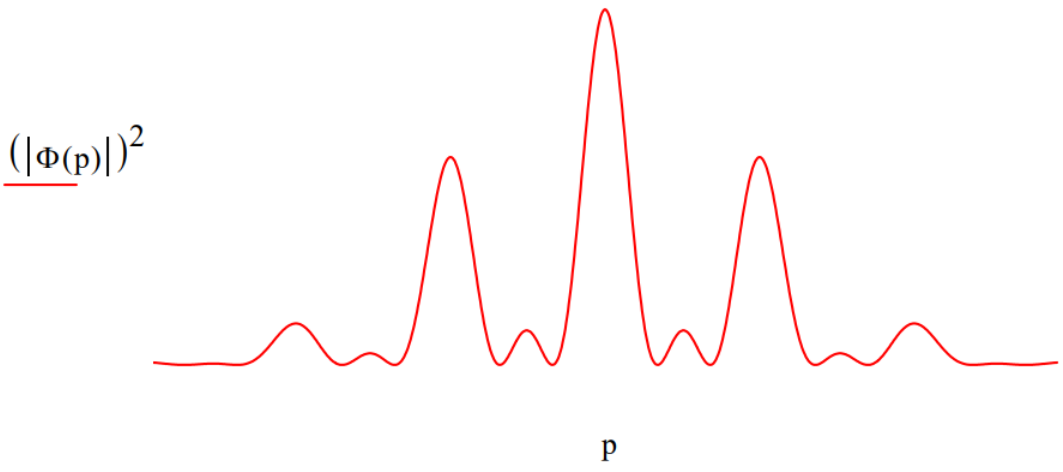
The slit-screen geometry and therefore the coordinate wavefunction is modeled as a superposition of three Gaussian functions.

$$\Psi(x) := \exp\left[-4 \cdot (x-3)^2\right] + \exp\left(-4 \cdot x^2\right) + \exp\left[-4 \cdot (x+3)^2\right]$$



The coordinate wavefunction is Fourier transformed into momentum space to yield the diffraction pattern. Note that this calculation is in agreement with the expectation that the number of minor maxima appearing between the major maxima is given by the number of slits minus 2.

$$\Phi(\mathrm{p}) := \frac{1}{\sqrt{2 \cdot \pi}} \int_{-6}^{6} \exp(-\mathrm{i} \cdot \mathrm{p} \cdot \mathrm{x}) \cdot \Psi(\mathrm{x}) \mathrm{dx}$$

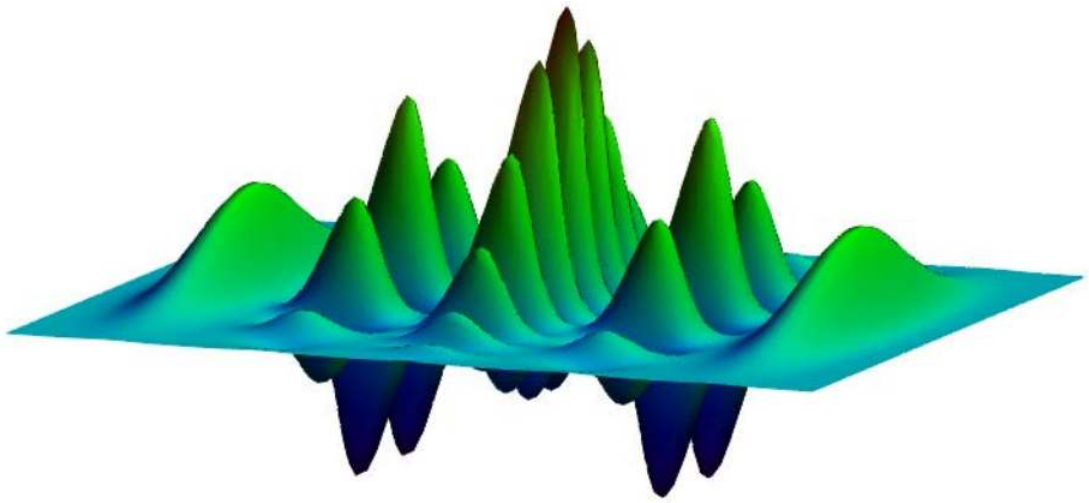


The Wigner function is a phase-space distribution that is obtained by the Fourier transform of either the coordinate or momentum wavefunction. We use the coordinate wavefunction.

$$W(x,p) := \frac{1}{\pi^{\frac{3}{2}}} \cdot \int_{-\infty}^{\infty} \Psi\left(x + \frac{s}{2}\right) \cdot \exp(i \cdot s \cdot p) \cdot \Psi\left(x - \frac{s}{2}\right) ds$$

$$N := 100 \qquad i := 0 \ldots N \qquad x_i := -4 + \frac{8 \cdot i}{N}$$

$$j := 0 \ldots N \qquad p_j := -6 + \frac{12 \cdot j}{N} \qquad Wigner_{i,j} := W\left(x_i, p_j\right)$$

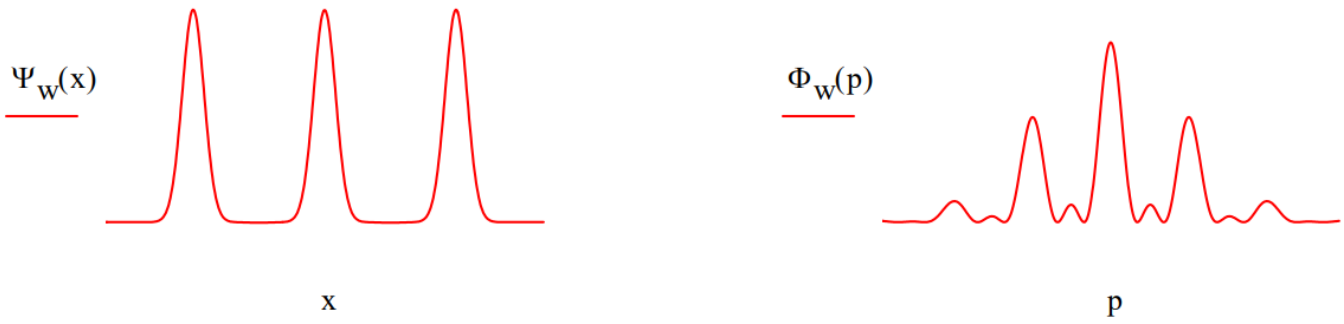


Wigner

The Wigner distribution is frequently called a quasi-probability distribution because, as can be seen in the display above, it can have negative values. Integration of the Wigner function with respect to momentum recovers the coordinate wavefunction and integration with respect to position yields the momentum wavefunction.

$$\Psi_w(x) := \int_{-6}^{6} W(x,p)dp \qquad x := -5, -4.98 \ldots 5$$

$$\Phi_w(p) := \int_{-5}^{5} W(x,p)dx \qquad p := -6, -5.98 \ldots 6$$



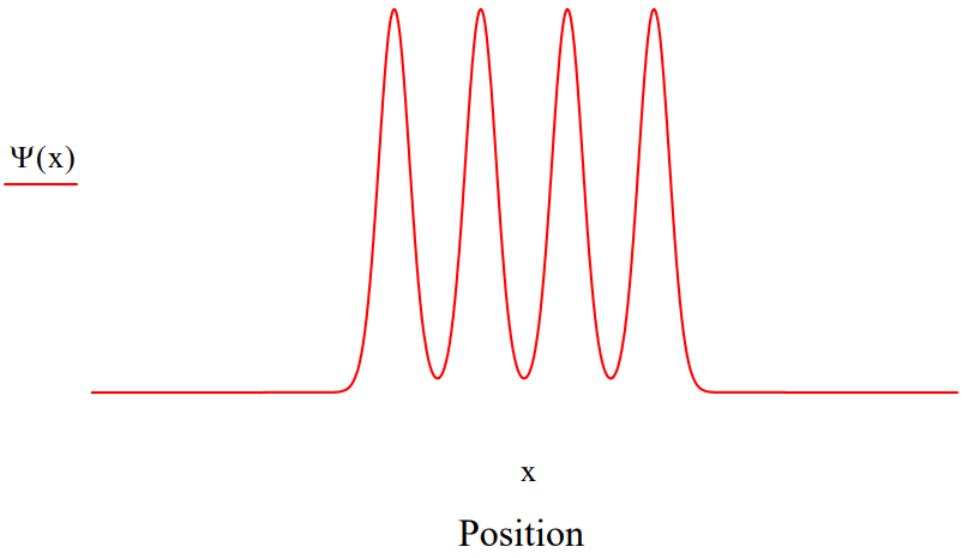
This page titled 1.65: Wigner Distribution for the Triple Slit Experiment is shared under a CC BY 4.0 license and was authored, remixed, and/or curated by Frank Rioux via source content that was edited to the style and standards of the LibreTexts platform.

1.66: Wigner Distribution for the Quadruple Slit Experiment

The quantum mechanical interpretation of the quadruple-slit experiment is that position is measured at the slit screen and momentum is measured at the detection screen. Position and momentum are conjugate observables connected by a Fourier transform and governed by the uncertainty principle. Knowing the slit screen geometry makes it possible to calculate the momentum distribution at the detection screen.

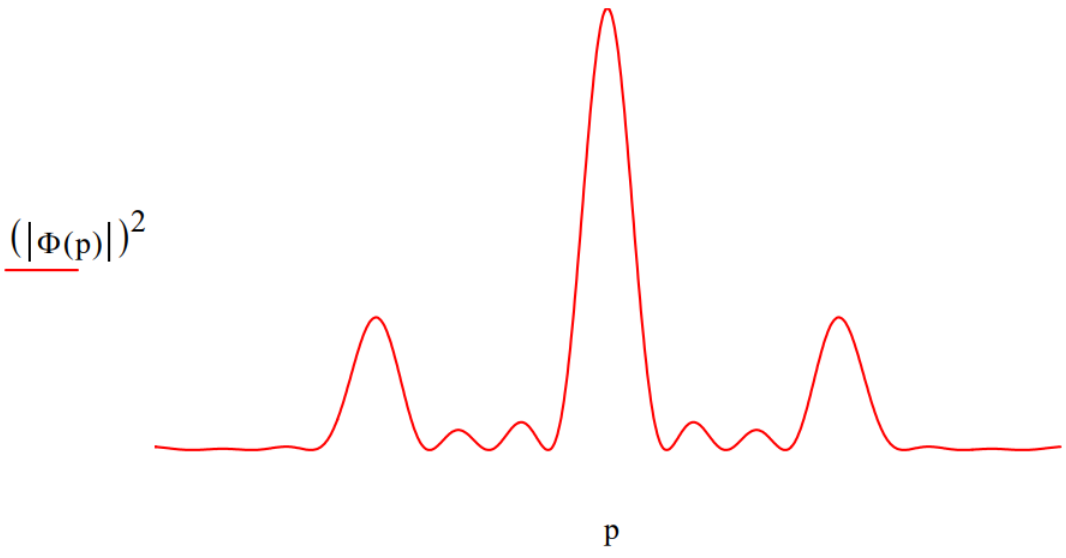
The slit-screen geometry and therefore the coordinate wavefunction is modeled as a superposition of three Gaussian functions.

$$\Psi(x) = \exp\left[-4 \cdot (x-3)^2\right] + \exp\left[-4 \cdot (x-1)^2\right] + \exp\left[-4 \cdot (x+1)^2\right] + \exp\left[-4 \cdot (x+3)^2\right]$$



The coordinate wavefunction is Fourier transformed into momentum space to yield the diffraction pattern. Note that this calculation is in agreement with the expectation that the number of minor maxima appearing between the major maxima is given by the number of slits minus 2.

$$\Phi(\mathrm{p}) := \frac{1}{\sqrt{2 \cdot \pi}} \cdot \int_{-8}^{8} \exp(-\mathrm{i} \cdot \mathrm{p} \cdot \mathrm{x}) \cdot \Psi(\mathrm{x}) \mathrm{dx}$$

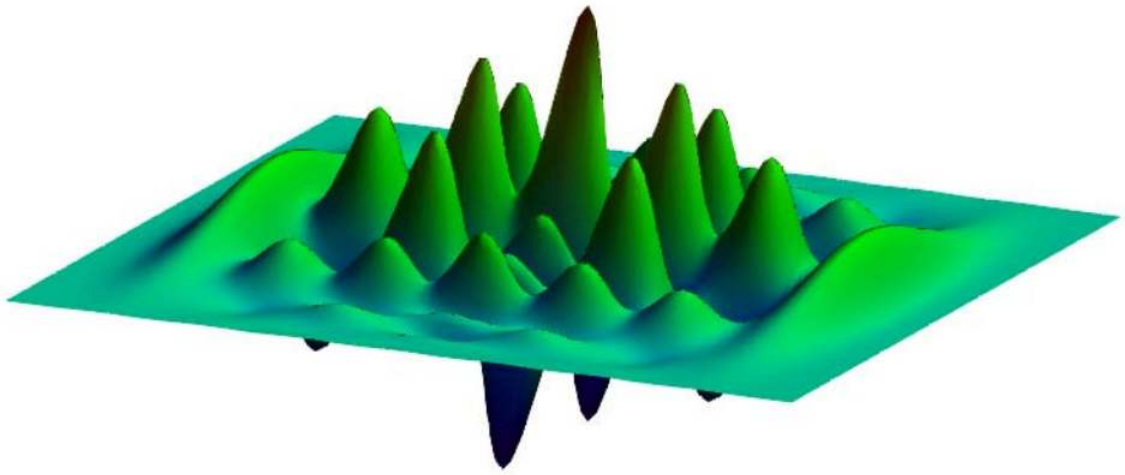


The Wigner function is a phase-space distribution that is obtained by the Fourier transform of either the coordinate or momentum wavefunction. We use the coordinate wavefunction.

$$W(x,p) := \frac{1}{\pi^{\frac{3}{2}}} \cdot \int_{-\infty}^{\infty} \Psi\left(x + \frac{s}{2}\right) \cdot \exp(i \cdot s \cdot p) \cdot \Psi\left(x - \frac{s}{2}\right) ds$$

$$N := 100 \qquad i := 0 \ldots N \qquad x_i := -4 + \frac{8 \cdot i}{N}$$

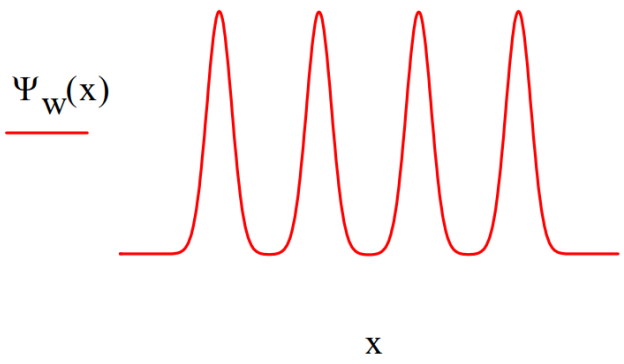
$$j := 0 \ldots N \qquad p_j := -6 + \frac{12 \cdot j}{N} \qquad Wigner_{i,j} := W\left(x_i, p_j\right)$$



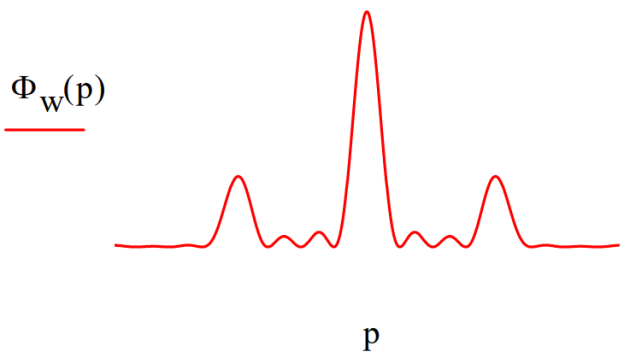
Wigner

The Wigner distribution is frequently called a quasi-probability distribution because, as can be seen in the display above, it can have negative values. Integration of the Wigner function with respect to momentum recovers the coordinate wavefunction and integration with respect to position yields the momentum wavefunction.

$$\Psi_w(x) := \int_{-6}^{6} W(x,p)dp \qquad x := -5, -4.98 \ldots 5$$



$$\Phi_w(p) := \int_{-5}^{5} W(x,p)dx \qquad p = -6, -5.98 \ldots 6$$



This page titled 1.66: Wigner Distribution for the Quadruple Slit Experiment is shared under a CC BY 4.0 license and was authored, remixed, and/or curated by Frank Rioux via source content that was edited to the style and standards of the LibreTexts platform.

1.67: Quantum Tunneling in Coordinate, Momentum and Phase Space

A study of quantum mechanical tunneling brings together the classical and quantum mechanical points of view. In this tutorial the harmonic oscillator will be used to analyze tunneling in coordinate-, momentum- and phase-space. The Appendix provides the position and momentum operators appropriate for these three representations.

The classical equation for the energy of a harmonic oscillator is,

$$E = \frac{p^2}{2 \cdot \mu} + \frac{1}{2} \cdot k \cdot x^2$$

The quantum mechanical counter part is Schrödinger's equation (in atomic units, h = 2 π),

$$\frac{-1}{2 \cdot \mu} \cdot \frac{d^2}{dx^2} \Psi(x) + \frac{1}{2} \cdot k \cdot x^2 \cdot \Psi(x) = E \cdot \Psi(x)$$

In atomic units the quantum mechanical wave function in coordinate space for the harmonic oscillator ground state with reduced mass μ and force constant k is given by,

$$\Psi(x, k, \mu) := \left(\frac{\sqrt{k \cdot \mu}}{\pi} \right)^{\frac{1}{4}} \cdot \exp\left(-\sqrt{k \cdot \mu} \cdot \frac{x^2}{2} \right)$$

In the interest of mathematical simplicity and expediency we will use k = μ =1. The normalized ground state wave function under these conditions is,

$$\Psi(x) := \left(\frac{1}{\pi} \right)^{\frac{1}{4}} \cdot \exp\left(\frac{-x^2}{2} \right) \qquad \int_{-\infty}^{\infty} \Psi(x)^2 dx = 1$$

Solving Schrödinger's equation for this wave function yields a ground state energy of 0.5 in atomic units.

$$\frac{-1}{2} \cdot \frac{d^2}{dx^2} \Psi(x) + \frac{1}{2} \cdot x^2 \cdot \Psi(x) = E \cdot \Psi(x) \text{ solve, } E \rightarrow \frac{1}{2}$$

Classically a harmonic oscillator, like a pendulum, has a turning point when kinetic energy is zero and the pendulum bob changes direction. The turning point is calculated as follows using the classical expression for the energy.

$$\frac{1}{2} = \frac{1}{2} \cdot x^2 \text{ solve, } x \rightarrow \begin{pmatrix} 1 \\ -1 \end{pmatrix}$$

Thus, the permissible range of position values is between -1 and +1. Position values outside this range are classically forbidden. However, quantum theory permits position values for which the total energy is less than the potential energy. This is referred to as quantum tunneling. The probability that tunneling is occurring is calculated below.

$$2 \cdot \int_{1}^{\infty} \Psi(x)^2 dx = 0.157$$

Next we move to a similar calculation in momentum space. First the coordinate wave function is Fourier transformed into momentum space and normalization is demonstrated.

$$\Phi(p) := \frac{1}{\sqrt{2 \cdot \pi}} \cdot \int_{-\infty}^{\infty} \exp(-i \cdot p \cdot x) \cdot \Psi(x) dx \rightarrow \frac{1}{\pi^{\frac{1}{4}}} \cdot e^{\frac{-1}{2} \cdot p^2} \qquad \int_{-\infty}^{\infty} (|\Phi(p)|)^2 dp = 1$$

Solving Schrödinger's equation in momentum space naturally gives the same energy eigenvalue.

$$\frac{p^2}{2} \cdot \Phi(p) - \frac{1}{2} \cdot \frac{d^2}{dp^2} \Phi(p) = E \cdot \Phi(p) \text{ solve, } E \rightarrow \frac{1}{2}$$

And we find that the classically permissible range of momentum values is the same given the reduced mass and force constant values used in these calculations.

$$\frac{1}{2} = \frac{p^2}{2} \text{ solve, } p \rightarrow \begin{pmatrix} 1 \\ -1 \end{pmatrix}$$

Next we see that the tunneling probability in momentum space is the same as it is in coordinate space.

$$2 \cdot \int_1^{\infty} \Phi(p)^2 dp = 0.157$$

Moving to phase space requires a distribution function that depends on both position and momentum. The Wigner function fits these requirements and is generated here using both the coordinate and momentum wave functions. Please see "Examining the Wigner Distribution Using Dirac Notation," arXiv: 0912.2333 (**2009**) for further detail.

$$W(x,p) := \frac{1}{2 \cdot \pi} \int_{-\infty}^{\infty} \Psi\left(x + \frac{s}{2}\right) \cdot \exp(i \cdot sp) \cdot \Psi\left(x - \frac{s}{2}\right) ds \rightarrow \frac{1}{\pi} \cdot e^{(-x^2)-p^2}$$

$$W(x,p) := \frac{1}{2 \cdot \pi} \int_{-\infty}^{\infty} \Phi\left(p + \frac{s}{2}\right) \cdot \exp(-i \cdot s \cdot x) \cdot \Phi\left(p - \frac{s}{2}\right) ds \rightarrow \frac{1}{\pi} \cdot e^{(-x^2)-p^2}$$

The Wigner function is normalized over position and momentum, and yields the appropriate energy expectation value for the ground state of the harmonic oscillator.

$$\int_{-\infty}^{\infty} \int_{-\infty}^{\infty} W(x,p) dx dp = 1 \qquad \int_{-\infty}^{\infty} \int_{-\infty}^{\infty} \left(\frac{p^2}{2} + \frac{x^2}{2}\right) \cdot W(x,p) dx dp = 0.5$$

Tunneling probability in phase space is calculated as follows:

$$\int_1^{\infty} \int_1^{\infty} W(x,p) dx dp = 0.025$$

This is in agreement with the separate coordinate and momentum space calculations which gave values of 0.157.

$$0.157 \cdot 0.157 = 0.025$$

Appendix

The table lists the forms of the position and momentum operators in the coordinate, momentum and phase space representations. Clearly the multiplicative character of the phase space operators appeals to our classical prejudices and intuition. However, we must remind ourselves that the phase space distribution function on which they "operate" is generated from either the coordinate or momentum wave function. In the coordinate representation the momentum operator is differential; in the momentum representation the coordinate operator is differential. As is shown in other tutorials in this series, the apparent "classical character" of the phase space representation only temporarily hides the underlying quantum weirdness.

$$\begin{pmatrix} \text{Operator} & \text{CoordinateSpace} & \text{MomentumSpace} & \text{PhaseSpace} \\ \text{position} & x \cdot \square & i \cdot \frac{d}{dp} \square & x \cdot \square \\ \text{momentum} & \frac{1}{i} \cdot \frac{d}{dx} \square & p \cdot \square & p \cdot \square \end{pmatrix}$$

This page titled 1.67: Quantum Tunneling in Coordinate, Momentum and Phase Space is shared under a CC BY 4.0 license and was authored, remixed, and/or curated by Frank Rioux via source content that was edited to the style and standards of the LibreTexts platform.

1.68: Another Look at the Wigner Function

The Wigner function, W(x,p), is a phase space distribution function which behaves similarly to the coordinate $(|\Psi(x)|^2)$ and momentum $\left(|\tilde{\Psi}(p)|^2\right)$ distribution functions. For example, its integral over phase space is normalized.

$$\iint W(x,p)dxdp = 1$$

In phase space, position and momentum are represented by multiplicative operators, so the calculation of their expectation values has a classical appearance. This, naturally, is part of the appeal of phase space quantum mechanical calculations.

$$\langle x \rangle = \iint xW(x,p)dxdp$$

$$\langle p \rangle = \iint pW(x,p)dxdp$$

While the Wigner function is real, unlike $|\Psi(x)|^2$ and $|\tilde{\Psi}(p)|^2$, it can take on negative values making it impossible to interpret it as a genuine probability distribution function. For this reason it is frequently referred to as a quasi-probability function, and loses some of its classical appeal. In any case, the Wigner function is redundant in the sense that it is generated from a Schrödinger coordinate or momentum wave equation.

In what follows, the quantum mechanical Wigner distribution function will be rationalized by reference to familiar classical concepts, such as position, momentum and trajectory.

In classical physics, a trajectory is a temporal sequence of position and momentum states. Let us try to represent a classical trajectory in a quantum mechanical formalism. Suppose a quantum mechanical object, a quon (thank you Nick Herbert), in state $|\Psi>$ moves from position x –s/2 to position x + s/2. We might represent this transition quantum mechanically as the product of two coordinate space probability amplitudes (reading from left to right).

$$\langle x - \frac{s}{2}|\Psi\rangle\langle\Psi|x + \frac{s}{2}\rangle$$

Thus far we have a coordinate representation of a transition from one spatial location to another. However, a phase space description also requires a dynamic (or motional) parameter such as momentum. We can introduce momentum by first rearranging the above product of amplitudes as follows.

$$\langle\Psi|x + \frac{s}{2}\rangle\langle x - \frac{s}{2}|\Psi\rangle$$

This convolution of positional states takes on the coherent character of a trajectory with the insertion of the following momentum projector (see Feynman Lectures Volume 3) coupling the two spatial states.

$$\langle x + \frac{s}{2}|p\rangle\langle p|x - \frac{s}{2}\rangle$$

This gives us a quantum trajectory expressed in the following product of Dirac brackets,

$$\langle\Psi|x + \frac{s}{2}\rangle\langle x + \frac{s}{2}|p\rangle\langle p|x - \frac{s}{2}\rangle\langle x - \frac{s}{2}|\Psi\rangle$$

The four Dirac brackets are read now from right to left as follows: (1) is the amplitude that a particle in the state Ψ has position (x - $\frac{s}{2}$)); (2) $is the amplitude that a particle with position (x - \(\frac{s}{2}$) has momentum p; (3) is the amplitude that a particle with momentum p has position (x + $\frac{s}{2}$); (4) is the amplitude that a particle with position (x + $\frac{s}{2}$) is (still) in the state Ψ.

Integration over s yields the Wigner distribution function, which is a superposition of all possible quantum trajectories of the state Ψ, which interfere constructively and destructively, providing a quasi-probability distribution in phase space.

$$\int\langle\Psi|x + \frac{s}{2}\rangle\langle x + \frac{s}{2}|p\rangle\langle p|x - \frac{s}{2}\rangle\langle x - \frac{s}{2}|\Psi\rangle ds = \frac{1}{h}\int \Psi(x + \frac{s}{2})^* \exp\left(i\frac{ps}{\hbar}\right)\Psi(x - \frac{s}{2})ds$$

given that

$$\langle x+\frac{s}{2}|p\rangle\langle p|x-\frac{s}{2}\rangle=\frac{1}{\sqrt{h}}\exp\left(i\frac{p(x+\frac{s}{2})}{\hbar}\right)\frac{1}{\sqrt{h}}\exp\left(-i\frac{p(x-\frac{s}{2})}{\hbar}\right)=\frac{1}{h}\exp\left(i\frac{ps}{\hbar}\right)$$

While the Wigner distribution is more than a quantum mechanical curiosity and plays an important role in current research (see references below), it is also true, as mentioned above, that it is redundant because it is generated from either a coordinate or momentum wave function. In Dan Styer's words it is useful in exploring the quantum/classical transition, but it does not eliminate quantum weirdness – it simply repackages it (see reference 12).

Having said this it should be acknowledged that the Wigner phase-space distribution has been measured for the double slit experiment using tomographic techniques (see references 17-19).

Literature references to the Wigner distribution function:

1. E. P. Wigner, "On the quantum correction for thermodynamic equilibrium," *Phys. Rev.* **40**, 749 – 759 (1932).
2. M. Hillery, R. F. O'Connell, M. O. Scully, and E. P. Wigner, "Distribution functions in physics: Fundamentals," *Phys. Rep.* **106**, 121 – 167 (1984).
3. Y. S. Kim and E. P. Wigner, "Canonical transformations in quantum mechanics," *Am. J. Phys.* **58**, 439 – 448 (1990).
4. J. Snygg, "Wave functions rotated in phase space," *Am. J. Phys.* **45**, 58 – 60 (1977).
5. J. Snygg, "Uses of operator functions to construct refined correspondence principle via the quantum mechanics of Wigner and Moyal," *Am. J. Phys.* **48**, 964 – 970 (1980).
6. N. Mukunda, "Wigner distribution for angle coordinates in quantum mechanics," *Am. J. Phys.* **47**, 192 – 187 (1979).
7. S. Stenholm, "The Wigner function: I. The physical interpretation," *Eur. J. Phys.* 1, 244 – 248 (1980).
8. G. Mourgues, J. C. Andrieux, and M. R. Feix, "Solutions of the Schrödinger equation for a system excited by a time Dirac pulse of pulse of potential. An example of the connection with the classical limit through a particular smoothing of the Wigner function," *Eur. J. Phys.* **5**, 112 – 118 (1984).
9. M. Casas, H. Krivine, and J. Martorell, "On the Wigner transforms of some simple systems and their semiclassical interpretations," *Eur. J.Phys.* **12**, 105 – 111 (1991).
10. R. A. Campos, "Correlation coefficient for incompatible observables of the quantum mechanical harmonic oscillator," *Am. J. Phys.* **66**, 712 – 718 (1998).
11. M. Belloni, M. A. Doncheski, and R. W. Robinett, "Wigner quasi-probability distribution for the infinite square well: Energy eigenstates and time-dependent wave packets," *Am. J. Phys.* **72**, 1183 – 1192 (2004).
12. D. F. Styer, et al., "Nine formulations of quantum mechanics," *Am. J. Phys.* **70**, 288 – 297 (2002).
13. H-W Lee, "Spreading of a free wave packet," *Am. J. Phys.* **50**, 438 – 440 (1982).
14. D. Home and S. Sengupta, "Classical limit of quantum mechanics," *Am. J. Phys.* **51**, 265 – 267 (1983).
15. W. H. Zurek, "Decoherence and the transition from quantum to classical," *Phys. Today* **44**, 36 – 44 (October 1991).
16. M. C. Teich and B. E. A. Saleh, "Squeezed and antibunched light," *Phys. Today* **43**, 26 – 34 (June 1990).
17. Ch. Kurtsiefer, T. Pfau, and J.Mlynek, "Measurement of the Wigner function of an ensemble of helium atoms," *Nature* **386**, 150-153 (1997).
18. M. Freyberger and W. P. Schleich, "True vision of a quantum state," *Nature* **386**, 121-122 (1997).
19. D. Leibfried, T. Pfau, and C. Monroe, "Shadows and mirrors: Reconstructing quantum states of motion," *Phys. Today* **51**, 22 – 28 (April 1998).
20. W. P. Schleich and G. Süssmann, "A jump shot at the Wigner distribution," *Phys. Today* **44**, 146 – 147 (October 1991).
21. R. A. Campos, "Correlation coefficient for incompatible observables of the quantum harmonic oscillator," *Am. J. Phys.* **66**, 712 – 718 (1998).
22. R. A. Campos, "Wigner quasiprobability distribution for quantum superpositions of coherent states, a Comment on 'Correlation coefficient for incompatible observables of the quantum harmonic oscillator,'" *Am. J. Phys.* **67**, 641 – 642 (1999).
23. C. C. Gerry and P. L. Knight, "Quantum superpositions and Schrödinger cat states in quantum optics," *Am. J. Phys.* **65**, 964 – 974 (1997).
24. K. Ekert and P. L. Knight, "Correlations and squeezing of two-mode oscillations," *Am. J. Phys.* **57**, 692 – 697 (1989).
25. W. B. Case, "Wigner functions and Weyl transforms for pedestrians," *Am. J. Phys.* **76**, 937 – 946 (2008).
26. M. G. Raymer, "Measuring the quantum mechanical wave function," *Contemp. Phys.* **38**, 343 – 355 (1997).
27. F. Rioux, "Illuminating the Wigner function with Dirac notation,"

28. F. Rioux, “The Wigner distribution for the double-slit experiment,” www.users.csbsju.edu/~frioux/wigner/DBL-SLIT-NEW.pdf
29. F. Rioux, “Basic quantum mechanics in coordinate space, momentum space and phase space,”
30. F. Rioux, “The Wigner distribution for the harmonic oscillator,”
31. F. Rioux, “The Wigner distribution for the particle in a box,”
32. F. Rioux, “The time-dependent Wigner distribution for harmonic oscillator transitions,”
33. F. Rioux, “The Wigner distribution distinguishes between a superposition and a mixture,”

This page titled 1.68: Another Look at the Wigner Function is shared under a CC BY 4.0 license and was authored, remixed, and/or curated by Frank Rioux via source content that was edited to the style and standards of the LibreTexts platform.

1.69: The Wigner Distribution Function for the Harmonic Oscillator

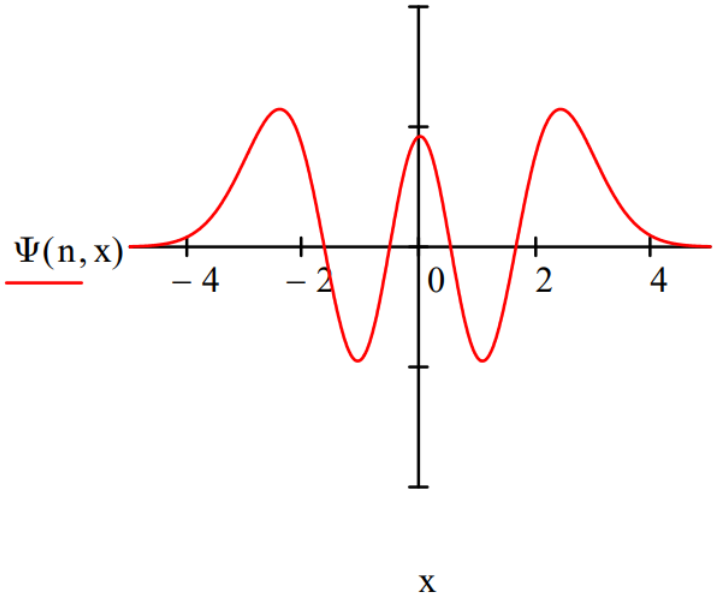
Given the quantum number this Mathcad file calculates the Wigner distribution function for the specified harmonic oscillator eigenstate using the coordinate wave function.

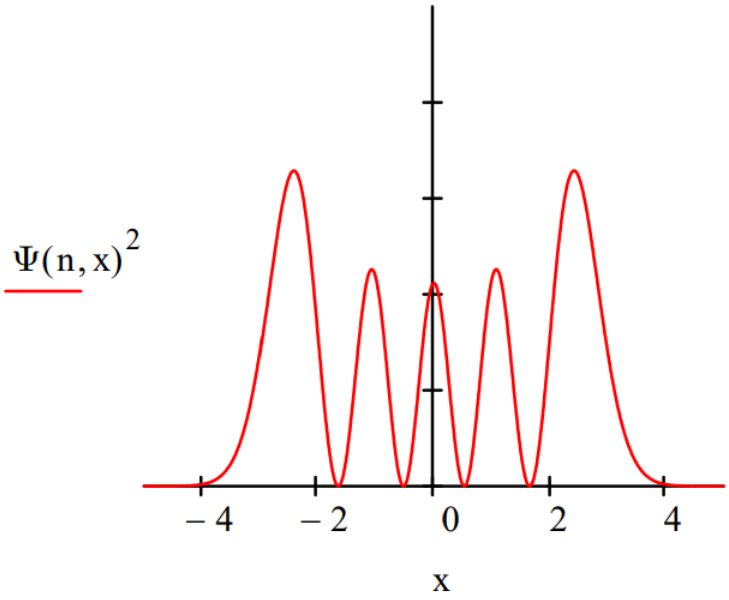
Quantum number: $n := 4$

Harmonic oscillator coordinate eigenstate:

$$\Psi(n, x) := \frac{1}{\sqrt{2^n \cdot n! \sqrt{\pi}}} \cdot \mathrm{Her}(n, x) \cdot \exp\left(-\frac{x^2}{2}\right)$$

Display coordinate wave function and distribution function:





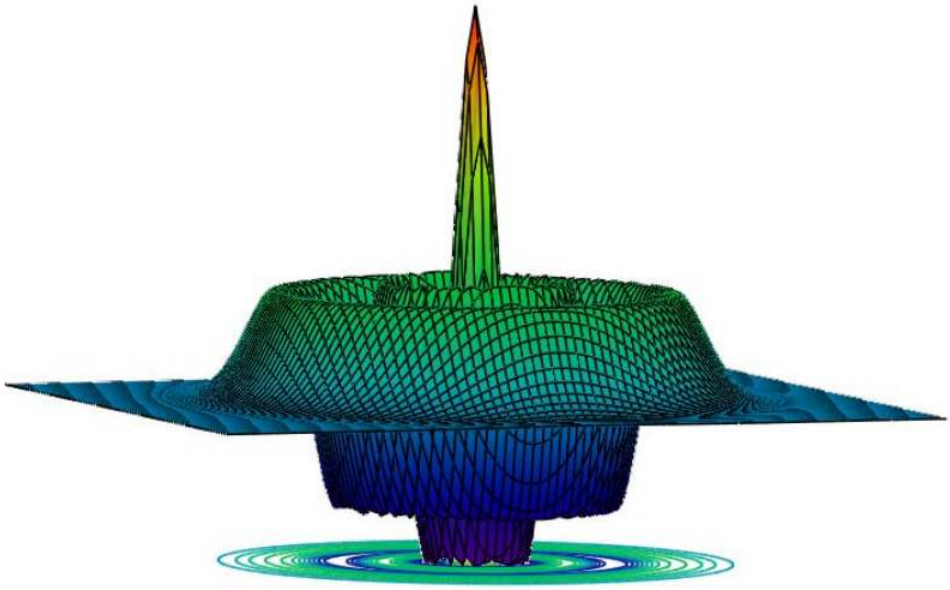
Calculate Wigner distribution:

$$W(n, x, p) := \frac{1}{\pi^{\frac{3}{2}}} \cdot \int_{-\infty}^{\infty} \Psi\left(n, x + \frac{s}{2}\right) \cdot \exp(i \cdot s \cdot p) \cdot \Psi\left(n, x - \frac{s}{2}\right) ds$$

Display Wigner distribution:

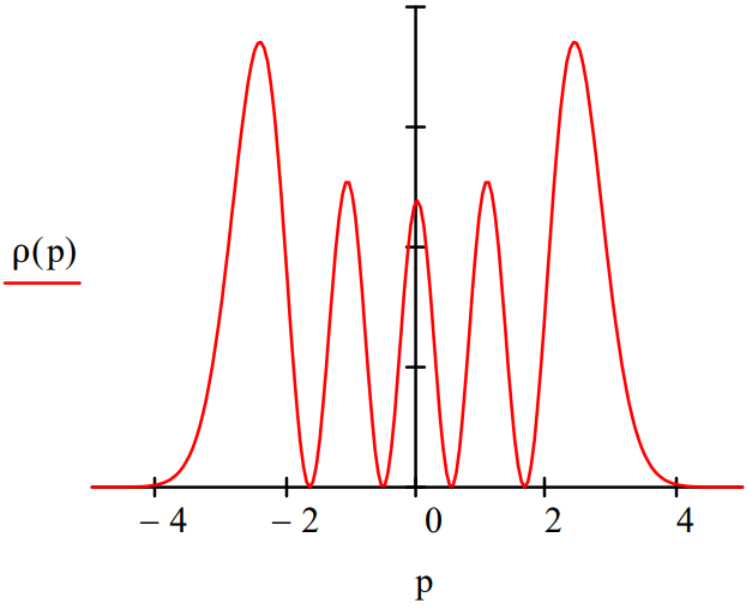
$$N := 80 \qquad i := 0 \ldots N \qquad x_i = -4 + \frac{8 \cdot i}{N}$$

$$j := 0 \ldots N \qquad p_j = -5 + \frac{10 \cdot j}{N} \qquad \text{Wigner}_{i,j} := W(n, x_i, p_j)$$



Calculate the momentum distribution function using the Wigner function:

$$\rho(p) := \int_{-\infty}^{\infty} W(n, x, p) dx \qquad p := -5, -4.95 \ldots 5$$



This page titled 1.69: The Wigner Distribution Function for the Harmonic Oscillator is shared under a CC BY 4.0 license and was authored, remixed, and/or curated by Frank Rioux via source content that was edited to the style and standards of the LibreTexts platform.

1.70: Wigner Distribution for the Particle in a Box

The Wigner function is a quantum mechanical phase-space quasi-probability function. It is called a quasi-probability function because it can take on negative values, which have no classical meaning in terms of probability.

The PIB eigenstates for a box of unit dimension are given by:

$$\Psi(x,n) := \sqrt{2}\cdot\sin(n\cdot\pi\cdot x)$$

For these eigenstates the Wigner distribution function is:

$$\mathrm{W(x,p,n)} := \frac{1}{\pi}\cdot\int_{-x}^{x}\sqrt{2}\cdot\sin[\mathrm{n}\cdot\pi\cdot(\mathrm{x}+\mathrm{s})]\cdot\exp(2\cdot\mathrm{i}\cdot\mathrm{s}\cdot\mathrm{p})\cdot\sqrt{2}\cdot\sin[\mathrm{n}\cdot\pi\cdot(\mathrm{x}-\mathrm{s})]\mathrm{ds}$$

Integration with respect to s yields the following function:

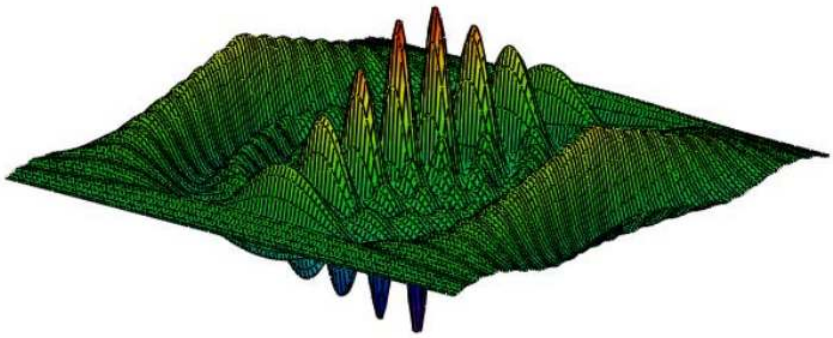
$$\mathrm{W(x,p,n)} := \frac{2}{\pi}\cdot\left[\frac{\sin[2\cdot(\mathrm{p}-\mathrm{n}\cdot\pi)\cdot\mathrm{x}]}{4\cdot(\mathrm{p}-\mathrm{n}\cdot\pi)}+\frac{\sin[2\cdot(\mathrm{p}+\mathrm{n}\cdot\pi)\cdot\mathrm{x}]}{4\cdot(\mathrm{p}+\mathrm{n}\cdot\pi)}-\cos(2\cdot\mathrm{n}\cdot\pi\cdot\mathrm{x})\cdot\frac{\sin(2\cdot p\cdot\mathrm{x})}{2\cdot p}\right]$$

The Wigner distribution for the nth eigenstate is calculated below:

$$\mathrm{n} := 10 \qquad \mathrm{N} := 115 \qquad \mathrm{i} := 0..\mathrm{N}$$

$$\mathrm{x_i} := \frac{\mathrm{i}}{\mathrm{N}} \qquad \mathrm{j} := 0..\mathrm{N} \qquad \mathrm{p_j} := -40+\frac{80\cdot\mathrm{j}}{\mathrm{N}}$$

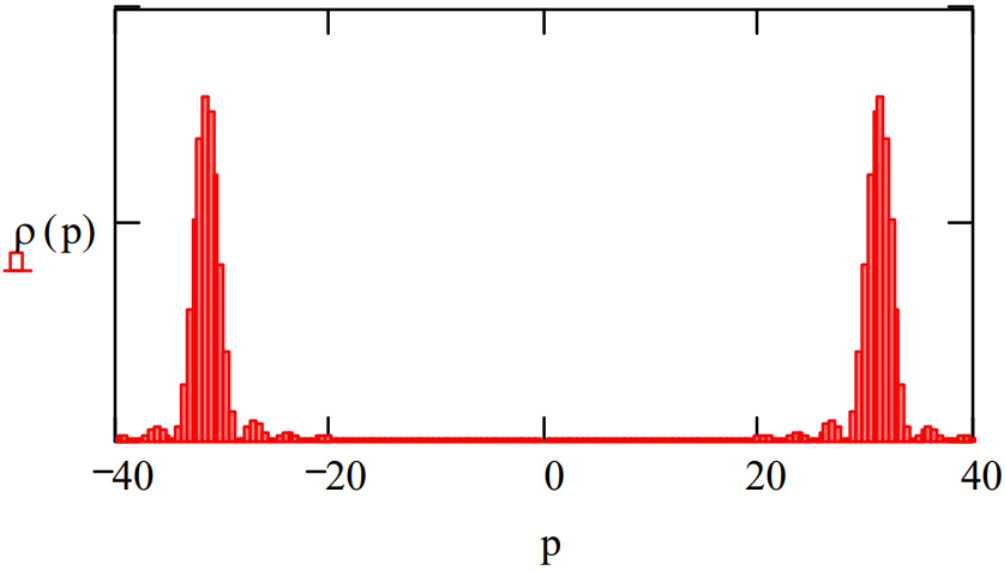
$$\mathrm{Wigner}_{i,j} := \mathrm{if}\left[x_i \le 0.5, W\left(x_i,p_j,n\right), W\left[\left(1-x_i\right),p_j,n\right]\right]$$



Wigner

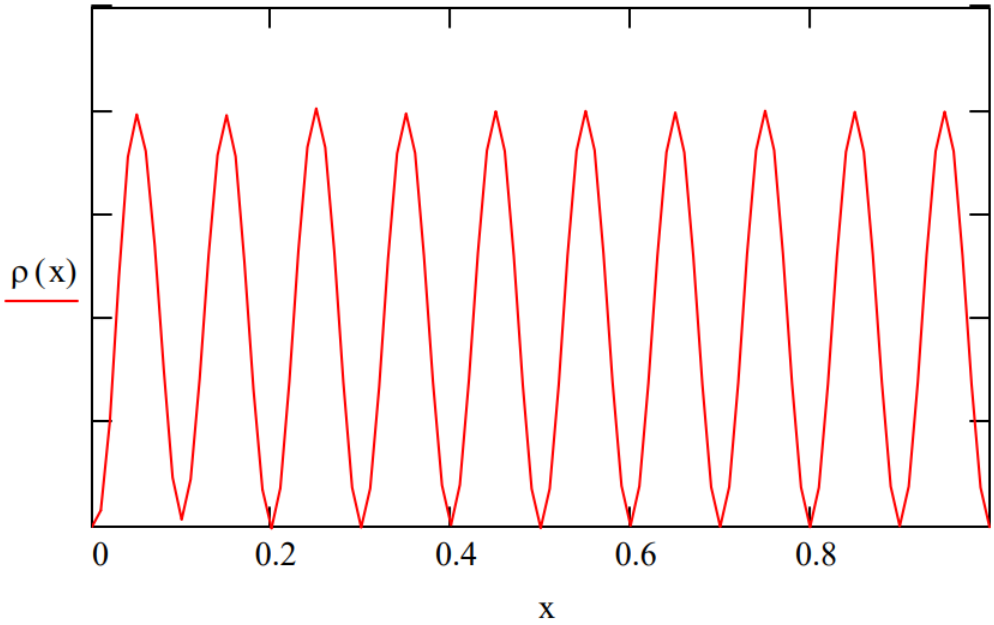
Integration of the Wigner function over the spatial coordinate yields the momentum distribution function as is shown below.

$$\rho(\mathrm{p}) := \int_{0}^{1}\mathrm{W(x,p,n)}\mathrm{dx} \qquad \mathrm{p} := -40,-39.5\ldots 40$$



Integration of the Wigner function over the momentum coordinate yields the spatial distribution function as is shown below.

$$\rho(x) := \int_{-51}^{50} W(x, p, n)dp \qquad x := 0, 01 \ldots 1$$



The Wigner distribution can be used to calculate the expectation values for position, momentum and kinetic energy.

$$x_{bar} = \int_{-\infty}^{\infty}\int_{0}^{1} W(x, p, 1) \cdot x \; dx \; dp \text{ simplify } \rightarrow x_{bar} = \frac{1}{2}$$

$$p_{bar} = \int_{-\infty}^{\infty}\int_{0}^{1} W(x, p, 1) \cdot pdx \; dp \text{ simplify } \rightarrow p_{bar} = 0$$

$$T_{bar} = \int_{-\infty}^{\infty}\int_{0}^{1} W(x, p, 1) \cdot \frac{p^2}{2} dx \; dp \text{ simplify } \rightarrow T_{bar} = \frac{1}{2} \cdot \pi^2$$

https://chem.libretexts.org/@go/page/156420

References:

"Wigner quasi-probability distribution for the infinite square well: Energy eigenstates and time-dependent wave packets," by Belloni, Docheski and Robinett; *American Journal of Physics* **72(9)**, 1183-1192 (2004).

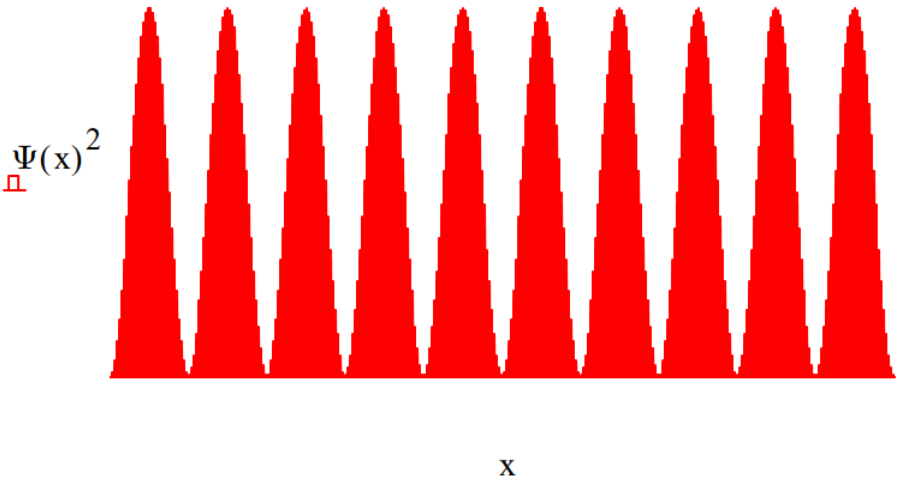
"Wigner functions and Weyl transforms for pedestrians," by William Case, *American Journal of Physics* **76(10)**, 937-946 (2008).

This page titled 1.70: Wigner Distribution for the Particle in a Box is shared under a CC BY 4.0 license and was authored, remixed, and/or curated by Frank Rioux via source content that was edited to the style and standards of the LibreTexts platform.

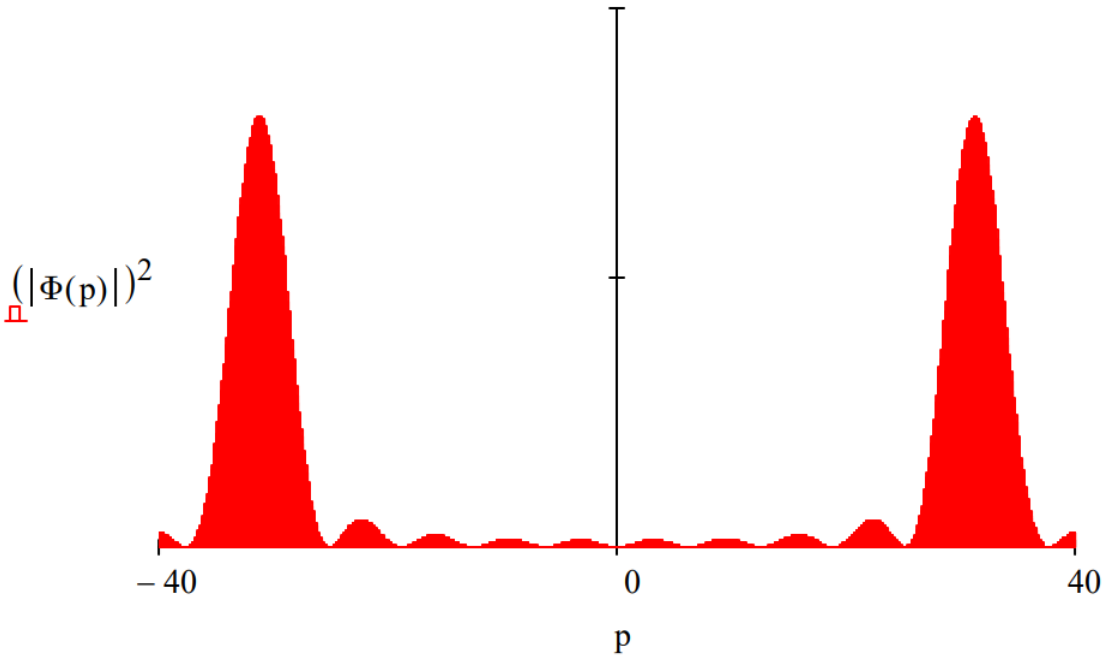
1.71: The Wigner Distribution for a Particle in a One-dimensional Box

The following outlines the calculation of the Wigner distribution for a particle in a one-dimensional box for the n = 10 state. First the coordinate wave function is Fourier transformed into momentum space. Following that the Wigner function is calculated using the momentum space wave function.

$$\Psi(x) := \sqrt{2} \cdot \sin(10 \cdot \pi \cdot x)$$



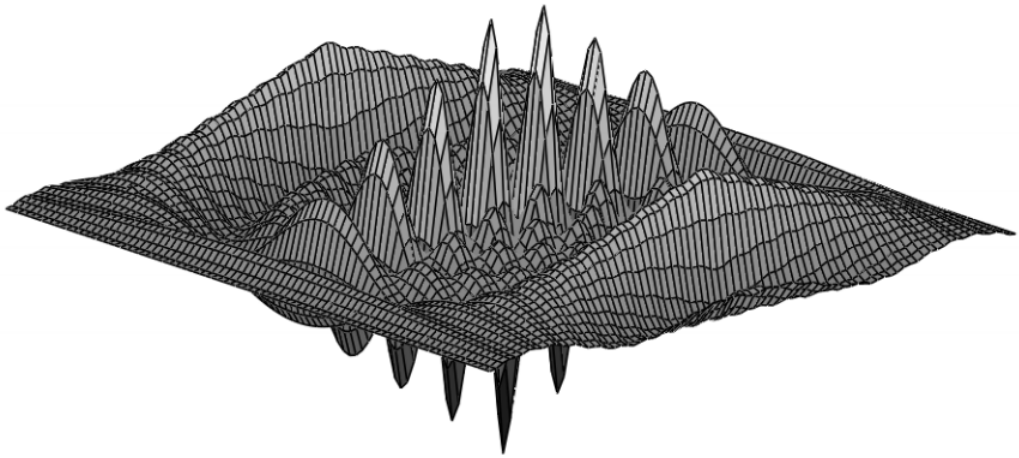
$$\Phi(p) := \frac{1}{\sqrt{2 \cdot \pi}} \cdot \int_0^1 \exp(-i \cdot p \cdot r) \cdot \Psi(x) dx \text{ simplify } \rightarrow -\frac{10 \cdot \sqrt{\pi} \cdot \left(e^{-p \cdot i} - 1\right)}{100 \cdot \pi^2 - p^2}$$



$$W(x, p) := \frac{1}{2 \cdot \pi} \cdot \int_{-\infty}^{\infty} \overline{\Phi\left(p + \frac{s}{2}\right)} \cdot \exp(-i \cdot s \cdot x) \cdot \Phi\left(p - \frac{s}{2}\right) ds$$

$$N := 80 \qquad i := 0 \ldots N \qquad x_i := \frac{i}{N}$$

$$j := 0 \ldots N \qquad p_j := -40 + \frac{80 \cdot j}{N} \qquad \text{Wigner}_{i,j} := W\left(x_i, p_j\right)$$



Wigner

This page titled 1.71: The Wigner Distribution for a Particle in a One-dimensional Box is shared under a CC BY 4.0 license and was authored, remixed, and/or curated by Frank Rioux via source content that was edited to the style and standards of the LibreTexts platform.

1.72: Superposition vs. Mixture

The Wigner function can be used to illustrate the difference between a superposition and a mixture. First consider the following linear superposition of Gaussian functions.

$$\Psi(x) := \exp\left[-(x-5)^2\right] + \exp\left[-(x+5)^2\right]$$

The Wigner distribution for this function is calculated and plotted below.

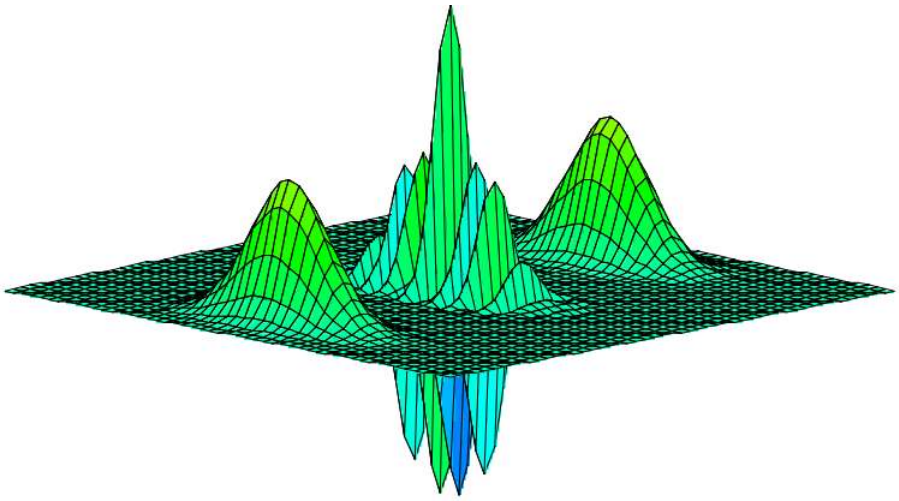
$$W(x,p) := \int_{-\infty}^{\infty} \left[\exp\left[-\left(x+\frac{s}{2}-5\right)^2\right] + \exp\left[-\left(x+\frac{s}{2}+5\right)^2\right]\right] \cdot \exp(i\cdot p\cdot s) \cdot \left[\exp\left[-\left(x-\frac{s}{2}-5\right)^2\right] + \exp\left[-\left(x-\frac{s}{2}+5\right)^2\right]\right] ds$$

Integration yields:

$$W(x,p) := \sqrt{2}\cdot\sqrt{\pi}\cdot\left(2\cdot\exp\left(-2\cdot x^2-\frac{1}{2}\cdot p^2\right)\cdot\cos(10\cdot p) + \exp\left(-2\cdot x^2+20\cdot x-50-\frac{1}{2}\cdot p^2\right) + \exp\left(-2\cdot x^2-20\cdot x-50-\frac{1}{2}\cdot p^2\right)\right)$$

$$N := 50 \qquad i := 0\ldots N \qquad x_i := -7+\frac{14\cdot i}{N}$$

$$j := 0\ldots N \qquad p_j := -6+\frac{12\cdot j}{N} \qquad Wigner_{i,j} := W(x_i, p_j)$$



Wigner

The signature of a superposition is the occurrence of interference fringes as seen in the center of the figure above.

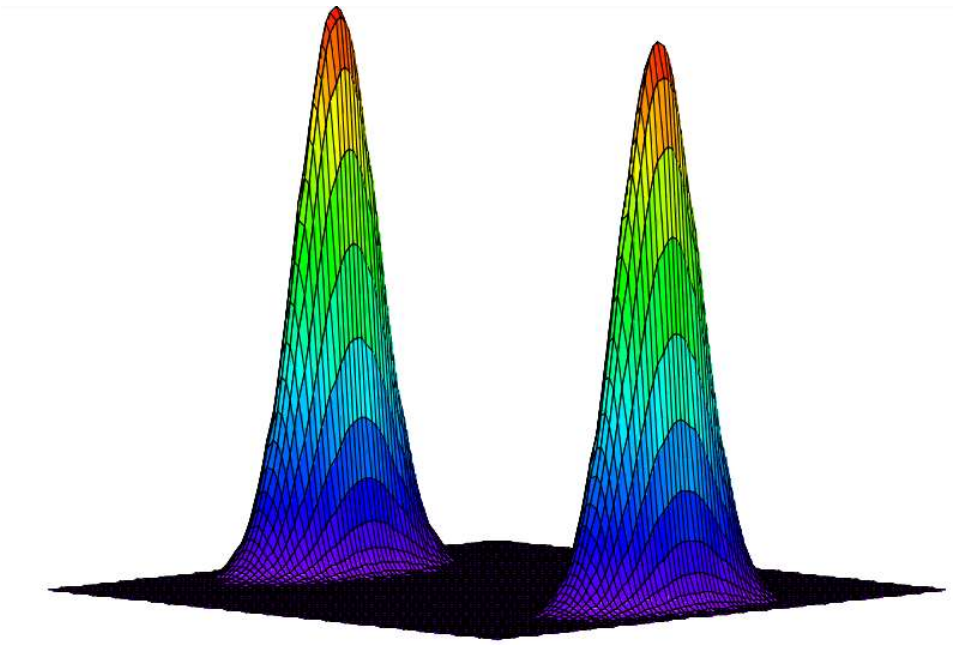
The Wigner function for a classical mixture is the sum of Wigner functions for each member of the mixture. The interference region is clearly absent in the figure shown below.

$$W(x,p) := \int_{-\infty}^{\infty} \exp\left[-\left(x+\frac{s}{2}-5\right)^2\right]\cdot\exp(i\cdot p\cdot s)\cdot\exp\left[-\left(x-\frac{s}{2}-5\right)^2\right] ds + \int_{-\infty}^{\infty} \exp\left[-\left(x+\frac{s}{2}+5\right)^2\right]\cdot\exp(i\cdot p\cdot s)\cdot\exp\left[-\left(x-\frac{s}{2}+5\right)^2\right] ds$$

Integration yields:

$$W(x,p) := \exp\left(-2\cdot x^2 + 20\cdot x - 50 - \frac{1}{2}\cdot p^2\right)\cdot\sqrt{2}\cdot\sqrt{\pi}$$
$$+ \exp\left(-2\cdot x^2 - 20\cdot x - 50 - \frac{1}{2}\cdot p^2\right)\cdot\sqrt{2}\cdot\sqrt{\pi}$$

$$N := 100 \qquad i := 0 \ldots N \qquad x_i := -7 + \frac{14\cdot i}{N}$$
$$j := 0 \ldots N \qquad p_j := -6 + \frac{12\cdot j}{N} \qquad Wigner_{i,j} := W\left(x_i, p_j\right)$$



Wigner

Reference: Decoherence and the Transition form Quantum to Classical, Wojciech Jurek, Physics Today, October 1991, pages 36-44.

This page titled 1.72: Superposition vs. Mixture is shared under a CC BY 4.0 license and was authored, remixed, and/or curated by Frank Rioux via source content that was edited to the style and standards of the LibreTexts platform.

1.73: Time-dependent Wigner Function for Harmonic Oscillator Transitions

Initial state:

$$m := 0 \qquad E_m := m + \frac{1}{2}$$

Final state:

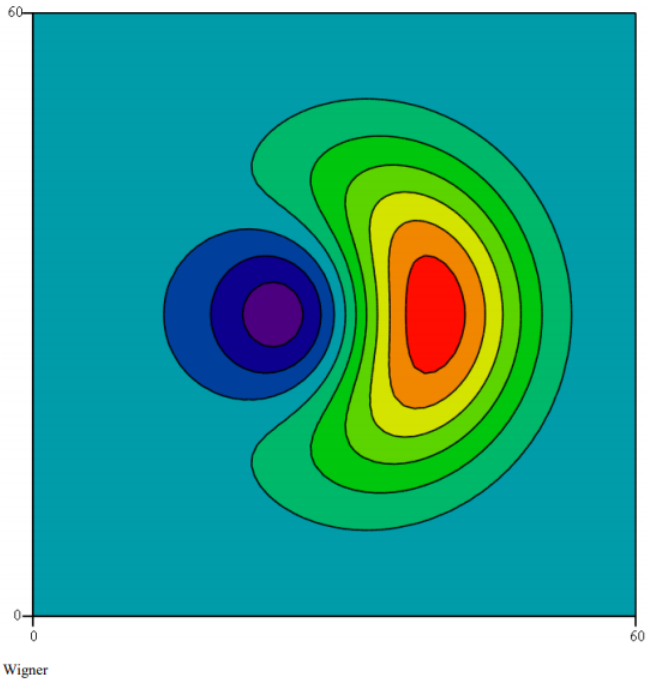
$$n := 1 \qquad E_n := n + \frac{1}{2} \qquad t := \text{FRAME}$$

Define Wigner distribution function for a linear superposition of the initial and final harmonic oscillator state.

$$W(x,p) := \frac{1}{\pi^{\frac{3}{2}}} \int_{-\infty}^{\infty} \left[\frac{1}{\sqrt{2^n \cdot n! \sqrt{\pi}}} \cdot \text{Her}\left(n, x + \frac{s}{2}\right) \cdot \exp\left[-\frac{\left(x + \frac{s}{2}\right)^2}{2} \right] \cdot \exp\left(i \cdot E_n \cdot t\right) \right.$$
$$\left. + \frac{1}{\sqrt{2^m \cdot m! \cdot \sqrt{\pi}}} \cdot \text{Her}\left(m, x + \frac{s}{2}\right) \cdot \exp\left[-\frac{\left(x + \frac{s}{2}\right)^2}{2} \right] \cdot \exp\left(i \cdot E_m \cdot t\right) \right]$$
$$\cdot \exp(i \cdot s \cdot p) \cdot \left[\frac{1}{\sqrt{2^n \cdot n! \cdot \sqrt{\pi}}} \cdot \text{Her}\left(n, x - \frac{s}{2}\right) \cdot \exp\left[-\frac{\left(x - \frac{s}{2}\right)^2}{2} \right] \cdot \exp\left(-i \cdot E_n \cdot t\right) \right.$$
$$\left. + \frac{1}{\sqrt{2^m \cdot m! \cdot \sqrt{\pi}}} \cdot \text{Her}\left(m, x - \frac{s}{2}\right) \cdot \exp\left[-\frac{\left(x - \frac{s}{2}\right)^2}{2} \right] \cdot \exp\left(-i \cdot E_m \cdot t\right) \right] ds$$

Display Wigner distribution:

$$N = 60 \qquad i := 0 \ldots N \qquad x_i := -2.5 + \frac{5 \cdot i}{N}$$
$$j := 0 \ldots N \qquad P_j := -2.5 + \frac{5j}{N} \qquad \text{Wigner}_{i,j} := W(x_i, p_j)$$



Wigner

This page titled 1.73: Time-dependent Wigner Function for Harmonic Oscillator Transitions is shared under a CC BY 4.0 license and was authored, remixed, and/or curated by Frank Rioux via source content that was edited to the style and standards of the LibreTexts platform.

1.74: Momentum Operator in Coordinate Space

Wave-particle duality is at the heart of quantum mechanics. A particle with wavelength λ has wave function (un-normalized)

$$\langle x|\lambda\rangle = \exp\left(i2\pi\frac{x}{\lambda}\right)$$

However, according to deBroglie's wave equation the particle's momentum is p = h/λ. Therefore the momentum wave function of the particle in coordinate space is

$$\langle x|p\rangle = \exp\left(\frac{ipx}{h}\right)$$

In momentum space the following eigenvalue equation holds: $\hat{p}|p\rangle = p|p\rangle$. Operating on the momentum eigenfunction with the momentum operator in momentum space returns the momentum eigenvalue times the original momentum eigenfunction. In other words, in its own space the momentum operator is a multiplicative operator (the same is true of the position operator in coordinate space). To obtain the momentum operator in coordinate space this expression can be projected onto coordinate space by operating on the left by $\langle x|$.

$$\langle x|\hat{p}|p\rangle = p\langle x|p\rangle = p\exp\left(\frac{ipx}{h}\right) = \frac{h}{i}\frac{d}{dx}\langle x|p\rangle$$

Comparing the first and last terms reveals that

$$\langle x|\hat{p} = \frac{h}{i}\frac{d}{dx}\langle x|$$

and that $\frac{h}{i}\frac{d}{dx}$ is the momentum operator in coordinate space.

The position wave function in momentum space is the complex conjugate of the momentum wave function coordinate space.

$$\langle p|x\rangle = \langle x|p\rangle^* = \exp\left(\frac{-ipx}{\hbar}\right)$$

Using the method outlined above it is easy to show that the position operator in momentum space is $-\frac{\hbar}{i}\frac{d}{dp}$.

This page titled 1.74: Momentum Operator in Coordinate Space is shared under a CC BY 4.0 license and was authored, remixed, and/or curated by Frank Rioux via source content that was edited to the style and standards of the LibreTexts platform.

1.75: Momentum Wave Functions for the Particle in a Box

Momentum-space wave functions frequently are most easily obtained by the Fourier transform of the already available position-space wave function. For the particle in a one-dimensional box the Fourier transform is given by the following equation:

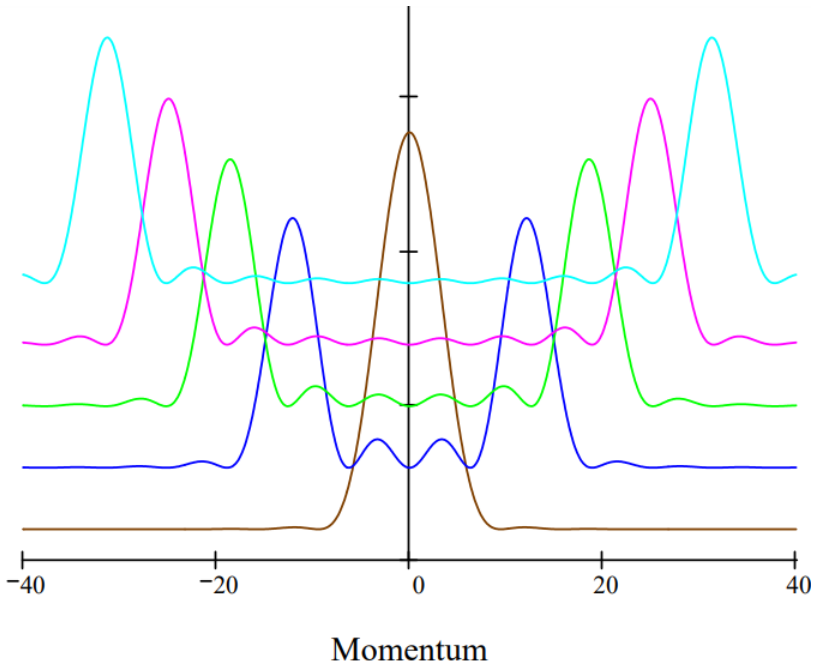
$$\Phi(n,p,a) := \frac{1}{\sqrt{2\cdot\pi}}\int_0^a \exp(-i-p-x)\cdot\sqrt{\frac{2}{a}}\cdot\sin\left(\frac{n\cdot\pi\cdot x}{a}\right)dx$$

Evaluation of this integral yields:

$$\Phi(\mathrm{n},\mathrm{p},\mathrm{a}) := \mathrm{n}\cdot\sqrt{\mathrm{a}\cdot\pi}\cdot\left[\frac{1-(-1)^{\mathrm{n}}\cdot\exp(-\mathrm{i}\cdot\mathrm{p}\cdot\mathrm{a})}{\mathrm{n}^2\cdot\pi^2-\mathrm{a}^2\cdot\mathrm{p}^2}\right]$$

Choose box dimension: $\mathrm{a} := 1$

The momentum-space probability distribution functions, $|\Phi(\mathrm{n,p})|^2$, for the n = 1, 4, 6, 8 and 10 energy levels of the particle in a one-dimensional box are displayed below. They show the probability that the particle will be found to have various momentum values in an experimental measurement. The distribution functions are offset by small increments for clarity presentation.



This figure illustrates the correspondence principle. As the **n** quantum number increases th momentum distribution appears more classical. For example, for n = 10 the momentum distribution has principle maxima around $\pm$ 30, suggesting a particle moving to the right and left with a specific momentum. This effect becomes more pronounced with higher n-values.

This page titled 1.75: Momentum Wave Functions for the Particle in a Box is shared under a CC BY 4.0 license and was authored, remixed, and/or curated by Frank Rioux via source content that was edited to the style and standards of the LibreTexts platform.

1.76: A Graphical Illustration of the Heisenberg Uncertainty Relationship

According to quantum mechanics position and momentum are conjugate variables; they cannot be simultaneously known with high precision. The uncertainty principle requires that if the position of an object is precisely known, its momentum is uncertain, and vice versa. This reciprocal relationship is captured by the well-known uncertainty relation, which says that the product of the uncertainties in position and momentum must be greater than or equal to Planck's constant divided by 4π.

$$\Delta x \cdot \Delta p \geq \frac{h}{4 \cdot \pi}$$

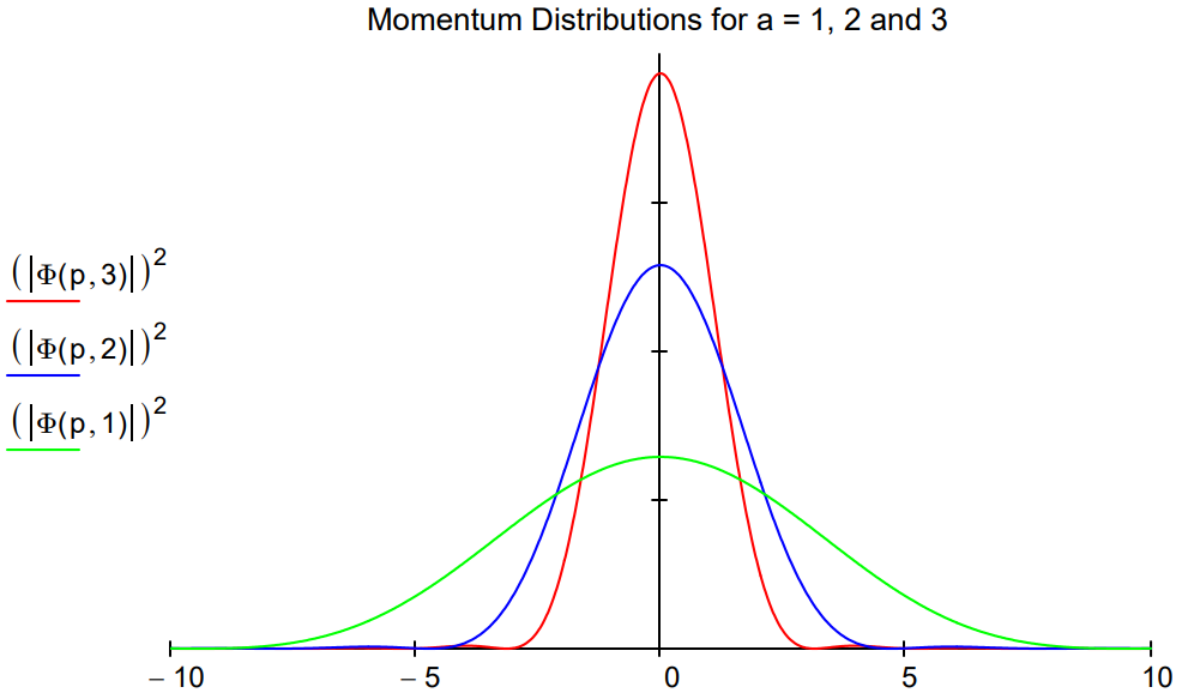
This simple mathematical relation can be visualized using the traditional work horse - the quantum mechanical particle in a box (infinite one-dimensional potential well). The particle's ground-state wave function in coordinate space for a box of width a is shown below.

$$\Psi(x, a) := \sqrt{\frac{2}{a}} \cdot \sin\left(\frac{\pi \cdot x}{a}\right)$$

To illustrate the uncertainty principle and the reciprocal relationship between position and momentum, Ψ(x,a) is Fourier transformed into momentum space yielding the particle's ground-state wave function in the momentum representation.

$$\Phi(p, a) := \sqrt{\frac{1}{2 \cdot \pi}} \cdot \int_0^a \exp(-i \cdot p \cdot x) \cdot \sqrt{\frac{2}{a}} \cdot \sin\left(\frac{\pi \cdot x}{a}\right) dx \text{ simplify} \rightarrow \frac{\pi \cdot a \cdot \left(e^{-a \cdot p \cdot i} + 1\right) \cdot \sqrt{\frac{1}{a}}}{\pi^{\frac{5}{2}} - \sqrt{\pi} \cdot a^2 \cdot p^2}$$

In the figure below, the momentum distribution, $|\Phi(p,a)|^2$, is shown for three sizes, a = 1,2 and 3. The uncertainty principle is illustrated as follows: as the box size increases the position uncertainty increases and momentum uncertainty decreases because the momentum distribution narrows.



This page titled 1.76: A Graphical Illustration of the Heisenberg Uncertainty Relationship is shared under a CC BY 4.0 license and was authored, remixed, and/or curated by Frank Rioux via source content that was edited to the style and standards of the LibreTexts platform.

1.77: The Quantum Harmonic Oscillator

The harmonic oscillator is frequently used by chemical educators as a rudimentary model for the vibrational degrees of freedom of diatomic molecules. Most often when this is done, the teacher is actually using a classical ball-and-spring model, or some hodge-podge hybrid of the classical and the quantum harmonic oscillator. Unfortunately these models are not accurate representations of the vibrational modes of molecules. To the extent that a simple harmonic potential can be used to represent molecular vibrational modes, it must be done in a pure quantum mechanical treatment based on solving the Schrödinger equation.

Schrödinger's equation in atomic units (h = 2π) for the harmonic oscillator has an exact analytical solution.

$$\frac{-1}{2\cdot\mu}\cdot\frac{d^2}{dx^2}\Psi(x)+\frac{1}{2}\cdot k\cdot x^2\cdot\Psi(x)=E\cdot\Psi(x)$$

Potential energy:

$$V(x,k):=\frac{1}{2}\cdot k\cdot x^2$$

Energy eigenstates:

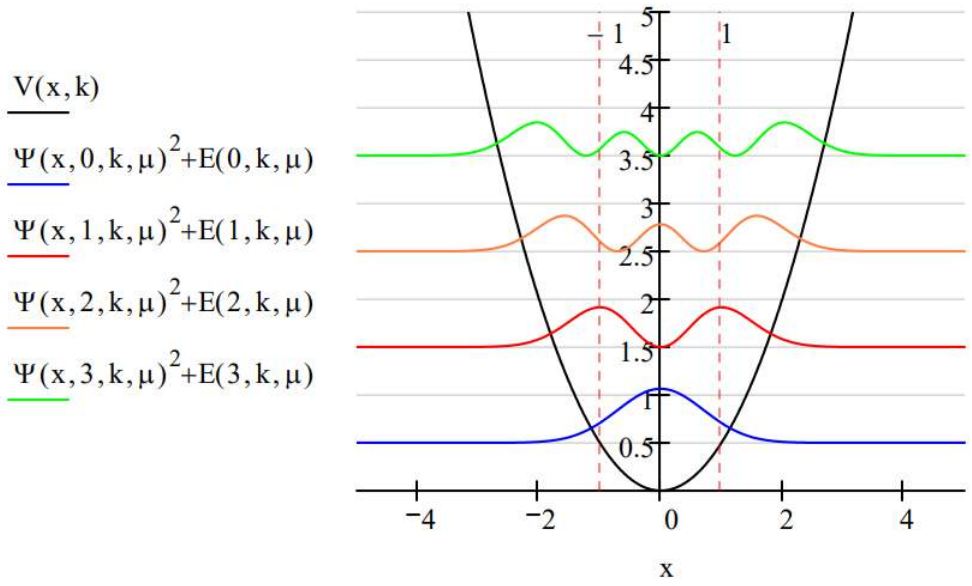
$$E(v,k,\mu):=\left(v+\frac{1}{2}\right)\cdot\sqrt{\frac{k}{\mu}}$$

Eigenfunctions:

$$\Psi(x,v,k,\mu):=\frac{(k\cdot\mu)^{\frac{1}{8}}}{\sqrt{2^v\cdot v!\cdot\sqrt{\pi}}}\cdot\mathrm{Her}\left[v,(k\cdot\mu)^{\frac{1}{4}}\cdot x\right]\cdot\exp\left(\frac{\sqrt{k\cdot\mu}\cdot x^2}{2}\right)$$

The probability distribution functions for k = μ = 1 for the first four eigenstates are shown graphically below.

Force constant: $k := 1$	Effective mass: $\mu := 1$



The harmonic oscillator eigenfunctions form an orthonormal basis set.

Normalized:

$$\int_{-\infty}^{\infty}\Psi(x,0,k,\mu)^2dx=1$$

Orthogonal:

$$\int_{-\infty}^{\infty} \Psi(x,1,k,\mu)\cdot\Psi(x,0,k,\mu)dx = 0$$

Several non-classical attributes of the quantum oscillator are revealed in the graph above. Perhaps most obvious is that energy is quantized. Another is that the allowed oscillator states are stationary states. There is no vibratory motion associated with these states. In these allowed states, the oscillator is in a weighted superposition of all values of the x-coordinate, which in this case is the internuclear separation. The only time oscillatory motion occurs in the quantum oscillator is when it is perturbed by, for example, external electromagnetic radiation and making a transition from one allowed energy state to another. For a detailed discussion of these points see "Coherent Superpositions for the Harmonic Oscillator". For a discussion of "The Harmonic Oscillator and the Uncertainty Principle" visit this tutorial.

Another non-classical feature of the quantum oscillator is tunneling. The vertical dashed lines in the figure show the classical turning points for the ground state of the quantum oscillator. The classical turning point is that value of the x-coordinate at which the potential energy is equal to the total energy, and therefore classically the system must reverse its direction of motion.

Classical turning point for v=0, k=μ=1:

$$\frac{1}{2}\cdot \mathrm{k}\cdot \mathrm{x}^2 = \left(\mathrm{v}+\frac{1}{2}\right)\cdot\sqrt{\frac{\mathrm{k}}{\mu}}\ \text{solve},x \rightarrow \begin{bmatrix} (2\cdot v+1)^{\frac{1}{2}} \\ -(2\cdot v+1)^{\frac{1}{2}} \end{bmatrix}\ \text{substitute},\mathrm{v}=0 \rightarrow \begin{pmatrix} 1 \\ -1 \end{pmatrix}$$

For v=0 the region beyond $\pm$1 is called the classically forbidden region because the oscillator does not have enough energy (E = 1/2) to be there because V > E. It implies a negative kinetic energy which does not make classical sense. Due to the symmetry of the potential well, the tunneling probability is calculated as follows.

$$2\cdot\int_{1}^{\infty}\Psi(x,0,k,\mu)^2dx = 0.157$$

It is easy to demonstrate that the tunneling probability decreases as the v quantum number increases. This might be considered a minor example of Bohr's correspondence principle: as the energy of a quantum system increases it appears to be more classical.

The fact that the wave functions of quantum states are superpositions is a fundamental idea in quantum theory. A quantum object (quon to use Nick Herbert's term) is not here or there, it is here and there. We can illuminate this idea by looking at a quantum oscillator's state operator, $|\Psi><\Psi|$. This is also called the density operator or density matrix. It is a very powerful concept which is not generally presented in undergraduate courses in quantum physics or chemistry.

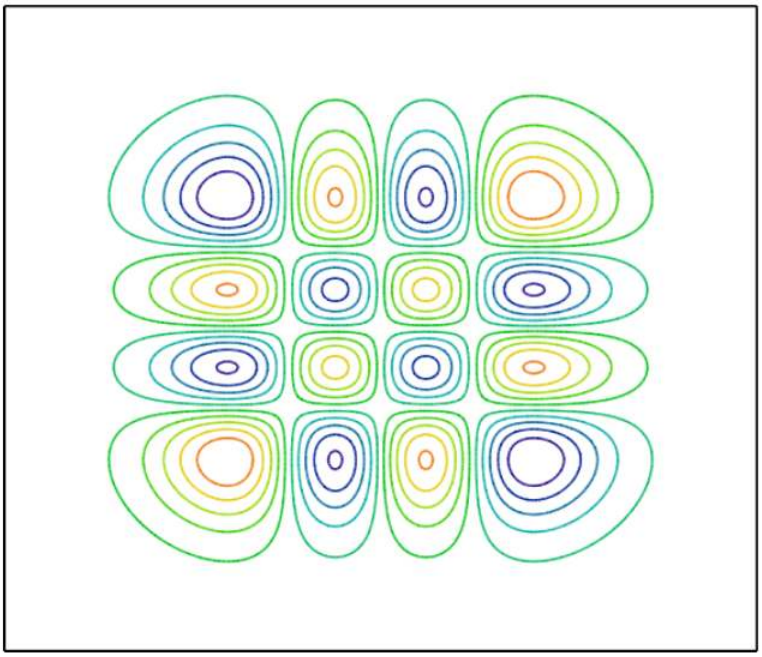
The state operator is now calculated and displayed for the v = 3 state. The state operator is a projection operator and its matrix elements, $<\mathrm{x}_1|\Psi><\Psi|x_2>$, are calculated and displayed below. These matrix elements are the probability amplitude that an oscillator in the state $|\Psi>$ is at both x_1 and x_2. This reveals the meaning of the quantum superposition as the quon being both here and there.

$$\mathrm{v}:=3 \quad \mathrm{Min}:=5 \quad \mathrm{N}:=200 \quad \mathrm{j}:=0\ldots\mathrm{N} \qquad \mathrm{k}:=0\ldots\mathrm{N}$$

$$x_{1_j}:=-\mathrm{Min}+\frac{2\cdot\mathrm{Min}\cdot\mathrm{j}}{\mathrm{N}} \qquad \mathrm{x}_{2_k}:=-\mathrm{Min}+\frac{2\cdot\mathrm{Min}\cdot\mathrm{k}}{\mathrm{N}}$$

$$\Psi(x_1,x_2):=\frac{1}{2^v\cdot v!\cdot\sqrt{\pi}}\cdot\mathrm{Her}(v,x_1)\cdot\mathrm{Her}(v,x_2)\cdot\exp\left[\frac{-\left(x_1^2+x_2^2\right)}{2}\right]$$

$$\Psi\Psi_{j,k}=\Psi(x_1,x_2)$$



$\Psi\Psi$

Viewing this as a graphical representation of the density matrix we clearly see the prominence of off-diagonal elements, elements with non-zero values for which x_1 is not equal to x_2. This is the signature of quantum mechanics. By comparison a classical system would have a diagonal density matrix - only the $x_1 = x_2$ elements would have non-zero values.

The following statements, modified slightly, are the best single-sentence descriptions of the meaning of the wave function I have read.

> *Quons are characterized by their entire distributions, called wave functions or orbitals, rather than by instantaneous positions and velocities: a quon may be considered always to be, with appropriate probability, at all points of its distribution, which does not vary with time. (F. E. Harris, Encyclopedia of Physics)*
>
> *From the quantum mechanical perspective, to measure the position of a quon is not to find out where it is, but to cause it to be somewhere. (Louisa Gilder, The Age of Entanglement)*

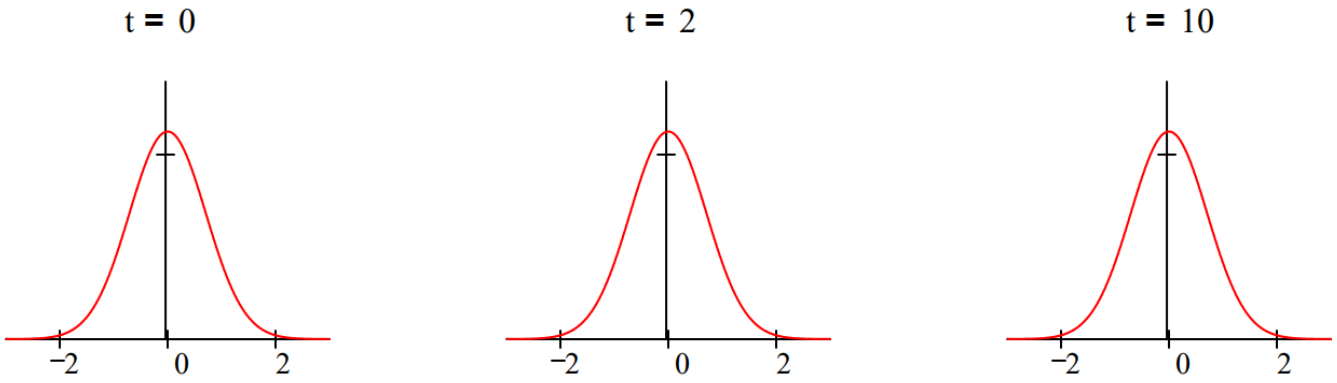
This page titled 1.77: The Quantum Harmonic Oscillator is shared under a CC BY 4.0 license and was authored, remixed, and/or curated by Frank Rioux via source content that was edited to the style and standards of the LibreTexts platform.

1.78: Coherent Superpositions for the Harmonic Oscillator

The quantum mechanical harmonic oscillator eigenstates are stationary states and therefore cannot be used individually to represent classical oscillatory motion. (Atomic units are used in this tutorial.)

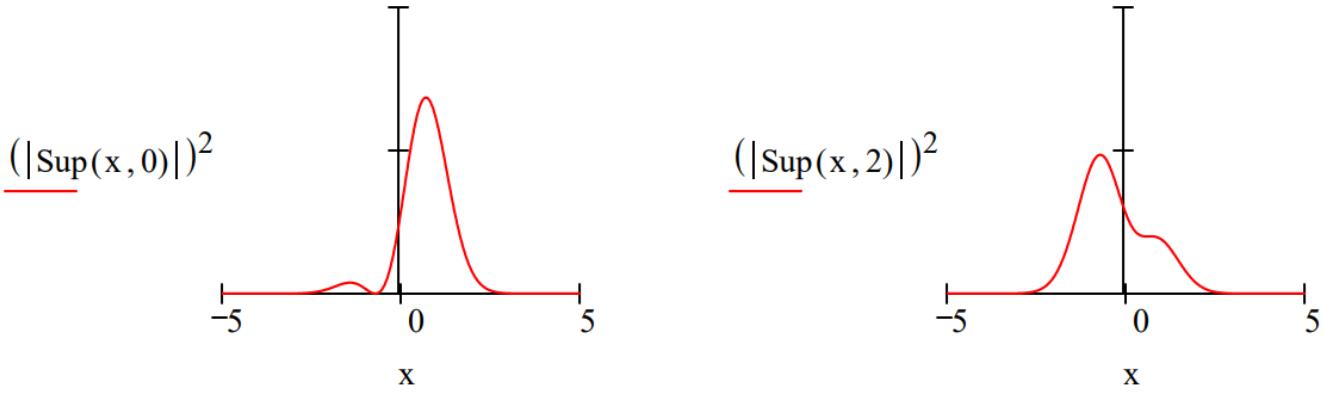
$$\Psi(v,x,t) := \frac{1}{\sqrt{2^v \cdot v! \cdot \sqrt{\pi}}} \cdot \mathrm{Her}(v,x) \cdot \exp\left(\frac{-x^2}{2}\right) \cdot \exp\left[-i \cdot \left(v + \frac{1}{2}\right) \cdot t\right]$$

For example, suppose we choose to represent the ground vibrational state of a homonuclear diatomic mole as a simple harmonic oscillator with vibrational quantum number v = 0. We see that probability distributio $|\Psi(0,x,t)|^2$, is independent of time. There is no oscillatory motion; the molecule is in a stationary state whic weighted superposition of all possible internuclear separations.



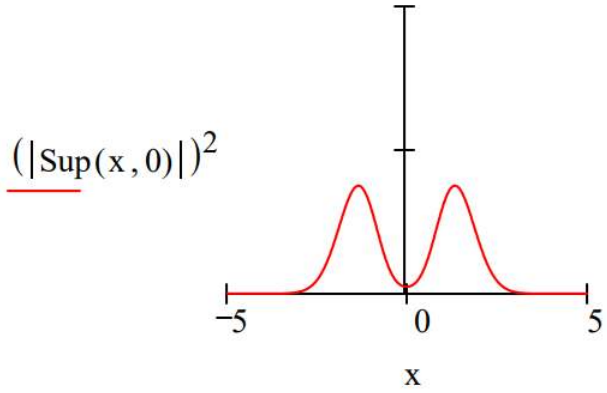
However, simple superpositions of the vibrational eigenstates do show oscillatory behavior. This is due to exponential term involving the vibrational energy, exp[-iE(v)t]. This term oscillates with a dependence on vibrational quantum number. Thus, the different eigenstates oscillate with different frequencies giving rise constructive and destructive intereference. The figures below show the time dependence of the v = 0/v =1 the v = 0/v = 2 superpositions. Both show oscillatory behavior, but the first is asymmetric and the second i symmetric. This has significance for harmonic oscillator selection rules, as will be discussed below.

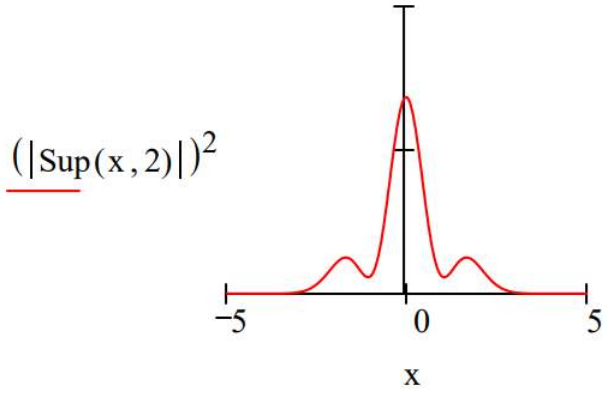
$$\mathrm{Sup}(x,t) := \frac{\Psi(0,x,t) + \Psi(1,x,t)}{\sqrt{2}}$$



The asymmetry of this time-dependent probability distribution gives it electric oscillating dipole character mechanism for coupling with the oscillating dipole of the electromagnetic field. Thus we could argue this i basis for the fact that the v = 0 to v = 1 vibrational transition is allowed.

$$\mathrm{Sup}(x,t) := \frac{\Psi(0,x,t) + \Psi(2,x,t)}{\sqrt{2}}$$





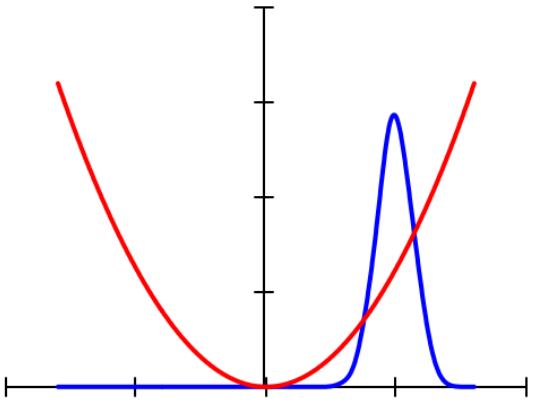
By comparison the symmetry of this time-dependent probability distribution does not have oscillatory dipo character, so there is no coupling with the external electromagnetic field. Therefore, the v = 0 to v = 2 vibrational transition is formally forbidden. Further detail on this interpretation of the "quantum jump" can found in the Spectroscopy section of Quantum Potpourri.

By comparison, coherent states (also called Glauber states) of the harmonic oscillator are more elaborate superpositions that maintain the well-defined shape of the ground state distribution while exhibiting the ki classical oscillatory motion that is absent in the previous examples. The time-dependence and "classical" oscillatory behavior of a coherent superposition of 25 vibrational eigenstates is illustrated below. See any contemporary text on quantum optics for further information on coherent states of the harmonic oscillator.

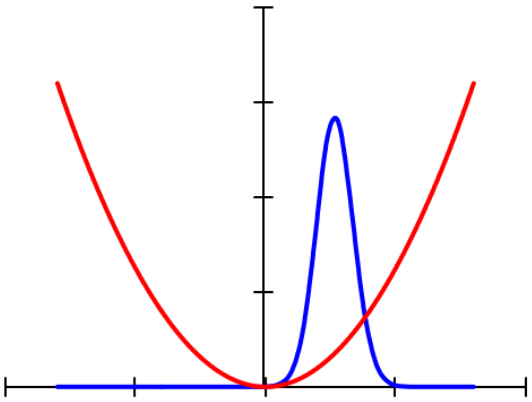
$$n := 25 \qquad x := -8, -7.98 \ldots 8 \qquad \alpha := 3.5$$

$$\Psi(x,t) := \frac{1}{\sqrt{n}} \cdot \exp\left(\frac{-x^2}{2}\right) \cdot \exp\left(\frac{-\alpha^2}{2}\right) \cdot \sum_{v=0}^{n} \left[\mathrm{Her}(v,x) \cdot \exp\left[-i \cdot \left(v + \frac{1}{2}\right) \cdot t\right] \cdot \frac{\alpha^v}{v! \cdot \sqrt{2^v \cdot \sqrt{2}}} \right]$$

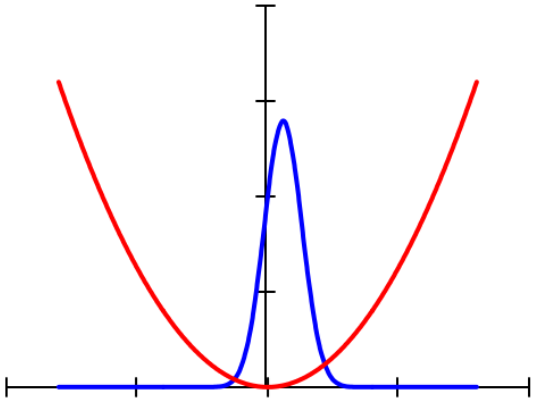
t = 0



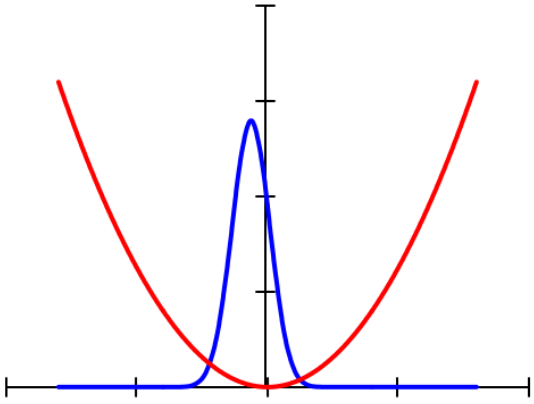
t = 1



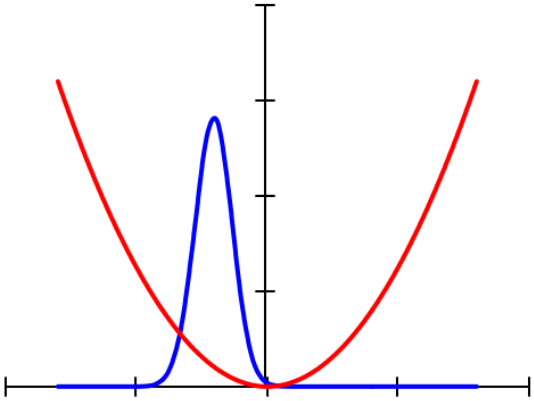
t = 1.45



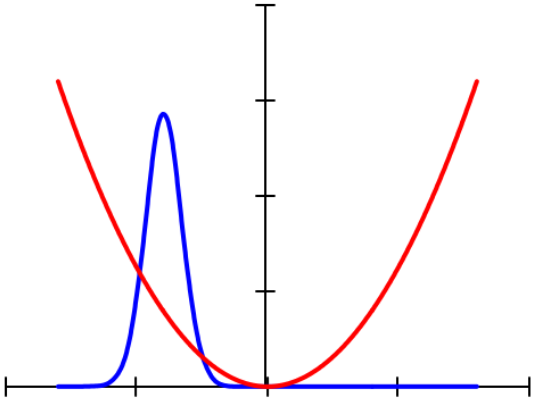
t = 1.7



t = 2



t = 2.5



Time-dependent superpositions of coherent states have been used to model Schrödinger cat states. Below w show the interaction of two coherent states moving in opposite directions from opposite sides of a harmoni potential well. The interference observed when they meet in the middle has been observed experimentally Bose-Einstein condensates.

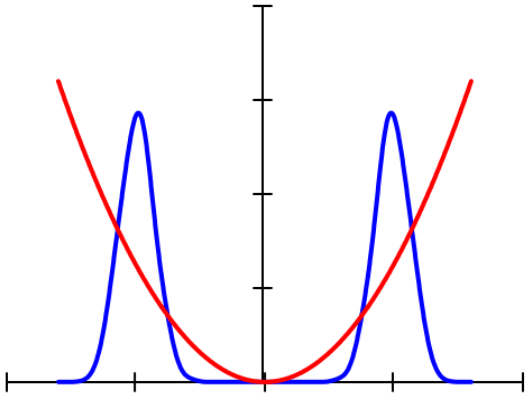
$$\alpha := 3.5 \qquad \beta := -3.5$$

$$\Psi(x,t)$$

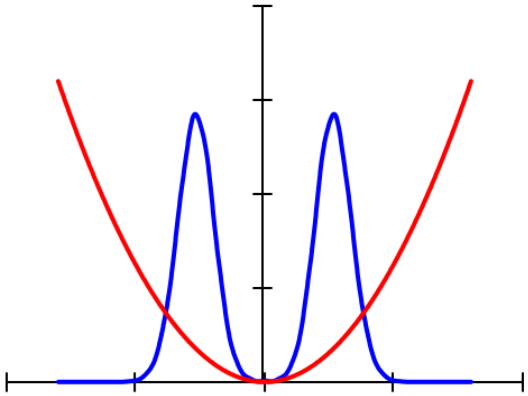
$$:= \frac{1}{\sqrt{n}} \cdot \exp\left(\frac{-x^2}{2}\right) \cdot \exp\left(\frac{-\alpha^2}{2}\right) \cdot \sum_{v=0}^{n} \left[\mathrm{Her}(v,x) \cdot \exp\left[-i \cdot \left(v + \frac{1}{2}\right) \cdot t\right] \cdot \frac{\alpha^v}{v! \cdot \sqrt{2^v \cdot \sqrt{2}}} \right]$$

$$+ \frac{1}{\sqrt{n}} \cdot \exp\left(\frac{-\mathrm{x}^2}{2}\right) \exp\left(\frac{-\beta^2}{2}\right) \cdot \sum_{\mathrm{v}=0}^{\mathrm{n}} \left[\mathrm{Her}(\mathrm{v},\mathrm{x}) \cdot \exp\left[-\mathrm{i} \cdot \left(\mathrm{v} + \frac{1}{2}\right) \cdot \mathrm{t}\right] \cdot \frac{\beta^{\mathrm{v}}}{\mathrm{v}! \cdot \sqrt{2^{\mathrm{v}} \cdot \sqrt{2}}} \right]$$

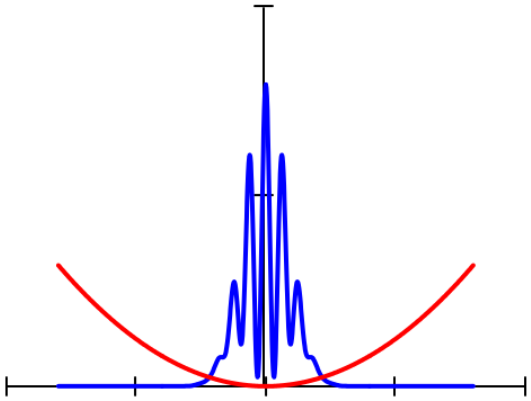
t = 0



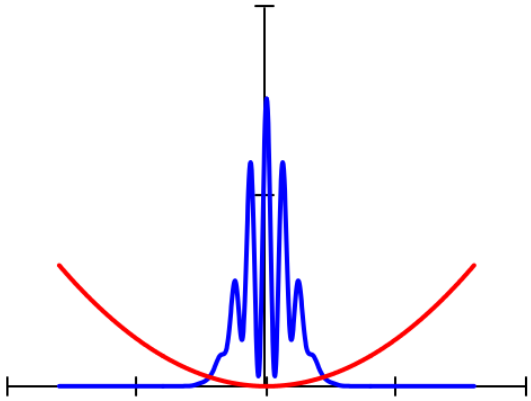
t = 1



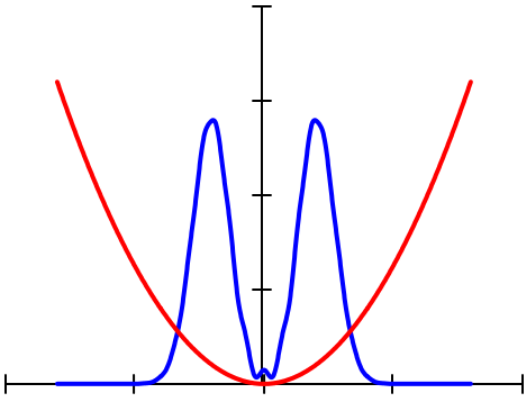
t = 1.45



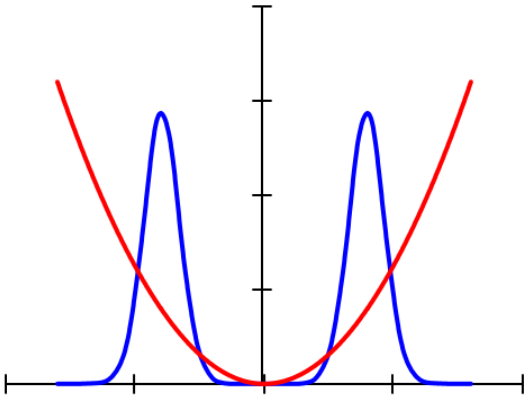
t = 1.7



t = 2



t = 2.5



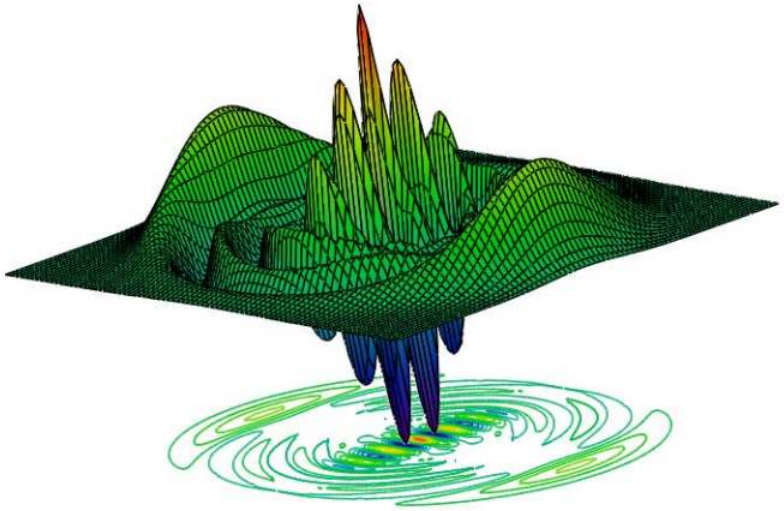
We finish with a calculation of the Wigner phase-space distribution for a Schrödinger cat state at t = 0. In t interest of computational expediency a superposition of only 10 harmonic eigenstates is calculated. The Wigner function is itself a superposition of all phase-space trajectories and is called a quasi probability distribution because it can take on negative values as is shown in the figure below. The interference fringe the center are closely related to those that appear in the figures above.

$$\Psi(x) := \frac{1}{\sqrt{n}} \cdot \exp\left(\frac{-x^2}{2}\right) \cdot \exp\left(\frac{-\alpha^2}{2}\right) \cdot \sum_{v=0}^{10} \left(Her(v,x) \cdot \frac{\alpha^v}{v! \cdot \sqrt{2^v \cdot \sqrt{2}}}\right)$$
$$+ \left[\frac{1}{\sqrt{n}} \cdot \exp\left(\frac{-x^2}{2}\right) \cdot \exp\left(\frac{-\beta^2}{2}\right) \cdot \sum_{v=0}^{10} \left(Her(v,x) \cdot \frac{\beta^v}{v! \cdot \sqrt{2^v \cdot \sqrt{2}}}\right)\right]$$

Wigner distribution:

$$W(x,p) := \frac{1}{\pi^{\frac{3}{2}}} \cdot \int_{-\infty}^{\infty} \Psi\left(x + \frac{s}{2}\right) \cdot \exp(i \cdot s \cdot p) \cdot \Psi\left(x - \frac{s}{2}\right) ds$$

$$N := 80 \qquad i := 0 \ldots N \qquad x_i := -5 + \frac{10 \cdot i}{N}$$
$$j := 0 \ldots N \qquad p_j := -5 + \frac{10 \cdot j}{N} \qquad Wigner_{i,j} := W(x_i, p_j)$$



Wigner, Wigner

This page titled 1.78: Coherent Superpositions for the Harmonic Oscillator is shared under a CC BY 4.0 license and was authored, remixed, and/or curated by Frank Rioux via source content that was edited to the style and standards of the LibreTexts platform.

1.79: The Harmonic Oscillator and the Uncertainty Principle

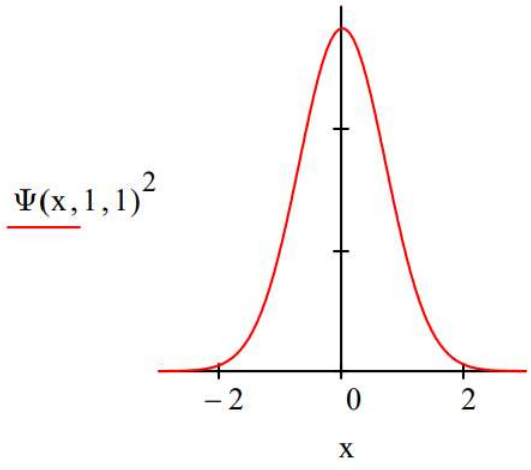
In atomic units the wave function in coordinate space for an harmonic oscillator with reduced mass, μ, equal to one and force constant k is given by,

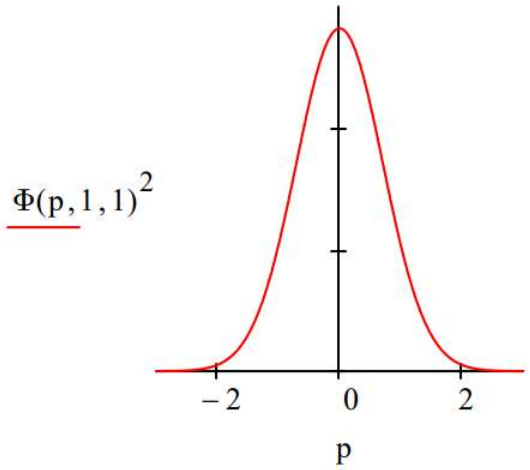
$$\Psi(x, k, \mu) := \left(\frac{\sqrt{k \cdot \mu}}{\pi}\right)^{\frac{1}{4}} \cdot \exp\left(-\sqrt{k \cdot \mu} \cdot \frac{x^2}{2}\right)$$

This function is easily Fourier transformed into momentum space:

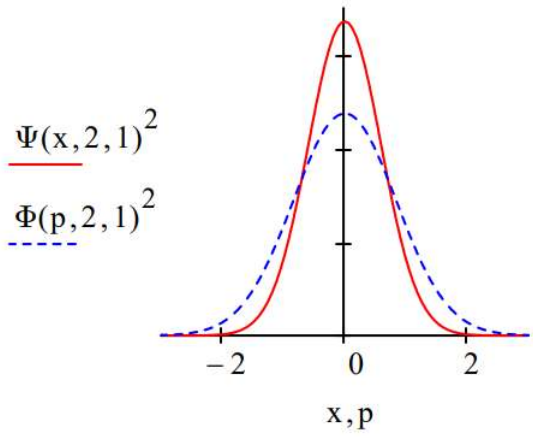
$$\Phi(p, k, \mu) := \frac{1}{\sqrt{2 \cdot \pi}} \cdot \int_{-\infty}^{\infty} \exp(-i \cdot p \cdot x) \cdot \Psi(x, k, \mu) dx \Bigg| \begin{array}{l} \text{assume, } k > 0 \\ \text{assume, } \mu > 0 \\ \text{simplify} \end{array} \rightarrow \frac{e^{-\frac{p^2}{2 \cdot \sqrt{\mu} \cdot \sqrt{k}}}}{\pi^{\frac{1}{4}} \cdot \mu^{\frac{1}{8}} \cdot k^{\frac{1}{8}}}$$

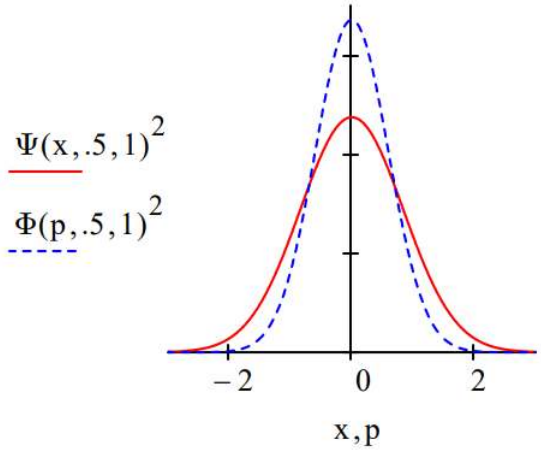
The force constant for μ=1 controls the probability distribution in coordinate ((\Psi\)(x)^2) and momentum ($\Phi(p)^2$) space. For k = 1 the coordinate and momentum distributions are identical as is shown below.





For larger values of k the coordinate-space distribution decreases in breadth while the momentum distribution increases. For values of k less than 1, the reverse occurs; the coordinate-space distribution increases in breadth while the momentum distribution becomes narrower.





This is an illustration of the Uncertainty Principle: the more sharply defined position is, the greater the uncertainty in momentum. Conversely, the greater the uncertainty in position, the more sharply the momentum is defined.

Tunneling occurs in the simple harmonic oscillator. The classical turning point is that position at which the total energy is equal to the potential energy. In other words kinetic energy is zero and the oscillators direction is going to reverse. For the ground state the classical turning point is,

$$E = \frac{1}{2}\cdot\sqrt{\frac{k}{\mu}} = \frac{p^2}{2\cdot\mu} + \frac{1}{2}\cdot k\cdot x^2$$

$$\frac{1}{2}\cdot\sqrt{\frac{k}{\mu}} = \frac{1}{2}\cdot k\cdot x^2 \text{ solve, } ,x \rightarrow \begin{bmatrix} \frac{\left(\frac{k}{\mu}\right)^{\frac{1}{4}}}{\sqrt{k}} \\ -\frac{\left(\frac{k}{\mu}\right)^{\frac{1}{4}}}{\sqrt{k}} \end{bmatrix}$$

The probability that tunneling occurs is independent of the values of **k** and μ.

$$2\cdot\left[\int_{\frac{1}{(k\cdot\mu)^{\frac{1}{4}}}}^{\infty} \Psi(x,k,\mu)^2 dx\right] \left| \begin{array}{l} \text{assume, } k > 0 \\ \text{assume, } \mu > 0 \rightarrow 1 - \operatorname{erf}(1) = 0.157 \\ \text{simplify} \end{array} \right.$$

It is also possible to calculate the tunneling probability using the momentum wave function. Classically the maximum magnitude of momentum is achieved when the potential energy is zero, so that the total energy is equal to the kinetic energy.

$$\frac{1}{2}\cdot\sqrt{\frac{k}{\mu}} = \frac{p^2}{2\cdot\mu} \text{ solve, } p \rightarrow \begin{bmatrix} \sqrt{\mu}\cdot\left(\frac{k}{\mu}\right)^{\frac{1}{4}} \\ -\sqrt{\mu}\cdot\left(\frac{k}{\mu}\right)^{\frac{1}{4}} \end{bmatrix}$$

Thus momentum can have values in the range shown above, depending on the magnitude of the potential energy. Values outside this range are classically forbidden. Therefore the tunneling probability in momentum space is,

$$2\cdot\int_{(k\cdot\mu)^{\frac{1}{4}}}^{\infty} \Phi(p,k,\mu)^2 dp \left| \begin{array}{l} \text{assume, } k > 0 \\ \text{assume, } \mu > 0 \rightarrow 1 - \operatorname{erf}(1) = 0.157 \\ \text{simplify} \end{array} \right.$$

It is not surprising that the momentum and coordinate calculations agree.

This page titled 1.79: The Harmonic Oscillator and the Uncertainty Principle is shared under a CC BY 4.0 license and was authored, remixed, and/or curated by Frank Rioux via source content that was edited to the style and standards of the LibreTexts platform.

1.80: Another view of the Harmonic Oscillator and the Uncertainty Principle

Schrödinger's equation in atomic units (h = 2π) for the harmonic oscillator has an exact analytical solution.

$$V(x,k) := \frac{1}{2}\cdot k\cdot x^2 \qquad \frac{-1}{2\cdot\mu}\cdot\frac{d^2}{dx^2}\Psi(x) + V(x)\cdot\Psi(x) = E\cdot\Psi(x)$$

The ground-state wave function (coordinate space) and energy for an oscillator with reduced mass μ and force constant **k** are as follows.

$$\Psi(x,k,\mu) := \left(\frac{\sqrt{k\cdot\mu}}{\pi}\right)^{\frac{1}{4}}\cdot\exp\left(-\sqrt{k\cdot\mu}\cdot\frac{x^2}{2}\right) \qquad E(k,\mu) := \frac{1}{2}\cdot\sqrt{\frac{k}{\mu}}$$

The first thing we want to illustrate is that tunneling occurs in the simple harmonic oscillator. The classical turning point is that position at which the total energy is equal to the potential energy. In other words, classically the kinetic energy is zero and the oscillator's direction is going to reverse. For the ground state the classical turning point is,

$$\frac{1}{2}\cdot\sqrt{\frac{k}{\mu}} = \frac{1}{2}\cdot k\cdot x^2 \quad \text{has solution(s)} \begin{pmatrix} \frac{-1}{k^{\frac{1}{4}}\cdot\mu^{\frac{1}{4}}} \\ \frac{1}{k^{\frac{1}{4}}\cdot\mu^{\frac{1}{4}}} \end{pmatrix}$$

From the quantum mechanical perspective the oscillator is not vibrating; it is in a stationary state. To the extent that the oscillator's wave function extends beyond the classical turning point, tunneling is occurring. The calculation below shows that the probability that tunneling occurs is independent of the values of k and μ for the ground state.

$$2\cdot\left[\int_{\frac{1}{(k\cdot\mu)^{\frac{1}{4}}}}^{\infty}\left[\left(\frac{\sqrt{k\cdot\mu}}{\pi}\right)^{\frac{1}{4}}\cdot\exp\left(-\sqrt{k\cdot\mu}\cdot\frac{x^2}{2}\right)\right]^2 dx\right]\Bigg|_{\text{simplify}}^{\text{assume},k>0,\ \mu>0} \rightarrow 1-\text{erf}(1) = 0.157$$

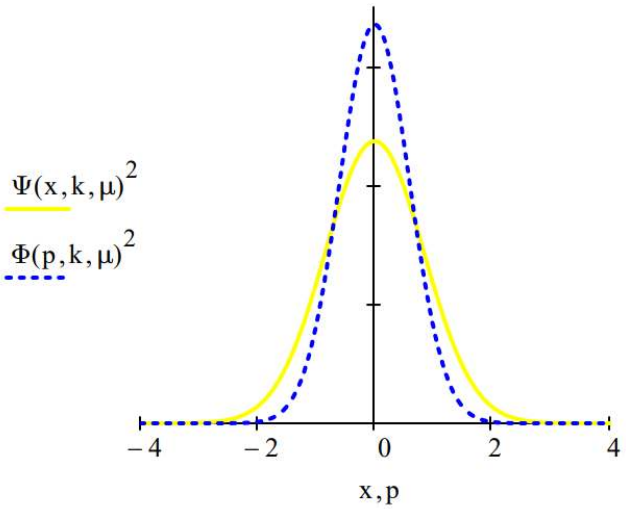
A Fourier transform of the coordinate wave function provides its counter part in momentum space.

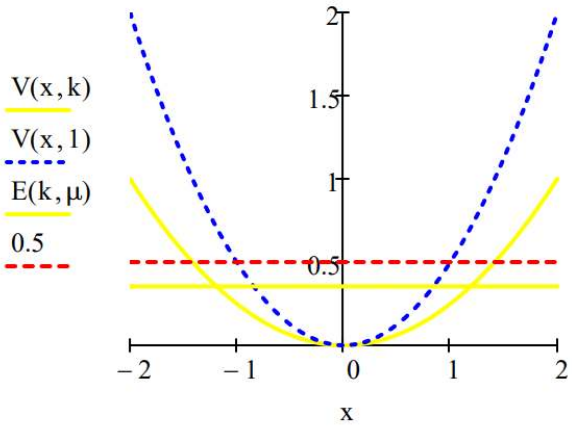
$$\Phi(p,k,\mu) := \frac{1}{\sqrt{2\cdot\pi}}\cdot\int_{-\infty}^{\infty}\exp(-i\cdot p\cdot x)\cdot\Psi(x,k,\mu)dx\Bigg|\begin{matrix}\text{assume, } k>0\\ \text{assume, } \mu>0\\ \text{simplify}\end{matrix} \rightarrow \frac{e^{-\frac{p^2}{2\cdot\sqrt{\mu}\cdot\sqrt{k}}}}{\pi^{\frac{1}{4}}\cdot\mu^{\frac{1}{8}}\cdot k^{\frac{1}{8}}}$$

The uncertainty principle can now be illustrated by comparing the coordinate and momentum wave functions for a variety values of **k** and μ. For the benchmark case, **k** = μ = **1**, we see that the coordinate and momentum wave functions are identical and the classical turning point (CTP) is 1. The classical turning point will be taken as a measure of the spatial domain of the oscillator.

- For k = 2 and μ =1, the force constant has doubled reducing the amplitude of vibration (CTP =0.841) and therefore the uncertainty in position. Consequently there is an increase in the uncertainty in momentum which is manifested by a broader momentum distribution function.
- For k = 1 and μ = 2, the increase in effective mass drops the oscillator in the potential well decreasing the vibrational amplitude (CTP = 0.841) causing a decrease in Δx and an increase in Δp.
- For k = 0.5 and μ = 1, the lower force constant causes a larger vibrational amplitude (CTP = 1.189) and an accompanying increase in Δx. Consequently Δp decreases.

Force constant: $k := 0.5$	Effective mass: $\mu := 1$
Energy: $E(k,\mu) = 0.354$	CTP: $\frac{1}{k^{\frac{1}{4}}\cdot\mu^{\frac{1}{4}}} = 1.189$





The uncertainties in position and momentum are calculated as shown below because for the harmonic oscillator <x> =

= 0.

$$\Delta x := \sqrt{\int_{-\infty}^{\infty} x^2 \cdot \Psi(x,k,\mu)^2 dx} = 0.841$$

$$\Delta p := \sqrt{\int_{-\infty}^{\infty} p^2 \cdot \Phi(p,k,\mu)^2 dp} = 0.595$$

$$\Delta x \cdot \Delta p = 0.5$$

A summary of the four cases considered is provided in the table below.

μ	k	CTP	Δx	Δp	$\Delta x \Delta p$
1	1	1.00	0.707	0.707	0.5
1	2	0.841	0.595	0.841	0.5
2	1	0.841	0.595	0.841	0.5
1	0.5	1.189	0.841	0.594	0.5

The Wigner function, W(x,p), is a phase-space distribution that can be used to provide an alternative graphical representation of the results calculated above. As shown below it can be generated using either the coordinate or momentum wave function.

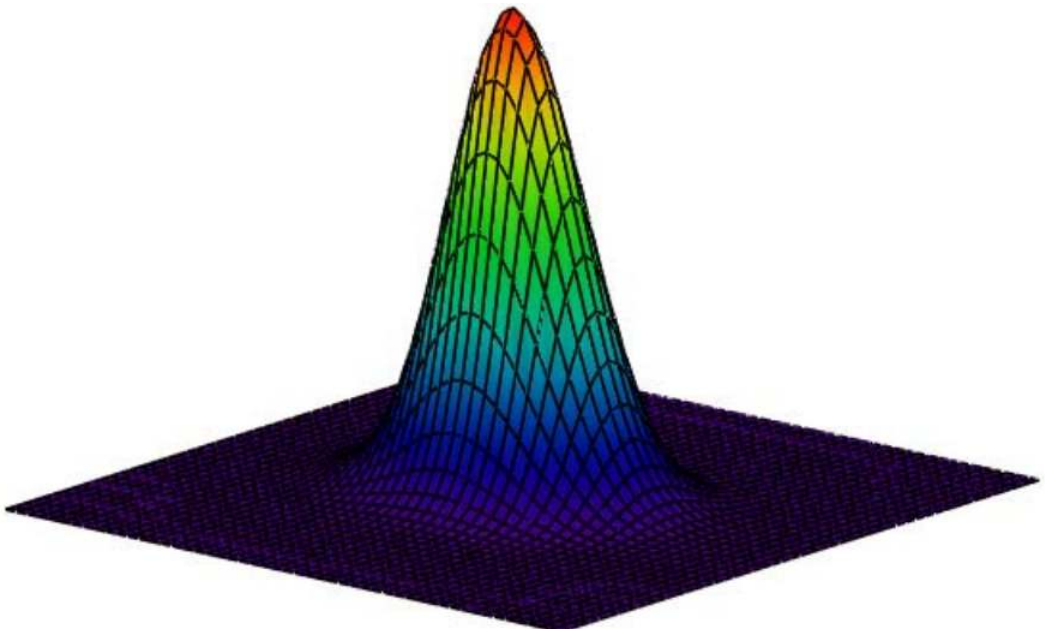
Calculate Wigner distribution:

$$W(x,p) := \frac{1}{\pi^{\frac{3}{2}}} \cdot \int_{-\infty}^{\infty} \Psi\left(x + \frac{s}{2}, k, \mu\right) \cdot \exp(i \cdot s \cdot p) \cdot \Psi\left(x - \frac{s}{2}, k, \mu\right) ds$$

Display Wigner distribution:

$$N := 50 \qquad i := 0 \ldots N \qquad x_i := -4 + \frac{8 \cdot i}{N}$$

$$j := 0 \ldots N \qquad p_j := -4 + \frac{8 \cdot j}{N} \qquad Wigner_{i,j} := W(x_i, p_j)$$



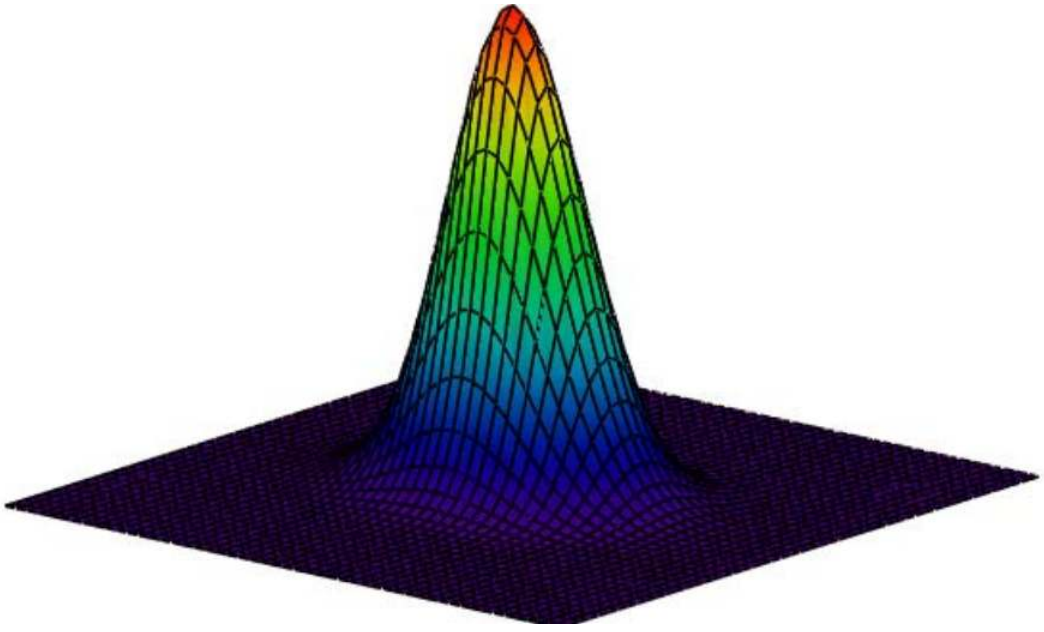
Calculate Wigner distribution:

$$W(x,p) := \frac{1}{\pi^{\frac{3}{2}}} \cdot \int_{-\infty}^{\infty} \Phi\left(p + \frac{s}{2}, k, \mu\right) \cdot \exp(i \cdot s \cdot x) \cdot \Phi\left(p - \frac{s}{2}, k, \mu\right) ds$$

Display Wigner distribution:

$$N := 50 \qquad i := 0 \ldots N \qquad x_i := -4 + \frac{8 \cdot i}{N}$$

$$j := 0 \ldots N \qquad p_j := -4 + \frac{8 \cdot j}{N} \qquad Wigner_{i,j} := W\left(x_i, p_j\right)$$



This page titled 1.80: Another view of the Harmonic Oscillator and the Uncertainty Principle is shared under a CC BY 4.0 license and was authored, remixed, and/or curated by Frank Rioux via source content that was edited to the style and standards of the LibreTexts platform.

1.81: Hydrogen Atom and Helium Ion Spatial and Momentum Distribution Functions Illustrate the Uncertainty Principle

The uncertainty principle is revealed by a comparison of the coordinate and momentum wave functions for one-electron species such as the hydrogen atom and the helium ion.

The coordinate 1s wave function for one-electron species as a function of nuclear charge is given by the following function.

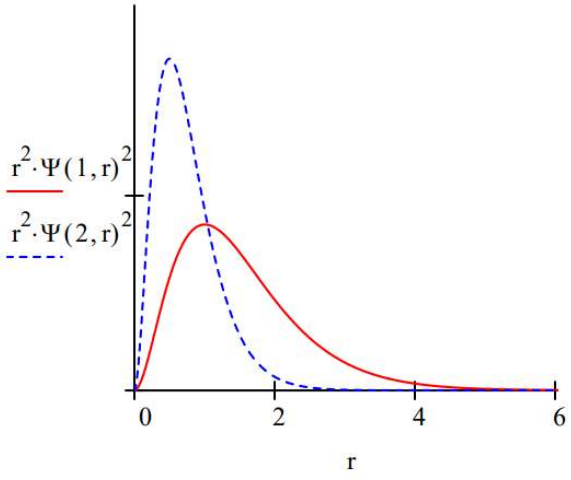
$$\Psi(z,r) := \sqrt{\frac{z^3}{\pi}} \cdot \exp(-z \cdot r)$$

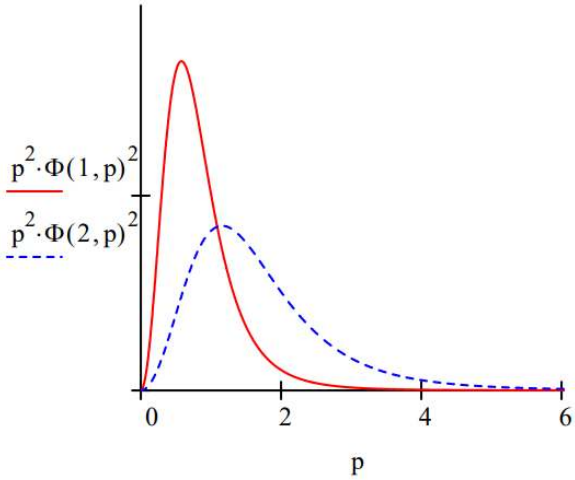
The Fourier transform of the coordinate wave function yields the momentum wave function.

$$\Phi(\mathrm{z},\mathrm{p}) := \frac{1}{\sqrt{8 \cdot \pi^3}} \cdot \int_0^{\infty} \int_0^{\pi} \int_0^{2 \cdot \pi} \Psi(\mathrm{z},\mathrm{r}) \cdot \exp(-\mathrm{i} \cdot \mathrm{p} \cdot \cos(\theta)) \cdot \mathrm{r}^2 \cdot \sin(\theta) \mathrm{d}\phi \mathrm{d}\theta \mathrm{dr}$$

$$\Big|^{\text{simplify}}_{\text{assume, } z>0} \rightarrow 2 \cdot \frac{2^{\frac{1}{2}}}{\pi} \cdot \frac{z^{\frac{5}{2}}}{z^4 + 2 \cdot z^2 \cdot p^2 + p^4}$$

Plots of the spatial and momentum radial distribution functions for the hydrogen atom (z=1) and helium ion (z=2) clearly illustrate the uncertainty principle.





Relative to the hydrogen atom, the helium ion′s coordinate distribution function is localized closer to the nucleus, meaning less uncertainty in electron position. Consequently, its momentum distribution is more delocalized than that for the hydrogen atom, meaning more uncertainty in electron momentum.

This page titled 1.81: Hydrogen Atom and Helium Ion Spatial and Momentum Distribution Functions Illustrate the Uncertainty Principle is shared under a CC BY 4.0 license and was authored, remixed, and/or curated by Frank Rioux via source content that was edited to the style and standards of the LibreTexts platform.

1.82: The Position-Momentum Uncertainty Relation in the Hydrogen Atom

The hydrogen atom coordinate and momentum wave functions can be used to illustrate the uncertainty relation involving position and momentum.

The 1s wave function is used to calculate the average distance of the electron from the nucleus.

$$\Psi_{1s}(\mathrm{r}) := \frac{1}{\sqrt{\pi}} \cdot \exp(-\mathrm{r}) \qquad \mathrm{r}_{1s} := \int_0^{\infty} \mathrm{r} \cdot \Psi_{1s}(\mathrm{r})^2 \cdot 4 \cdot \pi \cdot \mathrm{r}^2 \mathrm{dr} \qquad r_{1s} = 1.500$$

The Fourier transform of the 1s wave function yields the momentum wave function. The momentum wave function is used to calculate the average magnitude of the electron momentum.

$$\Phi_{1s}(\mathrm{p}) := \frac{1}{\sqrt{8 \cdot \pi^3}} \cdot \int_0^{\infty} \int_0^{\pi} \int_0^{2 \cdot \pi} \Psi_{1s}(\mathrm{r}) \cdot \exp(-\mathrm{i} \cdot \mathrm{p} \cdot \mathrm{r} \cdot \cos(\theta)) \cdot \mathrm{r}^2 \cdot \sin(\theta) \mathrm{d}\phi \mathrm{d}\theta \mathrm{dr}$$

$$\rightarrow 2 \cdot \frac{2^{\frac{1}{2}}}{\pi \cdot [(-1) + \mathrm{i} \cdot \mathrm{p}]^2 \cdot (1 + \mathrm{i} \cdot \mathrm{p})^2}$$

$$\mathrm{p}_{1s} := \int_0^{\infty} \mathrm{p} \cdot (|\Phi_{1s}(\mathrm{p})|)^2 \cdot 4 \cdot \pi \cdot \mathrm{p}^2 \mathrm{dp} \qquad \mathrm{p}_{1s} = 0.849$$

The 2s wave function is used to calculate the average distance of the electron from the nucleus.

$$\Psi_{2s}(r) := \frac{1}{\sqrt{32 \cdot \pi}} \cdot (2 - r) \cdot \exp\left(-\frac{r}{2}\right) \qquad \mathrm{r}_{2s} := \int_0^{\infty} \mathrm{r} \cdot \Psi_{2s}(\mathrm{r})^2 \cdot 4 \cdot \pi \cdot \mathrm{r}^2 \mathrm{dr} \qquad \mathrm{r}_{2s} = 6.000$$

The Fourier transform of the 2s wave function yields the momentum wave function. The momentum wave function is used to calculate the average magnitude of the electron momentum.

$$\Phi_{2s}(\mathrm{p}) := \frac{1}{\sqrt{8 \cdot \pi^3}} \cdot \int_0^{\infty} \int_0^{\pi} \int_0^{2 \cdot \pi} \Psi_{2s}(\mathrm{r}) \cdot \exp(-\mathrm{i} \cdot \mathrm{p} \cdot \cos(\theta)) \cdot \mathrm{r}^2 \cdot \sin(\theta) \mathrm{d}\phi \mathrm{d}\theta \mathrm{dr}$$

$$\rightarrow \frac{-16}{\pi} \cdot \frac{(-1) + 4 \cdot p^2}{[(-1) + 2 \cdot i \cdot p]^3 \cdot (1 + 2 \cdot i \cdot p)^3}$$

$$\mathrm{p}_{2s} := \int_0^{\infty} \mathrm{p} \cdot (|\Phi_{2s}(\mathrm{p})|)^2 \cdot 4 \cdot \pi \cdot \mathrm{p}^2 \mathrm{dp} \qquad \mathrm{p}_{2s} = 0.340$$

The 3s wave function is used to calculate the average distance of the electron from the nucleus

$$\Psi_{3s}(\mathrm{r}) := \frac{1}{81 \cdot \sqrt{3 \cdot \pi}} \cdot \left(27 - 18 \cdot \mathrm{r} + 2 \cdot \mathrm{r}^2\right) \exp\left(\frac{-\mathrm{r}}{3}\right)$$

$$r_{3s} := \int_0^{\infty} r \cdot \Psi_{3s}(r)^2 \cdot 4 \cdot \pi \cdot r^2 dr \qquad r_{3s} = 13.500$$

The Fourier transform of the 3s wave function yields the momentum wave function. The momentum wave function is used to calculate the average magnitude of the electron momentum.

$$\Phi_{3s}(\mathrm{p}) := \frac{1}{\sqrt{8 \cdot \pi^3}} \cdot \int_0^{\infty} \int_0^{\pi} \int_0^{2 \cdot \pi} \Psi_{3s}(\mathrm{r}) \cdot \exp(-\mathrm{i} \cdot \mathrm{p} \cdot \cos(\theta)) \cdot \mathrm{r}^2 \cdot \sin(\theta) \mathrm{d}\phi \mathrm{d}\theta \mathrm{dr}$$

$$\rightarrow 18 \cdot \frac{2^2}{\pi} \cdot 3^{\frac{1}{2}} \cdot \frac{1 - 30 \cdot \mathrm{p}^2 + 81 \cdot \mathrm{p}^4}{[(-1) + 3 \cdot \mathrm{i} \cdot \mathrm{p}]^4 \cdot (1 + 3 \cdot \mathrm{i} \cdot \mathrm{p})^4}$$

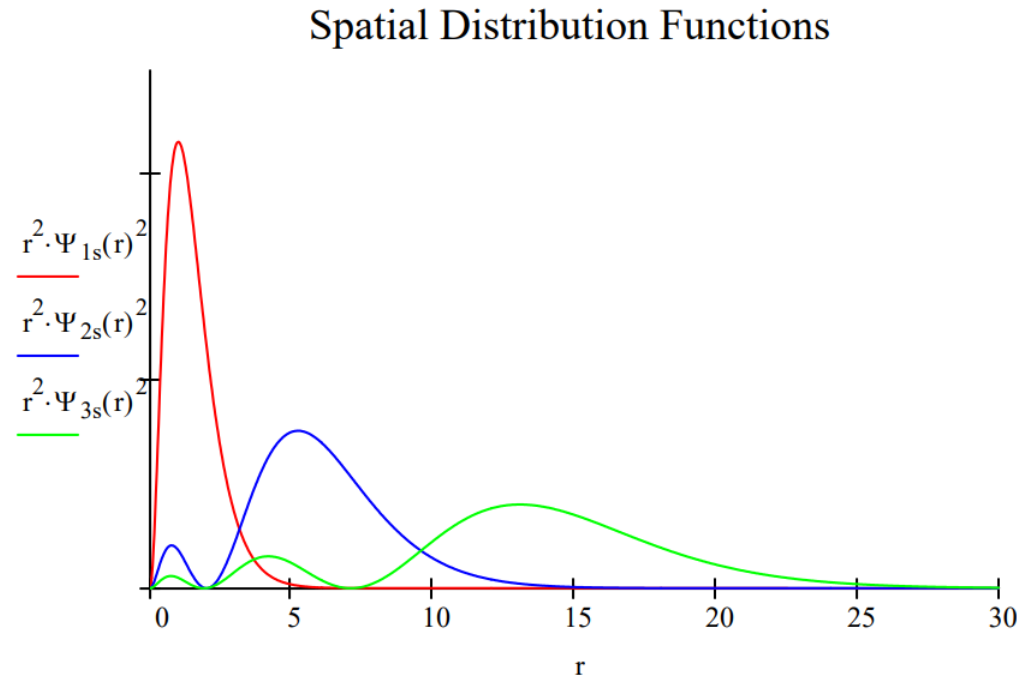
$$\mathrm{p}_{3s} := \int_0^{\infty} \mathrm{p} \cdot (|\Phi_{3s}(\mathrm{p})|)^2 \cdot 4 \cdot \pi \cdot \mathrm{p}^2 \mathrm{dp} \qquad \mathrm{p}_{3s} = 0.218$$

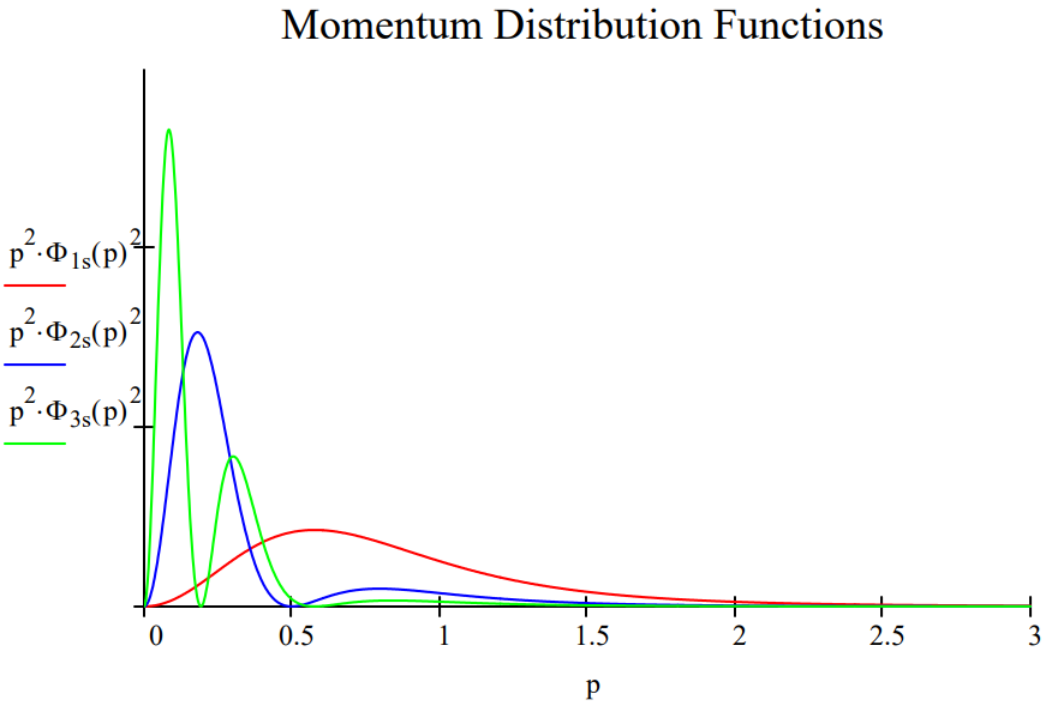
These results can be summarize in both tabular and graphical form.

Orbital	AveragePosition	AverageMomentum
1s	1.5	0.849
2s	6.0	0.340
3s	13.5	0.218

The table shows that the average distance of the electron from the nucleus increases from 1s to 3s, indicating an increase in the uncertainty in the location of the electron. At the same time the average magnitude of electron momentum decreases from 1s to 3s,

indicating a decrease in momentum uncertainty. The spatial and momentum distribution functions shown below illustrate this effect graphically.





This page titled 1.82: The Position-Momentum Uncertainty Relation in the Hydrogen Atom is shared under a CC BY 4.0 license and was authored, remixed, and/or curated by Frank Rioux via source content that was edited to the style and standards of the LibreTexts platform.

1.83: Demonstrating the Uncertainty Priniciple for Angular Momentum and Angular Position

The uncertainty relation between angular momentum and angular position can be derived from the more familiar uncertainty relation between linear momentum and position.

$$\Delta \mathrm{p} \cdot \Delta \mathrm{x} \geq \frac{\mathrm{h}}{4 \cdot \pi}$$

Consider a particle with linear momentum p moving on a circle of radius r. The particle′s angular momentum is given by equation (2).

$$\mathrm{L} = \mathrm{m} \cdot \mathrm{v} \cdot \mathrm{r} = \mathrm{p} \cdot \mathrm{r}$$

In moving a distance x on the circle the particle sweeps out an angle ϕ in radians.

$$\phi = \frac{x}{r}$$

Equations (2) and (3) suggest,

$$\Delta \mathrm{p} = \frac{\Delta \mathrm{L}}{\mathrm{r}} \qquad \Delta \mathrm{x} = \Delta \phi \cdot \mathrm{r}$$

Substitution of equations (4) into equation (1) yields the angular momentum, angular position uncertainty relation.

$$\Delta \mathrm{L} \cdot \Delta \phi \geq \frac{\mathrm{h}}{4 \cdot \pi}$$

In addition to the Heisenberg restrictions represented by equations (1) and (5), conjugate observables are related by Fourier transforms. For example, for position and momentum it is given by equation (6) in atomic units (h = 2π).

$$\langle p|x\rangle = \frac{1}{\sqrt{2\pi}} \exp(-ipx)$$

Equations (2) and (3) can be used with (6) to obtain the Fourier transform between angular momentum and angular position.

$$\langle L|\phi\rangle = \frac{1}{\sqrt{2\pi}} \exp(-iL\phi)$$

Equations (6) and (7) are mathematical dictionaries telling us how to translate from x language to p language, or ϕ language to L language. The complex conjugates of (6) and (7) translate in the reverse direction, from p to x and from L to ϕ.

The work-horse particle-in-a-box (PIB) problem can be used to provide a compelling graphical illustration of the position-momentum uncertainty relation. The position wave function for the ground state of a PIB in a box of length a is given below.

$$\langle x|\Psi\rangle = \sqrt{\frac{2}{a}} \sin\left(\frac{\pi x}{a}\right)$$

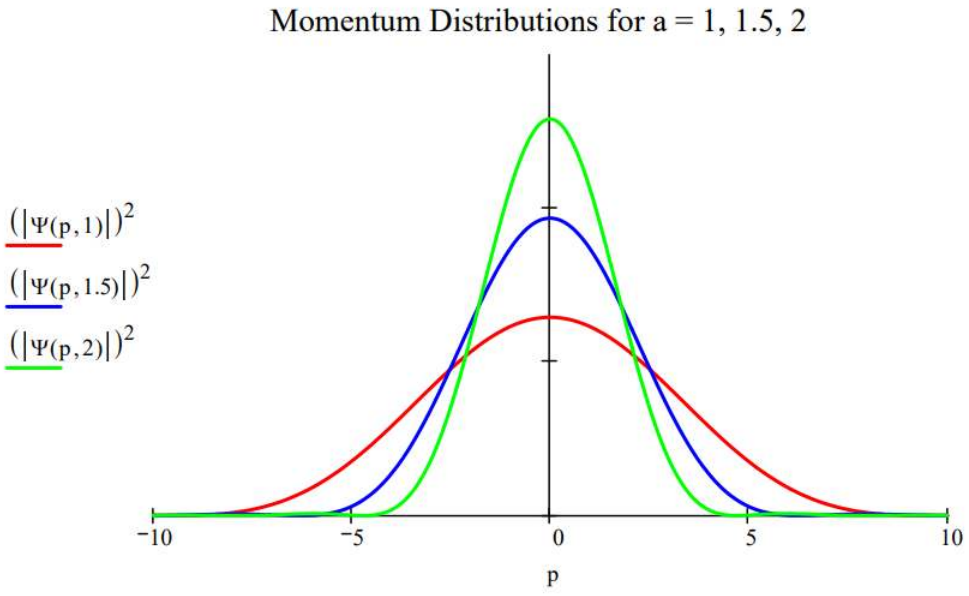
The conjugate momentum-space wave function is obtained by the following Fourier transform.

$$\langle p|\Psi\rangle = \int_0^a \langle p|x\rangle\langle x|\Psi\rangle dx = \frac{1}{\sqrt{\pi a}} \int_0^a \exp(-ipx) \sin\left(\frac{\pi x}{a}\right)$$

Evaluation of the integral in equation (9) yields,

$$\Psi(p,a) := \sqrt{a \cdot \pi} \cdot \frac{\exp(-i \cdot p \cdot a) + 1}{\pi^2 - p^2 \cdot a^2}$$

Plotting the momentum distribution function for several box lengths, as is done in the figure below, clearly reveals the position-momentum uncertainty relation. The greater the box length the greater the uncertainty in position. However, as the figure shows, the greater the box length the narrower the momentum distribution, and, consequently, the smaller the uncertainty in momentum.



A similar visualization of the angular-momentum/angular-position uncertainty relation is also possible. Suppose a particle on a ring is prepared in such a way that its angular wave function is represented by the following gaussian function,

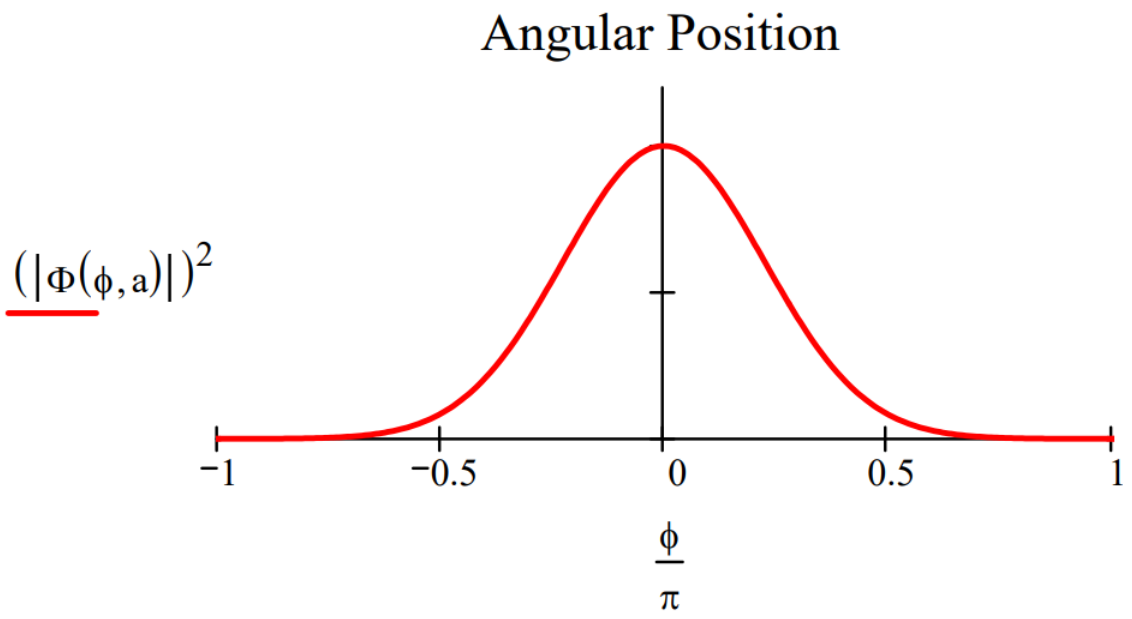
$$\langle \phi | \Psi \rangle = \exp\left(-a\phi^2\right)$$

where the parameter a controls the width of the angular distribution. The conjugate angular momentum wave function is obtained by the following Fourier transform.

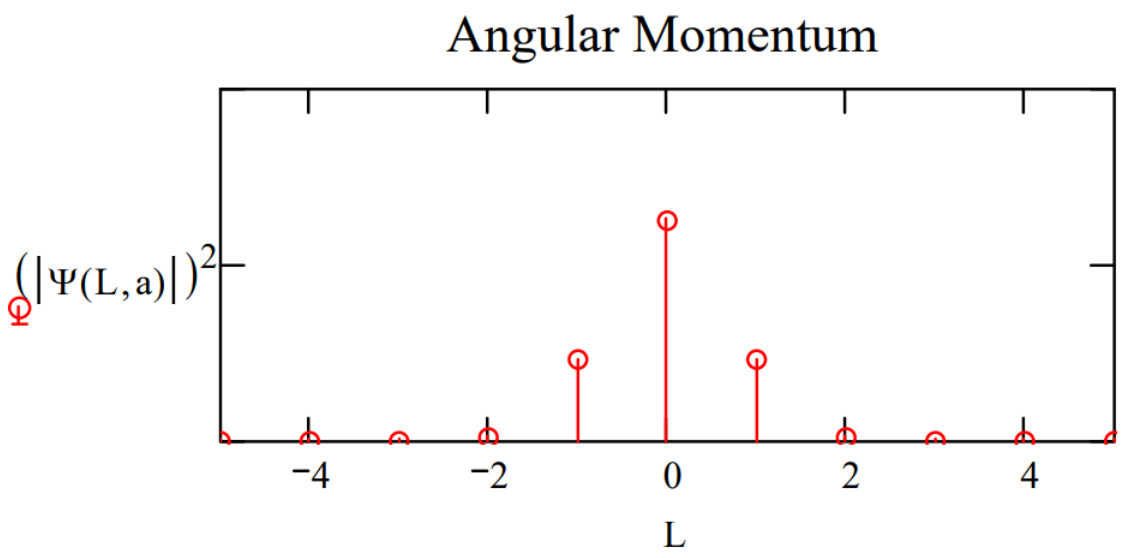
$$\langle L | \Psi \rangle = \int_{-\pi}^{\pi} \langle L | \phi \rangle \langle \phi | \Psi \rangle d\phi = \frac{1}{\sqrt{2\pi}} \int_{-\pi}^{\pi} \exp(-iL\phi) \exp\left(-a\phi^2\right) d\phi$$

Plots of $| < \phi | \Psi > |^2$ and $| < \mathrm{L} | \Psi > |^2$ shown below for two values of the parameter a illustrate the angular momentum/angular position uncertainty relation. The larger the value of a, the smaller the angular positional uncertainty and the greater the angular momentum uncertainty. In other words, the greater the value of a the greater the number of angular momentum eigenstates observed.

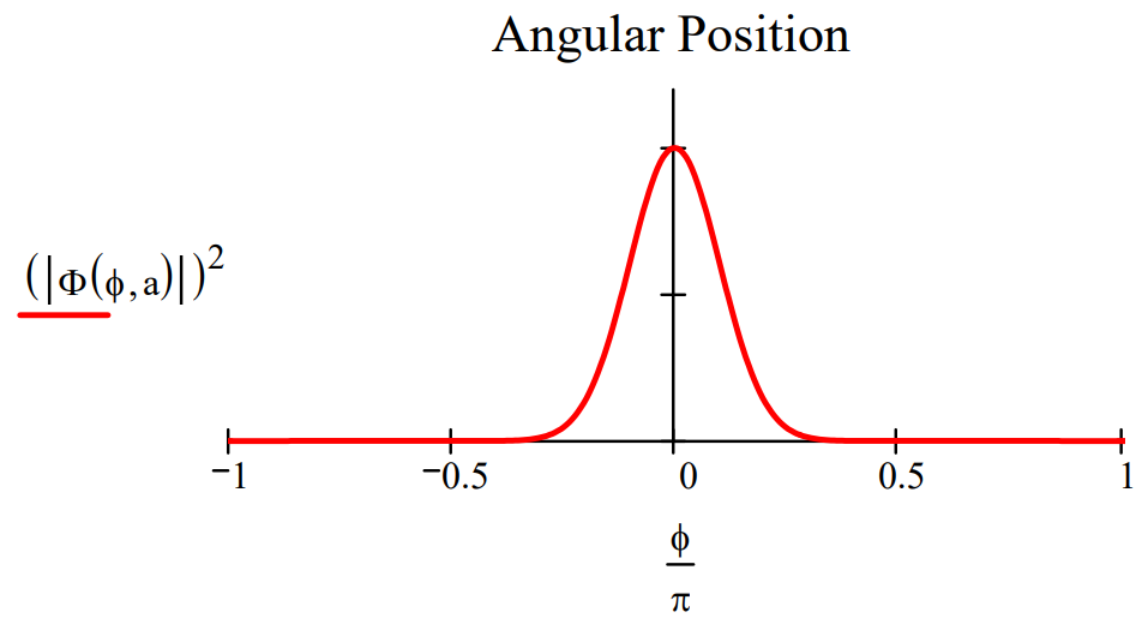
$$\mathrm{a} := 0.5 \qquad \Phi(\phi, \mathrm{a}) := \exp\left(-\mathrm{a} \cdot \phi^2\right)$$



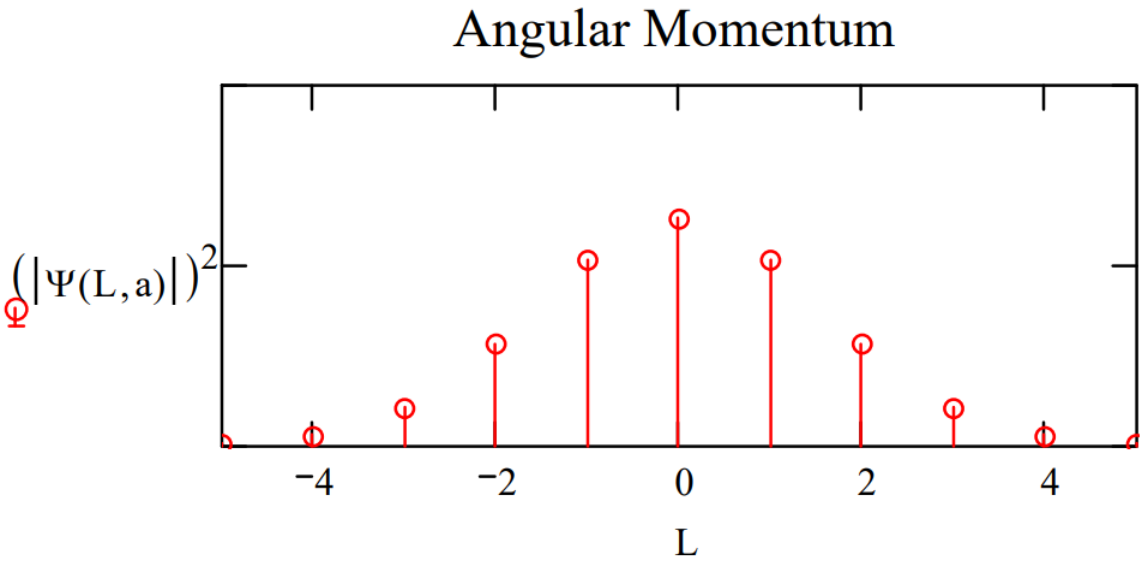
$$L := -5 \ldots 5 \qquad \Psi(L,a) := \int_{-\pi}^{\pi} \exp(-i \cdot L \cdot \phi)\Phi(\phi,a)d\phi$$



Make the angular position distribution narrower: $a := 2.5$



Observe a broader distribution in angular momentum.



The uncertainty relation between angular position and angular momentum as outlined above is a simplified version of that presented by S. Franke-Arnold et al. in *New Journal of Physics* **6**, 103 (2004).

This page titled 1.83: Demonstrating the Uncertainty Priniciple for Angular Momentum and Angular Position is shared under a CC BY 4.0 license and was authored, remixed, and/or curated by Frank Rioux via source content that was edited to the style and standards of the LibreTexts platform.

1.84: A Brief Tutorial on Wavepackets

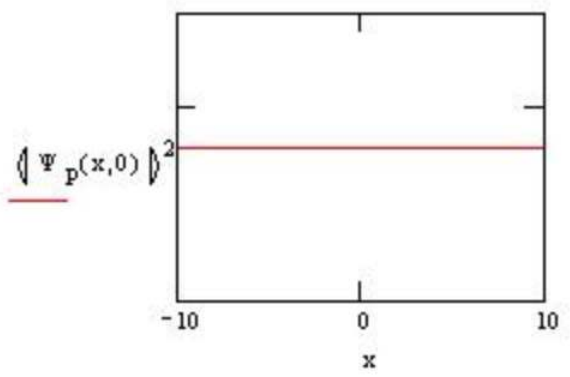
“A wavepaccket is a superposition of wavefunctions that is usually strongly peaked in one region of space and virtually zero elsewhere. The peak of the wavepacket denotes the most likely location of the particle; it occurs where the contributing wavefunctions are in phase and interfere constructively. Elsewhere the wavefunctions interfere destructively, and the net amplitude is small or zero.

A wavepacket moves because all the component functions change at different rates, and at different times the point of maximum constructive interference is in different locations. The motion of the wavepacket corresponds very closely to the motion predicted for a classical particle in the same potential. An important difference from classical physics is that the wavepacket spreads with time, but this tendency is very small for massive, slow particles.” P. W. Atkins, Quanta, page 395.

The time dependent coordinate-space wavefunction for a free particle with momentum p is, in atomic units:

$$m := 1 \qquad p := 1 \qquad x := -10, -9.95 \ldots 10$$

$$\Psi_p(x,t) := \frac{1}{\sqrt{2\cdot\pi}} \cdot \exp(i\cdot p\cdot x)\cdot \exp\left(\frac{-i\cdot p^2\cdot t}{2\cdot m}\right) \quad \text{where} \quad E_p = \frac{p^2}{2m}$$

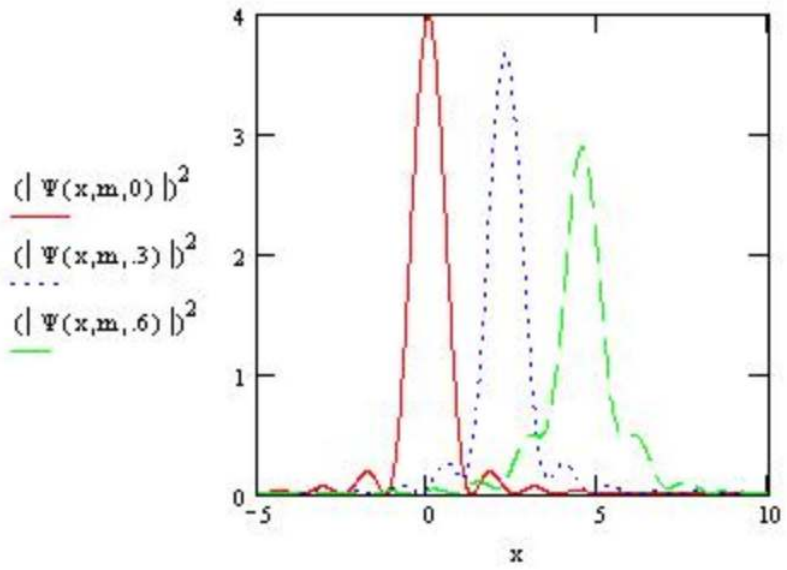


In quantum mechanics a state such as this with a precisely known momentum must have a completely uncertain position as is shown in the graph above for p=1. To use this wavefunction to model a particle it is necessary to form a linear superposition of momentum states. This adds enough uncertainty to momentum to localize the position of the particle to some degree. Because the momentum of a free particle is a continuous variable the discrete summation is replaced by the integral summation in forming the linear superpositon.

For example, the wavefunction for a particle of mass =1 moving to right with momentum between 5 and 10 atomic units is calculated below and the probability distribution is plotted for several times. Note that the wavepacket is indeed spreading as Atkins said it would.

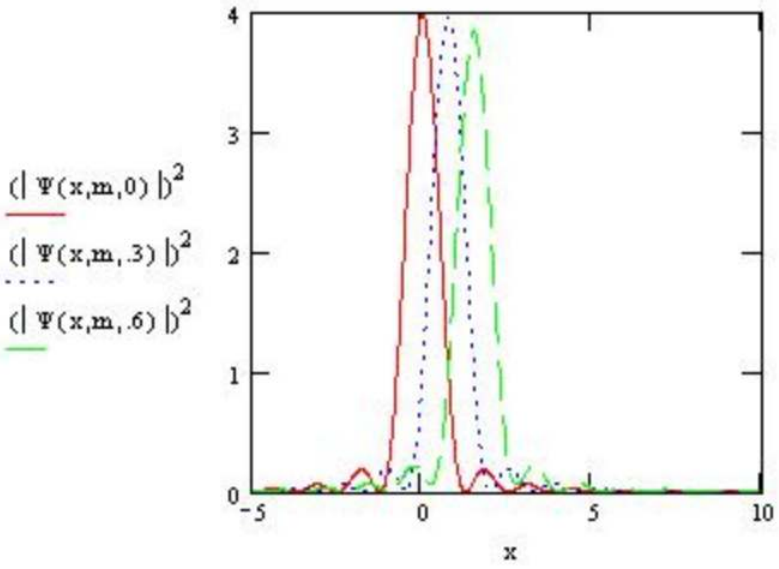
$$m := 1 \qquad x := -5, -4.98 \ldots 10$$

$$\Psi(x,m,t) := \frac{1}{\sqrt{2\cdot\pi}} \int_5^{10} \exp\left[i\cdot\left(p\cdot x - \frac{p^2\cdot t}{2\cdot m}\right)\right] dp$$



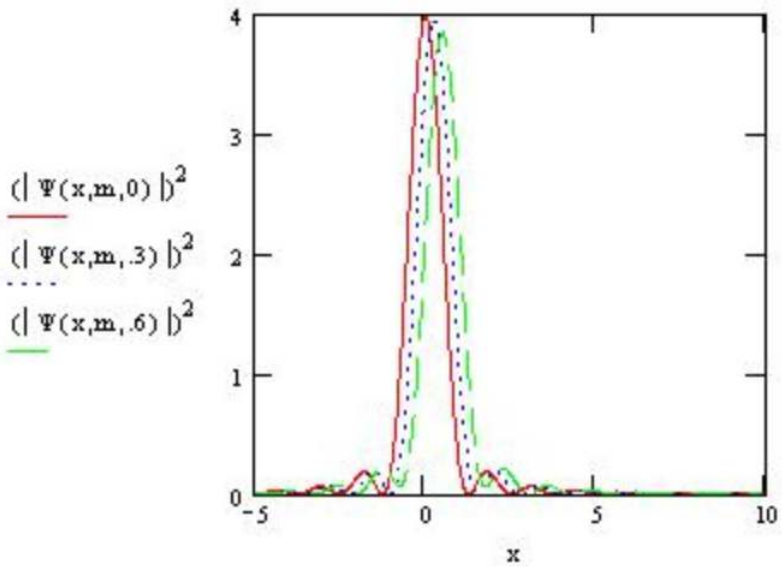
The spreading is not as great for more massive particles as can be seen by increasing the mass to 3.

$$m := 3$$



Atkins also said the spreading is not as great for slower participles. This is shown below by summing momentum values from 0 to 5 instead of 5 to 10.

$$\Psi(x,m,t) := \frac{1}{\sqrt{2\cdot\pi}} \int_0^5 \exp\left[i\cdot\left(p\cdot x - \frac{p^2 t}{2\cdot m}\right)\right] dp$$



This page titled 1.84: A Brief Tutorial on Wavepackets is shared under a CC BY 4.0 license and was authored, remixed, and/or curated by Frank Rioux via source content that was edited to the style and standards of the LibreTexts platform.

1.85: The Difference Between Fermions and Bosons

$$n_1 := 1 \qquad n_2 := 2$$
$$\Psi(x) := \sqrt{2} \cdot \sin(n_1 \cdot \pi \cdot x) \qquad \Phi(x) := \sqrt{2} \cdot \sin(n_2 \cdot \pi \cdot x)$$

Calculate the average separation, $|x_1 - x_2|$, for two fermions and two bosons in a 1D box of unit length.

Fermions have antisymmetric wave functions:

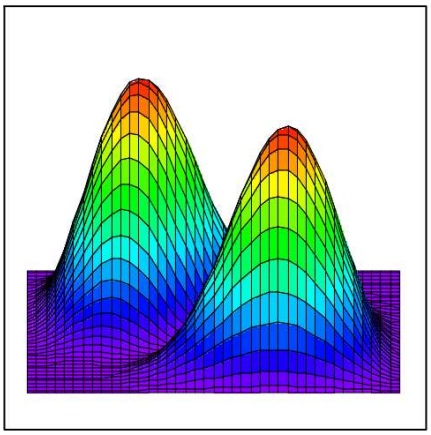
$$\Psi_f(x_1, x_2) := \frac{\Psi(x_1) \cdot \Phi(x_2) - \Psi(x_2) \cdot \Phi(x_1)}{\sqrt{2}}$$

The average particle separation for indistinquishable fermions:

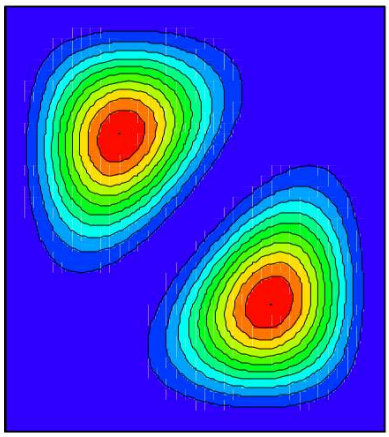
$$\int_0^1 \int_0^1 \Psi_f(x_1, x_2) \cdot |x_1 - x_2| \cdot \Psi_f(x_1, x_2)\, dx_1 dx_2 = 0.383$$

The particles are correlated so as to keep them apart.

$$N := 40 \qquad i := 0..N$$
$$x_{1_i} := \frac{1}{N} \quad j := 0 \ldots N \qquad x_2 := \frac{j}{N}$$
$$\Psi_{f_{i,j}} := \Psi_{f(x_{1_i}, x_{2_j})^2}$$



Ψ_f



x_2

Ψ_f

Bosons have symmetric wave functions:

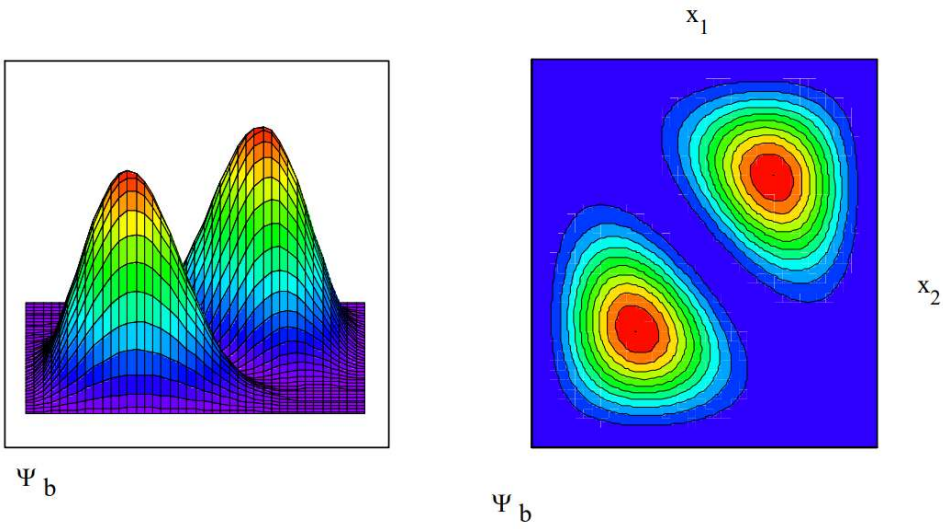
$$\Psi_b(x_1, x_2) = \frac{\Psi(x_1) \cdot \Phi(x_2) + \Psi(x_2) \cdot \Phi(x_1)}{\sqrt{2}}$$

The average particle separation for indistinquishable bosons:

$$\int_0^1 \int_0^1 \Psi_b(x_1, x_2) \cdot |x_1 - x_2| \cdot \Psi_b(x_1, x_2)\, dx_1 dx_2 = 0.157$$

The particles are correlated so as to bring them closer together.

$$N := 40 \qquad i := 0..N$$
$$x_{1_i} := \frac{1}{N} \quad j := 0 \ldots N \qquad x_2 := \frac{j}{N}$$
$$\Psi_{b_{i,j}} := \Psi_{b(x_{1_i}, x_{2_j})^2}$$



All fundamental particles (electrons, neutrons, protons, photons, etc.) are either bosons or fermions. Composite entities such as the elements also fall into these two categories. The fundamental distinction is spin: bosons have integer spin (0, 1, 2, ...) while fermions have half-integer spin (1/2, 3/2, ...).

The dramatic difference in behavior between bosons and fermions has led to a sociology of fundamental particles. Bosons are social and gregarious, while fermions are antisocial and aloof.

This page titled 1.85: The Difference Between Fermions and Bosons is shared under a CC BY 4.0 license and was authored, remixed, and/or curated by Frank Rioux via source content that was edited to the style and standards of the LibreTexts platform.

1.86: Quantum Corrals - Electrons within a Ring

"When electrons are confined to length scales approaching the de Broglie wavelength, their behavior is dominated by quantum mechanical effects. Here we report the construction and characterization of structures for confining electrons to this length scale. The walls of these "quantum corrals" are built from Fe atoms which are individually positioned on the Cu (111) surface by means of a scanning tunneling microscope (STM). These atomic structures confine surface state electrons laterally because of the strong scattering that occurs between surface state electrons and the Fe atoms. The surface state electrons are confined in the direction perpendicular to the surface because of intrinsic energetic barriers that exist in that direction."

This is the first paragraph of "Confinement of Electrons to Quantum Corrals on a Metal Surface," published by M. F. Crommie, C. P. Lutz, and D. M. Eigler in the October 8, 1993 issue of *Science Magazine*. They report the corraling of the surface electrons of Cu in a ring of radius 135 a0 created by 48 Fe atoms. The quantum mechanics for this form of electron confinement is well-known. Schroedinger's equation for a particle in a ring and its solution (in atomic units) are given below.

$$\frac{1}{2\mu}\frac{d^2}{d^2r}\Psi(r) - \frac{1}{2r\mu}\frac{d}{dr}\Psi(r) + \left(\frac{L^2}{2\mu r^2}\right)\Psi(r) = E\Psi(r) \tag{1.86.1}$$

with energies

$$E_{n,L} = \frac{Z_{n,L}^2}{2\mu R^2} \tag{1.86.2}$$

and the unnormalized wavefunctions

$$\Psi_{n,L} = J_z(Z_{n,L}, R) \tag{1.86.3}$$

J_L is the Lth order Bessel function, L is the angular momentum quantum number, n is the principle quantum number, Z n,L is the nth root of J_L, μ is the effective mass of the electron, and R is the corral (ring) radius. Dirac notation is used to describe the electronic states, $|n, L\rangle$. The roots of the Bessel function are given below in terms of the n and L quantum numbers.

L quantum number									
$Z :=$	0	1	2	3	4	5	6	7	$''n''$
	2.405	3.832	5.316	6.380	7.588	8.771	9.936	11.086	1
	5.5.20	7.016	8.417	9.761	11.065	12.339	13.589	14.821	2
	8.654	10.173	11.620	13.015	14.373	15.700	17.004	18.288	3
	11.792	13.324	14.796	16.223	17.616	18.980	20.321	21.642	4
	14.931	16.471	17.960	19.409	20.827	22.218	23.586	24.935	5
	180071	19.616	21.117	22.583	24.019	25.430	26.820	28.191	6

n quantum number

On the basis of Fermi energy considerations, Crombie, et al. identify the $|5, 0\rangle$, $|4, 2\rangle$ and $|2, 7\rangle$ as the most likely states contributing to the behavior of the surface electrons of Cu. A graphical comparison of the calculated surface electron density contributed by $|5, 0\rangle$ with the experimental data suggests that it is the dominant state in determining the surface electron density. The calculated results are displayed by plotting the wave function squared in Cartesian coordinates. The exponential term involving L and θ is discarded because $\left(\left|e^{i\cdot L\cdot\theta}\right|\right)^2 = 1$.

The theoretical results are displayed by plotting the wave function in Cartesian coordinates.

$$R = 135 \quad n = 5 \quad L = 0 \quad N = 100 \quad i = 0 \ldots N \quad j := 0 \ldots N$$

$$x_i = -R + \frac{2\cdot i}{N}\cdot R \qquad y_j := -R + \frac{2\cdot j}{N}\cdot R$$

$$\Psi(x,y) := \begin{cases} \mathrm{Jn}\left(L, Z_{n,L}\cdot\frac{\sqrt{x^2+y^2}}{R}\right) & \text{if } \sqrt{x^2+y^2}\le R \\ 0 & \text{otherwise} \end{cases} \qquad P_{i,j} = \Psi\left(x_i, y_j\right)^2$$

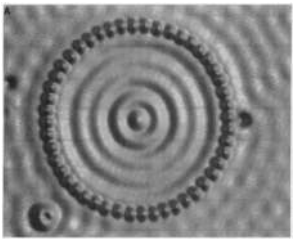
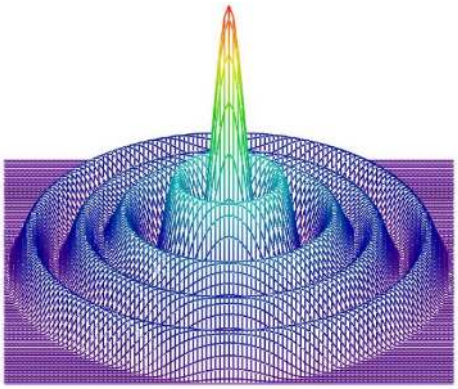


Figure 1: (left) The $|5, 0\rangle$ wavefunction of an electron in the 2D quantum corral. (Right) The experimental surface electron density reported by Crombie, et al. is shown below. The agreement between theory and experiment is very good.

However, Crommie, et al. noted that the $|5, 0\rangle$, $|4, 2\rangle$ and $|2, 7\rangle$ states are close in energy, being proportional to the squares of 14.931, 14.796 and 14.81 given in the table above. An even statistical mixture of these states would yield the surface electron density shown below, which is also visually in agreement with the experimental surface electron density.

$$\Psi'(x,y) := \begin{cases} \mathrm{Jn}\left(0, Z_{5,0}\cdot\frac{\sqrt{x^2+y^2}}{R}\right)^2 + \mathrm{Jn}\left(2, Z_{4,2}\cdot\frac{\sqrt{x^2+y^2}}{R}\right)^2 + \mathrm{Jn}\left(7, Z_{2,7}\cdot\frac{\sqrt{x^2+y^2}}{R}\right)^2 & \text{if } \sqrt{x^2+y^2}\le R \\ 0 & \text{otherwise} \end{cases} \qquad P_{i,j} := \Psi'\left(x_i, y_j\right)$$



P

References

1. M. F. Crommie, C. P. Lutz, and D. M. Eigler in the October 8, 1993 issue of Science Magazine

Contributors and Attributions

- Prof. Emeritus Frank Rioux (St. John's University and College of St. Benedict)

This page titled 1.86: Quantum Corrals - Electrons within a Ring is shared under a CC BY 4.0 license and was authored, remixed, and/or curated by Frank Rioux via source content that was edited to the style and standards of the LibreTexts platform.

1.87: Planck's Radiation Equation Fit to Experimental Data

https://chem.libretexts.org/@go/page/157655

$n := 42 \qquad i := 1..n$

$\rho_i :=$	$\lambda_i :=$
0.07	0.667
0.096	00.720
0.10	0.737
0.190	0.811
0.210	0.383
0.398	0.917
0.420	0.917
0.680	1.027
0.708	1.021
1.036	1.167
1.062	1.172
1.258	1.247
1.669	1.484
1.770	1.697
1.776	1.831
1.730	2.039
1.685	2.170
1.640	2.275
1.551	2.406
1.392	2.563
1.145	2.27
1.115	2.824
1.071	2.916
1.042	2.921
0.974	3.050
0.918	2.151
0.797	3.344
0.760	3.450
0.742	3.556
0.698	3.661
0.667	3.754
0.570	4.027

0.426	4.427
0.378	4.613
0.345	4.805
0.310	4.968
0.280	5.128
0.250	5.296
0.220	5.469
0.205	5.632
0.175	5.783
0.155	6.168

The data for this exercise is taken from page 19 of Eisberg and Resnick, *Quantum Physics.*

The values of rho are given in units of 10^3 joules/m^3 and the values of lambda are given in 10^{-6} m. The temperature is 1595 K.

Two pairs of data points are used to get approximate values for the parameters a and b in the Planck equation.

$$a := 1 \qquad b := 1$$

Given

$$\rho_{16} = \frac{a \cdot (\lambda_{16})^{-5}}{e^{\frac{b}{\lambda_{16}}}} \qquad \rho_{22} = \frac{a \cdot (\lambda_{22})^{-5}}{e^{\frac{b}{\lambda_{22}}} - 1}$$

$$\begin{pmatrix} a \\ b \end{pmatrix} := \text{Find}\,(a, b) \qquad a = 3.84 \times 10^3 \qquad b = 8.479$$

Planck's Equation is fit to data:

$$F(\lambda, a, b) := \frac{a \cdot \lambda^{-5}}{e^{\frac{b}{\lambda}} - 1}$$

$$SSD(a, b) := \sum_i \left(\rho_i - F\left(\lambda_i, a, b\right)\right)^2$$

Given

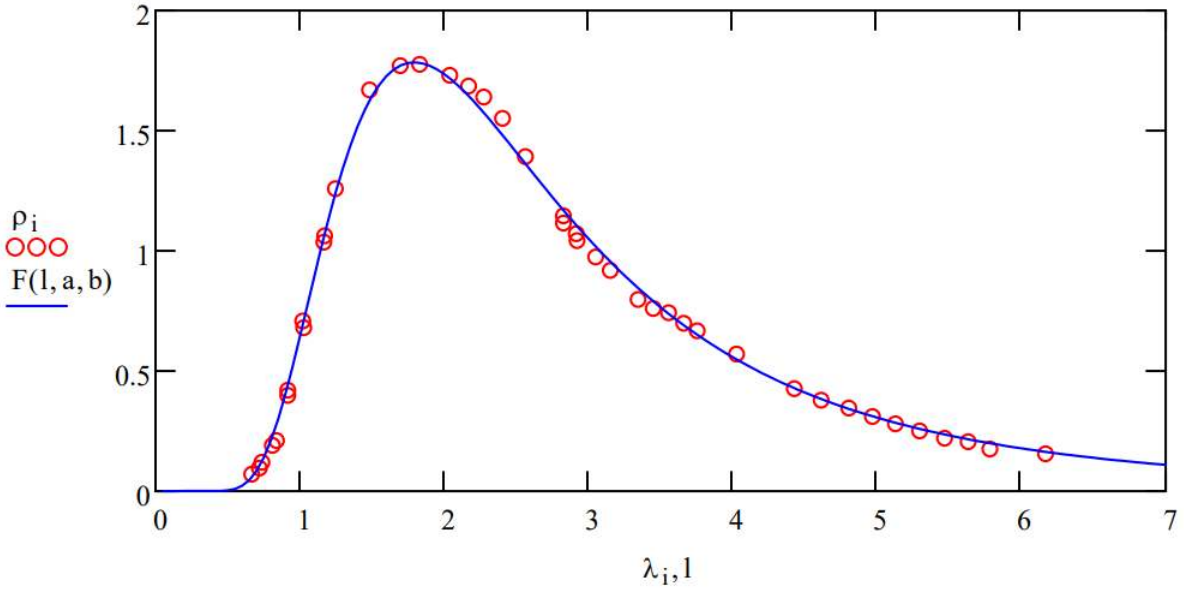
$$SSD(a, b) = 0 \qquad a > 0 \qquad b > 0 \qquad \begin{pmatrix} a \\ b \end{pmatrix} := \text{Minerr}(a, b)$$

Display optimum values of a and b:

$$a = 4.715 \times 10^3 \qquad b = 8.906$$

Plot of fit:

$$1 := 0.05, 0.1 \ldots 7$$



Calculate Planck's constant using the value of b, which is equal to (hc)/(kT).

$$h := \frac{b \cdot 10^{-6} \cdot 1.381 \cdot 10^{-23} \cdot 1595}{2.9979 \cdot 10^{8}} \qquad h = 6.544 \times 10^{-34}$$

This page titled 1.87: Planck's Radiation Equation Fit to Experimental Data is shared under a CC BY 4.0 license and was authored, remixed, and/or curated by Frank Rioux via source content that was edited to the style and standards of the LibreTexts platform.

1.88: Planck's Radiation Equation Fit to Experimental Data - Another Algorithm

https://chem.libretexts.org/@go/page/157656

$n := 42 \qquad i := 1..n$

$\rho_i :=$	$\lambda_i :=$
0.07	0.667
0.096	00.720
0.10	0.737
0.190	0.811
0.210	0.383
0.398	0.917
0.420	0.917
0.680	1.027
0.708	1.021
1.036	1.167
1.062	1.172
1.258	1.247
1.669	1.484
1.770	1.697
1.776	1.831
1.730	2.039
1.685	2.170
1.640	2.275
1.551	2.406
1.392	2.563
1.145	2.27
1.115	2.824
1.071	2.916
1.042	2.921
0.974	3.050
0.918	2.151
0.797	3.344
0.760	3.450
0.742	3.556
0.698	3.661
0.667	3.754
0.570	4.027

0.426	4.427
0.378	4.613
0.345	4.805
0.310	4.968
0.280	5.128
0.250	5.296
0.220	5.469
0.205	5.632
0.175	5.783
0.155	6.168

The data for this exercise is taken from page 19 of Eisberg and Resnick, *Quantum Physics.*

The values of rho are given in units of 10^3 joules/m^3 and the values of lambda are given in 10^{-6} m. The temperature is 1595 K.

Define Planck radiation function and first derivatives with respect to parameters a and b:

$$F(\lambda, a, b) := \begin{bmatrix} \frac{a \cdot \lambda^{-5}}{\left(\frac{b}{\lambda}\right)} \\ \frac{d}{da} \frac{a \cdot \lambda^{-5}}{\frac{b}{\lambda}} \\ \frac{d}{db} \frac{a \cdot \lambda^{-5}}{\left(e^{\frac{b}{\lambda}} - 1\right)} \end{bmatrix}$$

Carry out nonlinear regression using Mathcad's genfit algorithm:

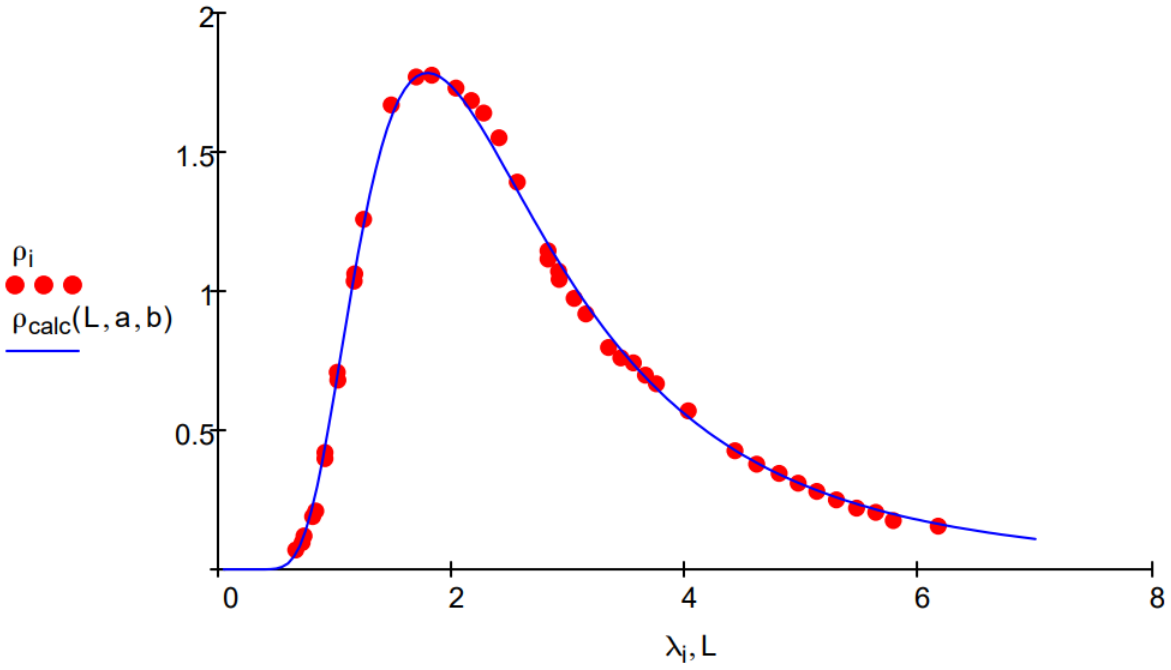
$$\text{seed} := \begin{pmatrix} 5 \cdot 10^3 \\ 10 \end{pmatrix} \qquad P := \text{genfit}\ (\lambda, \rho,\ \text{seed},\ F) \qquad P = \begin{pmatrix} 4.715 \times 10^3 \\ 8.906 \end{pmatrix} \qquad \begin{pmatrix} a \\ b \end{pmatrix} := P$$

Calculated radiation equation using output parameters:

$$\rho_{\text{calc}}(\mathrm{L}, a, b) = \frac{a \cdot L^{-5}}{\left(e^{\frac{b}{L}} - 1\right)}$$

Plot data and fit:

$$\mathrm{L} = 0.05, 0.1 \ldots 7$$



Calculate Planck's constant using the value of b, which is equal to (hc)/(kT).

$$h := \frac{b \cdot 10^{-6} \cdot 1.381 \cdot 10^{-23} \cdot 1595}{2.9979 \cdot 10^{8}} \qquad h = 6.544 \times 10^{-34}$$

This page titled 1.88: Planck's Radiation Equation Fit to Experimental Data - Another Algorithm is shared under a CC BY 4.0 license and was authored, remixed, and/or curated by Frank Rioux via source content that was edited to the style and standards of the LibreTexts platform.

1.89: Fitting Einstein's Heat Capacity Equation to Experimental Data for Silver

$n := 30 \qquad i := 1 \ldots n$

$T_i :=$	$C_i :=$
1	0.000818
3	0.0065
5	0.0243
8	0.0927
10	0.183
15	0.670
20	1.647
25	3.066
30	4.774
35	6.612
40	8.419
45	10.11
50	11.66
55	13.04
60	14.27
65	15.35
70	16.30
80	17.87
90	19.11
100	20.10
120	21.54
140	22.52
160	23.22
180	23.75
200	24.16
220	24.49
240	24.76
260	24.99
280	25.19
300	25.37

The heat capacity data were taken from the *Handbook of Physics and Chemistry* - 72nd Edition, page 5-71. The data are presented in units of Joules/mole/K.

Gas law constant:

$$R := 8.3145$$

Define Einstein function for heat capacity:

$$F(T, \Theta) := 3 \cdot R \cdot \left(\frac{\Theta}{T}\right)^2 \cdot \frac{\exp\left(\frac{\Theta}{T}\right)}{\left(\exp\left(\frac{\Theta}{T}\right) - 1\right)^2} \quad \text{where } \Theta = \frac{h \cdot v}{k}$$

Form the sum of the squares of the deviations:

$$SSD(\Theta) := \sum_i \left(C_i - F\left(T_i, \Theta\right)\right)^2$$

Minimize the sum of the squares of the deviations:

$$\Theta := 200$$

Given

$$SSD(\Theta) = 0 \qquad \Theta = Minerr(\Theta)$$

Einstein Temperature for best fit:

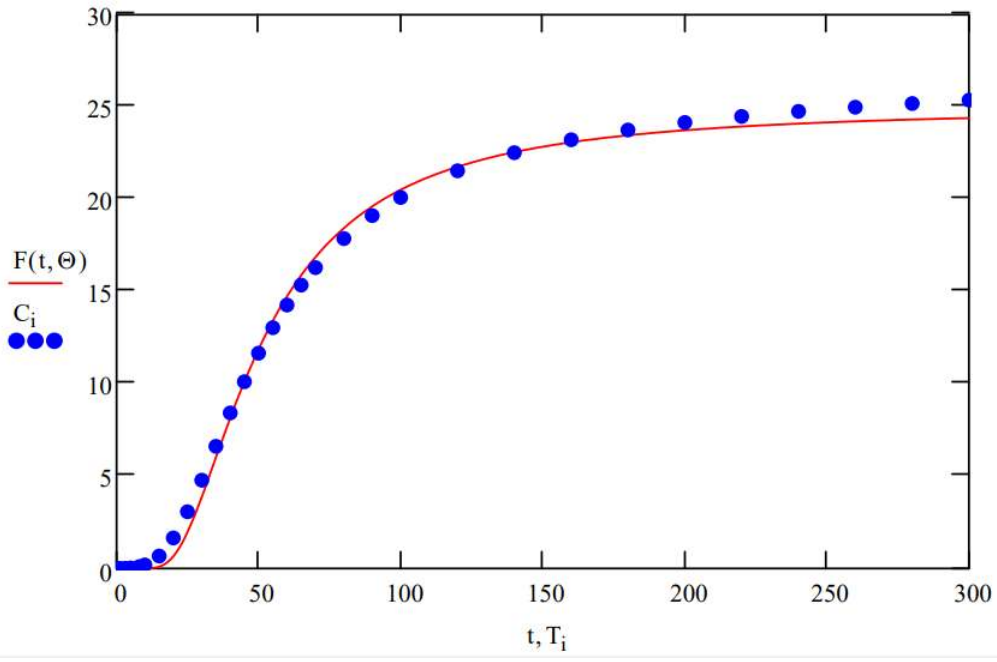
$$\Theta = 154.707$$

Mean squared error:

$$\frac{SSD(\Theta)}{(n-2)} = 0.319$$

Plot data and fit:

$$t := 1 \ldots 300$$



This page titled 1.89: Fitting Einstein's Heat Capacity Equation to Experimental Data for Silver is shared under a CC BY 4.0 license and was authored, remixed, and/or curated by Frank Rioux via source content that was edited to the style and standards of the LibreTexts platform.

1.90: Einstein's Heat Capacity Equation Fit to Experimental Data - Another Algorithm

$n := 30$ $\quad i := 1 \ldots n$

$T_i :=$	$C_i :=$
1	0.000818
3	0.0065
5	0.0243
8	0.0927
10	0.183
15	0.670
20	1.647
25	3.066
30	4.774
35	6.612
40	8.419
45	10.11
50	11.66
55	13.04
60	14.27
65	15.35
70	16.30
80	17.87
90	19.11
100	20.10
120	21.54
140	22.52
160	23.22
180	23.75
200	24.16
220	24.49
240	24.76
260	24.99
280	25.19
300	25.37

The heat capacity data were taken from the *Handbook of Physics and Chemistry* - 72nd Edition, page 5-71. The data are presented in units of Joules/mole/K.

$$R := 8.3145$$

Define Einstein function for heat capacity and first derivative with respect Θ:

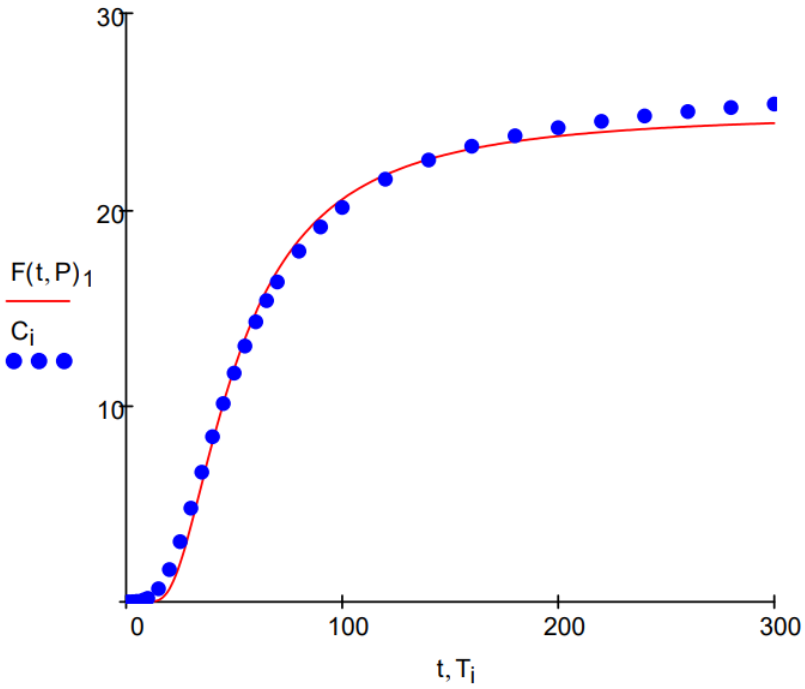
$$F(T,\Theta) := \begin{bmatrix} 3 \cdot R \cdot \left(\frac{\Theta}{T}\right)^2 \cdot \frac{\exp\left(\frac{\Theta}{T}\right)}{\left(\exp\left(\frac{\Theta}{T}\right)-1\right)^2} \\ \frac{d}{d\Theta}\left[3 \cdot R \cdot \left(\frac{\Theta}{T}\right)^2 \cdot \frac{\exp\left(\frac{\Theta}{T}\right)}{\left(\exp\left(\frac{\Theta}{T}\right)-1\right)^2}\right] \end{bmatrix}$$

Call genfit to do nonlinear regression analysis.

$$P := \text{genfit}\ (T, C, 200, F) \qquad P = 154.707$$

Plot data and fit:

$$t := 1 \ldots 300$$



This page titled 1.90: Einstein's Heat Capacity Equation Fit to Experimental Data - Another Algorithm is shared under a CC BY 4.0 license and was authored, remixed, and/or curated by Frank Rioux via source content that was edited to the style and standards of the LibreTexts platform.

1.91: Fitting Debye's Heat Capacity Equation to Experimental Data for Silver

$n := 30 \qquad i := 1 \ldots n$

$T_i :=$	$C_i :=$
1	0.000818
3	0.0065
5	0.0243
8	0.0927
10	0.183
15	0.670
20	1.647
25	3.066
30	4.774
35	6.612
40	8.419
45	10.11
50	11.66
55	13.04
60	14.27
65	15.35
70	16.30
80	17.87
90	19.11
100	20.10
120	21.54
140	22.52
160	23.22
180	23.75
200	24.16
220	24.49
240	24.76
260	24.99
280	25.19
300	25.37

The heat capacity data were taken from the *Handbook of Physics and Chemistry* - 72nd Edition, page 5-71. The data are presented in units of Joules/mole/K.

Gas law constant:

$$R := 8.31451$$

Define Debye function for heat capacity:

$$F(T, \Theta) := 9 \cdot R \cdot \left(\frac{T}{\Theta}\right)^3 \cdot \int_0^{\frac{\Theta}{T}} \frac{x^4 \cdot \exp(x)}{(\exp(x) - 1)^2} dx \quad \text{where} x = \frac{hv}{kT}$$

Form the sum of the squares of the deviations:

$$SSD(\Theta) := \sum_i \left(C_i - F\left(T_i, \Theta\right)\right)^2$$

Minimize the sum of the squares of the deviations:

$$\Theta := 200$$

Given

$$SSD(\Theta) = 0 \qquad \Theta := \text{Minerr}(\Theta)$$

Debye Temperature for best fit:

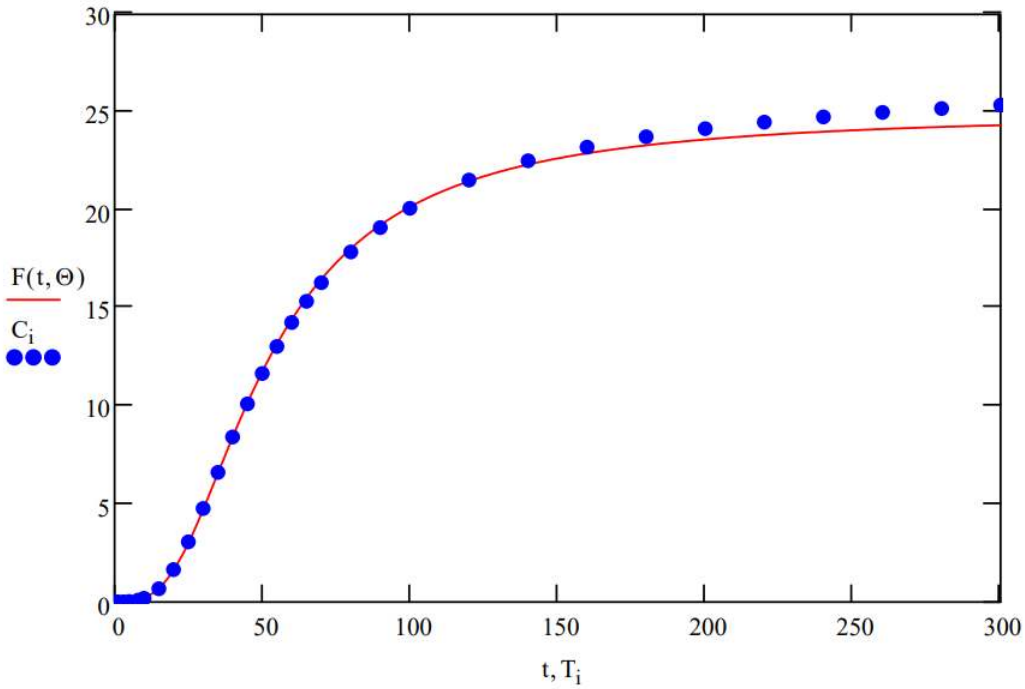
$$\Theta = 210.986$$

Mean squared error:

$$\frac{SSD(\Theta)}{(n-2)} = 0.16$$

Plot data and fit:

$$t := 1 \ldots 300$$



This page titled 1.91: Fitting Debye's Heat Capacity Equation to Experimental Data for Silver is shared under a CC BY 4.0 license and was authored, remixed, and/or curated by Frank Rioux via source content that was edited to the style and standards of the LibreTexts platform.

1.92: Debye's Heat Capacity Equation Fit to Experimental Data - Another Algorithm

$n := 30 \qquad i := 1 \ldots n$

$T_i :=$	$C_i :=$
1	0.000818
3	0.0065
5	0.0243
8	0.0927
10	0.183
15	0.670
20	1.647
25	3.066
30	4.774
35	6.612
40	8.419
45	10.11
50	11.66
55	13.04
60	14.27
65	15.35
70	16.30
80	17.87
90	19.11
100	20.10
120	21.54
140	22.52
160	23.22
180	23.75
200	24.16
220	24.49
240	24.76
260	24.99
280	25.19
300	25.37

The heat capacity data were taken from the *Handbook of Physics and Chemistry* - 72nd Edition, page 5-71. The data are presented in units of Joules/mole/K.

Gas law constant:

$$R := 8.31451$$

Define Einstein function for heat capacity and first derivative with respect Θ:

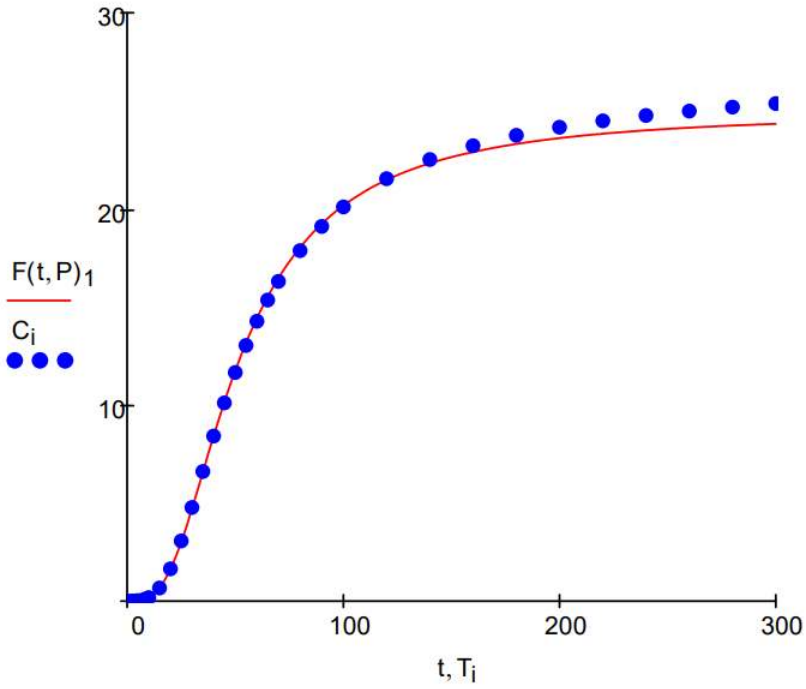
$$F(T,\Theta) = \begin{bmatrix} 9\cdot R\cdot\left(\frac{T}{\Theta}\right)^3\cdot\int_0^{\frac{\Theta}{T}}\frac{x^4\cdot\exp(x)}{(\exp(x)-1)^2}dx \\ \frac{d}{d\Theta}\left[9.R\cdot\left(\frac{T}{\Theta}\right)^3\cdot\int_0^{\frac{\Theta}{T}}\frac{x^4\cdot\exp(x)}{(\exp(x)-1)^2}dx\right] \end{bmatrix}$$

Call genfit to do nonlinear regression analysis.

$$P := \text{genfit}\ (T, C, 200, F) \qquad P = 210.985$$

Plot data and fit:

$$t := 1 \ldots 300$$



This page titled 1.92: Debye's Heat Capacity Equation Fit to Experimental Data - Another Algorithm is shared under a CC BY 4.0 license and was authored, remixed, and/or curated by Frank Rioux via source content that was edited to the style and standards of the LibreTexts platform.

1.93: Wave-particle Duality and the Uncertainty Principle

Nick Herbert, author of *Quantum Reality*, has proposed the name *quon* for "any entity that exhibits both wave and particle attributes in the peculiar quantum mechanical manner." Obvious examples of quons for chemists are the electron, proton, neutron and photon. The wave-particle duality of quons is captured succinctly by the deBroglie relation, which unites the wave property λ with the particle property mv in a reciprocal relationship mediated by the ubiqutous Planck's constant.

$$\lambda = \frac{\mathrm{h}}{\mathrm{mv}} = \frac{\mathrm{h}}{\mathrm{p}}$$

The most general momentum wave function for a quon in one-dimension is Euler's equation when it incorporates the deBroglie equation.

$$\langle x|p\rangle = \exp\left(i2\pi\frac{x}{\lambda}\right)\frac{\lambda = h/p}{\hbar = h/2\pi}\exp\left(\frac{ipx}{\hbar}\right) = \cos\left(\frac{px}{\hbar}\right) + i\sin\left(\frac{px}{\hbar}\right)$$
$$\Psi(p,x) := \exp(ip\cdot x)$$

The momentum wave function for a quon with a well-defined momentum (p = 7, for example) is shown below in atomic units (h = 2π). It clearly illustrates the uncertainty principle because the wave function is completely spatially delocalized.

Momentum:

$$\mathrm{p} := 7 \qquad \mathrm{j} := 0 \ldots 300$$

Axis of propagation:

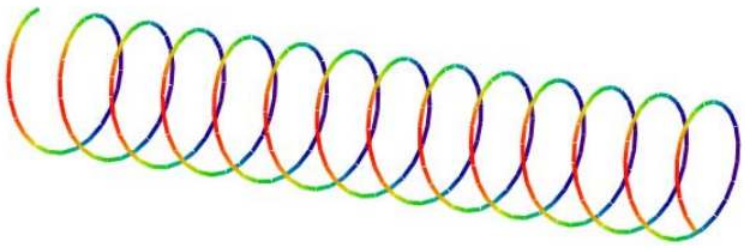
$$\mathrm{x_j} := \mathrm{j}\cdot 0.04$$

Real axis:

$$\mathrm{y_j} := \mathrm{Re}\left(\Psi\left(\mathrm{p}, \mathrm{x_j}\right)\right)$$

Imaginary axis:

$$z_{\mathrm{j}} := \mathrm{Im}\left(\Psi\left(\mathrm{p}, \mathrm{x_j}\right)\right)$$



$$(\mathrm{x}, \mathrm{y}, \mathrm{z})$$

As might be expected on the basis of the uncertainty principle, the particle-like character of a quon is revealed only when there is uncertainty in momentum. This can be demonstrated by plotting Euler's equation for a superposition of momentum states as shown below. This superposition (integrating, or summing over a range of momentum values) clearly reveals the incipient particle-like characteristics of a quon.

Axis of propagation:

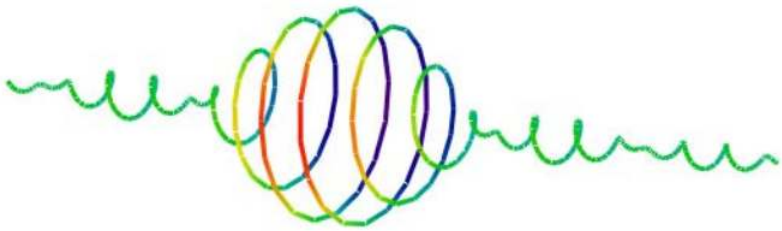
$$x_j := j \cdot 0.054 - 7$$

Real axis:

$$y_j := \int_6^8 \mathrm{Re}\left(\Psi\left(p, x_j\right)\right) dp$$

Imaginary axis:

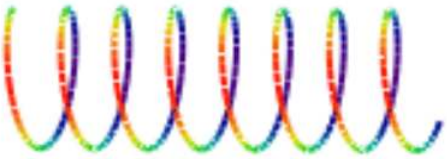
$$z_j := \int_6^8 \mathrm{Im}\left(\Psi\left(p, x_j\right)\right) dp$$



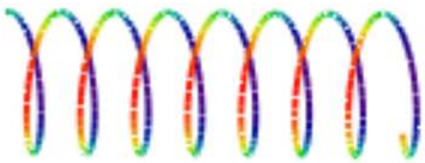
$$(x, y, z)$$

The form of Euler's equation we have been using, $< x|p >$, is the momentum eigenfunction in coordinate space. Its complex conjugate, $< p|x >$, is the position eigenfunction in momentum space. In other words, a quon with a well-defined position is delocalized in momentum space, just as a quon with a well-defined momentum is delocalized in coordinate space.

$$\langle x|p\rangle = \exp\left(\frac{ipx}{\hbar}\right)$$



$$\langle p|x\rangle = \exp\left(-\frac{ipx}{\hbar}\right)$$



These equations are simple Fourier transforms; they allow us to translate knowledge in one language (position or momentum) into the other language. They are a kind of mathematical dictionary. Richard Feynman claimed that Euler's equation is the most remarkable equation in mathematics and called it "our jewel." Because it is the kernel in Fourier transforms, it is ubiquitous in quantum mechanics.

This page titled 1.93: Wave-particle Duality and the Uncertainty Principle is shared under a CC BY 4.0 license and was authored, remixed, and/or curated by Frank Rioux via source content that was edited to the style and standards of the LibreTexts platform.

1.94: Wave-Particle Duality for Matter and Light

A wave is spatially delocalized



A particle is spatially localized



These incompatible concepts are united by the deBroglie wave equation with the wave property (wavelength) on the left and the particle property (momentum) on the right in a reciprocal relationship mediated by the ubiquitous Planck's constant.

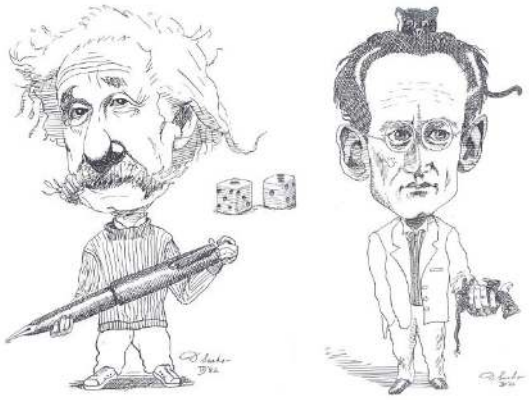
$$\lambda = \frac{h}{mv}$$

This page titled 1.94: Wave-Particle Duality for Matter and Light is shared under a CC BY 4.0 license and was authored, remixed, and/or curated by Frank Rioux via source content that was edited to the style and standards of the LibreTexts platform.

1.95: What Part of the Quantum Theory Don't You Understand?

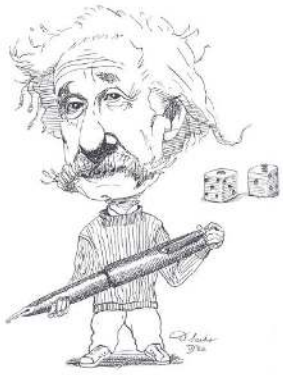
Quantum Mechanics and Mathematics According to Richard Feynman

- We have come to the conclusion that what are usually called the advanced parts of quantum mechanics are, in fact, quite simple.
- The mathematics that is involved is particularly simple, involving simple algebraic operations and no differential equations or at most very simple ones.



Einstein and Schrödinger

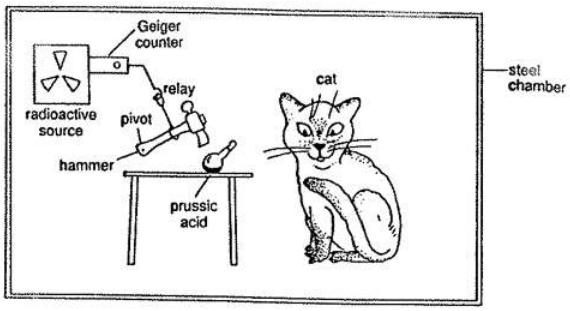
Gott würfelt nicht.

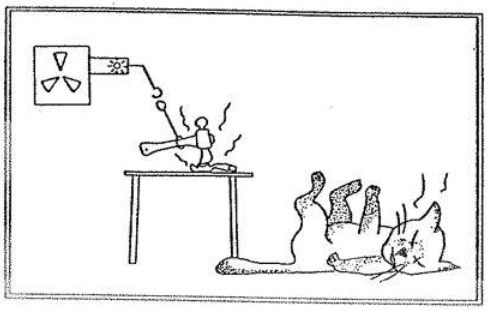


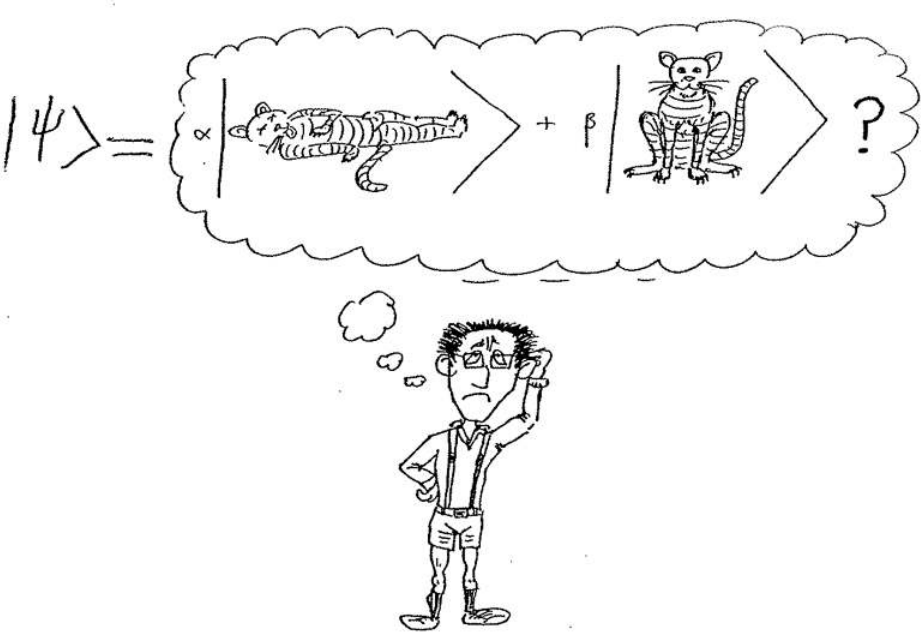
$$|\Psi\rangle = \frac{1}{\sqrt{6}}\left[\left| \boxed{\bullet} \right\rangle + \left| \boxed{\bullet\ \ \bullet} \right\rangle + \left| \boxed{\bullet\ \ \bullet} \right\rangle + \left| \boxed{\bullet\ \ \bullet} \right\rangle + \left| \boxed{\bullet\ \ \bullet} \right\rangle + \left| \boxed{\bullet\ \ \bullet} \right\rangle \right]$$



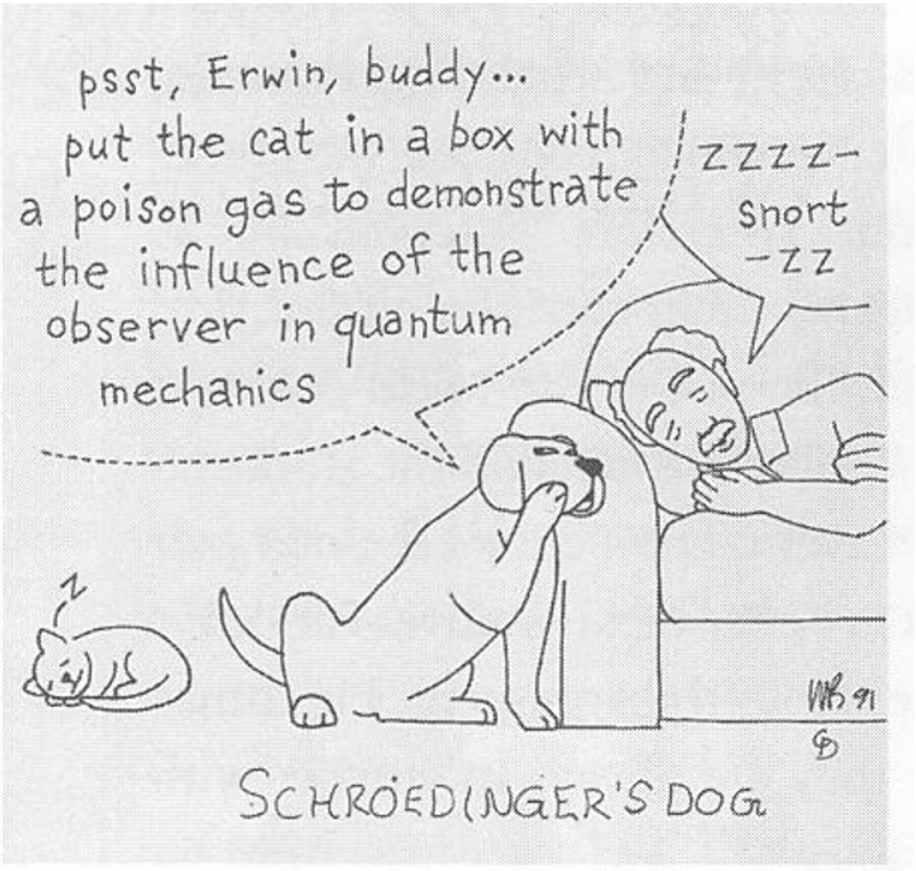
https://chem.libretexts.org/@go/page/158514

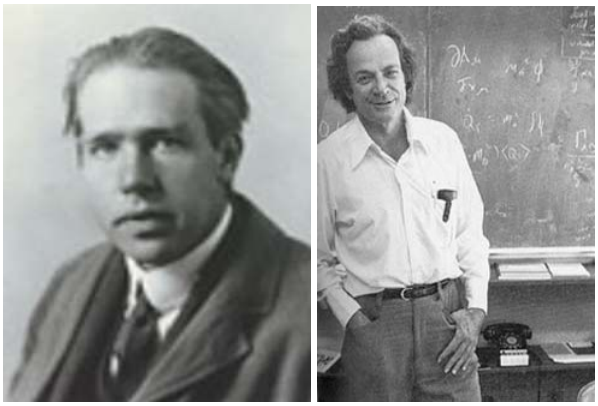






https://chem.libretexts.org/@go/page/158514





Bohr and Feynman

Quantum Quotes

- Quantum mechanics is certainly imposing. But an inner voice tells me that it is not yet the real thing. The theory says a lot, but does not really bring us any closer to the secret of the 'old one.' I, at any rate, am convinced that He is not playing at dice. (Einstein)
- I still believe in the possibility of a model of reality, that is to say, of a theory, which represents things themselves and not merely the probability of their occurrence. (Einstein)
- It is wrong to think that the task of physics is to find out how nature is. Physics concerns what we can say about nature. (Bohr)
- Quantum states are states of knowledge and not objective features of the systems they describe. (N. David Mermin)
- I remember discussions with Bohr which went through many hours till very late at night and ended almost in despair; and when at the end of the discussion I went alone for a walk in a neighboring park I repeated to myself again and again the question: **Can**

nature possibly be as absurd as it seemed to us in these atomic experiments? (Heisenberg)

After state preparation by the vertical polarizer, only two subsequent experiments have certain outcomes according to quantum mechanics.

1. The probability that the vertically polarized photons will pass a second vertical polarizer is 1.

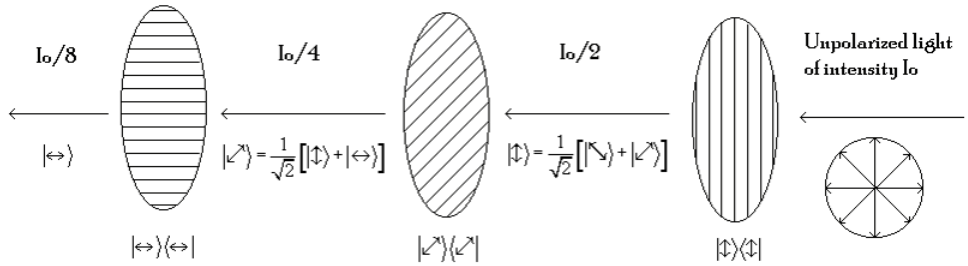
$$|\langle \updownarrow \mid \updownarrow \rangle|^2 = 1 \tag{1.95.1}$$

2. The probability that the vertically polarized photons will pass a second polarizer that is oriented horizontally is 0.

$$|\langle \leftrightarrow \mid \updownarrow \rangle|^2 = 0 \tag{1.95.2}$$

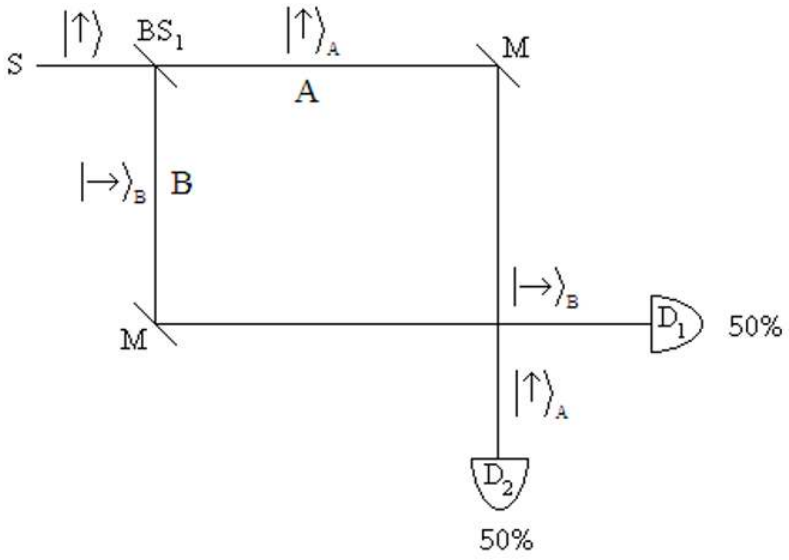
For all other experiments involving two polarizers only the probability of the outcome can be predicted, and this is $\cos^2(\theta)$, where θ is the relative angle of the polarizing films. For example,

$$\left|\left\langle \nearrow \middle| \updownarrow \right\rangle\right|^2 = \left|\frac{1}{\sqrt{2}}\right|^2 = \frac{1}{2}$$

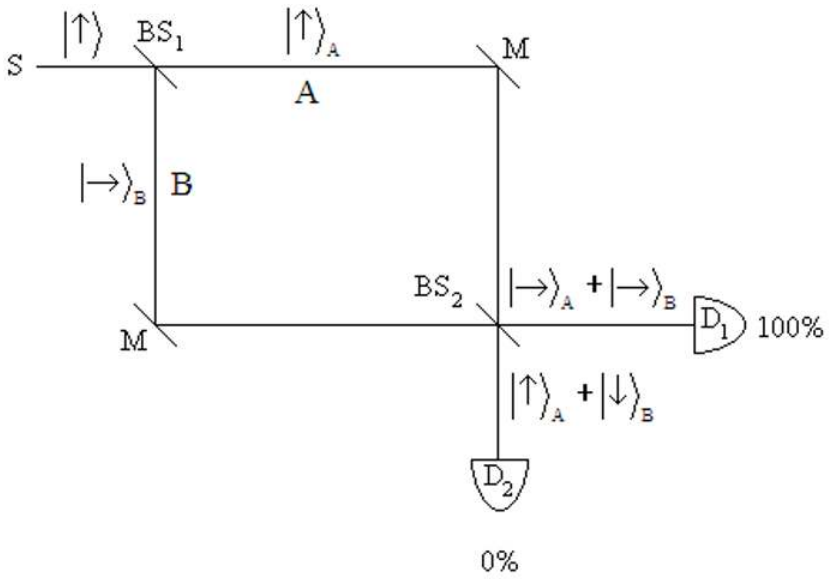


Feynman on the Significance of the Double-Slit Experiment

- We choose to examine a phenomenon which is impossible, *absolutely* impossible, to explain in any classical way, and which has in it the heart of quantum mechanics.
- In reality, it contains the *only* mystery.
- We cannot make the mystery go away by "explaining" how it works. We will just *tell* you how it works.
- In telling you how it works we will have told you about the basic peculiarities of all quantum mechanics.
- Any situation in quantum mechanics can always be explained by saying, "You remember the experiment with the two holes? It's the same thing."



$$|\uparrow\rangle_S \xrightarrow{\text{BS}_1} \frac{1}{\sqrt{2}}[|\uparrow\rangle_A + |\rightarrow\rangle_B]$$



$$|\uparrow\rangle_S \xrightarrow{\text{BS}_1} \frac{1}{\sqrt{2}}[|\uparrow\rangle_A + |\rightarrow\rangle_B]$$

$$|\uparrow\rangle_A \xrightarrow{\text{BS}_2} \frac{1}{\sqrt{2}}[|\rightarrow\rangle_{D_1} + |\uparrow\rangle_{D_2}] \qquad |\rightarrow\rangle_B \xrightarrow{\text{BS}_2} \frac{1}{\sqrt{2}}[|\rightarrow\rangle_{D_1} + |\downarrow\rangle_{D_2}]$$

$$|\uparrow\rangle_s \frac{\text{BS}_1}{\text{BS}_2} > \frac{1}{2}[|\rightarrow\rangle_{D_1} + |\uparrow\rangle_{D_2} + |\rightarrow\rangle_{D_1} + |\downarrow\rangle_{D_2}] = |\rightarrow\rangle_{D_1}$$

Experimental Realization of Wheeler's Delayed-Choice Gedanken Experiment

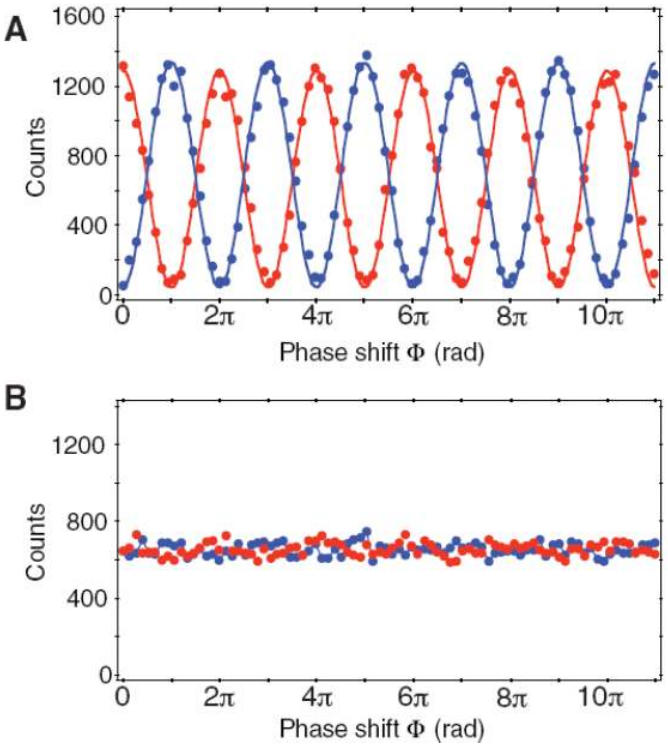
Vincent Jacques,[1] E Wu,[1,2] Frédéric Grosshans,[1] François Treussart,[1] Philippe Grangier,[3] Alain Aspect,[3] Jean-François Roch[1]*

Wave-particle duality is strikingly illustrated by Wheeler's delayed-choice gedanken experiment, where the configuration of a two-path interferometer is chosen after a single-photon pulse has entered it: Either the interferometer is closed (that is, the two paths are recombined) and the interference is observed, or the interferometer remains open and the path followed by the photon is measured. We report an almost ideal realization of that gedanken experiment with single photons allowing unambiguous which-way measurements. The choice between open and closed configurations, made by a quantum random number generator, is relativistically separated from the entry of the photon into the interferometer.

Young's double-slit experiment, realized with particles sent one at a time through an interferometer, is at the heart of quantum mechanics (*1*). The striking feature is that the phenomenon of interference, interpreted as a wave following two paths simultaneously, is incompatible with our common-sense representation of a particle following one route or the other but not both. Several single-photon interference experiments (*2*–*6*) have confirmed the wave-particle duality of the light field. To understand their meaning, consider the single-photon interference experiment sketched in Fig. 1. In the closed interferometer configuration, a single-photon pulse is split by a first beamsplitter BS_{input} of a Mach-Zehnder interferometer and travels through it until a second beamsplitter BS_{output} recombines the two interfering arms. When the phase shift Φ between the two arms is varied, interference appears as a modulation of the detection probabilities at output ports 1 and 2, respectively, as $\cos^2 \Phi$ and $\sin^2 \Phi$. This result is the one expected for a wave, and as Wheeler pointed out, "[this] is evidence … that each ar-

[1]Laboratoire de Photonique Quantique et Moléculaire, Ecole Normale Supérieure de Cachan, UMR CNRS 8537, 94235 Cachan, France. [2]Key Laboratory of Optical and Magnetic Resonance Spectroscopy, East China Normal University, 200062 Shanghai, China. [3]Laboratoire Charles Fabry de l'Institut d'Optique, Campus Polytechnique, UMR CNRS 8501, 91127 Palaiseau, France.

*To whom correspondence should be addressed. E-mail: roch@physique.ens-cachan.fr



Final Quantum Quotes

- If we want to describe what happens in an atomic event, we have to realize that the word "happens" can only apply to the observation, not to the state of affairs between two observations. [Werner Heisenberg]
- I think it is safe to say that no one understands quantum mechanics. Do not keep saying to yourself, if you can possibly avoid it, 'But how can it possibly be like that?' because you will go down the drain into a blind alley from which nobody has yet escaped. Nobody knows how it can be like that. [Richard Feynman]
- Any one who is not shocked by quantum mechanics has not fully understood it. [Niels Bohr]
- The mathematical predictions of quantum mechanics yield results that are in agreement with experimental findings. That is the reason we use quantum theory. That quantum theory fits experiment is what validates the theory, but why experiment should give such peculiar results is a mystery. This is the shock to which Bohr referred. [Marvin Chester with slight modifications by Frank Rioux]

- In the quantum world the present does not always have a unique past.

Feynman Poetry

> *We have always had a great deal of difficulty understanding the world view that quantum mechanics represents.*
>
> *At least I do, because I'm an old enough man that I haven't got to the point that this stuff is obvious to me.*
>
> *Okay, I still get nervous with it …*
>
> *You know how it always is, every new idea, it takes a generation or two until it becomes obvious that there's no real problem.*
>
> *I cannot define the real problem, therefore I suspect there's no real problem, but I'm not sure there's no real problem.*

This page titled 1.95: What Part of the Quantum Theory Don't You Understand? is shared under a CC BY 4.0 license and was authored, remixed, and/or curated by Frank Rioux via source content that was edited to the style and standards of the LibreTexts platform.

1.96: Quantum Potpourri - An Attempt to Demonstrate Two Fundamental Quantum Concepts- Wave-particle Duality and The Superposition Principle

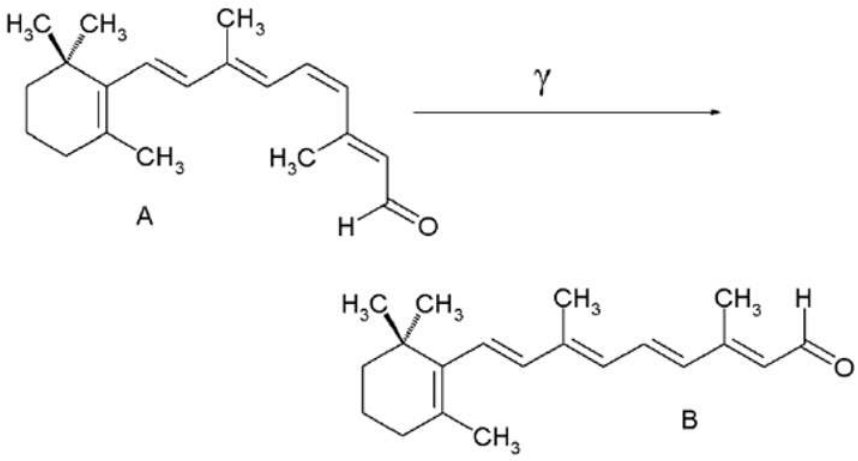
Wave-particle Duality

Quon

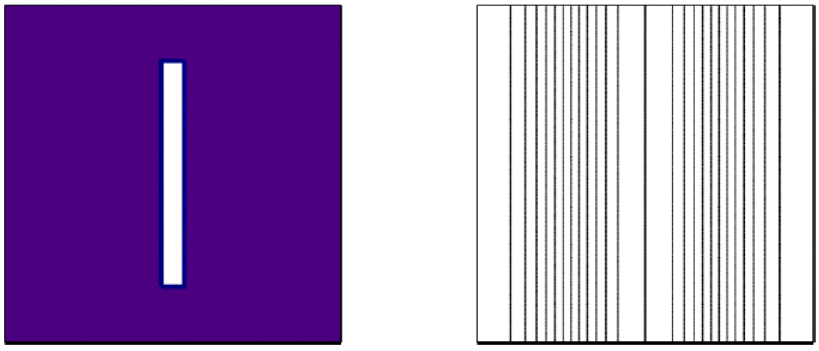
- An entity that exhibits both wave and particle behavior in the peculiar quantum mechanical manner. (Nick Herbert)
- Examples from chemistry:
  - Electrons
  - Protons
  - Neutrons
  - Photons

Wave-particle Duality Illustrated

- Source (light bulb, sun) emits light
- Interference fringes are observed suggesting wave-like behavior.
- However, the detector (eye) registers particles (retinal absorbs a photon and changes shape ultimately causing a signal to be sent to the brain via the optic nerve)
- We detect particles, but we predict what will happen, or interpret what happened, by assuming wave-like behavior
- “Everything in the future is a wave, everything in the past is a particle.” Lawrence Bragg



Retinal Absorbs a Photon



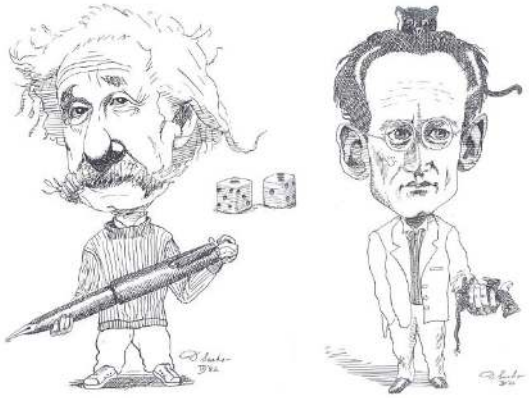
SlitPattern

DiffractionPattern

https://chem.libretexts.org/@go/page/158515

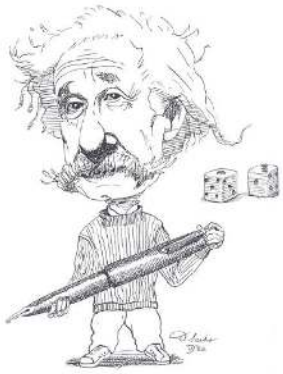
Other Diffraction Phenomena

- Optical Transforms
  - Hexagon
  - Pentagon
- X-ray Diffraction Pattern of DNA



Einstein and Schrödinger

Gott würfelt nicht.

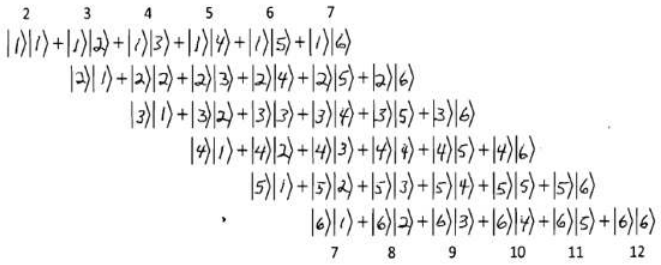


$$|\Psi\rangle = \frac{1}{\sqrt{6}}\left[\left| \boxed{\bullet} \right\rangle + \left| \begin{smallmatrix} \bullet & \\ & \bullet \end{smallmatrix} \right\rangle + \left| \begin{smallmatrix} \bullet & \\ \bullet & \bullet \end{smallmatrix} \right\rangle + \left| \begin{smallmatrix} \bullet & \bullet \\ \bullet & \bullet \end{smallmatrix} \right\rangle + \left| \begin{smallmatrix} \bullet & \bullet \\ \bullet & \bullet \\ \bullet & \bullet \end{smallmatrix} \right\rangle + \left| \begin{smallmatrix} \bullet & \bullet \\ \bullet & \bullet \\ \bullet & \bullet \end{smallmatrix} \right\rangle \right]$$

The Quantum View of Playing Dice

$$|\Psi\rangle_a|\Psi\rangle_b = \frac{1}{\sqrt{6}}[|1\rangle + |2\rangle + |3\rangle + |4\rangle + |5\rangle + |6\rangle]\frac{1}{\sqrt{6}}[|1\rangle + |2\rangle + |3\rangle + |4\rangle + |5\rangle + |6\rangle]$$

$$\begin{aligned}|\Psi\rangle_a|\Psi\rangle_b = \frac{1}{6}\,[&|1||1\rangle + |1||2\rangle + |1\rangle|3\rangle + |1\rangle|4\rangle + |1\rangle|5\rangle + |1\rangle|6\rangle \\ &+|2\rangle|1\rangle + |2\rangle|2\rangle + |2\rangle|3\rangle + |2\rangle|4\rangle + |2\rangle|5\rangle + |2\rangle|6\rangle \\ &+|3\rangle|1\rangle + |3\rangle|2\rangle + |3\rangle|3\rangle + |3\rangle|4\rangle + |3\rangle|5\rangle + |3\rangle|6\rangle \\ &+|4\rangle|1\rangle + |4||2\rangle + |4\rangle|3\rangle + |4\rangle|4\rangle + |4||5\rangle + |4\rangle|6\rangle \\ &+|5\rangle|1\rangle + |5\rangle|2\rangle + |5\rangle|3\rangle + |5\rangle|4\rangle + |5\rangle|5\rangle + |5\rangle|6\rangle \\ &+|6\rangle|1\rangle + |6\rangle|2\rangle + |6\rangle|3\rangle + |6\rangle|4\rangle + |6\rangle|5\rangle + |6\rangle|6\rangle]\end{aligned}$$

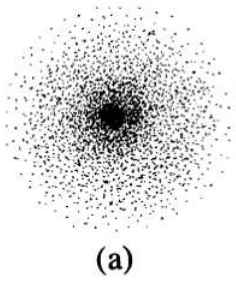


Electronic Structure and the Superposition Principle

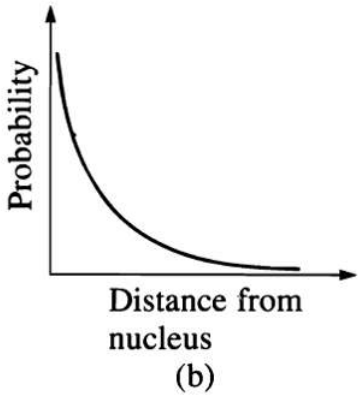
Electrons in atoms or molecules are characterized by their entire distributions, called wave functions or orbitals, rather than by instantaneous positions and velocities: an electron may be considered always to be, with appropriate probability, at all points of its distribution, which does not vary with time. (F. E. Harris)

For example, the hydrogen atom electron is in a stationary state which is a weighted superposition of all possible distances from the nucleus. The electron is not orbiting the nucleus; it does not execute a classical trajectory during its interaction with the nucleus.

From the quantum mechanical perspective, to measure the position of an electron is not to find out where it is, but to cause it to be somewhere. (Louisa Gilder)



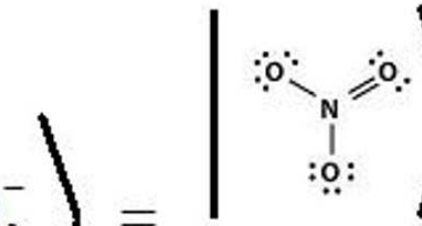
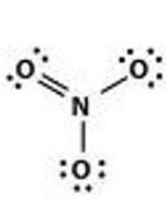
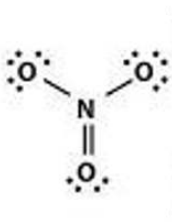
(a)



(b)

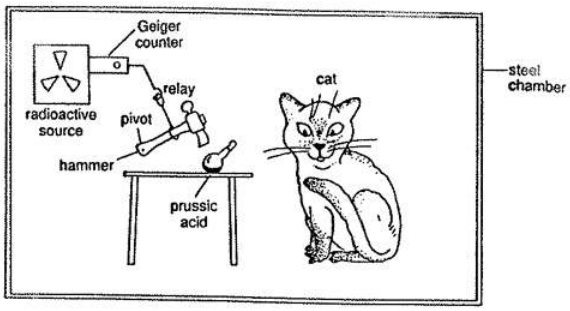
https://chem.libretexts.org/@go/page/158515

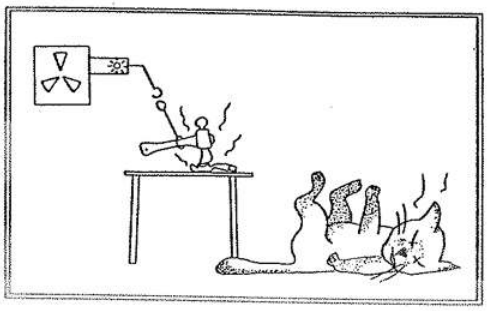
Resonance from the Quantum Mechanical Perspective

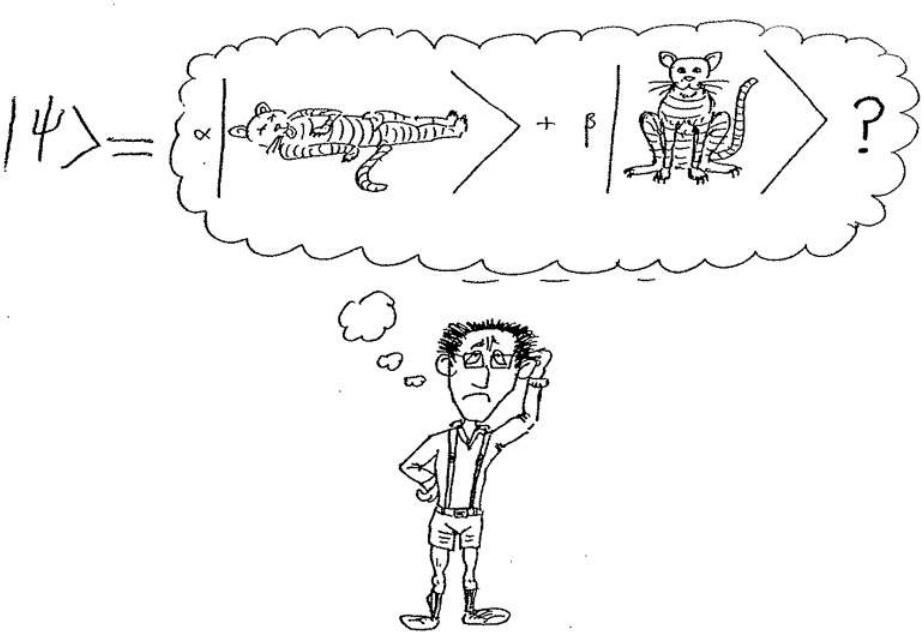
$$\left| NO_3^- \right\rangle = \frac{\left| \text{  } \right\rangle + \left| \text{  } \right\rangle + \left| \text{  } \right\rangle}{\sqrt{3}}$$

Schrödinger's Cat

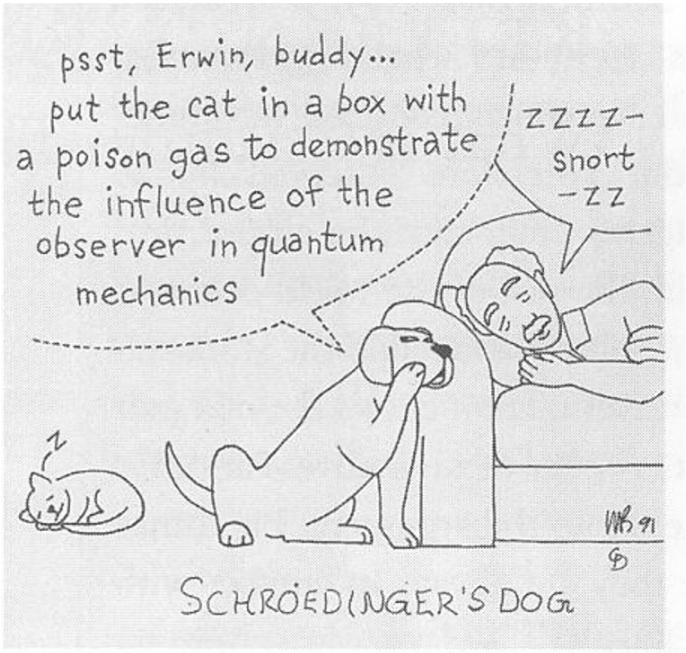




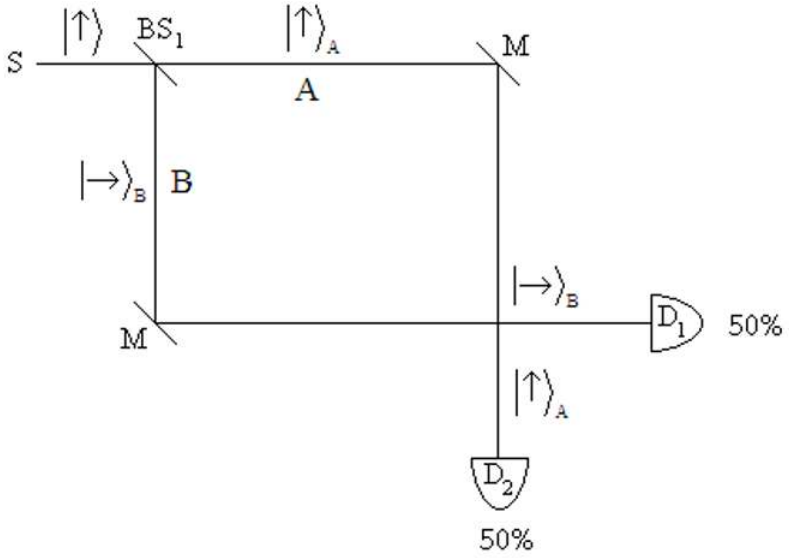




https://chem.libretexts.org/@go/page/158515



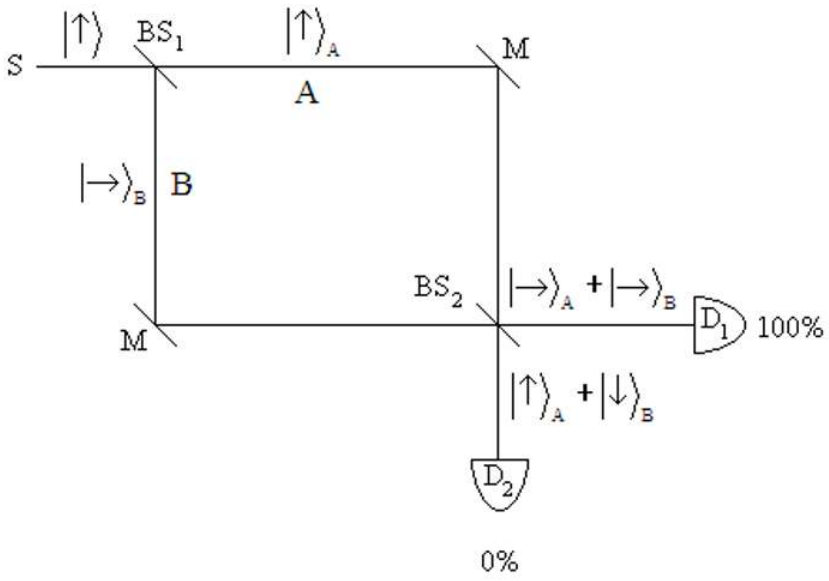
Another Example of the Superposition Principle



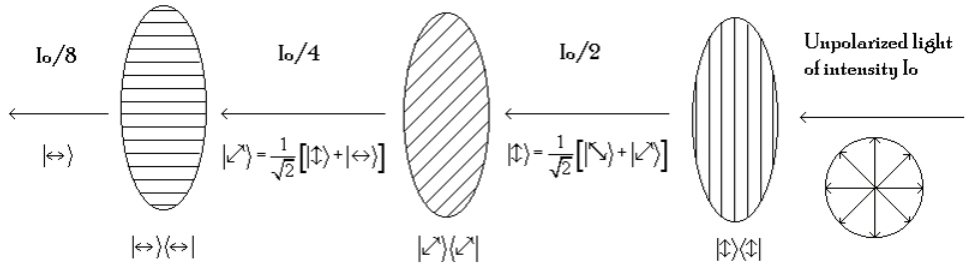
$$|\uparrow\rangle_s \xrightarrow{Bs_1} \frac{1}{\sqrt{2}}[|\uparrow\rangle_A + |\rightarrow\rangle_B]$$

https://chem.libretexts.org/@go/page/158515

Mach-Zehnder Interferometer



Quantum Mechanical Analysis of the Three Polarizer Paradox



Quantum Quotes

- If we want to describe what happens in an atomic event, we have to realize that the word “happens” can only apply to the observation, not to the state of affairs between two observations. [Werner Heisenberg]
- I think it is safe to say that no one understands quantum mechanics. Do not keep saying to yourself, if you can possibly avoid it, 'But how can it possibly be like that?' because you will go down the drain into a blind alley from which nobody has yet escaped. Nobody knows how it can be like that. [Richard Feynman]
- Any one who is not shocked by quantum mechanics has not fully understood it. [Niels Bohr]
- The mathematical predictions of quantum mechanics yield results that are in agreement with experimental findings. That is the reason we use quantum theory. That quantum theory fits experiment is what validates the theory, but why experiment should give such peculiar results is a mystery. This is the shock to which Bohr referred. [Marvin Chester with slight modifications by Frank Rioux]
- A philosopher once said, ‘It is necessary for the very existence of science that the same conditions always produce the same results.’ Well, they don’t! [Richard Feynman]
- After the first world war I gave a great deal of thought to the theory of quanta. It was then that I had a sudden inspiration. Einstein's wave-particle dualism for light was an absolutely general phenomenon extending to all physical nature. **De Broglie**
- He (de Broglie) has lifted one corner of the great veil. **Einstein**
- Everything in the future is a wave, everything in the past is a particle. **Lawrence Bragg**
- Something unknown is doing we don't know what. **Sir Arthur Eddington** commenting on the quantum mechanical view of the electron.

- Thirty-one years ago, Dick Feynman told me about his 'sum over histories' version of quantum mechanics. "The electron does anything it likes," he said. "It just goes in any direction at any speed, ...however it likes, and then you add up the amplitudes and it gives you the wave function." I said to him, "You're crazy." But he wasn't. **Freeman Dyson**
- I still believe in the possibility of a model of reality, that is to say, of a theory, which represents things themselves and not merely the probability of their occurrence. **Einstein**

This page titled 1.96: Quantum Potpourri - An Attempt to Demonstrate Two Fundamental Quantum Concepts- Wave-particle Duality and The Superposition Principle is shared under a CC BY 4.0 license and was authored, remixed, and/or curated by Frank Rioux via source content that was edited to the style and standards of the LibreTexts platform.

1.97: Quantum Dynamics- One Step at a Time

Integration of the time-dependent Schrödinger equation

$$i\hbar\frac{d|\Psi(t)\rangle}{dt} = H(\hat{p},\hat{x})|\Psi(t)\rangle$$

yields

$$|\Psi(t+\tau)\rangle = \exp\left(\frac{-iH(\hat{p},\hat{x})\tau}{\hbar}\right)|\Psi(t)\rangle = \exp\left(\frac{-iT(\hat{p})\tau}{\hbar}\right)\exp\left(\frac{-iV(\hat{x})\tau}{\hbar}\right)|\Psi(t)\rangle$$

The purpose of this tutorial is to show how this single time-step calculation is implemented. In the above equation, T ($\hat{p}$) and V ($\hat{x}$) are the kinetic and potential energy operators, and τ is the time increment. However, it is not immediately obvious how the exponential time-evolution operator operates on the wave function. For example, in the coordinate representation $\hat{x}$ is a multiplicative operator, but $\hat{p}$ is a differential operator (see any introductory quantum or physical chemistry textbook).

The tactic that will be employed is to carry out the potential energy operation in coordinate space where the position operator is multiplicative and Fourier transform the result to momentum space where the momentum operator is multiplicative. After operation by the kinetic energy operator the result is Fourier transformed back to coordinate space and displayed.

This procedure requires the following mathematical tools.

The coordinate-space eigenvalue equation and completeness relation:

$$\hat{x}|x\rangle = |x\rangle x \qquad \int |x\rangle\langle x|dx = 1$$

The momentum-space eigenvalue equation and completeness relation:

$$\hat{p}|p\rangle = |p\rangle p \qquad \int |p\rangle\langle p|dp = 1$$

The Fourier transforms between position and momentum:

$$\langle x|p\rangle = \langle p|x\rangle^* = \frac{1}{\sqrt{2\pi}}\exp\left(\frac{ipx}{\hbar}\right)$$

With these preliminaries out of the way the first step is to insert the coordinate completeness relation between the exponential potential energy operator and the wave function. In other words, we are going to work initially in coordinate space.

$$|\Psi(t+\tau)\rangle = \int \exp\left(\frac{-iT(\hat{p})\tau}{\hbar}\right)\exp\left(\frac{-iV(\hat{x})\tau}{\hbar}\right)|x|\langle x|\Psi(t)\rangle dx$$

The next step is to carry out a series expansion on the potential energy operator. To see what happens we will assume, for the sake of mathematical clarity, the potential energy operator is simply $\hat{x}$. Here we make use of the coordinate space eigenvalue equation to take the "hat" off the position operator.

$$\exp\left(-\frac{i\hat{x}\tau}{\hbar}\right)|x\rangle = \left(1-\frac{i\hat{x}\tau}{\hbar}-\frac{\hat{x}^2\tau^2}{2\hbar^2}+\cdots\right)|x\rangle = |x\rangle\left(1-\frac{ix\tau}{\hbar}-\frac{x^2\tau^2}{2\hbar^2}+\cdots\right) = |x\rangle\exp\left(-\frac{ix\tau}{\hbar}\right)$$

In general, for an operator operating in its "eigen space" we have,

$$\exp\left(-\frac{i\hat{\delta}\tau}{\hbar}\right)|o\rangle = |o\rangle\exp\left(-\frac{io\tau}{\hbar}\right)$$

The first two steps have brought us to this point.

$$|\Psi(t+\tau)\rangle = \int \exp\left(\frac{-iT(\hat{p})\tau}{\hbar}\right)|x\rangle\exp\left(\frac{-iV(x)\tau}{\hbar}\right)\langle x|\Psi(t)\rangle dx$$

Now we Fourier transform to momentum space by inserting the momentum completeness relation between the exponential kinetic energy operator and $|x\rangle$.

$$|\Psi(t+\tau)\rangle = \iint \exp\left(\frac{-iT(\hat{p})\tau}{\hbar}\right)|p\rangle\langle p|x\rangle \exp\left(\frac{-iV(x)\tau}{\hbar}\right)\langle x|\Psi(t)\rangle dxdp$$

The procedure used for the potential energy operator is repeated for kinetic energy using a series expansion and the momentum eigenvalue equation.

$$|\Psi(t+\tau)\rangle = \iint |p\rangle \exp\left(\frac{-iT(p)\tau}{\hbar}\right)\langle p|x\rangle \exp\left(\frac{-iV(x)\tau}{\hbar}\right)\langle x|\Psi(t)\rangle dxdp$$

This result is now projected back to the coordinate representation by employing a final Fourier transform.

$$\langle x'|\Psi(t+\tau)\rangle = \iint \langle x'|p\rangle \exp\left(\frac{-iT(p)\tau}{\hbar}\right)\langle p|x\rangle \exp\left(\frac{-iV(x)\tau}{\hbar}\right)\langle x|\Psi(t)\rangle dxdp$$

The last steps before actual calculation are to insert the mathematical expressions for the Fourier transforms (see above) and the kinetic and potential energy operators. In this exercise a harmonic oscillator potential will be used.

$$\langle x'|\Psi(t+\tau)\rangle$$
$$= \iint \frac{1}{\sqrt{2\pi}}\exp\left(\frac{ipx'}{\hbar}\right)\exp\left(\frac{-ip^2\tau}{2m\hbar}\right)\frac{1}{\sqrt{2\pi}}\exp\left(-\frac{ipx}{\hbar}\right)\exp\left(\frac{-ikx^2\tau}{2\hbar}\right)\langle x|\Psi(t)\rangle dxdp$$

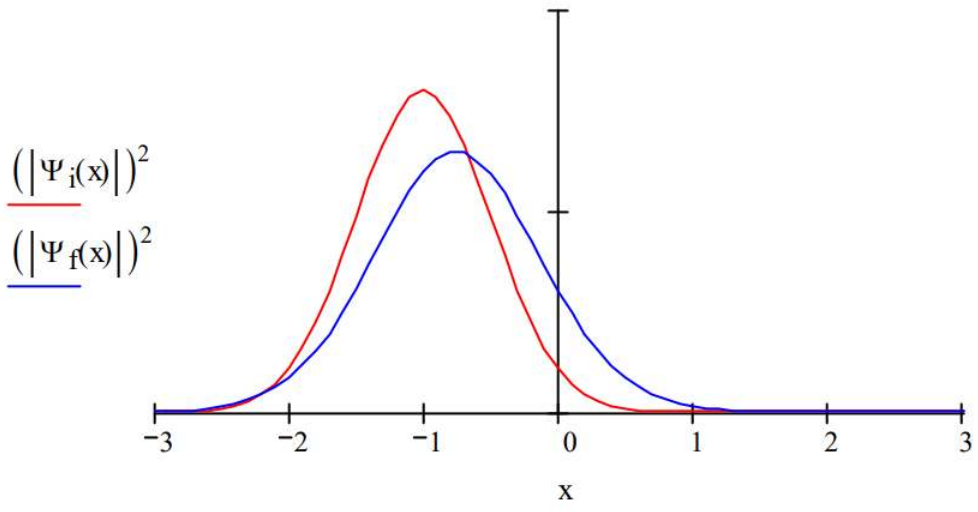
This algorithm advances the wave function in time from t to t+τ. It is only valid for one short time increment because the kinetic and potential energy operators do not commute (see reference 2, page 336 for further detail). For examples of accurate algorithms for the continued time-evolution of the wave function consult references 1 and 2.

The algorithm is now carried out in atomic units (h = 2π) in the Mathcad programming environment. In addition, mass and the force constant will be set to unity. The limits of integration are ± 4 atomic units for both position and momentum. A Gaussian initial wave function is assumed.

$$\Psi_i(x) := \left(\frac{2}{\pi}\right)^{\frac{1}{4}} \cdot \exp\left[-(x+1)^2\right]$$

$$\Psi_f(x') := \frac{1}{2\cdot\pi}$$
$$\cdot \int_{-4}^{4}\int_{-4}^{4} \exp(i\cdot p\cdot x')\cdot \exp\left(\frac{-i\cdot p^2\cdot\tau}{2}\right)\cdot\left[\exp(-i\cdot p\cdot x)\cdot\exp\left(\frac{-i\cdot x^2\cdot\tau}{2}\right)\cdot\Psi_i(x)\right] dxdp$$

$$\tau := 0.5 \qquad x := -3, -2.9 \ldots 3$$



The initial wave function centered at x = -1 moves to the right under the influence of the harmonic oscillator potential as expected.

References:

1. John J. Tanner, “A Computer-Based Approach to Teaching Quantum Dynamics,” *J. Chem. Educ.* **1990**, *67*, 917-921.
2. John C. Hansen; Donald J. Kouri; David K. Hoffman, “A Spreadsheet Template for Quantum Mechanical Wavepacket Propagation,” *J. Chem. Educ.* **1997**, *74*, 335-342.

This page titled 1.97: Quantum Dynamics- One Step at a Time is shared under a CC BY 4.0 license and was authored, remixed, and/or curated by Frank Rioux via source content that was edited to the style and standards of the LibreTexts platform.

1.98: Quantum Mechanical Pressure

Quantum mechanics is based on the concept of wave-particle duality, which for massive particles is expressed simply and succinctly by the de Broglie wave equation.

$$\lambda = \frac{h}{mv} = \frac{h}{p} \tag{1.98.1}$$

On the left side is the wave property, λ, and on the right the particle property, momentum. These incompatible concepts are united in a reciprocal relationship mediated by the ubiquitous Planck's constant. Using de Broglie's equation in the classical expression for kinetic energy, T converts it to its quantum mechanical equivalent.

$$T = \frac{p^2}{2m} = \frac{h^2}{2m\lambda^2} \tag{1.98.2}$$

Because objects with wave-like properties are subject to interference phenomena, quantum effects emerge when they are confined by some restricting potential energy function. For example, to avoid self-interference, a particle in an infinite one-dimensional square-well potential (PIB, particle in a box) of width a must form standing waves. The required restriction on the allowed wavelengths,

$$\lambda = \frac{2a}{n} \quad n = 1, 2, ... \tag{1.98.3}$$

quantizes the kinetic energy.

$$T(n) = \frac{n^2h^2}{8ma^2} \tag{1.98.4}$$

In addition to providing a simple explanation for the origin of energy quantization, the PIB model shows that reducing the size of the box **increases** the kinetic energy dramatically. This "repulsive" character of quantum mechanical kinetic energy is the ultimate basis for the stability of matter. It also provides, as we see now, a quantum interpretation for gas pressure. To show this we will consider a particle in the ground state of a three-dimensional box ($n_x = n_y = n_z = 1$) of width a and volume a^3. Its kinetic energy is,

$$T = \frac{3h^2}{8ma^2} = \frac{3h^2}{8mV^{2/3}} = \frac{A}{V^{2/3}} \tag{1.98.5}$$

According to thermodynamics, pressure is the negative of the derivative of energy with respect to volume.

$$P = -\frac{dT}{dV} = -\frac{2}{3}\frac{A}{V^{5/3}} \tag{1.98.6}$$

Using Equation 1.98.5 to eliminate A from Equation 1.98.6 yields,

$$P = \frac{2}{3}\frac{T}{V} \tag{1.98.7}$$

This result has the same form as that obtained by the kinetic theory of gases for an individual gas molecule.

Contributors and Attributions

- Prof. Emeritus Frank Rioux (St. John's University and College of St. Benedict)

This page titled 1.98: Quantum Mechanical Pressure is shared under a CC BY 4.0 license and was authored, remixed, and/or curated by Frank Rioux via source content that was edited to the style and standards of the LibreTexts platform.

1.99: Visualizing the Difference Between a Superposition and a Mixture

The superposition principle, as Feynman said, is at the heart of quantum mechanics. While its mathematical expression is simple, its true meaning is difficult to grasp. For example, given a linear superposition (not normalized) of two states,

$$|\Psi\rangle = |\phi_1\rangle + |\phi_2\rangle$$

one might assume that it represents a mixture of ϕ_1 and ϕ_2. In other words, half of the quons [1] are in state ϕ_1 and half in ϕ_2. However, the correct quantum mechanical interpretation of this equation is that the system represented by Ψ is simultaneously in the states ϕ_1 and ϕ_2, properly weighted.

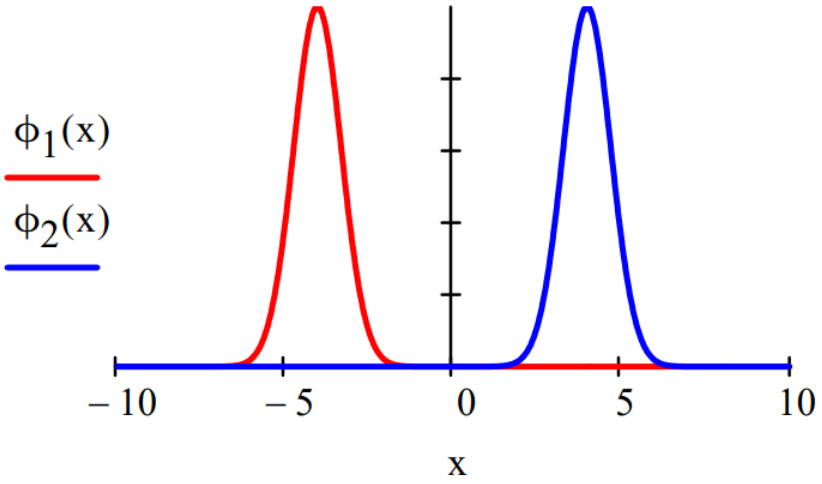
A mixture, half ϕ_1 and half ϕ_2, or any other ratio, cannot be represented by a wavefunction. It requires a density operator, which is a more general quantum mechanical construct that can be used to represent both pure states (superpositions) and mixtures, as shown below.

$$\hat{\rho}_{\max} = |\Psi\rangle\langle\Psi| \qquad \hat{\rho}_{\min d} = \sum p_i |\Psi_i\rangle\langle\Psi_i|$$

In the equation on the right, p_i is the fraction of the mixture in the state Ψ_i.

To illustrate how these equations distinguish between a mixture and a superposition, we will consider a superposition and a mixture of equally weighted gaussian functions representing one-dimensional wave packets. The normalization constants are omitted in the interest of mathematical clarity. The gaussians are centered at x = $\pm$ 4.

$$\phi_1(x) := \exp\left[-(x+4)^2\right] \qquad \phi_2(x) := \exp\left[-(x-4)^2\right]$$



To visualize how the density operator discriminates between a superposition and a mixture, we calculate its matrix elements in coordinate space for the 50-50 superposition and mixture of ϕ_1 and ϕ_2. The superposition is considered first.

$$\Psi(x) := \phi_1(x) + \phi_2(x)$$

The matrix elements of this pure state are calculated as follows.

$$\rho_{\text{pure}} = \langle x|\hat{\rho}_{\text{pure}}|x'\rangle = \langle x|\Psi\rangle\,\langle\Psi|x'\rangle$$

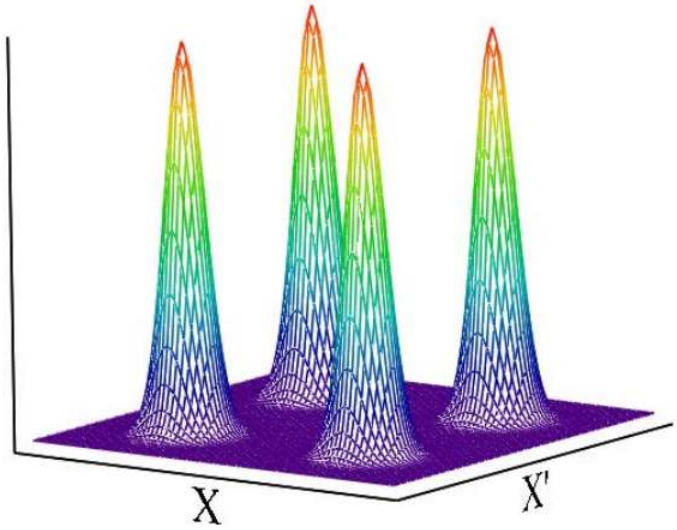
Looking at the right side we see that the matrix elements are the product of the probability amplitudes of a quon in state Ψ being at x and x′. Next we display the density matrix graphically.

$$\text{DensityMatrixPure}\,(x, x') := \Psi(x)\cdot\Psi\,(x')$$

$$x_0 = 8 \qquad N := 80 \qquad i := 0 \ldots N$$

$$x_i := -x_0 + \frac{2\cdot x_0 \cdot i}{N} \qquad j := 0 \ldots N \qquad x'_j := -x_0 + \frac{2\cdot x_0 \cdot j}{N}$$

$$\text{DensityMatrixPure}_{i,j} := \text{DensityMatrixPure}\,(x, x')$$



DensityMatrixPure

The presence of off-diagonal elements in this density matrix is the signature of a quantum mechanical superposition. For example, from the quantum mechanical perspective bi-location is possible.

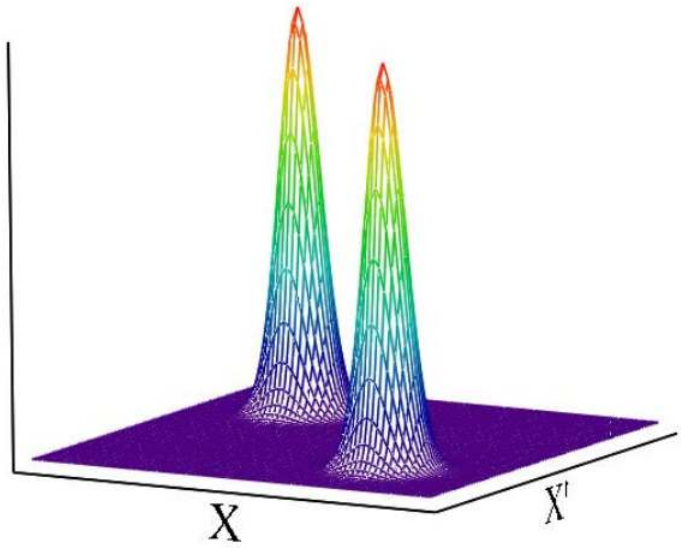
Now we turn our attention to the density matrix of a mixture of gaussian states.

$$\rho_{\text{mix}} = \langle x \left| \hat{\rho}_{\text{mix}} \right| x' \rangle = \sum_i p_i \langle x|\phi_i\rangle \langle \phi_i|x'\rangle = \frac{1}{2} \langle x|\phi_1\rangle \langle \phi_1|x'\rangle + \frac{1}{2} \langle x|\phi_2\rangle \langle \phi_2|x'\rangle$$

$$\text{DensityMatrixMix}(\text{x}, \text{x}') := \frac{\phi_1(\text{x}) \cdot \phi_1(\text{x}') + \phi_2(\text{x}) \cdot \phi_2\left(\text{x}''\right)}{2}$$

$$\text{DensityMatrixMix}_{i,j} := \text{DensityMatrixMix}\,(x, x')$$

https://chem.libretexts.org/@go/page/158605



DensityMatrixMix

The obvious difference between a superposition and a mixture is the absence of off-diagonal elements, $\phi_1(x) \cdot \phi_2(x') + \phi_2(x) \cdot \phi_1(x')$, in the mixed state. This indicates the mixture is in a definite but unknown state; it is an example of classical ignorance.

An equivalent way to describe the difference between a superposition and a mixture, is to say that to calculate the probability of measurement outcomes for a superpostion you add the probability amplitudes and square the sum. For a mixture you square the individual probability amplitudes and sum the squares.

1. Nick Herbert (*Quantum Reality*, page 64) suggested "quon" be used to stand for a generic quantum object. "A quon is any entity, no matter how immense, that exhibits both wave and particle aspects in the peculiar quantum manner.

This page titled 1.99: Visualizing the Difference Between a Superposition and a Mixture is shared under a CC BY 4.0 license and was authored, remixed, and/or curated by Frank Rioux via source content that was edited to the style and standards of the LibreTexts platform.

CHAPTER OVERVIEW

2: Atomic Structure

2.1: The de Broglie-Bohr Model for the Hydrogen Atom
2.2: The de Broglie-Bohr Model for the Hydrogen Atom - Version 3
2.3: The de Broglie-Bohr Model for the Hydrogen Atom - Version 3
2.4: A de Broglie-Bohr Model for Positronium
2.5: The de Broglie-Bohr Model for the Hydrogen Atom - Version 4
2.6: The de Broglie-Bohr Model for a Hydrogen Atom Held Together by a Gravitational Interaction
2.7: The de Broglie-Bohr Model for Positronium
2.8: The Bohr Model for the Earth-Sun System
2.9: Extracting Atomic and Molecular Parameters from the deBroglie-Bohn Model for the Atom
2.10: Electronic Structure and the Superposition Principle
2.11: Atomic Spectroscopy and the Correspondence Principle
2.12: Hydrogen-Like Calculations with Variable Lepton Mass
2.13: Atomic Stability
2.14: Quantum Mechanical Calculations for the One-Dimensional Hydrogen Atom
2.15: Quantum Mechanical Calculations for the Hydrogen Atom
2.16: Atomic Stability
2.17: Atomic Stability - Mathcad Version
2.18: 110. Critique of the Centrifugal Effect in the Hydrogen Atom
2.19: A Shorter Critique of the Centrifugal Effect in the Hydrogen Atom
2.20: Exploring the Role of Lepton Mass in the Hydrogen Atom
2.21: The Effect of Lepton Mass on the Energy and Bond Length of the Hydrogen Molecule Ion
2.22: The Hydrogen Atom with Finite Sized Nucleus
2.23: The Hyperfine Interaction in the Hydrogen Atom
2.24: Positronium Annihilation
2.25: Positronium Annihilation- Another View
2.26: Positronium Annihilation- Yet Another View
2.27: The Hyperfine Interaction in the Deutrium Atom
2.28: A Tensor Algebra Approach to Spin-Orbit Coupling
2.29: A Bohr Model for Multi-electron Atoms and Ions
2.30: Atomic Variational Calculations- Hydrogen to Boron
2.31: Some Calculations on the Lithium Atom Ground State
2.32: E. B. Wilson's Calculation on the Lithium Atom Ground State
2.33: The Importance of the Pauli Principle
2.34: Splitting the 2s-2p Degeneracy in the Lithium Atom
2.35: Addition of Spin Angular Momentum- A Tensor Algebra Approach
2.36: Hund's Rule
2.37: Hund's Rule - Singlet-Triplet Calculations with Mathcad
2.38: Electron Correlation in Two-electron Systems
2.39: First Trial Wave Function
2.40: Second Trial Wavefunction

2.41: Third Trial Wavefunction
2.42: 129.4 Fourth Trial Wavefunction
2.43: Fifth Trial Wavefunction and Summary
2.44: The Crucial Role of Kinetic Energy in Interpreting Ionization Energies
2.45: Quantum Dots Are Artificial Atoms
2.46: Calculating the Atomic Radius of Polonium
2.47: Calculating the Atomic Radius of Gold
2.48: How Many Bibles Can Fit on the Head of a Pin
2.49: Momentum Wavefunctions and Distributions for the Hydrogen Atom
2.50: The SCF Method for Two Electrons
2.51: Outline of the SCF Method for Two Electrons
2.52: The SCF Method for Two Electrons Using a Gaussian Wave Function
2.53: An Interactive SCF Calculation for the Helium Atom
2.54: Quantum Calculations on the Hydrogen Atom in Coordinate, Momentum and Phase Space
2.55: The Wigner Distribution for the 1s State of the 1D Hydrogen Atom
2.56: The Wigner Distribution for the 2s State of the 1D Hydrogen Atom
2.57: The Wigner Distribution for the 2p State of the 1D Hydrogen Atom
2.58: The Wigner Distribution for the 3s State of the 1D Hydrogen Atom
2.59: The Wigner Distribution for the 3p State of the 1D Hydrogen Atom
2.60: The Wigner Distribution for the 4s State of the 1D Hydrogen Atom
2.61: One-dimensional H-atom with Delta Function Potential
2.62: The Atomic Structure Factor in Coordinate and Momentum Space

---

This page titled 2: Atomic Structure is shared under a CC BY 4.0 license and was authored, remixed, and/or curated by Frank Rioux via source content that was edited to the style and standards of the LibreTexts platform.

2.1: The de Broglie-Bohr Model for the Hydrogen Atom

$\lambda = \frac{h}{mv}$ de Broglie's hypothesis that matter has wave-like properties.

$n\lambda = 2\pi r$ The consequence of de Broglie's hypothesis; an integral number of wavelengths must fit within the circumference of the orbit. This introduces the quantum number which can have values 1, 2, 3...

$mv = \frac{nh}{2\pi r}$ Substitution of the first equation into the second equation reveals that linear momentum is quantized.

$T = \frac{1}{2}mv^2 = \frac{n^2h^2}{8\pi^2 m_e r^2}$ If momentum is quantized, so it kinetic energy.

$E = T + V = \frac{n^2h^2}{8\pi^2 m_e r^2} - \frac{e^2}{4\pi\varepsilon_0 r}$ Which means that total energy is quantized.

Below the ground state energy and orbit radius of the electron in the hydrogen atom is found by plotting the energy as a function of the orbital radius. The ground state is the minimum in the curve.

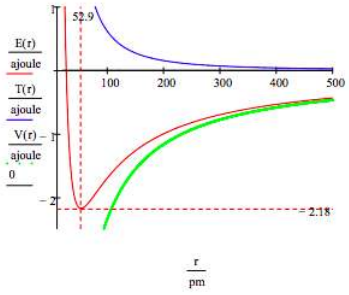
Fundamental constants: electron charge, electron mass, Planck's constant, vacuum permitivity.

$$e = 1.6021777(10)^{-19}\text{coul} \qquad m_e = 9.10939(10)^{-31}\text{kg}$$
$$h = 6.62608(10)^{-34}\text{joule sec} \qquad \varepsilon_0 = 8.85419(10)^{-12}\frac{\text{coul}^2}{\text{joule m}}$$

Quantum number and conversion factor between meters and picometers and joules and atto joules.

$$n = 1 \quad pm = 10^{-12}m \quad \text{ajoule} = 10^{-18}\text{joule}$$

$$r = 20pm,\ 20.5pm..500pm \quad T(r) = \frac{n^2h^2}{8\pi^2 m_e r^2} \quad V(r) = -\frac{e^2}{4\pi\varepsilon_0 r} \quad E(r) = T(r) + V(r)$$



This figure shows that atomic stability involves a balance between potential and kinetic energy. The electron is drawn toward the nucleus by the attractive potential energy interaction (~ -1/R), but is prevented from spiraling into the nucleus by the extremely large kinetic energy (~1/R2) associated with small orbits.

Prepared by Frank Rioux.

This page titled 2.1: The de Broglie-Bohr Model for the Hydrogen Atom is shared under a CC BY 4.0 license and was authored, remixed, and/or curated by Frank Rioux via source content that was edited to the style and standards of the LibreTexts platform.

2.2: The de Broglie-Bohr Model for the Hydrogen Atom - Version 3

$\lambda = \frac{h}{mv}$ de Broglie's hypothesis that matter has wave-like properties.

$n\lambda = 2\pi r$ The consequence of de Broglie's hypothesis; an integral number of wavelengths must fit within the circumference of the orbit. This introduces the quantum number, n, which can have values 1, 2, 3...

$mv = \frac{nh}{2\pi r}$ Substitution of the first equation into the second equation reveals that linear momentum is quantized.

$T = \frac{1}{2}mv^2 = \frac{n^2h^2}{8\pi^2 m_e r}$ If momentum is quantized, so is kinetic energy.

$E = T + V = \frac{n^2h^2}{8\pi^2 m_e r^2} - \frac{q^2}{4\pi\varepsilon_0 r}$ Which means that total energy is quantized.

Below the ground state energy and orbit radius of the electron in the hydrogen atom is found by plotting the energy as a function of the orbital radius. The ground state is the minimum in the curve.

Fundamental constants: electron charge, electron mass, Planck's constant, vacuum permitivity.

$$q = 1.6021777(10)^{-19}\text{coul} \qquad m_e = 9.10939(10)^{-31}\text{kg}$$
$$h = 6.62608(10)^{-34}\text{joule sec} \qquad \varepsilon_0 = 8.85419(10)^{-12}\frac{\text{coul}^2}{\text{joule m}}$$

Conversion factors between meters and picometers and joules and atto joules.

$$pm = 10^{-12}m \quad \text{ajoule} = 10^{-18}\text{joule} \quad eV = 1.602177(10)^{-19}\text{joule}$$

Setting the first derivative of the energy with respect to r equal to zero, yields the optimum value of r.

$$\frac{d}{dr}\left(\frac{n^2h^2}{8\pi^2 m_e r^2} - \frac{q^2}{4\pi\varepsilon_0 r}\right) = 0 \quad \text{has solution(s)} \quad n^2h^2\frac{\varepsilon_0}{q^2\pi m_e}$$

Substitution of this value of r back into the energy expression yields the energy gives the energy of the hydrogen atom in terms of the quantum number, n, and the fundamental constants.

$$E = \frac{n^2h^2}{8\pi^2 m_e r^2} - \frac{q^2}{4\pi\varepsilon_0 r} \quad \text{by substitution, yields} \quad E = \frac{-1}{8n^2h^2}\frac{m_e}{\varepsilon_0^2}q^4$$

Calculate the allowed energy levels for the hydrogen atom: n = 1 .. 5

$$E_n = \frac{-1}{8n^2h^2}\frac{m_e}{\varepsilon_0^2}q^4 \qquad \frac{E_n}{\text{ajoule}} = \begin{pmatrix} -2.18 \\ -0.545 \\ -0.242 \\ -0.136 \\ -0.087 \end{pmatrix} \qquad \frac{E_n}{eV} = \begin{pmatrix} -13.606 \\ -3.401 \\ -1.512 \\ -0.85 \\ -0.544 \end{pmatrix}$$

Prepared by Frank Rioux.

This page titled 2.2: The de Broglie-Bohr Model for the Hydrogen Atom - Version 3 is shared under a CC BY 4.0 license and was authored, remixed, and/or curated by Frank Rioux via source content that was edited to the style and standards of the LibreTexts platform.

2.3: The de Broglie-Bohr Model for the Hydrogen Atom - Version 3

The 1913 Bohr model of the hydrogen atom was replaced by Schrödinger's wave mechanical model in 1926. However, Bohr's model is still profitably taught today because of its conceptual and mathematical simplicity, and because it introduced a number of key quantum mechanical ideas such as the quantum number, quantization of observable properties, quantum jump and stationary state.

Bohr calculated the manifold of allowed electron energies by balancing the mechanical forces (centripetal and electron-nucleus) on an electron executing a circular orbit of radius R about the nucleus, and then arbitarily quantizing its angular momentum. Finally by fiat he declared that the electron was in a non-radiating stationary state because an orbiting (accelerating) charge radiates energy and will collapse into the oppositely charge nucleus.

In 1924 de Broglie postulated wave-particle duality for the electron and thereby provided the opportunity to take some of the arbitariness out of Bohr's model. An electron possessing wave properties is subject to constructive and destructive interference. As will be shown this leads naturally to quantization of electron momentum and kinetic energy, and consequently a manifold of allowed energy states for the electron relative to the nucleus.

The de Broglie-Bohr model of the hydrogen atom presented here treats the electron as a particle on a ring with wave-like properties. The electron's kinetic (confinement) energy is calculated using its momentum eigenfunction in the coordinate representation. This equation is obtained by substituting the de Broglie wave-particle equation (λ = h/p) into Euler's equation, the most general one-dimensional wavefunction.

$$\langle x|\lambda\rangle = \frac{1}{\sqrt{2\pi}}\exp\left(\frac{i2\pi x}{\lambda}\right) \quad \text{plus} \quad \lambda = \frac{h}{p} \quad \text{yields} \quad \langle x|p\rangle = \frac{1}{\sqrt{2\pi}}\exp$$

In order to avoid destructive interference, the electron's momentum wavefunction must be single-valued, which in this application requires a circular boundary condition: the wavefunction must match at points separated by one circumference, 2 πr. The mathematical consequence of satisfying this requirement leads to quantized momentum and the emergence of a quantum number, n.

$$\langle x + 2\pi r|p\rangle = \langle x|p\rangle$$

$$\exp\left(\frac{ip(x+2\pi r)}{\hbar}\right) = \exp\left(\frac{ipx}{\hbar}\right) \qquad \exp\left(\frac{ipx}{\hbar}\right)\exp\left(\frac{i2\pi pr}{\hbar}\right) = \exp\left(\frac{ipx}{\hbar}\right)$$

$$\exp\left(\frac{i2\pi pr}{\hbar}\right) = 1$$

The last equation succinctly states the boundary condition requirements and is satisfied when,

$$\frac{pr}{\hbar} = \frac{mvr}{\hbar} = n \quad \text{where} \quad n = 0, \ \pm 1, \ \pm 2...$$

This restriction quantizes the angular momentum and allows the conversion of classical kinetic energy into its quantum mechanical form. In this model, the +/- values suggest clockwise and counter-clockwise angular momentum.

$$T_n = \frac{p^2}{2m} = \frac{n^2\hbar^2}{2mr^2} \quad \text{where} \quad n = 0, \ \pm 1, \ \pm 2...$$

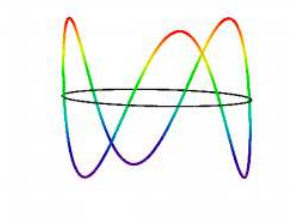
The wavefunctions associated with these quantized kinetic energies are obtained by using the quantum condition of equation 3 to eliminate momentum in equation 1, recognizing that in radians θ = x/R. (x is the linear distance on the ring from some reference point.)

$$\Psi_n(\theta) = \langle\theta|n\rangle = \frac{1}{\sqrt{2\pi}}\exp(in\theta)$$

The allowed electron wavefunctions are displayed graphically as follows.

$$\text{Quantum number:} \qquad n = 3$$

$$\text{numpts} = 200 \qquad i = 0...\text{numpts} \quad j = 0...\text{numpts} \quad \theta_i = \frac{2\pi i}{\text{numpts}}$$



(x, y, z) , (x, y, zz)

The quantum mechanical interpretation of these "Bohr orbits" is that they are stationary states. In spite of the fact that we use the expression kinetic energy, which implies electron motion, there is no motion. The electron occupies the orbit as a particle-wave, it is not orbiting the nucleus. If it was orbiting in a classical sense it would radiate energy and quickly collapse into the nucleus. Clearly the stability of matter requires the quantum mechanical version of kinetic energy.

We now place a proton at the center of the ring and calculate the potential energy using Coulombs law.

$$V = -\frac{e^2}{4\pi\varepsilon_0 r}$$

Adding the kinetic and potential energy terms yields the total energy. However, the n = 0 state is discarded because it has zero kinetic energy and therefore does not represent a stable atomic state.

$$E = T + V = \frac{n^2 h^2}{*\pi^2 m_e r^2} - \frac{e^2}{4\pi\varepsilon_0 r}$$

The ground state energy and orbit radius of the electron in the hydrogen atom is found by plotting the energy as a function of the orbital radius. The ground state is the minimum in the total energy curve. Naturally calculus can be used to obtain the same information by minimizing the energy with respect to the orbit radius. However, the graphical method has the virtue of illuminating the issue of atomic stability.

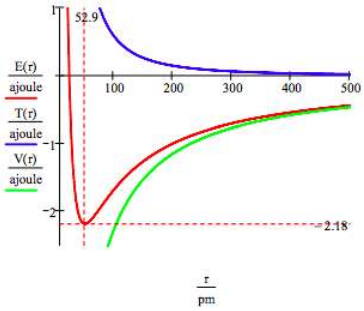
Fundamental constants: electron charge, electron mass, Planck's constant, vacuum permitivity.

$$e = 1.6021777(10)^{-19}\text{coul} \qquad m_e = 9.10939(10)^{-31}\text{kg}$$
$$h = 6.62608(10)^{-34}\text{joule sec} \qquad \varepsilon_0 = 8.85419(10)^{-12}\frac{\text{coul}^2}{\text{joule m}}$$

Quantum number and conversion factor between meters and picometers and joules and attojoules.

$$n = 1 \quad pm = (10)^{-12}m \quad \text{ajoule} = 10^{-18}\text{joule}$$

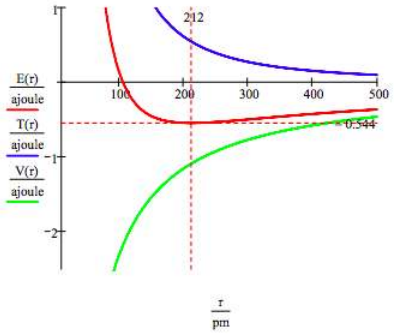
$$r = 20pm,\ 20.5pm..500pm \quad T(r) = \frac{n^2h^2}{8\pi^2 m_e r^2} \quad V(r) = -\frac{e^2}{4\pi\varepsilon_0 r} \quad E(r) = T(r) + V(r)$$



This figure shows that atomic stability involves a balance between potential and kinetic energy. The electron is drawn toward the nucleus by the attractive potential energy interaction (~ -1/R), but is prevented from collapsing into the nucleus by the extremely large kinetic energy (~1/R 2) associated with small orbits.

As shown below, the graphical approach can also be used to find the electronic excited states.

$$n = 2 \quad T(r) = \frac{n^2 h^2}{8\pi^2 m_e r^2} \quad V(r) = -\frac{e^2}{4\pi\varepsilon_0 r} \quad E(r) = T(r) + V(r)$$



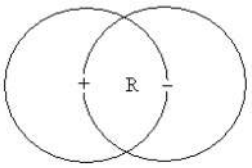
However, it is much easier to generate the manifold of allowed electron energies by minimizing the energy with respect to the orbit radius. This procedure yields,

$$E_n = -\frac{m_e e^4}{2(4\pi\varepsilon_0)^2 \hbar^2}\frac{1}{n} \quad \text{and} \quad r_n = \frac{4\pi\varepsilon_0 \hbar^2}{m_e e^2} n^2$$

This page titled 2.3: The de Broglie-Bohr Model for the Hydrogen Atom - Version 3 is shared under a CC BY 4.0 license and was authored, remixed, and/or curated by Frank Rioux via source content that was edited to the style and standards of the LibreTexts platform.

2.4: A de Broglie-Bohr Model for Positronium

Positronium is a metastable bound state consisting of an electron and its positron antiparticle. In other words it might be thought of as a hydrogen atom in which the proton is replaced by a positron. Naturally it decays quickly after formation due to electron-positron annihilation. However, it exists long enough for its ground state energy, \(-0.25 E_h\), to be determined. The purpose of this tutorial is to calculate this value using the Bohr model for positronium shown below.



The electron occupies a circular orbit of radius R which has a positron at its center. Likewise the positron occupies a circular orbit of radius R which has an electron at its center. Occupies has been emphasized to stress that there is no motion, no orbiting. Both particles are behaving as waves (this is the meaning of wave-particle duality) occupying the orbit. As waves they are subject to interference, and to avoid destructive interference the wavelength for the ground state is one orbit circumference.

$$\lambda = 2\pi R$$

Introducing the de Broglie relationship between wavelength and momentum,

$$\lambda = \frac{h}{p}$$

yields the following expression for momentum in atomic units (h = 2).

In atomic units $m_e = m_p = 1$. Therefore, the kinetic energy of each particle is,

$$T = \frac{p^2}{2m} = \frac{1}{2R^2}$$

The total energy of positronium is the sum of electron and positron kinetic energies and their Coulombic potential energy.

$$R = T + V \tag{2.4.1}$$

$$= \frac{1}{2R^2} + \frac{1}{2R^2} + \frac{1}{R} = \frac{1}{R^2} - \frac{1}{R} \tag{2.4.2}$$

Energy minimization with respect to the electron-positron distance R yields the following result.

$$\frac{d}{dR}\left(\frac{1}{R^2} - \frac{1}{R}\right) = 0$$

solve $R \to 2$.The optimum R value yields a ground state energy of $-0.25E_h$, in agreement with experiment.substitute $R = 2$

Including the symbols for mass in the kinetic energy contributions facilitates the introduction of the concept of effective mass of the composite system.

Contributors and Attributions

- Prof. Emeritus Frank Rioux (St. John's University and College of St. Benedict)

This page titled 2.4: A de Broglie-Bohr Model for Positronium is shared under a CC BY 4.0 license and was authored, remixed, and/or curated by Frank Rioux via source content that was edited to the style and standards of the LibreTexts platform.

2.5: The de Broglie-Bohr Model for the Hydrogen Atom - Version 4

The 1913 Bohr model of the hydrogen atom was replaced by Schrödinger′s wave mechanical model in 1926. However, Bohr′s model is still profitably taught today because of its conceptual and mathematical simplicity, and because it introduced a number of key quantum mechanical ideas such as the quantum number, quantization of observable properties, quantum jump and stationary state.

Bohr calculated the manifold of allowed electron energies by balancing the mechanical forces (centripetal and electron-nucleus) on an electron executing a circular orbit of radius R about the nucleus, and then arbitarily quantizing its angular momentum. Finally by fiat he declared that the electron was in a non-radiating stationary state because an orbiting (accelerating) charge radiates energy and will collapse into the oppositely charge nucleus.

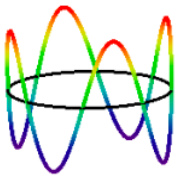
In 1924 de Broglie postulated wave-particle duality for the electron and other massive particles, thereby providing the opportunity to remove some of the arbitariness from Bohr′s model. For example, an electron possessing wave properties is subject to constructive and destructive interference. As will be shown this leads naturally to quantization of electron momentum and kinetic energy, and consequently a manifold of allowed energy states for the electron relative to the nucleus. The de Broglie-Bohr model of the hydrogen atom presented here treats the electron as a particle on a ring with wave-like properties.

$$\lambda = \frac{h}{m_e v}$$

de Broglie's hypothesis that matter has wave-like properties.

$$n\lambda = 2\pi r$$

The consequence of de Broglie′s hypothesis; an integral number of wavelengths must fit within the circumference of the orbit. This introduces the quantum number which can have values 1,2,3,... The n = 4 electron state is shown below.



$$m_e v = \frac{nh}{2\pi r}$$

Substitution of the first equation into the second equation reveals that momentum is quantized.

$$T = \frac{1}{2} m_e v^2 = \frac{n^2 h^2}{8\pi^2 m_e r^2}$$

If momentum is quantized, so is kinetic energy.

$$E = T + V = \frac{n^2 h^2}{8\pi^2 m_e r^2} - \frac{e^2}{4\pi\varepsilon_0 r}$$

Which means that total energy is quantized. The second term is the electron-proton electrostatic potential energy.

The quantum mechanical interpretation of these ″Bohr orbits″ is that they are stationary states. In spite of the fact that we use the expression kinetic energy, which implies electron motion, there is no motion. The electron occupies the orbit as a particle-wave, it is not orbiting the nucleus. If it was orbiting in a classical sense it would radiate energy and quickly collapse into the nucleus. Clearly the stability of matter requires the quantum mechanical version of kinetic energy.

The ground state energy and orbit radius of the electron in the hydrogen atom is found by plotting the energy as a function of the orbital radius. The ground state is the minimum in the total energy curve. Naturally calculus can be used to obtain the same information by minimizing the energy with respect to the orbit radius. However, the graphical method has the virtue of illuminating the issue of atomic stability.

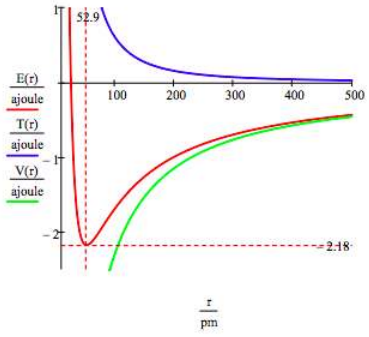
Fundamental constants: electron charge, electron mass, Planck's constant, vacuum permitivity.

$$e = 1.6021777(10)^{-19}\text{coul} \qquad m_e = 9.10939(10)^{-31}\text{kg}$$
$$h = 6.62608(10)^{-34}\text{joule sec} \quad \varepsilon_0 = 8.85419(10)^{-12}\frac{\text{coul}^2}{\text{joule m}}$$

Quantum number and conversion fact between meters and picometers and joules and attojoules.

$$n = 1 \quad pm = 10^{-12}m \quad \text{ajoule} = 10^{-18}\text{joule}$$

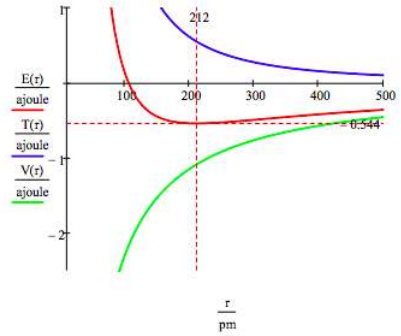
$$r = 20pm,\ 20.5pm,\ 500pm \quad T(r) = \frac{n^2h^2}{8\pi^2 m_e r^2} \quad V(r) = -\frac{e^2}{4\pi\varepsilon_0 r} \quad E(r) = T(r) + V(r)$$



This figure shows that atomic stability involves a balance between potential and kinetic energy. The electron is drawn toward the nucleus by the attractive potential energy interaction (~ -1/R), but is prevented from collapsing into the nucleus by the extremely large kinetic energy (~1/R2) associated with small orbits.

As shown below, the graphical approach can also be used to find the electronic excited states.

$$n = 2 \quad T(r) = \frac{n^2h^2}{8\pi^2 m_e r^2} \quad V(r) = -\frac{e^2}{4\pi\varepsilon_0 r} \quad E(r) = T(r) + V(r)$$

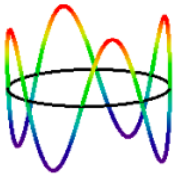


As mentioned earlier the manifold of allowed electron energies can also be obtained by minimizing the energy with respect to the orbit radius. This procedure yields,

$$E_n = -\frac{m_e e^4}{2(4\pi\varepsilon_0)^2\hbar^2}\frac{1}{n^2} \quad \text{and} \quad r_n = \frac{4\pi\varepsilon_0\hbar^2}{m_e e^2}n^2$$

This page titled 2.5: The de Broglie-Bohr Model for the Hydrogen Atom - Version 4 is shared under a CC BY 4.0 license and was authored, remixed, and/or curated by Frank Rioux via source content that was edited to the style and standards of the LibreTexts platform.

2.6: The de Broglie-Bohr Model for a Hydrogen Atom Held Together by a Gravitational Interaction



$$\lambda = \frac{h}{mv}$$

de Broglie's hypothesis that matter has wave-like properties.

$$n\lambda = 2\pi r$$

The consequence of de Broglie's hypothesis; an integral number of wavelengths must fit within the circumference of the orbit. This introduces the quantum number, n, which can have values 1,2,3,...

$$mv = \frac{nh}{2\pi r}$$

Substitution of the first equation into the second equation reveals that linear momentum is quantized.

$$T = \frac{1}{2}mv^2 = \frac{n^2h^2}{8\pi^2 m_e r^2}$$

If momentum is quantized, so is kinetic energy.

$$E = T + V = \frac{n^2h^2}{8\pi^2 m_e r^2} - \frac{Gm_p m_e}{r}$$

Which means that total energy is quantized, where $-\frac{Gm_p m_e}{r}$ is the gravitational potential energy interaction between a proton and an electron.

$$\frac{d}{dr}\left(\frac{n^2h^2}{8\pi^2 m_e r^2} - \frac{Gm_p m_e}{r}\right) = 0 \text{ solve, r} \rightarrow \frac{h^2n^2}{4\pi^2 G m_e^2 m_p}$$

Minimization of the energy with respect to orbit radius yields the optimum values of r. This expression is subtituted back in the energy expression below to find the allowed energies.

$$E = \frac{n^2h^2}{8\pi^2 m_e r^2} - \frac{Gm_p m_e}{r} \text{substitute, r} = \frac{h^2n^2}{4\pi^2 G m_e^2 m_p} \rightarrow E = \frac{2\pi^2 G^2 m_e^3 m_p^2}{h^2n^2}$$

$$\text{Fundamental constants:} \quad m_p = 1.67262(10)^{-27}\text{kg} \quad m_e = 9.10939(10)^{-31}\text{kg}$$
$$h = 6.62608(10)^{-34}\text{joule sec} \quad G = 6.67259(10)^{-11}\frac{m^3}{\text{kg s}^2}$$

Energy:

$$E(n) = -\frac{2\pi^2 G^2 m_e^3 m_p^2}{h^2n^2}$$

Orbit radius:

$$r(n) = \frac{h^2n^2}{4\pi^2 G m_e^2 m_p^2}$$

Calculate the first four energy levels and orbit radii.

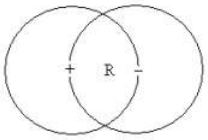
$$n = 1..4 \quad \frac{E(n)}{J} = \begin{pmatrix} -4.233 \times 10^{-97} \\ -1.058 \times 10^{-97} \\ -4.704 \times 10^{-98} \\ -2.646 \times 10^{-98} \end{pmatrix} \quad \frac{r(n)}{m} = \begin{pmatrix} 1.201 \times 10^{29} \\ 4.803 \times 10^{29} \\ 1.081 \times 10^{30} \\ 1.921 \times 10^{30} \end{pmatrix}$$

Prepared by Frank Rioux.

This page titled 2.6: The de Broglie-Bohr Model for a Hydrogen Atom Held Together by a Gravitational Interaction is shared under a CC BY 4.0 license and was authored, remixed, and/or curated by Frank Rioux via source content that was edited to the style and standards of the LibreTexts platform.

2.7: The de Broglie-Bohr Model for Positronium

Positronium is a metastable bound state consisting of an electron and its positron antiparticle. In other words it might be thought of as a hydrogen atom in which the proton is replaced by a positron. Naturally it decays quickly after formation due to electron-positron annihilation. However, it exists long enough for its ground state energy, -0.25 E_h, to be determined. The purpose of this tutorial is to calculate this value using the Bohr model for positronium shown below.



The electron occupies a circular orbit of radius R which has a positron at its center. Likewise the positron occupies a circular orbit of radius R which has an electron at its center. Occupies has been emphasized to stress that there is no motion, no orbiting. Both particles are behaving as waves (this is the meaning of wave-particle duality) occupying the orbit. As waves they are subject to interference, and to avoid destructive interference the wavelength for the ground state is one orbit circumference.

$$\lambda = 2\pi R$$

Introducing the de Broglie relationship between wavelength and momentum, $\lambda = \frac{h}{p}$, yields the following expression for momentum in atomic units (h = 2π).

$$p = \frac{h}{2\pi R} = \frac{1}{R}$$

In atomic units $m_e = m_p = 1$. Therefore, the kinetic energy of each particle is,

$$T = \frac{p^2}{2m} = \frac{1}{2R^2}$$

The total energy of positronium is the sum of electron and positron kinetic energies and their coulombic potential energy.

$$E = T_e + T_p + V_{ep} = \frac{1}{2R^2} + \frac{1}{2R^2} - \frac{1}{R} = \frac{1}{R^2} - \frac{1}{R}$$

Energy minimization with respect to the electron-positron distance R yields the following result.

$$\frac{d}{dR}\left(\frac{1}{R^2} - \frac{1}{R}\right) = 0 \text{ solve, } \mathrm{R} \rightarrow 2$$

The optimum R value yields a ground state energy of -0.25 Eh, in agreement with experiment.

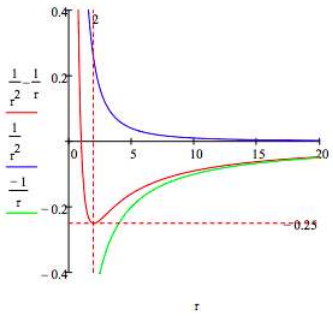
$$E = \frac{1}{R^2} - \frac{1}{R} \text{ substitute, } \mathrm{R} = 2 \rightarrow E = -\frac{1}{4}$$

Including the symbols for mass in the kinetic energy contributions facilitates the introduction of the concept of effective mass of the composite system.

$$T = \frac{1}{2m_eR^2} + \frac{1}{2m_pR^2} = \frac{1}{2R^2}\left(\frac{1}{m_e} + \frac{1}{m_p}\right) = \frac{1}{2R^2}\left(\frac{m_e + m_p}{m_em_p}\right) = \frac{1}{2\mu_{ep}R^2}$$

$$\mu_{ep} = \frac{m_em_p}{m_em_p} = \frac{(1)(1)}{1+1} = \frac{1}{2}$$

The positronium energy minimum can also be located graphically.



Plotting kinetic and potential energy along with total energy reveals that a ground state is achieved because beginning at R = 2, the kinetic energy is approaching positive infinity more quickly than the potential energy is approaching negative infinity.

This page titled 2.7: The de Broglie-Bohr Model for Positronium is shared under a CC BY 4.0 license and was authored, remixed, and/or curated by Frank Rioux via source content that was edited to the style and standards of the LibreTexts platform.

2.8: The Bohr Model for the Earth-Sun System

Data for the earth-sun system assuming a circular earth orbit:

Mass of the earth:	$Me = 5.974(10)^{24}\text{kg}$	Mass of the sun:	$Ms = 1.989(10)^{30}\text{kg}$
Earth orbit radius:	$r = 1.496(10)^{11}m$	Gravitational constant:	$G = 6.674(10)^{-11}\frac{\text{N m}^2}{\text{kg}^2}$
Planck's constant:	$h = 6.62608(10)^{-34}\text{J s}$		

Assuming the earth executes a circular orbit of radius r about the sun and has a deBroglie wavelength given by h/mv, yields a quantum mechanical kinetic energy for the earth which is the first term in the total energy expression below. The potential energy of the earth-sun interaction is well-known and is the second term in the total energy expression.

$$E = \frac{n^2h^2}{8\pi^2Mer^2} - \frac{GMeMs}{r} \quad \text{where n = 1, 2, 3, ...}$$

Setting the first derivative of the energy with respect to r equal to zero, yields the allowed values of r in terms of the quantum number, n.

$$\frac{d}{dr}\left(\frac{GMeMs}{r} - \frac{GMeMs}{r}\right) = 0 \quad \text{has solution(s)} \quad \frac{1}{4}n^2\frac{h^2}{G[Me^2(Ms\pi^2)]}$$

Substitution of this value of r in the total energy expression yields the energy of the earth-sun system as a function of the quantum number, n, Planck's constant, the gravitational constant, and the masses of the earth and the sun.

$$E = \frac{n^2h^2}{8\pi^2Mer^2} - \frac{GMeMs}{r} \quad \text{by substitution, yields} \quad E = \frac{-2}{n^2h^2}\pi^2Me^3G^2Ms^2$$

Given the radius of the earth's orbit listed above, calcuate the earth's quantum number.

$$r = \frac{1}{4}n^2\frac{h^2}{G[Me^2(Ms\pi^2)]} \quad \text{has solution(s)} \quad \begin{pmatrix} \frac{-2}{h}\sqrt{G}Me\sqrt{Ms}\pi\sqrt{r} \\ \frac{2}{h}\sqrt{G}Me\sqrt{Ms}\pi\sqrt{r} \end{pmatrix} = \begin{pmatrix} -2.524 \times 10^{74} \\ 2.524 \times 10^{74} \end{pmatrix}$$

The positive root n is used to calculate the energy of the earth-sun system.

$$n = 2.524(10)^{74} \quad E = \frac{-2}{n^2h^2}\pi^2Me^3G^2Ms^2 \quad E = -2.65 \times 10^{33}\text{J}$$

According to the virial theorem the classical expression for the energy of the earth-sun system with earth orbit radius r is half the potential energy. Note that this gives a value which is in agreement with the Bohr model for the earth-sun system. Is this a legitimate example of the correspondence principle?

$$E = -\frac{GMeMs}{2r} \quad E = -2.65 \times 10^{33}\text{J}$$

*Johnson and Pedersen, Problems and Solutions in Quantum Chemistry and Physics, pages 26-27.

This page titled 2.8: The Bohr Model for the Earth-Sun System is shared under a CC BY 4.0 license and was authored, remixed, and/or curated by Frank Rioux via source content that was edited to the style and standards of the LibreTexts platform.

2.9: Extracting Atomic and Molecular Parameters from the deBroglie-Bohn Model for the Atom

The 1913 Bohr model of the hydrogen atom was replaced by Schrödinger′s wave mechanical model in 1926. However, Bohr′s model is still profitably taught today because of its conceptual and mathematical simplicity, and because it introduced a number of key quantum mechanical ideas such as the quantum number, quantization of observable properties, quantum jump and stationary state. In addition it provided realistic values for such parameters as atomic and molecular size, electron ionization energy, and molecular bond energy.

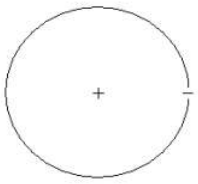
In his ″planetary″ model of the hydrogen atom Bohr began with a Newtonian analysis of the electron executing a circular orbit of radius R about a stationary nucleus, and then arbitrarily quantized the electron′s angular momentum. Finally, by fiat he declared that the electron was in a non-radiating stationary state because an orbiting (accelerating) charge radiates energy and will collapse into the oppositely charge nucleus.

In 1924 de Broglie postulated wave-particle duality for the electron and other massive particles, thereby providing the opportunity to remove some of the arbitrariness from Bohr′s model. For example, an electron possessing wave properties is subject to constructive and destructive interference. As will be shown this leads naturally to quantization of electron momentum and kinetic energy, and consequently to a stable ground state for the hydrogen atom.

The de Broglie-Bohr model of the hydrogen atom presented here treats the electron as a particle on a ring with wave-like properties. The key equation is wave-particle duality as expressed by the de Broglie equation. The particle concept momentum and the wave concept λ are joined in a reciprocal relationship mediated by the ubiquitous Planck′s constant.

$$p = \frac{h}{\lambda}$$

This equation will be used with the Bohr model of the hydrogen atom to explain atomic stability and to generate estimates of atomic size and electron binding energy in the atom.



In the de Broglie version of the Bohr hydrogen atom we say that the electron occupies a ring of radius R. It is not orbiting the nucleus, it is behaving as a stationary wave. In order to avoid self-interference the following wavelength restriction must be obeyed for the ground state of the hydrogen atom.

$$\lambda = 2\pi R$$

When combined with the de Broglie equation it reveals the following restriction on the electron's particle property, linear momentum.

$$p = \frac{h}{2\pi R}$$

This means that there is also a restriction on the electron's kinetic energy. Use of this equation in the classical expression for kinetic energy yields the quantum mechanical kinetic energy or more accurately electron confinement energy.

$$T = \frac{p^2}{2m} = \frac{h^2}{8\pi^2 m R^2} = \frac{1}{2R^2}$$

In this equation we have moved from the classical definition of kinetic energy to the quantum mechanical version expressed on the right in atomic units.

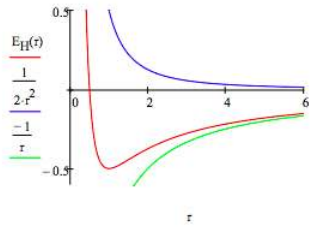
$$\frac{h}{2\pi} = m = e = 4\pi\varepsilon_0 = 1$$

The electrostatic potential energy retains its classical definition in quantum mechanics.

$$V = \frac{-e^2}{4\pi\varepsilon_0 R} = \frac{-1}{R}$$

The total electron energy, $E_H(R) = T(R) + V(R)$, is now minimized with respect to the ring or orbit radius, the only variational parameter in the model. The total energy, and kinetic and potential energy, are also displayed as a function of ring radius.

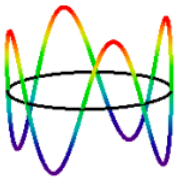
$$R = .5 \quad E_H(R) = \frac{1}{2R^2} - \frac{1}{R} \quad R = \text{Minimize}\,(E_H,\ R) \quad R = 1.000 \quad E_H(R) = -0.500$$



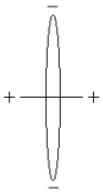
From this simple model we learn that it is the wave nature of the electron that explains atomic stability. The electron′s ring does not collapse into the nucleus because kinetic (confinement) energy goes to positive infinity (~R^{-2}) faster than potential energy goes to negative infinity (~$-R^{-1}$). This is seen very clearly in the graph. The ground state is due to the sharp increase in kinetic energy as the ring radius decreases. This is a quantum effect, a consequence of de Broglie′s hypothesis that electrons have wave-like properties. As Klaus Ruedenberg has written, ″There are no ground states in classical mechanics.″

The minimization process above the figure provides the ground state ring radius and electron energy in atomic units, a0 and Eh, respectively. R = 1 a_0 = 52.9 pm gives us the benchmark for atomic size. Tables of atomic and ionic radii carry entries ranging from approximately half this value to roughly five or six times it. The ground state (binding) energy, E = -0.5 E_h = -13.6 eV = -1312 kJ/mol, is the negative of the ionization energy. This value serves as a benchmark for how tightly electrons are held in atoms and molecules.

A more comprehensive treatment of the Bohr atom utilizing the restriction that an integral number of wavelengths must fit within the ring, nλ = 2πR , where n = 1, 2, 3, ... reveals a manifold of allowed energy states (-0.5 Eh/n2) and the basis for Bohr′s concept of the quantum jump which ″explained″ the hydrogen atom emission spectrum. Here for example is the n = 4 Bohr atom excited state.



Rudimentary estimates of some molecular parameters, the most important being bond energy and bond length, can be obtained using the following Bohr model for H2. The distance between the protons is D, the electron ring radius is R, and the bond axis is perpendicular to the plane of the ring.



There are eight contributions to the total molecular energy based on this model: electron kinetic energy (2), electron-proton potential energy (4), proton-proton potential energy (1) and electron-electron potential energy (1).

$$E_{H2}(R,\ D) = \frac{1}{R^2} = \frac{4}{\sqrt{R^2 + \left(\frac{D}{2}\right)^2}} + \frac{1}{D} + \frac{1}{2R}$$

Minimization of the energy with respect to ring radius and proton-proton distance yields the following results.

$$D = 2 \quad \begin{pmatrix} R \\ D \end{pmatrix} = \text{Minimize}\left(E_{H2},\ R,\ D\right) \quad \begin{pmatrix} R \\ D \end{pmatrix} = \begin{pmatrix} 0.953 \\ 1.101 \end{pmatrix} \quad E_{H2}(R,\ D) = -1.100$$

The H-H bond energy is the key parameter provided by this analysis. We see that it predicts a stable molecule and that the energy released on the formation of H2 is 0.1 Eh or 263 kJ/mol, compared with the experimental value of 458 kJ/mol. The model predicts a H-H bond length of 58 pm (D.52.9 pm), compared to the literature value of 74 pm. These results are acceptable given the primitive character of the model.

$$H + H = H_2$$

$$\Delta E_{bond} = E_{H2}(R,\ D) - 2E_H(1) \quad \Delta E_{bond} = -0.100$$

In addition to these estimates of molecular parameters, the model clearly shows that molecular stability depends on a balancing act between electron-proton attraction and the "repulsive" character of electron kinetic energy. Just as in the atomic case, it is the 1/R2 dependence of kinetic (confinement) energy on ring radius that prevents molecular collapse under electron-proton attraction. As the energy profile provided in the Appendix shows, the immediate cause of the molecular ground state is a rise in kinetic energy. Potential energy is still declining at this point and does not begin to rise until 0.55 a_0, well after the ground state is reached at 1.10 a_0.

Although the model is a relic from the early days of quantum theory it still has pedagogical value. Its mathematical simplicity clearly reveals the importance of the wave nature of matter, the foundational concept of quantum theory.

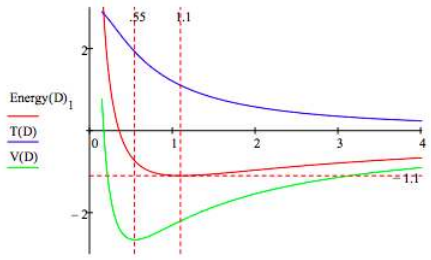
Two relatively recent appraisals of Bohr's models of atomic and molecular structure have been appeared in Physics Today:

- "Niels Bohr between physics and chemistry," by Helge Kragh, May 2013, 36-41.
- "Bohr's molecular model, a century later," by Anatoly Svidzinsky, Marlan Scully, and Dudley Herschbach, January 2014, 33-39.

Appendix

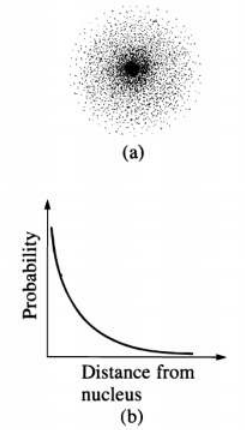
$$R = .1 \quad \text{Energy} = -1 \quad \text{Given} \quad \text{Energy} = E_{H2}(R,\ D) \quad \frac{d}{dR}E_{H2}(R,\ D) = 0 \quad \text{Energy(D)} = \text{Find(R, Energy)}$$

$$D = .15,\ .16..4 \quad T(D) = \frac{1}{(\text{Energy(D)}_0)^2} \quad V(D) = -\frac{4}{\sqrt{(\text{Energy(D)}_0)^2 + \left(\frac{D}{2}\right)^2}} + \frac{1}{D} + \frac{1}{2\text{Energy (D)}_0}$$



This page titled 2.9: Extracting Atomic and Molecular Parameters from the deBroglie-Bohn Model for the Atom is shared under a CC BY 4.0 license and was authored, remixed, and/or curated by Frank Rioux via source content that was edited to the style and standards of the LibreTexts platform.

2.10: Electronic Structure and the Superposition Principle



Electrons in atoms or molecules are characterized by their entire distributions, called wave functions or orbitals, rather than by instantaneous positions and velocities: an electron may be considered always to be, with appropriate probability, at all points of its distribution, which does not vary with time. (F. E. Harris)

For example, the hydrogen atom electron is in a stationary state which is a weighted superposition of all possible distances from the nucleus. The electron is not orbiting the nucleus; it does not execute a classical trajectory during its interaction with the nucleus.

From the quantum mechanical perspective, to measure the position of an electron is not to find out where it is, but to cause it to be somewhere. (Louisa Gilder)

This page titled 2.10: Electronic Structure and the Superposition Principle is shared under a CC BY 4.0 license and was authored, remixed, and/or curated by Frank Rioux via source content that was edited to the style and standards of the LibreTexts platform.

2.11: Atomic Spectroscopy and the Correspondence Principle

Bohr′s correspondence principle states that the predictions of classical and quantum mechanics agree in the limit of large quantum numbers (An Introduction to Quantum Physics, French and Taylor, p. 27). This principle can be illustrated using the Bohr model of the hydrogen atom, which is an ad hoc mixture of established classical and newly proposed quantum concepts.

On the basis of Rutherford′s nuclear model of the atom, Bohr envisioned the hydrogen atom′s electron executing circular orbits around the proton with quantized angular momentum. This gave rise to a manifold of allowed electron orbits with discrete (as opposed to continuous) radii and energies. By fiat Bohr called these stationary states, because the orbiting (accelerating) electron did not radiate energy as required by classical electromagnetic principles.

Initial speculation, however, suggested that the observed line spectrum of the hydrogen atom might be interpeted in terms of electromagnetic emissions related to orbital frequencies of the electron. Subsequently, Bohr achieved agreement with experiment by postulating that the observed frequencies were due to photon (hv) emissions as the electron made a quantum jump from one allowed orbit to another. As will be shown below these two explanations, the first classical and the second quantum mechanical, can be used to illustrate the correspondence principle.

The calculations below are carried out in the Mathcad programming environment using the following information.

Planck's constant:	$h = 6.62608(10)^{-34}$joule sec	Electron mass:	$m_e = 9.1093897(10)^{-31}$kg
Speed of light:	$c = 2.9979(10)^{8}\frac{m}{sec}$	Bohr radius:	$a_0 = 5.29177(10)^{-11}$m
Conversion factors:	$pm = 10^{-12}m$		$aJ = 10^{-18}$joule
Energy of a photon:	$E_{photon} = h\nu = \frac{hc}{\lambda}$		

Energy of the hydrogen atom's electron (n is a quantum number and can have integer values).

$$E_{atom} = \frac{-2.18aJ}{n^2}$$

Emission Spectroscopy

In emission spectroscopy a photon is created as the electron undergoes a transition from a higher to a lower energy state. Energy conservation requires

$$E_{atom}^{initial} = E_{atom}^{final} + E_{photon}$$

Using Bohr′s quantum jump model we calculate the frequency of the photon emitted when an electron undergoes a transition from the n=2 to the n=1 state.

$$n_i = 2 \quad n_f = 1 \qquad \frac{-2.178aJ}{n_i^2} = \frac{-2.178aJ}{n_f^2} + h\nu \;\Big|\; \begin{matrix} solve,\,\nu \\ float,\,3 \end{matrix} \rightarrow \frac{2.47e15}{sec}$$

This result is in agreement with the experimental hydrogen atom emission spectrum.

Next we calculate the orbital frequencies of these two quantum states. This requires knowing the classical orbital velocity and orbit circumference. These are most easily obtained by using postulates and results of the Bohr model.

Quantized orbital angular momentum: $m_e v r = \frac{nh}{2\pi}$

Allowed orbit radius: $r = n^2 a_0$

Orbit circumference: $C = 2\pi r$

Orbit frequency: $\nu = \frac{v}{C} \quad \nu(n) = \frac{h}{4\pi^2 m_e n^3 a_0^2}$

The classical orbital frequencies for the n = 1 and n = 2 orbits bracket the photon frequency, but are not in good agreement with the quantum result.

$$\nu(1) = 6.58 \times 10^{15}\frac{1}{s} \quad \nu(2) = 8.22 \times 10^{14}\frac{1}{s}$$

Next we explore high energy electronic states. Recently an electronic hydrogen atom emission transition was observed at 408.367 MHz in interstellar space. Assuming the transition occurs between adjacent states, calculate the quantum number of the destination

state.

$$\frac{-2.18aJ}{(n+1)^2} = \frac{-2.18aJ}{n^2} + h\frac{408.367(10)^6}{\text{sec}} \left| \begin{array}{l} \text{solve, n} \\ \text{float, 3} \end{array} \right. \rightarrow \begin{pmatrix} -0.5 \\ 252.0 \\ -127.0 - 219.0i \\ -127.0 + 219.0i \end{pmatrix}$$

Thus the transition is from n = 253 to n = 252. Below we see that the classical orbital frequencies for these states again bracket the quantum result, but now are in much closer agreement with it.

$$\nu(252) = 4.11 \times 10^8 \frac{1}{s} \quad \nu(253) = 4.06 \times 10^8 \frac{1}{s}$$

As the n quantum number increases the predictions of classical and quantum mechanics converge as required by Bohr′s correspondence principle.

This page titled 2.11: Atomic Spectroscopy and the Correspondence Principle is shared under a CC BY 4.0 license and was authored, remixed, and/or curated by Frank Rioux via source content that was edited to the style and standards of the LibreTexts platform.

2.12: Hydrogen-Like Calculations with Variable Lepton Mass

Under normal circumstances the the hydrogen atom consists of a proton and an electron. However, electrons are leptons and there are two other leptons which could temporarily replace the electron in the hydrogen atom. The other leptons are the muon and tauon, and their relevant properties, along with those of the electron, are given in the following table. The following calculations are carried out in atomic units (me = e = h/2π = 1) and are valid for any one-lepton atom or ion.

$$\begin{pmatrix} \text{Property} & e & \mu & \tau \\ \frac{\text{Mass}}{m_e} & 1 & 206.8 & 3491 \\ \frac{\text{EffectiveMass}}{m_e} & 1 & 185.86 & 1203 \\ \frac{\text{LifeTime}}{s} & \text{Stable} & 2.2(10)^{-6} & 3.0(10)^{-13} \end{pmatrix}$$

Coordinate-space calculations:

Energy operator:

$$H = -\frac{1}{2\mu}\frac{d^2}{dx^2}\blacksquare - \frac{1}{x}\blacksquare$$

Trial ground state wave function:

$$\Psi(x,\ \mu) = 2\mu^{\frac{3}{2}} x \exp(-\mu,\ x) \quad \int_0^\infty \Psi(x,\ \mu)^2 \text{dx assume}, \mu > 0 \to 1$$

Demonstrate that the wave function is an eigenfunction of the total energy operator, but not of the kinetic and potential energy operators individually:

$$-\frac{1}{2\mu}\frac{d^2}{dx^2}\Psi(x,\ \mu) - \frac{1}{x}\Psi(x,\ \mu) = E\Psi(x,\ \mu) \text{solve, E} \to \frac{-1}{2}\mu$$

$$\frac{-\frac{1}{2\mu}\frac{d^2}{dx^2}\Psi(x,\ \mu)}{\Psi(x,\ \mu)} \text{simplify} \to \frac{-1}{2}\frac{(-2)+\mu x}{x} \quad \frac{-\frac{1}{x}\Psi(x,\ \mu)}{\Psi(x,\ \mu)} \to \frac{-1}{x}$$

Calculate <T>:

$$\int_0^\infty \Psi(x,\ \mu) - \frac{1}{2\mu}\frac{d^2}{dx^2}\Psi(x,\ \mu) \text{dx assume}, \mu > 0 \to \frac{1}{2}\mu$$

Calculate <R>:

$$\int_0^\infty \Psi(x,\ \mu)\frac{-1}{x}\Psi(x,\ \mu)\ \text{dx assume}, \mu > 0 \to -\mu$$

Is the virial theorem satisfied? Yes.

$$< E >= \frac{< V >}{2} = - < T >= \frac{\mu}{2}$$

Calculate the classical turning point:

$$\frac{-\mu}{2} = \frac{-1}{x} \text{ solve, x} \to \frac{2}{\mu}$$

Calculate the probability that tunneling is occurring:

$$\int_{\frac{2}{\mu}}^\infty \Psi(x,\ \mu)^2\ \text{dx assume}, \mu > 0 \to 13e^{-4} = 0.238$$

Calculate <x>:

$$\int_0^\infty x\Psi(x,\ \mu)^2\ \text{dx assume}, \mu > 0 \to \frac{3}{2\mu}$$

Calculate <x^2>:

$$\int_0^\infty x^2 \Psi(x,\ \mu)^2 \text{ dx assume, } \mu > 0 \rightarrow \frac{3}{\mu^2}$$

Calculate the most probable position:

$$\frac{d}{dx}\Psi(x,\ \mu) = 0 \text{solve, x} \rightarrow \frac{1}{\mu}$$

Calculate the electron density at the most probable position:

$$\Psi\left(\tfrac{1}{\mu},\ \mu\right)^2 \rightarrow 4\mu\left(e^{-1}\right)^2 \quad 0.541\mu$$

Calculate the probability the electron is beyond the most probable position:

$$\int_{\frac{1}{\mu}}^\infty \text{ dx assume, } \mu > 0 \rightarrow 5e^{-2} = 0.677$$

Calculate

:

$$\int_0^\infty \Psi(x,\ \mu)\frac{1}{i}\frac{d}{dx}\Psi(x,\ \mu)\text{dx assume, } \mu > 0 \rightarrow$$

Calculate <p^2>:

$$\int_0^\infty \Psi(x,\ \mu) - \frac{d^2}{dx^2}\Psi(x,\ \mu) \text{ dx assume, } \mu > 0 \rightarrow \mu^2$$

Calculate the position-momentum commutator:

$$\frac{x\frac{1}{i}\frac{d}{dx}\Psi(x,\ \mu) - \frac{1}{i}\frac{d}{dx}(x\Psi(x,\ \mu))}{\Psi(x,\mu)}\text{simplify} \rightarrow i$$

Momentum-space calculations:

Generate the momentum wave function by Fourier transform of the coordinate-space wave function:

$$\Phi(p,\ \mu) = \int_0^\infty \frac{\exp(-ipx)}{\sqrt{2\pi}}\Psi(x,\ \mu) \text{ dx assume, } \mu > 0 \rightarrow 2^{\frac{1}{2}}\text{-}$$

Calculate <T>:

$$\int_{-\infty}^\infty \overline{\Phi(p,\ \mu)}\frac{p^2}{2\mu}\Phi(p,\ \mu) \text{ dp assume, } \mu > 0 \rightarrow \frac{1}{2}\mu$$

Calculate <x>:

$$\int_{-\infty}^\infty \overline{\Phi(p,\ u)}i\frac{d}{dp}\Phi(p,\ u)dp \left|\begin{array}{l}\text{assume, } \mu>0\\ \text{simplify}\end{array}\right. \rightarrow \frac{3}{\mu}$$

Calculate <x^2>:

$$\int_{-\infty}^\infty \overline{\Phi(p,\ u)} - \frac{d}{dp}\Phi(p,\ u)dp \left|\begin{array}{l}\text{assume, } \mu>0\\ \text{simplify}\end{array}\right. \rightarrow \frac{3}{\mu^2}$$

Calculate

:

$$\int_{-\infty}^\infty \overline{\Phi(p,\ u)}p\Phi(p,\ \mu) \text{ dp assume, } \mu > 0 \rightarrow 0$$

Calculate <p^2>:

$$\int_{-\infty}^\infty \overline{\Phi(p,\ u)}p^2\Phi(p,\ \mu) \text{ dp assume, } \mu > 0 \rightarrow \mu^2$$

Calculate Δx:

$$\sqrt{\frac{3}{\mu^2} - \left(\frac{3}{2\mu}\right)^2} = \frac{\sqrt{2}}{2\mu}$$

Calculate Δp:

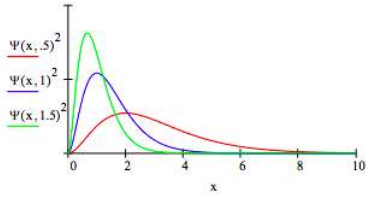
$$\sqrt{\mu^2} = \mu$$

Calculate ΔxΔp:

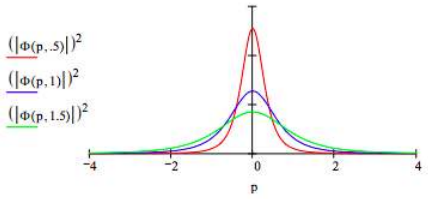
$$\frac{\sqrt{3}}{2} = 0.866$$

The uncertainty principle is obeyed because the result is greater than 0.5.

Spatial distribution as a function of μ:



Momentum distribution as a function of μ:



The spatial and momentum distributions provide a graphical illustration of the uncertainty principle.

This page titled 2.12: Hydrogen-Like Calculations with Variable Lepton Mass is shared under a CC BY 4.0 license and was authored, remixed, and/or curated by Frank Rioux via source content that was edited to the style and standards of the LibreTexts platform.

2.13: Atomic Stability

Neils Bohr once observed that from the perspective of classical physics that the stability of matter was a pure miracle. The problem, of course, is that two of the basic building blocks of matter are oppositely charged particles: the proton and the electron. Given Coulomb's Law, the troubling question is what keeps them from combining? Quantum mechanics is considered by many to be an abstract and esoteric science that does not have much to do with everyday life. Yet it provides an explanation for atomic and molecular stability, and classical physics fails at that task. Thus, to achieve some understanding of one of the basic facts about the macro-world requires quantum mechanical concepts and tools.

The issue of atomic stability will be explored with a quantum mechanical analysis of the two simplest elements in the periodic table - hydrogen and helium. Schrödinger's equation can be solved exactly for the hydrogen atom, but approximate methods are required for the helium atom. However, in the pursuit of an explanation for atomic stability, it is instructive to use an approximate method to study the hydrogen atom. The approximate method of choice for many quantum mechanical problems is the variational method.

Variational Treatment for the Hydrogen Atom

The Hamiltonian energy operator for the hydrogen atom in atomic units is,

$$\hat{H} = -\frac{1}{2}\nabla^2 - \frac{1}{r} \tag{2.13.1}$$

Using a scaled hydrogenic wavefunction as the trial wavelength ($\alpha = 1$ for the exact solution),

$$\Psi(r) = \sqrt{\frac{\alpha^3}{\pi}}\exp(-\alpha r) \tag{2.13.2}$$

in a variational calculation yields

$$\langle E_H \rangle = \langle \hat{H} \rangle = \langle T_E \rangle + \langle V_{NE} \rangle \tag{2.13.3}$$

where

$$\langle T_E \rangle = \frac{\alpha^3}{\pi}\int_o^\infty \exp(-\alpha r)\left(-\frac{1}{2}\nabla^2\right)\exp(-\alpha r)4\pi r^2 dr = \frac{\alpha^2}{2} \tag{2.13.4}$$

and

$$\langle V_{NE} \rangle = \frac{\alpha^3}{\pi}\int_o^\infty \exp(-\alpha r)\left(\frac{-Z}{r}\right)\exp(-\alpha r)4\pi r^2 dr = -\alpha Z \tag{2.13.5}$$

Z is the nuclear charge and the scale factor α is the variational parameter in this calculation. It is easy to see that it is a decay constant which controls how quickly the wavefunction goes to zero as a function of *r*, the distance from the nucleus. Therefore, it is also intimately related to the average distance of the electron from the nucleus. This is easily seen by calculating the expectation value for the distance of the electron from the nucleus:

$$\langle R \rangle = \frac{\alpha^3}{\pi}\int_o^\infty \exp(-\alpha r) r \exp(-\alpha r)4\pi r^2 dr = \frac{3}{2\alpha} \tag{2.13.6}$$

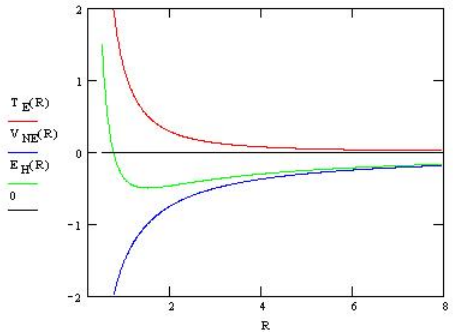
$\langle R \rangle$ is inversely proportional to α vice versa. The larger the value of α, the closer the electron is *on average* to the nucleus. Using this relationship $\langle R \rangle$ can be mapped into the variational parameter (instead of α) by combining Equations 2.13.3 - 2.13.6:

$$E_H = \langle T_E \rangle + \langle V_{NE} \rangle \tag{2.13.7}$$

$$= \frac{\alpha^2}{2} - \alpha \tag{2.13.8}$$

$$= \frac{9}{8R^2} - \frac{3}{2R} \tag{2.13.9}$$

The next step in elucidating the nature of atomic stability is to plot E_H vs R.



Imagine a hydrogen atom forming as an electron approaches a proton from a great distance. (Notice that we assume that the more massive proton is stationary.) The electron is drawn toward the proton by the Coulombic attractive interaction between the two opposite charges and the potential energy decreases like $\frac{-1}{R}$. The attractive potential energy interaction confines the electron to a smaller volume and according to de Broglie's wave hypothesis for matter the kinetic energy increases like $V^{-2/3}$ or as shown above like $\frac{-1}{R^2}$. Thus the kinetic energy goes to positive infinity faster than the potential energy goes to negative infinity and a total energy minimum (ground state) is achieved at $R = 1$, as shown in the figure above. The electron does not collapse into (coalesce with) the proton under the influence of the attractive Coulombic interaction because of the repulsive effect of the confinement energy - that is, kinetic energy. Kinetic energy, therefore, is at the heart of understanding atomic stability. But it is important to understand that this is quantum mechanical kinetic energy, or confinement energy. It is remarkably different than classical kinetic energy.

Variational Treatment for the Helium Atom

We now move on to the next most complicated element, helium, which has a nucleus of charge fo two ($Z = 2$) and two electrons. The Hamiltonian energy operator in atomic units is given by

$$\hat{H} = -\frac{1}{2}\nabla_1^2 - \frac{1}{2}\nabla_2^2 - \frac{2}{r_1} - \frac{2}{r_2} + \frac{1}{r_{12}} \tag{2.13.10}$$

There are five terms in the energy operator, but only one new type, the **electron-electron potential** energy term. When this interaction is calculated using the variational wavefunction in Equation 2.13.2, we have:

$$\langle R \rangle = \frac{\alpha^6}{\pi^2} \tag{2.13.11}$$

$$\int_0^\infty \int_0^\infty \exp(\alpha r_1)\exp(\alpha r_2)\left(\frac{1}{r_{12}}\right)\exp(\alpha r_1)\exp(\alpha r_2) 4\pi r_1^2 dr_1 4\pi r_2^2 dr_2 = \frac{5\alpha}{8}$$

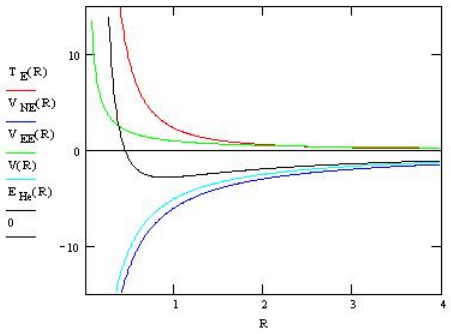
The total energy for helium atom can now be written as shown below because the same relationship applies between $\langle R \rangle$ and α ($\alpha = 3/2\langle R \rangle$).

$$E_{He} = 2\langle T_E \rangle + 2\langle V_{NE} \rangle + \langle V_{EE} \rangle \tag{2.13.12}$$

$$= \alpha^2 - 4\alpha + \frac{5\alpha}{8} \tag{2.13.13}$$

$$= \frac{9}{4R^2} - \frac{6}{R} + \frac{15}{16R} \tag{2.13.14}$$

Graphing E_{He} vs. $\langle R \rangle$ reveals again that kinetic energy (confinement energy) is the key to atomic stability. Several things should be noted in the graph shown below. First, that when the total energy minimum is achieved V_{NE} and V ($V_{NE} + V_{EE}$) are still in a steep decline. This is a strong indication that V_{EE} is really a rather feeble contribution to the total energy, increasing significantly only long after the energy minimum has been attained. Thus electron-electron repulsion cannot be used to explain atomic stability. The graph below clearly shows that on the basis of classical electrostatic interactions, the electron should collapse into the nucleus. This is prevented by the kinetic energy term for the same reasons as were given for the hydrogen atom.



Unfortunately chemists tend to give too much significance to electron-electron repulsion (see VSEPR for example) when it is really the least important term in the Hamiltonian energy operator. And to make matters worse they completely ignore kinetic energy as an important factor in atomic and molecular phenomena. It is becoming increasingly clear in the current literature that many well-established explanations for chemical phenomena based exclusively on electrostatic arguments are in need of critical re-evaluation.

Contributors and Attributions

- Prof. Emeritus Frank Rioux (St. John's University and College of St. Benedict)

This page titled 2.13: Atomic Stability is shared under a CC BY 4.0 license and was authored, remixed, and/or curated by Frank Rioux via source content that was edited to the style and standards of the LibreTexts platform.

2.14: Quantum Mechanical Calculations for the One-Dimensional Hydrogen Atom

The following exercises pertain to several of the 1 = 0 states of the one-dimensional hydrogen atom.

$1s \quad \Psi_1(x) = 2x\exp(-x) \qquad 2s \quad \Psi_2(x) = \frac{1}{\sqrt{8}}x(2-x)\exp\left(-\frac{x}{2}\right)$

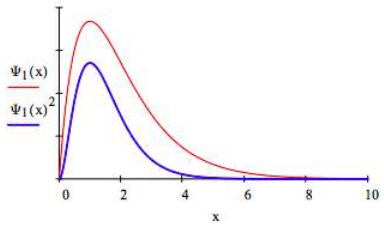
$3s \quad \Psi_3(x) = \frac{2}{243}\sqrt{3}x\left(27 - 18x + 2x^2\right)\exp\left(-\frac{x}{3}\right)$

Coordinate Space Calculations

Position operator: $x\blacksquare$ Momentum operator: $p = \frac{1}{i}\frac{d}{dx}\blacksquare$ Integral: $\int_0^\infty \blacksquare dx$

Kinetic energy operator: $KE = -\frac{1}{2}\frac{d^2}{dx^2}$ Potential energy operator: $PE = \frac{-1}{x}\blacksquare$

Plot Ψ(x) and Ψ(x)^2:



Show that this wave function is normalized:

$$\int_0^\infty \Psi_1(x)^2 dx \to 1 \quad \int_0^\infty \Psi_1(x)^2 dx = 1$$

Calculate the most probable position for the electron:

$$\frac{d}{dx}(2\text{x } \exp(\text{-x})) = 0 \text{solve, x} \to 1$$

Calculate the average value of the electron position:

$$\int_0^\infty \Psi_1(x) x \Psi_1(x) dx \to \frac{3}{2}$$

Calculate the probability density at both the most probable and average positions of the electron:

$$\text{Most probable:} \quad \Psi_1(x)^2 = 0.541 \quad \text{Average:} \quad \Psi_1\left(\tfrac{3}{2}\right)^2 = 0.448$$

Calculate the probability that the electron is between the nucleus and the most probable value of the electron position:

$$\int_0^1 \Psi_1(x)^2 \text{dx float, } 3 \to 0.323 \quad \int_0^1 \Psi_1(x)^2 dx = 0.323$$

Calculate the probability that the electron is between the nucleus and the average value of the electron position:

$$\int_0^{\frac{3}{2}} \Psi_1(x)^2 \text{dx float, } 3 \to 0.577 \quad \int_0^{\frac{3}{2}} \Psi_1(x)^2 dx = 0.577$$

Calculate the probability that the electron is beyond the most probable position:

$$\int_1^\infty \Psi_1(x)^2 \text{dx float, } 3 \to 0.677 \quad \int_1^\infty \Psi_1(x)^2 dx = 0.677$$

Calculate the probability that the electron will be found inside the nucleus. The nuclear dimension is approximately 2 x 10^{-5} a_o.

$$\int_0^{.00002} \Psi_1(x)^2 dx = 1.067 \times 10^{-14}$$

Calculate that position from the nucleus for which the probability of finding the electron is 0.95:

$$a = 2 \quad \text{Given} \quad \int_0^a \Psi_1(x)^2 dx = .95 \quad \text{Find(a)} = 3.148$$

Calculate the uncertainty in position:

$$\Delta x = \sqrt{\int_0^\infty \Psi_1(x) x^2 \Psi_1(x) dx - \left(\int_0^\infty \Psi_1(x) x \Psi_1(x) dx\right)^2} \text{ float, } 3 \rightarrow 0.866$$

Calculate the average value of the electronic momentum:

$$\int_0^\infty \Psi_1(x) \frac{1}{i} \frac{d}{dx} \Psi_1(x) dx \rightarrow 0$$

Calculate the uncertainty in momentum:

$$\Delta p = \sqrt{\int_0^\infty \Psi_1(x) - \frac{d^2}{dx^2} \Psi_1(x) dx - \left(\int_0^\infty \Psi_1(x) \frac{1}{i} \frac{d}{dx} \Psi_1(x) dx\right)^2} \rightarrow 1$$

Demonstrate that the position-momentum uncertainty relation is obeyed:

$$\Delta x \Delta p = 0.866$$

This value is greater than .5 as required.

Calculate the position-momentum commutator. Interpret the result.

$$\frac{x\left(\frac{1}{i}\frac{d}{dx}\Psi_1(x)\right) - \frac{1}{i}\frac{d}{dx}\left(x\Psi_1(x)\right)}{\Psi_1(x)} \text{simplify} \rightarrow i$$

Position and momentum measurements do not commute. The wave function is not an eigenfunction of the position and momentum operators.

Calculate the average value for kinetic energy:

$$\int_0^\infty \Psi_1(x) - \frac{1}{2}\frac{d^2}{dx^2}\Psi_1(x) dx \rightarrow \frac{1}{2} \quad \int_0^\infty \Psi_1(x) - \frac{1}{2}\frac{d^2}{dx^2}\Psi_1(x) dx = 0.5$$

Calculate the average value for potential energy:

$$\int_0^\infty \Psi_1(x) - \frac{1}{x}\frac{d^2}{dx^2}\Psi_1(x) dx \rightarrow -1 \quad \int_0^\infty \Psi_1(x) - \frac{1}{x}\frac{d^2}{dx^2}\Psi_1(x) dx = -1$$

Calculate the average value for the total energy: $\frac{1}{2} - 1 = -0.5$ or

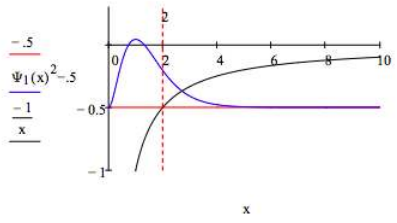
$$\int_0^\infty \Psi_1(x) - \frac{1}{2}\frac{d^2}{dx^2}\Psi_1(x) dx \rightarrow \frac{1}{2} \quad \int_0^\infty \Psi_1(x) - \frac{1}{x} dx \Psi_1(x) dx = -\frac{1}{2}$$

These results illustrate the virial theorem:

$$E = -T = \frac{V}{2}$$

Calculate the probability that the electron is in a classically forbidden region, that is a region for which E < V. First show that the classically forbidden region begins at x = 2, where E = V. For x larger than 2 the potential energy will be greater than the total energy. This is an example of quantum mechanical tunneling. Show the classically forbidden region graphically.

$$\frac{-1}{2} = \frac{-1}{x} \text{ solve, x } \rightarrow 2 \quad \int_2^\infty \Psi_1(x)^2 dx = 0.238$$



Demonstrate that the wave function is not an eigenfunction of the kinetic energy operator and comment on the significance of this result:

$$\frac{-\frac{1}{2}\frac{d^2}{dx^2}\Psi_1(x)-\frac{1}{x}\Psi_1(x)}{\Psi_1(x)}\text{simplify}\rightarrow\frac{1}{x}-\frac{1}{2}$$

Electron in the hydrogen atom does not have a well-defined value for kinetic energy.

Demonstrate that the wave function is not an eigenfunction of the potential energy operator and comment on the significance of this result:

$$\frac{-\frac{1}{2}\frac{d^2}{dx^2}\Psi_1(x)-\frac{1}{x}\Psi_1(x)}{\Psi_1(x)}\text{simplify}\ \rightarrow-\frac{1}{2}$$

In spite of not having a well-defined kinetic or potential energy, the electron in the hydrogen atom has a well-defined total energy.

$$-\frac{1}{2}\frac{d}{dx^2}\Psi_1(x)-\frac{1}{x}\Psi_1(x)=E\Psi_1(x)\text{ solve, E}\rightarrow-\frac{1}{2}$$

What is the energy eigenvalue and how does it compare to previous calculations in this exercise:

The energy eigenvalue is -0.5 which is in agreement with + calculated previously.

Calculate the overlap integral with the 2s orbital:

$$\int_0^\infty\Psi_1(x)\Psi_2(x)dx\rightarrow0$$

Interpret the result: the orbitals are orthogonal.

Calculate the kinetic, potential and total energy of a 2s electron and show that the virial theorem is satisfied.

$$\int_0^\infty\Psi_2(x)-\tfrac{1}{2}\tfrac{d^2}{dx^2}\Psi_2(x)dx\rightarrow\tfrac{1}{8}\quad\int_0^\infty\Psi_2(x)-\tfrac{1}{x}\Psi_2(x)dx\rightarrow-\tfrac{1}{4}\quad F=\tfrac{1}{8}-\tfrac{1}{4}\quad F\rightarrow-\tfrac{1}{8}$$

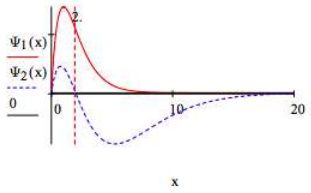
$$E=-T=\frac{V}{2}$$

Calculate the kinetic, potential and total energy of a 3s electron and show that the virial theorem is satisfied.

$$\int_0^\infty\Psi_3(x)-\tfrac{1}{2}\tfrac{d^2}{dx^2}\Psi_3(x)dx\rightarrow\tfrac{1}{18}\quad\int_0^\infty\Psi_3(x)-\tfrac{1}{x}\Psi_3(x)dx\rightarrow-\tfrac{1}{9}\quad E=\tfrac{1}{18}-\tfrac{1}{9}\quad E\rightarrow-\tfrac{1}{18}$$

$$E=-T=\frac{V}{2}$$

Plot the 1s and 2s orbitals on the same graph and explain the orthogonality or net zero overlap.



From x = 0 to 2 the overlap is positive, and x=2 to ∞ it is equal in magnitude but negative.

$$\int_0^2\Psi_1(x)\Psi_2(x)dx=0.188$$
$$\Psi_2^\infty\Psi_1(x)\Psi_2(x)dx=-0.188$$

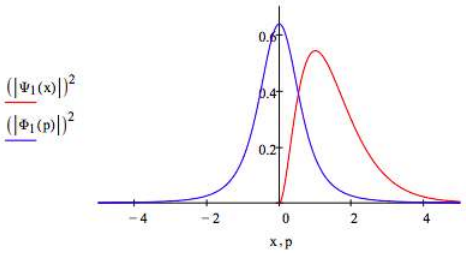
Momentum Space Calculations

Fourier transform the 1s coordinate-space wave function into momentum space.

$$\Phi_1(p)=\frac{1}{\sqrt{2\pi}}\left(\int_0^\infty\exp(-ipx)\Psi_1(x)dx\right)\rightarrow\frac{\sqrt{2}}{\sqrt{\pi}(1+pi)^2}$$

Plot $|\Psi(x)|^2$ and $|\Phi(p)|^2$ on the same graph:

$$p=-5,\ -4.99,...5\quad x=0,\ .01..5$$



Momentum space integral: $\int_{-\infty}^{\infty} \blacksquare\, dp$ Momentum operator: $p\blacksquare$

Kinetic energy operator: $\frac{p^2}{2}$ Position operator: $i\frac{d}{dp}\blacksquare$

Demonstrate that the 1s momentum wavefunction is normalized.

$$\int_{-\infty}^{\infty} \overline{\Phi_1(p)}\Psi_1(p)dp = 1 \quad \text{or} \quad \int_{-\infty}^{\infty} (|\Psi_1(p)|)^2 = 1$$

Calculate the average value of the momentum and compare it to value obtained with the coordinate space wave function.

$$\int_{-\infty}^{\infty} \overline{\Phi_1(p)}\Psi_1(p)dp = 1 \quad \text{Same value}$$

Calculate the average value of the kinetic energy and compare it to value obtained with the 1s coordinate space wave function.

$$\int_{-\infty}^{\infty} \overline{\Phi_1(p)}\frac{p^2}{2}\Psi_1(p)dp = 0.5 \quad \text{Same value}$$

Calculate the average value of the electron position and compare it to value obtained with the 1s coordinate space wave function.

$$\int_{-\infty}^{\infty} \overline{\Phi_1(p)}i\frac{p}{dp}\Psi_1(p)dp = 1.5 \quad \text{Same value}$$

Calculate the uncertainty in position using the momentum wave function:

$$\int_{-\infty}^{\infty} \overline{\Phi_1(p)} - \frac{d^2}{dp^2}\Phi_1(p)dp = 3 \quad \Delta x = \sqrt{3 - \left(\frac{3}{2}\right)^2} \quad \Delta x = 0.866$$

Calculate the uncertainty in momentum using the momentum wave function:

$$\int_{-\infty}^{\infty} \overline{\Phi_1(p)} - \frac{d^2}{dp^2}\Phi_1(p)dp = 3 \quad \Delta p = \sqrt{1 - 0} \quad \Delta p = 1$$

Demonstrate that the position-momentum uncertainty relation is satisfied:

$$\Delta x \Delta p = 0.866 \quad \text{Same value.}$$

Fourier transform the 2s wavefunction into momentum space:

$$\Phi_2(p) = \frac{1}{\sqrt{2\pi}}\int_0^{\infty} \exp(-ipx)\Psi_2(x)\text{dx simplify} \rightarrow \frac{2(-1+2ip)}{\sqrt{\pi}(1+2ip)^3}$$

Demonstrate the 2s wavefunction is normalized.

$$\int_{-\infty}^{\infty} (|\Phi_2(p)|)^2\, dp = 1$$

Demonstrate the 1s and 2s momentum wavefunctions are orthogonal.

$$\int_{\infty}^{\infty} \overline{\Phi_1(p)}\Phi_2(p)dp = 0$$

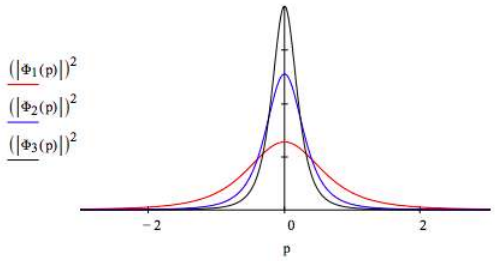
Fourier transform the 3s wavefunction into momentum space.

$$\Phi_3(p) = \frac{1}{\sqrt{2\pi}}\int_0^{\infty} \exp(-ipx)\Psi_3(x)\text{dx simplify} \rightarrow \frac{\sqrt{6}(-1+3ip)^2}{\sqrt{\pi}(1+3ip)^4}$$

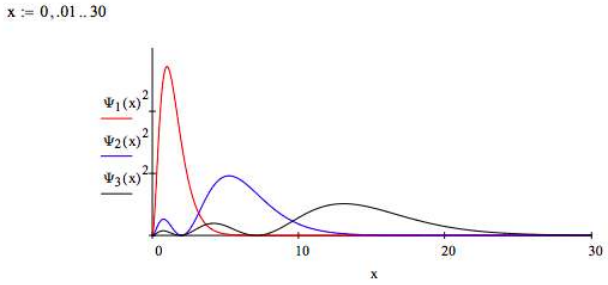
Demonstrate the 3s momentum wavefunction is normalized.

$$\int_{-\infty}^{\infty} (|\Phi_3(p)|)^2 \, dp = 1$$

Plot the 1s, 2s and 3s momentum wavefunctions and interpret the graph in terms of the uncertainty principle.



As shown below, as the principal quantum number increases, the spatial distribution of the electron becomes more delocalized. Therefore, according to the uncertainty principle, the momentum distribution must become more localized. The graph above shows a more localized momentum distribution as the principle quantum number increases.



This page titled 2.14: Quantum Mechanical Calculations for the One-Dimensional Hydrogen Atom is shared under a CC BY 4.0 license and was authored, remixed, and/or curated by Frank Rioux via source content that was edited to the style and standards of the LibreTexts platform.

2.15: Quantum Mechanical Calculations for the Hydrogen Atom

Full kinetic energy operator in spherical coordinates:

Kinetic energy operator for s states:

$$-\frac{1}{2r}\frac{d^2}{dr^2}\blacksquare$$

Kinetic energy operator for p states:

$$-\frac{1}{2r}\frac{d^2}{dr^2}r\blacksquare\ldots$$
$$+\frac{-1}{2r^2\sin(\theta)}\left[\frac{d}{d\theta}\left(\sin(\theta)\frac{d}{d\theta}\blacksquare\right)\right]\ldots$$
$$+\frac{-1}{2r^2\sin(\theta)^2}\frac{d^2}{d\phi^2}\blacksquare$$

Position operator: r

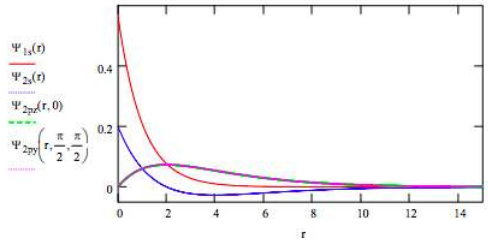
Potential energy operator: $-\frac{1}{r}$

Triple integral with volume element: $\int_0^{\infty}\int_0^{\pi}\int_0^{2\pi}\blacksquare r^2\sin(\theta)d\phi d\theta dr$

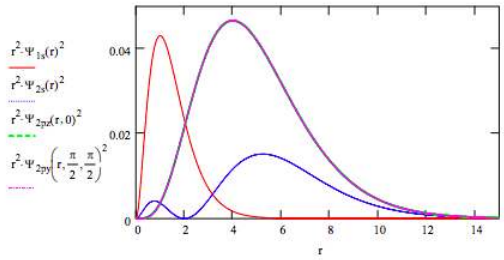
Orbitals:

$$\Psi_{1s}(r)=\frac{1}{\sqrt{\pi}}\exp(\text{-r}) \qquad \Psi_{2s}(r)=\frac{1}{\sqrt{32\pi}}(2-r)\exp\left(-\frac{r}{2}\right)$$
$$\Psi_{2pz}(r,\ \theta)=\frac{1}{\sqrt{32\pi}}\text{r}\ \exp\left(-\frac{r}{2}\right)\cos\theta \qquad \Psi_{2py}(r,\ \theta,\ \phi)=\frac{1}{\sqrt{32\pi}}\text{r}\ \exp\left(-\frac{r}{2}\right)\sin(\theta)\sin(\phi)$$

Plot the wave functions on the same graph:



Plot the radial distribution functions for each orbital on the same graph:



Demonstrate that the 1s orbital is normalized:

$$\int_0^{\infty}\int_0^{\pi}\int_0^{2\pi}\Psi_{1s}(r)^2r^2\sin(\theta)d\phi d\theta dr\rightarrow 1$$

Demonstrate that the 1s orbital is normalized:

$$\int_0^{\infty}\int_0^{\pi}\int_0^{2\pi}\Psi_{2s}(r)^2r^2\sin(\theta)d\phi d\theta dr\rightarrow 1$$

Demonstrate that the 2pz orbital is normalized:

$$\int_0^{\infty}\int_0^{\pi}\int_0^{2\pi}\Psi_{2pz}(r,\ \theta)^2 r^2\sin(\theta)d\phi d\theta dr \rightarrow 1$$

Demonstrate that the 1s and the 2pz orbitals are orthogonal:

$$\int_0^{\infty}\int_0^{\pi}\int_0^{2\pi}\Psi_{1s}(r)\Psi_{2pz}(r,\ \theta)^2 r^2\sin(\theta)d\phi d\theta dr \rightarrow 0$$

Demonstrate the 1s and 2s orbitals are orthogonal:

$$\int_0^{\infty}\int_0^{\pi}\int_0^{2\pi}\Psi_{1s}(r)\Psi_{2s}(r)^2 r^2\sin(\theta)d\phi d\theta dr \rightarrow 0$$

Demonstrate that the $2p_y$ and the $2p_z$ orbitals are orthogonal:

$$\int_0^{\infty}\int_0^{\pi}\int_0^{2\pi}\Psi_{2py}(r,\ \theta,\ \phi)\Psi_{2pz}(r,\ \theta)r^2\sin(\theta)d\phi d\theta dr \rightarrow 0$$

Determine the most probable value for r using the Trace function and calculus:

$$\frac{d}{dr}r^2\Psi_{1s}(r)^2 = 0 \text{ solve, r} \rightarrow \begin{pmatrix}0\\1\end{pmatrix}$$

Calculate the probability that an electron in the 1s orbital will be found within one Bohr radius of the nucleus.

$$\int_0^{1}\int_0^{\pi}\int_0^{2\pi}\Psi_{1s}(r)^2 r^2\sin(\theta)d\phi d\theta dr \text{ float, } 3 \rightarrow .325$$

Find the distance from the nucleus for which the probability of finding a 1s electron is 0.75.

$$a = 2 \quad \text{Given} \quad \int_0^a \Psi_{1s}(r)^2 4\pi r^2 dr = /75 \quad \text{Find(a)} = 1.96$$

Calculate <T>, <V>, and <r> for the 1s orbital. Is the virial theorem obeyed? Explain.

$$\int_0^{\infty}\int_0^{\pi}\int_0^{2\pi}\Psi_{1s}(r) - \frac{1}{2r}\frac{d^2}{dr^2}r\left(\Psi_{1s}(r)\right)r^2\sin(\theta)d\phi d\theta dr \rightarrow \frac{1}{2}$$

$$\int_0^{\infty}\int_0^{\pi}\int_0^{2\pi}\Psi_{1s}(r) - \frac{1}{r}\Psi_{1s}(r)r^2\sin(\theta)d\phi d\theta dr \rightarrow -1$$

$$\int_0^{\infty}\int_0^{\pi}\int_0^{2\pi}\Psi_{1s}(r)r\Psi_{1s}(r)r^2\sin(\theta)d\phi d\theta dr \rightarrow \frac{3}{2}$$

Calculate <T>, <V>, and <r> for the 2s orbital. Is the virial theorem obeyed? Explain.

$$\int_0^{\infty}\int_0^{\pi}\int_0^{2\pi}\Psi_{2s}(r) - \frac{1}{2r}\frac{d^2}{dr^2}r\Psi_{2s}(r)r^2\sin(\theta)d\phi d\theta dr \rightarrow \frac{1}{8}$$

$$\int_0^{\infty}\int_0^{\pi}\int_0^{2\pi}\Psi_{2s}(r) - \frac{1}{r}\Psi_{2s}(r)r^2\sin(\theta)d\phi d\theta dr \rightarrow -\frac{1}{4}$$

$$\int_0^{\infty}\int_0^{\pi}\int_0^{2\pi}\Psi_{2s}(r)r\Psi_{2s}(r)r^2\sin(\theta)d\phi d\theta dr \rightarrow 6$$

Calculate <T>, <V>, and <r> for the $2p_y$ orbital. Is the virial theorem obeyed? Explain.

$$\int_0^{\infty}\int_0^{\pi}\int_0^{2\pi}\Psi_{2py}(r,\ \theta,\ \phi)\begin{bmatrix}-\frac{1}{2r}\frac{d^2}{dr^2}r\Psi_{2py}(r,\ \theta,\ \phi)\ldots\\ +\frac{-1}{2r^2\sin(\theta)}\left[\frac{d}{d\theta}\left(\sin(\theta)\frac{d}{d\theta}\Psi_{2py}(r,\ \theta,\ \phi)\right)\right]\ldots\\ +\frac{-1}{2r^2\sin(\theta)^2}\frac{d^2}{d\phi^2}\Phi_{2py}(r,\ \theta,\ \phi)\end{bmatrix}r^2\sin(\theta)d\phi d\theta dr \rightarrow \frac{1}{8}$$

$$\int_0^{\infty}\int_0^{\pi}\int_0^{2\pi}\Psi_{2py}(r,\ \theta,\ \phi) - \frac{1}{r}\Psi_{2py}(r,\ \theta,\ \phi)r^2\sin(\theta)d\phi d\theta dr \rightarrow \frac{-1}{4}$$

$$\int_0^{\infty}\int_0^{\pi}\int_0^{2\pi}\Psi_{2py}(r,\ \theta,\ \phi)r\Psi_{2py}(r,\ \theta,\ \phi)r^2\sin(\theta)d\phi d\theta dr \rightarrow 5$$

Calculate <T>, <V>, and <r> for the 2pz orbital. Is the virial theorem obeyed? Explain.

$$\int_0^{\infty}\int_0^{\pi}\int_0^{2\pi}\Psi_{2pz}(r,\ \theta)\begin{bmatrix}-\frac{1}{2r}\frac{d^2}{dr^2}r\Psi_{2pz}(r,\ \theta)\ldots\\+\frac{-1}{2r^2\sin(\theta)}\left[\frac{d}{d\theta}\left(\sin(\theta)\frac{d}{d\theta}\Psi_{2pz}(r,\ \theta)\right)\right]\ldots\\+\frac{-1}{2r^2\sin(\theta)^2}\frac{d^2}{d\phi^2}\Phi_{2pz}(r,\ \theta)\end{bmatrix}r^2\sin(\theta)d\phi d\theta dr \rightarrow \frac{1}{8}$$

$$\int_0^{\infty}\int_0^{\pi}\int_0^{2\pi}\Psi_{2pz}(r,\ \theta)-\frac{1}{r}\Psi_{2pz}(r,\ \theta)r^2\sin(\theta)d\phi d\theta dr \rightarrow \frac{-1}{4}$$

$$\int_0^{\infty}\int_0^{\pi}\int_0^{2\pi}\Psi_{2pz}(r,\ \theta)r\Psi_{2pz}(r,\ \theta)r^2\sin(\theta)d\phi d\theta dr \rightarrow 5$$

Summarize your results in the following table:

Ψ	T	V	E	r
1s	0.5	−1	−0.5	1.5
2s	0.125	−0.25	−0.125	6
2pz	0.125	−0.25	−0.125	5
2py	0.125	−0.25	−0.125	5

Demonstrate that the 1s orbital is an eigenfunction of the energy operator. What is the eigenvalue?

$$T=-\frac{1}{2r}\frac{d^2}{dr^2}r\blacksquare \quad V=-\frac{1}{r} \quad H=T+V \quad \Psi(r)=\frac{1}{\sqrt{\pi}}\exp(-r)$$

$$\frac{-\frac{1}{2r}\frac{d^2}{dr^2}r\Psi_{1s}(r)-\frac{1}{r}\Psi_{2s}(r)}{\Psi_{1s}(r)}\ \text{simplify}\ \rightarrow \frac{-1}{2}$$

Demonstrate that the 2s orbital is an eigenfunction of the energy operator. What is the eigenvalue?

$$\frac{-\frac{1}{2r}\frac{d^2}{dr^2}r\Psi_{2s}(r)-\frac{1}{r}\Psi_{2s}(r)}{\Psi_{2s}(r)}\ \text{simplify}\ \rightarrow \frac{-1}{8}$$

Demonstrate that the 2py orbital is an eigenfunction of the energy operator. What is the eigenvalue?

$$\frac{\begin{bmatrix}-\frac{1}{2r}\frac{d^2}{dr^2}r\Psi_{2py}(r,\ \theta,\ \phi)\ldots\\+\frac{-1}{2r^2\sin(\theta)}\left[\frac{d}{d\theta}\left(\sin(\theta)\frac{d}{d\theta}\Psi_{2py}(r,\ \theta,\ \phi)\right)\right]\ldots\\+\frac{-1}{2r^2\sin(\theta)^2}\frac{d^2}{d\phi^2}\Phi_{2py}(r,\ \theta,\ \phi)\end{bmatrix}-\frac{1}{r}\Psi_{2py}(r,\ \theta,\ \phi)}{\Psi_{2py}(r,\ \theta,\ \phi)}\ \text{simplify}\ \rightarrow \frac{-1}{8}$$

This page titled 2.15: Quantum Mechanical Calculations for the Hydrogen Atom is shared under a CC BY 4.0 license and was authored, remixed, and/or curated by Frank Rioux via source content that was edited to the style and standards of the LibreTexts platform.

2.16: Atomic Stability

Neils Bohr once observed that from the perspective of classical physics the stability of matter was a pure miracle. The problem, of course, is that two of the basic building blocks of matter are oppositely charged particles - the proton and the electron. Given Coulomb's Law the troubling question is what keeps them from coaleseing?

Quantum mechanics is considered by many to be an abstract and esoteric science that doesn't have much to do with everyday life. Yet it provides an explanation for atomic and molecular stability, and classical physics fails at that task. Thus, to achieve some understanding of one of the basic facts about the macro-world requires quantum mechanical concepts and tools.

The issue of atomic stability will be explored with a quantum mechanical analysis of the two simplest elements in the periodic table - hydrogen and helium. Schrödinger's equation can be solved exactly for the hydrogen atom, but approximate methods are required for the helium atom. However, in the pursuit of an explanation for atomic stability it is instructive to use an approximate method to study the hydrogen atom. The approximate method of choice for many quantum mechanical problems is the variation method.

Variational Treatment for the Hydrogen Atom

The Hamiltonian energy operator for the hydrogen atom in atomic units is,

$$\hat{H} = -\frac{1}{2}\overline{V}^2 - \frac{1}{r}$$

Using a scaled hydrogenic wave function (a=1 for the exact solution),

$$\Psi(r) = \frac{\sqrt{\alpha^3}}{\pi}\exp(-\alpha r)$$

in a variational calculation yields

$$\langle E_H = \langle \Psi|\hat{H}|\Psi\rangle = \langle T_g\rangle + \langle V_{NE}\rangle$$

where

$$\langle T_E\rangle = \frac{\alpha^3}{\pi}\int_0^{\omega}\exp(-\alpha r)\left(-\frac{1}{2}\overline{V}^2\right)\exp(-\alpha r)4\pi r^2 dr = \frac{\alpha^2}{2}$$

and

$$\langle V_{NE}\rangle = \frac{\alpha^3}{\pi}\int_0^{\omega}\exp(-\alpha r)\left(\frac{-Z}{r}\right)\exp(-\alpha r)4\pi r^2 dr = -\alpha Z$$

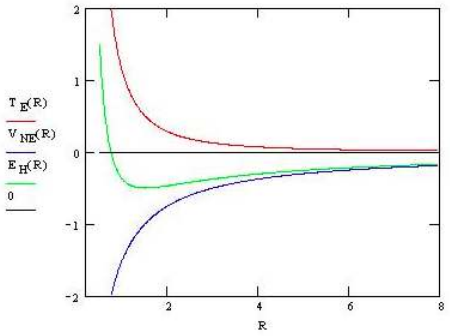
Z is the nuclear charge and the scale factor a is the variational parameter in this calculation. It is easy to see that it is a decay constant which controls how quickly the wave function goes to zero as a function of *r*, the distance from the nucleus. Therefore, it is also intimately related to the average distance of the electron from the nucleus. This is easily seen by calculating the expectation value for the distance of the electron from the nucleus.

$$\langle R\rangle = \frac{\alpha^3}{\pi}\int_0^{\omega}\exp(-\alpha r)r\exp(-\alpha r)4\pi r^2 dr = \frac{3}{2\alpha}$$

<R> is inversely proportional to a; a is inversely proportional to <R>. The larger the value of a, the closer the electron is on average to the nucleus. Using this relationship <R> can be made the variational parameter as is shown in the equation below.

$$E_H = \langle T_E\rangle + \langle N_{NE}\rangle = \frac{\alpha^2}{2} - \alpha = \frac{9}{8R^2} - \frac{3}{2R}$$

The next step in elucidating the nature of atomic stability is to plot E_H vs R.



Imagine a hydrogen atom forming as an electron approaches a proton from a great distance. (Notice that we assume that the more massive proton is stationary.) The electron is drawn toward the proton by the Coulombic attractive interaction between the two opposite charges and the potential energy decreases like $-R^{-1}$. The attractive potential energy interaction confines the electron to a smaller volume and according to deBroglie's wave hypothesis for matter the kinetic energy increases like $V^{-2/3}$ or as shown above like R^{-2}. Thus the kinetic energy goes to positive infinity faster than the potential energy goes to negative infinity and a total energy minimum (ground state) is achieved at R = 1, as shown in the figure above. The electron does not collapse into (coalesce with) the proton under the influence of the attractive Coulombic interaction because of the repulsive effect of the confinement energy - that is, kinetic energy. Kinetic energy, therefore, is at the heart of understanding atomic stability. But it is important to understand that this is quantum mechanical kinetic energy, or confinement energy. It is remarkably different than classical kinetic energy.

Variational Treatment for the Helium Atom

We now move on to the next most complicated element, helium. Helium has a nucleus of charge +2 and two valence electrons. The Hamiltonian energy operator in atomic units is given by,

$$\hat{H} = -\frac{1}{2}\overline{V}^2 - \frac{1}{2}\overline{V}^2 - \frac{2}{r_1} - \frac{2}{r_2} + \frac{1}{r_{12}}$$

There are five terms in the energy operator, but only one new type, the electron-electron potential energy term. When this interaction is calculated using the variational wave function given above we have,

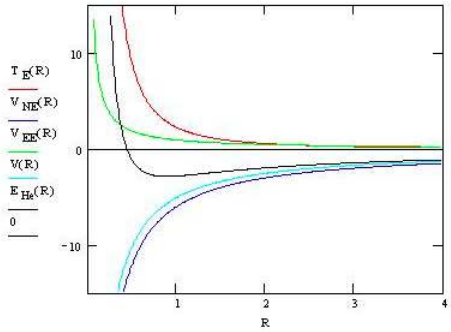
$$\langle V_{EE} \rangle = \frac{\alpha^6}{\pi^2} \int_0^{\omega} \int_0^{\omega} \exp(-\alpha r_1)\exp(-\alpha r_2) \left(\frac{1}{\overline{r}_{12}}\right) \exp(-\alpha r_1)\exp(-\alpha r_2) 4\pi r_1^2 dr_1 4\pi_2^2 dr_2 = \frac{5\alpha}{8}$$

The total energy for helium atom can now be written as shown below because the same relationship applies between <R> and a [a = 3/(2<R>)].

$$E_{HE} = 2\langle T_E \rangle + 2\langle V_{NE} \rangle + \langle V_{EE} \rangle = \alpha^2 - 4\alpha + \frac{5\alpha}{8} = \frac{9}{4R^2} - \frac{6}{R} + \frac{15}{16R}$$

Graphing E_{He} vs. <R> reveals again that kinetic energy (confinement energy) is the key to atomic stability. Several things should be noted in the graph shown below. First, that when the total energy minimum is achieved V_{NE} and V (V_{NE} + V_{EE}) are still in a steep decline. This is a strong indication that V_{EE} is really a rather feeble contribution to the total energy, increasing significantly only long after the energy minimum has been attained. Thus electron-electron repulsion cannot be used to explain atomic stability. The graph below clearly shows that on the basis of classical electrostatic interactions, the electron should collapse into the nucleus. This is prevented by the kinetic energy term for the same reasons as were given for the hydrogen atom.

Unfortunately chemists tend to give too much significance to electron-electron repulsion (see VSEPR for example) when it is really the least important term in the Hamiltonian energy operator. And to make matters worse they completely ignore kinetic energy as an important factor in atomic and molecular phenomena. It is becoming increasingly clear in the current literature that many well-established explanations for chemical phenomena based exclusively on electrostatic arguments are in need of critical re-evaluation.



This page titled 2.16: Atomic Stability is shared under a CC BY 4.0 license and was authored, remixed, and/or curated by Frank Rioux via source content that was edited to the style and standards of the LibreTexts platform.

2.17: Atomic Stability - Mathcad Version

Neils Bohr once observed that from the perspective of classical physics the stability of matter was a pure miracle. The problem, of course, is that two of the basic building blocks of matter are oppositely charged - the electron and the proton. Given Coulomb's Law the troubling question is what keeps them from coalescing?

Quantum mechanics is considered by many to be an abstract and esoteric science that doesn't have much to do with everyday life. Yet it provides an explanation for atomic and molecular stability, and classical physics fails at that task. Thus, to achieve some understanding of one of the basic facts about the macro-world requires quantum mechanical concepts and tools.

The issue of atomic stability will be explored with a quantum mechanical analysis of the two simplest elements in the periodic table - hydrogen and helium. They are also the two most abundant elements in the universe. Schrödinger's equation can be solved exactly for the hydrogen atom, but approximate methods are required for the helium atom. In this study, the variational method will be used for both hydrogen and helium.

Variational Method for the Hydrogen Atom

Normalized trial wave function:

\[\Psi (\alpha,~r) = \sqrt{ \frac{ \alpha^3}{ \pi}} \text{exp} (- \alpha,~r)

α is a scale-factor that controls the size of the wave function.

Integral:

$$\int_0^{\infty} \blacksquare 4\pi r^2 dr$$

Kinetic energy operator:

$$-\frac{1}{2r}\frac{d^2}{dr^2}(r\blacksquare)$$

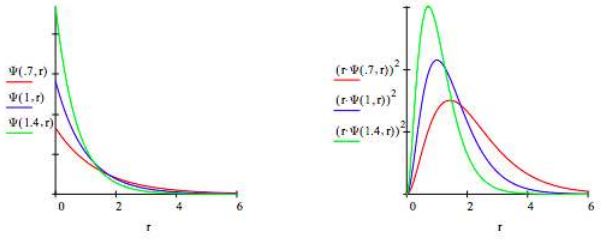
Potential energy operator:

$$\frac{-Z}{r}\blacksquare$$

Demonstrate that the trial function is normalized:

$$\int_0^{\infty} \Psi(\alpha,\ R)^2 4\pi r^2 \text{dr assume, } \alpha > 0 \rightarrow 1$$

Plot trial wave function for several values of α, the variational parameter:



Calculate the average value of the kinetic energy of the electron:

$$T(\alpha) = \int_0^{\infty} \Psi(\alpha,\ r) - \frac{1}{2r}\frac{d^2}{dr^2}(r\Psi(\alpha,\ r)) 4\pi r^2 \text{ dr assume, } \alpha > 0 \rightarrow \frac{\alpha^2}{2}$$

Calculate the average value of the potential energy of the electron:

$$V(\alpha,\ Z) = \int_0^{\infty} \Psi(\alpha,\ r) - \frac{Z}{r}\Psi(\alpha,\ r) 4\pi r^2 \text{ dr assume, } \alpha > 0 \rightarrow -Z\alpha$$

Calculate R, the average distance of the electron from the nucleus:

$$R(\alpha) = \int_0^\infty \Psi(\alpha,\ r) r \Psi(\alpha,\ r) 4\pi r^2 \text{ dr assume, } \alpha > 0 \rightarrow \frac{3}{2\alpha}$$

From this we find that:

$$E(\alpha) = T(\alpha) + V(\alpha,\ Z) = \frac{\alpha^2}{2} - \alpha Z$$

But from above we knew:

$$\alpha = \frac{3}{2R}$$

This allows us to express the total energy and its components in terms of R the average distance of the electron from the nucleus.

Total energy:

$$\text{E(R, Z)} = \frac{\alpha^2}{2} - \alpha Z \left| \begin{array}{l} \text{substitute, } \alpha = \frac{3}{2R} \\ \text{expand} \end{array} \right. \rightarrow \frac{9}{8R^2} - \frac{3Z}{2R}$$

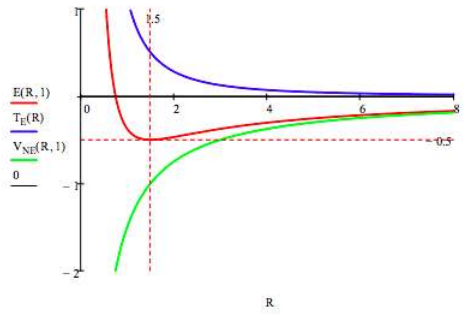
Electron kinetic energy:

$$T_E(R) = \frac{9}{8R^2}$$

Electron-nucleus potential energy:

$$V_{NE}(R,\ Z) = \frac{-3Z}{2R}$$

E, T_E and V_{NE} are graphed versus R for the hydrogen atom (Z = 1): R = 0, .01 ... 8



The hydrogen atom ground-state energy is determined by minimizing its energy with respect to R:

$$\text{R=R} \quad \text{R} = \frac{d}{dR}\text{E(R 1)} = \text{solve, R} \rightarrow \frac{3}{2} \quad \text{E(R, 1)} = \text{-0.5}$$

Imagine a hydrogen atom forming as an electron approaches a proton from a great distance. The electron is drawn toward the proton by the Coulombic attractive interaction between the two opposite charges and the potential energy decreases like -1/R. The attractive potential energy interaction confines the electron to a smaller volume and the kinetic energy increases as 1/R2. Thus the kinetic energy goes to positive infinity faster than the potential energy goes to negative infinity and a total energy minimum (ground state) is achieved at R = 1.5, as shown in the figure above.

The electron does not collapse into (coalesce with) the proton under the influence of the attractive Coulombic interaction because of the repulsive effect of the confinement energy - that is, kinetic energy. Kinetic energy, therefore, is at the heart of understanding atomic stability.

Variational Method for the Helium Atom

Now we will proceed to the He atom. There are five contributions to the total electronic energy: kinetic energy of each electron, the interaction of each electron with the nucleus, and the electron-electron interaction.The only new term is the last, electron-electron

potential energy. It is evaluated as follows for two electrons in 1s orbitals.

The electrostatic potential at r due to electron 1 is:

$$\Phi(\alpha,\ r) = \frac{1}{r}\int_0^r \Psi(\alpha,\ x)^2 4\pi x^2 dx + \int_r^\infty \frac{\Psi(\alpha,\ x)^2 4\pi x^2}{x} dx \ \Big|\ \begin{matrix}\text{assume, } \alpha>0 \\ \text{simplify}\end{matrix} \rightarrow -\frac{e^{-2\alpha r}+\alpha r e^{-2\alpha r}-1}{r}$$

The electrostatic interaction between the two electrons is:

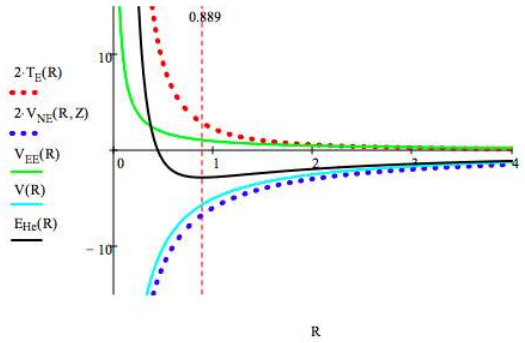
$$V_{EE} = \int_0^\infty \Phi(\alpha,\ r)\Psi(\alpha,\ r)^2 4\pi r^2 dr \ \Big|\ \begin{matrix}\text{assume, } \alpha>0 \\ \text{simplify}\end{matrix} \rightarrow \frac{5\alpha}{8}$$

In terms of R, the electron-electron potential energy is:

$$V_{EE}(R) = \frac{15}{16R}$$

$$Z = 2 \quad E_{He}(R) = 2T_E(R) + 2V_{NE}(R,\ Z) + V_{EE}(R) \quad V(R) = 2V_{NE}(R,\ Z) + V_{EE}(R)$$

The various contributions to the total electronic energy of the helium atom are plotted below. R = 0, .01 .. 4



The helium atom ground-state energy is determined by minimizing its energy with respect to R:

$$\mathrm{R} = \mathrm{R} \quad \mathrm{R} = \frac{d}{dR}E_{He}(R) = 0 \text{ solve, } \mathrm{R} \rightarrow \frac{8}{9} \quad \mathrm{R} = 0.889 \quad E_{He}(R) = -2.848$$

Graphing E_{He} vs. reveals again that kinetic energy (confinement energy) is the key to atomic stability. Several things should be noted in the graph shown above. First, that when the total energy minimum is achieved V_{NE} and V (V_{NE} + V_{EE}) are still in a steep decline. This is a strong indication that V_{EE} is really a rather feeble contribution to the total energy, increasing significantly only long after the energy minimum has been attained. Thus electron-electron repulsion cannot be used to explain atomic stability. The graph above clearly shows that on the basis of classical electrostatic interactions, the electron should collapse into the nucleus. This is prevented by the kinetic energy term for the same reasons as were given for the hydrogen atom.

Unfortunately chemists give too much significance to electron-electron repulsion (VSEPR for example) when it is really the least important term in the Hamiltonian energy operator. And to make matters worse they completely ignore kinetic energy as an important factor in atomic and molecular phenomena. It is becoming increasing clear in the current literature that many traditional explanations for chemical phenomena based exclusively on electrostatic arguments are in need of critical re-examination.

This page titled 2.17: Atomic Stability - Mathcad Version is shared under a CC BY 4.0 license and was authored, remixed, and/or curated by Frank Rioux via source content that was edited to the style and standards of the LibreTexts platform.

2.18: 110. Critique of the Centrifugal Effect in the Hydrogen Atom

Some quantum textbooks invoke the concept of effective potential energy when introducing the quantum mechanical treatment of the hydrogen atom to undergraduate audiences. I will show that this concept is deeply flawed and leads to an incorrect analysis of the energy contributions to the various electronic states of the hydrogen atom. We begin with the one-dimensional Schrödinger radial equation (French and Taylor, An Introduction to Quantum Physics, pages 519-523) expressed in atomic units (e = m_e = h/2π = $4\pi\varepsilon_o$ = 1).

$$H\Psi(r) = (T+V)\Psi(r) = E\Psi(r) \quad \text{where} \quad H = -\tfrac{1}{2}\tfrac{d^2}{dr^2}\blacksquare + \tfrac{L(L+1)}{2r^2}\blacksquare - \tfrac{1}{r}\blacksquare$$

Solving Schrödinger′s equation yields the eigenstates and their eigenvalues, along with the ability to calculate the expectation value for any observable for which the appropriate operator is known. The allowed energy values are $E(n) = -0.5n^{-2}$, where the quantum number, n, can take integer values beginning with unity. The quantized electronic energies for the one-electron hydrogen atom do not depend on the angular momentum quantum number, L.

The problem I wish to deal with involves the middle term in the Hamiltonian given above. Some authors call it the centrifugal potential, combine it with the third term which is the coulombic potential energy, and call the combination the effective potential energy. In support of this maneuver they invoke the idea of centrifugal force, which unfortunately for them is only an apparent force (actually it′s just plain fictitious). Centrifugal means moving away from the center and so one might assume (and some authors claim) that the greater the centrifugal effect (″force″), i.e. the larger the L quantum number, the farther from the nucleus the electron should be for any given value of the principal quantum number n.

This, unfortunately, simply isn′t the case. The radial expectation values for the hydrogen atom are given below, along with a table that shows that the larger the angular momentum quantum number, the closer on average the electron is to the nucleus for any given n quantum number. This effect is also shown graphically in the Appendix.

$$r(n,\ L) = \tfrac{3n^2 - L(L+1)}{2} \qquad \begin{pmatrix} \text{L} & 0 & 1 & 2 & 3 \\ n=1 & 1.5 & ' & ' & ' \\ n=2 & 6 & 5 & ' & ' \\ n=3 & 13.5 & 12.5 & 10.5 & ' \\ n=4 & 24 & 23 & 21 & 18 \end{pmatrix}$$

This is not the only difficulty with the effective potential energy approach. It also violates the virial theorem, which we all know is sacrosanct when it comes to quantum mechanical analyses. In other words, if your analysis or calculation violates the virial theorem discard it, because it′s wrong! The virial theorem for the hydrogen atom is <E>= -<T> = <V>/2. The expectation values for the centrifugal and coulombic contributions to the total energy are provided below. Note that I have used ″V″ for the centrifugal term, assuming that it really is a potential energy term. If this assignment is valid the virial theorem will be satisfied.

$$V_{centrifugal}(n,\ L) = \tfrac{L(L+1)}{2n^3(L+\frac{1}{2})} \qquad V_{coulomb}(n) = -\tfrac{1}{n^2}$$

Next the virial theorem is used as a check on this assignment using the version / = 0.5. What we see below is that the virial theorem is violated for all states for which L > 0. This strongly suggests that the centrifugal term is not a potential energy contribution, but a kinetic energy term.

$$\begin{array}{llll} 1s & n=1 & L=0 & \frac{E(n)}{V_{centrifugal}(n,\ L)+V_{coulomb}(n)} = 0.5 \\ 2s & n=2 & L=0 & \frac{E(n)}{V_{centrifugal}(n,\ L)+V_{coulomb}(n)} = 0.5 \\ 2p & n=2 & L=1 & \frac{E(n)}{V_{centrifugal}(n,\ L)+V_{coulomb}(n)} = 0.75 \\ 3s & n=3 & L=0 & \frac{E(n)}{V_{centrifugal}(n,\ L)+V_{coulomb}(n)} = 0.5 \\ 3p & n=3 & L=1 & \frac{E(n)}{V_{centrifugal}(n,\ L)+V_{coulomb}(n)} = 0.833 \\ 1s & n=3 & L=2 & \frac{E(n)}{V_{centrifugal}(n,\ L)+V_{coulomb}(n)} = 0.833 \end{array}$$

This suspicion is confirmed by recalculating the above results after taking out the centrifugal ″potential energy″ term.

$$1s \quad n=1 \quad L=0 \quad \frac{E(n)}{V_{coulomb}(n)} = 0.5$$
$$2s \quad n=2 \quad L=0 \quad \frac{E(n)}{V_{coulomb}(n)} = 0.5 \quad 2p \quad n=2 \quad L=1 \quad \frac{E(n)}{V_{coulomb}(n)} = 0.5$$
$$3s \quad n=3 \quad L=0 \quad \frac{E(n)}{V_{coulomb}(n)} = 0.5 \quad 3p \quad n=3 \quad L=1 \quad \frac{E(n)}{V_{coulomb}(n)} = 0.5$$
$$3d \quad n=3 \quad L=2 \quad \frac{E(n)}{V_{coulomb}(n)} = 0.5$$

While this is decisive, we will also show that the virial theorem (in the form <T>/<V> = -1/2) is satisfied with expectation value calculations using the correct kinetic energy operator.

$$T = -\frac{1}{2}\frac{d^2}{dr^2}\blacksquare + \frac{L(L+1)}{2r^2}\blacksquare$$

This will be demonstrated using the 3s, 3p and 3d eigenfunctions. The n = 1, 2 and 4 eigenfunctions are provided in the Appendix.

$$\Psi_{3s}(r) = \frac{2}{\sqrt{27}}\left(1 - \frac{2}{3}r + \frac{2}{27}r^2\right)\mathrm{r} \quad \Psi_{3p}(r) = \frac{8}{27\sqrt{6}}\left(1 - \frac{r}{6}\right)\mathrm{r}^2\,\exp\left(\frac{-r}{3}\right) \quad \Psi_{3d}(r) = \frac{4}{81\sqrt{30}}\mathrm{r}^2\,\exp\left(\frac{-r}{3}\right)$$
$$\exp\left(-\frac{2}{3}\right)$$

$$3s \quad L=0 \quad \frac{\int_0^\infty \Psi_{3s}(r)\frac{-1}{2}\frac{d^2}{dr^2}\Psi_{3s}(r)dr + \int_0 \frac{L(L+1)}{2r^2}\Psi_{3s}(r)^2 dr}{\int_0^\infty \frac{-1}{r}\Psi_{3s}(r)^2 dr} = -0.5$$
$$3p \quad L=1 \quad \frac{\int_0^\infty \Psi_{3p}(r)\frac{-1}{2}\frac{d^2}{dr^2}\Psi_{3p}(r)dr + \int_0 \frac{L(L+1)}{2r^2}\Psi_{3p}(r)^2 dr}{\int_0^\infty \frac{-1}{r}\Psi_{3p}(r)^2 dr} = -0.5$$
$$3d \quad L=2 \quad \frac{\int_0^\infty \Psi_{3s}(r)\frac{-1}{2}\frac{d^2}{dr^2}\Psi_{3d}(r)dr + \int_0 \frac{L(L+1)}{2r^2}\Psi_{3d}(r)^2 dr}{\int_0^\infty \frac{-1}{r}\Psi_{3d}(r)^2 dr} = -0.5$$

In summary, the "centrifugal effect" and the concept of "effective potential energy" are good examples of the danger in thinking classically about a quantum mechanical system. Furthermore, it's bad pedagogy to create fictitious forces and to mislabel energy contributions in a misguided effort to provide conceptual simplicity. Other concepts in this category, in my opinion, are screening and effective nuclear charge.

Appendix

The following calculations demonstrate that wave functions used are eigenfunctions of the energy operator.

$$1s \quad L=0 \quad \frac{-1}{2}\frac{d^2}{dr^2}\Psi_{1s}(r) + \frac{L(L+1)}{2r^2}\Psi_{1s}(r) - \frac{1}{r}\Psi_{1s}(r) = E_{1s}\Psi_{1s}(r)\text{solve, } E_{1s} \to -\frac{1}{2}$$
$$2s \quad L=0 \quad \frac{-1}{2}\frac{d^2}{dr^2}\Psi_{2s}(r) + \frac{L(L+1)}{2r^2}\Psi_{2s}(r) - \frac{1}{r}\Psi_{2s}(r) = E_{2s}\Psi_{2s}(r)\text{solve, } E_{2s} \to -\frac{1}{8}$$
$$2p \quad L=1 \quad \frac{-1}{2}\frac{d^2}{dr^2}\Psi_{2p}(r) + \frac{L(L+1)}{2r^2}\Psi_{2p}(r) - \frac{1}{r}\Psi_{2p}(r) = E_{2p}\Psi_{2p}(r)\text{solve, } E_{2p} \to -\frac{1}{8}$$
$$3s \quad L=0 \quad \frac{-1}{2}\frac{d^2}{dr^2}\Psi_{3s}(r) + \frac{L(L+1)}{2r^2}\Psi_{3s}(r) - \frac{1}{r}\Psi_{3s}(r) = E_{3s}\Psi_{3s}(r)\text{solve, } E_{3s} \to -\frac{1}{18}$$
$$3p \quad L=1 \quad \frac{-1}{2}\frac{d^2}{dr^2}\Psi_{3p}(r) + \frac{L(L+1)}{2r^2}\Psi_{3p}(r) - \frac{1}{r}\Psi_{3p}(r) = E_{3p}\Psi_{3p}(r)\text{solve, } E_{3p} \to -\frac{1}{18}$$
$$3d \quad L=2 \quad \frac{-1}{2}\frac{d^2}{dr^2}\Psi_{3d}(r) + \frac{L(L+1)}{2r^2}\Psi_{3d}(r) - \frac{1}{r}\Psi_{3d}(r) = E_{3d}\Psi_{3d}(r)\text{solve, } E_{3d} \to -\frac{1}{32}$$
$$4s \quad L=0 \quad \frac{-1}{2}\frac{d^2}{dr^2}\Psi_{4s}(r) + \frac{L(L+1)}{2r^2}\Psi_{4s}(r) - \frac{1}{r}\Psi_{4s}(r) = E_{4s}\Psi_{4s}(r)\text{solve, } E_{4s} \to -\frac{1}{32}$$
$$4p \quad L=1 \quad \frac{-1}{2}\frac{d^2}{dr^2}\Psi_{4p}(r) + \frac{L(L+1)}{2r^2}\Psi_{4p}(r) - \frac{1}{r}\Psi_{4p}(r) = E_{4p}\Psi_{4p}(r)\text{solve, } E_{4p} \to -\frac{1}{32}$$
$$4d \quad L=2 \quad \frac{-1}{2}\frac{d^2}{dr^2}\Psi_{4d}(r) + \frac{L(L+1)}{2r^2}\Psi_{4d}(r) - \frac{1}{r}\Psi_{4d}(r) = E_{4d}\Psi_{4d}(r)\text{solve, } E_{4d} \to -\frac{1}{32}$$
$$4f \quad L=3 \quad \frac{-1}{2}\frac{d^2}{dr^2}\Psi_{4f}(r) + \frac{L(L+1)}{2r^2}\Psi_{4f}(r) - \frac{1}{r}\Psi_{4f}(r) = E_{4f}\Psi_{4f}(r)\text{solve, } E_{4f} \to -\frac{1}{32}$$

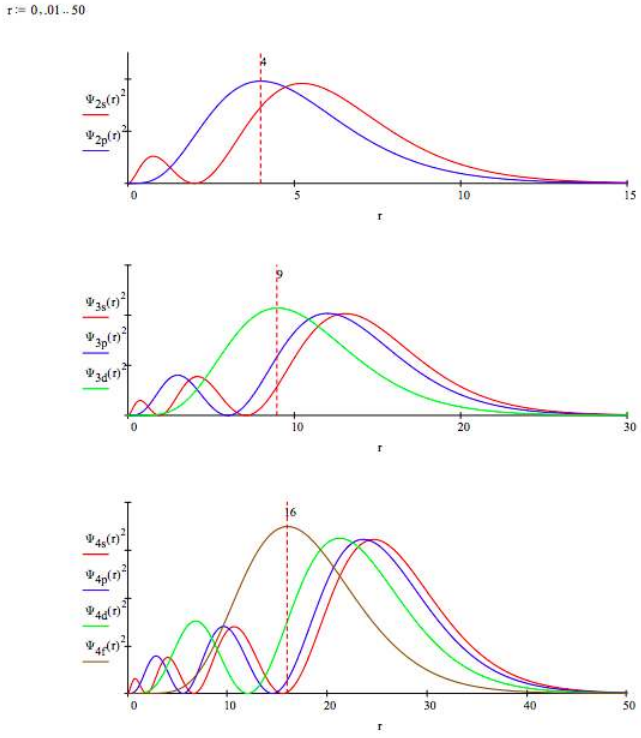
The computational results obtained using the three-dimensional Schrödinger equation,

$$\frac{-1}{2}\frac{d^2}{dr^2}(r,\ \Psi(\theta,\ \phi)) - \frac{1}{2r^2\sin(\theta)}\frac{d}{d\theta}\left(\sin(\theta)\frac{d}{d\theta}\Psi(r,\ \theta,\ \phi)\right)$$
$$-\frac{1}{2r^2\sin(\theta)^2}\frac{d^2}{d\phi^2}\Psi(r,\ \theta,\ \phi) - \frac{1}{r}(r,\ \theta,\ \phi) = E\Psi(r,\ \theta,\ \phi)$$

and its eigenfunctions are identical to those reported in this critique using the one-dimensional radial equation and its eigenfunctions.

Some authors call $\frac{L(L+1)}{2r^2}$ a centrifugal barrier because for L > 0 it prevents the electron from being very close the nucleus, without also noting that the greater the value of L the closer the electron is on average to the nucleus as this equation $r(n,\ L) = \frac{3n^2 - L(L+1)}{2}$ clearly shows. The radial distribution functions for n = 2, 3 and 4 clearly show this dual effect: as L increases for a given n the

average distance to the nucleus decreases as does the electron density in the region nearest the nucleus. The maximum value of the radial distribution function for the highest L state is indicated on each graph.



This page titled 2.18: 110. Critique of the Centrifugal Effect in the Hydrogen Atom is shared under a CC BY 4.0 license and was authored, remixed, and/or curated by Frank Rioux via source content that was edited to the style and standards of the LibreTexts platform.

2.19: A Shorter Critique of the Centrifugal Effect in the Hydrogen Atom

On page 174 of Quantum Chemistry & Spectroscopy, 3rd ed. Thomas Engel derives equation 9.5 which is presented in equivalent form in atomic units (e = me = h/2π = 4πε$_o$ = 1) here.

$$-\frac{1}{2r^2}\frac{d}{dr}\left(r^2\frac{d}{dr}R(r)\right)+\left[\frac{L(L+1)}{2r^2}-\frac{1}{r}\right]R(r)=ER(r)$$

At the bottom of the page he writes,

> Note that the second term (in brackets) on the left-hand side of Equation 9.5 can be viewed as a effective potential, $V_{eff}(r)$. It is made up of the centrifugal potential, which varies as $+1/r^2$, and the Coulomb potential, which varies as -1/r.

$$V_{eff}(r)=\frac{L(L+1)}{2r^2}-\frac{1}{r}$$

Engel notes that because of its positive mathematical sign, the centrifugal potential is repulsive, and goes on to say,

> The net result of this repulsive centrifugal potential is to force the electrons in orbitals with L > 0 (p, d, and f electrons) on average farther from the nucleus than s electrons for which L = 0.

This statement is contradicted by the radial distribution functions shown in Figure 9.10 on page 187, which clearly show the opposite effect. As L increases the electron is on average closer to the nucleus. It is further refuted by calculations of the average value of the electron position from the nucleus as a function of the n and L quantum numbers. For a given n the larger L is the closer on average the electron is to the nucleus. In other words, these calculations support the graphical representation in Figure 9.10.

$$r(n,\ L)=\tfrac{3n^2-L(L+1)}{2}\qquad\begin{pmatrix} \mathrm{L} & 0 & 1 & 2 & 3\\ n=1 & 1.5 & ' & ' & '\\ n=2 & 6 & 5 & ' & '\\ n=3 & 13.5 & 12.5 & 10.5 & '\\ n=4 & 24 & 23 & 21 & 18\end{pmatrix}$$

On page 180 in Example Problem 9.2, Engel introduces the virial theorem. For systems with a Coulombic potential energy, such as the hydrogen atom, it is <V>= 2<E> = -2<T>. We will work with the version <E>/<V> = 0.5. The values of the energy, the so called centrifugal potential energy and the Coulombic potential energy are as shown below as a function of the appropriate quantum numbers.

$$E(n)=\tfrac{-1}{2n^2}\quad V_{centrifugal}(n,\ L)=\tfrac{L(L+1)}{2n^3(L+\frac{1}{2})}\quad V_{coulomb}(n)=-\tfrac{1}{n^2}$$

The calculations below show that the virial theorem is violated for any state for which L > 0.

$$\begin{array}{llll} 1s & n=1 & L=0 & \frac{E(n)}{V_{centrifugal}(n,\ L)+V_{coulomb}(n)}=0.5\\ 2s & n=2 & L=0 & \frac{E(n)}{V_{centrifugal}(n,\ L)+V_{coulomb}(n)}=0.5\\ 2p & n=2 & L=1 & \frac{E(n)}{V_{centrifugal}(n,\ L)+V_{coulomb}(n)}=0.75\\ 3s & n=3 & L=0 & \frac{E(n)}{V_{centrifugal}(n,\ L)+V_{coulomb}(n)}=0.5\\ 3p & n=3 & L=1 & \frac{E(n)}{V_{centrifugal}(n,\ L)+V_{coulomb}(n)}=0.833\\ 1s & n=3 & L=2 & \frac{E(n)}{V_{centrifugal}(n,\ L)+V_{coulomb}(n)}=0.833 \end{array}$$

These calculations are now repeated eliminating the centrifugal term, showing that the virial theorem is satisfied and supporting the claim that the "centrifugal potential" is actually a kinetic energy term.

$$\begin{array}{llll} 1s & n=1 & L=0 & \frac{E(n)}{V_{coulomb}(n)}=0.5 \quad 2s \quad n=2 \quad L=0 \quad \frac{E(n)}{V_{coulomb}(n)}=0.5\\ 2p & n=2 & L=1 & \frac{E(n)}{V_{coulomb}(n)}=0.5 \quad 3s \quad n=3 \quad L=0 \quad \frac{E(n)}{V_{coulomb}(n)}=0.5\\ 3p & n=3 & L=1 & \frac{E(n)}{V_{coulomb}(n)}=0.5 \quad 3d \quad n=3 \quad L=2 \quad \frac{E(n)}{V_{coulomb}(n)}=0.5 \end{array}$$

We finish by rewriting the equation at the top with brackets showing that the first two terms are quantum kinetic energy and that the Coulombic term is the only potential energy term.

$$\left[-\frac{1}{2r^2}\frac{d}{dr}\left(r^2\frac{d}{dr}R(r)\right)+\frac{L(L+1)}{2r^2}R(r)\right]-\frac{1}{r}R(r)=ER(r)$$

In summary, the "centrifugal potential" and the concept of "effective potential energy" are good examples of the danger in thinking classically about a quantum mechanical system. Furthermore, it's bad pedagogy to create fictitious forces and to mislabel energy contributions in a misguided effort to provide conceptual simplicity.

This page titled 2.19: A Shorter Critique of the Centrifugal Effect in the Hydrogen Atom is shared under a CC BY 4.0 license and was authored, remixed, and/or curated by Frank Rioux via source content that was edited to the style and standards of the LibreTexts platform.

2.20: Exploring the Role of Lepton Mass in the Hydrogen Atom

Under normal circumstances the the hydrogen atom consists of a proton and an electron. However, electrons are leptons and there are two other leptons which could temporarily replace the electron in the hydrogen atom. The other leptons are the muon and tauon, and their fundamental properties, along with those of the electron, are given in the following table.

$$\begin{pmatrix} \text{Property} & e & \mu & \tau \\ \frac{\text{Mass}}{m_e} & 1 & 206.8 & 3491 \\ \frac{\text{Effective Mass}}{m_e} & 1 & 185.86 & 1203 \\ \frac{\text{Life Time}}{s} & \text{Stable} & 2.2(10)^{-6} & 3.0(10)^{-13} \end{pmatrix}$$

The purpose of this exercise is to demonstrate the importance of mass in atomic systems, and therefore also kinetic energy. Substitution of the deBroglie relation (λ = h/mv) into the classical expression for kinetic energy yields a quantum mechanical expression for kinetic energy. It is of utmost importance that in quantum mechanics, kinetic energy is inversely proportional to mass.

$$T = \frac{1}{2}mv^2 = \frac{h^2}{2m\lambda}$$

A more general and versatile quantum mechanical expression for kinetic energy is the differential operator shown below, where again mass appears in the denominator. An Approach to Quantum Mechanics outlines the origin of kinetic energy operator.

Atomic units ($e = m_e = h/2\pi = 4\pi\varepsilon_o = 1$) will be used in the calculations that follow. Please note that μ in the equations below is the effective mass and not a symbol for the muon.

Kinetic energy operator:

$$T = -\frac{1}{2\mu r}\frac{d^2}{dr^2}(r\blacksquare)$$

Potential energy operator:

$$V = -\frac{1}{r}\blacksquare$$

Variational trial wave function with variational parameter β:

$$\Psi(r,\ \beta) = \left(\frac{\beta^3}{\pi}\right)^{\frac{1}{2}} \exp(-\beta r)$$

Evaluation of the variational energy integral:

$$\begin{matrix} E(\beta,\ \mu) = \int_0^\infty \Psi(r,\ \beta)\left[-\frac{1}{2\mu r}\frac{d^2}{dr^2}(r\Psi(r,\ \beta))\right] 4\pi r^2 dr \ldots \\ + \int_0^\infty \Psi(r,\ \beta) - \frac{1}{r}\Psi(r,\ \beta) 4\pi r^2 dr \end{matrix} \left| \begin{matrix} \text{assume, } \beta>0 \\ \text{simplify} \end{matrix} \right. \rightarrow \frac{\beta^2}{2\mu} - \beta$$

Minimize the energy with respect to the variational parameter β.

$$\frac{d}{d\beta}E(\beta,\ \mu + 0 \text{ solve, } \beta \rightarrow \mu$$

Express energy in terms of reduced mass:

$$E(\beta,\ \mu) \text{ substitute, } \beta = \mu \rightarrow -\frac{\mu}{2}$$

Using the virial theorem, the kinetic and potential energy contributions are:

$$T = \tfrac{\mu}{2} \quad V = -\mu$$

Express the trial wave function in terms of reduced mass.

$$\Psi(r,\ \beta) \text{ substitute, } \beta = \mu \rightarrow \frac{e^{-\mu r}\sqrt{\mu^3}}{\sqrt{\pi}}$$

Demonstrate the effect of mass on the radial distribution function with plots of mass equal to 0.5, 1 and 2.

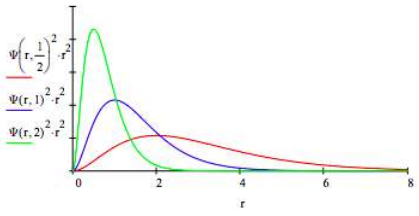


Figure 1

Calculate the expectation value for position to show that it is consistent with the graphical representation above. The more massive the lepton the closer it is on average to the proton.

$$\int_0^\infty \Psi(r,\ \mu) r \Psi(r,\ \mu) 4\pi r^2 \text{dr assume, } \mu > 0 \rightarrow \frac{3}{2\mu}$$

Summarize the calculated values for the physical properties of H_e, H_μ and H_τ.

Species	$\frac{E}{E_h}$	$\frac{T}{E_h}$	$\frac{V}{E_h}$	$\frac{r_{avg}}{a_o}$
H_e	$\frac{-1}{2}$	$\frac{1}{2}$	-1	$\frac{3}{2}$
H_μ	-92.93	92.93	-185.86	$8.07(10)^{-3}$
H_τ	-601.5	601.5	-1203	$1.25(10)^{-3}$

Now imagine that you have a regular hydrogen atom in its ground state and the electron is suddenly by some mechanism replaced by a muon. Nothing has changed from an electrostatic perspective, but the change in energy and average distance of the lepton from the proton are very large. The ground state energy and the average distance from the nucleus decrease by a factor of 185.6, the ratio of the effective masses of the electron and the muon.

This mass effect provides a challenge for those who think all atomic physical phenomena can be explained in terms of electrostatic potential energy effects. Of course, there is an even bigger problem for the potential energy aficionados, and that is the fundamental issue of atomic and molecular stability. Quantum mechanical kinetic energy effects are required to explain the stability of matter.

A Fourier transform of the coordinate wave function yields the corresponding momentum distribution and the opportunity to create a visualization of the uncertainty principle.

$$\Phi(p,\ \mu) = \frac{1}{4\sqrt{\pi^3}} \int_0^\infty \exp(\text{-i p r}) \Psi(r,\ \mu) 4\pi r^2 dr \left| \begin{array}{l} \text{assume, } \mu>0 \\ \text{simplify} \end{array} \right. \rightarrow \frac{2\mu^{\frac{3}{2}}}{\pi(\mu + p\ i)^3}$$

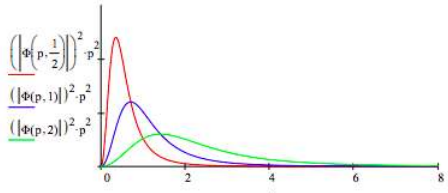


Figure 2

Figure 2 shows that the most massive particle has the most delocalized momentum distribution. This is consistent with the uncertainty principle which states less spatial uncertainty is accompanied by greater uncertainty in the momentum distribution.

Replacing the proton with a positron, the electron's anti-particle, creates another exotic atom, positronium (Ps). In its singlet ground state electron-positron annihilation occurs in 125 ps creating two γ rays. Positronium's (μ = 1/2) spatial and momentum distributions are shown in Figures 1 and 2. A revised table including positronium is provided below.

Species	$\frac{E}{E_h}$	$\frac{T}{E_h}$	$\frac{V}{E_h}$	$\frac{r_{avg}}{a_o}$
H_e	$\frac{-1}{2}$	$\frac{1}{2}$	-1	$\frac{3}{2}$
H_μ	-92.93	92.93	-185.86	$8.07(10)^{-3}$
H_τ	-601.5	601.5	-1203	$1.25(10)^{-3}$
Ps	$-\frac{1}{4}$	$\frac{1}{4}$	$-\frac{1}{2}$	3

This page titled 2.20: Exploring the Role of Lepton Mass in the Hydrogen Atom is shared under a CC BY 4.0 license and was authored, remixed, and/or curated by Frank Rioux via source content that was edited to the style and standards of the LibreTexts platform.

2.21: The Effect of Lepton Mass on the Energy and Bond Length of the Hydrogen Molecule Ion

There are many in the chemical education community who believe that chemical bonding is simply an electrostatic phenomenon. I and several others have argued against this incorrect, simplistic view on many occasions (most of my critiques can be found in this section of my tutorials). In this tutorial the simplistic electrostatic model is shown to be inadequate by consideration of the effect of lepton mass on the equilibrium geometry (bond length) and energy of the hydrogen molecule ion. The electron has several heavy weight cousins and in this analysis we will look at the effect of replacing the electron with the muon (207 m_e).

The molecular orbital for the hydrogen molecule ion is formed as a linear combination of scaled hydrogenic 1s orbitals centered on the nuclei, a and b.

$$\Psi = \frac{a+b}{\sqrt{2+2S}} \quad \text{where} \quad a = \sqrt{\frac{\alpha^3}{\pi}}\exp\left(-\alpha r_a\right) \quad b = \sqrt{\frac{\alpha^3}{\pi}}\exp\left(-\alpha r_b\right) \quad S = \int abd\tau$$

The molecular energy operator in atomic units:

$$H = \frac{-1}{2}\left[\frac{d}{dr}\left(r^2\frac{d}{dr}\blacksquare\right)\right] - \frac{1}{r_a} - \frac{1}{r_b} + \frac{1}{R}$$

The energy integral to be minimized by the variation method:

$$E = \frac{\int (a+b)H(a+b)d\tau}{2+2S}$$

When this integral is evaluated the following expression for the energy is obtained.

$$E(\alpha,\ m,\ R) = \frac{-\alpha^2}{2m} + \frac{\frac{\alpha^2}{m} - \alpha - \frac{1}{R} + \frac{1}{R}(1+\alpha R)\exp(-2\alpha R) + \alpha\left(\frac{\alpha}{m} - 2\right)(1+\alpha R)\exp(-\alpha R)}{1+\exp(-\alpha,\ R)\left(1+\alpha R+\frac{\alpha^2 R^2}{3}\right)} + \frac{1}{R}$$

Minimization of the energy of the hydrogen molecule ion for the electron follows. There are two variational parameters, the orbital scale factor and internuclear distance.

Electron mass: m = 1

Seed values for the variational parameter and internuclear separation:

$$\alpha = 1 \quad R = .1$$

$$\text{Given} \quad \frac{d}{d\alpha}(\alpha,\ m,\ R) = 0 \qquad \begin{matrix}\frac{d}{dR}\\ E(\alpha,\ m,\ R)\\ = 0\end{matrix} \qquad \begin{pmatrix}\alpha\\ R\end{pmatrix} = \text{Find}(\alpha,\ R) \qquad \begin{pmatrix}\alpha\\ R\end{pmatrix} = \begin{pmatrix}1.238\\ 2.0033\end{pmatrix} \qquad \begin{matrix}E(\alpha,\ m,\ R)\\ = -0.5865\end{matrix}$$

This result is well-known and can be found in any comprehensive quantum chemistry text. Next we replace the electron with the more massive muon and recalculate the ground-state energy.

Muon mass: m = 207

Seed values for the variational parameter and internuclear separation:

$$\alpha = 200 \quad R = .012$$

$$\text{Given} \quad \frac{d}{d\alpha}(\alpha,\ m,\ R) = 0 \qquad \begin{matrix}\frac{d}{dR}\\ E(\alpha,\ m,\ R)\\ = 0\end{matrix} \qquad \begin{pmatrix}\alpha\\ R\end{pmatrix} = \text{Find}(\alpha,\ R) \qquad \begin{pmatrix}\alpha\\ R\end{pmatrix} = \begin{pmatrix}256.2721\\ 0.0097\end{pmatrix} \qquad \begin{matrix}E(\alpha,\ m,\ R)\\ = -121.4068\end{matrix}$$

The results of the calculations are summarized in the following table.

$$\begin{pmatrix} \text{Lepton} & \frac{E}{E_h} & \frac{R}{a_o} \\ \text{Electron} & -0.5865 & 2.0033 \\ \text{Muon} & -121.41 & 0.0097 \end{pmatrix}$$

Now imagine that you have a regular hydrogen molecule ion in its ground state and the electron is suddenly by some mechanism replaced by a muon. Nothing has changed from an electrostatic perspective, but the changes in energy and internuclear distance (bond length) of the molecule are very large as is shown in the table. For example, in the muonium molecule the bond length decreases sharply bringing the nuclei 207 times closer than they are in the electron version of the molecule.

This mass effect provides a challenge for those who think chemical bond can be explained in terms of electrostatic potential energy effects. The mass change is important because quantum mechanical kinetic energy is inversely proportional to mass. By comparison classical kinetic energy is directly proportional to mass.*

Of course, there is an even bigger problem for the potential energy aficionados, and that is the fundamental issue of atomic and molecular stability. Quantum mechanical kinetic energy is required to explain the stability of matter and the physical nature of the chemical bond.

* The mass effect in the harmonic oscillator (kinetic isotope effect) is also a quantum kinetic energy phenomenon. See http://www.users.csbsju.edu/~frioux/sho/Uncertainty-SHO.pdf for calculations on the effect of mass in the harmonic oscillator.

This page titled 2.21: The Effect of Lepton Mass on the Energy and Bond Length of the Hydrogen Molecule Ion is shared under a CC BY 4.0 license and was authored, remixed, and/or curated by Frank Rioux via source content that was edited to the style and standards of the LibreTexts platform.

2.22: The Hydrogen Atom with Finite Sized Nucleus

This exercise explores the impact of nuclear size on the ground state energy of the hydrogen atom's electron. The traditional approach assumes that the proton is a dimensionless point charge, which is a very good approximation for the hydrogen atom. However, for heavy atoms with many protons and neutrons, the finite size of the nucleus has to be taken into consideration when the goal is exact results. If the proton has uniform charge density and is given a finite radius, the potential energy of the electron is as given below.

Nuclear radius: Rn = 0.1

Potential energy:

$$V(r) = \text{if}\left[r \le \text{Rn},\ \frac{-1}{\text{Rn}}\left(1.5 - \frac{r^2}{2Rn^2}\right),\ \frac{-1}{r}\right]$$

Numerical integration of Schrödinger's equation (see below) yields the following results.

$$\begin{pmatrix} \frac{\text{Nuclear Radius}}{a_o} & 0 & 0.1 & 0.2 & 0.5 & 1.0 & 2.0 \\ \frac{\text{Energy}}{E_h} & -0.500 & -0.496 & -0.488 & -0.450 & -0.385 & -0.293 \end{pmatrix}$$

A recommended exercise is to repeat these calculations for the 2s and 3s electronic states, and interpret the results.

Numerical integration of Schrödinger's equation:

$$\text{Given} \quad \frac{-1}{2\mu}\frac{d^2}{dr^2}\Psi(r) \quad -\frac{1}{r\mu}\frac{d}{dr}\Psi(r) + \left[\frac{L(L+1)}{2\mu r^2} + V(r)\right]\Psi(r) = E\Psi(r) \quad \Psi(.0001) = .1 \quad \Psi(.0001) = 0$$

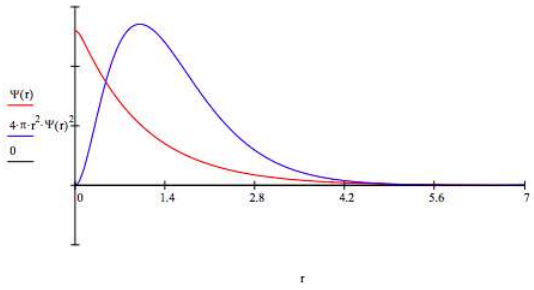
$$\Psi = \text{Odesolve}\,(r,\ r_{max})$$

Normalize the wave function:

$$\Psi(r) = \left(\int_0^{r_{max}} \Psi(r)^2 4\pi r^2 dr\right)^{-.5}\Psi(r)$$

Reduced mass: $\mu = 1$ Angular momentum: $L = 0$ Integration limit: $r_{max} = 7$

Energy guess: $E = -0.496$ $r = 0,\ .01..r_{max}$



This page titled 2.22: The Hydrogen Atom with Finite Sized Nucleus is shared under a CC BY 4.0 license and was authored, remixed, and/or curated by Frank Rioux via source content that was edited to the style and standards of the LibreTexts platform.

2.23: The Hyperfine Interaction in the Hydrogen Atom

The purpose of this tutorial is to provide a much abreviated version of the first three sections in Chapter 12 of Volume III of *The Feynman Lectures on Physics*. These sections deal with the hyperfine interaction in the hydrogen atom.

At the introductory quantum chemistry-physics level we treat the hydrogen atom using an energy operator consisting of a kinetic energy term and an electron-proton potential energy term and calculate the ground-state energy. These are clearly the most important terms in the total energy operator, but they are not the only terms. The proton and electron are spin-1/2 fermions and as such have magnetic moments which interact with one another. This means that the ground state that we have calculated consists of four terms which have slightly different energies due to the magnetic interaction between the electron and proton (hyperfine splitting).

For example, listing the electron spin first we have the following four electron-proton states in the z-basis: |++>, |+->, |-+> and |-->. The spin-spin operator is.

$$\hat{H}_{SpinSpin} = A\omega^e\omega^p = A\left(\omega_x^e\omega_x^p + \omega_y^e\omega_y^p + \omega_z^e\omega_z^p\right)$$

where the Pauli spin operators appear on the right side and represent the magnetic interaction between the electron and proton. The identity operator, on the right, will be needed later.

$$\omega_x = \begin{pmatrix} 0 & 1 \\ 1 & 0 \end{pmatrix} \quad \omega_y = \begin{pmatrix} 0 & -i \\ i & 0 \end{pmatrix} \quad \omega_z = \begin{pmatrix} 1 & 0 \\ 0 & -1 \end{pmatrix} \quad I = \begin{pmatrix} 1 & 0 \\ 0 & 1 \end{pmatrix}$$

Tensor multiplication is now used to represent the spin-spin operator in matrix format. In the interest of mathematical clarity the constant A a is set equal to unity.

$$H_{SpinSpin} = \left(\text{kronecker}\left(\omega_x,\ \omega_x\right) + \text{kronecker}\left(\omega_y,\ \omega_y\right) + \text{kronecker}\left(\omega_z,\ \omega_z\right)\right)$$

$$H_{SpinSpin} = \begin{pmatrix} 1 & 0 & 0 & 0 \\ 0 & -1 & 2 & 0 \\ 0 & 2 & -1 & 0 \\ 0 & 0 & 0 & 1 \end{pmatrix}$$

We know ask Mathcad to calculate the eigenvalues and eigenvectors of the spin-spin operator. These results are displayed by constructing a matrix which contains the eigenvalues in the top row, and their eigenvectors in the columns below the eigenvalues.

$$E = \text{eigenvals}\left(H_{SpinSpin}\right) \quad \text{EigenvalEigenvec} = \text{rsort}\left(\text{stack}\left(E^T,\ \text{eigenvecs}\left(H_{SpinSpin}\right)\right),\ 1\right)$$

$$\text{EigenvalEigenvec} = \begin{pmatrix} -3 & 1 & 1 & 1 \\ 0 & 0 & 0 & 1 \\ 0.707 & 0.707 & 0 & 0 \\ -0.707 & 0.707 & 0 & 0 \\ 0 & 0 & 1 & 0 \end{pmatrix}$$

These results are expressed in more familiar form below.

$$\begin{array}{ll} & |T\rangle_1 = |\uparrow\rangle_p|\uparrow\rangle_e \\ \text{Triplet state } \mathrm{E}_T = 1 & |T\rangle_0 = \frac{1}{\sqrt{2}}\left[|\uparrow\rangle_p|\downarrow\rangle_e + |\downarrow\rangle_p|\uparrow\rangle_e\right] \\ & |T\rangle_{-1} = |T\downarrow\rangle_p|\downarrow\rangle_e \\ \text{Singlet state } \mathrm{E}_s = -3 & |S\rangle_0 = \frac{1}{\sqrt{2}}\left[|\uparrow\rangle_p|\downarrow\rangle_e - |\downarrow\rangle_p|\uparrow\rangle_e\right] \end{array}$$

We can achieve the same result using these electron-proton states: |++>, |+->, |-+> and |-->.

First we write the spin states in vector format:

$$|+\rangle = \begin{pmatrix} 1 \\ 0 \end{pmatrix} \quad |-\rangle = \begin{pmatrix} 0 \\ 1 \end{pmatrix}$$

Next we write the four electron-proton spin states in tensor format.

$$|++\rangle = \begin{pmatrix}1\\0\end{pmatrix} \otimes \begin{pmatrix}1\\0\end{pmatrix} = \begin{pmatrix}1\\0\\0\\0\end{pmatrix} \quad |+-\rangle = \begin{pmatrix}1\\0\end{pmatrix} \otimes \begin{pmatrix}0\\1\end{pmatrix} = \begin{pmatrix}0\\1\\0\\0\end{pmatrix}$$

$$|-+\rangle = \begin{pmatrix}0\\1\end{pmatrix} \otimes \begin{pmatrix}1\\0\end{pmatrix} = \begin{pmatrix}0\\0\\1\\0\end{pmatrix} \quad |--\rangle = \begin{pmatrix}0\\1\end{pmatrix} \otimes \begin{pmatrix}0\\1\end{pmatrix} = \begin{pmatrix}0\\0\\0\\1\end{pmatrix}$$

These spin states are given the following labels to facilitate the calculation of energy matrix.

$$a = \begin{pmatrix}1\\0\\0\\0\end{pmatrix} \quad b = \begin{pmatrix}0\\1\\0\\0\end{pmatrix} \quad c = \begin{pmatrix}0\\0\\1\\0\end{pmatrix} \quad d = \begin{pmatrix}0\\0\\0\\1\end{pmatrix}$$

$$\text{eigenvals}\left(\begin{pmatrix} a^T H_{\text{SpinSpin}} a & a^T H_{\text{SpinSpin}} b & a^T H_{\text{SpinSpin}} c & a^T H_{\text{SpinSpin}} d \\ b^T H_{\text{SpinSpin}} a & b^T H_{\text{SpinSpin}} b & b^T H_{\text{SpinSpin}} c & b^T H_{\text{SpinSpin}} d \\ c^T H_{\text{SpinSpin}} a & c^T H_{\text{SpinSpin}} b & c^T H_{\text{SpinSpin}} c & c^T H_{\text{SpinSpin}} d \\ d^T H_{\text{SpinSpin}} a & d^T H_{\text{SpinSpin}} b & d^T H_{\text{SpinSpin}} c & d^T H_{\text{SpinSpin}} d \end{pmatrix}\right) = \begin{pmatrix}1\\-3\\1\\1\end{pmatrix}$$

$$\text{eigenvecs}\left(\begin{pmatrix} a^T H_{\text{SpinSpin}} a & a^T H_{\text{SpinSpin}} b & a^T H_{\text{SpinSpin}} c & a^T H_{\text{SpinSpin}} d \\ b^T H_{\text{SpinSpin}} a & b^T H_{\text{SpinSpin}} b & b^T H_{\text{SpinSpin}} c & b^T H_{\text{SpinSpin}} d \\ c^T H_{\text{SpinSpin}} a & c^T H_{\text{SpinSpin}} b & c^T H_{\text{SpinSpin}} c & c^T H_{\text{SpinSpin}} d \\ d^T H_{\text{SpinSpin}} a & d^T H_{\text{SpinSpin}} b & d^T H_{\text{SpinSpin}} c & d^T H_{\text{SpinSpin}} d \end{pmatrix}\right) = \begin{pmatrix} 0 & 0 & 1 & 0 \\ 0.707 & 0.707 & 0 & 0 \\ 0.707 & -0.707 & 0 & 0 \\ 0 & 0 & 0 & 1 \end{pmatrix}$$

Identical to the previous calculation, this method also yields an upper triplet state at E = 1 and a lower singlet at E = -3. Two of the four final states are superpositions of |+-> and |-+>. In other words, we have found the eigenstates of the spin-spin energy operator as is shown below. Using these states the spin-spin energy matrix is diagonal.

$$a = \begin{pmatrix}1\\0\\0\\0\end{pmatrix} \quad b = \begin{pmatrix}0\\\frac{1}{\sqrt{2}}\\\frac{1}{\sqrt{2}}\\0\end{pmatrix} \quad c = \begin{pmatrix}0\\0\\0\\1\end{pmatrix} \quad d = \begin{pmatrix}0\\\frac{1}{\sqrt{2}}\\-\frac{1}{\sqrt{2}}\\0\end{pmatrix}$$

$$\begin{pmatrix} a^T H_{\text{SpinSpin}} a & a^T H_{\text{SpinSpin}} b & a^T H_{\text{SpinSpin}} c & a^T H_{\text{SpinSpin}} d \\ b^T H_{\text{SpinSpin}} a & b^T H_{\text{SpinSpin}} b & b^T H_{\text{SpinSpin}} c & b^T H_{\text{SpinSpin}} d \\ c^T H_{\text{SpinSpin}} a & c^T H_{\text{SpinSpin}} b & c^T H_{\text{SpinSpin}} c & c^T H_{\text{SpinSpin}} d \\ d^T H_{\text{SpinSpin}} a & d^T H_{\text{SpinSpin}} b & d^T H_{\text{SpinSpin}} c & d^T H_{\text{SpinSpin}} d \end{pmatrix} = \begin{pmatrix}1&0&0&0\\0&1&0&0\\0&0&1&0\\0&0&0&-3\end{pmatrix}$$

The spin-spin hyperfine interaction is the basis of the hydrogen maser. The triplet state is selected using a Stern-Gerlach magnet and then 21 cm photons induce a triplet-singlet transition creating a coherent beam of photons.

The following table calculates expectation values for the z-direction spin for triplet and singlet states. In the first column, the expectation values for z-direction measurements jointly on the electron and proton are calculated. The next two columns calculate the z-direction expectation values for the electron and proton independently.

$$\begin{pmatrix} a^T \text{kronecker}(\sigma_z,\ \sigma_z)\, a & a^T \text{kronecker}(\sigma_z,\ I)\, a & a^T \text{kronecker}(I,\ \sigma_z)\, a \\ b^T \text{kronecker}(\sigma_z,\ \sigma_z)\, b & b^T \text{kronecker}(\sigma_z,\ I)\, b & b^T \text{kronecker}(I,\ \sigma_z)\, b \\ c^T \text{kronecker}(\sigma_z,\ \sigma_z)\, c & c^T \text{kronecker}(\sigma_z,\ I)\, c & c^T \text{kronecker}(I,\ \sigma_z)\, c \\ d^T \text{kronecker}(\sigma_z,\ \sigma_z)\, d & d^T \text{kronecker}(\sigma_z,\ I)\, d & d^T \text{kronecker}(I,\ \sigma_z)\, d \end{pmatrix} = \begin{pmatrix}1&1&1\\-1&0&0\\1&-1&-1\\-1&0&0\end{pmatrix}$$

The b and d states are entangled Bell states. Note that in these states the expectation values for the individual spins are 0, indicating complete randomness. Collectively, however, the electron and proton always show opposite spin states leading to a joint

expectation value of -1. In other words, the measurement result for the z-spin for either the electron or proton is completely random, but once the result for one of the particles is obtained, the other particle's spin state can be predicted with certainty.

This page titled 2.23: The Hyperfine Interaction in the Hydrogen Atom is shared under a CC BY 4.0 license and was authored, remixed, and/or curated by Frank Rioux via source content that was edited to the style and standards of the LibreTexts platform.

2.24: Positronium Annihilation

The following provides an alternative mathematical analysis of the annihilation of positronium as presented in section 18-3 in Volume III of *The Feynman Lectures on Physics*.

Positronium is an analog of the hydrogen atom in which the proton is replaced by a positron, the electron's anti-particle. The electron-positron pair undergoes annihilation in 10-10 seconds producing two γ-ray photons. Positronium's effective mass is 1/2, yielding a ground state energy (excluding the magnetic interactions between the spin 1/2 anti-particles) E = -0.5μE_h = -0.25 E_h. Considering spin the ground state is four-fold degenerate, but this degeneracy is split by the magnetic spin-spin hyperfine interaction shown below. See "The Hyperfine Splitting in the Hydrogen Atom" for further detail.

$$\hat{H}_{SpinSpin} = A\sigma^e\sigma^p = A\left(\sigma_x^e\sigma_x^p + \sigma_y^e\sigma_y^p + \sigma_z^e\sigma_z^p\right)$$

The spin-spin Hamiltonian has the following eigenvalues (top row) and eigenvectors (columns beneath the eigenvalues), showing a singlet ground state and triplet excited state. The electron-positron spin states are to the right of the table with their m quantum numbers, showing that the singlet (j = 0, m = 0) is a superposition state as is one of the triplet states (j = 1, m = 0). The parameter A is much larger for positronium than for the hydrogen atom because the positron has a much larger magnetic moment than the proton.

$$\begin{pmatrix} -3A & A & A & A \\ 0 & 0 & 0 & 1 \\ \frac{1}{\sqrt{2}} & \frac{1}{\sqrt{2}} & 0 & 0 \\ -\frac{1}{\sqrt{2}} & \frac{1}{\sqrt{2}} & 0 & 0 \\ 0 & 0 & 1 & 0 \end{pmatrix} \begin{matrix} |++\rangle\ m=1 \\ |+-\rangle\ m=0 \\ |-+\rangle\ m=0 \\ |--\rangle\ m=-1 \end{matrix}$$

Feynman shows that when the singlet ground state (J = 0, m = 0) annihilates, conservation of momentum requires that the photons emitted in opposite directions (A and B) must have the same circular polarization state, either both in the right or both in left circular state in their direction of motion. This leads to the following entangled superposition. The negative sign is required by parity conservation. The positronium ground state has negative parity (see above), therefore the final photon state must have negative parity.

$$|\Psi\rangle = \frac{1}{\sqrt{2}}\left[|R\rangle_A|R\rangle_B - |L\rangle_A|L\rangle_B\right] = \frac{1}{2\sqrt{2}}\left[\begin{pmatrix}1\\i\end{pmatrix}_A \otimes \begin{pmatrix}1\\i\end{pmatrix}_B - \begin{pmatrix}1\\-i\end{pmatrix}_A \otimes \begin{pmatrix}1\\-i\end{pmatrix}_B\right]$$
$$= \frac{1}{2\sqrt{2}}\left[\begin{pmatrix}1\\i\\i\\-1\end{pmatrix} - \begin{pmatrix}1\\-i\\-i\\-1\end{pmatrix}\right] = \frac{i}{\sqrt{2}}\begin{pmatrix}0\\1\\1\\0\end{pmatrix}$$

The circular polarization states are:

$$R = \frac{1}{\sqrt{2}}\begin{pmatrix}1\\i\end{pmatrix} \quad L = \frac{1}{\sqrt{2}}\begin{pmatrix}1\\-i\end{pmatrix}$$

The appropriate operators are formed below:

$$RC = R\left(\overline{R}\right)^T \rightarrow \begin{pmatrix}\frac{1}{2} & -\frac{1}{2}i\\ \frac{1}{2}i & \frac{1}{2}\end{pmatrix} \quad LC = L\left(\overline{L}\right)^T \rightarrow \begin{pmatrix}\frac{1}{2} & \frac{1}{2}i\\ -\frac{1}{2}i & \frac{1}{2}\end{pmatrix} \quad RLC = R\left(\overline{R}\right)^T - L\left(\overline{L}\right)^T \rightarrow \begin{pmatrix}0 & -i\\ i & 0\end{pmatrix}$$

RLC is the angular momentum operator for photons. Below it is shown that |R> and |L> are eigenstates with eigenvalues of +1 and -1, respectively.

$$\text{eigenvals(RLC)} = \begin{pmatrix}1\\-1\end{pmatrix} \quad \text{RLC R} \rightarrow \begin{pmatrix}\frac{\sqrt{2}}{2}\\ \frac{\sqrt{2}i}{2}\end{pmatrix} \quad \text{RLC L} \rightarrow \begin{pmatrix}-\frac{\sqrt{2}}{2}\\ \frac{\sqrt{2}i}{2}\end{pmatrix}$$

Now we can consider some of the measurements that Feynman discusses in his analysis of positronium annihilation. Because the photons in state Ψ are entangled the measurements of observers A and B are correlated. For example, if observers A and B both measure the circular polarization of their photons and compare their results they always agree that they have measured the same polarization state. Their composite expectation value is 1.

$$\Psi = \frac{i}{\sqrt{2}} \begin{pmatrix} 0 \\ 1 \\ 1 \\ 0 \end{pmatrix} \quad \left(\overline{\Psi}\right)^T \text{kronecker(RLC, RLC)}\Psi = 1$$

The identity operation, do nothing, is now needed:

$$I = \begin{pmatrix} 1 & 0 \\ 0 & 1 \end{pmatrix}$$

But their individual results are a random sequence of +1 and -1 outcomes averaging to an expectation value of zero.

$$\left(\overline{\Psi}\right)^T \text{kronecker(RLC, I)}\Psi = 0 \quad \left(\overline{\Psi}\right)^T \text{kronecker(I, RLC)}\Psi = 0$$

The probability that both observers will measure |R> or both measure |L> is 0.5. The probability that one will measure |R> and the other |L>, or vice versa is zero.

$$\left(\overline{\Psi}\right)^T \text{kronecker(RC, RC)}\Psi = 0.5 \quad \left(\overline{\Psi}\right)^T \text{kronecker(LC, LC)}\Psi = 0.5 \quad \left(\overline{\Psi}\right)^2 \text{kronecker(LC, RC)}\Psi = 0$$

Because |R> and |L> are superpositions of |V> and |H>, the photon wave function can also be written in the V-H plane polarization basis as is shown below. See the Appendix for an alternative justification.

$$|\Psi\rangle = \frac{i}{\sqrt{2}} \left[|V\rangle_A |H\rangle_B + |H\rangle_A |V\rangle_B\right] = \frac{i}{\sqrt{2}} \left[\begin{pmatrix} 1 \\ 0 \end{pmatrix}_A \otimes \begin{pmatrix} 0 \\ 1 \end{pmatrix}_B + \begin{pmatrix} 0 \\ 1 \end{pmatrix}_A \otimes \begin{pmatrix} 1 \\ 0 \end{pmatrix}_B\right]$$
$$= \frac{i}{\sqrt{2}} \left[\begin{pmatrix} 0 \\ 1 \\ 0 \\ 0 \end{pmatrix} + \begin{pmatrix} 0 \\ 0 \\ 1 \\ 0 \end{pmatrix}\right] = \frac{i}{\sqrt{2}} \begin{pmatrix} 0 \\ 1 \\ 1 \\ 0 \end{pmatrix}$$

The eigenstates for plane polarization are:

$$V = \begin{pmatrix} 1 \\ 0 \end{pmatrix} \quad H = \begin{pmatrix} 0 \\ 1 \end{pmatrix}$$

The appropriate measurement operators are:

$$Vop = \begin{pmatrix} 1 & 0 \\ 0 & 0 \end{pmatrix} \quad Hop = \begin{pmatrix} 0 & 0 \\ 0 & 1 \end{pmatrix} \quad VH = \begin{pmatrix} 1 & 0 \\ 0 & -1 \end{pmatrix}$$

As VH is diagonal it is obvious that its eigenvalues are +1 and -1, and that V is the eigenstate with eigenvalue +1 and H is the eigenstate with eigenvalue -1.

$$\text{VH V} = \begin{pmatrix} 1 \\ 0 \end{pmatrix} \quad \text{VH H} = \begin{pmatrix} 0 \\ -1 \end{pmatrix}$$

Just as for the circular polarization measurements, the observers individual plane polarization measurements are totally random, but when they compare their results they find perfect anti-correlation, always observing the opposite polarization state.

$$\left(\overline{\Psi}\right)^T \text{kronecker(VH, I)}\Psi = 0 \quad \left(\overline{\Psi}\right)^T \text{kronecker(I, VH)} = 0 \quad \left(\overline{\Psi}\right)^T \text{kronecker(VH, VH)}\Psi = -1$$

$$\left(\overline{\Psi}\right)^T \text{kronecker(Vop, Hop)}\Psi = 0.5 \quad \left(\overline{\Psi}\right)^T \text{kronecker(Hop, Vop)}\Psi = 0.5$$
$$\left(\overline{\Psi}\right)^T \text{kronecker(Vop, Vop)}\Psi = 0 \quad \left(\overline{\Psi}\right)^T \text{kronecker(Hop, Hop)}\Psi = 0$$

If one observer measures circular polarization and the other measures plane polarization the expectation value is 0. In other words there is no correlation between the measurements.

$$\left(\overline{\Psi}\right)^T \text{kronecker(RLC, VH)}\Psi = 0 \quad \left(\overline{\Psi}\right)^T \text{kronecker(VH, RLC)}\Psi = 0$$

Classical reasoning (according to Feynman) is in disagreement with the highlighted result. Earlier it was demonstrated that the photons are either |L> or |R> polarized. However, suppose photon A is measured in the V-H basis and found to be |V>, and given that B is either |L> or |R>, which are superpositions of |V> and |H> (see Appendix), measurement of B in the V-H basis should yield |V> 50% of the time and |H> 50% of the time. There should be no correlation between the A and B measurements. The expectation value should be zero.

Feynman put it this way (parenthetical material added):

> Surely you (A) cannot alter the physical state of his (B) photons by changing the kind of observation you make on your photons. No matter what measurements you make on yours, his must still be either RHC (|R>) or LHC (|L>).

But according to quantum mechanics the photons are entangled in the R-L and V-H bases as shown above, and therefore measurement of |V> at A collapses the wave function to |H> at B.

The highlighted prediction is confirmed experimentally leading to the conclusion that reasoning classically in this manner about the photons created in positronium annihilation is not valid.

While this analysis of positronium annihilation clarifies the conflict between quantum theory and classical realism, it does not lead to an experimental adjudication of the disagreement. In 1964 John Bell demonstrated that entangled systems, like the positronium decay products, could be used to decide the conflict one way or the other empirically. As is well known the subsequent experimental work based on Bell's theorem decided the conflict between the two views in favor of quantum theory.

Appendix

The relationships between place and circularly polarized light.

$$\begin{array}{cccc} IR> & IL> & |V> & |H> \\ \frac{1}{\sqrt{2}}(\text{V} + \text{iH}) \rightarrow \begin{pmatrix} \frac{\sqrt{2}}{2} \\ \frac{\sqrt{2}i}{2} \end{pmatrix} & \frac{1}{\sqrt{2}}(\text{V - iH}) \rightarrow \begin{pmatrix} \frac{\sqrt{2}}{2} \\ -\frac{\sqrt{2}i}{2} \end{pmatrix} & \frac{1}{\sqrt{2}}(\text{L} + \text{R}) \rightarrow \begin{pmatrix} 1 \\ 0 \end{pmatrix} & \frac{i}{\sqrt{2}}(\text{L - R}) \rightarrow \begin{pmatrix} 0 \\ 1 \end{pmatrix} \end{array}$$

Transforming Ψ from the R-L basis to the V-H basis using the superpositions above.

$$\psi = \frac{1}{\sqrt{2}}\left(R_A R_B - L_A L_B\right) \left| \begin{array}{l} \text{substitute, } \text{R}_A \frac{1}{\sqrt{2}}\left(V_A + iH_A\right) \\ \text{substitute, } \text{R}_B = \frac{1}{\sqrt{2}}\left(V_B + iH_B\right) \\ \text{substitute, } \text{L}_A = \frac{1}{\sqrt{2}}\left(V_A - iH_A\right) \\ \text{substitute, } \text{L}_B = \frac{1}{\sqrt{2}}\left(V_B - iH_B\right) \\ \text{simplify} \end{array} \right. \rightarrow \psi = \sqrt{2}\left(\frac{H_A V_B}{2} + \frac{H_B V_A}{2}\right) i$$

This page titled 2.24: Positronium Annihilation is shared under a CC BY 4.0 license and was authored, remixed, and/or curated by Frank Rioux via source content that was edited to the style and standards of the LibreTexts platform.

2.25: Positronium Annihilation- Another View

This tutorial provides an alternative analysis of the annihilation of positronium as presented in section 18-3 in Volume III of The Feynman Lectures on Physics. The calculations begin after the highlighted region which provides a justification for selecting an entangled singlet state for the two photons created in the decay event.

Positronium is an analog of the hydrogen atom in which the proton is replaced by a positron, the electron's anti-particle. The electron-positron pair undergoes annihilation in 10-10 seconds producing two γ-ray photons. Positronium's effective mass is 1/2, yielding a ground state energy (excluding the magnetic interactions between the spin 1/2 anti-particles) E = -0.5μE_h = -0.25 E_h. Considering spin the ground state is four-fold degenerate, but this degeneracy is split by the magnetic spin-spin hyperfine interaction shown below. See "The Hyperfine Splitting in the Hydrogen Atom" for further detail.

$$\hat{H}_{SpinSpin} = A\sigma^e\sigma^p = A\left(\sigma_x^e\sigma_x^p + \sigma_y^e\sigma_y^p + \sigma_z^e\sigma_z^p\right)$$

The spin-spin Hamiltonian has the following eigenvalues (top row) and eigenvectors (columns beneath the eigenvalues), showing a singlet ground state and triplet excited state. The electron-positron spin states are to the right of the table with their m quantum numbers, showing that the singlet (j = 0, m = 0) is a superposition state as is one of the triplet states (j = 1, m = 0). The parameter A is much larger for positronium than for the hydrogen atom because the positron has a much larger magnetic moment than the proton.

$$\begin{pmatrix} -3A & A & A & A \\ 0 & 0 & 0 & 1 \\ \frac{1}{\sqrt{2}} & \frac{1}{\sqrt{2}} & 0 & 0 \\ -\frac{1}{\sqrt{2}} & \frac{1}{\sqrt{2}} & 0 & 0 \\ 0 & 0 & 1 & 0 \end{pmatrix} \begin{matrix} \\ |++\rangle\ m=1 \\ |+-\rangle\ m=0 \\ |-+\rangle\ m=0 \\ |--\rangle\ m=-1 \end{matrix}$$

Feynman shows that when the singlet ground state (J = 0, m = 0) annihilates, conservation of momentum requires that the photons emitted in opposite directions (A and B) must have the same circular polarization state, either both in the right or both in left circular state in their direction of motion. This leads to the following entangled superposition. The negative sign is required by parity conservation. The positronium ground state has negative parity (see above), therefore the final photon state must have negative parity.

$$|\Psi\rangle = \frac{1}{\sqrt{2}}\left[|R\rangle_A|R\rangle_B - |L\rangle_A|L\rangle_B\right] = \frac{1}{2\sqrt{2}}\left[\begin{pmatrix}1\\i\end{pmatrix}_A \otimes \begin{pmatrix}1\\i\end{pmatrix}_B - \begin{pmatrix}1\\-i\end{pmatrix}_A \otimes \begin{pmatrix}1\\-i\end{pmatrix}_B\right]$$
$$= \frac{1}{2\sqrt{2}}\left[\begin{pmatrix}1\\i\\i\\-1\end{pmatrix} - \begin{pmatrix}1\\-i\\-i\\-1\end{pmatrix}\right] = \frac{i}{\sqrt{2}}\begin{pmatrix}0\\1\\1\\0\end{pmatrix}$$

The circular polarization states are:

$$R = \tfrac{1}{\sqrt{2}}\begin{pmatrix}1\\i\end{pmatrix} \quad L = \tfrac{1}{\sqrt{2}}\begin{pmatrix}1\\-i\end{pmatrix}$$

The appropriate operators are formed below:

$$RC = R\left(\overline{R}\right)^T \rightarrow \begin{pmatrix}\frac{1}{2} & -\frac{1}{2}i\\ \frac{1}{2}i & \frac{1}{2}\end{pmatrix} \quad LC = L\left(\overline{L}\right)^T \rightarrow \begin{pmatrix}\frac{1}{2} & \frac{1}{2}i\\ -\frac{1}{2}i & \frac{1}{2}\end{pmatrix} \quad RLC = R\left(\overline{R}\right)^T - L\left(\overline{L}\right)^T \rightarrow \begin{pmatrix}0 & -i\\ i & 0\end{pmatrix}$$

RLC is the angular momentum operator for photons. Below it is shown that |R> and |L> are eigenstates with eigenvalues of +1 and -1, respectively.

$$\text{eigenvals(RLC)} = \begin{pmatrix}1\\-1\end{pmatrix} \quad \text{RLC R} \rightarrow \begin{pmatrix}\frac{\sqrt{2}}{2}\\ \frac{\sqrt{2}i}{2}\end{pmatrix} \quad \text{RLC L} \rightarrow \begin{pmatrix}-\frac{\sqrt{2}}{2}\\ \frac{\sqrt{2}i}{2}\end{pmatrix}$$

Now we can consider some of the measurements that Feynman discusses in his analysis of positronium annihilation. Because the photons in state Ψ are entangled the measurements of observers A and B are correlated. For example, if observers A and B both measure the circular polarization of their photons and compare their results they always agree that they have measured the same polarization state. Their composite expectation value is 1.

$$\Psi = \frac{i}{\sqrt{2}} \begin{pmatrix} 0 \\ 1 \\ 1 \\ 0 \end{pmatrix} \quad \left(\overline{\Psi}\right)^T \text{kronecker(RLC, RLC)}\Psi = 1$$

The identity operation, do nothing, is now needed:

$$I = \begin{pmatrix} 1 & 0 \\ 0 & 1 \end{pmatrix}$$

But their individual results are a random sequence of +1 and -1 outcomes averaging to an expectation value of zero.

$$\left(\overline{\Psi}\right)^T \text{kronecker(RLC, I)}\Psi = 0 \quad \left(\overline{\Psi}\right)^T \text{kronecker(I, RLC)}\Psi = 0$$

The probability that both observers will measure |R> or both measure |L> is 0.5. The probability that one will measure |R> and the other |L>, or vice versa is zero.

$$\left(\overline{\Psi}\right)^T \text{kronecker(RC, RC)}\Psi = 0.5 \quad \left(\overline{\Psi}\right)^T \text{kronecker(LC, LC)}\Psi = 0.5 \quad \left(\overline{\Psi}\right)^2 \text{kronecker(LC, RC)}\Psi = 0$$

Because |R> and |L> are superpositions of |V> and |H>, the photon wave function can also be written in the V-H plane polarization basis as is shown below. See the Appendix for an alternative justification.

$$|\Psi\rangle = \frac{i}{\sqrt{2}} \left[|V\rangle_A |H\rangle_B + |H\rangle_A |V\rangle_B\right] = \frac{i}{\sqrt{2}} \left[\begin{pmatrix} 1 \\ 0 \end{pmatrix}_A \otimes \begin{pmatrix} 0 \\ 1 \end{pmatrix}_B + \begin{pmatrix} 0 \\ 1 \end{pmatrix}_A \otimes \begin{pmatrix} 1 \\ 0 \end{pmatrix}_B\right]$$
$$= \frac{i}{\sqrt{2}} \left[\begin{pmatrix} 0 \\ 1 \\ 0 \\ 0 \end{pmatrix} + \begin{pmatrix} 0 \\ 0 \\ 1 \\ 0 \end{pmatrix}\right] = \frac{i}{\sqrt{2}} \begin{pmatrix} 0 \\ 1 \\ 1 \\ 0 \end{pmatrix}$$

The eigenstates for plane polarization are:

$$V = \begin{pmatrix} 1 \\ 0 \end{pmatrix} \quad H = \begin{pmatrix} 0 \\ 1 \end{pmatrix}$$

The appropriate measurement operators are:

$$Vop = \begin{pmatrix} 1 & 0 \\ 0 & 0 \end{pmatrix} \quad Hop = \begin{pmatrix} 0 & 0 \\ 0 & 1 \end{pmatrix} \quad VH = \begin{pmatrix} 1 & 0 \\ 0 & -1 \end{pmatrix}$$

As VH is diagonal it is obvious that its eigenvalues are +1 and -1, and that V is the eigenstate with eigenvalue +1 and H is the eigenstate with eigenvalue -1.

$$\text{VH V} = \begin{pmatrix} 1 \\ 0 \end{pmatrix} \quad \text{VH H} = \begin{pmatrix} 0 \\ -1 \end{pmatrix}$$

Just as for the circular polarization measurements, the observers individual plane polarization measurements are totally random, but when they compare their results they find perfect anti-correlation, always observing the opposite polarization state.

$$\left(\overline{\Psi}\right)^T \text{kronecker(VH, I)}\Psi = 0 \quad \left(\overline{\Psi}\right)^T \text{kronecker(I, VH)} = 0 \quad \left(\overline{\Psi}\right)^T \text{kronecker(VH, VH)}\Psi = 1$$

$$\left(\overline{\Psi}\right)^T \text{kronecker(Vop, Hop)}\Psi = 0.5 \quad \left(\overline{\Psi}\right)^T \text{kronecker(Hop, Vop)}\Psi = 0.5$$
$$\left(\overline{\Psi}\right)^T \text{kronecker(Vop, Vop)}\Psi = 0 \quad \left(\overline{\Psi}\right)^T \text{kronecker(Hop, Hop)}\Psi = 0$$

If one observer measures circular polarization and the other measures plane polarization the expectation value is 0. In other words there is no correlation between the measurements.

$$\left(\overline{\Psi}\right)^T \text{kronecker(RLC, VH)}\Psi = 0 \quad \left(\overline{\Psi}\right)^T \text{kronecker(VH, RLC)}\Psi = 0$$

A realist believes that all observables have definite values independent of measurement and that measurement of one variable doesn't affect the value of another variable. Such a person might construct the following table which assigns specific polarization states to the photons in the R-L and V-H bases to explain the quantum mechanical calculations performed above.

$$\begin{pmatrix} \text{Photon A} & ' & \text{Photon B} & ' & \text{RL(A) RL(B)} & \text{VH(A) VH(B)} & \text{RL(A) VH(B)} & \text{VH(A) RL(B)} \\ \text{R V} & ' & \text{R H} & ' & 1 & -1 & -1 & 1 \\ \text{L V} & ' & \text{L H} & ' & 1 & -1 & 1 & -1 \\ \text{R H} & ' & \text{R V} & ' & 1 & -1 & -1 & 1 \\ \text{Expectation} & ' & \text{Value} & ' & 1 & -1 & 0 & 0 \end{pmatrix}$$

However, the quantum theorist objects that the operators representing rectilinear and circular polarization do not commute, which means that they represent incompatible observables which cannot simultaneously occupy well-defined states.

$$\text{RLC VH - VH RLC} = \begin{pmatrix} 0 & 2i \\ 2i & 0 \end{pmatrix}$$

As shown below |R> and |L> are superpositions of |V> and |H> and vice versa. This is another way of demonstrating that a photon cannot be in a well-defined circular polarization state, say |R>, and at the same time be definitely either |V> or |H>. |R> is a superposition of |V> and |H> and therefore its plane polarization state is completely undetermined. Thus the photon states in the table proposed by the realist are not valid from the quantum mechanical perspective. They have, therefore, no explanatory validity.

$$\begin{matrix} IR> & IL> & |V> & |H> \\ \frac{1}{\sqrt{2}}(\text{V + iH}) \rightarrow \begin{pmatrix} \frac{\sqrt{2}}{2} \\ \frac{\sqrt{2}i}{2} \end{pmatrix} & \frac{1}{\sqrt{2}}(\text{V - iH}) \rightarrow \begin{pmatrix} \frac{\sqrt{2}}{2} \\ -\frac{\sqrt{2}i}{2} \end{pmatrix} & \frac{1}{\sqrt{2}}(\text{L + R}) \rightarrow \begin{pmatrix} 1 \\ 0 \end{pmatrix} & \frac{i}{\sqrt{2}}(\text{L - R}) \rightarrow \begin{pmatrix} 0 \\ 1 \end{pmatrix} \end{matrix}$$

Appendix

Transforming Ψ from the R-L basis to the V-H basis using the superpositions above.

$$\psi = \frac{1}{\sqrt{2}}\left(R_A R_B - L_A L_B\right) \left| \begin{array}{l} \text{substitute, R}_A \frac{1}{\sqrt{2}}\left(V_A + iH_A\right) \\ \text{substitute, R}_B = \frac{1}{\sqrt{2}}\left(V_B + iH_B\right) \\ \text{substitute, L}_A = \frac{1}{\sqrt{2}}\left(V_A - iH_A\right) \\ \text{substitute, L}_B = \frac{1}{\sqrt{2}}\left(V_B - iH_B\right) \\ \text{simplify} \end{array} \right. \rightarrow \psi = \sqrt{2}\left(\frac{H_A V_B}{2} + \frac{H_B V_A}{2}\right) i$$

I thought it would be interesting to look at calculations that included measurement in the diagonal-slant rectilinear basis.

The diagonal and slant eigenvectors:

$$D = \frac{1}{\sqrt{2}}\begin{pmatrix} 1 \\ 1 \end{pmatrix} \quad S = \frac{1}{\sqrt{2}}\begin{pmatrix} 1 \\ -1 \end{pmatrix} \quad \frac{D-S}{\sqrt{2}} = \begin{pmatrix} 0 \\ 1 \end{pmatrix} \quad \frac{D+S}{\sqrt{2}} = \begin{pmatrix} 1 \\ 0 \end{pmatrix}$$

The original state function in the diagonal-slant basis:

$$\psi = \frac{i}{\sqrt{2}}\left(H_A V_B - V_A H_B\right) \left| \begin{array}{l} \text{substitute, H}_A \frac{1}{\sqrt{2}}\left(D_A + iS_A\right) \\ \text{substitute, H}_B = \frac{1}{\sqrt{2}}\left(D_B + iS_B\right) \\ \text{substitute, L}_A = \frac{1}{\sqrt{2}}\left(D_A - iS_A\right) \\ \text{substitute, L}_B = \frac{1}{\sqrt{2}}\left(D_B - iS_B\right) \\ \text{simplify} \end{array} \right. \rightarrow \psi = \sqrt{2}\left(\frac{D_A D_B}{2} - \frac{S_A S_B}{2}\right) i$$

$$\text{DS} = \begin{pmatrix} 0 & 1 \\ 1 & 0 \end{pmatrix} \quad \text{Dd} = \frac{1}{2}\begin{pmatrix} 1 & 1 \\ 1 & 1 \end{pmatrix} \quad \text{Ds} = \frac{1}{2}\begin{pmatrix} 1 & -1 \\ -1 & 1 \end{pmatrix} \quad \text{D D}^T - \text{S S}^T = \begin{pmatrix} 0 & 1 \\ 1 & 0 \end{pmatrix}$$

$$\left(\overline{\Psi}\right)^T \text{kronecker}(\text{DS, DS}) = 1 \quad \left(\overline{\Psi}\right)^T \text{kronecker}(\text{Dd, Dd})\Psi = 0.5 \quad \left(\overline{\Psi}\right)^T \text{kronecker}(\text{Ds, Ds}) = 0.5$$

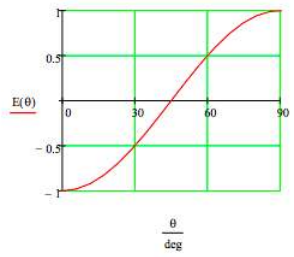
$$\left(\overline{\Psi}\right)^T \text{kronecker}(\text{Dd, Ds}) = 0 \quad \left(\overline{\Psi}\right)^T \text{kronecker}(\text{DS, RLC})\Psi = 0 \quad \left(\overline{\Psi}\right)^T \text{kronecker}(\text{DS, VH}) = 0$$

$$\text{VH D} - \text{DS VH} = \begin{pmatrix} 0 & 2 \\ -2 & 0 \end{pmatrix} \quad \text{RLC DS} - \text{DS RLC} = \begin{pmatrix} -2i & 0 \\ 0 & 2i \end{pmatrix}$$

All of the states below give expectation values that agree with quantum mechanics, but are not permissible in quantum mechanics because the operators do not commute.

PhotonA	PhotonB	RL(A) RL(B)	VH(A) VH(B)	RL(A) VH(B)	DS(A) DS(B)	RL(A) DS(B)	VH(A) DS(B)
RVD	RHD	1	−1	01	1	1	1
RVS	RHS	1	−1	−1	1	−1	−1
LVD	LHD	1	−1	1	1	−1	1
LVS	LHS	1	−1	1	1	1	−1
RHD	RVD	1	−1	1	1	−1	1
LHD	LVD	1	−1	−1	1	−1	−1
LHS	LVS	1	−1	−1	1	1	1
LHS	LVS	1	−1	−1	1	1	1
Expectation	Value	1	−1	0	1	0	0

$$E(\theta) = \left(\overline{\Psi}\right)^T \begin{pmatrix} \cos(2\theta) & \sin(2\theta) & 0 & 0 \\ \sin(2\theta) & -\cos(2\theta) & 0 & 0 \\ 0 & 0 & -\cos(2\theta) & -\sin(2\theta) \\ 0 & 0 & -\sin(2\theta) & \cos(2\theta) \end{pmatrix} \Psi \rightarrow -\cos(2\theta)$$



This page titled 2.25: Positronium Annihilation- Another View is shared under a CC BY 4.0 license and was authored, remixed, and/or curated by Frank Rioux via source content that was edited to the style and standards of the LibreTexts platform.

2.26: Positronium Annihilation- Yet Another View

The following provides an alternative mathematical analysis of the annihilation of positronium as presented in section 18-3 of Volume III of *The Feynman Lectures on Physics*. Positronium is an analog of the hydrogen atom in which the proton is replaced by a positron, the electron's anti-particle. The electron-positron pair undergoes annihilation in 10^{-10} seconds producing two γ-ray photons.

Feynman shows that when positronium annihilates, conservation of momentum requires that the photons emitted in opposite directions (A and B) must have the same circular polarization state, either both in the right or both in left circular state in their direction of motion. This leads to the following entangled superposition in the R-L basis. The negative sign is required by parity conservation.

$$|\Psi\rangle = \frac{1}{\sqrt{2}}\left[|R\rangle_A|R\rangle_B - |L\rangle_A|L\rangle_B\right] = \frac{1}{2\sqrt{2}}\left[\begin{pmatrix}1\\ i\end{pmatrix}_A \otimes \begin{pmatrix}1\\ i\end{pmatrix}_B - \begin{pmatrix}1\\ -i\end{pmatrix}_A \otimes \begin{pmatrix}1\\ -i\end{pmatrix}_B\right]$$
$$= \frac{1}{2\sqrt{2}}\left[\begin{pmatrix}1\\ i\\ i\\ -1\end{pmatrix} - \begin{pmatrix}1\\ -i\\ -i\\ -1\end{pmatrix}\right] = \frac{i}{\sqrt{2}}\begin{pmatrix}0\\ 1\\ 1\\ 0\end{pmatrix}$$

The circular polarization states are:

$$R = \tfrac{1}{\sqrt{2}}\begin{pmatrix}1\\ i\end{pmatrix} \quad L = \tfrac{1}{\sqrt{2}}\begin{pmatrix}1\\ -i\end{pmatrix}$$

The appropriate operators are formed below:

$$\mathrm{RC} = \mathrm{R}\left(\overline{R}\right)^T \rightarrow \begin{pmatrix}\frac{1}{2} & -\frac{1}{2}i\\ \frac{1}{2}i & \frac{1}{2}\end{pmatrix} \mathrm{LC} = \quad \mathrm{RLC} = \mathrm{R}\left(\overline{R}\right)^T - \mathrm{L}\left(\overline{L}\right)^T \rightarrow \begin{pmatrix}0 & -i\\ i & 0\end{pmatrix}$$
$$\mathrm{L}\left(\overline{L}\right)^T \rightarrow \begin{pmatrix}\frac{1}{2} & \frac{1}{2}i\\ -\frac{1}{2}i & \frac{1}{2}\end{pmatrix}$$

RLC is the angular momentum operator for photons. Below it is shown that |R> and |L> are eigenstates with eigenvalues of +1 and -1, respectively.

$$\mathrm{eigenvals}(\mathrm{RLC}) = \begin{pmatrix}1\\ -1\end{pmatrix} \quad \mathrm{RLC\ R} = \begin{pmatrix}0.707\\ 0.707i\end{pmatrix} \quad \mathrm{RLC\ L} = \begin{pmatrix}-0.707\\ 0.707i\end{pmatrix} \quad \tfrac{1}{\sqrt{2}} = 0.707$$

Now we can consider some of the measurements that Feynman discusses in his analysis of positronium annihilation. Because the photons in state Ψ are entangled the measurements of observers A and B are correlated. For example, if observers A and B both measure the circular polarization of their photons and compare their results they always agree that they have measured the same polarization state. Their composite expectation value is 1.

$$\Psi = \tfrac{i}{\sqrt{2}}\begin{pmatrix}0\\ 1\\ 1\\ 0\end{pmatrix} \quad \left(\overline{\Psi}\right)^T \mathrm{kronecker}(\mathrm{RLC},\ \mathrm{RLC})\Psi = 1$$

The identity operation, do nothing, is needed:

$$I = \begin{pmatrix}1 & 0\\ 0 & 1\end{pmatrix}$$

But their individual results are a random sequence of +1 and -1 outcomes averaging to an expectation value of zero.

$$\left(\overline{\Psi}\right)^2 \mathrm{kronecker}(\mathrm{RLC},\ \mathrm{I})\Psi = 0 \quad \left(\overline{\Psi}\right)^2 \mathrm{kronecker}(\mathrm{I},\ \mathrm{RLC})\Psi = 0$$

The probability that both observers will measure |R> or both measure |L> is 0.5. The probability that one will measure |R> and the other |L>, or vice versa is zero.

$\left(\overline{\Psi}\right)^2$ kronecker(RC, $\left(\overline{\Psi}\right)^2$ kronecker(LC, LC)$\Psi = 0.5$ $\left(\overline{\Psi}\right)^2$ kronecker(LC, RC)$\Psi = 0$ RC)$\Psi = 0.5$

Now suppose the observers measure photon polarization in the vertical/horizontal basis. The appropriate eigenstates and measurement operators needed are shown below.

The eigenstates for plane polarization are:

$$V = \begin{pmatrix}1\\0\end{pmatrix} \quad H = \begin{pmatrix}0\\1\end{pmatrix}$$

The needed measurement operators are:

$$Vop = \begin{pmatrix}1 & 0\\0 & 0\end{pmatrix} \quad Hop = \begin{pmatrix}0 & 0\\0 & 1\end{pmatrix} \quad VH = \begin{pmatrix}1 & 0\\0 & -1\end{pmatrix}$$

As VH is diagonal it is obvious that its eigenvalues are +1 and -1, and that V is the eigenstate with eigenvalue +1 and H is the eigenstate with eigenvalue -1.

$$\text{VH V} = \begin{pmatrix}1\\0\end{pmatrix} \quad \text{VH H} = \begin{pmatrix}0\\-1\end{pmatrix}$$

Just as for the circular polarization measurements, the observers individual polarization measurements are totally random, but when they compare their results they find perfect anti-correlation, always observing the opposite polarization state.

$$\left(\overline{\Psi}\right)^T \text{kronecker(VH, I)}\Psi = 0 \quad \left(\overline{\Psi}\right)^T \text{kronecker(I, VH)}\Psi = 0 \quad \left(\overline{\Psi}\right)^T \text{kronecker(VH, VH)}\Psi = -1$$

Local classical reasoning is in disagreement with the highlighted result. Earlier it was demonstrated that the photons are either |L> or |R> polarized. However, suppose photon A is measured in the V-H basis and found to be |V>, and given that B is either |L> or |R>, which are superpositions of |V> and |H> (as shown below), measurement of B in the V-H basis should yield |V> 50% of the time and |H> 50% of the time. There should be no correlation between the A and B measurements in the V-H basis. The expectation value should be zero.

$$|R> \quad \tfrac{1}{\sqrt{2}}(\text{V} + \text{iH}) = \begin{pmatrix}0.707\\0.707i\end{pmatrix} \quad |L> \quad \tfrac{1}{\sqrt{2}}(\text{V - iH}) = \begin{pmatrix}0.707\\-0.707i\end{pmatrix}$$

Arguing temporarily against non-local effects Feynman states: Surely you (A) cannot alter the physical state of his (B) photons by changing the kind of observation you make on your photons. No matter what measurements you make on yours, his must still be either RHC (|R>) or LHC (|L>).

However, because |R> and |L> are superpositions of |V> and |H>, the initial R-L wave function is also an entangled superposition in the V-H polarization basis.

$$|\Psi\rangle = \frac{1}{\sqrt{2}}\left[|V\rangle_A|H\rangle_B - |H\rangle_A|V\rangle_B\right] = \frac{i}{2\sqrt{2}}\left[\begin{pmatrix}1\\0\end{pmatrix}_A \otimes \begin{pmatrix}0\\1\end{pmatrix}_B + \begin{pmatrix}0\\1\end{pmatrix}_A \otimes \begin{pmatrix}1\\0\end{pmatrix}_B\right]$$
$$= \frac{i}{2}\sqrt{2}\left[\begin{pmatrix}0\\1\\0\\0\end{pmatrix} + \begin{pmatrix}0\\0\\1\\0\end{pmatrix}\right] = \frac{i}{\sqrt{2}}\begin{pmatrix}0\\1\\1\\0\end{pmatrix}$$

This wave function says a measurement of |V> at A collapses the wave function to |H> at B and a measurement of |H> at A collapses the wave function to |V> at B, in agreement with the highlighted expectation value. "A non-local interaction hooks up one location (A) with another (B) without crossing space, without decay, and without delay. A non-local event is, in short, unmediated, unmitigated and immediate." Quantum Reality by Nick Herbert, page 214.

$$\psi = \frac{1}{\sqrt{2}}\left(R_A R_B - L_A L_B\right), \quad \rightarrow \psi = \sqrt{2}\left(\frac{H_B V_A i}{2} + \frac{H_A V_B i}{2}\right)$$

The interference between the probability amplitudes after the RL to HV substitutions leading to the final state is shown below by a "hand" calculation. The unseen middle step.

$$\frac{1}{2\sqrt{2}}\left[V_AV_B + iV_AH_B + iH_AV_B - H_AH_B - V_AV_B - iV_AH_B + iH_AV_B + H_AH_B\right]$$
$$= \frac{i}{\sqrt{2}}\left[V_AH_B + H_AV_B\right]$$

This page titled 2.26: Positronium Annihilation- Yet Another View is shared under a CC BY 4.0 license and was authored, remixed, and/or curated by Frank Rioux via source content that was edited to the style and standards of the LibreTexts platform.

2.27: The Hyperfine Interaction in the Deutrium Atom

This tutorial is an addendum to the immediately preceeding one dealing with the hyperfine splitting in the hydrogen atom. It represents an alternative version of material that can be found in section 18.6 of Volume III of *The Feynman Lectures on Physics*.

The deuterium isotope of hydrogen consists of an electron, and a proton and neutron in the nucleus (a deuteron). All three fundamental particles are spin-1/2 fermions. However, the proton and the neutron in the nucleus collectively behave like a spin-1 particle in their magnetic interaction with the extra-nuclear electron. The spin-spin interaction between the electron and the nucleus is given below, where the superscript d refers to the proton-neutron nucleus.

$$\hat{H}_{SpinSpin} = A\left(J^d \sigma^e\right) = A\left(J_x^d \sigma_x^e + J_x^d \sigma_y^e + J_z^d \sigma_z^e\right)$$

The spin-1/2 and spin-1 operators required for this Hamiltonian are given below. The spin-1/2 operators are the familiar Pauli matrices. For a derivation of the spin-1 operators see *Quantum Mechanics Demystified* by David McMahon, chapter 10.

$$\sigma_x = \tfrac{1}{2}\begin{pmatrix} 0 & 1 \\ 1 & 0 \end{pmatrix} \qquad \sigma_y = \tfrac{1}{2}\begin{pmatrix} 0 & -i \\ i & 0 \end{pmatrix} \qquad \sigma_z = \tfrac{1}{2}\begin{pmatrix} 1 & 0 \\ 0 & -1 \end{pmatrix}$$

$$J_x = \tfrac{1}{\sqrt{2}}\begin{pmatrix} 0 & 1 & 0 \\ 1 & 0 & 1 \\ 0 & 1 & 0 \end{pmatrix} \quad J_y = \tfrac{1}{\sqrt{2}}\begin{pmatrix} 0 & -i & 0 \\ i & 0 & -i \\ 0 & i & 0 \end{pmatrix} \quad J_z = \begin{pmatrix} 1 & 0 & 0 \\ 0 & 0 & 0 \\ 0 & 0 & -1 \end{pmatrix}$$

Tensor multiplication is now used to represent the spin-spin operator in matrix format. In the interest of mathematical clarity the constant A a is set equal to unity.

$$H_{SpinSpin} = \text{kronecker}\left(J_x,\ \sigma_x\right) + \text{kronecker}\left(J_y,\ \sigma_y\right) + \text{kronecker}\left(J_x,\ \sigma_z\right)$$

We know ask Mathcad to calculate the eigenvalues and eigenvectors of the spin-spin operator. These results are displayed by constructing a matrix which contains the eigenvalues in the top row, and their eigenvectors in the columns below the eigenvalues.

$$\text{E} = \text{eigenvals}\left(H_{SpinSpin}\right) \quad \text{EigenvalEigenvec} = \text{rsort}\left(\text{stack}\left(E^T,\ \text{eigenvecs}\left(H_{SpinSpin}\right)\right),\ I\right)$$

$$\text{EigenvalEigenvec} = \begin{pmatrix} -1 & -1 & 0.5 & 0.5 & 0.5 & 0.5 \\ 0 & 0 & 0 & 0 & 0 & 1 \\ 0 & -0.816 & 0 & 0.577 & 0 & 0 \\ 0 & 0.577 & 0 & 0.816 & 0 & 0 \\ 0.577 & 0 & 0.816 & 0 & 0 & 0 \\ -0.816 & 0 & 0.577 & 0 & 0 & 0 \\ 0 & 0 & 0 & 0 & 1 & 0 \end{pmatrix}$$

These results are in agreement with Tables 18-5 and 18-6 in Feynman's text, a ground J = 1/2 state and an excited J = 3/2 state. We can go forward, as we did in the previous tutorial, by writing the electron and deuteron spin wavefunctions in vector format.

The spin states in vector format:

$$|+\rangle = \begin{pmatrix} 1 \\ 0 \end{pmatrix} \quad |-\rangle = \begin{pmatrix} 0 \\ 1 \end{pmatrix}$$

The deuteron spin states in vector format (see McMahon):

$$|d_1\rangle = \begin{pmatrix} 1 \\ 0 \\ 0 \end{pmatrix} \quad |d_0\rangle = \begin{pmatrix} 0 \\ 1 \\ 0 \end{pmatrix} \quad |d_{-1}\rangle \begin{pmatrix} 0 \\ 0 \\ 1 \end{pmatrix}$$

Next we write the six electron-deuteron spin states in tensor format.

$$|+d_1\rangle = \begin{pmatrix}1\\0\end{pmatrix} \otimes \begin{pmatrix}1\\0\\0\end{pmatrix} = \begin{pmatrix}1\\0\\0\\0\\0\\0\end{pmatrix} \quad |+d_0\rangle = \begin{pmatrix}1\\0\end{pmatrix} \otimes \begin{pmatrix}0\\1\\0\end{pmatrix} = \begin{pmatrix}0\\1\\0\\0\\0\\0\end{pmatrix} \quad |+d_{-1}\rangle = \begin{pmatrix}1\\0\end{pmatrix} \otimes \begin{pmatrix}0\\0\\1\end{pmatrix} = \begin{pmatrix}0\\0\\1\\0\\0\\0\end{pmatrix}$$

$$|-d_1\rangle = \begin{pmatrix}0\\1\end{pmatrix} \otimes \begin{pmatrix}1\\0\\0\end{pmatrix} = \begin{pmatrix}0\\0\\0\\1\\0\\0\end{pmatrix} \quad |-d_0\rangle = \begin{pmatrix}0\\1\end{pmatrix} \otimes \begin{pmatrix}0\\1\\0\end{pmatrix} = \begin{pmatrix}0\\0\\0\\0\\1\\0\end{pmatrix} \quad |-d_{-1}\rangle = \begin{pmatrix}0\\1\end{pmatrix} \otimes \begin{pmatrix}0\\0\\1\end{pmatrix} = \begin{pmatrix}0\\0\\0\\0\\0\\1\end{pmatrix}$$

These spin states are given the following labels to facilitate the calculation of energy matrix.

$$\mathrm{a} = \begin{pmatrix}1\\0\\0\\0\\0\\0\end{pmatrix} \quad \mathrm{b} = \begin{pmatrix}0\\1\\0\\0\\0\\0\end{pmatrix} \quad \mathrm{c} = \begin{pmatrix}0\\0\\1\\0\\0\\0\end{pmatrix} \quad \mathrm{d} = \begin{pmatrix}0\\0\\0\\1\\0\\0\end{pmatrix} \quad \mathrm{e} = \begin{pmatrix}0\\0\\0\\0\\1\\0\end{pmatrix} \quad \mathrm{f} = \begin{pmatrix}0\\0\\0\\0\\0\\1\end{pmatrix}$$

$$\mathrm{H} = \mathrm{H}_{SpinSpin}$$

$$\mathrm{eigenvals}\left(\begin{pmatrix} \mathrm{a}^T\mathrm{H}\,\mathrm{a} & \mathrm{a}^T\mathrm{H}\,\mathrm{b} & \mathrm{a}^T\mathrm{H}\,\mathrm{c} & \mathrm{a}^T\mathrm{H}\,\mathrm{d} & \mathrm{a}^T\mathrm{H}\,\mathrm{e} & \mathrm{a}^T\mathrm{H}\,\mathrm{f} \\ \mathrm{b}^T\mathrm{H}\,\mathrm{a} & \mathrm{b}^T\mathrm{H}\,\mathrm{b} & \mathrm{b}^T\mathrm{H}\,\mathrm{c} & \mathrm{b}^T\mathrm{H}\,\mathrm{d} & \mathrm{b}^T\mathrm{H}\,\mathrm{e} & \mathrm{b}^T\mathrm{H}\,\mathrm{f} \\ \mathrm{c}^T\mathrm{H}\,\mathrm{a} & \mathrm{c}^T\mathrm{H}\,\mathrm{b} & \mathrm{c}^T\mathrm{H}\,\mathrm{c} & \mathrm{c}^T\mathrm{H}\,\mathrm{d} & \mathrm{c}^T\mathrm{H}\,\mathrm{e} & \mathrm{c}^T\mathrm{H}\,\mathrm{f} \\ \mathrm{d}^T\mathrm{H}\,\mathrm{a} & \mathrm{d}^T\mathrm{H}\,\mathrm{b} & \mathrm{d}^T\mathrm{H}\,\mathrm{c} & \mathrm{d}^T\mathrm{H}\,\mathrm{d} & \mathrm{d}^T\mathrm{H}\,\mathrm{e} & \mathrm{d}^T\mathrm{H}\,\mathrm{f} \\ \mathrm{e}^T\mathrm{H}\,\mathrm{a} & \mathrm{e}^T\mathrm{H}\,\mathrm{b} & \mathrm{e}^T\mathrm{H}\,\mathrm{c} & \mathrm{e}^T\mathrm{H}\,\mathrm{d} & \mathrm{e}^T\mathrm{H}\,\mathrm{e} & \mathrm{e}^T\mathrm{H}\,\mathrm{f} \\ \mathrm{f}^T\mathrm{H}\,\mathrm{a} & \mathrm{f}^T\mathrm{H}\,\mathrm{b} & \mathrm{f}^T\mathrm{H}\,\mathrm{c} & \mathrm{f}^T\mathrm{H}\,\mathrm{d} & \mathrm{f}^T\mathrm{H}\,\mathrm{e} & \mathrm{f}^T\mathrm{H}\,\mathrm{f} \end{pmatrix}\right) = \begin{pmatrix}-1\\0.5\\0.5\\-1\\0.5\\0.5\end{pmatrix}$$

$$\mathrm{eigenvecs}\left(\begin{pmatrix} \mathrm{a}^T\mathrm{H}\,\mathrm{a} & \mathrm{a}^T\mathrm{H}\,\mathrm{b} & \mathrm{a}^T\mathrm{H}\,\mathrm{c} & \mathrm{a}^T\mathrm{H}\,\mathrm{d} & \mathrm{a}^T\mathrm{H}\,\mathrm{e} & \mathrm{a}^T\mathrm{H}\,\mathrm{f} \\ \mathrm{b}^T\mathrm{H}\,\mathrm{a} & \mathrm{b}^T\mathrm{H}\,\mathrm{b} & \mathrm{b}^T\mathrm{H}\,\mathrm{c} & \mathrm{b}^T\mathrm{H}\,\mathrm{d} & \mathrm{b}^T\mathrm{H}\,\mathrm{e} & \mathrm{b}^T\mathrm{H}\,\mathrm{f} \\ \mathrm{c}^T\mathrm{H}\,\mathrm{a} & \mathrm{c}^T\mathrm{H}\,\mathrm{b} & \mathrm{c}^T\mathrm{H}\,\mathrm{c} & \mathrm{c}^T\mathrm{H}\,\mathrm{d} & \mathrm{c}^T\mathrm{H}\,\mathrm{e} & \mathrm{c}^T\mathrm{H}\,\mathrm{f} \\ \mathrm{d}^T\mathrm{H}\,\mathrm{a} & \mathrm{d}^T\mathrm{H}\,\mathrm{b} & \mathrm{d}^T\mathrm{H}\,\mathrm{c} & \mathrm{d}^T\mathrm{H}\,\mathrm{d} & \mathrm{d}^T\mathrm{H}\,\mathrm{e} & \mathrm{d}^T\mathrm{H}\,\mathrm{f} \\ \mathrm{e}^T\mathrm{H}\,\mathrm{a} & \mathrm{e}^T\mathrm{H}\,\mathrm{b} & \mathrm{e}^T\mathrm{H}\,\mathrm{c} & \mathrm{e}^T\mathrm{H}\,\mathrm{d} & \mathrm{e}^T\mathrm{H}\,\mathrm{e} & \mathrm{e}^T\mathrm{H}\,\mathrm{f} \\ \mathrm{f}^T\mathrm{H}\,\mathrm{a} & \mathrm{f}^T\mathrm{H}\,\mathrm{b} & \mathrm{f}^T\mathrm{H}\,\mathrm{c} & \mathrm{f}^T\mathrm{H}\,\mathrm{d} & \mathrm{f}^T\mathrm{H}\,\mathrm{e} & \mathrm{f}^T\mathrm{H}\,\mathrm{f} \end{pmatrix}\right)$$

$$= \begin{pmatrix} 0 & 0 & 0 & 0 & 1 & 0 \\ 0 & 0 & 0.577 & -0.816 & 0 & 0 \\ 0 & 0 & 0.816 & 0.577 & 0 & 0 \\ 0.577 & 0.816 & 0 & 0 & 0 & 0 \\ -0.816 & 0.577 & 0 & 0 & 0 & 0 \\ 0 & 0 & 0 & 0 & 0 & 1 \end{pmatrix}$$

Appendix

While it's not directly pertinent to the subject of this tutorial, the interaction of two spin-1 systems is calculated below.

$$H_{SpinSpin} = (\mathrm{kronecker}\,(J_x,\ J_x) + \mathrm{kronecker}\,(J_y,\ J_y) + \mathrm{kronecker}\,(J_z,\ J_z))$$

$$H_{SpinSpin} = \begin{pmatrix} 1 & 0 & 0 & 0 & 0 & 0 & 0 & 0 & 0 \\ 0 & 0 & 0 & 1 & 0 & 0 & 0 & 0 & 0 \\ 0 & 0 & -1 & 0 & 1 & 0 & 0 & 0 & 0 \\ 0 & 1 & 0 & 0 & 0 & 0 & 0 & 0 & 0 \\ 0 & 0 & 1 & 0 & 0 & 0 & 1 & 0 & 0 \\ 0 & 0 & 0 & 0 & 0 & 0 & 0 & 1 & 0 \\ 0 & 0 & 0 & 0 & 1 & 0 & -1 & 0 & 0 \\ 0 & 0 & 0 & 0 & 0 & 1 & 0 & 0 & 0 \\ 0 & 0 & 0 & 0 & 0 & 0 & 0 & 0 & 1 \end{pmatrix}$$

We know ask Mathcad to calculate the eigenvalues and eigenvectors of the spin-spin operator.

$$\mathrm{E} = \mathrm{eigenvals}\left(H_{SpinSpin}\right) \quad \mathrm{EigenvalEigenvec} = \mathrm{rsort}\left(\mathrm{stack}\left(E^{T},\ \mathrm{eigenvecs}\left(H_{SpinSpin}\right)\right),\ 1\right)$$

$$\mathrm{EigenvalEigenvec} = \begin{pmatrix} -2 & -1 & -1 & -1 & 1 & 1 & 1 & 1 & 1 \\ 0 & 0 & 0 & 0 & 0 & 0 & 0 & 0 & 1 \\ 0 & 0.707 & 0 & 0 & -0.707 & 0 & 0 & 0 & 0 \\ 0.577 & 0 & 0 & -0.707 & 0 & -0.408 & 0 & 0 & 0 \\ 0 & -0.707 & 0 & 0 & -0.707 & 0 & 0 & 0 & 0 \\ -0.577 & 0 & 0 & 0 & 0 & -0.816 & 0 & 0 & 0 \\ 0 & 0 & -0.770 & 0 & 0 & 0 & 0.707 & 0 & 0 \\ 0.577 & 0 & 0 & 0.707 & 0 & -0.408 & 0 & 0 & 0 \\ 0 & 0 & 0.707 & 0 & 0 & 0 & 0.707 & 0 & 0 \\ 0 & 0 & 0 & 0 & 0 & 0 & 0 & 1 & 0 \end{pmatrix}$$

These results are in agreement with Table 18-7 of Feynman's text. Reading from the left we have a singly degenerate J = 0 state, a triply degenerate J = 1 state, and a five-fold degenerate J = 2 state.

This page titled 2.27: The Hyperfine Interaction in the Deutrium Atom is shared under a CC BY 4.0 license and was authored, remixed, and/or curated by Frank Rioux via source content that was edited to the style and standards of the LibreTexts platform.

2.28: A Tensor Algebra Approach to Spin-Orbit Coupling

The p^1, d^1 and f^1 electronic configurations have six, ten and fourteen microstates, respectively. The degeneracies of these microstates are split by the interaction between magnetic fields associated with spin and orbital angular momentum - the spin-orbit interaction. As is well know the p1 configuration gives rise to a $^2P_{3/2}(4)$ and $^2P_{1/2}(2)$ term under the Russell-Saunders coupling scheme. The d_1 configuration yields a $^2D_{5/2}(6)$ and $^2D_{3/2}(4)$ term. The f^1 configuration consists of $^2F_{7/2}(8)$ and $^2F_{5/2}(6)$ terms. The numbers in parentheses are the degeneracies associated with the term symbols.

In what follows, tensor algebra will be used to calculate the spin-orbit interaction in the p^1, d^1 and f^1 electronic configurations. An approximate energy level diagram for the three electronic configurations will also be presented. The required spin and angular momentum operators (in atomic units) are provided below.

Spin angular momentum operators for spin 1/2:

$$S_x = \tfrac{1}{2}\begin{pmatrix} 0 & 1 \\ 1 & 0 \end{pmatrix} \quad S_y = \tfrac{1}{2}\begin{pmatrix} 0 & -i \\ i & 0 \end{pmatrix} \quad S_z = \tfrac{1}{2}\begin{pmatrix} 1 & 0 \\ 0 & -1 \end{pmatrix}$$

Orbital angular momentum operators for L = 1 and 2 (see E. E. Anderson, *Modern Physics and Quantum Mechanics*, pp 298-300):

$$L1_x = \tfrac{1}{\sqrt{2}}\begin{pmatrix} 0 & 1 & 0 \\ 1 & 0 & 1 \\ 0 & 1 & 0 \end{pmatrix} \qquad L1_y = \tfrac{1}{\sqrt{2}}\begin{pmatrix} 0 & -i & 0 \\ i & 0 & -i \\ 0 & i & 0 \end{pmatrix} \qquad L1_z = \begin{pmatrix} 1 & 0 & 0 \\ 0 & 0 & 0 \\ 0 & 0 & -1 \end{pmatrix}$$

$$L2_x = \tfrac{1}{2}\begin{pmatrix} 0 & 2 & 0 & 0 & 0 \\ 2 & 0 & \sqrt{6} & 0 & 0 \\ 0 & \sqrt{6} & 0 & \sqrt{6} & 0 \\ 0 & 0 & \sqrt{6} & 0 & 2 \\ 0 & 0 & 0 & 2 & 0 \end{pmatrix} \qquad L2_y = \tfrac{i}{2}\begin{pmatrix} 0 & -2 & 0 & 0 & 0 \\ 2 & 0 & -\sqrt{6} & 0 & 0 \\ 0 & \sqrt{6} & 0 & -\sqrt{6} & 0 \\ 0 & 0 & \sqrt{6} & 0 & -2 \\ 0 & 0 & 0 & 2 & 0 \end{pmatrix} \qquad L2_z = \begin{pmatrix} 2 & 0 & 0 & 0 & 0 \\ 0 & 1 & 0 & 0 & 0 \\ 0 & 0 & 0 & 0 & 0 \\ 0 & 0 & 0 & -1 & 0 \\ 0 & 0 & 0 & 0 & -2 \end{pmatrix}$$

The spin-orbit Hamiltonian in tensor format to within a multiplicative constant which depends on the principle and angular momentum quantum numbers is as follows.

$$\hat{H}_{LS} = \hat{L} \otimes \hat{S} = \hat{L}_x \otimes \hat{S}_x + \hat{L}_y \otimes \hat{S}_y + \hat{L}_z \otimes \hat{S}_z$$

For the p^1 electronic configuration L = 1 and S = 1/2. The spin-orbit Hamiltonian and its eigenvalues are calculated as shown below. Kronecker is Mathcad's command for matrix tensor multiplication.

$$H_{LS} = \text{kronecker}\left(L1_x,\ S_x\right) + \text{kronecker}\left(L1_y,\ S_y\right) + \text{kronecker}\left(L1_z,\ S_z\right)$$

$$\text{E} = \text{sort}\left(\text{eigenvals}\left(H_{LS}\right)\right) \quad E^T = \begin{pmatrix} -1 & -1 & 0.5 & 0.5 & 0.5 & 0.5 \end{pmatrix}$$

We see that these results are as expected. We have two -1 eigenstates corresponding to the $^2P_{1/2}$ term and four 0.5 eigenstates corresponding to the $^2P_{3/2}$ term.

For the d^1 electronic configuration L = 2 and S = 1/2. The spin-orbit Hamiltonian and its eigenvalues are now calculated.

$$H_{LS} = \left(\text{kronecker}\left(L2_x,\ S_x\right) + \text{kronecker}\left(L2_y,\ S_y\right) + \text{kronecker}\left(L2_z,\ S_z\right)\right)$$

$$\text{E} = \text{sort}\left(\text{eigenvals}\left(H_{LS}\right)\right) \quad E^T = \begin{pmatrix} -1.5 & -1.5 & -1.5 & -1.5 & 1 & 1 & 1 & 1 & 1 & 1 \end{pmatrix}$$

Again the results are as expected. We have four -1.5 eigenstates corresponding to the $^2D_{3/2}$ term and a six-fold degenerate state at +1.0 corresponding to the $^2D_{5/2}$ term.

L = 3 for the f^1 configuration. The angular momentum operators for L = 3 were obtained by a study of the trends in the other angular momentum operators as L increased. To demonstrate that this procedure yielded the correct matrix operators it is shown that the x-y commutator for L = 3 is satisfied.

$$L3_x = \frac{1}{2}\begin{pmatrix} 0 & \sqrt{6} & 0 & 0 & 0 & 0 & 0 \\ \sqrt{6} & 0 & \sqrt{10} & 0 & 0 & 0 & 0 \\ 0 & \sqrt{10} & 0 & 0 & 0 & 0 & \\ 0 & 0 & \sqrt{12} & 0 & \sqrt{12} & 0 & 0 \\ 0 & 0 & 0\sqrt{120} & \sqrt{12} & 0 & & \\ 0 & 0 & 0 & 0 & \sqrt{10} & 0 & \sqrt{6} \\ 0 & 0 & 0 & 0 & 0 & \sqrt{6} & 0 \end{pmatrix}$$

$$L3_y = \frac{i}{2}\begin{pmatrix} 0 & -\sqrt{6} & 0 & 0 & 0 & 0 & 0 \\ \sqrt{6} & 0 & -\sqrt{10} & 0 & 0 & 0 & 0 \\ 0 & \sqrt{10} & 0 & -\sqrt{12} & 0 & 0 & 0 \\ 0 & 0 & \sqrt{12} & 0 & -\sqrt{12} & 0 & 0 \\ 0 & 0 & 0 & \sqrt{12} & 0 & -\sqrt{10} & 0 \\ 0 & 0 & 0 & 0\sqrt{10} & 0 & -\sqrt{10} & \end{pmatrix}$$

$$L3_z = \begin{pmatrix} 3 & 0 & 0 & 0 & 0 & 0 & 0 \\ 0 & 2 & 0 & 0 & 0 & 0 & 0 \\ 0 & 0 & 1 & 0 & 0 & 0 & 0 \\ 0 & 0 & 0 & 0 & 0 & 0 & 0 \\ 0 & 0 & 0 & 0 & -1 & 0 & 0 \\ 0 & 0 & 0 & 0 & 0 & -2 & 0 \\ 0 & 0 & 0 & 0 & 0 & 0 & -3 \end{pmatrix}$$

$$L3_x L3_y - L3_y L3_x$$

$$\rightarrow \begin{pmatrix} 3i & 0 & 0 & 0 & 0 & 0 & 0 \\ 0 & 2i & 0 & 0 & 0 & 0 & 0 \\ 0 & 0 & i & 0 & 0 & 0 & 0 \\ 0 & 0 & 0 & 0 & 0 & 0 & 0 \\ 0 & 0 & 0 & 0 & -i & 0 & 0 \\ 0 & 0 & 0 & 0 & 0 & -2i & 0 \\ 0 & 0 & 0 & 0 & 0 & 0 & -3i \end{pmatrix}$$

The spin-orbit Hamiltonian and its eigenvalues are now calculated.

$$H_{LS} = (\text{kronecker}\,(L3_x,\ S_x) + \text{kronecker}\,(L3_y,\ S_y) + \text{kronecker}\,(L3_z,\ S - z))$$

The six states at -2 correspond to a $^2F_{5/2}$ term and the eight states at 1.5 belong to a $^2F_{7/2}$ term. These results are in agreement with expectations.

Using these results and the hydrogen atom energy equation as a function of the n and j quantum numbers, we can construct a diagram of the spin-orbit fine structure and its j-level degeneracy for the n = 4 level.

$$E = -\frac{1}{2n^2}\left[1 + \frac{\alpha^2}{n^2}\left(\frac{n}{j+\frac{1}{2}} - \frac{3}{4}\right)\right]$$

$$4f^1 \rightarrow F_{7/2}$$
$$4d^1,\ 4f^1 \rightarrow\ ^2F_{5/2},\ ^2D_{5/2}$$
$$4p^1,\ 4d^1 \rightarrow\ ^2D_{3/2},\ ^2P_{3/2}$$
$$4s^1,\ 4p^1 \rightarrow\ ^2P_{1/2},\ ^2S_{1/2}$$

This page titled 2.28: A Tensor Algebra Approach to Spin-Orbit Coupling is shared under a CC BY 4.0 license and was authored, remixed, and/or curated by Frank Rioux via source content that was edited to the style and standards of the LibreTexts platform.

2.29: A Bohr Model for Multi-electron Atoms and Ions

Abstract

A deBroglie Bohr model is described that can be used to calculate the electronic energies of atoms or ions containing up to four electrons. Seven exercises are provided which can be used to give students training in doing energy audits, carrying out simple variational calculations and critically analyzing the calculated results.

This note builds on two publications in the pedagogical literature [1,2] that showed how extending the Bohr model to two- and three-electron atoms and ions could be used to enhance student understanding of atomic structure. A Bohr model, more correctly a deBroglie-Bohr model, is used here to calculate the total electronic energies of atoms and ions containing up to four electrons.

The Bohr model for the hydrogen atom is the prototype of the semi-classical approach to atomic and molecular structure. Although it was superseded by quantum mechanics many decades ago, it is still taught today because of its simplicity and because it introduced several important quantum mechanical concepts that have survived the model: quantum number, quantized energy, and quantum jump.

When applied to multi-electron atoms and ions, the Bohr model provides a pedagogical tool for improving students′ analytical and critical skills. As will be demonstrated, given a ″picture″ of an atom or ion, it is not unrealistic to expect an undergraduate student to identify all the contributions to the total electronic energy, carry out an energy minimization and interpret the results in a variety of ways. Seven student exercises, with answers, are provided to illustrate how this might be accomplished.

We begin with a review of the deBroglie-Bohr model for the hydrogen atom. Working in atomic units ($h = 2\pi$, $m_e = e = 4\pi\varepsilon_0 = 1$), and using the deBroglie-Bohr restriction on electron orbits ($n\lambda = 2\pi R_n$, where n = 1, 2, 3, ...), the deBroglie wave equation ($\lambda = h/mv$) and Coulomb′s law the total electron energy is the following sum of its kinetic and potential energy contributions.

$$E_n = \frac{n^2}{2R_n^2} - \frac{1}{R_n}$$

Minimization of the energy with respect to the variational parameter Rn yields the allowed orbit radii and energies.

$$R_n = n^2 a_0$$
$$E_n = \frac{-0.5E_h}{n^2}$$

where a_0 = 52.9 pm and Eh = 4.36 x 10^{-18} joule.

The model shown in the figure below is for the beryllium atom or any four-electron ion. Note that the occupancy of the inner orbit is restricted to two electrons (Pauli Principle) and that the orbit radii are constrained by the hydrogen atom result ($R_2 = 4R_1$) leaving only one variational parameter, the radius of the n = 1 orbit.

With these model elements and a little geometry [2] it is easy to specify the kinetic and potential energy contributions to the total energy. The numeric subscripts refer to the quantum number of the orbit. Thus T_1 is the kinetic energy of an electron in the n = 1 orbit, V_{N1} is the potential energy interaction of an electron in the n = 1 orbit with the nucleus, and V_{12} is the potential energy interaction of an electron in the n = 1 orbit with an electron in the n = 2 orbit.

The recommended student calculations described below are carried out in the Mathcad programming environment [3]. A Mathcad file for doing the exercises is available for download on the Internet [4]. The calculation for the beryllium atom is carried out as shown below. Required student input is indicated by the highlighted regions.

Enter nuclear charge: Z = 4

Kinetic energy:

$$T_1(R_1) = \frac{1}{2R_1^2} \quad T_2(R_1) = \frac{1}{8R_1^2}$$

Electron-nucleus potential energy:

$$V_{N1}(R_1) = \frac{-Z}{R_1} \quad V_{N2}(R_1) = \frac{-Z}{4R_1}$$

Electron-electron potential energy:

$$V_{11}(R_1) = \frac{1}{2R_1} \quad V_{22}(R_1) = \frac{1}{8R_1} \quad V_{12}(R_1) = \frac{1}{\sqrt{17}R_1}$$

The next step is to do an energy audit for the atom or ion under consideration. The student is prompted to weight each of the contributions to the total electronic energy. The entries given below are appropriate for the Bohr beryllium atom shown in the figure above.

Enter coefficients for each contribution to the the total energy:

$T_1(R_1)$	$T_2(R_1)$	$V_{N1}(R_1)$	$V_{N2}(R_1)$	$V_{11}(R_1)$	$V_{22}(R_1)$	$V_{12}(R_1)$
a = 2	b = 2	c = 2	d = 2	e = 1	f = 1	g = 4

The energy of the Bohr atom/ion in terms of the variational parameter R1, the radius of the inner electron orbit, and the various kinetic and potential energy contributions is:

$$E(R_1) = aT_1(R_1) + bT_2(R_1) + cV_{N1}(R_1) + dV_{N2}(R_1) + eV_{11}(R_1) + fV_{22}(R_1) + gV_{12}(R_1)$$

Minimization of the electronic energy of the Bohr atom/ion with respect to R1 yields the optimum inner orbit radius and ground-state energy

$$R_1 = \frac{d}{dR_1}E(R_1) = 0 \;\Big|\; \begin{matrix}\text{solve, } R_1 \\ \text{float, } 5\end{matrix} \rightarrow .29744 \qquad E(R_1) = -14.128$$

Thus, this model predicts a stable beryllium atom with an electronic energy in error by less than 4%. However, it must be stressed that the main purpose of the exercises presented is not to promote the Bohr model as such, but to use it as a vehicle for providing students with training in doing energy audits, carrying out simple variational calculations and critically analyzing the calculated results.

In the student exercises critical analysis will involve assessing the level of agreement with experimental results, and whether or not the variational principle and the virial theorem are satisfied. Because the second exercise involves the virial theorem as criterion for validity, it is recommended that the first and second exercises be done in tandem.

Student Exercises

Exercise 1: Use this worksheet to calculate the ground state energy for H, He, Li and Be, and confirm all the entries in the table below. The experimental ground state energy of an atom is the negative of the sum of the successive ionization energies given in the data table in the Appendix A.

Element	$\frac{\text{E(calc)}}{E_h}$	$\frac{\text{E(exp)}}{E_h}$	%Error
H	−0.500	−0.500	0
He	−3.062	−2.904	5.46
Li	−7.385	−7.480	1.26
Be	−14.128	−14.672	3.71

This assignment shows that, given its simplicity, the Bohr model achieves acceptable results. However, the students should note that the He result violates the variational theorem. In other words, the calculated energy is lower than the experimental energy.

Exercise 2: An important criterion for the validity of a quantum mechanical calculation is satisfying the virial theorem which for atoms and ions requires: E = -T = V/2. Demonstrate whether or not the virial theorem is satisfied for the elements in the first exercise.

Calculate the kinetic energy:

$$T(R_1) = aT_1(R_1) + bT_2(R_1) \quad T(R_1) = 14.129$$

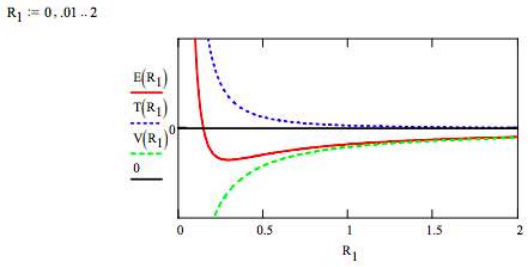
Calculate potential energy:

$$V(R_1) = E(R_1) - T(R_1) \quad V(R_1) = -28.257 \quad \frac{V(R_1)}{2} = -14.129$$

Element	$\frac{E(calc)}{E_h}$	$\frac{-T(calc)}{2E_h}$	VTSatisfied	
H	−0.500	−0.500	−0.500	Yes
He	−3.062	−3.062	−3.062	Yes
Li	−7.385	−7.385	−7.385	Yes
Be	−14.128	−14.129	−14.129	Yes

The Bohr model satisfies the virial theorem for all atomic calculations (atoms and ions). This does not guarantee the validity of the model. However, any model calculation that violates the virial theorem indicates that the model is not quantum mechanically valid.

Exercise 3: Plot the total energy, and the kinetic and potential energy components on the same graph for beryllium and interpret the results.



This graph clearly shows that atomic stability is the result of two competing energy terms. The attractive coulombic potential energy interaction draws the electrons toward the nucleus. At large R_1 values this term dominates and the electron orbits gets smaller. However, this attractive interaction is overcome at small R_1 values by the "repulsive" character of kinetic energy term that dominates at small R_1 values and an energy minimum, a ground-state is achieved.

Exercise 4: Calculate the ground state energies of some cations (He^+, Li^+, Be^+, B^+, C^{2+}) and compare your calculations with experimental results using the data table in Appendix A.

Cation	$\frac{E(calc)}{E_h}$	$\frac{E(exp)}{E_h}$	%Error
He^1	−2.000	−2.000	0
Li^1	−7.562	−7.282	3.70
Be^1	−14.275	−14.329	0.38
B^1	−23.782	−24.348	2.33
C^2	−35.938	−36.613	1.88

Just as in the first exercise, the one-electron species He+1 is in exact agreement with experiment and the two-electron ion, Li^+, violates the variational theorem.

Exercise 5: Use the results of exercises 1 and 3 to calculate the first ionization energies of H, He, Li and Be and compare your results with the experimental data available in Appendix A.

Element	$\frac{E(atom)}{E_h}$	$\frac{E(ion)}{E_h}$	$\frac{IE(calc)}{E_h}$	$\frac{IE(exp)}{E_h}$
H	−0.500	0	0.500	0.500
He	−3.063	−2.000	1.063	0.904
Li	−7.385	−7.562	−0.177	0.198
Be	−14.128	−14.275	−0.147	0.343

The results for H and He are acceptable, but both Li and Be have negative ionization energies.

Exercise 6: Are the anions of H, He and Li stable? In other words, do they have energies lower than the neutral species?

Anion	$\frac{Eion(calc)}{E_h}$	$\frac{Eatom(exp)}{E_h}$	Stable				
H^{-1}	−0.562	−0.500	Yes	He^{-1}	−2.745	−2.904	No
Li^{-1}	−6.681	−7.480	No				

The Bohr model gets these results correct. However, it should be noted that Li-1 is stable in liquid ammonia.

Exercise 7: Do a two-parameter variational calculation on the beryllium atom shown in the Figure. In other words, minimize the total electronic energy of a beryllium atom that has two electrons in an orbit of radius R_1 and two electrons in another orbit of radius R_2.

As outlined in Appendix B this calculation yields the following results: $R_1 = R_2 = 0.329\ a_0$ and $E(R_1, R_2) = -18.518\ E_h$, an energy significantly lower than calculated for beryllium in Exercise 1. Thus, in the absence of the orbital occupancy restriction of the exclusion principle, energy minimization places all electrons in the ground state orbit. It was a realization of this that lead Pauli in part to formulate the exclusion principle.

In summary, the purpose of this note is to use the Bohr model as an initial vehicle to help students develop skill in carrying out basic atomic structure calculations and to critically analyze the results of those calculations.

Appendix A

Data: Successive Ionization Energies for the First Six Elements

Element	IE_1	IE_2	IE_3	IE_4	IE_5	IE_6
H	0.500	x	x	x	x	x
He	0.904	2.000	x	x	x	x
Li	0.198	2.782	4.500	x	x	x
Be	0.343	0.670	5.659	8.000	x	x
B	0.305	0.926	1.395	9.527	12.500	x
C	0.414	0.896	1.761	2.370	14.482	18.000

Appendix B

Energy contributions for the two-parameter Bohr calculation:

$$T_1(R_1) = \frac{1}{2R_1^2} \quad T_2(R_2) = \frac{1}{2R_2^2} \quad V_{N1}(R_1) = \frac{-Z}{R_1} \quad V_{N2}(R_2) = \frac{-Z}{R_2}$$
$$V_{11}(R_1) = \frac{1}{2R_1} \quad V_{22}(R_2) = \frac{1}{2R_2} \quad V_{12}(R_1,\ R_2) = \frac{1}{\sqrt{R_1^2+R_2^2}}$$

$$E(R_1,\ R_2) = 2T_1(R_1) + 2T_2(R_2) + 2V_{N1}(R_1) + 2V_{N2}(R_2) + V_{11}(R_1) + V_{22}(R_2) + 4V_{12}(R_1,\ R_2)$$

Minimization of the electronic energy with respect to R_1 and R_2:

$$\begin{pmatrix} R_1 \\ R_2 \end{pmatrix} = \begin{pmatrix} 1 \\ 4 \end{pmatrix} \quad \begin{pmatrix} R_1 \\ R_2 \end{pmatrix} = \text{Minimize}(E,\ R_1,\ R_2) \quad \begin{pmatrix} R_1 \\ R_2 \end{pmatrix} = \begin{pmatrix} 0.329 \\ 0.329 \end{pmatrix} \quad \text{E}(R_1,\ R_2) = -18.518$$

Literature cited:

1. Bagchi, B.; Holody, P. "An interesting application of Bohr theory," Am. J. Phys. 1988, 56, 746.
2. Saleh-Jahromi, A. "Ground State Energy of Lithium and Lithium-like Atoms Using the Bohr Theory," The Chemical Educator, 2006, 11, 333-334.
3. Mathcad is a product of Mathsoft, 101 Main Street, Cambridge, MA 02142
4. www.users.csbsju.edu/~frioux/stability/BohrAtoms.mcd

This page titled 2.29: A Bohr Model for Multi-electron Atoms and Ions is shared under a CC BY 4.0 license and was authored, remixed, and/or curated by Frank Rioux via source content that was edited to the style and standards of the LibreTexts platform.

2.30: Atomic Variational Calculations- Hydrogen to Boron

The purpose of this tutorial is to calculate the ground-state energies of simple multi-electron atoms and ions using the variational method. In the interest of mathematical and computational simplicity the single parameter, orthonormal hydrogenic wave functions shown below will be used. The method will be illustrated for boron, but can be used for any atomic or ionic species with five or less electrons.

Using the following orthonormal trial wave functions, the various contributions to the total electronic energy of a multi-electron atom are given below in terms of the variational parameter, α. For further detail see: "Atomic Variational Calculations: Hydrogen to Boron," The Chemical Educator 1999, 4, 40-43. It should be pointed out that in these calculations the exchange interaction is ignored. Including exchange generally improves the results by about 1%.

$$\Psi_{1s}(\alpha,\ \mathrm{r}) = \sqrt{\frac{\alpha^3}{\pi}}\exp(-\alpha,\ \mathrm{r}) \qquad \Psi_{2s}(\alpha,\ \mathrm{r}) = \sqrt{\frac{\alpha^3}{32\pi}}(2-\alpha\mathrm{r})\exp\left(\frac{-\alpha r}{2}\right) \qquad \Psi_{2p}(\alpha,\ r,\ \theta) = \sqrt{\frac{\alpha^3}{32\pi}}\alpha\mathrm{r}\exp\left(\frac{-\alpha\mathrm{r}}{2}\right)\cos(\theta)$$

The method will be illustrated with boron which has the electronic structure $1s^2 2s^2 2p^1$.

Nuclear charge: Z = 5

Seed value for variational parameter α: α = Z

Kinetic energy integrals:

$$T_{1s}(\alpha) = \frac{\alpha^2}{2} \quad T_{2s}(\alpha) = \frac{\alpha^2}{8} \quad T_{2p}(\alpha) = \frac{\alpha^2}{8}$$

Electron-nucleus potential energy integrals:

$$V_{N1s}(\alpha) = -Z\alpha \quad V_{N2s}(\alpha) = -\frac{Z}{4}\alpha \quad V_{N2p}(\alpha) = -\frac{Z}{4}\alpha$$

Electron-electron potential energy integrals:

$$V_{1s1s}(\alpha) = \frac{5}{8}\alpha \quad V_{1s2s}(\alpha) = \frac{17}{81}\alpha \quad V_{1s2p}(\alpha) = \frac{59}{243}\alpha \quad V_{2s2s}(\alpha) = \frac{77}{512}\alpha \quad V_{2s2p}(\alpha) = \frac{83}{512}\alpha$$

Enter coefficients for each contribution to the total energy:

T_{1s}	T_{2s}	T_{2p}	V_{N1s}	V_{N2s}	V_{N2p}	V_{1s1s}	V_{1s2s}	V_{1s2p}	V_{2s2s}	V_{2s2p}
a = 2	b = 2	c = 1	d = 2	e = 2	f = 1	g = 1	h = 4	i = 2	j = 1	k = 2

Variational energy equation:

$$E(\alpha) = \frac{\mathrm{a}T_{1s}(\alpha) + \mathrm{b}T_{2s}(\alpha) + \mathrm{c}T_{2p}(\alpha) + \mathrm{d}V_{N1s}(\alpha) + \mathrm{e}V_{n2s}(\alpha) + \mathrm{f}V_{N2p}(\alpha)\ldots}{\mathrm{g}V_{1s1s}(\alpha) + \mathrm{h}V_{1s2s}(\alpha) + \mathrm{i}V_{1s2s}(\alpha) + \mathrm{j}V_{2s2s}(\alpha) + \mathrm{k}V_{2s2p}(\alpha)}$$

Minimize energy with respect to the variational parameter, α.

$$\alpha = \mathrm{Minimize}(E,\ \alpha) \quad \alpha = 4.118 \quad E(\alpha) = -23.320$$

The experimental ground state energy is the negative of the sum of the successive ionization energies of the atom or ion (see table of experimental data below):

$$\mathrm{SumIE} = 0.305 + 0.926 + 1.395 + 9.527 + 12.500 \quad E_{exp} = \mathrm{SumIE} \quad E_{exp} = -24.653$$

Compare theory and experiment:

$$\left|\frac{E(\alpha) - E_{exp}}{E_{exp}}\right| = 5.405\%$$

Calculate orbital energies of a 1s, 2s and 2p electron by filling the place holders with the appropriate coefficients (0, 1, 2, ...). Compare the calculated results with experimental values (see table below):

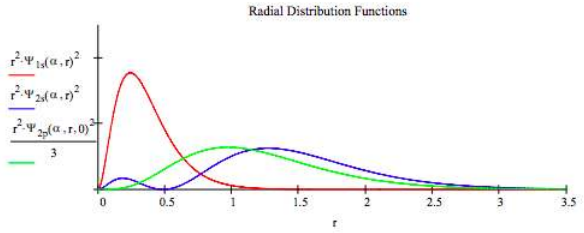
$$
\begin{aligned}
E_{1s}(\alpha) = \; & 1T_{1s}(\alpha) + 0T_{2s}(\alpha) + 0T_{2p}(\alpha) + 1V_{N1s}(\alpha)\ldots \\
& +0V_{N2s}(\alpha) + 0V_{N2p}(\alpha) + 1V_{1s1s}(\alpha) + 2V_{1s2s}(\alpha)\ldots \quad E_{1s}(\alpha) = -6.809 \quad \text{Exp} = -7.355 \\
& +1V_{1s2p}(\alpha) + 0V_{2s2s}(\alpha) + 0V_{2s2p}(\alpha) \\
E_{2s}(\alpha) = \; & 0T_{1s}(\alpha) + 1T_{2s}(\alpha) + 0T_{2p}(\alpha) + 0V_{N1s}(\alpha)\ldots \\
& +1V_{N2s}(\alpha) + 0V_{N2p}(\alpha) + 0V_{1s1s}(\alpha) + 2V_{1s2s}(\alpha)\ldots \quad E_{2s}(\alpha) = -0.012 \quad \text{Exp} = -0.518 \\
& +0V_{1s2p}(\alpha) + 1V_{2s2s}(\alpha) + 1V_{2s2p}(\alpha) \\
E_{1s}(\alpha) = \; & 0T_{1s}(\alpha) + 0T_{2s}(\alpha) + 1T_{2p}(\alpha) + 0V_{N1s}(\alpha)\ldots \\
& +0V_{N2s}(\alpha) + 1V_{N2p}(\alpha) + 0V_{1s1s}(\alpha) + 0V_{1s2s}(\alpha)\ldots \quad E_{2p}(\alpha) = 0.307 \quad \text{Exp} = -0.305 \\
& +2V_{1s2p}(\alpha) + 0V_{2s2s}(\alpha) + 2V_{2s2p}(\alpha)
\end{aligned}
$$

Successive Ionization Energies for the First Six Elements

Element	IE_1	IE_2	IE_3	IE_4	IE_5	IE_6
H	0.500	x	x	x	x	x
He	0.904	2.000	x	x	x	x
Li	0.198	2.782	4.500	x	x	x
Be	0.343	0.670	5.659	8.000	x	x
B	0.305	0.926	1.395	9.527	12.500	x
C	0.414	0.896	1.761	2.370	14.482	18.000

Orbital Energies for the First Six Atoms

Element	$1s$	$2s$	$2p$
H	-0.500	x	x
He	-0.904	x	x
Li	-2.386	-0.198	x
Be	-4.383	-0.343	x
B	-7.355	-0.518	-0.305
C	-10.899	-0.655	-0.414



Interpretation of results:

With this model for atomic structure we are able to compare theory with experiment in two ways. The calculated ground-state energy is compared to the negative of the sum of the successive ionization energies. This comparison shows that theory is in error by 5.4% - not bad for a one-parameter model for a five-electron atom.

However, the comparison of the calculated orbital energies with the negative of the orbital ionization energies is not so favorable. It is clear that the one-parameter model used in this calculation does not do a very good job on the valence electrons. For example, the 2s electrons are barely bound and the 2p electron is not bound at all.

The total energy (ground-state energy) comparison is more favorable because the model does a decent job on the non-valence electrons where the vast majority of the energy resides. Chemistry, however, is dictated by the behavior of the valence electrons, so the failure of the model to calculate good orbital energies, and therefore good wave functions, for the valence electrons is a serious problem. This is a common problem in atomic and molecular calculations; finding wave functions that effectively model the behavior of both the core and the valence electrons.

Suggested additional problems: H, H^-, Li, Li^+, Be, C^+, and Li atom excited state $1s^2 2p^1$.

This page titled 2.30: Atomic Variational Calculations- Hydrogen to Boron is shared under a CC BY 4.0 license and was authored, remixed, and/or curated by Frank Rioux via source content that was edited to the style and standards of the LibreTexts platform.

2.31: Some Calculations on the Lithium Atom Ground State

The purpose of this tutorial is to point out that if all that mattered in the determination of atomic structure was energy minimization, the electronic structure of lithium would be $1s_3$, rather than $1s^2 2s^1$.

To deal with this issue we choose the following scaled hydrogenic orbitals for the lithium atom's electrons:

$$\Psi_{1s} = \sqrt{\frac{\alpha^3}{\pi}} \exp(-\alpha,\ \mathrm{r}) \quad \Psi_{2s} = \sqrt{\frac{\alpha^3}{32\pi}} (2 - \alpha \mathrm{r}) \exp\left(\frac{-\alpha \mathrm{r}}{2}\right)$$

Using this basis set we find the following expressions (in terms of the variational parameter α) for the expectation values for the various contributions to the electronic energy of the lithium atom.

Nuclear charge:

$$Z = 3$$

Kinetic energy integrals:

$$T_{1s}(\alpha) = \frac{\alpha^2}{2} \quad T_{2s}(\alpha) = \frac{\alpha^2}{8}$$

Electron-nucleus potential energy integrals:

$$V_{N1s}(\alpha) = -Z\alpha \quad V_{N2s}(\alpha) = -\frac{Z}{4}\alpha$$

Electron-electron potential energy integrals:

$$V_{1s1s}(\alpha) = \frac{5}{8}\alpha \quad V_{1s2s}(\alpha) = \frac{17}{81}\alpha$$

We now calculate the ground-state energy of lithium assuming it has the 1s 22s1 electronic configuration. The total electronic energy consists of nine contributions: three kinetic energy terms, three electron-nucleus potential energy terms, and three electron-electron potential energy contriubtions.

$$E_{Li}(\alpha) = 2T_{1s}(\alpha) + 2V_{N1s}(\alpha) + V_{1s1s}(\alpha) + 2T_{2s}(\alpha) + V_{N2s}(\alpha) + 2V_{1s2s}(\alpha)$$

Minimization of the energy with respect to the variational parameter, α, yields the following result:

$$\alpha = \frac{d}{d\alpha} E_{Li}(\alpha) = 0 \ \Big|\ \substack{\text{solve, } \alpha \\ \text{float, } 4} \rightarrow 2.536 \quad E_{Li}(\alpha) = -7.2333$$

Compared to the experimental ground-state energy -7.478 E_h (the negative of the successive ionization energies of the lithium atom) this result is in error by 3.3%. This result is satisfactory, indicating that the theoretical model has some merit. We could do better, of course, but it would cost something in terms of computational effort and simplicity of the model.

Now we calculate the energy of the hypothetical $1s^3$ electronic configuration for lithium using the same basis functions. Again, the total electronic energy consists of nine contributions: three kinetic energy terms, three electron-nucleus potential energy terms, and three electron-electron potential energy contributions.

$$E_{Li}(\alpha) = 2T_{1s}(\alpha) + 3V_{N1s}(\alpha) + 3V_{1s1s}(\alpha)$$

Minimization of the energy with respect to the variational parameter, α, yields the following result:

First reset the value of α:

$$\alpha = \alpha \quad \alpha = \frac{d}{d\alpha} E_{Li}(\alpha) = 0 \ \Big|\ \substack{\text{solve, } \alpha \\ \text{float, } 4} \rightarrow 2.375 \qquad E_{Li}(\alpha) = -8.4609$$

This electronic configuration has a lower energy than that for $1s^2 2s^1$, and also lower than the experimental value in clear violation of the variational principle.

Electrons are fermions and subject to the Pauli exclusion principle which prevents two electrons from having the same set of quantum numbers. Thus, while the $1s^3$ electronic configuration has a lower energy its existence is prevented by the Pauli principle.

This page titled 2.31: Some Calculations on the Lithium Atom Ground State is shared under a CC BY 4.0 license and was authored, remixed, and/or curated by Frank Rioux via source content that was edited to the style and standards of the LibreTexts platform.

https://chem.libretexts.org/@go/page/156473

2.32: E. B. Wilson's Calculation on the Lithium Atom Ground State

The electronic structure of lithium is $1s^1 2s^1$. The hydrogenic 1s and 2s orbitals are as follows:

$$\Psi(1s) = \sqrt{\frac{\alpha^3}{\pi}}\exp(-\alpha r) \quad \Psi(2s) = \sqrt{\frac{\alpha^3}{32\pi}}(2-\alpha r)\exp\left(\frac{-\alpha r}{2}\right)$$

If these orbitals are used the variational expression for the lithium atom energy is given below.

Nuclear charge:

$$Z = 3$$

Seed value for α:

$$\alpha = Z$$

Define variational integral for lithium:

$$E(\alpha) = \alpha^2 - 2Z\alpha + \frac{5}{8}\alpha + \frac{\alpha^2}{8} - \frac{Z\alpha}{4} + \frac{34\alpha}{81}$$

Minimize energy with respect to the variational parameter, α:

$$\text{Given}\ \frac{d}{d\alpha}E(\alpha) = 0 \quad \alpha = \text{Find}(\alpha) \quad \alpha = 2.5357 \quad E(\alpha) = -7.2333$$

This one-parameter variational calculation is in error by 3.27%. The ground state energy is the negative of the sum of the ionization energies.

$$E_{exp} = \frac{-5.392 - 75.638 - 122.451}{27.2114} \quad E_{exp} = -7.4778 \quad \left|\frac{E(\alpha) - E_{exp}}{E_{exp}}\right| = 3.2695\%$$

It is possible to improve the results by using a two-parameter calculation in which the 2s electron has a different scale factor that the 1s electrons. In other words the electronic structure would be $1s(\alpha)^2 2s(\beta)^1$.

$$\Psi_{1s}(r,\ \alpha) = \sqrt{\frac{\alpha^3}{\pi}}\exp(-\alpha,\ r) \quad \Psi_{2s}(r,\ \beta) = \sqrt{\frac{\beta^3}{32\pi}}(2-\beta r)\exp\left(\frac{-\beta r}{2}\right)$$

This calculation was first published by E. Bright Wilson (*J. Chem. Phys* **1**, 210 (1933)) in 1933. Levine's Quantum Chemistry (6th ed. p 299) contains a brief summary of the calculation.

Nuclear charge:

$$Z = 3$$

Seed values for α and β:

$$\alpha = Z \quad \beta = Z - 1$$

When the wave function for the $1s(\alpha)^2 2s(\beta)$ electron configuration is written as a Slater determinant, the following variational integrals arise.

$$T_{1s}(\alpha) = \frac{\alpha^2}{2} \quad T_{2s}(\beta) = \frac{\beta^2}{2} \quad V_{N1s}(\alpha) = -Z\alpha \quad V_{N2s}(\beta) = \frac{-Z\beta}{4}$$

$$V_{1s1s}(\alpha) = \frac{5}{8}\alpha \qquad V_{1s2s}(\alpha,\ \beta) = \frac{\beta^4 + 10\alpha\beta + 8\alpha^4 + 20\alpha^3\beta + 12\alpha^2\beta^2}{(2\alpha+\beta)^5}$$

$$T_{1s2s}(\alpha,\ \beta) = -4\sqrt{4}\alpha^{\frac{5}{2}}\beta^{\frac{5}{2}}\frac{\beta - 4\alpha}{(2\alpha+\beta)^4} \quad V_{N1s2s}(\alpha,\ \beta) = -Z4\sqrt{2}\alpha^{\frac{3}{2}}\beta^{\frac{3}{2}}\frac{2\alpha - \beta}{(2\alpha+\beta)^3}$$

$$V_{1112}(\alpha,\ \beta) = 32\sqrt{2}\beta^{\frac{3}{2}}\alpha^{\frac{5}{2}}\frac{-28\alpha^3\beta + 264\alpha^4 - 21\alpha\beta^3 - \beta^4 - 86\alpha^2\beta^2}{(2\alpha\beta)^3(\beta+6\alpha)^4}$$

$$V_{1212}(\alpha,\ \beta) = 16\alpha^3\beta^3\frac{13\beta^2 + 20\alpha^2 - 30\beta\alpha}{(\beta+2\alpha)^7} \quad S_{1s2s}(\alpha,\ \beta) = 32\sqrt{2}\alpha^{\frac{3}{2}}\beta^{\frac{3}{2}}\frac{\alpha-\beta}{(2\alpha+\beta)^4}$$

The next step in this calculation is to collect these terms in an expression for the total energy of the lithium atom and then minimize it with respect to the variational parameters, α and β. The results of this minimization procedure are shown below.

$$E(\alpha,\ \beta) = \frac{\begin{array}{l} 2T_{1s}(\alpha) + T_{2s}(\beta) - T_{1s}(\alpha)S_{1s2s}(\alpha,\ \beta)^2 - 2T_{1s2s}(\alpha,\ \beta)S_{1s2s}(\alpha,\ \beta)... \\ +2V_{N1s}(\alpha) + V_{N2s}(\beta) - V_{N1s}(\alpha)S_{1s2s}(\alpha,\ \beta)^2 - 2V_{N1s2s}(\alpha,\ \beta)S_{1s2s}(\alpha,\ \beta)... \\ +2V_{1s2s}(\alpha,\ \beta) + V_{1s1s}(\alpha) - 2V_{1112}(\alpha,\ \beta)S_{1s2s}(\alpha,\ \beta) - V_{1212}(\alpha,\ \beta) \end{array}}{1 - S_{1s2s}(\alpha,\ \beta)^2}$$

Minimization of E(α, β) simultaneously with respect to α and β.

$$\text{Given} \quad \frac{d}{d\alpha}E(\alpha,\ \beta) = 0 \quad \frac{d}{d\beta}E(\alpha,\ \beta) = 0$$

$$\begin{pmatrix}\alpha\\ \beta\end{pmatrix} = \text{Find}(\alpha,\ \beta) \quad \begin{pmatrix}\alpha\\ \beta\end{pmatrix} = \begin{pmatrix}2.6797\\ 1.8683\end{pmatrix} \quad E(\alpha,\ \beta) = -7.3936$$

Comparison with experiment (ground state energy is the negative of the sum of the ionization energies):

$$E_{exp} = \frac{-5.392 - -75.638 - 122.451}{27.2114} \quad E_{exp} = -7.4778 \quad \left|\frac{E(\alpha,\ \beta) - E_{exp}}{E_{exp}}\right| = 1.1258\%$$

This result is slightly different from that reported by Wilson in 1933. He found that the energy was minimized at -7.3922 E_h, with parameters α = 2.686 and β = 1.776. When I use his parameters with my equation for the energy I get Wilson's energy value, so I can only conclude that he did not quite find the energy minimum.

$$\alpha = 2.686 \quad \beta = 1.776 \quad E(\alpha,\ \beta) = -7.3922$$

This page titled 2.32: E. B. Wilson's Calculation on the Lithium Atom Ground State is shared under a CC BY 4.0 license and was authored, remixed, and/or curated by Frank Rioux via source content that was edited to the style and standards of the LibreTexts platform.

2.33: The Importance of the Pauli Principle

In a provacative article published in *Science* (21 February 1975) with the title "Of Atoms, Mountains and Stars: A Study in Qualitative Physics," Victor Weisskopf illustrates the importance of quantum mechanics in understanding not only the nanoscopic world of atoms and molecules, and our macroworld of mountains, but also the cosmological world of stars and galaxies. Weisskopf's paper presents an analysis of material science in terms of two fundamental ideas: wave-particle duality for matter and light, and the Pauli exclusion principle for the basic building blocks of matter (electrons, protons and neutrons, all fermions).

Regarding the Pauli principle Weisskopf writes:

> If the Pauli principle did not hold, all electrons would be allowed to be in the lowest quantum state. That would mean that the ground states of all atoms would be similar: the atomic electrons would all assemble in the lowest and simplest quantum state. All atoms would exhibit essentially the same properties, a most uninteresting world. We owe the variety of nature largely to the exclusion principle.

The purpose of this tutorial is to illustrate what Weisskopf is saying in this paragraph. Using the following trial wave function, a general variational calculation will be carried out assuming all atomic electrons are resident in the ground 1s quantum level.

$$\Psi(\alpha) = \sqrt{\frac{\alpha^3}{\pi}}\exp(-\alpha r)$$

The calculation of the energy of the $1s^Z$ electronic configuration assuming this trial wave function yields.

$$\mathrm{E} = \mathrm{Z}\frac{\alpha^2}{2} - \mathrm{Z}^2\alpha + \frac{\mathrm{Z}(\mathrm{Z}-1)}{2}\frac{5}{8}\alpha$$

Minimization of E with respect to α gives

$$\frac{d}{d\alpha}\left[\mathrm{Z}\frac{\alpha^2}{2} - \mathrm{Z}^2\alpha + \frac{\mathrm{Z}(\mathrm{Z}-1)}{2}\frac{5}{8}\alpha\right] = 0 \text{ solve, } \alpha \rightarrow \frac{11}{16}\mathrm{Z} + \frac{5}{16}$$

Substitution of the optimum value for α into E yields the energy $1s^Z$ electronic configuration:

$$\mathrm{E}(\mathrm{Z}) = \mathrm{Z}\tfrac{\alpha^2}{2} - \mathrm{Z}^2\alpha + \tfrac{\mathrm{Z}(\mathrm{Z}-1)}{2}\tfrac{5}{8}\alpha \;\Big|\; \begin{matrix}\text{substitute, } \alpha=\frac{11}{16}\mathrm{Z}+\frac{5}{16} \\ \text{simplify}\end{matrix} \rightarrow \tfrac{-121}{512}\mathrm{Z}^3 - \tfrac{55}{256}\mathrm{Z}^2 - \tfrac{25}{512}\mathrm{Z}$$

Comparing this result for the energy as a function of atomic number with the actual ground state energies of the elements confirms Weisskopf's statement. The energy result ignoring the Pauli principle presented here is lower than the experimental energies for elements beyond He.

Z	E(Z)	E(experimental)
1	−0.500	−0.500
2	−2.484	−2.903
3	−8.461	−7.478
4	−18.758	−14.668
5	−35.156	−24.658
6	−59.074	−37.855
7	−91.930	−54.609
8	−135.141	−75.106
9	−190.125	−99.801
10	−258.301	−129.044

This page titled 2.33: The Importance of the Pauli Principle is shared under a CC BY 4.0 license and was authored, remixed, and/or curated by Frank Rioux via source content that was edited to the style and standards of the LibreTexts platform.

2.34: Splitting the 2s-2p Degeneracy in the Lithium Atom

In lithium the ground state electronic configuration is $1s^2 2s^1$. $1s^2 2p^1$ is an excited state because the s-p degeneracy of the one-electron hydrogen atom has been split by the presence of the core ($1s^2$) electrons. A simple variational calculation on Li^+ using $\Psi(r) = (\alpha^3/\pi)^{1/2}\exp(-\alpha r)$ to represent the core electrons yields the following optimum for the variational parameter $\alpha = 2.6875$.

We can model the behavior of the 2s electron by assuming that is attracted to the nucleus and repelled by the core electrons. The attraction for the nucleus is simply the familiar -Z/r coulombic interaction. The electrostatic interaction with the core electrons is given by,

$$V_{core} = 2\left(\frac{1-\exp(-2\alpha r}{r} - \alpha\exp(-2\alpha r)\right)$$

The next steps are to calculate the orbital energies of the 2s and 2p states by numerical integration of Schrödinger's equation. First, the 2s orbital energy.

Reduced mass: $\mu = 1$ Nuclear charge: $Z = 3$ Integration limit: $r_{max} = 12$

Angular momentum: $L = 0$ Energy guess: $Es = -.1748$ $r = 0,\ .01..r_{max}$

$$\text{Given} \quad \frac{-1}{2\mu}\frac{d^2}{dr^2}\Psi s(r) - \frac{1}{r\mu}\frac{d}{dr}\Psi s(r) + \left[2\left(\frac{1-\exp(-2\alpha r}{r} - \alpha\exp(-2\alpha r)\right) + \frac{L(L+1)}{2\mu r^2} - \frac{Z}{r}\right]\Psi s(r) = Es\Psi s(r)$$

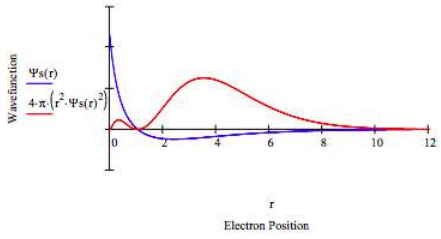
Seed values for wave function and its first derivative:

$$\Psi s(.001) = 1 \quad \Psi(.001) = 0.1$$

$$\Psi s = \text{Odesolve}\,(r,\ r_{max})$$

Normalize the wavefunction:

$$\Psi s(r) = \left(\int_0^{r_{max}} \Psi(r)^2 4\pi r^2 dr\right)^{-0.5} \Psi s(r)$$



Setting L = 1 above demonstrates that the 2p state does not have the same energy as the 2s state. The next step is to demonstrate that the 2p energy is -0.1259 E_h.

Integration limit: $r_{max} = 20$ Angular momentum: $L = 1$ Energy guess: $Ep = -.1259$

$$\text{Given} \quad \frac{-1}{2\mu}\frac{d^2}{dr^2}\Psi p(r) - \frac{1}{r\mu}\frac{d}{dr}\Psi p(r) + \left[2\frac{1-\exp(-2\alpha r}{r} - \alpha\exp(-2\alpha r)\right]\Psi p(r) = Ep\Psi p(r)$$

Seed values for wave function and its first derivative:

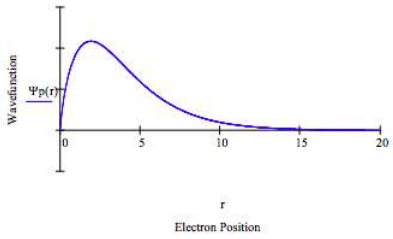
$$\Psi p(.001) = 0 \quad \Psi p(.001) = 0.001$$

$$\Psi p = \text{Odesolve}\,(r,\ r_{max})$$

Normalize the wavefunction:

$$\Psi p(r) = \left(\int_0^{r_{max}} \Psi p(r)^2 4\pi r^2 dr\right)^{-0.5} \Psi p(r)$$

$$r = 0,\ .01..r_{max}$$



Note that 2s-2p degeneracy has indeed been split. The splitting, E2p - E2s = .0488 hartree = 1.33 eV. Herzberg reports an experimental splitting of 1.85 eV. The results of this model could be improved by treating α, the core electron scale factor, as an adjustable parameter.

This page titled 2.34: Splitting the 2s-2p Degeneracy in the Lithium Atom is shared under a CC BY 4.0 license and was authored, remixed, and/or curated by Frank Rioux via source content that was edited to the style and standards of the LibreTexts platform.

2.35: Addition of Spin Angular Momentum- A Tensor Algebra Approach

In this entry I work through section 4.4.3 of David Griffiths' *Introduction to Quantum Mechanics* (2nd ed.) in which he treats the addition of angular momentum for two identical spin-1/2 particles. The tensor algebra approach is illustrated.

The four spin states of two spin-1/2 particles are written below in the spin-z basis in tensor format.

$$|\uparrow\rangle = \begin{pmatrix}1\\0\end{pmatrix} \quad |\downarrow\rangle = \begin{pmatrix}0\\1\end{pmatrix}$$

$$|\uparrow\uparrow\rangle = \begin{pmatrix}1\\0\end{pmatrix}\otimes\begin{pmatrix}1\\0\end{pmatrix} = \begin{pmatrix}1\\0\\0\\0\end{pmatrix} \quad |\uparrow\downarrow\rangle = \begin{pmatrix}1\\0\end{pmatrix}\otimes\begin{pmatrix}0\\1\end{pmatrix} = \begin{pmatrix}0\\1\\0\\0\end{pmatrix} \quad |\downarrow\uparrow\rangle = \begin{pmatrix}0\\1\end{pmatrix}\otimes\begin{pmatrix}1\\0\end{pmatrix} = \begin{pmatrix}0\\0\\1\\0\end{pmatrix} \quad |\downarrow\downarrow\rangle = \begin{pmatrix}0\\1\end{pmatrix}\otimes\begin{pmatrix}0\\1\end{pmatrix} = \begin{pmatrix}0\\0\\0\\1\end{pmatrix}$$

The two middle states are not permissible because they distinguish between identical particles. The solution is to form symmetric and anti-symmetric superpositions of them, but let's follow Griffith's approach for the time being. The four spin states are labeled as shown below.

$$\mathrm{a} = \begin{pmatrix}1\\0\\0\\0\end{pmatrix} \quad \mathrm{b} = \begin{pmatrix}0\\1\\0\\0\end{pmatrix} \quad \mathrm{c} = \begin{pmatrix}0\\0\\1\\0\end{pmatrix} \quad \mathrm{d} = \begin{pmatrix}0\\0\\0\\1\end{pmatrix}$$

The identity and spin operators in units of h/2π are now defined. The final two are the up and down spin ladder operators.

$$I = \begin{pmatrix}1&0\\0&1\end{pmatrix} \quad S_x = \tfrac{1}{2}\begin{pmatrix}0&1\\1&0\end{pmatrix} \quad S_y = \tfrac{1}{2}\begin{pmatrix}0&-i\\i&0\end{pmatrix} \quad S_z = \tfrac{1}{2}\begin{pmatrix}1&0\\0&-1\end{pmatrix} \quad S = S_x + S_y + S_z$$

$$S_u = \begin{pmatrix}0&1\\0&0\end{pmatrix} \quad S_d = \begin{pmatrix}0&0\\1&0\end{pmatrix}$$

Next the total spin operator and total spin operator in the z-direction are defined using kronecker, Mathcad's command for tensor matrix multiplication.

$$S_{tot} = \mathrm{kronecker(S,\,I)} + \mathrm{kronecker(I,\,S)} \quad Sz_{tot} = \mathrm{kronecker}\,(S_z,\ I) + \mathrm{kronecker}\,(I,\ S_z)$$

Calculation of the expectation values for total spin in the z-direction for spin states a, b, c and d reveals the problem mentioned above. For S = 1 we expect S_z values of -1, 0 and 1. The extra value for Sz = 0 indicates an interpretive problem.

$$\mathrm{a}^T Sz_{tot}\mathrm{a} = 1 \quad \mathrm{b}^T Sz_{tot}\mathrm{b} = 0 \quad \mathrm{c}^T Sz_{tot}\mathrm{c} = 0 \quad \mathrm{d}^T Sz_{tot}\mathrm{d} = -1$$

Griffiths solves the problem by operating with the lowering operator on spin state a, which yields an in-phase superposition (unnormalized) of spin states b and c.

$$(\mathrm{kronecker}\,(S_d,\ I) + \mathrm{kronecker}\,(I,\ S_d))\begin{pmatrix}1\\0\\0\\0\end{pmatrix} = \begin{pmatrix}0\\1\\1\\0\end{pmatrix}$$

Repeating with the result from above yields an unnormalized d spin state.

$$(\mathrm{kronecker}\,(S_d,\ I) + \mathrm{kronecker}\,(I,\ S_d))\begin{pmatrix}0\\1\\1\\0\end{pmatrix} = \begin{pmatrix}0\\0\\0\\2\end{pmatrix}$$

Operating on the unnormalized d spin state yield a null vector suggesting that the original spin states might be reformulated as triplet and singlet states.

$$(\text{kronecker}(S_d,\ I) + \text{kronecker}(I,\ S_d)) \begin{pmatrix} 0 \\ 0 \\ 0 \\ 2 \end{pmatrix} = \begin{pmatrix} 0 \\ 0 \\ 0 \\ 0 \end{pmatrix}$$

Given this hint and the fact that the initial spin states are orthonormal, we preserve this property in the new spin states by constructing an out-of-phase superposition of b and c. This give us a revised set of orthonormal spin vectors. In conventional notation these states are |11 >, |10 >, |1-1 > and |00 >, where the first number is total spin value and the second the spin in the z-direction. Thus, we have a triplet and a singlet state as will be confirmed below.

$$\Psi_{1p1} = \begin{pmatrix} 1 \\ 0 \\ 0 \\ 0 \end{pmatrix} \quad \Psi_{10} = \begin{pmatrix} 0 \\ \frac{1}{\sqrt{2}} \\ \frac{1}{\sqrt{2}} \\ 0 \end{pmatrix} \quad \Psi_{1m1} = \begin{pmatrix} 0 \\ 0 \\ 0 \\ 1 \end{pmatrix} \quad \Psi_{00} = \begin{pmatrix} 0 \\ \frac{1}{\sqrt{2}} \\ \frac{-1}{\sqrt{2}} \\ 0 \end{pmatrix}$$

We now establish by calculation of expectation values for S^2 (constructed below) and S_z that the first three spin states are members of a triplet state (S = 1) and the final spin state is a singlet (S = 0). The eigenvalues for the S^2 operator are S(S + 1) which is 2 for the triplet state and 0 for the singlet state.

$$\begin{aligned} \text{SS} = {} & \text{kronecker}(S^2,\ I) + \text{kronecker}(I,\ S^2) + 2\text{kronecker}(S_x,\ S_x) \\ & + \text{kronecker}(S_y,\ S_y) + \text{kronecker}(S_z,\ S_z) \end{aligned}$$

$$\begin{array}{llll} (\Psi_{1p1})^T \text{SS}\Psi_{1p1} = 2 & (\Psi_{10})^T \text{SS}\Psi_{10} = 2 & (\Psi_{1m1})^T \text{SS}\Psi_{1m1} = 2 & (\Psi_{00})^T \text{SS}\Psi_{00} = 0 \\ (\Psi_{1p1})^T Sz_{tot}\Psi_{1p1} = 1 & (\Psi_{10})^T Sz_{tot}\Psi_{10} = 0 & (\Psi_{1m1})^T Sz_{tot}\Psi_{1m1} = -1 & (\Psi_{00})^T Sz_{tot}\Psi_{00} = 0 \end{array}$$

Next, we look at this problem from the energy perspective and use the spin-spin interaction Hamiltonian to calculate the energy eigenvalues and eigenvectors for the two spin-1/2 particle system

$$H_{SpinSpin} = \text{kronecker}(S_x,\ S_x) + \text{kronecker}(S_y,\ S_y) + \text{kronecker}(S_z,\ S_z)$$

$$H_{SpinSpin} = \begin{pmatrix} 0.25 & 0 & 0 & 0 \\ 0 & -0.25 & 0.5 & 0 \\ 0 & 0.5 & -0.25 & 0 \\ 0 & 0 & 0 & 0.25 \end{pmatrix}$$

We now ask Mathcad to calculate the eigenvalues and eigenvectors of the spin-spin operator. These results are displayed by constructing a matrix which contains the eigenvalues in the top row, and their eigenvalues in the columns below the eigenvalues.

$$i = 1..4 \quad \text{E} = \text{eigenvals}(H_{SpinSpin}) \quad \text{EigenvalsEigenvec} = \text{rsort}(\text{stack}(E^T,\ \text{eigenvecs}(H_{SpinSpin})),\ 1)$$

$$\text{EigenvalEigenvec} = \begin{pmatrix} -0.75 & 0.25 & 0.25 & 0.25 \\ 0 & 1 & 0 & 0 \\ 0.707 & 0 & 0 & 0.707 \\ -0.707 & 0 & 0 & 0.707 \\ 0 & 0 & 1 & 0 \end{pmatrix}$$

These calculations are consistent with those that preceded and with the results presented on page 284 of Griffiths′ text.

This page titled 2.35: Addition of Spin Angular Momentum- A Tensor Algebra Approach is shared under a CC BY 4.0 license and was authored, remixed, and/or curated by Frank Rioux via source content that was edited to the style and standards of the LibreTexts platform.

2.36: Hund's Rule

In a recent discussion of the role of electron–electron repulsion in interpreting chemical reaction mechanisms and spectroscopic phenomena, Liu (*1*) gives an incorrect answer to the question, Why is the triplet state lower in energy than the corresponding singlet state?

After reviewing the mathematical form of the singlet and triplet wave functions for a two-electron system, Liu presents the plausible and frequently used explanation that the antisymmetric triplet spatial wave function keeps electrons apart while the symmetric singlet spatial wave function permits electrons to be close together. Therefore it follows that electron–electron repulsion must be lower in the triplet state, giving it a lower total energy, *E*, than the singlet state, which clearly must have greater interelectron repulsion.

Snow and Bills (2) challenged this explanation over thirty years ago with a review of low- and high-level calculations on the $1s^12s^1$ and $1s^12p^1$ excited states of the helium atom available in the research literature. The most accurate calculations (for all practical purposes exact) available for the helium $1s^12s^1$ excited state are shown in Table 1.1 All numerical results are reported in atomic units. (Energy: E_h = 2.626 MJ mol1; distance: a_0 = 52.9 pm).

It is obvious that the explanation Liu offers for the relative stability of the triplet state is not supported by accurate quantum mechanical calculations. The electrons are actually closer on average in the triplet state (smaller r_{12}), and consequently electron–electron repulsion (V_{ee}) and electron kinetic energy (T) are higher in the triplet state.[2] As the table shows the real reason that the triplet state lies low is due to greater electron–nucleus attraction (V_{ne}). In other words, V_{ne} decreases more than V_{ee} and T increase leading to a more stable triplet state.

Table 1. Expectation Values for the Singlet and Triplet States of the Helium $1s^12s^1$ Excited State Calculated Using the Exact Wave Function

Property	^1S	Δ	^3S
$\langle E \rangle$	−2.146	−0.029	−2.175
$\langle T \rangle$	2.146	0.029	2.175
$\langle V_{ne} \rangle$	−4.541	−0.078	−4.619
$\langle V_{ee} \rangle$	0.250	0.018	0.268
$\langle r_{12} \rangle$	5.270	−0.822	4.448

Note: All numerical results are reported in atomic units (Energy: E_h = 2.626 MJ mol^{-1}; distance: a_0 = 52.9 pm). $\Delta = {}^3S - {}^1S$.

Two questions emerge at this point:

- What is the origin of the incorrect explanation that the results in Table 1 refute?
- How do we “explain” the results in Table 1?

The answer to the first question seems clear in Snow and Bills’ article—first-order perturbation theory. Using zero-order wave functions (the He^+ 1s and 2s eigenfunctions) to calculate the singlet and triplet energies of the helium $1s^12s^1$ excited state yields the results shown in Table 2. While this simple calculation correctly shows that the triplet state is more stable than the singlet state, it cannot be safely used for interpretive purposes because it violates the virial theorem, which requires \(\langle E \rangle = - \langleT \rangle = \frac{1}{2} \left[V_{ \text{ne}} + V_{ \text{ee}} \right]. In other words, no physical significance should be attached to the lower interelectron repulsion it yields for the triplet state.

Table 2. Expectation Values for the Singlet and Triplet States of the Helium $1s^12s^1$ Excited State Calculated Using the Zero-Order Wave Function

Property	^1S	Δ	^3S
$\langle E \rangle$	−2.036	−0.088	−2.124
$\langle T \rangle$	2.500	0	2.500
$\langle V_{ne} \rangle$	−5.000	0	−5.000
$\langle V_{ee} \rangle$	0.464	−0.088	0.376
$\langle r_{12} \rangle$	3.085	0.046	3.131

In the search for an answer to the second question, we accept guidance from Robert Mulliken's famous remark (*3*): "... the more accurate the calculations became, the more the concepts tended to vanish into thin air." In other words, we seek a level of theory that is quantum mechanically sound and also comprehensible in terms of traditional chemical concepts such as orbitals. The best way to find this theoretical level is to move up gradually from the first-order perturbation theory calculation summarized in Table 2. The calculations that follow have been carried out in the Mathcad programming environment and are available on the Internet (*4*).

An obvious improvement to the first-order perturbation theory calculation is to add a variational parameter, α, to the 1s and 2s wave functions:

$$\Psi_{1s} = \sqrt{\frac{\alpha^3}{\pi}}\exp(\alpha r)$$

$$\Psi_{2s} = \sqrt{\frac{\alpha^3}{2\pi}}(2-\alpha r)\exp\left(-\frac{\alpha r}{2}\right)$$

Results for such a variational calculation on the $1s^1 2s^1$ singlet and triplet states of He and Li^+ are shown in Table 3.

Table 3. One-Parameter Variational Calculations on He and Li^+ Singlet and Triplet States

Property	Helium Atom			Lithium Ion		
	^1S	Δ	^3S	^1S	Δ	^3S
α	1.815	0.035	1.850	2.185	0.035	2.850
$\langle E\rangle$	−2.058	−0.080	−2.138	−4.951	−0.124	−5.075
$\langle T\rangle$	2.508	0.088	2.138	4.951	0.124	5.075
$\langle V_{ne}\rangle$	−4.536	−0.088	−4.624	−10.555	−0.131	−10.686
$\langle V_{ee}\rangle$	0.421	−0.106	0.315	0.653	−0.117	0.536

This calculation shows that the triplet state has a lower energy because both Vne and Vee have lower values in the triplet state. This is a hint that the simple notion that only Vee counts is not valid. This calculation also correctly shows that the triplet state species is smaller (has a larger decay constant α) than the singlet state.

The next step is obvious—a two-parameter calculation that assigns the 2s orbital an independent variational parameter β. The results for this calculation are shown in Table 4. The first thing to note is that this wave function is not quite good enough for He. It shows the singlet state slightly lower in energy than the triplet, but it does show, in agreement with the exact calculations, that V_{ee} is higher for the triplet state. Everything is in order for Li+, showing that V_{ne} is the reason the triplet state lies lower in energy than the singlet because it overwhelms the increases in T and V_{ee}. Additional calculations on Be^{2+}, B^{3+}, and so forth are consistent with the lithium ion results. Given this success it appears justified to use the two-parameter wave function to formulate an answer to the second question.

Table 4. Two-Parameter Variational Calculations on He and Li + Singlet and Triplet States

Property	Helium Atom			Lithium Ion		
	^1S	Δ	^3S	^1S	Δ	^3S
$1s(\alpha)$	2.013	−0.019	1.994	3.019	−0.020	2.999
$2s(\beta)$	0.925	0.626	1.551	1.681	0.889	2.570
$\langle E\rangle$	−2.170	0.003	−2.167	−5.091	−0.012	−5.103
$\langle T\rangle$	2.170	−0.003	2.167	5.091	0.012	5.103
$\langle V_{ne}\rangle$	−4.594	−0.026	−4.620	−10.629	−0.055	−10.684
$\langle V_{ee}\rangle$	0.254	0.033	0.287	0.448	0.031	0.479
$\langle r_{1s}\rangle$	0.745	0.007	0.752	0.497	0.003	0.500
$\langle r_{2s}$	6.489	−2.620	3.869	3.569	−1.235	2.334

These calculations show that V_{ee} increases and V_{ne} decreases in going from the singlet to the triplet state. The results also reveal a sharp decrease in the average orbital radius for the 2s electron in the triplet state. These findings are selfconsistent; the antisymmetric character of the triplet state spatial wave function permits a sharp contraction of the 2s orbital increasing the interelectronic repulsion with the 1s electron, but at the same time greatly increasing the favorable attractive interaction between

the 2s electron and the nucleus. Shenkuan previously offered a similar analysis on the basis of fourth-order perturbation theory calculations (*5*). He summarized the results of his study as follows:

> In neutral atoms, in many positive ions, and in small molecules, the energy differences among multiplets are dominated by the energy differences in electron–nuclear attractions—not by the energy differences of interelectron repulsions, which was held traditionally.

The singlet–triplet energy difference can be examined further by consideration of the following two-step mechanism using the lithium ion calculation as an example:

$$\begin{aligned} {}^1S \qquad & (\alpha = 3.019,\ \beta = 1.681) \\ \rightarrow\ & {}^3S^*\,(\alpha = 3.019,\ \beta = 1.681) \\ \rightarrow\ & {}^3S\,(\alpha = 2.999,\ \beta = 2.570) \end{aligned}$$

In the singlet–triplet transition two things change: spatial symmetry and orbital size. In the first step the spatial symmetry changes (symmetric to antisymmetric) while the orbitals are frozen at singlet-state size. As shown in Table 5, kinetic energy and electron–electron repulsion decrease, while electron–nucleus and total energy increase. In the second step the orbitals relax to their optimum triplet-state sizes. This net orbital contraction increases kinetic energy and electron–electron repulsion, and decreases electron–nucleus and total energy.

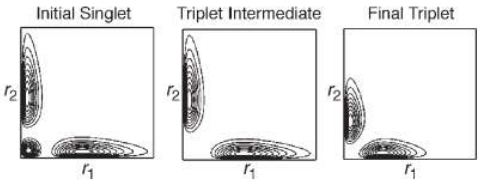


Figure 1. Contour representations of the radial distribution functions graphed versus the coordinates of both electrons.

This mechanism is visualized in Figure 1 in which the radial distribution functions[3] for the three states are graphed versus the coordinates of both electrons in contour format. The three panes of the figure clearly show the symmetry change and the subsequent orbital contraction, providing visual support for the numeric results presented in Table 5.

Table 5. Mechanism for a Singlet–Triplet Transition for the $1s^12s^2$ Excited State of Li^+

Property	^1S	Δ	Intermediate	Δ	^3S
$1s(\alpha)$	3.019	0	3.019	−0.020	2.999
$2s(\beta)$	1.681	0	1.681	0.889	2.570
$\langle E\rangle$	−5.091	0.131	−4.960	−0.143	−5.103
$\langle T\rangle$	5.091	−0.376	4.715	0.388	5.103
$\langle V_{ee}\rangle$	0.448	−0.142	0.306	0.173	0.479
$\langle V_{ne}\rangle$	−10.629	0.649	−9.980	−0.704	−10.684

Summary

This example teaches the important lesson that an intuitively plausible qualitative explanation may not be correct. Qualitative models for atomic and molecular phenomena require validation by rigorous calculations based on quantum mechanical principles. For example, for the electronic states examined in this study V_{ee} represents less than 4% of the total energy. V_{ne}, the only negative contribution, dominates at about 69% while kinetic energy contributes 31%. In the light of this breakdown it is not surprising that V_{ee} is not the reason for the greater stability of the triplet state.

Notes

1. Please consult ref *2* for the appropriate references to the original literature. These can be found in Tables 1 and 2.
2. The smaller value for the average interelectron separation for the triplet state implies a smaller atomic volume. Therefore, kinetic energy increases from singlet to triplet because it scales as $V^{-2/3}$.
3. For example, the singlet state spatial wave function can be written as

$$\Psi_s = (r_1,\ r_2) = N_s\left[1s\,(r_1)\,2s\,(r_2) + 2s\,(r_1)\,1s\,(r_2)\right]$$

where r_1 and r_2 are the coordinates of the electrons and N_S is the normalization constant. The singlet state distribution function is

$$R_s(r_1,\ r_2) \approx \Psi_s(r_1,\ r_2)^2 r_1^2 r_2^2$$

Similar arguments yield the triplet state distribution function.

Literature Cited

1. Liu, R. S. H. *J. Chem. Educ*. 2005, 82, 558–560.
2. Snow, R. L.; Bills, J. L. *J. Chem. Educ.* **1974**, 51, 585–586.
3. Mulliken, R. S. *J. Chem. Phys.* **1965**, 43, S2.
4. Mathcad is a product of Mathsoft Engineering & Education, Inc., 101 Main Street, Cambridge, MA 02142. www.mathsoft.com/. The Mathcad file is available at www.users. csbsju.edu/~frioux/stability/HundsRuleCalc.pdf/.
5. Shenkuan, N. *J. Chem. Educ.* **1992**, 69, 800–803.

This page titled 2.36: Hund's Rule is shared under a CC BY 4.0 license and was authored, remixed, and/or curated by Frank Rioux via source content that was edited to the style and standards of the LibreTexts platform.

2.37: Hund's Rule - Singlet-Triplet Calculations with Mathcad

Two-parameter Study of the 1s2s Excited State of He and Li^+ - Hund's Rule

The trial variational wave functions for the $1s^12s^1$ excited state of helium atom and lithium ion are scaled hydrogen 1s and 2s orbitals:

$$\Psi_{1s}(r,\ \alpha) = \sqrt{\frac{\alpha^3}{\pi}}\exp(-\alpha r) \quad \Psi_{2s}(r,\ \beta) = \sqrt{\frac{\beta^3}{32\pi}}(2-\beta r)\exp\left(\frac{-\beta r}{2}\right)$$

Nuclear charge: Z = 3

Seed values for α and β: $\alpha = Z + 1 \quad \beta = Z - 1$

The purpose of this analysis is to illustrate Hund's rule by calculating the energy of the singlet and triplet states for the $1s^12s^1$ electronic configuration. The singlet state has a symmetric orbital wave function and the triplet state has an antisymmetric orbital wave function:

$$\Psi_S = \frac{1s(1)2s(2)+1s(2)2s(1)}{\sqrt{2+2S_{1s2s}^2}} \quad \Psi_T = \frac{1s(1)2s(2)-1s(2)2s(1)}{\sqrt{2-2S_{1s2s}^2}}$$

The integrals required for variational calculations on these states are given below:

$$T_{1s}(\alpha) = \frac{\alpha^2}{2} \quad T_{2s}(\beta) = \frac{\beta^2}{8} \quad V_{N1s}(\alpha) = -Z\alpha \quad V_{N2s}(\beta) = \frac{-Z\beta}{4}$$

$$T_{1s2s}(\alpha,\ \beta) = -4\sqrt{2\alpha^5\beta^5}\frac{\beta-4\alpha}{(\beta+2\alpha)^4} \qquad V_{N1s2s}(\alpha,\ \beta) = 4Z\sqrt{2\alpha^3\beta^3}\frac{-2\alpha+\beta}{(\beta+2\alpha)^3}$$

$$V_{1212}(\alpha,\ \beta) = 16\alpha^3\beta^3\frac{13\beta^2+20\alpha^2-30\beta\alpha}{(\beta+2\alpha)^7} \qquad S_{1s2s}(\alpha,\ \beta) = 32\sqrt{2\alpha^3\beta^3}\frac{\alpha-\beta}{(\beta+2\alpha)^4}$$

$$V_{1122}(\alpha,\ \beta) = \beta\alpha\frac{\beta^4+10\beta^3\alpha+8\alpha^4+20\alpha^3\beta+12\beta^2\alpha^2}{(\beta+2\alpha)^5}$$

The next step in this calculation is to collect these terms in an expression for the energy of the singlet and triplet states and then minimize the energy with respect to the variational parameters, α and β. The results of this minimization procedure are shown below.

Singlet state calculation:

Illegal pream-token (T)

$$\begin{pmatrix}\alpha\\ \beta\end{pmatrix} = \text{Minimize}\,(E_s,\ \alpha,\ \beta) \quad \begin{pmatrix}\alpha\\ \beta\end{pmatrix} = \begin{pmatrix}3.019\\ 1.681\end{pmatrix}$$

Break down the total energy into kinetic, electron-nuclear potential, and electron-electron potential energy.

$$T = \frac{T_{1s}(\alpha) + T_{2s}(\beta)\ldots}{1 + S_{1s2s}(\alpha,\ \beta)^2} \quad \frac{+2T_{1s2s}(\alpha,\ \beta)S_{1s2s}(\alpha,\ \beta)}{1 + S_{1s2s}(\alpha,\ \beta)^2}$$

$$= \frac{V_{ne}}{1 + S_{1s2s}(\alpha,\ \beta)^2} \quad \frac{V_{N1s}(\alpha) + V_{N2s}(\beta)\ldots}{1 + S_{1s2s}(\alpha,\ \beta)^2} \quad \frac{+2V_{N1s2s}(\alpha,\ \beta)S_{1s2s}(\alpha,\ \beta)}{1 + S_{1s2s}(\alpha,\ \beta)^2}$$

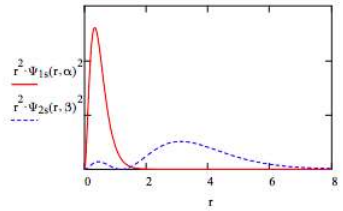
$$V_{ee} = \frac{V_{1122}(\alpha,\ \beta) + V_{1212}(\alpha,\ \beta)}{1 + S_{1s2s}(\alpha,\ \beta)^2}$$

$$T = 5.091 \quad V_{ne} = -10.629 \quad V_{ee} = 0.448 \quad E_s(\alpha,\ \beta) = -5.091$$

Calculate <r_{1s}>, <r_{2s}> and the absolute magnitude of the 1s-2s overlap:

$$\int_0^\infty r\Psi_{1s}(r,\ \alpha)^2 4\pi r^2 dr = 0.497 \quad \int_0^\infty r\Psi_{2s}(r,\ \beta)^2 4\pi r^2 dr = 3.569 \quad \int_0^\infty |\Psi_{1s}(r,\ \alpha)\Psi_{2s}(r,\ \beta)|\, 4\pi r^2 dr = 0.251$$

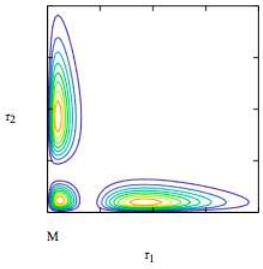
Display the radial distribution function for the 1s and 2s orbitals:



Display contour plot of singlet wave function:

$$i = 0..80 \quad r1_i = .085i \quad j = 0..80 \quad r2_j = .085j$$

$$\Psi(r1,\ r2) = \frac{\Psi_{1s}(r1,\ \alpha)\Psi_{2s}(r2,\ \beta)+\Psi_{1s}(r2,\ \alpha)\Psi_{2s}(r1,\ \beta)}{\sqrt{2(1+S_{1s2s}(\alpha,\ \beta)^2)}} r1r2 \quad M_{i,\ j} = \Psi\left(r1_i,\ r2_j\right)^2$$



Triplet state calculation:

Illegal pream-token (T)

Minimization of E(α, β) simultaneously with respect to α and β. $\alpha = Z \quad \beta = Z - 1$

$$\begin{pmatrix}\alpha\\ \beta\end{pmatrix} = \text{Minimize}\left(E_T,\ \alpha,\ \beta\right) \quad \begin{pmatrix}\alpha\\ \beta\end{pmatrix} = \begin{pmatrix}2.999\\ 2.570\end{pmatrix}$$

Break down the total energy into kinetic, electron-nuclear potential, and electron-electron potential energy.

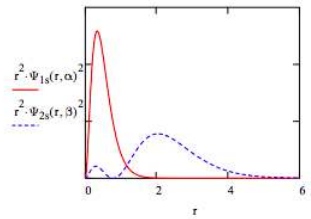
$$\begin{matrix} T \\ T_{1s}(\alpha) + T_{2s}(\beta)... \\ = \ +- 2T_{1s2s}(\alpha,\ \beta)S_{1s2s}(\alpha,\ \beta) \\ 1 - S_{1s2s}(\alpha,\ \beta)^2 \end{matrix} \quad \begin{matrix} V_{ne} \\ V_{N1s}(\alpha) + V_{N2s}(\beta)... \\ = \ +- 2V_{N1s2s}(\alpha,\ \beta)S_{1s2s}(\alpha,\ \beta) \\ 1 - S_{1s2s}(\alpha,\ \beta)^2 \end{matrix} \quad V_{ee} = \frac{V_{1122}(\alpha,\ \beta) + V_{1212}(\alpha,\ \beta)}{1 - S_{1s2s}(\alpha,\ \beta)^2}$$

$$T = 5.103 \quad V_{ne} = -10.684 \quad V_{ee} = 0.479 \quad E_T(\alpha,\ \beta) = -5.103$$

Calculate <r_{1s}>, <r_{2s}> and the absolute magnitude of the 1s-2s overlap:

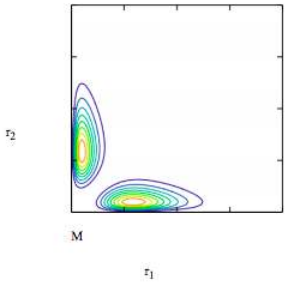
$$\int_0^\infty r\Psi_{1s}(r,\ \alpha)^2 4\pi r^2 dr = 0.500 \quad \int_0^\infty r\Psi_{2s}(r,\ \beta)^2 4\pi r^2 dr = 2.334 \quad \int_0^\infty \left|\Psi_{1s}(r,\ \alpha)\Psi_{2s}(r,\ \beta)\right| 4\pi r^2 dr = 0.328$$

Display the radial distribution function for the 1s and 2s orbitals:



Display contour plot of singlet wave function:

$$\Psi(r1,\ r2) = \frac{\Psi_{1s}(r1,\ \alpha)\Psi_{2s}(r2,\ \beta) - \Psi_{1s}(r2,\ \alpha)\Psi_{2s}(r1,\ \beta)}{\sqrt{2(1 - S_{1s2s}(\alpha,\ \beta)^2)}} r1r2 \quad M_{i,\ j} = \Psi\left(r1_i,\ r2_j\right)^2$$



Summary of the calculations for the helium atom and lithium ion:

HundsRule	Helium	o	Atom	Lithium	o	Ion
Property	Singlet	Δ	Triplet	Singlet	Δ	Triplet
α	2.013	−0.019	1.994	3.019	−0.020	2.999
β	0.925	0.626	1.551	1.681	0.889	2.570
E	−2.170	0.003	−2.167	−5.091	−0.012	−5.103
V_{ne}	−4.594	−0.026	−4.260	−10.629	−0.055	−10.684
V_{ee}	0.254	0.033	0.287	0.448	0.031	0.479
r_{1s}	0.745	0.007	0.752	0.497	0.003	0.500
r_{2s}	6.489	−2.620	3.869	3.569	−1.235	2.334
$\int \lvert 1s2s \rvert d\tau$	0.232	0.072	0.304	0.251	0.077	0.328

- The triplet state has a lower energy than the singlet state because electron-nuclear attraction increases more than electron-electron repulsion.
- Atomic size decreases in the triplet state due to the large decrease in the size of the 2s orbital. The 1s orbital's size is basically the same in the singlet and triplet states.
- The sharp decrease in the size of the 2s orbital is responsible for the increase in the electron-nuclear attraction, electron-electron repulsion and the absolute magnitude of the 1s-2s orbital overlap.

Note that this two-parameter calculation does not show the He triplet state lower in energy than the singlet state. However, it does show that the absolute magnitudes of V_{ne} and V_{ee} are greater in the triplet state. This is important because this is the trend that the exact wave function (see reference) reveals (V_{ee}: 0.250 vs 0.268; V_{ne}: -4.541 vs -4.619).

The calculation for the lithium ion does show the triplet state lower in energy and the same trend in V_{ne} and V_{ee} as for the helium atom and the exact calculation. In other words, both electron-electron repulsion and electron-nuclear attraction are stronger in the triplet state, and the real reason the triplet state lies below the singlet in energy is because the decrease in V_{ne} overwhelms the increase in V_{ee}. Thus, the common explanation that the triplet state is favored because of reduced electron-electron repulsion is without merit.

The key phenomenon that accounts for these effects is the dramatic decrease in the size of the 2s orbital in going from the singlet to the triplet state. This accounts for the increases electron-electron repulsion and electron-nuclear attraction. The size of the 1s orbital is about the same in the singlet and triplet states. The significant increase in the absolute magnitude of the overlap integral in the triplet state is consistent with its higher electron-electron repulsion.

Reference: Snow, R. L.; Bills, J. L. "The Pauli Principle and Electron Repulsion in Helium," *Journal of Chemical Education* **1974**, 51 585.

Property	$\frac{\text{Singlet}}{\text{Initial}}$	Δ	$\frac{\text{Singlet}}{\text{Intermediate}}$	Δ	$\frac{\text{Triplet}}{\text{Final}}$
α	3.019	−0.020	2.999	0	2.999
β	1.681	0.889	2.570	0	2.570
T	5.091	0.450	5.541	−0.438	5.103
V_{ne}	−10.629	−0.534	−11.163	0.479	−10.684
V_{ee}	0.448	0.174	0.622	−0.143	0.479
E	−5.091	0.091	−5.000	−0.103	−5.103

- Singlet to singlet with 2s orbital contraction: T, V_{ee} and E increase while V_{ne} decreases.
- Singlet to triplet with frozen orbitals: T, V_{ee} and E decrease while Vne increases.

Property	$\frac{\text{Singlet}}{\text{Initial}}$	Δ	$\frac{\text{Singlet}}{\text{Intermediate}}$	Δ	$\frac{\text{Triplet}}{\text{Final}}$
α	3.019	0	3.019	−0.020	2.999
β	1.681	0	1.681	0.889	2.570
T	5.091	−0.376	4.715	0.388	5.103
V_{ne}	−10.629	0.649	−9.980	−0.704	−10.684
V_{ee}	0.448	−0.142	0.306	0.173	0.479
E	−5.091	0.131	−4.960	−0.143	−5.103

- Singlet to triplet with frozen orbitals: T and V_{ee} decrease while V_{ne} and E increase.
- Triplet to triplet with 2s orbital contraction: T and V_{ee} increase while V_{ne} and E decrease.

This page titled 2.37: Hund's Rule - Singlet-Triplet Calculations with Mathcad is shared under a CC BY 4.0 license and was authored, remixed, and/or curated by Frank Rioux via source content that was edited to the style and standards of the LibreTexts platform.

2.38: Electron Correlation in Two-electron Systems

The purpose of this exercise is to examine five trial wavefunctions for the helium atom and several two-electron ions. The calculations begin with an uncorrelated wavefunction in which both electrons are placed in a hydrogenic orbital with scale factor α. The next four trial functions use several methods to increase the amount of electron correlation in the wave function. As the summary of results that is appended shows this gives increasingly more favorable agreement with the experimentally determined value for the ground state energy of the species under study. The detailed calculations show that the reason for this improved agreement with experiment is due to a reduction in electron-electron repulsion.

Because of the electron-electron interaction Schrödinger's equation cannot be solved exactly for the helium atom or more complicated atomic or ionic species. However, the ground state energy of the helium atom can be calculated using approximate methods. One of these is the variation method which requires the evaluation of the following variational integral.

$$E = \frac{\int_0^\infty \Psi_{\text{trial}} \mathrm{H} \Psi_{\text{trial}} d\tau}{\int_0^\infty \Psi_{\text{trial}}^2 d\tau}$$

First Trial Wavefunction

The variation method is discussed in all of the standard physical chemistry textbooks. As is clear from the expression above this method requires that a trial wavefunction with one or more adjustable parameters be chosen. A logical first choice for such a function would be to assume that the electrons in the helium atom occupy scaled hydrogen 1s orbitals.

$$\Psi(1,\ 2) = \Phi(1)\Phi(2) = \exp\left[-\alpha\left(r_1,\ r_2\right)\right]$$

He1ans.mcd illustrates how the ground state energy and the optimum value for the scale factor, α, can be found using Mathcad. The value of -2.8477 hartrees is within 2% of the known ground state energy of the helium atom. The error in the calculation is attributed to the fact that the wavefunction is based on the orbital approximation and, therefore, does not adequately take electron correlation into account. In other words, this wavefunction gives the electrons too much independence, given that they have like charges and tend to avoid one another.

Second Trial Wavefunction

Some electron correlation can be built into the wavefunction by assuming that each electron is in an orbital which is a linear combination of two scaled hydrogen 1s orbital.

$$\Phi = \exp(-\alpha r) + \exp(-\beta r)$$

Under the orbital approximation this assumption gives a trial wavefunction of the form

$$\begin{aligned}\Psi(1,\ 2) = \Phi(1)\Phi(2) = &\exp\left(-\alpha r_1\right)\exp\left(-\alpha r_2\right) + \exp\left(-\alpha r_1\right)\exp\left(-\beta r_2\right) \\ &+ \exp\left(-\beta r_1\right)\exp\left(-\alpha r_2\right) + \exp\left(-\beta r_1\right)\exp\left(-\beta r_2\right)\end{aligned}$$

Inspection of this wavefunction indicates that 50% of the time the electrons are in different orbitals, while for the first trial wavefunction the electrons were in the same orbital 100% of the time. He2ans.mcd illustrates how this calculation would be executed. Notice the enormous increase in the complexity of the variational expression for the energy. However, also notice that the calculation is very similar to that using the previous trial wavefunction. The differences are that in this case the expression for the energy is more complex and that it is being minimized simultaneously with respect to two parameters rather than just one. It is also clear that introducing some electron correlation into the trial wavefunction has improved the agreement between theory and experiment.

Third Trial Wavefunction

The extent of electron correlation can be increased further by eliminating the first and last term in the second wavefunction. This yields a wavefunction of the form,

$$\Psi(1,\ 2) = \exp\left(\alpha r_1\right)\exp\left(-\beta r_2\right) + \exp\left(-\beta r_1\right)\exp\left(-\alpha r_2\right)$$

This trial wavefunction places the electrons in different scaled hydrogen 1s orbitals 100% of the time and He3ans.mcd shows that further improvement in the agreement with the literature value of the ground state energy is obtained. This result is within 1% of the actual ground state energy of the helium atom.

Fourth Trial Wavefunction

The third trial wavefunction, however, still rests on the orbital approximation and, therefore, doesn't treat electron correlation adequately. Hylleraas took the calculation a step further by introducing electron correlation directly into the wavefunction by adding a term, r_{12}, involving the inter-electron separation.

$$\Psi(1,\ 2) = \exp\left[-\alpha\left(r_1 + r_2\right)\right]\left[1 + \beta r_{12}\right]$$

In the trial wavefunction shown above, if the electrons are far apart r_{12} is large and the magnitude of the wave function increases favoring that configuration. He4ans.mcd shows that this modification of the trial wavefunction has further improved the agreement between theory and experiment to within 0.5%.

Fifth Trial Wavefunction

Chandrasakar brought about further improvement by adding Hylleraas's r_{12} term to the third trial wave function as shown here.

$$\Psi(1,\ 2) = \left[\exp\left(-\alpha r_1\right)\exp\left(-\beta r_2\right) + \exp\left(-\beta r_1\right)\exp\left(-\alpha r_2\right)\right]\left[1 + b r_{12}\right]$$

As can be seen in He5ans.mcd Chandrasakar's three parameter wavefunction gives rise to a fairly complicated variational expression for ground state energy. However it also gives a result for helium that is within .07% of the experimental value for the ground state energy. The experimental value for the ground state energy of the helium atom is 2.90372 E_h.

The calculations that have been outlined here for the helium atom can be repeated for H^-, Li^+, Be^{++} , etc. The hydride anion is a particularly interesting case because the first two trial wavefunctions do not predict a stable ion. This indicates that electron correlation is an especially important issue for atoms and ions with small nuclear charge.

Summary of the Results for the Helium Atom

$$\Psi = \frac{\alpha^3}{\pi}\exp\left(-\alpha r_1\right)\exp\left(-\alpha r_2\right)$$
$$E = -2.84766$$
$$\Psi = \exp\left(-\alpha r_1\right)\exp\left(-\alpha r_2\right) + \exp\left(-\alpha r_1\right)\exp\left(-\beta r_1\right)\exp\left(-\alpha r_2\right) + \exp\left(-\beta r_1\right)\exp\left(-\beta r_2\right)$$
$$E = -2.86035$$
$$\Psi = \exp\left(-\alpha r_1\right)\exp\left(-\beta r_2\right) + \exp\left(-\beta r_1\right)\exp\left(-\alpha r_2\right)$$
$$E = -2.87566$$
$$\Psi = \exp\left[-\alpha\left(r_1 + r_2\right)\right]\left(1 + \beta r_{12}\right)$$
$$E = -2.89112$$
$$\Psi = \left(\exp\left(-\alpha r_1\right)\exp\left(-\beta r_2\right) + \exp\left(-\beta r_1\right)\exp\left(-\alpha r_2\right)\right)\left(1 + b r_{12}\right)$$
$$E = -2.90143$$

Experimentally Determined Ground State Energy

$$E_{exp} = -2.90372$$

This page titled 2.38: Electron Correlation in Two-electron Systems is shared under a CC BY 4.0 license and was authored, remixed, and/or curated by Frank Rioux via source content that was edited to the style and standards of the LibreTexts platform.

2.39: First Trial Wave Function

The first trial wavefunction is based on the orbital concept - electrons have wavefunctions that are independent of the coordinates of other electrons. Since it does not provide for electron correlation it will serve as the benchmark in the subsequent series of calculations. The remaining trail wavefunctions will include electron correlation to an increasing degree.

$$\Psi(1,\ 2) = \frac{\alpha^3}{\pi}\exp\left(-\alpha r_1\right)\exp\left(-\alpha r_2\right)$$

When this wavefunction is used in a variational calculation for the ground state energy for two-electron atoms or ions the expression shown below for the energy, E(α), is obtained. This equation is then minimized with respect to the adjustable parameter, α. The calculation for He is shown below.

Nuclear charge: Z = 2

Seed value for scale factor: $\alpha = 2$

Contributions to total energy:

$$T(\alpha) = \alpha^2 \quad V_{ne}(\alpha) = -2Z\alpha \quad V_{ee}(\alpha) = \tfrac{5}{8}\alpha$$

Minimization of the total energy with respect to the variational parameter:

$$E(\alpha) = T(\alpha) + V_{ne}(\alpha) + V_{ee}(\alpha) \quad \alpha = \text{Minimize}(E,\ \alpha) \quad \alpha = 1.6875 \quad E(\alpha) = -2.8477$$

Calculate the orbital energy:

$$\varepsilon = \tfrac{\alpha^2}{2} - Z\alpha + \tfrac{5}{8}\alpha \quad \varepsilon = -0.8965$$

Compare the results of this calculation to experiment in two ways. [1] Minus the sum of the ionization energies is equal to the experimental ground state energy (you should show this). [2] The orbital energy is a good approximation to the first ionization energy. Repeat this exercise for H^- , Li^+ and Be^{2+}. Present your results and the comparison with experimental results in tabular form.

$H\Psi = E\Psi$	H	He	Li	Be
α	0.6875	1.6875	2.6875	3.6875
ε	−0.0215	−0.8965	2.7715	−5.6465
$-IP_1$	−0.0277	−0.904	−2.781	−5.658
%Error	22.4	0.83	0.34	0.20
E_{atom}	−0.4727	−2.8477	−7.2227	−13.5977
$-(IP_1 + IP_2)$	−0.5277	−2.9037	−7.2838	−13.6640
%Error	10.4	1.94	0.80	0.40

- Demonstrate that the virial theorem is satisfied for each calculation: <E> = <V>/2 = -<T>

$$E(\alpha) = -2.8477 \quad \tfrac{-2Z\alpha + \frac{5}{8}\alpha}{2} = -2.8477 \quad -\alpha^2 = -2.8477$$

- Complete the table below which breaks down the various contributions to the total energy.

Element	%T	$\%V_{ne}$	$\%V_{ee}$
H	20.8	60.4	18.9
He	26.7	63.4	9.9
Li	28.9	64.4	6.7
Be	29.9	65.0	5.1

Absolute value of energy:

$$E_{abs} = \alpha^2 + 2Z\alpha + \frac{5}{8}\alpha$$

Percent kinetic energy contribution to total energy:

$$\frac{T(\alpha)}{E_{abs}(\alpha)} = 26.7\%$$

Percent electron-nuclear potential energy contribution to total energy:

$$\frac{|V_{ne}(\alpha)|}{E_{abs}(\alpha)} = 63.4\%$$

Percent electron-electron potential energy contribution to total energy:

- Demonstrate that this wave function does not predict a stable hydride ion.
  - The hydride anion has a higher energy (-0.4727 E_h) than the hydrogen atom (-0.5000 E_h).
- Identify a deficiency in the wave function that might explain why it does not predict a stable hydride ion.
  - The wave function does not allow adequately for electron-electron correlation in a case where the nuclear charge is only +1.
- Explain the improved agreement between theory and experiment as the nuclear charge increases.
  - Nuclear-electron potential energy becomes increasingly important overwhelming electron-electron potential energy. The inadequacies of the wave function are becoming less important.
- Complete the summary table below. You will be asked to do this for each trial wave function we use in this exercise and subsequently compare the results.

$$E(\alpha) = -2.8477 \quad T(\alpha) = 2.8477 \quad V_{ne}(\alpha) = -6.7500 \quad V_{ee}(\alpha) = 1.0547$$

WF1	E	T	V_{ne}	V_{ee}
H	−0.4727	0.4727	−1.375	0.4297
He	−2.8477	2.8477	−6.7500	1.0547
Li	−7.2227	7.2227	−16.1250	1.6797
Be	−13.5977	13.5977	−29.5000	2.3047

This table shows that Vee increases in magnitude from H^- to Be^{2+}. Earlier, however, we saw that its percentage contribution to the total energy decreases in this series.

- You should also fill in the following tables for each of the elements and carry them forward to the next Mathcad document.

H	E	T	V_{ne}	V_{ee}
WF1	−0.4727	0.4727	−1.375	0.4297
WF2	■	■	■	■
WF3	■	■	■	■
WF4	■	■	■	■
WF5	■	■	■	■

He	E	T	V_{ne}	V_{ee}
WF1	−2.8477	2.8477	−6.7500	1.05447
WF2	■	■	■	■
WF3	■	■	■	■
WF4	■	■	■	■
WF5	■	■	■	■

Li	E	T	V_{ne}	V_{ee}
WF1	−7.2227	7.2227	−16.1250	1.6797
WF2	■	■	■	■
WF3	■	■	■	■
WF4	■	■	■	■
WF5	■	■	■	■

H	E	T	V_{ne}	V_{ee}
WF1	−13.5977	13.5977	−29.5000	2.3047
WF2	■	■	■	■
WF3	■	■	■	■
WF4	■	■	■	■
WF5	■	■	■	■

This page titled 2.39: First Trial Wave Function is shared under a CC BY 4.0 license and was authored, remixed, and/or curated by Frank Rioux via source content that was edited to the style and standards of the LibreTexts platform.

2.40: Second Trial Wavefunction

$$\Psi = \exp(-\alpha r_1)\exp(-\alpha r_2) + \exp(-\alpha r_1)\exp(-\beta r_2) + \exp(-\beta r_1)\exp(-\alpha r_2) + \exp(-\beta r_1)\exp(-\beta r_2)$$

When the wavefunction shown above is used in a variational method calculation for the ground state energy for two-electron atoms or ions the two-parameter equation shown below for the energy is obtained. This equation is then minimized simultaneously with respect to the adjustable parameters, α and β.

Nuclear charge: Z = 2

Seed values for scale factors: $\alpha = 2 \quad \beta = Z + 1$

Variational energy expression:

$$E(\alpha,\ \beta) = \frac{\left[\frac{\frac{\alpha^2+\beta^2}{2} - Z(\alpha+\beta) - \frac{8\alpha^{1.5}\beta^{1.5}}{(\alpha+\beta)^2}\left(Z - \frac{\alpha\beta}{\alpha+\beta}\right)}{1+\frac{8\alpha^{1.5}\beta^{1.5}}{(\alpha+\beta)^3}}\right]\ldots + \frac{5}{8}(\alpha+\beta) + \frac{2\alpha\beta(\alpha^2+3\alpha\beta+\beta^2)}{(\alpha+\beta)^3} + 4\left[\begin{array}{c}\frac{8\alpha^{2.5}\beta^{1.5}(11\alpha^2+8\alpha\beta+\beta^2)}{(\alpha+\beta)^2(3\alpha+\beta)^3}\ldots \\ +\frac{8\alpha^{1.5}\beta^{2.5}(11\beta^2+8\alpha\beta+\alpha^2)}{(\alpha+\beta)^2(3\beta+\alpha)^3}\ldots \\ \frac{20\alpha^3\beta^3}{(\alpha+\beta)^5}\end{array}\right]}{4\left[1+\frac{8\alpha^{1.5}\beta^{1.5}}{(\alpha+\beta)^3}\right]^2}$$

$$\begin{pmatrix}\alpha\\ \beta\end{pmatrix} = \text{Minimize}(E,\ \alpha,\ \beta) \quad \begin{pmatrix}\alpha\\ beta\end{pmatrix} = \begin{pmatrix}1.2141\\ 2.1603\end{pmatrix} \quad E(\alpha,\ \beta) = -2.8603$$

Experimental ground state energy:

$$E_{exp} = -2.9037$$

Calculate error in calculation:

$$\text{Error} = \left|\frac{E_{exp} - E(\alpha,\ \beta)}{E_{exp}}\right| \quad \text{Error} = 1.4931\%$$

Fill in the table and answer the questions below:

Ψ	H	He	Li	Be
α	0.3703	1.2141	2.0969	2.9993
β	1.0001	2.1603	3.2778	4.3756
E_{atom}	−0.487	−2.8603	−7.235	−13.6098
E_{atom}(exp)	−0.5277	−2.9037	−7.2838	−13.6640
%Error	7.72	1.49	0.670	0.397

Fill in the table below and explain why this trial wave function gives better results than the first trial wave function.

$$T(\alpha,\ \beta) = \left[\frac{\frac{\alpha^2+\beta^2}{2} + \frac{8\alpha^{1.5}\beta^{1.5}}{(\alpha+\beta)^2}\left(\frac{\alpha\beta}{\alpha+\beta}\right)}{1+\frac{8\alpha^{1.5}\beta^{1.5}}{(\alpha+\beta)^2}}\right] \quad V_{ne}(\alpha,\ \beta) = \left[\frac{-Z(\alpha+\beta) - \frac{8\alpha^{1.5}\beta^{1.5}}{(\alpha+\beta)^2}Z}{1+\frac{8\alpha^{1.5}\beta^{1.5}}{(\alpha+\beta)^3}}\right]$$

$$T(\alpha,\ \beta) = 2.8603 \qquad V_{ne} = -6.7488$$

$$V_{ee}(\alpha,\ \beta) = E(\alpha,\ \beta) - T(\alpha,\ \beta) - V_{ne}(\alpha,\ \beta) \quad V_{ee}(\alpha,\ \beta) = 1.0281$$

WF2	E	T	V_{ne}	V_{ee}
H	−0.4870	0.4780	−1.3705	0.3965
He	−2.8603	2.8603	−6.7488	1.0281
Li	−7.2350	7.2350	−16.1243	1.6544
Be	−13.6098	13.6098	−29.4995	2.2799

Demonstrate that the virial theorem is satisfied.

$$E(\alpha,\ \beta) = -2.8603 \quad -T(\alpha,\ \beta) = -2.8603 \quad \frac{V_{ne}(\alpha,\ \beta) + V_{ee}(\alpha,\ \beta)}{2} = -2.8603$$

Add the results for this wave function to your summary table for all wave functions.

$$\begin{pmatrix} \text{H} & \text{E} & \text{T} & \text{V}_{ne} & \text{V}_{ee} \\ \text{WF1} & -0.4727 & 0.4727 & -1.375 & 0.4297 \\ \text{WF2} & -0.4870 & 0.4870 & -1.3705 & 0.3965 \end{pmatrix} \quad \begin{pmatrix} \text{He} & \text{E} & \text{T} & \text{V}_{ne} & \text{V}_{ee} \\ \text{WF1} & -2.8477 & 2.8477 & -6.7500 & 1.0547 \\ \text{WF2} & -2.8603 & 2.8603 & -6.7488 & 1.0281 \end{pmatrix}$$

$$\begin{pmatrix} \text{Li} & \text{E} & \text{T} & \text{V}_{ne} & \text{V}_{ee} \\ \text{WF1} & -7.2227 & 7.2227 & -16.1250 & 1.6797 \\ \text{WF2} & -7.2350 & 7.2350 & -16.1243 & 1.6544 \end{pmatrix} \quad \begin{pmatrix} \text{Be} & \text{E} & \text{T} & \text{V}_{ne} & \text{V}_{ee} \\ \text{WF1} & -13.5977 & 13.5977 & -29.5000 & 2.3047 \\ \text{WF2} & -13.6098 & 13.6098 & -29.4995 & 2.2799 \end{pmatrix}$$

These tables show that the improved agreement with experimental results (the lower total energy), is due to a reduction in electron-electron repulsion.

This page titled 2.40: Second Trial Wavefunction is shared under a CC BY 4.0 license and was authored, remixed, and/or curated by Frank Rioux via source content that was edited to the style and standards of the LibreTexts platform.

2.41: Third Trial Wavefunction

$$\Psi = \exp(-\alpha r_1)\exp(-\beta r_2) + \exp(-\beta r_1)\exp(-\alpha r_2)$$

When the wavefunction shown above is used in a variational method calculation for the ground state energy for two-electron atoms or ions the two-parameter equation shown below for the energy is obtained. This equation is then minimized simultaneously with respect to the adjustable parameters, α and β.

Nuclear charge: Z = 2

Seed values for scale factors: $\alpha = Z \quad \beta = Z + 1$

Variational energy expression:

$$E(\alpha,\ \beta) = \frac{64\alpha^3\beta^3[\alpha\beta - Z(\alpha+\beta)]\frac{\alpha\beta}{\alpha+\beta} + \frac{\alpha^2 beta^2}{(\alpha+\beta)^3} + \frac{20\alpha^3\beta^3}{(\alpha+\beta)^5}}{1 + \frac{64\alpha^3\beta^3}{(\alpha+\beta)^6}}$$

$$\begin{pmatrix}\alpha\\ \beta\end{pmatrix} = \text{Minimize}(E,\ \alpha,\ \beta) \quad \begin{pmatrix}\alpha\\ \beta\end{pmatrix} = \begin{pmatrix}1.1885\\ 2.1832\end{pmatrix} \quad E(\alpha,\ \beta) = -2.8757$$

Experimental ground state energy:

$$E_{exp} = -2.9037$$

Calculate error in calculation:

$$\text{Error} = \left|\frac{E_{exp} - E(\alpha,\ \beta)}{E_{exp}}\right| \quad \text{Error} = 0.9656\%$$

Summarize the calculations in the following table.

Ψ	H	He	Li	Be
α	0.28322	1.18853	2.07898	2.98472
β	1.023923	2.18317	3.29491	4.38972
E_{atom}	−0.5133	−2.8757	−7.2488	−13.6230
E_{atom}(exp)	−5.277	−2.9037	−7.2838	−13.6640
%Error	2.73	0.964	0.481	0.300

Fill in the table below and explain why this trial wave function gives better results than the previous trial wave function.

$$T(\alpha,\ \beta) = \frac{\frac{\alpha^2+\beta^2}{2} + \frac{64\alpha^3\beta^3(\alpha\beta)}{(\alpha+\beta)^6}}{1+\frac{64\alpha^3\beta^3}{(\alpha+\beta)^6}} \qquad V_{ne}(\alpha,\ \beta) = \frac{-Z(\alpha+\beta) + \frac{64\alpha^3\beta^3(\alpha\beta)}{(\alpha+\beta)^6}}{1+\frac{64\alpha^3\beta^3[-Z(\alpha+\beta)]}{(\alpha+\beta)^6}}$$

$$V_{ee}(\alpha,\ \beta) = \frac{\frac{\alpha\beta}{\alpha+\beta} + \frac{\alpha^2\beta^2}{(\alpha+\beta)^3} + \frac{20\alpha^3\beta^3}{(\alpha+\beta)^5}}{1+\frac{64\alpha^3\beta^3}{(\alpha+\beta)^6}}$$

$$T(\alpha,\ \beta) = 2.8757$$
$$V_{ne}(\alpha,\ \beta) = -6.7434$$
$$V_{ee}(\alpha,\ \beta) = 0.9921$$

WF3	E	T	V_{ne}	V_{ne}
H	−0.5133	0.5133	−1.3225	0.2958
He	−2.8757	2.8757	−6.7434	0.9921
Li	−7.2487	7.2487	−16.1217	1.6242
Be	−13.6230	13.620	−29.4978	2.2519

Demonstrate that the virial theorem is satisfied.

$$E(\alpha,\ \beta) = -2.8757 \quad -T(\alpha,\ \beta) = -2.8757 \quad \frac{V_{ne}(\alpha,\ \beta) + V_{ee}(\alpha,\ \beta)}{2} = -2.8757$$

Add the results for this wave function to your summary table for all wave functions.

H	E	T	V_{ne}	V_{ee}
WF1	−0.4727	0.4727	−1.375	0.4297
WF2	−0.4870	0.4870	−1.3705	0.3965
WF3	−0.5133	0.5133	−1.3225	0.2958

He	E	T	V_{ne}	V_{ee}
WF1	−2.8477	2.8477	−6.7500	1.0547
WF2	−2.8603	2.8603	−6.7488	1.0281
WF3	−2.8757	2.8757	−6.7434	0.9921

Li	E	T	V_{ne}	V_{ee}
WF1	−7.2227	7.2227	−16.1250	1.6797
WF2	−7.2350	7.2350	−16.1243	1.6544
WF3	−7.2487	7.2487	−16.1217	1.6242

Be	E	T	V_{ne}	V_{ee}
WF1	−13.5977	13.5977	−29.5000	2.3047
WF2	−13.6098	13.6098	−29.4995	2.2799
WF3	−13.6230	13.6230	−29.4978	2.2519

These tables show that the improved agreement with experimental results (the lower total energy), is due to a reduction in electron-electron repulsion.

This page titled 2.41: Third Trial Wavefunction is shared under a CC BY 4.0 license and was authored, remixed, and/or curated by Frank Rioux via source content that was edited to the style and standards of the LibreTexts platform.

2.42: 129.4 Fourth Trial Wavefunction

$$\Psi(r) = \exp\left[-\alpha\left(r_1 + r_2\right)\right]\left(1 + \beta r_{12}\right)$$

When the wavefunction shown above is used in a variational method calculation for the ground state energy for two-electron atoms or ions the two-parameter equation shown below for the energy is obtained. This equation is then minimized simultaneously with respect to the adjustable parameters, α and b.

Nuclear charge: Z = 1

Seed values for scale factors: $\alpha = Z \quad \beta = .7$

Contributions to total energy:

$$T(\alpha,\ \beta) = \frac{\frac{1}{2} + \frac{25\beta}{16\alpha} + \frac{2\beta^2}{\alpha^2}}{\frac{1}{2\alpha^2} + \frac{35\beta}{16\alpha^3} + \frac{3\beta^2}{\alpha^4}} \quad V_{ne}(\alpha,\ \beta) = \frac{-\frac{Z}{\alpha} - \frac{15Z\beta}{4\alpha^2} - \frac{9Z\beta^2}{2\alpha^3}}{\frac{1}{2\alpha^2} + \frac{35\beta}{16\alpha^3} + \frac{3\beta^2}{\alpha^4}} \quad V_{ee}(\alpha,\ \beta) = \frac{-\frac{5}{16\alpha} - \frac{\beta}{\alpha^2} - \frac{35\beta^2}{32\alpha^3}}{\frac{1}{2\alpha^2} + \frac{35\beta}{16\alpha^3} + \frac{3\beta^2}{\alpha^4}}$$

Minimization of the total energy with respect to the variational parameters:

$$E(\alpha,\ \beta) = T(\alpha,\ \beta) + V_{ne}(\alpha,\ \beta) + V_{ee}(\alpha,\ \beta) \quad \begin{pmatrix}\alpha\\ \beta\end{pmatrix} = \text{Minimize}(E,\ \alpha,\ \beta) \quad \begin{pmatrix}\alpha\\ \beta\end{pmatrix} = \begin{pmatrix}0.8257\\ 0.4934\end{pmatrix} \quad E(\alpha,\ \beta) = -0.5088$$

Experimental ground state energy:

$$E_{exp} = -2.9037$$

Calculate error in calculation:

$$\text{Error} = \left|\frac{E_{exp} - E(\alpha,\ \beta)}{E_{exp}}\right| \quad \text{Error} = 82.4782\%$$

Fill in the table and answer the questions below:

Ψ	H	He	Li	Be
α	0.8257	1.8497	2.8564	3.8592
β	0.4934	0.3658	0.3354	0.3213
E_{atom}	−0.5088	−2.8911	−7.2682	−13.6441
$E_{atom}(\text{exp})$	−0.5277	−2.9037	−7.2838	−13.6640
%Error	3.59	0.433	0.215	0.146

Fill in the table below and explain why this trial wave function gives better results than the previous trial wave function.

WF4	E	T	V_{ne}	V_{ee}
H	−0.5088	0.5088	−1.3907	0.3731
He	−2.8911	2.8911	−6.7565	0.9743
Li	−7.2682	7.2682	−16.1288	1.5924
Be	−13.6441	13.6441	−29.5025	2.2144

$$T(\alpha,\ \beta) = 0.5088 \quad V_{ne}(\alpha,\ \beta) = -1.3907 \quad V_{ee}(\alpha,\ \beta) = 0.3731$$

Explain the importance of the parameter β. Why does its magnitude decrease as the nuclear charge increases?

The parameter β adds weight to the r_{12} term which most directly represents electron correlation in the wavefunction. As the nuclear charge increases, as we have previously seen, V_{ee} becomes less important as a percentage of the total energy. Thus, the impact of the electron correlation term becomes less significant.

Demonstrate that the virial theorem is satisfied.

$$E(\alpha,\ \beta) = -0.5088 \quad -T(\alpha,\ \beta) = -0.5088 \quad \frac{V_{ne}(\alpha,\ \beta) + V_{ee}(\alpha,\ \beta)}{2} = -0.5088$$

Add the results for this wave function to your summary table for all wave functions.

H	E	T	V_{ne}	V_{ee}
WF1	−0.4727	0.4727	−1.375	0.4297
WF2	−0.4870	0.4870	−1.3705	0.3965
WF3	−0.5133	0.5133	−1.3225	0.2958
WF4	−0.5088	0.5088	−1.3907	0.3731

He	E	T	V_{ne}	V_{ee}
WF1	−2.8477	2.8477	−6.7500	1.0547
WF2	−2.8603	2.8603	−6.7488	1.0281
WF3	−2.8757	2.8757	−6.7434	0.9921
WF4	−2.8911	2.8911	−6.7565	0.9743

Li	E	T	V_{ne}	V_{ee}
WF1	−7.2227	7.2227	−16.1250	1.6797
WF2	−7.2350	7.2350	−16.1243	1.6544
WF3	−7.2487	7.2487	−16.1217	1.6242
WF4	−7.2682	7.2682	−16.1288	1.5924

Be	E	T	V_{ne}	V_{ee}
WF1	−13.5977	13.5977	−29.5000	2.3047
WF2	−13.6098	13.6098	−29.4995	2.2799
WF3	−13.6230	13.6230	−29.4978	2.2519
WF4	−13.6441	13.6441	−29.5025	2.2144

Except for a hiccup in the hydrogen anion results for WF4, these tables show that the improved agreement with experimental results (the lower total energy), is due to a reduction in electron-electron repulsion.

This page titled 2.42: 129.4 Fourth Trial Wavefunction is shared under a CC BY 4.0 license and was authored, remixed, and/or curated by Frank Rioux via source content that was edited to the style and standards of the LibreTexts platform.

2.43: Fifth Trial Wavefunction and Summary

$$\Psi = \left(\exp\left(-\alpha r_1\right)\exp\left(-\beta r_2\right) + \exp\left(-\beta r_1\right)\exp\left(-\alpha r_2\right)\right)\left(1 + b r_{12}\right)$$

When Chandrasakar's wavefunction is used in a variational calculation on a two-electron atom or ion the following expressions are obtained.

Enter the nuclear charge: Z = 2

Enter initial values for α. β, and b (use results from previous calculations):

$$\alpha = Z \quad \beta = Z + 1 \quad b = 0.3 \quad c = \frac{\alpha+\beta}{2} \quad d = \frac{|\alpha-\beta|}{2}$$

Define the normalization constant:

$$N(b,\ c,\ d) = \frac{\begin{bmatrix}-8d^{10} + \left[40d^8 + \left[-80d^6\left[88d^4 + \left(-56d^2 16c^2\right)c^2\right]c^2\right]c^2\right]c^2 \ldots \\ + \left[\left[-35d^{10} + \left[\begin{matrix}175d^8 + \left[-349d^6 + \left[335d^4 + \left(-196d^2 + 70c^2\right)c^2\right]c^2\right]c^2 c^2 c \ldots \\ + \left[-48d^{10} + \left[240d^8 + \left[-480d^6\left[480d^4 + \left(-192d^2 + 96c^2\right)c^2\right]c^2\right]c^2\right]c^2\right]b\end{matrix}\right]b\right]\right]}{8(c+d)^5(c-d)^5c^8}$$

Define the electron kinetic energy:

$$T(b,\ c,\ d) = \frac{\begin{bmatrix}8d^{12} + \left[-48d^{10} + \left[120d^8 + \left[-152d^6 + \left[112d^4 + \left(-56d^2 + 16c^2\right)c^2\right]c^2\right]c^2\right]c^2\right]c^2 \ldots \\ + \left[\begin{matrix}\left[35d^{12} + \left[-200d^{10} + \left[474d^8 + \left[-598d^6 + \left[353d^4 + \left(-114d^2 + 50c^2\right)c^2\right]c^2\right]c^2\right]c^2\right]c^2\right]c \ldots \\ + \left[48d^{12} + \left[-272d^{10} + \left[640d^8 + \left[-800d^6 + \left[592d^4 + \left(\begin{matrix}-80d^2 \ldots \\ +64c^2\end{matrix}\right)c^2\right]c^2\right]c^2\right]c^2\right]c^2\right]b\end{matrix}\right]b\end{bmatrix}}{\left[8(c+d)^5(c-d)^5c^8\right]N(b,\ c,\ d)}$$

Define electron-nucleus potential energy:

Illegal pream-token (\)

Define electron-electron potential energy:

$$VE(b,\ c,\ d) = \frac{\begin{bmatrix}10d^8 + \left[-42d^6 + \left[74d^4 + \left(-62d^2 + 20c^2\right)c^2\right]c^2\right]c^2\right]c^2 \ldots \\ + \left[\begin{matrix}\left[32d^8 + \left[-128d^6 + \left[192d^4 + \left(-160d^2 + 64c^2\right)c^2\right]c^2\right]c^2\right]c \ldots \\ + \left[35d^8 + \left[-140d^6 + \left[209d^4 + \left(-126d^2 + 70c^2\right)c^2\right]c^2\right]c^2\right]b\end{matrix}\right]b\end{bmatrix}}{\left[16(c+d)^4(c-d)^4c^7\right]N(b,\ c,\ d)}$$

Define total energy:

$$\mathrm{E(b,\ c,\ d)} = \mathrm{T(b,\ c,\ d)} + \mathrm{VN(b,\ c,\ d)} + \mathrm{VE(b,\ c,\ d)}$$

Minimize total energy simultaneously with respect to the parameters, b, c, d:

$$\begin{pmatrix} b \\ c \\ d \end{pmatrix} = \mathrm{Minimize(E,\ b,\ c,\ d)} \quad \begin{pmatrix} b \\ c \\ d \end{pmatrix} = \begin{pmatrix} 0.2934 \\ 1.8226 \\ 0.3862 \end{pmatrix} \quad \mathrm{E(b,\ c,\ d)} = \text{-}2.9014$$

Experimental ground state energy: E_{exp} = -2.9037

Calculate error in calculation:

$$\text{Error} = \left|\frac{E_{exp} - E(b,\ c,\ d)}{E_{exp}}\right| \quad \text{Error} = 0.0782\%$$

Calculate α and β from the values of c and d:

\alpha is only supported in math mode

Fill in the table and answer the questions below:

Ψ	H	He	Li	Be
α	0.4925	1.4364	2.3616	3.2932
β	1.0744	2.2088	3.2996	4.3745
b	0.3326	0.2934	0.2769	0.2687
E_{atom}	−0.5255	2.9014	−7.227	−13.6525
$E_{atom}(\text{exp}) - 0.5277$	−2.9037	−7.2838	−13.6640	
%Error	0.4090	0.0792	.0909	0.0838

Explain the importance of the parameter b. Why does its magnitude decrease as the nuclear charge increases?

The parameter b adds weight to the r_{12} term which most directly represents electron correlation in the wavefunction. As the nuclear charge increases, as we have previously seen, V_{ee} becomes less important as a percentage of the total energy. Thus, the impact of the electron correlation term becomes less significant.

Fill in the table below and explain why this trial wave function gives better results than the previous trial wave function.

$$E(b,\ c,\ d) = -2.9014 \quad T(b,\ c,\ d) = 2.9017 \quad VN(b,\ c,\ d) = -6.7524 \quad VE(b,\ c,\ d) = 0.9492$$

WF5	E	T	V_{ne}	V_{ee}
H	−0.5275	0.5275	−1.3738	0.3208
He	−2.9017	2.9017	−6.7524	0.9492
Li	−7.2772	7.2772	−16.1265	1.5721
Be	−13.6525	13.6525	−29.5011	2.1960

Demonstrate that the virial theorem is satisfied for the helium atom:

$$E(b,\ c,\ d) = -2.9014 \quad T(b,\ c,\ d) = 2.9017 \quad \frac{VN(b,\ c,\ d) + VE(b,\ c,\ d)}{2} = -2.9016$$

Add the results for this wave function to your summary table for all wave functions.

H	E	T	V_{ne}	V_{ee}
WF1	−0.4727	0.4727	−1.375	0.4297
WF2	−0.4870	0.4870	−1.3705	0.3965
WF3	−0.5133	0.5133	−1.3225	0.2958
WF4	−0.5088	0.5088	−1.3907	0.3731
WF5	−0.5275	0.5275	−1.3738	0.3208

He	E	T	V_{ne}	V_{ee}
WF1	−2.8477	2.8477	−6.7500	1.0547
WF2	−2.8603	2.8603	−6.7488	1.0281
WF3	−2.8757	2.8757	−6.7565	0.9743
WF4	−2.8911	2.8911	−6.7565	0.9743
WF5	−2.9017	2.9017	−6.7424	0.9492

Li	E	T	V_{ne}	V_{ee}
WF1	−7.2227	7.2227	−16.1250	1.6797
WF2	−7.2350	7.2350	−16.1243	1.6544
WF3	−7.2487	7.2487	−16.1217	1.6242
WF4	−7.2682	7.2682	−16.1288	1.5924
WF5	−7.2227	7.2227	−16.1265	1.5721

Be	E	T	V_{ne}	V_{ee}
WF1	−13.5977	13.5977	−29.5000	2.3047
WF2	−13.6098	13.6098	−29.4995	2.2799
WF3	−13.6230	13.6230	−29.4978	2.2519
WF4	−13.6441	13.6441	−29.5025	2.2144
WF5	−13.6526	13.6525	−29.5011	2.1960

Except for a hiccup in the hydrogen anion results for WF4, these tables show that the improved agreement with experimental results (the lower total energy), is due to a reduction in electron-electron repulsion through the use of trial wavefunctions that improve electron correlation.

This page titled 2.43: Fifth Trial Wavefunction and Summary is shared under a CC BY 4.0 license and was authored, remixed, and/or curated by Frank Rioux via source content that was edited to the style and standards of the LibreTexts platform.

2.44: The Crucial Role of Kinetic Energy in Interpreting Ionization Energies

This Journal has recently published a series of four articles by Gillespie, Spencer, and Moog under the banner of “Demystifying Introductory Chemistry”, an effort supported by the Task Force on General Chemistry (*1*). In their opening remarks they make the following statement (*1a*):

In our opinion we make chemistry seem more abstract, more mysterious, and more esoteric than necessary. Chemistry is certainly a complicated subject, but shrouding it in esoteric jargon and impenetrable theory makes it seem much more difficult than it really is.

We accept many of the excellent recommendations the authors make for improving the general chemistry sequence, but we have serious reservations about one of their arguments. In their attempt to draw back the quantum mechanical veil shrouding introductory chemistry they offer an incorrect interpretation of the trend of ionization energies for the first two elements of the periodic table and carry this form of reasoning forward to Li and Be. We quote one of their paragraphs (*1a*) in its entirety and then proceed to our objections and a quantum mechanical analysis.

The first ionization energy of helium (2.37 MJ mol^{-1}) is nearly twice that of hydrogen (1.31 MJ mol^{-1}); thus, these ionization energies are consistent with the two electrons in helium being at about the same distance from the nucleus as the single electron in hydrogen. These two electrons occupy a spherical region around the nucleus— the first (n = 1) shell. The ionization energy of helium is slightly less than twice the ionization energy of hydrogen because of the repulsion between the two electrons in helium.

We find two problems with this paragraph. The first is the statement that the two electrons in helium are about the same distance from the nucleus as the hydrogen electron. We do not believe the experimental ionization energies themselves provide support for this assertion. Furthermore, we do not believe there is other reliable experimental or theoretical evidence that supports the assertion. The second is the fact that the authors have used a classical explanation that is based solely on potential energy (Coulomb’s law, potential energy = $-Ze^2/r$): the electrons are about the same distance from the nucleus, the nuclear charge increases by a factor of two, so the attraction to the nucleus increases by a factor of two, but the ionization energy increases by a factor of only 1.81 because of electron–electron repulsion. What is missing in the above potential energy argument is the fact that kinetic energy is an important factor in the quantum world of atoms and molecules, and cannot be ignored. More than three decades ago Ruedenberg (*2*) demonstrated the crucial importance of electron kinetic energy in understanding the physical nature of the chemical bond. Unfortunately, in spite of discussion of this profoundly important analysis in the pedagogical literature (*3–5*) and review journals (*2b*, *6*), Ruedenberg’s work has been largely ignored by the undergraduate chemistry community. We hope that the quantum mechanical treatment that we present will help to underline the role of kinetic energy in understanding atomic structure and stability, and in particular its importance in understanding the ionization energy ratio of 1.81 mentioned above.

The hydrogen atom problem can be solved exactly, but the two-electron helium atom cannot. However, it can be solved to an arbitrary degree of accuracy by approximate methods. So the first issue is what level of theory should be employed in order to achieve an understanding of the problem under study. In our analysis, hydrogenic 1s orbitals

$$\Psi = \sqrt{\frac{\alpha^3}{\pi}}\exp(-\alpha r)$$

will be used with the variational principle to obtain the electron orbital energies for the hydrogen and helium atoms. The orbital energies will be used because Koopmans’ theorem (7) states that the ionization energy can be approximated as the negative of the orbital energy. This is correct for the hydrogen atom, but approximate for the helium atom. However, as we shall see, the error introduced by this approximation is relatively small. We show that this simple quantum mechanical analysis gives satisfactory agreement with experimental results and provides a basis from which to reach an interpretation of the relative values of the ionization energies of hydrogen and helium.

Use of the trial wave function chosen above with the variational theorem yields the results given in the tables. Table 1 shows the expressions for the total electron energy, the electron orbital energies, and the optimum values of obtained when the variational principle is applied to the total energy. Table 2 gives the results of the variational calculation for the electronic orbital energy for hydrogen and helium.

Table 1. Total Electron and Electron Orbital Energy for H and He

Element	Total Electron Energy	Electron Orbital Energy	Optimum α
$H\ (Z=1)$	$E_H = \frac{\alpha^2}{2} - Z_\alpha$	$\varepsilon = \frac{\alpha^2}{2} - Z_\alpha$	$\alpha = 1$
$He\ (Z=2)$	$E_{He} = \alpha^2 - 2Z_\alpha + \frac{5\alpha}{8}$	$\varepsilon_{He} = \frac{\alpha^2}{2} - Z_\alpha + \frac{5\alpha}{8}$	$\alpha = 1.6875$

The orbital energies are important because we will make use of Koopmans' theorem in our analysis. Appendix A provides a brief discussion of the use of Koopmans' theorem in interpreting the ionization energy of the helium atom. Atomic units have been used because they are properly scaled for atomic calculations. The conversion factor to SI units is 1 hartree = 2.6255 MJ mol^{-1} (*8*).

We now discuss the entries in these tables. For the hydrogen atom there are two contributions to the electronic energy, EH: kinetic energy ($\alpha^2/2$) and the electrostatic interaction with the nucleus ($-Z_\alpha$). Because there is only one electron in the hydrogen atom, this is also the expression for the electron orbital energy. Minimization of EH with respect to α yields α = 1, E_H = -0.5 hartree, and εH = -0.5 hartree. Applying Koopmans' theorem (IE = $-\varepsilon_H$) yields an ionization energy of 0.5 hartree, which is in agreement with experiment. The evaluation of the variational integrals that appear in the hydrogen and helium calculations outlined in this paper can be found in papers previously published in this Journal (*9*, *10*).

For the helium atom with two electrons there are five contributions to the total electronic energy, E_{He}: the kinetic energy of each electron ($\alpha^2/2$), the electrostatic interaction of each electron with the nucleus ($-Z_\alpha$), and the electrostatic interaction of the electrons with each other (5α/8). The electron orbital energy for the helium atom, ε_{He}, is simply those energy contributions that an individual electron experiences: kinetic energy ($\alpha^2/2$), electrostatic interaction with the nucleus ($-Z_\alpha$), and the electrostatic interaction with the other electron (5α/8). Minimization of EHe with respect to α yields α = 1.6875, E_{He} = -2.848 hartree, and ε_{He} = -0.8965 hartree. Appendix B provides a graphical representation of the variational procedure. Thus, the predicted ionization energy using Koopmans' theorem is 0.8965 hartree. The experimental ionization energy is 0.9037 hartree, so this result is not exact; but it is reasonably close, given the simplicity of the wave function chosen.

The first thing to note is that this analysis yields a ratio of ionization energies (IE ≈ -ε) of 1.79, as compared with the experimental value of 1.81. This gives us some confidence that we have chosen a reliable level of theory to deal with the question at hand. Note also that this quantum mechanical treatment brings into serious question the assumption (*1a*) that the electrons are about the same distance from the nucleus in the hydrogen atom and the helium atom. The last row of the second table shows that the ratio of , the quantum mechanically calculated average radial distance from the nucleus, is 0.59 which is considerably different from 1.0.

Continuing with the results given in the second table, we note that in going from H to He the orbital potential energy more than doubles (2.32). The orbital potential energy in He is the sum of the electron–nuclear attraction (-2α = -3.375 hartree) and the electron–electron repulsion (5α/8 = 1.055 hartree) terms. Thus we see that the electron–nuclear attraction more than triples, but the total potential energy increases by a factor of only 2.32 because of electron–electron repulsion. Coming back to the original issue, that the ionization energy increases by a factor of only 1.81 from H to He, we can now see that the explanation must lie in the kinetic energy term. Table 2 shows that the orbital kinetic energy almost triples (2.85) in going from H to He. Thus, the reason for the less than doubling of the ionization energy cannot be found by considering only potential energy, which alone predicts more than a doubling of the ionization energy. The explanation for the less than doubling of the ionization energy actually lies in the large increase in electron kinetic energy as the electrons are drawn closer to the nucleus by the increase in nuclear charge from H to He.

Table 2. Variational Results for Hydrogen and Helium

Parameter	Hydrogen	Helium	Ratio, He/H
Electron orbital energy	$\varepsilon_H = \alpha^2/2 - \alpha$	$\varepsilon_{He} = \frac{\alpha^2}{2} - 2\alpha + \frac{5\alpha}{8}$	
Optimum, α	1.0	1.6875	1.6875
Exp. ionization energy	0.5	0.9037	1.81
ε (orbital energy)	-0.5	-0.8965	1.79
Kinetic energy	0.5	1.424	2.85
Potential energy	-1.0	$-3.375 + 1.055 = -2.32$	2.32
$\langle R \rangle$	1.5	0.89	0.59

Earlier we referenced Ruedenberg's analysis of the physical nature of the chemical bond. What he said about molecular bonding also pertains to atomic electronic structure (*2c*):

Finally, it should be emphasized that the phenomenon of the eigenstate is intimately related to the fact that molecules are subject to the laws of quantum mechanics; there are no ground states in classical mechanics or electrostatics [emphasis added]. Consequently, a physical picture seeking to describe chemical bonding must necessarily incorporate features which distinguish quantum mechanics from classical mechanics and electrostatics…It may be added that the existence of a ground state is intrinsically connected with the fact that the variation integral contains both kinetic and potential energy…Omission of one or the other from consideration cannot, therefore, lead to a full interpretation of binding.

We have seen that one needs to use a quantum chemical treatment to understand the ratio of ionization energies for H and He. We wish to point out that interpreting the ionization of any atom or molecule requires quantum chemical tools and a consideration of both kinetic and potential energy.

While the quantum mechanical arguments outlined here may be used with undergraduate physical chemistry students, they are obviously too advanced for introductory students. However, we also should not use incorrect classical models. This leaves us with the important task of deciding what we can say to introductory students about the details of the periodicity of physical properties, such as ionization energies, that is both correct and understandable.

Literature Cited

1. (a) Gillespie, R. J.; Spencer, J. N.; Moog, R. S. *J. Chem. Educ.* **1996**, 73, 617. (b) Gillespie, R. J.; Spencer, J. N.; Moog, R. S. Ibid., 622. (c) Spencer, J. N.; Moog, R. S.; Gillespie, R. J. Ibid., 627. (d) Spencer, J. N.; Moog, R. S.; Gillespie, R. J. Ibid., 631.
2. (a) Ruedenberg, K. *Rev. Mod. Phys.* **1962**, 34, 326. (b) Feinberg, M. J.; Ruedenberg, K.; Mehler, E. L. *Adv. Quantum Chem.* **1970**, 5, 27. (c) Ruedenberg, K. In *Localization and Delocalization in Quantum Chemistry*, Vol. I; O. Chalvet et al., Eds.; D. Reidel: Dordrecht, **1975**; pp 223–245.
3. Baird, N. C. *J. Chem. Educ.* **1986**, 63, 660.
4. DeKock, R. L. J. Chem. Educ. **1987**, 64, 934.
5. Harcourt, R. D. Am. J. Phys. **1988**, 56, 660.
6. Kutzelnigg, W. Angew. Chem. Int. Ed. Eng. **1973**, 12, 546.
7. Koopmans, T. A. Physica 1933, 1, 104. Lowe, J. P. *Quantum Chemistry*, 2nd ed.; Academic: New York, **1993**; pp 361–363.
8. International Union of Pure and Applied Chemistry. *Quantities, Units, and Symbols in Physical Chemistry*, 2nd ed.; Blackwell Scientific: Oxford, 1993. Almost any physical chemistry or quantum chemistry textbook will also make reference to “atomic units”, for which the energy unit is called the “hartree.”
9. Snow, R. L.; Bills, J. L. *J. Chem. Educ.* **1975**, 52, 506.
10. Lee, S.-Y. *J. Chem. Educ.* **1983**, 60, 935.
11. Linnett, J. W. *Wave Mechanics and Valency*; Methuen: London, **1960**; pp 1–2.
12. Atkins, P. W. *Physical Chemistry*, 5th ed.; Freeman: New York, **1994**; p 371.

Appendix

A. Employing Koopmans’ theorem at the Hartree-Fock level to interpret the helium atom ionization energy breaks the ionization process into two steps: (1) frozen ionization (constant α) followed by (2) relaxation to the He+ ground state:

$$He(\alpha = 1.6875) \rightarrow He^{+}(\alpha = 1.6875);\ \Delta E = -\varepsilon = 0.89648 \text{ hartree}$$

$$He^{+}(\alpha = 1.6875) \rightarrow He^{+}(\alpha = 2);\ \Delta E = -0.0488 \text{ hartree}$$

One reason Koopmans’ theorem is successful in approximating the ionization in this way is that the energy change accompanying relaxation to the true ground state of the helium ion is small. Another reason is that Hartree–Fock calculations ignore electron correlation. With the wave function used in this study the correlation energy, EC , is

$$E_C = IT_{exp} - (E_{He+} - E_{He}) = 0.9037 - (-2.0000 + 2.8478) = 0.0560 \text{ hartree}$$

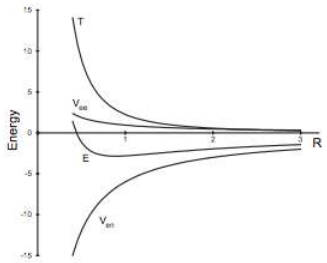
Thus, the correlation (0.0560 hartree) and relaxation ({0.0488 hartree) energy nearly cancel. This cancellation of terms accounts for the better-than-expected agreement between theory and experiment, given the simplicity of the wave function chosen. B. The variational expression for the helium atom energy using the wave function chosen in this study is

$$E(\alpha) = \alpha^2 - 4\alpha + \frac{5\alpha}{8}$$

Using the fact that the average radial distance of the electrons from the nucleus is inversely proportional to the scale factor α, = 1.5/α, R becomes the variational parameter and the variation integral becomes

$$E(R) = \frac{9}{4R^2} - \frac{6}{R} + \frac{15}{16R} = T(R) + V_{en}(R) + V_{ee}(R)$$

The figure below provides a graphical representation of the variation method (minimization of E with respect to R) and shows the behavior of the kinetic energy (T), electron–nuclear potential energy (V_{en}), electron–electron potential energy (V_{ee}), and total electronic energy (E) as a function of , the average radial distance of the helium atom electrons from the nucleus.



Contributions to the electronic energy of the He atom

Note the relative insignificance of V_{ee} compared to T and V_{en}. In other words, T and Ven are the dominant terms contributing to the ground state of the helium atom. This figure also clearly illustrates that the existence of a ground state (2) depends on the kinetic energy term. Atomic and molecular stability, therefore, can only be understood in quantum mechanical terms, and the foundation of all quantum mechanics is de Broglie's hypothesis that matter has wavelike properties, λ = h/mv. For one-dimensional problems it is easy to show the relationship between Schrödinger's equation and de Broglie's wave equation (*11, 12*).

This page titled 2.44: The Crucial Role of Kinetic Energy in Interpreting Ionization Energies is shared under a CC BY 4.0 license and was authored, remixed, and/or curated by Frank Rioux via source content that was edited to the style and standards of the LibreTexts platform.

2.45: Quantum Dots Are Artificial Atoms

"A quantum dot (QD) is a nanostructure that can confine the motion of an electron in all three spatial dimensions. This gives rise to a set of discrete and narrow electronic energy levels, similar to those of atomic physics (1)."

"Essentially, artificial atoms (quantum dots) are small boxes about 100 nm on a side, contained in a semiconductor, and holding a number of electrons that may be varied at will. As in real atoms, the electrons are attracted to a central location. In a natural atom, this central location is a positively charged nucleus; in an artificial atom, electrons are typically trapped in a bowl-like parabolic potential well in which electrons tend to fall in towards the bottom of the bowl (2)."

In most cases the nanostructures resemble "pancakes" in which the electrons are restricted to motion in the x-y plane. Thus the appropriate potential is the two-dimensional harmonic oscillator.

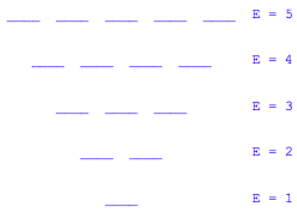
Schrödinger's equation can be solved for this potential in both cartesian and circuluar coordinates, yielding the following expressions (in units of hν) for the quantized energy levels. For an excellent introduction to the quantum mechanics of the two-dimensional harmonic oscillator see French & Taylor, "An Introduction to Quantum Physics," pp 454 - 463, plus three exercises on page 469.

$$\mathrm{E}\,(\mathrm{n}_x,\ \mathrm{n}_y) = \mathrm{n}_x + \mathrm{n}_y + 1 \quad \text{where} \quad \mathrm{n}_x = 0,\ 1,\ 2,\ 3... \quad \text{and} \quad \mathrm{n}_y = 0,\ 1,\ 2,\ 3...$$
$$\mathrm{E}(n,\ l) = 2n + |l| + 1 \quad \text{where} \quad n = 0,\ 1,\ 3... \quad \text{and} \quad l = 0,\ \pm 1,\ \pm 2...$$

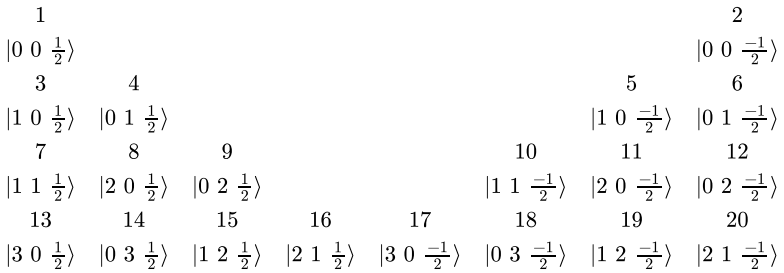
The quantum numbers and energies of the first ten states are shown in tabular format below.

n_x	n_y	E		n	l	E
0	0	1		0	0	1
1	0	2		0	+1	2
0	1	2		0	−1	2
1	1	3		0	+2	3
2	0	3		0	−2	3
0	2	3		1	0	3
3	0	4		0	+3	4
0	3	4		0	−3	4
1	2	4		1	+1	4
2	1	4		1	−1	4

The magnitude of the energy level spacing (hν) depends on the size of the quantum dot. Each level in the diagram below can be thought of as an electronic shell and when a level is filled a new row is started in the periodic table.



According to the Pauli Exclusion principle, the first four energy levels have a capacity for 20 electrons. Assuming that there is no splitting of energy level degeneracy in multi-electron atoms, the aufbau principle would give the following structure for the periodic table for a world made up of such "pancake" atoms. The quantum numbers of the last electron added to the "atom." For example atom 4 would have four electrons and their quantum numbers would be |0 0 ½>, |0 0 - ½>, |1 0 ½>, and |0 1 ½>.



To down-load a Mathcad file which will carry out a numerical integration of Schrödinger's equation click here.

To see representative wave functions click on the states shown below:

|0 0 ½>

|0 3 ½>

|1 1 ½>

References:

1. E. E. Vdovin, *Science*, **2000**, 290, 122.
2. R. C. Ashoori, *Nature*, **1996**, 379, 413.

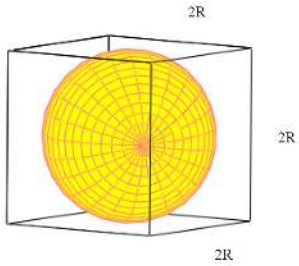
This page titled 2.45: Quantum Dots Are Artificial Atoms is shared under a CC BY 4.0 license and was authored, remixed, and/or curated by Frank Rioux via source content that was edited to the style and standards of the LibreTexts platform.

2.46: Calculating the Atomic Radius of Polonium

Three experimental facts are required to determine the atomic radius of a metallic element such as polonium:

1. density,
2. molar mass and
3. crystal structure.

The crystal structure of room temperature polonium is simple cubic, the only metallic element in the periodic table with this structure. Its unit cell, or basic repeating unit, is shown below.



As noted above, this calculation will require, in addition to the crystal structure, the density and molar mass of polonium, which are given below along with Avogadro′s number.

- Density: $\rho = 9.32\ g/cm^3$
- Molar Mass (MM): $208.98\ g/mol$
- Atoms per mole: $N_a = 6.023 \times 10^{23}$

Assuming that atomic polonium is a sphere, as shown above, we can calculate its atomic volume.

Atomic volume

$$V_{atomic} = \frac{4}{3}\pi R^3 \tag{2.46.1}$$

However, as the unit cell (basic building block) shows, the effective volume of a polonium atom is a cube of side $2R$. Therefore the effective volume of an atom of polonium is R^3.

Effective atomic volume

$$V_{effective} = (2R)^3 = 8R^3 \tag{2.46.2}$$

The next step involves calculating the packing efficiency of the simple cubic structure - in other words, the ratio of the atomic and effective volumes.

Ratio of atomic and effective volumes

$$\frac{V_{atomic}}{V_{effective}} = \frac{\frac{4}{3}\pi R^3}{8R^3} \tag{2.46.3}$$

$$= 0.524 \tag{2.46.4}$$

We see that only 52.4% of the space is occupied by polonium atoms. Next the reciprocal of the density, along with the molar mass and Avogadro′s number is used to calculate the effective volume of an individual polonium atom.

Experimental effective volume

Multiple \label

The atomic volume is 52.4% of the effective volume.

$$V_{atomic} = 0.524 V_{effective} = 0.195 \times 10^{-22} cm^3 \tag{2.46.5}$$

This allows the calculation of the atomic radius of polonium.

Multiple \label

This is in agreement with the literature value.

Contributors and Attributions

- Prof. Emeritus Frank Rioux (St. John's University and College of St. Benedict)

This page titled 2.46: Calculating the Atomic Radius of Polonium is shared under a CC BY 4.0 license and was authored, remixed, and/or curated by Frank Rioux via source content that was edited to the style and standards of the LibreTexts platform.

2.47: Calculating the Atomic Radius of Gold

Three experimental facts are required to determine the atomic radius of a metallic element such as gold: density, molar mass and crystal structure.

The crystal structure of gold is face-centered cubic. Its unit cell, or basic repeating unit, shows that it contains four gold atoms and that the gold atoms touch along the face diagonal. In terms of the gold atom radius, the unit cell dimension is $2\sqrt{2}\mathrm{R}$.

As noted above, this calculation will require, in addition to the crystal structure, the density and molar mass of gold, which are given below along with Avogadro′s number.

- Density: $19.32\frac{\mathrm{gm}}{\mathrm{cm}^3}$
- Molar mass: $197.0\mathrm{gm}$
- Atoms per mole: $6.022(10)^{23}$

Assuming that atomic gold is a sphere, as shown above, we can calculated its atomic volume.

- Atomic volume: $V_{Atom} = \frac{4}{3}\pi\mathrm{R}^3$

However, the effective volume of a gold atom is 25% of the unit cell volume, $(2\sqrt{2}\mathrm{R})^3$.

- Effective atomic volume: $V_{Aeffective} = \frac{(2\sqrt{2}\mathrm{R})^3}{4} \rightarrow V_{Aeffective} = 4(2)^{\frac{1}{2}}\mathrm{R}^3$

The next step involves calculating the packing efficiency of the face-centered cubic structure - in other words, the ratio of the atomic and effective atomic volumes. We see that only 74% of the space is occupied by gold atoms.

- Ratio of atomic and effective atomic volumes according to the fcc model:

$$\frac{V_{Atom}}{V_{Aeffective}} = \frac{\frac{4}{3}\pi\mathrm{R}^3}{4 \times 2^{\frac{1}{2}}\mathrm{R}^3}\mathrm{float},\ 2 \rightarrow \frac{V_{Atom}}{V_{Aeffective}} = .74$$

Next the reciprocal of the density, along with the molar mass and Avogadro′s number is used to calculate the experimental effective volume of an individual gold atom.

- Experimental effective atomic volume:

$$V_{ExEffective} = \frac{1cm^3}{19.32gm}\frac{197.0gm}{6.022\ 10^{23}} \quad V_{ExEffective} = 1.693 \times 10^{-23}cm^3$$

According to the fcc model the atomic volume is 74% of the experimental effective atomic volume. This allows the calculation of the atomic radius of gold.

$$\frac{4}{3}\pi\mathrm{R}^3 = 0.74V_{ExEffective} \quad R = \left(\frac{0.74V_{ExEffective}}{\frac{4}{3}\pi}\right)^{\frac{1}{3}} \quad \mathrm{R} = 144\mathrm{pm}$$

This is in agreement with the literature value (see Figure 5.19 page 176 in Chemistry, 5th edition, by McMurry and Fay).

- Define picometer: $\mathrm{pm} = 10^{-12}\mathrm{m}$

This page titled 2.47: Calculating the Atomic Radius of Gold is shared under a CC BY 4.0 license and was authored, remixed, and/or curated by Frank Rioux via source content that was edited to the style and standards of the LibreTexts platform.

2.48: How Many Bibles Can Fit on the Head of a Pin

On December 29, 1959 Richard Feynman gave an address (There′s Plenty of Room at the Bottom) in which he calculated how many Encyclopedia Britannicas could fit on the head of a pin. Legend identifies this event as the beginning of the field of theoretical nanotechnology.

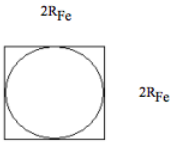
To illustrate to general chemistry students how small nanoscopic entities, such as atoms, are I calculate with the following simple model how many bibles can fit on the head of a pin.

The model assumes that the pinhead surface is made up of Fe atoms packed in a simple squaric array. It further assumes that letters would be made by placing adatoms in the pockets created by the surface Fe atoms using a scanning tunneling microscope, and that 100 pinhead surface Fe atoms would be required to form a letter.

The first step is to calculate the number of Fe atoms on the pinhead.

$$\begin{array}{lll} \text{Radium of pinhead:} & R_{PH} = \frac{1}{32} in & R_{PH} = 7.94 \times 10^{8} pm \\ \text{Area of pinhead:} & \text{Area}_{PH} = \pi R_{PH}^2 & \text{Area}_{PH} = 1.98 \times 10^{18} \text{pm}^3 \\ \text{Radius of Fe:} & \text{R}_{Fe} = 126\text{pm} & \text{R}_{Fe} = 1.26 \times 10^{-10} \text{pm} \\ \text{Area of Fe atom:} & \text{Area}_{Fe} = \pi \text{R}_{Fe}^2 & \text{Area}_{Fe} = 4.99 \times 10^{4} \text{pm}^2 \end{array}$$

Effective area of Fe atom:



$$\text{EffectiveArea}_{Fe} = 4\text{R}_{Fe}^2$$
$$\text{EffectiveArea}_{Fe} = 6.35 \times 10^{4} \text{pm}^2$$

Fe atoms per pinhead:

$$\text{FeAtomsPerPinHead} = \frac{\text{Area}_{PH}}{\text{EffectiveArea}_{Fe}} \quad \text{FeAtomsPerPinHead} = 3.12 \times 10^{13}$$

A typical family Bible consists of 1,000 pages with an average of 5,000 characters and spaces per page. If it takes 100 Fe atoms to define a character, how many Bibles can fit on the head of a pin?

$$\text{PagesPerBible} = 1000 \quad \text{CharactersPerPage} = 5000 \quad \text{FeAtomsPerCharacter} = 100$$

Fe atoms required per bible:

$$\text{FeAtomsPerCharacter CharactersPerPage PagesPerBible} = 5 \times 10^{8}$$
$$\text{BiblesPerPinHead} = \frac{\text{FeAtomsPerPinHead}}{\text{FeAtomsPerCharacter CharactersPerPage PagesPerBible}}$$
$$\text{BiblesPerPinHead} = 6.2 \times 10^{4}$$

Define picometer: $\text{pm} = 10^{-12}\text{m}$

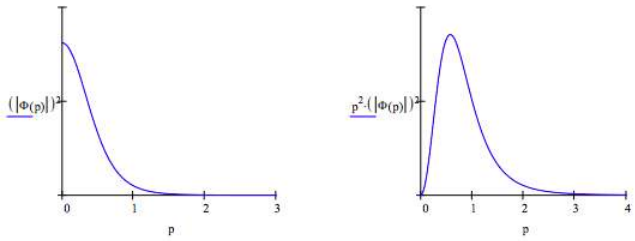
This page titled 2.48: How Many Bibles Can Fit on the Head of a Pin is shared under a CC BY 4.0 license and was authored, remixed, and/or curated by Frank Rioux via source content that was edited to the style and standards of the LibreTexts platform.

2.49: Momentum Wavefunctions and Distributions for the Hydrogen Atom

The Fourier transform for the 1s orbital

$$\Phi(p) = \frac{1}{\sqrt{8\pi^4}} \int_0^{\infty} \int_0^{\pi} \int_0^{2\pi} \exp(\text{-r})\ \exp\left(-\text{i p r}\cos(\theta)\right) r^2 \sin(\theta)\, d\phi d\theta dr \rightarrow \frac{2^{\frac{1}{2}}}{\pi\left[(-1)+\text{i p}\right]^2 (1+\text{i p}^2}$$

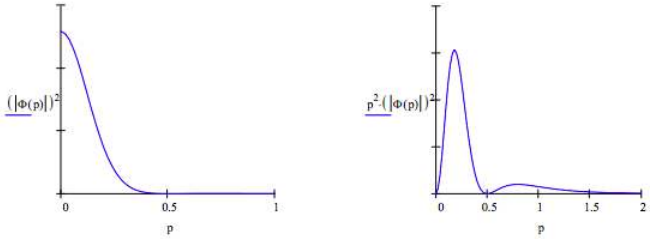
p = 0, .02 .. 5



The Fourier transform for the 2s orbital

$$\Phi(p) = \frac{1}{16\pi^2} \int_0^{\infty} \int_0^{\pi} \int_0^{2\pi} (2-r)\exp\left(-\frac{r}{2}\right) \exp\left(\text{-i p r}\cos(\theta)\right) r^2 \sin(\theta) d\phi d\theta dr$$

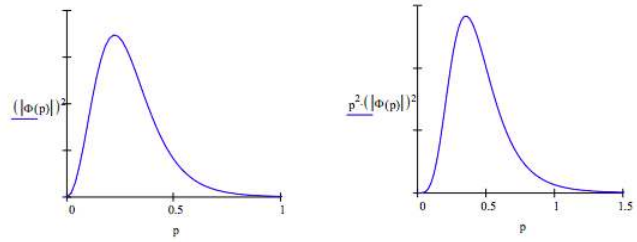
$$\text{yields} \quad \Phi(p) = \frac{-16}{\pi} \frac{(-1)+4p^2}{\left[(-1)+2\text{i p}\right]^3 (1+2\text{i p})^3} \quad p = 0, .02..2$$



The Fourier transform for the $2p_z$ orbital

$$\Phi(p) = \frac{1}{16\pi^2} \int_0^{\infty} \int_0^{\pi} \int_0^{2\pi} \text{r}\ \exp\left(-\frac{r}{2}\right) \exp\left(\text{-i p r}\cos(\theta)\right) r^2 \sin(\theta) d\phi d\theta dr$$

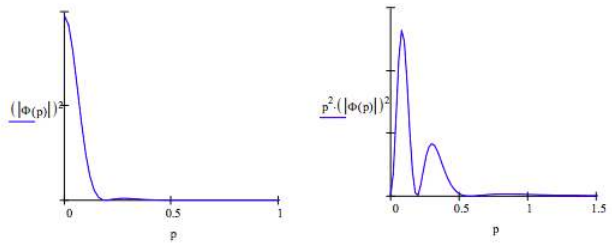
$$\text{yields} \quad \Phi(p) = 64\frac{i}{\pi} \frac{p}{\left[(-1)+2\text{i p}^3 (1+2\text{i p}^3\right.}$$



The Fourier transform for the 3s orbital

$$\Phi(p) = \frac{1}{162\sqrt{2}\pi^2} \int_0^{\infty} \int_0^{\pi} \int_0^{2\pi} \left(27-18r+2r^2\right) \exp\left(-\frac{r}{3}\right) \exp\left(\text{-i p r}\cos(\theta)\right) r^2 \sin(\theta) d\phi d\theta dr$$

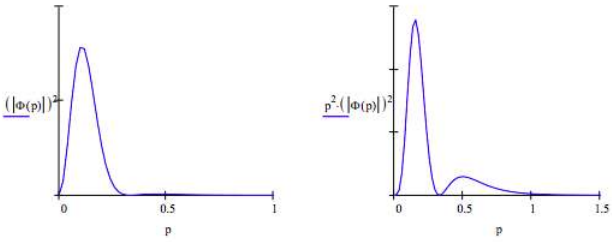
$$\text{yields} \quad \Phi(p) = 18\frac{6^{\frac{1}{2}}}{\pi} \frac{(-30)p^2+1+81p^4}{\left[(-1)+3\text{i p}\right]^4 (1+3\text{i p})^4}$$



The Fourier transform for the $3p_z$ orbital

$$\Phi(p) = \frac{1}{162\pi^2} \int_0^{\infty} \int_0^{\pi} \int_0^{2\pi} \left(6r - r^2\right) \exp\left(-\frac{r}{3}\right) \exp\left(\text{-i p r} \cos(\theta)\right) \cos(\theta)\, r^2 \sin(\theta) d\phi d\theta dr$$

$$\text{yields} \quad \Phi(p) = (-432)\frac{i}{\pi} p \frac{9p^2-1}{[(-1)+3\text{i p}]^4(1+3\text{i p})^4}$$



This page titled 2.49: Momentum Wavefunctions and Distributions for the Hydrogen Atom is shared under a CC BY 4.0 license and was authored, remixed, and/or curated by Frank Rioux via source content that was edited to the style and standards of the LibreTexts platform.

2.50: The SCF Method for Two Electrons

Self-consistent field calculations have great historical significance and play a major role in contemporary quantum chemistry. Therefore, the purpose of this exercise is to illustrate with an interactive example the simplest possible self-consistent field calculation for atomic systems. The SCF method is particularly transparent in the Mathcad programming environment as will be shown below.

Under the orbital approximation [Φ(1,2) = Ψ(1)Ψ(2)] the two-electron Schrödinger Equation can be decoupled into two one-electron equations with effective Hamiltonian operators of the form,

$$H_i = -\frac{1}{2r_1}\frac{d^2}{dr_i^2}r_i - \frac{Z}{r_i} + \int_0^\infty \Psi_j \frac{1}{r_j} d\tau_j$$

Here the subscripts i and j are used to distinguish the two electrons.

The first term on the right side represents the kinetic energy of the ith electron, the second term is its interaction with the nucleus, and the third term is its average interaction with the jth electron. If it is assumed that the jth electron is in a Slater-type orbital with scale factor β,

$$\Psi_j = \sqrt{\frac{\beta^3}{\pi}}\exp\left(-\beta r_j j\right)$$

the effective Hamiltonian for the ith electron becomes,

$$H_i = -\frac{1}{2r_1}\frac{d^2}{dr_i^2} - \frac{Z}{r_1} + \frac{1}{r_1}\left[1 - (1+\beta r_1)\exp\left(-2\beta r_i\right)\right]$$

This Hamiltonian is then used with the variational method to calculate the orbital energy of the ith electron,

$$\varepsilon_i = \int_0^\infty \Psi_i H_i \Psi_i d\tau_i$$

If the ith electron is also assumed to be in a Slater-type orbital but with a different scale factor α,

$$\Psi_i = \sqrt{\frac{\alpha^3}{\pi}}\exp\left(-\alpha r_i\right)$$

the variational integral for the orbital energy upon evaluation is,

$$\varepsilon_i = \frac{\alpha^2}{2} - Z\alpha + \frac{\alpha\beta\left(\alpha^2 + 3\alpha\beta + \beta^2\right)}{(\alpha+\beta)^3}$$

The SCF calculation proceeds by minimizing εi with respect to α given an initial value for β. This amounts to finding the orbital energy and wavefunction of the ith electron in the average electrostatic field created by the jth electron. Now we turn our attention to the jth electron. By identical arguments to those given above for the ith electron, it can be shown that the orbital energy of the jth electron is

$$\varepsilon_j = \frac{\beta^2}{2} - Z\beta + \frac{\alpha\beta\left(\alpha^2 + 3\alpha\beta + \beta^2\right)}{(\alpha+\beta)^3}$$

The value of α just obtained for the ith electron serves as the seed value as εj is minimized with respect to β in order to obtain the orbital energy and wavefunction of the jth electron. One cycle has now been completed and this procedure is continued until self-consistency is achieved. This occurs when the orbital energies and the wavefunctions of the two electrons converge to the same values. After each iteration the energy of the atom or ion is calculated as the sum of orbital energy of one of the electrons plus the kinetic and nuclear potential energy of the other electron.

$$E_{atom} = \varepsilon_i + \frac{\beta^2}{2} - Z\beta$$

To summarize: After making a guess for the wavefunction of the jth electron the variation method is used to determine the orbital energy and wavefunction of the i^{th} electron. Using this output wavefucntion as the input wavefunction in the second iteration, the orbital energy and wavefunction of the j^{th} electron is calculated. The procedure is repeated until self-consistency is achieved; that is until $\Psi_i = \Psi_j$ and $\varepsilon_i = \varepsilon_j$. This is also the point at which the energy of the atom has achieved a minimum value in compliance with the variational theorem. This is clearly shown in the output of the third method.

Note that the final SCF result is the same as that achieved in a variational calculation which places both electrons in the same Slater orbital from the beginning. This calculation results in the familiar expression

$$E = \alpha^2 - \left(2Z - \frac{5}{8}\right)\alpha$$

which when minimized with respect to α yields, α = Z - 5/16 and $E_{atom} = -\alpha^2$.

The reason for using the indirect procedure outlined here is that it provides an unusually simple and direct example of the SCF method. This example should be helpful in understanding what is going on behind the scenes in much more complicated quantum mechanical calculations performed with comprehensive commercial programs like Spartan.

SCF Calculation for Two Electron Atoms and Ions

1. Supply nuclear charge and an input value for β:

$$Z = 2 \quad \beta = 2 \quad \alpha = Z$$

2. Define orbital energies of the electrons in terms of the variational parameters:

$$\varepsilon_{1s\alpha}(\alpha,\ \beta) = \frac{\alpha^2}{2} - Z\alpha + \frac{\alpha\beta(\alpha^2+3\alpha\beta+\beta^2)}{(\alpha+\beta)^3} \quad \varepsilon_{1s\beta}(\alpha,\ \beta) = \frac{\beta^2}{2} - Z\beta + \frac{\alpha\beta(\alpha^2+3\alpha\beta+\beta^2)}{(\alpha+\beta)^3}$$

3. Minimize orbital energies with respect to α and β:

$$\begin{array}{llllll} \text{Given} & \frac{d}{d\alpha}\varepsilon_{1s\alpha}(\alpha,\ \beta) = 0 & \alpha = \text{Find}(\alpha) & \alpha = 1.5999 & \varepsilon_{1s\alpha}(\alpha,\ \beta) = -0.8116 \\ \text{Given} & \frac{d}{d\beta}\varepsilon_{1s\alpha}(\alpha,\ \beta) = 0 & \beta = \text{Find}(\beta) & \beta = 1.5999 & \varepsilon_{1s\beta}(\alpha,\ \beta) = -0.9250 \end{array}$$

4. Calculate the energy of the atom:

$$E_{atom} = \frac{\alpha^2}{2} + \frac{\beta^2}{2} - Z\alpha - Z\beta + \frac{\alpha\beta(\alpha^2+3\alpha\beta+\beta^2)}{(\alpha+\beta)^3} \quad E_{atom} = -2.8449$$

5. Record results of the SCF cycle and return to step 1 with the new and improved input value for β.
6. Continue until self-consistency is achieved.
7. Verify the results shown below for He. Repeat for Li^+, Be^{2+} and B^{3+}.

Recommend tabular form for results of each SCF cycle:

$$\begin{pmatrix} \beta(\text{input}) & \alpha & \varepsilon_{1s\alpha} & \beta & \varepsilon_{1s\beta} & E_{atom} \\ 2.000 & 1.5999 & -0.8116 & 1.7126 & -0.9250 & -2.8449 \\ 1.7126 & 1.6803 & -0.8887 & 1.6895 & -0.8987 & -2.8476 \\ 1.6895 & 1.6869 & -0.8959 & 1.6877 & -0.8967 & -2.8477 \\ 1.6877 & 1.6874 & -0.8964 & 1.6875 & -0.8965 & -2.8477 \\ 1.6875 & 1.6875 & -0.8965 & 1.6875 & -0.8965 & -2.8477 \end{pmatrix}$$

This page titled 2.50: The SCF Method for Two Electrons is shared under a CC BY 4.0 license and was authored, remixed, and/or curated by Frank Rioux via source content that was edited to the style and standards of the LibreTexts platform.

2.51: Outline of the SCF Method for Two Electrons

Trial Wave Function:

$$\Psi(r,\ \beta) = \sqrt{\frac{\beta^3}{\pi}}\exp(-\beta r)$$

Calculate kinetic energy:

$$T_e(\beta) = \int_0^\infty \Psi(r,\ \beta)\left[-\frac{1}{2r}\frac{d^2}{dr^2}(r\Psi(r,\ \beta))\right]4\pi r^2 dr \ \Big|\ \begin{matrix}\text{assume, } \beta>0\\ \text{simplify}\end{matrix} \rightarrow (-\beta)Z$$

Calculate electron-nucleus potential energy:

$$V_{ne}(\beta,\ Z) = \int_0^\infty \Psi(r,\ \beta)\frac{-Z}{r}4\pi r^2 dr \ \Big|\ \begin{matrix}\text{assume, } \beta>0\\ \text{simplify}\end{matrix} \rightarrow (-\beta)Z$$

Calculation of electron-electron potential energy:

a. Calculate the electrostatic potential due to the β electron:

$$\Phi(\beta,\ r) = \begin{matrix}\frac{1}{r}\int_0^r \Psi(x,\ \beta)^2 4\pi x^2 dx... \\ +\int_r^\infty \frac{\Psi(x,\ \beta)^2 4\pi x^2 dx}{x}dx\end{matrix} \ \Big|\ \begin{matrix}\text{assume, } \beta>0\\ \text{simplify}\end{matrix} \rightarrow \frac{-\left[e^{(-2)r\beta}\beta r + e^{(-2)r\beta} - 1\right]}{r}$$

b. Calculate the electron-electron potential energy of the α and β electrons using result of part a:

$$V_{ee}(\alpha,\ \beta) = \int_0^\infty \Psi(r,\ \alpha)^2\Phi(\beta,\ r)4\pi r^2 dr \ \Big|\ \begin{matrix}\text{assume, } \beta>0,\ \alpha>0\\ \text{simplify}\end{matrix} \rightarrow \alpha\beta\frac{\alpha^2+3\alpha\beta+\beta^2}{(\alpha^2+2\beta\alpha+\beta^2)(\beta+\alpha)}$$

SCF Calculation

1. Supply nuclear charge and an input value for β:

$$Z = 2 \quad \beta = 2.0 \quad \alpha = Z$$

2. Define orbital energies of the electrons in terms of the variational parameters:

$$\begin{matrix}\text{Orbital energy of the } \alpha \text{ electron:} & \varepsilon_{1s\alpha}(\alpha,\ \beta) = T_e(\alpha) + V_{ne}(\alpha,\ Z) + V_{ee}(\alpha,\ \beta)\\ \text{Orbital energy of the } \beta \text{ electron:} & \varepsilon_{1s\beta}(\alpha,\ \beta) = T_e(\beta) + V_{ne}(\beta,\ Z) + V_{ee}(\alpha,\ \beta)\end{matrix}$$

3. Minimize orbital energies with respect to α and β:

$$\begin{matrix}\text{Given} & \frac{d}{d\alpha}\varepsilon_{1s\alpha}(\alpha,\ \beta) = 0 & \alpha = \text{Find}(\alpha) & \alpha = 1.5999 & \varepsilon_{1s\alpha}(\alpha,\ \beta) = -0.8116\\ \text{Given} & \frac{d}{d\beta}\varepsilon_{1s\beta}(\alpha,\ \beta) = 0 & \beta = \text{Find}(\beta) & \beta = 1.7126 & \varepsilon_{1s\beta}(\alpha,\ \beta) = -0.9250\end{matrix}$$

4. Calculate the energy of the atom:

$$E_{atom} = T_e(\alpha) + V_{ne}(\alpha,\ Z) + T_e(\beta) + V_{ne}(\beta,\ Z) + V_{ee}(\alpha,\ \beta) \quad E_{atom} = -2.8449$$

5. Record results of the SCF cycle and return to step 1 with the new and improved input value for β.
6. Continue until self-consistency is achieved.
7. Verify the results shown below for He. Repeat for Li^+, Be^{2+} and B^{3+}

$$\begin{pmatrix}\beta\ (\text{input}) & \alpha & \varepsilon_{1s\alpha} & \beta & \varepsilon_{1s\beta} & E_{atom}\\ 2.000 & 1.5999 & -0.8116 & 1.7126 & -0.9250 & -2.8449\\ 1.7126 & 1.6803 & -0.8887 & 1.6895 & -0.8987 & -2.8476\\ 1.6895 & 1.6869 & -0.8959 & 1.6877 & -0.8967 & -2.8477\\ 1.6877 & 1.6874 & -0.8964 & 1.6875 & -0.8965 & -2.8477\\ 1.6875 & 1.6875 & -0.8965 & 1.6875 & -0.8965 & -2.8477\end{pmatrix}$$

This page titled 2.51: Outline of the SCF Method for Two Electrons is shared under a CC BY 4.0 license and was authored, remixed, and/or curated by Frank Rioux via source content that was edited to the style and standards of the LibreTexts platform.

2.52: The SCF Method for Two Electrons Using a Gaussian Wave Function

Gaussian Trial Wave Function:

$$\Psi(r,\ \beta) = \left(\frac{2\beta}{\pi}\right)^{\frac{3}{4}} \exp\left(-\beta r^2\right)$$

Calculate kinetic energy:

$$\int_0^\infty \Psi(r,\ \beta)\left[-\frac{1}{2r}\frac{d^2}{dr^2}(r\Psi(r,\ \beta))\right] 4\pi r^2 dr \ \Big|\ \begin{matrix}\text{assume, } \beta>0\\ \text{simplify}\end{matrix} \rightarrow \frac{3}{2}\beta$$

Calculate electron-nucleus potential energy:

a. Calculate the electric potential of one of the electrons in the presence of the other:

$$\frac{1}{r}\int_0^r \Psi(x,\ \beta)^2 4\pi x^2 dx + \int_r^\infty \frac{\Psi(x,\ \beta)^2 4\pi x^2}{x} dx \ \Big|\ \begin{matrix}\text{assume, } \beta>0\\ \text{simplify}\end{matrix} \rightarrow \frac{\operatorname{erf}\left(r 2^{\frac{1}{2}} \beta^{\frac{1}{2}}\right)}{r}$$

b. Calculate the electron-electron potential energy using the result of part a:

Illegal pream-token (\)

SCF Calculation

1. Supply nuclear charge and an input value for β:

$$Z = 2 \quad \beta = 0.767 \quad \alpha = Z$$

2. Define orbital energies of the electrons in terms of the variational parameters:

$$\text{Orbital energy of the } \alpha \text{ electron:} \quad \varepsilon_{1s\alpha}(\alpha,\ \beta) = \frac{3\alpha}{2} - Z\sqrt{\frac{8\alpha}{\pi}} + \sqrt{\frac{8\alpha\beta}{\pi(\alpha+\beta)}}$$

$$\text{Orbital energy of the } \beta \text{ electron:} \quad \varepsilon_{1s\beta}(\alpha,\ \beta) = \frac{3\beta}{2} - Z\sqrt{\frac{8\beta}{\pi}} + \sqrt{\frac{8\alpha\beta}{\pi(\alpha+\beta)}}$$

3. Minimize orbital energies with respect to α and β:

$$\text{Given} \quad \frac{d}{d\alpha}\varepsilon_{1s\alpha}(\alpha,\ \beta) = 0 \quad \alpha = \text{Find}(\alpha) \quad \alpha = 0.7670 \quad \varepsilon_{1s\alpha}(\alpha,\ \beta) = -0.6564$$

$$\text{Given} \quad \frac{d}{d\beta}\varepsilon_{1s\beta}(\alpha,\ \beta) = 0 \quad \beta = \text{Find}(\beta) \quad \beta = 0.7670 \quad \varepsilon_{1s\beta}(\alpha,\ \beta) = -0.6564$$

4. Calculate the energy of the atom:

$$E_{atom} = \frac{3\alpha}{2} \quad \frac{3\beta}{2} - Z\sqrt{\frac{8\alpha}{\pi}} - Z\sqrt{\frac{8\beta}{\pi}} + \sqrt{\frac{8\alpha\beta}{\pi(\alpha+\beta)}} \quad E_{atom} = -2.3010$$

5. Record results of the SCF cycle and return to step 1 with the new and improved input value for β.
6. Continue until self-consistency is achieved.
7. Verify the results shown below for He. Repeat for Li^+, Be^{2+} and B^{3+}.

$$\begin{pmatrix} \beta(\text{input}) & \alpha & \varepsilon_{1s\alpha} & \beta & \varepsilon_{1s\beta} & E_{atom} \\ 2.000 & 0.4514 & -0.4988 & 0.9303 & -0.8031 & -2.2703 \\ 0.9303 & 0.6943 & -0.6117 & 0.8023 & -0.6816 & -2.2996 \\ 0.8023 & 0.7504 & -0.6454 & 0.7749 & -0.6618 & -2.3009 \\ 0.7749 & 0.7633 & -0.6539 & 0.7688 & -0.6576 & -2.3010 \\ 0.7688 & 0.7661 & -0.6588 & 0.7674 & -0.6567 & -2.3010 \\ 0.7674 & 0.7668 & -0.6563 & 0.7671 & -0.6564 & -2.3010 \\ 0.7671 & 0.7669 & -0.6564 & 0.7670 & -0.6564 & -2.3010 \\ 0.7670 & 0.7670 & -0.6564 & 0.7670 & -0.6564 & -2.3010 \end{pmatrix}$$

This page titled 2.52: The SCF Method for Two Electrons Using a Gaussian Wave Function is shared under a CC BY 4.0 license and was authored, remixed, and/or curated by Frank Rioux via source content that was edited to the style and standards of the LibreTexts platform.

2.53: An Interactive SCF Calculation for the Helium Atom

This is an outline of the Mathcad implementation of a two-electron SCF calculation published in JCE by Snow and Bills. [Snow, R. L.; Bills, J. L. *J. Chem. Educ.* 1975, 52, 506.]

Under the orbital approximation, Ψ(1,2) = Φ(1)Φ(2), the two-electron Schrödinger equation for helium can be decoupled into two, one-electron Hartree differential equations.The individual helium atom electrons are assumed to occupy an orbital which is a linear combination of two Slater 1s orbitals,

$$\Phi = C_1 f_1 + C_2 f_2$$

$$f_1 = \sqrt{\frac{\alpha^3}{\pi}} \exp(-\alpha r) \quad \text{and} \quad f_2 = \sqrt{\frac{\beta^3}{\pi}} \exp(-\beta r)$$

The effective Hamiltonian for the ith electron is,

$$H_i = -\frac{1}{2r^2}\frac{d}{dr}\left(r^2 \frac{d}{dr}\blacksquare\right) - \frac{2}{r_i} + \int_0^\infty (C_{j1} f_1 + C_{j2} f_2)\frac{1}{r_{ij}}(C_{j1} f_1 + C_{j2} f_2)\, d\tau$$

where the Cjs are the coefficients of the jth electron.

Assuming that the ith electron is also in an orbital of the form given in equation (1), the variational method yields the following expression for the energy of the ith electron.

$$\varepsilon_i = \frac{\int_0^\infty (C_{j1} f_1 + C_{j2} f_2) H_i (C_{j1} f_1 + C_{j2} f_2)\, d\tau}{\int_0^\infty (C_{j1} f_1 + C_{j2} f_2)^2\, d\tau} = \frac{Ci_1^2 + H_{11} 2Ci_i Ci_2 H_{12} + Ci_2^2 H_{22}}{Ci_1^2 + 2Ci_1 Ci_2 S_{12} + Ci_2^2}$$

The optimum values for the orbital scale factors are given below. The user can change these values to demonstrate that they do indeed yield a minimum energy for the trial wavefunction chosen.

$$\alpha = 1.45 \quad \beta = 2.90$$

Evaluation of integrals given values for the scale factors, α and β, of the Slater type orbitals follows (See Snow and Bills for details):

$$\tau = \frac{\alpha-\beta}{\alpha+\beta} \quad \tau 1 = \frac{\alpha-\beta}{3\alpha+\beta} \quad \tau 2 = \frac{\alpha-\beta}{\alpha+3\beta}$$

Kinetic energy integrals:

$$T_{11} = \frac{\alpha^2}{2} \quad T_{22} = \frac{\beta^2}{2} \quad T_{12} = \frac{1}{8}(\alpha+\beta)^2 (1-\tau^2)^{2.5}$$

Electron-nucleus potential energy integrals:

$$V_{11} = -2\alpha \quad V_{22} = -2\beta \quad V_{12} = -(\alpha+\beta)(1-\tau)^{1.5}$$

Electron-electron repulsion integrals:

$$V_{1111} = \frac{5}{8}\alpha \quad V_{2222} = \frac{5}{8}\alpha \quad V_{1212} = \frac{5}{16}(1-\tau^2)^3 (\alpha+\beta)$$

$$V_{1122} = \frac{1}{16}(1-\tau^2)(5-\tau^2)(\alpha+\beta) \qquad V_{1222} = \frac{1}{32}(1-\tau^2)^{1.5}(1-tau2^2)(5-\tau 2^2)(\alpha+3\beta)$$

$$V_{1112} = \frac{1}{32}(1-\tau^2)^{1.5}(1-\tau 1^2)(5-\tau 1^2)(3\alpha+\beta) \qquad \text{Overlap integral: } S_{12} = (1-\tau^2)^{1.5}$$

Having evaluated the integrals, the next step is the calculation of the matrix elements that appear in equation (4).

$$H_{11} = T_{11} + V_{11} + Cj_1^2 V_{1111} + 2Cj_1 Cj_2 V_{1112} + Cj_2^2 V_{1122}$$
$$H_{12} = T_{12} + V_{12} + Cj_1^2 V_{1112} + 2Cj_1 Cj_2 V_{1212} + Cj_2^2 V_{1222}$$
$$H_{22} = T_{22} + V_{22} + Cj_1^2 V_{1122} + 2Cj_1 Cj_2 V_{1222} + Cj_2^2 V_{2222}$$

Given initial values for the coefficients of the jth electron (these are declared below in a more convient location using Mathcad′s global equal sign), minimization of the orbital energy simultaneously with respect to the coefficients of the ith electron yields the

orbital energy of the ith electron and its coefficients. These output coefficients become the input coefficients of the next iteration when the orbital energy of the j th electron is calculated. The procedure is repeated until self-consistency is achieved. This occurs when the output coefficients are equal to the input coefficients, or to put it another way, when the coefficients of the two electrons are identical.

In the numeric mode Mathcad requires seed values for all variable which appear in the expression to be evaluated in a Given/Find solve block. The seed values for the coefficients shown below are arbitrarily set at 0.5.

$$Ci_1 = .5 \quad Ci_2 = .5$$

The variational integral for the electron orbital energy:

$$\varepsilon\left(Ci_1,\ Ci_2\right) = \frac{Ci_1^2 H_{11} + 2Ci_1 H_{12} + Ci_2^2 H_{22}}{Ci_1^2 + 2Ci_1 Ci_2 S_{12} + Ci_2^2}$$

Minimization of the variational integral simultaneously with respect to the coefficients plus the normalization condition

$$\text{Given} \quad \frac{d}{dCi_1}\varepsilon\left(Ci_1,\ Ci_2\right) = 0 \quad \frac{d}{dCi_2}\varepsilon\left(Ci_1,\ Ci_2\right) = 0 \quad Ci_1^2 + 2Ci_1 Ci_2 S_{12} + Ci_2^2 = 1$$

yields the output coefficients and the orbital energy:

$$\begin{pmatrix} Ci_1 \\ Ci_2 \end{pmatrix} = \text{Find}\left(Ci_1,\ Ci_2\right) \quad \begin{pmatrix} Ci_1 \\ Ci_2 \end{pmatrix} = \begin{pmatrix} 0.809249 \\ 0.219060 \end{pmatrix}$$

In the SCF method the output coefficients become the input coefficients in the next iteration.

Display the orbital energy:

$$\varepsilon\left(Ci_1,\ Ci_2\right) = -0.984326$$

The energy of the atom at this point in the calculation is the orbital energy of the ith electron plus the kinetic and nuclear potential energy of the jth electron.

$$E_{atom} \qquad\qquad E_{atom} = -2.833076$$
$$= \varepsilon\left(Ci_1,\ Ci_2\right) + Cj_1^2\left(T_{11} + V_{11}\right) + 2C_1 Cj_2\left(T_{12} + V_{12}\right) + Cj_2^2\left(T_{22} + V_{22}\right)$$

Input coefficients:

$$\begin{pmatrix} Cj_1 \\ Cj_2 \end{pmatrix} = \begin{pmatrix} 1 \\ 0 \end{pmatrix}$$

Paste new input coefficients after each iteration.

Summary of the SCF results for the following initial input coefficients:

$$\begin{pmatrix} Cj_1 \\ Cj_2 \end{pmatrix} = \begin{pmatrix} 1 \\ 0 \end{pmatrix}$$

Iteration	Ci_1	Ci_2	$\varepsilon\left(Ci_1,\ Ci_2\right)$	E_{atom}
1	0.809249	0.21906	−0.984326	−2.833076
2	0.847034	0.176951	−0.90556	−2.860616
3	0.839638	0.185241	−0.920653	−2.86163
4	0.841091	0.183615	−0.917676	−2.86167
5	0.840806	0.183934	−0.918258	−2.861672
6	0.840862	0.183871	−0.918144	−2.861672
7	0.840851	0.183884	−0.918167	−2.861672
8	0.840852	0.183881	−0.918161	−2.861673
9	0.840852	0.183882	−0.918164	−2.861672
10	0.840852	0.183882	−0.918164	−2.861672

This page titled 2.53: An Interactive SCF Calculation for the Helium Atom is shared under a CC BY 4.0 license and was authored, remixed, and/or curated by Frank Rioux via source content that was edited to the style and standards of the LibreTexts platform.

2.54: Quantum Calculations on the Hydrogen Atom in Coordinate, Momentum and Phase Space

Coordinate Space Operators

Position operator: $x \cdot \square$	Momentum operator: $\mathrm{p} = \frac{1}{\mathrm{i}} \cdot \frac{\mathrm{d}}{\mathrm{dx}} \square$	Integral: $\int_0^\infty \square dx$

Kinetic energy operator: $\mathrm{KE} = -\frac{1}{2} \cdot \frac{\mathrm{d}^2}{\mathrm{dx}^2} \square$	Potential energy operator: $\mathrm{PE} = \frac{-1}{\mathrm{x}} \square$

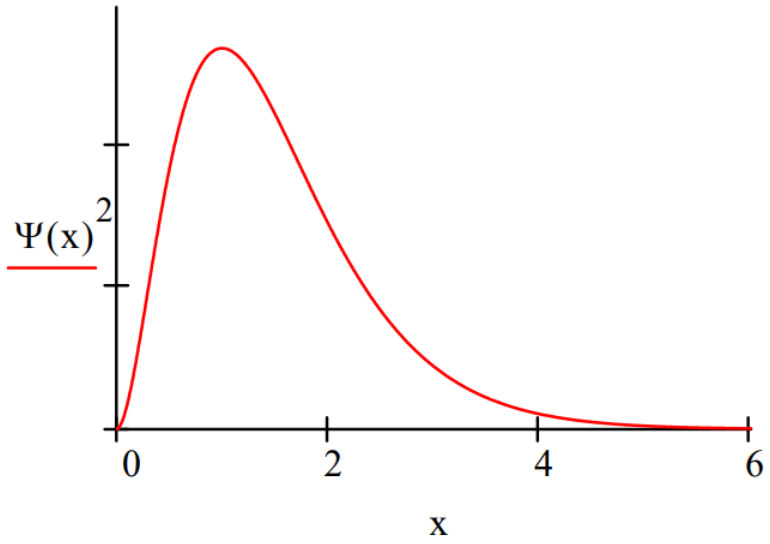
The energy operator for the one-dimensional hydrogen atom in atomic units is:

$$\frac{-1}{2} \cdot \frac{\mathrm{d}^2}{\mathrm{dx}^2} \square - \frac{1}{\mathrm{x}} \cdot \square$$

The ground state wave function in coordinate space is:

$$\Psi(x) := 2 \cdot x \cdot \exp(-x)$$

Display the coordinate-space distribution function:



The ground state energy is -0.5 E_h.

$$\frac{-1}{2} \cdot \frac{\mathrm{d}^2}{\mathrm{dx}^2} \Psi(\mathrm{x}) - \frac{1}{\mathrm{x}} \cdot \Psi(\mathrm{x}) = \mathrm{E} \cdot \Psi(\mathrm{x}) \text{ solve, } \mathrm{E} \rightarrow \frac{-1}{2}$$

The coordinate wave function is normalized:

$$\int_0^\infty \Psi(x)^2 dx = 1$$

The expectation value for position:

$$\int_0^\infty x \cdot \Psi(x)^2 dx = 1.5$$

The expectation value for momentum:

$$\int_0^\infty \Psi(x) \cdot \frac{1}{i} \cdot \frac{d}{dx} \Psi(x) dx = 0$$

The expectation value for kinetic energy:

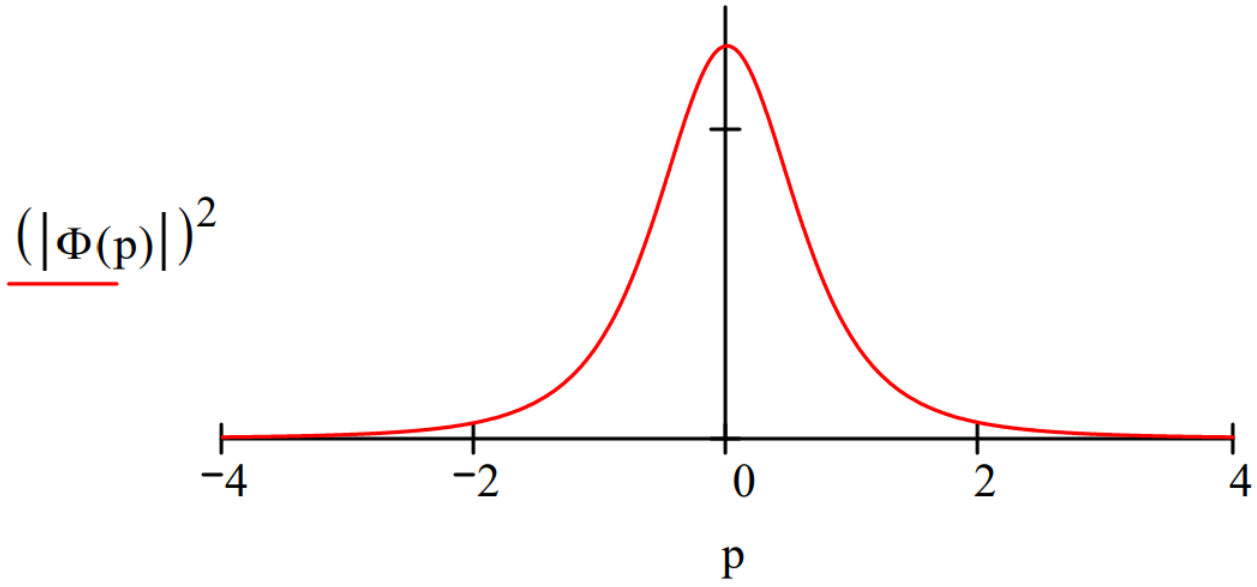
$$\int_0^\infty \Psi(x) \cdot \frac{-1}{2} \cdot \frac{d^2}{dx^2}\Psi(x)dx = 0.5$$

The expectation value for potential energy:

$$\int_0^\infty \frac{-1}{x} \cdot \Psi(x)^2 dx = -1$$

The momentum wave function is generated by the following Fourier transform of the coordinate space wave function.

$$\Phi(p) := \frac{1}{\sqrt{2 \cdot \pi}} \int_0^\infty \exp(-i \cdot p \cdot x) \cdot \Psi(x)dx \rightarrow \frac{2^{\frac{1}{2}}}{\pi^{\frac{1}{2}} \cdot (i \cdot p + 1)^2}$$



Momentum Space Operators

Momentum space integral: $\int_{-\infty}^{\infty} \square \mathrm{dp}$	Momentum operator: $p \cdot \square$
Kinetic energy operator: $\frac{\mathrm{p}^2}{2}$	Position operator: $i \cdot \frac{\mathrm{d}}{\mathrm{dp}} \square$

The same calculations made with the momentum space wave function:

The momentum wave function is normalized:

$$\int_{-\infty}^{\infty} (|\Phi(p)|)^2 dp = 1$$

The expectation value for position:

$$\int_{-\infty}^{\infty} \overline{\Phi(p)} \cdot i \cdot \frac{d}{dp}\Phi(p)dp = 1.5$$

The expectation value for momentum:

$$\int_{-\infty}^{\infty} p \cdot (|\Phi(p)|)^2 dp = 0$$

The expectation value for kinetic energy:

$$\int_{-\infty}^{\infty} \frac{\mathrm{p}^2}{2} \cdot (|\Phi(\mathrm{p})|)^2 \mathrm{dp} = 0.5$$

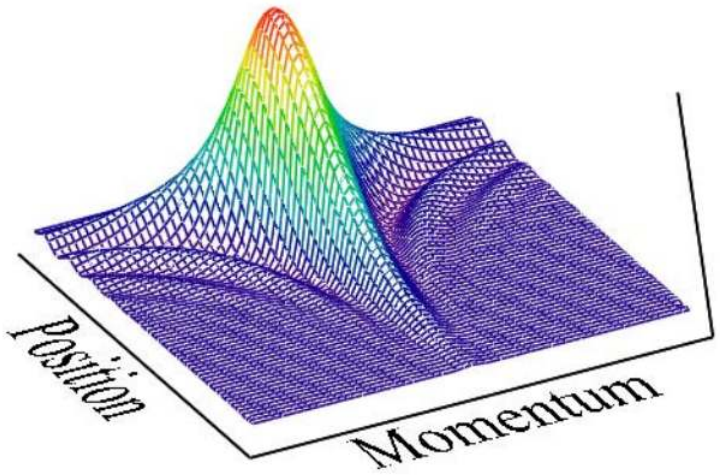
The Wigner function for the hydrogen atom ground state is generated using the momentum wave function.

$$W(x,p) := \frac{1}{2\cdot\pi}\cdot\int_{-\infty}^{\infty}\overline{\Phi\left(p+\frac{s}{2}\right)}\cdot\exp(-i\cdot s\cdot x)\cdot\Phi\left(p-\frac{s}{2}\right)ds$$

The Wigner distribution is displayed graphically.

$$N := 60 \qquad i := 0..N \qquad x_i := \frac{6\cdot i}{N}$$

$$j := 0..N \qquad p_j := -5+\frac{10\cdot j}{N} \qquad Wigner_{i,j} := W(x_i, p_j)$$



Wigner

One of the interesting features of doing quantum mechanics with the Wigner distribution is that the position and momentum operators retain their classical forms; they are both multiplicative operators. By comparison in the coordinate representation position is multiplicative and momentum is differential. In the momentum representation it's the reverse. This is illustrated below with the following calculations.

Phase space integral: $\int_{-\infty}^{\infty}\int_{0}^{\infty}\square dxdp$	Position operator: $x\cdot\square$	Momentum operator: $p\cdot\square$

Kinetic energy operator: $\mathrm{KE}=\frac{p^2}{2}\cdot\square$	Potential energy operator: $\mathrm{PE}=\frac{-1}{x}\cdot\square$

Phase space calculations using the Wigner distribution:

The Wigner distribution is normalized:

$$\int_{-\infty}^{\infty}\int_{0}^{\infty}W(x,p)dxdp=1$$

The expectation value for position:

$$\int_{-\infty}^{\infty}\int_{0}^{\infty}x\cdot W(x,p)dxdp=1.5$$

The expectation value for momentum:

$$\int_{-\infty}^{\infty}\int_{0}^{\infty}p\cdot W(x,p)dxdp=0$$

The expectation value for kinetic energy:

$$\int_{-\infty}^{\infty}\int_{0}^{\infty}\frac{p^2}{2}\cdot W(x,p)dxdp=0.5$$

The expectation value for potential energy:

$$\int_{-\infty}^{\infty}\int_{0}^{\infty}\frac{-1}{x}\cdot W(x,p)dxdp=-1$$

This page titled 2.54: Quantum Calculations on the Hydrogen Atom in Coordinate, Momentum and Phase Space is shared under a CC BY 4.0 license and was authored, remixed, and/or curated by Frank Rioux via source content that was edited to the style and standards of the LibreTexts platform.

2.55: The Wigner Distribution for the 1s State of the 1D Hydrogen Atom

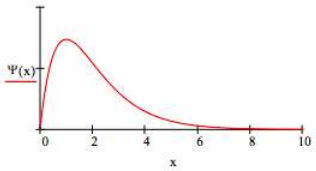
This tutorial presents three pictures of the 1s state of the one-dimensional hydrogen atom using its position, momentum and phase-space representations.

The energy operator for the one-dimensional hydrogen atom in atomic units is:

$$\frac{-1}{2}\frac{d^2}{dx^2}\blacksquare - \frac{1}{x}\blacksquare$$

The ground state eigenstate is:

$$\Psi(x) = 2x\exp(-x) \quad \int_0^\infty \Psi(x)^2 dx = 1$$

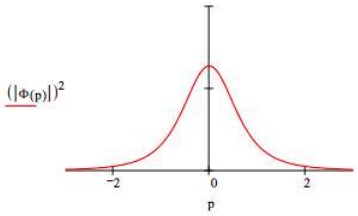


The ground state energy is -0.5 E_h.

$$\frac{-1}{2}\frac{d^2}{x^2}\Psi(x) - \frac{1}{x}\Psi(x) = E\Psi(x) \text{ solve, E} \rightarrow \frac{-1}{2}$$

The momentum wave function is generated by the following Fourier transform of the coordinate space wave function.

$$\Phi(p) = \frac{1}{\sqrt{2\pi}}\int_0^\infty \exp(\text{-i p x})\Psi(x)dx \rightarrow \frac{2^{\frac{1}{2}}}{(\text{i p} + 1)\pi^{\frac{1}{2}}}$$

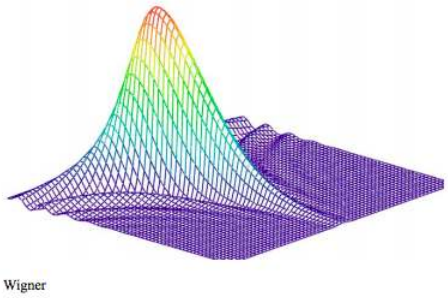


The Wigner function for the hydrogen atom ground state is generated using the momentum wave function.

$$\text{W(x, p)} = \frac{1}{2\pi}\int_{-\infty}^{\infty} \overline{\Phi\left(\text{p} + \frac{\text{s}}{2}\right)}\exp(\text{-i s x})\Phi\left(\text{p} - \frac{\text{s}}{2}\right)\text{ds}$$

The Wigner distribution is displayed graphically.

$$N = 60 \quad i = 0..N \quad x_i = \frac{6i}{N} \quad j = 0..N \quad p_j = -5 + \frac{10j}{N} \quad \text{Wigner}_{i,\,j} = \text{W}\left(x_i,\ p_j\right)$$



This page titled 2.55: The Wigner Distribution for the 1s State of the 1D Hydrogen Atom is shared under a CC BY 4.0 license and was authored, remixed, and/or curated by Frank Rioux via source content that was edited to the style and standards of the LibreTexts platform.

2.56: The Wigner Distribution for the 2s State of the 1D Hydrogen Atom

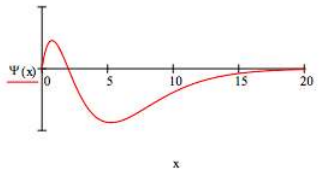
This tutorial presents three pictures of the 2s state of the one-dimensional hydrogen atom using its position, momentum and phase-space representations.

The energy operator for the one-dimensional hydrogen atom in atomic units is:

$$\frac{-1}{2}\frac{d^2}{dx^2}\blacksquare - \frac{1}{x}\blacksquare$$

The 2s wave function is:

$$\Psi(x) = \frac{1}{\sqrt{8}}\mathrm{x}(2-\mathrm{x})\exp\left(-\frac{x}{2}\right) \quad \int_0^\infty \Psi(x)^2 dx = 1$$

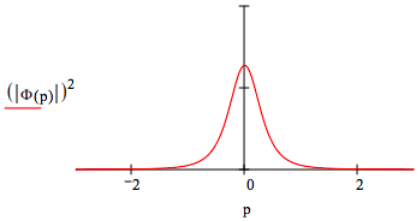


The 2s state energy is -0.125 E_h.

$$\frac{\frac{-1}{2}\frac{d^2}{dx^2}\Psi(x) - \frac{1}{x}\Psi(x)}{\Psi(x)}\text{simplify} \rightarrow \frac{-1}{8}$$

The momentum wave function is generated by the following Fourier transform of the coordinate space wave function.

'^' allowed only in math mode

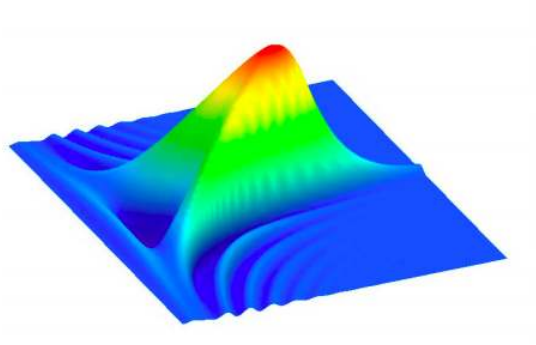


The Wigner function (phase-space representation) for the 2s state is generated using the momentum wave function.

$$\mathrm{W(x,\ p)} = \frac{1}{2\pi}\int_{-\infty}^{\infty} \overline{\Phi\left(\mathrm{p}+\frac{\mathrm{s}}{2}\right)}\exp(\text{-i s x})\Phi\left(\mathrm{p}-\frac{\mathrm{s}}{2}\right)\mathrm{ds}$$

The Wigner distribution is displayed graphically.

$$N = 100 \quad i = i..N \quad x_i = \frac{15i}{N} \quad j = 0..N \quad p_j = -3\frac{6j}{N} \quad \mathrm{Wigner}_{i,\,j} = \mathrm{W}\left(x_i,\ p_j\right)$$



Wigner

If we rotate this figure to look below the plane, we see that for the 2s state of the 1D hydrogen atom the Wigner distribution takes on negative values.

This page titled 2.56: The Wigner Distribution for the 2s State of the 1D Hydrogen Atom is shared under a CC BY 4.0 license and was authored, remixed, and/or curated by Frank Rioux via source content that was edited to the style and standards of the LibreTexts platform.

2.57: The Wigner Distribution for the 2p State of the 1D Hydrogen Atom

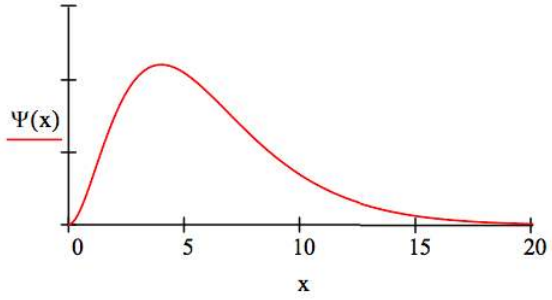
This tutorial presents three pictures of the 2p state of the one-dimensional hydrogen atom using its position, momentum and phase-space representations.

The energy operator for the one-dimensional hydrogen atom in atomic units is:

$$\frac{-1}{2}\frac{d^2}{dx^2}\blacksquare + \frac{\mathrm{L(L+1)}}{2x^2}\blacksquare - \frac{1}{x}\blacksquare$$

The 2p wave function is:

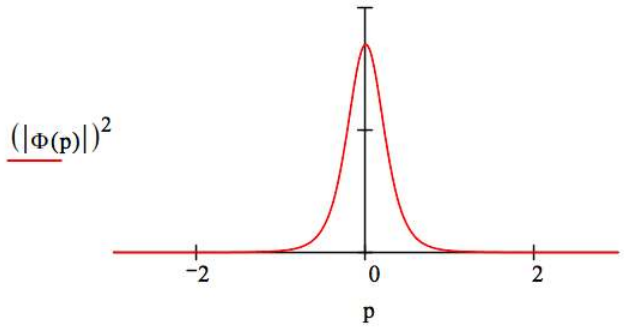
$$\Psi(x) = \frac{1}{\sqrt{24}}x^2\exp\left(-\frac{x}{2}\right) \quad \int_0^\infty \Psi(x)^2 dx = 1$$



The 2p state energy is -0.125 E_h.

$$\frac{-1}{2}\frac{d^2}{dx^2}\Psi(x) + \frac{1}{x^2}\Psi(x) - \frac{1}{x}\Psi(x) = \mathrm{E}\Psi(x)\text{solve, E} \rightarrow \frac{-1}{8} = -0.125$$

The momentum wave function is generated by the following Fourier transform of the coordinate space wave function.

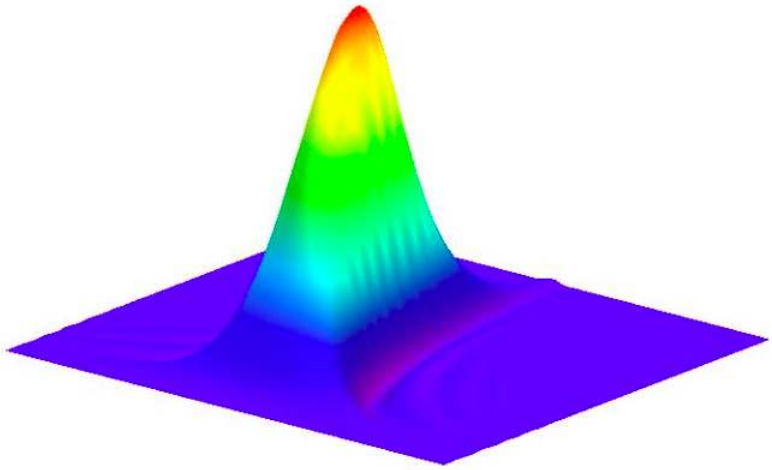


The Wigner function (phase-space representation) for the 2p state is generated using the momentum wave function.

$$\mathrm{W(x,\ p)} = \frac{1}{2\pi}\int_{-\infty}^{\infty}\overline{\left(\mathrm{p}+\frac{\mathrm{s}}{2}\right)}\exp(\text{-i s x})\Phi\left(\mathrm{p}-\frac{\mathrm{s}}{2}\right)\mathrm{ds}$$

The Wigner distribution is displayed graphically.

$$N = 100 \quad i = 0..N \quad x_i = \frac{15i}{N} \quad j = 0..N \quad p_j = -3 + \frac{6j}{N} \quad \mathrm{Wigner}_{i,\,j} = \mathrm{W}\left(x_i,\ p_j\right)$$



Wigner

This page titled 2.57: The Wigner Distribution for the 2p State of the 1D Hydrogen Atom is shared under a CC BY 4.0 license and was authored, remixed, and/or curated by Frank Rioux via source content that was edited to the style and standards of the LibreTexts platform.

2.58: The Wigner Distribution for the 3s State of the 1D Hydrogen Atom

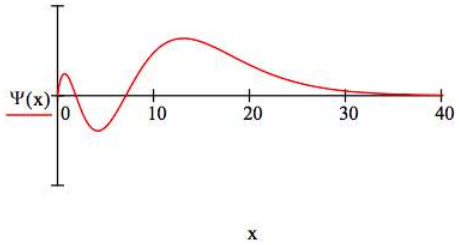
This tutorial presents three pictures of the 3s state of the one-dimensional hydrogen atom using its position, momentum and phase-space representations.

The energy operator for the one-dimensional hydrogen atom in atomic units is:

$$\frac{-1}{2}\frac{d^2}{dx^2}\blacksquare - \frac{1}{x}\blacksquare$$

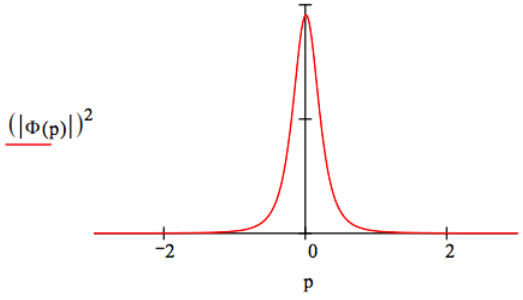
The position 3s wave function is:

$$\Psi(x) = \tfrac{2}{243}\sqrt{3}\mathrm{x}\left(27 - 18x + 2x^2\right)\exp\left(-\tfrac{x}{3}\right) \quad \int_0^\infty \Psi(x)^2 dx = 1$$



The 3s energy is -0.065 E_h.

$$\Phi(p) = \frac{1}{\sqrt{2\pi}}\int_0^\infty \exp(\text{-i p x})\Psi(x)\mathrm{dx} \rightarrow \left(-2^{\frac{1}{2}}\right)3^{\frac{1}{2}}\frac{9p^2 + 6ip - 1}{(3ip+1)^4\pi^{\frac{1}{2}}}$$

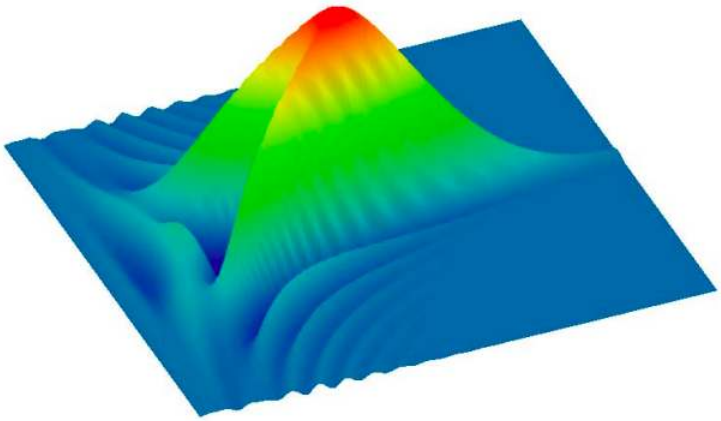


The Wigner function (phase-space representation) for the hydrogen atom 3s state is generated using the momentum wave function.

$$\mathrm{W(x,\ p)} = \frac{1}{2\pi}\int_{-\infty}^{\infty}\overline{\Phi\left(\mathrm{p} + \frac{\mathrm{s}}{2}\right)}\exp(\text{-i s x})\Phi\left(\mathrm{p} - \frac{\mathrm{s}}{2}\right)\mathrm{ds}$$

The Wigner distribution is displayed graphically.

$$N = 100 \quad i = 0..N \quad x_i = \tfrac{30i}{N} \quad j = 0..N \quad p_j = -2 + \tfrac{4j}{N} \quad \mathrm{Wigner}_{i,\,j} = \mathrm{W}\left(x_i,\ p_j\right)$$



Wigner

Just as for the 2s state, the Wigner distribution for the 3s state takes on negative values.

This page titled 2.58: The Wigner Distribution for the 3s State of the 1D Hydrogen Atom is shared under a CC BY 4.0 license and was authored, remixed, and/or curated by Frank Rioux via source content that was edited to the style and standards of the LibreTexts platform.

2.59: The Wigner Distribution for the 3p State of the 1D Hydrogen Atom

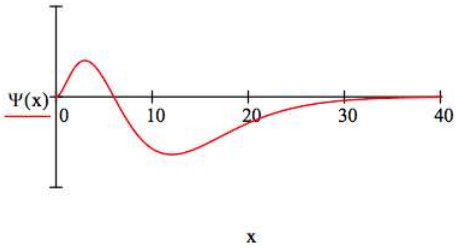
This tutorial presents three pictures of the 3p state of the one-dimensional hydrogen atom using its position, momentum and phase-space representations.

The energy operator for the one-dimensional hydrogen atom in atomic units is:

$$\frac{-1}{2}\frac{d^2}{dx^2}\blacksquare + \frac{\mathrm{L(L+1)}}{2x^2}\blacksquare - \frac{1}{x}\blacksquare$$

The 3p wave function is:

$$\Psi(x) = \frac{8}{27\sqrt{6}}\left(1-\frac{x}{6}\right)x^2\exp\left(\frac{-x}{2}\right) \quad \int_0^\infty \Psi(x)^2 dx = 1$$

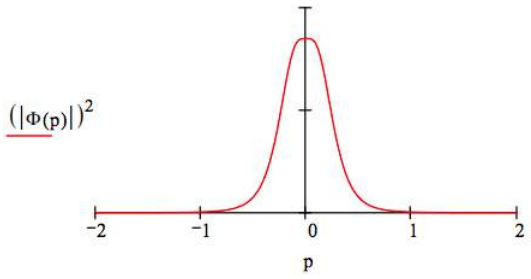


The 3p state energy is -0.0556 E_h.

$$\frac{-1}{2}\frac{d^2}{dx^2}\Psi(x) + \frac{1}{x^2}\Psi(x) - \frac{1}{x}\Psi(x) = \mathrm{E}\Psi(x) \text{ solve, } \mathrm{E} \to \frac{-1}{18} = -0.0556$$

The momentum wave function is generated by the following Fourier transform of the coordinate space wave function.

$$\Phi(p) = \frac{1}{\sqrt{2\pi}}\int_0^\infty \exp(\text{-i p x})\Psi(x)dx \to \frac{2}{3}2^{\frac{1}{2}}6^{\frac{1}{2}}\frac{(-1)+6\text{i p}}{(3\text{i p}+1)^4\pi^{\frac{1}{2}}}$$

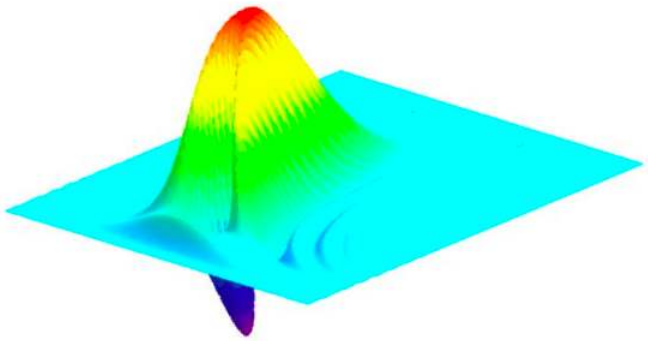


The Wigner function (phase-space representation) for the 3p state is generated using the momentum wave function.

$$\mathrm{W(x,\ p)} = \frac{1}{2\pi}\int_{-\infty}^{\infty}\overline{\Phi\left(\mathrm{p}+\frac{\mathrm{s}}{2}\right)}\exp(\text{-i s x})\Phi\left(\mathrm{p}-\frac{\mathrm{s}}{2}\right)\mathrm{ds}$$

The Wigner distribution is displayed graphically.

$$N = 150 \quad i = 0..N \quad x_i = \frac{35i}{N} \quad j = 0..N \quad p_j = -2 + \frac{4j}{N} \quad \mathrm{Wigner}_{i,\,j} = \mathrm{W}\left(x_i,\ p_j\right)$$



Wigner

This page titled 2.59: The Wigner Distribution for the 3p State of the 1D Hydrogen Atom is shared under a CC BY 4.0 license and was authored, remixed, and/or curated by Frank Rioux via source content that was edited to the style and standards of the LibreTexts platform.

2.60: The Wigner Distribution for the 4s State of the 1D Hydrogen Atom

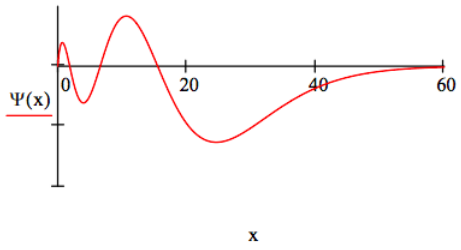
This tutorial presents three pictures of the 4s state of the one-dimensional hydrogen atom using its position, momentum and phase-space representations.

The energy operator for the one-dimensional hydrogen atom in atomic units is:

$$\frac{-1}{2}\frac{d^2}{dx^2}\blacksquare - \frac{1}{x}\blacksquare$$

The position 4s wave function is:

$$\Psi(x) = \tfrac{x}{4}\left(1 - \tfrac{3}{4}x + \tfrac{1}{8}x^2 - \tfrac{1}{192}x^3\right)\exp\left(\tfrac{-x}{4}\right) \quad \int_0^\infty \Psi(x)^2 \mathrm{dx} = 1$$

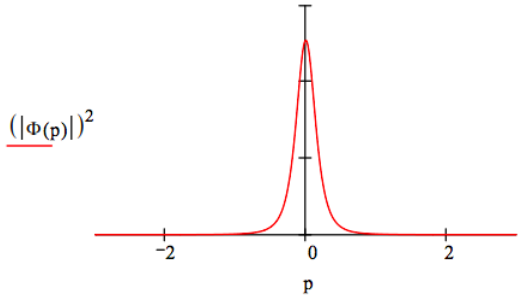


The 4s energy is -0.03125 E_h.

$$\frac{-1}{2}\frac{d^2}{dx^2}\Psi(x) - \frac{1}{x}\Psi(x) = \mathrm{E}\Psi(x)\text{solve, E} \rightarrow \frac{-1}{32} = -0.03125$$

The momentum wave function is generated by the following Fourier transform of the coordinate wave function.

$$\Phi(p) = \frac{1}{\sqrt{2\pi}}\int_0^\infty \exp(\text{-i p x})\Psi(x)dx \rightarrow (-2)2^{\frac{1}{2}}\frac{64\text{i p}^3 - 48\text{p}^2 - 12\text{i p} + 1}{(4\text{i p} + 1)^5\pi^{\frac{1}{2}}}$$

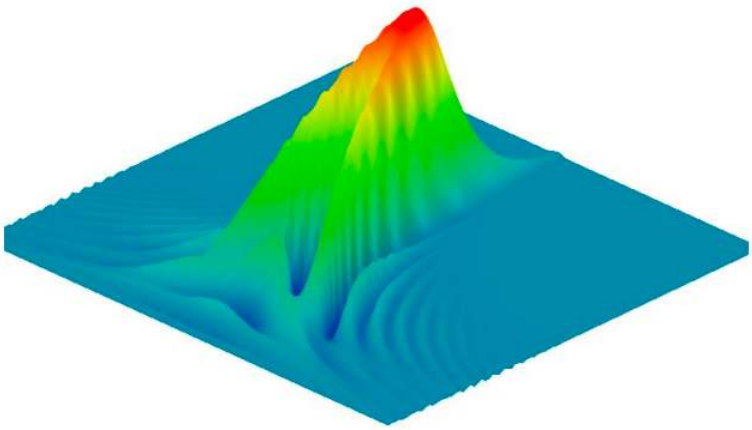


The Wigner function (phase-space representation) for the hydrogen atom 4s state is generated using the momentum wave function.

$$\mathrm{W(x,\ p)} = \frac{1}{2\pi}\int_{-\infty}^{\infty}\overline{\Phi - \left(\mathrm{p} + \frac{\mathrm{s}}{2}\right)}\exp(\text{-i s x})\Phi\left(\mathrm{p} - \frac{\mathrm{s}}{2}\right)\mathrm{ds}$$

The Wigner distribution is displayed graphically.

$$N = 100 \quad i = 0..N \quad x_i = \tfrac{50i}{N} \quad j = 0..N \quad p_j = -2 + \tfrac{4j}{N} \quad \mathrm{Wigner}_{i,\,j} = \mathrm{W}\left(x_i,\ p_j\right)$$



Wigner

Just as for the 2s and 3s states, the Wigner distribution for the 4s state takes on negative values.

This page titled 2.60: The Wigner Distribution for the 4s State of the 1D Hydrogen Atom is shared under a CC BY 4.0 license and was authored, remixed, and/or curated by Frank Rioux via source content that was edited to the style and standards of the LibreTexts platform.

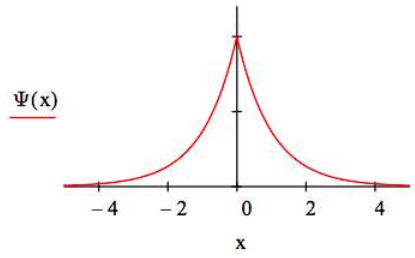
2.61: One-dimensional H-atom with Delta Function Potential

The One-dimensional Hydrogen Atom with a Delta Function Potential Energy Interaction Between the Proton and Electron

The energy Hamiltonian and a normalized wave function for the hydrogen atom with delta function interaction between the electron and proton is given below.

$$\mathrm{H} = -\frac{1}{2}\frac{d^2}{dx^2}\blacksquare - \Delta(x)\blacksquare \quad \Psi(x) = \exp(-|x|) \quad \int_{-\infty}^{\infty} \Psi(x)^2 dx \to 1$$

The wave function is not well-behaved in coordinate space making the evaluation of kinetic energy tricky. However, the evaluation of potential energy is straight forward. So the strategy is to evaluate potential energy in coordinate space and kinetic energy in momentum space. The latter requires a Fourier transform of the coordinate space wave function.



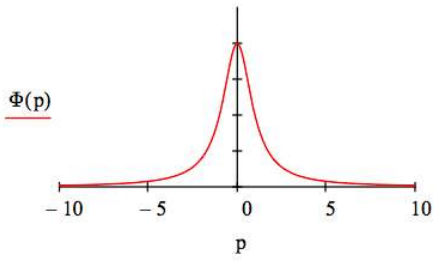
Calculation of Potential Energy in Coordinate Space

$$V = \int_{-\infty}^{\infty} \Psi(x) - \Delta(x)\Psi(x)\mathrm{dx} \to -1$$

Fourier Transform of the Coordinate Wave Function into Momentum Space

$$\Psi(p) = \int_{-\infty}^{\infty} \frac{\exp(\text{-i p x})}{\sqrt{2\pi}}\Psi(x)\mathrm{dx} \text{ simplify} \to \frac{\sqrt{2}}{\sqrt{\pi}\,(p^2+1)}$$

Display the Momentum Wave Function to Show it is Well-behaved



Calculation of Kinetic Energy in Momentum Space

$$\mathrm{T} = \int_{-\infty}^{\infty} \Phi(p)\frac{p^2}{2}\Phi(p)\mathrm{dp} \text{ simplify} \to \frac{1}{2}$$

Calculation of Total Energy

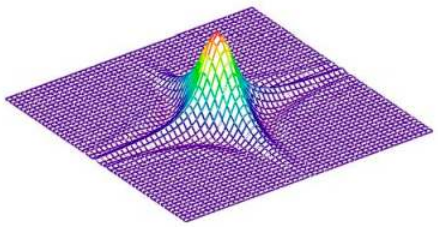
$$\mathrm{E} = \mathrm{T} + \mathrm{V} \to \mathrm{E} = -\frac{1}{2}$$

The Wigner Function

The Wigner phase-space distribution function is calculated using the momentum wave function.

$$\mathrm{W(x,\ p)} = \frac{1}{2\pi}\int_{-\infty}^{\infty} \overline{\Phi\left(\mathrm{p}+\frac{\mathrm{s}}{2}\right)}\exp(\text{-i s x})\Phi\left(\mathrm{p}-\frac{\mathrm{s}}{2}\right)\mathrm{ds}$$

$$N = 50 \quad i = 0..N \quad x_i = -4 + \frac{8i}{N} \quad j = 0..N \quad p_j = -7 + \frac{14j}{N} \quad \mathrm{Wigner}_{i,\,j} = \mathrm{W}\left(x_i,\ p_j\right)$$



Wigner

Next we look at two variational calculations on the same system. The first involves a gaussian trial wave function, and the second a trigonmetric trial wave function.

Gaussian Trial Wave Function

$$\Psi_1(x,\ \beta) = \left(\frac{2\beta}{\pi}\right)^{\frac{1}{4}}\exp\left(-\beta x^2\right) \quad \int_{-\infty}^{\infty}\Psi_1(x,\ \beta)^2\mathrm{dx}\ \text{assume, } \beta > 0 \rightarrow 1$$

Evaluation of Variational Energy Integral

$$\mathrm{E}(\beta) = \int_{-\infty}^{\infty}\Psi_1(x,\ \beta) - \frac{1}{2}\frac{d^2}{dx^2}\Psi(x,\ \beta)\mathrm{dx}...$$
$$\text{assume, } \beta > 0 \rightarrow \frac{\beta}{2} - \frac{\sqrt{2}\sqrt{3}}{\sqrt{\pi}} + \int_{-\infty}^{\infty} -\Delta(x)\Psi_1(x,\ \beta)^2 dx$$

Energy Minimization With Respect to Variational Parameter

$$\frac{d}{d\beta}\mathrm{E}(\beta = 0 \text{ solve, } \beta \rightarrow \tfrac{2}{\pi} \quad \mathrm{E}(\beta)\ \Big|\ \substack{\text{substitute, } \beta=\frac{2}{\pi} \\ \text{simplify}} \rightarrow -\tfrac{1}{\pi} = -0.318$$

Error

$$\left|\frac{-.318 + .5}{-.5}\right| = 36.4\%$$

Trigonometric Trial Wave Function

$$\Psi_2(\mathrm{x},\ \beta) = \sqrt{\tfrac{\beta}{2}}\mathrm{sech}(\beta\mathrm{x})$$

Evaluation of Variational Energy Integral

$$\mathrm{E}(\beta) = \begin{array}{c}\int_{-\infty}^{\infty}\Psi_2(\mathrm{x},\ \beta) - \frac{1}{2}\frac{d^2}{dx^2}\Psi_2(\mathrm{x},\ \beta)dx... \\ +\int_{-\infty}^{\infty} -\Delta(\mathrm{x})\Psi_2(\mathrm{x},\ \beta)^2 dx\end{array}\ \Big|\ \substack{\text{assume, } \beta>0 \\ \text{simplify}} \rightarrow \frac{\beta(\beta-3}{6}$$

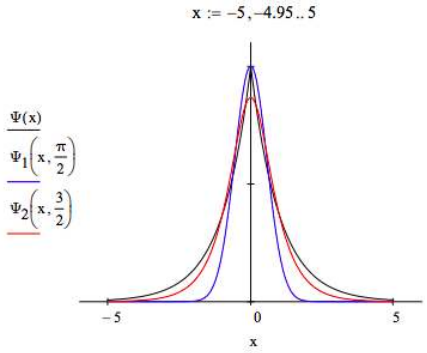
Energy Minimization With Respect to Variational Parameter

$$\frac{d}{d\beta}\mathrm{E}(\beta) = 0 \text{ solve, } \beta \rightarrow \tfrac{3}{2} \quad \mathrm{E}(\beta)\ \Big|\ \substack{\text{substitute, } \beta=\frac{3}{2} \\ \text{simplify}} \rightarrow -\tfrac{3}{8} = -0.375$$

Error

$$\left|\frac{-.375+.5}{-.5}\right| = 25\%$$

Graphical Comparison of Exact Wave Function with Trial Wave Function



This graphical comparison is consistent with the variational results presented above. The trigonometric trial function more closely resembles the exact wave function.

This page titled 2.61: One-dimensional H-atom with Delta Function Potential is shared under a CC BY 4.0 license and was authored, remixed, and/or curated by Frank Rioux via source content that was edited to the style and standards of the LibreTexts platform.

2.62: The Atomic Structure Factor in Coordinate and Momentum Space

The following expression for the atomic structure factor in the coordinate and momentum representations can be found in a paper by Fearnside and Matthew [AJP 65(8), 795-796 (1997)].

$$f(\mu) = \int \exp(i\mu\ r)|\Psi(r)|^2 dr = \int \Psi(p)\Psi^*(P+\mu)dp$$

The purpose of this tutorial is to establish the validity of this equation using Dirac notation and actual calculations using the hydrogen atom ground state eigenfunction in the position and momentum representations. See the Appendix for a graphical representation of what follows.

$$\begin{gathered}\int \exp(i\mu\ r)|\Psi(r)|^2 dr = \int \langle\Psi|r\rangle\langle r|\mu\rangle\langle r|\Psi\rangle dr \\ = \int\int \langle\Psi|r\rangle\langle r|\mu\rangle\langle r|p\rangle\langle p|\Psi\rangle dr dp \int\int \langle\Psi|r\rangle\langle r|\mu\rangle\langle r|p\rangle\langle p|\Psi\rangle dr dp \\ = \int\int \langle p|\Psi\rangle\langle\Psi|r\rangle\langle r|p+\mu\rangle dr dp = \int\int \langle p|\Psi\rangle\langle\Psi|p+\mu\rangle dp\end{gathered}$$

The following expressions have been used in mathematical manipulations alone.

$$\int |p\rangle\langle p| dp = 1 \quad \int |r\rangle\langle r| dr = 1 \quad \langle r|\mu\rangle\langle r|p\rangle = \langle r|p+\mu\rangle$$

Detail on the latter relationship is as follows.

$$\langle r|mu\rangle\langle r|p\rangle = \exp(i\mu\ r)\exp(ip\ r) = \exp(i(p+\mu)r) = \langle r|p+\mu\rangle$$

Now for the actual calculations (in atomic units) using the hydrogen atom ground state.

Ground state in the coordinate representation:

$$\Psi(r) = \frac{1}{\sqrt{\pi}}\exp(-r)$$

$$f(\mu) = \int_0^\infty \int_0^\pi \int_0^{2\pi} \Psi(r)^2 \exp(i\cos r\cos(\theta)) r^2 \sin(\theta) d\phi d\theta dr \ \Big|\ \begin{smallmatrix}\text{complex}\\ \text{simplify}\end{smallmatrix} \rightarrow \frac{16}{16+8\mu^2+\mu^4}$$

Ground state in the momentum representation:

$$\Psi(p) = \frac{2\sqrt{2}}{\pi}\frac{1}{(1+p^2)^2}$$

Illegal pream-token (f)

where

$$\Psi(p+\mu) = \frac{2\sqrt{2}}{\pi}\frac{1}{[1+(p^2+\mu^2+2p\mu\cos(\theta))]^2}$$

Appendix

$$\begin{array}{ccc} \int \Psi(p)\Psi^*(p+\mu)dp & = & \int \Psi^*(r)\exp(i\mu r)\Psi(r)dr \\ \updownarrow (Dirac) & & \updownarrow (Dirac) \\ \int \langle p|\Psi\rangle\langle\Psi|p+\mu\rangle dp & & \int \langle\Psi|r\rangle\langle r|\mu\rangle\langle r|\Psi\rangle dr \\ \updownarrow \left(\int |r\rangle\langle r| dr = 1\right) & & \updownarrow \left(\int |p\rangle\langle p| dp = 1\right) \\ \int\int \langle\Psi|r\rangle\langle r|p+\mu\rangle\langle p|\Psi\rangle dp dr & \overset{\langle r|p+\mu\rangle = \langle r|\mu\rangle\langle r|p\rangle}{\longleftrightarrow} & \int\int \langle\Psi|r\rangle\langle r|\mu\rangle\langle r|p\rangle\langle p|\Psi\rangle dp dr \end{array}$$

This page titled 2.62: The Atomic Structure Factor in Coordinate and Momentum Space is shared under a CC BY 4.0 license and was authored, remixed, and/or curated by Frank Rioux via source content that was edited to the style and standards of the LibreTexts platform.

CHAPTER OVERVIEW

3: Chemical Bonding

3.1: The Covalent Bond and Quantum Mechanics
3.2: The Covalent Bond in the Hydrogen Molecule
3.3: The Covalent Bond Clarified Through the Use of the Virial Theorem
3.4: Brief Version of the Covalent Bond Clarified Through the Use of the Virial Theorem
3.5: The H2 Covalent Bond and the Virial Theorem
3.6: The Covalent Bond According to Slater and Ruedenberg
3.7: Slater's Analysis of the Covalent Bond using the Virial Theorem
3.8: Two Analyses of the Covalent Bond using the Virial Theorem
3.9: A Simple Charge Cloud Model for Molecular Hydrogen- Or, Is It a DFT Model?
3.10: Three Mechanisms for Bond Formation in the Hydrogen Molecule Ion
3.11: A Mechanistic Approach to Bond Formation in the Hydrogen Molecule Ion
3.12: A Lite Version of Ruedenberg's Analysis of the Covalent Bond in the Hydrogen Molecule Ion
3.13: Molecular Orbital Analysis for the Hydrogen Molecule Ion Bond
3.14: A One-dimensional Model for the Covalent Bond in the Hydrogen Molecule Ion
3.15: Localized and Delocalized Molecular Orbitals
3.16: Two Perspectives on the Bonding in Water
3.17: Covalent Bonding in Ammonia from Several Perspectives
3.18: A Molecular Orbital Approach to Bonding in Methane
3.19: A Simple Calculation of the Lattice Energy of LiH
3.20: An Even Simpler LiH Lattice Energy Calculation
3.21: Charge Cloud Models for Some Simple Atomic, Molecular and Solid Systems
3.22: A Critique of the Valence Shell Electron Pair Repulsion Model
3.23: A Simple Electrostatic Critique of VSEPR
3.24: Another Critique of VSEPR
3.25: Why Nonbonding Electrons Occupy the Equatorial Position in Trigonal Bipyramidal Geometry
3.26: A Modified Tangent Spheres Model Analysis of Trigonal Bipyramidal Geometry
3.27: A Symbolic Huckel MO Calculation Using Mathcad
3.28: A Numeric Huckel MO Calculation Using Mathcad
3.29: A Numerical Huckel MO Calculation on C60
3.30: Chemical Bonding and Electronic Structure of Buckminsterfullerene
3.31: Quantum Mechanics, Group Theory and C60
3.32: A Numerical Huckel Calculation on Anthracene and Phenanthrene
3.33: A Numerical Huckel Calculation on C10H8 Isomers
3.34: Semi-empirical Molecular Orbital Calculation on HF
3.35: Semi-empirical Molecular Orbital Calculation on XeF2
3.36: Posch-Teller Potential Model for Metals

This page titled 3: Chemical Bonding is shared under a CC BY 4.0 license and was authored, remixed, and/or curated by Frank Rioux via source content that was edited to the style and standards of the LibreTexts platform.

3.1: The Covalent Bond and Quantum Mechanics

The behavior of electrons in molecules and atoms is described by quantum mechanics; classical (Newtonian) mechanics cannot be used because the de Broglie wavelengths (λ=h/mv) of the electrons are comparable with molecular (and atomic) dimensions.

The relevant quantum-mechanical ideas are as follows:

- Electrons are characterized by their entire distributions (called wave functions or orbitals) rather than by instantaneous positions and velocities: an electron may be considered always to be (with appropriate probability) at all points of its distribution (which does not vary with time).
- The kinetic energy of an electron decreases as the volume occupied by the bulk of its distribution increases, so delocalization lowers its kinetic energy.

$$KE = \frac{p^2}{2m} = \frac{h^2}{2m\lambda^2} \approx \frac{A}{D^2} \approx \frac{A}{V^{\frac{2}{3}}}$$

- The potential energy of interaction between an electron and other charges is as calculated by classical physics, using the appropriate distribution (wave function) for the electron: an electron distribution is therefore attracted by nuclei and its potential energy decreases as the average electron-nuclear distance decreases.

$$PE \approx -\frac{B}{D} \approx -\frac{B}{V^{\frac{2}{3}}}$$

- A minimum-energy electron distribution represents the best compromise between concentration near the nuclei (to reduce potential energy) and delocalization (to reduce kinetic energy).

$$E \approx KE + PE \approx \frac{A}{V^{\frac{2}{3}}} - \frac{B}{V^{\frac{2}{3}}}$$

A bond will form between two atoms when the electron distribution of the combined atoms (molecular orbital) yields a significantly lower energy than the separate-atom distributions (atomic orbitals). An example is a covalent bond, in which two electrons, one originally on each atom, change their distributions so that each extends over both atoms.

*Taken from "Molecules" in The Encyclopedia of Physics by Frank E. Harris (with some additions and modifications by Frank Rioux)

This page titled 3.1: The Covalent Bond and Quantum Mechanics is shared under a CC BY 4.0 license and was authored, remixed, and/or curated by Frank Rioux via source content that was edited to the style and standards of the LibreTexts platform.

3.2: The Covalent Bond in the Hydrogen Molecule

Introduction

The covalent chemical bond is a difficult concept that is frequently oversimplified as a purely electrostatic phenomenon in textbooks at all levels of the undergraduate chemistry curriculum. Therefore, the purpose of this paper is to provide an elementary quantum-mechanical analysis of the covalent bond appropriate for an undergraduate course in physical or advanced inorganic chemistry. It is important to emphasize that there is no acceptable classical electrostatic explanation for the covalent bond, just as there is no classical explanation for atomic stability or atomic structure. Quantum-mechanical principles are required to understand atomic and molecular stability and structure.

Background

Forty years ago, Ruedenberg and his collaborators undertook a detailed study of the covalent bond in H_2^+ [1-3]. This thorough and incisive theoretical analysis revealed that chemical-bond formation was not simply an electrostatic phenomenon as commonly thought, but that electron kinetic energy also played an essential role. Ruedenberg's contribution to our current understanding of the physical nature of the chemical bond has been discussed in a number of publications in the pedagogical literature in chemistry and physics [4-9]. In addition, there are excellent critiques and summaries elsewhere that are accessible to the interested nonspecialist [10-12]. It should be noted that Slater also recognized the importance of electron kinetic energy in chemical bond formation in a benchmark paper published in the inaugural volume of the *Journal of Chemical Physics* [13]. He returned to the subject subsequently [14], but never pursued it at the depth that Ruedenberg and his colleagues did.

Ruedenberg chose to study H_2^+ because, as the simplest molecule, he could easily extract detailed information about all the contributions to the total energy from its one electron wave function. In the present study the simplest electron-pair bond, H_2, will be examined. The analysis is carried out at a much more elementary level, but the same message emerges-electron kinetic energy plays a crucial role in chemical bond formation. Theoretical analysis shows that H-H bond formation, $2H \rightarrow H_2$, is an exothermic process that obeys the virial theorem: $\Delta E = \Delta V/2 = -\Delta T$ [15]. Noncritical use of the virial theorem, therefore, may lead one to believe that stable bond formation is solely an electrostatic potential-energy effect, and that consideration of kinetic energy is neither relevant nor necessary. However, H-H bond formation can be thought of as a very simple chemical reaction, and we know that it is never justified to assume that the balanced chemical equation is also the mechanism for the reaction. For example, even a simple first-order isomerization reaction ($R \rightarrow P$) requires the formation of an activated form of the reactant ($R \rightarrow R^* \rightarrow P$).

Similarly, to study the covalent bond it is instructive to postulate a "mechanism" for bond formation, a sequence of hypothetical steps that are equivalent to the overall process $2H \rightarrow H_2$. Unlike a traditional chemical mechanism, it cannot be tested empirically and, therefore, its value or validity rests on the clarity and cogency of its basic premises. There are actually several plausible mechanisms, but our attention will be restricted to one that might appear especially cogent to undergraduate audiences. For example, when we describe the bonding in methane to students, we generally invoke a mechanism that uses the concepts of atomic promotion [$2s^2 2p^2 \rightarrow 2s^1 2p^3$], hybridization [$2s^1 2p^3 \rightarrow (sp^3 \text{ hybrids})^4$], and bond formation through the overlap of atomic orbitals. The H2 bond-formation mechanism described in this paper will consist of two steps: atomic promotion and overlap of atomic orbitals ($2H \rightarrow 2H^* \rightarrow H2$). This simple mechanism has previously been used to analyze the bonding in H_2^+ [12]. It should be noted that the individual steps of the mechanism do not satisfy the virial theorem, but, of course, collectively they do. To carry out a quantum-mechanical analysis of bond formation in H_2, it is necessary to decide at what level of theory to work. In this analysis scaled hydrogenic 1s orbitals will be used for the atomic orbitals. At the molecular level, both molecular orbital (MO) and valence bond (VB) wave functions will be considered. Labeling the nuclei a and b, and the electrons 1 and 2, the atomic orbitals are,

$$1s_a = \sqrt{\frac{\alpha^3}{\pi}}\exp(-\alpha r_a) \quad 1s_b = \sqrt{\frac{\alpha^3}{\pi}}\exp(-\alpha r_b)$$

Table 1. Variational Results for the MO and VB Wave Functions

	MO	VB
α	1.197	1.166
T/E_b	1.1282	1.1389
V/E_b	-2.2564	-2.2778
E/E_b	-1.1282	-1.1389
% Error	3.95	3.04
R_e/α_0	1.38	1.41
% Error	1.43	0.71

Table 2. Bond Formation Mechanism Results for the Molecular Orbital Wave Function

	2 H(α=1)		2H*(α=1.197)[a]		H_2(α=1.197)
T/E_h	1.00	0.4328	1.4328	-0.3046	1.1282
V/E_h	-2.00	-0.3940	-2.3940	0.1376	-2.2564
E/E_h	-1.00	0.0388	-0.9612	-0.1670	-1.1282

[a]Eq 4 is used to calculate the entries in this column.

Table 3. Bond Formation Mechanism Results for the Valence Bond Wave Function

	2 H(α=1)		2H*(α=1.166)[a]		H_2(α=1.166)
T/E_h	1.00	0.3596	1.3596	-0.2207	1.1389
V/E_h	-2.00	-0.3320	-2.3320	0.0542	-2.2778
E/E_h	-1.00	0.0276	-0.9724	-0.1665	-1.1389

[a]Eq 4 is used to calculate the entries in this column.

Using this basis set, the MO and VB wave functions are (neglecting spin),

$$\Psi_{MO} = N_{MO}\left[1s_a(1) + 1s_b(1)\right]\left[1s_a(2) + 1s_b(2)\right]$$

$$\Psi_{VB} = N_{VB}\left[1s_a(1)1s_b(2) + 1s_a(2)1s_b(1)\right]$$

In these equations the scale factor, α is a variational parameter which controls how rapidly the atomic wave function decays to zero, and N_{MO} and N_{VB} are the appropriate normalization constants.

The Hydrogen Atom

Using a scaled hydrogenic wave function (see eq 1) in a variational calculation for the hydrogen atom yields the following expression for the energy in atomic units ($m_e = e = \hbar = 1$),

$$E_H = \frac{\alpha^2}{2} - \alpha$$

where the first term is the electron kinetic energy, and the second term is the electron-nucleus potential energy. Minimization of E_H with respect to α yields,

$$\alpha = 1 \rightarrow E_H = < T > + < V > = \frac{1}{2} - 1 = -\frac{1}{2}$$

where and represent the expectation values for kinetic and potential energy, respectively.

The Hydrogen Molecule. The results for the variational calculations on the hydrogen molecule using the molecularorbital and valence-bond wave functions, and the Born-Oppenheimer energy operator,

$$\hat{H} = -\frac{1}{2}\nabla_1^2 - \frac{1}{2}\nabla_2^2 - \frac{1}{r_{a1}} - \frac{1}{r_{a2}} - \frac{1}{r_{b1}} - \frac{1}{r_{b2}} + \frac{1}{r_{12}} + \frac{1}{R_{ab}}$$

are presented in Table 1. The table provides the optimum value of α, the total energy, and the equilibrium bond length for both wave functions as reported in the literature [16]. The kinetic and potential contributions to the total energy are obtained using the virial theorem. The experimental values [17] for the ground-state energy and the equilibrium bond distance are, respectively, -1.1746 E_h (1 E_h = 27.2114 eV = 2.6255 MJ mol^{-1}) and 1.40 a_o (1 a_o = 52.92 pm).

The Mechanism

For both wave functions, the bond formation mechanism is the same. In the first step, atomic promotion, the hydrogen atom orbitals prepare for bonding by contracting from α = 1 to the optimum α value of the final molecular wave function. This step is atomic and endothermic, increasing the kinetic energy more than it decreases the potential energy. The potential energy decreases because the electrons move closer on average to their respective nuclei. The kinetic energy increases because of the greater confinement of the electrons in the contracted orbitalsókinetic energy is inversely proportional to the square of the average distance of the electron from the nucleus.

The second step consists of the formation of a molecular wave function by overlap of the promoted atomic orbitals. The constructive interference that accompanies orbital overlap brings about charge delocalization and charge redistribution. Charge delocalization distributes the electron density over the molecule as a whole (each electron now belongs to both nuclei) and brings about a significant decrease in kinetic energy. Charge redistribution transfers some electron density from the neighborhood of the nuclei into the inter-nuclear region, which involves an increase in electron potential energy. The second step is exothermic because kinetic energy decreases more than potential energy increases-charge delocalization funds the redistribution of charge from the area around the nuclei into the bond region. The results for both molecular wave functions are summarized in Tables 2 and 3. In summary, this simple two-step mechanism clearly shows that covalent bond formation in H_2 is driven by a decrease in kinetic energy brought about by the charge delocalization that accompanies the overlap of atomic orbitals. This is also the basic conclusion of Ruedenbergís more-detailed and sophisticated analysis for H_2^+.

Acknowledgment. I wish to acknowledge a number of very helpful recommendations made by an anonymous reviewer.

References and Notes

1. Ruedenberg, K. *Rev. Mod. Phys.* **1962**, 34, 326-352.
2. Feinberg, M. J.; Ruedenberg, K. *J. Chem. Phys.* **1971**, *54*, 1495-1511; Feinberg, M. J.; Ruedenberg, K. *J. Chem. Phys.* **1971**, *55*, 5804-5818.
3. Ruedenberg, K. In *Localization and Delocalization in Quantum Chemistry*, Vol I; Chalvet, O.; Daudel, R.; Diner, S.; Malrieu, J. P., Eds.; Reidel: Dordrecht, The Netherlands, 1975; Vol. I, pp 223-245.
4. Baird, N. C. *J. Chem. Educ.* **1986**, 63, 660-664.
5. Harcourt, R. D. *Am. J. Phys.* **1988**, 56, 660-661.
6. Nordholm, S. *J. Chem. Educ.* **1988**, 65, 581-584.
7. Bacskay, G. G.; Reimers, J. R.; Nordholm, S. J. Chem. Educ. 1997, 74, 1494-1502.
8. Rioux, F. *Chem. Educator* **1997**, 2 (6), S1430-4171(97)06153-2; DOI 10.1007/s00897970153a
9. Harcourt, R. D.; Solomon, H.; Beckworth, J.; Chislett, L. *Am. J. Phys.* **1982**, 50, 557-559.
10. Kutzelnigg, W. *Angew. Chem. Int. Ed. Eng.* **1973**, 12, 546-562.
11. Melrose, M. P.; Chauhan, M.; Kahn, F. *Theor. Chim. Acta* **1994**, 88, 311-324.
12. Gordon, M. S.; Jensen, J. H. *Theor. Chem. Acc.* **2000**, 103, 248-251.
13. Slater, J. C. *J. Chem. Phys.* **1933**, 1, 687-691.
14. Slater, J. C. *Quantum Theory of Matter*; Krieger Publishing: Huntington, NY, 1977; pp 405-408.
15. The full virial theorem for a diatomic molecule as a function of internuclear separation is 2 + + RdE/dR = 0. This expression takes the form used here when dE/dR = 0, which occurs at R = Re (at the equilibrium internuclear separation) and R = ∞ (the

separated atoms).
16. Levine, I. N. *Quantum Chemistry*, 4th Ed.; Prentice-Hall: Englewood Cliffs, NJ, 1991; pp 384-390. The primary literature reference for the MO calculation is Coulson, C. A. Trans. Faraday Soc. **1937**, 33, 1479; for the VB calculation it is Wang, S. C. Phys. Rev. **1928**, 31, 579.
17. Huber, K. P.; Herzberg, G. *Constants of Diatomic Molecules*, Vol. IV; Van Nostrand Reinhold: New York, 1979.

This page titled 3.2: The Covalent Bond in the Hydrogen Molecule is shared under a CC BY 4.0 license and was authored, remixed, and/or curated by Frank Rioux via source content that was edited to the style and standards of the LibreTexts platform.

3.3: The Covalent Bond Clarified Through the Use of the Virial Theorem

Abstract

Slater's method of analyzing the covalent bond using the virial theorem is presented for the hydrogen molecule. The overall conclusion reached is the same as that reached with Ruedenberg's well-known *abinitio* quantum mechanical study - electron kinetic energy plays an important role in chemical bond formation.

Introduction

In the second edition of his classic monograph, *Molecular Quantum Mechanics*, Peter Atkins begins the chapter on molecular structure with the following sentences (*1*),

> Now we come to the heart of chemistry. If we can understand what holds atoms together as molecules we may also start to understand why, under certain conditions, old arrangements change in favor of new ones. We shall understand structure, and through structure, the mechanism of change.

Few will argue with Atkins' eloquent assertion that the chemical bond is at the heart of chemistry, however finding a satisfactory discussion of chemistry's central concept is difficult. For example, a survey of widely adopted general chemistry texts showed the following errors in the description of the covalent bond to be prevalent. Surprisingly the origin of some of these errors can be traced to two authoritative monographs on chemical bonding of enormous influence (*2*).

- The covalent bond is presented as a purely electrostatic phenomenon. Electron kinetic energy is never mentioned, even though the total energy of a molecule is a sum of kinetic and potential energy contributions, and atomic and molecular stability cannot be understood solely in terms of potential energy.
- Closely related to this is that what is actually an energy curve is called a potential energy curve. What is shown in introductory texts is the total molecular energy as a function of internuclear separation under the Born-Oppenheimer approximation. In other words, nuclear kinetic energy is frozen, but electron kinetic energy contributes to the total molecular energy.
- It is claimed that the electron density in the inter-nuclear (bond) region has a lower potential energy because it is attracted to two nuclei. Actually using simple electrostatic arguments it is easy to show that the electron-nuclear potential energy is higher in the internuclear region than it is closer to the nuclei. On the basis of potential energy alone the electrons would prefer to be in the nucleus.
- An energy minimum, or molecular ground state, is achieved because of increases in nuclear-nuclear and electron-electron repulsions as the internuclear separation decreases. As will be shown later, the immediate cause of the molecular ground state is a sharp increase in electron kinetic energy.
- The amount of electron density transferred to the bonding region is greatly overstated, sometimes implying that a pair of electrons is shared **between** two nuclei rather than **by**two nuclei.

Unfortunately, to find accurate analyses of the physical origin of the covalent bond one must go to the research or pedagogical literature; chemistry textbooks will not, in general, provide enlightenment. In the 1960s and 70s Ruedenberg and his collaborators carried out a detailed quantum mechanical study of the covalent bond in H_2^+ (*4* - *6*). The most important conclusion of this thorough and insightful study was that electron kinetic energy plays a crucial role in the formation of a chemical bond. Ruedenberg's contributions to the understanding of the chemical bond have been summarized in the pedagogical literature (*7* - *12*) and in review articles (*13* - *15*). There are also at least two encyclopedia entries which give accurate and clear interpretations of covalent bond formation (*16*, *17*).

It is surprising that none of these efforts to make Ruedenberg's work accessible to the non-specialist have had any noticeable impact on the way chemical bonding is presented by the authors of chemistry textbooks currently used in the undergraduate curriculum. While physical chemistry texts avoid the errors cited above, they generally do not attempt to provide an "explanation" of the chemical bond. For example, after outlining the mathematical techniques required to solve Schr  dinger's equation for H_2^+ and H_2, physical chemistry texts do not interpret the calculations other than to say something to the effect that the stability of the chemical bond is a quantum mechanical effect that has no classical analog or explanation. Atkins' physical chemistry text is a notable exception; in a footnote he alerts the reader to the subtleties of the chemical bond and briefly outlines the interplay between kinetic and potential energy during the formation of the covalent bond in H_2^+(*3*).

It is not widely appreciated that John C. Slater used the virial theorem to come to a similar conclusion about the importance of electron kinetic energy in chemical bond formation in the early days of quantum mechanics. In a paper published in the inaugural volume of the *Journal of Chemical Physics* Slater pioneered the use of the virial theorem in interpreting the chemical bond. With regard to the virial theorem he said (*18*),

> "... this theorem gives a means of finding kinetic and potential energy separately for all configurations of the nuclei, as soon as the total energy is known, from **experiment** or **theory**." (emphasis added)

The purpose of this paper is to outline Slater's method of analysis for the hydrogen molecule, the simplest example of the traditional two-electron chemical bond.

Background Theory

The Hamiltonian energy operator (in atomic units) for the hydrogen molecule consists of the following ten contributions,

$$\hat{H} = -\frac{1}{2M}\nabla_a^2 - \frac{1}{2M}\nabla_b^2 - \frac{1}{2}\nabla_1^2 - \frac{1}{2}\nabla_2^2 - \frac{1}{r_{a1}} - \frac{1}{r_{a2}} - \frac{1}{r_{b1}} - \frac{1}{r_{b2}} + \frac{1}{r_{12}} + \frac{1}{R}$$

where *a* and *b* label the nuclei, *1* and *2* label the electrons, and $R = R_{ab}$, the internuclear separation. Under the Born-Oppenheimer approximation the nuclear kinetic energy operators drop out, and the molecular electronic energy as a function of internuclear separation, *E(R)*, can be obtained by solving Schr  dinger's equation variationally for the resulting eight-term electronic Hamiltonian, H_{el}, which in this analysis includes nuclear-nuclear repulsion.

$$E(R) = \frac{\langle \Psi(R;\ 1,2)|\hat{H}_{el}|\Psi(R;\ 1,2)\rangle}{\langle \Psi(R;\ 1,2)|\Psi(R;\ 1,2)\rangle}$$

Now one can return to equation (1) with the calculated *E(R)* and treat it as the molecular "potential" field in which the nuclei move. The nuclear kinetic energy operators are re-written in terms of the nuclear center-of-mass coordinate and the internal coordinate *R*. After discarding the term involving the motion of the center of mass, the Hamiltonian energy operator becomes

$$\hat{H} = -\frac{1}{2\mu}\nabla^2 + E(R)$$

Following Slater, a more empirical approach is taken here and the *ab initio E(R)* is replaced by an analytical surrogate such as the Morse function (*19*) which has a similar R-dependence (*20*).

$$E(R) = D_e\left[1 - \exp(-\beta(R - R_e))\right]^2 - D_e$$

In other words the Morse function represents the total energy of a diatomic molecule assuming the Born-Oppenheimer approximation.

Substitution of equation (4) into (3) yields an energy Hamiltonian for which Schrödinger's equation has an exact solution with the following quantized nuclear vibrational states (*2*),

$$G(v) = \left(v + \frac{1}{2}\right)\overline{\nu}_e - \left(v + \frac{1}{2}\right)^2 \overline{\nu}_e x_e$$

where v = 0, 1, 2, ..., and the Morse parameters, D_e and b, are defined as,

$$D_e = \frac{h c \overline{\nu}_e (1 - x_e^2)}{4 x_e} \qquad \beta = \sqrt{\frac{\mu}{D_e}}\pi \overline{\nu}_e c$$

Fitting equation (5) to spectroscopic data for H_2 yields the following values for the Morse parameters: $D_e = 7.92 \times 10^{-19}$ joule; b = 0.0191 pm^{-1}; and R_e = 74.1 pm (*21*).

The Virial Theorem

At this point the virial theorem is used to obtain a total energy profile for covalent bond formation in H_2. The first step in this approach is to acknowledge that the energy of a molecule is a sum of kinetic and potential energy contributions.

$$E(R) = T(R) + V(R)$$

The virial theorem for a diatomic molecule as a function of internuclear separation, *R*, is (*14*)

$$2T(R) + V(R) + R\frac{dE(R)}{dR} = 0$$

Equations (7) and (8) can now be used to obtain expressions for the kinetic and potential energy in terms of the total energy and its first derivative.

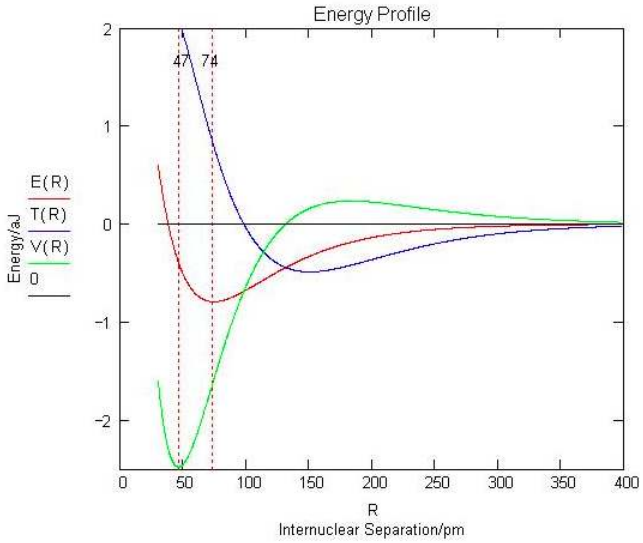
$$T(R) = -E(R) - R\frac{dE(R)}{dR}$$

$$V(R) = 2E(R) + R\frac{dE(R)}{dR}$$

Quoting Slater again (*18*)

> These important equations determine the mean kinetic and potential energies as a function of r, one might almost say, experimentally, directly from the curves of E as a function of r which can be found from band spectra. The theory is so simple and direct that one can accept the results without question, remembering only the limitation of accuracy mentioned above. (Here Slater is referring to the neglect of zero point vibration in his analysis.)

Thus, when equation (4), parameterized as indicated above, is used in equations (9) and (10) the energy profile for covalent bond formation in H_2 shown in Figure 1 is obtained.



Analysis

This energy profile shows that as the inter-nuclear separation decreases, the potential energy rises, falls, and then rises again. The kinetic energy first decreases and then increases at about the same value of R that the potential energy begins to decrease.

The quantum mechanical interpretation of the energy profile is as follows (*4*, *18*). As the molecular orbital is formed at large R constructive interference between the two overlapping atomic orbitals on the hydrogen atoms draws electron density away from the nuclear centers into the inter-nuclear region. The potential energy rises as electron density is removed from the region around the nuclei, but the total energy decreases because of a larger decrease in kinetic energy due to charge delocalization - the electrons now belong to the molecule and not the individual atoms. Thus, a decrease in kinetic energy funds the initial build-up of charge between the nuclei that is traditionally associated with chemical bond formation.

Following this initial phase, at an inter-nuclear separation of about 150 pm, the potential energy begins to decrease and the kinetic energy increases, both sharply eventually, while the total energy continues to decrease gradually. This is an atomic affect, not a molecular one, as Ruedenberg clearly showed. The initial transfer of charge away from the nuclei and into the bond region allows the atomic orbitals to contract causing a large decrease in potential energy because the electron density is moved, on average, closer

to the nuclei. The kinetic energy increases because the atomic orbitals are smaller and kinetic energy is inversely proportional to the square of the average orbital radius. This is an atomic affect because the orbital contraction actually causes some electron density to be withdrawn from the bonding region and returned to the nuclei.

An energy minimum is reached while the potential energy is still in a significant decline, indicating that kinetic energy, which is increasing rapidly, is the immediate cause of a stable bond and the molecular ground state in H_2. The final increase in potential energy which is mainly due to nuclear-nuclear repulsion doesn't begin until the inter-nuclear separation is less than 50 pm, while the equilibrium bond length is 74 pm. Thus the common explanation that an energy minimum is reached because of nuclear-nuclear and electron-electron repulsion does not have merit. As Ruedenberg (*4*) has noted "there are no ground states in classical mechanics or electrostatics."

Conclusion

In conclusion a review of some basic principles and some additional observations are offered. Under the Born-Oppenheimer approximation the quantum mechanical energy operator for H_2 consists of the final eight terms in equation (1), which fall into four types of energy contributions: electron kinetic energy, electron-electron, nuclear-nuclear, and electron-nuclear potential energy. Electron-nuclear potential energy is the only negative contribution to the total energy and is essential in understanding the stability of the chemical bond. H_2 is a stable molecule because it has a lower **total** energy than its constituent atoms, not simply because there is a build-up of charge in the inter-nuclear region. As shown above, by itself this charge build-up actually increases the energy rather than decreasing it as is popularly, but incorrectly, believed.

We all recognize that electron kinetic energy is important at the computational level through its presence in the energy operator given in equation (1). In other words ground states are calculated by minimizing the total energy, the sum of the kinetic and potential energy contributions. However, many ignore kienticenergy when it comes to interpretation because they believe it is irrelevant. The origin of this error is a common misapplication of the virial theorem.

For example, it is common to argue from the virial theorem in the form,

$$\Delta E = \frac{\Delta V}{2} = -\Delta T$$

that bond stability is due solely to potential energy, because it decreases with bond formation and kinetic energy actually increases by twice as much. However, this form of the virial theorem is valid only for R = R$_{\infty}$ and R = R_e, the initial and final states. It tells us nothing about what is occuring when the bond is actually being formed - for that you need equations (7 - 10). As has been shown above, what is actually occuring during bond formation is a rather subtle role reversal between kinetic and potential energy. It is ironic that Slater correctly used the virial theorem to show that electron kinetic energy is essential to understanding the chemical bond in the 1930s, while today many use it incorrectly to show that electron kinetic energy is irrelevant.

It has been known since the early years of the 20th century that no dynamic or static array of charged particles is stable on the basis of classical electrostatic principles alone. Therefore, the quantum mechanical picture of a wave-particle duality for the electron and the peculiar quantum mechanical nature of kinetic energy are essential in understanding atomic and molecular stability and structure. The importance of kinetic energy runs counter to conventional opinion regarding the covalent bond in two seemingly paradoxical ways. First, a **decrease** in kinetic energy due to incipient molecular orbital formation funds the transfer of charge density into the internuclear region, lowering the total energy. Second, a large **increase** in kinetic energy associated with the subsequent atomic orbital contraction prevents the collapse of the molecule and causes an energy minimum and a stable molecular ground state.

In a previous publication (*10b*) the formation of the covalent bond in H_2 was analyzed in terms of a two-step mechanism involving: a) orbital contraction ("hybridization") followed by b) orbital overlap (charge delocalization and redistribution). It was shown that step a) is an atomic and endothermic process, while b) is a molecular and exothermic effect. The present study is consistent with this prior analysis, but reverses the order of the contributing effects; atomic orbital overlap precedes atomic orbital contraction. Both mechanisms clearly reveal the important role that electron kinetic energy plays in chemical bond formation.

In summary I concur with Kutzelnigg's observation (*22*), "The chemical bond is a highly complex phenomenon which eludes all attempts at simple description." This means we must be careful how we teach the chemical bond to our students. It is not acceptable to present incorrect models of bonding to undergraduates because they are easier to understand and therefore easier to teach.

Literature Cited:

1. Atkins, P. W. *Molecular Quantum Mechanics*, Oxford University Press, Oxford, UK, 1983, p. 250.
2. Pauling, L. *The Nature of the Chemical Bond*, 3rd ed., Cornell University Press, Ithaca, 1960, pp. 19-21. Coulson, C. A. *Valence*, 2nd ed., Oxford University Press, London, 1961, pp. 85-86.
3. Atkins, P. W. *Physical Chemistry*, 6th ed., W. H. Freeman and Co., New York, 1998, p. 397.
4. Ruedenberg, K. *Rev. Mod. Phys.* **1962**, *34*, 326-352.
5. Feinberg, M. J.; Ruedenberg, K. *J. Chem. Phys.* **1971**, *54*, 1495-1511. Feinberg, M. J.; Ruedenberg, K. *J. Chem. Phys.* **1971**, *55*, 5804-5818.
6. Ruedenberg, K. In *Localization and Delocalization in Quantum Chemistry;* Chalvet, O. et al., Eds.; Reidel: Dordrecht, The Netherlands, **1975**; Vol. I, pp 223-245.
7. Baird, N. C. *J. Chem. Educ.* **1986**, *63*, 660-664.
8. Harcourt, R. D. *Am. J. Phys.* **1988**, *56*, 660-661.
9. Nordholm, S. *J. Chem. Educ.* **1988**, *65*, 581-584.
10. Bacskay, G. G.; Reimers, J. R.; Nordholm, S. *J. Chem. Educ.* **1997**, *74*, 1494-1502.
11. Rioux, F. a) *Chem. Educator* **1997**, *2(6)*, 1-14; *b) Chem. Educator* **2001**, *6(5)*, 288-290.
12. Harcourt, R. D.; Solomon, H.; Beckworth, J.; Chislett, L. *Am. J. Phys.* **1982**, *50*, 557-559.
13. Kutzelnigg, W. *Angew. Chem. Int. Ed. Eng.* **1973**, *12*, 546-562.
14. Melrose, M. P.; Chauhan, M.; Kahn, F. *Theor. Chim. Acta* **1994**, *88*, 311-324.
15. Gordon, M. S.; Jensen, J. H. *Theor. Chem. Acc.* **2000**, *103*, 248-251.
16. Gordon, M. S.; Jensen, J. H. *Encyclopedia of Computational Chemistry*, Schleyer, P. v. R., Ed.; John Wiley & Sons: New York, 1998, pp 3198-3214.
17. Harris, F. E. In *Encyclopedia of Physics*, 2nd Edition; Lerner, R. G.; Trig, G. L., Eds.; VCH Publishers, Inc.: New York, 1991, pp 762-764.
18. Slater, J. C. *J. Chem. Phys.* **1933**, *1*, 687-691.
19. Morse, P. M. *Phys. Rev.* **1929**, *34*, 57.
20. For a virial theorem analysis using the best *ab initio* results for H_2 see, Winn, J. S. *J. Chem. Phys.***1981**, *74*, 608-611.
21. Huber, K. P.; Herzberg *Molecular Spectra and Molecular Structure*, vol IV, *Constants of Diatomic Molecules*; Van Nostrand Reinhold: New York, 1979.
22. Kutzelnigg, W. *Angew. Chem. Int. Ed. Eng.* **1984**, *23*, 292.

This page titled 3.3: The Covalent Bond Clarified Through the Use of the Virial Theorem is shared under a CC BY 4.0 license and was authored, remixed, and/or curated by Frank Rioux via source content that was edited to the style and standards of the LibreTexts platform.

3.4: Brief Version of the Covalent Bond Clarified Through the Use of the Virial Theorem

Abstract: The chemical bond is a concept of unique importance in chemistry that students first study seriously in a college or university general chemistry course. At first glance, the descriptions of covalent bond formation found in general chemistry texts seem plausible and comprehensible; however, when they are examined more carefully, it is found that they violate both classical and quantum mechanical principles.

Introduction

In the second edition of his classic text, Molecular Quantum Mechanics, Peter Atkins begins the chapter on molecular structure with the following sentences [1]:

> Now we come to the heart of chemistry. If we can understand what holds atoms together as molecules we may also start to understand why, under certain conditions, old arrangements change in favor of new ones. We shall understand structure, and through structure, the mechanism of change.

Few will argue with Atkins' eloquent assertion that the chemical bond is at the heart of chemistry, but where do we find an accurate explanation of chemistry's central concept?-certainly not in chemistry textbooks written for undergraduate audiences. For example, a survey of widely adopted general chemistry texts showed the following errors in the description of the covalent bond to be prevalent.

- The covalent bond is presented as a purely electrostatic phenomenon. Electron kinetic energy is never mentioned, even though the total energy of a molecule is a sum of kinetic and potential energy contributions, and atomic and molecular stability cannot be understood solely in terms of potential energy.
- Closely related to this is what is actually an energy curve is called a potential energy curve. What is shown in introductory texts is the total molecular energy as a function of internuclear separation under the Born-Oppenheimer approximation. In other words, nuclear kinetic energy is frozen, but electron kinetic energy contributes to the total molecular energy.
- It is claimed that the electron density in the internuclear (bond) region has a lower potential energy because it is attracted to two nuclei. Actually using simple electrostatic arguments (see the appendix) it is easy to show that the electron-nuclear potential energy is higher in the internuclear region than it is closer to either of the nuclei. On the basis of potential energy alone the electrons would prefer to be in the nucleus.
- It is claimed that an energy minimum, or molecular ground state, is achieved because of increases in nuclear- nuclear and electron-electron repulsions as the internuclear separation decreases. As will be shown later, the immediate cause of the molecular ground state is a sharp increase in electron kinetic energy.
- The amount of electron density transferred to the bonding region is greatly overstated, sometimes implying that a pair of electrons is shared in the space between two nuclei rather than by two nuclei.

By comparison, these errors are not often found in physical chemistry textbooks. Most physical chemistry texts set up the Schrödinger equation for the H_2^+ and H_2 molecules and outline the solutions, but avoid interpreting the calculations other than saying something to the effect that the chemical bond is a quantum mechanical phenomenon that has no classical analog or explanation. A notable exception is the text by Atkins and de Paula, which gives a correct analysis of the bond in H_2^+ in a footnote and the text by Raff, which summarizes the best ab initio results for H_2 [2]. Thus, in order to find an accurate analysis of covalent bond formation, it is necessary to consult advanced quantum chemistry texts, the research literature, or the pedagogical literature.

In the 1960s and 70s Ruedenberg and his collaborators carried out a detailed quantum mechanical study of the covalent bond in H2 + [3-5]. The most important conclusion of this thorough and insightful study was that electron kinetic energy plays a crucial role in chemical bond formation. Ruedenberg's contributions to the understanding of the chemical bond have been summarized in the pedagogical literature [6-11] and in review articles [12-14]. It is unfortunate that none of these efforts to make Ruedenberg's work accessible to the nonspecialist have had any noticeable impact on the way chemical bonding is presented by authors of chemistry textbooks at the introductory or intermediate level.

It is not widely appreciated that John Slater came to similar conclusions about covalent bond formation thirty years before Ruedenberg using a more empirical approach based directly on the virial theorem [15-17]; therefore, the purpose of this paper is to

outline Slater's method for the hydrogen molecule, the simplest example of the traditional two-electron chemical bond. It should be noted, however, that Slaterís approach is appropriate for any diatomic molecule for which Morse parameters are available.

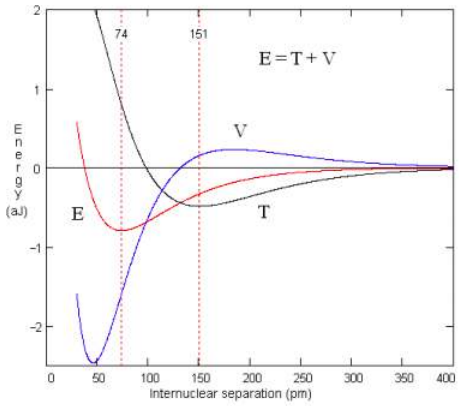


Figure 1. Energy profile for H_2 using the virial theorem and a Morse function with spectroscopic parameterization.

Background Theory

In the early days of the quantum revolution Slater used the virial theorem to analyze the chemical bond and was the first to notice the importance that electron kinetic energy played incovalent bond formation. With regard to the virial theorem he said [15]:

> ...this theorem gives a means of finding kinetic and potential energy separately for all configurations of the nuclei, as soon as the total energy is known, from experiment or theory.

Under the Born-Oppenheimer approximation, the molecular energy as a function of internuclear separation, E(R), is represented well by a Morse function [18] whose parameters for H2 are based on spectroscopic data: De = 7.93 aJ; β = 0.0190 pm^{-1}; Re = 74.1 pm [19].

$$E(R) = D_e \left[1 - \exp\left(-\beta(R - R_e)\right)\right]^2 - D_e$$

The virial theorem for diatomic molecules [15] can be used with eq 1 to obtain expressions for the average values of kinetic and potential energy as a functions of the internuclear separation, R.

$$T(R) = -E(R) - R\frac{dE(R)}{dR}$$

$$V(R) = 2E(R) + R\frac{dE(R)}{dR}$$

Quoting Slater again [15]:

> These important equations determine the mean kinetic and potential energies as functions of R, one might almost say, experimentally, directly from the curves of E as a function of R which can be found from band spectra. The theory is so simple and direct that one can accept the results without question...

When eq 1, parameterized as indicated earlier, is used in eqs 2 and 3, the energy profile for covalent bond formation in H2 shown in the Figure 1 is obtained.

Analysis

As Slater pointed out, the molecular energy curve can be obtained from experiment (spectroscopy) or theory (ab initio quantum mechanics). The energy profile obtained is similar in both approaches. For example, Winn [20] offered the following analysis of the ab initio results of Kolos and Wolniewicz [21] for H_2.

> As the atoms approach, the potential energy rises (electrons are moving away from nuclei) and the kinetic energy falls (as delocalization begins). In the vicinity of $R/R_e = 2$, this trend reverses. The kinetic energy increases as the electronic wave function is localized further, raising the momentum, but the potential energy falls, as charge is now brought nearer both

nuclei. Only at $R/R_e < 0.5$ does nuclear repulsion cause the potential energy to increase and contribute to the total repulsion energy.

This analysis will serve as the basis for a simple quantum mechanical model for covalent bond formation consistent with the spectroscopic energy profile shown in Figure 1 that uses qualitative concepts accessible to introductory students. It consists of two steps: (1) molecular orbital formation through the overlap of atomic orbitals, followed by (2) atomic orbital contraction. It is assumed step (1) ends as kinetic energy reaches a minimum (151 pm), and step (2) ends when the total energy reaches a minimum (74.1 pm). This approach yields the following quantitative analysis of bond formation in H_2.

	Step 1	Step 2	Overall
ΔT/aJ	-0.495	1.288	0.793
ΔV/aJ	0.159	-1.745	-1.586
ΔE/aJ	-0.336	-0.457	-0.793
R/pm	151	74.1	74.1

1. The constructive interference that accompanies molecular orbital formation brings about charge delocalization and charge redistribution. This step is molecular in character and is driven by a decrease in kinetic energy as the table above shows.

Charge delocalization occurs because each electron now belongs to both nuclei and occupies a larger volume than in the atomic state. This effect is accompanied by a significant decrease in electron kinetic energy [22]. Charge redistribution occurs because atomic overlap transfers some electron density away from the nuclear centers into the internuclear (overlap) region, which involves an increase in potential energy. Overall this step is exothermic because kinetic energy decreases more than potential energy increases. Thus, charge delocalization funds the redistribution of charge into the internuclear region that is normally associated with bond formation.

2. The reduction of electron density near the nuclei that occurs in step 1 allows the atomic orbitals to contract returning some electron density to the nuclear centers from the internuclear region. This step is atomic in character and is driven by a large decrease in potential energy.

The decrease in potential energy occurs because the electrons are brought closer to the nuclei, and the increase in kinetic energy occurs because orbital contraction has reduced the volume occupied by the electrons, thereby reducing the level of delocalization. It has been shown that at the equilibrium bond distance the net transfer of electron density into the internuclear region is only 16% [5].

According to the energy profile, an energy minimum is reached while the potential energy is still in a significant decline, showing that kinetic energy, which is increasing rapidly, is the immediate cause of a stable bond and molecular ground state in H_2. The final increase in potential energy, which is mainly due to nuclear-nuclear repulsion, doesn't begin until the internuclear separation is less than 50 pm and the equilibrium bond length is 74 pm. Thus, the common explanation that an energy minimum is reached because of nuclear-nuclear and electron-electron repulsion does not have merit. As Ruedenberg [5] has succinctly noted "there are no ground states in classical mechanics or electrostatics".

Conclusion

In summary, an "empirical" analysis of the covalent bond in H_2 has been presented based on the virial theorem and a Morse molecular energy function parameterized using spectroscopic data. This analysis shows that the role of electron kinetic energy in covalent bond formation runs counter to conventional wisdom in two seemingly paradoxical ways. First, a decrease in kinetic energy due to incipient molecular orbital formation funds the transfer of charge density into the internuclear region, lowering the total energy. Second, a large increase in kinetic energy accompanying the subsequent atomic orbital contraction prevents the collapse of the molecule, and causes an energy minimum and a stable molecular ground state.

Clearly, using rigorous quantum mechanics in introductory chemistry courses in order to avoid error in describing the chemical bond is not a practical solution; however, teaching simple, easily digestible, but incorrect models for the covalent bond is pedagogically unacceptable. It is therefore necessary to offer general chemistry students an explanation of the nature of the

covalent bond that is both correct and accessible. To achieve this end a rudimentary two-step quantum mechanical mechanism for covalent bond formation in H_2 has been proposed.

Appendix

When asked what motivated the creation of his famous model of the atom Bohr replied "the stability of matter, a pure miracle when considered from the standpoint of classical physics." The following simple calculation will demonstrate what Bohr meant by this statement. This calculation will be carried out in atomic units where the charge on the electron is ñ1, the charge on the nucleus +1, and distances are measured in bohr, a_o.

Two nuclei (Z = 1) are placed at x = 0.0 and 2.0, respectively. An electron is located exactly between them at x = 1.0, where we instinctively, but incorrectly, think it would want to be on the basis of electrostatic considerations. The potential energy consists of three interactions (nuclear-nuclear repulsion and two electron-nuclear attractions) and is calculated as follows:

$$V = \frac{(+1)(+1)}{2} + \frac{(-1)(+1)}{2} + \frac{(-1)(+1)}{1} = -1.50$$

Now move the electron 0.5 a_o closer to one of the nuclei.

$$V = \frac{(+1)(-1)}{2} + \frac{(-1)(+1)}{0.5} + \frac{(-1)(+1)}{1.5} = -2.17$$

And so it goes, on the basis of electrostatic considerations, until the electron is inside one nucleus or the other. Although the electron was treated as a point charge in this calculation, a rigorous quantum mechanical calculation tells the same story-moving charge to the internuclear region increases electrostatic potential energy.

References and Notes

1. Atkins, P. W. *Molecular Quantum Mechanics*; Oxford University Press, Oxford, UK, 1983, p. 250.
2. (a) Atkins, P.; de Paula, J. *Physical Chemistry*, 7th ed.; W. H. Freeman and Co.: New York, 2002; p 420; (b) Raff, L. M. *Principles of Physical Chemistry*; Prentice Hall: Upper Saddle River, NJ, 2000; pp 761-764.
3. Ruedenberg, K. *Rev. Mod. Phys.* **1962**, *34*, 326-352.
4. Feinberg, M. J.; Ruedenberg, K. *J. Chem. Phys.* **1971**, *54*, 1495-1511; Feinberg, M. J.; Ruedenberg, K. *J. Chem. Phys*. **1971**, 55, 5804-5818.
5. Ruedenberg, K. In *Localization and Delocalization in Quantum Chemistry*, Vol. I; Chalvet, O. ; Daudel, R.; Diner, S.; Malrieu, J. P., Eds.; Reidel: Dordrecht, The Netherlands, 1975; pp 223-245.
6. Baird, N. C. *J. Chem. Educ.* **1986**, 63, 660-664.
7. Harcourt, R. D. *Am. J. Phys.* **1988**, 56, 660-661.
8. Nordholm, S. *J. Chem. Educ.* **1988**, 65, 581-584.
9. Bacskay, G. G.; Reimers, J. R.; Nordholm, S. *J. Chem. Educ.* **1997**, *74*, 1494-1502.
10. Rioux, F. *Chem. Educator* **1997**, *2(6)*, S1430-4171(97)06153-2; DOI 10.1007/s00897010153a.
11. Harcourt, R. D.; Solomon, H.; Beckworth, J.; Chislett, L. *Am. J. Phys.* 1982, 50, 557-559.
12. Kutzelnigg, W. Angew. *Chem. Int. Ed. Eng*. **1973**, *12*, 546-562.
13. Melrose, M. P.; Chauhan, M.; Kahn, F. *Theor. Chim. Acta* **1994**, *88*, 311-324.
14. Gordon, M. S.; Jensen, J. H. *Theor. Chem. Acc.* **2000**, *103*, 248-251.
15. Slater, J. C. *J. Chem. Phys.* **1933**, *1*, 687-691.
16. Slater, J. C. *Quantum Theory of Matter*; Krieger Publishing: Huntington, NY, 1977; pp 405-408.
17. For a thorough discussion of the virial theorem see: Levine, I. N. Quantum Chemistry, 4th ed.; Prentice Hall: Englewood Cliffs, NJ, 1991, Chapter 14.
18. Morse, P. M. *Phys. Rev.* **1929**, *34*, 57.
19. Huber, K. P.; Herzberg, G. *Molecular Spectra and Molecular Structure*, Vol IV; *Constants of Diatomic Molecules*; Van Nostrand Reinhold: New York, 1979.
20. Winn, J. S. *J. Chem. Phys.* **1981**, *74*, 608-611.
21. Kolos, W.; Wolniewicz, L. J. Chem. Phys. 1965, 43, 2429. 22. According to de Broglie, p = h/λ, which means T ~ λ^{-2}. Because the wavelength of a confined particle is proportional to the confinement dimension R, we have T ~ R^{-2} and in terms of

confinement volume $T \sim V^{-2/3}$.

This page titled 3.4: Brief Version of the Covalent Bond Clarified Through the Use of the Virial Theorem is shared under a CC BY 4.0 license and was authored, remixed, and/or curated by Frank Rioux via source content that was edited to the style and standards of the LibreTexts platform.

3.5: The H2 Covalent Bond and the Virial Theorem

Total energy: $E(R) = T(R) + V(R)$

Virial theorem: $2T(R) + V(R) = -R\frac{d}{dR}E(R)$

Morse parameters: $D_e = 0.761aJ \qquad \beta = 0.0193pm^{-1} \qquad R_e = 74.1pm$

These parameters are taken from Fig. 5.6 on page 165 of McQuarrie and Simon's *Physical Chemistry: A Molecular Approach*.

$$\text{Morse Function:} \quad E(R) = D_e\left[1 - \exp\left[-\beta\left(R - R_e\right)\right]\right]^2 - D_e$$

Using equation (1) to eliminate V(R) in equation (2) yields an equation for kinetic energy as a function of the internuclear separation.

$$\text{Kinetic energy:} \quad T(R) = -E(R) - R\frac{d}{dR}E(R)$$

Using equation (1) to eliminate T(R) in equation (2) yields an equation for potential energy as a function of the internuclear separation.

$$\text{Potential energy:} \quad T(R) = 2E(R) + R\frac{d}{dR}E(R)$$

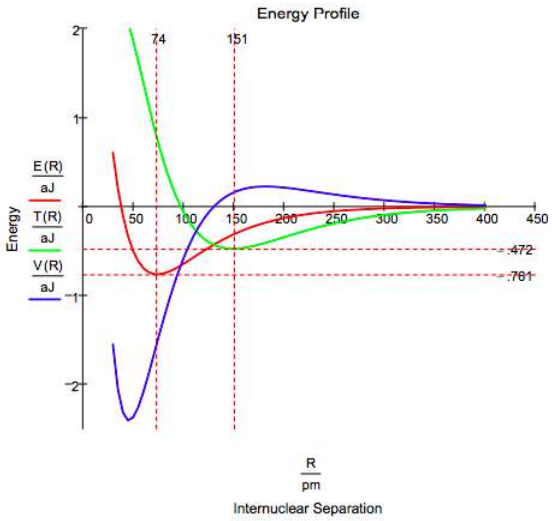
John C. Slater [*J.Chem. Phys.* **1933**, *1*, 687-691] used the virial theorem to analyze the chemical bond and was among the first to note the importance of kinetic energy in covalent bond formation. He wrote,

> ...this theorem gives a means of finding kinetic and potential energy separately for all configurations of the nuclei, as soon as the total energy is known, from experiment or theory.
>
> These important equations (4 and 5) determine the mean kinetic and potential energies as functions of R, one might almost say experimentally, directly from the curves of E as a function of R which can be found from band spectra. The theory is so simple and direct that one can accept the results without question....

John Winn [J. Chem. Phys. 1981, 74, 608-611] offered the following interpretation of the energy profile shown below.

> As the atoms approach, the potential energy rises (electrons are moving away from nuclei) and the kinetic energy falls (as delocalization begins). In the vicinity of R/Re = 2, this trend reverses. The kinetic energy increases as the wave function is localized ..., but the potential energy falls as the charge is now brought nearer both nuclei. Only at R/Re < 0.5 does nuclear repulsion cause the potential energy to increase and contribute to the total repulsion energy.

Plot range: $R = 30pm,\ 35pm..400pm$



The following table provides quantitative support for Winn's analysis.

o	Step 1	Step 2	Overall
$\frac{\Delta T}{aJ}$	-0.472	1.233	0.761
$\frac{\Delta V}{aJ}$	0.166	-1.688	-1.522
$\frac{\Delta E}{aJ}$	-0.306	-0.455	-0.761
$\frac{R}{pm}$	151	74.1	74.1
Type	Molecular	Atomic	Molecular + Atomic

This type of analysis is valid for any diatomic molecule for which Morse paramters are available.

$$\text{Conversion factors:} \quad pm = 10^{-12}m \quad aJ = 10^{-18}joule$$

This page titled 3.5: The H2 Covalent Bond and the Virial Theorem is shared under a CC BY 4.0 license and was authored, remixed, and/or curated by Frank Rioux via source content that was edited to the style and standards of the LibreTexts platform.

3.6: The Covalent Bond According to Slater and Ruedenberg

John Slater pioneered the use of the virial theorem in interpreting the chemical bond in a benchmark paper published in the inaugural volume of the *Journal of Chemical Physics* (1). This early study indicated that electron kinetic energy played an important role in bond formation. Thirty years later Klaus Ruedenberg and his collaborators published a series of papers (2,3,4) detailing the crucial role that kinetic energy plays in chemical bonding, thereby completing the project that Slater started. This Mathcad worksheet recapitulates Slater's use of the virial theorem in studying chemical bond formation and summarizes Ruedenberg final analysis.

Equation [1] gives the virial theorem for a diatomic molecule as a function of internuclear separation, while equation [2] is valid at the energy minimum.

$$2T(R) + V(R) == R\frac{d}{dR}E(R)$$

$$E\left(R_e\right) = \frac{V\left(R_e\right)}{2} = -T\left(R_e\right)$$

At non-equilibrium values for the internuclear separation the virial equation can be used, with E = T + V, to obtain equations for the kinetic and potential energy as a function of the inter-nuclear separation.

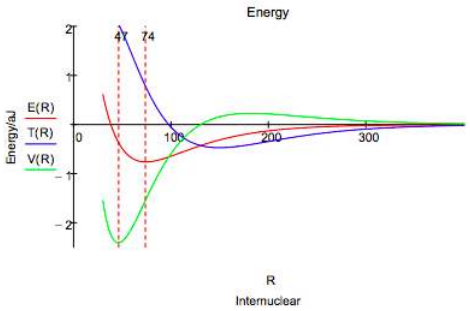
$$T(R) = -E(R) - R\frac{d}{dR}E(R)$$

$$V(R) = 2E(R) + R\frac{d}{dR}E(R)$$

Thus, if E(R) is known one can calculate T(R) and V(R) and provide a detailed energy profile for the formation of a chemical bond. E(R) can be provided from spectroscopic data or from ab initio quantum mechanics. In this examination of the chemical bond we employ the empirical approach and use spectroscopic data for the hydrogen molecule to obtain the parameters (highlighted below) for a model of the chemical bond based on the Morse function (5). However, it should be noted that quantum mechanics tells the same story and yields an energy profile just like that shown in the following figure.

$$R = 30, 30.2..400 \quad D_e = 0.761 \quad \beta = 0.0193 \quad R_e = 74.1 \qquad E(R) = \left[D_e\left[1 - \exp\left[-\beta\left(R - R_e\right)\right]\right]^2 - D_e\right]$$

The dissociation energy, De, is given in atta (10^{-18}) joules, the internuclear separation in picometers, and the constant β in inverse picometers.



This energy profile shows that as the internuclear separation decreases, the potential energy rises, falls, and then rises again. The kinetic energy first decreases and then increases at about the same internuclear distance that the potential energy begins to decrease.

As the molecular orbital is formed at large R constructive interference between the two overlaping atomic orbitals draws electron density away from the nuclear centers into the internuclear region. The potential energy rises as electron density is drawn away from the nuclei, but the total energy decreases because of a larger decrease in kinetic energy due to charge delocalization. Thus a decrease in kinetic energy funds the initial build up of charge between the nuclei that we normally associate with chemical bond formation.

Following this initial phase, at an internuclear separation of about 180 pm the potential energy begins to decrease and the kinetic energy increases, both sharply (eventually), while the total energy continues to decrease gradually. This is an atomic effect, not a molecular one as Ruedenberg so clearly showed. The initial transfer of charge away from the nuclei and into the bond region allows the atomic orbitals to contract significantly (α increases) causing a large decrease in potential energy because the electron density has moved, on average, closer to the nuclei. The kinetic energy increases because the orbitals are smaller and kinetic energy increases inversely with the square of the orbital radius.

An energy minimum is reached while the potential energy is still in a significant decline (6), indicating that kinetic energy is the immediate cause of a stable bond and the molecular ground state in H_2. The final increase in potential energy which is due mainly to nuclear-nuclear repulsion, and not electron-electron repulsion, doesn't begin until the internuclear separation is less than 50 pm, while the equilibrium bond length is 74 pm . Thus the common explanation that an energy minimum is reached because of nuclear-nuclear repulsion does not have merit.

The H2 ground state, E = -0.761 aJ, is reached at an internuclear separation of 74 pm (1.384 a_0). In light of the previous arguments it is instructive to partition the total H_2 electron density into atomic and molecular contributions. Each electron is in a molecular orbital which is a linear combination of hydrogenic 1s orbitals, as is shown below.

$$\Psi_{mo} = \frac{\Psi_{1sa}+\Psi_{1sb}}{\sqrt{2+2S_{ab}}} \quad \text{where} \quad \Psi_{1sa} = \sqrt{\frac{\alpha^3}{\pi}}\exp\left(-\alpha r_a\right) \quad \Psi_{1sb} = \sqrt{\frac{\alpha^3}{\pi}}\exp\left(-\alpha r_b\right)$$

The total electron density is therefore $2\Psi_{MO}^2$. The atomic, or non-bonding, electron density is given by the following equation, which represents the electron density associated with two non-interacting atomic orbitals.

$$\rho_n = 2\left(\left|\frac{\Psi_{1sa}+i\Psi_{1sb}}{\sqrt{2}}\right|\right) = \Psi_{1sa}^2 + \Psi_{1sb}^2$$

Clearly, the bonding electron density must be the difference between the total electron density and the non-bonding, or atomic, electron density.

$$\rho_b = \Psi_{MO}^2 - \rho_n = \rho_t - \rho_n$$

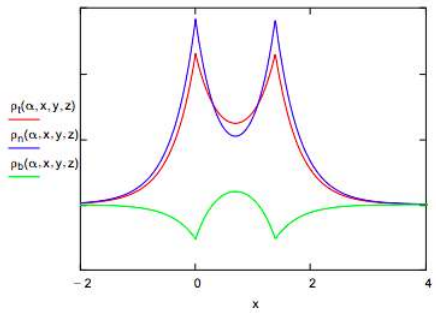
These three terms are plotted along the bond axis in the figure below. Alpha is the optimum orbital scale factor, S_{ab} is the overlap integral, and R is the equilibrium internuclear distance in atomic units.

$$\alpha = 1.197 \quad S_{ab} = 0.681 \quad R = 1.384 \quad y = 0 \quad z = 0 \quad x = -3, -2.99..5$$

$$\rho_t(\alpha,\ x,\ y,\ z) = \frac{\frac{\alpha^2}{\pi}\left[\exp\left(-\alpha\sqrt{x^2+y^2+z^2}\right)+\exp\left[-\alpha\sqrt{(x-R)^2+y^2+z^2}\right]\right]^2}{1+S_{ab}}$$

$$\rho_n(\alpha,\ x,\ y,\ z) = \frac{\alpha^2}{\pi}\left[\exp\left(-\alpha\sqrt{x^2+y^2+z^2}\right)+\exp\left[-\alpha\sqrt{(x-R)^2+y^2+z^2}\right]\right]^2$$

$$\rho_b(\alpha,\ x,\ y,\ z) = \rho_t(\alpha,\ x,\ y,\ z) - \rho_n(\alpha,\ x,\ y,\ z)$$



The bonding electron density illustrates that constructive interference accompanying atomic orbital overlap transfers charge from the nuclei into the internuclear region, while the non-bonding density clearly shows the subsequent atomic orbital contraction which draws some electron density back toward the nuclei.

Literature cited:

1. Slater, J. C. *J. Chem. Phys.* **1933**, *1*, 687-691.
2. Ruedenberg, K. *Rev. Mod. Phys.* **1962**, *34*, 326-352.
3. Feinberg, M. J.; Ruedenberg, K. *J. Chem. Phys.* **1971**, *54*, 1495-1511; 1971, 55, 5804-5818.
4. Feinberg, M. J.; Ruedenberg, K.; Mehler, E. L. *Adv. Quantum Chem.* **1970**, *5*, 27-98.
5. McQuarrie, D. A.; Simon, J. D. *Physical Chemistry: A Molecular Approach*, University Science Books, Sausalito, CA, 1997, p. 165.
6. Slater, J. C. *Quantum Theory of Matter*, Krieger Publishing, Huntington, N.Y., 1977, pp. 405-408.
7. Rioux, F. *The Chemical Educator*, **1997**, *2*, No. 6.

This page titled 3.6: The Covalent Bond According to Slater and Ruedenberg is shared under a CC BY 4.0 license and was authored, remixed, and/or curated by Frank Rioux via source content that was edited to the style and standards of the LibreTexts platform.

3.7: Slater's Analysis of the Covalent Bond using the Virial Theorem

John C. Slater [*J. Chem. Phys.* **1933**, *1*, 687-691] used the virial theorem to analyze the chemical bond and was the first to recognize the importance of kinetic energy in covalent bond formation. He wrote,

> ...this theorem gives a means of finding kinetic and potential energy separately for all configurations of the nuclei, as soon as the total energy is known, from experiment or theory.

The kinetic energy, potential energy and total energy of the hydrogen molecule are calculated as a function of R using the virial theorem and a Morse function for the total energy based on experimental parameters.

Total energy:

$$E(R) = T(R) + V(R)$$

Virial theorem:

$$2T(R) + V(R) = -R\frac{d}{dR}E(R)$$

Morse parameters:

$$D_e = 0.761aJ \quad \beta = 0.0193pm^{-1} \quad R_e = 74.1pm$$

These parameters are taken from Fig. 5.6 on page 165 of McQuarrie and Simon's *Physical Chemistry: A Molecular Approach*.

Morse function:

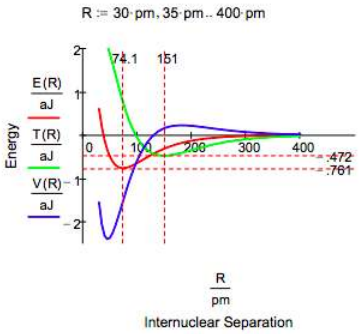
$$E(R) = D_e\left[1 - \exp\left[-\beta\left(R - R_e\right)\right]\right]^2 - D_e$$

Using equation (1) to eliminate V(R) in equation (2) yields an equation for kinetic energy as a function of the internuclear separation. Using equation (1) to eliminate T(R) in equation (2) yields an equation for potential energy as a function of the internuclear separation.

$$T(R) = -E(R) - R\frac{d}{dR}E(R)$$

$$V(R) = 2E(R) + R\frac{d}{dR}E(R)$$

These important equations determine the mean kinetic and potential energies as functions of R, one might almost say experimentally, directly from the curves of E as a function of R which can be found from band spectra. The theory is so simple and direct that one can accept the results without question....



The covalent bond in H2 can be thought of as arising from the overlap of 1s atomic orbitals forming a molecular orbital. As the atoms approach, the potential energy rises because constructive interference of the overlapping atomic orbitals draws electron density away from the nuclear centers into the bond region. Kinetic energy decreases due to delocalization of the electrons over the entire molecular orbital. At an inter-nuclear separation of 151 pm this trend reverses as the atomic orbitals shrink bringing electron density closer to both nuclei. It is the sharp increase in kinetic energy at 74.1 pm due to the shrinking of the molecular orbital that

causes the energy minimum and the formation of a stable bond; potential energy is still in a steep decline and doesn't begin to increase (mainly due to nuclear repulsion) until 40 pm. This analysis is based in part on a paper by John Winn [*J. Chem. Phys.* **1981**, *74*, 608-611].

The following table provides quantitative support for Winn's analysis. Step 1 occurs from large inter-nuclear separation to 151 pm and is molecular in character. Step 2 is the change from 151 pm to 74.1 pm and is basically atomic as electron density is drawn closer to the nuclei and out of the inter-nuclear bond region.

$$\begin{pmatrix} \prime & \text{Step 1} & \text{Step 2} & \text{Overall} \\ \frac{\Delta T}{aJ} & -0.472 & 1.233 & 0.761 \\ \frac{\Delta V}{aJ} & 0.166 & -1.688 & -1.522 \\ \frac{\Delta E}{aJ} & -0.306 & -0.455 & -0.761 \\ \frac{R}{pm} & 151 & 74.1 & 74.1 \\ \text{Type} & \text{Molecular} & \text{Atomic} & \text{Molecular + Atomic} \end{pmatrix}$$

Conversion factors:

$$pm = 10^{-12}m \quad aJ = 10^{-18}joule$$

This page titled 3.7: Slater's Analysis of the Covalent Bond using the Virial Theorem is shared under a CC BY 4.0 license and was authored, remixed, and/or curated by Frank Rioux via source content that was edited to the style and standards of the LibreTexts platform.

3.8: Two Analyses of the Covalent Bond using the Virial Theorem

Atomic and molecular stability and spectroscopy, and the nature of the chemical bond cannot be explained using classical physics: quantum mechanical principles are required. Bohr was a pioneer in an effort to apply an early version of quantum theory to these important issues with his models of the hydrogen atom and hydrogen molecule. Of course, Bohr's approach became "old" quantum mechanics and was abandoned in the 1920s with the creation of a "new" quantum mechanics by Heisenberg and Schrödinger and their collaborators. This tutorial deals exclusively with the chemical bond and summarizes Slater's contribution to our current understanding of the energetics of its formation using the virial theorem. Since the acceptance of the "new" quantum mechanics many others have contributed to the interpretation of chemical bond formation, but like Bohr, Slater was an insightful pioneer.

In a seminal paper, *J. Chem. Phys.* **1933**, *1*, 687-691, John C. Slater used the virial theorem to analyze chemical bond formation and was the first (in my opinion) to recognize the importance of kinetic energy in covalent bond formation. Regarding the universally valid virial theorem he wrote,

...this theorem gives a means of finding kinetic and potential energy separately for all configurations of the nuclei, as soon as the total energy is known, from experiment or theory.

The purpose of this tutorial is to demonstrate the validity of this assertion. The experimental method employs a Morse function for the energy of the hydrogen molecule ion parametrized using spectroscopic data. The theoretical approach is based on an ab initio LCAO-MO calculation of the energy based on a molecular orbital consisting a superposition of scaled hydrogen atomic orbitals.

Experimental Method

The kinetic energy, potential energy and total energy of the hydrogen molecule ion are calculated as a function of R using the virial theorem and a Morse function for the total energy based on experimental parameters.

Total energy:

$$E(R) = T(R) + V(R)$$

Virial theorem:

$$2T(R) + V(R) = -R\frac{d}{dR}E(R)$$

Morse parameters:

$$D_e = 0.103E_h \quad R_e = 2.003a_0 \quad \beta = 0.708a_0^{-1}$$

These parameters are from Levine, I. N. *Quantum Chemistry*, 6th ed., p. 400.

Morse function:

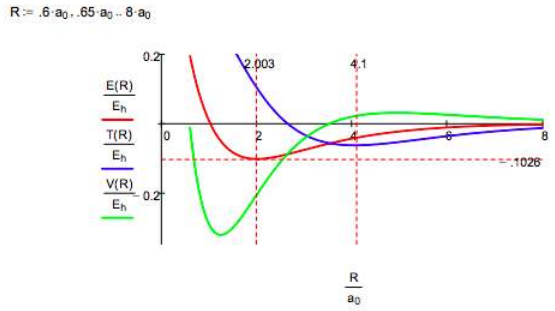
$$E(R) = D_e\left[1 - \exp\left[-\beta\left(R - R_e\right)\right]\right]^2 - D_e$$

Using equation (1) to eliminate V(R) in equation (2) yields an equation for kinetic energy as a function of the internuclear separation. Using equation (1) to eliminate T(R) in equation (2) yields an equation for potential energy as a function of the internuclear separation.

$$T(R) - = E(R) - R\frac{d}{dR}E(R)$$

$$V(R) = 2E(R) + R\frac{d}{dR}E(R)$$

> These important equations determine the mean kinetic and potential energies as functions of R, one might almost say experimentally, directly from the curves of E as a function of R which can be found from band spectra. The theory is so simple and direct that one can accept the results without question....



While the Morse calculation has an empirical flavor to it, its results are interpreted in terms of rudimentary quantum theory concepts. This energy profile shows that as the protons approach, the potential energy rises because molecular orbital formation (constructive interference) draws electron density away from the nuclei into the internuclear region. The kinetic energy decreases because molecular orbital formation brings about electron delocalization.

At about 4.1 a_0 this trend reverses as atomic orbital contraction begins. The kinetic energy rises because the volume occupied by the electron decreases and the potential energy decreases for the same reason: a smaller electronic volume brings the electron closer to the nuclei on average. Only at R ~ $1a_0$ does nuclear repulsion cause the total potential energy to increase and contribute to the repulsion energy of the molecule. In other words, the kinetic energy increase is the immediate cause of the energy minimum or ground state.

Theoretical Method

The following LCAO-MO calculation uses a superposition of scaled 1s atomic orbitals and yields the following result for the energy of the hydrogen molecule ion as a function of the internuclear distance and the orbital scale factor.

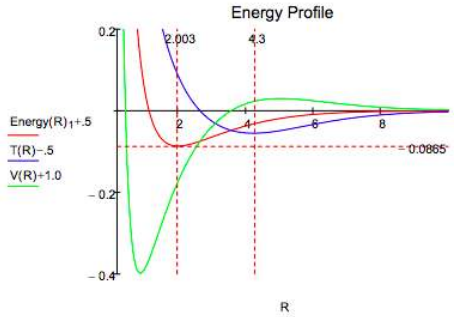
$$1s_a = \sqrt{\frac{\alpha^3}{\pi}\exp(-\alpha r_a)} \quad s_b = \sqrt{\frac{\alpha^3}{\pi}\exp(-\alpha r_b)} \quad S_{ab} = \int 1s_a 1s_b d\tau \quad \Psi_{mo} = \frac{1s_a + 1s_b}{\sqrt{2+2S_{ab}}}$$

$$E(\alpha,\ R) = \frac{-\alpha^2}{2} + \frac{\left[\alpha^2 - \alpha - \frac{1}{R} + \frac{1+\alpha R}{R}\exp(-2\alpha R) + \alpha(\alpha-2)(1+\alpha R)\exp(-\alpha R)\right]}{\left[1+\exp\left(-\alpha,\ R\right)\left(1+\alpha R+\frac{\alpha^2 R^2}{3}\right)\right]} + \frac{1}{R}$$

$$\alpha = 1 \quad \text{Energy} = \text{-2} \quad \text{Given} \quad \text{Energy} = E(\alpha,\ R) \quad \frac{d}{d\alpha}E(\alpha,\ R) = 0 \quad \text{Energy(R)} = \text{Find}(\alpha,\ \text{Energy})$$

As noted above, using $E = T + V$ with the virial theorem $2T + V = -R\frac{d}{dR}E$ leads to the following expressions for T and V.

$$T(R) = -\text{Energy}(R)_1 - R\frac{d}{dR}\text{Energy}(R)_1 \qquad V(R) = 2\text{Energy}(R)_1 + R\frac{d}{dR}\text{Energy}(R)_1 \quad R = .2, .25..10$$



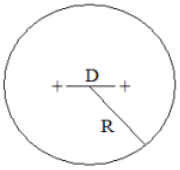
It is clear that both methods lead to very similar energy profiles. The only significant difference is that the Morse calculation leads to a lower energy minimum, -0.1026 Eh versus -0.0865 Eh for the molecular orbital calculation. Therefore, the interpretation provided for the Morse energy profile is valid for the LCAO-MO profile.

Conversion factors: $a_o = 5.29177(10)^{-11}m \quad E_h = 4.359748(10)^{-18}$ joule

This page titled 3.8: Two Analyses of the Covalent Bond using the Virial Theorem is shared under a CC BY 4.0 license and was authored, remixed, and/or curated by Frank Rioux via source content that was edited to the style and standards of the LibreTexts platform.

3.9: A Simple Charge Cloud Model for Molecular Hydrogen- Or, Is It a DFT Model?

A simple charge cloud model for H2 is shown below (1,2). Two protons, separated by distance D, are symmetrically embedded in a uniform-density, two-electron spherical charge cloud of radius R.



In atomic units ($h/2\pi = m_e = e = 4\pi\varepsilon_0 = 1$) the total electronic energy based on this model is,

$$E = \frac{9}{4R^2} - \frac{24}{5R} + \frac{D^2}{2R^3} + \frac{1}{D}$$

The various energy components are identified below (3).

$$\begin{aligned} &\text{Electron kinetic energy:} && T = \tfrac{9}{4R^2} \\ &\text{Electron-nucleus potential energy:} && V_{ne} = \tfrac{-6}{R} + \tfrac{D^2}{2R^3} \\ &\text{Electron-electron potential energy:} && V_{ee} = \tfrac{6}{5R} \\ &\text{Nucleus-nucleus potential energy:} && V_{nn} = \tfrac{1}{D} \end{aligned}$$

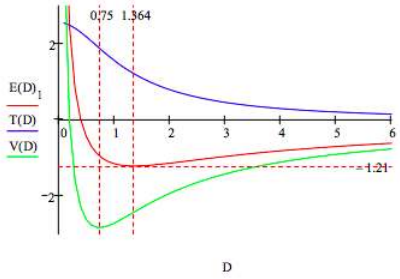
The total electronic energy is minimized with respect to R for a series of internuclear separations, D, to generate an energy curve that can be used with the virial theorem to generate kinetic and potential energy contributions.

$$\text{Seed values for the minimization algorithm:} \quad R = 1 \quad E = -2$$

$$\text{Given} \quad E = \tfrac{9}{4R^2} - \tfrac{24}{5R} + \tfrac{D^2}{2R^3} + \tfrac{1}{D} \quad \tfrac{d}{dR}\left(\tfrac{9}{4R^2} - \tfrac{24}{5R} + \tfrac{D^2}{2R^3} + \tfrac{1}{D}\right) = 0 \quad \text{E(D)} = \text{Find(R, E)}$$

Substitution of $E(D) = T(D) + V(D)$ into the virial relation $2T(D) + V(D) = -D\frac{d}{dD}E(D)$ yields expressions for the kinetic and potential energies given below.

$$\begin{aligned} D = .1, .2..6 \quad &\text{Kinetic energy:} && T(D) = -E(D)_1 - D\tfrac{d}{dD}E(D)_1 \\ &\text{Potential energy:} && V(D) = 2E(D)_1 + D\tfrac{d}{dD}E(D)_1 \end{aligned}$$



This graphic display of the total energy and its kinetic and potential energy components clearly shows that molecular stability depends on electron kinetic energy. The immediate cause of the total energy minimum is a rise in electron kinetic energy. In other words potential energy is still decreasing at D = 1.364, and doesn't start to rise sharply, due to electron and nuclear repulsion, until D = 0.75. So, although it is commonly thought and taught, electron and nuclear repulsion are not the immediate cause of atomic and molecular stability.

Minimization of the total energy simultaneously with respect to D and R locates the energy ground state and the equilibrium values of D and R precisely.

$$\text{Seed values for the energy minimization:} \quad D = 1 \quad R = 3$$

$$E(R,\ D) = \frac{9}{4R^2} - \frac{24}{5R} + \frac{D^2}{2R^3} + \frac{1}{D} \qquad \begin{pmatrix} R \\ D \end{pmatrix} = \text{Minimize(E, R, D)} \qquad \begin{pmatrix} R \\ D \end{pmatrix} = \begin{pmatrix} 1.364 \\ 1.364 \end{pmatrix} \qquad \text{E(R, D)} = \text{-1.21}$$

Show that the virial theorem is obeyed:

$$\left| \frac{V(R)}{T(D)} \right| = 2$$

The calculated internuclear separation, 1.364 a_0, is in good agreement with the experimental bond length of 1.40 a_0. However, the calculated ground state energy -1.21 E_h is lower than the experimental value -1.17 E_h. Thus in this calculation the virial theorem is satisfied, but the variational principle is violated.

It is the author′s opinion that the charge cloud approach is a primitive version of density functional theory (DFT), because as can be seen above, all energy components are calculated in terms of the electron density, the signature of the DFT method.

Literature cited:

1. G. F. Neumark, *Microfilm Abstr*. **11**, 834 (1951).
2. L. M. Kleiss, *Diss. Abstr.* **14**, 1562 (1954).
3. F. Rioux, *Am. J. Phys.* **44**, 56 (1976)

This page titled 3.9: A Simple Charge Cloud Model for Molecular Hydrogen- Or, Is It a DFT Model? is shared under a CC BY 4.0 license and was authored, remixed, and/or curated by Frank Rioux via source content that was edited to the style and standards of the LibreTexts platform.

3.10: Three Mechanisms for Bond Formation in the Hydrogen Molecule Ion

Introduction

Ruedenberg′s innovative analysis of the covalent bond (1-2) has received considerable attention in the pedagogical literature (3-13) as well as a number of excellent reviews in the primary literature that are accessible to non-specialists (14-16). The purpose of this study is analyze three mechanisms for covalent bond formation in H_2^+ that are suitable for an undergraduate course in quantum chemistry and reveal Ruedenberg′s central message - a full understanding of the nature of the chemical bond requires consideration of the role of electron kinetic energy.

All three mechanisms postulate a single intermediate state for the reaction for H_2^+ bond formation.

$$H + H^+ \rightarrow H_2^+$$

Scaled hydrogenic wave functions will be used to calculate the initial atomic state, the final molecular state and the intermediate states. Mathematical details can be found in the Appendix.

The Hydrogen Atom

Using the following 1s orbital

$$1s(\alpha,\ R) = \sqrt{\frac{\alpha^3}{\pi}}\exp(-\alpha,\ R)$$

in a variational calculation on the hydrogen atom yields the following result for the energy in atomic units.

$$E_H = \frac{\alpha^2}{2} - \alpha$$

The first term is electron kinetic energy and the second term is electron-nucleus potential energy. Minimization of EH with respect to α yields α = 1, and the following result for the ground state energy.

$$E_H = T + V = 0.50 - 1.0 = -0.50$$

The Hydrogen Ion Molecule

The H_2^+ molecular orbital is written as a linear superposition of scaled hydrogenic orbitals centered on the two hydrogen nuclei, a and b.

$$\Psi_{bmo} = \frac{1s_a(\alpha,\ r_a) + 1s_b(\alpha,\ r_b)}{\sqrt{2 + 2S_{ab}(\alpha,\ R_{ab})}}$$

S_{ab} is the overlap integral,

$$S_{ab}(\alpha,\ R_{ab} = \exp\left(-\alpha R_{ab}\right)\left[1 + \alpha R_{ab} + \frac{\alpha^2 R^2}{3}\right]$$

A variational calculation using Ψ_{bmo} yields the results in the following table.

o	$\frac{\text{Initial}}{\text{Atomic State}}$	o	$\frac{\text{Final}}{\text{Molecular State}}$
o	$H_{atom} + H_{ion}$	o	$\Psi_{mo} = \frac{a+b}{\sqrt{2+2S}}$
o	$\alpha = 1$	Δ	$\frac{\alpha=1.238}{R=2.003}$
T	0.5	0.0865	0.5865
V	−1.0	−0.1730	−1.1730
V_{ne}	−1.0	−0.6723	−1.623
V_{nn}	0	0.4993	0.4993
E	−0.50	−0.0865	−0.5865

Table 1 shows that the atomic and molecular states individually satisfy the virial theorem (E = V/2 = -T), as does the bond formation process (ΔE = ΔV/2 = -ΔT). At first glance Table 1 and the virial theorem suggest that chemical bonding is governed

solely by electrostatics. In bond formation, in the transition from atoms to a molecule, kinetic energy increases, potential energy decreases, and total energy decreases. From this perspective, clearly potential energy must be the key factor in the formation of a stable molecule, because it has the same sign as the change in total energy, and a decrease in energy is the signature of stability. That this sort of reasoning leads to an incorrect interpretation of the covalent bond will be illustrated by the mechanistic analyses that follow.

Mechanism I

The first mechanism is one that might appear familiar to general chemistry students. For example, when we describe the bonding in methane to undergraduates we generally invoke a mechanism that uses the concepts of atomic promotion [$2s^2 2p^2$ --> $2s^1 2p^3$], hybridization [$2s^1 2p^3$ --> (sp^3 hybrids)^4], and bond formation through the overlap of atomic orbitals. The H_2^+ bond formation mechanism described here consist of just two steps: atomic promotion and covalent bond formation ($H + H^+$ --> $H^* + H^+$ --> H_2^+). This simple mechanism has previously been discussed in the review literature (16) and has been invoked in a study of the covalent bond in H_2 (10).

$$H(\alpha = 1) + H^+ \rightarrow (\alpha = 1.238) + H^+ \rightarrow H_2^+(\alpha = 1.238,\ R = 2.003)$$

$$\begin{pmatrix} o & \frac{\text{Initial}}{\text{Atomic State}} & o & \frac{\text{Intermediate}}{\text{Excited Atomic State}} & o & \frac{\text{Final}}{\text{Molecular State}} \\ o & H_{atom} + H_{ion} & o & H_{atom} + H_{ion} & o & \Psi_{mo} = \frac{a+b}{\sqrt{2+2S}} \\ o & \alpha = 1 & \Delta & \alpha = 1.238 & \Delta & \frac{\alpha=1.238}{R=2.003} \\ T & 0.50 & 0.2663 & 0.7663 & -0.1798 & 0.5865 \\ V & -1.0 & -0.2380 & -1.2380 & 0.0650 & -1.1730 \\ V_{ne} & -1.0 & -0.2380 & -1.2380 & -0.4343 & -1.6723 \\ V_{nn} & 0 & 0 & 0 & 0.4993 & 0.4993 \\ E & -0.50 & 0.0283 & -0.4717 & -0.1148 & -0.5865 \end{pmatrix}$$

In the first step the hydrogen atom orbitals prepare for bonding by contracting from α = 1 to α = 1.238, the optimum value of the final molecular wave function. This step is atomic and endoergic (+0.0283 E_h), increasing the kinetic energy more (+0.2663 E_h) than it decreases the potential energy (-0.2380 E_h). The potential energy decreases because the electron is drawn closer to the nucleus. The kinetic energy increases because of the increased confinement of the electron in the contracted atomic orbital - kinetic energy is inversely proportional to the square of the average distance of the electron from the nucleus, or inversely proportional to volume of the electron distribution raised to the 2/3 power, $V^{-2/3}$.

The second step consists of the formation of a molecular wave function by the superposition (linear combination) of the promoted atomic orbitals. The electron density of this molecular orbital is,

$$(|\Psi_{bmo}|)^2 = \left(\left|\frac{a+b}{\sqrt{2+2S}}\right|\right)^2 = \frac{a^2+2ab+b^2}{2+2s}$$

Molecular orbital formation distributes the electron density over the entire molecule and this charge delocalization brings about a significant decrease in kinetic energy (-0.1798 E_h). Potential energy increases slightly (0.0650 E_h) because nuclear repulsion (0.4993 E_h) more than offsets the increase in electron-nuclear attraction (-0.4343 E_h) due to the fact that the electron now interacts with both nuclei. This step is exoergic (-0.1148 Eh) because kinetic energy decreases more than potential energy increases. In other words, in this mechanism charge delocalization funds (drives) the formation of the chemical bond.

Mechanism II

Mechanism II postulates an intermediate non-bonding molecular state that has the equilibrium values of α and R. The non-bonding character this state is revealed by examining its electron density.

$$(|\Psi_{nmo}|)^2 = \left(\left|\frac{a+ib}{\sqrt{2}}\right|\right)^2 = \frac{a^2}{2} + \frac{b^2}{2}$$

The electron density has no interference term and simply places half the electron density in each atomic orbital. The energy of the non-bonding state as a function of α and R and is provided in the Appendix. This intermediate state subsequently relaxes to the final molecular bonding state. The calculations for this mechanism are summarized in Table III.

o	$\frac{\text{Initial}}{\text{Atomic State}}$	o	$\frac{\text{Intermediate}}{\text{Non Bonding State}}$	o	$\frac{\text{Final}}{\text{Molecular State}}$
o	$H_{atom}+H_{ion}$	o	$\Psi_{nmo}=\frac{a+ib}{\sqrt{2}}$	o	$\Psi_{mo}=\frac{a+b}{\sqrt{2+2S}}$
o	$\alpha=1$	Δ	$\frac{\alpha=1.238}{R=2.003}$	Δ	$\frac{\alpha=1.238}{R=2.003}$
T	0.50	0.2663	0.7663	−0.1798	0.5865
V	−1.0	−0.2258	−1.2258	0.0528	−1.1730
V_{ne}	−1.0	−0.7251	−1.7251	0.0528	−1.6723
V_{nn}	0	0.4993	0.4993	0	0.4993
E	−0.50	0.0407	−0.4595	−0.1270	−0.5865

Formation of the non-bonding molecular state is endoergic (+0.0407 E_h) because orbital contraction increases kinetic energy (+0.2664 E_h) more than it decreases potential energy (-0.2258 E_h). The kinetic energy increase for this intermediate state is identical to that in Mechanism I. The potential energy decrease is less than that for Mechanism I because nuclear-nuclear repulsion (+0.4993 E_h) in the intermediate state is greater than "electron-other-nucleus" attraction [-0.4871 E_h = -0.7251 E_h - (-0.2380 E_h)]

The subsequent relaxation to the bonding molecular state is exoergic (-0.1270 E_h) because charge delocalization decreases kinetic energy (-0.1799 E_h) more than charge redistribution to the bond region increases electron-nucleus potential energy (+0.0528 E_h). As in Mechanism I we have an endoergic atomic step followed by a exoergic molecular step.

This mechanism clarifies an important issue. It is commonly thought, and frequently taught, that from a potential energy point of view the internuclear region is the most favorable place for electron density because it is midway between to nuclei. However, this mechanism clearly shows that the redistribution of charge into the internuclear region due to the interference term in the bonding electron density occurs with an increase in potential energy. That this is not some arcane quantum mechanical phenomenon is revealed by a simple classical electrostatic calculation [11]. From a purely electrostatic perspective the prefered location for an electron is in the nucleus.

If a stable chemical bond is due to the build-up of charge density in the internuclear region, then this mechanism shows that kinetic energy plays a crucial role in bringing about this effect.

Mechanism III

The third mechanism postulates an initial molecular state, rather than a promoted atomic state or a non-bonding molecular state for the intermediate. The initial molecular state has the equilibrium bond length, but the atomic value for the orbital scale factor, α. The calculations based on this mechanism are shown below.

$$H(\alpha=1)+H^+ \rightarrow H_2^+(\alpha=1,\ R=2.003) \rightarrow H_2^+(\alpha=1.238,\ R=2.003)$$

o	$\frac{\text{Initial}}{\text{Atomic State}}$	o	$\frac{\text{Intermediate}}{\text{Bonding State}}$	o	$\frac{\text{Final}}{\text{Molecular State}}$
o	$H_{atom}+H_{ion}$	o	$\Psi_{imo}=\frac{a+b}{\sqrt{2+2S}}$	o	$\Psi_{mo}=\frac{a+b}{\sqrt{2+2S}}$
o	$\alpha=1$	Δ	$\frac{\alpha=1}{R=2.003}$	Δ	$\frac{\alpha=1.238}{R=2.003}$
T	0.50	−0.1138	0.3862	0.2003	0.5865
V	−1.0	0.0599	−0.9401	−0.2329	−1.1730
V_{ne}	−1.0	−0.4394	−1.4394	−0.2329	−1.6723
V_{nn}	0	0.4993	0.4993	0	0.4993
E	−0.5	−0.0539	−0.5539	−0.0326	−0.5865

The intermediate molecular state is calculated at the equilibrium bond length (R = 2.003 a_o) for a molecular orbital with α = 1.0. Charge delocalization over the two nuclear centers on the formation of the molecular orbital brings about a large decrease in kinetic energy (-0.1138 E_h). Potential energy (+0.0599 E_h) increases because nuclear repulsion (0.4993 E_h) is larger, as in Mechanism II, than electron-other-nucleus attraction (-0.4394 E_h). This step is exoergic and we see again that it is kinetic energy drives covalent bond formation.

In the second step of this mechanism the atomic orbitals making up the molecular orbital contract (α increases from 1 to 1.238) to achieve the final equilibrium molecular state. This orbital contraction decreases electron-nucleus potential energy (-0.2329 E_h) more than it increases kinetic energy (+0.2003 E_h), so this step is also exoergic. However, as Ruedenberg pointed out, this step is essentially atomic in character. Orbital contraction draws electron density out of the bond region back toward the nuclei. In other words it returns some of the charge density transferred to the bond region in the first step back to the nuclear centers.

Summary

The three mechanisms examined postulate three different intermediate states: (1) promoted atomic; (2) non-bonding molecular; (3) intermediate molecular. However, they all tell the same story; kinetic energy plays a crucial role in chemical bond formation, and therefore viable models for the covalent bond require a consideration of both kinetic and potential energy. The virial theorem notwithstanding (as Ruedenberg has said), the formation of a chemical bond is not simply an electrostatic phenomena.

Appendix: Computational Details

Atomic energy contributions

$$E_H(\alpha) = \frac{\alpha^2}{2} - \alpha \quad T_H(\alpha) = \frac{\alpha^2}{2} \quad V_H(\alpha) = -\alpha$$

Bonding molecular energy contributions:

$$S(\alpha,\ R) = \exp(-\alpha,\ R)\left(1 + \alpha R + \frac{\alpha^2 R^2}{3}\right) \quad T_{bmo}(\alpha,\ R) = \frac{\alpha^2}{2}\frac{1+\exp(-\alpha,\ R)\left(1+\alpha R - \frac{\alpha^2 R^2}{3}\right)}{1+S(\alpha,\ R)}$$

$$V_{bmo}(\alpha,\ R) = \frac{-\alpha - \frac{1}{R} + \frac{1}{R}(1+\alpha R)\exp(-2\alpha R) - 2\alpha(1+\alpha R_{\exp}(-\alpha R)}{1+S(\alpha,\ R)} + \frac{1}{R}$$

$$E_{bmo}(\alpha,\ R) = T_{bmo}(\alpha,\ R) + V_{bmo}(\alpha,\ R)$$

Non-bonding molecular energy contributions:

$$T_{nbmo}(\alpha,\ R) = \frac{\alpha^2}{2} \quad V_{nbmo}(\alpha,\ R) = -\alpha + \left(\alpha + \frac{1}{R}\right)\exp(-2\alpha R) \quad E_{nbmo}(\alpha,\ R) = T_{nbmo}(\alpha,\ R) + V_{nbmo}(\alpha,\ R)$$

Initial Atomic State

$$T_H(1) = 0.5000 \quad V_H(1) = -1.0000 \quad E_H(1) = -0.5000$$

Final Molecular State:

$$T_{bmo}(1.238,\ 2.003) = 0.5865 \quad V_{bmo}(1.238,\ 2.003) = -1.1730$$
$$E_{bmo}(1.238,\ 2.003) = -0.5865$$

Mechanism I - Intermediate - Excited Atomic State

$$T_H(1.238) = 0.7663 \quad V_H(1.228) = -1.2380 \quad E_H(1.238) = -0.4717$$

Mechanism II - Intermediate = Nonbonding Molecular State

$$E_{nbmo}(1.238,\ 2.0033) = -0.4595 \quad T_{nbmo}(1.238,\ 2.0033) = 0.7663 \quad V_{nbmo}(1.238,\ 2.0033) = -1.2258$$

Mechanism III - Intermediate Bonding Molecular State

$$T_{bmo}(1,\ 2.003) = 0.3862 \quad V_{bmo}(1,\ 2.003) = -0.9401 \quad E_{bmo}(1,\ 2.003) = -0.5539$$

Literature cited:

1. Ruedenberg, K. *Rev. Mod. Phys.* **1962**, 34, 326-352. Feinberg, M. J.; Ruedenberg, K. *J. Chem. Phys.* **1971**, 54, 1495-1511. Feinberg, M. J.; Ruedenberg, K. *J. Chem. Phys.* **1971**, *55*, 5804-5818.
2. Ruedenberg, K. In *Localization and Delocalization in Quantum Chemistry*; Chalvet, O. et al., Eds.; Reidel: Dordrecht, The Netherlands, **1975**; Vol. I, pp 223-245.
3. Harcourt, R. D.; Solomon, H.; Beckworth. *J. Am. J. Phys.* **1982**, *50*, 557-559.
4. Baird, N. C. J. Chem. Educ. 1986, *63*, 660-664.
5. Harcourt, R. D. Am. J. Phys. 1988, *56*, 660-661.
6. Nordholm, S. J. Chem. Educ. 1988, *65*, 581-584.
7. Bacskay, G. G.; Reimers, J. R.; Nordholm, S. *J. Chem. Educ.* **1997**, *74*, 1494-1502.
8. Weinhold, F. *J. Chem. Educ.* **1999**, *76(8)*, 1141-1145.
9. Rioux, F. *Chem. Educator* **1997**, *2(6)*, 1-14.
10. Rioux, F. *Chem. Educator* **2001**, *6(6)*, 288-290.

11. Rioux, F. *Chem. Educator* **2003**, *8(1)*, 10-12.
12. Ashkenazai, G; Kosloff, R. *Chem. Educator* **2006**, *11(2)*, 1-10.
13. Nordholm, S.; Back, A.; Bacskay, G. B. *J. Chem. Educ.* **2007**, *84(7)*, 1201-1203.
14. Kutzelnigg, W. *Angew. Chem. Int. Ed. Eng.* **1973**, *12*, 546-562.
15. Melrose, M. P.; Chauhan, M.; Kahn, F. *Theor. Chim. Acta* **1994**, 88, 311-324.
16. Gordon, M. S.; Jensen, J. H. *Theor. Chem. Acc.* **2000**, 103, 248-251.

Added references: Recently Klaus Ruedenberg and former student (now colleague) Mike Schmidt published two exhaustive studies on the quantum mechanical principles of the covalent bond.

- ″Why Does Electron Sharing Lead to Covalent Bonding? A Variational Analysis″ *J. Comput. Chem.* **2007**, *28*, 391-410.
- ″Physical Understanding through Variational Reasoning: Electron Sharing and Covalent Bonding″ *J. Phys. Chem.* A, **2009**. *113(10)*, 1954-1968.

This page titled 3.10: Three Mechanisms for Bond Formation in the Hydrogen Molecule Ion is shared under a CC BY 4.0 license and was authored, remixed, and/or curated by Frank Rioux via source content that was edited to the style and standards of the LibreTexts platform.

3.11: A Mechanistic Approach to Bond Formation in the Hydrogen Molecule Ion

The centrality of the covalent bond to chemistry is captured in a short and eloquent statement by Peter Atkins [1].

> Now we come to the heart of chemistry. If we can understand what holds atoms together as molecules we may also start to understand why, under certain conditions, old arrangements change in favor of new ones. We shall understand structure, and through structure, the mechanism of change.

The barrier to understanding is that, in spite of what our textbooks teach, "The chemical bond is a highly complex phenomenon which eludes all attempts at simple description [2]." Charles Coulson, one of the pioneering theorists in the application of quantum mechanics to the study of chemical bonding wrote the following [3].

> Sometimes it seems to me that a bond between two atoms has become so real, so tangible, so friendly that I can almost see it. And then I awake with a little shock: for a chemical bond is not a real thing: it does not exist: no one has ever seen it, no one ever can. It is a figment of our own imagination.... Here is a strange situation. The tangible, the real, the solid, is explained by the intangible, the unreal, the purely mental.

Many chemists and physicists have grappled with the intellectual challenge of understanding the chemical bond. Among those who have made significant contributions are Hellmann [4], Pauling [5], Slater [6, 7], Coulson [8] and Ruedenberg [9-12]. Among these, Ruedenberg's work is the most comprehensive and cogent. It has received considerable attention in the pedagogical literature [13-23] as well as a number of excellent reviews in the primary literature that are accessible to non specialists [24-26].

Unfortunately none of these efforts to make Ruedenberg's analysis of the covalent bond accessible to educators has had any noticeable affect on the way the chemical bond is presented in introductory and intermediate level undergraduate textbooks [27]. Therefore, the purpose of this paper is to try again by providing a simple two-step mechanistic approach to covalent bond formation in H_2^+ that reveals Ruedenberg's central message - a full understanding of the nature of the chemical bond requires consideration of the role of electron kinetic energy, or more appropriately confinement energy [28].

The mechanism postulates a single intermediate molecular state for the H_2^+ bond formation reaction.

$$H + H^+ \rightarrow H_2^+$$

Scaled hydrogenic wave functions will be used to calculate the initial atomic state, and the intermediate and final molecular states. Computational details for the intermediate and final molecular states are available in the appendix.

The Initial State

Schrödinger's equation for the hydrogen atom, of course, is exactly soluble and the result in atomic units ($h/2\pi = m_e = e = 4\pi\varepsilon_0 = 1$; $E_h = 4.3597 \times 10^{-18}$ J) is given below. By convention the energy of the hydrogen ion is zero.

$$E_H = T + V = 0.50E_h - 1.0E_h = -0.50E_h$$

The Hydrogen Molecule Ion

The H_2^+ molecular orbital is written as a linear superposition of scaled hydrogenic orbitals centered on the two hydrogen nuclei, where S is the overlap integral. (a and b label the atomic orbitals, A and B the nuclear centers which are separated by a distance R.

$$\Psi_{mo} = \frac{a+b}{\sqrt{2+2S}}$$

where

$$a = \sqrt{\tfrac{\alpha^3}{\pi}}\exp(-\alpha r_A) \quad b = \sqrt{\tfrac{\alpha^3}{\pi}}\exp(-\alpha r_B) \quad S = \int abd\tau$$

This trial wave function and the appropriate energy operator lead to the following variational energy integral, expressed in Dirac notation.

$$E = \left(a+b\left|T - \frac{1}{r_A} - \frac{1}{r_B} + \frac{1}{R}\right|a+b\right)[2(1+S)]^{-1}$$

Expansion, after symmetry considerations, yields the following expression,

$$E = \frac{(a|T|a) + (a|T|b) + \left(a\left|\frac{-1}{r_A}\right|a\right) + \left(b\left|\frac{-1}{r_A}\right|b\right) + 2\left(a\left|\frac{-1}{r_A}\right|b\right)}{1+S} + \frac{1}{R}$$

which is written below in short-hand notation.

$$E = \frac{T_{aa} + T_{ab} + V_{Aaa} + V_{Abb} + 2V_{Vab}}{1+S} + \frac{1}{R}$$

Minimization of the energy of H_2^+ yields the optimum values for α and R, its ground state energy and energy components. Table 1 summarizes the results for the formation of the molecule ion from a hydrogen atom and hydrogen ion.

o	$\frac{\text{Initial}}{\text{Atomic State}}$	o	$\frac{\text{Final}}{\text{Molecular State}}$
o	$H_{atom} + H_{ion}$	o	$\Psi_{mo} = \frac{a+b}{\sqrt{2+2S}}$
o	$\alpha = 1$	Δ	$\frac{\alpha=1.238}{R=2.003}$
T	0.5	0.0865	0.5865
V	−1.0	−0.1730	−1.1730
V_{ne}	−1.0	−0.6723	−1.6723
$V_{ne}(Aaa)$	−1.0	0.1539	−0.8461
$V_{ne}(Abb)$	0	−0.3329	−0.3329
$V_{ne}(Aab)$	0	−0.4933	−0.4933
V_{nn}	0	0.4993	0.4993
E	−0.5	−0.0865	−0.5865

V_{ne}(Aaa) is the interaction of the electron density centered on nucleus A with nucleus A. V_{ne}(Abb) is the interaction of the electron density centered on nucleus B with nucleus A. V_{ne}(Aab) is the interaction of the overlap electron density with nucleus A. These energy contributions include the companion terms involving nucleus B as justified by molecular symmetry.

Table 1 shows that the atomic and molecular states individually satisfy the virial theorem (E = V/2 = -T), and therefore so does the bond formation process (ΔE = ΔV/2 = -ΔT). At first glance Table 1 and the virial theorem suggest that chemical bonding is governed solely by electrostatics. In bond formation, in the transition from atoms to a molecule, kinetic energy increases, potential energy decreases, and total energy decreases. From this perspective it appears that potential energy must be the key factor in the formation of a stable molecule, because it has the same sign as the change in total energy, and a decrease in energy is the signature of stability. That this view is an over-simplification is shown by the energy profile (in atomic units) provided by an ab initio calculation of covalent bond formation in the hydrogen molecule ion using the trial molecular orbital given above.

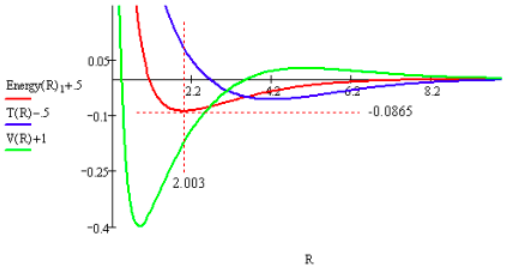


Figure 1. Ab initio energy profile for the formation the hydrogen molecule ion.

This energy profile shows that consideration of kinetic energy is essential in understanding bond formation and molecular stability. First, the initial drop in total energy as the nuclei approach each other is due to a decrease in kinetic energy, because the potential energy initially increases. Second, the energy minimum (ground state) is achieved while potential energy is in a steep decline. It is a sharp increase in kinetic energy that causes the energy minimum and provides the "repulsive" effect necessary to counter the (still) attractive potential energy term. As the profile shows nuclear repulsion doesn't become dominant until well after the energy minimum has been reached. Clearly a valid model for the covalent bond requires consideration of both kinetic and potential energy.

These *ab initio* results are supported by a more empirical approach based on the virial theorem, a method of analysis first demonstrated by Slater in 1933 [5]. A serviceable representation of molecular energy for diatomic molecules (excluding nuclear kinetic energy, i.e. vibrational degrees of freedom) is provided by the Morse function.

$$E(R) = D_e \left[1 - \exp\left[-\beta\left(R - R_e\right)\right]\right]^2 - D_e$$

The Morse parameters (De, Re and β) can be obtained from analysis of spectroscopic data. Therefore, using the Morse function with the general expression for the virial theorem (valid for both the classical and quantum mechanical domains)

$$2T(R) + V(R) = -R\frac{d}{dR}E(R)$$

and the expression for total energy

$$E(R) = T(R) + V(R)$$

leads to the following equations for kinetic and potential energy as a function of internuclear separation.

$$T(R) = -E(R) - R\tfrac{d}{dR}E(R) \quad V(R) = 2E(R) + R\tfrac{d}{dR}E(R)$$

Using spectroscopic parameters from the literature [29] for H_2^+ allows the generation of the following energy profile in atomic units.

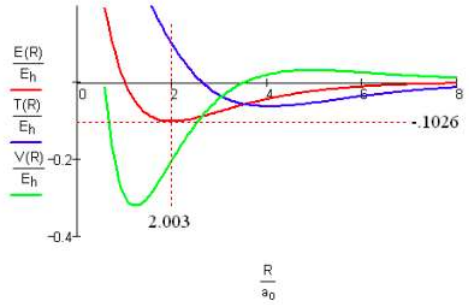


Figure 2. Energy profile for the formation of the hydrogen molecule ion based on the virial theorem.

The basic agreement between Figure 1 (theoretical, ab initio) and Figure 2 (experimental, spectroscopic) supports the view that both kinetic and potential energy considerations are required for a viable model of the covalent bond; models that consider only electrostatic potential energy effects are invalid and misleading.

In Figures 1 and 2 the fact that the potential energy increases, then decreases, and finally increases again as R decreases suggests that it can be partitioned into three terms. The initial decrease in kinetic energy is followed by an increase indicating that it consists of two opposing contributions. Thus, Ruedenberg analyzed the H_2^+ bond formation in terms of five contributions to the binding energy. In an effort to make Ruedenberg′s ideas accessible to undergraduates, a simple two-step mechanistic approach will be used to interpret covalent bond formation.

As shown below, the mechanism postulates an intermediate molecular state at the equilibrium bond length, but with the atomic value for the orbital scale factor, α. Computational details on the intermediate state are provided in the appendix.

$$H(\alpha = 1) + H^+ \rightarrow H_2^+(\alpha = 1,\ R = 2.003) \rightarrow H_2^+(\alpha = 1.238,\ R = 2.003)$$

$$\begin{pmatrix}
o & \frac{\text{Initial}}{\text{Atomic State}} & o & \frac{\text{Intermediate}}{\text{Molecular State}} & o & \frac{\text{Final}}{\text{Molecular State}} \\
o & H_{atom} + H_{ion} & o & \Psi_{imo} = \frac{a+b}{\sqrt{2+2S}} & o & \Psi_{mo} = \frac{a+b}{\sqrt{2+2S}} \\
o & \alpha = 1 & \Delta & \frac{\alpha=1}{R=2.003} & \Delta & \frac{\alpha=1.238}{R=2.003} \\
T & 0.5 & -0.1138 & 0.3862 & 0.2003 & 0.5865 \\
V & -1.0 & 0.0599 & -0.9401 & -0.2329 & -1.1730 \\
V_{ne} & -1.0 & -0.4394 & -1.4394 & -0.2329 & -1.6723 \\
V_{ne}(Aaa) & -1.0 & 0.36937 - 0.6307 & -0.2154 & -0.8461 & \\
V_{ne}(Abb) & 0 & -0.2976 & -0.2976 & -0.0353 & -0.3329 \\
V_{ne}(Aab)0 & -0.511 & -0.511 & 0.0178 & -0.4933 & \\
V_{nn}0 & 0.4993 & 0.4993 & 0 & 0.4993 & \\
E & -0.5 & -0.0539 & -0.5539 & -0.0326 & -0.5865
\end{pmatrix}$$

The first step is exoergic and is driven by a decrease in electron kinetic energy. Charge delocalization over the two nuclear centers on the formation of the molecular orbital brings about a large decrease in kinetic energy (-0.1138 E_h) because of the larger molecular volume now available to the electron [28]. Potential energy increases (+0.0599 E_h) because nuclear repulsion (+0.4993 E_h) is larger than the decrease electron-nucleus potential energy (-0.4394 E_h), which consists of the three contributions shown in Table 2. Constructive interference between atomic orbitals during molecular orbital formation draws some electron density into the internuclear region where potential energy is higher than in the region around the nucleus. Thus, the significant increase in Vne(Aaa) (+0.3693 E_h) is the main reason that the decrease in the attractive V_{ne} term is less than the increase in the repulsive V_{nn} term.

The second step is also exoergic, but is driven by a decrease in potential energy. In this step the atomic orbitals making up the molecular orbital contract (α increases from 1 to 1.238) to achieve the final equilibrium molecular state. Orbital contraction draws electron density from the bond region back toward the nuclei - it returns some of the charge density transferred to the bond region in the first step back to the nuclear centers. This is evidenced by the significant decrease in V_{ne}(Aaa) (-0.2154 E_h) and the change in the overlap integral from 0.5856 for α = 1 to 0.4632 for α = 1.238 (see the appendix). The changes in V_{ne}(Abb) and V_{ne}(Aab) are relatively minor in this step. Potential energy decreases (-0.2329 E_h) because the electron is on average closer to the nuclei. Kinetic energy increases (+0.2003 E_h) because orbital contraction decreases the volume occupied by the electron [28].

This mechanism is consistent with the computational results summarized in Figures 1 and 2, and therefore, reiterates that a consideration of both kinetic and potential energy effects are required to understand the nature of the covalent bond. Electron-nucleus potential energy is the only negative (attractive) energy term and is the "glue" that holds the molecule together. Paradoxically kinetic energy plays two contradictory roles in covalent bond formation. Its initial decrease due to charge delocalization funds the build up of charge in the internuclear region and is responsible for the early drop in total energy, while its subsequent sharp increase due to orbital contraction insures a ground state and a stable molecular entity.

To summarize further we can say that the first step is molecular in character and is driven by a decrease in electron kinetic energy. The second step, orbital contraction, is atomic in character (drawing electron density back to the nuclei) and driven by a decrease in electron-nucleus potential energy.

Literature cited:

1. Atkins, P. W. *Molecular Quantum Mechanics*, 2nd ed.; Oxford University Press, Oxford, UK, 1983, p.250.
2. Kutzelnigg, W. *Angew. Chem. internat. Edit.* **1973**, *12*, 546-562.
3. Coulson, C. A. *J. Chem. Soc.* **1955**, 2069.
4. Hellmann, H. Z. *Phys.* **1933**, *35*, 180.
5. Pauling, L. *The Nature of the Chemical Bond*, 3rd ed.; Cornell University Press, Ithaca, NY, 1960.
6. Slater, J. C. *J. Chem. Phys.* **1933**, *1*, 687-691.
7. Slater, J. C. *Quantum Theory of Matter*, Krieger Publishing: Untington, NY, 1977; pp 405-408.
8. Coulson, C. A. *Valence*, 2nd ed.; Oxford University Press, Oxford, UK, 1961.
9. Ruedenberg, K. *Rev. Mod. Phys.* **1962**, *34*, 326-352.
10. Feinberg, M. J.; Ruedenberg, K. *J. Chem. Phys.* **1971**, *54*, 1495-1511. Feinberg, M. J.; Ruedenberg, K. *J. Chem. Phys.* **1971**, *55*, 5804-5818.
11. Ruedenberg, K. In *Localization and Delocalization in Quantum Chemistry*; Chalvet, O. et al., Eds.; Reidel: Dordrecht, The Netherlands, 1975; Vol. I, pp 223-245.
12. Ruedenberg, K.; Schmidt, M. W. *J. Comput. Chem.* **2007**, *28*, 391-410. Ruedenberg, K.; Schmidt, M. W. *J. Phys. Chem. A* **2009**, *113*, 1954-1968.
13. Harcourt, R. D.; Solomon, H.; Beckworth. *J. Am. J. Phys.* **1982**, *50*, 557-559.
14. Baird, N. C. *J. Chem. Educ.* **1986**, *63*, 660-664.
15. Harcourt, R. D. *Am. J. Phys.* **1988**, *56*, 660-661.
16. Nordholm, S. *J. Chem. Educ.* **1988**, *65*, 581-584.
17. Bacskay, G. G.; Reimers, J. R.; Nordholm, S. *J. Chem. Educ.* **1997**, *74*, 1494-1502.
18. Weinhold, F. *J. Chem. Educ.* **1999**, *76(8)*, 1141-1145.
19. Rioux, F. *Chem. Educator* **1997**, *2(6)*, 1-14.
20. Rioux, F. *Chem. Educator* **2001**, *6(5)*, 288-290.

21. Rioux, F. *Chem. Educator* **2003**, *8(1)*, 10-12.
22. Ashkenazi, G; Kosloff, R. *Chem. Educator* **2006**, *11(2)*, 67-76.
23. Nordholm, S.; Back, A.; Bacskay, G. B. *J. Chem. Educ.* **2007**, *84*, 1201-1203.
24. Kutzelnigg, W. *Angew. Chem. Int. Ed. Eng.* **1973**, *12*, 546-562.
25. Melrose, M. P.; Chauhan, M.; Kahn, F. *Theor. Chim. Acta* **1994**, *88*, 311-324.
26. Gordon, M. S.; Jensen, J. H. *Theor. Chem. Acc.* **2000**, *103*, 248-251.
27. An exception is the physical chemistry text by Jeff Davis which provides a concise and coherent quantum mechanically correct interpretation of the covalent bond. Unfortunately it is long out of print. Davis, J. C., *Advanced Physical Chemistry: Molecules, Structure, and Spectra*; The Ronald Press, New York, 1965; pp 427-428.
28. Electrons confined by attractive interaction with nuclei in atoms and molecules occupy, due to their wave nature, stationary states. They are not executing classical trajectories and consequently the term kinetic energy is inappropriate. Substitution of the de Broglie relation (p = h/λ) into the classical expression for kinetic energy yields the electron′s confinement energy, $h^2/2m\lambda^2$. Because the wavelength of a confined electron is proportional to the confinement dimension, it is also proportional to cube root of the confinement volume, V1/3. Therefore the electron′s confinement energy is proportional to $V^{-2/3}$.
29. Levine, I. N. *Quantum Chemistry*, 6th ed., Pearson Prentice Hall, Upper Saddle River, NJ, 2009; p 400.

Appendix

Overlap integral:

$$S(\alpha,\ R) = \exp(-\alpha,\ R)\left(1 + \alpha R + \frac{\alpha^2 R^2}{3}\right)$$

Kinetic energy integrals:

$$Taa(\alpha,\ R) = \frac{\frac{1}{2}\alpha^2}{1+S(\alpha,\ R)} \quad Tab(\alpha,\ R) = \frac{\frac{\alpha^2}{2}\exp(-\alpha R)\left(1+\alpha R-\frac{\alpha^2 R^2}{3}\right)}{1+S(\alpha,\ R)}$$

Potential energy integrals: $VAaa(\alpha,\ R) = \frac{-\alpha}{1+S(\alpha,\ R)}$

$$VAbb(\alpha,\ R) = \frac{-\alpha\left[\frac{1}{\alpha R}-\exp(-2\alpha R)\left(1+\frac{1}{\alpha R}\right)\right]}{1+S(\alpha,\ R)} \quad VAab(\alpha,\ R) = \frac{-\alpha\exp(-\alpha R)(1+\alpha R)}{1+S(\alpha,\ R)}$$

Intermediate Molecular State

Values of variational parameters: $\alpha = 1 \quad R = 2.003$ Overlap integral: $S(\alpha,\ R) = 0.5856$

Total energy: $Taa(\alpha,\ R) + Tab(\alpha,\ R) + VAaa(\alpha,\ R) + VAbb(\alpha,\ R) + 2VAab(\alpha,\ R) + \frac{1}{R} = -0.5539$

Kinetic energy: $Taa(\alpha,\ R) + Tab(\alpha,\ R) = 0.3862 \quad Taa(\alpha,\ R) = 0.3153 \quad Tab(\alpha,\ R) = 0.0709$

Electron-nucleus potential energy: $VAaa(\alpha,\ R) + VAbb(\alpha,\ R) + 2VAab(\alpha,\ R) = -1.4394$

$VAaa(\alpha,\ R) == 0.6307 \quad VAbb(\alpha,\ R) = -0.2976 \quad 2VAab(\alpha,\ R) = -0.5111$

Nuclear potential energy: $\frac{1}{R} = 0.4993$

Total potential energy: $VAaa(\alpha,\ R) + VAbb(\alpha,\ R) + 2VAab(\alpha,\ R) + \frac{1}{R} = -0.9401$

Final Molecular State

Values of variational parameters: $\alpha = 1.238 \quad R = 2.003$ Overlap integral: $S(\alpha,\ R) = 0.4632$

Total Energy: $Taa(\alpha,\ R) + Tab(\alpha,\ R) + VAaa(\alpha,\ R) + VAbb(\alpha,\ R) + 2VAab(\alpha,\ R) + \frac{1}{R} = -0.5865$

Kinetic energy: $Taa(\alpha,\ R) + Tab(\alpha,\ R) = 0.5865 \quad Taa(\alpha,\ R) = 0.5237 \quad Tab(\alpha,\ R) = 0.0627$

Electron-nucleus potential energy: $Vaa(\alpha,\ R) + VAbb(\alpha,\ R) + 2VAab(\alpha,\ R) = -1.6722$

$$VAaa(\alpha,\ R) = -0.8461 \quad VAbb(\alpha,\ R) = -0.3329 \quad 2VAab(\alpha,\ R) = -0.4933$$

Nuclear potential energy:	$\frac{1}{R} = 0.4993$
Total potential energy:	$VAaa(\alpha,\ R) + VAbb(\alpha,\ R) + 2VAab(\alpha,\ R) + \frac{1}{R} = -1.1730$

This page titled 3.11: A Mechanistic Approach to Bond Formation in the Hydrogen Molecule Ion is shared under a CC BY 4.0 license and was authored, remixed, and/or curated by Frank Rioux via source content that was edited to the style and standards of the LibreTexts platform.

3.12: A Lite Version of Ruedenberg's Analysis of the Covalent Bond in the Hydrogen Molecule Ion

Appendix

This study of the nature of the H_2^+ covalent bond forms a molecular orbital as a linear combination of scaled hydrogenic orbitals, LCAO-MO. The quantum mechanical integrals necessary to carry out the required calculations are provided immediately below. Consult the first five sections of Chapter 23 of our textbook for an overview of the covalent bond in the hydrogen molecule ion. The reaction for its formation is,

$$H + H^+ \rightarrow H_2^+$$

For the hydrogen atom: <E> = -0.5; <T> = 0.5; <V> = -1.0.

The Virial Theorem is expressed in a variety of ways:

$$\left|\frac{\Delta V}{\Delta T}\right| = 2 \quad \left|\frac{\Delta E}{\Delta T}\right| = 1 \quad \frac{\Delta E}{\Delta V} = \frac{1}{2}$$

The evaluated integrals required for this exercise are provided below:

Overlap integral:

$$S(\alpha,\ R) = \exp(-\alpha,\ R)\left(1 + \alpha R + \frac{\alpha^2 R^2}{3}\right)$$

Kinetic energy integrals:

$$Taa(\alpha,\ R) = \frac{\alpha^2}{2} \quad Tab(\alpha,\ R) = \frac{\alpha^2}{2}\exp(-\alpha,\ R)\left(1 + \alpha R - \frac{\alpha^2 R^2}{3}\right)$$

Potential energy integrals:

$$Vaa(\alpha,\ R) = -\left[\alpha - \exp(-2\alpha R)\left(\frac{1}{R} + \alpha\right)\right]$$

Total energy integral:

$$E(\alpha,\ R) = \frac{Haa(\alpha,\ R) + Hab(\alpha,\ R)}{1 + S(\alpha,\ R)}$$

Bonding molecular orbital:

$$\Psi_{bmo}(\alpha,\ x,\ y,\ z,\ R) = \frac{\sqrt{\frac{\alpha^3}{\pi}}\left[\exp\left[-\alpha\sqrt{\left(x - \frac{R}{2}\right)^2 + y^2 + z^2}\right] + \exp\left[-\alpha\sqrt{\left(x + \frac{R}{2}\right)^2 + y^2 + z^2}\right]\right]}{\sqrt{2 + 2S(\alpha,\ R)}}$$

Demonstrate wavefunction is normalized:

$$\int_{-\infty}^{\infty}\int_{-\infty}^{\infty}\int_{-\infty}^{\infty} \Psi_{bmo}(1,\ x,\ y,\ z,\ 2)^2 \mathrm{dx\ dy\ dz} = 1.0000$$

Anti-bonding molecular orbital:

$$\Psi_{amo}(\alpha,\ x,\ y,\ z,\ R) = \frac{\sqrt{\frac{\alpha^3}{\pi}}\left[\exp\left[-\alpha\sqrt{\left(x - \frac{R}{2}\right)^2 + y^2 + z^2}\right] - \exp\left[-\alpha\sqrt{\left(x + \frac{R}{2}\right)^2 + y^2 + z^2}\right]\right]}{\sqrt{2 - 2S(\alpha,\ R)}}$$

Demonstrate wavefunction is normalized:

$$\int_{-\infty}^{\infty}\int_{-\infty}^{\infty}\int_{-\infty}^{\infty} \Psi_{amo}(1,\ x,\ y,\ z,\ 2)^2 \mathrm{dx\ dy\ dz} = 1.0000$$

Non-bonding molecular orbital:

$$\Psi_{nmo}(\alpha,\ x,\ y,\ z,\ R) = \frac{\sqrt{\frac{\alpha^3}{\pi}}\left[\exp\left[-\alpha\sqrt{\left(x-\frac{R}{2}\right)^2+y^2+z^2}\right]+\mathrm{i}\,\exp\left[-\alpha\sqrt{\left(x+\frac{R}{2}\right)^2+y^2+z^2}\right]\right]}{\sqrt{2}}$$

Demonstrate wavefunction is normalized:

$$\int_{-\infty}^{\infty}\int_{-\infty}^{\infty}\int_{-\infty}^{\infty}(|\Psi_{nmo}(1,\ x,\ y,\ z,\ 2)^2|)^2 \mathrm{dx}\ \mathrm{dy}\ \mathrm{dz} = 1.0000$$

The Covalent Bond in H_2^+

Variational Calculation of the Molecular Ground State and Bond Energy

The molecular orbital for the hydrogen molecule ion is formed as a linear combination of scaled hydrogenic 1s orbitals centered on the nuclei, a and b.

$$\Psi = \frac{a+b}{\sqrt{2+2S}}$$

where

$$a = \sqrt{\frac{\alpha^3}{\pi}}\exp(-\alpha r_a) \quad b = \sqrt{\frac{\alpha^3}{\pi}}\exp(-\alpha r_b) \quad S = \int a\ b\ d\tau$$

The energy operator:

$$H = \frac{-1}{2}\left[\frac{d}{dR}\left(r^2\frac{d}{dR}\blacksquare\right)\right] - \frac{1}{r_a} - \frac{1}{r_b} + \frac{1}{R}$$

The energy integral to be minimized by the variation method:

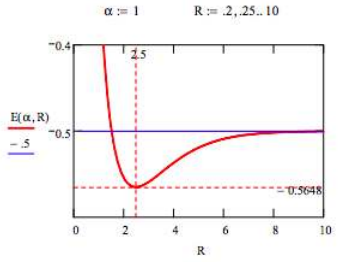
$$E = \frac{\int (a+b)H(a+b)d\tau}{2+2S} = \frac{Haa+Hab}{1+S}$$

where

$$Haa = (a|T|a) + \left(a\left|\tfrac{-1}{r_a}\right|a\right) + \left(a\left|\tfrac{-1}{r_b}\right|a\right) + \left(a\left|\tfrac{1}{R}\right|a\right)$$
$$Hab = (a|T|b) + \left(a\left|\tfrac{-1}{r_a}\right|b\right) + \left(a\left|\tfrac{-1}{r_b}\right|b\right) + \left(a\left|\tfrac{1}{R}\right|b\right)$$

and Haa = Taa + Vaa and Hab = Tab + Vab and Hba = Hab. These integrals and the overlap integral S can be found in the appendix above.

1. Plot E(α,R) vs R, for α = 1 for values of R ranging from 0.2 to 10 in increments of 0.05. You can make space by pressing . You can eliminate space by pressing . Use the markers for the x- and y-axis to find the optimum internuclear separation, R, and the ground-state energy.



Notice how shallow the energy minimum initially is. You can exagerate the minimum by plotting from -0.6 to -0.4 on the y-axis.

2. Minimize the energy with respect to R with α = 1. This will require a Given/Find solve block and seed values for α and R. Report the optimum R value (equilibrium bond distance) and the ground-state energy. Compare these calculated values to the literature values of 2.00 ao for R and -0.6029 Eh for the E.

$$\alpha = 1 \quad R = 2 \quad \text{Given } \frac{d}{dR}E(\alpha,\ R) = 0 \quad \text{R} = \text{Find(R)} \quad R = 2.4928 \quad E(\alpha,\ R) = -0.5648$$

$$\frac{R-2.00}{2.00} = 24.6415\% \qquad \left|\frac{E(\alpha,\ R)+.6029)}{-.6029}\right| = 6.3143\% \quad \frac{E(\alpha,\ R)}{-.6029} = 93.6875\%$$

Demonstrate that the calculated hydrogen molecule ion energy does not satisfy the Virial Theorem.

$$T = \frac{Taa(\alpha,\ R)+Tab(\alpha,\ R)}{1+S(\alpha,\ R)} \qquad T = 0.3827 \qquad V = \frac{Vaa(\alpha,\ R)+Vab(\alpha,\ R)}{1+S(\alpha,\ R)} \quad V = -0.9475$$

$$\left|\frac{V}{T}\right| = 2.4759 \qquad \left|\frac{E(\alpha,\ R)}{T}\right| = 1.4759 \qquad \left|\frac{E(\alpha,\ R)}{V}\right| = 0.5961$$

3. Write the equation for breaking the H_2^+ bond. Then use the theoretical value of the ground state energy to calculate the bond energy of the hydrogen molecule ion and compare it to the experimental value, 0.1029 E_h. You may recall that the hydrogen atom ground state energy is -0.5 hartree.

$$\begin{matrix}\text{Hydrogen molecule ion} = & \text{Hydrogen atom} + & \text{Hydrogen ion} & \\ -0.5648 & -0.500 & 0 & \text{Bond energy} = 0.0648\end{matrix}$$

4. The first three exercises refer to a variational calculation based on the hydrogen 1s orbital (α = 1). Now treat both α and R as variational by minimizing the energy simultaneously with respect to α and R.

$$\text{Given} \quad \frac{d}{dR}E(\alpha,\ R) = 0 \quad \begin{pmatrix}\alpha \\ R\end{pmatrix} = \text{Find}(\alpha,\ R) \quad \begin{pmatrix}\alpha \\ R\end{pmatrix} = \begin{pmatrix}1.2380 \\ 2.0033\end{pmatrix} \quad E(\alpha,\ R) = -0.5865$$

Demonstrate that the calculated hydrogen molecule ion energy does satisfy the Virial Theorem.

$$T = \frac{Taa(\alpha,\ R)+Tab(\alpha,\ R)}{1+S(\alpha,\ R)} \qquad T = 0.5865 \qquad V = \frac{Vaa(\alpha,\ R)+Vab(\alpha,\ R)}{1+S(\alpha,\ R)} \quad V = -1.1730$$

$$\left|\frac{V}{T}\right| = 2.0000 \qquad \left|\frac{E(\alpha,\ R)}{T}\right| = 1.0000 \qquad \left|\frac{E(\alpha,\ R)}{V}\right| = 0.5000$$

5. Compare E and R with the literature values. Recalculate the H2 + bond energy and compare it with the experimental value. Comment on the agreement between theory and experiment as compared with that found in part 3.

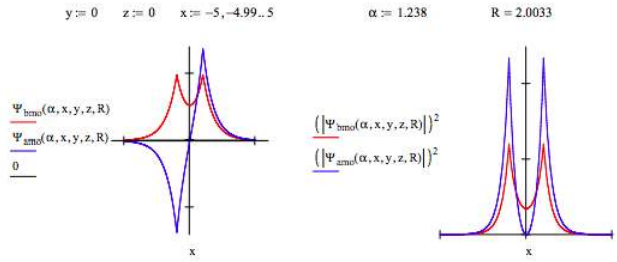
$$\begin{matrix}\text{Hydrogen Molecule Ion} = & \text{Hydrogen Atom} + & \text{Hydrogen Ion} & & \\ -0.5865 & -0.5000 & 0 & \text{Bond Energy} = 0.0865\end{matrix}$$

$$\frac{.1029-.0865}{.1029} = 15.9378\% \quad \frac{.0865}{.1029} = 84/0622\% \quad \left|\frac{E(\alpha,\ R)+.6029}{-.6029}\right| = 2.7191\%$$

6. The vibrational force constant is the second derivative of the energy with respect to R evaluated at the energy minimum. Calculate the force constant and compare it to the experimental value of .103 in atomic units.

$$k = \frac{d^2}{dR^2}E(\alpha,\ R) \quad k = 0.1409 \quad \frac{k}{.103} = 136.8240\%$$

7. The appendix contains the bonding and antibonding orbitals for H_2^+. On one graph plot Ψ for the bonding and antibonding orbitals along the bond axis (i.e. set y and z to zero). On another graph plot Ψ_2 for the bonding and antibonding orbitals. Compare these orbitals.



These figures show that the electron density is greatest at the nuclear centers, and that the bonding molecular orbital has significant electron density in the internuclear region. Just how much charge is transferred to the bond region will be calculated later. The antibonding molecular orbital has a node exactly between the two nuclei and thus removes charge from the internuclear region. This, of course, is why it called an anti-bonding molecular orbital.

A Mechanism for Covalent Bond Formation in H2+

The following two-step mechanism is proposed for covalent bond formation:

- The hydrogen atom and proton form an intermediate, nonbonding state at the equilibrium bond length (R= 2.0033) with the optimum value of the decay constant (α = 1.238).
- The non-bonding state, N_{nmo}(a + ib), morphs into the final molecular state, N_{bmo} (a + b).

$$\begin{pmatrix} \frac{\text{Initial}}{\text{Atomic State}} & o & \frac{\text{Intermediate}}{\text{Non Bonding State}} & o & \frac{\text{Final}}{\text{Molecular State}} \\ H_{atom}+H_{ion} & o & \Psi_{nmo}=\frac{a+ib}{\sqrt{2}} & o & \Psi_{bmo}=\frac{a+b}{\sqrt{2+2S}} \end{pmatrix}$$

8. We now calculate the kinetic (T), potential (V) and total energy (E) for each of the species involved in the mechanism.

In previous work we calculated the following values for the hydrogen atom. (The energy of the hydrogen ion by convention is 0).

$$E_h=\frac{-1}{2} \quad T_h=\frac{1}{2} \quad V_h=-1$$

The energy of the non-bonding intermediate state is calculated as follows.

$$E_{nb}=\int \frac{a-ib}{\sqrt{2}} H \frac{a+ib}{\sqrt{2}} d\tau = \frac{1}{2}\left(\int aHad\tau + \int bHbd\tau\right) = Haa = Taa + Vaa$$

because

$$Hbb = Haa$$

$$\begin{array}{lll} \text{Total: } Haa(\alpha,\ R) = -0.4594 & \text{Kinetic: } Taa(\alpha,\ R) = 0.7663 & \text{Potential: } Vaa(\alpha,\ R) = -1.2258 \\ & \text{Nuclear potential energy: } \frac{1}{R} = 0.4992 & \end{array}$$

In exercise 4 we calculated the energy contributions of the final molecular state of H_2^+.

$$\begin{array}{lll} \text{Total:} & \text{Kinetic:} & \text{Potential:} \\ E(\alpha,\ R) == 0.5865 & \frac{Taa(\alpha,\ R)+Tab(\alpha,\ R)}{1+S(\alpha,\ R)} = 0.5865 & \frac{Vaa(\alpha,\ R)+Vab(\alpha,\ R)}{1+S(\alpha,\ R)} = -1.1730 \end{array}$$

Nuclear potential energy:

$$\frac{1}{R} = 0.4992$$

We are now in a position to construct the following quantitative summary of the mechanism.

$$\begin{pmatrix} o & \frac{\text{Initial}}{\text{Atomic State}} & o & \frac{\text{Intermediate}}{\text{Non Bonding State}} & o & \frac{\text{Final}}{\text{Molecular State}} & o \\ o & H_{atom}+H_{ion} & o & \Psi_{nmo}=\frac{a+ib}{\sqrt{2}} & o & \Psi_{bmo}=\frac{a+b}{\sqrt{2+2S}} & \\ o & \alpha=1 & \Delta & \frac{\alpha=1.238}{R=2.003} & \Delta & \frac{\alpha=1.238}{R=2.003} & \\ T & 0.50 & 0.2663 & 0.7663 & -0.1798 & 0.5865 & \\ V & -1.0 & -0.2258 & -1.2258 & 0.0528 & -1.1730 & \\ V_{ne} & -1.0 & -0.7250 & -1.7250 & 0.0528 & -1.6722 & \\ V_{nn} & 0 & 0.4992 & 0.4992 & 0 & 0.4992 & \\ E & -0.50 & 0.0407 & -0.4595 & -0.1270 & -0.5865 & \end{pmatrix}$$

Interpretation of the Mechanism

The first step is atomic and endoergic. It is atomic because there is no constructive interference between the atomic orbitals. It is endoergic because kinetic energy increases more than potential energy decreases. The increase in kinetic energy and the decrease in potential energy are due predominantly to atomic orbital contraction from α = 1 in the hydrogen atom to α = 1.238 in the hydrogen molecule ion.

The second step is exoergic and molecular. The atomic orbitals form a molecular orbital leading to charge redistribution relative to the non-bonding intermediate state. This redistribution causes a decrease in kinetic energy because the electron is now more

delocalized, and an increase in potential energy because the electron is drawn away from the nuclear centers into the high-potential energy internuclear region.

Overall the kinetic energy increases and potential energy decreases on bond formation, and the virial theorem is satisfied. This is the source of the conclusion that covalent bonding is a potential energy effect. However, as this analysis shows, both kinetic and potential energy play important roles in covalent bond formation.

This mechanism clarifies an important issue. It is commonly thought, and frequently taught, that from a potential energy point of view the internuclear region is the most favorable place for electron density because it is midway between to nuclei. However, this mechanism clearly shows that the redistribution of charge into the internuclear region due to the interference term in the bonding electron density occurs with an increase in potential energy (0.0528 Eh). From a purely electrostatic perspective the prefered location for an electron is in the nucleus.

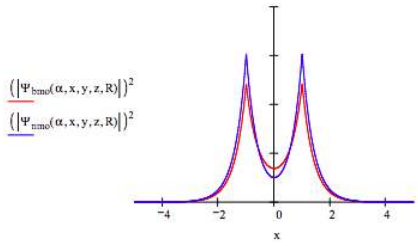
The Bonding Electron Density

9. How much of the total electron density, Ψ_{bmo}^2, actually contributes to covalent bonding? This question can be answered by comparing the electron density in the intermediate non-bonding state with that of the final molecular state. First we will demonstrate that $\Psi_{nmo}^2 = (a^2 + b^2)/2$ and that this wave function is normalized because a and b are normalized.

$$\Psi_{nmo} = \frac{a+ib}{\sqrt{2}} \quad \left(\left|\frac{a+ib}{\sqrt{2}}\right|\right)^2 \rightarrow \frac{1}{2}a^2 + \frac{1}{2}b^2 \quad \int \frac{a-ib}{\sqrt{2}}\frac{a+ib}{\sqrt{2}}d\tau = \frac{1}{2}\left(\int a^2 d\tau + \int b^2 d\tau\right) = 1$$

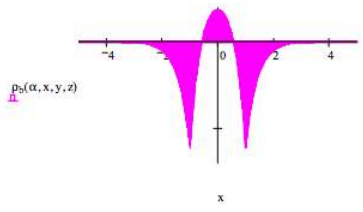
Ψ_{nmo}^2 shows the "atomic" electron density - the electron density that would exist in the absence of constructive interference between the two atomic orbitals, 1sa and 1sb.

The non-bonding wave function is given in the appendix. Graph $|\Psi_{bmo}|^2$ and $|\Psi_{nmo}|^2$ along the bond axis and compare them.



10. The question posed in section 9 can now be answered. The bonding electron density can be defined as the charge redistribution that occurs in step 2 of the mechanism. Plot the difference between the total electron density and the non-bonding electron density along the bond axis. Interpret the plot. For example, where does the electron density in the internuclear region come from? What is the sign on the potential energy term for this transfer of electron density to the internuclear region? If this is an endoergic process, how is it funded?

$$\rho_b(\alpha,\ x,\ y) = (|\Psi_{bmo}(\alpha,\ x,\ y,\ z,\ R)|)^2 - (|\Psi_{nmo}(\alpha,\ x,\ y,\ z,\ R)|)^2$$



This graph shows that electron density is being transferred from the nuclear centers (low potential energy) to the internuclear region (high potential energy). This explains why potential energy increases during step 2. The kinetic energy decreases more because this redistribution of charge also involves charge delocalization, so it is the larger decrease in kinetic energy that funds the transfer of charge to the internuclear region.

11. The electron density in the internuclear region is equal to a polynomial in the overlap integral S and is given by 0.738S(1 - S)(1 - 0.577S^2). Use the value of S you calculated earlier to evaluate the amount of charge in the bonding region of H_2^+. Comment on this value. For example, how does its value compare with a literal interpretation of the Lewis electron pair model of chemical bonding that says that chemical bonds are formed by sharing electrons between two nuclei.

$$0.738S(\alpha,\ R)(1-S(\alpha,\ R))\left(1-0.577S(\alpha,\ R)^2\right)=16.1\%$$

This page titled 3.12: A Lite Version of Ruedenberg's Analysis of the Covalent Bond in the Hydrogen Molecule Ion is shared under a CC BY 4.0 license and was authored, remixed, and/or curated by Frank Rioux via source content that was edited to the style and standards of the LibreTexts platform.

3.13: Molecular Orbital Analysis for the Hydrogen Molecule Ion Bond

In this analysis the molecular orbital for the hydrogen molecule ion is formed as a linear combination of scaled hydrogenic 1s orbitals centered on the nuclei, a and b.

$$\Psi_{MO} = \frac{a+b}{\sqrt{2+2S}} \quad \text{where} \quad a = \sqrt{\frac{\alpha^3}{\pi}}\exp(-\alpha,\ r_a) \quad b = \sqrt{\frac{\alpha^3}{\pi}}\exp(-\alpha,\ r_b) \quad S = \int abd\tau$$

The molecular energy operator in atomic units:

$$H = \frac{-1}{2}\left[\frac{d}{dr}\left(r^2\frac{d}{dr}\blacksquare\right)\right] - \frac{1}{r_a} - \frac{1}{r_b} + \frac{1}{R}$$

The energy integral to be minimized by the variation method:

$$E = \frac{\int (a+b)H(a+b)d\tau}{2+2S} = \frac{Haa + Hab}{1+S}$$

When this integral is evaluated a two-parameter variational expression for the energy (highlighted below) is obtained.

Electron mass:

m = 1

Seed values for the variational parameter and internuclear separation:

$$\alpha = 1 \quad R = .1$$

$$E(\alpha,\ R) = \frac{-\alpha^2}{2m} + \frac{\frac{\alpha^2}{m} - \alpha - \frac{1}{R} + \frac{1}{R}(1+\alpha R)\exp(-2\alpha R) + \alpha\left(\frac{\alpha}{m} - 2\right)(1+\alpha R)\exp(-\alpha R)}{1+\exp(-\alpha R)\left(1+\alpha R+\frac{\alpha^2 R^2}{3}\right)} + \frac{1}{R}$$

Minimization of the energy of the hydrogen molecule ion follows. There are two variational parameters, the orbital scale factor and the internuclear distance.

$$\text{Given} \quad \frac{d}{d\alpha}E(\alpha,\ R) = 0 \quad \frac{d}{dR}E(\alpha,\ R) = 0 \quad \begin{pmatrix}\alpha\\ R\end{pmatrix} = \text{Find}(\alpha,\ R) \quad \begin{pmatrix}\alpha\\ R\end{pmatrix} = \begin{pmatrix}1.23803\\ 2.0033\end{pmatrix} \quad E(\alpha,\ R) = -0.58651$$

The calculation yields a stable molecule ion as is shown here.

	Hydrogen Molecule Ion =	Hydrogen Atom+	Hydrogen Ion	
Theory	−0.5865	−0.5000	0	Bond Energy = 0.0865
Experiment	−0.6029	−0.5000	0	Bond Energy = 0.1029

The experimental ground state energy is -0.6029 E_h. The error in this calculation is calculate two ways: error in bond energy and error in total ground state energy.

$$\frac{.1029-.0865}{.1029} = 15.9378\% \quad \left|\frac{E(\alpha,\ R)+.6029}{-.6029}\right| = 2.71911\%$$

It is instructive to calculate the kinetic and potential energy contributions to the total energy.

$$E = \int \Psi_{MO}(T+V)\Psi_{MO}d\tau = Taa + Tab + Vaa + Vab$$

$$Taa(\alpha,\ R) = \frac{\frac{\alpha^2}{2m}}{1+\exp(-\alpha,\ R)\left(1+\alpha R+\frac{\alpha^2R^2}{3}\right)} \quad Tab(\alpha,\ R) = \frac{\frac{\alpha^2}{2m}\exp(-\alpha,\ R)\left(1+\alpha R-\frac{\alpha^2R^2}{3}\right)}{1+\exp(-\alpha,\ R)\left(1+\alpha R+\frac{\alpha^2R^2}{3}\right)}$$

$$Vaa(\alpha,\ R) = \frac{\left(\frac{1}{R}+\alpha\right)\exp(-2\alpha R)-\alpha}{1+\exp(-\alpha,\ R)\left(1+\alpha R+\frac{\alpha^2R^2}{3}\right)} \quad Taa(\alpha,\ R) = \frac{\frac{-1}{3}\exp(\alpha,\ R)\frac{3\alpha R+5\alpha^2R^2-3}{R}}{1+\exp(-\alpha,\ R)\left(1+\alpha R+\frac{\alpha^2R^2}{3}\right)}$$

First we establish that these terms are correct by showing that they sum to the correct ground state energy calculated earlier.

$$Taa(\alpha,\ R) + Tab(\alpha,\ R) + Vaa(\alpha,\ R) + Vab(\alpha,\ R) = -0.58651$$

Next we establish that the virial theorem is obeyed. Quantum mechanical calculations that violate the appropriate virial theorem are not valid. For atomic and molecular systems the virial theorem is: <E> = -<T> = <V>/2.

Electron Kinetic Energy	Total Potential Energy	Virial Theorem Satisfied
$Taa(\alpha,\ R) + Tab(\alpha,\ R) = 0.58651$	$Vaa(\alpha,\ R) + Vab(\alpha,\ R) = -1.17301$	$\frac{\lvert Vaa(\alpha,\ R)+Vab(\alpha,\ R)\rvert}{Taa(\alpha,\ R)+Tab(\alpha,\ R)} = 2$

Next we separate the nuclear potential energy into its two components: electron-nucleus and nucleus-nucleus.

Electron Kinetic Energy	Electron-Nucleus Potential Energy	Nucleus-Nucleus Potential Energy
$T = Taa(\alpha,\ R) + Tab(\alpha,\ R)$	$Ven = Vaa(\alpha,\ R) + Vab(\alpha,\ R) - \frac{1}{R}$	$Vnn = \frac{1}{R}$
$T = 0.58651$	$Ven = -1.67219$	$Vnm = 0.49918$
$\frac{T}{T+\lvert Ven\rvert+Vnn} = 21.27\%$	$\frac{\lvert Ven\rvert}{T+\lvert Ven\rvert+Vnn} = 60.63\%$	$\frac{Vnn}{T+\lvert Ven\rvert+Vnn} = 18.10\%$

In light of these calculations the following comments on the covalent bond in the H_2^+ are made. Ven is the largest and only negative term, and might be thought of as the glue holding the H_2^+ molecule together. However, a ground state (stable molecule) requires "energetic" opposition to the attractive Ven, otherwise molecular collapse occurs. This opposition is provided by T and Vnn. It might surprise those who think that chemical bonding is simply an electrostatic phenomenon, that nuclear repulsion makes a smaller contribution to molecular stability than electron kinetic energy.

This page titled 3.13: Molecular Orbital Analysis for the Hydrogen Molecule Ion Bond is shared under a CC BY 4.0 license and was authored, remixed, and/or curated by Frank Rioux via source content that was edited to the style and standards of the LibreTexts platform.

3.14: A One-dimensional Model for the Covalent Bond in the Hydrogen Molecule Ion

The covalent bond is a very challenging concept which few chemistry textbooks treat adequately. The simplest example of a covalent bond is the one-electron bond in the hydrogen molecule ion. It plays the same role in the study of chemical bonding that the hydrogen atom plays in the study of atomic structure. The most penetrating, extensive, and perhaps controversial, analysis of the H_2^+ bond was provided by Ruedenberg over forty years ago (*Rev. Mod. Phys.* **1962**, *34*, 326-352). The goal of this tutorial is quite modest in comparison; here an attempt is made to capture several of the basic features of the covalent bond with a simple, and yet plausible, one-dimensional model.

This tutorial uses a one-dimensional, double-well potential (double Posch-Teller potential) to model the H_2^+ covalent bond. Schrödinger′s equation is solved numerically for the two lowest energy states using Mathcad′s ordinary differential equation solver, and the numerical results are displayed graphically and interpreted. The calculations are carried out in atomic units: e = m_e = h/2π = 1.

As a numerical model, this approach is not based on the molecular orbital method (LCAO - linear combination of atomic orbitals), but as we will see its results are consistent with the LCAO-MO model for chemical bonding.

ODE Numerical Integration Algorithm

The Posch-Teller parameters were determined by adjusting V0 so that it gave the correct H_2^+ ground state energy (-0.6029 E_h) at the equilibrium bond length (2.00 a_0).

$$\text{Parameters:} \quad m = 1 \quad x_{max} = 8 \quad V_o = -1.11223 \quad \alpha = 1.5 \quad d = 1$$

$$\text{Potential energy:} \quad V(x) = V_o \left[\frac{1}{\cosh\left[\alpha(x-d)\right]^2} + \frac{1}{\cosh\left[\alpha(x+d)\right]^2} \right]$$

Solve Schrödinger′s equation numerically, and normalize and display the solution:

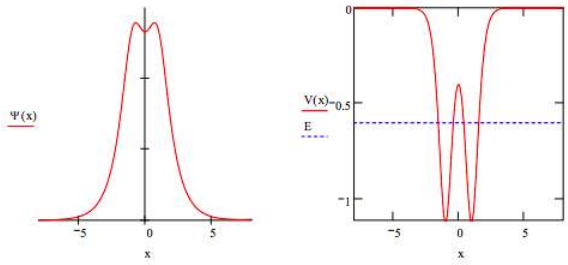
\[

$$\text{Given} \quad \frac{-1}{2m}\frac{d^2}{dx^2}\Psi(x) + V(x)\Psi(x) = E\Psi(x) \quad \Psi\left(-x_{max}\right) = 0 \quad \Psi'\left(-x_{max}\right) = 0.1 \tag{3.14.1}$$

\ & \Psi = \text{Odesolve} \left(x,~x_{max} \right) &

N = \frac{1}{ \sqrt{ \int_{-x_{max}}^{x_{max}} \Psi (x)^2 dx}} & \Psi (x) = N \Psi(x) \end{matrix} \nonumber \]

Enter energy: E = =0.6029

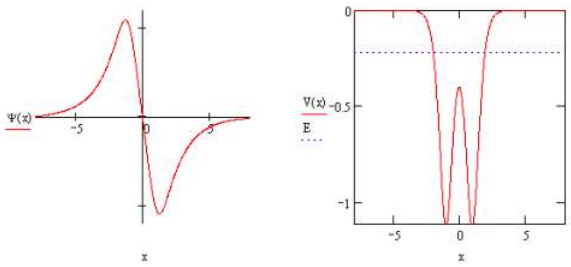


This result for the ground state correctly shows that the electron density is delocalized over both nuclear centers forming a molecular state. It also shows that the electron density is greatest at the nuclear centers where the electron-nucleus potential energy is lowest, and dips somewhat in the "bond region" where the potential energy is much higher. It also shows that tunneling is occurring because the electron is present in regions where its total energy is lower than the local potential energy. Inspection of the right-hand figure above shows that tunneling occurs for the following situations: x < -1.55, x > 1.55, and -0.396 < x < 0.396. The probability that tunneling is occuring is calculated below.

$$\int_{-1.56}^{x_{max}} \Psi(x)^2 dx + \int_{-0.396}^{0.396} \Psi(x)^2 dx + \int_{1.56}^{x_{max}} \Psi(x)^2 dx = 0.229$$

The next allowed state with energy E = -0.2222 E_h is clearly anti-bonding because of the node in the internuclear region. The model also shows that this anti-bonding state is unstable relative to a hydrogen atom and hydrogen ion which collectively have an

energy of -0.500 E_h.

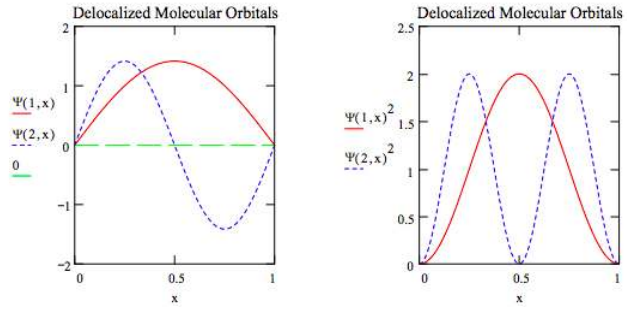


This page titled 3.14: A One-dimensional Model for the Covalent Bond in the Hydrogen Molecule Ion is shared under a CC BY 4.0 license and was authored, remixed, and/or curated by Frank Rioux via source content that was edited to the style and standards of the LibreTexts platform.

3.15: Localized and Delocalized Molecular Orbitals

The generation of localized molecular orbitals (LMOs) from canonical or delocalized molecular orbitals (DMOs) will be illustrated by modeling the π-electrons of 1,3-butadiene as particles in a one-dimensional box (PIB). Solving Schrödinger's equation for this application yields the familiar sine function for the canonical orbitals. The n = 1 and n = 2 states are occupied by two π-electrons each; Ψ and Ψ2 for both states are graphed below.

$$\Psi(n,\ x) = \sqrt{2}\sin(n\pi x) \quad x = 0, .01..1$$



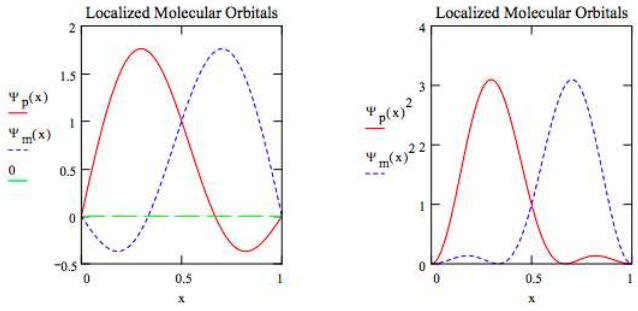
These canonical, delocalized wave functions present a problem for chemists who are accoustomed to localizing the π-electrons of butadiene between carbons 1 and 2, and carbons 3 and 4 with the Lewis structure shown below. In contradiction to this view, the DMOs clearly distribute the π-electron density over the entire carbon backbone

$$H_2C{=}CH{-}CH{=}CH_2$$

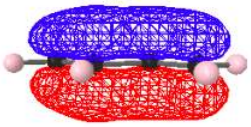
The chemist's localized-electron-pair model can be recovered to some extent from the delocalized, canonical wave functions by invoking the quantum mechanical superposition principle. The superposition principle teaches that any linear combination of the canonical solutions is also a valid wave function as long as they are only used to interpret physical properties that depend on the total electron density. The canonical DMOs are required for single-electron phenomena such as electronic spectroscopy and ionization phenomena.

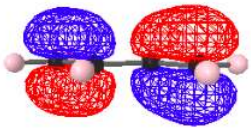
Thus, it is easy to show that simply adding (Ψ_p) and subtracting (Ψ_m) the canonical wave functions yields LMOs in this simple example involving a particle-in-a-box model for the π-electrons of butadiene. Ψp shifts electron density to the left closer to the bond region between carbon atoms 1 and 2, while Ψ_m shows the electron density closer to the bond region between carbon atoms 3 and 4. Naturally, for more complicated molecular situations a more sophisticated protocol is required to generate LMOs.

$$\Psi_p(x) = \frac{1}{\sqrt{2}}(\Psi(1,\ x) + \Psi(2,\ x)) \quad \Psi_m(x) = \frac{1}{\sqrt{2}}(\Psi(1,\ x) - \Psi(2,\ x))$$



For example, raising the level of theory from PIB to a low-level ab initio quantum mechanical basis set (STO-3G) yields the following HOMO-1 and HOMO for butadiene. These, of course, are the two occupied π molecular orbitals that are equivalent to the n = 1 and n =2 states for the PIB model. Just as for the PIB model the HOMO-1 has no nodes, while the HOMO has one node.





As noted above there are a variety of protocols in use to provide LMOs from the canonical DMOs. A method in wide-spread use forms LMOs from linear combinations of the DMOs by maximizing intra-orbital electron repulsion. This protocol yields the following LMOs for the π electrons in butadiene.



For a more detailed discussion of this subject and useful references to the pedagogical and primary literature consult the following reference. R. Bruce Martin, "Localized and Spectroscopic Orbitals: Squirrel Ears on Water," *Journal of Chemical Education*, **65(8)**, 668-670 (1988).

This page titled 3.15: Localized and Delocalized Molecular Orbitals is shared under a CC BY 4.0 license and was authored, remixed, and/or curated by Frank Rioux via source content that was edited to the style and standards of the LibreTexts platform.

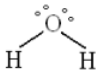
3.16: Two Perspectives on the Bonding in Water

Chemists use a variety of models to describe the electronic structure of molecules. The oldest and most rudimentary model which is still in widespread use, and is taught at all levels of the chemistry curriculum, is the localized electron pair model proposed by G. N. Lewis in 1916. This pre-quantum approach to chemical bonding was stimulated in part by the observation that half the elements in the periodic table have an odd number of electrons, but very few molecules do.

Today we know that the importance of the electron pair is explained by the Pauli Exclusion Principle. Electrons, as fermions, cannot have the same set of quantum numbers. Therefore, if the three spatial quantum numbers are the same the spin quantum number must be different, and the spin quantum number has only two allowed values - plus or minus 1/2. Thus only two electrons can occupy an orbital - a region of space.

Molecular orbital theory, a successor to the Lewis model, is based on the Exclusion Principle and the postulates of quantum mechanics. Thus it retains the concept of the electron pair but, due to the wave nature of quantum theory, it abandons spatial localization. This is perhaps the most challenging concept that quantum mechanics offers chemists, the delocalization of the electron pair over the entire molecule.

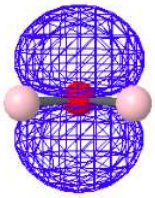
To emphasize the difference between the Lewis and MO approaches the bonding in water will be considered. The traditional Lewis structure for water is shown below. There are two equivalent bonding electron pairs and two equivalent non-bonding electron pairs.



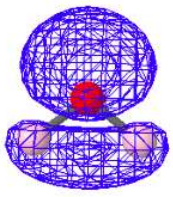
Therfore, according to the Lewis localized electron pair bonding model there should be two bands in the experimental photoelectron spectrum of equal weight. However, the actual spectrum shows four distinct bands, indicating that there are four types of valence electrons in the water molecule, not two.

The quantum mechanical treatment of bonding is based primarily on the LCAO-MO approach where a molecular orbital is formed as a linear combination of atomic orbitals. A quantum mechanical calculation for water yields the following valence electron molecular orbitals. Note that there are four distinctly different molecular orbitals in agreement with the spectroscopic data mentioned above. Note also that the electron density is distributed over the molecule as a whole.

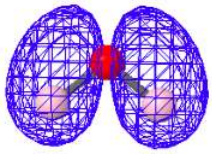
The canonical molecular orbitals are arranged on a relative energy scale below with comments.



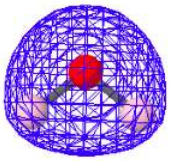
Highest Occupied Molecular Orbital - HOMO: Non-bonding



HOMO-1: Also non-bonding with regard to oxygen and hydrogen



HOMO-2: Bonding - charge density present between oxygen and hydrogen.

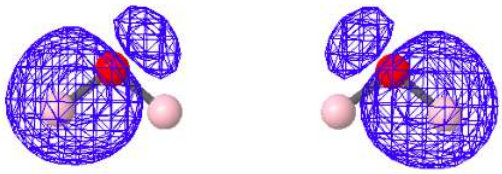


HOMO-3: Bonding-charge density present between oxygen and hydrogen.

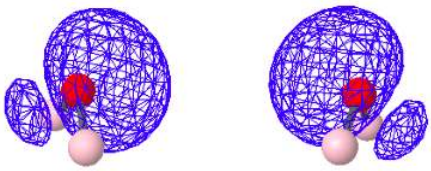
The fact that the delocalized molecular orbitals are in agreement with experimental data but the localized electron pair model is not presents a challenge for the chemist who is accustomed to placing confidence in the value of the Lewis model. However, the quantum mechanical superposition principle allows one to construct localized molecular orbitals (LMOs) from the canonical delocalized molecular orbitals (DMOs). In other words, quantum mechanics itself provides the justification for placing confidence in the utility of the Lewis electron-pair model.

There are a variety of computational protocols for generating LMOs from DMOs. The following LMOs were calculated using a method developed by Ruedenberg in which intra-orbital electron repulsions are maximized. It is clear that the four LMOs generated by this protocol bear a strong relationship to the simple localized electron pair model of Lewis for water shown above.

Bonding LMOs



Non-Bonding LMOs

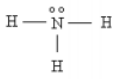


This page titled 3.16: Two Perspectives on the Bonding in Water is shared under a CC BY 4.0 license and was authored, remixed, and/or curated by Frank Rioux via source content that was edited to the style and standards of the LibreTexts platform.

3.17: Covalent Bonding in Ammonia from Several Perspectives

Chemists use a variety of models to describe the electronic structure of molecules. The oldest and most rudimentary model which is still in widespread use, and is taught at all levels of the chemistry curriculum, is the localized electron pair model proposed by G. N. Lewis in 1916. This pre-quantum approach to chemical bonding was stimulated in part by the observation that half the elements in the periodic table have an odd number of electrons, but very few molecules do.

For example ammonia, NH_3, has four atoms each with an odd number of valence electrons (5,1,1,1), giving the molecule the magic number of eight valence electrons or four pairs in the Lewis formulation. In the non-geometrical representation shown below, Lewis has the nitrogen sharing a pair of electrons with each hydrogen, and keeping a lone-pair for itself.

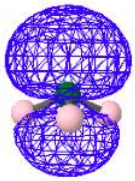


In a proper three-dimensional representation the ammonia molecule has C_{3v} symmetry and looks like a camera tripod with the lone pair occupying the position of the camera.

However there is a serious problem with this simple model for the electronic structure of ammonia, and that is that it suggests that there are two types of valence electrons - three equivalent bonding pairs and one non-bonding pair. Unfortunately, there are three bands in ammonia's photoelectron spectrum, indicating that there are actually three types of valence electrons.

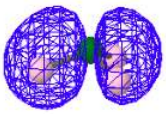
Quantum mechanical calculations based on the molecular orbital approach to chemical bonding (MO - LCAO; molecular orbitals formed as a linear combination of atomic orbitals) yield the following molecular orbitals which are in agreement with the experimental spectroscopic data.

Highest Occupied Molecular Orbital - HOMO

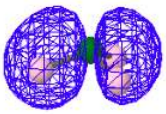


This MO is clearly non-bonding and represents the lone-pair electrons on the nitrogen.

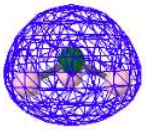
The next three MOs, a degenerate pair and a single ground-state MO, represent the three bonding pairs of electrons. However they are not localized between the nitrogen and hydrogens as suggested by the simple Lewis structure shown above. They are indeed molecular orbitals, delocalizing the bonding electron density over the whole molecule.



HOMO-1



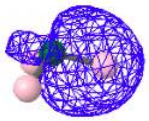
HOMO-2



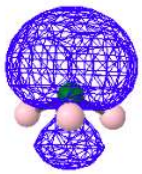
HOMO-3

Thus the delocalized canonical molecular orbitals provided by ab initio quantum mechanics do not directly support the concept of the localized electron pair model of Lewis that has proven so useful to chemists. However, the quantum mechanical superposition principle allows one to construct localized molecular orbitals (LMOs) from the canonical delocalized molecular orbitals (DMOs).

In other words, using appropriate protocols linear combinations of the canonical MOs shown above yield the LMOs shown below which are consistent with the rudimentary Lewis structure shown above.



There are three localized bonding MOs like this, one for each N - H bond.



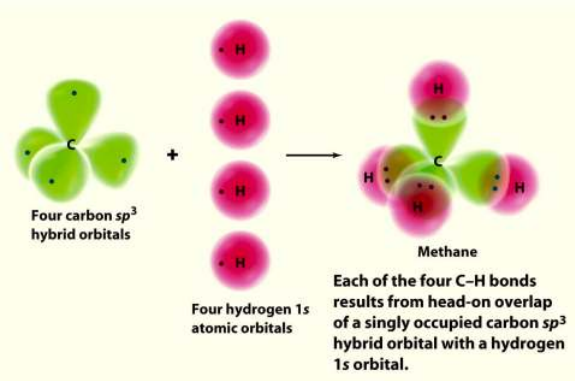
And one non-bonding MO like this.

This page titled 3.17: Covalent Bonding in Ammonia from Several Perspectives is shared under a CC BY 4.0 license and was authored, remixed, and/or curated by Frank Rioux via source content that was edited to the style and standards of the LibreTexts platform.

3.18: A Molecular Orbital Approach to Bonding in Methane

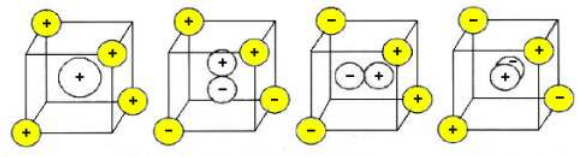
Most general chemistry textbooks invoke sp^3 hybridization to explain the bonding in the tetrahedral methane (CH_4) molecule. The idea (valence bond theory, VBT) is that good overlap between the atomic orbitals centered on carbon and hydrogen leads to strong bonds. The problem is that the carbon 2s and 2p valence orbitals don't point in the tetrahedral directions occupied by the hydrogen 1s valence orbitals. Linus Pauling solved this problem in 1931 by mathematically hybridizing carbon's 2s and 2p orbitals so that the resulting hybrids (linear combinations) point toward the hydrogen 1s orbitals.

A typical representation of the valence bond approach to methane bonding is shown in the following graphic taken from the 5th edition of McMurray and Fay's General Chemistry text.

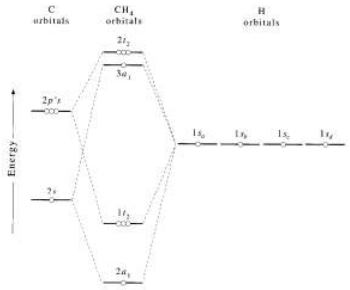


It might be assumed that the tetrahedral geometry of methane requires sp^3 hybridization of the carbon 2s and 2p valence atomic orbitals. However, this is not the case because there is a perfectly valid alternative bonding model, molecular orbital theory, which has solid empirical support.

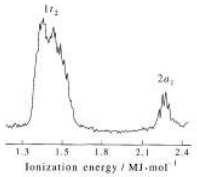
Molecular orbital theory (MOT) for methane forms bonding molecular orbitals involving linear combinations of the unhybridized carbon 2s and 2p valence orbitals with the hydrogen 1s orbitals as shown in the graphic below. The plus and minus signs signify phase, not electrical charge.



A molecular orbital diagram showing both the bonding and anti-bonding molecular energy levels is provided below. (McQuarrie & Simon, Physical Chemistry: A Molecular Approach, p. 388)



Methane has eight valence electrons, so according to the aufbau and Pauli exclusion principles the two lowest energy molecular orbitals (2a1 and 1t2) are fully occupied with electrons. This is consistent with the experimental valence electron ionization spectrum for methane shown below. (McQuarrie & Simon, Physical Chemistry: A Molecular Approach, p. 388)



The VBT model appears to predict only one valence electron ionization energy for methane, because there is only one kind of bonding electron – an electron in a carbon sp3 hybridized orbital which overlaps with a tetrahedrally located hydrogen 1s orbital. To see how VBT accounts for two ionization energies see the following reference: *Journal of Chemical Education*, **89**, 570-572 (2012).

This page titled 3.18: A Molecular Orbital Approach to Bonding in Methane is shared under a CC BY 4.0 license and was authored, remixed, and/or curated by Frank Rioux via source content that was edited to the style and standards of the LibreTexts platform.

3.19: A Simple Calculation of the Lattice Energy of LiH

Lithium hydride is a white crystalline solid with the face-centered cubic crystal structure (see lattice shown below). The model for LiH(s) proposed in this study constists of the following elements:

1. The bonding in LiH(s) is completely ionic. The lattice sites are occupied by the spherical, two-electron ions, Li^+ and H^-.

2. The electrons of Li^+ and H^- occupy hydrogenic 1s atomic orbitals with adjustable scale factors α and β, respectively. Expressed in atomic units the wavefunctions have the form,

$$\Psi(1,2) = 1s(1)1s(2) = (\alpha^3/\pi)\exp[-\alpha(r_1 + r_2)]$$

The scale factor determines how rapidly the wavefunction (and, therefore, the electron density) diminishes as the distance from the nucleus increases. α and β are, therefore, inversely related to the atomic radius. The larger α and β, the smaller the ionic radii are.

3. The average distance of an electron from the nucleus, <r>, in a scaled 1s orbital is 1.5/α. Therefore, it seems reasonable to take 2, or 3/α as the effective ionic radius in the solid. It is easy to show that 94% of the charge is contained within this radius. (See Appendix)

4. Van der Waals interations between the electron clouds of the ions and the quantum mechanical zero-point energy of the lattice are neglected.

To check the validity of this model the lattice energy of LiH(s) will be calculated and compared to the value obtained by a Born-Haber analysis. The lattice energy is defined as the energy required to bring about the following process,

$$LiH(s) \text{ ----> } Li^+(g) + H^-(g)$$

The determination of the lattice energy on the basis of the proposed model, therefore, proceeds by calculating the ground state energies of $Li^+(g)$ and $H^-(g)$. and subtracting from them the ground state energy of LiH(s). Since terms for the kinetic energy of the ions are not included, the calculations refer to absolute zero.

$Li^+(g)$ and $H^-(g)$

The calculations for the ground-state energies of Li^+ (g) and $H^-(g)$ are similar to that of He. The energy operators consist of five terms: kinetic energy operators for each of the electrons, electron-nuclear potential energy operators for each of the electrons, and an electron-electron potential energy operator.

$$H_{Li} = -\frac{1}{2r_1}\frac{d^2}{dr_1^2}r_1 - \frac{1}{2r_2}\frac{d^2}{dr_2^2}r_2 - \frac{3}{r_1} - \frac{3}{r_2} + \frac{1}{r_{12}}$$
$$H_H = -\frac{1}{2r_1}\frac{d^2}{dr_1^2}r_1 - \frac{1}{2r_2}r_2 - \frac{1}{r_1} - \frac{1}{r_2} + \frac{1}{r_{12}}$$

When the trial wavefunction and the appropriate energy operator is used in the variational integral,

$$E = \int_0^\infty \Psi(1,\ 2)H\Psi(1,\ 2)d\tau_1 d\tau_2$$

the following expression result (see Appendix for details):

$$E_{Li} = \alpha^2 - 6\alpha + \frac{5}{8}\alpha \quad E_H = \beta^2 - 2\beta + \frac{5}{8}\beta$$

Minimization of the energy with respect to the scale factors to obtain the ground state energies of the gas-phase ions is the next step.

Calculation of the energies of the gas phase ions:

Seed value for the cation scale factor: α = 3

Calculate the energy and radius of the gase phase cation: $E_{Li}(\alpha) = \alpha^2 - 5.375\alpha$

$$\alpha = \text{Minimize}\,(E_{Li},\ \alpha) \quad E_{Li}(\alpha) = -7.2227 \quad E_{Li} = E_{Li}(\alpha) \quad R_{Li}(\alpha) \quad R_{Li} = \frac{3}{\alpha} \quad R_{Li} = 1.1163$$

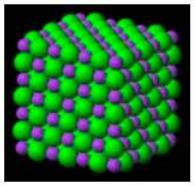
Seed value for the anion scale factor: β = 1

Calculate the energy and radius of the gas phase anion: $E_{Li}(\beta) = \beta^2 - 1.375\beta$

$$\beta = \text{Minimize}\,(E_H,\ \beta) \quad \beta = 0.6875 \quad E_H(\beta) = -0.4727 \quad E_H = E_H(\beta) \quad R_H = \frac{3}{\beta} \quad R_H = 4.3636$$

Lithium hydride solid - LiH(s)

As noted above, LiH has the face-centered cubic structure shown below.



The ground state energy of LiH(s) consists of three terms: the internal energy of Li^+, the internal energy of H^-, and the coulombic interaction energy of the ions occupying the lattice sites.

$$E_{LiH} = E_{Li} + E_H + E_{coul}$$

where

$$E_{coul} = -\frac{1.748}{R_c + R_a} \quad \text{for } \frac{R_c}{R_a} >= .414 \quad E_{coul} = -\frac{1.748}{\sqrt{2}R_a} \quad \text{for } \frac{R_c}{R_a} < 0.414$$

Here 1.748 is the Madelung constant for the face-centered cubic structure for singly charged ions. Rc and Ra are the radii of the cation and anion. (R_c + R_a) is the inter-ionic separation for situations (R_c/R_a >= .414) in which there is cation-anion contact, while 1.414Ra is the inter-ionic separation for those circumstances (R_c/R_a < .414) in which there is only anion-anion contact. On the basis of assumption 3 of the model, Rc and Ra are replaced by 3/α and 3/β, the effective ionic radii of the cation and the anion. The coulombic contribution now has the form

$$E_{coul} = -\frac{1.478}{\frac{3}{\alpha} + \frac{3}{\beta}} \quad \text{for } \frac{\beta}{\alpha} >= .414 \quad E_{coul} = -\frac{1.748}{\frac{\sqrt{2}3}{\beta}} \quad \text{for} \frac{\beta}{\alpha} < .414$$

Minimization of the energy of the solid simultaneously with respect to α and β is outlined below.

Energy of the solid assuming anion-cation contact. $f(\alpha,\ \beta) = \alpha^2 - 5.375\alpha + \beta^2 - 1.375\beta - \frac{1.748}{\frac{3}{\alpha} + \frac{3}{\beta}}$

Energy of the solid assuming anion-anion contact and that the cation rattles in the octahedral hole. $g(\alpha,\ \beta) = \alpha^2 - 5.375\alpha + \beta^2 - 1.375\beta - \frac{1.748\beta}{3\sqrt{2}}$

Composite expression for the energy of the solid using a conditional statement. $E_{LiH}(\alpha,\ \beta) = \text{if}\left(\frac{\beta}{\alpha} \geq .414,\ f(\alpha,\ \beta),\ g(\alpha,\ \beta)\right)$

Minimization of the energy of LiH with respect to the parameters α and β.

$$\begin{pmatrix} \alpha \\ \beta \end{pmatrix} = \text{Minimize}\,(E_{Li},\ \alpha,\ \beta)$$

$$\alpha = 2.6875 \quad R_c = \frac{3}{\alpha} \quad R_c = 1.1163 \quad \text{R}_c\ \text{(experimental)} = 1.134$$
$$\beta = 0.8935 \quad R_a = \frac{3}{\beta} \quad R_a = 3.3576 \quad \text{R}_a\ \text{(experimental)} = 3.931$$

$$E_{LiH}(\alpha,\ \beta) = -8.0210 \quad E_{LiH} = E_{LiH}(\alpha,\ \beta)$$

Comparison of gas-phase and solid-state ion energies (see Appendix for interpretation):

$$\begin{array}{lllll} \text{Cation:} & E_{Lis} = \alpha^2 - 5.375\alpha & E_{Lis} = -7.227 & E_{Li} = -7.227 & \text{Cation energy doesn't change.} \\ \text{Anion:} & E_{Hs} = \beta^2 - 1.375\beta & E_{Hs} = -0.4032 & E_H = -0.4727 & \text{Anion energy increases.} \end{array}$$

$$\begin{array}{ll} \text{Coulomb energy in solid state:} & E_{LiH} - E_{Lis} - E_{Hs} = -0.3681 \\ \text{The calculated lattice energy for LiH(s):} & U_{Lattice} = E_{Li} + E_H - E_{LiH} \quad U_{Lattice} = 0.3257 \end{array}$$

This result in atomic units is equivalent to a lattice energy expressed in SI units of 856 kJ/mol. A Born-Haber analysis (see below) yields a lattice energy of 912 kJ/mol. Thus, the calculated result of the proposed model is in error by only 6%. The errors for the

solid-state ionic radii are 1.6% (cation) and 14.6% (anion). Given the simplicity of the model these comparisons with experimental data are encouraging. For further details on this model see the reference cited below.

$$\mathrm{LiH(s)} \xrightarrow{-\Delta H^{\circ}_{form}=90.4kJ} \mathrm{Li(s)} + \frac{1}{2}\mathrm{H_2(g)} \xrightarrow[\frac{1}{2}BDE=218kJ]{\Delta H_{sub}=155kJ} \mathrm{Li(g)} + \mathrm{H(g)} \xrightarrow[EA=-72kJ]{IE=520kJ} \mathrm{Li^{+}(g)} + \mathrm{H^{-}(g)}$$

F. Rioux, "Simple Calculation of the Lattice Energy of Lithium Hydride," *Journal of Chemical Education* **54**, 555 (1977).

Appendix:

$$\int_0^{\frac{3}{\alpha}} \left(\sqrt{\frac{\alpha^3}{\pi}} \exp(-\alpha,\ R) \right) 4\pi r^2 dr = 93.8\%$$

The table below provides a summary of the lattice energy calculation carried out in this tutorial.

Property	Gas Phase	Solid State
Cation, α	2.6875	2.6875
Cation Radius	1.1163	1.163
Cation Energy	−7.2227	−7.2227
Anion, β	0.6875	0.8935
Anion Radius	4.364	3.3576
Anion Energy	−0.4727	−0.4302
$\frac{\text{Inter Ion}}{\text{Coulomb Energy}}$	x	−0.3681
Total Energy	−7.6953	−8.0210
Lattice Energy	x	0.3257

From the table it is clear that in the formation of LiH solid, the hydride anion contracts significantly from its gas-phase size. This increases its energy (-0.4302+0.4727=0.0425). The increase in anion energy is more than offset by the attractive inter-ion coulombic energy (-0.3681). In other words, the anion suffers a modest increase in energy by shrinking in size so that it can be on-average closer to the cation, thereby increasing the coulombic attraction between the ions and leading to a stable ionic solid.

Most of the integrals required in the analysis above are now evaluated.

Previous memory of α and β values is cleared: $\alpha = \alpha \quad \beta = \beta$

Trial one-electron wavefunction:

$$\Psi(r,\ \beta = \sqrt{\frac{\beta^3}{\pi}} \exp(-\beta,\ r)$$

Demonstrate that is is normalized:

$$\int_0^{\infty} \Psi(r,\ \beta)^2 4\pi r^2 dr \text{ assume, } \beta > 0 \rightarrow 1$$

Calculate the average value of the electron's distance from the nucleus:

$$R(\beta) = \int_{)}^{\infty} \Psi(r,\ \beta) r \Psi(r,\ \beta) 4\pi r^2 dr \text{ assume, } \beta > 0 \rightarrow \frac{3}{2\beta}$$

Calculate the average value of the kinetic energy of the electron:

$$T(\beta) = \int_0^{\infty} \Psi(r,\ \beta) - \frac{1}{2r}\frac{d^2}{dr^2}(r\Psi(r,\ \beta)) 4\pi r^2 dr \text{ assume, } \beta > 0 \rightarrow \frac{\beta^2}{2}$$

Calculate the average value of the electron-nucleus potential energy:

$$V(\beta,\ Z) = \int_0^{\infty} \Psi(r,\ \beta) - \frac{Z}{r}\Psi(r,\ \beta) 4\pi r^2 dr \text{ assume, } \beta > 0 \rightarrow -Z\beta$$

Calculate the average value of the electron-electron potential energy in two steps:

1. The electrostatic potential at r due to electron 1 is:

$$\Phi(r,\ \beta_{=}\frac{1}{r}\int_0^r \Psi(x,\ \beta)^2 4\pi x^2 dx + \int_r^\infty \frac{\Psi(x,\ \beta)^2 4\pi x^2}{x} dx \ \Big|\ \substack{\text{assume, } \beta>0 \\ \text{simplify}} \rightarrow -\frac{e^{-2\beta r}+\beta r e^{-2\beta r}-1}{r}$$

2. The electrostatic interaction between the two electrons is:

$$V_{EE}(\beta) = \int_0^\infty \Phi(r,\ \beta)\Psi(r,\ \beta)^2 4\pi r^2 dr \ \Big|\ \substack{\text{assume, } \beta>0 \\ \text{simplify}} \rightarrow \frac{5\beta}{8}$$

To summarize, the trial wavefunction chosen for two electron systems lead to the following expression for the energy.

$$E(Z,\ \beta) = \beta^2 - 2Z\beta + \frac{5}{8}\beta = \beta^2 - 2\beta\left(Z - \frac{5}{16}\right)$$

Minimization of the energy with respect to the variational parameter β yields: $\beta = Z - \frac{5}{16}$

Ground state energy:

$$E(Z) = -\left(Z - \frac{5}{16}\right)^2$$

Ionic radius:

$$R_Z = \frac{3}{Z - \frac{5}{16}}$$

This page titled 3.19: A Simple Calculation of the Lattice Energy of LiH is shared under a CC BY 4.0 license and was authored, remixed, and/or curated by Frank Rioux via source content that was edited to the style and standards of the LibreTexts platform.

3.20: An Even Simpler LiH Lattice Energy Calculation

Lithium hydride is a white crystalline solid with the face-centered cubic crystal structure (see lattice shown below). The model for LiH(s) proposed in this study constists of the following elements:

1. The bonding in LiH(s) is completely ionic. The lattice sites are occupied by the spherical, two-electron ions, Li^+ and H^-.

2. The electrons of Li^+ and H^- occupy hydrogenic 1s atomic orbitals with adjustable scale factor α. Expressed in atomic units the wavefunctions have the form,

$$\Psi(1,2) = 1s(1)1s(2) = (\alpha^3/\pi)\exp[-\alpha(r_1 + r_2)]$$

The scale factor determines how rapidly the wavefunction (and, therefore, the electron density) diminishes as the distance from the nucleus increases. α and β are, therefore, inversely related to the atomic radius. The larger α and β, the smaller the ionic radii are.

3. The average distance of an electron from the nucleus, <r>, in a scaled 1s orbital is 1.5/α. Therefore, it seems reasonable to take 2, or 3/α as the effective ionic radius in the solid. It is easy to show that 94% of the charge is contained within this radius. (See Appendix)

4. It is also assumed that the Li^+ and H^- ions in the solid have the same α value, energy and radius as they do in the gas phase. Under this assumption the lattice energy is the negative of the inter-ion coulombic energy in the solid state.

To check the validity of this model the calculated lattice energy of LiH(s) will be compared to the value obtained from a Born-Haber analysis. The lattice energy is defined as the energy required to bring about the following process,

$$LiH(s) \text{ ----> } Li^+(g) + H^-(g)$$

The determination of the lattice energy on the basis of the proposed model, therefore, proceeds by calculating the ground state energies of $Li^+(g)$ and $H^-(g)$. and subtracting from them the ground state energy of LiH(s). Since terms for the kinetic energy of the ions are not included, the calculations refer to absolute zero.

$Li^+(g)$ and $H^-(g)$

We begin with variational calculations for the ground-state energies of Li^+ (g) and H^- (g). These calculations will yield the ionic radii which will subsequently be used to calculate the LiH lattice energy.

The energy operators consist of five terms: kinetic energy operators for each of the electrons, electron-nuclear potential energy operators for each of the electrons, and an electron-electron potential energy operator.

$$H_{Li} = -\frac{1}{2r_1}\frac{d^2}{dr_1^2}r_1 - \frac{1}{2r_2}\frac{d^2}{dr_2^2}r_2 - \frac{3}{r_1} - \frac{3}{r_2} + \frac{1}{r_{12}}$$
$$H_H = -\frac{1}{2r_1}\frac{d^2}{dr_1^2}r_1 - \frac{1}{2r_2}r_2 - \frac{1}{r_1} - \frac{1}{r_2} + \frac{1}{r_{12}}$$

When the trial wavefunction and the appropriate energy operator is used in the variational integral,

$$E = \int_0^\infty \Psi(1,\ 2)H\Psi(1,\ 2)d\tau_1 d\tau_2$$

the following expression result (see the appendix for computational details):

$$E_{Li} = \alpha^2 - 6\alpha + \frac{5}{8}\alpha \quad E_H = \beta^2 - 2\beta + \frac{5}{8}\beta$$

Minimization of the energy with respect to the scale factors to obtain the ground state energies and radii of the ions is shown below.

Calculation of the energies of the gas phase ions:

Seed value for the cation scale factor: α = 3

Calculate the energy and radius of the gase phase cation: $E_{Li}(\alpha) = \alpha^2 - 5.375\alpha$

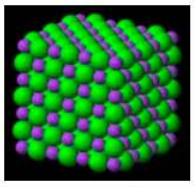
$$\alpha = \text{Minimize}\,(E_{Li},\ \alpha) \quad E_{Li}(\alpha) = -7.2227$$
$$R_{Li} = \frac{3}{\alpha} \qquad R_{Li} = 1.1163$$

Energy and radius of the gas phase anion: $E_{Li}(\alpha) = \beta^2 - 1.375\beta$

$$\alpha = \text{Minimize}(E_H,\ \alpha) \quad \alpha = 0.6875 \quad E_H(\alpha) = -0.4727$$
$$R_H = \frac{3}{\alpha} \quad R_H = 4.3636$$

Lithium hydride solid - LiH(s)

As noted above, LiH has the face-centered cubic structure shown below.



The ground state energy of LiH(s) consists of three terms: the internal energy of Li^+, the internal energy of H^-, and the coulombic interaction energy of the ions occupying the lattice sites.

$$E_{LiH} = E_{Li} + E_H + E_{coul}$$

Assuming a face-centered structure (Madelund constant = 1.748) with cation-anion and anion-anion contact, the coulombic term is as shown below.

$$E_{Li}(2.6875) + E_H(0.6875) - \frac{1.748}{R_{Li} + R_H} = -8.0143$$

Since it has been assumed that the Li^+ (g) and H^- (g) ions are the same in the gas phase and the solid state, the lattice energy is the negative of E_{coul}.

$$U_{Lattice} = \frac{1.748}{R_{Li}+R_H} \quad U_{Lattice} = 0.319$$

This result in atomic units is equivalent to a lattice energy expressed in SI units of 838 kJ/mol. The Born-Haber analysis shown below yields a lattice energy of 912 kJ/mol. Thus, the calculated result of the proposed model is in error by 8%.

$$\text{LiH(s)} \xrightarrow{-\Delta H^{\circ}_{form}=90.4kJ} \text{Li(s)} + \frac{1}{2}\text{H}_2\text{(g)} \xrightarrow[\frac{1}{2}BDE=218kJ]{\Delta H_{sub}=155kJ} \text{Li(g)} + \text{H(g)} \xrightarrow[EA=-72kJ]{IE=520kJ} \text{Li}^+\text{(g)} + \text{H}^-\text{(g)}$$

Improved results can be obtained by allowing the gas phase ions to change size on the formation of the solid under the influence of the inter-ion coulombic interaction, and by abandoning the simplifying restriction of cation-anion and anion-anion contact. See the reference below for an outline of such a calculation.

F. Rioux, "Simple Calculation of the Lattice Energy of Lithium Hydride," *Journal of Chemical Education* **54**, 555 (1977).

Appendix:

Because this is a live Mathcad document and the scale factor, α, has been used above, β will be used for the calculations outlined below.

Trial one-electron wavefunction:

$$\Psi(r,\ \beta) = \sqrt{\frac{\beta^3}{\pi}}\exp(-\beta,\ r)$$

Demonstrate that is is normalized:

$$\int_0^{\infty} \Psi(r,\ \beta)^2 4\pi r^2 dr \text{ assume, } \beta > 0 \rightarrow 1$$

Calculate the average value of the electron's distance from the nucleus:

$$R(\beta) = \int_0^{\infty} \Psi(r,\ \beta) r \Psi(r,\ \beta) 4\pi r^2 dr \text{ assume, } \beta > 0 \rightarrow \frac{3}{2\beta}$$

Demonstrate 94% of electron density is contained within 2<r>: \(\int_0 ^{ \frac{3}{ \beta}} \Psi (r,~ \beta)^2 4 \pi r^2 dr \text{ assume, } \beta >0 \rightarrow (-25)e^{-6} + 2 = 93.8 \% \nonumber \]

Calculate the average value of the kinetic energy of the electron:

$$T(\beta) = \int_0^{\infty} \Psi(r,\ \beta) - \frac{1}{2r}\frac{d^2}{dr^2}(r\Psi(r,\ \beta))4\pi r^2 dr \text{ assume, } \beta > 0 \rightarrow \frac{1}{2}\beta^2$$

Calculate the average value of the electron-nucleus potential energy:

$$V(\beta,\ Z) = \int_0^{\infty} \Psi(r,\ \beta) - \frac{Z}{r}\Psi(r,\ \beta)4\pi r^2 dr \text{ assume, } \beta > 0 \rightarrow (-\beta)Z$$

Calculate the average value of the electron-electron potential energy in two steps:

1. The electrostatic potential at r due to electron 1 is:

$$\Phi(r,\ \beta = \frac{1}{r}\int_0^r \Psi(x,\ \beta)^2 4\pi x^2 dx + \int_r^{\infty} \frac{\Psi(x,\ \beta)^2 4\pi x^2}{x} dx \ \Big|\ \substack{\text{assume, } \beta>0 \\ \text{simplify}} \rightarrow \frac{-\left[e^{-2\beta r} + \beta r e^{-2\beta r} - 1\right]}{r}$$

2. The electrostatic interaction between the two electrons is:

$$V_{EE}(\beta) = \int_0^{\infty} \Phi(r,\ \beta)\Psi(r,\ \beta)^2 4\pi r^2 dr \ \Big|\ \substack{\text{assume, } \beta>0 \\ \text{simplify}} \rightarrow \frac{5\beta}{8}$$

To summarize, the trial wavefunction chosen for two electron systems lead to the following expression for the energy.

$$E(Z,\ \beta) = \beta^2 - 2Z\beta + \frac{5}{8}\beta = \beta^2 - 2\beta\left(Z - \frac{5}{16}\right)$$

Minimization of the energy with respect to the variational parameter β yields: $\beta = Z - \frac{5}{16}$

Ground state energy:

$$E(Z) = -\left(Z - \frac{5}{16}\right)^2$$

Ionic radius:

$$R_Z = \frac{3}{Z - \frac{5}{16}}$$

This page titled 3.20: An Even Simpler LiH Lattice Energy Calculation is shared under a CC BY 4.0 license and was authored, remixed, and/or curated by Frank Rioux via source content that was edited to the style and standards of the LibreTexts platform.

3.21: Charge Cloud Models for Some Simple Atomic, Molecular and Solid Systems

The charge cloud model for atomic and molecular systems was developed in the early 1950s by George Kimball and his graduate students Gertrude Neumark and Lee Kleiss. Unfortunately their research was only published through University Microfilms at the University of Michigan.

I took an interest in the charge cloud model for pedagogical reasons in the 70s and 80s. I believed it could be used to introduce students to the quantum mechanical explanation for atomic and molecular stability and structure using only the most rudimentary mathematical tools - algebra, geometry and basic calculus.

I will present in skeletal form the calculations that appear in the following publications. Please consult these references for more details on the calculations such as comparisons with available experimental data.

"The Stability of the Hydrogen Atom," Frank Rioux, *J. Chem. Educ.* **50**, 550 (1973).

"Charge cloud study of atomic and molecular structure," Frank Rioux and Peter Kroger, *Am. J. Phys.* **44**, 56 (1976).

"An Ionic Model for Metallic Bonding," Frank Rioux, *J. Chem. Educ.* **62**, 383 (1985).

A thorough and insightful historical review of the charge cloud model appeared recently in the *Journal of Chemical Education*.

"The Kimball Free-Cloud Model: A Failed Innovation in Chemical Education?," William B. Jensen, *J. Chem. Educ.* **91**, 1106 (2014).

The basic building block of the charge cloud model is a spherical electron charge cloud of radius R and uniform charge distribution. This is the wave function of the electron. Its use leads to the following expressions for electron kinetic energy, electron-nucleus potential energy when the nucleus is in the center of the charge cloud, and electron-electron potential energy for two concentric interpenetrating charge clouds. All charge cloud calculations satisfy the virial theorem. The highlighted calculations do not predict stable species. The calculations are carried out in atomic units: $h/2\pi = m_e = e = a_o = 4\pi\varepsilon_o = 1$.

$$T = \frac{9}{8R^2} \quad V_{ne} = \frac{-3Z}{2R} \quad V_{ee} = \frac{6}{5R}$$

Hydrogen atom: point charge proton surrounded by a spherical electron charge cloud of radius R and even charge distribution throughout.

$$E_H(R) = \frac{9}{8R^2} - \frac{3}{2R} \qquad R = \frac{d}{dR}E_H(R) = 0 \;\Big|\; \substack{\text{solve, R}\\ \text{float, 5}} \rightarrow 1.5 \qquad E_H(R) = -0.5$$

Hydride anion: point charge proton surrounded by two spherical electron charge clouds of radius R and even charge distribution throughout. It is not stable on the basis of the charge cloud model.

$$\text{Reset R:} \quad E_{H'}(R) = \frac{9}{4R^2} + \frac{6}{5R} - \frac{3}{R} \qquad R = \frac{d}{dR}E_{H'}(R) = 0 \;\Big|\; \substack{\text{solve, R}\\ \text{float, 5}} \rightarrow 3.5 \qquad E_{H'}(R) = -0.36$$

Positronium: two oppositely charged concentric interpenetrating charge clouds. The correct ground state energy is -0.25 au.

$$\text{R = R} \quad E_p(R) = \frac{9}{4R^2} - \frac{6}{5R} \qquad R = \frac{d}{dR}E_p(R) = 0 \;\Big|\; \substack{\text{solve, R}\\ \text{float, 5}} \rightarrow 3.75 \qquad E_{H'}(R) = -0.16$$

Helium ion: spherical electron charge cloud with +2 nuclear point charge at the center.

$$\text{R = R} \quad E_{He'}(R) = \frac{9}{8R^2} - \frac{3}{R} \qquad R = \frac{d}{dR}E_{He'}(R) = 0 \;\Big|\; \substack{\text{solve, R}\\ \text{float, 3}} \rightarrow 0.75 \qquad E_{He'}(R) = -2$$

Helium atom: two concentric electron charge clouds with a +2 nuclear point charge at the center.

$$\text{R = R} \quad E_{He}(R) = \frac{9}{4R^2} - \frac{6}{R} + \frac{6}{5R} \qquad R = \frac{d}{dR}E_{He}(R) = 0 \;\Big|\; \substack{\text{solve, R}\\ \text{float, 3}} \rightarrow 0.937 \qquad E_{He}(R) = -2.56$$

First ionization energy: $E_{He'}(0.75) - E_{He}(R) = 0.56$

Hydrogen molecule ion: a spherical electron charge cloud with two protons positioned at +/- r from the center. The electron-proton and proton-proton potential energies for this configuration are:

$$V_{en} = \frac{-3}{2R} + \frac{r^2}{2R^3} \quad V_{nn} = \frac{1}{2r}$$

$$E_{H2'}(R,\ r) = \frac{9}{8R^2} - \frac{3}{R} + \frac{r^2}{R^3} + \frac{1}{2r}$$

$$R = 1 \quad r = .2 \quad \begin{pmatrix} R \\ r \end{pmatrix} = \text{Minimize}\left(E_{H2'},\ R,\ r\right) \quad \begin{pmatrix} R \\ r \end{pmatrix} = \begin{pmatrix} 1.243 \\ 0.783 \end{pmatrix} \quad E_{H2'}(R,\ r) = -0.728$$

Bond energy: $2E_H(1.5) - E_{H2}(R,\ r) = 0.21$

Hydrogen molecule: two concentric electron charge clouds with protons positioned at +/- r from the center.

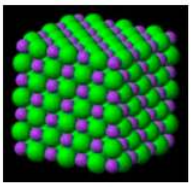
$$E_{H2}(R,\ r) = \frac{9}{4R^2} - \frac{6}{R} + \frac{2r^2}{R^3} + \frac{6}{5R} + \frac{1}{2r}$$

$$\left(E_{H2},\ R,\ r\right) \quad \begin{pmatrix} R \\ r \end{pmatrix} = \begin{pmatrix} 1.364 \\ 0.682 \end{pmatrix} \quad E_{H2}(R,\ r) = -1.21$$

Bond energy:

$$2E_H(1.5) - E_{H2}(R,\ r) = 0.21$$

LiH(s): This simple ionic solid has a face-centered cubic lattice structure shown below. It's lattice sites are occupied by the two-electron ions, $Li^+(1s2)$ and H^- $(1s^2)$. Since the ions are isoelectronic it is clear that the small spheres must be the lithium cation with nuclear charge +3, and the large spheres are the hydride anion with nuclear charge +1.



The total energy of LiH consists of three terms: the energy of the lithium cation, the energy of the hydride anion and the coulombic potential energy between the ions. As indicated below the cation-anion potential energy depends on the relative size of ions.

$$E_{cation} = \frac{9}{4R_c^2} - \frac{3Z_c}{R_c} + \frac{6}{5R_c} \quad E_{anion} = \frac{9}{4R_a^2} - \frac{3Z_a}{R_a} + \frac{6}{5R_a}$$

$$\frac{R_c}{R_a} \geq 0.414 \quad E_{coul} = \frac{-1.748}{R_a + R_c} \quad \frac{R_c}{R_a} < 0.414 \quad E_{coul} = \frac{-1.748}{\sqrt{2}R_a}$$

Nuclear charges: $Z_a = 1 \quad Z_c = 3$

Seed values for the ionic radii: $R_a = .5 \quad R_c = .5$

$$E_{LiH}\left(R_c,\ R_a\right) = \left| \begin{array}{l} \frac{9}{4R_c^2} - \frac{3Z_c}{R_c} + \frac{6}{5R_c} + \frac{9}{4R_a^2} - \frac{3Z_a}{R_a} + \frac{6}{5R_a} - \frac{1.748}{R_a + R_c} \text{ if } \frac{R_c}{R_a} \geq 0.414 \\ \frac{9}{4R_c^2} - \frac{3Z_c}{R_c} + \frac{6}{5R_c} + \frac{9}{4R_a^2} - \frac{3Z_a}{R_a} + \frac{6}{5R_a} - \frac{1.748}{R_a + R_c} \text{ otherwise} \end{array} \right.$$

$$\begin{pmatrix} R_c \\ R_a \end{pmatrix} = \text{Minimize}\left(E_{LiH},\ R_c,\ R_a\right) \quad \begin{pmatrix} R_c \\ R_a \end{pmatrix} = \begin{pmatrix} 0.577 \\ 1.482 \end{pmatrix} \quad E_{LiH}\left(R_c,\ R_a\right) = -7.784$$

Calculation of the energies of the gas-phase ions:

$$E_c\left(R_c\right) = \frac{9}{4R_c^2} - \frac{3Z_c}{R_c} + \frac{6}{5R_c} \quad R_c = \text{Minimize}\left(E_c,\ R_c\right) \quad R_c = 0.577 \quad E_c\left(R_c\right) = -6.76$$

$$E_c\left(R_c\right) = \frac{9}{4R_a^2} - \frac{3Z_a}{R_a} + \frac{6}{5R_a} \quad R_a = \text{Minimize}\left(E_a,\ R_a\right) \quad R_a = 2.500 \quad E_a\left(R_a\right) = -0.360$$

Lattice energy calculation: LiH (s) --> Li^+ (g) + H^- (g)

$$E_c\left(R_c\right) + E_a\left(R_a\right) - E_{LiH}\left(R_c,\ R_a\right) = 0.494$$

Li(s): Lithium metal is modeled as an ionic solid with the same face-centered structure as used for LiH. The small spheres in the figure above are again the lithium cations and the large spheres are the electride anions, spherical electron charge clouds of radius Ra.

$$E_{LiH}(R_c,\ R_a) = \begin{vmatrix} \frac{9}{4R_c^2} - \frac{3Z_c}{R_c} + \frac{6}{5R_c} + \frac{9}{8R_a^2} - \frac{1.748}{R_a+R_c} \text{ if } \frac{R_c}{R_a} \geq 0.414 \\ \frac{9}{4R_c^2} - \frac{3Z_c}{R_c} + \frac{6}{5R_c} + \frac{9}{8R_a^2} - \frac{1.748}{\sqrt{2}R_a} \text{ otherwise} \end{vmatrix}$$

$$\begin{pmatrix} R_c \\ R_a \end{pmatrix} = \text{Minimize}(E_{Li},\ R_c,\ R_a) \quad \begin{pmatrix} R_c \\ R_a \end{pmatrix} = \begin{pmatrix} 0.577 \\ 1.82 \end{pmatrix} \quad E_{Li}(R_c,\ R_a) = -7.1$$

Lattice energy calculation for lithium metal assuming that the energy of a gas-phase electron is zero: Li(s) ---> Li^+(g) + e^- (g)

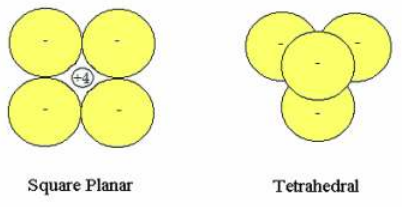
$$E_c(R_c) + 0 = E_{Li}(R_c,\ R_a) = 0.34$$

Calculation of the enthalpy of formation of LiH(s) using the results of previous calculations: Li(s) + 1/2 H_2(g) ---> LiH(s)

$$-7.784 - \left(-7.1 - \frac{121}{2}\right) = -0.079$$

Methane: Two ionic models for methane are proposed in order to show that VSEPR′s explanation for the greater stability of tetrahedral methane is spurious. Gillespie′s Valence Shell Electron Pair Repulsion (VSEPR) theory [*J. Chem. Educ.* **40**, 295 (1963)] holds that the configuration of valence electron pairs surrounding a central nonvalence nuclear kernel is determined by minimization of electron-electron potential energy.

In the ionic models considered here the +4 carbon kernel (nucleus and nonvalence electrons) is treated as a point charge which interacts electrostatically with four unpolarized hydride anions of radius R in both the square planar (D4h) and tetrahedral (Td) arrangement. In Td methane the carbon kernel occupies the tetrahedral hole and is not visible in the figure below. The energy of the hydride anion as a function of charge cloud radius was calculated previously.



D4h: In the energy expression for square planar geometry the first term in brackets multiplied by four is the hydride ion energy contribution, the next two are the repulsive interactions between the hydrides and the final term is the attractive hydride-kernel potential energy.

$$E_{D4h}(R) = 4\left(\frac{9}{4R^2} + \frac{6}{5R} - \frac{3}{R}\right) + \frac{2}{R} + \frac{1}{\sqrt{2}R} - \frac{16}{\sqrt{2}R}$$

$$R = R \quad R = \frac{d}{dR}E_{D4h}(R) = 0 \left| \begin{matrix} \text{solve, R} \\ \text{float, 5} \end{matrix} \right. \rightarrow 1.1388 \quad E_{D4h}(R) = -6.94$$

$$V_{hh} = \frac{2}{R} + \frac{1}{\sqrt{2}R} = 2.377 \quad V_{hk} = -\frac{16}{\sqrt{2}R} = -9.935$$

Td: In the energy expression for tetrahedral geometry the repulsive interaction between the hydrides and the attractive hydride-kernel potential energy follow the hydride ions energy contribution.

$$E_{Td}(R) = 4\left(\frac{9}{4R^2} + \frac{6}{5R} - \frac{3}{R}\right) - \frac{16}{\sqrt{\frac{3}{2}}R}$$

$$R = R \quad R = \frac{d}{dR}E_{Td}(R) = 0 \left| \begin{matrix} \text{solve, R} \\ \text{float, 5} \end{matrix} \right. \rightarrow 1.0426 \quad E_{Td}(R) = -8.279$$

$$V_{hh} = \frac{3}{R} = 2.877 \quad V_{hk} = -\frac{16}{\sqrt{2}R} = -10.851$$

These calculations show that indeed tetrahedral methane is the energetically preferred geometry and that the reason for this is the stronger hydride-kernel attractive interaction, which is due to its smaller charge cloud radius and the close packing of the charge clouds around the nuclear kernel. The repulsive interaction between the hydride anions is actually higher in tetrahedral methane. In

other words, molecular geometry is driven by maximizing the attractive electron-nuclear interactions and not by minimizing the electron-electron repulsive interactions.

This page titled 3.21: Charge Cloud Models for Some Simple Atomic, Molecular and Solid Systems is shared under a CC BY 4.0 license and was authored, remixed, and/or curated by Frank Rioux via source content that was edited to the style and standards of the LibreTexts platform.

3.22: A Critique of the Valence Shell Electron Pair Repulsion Model

During the last three decades the emphasis on teaching VSEPR theory in the general chemistry sequence has increased dramatically. In fact in the area of molecular structure it might be described as the theory of choice at the introductory level of the chemistry curriculum. However given long-term reservations in some quarters (see quotes below) regarding its validity, and given the tightness of the general chemistry curriculum the question of whether or not its use is justified should be a matter of discussion. This is an important issue because VSEPR is generally taught at the expense of more comprehensive and important bonding theories such as molecular orbital theory. I think it is important for the community of undergraduate chemistry teachers to discuss the question of whether or not VSEPR belongs in the chemistry curriculum.

Recently I analyzed the VSEPR model quantitatively using a simple quantum mechanical model for bonding created by Henry Bent (*1*) in the 1960s called the Tangent Spheres Model (TSM). The purpose of this paper is to share the results of my analysis with the general chemistry faculty in order to facilitate a discussion of the role VSEPR should play in the general chemistry curriculum. TSM is a rudimentary quantum mechanical model that yields quantitative predictions for molecular geometries with relative ease. Because of its simplicity as an electronic structure model, the conclusions drawn from an analysis of its results need to be validated by higher level quantum mechanical calculations. In other words the TSM can point us in the direction of further study.

Before proceeding to the TSM calculations, I would like to review a sample of the concerns that have been voiced about teaching and using VSEPR in the recent literature. As can be seen by the dates of these citations, there have been periodic expressions of caution about the use and interpretation of VSEPR since its first appearance in the chemistry curriculum.

Recent articles in the literature have championed the use of the valence shell electron pair repulsion, VSEPR, approach to predicting molecular structure. Recently, the authors of general chemistry textbooks have grasped this idea and incorporated it into the curriculum. This approach leads to the impression that electron-electron repulsions determine the geometries of molecules, because the model is presented in the form of an explanation and structures are used to confirm the model. The factors that influence the geometry of molecules are much more complicated than the VSEPR model leads one to believe. ***Drago, JCE 50, 244 (1973)****.*

In teaching VSEPR theory, as in teaching any other simple model, the student should understand that such a simple approach neglects many other factors in bonding. Its emphasis on interelectronic repulsions rather than on bond formation contrasts sharply with other models in which replusions are considered only to refine structural details. VSEPR theory like most simple models, produces mostly correct predictions. However, such a simple theory can easily be misused or overused. It should be stressed that although VSEPR theory is an easy-to-use tool, such a simple tool - by the very nature of its simplicity - may not be as accurate as necessary. ***McKenna and McKenna, JCE 61, 771 (1984)****.*

On the whole, the VSEPR method predicts the geometries of main group compounds and complexes rather well. This is not the same thing as saying that it provides a correct explanation of molecular geometry. Indeed, in the opinion of some, its status and use is just that of prediction, that of an aid to getting the right answer. One is forced to remember a difficult lesson: a model that leads to a correct prediction is not necessarily a correct model. ***Kettle, Physical Inorganic Chemistry, University Science Books, 1996, Appendix 2****.*

Among my concerns is the fact that much of the caution that is voiced in these quotations appears to be absent in our general chemistry textbooks. If it isn't stated explicitly, the impression one is left with after reading textbook presentations of VSEPR is that it is not just a predictive devise, but an explanation for the equilibrium geometries that molecules achieve. I will argue below that it does not have explanatory success because it is concerned only with electron-electron repulsions and they represent a relatively minor contribution to the total molecular energy.

The Tangent Spheres Model

The Tangent Spheres Model assumes electron pairs are spheres of radius R (an adjustable or variational parameter) and that the electron density within the spheres is uniform. As described, the TSM might be viewed as a primitive precursor of the current density functional theory (DFT). The Pauli Exclusion Principle is incorporated into the model by assuming that spheres are hard, that is that they occupy space to the exclusion of other spherical electron pairs. Quantum mechanics enters TSM through a $1/R^2$ dependence for electron kinetic energy. All potential energy contributions are calculated classically, as they are in any *ab*

*initio*quantum mechanical calculation. In other words, quantum mechanics always manifests itself in the kinetic energy term. The consequence of de Broglie's hypothesis of wave-particle duality for matter is a non-classical expression for the kinetic energy of material objects such as the electron.

To take a specific example, VSEPR predicts tetrahedral geometry for methane because this geometry puts the electron pairs farthest apart and therefore minimizes valence electron repulsions. To challenge this approach the valence energy of methane was calculated assuming both square planar and tetrahedral geometry using the Tangent Spheres method. To build square planar or tetrahedral methane using TSM requires five spheres. A small sphere represents the nuclear kernel - the nucleus and non-valence electrons and carries a net +4 charge. Four larger spheres contain the four pairs of valence electrons each with a proton imbedded in the center. Each valence sphere, therefore, carries a net charge of -1. The arrangement of the spheres for the two geometries is shown schematically in the accompanying Mathcad worksheet showing the computational details.

As we shall see below, TSM also predicts tetrahedral geometry for methane, but clearly identifies electron-nuclear attractions as the driving force in determining the equilibrium geometry. The entire TSM calculation is appended as a Mathcad worksheet as mentioned above. For computational details **click here**.

In the TSM approach the total molecular energy for methane is partitioned into the following contributions:

- Electron kinetic energy: $9/(8R^2)$
- Intra-pair electron-electron repulsion: 6/(5R)
- Inter-pair electron-electron repulsion: Coulomb's Law using point charges
- Nuclear-nuclear repulsion: Coulomb's Law using point charges
    - Hydrogen - hydrogen
    - Carbon - hydrogen
- Electron-nuclear attraction
    - For carbon: Coulomb's Law using point charges
    - For hydrogen: -3/(2R)

The results are summarized below in tabular form. The various energy contributions are reported in hartrees (1 hartree = 27.2 eV = 2.6255 MJ/mol). The results in the table show that the TSM calculations satisfy the virial theorem. That is total energy is half the potential energy and the kinetic energy is the negative of the total energy.

Methane	Square Planar	Tetrahedral	Difference
Electron kinetic energy	6.94	8.28	1.34
Electron-electron repulsion, total	13.73	16.11	2.38
Intra-pair electron repulsion	4.22	4.60	0.38
Inter-pair electron repulsion	9.51	11.51	2.00
Nuclear-nuclear repulsion, total	12.31	15.41	3.1
Nuclear-nuclear repulsion: H-H	2.38	2.88	0.50
Nuclear-nuclear repulsion: C-H	9.94	12.53	2.60
Electron-nuclear attraction, total	-39.92	-48.08	-8.16
Electron-carbon attraction	-19.87	-25.06	-5.19
Electron-hydrogen attraction: molecular	-9.51	-11.51	-2.00
Electron-hydrogen attraction: atomic	-10.54	-11.51	-0.97
Total energy	-6.94	-8.28	-1.34
Sphere radius	1.14	1.04	-0.10

In *ab initio* quantum mechanical geometry optimizations the total energy is minimized, thus, the VSEPR model seems suspect in concentrating on a single energy contribution to predict molecular geometry. The rudimentary quantum mechanical results provided in the table seem to support this suspicion. Nothing the VSEPR theory claims to be important is supported by the calculations based on TSM. For example, in going from square planar to tetrahedral geometry:

- inter-pair electronic repulsions increase rather than decrease
- the valence electrons get closer together rather than farther apart (see R in table)
- the inter-pair electron repulsion term is much smaller than the valence electron attraction for the carbon nucleus

In fact it can be stated that on the basis of the TSM analysis it appears that the major driving force for molecular geometry appears to be maximizing electron-nuclear attractions, not minimizing electron-electron repulsions. TSM suggest, therefore, that the acronym should be VSEPNA (valence shell electron pair nuclear attraction). According to TSM that geometry is best which allows electrons to get closest to the nucleus. This is, of course, a packing problem. In this example, the tetrahedral hole is clearly smaller than the square planar (octahedral) hole, allowing the negatively charged valence electrons to get closer to the positively charged nucleus. Or we could argue that the tetrahedral arrangement of valence electron pairs is close packing and the square planar arrangement isn't.

Reference:

1. Bent, H. A. *J. Chem. Educ.* **40**, 446-452 (1963).

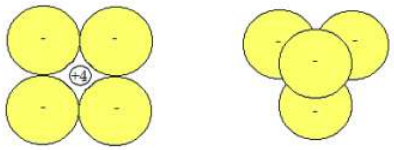
This page titled 3.22: A Critique of the Valence Shell Electron Pair Repulsion Model is shared under a CC BY 4.0 license and was authored, remixed, and/or curated by Frank Rioux via source content that was edited to the style and standards of the LibreTexts platform.

3.23: A Simple Electrostatic Critique of VSEPR

In a previous tutorial [1] it was shown that the reason methane is tetrahedral (T_d) rather than square planar (D_{4h}) is because electron-nucleus attractions are greater for the tetrahedral geometry. VSEPR teaches (incorrectly) that minimization of electron-electron potential energy drives molecular geometry. However, the previous variational calculation showed that electron-electron repulsion is actually higher in T_d methane than it is in the D_{4h} molecule.

In what follows a simple electrostatic calculation will be presented which reaches the same conclusion as the more elaborate and rigorous variational calculation based on Henry Bent's [2] Tangent Spheres Model (TSM) of chemical bonding and molecular geometry. This calculation was suggested to the author in a private communication from Henry Bent.

A simple ionic model is proposed for the bonding in methane. The +4 carbon kernel (nucleus and nonvalence electrons) is treated as a point charge which interacts electrostatically with four unpolarized hydride anions of unit diameter in either a square planar or tetrahedral arrangement. In tetrahedral methane the +4 kernel occupies the tetrahedral hole and is not visible in the diagram shown below.



Square Planar Tetrahedral

Rudimentary geometrical considerations provide the necessary molecular parameters in the following table.

Molecular Parameter	D_{4h}	T_d
Hydride-Hydride Distance	4 @ 1 and 2 @ √2	6 @ 1
Hydride-Nucleus Distance	4 @ √2/2	4 @ √(3/8)

From an electrostatic perspective a hydride anion is equivalent to an electron. Therefore, the calculation of the potential energy will be expressed in terms of electron-electron potential energy and electronnucleus potential energy. Using the molecular parameters listed in the table above we calculate the potential energy contributions for both geometries as follows.

Square Planar Methane

$$\begin{pmatrix} V_{ee} = 4\frac{(-1)(-1)}{1} + 2\frac{(-1)(-1)}{\sqrt{2}} = 5.41 \\ V_{en} = 4\frac{(-1)(+4)}{\frac{\sqrt{2}}{2}} = -22.63 \end{pmatrix}$$

Tetrahedral Methane

$$V_{ee} = 6\frac{(-1)(-1)}{1} = 6.00$$
$$V_{en} = 4\frac{(-1)(+4)}{\sqrt{\frac{3}{8}}} = -26.13$$

These results are summarized in the following table.

Energy Contribution	D_{4h}	T_d
V_{ee}	5.41	6.00
V_{en}	-22.63	-26.13
V_{tot}	-17.22	-20.13

The results of this simple electrostatic calculation contradict the VSEPR model in two significant ways:

1. Electron-electron repulsions are greater for tetrahedral geometry than they are for square planar geometry.
2. T_d is favored over D_{4h} because of electron-nucleus attractions. In other words, electron-nuclear attractions are the most important energy contribution in determining molecular geometry.

The latter conclusion should not be surprising. There are four types of energy contributions in a molecule under the Born-Oppenheimer approximation: (1) electron kinetic energy; (2) electron-nucleus potential energy; (3) electron-electron potential energy; (4) nucleus-nucleus potential energy. Electronnucleus potential energy is the only attractive term, and electron-electron potential energy is the smallest of the “repulsive” terms. Clearly electron-nucleus attraction is the single most important term in determining molecular geometry.

Furthermore, this guarantees that electron-electron potential energy will track in the opposite direction. Electron domains get closer to nuclei in two ways: by adopting a close-packed geometry (T_d versus D_{4h}) and by shrinking in size. Both lead to larger electron-electron potential energy and lower (more negative) electron-nucleus potential energy.

For the reasons enumerated above, chemical educators should recall VSEPR. It is not a valid model for molecular geometry and takes up space in textbooks that would be better devoted to viable quantum mechanical models of molecular geometry such as TSM [1, 2] or molecular orbital theory. Even in those textbooks in which it is juxtaposed with more credible models it distracts attention from them because of its specious predictive methodology.

1. Rioux, F. http://www.users.csbsju.edu/~frioux/vsepr/NVSEPR.htm
2. Bent, H. A. *J. Chem. Educ.* **40**, 446-452 (1963).

This page titled 3.23: A Simple Electrostatic Critique of VSEPR is shared under a CC BY 4.0 license and was authored, remixed, and/or curated by Frank Rioux via source content that was edited to the style and standards of the LibreTexts platform.

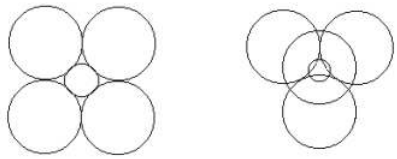
3.24: Another Critique of VSEPR

Gillespie's Valence Shell Electron Pair Repulsion (VSEPR) theory holds that the configuration of valence electron pairs surrounding a central nonvalence nuclear kernel is determined by minimization of electron-electron potential energy. The following summary statement by Gillespie is taken from *J. Chem. Educ.* **40**, 295 (1963).

> The theory proposes that the stereochemistry of an atom is determined primarily by the repulsive interactions between the electron pairs in a valence shell. The electrons in a valence shell are regarded as occupying essentially localized orbitals that are oriented in space around the nucleus and completed inner electron shells (nuclear kernel) so that their average distance apart is maximized. The tendency of electrons in a pair in a valence-shell to adopt an arrangement which maximizes their distance apart may be regarded as arising from repulsive interactions between the electron pairs.

However, quantum theory teaches that minimization of the total energy determines electronic structure. The following analysis will show that the VSEPR short-cut is specious; electron-nucleus attraction is the most important factor in determining electronic geometry and electron-electron repulsion actually increases in the transition from square planar to the more stable tetrahedral geometry in the system examined. If VSEPR gets the right answer, it does so for the wrong reason.

For the sake of mathematical simplicity the calculation of the total energy of an atomic configuration of charges will be used to refute the VSEPR theory that electron-electron repulsion determines geometry. Consider a +8 charge nuclear kernel interacting with four spherical two-electron charge clouds of uniform density and radius R in both square-planar and tetrahedral geometry. The kinetic energy of a uniform single electron charge cloud of radius R is 9/8R2. The intra-pair repulsion is 6/5R and the other electrostatic contributions to the total energy also go like +/- 1/R and are easily determined using elementary geometry. The large spheres in the figures shown below contain two electrons and the small sphere represents the +8 nuclear kernel which is assumed to have the same total energy in both geometries. Further computational detail can be found at http://www.users.csbsju.edu/~frioux/...loudModels.pdf.



Square Planar Tetrahedral

For each geometry the total energy will be minimized with respect to the charge cloud radius using the Mathcad programming environment.

The calculations are carried out in atomic units: h/2π = me = e = a_o = $4\pi\varepsilon_o$ = 1.

Square Planar Geometry

Total energy as a function of R: $E_D(R) := \frac{9}{R^2} + \frac{8}{R} + \frac{4}{\sqrt{2}R} + 4\frac{6}{5R} - \frac{64}{\sqrt{2}R}$

Minimize energy with respect to R: $R := \frac{d}{dR}E_D(R) = 0 \;\Big|\; \begin{matrix}\text{solve, R}\\ \text{float, 4}\end{matrix} \rightarrow 0.6076 \qquad E_D(R) = -24.381$

Kinetic energy: $\frac{9}{R^2} = 24.378$

Electron-Electron Repulsion: $\frac{8}{R} + \frac{4}{\sqrt{2}R} + 4\frac{6}{5R} = 25.722$

Electron-nucleus attraction: $-\frac{64}{\sqrt{2}R} = -74.481$

Total potential energy: $25.722 - 74.481 = -48.759$

Average electron-nucleus distance: $\sqrt{2}R = 0.859$

Clear R memory: $R := R$

Tetrahedral Geometry

Total energy as a function of R: $E_T(R) = \frac{9}{R^2} + \frac{12}{R} + 4\frac{6}{5R} - \frac{64}{\sqrt{\frac{3}{2}}R}$

Minimize energy with respect to R: $R = \frac{d}{dR}E_T(R) = 0 \left| \begin{matrix} \text{solve, R} \\ \text{float, 4} \end{matrix} \right. \rightarrow 0.5077 \quad E_T(R) = -34.920$

Kinetic energy: $\frac{9}{R^2} = 34.916$

Electron-electron repulsion: $\frac{12}{R} + 4\frac{6}{5R} = 33.090$

Electron-nucleus attraction: $-\frac{64}{\sqrt{\frac{3}{2}}R} = -102.926$

Total potential energy: $33.090 - 102.926 = -69.836$

Average electron-nucleus distance: $\sqrt{\frac{3}{2}}R = 0.622$

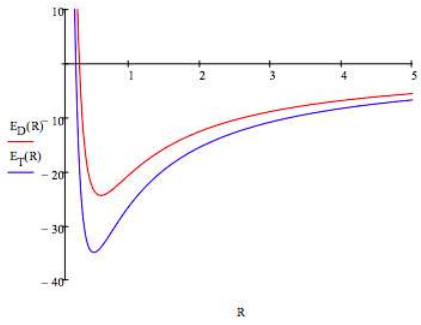
These calculations are now summarized in tabular format.

Energy Contribution	Square Planar	Tetrahedral	Change
Kinetic Energy	24.378	34.916	10.538
Electron electron potential energy	25.722	33.090	7.368
Electron nucleus potential energy	−74.481	−102.926	−28.445
Total energy	−24.381	−34.920	−10.539
Electron nucleus distance	0.859	0.622	−0.237

Of the three contributions to the total energy, electron-nucleus potential energy has the largest magnitude and is the only negative term. Kinetic energy and electron-electron potential energy have "repulsive" character and are of similar magnitudes for both geometries. They both increase in going from square-planar to tetrahedral geometry, but are overwhelmed by the very large decrease in electron-nuclear potential energy due to the closer proximity of the electrons to the nuclear kernel in the tetrahedral configuration shown in the bottom line of the table. The only conclusion that can be drawn from these calculations is that electron-nuclear attraction determines the configuration of valence electron density around a nonvalence nuclear kernel. And tetrahedral geometry is more stable because it is close-packed and brings the electrons closer to the nucleus than the square planar arrangement.

Further insight can be obtained by graphing the total energy as a function of R for both geometries.

$$R = .2, .21..5 \quad E_D(R) = \frac{9}{R^2} - \frac{29.626}{R} \quad E_T(R) = \frac{9}{R^2} - \frac{35.456}{R}$$



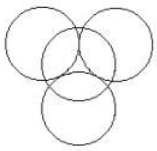
Both the square planar and tetrahedral examples show that it is kinetic energy that is responsibility for the stability of matter. While potential energy is going to negative infinity like -1/R as R decreases, kinetic energy is going to positive infinity like $1/R^2$.

This page titled 3.24: Another Critique of VSEPR is shared under a CC BY 4.0 license and was authored, remixed, and/or curated by Frank Rioux via source content that was edited to the style and standards of the LibreTexts platform.

3.25: Why Nonbonding Electrons Occupy the Equatorial Position in Trigonal Bipyramidal Geometry

Why do non-bonding electron pairs occupy the equatorial rather than the axial positions in trigonal bipyramidal geometry? VSEPR teaches that it is because they have more room in the equatorial positions and this leads to lower electron-electron repulsion. The Tangent Spheres Model (TSM) [Bent, H. A. *J. Chem. Educ.* **40**, 446-452 (1963)] calculation below shows that equatorial electrons indeed have a lower energy than the axial electrons, but not for the reason VSEPR postulates.

In the TSM approach electron pairs are represented as non-penetrating spherical charge clouds of radius R and uniform charge density. These Pauli spheres are surogates for the hybridized atomic orbitals that are frequently invoked in VSEPR explanations. There are five such pairs (three equatorial and two axial) in trigonal bipyramidal geometry. The trigonal planar hole created by the equatorial electron pairs is occupied by the nuclear kernel (nucleus plus non-valence electrons). The pockets created by the trigonal planar spheres are occupied by the two axial pairs of electrons. The equatorial electrons and one of the axial pairs is shown in the figure below.



In the calculations carried out here, the equatorial and axial electron spheres are allowed to have different radii. The nuclear kernel is treated as +10 point charge centered in the trigonal planar hole, and its electrostatic interaction with the valence electrons is its only contribution to the total energy. The contributions to the energy are identified in the table below. These Mathcad calculations are carried out using atomic units.

$$\begin{bmatrix} \text{Energy Contribution} & \text{Trigonal Bipyramidal Geometry} \\ \text{Electron Kinetic Energy} & 6\frac{6}{8R_e^2}+4\frac{9}{8R_a^2} \\ \text{Intra Pair Electron Repulsion} & 3\frac{6}{5R_e}+2\frac{6}{5R_a} \\ \text{Inter Pair Electron Repulsion} & 3\frac{-2(-2)}{2R_e}+6\frac{-2(-2)}{R_e+R_a}+\frac{-2(-2)}{2\sqrt{(R_e+R_a)^2-\frac{4}{3}R_e^2}} \end{bmatrix}$$

Seed values for the equatorial and axial radii: $R_e = .2 \quad R_a = R_e$

Minimization of the energy with respect to the equatorial and axial radii:

$$E(R_e,\ R_a) = 6\frac{9}{8R_e^2}+4\frac{9}{8R_a^2}+3\frac{6}{5R_e}+2\frac{6}{5R_a}+3\frac{(-2)(-2)}{2R_e}+6\frac{(-2)(-2)}{R_e+R_a}\ldots$$
$$\frac{(-2)(-2)}{\sqrt{(R_e+R_a)^2-\frac{4}{3}R_e^2}}+3\frac{(-2)10}{\frac{2}{3}\sqrt{3}R_e}+2\frac{(-2)10}{\sqrt{(R_e+R_a)^2-\frac{4}{3}R_e^2}}$$

$$\text{Given} \qquad \frac{d}{dR_e}E(R_e,\ R_a)=0 \qquad \frac{d}{dR_a}E(R_e,\ R_a)=0$$

$$\begin{pmatrix} R_e \\ R_a \end{pmatrix} = \text{Find}(R_e,\ R_a) \quad R_e = 0.317 \ R_a = 1.057 \quad E(R_e,\ R_a) = -71.389$$

In what follows the results of this calculation will be broken down into separate contributions for interpretive purposes. The first thing to note is that TSM predicts that the equatorial electrons are smaller than the axial electrons and, therefore, close to one another. This contradicts the VESPR idea that the equatorial position offers nonbonding electron pairs require more space.

The calculation immediately below shows that equatorial electrons have a lower energy than axial electrons. The question is why do they have a lower energy; is it because of reduced electron-electron repulsion or some other factor contributing to the energy. The smaller radius of the equatorial electrons not only brings them closer to each other (increasing electron-electron repulsion) it also brings them closer to the nuclear kernel (increasing nuclear-electron attraction).

Individual equatorial electron energy:

$$\varepsilon(R_e,\ R_a) = \frac{9}{8R_e^2}+\frac{6}{5R_e}+4\left(\frac{(-1)(-1)}{2R_e}\right)+4\left(\frac{(-1)(-1)}{R_e+R_a}\right)+\frac{(-1)(10)}{\frac{2}{3}\sqrt{3}R_e} \quad \varepsilon(R_e,\ R_a) = -3.111$$

Individual axial electron energy:

$$\gamma\left(R_e,\ R_a\right) = \begin{array}{c} \frac{9}{8R_a^2} + \frac{6}{5R_a} + 6\frac{(-1)(-1)}{R_e+R_a}\ldots \\ +\frac{(-1)(-2)}{2\sqrt{(R_e+R_a)^2-\frac{4}{3}R_e^2}} + \frac{(-1)(10)}{\sqrt{(R_e+R_a)^2-\frac{4}{3}R_e^2}} \end{array} \qquad \gamma\left(R_e,\ R_a\right) = -0.287$$

To determine why the equatorial electrons have a lower energy than the axial electrons requires that the total equilibrium energy be broken down to its constituent parts. The relative importance of each energy type (kinetic, electron-nucleus potential, electron-electron potential) is calculated as the percentage of its magnitude to the sum of the magnitudes of all energy contributions.

Equatorial-equatorial electron repulsion:

$$3\frac{6}{5R_e} + 3\frac{(-2)(-2)}{2R_e} = 30.327$$

Axial-equatorial electron repulsion:

$$6\frac{(-2)(-2)}{R_e+R_a} = 17.469$$

Axial-axial electron repulsion:

$$2\frac{6}{5R_a} + \frac{(-2)(-2)}{2\sqrt{\left(R_e+R_a\right)^2-\frac{4}{3}R_e^2}} = 3.78$$

Total electron-electron repulsion:

$$30.327 + 17.469 + 3.78 = 51.576 \quad 16.3$$

Equatorial electron-nuclear kernel attraction:

$$3\frac{(-2)(10)}{\frac{2}{3}\sqrt{3}R_e} = -164.151$$

Axial electron-nuclear kernel attraction:

$$2\frac{(-2)(10)}{\sqrt{\left(R_e+R_a\right)^2-\frac{4}{3}R_e^2}} = -30.203$$

Total electron-nuclear attraction:

$$-164.151 - 30.203 = -194.354 \quad 61.2$$

Equatorial electron kinetic energy:

$$6\frac{9}{8R_e^2} = 67.364$$

Axial electron kinetic energy:

$$4\frac{9}{8R_a^2} = 4.025$$

Total electron kinetic energy:

$$67.364 - 4.025 = 71.389 \quad 22.5$$

Every detail of this calculation contradicts the VSEPR dogma. First, electron-electron repulsion is the least important contribution to the total energy, significantly below electron kinetic energy. Second, equatorial-equatorial electron repulsion is larger than equatorial-axial and axial-axial electron repulsion. Third, VSEPR completely ignores the most important contribution to the total energy in its prediction of molecular geometry - electron-nuclear potential energy. It also ignores the importance of kinetic energy in determining molecular stability and geometry.

The validity of this TSM calculation can be tested by other calculations in which protons are imbedded in the axial or equatorial electron pairs. Energy minimization with respect to the sphere radii (axial, equatorial, imbedded) should show a lower energy for the structure in which the axial electron pair has the imbedded proton.

This page titled 3.25: Why Nonbonding Electrons Occupy the Equatorial Position in Trigonal Bipyramidal Geometry is shared under a CC BY 4.0 license and was authored, remixed, and/or curated by Frank Rioux via source content that was edited to the style and standards of the LibreTexts platform.

3.26: A Modified Tangent Spheres Model Analysis of Trigonal Bipyramidal Geometry

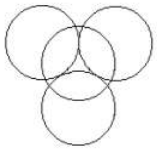
Why do non-bonding electron pairs occupy the equatorial rather than the axial positions in trigonal bipyramidal geometry? VSEPR teaches that it is because they have more room in the equatorial positions and this leads to lower electron-electron repulsion. The modified Tangent Spheres Model (TSM) [see Bent, H. A. *J. Chem. Educ.* **40**, 446-452 (1963) for an introduction] calculation below shows that equatorial electrons indeed have a lower energy than the axial electrons, but not for the reason VSEPR postulates.

In this modified TSM approach an electron is represented as a particle in a sphere of radius R. The wave function for such an electron is the eigenfunction of the kinetic energy operator in spherical coordinates, with energy $\pi^2/(2R^2)$ in atomic units, as is shown below.

$$\Phi(r,\ R) = \frac{1}{\sqrt{2\pi R}}\frac{\sin\left(\frac{\pi r}{R}\right)}{r} \qquad \frac{-\frac{1}{2r}\frac{d^2}{dr^2}(r\Phi(r,\ R))}{\Phi(r,\ R)} \rightarrow \frac{1}{2}\frac{\pi^2}{R^2}$$

According to the Pauli Exclusion Principle each spherical wave function (orbital) can accomodate two electrons. These non-interpenetrating Pauli spheres are surogates for the hybridized atomic orbitals that are frequently invoked in VSEPR explanations.

There are five such pairs (three equatorial and two axial) in trigonal bipyramidal geometry. The trigonal planar hole created by the equatorial electron pairs is occupied by the nuclear kernel (nucleus plus non-valence electrons). The pockets created by the trigonal planar spheres are occupied by the two axial pairs of electrons. The equatorial electrons and one of the axial pairs is shown in the figure below.



In the calculations carried out here, the equatorial and axial electron spheres are allowed to have different radii. This means there are two variational parameters in the energy calculation, the radii of the axial and equatorial spherical electron clouds. The nuclear kernel is treated as +10 point charge centered in the trigonal planar hole, and its electrostatic interaction with the valence electrons is its only contribution to the total energy. The contributions to the energy are identified in the table below. These Mathcad calculations are carried out using atomic units.

Energy Contribution	Trigonal Bipyramidal Geometry
Electron Kinetic Energy	$6\frac{\pi^2}{2R_e^2} + 4\frac{\pi^2}{2R_a^2}$
Intra Pair Electron Repulsion	$3\frac{1.786}{R_e} + 2\frac{1.786}{R_a}$
Inter Pair Electron Repulsion	$3\frac{(-2)(-2)}{2R_e} + 6\frac{(-2)(-2)}{R_e+R_a} + \frac{(-2)(-2)}{2\sqrt{(R_e+R_a)^2-\frac{4}{3}R_e^2}}$
Electron Kernel Attraction	$3\frac{(-2)(10)}{\frac{2}{3}\sqrt{3}R_e} + 2\frac{(-2)(10)}{\sqrt{(R_e+R_a)^2-\frac{4}{3}R_e^2}}$

Seed values for the equatorial and axial radii: $R_e = .2 \quad R_a = R_e$

$$E(R_e,\ R_a) = 6\frac{\pi^2}{2R_e^2} + 4\frac{\pi^2}{2R_a^2} + 3\frac{1.786}{R_e} + 2\frac{1.786}{R_a} + 3\frac{(-2)(-2)}{2R_e} + 6\frac{(-2)(-2)}{R_e+R_a} \ldots + \frac{(-2)(-2)}{2\sqrt{(R_e+R_a)^2-\frac{4}{3}R_e^2}} + 3\frac{(-2)(10)}{\frac{2}{3}\sqrt{3}R_e} + 2\frac{(-2)(10)}{\sqrt{(R_e+R_a)^2-\frac{4}{3}R_e^2}}$$

Given $\quad \frac{d}{dR_e}E(R_e,\ R_a) = 0 \quad \frac{d}{dR_a}E(R_e,\ R_a) = 0$

$$\begin{pmatrix} R_e \\ R_a \end{pmatrix} = \text{Find}(R_e,\ R_a) \quad R_e = 1.449 \ R_a = 5.331 \quad E(R_e,\ R_a) = -14.799$$

In what follows the results of this calculation will be broken down into separate contributions for interpretive purposes. The first thing to note is that TSM predicts that the equatorial electrons are smaller than the axial electrons and, therefore, close to one another. This contradicts the VESPR idea that the equatorial position offers nonbonding electron pairs require more space.

The calculation immediately below shows that equatorial electrons have a lower energy than axial electrons. The question is why do they have a lower energy; is it because of reduced electron-electron repulsion or some other factor contributing to the energy.

The smaller radius of the equatorial electrons not only brings them closer to each other (increasing electron-electron repulsion) it also brings them closer to the nuclear kernel (increasing nuclear-electron attraction).

Individual equatorial electron energy:

$$\varepsilon\left(R_e,\ R_a\right)=\frac{\pi^2}{2R_e^2}+\frac{1.786}{R_e}+4\left(\frac{(-1)(-1)}{R_e}\right)+4\left(\frac{(-1)(-1)}{R_e+R_a}\right)+\frac{(-1)(10)}{\frac{2}{3}\sqrt{3}R_e}\quad \varepsilon\left(R_e,\ R_a\right)=-0.423$$

Individual axial electron energy:

$$\gamma\left(R_e,\ R_a\right)=\begin{array}{c}\frac{\pi^2}{2R_a^2}+\frac{1.786}{R_a}+6\frac{(-1)(-1)}{R_e+R_a}\ldots \\ +\frac{(-1)(-2)}{2\sqrt{\left(R_e+R_a\right)^2-\frac{4}{3}R_e^2}}+\frac{(-1)(10)}{\sqrt{\left(R_e+R_a\right)^2-\frac{4}{3}R_e^2}}\end{array}\qquad \gamma\left(R_e,\ R_a\right)=0.024$$

To determine why the equatorial electrons have a lower energy than the axial electrons requires that the total equilibrium energy be broken down to its constituent parts. The relative importance of each energy type (kinetic, electron-nucleus potential, electron-electron potential) is calculated as the percentage of its magnitude to the sum of the magnitudes of all energy contributions.

Equatorial-equatorial electron repulsion:

$$3\frac{1.786}{R_e}+3\frac{(-2)(-2)}{2R_e}=7.839$$

Axial-equatorial electron repulsion:

$$6\frac{(-2)(-2)}{R_e+R_a}=3.54$$

Axial-axial electron repulsion:

$$2\frac{1.786}{R_a}+\frac{(-2)(-2)}{2\sqrt{\left(R_e+R_a\right)^2-\frac{4}{3}R_e^2}}=0.974$$

Total electron-electron repulsion:

$$7.839+3.54+0.974=12.353\quad 17.9$$

Equatorial electron-nuclear kernel attraction:

$$3\frac{(-2)(10)}{\frac{2}{3}\sqrt{3}R_e}=-35.863$$

Axial electron-nuclear kernel attraction:

$$2\frac{(-2)(10)}{\sqrt{\left(R_e+R_a\right)^2-\frac{4}{3}R_e^2}}=-6.088$$

Total electron-nuclear attraction:

$$-35.863-6.088=-41.951\quad 60.7$$

Equatorial electron kinetic energy:

$$6\frac{\pi^2}{2R_e^2}=14.104$$

Axial electron kinetic energy:

$$4\frac{\pi^2}{2R_a^2}=0.695$$

Total electron kinetic energy:

$$14.104+0.695=14.799\quad 21.4$$

Every detail of this calculation contradicts the VSEPR dogma. First, electron-electron repulsion is the least important contribution to the total energy, significantly below electron kinetic energy. Second, equatorial-equatorial electron repulsion is larger than equatorial-axial and axial-axial electron repulsion. Third, VSEPR completely ignores the most important contribution to the total energy in its prediction of molecular geometry - electron-nuclear potential energy. It also ignores the importance of kinetic energy in determining molecular stability and geometry.

Appendix: Calculation of intra-pair electron repulsion for sphere of unit radius.

$$R = 1 \quad \int_0^R \Psi(r,\ R)^2 \left(\frac{1}{r} \int_0^r \Phi(x,\ R)^2 4\pi x^2 dx + \int_0^R \frac{\phi(x,\ R)^2 4\pi x^2}{x} dx \right) 4\pi r^2 dr = 1.786$$

This page titled 3.26: A Modified Tangent Spheres Model Analysis of Trigonal Bipyramidal Geometry is shared under a CC BY 4.0 license and was authored, remixed, and/or curated by Frank Rioux via source content that was edited to the style and standards of the LibreTexts platform.

3.27: A Symbolic Huckel MO Calculation Using Mathcad

Enter and solve the butadiene Huckel determinant for energy eigenvalues.

$$\left|\begin{pmatrix}\alpha-E & \beta & 0 & 0\\ \beta & \alpha-E & \beta & 0\\ 0 & \beta & \alpha-E & \beta\\ 0 & 0 & \beta & \alpha-E\end{pmatrix}\right| = 0 \left|\begin{array}{l}\text{solve, E}\\ \text{float, 4}\end{array}\right. \rightarrow \begin{pmatrix}\alpha+.6180\beta\\ \alpha-1.618\beta\\ \alpha+1.618\beta\\ \alpha-.6180\beta\end{pmatrix}$$

Calculate the eigenvectors:

$$\text{eigenvecs}\left(\begin{pmatrix}\begin{pmatrix}\alpha-E & \beta & 0 & 0\\ \beta & \alpha-E & \beta & 0\\ 0 & \beta & \alpha-E & \beta\\ 0 & 0 & \beta & \alpha-E\end{pmatrix}\\ \end{pmatrix} = 0\right) \left|\begin{array}{l}\text{simplify}\\ \text{float, 4}\end{array}\right. \rightarrow \begin{pmatrix}.317 & .6013 & -.6013 & -.3717\\ .6014 & -.3716 & .3716 & .6014\\ .6014 & .3716 & .3716 & -.6014\\ .3717 & .6013 & .6013 & .3717\end{pmatrix}$$

Construct an energy level diagram and show the occupied levels.

Energy	Occupancy	Wave function coefficients
$\alpha-0.618\beta$	–	$(-.3717 \quad .6014 \quad -.6014 \quad .3717)$
$\alpha-0.618\beta$	–	$(-.6014 \quad .3717 \quad .3717 \quad -.6014)$
$\alpha+0.618\beta$	$_xo_$	$(-.6013 \quad -.3716 \quad .3716 \quad .6013)$
$\alpha+1.618\beta$	$_xo_$	$(.3717 \quad .6013 \quad .6013 \quad .3717)$

Calculate the π-electron energy:

$$E_\pi = [2(\alpha+1.618\beta)+2(\alpha+0.618\beta)] \rightarrow E_\pi = 4\alpha+4.472\beta$$

Calculate the delocalization energy:

$$E_d = [4\alpha+4.472\beta-2(2\alpha+2\beta)] \rightarrow E_d = .472\beta$$

Calculate the wavelength of the photon required for the HOMO-LUMO transition.

$$\frac{hc}{\lambda} = (\alpha-0.618\beta)-(\alpha+0.618\beta) \left|\begin{array}{l}\text{solve, }\lambda\\ \text{float, 3}\end{array}\right. \rightarrow -.809h\frac{c}{\beta}$$

This page titled 3.27: A Symbolic Huckel MO Calculation Using Mathcad is shared under a CC BY 4.0 license and was authored, remixed, and/or curated by Frank Rioux via source content that was edited to the style and standards of the LibreTexts platform.

3.28: A Numeric Huckel MO Calculation Using Mathcad

Enter the number of carbon atoms. $\text{Natoms} = 4$

Enter the number of occupied molecular orbitals. $\text{Nocc} = 2$

Enter the Huckel matrix.

$$H = \begin{pmatrix} 0 & 1 & 0 & 0 \\ 1 & 0 & 1 & 0 \\ 0 & 1 & 0 & 1 \\ 0 & 0 & 1 & 0 \end{pmatrix} \quad H = -H$$

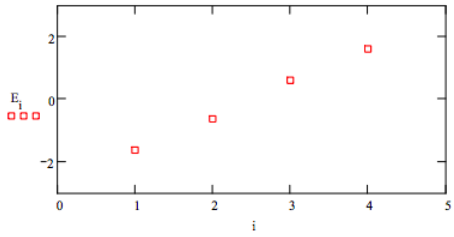
Calculate eigenvalues and eigenvectors:

$$E = \text{eigenvals(H)} \quad \text{Display} = \text{rsort}\left(\text{stack}\left(E^T,\ \text{eigenvecs(H)}\right),\ 1\right)$$

Display eigenvalues and eigenvectors:

$$\text{Display} = \begin{pmatrix} -1.618 & -0.618 & 0.618 & 1.618 \\ 0.372 & -0.602 & 0.602 & -0.372 \\ 0.602 & -0.372 & -0.372 & 0.602 \\ 0.602 & 0.372 & -0.372 & -0.602 \\ 0.372 & 0.602 & 0.602 & 0.372 \end{pmatrix}$$

Display energy level diagram. $\text{E} = \text{sort(E)} \quad \text{i} = 1 \ldots \text{Natoms}$



Calculate total π-electronic energy:

$$E_\pi = 2\sum_{i=1}^{\text{Nocc}} E_i \quad E_\pi = -4.472$$

Calculate the delocalization energy:

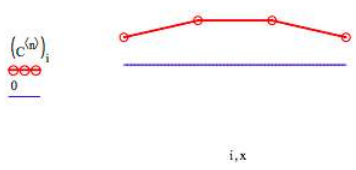
$$E_{deloc} = E_\pi + 2\text{Nocc} \quad E_{deloc} = -0.472$$

Calculate the delocalization energy per atom:

$$\frac{\text{E}_{deloc}}{\text{Natoms}} = -0.118$$

$$C = \text{submatrix}\ (\text{Display},\ 2,\ \text{Natoms} + 1,\ 1,\ \text{Natoms})$$

Enter the number of the molecualr orbital to be plotted.

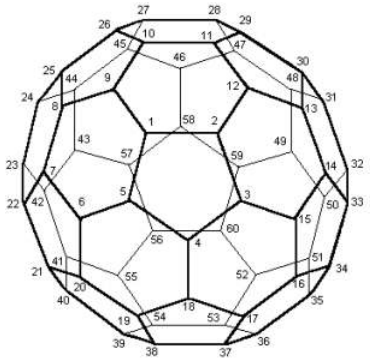


$$r = 1 \quad s = 1 \quad 2\sum_{i=1}^{Nocc}\left[\left(C^{<i>}\right)_r\left(C^{<i>}\right)_s\right] = 1 \quad \pi - \text{electron density on carbon 1}$$
$$r = 1 \quad s = 2 \quad 2\sum_{i=1}^{Nocc}\left[\left(C^{<i>}\right)_r\left(C^{<i>}\right)_s\right] = 0.894 \quad \pi - \text{bond order between carbons 1 and 2}$$
$$r = 2 \quad s = 3 \quad 2\sum_{i=1}^{Nocc}\left[\left(C^{<i>}\right)_r\left(C^{<i>}\right)_s\right] = 0.447 \quad \pi - \text{bond order between carbons 2 and 3}$$
$$r = 3 \quad s = 4 \quad 2\sum_{i=1}^{Nocc}\left[\left(C^{<i>}\right)_r\left(C^{<i>}\right)_s\right] = 1 \quad \pi - \text{bond order between carbons 3 and 4}$$

This page titled 3.28: A Numeric Huckel MO Calculation Using Mathcad is shared under a CC BY 4.0 license and was authored, remixed, and/or curated by Frank Rioux via source content that was edited to the style and standards of the LibreTexts platform.

3.29: A Numerical Huckel MO Calculation on C60

1. Number the carbons after inspection of the molecular structure and fill in data needed below.



$$\text{Natoms} = 60 \quad \text{the number of carbon atoms and } \pi - \text{electrons}$$
$$\text{Nocc} = 30 \quad \text{the number of occupied molecular occupied}$$

2. Create a 60 x 60 null matrix.

$$\text{i} = 1 \,..\, \text{Natoms} \quad \text{j} = 1 \,..\, \text{Natoms} \quad \text{H}_{i,\,j} = 0$$

3. Form the Huckel matrix from the null matrix using the results of part 1.

$$\text{k} = 1 \,..\, \text{Natoms - 1} \quad \text{H}_{k,\,k+1} = 1$$

$$\begin{array}{lllllll} H_{1,\,5} = 1 & H_{1,\,9} = 1 & H_{2,\,12} = 1 & H_{3,\,15} = 1 & H_{4,\,18} = 1 & H_{6,\,20} = 1 & H_{7,\,22} = 1 \\ H_{8,\,25} = 1 & H_{10,\,26} = 1 & H_{11,\,29} = 1 & H_{13,\,30} = 1 & H_{14,\,33} = 1 & H_{16,\,34} = 1 & H_{17,\,37} = 1 \\ H_{19,\,38} = 1 & H_{21,\,40} = 1 & H_{23,\,42} = 1 & H_{24,\,44} = 1 & H_{27,\,45} = 1 & H_{28,\,47} = 1 & H_{31,\,48} = 1 \\ H_{32,\,50} = 1 & H_{35,\,51} = 1 & H_{36,\,53} = 1 & H_{39,\,54} = 1 & H_{41,\,55} = 1 & H_{43,\,57} = 1 & H_{46,\,58} = 1 \\ H_{49,\,59} = 1 & H_{52,\,60} = 1 & H_{56,\,60} = 1 & H_{j,\,i} = H_{i,\,j} & H = -H & & \end{array}$$

4. Calculate the eigenvalues and eigenvectors. It is not feasible to look at the eigenvectors as a group because that would require displaying a 60 x 60 matrix. The eigenvalues will be displayed later.

$$\text{E} = \text{eigenvals(H)} \quad \text{C} = \text{submatrix}\left(\text{rsort}\left(\text{stack}\left(\text{E}^{T},\ \text{eigenvecs(H)}\right),\ 1\right),\ 2\text{Natoms} + 1,\ 1,\ \text{Natoms}\right)$$

5. Use the eigenvectors to calculate selected π-electron densities and π-bond orders. If r = s you are calculating the π-electron density on carbon r. If r is not equal to s you are calculating the r-s π-bond order. Several examples are given below. These calculations can be used to show that all the carbons have the same π-electron density and that there are only two physically meaningful π-bond orders.

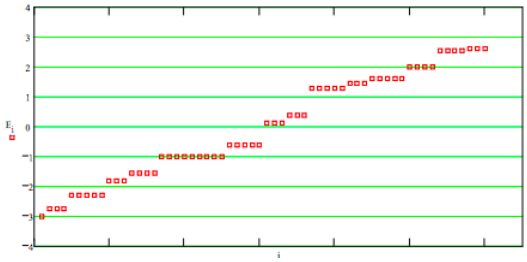
$$\begin{array}{llll} r = 1 & s = 1 & 2\sum_{i=1}^{\text{Nocc}} \left(C^{<i>}\right)_r,\ \left(C^{<i>}\right)_s = 1 & \pi - \text{electron density on carbon 1} \\ r = 1 & s = 2 & 2\sum_{i=1}^{\text{Nocc}} \left(C^{<i>}\right)_r,\ \left(C^{<i>}\right)_s = 0.476 & \pi - \text{bond order between carbons 1 and 2} \\ r = 1 & s = 5 & 2\sum_{i=1}^{\text{Nocc}} \left(C^{<i>}\right)_r,\ \left(C^{<i>}\right)_s = 0.476 & \pi - \text{bond order between carbons 1 and 5} \\ r = 1 & s = 9 & 2\sum_{i=1}^{\text{Nocc}} \left(C^{<i>}\right)_r,\ \left(C^{<i>}\right)_s = 0.601 & \pi - \text{bond order between carbons 1 and 9} \end{array}$$

Note that the π-bond order is higher for bonds that fuse two hexagons compared to bonds that fuse a hexagon and a pentagon.

6. Display the energy eigenvalues: $\text{E} = \text{sort(E)}$

$i = 1..15$	E_i	$i = 16..30$	E_i	$i = 31..45$	E_i	$i = 46..60$	E_i
	−3		−1.562		0.139		1.618
	−2.757		−1		0.139		1.618
	−2.757		−1		0.139		1.618
	−2.757		−1		0.382		1.618
	−2.303		−1		0.382		2
	−2.303		−1		0.382		2
	−2.303		−1		1.303		2
	−2.303		−1		1.303		2
	−2.303		−1		1.303		2.562
	−1.82		−1		1.303		2.562
	−1.82		−0.618		1.303		2.562
	−1.82		−0.618		1.438		2.562
	−1.562		−0.618		1.438		2.618
	−1.562		−0.618		1.438		2.618
	−1.562		−0.618		1.618		2.618

The energy eigenvalues can also be displayed graphically as follows: $i = 1..60$



Attention should be drawn to the nine-fold degenerate state at E = -1. C_{60} belongs to the icosahedral point group and the largest degeneracy permitted is 5-fold. Thus, this state is an example of the accidental degeneracy of a 5-fold degenerate state and a 4-fold degenerate state.

7. It is easy to show that this manifold of energy states is in agreement with the basic facts about C_{60}. For example, it is diamagnetic and a non-conductor. Placing the 60 π-electrons is the lowest available energy states completely fills all the bonding molecular orbitals. The HOMO has an energy of -.618 |β| and contains ten paired electrons giving a diamagnetic and non-conducting electronic structure. The LUMO is three-fold degenerate and not far away in energy. This is consistent with the fact that C_{60} has a high electron affinity and forms ionic compounds with alkali metals such as potassium. For example, K_3C_{60} (three unpaired electrons in the LUMO) is a conductor and becomes a superconductor at low temperatures, while K_6C_{60} (six paired electrons in the LUMO) is a non-conductor.

The Huckel calculation can be extended with a simple example of modeling. Since the results of the following calculation require the assignment of a value for β, the results should not be taken too seriously. The HOMO-LUMO gap is .757 |β|. Giving |β| a typical value 2.5 eV enables one to calculate the wavelength of light required to promote an electron from the HOMO to the LUMO.

$$eV = 1.6021777(10)^{-19}\text{joule} \quad h = 6.62608(10)^{-34}\text{joule sec} \quad c = 2.99792458(10)^{8}\frac{m}{sec}$$

$$\beta = 2.5eV \quad nm = 10^{-9}m \quad \lambda = 1nm$$

$$\text{Given} \quad \frac{hc}{\lambda} = .757|\beta| \quad \text{Find}(\lambda) = 655nm$$

This result is just barely within the visible region and not in particularly good agreement with a known visible transition around 400 nm. However, it should be noted that the HOMO-LUMO transition is formally forbidden. The HOMO-LUMO+1 is allowed and the energy gap is |β| which would give an optical transition at 496 nm, in better agreement with the experimental value.

There are a number of very weak features in the visible spectrum between 440 and 670 nm any of which may be attributable to the forbidden HOMO-LUMO transtion. However, it is also true that small amounts of other fullerenes may be contributing to this part of the visible spectrum.

8. Calculate the π-electron stabilization energy per carbon atom. This is calculated by summing the energies of the occupied orbitals and multiplying by two. Subtract from this the π-electron binding energy of the equivalent number of ethylene molecules and divide by the number of carbon atoms, which is the same as the number of π-electrons.

$$\Delta E_\pi = \frac{2\sum_{i-1}^{\text{Nocc}}|E_i| - \text{Natoms}}{\text{Natoms}} \quad \Delta E_\pi = 0.553$$

Recall that the π-electron stabilization energy per carbon atom for benzene is 0.333.

This page titled 3.29: A Numerical Huckel MO Calculation on C60 is shared under a CC BY 4.0 license and was authored, remixed, and/or curated by Frank Rioux via source content that was edited to the style and standards of the LibreTexts platform.

3.30: Chemical Bonding and Electronic Structure of Buckminsterfullerene

As is well-known C_{60} resembles an American soccerball, containing 12 pentagons and 20 hexagons (see Figure 1). Removing the leather, but keeping the seams, leaves 60 vertices for the carbon atoms and 90 covalent bonds between them, 60 single bonds and 30 double bonds.



Figure 1

Figure 2. Curly and Smalley (see Scientific American, October 1991, pp 54-63) have described it as the "roundest molecule that can possible exist."

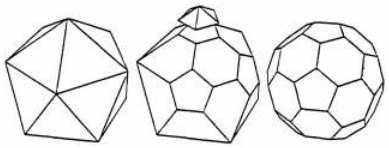


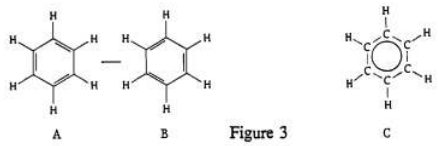
Figure 2

Figure 1.

However, we should note that the actual bonding in C60 is somewhat more complex. The reason for this is that sp^2 hybrid orbitals all lie in the same plane, but inspection of any model of buckminsterfullerene clearly shows that the environment at each carbon is not planar. So the hybridization at each carbon cannot be pure sp^2, and current research indicates that the actual hybridization is $sp^{2.3}$. Since we are trying to develop a simple, but serviceable, model of the bonding and electronic structure of C_{60}, we will assume sp^2 hybridization as a first approximation. It might be a good idea at this point to review what Zumdahl has to say about models on pages 362 to 364 in his textbook.

In chapter 8 we spent a fair amount of time drawing resonance structures for molecules and ions that had more than one correct Lewis structure. C_{60} is such a molecule and, as a matter of fact, it has 12,500 resonance structures! Try drawing at least two resonance structures, one in which all double bonds are in the hexagons, and one in which the pentagons have double bonds.

Associated with the concept of resonance is the idea of delocalization of electrons. For example, for a molecule with two resonance structures of equal plausibility (review formal charge arguments) we would say that the molecule's electronic structure is not correctly represented by either one or the other, but an average of the two (see Zumdahl's discussion of resonance in section 8.12). The fact that more than one Lewis structure can be written for a molecule is an indication of weakness in the Lewis' localized electron pair model of chemical bonding, because the existence of resonance structures actually delocalizes the r-electrons over the molecule as a whole. Benzene is, perhaps, the best example of this. Rather than writing structures A or B below, we write C and think Figure 9.48b in Zumdahl.



A B Figure 3 C

Since C_{60} has 12,500 resonance structures involving its 60 r-electrons we may profitably consider the r-electrons to be particles delocalized over a sphere. The solution of Schrödinger's equation for a particle on a sphere is well known. Since a particle on a sphere is restricted to move in two directions, in spherical polar coordinates its position can be described by two angles, θ and ϕ. Thus, two spatial quantum numbers are required and they are the old familiar 1 and m_1 of Chapter 7 of Zumdahl. Since the particles in question are electrons, the spin quantum number, m_s, is also required. The rules for the quantum numbers are as stated in Chapter 7: 1 can have integer values starting with 0; m_1 can have integer values ranging from -1 to +1; m_s, can have the values of $\pm 1/2$.

Using the rules for the 1 and m_1 quantum numbers makes it possible to construct an energy level diagram for an electron on a sphere. This is shown in Figure 4.

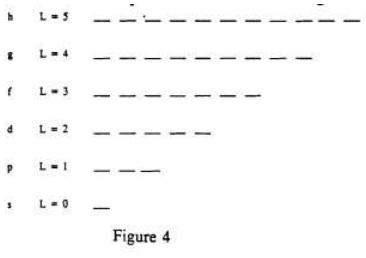


Figure 4

Figure 5.

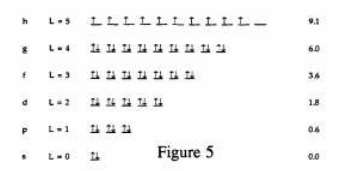


Figure 5

This figure shows 10 unpaired electrons (Hund's Rule) in the highest occupied energy level. This would suggest that C_{60} is paramagnetic and perhaps a conductor of electricity. In fact C_{60} is diamagnetic (no unpaired electrons) and does not conduct electricity. Thus, this initial model for the bonding and electronic structure of C_{60} is not correct.

A way out of this difficulty is to recall that C_{60} is not a sphere, but a truncated iscosohedron. The symmetry of the truncated icosohedron is high, but not as high as a perfect sphere. The main consequence of this is that the degeneracies of some of the higher energy levels are split by the lower iscosahedral symmetry. You will see more of this in CHEM 234 when we study transition metal complexes and crystal field theory. Figure 6 shows what happens to the energy levels under icosahedral symmetry and how they are filled with 60 electrons.

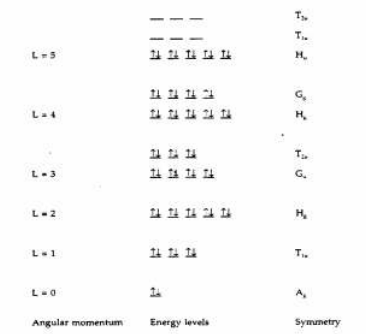


Figure 6

Note that this energy level diagram is in agreement with the basic facts about C_{60}. It is a non-conductor and diamagnetic. In addition, it suggests that C_{60} might have a fairly high electron affinity because it has a low-lying unoccupied energy level with room for six electrons. This is consistent with the fact that K_3C_{60} is known and is a conductor and passes into a super-conducting state at low temperature. The electro-positive potassium atoms supply three electrons which half-fill the lowest unoccupied energy level. K_6C_{60} is also known and is a non-conductor. This too is consistent with the model as the potassiums supply six valence electrons completely filling the C_{60}'s lowest unoccupied energy level.

In Chapter 10 we will see that the crystal structures of solid C_{60}, K_3C_{60}, and K_6C_{60} can be described using the same concepts as are used to describe the more familiar structures of NaCl, $CsCl_2$, and CaF_2. For now we can say, for example, that solid buckminsterfullerene consists of a face-centered cubic packing of spherical C_{60} molecules (see Figures 10.15 and 10.17 in Zumdahl). K_3C_{60} can be described as face-centered cubic C_{60}^{3-} ions with K^+ ions in all the tetrahedral and octahedral holes (see Figure 10.33 in Zumdahl for an illustration of tetrahedral and octahedral holes). You should confirm that this structure gives the correct stoichiometric ratios for the ions. By contrast K_6C_{60} is body centered C_{60}^{3-} ions with four K^+ ions in each of the six cube

faces as shown in Figure 7 below. Again you should confirm that this structure gives the correct ratio of the stoichiometric coefficients.

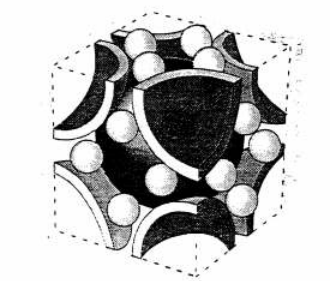


Figure 7

While it is not possible to go into detail at this point, it is also the case that the model presented here for the bonding and electronic structure of buckminsterfullerene is consistent with the absorption spectra of C_{60} in the ultraviolet, visible, and infrared regions of the electromagnetic spectrum.

This page titled 3.30: Chemical Bonding and Electronic Structure of Buckminsterfullerene is shared under a CC BY 4.0 license and was authored, remixed, and/or curated by Frank Rioux via source content that was edited to the style and standards of the LibreTexts platform.

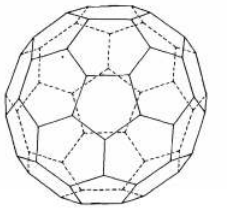
3.31: Quantum Mechanics, Group Theory and C60

The recent discovery of a new allotropic form of carbon[1] and its production in macroscopic amounts[2] has generated a tremendous amount of research activity in chemistry, physics and material science.[3] Among the areas of current interest are the electronic properties of the fullerenes and this note describes a simple model for the electronic structure of Coo that is consistent with recent experimental findings. It is based on the most elementary principles of quantum mechanics and group theory.

After the soccer-ball structure for C_{60} was first suggested in 1985 it became important to obtain as much independent supporting evidence as possible. This came in the areas of nmr, IR, and Raman spectroscopy. The nmr spectrum showed a single resonance indicating 60 equivalent carbon atoms in the structure. The IR spectrum was found to have four lines, while Raman spectroscopy yielded ten lines. The second half of this paper will use group theory to demonstrate that a C_{60} molecule with a soccer-ball structure must have four IR active and ten Raman active vibrational modes.

Electronic Structure

As is well-known C_{60} is a carbon cage consisting of 20 hexagons and 12 pentagons and resembles a soccerball. Removing the leather, but keeping the seams, leaves 60 vertices for the carbon atoms and 90 covalent bonds between them. Actually C_{60} has spheroidal geometry and belongs to the truncated icosahedral symmetry group, l_h. Curly and Smalley, codiscoverers of buckminsterfullerene, have described it as the "roundest molecule that can possibly exist"[4] so the model presented here assumes, initially, that Coo is a perfect sphere. Each carbon is sigma bonded to three other carbons using three of its four valence electrons to form these bonds. The remaining electron is considered to be delocalized on the surface of the sphere created by the 60 atom carbon cage.



1

The quantum mechanical behavior of an individual electron restricted to the surface of a sphere is well-known.[5] Solving Schrödinger's equation for a particle on a sphere yields the spherical harmonic wavefunctions, pictures of which can be found in Atkins' physical chemistry textbook. The energy levels associated with the spherical harmonic states are a function of the radius of the sphere and the angular momentum quantum number.

$$E_L = \frac{h^2}{8\pi^2 m_e R^2} L(L+1)$$

Just as the quantum mechanical solution for the one-electron hydrogen atom can be adapted for qualitative treatments of the electronic structure of multi-electron atoms, so the energy level diagram for the electron moving on a sphere can be used to describe the electronic structure of C_{60}. The energy level diagram shown in Figure 1 provides a qualitative description of the electronic structure obtained when one applies the aufbau principle, the Pauli exclusion principle, and Hund' s rule to the addition of 60 electrons to the available spherical harmonic energy levels.

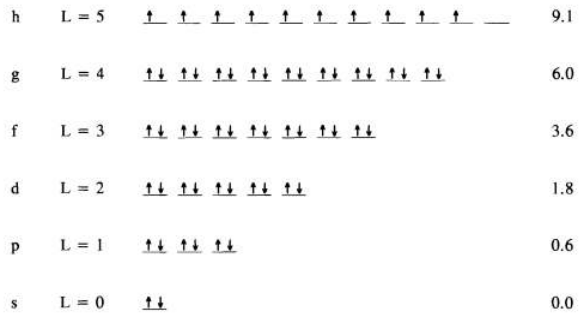


Figure 1. Sixty electrons placed in the lowest available energy levels according to the aufbau principle, the Pauli exclusion principle, and Hund's rule. The energies for the individual levels shown on the right are in eV and were calculated using equation 1.

As it stands this is not a satisfactory picture because pristine C_{60} is an insulator and has no un-paired electrons. This difficulty is resolved by recalling that C_{60} is not a perfect sphere, but has the lower symmetry of the icosahedral group. Invoking icosahedral symmetry at this point splits the degeneracies of all levels above L = 2. However, initially it is only necessary to examine what happens to the highest occupied level, L = 5, since all other levels are completely filled.

Using traditional group theoretical methods[6], it can be shown that the L = 5 spherical harmonics transform under the rotations of the icosahedral symmetry group as shown in the last row of the icosahedral character table shown below. The behavior of the spherical harmonics under the rotations of the icosahedral group is given by

$$\chi\left(c_\alpha\right)=\frac{\sin\left(L+\frac{1}{2}\right)\alpha}{\sin\frac{\alpha}{2}}$$

I_h	E	$12C_5$	$12C_5^2$	$20C_3$	$15C_2$
A	1	1	1	1	1
T_1	3	1.618	-.618	0	-1
T_2	3	-.618	1.618	0	-1
G	4	-1	-1	1	0
H	5	0	0	-1	1
L=5	11	1	1	-1	-1

It is easy to show that this reducible representation is a linear combination of the fivefold degenerate H_u, an the two three-fold degenergate, T_{1u} and T_{2u} irreducible representations of the icosahedral group. Group theory doesn't predict the order of the levels, but Figure 2 shows that if the five-fold degenerate level is placed lowest, an energy level diagram that captures the essentials of the known electronic structure of C_{60} is obtained.[7,8] This assignment is consistent with HOMO, LUMO, and LUMO+ 1 levels of the Huckel molecular orbital calculation on C_{60}.[8,9] In addition, if the splittings of the L = 3 and L = 4 states are also examined in the manner outlined above, the complete energy level diagram for the π-electrons of C_{60} shown in Figure 3 is obtained. This set of π-electron levels is qualitatively consistent with the results of an ab initio calculation based on the pseudopotentiallocal density method.[10]

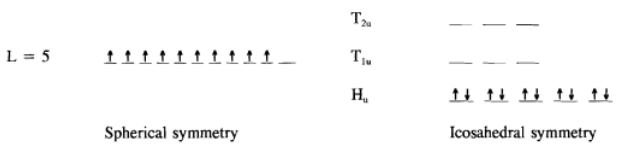


Figure 2. The splitting of the L = 5 energy level under icosahedral symmetry.

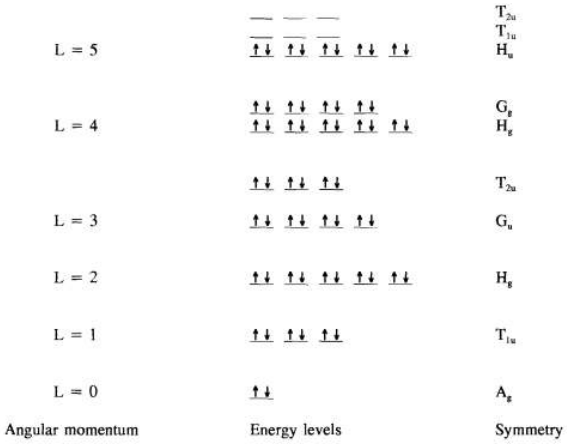


Figure 3. A complete energy level diagram for the π-*electrons of C60 showing the splitting of the relevant angular momentum states under icosahedral symmetry.*

The HOMO-LUMO energy gap is known to be 1.5 eV. However, the HOMO -> LUMO electronic transition is optically forbidden. Because H_u level is full, $(H_u)^{10}$, the ground electronic state has A_g symmetry. The first excited state $(H_u)^9(T_{1u})^1$ produces the reducible representation shown in the table below. This is obtained by taking the direct product of the H_u and T_{1u} irreducible representations ($H_u x T_{1u}$). The reducible representation of the second excited state, $(H_u)^9(T_{1g})^1$ is also shown in the table. It is important to note that both excited states are 15-fold degenerate.

	E	$12C_5$	$12C_5^2$	$20C_3$	$15C_2$	i	$12S_{10}$	$12S_{10}^2$	$20S_6$	15 σ
H_uT_{1u}	15	0	0	0	-15	15	0	0	0	15
H_uT_{1g}	15	0	0	0	-15	-15	0	0	0	15

Employing the usual methods it is not difficult to show that the first and second excited electronic configurations contain the following irreducible representations.

$$(H_u)^9\,(T_{1u})^1 \rightarrow T_{1g} + T_{2g} + G_g + H_g$$
$$(H_u)^9\,(T_{1g})^1 \rightarrow T_{1u} + T_{2u} + G_u + H_u$$

Thus, it can be seen that the excited electronic configurations each give rise to four excited states. In order for a transition to any of these states from the ground state to be allowed, the transition probability integral $\int \Psi_i \mu \Psi_f d\tau$ must be non-zero. For this integral to be non-zero the direct product of the irreducible representations for the ground electronic state, the electric dipole operator, and the excited electronic state must contain the totally symmetric irreducible representation A_g. Because the ground state itself has A_g symmetry and the electric dipole operator has T_{1u} symmetry, only an excited state with T_{1u} symmetry will lead to a direct product which contains the A_g irreducible representation.

Inspection of the irreducible representations for the first and second exited electronic configurations shows that only the second excited electronic configuration contains the T_{1u} irreducible representation. Thus, while the HOMO → LUMO transition is forbidden, the HOMO → LUMO+ 1 transition is allowed. This result is consistent with the visible spectrum of the free molecule.[9]

A further comment on the magnitude of the HOMO-LUMO gap might be made at this point. The energies of the spherical harmonic states shown in Figure 1 were calculated using equation (1) and a value of 710 pm for the diameter of the carbon cage. At the L = 5 level the energy difference between adjacent states is 3.1 and 3.6 eV. While the model doesn't provide a detailed quantitative analysis of.the splitting of the L = 5 level, using reasonable assumptions one can obtain a value for the HOMO-LUMO gap that is "in the ball park. "

In summary, this analysis provides a simple interpretation of the fact that C_{60} is an insulator. The model also provides low-lying, un-occupied orbitals to form conduction bands and receive electrons from donors such as potassium. Furthermore, the fact that the LUMO is triply degenerate is consistent with the experimental evidence that K_3C_{60} is a conductor and K_6C_{60} is an insulator.[7] While

this simple model is not a rival to the more sophisticated molecular orbital or band theory calculations, it does provide the non-specialist with an appealing and simple alternative.

Vibrational Spectroscopy

To analyze the vibrational modes of C_{60} using group theory it is necessary to determine how the 180 degrees of freedom of the C_{60} molecule transform under the symmetry operations of the I_h group. This is actually quite easily done because the rotations and the inversion symmetry operation move all the carbon atoms and, therefore, have characters of O. The identity operation leaves all carbons unmoved for a character of 180, while the 15 planes of symmetry contain four carbon atoms each and can be shown to have a character of 4. The model of C_{60} on the first page shows one of these planes. It is perpendicular to the plane of the paper and clearly contains four carbon atoms, two at the top and two at the bottom.

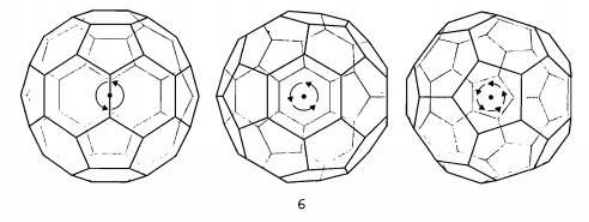
This makes it very easy to decompose the reducible representation, Γ_{tot}, into its irreducible representations by the usual methods. This is summarized in the table on the next two pages. For simplicity only the E and cr symmetry operations are shown, but it must be remembered that there are 120 symmetry operations total. For example, the occurrence of H_g is calculated as follows:

$$\Lambda_{tot} \cdot H_g = \frac{[(1)(180)(5) + (15)(4)(1)]}{120} = 8$$

After translation and rotation are subtracted from the total, 174 vibrational degrees of freedom remain. However, group theory shows that many vibrational modes are degenerate. In fact, as the table below shows, there are only 46 distinct vibrational frequencies.

$$\Lambda_{vib} = 2A_g + 3T_{1g} + 4T_{2g} + 6G_g + 8H_g + A_u + 4T_{1u} + 5T_{2u} + 6G_u + 7H_u$$

Of these, the table indicates that only the four triply degenerate T_{1u} modes are IR active while ten vibrational modes ($2A_g + 8H_g$) are Raman active. This analysis is in complete agreement with the experimental measurements[11] and was considered to be crucial evidence in support of the proposed soccer-ball structure for C_{60}. Several of the rotational axes for C_{60} are shown below to illustrate that they do move all atoms.



I_h	E	15σ	Occurrence	h = 120
Γ_{xyz}	180	4		
A_g	1	1	2	Raman active
T_{1g}	3	-1	4	R_x, R_y, R_z
T_{2g}	3	-1	4	
G_g	4	0	6	
H_g	5	1	8	Raman active
A_u	1	-1	1	
T_{1u}	3	1	5	T_x, T_y, T_z /IR
T_{2u}	3	1	5	
G_u	4	0	6	
H_u	5	-1	7	

Literature cited:

1. Kroto, H. W.; Heath, J. R.; O'Brien, S. C.; Curl, R. F.; Smalley, R. E. *Nature* **1985**, *318*, 162-164.
2. Kratschmer, W.; Lamb, L. D.; Fostiropolous, K.; and Huffman, D. R., *Nature* **1990**, *347*, 354.
3. *Accounts of Chemical Research* **1992**, 25 , number 3.
4. Curl, R.F.; Smalley, R. E. *Sci. Am.* **1991**, *10*, 54-63.
5. Atkins, P. W. *Physical Chemistry*, **1990** (W. H. Freeman and Company, New York, 4th edition, Chapter 12, pages 336-338).
6. Atkins, P. W. *Molecular Quantum Mechanics*, **1983** (Oxford University Press, Oxford, New York, 2nd Edition, Chapter 7, pages 163-167).
7. Weaver, J. H., et al. *Phys. Rev. Lett.* **1991**, *66*, 1741-1744.
8. Haddon, R. C., *Accounts of Chemical·Research* **1992**, *25*, 127-133.
9. Hebard, A. F., *Physics Today* **1992**, *11*, 26-32.
10. Martins, J. L.; Troullier, N.; Weaver, J. H., *Chem. Phys. Lett.* **1991**, *180*, 457-60.
11. Chung, F.; Sternberg, S., *American Scientist* **1993**, *81*, 56-71.

This page titled 3.31: Quantum Mechanics, Group Theory and C60 is shared under a CC BY 4.0 license and was authored, remixed, and/or curated by Frank Rioux via source content that was edited to the style and standards of the LibreTexts platform.

3.32: A Numerical Huckel Calculation on Anthracene and Phenanthrene

High level quantum mechanical calculations reveal that phenanthrene is more stable than anthracene, and that the enhanced stability has its origin in the energy of the π-electron density. This tutorial shows that even a simple Huckel molecular orbital calculation predicts the greater stability of phenanthrene.

Huckel calculations can be carried out in several ways; perhaps the most economical and revealing is the numeric method which is based on a connectivity matrix. Anthracene and phenanthrene, shown below, have 14 carbon atoms, so the connectivity matrix is 14 x 14. The only non-zero matrix elements contain the integer 1 indicating adjacent (bonded) carbons. For example, using the numbering scheme shown below carbon 1 is bonded to carbons 2 and 14 in both molecules, and this connectivity (bonding) is registered in the first row of the respective Huckel matirices shown below.



anthracene phenanthrene

The Huckel connectivity matrices for anthracene and phenanthrene are,

$$Ha = \begin{pmatrix} 0 & 1 & 0 & 0 & 0 & 0 & 0 & 0 & 0 & 0 & 0 & 0 & 0 & 1 \\ 1 & 0 & 1 & 0 & 0 & 0 & 0 & 0 & 0 & 0 & 1 & 0 & 0 & 0 \\ 0 & 1 & 0 & 1 & 0 & 0 & 0 & 0 & 0 & 0 & 0 & 0 & 0 & 0 \\ 0 & 0 & 1 & 0 & 1 & 0 & 0 & 0 & 1 & 0 & 0 & 0 & 0 & 0 \\ 0 & 0 & 0 & 1 & 0 & 1 & 0 & 0 & 0 & 0 & 0 & 0 & 0 & 0 \\ 0 & 0 & 0 & 0 & 1 & 0 & 1 & 0 & 0 & 0 & 0 & 0 & 0 & 0 \\ 0 & 0 & 0 & 0 & 0 & 1 & 0 & 1 & 0 & 0 & 0 & 0 & 0 & 0 \\ 0 & 0 & 0 & 0 & 0 & 0 & 1 & 0 & 1 & 0 & 0 & 0 & 0 & 0 \\ 0 & 0 & 0 & 1 & 0 & 0 & 0 & 1 & 0 & 1 & 0 & 0 & 0 & 0 \\ 0 & 0 & 0 & 0 & 0 & 0 & 0 & 0 & 1 & 0 & 1 & 0 & 0 & 0 \\ 0 & 1 & 0 & 0 & 0 & 0 & 0 & 0 & 0 & 1 & 0 & 1 & 0 & 0 \\ 0 & 0 & 0 & 0 & 0 & 0 & 0 & 0 & 0 & 0 & 1 & 0 & 1 & 0 \\ 0 & 0 & 0 & 0 & 0 & 0 & 0 & 0 & 0 & 0 & 0 & 1 & 0 & 1 \\ 1 & 0 & 0 & 0 & 0 & 0 & 0 & 0 & 0 & 0 & 0 & 0 & 1 & 0 \end{pmatrix} \quad Hp = \begin{pmatrix} 0 & 1 & 0 & 0 & 0 & 0 & 0 & 0 & 0 & 0 & 0 & 0 & 0 & 1 \\ 1 & 0 & 1 & 0 & 0 & 0 & 0 & 0 & 0 & 0 & 1 & 0 & 0 & 0 \\ 0 & 1 & 0 & 1 & 0 & 0 & 0 & 0 & 0 & 0 & 0 & 0 & 0 & 0 \\ 0 & 0 & 1 & 0 & 1 & 0 & 0 & 0 & 1 & 0 & 0 & 0 & 0 & 0 \\ 0 & 0 & 0 & 1 & 0 & 1 & 0 & 0 & 0 & 0 & 0 & 0 & 0 & 0 \\ 0 & 0 & 0 & 0 & 1 & 0 & 1 & 0 & 0 & 0 & 0 & 0 & 0 & 0 \\ 0 & 0 & 0 & 0 & 0 & 1 & 0 & 1 & 0 & 0 & 0 & 0 & 0 & 0 \\ 0 & 0 & 0 & 0 & 0 & 0 & 1 & 0 & 1 & 0 & 0 & 0 & 0 & 0 \\ 0 & 0 & 0 & 1 & 0 & 0 & 0 & 1 & 0 & 1 & 0 & 0 & 0 & 0 \\ 0 & 0 & 0 & 0 & 0 & 0 & 0 & 0 & 1 & 0 & 1 & 0 & 0 & 0 \\ 0 & 1 & 0 & 0 & 0 & 0 & 0 & 0 & 0 & 1 & 0 & 1 & 0 & 0 \\ 0 & 0 & 0 & 0 & 0 & 0 & 0 & 0 & 0 & 0 & 1 & 0 & 1 & 0 \\ 0 & 0 & 0 & 0 & 0 & 0 & 0 & 0 & 0 & 0 & 0 & 1 & 0 & 1 \\ 1 & 0 & 0 & 0 & 0 & 0 & 0 & 0 & 0 & 0 & 0 & 0 & 1 & 0 \end{pmatrix}$$

The energy eigenvalues are the negatives of the eigenvalues of the connectivity matrices. The energy eigenvalues, π−electron energy and the π−delocalization energy are calculated for each molecule below. There are seven doubly occupied molecular orbitals for each molecule and the energy of a localized π electron pair (ethene) is -2. Thus the π-electron energy is twice the sum of the occupied energy levels. The delocalization energy is the π-electron energy minus the energy of an equivalent number of localized π-electron pairs. See the appendix for the calculation of the ethene (localized) π-electron energy.

Anthracene

$$\text{Ha} = \text{-Ha} \quad \text{Ea} = \text{eigenvals(Ha)} \quad \text{Ea} = \text{sort(Ea)}$$

$$Ea^T = (-2.414 \quad -2 \quad -1.414 \quad -1.414 \quad -1 \quad -1 \quad -0.414 \quad 0.414 \quad 1 \quad 1 \quad 1.414 \quad 1.414 \quad 2 \quad 2.414)$$

$$E_{\pi a} = 2\sum_{i=1}^{7} Ea_i \quad E_{\pi a} = -19.314 \quad Ea_{deloc} = E_{\pi a} - 7(-2) \quad Ea_{deloc} = -5.314$$

Phenanthrene

$$\text{Hp} = \text{-Hp} \quad \text{Ep} = \text{eigenvals}(\text{Hp}) \quad \text{Ep} = \text{sort}(\text{Ep})$$

$$Ep^T =$$
$$(-2.435 \quad -1.951 \quad -1.516 \quad -1.306 \quad -1.142 \quad -0.769 \quad -0.605 \quad 0.605 \quad 0.769 \quad 1.142 \quad 1.306 \quad 1.516 \quad 1.951 \quad 2.414)$$

$$E_{\pi p} = 2\sum_{i=1}^{7} Ep_i \quad E_{\pi p} = -19.448 \quad Ep_{deloc} = E_{\pi p} - 7(-2) \quad Ep_{deloc} = -5.448$$

Summary

$$\begin{pmatrix} \text{Molecule} & E_\pi & E_{deloc} \\ \text{Anthracene} & -19.314 & -5.314 \\ \text{Phenanthrene} & -19.448 & -5.448 \end{pmatrix}$$

According to the Huckel model for π-electron energy phenanthrene is more stable than anthracene. This result is in agreement with higher level quantum mechanical calculations and the enthalpies of formation of anthracene and phenanthrene, 227 and 201 kJ/mol, respectively.

Appendix

Ethene is the bench mark for a localized pair of π electrons. As shown below, the eigenvalues for the Huckel connectivity matrix for ethene are -1 and +1. Thus a localized pair of π electrons has an energy of -2.

$$He = \begin{pmatrix} 0 & 1 \\ 1 & 0 \end{pmatrix} \quad \text{He} = \text{-He} \quad \text{Ee} = \text{eigenvals}(\text{He}) \quad \text{Ee} = \text{sort}(\text{Ee}) \quad Ee^T = (-1 \quad 1)$$

References

See problem 14.16 on page 469 of Atkins and de Paula, *Physical Chemistry*, 7th edition.

For results of high level calculations see, Poater, J. *Journal of Organic Chemistry*, **2007**, 72, 1134.

This page titled 3.32: A Numerical Huckel Calculation on Anthracene and Phenanthrene is shared under a CC BY 4.0 license and was authored, remixed, and/or curated by Frank Rioux via source content that was edited to the style and standards of the LibreTexts platform.

3.33: A Numerical Huckel Calculation on C10H8 Isomers

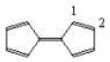
The numeric version of the Huckel molecular orbital theory (HMOT) is based on a connectivity matrix which records which atoms are bonded to each other. The eigenvalues of this matrix provide the HMOT energy levels and the HMOT wave functions.

The purpose of this exercise is to see what HMOT has to say about the relative stability of the $C_{10}H_8$ isomers shown below.

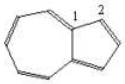
Napthalene



Fulvalene



Azulene



Napthalene calculation: $\mathrm{Natoms} = 10 \quad \mathrm{Nocc} = 5$

$$H = \begin{pmatrix} 0 & 1 & 0 & 0 & 0 & 1 & 0 & 0 & 0 & 1 \\ 1 & 0 & 1 & 0 & 0 & 0 & 0 & 0 & 0 & 0 \\ 0 & 1 & 0 & 1 & 0 & 0 & 0 & 0 & 0 & 0 \\ 0 & 0 & 1 & 0 & 1 & 0 & 0 & 0 & 0 & 0 \\ 0 & 0 & 0 & 1 & 0 & 1 & 0 & 0 & 0 & 0 \\ 1 & 0 & 0 & 0 & 1 & 0 & 1 & 0 & 0 & 0 \\ 0 & 0 & 0 & 0 & 0 & 1 & 0 & 1 & 0 & 0 \\ 0 & 0 & 0 & 0 & 0 & 0 & 1 & 0 & 1 & 0 \\ 0 & 0 & 0 & 0 & 0 & 0 & 0 & 1 & 0 & 1 \\ 1 & 0 & 0 & 0 & 0 & 0 & 0 & 0 & 1 & 0 \end{pmatrix}$$

Calculate the eigenvalues and eigenvectors: $\mathrm{E} = \mathrm{eigenvals}(\mathrm{H}) \quad \mathrm{E} = \mathrm{sort}(\mathrm{E})$

$$E^T = (-2.303 \quad -1.618 \quad -1.303 \quad -1 \quad -0.618 \quad 0.618 \quad 1 \quad 1.303 \quad 1.618 \quad 2.303)$$

Calculate total π-electronic energy: $E_\pi = 2\sum_{i=1}^{\mathrm{Nocc}} E_i \quad E_\pi = -13.683$

Calculate the delocalization energy: $E_{deloc} = E_\pi + 2\mathrm{Nocc} \quad E_{deloc} = -3.683$

Calculate the delocalization energy per atom: $\frac{E_{deloc}}{Natoms} = -0.368$

Fulvalene calculation:

$$H = \begin{pmatrix} 0 & 1 & 0 & 0 & 1 & 0 & 0 & 0 & 0 & 0 \\ 1 & 0 & 1 & 0 & 0 & 0 & 0 & 0 & 0 & 0 \\ 0 & 1 & 0 & 1 & 0 & 0 & 0 & 0 & 0 & 0 \\ 0 & 0 & 1 & 0 & 1 & 0 & 0 & 0 & 0 & 0 \\ 1 & 0 & 0 & 1 & 0 & 1 & 0 & 0 & 0 & 0 \\ 0 & 0 & 0 & 0 & 1 & 0 & 1 & 0 & 0 & 1 \\ 0 & 0 & 0 & 0 & 0 & 1 & 0 & 1 & 0 & 0 \\ 0 & 0 & 0 & 0 & 0 & 0 & 1 & 0 & 1 & 0 \\ 0 & 0 & 0 & 0 & 0 & 0 & 0 & 1 & 0 & 1 \\ 0 & 0 & 0 & 0 & 0 & 1 & 0 & 0 & 1 & 0 \end{pmatrix}$$

Calculate the eigenvalues and eigenvectors: $\mathrm{E} = \mathrm{eigenvals}(\mathrm{H}) \quad \mathrm{E} = \mathrm{sort}(\mathrm{E})$

$$E^T = (-2.115 \quad -1.618 \quad -1.618 \quad -1.303 \quad 0.254 \quad 0.618 \quad 0.618 \quad 1 \quad 1.861 \quad 2.303)$$

Calculate the total π-electronic energy: $E_\pi = 2\sum_{i=1}^{\mathrm{Nocc}} E_i \quad E_\pi = -12.799$

Calculate the delocalization energy: $E_{\mathrm{deloc}} = E_\pi + 2\mathrm{Nocc} \quad E_{deloc} = -2.799$

Calculate the delocalization energy per atom: $\frac{E_{deloc}}{Natoms} = -0.28$

Azulene calculation:

$$H = \begin{pmatrix} 0 & 1 & 0 & 0 & 1 & 0 & 0 & 0 & 0 & 1 \\ 1 & 0 & 1 & 0 & 0 & 0 & 0 & 0 & 0 & 0 \\ 0 & 1 & 0 & 1 & 0 & 0 & 0 & 0 & 0 & 0 \\ 0 & 0 & 1 & 0 & 1 & 0 & 0 & 0 & 0 & 0 \\ 1 & 0 & 0 & 1 & 0 & 1 & 0 & 0 & 0 & 0 \\ 0 & 0 & 0 & 0 & 1 & 0 & 1 & 0 & 0 & 0 \\ 0 & 0 & 0 & 0 & 0 & 1 & 0 & 1 & 0 & 0 \\ 0 & 0 & 0 & 0 & 0 & 0 & 1 & 0 & 1 & 0 \\ 0 & 0 & 0 & 0 & 0 & 0 & 0 & 1 & 0 & 1 \\ 1 & 0 & 0 & 0 & 0 & 0 & 0 & 0 & 1 & 0 \end{pmatrix}$$

Calculate the eigenvalues and eigenvectors: $\mathrm{E} = \mathrm{eigenvals}(\mathrm{H}) \quad \mathrm{E} = \mathrm{sort}(\mathrm{E})$

Calculate the total π-electronic energy: $E_\pi = 2\sum_{i=1}^{\mathrm{Nocc}} E_i \quad E_\pi = -13.364$

Calculate the delocalization energy per atom: $\frac{E_{deloc}}{Natoms} = -0.336$

The HMOT calculations indicate that napthalene has the largest delocalization energy and fulvalene has the smallest delocalization energy.

Molecule	E_π	E_{deloc}	$\frac{E_{deloc}}{atom}$
Napthalene	−13.683	−3.683	−0.368
Azulene	−13.364	−3.364	−0.336
Fulvalene	−12.799	−2.799	−0.280

The enthalpies of formation are available for napthalene and azulene and are 150 and 280 kJ/mol, respectively. Thus the rudimentary Huckel calculation is consistent with the thermodynamic data.

This page titled 3.33: A Numerical Huckel Calculation on C10H8 Isomers is shared under a CC BY 4.0 license and was authored, remixed, and/or curated by Frank Rioux via source content that was edited to the style and standards of the LibreTexts platform.

3.34: Semi-empirical Molecular Orbital Calculation on HF

Calculate the wavefunctions and energies of the σ orbitals in the HF molecule, taking β = -1.0 eV. The values of the Coulomb integrals αH and αF are taken as the negatives of the orbital ionization energies of the atoms.

The molecular orbital is formed as a linear combination of the valence orbitals of H and F.

$$\Psi = C_h\Psi_h + C_f\Psi_f$$

where

$$\Psi_h = 1s(h) and \Psi_f = 2p_z(f)$$

The variational integral for this calculation is,

$$E = \frac{\int_0^\infty (C_h\Psi_h + C_f\Psi_f)\, H\, (C_h\Psi_h + C_h\Psi_f)\, d\tau}{\int_0^\infty (C_h\Psi_h + C_f\Psi_f)^2\, d\tau}$$

Minimization of the variational energy integral simultaneously with respect to Ch and Cf yields two linear homogeneous equations (see McQuarrie and Simon, section 7-2, for details).

$$C_h\,[H_{hh} - ES_{hh}] + C_f\,[H_{hf} - ES_{hf}] = 0$$
$$C_h\,[H_{hf} - ES_{hf}] + C_f\,[H_{ff} - ES_{ff}] = 0$$

where the integral and their parameterizations are presented below.

$$H_{hh} = \int_0^\infty \Psi_h H \Psi_h d\tau = -13.6 \qquad S_{hh} = \int_0^\infty \Psi_h^2 d\tau = 1$$
$$H_{ff} = \int_0^\infty \Psi_f H \Psi_f d\tau = \alpha_f = -18.6 \qquad S_{ff} = \int_0^\infty \Psi_f^2 d\tau = 1$$
$$H_{hf} = \int_0^\infty \Psi_h H \Psi_f d\tau = \beta = -1 \qquad Shf = \int_0^\infty \Psi_h \Psi_f d\tau = 0$$

In matrix form equations (4) can be written as,

$$\begin{pmatrix} \alpha_h - E & \beta \\ \beta & \alpha_f - E \end{pmatrix} \begin{pmatrix} C_h \\ C_f \end{pmatrix} = \begin{pmatrix} 0 \\ 0 \end{pmatrix}$$

or, as an eigenvalue equation,

$$\begin{pmatrix} \alpha_h & \beta \\ \beta & \alpha_f \end{pmatrix} \begin{pmatrix} C_h \\ C_f \end{pmatrix} = \begin{pmatrix} E & 0 \\ 0 & E \end{pmatrix} \begin{pmatrix} C_h \\ C_f \end{pmatrix}$$

Mathcad can now be used to find the eigenvalues and eigenvectors of (6). First we must give it the values for all the parameters.

$$\alpha_f = -18.6 \quad \alpha_h = -13.6 \quad \beta = -1$$

Define the variational matrix shown on the left side of equation (6):

$$H = \begin{pmatrix} \alpha_h & \beta \\ \beta & \alpha_f \end{pmatrix}$$

Find the eigenvalues:

$$\mathrm{E} = \mathrm{sort}(\mathrm{eigenvals}(\mathrm{H})) \quad \mathrm{E}_0 = -18.79 \quad E_1 = -13.41$$

Now find the eigenvectors:

$$\text{The bonding MO is:} \quad \Psi_h = \mathrm{eigenvec}\,(H,\ E_0) \quad \Psi_b = \begin{pmatrix} 0.19 \\ 0.98 \end{pmatrix} \quad \overrightarrow{(\Psi_b^2)} = \begin{pmatrix} 0.04 \\ 0.96 \end{pmatrix}$$
$$\text{The anti-bonding MO is:} \quad \Psi_h = \mathrm{eigenvec}\,(H,\ E_1) \quad \Psi_b = \begin{pmatrix} -0.98 \\ 0.19 \end{pmatrix} \quad \overrightarrow{(\Psi_a^2)} = \begin{pmatrix} 0.96 \\ 0.04 \end{pmatrix}$$

Squaring the coefficients of the wavefunction we find that an electron in the bonding molecular orbital spends 96% of its time on the fluorine atom and 4% of its time on the hydrogen atom. Because fluorine has a kernel charge (nuclear charge minus two non-valence electrons) of +7 and gets credit, according to the appended MO diagram for six non-bonding electrons, plus 96% of the two

bonding electrons, the net charge on flourine can be shown to be -.92. This value indicates that the H-F bond is quite polar, which is consistent with the high electronegativity of the flourine atom.

On the Pauling scale the electronegativities of H and F are 2.1 and 4.0, respectively. The partial charge on H is calculated as: nuclear charge - non-valence electrons - unshared valence electrons - bonding electrons times $\chi_H/(\chi_H + \chi_F)$. As shown below these formal charge calculations do not give fluorine such a high negative charge.

$$\begin{array}{cccc} Z_H = 1 & _F = 9 & \chi_H = 2.1 & \chi_F = 4.0 \\ \delta_H = 1 - 0 - 0 - 2\frac{\chi_H}{\chi_H + \chi_F} & \delta_H = 0.31 & \delta_F = 9 - 2 - 6 - 2\frac{\chi_F}{\chi_H + \chi_F} & \delta_F = -0.31 \end{array}$$

Mathcad offers another way of performing the variational calculation. The variational integral given in equation (3) can also be written in the following form in which the integrals have been replaced by the experimental parameters used to replace them.

$$E = \frac{C_h^2\alpha_h + C_f^2\alpha_f + 2C_hC_f\beta}{C_h^2 + C_f^2 + 2C_hC_fS_{hf}}$$

This expression can be minimized simultaneously with respect to C_h and C_f in a Given/Find solve block. As is usually the case, Mathcad requires seed values or actual values for all the variables that appear in the solve block. There are two solutions, the ground state and the excited state. That is, the bonding molecular orbital and the anti-bonding molecular orbital. Within the solve block we have the equation for the energy, its first derivative with respect to C_h and C_f each set equal to zero, and the normalization requirement. To find the ground state we chose initial values of the coefficients that favor the fluorine $2p_z$ orbital.

$$C_h = 0.1 \quad C_f = .9 \quad \alpha_h = -13.6 \quad \alpha_f = -18.6 \quad \beta = -7 \quad S_{hf} = 0 \quad E = -10$$

Given

$$\begin{array}{cc} E = \frac{C_h^2\alpha_h + C_f^2\alpha_f + 2C_hC_f\beta}{C_h^2 + C_f^2 2C_hS_{hf}} & \frac{d}{dC_h}\frac{C_h^2\alpha_h + C_f^2\alpha_f + 2C_hC_f\beta}{C_h^2 + C_f^2 2C_hS_{hf}} = 0 \\ \frac{d}{dC_f}\frac{C_h^2\alpha_h + C_f^2\alpha_f + 2C_hC_f\beta}{C_h^2 + C_f^2 2C_hS_{hf}} = 0 & C_h^2 + C_f^2 + 2C_hC_fS_{hf} = 1 \end{array}$$

Given these constraints, we ask Mathcad to find a solution. The solution yields wavefunction coefficients and the ground-state energy.

$$\text{Find}\,(C_h,\ C_f,\ E) = \begin{pmatrix} 0.19 \\ 0.98 \\ -18.79 \end{pmatrix}$$

To find the anti-bonding state, we choose initial coefficients that favor the hydrogen 1s orbital.

$$C_h = .9 \quad C_f = 0.1 \quad \alpha = -13.6 \quad \alpha_f = -18.6 \quad \beta = -1 \quad S_{hf} = 0 \quad E = -10$$

Given

$$\begin{array}{cc} E = \frac{C_h^2\alpha_h + C_f^2\alpha_f + 2C_hC_f\beta}{C_h^2 + C_f^2 2C_hS_{hf}} & \frac{d}{dC_h}\frac{C_h^2\alpha_h + C_f^2\alpha_f + 2C_hC_f\beta}{C_h^2 + C_f^2 2C_hS_{hf}} = 0 \\ \frac{d}{dC_f}\frac{C_h^2\alpha_h + C_f^2\alpha_f + 2C_hC_f\beta}{C_h^2 + C_f^2 2C_hS_{hf}} = 0 & C_h^2 + C_f^2 + 2C_hC_fS_{hf} = 1 \end{array}$$

Given these constraints, we ask Mathcad to find a solution.

$$\text{Find}\,(C_h,\ F_f,\ E) = \begin{pmatrix} 0.98 \\ -0.19 \\ -13.41 \end{pmatrix}$$

There is yet another way that Mathcad can do this calculation that requires that the symbolic processor be loaded. Equation (5) in matrix form has a non-trivial solution only if the determinant of the coefficient matrix is equal to zero.

$\begin{pmatrix} \alpha_h - E & \beta \\ \beta & \alpha_f - E \end{pmatrix}$ has determinant $\alpha_h - \alpha_f - \alpha_h E - E\alpha_f + E^2 - \beta^2$ which has solution(s)

$$\begin{pmatrix} \frac{1}{2}\alpha_h + \frac{1}{2}\alpha_f + \frac{1}{2}\sqrt{\alpha_h^2 - 2\alpha_h\alpha_f + \alpha_f^2 + 4\beta^2} \\ \frac{1}{2}\alpha_h + \frac{1}{2}\alpha_f + \frac{1}{2}\sqrt{\alpha_h^2 - 2\alpha_h\alpha_f + \alpha_f^2 + 4\beta^2} \end{pmatrix} = \begin{pmatrix} -13.41 \\ -18.79 \end{pmatrix}$$

Find the bonding molecular orbital:

E = -18.793

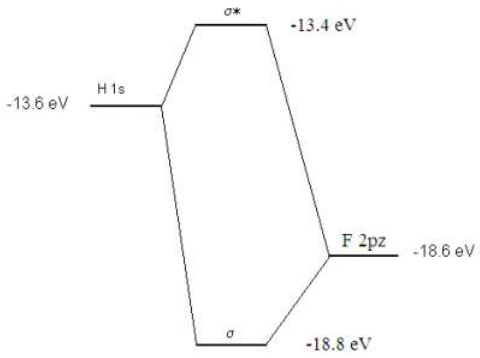
Given $(\alpha_h - E)\, C_h + \beta C_f = 0$ and $C_h^2 + C_f^2 + 2C_hC_fS_{hf} = 1 \quad \text{Find}\,(C_h,\ C_f) = \begin{pmatrix} 0.19 \\ 0.98 \end{pmatrix}$

Find the anti-bonding molecular orbital:

E = -13.407

Given $(\alpha_h - E)\, C_h + \beta C_f = 0$ and $C_h^2 + C_f^2 + 2C_hC_fS_{hf} = 1 \quad \text{Find}\,(C_h,\ C_f) = \begin{pmatrix} 0.98 \\ -0.19 \end{pmatrix}$

The molecular orbital calculation can be summarized graphically as shown below.



Reference: See page 428 of Atkins and de Paula, *Physical Chemistry*, 7th edition.

This page titled 3.34: Semi-empirical Molecular Orbital Calculation on HF is shared under a CC BY 4.0 license and was authored, remixed, and/or curated by Frank Rioux via source content that was edited to the style and standards of the LibreTexts platform.

3.35: Semi-empirical Molecular Orbital Calculation on XeF2

The bonding in XeF_2 can be interpreted in terms the three-center four-electron bond. In linear XeF_2 the molecular orbital can be considered to be a linear combination of the fluorine 2p orbitals and the central xenon 5p.

$$\Psi = C_{F1}\Psi_{F1} + C_{Xe}\Psi_{Xe} + C_{F2}\Psi_{F2}$$

Minimization of the variational integral

$$E = \frac{\int \left(C_{F1}\Psi_{F1} + C_{Xe}\Psi_{Xe} + C_{F2}\Psi_{F2}\right) H \left(C_{F1}\Psi_{F1} + C_{Xe}\Psi_{Xe} + C_{F2}\Psi_{F2}\right) d\tau}{\int \left(C_{F1}\Psi_{F1} + C_{Xe}\Psi_{Xe} + C_{F2}\Psi_{F2}\right)^2 d\tau}$$

yields the following 3 x 3 Huckel matrix

$$H = \begin{pmatrix} \alpha_F & \beta & 0 \\ \beta & \alpha_{Xe} & \beta \\ 0 & \beta & \alpha_F \end{pmatrix}$$

All overlap integrals are zero. The Coulomb integrals are parameterized as the negative of the valence orbital ionization energies (-12.13 eV for the Xe 5p orbital, -17.42 eV for the F 2p). The non-zero resonance integral is given a value of -2.0 eV.

$$\alpha_{F1} = \alpha_F = \int \Psi_{F1} H \Psi_{F1} d\tau = -17.42 \quad \alpha_{F2} = \alpha_F = \int \Psi_{F2} H \Psi_{F2} d\tau = -17.42$$
$$\alpha_{Xe} = \int \Psi_{Xe} H \Psi_{Xe} d\tau = -12.13 \qquad \beta = \int \Psi_{Xe} H \Psi_F d\tau = -2$$

Mathcad can now be used to find the eigenvalues and eigenvectors of H. First we must give it the values for all of the parameters.

$$\alpha_F = -17.42 \quad \alpha_{Xe} = -12.13 \quad \beta = -2.00$$

Define the variational matrix shown on the left side of equation (6):

$$H = \begin{pmatrix} \alpha_F & \beta & 0 \\ \beta & \alpha_{Xe} & \beta \\ 0 & \beta & \alpha_F \end{pmatrix}$$

Find the eigenvalues: $\mathrm{E} = \mathrm{sort}(\mathrm{eigenvals}(\mathrm{H}))$ $\quad E_0 = -18.647 \quad E_1 = -17.42 \quad E_2 = -10.903$

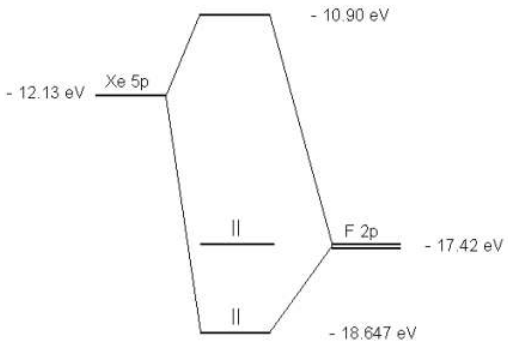
Now find the eigenvectors:

$$\text{The bonding MO is:} \quad \Psi_b = \mathrm{eigenvec}\left(H,\ E_0\right) \quad \Psi_b = \begin{pmatrix} 0.649 \\ 0.389 \\ 0.649 \end{pmatrix} \quad \overrightarrow{(\Psi_b)^2} = \begin{pmatrix} 0.421 \\ 0.158 \\ 0.421 \end{pmatrix}$$

$$\text{The non-bonding MO is:} \quad \Psi_{nb} = \mathrm{eigenvec}\left(H,\ E_1\right) \quad \Psi_{nb} = \begin{pmatrix} -0.707 \\ 0 \\ 0.707 \end{pmatrix} \quad \overrightarrow{(\Psi_{nb})^2} = \begin{pmatrix} 0.5 \\ 0 \\ 0.5 \end{pmatrix}$$

$$\text{The anti-bonding MO is:} \quad \Psi_a = \mathrm{eigenvec}\left(H,\ E_2\right) \quad \Psi_b = \begin{pmatrix} -0.282 \\ 0.917 \\ -0.282 \end{pmatrix} \quad \overrightarrow{(\Psi_a)^2} = \begin{pmatrix} 0.079 \\ 0.842 \\ 0.079 \end{pmatrix}$$

The molecular orbital diagram for this system is shown below.



Is the molecule stable? The diagram shows two electrons each in the bonding and non-bonding orbitals for a total energy of -72.14 eV. The energy of the isolated atoms is 2(-12.13 eV) + 2(-17.42 eV) = - 59.1 eV. Thus, the molecule is more stable than the isolated atoms according to this crude semi-empirical model.

The partial charges are calculated next. The fluorine atoms have a kernel charge of +7. They get credit for 6 non-bonding atomic electrons, 42.1% of the two electrons in the bonding MO, and 50% of the two electrons in the non-bonding MO. This gives a partial charge of (7 - 6 - 2(.421) - 2(.50)) -0.842.

The xenon atom has a kernel charge of +8. It gets credit for 6 non-bonding atomic electrons, 15.8% of the two electrons in the bonding MO, and no credit for the two electrons in non-bonding MO. This yields a partial charge of (8 - 6 - 2(.158)) +1.684. This value is reasonable because xenon is bonded to the most electronegative element in the periodic table.

This page titled 3.35: Semi-empirical Molecular Orbital Calculation on XeF2 is shared under a CC BY 4.0 license and was authored, remixed, and/or curated by Frank Rioux via source content that was edited to the style and standards of the LibreTexts platform.

3.36: Posch-Teller Potential Model for Metals

The purpose of this tutorial is to use a one-dimensional Posch-Teller potential to model the electronic behavior of metals. Schrödinger′s equation is integrated numerically for the first six energy states, producing two bands of bound states separated by a significant band gap. The integration algorithm is taken from J. C. Hansen, *J. Chem. Educ. Software*, 8C2, 1996.)

$$\text{Set parameters:} \quad n = 200 \quad xmin = -6 \quad xmax = 6 \quad \Delta = \frac{xmax - xmin}{n-1}$$
$$\mu = 1 \qquad Vo = -10 \qquad \alpha = 2 \qquad d = 2 \qquad a = 1$$

Calculate the position vector, the potential energy matrix, and the kinetic energy matrix. Then combine them into a total energy matrix.

$$i = 1..n \quad j = 1..n \quad x_i = xmin + (i-1)\Delta$$

$$V_{i,\,j} = \text{if}\,[\,] \quad T_{i,\,j} = \text{if}\left[i = j,\ \frac{\pi^2}{6\mu\Delta^2},\ \frac{(-1)^{i-j}}{(i-j)^2\mu\Delta^2}\right]$$

Total energy matrix: H = T + V

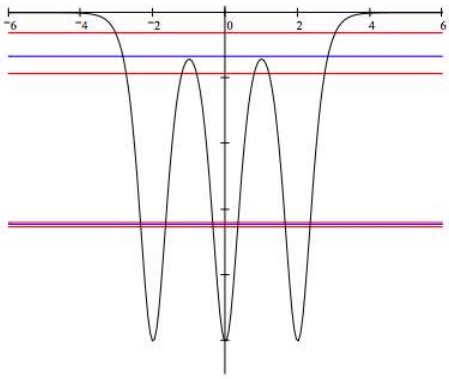
Calculate eigenvalues: $\mathrm{E} = \mathrm{sort}(\mathrm{eigenvals}(\mathrm{H}))$

Display selected eigenvalues: m = 1 .. 6

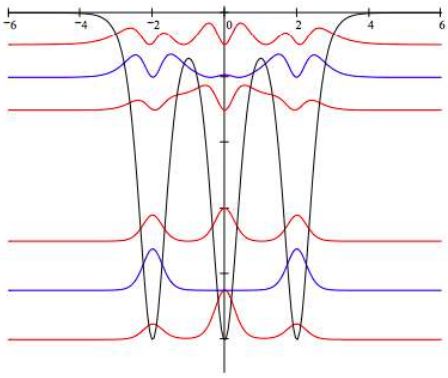
$$E_m = \begin{bmatrix} -6.5283 \\ -6.4484 \\ -6.3942 \\ -1.8562 \\ -1.3274 \\ -0.6173 \end{bmatrix}$$

Calculate eigenvectors: $k = 1..6 \quad \Psi(k) = \mathrm{eigenvec}\,(H,\ E_k)$

Display the potential energy and energy eigenvalues to show band formation:



Display the potential energy and electron density distributions offset by an arbitrary amount for purposes of clarity:



Discussion of the model: The metal cations occupy the potential energy minima. The electron density distributions show that the allowed valence electron states are delocalized over the metal structure. Delocalization is achived (especially for the lower energy band) by quantum tunneling through the internal energy barriers representing the inter-nuclear regions.

Bunching of the allowed energy states into two ″bands″ separated by a significant band gap occurs because the states have different electron densities at the locations of the potential energy minima and maxima, in addition to the fact that kinetic energy increases with increasing quantum number. This is illustrated by the following table in which the expectation values for kinetic and potential energy are calculated. Note that the kinetic energy always increases with increasing quantum number, but within a band the potential energy actually decreases slightly.

$$\begin{pmatrix} \text{"Kinetic Energy"} & \text{"Potential Energy"} & \text{"Total Energy"} \\ \Psi(1)^T T \Psi(1) & \Psi(1)^T V \Psi(1) & E_1 \\ \Psi(2)^T T \Psi(2) & \Psi(2)^T V \Psi(2) & E_2 \\ \Psi(3)^T T \Psi(3) & \Psi(3)^T V \Psi(3) & E_3 \\ \Psi(4)^T T \Psi(4) & \Psi(4)^T V \Psi(4) & E_4 \\ \Psi(5)^T T \Psi(5) & \Psi(5)^T V \Psi(5) & E_5 \\ \Psi(6)^T T \Psi(6) & \Psi(6)^T V \Psi(6) & E_6 \end{pmatrix}$$

$$= \begin{pmatrix} \text{"Kinetic Energy"} & \text{"Potential Energy"} & \text{"Total Energy"} \\ 1.1917 & -7.7201 & -6.5283 \\ 1.3766 & -7.8251 & -6.4484 \\ 1.5634 & -7.9576 & -6.3942 \\ 1.924 & -3.7855 & -1.8562 \\ 2.4726 & -3.8000 & -1.3274 \\ 3.2362 & -3.8535 & -0.6173 \end{pmatrix}$$

This page titled 3.36: Posch-Teller Potential Model for Metals is shared under a CC BY 4.0 license and was authored, remixed, and/or curated by Frank Rioux via source content that was edited to the style and standards of the LibreTexts platform.

CHAPTER OVERVIEW

4: Spectroscopy

4.1: Rudiments of Atomic Spectroscopy Using Mathcad
4.2: A Particle-in-a-Box Model for Color Centers
4.3: Cyanine Dyes as Two-State Electronic Systems
4.4: The Ammonia Inversion and the Maser
4.5: A Symmetric Double Well Potential Illustrating Tunneling
4.6: Analyses of the Pure Rotational Spectrum of HCl
4.7: A Rudimentary Analysis of the Vibrational-Rotational HCl Spectrum
4.8: Visualizing the Formally Forbidden Overtone Vibrational Transitions in HCl
4.9: The Quantum Jump
4.10: Another Look at the Quantum Jump
4.11: Quantum Beats
4.12: The 1s-2s Electronic Transition in the 1D Hydrogen Atom
4.13: The Quantum Jump in Momentum Space
4.14: The Harmonic Oscillator Quantum Jump
4.15: Coherent States of the Harmonic Oscillator
4.16: Analysis of the Electronic Spectrum of Ti(H2O)3+
4.17: Quantum Jumps for an Electron on a Ring
4.18: Analysis of the Vibrational and Electronic Spectrum of Benzene
4.19: NMR - Quantum Mechanics of a Three Proton System
4.20: AB Proton NMR Using Tensor Algebra
4.21: Calculating the AB Proton NMR Using Tensor Algebra
4.22: AB Proton NMR Analysis for 2,3-dibromothiophene
4.23: ABC Proton NMR Using Tensor Algebra
4.24: AB2 Proton NMR Using Tensor Algebra
4.25: AB3 Proton NMR Using Tensor Algebra
4.26: HD-Like NMR Spectrum Calculated Using Tensor Algebra
4.27: The Michelson Interferometer and Fourier Transform Spectroscopy
4.28: A Sum Over Histories Approach to Fourier Transform Infrared Spectroscopy
4.29: Modeling the Pi-electrons of Benzene as Particles on a Ring
4.30: Modeling the Pi-electrons of Benzene as Particles on a Ring - Version 2
4.31: Calculating the Pi-electron HOMO-LUMO Electronic Transition for Benzene
4.32: Modeling the Pi-electrons of Benzene as Particles in a Ring
4.33: Modeling the Pi-electrons of Corannulene as Particles in a Ring
4.34: The Vibrational and Electronic States of C60

This page titled 4: Spectroscopy is shared under a CC BY 4.0 license and was authored, remixed, and/or curated by Frank Rioux via source content that was edited to the style and standards of the LibreTexts platform.

4.1: Rudiments of Atomic Spectroscopy Using Mathcad

Planck's constant: $h = 6.6260810^{-34}$ Speed of light: $c = 2.997910^{8}\,\frac{m}{sec}$

Conversion factors: $nm = 10^{-9}m$ $pm = 10^{-12}m$ $aJ = 10^{-18}\text{Joule}$

Energy of a photon: $E_{photon} = h\nu = \frac{hc}{\lambda}$

Energy of the hydrogen atom: where n is a quantum number and can have integer values.

$$E_{atom} = \frac{-2.178aJ}{n^2}$$

Emission Spectroscopy

In emission spectroscopy a photon is created as the electron undergoes a transition from a higher to a lower energy state. Energy conservation requires

$$E_{atom}{}^{initial} = E_{atom}{}^{final} + E_{photon}$$

Example: Calculate the frequency, wavelength, and energy of the photon emitted when an electron undergoes a transition from the n=2 to the n=1 state.

$$n_i = 2 \quad n_f = 1 \quad \nu = \frac{-2.178aJ}{n_i^2} = \frac{-2.178aJ}{n_f^2} + h\nu \;\Big|\; \begin{matrix} solve,\ \nu \\ float,\ 4 \end{matrix} \rightarrow \frac{0.2465e16}{sec}$$

Calculate the wavelength of the photon: $\lambda = \frac{c}{\nu}$ $\lambda = 121.619nm$

Calculate the energy of the photon: $h\nu = 1.633aJ$

Absorption Spectroscopy

In absorption spectroscopy a photon is absorbed and an electron is promoted to a higher energy level. Energy conservation requires

$$E_{atom}{}^{initial} = E_{atom}{}^{final} + E_{photon}$$

Example: Calculate the frequency, wavelength, and energy of the photon required to promote the electron from the n=1 to the n=3 level.

$$\nu = \nu \quad n_i = 1 \quad n_f = 3 \quad \nu = \frac{-2.178aJ}{n_i^2} + h\nu = \frac{-2.178aJ}{n_f^2} \;\Big|\; \begin{matrix} solve,\ \nu \\ float,\ 4 \end{matrix} \rightarrow \frac{0.2922e16}{sec}$$

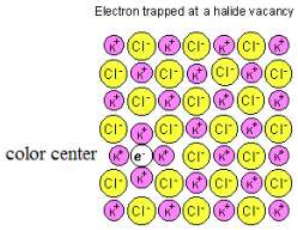
Calculate the wavelength of the photon: $\lambda = \frac{c}{\nu}$ $\lambda = 102.598nm$

Calculate the energy of the photon: $h\nu = 1.936aJ$

This page titled 4.1: Rudiments of Atomic Spectroscopy Using Mathcad is shared under a CC BY 4.0 license and was authored, remixed, and/or curated by Frank Rioux via source content that was edited to the style and standards of the LibreTexts platform.

4.2: A Particle-in-a-Box Model for Color Centers

Electrons trapped (see figure below) in anion vacancies of alkali halide salts absorb visible radiation and cause the typically white solids to appear colored.* A simple explanation of this phenomenon is that due to the wave nature of matter (the basic postulate of quantum theory), the energy of a trapped particle, such as an electron, is quantized. This permits a simple interpretation of the absorption spectra (and, therefore, the color) of F-centers. It is assumed that a photon of visible light promotes the trapped electron from its ground state to its first excited state.



This simplest model for the electron under these conditions is to assume that it behaves like a particle in a cubic box. The allowed energy levels of an electron in a cubic box are,

$$E = \frac{h^2}{8ma^2}\left[(n_x)^2 + (n_y)^2 + (n_z)^2\right]$$

where, h is Planck′s constant, m is the electron mass, a is the box dimension, and n_x, n_y, and n_z are quantum numbers.

On the basis of this simple model the first allowed transition is given by

$$\Delta E = \frac{hc}{\lambda} = E_f - E_i = \frac{h^2}{8ma^2}\left[(2^2 + 1^2 + 1^2) - (1^2 + 1^2 + 1^2)\right]$$

where c is the speed of light and λ is the wavelength of the photon of light absorbed. This expression can be re-written as follows:

$$\lambda = \frac{8mc}{3h}a^2 = 1099a^2 \quad \text{(where } \lambda \text{ and a are given in nanometers)}$$

As equation (3) shows, the model predicts that the wavelength maximum is directly proportional to the box dimension squared.

Reasonable agreement between experimental absorbance maxima and the model can be obtained by assuming that the electron is restricted to a cube the size of one unit cell. This is shown below by doing a linear regression analysis on equation (3) assuming that the exponent of a is an adjustable parameter. In other words, it is assumed that the wavelength maximum is directly proportional to a^n, where a is the lattice constant and n is the parameter to be determinded.

The data below are the lattice constant and wavelength maximum for the following alkali halides: LiF, NaF, LiCl, KF, NaCl, NaBr, KCl, NaI, RbCl, KBr, RbBr, KI, and RbI.

i = 1 .. 13

$a_i =$	$\lambda_i =$
.402	250
.462	341
.514	385
.534	455
.562	458
.596	540
.628	556
.646	588
.654	609
.658	625
.686	694
.706	689
.732	756

Equation (3) is transformed into a linear function by taking the logarithm of both sides of the equation. This yields: ln(λ) = n ln(a) + ln(1099). This is, of course, the familiar: y = slope*x + intercept.

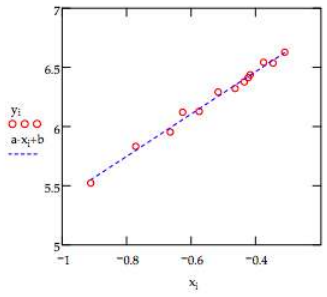
$$y_i = \ln(\lambda_i) \qquad x_i = \ln(a_i)$$

$$\text{a} = \text{slope(x, y)} \qquad \text{b} = \text{slope(x, y)} \qquad \text{c} = \text{corr(x, y)}$$

$$\text{Slope:} \quad a = 1.7943 \qquad \text{Intercept:} \quad b = 7.1841$$

$$\text{Correlation coefficient:} \quad c = 9.9499 \times 10^{-1}$$

The data and the fit to the data are displayed below. The fit is good and the optimum value of n is reasonably close to the theoretical value of 2. Ways to increase the sophistication of the model are discussed below.



It is clear from the figure above that the simple model employed here accounts for the trend in the data. More sophisticated models would assume that the electron occupied a finite potential well. In other words that some tunneling into the potential barrier would be permitted. In addition to cubic wells, it would not be difficult to perform an analysis assuming that the trapped electrons occupy finite spherical potential wells.

*The F-center (electron trapped in an anion vacancy) can be formed by the ionization of the halide anion as follows: X- + hν -------> X + e-. The neutral X drifts away and the negatively charged electron takes its place as the anion in the crystal structure.

Reference: G. P. Hughes, "Color Centers: An example of a particle trapped in a finite potential well", *American Journal of Physics* **45**, 948, (1977).

This page titled 4.2: A Particle-in-a-Box Model for Color Centers is shared under a CC BY 4.0 license and was authored, remixed, and/or curated by Frank Rioux via source content that was edited to the style and standards of the LibreTexts platform.

4.3: Cyanine Dyes as Two-State Electronic Systems

Using the particle-in-a-box (PIB) approximation or Hückel molecular orbital theory (HMOT) to model the π-electrons of various dyes is a standard lecture/lab exercise in the traditional undergraduate physical chemistry curriculum (1-8). In Volume III of his celebrated *The Feynman Lectures on Physics*, Richard Feynman offers a different approach by considering such dyes as examples of two-state electronic systems (9). Other examples of two-state systems that Feynman presents are photon polarization, the ammonia inversion, bonding in the hydrogen molecular ion and the hydrogen molecule, spin ½ systems, the strong nuclear force, and other more esoteric nuclear phenomena.

The PIB and HMOT models provide a manifold of quantized π-electron energy levels which are then populated with electrons. A HOMO-LUMO electronic transition provides the mechanism for the absorption of a photon of light and the origin of the dye color. These models each have one parameter: box length for PIB and the resonance integral, β, for HMOT.

Both models also start with Lewis structures, as does the Feynman approach. Two equivalent resonance structures can be written for the symmetric cyanine dyes, the subject of this tutorial.

$$R_2\ddot{N}[CH=CH]_nCH= \ ^+NR_2 \leftrightarrow R_2N^+=CH[CH=CH]_n\ddot{N}R_2$$

The resonance structures are used to determine the box length for the PIB model and to construct the energy matrix for the HMOT calculation.

Feynman, however, considers the resonance structures as base states in a simple quantum mechanical analysis.

$$|1\rangle = |R_2\ddot{N}[CH=CH]_nCH= \ ^+NR_2\rangle \quad |2\rangle = |R_2N^+=CH[CH=CH]_n\ddot{N}R_2\rangle$$

The energy matrix for these base states is shown below. The presence of off-diagonal elements indicates that these base states are not stationary states of the energy operator.

$$\begin{bmatrix} E^0 & A \\ A & E^0 \end{bmatrix}$$

Here E^0 and A are negative quantities, which are generally approximated by an appeal to experimental data.

$$\langle 1|\hat{H}|1\rangle = \langle 2|\hat{H}|2\rangle = E^0 \quad \langle 1|\hat{H}|2\rangle = \langle 2|\hat{H}|1\rangle = A$$

The following quantum mechanical superpositions of the base states diagonalize the energy matrix and are, therefore, stationary states.

$$|\Psi^{\pm}_{elec}\rangle$$

$$= \frac{1}{\sqrt{2}}\left[\left|R_2\ddot{N}[CH=CH]_nCH= \ ^+NR_2\right\rangle \pm \left|R_2N^+=CH[CH=CH]_n\ddot{N}R_2\right\rangle\right] = \frac{1}{\sqrt{2}}\left[|1\rangle \pm |2\rangle\right]$$

$$\begin{bmatrix} E^0+A & 0 \\ 0 & E^0-A \end{bmatrix}$$

$$\langle \Psi^+_{elec}|\hat{H}|\Psi^+_{elec}\rangle = E^0+A \quad \langle \Psi^-_{elec}|\hat{H}|\Psi^-_{elec}\rangle = E^0-A \quad \langle \Psi^-_{elec}|\hat{H}|\Psi^+_{elec}\rangle = \langle \Psi^+_{elec}|\hat{H}|\Psi^-_{elec}\rangle = 0$$

The in-phase superposition represents the ground electric state, while the anti-symmetric superposition represents the excited electronic state.

It must be stressed that a superposition is not a mixture. The dye is not a 50-50 mixture of two equivalent structures, nor is it rapidly oscillating back and forth between two equivalent structures. According to quantum mechanics the dye is simultaneously in both electronic base states.

To proceed to the issue of experimental validation, we need to recognize that the values of the matrix elements will depend on n, the length of the dye chromophore. This can be accomplished by adding subscripts in the energy matrix shown above.

$$\begin{bmatrix} E^0_n+A_n & 0 \\ 0 & E^0_n-A_n \end{bmatrix}$$

This leads to the following picture of the absorption of visible light by the dyes.

$$|\Psi^{-}_{elec}\rangle_n - - - - - - E^0_n - A_n$$
$$\uparrow$$
$$|\Psi^{+}_{elec}\rangle_n - - - - - - E^0_n + A_n$$

The wavelength of the photon required for this electronic excitation is,

$$\lambda_n = -\frac{hc}{2A_n}$$

It is clear from this result that two experimental photon wavelengths are required to calibrate the model. These can be used to calculate the photon wavelength of a third dye. In general this would be formulated as follows.

$$\frac{\lambda_{n+1}}{\lambda_n} = \frac{A_n}{A_{n+1}} \xrightarrow[implies]{constant\ ratio} \lambda_{n+2} = \lambda_{n+1}\left(\frac{\lambda_{n+1}}{\lambda_n}\right)$$

Due to rotational and vibrational fine structure, and other complications, the visible spectra of dyes exhibit broad electronic absorption bands. The theoretically calculated wavelength is therefore compared to the longest wavelength absorption maximum, λ_{max}, in the UV-VIS spectrum. The table below compares calculated photon wavelengths with experimental λ_{max} values for a series of symmetric cyanine dyes (8), and shows that Feynman's two-state model gives modest agreement with experimental results. This generally is also the level of success achieved by the PIB and HMOT models.

	Symmetric Cyanine Dye Results			
n	1	2	3	4
Experimental λ_{max}/nm	313	416	519	625
Theoretical Prediction			553	647

The interaction of the dye chromophores with electromagnetic radiation is a complicated process, so simple models such as PIB, HMOT and Feynman's two-state approach which isolate the electronic event from other degrees of freedom can only be expected to give "ball park" quantitative agreement with experimental results. However, conceptually we believe that these simple models capture the essence of the photon absorption process. From a pedagogical perspective it is valuable to have three complementary models for the same physical phenomenon.

Literature cited:

1. Gerkin, R. E. *J. Chem. Educ.* **1965**, 42, 490-491.
2. Farrell, J. J. *J. Chem. Educ.* **1985**, 62, 351-352.
3. Shoemaker, D. P.; Garland, C. W.; Nibler, J. W. *Experiments in Physical Chemistry*, 5th ed.; McGraw-Hill: New York, 1989, pp 440-445.
4. Sime, R. J. *Physical Chemistry: Methods, Techniques, and Experiments*; Saunders: Philidelphia, 1990; pp 687-694.
5. Moog, R. S. *J. Chem. Educ.* **1991**, 68, 506-508.
6. Bahnick, D. A. *J. Chem. Educ.* **1994**, 71, 171-173.
7. Anderson, B. D. J. Chem. Educ. **1997**, 74, 985.
8. Autschbach, J. *J. Chem. Educ.* **2007**, 84, 1840-1845.
9. Feynman, R. P.; Leighton, R. B.; Sands, M. *The Feynman Lectures on Physics*; Addison-Wesley Publishing Co.: Reading MA, 1965; p. 10-12.

This page titled 4.3: Cyanine Dyes as Two-State Electronic Systems is shared under a CC BY 4.0 license and was authored, remixed, and/or curated by Frank Rioux via source content that was edited to the style and standards of the LibreTexts platform.

4.4: The Ammonia Inversion and the Maser

Abstract:

The umbrella inversion in ammonia is modeled as a harmonic potential with an internal Gaussian barrier to inversion. The allowed vibrational eigenstates are calculated by numerical integration of Schrödinger's equation. The significance of the inversion in the operation of the maser is stressed.

Ammonia has four IR active vibrational modes occurring at 3444, 3337, 1627, and 950 cm^{-1}. The umbrella-like bending mode at 950 cm^{-1} is modeled by a harmonic potential well with a Gaussian internal barrier. [See for example: Swallen and Ibers, *J. Chem. Phys.* **36**, 1914 (1962).]

$$V = \frac{1}{2}kx^2 + b\exp(-cx^2)$$

The presence of the Gaussian barrier within the dominant harmonic potential causes a bunching between adjacent symmetric (+) and anti-symmetric (-) states. All states are raised in energy by the presence of the barrier, but the (-) states are elevated less than the (+) states because they have a node in the barrier and the (+) states do not.

Below Schrödinger's equation is integrated numerically for the first four energy states and the results compared with experimental spectroscopic data. (Integration algorithm taken form J. C. Hansen, *J. Chem. Educ.* Software, **8C2**, 1996.)

Set parameters (atomic units are used):

$$n = 99 \quad xmin = -2 \quad xmax = 2 \quad \Delta = \frac{xmax - xmin}{n}$$
$$\mu = 4668 \quad k = .07598 \quad b = .05684 \quad c = 1.36696$$

Calculate position vector, the potential energy matrix, and the kinetic energy matrix. Then combine them into a total energy matrix.

$$i = 0..n \quad j = 0..n \quad x_i = xmin + (i)\Delta$$

$$V_{i,\,j} = \text{if}\left[i = j,\ \left[\tfrac{1}{2}k(x_i)^2 + b\exp\left[-c(x_i)^2\right]\right],\ 0\right] \quad T_{i,\,j} = \text{if}\left[i - j,\ \tfrac{\pi^2}{6\mu\Delta^2},\ \tfrac{(-1)^{i-j}}{(i-j)^2\mu\Delta^2}\right]$$

Hamiltonian matrix: H = T + V

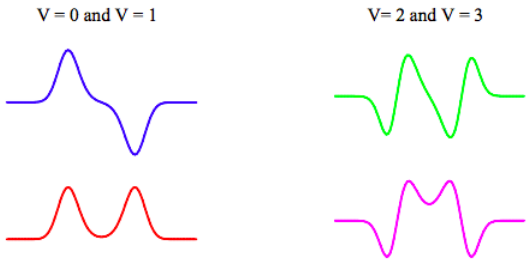
Find eigenvalues: E = sort(eigenvals(H))

Selected eigenvales: m = 0 .. 3

$$E_m = \begin{bmatrix} 0.04996046 \\ 0.04996492 \\ 0.05418694 \\ 0.05435966 \end{bmatrix}$$

Find selected eigenevectors: $\Psi(m) = \text{eigenvec}(H,\ E_m)$

Plot selected eigenfunctions: $V_{poti} = V_{i,\,i}$



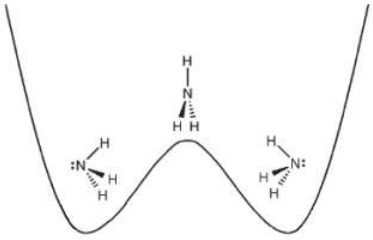
The selection rule for transitions between the manifold of energy levels obtained with this potential is (+ --> -) or (- --> +). A comparison of the first four calculated energy levels with experimental spectroscopic data shows that the Gaussian potential is a good model for the ammonia inversion.

According to the selection rule, there are four allowed transitions between these energy states. Two transitions (E_0 ---> E_1 and E_2 ---> E_3) occur in the microwave region at 0.79 and 36 cm^{-1}. The E_1 ---> E_0 transition is, of course, the basis for the ammonia maser. The other allowed transitions (E_0 ---> E_3 and E_1 ---> E_2) appear in the infra-red region at 968.3 and 932.5 cm^{-1}. The E_0 ---> E_2 and E_1 ---> E_3 transitions are forbidden. A comparison between the experimental and calculated frequencies for the allowed transitions is given below.

Transition	Theory/cm^{-1}	Experiment/cm^{-1}
$E_0 \rightarrow E_1$	$(E_1 - E_0)2.1947463 \times 10^5 = 0.98$	0.79
$E_2 \rightarrow E_3$	$(E_3 - E_2)2.1947463 \times 10^5 = 37.9$	36.0
$E_1 \rightarrow E_2$	$(E_1 - E_2)2.1947463 \times 10^5 = 926.6$	932.5
$E_0 \rightarrow E_3$	$(E_13 - E_0)2.1947463 \times 10^5 = 965.5$	968.3

The criteria for allowed transitions are that the photon must satisfy the Bohr frequency condition and that the time-dependent superposition involving the initial and final states must exhibit asymmetric oscillating dipole character. The animation provided in the Appendix allows one to confirm the allowed and forbidden transitions listed above.

The harmonic potential with internal Gaussian function representing the barrier to inversion is shown below:



The nitrogen is to the left of the plane of hydrogens in the left-hand well, NH_3, and to the right in the right-hand well H_3N. It is clear from the plots above that the v = 0 and v = 1 wave functions are linear superpositions of these states:

$$|\Psi\rangle_0 = \frac{1}{\sqrt{2}}\left[|\ddot{N}H_3\rangle + |H_3\ddot{N}\rangle\right] \quad |\Psi\rangle_1 = \frac{1}{\sqrt{2}}\left[|\ddot{N}H_3\rangle + |H_3\ddot{N}\rangle\right]$$

These states are equally populated at room temperature because the energy difference separating them is less than 1 cm^{-1}. However they can be separated electrostatically because they have different dipole moments. The |Ψ>1 state is isolated in a resonant cavity and the v =1 ----> v = 0 transition is induced by 24 GHz micro-waves (see "The Maser", J. P. Gordon, Scientific American, Dec. 1958, page 42).

A few additional comments are in order, because by and large most of the time the ammonia inversion phenomenon is interpreted using classical concepts. In his Scientific American article Gordon juxtaposes the (incorrect) classical explanation with the (correct) quantum mechanical explanation.

For example, regarding molecular vibration Gordon says "The molecule does not vibrate; the broken circles (shown in figures on page 44) merely indicate that the atoms are regarded as simultaneously occupying a number of positions." In other words, each vibrational degree of freedom is represented by a wave function which is a weighted superposition of all possible positions. The molecule is in a stationary state; movement only occurs when the vibrational state is perturbed by electromagnetic radiation.

Regarding the inversion phenomenon Gordon writes the following. "On the classical theory we picture the nitrogen atom flipping back and forth at a characteristic frequency of about 24,000 million vibrations per second, or 24,000 megacycles per second. At any given instant the nitrogen atom is on one side of the hydrogens or on the other. From the quantum point of view the nitrogen has at a given time a certain probability of being on either side - in a sense it is partly on both sides. Moreover, the molecule as a whole has two distinct energy states (see calculations above). The difference in energy between the states equals the energy of a photon with frequency of 24,000 megacycles per second."

In other words, the quantum view states that the so-called inversion frequency is actually the frequency of the photon required to induce a transition between the v = 0 and v = 1 states calculated above.

There is at least one other major misconception regarding the inversion phenomenon -- this is the concept of inversion doubling. Harris and Bertolucci, in their otherwise excellent monograph "Symmetry and Spectroscopy", write "The quantum mechanical consequence of a mutiple-minimum potential well is that there are two states for every one state of the single-minimum state." This certainly seems to imply that you are getting two for the price of one, that the internal barrier is creating new vibrational states.

Actually all that is going on is a bunching of existing states. Sketch the harmonic oscillator eigenfunctions and then compare them with the eigenfunctions for harmonic oscillator with Gaussian internal barrier. The presence of the barrier raises the energy of all states, but raises the energy of the symmetric states more than the antisymmetric states because the antisymmetric states have a node (zero probability) in the barrier and the symmetric states don't have a node.

In summary, the ammonia maser is a stunning illustration of quantum mechanics in action. We should teach the maser phenomenon from the quantum mechanical point of view: classical models are more easily digestable, but unfortunately they are incorrect.

Appendix

The selection rule stated above can be illustrated with an animation of the time-dependent superposition involving the two states involved in a transition. McMillin [J. Chem. Ed. 55, 7 (1978)] has described an appealing model for "quantum jumps" that is referred to as the fluctuating dipole mechanism. The animation shown below is based on McMillin's dipole mechanism. Several other "quantum jump" tutorials on this page are also based on McMillin's mechanism.

The v = 0 to v = 1 transition is allowed because the time-dependent superposition involving these states exhibits oscillating dipole character. The ammonia molecule oscillates asymmetrically in time within the left and right potential wells providing a mechanism for coupling with the oscillating electromagnetic field as long as the Bohr frequency condition is satisfied.

The v = 0 to v = 2 transition is forbidden because the time-dependent superposition involving these states does not exhibit oscillating dipole character. The ammonia molecule oscillates symmetrically in time within the left and right potential well and does not provide a mechanism for coupling with the external electromagnetic field.

Select quantum numbers of initial and final states:

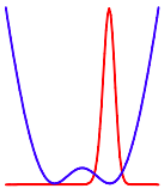
$$vi = 0 \quad vf = 1$$

$$\text{Energy of transition:} \quad \Delta E = E_{vf} - E_{vi} \quad \Delta E = 4.45734266 \times 10^{-6} \quad t = \frac{\text{FRAME}}{10^{-8}}$$

Time-dependent superposition of initial and final states:

$$\Phi_i = \frac{\Psi(vi)_i exp(-iE_{vi}t) + \Psi(vf)_i exp(-iE_{vf}t)}{\sqrt{2}}$$

To animate click on Tools, Animation, Record and follow the instructions in the dialog box. Recommended setting: From 0 To 40 in 10 Frames/Sec.



This page titled 4.4: The Ammonia Inversion and the Maser is shared under a CC BY 4.0 license and was authored, remixed, and/or curated by Frank Rioux via source content that was edited to the style and standards of the LibreTexts platform.

4.5: A Symmetric Double Well Potential Illustrating Tunneling

Schrödinger's equation is solved numerically for a symmetric double well potential: $V = bx^4 - cx^2$, which resembles the double-well potential used to model the ammonia inversion in the previous tutorial. The integration algorithm is taken from J. C. Hansen, *J. Chem. Educ. Software*, **8C2**, 1996.

Set parameters:

$$\begin{array}{llllll} \text{Increments:} & n = 100 & \text{Integration limits:} & xmin = 4 & \Delta = \frac{xmax - xmin}{n-1} \\ \text{Effective mass:} & \mu = 1 & \text{Constants:} & b = 1 & c = 6 \end{array}$$

Calculate position vector, the potential energy matrix, and the kinetic energy matrix. Then combine them into a total energy matrix.

$$i = 1..n \quad j = 1..n \quad x_i = xmin + (i-1)\Delta$$

$$V_{i,\,j} = \text{if}\left[i = j,\ b(x_i)^4 - c(x_j)^2,\ 0\right] \quad T_{i,\,j} = \text{if}\left[i = j,\ \frac{\pi^2}{6\mu\Delta^2},\ \frac{(-1)^{i-j}}{(i-j)^2\mu\Delta}\right]$$

Hamiltonian matrix:

$$H = T + V$$

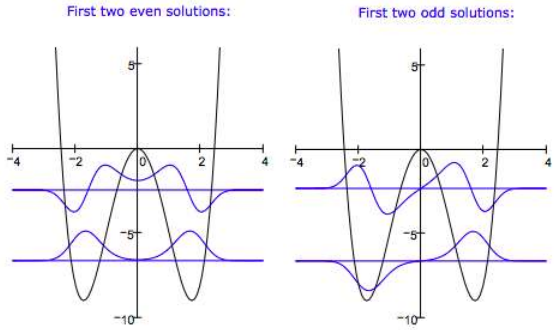
Calculate eigenvalues: E = sort(eigenvals(H))

Display selected eigenvalues: m = 1 .. 6

$$E_m = \begin{array}{|c|}\hline -6.6427 \\ \hline -6.6406 \\ \hline -2.4512 \\ \hline -2.3156 \\ \hline 0.4156 \\ \hline 1.6785 \\ \hline \end{array}$$

Calculate selected eigenvectors: k = 1 .. 4 Ψ(k) = eigenvec(H, E_k)

Display the results graphically:



The numerical results show that the energy eigenvalues are paired due to the presence of the central barrier because the odd energy states have a node at the center of the internal potential barrier. The canonical solutions to Schrödinger's equation (stationary states) show that the wave functions are delocalized over the entire potential well and that tunneling is occurring because of the probability of being in a barrier of greater potential energy than that of the total eigenstate energy. But at this point tunneling does not imply motion, just a violation of a very important classical concept - kinetic energy cannot be negative!

We also see that the ground and first-excited states are very nearly degenerate. In the presence of a small perturbing electromagnetic field, the system would be forced into a superposition of these states which would exhibit oscillatory behavior. This effect is now demonstrated for the two lowest energy states. In the presence of this perturbation we see movement from one well to the other because the system is no longer in a stationary state.

This effect is demonstrated using Mathcad's animation capabilities.

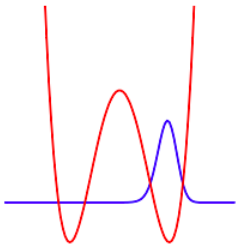
Select quantum numbers of superposition states:

$$vi = 1 \quad vf = 2 \quad t = \frac{\text{FRAME}}{0.005}$$

Timed-dependent superposition of these states:

$$Phi_i = \frac{\Psi(vi)_i exp(-iE_{vi}t) + \Psi(vf)_i exp(-iE_{vf}t)}{\sqrt{2}}$$

To animate click on Tools, Animation, Record and follow the instructions in the dialog box. Recommended setting: From 0 To 40 in 5 Frames/Sec.



This page titled 4.5: A Symmetric Double Well Potential Illustrating Tunneling is shared under a CC BY 4.0 license and was authored, remixed, and/or curated by Frank Rioux via source content that was edited to the style and standards of the LibreTexts platform.

4.6: Analyses of the Pure Rotational Spectrum of HCl

This exercise deals with simple algebraic analyses of the microwave spectrum of HCl. This problem is dealt with in a number of current physical chemistry texts. Here the rigid rotor and non-rigid rotor models will be used to analyze the data that follows.

Rotational absorption lines from $H^{35}Cl$ were found at the following wavenumbers (cm^{-1}): 83.32, 104.13, 124.73, 145.37, 165.89, 186.23, 206.60, and 226.86. Given this data our goal is to calculate the rotational constant, the bond length and the centrifugal distortion constant. We also want to assign J quantum numbers to each of the transitions.

Rigid Rotor Model for HCl

For the rigid rotor model the rotational energy levels (in cm-1) are given by the following equation.

$$E_J = BJ(J+1)$$

where

$$B = \frac{h}{8\pi^2 c\mu r^2}$$

For absorption spectroscopy, the rotational selection rule is $\Delta J = \pm 1$. Therefore, the energies of the allowed rotational transitions are,

$$\Delta E(J) = B(J+1)(J+2) - BJ(J+1) \text{ simplify } \rightarrow \Delta E(J) = 2BJ + 2B$$
$$\Delta E(J) = 2B(J+1)$$

We do not know if the first frequency listed above (83.32 cm^{-1}) is the J = 0 to J = 1 transition. However, we do know that the frequencies represent adjacent transitions. So we can use the first two transitions to calculate both J and B.

$$h = 6.62608(10)^{-34}\text{joule sec} \quad c = 2.99792458(10)^{8}\frac{m}{sec} \quad u = 1.66054(10)^{-27}kg$$
$$m_H = 1.0078u \quad m_{Cl} = 34.9688u \quad pm = 10^{-12}m$$

Calculate the reduced mass:

$$\mu = \frac{m_H m_{Cl}}{m_H + m_{Cl}} \quad \mu = 1.62661 \times 10^{-27}kg$$

Calculate the bond length:

$$B = \frac{h}{8\pi^2 c\mu r^2} \left| \begin{matrix} solve,\ r \\ float,\ 4 \end{matrix} \rightarrow \left[\begin{matrix} \frac{.1286e-8}{\text{m kg}}(\text{m kg joule cm})^{\frac{1}{2}}\text{sec} \\ \frac{-.1286e-8}{\text{m kg}}(\text{m kg joule cm})^{\frac{1}{2}}\text{sec} \end{matrix} \right] \right. = \begin{pmatrix} 128.6 \\ -128.6 \end{pmatrix} pm$$

Clear memory of J and B to facilitate subsequent calculations:

$$J = J \quad B = B$$

Non-Rigid Rotor Model for HCl

The non-rigid rotor model adds a centrifugal distortion term to accommodate the classical idea that the H-Cl bond will stretch as the rotational energy increases causing the rotational states to become closer together at higher J values.

The rotational energy levels (in cm^{-1}) for the non-rigid rotor are given by,

$$E(J) = BJ(J+1) - DJ^2(J+1)^2$$

The rotational transitions, therefore, appear at the following energies

$$\Delta E(J) = E(J+1) - E(J) \text{ simplify } \rightarrow 2B(J+1) = 2BJ + 2B - 4DJ^3 - 12DJ^2 - 12DJ - 4D$$
$$\Delta E(J) = 2BJ + 2B - 4DJ^3 - 12DJ^2 - 12DJ - 4D$$

Because J values have now been assigned to the rotational transitions, we can use two of them to calculate B and D.

$$(B\ D) = \begin{pmatrix} \Delta E(3) = 83.2 cm^{-1} \\ \Delta E(4) = 104.13 cm^{-1} \end{pmatrix} \left| \begin{matrix} solve, \begin{pmatrix} B \\ D \end{pmatrix} \\ float,\ 4 \end{matrix} \right. \rightarrow \begin{pmatrix} \frac{10.42}{cm} \\ \frac{.1111e-3}{cm} \end{pmatrix}$$

Next we calculate the HCl bond length under the non-rigid rotor approximation.

$$B = \frac{h}{8\pi^2 c \mu r^2} \left| \begin{matrix} solve,\ r \\ float,\ 4 \end{matrix} \right. \rightarrow \begin{bmatrix} \frac{.1285e-8}{\text{m kg}} (\text{m kg joule cm})^{\frac{1}{2}} \text{sec} \\ \frac{-.1285e-8}{\text{m kg}} (\text{m kg joule cm})^{\frac{1}{2}} \text{sec} \end{bmatrix} = \begin{pmatrix} 128.5 \\ -128.5 \end{pmatrix} pm$$

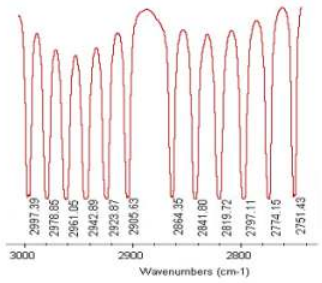
Finally we summarize the calculated results and compare them to the literature values. Given the simplicity of the models and the rudimentary method of analysis, the comparisons are satisfactory. The large error in D is not surprising given its small magnitude.

Molecular Parameter	Rigid Rotor	Nonrigid Rotor	Literature
$\frac{\text{Rotational Constant}}{cm^{-1}}$	10.41	10.42	10.59
$\frac{\text{Bond Length}}{pm}$	128.6	128.5	127.5
$\frac{\text{Centrifugal Distortion Constant}}{cm^{-1}}$	.	$1.11(10)^{-4}$	$5.32(10)^{-4}$

This page titled 4.6: Analyses of the Pure Rotational Spectrum of HCl is shared under a CC BY 4.0 license and was authored, remixed, and/or curated by Frank Rioux via source content that was edited to the style and standards of the LibreTexts platform.

4.7: A Rudimentary Analysis of the Vibrational-Rotational HCl Spectrum

This analysis assumes an harmonic-oscillator, non-rigid rotor model for the vibrational and rotational degrees of freedom of gas-phase HCl. In other words, the magnitude of the rotational constant depends on the vibrational state of the molecule. Using the portion of the $H^{35}Cl$ vibrational-rotational spectrum provided below, this model will be used to calculate the following molecular parameters: ν_0, B_0, B_1, B_e, α_e, r_0, r_1, r_e, and k.



A simple algebraic method, rather than a sophisticated statistical analysis, will be used to extract HCl′s molecular parameters from the spectroscopic data. We will see that although the model and the method of analysis are rudimentary, the results compare rather well with literature values for the molecular parameters. This exercise might serve as an introduction to a more rigorous and thorough statistical analysis. The equations for the **R-branch** and **P-branch** transitions appropriate for this model are given below.

$$\nu_R(J) = \nu_0 B_1(J+1)(J+2) - B_0 J(J+1) \quad \nu_p(J) = \nu_0 + B_1(J-1)J - B_0 J(J+1)$$

where

$$B_\nu = \frac{h}{8\pi^2 c\mu r_\nu^2} \quad B_\nu = B_e - \alpha_e\left(\nu + \tfrac{1}{2}\right)$$

Fundamental constants, conversion factors and atomic masses:

$$h = 6.6260755(10)^{-34}\text{joule sec} \quad c = 2.99792458(10)^8 \frac{m}{sec} \quad u = 1.6605410^{-27}kg \quad pm = 10^{-12}m$$
$$m_H = 1.0078u \qquad m_{Cl} = 34.9688u$$

Calculate the reduced mass of HCl:

$$\mu = \frac{m_H + m_{Cl}}{m_H + m_{Cl}} \quad \mu = 1.627 \times 10^{-27}kg$$

Obtain several P- and R-branch transitions from the spectrum:

$$\begin{pmatrix} \text{Transition} & P(2) & P(1) & R(0) & R(1) \\ \frac{\text{Frequency}}{cm^{-1}} & 2841.80 & 2864.35 & 2905.63 & 2923.87 \end{pmatrix}$$

Set up and solve a system of equations to calculate ν_0, B_0 and B_1 by selecting data from the table above.

$$\begin{pmatrix} \nu_0 & B_0 & B_1 \end{pmatrix} = \begin{pmatrix} \nu_p(2) = 2841.80cm^{-1} \\ \nu_p(1) = 2864.35cm^{-1} \\ \nu_R(0) = 2905.63cm^{-1} \end{pmatrix} \left| \begin{matrix} solve, \begin{pmatrix} \nu_0 \\ B_0 \\ B_1 \end{pmatrix} \\ float,\ 5 \end{matrix} \right. \rightarrow \begin{pmatrix} \frac{2885.6}{cm} \\ \frac{10.638}{cm} \\ \frac{10.002}{cm} \end{pmatrix}$$

Use the values of B_0 and B_1 to calculate B_e and α_e:

$$\begin{pmatrix} B_e & \alpha_e \end{pmatrix} = \begin{pmatrix} B_0 = B_e - \alpha_e \frac{1}{2} \\ B_1 = B_e - \alpha_e \frac{3}{2} \\ \nu_R(0) = 2905.63cm^{-1} \end{pmatrix} \left| \begin{matrix} solve, \begin{pmatrix} B_e \\ \alpha_e \end{pmatrix} \\ float,\ 5 \end{matrix} \right. \rightarrow \begin{pmatrix} \frac{10.956}{cm} \\ \frac{.63600}{cm} \end{pmatrix}$$

Now calcuate r_0, r_1, and r_e using the values of B_0, B_1 and B_e.

$$r_0 = \sqrt{\frac{h}{8\pi^2 c\mu B_0}} \quad r_0 = 127.189pm \quad r_1 = \sqrt{\frac{h}{8\pi^2 c\mu B_1}} \quad r_1 = 131.171pm$$
$$r_e = \sqrt{\frac{h}{8\pi^2 c\mu B_e}} \quad r_e = 125.33pm$$

Calculate the force constant using the value of ν_0.

$$k = \nu_0 = \frac{1}{2\pi c}\sqrt{\frac{k}{\mu}} \;\Big|\; \substack{solve,\ k \\ float,\ 4} \rightarrow .4806e-1\frac{m^2}{sec^2 cm^2}kg \quad k = 480.6\frac{newton}{m}$$

Compare the calculated parameter values with the literature values.

Molecular Parameter	Calcuated Value	Literature Value	%Error
$\frac{\nu_0}{cm^{-1}}$	2885.6	2886	0.014
$\frac{B_0}{cm^{-1}}$	10.638	10.440	1.90
$\frac{B_1}{cm^{-1}}$	10.002	10.136	1.32
$\frac{B_e}{cm^{-1}}$	10.956	10.593	3.43
$\frac{\alpha_e}{cm_{-1}}$	0.6360	0.307	107
$\frac{r_0}{pm}$	127.2	128.3	0.86
$\frac{r_1}{pm}$	131.2	130.2	0.77
$\frac{r_e}{pm}$	125.3	127.4	1.65
$\frac{k}{newton\ m^{-1}}$	480.6	516.3	6.92

Summary: Given the simplicity of the model (harmonic-oscillator, non-rigid rotor) and the rudimentary algebraic (as opposed to rigorous statistical) method of analysis, the results are quite respectable. Naturally, results will vary depending on the P- and R-branch transitions used to calculate the molecular parameters.

This page titled 4.7: A Rudimentary Analysis of the Vibrational-Rotational HCl Spectrum is shared under a CC BY 4.0 license and was authored, remixed, and/or curated by Frank Rioux via source content that was edited to the style and standards of the LibreTexts platform.

4.8: Visualizing the Formally Forbidden Overtone Vibrational Transitions in HCl

Using the harmonic oscillator model, the selection rule for molcecular vibrations is Δv = +/- 1. However, overtone transitions (Δv = 2, 3, ..) are observed experimentally. In what follows it will be shown that under the Morse oscillator (anharmonic) model, overtone vibrational transitions are weakly allowed.

Schroedinger's equation for the Morse oscillator model for Extra close brace or missing open brace is integrated numerically for the first five energy states. (Integration algorithm taken from J. C. Hansen, *J. Chem. Educ. Software*, **8C2**, 1996.)

Set integration parameters (in atomic units):

$$n = 150 \quad xmin = 1.4 \quad xmax = 8 \quad \Delta = \frac{xmax - xmin}{n-1}$$

Enter the Morse parameters for HCl (in atomic units):

$$\mu = 1785.64 \quad D = .1655 \quad \beta = 1.0051 \quad x_e = 2.4086$$

Calculate position vector, the potential energy matrix, and the kinetic energy matrix. Then combine them into a total energy matrix.

$$i = 1..n \quad j = 1..n \quad x_i = xmin + (i-1)\Delta$$

$$V_{i,\,j} = \text{if}\left[i = j,\ D\left[1 - exp\left[-\beta(x_i - x_e)\right]\right]^2,\ 0\right] \quad T_{i,\,j} = \text{if}\left[i = j,\ \frac{\pi^2}{6\mu\Delta^2},\ \frac{(-1)^{i-j}}{(i-j)^2\mu\Delta}\right]$$

Hamiltonian matrix: H = T + V

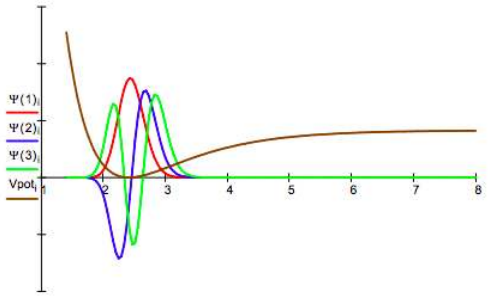
Calculate eigenvalues: E = sort(eigenvals(H))

Display selected eigenvalues: m = 1 .. 6

$$E_m = \begin{bmatrix} 0.00677149 \\ 0.01989016 \\ 0.03244307 \\ 0.04443024 \\ 0.05585166 \end{bmatrix}$$

Calculate selected eigenvectors: Ψ(k) = eigenvec(H, E_k)

Plot diagonal elements of potential energy matrix and selected eigenfunctions: $Vpot_i = V_{i,\,i}$



Because of the way the integration algorithm is implemented the initial index is m = 1. This corresponds to the v = 0 vibrational ground state. In other words, subtract 1 from the m index to get the v quantum number.*

Demonstrate numerically that the solutions form an orthonormal set:

$$\sum_i (\Psi(1)_i)^2 = 1.00 \quad \sum_i (\Psi(2)_i)^2 = 1.00 \quad \sum_i (\Psi(3)_i)^2 = 1.00$$
$$\sum_i (\Psi(1)_i \Psi(2)_i) = 0.00 \quad \sum_i (\Psi(1)_i \Psi(3)_i) = 0.00 \quad \sum_i (\Psi(2)_i \Psi(3)_i) = 0.00$$

Calculate the transition dipole moment to demonstrate that the v = 0 to v = 2 transition, which is forbidden for the harmonic oscillator, is (slightly) allowed. Compare this result to v = 0 to v = 1, v = 1 to v=2 transitions which are allowed. (See * above.)

$$\sum_i (\Psi(1)_i x_i \Psi(3)_i) = -0.01 \quad \sum_i (\Psi(1)_i x_i \Psi(2)_i) = 0.14 \quad \sum_i (\Psi(2)_i x_i \Psi(3)_i) = 0.21$$

Animate these transitions to confirm that they lead to oscillating dipole character.

Select quantum numbers of initial and final states:

$$v_i = 1 \quad v_f = 3$$

Energy of transition:

$$\Delta E = E_{vf} - E_{vi} \quad \Delta E = 0.02567158$$

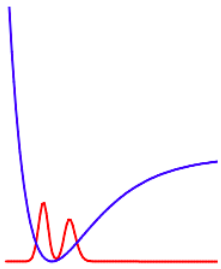
Define animation parameter:

$$t = \frac{\text{FRAME}}{10^{-8}}$$

Time-dependent superposition of initial and final states:

$$\Phi_i = \frac{\Psi(vi)_i exp(-iE_{vi}t) + \Psi(vf)_i exp(-iE_{vf}t)}{\sqrt{2}}$$

To animate click on Tools, Animation, Record and follow the instructions in the dialog box. Recommended setting: From 0 To 40 in 5 Frames/Sec.



This page titled 4.8: Visualizing the Formally Forbidden Overtone Vibrational Transitions in HCl is shared under a CC BY 4.0 license and was authored, remixed, and/or curated by Frank Rioux via source content that was edited to the style and standards of the LibreTexts platform.

4.9: The Quantum Jump

Quantum Jumps for an Electron in a One-dimensional Box

The phrases "quantum jump" and "quantum leap" are used in everyday discourse. This disguises the fact that scientists have always been somewhat troubled by the nature of the process by which a quantum system passes from one allowed energy state to another. McMillin [J. Chem. Ed. 55, 7 (1978)] has described an appealing model for "quantum jumps" that is referred to as the fluctuating dipole mechanism. This mechanism will be illustrated by considering spectroscopic transitions for an electron in a one-dimensional box of length a_o. Since only a brief outline of the mechanism can be provided here, please consult this reference for a thorough presentation of the theoretical background.

In order for an electron in a one-dimensional box to undergo a transition from one allowed energy state to another under the influence of electromagnetic radiation two criteria must be met according to the mechanism described by McMillin. First, the photons of the electromagnetic field must satisfy the Bohr frequency condition and have an energy which equals the difference in energy between the two states under consideration. Second, there must be a dipolar coupling between the electromagnetic field and the oscillating electron density in the box. This later criterion is, of course, the selection rule for the transition.

According to this model, when an electron in a box is subjected to a perturbation such as electromagnetic radiation, the electron responds by going into a state which is a linear superposition of the unperturbed states.

$$\Psi(x,\ t) = \sum_i \psi_i \exp\left(-\frac{iEt}{\hbar}\right)$$

If the square modulus, Ψ(x,t)*Ψ(x,t), of the time-dependent wavefunction associated with this linear superposition exhibits an asymmetric fluctuating charge density (an oscillating dipole moment) in the box, a coupling with the dipolar character of the electromagnetic field exists and a transition can occur. If the linear combination of states leads to a symmetric fluctuating charge density there is no coupling between the field and the electron density in the box and a transition is not possible.

The model is illustrated below first for the n = 1 to n = 2 allowed transition for the electron in a one- dimensional box. Note that for the 1 ---> 2 transition, shown immediately below, the electron density does oscillates from one side of the box to the other satisfying the mechanism's criterion for coupling with the external electromagnetic field.

The n = 1 to n = 2 Transition for the Particle in a Box is Allowed

In the space immediately below the wavefunction for the linear superposition of states is calculated and Ψ*Ψ is plotted to demonstrate that the 1 ---> 2 transition is allowed.

Initial and final energy states for the transition under study

$$n_i = 1 \quad n_f = 2 \quad E_i = \frac{n_i^2\pi^2}{2} \quad E_f = \frac{n_f^2\pi^2}{2}$$

Plot the wavefunction:

$$j = 0..40 \quad x_j = \frac{j}{40} \quad k = 0..40 \quad t_k = \frac{k}{40}$$

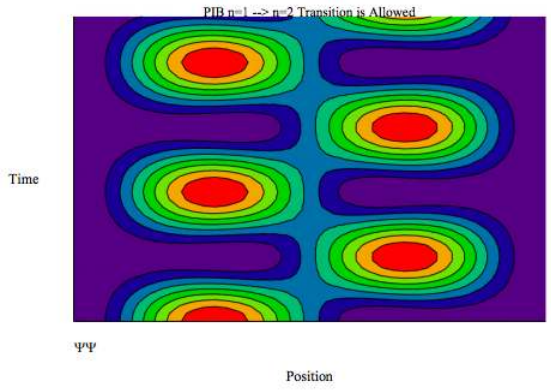
Linear combination of ground state and excited states:

$$\Psi(x,\ t) = \sin(n_i\pi x)exp(-iE_it) + \sin(n_f\pi x)exp(-iE_ft)$$

Calculate and plot Ψ*Ψ:

$$\Psi\Psi_{(j,\ k)} = \overline{\Psi(x_j,\ t_k}\Psi(x_j,\ t_k)$$

In this contour plot the horizontal axis is the spatial axis and time is graphed on the vertical axis.



The n = 1 to n = 3 Transition for the Particle in a Box is Forbidden

However, for the 1 ---> 3 transition the electron density fluctuates symmetrically about the center of the box, and, therefore does not provide a mechanism for coupling with the external electromagnetic field.

Initial and final energy states for the transition under study

$$n_i = 1 \quad n_f = 3 \quad E_i = \frac{n_i^2 \pi^2}{2} \quad E_f = \frac{n_f^2 \pi^2}{2}$$

Plot the wavefunction:

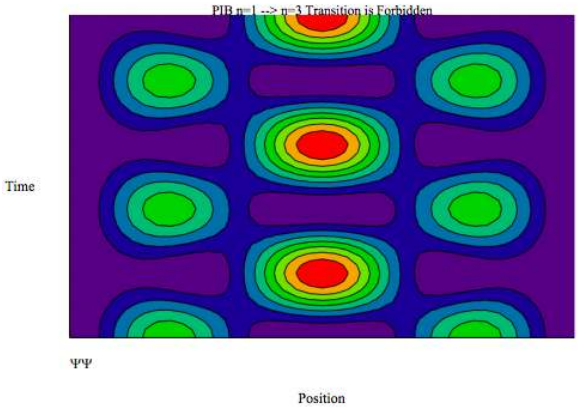
$$j = 0..40 \quad x_j = \frac{j}{40} \quad k = 0..40 \quad t_k = 4\frac{k}{40}$$

Linear combination of ground state and excited states:

$$\Psi(x,\ t) = \sin(n_i \pi x) exp(-iE_i t) + \sin(n_f \pi x) exp(-iE_f t)$$

Calculate and plot Ψ*Ψ:

$$\Psi\Psi_{(j,\ k)} = \overline{\Psi(x_j,\ t_k}\Psi(x_j,\ t_k)$$



This page titled 4.9: The Quantum Jump is shared under a CC BY 4.0 license and was authored, remixed, and/or curated by Frank Rioux via source content that was edited to the style and standards of the LibreTexts platform.

4.10: Another Look at the Quantum Jump

Consider an electron in a one-bohr, one-dimensional box. This tutorial will explore, in an elementary way, the selection rule for the transition of the electron from one allowed energy level to another. The condition for an allowed transition is two-fold: the photon exciting the transition must satisfy the Bohr frequency condition [hν = Ef - Ei] and the expectation value for the position of the electron must exhibit oscillatory dipole character as a function of time. This latter requirement provides a coupling mechanism between the oscillating electromagnetic field and the oscillating charge density of the electron in the box.

Assuming that the Bohr frequency condition is met we will look at the second at the second criterion for a number of possible electronic transitions or "quantum jumps." Consider first the transition from the ground state to the first excited state.

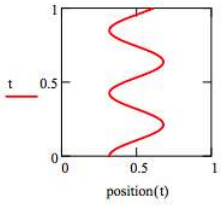
$$\text{Initial state:} \quad n_i = 1 \quad E_i = \frac{n_i^2 \pi^2}{2} \quad \text{Final state:} \quad n_f = 2 \quad E_f = \frac{n_f^2 \pi^2}{2}$$

Time-dependent superposition of initial and final states:

$$\Psi(x,\ t) = \sin(n_i \pi x) exp(-iE_i t) + \sin(n_f \pi x) exp(-iE_f t)$$

Time-dependent expectation value for position:

$$\text{position(t)} = \int_0^1 x(|\Psi(\text{x},\ \text{t})|)^2 dx \quad t = 0, .001..1$$



Since the expectation value for position fluctuates in time (has time dependence) the transition between the n =1 and n = 2 states is allowed.

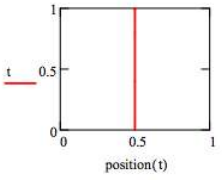
Now consider the n = 1 to n = 3 electronic transition.

$$\text{Initial state:} \quad n_i = 1 \quad E_i = \frac{n_i^2 \pi^2}{2} \quad \text{Final state:} \quad n_f = 3 \quad E_f = \frac{n_f^2 \pi^2}{2}$$

Time-dependent superposition of initial and final states:

$$\Psi(x,\ t) = \sin(n_i \pi x) exp(-iE_i t) + \sin(n_f \pi x) exp(-iE_f t)$$

$$\text{position}(t) = \int_0^1 x(|\Psi(x,\ t)|)^2 dx \quad t = 0, .002..1$$



For this case the expectation value for position does not fluctuate with time, providing no mechanism for coupling with the oscillating dipole character of the electromagnetic field. Therefore, the n = 1 to n = 3 electronic transition is not allowed. The selection rule that emerges after study of more cases is that Δn = an odd integer.

Simple Harmonic Oscillator

The same method is now used to look at allowed and forbidden transitions for the simple harmonic oscillator.

$$\text{Initial state:} \quad E_i = \nu_i + \tfrac{1}{2} \quad \text{Final state:} \quad E_f = \nu_f + \tfrac{1}{2} \quad nu = 0,\ 1, \text{etc.}$$

Time-dependent superposition of initial and final harmonic oscillator states:

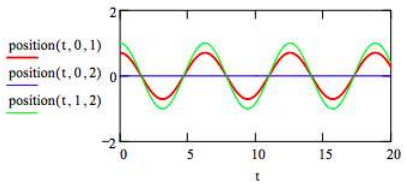
$$\Psi(x,\ t,\ \nu_i,\ \nu_f)$$

$$= \frac{1}{\sqrt{2}}\exp\left(-\frac{x^2}{2}\right)\left[\frac{\mathrm{Her}(\nu_i,\ x)\exp\left[-i\left(\nu_i+\frac{1}{2}\right)t\right]}{\sqrt{\nu_i!2^{\nu_i}\sqrt{\pi}}}+\frac{\mathrm{Her}(\nu_f,\ x)\exp\left[-i\left(\nu_f+\frac{1}{2}\right)t\right]}{\sqrt{\nu_f!2^{\nu_f}\sqrt{\pi}}}\right]$$

Time-dependent expectation value for position:

$$\mathrm{position}\,(t,\ \nu_i,\ \nu_f) = \int_{-\infty}^{\infty} x\left(\left|\Psi(x,\ t,\ \nu_i,\ \nu_f)\right|\right)^2 dx \quad t = 0,\ .05..20$$

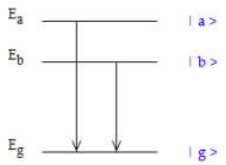
Plot the time-dependent position expectation value for three transitions: 0-1; 0-2; 1-2. The 0-1 and 1-2 transitions are allowed and the 0-2 transition is forbidden.



This page titled 4.10: Another Look at the Quantum Jump is shared under a CC BY 4.0 license and was authored, remixed, and/or curated by Frank Rioux via source content that was edited to the style and standards of the LibreTexts platform.

4.11: Quantum Beats

Quantum beats are the oscillatory behavior in the intensity of radiation emitted by atomic or molecular systems that are in a superposition of excited states created by off-resonance excitation. The quantum mechanical analysis of quantum beats is essentially the same as it is for the double-slit experiment. In the double-slit experiment there are two paths to each position on the detector and the probability amplitudes for these paths interfere. As shown in the figure below, in this example the ground-state can be reached from two excited states having different energies. The probability amplitudes for these paths to the ground state (| a > ---> | g > and | b > ---> | g >) also interfere constructively and destructively causing oscillations in the intensity of the emitted radiation.



The superposition of transitions to the ground state in the time domain is as follows,

$$\langle g|t\rangle\langle t|a\rangle + \langle g|t\rangle\langle t|b\rangle$$

where, for example, the Dirac brackets in atomic units are of the form

$$\langle t|a\rangle = \langle a|t\rangle* = \exp(-iE_at)$$

Using relations of the type given in equation (2) we can write equation (1) as

$$\exp(iE_gt)\exp(-iE_at) + \exp(iE_gt)\exp(-iE_bt)$$

This equation can be simplified by using the ground state as a reference by setting $E_g = 0$.

$$\exp(-iE_at) + \exp(-iE_bt)$$

The excited states decay exponentially, but not necessarily with the same decay constant. The fraction of the atoms or molecules not decayed at time t is given by first-order kinetics.

$$\frac{A_t}{A_0} = \exp(-k_at)$$

Thus, each term in equation (4) is weighted by the probability that state exists at time t.

$$\exp(-iE_at)\exp(-k_at) + \exp(-iE_bt)\exp(-k_bt)$$

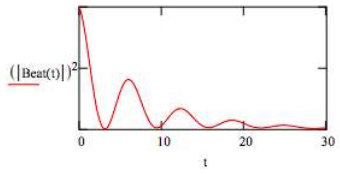
The time-dependence of the intensity of the emitted radiation is proportional to the square of the absolute magnitude of equation (6)

$$|\exp(-iE_at)\exp(-k_at) + \exp(-iE_bt)\exp(-k_bt)|^2$$

The time-dependence as calculated below for arbitrary values for the parameters clearly shows the oscillatory character of the intensity of the emitted radiation.

$$E_a = 1 \quad k_a = .1 \quad E_b = 2 \quad k_b = .05$$

$$\text{Beat(t)} = \exp(-iE_bt)\exp(-k_bt) + \exp(-iE_at)\exp(-k_at)$$



This page titled 4.11: Quantum Beats is shared under a CC BY 4.0 license and was authored, remixed, and/or curated by Frank Rioux via source content that was edited to the style and standards of the LibreTexts platform.

4.12: The 1s-2s Electronic Transition in the 1D Hydrogen Atom

This tutorial examines the 1s-2s electronic transition in the hydrogen atom. These L = 0 states of the hydrogen atom can be written as one-dimensional, time-dependent wave functions as shown below.

The condition for an allowed electronic transition is two-fold:

1. the photon exciting the transition must satisfy the Bohr frequency condition [hν = E_f - E_i] and
2. the expectation value for the position of the electron must exhibit oscillatory dipole character as a function of time.

This latter requirement provides a coupling mechanism between the oscillating electromagnetic field and the oscillating charge density of the electron. For further details see McMillin *J. Chem. Ed.* 55, 7 (1978).

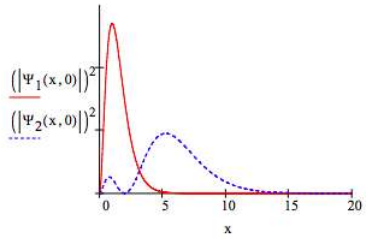
The subsequent calculations are carried out using atomic units: $h = 2\pi$; $m_e = 1$.

$$\text{Initial state:} \quad n_i = 1 \quad E_i = \frac{-0.5}{n_i^2} \quad \text{Final state:} \quad n_f = 2 \quad E_f = \frac{-0.5}{n_f^2}$$

Time-dependent 1s and 2s electron wave functions:

$$\Psi_1(x,\ t) = 2x\exp(-x)\exp(-iE_i t) \quad \Psi_2(x,\ t) = \frac{1}{\sqrt{8}}x(2-x)\exp\left(-\frac{x}{2}\right)\exp(-iE_f t)$$

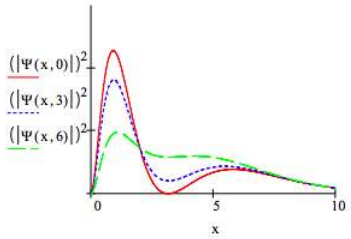
The following graphic shows the separate 1s and 2s electron densities at $t = 0$.



In the presence of a perturbing electromagnetic field the hydrogen atom electron is no longer in a stationary state and is represented by the following time-dependent superposition of the 1s and 2s electronic states.

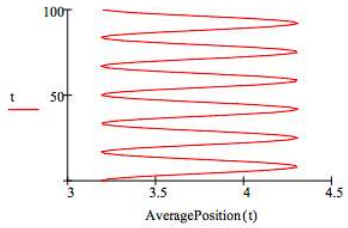
$$\Psi(x,\ t) = \frac{1}{\sqrt{2}}\left(\Psi_1(x,\ t) + \Psi_2(x,\ t)\right)$$

The square of the absolute magnitude for this time-dependent superposition is shown below for three time values. It clearly shows the oscillatory character of the perturbed electron density, and it appears that the oscillations have dipole character.



That the oscillations of the electron density do indeed have dipole character can also be seen by plotting the average position of the electron from the nucleus as a function of time.

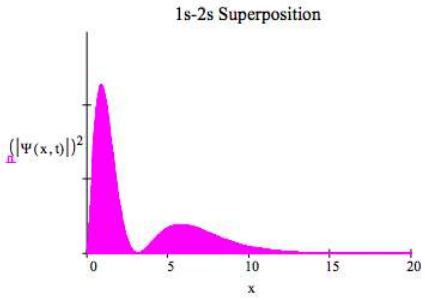
$$\text{Average Position(t)} = \int_0^\infty x\left(|\Psi(x,\ t)|\right)^2 dx \quad t = 0..100$$



Since the expectation value for position fluctuates in time creating an oscillating dipole the transition between the $n = 1$ and $n = 2$ states is allowed.

It is also possible to animate the time-dependent superposition. Click on Tools, Animation, Record and follow the instructions in the dialog box. Choose From: 0, To: 100, At: 10 Frames/Sec .

t = FRAME



This page titled 4.12: The 1s-2s Electronic Transition in the 1D Hydrogen Atom is shared under a CC BY 4.0 license and was authored, remixed, and/or curated by Frank Rioux via source content that was edited to the style and standards of the LibreTexts platform.

4.13: The Quantum Jump in Momentum Space

This tutorial is a companion to "The Quantum Jump" which deals with the quantum jump from the perspective of the coordinate-space wave function. This tutorial accomplishes the same thing in momentum space.

The time-dependent momentum wave function for a particle in a one-dimensional box of width $1a_0$ is shown below.

$$\psi(n,\ p,\ t) = n\sqrt{\pi}\left[\frac{1-(-1)^n\exp(-ip)}{n^2-\pi^2-p^2}\right]\exp(-iE_it)$$

The n = 1 to n = 2 Transition for the Particle in a Box is Allowed

This transition is allowed because it yields a momentum distribution that is asymmetric in time as is shown in the figure below. Consequently it allows for coupling with the perturbing electromagnetic field.

Momentum increment $P = 100$ Time Increment $T = 100$ Initial $n_i = 1$ Final state $n_f = 2$

Initial and final energy states for the transition under study:

$$E_i = \frac{n_i^2\pi^2}{2} \quad E_f = \frac{n_f^2\pi^2}{2}$$

Plot the wavefunction:

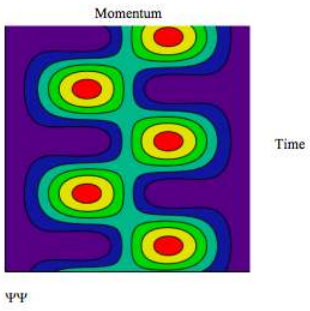
$$j = 0..P \quad p_j = -10 + \frac{20j}{P} \quad k = 0..T \quad t_k = \frac{k}{T}$$

In the presence of electromagnetic radiation the particle in the box goes into a linear superposition of the stationary states. The linear superposition for the n = 1 and n = 2 states is given below.

$$\Psi(p,\ t) = n_i\sqrt{\pi}\left[\frac{1-(-1)^{n_i}\exp(-ip)}{n_i^2\pi^2-p^2}\right]\exp(-iE_it) + n_f\sqrt{\pi}\left[\frac{1-(-1)^{n_f}\exp(-ip)}{n_f^2\pi^2-p^2}\right]\exp(-iE_ft)$$

Calculate and plot the momentum distribution: Ψ*Ψ:

$$\Psi\Psi_{(j,\ k)} = \left(|\Psi(p_j,\ t_k)|\right)^2$$



The n = 1 to n = 3 Transition for the Particle in a Box is Not Allowed

This transition is allowed because it yields a momentum distribution that is symmetric in time as is shown in the figure below. Consequently it does not allow for coupling with the perturbing electromagnetic field.

Momentum increment $P = 100$ Time Increment $T = 100$ Initial $n_i = 1$ Final state $n_f = 3$

Initial and final energy states for the transition under study:

$$E_i = \frac{n_i^2\pi^2}{2} \quad E_f = \frac{n_f^2\pi^2}{2}$$

Plot the wavefunction:

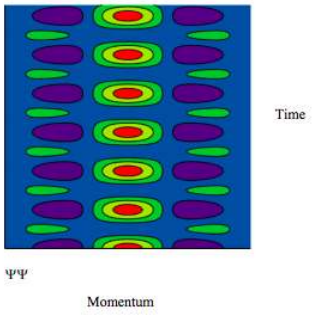
$$j = 0..P \quad p_j = -10 + \frac{20j}{P} \quad k = 0..T \quad t_k = \frac{k}{T}$$

In the presence of electromagnetic radiation the particle in the box goes into a linear superposition of the stationary states. The linear superposition for the n = 1 and n = 3 states is given below.

$$\Psi(p,\ t) = n_i\sqrt{\pi}\left[\frac{1-(-1)^{n_i}\exp(-ip)}{n_i^2\pi^2 - p^2}\right]\exp(-iE_i t) + n_f\sqrt{\pi}\left[\frac{1-(-1)^{n_f}\exp(-ip)}{n_f^2\pi^2 - p^2}\right]\exp(-iE_f t)$$

Calculate and plot the momentum distribution: Ψ*Ψ:

$$\Psi\Psi_{(j,\ k)} = \left(\left|\Psi(p_j,\ t_k)\right|\right)^2$$



This page titled 4.13: The Quantum Jump in Momentum Space is shared under a CC BY 4.0 license and was authored, remixed, and/or curated by Frank Rioux via source content that was edited to the style and standards of the LibreTexts platform.

4.14: The Harmonic Oscillator Quantum Jump

This Mathcad worksheet determines whether an SHO spectroscopic transition is allowed assuming that the Bohr frequency condition is satisfied. It requires only the quantum numbers of the initial and final states.

The $v = 0$ to $v = 1$ transition is allowed because the position distribution function, Y^*Y, exhibits oscillating dipole character.

$$\text{Initial State:} \quad v_i = 0 \quad E_i = v_i + \tfrac{1}{2} \quad \text{Final state:} \quad v_f = 1 \quad E_f = v_f + \tfrac{1}{2}$$

$$\text{Set plot parameters:} \quad \text{Space} = 60 \quad \text{Time} = 10 \quad \text{Xmin} = 3$$
$$j = 0..\text{Space} \quad x_j = -\text{Xmin} + \tfrac{2\text{Xmin}j}{\text{Space}} \quad k = 0..\text{Time} \quad t_k = \tfrac{k20}{\text{Time}}$$

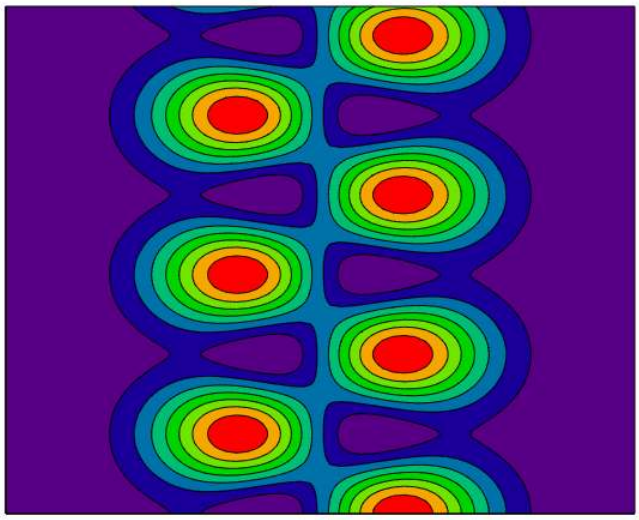
Construct time-dependent superposition of the initial and final states:

$$\Psi(x,\ t) = \exp\left(-\frac{x^2}{2}\right)(\text{Her}(v_i,\ x)\exp(-iE_it) + \text{Her}(v_f,\ x)\exp(-iE_ft))$$

Calculate and plot Y*Y:

$$\Psi\Psi_{(j,\ k)} = \overline{\Psi(x_j,\ t_k)}\Psi(x_j,\ t_k)$$

In this contour plot the horizontal axis is the spatial axis. Time is graphed on the veritcal axis. If Y^*Y asymmetric in time the transition is allowed.



The v = 0 to v = 2 transition is allowed because the position distribution function, Y^*Y, does not exhibit oscillating dipole character.

$$\text{Initial State:} \quad v_i = 0 \quad E_i = v_i + \tfrac{1}{2} \quad \text{Final state:} \quad v_f = 1 \quad E_f = v_f + \tfrac{1}{2}$$

$$\text{Set plot parameters:} \quad \text{Space} = 60 \quad \text{Time} = 150 \quad \text{Xmin} = 3$$
$$j = 0..\text{Space} \quad x_j = -\text{Xmin} + \tfrac{2\text{Xmin}j}{\text{Space}} \quad k = 0..\text{Time} \quad t_k = \tfrac{k20}{\text{Time}}$$

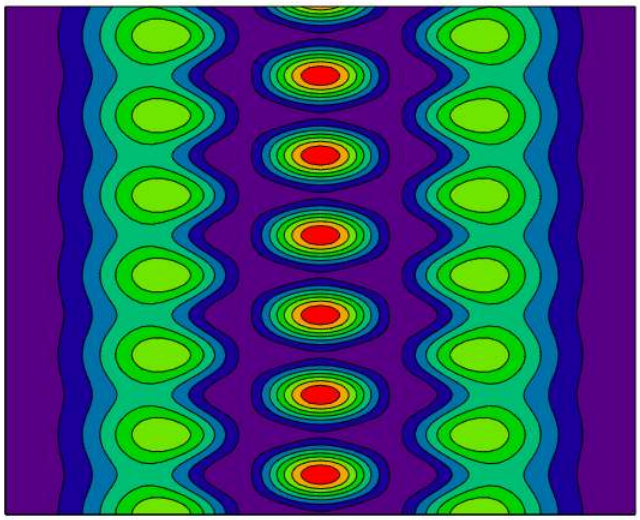
Construct time-dependent superposition of the initial and final states:

$$\Psi(x,\ t) = \exp\left(-\frac{x^2}{2}\right)(\text{Her}(v_i,\ x)\exp(-iE_it) + \text{Her}(v_f,\ x)\exp(-iE_ft))$$

Calculate and plot Y*Y:

$$\Psi\Psi_{(j,\,k)} = \overline{\Psi(x_j,\ t_k)}\Psi(x_j,\ t_k)$$

In this contour plot the horizontal axis is the spatial axis. Time is graphed on the vertical axis. If $\Upsilon^*\Upsilon$ asymmetric in time the transition is allowed.



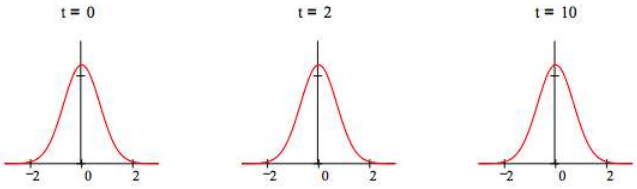
This page titled 4.14: The Harmonic Oscillator Quantum Jump is shared under a CC BY 4.0 license and was authored, remixed, and/or curated by Frank Rioux via source content that was edited to the style and standards of the LibreTexts platform.

4.15: Coherent States of the Harmonic Oscillator

The quantum mechanical harmonic oscillator eigenstates are stationary states and therefore cannot be used individually to represent classical oscillatory motion. (Atomic units are used in this tutorial.)

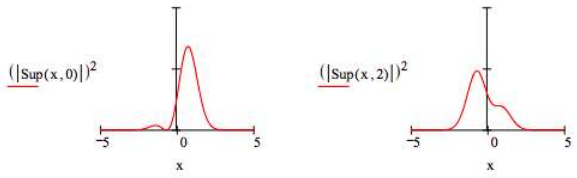
$$\Psi(v,\ x,\ t) = \frac{1}{\sqrt{2^v v\ \sqrt{\pi}}} \mathrm{Her}(v,\ x) \exp\left(\frac{-x^2}{2}\right) \exp\left[-i\left(v + \frac{1}{2}\right) t\right]$$

For example, suppose we choose to represent the ground vibrational state of a homonuclear diatomic molecule as a simple harmonic oscillator with vibrational quantum number v = 0. We see that probability distribution |Ψ(0,x,t)|2, is independent of time. There is no oscillatory motion; the molecule is in a stationary state which weighted superposition of all possible internuclear separations.



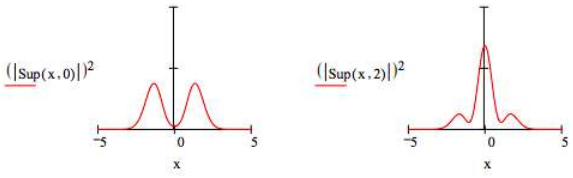
However,simple superpositions of the vibrational eigenstates do show oscillatory behavior. This is due to exponential term involving the vibrational energy, exp[-iE(v)t]. This term oscillates with a dependence on vibrational quantum number. Thus, the different eigenstates oscillate with different frequencies giving rise constructive and destructive interference. The figures below show the time dependence of the v = 0/v =1 the v = 0/v = 2 superpositions. Both show oscillatory behavior, but the first is asymmetric and the second i symmetric. This has significance for harmonic oscillator selection rules, as will be discussed below.

$$\mathrm{Sup(x,\ t)} = \frac{\Psi(0,\ x,\ t) + \Psi(1,\ x,\ t)}{\sqrt{2}}$$



The asymmetry of this time-dependent probability distribution gives it electric oscillating dipole character mechanism for coupling with the oscillating dipole of the electromagnetic field. Thus we could argue this i basis for the fact that the v = 0 to v = 1 vibrational transition is allowed.

$$\mathrm{Sup(x,\ t)} = \frac{\Psi(0,\ x,\ t) + \Psi(2,\ x,\ t)}{\sqrt{2}}$$



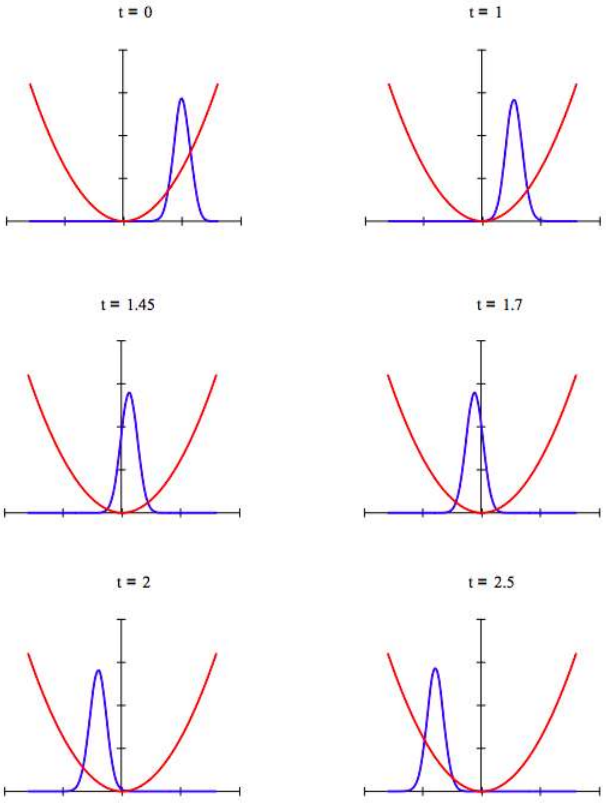
By comparison the symmetry of this time-dependent probability distribution does not have oscillatory dipole character, so there is no coupling with the external electromagnetic field. Therefore, the v = 0 to v = 2 vibrational transition is formally forbidden. Further detail on this interpretation of the "quantum jump" can found in the Spectroscopy section of Quantum Potpourri.

By comparison, coherent states (also called Glauber states) of the harmonic oscillator are more elaborate superpositions that maintain the well-defined shape of the ground state distribution while exhibiting the kind of classical oscillatory motion that is

absent in the previous examples. The time-dependence and "classical" oscillatory behavior of a coherent superposition of 25 vibrational eigenstates is illustrated below. See any contemporary text on quantum optics for further information on coherent states of the harmonic oscillator.

$$n = 25 \quad x = -8, -7.98..8 \quad \alpha = 3.5$$

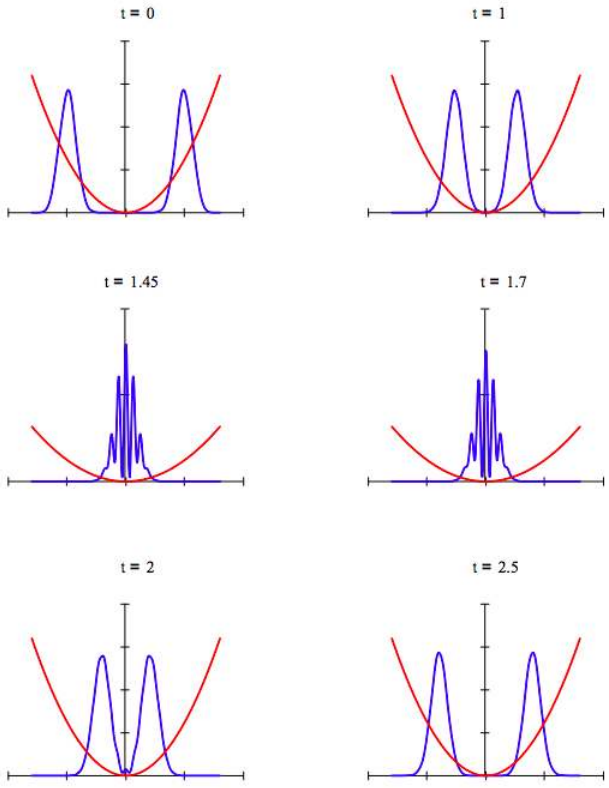
$$\Psi(x,\ t) = \frac{1}{\sqrt{n}} \exp\left(\frac{-x^2}{2}\right) \exp\left(\frac{-\alpha^2}{2}\right) \sum_{v=0}^{n} \left[\mathrm{Her(v,\ x)}\ \exp\left[-i\left(v + \frac{1}{2}\right)t\right] \frac{\alpha^v}{v!\sqrt{2^v\sqrt{2}}} \right]$$



Time-dependent superpositions of coherent states have been used to model Schrödinger cat states. Below show the interaction of two coherent states moving in opposite directions from opposite sides of a harmonic potential well. The interference observed when they meet in the middle has been observed experimentally Bose-Einstein condensates.

$$\alpha = 3.5 \quad \beta = -3.5$$

$$\begin{aligned}\Psi(x,\ t) = \ & \frac{1}{\sqrt{n}} \exp\left(\frac{-x^2}{2}\right) \exp\left(\frac{-\alpha^2}{2}\right) \sum_{v=0}^{n} \left[\mathrm{Her(v,\ x)}\ \exp\left[-i\left(v + \frac{1}{2}\right)t\right] \frac{\alpha^v}{v\ \sqrt{2^v\sqrt{2}}} \right] \ldots \\ & + \frac{1}{\sqrt{n}} \exp\left(\frac{-x^2}{2}\right) \exp\left(\frac{-\beta^2}{2}\right) \sum_{v=0}^{n} \left[\mathrm{Her(v,\ x)}\ \exp\left[-i\left(v + \frac{1}{2}\right)t\right] \frac{\beta^v}{v\ \sqrt{2^v\sqrt{2}}} \right]\end{aligned}$$



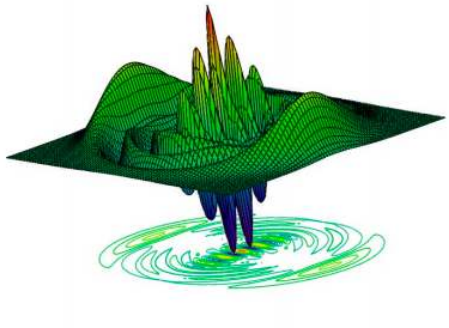
We finish with a calculation of the Wigner phase-space distribution for a Schrödinger cat state at t = 0. In t interest of computational expediency a superposition of only 10 harmonic eigenstates is calculated. The Wigner function is itself a superposition of all phase-space trajectories and is called a quasi probability distribution because it can take on negative values as is shown in the figure below. The interference fringe the center are closely related to those that appear in the figures above.

$$\Psi(x) = \frac{1}{\sqrt{n}}\exp\left(\frac{-x^2}{2}\right)\exp\left(\frac{-\alpha^2}{2}\right)\sum_{v=0}^{10}\left(\mathrm{Her(v,\ x)}\frac{\alpha^v}{v\sqrt{2^v\sqrt{2}}}\right)\ldots + \left[\frac{1}{\sqrt{n}}\exp\left(\frac{-x^2}{2}\right)\exp\left(\frac{-\beta^2}{2}\right)\sum_{v=0}^{10}\left(\mathrm{Her(v,\ x)}\frac{\beta^v}{v\sqrt{2^v\sqrt{2}}}\right)\right]$$

Wigner distribution:

$$\mathrm{W(x,\ p)} = \frac{1}{\pi^{\frac{3}{2}}}\int_{-\infty}^{\infty}\Psi\left(x+\frac{s}{2}\right)\exp(\mathrm{i\ s\ p})\Psi\left(x-\frac{s}{2}\right)ds$$

$$N = 80 \quad i = 0..N \quad x_i = -5 + \frac{10i}{N} \quad j = 0..N \quad p_j = -5 + \frac{10j}{N} \quad \mathrm{Wigner}_{i,\,j} = W(x_i,\ p_j)$$



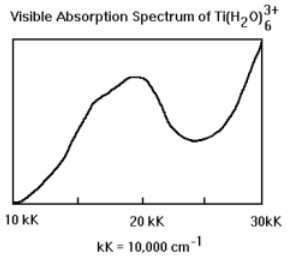
Wigner, Wigner

https://chem.libretexts.org/@go/page/150727

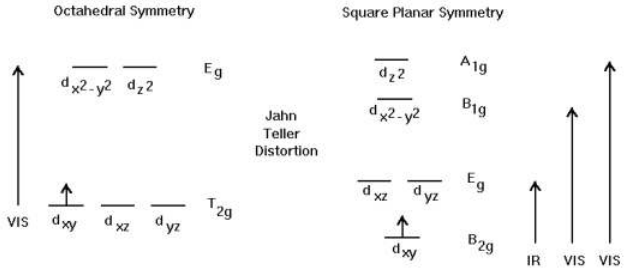
This page titled 4.15: Coherent States of the Harmonic Oscillator is shared under a CC BY 4.0 license and was authored, remixed, and/or curated by Frank Rioux via source content that was edited to the style and standards of the LibreTexts platform.

4.16: Analysis of the Electronic Spectrum of Ti(H2O)3+

This spectroscopy exercise deals with the interpretation of the visible spectrum of $Ti(H_2O)_6^{3+}$ shown below.



The analysis begins with the assumption that $Ti(H_2O)_6^{3+}$ has octahedral, O_h, symmetry. This assumption accounts for the gross features of the spectrum, but does not explain the shoulder that appears on the main absorption peak. The hexaaquatitanium(III) complex is orbitally degenerate and is therefore subject to a Jahn-Teller distortion which reduces the symmetry from octahedral to square planar. It will be shown that D_{4h} symmetry is fully consistent with the experimental spectrum. The d-orbital energy level diagrams for Oh and D4h symmetry are shown below and will be referred to later in the analysis.



On the basis of these energy level diagrams the following predictions would be plausible. For octahedral symmetry there is one electronic transition in the visible region. For square planar symmetry there are two electronic transitions in the visible region and one in the infrared. In the analysis that follows it will be shown that none of the predicted electronic transitions is orbitally allowed, but they are observed through the agency of vibronic coupling. Furthermore the square planar geometry is in better agreement with the experimental spectrum than octahedral symmetry.

Because of the importance of vibronic coupling to electronic transitions in this example the determination of the symmetry of the vibrational degrees of freedom is essential. In the vibrational analysis the water ligands will be treated as composite entities. We will only consider the titanium water molecule vibrational modes and ignore the internal vibrations of the water molecule.

$Ti(H_2O)_6^{3+}$ - Octahedral Symmetry

Illegal pream-token (E)

$$\begin{array}{lllll} A_{1g} = (C_{Oh}^T)^{<1>} & A_{2g} = (C_{Oh}^T)^{<2>} & E_g = (C_{Oh}^T)^{<3>} & T_{1g} = (C_{Oh}^T)^{<4>} & T_{2g} = (C_{Oh}^T)^{<5>} \\ A_{1u} = (C_{Oh}^T)^{<6>} & A_{2u} = (C_{Oh}^T)^{<7>} & E_u = (C_{Oh}^T)^{<8>} & T_{1u} = (C_{Oh}^T)^{<9>} & T_{2u} = (C_{Oh}^T)^{<10>} \end{array}$$

$$\Gamma_{tot}^T = (21 \quad 0 \quad -1 \quad 3 \quad -3 \quad -3 \quad -1 \quad 0 \quad 5 \quad 3) \quad \Gamma_{vib} = \Gamma_{tot} - T_{1u} - T_{1g}$$

Determine which irreducible representations contribute to Γ_{vib}.

Illegal pream-token (\)

Thus we see that the vibrational modes have the following symmetry:

$$\Gamma_{vib} = A_{1g} + E_g + T_{2g} + 2T_{1u} + T_{2u}$$

Inspection of the character table shows that in octahedral symmetry the degeneracy of the d-orbitals is split into a three-fold degenerate T_{2g} (d_{xy}, d_{xz}, d_{yz}) level and a two-fold degenerate E_g (d_{z2}, $d_{x2\ -\ y2}$) level. Electrostatic arguments (see your general

chemistry text) predict that the T_{2g} level is lower in energy. Thus, according to this model Ti^{3+} has one d-electron in the T_{2g} level. As the spectrum above shows, the complex absorbs in the visible region at 20,000 cm^{-1} (500 nm). However, the T_{2g} ---> E_g transition is orbitally forbidden as is shown below.

$$\int \Psi_{ex}\mu_e\Psi_{eg}d\tau_e = 0 \quad \frac{\sum\overrightarrow{(OhE_gT_{1u}T_{2g})}}{h} = 0$$

On the left we have the transition moment integral expressed in the language of integral calculus (see any quantum chemistry text) and on the right we have the same integral in the group-theoretical vector-matrix representation.

In calculating the transition moment for T_{2g} ---> E_g electronic transition it has been assumed that there was no change in the vibrational state of the molecule. However, it is possible for formally forbidden electronic transitions to become allowed through coupling to changes in the vibrational state of the molecule. In other words pure electronic transitions do not actually occur, because the vibrational (and rotational) states of the molecule change at the same time. These are called vibronic transitions and they are allowed if the integral shown below is nonzero.

$$\int\int \Psi_{ex}\Psi_{vx}\mu_e\Psi_{eg}\Psi_{vg}d\tau_e d\tau_v$$

The calculations below show that vibronic transitions involving the T_{1u} and T_{2u} vibrational modes are allowed because the transition moment is not zero. It is important to note that the ground states of all vibrational modes of all point groups have A1g symmetry. (See F. A. Cotton, *Chemical Applications of Group Theory*, J. Wiley, 1963, p. 262.)

$$\frac{\sum\overrightarrow{(OhT_{1u}E_gT_{1u}T_{2g}A_{1g})}}{h} = 2 \quad \frac{\sum\overrightarrow{(OhT_{2u}E_gT_{1u}T_{2g}A_{1g})}}{h} = 2$$

The A_{1g}, E_g, and T_{2g} modes do not provide vibrational assistance as is shown below.

$$\frac{\sum\overrightarrow{(OhA_{1g}E_gT_{1u}T_{2g}A_{1g})}}{h} = 0 \quad \frac{\sum\overrightarrow{(OhE_gE_gT_{1u}T_{2g}A_{1g})}}{h} = 0 \quad \frac{\sum\overrightarrow{(OhT_{2g}E_gT_{1u}T_{2g}A_{1g})}}{h} = 0$$

At this point we have shown that the vibrationally assisted T_{2g} ---> E_g electronic transition is allowed. However, the shoulder on the experimental spectrum suggest that more than one electronic transition is occurring. In the next section we will see that a reduction to square planar symmetry under the Jahn-Teller effect leads to a d-orbital energy level diagram that is consistent with the experimental spectrum.

$Ti(H_2O)_6^{3+}$ - Square Planar Symmetry

The Jahn-Teller effect predicts a tetragonal distortion of the octahedral complex to the lower D_{4h} square planar symmetry. The energy level diagram is shown above - essentially the ligands on the z-axis move in toward the titanium ion.

Illegal pream-token (E)

$$\begin{array}{lllll} A_{1g} = (CD4h^T)^{<1>} & A_{2g} = (CD4h^T)^{<2>} & B_{1g} = (CD4h^T)^{<3>} & B_{2g} = (CD4h^T)^{<4>} & E_g = (CD4h^T)^{<5>} \\ A_{1u} = (CD4h^T)^{<6>} & A_{2u} = (CD4h^T)^{<7>} & B_{1u} = (CD4h^T)^{<8>} B_{2u} = (CD4h^T)^{<9>} & E_u = (CD4h^T)^{<10>} & \end{array}$$

$$h = \sum D4h \quad \Gamma_{tot} = \overrightarrow{(\Gamma_{uma}(A2u + Eu))} \quad \Gamma_{tot}^T = (21 \quad 3 \quad -3 \quad -3 \quad -1 \quad -3 \quad -1 \quad 5 \quad 5 \quad 3)$$

Symmetry of the vibrational modes.

$$\Gamma_{vib} = \Gamma_{tot} - A_{2g} - E_g - A_{2u} - E_u$$

Illegal pream-token (A)

$$\Gamma_{vib} = 2A_{1g} + B_{1g} + B_{2g} + E_g + 2A_{2u}B_{2u} + 3E_u$$

The D_{4h} energy level diagram shows three possible electronic transitions, one IR transition and two transitions in visible region of the spectrum. The following calculations show that all three are formally forbidden. Again, vibronic coupling is invoked to explain the appearance of the two electronic transitions in the visible region.

$$\frac{\sum \overrightarrow{(D4h\ E_g(A_{2u}+E_u)B_{2g})}}{h} = 0 \quad \frac{\sum \overrightarrow{(D4h\ B_{1g}(A_{2u}+E_u)B_{2g})}}{h} = 0 \quad \frac{\sum \overrightarrow{(D4h\ A_{1g}(A_{2u}+E_u)B_{2g})}}{h} = 0$$

An A_{1u} or E_u vibrational mode can provide vibronic coupling for the B_{2g} --> B_{1g} transition. Again it is important to recall that the ground states of all vibrational modes have A_{1g} symmetry.

$$\frac{\sum \overrightarrow{(D4h\ A_{1u}\ B_{1g}(A_{2u}+E_u)B_{2g}\ A_{1g})}}{h} = 1 \quad \frac{\sum \overrightarrow{(D4h\ E_u\ B_{1g}(A_{2u}+E_u)B_{2g}\ A_{1g})}}{h} = 1$$

A B_{1u} or E_u vibrational mode can provide vibronic coupling for the B_{2g} --> A_{1g} transition.

$$\frac{\sum \overrightarrow{(D4h\ B_{1u}\ A_{1g}(A_{2u}+E_u)B_{2g}\ A_{1g})}}{h} = 1 \quad \frac{\sum \overrightarrow{(D4h\ E_u\ A_{1g}(A_{2u}+E_u)B_{2g}\ A_{1g})}}{h} = 1$$

A close examination of the experimental spectrum indicates the presence of two electronic transitions of similar energy (shoulder). So the energy level diagram and the vibronic analysis are consistent with the actual spectrum.

Primary reference: Daniel C. Harris and Michael D. Bertolucci, "Symmetry and Spectroscopy: An Introduction to Vibrational and Electronic Spectroscopy." Dover Publications, Inc., New York, 1989.

This page titled 4.16: Analysis of the Electronic Spectrum of Ti(H2O)3+ is shared under a CC BY 4.0 license and was authored, remixed, and/or curated by Frank Rioux via source content that was edited to the style and standards of the LibreTexts platform.

4.17: Quantum Jumps for an Electron on a Ring

In spite of Max Born's warning, we are going to present a simple model for a quantum jump that is based on visualization.

This tutorial deals with the quantum mechanical particle (quon to use Nick Herbert's term) on a ring. Previously the behavior of the π-electrons of benzene were analyzed using this model. Links to the tutorials are provided below.

http://www.users.csbsju.edu/~frioux/...enzene-por.pdf

http://www.users.csbsju.edu/~frioux/...onsBenzene.pdf

In the absence of perturbations, such as oscillating electromagnetic fields, quantum systems are in the stationary states obtained from the solution of the time-independent Schrödinger equation. When a quantum system is subject to a perturbation such as an oscillating electromagnetic field it is forced into a time-dependent superposition of its stationary states.

$$\Psi(q,\ t) = \sum_n \left(\psi_n(q)\exp\left(-i\frac{2\pi E_n t}{h}\right)\right)$$

For the system to absorb energy from the electromagnetic field and undergo a transition from one allowed energy state to another two conditions must be met. First, the photons of the electromagnetic field must satisfy the Bohr frequency condition by having an energy which equals the energy difference between the two states under consideration. Second, there must be a dipolar coupling between the electromagnetic field and the oscillating electron density of the system. This later criterion is, of course, the selection rule for the transition.

According to this model, when an electron on a ring is subjected to a electromagnetic perturbation, the electron responds by going into a state which is a linear superposition of the unperturbed stationary states. Assuming the Bohr frequency condition is satisfied for two states, if the square modulus, $|\Psi(x,t)|^2$, of the time-dependent wavefunction associated with this linear superposition exhibits an asymmetric fluctuating charge density (an oscillating dipole moment) on the ring, a coupling with the dipolar character of the electromagnetic field exists and a transition can occur. If the linear combination of states leads to a symmetric fluctuating charge density there is no coupling between the field and the electron density in the box and a transition is not possible.

The model is illustrated below for several possible transitions for an electron on a ring and the selection rule determined. Previously this model was used for the particle in a box and the harmonic oscillator. Links to these tutorials are provided below.

http://www.users.csbsju.edu/~frioux/q-jump/njump.pdf

http://www.users.csbsju.edu/~frioux/...mp/jumpsho.htm

http://www.users.csbsju.edu/~frioux/q-jump/p-jump.htm

Set up for graphics:

$$\text{numpts} = 100 \quad i = 0..\text{numpts} \quad j = 0..\text{numpts} \quad \phi_i = \frac{2\pi i}{\text{numpts}}$$
$$x_{i,\,j} = \cos(\phi_i) \quad y_{i,\,j} = \sin(\phi_i) \quad z_{i,\,j} = 0 \quad t = \frac{\text{FRAME}}{3}$$

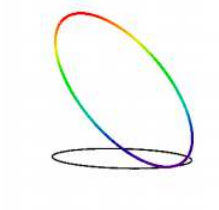
Form the time-dependent superposition of initial and final states:

$$\text{Initial state:} \quad n_i = 0 \quad E_i = 2n_i^2\pi^2 \quad \text{Final state:} \quad n_f = 1 \quad E_f = 2n_f^2\pi^2$$

$$\Psi_{i,\,j} = \frac{1}{2\sqrt{\pi}}\left(\left|\exp(in_1\phi_i)\exp(-iE_i t) + \exp(in_f\phi_i)\exp(-iE_f t)\right|\right)^2$$

Select Animation and then Record from the Tools menu and follow instructions. Choose from 0 to 30 at 3 frames/sec for a reasonable animated display.

Before running the animation note that this superposition shows dipole character in that the electron density is a minimum at the opposite side of the ring at which it is a maximum. This dipole rotates around the ring during the animation, providing a mechanism for coupling with the electromagnetic field illuminating the particle on a ring, if the Bohr frequency condition is satisfied. Thus the transition from the n = 0 state to the n = 1 state is allowed. It is easy to show in this way that any transition for which Δn = +/- 1 is allowed.

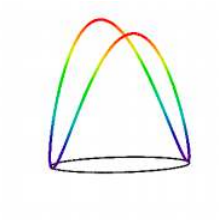


$(x,y,\Psi)_{,(x,y,z)}$

Now we look at a transition for which Δn = 2. It is clear from the symmetry of the superposition wave function that the electron density distribution does not have dipole character, and, therefore, there is no mechanism for coupling with the electromagnetic field. It is easy to show that the same is true for Δn = +/- 3, 4, etc.

$$\text{Initial state:} \quad n_i = 1 \quad E_i = 2n_i^2\pi^2 \quad \text{Final state:} \quad n_f = 3 \quad E_f = 2n_f^2\pi^2$$

$$\Psi_{i,\,j} = \frac{1}{2\sqrt{\pi}}(|\exp(in_i\phi_i)\exp(-iE_it) + \exp(in_f\phi_i)\exp(-iE_ft)|)^2$$



$(x,y,\Psi)_{,(x,y,z)}$

It is easy to show that while n = 1 to 2 and n = -1 to -2 transitions are allowed, the n = 1 to -2 and n = -1 to 2 transitions are forbidden, even though all of these transitions involve the same energy change.

Acknowledgement

The preparation of this tutorial and others on my page dealing with quantum jumps was stimulated by reading "Fluctuating Electric Dipoles and the Absorption of Light," by David R. McMillin [J. Chem. Ed. 55, 7 (1978)] .

This page titled 4.17: Quantum Jumps for an Electron on a Ring is shared under a CC BY 4.0 license and was authored, remixed, and/or curated by Frank Rioux via source content that was edited to the style and standards of the LibreTexts platform.

4.18: Analysis of the Vibrational and Electronic Spectrum of Benzene

This tutorial deals with the interpretation of the vibrational and electronic spectra of benzene using group theory.

Analysis of the Vibrational Spectrum

The vibrational analysis uses the method of unmoved atoms (uma). The number of unmoved atoms for each symmetry operation is stored in a vector, Γ_{uma}. This is converted into a reducible representation (Γ_{vib}) for the vibrational degrees of freedom in several steps as is shown below. Next the irreducible representations that contribute to Γ_{vib} is determined.

$$D6h = (1 \quad 2 \quad 2 \quad 1 \quad 3 \quad 3 \quad 1 \quad 2 \quad 2 \quad 1 \quad 3 \quad 3) \quad D6h = D6h^T \quad h = \sum D6h \quad h = 24$$

Illegal pream-token (E)

$$\Gamma_{trans} = (CD6h^T)^{<g>} + (CD6h^T)^{<11>} \quad \Gamma_{rot} = (CD6h^T)^{<2>} + (CD6h^T)^{<5>} \quad \Gamma_{tot} = \overrightarrow{(\Gamma_{uma}\Gamma_{trans})}$$

$$\Gamma_{vib} = \Gamma_{rot} - \Gamma_{trans} - \Gamma_{rot} \quad i = 1..12 \quad \mathrm{Vib}_i = \frac{\sum\overrightarrow{[D6h(CD6h^T)^{<i>}\Gamma_{vib}]}}{h}$$

$$\mathrm{Vib}^T = (2 \quad 1 \quad 0 \quad 2 \quad 1 \quad 4 \quad 0 \quad 1 \quad 2 \quad 2 \quad 3 \quad 2)$$

$$\Gamma_{vib} = 2A_{1g} + A_{2g} + 2B_{2g} + E_{1g} + 4E_{2g} + A_{2u} + 2B_{1u} + 1B_{2u} + 3E_{1u} + 2E_{2u}$$

The symmetry of the vibrational modes and their IR and Raman activity are given below:

IR active: A_{2u} and $3E_{1u}$

Raman active: $2A_{1g}$, E_{1g}, and $4E_{2g}$

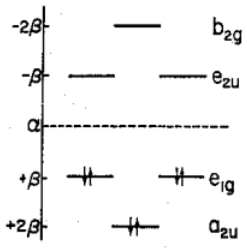
IR active modes are observed at 675, 1035, 1479, and 3036 cm^{-1}, which is consistent with the above analysis. The Raman spectrum is not as clearly resolved.

Analysis of the Electronic Spectrum

The electronic spectrum to be analyzed (see below) is due to transitions involving benzene's π electrons. The symmetry of the relevant π−electron molecular orbitals is determined by examining how the π orbitals transform under the symmetry operations of the D_{6h} group.

$$\Gamma_\pi = (6 \quad 0 \quad 0 \quad -2 \quad 0 \quad 0 \quad 0 \quad -6 \quad 0 \quad 2) \quad \Pi_i = \frac{\sum\overrightarrow{[D6h(CD6h^T)^{<i>}\tau_\pi^T]}}{h}$$

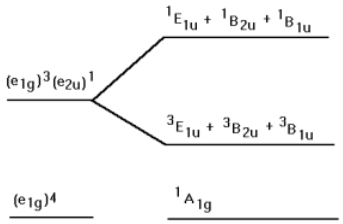
Illegal pream-token (\\)



The symmetry of the π-molecular orbitals is Γ_π = B_{2g} + E_{1g} + A_{2u} + E_{2u}. The order of the levels from a Huckel calculation is as shown above: A_{2u}, E_{1g}, E_{2u}, and B_{2g}. The ground electronic state is $A_{2u}(2)$, $E_{1g}(4)$ and has A_{1g} symmetry because the A_{2u} and E_{1g} orbitals are full. The first electronic excited state is $A_{2u}(2)$, $E_{1g}(3)$, $E_{2u}(1)$. This has the symmetry properties of $E_{1g}(1)E_{2u}(1)$ which gives rise to the manifold of states: B_{1u}, B_{2u}, and E_{1u} as is shown below.

$$X_i = \frac{\sum\overrightarrow{[D6h(CD6h^T)^{<i>}(CD6h^T)^{<5>}(CD6h^T)^{<12>}]}}{h} \quad X^T = (0 \quad 0 \quad 0 \quad 0 \quad 0 \quad 0 \quad 0 \quad 0 \quad 1 \quad 1 \quad 1 \quad 0)$$

The electronic energy level diagram consistent with this analysis is shown below. Note that the excited state splits into a set of singlet and triplet exited states. Transitions from the singlet ground state to the triplet excited states are formally forbidden.



For an electronic transition to be allowed the transition moment integral must be greater than zero.

$$\int \Psi_{ex}\mu_e\Psi_{eg}d\tau_e > 0$$

Only the A_{1g} ---> E_{1u} transition is orbitally allowed as is shown below.

$$A_{1g} \rightarrow B_{1u} \quad \frac{\sum\overrightarrow{[D6h(CD6h^T)^{<9>}[(CD6h^T)^{<g>}+(CD6h^T)^{<11>}](CD6h^T)^{<1>}]}}{h} = 0$$

$$A_{1g} \rightarrow B_{2u} \quad \frac{\sum\overrightarrow{[D6h(CD6h^T)^{<10>}[(CD6h^T)^{<g>}+(CD6h^T)^{<11>}](CD6h^T)^{<1>}]}}{h} = 0$$

$$A_{1g} \rightarrow E_{1u} \quad \frac{\sum\overrightarrow{[D6h(CD6h^T)^{<11>}[(CD6h^T)^{<g>}+(CD6h^T)^{<11>}](CD6h^T)^{<1>}]}}{h} = 0$$

Electronic transitions that are orbitally forbidden can occur if they are properly coupled to vibrational transitions. This occurs when the following integral is non-zero. These are called vibronic or vibrationally assisted electronic transitions.

$$\int\int \Psi_{ex}\Psi_{vx}\mu_e\Psi_{eg}\Psi_{vg}d\tau_e d\tau_v$$

The orbitally forbidden A_{1g} --> B_{1u} is vibronically assisted by B_{2g} or E_{2g} vibrations.

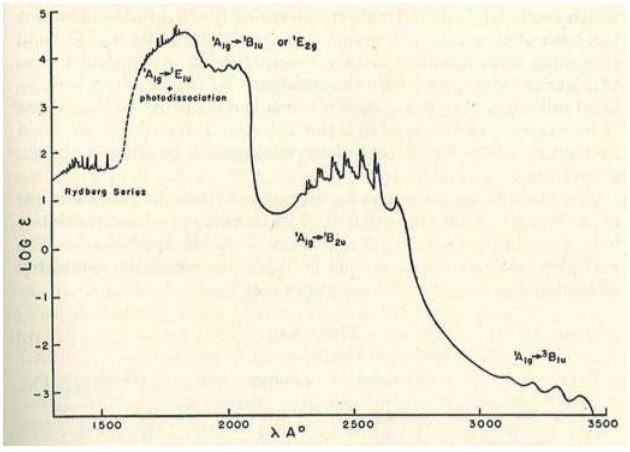
$$X_i = \frac{\sum\overrightarrow{[D6h(CD6h^T)^9(CD6h^T)^i[(CD6h^T)^g+(CD6h^T)^{11}](CD6h^T)^1(CD6h^T)^1]}}{h}$$

$$X^T = (0 \quad 0 \quad 0 \quad 1 \quad 0 \quad 1 \quad 0 \quad 0 \quad 0 \quad 0 \quad 0 \quad 0)$$

The orbitally forbidden A_{1g} --> B_{2u} is vibronically assisted by B_{1g} or E_{2g} vibrations. However there is no B_{1g} vibration.

$$X_i = \frac{\sum\overrightarrow{[D6h(CD6h^T)^{10}(CD6h^T)^i[(CD6h^T)^g+(CD6h^T)^{11}](CD6h^T)^1(CD6h^T)^1]}}{h}$$

$$X^T = (0 \quad 0 \quad 1 \quad 0 \quad 0 \quad 1 \quad 0 \quad 0 \quad 0 \quad 0 \quad 0 \quad 0)$$



The fully allowed A_{1g} ---> E_{1u} transition is assigned to the most intense transition which occurs at 180 nm. The vibronically assisted A_{1g} --> B_{1u} and A_{1g} --> B_{2u} transitions are assigned to the less intense bands at 200 and 260 nm, respectively. The spin-forbidden 1 A_{1g} --> 3 B_{1u} is assigned to the lowest energy and lowest intensity transition at 340 nm.

This page titled 4.18: Analysis of the Vibrational and Electronic Spectrum of Benzene is shared under a CC BY 4.0 license and was authored, remixed, and/or curated by Frank Rioux via source content that was edited to the style and standards of the LibreTexts platform.

4.19: NMR - Quantum Mechanics of a Three Proton System

In this computer/spectroscopy lab the variational method is used to determine the nuclear spin states and allowed transitions in a three proton spin system. The theoretical procedure is essentially the same as that used in the other applications of the variational method that we have studied (LCAO-MO for H_2^+, Roothaan SCF, and various examples presented in class).

To prepare for this lab study the section on NMR in your textbook and review your class notes on the quantum mechanical treatment of the NMR spectroscopy of one- and two-proton systems. This lab will compare the low field NMR spectra of vinyl acetate and acrylonitrile. The high field (300 MHz) NMR spectrum of acrylonitrile will be measured and analyzed, and compared to the 60 MHz spectra of vinyl acetate and acrylonitrile.

The major steps in this exercise are listed below. Further detail is provided following the list. As you examine this sequence of steps you will see the similarities with previous variational calculations that we have looked at in class and lab.

1. Choose a trial nuclear spin wavefunction.
2. Write the energy operator for the three spin system which includes all the pertinent interactions.
3. Input parameters (in this case chemical shifts and coupling constants) and evaluate the matrix elements of the secular determinant for the system.
4. Solve the secular determinant for the energy eigenvalues and eigenfunctions.
5. Using the appropriate selection rule, DI_z = ± 1, construct a transition probability matrix.
6. Using the results from parts 4 and 5 above, calculate the allowed transitions and their intensities and then generate a model spectrum.
7. Compare the theoretical generated spectrum with the experimentally determined NMR spectrum.

Fortunately for us, the computer does most of the work and certainly all the difficult math in this exercise.

1. A molecule with three protons can be in any of eight possible spin states. To determine these states we choose as our trial wavefunction the following linear combination.

$$|\Psi_{spin}\rangle = c_1|\alpha\alpha\alpha\rangle + c_2|\alpha\alpha\beta\rangle + c_3|\alpha\beta\alpha\rangle + c_4|\beta\alpha\alpha\rangle + c_5|\alpha\beta\beta\rangle + c_6|\beta\alpha\beta\rangle + c_7|\beta\beta\alpha\rangle + c_8|\beta\beta\beta\rangle$$

   In this particular notation, |aaa> stands for all three nuclear spins in the spin-up (I_z = +±) spin state, while |aba> indicates that nuclei 1 and 3 are in the spin-up state and nucleus 2 is in the spin-down state (I_z = -±). In the absence of an external magnetic field and any interaction between the protons, all eight states have the same energy.
2. The complete energy operator is the sum of equations (3) and (4). There is a term like (3) for each proton and there is a term like (4) for each distinct pair of protons. For a three proton system, ABC, we have,

$$\hat{H}_{mag} = -g_n\beta_n\hat{B}_z\left[(1-\sigma_a)\hat{I}_z(a) + (1-\sigma_b)\hat{I})_z(b) + (1-\sigma_c)\hat{I}_z(c)\right] + \hat{J}_{ab}\hat{I}_a\hat{I}_b + J_{ac}\hat{I}_a\hat{I}_c + J_{bc}\hat{I}_b\hat{I}_c$$

3. We are now ready to apply the variational method as outlined earlier in your text. The variational integral for this application is

$$E = \langle\Psi_{spin}|\hat{H}_{mag}|\Psi_{spin}\rangle$$

   Treatment of this integral by the usual techniques yields an 8 x 8 secular determinant of the form:

$$\begin{vmatrix} H_{11}-E & 0 & 0 & 0 & 0 & 0 & 0 & 0 \\ 0 & H_{22}-E & \frac{J_{bc}}{2} & \frac{J_{ac}}{2} & 0 & 0 & 0 & 0 \\ 0 & \frac{J_{bc}}{2} & H_{33}-E & \frac{J_{ab}}{b} & 0 & 0 & 0 & 0 \\ 0 & \frac{J_{ac}}{2} & \frac{J_{ab}}{2} & H_{44}-E & 0 & 0 & 0 & 0 \\ 0 & 0 & 0 & 0 & H_{55}-E & \frac{J_{ab}}{2} & \frac{J_{ac}}{2} & 0 \\ 0 & 0 & 0 & 0 & \frac{J_{ab}}{2} & H_{66}-E & \frac{J_{bc}}{2} & 0 \\ 0 & 0 & 0 & 0 & \frac{J_{ac}}{2} & \frac{J_{bc}}{2} & H_{\eta}-E & 0 \\ 0 & 0 & 0 & 0 & 0 & 0 & 0 & H_{88}-E \end{vmatrix} = 0$$

   where the diagonal matrix elements are, for example, of the form

$$H_{11} = \frac{1}{2}\left[v_a + v_b + v_c\right] + \frac{1}{4}\left[J_{ab} + J_{ac} + J_{bc}\right]$$
$$H_{22} = \frac{1}{2}\left[v_a + v_b - v_c\right] + \frac{1}{4}\left[J_{ab} - J_{ac} - J_{bc}\right]$$
$$\vdots$$
$$H_{88} = \frac{1}{2}\left[-v_a - v_b - v_c\right] + \frac{1}{4}\left[J_{ab} + J_{ac} + J_{bc}\right]$$

Here the n_i represent the terms g_n b_n (1 - s_i) B_z which are the resonant frequencies of the protons in their respective chemical environments. The various matrix elements can be evaluated once the chemical shifts and coupling constants are supplied.

4. The Mathcad document which is appended solves the secular determinant (7) after chemical shifts and coupling constants are provided. It yields the nuclear spin energy levels, their associated wavefunctions, the allowed transitions between these levels, the frequencies at which the transitions occur and their intensities. It also generates a model spectrum. Study the Mathcad document to make certain you understand each of the steps in this quantum mechanical calculation.
5. The calculation of the allowed transitions deserves further comment. Because the three proton system has eight spin states, there are 28 potential transitions amongst these energy levels. How many transitions are actually observed and at what intensities is determined by the selection rule for NMR spectroscopy. This selection rule states that only one spin can be *flipped* in any given transition. In other words D I_z = **?** 1.

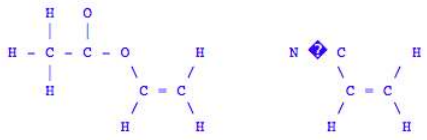
   A transition is allowed if the product of the three matrices shown below is non-zero. The intensity of the transition is equal to the square of the product of these matrices.

$$\begin{pmatrix} c_1 & c_2 & c_3 & c_4 & c_5 & c_6 & c_7 & c_8 \end{pmatrix} \begin{pmatrix} 0 & 1 & 1 & 1 & 0 & 0 & 0 & 0 \\ 1 & 0 & 0 & 0 & 1 & 1 & 0 & 0 \\ 1 & 0 & 0 & 0 & 1 & 0 & 1 & 0 \\ 1 & 0 & 0 & 0 & 0 & 1 & 1 & 0 \\ 0 & 1 & 1 & 0 & 0 & 0 & 0 & 1 \\ 0 & 1 & 0 & 1 & 0 & 0 & 0 & 1 \\ 0 & 0 & 1 & 1 & 0 & 0 & 0 & 1 \\ 0 & 0 & 0 & 0 & 1 & 1 & 1 & 0 \end{pmatrix} \begin{pmatrix} c`_1 \\ c`_2 \\ c'_3 \\ c`_4 \\ c`_5 \\ c`_6 \\ c`_7 \\ c`_8 \end{pmatrix}$$

   For example this matrix determines whether the transition from state 1 to state 2 is allowed. The matrix on the left contains the coefficients of the wavefunction of state 1 written in row-matrix form, while the matrix on the right contains the coefficients of the wavefunction of state 2 written in column-matrix form. The center matrix is the transition matrix and is an 8x8 square matrix which summarizes the allowed transitions. For example, the (1,1) matrix element represents the |aaa> ---> |aaa> transition and is 0 because it violates the selection rule (no spins are flipped). However, the (1,2) matrix element is 1 because the transition |aaa> ---> |aab> is allowed (only one spin is flipped). Following the rules of matrix multiplication, Mathcad examines each possible transition. If its intensity is non-zero it makes a record of it and later displays the transition in tabular and graphical form. For example, the matrix product shown below indicates that the |aaa> ---> |bbb> transition is forbidden.

Experimental:

The 300 MHz NMR spectrum of acrylonitrile will be measured and compared to its 60 MHz NMR and also to the 60 MHz spectrum of vinyl acetate.



The methyl protons are not coupled to the vinyl protons so it is possible to treat the vinyl protons as an ABC system. The low field (60 MHz) NMR spectra of acrylonitrile and vinyl acetate are shown below.

Interpretation of the Spectrum

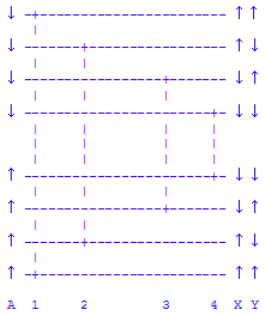
Acrylonitrile is a true ABC system while the vinyl protons of vinyl acetate behave like an ABC system because they are not coupled to the methyl protons. Vinyl acetate presents a classic ABC spectrum. Each proton has a distinct chemical shift and each proton's resonance is split by the two other protons. Thus what is observed is a spectrum which consists of three separate

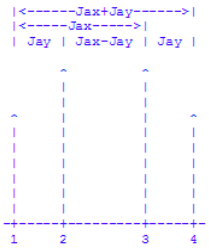
resonances each of which is a quartet of peaks (a doublet of doublets). The chemical shifts are obtained by locating the center of the doublet of doublets. The determination of the coupling constants is described below.

In the absence of any coupling the resonance of an individual proton, A, would appear as a singlet.



The presence of two non-equivalent protons, X and Y , splits A's singlet into a quartet of peaks as shown in the diagram below. This occurs because there are four possible orientations of the non-equivalent protons (up-up, up-down, down-up, down-down) and, therefore, both the ground state and excited state of proton A are split into four levels.



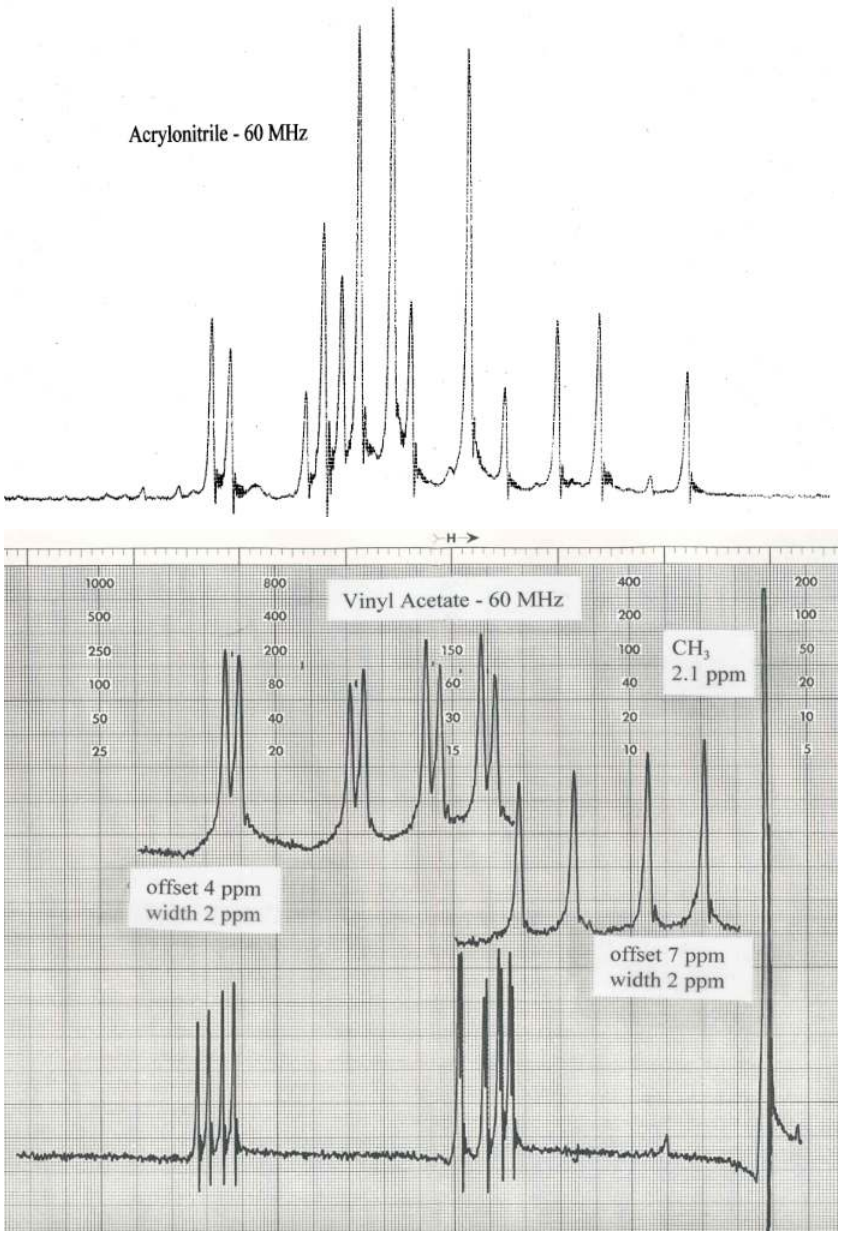


Remember that it is proton A that is undergoing the resonance and that the spins of X and Y don't flip during A's resonance. That is why there are only four transitions amongst these eight states. Note that the difference between transition 1 and 2 is the spin state of proton Y. Thus the frequency difference between these peaks is the coupling constant J_{ay} expressed in hertz. Similarly, the difference between 3 and 4 is J_{ay}, the difference between 1 and 3 is J_{ax}, the difference between 2 and 4 is J_{ax}, the difference between 1 and 4 is $J_{ax} + J_{ay}$, and the difference between 2 and 3 is $J_{ax} - J_{ay}$. Similar arguments would be used to discuss the resonances of protons B and C.

To obtain the three coupling constants for vinyl acetate use the following procedure. Label the doublet of doublets farthest down field "A", the middle one "B" and the last one "C". The analysis described above provides you with two direct measurements of two coupling constants. For example, J_{ab} and J_{ac} can be obtained from the analysis of the "A" resonance but you don't know which proton is "B" and which one is "C" at this point. However, the analysis of the "B" resonance provides determinations of J_{ab} and J_{bc}. Comparison of the results for "A" and "B" enable you to assign values to J_{ab}, J_{ac}, and J_{bc}. Use the average of the four values for J_{ab}, but hold off on J_{ac} and J_{bc} until you have analyzed the resonance of proton "C". This proceedure provides you with four determinations of J_{ac} and J_{bc}. Use the average values for each of these parameters.

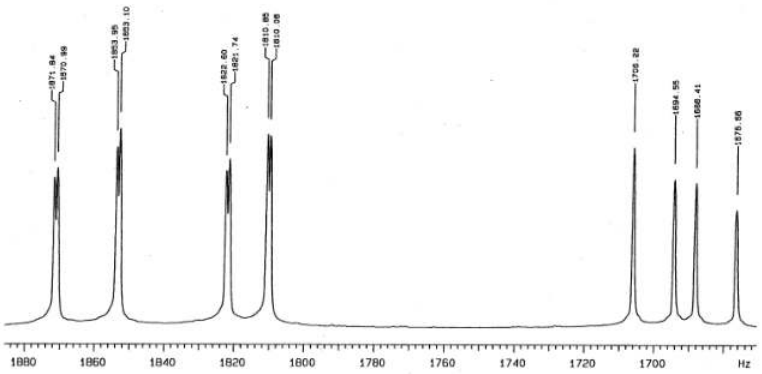
Assignment

1. First compare the 60 MHz NMR spectra of acrylonitrile and vinyl acetate shown below. Notice the difference in appearance of the spectra in spite of the fact that both spectra show the resonances of three vinyl protons.



2. Use the methods outlined above to obtain chemical shifts and coupling constants from the vinyl acetate NMR spectrum.
3. With assistance, obtain the 300 MHz spectrum of acrylonitile. Note its basic similarity to the low field vinyl acetate spectrum. Explain why increasing the magnetic field simplifies the acrylonitrile spectrum. Analyze the spectrum to obtain the chemical

Acrylonitrile - 300 MHz



shifts and coupling constants.

4. Run the Mathcad program supplied for the low field NMR spectrum of vinyl acetate.
    1. Use the eigenvalues and eigenvectors generated by Mathcad to construct an energy level diagram for the eight allowed spin states. Use the format indicated below for each energy level.

        E_8 ..... Y_8

        E_7 ..... Y_7

        E_6 ..... Y_6

        E_5 ..... Y_5

        E_4 ..... Y_4

        E_3 ..... Y_3

        E_2 ..... Y_2

        E_1 ..... Y_1

    2. Now use the intensity matrix generated by Mathcad to sketch in the allowed transitions on the diagram above.
    3. Also prepare a table which compares the experimental transition frequencies with the computer generated frequencies given in the frequency matrix. If you do not find a favorable comparison it means either that the theoretical model used in this exercise does not adequately represent the vinyl acetate nuclear spin system or that you have misread your spectrum.
    4. Qualitatively compare the appearance of the experimental spectrum with the model spectrum generated by Mathcad. In other words do you find satisfactory agreement for the relative values of the frequencies and intensities for each resonance. Explain.
5. Run the Mathcad program supplied for the high field NMR spectrum of acrylonitrile.
    1. Use the eigenvalues and eigenvectors generated by Mathcad to construct an energy level diagram for the eight allowed spin states. Use the format given in 4.1 for each energy level.
    2. Now use the intensity matrix generated by Mathcad to sketch in the allowed transitions on the diagram from part 4.1 above.
    3. Also prepare a table which compares the experimental transition frequencies with the computer generated frequencies given in the frequency matrix. If you do not find a favorable comparison it means either that the theoretical model used in this exercise does not adequately represent the acrylonitrile nuclear spin system or that you have misread your spectrum.
    4. Qualitatively compare the appearance of the experimental spectrum with the model spectrum generated by Mathcad. In other words do you find satisfactory agreement for the relative values of the frequencies and intensities for each resonance. Explain.
6. Run the Mathcad program to simulate the low field (60 MHz) spectrum of acrylonitrile. Do this by dividing the high field chemical shifts by 5 (60 = 300/5). Compare the Mathcad model spectrum with the experimental 60 MHz spectrum provided.

1. Use the eigenvalues and eigenvectors generated by Mathcad to construct an energy level diagram for the eight allowed spin states. Use the format given in 4.1 for each energy level.
2. Now use the intensity matrix generated by Mathcad to sketch in the allowed transitions on the diagram from part 4.1 above.
3. Qualitatively compare the appearance of the experimental spectrum with the model spectrum generated by Mathcad. In other words do you find satisfactory agreement for the relative values of the frequencies and intensities for each resonance. Explain.
4. Before the existence of high field nmr an analysis of the 60 MHz spectrum of acrylonitrile yielded the following chemical shifts and coupling constants in Hz: s_a = 372.2; s_b = 364.4; s_c= 342.0; J_{ab} = 0.91; J_{ac} = 17.90; J_{bc} = 11.75. Compare your values for the chemical shifts and coupling constants with these values.

7. The low-field acrylonitrile spectrom shows that 14 resonances are observed [a 15th resonance (see intensity matrix) is too weak to be seen experimentally]. The high-field acrylonitrile and low-field vinyl acetate spectra show 12 resonances. Examine the nuclear spin wave functions for all three cases and use the superposition principle to explain these differences.

This page titled 4.19: NMR - Quantum Mechanics of a Three Proton System is shared under a CC BY 4.0 license and was authored, remixed, and/or curated by Frank Rioux via source content that was edited to the style and standards of the LibreTexts platform.

4.20: AB Proton NMR Using Tensor Algebra

The purpose of this tutorial is to deviate from the traditional matrix mechanics approach to the AB proton nmr system in order to illustrate a related method of analysis which uses tensor algebra.

The nuclear magnetic energy operator for the AB system is given below.

$$\hat{H}_{mag} = -\nu_A \hat{I}_z^A - \nu_B \hat{I}_z^B + J_{AB} \hat{I}^A \hat{I}^B \quad \text{where} \quad \nu_A = g_n \beta_n B_n (1-\sigma_A) \hat{I}_z^A \quad \nu_B = g_n \beta_n B_z (1-\sigma_B) \hat{I}_z^B$$

$$\text{and} \quad \hat{I}^A \hat{I}^B = \hat{I}_x^A \hat{I}_x^B + \hat{I}_y^A \hat{I}_y^B + \hat{I}_z^A \hat{I}_z^B$$

The customary matrix mechanics analysis requires the following mathematical structures.

- Nuclear spin wave function:

$$|\Psi_{mag}\rangle = c_1|\alpha_A\alpha_B\rangle + c_2|\alpha_A\beta_B\rangle + c_3|\beta_A\alpha_B\rangle + c_4|\beta_A\beta_B\rangle = c_1|\alpha_A\rangle|\alpha_B\rangle + c_2|\alpha_A\rangle|\beta_B\rangle + c_3|\beta_A\rangle|\alpha_B\rangle + c_4|\beta_A\rangle|\beta_B\rangle$$

- Spin operators (using atomic units, h = 2 π) in the x-, y- and z-directions, plus the identity operator (needed later):

$$I_x = \tfrac{1}{2}\begin{pmatrix} 0 & 1 \\ 1 & 0 \end{pmatrix} \quad I_y = \tfrac{1}{2}\begin{pmatrix} 0 & -i \\ i & 0 \end{pmatrix} \quad I_z = \tfrac{1}{2}\begin{pmatrix} 1 & 0 \\ 0 & -1 \end{pmatrix} \quad I = \begin{pmatrix} 1 & 0 \\ 0 & 1 \end{pmatrix}$$

- Spin eigenfunctions in the x-, y- and z-directions:

$$\alpha_a = \begin{pmatrix} 1 \\ 0 \end{pmatrix} \quad \beta_z = \begin{pmatrix} 0 \\ 1 \end{pmatrix} \quad \alpha_x = \tfrac{1}{\sqrt{2}}\begin{pmatrix} 1 \\ 1 \end{pmatrix} \quad \beta_x = \tfrac{1}{\sqrt{2}}\begin{pmatrix} -1 \\ 1 \end{pmatrix} \quad \alpha_y = \tfrac{1}{\sqrt{2}}\begin{pmatrix} 1 \\ i \end{pmatrix} \quad \beta_y = \tfrac{1}{\sqrt{2}}\begin{pmatrix} 1 \\ -i \end{pmatrix}$$

Note that while the spin wave function is a linear combination of four spin states, the operators are 2x2 matrices. This requires that special care is taken to insure that the operator is operating on the correct spin wave function component. This can be avoided by writing both the spin states and magnetic operator in tensor format.

First tensor vector multiplication is used to construct the nuclear spin states.

$$|\alpha\alpha\rangle = |\alpha\rangle|\alpha\rangle = \begin{pmatrix} 1 \\ 0 \end{pmatrix} \otimes \begin{pmatrix} 1 \\ 0 \end{pmatrix} = \begin{pmatrix} 1\begin{pmatrix} 1 \\ 0 \end{pmatrix} \\ 0\begin{pmatrix} 1 \\ 0 \end{pmatrix} \end{pmatrix} = \begin{pmatrix} 1 \\ 0 \\ 0 \\ 0 \end{pmatrix} \quad |\alpha\beta\rangle = |\alpha\rangle|\beta\rangle = \begin{pmatrix} 1 \\ 0 \end{pmatrix} \otimes \begin{pmatrix} 0 \\ 1 \end{pmatrix} = \begin{pmatrix} 1\begin{pmatrix} 1 \\ 0 \end{pmatrix} \\ 0\begin{pmatrix} 0 \\ 1 \end{pmatrix} \end{pmatrix} = \begin{pmatrix} 0 \\ 1 \\ 0 \\ 0 \end{pmatrix}$$

$$|\beta\alpha\rangle = |\beta\rangle|\alpha\rangle = \begin{pmatrix} 0 \\ 1 \end{pmatrix} \otimes \begin{pmatrix} 1 \\ 0 \end{pmatrix} = \begin{pmatrix} 0\begin{pmatrix} 1 \\ 0 \end{pmatrix} \\ 1\begin{pmatrix} 1 \\ 0 \end{pmatrix} \end{pmatrix} = \begin{pmatrix} 0 \\ 0 \\ 1 \\ 0 \end{pmatrix} \quad |\beta\beta\rangle = |\beta\rangle|\beta\rangle = \begin{pmatrix} 0 \\ 1 \end{pmatrix} \otimes \begin{pmatrix} 0 \\ 1 \end{pmatrix} = \begin{pmatrix} 0\begin{pmatrix} 0 \\ 1 \end{pmatrix} \\ 1\begin{pmatrix} 0 \\ 1 \end{pmatrix} \end{pmatrix} = \begin{pmatrix} 0 \\ 0 \\ 0 \\ 1 \end{pmatrix}$$

We now write these spin states in the Mathcad code.

$$\alpha\alpha = \begin{pmatrix} 1 \\ 0 \\ 0 \\ 0 \end{pmatrix} \quad \alpha\beta = \begin{pmatrix} 0 \\ 1 \\ 0 \\ 0 \end{pmatrix} \quad \beta\alpha = \begin{pmatrix} 0 \\ 0 \\ 1 \\ 0 \end{pmatrix} \quad \beta\beta = \begin{pmatrix} 0 \\ 0 \\ 0 \\ 1 \end{pmatrix}$$

Next, tensor matrix multiplication is used to construct the magnetic energy operator.

$$-\nu_A \hat{I}_z^A \rightarrow -\nu_A \hat{I}_z^A \otimes \hat{I} = \frac{-\nu_A}{2} \begin{pmatrix} 1 & 0 \\ 0 & -1 \end{pmatrix} \otimes \begin{pmatrix} 1 & 0 \\ 0 & 1 \end{pmatrix}$$

$$= \frac{-\nu_A}{2} \begin{pmatrix} 1\begin{pmatrix} 1 & 0 \\ 0 & 1 \end{pmatrix} & 0\begin{pmatrix} 1 & 0 \\ 0 & 1 \end{pmatrix} \\ 0\begin{pmatrix} 1 & 0 \\ 0 & 1 \end{pmatrix} & -1\begin{pmatrix} 1 & 0 \\ 0 & 1 \end{pmatrix} \end{pmatrix} = \frac{-\nu_A}{2} \begin{pmatrix} 1 & 0 & 0 & 0 \\ 0 & 1 & 0 & 0 \\ 0 & 0 & -1 & 0 \\ 0 & 0 & 0 & -1 \end{pmatrix}$$

$$-\nu_B \hat{I}_z^B \rightarrow -\nu_B \hat{I}_z^B \otimes \hat{I} = \begin{pmatrix} 1 & 0 \\ 0 & 1 \end{pmatrix} \otimes \frac{-\nu_B}{2} \begin{pmatrix} 1 & 0 \\ 0 & -1 \end{pmatrix}$$

$$= \frac{-\nu_B}{2} \begin{pmatrix} 1\begin{pmatrix} 1 & 0 \\ 0 & -1 \end{pmatrix} & 0\begin{pmatrix} 1 & 0 \\ 0 & -1 \end{pmatrix} \\ 0\begin{pmatrix} 1 & 0 \\ 0 & -1 \end{pmatrix} & 1\begin{pmatrix} 1 & 0 \\ 0 & -1 \end{pmatrix} \end{pmatrix} = \frac{-\nu_B}{2} \begin{pmatrix} 1 & 0 & 0 & 0 \\ 0 & -1 & 0 & 0 \\ 0 & 0 & 1 & 0 \\ 0 & 0 & 0 & -1 \end{pmatrix}$$

$$J_{AB} \hat{I}_x^A \otimes \hat{I}_x^B = \frac{J_{AB}}{4} \begin{pmatrix} 0 & 1 \\ 1 & 0 \end{pmatrix} \otimes \begin{pmatrix} 0 & 1 \\ 1 & 0 \end{pmatrix} = \frac{J_{AB}}{4} \begin{pmatrix} 0\begin{pmatrix} 0 & 1 \\ 1 & 0 \end{pmatrix} & 1\begin{pmatrix} 0 & 1 \\ 1 & 0 \end{pmatrix} \\ 1\begin{pmatrix} 0 & 1 \\ 1 & 0 \end{pmatrix} & 0\begin{pmatrix} 0 & 1 \\ 1 & 0 \end{pmatrix} \end{pmatrix} = \frac{J_{AB}}{4} \begin{pmatrix} 1 & 0 & 0 & 0 \\ 0 & -1 & 0 & 0 \\ 0 & 0 & 1 & 0 \\ 0 & 0 & 0 & -1 \end{pmatrix}$$

$$J_{AB} \hat{I}_y^A \otimes \hat{I}_y^B = \frac{J_{AB}}{4} \begin{pmatrix} 0 & -i \\ i & 0 \end{pmatrix} \otimes \begin{pmatrix} 0 & -i \\ i & 0 \end{pmatrix}$$

$$= \frac{J_{AB}}{4} \begin{pmatrix} 0\begin{pmatrix} 0 & -i \\ i & 0 \end{pmatrix} & -i\begin{pmatrix} 0 & -i \\ i & 0 \end{pmatrix} \\ i\begin{pmatrix} 0 & -i \\ i & 0 \end{pmatrix} & 0\begin{pmatrix} 0 & -i \\ i & 0 \end{pmatrix} \end{pmatrix} = \frac{J_{AB}}{4} \begin{pmatrix} 0 & 0 & 0 & -1 \\ 0 & 0 & 1 & 0 \\ 0 & 1 & 0 & 0 \\ -1 & 0 & 0 & 0 \end{pmatrix}$$

$$J_{AB} \hat{I}_z^A \otimes \hat{I}_z^B = \frac{J_{AB}}{4} \begin{pmatrix} 1 & 0 \\ 0 & -1 \end{pmatrix} \otimes \begin{pmatrix} 1 & 0 \\ 0 & -1 \end{pmatrix}$$

$$= \frac{J_{AB}}{4} \begin{pmatrix} 1\begin{pmatrix} 1 & 0 \\ 0 & -1 \end{pmatrix} & 0\begin{pmatrix} 1 & 0 \\ 0 & -1 \end{pmatrix} \\ 0\begin{pmatrix} 1 & 0 \\ 0 & -1 \end{pmatrix} & -1\begin{pmatrix} 1 & 0 \\ 0 & -1 \end{pmatrix} \end{pmatrix} = \frac{J_{AB}}{4} \begin{pmatrix} 1 & 0 & 0 & 0 \\ 0 & -1 & 0 & 0 \\ 0 & 0 & -1 & 0 \\ 0 & 0 & 0 & 1 \end{pmatrix}$$

$$J_{AB}() = J_{AB} \hat{I}^A \otimes \hat{I}^B = \frac{J_{AB}}{4} \begin{pmatrix} 1 & 0 & 0 & 0 \\ 0 & -1 & 2 & 0 \\ 0 & 2 & -1 & 0 \\ 0 & 0 & 0 & 1 \end{pmatrix}$$

The magnetic Hamiltonian can now be written in Mathcad code.

$$\text{IzAIzB} = \frac{-1}{2} \begin{pmatrix} \nu_A + \nu_B & 0 & 0 & 0 \\ 0 & \nu_A - \nu_B & 0 & 0 \\ 0 & 0 & -\nu_A + \nu_B & 0 \\ 0 & 0 & 0 - \nu_A - \nu_B & \end{pmatrix} \qquad \text{IAIB} = \frac{J_{AB}}{4} \begin{pmatrix} 1 & 0 & 0 & 0 \\ 0 & -1 & 2 & 0 \\ 0 & 2 & -1 & 0 \\ 0 & 0 & 0 & 1 \end{pmatrix} \qquad H_{mag} = IzAIzIzB + \text{IAIB}$$

$$\rightarrow \begin{matrix} \\ \\ \\ \\ \end{matrix} \begin{matrix} H_{mag} \\ \end{matrix}$$

$$\begin{pmatrix} \frac{-1}{2}\nu_A - \frac{1}{2}\nu_B + \frac{1}{4}J_{AB} & 0 & 0 & 0 \\ 0 & \frac{-1}{2}\nu_A + \frac{1}{2}\nu_B - \frac{1}{4}J_{AB} & \frac{1}{2}J_{AB} & 0 \\ 0 & \frac{1}{2}J_{AB} & \frac{1}{2}\nu_A - \frac{1}{2}\nu_B - \frac{1}{4}J_{AB} & 0 \\ 0 & 0 & 0 & \frac{1}{2}\nu_A + \frac{1}{2}\nu_B + \frac{1}{4}J_{AB} \end{pmatrix}$$

The eigenvaues of the magnetic energy matrix can now be calculated.

$$\text{eigenvals}(H_{mag}) \rightarrow \begin{bmatrix} \frac{-1}{2}\nu_A - \frac{1}{2}\nu_B + \frac{1}{4}J_{AB} \\ \frac{1}{2}\nu_A + \frac{1}{2}\nu_B + \frac{1}{4}J_{AB} \\ \frac{-1}{4}J_{AB} + \frac{1}{2}\left(J_{AB}^2 + \nu_A^2 - 2\nu_A\nu_B + \nu_B^2\right)^{\frac{1}{2}} \\ \frac{-1}{4}J_{AB} - \frac{1}{2}\left(J_{AB}^2 + \nu_A^2 - 2\nu_A\nu_B + \nu_B^2\right)^{\frac{1}{2}} \end{bmatrix}$$

We can also calculate the magnetic energy matrix elements individually, as follows.

$$\begin{array}{llll} \alpha\alpha^T H_{mag}\alpha\alpha & \alpha\beta H_{mag}\alpha\alpha \rightarrow 0 & \beta\alpha^T H_{mag}\alpha\alpha \rightarrow 0 & \beta\beta^T H_{mag}\alpha\alpha \rightarrow 0 \\ \rightarrow \frac{-1}{2}\nu_A - \frac{1}{2}\nu_B + \frac{1}{4}J_{AB} & & & \\ \alpha\beta^T H_{mag}\alpha\beta \rightarrow \frac{-1}{2}\nu_A + \frac{1}{2}\nu_B - \frac{1}{4}J_{AB} & \beta\alpha H_{mag}\alpha\beta \rightarrow \frac{1}{2}J_{AB} & \beta\beta^T H_{mag}\alpha\beta \rightarrow 0 & \\ \beta\alpha^T H_{mag}\beta\alpha \rightarrow \frac{1}{2}\nu_A - \frac{1}{2}\nu_B - \frac{1}{4}J_{AB} & \alpha\beta H_{mag}\beta\alpha \rightarrow \frac{1}{2}J_{AB} & \beta\beta^T H_{mag}\beta\alpha \rightarrow 0 & \\ \beta\beta^T H_{mag}\beta\beta \rightarrow \frac{1}{2}\nu_A + \frac{1}{2}\nu_B + \frac{1}{4}J_{AB} & & & \end{array}$$

This page titled 4.20: AB Proton NMR Using Tensor Algebra is shared under a CC BY 4.0 license and was authored, remixed, and/or curated by Frank Rioux via source content that was edited to the style and standards of the LibreTexts platform.

4.21: Calculating the AB Proton NMR Using Tensor Algebra

The purpose of this tutorial is to deviate from the usual matrix mechanics approach to the ABC proton nmr system in order to illustrate a related method of analysis which uses tensor algebra. For a discussion of the traditional approach for the ABC system visit http://www.users.csbsju.edu/~frioux/nmr/Speclab4.htm. This site also provides general information on the quantum mechanics of nmr spectroscopy.

$$\text{Nuclear spin and identity operators:} \quad I_x = \tfrac{1}{2}\begin{pmatrix}0 & 1\\ 1 & 0\end{pmatrix} \quad I_y = \tfrac{1}{2}\begin{pmatrix}0 & -i\\ i & 0\end{pmatrix} \quad I_z = \tfrac{1}{2}\begin{pmatrix}1 & 0\\ 0 & -1\end{pmatrix} \quad I = \begin{pmatrix}1 & 0\\ 0 & 1\end{pmatrix}$$

$$\text{Chemical shifts:} \quad \nu_A = 250 \qquad \nu_B = 300 \qquad \text{Coupling constant:} \quad \text{Jab} = 10$$

Hamiltonian representing the interaction of nuclear spins with the external magnetic field in tensor format:

$$\hat{H}_{mag} = \nu_A \hat{I}_z^A - \nu_B \hat{I}_z^B = -\nu_A \hat{I}_z^A \otimes \hat{I} + \hat{I} \otimes \left(-\nu_B \hat{I}_z^B\right) \quad \text{where, for example,} \quad \nu_A = g_n \beta_n B_z (1 - \sigma_A)$$

Implementing the operator using Mathcad's command for the tensor product, kronecker, is as follows.

$$H_{mag} = -\nu_A \text{kronecker}(I_z,\ I) - \nu_B \text{kronecker}(I,\ I_z)$$

Hamiltonian representing the interaction of nuclear spins with each other in tensor format:

$$\hat{H}_{spin} = Jab\left(\hat{I}_x^A \otimes \hat{I}_x^B + \hat{I}_y^B \otimes \hat{I}_y^B + \hat{I}_z^A \otimes \hat{I}_z^B\right)$$

Implementation of the operator in the Mathcad programming environment:

$$H_{spin} = Jab\left(\text{kronecker}(I_x,\ I_x) + \text{kronecker}(I_y,\ I_y) + \text{kronecker}(I_z,\ I_z)\right)$$

The total Hamiltonian spin operator is now calculated and displayed.

$$H = H_{mag} + H_{spin}$$

Illegal pream-token (\)

Calculate and display the energy eigenvalues and associated eigenvectors of the Hamiltonian.

$$i = 1..4 \quad E = \text{sort}(\text{eigenvals}(\text{H})) \quad C^{<i>} = \text{eigenvec}(H,\ E_i)$$

Illegal pream-token (\)

The nmr selection rule is that only one nuclear spin can flip during a transition. Therefore, the transition probability matrix for the AB spin system is:

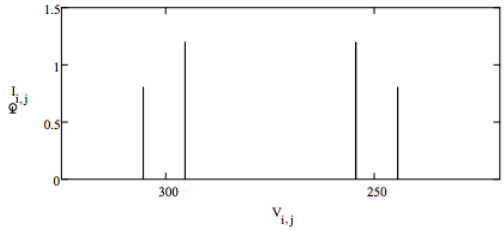
$$T = \begin{pmatrix}' & \alpha\alpha & \alpha\beta & \beta\alpha & \beta\beta\\ \alpha\alpha & 0 & 1 & 1 & 0\\ \alpha\beta & 1 & 0 & 0 & 1\\ \beta\alpha & 1 & 0 & 0 & 1\\ \beta\beta & 0 & 1 & 1 & 0\end{pmatrix} \quad T = \begin{pmatrix}0 & 1 & 1 & 0\\ 1 & 0 & 0 & 1\\ 1 & 0 & 0 & 1\\ 0 & 1 & 1 & 0\end{pmatrix}$$

Calculate the intensities and frequencies of the allowed transitions.

$$i = 1..4 \quad j = 1..4 \quad I_{i,\,j} = \left[C^{<i>}\left(TC^{<j>}\right)\right]^2 \quad V_{i,\,j} = \text{if}\left(I_{i,\,j} > .001,\ \left|E_i - E_j\right|,\ 0\right)$$

$$\text{Intensity matrix:} \quad I = \begin{pmatrix}0 & 0.8 & 1.2 & 0\\ 0.8 & 0 & 0 & 0.8\\ 1.2 & 0 & 0 & 1.2\\ 0 & 0.8 & 1.2 & 0\end{pmatrix} \quad \text{Frequency matrix:} \quad V = \begin{pmatrix}0 & 244.5 & 295.5 & 0\\ 244.5 & 0 & 0 & 244.5\\ 295.5 & 0 & 0 & 254.5\\ 0 & 305.5 & 254.5 & 0\end{pmatrix}$$

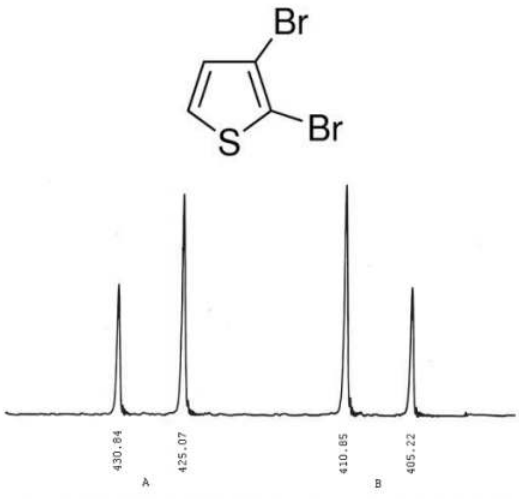
Display the calculated AB nmr spectrum:



This page titled 4.21: Calculating the AB Proton NMR Using Tensor Algebra is shared under a CC BY 4.0 license and was authored, remixed, and/or curated by Frank Rioux via source content that was edited to the style and standards of the LibreTexts platform.

4.22: AB Proton NMR Analysis for 2,3-dibromothiophene

The chemical shifts and the coupling constant for the two protons in 2,3-dibromothiophene are obtained from its nmr spectrum. These paramaters serve as inputs to a quantum mechanical calculation of the nmr spectrum. The theoretically generated spectrum is in good agreement with experiment, justifying the Hamiltonian operator chosen to represent the interaction of the protons with the external magnetic field and with each other.



Theory

Nuclear spin and identity operators:

$$I_x = \frac{1}{2}\begin{pmatrix}0 & 1\\ 1 & 0\end{pmatrix} \quad I_y = \frac{1}{2}\begin{pmatrix}0 & -i\\ i & 0\end{pmatrix} \quad I_z = \frac{1}{2}\begin{pmatrix}1 & 0\\ 0 & -1\end{pmatrix} \quad I = \begin{pmatrix}1 & 0\\ 0 & 1\end{pmatrix}$$

$$\text{Chemical shifts:} \quad \nu_A = 427.57 \quad \nu_B = 408.42 \quad \text{Coupling constant:} \quad J_{AB} = 5.70$$

Hamiltonian representing the interaction of nuclear spins with the external magnetic field in tensor format:

$$\begin{aligned}\hat{H}_{mag} &= -\nu_A \hat{I}_z^A - \nu_B \hat{I}_z^B \qquad \text{where for example,} \quad \nu_A = g_n \beta_n B_z (1-\sigma_A)\\ &= -\nu_A \hat{I}_z^A \otimes \hat{I} + \hat{I} \otimes \left(-\nu_B \hat{I}_z^B\right)\end{aligned}$$

Implementing the operator using Mathcad's command for the tensor product, kronecker, is as follows.

$$H_{mag} = \nu_A \text{kronecker}\,(I_z,\ I) - \nu_B \text{kronecker}\,(I,\ I_z)$$

Hamiltonian representing the interaction of nuclear spins with each other in tensor format:

$$\widehat{H}_{spin} = J_{AB}\left(\hat{I}_x^A \otimes \hat{I}_x^B + \hat{I}_y^A \otimes \hat{I}_y^B + \hat{I}_z^A \otimes \hat{I}_z^B\right)$$

Implementation of the operator in the Mathcad programming environment:

$$H_{spin} = J_{AB}\left(\text{kronecker}\,(I_x,\ I_x) + \text{kronecker}\,(I_y,\ I_y) + \text{kronecker}\,(I_z,\ I_z)\right)$$

The total Hamiltonian spin operator is now calculated and displayed.

$$H = H_{mag} + H_{spin}$$

Illegal pream-token (\)

Calculate and display the energy eigenvalues and associated eigenvectors of the Hamiltonian.

$$i = 1..4 \quad E = \text{sort}(\text{eigenvals}(\text{H})) \quad C^{<i>} = \text{eigenvec}(H,\ E_i)$$

Illegal pream-token (\)

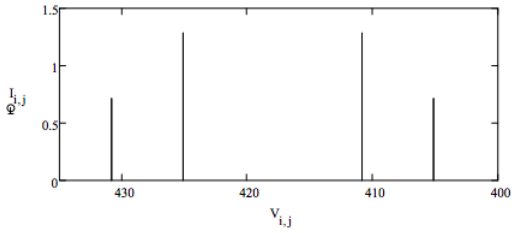
The nmr selection rule is that only one nuclear spin can flip during a transition. Therefore, the transition probability matrix for the two spin system is:

$$T = \begin{pmatrix} ' & \alpha\alpha & \alpha\beta & \beta\alpha & \beta\beta \\ \alpha\alpha & 0 & 1 & 1 & 0 \\ \alpha\beta & 1 & 0 & 0 & 1 \\ \beta\alpha & 1 & 0 & 0 & 1 \\ \beta\beta & 0 & 1 & 1 & 0 \end{pmatrix} \quad T = \begin{pmatrix} 0 & 1 & 1 & 0 \\ 1 & 0 & 0 & 1 \\ 1 & 0 & 0 & 1 \\ 0 & 1 & 1 & 0 \end{pmatrix}$$

Calculate the transition intensities and frequencies.

$$i = 1..4 \quad j = 1..4 \quad I_{i,\,j} = \left[C^{<i>}\left(TC^{<j>}\right)\right]^2 \quad V_{i,\,j} = |E_i - E_j|$$

Display the calculated 2,3-dibromothiophene nmr spectrum:



This page titled 4.22: AB Proton NMR Analysis for 2,3-dibromothiophene is shared under a CC BY 4.0 license and was authored, remixed, and/or curated by Frank Rioux via source content that was edited to the style and standards of the LibreTexts platform.

4.23: ABC Proton NMR Using Tensor Algebra

The purpose of this tutorial is to deviate from the usual matrix mechanics approach to the ABC proton nmr system in order to illustrate a related method of analysis which uses tensor algebra. For a discussion of the traditional approach visit http://www.users.csbsju.edu/~frioux/nmr/Speclab4.htm. This site also provides general information on the quantum mechanics of nmr spectroscopy.

Nuclear spin operators and identity:

$$I_x = \tfrac{1}{2}\begin{pmatrix}0 & 1\\ 1 & 0\end{pmatrix} \quad I_y = \tfrac{1}{2}\begin{pmatrix}0 & -i\\ i & 0\end{pmatrix} \quad I_z = \tfrac{1}{2}\begin{pmatrix}1 & 0\\ 0 & -1\end{pmatrix} \quad I = \begin{pmatrix}1 & 0\\ 0 & 1\end{pmatrix}$$

The following experimentally determined chemical shifts and coupling constants (both in Hz) are for the vinyl protons of vinyl acetate at 60 MHz.

$$\begin{array}{lcccc} \text{Chemical shifts:} & \nu_A = 345.6 & \nu_B = 237.6 & Jab = 6.1 \\ \text{Coupling constants:} & Jab = 7.00 & Jbc = 1.50 & Jac = 15.00 \end{array}$$

Hamiltonian representing the interaction of nuclear spins with the external magnetic field in tensor format:

$$\widehat{H}_{mag} = -\nu_A \hat{I}_z^A - \nu_B \hat{I}_z^B - \nu_C \hat{I}_z^C = -\nu_A \hat{I}_z^A \otimes \hat{I} \otimes \hat{I} + \hat{I} \otimes \left(-\nu_B \hat{I}_z^B\right) \otimes \hat{I} + \hat{I} \otimes \hat{I} \otimes \left(-\nu_B \hat{I}_z^B\right)$$

where, for example,

$$\nu_A = g_n \beta_n B_z (1 - \sigma_A)$$

Implementing the operator using Mathcad's command for the tensor product, kronecker, is as follows.

$$\begin{aligned} H_{mag} = &-\nu_A \text{kronecker}\left(I_z,\ \text{kronecker}(\text{I},\ \text{I})\right) - \nu_B \text{kronecker}\left(I,\ \text{kronecker}\left(I_z,\ I\right)\right) \\ &- \nu_B \text{kronecker}\left(I,\ \text{kronecker}\left(I,\ I_z\right)\right) \end{aligned}$$

Hamiltonian representing the interaction of nuclear spins with each other in tensor format:

$$\begin{aligned} \widehat{H}_{spin} = {} & J_{AB}\left(\hat{I}_x^A \otimes \hat{I}_x^B \otimes \hat{I} + \hat{I}_y^A \otimes \hat{I}_y^B \otimes \hat{I} + \hat{I}_z^A \otimes \hat{I}_z^B \otimes \hat{I}\right) \\ & + J_{AB}\left(\hat{I}_x^A \otimes \hat{I} \otimes \hat{I}_x^B + \hat{I}_y^A \otimes \hat{I} \otimes \hat{I}_y^B + \hat{I}_z^A \otimes \hat{I} \otimes \hat{I}_z^B\right) \\ & + J_{BC}\left(\hat{I} \otimes \hat{I}_x^B \otimes \hat{I}_x^C + \hat{I} \otimes \hat{I}_y^{\otimes} \hat{I}_y^C + \hat{I} \otimes \hat{I}_z^B \otimes \hat{I}_z^C\right) \end{aligned}$$

Implementation of the operator in the Mathcad programming environment:

$$H_{spin} = \begin{aligned} & Jab\left(\text{kronecker}\left(I_x,\ \text{kronecker}\left(I_x,\ I\right)\right)\text{kronecker}\left(I_y,\ \text{kronecker}\left(I_y,\ I\right)\right)\right. \\ & \left. + \text{kronecker}\left(I_z,\ \text{kronecker}\left(I_z,\ I\right)\right)\right) \ldots \\ & + \begin{bmatrix} Jab\left(\text{kronecker}\left(I_x,\ \text{kronecker}\left(I,\ I_x\right)\right) + \text{kronecker}\left(I_y,\ \text{kronecker}\left(I,\ I_y\right)\right)\right. \\ \left. + \text{kronecker}\left(I_z,\ \text{kronecker}\left(I,\ I_z\right)\right)\right) \ldots \\ +Jbc\left(\text{kronecker}\left(I,\ \text{kronecker}\left(I_x,\ I_x\right)\right) + \text{kronecker}\left(I,\ \text{kronecker}\left(I_y,\ I_y\right)\right)\right. \\ \left. + \text{kronecker}\left(I,\ \text{kronecker}\left(I_z,\ I_z\right)\right)\right) \end{bmatrix} \end{aligned}$$

The total Hamiltonian spin operator is now calculated and displayed.

$$H = H_{mag} + H_{spin}$$

The indexing of the matrix elements of the Hamiltonial spin operator is discussed in the Appendix.

i = 1 .. 8

Illegal pream-token (\)

Calculate and display the energy eigenvalues and associated eigenvectors of the Hamiltonian.

$$E = \text{sort}(\text{eigenvals}(\text{H})) \quad C^{<i>} = \text{eigenvec}\left(H,\ E_i\right)$$

Illegal pream-token (\)

Notice that the ground state |ααα> and the highest excited state |βββ> are pure states. The other six states are strictly speaking superpositions.

The nmr selection rule is that only one nuclear spin can flip during a transition. Therefore, the transition probability matrix for the ABC spin system is:

Illegal pream-token (\)

Calculate the intensities and frequencies of the allowed transitions.

$$i = 1..8 \quad j = 1..8 \quad I_{i,\,j} = \left[C^{\langle i \rangle}\,(TC^{\langle j \rangle})\right]^2 \quad V_{i,\,j} = \ \text{if}(I_{i,\,j}..001,\ \ |E_i - E_j|\,,\ 0)$$

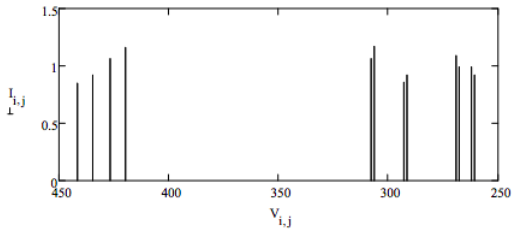
Intensity matrix:

$$i = \begin{pmatrix} 0 & 0.92 & 0.92 & 1.16 & 0 & 0 & 0 & 0 \\ 0.92 & 0 & 0 & 0 & 0.86 & 1.07 & 0 & 0 \\ 0.92 & 0 & 0 & 0 & 1 & 0 & 0.92 & 0 \\ 1.16 & 0 & 0 & 0 & 0 & 0.99 & 1.17 & 0 \\ 0 & 0.86 & 1 & 0 & 0 & 0 & 0 & 0.85 \\ 0 & 1.07 & 0 & 0.99 & 0 & 0 & 0 & 1.06 \\ 0 & 0 & 0.92 & 1.17 & 0 & 0 & 0 & 1.09 \\ 0 & 0 & 0 & 0 & 0.85 & 1.06 & 1.09 & 0 \end{pmatrix}$$

Frequency matrix:

$$\mathrm{V} = \begin{pmatrix} 0 & 260.66 & 291.32 & 419.52 & 0 & 0 & 0 & 0 \\ 260.66 & 0 & 0 & 0 & 292.85 & 426.49 & 0 & 0 \\ 291.32 & 0 & 0 & 0 & 262.19 & 0 & 434.52 & 0 \\ 419.52 & 0 & 0 & 0 & 0 & 267.63 & 306.32 & 0 \\ 0 & 292.85 & 262.19 & 0 & 0 & 0 & 0 & 441.49 \\ 0 & 426.49 & 0 & 267.63 & 0 & 0 & 0 & 269.16 \\ 0 & 0 & 434.52 & 306.32 & 0 & 0 & 0 & 269.16 \\ 0 & 0 & 0 & 0 & 441.49 & 307.85 & 269.16 & 0 \end{pmatrix}$$

Display the calculated vinyl acetate nmr spectrum:



The calculated spectrum compares favorably with experimental spectrum, indicating that the spin Hamiltonian used adequately represents the magnetic interaction of the vinyl protons in vinyl acetate. By comparison, acrylonitrile, a pure ABC system, has a very complicated 60 MHz spectrum. See the link provide above for a quantum mechanical explanation for the greater complexity of the acrylonitrile spectrum.

Appendix

The tensor product of three spinors is shown below.

$$\begin{pmatrix} a \\ b \end{pmatrix} \otimes \begin{pmatrix} c \\ d \end{pmatrix} \otimes \begin{pmatrix} e \\ f \end{pmatrix} = \begin{pmatrix} a \\ b \end{pmatrix} \otimes \begin{pmatrix} ce \\ cf \\ de \\ df \end{pmatrix} = \begin{pmatrix} ace \\ acf \\ ade \\ adf \\ bce \\ bcf \\ bde \\ bdf \end{pmatrix}$$

Mathcad does not have a command for this type of vector tensor product, so it is necessary to develop a way of implementing it using kronecker, which requires square matrices. For this reason the spin vector is stored in the left column of a 2x2 matrix by augmenting the spin vector with the null vector. After all the matrix tensor products have been carried out using kronecker the final spin vector resides in the left column of the final square matrix. Next the submatrix cammand is used to save this column, discarding the rest of the matrix.

$$\text{Spin-up in the z-direction:} \quad \alpha = \begin{pmatrix} 1 \\ 0 \end{pmatrix} \quad \text{Spin-down in the z-direction:} \quad \beta = \begin{pmatrix} 0 \\ 1 \end{pmatrix} \quad \text{Null vector:} \quad N = \begin{pmatrix} 0 \\ 0 \end{pmatrix}$$

The eight possible spin states of a three-proton system are calculated as shown below.

$$\Psi(\text{a, b, c}) = \text{submatrix}(\text{kronecker}(\text{augment}(\text{a, N}),\ \text{kronecker}(\text{augment}(\text{b, N}),\ \text{augment}(\text{c, N}))),\ 1,\ 8,\ 1,\ 1)$$

$$\Psi(\alpha,\alpha,\alpha)^T = (1\ 0\ 0\ 0\ 0\ 0\ 0\ 0) \quad \Psi(\alpha,\alpha,\beta)^T = (0\ 1\ 0\ 0\ 0\ 0\ 0\ 0)$$
$$\Psi(\alpha,\beta,\alpha)^T = (0\ 0\ 1\ 0\ 0\ 0\ 0\ 0) \quad \Psi(\alpha,\beta,\beta)^T = (0\ 0\ 0\ 1\ 0\ 0\ 0\ 0)$$
$$\Psi(\beta,\alpha,\alpha)^T = (0\ 0\ 0\ 0\ 1\ 0\ 0\ 0) \quad \Psi(\beta,\alpha,\beta)^T = (0\ 0\ 0\ 0\ 1\ 0\ 0\ 0)$$
$$\Psi(\beta,\beta,\alpha)^T = (0\ 0\ 0\ 0\ 0\ 0\ 1\ 0) \quad \Psi(\beta,\beta,\beta)^T = (0\ 0\ 0\ 0\ 0\ 0\ 0\ 1)$$

Thus the indexing in Hamiltonian matrix is: |ααα>, |ααβ>, |αβα>, |αββ>, |βαα>, |βαβ>, |ββα>, |βββ>.

This page titled 4.23: ABC Proton NMR Using Tensor Algebra is shared under a CC BY 4.0 license and was authored, remixed, and/or curated by Frank Rioux via source content that was edited to the style and standards of the LibreTexts platform.

4.24: AB2 Proton NMR Using Tensor Algebra

The purpose of this tutorial is to deviate from the usual matrix mechanics approach to the ABC proton nmr system in order to illustrate a related method of analysis which uses tensor algebra. For a discussion of the traditional approach visit http://www.users.csbsju.edu/~frioux/nmr/Speclab4.htm. This site also provides general information on the quantum mechanics of nmr spectroscopy.

Nuclear spin operators and identity:

$$I_x = \frac{1}{2}\begin{pmatrix} 0 & 1 \\ 1 & 0 \end{pmatrix} \quad I_y = \frac{1}{2}\begin{pmatrix} 0 & -i \\ i & 0 \end{pmatrix} \quad I_z = \frac{1}{2}\begin{pmatrix} 1 & 0 \\ 0 & -1 \end{pmatrix} \quad I = \begin{pmatrix} 1 & 0 \\ 0 & 1 \end{pmatrix}$$

The following experimentally determined chemical shifts and coupling constant (all in Hz) are for the AB_2 proton system 1,1,2-trichloroethane at 60 MHz.

$$\text{Chemical shifts:} \quad \nu_A = 345.6 \quad \nu_B = 237.6 \quad Jab = 6.1$$

Hamiltonian representing the interaction of nuclear spins with the external magnetic field in tensor format:

$$\widehat{H}_{mag} = -\nu_A \hat{I}_z^A - \nu_B \hat{I}_z^B - \nu_C \hat{I}_z^C = \nu_A \hat{I}_z^A \otimes \hat{I} \otimes \hat{I} + \hat{I} \otimes \left(-\nu_B \hat{I}_z^B\right) \otimes \hat{I} + \hat{I} \otimes \hat{I} \otimes \left(-\nu_B \hat{I}_z^B\right)$$

where, for example,

$$\nu_A = g_n \beta_n B_z (1 - \sigma_A)$$

Implementing the operator using Mathcad's command for the tensor product, kronecker, is as follows.

$$H_{mag} = -\nu_A \text{kronecker}\left(I_z,\ \text{kronecker}(\text{I},\ \text{I})\right) - \nu_B \text{kronecker}\left(I,\ \text{kronecker}\left(I_z,\ I\right)\right) - \nu_B \text{kronecker}\left(I,\ \text{kronecker}\left(I,\ I_z\right)\right)$$

Hamiltonian representing the interaction of nuclear spins with each other in tensor format:

$$\widehat{H}_{spin} = J_{AB}\left(\hat{I}_x^A \otimes \hat{I}_x^B \otimes \hat{I} + \hat{I}_y^A \otimes \hat{I}_y^B \otimes \hat{I} + \hat{I}_z^A \otimes \hat{I}_z^B \otimes \hat{I}\right) + J_{AB}\left(\hat{I}_x^A \otimes \hat{I} \otimes \hat{I}_x^B + \hat{I}_y^A \otimes \hat{I} \otimes \hat{I}_y^B + \hat{I}_z^A \otimes \hat{I} \otimes \hat{I}_z^B\right)$$

Implementation of the operator in the Mathcad programming environment:

$$H_{spin} = \begin{matrix} Jab\left(\text{kronecker}\left(I_x,\ \text{kronecker}\left(I_x,\ I\right)\right)\text{kronecker}\left(I_y,\ \text{kronecker}\left(I_y,\ I\right)\right)\right. \\ \left. + \text{kronecker}\left(I_z,\ \text{kronecker}\left(I_z,\ I\right)\right)\right) \ldots \\ + \left[Jab\left(\text{kronecker}\left(I_x,\ \text{kronecker}\left(I,\ I_x\right)\right) + \text{kronecker}\left(I_y,\ \text{kronecker}\left(I,\ I_y\right)\right)\right. \\ \left. + \text{kronecker}\left(I_z,\ \text{kronecker}\left(I,\ I_z\right)\right)\right)\Bigg] \end{matrix}$$

The total Hamiltonian spin operator is now calculated and displayed.

$$H = H_{mag} + H_{spin}$$

The indexing of the matrix elements of the Hamiltonial spin operator is discussed in the Appendix.

i = 1 .. 8

$$H = \begin{pmatrix} -407.35 & 0 & 0 & 0 & 0 & 0 & 0 & 0 \\ 0 & -172.8 & 0 & 0 & 3.05 & 0 & 0 & 0 \\ 0 & 0 & -172.8 & 0 & 3.05 & 0 & 0 & 0 \\ 0 & 3.05 & 3.05 & 0 & -67.85 & 0 & 0 & 0 \\ 0 & 0 & 0 & 3.05 & 0 & 172.8 & 0 & 0 \\ 0 & 0 & 0 & 3.5 & 0 & 234.13 & 0.75 & 0 \\ 0 & 0 & 0 & 3.05 & 0 & 0 & 172.8 & 0 \\ 0 & 0 & 0 & 0 & 0 & 0 & 0 & 413.45 \end{pmatrix}$$

Calculate and display the energy eigenvalues and associated eigenvectors of the Hamiltonian.

$$E = \text{sort}(\text{eigenvals}(\text{H})) \quad C^{<i>} = \text{eigenvec}\left(H,\ E_i\right)$$

Illegal pream-token (\)

Notice that the ground state |ααα> and the highest excited state |βββ> are pure states. The other six states are strictly speaking superpositions.

The nmr selection rule is that only one nuclear spin can flip during a transition. Therefore, the transition probability matrix for the ABC spin system is:

Illegal pream-token (\)

Calculate the intensities and frequencies of the allowed transitions.

$$i = 1..8 \quad j = 1..8 \quad I_{i,j} = \left[C^{\langle i \rangle} \left(TC^{\langle j \rangle}\right)\right]^2 \quad V_{i,j} = \text{if}(I_{i,j}..001,\ |E_i - E_j|,\ 0)$$

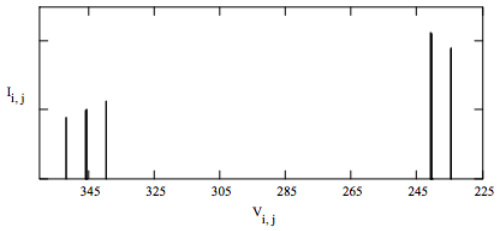
Intensity matrix:

$$i = \begin{pmatrix} 0 & 1.88 & 0 & 1.12 & 0 & 0 & 0 & 0 \\ 1.88 & 0 & 0 & 0 & 1.89 & 0 & 0.99 & 0 \\ 0 & 0 & 0 & 0 & 0 & 1 & 0 & 0 \\ 1.12 & 0 & 0 & 0 & 0 & 0 & 2.12 & 0 \\ 0 & 1.89 & 0 & 0 & 0 & 0 & 0 & 0.89 \\ 0 & 0 & 1 & 0 & 0 & 0 & 0 & 0 \\ 0 & 0.99 & 0 & 2.12 & 0 & 0 & 0 & 2.11 \\ 0 & 0 & 0 & 0 & 0.89 & 0 & 2.11 & 0 \end{pmatrix}$$

Frequency matrix:

$$\mathrm{V} = \begin{pmatrix} 0 & 234.37 & 234.55 & 339.68 & 468.93 & 580.15 & 580.32 & 820.8 \\ 234.37 & 0 & 0.18 & 105.3 & 234.56 & 345.78 & 345.94 & 586.43 \\ 234.55 & 0.18 & 0 & 105.13 & 234.38 & 345.6 & 345.77 & 586.25 \\ 339.68 & 105.3 & 105.13 & 0 & 129.26 & 240.47 & 240.64 & 481.12 \\ 468.93 & 234.56 & 234.38 & 129.26 & 0 & 111.22 & 111.38 & 351.87 \\ 580.15 & 345.78 & 345.6 & 240.47 & 111.22 & 0 & 0.17 & 240.65 \\ 580.32 & 345.94 & 345.77 & 240.64 & 111.38 & 0.17 & 0 & 240.48 \\ 820.8 & 586.43 & 586.25 & 481.12 & 351.87 & 240.65 & 240.48 & 0 \end{pmatrix}$$

Display the calculated vinyl acetate nmr spectrum:



The calculated spectrum compares favorably with experimental spectrum, indicating that the spin Hamiltonian used adequately represents the magnetic interaction of the protons in 1,1,2-trichloroethane at 60 MHz.

Appendix

The tensor product of three spinors is shown below.

$$\begin{pmatrix} a \\ b \end{pmatrix} \otimes \begin{pmatrix} c \\ d \end{pmatrix} \otimes \begin{pmatrix} e \\ f \end{pmatrix} = \begin{pmatrix} a \\ b \end{pmatrix} \otimes \begin{pmatrix} ce \\ cf \\ de \\ df \end{pmatrix} = \begin{pmatrix} ace \\ acf \\ ade \\ adf \\ bce \\ bcf \\ bde \\ bdf \end{pmatrix}$$

Mathcad does not have a command for this type of vector tensor product, so it is necessary to develop a way of implementing it using kronecker, which requires square matrices. For this reason the spin vector is stored in the left column of a 2x2 matrix by augmenting the spin vector with the null vector. After all the matrix tensor products have been carried out using kronecker the final spin vector resides in the left column of the final square matrix. Next the submatrix cammand is used to save this column, discarding the rest of the matrix.

Spin-up in the z-direction: $\alpha = \begin{pmatrix} 1 \\ 0 \end{pmatrix}$ Spin-down in the z-direction: $\beta = \begin{pmatrix} 0 \\ 1 \end{pmatrix}$ Null vector: $N = \begin{pmatrix} 0 \\ 0 \end{pmatrix}$

The eight possible spin states of a three-proton system are calculated as shown below.

$$\Psi(a, b, c) = \text{submatrix}(\text{kronecker}(\text{augment}(a, N), \text{kronecker}(\text{augment}(b, N), \text{augment}(c, N))), 1, 8, 1, 1)$$

$$\Psi(\alpha,\alpha,\alpha)^T = (1\ 0\ 0\ 0\ 0\ 0\ 0\ 0) \quad \Psi(\alpha,\alpha,\beta)^T = (0\ 1\ 0\ 0\ 0\ 0\ 0\ 0)$$
$$\Psi(\alpha,\beta,\alpha)^T = (0\ 0\ 1\ 0\ 0\ 0\ 0\ 0) \quad \Psi(\alpha,\beta,\beta)^T = (0\ 0\ 0\ 1\ 0\ 0\ 0\ 0)$$
$$\Psi(\beta,\alpha,\alpha)^T = (0\ 0\ 0\ 0\ 1\ 0\ 0\ 0) \quad \Psi(\beta,\alpha,\beta)^T = (0\ 0\ 0\ 0\ 1\ 0\ 0\ 0)$$
$$\Psi(\beta,\beta,\alpha)^T = (0\ 0\ 0\ 0\ 0\ 0\ 1\ 0) \quad \Psi(\beta,\beta,\beta)^T = (0\ 0\ 0\ 0\ 0\ 0\ 0\ 1)$$

Thus the indexing in Hamiltonian matrix is: |ααα>, |ααβ>, |αβα>, |αββ>, |βαα>, |βαβ>, |ββα>, |βββ>.

This page titled 4.24: AB2 Proton NMR Using Tensor Algebra is shared under a CC BY 4.0 license and was authored, remixed, and/or curated by Frank Rioux via source content that was edited to the style and standards of the LibreTexts platform.

4.25: AB3 Proton NMR Using Tensor Algebra

The purpose of this tutorial is to calculate the NMR spectrum of a four proton AB_3 system.

Nuclear spin operators and identity: $I_x = \frac{1}{2}\begin{pmatrix}0 & 1\\ 1 & 0\end{pmatrix}$ $I_y = \frac{1}{2}\begin{pmatrix}0 & -i\\ i & 0\end{pmatrix}$ $I_z = \frac{1}{2}\begin{pmatrix}1 & 0\\ 0 & -1\end{pmatrix}$ $I = \begin{pmatrix}1 & 0\\ 0 & 1\end{pmatrix}$

The following experimentally determined chemical shifts and coupling constant (all in Hz) are for the AB3 proton system 1,1-dichloroethane at 60 MHz.

$$]nu_A = 350.0 \quad \nu_B = 120.0 \quad Jab = 10.00$$

Hamiltonian representing the interaction of nuclear spins with the external magnetic field in tensor format:

$$\begin{aligned} H_{mag} \quad &= -\nu_A \text{kronecker}\left(I_z,\ \text{kronecker}(\text{I},\ \text{kronecker}(\text{I},\ \text{I}))\right) \\ &\quad - \nu_B \text{kronecker}\left(\text{I},\ \text{kronecker}\left(I_z,\ \text{kronecker}(\text{I},\ \text{I})\right)\right) \ldots \\ &\quad + - \nu_B \text{kronecker}\left(\text{I},\ \text{kronecker}\left(\text{I},\ \text{kronecker}\left(I_z,\ I\right)\right)\right) \\ &\quad - \nu_B \text{kronecker}\left(\text{I},\ \text{kronecker}\left(\text{I},\ \text{kronecker}\left(I,\ I_z\right)\right)\right) \end{aligned}$$

Hamiltonian representing the nuclear spin-spin interaction in tensor format:

$$\begin{aligned} H_{spin} &= Jab \\ &\left(\text{kronecker}\left(I_x,\ \text{kronecker}\left(I_x,\ \text{kronecker}(\text{I},\ \text{I})\right)\right) + \text{kronecker}\left(I_y,\ \text{kronecker}\left(I_y,\ \text{kronecker}(\text{I},\ \text{I})\right)\right) \ldots\right) \\ &\ldots \\ &+ Jab \begin{pmatrix} \text{kronecker}\left(I_x,\ \text{kronecker}\left(I,\ \text{kronecker}(I_x,\ I)\right)\right) \\ + \text{kronecker}\left(I_y,\ \text{kronecker}\left(I,\ \text{kronecker}\left(I_y,\ I\right)\right)\right) \ldots \end{pmatrix} \ldots \\ &+ Jab \begin{pmatrix} \text{kronecker}\left(I_x,\ \text{kronecker}\left(I,\ \text{kronecker}(I,\ I_x)\right)\right) \\ + \text{kronecker}\left(I_y,\ \text{kronecker}\left(I,\ \text{kronecker}\left(I,\ I_y\right)\right)\right) \ldots \end{pmatrix} \end{aligned}$$

Total Hamiltonian operator: $H = H_{mag} + H_{spin}$ $i = 1..16$ $E = \text{sort}(\text{eigenvals}(\text{H}))$ $C^{<i>} = \text{eigenvec}\left(H,\ E_i\right)$

The first half of the results matrix:

$$\text{augment}\left(E,\ C^{T}\right)^{T}$$

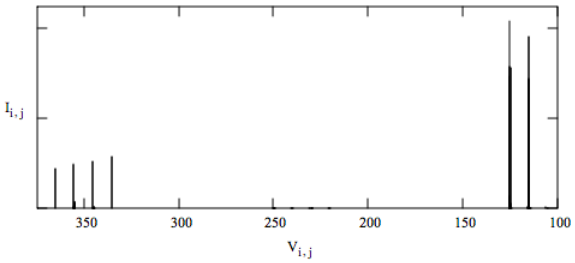
$$=\begin{array}{|c|c|c|c|c|c|c|c|c|}\hline -347.5 & 232.84 & -232.5 & -232.5 & -117.93 & -117.61 & -117.61 & -12.16 & -2.81 \\ \hline 1 & 0 & 0 & 0 & 0 & 0 & 0 & 0 & 0 \\ \hline 0 & 0.58 & -0.76 & -0.76 & 0 & 0 & 0 & 0.02 & 0 \\ \hline 0 & 0.58 & 0.11 & 0.11 & 0 & 0 & 0 & 0.02 & 0 \\ \hline 0 & 0 & 0 & 0 & 0.58 & -0.18 & -0.18 & 0 & 0 \\ \hline 0 & 0.58 & 0.64 & 0.64 & 0 & 0 & 0 & 0.02 & 0 \\ \hline 0 & 0 & 0 & 0 & 0.58 & -0.6 & -0.6 & 0 & 0 \\ \hline 0 & 0 & 0 & 0 & 0.58 & 0.78 & 0.78 & 0 & 0 \\ \hline 0 & 0 & 0 & 0 & 0 & 0 & 0 & 0 & 1 \\ \hline 0 & -0.04 & 0 & 0 & 0 & 0 & 0 & 1 & 0 \\ \hline 0 & 0 & 0 & 0 & -0.03 & 0.02 & 0.02 & 0 & 0 \\ \hline 0 & 0 & 0 & 0 & -0.03 & -0.01 & -0.01 & 0 & 0 \\ \hline 0 & 0 & 0 & 0 & 0 & 0 & 0 & 0 & -0.02 \\ \hline 0 & 0 & 0 & 0 & -0.03 & -0 & -0 & 0 & 0 \\ \hline 0 & 0 & 0 & 0 & 0 & 0 & 0 & 0 & -0.02 \\ \hline 0 & 0 & 0 & 0 & 0 & 0 & 0 & 0 & -0.02 \\ \hline\end{array}$$

The nmr selection rule is that only one nuclear spin can flip during a transition. Therefore, the transition probability matrix for the four spin system is shown below. See the Appendix for detail on how this matrix is constructed.

$$T=\begin{pmatrix} 0 & 1 & 1 & 0 & 1 & 0 & 0 & 0 & 1 & 0 & 0 & 0 & 0 & 0 & 0 & 0 \\ 1 & 0 & 0 & 1 & 0 & 1 & 0 & 0 & 0 & 1 & 0 & 0 & 0 & 0 & 0 & 0 \\ 1 & 0 & 0 & 1 & 0 & 0 & 1 & 0 & 0 & 0 & 1 & 0 & 0 & 0 & 0 & 0 \\ 0 & 1 & 1 & 0 & 0 & 0 & 0 & 1 & 0 & 0 & 0 & 1 & 0 & 0 & 0 & 0 \\ 1 & 0 & 0 & 0 & 0 & 1 & 1 & 0 & 0 & 0 & 0 & 0 & 1 & 0 & 0 & 0 \\ 0 & 1 & 0 & 0 & 1 & 0 & 0 & 1 & 0 & 0 & 0 & 0 & 0 & 1 & 0 & 0 \\ 0 & 0 & 1 & 0 & 1 & 0 & 0 & 1 & 0 & 0 & 0 & 0 & 0 & 0 & 1 & 0 \\ 0 & 0 & 0 & 1 & 0 & 1 & 1 & 0 & 0 & 0 & 0 & 0 & 0 & 0 & 0 & 1 \\ 1 & 0 & 0 & 0 & 0 & 0 & 0 & 0 & 0 & 1 & 1 & 0 & 1 & 0 & 0 & 0 \\ 0 & 1 & 0 & 0 & 0 & 0 & 0 & 0 & 1 & 0 & 0 & 1 & 0 & 1 & 0 & 0 \\ 0 & 0 & 1 & 0 & 0 & 0 & 0 & 0 & 1 & 0 & 0 & 1 & 0 & 0 & 1 & 0 \\ 0 & 0 & 0 & 1 & 0 & 0 & 0 & 0 & 0 & 1 & 1 & 0 & 0 & 0 & 0 & 1 \\ 0 & 0 & 0 & 0 & 1 & 0 & 0 & 0 & 1 & 0 & 0 & 0 & 0 & 1 & 1 & 0 \\ 0 & 0 & 0 & 0 & 0 & 1 & 0 & 0 & 0 & 1 & 0 & 0 & 1 & 0 & 0 & 1 \\ 0 & 0 & 0 & 0 & 0 & 0 & 1 & 0 & 0 & 0 & 1 & 0 & 0 & 0 & 0 & 1 \\ 0 & 0 & 0 & 0 & 0 & 0 & 0 & 1 & 0 & 0 & 0 & 1 & 0 & 1 & 1 & 0 \end{pmatrix}$$

Calculate the intensities and frequencies of the allowed transitions, and display the spectrum.

$$i=1..16 \quad j=1..16 \quad I_{i,\,j}=\left[C^{\langle i\rangle}\left(TC^{\langle i\rangle}\right)\right] \quad V_{i,\,j}=\left|E_i-E_j\right|$$



Appendix

The construction of the transition probability matrix requires the proper indexing of the 16 spin states of the four proton system. In tensor format the states are represented in this manner.

$$\begin{pmatrix} a \\ b \end{pmatrix} \otimes \begin{pmatrix} c \\ d \end{pmatrix} \otimes \begin{pmatrix} e \\ f \end{pmatrix} \otimes \begin{pmatrix} g \\ h \end{pmatrix} = \begin{pmatrix} a \\ b \end{pmatrix} \otimes \begin{pmatrix} c \\ d \end{pmatrix} \otimes \begin{pmatrix} eg \\ eh \\ fg \\ fh \end{pmatrix} = \begin{pmatrix} aceg \\ aceh \\ acfg \\ acfh \\ adeg \\ adeh \\ adfg \\ adfh \\ bceg \\ bceh \\ bcfg \\ bcfh \\ bdeg \\ bedh \\ bdfg \\ bdfh \end{pmatrix}$$

Mathcad does not have a command for this type of vector tensor product, so it is necessary to develop a way of implementing it using kronecker, which requires square matrices. For this reason the spin vector is stored in the left column of a 2x2 matrix by augmenting the spin vector with the null vector. After all the matrix tensor products have been carried out using kronecker the final spin vector resides in the left column of the final square matrix. Next the submatrix cammand is used to save this column, discarding the rest of the matrix.

Spin-up in the z-direction: $\alpha = \begin{pmatrix} 1 \\ 0 \end{pmatrix}$ Spin-down in the z-direction: $\beta = \begin{pmatrix} 0 \\ 1 \end{pmatrix}$ Null vector: $N = \begin{pmatrix} 0 \\ 0 \end{pmatrix}$

The 16 possible spin states of a three-proton system are calculated as shown below.

$$\Psi(a, b, c, d) = \text{submatrix}(\text{kronecker}\ (\text{augment}(b, N), \text{kronecker}(\text{augment}(c, N), \text{augment}(d, N)))), 1, 16, 1, 1)$$

Representing the spin states in tensor format facillitates their proper indexing and the formation of the transition probability matrix.

$$\begin{pmatrix} \Psi(\alpha,\ \alpha,\ \alpha,\ \alpha)^T \\ \Psi(\alpha,\ \alpha,\ \alpha,\ \beta)^T \\ \Psi(\alpha,\ \alpha,\ \beta,\ \alpha)^T \\ \Psi(\alpha,\ \alpha,\ \beta,\ \beta)^T \\ \Psi(\alpha,\ \beta,\ \alpha,\ \alpha)^T \\ \Psi(\alpha,\ \beta,\ \alpha,\ \beta)^T \\ \Psi(\alpha,\ \beta,\ \beta,\ \alpha)^T \\ \Psi(\beta,\ \alpha,\ \alpha,\ \alpha)^T \\ \Psi(\beta,\ \alpha,\ \alpha,\ \beta)^T \\ \Psi(\beta,\ \alpha,\ \beta,\ \alpha)^T \\ \Psi(\beta,\ \alpha,\ \beta,\ \beta)^T \\ \Psi(\beta,\ \beta,\ \alpha,\ \alpha)^T \\ \Psi(\beta,\ \beta,\ \alpha,\ \beta)^T \\ \Psi(\beta,\ \beta,\ \beta,\ \alpha)^T \\ \Psi(\beta,\ \beta,\ \beta,\ \beta)^T \end{pmatrix} = \begin{bmatrix} (1 & 0 & 0 & 0 & 0 & 0 & 0 & 0 & 0 & 0 & 0 & 0 & 0 & 0 & 0 & 0) \\ (0 & 1 & 0 & 0 & 0 & 0 & 0 & 0 & 0 & 0 & 0 & 0 & 0 & 0 & 0 & 0) \\ (0 & 0 & 1 & 0 & 0 & 0 & 0 & 0 & 0 & 0 & 0 & 0 & 0 & 0 & 0 & 0) \\ (0 & 0 & 0 & 1 & 0 & 0 & 0 & 0 & 0 & 0 & 0 & 0 & 0 & 0 & 0 & 0) \\ (0 & 0 & 0 & 0 & 1 & 0 & 0 & 0 & 0 & 0 & 0 & 0 & 0 & 0 & 0 & 0) \\ (0 & 0 & 0 & 0 & 0 & 1 & 0 & 0 & 0 & 0 & 0 & 0 & 0 & 0 & 0 & 0) \\ (0 & 0 & 0 & 0 & 0 & 0 & 1 & 0 & 0 & 0 & 0 & 0 & 0 & 0 & 0 & 0) \\ (0 & 0 & 0 & 0 & 0 & 0 & 0 & 1 & 0 & 0 & 0 & 0 & 0 & 0 & 0 & 0) \\ (0 & 0 & 0 & 0 & 0 & 0 & 0 & 0 & 1 & 0 & 0 & 0 & 0 & 0 & 0 & 0) \\ (0 & 0 & 0 & 0 & 0 & 0 & 0 & 0 & 0 & 1 & 0 & 0 & 0 & 0 & 0 & 0) \\ (0 & 0 & 0 & 0 & 0 & 0 & 0 & 0 & 0 & 0 & 1 & 0 & 0 & 0 & 0 & 0) \\ (0 & 0 & 0 & 0 & 0 & 0 & 0 & 0 & 0 & 0 & 0 & 1 & 0 & 0 & 0 & 0) \\ (0 & 0 & 0 & 0 & 0 & 0 & 0 & 0 & 0 & 0 & 0 & 0 & 1 & 0 & 0 & 0) \\ (0 & 0 & 0 & 0 & 0 & 0 & 0 & 0 & 0 & 0 & 0 & 0 & 0 & 1 & 0 & 0) \\ (0 & 0 & 0 & 0 & 0 & 0 & 0 & 0 & 0 & 0 & 0 & 0 & 0 & 0 & 1 & 0) \\ (0 & 0 & 0 & 0 & 0 & 0 & 0 & 0 & 0 & 0 & 0 & 0 & 0 & 0 & 0 & 1) \end{bmatrix}$$

$$\begin{pmatrix} ' & \begin{matrix}\alpha\alpha\\\alpha\alpha\end{matrix} & \begin{matrix}\alpha\alpha\\\alpha\beta\end{matrix} & \begin{matrix}\alpha\alpha\\\beta\alpha\end{matrix} & \begin{matrix}\alpha\alpha\\\beta\beta\end{matrix} & \begin{matrix}\alpha\beta\\\alpha\alpha\end{matrix} & \begin{matrix}\alpha\beta\\\alpha\beta\end{matrix} & \begin{matrix}\alpha\beta\\\beta\alpha\end{matrix} & \begin{matrix}\alpha\beta\\\beta\beta\end{matrix} & \begin{matrix}\beta\alpha\\\alpha\alpha\end{matrix} & \begin{matrix}\beta\alpha\\\alpha\beta\end{matrix} & \begin{matrix}\beta\alpha\\\beta\alpha\end{matrix} & \begin{matrix}\beta\alpha\\\beta\beta\end{matrix} & \begin{matrix}\beta\beta\\\alpha\alpha\end{matrix} & \begin{matrix}\beta\beta\\\alpha\beta\end{matrix} & \begin{matrix}\beta\beta\\\beta\alpha\end{matrix} & \begin{matrix}\beta\beta\\\beta\beta\end{matrix} \\ \begin{matrix}\alpha\alpha\\\alpha\alpha\end{matrix} & 0 & 1 & 1 & 0 & 1 & 0 & 0 & 0 & 1 & 0 & 0 & 0 & 0 & 0 & 0 & 0 \\ \begin{matrix}\alpha\alpha\\\alpha\beta\end{matrix} & 1 & 0 & 0 & 1 & 0 & 1 & 0 & 0 & 0 & 1 & 0 & 0 & 0 & 0 & 0 & 0 \\ \begin{matrix}\alpha\alpha\\\beta\alpha\end{matrix} & 1 & 0 & 0 & 1 & 0 & 0 & 1 & 0 & 0 & 0 & 1 & 0 & 0 & 0 & 0 & 0 \\ \begin{matrix}\alpha\alpha\\\beta\beta\end{matrix} & 0 & 1 & 1 & 0 & 0 & 0 & 0 & 1 & 0 & 0 & 0 & 1 & 0 & 0 & 0 & 0 \\ \begin{matrix}\alpha\beta\\\alpha\beta\end{matrix} & 0 & 1 & 0 & 0 & 1 & 0 & 0 & 1 & 0 & 0 & 0 & 0 & 0 & 1 & 0 & 0 \\ \begin{matrix}\alpha\beta\\\beta\alpha\end{matrix} & 0 & 0 & 1 & 0 & 1 & 0 & 0 & 1 & 0 & 0 & 0 & 0 & 0 & 0 & 1 & 0 \\ \begin{matrix}\alpha\beta\\\beta\beta\end{matrix} & 0 & 0 & 0 & 1 & 0 & 1 & 1 & 0 & 0 & 0 & 0 & 0 & 0 & 0 & 0 & 1 \\ \begin{matrix}\beta\alpha\\\alpha\alpha\end{matrix} & 1 & 0 & 0 & 0 & 0 & 0 & 0 & 0 & 0 & 1 & 1 & 0 & 1 & 0 & 0 & 0 \\ \begin{matrix}\beta\alpha\\\alpha\beta\end{matrix} & 0 & 1 & 0 & 0 & 0 & 0 & 0 & 0 & 1 & 0 & 0 & 1 & 0 & 1 & 0 & 0 \\ \begin{matrix}\beta\alpha\\\beta\alpha\end{matrix} & 0 & 0 & 1 & 0 & 0 & 0 & 0 & 0 & 1 & 0 & 0 & 1 & 0 & 0 & 1 & 0 \\ \begin{matrix}\beta\alpha\\\beta\beta\end{matrix} & 0 & 0 & 0 & 1 & 0 & 0 & 0 & 0 & 0 & 1 & 1 & 0 & 0 & 0 & 0 & 1 \\ \begin{matrix}\beta\beta\\\alpha\alpha\end{matrix} & 0 & 0 & 0 & 0 & 1 & 0 & 0 & 0 & 1 & 0 & 0 & 0 & 0 & 1 & 1 & 0 \\ \begin{matrix}\beta\beta\\\alpha\beta\end{matrix} & 0 & 0 & 0 & 0 & 0 & 1 & 0 & 0 & 0 & 1 & 0 & 0 & 1 & 0 & 0 & 1 \\ \begin{matrix}\beta\beta\\\beta\alpha\end{matrix} & 0 & 0 & 0 & 0 & 0 & 0 & 1 & 0 & 0 & 0 & 1 & 0 & 0 & 0 & 0 & 1 \\ \begin{matrix}\beta\beta\\\beta\beta\end{matrix} & 0 & 0 & 0 & 0 & 0 & 0 & 0 & 1 & 0 & 0 & 0 & 1 & 0 & 1 & 1 & 0 \end{pmatrix}$$

This page titled 4.25: AB3 Proton NMR Using Tensor Algebra is shared under a CC BY 4.0 license and was authored, remixed, and/or curated by Frank Rioux via source content that was edited to the style and standards of the LibreTexts platform.

4.26: HD-Like NMR Spectrum Calculated Using Tensor Algebra

In section 7.12.3 of *Atoms and Molecules*, Karplus and Porter consider the nuclear magnetic resonance of HD. In this tutorial it is treated as analogous to the traditional AB system, except that HD consists of a spin 1/2 nucleus interacting with a spin 1 nucleus. Using arbitrary values for the chemical shifts and coupling constant, a tensor algebra calculation yields a model nmr spectrum. Related tutorials on the AB and ABC systems are also available in this tutorial section.

$$\text{Chemical shifts:}\quad \nu_H := 400 \quad \nu_D := 200 \quad \text{Coupling constant:}\quad J_{HD} := 30$$

Nuclear spin and identity operators for the proton (the proton is a spin 1/2 particle):

$$IH_x := \tfrac{1}{2}\begin{pmatrix}0 & 1\\ 1 & 0\end{pmatrix} \quad IH_y := \tfrac{1}{2}\begin{pmatrix}0 & -i\\ i & 0\end{pmatrix} \quad IH_z := \tfrac{1}{2}\begin{pmatrix}1 & 0\\ 0 & -1\end{pmatrix} \quad IH := \begin{pmatrix}1 & 0\\ 0 & 1\end{pmatrix}$$

Nuclear spin and identity operators for the deuteron (the deuteron is a spin 1 particle):

$$ID_x := \tfrac{1}{\sqrt{2}}\begin{pmatrix}0 & 1 & 0\\ 1 & 0 & 1\\ 0 & 1 & 0\end{pmatrix} \quad ID_y := \tfrac{1}{\sqrt{2}}\begin{pmatrix}0 & -i & 0\\ i & 0 & -i\\ 0 & i & 0\end{pmatrix} \quad ID_z := \begin{pmatrix}1 & 0 & 0\\ 0 & 0 & 0\\ 0 & 0 & -1\end{pmatrix} \quad ID := \begin{pmatrix}1 & 0 & 0\\ 0 & 1 & 0\\ 0 & 0 & 1\end{pmatrix}$$

Hamiltonian representing the interaction of nuclear spins with the external magnetic field in tensor format:

$$\hat{h}_{MagField} = -\nu_H \hat{I}_z^H - \nu_D \hat{I}_z^H = -\nu_H \hat{I}_z^H \otimes \hat{I}_D - \nu_D \hat{I}_H \otimes \hat{I}_z^D$$

Implementing the operator using Mathcad′s command for the tensor product, kronecker, is as follows.

$$H_{MagField} := -\nu_H \text{kronecker}\left(IH_z,\ ID\right) - \nu_D \text{kronecker}\left(IH,\ ID_z\right)$$

Hamiltonian representing the interaction of nuclear spins with each other in tensor format:

$$\hat{H}_{SpinSpin} = J_{HD}\left(\hat{I}_x^H \otimes \hat{I}_x^D + \hat{I}_y^H \otimes \hat{I}_y^D + \hat{I}_z^H \otimes \hat{I}_z^D\right)$$

Implementation of the operator in the Mathcad programming environment:

$$H_{SpinSpin} := J_{HD}\left(\text{kronecker}\left(IH_x,\ ID_x\right) + \text{kronecker}\left(IH_y,\ ID_y\right) + \text{kronecker}\left(IH_z,\ ID_z\right)\right)$$

The total Hamiltonian spin operator is now calculated and displayed.

$$H := H_{MagField} + H_{SpinSpin}$$

$$H = \begin{pmatrix}-385 & 0 & 0 & 0 & 0 & 0\\ 0 & -200 & 0 & 21.213 & 0 & 0\\ 0 & 0 & -15 & 0 & 21.213 & 0\\ 0 & 21.213 & 0 & -15 & 0 & 0\\ 0 & 0 & 21.213 & 0 & 200 & 0\\ 0 & 0 & 0 & 0 & 0 & 415\end{pmatrix}$$

Calculate and display the energy eigenvalues and associated eigenvectors of the Hamiltonian.

$$i := 1..6 \quad E := \text{sort}(\text{eigenvals}(\text{H})) \quad C^{<i>} := \text{eigenvec}\left(H,\ E_i\right)$$

$$\text{augment}\left(E,\ C^T\right)^T = \begin{pmatrix}-385 & -202.401 & -17.073 & -12.599 & 202.073 & 415\\ 1 & 0 & 0 & 0 & 0 & 0\\ 0 & 0.994 & 0 & 0.112 & 0 & 0\\ 0 & 0 & 0.995 & 0 & 0.097 & 0\\ 0 & -0.112 & 0 & 0.994 & 0 & 0\\ 0 & 0 & -0.097 & 0 & 0.995 & 0\\ 0 & 0 & 0 & 0 & 0 & 1\end{pmatrix}$$

The HD composite nuclear spin states expressed in tensor format are as follows:

$$|\tfrac{1}{2},\ 1\rangle = \begin{pmatrix}1\\0\end{pmatrix} \otimes \begin{pmatrix}1\\0\\0\end{pmatrix} = \begin{pmatrix}1\\0\\0\\0\\0\\0\end{pmatrix} \qquad |\tfrac{1}{2},\ 0\rangle = \begin{pmatrix}1\\0\end{pmatrix} \otimes \begin{pmatrix}0\\1\\0\end{pmatrix} = \begin{pmatrix}0\\1\\0\\0\\0\\0\end{pmatrix} \qquad |\tfrac{1}{2},\ -1\rangle = \begin{pmatrix}1\\0\end{pmatrix} \otimes \begin{pmatrix}0\\0\\1\end{pmatrix} = \begin{pmatrix}0\\0\\1\\0\\0\\0\end{pmatrix}$$

$$|-\tfrac{1}{2},\ 1\rangle = \begin{pmatrix}0\\1\end{pmatrix} \otimes \begin{pmatrix}1\\0\\0\end{pmatrix} = \begin{pmatrix}0\\0\\0\\1\\0\\0\end{pmatrix} \qquad |-\tfrac{1}{2},\ 0\rangle = \begin{pmatrix}0\\1\end{pmatrix} \otimes \begin{pmatrix}0\\1\\0\end{pmatrix} = \begin{pmatrix}0\\0\\0\\1\\0\\0\end{pmatrix} \qquad |-\tfrac{1}{2},\ -1\rangle = \begin{pmatrix}0\\1\end{pmatrix} \otimes \begin{pmatrix}0\\0\\1\end{pmatrix} = \begin{pmatrix}0\\0\\0\\0\\0\\1\end{pmatrix}$$

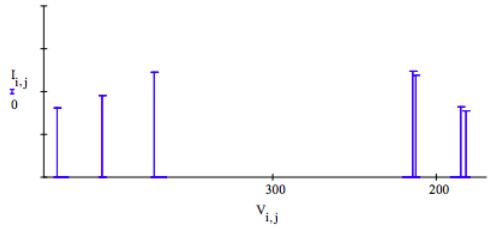
The nmr selection rule is that only one nuclear spin can flip during a transition and that ΔI = +/- 1. Therefore, the transition probability matrix given the above nuclear spin assignments for the HD system is:

$$T = \begin{pmatrix}0&1&0&1&0&0\\1&0&1&0&1&0\\0&1&0&0&0&1\\1&0&0&0&1&0\\0&1&0&1&0&1\\0&0&1&0&1&0\end{pmatrix}$$

Calculate the transition intensities and frequencies.

$$i = 1..6 \quad j = 1..6 \quad I_{i,\,j} = [C^{<i>T}\,(TC^{<j>})] \quad V_{i,\,j} = |E_i - E_j|$$

Display the calculated HD nmr spectrum:



As expected, we see that the single proton resonance on the left is split into three transitions due to the three deuteron spin orientations, and that the two deuteron resonances are each split into two transitions due to the two proton spin orientations.

The frequencies of all possible transitions are presented in the following matrix.

$$V = \begin{pmatrix}0&182.599&367.927&372.401&587.073&800\\182.599&0&185.328&189.803&404.474&617.401\\367.927&185.328&0&4.474&219.146&432.073\\372.401&189.803&4.474&0&214.672&427.599\\587.073&404.474&219.146&214.672&0&212.927\\800&617.401&432.073&427.599&212.927&0\end{pmatrix}$$

Some of these transitions are forbidden by the selection rule as can be seen in the following intensity matrix.

$$I = \begin{pmatrix} 0 & 0.776 & 0 & 1.224 & 0 & 0 \\ 0.776 & 0 & 0.816 & 0 & 0.948 & 0 \\ 0 & 0.816 & 0 & 1.903 \times 10^{-5} & 0 & 0.806 \\ 1.224 & 0 & 1.903 \times 10^{-5} & 0 & 1.236 & 0 \\ 0 & 0.948 & 0 & 1.236 & 0 & 1.194 \\ 0 & 0 & 0.806 & 0 & 1.194 & 0 \end{pmatrix}$$

On the basis of the frequency and intensity tables we make the following assignments for the various allowed transition for the proton and deuteron.

$$\left|\tfrac{1}{2},\ -1\right\rangle \qquad \left|\tfrac{1}{2},\ 0\right\rangle \xrightarrow{404.5} \left|\tfrac{-1}{2},\ 0\right\rangle \qquad \left|\tfrac{1}{2},\ 1\right\rangle \xrightarrow{372.4} \left|\tfrac{-1}{2},\ 1\right\rangle$$

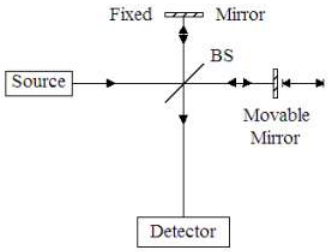
$$\xrightarrow{432.1} \left|\tfrac{-1}{2},\ -1\right\rangle$$

$$\left|\tfrac{-1}{2},\ 1\right\rangle \xrightarrow{214.7} \left|\tfrac{-1}{2},\ 0\right\rangle \quad \left|\tfrac{1}{2},\ 0\right\rangle \xrightarrow{212.9} \left|\tfrac{-1}{2},\ -1\right\rangle \quad \left|\tfrac{1}{2},\ 0\right\rangle \xrightarrow{185.3} \left|\tfrac{1}{2},\ -1\right\rangle \quad \left|\tfrac{1}{2},\ 1\right\rangle \xrightarrow{182.6} \left|\tfrac{-1}{2},\ 0\right\rangle$$

This page titled 4.26: HD-Like NMR Spectrum Calculated Using Tensor Algebra is shared under a CC BY 4.0 license and was authored, remixed, and/or curated by Frank Rioux via source content that was edited to the style and standards of the LibreTexts platform.

4.27: The Michelson Interferometer and Fourier Transform Spectroscopy

A Michelson interferometer with a movable mirror in one arm is an essential element in Fourier Transform (FT) spectroscopy.



A source illuminates a 50-50 beam splitter (BS). After the beam splitter the photons are in a linear superposition of being both transmitted and reflected. By convention a 90º phase shift is assigned to the reflected beam.

$$|S\rangle \rightarrow \frac{1}{\sqrt{2}}\left[|T\rangle + i|R\rangle\right]$$

Mirrors return the reflected and transmitted photons to the beam splitter where they evolve into the following superpositions.

$$|R\rangle \rightarrow \frac{1}{\sqrt{2}}\left[|D\rangle + i|S\rangle\right]$$

$$|T\rangle \rightarrow \frac{\exp\left(i\frac{2\pi\delta}{\lambda}\right)}{\sqrt{2}}\left[S\rangle + i|D\rangle\right]$$

The reflected beam is in a superposition of being transmitted to the detector and reflected back to the source, while the transmitted beam is in a superposition of being transmitted to the source and reflected to the detector. The exponential term in equation (3) is the phase shift acquired by the transmitted beam due to any path difference between the two arms created by the movable mirror.

The history of the source photons is obtained by substitution of equations (2) and (3) into equation (1).

$$|S\rangle \rightarrow \frac{1}{2}\left[\left(\exp\left(i\frac{2\pi\delta}{\lambda}\right)-1\right)|S\rangle + i\left(\exp\left(i\frac{2\pi\delta}{\lambda}\right)+1\right)|D\rangle\right]$$

The intensity of the radiation arriving at the detector (D) is the absolute magnitude squared of its coefficient in equation(4).

$$I_D(\delta) = \left|i\left(\exp\left(i\frac{2\pi\delta}{\lambda}\right)+1\right)\right|^2 = \frac{1}{2}\left[\cos\frac{2\pi\delta}{\lambda}+1\right]$$

Thus for a single-frequency source the intensity at the detector as a function of δ traces a cosine function.

In FT-IR spectroscopy the source is a "glower" that emits a broad range of infrared frequencies. In this case the signal at the detector is the sum of of intensities of the individual photons. This is called an interferogram and has the following mathematical form.

$$I(\delta) = \sum_j \left|i\left(\exp\left(i\frac{2\pi\delta}{\lambda_j}\right)+1\right)\right|^2 = \sum_j \frac{1}{2}\left[\cos\left(\frac{2\pi\delta}{\lambda_j}\right)+1\right]$$

The interferogram is obtained by measuring the intensity at the detector as a function of the path difference (δ) also called the retardation. In the next step the intensity of the frequencies present in the source beam are recovered by the following Fourier Transform.

$$B(\nu) = \int I(\delta)\exp(i2\pi\delta\nu)d\delta$$

To illustrate the FT method we will assume that the source beam only contains four wavelengths or frequencies.

Wavelength: $\lambda_1 = 20 \quad \lambda_2 = 10 \quad \lambda_3 = 5 \quad \lambda_4 = 2.5$

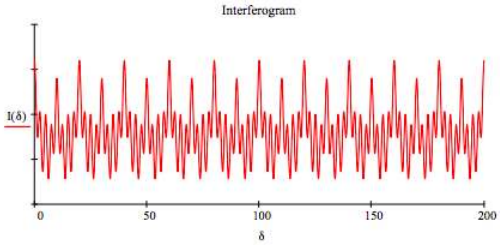
Intensities: $B_1 = 2 \quad B_2 = 5 \quad B_3 = 3 \quad B_4 = 6$ Frequencies: $\frac{1}{\lambda_1} = 0.05 \quad \frac{1}{\lambda_2} = 0.1 \quad \frac{1}{\lambda_3} = 0.2 \quad \frac{1}{\lambda_4} = 0.4$

Generate interferogram:

$$I(\delta) = \tfrac{1}{2}\left(\cos\left(2\pi\tfrac{\delta}{\lambda_1}\right)+1\right)B_1 + \tfrac{1}{2}\left(\cos\left(2\pi\tfrac{\delta}{\lambda_2}\right)+1\right)B_2 \ldots$$
$$+\tfrac{1}{2}\left(\cos\left(2\pi\tfrac{\delta}{\lambda_3}\right)+1\right)B_3 + \tfrac{1}{2}\left(\cos\left(2\pi\tfrac{\delta}{\lambda_4}\right)+1\right)B_4$$

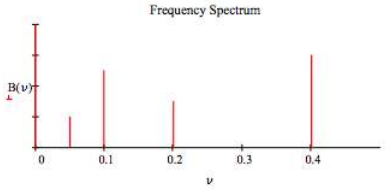
Display interferogram:

$$\delta = 0, .1 \ldots 200$$



Fourier transform interferogram to recover frequencies and intensities:

$$B(\nu) = \int_0^{200} I(\delta)\exp(i2\pi\delta\nu)d\delta \quad \nu = 0, 0.005 \ldots 5$$

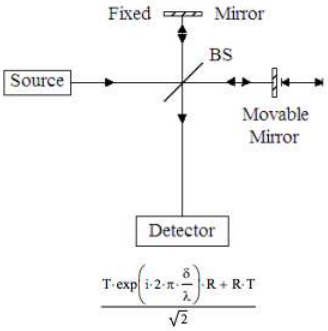


This calculation reveals how a Michelson interferometer is used to measure the wavelengths or frequencies present in the source beam. In a FT-IR instrument the source ideally contains all the IR frequencies. The sample is placed between the beam splitter and the detector and an absorption spectrum is measured.

This page titled 4.27: The Michelson Interferometer and Fourier Transform Spectroscopy is shared under a CC BY 4.0 license and was authored, remixed, and/or curated by Frank Rioux via source content that was edited to the style and standards of the LibreTexts platform.

4.28: A Sum Over Histories Approach to Fourier Transform Infrared Spectroscopy

A Michelson interferometer with a movable mirror in one arm is an essential element in a Fourier transform infrared (FTIR) spectrophotometer. Feynman's "sum over histories" approach to quantum mechanics will be used to analyze its operation. The analysis is similar to that used for the Mach-Zehnder interferometer in Chapter 6.



There are two photon paths (histories) to the detector from the source. The photon can be transmitted by the beam splitter into the arm with the movable mirror, returned to the beam splitter by the mirror, and then reflected at the beam splitter to the detector. And it can be reflected at the beam splitter into the arm with the fixed mirror, returned to the beam splitter, and then transmitted to the detector. The probability amplitudes for transmission and reflection at the beam splitter are given below, along with the phase shift that occurs due to any path difference in the arms of the interferometer.

Probability amplitude for photon transmission at a 50-50 beam splitter: $\langle T|S\rangle = \frac{1}{\sqrt{2}}$

Probability amplitude for photon reflection at a 50-50 beam splitter: $\langle R|S\rangle = \frac{i}{\sqrt{2}}$

Phase shift due to the path difference between the beam splitter arms: $\exp\left(i2\pi\frac{\delta}{\lambda}\right)$

The probability amplitude for photon detection is given below the figure. Using the information above yields the following expression.

$$\frac{1}{\sqrt{2}}\exp\left(i2\pi\frac{\delta}{\lambda}\right)\frac{i}{\sqrt{2}}+\frac{i}{\sqrt{2}}\frac{1}{\sqrt{2}}$$

The probability the photon will arrive at the detector is the magnitude squared of the probability amplitude.

$$\left(\left|\frac{1}{\sqrt{2}}\exp\left(i2\pi\frac{\delta}{\lambda}\right)\frac{i}{\sqrt{2}}+\frac{i}{\sqrt{2}}\frac{1}{\sqrt{2}}\right|\right)^2 \text{ simplify } \rightarrow \frac{1}{2}\cos\left(2\pi\frac{\delta}{\lambda}\right)+\frac{1}{2}$$

For a single wavelength source the intensity at the detector as a function of δ traces a cosine.

In FTIR spectroscopy the source is a "glower" that emits a broad range of infrared frequencies. In this case the signal at the detector is the sum of of intensities of the individual photons. This is called an interferogram and has the following mathematical form.

$$I(\delta)=\sum_j\left(\frac{1}{2}\cos\left(2\pi\frac{\delta}{\lambda_j}\right)+\frac{1}{2}\right)$$

The interferogram is obtained by measuring the intensity at the detector as a function of the path difference (δ) also called the retardation. In the next step the intensity of the frequencies present in the source beam are recovered by the following Fourier transform. The mirror moves at a constant speed, so δ is proportional to time. Therefore, this is a time-frequency Fourier transform.

$$B(\nu)=\int I(\delta)\exp(i2\pi\delta\nu)d\delta$$

To illustrate the FT method we will assume that the source beam only contains four wavelengths or frequencies.

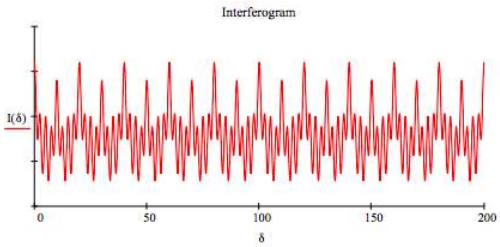
Wavelengths:	$\lambda_1=20$	$\lambda_2=10$	$\lambda_3=5$	$\lambda_4=2.5$
Intensities:	$B_1=3$	$B_2=5$	$B_3=4$	$B_4=6$
Frequencies:	$\frac{1}{\lambda_1}=0.05$	$\frac{1}{\lambda_2}=0.1$	$\frac{1}{\lambda_3}=0.2$	$\frac{1}{\lambda_4}=0.4$

Generate interferogram:

$$I(\delta) = \tfrac{1}{2}\left(\cos\left(2\pi\tfrac{\delta}{\lambda_1}\right)+1\right)B_1 + \tfrac{1}{2}\left(\cos\left(2\pi\tfrac{\delta}{\lambda_2}\right)+1\right)B_2 \ldots$$
$$+\tfrac{1}{2}\left(\cos\left(2\pi\tfrac{\delta}{\lambda_3}\right)+1\right)B_3 + \tfrac{1}{2}\left(\cos\left(2\pi\tfrac{\delta}{\lambda_4}\right)+1\right)B_4$$

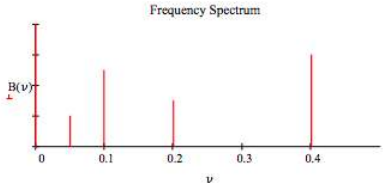
Display interferogram:

$$\delta = 0, .1..200$$



Fourier transform interferogram to recover frequencies and intensities:

$$B(\nu) = \int_0^{200} I(\delta)\exp(i2\pi\delta\nu)d\delta \quad \nu = 0, .005..5$$



This calculation reveals how a Michelson interferometer is used to measure the wavelengths or frequencies present in the source beam. In a FT-IR instrument the source ideally contains all the IR frequencies. The sample is placed between the beam splitter and the detector and an absorption spectrum is measured.

This page titled 4.28: A Sum Over Histories Approach to Fourier Transform Infrared Spectroscopy is shared under a CC BY 4.0 license and was authored, remixed, and/or curated by Frank Rioux via source content that was edited to the style and standards of the LibreTexts platform.

4.29: Modeling the Pi-electrons of Benzene as Particles on a Ring

From previous work we know that the momentum eigenfunction in coordinate space is given by

$$\langle x|p\rangle = \frac{1}{\sqrt{2\pi}}\exp\left(\frac{ipx}{\hbar}\right)$$

Quantum mechanical wave functions must be single-valued, which in this application (electron on a ring) requires a cyclical boundary condition: the wave function must match at points separated by one circumference, C = 2πR.

$$\langle x + C|p\rangle = \langle x|p\rangle$$
$$\exp\left(\tfrac{pi(x+C)}{\hbar}\right) = \exp\left(\tfrac{ipx}{\hbar}\right)$$
$$\exp(\text{-})\exp\left(\tfrac{pix}{\hbar}\right) = \exp\left(\tfrac{ipC}{\hbar}\right)$$
$$\exp\left(\tfrac{ipC}{\hbar}\right) = 1$$

This equation is satisfied if $\frac{pC}{\hbar} = 2\pi m$ where $m = 0, \pm1, \pm2...$ You can easily verify this with Mathcad. Thus the quantum number is required in order to satisfy the cyclic boundary condition. Next we calculate the kinetic energy and express it in terms of the circumference of the ring.

$$T_m = \frac{p^2}{2m_e} = \frac{m^2h^2}{2m_eC^2} \quad \text{where } m = 0, \pm1, \pm2...$$

Substitution of $\frac{2\pi m\hbar}{C}$ for *p* and recognizing that $\phi = \frac{2\pi x}{C}$ allow one to transform the first equation to,

$$\langle \phi|m\rangle = \frac{1}{\sqrt{2\pi}}\exp(im\backslash\text{hi})$$

1. Sketch an energy level diagram for a particle on a ring.
2. Use the aufbau principle and the Pauli exclusion principle to place the π-electrons of benzene in the allowed energy levels.
3. Calculate the wavelength of the lowest allowed electronic transition (HOMO ÷ LUMO). The average c - c bond length in benzene is 140 pm.

This page titled 4.29: Modeling the Pi-electrons of Benzene as Particles on a Ring is shared under a CC BY 4.0 license and was authored, remixed, and/or curated by Frank Rioux via source content that was edited to the style and standards of the LibreTexts platform.

4.30: Modeling the Pi-electrons of Benzene as Particles on a Ring - Version 2

Wave-particle duality for massive objects as expressed by the de Broglie equation (λ = h/mv = h/p) is a foundational concept of quantum theory. Classical potential energy carries over to quantum mechanics unchanged, but classical kinetic energy is, as shown below, transformed into a quantum mechanical confinement energy by the de Broglie relation. Confined objects with wave properties are subject to interference which restricts the allowed values of λ, which in turn leads to energy quantization.

$$T = \frac{p^2}{2m} \xrightarrow{p=\frac{h}{\lambda}} \frac{h^2}{2m\lambda^2}$$

A general one-dimensional function, $\Psi(x) = \frac{1}{\sqrt{2\pi}}\exp\left(i2\pi\frac{x}{\lambda}\right)$, is used to represent the wave character of a particle on a ring (POR) where in order to avoid self-interference the head and tail of the wave function must match after one revolution.

$$\Psi(x) = \Psi(x + C) \quad C = 2\pi R$$

This requirement restricts the allowed values of the wavelength and leads to a manifold of quantized energies as is now demonstrated. The structure of the manifold of allowed energies depends on the nature of the confinement, each problem gives a characteristic energy manifold. For the particle on a ring we find,

$$\frac{1}{\sqrt{2\pi}}\exp\left(i2\pi\frac{x}{\lambda}\right) = \frac{1}{\sqrt{2\pi}}\exp\left(i2\pi\frac{x+C}{\lambda}\right) = \frac{1}{\sqrt{2\pi}}\exp\left(i2\pi\frac{x}{\lambda}\right)\frac{1}{\sqrt{2\pi}}\exp\left(i2\pi\frac{C}{\lambda}\right)$$

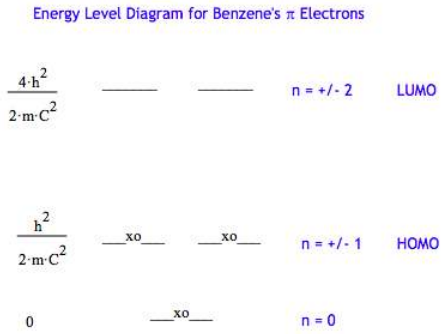
$$\text{It follows that} \quad \frac{1}{\sqrt{2\pi}}\exp\left(i2\pi\frac{C}{\lambda}\right) = 1 \quad \text{which requires} \quad \lambda = \frac{C}{n} \quad \text{where n} = 0,\ \pm 1,\ \pm 2...$$

Substitution of this restriction for λ into the quantum expression for kinetic energy yields an equation for the allowed energy states in terms of Planck's constant, the particle mass, the ring circumference and the quantum number, n.

$$T = \frac{h^2}{2m\lambda^2} \text{substitute, } \lambda = \frac{C}{n} \rightarrow T = \frac{h^2n^2}{2C^2m}$$

An obvious POR application is to treat the π-electrons of benzene as particles on a ring. The energy level diagram is constructed using the above energy expression and the allowed values for the quantum number, n. Then the energy level diagram is populated with six π-electrons using the aufbau principle and the Pauli exclusion principle.

The validity of the model is tested by calculating the wavelength of the photon required for the HOMO-LUMO transition. The average c-c bond length in benzene is 140 pm, so the ring circumference is approximated as 6x140 pm. As shown below the photon wavelength required for the HOMO-LUMO transition is 194 nm, a value that might be described as "in the ball park."



Energy conservation for the HOMO-LUMO transition requires:

$$\frac{n_i^2h^2}{2m_eC^2} + \frac{hc}{\lambda} = \frac{n_f^2h^2}{2m_eC^2}$$

Fundamental constants and conversion factors:

$$pm = 10^{-12}m \quad aJ = 10^{-18}J$$

$$h = 6.626 - 755(10^{-34}\text{joule sec} \quad c = 2.99792458(10^{8})\frac{m}{sec} \quad m_e = 9.1093897(10^{-31})kg$$

Calculate the photon wavelength for the HOMO-LUMO electronic transition.

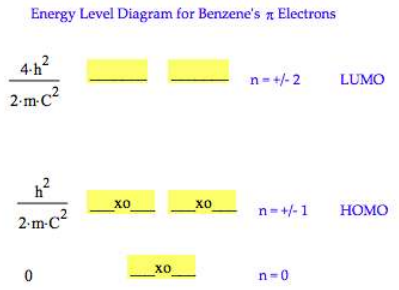
$$\text{HOMO:} \quad n_i = 1 \quad \text{LUMO:} \quad n_f = 2 \quad \text{Benzene circumference:} \quad C = 6(140)pm$$

$$\lambda = \frac{n_i^2 h^2}{2m_e C^2} + \frac{hc}{\lambda} = \frac{n_f^2 h^2}{2m_e C^2} \left| \begin{array}{l} \text{float, 3} \\ \text{solve, } \lambda \end{array} \right. \rightarrow \frac{1.94e{-}7\text{kg m}^3}{\text{joule sec}^2} \quad \lambda = 194nm$$

This page titled 4.30: Modeling the Pi-electrons of Benzene as Particles on a Ring - Version 2 is shared under a CC BY 4.0 license and was authored, remixed, and/or curated by Frank Rioux via source content that was edited to the style and standards of the LibreTexts platform.

4.31: Calculating the Pi-electron HOMO-LUMO Electronic Transition for Benzene

Calculate the wavelength of the photon required for the first allowed (HOMO-LUMO) electronic transition involving the π−electrons of benzene.



Energy conservation requirements:

$$\frac{n_i^2 h^2}{2m_e C^2} + \frac{hc}{\lambda} = \frac{n_f^2 h^2}{2m_e C^2}$$

Fundamental constants and conversion factors:

$$pm = 10^{-12}m \quad aJ = 10^{-18}J$$

$$h = 6.6260755(10^{-34})\text{joule sec} \quad c = 2.99792458(10^{8})\frac{m}{sec} \quad m_e = 9.1093897(10^{-31})kg$$

Calculate the photon wavelength for the HOMO-LUMO electronic transition.

$$\text{HOMO:} \quad n_i = 1 \quad \text{LUMO:} \quad n_f = 2 \quad \text{Benzene circumference:} \quad C = 6(140)pm$$

$$\lambda = \frac{n_i^2 h^2}{2m_e C^2} + \frac{hc}{\lambda} = \frac{n_f^2 h^2}{2m_e C^2} \;\Big|\; \begin{matrix}\text{float, 3}\\ \text{solve, } \lambda\end{matrix} \rightarrow .194e-6m^3\frac{kg}{joule\ sec^2} \quad \lambda = 194nm$$

Calculate the photon energy and frequency.

$$\text{energy} \quad \frac{c}{\lambda} = 1.024aJ \quad \text{frequency} \quad \frac{c}{\lambda} = 1.545 \times 10^{15}Hz$$

Plot Wave Functions

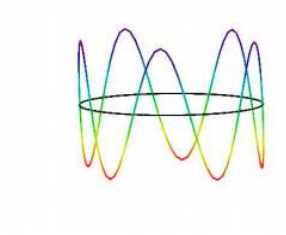
See Figure 7.6 (page 111) in *Quantum Chemistry and Spectroscopy*, by Engel.

The real part of the wave function is plotted below.

Quantum number: n = 5

$$\text{numpts} = 100 \quad i = 0..\text{numpts} \quad j = 0..\text{numpts} \quad \phi_i = \frac{2\pi i}{\text{numpts}}$$

$$x_{i,\,j} = \cos(\phi_i) \quad y_{i,\,j} = \sin(\phi_i) \quad z_{i,\,j} = \frac{1}{\sqrt{2\pi}}\exp(in\phi_i) \quad zz_{i,\,j} = 0$$



The square of the absolute magnitude for all the wave functions (for all values of the quantum number n) is 1/2π, as shown below.

$$\left(\left|\frac{1}{\sqrt{2\pi}}\exp(in\phi)\right|\right)^2 \quad \text{simplifies to} \quad \frac{1}{2\pi}$$

The wave functions for the electron on a ring are eigenstates of the momentum operator. In other words the momentum is precisely known: p = nh/C, where n is the quantum number and C is the ring circumference. According to the uncertainty principle, the elctron position must be uncertain. The result above confirms this; the electron density is distributed uniformly over the entire ring.

This page titled 4.31: Calculating the Pi-electron HOMO-LUMO Electronic Transition for Benzene is shared under a CC BY 4.0 license and was authored, remixed, and/or curated by Frank Rioux via source content that was edited to the style and standards of the LibreTexts platform.

4.32: Modeling the Pi-electrons of Benzene as Particles in a Ring

In this exercise benzene's six π electrons will be modeled as particles in a ring or circular corral. Schrödinger's equation in plane polar coordinates and its energy eigenvalues are given below. R is the ring radius and C the ring circumference.

$$\frac{-h^2}{8\pi^2 m_e}\left(\frac{d^2}{dr^2}\Psi(r)+\frac{1}{r}\frac{d}{dr}\Psi(r)-\frac{L^2}{r^2}\Psi(r)\right)=E\Psi(r) \quad E_{n,\,L}=\frac{(Z_{n,\,L})^2h^2}{8\pi^2 m_e R^2}=\frac{(Z_{n,\,L})^2n^2}{2m_eC^2}$$

J_L is the L^{th} order Bessel function, L is the angular momentum quantum number, n is the principle quantum number, $Z_{n,L}$ is the n^{th} root of J_L. Dirac notation is used to describe the electronic states, |n,L>. The roots of the Bessel function are given below in terms of the n and L quantum numbers.

Illegal pream-token (&)

The manifold of allowed energy levels up to the LUMO is shown below and is populated with 6 π electrons. Note that the states with L > 0 are doubly degenerate.

					$Z_{n,L}$	
LUMO	(1,2)	(1,−2)	___	___	5.316	
HOMO	(1,1)	(1,−1)	_xo_	_xo_	3.832	6
	(1,0)		_xo_		2.405	2

The photon wavelength required for the first electronic transition involving the π electrons is now calculated. The ring circumference is approximated as six benzene carbon-carbon bond lengths.

$$h = 6.6260755(10^{-34})\text{joule sec} \qquad c = 2.99792458(10^8)\frac{m}{sec} \quad m_e = 9.1093897(10^{-31})kg \quad pm = 10^{-12}m$$

$$C = 6(140)pm \qquad \frac{(Z_{1,\,1})^2h^2}{2m_eC^2}+\frac{hc}{\lambda}=\frac{(Z_{1,\,2})^2h^2}{2m_eC^2}\ \Big|\ \begin{matrix}\text{float, 3}\\ \text{solve, }\lambda\end{matrix}\rightarrow \frac{4.28e{-}8kg\ m^3}{joule\ sec^2}=42.8nm$$

Benzene has a strong electronic transition at about 200 nm.

This page titled 4.32: Modeling the Pi-electrons of Benzene as Particles in a Ring is shared under a CC BY 4.0 license and was authored, remixed, and/or curated by Frank Rioux via source content that was edited to the style and standards of the LibreTexts platform.

4.33: Modeling the Pi-electrons of Corannulene as Particles in a Ring

In this exercise the 20 π electrons of corannulene will be modeled as particles in a ring or circular corral. Corannulene is bowl-shaped not planar, so the model has some initial difficiencies.

Schrödinger's equation in plane polar coordinates and its energy eigenvalues are given below. R is the ring radius and C the ring circumference.

$$\frac{-h^2}{8\pi^2 m_e}\left(\frac{d^2}{dr^2}\Psi(r)+\frac{1}{r}\frac{d}{dr}\Psi(r)-\frac{L^2}{r^2}\Psi(r)\right)=E\Psi(r)\quad E_{n,\,L}=\frac{(Z_{n,\,L})^2h^2}{8\pi^2 m_e R^2}=\frac{(Z_{n,\,L})^2h^2}{2m_e C^2}$$

J_L is the L^{th} order Bessel function, L is the angular momentum quantum number, n is the principle quantum number, $Z_{n,L}$ is the n^{th} root of J_L. Dirac notation is used to describe the electronic states, |n,L>. The roots of the Bessel function are given below in terms of the n and L quantum numbers.

Illegal pream-token (&)

The manifold of allowed energy levels up to the LUMO is shown below and is populated with 20 π electrons. Note that the states with L > 0 are doubly degenerate.

					$Z_{n,L}$	
LUMO	(1,4)	(1,-4)	___	___	7.588	
HOMO	(2,1)	(2,-1)	_xo_	_xo_	7.016	20
	(1,3)	(1,-3)	_xo_	_xo_	6.380	16
	(2,0)		_xo_		5.520	12
	(1,2)	(1,-2)	_xo_	_xo_	5.316	10
	(1,1)	(1,-1)	_xo_	_xo_	3.832	6
	(1,0)		_xo_		2.405	2

Corannulene has a strong electronic transition at 280 nm. This information will be used to calculate its circumference.

$$h = 6.6260755(10^{-34})\text{joule sec}\qquad c=2.99792458(10^8)\frac{m}{sec}\quad m_e=9.1093897(10^{-31})kg\quad pm=10^{-12}m$$

$$\lambda=280nm\qquad \frac{(Z_{2,\,1})^2h^2}{2m_eC^2}+\frac{hc}{\lambda}=\frac{(Z_{1,\,4})^2h^2}{2m_eC^2}\;\Bigg|\;\begin{matrix}\text{float, 3}\\ \text{solve, C}\end{matrix}\rightarrow\begin{pmatrix}-\frac{0.0000533\sqrt{joule}\sqrt{nm}sec}{\sqrt{kg}\sqrt{m}}\\ \frac{0.0000533\sqrt{joule}\sqrt{nm}sec}{\sqrt{kg}\sqrt{m}}\end{pmatrix}=\begin{pmatrix}-1.685\times10^3\\ 1.685\times10^3\end{pmatrix}pm$$

The result is reasonable given that there are 15 c-c bonds on the circumference:

$$15(140)pm=2.1\times10^3pm$$

This page titled 4.33: Modeling the Pi-electrons of Corannulene as Particles in a Ring is shared under a CC BY 4.0 license and was authored, remixed, and/or curated by Frank Rioux via source content that was edited to the style and standards of the LibreTexts platform.

4.34: The Vibrational and Electronic States of C60

The first step in using Mathcad to do group theory is to enter the character table in matrix form for the symmetry under study. In this example we shall be looking at C_{60} and so the character table for the icosahedral point group has been entered in the matrix C_{Ih} below. The icosahedhral group has 120 symmetry operations which fall into ten classes. Ih is a vector containing the number of symmetry operations in each of the ten classes. Γ_{uma} (unmoved atoms) is a reducible representation showing the behavior of the atoms under the symmetry operations of the icosahedral group.[2] In particular it records the number of atoms that are unmoved by the symmetry operations of the group. Because C_{60} is a cage molecule with no central atom, only the identity operation and the symmetry planes leave atoms unmoved. Obviously the identity operation leaves all sixty carbon atoms unmoved and inspection of the molecule shows that the symmetry planes each contain four atoms which are unmoved by reflection in the plane.

Illegal pream-token (E)

$$Ih = \begin{pmatrix} 1 \\ 12 \\ 12 \\ 20 \\ 15 \\ 1 \\ 12 \\ 12 \\ 20 \\ 15 \end{pmatrix} \quad \Gamma_{uma} = \begin{pmatrix} 60 \\ 0 \\ 0 \\ 0 \\ 0 \\ 0 \\ 0 \\ 0 \\ 0 \\ 4 \end{pmatrix}$$

At this point it is necessary to identify the irreducible representations with a row in the matrix representing the character table for the icosahedral group. It should be noted that these irreducible representations could also have been entered individually as column or row vectors.

$$Ag = (CIh^T)^{<1>} \quad T1g = (CIh^T)^{<2>} \quad T2g = (CIh^T)^{<3>} \quad Gg = (CIh^T)^{<4>} \quad Hg = (CIh^T)^{<5>}$$
$$Ag = (CIh^T)^{<1>}$$
$$Au = (CIh^T)^{<6>} \quad T1u = (CIh^T)^{<7>} \quad T2u = (CIh^T)^{<8>} \quad Gu = (CIh^T)^{<9>} \quad Hu = (CIh^T)^{<10>}$$

The order of the group (the normalization constant) is the sum of the total number of symmetry operations.

$$h = \sum Ih \quad h = 120$$

The irreducible representations are a set of orthonormal basis vectors that span the Ih space. This is demonstrated below for several cases.

$$\frac{\sum \overrightarrow{(IhAgAg)}}{h} = 1 \quad \frac{\sum \overrightarrow{(IhT1gT1g)}}{h} = 1 \quad \frac{\sum \overrightarrow{(IhAgT1u)}}{h} = 0 \quad \frac{\sum \overrightarrow{(IhGuHu)}}{h} = 0$$

These vector operations are the symmetry equivalent of the quantum mechanical overlap integrals.

Vibrational Spectroscopy

One of the major goals of a symmetry analysis is to determine how the individual degrees of freedom of the molecule behave under the symmetry operations of the group. This is particularly important in interpreting or predicting the infrared or Raman spectrum of a molecule. The easiest way to find the behavior (reducible representation) of C60's 180 degrees of freedom under the symmetry operations of the Ih group is to take the direct product of Γ_{uma} with the T_{1u} irreducible representation for translation in the x, y, and z directions.[2]

$$\Gamma_{tot} = \overrightarrow{(\Gamma_{uma} T1u)} \quad \Gamma_{tot}^T = (180 \quad 0 \quad 0 \quad 0 \quad 0 \quad 0 \quad 0 \quad 0 \quad 0 \quad 4)$$

Now it is possible to find which irreducible representations contribute to Γ_{tot} by calculating the normalized vector sums shown below.[3] The irreducible representations are the unit vectors of Ih space and any other vector in that space can be written as a linear

combination of the unit vectors. Taking the product of each irreducible representation with the reducible representation, Γ_{tot}, yields the appropriate coefficient in the linear combination.

$$\frac{\sum\overrightarrow{(IhAg\Gamma_{tot})}}{h}-2 \quad \frac{\sum\overrightarrow{(IhT1g\Gamma_{tot})}}{h}-4 \quad \frac{\sum\overrightarrow{(IhAg\Gamma_{tot})}}{h}-4 \quad \frac{\sum\overrightarrow{(IhGu\Gamma_{tot})}}{h}-6 \quad \frac{\sum\overrightarrow{(IhHg\Gamma_{tot})}}{h}-8$$
$$\frac{\sum\overrightarrow{(IhAu\Gamma_{tot})}}{h}=1 \quad \frac{\sum\overrightarrow{(IhT1u\Gamma_{tot})}}{h}=5 \quad \frac{\sum\overrightarrow{(IhT2u\Gamma_{tot})}}{h}=5 \quad \frac{\sum\overrightarrow{(IhGu\Gamma_{tot})}}{h}=6 \quad \frac{\sum\overrightarrow{(IhHu\Gamma_{tot})}}{h}=7$$

This result can also be computed more compactly as follows:

$$i=1..10 \quad X_i=\frac{\sum\left(\overrightarrow{\left[Ih(CIh^T)^{<i>}\Gamma_{tot}\right]}\right)}{h} \quad X^T=(2 \quad 4 \quad 4 \quad 6 \quad 8 \quad 1 \quad 5 \quad 5 \quad 6 \quad 7)$$

Of the 180 degrees of freedom that C_{60} has, three are due to translation of the center of mass in Cartesian space (T_{1u}) and three are due to rotation about the Cartesian axes (T_{1g}). This leaves 174 vibrational degrees of freedom. They have the following symmetry properties.

$$\Gamma_{vib}=\Gamma_{tot}-T1u-T1g$$

$$i=1..10 \quad X_i=\frac{\sum\left(\overrightarrow{\left[Ih(CIh^T)^{<i>}\Gamma_{vib}\right]}\right)}{h} \quad X^T=(2 \quad 3 \quad 4 \quad 6 \quad 8 \quad 1 \quad 4 \quad 5 \quad 6 \quad 7)$$

One important consequence of the high symmetry of C_{60} is that many of the vibrational modes are degenerate. As the result above shows there are only 46 distinct vibrational modes. Another consequence of the symmetry of C_{60} is that most of these modes are not IR or Raman active.4 In fact only the four T_{1u} vibrational modes are IR active and they appear at 528, 577, 1180, and 1430 cm-1 with varying intensities. Sample calculations for the transition moment for IR transitions are shown below. Those with transition moments of zero are forbidden.

$$\frac{\sum\overrightarrow{(IhT1gT1uAg)}}{h}=1 \quad \frac{\sum\overrightarrow{(IhT1uT1uAg)}}{h}=1 \quad \frac{\sum\overrightarrow{(IhGgT1uAg)}}{h}=0 \quad \frac{\sum\overrightarrow{(IhHuT1uAg)}}{h}=0$$

These vector multiplications are the symmetry representations of the quantum mechanical integrals for transition moments. For the transition moment to have a non-zero value, the vector product must span the totally symmetric irreducible representation, Ag. In the examples shown above Ag is the symmetry of the ground vibrational state for all vibrational modes, T_{1u} is the symmetry of the electric dipole operator, and T_{1g}, T_{1u}, G_g, and H_u are the irreducible representations for the vibrational states to be excited by the infrared radiation. As these calculations show, only the T_{1u} vibrational modes have a non-zero transition moment.

However, it is important to realize that the group theoretical analysis given above, and those that follow, can only decide which transitions are forbidden. They do not provide the transition probabilities of the transitions which are not forbidden. For example, the fact that the second vector sum above is 1 says nothing about the intensity of the actual absorption in the infrared, only that the vibrational modes with T_{1u} symmetry are not forbidden.

There are ten Raman active modes, two modes with Ag symmetry and eight with Hg symmetry. They appear at the following frequencies: 273, 436, 496, 710, 773, 1100, 1250, 1435, 1470, and 1570 cm^{-1}. 4 The calculation is similar to that for IR activity except that the operators for the Raman interaction are the quadratic forms (the components of the polarizability tensor) which transform as Ag and Hg, as shown in the Ih character table.

$$\frac{\sum\overrightarrow{(IhAgAgAg)}}{h}=1 \quad \frac{\sum\overrightarrow{(IhT1uAgAg)}}{h}=0 \quad \frac{\sum\overrightarrow{(IhT1uHgAg)}}{h}=0 \quad \frac{\sum\overrightarrow{(IhHgHgAg)}}{h}=1$$

In these sample calculations we see the basis for the widely used generalization that for a vibrational mode to be IR active it must have the same symmetry as one of the Cartesian coordinates and to be Raman active it must have the same symmetry as one of the components of the polarizability tensor. We also see quite clearly that for a molecule with a center of inversion there is no overlap between the IR and Raman active vibrational modes. In the appendix it is shown that three of the IR active modes and seven of the Raman active modes are stretching vibrations.

Electronic States of the π Electrons

To a first approximation the bonding in C_{60} might be described as follows: each carbon forms σ bonds to its three neighboring carbon atoms using sp^2 hybridized orbitals with the remaining p orbital on each carbon available for π bonding. It is customary in approximate models to treat the π electrons independently of the σ electrons, just as chemists generally assume that they can treat

valence electrons independently of the core electrons. The behavior of the π electrons under the symmetry operations of the icosahedral point group is easy to determine. Because the π orbitals are centered on the carbon atoms and are perpendicular to the sp^2 "plane", they have the same symmetry properties as the carbon atoms.

$$\Gamma\pi = \Gamma_{uma}$$

We now decompose Γ_π into its irreducible representations using the method outlined above.

$$\frac{\sum\overrightarrow{IhAg\Gamma_\pi}}{h}=1 \quad \frac{\sum\overrightarrow{IhT1g\Gamma_\pi}}{h}=1 \quad \frac{\sum\overrightarrow{IhT2g\Gamma_\pi}}{h}=1 \quad \frac{\sum\overrightarrow{IhAg\Gamma_\pi}}{h}=1 \quad \frac{\sum\overrightarrow{IhGg\Gamma_\pi}}{h}=2 \quad \frac{\sum\overrightarrow{IhHg\Gamma_\pi}}{h}=3$$
$$\frac{\sum\overrightarrow{IhAu\Gamma_\pi}}{h}=0 \quad \frac{\sum\overrightarrow{IhT1u\Gamma_\pi}}{h}=2 \quad \frac{\sum\overrightarrow{IhT2u\Gamma_\pi}}{h}=2 \quad \frac{\sum\overrightarrow{IhGu\Gamma_\pi}}{h}=2 \quad \frac{\sum\overrightarrow{IhHu\Gamma_\pi}}{h}=2$$

Or calculated more compactly:

$$i = 1..10 \quad X_i = \frac{\sum\left(\overrightarrow{\left[Ih(CIh^T)^{<i>}\Gamma_{uma}\right]}\right)}{} \quad X^T$$

$$Gamma_{uma} = Ag + T1g + T2g + 2Gg + 3Hg + 2T1u + 2T2u + 2Gu + 2Hu$$

Just as symmetry arguments cannot predict the actual intensities of allowed infrared or Raman transitions, they also can't predict the energy order of these π electron energy levels. However, group theory combined with a Huckel calculation yields the following order.[5]

Ag < T1u < Hg < T2u < Gu < (Gg + Hg) < Hu < T1u < T1g < Hg < T2u < Hu < Gg < Gu < T2g

With 60 π electrons to distribute in accordance with the Aufbau and Exclusion Principles, the H_u level is the HOMO, the T_{1u} level is the LUMO, and the T_{1g} level is the LUMO +1. This ordering of the levels is consistent with the basic magnetic and electronic properties of C_{60}. For example, it is diagmagnetic with a completely filled HOMO level and it has a reasonably high electron affinity because of the low lying LUMO. The three-fold orbital degeneracy of the LUMO is consistent with the fact that K_3C_{60} and K_6C_{60} are both known, and K_3C_{60} is paramagnetic while K_6C_{60} is diamagnetic. K_4C_{60} is also known and is diamagnetic due to a Jahn-Teller distortion that splits the T_{1u} level into a lower two-fold degenerate level and a higher singlet level.

Calculation of the transition moments for electronic transitions is similar to that for IR and Raman interactions with electromagnetic radiation. The HOMO ---> LUMO electronic transition in C_{60} involves the following change in electronic structure: H_u^{10} ---> $H_u^9\ T_{1u}^1$. The ground state, H_u^{10}, has A_g symmetry as a fully filled level. The transition moment between this state and $H_u^9\ T_{1u}^1$ configuration is formulated as shown below because H_u^9 has the same symmetry as H_u^1. Starting at the right Ag is the symmetry of the ground electronic state, T_{1u} is the symmetry of the electric dipole operator, (H_uT_{1u}) represents the symmetry of the manifold of excited electronic states associated with the $H_u^9T_{1u}^1$ electronic configuration (see appendix), and I_h is, as mentioned earlier, the vector containing the number of symmetry operations in each symmetry class.

$$\frac{\sum\overrightarrow{[Ih(HuT1u)T1uAg]}}{h}=0$$

Thus the HOMO ---> LUMO electronic transition is formally forbidden. However, the HOMO ----> LUMO+1 is allowed as is shown below. In other words the transition moment for this electronic transition spans the A_g irreducible representation

$$\frac{\sum\overrightarrow{[Ih(HuT1g)T1uAg]}}{h}=1$$

The ($H_u^9T_{1g}^1$) excited state consists of 15 microstates with symmetry T_{1u}, T_{2u}, G_u, and Hu (see appendix). Only the transition to the T_{1u} state is allowed and it occurs at 408 nm.[6] In calculating the transition moment for HOMO --> LUMO electronic transition it has been assumed that there was no change in the vibrational state of the molecule. However, it is possible for forbidden electronic transitions to become weakly allowed through coupling to changes in vibrational state. These are called vibronic transitions and they are allowed if the integral shown below is nonzero.

$$\int\int \Psi ex \Psi vx \mu e \Psi eg \Psi vg\ d\tau e\ d\tau v$$

For example, if the formally forbidden HOMO ---> LUMO electronic transition is accompanied by a vibrational transition of A_u, T_{1u}, T_{2u}, G_u, or H_u symmetry the transition may be allowed (see appendix). The vibronic transition moment would be calculated as follows.

$$\frac{\sum \overrightarrow{[Ih(HuT1u)AuT1uAgAg]}}{h} = 1$$

Here (H_uT_{1u}) is the manifold of excited electronic states, A_u is the excited vibrational state, T_{1u} is the electric dipole operator, A_g is the ground electronic state, and A_g is the ground vibrational state.

Thus while formally forbidden, the HOMO ---> LUMO transition is weakly allowed through vibronic coupling. This type of mechanism has been used to interpret the visible spectrum of C_{60} and recent analyses have put the lowest spin-allowed, vibronically assisted HOMO ----> LUMO transition at 620 nm.[6]

As can be seen, Mathcad provides an efficient programming environment for performing symmetry analyses with any of the finite point groups. Once a Mathcad worksheet is prepared for one molecule it serves as a template for all other molecules with that symmetry. The only changes that need to be made are to the vector Γ_{uma} which records how many atoms are unmoved by the symmetry operations of the group. Recently, Greathouse has demonstrated how molecules that belong to the infinite point groups can be analyzed numerically.[7]

Literature Cited:

1. Mathcad is a product of MathSoft Inc., 101 Main Street, Cambridge, MA 02142.
2. Harris, D. C.; Bertolucci, M. D. *Symmetry and Spectroscopy: An Introduction to Vibrational and Electronic Spectroscopy*, Dover Publications, Inc.: New York, 1989; Chater 3, pp. 140-142.
3. Ibid, Chapter 1, page 56.
4. Bethume, D. S.; et. al. *Chem. Phys. Lett.* **1991**, 179, 181-186.
5. Hebard, A. F. *Physics Today* **1992**, *45(11)*, 29.
6. Leach, S.; et, al. *Chem. Phys.* **1992**, *160*, 451-466.
7. Greathouse, J. A. *The Chemical Educator* 1996, Vol. 1, No. 1.

Appendix

This is a demonstration that the $H_u^9 T_{1u}^1$ configuration yields the manifold of states, T_{1g}, T_{2g}, G_g, and H_g.

$$i = 1..10 \quad X_i = \frac{\sum \overrightarrow{[Ih(CIh^T)^{<i>}(HuT1u)]}}{h} \quad X^T = (0 \quad 1 \quad 1 \quad 1 \quad 1 \quad 0 \quad 0 \quad 0 \quad 0 \quad 0)$$

This is a demonstration that the $H_u^9 T_{1g}^1$ configuration yields the manifold of states, T_{1u}, T_{2u}, G_u, and H_u.

$$X_i = \frac{\sum \overrightarrow{[Ih(CIh^T)^{<i>}(HuT1g)]}}{h} \quad X^T = (0 \quad 0 \quad 0 \quad 0 \quad 0 \quad 0 \quad 1 \quad 1 \quad 1 \quad 1)$$

As shown earlier the vibrational modes span all of the irreducible representations. This calculation shows which of those modes provide vibrational coupling for the formally forbidden HOMO ---> LUMO electronic transition.

$$X_i = \frac{\sum \overrightarrow{[Ih(HuT1u)(CIh^T)^{<i>}T1uAgAg]}}{h} \quad X^T = (0 \quad 0 \quad 0 \quad 0 \quad 0 \quad 0 \quad 1 \quad 2 \quad 3 \quad 4)$$

This page titled 4.34: The Vibrational and Electronic States of C60 is shared under a CC BY 4.0 license and was authored, remixed, and/or curated by Frank Rioux via source content that was edited to the style and standards of the LibreTexts platform.

CHAPTER OVERVIEW

5: Diffraction Phenomena

5.1: Using Optical Transforms to Teach Quantum Mechanics
5.2: Single-slit Diffraction and the Uncertainty Principle
5.3: Single-slit Diffraction and the Uncertainty Principle (Mathcad Version)
5.4: Simulating DNA's Diffraction Pattern
5.5: Simulating DNA's Diffraction Pattern with a More Realistic Model
5.6: Simulating DNA's Diffraction Pattern - Short Version
5.7: A Model Graphene Diffraction Pattern
5.8: Is a Two-dimensional Fibonacci Array a Quasilattice?
5.9: Calculating Diffraction Patterns
5.10: Modeling the C60 Diffraction Pattern
5.11: Diffraction Pattern for Pentagonal Point Scatterers
5.12: Diffraction Pattern for Pentagonal Finite Point Scatterers
5.13: Pentagram Diffraction Pattern
5.14: Model Diffraction Pattern for Napthalene
5.15: Calculating the Airy Diffraction Pattern
5.16: Diffraction Pattern for Two Concentric Rings
5.17: Density Operator Approach to the Double-Slit Experiment
5.18: Another Look at the Double-Slit Experiment
5.19: A Quantum Mechanical Interpretation of Diffraction
5.20: Electron Diffraction at Multiple Slits
5.21: Multiple Slit Diffraction and the Fourier Transform
5.22: The Double-Slit Experiment with C60 Molecules
5.23: Crystal Structure, Rotational Symmetry, and Quasicrystals
5.24: X-ray Crystallography from a Quantum Mechanical Perspective
5.25: Holography Involves Single Photon Interference
5.26: X-ray Diffraction
5.27: Holography Involves Single Photon Interference

This page titled 5: Diffraction Phenomena is shared under a CC BY 4.0 license and was authored, remixed, and/or curated by Frank Rioux via source content that was edited to the style and standards of the LibreTexts platform.

5.1: Using Optical Transforms to Teach Quantum Mechanics

Abstract: Wave-particle duality, the superposition principle, the uncertainty principle, and single-particle interference are the most fundamental quantum mechanical concepts. The purpose of this paper is to demonstrate that these quantum mechanical principles are illuminated by a study of diffraction patterns created with laser light and a variety of two-dimensional masks.

The principles of X-ray crystallography are generally taught using the Bragg model in which X-rays irradiating a crystal behave as classical waves reflected by planes of atoms producing a characteristic diffraction pattern determined by the Bragg interference condition. Optical transform kits developed by the Institute for Chemical Education [1-4] and similar resources [5] have been used to teach these principles through classroom demonstrations of the diffraction patterns generated by laser light and two-dimensional masks. The purpose of this paper is to show that these same teaching aids can be used to teach quantum mechanical principles to chemistry majors in upper-division courses. The quantum concepts illuminated in this approach are

• wave-particle duality,

• the superposition principle,

• the uncertainty principle,

• single-particle interference,

• the quantum mechanical view of experimentation.

Our approach to using optical transforms is an extension of the method Marcella used recently to analyze the famous double-slit experiment [6, 7]. In what follows, the relationship of optical transforms to the quantum mechanical principles listed above is presented as concisely as possible while supporting information is relegated to footnotes and appendices.

Marcella identified three steps in a quantum mechanical experiment: (1) state preparation, (2) measurement of an observable property, and (3) comparison of experimental results with theoretical calculations. We will introduce Marcella's method with a review of the double-slit experiment and then extend this approach to optical transforms of other two-dimensional masks.

According to Richard Feynman the double-slit experiment is the paradigm for all quantum mechanics because it is a simple manifestation of the superposition principle, which is quantum theory is "only mystery" [8]. Stressing the fundamental importance of the double-slit experiment he said that any question in quantum mechanics could always be answered with the response, "You remember the experiment with the two holes? It is the same thing" [9].

In the double-slit experiment the apparatus consists of a source of particles (photons, electrons, neutrons, He atoms, C_{60} molecules, etc.; see reference 14 and papers cited therein), a slit-screen, and a detection screen. Wave-particle duality is manifested in this experiment as follows. The source creates particles and the detector registers particles, but between source and detector the behavior is wave-like. This is the underlying structure for all quantum mechanical experiments.

State preparation occurs at the slit screen where the particle is position is localized at holes or slits. According to quantum mechanical principles the coordinate-space wave function at the slit screen is a linear superposition describing the particle as present at both slits simultaneously. To begin we will treat the slits as point holes in a screen at (x1, y1) and (x2, y2). This view yields the following coordinate-space wave function [10].

$$|\Psi\rangle = \frac{1}{\sqrt{2}}\left[|x_1,\ y_1\rangle + |x_2,\ y_2\rangle\right] = \frac{1}{\sqrt{2}}\sum_{i=1}^{2}|x_i,\ y_i\rangle$$

In Marcella's quantum mechanical analysis of the double slit experiment, what is subsequently measured at the detection screen is actually the particle's momentum. In other words, the well-known diffraction pattern created by the double-slit geometry is the particle's momentum distribution in the plane of the detection screen. Therefore, to calculate the diffraction pattern one needs a momentum wave function, and this is obtained by a Fourier transform of eq 1 into momentum space. The primary dynamical variables of position and momentum have a conjugate relationship expressed by the Fourier transform (see Appendix A) shown in eq 2.

$$\langle p|\Psi\rangle = \frac{1}{\sqrt{2}}\sum_{i=1}^{2}\langle p_x|x_i\rangle\langle p_y|y_i\rangle = \frac{1}{2\pi h\sqrt{2}}\sum_{i=1}^{2} exp\left(-\frac{ip_x x_i}{h}\right) exp\left(-\frac{ip_y y_i}{h}\right)$$

where $\langle p_q|q_i\rangle = \frac{1}{\sqrt{2\pi\hbar}} exp\left(-\frac{ip_q q_i}{\hbar}\right)$ are the position eigenfunctions in the momentum representation.

In summary, during propagation to the detection screen the particle is in a superposition of momentum states determined by the hole configuration of the slit screen. The square of the absolute magnitude of eq 2, the momentum probability distribution in the xy plane, is, therefore, the diffraction pattern. If this were calculated using eq 2, it would not resemble the actual diffraction because it has been assumed, initially, that the slits are infinitesimally small holes; however, if the holes are given a width d in both directions, the Fourier transform is given by eq 3.

$$\langle p|\Psi\rangle = \frac{1}{2\pi\hbar d\sqrt{N}} \sum_{i=1}^{N} \int_{x_i-\frac{d}{2}}^{x_i+\frac{d}{2}} exp\left[-\frac{ip_x x_i}{\hbar}\right] dx \int_{y_i-\frac{d}{2}}^{y_i+\frac{d}{2}} exp\left[-\frac{ip_y y_i}{\hbar}\right] dy$$

In the present case, N = 2, and for two "holes" with dimension 0.3 a_0 [11], separated by 1.0 a_0 along the x axis, the diffraction pattern is shown in Figure 1. This pattern is in agreement with the diffraction from a two-hole mask as shown on plate 2, panel 3 of reference 5. It is interpreted here using both the uncertainty and superposition principles. The particle is localized in space by the holes in the slit screen, and this leads, according to the uncertainty principle, to a delocalization of the x and y components of the particle's momentum. The figure clearly shows this delocalization in the momentum components. In addition, because the particle is localized at two positions in the x direction, the superposition principle demands constructive and destructive interference in the x component of the momentum. This effect is also clearly shown in Figure 1.

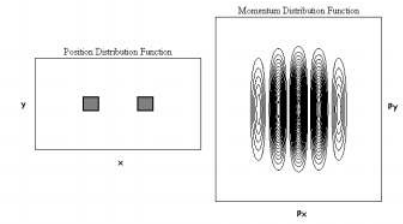


Figure 1. Hole positions are as described in the text. The momentum range is ± 25 a_0^{-1} from border to border for p_x and p_y.

The complementary relationship between position and momentum required by the uncertainty principle is illustrated further in Figure 2, where the position and momentum distributions are shown for holes of dimension 0.5 a_0. Clearly, the decreased localization in coordinate space has led to an increased localization in momentum space. Similar quantitative arguments relating the uncertainty principle to slit width and momentum distribution have recently been made in both the pedagogical [12] and research [13] literature for single-slit diffraction phenomena.

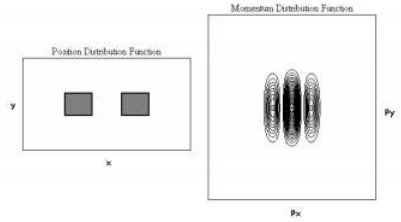


Figure 2. Hole positions are as described in the text. The momentum range is ± 25 a_0^{-1} from border to border for p_x and p_y.

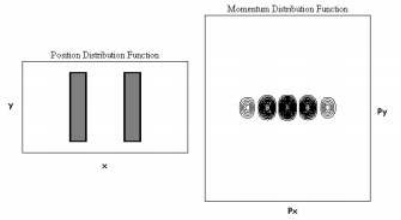


Figure 3. Hole positions are as described in the text. The momentum range is ± 25 a_0^{-1} from border to border for p_x and p_y.

We can change the two holes to two slits by increasing the y dimension of the holes. For example, holding the x dimension constant at 0.3 a0 while increasing the y dimension to 1.5 a_0 yields the diffraction pattern shown in Figure 3. This result is in agreement with the diffraction pattern obtained using the multislit mask on panel b of the Discovery Slide of reference 2. Comparing Figures 1 and 3, nothing has changed in the x direction, but the particle is partially delocalized in the y direction at the slit screen in Figure 3.

According to the uncertainty principle, its momentum in the y direction will become more localized the spread in observed momentum values will decrease. To summarize, spatial localization leads to a delocalized momentum distribution that is projected onto the detection screen and is calculated as $|\langle p|\Psi\rangle|^2$ using eq 3. Furthermore, spatial localization at more than one position in a particular direction leads to interference effects in the momentum distribution in that direction.

It should also be pointed out that the double-slit experiment has been carried out at low source intensity such that there is only one particle in the apparatus at a time [14]. The resulting diffraction pattern is the same as that observed with intense sources; it just takes longer to record to the same number of observations. This confirms the quantum mechanical view that wave functions 1 and 2 represent individual particles rather than an ensemble of particles. According to quantum mechanical principles the particles can be placed in a well defined state by the slit screen, but the outcome of a subsequent measurement, momentum in this case, is not uniquely determined. All we can do is calculate the probability that a particular momentum state will be observed. The mechanism, therefore, is single-particle, or self-interference; two particles do not interfere with each other [14, 15].

With this introduction it is easy to move to a general treatment of diffraction by two-dimensional masks. Following eq 1, for a mask consisting of N scatterers the coordinate wave function is given by eq 4 below, and the momentum wave function is given by eq 3.

$$|\Psi\rangle = \frac{1}{\sqrt{N}} \sum_{i=1}^{N} |x_i,\ y_i\rangle$$

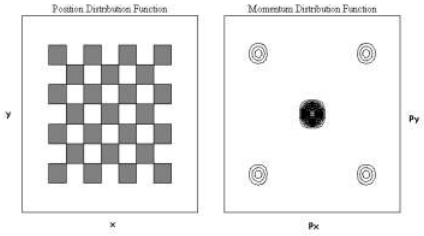


Figure 4. Hole dimension are 0.5 a_0 on a side with horizontal hole centers separated by 1.0 a_0. The momentum range is ± 10 a_0^{-1} from border to border for p_x and p_y.

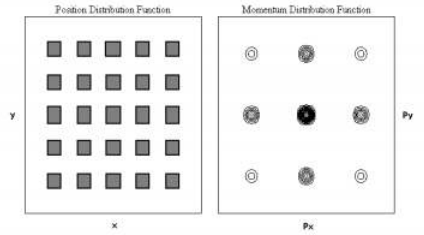


Figure 5. Hole dimensions are 0.5 a_0 with horizontal and vertical centers separated by 1.0 a_0. The momentum range is ± 10 a_0^{-1} from border to border for p_x and p_y.

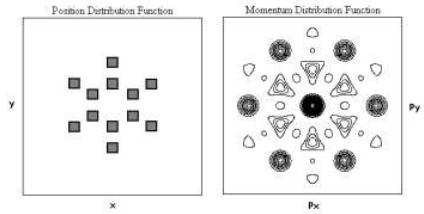


Figure 6. The hole dimensions are 0.5 a_0 on a side with an inner ring of radius 1.0 a_0 and an outer ring of radius 2.0 a_0. The momentum range is ± 10 a_0^{-1} from border to border for p_x and p_y.

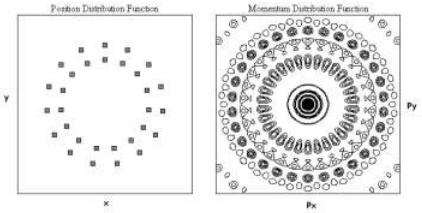


Figure 7. The hole dimensions are 0.1 a_0 on a side with an inner ring of radius 0.9 a_0 and an outer ring of radius 1.2 a_0. The momentum range is ± 30 a_0^{-1} from border to border for p_x and p_y.

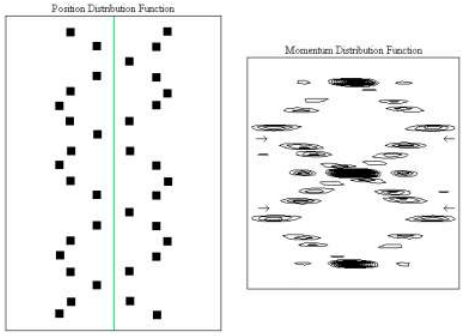


Figure 8. Simulation of DNA diffraction pattern. The arrows indicate the missing fourth layers.

Figure 4 shows the diffraction pattern for a face-centered squaric arrangement of 25 holes (the two-dimensional analog of face-centered cubic), while Figure 5 was created with a simple squaric arrangement of 25 holes (the two-dimensional analog of simple cubic). Both calculated diffraction patterns are in excellent agreement with the experimental results shown in Figure 3a and b of reference 1. These examples show that the addition of a scatterer to the unit cell increases destructive interference and fewer momentum states are observed at the Figure 5. Hole dimensions are 0.5 a0 with horizontal and vertical detector.

Figures 6 and 7 show the calculated diffraction patterns for two concentric hexagons and two concentric pentadecagons, respectively. These calculated diffraction patterns are in excellent agreement with the experimental patterns found in Plates 10 and 12 in reference 5. Given the recently celebrated 50^{th} anniversary of the publication of the DNA double helix structure [16] it is appropriate to draw special attention to references 3 and 4, which provide optical transforms that simulate DNA's experimental X-ray diffraction pattern.

Using the theoretical methods outlined above, it is possible to calculate in a rudimentary way several of the characteristic features of the DNA diffraction pattern. For example, representing DNA solely by a planar double strand of phosphate backbone groups as shown on the left side of Figure 8 generates the diffraction pattern shown on the right side. The essential features captured by this naive model are the characteristic X-shaped cross of the diffraction pattern and the missing fourth horizontal layer. Additional discussion on this rudimentary model is available in references 3 and 4.

The diffraction patterns presented in this paper have been calculated using Mathcad Plus 5.0. Naturally, once a calculation for one mask geometry has been programmed, it can serve as a template for other calculations with minor editing. Such a Mathcad file for calculating diffraction patterns for two-dimensional masks is available for download [17].

The conceptual and computational simplicity of the approach presented here makes it possible to bring experiment and theory together in the classroom in order to gain insight into the physical nature of diffraction phenomena from the quantum mechanical perspective.

Appendix A. The Fourier Transform

Wave-particle duality, as expressed by de Broglie's wave equation, is at the heart of quantum mechanics.

$$\lambda = \frac{h}{p}$$

On the left side we have the wave property, wavelength, and on the right momentum, the particle property; thus, (A.1) shows wave and particle properties in one equation united by the ubiquitous Planck's constant.

The most general coordinate-space wave function for a free particle with wavelength λ is the complex Euler function shown below in Dirac notation.

$$\langle x|\lambda\rangle = exp\left(i\frac{2pix}{\lambda}\right)$$

Substitution of eq A.1 into eq A.2 yields the momentum wave function in the coordinate representation.

$$\langle x|p\rangle = exp\left(\frac{ipx}{\hbar}\right)$$

The complex conjugate of eq A.3, $\langle x|p\rangle = \langle p|x\rangle$, is the coordinate wave function in the momentum representation.

$$\langle p|x\rangle = exp\left(-\frac{ipx}{\hbar}\right)$$

These equations are extremely useful in quantum mechanics in translating coordinate-space information into the momentum representation, and vice versa.

For example, if a system is in a well-defined state, $|\Psi\rangle$, it might be expressed in coordinate language as $\langle x|\Psi\rangle$ or momentum language as $\langle p|\Psi\rangle$. If one is known, the other can be found by a Fourier transform because both representations contain the same state information. As shown below, the overlap integral between $\langle x|\Psi\rangle$ and $\langle p|x\rangle$ in coordinate space is the momentum wavefunction, and the overlap between $p|\Psi\rangle$ and $\langle x|p\rangle$ in momentum space is the position wavefunction.

$$\langle p|\Psi\rangle = \int \langle p|x\rangle\langle x|\Psi\rangle dx = \frac{1}{\sqrt{2pi\hbar}}\int exp\left(-\frac{ipx}{\hbar}\right)\Psi(x)dx$$

$$\langle x|\Psi\rangle = \int \langle x|p\rangle\langle p|\Psi\rangle dx = \frac{1}{\sqrt{2pi\hbar}}\int exp\left(-\frac{ipx}{\hbar}\right)\Psi(p)dp$$

In these equations $(2\pi\hbar)^{-\frac{1}{2}}$ is the normalization constant for $\langle x|p\rangle$ and $\langle p|x\rangle$.

In our analysis of diffraction phenomena, eq A.5 is used because state preparation occurs in coordinate space at the slit screen yielding $\langle x|\Psi\rangle$, which is then projected into momentum space, $\langle p|\Psi\rangle$, to calculate the diffraction pattern, $|\langle p|\Psi\rangle|^2$, at the detection screen.

Appendix B. Bragg's Law

The reader will have noticed that we only made brief mention of Bragg's Law in our presentation. This is because we prefer, for pedagogical reasons, Marcella's quantum mechanical approach with its roots in von Laue's early classical analysis of X-ray diffraction as a scattering phenomenon. The following quotation from French and Taylor's excellent text reveals the connection between von Laue and Bragg in the pre-quantum mechanical era [18].

> The original analysis by von Laue treated the problem (X-ray diffraction), as basically one must, in terms of the scattering of an incident X-ray beam by all the individual atoms in the three-dimensional lattice making up the crystal. This is somewhat formidable, but very soon afterwards (in 1913), W. L. Bragg showed that the results of the analysis are the same as if one regarded the x-rays as being reflected at sets of parallel planes that include many atoms.

Reflection, therefore, is a conceptual device that simplifies analysis; diffraction is really a scattering phenomenon that behaves as if it were reflection for simple systems. While Bragg's approach simplifies analysis in simple cases, it does so at the expense of providing an incorrect physical picture of what is actually occurring. It has also led to abstract concepts such as the reciprocal lattice and Miller indices which students and teachers alike find difficult to understand. In our teaching we prefer the more direct appeal to the physical concepts of position and momentum, united as they always are by the uncertainty principle.

References and Notes

1. Lisensky, G. C.; Kelly, T. F.; Neu, D. R.; Ellis, A. B. The Optical Transform: Simulating Diffraction Experiments in Introductory Courses. *J. Chem. Educ.* **1991**, 68, 91-96.

2. Lisensky, G. C.; Ellis, A. B.; Neu, D. R. Optical Transform Kit, 2nd Ed.; Institute for Chemical Education: University of Wisconsin, Madison, WI, 1994.
3. Lucas, A. A.; Lambin, Ph.; Mairesse, R.; Mathot, M. Revealing the Backbone Structure of B-DNA from Laser Optical Simulations of Its 1 X-ray Diffraction Diagram. *J. Chem. Educ.* **1999**, 76, 378ñ383.
4. Lisensky, G. C.; Lucas A. A.; Nordell, K. J.; Jackelen, A. L.; Condren, S. M.; Tobe, R. H.; Ellis, A. B. *DNA Optical Transform Kit*; Institute for Chemical Education: University of Wisconsin, Madison, WI, 1999.
5. Harburn, G.; Taylor, C. A.; Welberry, T. R. *Atlas of Optical Transforms*; Cornell University Press: Ithaca, NY, 1975.
6. Marcella, T. V. Quantum interference with slits. *Eur. J. Phys*. **2002**, 23, 615-621.
7. Rioux, F. Calculating diffraction patterns. *Eur. J. Phys*. **2003**, 24, N1-N3.
8. Feynman, R. P.; Leighton, R. B.; Sands, M. *The Feynman Lectures on Physics*; Addison-Wesley: Reading, 1965; Vol 3.
9. Feynman, R. P. *The Character of Physical Law*; MIT Press: Cambridge, 1967; p 130.
10. Dirac bracket notation is used exclusively in this paper because it is a concise and coherent language in which to express quantum mechanical concepts. For further examples of its use see reference 8 or visit http://www.users.csbsju.edu/~frioux/dirac/dirac.pdf (accessed Dec 2003).
11. Atomic units are used in these calculations: $(\hbar = m_e = e = 1)$. The atomic unit of distance is the bohr, a_0. 1 a_0 = 52.9 pm.
12. Muino, P. L. Introducing the Uncertainty Principle Using Diffraction of Light Waves. J. Chem. Educ. **2000**, 77, 1025-1027.
13. Nairz, O.; Arndt, M.; Zeilinger, A. Experimental verification of the Heisenberg uncertainty principle for hot fullerene molecules. *Phys. Rev. A.* **2002**, 65, 032109.
14. Nairz, O.; Arndt, M.; Zeilinger, A. Quantum interference experiments with large molecules, *Am. J. Phys.* **2003**, 71, 319-325.
15. "Each photon then interferes only with itself. Interference between two different photons never occurs." From Dirac, P. A. M. *The Principles of Quantum Mechanics*, 4th ed.; Oxford University Press: Oxford, 1958, p 9.
16. Watson, J. D.; Crick, F. H. C. Molecular Structure of Nucleic Acids: A Structure for Deoxyribose Nucleic Acid. *Nature* **1953**, 171, 737.
17. www.users.csbsju.edu/~frioux/...n/template.mcd (accessed Dec 2003).
18. French, A. P.; Taylor, E. F. An Introduction to Quantum Physics; W. W. Norton & Co. Inc.: New York, 1978, p 41.

This page titled 5.1: Using Optical Transforms to Teach Quantum Mechanics is shared under a CC BY 4.0 license and was authored, remixed, and/or curated by Frank Rioux via source content that was edited to the style and standards of the LibreTexts platform.

5.2: Single-slit Diffraction and the Uncertainty Principle

Muiño has used single-slit diffraction to provide an introduction to the uncertainty principle suitable for an undergraduate physical chemistry course (1). His article provided both a theoretical analysis of single-slit diffraction and a lecture demonstration of the phenomenon using readily-available equipment. In the current research literature Nairz and colleagues have confirmed the uncertainty principle in a single-slit diffraction experiment with a beam of C70 molecules (2). And, quite recently, a research team led by Marcus Arndt and Anton Zeilinger performed multi-slit experiments demonstrating wave-particle behavior for tetraphenylporphyrin and a fluorinated fullerene, $C_{60}F_{48}$ (3). The significance of these results is that tetraphenylporphyrin is an important biomolecule and C60F48 is the most massive particle to demonstrate wavelike properties to date.

The purpose of this short article is to provide an alternative theoretical analysis of single-slit diffraction based on the Fourier transform between coordinate and momentum space. This approach was recently used by Marcella (4) to analyze single- and double-slit diffraction and has been extended by the author to more complicated slit geometries (5). Quantum experiments have three parts: (i) state preparation; (ii) subsequent measurement of an observable; and (iii) theoretical interpretation of experimental results. In diffraction experiments, passage through the slit screen represents a position measurement that establishes the state of the system in coordinate space. The coordinate-space wave function for a photon or massive particle that has passed a screen with a slit of width w centered at x = 0 is

$$\Psi(x,w) = \left\{ \begin{array}{c} 0 \text{ for } x < -\frac{w}{2} \\ \frac{1}{\sqrt{w}} \text{ for } -\frac{w}{2} \le x \le \frac{w}{2} \\ 0 \text{ for } x > \frac{w}{2} \end{array} \right\}$$

The quantum mechanical interpretation of diffraction is that the physical property recorded at the detection screen is the momentum distribution of the diffracted particle.

A Fourier transform of Ψ(x, w) into the momentum representation yields the momentum-space wave function

$$\Phi(p_x,\ w) = \int_{-\frac{w}{2}}^{\frac{w}{2}} \frac{1}{\sqrt{2pi\hbar}} exp\left(-\frac{ip_x x}{\hbar}\right) \frac{1}{\sqrt{w}} dx = \sqrt{\frac{2\hbar}{\pi w}} \frac{\sin\left(\frac{p_x w}{2\hbar}\right)}{p_x}$$

where p_x is the x-direction momentum. Thus, according to quantum mechanics, the diffraction pattern observed is the square of the absolute magnitude of the momentum wave function, $|\Phi(p_x, w)|^2$. This is shown in Figure 1 for two slit widths.

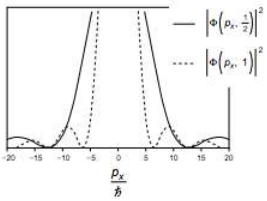


Figure 1. Momentum distribution at the slit screen for slit widths of 0.5 and 1.0 a_0 (1 a_0 = 52.9 pm).

The uncertainty principle is clearly revealed—the narrow slit produces a broader momentum distribution. In other words, localization in coordinate space leads to delocalization in momentum space. However, we can also treat this effect in a more quantitative manner.

Following Muiño we will assume that the uncertainty in position is the slit width, w. The uncertainty in momentum is defined as half the width of the momentum distribution of the central diffraction band (2). As the momentum distribution is zero for

$$\frac{p_x w}{2\hbar} = \pm n\pi$$

it is easy to show that using this criterion the uncertainty in momentum is $\frac{2\pi\hbar}{w}$. Therefore, the product of the uncertainty in position and momentum is greater than \(\frac{ \hbar}{2}} as required by the uncertainty principle.

$$\Delta x \Delta p_x = w\frac{2pi\hbar}{w} = 2\pi\hbar$$

The Fourier transform connecting complementary observables is ubiquitous in quantum theory (and, of course, in our laboratory instruments). Here the transform between position and momentum has been used to illuminate the intimate relationship between single-slit diffraction and the uncertainty principle.

Literature Cited

1. Muiño, P. L. *J. Chem. Educ*. **2000**, 77, 1025–1027.
2. Nairz, O.; Arndt, M.; Zeilinger, *A. Phys. Rev. A*, **2002**, 65, 032109.
3. Hackermüller, L.; Uttenhaler, S.; Hornberger, K.; Reiger, E.; Brezger, B.; Zeilinger, A.; Arndt, *M. Phys. Rev. L.* **2003**, 91, 090408.
4. Marcella, T. V. *Eur. J. Phys.* **2002**, 23, 615–621. Also see: French, A. P.; Taylor, E. F. *An Introduction to Quantum Physics*; W. W. Norton and Co. Inc.: New York, 1978; pp 331–336.
5. Rioux, F. *Eur. J. Phys*. **2003**, 24, N1–N3

This page titled 5.2: Single-slit Diffraction and the Uncertainty Principle is shared under a CC BY 4.0 license and was authored, remixed, and/or curated by Frank Rioux via source content that was edited to the style and standards of the LibreTexts platform.

5.3: Single-slit Diffraction and the Uncertainty Principle (Mathcad Version)

Diffraction has a simple quantum mechanical interpretation based on the uncertianty principle. Or we could say diffraction is an excellent way to illustrate the uncertainty principle.

A screen with a single slit of width, w, is illuminated with a coherent photon or particle beam. The normalized coordinate-space wave function at the slit screen is,

$$w = 1 \quad \Psi(x, w) = \text{if}\left[(x \geq -\tfrac{w}{2})\,(x \leq \tfrac{w}{2}),\ \tfrac{1}{\sqrt{w}},\ 0\right] \quad x = \tfrac{-w}{2},\ \tfrac{+w}{2} + 0.005\,..\,\tfrac{w}{2}$$

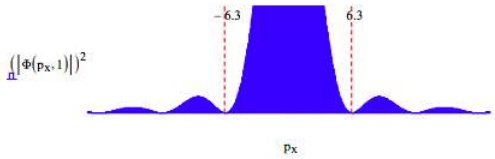
The coordinate-space probability density, $|\Psi(x,\ w)|^2$, is displayed for a slit of unit width below



The slit-screen measures position, it localizes the incident beam in the x-direction. According to the uncertainty principle, because position and momentum are complementary, or conjugate, observables, this measurement must be accompanied by a delocalization of the x-component of the momentum. This can be seen by a Fourier transform of Ψ(x,w) into momentum space to obtain the momentum wave function, $\Phi(p_x,w)$.

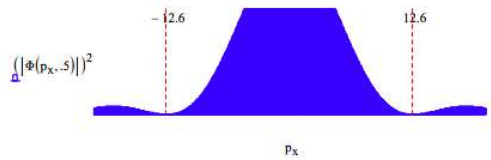
$$\Psi(p_x,\ w) = \frac{1}{\sqrt{2\pi}} \int_{-\frac{w}{2}}^{\frac{w}{2}} exp(-i\ p_x\ x)\frac{1}{\sqrt{w}}dx \text{ simplify } \rightarrow \frac{\sqrt{2}\sin\left(\frac{p_x w}{2}\right)}{\sqrt{\pi}p_x\sqrt{w}}$$

It is the momentum distribution, $|\Phi(p_x,\ w)|^2$, shown histographically below that is projected onto the detection screen. Thus, a position measurement at the detection screen is also effectively a measure of the x-component of the particle momentum.

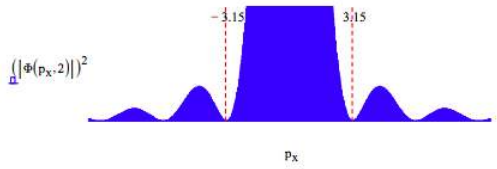


In this figure we see the spread in momentum required by the uncertainty principle, plus interference fringes due to the fact that the incident beam can imerge from any where within the slit, allowing for constructive and destructive interference at the detection screen. If the slit width is decreased the position is more precisely known and the uncertainty principle demands a broadening in the momentum distribution as shown below.

Equating uncertainty in position with slit width and uncertainty in momentum with the width of the intense center of the diffraction pattern, we have in atomic units: $\Delta x \Delta p_x$ = 12.6. If the slit width is decreased the position is more precisely known and the uncertainty principle demands a broadening in the momentum distribution as shown below. For slit width 0.5 we again find the product of the uncertainties is 12.6.



Naturally if the slit width is increased to 2.0 the position uncertainty increases and the uncertainty in momentum decreases yielding again $\Delta x \Delta p_x$ = 12.6.

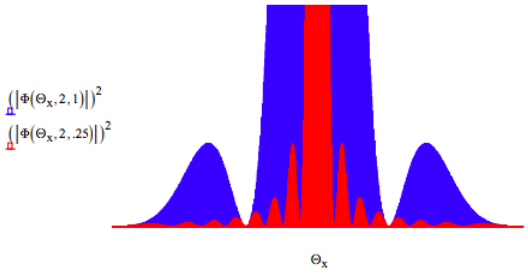


The x-direction momentum can be expressed in terms of the wavelength of the illuminating beam and the diffraction angle using the following sequence of equations of which the second is the de Broglie relation in atomic units (h = 2π).

$$p_x = p\sin(\Theta) \quad p = \frac{2\pi}{\lambda} \quad p_x = \frac{2\pi}{\lambda}\sin(\Theta)$$

$$\Phi(\Theta_x,\ w,\ \lambda) = \sqrt{\frac{2}{\pi w}}\frac{\sin\left(\frac{\pi w}{\lambda}\sin(\Theta_x)\right)}{\frac{2\pi}{\lambda}\sin(\Theta_x)}$$

This allows one to explore the effect of the wavelength of the illuminating beam on the diffraction pattern. The figure below shows that a short wavelength (high momentum) illuminating beam gives rise to a narrower diffraction pattern.



The method used here to calculate single-slit diffraction patterns (momentum-space distribution functions) is easily extended to multiple slits, and also to diffraction at two-dimensional masks with a variety of hole geometries.

Relevant literature:

Primary source: "Quantum interference with slits," Thomas Marcella which appeared in *European Journal of Physics* **23**, 615-621 (2002).

See also: "Calculating diffraction patterns," F. Rioux in *European Journal of Physics*, **24**, N1-N3 (2003). "Using Optical Transforms to Teach Quantum Mechanics," F. Rioux; B. J. Johnson, *The Chemical Educator*, **9**, 12-16 (2004). "Single-slit Diffraction and the Uncertainty Prinicple," F. Rioux in *Journal of Chemical Education*, **82**, 1210 (2005).

"Experimental verification of the Heisenberg uncertainty principle for hot fullerene molecules", O. Nairz, M. Arndt, and A. Zeilinger, *Phys. Rev. A*, **65**, 032109 (2002).

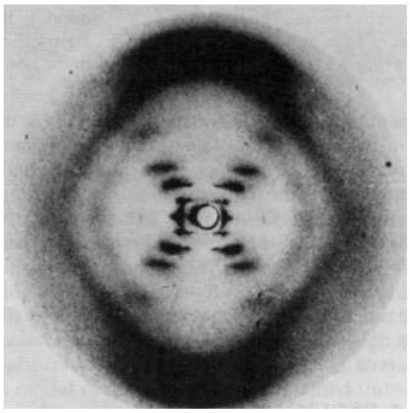
"Introducing the Uncertainty Principle Using Diffraction of Light Waves," Pedro L. Muino, *Journal of Chemical Education*, **77**, 1025-1027 (2000).

This page titled 5.3: Single-slit Diffraction and the Uncertainty Principle (Mathcad Version) is shared under a CC BY 4.0 license and was authored, remixed, and/or curated by Frank Rioux via source content that was edited to the style and standards of the LibreTexts platform.

5.4: Simulating DNA's Diffraction Pattern

The publication of the DNA double-helix structure by x-ray diffraction in 1953 is one the most significant scientific events of the 20th century (*1*). Therefore, it is important that science students and their teachers have some understanding of how this great achievement was accomplished. X-ray diffraction is conceptually simple: a source of X-rays illuminates a sample which scatters the x-rays, and a detector records the arrival of the scattered x-rays (diffraction pattern). However, the mathematical analysis required to extract from diffraction pattern the molecular geometry of the sample that caused the diffraction pattern is quite formidable. Therefore, the purpose of this tutorial is to illustrate some of the elements of the mathematical analysis required to solve a structure.

The famous X-ray diffraction pattern obtained by Rosalind Franklin is shown below (*2*).



This X-ray picture stimulated Watson and Crick to propose the now famous double-helix sturcture for DNA. It was surely fortuitous that Crick had recently completed an unrelated study of the diffraction patterns of helical molecules (*3*).

To gain some understanding of how the experimental pattern led to the hypothesis of a double-helical structure we will work in reverse. We will assume the double-helix structure, calculate the diffraction pattern, and compare it with the experimental result. This, therefore, is a deductive exercise as opposed to the brilliant inductive accomplishment of Watson and Crick in determining the DNA structure from Franklin's experimental X-ray pattern.

The experimental pattern will be simulated by modeling DNA solely as a planar double strand of sugar-phosphate backbone groups shown below. Reference 4 provides the justification and the limitations in using two-dimensional models for three-dimensional structures when simulating X-ray diffraction experiments.

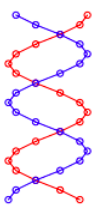
The double-strand geometry shown below was created using the following mathematics. Calculations are carried out in atomic units.

Sugar-phosphate groups per strand: $A = 20$ Strand radius: $R = 1$ Phase difference between strands: 0.8π

First strand: $m = 1..A$ $\Theta_m = \frac{4\pi m}{A}$ $y_m = m$ $x_m = R\cos(\Theta_m)$

Second strand: $m = 21..40$ $\Theta_m = \frac{4\pi(m-A)}{A}$ $y_m = (m - A)$ $x_m = R\cos(\Theta_m + 0.8\pi)$

$m = 1..20$ $n = 21..40$



According to quantum mechanical principles, the photons illuminating this geometrical arrangement interact with all its members simultaneously thus being cast into the spatial superposition, Ψ, given below.

$$|\Psi\rangle = \frac{1}{\sqrt{N}} \sum_{i=1}^{N} |x_i,\ y_i\rangle$$

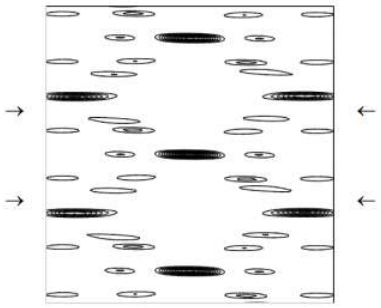
This spatial wave function is then projected into momentum space by a Fourier transform to yield the theoretical diffraction pattern. What is measured at the detector according to quantum mechanics is the two-dimensional momentum distribution created by the spatial localization that occurs during illumination of the structure. If the sugar-phosphate groups are treated as point scatterers the momentum wave function is given by the following Fourier transform.

$$\Theta(p_x,\ p_y) = \frac{1}{2\pi} \sum_{m=1}^{40} exp(-i\ p_x\ x_m) exp(-i\ p_y\ y_m)$$

The theoretical diffraction pattern can now be displayed as the absolute magnitude squared of the momentum wave function.

$$\Delta = 8 \quad N = 200 \quad j = 0..N \quad px_j = -\Delta + \frac{2\Delta j}{N} \quad k = 0..N \quad py_k = -\Delta + \frac{2\Delta k}{N}$$

$$\text{Diffraction pattern}_{j,\,k} = \left(|\Phi\,(px_j,\ y_k)|\right)^2$$



DiffractionPattern

Clearly the naive model diffraction pattern presented here captures several important features of the experimental diffraction pattern. Among those are the characteristic X-shaped cross of the diffraction pattern and the missing fourth horizontal layer (indicated by arrows).

Lucas, Lisensky, and co-workers (4, 5) have simulated the DNA diffraction pattern using the optical transform method. This tutorial might therefore be considered to be a theoretical companion to their more empirical approach to the subject.

References:

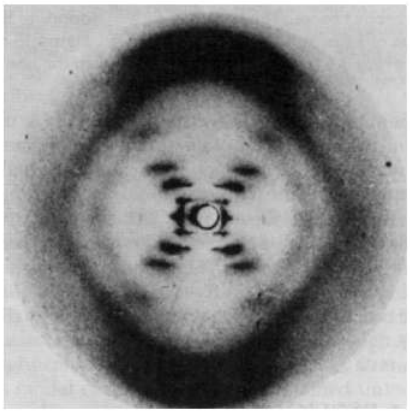
1. Watson, J. D.; Crick, F. H. C. *Nature* **1953**, 171, 737.
2. Franklin, R. E.; Gosling, R. G. *Nature* **1953**, 171, 740.
3. Cochran, W.; Crick, F. H. C.; Vand, V. *Acta Crystallogr*. **1952**, 5, 581.
4. Lucas, A. A.; Lambin, Ph.; Mairesse, R.; Mathot, M. *J. Chem. Educ.* **1999**, 76, 378.
5. Lisensky, G. C.; Lucas, A. A.; Nordell, K. J.; Jackelen, A. L.; Condren, S. M.; Tobe, R. H.; Ellis, A. B. DNA Optical Transform Kit; Institute for Chemical Education: University of Wisconsin, WI, 1999.

This page titled 5.4: Simulating DNA's Diffraction Pattern is shared under a CC BY 4.0 license and was authored, remixed, and/or curated by Frank Rioux via source content that was edited to the style and standards of the LibreTexts platform.

5.5: Simulating DNA's Diffraction Pattern with a More Realistic Model

The publication of the DNA double-helix structure by x-ray diffraction in 1953 is one the most significant scientific events of the 20th century (*1*). Therefore, it is important that science students and their teachers have some understanding of how this great achievement was accomplished. X-ray diffraction is conceptually simple: a source of X-rays illuminates a sample which scatters the x-rays, and a detector records the arrival of the scattered x-rays (diffraction pattern). However, the mathematical analysis required to extract from diffraction pattern the molecular geometry of the sample that caused the diffraction pattern is quite formidable. Therefore, the purpose of this tutorial is to illustrate some of the elements of the mathematical analysis required to solve a structure.

The famous X-ray diffraction pattern obtained by Rosalind Franklin is shown below (*2*).



This X-ray picture stimulated Watson and Crick to propose the now famous double-helix sturcture for DNA. It was surely fortuitous that Crick had recently completed an unrelated study of the diffraction patterns of helical molecules (*3*).

To gain some understanding of how the experimental pattern led to the hypothesis of a double-helical structure we will work in reverse. We will assume the double-helix structure, calculate the diffraction pattern, and compare it with the experimental result. This, therefore, is a deductive exercise as opposed to the brilliant inductive accomplishment of Watson and Crick in determining the DNA structure from Franklin′s experimental X-ray pattern.

The experimental pattern will be simulated by modeling DNA solely as a planar double strand of sugar-phosphate backbone groups shown below. Reference 4 provides the justification and the limitations in using two-dimensional models for three-dimensional structures when simulating X-ray diffraction experiments.

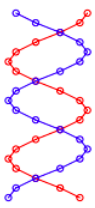
The double-strand geometry shown below was created using the following mathematics. Calculations are carried out in atomic units.

Sugar-phosphate groups per strand: $A = 20$ Strand radius: $R = 1$ Phase difference between strands: 0.8π

First strand: $m = 1..A$ $\Theta_m = \frac{4\pi m}{A}$ $y_m = m$ $x_m = R\cos(\Theta_m)$

Second strand: $m = 21..40$ $\Theta_m = \frac{4\pi(m-A)}{A}$ $y_m = (m-A)$ $x_m = R\cos(\Theta_m + 0.8\pi)$

$m = 1..20$ $n = 21..40$



According to quantum mechanical principles, the photons illuminating this geometrical arrangement interact with all its members simultaneously thus being cast into the spatial superposition, Ψ, given below.

$$|\Psi\rangle = \frac{1}{\sqrt{N}} \sum_{i=1}^{N} |x_i,\ y_i\rangle$$

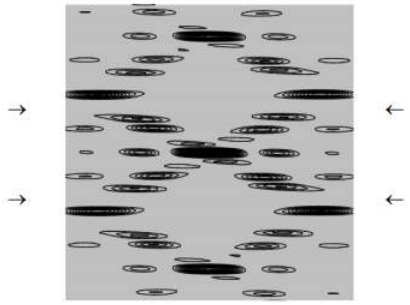
This spatial wave function is then projected into momentum space by a Fourier transform to yield the theoretical diffraction pattern. What is measured at the detector according to quantum mechanics is the two-dimensional momentum distribution created by the spatial localization that occurs during illumination of the structure. If the sugar-phosphate groups are treated as scatterers of dimension d the momentum wave function is given by the following Fourier transform.

$$d = 0.4 \quad \Phi(p_x,\ p_y) = \sum_{m=1}^{40} \left(\int_{y_m - \frac{d}{2}}^{y_m + \frac{d}{2}} \exp(-i\ p_y\ y) dy \right)$$

The theoretical diffraction pattern can now be displayed as the absolute magnitude squared of the momentum wave function.

$$\Delta = 8 \quad N = 200 \quad j = 0..N \quad px_j = -\Delta + \frac{2\Delta j}{N} \quad k = 0..N \quad py_k = -\Delta + \frac{2\Delta k}{N}$$

$$\text{Diffraction Pattern}_{j,\,k} = \left(|\Phi(px_j,\ py_k)|\right)^2$$



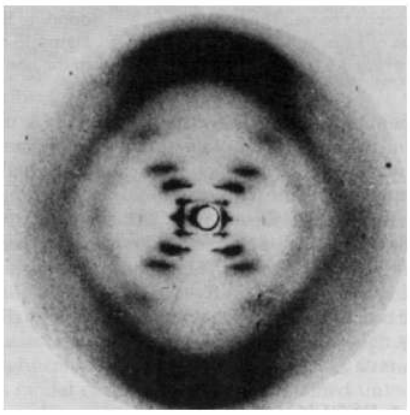
Clearly the naive model diffraction pattern presented here captures several important features of the experimental diffraction pattern. Among those are the characteristic X-shaped cross of the diffraction pattern and the missing fourth horizontal layer (indicated by arrows). Lucas, Lisensky, and co-workers (4, 5) have simulated the DNA diffraction pattern using the optical transform method. This tutorial might therefore be considered to be a theoretical companion to their more empirical approach to the subject.

References:

1. Watson, J. D.; Crick, F. H. C. *Nature* **1953**, 171, 737.
2. Franklin, R. E.; Gosling, R. G. *Nature* **1953**, 171, 740.
3. Cochran, W.; Crick, F. H. C.; Vand, V. *Acta Crystallogr*. **1952**, 5, 581.
4. Lucas, A. A.; Lambin, Ph.; Mairesse, R.; Mathot, M. *J. Chem. Educ.* **1999**, 76, 378.
5. Lisensky, G. C.; Lucas, A. A.; Nordell, K. J.; Jackelen, A. L.; Condren, S. M.; Tobe, R. H.; Ellis, A. B. DNA Optical Transform Kit; Institute for Chemical Education: University of Wisconsin, WI, 1999.

This page titled 5.5: Simulating DNA's Diffraction Pattern with a More Realistic Model is shared under a CC BY 4.0 license and was authored, remixed, and/or curated by Frank Rioux via source content that was edited to the style and standards of the LibreTexts platform.

5.6: Simulating DNA's Diffraction Pattern - Short Version

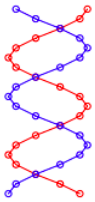


Sugar-phosphate groups per strand: $A = 20$ Strand radius: $R = 1$ Phase difference between strands: 0.8π

First strand: $m = 1..A$ $\Theta_m = \frac{4\pi m}{A}$ $y_m = m$ $x_m = R\cos(\Theta_m)$

Second strand: $m = 21..40$ $\Theta_m = \frac{4\pi(m-A)}{A}$ $y_m = (m - A)$ $x_m = R\cos(\Theta_m + 0.8\pi)$

$m = 1..20$ $n = 21..40$



Coordinate space wave function:

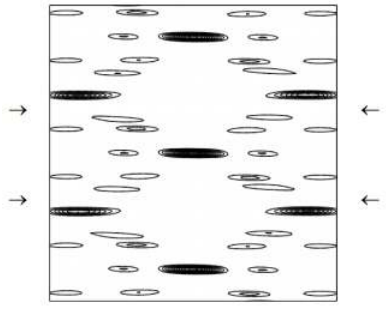
$$|\Psi\rangle = \frac{1}{\sqrt{N}} \sum_{i=1}^{N} |x_i,\ y_1\rangle$$

Momentum space wave function:

$$\Phi(p_x,\ p_y) = \frac{1}{2\pi} \sum_{m=1}^{40} exp(-ip_x x_m) exp(-ip_y y_m)$$

$$\Delta = 8 \quad N = 200 \quad j = 0..N \quad px_j = -\Delta + \frac{2\Delta j}{N} \quad k = 0..N \quad py_k = -\Delta + \frac{2\Delta k}{N}$$

$$\text{Diffraction Pattern}_{j,\,k} = (|\Phi(px_j,\ py_k)|)^2$$



DiffractionPattern

This page titled 5.6: Simulating DNA's Diffraction Pattern - Short Version is shared under a CC BY 4.0 license and was authored, remixed, and/or curated by Frank Rioux via source content that was edited to the style and standards of the LibreTexts platform.

5.7: A Model Graphene Diffraction Pattern

The purpose of this tutorial is to model graphene as seven fused benzene rings (see below) and use a Fourier transform of the atomic positions to calculate its diffraction pattern.

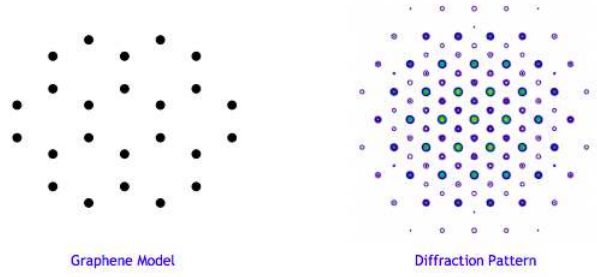
Number of atoms:	$A = 24$	Atomic dimension:	$d = .25$	Atomic positions:	
$x_1 = 0$	$y_1 = 1.386$	$x_2 = 0$	$y_2 = -1.386$	$x_{15} = 0$	$y_{15} = 2.772$
$x_3 = -1.2$	$y_3 = 0.693$	$x_4 = 1.2$	$y_4 = 0.693$	$x_{16} = 1.2$	$y_{16} = 3.465$
$x_5 = 1.2$	$y_5 = -0.693$	$x_6 = -1.2$	$y_6 = -0.693$	$x_{17} = 2.4$	$y_{17} 2.772$
$x_7 = 2.4$	$y_7 = 1.386$	$x_8 = 3.6$	$y_8 = 0.693$	$x_{18} = 0$	$y_{18} = -2.772$
$x_9 = 3.6$	$y_9 = -0.693$	$x_{10} = 2.4$	$y_{10} = -1.386$	$x_{19} = 1.2$	$y_{19} = -3.465$
$x_{11} = -2.4$	$y_{11} = 1.368$	$x_{12} = -3.6$	$y_{12} = 0.693$	$x_{20} = 2.4$	$y_{20} = -2.772$
$x_{13} = -3.6$	$y_{13} = -0.693$	$x_{14} = -2.4$	$y_{14} = -1.386$	$x_{21} = -2.4$	$y_{21} = 2.772$
$x_{22} = -1.2$	$y_{22} = 3.465$	$x_{23} = -2.4$	$y_{23} = -2.772$	$x_{24} = -1.2$	$y_{24} = -3.465$

The diffraction pattern is the Fourier transform of the atomic positions into momentum space.

$$\Delta = 20 \quad N = 200 \quad j = 0..N \quad px_j = -\Delta + \frac{2\Delta j}{N} \quad k = 0..N \quad py_k = -\Delta + \frac{2\Delta k}{N}$$

$$\Psi(p_x,\ p_y) = \sum_{m=1}^{A} \left(\int_{x_m - \frac{d}{2}}^{x_m + \frac{d}{2}} exp(-ip_x x)dx \int_{y_m - \frac{d}{2}}^{y_m + \frac{d}{2}} exp(-ip_y y)dx \right) \quad p_{j,\,k} = \left(|\Psi(px_j,\ py_j)|\right)^2$$

$i = 1..A$



This page titled 5.7: A Model Graphene Diffraction Pattern is shared under a CC BY 4.0 license and was authored, remixed, and/or curated by Frank Rioux via source content that was edited to the style and standards of the LibreTexts platform.

5.8: Is a Two-dimensional Fibonacci Array a Quasilattice?

A two-dimensional Fibonacci lattice lacks translational periodicity but has a discrete diffraction pattern, just like a quasicrystal. However, it does not fit the definition of a quasilattice because it does not posses one of the 'forbidden' n-fold rotational symmetries (n = 5 or greater than 6) that are characteristic of quasicrystals and incompatible with translational periodicity. R. Lifshitz1, therefore, recommends that the symmetry requirement be relaxed so that two- and three-dimensional Fibonacci lattices can have quasilattice stature.

A one-dimensional Fibonacci grid consists of a sequence of long (L) and short (S) segments such as LSLLSLSLLS.... with L/S = 1.618, the golden ratio. A two-dimensional array is created by superimposing two such grids at a 90^o angle and placing atomic scatterers at the vertices.

$$\text{Dimension of grid:} \quad A = 10 \quad m = 1..A \quad n = 1..A \quad \tau = \frac{1+\sqrt{5}}{2}$$

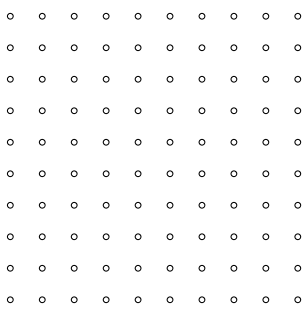
Calculate the coordinates of the Fibonacci vertices in a two-dimensional lattice (see Lifshitz).

$$x_m = \text{floor}\left(\frac{m}{\tau}\right)\tau + \left(m - \text{floor}\left(\frac{m}{\tau}\right)\right) - 1 \quad y_n = \text{floor}\left(\frac{n}{\tau}\right)\tau + \left(n - \text{floor}\left(\frac{n}{\tau}\right)\right) - 1$$

$$x^T = (0 \quad 1.618 \quad 2.618 \quad 4.236 \quad 5.854 \quad 6.854 \quad 8.472 \quad 9.472 \quad 11.09 \quad 12.708)$$
$$y^T = (0 \quad 1.618 \quad 2.618 \quad 4.236 \quad 5.854 \quad 6.854 \quad 8.472 \quad 9.472 \quad 11.09 \quad 12.708)$$

Display the two-dimensional Fibonacci array:

2D Fibonacci Lattice



The diffraction pattern is the Fourier transform of the spatial Fibonacci array into the momentum representation.

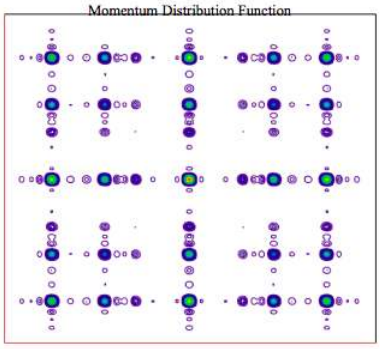
Calculate momentum-space wave function:

$$\Phi(p_x,\ p_y) = \frac{1}{2\pi}\sum_{m=1}^{A} exp(-ip_x x_m)\sum_{n=1}^{A} exp(-ip_y y_n)$$

Display momentum-space distribution function (diffraction pattern).

$$\Delta = 10 \quad N = 200 \quad j = 1..N \quad px_j = -\Delta + \frac{2\Delta j}{N} \quad k = 1..N \quad py_k = -\Delta + \frac{2\Delta k}{N}$$

$$\text{Diffraction Pattern}_{j,\,k} = \left(|\Phi(px_j,\ py_k)|\right)^2$$



DiffractionPattern

1. R. Lifshitz, "The square Fibonacci tiling," Journal of Alloys and Compounds 342, 186-190 (2002).

This page titled 5.8: Is a Two-dimensional Fibonacci Array a Quasilattice? is shared under a CC BY 4.0 license and was authored, remixed, and/or curated by Frank Rioux via source content that was edited to the style and standards of the LibreTexts platform.

5.9: Calculating Diffraction Patterns

I wish to describe a simple extension of Marcella's [1] recent analysis of the double-slit experiment to two dimensions.

The essential point Marcella makes in his unique treatment of this well-known experiment is that the diffraction pattern at the detection screen is actually a measurement of the momentum distribution of the diffracted particles. Therefore the calculated diffraction pattern is simply obtained from the Fourier transform of the coordinate space wave function (the double-slit geometry) into momentum space. Marcella considered two spatial models: (1) infinitesimally thin slits represented by Dirac delta functions, and (2) slits of finite width.

About sixty years ago Sir Lawerence Bragg [2] proposed the optical transform as an aid in the interpretation of the x-ray diffraction patterns of crystals. This required the fabrication of two-dimensional masks of various crystal or molecular geometries and the generation of the diffraction pattern using visible electromagnetic radiation. Present day laser technology has made the generation of such diffraction patterns routine, even in the classroom.

In addition, Marcella's computational approach makes calculating the diffraction patterns conceptually and mathematically straightforward. If one considers the mask as consisting of point scatterers (model 1), the coordinate space wave function is a linear superposition of the scattering positions,

$$|\Psi\rangle = \frac{1}{\sqrt{N}} \sum_{i=1}^{N} |x_i,\ y_1\rangle$$

where N is the number of point scatterers.

The Fourier transform into the momentum representation yields,

$$\langle p|\Psi\rangle = \frac{1}{\sqrt{N}} \sum_{i=1}^{N} \langle p_x|x_i\rangle\langle p_y|y_i\rangle = \frac{1}{2\pi h\sqrt{N}} \sum_{i=1}^{N} exp\left[-\frac{i}{h}(p_x x_i + p_y y_i)\right]$$

For model 2, which assumes finite-sized scatterers, equation (2) becomes,

$$\langle p|\Psi\rangle = \frac{1}{2\pi hr\sqrt{N}} \sum_{i=1}^{N} \int_{x_i-\frac{r}{2}}^{x_i+\frac{r}{2}} exp\left[-\frac{ip_x x}{h}\right] dx \int_{y_i-\frac{r}{2}}^{y_i+\frac{r}{2}} exp\left[-\frac{ip_y y}{h}\right] dy$$

where *r* is the spatial dimension of the scatterers. In the interest of mathematical simplicity, the scatterers are assumed to be small squares rather than circles.

Figure 1 shows the diffraction pattern, $|\langle p|\Psi\rangle|^2$, for a hexagonal arrangement of six point scatterers calculated using equation (2), while figure 2 shows the pattern obtained with equation (3) for six finite hexagonal scatterers. The calculated diffraction pattern shown in figure 2 is in excellent agreement with the experimental diffraction pattern available in the literature [3]. The calculations [4] of the diffraction patterns were carried out in atomic units (h = 2π) so that positions are given in a0 and momenta in a0 -1. The distance between adjacent scatters is 1.4 a0 and their spatial dimension is 0.3 a0 on a side.

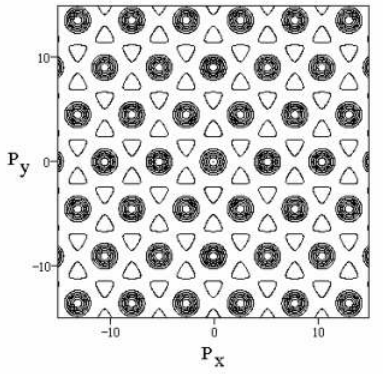


Figure 1. Diffraction pattern for a hexagonal arrangement of six point scatterers.

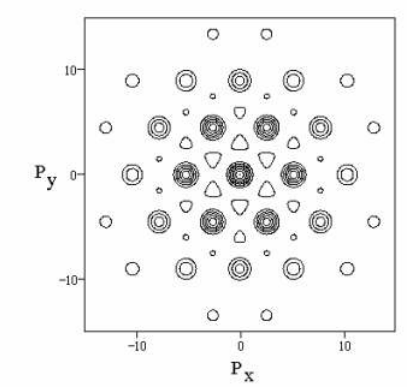


Figure 2. Diffraction pattern for a hexagonal arrangement of six finite scatterers.

In addition to showing the interference effects accompanying scattering from multiple positions, the figures also illustrate the uncertainty principle. Figure 1 shows no attenuation of the diffraction pattern at extreme values of momentum because the point scatterers sharply localize the particle being scattered in coordinate space, leading to a delocalized momentum distribution as required by the position-momentum uncertainty relation. By comparison the finite scatterers of figure (2) lead to some uncertainty in position and, therefore, less uncertainty in momentum. Therefore the diffraction pattern is attenuated at large values for both the x- and y-momentum components.

References

1. Marcella T V 2002 *Eur. J. Phys.* **23** 615-621
2. Bragg L 1944 *Nature* **154** 69-72
3. Harburn G, Taylor C A and Welberry T R 1975 *Atlas of Optical Transforms* (Ithaca, NY: Cornell University Press) Plates 4 and 5.
4. The Mathcad 5.0 files used to generate Figures 1 and 2 are available for download at ww.users.csbsju.edu/frioux/di.../hex-point.mcd and ~/hex-finite.mcd.

This page titled 5.9: Calculating Diffraction Patterns is shared under a CC BY 4.0 license and was authored, remixed, and/or curated by Frank Rioux via source content that was edited to the style and standards of the LibreTexts platform.

5.10: Modeling the C60 Diffraction Pattern

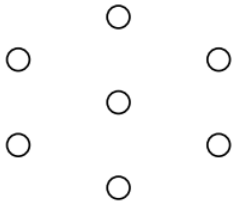
In this tutorial a model diffraction pattern for C_{60} is calculated and compared with the experimental diffraction pattern.

Solid C_{60} has the cubic close-packed crystal structure. For the sake of computational convenience this structure will be modeled as a planar close-packed array consisting of seven C_{60} molecules represented by squares (see the mask geometry shown below). According to quantum mechanical principles, radiat illuminating this geometrical arrangement interacts with all its members simultaneously thus being cas the spatial superposition, Ψ, given below. This spatial wave function is then projected into momentum space by a Fourier transform. Therefore what is measured at the detector can be interpreted as the two-dimensional momentum distribution created by the spatial localization that occurs at the mask up illumination.

Create mask geometry: $A = 6$ $R = 1.4$ $m = 1..A$ $\Theta_m = \frac{2\backslash pm}{A}$

$x_m = R\sin(\Theta_m)$ $y_m = R\cos(\Theta_m)$ $x_7 = 0$ $y_7 = 0$ Molecule size: $d = 3$

Display coordinate wave function (mask geometry): $m = 1..7$



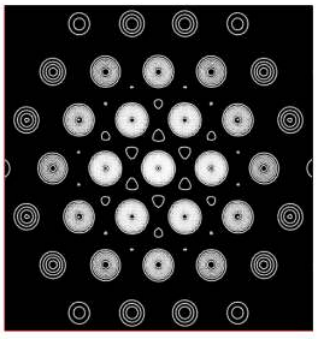
Fourier transform the coordinate wave function into the momentum representation:

$$\Phi(p_x,\ p_y) = \sum_{m=1}^{A+1} \int_{x_m-\frac{d}{2}}^{x_m+\frac{d}{2}} exp(-p\ p_x\ x)dx \int_{y_m-\frac{d}{2}}^{y_m+\frac{d}{2}} exp(-i\ p_y\ y)dy$$

Display diffraction pattern:

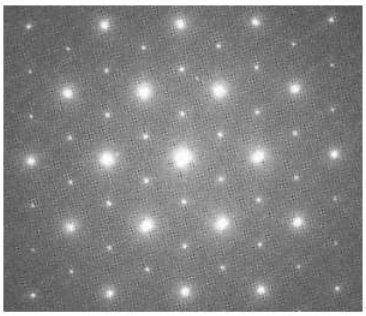
$$\Delta = 15 \quad N = 100 \quad j = 0..N \quad px_j = -\Delta + \frac{2\Delta j}{N} \quad k = 0..N \quad py_k = -\Delta + \frac{2\Delta k}{N}$$

$$\text{Diffraction Pattern}_{j,\,k} = \left(|\Phi(px_j,\ py_k)|\right)^2$$



DiffractionPattern

The calculated diffraction pattern above compares favorably with the experimental diffraction pattern shown below, indicating that the simple planar model proposed for C_{60} captures the essential element the actual solid structure. See page 154 of *Perfect Symmetry* by Jim Baggot for further information.



This page titled 5.10: Modeling the C60 Diffraction Pattern is shared under a CC BY 4.0 license and was authored, remixed, and/or curated by Frank Rioux via source content that was edited to the style and standards of the LibreTexts platform.

5.11: Diffraction Pattern for Pentagonal Point Scatterers

Establish mask geometry:

$$R = 2 \quad m = 1..A \quad \Theta_m = \frac{2\pi m}{A} \quad x_m = R\sin(\Theta_m) \quad y_m = R\cos(\Theta_m)$$

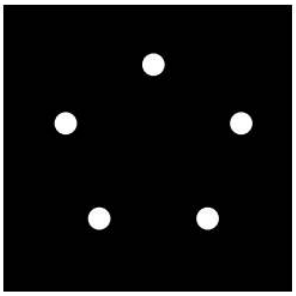
Fourier transform of position wave function (mask geometry) into the momentum representation:

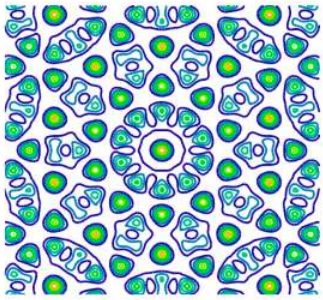
$$\Phi(p_x,\ p_y) = \frac{1}{2\pi\sqrt{A}} \sum_{m=1}^{A} (exp(-ip_x x_m) exp(-ip_y y_m))$$

Display mask geometry and diffraction pattern: $A \equiv 5$

$$N = 100 \quad \Delta p = 12 \quad j = 0..N \quad k = 0..N \quad px_j = -\Delta p + \frac{2\Delta p j}{N} \quad py_k = -\Delta p + \frac{2\Delta p\, k}{N}$$

$$\text{Diffraction Pattern}_{j,\,k} = \left(|\Phi(px_j,\ py_k)|\right)^2$$





This page titled 5.11: Diffraction Pattern for Pentagonal Point Scatterers is shared under a CC BY 4.0 license and was authored, remixed, and/or curated by Frank Rioux via source content that was edited to the style and standards of the LibreTexts platform.

5.12: Diffraction Pattern for Pentagonal Finite Point Scatterers

Establish mask geometry:

$$R = 2 \quad m = 1..A \quad \Theta_m = \frac{2\pi m}{A} \quad x_m = R\sin(\Theta_m) \quad y_m = R\cos(\Theta_m)$$

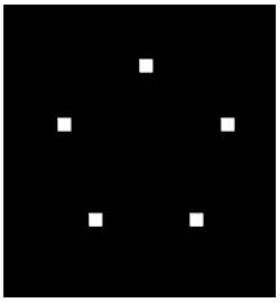
Fourier transform of position wave function (mask geometry) into the momentum representation:

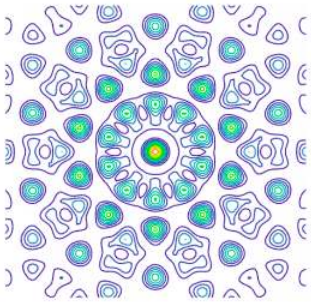
$$\Phi(p_x,\ p_y) = \frac{1}{2\pi d\sqrt{A}} \left[\sum_{m=1}^{A} \left(\int_{x_m - \frac{d}{2}}^{x_m + \frac{d}{2}} exp(-ip_x x)dx \int_{y_m - \frac{d}{2}}^{y_m + \frac{d}{2}} exp(-ip_y y)dy \right) \right]$$

Display mask geometry and diffraction pattern: $A = 5 \quad d = .3$

$$N = 100 \quad \Delta p = 10 \quad j = 0..N \quad k = 0..N \quad px_j = -\Delta + \frac{2\Delta pj}{N} \quad py_k = -\Delta p + \frac{2\Delta pk}{N}$$

$$\text{Diffraction pattern}_{j,\,k} = (|\Phi(px_j,\ py_k)|)^2$$





This page titled 5.12: Diffraction Pattern for Pentagonal Finite Point Scatterers is shared under a CC BY 4.0 license and was authored, remixed, and/or curated by Frank Rioux via source content that was edited to the style and standards of the LibreTexts platform.

5.13: Pentagram Diffraction Pattern

Establish mask geometry:

$$R = 2 \quad m = 1..5 \quad \Theta_m = \frac{2\pi m}{5} \quad x_m = R\sin(\Theta_m) \quad y_m = R\cos(\Theta_m)$$
$$R = 0.75 \quad m = 6..10 \quad \Theta_m = \frac{2\pi(m-0.5)}{5} \quad x_m = R\sin(\Theta_m) \quad y_m = R\cos(\Theta_m)$$

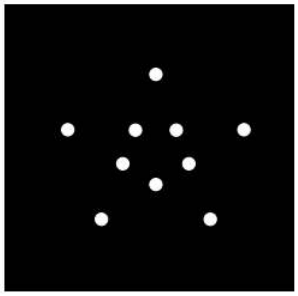
Fourier transform of position wave function (mask geometry) into the momentum representation: $m = 1..10$

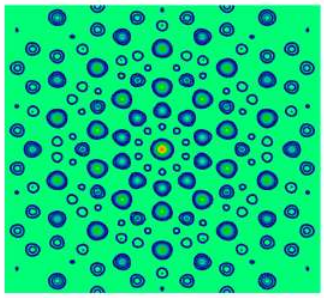
$$d = .15 \quad \Phi(p_x,\ p_y) = \frac{1}{2\pi d\sqrt{10}} \left[\sum_{m=1} \left(\int_{x_m-\frac{d}{2}}^{x_m+\frac{d}{2}} exp(-ip_x x)dx \int_{y_m-\frac{d}{2}}^{y_m+\frac{d}{2}} exp(-ip_y y)dy\right)\right]$$

Display mask geometry and diffraction pattern:

$$N = 100 \quad \Delta p = 20 \quad j = 0..N \quad k = 0..N \quad px_j = -\Delta + \frac{2\Delta pj}{N} \quad py_k = -\Delta p + \frac{2\Delta pk}{N}$$

$$\text{Diffraction pattern}_{j,\,k} = (|\Phi(px_j,\ py_k)|)^2$$





This page titled 5.13: Pentagram Diffraction Pattern is shared under a CC BY 4.0 license and was authored, remixed, and/or curated by Frank Rioux via source content that was edited to the style and standards of the LibreTexts platform.

5.14: Model Diffraction Pattern for Napthalene

Ten holes in a two-dimensional mask are used to model the diffraction pattern for napthalene. It is assumed that only the carbon atoms scatter radiation.

Establish mask geometry:

$$R = 2 \quad m = 1..6 \quad \Theta_m = \frac{2\pi m}{6} \quad x_m = R\sin(\Theta_m) - \sqrt{3} \quad y_m = R\cos(\Theta_m)$$
$$m = 7..10 \quad \Theta_m = \frac{2\pi(m-0.5)}{6} \quad x_m = R\sin(\Theta_m) + \sqrt{3} \quad y_m = R\cos(\Theta_m - \frac{\pi}{\sqrt{3}})$$

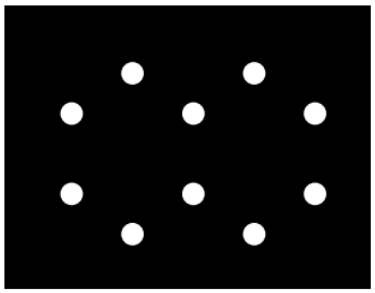
Fourier transform of position wave function (mask geometry) into the momentum representation. Initially the carbon atoms are considered to be point scatterers.

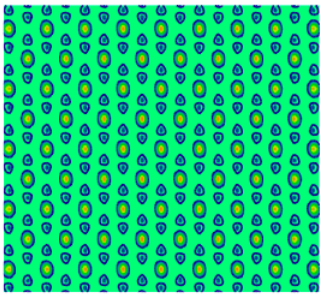
$$m = 1..10 \quad \Phi(p_x,\ p_y) = \frac{1}{2\pi d\sqrt{10}} \left[\sum_{m=1} \left(\int_{x_m-\frac{d}{2}}^{x_m+\frac{d}{2}} exp(-ip_x x)dx \int_{y_m-\frac{d}{2}}^{y_m+\frac{d}{2}} exp(-ip_y y)dy\right)\right]$$

Display mask geometry and diffraction pattern:

$$N = 100 \quad \Delta p = 15 \quad j = 0..N \quad k = 0..N \quad px_j = -\Delta + \frac{2\Delta pj}{N} \quad py_k = -\Delta p + \frac{2\Delta pk}{N}$$

$$\text{Diffraction pattern}_{j,\,k} = \left(|\Phi(px_j,\ py_k)|\right)^2$$



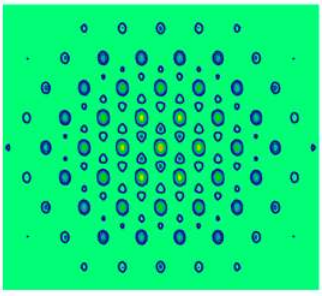


This calculation illustrates the uncertainty principle. There is no attenuation in the diffraction pattern (momentum distribution) because there is no uncertainty in the carbon atom positions.

Now the diffraction pattern is recalculated assuming an arbitrary finite dimension for the carbon atoms.

$$r = .15 \quad \Phi(p_x,\ p_y) = \frac{1}{2\pi d\sqrt{10}} \left[\sum_{m=1} \left(\int_{x_m-r}^{x_m+r} exp(-ip_x x)dx \int_{y_m-r}^{y_m+r} exp(-ip_y y)dy\right)\right]$$

$$\text{Diffraction pattern}_{j,\,k} = \left(|\Phi(px_j,\ py_k)|\right)^2$$

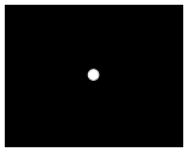


There is attenuation in the momentum distribution (less uncertainty) because there is more uncertainty in the carbon atom positions.

This page titled 5.14: Model Diffraction Pattern for Napthalene is shared under a CC BY 4.0 license and was authored, remixed, and/or curated by Frank Rioux via source content that was edited to the style and standards of the LibreTexts platform.

5.15: Calculating the Airy Diffraction Pattern

The Airy diffraction pattern is created by illuminating a screen containing a circular hole with photons. The experiment can be performed with weak sources such that there is only one photon interacting with the screen at a time. This photon-screen interaction constitutes a position measurement.



The position wave function has a constant amplitude within the area of the hole and is shown to be normalized.

$$\Psi(x,\ y) = \frac{1}{\sqrt{\pi R^2}} \quad R^2 = x^2 + y^2 \quad \int_{-R}^{R} \int_{-\sqrt{R^2-x^2}}^{\sqrt{R^2-x^2}} \Psi(x,\ y)^2 dy dx = 1$$

The Airy diffraction pattern is the Fourier transform of the position wave function into the momentum representation. In other words, the interference pattern at the detection screen actually represents a momentum measurement. The following calculations are carried out in atomic units using a hole radius of 0.2.

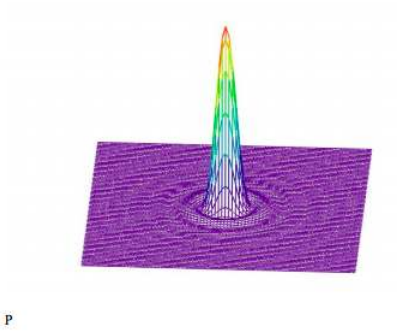
Hole radius: R = .2

Calculate the Airy diffraction pattern:

$$\Delta = 100 \quad N = 80 \quad j = 0..N \quad px_j = -\Delta + \frac{2\Delta j}{N} \quad k = 0..N \quad py_k = -\Delta + \frac{2\Delta k}{N}$$

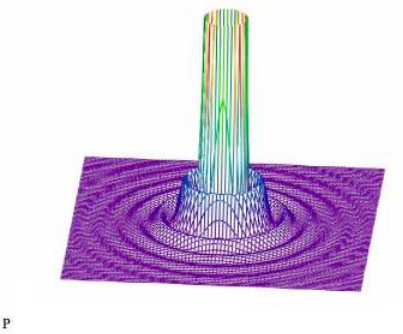
$$\Phi(p_x,\ p_y) = \frac{1}{\pi} \int_{R}^{R} \int_{-\sqrt{R^2-x^2}}^{\sqrt{R^2-x^2}} \frac{1}{\sqrt{\pi R^2}} exp(-ip_x x) exp(-ip_y y) dy dx \quad P_{j,\,k} = \left(|\Phi(px_j,\ py_k)|\right)^2$$

Display the Airy diffraction pattern.



P

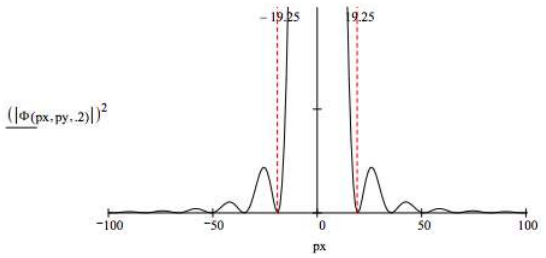
Truncating the high intensity central disk provides a better picture of the outer maxima and minima.



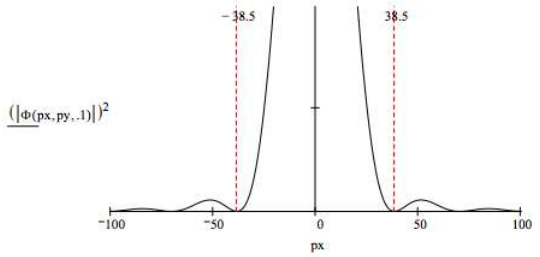
P

Examining a radial slice of the Airy diffraction pattern provides a simple illustration of the uncertainty principle. Assume that the position uncertainty is given by the diameter of the hole and that the momentum uncertainty is given by the momentum range of the central disk.

$$py = 0 \quad px = -100, \ -99, ..100 \qquad \Phi(px,\ py\ R)$$
$$= \frac{1}{\pi} \int_{-R}^{R} \int_{-\sqrt{R^2-x^2}}^{\sqrt{R^2-x^2}} \frac{1}{\sqrt{\pi R^2}} exp(-ipxx) exp(-ipyy) dydx$$



For a diameter of 0.4the position-momentum uncertainty product is: $0.4\ 38.5 = 15.4$



For a diameter of 0.2 the position-momentum uncertainty product is: $.2\ 77.0 = 15.4$

The reciprocal relationship between the uncertainty in position and momentum is clearly revealed in this example.

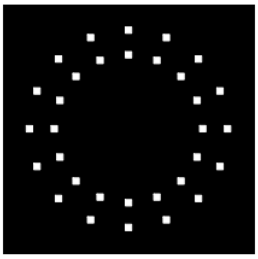
This page titled 5.15: Calculating the Airy Diffraction Pattern is shared under a CC BY 4.0 license and was authored, remixed, and/or curated by Frank Rioux via source content that was edited to the style and standards of the LibreTexts platform.

5.16: Diffraction Pattern for Two Concentric Rings

Create hole positions:

$$A = 32 \quad R = 1.2 \quad m = 1..16 \quad \Theta_m = \frac{2\pi m}{16} \quad x_m = R\sin(\Theta_m) \quad y_m = R\cos(\Theta_m)$$
$$R = .9 \quad m = 17..A \quad \Theta_m = \frac{2\pi m}{16} \quad x_m = R\sin(\Theta_m) \quad y_m = R\cos(\Theta_m)$$

Display coordinate-space wave function (mask geometry): $m = 1..A$



Fourier transform position wave function into the momentum representation:

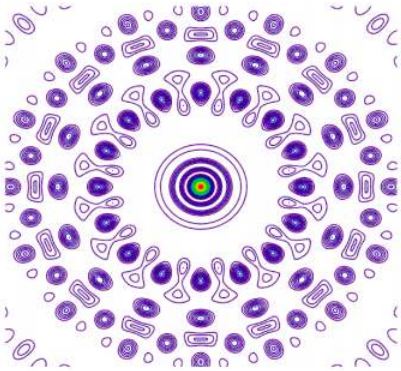
$$\Delta = 30 \quad N = 200 \quad j = 0..N \quad px_j = -\Delta + \frac{2\Delta j}{N} \quad k = 0..N \quad py_k = -\Delta + \frac{2\Delta k}{N}$$

Hole dimension:

$$d = .1 \quad \Psi(p_x,\ p_y) = \frac{1}{2\pi d\sqrt{A}} \sum_{m=1}^{A} \left(\int_{x_m - \frac{d}{2}}^{x_m + \frac{d}{2}} exp(-ip_x x)dx \int_{y_m - \frac{d}{2}}^{y_m + \frac{d}{2}} exp(-ip_y y)dy \right)$$

Display diffraction pattern:

$$P_{j,\,k} = \left(|\Psi(x_j,\ Py_k)|\right)^2$$



P

This page titled 5.16: Diffraction Pattern for Two Concentric Rings is shared under a CC BY 4.0 license and was authored, remixed, and/or curated by Frank Rioux via source content that was edited to the style and standards of the LibreTexts platform.

5.17: Density Operator Approach to the Double-Slit Experiment

A sharply focused particle beam (photons, electrons, molecules, etc.) is incident on a screen with two slits. According to quantum mechanics the individual particles are represented by a coherent superposition of being simultaneously at both slits.

$$|\Psi\rangle = \frac{1}{\sqrt{2}}\left[|1\rangle + |2\rangle\right]$$

In the interest of mathematical simplicity, *1* and *2* label slits that are infinitesimally narrow in the x-direction and infinitely long in the y-direction. The density operator for this state is

$$\hat{\rho} = |\Psi\rangle\langle\Psi| = \frac{1}{2}\left[|1\rangle + |2\rangle\right]\left[\langle 1| + \langle 2|\right] = \frac{1}{2}\left[|1\rangle\langle 1| + |1\rangle\langle 2| + |2\rangle\langle 1| + |2\rangle\langle 2|\right]$$

The expectation value for the arrival of a particle at position *x* on the detection screen is

$$\langle x|\hat{\rho}|x\rangle = \frac{1}{2}\left[\langle x|1\rangle\langle 1|x\rangle + \langle x|1\rangle\langle 2|x\rangle + \langle x|2\rangle\langle 1|x\rangle + \langle x|2\rangle\langle 2|x\rangle\right]$$

Rearrangement yields,

$$\langle x|\hat{\rho}|x\rangle = \frac{1}{2}\left[|\langle x|1\rangle|^2 + |\rangle x|2\rangle|^2 + \langle x|1\rangle\langle x|2\rangle * + \langle x|2\rangle\langle x|1\rangle *\right]$$

The probability amplitudes in this equation represent the phase of a particle on arrival at position x from slits 1 and 2. For example, using Euler's equation we calculate the phase of a particle arriving at x from slit 1 as follows,

$$\langle x|1\rangle = \frac{1}{\sqrt{2\pi r}} exp\left(i2\pi\frac{\delta x_1}{\lambda}\right)$$

where δx_1 is the distance from slit 1 to position x on the detection screen and λ is the de Broglie wavelength of the particle.

Using this form for the probability amplitudes we can write the expectation value in terms of the distances to x from slits 1 and 2.

$$\begin{aligned}\langle x|\hat{\rho}|x\rangle &= \frac{1}{4\pi}\left[2 + exp\left(i2\pi\frac{(\delta x_1 - \delta x_2)}{\lambda}\right) + exp\left(-i2\pi\frac{(\delta x_1 - \delta x_2)}{\lambda}\right)\right] \\ &= \frac{1}{2\pi}\left[1 + \cos\left(\frac{(\delta x_1 - \delta x_2)}{\lambda}\right)\right]\end{aligned}$$

Clearly $\frac{(\delta x_1 - \delta x_2)}{\lambda}$ will vary continuously along the x-axis of the detector from large negative values at one end to large positive values at the other end leading to minima and maxima in the cosine term and therefore $\langle x|\hat{\rho}|x\rangle$, thereby yielding the well-known interference fringes associated with the double-slit experiment. Naturally a more realistic slit geometry will lead to a mathematically more complicated expression for the expectation value.

If one takes a classical view of the double-slit experiment that assumes the particle goes through one slit or the other, and has a 50% chance of going through either slit, the coherent superposition,

$$\hat{\rho} = \frac{1}{2}|1\rangle\langle 1| + \frac{1}{2}|2\rangle\langle 2|$$

The expectation value for the arrival of the particle at x on the detection screen is now,

$$\langle x|\hat{\rho}_{cl}|x\rangle = \frac{1}{2}\langle x|1\rangle\langle 1|x\rangle + \frac{1}{2}\langle x|2\rangle\langle 2|x\rangle = \frac{1}{2}|\langle x|1\rangle|^2 + \frac{1}{2}|\langle x|2\rangle|^2 = \text{ constant}$$

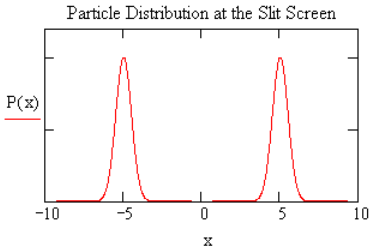
which has a constant value with no oscillations in arrival probability as a function of x. In other words, no interference fringes.

This page titled 5.17: Density Operator Approach to the Double-Slit Experiment is shared under a CC BY 4.0 license and was authored, remixed, and/or curated by Frank Rioux via source content that was edited to the style and standards of the LibreTexts platform.

5.18: Another Look at the Double-Slit Experiment

Illumination of a double-slit screen with a coherent particle beam leads to a Schrödinger "cat state" that can be represented by a linear superposition (unnormalized) of two Gaussian wavepackets. The probability distribution function in coordinate space, $|\Psi(x)|^2$, at the slit-screen for this "cat state" is shown below.

$$x = -10,\ -9.99..10 \quad \Psi(x) = exp\left[-(x-5)^2\right] + exp\left[-(x+5)^2\right] \quad P(x) = (|\Psi(x)|)^2$$



The slits localize the particle in the x-direction which leads to a spread in the x-component of the momentum required by the uncertainty principle, $\Delta x \Delta p_x > h/4\pi$. The momentum wave function is obtained by a Fourier transform of the coordinate-space wave function.

$$\Phi(p_x) = \frac{1}{\sqrt{2\pi}}\left[\int_{-\infty}^{\infty} exp(-ip_x x)\left[exp\left[-(x-5)^2\right] + exp\left[-(x+5)^2\right]\right] dx\right]$$

Evaluation of the integral yields,

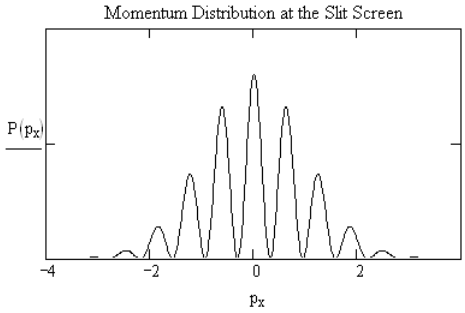
$$\Phi(p_x) = \frac{1}{\sqrt{2}}\left[exp\left[\frac{-1}{4}p_x(p_x + 20i)\right] + exp\left[\frac{-1}{4}p_x(p_x - 20i\right]\right]$$

The momentum probability function in the x-direction is $|\Phi(p_x)|^2$ and simplifies to the expression given below when evaluated.

$$P(p_x) = 2exp\left(\frac{-1}{2}p_x^2\right)\cos\left(5p_x\right)^2$$

This momentum probability function is displayed below.

$$p_x = -4, -3.99..4$$



Because the arrival at position x on the detection screen is proportional to p_x it is also proportional to $|\Phi(p_x)|^2$. In other words, the particle distribution at the detection screen is determined by the momentum distribution at the slit screen. This means the position measurement at the detection screen is effectively a measurement of the p_x. Therefore, the particle distribution at the detector screen will have the same shape as shown in the figure above.

In summary, the double-slit experiment clearly reveals the three essential steps in a quantum mechanical experiment:

1. State preparation (interaction of the incident beam with the slit-screen)
2. Measurement of an observable (arrival of scattered beam at the detection screen)
3. Calculation of expected results of the measurement step

*The preparation of this tutorial was stimulated by reading "Quantum interference with slits" by Thomas Marcella which appeared in *European Journal of Physics* **23**, 615-621 (2002). This paper offers a lucid and novel quantum mechanical analysis of a very important experiment.

Additional references:

R. P. Feynman, R. B. Leighton, and M.Sands, *The Feynman Lectures on Physics*, Volume 3; Addison-Wesley; Reading, 1965, Chapters 1 and 3.

R. P. Feynman, *The Character of Physical Law*; MIT Press: Cambridge, 1967, Chapter 6.

A. Tonomura, J. Endo, T. Matsuda, T. Kawasaki, and H. Exawa, "Demonstration of single-electron buildup of an interference pattern" *Am. J. Phys*. **57**, 117-120 (1989).

D. Leibfried, T. Pfau, and C. Monroe, "Shadows and Mirrors: Reconstructing Quantum States of Atom Motion" *Phys. Today* **51(4)**, 22-28 (1998).

The double-slit experiment with single electrons was recently selected (informally) as physics most beautiful experiment. The following web reference traces the history of double-slit interference experiments from the time of Thomas Young to the present, presenting numerous literature references in the process: http://physicsweb.org/article/world/15/9/1.

This page titled 5.18: Another Look at the Double-Slit Experiment is shared under a CC BY 4.0 license and was authored, remixed, and/or curated by Frank Rioux via source content that was edited to the style and standards of the LibreTexts platform.

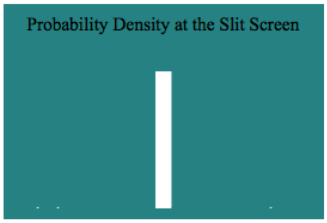
5.19: A Quantum Mechanical Interpretation of Diffraction

Diffraction has a simple quantum mechanical interpretation based on the uncertianty principle. Or we could say diffraction is an excellent way to illustrate the uncertainty principle.

A screen with a single slit of width, w, is illuminated with a coherent photon or particle beam. The normalized coordinate-space wave function at the slit screen is,

$$\Psi(x,\ w) = \begin{vmatrix} \frac{1}{\sqrt{w}} \text{if}\left(x \geq -\frac{w}{2}\right)\left(x \leq \frac{w}{2}\right) \\ 0 \text{ otherwise} \end{vmatrix}$$

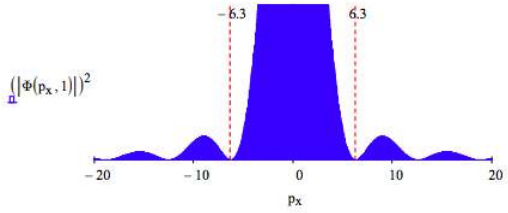
The coordinate-space probability density, $|\Psi(x,w)|^2$, is displayed for a slit of unit width below



The slit-screen measures position, it localizes the incident beam in the x-direction. According to the uncertainty principle, because position and momentum are complementary, or conjugate, observables, this measurement must be accompanied by a delocalization of the x-component of the momentum. This can be seen by a Fourier transform of $\Psi(x,w)$ into momentum space to obtain the momentum wave function, $\Phi(p_x,w)$.

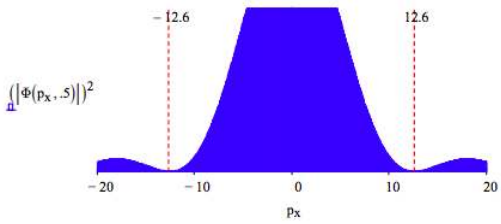
Extra \left or missing \right

It is the momentum distribution, $|\Psi(px\ ,w)|^2$, shown below that is projected onto the detection screen. Thus, a position measurement at the detection screen is also effectively a measure of the x-component of the particle momentum.

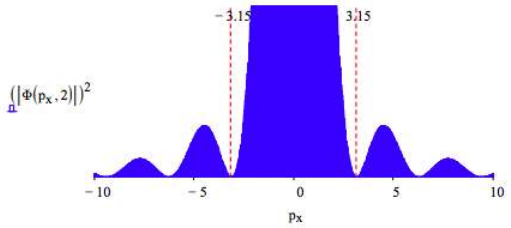


In this figure we see the spread in momentum required by the uncertainty principle, plus interference fringes due to the fact that the incident beam can imerge from any where within the slit, allowing for constructive and destructive interference at the detection screen. If the slit width is decreased the position is more precisely known and the uncertainty principle demands a broadening in the momentum distribution as shown below.

Equating uncertainty in position with slit width and uncertainty in momentum with the width of the intense center of the diffraction pattern, we have in atomic units: $\Delta x \Delta p_x$ = 12.6. If the slit width is decreased the position is more precisely known and the uncertainty principle demands a broadening in the momentum distribution as shown below. For slit width 0.5 we again find the product of the uncertainties is 12.6.



Naturally if the slit width is increased to 2.0 the position uncertainty increases and the uncertainty in momentum decreases yielding again $\Delta x \Delta p_x = 12.6$.

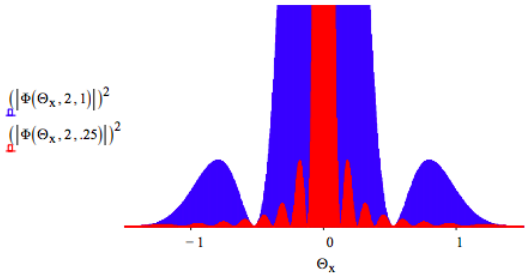


The x-direction momentum can be expressed in terms of the wavelength of the illuminating beam and the diffraction angle using the following sequence of equations of which the second is the de Broglie relation in atomic units (h = 2π).

$$p_x = p\sin(\Theta) \quad p = \frac{2\pi}{\lambda} \quad p_x = \frac{2\pi}{\lambda}\sin(\Theta)$$

$$\Phi(\Theta_x,\ w,\ \lambda) = \sqrt{\frac{2}{\pi w}}\,\frac{\sin\left(\frac{\pi w}{\lambda}\sin(\Theta_w)\right)}{\frac{2\pi}{\lambda}\sin(\Theta_w)}$$

This allows one to explore the effect of the wavelength of the illuminating beam on the diffraction pattern. The figure below shows that a short wavelength (high momentum) illuminating beam gives rise to a narrower diffraction pattern.



The method used here to calculate single-slit diffraction patterns (momentum-space distribution functions) is easily extended to multiple slits, and also to diffraction at two-dimensional masks with a variety of hole geometries.

Primary source: "Quantum interference with slits," Thomas Marcella which appeared in *European Journal of Physics* **23**, 615-621 (2002).

See also: "Calculating diffraction patterns," F. Rioux in *European Journal of Physics*, **24**, N1-N3 (2003). "Single-slit Diffraction and the Uncertainty Principle," F. Rioux in *Journal of Chemical Education*, **82**, 1210 (2005).

"Experimental verification of the Heisenberg uncertainty principle for hot fullerene molecules", O. Nairz, M. Arndt, and A. Zeilinger, *Phys. Rev. A*, **65**, 032109 (2002).

"Introducing the Uncertainty Principle Using Diffraction of Light Waves," Pedro L. Muino, *Journal of Chemical Education*, **77**, 1025-1027 (2000).

This page titled 5.19: A Quantum Mechanical Interpretation of Diffraction is shared under a CC BY 4.0 license and was authored, remixed, and/or curated by Frank Rioux via source content that was edited to the style and standards of the LibreTexts platform.

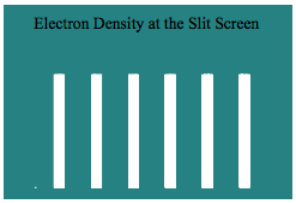
5.20: Electron Diffraction at Multiple Slits

The American Journal of Physics published a translation of Claus Jonsson's paper "Electron Diffraction at Multiple Slits" in *American Journal of Physics* **42**, 4-11 (1974). The following calculations are in agreement with the diffraction patterns reported by Jonsson.

$$\begin{array}{llllllll} \text{Number of slits:} & n=6 & \text{Slit width:} & w=.5 & & & & \\ \text{Slit locations:} & s_1=0 & s_2=2 & s_3=4 & s_4=6 & s_5=8 & s_6=10 \end{array}$$

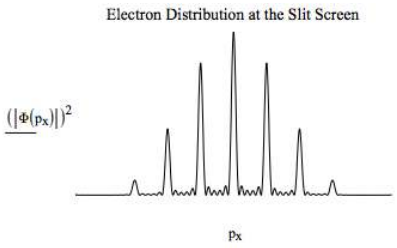
Normalized coordinate-space wave function at the slit screen:

$$\Psi(x)=\frac{1}{\sqrt{N}}\begin{vmatrix} \frac{1}{\sqrt{w}} \text{ if } \sum_{j=1}^{n}\left[(x\geq -s_j)(x\leq s_j+w)\right] \\ 0 \text{otherwise} \end{vmatrix}$$



Fourier transform the position wave function into the momentum representation:

$$\Phi(p_x)=\frac{1}{\sqrt{2\pi}}\int_0^{s_n+w} exp(-ip_x x)\Psi(x)dx$$



This page titled 5.20: Electron Diffraction at Multiple Slits is shared under a CC BY 4.0 license and was authored, remixed, and/or curated by Frank Rioux via source content that was edited to the style and standards of the LibreTexts platform.

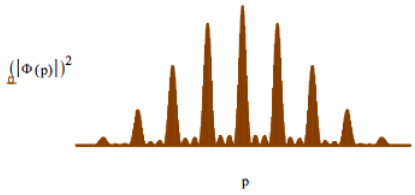
5.21: Multiple Slit Diffraction and the Fourier Transform

The American Journal of Physics published a translation of Claus Jonsson′s paper ″Electron Diffraction at Multiple Slits″ in *American Journal of Physics* **42**, 4-11 (1974). The following calculation is in agreement with the diffraction pattern reported by Jonsson.

A four slit geometry is created. This represents the coordinate space wave function. It is Fourier transformed into the momentum representation to generate its diffraction pattern.

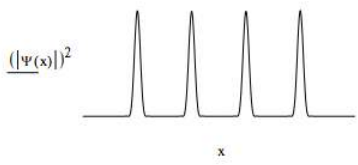
Number of slits: $n = 4$ Slit positions: $j = 1..n$ $x_j = j$ Slit width: $\delta = .2$

$$\Phi(p) = \frac{\sum_{j=1}^{n} \int_{x_j - \frac{\delta}{2}}^{x_j + \frac{\delta}{2}} \frac{1}{\sqrt{2\pi}} exp(-ipx) \frac{1}{\sqrt{\delta}} dx}{\sqrt{n}}$$



The momentum wave function is Fourier transformed back to coordinate space to generate the spatial wave function or slit geometry.

$$x = 0, .01..5 \quad \Psi(x) = \frac{1}{\sqrt{2\pi}} \int_{-30}^{30} exp(ipx)\Phi(p)dp$$



This page titled 5.21: Multiple Slit Diffraction and the Fourier Transform is shared under a CC BY 4.0 license and was authored, remixed, and/or curated by Frank Rioux via source content that was edited to the style and standards of the LibreTexts platform.

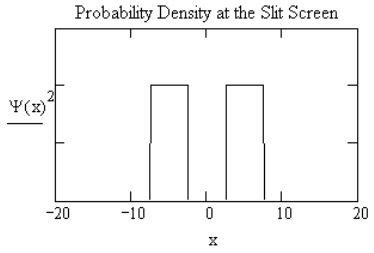
5.22: The Double-Slit Experiment with C60 Molecules

This is an attempt to capture with a simple model the behavior of C_{60} molecules in a double-slit experiment as reported in Nature Magazine (14 OCT 1999, pp 680-682). See *Eur. J. Phys.* **23**, 615-621 (2002) for the origin of the model.

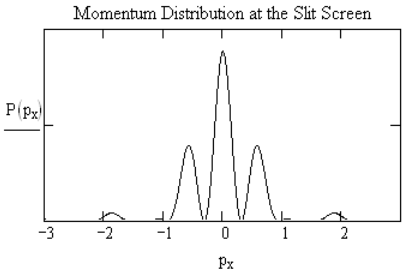
The C_{60} wave function at the slit screen is shown below. This coordinate-space wave function is Fourier transformed into momentum space to obtain the momentum distribution at the slit screen. This momentum distribution is ultimately projected onto the detection screen.

In the work reported in Nature the slit width and the distance between slits was equal (50 nm). Arbitrary distance units are used here to illustrate the effect. The slit screen is actually a diffraction grating, but the researchers assumed the interference effect was caused by adjacent slits.

$$x = -20, -19.99, ..20 \quad \Psi(x) = \text{if}\left[(x \geq -7.5)(x \leq -2.5) + (x \geq 2.5)(x \leq 7.5),\ \tfrac{1}{\sqrt{10}},\ 0\right]$$



$$P(p_x) = \left(\left|\tfrac{1}{\sqrt{2\pi}} \int_{-10}^{10} exp(-ip_x x)\Psi(x)dx\right|\right)^2 \quad p_x = -3, -2.99, ..3$$



This page titled 5.22: The Double-Slit Experiment with C60 Molecules is shared under a CC BY 4.0 license and was authored, remixed, and/or curated by Frank Rioux via source content that was edited to the style and standards of the LibreTexts platform.

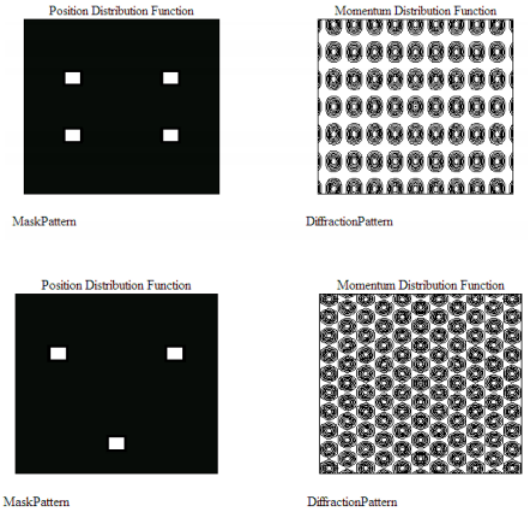
5.23: Crystal Structure, Rotational Symmetry, and Quasicrystals

Prior to 1991 crystals were defined to be solids having only 2-, 3-, 4- and 6-fold rotational symmetry because only these rotational symmetries have the required translational periodicity to build the long-range order of a crystalline solid. Long-range order is synonymous with periodicity, requiring some unit structure which repeats itself by translation in all directions infinitely. It is easy to demonstrate that a pentagon, with 5-fold rotational symmetry cannot be used as a unit cell to create long-range order in a plane or in three-dimensions.

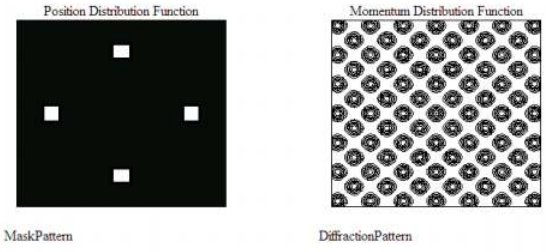
The justification for this definition was that solid structures with 2-, 3-, 4- and 6-fold rotational symmetry yield discrete diffraction patterns that also have translational periodicity. Another way to put this is to say that solid structures with 2-, 3-, 4- and 6-fold rotational symmetry have reciprocal lattices that also have translational periodicity. Yet, another way to put this, of course, is that the Fourier transforms of geometries with 2-, 3-, 4- and 6-fold rotational symmetry yield lattice-like momentum distributions with translational periodicity. This latter statement is preferred by the author because it emphasizes that diffraction patterns are actually the momentum distributions of the diffracted particles.

The key in this latter interpretation is that diffraction experiments involve an initial spatial localization of the radiation through interaction with the crystal lattice, followed as required by the uncertainty principle, a delocalization of the momentum distribution in the detection plane.

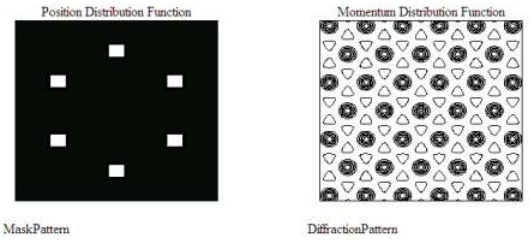
Let's look at some examples. First we examine the Fourier transforms of two mini-lattices with two- and three-fold rotational symmetry.



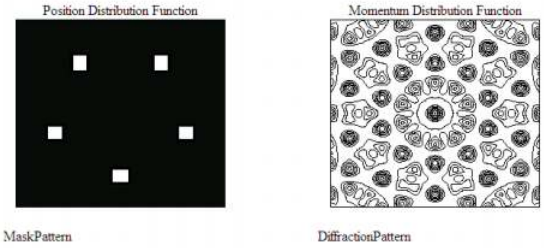
Clearly both diffraction patterns exhibit translational periodicity, their repeating units being a 90 degree rotation of the spatial structure. Next we look at four-fold rotational symmetry and see that the unit cell is obvious.



Six-fold rotational symmetry is more interesting than the previous three examples, but again the unit cell is easy to find.



Now look at what happens when we consider 5-fold symmetry – the diffraction pattern generated by a pentagon.



The unit cell, the universal repeating unit, is gone. The diffraction pattern is well-defined, it has rotational symmetry and it is appealing, but it does not satisfy the criterion for translational periodicity. That's why 5-fold rotational symmetry is excluded from the list of symmetries that can generate diffraction patterns that have translational periodicity, and why by definition crystalline solids are not supposed to have 5-fold axes, or rotational axes greater than order six.

However, in 1984 an international research team consisting of D. Shechtman, I. Blech, D. Gratias and J. W. Cahn, published "Metallic phase with long-range orientational order and no translational symmetry" in Physical Review Letters 53, 1951-1953 (1984). The crystalline metallic phases they studied produced discrete diffraction patterns that were characteristic of the 5- and 10-fold rotational symmetry axes that were prohibited by the accepted definition of a crystalline solid.

In the face of this contradictory evidence, 5-fold rotational symmetry and a well-defined diffraction pattern, the International Union of Crystallography in 1991 redefined crystal to mean any solid having a discrete diffraction pattern. However, the solid phases discovered by Shechtman and his co-workers go by the name quasicrystals, indicating that they don't quite have the same stature as those that don't violate the rotational symmetry rule.

This page titled 5.23: Crystal Structure, Rotational Symmetry, and Quasicrystals is shared under a CC BY 4.0 license and was authored, remixed, and/or curated by Frank Rioux via source content that was edited to the style and standards of the LibreTexts platform.

5.24: X-ray Crystallography from a Quantum Mechanical Perspective

According to Richard Feynman1 the double-slit experiment is the paradigm for all of quantum mechanics because it is a simple manifestation of the superposition principle, which is quantum theory's "only mystery." In an interesting quantum mechanical analysis of Young's double-slit experiment, Marcella2 writes the coordinate wave function of the particle interacting with the slit-screen as a linear superposition of being at both slits,

$$|\Psi\rangle = \frac{1}{\sqrt{2}}\left[|x_1\rangle + |x_2\rangle\right]$$

where x_1 and x_2 are the positions of two infinitesimally thin slits. The diffraction pattern at the detection screen is determined by the momentum distribution at the slit screen. The momentum wave function is obtained by projecting equation (1) into momentum space,

$$\langle p_x|\Psi\rangle = \frac{1}{\sqrt{2}}\left[\langle p_x|x_1\rangle + \langle p_x|x_2\rangle\right] = \frac{1}{2\sqrt{\pi h}}\left[exp\left(-\frac{ip_x x_1}{h}\right) + exp\left(-\frac{ip_x x_2}{h}\right)\right]$$

where the $\langle p_x|x_1\rangle$ are the position eigenfunctions in the momentum representation. The square of the absolute magnitude of this function is shown in Figure 1.

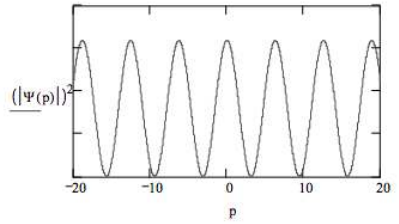
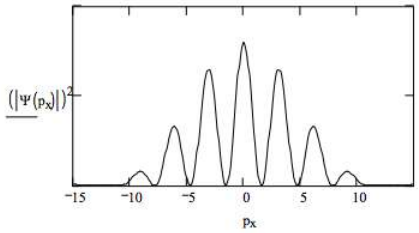


Figure 2.



Figures 1 and 2. In addition, because the particle has been localized at two positions interference effects are prominent in its momentum distribution.

Like the double-slit phenomenon, x-ray diffraction by crystals is also based on the linear superposition principle. For the sake of simplicity attention will be restricted to two-dimensional crystals. Also, following Marcella's first model, the atoms or ions occupying the lattice sites are considered to be point scatterers. Under these assumptions, the coordinate-space wave function of a photon illuminating a crystal is a superposition of the atomic scattering positions.

$$|\Psi = \frac{1}{\sqrt{N}}\sum_{i=1}^{N}|x_i,\ y_i\rangle$$

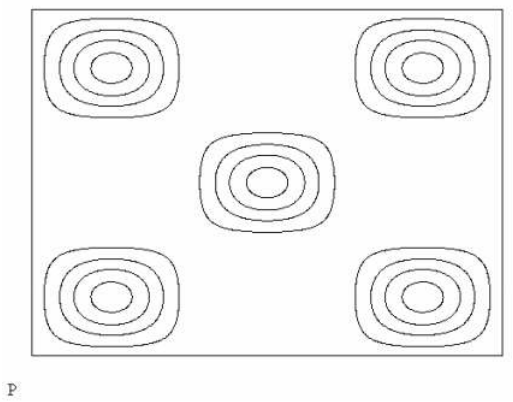
As we wish to know the diffraction pattern that will be found at the detector, we express this superposition in the momentum representation as follows.

$$\langle p|\Psi\rangle = \frac{1}{\sqrt{N}}\sum_{i=1}^{N}\langle p_x|x_i\rangle\langle p_y|y_i\rangle$$

Employing the expression for the position wave function in the momentum representation we can convert equation (4) to

$$\langle p|\Psi\rangle = \frac{1}{\sqrt{N}(2\pi h)}\sum_{i=1}^{N} f_i\ \exp\left[-\frac{i}{h}(p_x x_i + p_y y_i)\right]$$

where the fi are the atomic scattering factors. A face-centered “squaric” arrangement of five atomic point scatterers yields the following diffraction pattern, 2 p Ψ .



The Mathcad document used to generate this diffraction pattern is shown in the Appendix.

Literature cited:

1. R. P. Feynman, R. B. Leighton, and M. Sands, *The Feynman Lectures on Physics*, Vol. 3; Addison-Wesley: Reading, 1965.
2. T. V. Marcella, “Quantum interference with slits,” *European Journal of Physics* 23, 615-621 (2002).

Appendix

Number of atoms: $A = 5$ Atomic positions and relative scattering factors:

$$\begin{array}{lll} x_1 = 0 & y_1 = 0 & f_1 = \frac{1}{4} \\ x_3 = 1 & y_3 = 0 & f_3 = \frac{1}{4} \\ x_5 = \frac{1}{2} & y_5 = \frac{1}{2} & f_5 = \frac{1}{2} \end{array} \qquad \begin{array}{lll} x_2 = 0 & y_2 = 1 & f_2 = \frac{1}{4} \\ x_4 = 1 & y_4 = 1 & f_4 = \frac{1}{4} \end{array}$$

$$\Delta = 10 \quad N = 200 \quad j = 0..N \quad px_j = -\Delta + \frac{2\Delta j}{N} \quad k = 0..N \quad py_k = -\Delta + \frac{2\Delta k}{N}$$

Fourier transform of position wave function into the momentum representation:

$$\Psi(p_x,\ p_y) = \sum_{m=1}^{A} f_m exp(-ip_x x_m - ip_y y_m) \quad P_{j,\,k} = (|\Psi\,(px_j,\ py_k)|)^2$$

This page titled 5.24: X-ray Crystallography from a Quantum Mechanical Perspective is shared under a CC BY 4.0 license and was authored, remixed, and/or curated by Frank Rioux via source content that was edited to the style and standards of the LibreTexts platform.

5.25: Holography Involves Single Photon Interference

Recently I was reading an encyclopedia article [McMillan Encyclopedia of Physics, John Rigden, Editor, page 716] about holography...

The word "holography" is derived from Greek roots that literally mean "entire picture." The act of doing holograhpy is to make holograms. There are many different types of holograms, but they all share one common distinguishing feature, they recreate truly three-dimensional imgages of original objects.

The field of holography was originally discovered by Dennis Gabor in 1947. He was awarded the Nobel Prize for physics in 1971. In the early 1960s, Emmett N. Leith and Juris Upatinieks of the United States and Yu. Denisyuk of Russia independently discovered additional methods in using laser light to make holograms.

What is a hologram? A hologram is a recording on a lightsensitive medium (e.g. photographic emulsion) of interference patterns formed between two or more beams of light derived from the same laser.

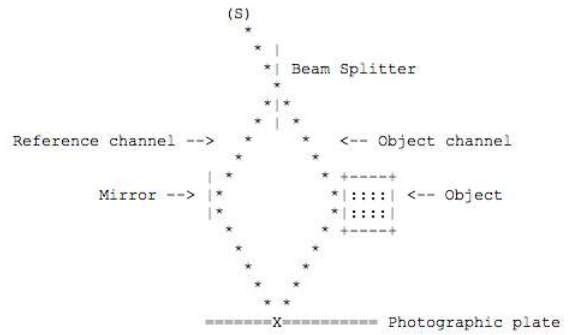
In holography, as the figure below shows, a laser beam is split by a beam splitter with one arm going to the object and the other going to a mirror. The beam arms recombine at the detector, in this case a photographic plate, and constructive or destructive interference occurs.

Although it isn't stated explicitly above, I assume that holography is an example of single-photon interference, and that the same can be said about any diffraction phenomenon - X-ray, electron, neutron, etc. To support this assumption I quote the celebrated remark by Dirac, "Each photon then interferes only with itself. Interference between two different photons never occurs." [I am aware of Roy Glauber's cautionary remarks about the second sentence - American Journal of Physics 63, 12 (1995). For example, two-photon interference can be observed if the photons are created in an entangled state.]

According to this single-particle mechanism, after the beam splitter each photon is considered to be in a linear superposition of being transmitted (toward object) and reflected (toward mirror). At the detector the probability amplitudes for these paths interfere (constructively or destructively) giving an interference pattern characteristic of the object. In Dirac notation, the probability of detection at some point x on the photographic film is,

$$P(x) = |\langle \text{Detector(x)} \mid \text{Mirror}\rangle\langle \text{Mirror}|\text{Source}\rangle + \langle \text{Detector(x)}|\text{Object}\rangle\langle \text{Object}|\text{Source}\rangle|^2$$

This is a clear example of quantum mechanical wave-particle duality; the photon is created by the source as a particle, behaves like a wave, and is detected at the photographic plate as a particle.



I would like to add further support the underlying assumption of this tutorial that holography is an example of single-particle interference with the following excerpt from Volume 23 of the *Encyclopedia Britannica*, 15th Edition, pages 20- 21.

It was at one time suggested that interference and diffraction phenomena are caused by collisions between photons considered as small particles, or at least to some kind of complex interaction between photons. A simple experiment performed by a British physicist, Geoffrey Ingram Taylor, in 1908 excludes this possibility. He photographed the diffraction pattern of a needle and reduced the illumination until long exposures were needed to obtain an image. When the chance of two or more energy quanta passing through the apparatus simultaneously was made extremely small, the diffraction pattern was exactly the same as that obtained with a strong source of light.

This experiment is supported by many later experiments, showing that interference and diffraction are to be associated with single photons. The discussion in the section on coherence above implies that when ordinary sources of light are used each photon can interfere only with itself and not with any other photon. An interference pattern can, of course, be photographed only by recording the effects of many photons because one photon can activate only one grain on the photographic plate, but it does not matter whether the photons all arrive over a time span of a microsecond or of several weeks.

The photograph of an interference pattern is both a wave phenomenon because it shows the characteristic spatial periodicity and a quantum phenomenon because the whole energy of a photon can be used to activate a single grain. It is not possible to trace the path of one photon (regarded as a particle) through the apparatus and, at the same time, obtain the interference pattern. In Young's experiment there is no way of finding out through which slit a given photon passes--except by covering one slit and thus losing the interference fringes.

For a discussion of the related double-slit experiment see the related tutorial: Calculating the Double-Slit Interference Pattern. To learn about contemporary applications of holographic techniques at the atomic level see "Optics: Holograms of Atoms," *Nature* **410**, 1037-1040 (2001) and references cited therein.

This page titled 5.25: Holography Involves Single Photon Interference is shared under a CC BY 4.0 license and was authored, remixed, and/or curated by Frank Rioux via source content that was edited to the style and standards of the LibreTexts platform.

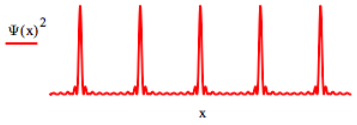
5.26: X-ray Diffraction

This tutorial on X-ray diffraction was stimulated by an appendix in the first edition of Peter Atkins′ celebrated physical chemistry text (pp. 734-739) titled ″Diffraction as a particle property.″ In exploring this approach we will work in one dimension in the interests of mathematical and conceptual simplicity.

Modeling the periodicity of the electron density in a one-dimensional atomic lattic requires the superposition of many electron wavelengths and, therefore, by the de Broglie relation (λ = h/p) many electron momentum states. For example, a superposition of eight cosine functions yields the sharply defined electron density distribution with lattice spacing d shown below.

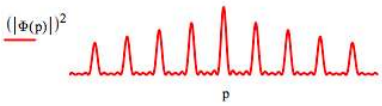
$$d = 1 \quad \Psi(x) = \sum_{n=1}^{8} \cos\left(n 2\pi \frac{x}{d}\right)$$

where *d* is the lattice spacing and λ = d/n with *n* = 1, 2, 3...



According to the quantum mechanical interpretation of diffraction, when this one-dimensional electron density distribution interacts with an X-ray source the individual photons are temporarily localized simultaneously at all lattice sites. The uncertainty principle requires that spatial localization leads to a delocalization (scattering) of the momentum distribution and the appearance of interference fringes because the spatial localization occurs at multiple sites. The resulting momentum distribution is the diffraction pattern and is calculated by a Fourier transform of the electron density distribution, $\Psi(x)^2$, into momentum space as is shown below (in atomic units: h = 2π).

$$\Phi(p) = \frac{1}{\sqrt{2\pi}} \int_{-.5}^{4.5} \Psi(x)^2 exp(ipx) dx$$



The approach adopted by Atkins is to model diffraction as an elastic particle-like collision between the X-ray photon and the electron distribution of the lattice. In this view one asks what momenta the lattice can transfer to the incident particle (photon). The quantum mechanical answer to this question is provided by the scattering amplitude or structure factor shown in the following equation.

$$F(p') = \int \langle p - p' | \Psi \rangle \langle \Psi | p \rangle dp$$

Reading the Dirac brackets above from right to left, this expression is the scattering amplitude or the ″possibility″ that an electronic state Ψ with momentum p can transfer momentum p′ to the scattered particle. Integrating the brackets over p yields all the ways that the electron distribution represented by Ψ can transfer momentum p′ to the incident photon.

The structure factor can be cast into the coordinate representation by applying the completeness relation

$$\int |x\rangle\langle x| dx = 1$$

to the left bracket in the integral followed by rearrangement.

$$F(p') = \int \int \langle p - p' | x \rangle \langle x | \Psi \rangle \langle \Psi | p \rangle dx dp$$

Using the momentum eigenfunction in the coordinate representation and the position eigenfunction in the momentum representation (normalization constants are ignored throughout this treatment),

$$\langle x|p\rangle = \langle p|x\rangle* = \exp\left(\frac{ipx}{\hbar}\right)$$

we see that the middle bracket on the right can be transformed as follows,

$$\langle p-p''|x\rangle = \exp\left(\frac{-i(p-p')x}{\hbar}\right) = \exp\left(-\frac{ipx}{\hbar}\right)\exp\left(\frac{ip'x}{\hbar}\right) = \langle p|x\rangle\langle x|p'\rangle$$

F(p') can now be written as

$$F(p') = \int\int \langle\Psi|p\rangle\langle p|x\rangle\langle x|p'\rangle\langle x|\Psi\rangle dxdp$$

Using the momentum-space completeness relation,

$$\int |p\rangle\langle p|dp = 1$$

we find,

$$F(p') = \int \langle\Psi|x\rangle\langle x|p'\rangle\langle x|\Psi\rangle dx$$

Expressing F(p') in traditional notation yields,

$$F(p') = \int \Psi*(x)\exp\left(\frac{ip'x}{\hbar}\right)\Psi(x)dx = \int \rho(x)\exp\left(\frac{ip'x}{\hbar}\right)dx$$

Note that we have reached the same point as in our initial approach: Fourier transform the electron density into the momentum representation to calculate the diffraction pattern.

We conclude by recovering the traditional form of the structure factor found in all physical chemistry texts and books dealing with X-ray crystallography. The momenta, p′, that the electron distribution can transfer to the incident photon are the momenta that it has.

Earlier it was noted that to build a one-dimensional electron density distribution with lattice spacing d requires the superposition of wavelengths restricted by the relation λ = d/n, where n = 1,2,3, ... This requires, by de Broglie′s wave equation, a superposition of quantized momentum states given by p′ = nh/d. Substitution of this equation into F(p′) yields

$$F(n) = \int \rho\exp\left(2\pi i\frac{nx}{d}\right)dx$$

where n is the Miller index that normally goes by the designation h. The extension to three dimensions using the traditional (h, k, l) designation for the Miller indices, and a, b and c for the lattice constants is straightforward.

This page titled 5.26: X-ray Diffraction is shared under a CC BY 4.0 license and was authored, remixed, and/or curated by Frank Rioux via source content that was edited to the style and standards of the LibreTexts platform.

5.27: Holography Involves Single Photon Interference

Your page has been created!

Remove this content and add your own.

Edit page

Click the Edit page button in your user bar. You will see a suggested structure for your content. Add your content and hit Save.

Tips:

Drag and drop

Drag one or more image files from your computer and drop them onto your browser window to add them to your page.

Classifications

Tags are used to link pages to one another along common themes. Tags are also used as markers for the dynamic organization of content in the NiCE Knowledge Management framework.

Working with templates

NiCE Knowledge Management templates help guide and organize your documentation, making it flow easier and more uniformly. Edit existing templates or create your own.

Visit for all help topics.

This page titled 5.27: Holography Involves Single Photon Interference is shared under a CC BY 4.0 license and was authored, remixed, and/or curated by Frank Rioux via source content that was edited to the style and standards of the LibreTexts platform.

CHAPTER OVERVIEW

6: Group Theory with Mathcad

6.1: Group Theory Principles Applied to H2O
6.2: Dodecahedrane
6.3: Xenon Tetrafluoride
6.4: Diborane
6.5: Cubane
6.5.1: Buckminsterfulerene
6.6: BCl3
6.7: Ti(H2O)6 3+
6.8: CH_4
6.9: P_4
6.10: Tetrahedrane
6.11: PH3
6.12: Cyclopropane
6.13: An Extensive Set of Group Theory Problems for Chemists
Index

This page titled 6: Group Theory with Mathcad is shared under a CC BY 4.0 license and was authored, remixed, and/or curated by Frank Rioux via source content that was edited to the style and standards of the LibreTexts platform.

CHAPTER OVERVIEW

Front Matter

TitlePage
InfoPage

College of Saint Benedict/Saint John's University

Group Theory with Mathcad

Frank Rioux

This text is disseminated via the Open Education Resource (OER) LibreTexts Project (https://LibreTexts.org) and like the thousands of other texts available within this powerful platform, it is freely available for reading, printing, and "consuming."

The LibreTexts mission is to bring together students, faculty, and scholars in a collaborative effort to provide an accessible, and comprehensive platform that empowers our community to develop, curate, adapt, and adopt openly licensed resources and technologies; through these efforts we can reduce the financial burden born from traditional educational resource costs, ensuring education is more accessible for students and communities worldwide.

Most, but not all, pages in the library have licenses that may allow individuals to make changes, save, and print this book. Carefully consult the applicable license(s) before pursuing such effects. Instructors can adopt existing LibreTexts texts or Remix them to quickly build course-specific resources to meet the needs of their students. Unlike traditional textbooks, LibreTexts' web based origins allow powerful integration of advanced features and new technologies to support learning.



LibreTexts is the adaptable, user-friendly non-profit open education resource platform that educators trust for creating, customizing, and sharing accessible, interactive textbooks, adaptive homework, and ancillary materials. We collaborate with individuals and organizations to champion open education initiatives, support institutional publishing programs, drive curriculum development projects, and more.

The LibreTexts libraries are Powered by NICE CXone Expert and was supported by the Department of Education Open Textbook Pilot Project, the California Education Learning Lab, the UC Davis Office of the Provost, the UC Davis Library, the California State University Affordable Learning Solutions Program, and Merlot. This material is based upon work supported by the National Science Foundation under Grant No. 1246120, 1525057, and 1413739.

Any opinions, findings, and conclusions or recommendations expressed in this material are those of the author(s) and do not necessarily reflect the views of the National Science Foundation nor the US Department of Education.

Have questions or comments? For information about adoptions or adaptions contact info@LibreTexts.org or visit our main website at https://LibreTexts.org.

This text was compiled on 05/10/2026

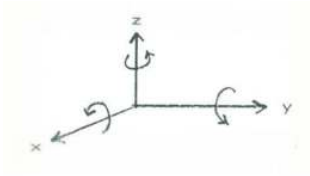
6.1: Group Theory Principles Applied to H2O

Symmetry Analysis for H_2O

Water belongs to the C_{2v} symmetry group and has the following symmetry elements: E, C_2^z, σ_{xz}, and σ_{yz}. Its character table is shown below.

C_{2v}	E	C_2^z	σ_{xz}	σ_{yz}	h = 4
A_1	1	1	1	1	$z,\ x^2,\ y^2,\ z^2$
A_2	1	1	−1	−1	xy, R_z
B_1	1	−1	1	−1	x, xz, R_y
B_2	1	−1	−1	1	y, yz, R_x
Γ_{tot}	−9	−1	1	3	

The C_{2v} symmetry group has four symmetry elements and four associated symmetry operations. It can be thought of as a four dimensional space with the A_1, A_2, B_1, and B_2 irreducible representations playing the role of unite vectors of vector algebra. The irreducible representations span the space and any other vector or representation in that space can be written as a linear combination of them. For simple groups like this character table can be generated by examining how translations along the x-, y-, and z-axes and rotations about these axes transform under the symmetry operations of the group. Using the figure show below you should be able to confirm the designations shown in the right-hand column of the character table. That is the translation in the z-direction transforms like A_1, rotation about the z-axis transforms like A_2, translation in the x-direction and rotation about the y-axis have symmetry properties represented by B_1, and translation in the y-direction and rotation about the x-axis have B_2 symmetry. In doing this note (see Atkins) that you record +1 if something is transformed into itself, -1 if it is transformed into minus itself, and 0 if it is transformed into something else under the symmetry operations of the group.



Note that just like the unit vectors in the Cartesian coordinate system, these irreducible representations are orthogonal. That is they have zero overlap.

$$A_1B_2 = \frac{[(-1)(1) + (1)(-1) + (1)(-1) + (1)(1)]}{4} = 0$$

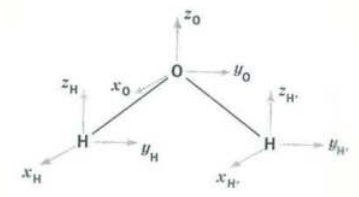
$$A_2B_1 = \frac{[(1)(1) + (1)(-1) + (-1)(1) + (-1)(-1)]}{4} = 0$$

Dividing by 4, the order of the group, normalizes the calculation. We can also show that all of the irreducible representation are normalized or have an overlap of 1.

$$A_2A_2 = \frac{[(1)(1) + (1)(1) + (-1)(-1) + (-1)(-1)]}{4} = 1$$

Note that these vector operations are exactly equivalent to evaluating quantum mechanical overlap integrals $\int \Psi_1 \Psi_2 d\tau$.

Since H_2O is a triatomic molecule it has a total of 9 degrees of freedom - three for each atom in the molecule. These are the x-, y-, and z-coordinates of the individual atoms and are shown as small vectors located on each of the atoms in the figure below.



A symmetry analysis for water begins by determining how these 9 coordinates behave under the symmetry operations of the C_{2v} group. You should be able to show that this generates the reducible representation Γ_{tot}, which is given in the last row of the character table shown above. Γ_{tot} can also be calculated as Γ_{uma} (Γ_x + Γ_y + Γ_z), where Γ_{uma} is the behavior of the atoms under the symmetry operations of the group. Of the 9 degrees of freedom possessed by the water molecule, three are for translation of the center of mass in the x-, y- and z-directions, and three are related to rotation about the x-, y-, and z-axes. This leaves three vibrational degrees of freedom. To determine the symmetry of the vibrational modes we decompose Γ_{tot} into the unit vectors or irreducible representations of the C_{2v} character table. This involves taking the dot product of Γ_{tot} with each of the irreducible representations of the C_{2v} symmetry.

$$\Gamma_{tot}\mathrm{A}_1 = \frac{[(9)(1) + (-1)(1) + (1)(1) + (3)(1)]}{4} = 3$$
$$\Gamma_{tot}\mathrm{A}_2 = \frac{[(9)(1) + (-1)(1) + (1)(-1) + (3)(-1)]}{4} = 1$$
$$\Gamma_{tot}\mathrm{B}_1 = \frac{[(9)(1) + (-1)(-1) + (1)(1) + (3)(-1)]}{4} = 2$$
$$\Gamma_{tot}\mathrm{B}_2 = \frac{[(9)(1) + (-1)(-1) + (1)(-1) + (3)(1)]}{4} = 3$$

This procedure has revealed the that the reducible representation, Γ_{tot}, is composed of the following irreducible representations:

$$\Gamma_{tot} = 3\mathrm{A}_1 + \mathrm{A}_2 + 2\mathrm{B}_1 + 3\mathrm{B}_2$$

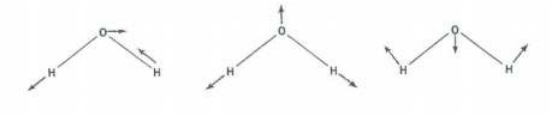
From the right side of the character table we see that translation and rotation have the following symmetry properties:

$$\Gamma_{trans} = \mathrm{A}_1 + \mathrm{B}_1 + \mathrm{B}_2$$
$$\Gamma_{rot} = \mathrm{A}_2 + \mathrm{B}_1 + \mathrm{B}_2$$

From this information we can determine the symmetry properties of the vibrational modes of the water molecule.

$$\Gamma_{vib} = \Gamma_{tot} - \Gamma_{trans} - \Gamma_{rot} = 2\mathrm{A}_1 + \mathrm{B}_2$$

There are three vibrational fundamentals. And, since there are two bonds there will be two stretching vibrations and one bending vibration. To determine which symmetry classification the bend belongs to, examine how the H-O-H bond angle transforms under the symmetry operations of the C_{2v} group.



The vibrational modes are shown above. Convince yourself that their symmetry properties are captured in the table below.

C_{2v}	E	C_2^z	σ_{xz}	σ_{yz}	
Γ_{bend}	1	1	1	1	A_1
$\Gamma_{stretch}$	1	1	1	1	A_1
$\Gamma_{stretch}$	1	−1	−1	1	B_2

Whether any of these modes is active in the infrared region of the spectrum is another question. This is determined by evaluating the quantum mechanical transition probability integral,

$$P = e\int \Psi^f(vib)\hat{q}\Psi^i(vib)d\tau$$

where q is the spatial coordinate and is either x, y, or z. If this integral is non-zero the transition is allowed. Group theory enables us to determine if the integral is non-zero as follows. We evaluate the direct product (note the similarity to the quantum mechanical transition probability integral) $\Gamma_{vib}{}^f\Gamma_q\Gamma_{vib}{}^i$ and if it turns out to be equal to, or contain, the irreducible representation A_1 then the transition is allowed. If the direct product isn't equal to or contain A_1 then the transition is forbidden.

$\Gamma_{vib}{}^i$, the representation for the ground state is always equal to A_1 and $\Gamma_{vib}{}^f$ is always equal to A_1 and $\Gamma_{vib}{}^f$ has the symmetry of the vibrational mode being excited, which in our case is either A_1 or B_2. Thus we can see that a vibrational mode will be infrared active

if it belongs to the same symmetry species as one of the Cartesian coordinates. You should verify that this is correct and also be able to show that all three vibrational modes of the water molecule are infrared active.

Group theory is also very helpful in constructing molecular orbitals from linear combinations of atomic orbitals. For the water molecule the atomic orbitals are the hydrogen 1s orbitals and the 2s and three 2p orbitals on the oxygen atom. We proceed by examining how the orbitals transform under the symmetry operations of the group. This is shown in the table below.

C_{2v}	E	C_2^z	σ_{xz}	σ_{yz}
H_1	H_1	H_2	H_2	H_1
O_{2s}	O_{2s}	O_{2s}	O_{2s}	O_{2s}
O_{2px}	O_{2px}	$-O_{2px}$	O_{2px}	$-O_{2px}$
O_{2py}	O_{2py}	$-O_{2py}$	$-O_{2py}$	O_{2py}
O_{2pz}	O_{2pz}	O_{2pz}	O_{2pz}	O_{2pz}
A_1	1	1	1	1
A_2	1	1	−1	−1
B_1	1	−1	1	−1
B_2	1	−1	−1	1

To find the molecular orbital with A_1 symmetry take the sum of the dot product of the A_1 irreducible representation with each of the representations in the top half of the table. This is $2(H_1 + H_2) + 4O_{2s} + 4O_{2pz}$. This indicates that the molecular orbital will consist of a linear combination of four of the six orbitals shown in the table above.

$$\Psi(A_1) = c_h\left[\psi(H_1) + \psi(H_2)\right] + c_o\psi(O_{2s}) + c_o\psi(O_{2pz})$$

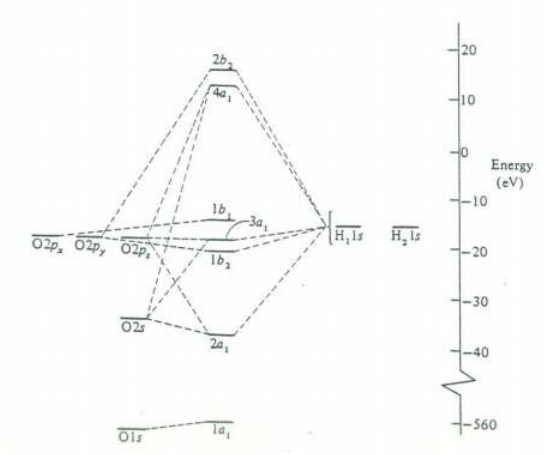
When this is done for A_2 symmetry it is found that the sum is zero, indicating that there is no molecular orbital with A_2 symmetry. Repeating this process for B_1 symmetry yields $4O_{2px}$. This means $\Psi(B_2) = \Psi(O_{2px})$ and we say that the oxygen $2p_x$ orbital is non-bonding because there are hydrogen orbitals with the same symmetry. This is easily seen by inspection of the water molecule when placed in a Cartesian coordinate system as shown in the figure above.

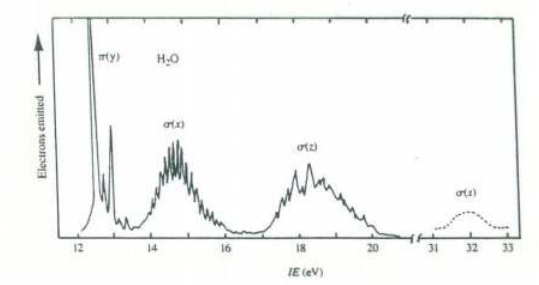
For B_2 symmetry the result is $2(H_1 - H_2) + 4O_{2py}$. This is clearly another bonding molecular orbital.

$$\Psi(B_2) = c_h\left[\psi(H_1) - \psi(H_2)\right] + c_o\psi(O_{2py})$$

The next step is to use the molecular orbitals from this symmetry analysis as the basis for a self-consistent field calculation on the water molecule. This will yield a set of coefficients for the molecular orbitals and a molecular orbital energy level diagram. This results are given below. You should compare these results with the traditional valence bond (Lewis structure) formulation of the bonding in H_2O.

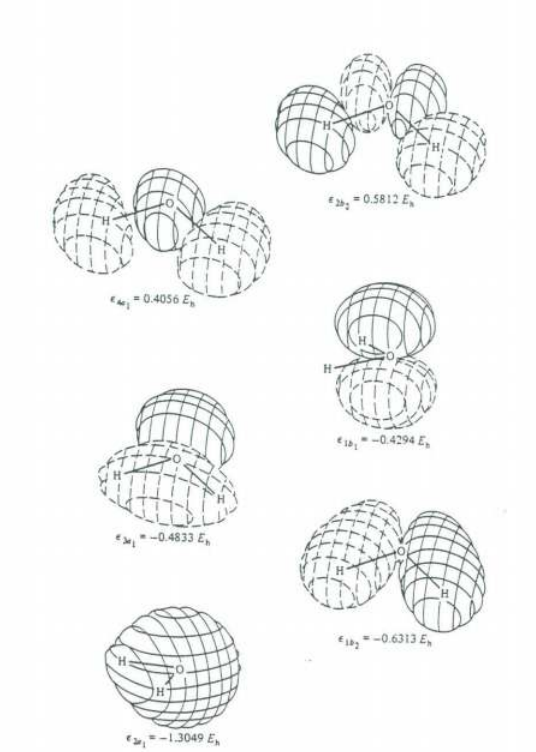
$$\begin{gathered}
\Psi(A_1) = 0.15\left[\psi(H_1) + \psi(H_2)\right] + 0.82\psi(O_{2s}) + 0.13\psi(O_{2pz}) \\
\Psi(B_2) = 0.42\left[\psi(H_1) - \psi(H_2)\right] + 0.62\psi(O_{2py}) \\
\Psi(A_1) = 0.26\left[\psi(H_1) + \psi(H_2)\right] - 0.50\psi(O_{2s}) + 0.79\psi(O_{2pz}) \\
\Psi(B_1) = \Psi(O_{2px}) \\
\Psi(A_1) = 0.75\left[\psi(H_1) + \psi(H_2)\right] - 0.84\psi(O_{2s}) - 0.70\psi(O_{2pz}) \\
\Psi(B_2) = 0.89\left[\psi(H_1) - \psi(H_2)\right] - 0.99\psi(O_{2py})
\end{gathered}$$



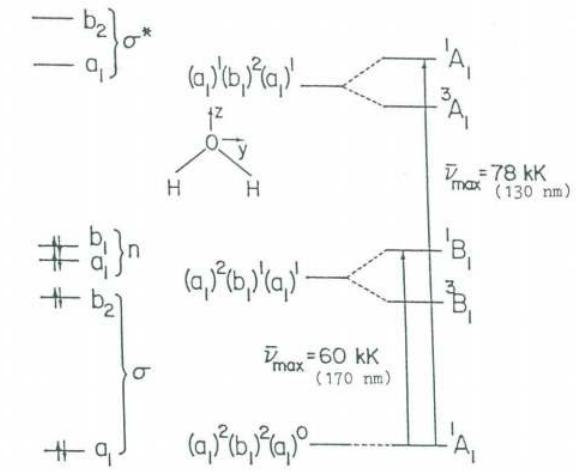


The $1a_1$ MO is, as would be expected, the oxygen non-valence 1s orbital. The $2a_1$ MO is mainly a linear combination of the hydrogen 1s and the 2s on oxygen. The $1b_2$ MO is entirely the oxygen $2p_y$ and the hydrogen 1s atomic orbitals. The $3a_1$ MO and the $1b_1$ MO correspond to the two long pairs. The $3a_1$ MO and the $1b_1$ MO correspond to the two long pairs. The $3a_1$ MO consists mainly of the oxygen 2s and $2p_z$ and the hydrogen 1s atomic orbitals and has its maximum value in the +z direction. The $1b_1$ is entirely oxygen $2p_x$ and thus is directed at right angles to the plane of the molecule; the lone pairs thus have their maxima in the xz plane.

https://chem.libretexts.org/@go/page/149257



The first two electronic transitions in water occur at 170 and 130 nm. The molecular orbital diagram obtained previously and the principles of group theory can be used to intepret the electronic spectrum as is shown in the figure below.



Molecular orbital scheme and state diagram for H_2O.

By analogy with IR spectroscopy those electronic transitions are allowed for which the transition moment integral is non-zero.

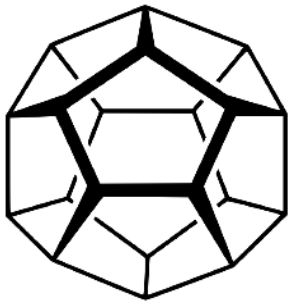
$$M = e \int \Psi^f(elec)\hat{q}\Psi^i(elec)d\tau$$

As in the case of IR spectroscopy, this integral can be non-zero if and only if $\Gamma_{vib}{}^f\Gamma_q\Gamma_{vib}{}^i$ is equal to or contains the totally symmetric irreducible representation, A_1. The figure shows that the electronic ground state has A_1 symmetry while the electric dipole operator (μ=eq) has the symmetry of the Cartesian coordinates (A_1, B_1, B_2). Thus $\Gamma_{vib}{}^f\Gamma_q\Gamma_{vib}{}^i$ will equal A_1 if the excited state has A_1, B_1, or B_2 symmetry. If this is the case then the transition is said to be orbitally allowed. Note that several orbitally allowed transitions are spin-forbidden (involve a change in spin multiplicity) and therefore do not occur.

This page titled 6.1: Group Theory Principles Applied to H2O is shared under a CC BY 4.0 license and was authored, remixed, and/or curated by Frank Rioux via source content that was edited to the style and standards of the LibreTexts platform.

6.2: Dodecahedrane

When Paquette's group synthesized dodecahedrane, $C_{20}H_{20}$, they measured its infrared and Raman spectra (JACS 1983, 105, 5446-5450).



Dodecahedrane: (Public Domain; Yikrazuul).

They found three IR active bands at 2945, 1298, and 728 cm^{-1} and eight Raman frequencies at 2924, 2938, 1324, 1164, 1092, 840, 676, and 480 cm^{-1}. Use group theory to show that these data are consistent with the fact that dodecahedrane has icosahedral symmetry.

Illegal pream-token (E)

$$\mathrm{Ih} = \qquad \mathrm{Ih} = \mathrm{Ih}^T \qquad \Gamma\mathrm{uma} = \qquad \Gamma\mathrm{uma} = \Gamma\mathrm{uma}^T$$
$$(1 \quad 12 \quad 12 \quad 20 \quad 15 \quad 1 \quad 12 \quad 12 \quad 20 \quad 15) \qquad (40 \quad 0 \quad 0 \quad 4 \quad 0 \quad 0 \quad 0 \quad 0 \quad 0 \quad 8)$$

$$\mathrm{Ag} = (\mathrm{CIh}^T)^{<1>} \quad \mathrm{T1g} = (\mathrm{CIh}^T)^{<2>} \quad \mathrm{T2g} = (\mathrm{CIh}^T)^{<3>} \quad \mathrm{Gg} = (\mathrm{CIh}^T)^{<4>} \quad \mathrm{Hg} = (\mathrm{CIh}^T)^{<5>}$$
$$\mathrm{Au} = (\mathrm{CIh}^T)^{<6>} \quad \mathrm{T1u} = (\mathrm{CIh}^T)^{<7>} \quad \mathrm{T2u} = (\mathrm{CIh}^T)^{<8>} \quad \mathrm{Gu} = (\mathrm{CIh}^T)^{<9>} \quad \mathrm{Hu} = (\mathrm{CIh}^T)^{<10>}$$

$$h = \sum Ih \quad h = 120 \quad \Gamma_{tot} = \overrightarrow{(\Gamma T1u)} \quad \Gamma_{vib} = \Gamma_{tot} - T1g - T1u \quad \Gamma_{bend} = \Gamma_{vib} - \Gamma_{stretch} \quad i = 1..10$$

$$\mathrm{Vib}_i = \frac{\overrightarrow{[\mathrm{Ih}(\mathrm{CIh}^T)^{<i>}\Gamma\mathrm{vib}]}}{h} \quad \mathrm{Stretch}_i = \frac{\overrightarrow{[\mathrm{Ih}(\mathrm{CIh}^T)^{<i>}\Gamma\mathrm{stretch}]}}{h} \quad \mathrm{Bend}_i = \frac{\overrightarrow{[\mathrm{Ih}(\mathrm{CIh}^T)^{<i>}\Gamma\mathrm{bend}]}}{h}$$

Illegal pream-token (\)

Illegal pream-token (\)

According to the usual selection rules only the three T_{1u} vibrations are IR active. The A_g and H_g vibrations are Raman active giving a total of eigth frequencies in the Raman spectra. This analysis is in agreement with the experimental spectroscopic results quoted by Paquette. Note also that, as is usual for molecules with a center of inversion, there are no coincidences between the IR and Raman active modes.

This page titled 6.2: Dodecahedrane is shared under a CC BY 4.0 license and was authored, remixed, and/or curated by Frank Rioux via source content that was edited to the style and standards of the LibreTexts platform.

6.3: Xenon Tetrafluoride

Xenon tetrafluoride is a chemical compound with chemical formula XeF_4. It was the first discovered binary compound of a noble gas. It is produced by the chemical reaction of xenon with fluorine, F_2, according to the chemical equation:

$$Xe + 2\,F_2 \longrightarrow XeF_4$$

The infrared spectrum of XeF_4 has absorptions at 161, 291, and 586 cm^{-1} (two bends, one stretch), while the Raman spectrum has peaks at 218, 524, and 554 cm^{-1} (one bend, two stretches). Is its molecular structure tetrahedral or square planar?

Tetrahedral Symmetry - T_d

Illegal pream-token (E)

$$A_1 = (C_{Td}^T)^{<1>} \quad A_2 = (C_{Td}^T)^{<2>} \quad E = (C_{Td}^T)^{<3>} \quad T_1 = (C_{Td}^T)^{<4>}$$
$$T_2 = (C_{Td}^T)^{<5.} \quad \Gamma_{tot} = \overrightarrow{\Gamma_{uma} T_2} \quad h = \sum Td \quad \Gamma_{tot}^T = (15 \quad 0 \quad -1 \quad -1 \quad 3)$$

Illegal pream-token (\)

This analysis predicts two IR active modes ($2T_2$) and four Raman active modes (A_1, E, $2T_2$). It also suggests that the IR and Raman should have the two T_2 modes in common. Thus, tetrahedral geometry is not consistent with the spectroscopic data. Further detail can be obtained by noting that the stretching vibrations have the same symmetry properties as the chemical bonds. This allows the vibrational modes to be decomposed further into the symmetry of the stretches and bends.

Square Planar Geometry - D_{4H}

Illegal pream-token (E)

$$A_{1g} = (C_{D4h}^T)^{<1>} \quad A_{2g} = (C_{D4h}^T)^{<2>} \quad B_{1g} = (C_{D4h}^T)^{<3>} \quad B_{2g} = (C_{D4h}^T)^{<4>} \quad E_g = (C_{D4h}^T)^{<5>}$$
$$A_{1u} = (C_{D4h}^T)^{<6>} \quad A_{2u} = (C_{D4h}^T)^{<7>} \quad B_{1u} = (C_{D4h}^T)^{<8>} \quad B_{2u} = (C_{D4h}^T)^{<9>} \quad E_u = (C_{D4h}^T)^{<10>}$$

$$h = \sum D4h \quad \Gamma_{trans} = A_{2u} + E_u \quad \Gamma_{rot} = A_{2g} + E_g \quad \Gamma_{tot} = \overrightarrow{(\Gamma_{uma} \Gamma_{trans})}$$

$$\Gamma_{vib} = \Gamma_{tot} - \Gamma_{trans} - \Gamma_{rot} \quad \Gamma_{stretch} = \Gamma_{bonds} \quad \Gamma_{bend} = \Gamma_{vib} - \Gamma_{stretch} \quad i = 1..10$$

$$\mathrm{Vib}_i = \frac{\sum \overrightarrow{[D4h(C_{D4h}^T)^{<i>} \Gamma_{vib}]}}{h} \quad \mathrm{Stretch}_i = \frac{\sum \overrightarrow{[D4h(C_{D4h}^T)^{<i>} \Gamma_{stretch}]}}{h} \quad \mathrm{Bend}_i = \frac{\sum \overrightarrow{[D4h(C_{D4h}^T)^{<i>} \Gamma_{bend}]}}{h}$$

Illegal pream-token (\)

This analysis predicts three IR active modes (A_{2u}, $2E_u$) and three Raman active modes (A_{1g}, B_{1g}, B_{2g}). It also indicates that there are no coincidences between the IR and Raman spectra. Thus, square planar geometry is consistent with the spectroscopic data. Examining the symmetry of the stretches and bends adds further support to this conclusion.

This analysis also predicts two Raman (A_{1g}, B_{1g}) and one IR (E_u) active stretches, and two IR (A_{2u}, E_u) and one Raman (B_{2g}) active bends. This is also consistent with the experiemental data.

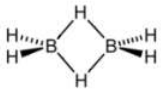
References

- *J. Am. Chem. Soc*. **1963**, *85*, 1927;
- *J. Phys. Chem*. **1971**, *54*, 5247.

This page titled 6.3: Xenon Tetrafluoride is shared under a CC BY 4.0 license and was authored, remixed, and/or curated by Frank Rioux via source content that was edited to the style and standards of the LibreTexts platform.

6.4: Diborane

Diborane - D_{2h} Symmetry



Diborane has 18 vibrational degrees of freedom. Nine modes are Raman active and eight are IR active. The experimental results are provided in the table below. Do a symmetry analysis to confirm the assignments given below, and identify stretches and bends.

$$\begin{pmatrix} D_{2h} & A_g & A_g & A_g & A_g & B_{1g} & B_{1g} & B_{2g} & B_{2g} & B_{3g} \\ \frac{\text{Raman}}{\text{cm}} & 2524 & 2104 & 1180 & 794 & 1768 & 1035 & 2591 & 920 & 1012 \\ D_{2h} & A_u & B_{1u} & B_{1u} & B_{1u} & B_{2u} & B_{2u} & B_{3u} & B_{3u} & B_{3u} \\ \frac{\text{IR}}{\text{cm}} & 0 & 2612 & 950 & 368 & 1915 & 973 & 2525 & 1606 & 1177 \end{pmatrix}$$

Illegal pream-token (E)

$$\begin{array}{llll} \mathrm{A}_g = (\mathrm{C}_{D4h}^T)^{<1>} & \mathrm{B}_{2g} = (\mathrm{C}_{D4h}^T)^{<2>} & \mathrm{B}_{2g} = (\mathrm{C}_{D4h}^T)^{<3>} & \mathrm{B}_{3g} = (\mathrm{C}_{D4h}^T)^{<4>} \\ \mathrm{A}_u = (\mathrm{C}_{D4h}^T)^{<5>} & \mathrm{B}_{1u} = (\mathrm{C}_{D4h}^T)^{<6>} & \mathrm{B}_{2u} = (\mathrm{C}_{D4h}^T)^{<7>} & \mathrm{B}_{3u} = (\mathrm{C}_{D4h}^T)^{<8>} \quad h = \sum \mathrm{D2h} \end{array}$$

$$\begin{array}{lll} \Gamma_{trans} = B_{1u} + B_{2u} + B_{3u} & \Gamma_{tot} = B_{1g} + B_{2g} + B_{3g} & \Gamma_{tot} = \overrightarrow{(\Gamma_{uma}\Gamma_{trans})} \\ \Gamma_{vib} = \Gamma_{tot} - \Gamma_{trans} - \Gamma_{rot} & \Gamma_{vib}^T = (18 \quad 2 \quad 0 \quad 0 \quad 0 \quad 4 \quad 6 \quad 2) & i = 1..8 \\ \Gamma_{stretch} = \Gamma_{bonds} & \Gamma_{bend} = \Gamma_{vib} - \Gamma_{stretch} & \end{array}$$

$$\mathrm{Vib}_i = \frac{\sum \overrightarrow{[D2h(C_{D2h}^T)^{<i>}\Gamma_{vib}]}}{h} \quad \mathrm{Stretch}_i = \frac{\sum \overrightarrow{[D2h(C_{D2h}^T)^{<i>}\Gamma_{stretch}]}}{h} \quad \mathrm{Bend}_i = \frac{\sum \overrightarrow{[D2h(C_{D2h}^T)^{<i>}\Gamma_{bend}]}}{h}$$

Illegal pream-token (\)

This analysis is in agreement with the experimental data. There are 9 Raman active modes and 8 IR active modes. Furthermore there are 4 Raman stretches at 2524 (Ag), 2104 (Ag), 1768 (B1g), and 2591 (B2g). The five Raman bends occur at 1180 (Ag), 794 (Ag), 1035 (B1g), 920 (B2g), and 1012 (B3g).

The 4 IR stretches occur at 2612 (B1u), 1915 (B2u), 2525 (B3u), and 1606 (B3u). The bends appear at 950 (B1u), 368 (B1u), 973 (B2u), 1177 (B3u).

This page titled 6.4: Diborane is shared under a CC BY 4.0 license and was authored, remixed, and/or curated by Frank Rioux via source content that was edited to the style and standards of the LibreTexts platform.

6.5: Cubane

Cubane, C_8H_8, has 42 vibrational degrees of freedom, but only three IR active modes. Cubane belongs to the octahedral point group. Show that group theory predicts three IR active modes. Determine how many vibrational modes will be Raman active. Will there be any coincidences between the IR and Raman active modes? The synthesis and characterization of cubane was reported in 1964 by Philip Eaton and Thomas Cole in JACS **1964**, *86*, 3157-3158. They reported three IR bands at 3000, 1231, and 851 cm^{-1}.

Illegal pream-token (E)

$$\mathrm{Ag} = (\mathrm{C}_{Oh}^{T})^{<1>} \quad \mathrm{A}_{2g} = (\mathrm{C}_{Oh}^{T})^{<2>} \quad \mathrm{E}_{g} = (\mathrm{C}_{Oh}^{T})^{<3>} \quad \mathrm{T}_{1g} = (\mathrm{C}_{Oh}^{T})^{<4>} \quad \mathrm{T}_{2g} = (C_{Oh}^{T})^{<5>}$$
$$\mathrm{A}_{1u} = (\mathrm{C}_{Oh}^{T})^{<6>} \quad \mathrm{A}_{2u} = (\mathrm{C}_{Oh}^{T})^{<7>} \quad \mathrm{E}_{u} = (\mathrm{C}_{Oh}^{T})^{<8>} \quad \mathrm{T}_{1u} = (\mathrm{C}_{Oh}^{T})^{<9>} \quad \mathrm{T}_{2u} = (C_{Oh}^{T})^{<10>}$$

$$\mathrm{Vib}_i = \frac{\sum \overrightarrow{[Oh(C_{Oh}^{T})^{<i>}\Gamma_{vib}]}}{h} \quad \mathrm{Stretch}_i = \frac{\sum \overrightarrow{[Oh(C_{Oh}^{T})^{<i>}\Gamma_{stretch}]}}{h} \quad \mathrm{Bend}_i = \frac{\sum \overrightarrow{[Oh(C_{Oh}^{T})^{<i>}\Gamma_{bend}]}}{h}$$

Illegal pream-token (\\)

Only the three T_{1u} vibrational modes are IR active, which is consistent with the spectroscopic data. The character table indicates that the A_{1g}, E_g, and T_{2g} modes are Raman active. Thus there should be 8 Raman active modes. These have been observed at 2996, 2978, 1185, 1081, 1002, 912, 826, and 665 cm^{-1} (*J. Phys. Chem.* **1981**, 85, 2186). There should be no coincidences between the IR and Raman modes because cubane has a center of inversion.

The vibrational modes can be sorted into stretches and bends by determining how the chemical bonds transform under the symmetry operations of the octahedral group. The symmetry of the stretching modes is the same as the symmetry of the bonds.

This analysis tells us that there are two IR active stretches ($2T_{1u}$) and five Raman active stretches ($2A_{1g}$, E_g, and $2T_{2g}$). This is consistent with the experimental spectra in that stretches generally occur at a higher frequency than bends.

This page titled 6.5: Cubane is shared under a CC BY 4.0 license and was authored, remixed, and/or curated by Frank Rioux via source content that was edited to the style and standards of the LibreTexts platform.

6.5.1: Buckminsterfulerene

C_{60} Has Icosahedral Symmetry

Buckminsterfulerene has four IR active vibrational modes (528, 577, 1180, 1430 cm^{-1}) and ten Raman active modes (273, 436, 496, 710, 773, 110, 1250, 1435, 1470, 1570 cm^{-1}). Demonstrate that the assumption of icosahedral symmetry for C_{60} is consistent with this data.

Illegal pream-token (E)

$$\text{Ih:} \quad \text{Ih} = \text{Ih}^T \quad \Gamma_{uma} = \quad \Gamma_{uma} = \Gamma_{uma}^T$$

$$(1 \quad 12 \quad 12 \quad 20 \quad 15 \quad 1 \quad 12 \quad 12 \quad 20 \quad 15) \qquad (60 \quad 0 \quad 0 \quad 0 \quad 0 \quad 0 \quad 0 \quad 0 \quad 0 \quad 4)$$

$$\Gamma_{bonds} = \quad \Gamma_{bonds} = \Gamma_{bonds}^T \quad \Gamma_{stretch} = \Gamma_{bonds}$$

$$(90 \quad 0 \quad 0 \quad 0 \quad 2 \quad 0 \quad 0 \quad 0 \quad 0 \quad 8)$$

$$\text{Ag} = (\text{CIh}^T)^{<1>} \quad \text{T}_{1g} = (\text{CIh}^T)^{<2>} \quad \text{T}_{2g} = (\text{CIh}^T)^{<3>} \quad \text{G}_g = (\text{CIh}^T)^{<4>} \quad \text{H}_g = (\text{CIh}^T)^{<5>}$$

$$\text{A}_u = (\text{CIh}^T)^{<6>} \quad \text{T}_{1u} = (\text{CIh}^T)^{<7>} \quad \text{A}_u = (\text{CIh}^T)^{<8>} \quad \text{G}_u = (\text{CIh}^T)^{<9>} \quad \text{H}_u = (\text{CIh}^T)^{<10>}$$

$$h = \sum \text{Ih} \quad h = 120 \quad \Gamma_{tot} = \overrightarrow{(\Gamma_{uma} T1u)} \quad \Gamma_{vib} = \Gamma_{tot} - T1g - T1u \quad \Gamma_{bend} = \Gamma_{vib} - \Gamma_{stretch} \quad i = 1..10$$

Illegal pream-token (\)

The 4 T_{1u} modes are IR active and the 2 A_g and 8 H_g modes are Raman active. Also there are no coincidences. Thus the assumption of icosahedral symmetry is consistent with the spectroscopic data.

This page titled 6.5.1: Buckminsterfulerene is shared under a CC BY 4.0 license and was authored, remixed, and/or curated by Frank Rioux via source content that was edited to the style and standards of the LibreTexts platform.

6.6: BCl3

C_{3v} Symmetry - BCl_3

The infrared spectrum of BCl_3 shows vibrational bands at 995, 480, and 244 cm^{-1}, while Raman bands appear at 995, 471, and 244 cm^{-1}. Is the geometry of the molecule trigonal pyramid (C_{3v}) or trigonal planar (D_{3h})? Is your answer to this question consistent with chemical bonding principles (VSEPR)? Assign symmetry labels to the vibrational bands and identify the stretches and bends.

Illegal pream-token (E)

$$A_1 = (C^T_{C3v})^{<1>} \quad A_2 = (C^T_{C3v})^{<2>} \quad E = (C^T_{C3v})^{<3>} \quad h = \sum C3v$$

$$\Gamma_{tot} = \overrightarrow{[\Gamma_{uma}(A_1 + E)]} \quad \Gamma^T_{tot} = (12 \quad 0 \quad 2) \quad \Gamma_{vib} = \Gamma_{tot} - A_1 - A_2 - 2E$$

Illegal pream-token (A)

This analysis predicts that there should be 4 IR and 4 Raman active vibrations. It also predicts that the IR and Raman vibrations should be coincident. This is not in agreement with the experimental data, so BCl3 does not have trigonal pyramidal geometry.

This analysis also predicts that the stretches should have A1 and E symmetry, but since it has already been concluded that the molecule does not have C_{3v} symmetry this result will not be discussed further.

D_{3h} Symmetry - BCl_3

Illegal pream-token (E)

$$A_1 = (C^T_{D3h})^{<1>} \quad A_2 = (C^T_{D3h})^{<2>} \quad E = (C^T_{D3h})^{<3>} \quad A_{11} = (C^T_{D3h})^{<4>}$$
$$A_{21} = (C^T_{D3h})^{<5>} \quad E_1 = (C^T_{D3h})^{<6>} \quad h = \sum D3h \quad \Gamma_{tot} = \overrightarrow{[\Gamma_{uma}(A_{21} + E)]}$$

$$\Gamma^T_{tot} = (12 \quad 0 \quad -2 \quad 4 \quad -2 \quad 2) \quad \Gamma_{vib} = \Gamma_{tot} - A_2 - E - A_{21} - E_1 \quad i = 1..6$$
$$\Gamma_{stretch} = \Gamma_{bonds} \qquad \Gamma_{bend} = \Gamma_{vib} - \Gamma_{stretch}$$

Illegal pream-token (A)

This analysis shows that there are 3 IR active modes (2E', A2") and 3 Raman active modes (A1', E'). It also show that there are two coincidences (2E'). Thus, D_{3h} symmetry for BCl_3 is consistent with the spectroscopic data.

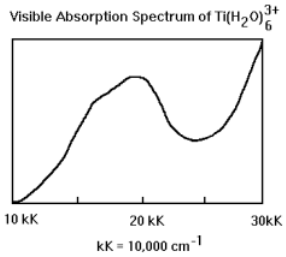
Thus the specific assignments are: A1' = 471; A2" = 480; E' = 995; E' = 244. From the analysis above it can be seen that the stretches occur at 995 and 471, and the bends are at 480 and 244 cm^{-1}.

VSEPR theory would predict a trigonal planar arrangement of chlorine atoms around the electron deficient boron, so the symmetry analysis and the bonding theory are in agreement with each other and the spectroscopic measurements.

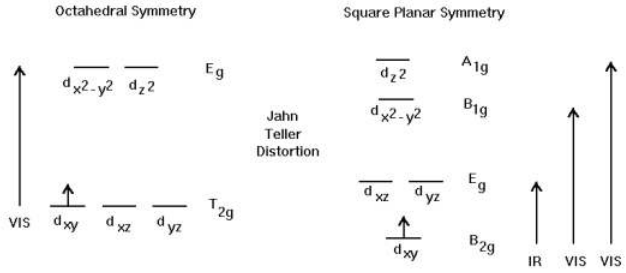
This page titled 6.6: BCl3 is shared under a CC BY 4.0 license and was authored, remixed, and/or curated by Frank Rioux via source content that was edited to the style and standards of the LibreTexts platform.

6.7: Ti(H2O)6 3+

This exercise has to do with the interpretation of the visible spectrum $Ti(H_2O)_6^{3+}$ which is shown below.



The analysis will begin by assuming that $Ti(H_2O)_6^{3+}$ has octahedral symmetry. This assumption accounts for the gross features of the spectrum, but does not explain the shoulder that appears on the main absorption peak. The hexaaquatitanium(III) complex is orbitally degenerate and is therefore subject to a Jahn-Teller distortion which reduces the symmetry to square planar. It will be shown that D_{4h} symmetry is fully consistent with the experimental spectrum. The d-orbital energy level diagrams for O_h and D_{4h} symmetry are shown below and will be referred to later in the analysis.



On the basis of these energy level diagrams we would make the following predictions. For octahedral symmetry there is one electronic transition in the visible region. For square planar symmetry there are two electronic transitions in the visible region and one in the infrared. In the analysis that follows it will be shown that none of the electronic transitions is orbitally allowed, but they are allowed through vibronic coupling. Further more the square planar geometry is in better agreement with the experimental spectrum than octahedral symmetry.

$Ti(H_2O)_6^{3+}$ - Octahedral Symmetry

Illegal pream-token (E)

$$\begin{array}{llll} \mathrm{Ag} = (\mathrm{C}_{Oh}^{T})^{<1>} & \mathrm{A}_{2g} = (\mathrm{C}_{Oh}^{T})^{<2>} & \mathrm{E}_{g} = (\mathrm{C}_{Oh}^{T})^{<3>} & \mathrm{T}_{1g} = (\mathrm{C}_{Oh}^{T})^{<4>} \\ \mathrm{T}_{2g} = (\mathrm{C}_{Oh}^{T})^{<5>} & \mathrm{A}_{1u} = (\mathrm{C}_{Oh}^{T})^{<6>} & \mathrm{A}_{2u} = (\mathrm{C}_{Oh}^{T})^{<7>} & \mathrm{E}_{u} = (\mathrm{C}_{Oh}^{T})^{<8>} \\ \mathrm{T}_{1u} = (\mathrm{C}_{Oh}^{T})^{<9>} & \mathrm{T}_{2u} = (\mathrm{C}_{Oh}^{T})^{<10>} & h = \sum \mathrm{Oh} & \Gamma_{tot} = \overrightarrow{(\Gamma_{uma} T1u)} \end{array}$$

$$\Gamma_{tot}^{T} = (21 \quad 0 \quad -1 \quad 3 \quad -3 \quad -3 \quad -1 \quad 0 \quad 5 \quad 3) \quad \Gamma_{vib} = \Gamma_{tot} - T1u - T1g$$

Determine which irreducible representations contribute to Γ_{vib}:

$$i = 1..10 \quad X_i = \frac{\sum \overrightarrow{[Oh(COh^T)^{<i>}\Gamma_{vib}]}}{h} \quad X^T = (1 \quad 0 \quad 1 \quad 0 \quad 1 \quad 0 \quad 0 \quad 0 \quad 2 \quad 1)$$

Thus we see that: $\Gamma_{vib} = A1g + Eg + T2g + 2T1u + 2T2u$

Inspection of the character table shows that in octahedral symmetry the d-orbitals are split into a lower T_{2g} (d_{xy}, d_{xz}, d_{yz}) level and an upper Eg (d_{z^2}, $d_{x^2-y^2}$) level. Ti^{3+} has one d-electron in the T_{2g} level. As the spectrum below shows, the complex absorbs in the visible region at 20,000 cm^{-1} (500 nm). However the T_{2g} ---> E_g transition is orbitally forbidden as is shown below.

$$\int \Psi_{ex} \mu_e \Psi_{eg} d\tau_e = 0 \quad \frac{\sum \overrightarrow{(Oh\ Eg\ T1u\ T2g)}}{h} = 0$$

In calculating the transition moment for T_{2g} ---> E_g electronic transition it has been assumed that there was no change in the vibrational state of the molecule. However, it is possible for formally forbidden electronic transitions to become allowed through coupling to changes in vibrational state. In other words pure electronic transitions do not actually occur, because the vibrational (and rotational) states of the molecule change at the same time. These are called vibronic transitions and they are allowed if the integral shown below is nonzero.

$$\int\int(\Psi_{ex}\Psi_{vx}\mu_e\Psi_{eg}\Psi_{vg})d\tau_e d\tau v$$

The calculations below show that vibronic calculations involving the T_{1u} and T_{2u} vibrational modes are allowed because the transition moment is not zero.

$$\frac{\sum\overrightarrow{(Oh\ T1u\ Eg\ T1u\ T2g\ A1g)}}{h}=2\quad\frac{\sum\overrightarrow{(Oh\ T1u\ Eg\ T1u\ T2g\ A1g)}}{h}=2$$

At this point we have shown that the vibrationally assisted T_{2g} ---> E_g electronic transition is allowed. However, the shoulder on the experimental spectrum suggest that more than one electronic transition is occuring. In the next section we will see that a reduction to square planar symmetry under the Jahn-Teller effect leads to an d-orbital energy level diagram that is consistent with the experimental spectrum.

Ti(H_2O)63+ - Square Planar Symmetry

The Jahn-Teller effect predicts a tetragonal distortion of the octahedral complex to the lower D_{4h} square planar symmetry. The energy level diagram is shown above - essentially the ligands on the z-axis move in toward the titanium ion.

Illegal pream-token (E)

$$\begin{array}{llll}\text{A1g} & \text{A2g} & \text{B1g}=(\text{CD4h}^T)^{<3>} & \text{B2g}=(\text{CD4h}^T)^{<4>}\quad\text{Eg}=(\text{CD4h}^T)^{<5>}\\ =(\text{CD4h}^T)^{<1>} & =(\text{CD4h}^T)^{<2>} & & \\ \text{A1u} & \text{A2u} & \text{B1u}=(\text{CD4h}^T)^{<8>} & \\ =(\text{CD4h}^T)^{<6>} & =(\text{CD4h}^T)^{<7>} & & \\ \text{B2u} & \text{Eu} & & \\ =(\text{CD4h}^T)^{<9>} & =(\text{CD4h}^T)^{<10>} & & \end{array}$$

$$h=\sum\text{D4h}\quad\Gamma_{tot}=\overrightarrow{(\Gamma_{uma}(A2u+Eu))}\quad\Gamma_{tot}^T=(15\quad1\quad-1\quad-3\quad-1\quad-3\quad-1\quad5\quad3\quad1)$$

Symmetry of the vibrational modes.

$$\Gamma_{vib}=\Gamma_{tot}-A2g-Eg-A2u-Eu\qquad i=1..10\qquad Y_i=\frac{\sum\overrightarrow{[D4h(CD4h^T)^{<i>}\Gamma_{vib}]}}{h}$$

$$Y^T=(1\quad0\quad1\quad1\quad0\quad0\quad1\quad0\quad1\quad2)$$

$$\Gamma_{vib}=A1g+B1g+B2g+A2u+B2u+2Eu$$

The energy level diagram above shows three possible electronic transitions, one IR transition and two transitions in visible region of the spectrum. The calculations below show that all three are formally forbidden. Vibronic coupling is invoked to explain the appearance of the two electronic transitions in the visible region.

$$\frac{\sum\overrightarrow{(D4h\ Eg(A2u+Eu)B2g))}}{h}=0\quad\frac{\sum\overrightarrow{(D4h\ B1g(A2u+Eu)B2g))}}{h}=0\quad\frac{\sum\overrightarrow{(D4h\ A1g(A2u+Eu)B2g))}}{h}=0$$

A A_{1u} or E_u vibrational mode can provide vibronic coupling for the B_{2g} --> B_{1g} transition.

$$\frac{\sum\overrightarrow{(D4h\ A1u\ B1g(A2u+Eu)B2g\ A1g))}}{h}=1\quad\frac{\sum\overrightarrow{(D4h\ Eu\ B1g(A2u+Eu)B2g\ A1g))}}{h}=1$$

A B_{1u} or E_u vibrational mode can provide vibronic coupling for the B_{2g} --> A_{1g} transition.

$$\frac{\sum\overrightarrow{(D4h\ B1u\ A1g(A2u+Eu)B2g\ A1g))}}{h}=1\quad\frac{\sum\overrightarrow{(D4h\ Eu\ A1g(A2u+Eu)B2g\ A1g))}}{h}=1$$

A close examination of the experimental spectrum indicates the presence of two electronic transitions of similar energy (shoulder). So the energy level diagram and the vibronic analysis are consistent with the actual spectrum.

This page titled 6.7: Ti(H2O)6 3+ is shared under a CC BY 4.0 license and was authored, remixed, and/or curated by Frank Rioux via source content that was edited to the style and standards of the LibreTexts platform.

6.8: CH_4

Tetrahedral Symmetry for Methane

The infrared spectrum of methane shows two absorptions: a bend at 1306 cm^{-1} and a stretch at 3019 cm^{-1}. Demonstrate that a symmetry analysis assuming tetrahedral symmetry for methane is consistent with this spectroscopic data. Also predict how many Raman active modes methane should have.

Illegal pream-token (E)

$$A_1 = (C_{Td}^T)^{<1>} \quad A_2 = (C_{Td}^T)^{<2>} \quad E = (C_{Td}^T)^{<3>} \quad T_1 = (C_{Td}^T)^{<4>}$$
$$T_2 = (C_{Td}^T)^{<5>} \quad \Gamma_{tot} = \overrightarrow{(\Gamma_{uma} T_2)} \quad h = \sum Td \quad \Gamma_{tot}^T = (15 \quad 0 \quad -1 \quad -1 \quad 3) \quad i = 1..5$$

Illegal pream-token (A)

Thus the vibrational modes have A_1, E, and T_2 symmetry. Only the two T_2 modes are infrared active which is consistent with the experimental data quoted above. One of the T_2 modes is a stretch (3019 cm^{-1}) and the other is a bend (1306 cm^{-1}).

This symmetry analysis predicts that all of vibrational modes are Raman active - one singly degenerate mode (A_1), one doubly degenerate mode (E), and two triply degenerate modes (T_2). Indeed four Raman active modes are found at 3019, 2917, 1534, and 1306 cm^{-1}. Note, as expected from the symmetry analysis, there are two coincidences between the IR and Raman spectra.

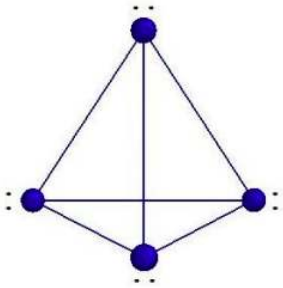
This page titled 6.8: CH_4 is shared under a CC BY 4.0 license and was authored, remixed, and/or curated by Frank Rioux via source content that was edited to the style and standards of the LibreTexts platform.

6.9: P_4

T_d - Tetrahedral Symmetry for P_4

The following Raman and IR frequencies have been observed for the tetrahedral P_4 molecule. Is the assignment of tetrahedral geometry to this molecule in agreement with the spectroscopic data? Explain.

$$\begin{pmatrix} R & R & R, IR \\ \frac{614}{\text{cm}} & \frac{372}{\text{cm}} & \frac{466}{\text{cm}} \end{pmatrix}$$



Illegal pream-token (E)

$$A_1 = (C_{Td}^T)^{<1>} \quad A_2 = (C_{Td}^T)^{<2>} \quad E = (C_{Td}^T)^{<3>} \quad T_1 = (C_{Td}^T)^{<4>}$$
$$T_2 = (C_{Td}^T)^{<5>} \quad \Gamma_{tot} = \overrightarrow{(\Gamma_{uma} T_2)} \quad h = \sum Td \quad \Gamma_{tot}^T = (12 \quad 0 \quad 0 \quad 0 \quad 2) \quad i = 1..5$$

Illegal pream-token (A)

The group theoretical analysis assuming tetrahedral geometry is in excellent agreement with the spectroscopic data. Group theory predicts one IR active mode, and that it is coincident with a Raman frequency. This is observed with the T_2 vibration. In addition theory predicts that there are two additional Raman active modes A_1 and E.

This page titled 6.9: P_4 is shared under a CC BY 4.0 license and was authored, remixed, and/or curated by Frank Rioux via source content that was edited to the style and standards of the LibreTexts platform.

6.10: Tetrahedrane

Symmetry Analysis for Tetrahedrane

Tetrahedrane, C_4H_4, belongs to the Td point group. Use group theory to predict the number of IR and Raman acitive vibrational modes it has. To date tetrahedrane has not been synthesized.

Illegal pream-token (E)

$$A_1 = (C_{Td}^T)^{<1>} \quad A_2 = (C_{Td}^T)^{<2>} \quad E = (C_{Td}^T)^{<3>} \quad T_1 = (C_{Td}^T)^{<4>}$$

$$T_2 = (C_{Td}^T)^{<5>} \quad \Gamma_{tot} = \overrightarrow{(\Gamma_{uma} T_2)} \quad h = \sum Td \quad \Gamma_{tot}^T = (20 \quad 0 \quad 0 \quad 0 \quad 4)$$

$$i = 1..5$$

Illegal pream-token (A)

According to the selection rules, tetrahedrane should have three IR active modes ($3T_2$) and seven Raman active modes ($2A_1$ + 2E + $3T_2$). Two of the IR modes are stretches, while five of the Raman modes are stretches.

This page titled 6.10: Tetrahedrane is shared under a CC BY 4.0 license and was authored, remixed, and/or curated by Frank Rioux via source content that was edited to the style and standards of the LibreTexts platform.

6.11: PH3

C_{3v} Symmetry - PH_3

PH_3 (pyramidal) has IR and Raman active vibrations at 2421, 2327, 1121, and 991 cm^{-1}. Make assignments in terms of stretches and bends.

Illegal pream-token (~)

$$A_1 = (C^T_{C3v})^{<1>} \qquad A_2 = (C^T_{C3v})^{<2>} \qquad E = (C^T_{C3v})^{<3>} \qquad h = \sum C3v$$

$$\Gamma_{tot} = \overrightarrow{[\Gamma_{uma}(A_1 + E)]} \quad \Gamma^T_{tot} = (12 \quad 0 \quad 2) \quad \Gamma_{vib} = \Gamma_{tot} - A_1 - A_2 - 2E$$

Illegal pream-token (A)

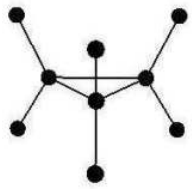
Group theory predicts two singly degenerate (A_1) vibrational modes and two doubly degenerate (E) vibrational modes. This is consistent with the appearance of four fundamentals in the experimental IR and Raman spectra. It further predicts that there are two stretches and two bends. This is also consistent with the experimental data.

This page titled 6.11: PH3 is shared under a CC BY 4.0 license and was authored, remixed, and/or curated by Frank Rioux via source content that was edited to the style and standards of the LibreTexts platform.

6.12: Cyclopropane

D_{3h} Symmetry - C_3H_6

The following IR and Raman spectroscopic data is available for cyclopropane, C_3H_6. Demonstrate that this data is consistent with a D_{3h} symmetry assignment for cyclopropane.



Frequency	3038	1479	1188	3025	1438	1029	866	3103	854	3082	1188	734
Activity	R	R	R	R, IR	R, IR	R, IR	R, IR	IR	IR	R	R	R
Type	■	■	■	■	■	■	■	■	■	■	■	■
Symmetry	■	■	■	■	■	■	■	■	■	■	■	■

Illegal pream-token (E)

$$A_1 = (C^T_{D3h})^{<1>} \quad A_2 = (C^T_{D3h})^{<2>} \quad E = (C^T_{D3h})^{<3>} \quad A_{11} = (C^T_{D3h})^{<4>}$$

$$A_{21} = (C^T_{D3h})^{<5>} \quad E_1 = (C^T_{D3h})^{<6>} \quad h = \sum D3h \quad \Gamma_{tot}\,\overrightarrow{[\Gamma_{uma}(A_{21}+E)]}$$

$$\Gamma^T_{tot} = (27 \quad 0 \quad -1 \quad 3 \quad 0 \quad 3) \quad \Gamma_{vib} = \Gamma_{tot} - A_2 - E - A_{21} - E_1 \quad i = 1..6$$

$$\Gamma_{stretch} = \Gamma_{bonds} \qquad \Gamma_{bend} = \Gamma_{vib} - \Gamma_{stretch}$$

Illegal pream-token (A)

Frequency	3038	1479	1188	3025	1438	1029	866	3103	854	3082	1188	734
Activity	R	R	R	R, IR	R, IR	R, IR	R, IR	IR	IR	R	R	R
Type	S	S	B	S	S	B	B	S	B	S	B	B
Symmetry	$A1'$	$A1'$	$A1'$	E'	E'	E'	E'	$A2''$	$A2''$	E''	E''	E''

There are 9 Raman active modes, 2 IR active modes, 8 IR/Raman active, and 2 modes that are neither Raman or IR active. This gives a total of 21 vibrational modes which is consistent with the total degrees of freedom (27=3x9) minus 6 for translation and rotation.

This page titled 6.12: Cyclopropane is shared under a CC BY 4.0 license and was authored, remixed, and/or curated by Frank Rioux via source content that was edited to the style and standards of the LibreTexts platform.

6.13: An Extensive Set of Group Theory Problems for Chemists

The following table shows the vibrational frequencies of CH_4. Assuming CH_4 belongs to the T_d point group, fill in the gaps in the table. Use S for stretch and B for bend to designate type of vibration.

Frequency	$2917cm^{-1}$	$1534cm^{-1}$	$3019cm^{-1}$	$1306cm^{-1}$
Stretch or Bend	■	■	■	■
Symmetry	■	■	■	■
$\frac{\text{Activity}}{\text{IR or Raman}}$	■	■	■	■

The following table shows the vibrational frequencies of CD_4. Assuming CD_4 belongs to the T_d point group, fill in the gaps in the table. Use S for stretch and B for bend to designate type of vibration.

Frequency	$2109cm^{-1}$	$1092cm^{-1}$	$2259cm^{-1}$	$966cm^{-1}$
Stretch or Bend	■	■	■	■
Symmetry	■	■	■	■
$\frac{\text{Activity}}{\text{IR or Raman}}$	■	■	■	■

The following table summarizes the infrared activity CH_2D_2. Assuming it belongs to the C_{2v} point group, complete the table. Use S for stretch and B for bend to designate the type of vibration.

Frequency	2974	2202	1436	1033	1333	3013	1090	2234	1155
Stretch or Bend	■	■	■	■	■	■	■	■	■
Symmetry	■	■	■	■	■	■	■	■	■
$\frac{\text{Activity}}{\text{IR or Raman}}$	■	■	■	■	■	■	■	■	■

The following table summarizes the infrared activity of CH_3D. Assuming CH_3D belongs to the C_{3v} point group, fill in the gaps in the table. Use S for stretch and B for bend to designate type of vibration.

Frequency	$2945cm^{-1}$	$2200cm^{-1}$	$1300cm^{-1}$	$3017cm^{-1}$	$1471cm^{-1}$	$1155cm^{-1}$
Stretch or Bend	■	■	■	■	■	■
Symmetry	■	■	■	■	■	■
$\frac{\text{Activity}}{\text{IR or Raman}}$	■	■	■	■	■	■

Formaldehde has vibrational frequencies at 2843, 2776, 1501, 1251, 1746, and 1167 cm^{-1}. How many are IR active and how many are Raman active. Separate them into bends and stretches.

Frequency	2843	2776	1501	1251	1746	1167
Stretch or Bend	A_1	A_1	A_1	B_1	B_2	B_2
Symmetry	Stretch	Stretch	Bend	Bend	Stretch	Bend
$\frac{\text{Activity}}{\text{IR or Raman}}$	IR, R	IR, R	IR, R	IR, R	IR, R	IR, R

PH_3 (C_{3v}) has IR and Raman active vibrations at 2421, 2327, 1121, and 991 cm^{-1}. PD_3 has IR and Raman active vibrations at 1698, 1694, 806 and 730 cm^{-1}. Make assignments in terms of stretches and bends.

The infrared spectrum of BCl3 shows vibrational bands at 995, 480, and 244 cm^{-1}, while Raman bands appear at 995, 471, and 244 cm^{-1}. Is the geometry of the molecule trigonal pyramid (C_{3v}) or trigonal planar (D_{3h})? Is your answer to this question consistent with chemical bonding principles? Assign symmetry labels to the vibrational bands and identify the stretches and bends.

Frequency	$995cm^{-1}$	$480cm^{-1}$	$471cm^{-1}$	$224cm^{-1}$
$\frac{\text{Activity}}{\text{IR or Raman}}$	IR, R	IR	R	IR, R
Symmetry	■	■	■	■
Stretch or Bend	■	■	■	■

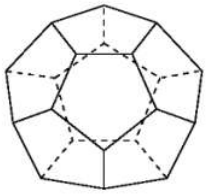
CH_3CN has 12 vibrational degrees of freedom, but 8 fundamental vibrational frequencies appear in the infrared at 2999, 2942, 2249, 1440, 1376, 1124, 918, and 380 cm^{-1}. Explain.

The infrared spectrum of methane shows two absorptions: a bend at 1306 cm^{-1} and a stretch at 3019 cm^{-1}. Demonstrate that a symmetry analysis assuming tetrahedral symmetry for methane is consistent with this spectroscopic data. Also predict how many Raman active modes methane should have.

The infrared spectrum of XeF_4 has absorptions at 161, 291, and 586 cm^{-1} (two bends, one stretch), while the Raman spectrum has peaks at 218, 524, and 554 cm^{-1} (one bend, two stretches). Is its molecular structure tetrahedral or square planar? References: *J. Am. Chem. Soc.* **1963**, 85, 1927; *J. Phys. Chem.* **1971**, 54, 5247.

Cubane, C_8H_8, has 42 vibrational degrees of freedom, but only three IR active modes. Cubane belongs to the octahedral point group. Show that group theory predicts three IR active modes. Determine how many vibrational modes will be Raman active. Will there be any coincidences between the IR and Raman active modes? The synthesis and characterization of cubane was reported in 1964 by Philip Eaton and Thomas Cole in JACS **1964**, 86, 3157-3158. They reported three IR bands at 3000, 1231, and 851 cm^{-1}.

When Paquette's group synthesized dodecahedrane, $C_{20}H_{20}$, they measured its infrared and Raman spectra (JACS 1**983**, 105, 5446-5450). They found three IR active bands at 2945, 1298, and 728 cm^{-1} and eight Raman frequencies at 2924, 2938, 1324, 1164, 1092, 840, 676, and 480 cm^{-1}. Use group theory to show that these data are consistent with the fact that dodecahedrane has icosahedral symmetry.



Frequency cm	2938	2924	1324	1164	1092	840	676	480	2945	1298	728
Symmetry	A_g	A_g	H_g	H_g	H_g	H_g	H_g	H_g	T_{1u}	T_{1u}	T_{1u}
$\frac{\text{IR, R}}{\text{Activity}}$	R	R	R	R	R	R	R	R	IR	IR	IR
Stretch or Bend	stretch	stretch	stretch	stretch	stretch	bend	bend	bend	stretch	stretch	bend

Sulfur tetrafluoride represents a difficult case which can't be resolved to complete satisfaction on the basis of IR and Raman data alone. The experimental spectra show eight (five certain and three likely) IR bands and eight (five certain and three likely) Raman bands, and eight (five certain and three likely) coincidences between the two. This information plus nmr spectra lead to the conclusion that the symmetry is C_{2v} or the see-saw structure predicted by VSEPR.

The March 28, 2003 issue of Science reported the synthesis and characterization of Al_2H_6, the aluminum analog of diborane (therefore, dialane). The researchers reported the following experimental IR frequencies in cm^{-1}: B_{1u} (1932, 836); B_{2u} (1268, 632); B_{3u} (1915, 1408,702). Do a symmetry analysis of Al_2H_6 which belongs to the D_{2h} point group. How many vibrational modes are there? Which ones are IR active and what are their symmetry designations. The researchers reported that one of the expected low frequency vibrations (~200 cm^{-1}) was not observed. What is the symmetry of this vibrational mode?

Buckminsterfullerene (C60) has four IR active vibrational modes (528, 577, 1180, 1430 cm^{-1}) and ten Raman active modes (273, 436, 496, 710, 773, 110, 1250, 1435, 1470, 1570 cm^{-1}). Demonstrate that the assumption of icosahedral symmetry for C_{60} is consistent with this data.

Do a symmetry analysis of the 60π orbitals of C_{60} and show that the results are in agreement with a Huckel calculation.

The following Raman and IR frequencies have been observed for the tetrahedral P_4 molecule. Is the assignment of tetrahedral geometry to this molecule in agreement with the spectroscopic data? Explain.

R	R	R, IR
$\frac{614}{cm}$	$\frac{372}{cm}$	$\frac{466}{cm}$

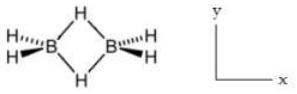
Isotopic subsitution for one of the ^{31}P atoms with a ^{32}P atom reduces the symmetry to C_{3v}. Redo the symmetry analysis and predict the number of IR and Raman active vibrational modes.

Tetrahedrane, C_4H_4, belongs to the T_d point group. Use group theory to predict the number of IR and Raman active vibrational modes it has. Predict also the number of stretches and bends will appear in each type of spectroscopy. To date tetrahedrane has not been synthesized.

Do symmetry analyses on cis-difluoroethene (C_{2v}) and trans-difluoroethene (C_{2h}). Can spectroscopic methods (IR and Raman) be used to distinquish between these isomers. Explain. What about 1,1 difluoroethene? What point group does it belong to? Can spectroscopic methods distinguish it from the cis and trans isomers examined above? Cis-MA_2B_2 has C_{2v} symmetry and trans-MA_2B_2 has D_{2h} symmetry. Determine the IR and Raman active modes for each molecule and discuss how such spectroscopic evidence can be used to distinguish the two isomers.

CH_3Cl has IR and Raman active modes at 3017, 2937, 1452, 1355, 1017, and 732 cm^{-1}. Is this data consistent with C3v symmetry assignment for chloromethane?

Diborane, D2h, has 18 vibrational degrees of freedom. Nine modes are Raman active and nine are IR active. There are no coincidences. Do a symmetry analysis of diborane to confirm the assignments made in the table below. Identify stretches and bends. The xy plane is the plane of the paper. The four terminal H atoms of diborane lie in the xz plane and the two bridging atoms lie in the xy plane.

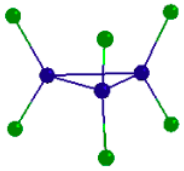


D_{2h}	A_g	A_g	A_g	A_g	B_{1g}	B_{1g}	B_{2g}	B_{2g}	B_{3g}
$\frac{\text{Raman}}{\text{cm}}$	2524	2104	1180	794	1768	1035	2591	920	1012
Stretch or Bend	S	S	B	B	S	B	S	B	B
D_{2h}	A_u	B_{1u}	B_{1u}	B_{1u}	B_{2u}	B_{2u}	B_{3u}	B_{3u}	B_{3u}
$\frac{\text{IR}}{\text{cm}}$	ia	2612	950	368	1915	973	2525	1606	1177
Stretch or Bend	B	S	B	B	S	B	S	S	B

The following IR and Raman spectroscopic data is available for cyclopropane, C_3H_6. Demonstrate that this data is consistent with a D_{3h} symmetry assignment for cyclopropane. In addition complete the table below.

$\frac{\text{Frequency}}{\text{cm}^{-1}}$	3038	1479	1188	3025	1438	1029	866	3103	854	3082	188	734
Activity	IR	IR	IR	R, IR	R, IR	R, IR	R, IR	IR	IR	R	R	R
Symmetry	■	■	■	■	■	■	■	■	■	■	■	■
Stretch or Bend	■	■	■	■	■	■	■	■	■	■	■	■

$\frac{\text{Frequency}}{\text{cm}^{-1}}$	3038	1479	1188	3025	1438	1029	866	3103	854	3082	188	734
Activity	IR	IR	IR	R, IR	R, IR	R, IR	R, IR	IR	IR	R	R	R
Symmetry	S	S	B	S	S	B	B	§	B	S	B	B
Stretch or Bend	$A1'$	$A1'$	$A1'$	E'	E'	E'	E'	$A2''$	$A2''$	E''	E''	E''



PX_5 has trigonal bipyramidal geometry and therefore belongs to the D_{3h} point group. Use the model provided to do a symmetry analysis of PX_5 by determining Γ_{uma} and Γ_{bonds}.

The following spectroscopic information is available.

Frequency	$816cm^{-1}$	$648cm^{-1}$	$947cm^{-1}$	$525cm^{-1}$	$1024cm^{-1}$	$533cm^{-1}$	$174cm^{-1}$	$520cm^{-1}$
Activity	R	R	IR	IR	R, IR	R, IR	R, IR	R
Symmetry	■	■	■	■	■	■	■	■
Stretch or Bend	■	■	■	■	■	■	■	■

Is the symmetry analysis consistent with the spectroscopic data? Explain in detail.

Frequency	$816cm^{-1}$	$648cm^{-1}$	$947cm^{-1}$	$525cm^{-1}$	$1024cm^{-1}$	$533cm^{-1}$	$174cm^{-1}$	$520cm^{-1}$
Activity	R	R	IR	IR	R, IR	R, IR	R, IR	R
Symmetry	A_1	A_1	A_2	A_2	E	E	E	E
Stretch or Bend	S	S	S	B	S	B	B	B

The following IR and Raman vibrational data is available for tetrahedral methane. Complete the table. Also show that vibrational data is not consistent with a square planar (D_{4h}) or square pyramid (C_{4v}) geometry.

Frequency	$3019cm^{-1}$	$2717cm^{-1}$	$1534cm^{-1}$	$1306cm^{-1}$
Activity	IR, R	R	R	IR, R
Symmetry	■	■	■	■
Stretch or Bend	■	■	■	■

The following IR and Raman spectroscopic data is available for ethene, C_2H_4. Demonstrate that this data is consistent with a D_{2h} symmetry assignment for ethene. In addition complete the table below.

Frequency	3018	3106	3019	2990	1623	1444	1342	1236	949	943	810
Activity	R	IR	R	IR	R	IR	R	R	R	IR	IR
Stretch or Bend	S	S	S	S	S	B	B	B	B	B	B
Symmetry	Ag	$B2u$	Ag	$B3u$	$B1g$	$B1u$	Ag	$B1g$	$B2g$	$B2u$	$B3u$

IR and Raman data for$XeOF_4$, which has C_{4v} symmetry. Establish that the symmetry assignment is correct.

Frequency cm	926	576	286	232	220	527	609	364	161
Activity	R, IR	R, IR	R, IR	R	R	R	R, IR	R, IR	R, IR
Symmetry	A_1	A_1	A_1	$\frac{B_1}{B_2}$	$\frac{B_1}{B_2}$	B_1	E	E	E
Stretch or Bend	S	S	B	B	B	S	S	B	B

IR and Raman data for $[PtCl_4]^{2-}$ which has D_{4h} symmetry. Establish that the symmetry assignment is correct.

Frequency	$332cm^{-1}$	$320cm^{-1}$	$314cm^{-1}$	$183cm^{-1}$	$170cm^{-1}$	$93cm^{-1}$
Activity	R	IR	R	IR	R	IR
Symmetry	A_{1g}	E_u	B_{1g}	E_u	B_{2g}	A_{2u}
Stretch or Bend	S	S	S	B	B	B

The vibrational modes of the ions $[BrF_2]^-$ and $[BrF_2]^+$ are given below. Identify which one is A and which one is B.

A	B
$596(IR)$	$715(IR, R)$
$442(R)$	$706(IR, R)$
$198(IR)$	$366(IR, R)$

The following spectroscopic data for $[ClO_4]^-$ is available. Show that it is consistent with T_d symmetry.

Frequency	$1102cm^{-1}$	$935cm^{-1}$	$628cm^{-1}$	$462cm^{-1}$
Activity	IR, R	R	IR, R	R
Symmetry	■	■	■	■
Stretch or Bend	■	■	■	■

MoF_5 has trigonal bipyramidal geometry and therefore belongs to the D_{3h} point group. Use the model provided to do a symmetry analysis of MoF_5 by determining Γ_{uma} and Γ_{bonds}. The following spectroscopic information is available.

Frequency	$747cm^{-1}$	$732cm^{-1}$	$703cm^{-1}$	$685cm^{-1}$	$500cm^{-1}$	$440cm^{-1}$	$239cm^{-1}$	$203cm^{-1}$
Activity	R	IR, R	R	IR	IR	R	IR, R	IR, R
Symmetry	■	■	■	■	■	■	■	■
Stretch or Bend	■	■	■	■	■	■	■	■

The Raman and IR spectra of a sample of N_2F_2 are measured and the results are shown below. Is the sample cis-difluordiazine (C_{2v}) or trans-difluordiazine (C_{2h})?

Frequency	$1636cm^{-1}$	$1010cm^{-1}$	$989cm^{-1}$	$592cm^{-1}$	$412cm^{-1}$	$360cm^{-1}$
Activity	R	R	IR	R	IR	IR
Symmetry	■	■	■	■	■	■
Stretch or Bend	■	■	■	■	■	■

Benzene has IR active modes at 675, 1035, 1479, and 3036 cm^{-1}. Demonstrate that this is consistent with D_{6h} symmetry. Separate the vibrations into stretches and bends.

Do a symmetry analysis of the π orbitals of benzene and show that it is consistent with the results of a Huckel calculation on benzene.

Allene, C_3H_4, belongs to the D_{2d} point group.

$\frac{\text{Frequency}}{cm^{-1}}$	3015	1443	1073	865	3007	1957	1398	3086	999	841	355
Symmetry	A_1	A_1	A_1	B_1	B_2	B_2	B_2	E	E	E	E
Bend or Stretch	S	S	B	B	S	S	B	S	B	B	B

The following data is available for ethene and deuterated ethene which have D_{2h} symmetry. To each of the vibrational modes determine whether it is a stretch or a bend and its symmetry.

C_2H_4	C_2D_4	Activity	$\frac{\text{Stretch}}{\text{Bend}}$	Symmetry
3108	2304	R	■	■
3106	2345	IR	■	■
3018	2251	R	■	■
2990	2200	IR	■	■
1623	1515	R	■	■
1444	1078	IR	■	■
1342	981	R	■	■
1236	1009	R	■	■
1007	726	IA	■	■
949	721	R	■	■
943	780	IR	■	■
810	586	IR	■	■

BH_3 has D_{3h} symmetry. Determine the reducible representation for the hydrogen 1s orbitals (collectively). What linear combination of boron valence orbitals has the same symmetry.

CH_4 has T_d symmetry. Determine the reducible representation for the hydrogen 1s orbitals (collectively). What linear combination of carbon valence orbitals has the same symmetry.

The following vibrational frequencies are available for cis-dichloroethene. Complete the table assuming that the molecule has C_{2v} symmetry.

Frequency cm	3077	1587	1179	711	173	876	406	697	3072	1303	857	571
Symmetry	A_1	A_1	A_1	A_1	A_1	A_2	A_2	B_1	B_2	B_2	B_2	B_2
$\frac{\text{IR}}{\text{Activity}}$	yes	yes	yes	yes	yes	no	no	yes	yes	yes	yes	yes
$\frac{\text{Raman}}{\text{Activity}}$	yes	yes	yes	yes	yes	yes	yes	yes	yes	yes	yes	yes
Type	stretch	stretch	stretch	bend	bend	bend	bend	bend	bend	bend	stretch	bend

The following vibrational frequencies are available for trans-dichloroethene. Complete the table assuming that the molecule has C_{2h} symmetry.

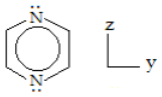
Frequency cm	3073	1578	1274	846	350	763	900	227	3090	1200	828	250
Symmetry	A_g	A_g	A_g	A_g	A_g	B_g	A_u	A_u	B_u	B_u	B_u	B_u
$\frac{\text{IR}}{\text{Activity}}$	no	no	no	no	no	no	yes	yes	yes	yes	yes	yes
$\frac{\text{Raman}}{\text{Activity}}$	yes	yes	yes	yes	yes	yes	no	no	no	no	no	no
Type	stretch	stretch	stretch	bend	bend	bend	bend	bend	bend	bend	stretch	bend

The following vibrational frequencies are available for 1,1-dichloroethene. Complete the table assuming that the molecule has C_{2v} symmetry.

Frequency cm	3035	1627	1400	603	299	686	875	460	3130	1095	800	372
Symmetry	A_1	A_1	A_1	A_1	A_1	A_2	A_2	B_1	B_2	B_2	B_2	B_2
$\frac{\text{IR}}{\text{Activity}}$	yes	yes	yes	yes	yes	no	no	yes	yes	yes	yes	yes
$\frac{\text{Raman}}{\text{Activity}}$	yes	yes	yes	yes	yes	yes	yes	yes	yes	yes	yes	yes
Type	stretch	stretch	stretch	bend	bend	bend	bend	bend	bend	bend	stretch	bend

Pyrazine has D_{2h} symmetry. Confirm the entries in the following table.

Symmetry	A_g	A_g	A_g	A_g	A_g	B_{1g}	B_{2g}	B_{2g}	B_{3g}	B_{3g}	B_{3g}	B_{3g}
Frequency cm	3054	1578	1230	1015	596	757	919	703	3041	1524	1118	641
Type	Stretch	Stretch	Stretch	Bend	Bend	Bend	Bend	Stretch	Stretch	Bend	Bend	
$\frac{\text{Ir, R}}{\text{Activity}} R$	R	R	R	R	R	R	R	R	R	R	R	
∘	∘	∘	∘	∘	∘	∘	∘	∘	∘	∘	∘	∘
Symmetry	A_u	A_u	B_{1u}	B_{1u}	B_{1u}	B_{1u}	B_{2u}	B_{2u}	B_{2u}	B_{2u}	B_{3u}	B_{3u}
Frequency cm	na	363	3066	1484	1135	1021	3066	1418	1346	1063	804	416
Type	Bend	Bend	Stretch	Stretch	Bend	Bend	Stretch	Stretch	Stretch	Bend	Bend	Bend
$\frac{\text{IR,R}}{\text{Activity}}$	IR	IR	IR	IR	IR	IR	IR	IR	IR	IR	IR	IR



Is the following spectroscopic data consistent with the assignment of D_{4h} symmetry to tetrachloroplatinate, $PtCl_4^{2-}$?

Frequency	$332cm^{-1}$	$314cm^{-1}$	$170cm^{-1}$	$320cm^{-1}$	$183cm^{-1}$	$93cm^{-1}$
Activity	R	R	R	IR	IR	IR
Symmetry	■	■	■	■	■	■
Stretch or Bend	■	■	■	■	■	■

Frequency	$332cm^{-1}$	$314cm^{-1}$	$170cm^{-1}$	$320cm^{-1}$	$183cm^{-1}$	$93cm^{-1}$
Activity	R	R	R	IR	IR	IR
Symmetry	A_{1g}	B_{1g}	B_{2g}	E_u	A_{2u}	B_{2u}
Stretch or Bend	S	S	B	S	B	B

Given the following spectroscopic data determine the whether $InCl_5^{2-}$ has C_{4v} or D_{3h} symmetry.

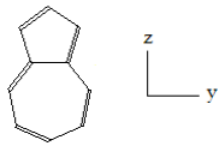
Frequency cm	294	287	283	274	193	165	143	140	108
Activity	IR, R	R	IR, R	IR, R	R	R	IR, R	IR, R	IR, R
Symmetry	■	■	■	■	■	■	■	■	■
Stretch or Bend	■	■	■	■	■	■	■	■	■

Symmetry analysis supports C_{4v} symmetry as indicated below.

Activity	IR	R	Coincidences
Exp	6	9	6
C_{4v}	6	9	6
D_{3h}	5	6	3

Do symmetry analyses on the three $C_{10}H_8$ isomers: azulene (C_{2v}), fulvalene (D_{2h}) and napthalene (D_{2h}). Determine whether IR and Raman spectroscopy can be used to distinguish between the isomers. Completing the table below should facilitate answering the question.

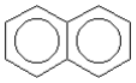
Azulene



Fulvalene

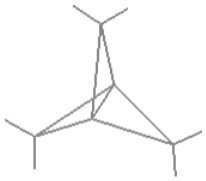


Napthalene



Molecule	$\frac{\text{IR}}{\text{Stretches}}$	$\frac{\text{Raman}}{\text{Stretches}}$	Coincidences	$\frac{\text{IR}}{\text{bends}}$	$\frac{\text{Raman}}{\text{Bends}}$	Coincidences	$\frac{\text{InActive}}{\text{Modes}}$
Azulene	19	19	19	23	29	23	0
Fulvalene	9	10	0	11	14	0	4
Napthalene	9	10	0	11	14	0	4

Propellane has, as shown below, has D_{3h} symmetry. To date it hasn't been synthesized, but theoreticians debate whether or not it has a bridging carbon-carbon bond as shown in the figure. Do a symmetry analysis with and without the bridging bond to determine whether vibrational spectroscopy could decide the issue if the molecule ever became available.



Propellane	$\frac{\text{IR}}{\text{Stretches}}$	$\frac{\text{Raman}}{\text{Stretches}}$	$\frac{\text{IR}}{\text{Bends}}$	$\frac{\text{Raman}}{\text{Bends}}$	$\frac{\text{InActive}}{\text{Modes}}$
Bond	4	9	4	6	3
No Bond	4	8	4	7	3

Raman spectroscopy would be required to answer this question, because it indicates one less stretch and one more bend in the vibrational spectroscopy. This makes sense since the number of vibrational degrees of freedom must be conserved. If there is one less bond, there must be one less stretch and therefore one more bend. In this case, the change is observable (hypothetically) in Raman spectroscopy.

This page titled 6.13: An Extensive Set of Group Theory Problems for Chemists is shared under a CC BY 4.0 license and was authored, remixed, and/or curated by Frank Rioux via source content that was edited to the style and standards of the LibreTexts platform.

CHAPTER OVERVIEW

Back Matter

Index

Index

A

Airy pattern
- 1.14: Quantum Mechanics and the Fourier Transform

alpha decay
- 10.4: A Rudimentary Model for Alpha Particle Decay

atomic properties
- 11.3: Commentary on “Probing the Orbital Energy of an Electron in an Atom”

Atomic volume
- 2.46: Calculating the Atomic Radius of Polonium

B

Bell states
- 1.7: Quantum Computation- A Short Course
- 8.53: Bell State Exercises

Bell Theorem
- 8.45: Yet Another Assault on Local Realism - A Matrix/Tensor Algebra Approach
- 8.46: Jim Baggott's Bell Theorem Analysis
- 8.48: Another Bell Theorem Analysis - Shorter Version

Bell’s theorem
- 1.5: Quantum Computation - A Short Course

C

Circularly polarized light
- 7.14: Matrix Mechanics Approach to Polarized Light
- 7.15: Matrix Mechanics Approach to Polarized Light - Version 2
- 7.24: Optical Activity - A Quantum Perspective

confinement energy
- 1.3: Atomic and Molecular Stability

cosmic microwave background radiation
- 11.19: Age of the Elements

Cosmic Radiation
- 11.18: Cosmic Background Radiation

cyanine dyes
- 4.3: Cyanine Dyes as Two-State Electronic Systems

D

Degenerate Perturbation Theory
- 10.35: First Order Degenerate Perturbation Theory - the Stark Effect of the Hydrogen Atom

density operator
- 7.9: Pure States, Mixtures and the Density Operator

Deutsch-Jozsa Algorithm
- 1.8: Quantum Computation- A Short Course

Deutsch's Problem
- 8.68: A Simple Solution to Deutsch's Problem

diffraction pattern
- 1.14: Quantum Mechanics and the Fourier Transform
- 5.9: Calculating Diffraction Patterns

Dirac delta function
- 1.25: The Dirac Delta Function

Dirac equation
- 1.36: Aspects of Dirac's Relativistic Matrix Mechanics

Dirac Notation
- 1.26: Elements of Dirac Notation

dodecahedrane
- 6.2: Dodecahedrane

down converter
- 7.39: Analysis of a Two-photon Quantum Eraser

downconversion
- 7.26: Two Photon Interference - The Creation of an Entangled Superposition

E

effective potential energy
- 1.3: Atomic and Molecular Stability

Electrons within a Ring
- 1.86: Quantum Corrals - Electrons within a Ring

Entangled Bipartate Superposition
- 8.64: Examining the Local States of an Entangled Bipartate Superposition

entanglement
- 1.7: Quantum Computation- A Short Course
- 8.59: An Entanglement Swapping Protocol

expectation value
- 7.10: Using the Trace Function to Calculate Expectation Values

F

Feshbach Potential
- 10.33: Variational Method for the Feshbach Potential
- 10.42: Variation Method Using the Wigner Function - The Feshbach Potential

G

GHZ Entanglement
- 8.16: GHZ Entanglement - A Tensor Algebra Analysis

Grover Search Algorithm
- 1.10: Quantum Computation- A Short Course

H

Hadamard gate
- 8.53: Bell State Exercises

Hardy's Paradox
- 8.52: Hardy's Paradox

L

ladder operators
- 1.28: Raising and Lowering; Creating and Annihilating
- 7.4: Single Photon Interference - Fourth Version

linearly polarized light
- 7.24: Optical Activity - A Quantum Perspective

locality
- 8.14: Greenaberger-Hrne-Zeilinger (GHZ) Entanglement and Local Realism

M

Mach-Zehnder interferometer
- 7.22: A Quantum Circuit for a Michelson Interferometer

maser
- 4.4: The Ammonia Inversion and the Maser

Matrix Mechanics
- 1.33: Basic Matrix Mechanics
- 1.35: Matrix Mechanics
- 7.16: Matrix Mechanics Exercises Using Polarized Light

methane
- 6.8: CH_4

Michelson Interferometer
- 7.21: Two Analyses of the Michelson Interferometer

Mixed states
- 7.9: Pure States, Mixtures and the Density Operator

Morse potential
- 4.8: Visualizing the Formally Forbidden Overtone Vibrational Transitions in HCl
- 9.12: Numerical Solutions for Morse Oscillator

N

Neutron Interferometry
- 7.18: Neutron Interferometry with Polarized Spin States

Numerical Solutions
- 9: Numerical Solutions for Schrödinger's Equation

O

optical activity
- 7.24: Optical Activity - A Quantum Perspective

Overlap integral
- 1.26: Elements of Dirac Notation

overtones
- 4.8: Visualizing the Formally Forbidden Overtone Vibrational Transitions in HCl

P

parametric down converter
- 1.7: Quantum Computation- A Short Course
- 7.27: Two-particle Interference for Bosons and Fermions

path integrals
- 1.9: Quantum Computation- A Short Course

Planck Distribution
- 11.18: Cosmic Background Radiation

Polarizability
- 10.36: Variational Calculation for the Polarizability of the Hydrogen Atom

Polarizing Beam Splitter
- 7.6: The Polarizing Beam Splitter and the Superposition Principle

polonium
- 2.46: Calculating the Atomic Radius of Polonium

Positronium
- 1.4: Atomic and Molecular Stability
- 2.4: A de Broglie-Bohr Model for Positronium

Positronium Annihilation
- 8.34: Positronium Annihilation

Pure state
- 7.9: Pure States, Mixtures and the Density Operator

Q

Quantum Beats
- 4.11: Quantum Beats

Quantum centrifugal potential
1.3: Atomic and Molecular Stability
quantum chemistry
11.3: Commentary on “Probing the Orbital Energy of an Electron in an Atom”
quantum cloning
1.6: Quantum Computation- A Short Course
Quantum Computation
1.5: Quantum Computation - A Short Course
1.6: Quantum Computation- A Short Course
1.7: Quantum Computation- A Short Course
1.8: Quantum Computation- A Short Course
quantum error correction
1.10: Quantum Computation- A Short Course
quantum pressure
1.98: Quantum Mechanical Pressure
Quantum Teleportation
1.6: Quantum Computation- A Short Course
8: Quantum Teleportation
8.2: Quantum Teleportation - A Brief Introduction
Quartic Oscillator
9.11: Numerical Solutions for the Quartic Oscillator
10.8: Variation Method for the Quartic Oscillator
10.41: Variation Method Using the Wigner Function - The Quartic Oscillator
qubits
8.65: A Brief Introduction to the Quantum Computer
quon
1.9: Quantum Computation- A Short Course

R

radioactive dating
11.19: Age of the Elements
Ramsey Atomic Interferometer
7.23: The Ramsey Atomic Interferometer
realism
8.14: Greenaberger-Hrne-Zeilinger (GHZ) Entanglement and Local Realism
Rotational Spectroscopy of Diatomic Molecules
4.6: Analyses of the Pure Rotational Spectrum of HCl
Rydberg Potential
10.7: Variation Method for the Rydberg Potential

S

Schrödinger equation
1.18: Exploring the Origin of Schrödinger’s Equations
Shor’s algorithm
1.7: Quantum Computation- A Short Course
Simon’s algorithm
1.10: Quantum Computation- A Short Course
Single Photon Interference
7.4: Single Photon Interference - Fourth Version
Slanted Well Potential
9.7: Particle in a Slanted Well Potential
10.11: Linear Variational Method for a Particle in a Slanted 1D Box
Stark Effect
10.35: First Order Degenerate Perturbation Theory - the Stark Effect of the Hydrogen Atom
superposition principle
1.24: Getting Accustomed to the Superposition Principle
7.6: The Polarizing Beam Splitter and the Superposition Principle

T

theoretical chemistry
11.3: Commentary on “Probing the Orbital Energy of an Electron in an Atom”
three polarizer paradox
7.14: Matrix Mechanics Approach to Polarized Light
7.15: Matrix Mechanics Approach to Polarized Light - Version 2
trace (matrix)
7.10: Using the Trace Function to Calculate Expectation Values
tunneling
4.5: A Symmetric Double Well Potential Illustrating Tunneling
Two Photon Interference
7.26: Two Photon Interference - The Creation of an Entangled Superposition

V

Variational Method
10.5: Variational Method for a Particle in a Finite Potential Well
Variational Theorem
10.3: The Variation Theorem in Dirac Notation
virial theorem
1.3: Atomic and Molecular Stability

W

Wheeler-type delayed-choice experiment
7.41: A Quantum Delayed-Choice Experiment
Wigner Function
10.38: Variation Method Using the Wigner Function- Finite Potential Well
10.39: 455. Variation Method Using the Wigner Function- V(x) = |x|

X

Xenon Tetrafluoride
6.3: Xenon Tetrafluoride

CHAPTER OVERVIEW

7: Quantum Optics

7.1: Single-Photon Interference - First Version
7.2: Single-Photon Interference - Second Version
7.3: Single-photon Interference - Third Version
7.4: Single Photon Interference - Fourth Version
7.5: Single Photon Interference - Mathcad version
7.6: The Polarizing Beam Splitter and the Superposition Principle
7.7: Mach-Zehner Polarization Interferometer Analyzed Using Tensor Algebra
7.8: Illustrating the Superposition Principle with Single Photon Interference
7.9: Pure States, Mixtures and the Density Operator
7.10: Using the Trace Function to Calculate Expectation Values
7.11: Polarized Light and Quantum Superposition
7.12: Polarized Light and Quantum Mechanics
7.13: The Three-Polarizer Paradox
7.14: Matrix Mechanics Approach to Polarized Light
7.15: Matrix Mechanics Approach to Polarized Light - Version 2
7.16: Matrix Mechanics Exercises Using Polarized Light
7.17: Polarized Light and Quantum Mechanics
7.18: Neutron Interferometry with Polarized Spin States
7.19: Interaction Free Measurement - Seeing in the Dark
7.20: Quantum Seeing in the Dark - A Matrix-Tensor Analysis
7.21: Two Analyses of the Michelson Interferometer
7.22: A Quantum Circuit for a Michelson Interferometer
7.23: The Ramsey Atomic Interferometer
7.24: Optical Activity - A Quantum Perspective
7.25: A Quantum Optical Cheshire Cat
7.26: Two Photon Interference - The Creation of an Entangled Superposition
7.27: Two-particle Interference for Bosons and Fermions
7.28: Analysis of a Two-photon Interferometer
7.29: Two-photon Interferometry
7.29.1: Another Two Photon Interference Experiment
7.30: Another Two Photon Interference Experiment
7.31: Quantum Correlations Illuminated with Tensor Algebra
7.32: Two Photon Entanglement - A Tensor Algebra Analysis
7.33: Two Photon Interference - Matrix Mechanics Approach
7.34: Two-electron Interference
7.35: Bosonic and Fermionic Photon Behavior at Beam Splitters
7.36: Bosonic and Fermionic Photon Behavior at Beam Splitters- A Tensor Algebra Analysis
7.37: Entangled Photons Can Behave Like Fermions
7.38: Analyzing Two-photon Interferometry Using Mathcad and Tensor Algebra
7.39: Analysis of a Two-photon Quantum Eraser

7.40: Another Example of a Two-photon Quantum Eraser
7.41: A Quantum Delayed-Choice Experiment
7.42: A Quantum Delayed-Choice Experiment
Index

This page titled 7: Quantum Optics is shared under a CC BY 4.0 license and was authored, remixed, and/or curated by Frank Rioux via source content that was edited to the style and standards of the LibreTexts platform.

CHAPTER OVERVIEW

Front Matter

TitlePage
InfoPage

College of Saint Benedict/Saint John's University

Quantum Optics

Frank Rioux

This text is disseminated via the Open Education Resource (OER) LibreTexts Project (https://LibreTexts.org) and like the thousands of other texts available within this powerful platform, it is freely available for reading, printing, and "consuming."

The LibreTexts mission is to bring together students, faculty, and scholars in a collaborative effort to provide an accessible, and comprehensive platform that empowers our community to develop, curate, adapt, and adopt openly licensed resources and technologies; through these efforts we can reduce the financial burden born from traditional educational resource costs, ensuring education is more accessible for students and communities worldwide.

Most, but not all, pages in the library have licenses that may allow individuals to make changes, save, and print this book. Carefully consult the applicable license(s) before pursuing such effects. Instructors can adopt existing LibreTexts texts or Remix them to quickly build course-specific resources to meet the needs of their students. Unlike traditional textbooks, LibreTexts' web based origins allow powerful integration of advanced features and new technologies to support learning.



LibreTexts is the adaptable, user-friendly non-profit open education resource platform that educators trust for creating, customizing, and sharing accessible, interactive textbooks, adaptive homework, and ancillary materials. We collaborate with individuals and organizations to champion open education initiatives, support institutional publishing programs, drive curriculum development projects, and more.

The LibreTexts libraries are Powered by NICE CXone Expert and was supported by the Department of Education Open Textbook Pilot Project, the California Education Learning Lab, the UC Davis Office of the Provost, the UC Davis Library, the California State University Affordable Learning Solutions Program, and Merlot. This material is based upon work supported by the National Science Foundation under Grant No. 1246120, 1525057, and 1413739.

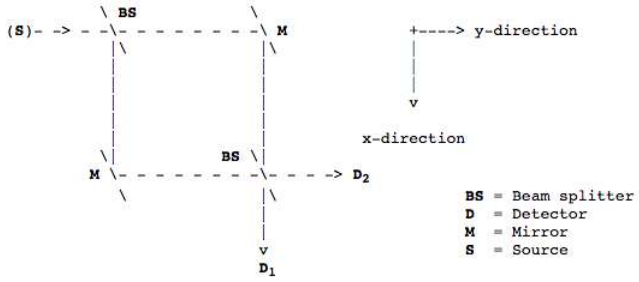
Any opinions, findings, and conclusions or recommendations expressed in this material are those of the author(s) and do not necessarily reflect the views of the National Science Foundation nor the US Department of Education.

Have questions or comments? For information about adoptions or adaptions contact info@LibreTexts.org or visit our main website at https://LibreTexts.org.

This text was compiled on 05/10/2026

7.1: Single-Photon Interference - First Version

The schematic diagram below shows a Mach-Zehnder interferometer for photons. When the experiment is run so that there is only one photon in the apparatus at any time, the photon is always detected at D_2 and never at D_1.(1,2,3) The qualitative explanation is that there are two paths to each detector and, therefore, the probability amplitudes for these paths may interfere constructively or destructively. For detector D_2 the probability amplitudes for the two paths interfere *constructively*, while for detector D_1 they interfere *destructively*.



A quantitative quantum mechanical analysis of this striking phenomenon is outlined below. The photon leaves the source, S, traveling in the y-direction. Whether the photon takes the upper or lower path it interacts with a beam splitter, a mirror, and another beam splitter before reaching the detectors.

Orthonormal basis states: (1 x 2 vectors)

Photon moving in the x-direction: $|x>= \begin{vmatrix} 1 \\ 0 \end{vmatrix} \quad < x| = (1 \quad 0) \quad < x|x >= 1$

Photon moving in the y-direction: $|y>= \begin{vmatrix} 0 \\ 1 \end{vmatrix} \quad < y| = (0 \quad 1) \quad < y|y >= 1$

< y | x > = < x | y > = 0

Operators: (2 x 2 matrices)

Operator for photon interaction with the mirror:

$$\hat{M} = \backslash(\begin{vmatrix} 0 & 1 \\ 1 & 0 \end{vmatrix}$$

Operator for photon interaction with the beam splitter:

$$\hat{BS} = \backslash(\begin{vmatrix} T & iR \\ iR & T \end{vmatrix}$$

T and R are the transmission and reflection amplitudes. For the half-silvered mirrors used in this example they are:

$$T = R = \left(\frac{1}{2}\right)^{\frac{1}{2}} = 0.707$$

Operations:

After interacting with a beam splitter, a photon is in a linear superposition of |x> and |y> in which the components are 90 degrees out of phase.

$$\hat{BS}|x\rangle = \frac{[|x + i|y]^{\frac{1}{2}}}{2}$$

$$\hat{BS}|y\rangle = \frac{[i|x + i|y]^{\frac{1}{2}}}{2}$$

BS M BS|y > = i|y>

Interaction with the mirror merely changes the direction of the photon.

$$\hat{M}|x\rangle = |y\rangle$$

$$\hat{M}|y\rangle = |x\rangle$$

Matrix elements:

$$< x \mid \mathbf{M} \mid x > = 0 < y \mid \mathbf{M} \mid x > = 1 < x \mid \mathbf{M} \mid y > = 1 < y \mid \mathbf{M} \mid y > = 0$$

$$< x \mid \mathbf{BS} \mid x > = < y \mid \mathbf{BS} \mid y > = \tfrac{1}{2}^{\frac{1}{2}} < y \mid \mathbf{BS} \mid x > = < x \mid \mathbf{BS} \mid y > = \tfrac{i}{2}^{\frac{1}{2}}$$

Dirac brackets are read from right to left. In Dirac's notation < x | **M** | y > is the amplitude that a photon initially moving in the y-direction will be moving in the x-direction after interacting with the mirror. $|< x \mid \mathbf{M} \mid y >|^2$ is the probability that a photon initially moving in the y-direction will be moving in the x-direction after interacting with the mirror. $|< y \mid \mathbf{BS} \mid y >|^2$ is the probability that a photon initially moving in the y-direction will be found moving in the y-direction after interacting with the beam splitter.

(A) For the photon to be detected at D_1 it must be in the state |x> after interacting with two beam splitters and a mirror in the configuration shown above. The probability that a photon will be detected at D1:

$$< x \mid \mathbf{BS\ M\ BS} \mid y > = 0 \text{ thus } |< x \mid \mathbf{BS\ M\ BS} \mid y>|2 = 0$$

(B) For the photon to be detected at D2 it must be in the state |y> after interacting with two beam splitters and a mirror in the configuration shown above. The probability that a photon will be detected at D_2:

$$< y \mid \text{BS M BS} \mid y > = i \text{ thus } |< y \mid \text{BS M BS} \mid y >|2 = 1$$

It is also instructive to use Dirac's notation to examine upper and lower paths.

(A')

$$\langle D_1|y\rangle = \langle D_1|y\rangle_{upper} + \langle D_1|y\rangle_{lower} \tag{7.1.1}$$

$$= \langle x|\mathbf{BS}|x\rangle\langle x|\mathbf{M}|y\rangle\langle y|\mathbf{BS}|y\rangle + \langle x|\mathbf{BS}|y\rangle\langle y|\mathbf{M}|x\rangle\langle x|\mathbf{BS}|y> \tag{7.1.2}$$

$$= \frac{i}{2}^{\frac{1}{2}} \times 1 \times \frac{i}{2}^{\frac{1}{2}} + \frac{i}{2}^{\frac{1}{2}} \times 1 \times \frac{i}{2}^{\frac{1}{2}} \tag{7.1.3}$$

$$= \frac{i}{2} - \frac{i}{2} = i \tag{7.1.4}$$

This shows that upper and lower paths have the photon arriving 180 degrees out of phase. Thus the photon suffers destructive interference at D1.

(B') $< D_2 \mid y > = < D_2 \mid y >_{\text{upper}} + < D_2 \mid Y >_{\text{lower}}$

$= < y \mid \mathbf{BS} \mid x >< x \mid \mathbf{M} \mid y >< y \mid \mathbf{BS} \mid y > + < y \mid \mathbf{BS} \mid y >< y \mid \mathbf{M} \mid x >< x \mid \mathbf{BS} \mid y >$

$= \tfrac{i}{2}^{\frac{1}{2}} \times 1 \times \tfrac{i}{2}^{\frac{1}{2}} + \tfrac{i}{2}^{\frac{1}{2}} \times 1 \times \tfrac{i}{2}^{\frac{1}{2}}$

$= \frac{i}{2} - \frac{i}{2} = i$ i

Thus, $|< D_2 \mid y >|2 = 1$

This calculation shows that the upper and lower paths have the photon arriving in phase at D_2.

If either path (upper or lower) is blocked the interference no longer occurs and the photon reaches D1 25% of the time and D2 25%. Of course, 50% of the time it is absorbed by the blocker.

Lower path blocked:

Probability photon reaches D_1: |< x | **BS** | x >< x | **M** | y >< y | **BS** | y >|2 = $\frac{1}{4}$

Probability photon reaches D_2: |< y | **BS** | x >< x | **M** | y >< y | **BS** | y >|2 = $\frac{1}{4}$

Upper path blocked:

Probability photon reaches D_1: |< x | **BS** | y >< y | **M** | x >< x | **BS** | y >|2 = $\frac{1}{4}$

Probability photon reaches D_2: |< y | **BS** | y >< y | **M** | x >< x | **BS** | y >|2 = $\frac{1}{4}$

References:

1. P. Grangier, G. Roger, and A. Aspect, "Experimental Evidence for Photon Anticorrelation Effects on a Beam Splitter: A New Light on Single Photon Interferences," Europhys. Lett. 1, 173-179 (1986).
2. V. Scarani and A. Suarez, "Introducing Quantum Mechanics: One-particle Interferences," Am. J. Phys. 66, 718-721 (1998).
3. Kwiat, P, Weinfurter, H., and Zeilinger, A, "Quantum Seeing in the Dark," Sci. Amer. Nov. 1996, pp 72-78.

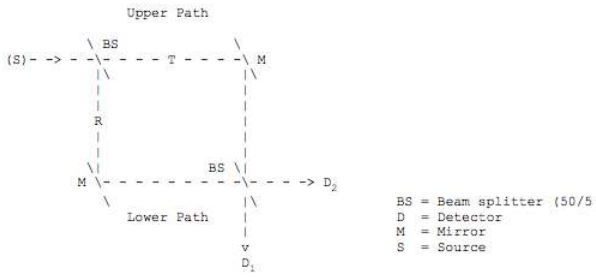
This page titled 7.1: Single-Photon Interference - First Version is shared under a CC BY 4.0 license and was authored, remixed, and/or curated by Frank Rioux via source content that was edited to the style and standards of the LibreTexts platform.

7.2: Single-Photon Interference - Second Version

Using Dirac Notation to Analyze Single Particle Interference

The schematic diagram below shows a Mach-Zehnder interferometer for photons. When the experiment is run so that there is only one photon in the apparatus at any time, the photon is always detected at D_2 and never at D_1. (1,2,3)

The quantum mechanical analysis of this striking phenomenon is outlined below. The photon leaves the source, S, and whether it takes the upper or lower path it interacts with a beam splitter, a mirror, and another beam splitter before reaching the detectors. At the beam splitters there is a 50% chance that the photon will be transmitted and a 50% chance that it will be reflected.



After the first beam splitter the photon is in an even linear superposition of being transmitted and reflected. Reflection involves a 90^o ($\pi/2$) phase change which is represented by $\exp(i\pi/2) = i$, where $i = (-1)1/2$. (See the appendix for a simple justification of the 90^o phase difference between transmission and reflection.) Thus the state after the first beam is given by equation 257.1.

$$|\psi = \left(\frac{[|T> + i|R]}{2}\right)^{\frac{1}{2}}$$

Now |T> and |R> will be written in terms of $|D_1>$ and $|D_2>$ the states they evolve to at detection. |T> reaches $|D_1>$ by transmission and $|D_2>$ by reflection.

$$|T> = \left(\frac{[|D1> + i|D2>]}{2}\right)^{\frac{1}{2}}$$

|R> reaches $|D_1>$ by reflection and $|D_2>$ by transmission.

$$|R> = \left(\frac{[i|D1> + |D2>]}{2}\right)^{\frac{1}{2}}$$

Equations 257.2 and 257.3 are substituted into equation 257.1.

$$|\psi> = \frac{[|D1> + i|D2> + i2|D1> + i|D2>]}{2}$$

It is clear ($i^2 = -1$) that the first and third terms cancel (the amplitudes are 180^o out of phase), so that we end up with a final state given by equation 257.5.

$$|\psi> = i|D_2>$$

The probability of an event is the square of the absolute magnitude of the probability amplitude.

$$P(D_2) = |i|^2 = 1$$

Thus this analysis is in agreement with the experimental outcome that no photons are ever detected at D_1.

Appendix:

Suppose there is no phase difference between transmission and reflection. Then equations 257.1, 257.2, and 257.3 become

$$|\psi = \left(\frac{[|T> + |R>]}{2}\right)^{\frac{1}{2}}$$

$$|T>=\left(\frac{[|D1>+|D2>]}{2}\right)^{\frac{1}{2}}$$

$$|\psi=\left(\frac{[|D_1>+|D_2>|D_1>+D_2>]}{2}\right)^{\frac{1}{2}}$$

Substitution of equations 257.8 and 257.9 into equation 257.7 yields

$$|\psi>=|D_1>+|D_2>$$

Thus, the detection probabilities at the two detectors are:

$$P(D_1)=1 and P(D_2)=1$$

This result violates the principle of conservation of energy because the original photon has a probability of 1 of being detected at D_1 and also a probability of 1 of being detected at D_2. In other words, the number of photons has doubled. Thus, there must be a phase difference between transmission and reflection, and a 90^o phase difference, as shown above, conserves energy.

References:

1. P. Grangier, G. Roger, and A. Aspect, "Experimental Evidence for Photon Anticorrelation Effects on a Beam Splitter: A New Light on Single Interferences," Europhys. Lett. 1, 173-179 (1986).

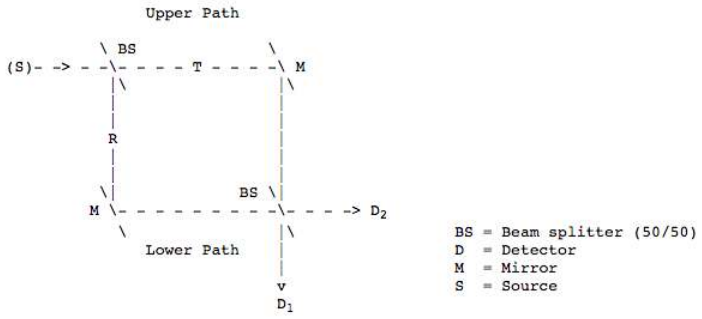
2. V. Scarani and A. Suarez, "Introducing Quantum Mechanics: One-particle Interferences," Am. J. Phys. 66, 718-721 (1998).

3. Kwiat, P, Weinfurter, H., and Zeilinger, A, "Quantum Seeing in the Dark, Sci. Amer. Nov. 1996, pp 72-78.

This page titled 7.2: Single-Photon Interference - Second Version is shared under a CC BY 4.0 license and was authored, remixed, and/or curated by Frank Rioux via source content that was edited to the style and standards of the LibreTexts platform.

7.3: Single-photon Interference - Third Version

The schematic diagram below shows a Mach-Zehnder interferometer for photons. When the experiment is run so that there is only one photon in the apparatus at any time, the photon is always detected at D_2 and never at D_1.(1,2,3) The quantum mechanical analysis of this striking phenomenon is outlined below. There are two paths (upper and lower) to each detector, and they both contain a beam splitter, a mirror, and another beam splitter before the detectors are reached. At the beam splitters the the probability amplitude for transmission is $\left(\frac{1}{2}\right)^{\frac{1}{2}}$, while for reflection it is $\left(\frac{i}{2}\right)^{\frac{1}{2}}$. The origin of the 90° phase difference between transmission and reflection is found in the principle of energy conservation.



Because there are two paths to each detector the probability amplitudes for these paths may interfere constructively or destructively when added. For detector D_2 the probability amplitudes for the two paths interfere constructively, while for detector D_1 they interfere destructively.

For example, the probability for the photon being detected at D_2 is calculated as follows:

$$P(D_2) = |< D_2|S >|^2 = |< D_2|T >< T|S > + < D_2|R >< R|S >|^2 \tag{7.3.1}$$
$$= \left| \left(\frac{i}{2}\right)^{\frac{1}{2}} \left(\frac{1}{2}\right)^{\frac{1}{2}} + \left(\frac{1}{2}\right)^{\frac{1}{2}} \left(\frac{i}{2}\right)^{\frac{1}{2}} \right|^2 = 1$$

The probability that the photon will be detected at D_1 is:

$$P(D_1) = |< D_1|S >|^2 = |< D_1|T >< T|S > + < D_1|R >< R|S >|^2 \tag{7.3.2}$$
$$= \left| \left(\frac{1}{2}\right)^{\frac{1}{2}} \left(\frac{1}{2}\right)^{\frac{1}{2}} + \left(\frac{i}{2}\right)^{\frac{1}{2}} \left(\frac{i}{2}\right)^{\frac{1}{2}} \right|^2 = 0$$

energy conservation

Suppose there is no phase difference between transmission and reflection. Then the probability amplitudes for transmission and reflection are both $\left(\frac{1}{2}\right)^{\frac{1}{2}}$. Under these circumstances Equations 7.3.1 and 7.3.2 become

$$P(D_2) = \left| \left(\frac{1}{2}\right)^{\frac{1}{2}} \left(\frac{1}{2}\right)^{\frac{1}{2}} + \left(\frac{1}{2}\right)^{\frac{1}{2}} \left(\frac{1}{2}\right)^{\frac{1}{2}} \right|^2 = 1$$

$$P(D_1) = \left| \left(\frac{1}{2}\right)^{\frac{1}{2}} \left(\frac{1}{2}\right)^{\frac{1}{2}} + \left(\frac{1}{2}\right)^{\frac{1}{2}} \left(\frac{1}{2}\right)^{\frac{1}{2}} \right|^2 = 1$$

This result violates the principle of conservation of energy because the original photon has a probability of 1 of being detected at D_1 and also a probability of 1 of being detected at D_2. In other words, the number of photons has **doubled**. Thus, there must be a phase difference between transmission and reflection, and a 90^o phase difference, as shown above, conserves energy.

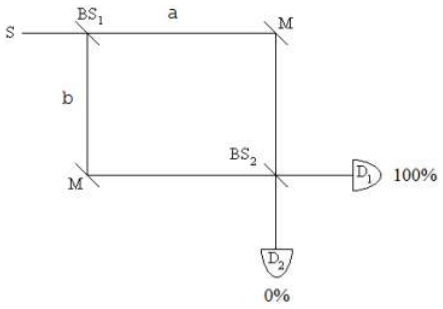
References

1. P. Grangier, G. Roger, and A. Aspect, "Experimental Evidence for Photon Anticorrelation Effects on a Beam Splitter: A New Light on Single Photon Interferences," Europhys. Lett. 1, 173-179 (1986).
2. V. Scarani and A. Suarez, "Introducing Quantum Mechanics: One-particle Interferences," Am. J. Phys. 66, 718-721 (1998).
3. Kwiat, P, Weinfurter, H., and Zeilinger, A, "Quantum Seeing in the Dark," Sci. Amer. Nov. 1996, pp 72-78.

This page titled 7.3: Single-photon Interference - Third Version is shared under a CC BY 4.0 license and was authored, remixed, and/or curated by Frank Rioux via source content that was edited to the style and standards of the LibreTexts platform.

7.4: Single Photon Interference - Fourth Version

This analysis of the operation of a Mach-Zehnder Interferometer (MZI) will use tensor algebra and the creation and annihilation operators.



An interferometer arm can be occupied or unoccupied. These states are represented by the following vectors.

$$Unoccupied: |0\rangle = \begin{pmatrix} 1 \\ 0 \end{pmatrix}$$

$$Occupied: |1\rangle = \begin{pmatrix} 0 \\ 1 \end{pmatrix}$$

After the first beam splitter the photon is in an even superposition of being in both arms of the interferometer. By convention a 90 degree phase shift is assigned to arm b to preserve probability. In terms of the concept of occupation, the superposition takes the following form in tensor algebra.

$$|S\rangle \xrightarrow{i} \frac{1}{\sqrt{2}}[|1\rangle_a|0\rangle_b + i|0\rangle_a 1|\rangle_b] = \frac{1}{\sqrt{2}}\left[\begin{pmatrix} 0 \\ 1 \end{pmatrix}_a \otimes \begin{pmatrix} 1 \\ 0 \end{pmatrix}_b + i \begin{pmatrix} 1 \\ 0 \end{pmatrix}_a \otimes \begin{pmatrix} 0 \\ 1 \end{pmatrix}_b \right] = \frac{1}{\sqrt{2}} \begin{pmatrix} 0 \\ i \\ 1 \\ 0 \end{pmatrix}$$

$$\Psi = \frac{1}{\sqrt{2}} \begin{pmatrix} 0 \\ i \\ 1 \\ 0 \end{pmatrix}$$

The matrix operators required for this analysis are as follows.

Creation:

$$C = \begin{pmatrix} 0 & 0 \\ 1 & 0 \end{pmatrix}$$

Annihilation:

$$A = \begin{pmatrix} 0 & 0 \\ 1 & 0 \end{pmatrix}$$

Number:

$$N = \begin{pmatrix} 0 & 0 \\ 1 & 0 \end{pmatrix}$$

Identity:

$$I = \begin{pmatrix} 0 & 0 \\ 1 & 0 \end{pmatrix}$$

The effect of the creation, annihilation and number operators on |0> and |1>:

$$C\begin{pmatrix}1\\0\end{pmatrix}=\begin{pmatrix}0\\1\end{pmatrix}$$

$$A\begin{pmatrix}0\\1\end{pmatrix}=\begin{pmatrix}1\\0\end{pmatrix}$$

$$N\begin{pmatrix}1\\0\end{pmatrix}=\begin{pmatrix}0\\0\end{pmatrix}$$

$$N\begin{pmatrix}0\\1\end{pmatrix}=\begin{pmatrix}0\\1\end{pmatrix}$$

The creation operator is the Hermitian adjoint of the annihilation operator and the annihilation operator is the Hermitian adjoint of the creation operator.

$$\overline{(A^T)}=\begin{pmatrix}0&0\\1&0\end{pmatrix}$$

$$\overline{(C^T)}=\begin{pmatrix}0&1\\0&0\end{pmatrix}$$

The number operator is the product of the creation and annihilation operators.

$$CA=\begin{pmatrix}0&0\\0&1\end{pmatrix}$$

$$\overline{(A^T)}A=\begin{pmatrix}0&0\\0&1\end{pmatrix}$$

$$\overline{(C^T)}C=\begin{pmatrix}0&0\\0&1\end{pmatrix}$$

The eigenvectors of the number operator are |0> and |1> with eigenvalues 0 and 1, respectively:

$$eigenvecs(N)=\begin{pmatrix}1&0\\0&1\end{pmatrix}$$

$$eigenvals(N)=\begin{pmatrix}0\\1\end{pmatrix}$$

There are two paths to each detector. This provides the opportunity for constructive and destructive interference. To arrive at D_1 the a-arm photon state is reflected (90 degree phase shift) at BS_2 and the b-arm photon state is transmitted at BS_2. Therefore, photon detection requires the annihilation of the superposition of these paths to D_1. The annihilation is achieved with the following operator.

$$\frac{iA_a+A_b}{\sqrt{2}}$$

The product of this operator with its Hermitian conjugate (see above) creates the number operator for photon detection at D1.

$$N_{D1}=\frac{iC_a+C_b}{\sqrt{2}}+\frac{iA_a+A_b}{\sqrt{2}}$$

The D_1 number operator is formed using Mathcad's kronecker command as follows:

N_{D1} = $\frac{1}{2}$ (-i kronecker (C, I) + kronecker (I, C)) (i kronecker (A,I) + kronecker (I, A))

To arrive at D_2 the a-arm photon state is transmitted at BS_2 and the b-arm photon state is reflected (90 degree phase shift) at BS_2. Photon detection at D_2 requires the annihilation of the superposition of these paths to the detector. The annihilation is represented the following operator.

$$\frac{iA_a+A_b}{\sqrt{2}}$$

Therefore, the number operator for photon detection at D_2 is:

$$N_{D2} = \frac{C_a + iC_b}{\sqrt{2}} \frac{A_a + iA_b}{\sqrt{2}}$$

The D_2 number operator is formed using Mathcad's kronecker command as follows.

$N_{D2} = \frac{1}{2}$ (kronecker (C, I) - i kronecker (I, C)) (kronecker (A,I) + i kronecker (I, A))

We now show that the photon always arrives at D_1 and never at D_2 for an equal arm MZI.

Expectation value for photon detection at D_1:

$$\overline{\Psi^T} N_{D1} \Psi = 1$$

Expectation value for photon detection at D_2:

$$\overline{\Psi^T} N_{D2} \Psi = 1$$

Equivalent results can be obtained algebraically. Operating on Ψ with the D_1 number operator yields Ψ. In other words, Ψ is an eigenfunction of N_{D1} with eigenvalue 1.

$$\left[\frac{-C_a + C_b}{\sqrt{2}} \frac{iA_a + A_b}{\sqrt{2}}\right] \frac{1}{\sqrt{2}} \left[|1\rangle_a |0\rangle_b + i|0\rangle_a |1\rangle_b\right] = \frac{1}{\sqrt{2}} \left[|1\rangle_a |0\rangle_b + i|0_a |1\rangle_b\right]$$

Operating on Ψ with the D_2 number operator yields 0.

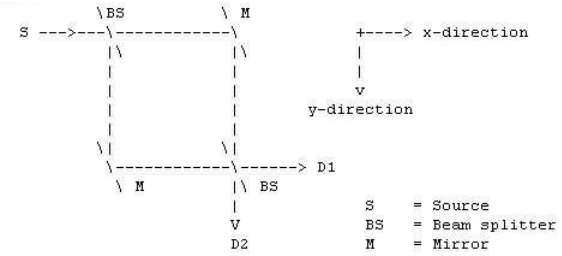
$$\left[\frac{C_a - iC_b}{\sqrt{2}} \frac{A_a + iA_b}{\sqrt{2}}\right] \frac{1}{\sqrt{2}} \left[|1\rangle_a |0\rangle_b + i|0\rangle_a |1\rangle_b\right] = 0$$

This page titled 7.4: Single Photon Interference - Fourth Version is shared under a CC BY 4.0 license and was authored, remixed, and/or curated by Frank Rioux via source content that was edited to the style and standards of the LibreTexts platform.

7.5: Single Photon Interference - Mathcad version

The schematic diagram below shows a Mach-Zehnder interferometer for photons. When the experiment is run so that there is only one photon in the apparatus at any time, the photon is always detected at D_1 and never at D_2.

This surprising phenomenon will be analyzed using matrix mechanics. State vectors for photon motion in the x- and y-direction, plus matrix operators for beam splitters and mirrors are defined below. For background and references to the primary literature see: V. Scarani and A. Suarez, "Introducing Quantum Mechanics: One-particle Interferences," Am. J. Phys. 66, 718-721 (1998).



Orthonormal basis states:

Photon moving in x-direction:

$$x = \begin{bmatrix} 1 \\ 0 \end{bmatrix} \quad x^T x = 1$$

Photon moving in y-direction:

$$y = \begin{bmatrix} 0 \\ 1 \end{bmatrix} \quad y^T y = 1 \quad x^T y = 0 \quad y^T x = 0$$

Operators:

Operator for interaction with the mirror:

$$M = \begin{bmatrix} 0 & 1 \\ 1 & 0 \end{bmatrix}$$

Operator for interaction with a 50/50 beam splitter:

$$BS = \frac{1}{\sqrt{2}} \begin{bmatrix} 1 & i \\ i & 1 \end{bmatrix}$$

Operations:

$$M(x) = \begin{bmatrix} 0 \\ 1 \end{bmatrix} \quad M(y) = \begin{bmatrix} 1 \\ 0 \end{bmatrix} \quad BS(x) = \begin{bmatrix} 0.707 \\ 0.707i \end{bmatrix} \quad BS(y) = \begin{bmatrix} 0.707i \\ 0.707 \end{bmatrix} \quad BS(M)BS(x) = \begin{bmatrix} i \\ 0 \end{bmatrix}$$

Quantum Mechanical Calculation of Experimental Results:

To be detected at D_1 the photon must be moving in the x-direction (photon state = |x>). To be detected at D_2 the photon must be moving in the y-direction (photon state = |y>). It is shown below that the probability the photon is moving in the x-direction is 1 and the probability it is moving in the y-direction is 0. In its course from source to detector the photon encounters a beam splitter, a mirror, and another beam splitter. Thus,

Probability photon will arrive at detector D_1:

$$(|x^T BS(M)BS(x)|)^2 = 1$$

Probability photon will arrive at detector D_2:

$$(|x^T BS(M)BS(x)|)^2 = 1$$

Further analysis:

The photon leaves the source traveling in the x-direction. Interaction with the beam splitter puts the photon in an even linear superposition of traveling in the x- and y-directions with a 90° phase shift ($\frac{\pi}{2}$ or i) assigned by convention to motion in the y-direction (see note below).

$$BS(x) = \begin{bmatrix} 0.707 \\ 0.707i \end{bmatrix} \quad \frac{x + iy}{\sqrt{2}} = \begin{bmatrix} 0.707 \\ 0.707i \end{bmatrix}$$

The interaction of this state with the mirrors transfers the 90° phase shift to motion in the x-direction.

$$(M)BS(x) = \begin{bmatrix} 0.707i \\ 0.707 \end{bmatrix} = \frac{ix + y}{\sqrt{2}} = \begin{bmatrix} 0.707i \\ 0.707 \end{bmatrix}$$

Finally the interaction of this state with the second beam splitter yields a 90° phase-shifted photon travelling in the x-direction.

$$BS(M)BS(x) = \begin{bmatrix} i \\ 0 \end{bmatrix} \quad ix = \begin{bmatrix} i \\ 0 \end{bmatrix}$$

Thus, the probability amplitude that it will be detected at D_1 is i and the probability amplitude that it will be detected at D_2 is 0.

$$x^T BS(M)BS(x) = (i) \quad y^T BS(M)BS(x) = (0)$$

The probability for an event is the square of the absolute magnitude of the probability amplitude, so the probability that the photon will be detected at D_1 is 1.

Note: The justification for the 90 ($\frac{\pi}{2}$ or i) phase shift between transmission and reflection at the beam splitter is conservation of energy. Assuming there is no phase shift requires that the BS operator be defined as:

$$BS = \frac{1}{\sqrt{2}} \begin{bmatrix} 1 & 1 \\ 1 & 1 \end{bmatrix}$$

This leads to the following calculation for the probability of the detection events:

Probability photon will arrive at detector D_1: $(|x^T BS(M)BS(x)|)^2 = 1$

Probability photon will arrive at detector D_2: $(|y^T BS(M)BS(x)|)^2 = 1$

According to this analysis, the single photon leaving the source has arrived at both detectors. One photon has become two, an obvious violation of the energy conservation principle.

This page titled 7.5: Single Photon Interference - Mathcad version is shared under a CC BY 4.0 license and was authored, remixed, and/or curated by Frank Rioux via source content that was edited to the style and standards of the LibreTexts platform.

7.6: The Polarizing Beam Splitter and the Superposition Principle

A polarizing beam splitter (PBS) and PBS interferometer (PBSI) can be used to illustrate the superposition principle. In this analysis the quantum math explaining the operation of a PBSI is presented.

A PBS transmits vertically polarized photons, $|v\rangle$, and reflects horizontally polarized photons, |h>. As the diagrams below show, the photons propagate in the x- or y-directions, $|x\rangle$ and $|y\rangle$. The interaction of $|v\rangle$ and $|h\rangle$ photons emitted by the source in the x-direction, $|x\rangle$, with the PBS is summarized in the two equations below. Note that we need to keep track of two degrees of freedom, direction of propagation and polarization state. This information is stored in the product of two Dirac kets, | >| >.

$$S \rightarrow |x\rangle|v\rangle \xrightarrow{PBS} |x\rangle|v\rangle$$

$$S \rightarrow |x\rangle|h\rangle \xrightarrow{PBS} |y\rangle|h\rangle$$

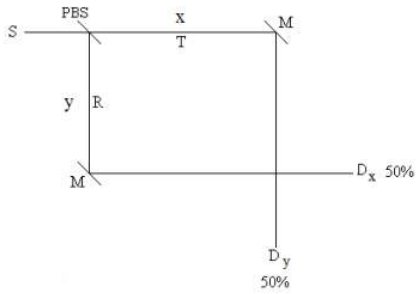
We will proceed with our analysis assuming that the source emits a diagonally polarized photon, |x>|d>. A diagonally polarized photon is an even superposition of being vertically and horizontally polarized. Thus the photon state incident on the PBS is,

$$S \rightarrow |x\rangle|d\rangle = |x\rangle\left[\frac{1}{\sqrt{2}}|v\rangle + \frac{1}{\sqrt{2}}|h\rangle\right] = \frac{1}{\sqrt{2}}|x\rangle|v\rangle + \frac{1}{\sqrt{2}}|x\rangle|h\rangle$$

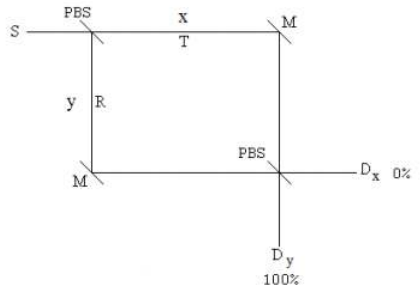
After the interaction with the PBS and the mirrors the photon state is,

$$\frac{1}{\sqrt{2}}|x\rangle|v\rangle + \frac{1}{\sqrt{2}}|x\rangle|h\rangle \xrightarrow{PBS} \frac{1}{\sqrt{2}}|x\rangle|v\rangle + \frac{1}{\sqrt{2}}|y\rangle|h\rangle \xrightarrow{M} \frac{1}{\sqrt{2}}|y\rangle|v\rangle + \frac{1}{\sqrt{2}}|x\rangle|h\rangle$$

The photon is in an even superposition of moving in the y-direction with vertical polarization and moving in the x-direction with horizontal polarization. For a statistically meaningful number of experiments, this analysis predicts that in 50% of the experiments the photon will appear at D_x with horizontal polarization and in 50% it will appear at D_y with vertical polarization. This is confirmed by experiment.



Now, at the photon path intersection just before the detectors a second PBS is inserted as shown below. This second PBS recombines the photon paths and creates a PBSI.



The interaction of the photon with the second PBS yields the following state.

$$\frac{1}{\sqrt{2}}|y\rangle|v\rangle + \frac{1}{\sqrt{2}}|x\rangle|h\rangle \xrightarrow{PBS} \frac{1}{\sqrt{2}}|y\rangle|v\rangle + \frac{1}{\sqrt{2}}|y\rangle|h\rangle = |y\rangle\left[\frac{1}{\sqrt{2}}|v\rangle + \frac{1}{\sqrt{2}}|h\rangle\right] = |y\rangle|d\rangle$$

The photon is always detected at Dy with diagonal polarization.

In summary, the source emits a photon in the x-direction in a v-h superposition state. Inside the interferometer the photon is in a superposition of both direction of propagation and polarization state. It emerges from the interferometer in the original polarization state |d>, but moving in the y-direction.

$$|x\rangle|d\rangle = |x\rangle\left[\frac{1}{\sqrt{2}}|v\rangle + \frac{1}{\sqrt{2}}|h\rangle\right] = \frac{1}{\sqrt{2}}|x\rangle|v\rangle + \frac{1}{\sqrt{2}}|x\rangle|h\rangle$$

PBS

$$\frac{1}{\sqrt{2}}|x\rangle|v\rangle + \frac{1}{\sqrt{2}}|y\rangle|h\rangle$$

M

$$\frac{1}{\sqrt{2}}|y\rangle|v\rangle + \frac{1}{\sqrt{2}}|x\rangle|h\rangle$$

PBS

$$\frac{1}{\sqrt{2}}|y\rangle|v\rangle + \frac{1}{\sqrt{2}}|y\rangle|h\rangle = |y\rangle\left[\frac{1}{\sqrt{2}}|v\rangle + \frac{1}{\sqrt{2}}|h\rangle\right] = |y\rangle|d\rangle$$

For an arbitrary polarization state |θ> we have,

$$|x\rangle|\theta\rangle = |x\rangle\left[\cos\theta|v\rangle + \sin\theta|h\rangle\right] = |x\rangle\cos\theta|v\rangle + |x\rangle\sin\theta|h\rangle$$

PBS

$$|x\rangle\cos\theta|v\rangle + |y\rangle\sin\theta|h\rangle$$

M

$$|x\rangle\cos\theta|v\rangle + |x\rangle\sin\theta|h\rangle$$

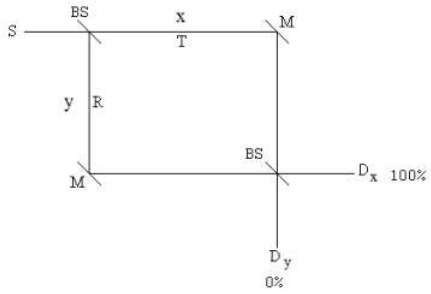
PBS

$$|y\rangle\cos\theta|v\rangle + |y\rangle\sin\theta|h\rangle = |y\rangle\left[\cos\theta|v\rangle + \sin\theta|h\rangle\right] = |y\rangle\theta\rangle$$

This page titled 7.6: The Polarizing Beam Splitter and the Superposition Principle is shared under a CC BY 4.0 license and was authored, remixed, and/or curated by Frank Rioux via source content that was edited to the style and standards of the LibreTexts platform.

7.7: Mach-Zehner Polarization Interferometer Analyzed Using Tensor Algebra

The purpose of this tutorial is to analyze a Mach-Zehnder (MZ) interferometer with polarizing beam splitters (PBS) using tensor algebra. First we will review the traditional MZ with non-polarizing beam splitters using matrix algebra.



The source emits photons in the x-direction illuminating a 50-50 beam splitter which splits the beam into a superposition of motion in the x- and y-directions. The reflected beam collects a $\frac{\pi}{2}$ (i) phase shift relative to the transmitted beam. Mirrors redirect the two beams to a second 50-50 BS. For the ideal case of an equal arm interferometer the photons are always registered at D_x and never at D_y. One way to explain this is shown on the figure above. Each photon has two paths to each of the detectors. At D_x the photon's paths add in phase each being shifted by $\frac{\pi}{2}$, resulting in constructive interference. At D_y the photon's paths are 180 degrees out of phase causing destructive interference.

The matrix analysis requires vectors to represent photon states, direction of propagation and polarization, and matrices to represent the devices that the photon interacts with, such as beam splitters and mirrors. The vectors representing direction of propagation are,

$$x = \begin{pmatrix} 1 \\ 0 \end{pmatrix} \quad y = \begin{pmatrix} 0 \\ 1 \end{pmatrix}$$

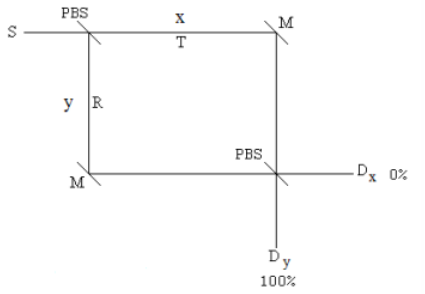
The beam splitters and mirrors are represented by the following matrices which operate on the motional states.

$$BS = \frac{1}{\sqrt{2}} \begin{pmatrix} 1 & i \\ i & 1 \end{pmatrix} \quad M = \begin{pmatrix} 0 & 1 \\ 1 & 0 \end{pmatrix}$$

The probability that the photon will be moving in the x-direction after the second BS and therefore detected at D_x is 1. The probability it will be registered at D_y is 0.

$$\left(|x^T BS(M) BS(x)|\right)^2 = 1 \quad \left(|y^T BS(M) BS(x)|\right)^2 = 0$$

In a polarization MZ interferometer the traditional beam splitters are replaced with polarizing beam splitters, which in this case transmit horizontal polarization and reflect vertical polarization.



Now in addition the direction of propagation, the photons have a polarization state which is initially restricted to horizontal or vertical polarization.

$$h = \begin{pmatrix} 1 \\ 0 \end{pmatrix} \quad v = \begin{pmatrix} 0 \\ 1 \end{pmatrix}$$

There are now four photon states: |xh>, |xv>, |yh> and |yv>, which can also be written |x>|h>, |x>|v>, |y>|h> and |y>|v>. These are vector tensor products and they take us from the two-dimensional space of the previous example to a four-dimensional Hilbert space.

$$|xh\rangle = |x\rangle|h\rangle = \begin{pmatrix}1\\0\end{pmatrix} \otimes \begin{pmatrix}1\\0\end{pmatrix} = \begin{pmatrix}1\\0\\0\\0\end{pmatrix} \quad |xv\rangle = |x\rangle|v\rangle = \begin{pmatrix}1\\0\end{pmatrix} \otimes \begin{pmatrix}0\\1\end{pmatrix} = \begin{pmatrix}0\\1\\0\\0\end{pmatrix}$$

$$|yh\rangle = |y\rangle|h\rangle = \begin{pmatrix}0\\1\end{pmatrix} \otimes \begin{pmatrix}1\\0\end{pmatrix} = \begin{pmatrix}0\\0\\1\\0\end{pmatrix} \quad |yv\rangle = |y\rangle|v\rangle = \begin{pmatrix}0\\1\end{pmatrix} \otimes \begin{pmatrix}0\\1\end{pmatrix} = \begin{pmatrix}0\\0\\0\\1\end{pmatrix}$$

$$xh = \begin{pmatrix}1\\0\\0\\0\end{pmatrix} \quad xv = \begin{pmatrix}0\\1\\0\\0\end{pmatrix} \quad yh = \begin{pmatrix}0\\0\\1\\0\end{pmatrix} \quad yv = \begin{pmatrix}0\\0\\0\\1\end{pmatrix}$$

As mentioned previously the PBS transmits horizontal polarization and reflects vertical polarization. Unlike the nonpolarizing BS, there is no phase change on reflection. The matrix representing a PBS can be constructed by considering the fate of the individual photon states encountering a PBS.

$$\widehat{PBS} = |xh\rangle\langle xh| + |yv\rangle\langle xv| + |yh\rangle\langle yh| + |xv\rangle\langle yv|$$

$$PBS: \begin{pmatrix}1\\0\\0\\0\end{pmatrix}(1\quad 0\quad 0\quad 0) + \begin{pmatrix}0\\0\\0\\1\end{pmatrix}(0\quad 1\quad 0\quad 0) + \begin{pmatrix}0\\0\\1\\0\end{pmatrix}(0\quad 0\quad 1\quad 0) + \begin{pmatrix}0\\1\\0\\0\end{pmatrix}(0\quad 0\quad 0\quad 1)$$

$$PBS = \begin{pmatrix}1&0&0&0\\0&0&0&1\\0&0&1&0\\0&1&0&0\end{pmatrix}$$

This gives us the PBS operator in the four-dimensional Hilbert space. Next we construct the matrix for the mirror in this space. The matrices representing the various photon interactions must be 4x4 because the photon vector states are 1x4. The mirror only affects the direction of propagation and not the polarization state of the photon. Since the motional state appears first in the kets, we form the 4-D mirror matrix by the following tensor (Kronecker) product of M and the identity matrix.

$$\widehat{M'} = \widehat{M} \otimes \hat{I} = \begin{pmatrix}0&0&1&0\\0&0&0&1\\1&0&0&0\\0&1&0&0\end{pmatrix}$$

$$M' = kronecker\left[M, \begin{pmatrix}1&0\\0&1\end{pmatrix}\right] \quad M' = \begin{pmatrix}0&0&1&0\\0&0&0&1\\1&0&0&0\\0&1&0&0\end{pmatrix}$$

As constructed this matrix changes the photon's direction of propagation with out affecting its state of polarization.

Now suppose that the source emits a horizontally polarized photon, |xh>. Calculation shows that it arrives at D_y with horizontal polarization,|yh>, 100% of the time.

$$\left(|yh^T PBS(M')PBS(xh)|\right)^2 = 1$$

If the source emits a vertically polarized photon, |xv>. Calculation shows that it arrives at D_y with vertical polarization,|yv>, 100% of the time.

$$\left(|yv^T PBS(M')PBS(xv)|\right)^2 = 1$$

A photon emitted by the source polarized at an angle of θ relative to the horizontal has the following state vector.

$$|x\theta\rangle = \begin{pmatrix}1\\0\end{pmatrix} \otimes \begin{pmatrix}\cos\theta\\ \sin\theta\end{pmatrix} = \begin{pmatrix}\cos\theta\\ \sin\theta\\ 0\\ 0\end{pmatrix}$$

It is easy to show that in the MZ polarization interferometer, the polarization state of the source photon is preserved while the direction of propagation changes.

$$|y\theta\rangle = \begin{pmatrix}0\\1\end{pmatrix} \otimes \begin{pmatrix}\cos\theta\\ \sin\theta\end{pmatrix} = \begin{pmatrix}0\\0\\ \cos\theta\\ \sin\theta\end{pmatrix}$$

$$\left|\langle y\theta|\widehat{PBSM'PBS}|x\theta\rangle\right|^2 = 1$$

$$\left[\left|\begin{pmatrix}0 & 0 & \cos\theta & \sin\theta\end{pmatrix}\begin{pmatrix}1&0&0&0\\0&0&0&1\\0&0&1&0\\0&1&0&0\end{pmatrix}\begin{pmatrix}0&0&1&0\\0&0&0&1\\1&0&0&0\\0&1&0&0\end{pmatrix}\begin{pmatrix}1&0&0&0\\0&0&0&1\\0&0&1&0\\0&1&0&0\end{pmatrix}\begin{pmatrix}\cos\theta\\ \sin\theta\\ 0\\ 0\end{pmatrix}\right|\right]^2 simplify \rightarrow 1$$

This is an excellent example of the superposition principle. The first PBS creates a x-h, y-v superposition state.

$$\begin{pmatrix}1&0&0&0\\0&0&0&1\\0&0&1&0\\0&1&0&0\end{pmatrix}\begin{pmatrix}\cos\theta\\ \sin\theta\\ 0\\ 0\end{pmatrix} \rightarrow \begin{pmatrix}\cos\theta\\ 0\\ 0\\ \sin\theta\end{pmatrix}$$

$$\begin{pmatrix}1\\0\end{pmatrix}\begin{pmatrix}\cos\theta\\ 0\end{pmatrix} + \begin{pmatrix}0\\1\end{pmatrix}\begin{pmatrix}0\\ \sin\theta\end{pmatrix} = \begin{pmatrix}\cos\theta\\ 0\\ 0\\ \sin\theta\end{pmatrix}$$

The mirror changes this to a y-h, x-v superposition.

$$\begin{pmatrix}0&0&1&0\\0&0&0&1\\1&0&0&0\\0&1&0&0\end{pmatrix}\begin{pmatrix}\cos\theta\\ 0\\ 0\\ \sin\theta\end{pmatrix} \rightarrow \begin{pmatrix}0\\ \sin\theta\\ \cos\theta\\ 0\end{pmatrix}$$

$$\begin{pmatrix}0\\1\end{pmatrix}\begin{pmatrix}\cos\theta\\ 0\end{pmatrix} + \begin{pmatrix}1\\0\end{pmatrix}\begin{pmatrix}0\\ \sin\theta\end{pmatrix} = \begin{pmatrix}0\\ \sin\theta\\ \cos\theta\\ 0\end{pmatrix}$$

The second PBS restores the original polarization state, but changes the direction of propagation.

$$\begin{pmatrix}1&0&0&0\\0&0&0&1\\0&0&1&0\\0&1&0&0\end{pmatrix}\begin{pmatrix}0\\ \sin\theta\\ \cos\theta\\ 0\end{pmatrix} \rightarrow \begin{pmatrix}0\\0\\ \cos\theta\\ \sin\theta\end{pmatrix}$$

$$\begin{pmatrix}0\\1\end{pmatrix}\begin{pmatrix}\cos\theta\\ 0\end{pmatrix} + \begin{pmatrix}0\\1\end{pmatrix}\begin{pmatrix}0\\ \sin\theta\end{pmatrix} = \begin{pmatrix}0\\1\end{pmatrix}\begin{pmatrix}\cos\theta\\ \sin\theta\end{pmatrix} = \begin{pmatrix}0\\0\\ \cos\theta\\ \sin\theta\end{pmatrix}$$

This page titled 7.7: Mach-Zehner Polarization Interferometer Analyzed Using Tensor Algebra is shared under a CC BY 4.0 license and was authored, remixed, and/or curated by Frank Rioux via source content that was edited to the style and standards of the LibreTexts platform.

7.8: Illustrating the Superposition Principle with Single Photon Interference

Abstract

Single-photon interference in a Mach-Zehnder interferometer is used to illustrate the superposition principle. Three methods of analysis of an historically important experiment are presented at a level appropriate for an undergraduate course in quantum chemistry or physics. The importance of the superposition principle in chemistry is also discussed.

Introduction

Introducing the double-slit experiment as paradigmatic of the bizarre nature of quantum mechanical behavior, Richard Feynman wrote,

> We choose to examine a phenomenon which is impossible, absolutely impossible, to explain in any classical way, and which has in it the heart of quantum mechanics. In reality, it contains the only mystery. We cannot make the mystery go away by "explaining" how it works. We will just tell you how it works. In telling you how it works we will have told you about the basic peculiarities of all quantum mechanics.*(1)*

Amplifying the last sentence of this quotation Feynman said the double-slit experiment is so fundamental that if asked a question about quantum mechanics one can always reply, "You remember the case of the experiment with the two holes? It's the same thing."*(2)* The crucial point being made is that the double-slit experiment is the simplest manifestation of the ubiquitous superposition principle and its attendant interference effects. The superposition principle, according to Feynman, permeates quantum mechanics, and is the origin of the strangeness we associate with quantum mechanical phenomena.

Having identified the mystery and conceptual difficulty of quantum mechanics Feynman went on to point out that computationally it was frequently quite simple.

> We have come to the conclusion that what are usually called the advanced parts of quantum mechanics are, in fact, quite simple. The mathematics that is involved is particularly simple, involving simple algebraic operations and no differential equations or at most very simple ones. *(3)*

Single-Photon Interference

Recently Scarani and Suarez *(4)* illustrated this mathematical simplicity by providing an elementary quantum mechanical analysis of an historically important experiment *(5)* that is a close relative of the famous double-slit experiment. Fig. 1 shows a schematic diagram of an equal-arm Mach-Zehnder interferometer consisting of two 50-50 beam splitters and two mirrors. The experiment is run at low source intensity such that there is only one photon in the interferometer at a time.

Three idealized experiments are considered for pedagogical purposes. (I) If either path is blocked 50% of the photons get through, and 25% reach D_1 and 25% reach D_2. (II) In the absence of the second beam splitter (BS_2) 50% of the time the photon is detected at D_1 and 50% of the time it is detected at D_2. (III) However, in the presence of BS_2 the photon is always detected at D_1 and never at D_2. Three methods will be used to analyze the surprising result of experiment III. Of course the key will be that in this experiment each detector can be reached by two paths, whereas in experiments I and II there is only one path to each detector.

First Method

We will begin with a brief review of the analysis given by Scarani and Suarez for experiment III before presenting two alternative approaches. After the first beam splitter the photon is in an even linear superposition of being transmitted $|T\rangle$ and reflected $|R\rangle$.

$$|S\rangle \rightarrow \frac{1}{\sqrt{2}}\left[|T\rangle + i|R\rangle\right]$$

By convention a $\frac{\pi}{2}$ (i) phase shift is assigned to the reflected beam. More will be said about this below.

The mirrors *(6)* direct the two beams to the second beam splitter where, according to the superposition principle, $|T\rangle$ and $|R\rangle$ evolve as follows,

$$|T\rangle \rightarrow \frac{1}{\sqrt{2}}\left[i|D_1\rangle + |D_2\rangle\right]$$

$$|R\rangle \rightarrow \frac{1}{\sqrt{2}}\left[|D_1\rangle + i|D_2\rangle\right]$$

where again the $\frac{\pi}{2}$ phase shift is assigned to the reflection. Substitution of eqns (2) and (3) into (1) yields

$$|S\rangle \rightarrow i|D_1\rangle$$

Thus, the probability that the photon will arrive at D_1 is

$$\left|\langle D_1|S\rangle\right|^2 = 1$$

It is easy to show that if there is no phase difference between reflection and transmission 1 2 (i.e. replace *i* by 1 in equations (1), (2), and (3)) the probabilities for arrival at D_1 and D_2 are both 1. This is a clear violation of energy conservation because one photon has become two photons with no mechanism for a reduction of energy of the individual photons. Thus, conservation of energy is a compelling argument for a $\frac{\pi}{2}$ phase difference between transmission and reflection.

Second Method

The second method uses Dirac notation to enumerate the probability amplitudes for arrival at the two detectors. As in the above analysis, at the beam splitters the probability amplitude for transmission is $\frac{1}{\sqrt{2}}$, and for reflection it is $\frac{i}{\sqrt{2}}$. Because the photon path is not observed the probability is calculated as the square of the absolute magnitude of the sum of the probability amplitudes for each path. Thus, the probability amplitudes for the two paths may interfere constructively and destructively. As shown below the probability amplitudes to reach D_1 are in phase (TR+RT) and those to reach D_2 are 180° out of phase (TT+RR), so the photon is never detected at D_2.

$$\left|\langle D_1|S\rangle\right|^2 = \left|\langle D_1|T\rangle\langle T|S\rangle + \langle D_1|R\rangle\langle R|S\rangle\right|^2 = \left|\frac{i}{\sqrt{2}}\frac{1}{\sqrt{2}} + \frac{1}{\sqrt{2}}\frac{i}{\sqrt{2}}\right|^2 = 1$$

$$\left|\langle D_2|S\rangle\right|^2 = \left|\langle D_2|T\rangle\langle T|S\rangle + \langle D_2|R\rangle\langle R|S\rangle\right|^2 = \left|\frac{1}{\sqrt{2}}\frac{1}{\sqrt{2}} + \frac{i}{\sqrt{2}}\frac{i}{\sqrt{2}}\right|^2 = 0$$

While it is customary to refer to this experiment as an example of single-particle interference, Glauber *(7)* recommends more careful language.

> The things that interfere in quantum mechanics are not particles. They are probability amplitudes for certain events. It is the fact that probability amplitudes add up like complex numbers that is responsible for all quantum mechanical interferences.

What Glauber is saying here is clearly revealed in this second method of analysis.

Third Method

The third method illustrates how the experiment is analyzed using matrix mechanics.*(8)* In this approach the photon's translational states $|x\rangle$ (horizontal) and $|y\rangle$ (vertical) are represented by the orthonormal basis vectors shown below.

$$|x\rangle = \begin{pmatrix}1\\0\end{pmatrix} \quad |y\rangle = \begin{pmatrix}0\\1\end{pmatrix} \quad \langle x| = \begin{pmatrix}1 & 0\end{pmatrix} \quad \langle y| = \begin{pmatrix}0 & 1\end{pmatrix}$$

The operators for the interaction of the photon with a 50-50 beam splitter and a mirror *(6)* are represented by the following matrices.

$$BS = \frac{1}{\sqrt{2}}\begin{pmatrix}1 & i\\ i & 1\end{pmatrix} \quad M = \begin{pmatrix}0 & 1\\ 1 & 0\end{pmatrix}$$

To be detected at D_1 a photon must be in the translational state $|x\rangle$ after interacting with two beam splitters and a mirror in the configuration shown in Fig. 1. To be detected at D_2 it must be in the translational state $|y\rangle$. The probabilities for these outcomes are calculated using equations (8) and (9) as follows:

$$\left|\langle x|BS(M)BS|x\rangle\right|^2 = 1 \quad \left|\langle y|BS(M)BS|x\rangle\right|^2 = 0$$

It is easy to confirm the rest by hand calculation.

Recapitulation

Dirac emphasized the unique role of the superposition principle in his seminal treatise on quantum mechanics by saying, “There is an entirely new idea involved, to which one must get accustomed and in terms of which one must proceed to build up an exact mathematical theory, without having any detailed classical picture.”*(9)*

The best way to get accustomed to the ubiquitous, but non-classical nature of the quantum mechanical superposition is through the study of those phenomena where it reveals itself most directly. Single-photon interference in a Mach-Zehnder interferometer provides a very simple example of the superposition principle in action, and is therefore suitable for presentation to undergraduates studying quantum chemistry or quantum physics. The same is true, of course, for the more widely known double-slit experiment.

The Superposition Principle in Chemistry

Having introduced the superposition with three analyses of an experiment in quantum optics, we will now briefly review its importance in chemistry. The superposition principle informs the chemists view of atomic and molecular structure, and is especially important in unifying the many facets of chemical bonding *(10)*.

For example, an electronic wave function, whether atomic or molecular, is a weighted linear superposition. In atoms and molecules...

> Electrons are characterized by their entire distributions (called wave functions or orbitals) rather than by instantaneous positions and velocities: an electron may be considered always to be (with appropriate probability) at all points of its distribution (which does not vary with time). *(11)*

Electrons confined in atoms and molecules are not moving in a classical sense; if they were they would radiate energy continuously, and atomic and molecular stability would be raised to the status of a scientific miracle. Atomic and molecular electrons are not here and later there, rather they are, at the same time, here and there. Just as the photon is present simultaneously in both arms of the Mach-Zehnder interferometer, the electron is present at all possible locations (properly weighted) in atoms and molecules. The confined electron is in an atomic or molecular stationary state.

Similar arguments pertain to molecular vibrations *(12)* and rotations. In the absence of external perturbations, such as electromagnetic radiation, molecules do not really vibrate and rotate about their centers of mass for the same reason electrons do not orbit the nucleus; such behavior would lead to the continuous emission of electromagnetic radiation, and again call into question the stability of matter. In the nanoscopic world of atoms and molecules motion only occurs during transitions from one stationary state to another – during the so called *quantum jump*.

The superposition principle also provides a viable model for this *quantum jump*, the transition between quantized stationary states, which is the essential process in all forms of spectroscopy. *(13)* Under the influence of an electromagnetic perturbation, a molecule or atom in an initial stationary state may move into a time-dependent linear superposition of the initial state and some final state.

$$\Psi(r,t) = c_i(t)\Psi_i(r,t)exp\left(-\frac{iE_it}{\hbar}\right) + c_f(t)\Psi_f(r,t)exp\left(-\frac{iE_ft}{\hbar}\right)$$

If the Bohr frequency condition is met, $v = \frac{E_f - E_i}{\hbar}$, and $|\Psi(r,t)|^2$ exhibits oscillating electric dipole character, the transition may occur, otherwise it is forbidden. In summary, the superposition principle provides an interpretation of quantized stationary states and the transitions between them induced by electromagnetic radiation.

Conclusion

Feynman has identified the superposition principle as the fundamental mystery of quantum mechanics. Accepting this view is good pedagogy, because it helps us teachers to see the coherence of this strange and awesome subject, and hopefully to pass that vision on to our students. It is characteristic of great thinkers, like Feynman, that they see the threads that make the tapestry.

Literature cited

1. Feynman, R. P.; Leighton, R. B.; Sands, M., *The Feynman Lectures on Physics, Vol. 3*; Addison-Wesley: Reading, 1965, p. 1-1.

2. Feynman, R. P. *The Character of Physical Law*; MIT Press: Cambridge, 1967; p. 130.

3. Feynman, R. P.; Leighton, R. B.; Sands, M., *The Feynman Lectures on Physics, Vol. 3*; Addison-Wesley: Reading, 1965, p. 3-1.

4. Scarani, V.; Suarez, A. “Introducing quantum mechanics: One-particle interferences,” *Am. J. Phys.* **1998**, 66, 718-721.

5. Grangier, P.; G. Roger, G.; Aspect, A. “Experimental Evidence for Photon Anticorrelation Effects on a Beam Splitter: A New Light on Single-Photon Interferences,” *Europhys. Lett* **1986**, 1, 173-179.

6. The $\frac{\pi}{2}$ phase shift accompanying reflection at the mirrors can be ignored because there are mirrors in both arms of the interferometer.

7. Glauber, R. J. “Dirac’s famous dictum,” *Am. J. Phys.* **1995**, 63, 12.

8. This suggestion was made to the author by V. Scarani in a private communication.

9. Dirac, P. A. M. *Principles of Quantum Mechanics*, 4th ed.; Oxford U. P.: London, 1958, p.12.

10. Weinhold, F. A. “Chemical Bonding as a Superposition Phenomenon,” *J. Chem. Educ.* **1999**, 76, 1141-1146.

11. Harris, F. E. “Molecules,” *The Encyclopedia of Physics*, 2nd ed.; R. G. Lerner, Ed. New York, VCH Publishers, 1990, p. 763.

12. Baskin, J. S.; Zewail, A. H. “Freezing Atoms in Motion: Principles of Femtochemistry and Demonstration by Laser Stroboscopy,” *J. Chem. Educ*. 2001, 78, 737-751.

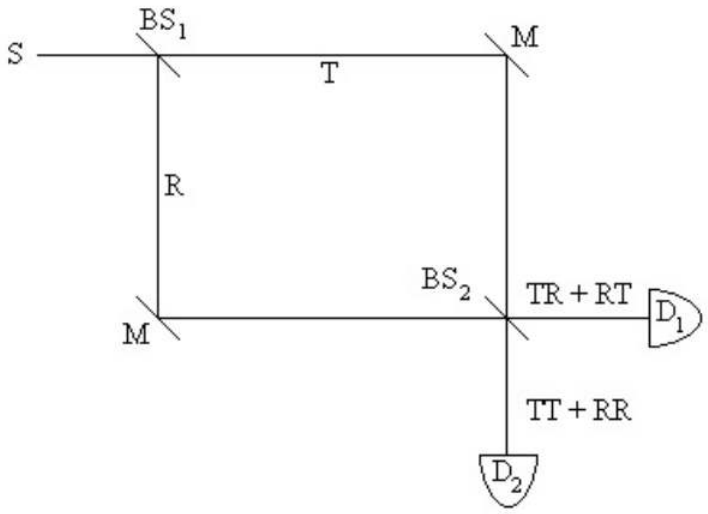


Fig. 1 Schematic diagram of a Mach-Zehnder interferometer. S = source; BS = beam splitter; M = mirror 1 ; R = reflected; T = transmitted; D = detector; TT = transmitted at BS and 2 1 2 transmitted at BS ; TR = transmitted at BS and reflected at BS ; etc.

This page titled 7.8: Illustrating the Superposition Principle with Single Photon Interference is shared under a CC BY 4.0 license and was authored, remixed, and/or curated by Frank Rioux via source content that was edited to the style and standards of the LibreTexts platform.

7.9: Pure States, Mixtures and the Density Operator

Calculations with polarized and un-polarized light will be used to illustrate the difference between pure states and mixtures, and to demonstrate the utility of the density operator.

In Heisenberg's matrix mechanics pure states are represented by vectors and operators by matrices. For example, light polarized at an angle 2 relative to the vertical is represented by the following Dirac ket vector,

$$|\theta\rangle = \begin{pmatrix} \cos\theta \\ \sin\theta \end{pmatrix}$$

The matrix operator for a polarizer oriented at an angle 2 relative to the vertical in Dirac notation is represented by a ket-bra product (outer product).

$$\hat{\theta} = |\theta\rangle\langle\theta| = \begin{pmatrix} \cos\theta \\ \sin\theta \end{pmatrix} \cos\theta \quad \sin\theta = \begin{pmatrix} \cos^2\theta & \cos\theta\sin\theta \\ \cos\theta\sin\theta & \sin^2\theta \end{pmatrix}$$

The state vector is normalized because the bra-ket product, or inner product, is unity.

$$\langle\theta|\rangle\theta = \cos\theta \quad \sin\theta \begin{pmatrix} \cos\theta \\ \sin\theta \end{pmatrix} = \cos^2\theta + \sin^2\theta = 1$$

Clearly the state vector is an eigenstate of the operator with unit eigenvalue.

$$\hat{\theta}|\theta\rangle = |\theta\rangle\langle\theta|\theta\rangle = |\theta\rangle$$

Un-polarized light from an incandescent bulb is incident upon a polarizing film oriented at an angle θ relative to the vertical producing 2-polarized light, $|\theta\rangle$. State preparation, such as this, is an essential first step in any quantum mechanical analysis.

As shown below, the expectation value for the passage of this 2-polarized light through a vertical polarizer is $\cos^2\theta$.

$$\langle V\rangle = \langle\theta|\hat{V}|\theta\rangle = \cos\theta \quad \sin\theta \begin{pmatrix} 1 & 0 \\ 0 & 0 \end{pmatrix} \begin{pmatrix} \cos\theta \\ \sin\theta \end{pmatrix} = \cos^2\theta$$

We can also argue that θ-polarized light is a coherent superposition of vertically and horizontally polarized light.

$$|\theta\rangle = |v\rangle\langle v|\theta\rangle + |h\rangle\langle H|\theta\rangle = \cos\theta|v\rangle + \sin\theta|h\rangle = \cos\theta \begin{pmatrix} 1 \\ 0 \end{pmatrix} + \sin\theta \begin{pmatrix} 0 \\ 1 \end{pmatrix}$$

where

$$|v\rangle\langle v| + |h\rangle\langle h| = 1$$

is the identity operator. In other words, $|v\rangle$ and $|h\rangle$ are an orthonormal basis for linear polarization. Any linear polarization state can be expressed as a superposition of these basis vectors.

The probability that a θ-polarized photon will pass a vertical polarizer in this approach is the probability amplitude for that event squared, $|\langle v|\theta\rangle|^2 = \cos^2\theta$.

The calculation for the expectation value $\langle\theta|\hat{V}|\theta\rangle$ can also be re-cast in terms of $\hat{\theta}$ by exploiting the idempotency of $\hat{V}$.

$$\hat{V}\hat{V} = \hat{V}|v\rangle\langle v| = |v\rangle\langle v|v\rangle\langle v| = |v\rangle\langle v| = \hat{V}$$

Using $\hat{V} = \hat{V}\hat{V}$ we find

$$\langle V\rangle = \langle\theta|\hat{V}\hat{V}|\theta\rangle = \langle\theta\hat{V}|v\rangle\langle v|\theta\rangle = \langle v|\theta\rangle\langle\theta|\hat{V}|v\rangle = \langle v|\hat{\theta}\hat{V}|v\rangle = Trace(\hat{\theta}\hat{V}$$

where *Trace* signifies the sum of the diagonal elements of the product matrix. By substituting $\hat{\theta}$ and $\hat{V}$ we find agreement with the previous method of calculating the expectation value.

$$\langle V\rangle = Trace\left[\begin{pmatrix} \cos^2\theta & \cos\theta\sin\theta \\ \cos\theta\sin\theta & \sin^2\theta \end{pmatrix} \begin{pmatrix} 1 & 0 \\ 0 & 0 \end{pmatrix}\right] = \cos^2\theta$$

This approach, while mathematically interesting, is non-intuitive compared with the previous traditional method. One might question its utility in the face of the more direct method of calculating expectation values. The utility of this method is apparent when one considers the calculation of the expectation values for a mixture – such as un-polarized light. Un-polarized light is an even mixture of all possible polarization states. However, it can be treated as a 50-50 mixture of any two orthogonal polarization states. Such a mixture cannot be represented by a single wavefunction,

$$|\psi\rangle = \frac{1}{\sqrt{2}}\left(|\theta\rangle + |\theta + \frac{\pi}{2}\right\rangle\Big)$$

because in quantum mechanical notation this represents a pure state, a coherent superposition of two orthogonal polarization states.

Density Operators

Rather, a mixture must be represented by a **density operator** (sometimes calld a density matrix), which is a weighted sum of the operators representing the states making up the mixture. The density operator for un-polarized light is,

$$\hat{\rho} = \frac{1}{2}|\theta\rangle\langle\theta| + \frac{1}{2}\left|\theta + \frac{\pi}{2}\right\rangle\left\langle\theta + \frac{\pi}{2}\right|$$

The expectation value for un-polarized light to pass a vertical polarizer according to the last method is

$$\langle V\rangle = Trace\left[\frac{1}{2}\right.$$
$$\left.\left(\begin{pmatrix}\cos^2\theta & \cos\theta\sin\theta\\ \cos\theta\sin\theta & \sin^2\theta\end{pmatrix} + \begin{pmatrix}\cos^2(\theta+\frac{\pi}{2}) & \cos(\theta+\frac{\pi}{2})\sin(\theta+\frac{\pi}{2})\\ \cos(\theta+\frac{\pi}{2})\sin(\theta+\frac{\pi}{2}) & \sin^2(\theta+\frac{\pi}{2})\end{pmatrix}\right)\begin{pmatrix}1 & 0\\ 0 & 0\end{pmatrix}\right] = \frac{1}{2}$$

This method can be used to derive an alternative method for calculating the expectation value for a mixture.

$$\langle V\rangle = Trace\left[\hat{\rho}\hat{V}\right] = \langle|\hat{\rho}\hat{V}|v\rangle \tag{7.9.1}$$

$$= \langle v|\left(\frac{1}{2}|\theta\rangle\langle\theta| + \frac{1}{2}\left|\theta + \frac{\pi}{2}\right\rangle\left\langle\theta + \frac{\pi}{2}\right|\right)\hat{V}|v\rangle \tag{7.9.2}$$

$$= \frac{1}{2}\langle v|\theta\rangle\langle\theta|v\rangle + \frac{1}{2}\left\langle v\left|\theta + \frac{\pi}{2}\right\rangle\right\langle\theta + \frac{\pi}{2}\left|v\right\rangle\right.$$

$$= \frac{1}{2}\langle\theta|v\rangle\langle v|\theta\rangle + \frac{1}{2}\left\langle\theta + \frac{\pi}{2}\left|v\right\rangle\right\langle v\left|\theta + \frac{\pi}{2}\right\rangle = \frac{1}{2}\langle\theta|\hat{V}|\theta\rangle + \frac{1}{2}\left\langle\theta + \frac{\pi}{2}\left|\hat{V}\right|\theta + \frac{\pi}{2}\right\rangle \tag{7.9.3}$$

$$= \frac{1}{2}\cos^2\theta + \frac{1}{2}\cos^2(\theta + \frac{\pi}{2}) = \frac{1}{2} \tag{7.9.4}$$

In general, for a mixture the expectation value is calculated as

$$\langle V\rangle = \sum_i p_i\langle\psi_i|\hat{V}|\psi_i\rangle$$

where p_i is the probability associated with the state $|\psi_i\rangle$.

This page titled 7.9: Pure States, Mixtures and the Density Operator is shared under a CC BY 4.0 license and was authored, remixed, and/or curated by Frank Rioux via source content that was edited to the style and standards of the LibreTexts platform.

7.10: Using the Trace Function to Calculate Expectation Values

Starting with the traditional expression for the calculation of the expectation value, the identity operator is inserted between the measurement operator and the ket containing the wave function. Rearranging terms gives the trace function operating on the product of the state's density operator and the measurement operator.

$$\begin{aligned}\langle\psi|\hat{O}|\psi\rangle &= \sum_i \langle\psi|\hat{O}|i\rangle\langle i|\psi\rangle \\ &= \sum_i \langle i|\psi\rangle\langle\psi|\hat{O}|i\rangle \\ &= Trace\left(|\psi\rangle\langle\psi|\hat{O}\right)\end{aligned}$$

where

$$\sum_i |i\rangle\langle i| = identity$$

Next this transition is carried out in detail using matrix algebra.

$$\begin{pmatrix}a & b\end{pmatrix}\begin{pmatrix}0 & 1\\ 1 & 0\end{pmatrix}\begin{pmatrix}a\\ b\end{pmatrix} = \begin{pmatrix}a & b\end{pmatrix}\begin{pmatrix}0 & 1\\ 1 & 0\end{pmatrix}\begin{pmatrix}1 & 0\\ 0 & 1\end{pmatrix}\begin{pmatrix}a\\ b\end{pmatrix}$$

$$= \begin{pmatrix}a & b\end{pmatrix}\begin{pmatrix}0 & 1\\ 1 & 0\end{pmatrix}\left[\begin{pmatrix}1\\ 0\end{pmatrix}\begin{pmatrix}1 & 0\end{pmatrix} + \begin{pmatrix}0\\ 1\end{pmatrix}\begin{pmatrix}0 & 1\end{pmatrix}\right]\begin{pmatrix}a\\ b\end{pmatrix} = 2ab$$

$$\begin{pmatrix}a & b\end{pmatrix}\begin{pmatrix}0 & 1\\ 1 & 0\end{pmatrix}\begin{pmatrix}1\\ 0\end{pmatrix}\begin{pmatrix}1 & 0\end{pmatrix}\begin{pmatrix}a\\ b\end{pmatrix} = \begin{pmatrix}a & b\end{pmatrix}\begin{pmatrix}0 & 1\\ 1 & 0\end{pmatrix}\begin{pmatrix}0\\ 1\end{pmatrix}\begin{pmatrix}0 & 1\end{pmatrix}\begin{pmatrix}a\\ b\end{pmatrix} = 2ab$$

$$\begin{pmatrix}1 & 0\end{pmatrix}\begin{pmatrix}a\\ b\end{pmatrix}\begin{pmatrix}a & b\end{pmatrix}\begin{pmatrix}0 & 1\\ 1 & 0\end{pmatrix}\begin{pmatrix}1\\ 0\end{pmatrix} + \begin{pmatrix}0 & 1\end{pmatrix}\begin{pmatrix}a\\ b\end{pmatrix}\begin{pmatrix}a & b\end{pmatrix}\begin{pmatrix}0 & 1\\ 1 & 0\end{pmatrix}\begin{pmatrix}0\\ 1\end{pmatrix} = 2ab$$

$$\begin{pmatrix}1 & 0\end{pmatrix}\begin{pmatrix}a^2 & ab\\ ab & b^2\end{pmatrix}\begin{pmatrix}0 & 1\\ 1 & 0\end{pmatrix}\begin{pmatrix}1\\ 0\end{pmatrix} + \begin{pmatrix}0 & 1\end{pmatrix}\begin{pmatrix}a^2 & ab\\ ab & b^2\end{pmatrix}\begin{pmatrix}0 & 1\\ 1 & 0\end{pmatrix}\begin{pmatrix}0\\ 1\end{pmatrix} = 2ab$$

$$\begin{pmatrix}1 & 0\end{pmatrix}\begin{pmatrix}ab & a^2\\ b^2 & ab\end{pmatrix}\begin{pmatrix}1\\ 0\end{pmatrix} + \begin{pmatrix}0 & 1\end{pmatrix}\begin{pmatrix}ab & a^2\\ b^2 & ab\end{pmatrix}\begin{pmatrix}0\\ 1\end{pmatrix} = ab + ab = Trace\begin{pmatrix}ab & a^2\\ b^2 & ab\end{pmatrix}$$

$$\begin{pmatrix}a & b\end{pmatrix}\begin{pmatrix}0 & 1\\ 1 & 0\end{pmatrix}\begin{pmatrix}a\\ b\end{pmatrix} \rightarrow 2ab \quad \begin{pmatrix}a & b\end{pmatrix}\begin{pmatrix}0 & 1\\ 1 & 0\end{pmatrix}\begin{pmatrix}1 & 0\\ 0 & 1\end{pmatrix}\begin{pmatrix}a\\ b\end{pmatrix} \rightarrow 2ab$$

$$\begin{pmatrix}1\\ 0\end{pmatrix}\begin{pmatrix}1 & 0\end{pmatrix} + \begin{pmatrix}0\\ 1\end{pmatrix}\begin{pmatrix}0 & 1\end{pmatrix} \rightarrow \begin{pmatrix}1 & 0\\ 0 & 1\end{pmatrix}$$

$$\begin{pmatrix}a & b\end{pmatrix}\begin{pmatrix}0 & 1\\ 1 & 0\end{pmatrix}\begin{pmatrix}1\\ 0\end{pmatrix}\begin{pmatrix}1 & 0\end{pmatrix}\begin{pmatrix}a\\ b\end{pmatrix} + \begin{pmatrix}a & b\end{pmatrix}\begin{pmatrix}0 & 1\\ 1 & 0\end{pmatrix}\begin{pmatrix}0\\ 1\end{pmatrix}\begin{pmatrix}0 & 1\end{pmatrix}\begin{pmatrix}a\\ b\end{pmatrix} \rightarrow 2ab$$

$$\begin{pmatrix}1 & 0\end{pmatrix}\begin{pmatrix}a\\ b\end{pmatrix}\begin{pmatrix}a & b\end{pmatrix}\begin{pmatrix}0 & 1\\ 1 & 0\end{pmatrix}\begin{pmatrix}1\\ 0\end{pmatrix} + \begin{pmatrix}0 & 1\end{pmatrix}\begin{pmatrix}a\\ b\end{pmatrix}\begin{pmatrix}a & b\end{pmatrix}\begin{pmatrix}0 & 1\\ 1 & 0\end{pmatrix}\begin{pmatrix}0\\ 1\end{pmatrix} \rightarrow 2ab$$

$$tr\left[\begin{pmatrix}a\\ b\end{pmatrix}\begin{pmatrix}a & b\end{pmatrix}\begin{pmatrix}0 & 1\\ 1 & 0\end{pmatrix}\right] \rightarrow 2ab \quad tr\left[\begin{pmatrix}0 & 1\\ 1 & 0\end{pmatrix}\begin{pmatrix}a\\ b\end{pmatrix}\begin{pmatrix}a & b\end{pmatrix}\right] \rightarrow 2ab$$

The last calculation on the right is justified by the following:

$$\langle\psi|\hat{O}|\psi\rangle = \sum_i \langle\psi|i\rangle\langle i|\hat{O}|\psi\rangle = \sum_i \langle i|\hat{O}|\psi\rangle\langle\psi|i\rangle = Trace\left(\hat{O}|\psi\rangle\langle\psi|\right)$$

This page titled 7.10: Using the Trace Function to Calculate Expectation Values is shared under a CC BY 4.0 license and was authored, remixed, and/or curated by Frank Rioux via source content that was edited to the style and standards of the LibreTexts platform.

7.11: Polarized Light and Quantum Superposition

The superposition principle is a deep and difficult quantum mechanical concept. There is no classical analog to lean on in probing its meaning, because it is impossible to simulate it with classical models. And yet because it pervades quantum mechanics we must find ways to present it to students that have some probability of success in revealing its significance.

The title of the first chapter in Dirac's famous treatise *The Principles of Quantum Mechanics* (Clarendon Press, Oxford) is The Principle of Superposition. On page 12 of the 4th edition he wrote,

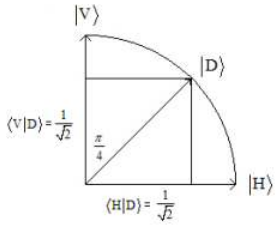
> The nature of the relationships which the superposition principle requires to exist between the states of any system is of a kind that cannot be explained in terms of familiar physical concepts. One cannot in the classical sense picture a system being partly in each of two states and see the equivalence of this to the system being completely in some other state. There is an entirely new idea involved, to which one must get accustomed and in terms of which one must proceed to build up an exact mathematical theory, without having any detailed classical picture.

Perhaps the easiest way to illustrate the superposition principle mathematically is with demonstrations using polarizing films. Suppose unpolarized light illuminates a polarizer oriented at 45º to the vertical creating a beam of diagonally polarized photons, $|D\rangle$. If the diagonally polarized beam now illuminates a second polarizer oriented in the vertical or horizontal direction, 50% of the photons are transmitted.

The quantum mechanical explanation for these results is to write the wave function of a diagonally polarized photon as a superposition in the V-H basis, $\langle v|v\rangle = \langle H|H\rangle = 1; \langle v|H\rangle\langle H|V\rangle = 0$.

$$|D\rangle = \frac{1}{\sqrt{2}}\left[|V\rangle + |H\rangle\right]$$

This superposition is illustrated graphically as follows.



Using either equation or figure we have, $|\langle V|D\rangle|^2 = |\langle H|D\rangle|^2 = \frac{1}{2}$, in agreement with the demonstration.

The same result would occur if the diagonally polarized beam was assumed to be a 50- 50 mixture of vertical and horizontal photons rather than a superposition. However, according to quantum mechanical principles, a mixture is represented by a density operator rather than by a wave function. In this case the appropriate density operator is

$$\hat{\rho}_{mix} = \frac{1}{2}|V\rangle\langle V| + \frac{1}{2}|H\rangle\langle H|$$

The probability (expectation value) that a 50-50 mixture of V-H photons will pass a vertical or horizontal polarizer is easily calculated.

$$\langle V|\hat{\rho}_{mix}|V\rangle = \langle H|\hat{\rho}_{mix}|H\rangle = \frac{1}{2}$$

At this point, the superposition and mixture models give the same result for what happens in the presence of the second (H or V) polarizer. However, it is not difficult to demonstrate that diagonally polarized light is not a mixture of vertical and horizontally polarized photons. If the second polarizer is replaced with another diagonally oriented polarizer, 100% of the photons are transmitted. This is because a diagonally polarized photon is an eigenstate of the diagonal polarization measurement operator.

The expectation value for a 50-50 mixture is not in agreement with this outcome. It predicts that only 50% of the photons will pass the diagonal oriented polarizing film.

$$\langle D|\hat{\rho}_{mix}|D\rangle = \frac{1}{2}\langle D|V\rangle\langle V|D\rangle + \frac{1}{2}\langle D|H\rangle\langle H|D\rangle = \frac{1}{2}\left(\frac{1}{\sqrt{2}}\right)^2 + \frac{1}{2}\left(\frac{1}{\sqrt{2}}\right)^2 = \frac{1}{2}$$

This result will seem more plausible when written in the following equivalent form.

$$\langle D|\hat{\rho}_{mix}|D\rangle = \frac{1}{2}\langle D|V\rangle\langle V|D\rangle + \frac{1}{2}\langle D|H\rangle\langle H|D\rangle$$
$$= \frac{1}{2}\langle V|D\rangle\langle D|V\rangle + \frac{1}{2}\langle H|D\rangle\langle D|H\rangle = \frac{1}{2}\langle V|\hat{D}|H\rangle = \frac{1}{2}$$

It is instructive to repeat these calculations using matrix mechanics. In this approach to quantum mechanics states are represented by vectors and operators by matrices. For example, the vector representations for the vertical, horizontal and diagonal polarization states are given below.

$$|V\rangle = \begin{pmatrix}1\\0\end{pmatrix} \quad |H\rangle = \begin{pmatrix}0\\1\end{pmatrix} \quad |D\rangle = \frac{1}{\sqrt{2}}\begin{pmatrix}1\\1\end{pmatrix}$$

With vector algebra it is easy to show that a diagonally polarized photon is a weighted superposition of the vertical and horizontal polarization states.

$$|D\rangle = \frac{1}{\sqrt{2}}\begin{pmatrix}1\\1\end{pmatrix} = \frac{1}{\sqrt{2}}\left[\begin{pmatrix}1\\0\end{pmatrix} + \begin{pmatrix}0\\1\end{pmatrix}\right]$$

The operators representing the various orientations of the polarizing films are as follows.

$$\hat{V} = |V\rangle\langle V| = \begin{pmatrix}1\\0\end{pmatrix}\begin{pmatrix}1 & 0\end{pmatrix} = \begin{pmatrix}1 & 0\\0 & 0\end{pmatrix}$$

$$\hat{H} = |H\rangle\langle H| = \begin{pmatrix}0\\1\end{pmatrix}\begin{pmatrix}0 & 1\end{pmatrix} = \begin{pmatrix}0 & 0\\0 & 1\end{pmatrix}$$

$$\hat{D} = |D\rangle\langle D| = \begin{pmatrix}\frac{1}{\sqrt{2}}\\\frac{1}{\sqrt{2}}\end{pmatrix}\begin{pmatrix}\frac{1}{\sqrt{2}} & \frac{1}{\sqrt{2}}\end{pmatrix} = \begin{pmatrix}\frac{1}{2} & \frac{1}{2}\\\frac{1}{2} & \frac{1}{2}\end{pmatrix}$$

With these vectors (polarization states) and matrices (measurement operators) it is straight forward to reproduce the previous calculations. For example, the probability that a diagonally polarized photon will pass a vertical polarizer is calculated as follows.

$$\langle D|\hat{V}|D\rangle = \begin{pmatrix}\frac{1}{\sqrt{2}} & \frac{1}{\sqrt{2}}\end{pmatrix}\begin{pmatrix}1 & 0\\0 & 0\end{pmatrix}\begin{pmatrix}\frac{1}{\sqrt{2}}\\\frac{1}{\sqrt{2}}\end{pmatrix} = \frac{1}{2} = |\begin{pmatrix}1 & 0\end{pmatrix}\begin{pmatrix}\frac{1}{\sqrt{2}}\\\frac{1}{\sqrt{2}}\end{pmatrix}|^2$$
$$= |\langle V|D\rangle|^2 = \langle D|V\rangle\langle V|D\rangle = \langle D|\hat{V}|D\rangle$$

The density operator representing the mixture is constructed as follows,

$$\hat{\rho}_{mix} = \frac{1}{2}|V\rangle\langle V| + \frac{1}{2}|H\rangle\langle H| = \frac{1}{2}\begin{pmatrix}1 & 0\\0 & 0\end{pmatrix} + \frac{1}{2}\begin{pmatrix}0 & 0\\0 & 1\end{pmatrix} = \begin{pmatrix}\frac{1}{2} & 0\\0 & \frac{1}{2}\end{pmatrix}$$

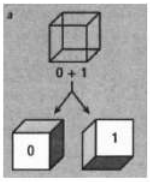
Therefore the expectation value for a 50-50 V-H mixture to pass a diagonal polarizer is as determined previously, ½.

$$\langle D|\hat{\rho}_{mix}|D\rangle = \begin{pmatrix}\frac{1}{\sqrt{2}} & \frac{1}{\sqrt{2}}\end{pmatrix}\begin{pmatrix}\frac{1}{2} & 0\\0 & \frac{1}{2}\end{pmatrix} = \begin{pmatrix}\frac{1}{\sqrt{2}}\\\frac{1}{\sqrt{2}}\end{pmatrix} = \frac{1}{2}$$

With regard to our desire for classical pictures,

> Dirac said, ...the main object of physical science is not the provision of pictures, but is the formulation of laws governing phenomena and application of these laws to the discovery of new phenomena. If a picture exists, so much the better; but whether a picture exists or not is a matter of only secondary importance. In the case of atomic phenomena no picture can be expected to exist in the usual sense of the word 'picture' by which is meant a model functioning essentially on classical lines.

In the August 2008 (page 66) issue of *Scientific American*, Monroe and Wineland attempted to provide a "picture" of the superposition with a figure of the "ambiguous" cube.



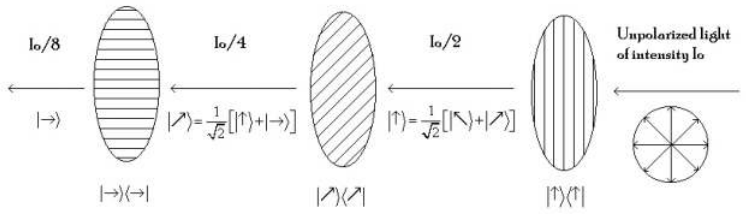
This page titled 7.11: Polarized Light and Quantum Superposition is shared under a CC BY 4.0 license and was authored, remixed, and/or curated by Frank Rioux via source content that was edited to the style and standards of the LibreTexts platform.

7.12: Polarized Light and Quantum Mechanics

Readily available and inexpensive polarizing films can be used to illustrate many fundamental quantum mechanical concepts. The purpose of this tutorial is to use polarized light to illustrate one of quantum theory's deepest and most challenging concepts - the linear superposition. According to Richard Feynman the superposition principle "has in it the heart of quantum mechanics" and is its "only mystery." *(1)*

Three Polarizer "Paradox"

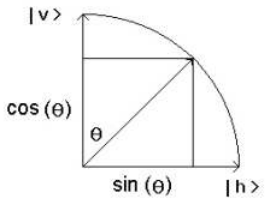
If two polarizing films are aligned in the same direction light from the first polarizer passes through the second. If the polarizers are opposed at a 90° angle, the polarized light from the first polarizer is stopped by the second. If a third polarizer is sandwiched between the two opposed polarizers at a 45° angle some light gets through the last polarizer.*(2, 3)* The analysis that follows is based on the quantum mechanical superposition principle. A graphical representation is shown below.



Quantum Mechanical Analysis

A photon polarized at an angle 2 with respect to the vertical can be written as a linear combination (superposition) of a vertically polarized photon, $|v\rangle$, and a horizontally polarized photon, $|h\rangle$. We say $|v\rangle$ and $|h\rangle$ are the polarization basis states, which means $\langle v|v\rangle = \langle h|h\rangle = 1$ and $\langle v|h\rangle = \langle h|v\rangle = 0$.

$$|\Theta\rangle = |v\rangle\langle v|\Theta\rangle + |h\rangle\langle h|\Theta\rangle$$



From this figure we see that the projections of $|\Theta\rangle$, onto $|v\rangle\langle\langle v|\Theta\rangle\rangle$ and $|h\rangle\langle\langle h|\Theta\rangle\rangle$ are $\cos\Theta$ and $\sin\Theta$, respectively.

$$|\Theta\rangle = |v\rangle\cos\Theta + |h\rangle\sin\Theta$$

The probability that a photon polarized at an angle Θ will pass a vertical polarizer is

$$|\langle v|\Theta\rangle|^2 = \cos^2\Theta$$

The light incident on the first polarizer is unpolarized, but the photons that pass the vertical polarizer are vertically polarized. In other words the photons are eigenfunctions of the measurement operator, which in this case is a vertically oriented linear polarizer. At this point only two experiments have definite outcomes.

1. The probability that vertically polarized photons will pass a second filter that is also vertically polarized is one. It is certain that a vertically polarized photon will pass a vertically polarized filter.

$$|\langle v|v\rangle|^2 = \cos^2 0 = 1$$

2. The probability that vertically polarized photons will pass a second filter that is horizontally polarized is zero. It is certain that a vertically polarized photon will not pass a horizontally polarized filter.

$$|\langle h|v\rangle|^2 = \cos^2 90 = 0$$

For any other orientation of the second filter, quantum mechanics can only predict the probability that a vertically polarized photon will pass, and that probability is, of course,

$$|\langle \Theta|v\rangle|^2 = \cos^2 \Theta$$

Now a vertically polarized photon may be written as a linear superposition of any other orthogonal basis states, for example $|45^o\rangle$, and $|-45^o\rangle$.

$$|v\rangle = |45^o\rangle\langle 45^o|v\rangle + |-45^o\rangle\langle -45^o|v\rangle \tag{7.12.1}$$

$$= |45^o\rangle \cos 45^o + |-45^o\rangle \cos 45^o \tag{7.12.2}$$

$$= |45^o\rangle 0.707 + |-45^o\rangle 0.707 \tag{7.12.3}$$

If a 45° polarizer is inserted between the vertical and horizontal polarizers photons get through the horizontal polarizer that stopped them previously. Here is the quantum mechanical explanation. The probability that a vertically polarized photon will get through a polarizer oriented at an angle of 45° is, by eqns (7), 1/2.

$$|\langle 45^o|v\rangle|^2 = \cos^2 45^o = \frac{1}{2}$$

At this point the photon is in the state $|45^o\rangle$, and according to the superposition principle a photon in this state can be written as a linear combination of $|v\rangle$ and $|h\rangle$.

$$|45^o\rangle = |v\rangle\langle v|45^o\rangle + |h\rangle\langle h + 45^o\rangle$$

$$|45^o\rangle = |v\rangle \cos 45^o + |h\rangle \sin 45^o$$

Therefore, the probability that this photon will pass the final horizontally oriented polarizer is

$$|\langle h|45^o\rangle|^2 = \sin^2 45^o = \frac{1}{2}$$

Alternatively, the probability that a photon emerging from the vertical polarizer will pass through the final horizontal polarizer in the presence of an intermediate 45° polarizer can be calculated as follows:

$$|\langle h|45^o\rangle\langle 45^o|v\rangle|^2 = |\sin^2 45^o \cos^2 45^o|^2 = \frac{1}{4}$$

In other words, half of the photons that emerge from the vertical polarizer pass the 45° polarizer, and half of those pass the final horizontal polarizer. So 25% of the photons that pass the initial vertical polarizer also pass the final horizontal polarizer.

Unpolarized Light

The unpolarized light illuminating the first polarizer is a 50-50 mixture of any orthogonal set of polarizer angles – (0°, 90°), (-45°, 45°), or in the general case $(\Theta, \Theta + \frac{\pi}{2})$.(4) A mixture cannot be represented by a single wave function, so the expectation value for a mixture of unpolarized photons to pass a vertical polarizer is calculated as follows:

$$\langle V\rangle = \sum_i p_i \langle \Psi_i|\hat{V}|\Psi_i\rangle$$

where V represents the operator associated with the vertical polarizer, and p_i is the fraction of photons in the state $|\Psi_i\rangle$.

For the general case of a beam of unpolarized light incident on a vertical polarizer the expectation value for transmission is,

$$\langle V\rangle = \frac{1}{2}\langle \Theta|\hat{V}|\Theta\rangle + \frac{1}{2}\left\langle \Theta + \frac{\pi}{2}\middle|\hat{V}\middle|\Theta + \frac{\pi}{2}\right\rangle \tag{7.12.4}$$

Since $\hat{V} = |v\rangle\langle v|$, Equation 7.12.4 can be written as,

$$\langle V\rangle = \frac{1}{2}\langle \Theta|v\rangle\langle v|\Theta\rangle + \frac{1}{2}\left\langle \Theta + \frac{\pi}{2}|v\right\rangle\left\langle v|\Theta + \frac{\pi}{2}\right\rangle$$

This expression simplifies to,

$$\langle V \rangle = \frac{1}{2}\left[\cos^2\Theta + \cos^2\left(\Theta + \frac{\pi}{2}\right)\right] = \frac{1}{2}$$

References

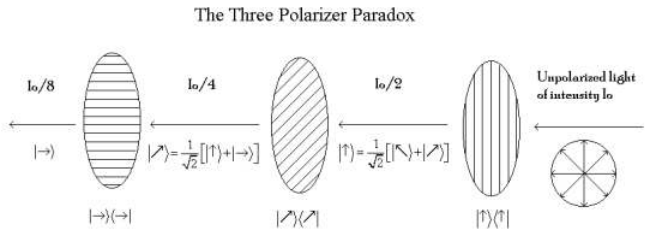
1. Feynman, R. P.; Leighton, R. B.; Sands, M. *The Feynman Lectures on Physics, Vol. 3*; Addison-Wesley: Reading, 1965
2. N. David Mermin, "Spooky Action at a Distance: Mysteries of the Quantum Theory," in *The Great Ideas Today 1988*, Encyclopedia Britannica, Inc., Chicago, pp 2-53.
3. Nick Herbert, *Quantum Reality: Beyond the New Physics*, Anchor Books, New York, 1985, pp 182-185.
4. H. J. Lipkin, *Quantum Mechanics*, North-Holland, Amsterdam, 1973, pp 12-14.

This page titled 7.12: Polarized Light and Quantum Mechanics is shared under a CC BY 4.0 license and was authored, remixed, and/or curated by Frank Rioux via source content that was edited to the style and standards of the LibreTexts platform.

7.13: The Three-Polarizer Paradox

A beam of unpolarized light illuminates a vertical polarizer and 50% of the light emerges vertically polarized. This light beam encounters a diagonal polarizer oriented at a 45 degree angle to the original vertical polarizer and 50% of it emerges as diagonally polarized light. Finally 50% of the diagonally polarized light passes a horizontally oriented polarizer. In other words 12.5% of the light illuminating the first vertical polarizer passes the final horizontal polarizer. However, if the diagonal polarizer sandwiched between the vertical and horizontal polarizers is removed, no light emerges form the final horizontal polarizer.

Using the figure below vector algebra will be used to analyze this so-called "three-polarizer paradox." The paradox being that it is surprising that the insertion of the diagonal polarizer between crossed polarizers allows photons to pass the final horizontal polarizer.



Eigenstate for a Θ-polarized photon:

$$\Theta(\theta) = (\cos\theta \sin\theta) \quad (\cos\theta \quad \sin\theta)\begin{pmatrix}\cos\theta \\ \sin\theta\end{pmatrix} simplify \rightarrow 1$$

Eigenstates for vertically, horizontally and diagonally polarized light (S (slant) represents D's orthogonal partner, just as V and H are orthogonal partners, or basis states):

$$V = \Theta(0) \rightarrow \begin{pmatrix}1 \\ 0\end{pmatrix}$$

$$H = \Theta(0)\left(\frac{\pi}{2}\right) \rightarrow \begin{pmatrix}0 \\ 1\end{pmatrix}$$

$$D = \Theta(0)\left(\frac{\pi}{4}\right) float,\ 4 \rightarrow \begin{pmatrix}0.7071 \\ 0.7071\end{pmatrix}$$

$$S = \Theta(0)\left(-\frac{\pi}{4}\right) float,\ 4 \rightarrow \begin{pmatrix}0.7071 \\ -0.7071\end{pmatrix}$$

Confirm with vector addition the superpositions shown in the figure:

$$\frac{D+S}{\sqrt{2}} = \begin{pmatrix}1 \\ 0\end{pmatrix}$$

$$\frac{D-S}{\sqrt{2}} = \begin{pmatrix}0 \\ 1\end{pmatrix}$$

$$\frac{V+H}{\sqrt{2}} = \begin{pmatrix}0.707 \\ 0.707\end{pmatrix}$$

$$\frac{V-H}{\sqrt{2}} = \begin{pmatrix}0.707 \\ -0.707\end{pmatrix}$$

The polarizers are operators, and their matrices are the outer products of their polarization vectors:

$$|\rightarrow\rangle\langle\rightarrow| \quad HH^T = \begin{pmatrix}0 & 0 \\ 0 & 1\end{pmatrix}$$

$$|\nearrow\rangle\langle\nearrow| \quad DD^T = \begin{pmatrix} 0.5 & 0.5 \\ 0.5 & 0.5 \end{pmatrix}$$

$$|\uparrow\rangle\langle\uparrow| \quad VV^T = \begin{pmatrix} 1 & 0 \\ 0 & 0 \end{pmatrix}$$

Unpolarized light is an even mixture of all polarization angles between 0 and $\frac{\pi}{2}$ radians. Probability is the absolute magnitude squared of the probability amplitude. The fraction of a beam of unpolarized light that will pass a vertically oriented polarizer is 0.5. To confirm this result we must integrate over all possible polarization angles, summing the squares of the probability amplitudes for each angle . The factor $\frac{2}{\pi}$ [(π/2)$^{-1}$] normalizes the calculation.

Probability Amplitude:

$$\langle V|\Theta\rangle \quad V^T\Theta(\theta) \rightarrow \cos\theta$$

Probability:

$$\frac{2}{\pi}\int_0^{\frac{\pi}{2}} |\langle V|\Theta\rangle|^2 d\Theta$$

$$\frac{2}{\pi}\int_0^{\frac{\pi}{2}} \left(V^T\Theta(\theta)\right)^2 d\theta = 0.5$$

As is well known, and easy to demonstrate, the probability that unpolarized light (or light of any polarization) will pass two crossed polarizing films (vertical followed by horizontal for example) is 0.

Probability Amplitude:

$$\langle H|V\rangle\langle V|\Theta\rangle \quad H^TVV^T\Theta(\theta) \rightarrow 0$$

Probability:

$$\frac{2}{\pi}\int_0^{\frac{\pi}{2}} |\langle H|V\rangle\langle V|\Theta\rangle|^2 d\Theta$$

$$\frac{2}{\pi}\int_0^{\frac{\pi}{2}} \left(H^TVV^T\Theta(\theta)\right)^2 d\theta = 0$$

However, if a polarizing film oriented diagonally at a 45 degree angle is inserted between the crossed polarizers light gets through the final horizontal filter. The following calculation shows that 12.5% of the unpolarized light illuminating the initial vertical filter gets through this arrangement of polarizing films in agreement with the figure above and experience.

Probability Amplitude:

$$\langle H|V\rangle\langle D|V\rangle\langle V|\Theta\rangle \quad H^TDD^TVV^T\Theta(\theta)\ float,\ 1 \rightarrow 0.5\cos\theta$$

Probability:

$$\frac{2}{\pi}\int_0^{\frac{\pi}{2}} |\langle H|V\rangle\langle D|V\rangle\langle V|\Theta\rangle|^2 d\Theta$$

$$\frac{2}{\pi}\int_0^{\frac{\pi}{2}} \left(|\, H^TDD^TVV^T\Theta(\theta)\,|\right)^2 d\theta = 0.125$$

The three probabilities can be also calculated by an equivalent method that explicitly treats the polarizers as measurement operators. From above we see that, $V_{op} = VV^T$, $H_{op} = HH^T$, $D_{op} = DD^T$, and write the probability calculations as follows.

$$\frac{2}{\pi}\int_0^{\frac{\pi}{2}} \left(V^TV_{op}\Theta(\theta)\right)^2 d\theta = 0.5$$

$$\frac{2}{\pi}\int_0^{\frac{\pi}{2}} \left(H^TV_{op}\Theta(\theta)\right)^2 d\theta = 0$$

$$\frac{2}{\pi}\int_0^{\frac{\pi}{2}}\left(H^T D_{op} V_{op} \Theta(\theta)\right)^2 d\theta = 0.125$$

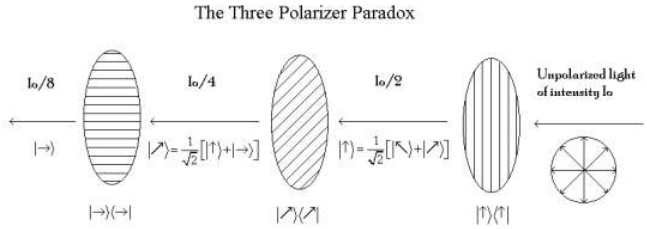
This page titled 7.13: The Three-Polarizer Paradox is shared under a CC BY 4.0 license and was authored, remixed, and/or curated by Frank Rioux via source content that was edited to the style and standards of the LibreTexts platform.

7.14: Matrix Mechanics Approach to Polarized Light

It is convenient to use matrix mechanics to describe experiments with polarized light. In this tutorial we will restrict our attention to plane polarized light. However, it would be just as easy to use matrix mechanics to describe the behavior of circularly polarized light.

The Three Polarizer Paradox

If two polarizing films are aligned in the same direction light from the first polarizer passes through the second. If the polarizers are opposed at a 90º angle, the polarized light transmitted from the first polarizer is absorbed by the second. If a third polarizer is sandwiched between the two opposed polarizers at a 45º angle some light gets through the last polarizer. This is illustrated below using Dirac notation for both the photons and the polarizers.



In what follows this demonstration is analyzed using the principles of matrix mechanics. Light polarized in the vertical and horizontal directions, and at an angle θ relative to the vertical can be represented by the following vectors,

$$|v\rangle = \begin{pmatrix} 1 \\ 0 \end{pmatrix} \quad |h\rangle = \begin{pmatrix} 0 \\ 1 \end{pmatrix} |\Theta\rangle = \begin{pmatrix} \cos\theta \\ \sin\theta \end{pmatrix}$$

The graphical representation between $|v\rangle$, $|h\rangle$ and $|\theta\rangle$ is shown below.

As can be seen in this figure, | v ⟩ and | h ⟩ represent an orthonormal basis set, and | θ ⟩ represents a general vector in the space defined by | v ⟩ and | h ⟩. As is shown below it is a normalized state vector.

$$\begin{pmatrix} \cos\theta & \sin\theta \end{pmatrix} \begin{pmatrix} \cos\theta \\ \sin\theta \end{pmatrix} = \cos^2\theta + \sin^2\theta = 1$$

Naturally | θ ⟩ can be written as a linear superposition of the polarization base states:

$$|\Theta\rangle = |v\rangle\langle v|\Theta\rangle + |h\rangle\langle h|\Theta\rangle = |v\rangle\cos\theta + |h\rangle\sin\theta$$

A polarizing filter (film) oriented in the veritcal direction in this basis can be represented by the following matrix operator.

$$\hat{V} = \begin{pmatrix} 1 & 0 \\ 0 & 0 \end{pmatrix}$$

Note the results of the following measurements on the three previously defined polarization states using this measurement operator.

$$\begin{pmatrix} 1 & 0 \\ 0 & 0 \end{pmatrix} \begin{pmatrix} 1 \\ 0 \end{pmatrix} = \begin{pmatrix} 1 \\ 0 \end{pmatrix}$$

$$\begin{pmatrix} 1 & 0 \\ 0 & 0 \end{pmatrix} \begin{pmatrix} 0 \\ 1 \end{pmatrix} = \begin{pmatrix} 0 \\ 0 \end{pmatrix}$$

$$\begin{pmatrix} 1 & 0 \\ 0 & 0 \end{pmatrix} \begin{pmatrix} \cos\theta \\ \sin\theta \end{pmatrix} = \begin{pmatrix} \cos\theta \\ 0 \end{pmatrix}$$

Vertically polarized light passes the vertical polarizer, horizontally polarized light is absorbed (annihilated), and θ-polarized light, if it passes, becomes vertically polarized with reduced intensity. The probability that it will pass the vertical polarizer is $\cos^2\theta$.

The operators associated with a horizontal filter and a filter oriented at an angle θ relative to the vertical are given below.

$$\hat{H} = \begin{pmatrix} 0 & 0 \\ 0 & 1 \end{pmatrix}$$

$$\hat{\Theta} = \begin{pmatrix} \cos^2\theta & \sin\theta\cos\theta \\ \sin\theta\cos\theta & \sin^2\theta \end{pmatrix}$$

The operator associated with a filter oriented at an angle θ relative to the vertical is generated as shown below.

$$\hat{\theta} = |\theta\rangle\langle\theta| = \begin{pmatrix} \cos\theta \\ \sin\theta \end{pmatrix} (\cos\theta \quad \sin\theta) = \begin{pmatrix} \cos^2\theta & \cos\theta\sin\theta \\ \sin\theta\cos\theta & \sin^2\theta \end{pmatrix}$$

We now have the mathematical apparatus in place to examine the three-polarizer paradox using the basic principles of matrix mechanics. Unpolarized light, such as that coming from an incandecent light bulb, might be considered to be a mixture of all polarization angles between 0 and π radians. Assuming this, the probability amplitude that a θ-polarized photon will pass a vertically oriented filter is,

$$(1 \quad 0) \begin{pmatrix} 1 & 0 \\ 0 & 0 \end{pmatrix} \begin{pmatrix} \cos\theta \\ \sin\theta \end{pmatrix}$$

The probability is the square of the absolute magnitude of the probability amplitude. Thus the fraction of a beam of unpolarized photons that will pass a vertically oriented polarizer is 0.5. To achieve this result we must integrate over all possible polarization angles. The normalization constant for this calculation is 2/π.

$$\frac{2}{\pi}\int_0^{\frac{\pi}{2}} \left| (1 \quad 0) \begin{pmatrix} 1 & 0 \\ 0 & 0 \end{pmatrix} \begin{pmatrix} \cos\theta \\ \sin\theta \end{pmatrix} \right|^2 d\theta = 0.5$$

As is well known, and easy to demonstrate, the probability that unpolarized light (or light of any polarization) will pass two crossed polarizing films (vertical followed by horizontal, for example) is zero.

$$\frac{2}{\pi}\int_0^{\frac{\pi}{2}} \left| (0 \quad 1) \begin{pmatrix} 0 & 0 \\ 0 & 1 \end{pmatrix} \begin{pmatrix} 1 & 0 \\ 0 & 0 \end{pmatrix} \begin{pmatrix} \cos\theta \\ \sin\theta \end{pmatrix} \right|^2 d\theta = 0$$

However, if a polarizing film oriented at a 45° angle is inserted between the crossed polarizers light gets through the final horizontal filter. The operator for a 45° polarizer is obtained as follows:

$$\theta = \frac{\pi}{4}$$

$$\hat{\Theta} = \begin{pmatrix} \cos^2\theta & \sin\theta\cos\theta \\ \sin\theta\cos\theta & \sin^2\theta \end{pmatrix} = \begin{pmatrix} \frac{1}{2} & \frac{1}{2} \\ \frac{1}{2} & \frac{1}{2} \end{pmatrix}$$

The following calculation shows that 12.5% of the unpolarized light illuminating the initial vertical polarizer is transmitted through this arrangement of polarizing films.

$$\frac{2}{\pi}\int_0^{\frac{\pi}{2}} \left| (0 \quad 1) \begin{pmatrix} 0 & 0 \\ 0 & 1 \end{pmatrix} \begin{pmatrix} \frac{1}{2} & \frac{1}{2} \\ \frac{1}{2} & \frac{1}{2} \end{pmatrix} \begin{pmatrix} 1 & 0 \\ 0 & 0 \end{pmatrix} \begin{pmatrix} \cos\theta \\ \sin\theta \end{pmatrix} \right|^2 d\theta = 0.125$$

It is easy to see that if the positions of the diagonal and horizontal polarizers are interchanged no light would be transmitted because the first and second polarizers would be crossed. This illustrates that the horizontal and diagonal polarization measurements do not commute; the outcome is dependent on the order of the measurements.

$$\frac{2}{\pi}\int_0^{\frac{\pi}{2}} \left| (0 \quad 1) \begin{pmatrix} \frac{1}{2} & \frac{1}{2} \\ \frac{1}{2} & \frac{1}{2} \end{pmatrix} \begin{pmatrix} 0 & 0 \\ 0 & 1 \end{pmatrix} \begin{pmatrix} 1 & 0 \\ 0 & 0 \end{pmatrix} \begin{pmatrix} \cos\theta \\ \sin\theta \end{pmatrix} \right|^2 d\theta = 0$$

This page titled 7.14: Matrix Mechanics Approach to Polarized Light is shared under a CC BY 4.0 license and was authored, remixed, and/or curated by Frank Rioux via source content that was edited to the style and standards of the LibreTexts platform.

7.15: Matrix Mechanics Approach to Polarized Light - Version 2

It is convenient and illustrative of quantum mechanical principles to use matrix mechanics to describe experiments with polarized light. In this tutorial we will restrict our attention to plane polarized light. However, it would be just as easy to use matrix mechanics to describe the behavior of circularly polarized light (see appendix).

In matrix mechanics we use vectors to represent states and matrices to represent measurement operator Light polarized in the vertical and horizontal directions will serve as base states and will be represented the following vectors. As will be shown shortly any other polarization state can be written as a linear superposition of these basis vectors.

$$v = \begin{pmatrix} 1 \\ 0 \end{pmatrix} \quad h = \begin{pmatrix} 0 \\ 1 \end{pmatrix}$$

$$\begin{pmatrix} 1 & 0 \end{pmatrix} \begin{pmatrix} 1 \\ 0 \end{pmatrix} \rightarrow 1 \quad \begin{pmatrix} 0 & 1 \end{pmatrix} \begin{pmatrix} 0 \\ 1 \end{pmatrix} \rightarrow 1 \quad \begin{pmatrix} 1 & 0 \end{pmatrix} \begin{pmatrix} 0 \\ 1 \end{pmatrix} \rightarrow 0$$

$$v^T v \rightarrow 1 \quad h^T h \rightarrow 1 \quad v^T h \rightarrow 0$$

Note from above that |v> and |h> form an orthonormal basis set for this two-dimensional vector space. Light polarized at an angle θ relative to the verticle can be written as

$$\Theta(\theta) = \begin{pmatrix} \cos\theta \\ \sin\theta \end{pmatrix}$$

It is easy to show that this state is normalized

$$\begin{pmatrix} \cos\theta & \sin\theta \end{pmatrix} \begin{pmatrix} \cos\theta \\ \sin\theta \end{pmatrix} \rightarrow \cos\theta^2 + \sin\theta^2 simplify \rightarrow 1$$

In addition, $|\theta\rangle$ can be written as a linear superposition of the polarization base states:

$$|\theta\rangle = |v\rangle\langle v|\theta\rangle + |h\rangle\langle h|\theta\rangle = |v\rangle\cos\theta + |h\rangle\sin\theta$$

$$v\cos\theta + h\sin\theta \rightarrow \begin{pmatrix} \cos\theta \\ \sin\theta \end{pmatrix}$$

A polarizing filter oriented in the vertical position in this basis can be represented by the following mat operator - |v><v|.

$V_{op} = \begin{pmatrix} 1 \\ 0 \end{pmatrix} \begin{pmatrix} 1 & 0 \end{pmatrix} \rightarrow \begin{pmatrix} 1 & 0 \\ 0 & 0 \end{pmatrix}$ which can also be accomplished this way $vv^T \rightarrow \begin{pmatrix} 1 & 0 \\ 0 & 0 \end{pmatrix}$

Note the results of the following measurements on the three defined polarization states using this operator

$$\begin{pmatrix} 1 & 0 \\ 0 & 0 \end{pmatrix} \begin{pmatrix} 1 \\ 0 \end{pmatrix} \rightarrow \begin{pmatrix} 1 \\ 0 \end{pmatrix}$$

$$\begin{pmatrix} 1 & 0 \\ 0 & 0 \end{pmatrix} \begin{pmatrix} 0 \\ 1 \end{pmatrix} \rightarrow \begin{pmatrix} 0 \\ 0 \end{pmatrix}$$

$$\begin{pmatrix} 1 & 0 \\ 0 & 0 \end{pmatrix} \begin{pmatrix} \cos\theta \\ \sin\theta \end{pmatrix} \rightarrow \begin{pmatrix} \cos\theta \\ 0 \end{pmatrix}$$

$$V_{op} v \rightarrow \begin{pmatrix} 1 \\ 0 \end{pmatrix}$$

$$V_{op} h \rightarrow \begin{pmatrix} 0 \\ 0 \end{pmatrix}$$

$$V_{op} \Theta(\theta) \rightarrow \begin{pmatrix} \cos\theta \\ 0 \end{pmatrix}$$

Vertically polarized light passes the vertical polarizer, horizontally polarized light is absorbed (anihilated and θ-polarized light, if it passes, becomes vertically polarized with reduced intensity. The probability will pass the vertical polarizer is $\cos^2\theta$. The operators

associated with a horizontal filter and a filter oriented at an angle θ relative to the vertical shown below. The latter is, of course, general and can be used to represent any operator by putting in the appropriate value for θ as is shown below.

$$H_{op} = \begin{pmatrix} 0 \\ 1 \end{pmatrix} \begin{pmatrix} 0 & 1 \end{pmatrix} \rightarrow \begin{pmatrix} 0 & 0 \\ 0 & 1 \end{pmatrix}$$

$$\Theta_{op}(\theta) = \begin{pmatrix} \cos\theta \\ \sin\theta \end{pmatrix} \begin{pmatrix} \cos\theta & \sin\theta \end{pmatrix} \rightarrow \begin{pmatrix} \cos\theta^2 & \cos\theta\sin\theta \\ \cos\theta\sin\theta & \sin\theta^2 \end{pmatrix}$$

The operators for vertical, diagonal and horizontal polarizers are shown below using the general operator

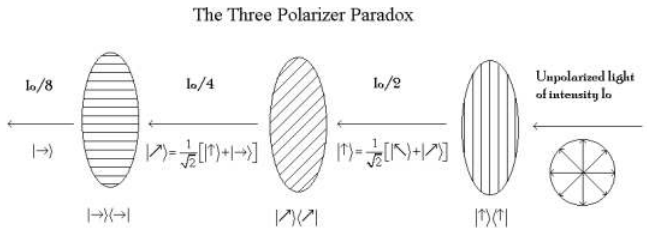
$$\Theta_{op}(0) \rightarrow \begin{pmatrix} 1 & 0 \\ 0 & 0 \end{pmatrix}$$

$$\Theta_{op}\left(\frac{\pi}{4}\right) \; float, \; 1 \rightarrow \begin{pmatrix} 0.5 & 0.5 \\ 0.5 & 0.5 \end{pmatrix}$$

$$\Theta_{op}\left(\frac{\pi}{2}\right) \rightarrow \begin{pmatrix} 0 & 0 \\ 0 & 1 \end{pmatrix}$$

We now examine the three polarizer paradox illustrated in the figure below. Unpolarized light illuminates vertical polarizer and 50% of the light emerges as vertically polarized light. This light encounters a diagonal polarizer oriented at a 45^o angle to the original vertical polarizer and 50% of it emerges as diagonally polarized light. Finally 50% of the diagonally polarized light passes a horizontally oriented polarizer. In other words 12.5% of the light illuminating the first vertical polarizer passes the final horizontal polarizer. However, if the diagonal polarizer sandwiched between the vertical and horizontal polarizers is remove no light emerges form the final horizontal polarizer.

Matrix mechanics will now be used to examine the so-called "three polarizer paradox." Please note that figure offers an alternative analysis based on Dirac bracket notation and the superposition principle.



Unpolarized light, such as that coming from an incandescent light bulb, might be considered to be an be mixture of all polarization angles between 0 and $\frac{\pi}{2}$ radians. The probability amplitude that a θ-polarized photon will pass a vertical filter is

$$\begin{pmatrix} 1 & 0 \end{pmatrix} \begin{pmatrix} 1 & 0 \\ 0 & 0 \end{pmatrix} \begin{pmatrix} \cos\theta \\ \sin\theta \end{pmatrix}$$

The probability is the square of the absolute magnitude of the probability amplitude. Thus the fraction of a beam of unpolarized light that will pass a vertically oriented polarizer is 0.5. To achieve this result we must integrate over all possible polarization angles. The factor $2/\pi$ $[(\pi/2)^{-1}]$ normalizes the calculation.

$$\frac{2}{\pi}\int_0^{\frac{\pi}{2}} \left[\begin{pmatrix} 1 & 0 \end{pmatrix} \begin{pmatrix} 1 & 0 \\ 0 & 0 \end{pmatrix} \begin{pmatrix} \cos\theta \\ \sin\theta \end{pmatrix} \right]^2 d\theta = 0.5$$

$$\frac{2}{\pi}\int_0^{\frac{\pi}{2}} \left(v^T V_{op} \Theta(\theta) \right)^2 d\theta = 0.5$$

As is well known, and easy to demonstrate, the probability that unpolarized light (or light of any polarization) will pass two crossed polarizing films (vertical followed by horizontal for example) is 0.

$$\frac{2}{\pi}\int_0^{\frac{\pi}{2}} \left[\begin{pmatrix} 0 & 1 \end{pmatrix} \begin{pmatrix} 0 & 0 \\ 0 & 1 \end{pmatrix} \begin{pmatrix} 1 & 0 \\ 0 & 0 \end{pmatrix} \begin{pmatrix} \cos\theta \\ \sin\theta \end{pmatrix} \right]^2 d\theta = 0$$

$$\frac{2}{\pi}\int_0^{\frac{\pi}{2}}\left(v^T H_{op} V_{op}\Theta(\theta)\right)^2 d\theta = 0.5$$

However, if a polarizing film oriented diagonally at a 45° angle is inserted between the crossed polarizers light gets through the final horizontal filter. The operator for a 45° polarizer is obtained from Θ_{op}.

$$\Theta_{op}\frac{\pi}{4} = \begin{pmatrix} 0.5 & 0.5 \\ 0.5 & 0.5 \end{pmatrix}$$

The following calculation shows that 12.5% of the unpolarized light illuminating the initial vertical filter gets through this arrangement of polarizing films in agreement with the figure above and experience.

$$\frac{2}{\pi}\int_0^{\frac{\pi}{2}}\left[\begin{pmatrix}0 & 1\end{pmatrix}\begin{pmatrix}0 & 0\\ 0 & 1\end{pmatrix}\begin{pmatrix}0.5 & 0.5\\ 0.5 & 0.5\end{pmatrix}\begin{pmatrix}1 & 0\\ 0 & 0\end{pmatrix}\begin{pmatrix}\cos\theta\\ \sin\theta\end{pmatrix}\right]^2 d\theta = 0.125$$

$$\frac{2}{\pi}\int_0^{\frac{\pi}{2}}\left(h^T\Theta_{op}\frac{\pi}{2}\Theta_{op}\frac{\pi}{4}\Theta_{op}(0)\Theta(\theta)\right)^2 d\theta \to \frac{1}{8}$$

In addition, the non-commutivity rule can be demonstrated by switching the second and third filters. When this is done no photons emerge from the apparatus for obvious reasons; the first two filters are crossed.

$$\frac{2}{\pi}\int_0^{\frac{\pi}{2}}\left[\begin{pmatrix}0 & 1\end{pmatrix}\begin{pmatrix}0.5 & 0.5\\ 0.5 & 0.5\end{pmatrix}\begin{pmatrix}0 & 0\\ 0 & 1\end{pmatrix}\begin{pmatrix}1 & 0\\ 0 & 0\end{pmatrix}\begin{pmatrix}\cos\theta\\ \sin\theta\end{pmatrix}\right]^2 d\theta = 0$$

$$\frac{2}{\pi}\int_0^{\frac{\pi}{2}}\left(h^T\Theta_{op}\frac{\pi}{4}\Theta_{op}\frac{\pi}{2}\Theta_{op}(0)\Theta(\theta)\right)^2 d\theta \to 0$$

Appendix:

The base states for circularly polarized light are given below, along with their superpositions in the h-v representation.

$$L = \frac{1}{\sqrt{2}}\begin{pmatrix}1\\ i\end{pmatrix} \quad \frac{1}{\sqrt{2}}(v+ih) = \begin{pmatrix}0.707\\ 0.707i\end{pmatrix}$$

$$R = \frac{1}{\sqrt{2}}\begin{pmatrix}1\\ -i\end{pmatrix} \quad \frac{1}{\sqrt{2}}(v-ih) = \begin{pmatrix}0.707\\ -0.707i\end{pmatrix}$$

Left and right circularly polarized light also form an orthonormal basis set.

$$\overline{L^T}L \to 1$$

$$\overline{R^T}R \to 1$$

$$\overline{L^T}R \to 0$$

$$\overline{R^T}L \to 0$$

The appropriate operators are:

$$L_{op} = L\overline{L^T}\ float,\ 1 \to \begin{pmatrix}0.5 & -0.5i\\ 0.5i & 0.5\end{pmatrix}$$

$$R_{op} = R\overline{R^T}\ float,\ 1 \to \begin{pmatrix}0.5 & 0.5i\\ -0.5i & 0.5\end{pmatrix}$$

Vertically and horizontally polarized light can be written as superpositions of circularly polarized light

$$v = \frac{1}{\sqrt{2}}(L+R) \to \begin{pmatrix}1\\ 0\end{pmatrix}$$

$$h = \frac{i}{\sqrt{2}}(R-L) \to \begin{pmatrix}0\\ 1\end{pmatrix}$$

Earlier unpolarized light was considered to be an even mixture of all polarization angles between 0^o and Another approach is to consider it to be a 50-50 mixture of any two orthogonal polarization angles. The expectation value for unpolarized light passing a vertical polarizer under this model is outlined below.

$$\langle V\rangle = \sum_i p_i \langle\psi_i|\hat{V}|\psi_i\rangle = \frac{1}{2}\langle\Theta|\hat{V}|\Theta\rangle + \frac{1}{2}\left\langle\Theta+\frac{\pi}{2}\right|\hat{V}\left|\Theta+\frac{\pi}{2}\right\rangle$$
$$= \frac{1}{2}\langle\Theta|v\rangle\langle v|\Theta\rangle + \frac{1}{2}\left\langle\Theta+\frac{\pi}{2}|v\right\rangle\left\langle v|\Theta+\frac{\pi}{2}\right\rangle$$

Just as calculated earlier 50% of the unpolarized light passes the vertical polarizer.

$$\frac{1}{2}\Theta(\theta)^T V_{op}\Theta(\theta) + \frac{1}{2}\Theta\left(\theta+\frac{\pi}{2}\right)V_{op}\Theta\left(\theta+\frac{\pi}{2}\right)\ simplify \rightarrow \frac{1}{2}$$

Unpolarized light can also be represented by the density operator shown below.

$$\hat{\rho} = \frac{1}{2}|\Theta\rangle\langle\Theta| + \frac{1}{2}\left|\Theta+\frac{\pi}{2}\right\rangle\left\langle\Theta+\frac{\pi}{2}\right|$$

$$\rho = \frac{1}{2}\Theta_{op}(\theta) + \frac{1}{2}\Theta_{op}\left(\theta+\frac{\pi}{2}\right)\ simplify\ \rightarrow \begin{pmatrix}\frac{1}{2} & 0\\ 0 & \frac{1}{2}\end{pmatrix}$$

It is not difficult to show that the expectation value for unpolarized light passing a verticle polarizer can be calculated as the trace of the product of this operator with the vertical polarization operator.

$$Tr\left[\left(\frac{1}{2}|\theta\rangle\langle\Theta\left|\Theta+\frac{\pi}{2}\right\rangle\left\langle\Theta+\frac{\pi}{2}\right|\right)\hat{V}\right] = \frac{1}{2}$$

$$tr(\rho V_{op})\ simplify\ \rightarrow \frac{1}{2}$$

Of course there is nothing special about the vertical direction. Unpolarized light has a 50% probability passing a polarizer of any other orientation.

$$tr(\rho H_{op}) = 0.5$$

$$tr(\rho L_{op}) = 0.5$$

$$tr(\rho R_{op}) = 0.5$$

$$tr\left(\rho\Theta_{op}\left(\frac{\pi}{3}\right)\right) = 0.5$$

$$tr\left(\rho\Theta_{op}\left(\frac{\pi}{4}\right)\right) = 0.5$$

$$tr\left(\rho\Theta_{op}\left(\frac{\pi}{8}\right)\right) = 0.5$$

In other words, the intensity of light passing a polarizer from an unpolarized source is independent of t orientation of the polarizer. Finally, the result of the three-polarizer demonstration is recalculated using the density matrix approach.

$$D_{op} = \Theta\left(\frac{\pi}{4}\right)$$

$$tr(H_{op}D_{op})tr(D_{op}V_{op})tr(V_{op}\rho) \rightarrow \frac{1}{8}$$

This page titled 7.15: Matrix Mechanics Approach to Polarized Light - Version 2 is shared under a CC BY 4.0 license and was authored, remixed, and/or curated by Frank Rioux via source content that was edited to the style and standards of the LibreTexts platform.

7.16: Matrix Mechanics Exercises Using Polarized Light

Eigenstates and operators are provided for a series of matrix mechanics exercises involving polarized light.

Eigenstate for a θ-polarized light:

$$\Theta(\theta) = \begin{pmatrix} \cos\theta \\ \sin\theta \end{pmatrix}$$

$$\begin{pmatrix} \cos\theta & \sin\theta \end{pmatrix} \begin{pmatrix} \cos\theta \\ \sin\theta \end{pmatrix} \; simplify \; \rightarrow 1$$

$$|\theta\rangle = \begin{pmatrix} \cos\theta \\ \sin\theta \end{pmatrix}$$

$$\langle\theta|\theta\rangle = \begin{pmatrix} \cos\theta & \sin\theta \end{pmatrix} \begin{pmatrix} \cos\theta \\ \sin\theta \end{pmatrix} = 1$$

Operator for a θ-oriented polarizer:

$$\Theta_{op}(\theta) = \begin{pmatrix} \cos\theta \\ \sin\theta \end{pmatrix} \begin{pmatrix} \cos\theta & \sin\theta \end{pmatrix} \rightarrow \begin{pmatrix} \cos\theta^2 & \cos\theta\sin\theta \\ \cos\theta & \sin\theta^2 \end{pmatrix}$$

$$\hat{\Theta}|\theta\rangle\langle\theta| = \begin{pmatrix} \cos\theta \\ \sin\theta \end{pmatrix} \begin{pmatrix} \cos\theta & \sin\theta \end{pmatrix}$$

Eigenstates for vertically, horizontally, and diagonally polarized light:

Vertically:

$$V = \Theta(0) \rightarrow \begin{pmatrix} 1 \\ 0 \end{pmatrix}$$

$$V^T \rightarrow \begin{pmatrix} 1 & 0 \end{pmatrix}$$

$$|V\rangle = \begin{pmatrix} 1 \\ 0 \end{pmatrix} \quad \langle V| = \begin{pmatrix} 1 & 0 \end{pmatrix}$$

Horizontally:

$$H = \Theta\left(\frac{\pi}{2}\right) \rightarrow \begin{pmatrix} 0 \\ 1 \end{pmatrix}$$

$$H^T \rightarrow \begin{pmatrix} 0 & 1 \end{pmatrix}$$

$$|H\rangle = \begin{pmatrix} 0 \\ 1 \end{pmatrix} \quad \langle H| = \begin{pmatrix} 0 & 1 \end{pmatrix}$$

Diagonally:

$$D = \Theta\left(\frac{\pi}{4}\right) \; float, \; 4 \; \rightarrow \begin{pmatrix} 0.7071 \\ 0.7071 \end{pmatrix}$$

$$D^T \rightarrow \begin{pmatrix} 0.7071 & 0.7071 \end{pmatrix}$$

$$|D\rangle = \begin{pmatrix} 0.707 \\ 0.707 \end{pmatrix} \quad \langle D| = \begin{pmatrix} 0.707 & 0.707 \end{pmatrix}$$

Operators for vertically, horizontally, and diagonally oriented polarizers:

Vertically:

$$V_{op} = \Theta_{op}(0) \rightarrow \begin{pmatrix} 1 & 0 \\ 0 & 0 \end{pmatrix}$$

$$\hat{V} = |V\rangle\langle V|$$

Horizontally:

$$H_{op} = \Theta_{op}\left(\frac{\pi}{2}\right) \rightarrow \begin{pmatrix} 0 & 0 \\ 0 & 1 \end{pmatrix}$$

$$\hat{H} = |H\rangle\langle H|$$

Diagonally:

$$D_{op} = \Theta_{op}\left(\frac{\pi}{4}\right)\ float,\ 1\ \rightarrow \begin{pmatrix} 0.5 & 0.5 \\ 0.5 & 0.5 \end{pmatrix}$$

$$\hat{D} = |D\rangle\langle D|$$

Demonstrate that a θ-polarized photon is an eigenfunction of a θ-oriented polarizer, with eigenvalue 1.

$$\begin{pmatrix} \cos\theta^2 & \cos\theta\sin\theta \\ \cos\theta\sin\theta & \sin\theta^2 \end{pmatrix}\begin{pmatrix} \cos\theta \\ \sin\theta \end{pmatrix}\ simplify \rightarrow \begin{pmatrix} \cos\theta \\ \sin\theta \end{pmatrix}$$

$$\hat{\Theta}|\theta\rangle = |\theta\rangle$$

or

$$\Theta_{op}(\theta)\Theta(\theta) simplify\ \rightarrow \begin{pmatrix} \cos\theta \\ \sin\theta \end{pmatrix}$$

Demonstrate that a θ-polarized photon is a linear superposition of the vertical and horizontal polarization states.

$$\cos\theta\begin{pmatrix} 1 \\ 0 \end{pmatrix} + \sin\theta\begin{pmatrix} 0 \\ 1 \end{pmatrix} \rightarrow \begin{pmatrix} \cos\theta \\ \sin\theta \end{pmatrix}$$

Demonstrate that a vertically polarized photon is a linear superposition of the $\pi/4$ and -$\pi/4$ polarization states.

$$\frac{1}{\sqrt{2}}\left[\begin{pmatrix} \cos\frac{\pi}{4} \\ \sin\frac{\pi}{4} \end{pmatrix} + \begin{pmatrix} \cos\frac{\pi}{4} \\ \sin\frac{-\pi}{4} \end{pmatrix}\right] \rightarrow \begin{pmatrix} 1 \\ 0 \end{pmatrix}$$

Calculate the probability amplitude and probability that a $\pi/3$ (60 degree) polarized photon will pass a vertical polarizer.

$$V^T\Theta\frac{\pi}{3} = 0.5$$

$$\left(\left|V^T\Theta\left(\frac{\pi}{3}\right)\right|\right) = 0.25$$

or

$$\Theta\left(\frac{\pi}{3}\right)^T V_{op}\Theta\left(\frac{\pi}{3}\right) = 0.25$$

$$\left\langle V|\frac{\pi}{3}\right\rangle = 0.5$$

$$\left|\left\langle V|\frac{\pi}{3}\right\rangle\right|^2 = 0.5$$

$$\left\langle\frac{\pi}{3}\left|\hat{V}\right|\frac{\pi}{3}\right\rangle = \left\langle\frac{\pi}{3}|V\right\rangle\left\langle V|\frac{\pi}{3}\right\rangle = \left|\left\langle V|\frac{\pi}{3}\right\rangle\right|^2 = 0.25$$

Calculate the probability amplitude and probability that vertically polarized photon will pass a $\pi/3$ (60 degree) polarizer.

$$\Theta\left(\frac{\pi}{3}\right)V = 0.5$$

$$\left(\left|\Theta\left(\frac{\pi}{3}\right)^T V\right|\right)^2 = 0.25$$

or

$$V^T \Theta_{op} \left(\frac{\pi}{3}\right) V = 0.25$$

Calculate the probability amplitude and probability that a π/3 (60 degree) polarized photon will pass a diagonal polarizer.

$$D^T \Theta \left(\frac{\pi}{3}\right) = 0.966$$

$$\left(\left| D^T \Theta \left(\frac{\pi}{3}\right)\right|\right)^2 = 0.933$$

or

$$\Theta \left(\frac{\pi}{3}\right) D_{op} \Theta \left(\frac{\pi}{3}\right) = 0.933$$

Calculate the probability that a π/3 (60 degree) polarized photon will pass the following sequence of polarizers: vertical, diagonal, horizontal.

$$\left(\left| H^T H_{op} D_{op} V_{op} \Theta \left(\frac{\pi}{3}\right)\right|\right)^2 = 0.063$$

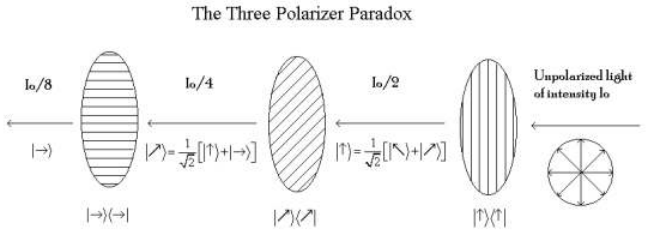
$$\left|\langle H | \hat{H} \hat{D} \hat{V} \left| \frac{\pi}{3} \right\rangle\right|^2 = 0.063$$

Calculate the probability that a π/3 (60 degree) polarized photon will pass the following sequence of polarizers: vertical, horizontal, diagonal. Explain the result.

$$\left(\left| D^T D_{op} H_{op} V_{op} \Theta \left(\frac{\pi}{3}\right)\right|\right)^2 = 0$$

With this sequence the first two polarizers are crossed (have a 90 degree relative angle). Thus the vertically polarized photon emerging from the first polarizer is stopped by the second polarizer.

Confirm the results shown in the diagram shown below. In other words, show that 12.5% of the incident unpolarized light will pass an arrangement of vertical, diagonal and horizontal polarizers.



$$\frac{2}{\pi} \int_0^{\frac{\pi}{2}} \left(\left| H^T H_{op} D_{op} V_{op} \Theta(\theta 0)\right|\right)^2 d\theta = 0.125$$

$$\frac{2}{\pi} \int_0^{\frac{\pi}{2}} |\langle H | \hat{H} \hat{D} \hat{V} | \theta \rangle|^2 d\theta$$

This calculation can also be performed assuming that unpolarized light is a 50-50 mixture of vertically and horizontally polarized light.

$$\frac{1}{2}(|H^T H_{op} D_{op} V_{op} V|)^2 + \frac{1}{2}(|H^T H_{op} D_{op} V_{op} H|)^2 = 0.125$$

Now a π/6 polarizer is placed between the vertical and diagonal polarizers, and a π/3 polarizer is placed between the diagonal and horizontal polarizer. Calculate the fraction of light that emerges from the final horizontal polarizer and explain the result.

$$\frac{2}{\pi} \int_0^{\frac{\pi}{2}} \left(\left| H^T H_{op} \Theta_{op} \left(\frac{\pi}{3}\right) D_{op} \Theta_{op} \left(\frac{\pi}{6}\right) V_{op} \Theta(\theta)\right|\right)^2 d\theta = 0.245$$

This calculation can also be performed assuming that unpolarized light is a 50-50 mixture of vertically and horizontally polarized light.

$$\frac{1}{2}\left(\left|H^T H_{op}\Theta_{op}\left(\frac{\pi}{3}\right)D_{op}\Theta_{op}\left(\frac{\pi}{6}\right)V_{op}V\right|\right)^2+\frac{1}{2}\left(\left|H^T H_{op}\Theta_{op}\left(\frac{\pi}{3}\right)D_{op}\Theta_{op}\left(\frac{\pi}{6}\right)V_{op}H\right|\right)^2=0.245$$

The initial and final polarizers are crossed and will not transmit light. A single p/4 polarizer sandwiched in between allows light through for the reasons presented earlier. The addition of two more polarizers increases the fraction of transmitted light because the relative angles between successive polarizers has been reduced. Significantly more light gets through each set of polarizers because the angle between them is smaller.

Calculate the probability that unpolarized light will pass the following sequence of polarizers: vertical, π/3 (60 degree), diagonal.

$$\frac{2}{\pi}\int_0^{\frac{\pi}{2}}\left(\left|D^T D_{op}\Theta_{op}\left(\frac{\pi}{3}\right)V_{op}\Theta(\theta)\right|\right)^2 d\theta=0.117$$

or

$$\frac{2}{\pi}\int_0^{\frac{\pi}{2}}\left(\left|D^T \Theta_{op}\left(\frac{\pi}{3}\right)V_{op}\Theta(\theta)\right|\right)^2 d\theta=0.117$$

Calculate the probability that unpolarized light will pass the following sequence of polarizers: vertical, diagonal, π/3 (60 degree). Explain the difference in the results.

$$\frac{2}{\pi}\int_0^{\frac{\pi}{2}}\left(\left|\Theta\left(\frac{\pi}{3}\right)^T\Theta_{op}\left(\frac{\pi}{3}\right)D_{op}V_{op}\Theta(\theta)\right|\right)^2 d\theta=0.233$$

or

$$\frac{2}{\pi}\int_0^{\frac{\pi}{2}}\left(\left|\Theta\left(\frac{\pi}{3}\right)^T D_{op}V_{op}\Theta(\theta)\right|\right)^2 d\theta=0.233$$

The operators representing the measurement of diagonal and 60 degree polarization do not commute.

Calculate the polarization of the incident photon such that the probability it will pass three polarizers (vertical, horizontal, diagonal) is 0.10

$$\theta=75\ deg$$

Given

$$\left(\left|H^T H_{op}D_{op}V_{op}\Theta(\theta)\right|\right)^2=.10$$

Find (θ) = 50.768 deg

The next few exercises involve circularly polarized light.

The base states for circularly polarized light are:

$$L=\frac{1}{\sqrt{2}}\begin{pmatrix}1\\ i\end{pmatrix}$$

$$R=\frac{1}{\sqrt{2}}\begin{pmatrix}1\\ -i\end{pmatrix}$$

Show that they form an orthonormal basis set:

$$\overline{L^T}L\rightarrow 1$$

$$\overline{R^T}R\rightarrow 1$$

$$\overline{L^T}R\rightarrow 0$$

$$\overline{R^T}L\rightarrow 0$$

Show that they are linear superpositions of the vertical and horizontal polarization states:

\[\frac{1}{ \sqrt{2}}\ (V + iH) =

$$\begin{pmatrix} 0.707 \\ 0.707i \end{pmatrix} \tag{7.16.1}$$

]

\[\frac{1}{ \sqrt{2}}\ (V - iH) =

$$\begin{pmatrix} 0.707 \\ -0.707i \end{pmatrix} \tag{7.16.2}$$

]

Show that vertically and horizontally polarized light can be written as superpositions of circularly polarized light:

\[\frac{1}{ \sqrt{2}}\ (L + R) =

$$\begin{pmatrix} 1 \\ 0 \end{pmatrix} \tag{7.16.3}$$

]

\[\frac{i}{ \sqrt{2}}\ (R - L) =

$$\begin{pmatrix} 0 \\ 1 \end{pmatrix} \tag{7.16.4}$$

]

T**he angular momentum operator in atomic units is**:

$$Pang = \begin{pmatrix} 0 & -i \\ i & 0 \end{pmatrix}$$

Calculate the expectation value for angular momentum for a vertical, horizontal and diagonal polarized photon.

$$V^T Pang(V) = 0$$

$$H^T Pang(H) = 0$$

$$D^T Pang(D) = 0$$

Calculate the expectation value for angular momentum for a θ polarized photon.

$$\Theta(\theta)^T Pang \Theta(\theta) = 0$$

Calculate the expectation value for angular momentum for left and right circularly polarized photons.

$$\overline{L^T} Pang(L) = 1$$

$$\overline{R^T} Pang(R) = -1$$

The remaining exercises deal with the effects of half and quarter wave plates.

The remaining exercises deal with the effects of half and quarter wave plates.

$$W_2 = \begin{pmatrix} 1 & 0 \\ 0 & -1 \end{pmatrix}$$

$$W_2(\theta) = \begin{pmatrix} \cos(2\theta) & \sin(2\theta) \\ \sin(2\theta) & -\cos(2\theta) \end{pmatrix}$$

Quarter wave plate and π/4 rotated quarter wave plate (which has the same effect as a 50-50 beam splitter):

$$W_4 = \begin{pmatrix} 1 & 0 \\ 0 & -i \end{pmatrix}$$

$$BS = \begin{pmatrix} \frac{1}{\sqrt{2}} & \frac{1}{\sqrt{2}} \\ \frac{1}{\sqrt{2}} & \frac{1}{\sqrt{2}} \end{pmatrix}$$

Show that,

When a half wave plate is placed between aligned polarizers all the light gets through.

$$\left(\left|V^T W_2(0) H\right|\right)^2 = 0$$

$$\left(\left|V^T W_2(0) V\right|\right)^2 = 1$$

When a half wave plate is placed between crossed polarizers no light gets through.

$$\left(\left|V^T W_2(0) H\right|\right)^2 = 0$$

When the half wave plate is rotated by an angle of $\pi/4$ all the light gets through.

$$\left(\left|V^T W_2\left(\frac{\pi}{4}\right) H\right|\right)^2 = 1$$

When the half wave plate is rotated by an additional angle of $\pi/4$ no light gets through.

$$\left(\left|V^T W_2\left(\frac{\pi}{2}\right) H\right|\right)^2 = 0$$

When a half wave plate rotated by $\pi/4$ is placed between two vertical or horizontal polarizers no light gets through.

$$\left(\left|V^T W_2\left(\frac{\pi}{4}\right) V\right|\right)^2 = 0$$

$$\left(\left|H^T W_2\left(\frac{\pi}{4}\right) H\right|\right)^2 = 0$$

There is no effect when a quarter wave plate is inserted between either aligned or crossed polarizers.

$$\left(\left|V^T W_4 V\right|\right)^2 = 1$$

$$\left(\left|H^T W_4 V\right|\right)^2 = 1$$

If the quarter wave plate is rotated by $\pi/4$ 50% of the light gets through.

$$\left(\left|V^T BS(V)\right|\right)^2 = 0.5$$

$$\left(\left|H^T BS(V)\right|\right)^2 = 0.5$$

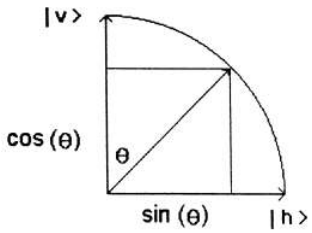
This page titled 7.16: Matrix Mechanics Exercises Using Polarized Light is shared under a CC BY 4.0 license and was authored, remixed, and/or curated by Frank Rioux via source content that was edited to the style and standards of the LibreTexts platform.

7.17: Polarized Light and Quantum Mechanics

The Linear Superposition

Unpolarized light consists of photons of all possible polarization angles. A photon polarized at an angle θ with respect to the vertical can be written as a linear superposition of a vertically polarized photon, $|v\rangle$, and a horizontally polarized photon, $|h\rangle$. $|v\rangle$ and $|h\rangle$ are the polarization basis states.

$$|\theta\rangle = |v\rangle\langle v|\theta\rangle + |h\rangle\langle h|\theta\rangle$$



From the figure above it can be seen that the projection of $|\theta\rangle$ onto $|v\rangle$ and $|h\rangle$ are $\cos\theta$ and $\sin\theta$ respectively.

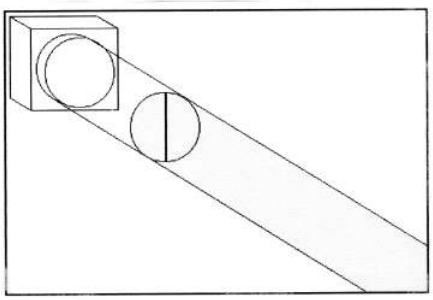
$$|\theta\rangle = |v\rangle\cos\theta + |h\rangle\sin\theta$$

The probability that a photon polarized at an angle θ will pass a vertical polarizer is

$$|\langle|\theta\rangle|^2 = \cos^2\theta$$

By integrating this function over all possible angles we find that half of the incident light passes through a vertical polarizer. See the figure below.

$$\frac{\int_0^{2\pi}\cos^2\theta d\theta}{2\pi} = 0.5$$



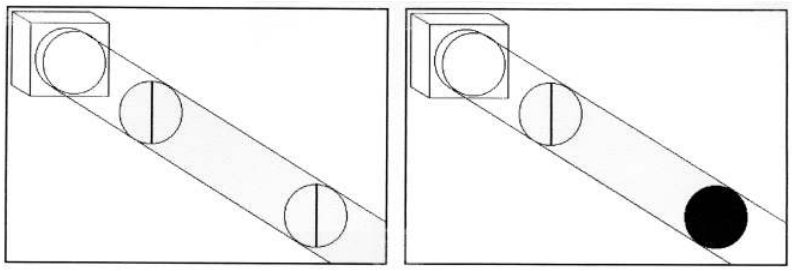
The photons that pass the vertical polarizer are now vertically polarized. That is they are eigenfunctions of that measurement operator.

The probability that a vertically polarized photon will pass a second filter that is vertically polarized is one.

$$|\langle v|v\rangle|^2 = \cos^2 0^o = 1$$

The probability that a vertically polarized photon will pass a second filter that is horizontally polarized is zero.

$$|\langle h|v\rangle|^2 = \cos^2 90^o = 0$$



The vertically polarized photon can be written as linear superposition of any other set of orthogonal basis states, for example $|45^o\rangle$ and $|-45^o\rangle$.

$$|v\rangle = |45^o\rangle\langle 45^o|v\rangle + |-45^o\rangle\langle -45^o|v\rangle$$

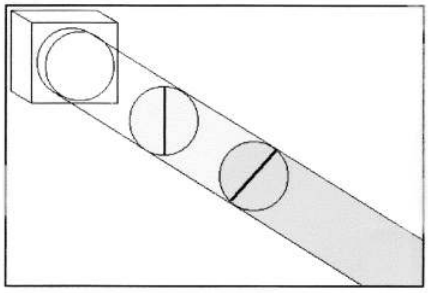
$$|v\rangle = |45^o\rangle \cos 45^o + |-45^o\rangle \cos -45^o$$

$$|v\rangle = |45^o\rangle 0.707 + |-45^o\rangle 0.707$$

Now if a 45° polarizer is inserted in between the vertical and horizontal polarizers photons get through the horizontal polarizer that stopped them previously (see the last figure).

Here's the explanation. The probability that a vertically polarized photon will get through a polarizer oriented at an angle of 45° is 0.5. See the figure below.

$$|\langle 45^o|v\rangle|^2 = \cos^2 45^o = 0.5$$



Now the photon is in the state of $|45^o\rangle$ which can be written as a linear superposition of $|v\rangle$ and \h$\rangle$.

$$|45^o\rangle = |v\rangle\langle v|45^o\rangle + |h\rangle\langle h|45^o\rangle$$

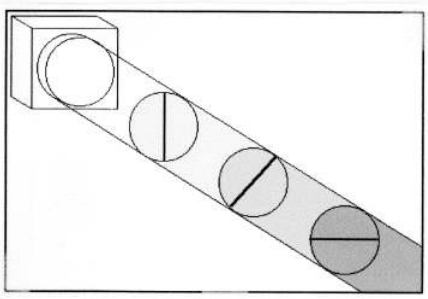
$$|45^o\rangle = |v\rangle \cos 45^o + |h\rangle \sin 45^o$$

$$|45^o\rangle = |v\rangle 0.707 + |h\rangle 0.707$$

Thus, the probability that this photon will pass the final horizontally oriented polarizer is

$$|\langle H|45^o\rangle|^2 = \sin^2 45^o = 0.5$$

See the figure below.



In this last figure the intensity of the light emerging from the final horizontal polarizing filter can be calculated compactly as

$$\frac{\int_0^{2\pi} |\langle h|45^o\rangle\langle 45^o|v\rangle\langle v|\theta\rangle|^2 d\theta}{2\pi} = \frac{1}{8}$$

The term inside the integral is the probability that a photon with polarization θ will pass through the three filters. This expression is integrated over all values of θ.

This page titled 7.17: Polarized Light and Quantum Mechanics is shared under a CC BY 4.0 license and was authored, remixed, and/or curated by Frank Rioux via source content that was edited to the style and standards of the LibreTexts platform.

7.18: Neutron Interferometry with Polarized Spin States

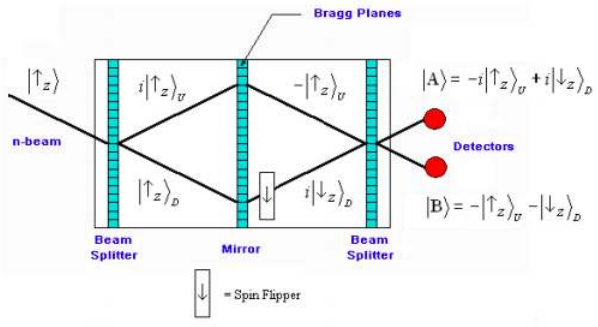
The following paragraph appears in an encyclopedia entry on neutron optics.***(1)*** A description of the original experiment is available in the physics research literature. ***(2)*** It is the purpose of this tutorial to work through the quantum math of the neutron interferometry experiment described here.

> One of the most important properties of quantum theory is the superposition principle, according to which the wave functions of coherent states combine additively. One of the most simple, yet most profound examples of this involves the spin for spin-½ particles. Such particles have two spin states, spin "up" (spin is directed upward along the ***z*** axis, s_z = + ½), and spin "down" (s_z = −½). If the ***z*** component of spin is measured, it is found that the particle is either spin up or spin down. Yet a spin along the ***x*** axis can be described as a linear combination of these two states. By a judicious use of magnetic fields, the neutron was polarized so that it was spin up in one leg of the interferometer and spin down in the other. Then when these two beams of equal amplitude, each polarized along the ***z*** axis, were recombined after passing through the interferometer, it was seen that they were polarized in the ***x***-***y*** plane, exactly according to the laws of quantum theory. This polarization was perpendicular to that of either of the beams separately, which proved both the coherence of the beam and the superposition principle for spin. This is the first time a beam of spin-½ particles has ever been spatially separated and then coherently recombined in this fashion.

The figure shows a simplified schematic of the neutron interferometer and the spin states of the neutron in each leg of the interferometer. The labels **U** and **D** refer to the upper and lower arms of the interferometer. The interferometer is fabricated out of a perfect single crystal and the Bragg planes of the crystal function as beam splitters, permitting both transmission and reflection. The middle element, which is labeled as a mirror, is actually another beam splitter; the neutrons transmitted in the upper and lower arms are discarded. The following conventions and simplifications are adopted:

1. It is assumed that the diagram describes the history of an individual neutron.
2. The paths to the detectors are of equal distance, meaning that the neutron beam is recombined at the final beam splitter in such a way that the labels U and D become meaningless at the detectors. They are retained in the diagram so the reader can more readily follow the math.
3. At the beam splitters reflection is assigned a 90° (= π/2 = ***i***) phase shift relative to transmission. (Reminder; the mirror is actually another beam splitter.)
4. In the interest of mathematical economy normalization constants are omitted.

In this experiment neutrons polarized spin-up in the z-direction illuminate a beam splitter creating a superposition of being transmitted (**D**) and reflected (**U**). A second beam splitter (mirror) redirects the beam to a third beam splitter which recombines the **D** and **U** branches before detection at **A** and **B**. But prior to recombination, the lower branch spin state is flipped to spin-down in the z-direction. Recombination at the final beam splitter leads to the superposition states at **A** and **B** shown in the figure below.



It is easy to show that these superposition states at **A** and **B** are actually spin-down and spin-up in the x-direction. This is because x-direction spin states can be written as linear superpositions of the z-direction spin states. As previously, normalization constants are omitted.

$$|\uparrow_x\rangle = |\uparrow_z\rangle + |\downarrow_z rangle$$

and

$$|\downarrow_x\rangle = -|\uparrow_z\rangle + |\downarrow_z rangle$$

Using these superpositions it is easy to show that the detected spin polarizations are $|\downarrow_x\rangle$ at **A** and $|\uparrow_x\rangle$ at **B**.

$$|A\rangle = i|\downarrow_x\rangle$$

and

$$|B\rangle = -|\uparrow_x\rangle$$

In summary, this experiment is a “textbook” illustration of the quantum mechanical superposition principle.

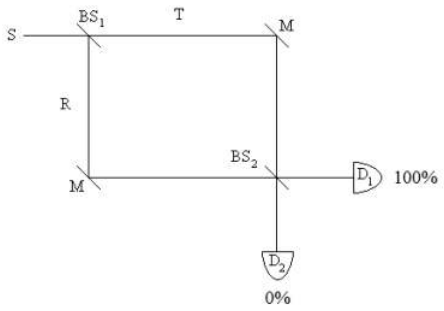
References

1. Daniel M. Greenberger, "Neutron optics", in AccessScience@McGraw-Hill, http://www.accessscience.com, DOI 10.1036/1097-8542.451000.
2. J. Summhammer, et al. “Direct observation of fermion spin superposition by neutron interferometry,” ***Physical Review A*. 27**, 2523-2532 (1983).

This page titled 7.18: Neutron Interferometry with Polarized Spin States is shared under a CC BY 4.0 license and was authored, remixed, and/or curated by Frank Rioux via source content that was edited to the style and standards of the LibreTexts platform.

7.19: Interaction Free Measurement - Seeing in the Dark

The illustration of the concept of interaction-free measurement requires the use of an interferometer. A simple illustration employs a Mach-Zehnder interferometer (MZI) like the one shown here.



This equal-arm MZI consists of two 50-50 beam splitters (BS_1, BS_2), two mirrors (M) and two detectors (D_1, D_2). A source emits a photon which interacts with BS_1 producing the following superposition. (By convention a 90 degree (i) phase shift is assigned to reflection.

$$S = \frac{1}{\sqrt{2}}(T + iR) \tag{7.19.1}$$

The transmitted and reflected branches are united at BS_2 by the mirrors, where they evolve into the following superpositions in the basis of the detectors.

$$T = \frac{1}{\sqrt{2}}(iD_1 + D_2) \tag{7.19.2}$$

$$R = \frac{1}{\sqrt{2}}(D_1 + iD_2) \tag{7.19.3}$$

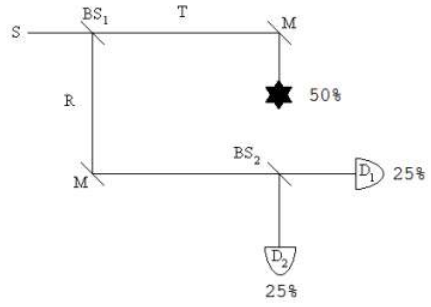
Substitution of Equations 7.19.2 and 7.19.3 into Equation 7.19.1 reveals that the output photon is always registered at D_1. There are two paths to each detector and constructive interference occurs at D_1 and destructive interference at D_2.

$$S = \frac{1}{\sqrt{2}}(T + iR)\Big|^{substitute\ T=\frac{1}{\sqrt{2}}(iD_1+D_2)}_{substitute,\ R=\frac{1}{\sqrt{2}}(D_1+iD_2)} \rightarrow \tag{7.19.4}$$

$$= D_1 i \tag{7.19.5}$$

Probability at D_1: $(|i|)^2 = 1$

The MZI provides a rudimentary method of determining whether an obstruction is present in its upper arm without actually interacting with it. As we shall see, it is not an efficient method, but it does clearly illustrate the principle involved which then can be used in a more elaborate and sophisticated interferometer to yield better results.



In the presence of the obstruction, Equation 7.19.2 becomes $T = \gamma_{Absorbed}$. This leads to the following result at the detectors.

$$S = \frac{1}{\sqrt{2}}(T + iR)\Big|_{substitute,\ R=\frac{1}{\sqrt{2}}(D_1+iD_2)}^{substitute\ T=\gamma_{Absorbed}} \rightarrow \tag{7.19.6}$$

$$= \frac{\sqrt{2}\gamma_{Absorbed}}{2} - \frac{D_2}{2} + \frac{D_1 i}{2} \tag{7.19.7}$$

Quantum mechanics predicts that for a large number of experiments 50% of the photons will be absorbed by the obstruction, 25% will be detected at D_1 and 25% will be detect at D_2. This later result is the signature of interaction-free measurement. Even if the photon is not absorbed, the mere presence of the obstruction causes the probability of detection at D_2 to go from zero to 25%. The photon's arrival at D_2 signals the presence of an obstruction in the upper arm of the MZI, and the obstruction is detected without an interaction.

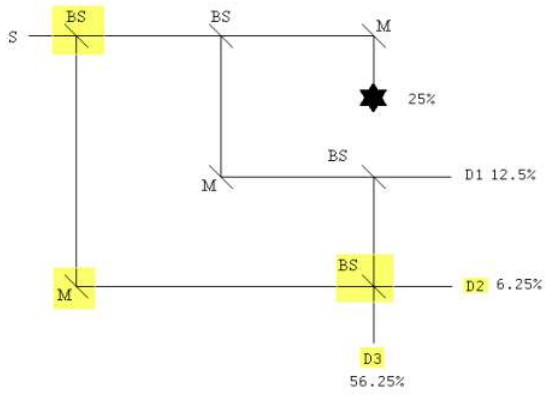
Of course, 25% is not great efficiency, so this is "a proof of principle" example. However, with a little ingenuity the probability of interaction-free detection can be increased dramatically. To see how this can be accomplished read "Quantum Seeing in the Dark" by Kwiat, Weinfurter and Zeilinger in the November 1996 issue of *Scientific American*.

However, it is possible to improve performance significantly by using a system of nested MZIs which is only slightly more complicated than the simple MZI used earlier. To simplify analysis Feynman's "sum over histories" approach to quantum mechanics will be used. The probability amplitudes for transmission and reflection at the beam splitters are required.

$$T = \frac{1}{\sqrt{2}}$$

$$R = \frac{i}{\sqrt{2}}$$

Placing an additional BS before the original MZI and another BS before D_2 and renaming it D_3, plus an additional mirror and new detector D_2, yields a nested interferometer configuration that significantly increases the probability of interaction-free detection of the obstruction.



To interact with the obstruction a photon must be transmitted at the first and second beam splitters. In this case there is only one history and the probability of the interaction occurring is the square of its absolute magnitude.

$$(|TT|)^2 \rightarrow \frac{1}{4} = 25 \tag{7.19.8}$$

The probabilities of detectors 1, 2 and 3 firing are calculated using the same methodology.

The probability D_1 registers a photon:

$$(|TRT|)^2 \rightarrow \frac{1}{8} = 12.5 \tag{7.19.9}$$

The probability D_2 registers a photon:

$$(|TRRR + RT|)^2 \rightarrow \frac{1}{16} = 6.25 \tag{7.19.10}$$

The probability D_3 registers a photon:

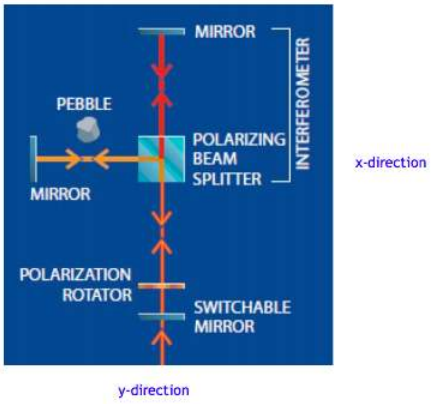
$$(|TRRT + RR|)^2 = \frac{9}{16} = 56.25 \tag{7.19.11}$$

With the modified interferometer detecting the presence of the obstruction without interacting with it increases from 25% to 56.25%.

This page titled 7.19: Interaction Free Measurement - Seeing in the Dark is shared under a CC BY 4.0 license and was authored, remixed, and/or curated by Frank Rioux via source content that was edited to the style and standards of the LibreTexts platform.

7.20: Quantum Seeing in the Dark - A Matrix-Tensor Analysis

The following device consisting of an equal-arm polarization interferometer, a switchable mirror and a polarization rotator appears in "Quantum Seeing in the Dark" by Kwiat, Weinfurter and Zeilinger in the November 1996 issue of Scientific American. It is used to illustrate the concept of interaction-free measurement. In what follows I analyze its operation using matrix and tensor algebra.



The polarizing beam splitter transmits horizontally polarized photons and reflects those that are vertically polarized. Therefore, vector states which contain direction of motion and polarization information of the photons are required. This is accomplished using vector tensor multiplication.

Vertical motion:

$$x = \begin{pmatrix} 1 \\ 0 \end{pmatrix}$$

Horizontal motion:

$$x = \begin{pmatrix} 0 \\ 1 \end{pmatrix}$$

Horizontal polarization:

$$x = \begin{pmatrix} 1 \\ 0 \end{pmatrix}$$

Vertical polarization:

$$x = \begin{pmatrix} 0 \\ 1 \end{pmatrix}$$

Photon direction of propagation and polarization states:

$$xh = \begin{pmatrix} 1 \\ 0 \end{pmatrix} \begin{pmatrix} 1 \\ 0 \end{pmatrix}$$

$$xh = \begin{pmatrix} 1 \\ 0 \\ 0 \\ 0 \end{pmatrix}$$

$$xv = \begin{pmatrix} 1 \\ 0 \end{pmatrix} \begin{pmatrix} 0 \\ 1 \end{pmatrix}$$

$$xv = \begin{pmatrix} 0 \\ 1 \\ 0 \\ 0 \end{pmatrix}$$

$$yh = \begin{pmatrix}0\\1\end{pmatrix}\begin{pmatrix}1\\0\end{pmatrix}$$

$$yh = \begin{pmatrix}0\\0\\1\\0\end{pmatrix}$$

$$yv = \begin{pmatrix}0\\1\end{pmatrix}\begin{pmatrix}0\\1\end{pmatrix}$$

$$yv = \begin{pmatrix}0\\0\\0\\1\end{pmatrix}$$

Now the matrix which represents a polarizing beam splitter which transmits horizontally polarized photons and reflects vertically polarized photons is constructed.

$$PBS = (xh)xh^T + (yv)xv^T + (yh)yh^T + (xv)yv^T$$

$$PBS = \begin{pmatrix}1&0&0&0\\0&0&0&1\\0&0&1&0\\0&1&0&0\end{pmatrix}$$

The matrix representing the polarization rotator is:

$$Rot(\theta) = \begin{pmatrix}\cos\theta & -\sin\theta & 0 & 0\\ \sin\theta & \cos\theta & 0 & 0\\ 0 & 0 & \cos\theta & -\sin\theta\\ 0 & 0 & \sin\theta & \cos\theta\end{pmatrix}$$

It is unnecessary to include matrices representing the mirrors because they simply reflect the photon back to the beam splitter for a second encounter. First consider the case in which there is no obstructing pebble in the y-branch of the interferometer. A horizontally polarized photon enters the system and the polarization rotator rotates the polarization by 15 degrees (π/12) toward the vertical. This results in a superposition of |xh> and |xv>. This photon state enters the interferometer, |xh> and |xv> are temporarily split, and then recombined to reform the entering superposition. After one cycle the photon's polarization state is as follows.

$$\left(PBS(PBS)Rot\left(\frac{\pi}{12}\right)\right)^1 xh = \begin{pmatrix}0.966\\0.259\\0\\0\end{pmatrix}$$

$$0.966xh + 0.259xv = \begin{pmatrix}0.966\\0.259\\0\\0\end{pmatrix}$$

The bottom mirror reflects the photon back to the polarization rotator for another pass through the interferometer. After six cycles the switchable mirror at the bottom of the device releases a vertically polarized photon. In other words, if the equal arm interferometer does not have an obstruction in the y-branch, the initial horizontally polarized photon is rotated stepwise to the vertical polarization state.

$$\left(PBS(PBS)Rot\left(\frac{\pi}{12}\right)\right)^6 xh = \begin{pmatrix}0\\1\\0\\0\end{pmatrix}$$

$$\left[\left|xv^T\left(PBS(PBS)Rot\left(\frac{\pi}{12}\right)\right)^6 xh\right|\right]^2 = 1$$

Practically this would be confirmed by having a polarizing beam splitter (PBS) at the output channel of the device. As shown below the photon will be detected at the vertical (y-direction) port and not the horizontal (x-direction) port.

$$\left[\left|yv^T PBS\left(PBS(PBS)Rot\left(\frac{\pi}{12}\right)\right)^6 xh\right|\right]^2 = 1$$

$$\left[\left|xh^T PBS\left(PBS(PBS)Rot\left(\frac{\pi}{12}\right)\right)^6 xh\right|\right]^2 = 0$$

The presence of the pebble takes the y-branch of the interferometer "out of play." Under these circumstances the polarizing beam splitter is represented by the following matrix.

$$PBS' = (xh)xh^T$$

$$PBS' = \begin{pmatrix} 1 & 0 & 0 & 0 \\ 0 & 0 & 0 & 0 \\ 0 & 0 & 0 & 0 \\ 0 & 0 & 0 & 0 \end{pmatrix}$$

Now after six cycles there is a 66% probability that the mirror will release a horizontally polarized photon. The other 34% of the time the photon will be absorbed by the pebble.

$$\left(PBS'(PBS')Rot\left(\frac{\pi}{12}\right)\right)^6 xh = \begin{pmatrix} 0.812 \\ 0 \\ 0 \\ 0 \end{pmatrix}$$

$$\left[\left|xh^T\left(PBS'(PBS')Rot\left(\frac{\pi}{12}\right)\right)^6 xh\right|\right]^2 = 0.66$$

As noted earlier, the actual device would have a final PBS after the switchable mirror, showing that a vertical photon is never detected (it has been absorbed) and a horizontal photon is recorded with a 0.66 probability.

$$\left[\left|yv^T PBS\left(PBS'(PBS')Rot\left(\frac{\pi}{12}\right)\right)^6 xh\right|\right]^2 = 0$$

$$\left[\left|xh^T PBS\left(PBS'(PBS')Rot\left(\frac{\pi}{12}\right)\right)^6 xh\right|\right]^2 = 0.66$$

Recall that in the absence of the obstruction the mirror releases a vertically polarized photon 100% of the time. The detection of a horizontally polarized photon indicates the presence of the pebble without an interaction with the pebble. With six cycles interaction-free measurement occurs about two thirds of the time. Increasing the number of cycles increases the utility of the device. For thirty cycles (a π/60 polarization rotation per cycle) a horizontally polarized photon is detected 92% of the time: interaction-free measurement occurs 92% of the time.

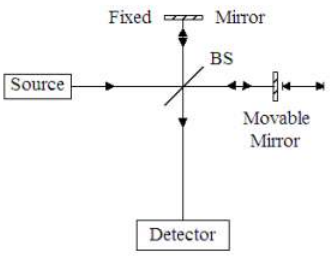
$$\left[\left|xh^T\left(PBS'(PBS')Rot\left(\frac{\pi}{60}\right)\right)^{30} xh\right|\right]^2 = 0.92$$

$$\left[\left|xh^T PBS\left(PBS'(PBS')Rot\left(\frac{\pi}{60}\right)\right)^{30} xh\right|\right]^2 = 0.92$$

Increasing the number of cycles increases the reliability of the method, but is also experimentally very challenging.

This page titled 7.20: Quantum Seeing in the Dark - A Matrix-Tensor Analysis is shared under a CC BY 4.0 license and was authored, remixed, and/or curated by Frank Rioux via source content that was edited to the style and standards of the LibreTexts platform.

7.21: Two Analyses of the Michelson Interferometer



Path difference between interferometer arms is δ. Phase accumulated due to path difference: $exp\left(i\frac{2\pi\delta}{\lambda}\right)$

S stands for source, **D** for detector, **T** for transmitted and **R** for reflected. The evolution of the photon wave function at various stages is given below.

$$S = \frac{1}{\sqrt{2}}(T + iR)$$

$$T = \frac{exp\left(i\frac{2\pi\delta}{\lambda}\right)}{\sqrt{2}}(iD + S)$$

$$R = \frac{1}{\sqrt{2}}(D + iS)$$

$$S = \frac{1}{\sqrt{2}}(T + iR)\Big|_{substitute,\ R=\frac{1}{\sqrt{2}}(D+iS)}^{substitute,\ T=\frac{exp\left(i\frac{2\pi\delta}{\lambda}\right)}{\sqrt{2}}(iD+S)} \rightarrow S = -\frac{S}{2} + \frac{Se^{\frac{2i\pi\delta}{\lambda}}}{2} + \frac{De^{\frac{2i\pi\delta}{\lambda}}}{2} + \frac{Di}{2}$$

The probability the photon will arrive at the detector is the square of the absolute magnitude of the coefficient of D.

$$\frac{-1}{2}\left(e^{\frac{-2i\pi\delta}{\lambda}}\right)\frac{1}{2}\left(e^{\frac{-2i\pi\delta}{\lambda}}\right) simplify \rightarrow \sin\left(\frac{\pi\delta}{\lambda}\right)^2$$

The same results are now illustrated using a matrix mechanics approach. Horizontal and vertical motion of the photon are represented by vectors. The source emits a horizontal photon, the detector receives a vertical photon. The beam splitter and the phase shift due to path length difference are represented by matrices. A matrix representation for the mirrors is unnecessary because the simply return the photon to the beam splitter.

Horizontal motion: $\begin{pmatrix}1\\0\end{pmatrix}$

Vertical motion: $\begin{pmatrix}0\\1\end{pmatrix}$

Beam splitter:

$$BS = \begin{pmatrix}\frac{1}{\sqrt{2}} & \frac{1}{\sqrt{2}}\\ \frac{1}{\sqrt{2}} & \frac{1}{\sqrt{2}}\end{pmatrix}$$

Phase shift:

$$A(\delta) = \begin{pmatrix}e^{2i\pi\frac{\delta}{\lambda}} & 0\\ 0 & 1\end{pmatrix}$$

Calculate the probability amplitude and probability that the photon will arrive at the detector

$$\begin{pmatrix}0 & 1\end{pmatrix} BS \begin{pmatrix}e^{2i\pi\frac{\delta}{\lambda}} & 0\\ 0 & 1\end{pmatrix} BS \begin{pmatrix}1\\0\end{pmatrix} \rightarrow \frac{e^{\frac{2i\pi\delta}{\lambda}}}{2} + \frac{1}{2}i$$

$$\left(\frac{e^{\frac{-2i\pi\delta}{\lambda}(-i)}}{2} + \frac{1}{2}(-i)\right)\left(\frac{e^{\frac{2i\pi\delta}{\lambda}(i)}}{2} + \frac{1}{2}i\right) simplify \rightarrow \cos\left(\frac{\pi\delta}{\lambda}\right)^2$$

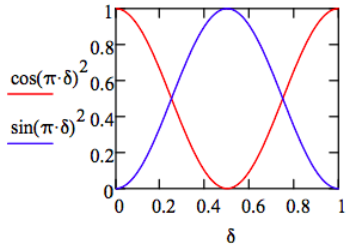
Calculate the probability amplitude and probability that the photon will be returned to the source.

$$(1 \quad 0)\, BS \begin{pmatrix} e^{2i\pi\frac{\delta}{\lambda}} & 0 \\ 0 & 1 \end{pmatrix} BS \begin{pmatrix} 1 \\ 0 \end{pmatrix} \rightarrow \frac{e^{\frac{2i\pi\delta}{\lambda}}}{2} - \frac{1}{2}$$

$$\left(\frac{e^{\frac{-2i\pi\delta}{\lambda}}}{2} - \frac{1}{2}\right)\left(\frac{e^{\frac{2i\pi\delta}{\lambda}}}{2} - \frac{1}{2}\right) simplify \rightarrow \sin\left(\frac{\pi\delta}{\lambda}\right)^2$$

Plotting these results in units of λ yields:

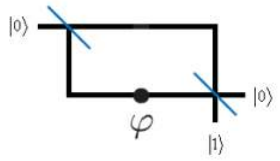
$$\delta = 0, .01..1$$



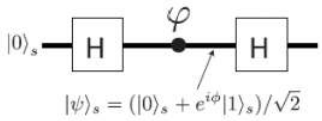
This page titled 7.21: Two Analyses of the Michelson Interferometer is shared under a CC BY 4.0 license and was authored, remixed, and/or curated by Frank Rioux via source content that was edited to the style and standards of the LibreTexts platform.

7.22: A Quantum Circuit for a Michelson Interferometer

Schematic diagram of a Mach-Zehnder interferometer (MZI).



The following quantum circuit simulates the MZI.



The arms of the MZI are represented by the following orthonormal basis.

$$|0\rangle = \begin{pmatrix} 1 \\ 0 \end{pmatrix}$$

$$|1\rangle = \begin{pmatrix} 0 \\ 1 \end{pmatrix}$$

The matrices representing the Hadamard and phase shift gates are:

$$H = \frac{1}{\sqrt{2}} \begin{pmatrix} 1 & 1 \\ 1 & -1 \end{pmatrix}$$

$$A(\theta) = \begin{pmatrix} 1 & 0 \\ 0 & e^{i\phi} \end{pmatrix}$$

Step-by-step through the circuit. The first Hadamard gate creates a superposition of the |0 > and |1 > states. The phase shifter operates on the lower arm of the MZI. The final Hadamard gate allows interference between the two arms of the MZI.

$$H \begin{pmatrix} 1 \\ 0 \end{pmatrix} \rightarrow \begin{pmatrix} \frac{\sqrt{2}}{2} \\ \frac{\sqrt{2}}{2} \end{pmatrix}$$

$$A(\phi) H \begin{pmatrix} 1 \\ 0 \end{pmatrix} \rightarrow \begin{pmatrix} \frac{\sqrt{2}}{2} \\ \frac{\sqrt{2} e^{\phi i}}{2} \end{pmatrix}$$

$$HA(\phi) H \begin{pmatrix} 1 \\ 0 \end{pmatrix} \rightarrow \begin{pmatrix} \frac{e^{\phi i}}{2} + \frac{1}{2} \\ \frac{1}{2} - \frac{e^{\phi i}}{2} \end{pmatrix}$$

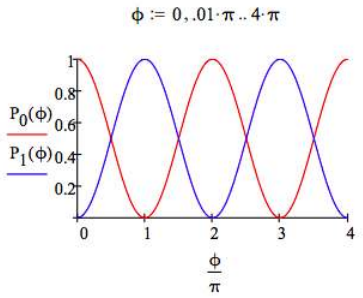
Probability of detection at the |0 > port:

$$P_0(\phi) = \left[\left| \begin{pmatrix} 1 & 0 \end{pmatrix} HA(\phi) H \begin{pmatrix} 1 \\ 0 \end{pmatrix} \right| \right]^2 \Big|_{simplify}^{assume,\ \phi=real} \rightarrow \frac{\cos\phi}{2} + \frac{1}{2}$$

Probability of detection at the |1 > port:

$$P_1(\phi) = \left[\left| \begin{pmatrix} 0 & 1 \end{pmatrix} HA(\phi) H \begin{pmatrix} 1 \\ 0 \end{pmatrix} \right| \right]^2 \Big|_{simplify}^{assume,\ \phi=real} \rightarrow \frac{1}{2} - \frac{\cos\phi}{2}$$

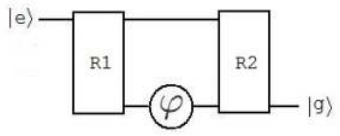
A graphical representation of the above calculations shows the interference effects as a function of ϕ.



This page titled 7.22: A Quantum Circuit for a Michelson Interferometer is shared under a CC BY 4.0 license and was authored, remixed, and/or curated by Frank Rioux via source content that was edited to the style and standards of the LibreTexts platform.

7.23: The Ramsey Atomic Interferometer

The Ramsey interferometer, which closely resembles the Mach-Zehnder interferometer, is constructed using two π/2 Rabi pulses (R1 and R2) separated by a phase shifter in the lower arm, as shown below.



where

$$|e\rangle = \begin{pmatrix} 1 \\ 0 \end{pmatrix}$$

$$|g\rangle = \begin{pmatrix} 0 \\ 1 \end{pmatrix}$$

The matrix representations of the phase shifter and the Rabi elements are as follows:

$$PhaseShift(\phi) = \begin{pmatrix} 1 & 0 \\ 0 & e^{i\phi} \end{pmatrix}$$

$$Rabi(\phi) = \begin{pmatrix} \cos\left(\frac{\theta}{2}\right) & -\sin\left(\frac{\theta}{2}\right) \\ \sin\left(\frac{\theta}{2}\right) & \cos\left(\frac{\theta}{2}\right) \end{pmatrix}$$

$$Rabi\left(\frac{\pi}{2}\right) = \begin{pmatrix} 0.707 & -0.707 \\ 0.707 & 0.707 \end{pmatrix}$$

The input to the interferometer is the upper state |e> of a two-state atom. The first pulse behaves like a Hadamard gate creating a coherent superposition of |e> and the lower state of the atom, |g>.

$$Rabi\left(\frac{\pi}{2}\right)\begin{pmatrix} 1 \\ 0 \end{pmatrix} \rightarrow \begin{pmatrix} \frac{1}{2}2^{\frac{1}{2}} \\ \frac{1}{2}2^{\frac{1}{2}} \end{pmatrix}$$

$$\frac{1}{\sqrt{2}}\begin{pmatrix} 1 \\ 1 \end{pmatrix}$$

The phase shifter alters the superposition by adding a phase to |g>.

$$PhaseShift(\phi)Rabi\left(\frac{\pi}{2}\right)\begin{pmatrix} 1 \\ 0 \end{pmatrix} \rightarrow \begin{pmatrix} \frac{1}{2}2^{\frac{1}{2}} \\ \frac{1}{2}e^{i\phi}2^{\frac{1}{2}} \end{pmatrix}$$

$$\frac{1}{\sqrt{2}}\begin{pmatrix} 1 \\ e^{i\phi} \end{pmatrix}$$

In the absence of a phase shift (ϕ = 0) the two π/2 pulses behave like a not gate yielding |g> at the output channel.

$$Rabi\left(\frac{\pi}{2}\right)PhaseShift(0)Rabi\left(\frac{\pi}{2}\right)\begin{pmatrix} 1 \\ 0 \end{pmatrix} \rightarrow \begin{pmatrix} 0 \\ 1 \end{pmatrix}$$

However if ϕ = π, the interferometer is equivalent to the identity operator and the output is |e>.

$$Rabi\left(\frac{\pi}{2}\right)PhaseShift(\pi)Rabi\left(\frac{\pi}{2}\right)\begin{pmatrix} 1 \\ 0 \end{pmatrix} \rightarrow \begin{pmatrix} 1 \\ 0 \end{pmatrix}$$

In general, the result is a superposition of |e> and |g>.

$$Rabi\left(\frac{\pi}{2}\right)PhaseShift(\phi)Rabi\frac{\phi}{2}\begin{pmatrix} 1 \\ 0 \end{pmatrix} \rightarrow \begin{pmatrix} \frac{1}{2} - \frac{1}{2}e^{i\phi} \\ \frac{1}{2} + \frac{1}{2}e^{i\phi} \end{pmatrix}$$

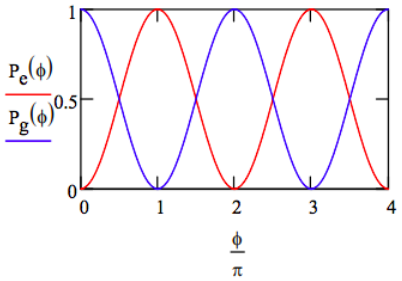
$$\begin{pmatrix} e \\ g \end{pmatrix} = \frac{1}{2}\begin{pmatrix} 1 - e^{i\phi} \\ 1 + e^{i\phi} \end{pmatrix}$$

The probabilities of detecting |e> and |g> at the output channel depend on the phase ϕ, exhibiting interference effects as in the Mach-Zehnder interferometer with a phase shifter in the lower arm. This is shown below both algebraically and graphically.

$$P_e(\phi) = \left[\left| \begin{pmatrix} 1 \\ 0 \end{pmatrix}^T Rabi\left(\frac{\pi}{2}\right) PhaseShift(\phi) Rabi\left(\frac{\pi}{2}\right) \begin{pmatrix} 1 \\ 0 \end{pmatrix} \right|\right]^2 \; simplify \rightarrow \frac{1}{2} - \frac{1}{2}\cos\phi$$

$$P_g(\phi) = \left[\left| \begin{pmatrix} 0 \\ 1 \end{pmatrix}^T Rabi\left(\frac{\pi}{2}\right) PhaseShift(\phi) Rabi\left(\frac{\pi}{2}\right) \begin{pmatrix} 1 \\ 0 \end{pmatrix} \right|\right]^2 \; simplify \rightarrow \frac{1}{2} + \frac{1}{2}\cos\phi$$

$\phi := 0, .01 \cdot \pi .. 4 \cdot \pi$



This page titled 7.23: The Ramsey Atomic Interferometer is shared under a CC BY 4.0 license and was authored, remixed, and/or curated by Frank Rioux via source content that was edited to the style and standards of the LibreTexts platform.

7.24: Optical Activity - A Quantum Perspective

Optical activity is the rotation of linearly polarized light as it advances through a chiral medium. The quantum explanation for optical rotation is based on the fact that linearly polarized light can be written as a superposition of left and right circularly polarized light, which possess angular momentum (see Appendix).

$$L = \frac{1}{\sqrt{2}}\begin{pmatrix}1\\-i\end{pmatrix}$$

$$R = \frac{1}{\sqrt{2}}\begin{pmatrix}1\\i\end{pmatrix}$$

This is demonstrated for vertical, horizontal and Θ polarized light.

$$V = \begin{pmatrix}1\\0\end{pmatrix}$$

$$\frac{1}{\sqrt{2}}(R+L) \rightarrow \begin{pmatrix}1\\0\end{pmatrix}$$

$$H = \begin{pmatrix}0\\1\end{pmatrix}$$

$$\frac{i}{\sqrt{2}}(L-R) \rightarrow \begin{pmatrix}0\\1\end{pmatrix}$$

$$\Theta = \begin{pmatrix}\cos\theta\\\sin\theta\end{pmatrix}$$

$$\frac{1}{\sqrt{2}}(e^{-i\theta}R + e^{i\theta}L)\ simplify \rightarrow \begin{pmatrix}\cos\theta\\\sin\theta\end{pmatrix}$$

To proceed to a quantum interpretation for optical activity, we assume that $|\theta\rangle$ polarized light entering a chiral medium will be in the state $|\theta + \alpha x\rangle$ after traveling a distance x, where α is the optical activity. Our immediate goal is to find the quantum operator for such a process. By analogy with the time-dependent Schrödinger equation, $i\frac{h}{2\pi}\frac{d}{dt}\Psi = H\Psi$, R. L. Martin (*Basic Quantum Mechanics*, page 30) suggests the following differential equation to describe the spatial evolution of polarization in a chiral medium.

$$i\frac{d}{dx}\Psi(\theta,\alpha,x) = K\Psi(\theta,\alpha,x)$$

where

$$\Psi(\theta,\alpha,x) = \begin{pmatrix}\cos(\theta+\alpha x)\\\sin(\theta+\alpha x)\end{pmatrix}$$

Since αx is an angle, id/dx is an angular momentum operator and what follows determines its matrix representation. Consulting the Appendix we see that it is α times the photon angular momentum operator.

Substitution of ψ yields,

$$i\alpha\begin{pmatrix}-\sin(\theta+\alpha x)\\\cos(\theta+\alpha x)\end{pmatrix} = K\begin{pmatrix}\cos(\theta+\alpha x)\\\sin(\theta+\alpha x)\end{pmatrix}$$

which requires

$$K = \begin{pmatrix}0 & -i\alpha\\ i\alpha & 0\end{pmatrix}$$

$$i\frac{d}{dx}\begin{pmatrix}\cos(\theta+\alpha x)\\\sin(\theta+\alpha x)\end{pmatrix} \rightarrow \begin{pmatrix}-\alpha\sin(\theta+\alpha x)\\\alpha\cos(\theta+\alpha x)\end{pmatrix}$$

$$\begin{pmatrix} 0 & -i\alpha \\ i\alpha & 0 \end{pmatrix} \begin{pmatrix} \cos(\theta+\alpha x) \\ \sin(\theta+\alpha x) \end{pmatrix} \rightarrow \begin{pmatrix} -\alpha\sin(\theta+\alpha x) \\ \alpha\cos(\theta+\alpha x) \end{pmatrix}$$

Because they play an essential role in understanding optical rotation, we pause briefly to show that |R > and |L > are eigenvectors of K with eigenvalues α and -α respectively.

$$\begin{pmatrix} 0 & -i\alpha \\ i\alpha & 0 \end{pmatrix} R \rightarrow \begin{pmatrix} \frac{\sqrt{2}\alpha}{2} \\ \frac{\sqrt{2}\alpha i}{2} \end{pmatrix}$$

$$\alpha\frac{1}{\sqrt{2}}\begin{pmatrix} 1 \\ i \end{pmatrix}$$

$$\begin{pmatrix} 0 & -i\alpha \\ i\alpha & 0 \end{pmatrix} L \rightarrow \begin{pmatrix} -\frac{\sqrt{2}\alpha}{2} \\ \frac{\sqrt{2}\alpha i}{2} \end{pmatrix}$$

$$-\alpha\frac{1}{\sqrt{2}}\begin{pmatrix} 1 \\ -i \end{pmatrix}$$

Integration of the differential equation describing the change in polarization during propagation through an optically active medium yields the sought after polarization spatial evolution operator.

$$\Psi_{final} = e^{-iKx}\Psi_{initial} = e^{-i\begin{pmatrix} 0 & -i\alpha \\ i\alpha & 0 \end{pmatrix}x}\Psi_{initial}$$

where

$$e^{-i\begin{pmatrix} 0 & -i\alpha \\ i\alpha & 0 \end{pmatrix}x} \; simplify \; \rightarrow \begin{pmatrix} \cos(\alpha x) & -\sin(\alpha x) \\ \sin(\alpha x) & \cos(\alpha x) \end{pmatrix}$$

This demonstrates that the spatial evolution operator is a matrix which rotates the plane of polarization by an angle αx. Now the effect of the operator on vertical, horizontal and Θ polarized light is demonstrated.

$$e^{-i\begin{pmatrix} 0 & -i\alpha \\ i\alpha & 0 \end{pmatrix}x}\begin{pmatrix} 1 \\ 0 \end{pmatrix} \; simplify \; \rightarrow \begin{pmatrix} \cos(\alpha x) \\ \sin(\alpha x) \end{pmatrix}$$

$$e^{-i\begin{pmatrix} 0 & -i\alpha \\ i\alpha & 0 \end{pmatrix}x}\begin{pmatrix} 0 \\ 1 \end{pmatrix} \; simplify \; \rightarrow \begin{pmatrix} -\sin(\alpha x) \\ \cos(\alpha x) \end{pmatrix}$$

$$e^{-i\begin{pmatrix} 0 & -i\alpha \\ i\alpha & 0 \end{pmatrix}x}\begin{pmatrix} \cos\theta \\ \sin\theta \end{pmatrix} \; simplify \; \rightarrow \begin{pmatrix} \cos(\theta+\alpha x) \\ \sin(\theta+\alpha x) \end{pmatrix}$$

Next the circular polarization states are operated on.

$$e^{-i\begin{pmatrix} 0 & -i\alpha \\ i\alpha & 0 \end{pmatrix}x}\frac{1}{\sqrt{2}}\begin{pmatrix} 1 \\ i \end{pmatrix} \; simplify \; \rightarrow \begin{pmatrix} \frac{\sqrt{2}e^{-\alpha xi}}{2} \\ \frac{\sqrt{2}e^{-\alpha xi}i}{2} \end{pmatrix}$$

or

$$e^{-i\alpha x}\frac{1}{\sqrt{2}}\begin{pmatrix} 1 \\ i \end{pmatrix}$$

$$e^{-i\begin{pmatrix} 0 & -i\alpha \\ i\alpha & 0 \end{pmatrix}x}\frac{1}{\sqrt{2}}\begin{pmatrix} 1 \\ -i \end{pmatrix} \; simplify \; \rightarrow \begin{pmatrix} \frac{\sqrt{2}e^{\alpha xi}}{2} \\ -\frac{\sqrt{2}e^{-\alpha xi}i}{2} \end{pmatrix}$$

or

$$e^{i\alpha x}\frac{1}{\sqrt{2}}\begin{pmatrix}1\\-i\end{pmatrix}$$

We see that propagation through the chiral medium causes a phase shift in the circular polarization states. This turns out to be of essential importance in understanding the rotation of plane polarized light which occurs during propagation. It was shown previously, that plane polarized light can be expressed as a superposition of left and right circularly polarized light. Let′s rewrite that superposition using the phase relation just demonstrated. For the sake of computational simplicity we will use α = 1, and because the phase factor is a trigonometric function we will express distance in units of π.

Our example involves a vertically polarized light source illuminating a chiral medium. At the point of entry, x = 0, we show that the light is indeed vertically polarized.

$x = 0$:

$$\frac{1}{2}\left[exp(-i\alpha x)\begin{pmatrix}1\\i\end{pmatrix}+exp(i\alpha x)\begin{pmatrix}1\\-i\end{pmatrix}\right]=\begin{pmatrix}1\\0\end{pmatrix}$$

This formulation shows that as light penetrates the chiral medium, the vertically polarized photon is rotated.

$x = \frac{\pi}{4}$:

$$\frac{1}{2}\left[exp(-i\alpha x)\begin{pmatrix}1\\i\end{pmatrix}+exp(i\alpha x)\begin{pmatrix}1\\-i\end{pmatrix}\right]=\begin{pmatrix}0.707\\0.707\end{pmatrix}$$

$x = \frac{\pi}{2}$:

$$\frac{1}{2}\left[exp(-i\alpha x)\begin{pmatrix}1\\i\end{pmatrix}+exp(i\alpha x)\begin{pmatrix}1\\-i\end{pmatrix}\right]=\begin{pmatrix}0\\1\end{pmatrix}$$

Of course, the same results are obtained by operating directly on |v >.

$x = 0$:

$$e^{-i\begin{pmatrix}0&-i\alpha\\i\alpha&0\end{pmatrix}x}\begin{pmatrix}1\\0\end{pmatrix}\ simplify\ \rightarrow\begin{pmatrix}1\\0\end{pmatrix}$$

$x = \frac{\pi}{4}$:

$$e^{-i\begin{pmatrix}0&-i\alpha\\i\alpha&0\end{pmatrix}x}\begin{pmatrix}1\\0\end{pmatrix}\ simplify\ \rightarrow\begin{pmatrix}\frac{\sqrt{2}}{2}\\\frac{\sqrt{2}}{2}\end{pmatrix}=\begin{pmatrix}0.707\\0.707\end{pmatrix}$$

$x = \frac{\pi}{2}$:

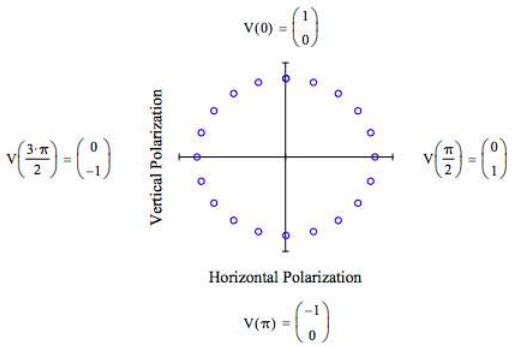
$$e^{-i\begin{pmatrix}0&-i\alpha\\i\alpha&0\end{pmatrix}x}\begin{pmatrix}1\\0\end{pmatrix}\ simplify\ \rightarrow=\begin{pmatrix}0\\1\end{pmatrix}$$

The juxtaposition of the two sets of calculations suggests that the rotation of plane polarized light in a chiral medium is due to phase changes in its left, |L >, and right, |R >, circularly polarized components during propagation. Couching the explanation in terms of |L > and |R > is further justified by the fact that they are the eigenstates of the Hermitian K matrix which produces the rotation. A picture of the progression of the angle of rotation as light advances through a chiral medium can be created by plotting the vertical vs horizontal components of the polarization vector as a function of x.

$x = 0, .1\pi..2\pi$:

$$V(x)=e^{-i\begin{pmatrix}0&-i\alpha\\i\alpha&0\end{pmatrix}x}\begin{pmatrix}1\\0\end{pmatrix}\ simplify\ \rightarrow\begin{pmatrix}\cos x\\\sin x\end{pmatrix}$$

for α = 1.



Appendix

The angular momentum operator for photons in atomic units is $M = \begin{pmatrix} 0 & -i \\ i & 0 \end{pmatrix}$, which means, of course, that K = αM. |R > and |L > are eigenvectors of M with eigenvalues +1 and -1, respectively. As shown earlier they are eigenvectors of K with eigenvalues α and -α, respectively.

$$MR = \begin{pmatrix} 0.707 \\ 0.707i \end{pmatrix}$$

$$\frac{1}{\sqrt{2}} \begin{pmatrix} 1 \\ i \end{pmatrix}$$

$$ML = \begin{pmatrix} -0.707 \\ 0.707i \end{pmatrix}$$

$$-\frac{1}{\sqrt{2}} \begin{pmatrix} 1 \\ -i \end{pmatrix}$$

The linearly polarized states are not eigenvectors of M and have angular momentum expectation values of zero.

$$(1 \quad 0)\, M \begin{pmatrix} 1 \\ 0 \end{pmatrix} = 0$$

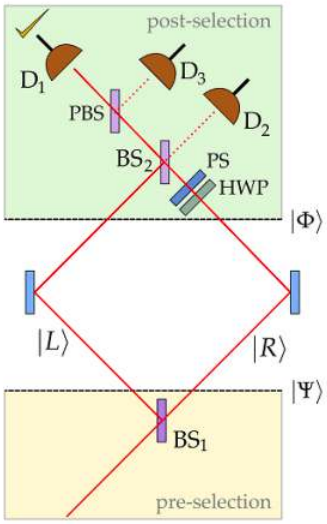
$$(0 \quad 1)\, M \begin{pmatrix} 0 \\ 1 \end{pmatrix} = 0$$

$$(\cos\theta \quad \sin\theta)\, M \begin{pmatrix} \cos\theta \\ \sin\theta \end{pmatrix} \rightarrow 0$$

This page titled 7.24: Optical Activity - A Quantum Perspective is shared under a CC BY 4.0 license and was authored, remixed, and/or curated by Frank Rioux via source content that was edited to the style and standards of the LibreTexts platform.

7.25: A Quantum Optical Cheshire Cat

The following is a summary of "Quantum Cheshire Cats" by Aharonov, Popescu, Rohrlich and Skrzypczyk which was published in the ***New Journal of Physics* 15**, 113015 (2013) and can also be accessed at: arXiv:1202.0631v2.



In the absence of the half-wave plate (HWP) and the phase shifter (PS) a horizontally polarized photon entering the interferometer from the lower left (propagating to the upper right) arrives at D_2 with a 90 degree (π/2, i) phase shift. (By convention reflection at a beam splitter introduces a 90 degree phase shift.)

$$|R\rangle|H\rangle \xrightarrow{BS_1} \frac{1}{\sqrt{2}}[i|L\rangle + |R\rangle]|H\rangle \xrightarrow{BS_2} i|D_2\rangle|H\rangle$$

The state immediately after the first beam splitter is the pre-selected state.

$$|Psi\rangle = \frac{1}{\sqrt{2}}\left[i|L\rangle + |R\rangle\right]|H\rangle$$

The post-selected state is,

$$|\Phi\rangle = \frac{1}{\sqrt{2}}\left[|L\rangle|H\rangle + |R\rangle|V\rangle\right]$$

The HWP (converts |V> to |H> in the R-branch) and PS transform this state to,

$$|\Phi\rangle \xrightarrow[PS]{HWP} \frac{1}{\sqrt{2}}\left[|L\rangle + i|R\rangle\right]|H\rangle$$

which exits the second beam splitter through the left port to encounter a polarizing beam splitter which transmits horizontal polarization and reflects vertical polarization. Thus, the post-selected state is detected at D_1. The evolution of the post-selected state is summarized as follows:

$$|\Phi\rangle = \frac{1}{\sqrt{2}}\left[|L\rangle|H\rangle + |R\rangle|V\rangle\right] \xrightarrow[PS]{HWP} \frac{1}{\sqrt{2}}\left[|L\rangle + i|R\rangle\right]|H\rangle \xrightarrow{BS_2} i|L\rangle|H\rangle \xrightarrow{PBS} i|D_1\rangle|H\rangle$$

The last term on the right side below is the weak value of A multiplied by the probability of its occurrence for the preselected state Ψ and the post-selected state Φ.

$$\langle\Psi|\hat{A}|\Psi\rangle = \sum_j \langle\Psi|\Phi_j\rangle\langle\Phi_j|\hat{A}|\Psi\rangle = \sum_j \langle\Psi|\Phi_j\rangle\langle\Phi_j|\Psi\rangle \frac{\langle\Phi_j|\hat{A}|\Psi\rangle}{\langle\Phi_j|\Psi\rangle} = \sum_j p_j \frac{\langle\Phi_j|\hat{A}|\Psi\rangle}{\langle\Phi_j|\Psi\rangle}$$

The weak value calculations are carried out in a 4-dimensional Hilbert space created by the tensor product of the photon's direction of propagation and polarization vectors.

Direction of propagation vectors:

$$L = \begin{pmatrix} 1 \\ 0 \end{pmatrix}$$

$$R = \begin{pmatrix} 0 \\ 1 \end{pmatrix}$$

Polarization state vectors:

$$H = \begin{pmatrix} 1 \\ 0 \end{pmatrix}$$

$$V = \begin{pmatrix} 0 \\ 1 \end{pmatrix}$$

Pre-selected state:

$$\Psi = \frac{1}{\sqrt{2}}(iL + R)H = \frac{1}{\sqrt{2}}\left[i\begin{pmatrix} 1 \\ 0 \end{pmatrix} + \begin{pmatrix} 0 \\ 1 \end{pmatrix}\right] + \begin{pmatrix} 1 \\ 0 \end{pmatrix} = frac1\sqrt{2}\begin{pmatrix} i \\ 1 \end{pmatrix}\begin{pmatrix} 1 \\ 0 \end{pmatrix}$$

$$\Psi = \frac{1}{\sqrt{2}}\begin{pmatrix} i \\ 0 \\ 1 \\ 0 \end{pmatrix}$$

Post-selected state:

$$\Phi = \frac{1}{\sqrt{2}}(LH + RV) = \frac{1}{\sqrt{2}}\left[\begin{pmatrix} 1 \\ 0 \end{pmatrix} + \begin{pmatrix} 1 \\ 0 \end{pmatrix} + \begin{pmatrix} 0 \\ 1 \end{pmatrix} + \begin{pmatrix} 0 \\ 1 \end{pmatrix}\right]$$

$$\Phi = \frac{1}{\sqrt{2}}\begin{pmatrix} 1 \\ 0 \\ 0 \\ 1 \end{pmatrix}$$

Direction of propagation operators:

$$Left = \begin{pmatrix} 1 \\ 0 \end{pmatrix}\begin{pmatrix} 1 & 0 \end{pmatrix} \rightarrow \begin{pmatrix} 1 & 0 \\ 0 & 0 \end{pmatrix}$$

$$Right = \begin{pmatrix} 0 \\ 1 \end{pmatrix}\begin{pmatrix} 0 & 1 \end{pmatrix} \rightarrow \begin{pmatrix} 0 & 0 \\ 0 & 1 \end{pmatrix}$$

Photon angular momentum operator:

$$Pang = \begin{pmatrix} 0 & -i \\ i & 0 \end{pmatrix}$$

Identity operator:

$$I = \begin{pmatrix} 1 & 0 \\ 0 & 1 \end{pmatrix}$$

The following weak value calculations show that for the pre- and post-selection ensemble of observations the photon is in the left arm of the interferometer while its angular momentum is in the right arm. Like the case of the Cheshire cat, a photon property has been separated from the photon.

$$\begin{pmatrix} "" & "Left\ Arm" & "Right\ Arm" \\ "Arm" & \frac{\Phi^T kronecker(Left,\ I)\Psi}{\Phi^T\Psi} & \frac{\Phi^T kronecker(Right,\ I)\Psi}{\Phi^T\Psi} \\ "Pang" & \frac{\Phi^T kronecker(Left,\ Pang)\Psi}{\Phi^T\Psi} & \frac{\Phi^T kronecker(Right,\ Pang)\Psi}{\Phi^T\Psi} \end{pmatrix}$$
$$= \begin{pmatrix} "" & "Left\ Arm" & "Right\ Arm" \\ "Arm" & 1 & 0 \\ "Pang" & 0 & 1 \end{pmatrix}$$

The following shows the evolution of the pre-selected state to the final state at the detectors. The intermediate is the state illuminating BS_2. The polarization state at the detectors is ignored.

$$|\Psi\rangle \rightarrow \frac{i}{\sqrt{2}}\left[|L\rangle|H\rangle + |R\rangle|V\rangle\right] \rightarrow -\frac{1}{2}|D_1\rangle + \frac{i}{2}|D_3\rangle + \frac{(i-1)}{2}|D_2\rangle$$

Squaring the magnitude of the probability amplitudes shows that the probabilities that D_1, D_3 and D_2 will fire are 1/4, 1/4 and 1/2, respectively. The probability at D_1 is consistent with the probability that the post-selected state is contained in the pre-selected state. A photon in the post-selected state has a probability of 1 of reaching D_1 and it represents a 25% contribution to the pre-selected state.

$$(|\Phi^T\Psi|)^2 \rightarrow \frac{1}{4}$$

Note that the expectation values for the pre-selected state show no path-polarization separation.

$$\begin{pmatrix} "" & "Left\ Arm" & "Right\ Arm" \\ "Arm" & (\overline{\Psi})^T kronecker(Left,\ I)\Psi & (\overline{\Psi})^T kronecker(Right,\ I)\Psi \\ "Pang" & (\overline{\Psi})^T kronecker(Left,\ Pang)\Psi & (\overline{\Psi})^T kronecker(Right,\ Pang)\Psi \\ "Hop" & (\overline{\Psi})^T kronecker(Left,\ HH^T)\Psi & (\overline{\Psi})^T kronecker(Right,\ HH^T)\Psi \\ "Vop" & (\overline{\Psi})^T kronecker(Left,\ VV^T)\Psi & (\overline{\Psi})^T kronecker(Right,\ VV^T)\Psi \end{pmatrix}$$
$$= \begin{pmatrix} "" & "Left\ Arm" & "Right\ Arm" \\ "Arm" & 0.5 & 0.5 \\ "Pang" & 0 & 0 \\ "Hop" & 0.5 & 0.5 \\ "Vop" & 0 & 0 \end{pmatrix}$$

In addition the following table shows that linear polarization (HV) is not separated from the photon's path.

$$HV = \begin{pmatrix} 1 & 0 \\ 0 & -1 \end{pmatrix}$$

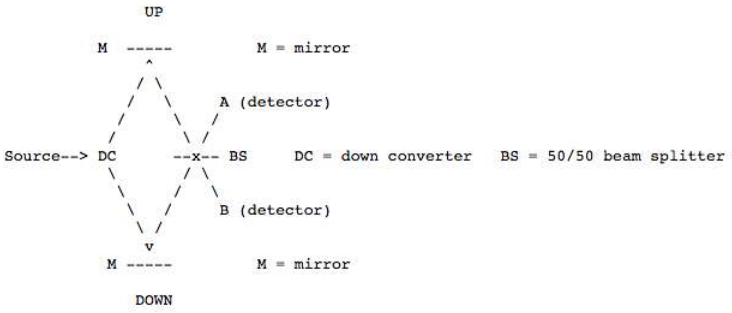
$$\begin{pmatrix} "" & "Left\ Arm" & "Right\ Arm" \\ "Arm" & \frac{\Phi^T kronecker(Left,\ I)\Psi}{\Phi^T\Psi} & \frac{\Phi^T kronecker(Right,\ I)\Psi}{\Phi^T\Psi} \\ "HV" & \frac{\Phi^T kronecker(Left,\ HV)\Psi}{\Phi^T\Psi} & \frac{\Phi^T kronecker(Right,\ HV)\Psi}{\Phi^T\Psi} \end{pmatrix}$$
$$= \begin{pmatrix} "" & "Left\ Arm" & "Right\ Arm" \\ "Arm" & 1 & 0 \\ "HV" & 1 & 0 \end{pmatrix}$$

The "Complete Quantum Cheshire Cat" by Guryanova, Brunner and Popescu (arXiv 1203.4215) provides an optical set-up which achieves complete path-polarization separation for the photon.

This page titled 7.25: A Quantum Optical Cheshire Cat is shared under a CC BY 4.0 license and was authored, remixed, and/or curated by Frank Rioux via source content that was edited to the style and standards of the LibreTexts platform.

7.26: Two Photon Interference - The Creation of an Entangled Superposition

In this experiment a down converter, DC, converts an incident photon into two lower energy photons. One photon takes the upper path and the other the lower path. The results of this experiment are that both photons are detected at either A or B. One photon is never detected at A while the other is detected at B. A quantum mechanical analysis of this phenomena is provided below.



After the down converter the initial photon leaving the source has evolved into a state which is an entangled linear superposition.

$$|Source\rangle \frac{[|up\rangle_1|down\rangle_2+|down\rangle_1|up\rangle_2]}{2^{\frac{1}{2}}} \tag{7.26.1}$$

This is an entangled state (non-factorable) because it acknowledges that it is unknown which photon takes which path. It also incorporates the fact that photons are bosons and consequently the state function must be symmetric with respect to interchange of the coordinates (paths) of the photons. If photons were fermions, |Source> would have to be antisymmetric with respect interchange of coordinates and the positive sign in Equation ??? would be replaced with a negative sign.

A photon that takes the upper path has a 50% chance of being detected at A or B. To reach A it must be reflected at the beam splitter and to reach B is must be transmitted. Conservation of energy requires a 90 degree phase difference between transmission and reflection, and by convention this phase difference is assigned to reflection. To reach detector A the upper photon must undergo a reflection at the beam splitter and its phase shift is recorded by multiplying |A> by i $[(-1)^{1/2}]$. Thus in terms of the detector states |A> and |B> the photon taking the upper path evolves into the state shown in Equation 7.26.2.

$$|up\rangle \frac{[i|A\rangle+|B\rangle]}{2^{\frac{1}{2}}} \tag{7.26.2}$$

Similar arguments show that the photon taking the lower path will evolve to the state given by Equation 7.26.3.

$$|down\rangle \frac{[i|A\rangle+|B\rangle]}{2^{\frac{1}{2}}} \tag{7.26.3}$$

When Equations 7.26.2 and 7.26.3 are substituted into Equation 7.26.1, the following final state results (A and B represent the detectors, while 1 and 2 designate the photons):

$$|Source\rangle$$
$$\frac{[i|A\rangle_1|A\rangle_2 + i^2|A\rangle_1 B\rangle_2 + |B\rangle_1|A\rangle_2 + i|B\rangle_1|B\rangle_2 + i|A\rangle_1|A\rangle_2 + |A\rangle_1|B\rangle_2 + i^2|B\rangle_1|A\rangle_2 + i|B\rangle_1|B\rangle_2]}{2^{\frac{3}{2}}}$$

Thus there eight final probability amplitudes, and they come in four pairs as can be seen above. However, two of the pairs destructively interfer (see note below) with each other and the final state is,

$$|Source\rangle \frac{[i|A\rangle_1|A\rangle_2 + i|B\rangle_1|B\rangle_2]}{2^{\frac{1}{2}}}$$

The probability of an outcome is found by taking the square of the absolute magnitude of its probability amplitude. Thus the probability that both photons will be recorded at A or both photons will be recorded at B is calculated as follows:

$$P(AA) = \left|\frac{i}{2}^{\frac{1}{2}}\right|^2 = \frac{1}{2}$$

$$P(BB) = \left| \frac{i}{2}^{\frac{1}{2}} \right|^2 = \frac{1}{2}$$

It was noted earlier that fermions require anti-symmetric state functions. So if this experiment **could** be performed with fermions Equation 7.26.1 would become,

$$|Source\rangle \frac{[|up\rangle_1 |down\rangle_2 - |down\rangle_1 |up\rangle_2]}{2^{\frac{1}{2}}} \tag{7.26.4}$$

After substitution of Equations 7.26.2 and 7.26.3 into Equation 7.26.4, we find

$$|Source\rangle \frac{[B\rangle_1 |A\rangle_2 - |A\rangle_1 |B\rangle_2]}{2^{\frac{1}{2}}}$$

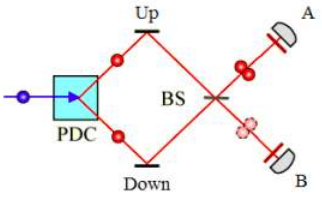
In other words the fermions are always detected at different detectors and are never found at the same detector at the same time. In summary, the sociology of bosons and fermions can be briefly stated: bosons are gregarious and enjoy company; fermions are antisocial and prefer solitude.

Note: "The things that interfere in quantum mechanics are not particles. They are probability amplitudes for certain events. It is the fact that probability amplitudes add up like complex numbers that is responsible for all quantum mechanical interferences." Roy J. Glauber, *American Journal of Physics*, **63(1)**, 12 (1995).

Reference: Greenberger, D. M.; Horne, M. A.; Zeilinger, A. *Physics Today*, **1993**, *44(8)*, 22.

This page titled 7.26: Two Photon Interference - The Creation of an Entangled Superposition is shared under a CC BY 4.0 license and was authored, remixed, and/or curated by Frank Rioux via source content that was edited to the style and standards of the LibreTexts platform.

7.27: Two-particle Interference for Bosons and Fermions



A parametric down converter, PDC, transforms an incident photon into two lower energy photons. One photon takes the upper path and the other the lower path or vice versa. The principles of quantum mechanics require that the wave function for this event be written as the following entangled superposition.

Entangled superposition for **bosons**:

$$\frac{1}{\sqrt{2}}(U_1 D_2 + D_1 U_2)$$

At the beam splitter, BS, the probability amplitude for transmission is $\frac{1}{\sqrt{2}}$ and the probability amplitude for reflection is $\frac{i}{\sqrt{2}}$. Therefore, for the four possible arrivals at the detectors we have,

$$U_1 = \frac{1}{\sqrt{2}}(iA_1 + B_1)$$

$$D_1 = \frac{1}{\sqrt{2}}(A_1 + iB_1)$$

$$U_2 = \frac{1}{\sqrt{2}}(iA_2 + B_2)$$

$$D_2 = \frac{1}{\sqrt{2}}(A_2 + iB_2)$$

Bosons are always observed at the same detector.

$$\frac{1}{\sqrt{2}}\left[\frac{1}{\sqrt{2}(iA_1 + B_1\sqrt{2}(A_2 + iB_2 + \sqrt{2}(A_1 + iB_1\sqrt{2}(iA_2 + B_2}\right] \; simplify$$
$$\rightarrow \sqrt{2}\left(\frac{A_1 A_2}{2} + \frac{B_1 B_2}{2}\right) i$$

Entangled superposition for **fermions**:

$$\frac{1}{\sqrt{2}} U_1 D_2 - D_1 U_2$$

Fermions are never observed at the same detector.

$$\frac{1}{\sqrt{2}}\left[\frac{1}{\sqrt{2}(iA_1 + B_1\sqrt{2}(A_2 + iB_2 - \sqrt{2}(A_1 + iB_1\sqrt{2}(iA_2 + B_2}\right] \; simplify$$
$$\rightarrow \frac{\sqrt{2}A_2 B_1}{2} + \frac{\sqrt{2}A_1 B_2}{2}$$

In summary, the sociology of bosons and fermions can be briefly stated: bosons are gregarious and enjoy company; fermions are antisocial and prefer solitude.

Another way to do the calculation using Mathcad.

Bosons:

$$\frac{1}{\sqrt{2}}(U_1 D_2 + D_1 U_2) \left| \begin{array}{l} \text{substitute, } U_1 = \frac{1}{\sqrt{2}}(iA_1 + B_1) \\ \text{substitute, } D_2 = \frac{1}{\sqrt{2}}(A_2 + iB_2) \\ \text{substitute, } D_1 = \frac{1}{\sqrt{2}}(A_1 + iB_1) \\ \text{substitute, } U_2 = \frac{1}{\sqrt{2}}(iA_2 + B_2) \\ \text{simplify} \end{array} \right. \rightarrow \sqrt{2}\left(\frac{A_1 A_2}{2} + \frac{B_1 B_2}{2}\right) i$$

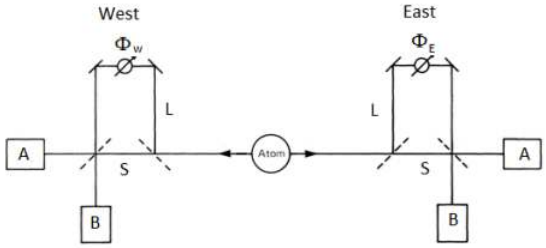
Fermions:

$$\frac{1}{\sqrt{2}}(U_1 D_2 - D_1 U_2) \left| \begin{array}{l} \text{substitute, } U_1 = \frac{1}{\sqrt{2}}(iA_1 + B_1) \\ \text{substitute, } D_2 = \frac{1}{\sqrt{2}}(A_2 + iB_2) \\ \text{substitute, } D_1 = \frac{1}{\sqrt{2}}(A_1 + iB_1) \\ \text{substitute, } U_2 = \frac{1}{\sqrt{2}}(iA_2 + B_2) \\ \text{simplify} \end{array} \right. \rightarrow \frac{\sqrt{2}A_2 B_1}{2} - \frac{\sqrt{2}A_1 B_2}{2}$$

This page titled 7.27: Two-particle Interference for Bosons and Fermions is shared under a CC BY 4.0 license and was authored, remixed, and/or curated by Frank Rioux via source content that was edited to the style and standards of the LibreTexts platform.

7.28: Analysis of a Two-photon Interferometer

In the two-photon interferometer shown below, an atom simultaneously emits identical photons to the east and west. Two paths (long and short) are available to detectors A and B in the east and west arms of the interferometer. The short paths are the same on both sides, but the long paths can have different lengths causing phase differences for the east and west directions.



Labeling the photons 1 and 2, and the directions W and E, the entangled photon wave function is:

$$\frac{1}{\sqrt{2}}(W_1E_2 + E_1W_2)$$

At the beam splitters (dashed diagonal lines), the probability amplitude for transmission is $\frac{1}{\sqrt{2}}$ and the probability amplitude for reflection is $\frac{1}{\sqrt{2}}$. By convention a π/2 phase shift is assigned to reflection. Armed with this information it in possible to trace the evolution of the initial entangled state. After the first beam splitter in each arm we have:

$$W_1 = \frac{1}{\sqrt{2}}(S_{w1} + iexp(i\phi_w)L_{w1})$$

$$E_1 = \frac{1}{\sqrt{2}}(S_{e1} + iexp(i\phi_e)L_{e1})$$

$$W_2 = \frac{1}{\sqrt{2}}(S_{w2} + iexp(i\phi_w)L_{w2})$$

$$E_2 = \frac{1}{\sqrt{2}}(S_{e2} + iexp(i\phi_e)L_{e2})$$

The second beam splitter has the following effect on the eight terms above:

$$S_{w1} = \frac{1}{\sqrt{2}}(A_{w1} + iB_{w1})$$

$$L_{w1} = \frac{1}{\sqrt{2}}(iA_{w1} + B_{w1})$$

$$S_{w2} = \frac{1}{\sqrt{2}}(A_{w2} + iB_{w2})$$

$$L_{w2} = \frac{1}{\sqrt{2}}(iA_{w2} + B_{w2})$$

$$S_{e1} = \frac{1}{\sqrt{2}}(A_{e1} + iB_{e1})$$

$$L_{e1} = \frac{1}{\sqrt{2}}(iA_{e1} + B_{e1})$$

$$S_{e2} = \frac{1}{\sqrt{2}}(A_{e2} + iB_{e2})$$

$$L_{e2} = \frac{1}{\sqrt{2}}(iA_{e2} + B_{e2})$$

Mathcad facilitates the substitution of these 12 expressions into the original entangled two-photon wave function as is shown below. To expedite interpretation we choose specific values for the relative phases of the photons in the branches of the interferometer. If the L paths both have ϕ = 0, they have the same length and the same length as the S paths. The photons always arrive at the B detectors. Other simple cases are summarized in the following table. However, most L-path phase relationships lead to complicated output wave functions.

$$\begin{bmatrix} \phi_w & \phi_e & WF \\ 0 & 0 & \frac{-1}{2}2^{\frac{1}{2}}(B_{w1}B_{e2}+B_{e1}B_{w2}) \\ 0 & \pi & \frac{1}{2}i2^{\frac{1}{2}}(B_{w1}A_{e2}+A_{e1}B_{w2}) \\ \pi & \pi & \frac{1}{2}2^{\frac{1}{2}}(A_{w1}A_{e2}+A_{e1}A_{w2}) \end{bmatrix}$$

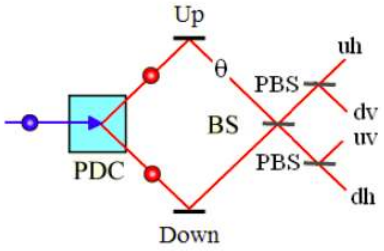
$$\phi_w = 0 \quad \phi_e = 0$$

$$\frac{1}{\sqrt{2}}(W_1E_2+E_1W_2) \left| \begin{array}{l} \text{substitute, } W_1 = \frac{1}{\sqrt{2}}(S_{w1}+iexp(i\phi_w)L_{w1}) \\ \text{substitute, } W_2 = \frac{1}{\sqrt{2}}(S_{w2}+iexp(i\phi_w)L_{w2}) \\ \text{substitute, } E_1 = \frac{1}{\sqrt{2}}(S_{e1}+iexp(i\phi_w)L_{e1}) \\ \text{substitute, } E_2 = \frac{1}{\sqrt{2}}(S_{e2}+iexp(i\phi_w)L_{e2}) \\ \text{substitute, } S_{w1} = \frac{1}{\sqrt{2}}(A_{w1}+iB_{w1}) \\ \text{substitute, } L_{w1} = \frac{1}{\sqrt{2}}(iA_{w1}+B_{w1}) \\ \text{substitute, } S_{w2} = \frac{1}{\sqrt{2}}(A_{w2}+iB_{w2}) \\ \text{substitute, } L_{w2} = \frac{1}{\sqrt{2}}(iA_{w2}+B_{w2}) \\ \text{substitute, } S_{e1} = \frac{1}{\sqrt{2}}(A_{e1}+iB_{e1}) \\ \text{substitute, } L_{e1} = \frac{1}{\sqrt{2}}(iA_{e1}+B_{e1}) \\ \text{substitute, } S_{e2} = \frac{1}{\sqrt{2}}(A_{e2}+iB_{e2}) \\ \text{substitute, } L_{e2} = \frac{1}{\sqrt{2}}(iA_{e2}+B_{e2}) \\ \text{simplify} \end{array} \right. \rightarrow \frac{-1}{2}2^{\frac{1}{2}}(B_{w1}B_{e2}+B_{e1}B_{w2})$$

This page titled 7.28: Analysis of a Two-photon Interferometer is shared under a CC BY 4.0 license and was authored, remixed, and/or curated by Frank Rioux via source content that was edited to the style and standards of the LibreTexts platform.

7.29: Two-photon Interferometry

In this experiment a parametric down converter, PDC, transforms an incident photon into two lower energy photons, one horizontally polarized and the other vertically polarized. One photon takes the upper path and the other the lower path or vice versa. The upper branch of the apparatus contains a polarization rotator, θ. The photon paths are combined at a 50-50 beam splitter, after which they interact with a polarizing beam splitter which separates horizontal (transmitted) and vertical (reflected) polarization. The results of this experiment are that no matter the angle θ both photons are detected at either the upper set of detectors (uh,dv) or the lower set of detectors (uv,dh). One photon is never detected at the upper set of detectors while the other is detected at the lower set of detectors. A quantum mechanical analysis of this phenomena is provided below.



PDC = Parametric Down Converter

BS = Beam Splitter

PBS = Polarizing Beam Splitter

uh = moving up, horizontal polarization

dv = moving down, vertical polarization

uv = moving up, vertical polarization

dh = moving down, horizontal polarization

θ = polarization rotator

The vectors representing the motional and polarization states of the photons are:

Motional states:

$$u = \begin{pmatrix} 1 \\ 0 \end{pmatrix}$$

$$d = \begin{pmatrix} 0 \\ 1 \end{pmatrix}$$

Polarization states:

$$h = \begin{pmatrix} 1 \\ 0 \end{pmatrix}$$

$$v = \begin{pmatrix} 0 \\ 1 \end{pmatrix}$$

There are four motional-polarization photon states after the PDC. These are formed by the tensor product of the appropriate motional and polarization vectors.

Combined motional and polarization states:

$$uh = \begin{pmatrix} 1 \\ 0 \\ 0 \\ 0 \end{pmatrix}$$

$$uv = \begin{pmatrix} 0 \\ 1 \\ 0 \\ 0 \end{pmatrix}$$

$$dh = \begin{pmatrix} 0 \\ 0 \\ 1 \\ 0 \end{pmatrix}$$

$$dv = \begin{pmatrix} 0 \\ 0 \\ 0 \\ 1 \end{pmatrix}$$

The optical devices are represented by matrices and operate on the vector states of the photons.

Rotation:

$$R(\theta) \begin{pmatrix} \cos\theta & -\sin\theta \\ \sin\theta & \cos\theta \end{pmatrix}$$

Beam splitter:

$$BS = \frac{1}{\sqrt{2}} \begin{pmatrix} 1 & i \\ i & 1 \end{pmatrix}$$

Polarizing beam splitter:

$$PBS = \begin{pmatrix} 1 & 0 & 0 & 0 \\ 0 & 0 & 0 & 1 \\ 0 & 0 & 1 & 0 \\ 0 & 1 & 0 & 0 \end{pmatrix}$$

An operator for the mirrors is not necessary, because if it is included it has no effect on the measurement results. The identity and a null matrix are also required as will be seen below.

Identity:

$$I = \begin{pmatrix} 1 & 0 \\ 0 & 1 \end{pmatrix}$$

Null matrix:

$$N = \begin{pmatrix} 0 & 0 & 0 \\ 0 & 0 & 0 \\ 0 & 0 & 0 \\ 0 & 0 & 0 \end{pmatrix}$$

The photon state after the PDC is a even superposition of all possible motional-polarization states.

$$|\Psi\rangle_i = \frac{1}{2}[|uh\rangle|dv\rangle + |uv\rangle|dh\rangle + |dh\rangle|uv\rangle + |dv\rangle|uh\rangle]$$

$$= \frac{1}{2}\left[\begin{pmatrix} 1 \\ 0 \\ 0 \\ 0 \end{pmatrix} \otimes \begin{pmatrix} 0 \\ 0 \\ 0 \\ 1 \end{pmatrix} + \begin{pmatrix} 0 \\ 1 \\ 0 \\ 0 \end{pmatrix} \otimes \begin{pmatrix} 0 \\ 0 \\ 1 \\ 0 \end{pmatrix} + \begin{pmatrix} 0 \\ 0 \\ 1 \\ 0 \end{pmatrix} \otimes \begin{pmatrix} 0 \\ 1 \\ 0 \\ 0 \end{pmatrix} + \begin{pmatrix} 0 \\ 0 \\ 0 \\ 1 \end{pmatrix} \otimes \begin{pmatrix} 1 \\ 0 \\ 0 \\ 0 \end{pmatrix}\right]$$

This state is formed as follows using Mathcad's kronecker command.

$$\Psi(a,b) = \text{submatrix}[\text{kronecker}[\text{augment}(a,N),\ (\text{augment}(b,N)), 1,\ 16,\ 1,\ 1]$$

$$\Psi_i = \frac{1}{2}\left(\Psi_{(uh,\ dv)} + \Psi_{(uv,\ dvh)} + \Psi_{(dh,\ uv)} + \Psi_{(dv,\ uh)}\right)$$

$$\Psi_i^T = (0 \quad 0 \quad 0 \quad 0.5 \quad 0 \quad 0 \quad 0.5 \quad 0 \quad 0 \quad 0.5 \quad 0 \quad 0 \quad 0.5 \quad 0 \quad 0 \quad 0)$$

The final state is calculated as a function of the orientation of the polarization rotator.

$$\Psi_f(\theta) = \text{kronecker}(PBS, PBS)\text{kronecker}(BS, \text{kronecker}(I, \text{kronecker}(BS,\ I)))$$
$$\text{kronecker}(I,\ \text{kronecker}(R, (\theta), \text{kronecker}(I,\ I)))\Psi_i$$

For θ = 0 the detected states are |uh>|dv>, |uv>|dh>, |dh>|uv> and |dv>|uh> each with a 25% probability of occurrence.

$$\begin{bmatrix} (|\Psi(uh,uh)\Psi_f(\theta)|)^2 & (|\Psi(uh,uv)\Psi_f(\theta)|)^2 & (|\Psi(uh,dh)\Psi_f(\theta)|)^2 & (|\Psi(uh,dv)\Psi_f(\theta)|)^2 \\ (|\Psi(uv,uh)\Psi_f(\theta)|)^2 & (|\Psi(uv,uv)\Psi_f(\theta)|)^2 & (|\Psi(uv,dh)\Psi_f(\theta)|)^2 & (|\Psi(uv,dv)\Psi_f(\theta)|)^2 \\ (|\Psi(dh,uh)\Psi_f(\theta)|)^2 & (|\Psi(dh,uv)\Psi_f(\theta)|)^2 & (|\Psi(dh,dh)\Psi_f(\theta)|)^2 & (|\Psi(dh,dv)\Psi_f(\theta)|)^2 \\ (|\Psi(dv,uh)\Psi_f(\theta)|)^2 & (|\Psi(dv,uv)\Psi_f(\theta)|)^2 & (|\Psi(dv,dh)\Psi_f(\theta)|)^2 & (|\Psi(dv,dv)\Psi_f(\theta)|)^2 \end{bmatrix}$$
$$= \begin{pmatrix} 0 & 0 & 0 & \frac{1}{4} \\ 0 & 0 & \frac{1}{4} & 0 \\ 0 & \frac{1}{4} & 0 & 0 \\ \frac{1}{4} & 0 & 0 & 0 \end{pmatrix}$$

For $\theta = \frac{\pi}{2}$ the detected states are |uh>|uh>, |uv>|uv>, |dh>|dh> and |dv>|dv> each with a 25% probability of occurrence.

$$\begin{bmatrix} (|\Psi(uh,uh)\Psi_f(\theta)|)^2 & (|\Psi(uh,uv)\Psi_f(\theta)|)^2 & (|\Psi(uh,dh)\Psi_f(\theta)|)^2 & (|\Psi(uh,dv)\Psi_f(\theta)|)^2 \\ (|\Psi(uv,uh)\Psi_f(\theta)|)^2 & (|\Psi(uv,uv)\Psi_f(\theta)|)^2 & (|\Psi(uv,dh)\Psi_f(\theta)|)^2 & (|\Psi(uv,dv)\Psi_f(\theta)|)^2 \\ (|\Psi(dh,uh)\Psi_f(\theta)|)^2 & (|\Psi(dh,uv)\Psi_f(\theta)|)^2 & (|\Psi(dh,dh)\Psi_f(\theta)|)^2 & (|\Psi(dh,dv)\Psi_f(\theta)|)^2 \\ (|\Psi(dv,uh)\Psi_f(\theta)|)^2 & (|\Psi(dv,uv)\Psi_f(\theta)|)^2 & (|\Psi(dv,dh)\Psi_f(\theta)|)^2 & (|\Psi(dv,dv)\Psi_f(\theta)|)^2 \end{bmatrix}$$
$$= \begin{pmatrix} \frac{1}{4} & 0 & 0 & 0 \\ 0 & \frac{1}{4} & 0 & 0 \\ 0 & 0 & \frac{1}{4} & 0 \\ 0 & 0 & 0 & \frac{1}{4} \end{pmatrix}$$

For $\theta = \frac{\pi}{4}$ the results of the previous examples occur with each state being observed with a probability of 12.5%.

$$\begin{bmatrix} (|\Psi(uh,uh)\Psi_f(\theta)|)^2 & (|\Psi(uh,uv)\Psi_f(\theta)|)^2 & (|\Psi(uh,dh)\Psi_f(\theta)|)^2 & (|\Psi(uh,dv)\Psi_f(\theta)|)^2 \\ (|\Psi(uv,uh)\Psi_f(\theta)|)^2 & (|\Psi(uv,uv)\Psi_f(\theta)|)^2 & (|\Psi(uv,dh)\Psi_f(\theta)|)^2 & (|\Psi(uv,dv)\Psi_f(\theta)|)^2 \\ (|\Psi(dh,uh)\Psi_f(\theta)|)^2 & (|\Psi(dh,uv)\Psi_f(\theta)|)^2 & (|\Psi(dh,dh)\Psi_f(\theta)|)^2 & (|\Psi(dh,dv)\Psi_f(\theta)|)^2 \\ (|\Psi(dv,uh)\Psi_f(\theta)|)^2 & (|\Psi(dv,uv)\Psi_f(\theta)|)^2 & (|\Psi(dv,dh)\Psi_f(\theta)|)^2 & (|\Psi(dv,dv)\Psi_f(\theta)|)^2 \end{bmatrix}$$
$$= \begin{pmatrix} \frac{1}{8} & 0 & 0 & \frac{1}{0} \\ 0 & \frac{1}{8} & \frac{1}{8} & 0 \\ 0 & \frac{1}{8} & \frac{1}{8} & 0 \\ \frac{1}{8} & 0 & 0 & \frac{1}{8} \end{pmatrix}$$

This page titled 7.29: Two-photon Interferometry is shared under a CC BY 4.0 license and was authored, remixed, and/or curated by Frank Rioux via source content that was edited to the style and standards of the LibreTexts platform.

7.29.1: Another Two Photon Interference Experiment

Your page has been created!

Remove this content and add your own.

Edit page

Click the Edit page button in your user bar. You will see a suggested structure for your content. Add your content and hit Save.

Tips:

Drag and drop

Drag one or more image files from your computer and drop them onto your browser window to add them to your page.

Classifications

Tags are used to link pages to one another along common themes. Tags are also used as markers for the dynamic organization of content in the NiCE Knowledge Management framework.

Working with templates

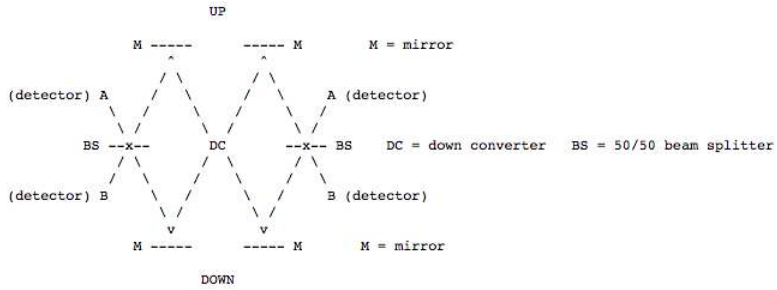
NiCE Knowledge Management templates help guide and organize your documentation, making it flow easier and more uniformly. Edit existing templates or create your own.

Visit for all help topics.

This page titled 7.29.1: Another Two Photon Interference Experiment is shared under a CC BY 4.0 license and was authored, remixed, and/or curated by Frank Rioux via source content that was edited to the style and standards of the LibreTexts platform.

7.30: Another Two Photon Interference Experiment

In this experiment a down converter, DC, converts an incident photon into two lower energy photons. One photon takes an upper path traveling left or right, and the other photon takes one of the lower paths traveling in the opposite direction. The results of this experiment are that both photons are recorded at either the A detectors or B detectors. One photon is never observed at an A detector while the other is observed at a B detector. A quantum mechanical analysis of this phenomena is provided below.



After the down converter the initial photon has evolved into a state which is an entangled linear superposition.

$$|DC\rangle \frac{[|up\rangle_1|down\rangle_2+|down\rangle_1|up\rangle_2]}{2^{\frac{1}{2}}}$$

This is an entangled state (non-factorable) because it acknowledges that it is unknown which photon takes which path. It also incorporates the fact that photons are bosons and consequently the state function must be symmetric with respect to interchange of the coordinates (paths) of the photons. If photons were fermions, |DC> would have to be antisymmetric with respect interchange of coordinates and the positive sign in equation (1) would be replaced with a negative sign.

A photon that takes one of the upper paths has a 50% chance of being recorded at an A or a B detector. To reach A it must be reflected at the beam splitter and to reach B is must be transmitted. Conservation of energy requires a 90 degree phase difference between transmission and reflection, and by convention this phase difference is assigned to reflection. To reach detector A the upper photon must undergo a reflection at the beam splitter and its phase shift is recorded by multiplying |A> by i $[(-1)^{1/2}]$. Thus in terms of the detector states |A> and |B> a photon taking an upper path evolves into the state shown in equation (2).

$$|up\rangle \frac{[i|A\rangle+|B\rangle]}{2^{\frac{1}{2}}}$$

Similar arguments show that a photon taking one of the lower paths will evolve into the state given by equation (3).

$$|down\rangle \frac{[|A\rangle + i|B\rangle]}{2^{\frac{1}{2}}}$$

When equations (2) and (3) are substituted into equation (1) the following final state results:

$$|Source\rangle$$
$$\frac{[i|A\rangle_1|A\rangle_2 + i^2|A\rangle_1|B\rangle_2+|B\rangle_1|A\rangle_2 + i|B\rangle_1|B\rangle_2 + i|A\rangle_1|A\rangle_2+|A\rangle_1|B\rangle_2 + i^2|B\rangle_1|A\rangle_2 + i|B\rangle_1|B\rangle_2]}{2^{\frac{3}{2}}}$$

Thus there are eight final probability amplitudes, and they come in four pairs as can be seen above. However, two of the pairs destructively interfer (see note below) with each other and the final state is,

$$|Source\rangle \frac{[i|A\rangle_1|A\rangle_2 + i|B\rangle_1|B\rangle_2]}{2^{\frac{1}{2}}}$$

The probability of an outcome is found by taking the square of the absolute magnitude of its probability amplitude. Thus the probability that both photons will be observed at A detectors, or both photons will be observed at B detectors is calculated as follows:

$$P(AA) = \left| \frac{1}{2}^{\frac{1}{2}} \right|^2 = \frac{1}{2}$$

$$P(BB) = \left| \frac{i}{2}^{\frac{1}{2}} \right|^2 = \frac{1}{2}$$

It was noted earlier that fermions require anti-symmetric state functions. So if this experiment **could** be performed with fermions the results would be P(AA) = P(BB) = 0, and P(AB) = P(BA) = 1/2.

Note: "The things that interfere in quantum mechanics are not particles. They are probability amplitudes for certain events. It is the fact that probability amplitudes add up like complex numbers that is responsible for all quantum mechanical interferences." Roy J. Glauber, *American Journal of Physics*, **63(1)**, 12 (1995).

Reference: Greenberger, D. M.; Horne, M. A.; Zeilinger, A. *Physics Today*, **1993**, *44(8)*, 22.

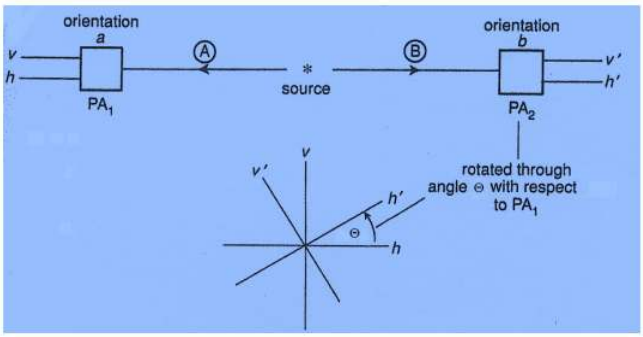
This page titled 7.30: Another Two Photon Interference Experiment is shared under a CC BY 4.0 license and was authored, remixed, and/or curated by Frank Rioux via source content that was edited to the style and standards of the LibreTexts platform.

7.31: Quantum Correlations Illuminated with Tensor Algebra

Jim Baggott's excellent text, *The Meaning of Quantum Theory*, deals with the fundamentals of quantum mechanics and its various philosophical interpretations. His demonstrations of computational methods (generally using Dirac algebra) are easy to follow and his summaries of the interpretive positions of Bohr, Einstein, Bohm, Everett, etc. are lucid. Of special note is the clarity with which he deals with the importance of the work of John S. Bell and the eponymous Bell's theorem.

In order to appreciate the significance of Bell's theorem you need to be willing to do some math. This tutorial deals with recasting the mathematics of Baggott's treatment of quantum correlations (pages 119 to 127) using tensor algebra. Not because there is any deficiency in his math, but simply to present another, related method.

The experiment analyzed involves the simultaneous release of two entangled photons in opposite directions as shown below, followed by measurement of their polarization state in the vertical/horizontal measurement basis. The experimental set-up allows for the rotation of the right-hand detector through an angle of Θ, in order to more thoroughly explore the consequences of photon entanglement.



The experiment involves measurement of the polarization states of the photon pairs (A,B) as diagramed above. The various polarization states involved are presented below in vector notation: v = vertical; h = horizontal; L = left circular; R = right circular.

$$|v\rangle = \begin{pmatrix} 1 \\ 0 \end{pmatrix}$$

$$|v'\rangle = \begin{pmatrix} \cos\theta \\ -\sin\theta \end{pmatrix}$$

$$|v\rangle = \begin{pmatrix} 0 \\ 1 \end{pmatrix}$$

$$|h'\rangle = \begin{pmatrix} \sin\theta \\ \cos\theta \end{pmatrix}$$

$$|L\rangle = \frac{1}{\sqrt{2}} \begin{pmatrix} 1 \\ i \end{pmatrix}$$

$$|R\rangle = \frac{1}{\sqrt{2}} \begin{pmatrix} 1 \\ -i \end{pmatrix}$$

The initial state (see Baggott for details) is the following entangled superposition. In other words, both photons, the one moving to the right and the one moving to the left are in the same circular polarization state.

$$|\Psi\rangle = \frac{1}{\sqrt{2}} \left[|L\rangle_A |L\rangle_B + |R\rangle_A |R\rangle_B \right]$$

This initial photon state is recast using the vector tensor product, which is formed as follows.

$$\begin{pmatrix} a \\ b \end{pmatrix} \otimes \begin{pmatrix} c \\ d \end{pmatrix} = \begin{pmatrix} ac \\ ad \\ bc \\ bd \end{pmatrix}$$

Therefore in the tensor format the initial state is,

$$|\Psi\rangle = \frac{1}{\sqrt{2}}\left[|L\rangle_A|L\rangle_B + |R\rangle_A|R\rangle_B\right] = \frac{1}{2\sqrt{2}}\left[\begin{pmatrix} 1 \\ i \end{pmatrix}_A \otimes \begin{pmatrix} 1 \\ i \end{pmatrix}_B + \begin{pmatrix} 1 \\ -i \end{pmatrix}_A \otimes \begin{pmatrix} 1 \\ -i \end{pmatrix}_B\right]$$
$$= \frac{1}{2\sqrt{2}}\left[\begin{pmatrix} 1 \\ i \\ i \\ -1 \end{pmatrix} + \begin{pmatrix} 1 \\ -i \\ -i \\ -1 \end{pmatrix}\right] = \frac{1}{\sqrt{2}}\begin{pmatrix} 1 \\ 0 \\ 0 \\ -1 \end{pmatrix}$$

There are four measurement outcomes for the photon pairs. Both photons can be detected in the vertical state, both in the horizontal state, A in the vertical state and B in the horizontal state, and vice versa. The measurement eigenstates are calculated below in tensor format.

$$|\psi'_{vv}\rangle = |v\rangle_A|v'\rangle_B = \begin{pmatrix} 1 \\ 0 \end{pmatrix} \otimes \begin{pmatrix} \cos\theta \\ -\sin\theta \end{pmatrix} = \begin{pmatrix} \cos\theta \\ -\sin\theta \\ 0 \\ 0 \end{pmatrix}$$

$$|\psi'_{vh}\rangle = |v\rangle_A|h'\rangle_B = \begin{pmatrix} 1 \\ 0 \end{pmatrix} \otimes \begin{pmatrix} \sin\theta \\ \cos\theta \end{pmatrix} = \begin{pmatrix} \sin\theta \\ \cos\theta \\ 0 \\ 0 \end{pmatrix}$$

$$|\psi'_{hv}\rangle = |h\rangle_A|v'\rangle_B = \begin{pmatrix} 0 \\ 1 \end{pmatrix} \otimes \begin{pmatrix} \cos\theta \\ -\sin\theta \end{pmatrix} = \begin{pmatrix} 0 \\ 0 \\ \cos\theta \\ -\sin\theta \end{pmatrix}$$

$$|\psi'_{hh}\rangle = |h\rangle_A|h'\rangle_B = \begin{pmatrix} 0 \\ 1 \end{pmatrix} \otimes \begin{pmatrix} \sin\theta \\ \cos\theta \end{pmatrix} = \begin{pmatrix} 0 \\ 0 \\ \sin\theta \\ \cos\theta \end{pmatrix}$$

The probability amplitudes for these experimental possibilities are found by calculating the projection of their eigenstates onto the initial state vector.

$$\langle\psi'_{vv}|\Psi\rangle \begin{pmatrix} \cos\theta & -\sin\theta & 0 & 0 \end{pmatrix} \frac{1}{\sqrt{2}}\begin{pmatrix} 1 \\ 0 \\ 0 \\ -1 \end{pmatrix} = \frac{1}{\sqrt{2}}\cos\theta$$

$$\langle\psi'_{vh}|\Psi\rangle \begin{pmatrix} \sin\theta & \cos\theta & 0 & 0 \end{pmatrix} \frac{1}{\sqrt{2}}\begin{pmatrix} 1 \\ 0 \\ 0 \\ -1 \end{pmatrix} = \frac{1}{\sqrt{2}}\sin\theta$$

$$\langle\psi'_{hv}|\Psi\rangle \begin{pmatrix} 0 & 0 & \cos\theta & -\sin\theta \end{pmatrix} \frac{1}{\sqrt{2}}\begin{pmatrix} 1 \\ 0 \\ 0 \\ -1 \end{pmatrix} = \frac{1}{\sqrt{2}}\sin\theta$$

$$\langle\psi'_{hh}|\Psi\rangle \begin{pmatrix} 0 & 0 & \sin\theta & \cos\theta \end{pmatrix} \frac{1}{\sqrt{2}}\begin{pmatrix} 1 \\ 0 \\ 0 \\ -1 \end{pmatrix} = -\frac{1}{\sqrt{2}}\cos\theta$$

This yields the following probabilities for the four experimental outcomes. (See Baggott's equation 4.16 on page 127 of his text.)

$$P_{vv}(\theta) = |\langle \psi'_{vv}|\Psi\rangle|^2 = \frac{1}{2}\cos^2\theta$$

$$P_{vh}(\theta) = |\langle \psi'_{vh}|\Psi\rangle|^2 = \frac{1}{2}\sin^2\theta$$

$$P_{hv}(\theta) = |\langle \psi'_{hv}|\Psi\rangle|^2 = \frac{1}{2}\sin^2\theta$$

$$P_{hh}(\theta) = |\langle \psi'_{hh}|\Psi\rangle|^2 = \frac{1}{2}\cos^2\theta$$

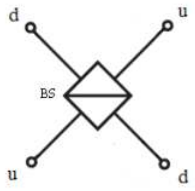
(Note that if Θ = 0, we get the results Baggott reports on page 122.)

Baggott goes on to show how this experiment and its more sophisticated successors, and their quantum mechanical analyses, illuminate the contradiction between the quantum and classical visions of reality. The purpose of this tutorial has been merely to present a somewhat different format for carrying out the quantum mechanical calculations.

This page titled 7.31: Quantum Correlations Illuminated with Tensor Algebra is shared under a CC BY 4.0 license and was authored, remixed, and/or curated by Frank Rioux via source content that was edited to the style and standards of the LibreTexts platform.

7.32: Two Photon Entanglement - A Tensor Algebra Analysis

Photons from separate sources, u and d, arrive simultaneously at the beam splitter shown in the figure below.



Because the photons arrive simultaneously at the beam splitter they are indistinguishable and don′t possess separate identities. We are forced by quantum mechanical principles to represent their collective state at the beam splitter (BS) by the following entangled wave function. The plus sign in this superposition indicates that photons are bosons; their wave functions are symmetric with respect to the interchange of the photon labels.

$$|\Psi_B\rangle = \frac{1}{\sqrt{2}}\left[|u\rangle_1|d\rangle_2 + |d\rangle_1|u\rangle_2\right]$$

The following vector representations are used for the photon motional states.

$$|u\rangle = \begin{pmatrix}1\\0\end{pmatrix}$$

$$|d\rangle = \begin{pmatrix}0\\1\end{pmatrix}$$

Writing Ψ_B in tensor format yields,

$$|\Psi_B\rangle = \frac{1}{\sqrt{2}}\left[\begin{pmatrix}1\\0\end{pmatrix}\otimes\begin{pmatrix}0\\1\end{pmatrix} + \begin{pmatrix}0\\1\end{pmatrix}\otimes\begin{pmatrix}1\\0\end{pmatrix}\right] = \frac{1}{\sqrt{2}}\left[\begin{pmatrix}0\\1\\0\\0\end{pmatrix} + \begin{pmatrix}0\\0\\1\\0\end{pmatrix}\right] = \frac{1}{\sqrt{2}}\begin{pmatrix}0\\1\\1\\0\end{pmatrix}$$

$$\Psi_B = \frac{1}{\sqrt{2}}\begin{pmatrix}0\\1\\1\\0\end{pmatrix}$$

Transmission and reflection occur at 50-50 beam splitters. By convention, reflection is assigned a π/2 (exp(iπ/2) = i) phase shift relative to transmission. The matrix representing a 50-50 beam splitter operating on an individual photon is given below, along with its effect on the u and d photon states.

$$BS = \frac{1}{\sqrt{2}}\begin{pmatrix}1 & i\\ i & 1\end{pmatrix}$$

$$BS\begin{pmatrix}1\\0\end{pmatrix} \rightarrow \begin{pmatrix}\frac{\sqrt{2}}{2}\\ \frac{\sqrt{2}i}{2}\end{pmatrix}$$

$$BS\begin{pmatrix}0\\1\end{pmatrix} \rightarrow \begin{pmatrix}\frac{\sqrt{2}i}{2}\\ \frac{\sqrt{2}}{2}\end{pmatrix}$$

This shows that the beam splitter converts pure states, u and d, into superpositions of u and d.

In this experiment the beam splitter operates on both photons, so in tensor format the operator representing the beam splitter becomes the following 4x4 matrix.

$$\hat{BS} = \hat{BS}_2 \otimes \hat{BS}_1 = \frac{1}{\sqrt{2}}\begin{pmatrix}1 & i\\ i & 1\end{pmatrix} \otimes \frac{1}{\sqrt{2}}\begin{pmatrix}1 & i\\ i & 1\end{pmatrix} \frac{1}{2}\begin{pmatrix}1\begin{pmatrix}1 & i\\ i & 1\end{pmatrix} & i\begin{pmatrix}1 & i\\ i & 1\end{pmatrix}\\ i\begin{pmatrix}1 & i\\ i & 1\end{pmatrix} & 1\begin{pmatrix}1 & i\\ i & 1\end{pmatrix}\end{pmatrix}$$

$$= \frac{1}{2}\begin{pmatrix}1 & i & i & -1\\ i & 1 & -1 & i\\ i & -1 & 1 & i\\ -1 & i & i & 1\end{pmatrix}$$

There are four possible photon output states after the beam splitter (|uu >, |ud >, |du >, |dd >), which are shown below in tensor format.

$$|uu\rangle = \begin{pmatrix}1\\0\end{pmatrix} \otimes \begin{pmatrix}1\\0\end{pmatrix} = \begin{pmatrix}1\\0\\0\\0\end{pmatrix}$$

$$uu = \begin{pmatrix}1\\0\\0\\0\end{pmatrix}$$

$$|ud\rangle = \begin{pmatrix}1\\0\end{pmatrix} \otimes \begin{pmatrix}0\\1\end{pmatrix} = \begin{pmatrix}0\\1\\0\\0\end{pmatrix}$$

$$ud = \begin{pmatrix}0\\1\\0\\0\end{pmatrix}$$

$$|du\rangle = \begin{pmatrix}0\\1\end{pmatrix} \otimes \begin{pmatrix}1\\0\end{pmatrix} = \begin{pmatrix}0\\0\\1\\0\end{pmatrix}$$

$$du = \begin{pmatrix}0\\0\\1\\0\end{pmatrix}$$

$$|dd\rangle = \begin{pmatrix}0\\1\end{pmatrix} \otimes \begin{pmatrix}0\\1\end{pmatrix} = \begin{pmatrix}0\\0\\0\\1\end{pmatrix}$$

$$dd = \begin{pmatrix}0\\0\\0\\1\end{pmatrix}$$

The output state created by the interaction of the initial entangled state with the beam splitter is,

$$\Psi_{Bout} = \frac{1}{2}\begin{pmatrix}1 & i & i & -1\\ i & 1 & -1 & i\\ i & -1 & 1 & i\\ -1 & i & i & 1\end{pmatrix} \frac{1}{\sqrt{2}}\begin{pmatrix}0\\1\\1\\0\end{pmatrix} \rightarrow \begin{pmatrix}\frac{\sqrt{2}i}{2}\\0\\0\\\frac{\sqrt{2}i}{2}\end{pmatrix}$$

By inspection we can see that the photons are always observed in the same output channel, either |uu > or |dd >, with equal probabilities of 0.5 ($|0.707i|^2$). Not surprisingly we see bosonic behavior by the photons. After the beam splitter they are in an even superposition of both being at u and both being at d. Unlike fermions bosons can be in the same state at the same time.

$$\left(\left|uu^T\Psi_{Bout}\right|\right)^2 \rightarrow \frac{1}{2}$$

$$\left(\left|dd^T\Psi_{Bout}\right|\right)^2 \rightarrow \frac{1}{2}$$

Naturally this means they are never observed in different output channels, |ud> or |du>.

$$\left(\left|ud^T\Psi_{Bout}\right|\right)^2 \rightarrow 0$$

$$\left(\left|du^T\Psi_{Bout}\right|\right)^2 \rightarrow 0$$

Now let's pretend that photons are fermions and examine the consequences for this experiment. Fermions have antisymmetric wave functions; the wave function changes sign on interchange of the constituents labels.

$$|\Psi_F\rangle = \frac{1}{\sqrt{2}}\left[|u\rangle_1|d\rangle_2 - |d\rangle_1|u\rangle_2\right]$$

Written in tensor format the antisymmetric wave function is

$$|\Psi_F\rangle = \frac{1}{\sqrt{2}}\left[\begin{pmatrix}1\\0\end{pmatrix}\otimes\begin{pmatrix}0\\1\end{pmatrix} - \begin{pmatrix}0\\1\end{pmatrix}\otimes\begin{pmatrix}1\\0\end{pmatrix}\right] = frac1\sqrt{2}\left[\begin{pmatrix}0\\1\\0\\0\end{pmatrix} - \begin{pmatrix}0\\0\\1\\0\end{pmatrix}\right] = \frac{1}{\sqrt{2}}\begin{pmatrix}0\\1\\-1\\0\end{pmatrix}$$

$$\Psi_F = \frac{1}{\sqrt{2}}\begin{pmatrix}0\\1\\-1\\0\end{pmatrix}$$

Now the interaction with the beam splitter yields the following result.

$$|Psi_{Fout} = \frac{1}{2}\begin{pmatrix}1 & i & i & 1\\ i & 1 & -1 & i\\ i & -1 & 1 & i\\ -1 & i & i & 1\end{pmatrix}\frac{1}{\sqrt{2}}\begin{pmatrix}0\\1\\-1\\0\end{pmatrix} \rightarrow \begin{pmatrix}0\\\frac{\sqrt{2}}{2}\\-\frac{\sqrt{2}}{2}\\0\end{pmatrix}$$

We see by inspection or calculation that fermionic photons are never observed in the same output channel after interaction with the beam splitter.

$$\left(\left|uu^T\Psi_{Fout}\right|\right)^2 \rightarrow 0$$

$$\left(\left|dd^T\Psi_{Fout}\right|\right)^2 \rightarrow 0$$

Naturally this means they are always observed in different output channels, |ud > or |du>.

$$\left(\left|ud^T\Psi_{Fout}\right|\right)^2 \rightarrow \frac{1}{2}$$

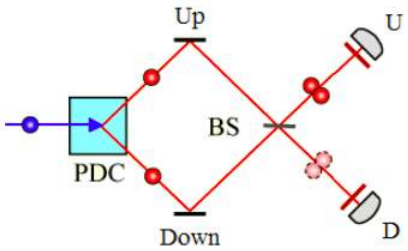
$$\left(\left|du^T\Psi_{Fout}\right|\right)^2 \rightarrow \frac{1}{2}$$

In summary, the sociology of bosons and fermions can be briefly stated: bosons are gregarious and enjoy company; fermions are antisocial and prefer solitude.

This page titled 7.32: Two Photon Entanglement - A Tensor Algebra Analysis is shared under a CC BY 4.0 license and was authored, remixed, and/or curated by Frank Rioux via source content that was edited to the style and standards of the LibreTexts platform.

7.33: Two Photon Interference - Matrix Mechanics Approach

In this experiment a down converter, DC, transforms an incident photon into two lower energy photons. One photon takes the upper path and the other the lower path or vice versa. The results of this experiment are that both photons are detected at either U or D. One photon is never detected at U while the other is detected at D. A quantum mechanical analysis of this phenomena is provided below.



Orthonormal basis states:

Photon moving in up-direction:

$$u = \begin{pmatrix} 1 \\ 0 \end{pmatrix}$$

$$u^T u = 1$$

Photon moving in down-direction:

$$d = \begin{pmatrix} 0 \\ 1 \end{pmatrix}$$

$$d^T d = 1$$

$$u^T d = 0$$

Operators:

Operator for interaction with the mirror:

$$M = \begin{pmatrix} 0 & 1 \\ 1 & 0 \end{pmatrix}$$

Operator for interaction with a 50/50 beam splitter:

$$BS = \frac{1}{\sqrt{2}} \begin{pmatrix} 1 & i \\ i & 1 \end{pmatrix}$$

A 90^o phase shift between transmission and reflection at the beam splitter is required to satisfy energy conservation. By convention the phase shift is assigned to reflection.

The down-converter creates the following entangled state:

$$|Psi_b\rangle = \frac{[|u\rangle_1 |d\rangle_2 + d\rangle_1 u\rangle_2]}{2^{\frac{1}{2}}}$$

This is a symmetric state because photons are bosons.

After creation in the down-converter, both photons interact with a mirror and a beam splitter before reaching a detector, either U or D. To be detected at the U-detector the photon must be moving in the up-direction (photon state = |u>). To be detected at the D-detector the photon must be moving in the down-direction (photon state = |d>). The probabilities for the four possible experimental outcomes are calculated below.

Both photons arrive at the U-detector: $|_1\langle u|_2\langle u|\mathbf{BS}\quad \mathbf{M}|\Psi_b\rangle|^2$.

$$\left[\left|\frac{(u^TBSMu)(u^TBSMd)+(u^TBSMd)(u^TBSMu)}{\sqrt{2}}\right|\right]^2=0.5$$

Both photons arrive at the D-detector: $|_1\langle d|_2\langle d|\mathbf{BS}\quad \mathbf{M}|\Psi_b\rangle|^2$.

$$\left[\left|\frac{(d^TBSMu)(d^TBSMd)+(d^TBSMd)(d^TBSMu)}{\sqrt{2}}\right|\right]^2=0.5$$

Photon 1 arrives at the U-detector and photon 2 arrives at the D-detector: $|_1\langle u|_2\langle d|\mathbf{BS}\quad \mathbf{M}|\Psi_b\rangle|^2$.

$$\left[\left|\frac{(u^TBSMu)(d^TBSMd)+(u^TBSMd)(d^TBSMu)}{\sqrt{2}}\right|\right]^2=0$$

Photon 1 arrives at the D-detector and photon 2 arrives at the U-detector: $|_1\langle d|_2\langle u|\mathbf{BS}\quad \mathbf{M}|\Psi_b\rangle|^2$.

$$\left[\left|\frac{(d^TBSMu)(u^TBSMd)+(d^TBSMd)(u^TBSMu)}{\sqrt{2}}\right|\right]^2=0$$

If the experiment could be performed with fermions, they would be created in the following anti-symmetric entangled state:

$$|Psi_f\rangle=\frac{[|u\rangle_1|d\rangle_2-d\rangle_1u\rangle_2]}{2^{\frac{1}{2}}}$$

As the analysis below shows, the results for fermions would be exactly opposite to those for bosons. Two fermions would never arrive at the same detector.

Both fermions arrive at the U-detector: $|_1\langle u|_2\langle u|\mathbf{BS}\quad \mathbf{M}|\Psi_f\rangle|^2$

$$\left[\left|\frac{(u^TBSMu)(u^TBSMd)-(u^TBSMd)(u^TBSMu)}{\sqrt{2}}\right|\right]^2=0$$

Both fermions arrive at the D-detector: $|_1\langle d|_2\langle d|\mathbf{BS}\quad \mathbf{M}|\Psi_f\rangle|^2$

$$\left[\left|\frac{(d^TBSMu)(d^TBSMd)-(d^TBSMd)(d^TBSMu)}{\sqrt{2}}\right|\right]^2=0$$

Fermion 1 arrives at the U-detector and fermion 2 arrives at the D-detector: $|_1\langle u|_2\langle d|\mathbf{BS}\quad \mathbf{M}|\Psi_f\rangle|^2$

$$\left[\left|\frac{(u^TBSMu)(d^TBSMd)-(u^TBSMd)(d^TBSMu)}{\sqrt{2}}\right|\right]^2=0.5$$

Fermion 1 arrives at the D-detector and fermion 2 arrives at the U-detector: $|_1\langle d|_2\langle u|\mathbf{BS}\quad \mathbf{M}|\Psi_f\rangle|^2$

$$\left[\left|\frac{(d^TBSMu)(u^TBSMd)-(d^TBSMd)(u^TBSMu)}{\sqrt{2}}\right|\right]^2=0.5$$

The results of this tutorial enable us to formulate a sociology for bosons and fermions: bosons are gregarious and enjoy companionship; fermions are anti-social and prefer solitude.

But why do bosons always end up at the same detector and fermions (hypothetically) always end up at different detectors? Why in both cases do half of the possible outcomes not occur? Are the bosons and fermions interfering with each other directly? Is there a subtle attractive interaction between bosons and an equally subtle, non-electrostatic, repulsive interaction between fermions?

Not according to Roy Glauber who said, "The things that interfere in quantum mechanics are not particles. They are probability amplitudes for certain events. It is the fact that probability amplitudes add up like complex numbers that accounts for all quantum mechanical interferences." [American Journal of Physics **63**, 12 (1995)]

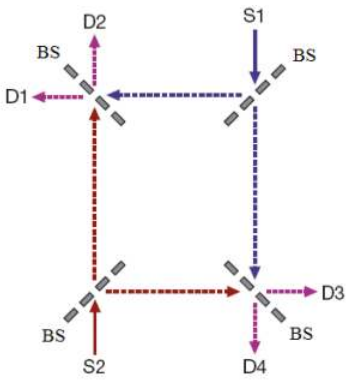
The analysis used in this tutorial clearly illustrates Glauber's assertion.

Reference: Greenberger, D.M.; Horne, M.A.; Zeilinger, A. *Physics Today*, **1993**, *44(8)*, *22*.

This page titled 7.33: Two Photon Interference - Matrix Mechanics Approach is shared under a CC BY 4.0 license and was authored, remixed, and/or curated by Frank Rioux via source content that was edited to the style and standards of the LibreTexts platform.

7.34: Two-electron Interference

This tutorial provides a simplified analysis of a recent experiment describing the "interference between two indistinguishable electrons from independent sources."*(1)* A schematic of the interferometer used in this experiment is shown below.



S1 and S2 are the electron sources, BS labels the four 50-50 beam splitters and D1, D2, etc. are the electron detectors.

To simplify the analysis it will be assumed that the arms of the interferometer are of equal length. This will make it unnecessary to consider the accumulation of phase differences due to unequal path distances to the detectors.

The sources simultaneously inject electrons into the interferometer. The presence of the beam splitters provides each source beam access to all four detectors. For example, the source wave functions written in the basis of the detectors are,

$$|S1\rangle \rightarrow \frac{1}{2}[i|D1\rangle - |D2\rangle + i|D3\rangle + |D4\rangle]$$

$$|S2\rangle \rightarrow \frac{1}{2}[i|D1\rangle + |D2\rangle + i|D3\rangle - |D4\rangle]$$

Following the usual convention a π/2 phase shift (represented by i) is assigned to reflection at the beam splitter. It should be noted that there is no opportunity for electron self-interference because the individual electron beams are not recombined. This means the source of interference in this experiment is due to the indistinguishability of the electrons and the fermionic character of the total wave function which is an entangled two-electron state.

$$|\Psi\rangle_{tot} = \frac{1}{\sqrt{2}}[|S1\rangle_a|S2\rangle_b - |S2\rangle_a|S1\rangle_b]$$

Substitution of the first two equations into the third yields,

$$|\Psi\rangle_{tot} = \frac{i\sqrt{2}}{4}[|D1\rangle_a|D2\rangle_b - |D2\rangle_a|D1\rangle_b - |D2\rangle_a|D3\rangle_b - D1\rangle_a|D4\rangle_b - D3\rangle_a|D4\rangle_b + |D4\rangle_a|D1\rangle_b + |D3\rangle_a|D2\rangle_b + |D4\rangle_a|D3\rangle_b]$$

where the subscripts $a$and b label the electrons.

This result predicts that the electrons never arrive at the same detector, and that the D1-D3 and D2-D4 coincidences are not observed. This is in agreement with the more general results reported by Neder, et al. *(1)* See, for example, their Equation 3 for $\phi 1 = \phi 2 = \phi 3 = \phi 4 = 0$.

Neder, et al. comment as follows on the distinction between single- and two-particle interference.

> Very much like the ubiquitous quantum interference of a single particle with itself, quantum interference of two independent, but indistinquishable, particles is also possible. For a single particle, the interference is between the amplitudes of the particle's wave function, whereas the interference between two particles is a direct result of quantum exchange statistics. Such interference is observed only in the joint probability of finding the particles in two separated detectors, after they were injected from spatially separated and independent sources.

While it is customary to talk about particle interference, as these authors do, Nobel Laureate Roy Glauber recommended more careful language. *(2)*

The things that interfere in quantum mechanics are not particles. They are probability amplitudes for certain events. It is the fact that probability amplitudes add up like complex numbers that is responsible for all quantum mechanical interferences.

The insightfulness of this observation is clearly revealed in the mathematical underpinnings of this experiment.

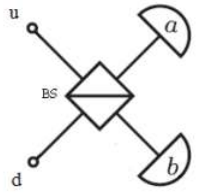
References

1. Neder, I. *et al. Nature* **448**, 333-337 (2007)
2. Glauber, J. *American Journal of Physics*, **63(1)**, 12 (1995).

This page titled 7.34: Two-electron Interference is shared under a CC BY 4.0 license and was authored, remixed, and/or curated by Frank Rioux via source content that was edited to the style and standards of the LibreTexts platform.

7.35: Bosonic and Fermionic Photon Behavior at Beam Splitters

Photons from separate sources, u and d, arrive simultaneously at the beam splitter shown in the figure below.



Because these photons are indistinguishable they do not possess separate identities, and we are forced by quantum mechanical principles to represent their collective state at the beam splitter (BS) by the following entangled wave function. The plus sign in this superposition indicates that photons are bosons; their wave functions are symmetric with respect to the interchange of the photon labels.

$$\Psi = \frac{1}{\sqrt{2}}(u_1 d_2 + d_1 u_2)$$

Transmission and reflection occur at the 50-50 beam splitters. By convention, reflection is assigned a π/2 phase shift relative to transmission. Thus, in the basis of the detectors, a and b, the photons originating in ports u and d evolve as follows.

$$u = \frac{1}{\sqrt{2}}(ia + b)$$

$$d = \frac{1}{\sqrt{2}}(a + ib)$$

Adding photon labels we have:

$$u_1 = \frac{1}{\sqrt{2}}(ia_1 + b_1)$$

$$u_2 = \frac{1}{\sqrt{2}}(ia_2 + b_2)$$

$$d_1 = \frac{1}{\sqrt{2}}(ia_1 + b_1)$$

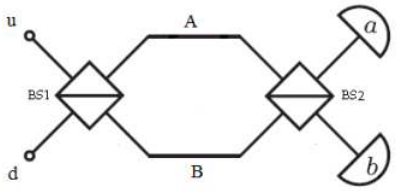
$$d_2 = \frac{1}{\sqrt{2}}(ia_2 + b_2)$$

Substitution of these states into Ψ yields,

$$\Psi = \frac{1}{\sqrt{2}}(u_1 d_2 + d_1 u_2) \left| \begin{array}{l} \text{substitute, } u_1 = \frac{1}{\sqrt{2}}(ia_1 + b_1) \\ \text{substitute, } u_2 = \frac{1}{\sqrt{2}}(ia_2 + b_2) \\ \text{substitute, } d_1 = \frac{1}{\sqrt{2}}(a_1 + ib_1) \\ \text{substitute, } d_2 = \frac{1}{\sqrt{2}}(a_2 + ib_2) \\ \text{simplify} \end{array} \right. \rightarrow \Psi = \sqrt{2}\left(\frac{a_1 a_2}{2} + \frac{b_1 b_2}{2}\right) i$$

Not surprisingly we see bosonic behavior by the photons. They both arrive at the same detector - 50% of the time at detector a and 50% of the time at detector b.

However, recombining the photon beams at a second beam splitter before the detectors (see figure below) appears to invest them with fermionic character.



As was the case above, the entangled two-photon state at BS1 is,

$$\Psi = \frac{1}{\sqrt{2}}(u1d2 + d1u2)$$

In terms of the BS1 output arms A and B, the photons originating in ports u and d evolve as,

$$u = \frac{1}{\sqrt{2}}(iA + B)$$

$$d = \frac{1}{\sqrt{2}}(A + iB)$$

While in terms of the detectors a and b, A and B in the presence of BS2 evolve as:

$$A = \frac{1}{\sqrt{2}}(ia + b)$$

$$B = \frac{1}{\sqrt{2}}(a + ib)$$

Thus, overall in the basis of the detectors, u and d evolve as follows.

$$u = \frac{1}{\sqrt{2}}\left[i\left[\frac{1}{\sqrt{2}}(ia + b)\right] + \frac{1}{\sqrt{2}}(a + ib)\right] = ib$$

$$d = \frac{1}{\sqrt{2}}\left[\frac{1}{\sqrt{2}}(ia + b) + \left[\frac{1}{\sqrt{2}}(a + ib)\right]\right] = ia$$

Attaching photon labels to u and d and substituting into Ψ yields:

$$\Psi = -\frac{1}{\sqrt{2}}(a_1 b_2 + b_1 a_2)$$

Now we see fermionic behavior for the photons. They always arrive at different detectors.

This result can also be achieved as follows:

$$\Psi = \frac{i}{\sqrt{2}}(A_1 A_2 + B_1 B_2) \left| \begin{array}{l} \text{substitute, } A_1 = \frac{1}{\sqrt{2}}(ia_1 + b_1) \\ \text{substitute, } A_2 = \frac{1}{\sqrt{2}}(ia_2 + b_2) \\ \text{substitute, } B_1 = \frac{1}{\sqrt{2}}(a_1 + ib_1) \\ \text{substitute, } B_2 = \frac{1}{\sqrt{2}}(a_2 + ib_2) \\ \text{simplify} \end{array} \right. \rightarrow \Psi = \frac{\sqrt{2}a_1 b_2 + a_2 b_1}{2}$$

The two examples can also be analyzed using matrix algebra. Below we have the vectors for photon direction of propagation, the initial two-photon entangled state, and the matrix representing a beam splitter.

$$u = \begin{pmatrix} 1 \\ 0 \end{pmatrix}$$

$$d = \begin{pmatrix} 0 \\ 1 \end{pmatrix}$$

$$\Psi = \frac{1}{\sqrt{2}}\left[\begin{pmatrix} 1 \\ 0 \end{pmatrix}\begin{pmatrix} 0 \\ 1 \end{pmatrix} + \begin{pmatrix} 0 \\ 1 \end{pmatrix}\begin{pmatrix} 0 \\ 1 \end{pmatrix}\right]$$

After the second beam splitter they propagate in opposite directions, behaving like fermions.

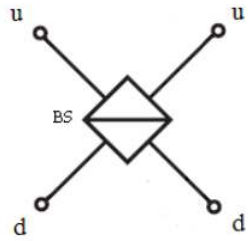
$$\text{kronecker}(BS,\ BS)\text{kronecker}(BS,\ BS)\Psi = \begin{pmatrix} 0 \\ -0.707 \\ -0.707 \\ 0 \end{pmatrix}$$

Unknown environment 'pmarix'

This page titled 7.35: Bosonic and Fermionic Photon Behavior at Beam Splitters is shared under a CC BY 4.0 license and was authored, remixed, and/or curated by Frank Rioux via source content that was edited to the style and standards of the LibreTexts platform.

7.36: Bosonic and Fermionic Photon Behavior at Beam Splitters- A Tensor Algebra Analysis

Photons from separate sources, u and d, arrive simultaneously at the beam splitter shown in the figure below.



Because these photons are indistinguishable they don′t possess separate identities, and we are forced by quantum mechanical principles to represent their collective state at the beam splitter (BS) by the following entangled wave function. The plus sign in this superposition indicates that photons are bosons; their wave functions are symmetric with respect to the interchange of the photon labels.

$$|\Psi_B\rangle = \frac{1}{\sqrt{2}}\left[|u\rangle_1|d\rangle_2 + |d\rangle_1|u\rangle_2\right]$$

The following vector representations are used for the photon states.

$$|u\rangle = \begin{pmatrix}1\\0\end{pmatrix}$$

$$|d\rangle = \begin{pmatrix}0\\1\end{pmatrix}$$

In tensor format this entangled state becomes,

$$\Psi_B\rangle = \frac{1}{\sqrt{2}}\left[\begin{pmatrix}1\\0\end{pmatrix}\otimes\begin{pmatrix}0\\1\end{pmatrix} + \begin{pmatrix}0\\1\end{pmatrix}\otimes\begin{pmatrix}1\\0\end{pmatrix}\right] = \frac{1}{\sqrt{2}}\left[\begin{pmatrix}0\\1\\0\\0\end{pmatrix} + \begin{pmatrix}0\\0\\1\\0\end{pmatrix}\right] = \frac{1}{\sqrt{2}}\begin{pmatrix}0\\1\\1\\0\end{pmatrix}$$

Transmission and reflection occur at the 50-50 beam splitters. By convention, reflection is assigned a π/2 phase shift relative to transmission. The matrix representing a 50-50 beam splitter operating on an individual photon is given below, along with its effect on the u and d photon states.

$$\frac{1}{\sqrt{2}}\begin{pmatrix}1 & i\\ i & 1\end{pmatrix}$$

$$\frac{1}{\sqrt{2}}\begin{pmatrix}1 & i\\ i & 1\end{pmatrix}\begin{pmatrix}1\\0\end{pmatrix} \rightarrow \begin{pmatrix}\frac{\sqrt{2}}{2}\\ \frac{\sqrt{2}i}{2}\end{pmatrix}$$

$$\frac{1}{\sqrt{2}}\begin{pmatrix}1 & i\\ i & 1\end{pmatrix}\begin{pmatrix}0\\1\end{pmatrix} \rightarrow \begin{pmatrix}\frac{\sqrt{2}i}{2}\\ \frac{\sqrt{2}}{2}\end{pmatrix}$$

This result clearly shows that the beam splitter converts pure states (u and d) into superpositions of u and d.

In this experiment the beam splitter operates on both photons, and in tensor format the operator becomes the following 4x4 matrix operator.

$$\hat{BS} = \hat{BS}_1 \otimes \hat{BS}_2 = \frac{1}{\sqrt{2}}\begin{pmatrix} 1 & i \\ i & 1 \end{pmatrix} \otimes \frac{1}{\sqrt{2}}\begin{pmatrix} 1 & i \\ i & 1 \end{pmatrix}$$
$$= \frac{1}{2}\begin{pmatrix} 1\begin{pmatrix} 1 & i \\ i & 1 \end{pmatrix} & i\begin{pmatrix} 1 & i \\ i & 1 \end{pmatrix} \\ i\begin{pmatrix} 1 & i \\ i & 1 \end{pmatrix} & 1\begin{pmatrix} 1 & i \\ i & 1 \end{pmatrix} \end{pmatrix} = \frac{1}{2}\begin{pmatrix} 1 & i & i & -1 \\ i & 1 & -1 & i \\ i & -1 & 1 & i \\ -1 & i & i & 1 \end{pmatrix}$$

Temporarily thinking of the photon as generic quantum particle (quon to use Nick Herbert's phrase), we can identify four possible photon states after the beam splitter, which are shown below in tensor format.

$$|uu\rangle = \begin{pmatrix} 1 \\ 0 \end{pmatrix} \otimes \begin{pmatrix} 0 \\ 1 \end{pmatrix} = \begin{pmatrix} 1 \\ 0 \\ 0 \\ 0 \end{pmatrix}$$

$$|ud\rangle = \begin{pmatrix} 1 \\ 0 \end{pmatrix} \otimes \begin{pmatrix} 0 \\ 1 \end{pmatrix} = \begin{pmatrix} 0 \\ 1 \\ 0 \\ 0 \end{pmatrix}$$

$$|du\rangle = \begin{pmatrix} 0 \\ 1 \end{pmatrix} \otimes \begin{pmatrix} 1 \\ 0 \end{pmatrix} = \begin{pmatrix} 0 \\ 0 \\ 1 \\ 0 \end{pmatrix}$$

$$|dd\rangle = \begin{pmatrix} 0 \\ 1 \end{pmatrix} \otimes \begin{pmatrix} 0 \\ 1 \end{pmatrix} = \begin{pmatrix} 0 \\ 0 \\ 0 \\ 1 \end{pmatrix}$$

The actual result of the interaction of the initial entangled state with the beam splitter is,

$$\frac{1}{2}\begin{pmatrix} 1 & i & i & -1 \\ i & 1 & -1 & i \\ i & -1 & 1 & i \\ -1 & i & i & 1 \end{pmatrix} \frac{1}{\sqrt{2}}\begin{pmatrix} 0 \\ 1 \\ 1 \\ 0 \end{pmatrix} \rightarrow \begin{pmatrix} \frac{\sqrt{2}i}{2} \\ 0 \\ 0 \\ \frac{\sqrt{2}i}{2} \end{pmatrix}$$

By inspection we can see that the photons are always observed in the same output channel, either |uu > or |dd >, with equal probabilities of 0.5. Not surprisingly we see bosonic behavior by the photons.

$$\left[\left|(1 \quad 0 \quad 0 \quad 0)\frac{1}{2}\begin{pmatrix} 1 & i & i & -1 \\ i & 1 & -1 & i \\ i & -1 & 1 & i \\ -1 & i & i & 1 \end{pmatrix} \frac{1}{\sqrt{2}}\begin{pmatrix} 0 \\ 1 \\ 1 \\ 0 \end{pmatrix}\right|\right]^2 \rightarrow \frac{1}{2}$$

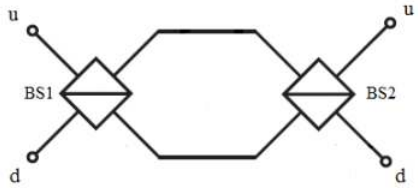
$$\left[\left|(0 \quad 0 \quad 0 \quad 1)\frac{1}{2}\begin{pmatrix} 1 & i & i & -1 \\ i & 1 & -1 & i \\ i & -1 & 1 & i \\ -1 & i & i & 1 \end{pmatrix} \frac{1}{\sqrt{2}}\begin{pmatrix} 0 \\ 1 \\ 1 \\ 0 \end{pmatrix}\right|\right]^2 \rightarrow \frac{1}{2}$$

Naturally this means they are never observed in different output channels, |ud > or |du>. The photons are not exhibiting fermionic behavior (so far).

$$\left[\left|(0 \quad 1 \quad 0 \quad 0)\frac{1}{2}\begin{pmatrix} 1 & i & i & -1 \\ i & 1 & -1 & i \\ i & -1 & 1 & i \\ -1 & i & i & 1 \end{pmatrix} \frac{1}{\sqrt{2}}\begin{pmatrix} 0 \\ 1 \\ 1 \\ 0 \end{pmatrix}\right|\right]^2 \rightarrow 0$$

$$\left[\left|\begin{pmatrix}0&0&1&0\end{pmatrix}\frac{1}{2}\begin{pmatrix}1&i&i&-1\\i&1&-1&i\\i&-1&1&i\\-1&i&i&1\end{pmatrix}\frac{1}{\sqrt{2}}\begin{pmatrix}0\\1\\1\\0\end{pmatrix}\right|\right]^2\rightarrow 0$$

However, recombining the photon beams at a second beam splitter appears to invest them with fermionic character.



As is shown below, the addition of a second beam splitter is easily implemented in the tensor format.

$$\frac{1}{2}\begin{pmatrix}1&i&i&-1\\i&1&-1&i\\i&-1&1&i\\-1&i&i&1\end{pmatrix}\frac{1}{2}\begin{pmatrix}1&i&i&-1\\i&1&-1&i\\i&-1&1&i\\-1&i&i&1\end{pmatrix}\frac{1}{\sqrt{2}}\begin{pmatrix}0\\1\\1\\0\end{pmatrix}\rightarrow\begin{pmatrix}0\\-\frac{\sqrt{2}}{2}\\-\frac{\sqrt{2}}{2}\\0\end{pmatrix}$$

Now we see (by inspection or calculation) fermionic behavior. The photons never appear in the same output channel.

$|uu\rangle$

$$\left[\left|\begin{pmatrix}1&0&0&0\end{pmatrix}\frac{1}{2}\begin{pmatrix}1&i&i&-1\\i&1&-1&i\\i&-1&1&i\\-1&i&i&1\end{pmatrix}\frac{1}{2}\begin{pmatrix}1&i&i&-1\\i&1&-1&i\\i&-1&1&i\\-1&i&i&1\end{pmatrix}\frac{1}{\sqrt{2}}\begin{pmatrix}0\\1\\1\\0\end{pmatrix}\right|\right]^2\rightarrow 0$$

$|dd\rangle$

$$\left[\left|\begin{pmatrix}0&0&0&1\end{pmatrix}\frac{1}{2}\begin{pmatrix}1&i&i&-1\\i&1&-1&i\\i&-1&1&i\\-1&i&i&1\end{pmatrix}\frac{1}{2}\begin{pmatrix}1&i&i&-1\\i&1&-1&i\\i&-1&1&i\\-1&i&i&1\end{pmatrix}\frac{1}{\sqrt{2}}\begin{pmatrix}0\\1\\1\\0\end{pmatrix}\right|\right]^2\rightarrow 0$$

They always appear in different output channels, now behaving like fermions.

$|ud\rangle$

$$\left[\left|\begin{pmatrix}0&1&0&0\end{pmatrix}\frac{1}{2}\begin{pmatrix}1&i&i&-1\\i&1&-1&i\\i&-1&1&i\\-1&i&i&1\end{pmatrix}\frac{1}{2}\begin{pmatrix}1&i&i&-1\\i&1&-1&i\\i&-1&1&i\\-1&i&i&1\end{pmatrix}\frac{1}{\sqrt{2}}\begin{pmatrix}0\\1\\1\\0\end{pmatrix}\right|\right]^2\rightarrow \frac{1}{2}$$

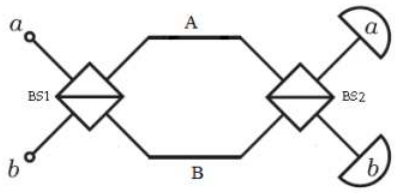
$|du\rangle$

$$\left[\left|\begin{pmatrix}0&0&1&0\end{pmatrix}\frac{1}{2}\begin{pmatrix}1&i&i&-1\\i&1&-1&i\\i&-1&1&i\\-1&i&i&1\end{pmatrix}\frac{1}{2}\begin{pmatrix}1&i&i&-1\\i&1&-1&i\\i&-1&1&i\\-1&i&i&1\end{pmatrix}\frac{1}{\sqrt{2}}\begin{pmatrix}0\\1\\1\\0\end{pmatrix}\right|\right]^2\rightarrow \frac{1}{2}$$

This page titled 7.36: Bosonic and Fermionic Photon Behavior at Beam Splitters- A Tensor Algebra Analysis is shared under a CC BY 4.0 license and was authored, remixed, and/or curated by Frank Rioux via source content that was edited to the style and standards of the LibreTexts platform.

7.37: Entangled Photons Can Behave Like Fermions

As shown in the figure, photons from separate sources, a and b, arrive simultaneously at the first beam splitter of a Mach-Zehnder interferometer (MZI).



Because the photons are indistinguishable they don't possess separate identities, and we are forced by quantum mechanical principles to represent their collective state at the beam splitter (BS) by the following entangled wave function. The plus sign in this superposition indicates that photons are bosons; their wave functions are symmetric with respect to the interchange of the photon labels.

$$|\Psi\rangle = \frac{1}{\sqrt{2}}\left[|a\rangle_1|b\rangle_2 + |b\rangle_1|a\rangle_2\right]$$

The following vector representations are used for the photon states, |a> representing presence in the upper arm of the MZI and |b> presence in its lower arm.

$$|a\rangle = \begin{pmatrix}1\\0\end{pmatrix}$$

$$|b\rangle = \begin{pmatrix}0\\1\end{pmatrix}$$

Writing Ψ in tensor format yields,

$$|\Psi\rangle = \frac{1}{\sqrt{2}}\left[\begin{pmatrix}1\\0\end{pmatrix}\otimes\begin{pmatrix}0\\1\end{pmatrix} + \begin{pmatrix}0\\1\end{pmatrix}\otimes\begin{pmatrix}1\\0\end{pmatrix}\right] = \frac{1}{\sqrt{2}}\left[\begin{pmatrix}0\\1\\0\\0\end{pmatrix} + \begin{pmatrix}0\\0\\1\\0\end{pmatrix}\right] = \frac{1}{\sqrt{2}}\begin{pmatrix}0\\1\\1\\0\end{pmatrix}$$

$$\Psi = \frac{1}{\sqrt{2}}\begin{pmatrix}0\\1\\1\\0\end{pmatrix}$$

There are four detector states after the exit channels of the MZI (|aa>, |ab>, |ba>, |bb>), which are shown below in tensor format.

$$|aa\rangle = \begin{pmatrix}1\\0\end{pmatrix}\otimes\begin{pmatrix}1\\0\end{pmatrix} = \begin{pmatrix}1\\0\\0\\0\end{pmatrix}$$

$$aa = \begin{pmatrix}1\\0\\0\\0\end{pmatrix}$$

$$|ab\rangle = \begin{pmatrix}1\\0\end{pmatrix}\otimes\begin{pmatrix}0\\1\end{pmatrix} = \begin{pmatrix}0\\1\\0\\0\end{pmatrix}$$

$$ab = \begin{pmatrix} 0 \\ 1 \\ 0 \\ 0 \end{pmatrix}$$

$$|ba\rangle = \begin{pmatrix} 0 \\ 1 \end{pmatrix} \otimes \begin{pmatrix} 1 \\ 0 \end{pmatrix} = \begin{pmatrix} 0 \\ 0 \\ 1 \\ 0 \end{pmatrix}$$

$$ba = \begin{pmatrix} 0 \\ 0 \\ 1 \\ 0 \end{pmatrix}$$

$$|bb\rangle = \begin{pmatrix} 0 \\ 1 \end{pmatrix} \otimes \begin{pmatrix} 0 \\ 1 \end{pmatrix} = \begin{pmatrix} 0 \\ 0 \\ 0 \\ 1 \end{pmatrix}$$

$$bb = \begin{pmatrix} 0 \\ 0 \\ 0 \\ 1 \end{pmatrix}$$

The matrix operator representing the beam splitter:

$$BS = \frac{1}{\sqrt{2}} \begin{pmatrix} 1 & i \\ i & 1 \end{pmatrix}$$

The following calculations show fermionic behavior for the photons. They never arrive at the same detector. (Kronecker is Mathcad's command for tensor matrix multiplication.)

$$\left(\left|aa^T \text{kronecker}(BS,\ BS)\text{kronecker}(BS,\ BS)\Psi\right|\right)^2 = 0$$

$$\left(\left|ab^T \text{kronecker}(BS,\ BS)\text{kronecker}(BS,\ BS)\Psi\right|\right)^2 = 0.5$$

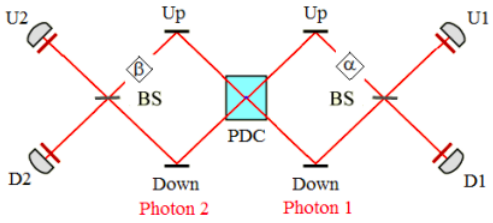
$$\left(\left|ba^T \text{kronecker}(BS,\ BS)\text{kronecker}(BS,\ BS)\Psi\right|\right)^2 = 0.5$$

$$\left(\left|bb^T \text{kronecker}(BS,\ BS)\text{kronecker}(BS,\ BS)\Psi\right|\right)^2 = 0$$

This page titled 7.37: Entangled Photons Can Behave Like Fermions is shared under a CC BY 4.0 license and was authored, remixed, and/or curated by Frank Rioux via source content that was edited to the style and standards of the LibreTexts platform.

7.38: Analyzing Two-photon Interferometry Using Mathcad and Tensor Algebra

Greenberger, Horne and Zeilinger (GHZ) surveyed the then relatively new field of multiparticle interferometry in their August 1993 Physics Today article, "Multiparticle Interferometry and the Superposition Principle." This tutorial will use Mathcad and tensor algebra to analyze the results associated with their Figure 2, shown below.



Richard Feynman identified the superposition principle, as manifested in the double-slit experiment, as the heart of quantum mechanics and its only mystery. Indeed that simple example of a single-photon superposition illustrates a number of quantum fundamentals, but as GHZ point out multi-photon entangled superpositions reveal additional mysteries like quantum correlations that challenge philosophical positions such as local realism.

The operators required to analyze this two-photon interferometer are defined below. α and β are phase shifters.

Identity:

$$I = \begin{pmatrix} 1 & 0 \\ 0 & 1 \end{pmatrix}$$

Mirror:

$$M = \begin{pmatrix} 0 & 1 \\ 1 & 0 \end{pmatrix}$$

Phase shift:

$$A(\delta) = \begin{pmatrix} e^{i\delta} & 0 \\ 0 & 1 \end{pmatrix}$$

Beam splitter:

$$BS = \sqrt{\frac{1}{2}} \begin{pmatrix} 1 & i \\ i & 1 \end{pmatrix}$$

The parametric down converter (PDC) creates two photons traveling in opposite directions in the arms of the interferometer, with photon 1 moving to the right and photon 2 to the left. The initial state is the following entangled superposition.

$$|\Psi\rangle = \frac{1}{\sqrt{2}} \left[|u_1\rangle |d_2\rangle + |d_1\rangle |u_2\rangle \right]$$

$$|\Psi\rangle = \frac{1}{\sqrt{2}} \left[\begin{pmatrix} 1 \\ 0 \end{pmatrix} \otimes \begin{pmatrix} 0 \\ 1 \end{pmatrix} + \begin{pmatrix} 0 \\ 1 \end{pmatrix} \otimes \begin{pmatrix} 1 \\ 0 \end{pmatrix} \right] = \frac{1}{\sqrt{2}} \left[\begin{pmatrix} 0 \\ 1 \\ 0 \\ 0 \end{pmatrix} + \begin{pmatrix} 0 \\ 0 \\ 1 \\ 0 \end{pmatrix} \right] = \frac{1}{\sqrt{2}} \begin{pmatrix} 0 \\ 1 \\ 1 \\ 0 \end{pmatrix}$$

There are four output states. The appendix shows how the input and output states are constructed in Mathcad.

$$|uu\rangle = \begin{pmatrix} 1 \\ 0 \end{pmatrix} \otimes \begin{pmatrix} 1 \\ 0 \end{pmatrix} = \begin{pmatrix} 1 \\ 0 \\ 0 \\ 0 \end{pmatrix}$$

$$|ud\rangle = \begin{pmatrix}1\\0\end{pmatrix} \otimes \begin{pmatrix}0\\1\end{pmatrix} = \begin{pmatrix}0\\1\\0\\0\end{pmatrix}$$

$$|du\rangle = \begin{pmatrix}0\\1\end{pmatrix} \otimes \begin{pmatrix}1\\0\end{pmatrix} = \begin{pmatrix}0\\0\\1\\0\end{pmatrix}$$

$$|dd\rangle = \begin{pmatrix}0\\1\end{pmatrix} \otimes \begin{pmatrix}0\\1\end{pmatrix} = \begin{pmatrix}0\\0\\0\\1\end{pmatrix}$$

The input and output states are defined in Mathcad syntax.

$$u = \begin{pmatrix}1\\0\end{pmatrix}$$

$$d = \begin{pmatrix}0\\1\end{pmatrix}$$

$$\Psi = \frac{1}{\sqrt{2}}\begin{pmatrix}0\\1\\1\\0\end{pmatrix}$$

$$u1u2 = \begin{pmatrix}1\\0\\0\\0\end{pmatrix}$$

$$u1d2 = \begin{pmatrix}0\\1\\0\\0\end{pmatrix}$$

$$d1u2 = \begin{pmatrix}0\\0\\1\\0\end{pmatrix}$$

$$d1d2 = \begin{pmatrix}0\\0\\0\\1\end{pmatrix}$$

The four outcome probabilities are now calculated. The appendix shows how Mathcad is used to carry out the tensor product of two matrices.

$$Pu1u2(\alpha,\beta) = \left(\left|u1u2^{T}\text{kronecker}(BS,\ BS)\text{kronecker}(A(\alpha),A(\beta))\text{kronecker}(M,\ M)\Psi\right|\right)^{2}$$

$$Pu1d2(\alpha,\beta) = \left(\left|u1d2^{T}\text{kronecker}(BS,\ BS)\text{kronecker}(A(\alpha),A(\beta))\text{kronecker}(M,\ M)\Psi\right|\right)^{2}$$

$$Pd1u2(\alpha,\beta) = \left(\left|d1u2^{T}\text{kronecker}(BS,\ BS)\text{kronecker}(A(\alpha),A(\beta))\text{kronecker}(M,\ M)\Psi\right|\right)^{2}$$

$$Pd1d2(\alpha,\beta) = \left(\left|d1d2^{T}\text{kronecker}(BS,\ BS)\text{kronecker}(A(\alpha),A(\beta))\text{kronecker}(M,\ M)\Psi\right|\right)^{2}$$

The probability that the individual detectors will fire is given by the following sums.

$$P_{u1} = P_{u1u2} + P_{u1d2}$$

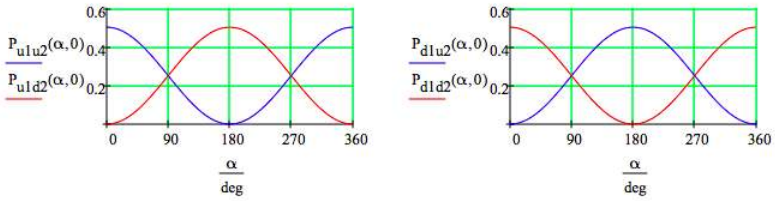
$$P_{d1} = P_{d1d2} + P_{d1u2}$$

$$P_{u2} = P_{u1u2} + P_{d1u2}$$

$$P_{d2} = P_{d1d2} + P_{u1d2}$$

Because only the phase difference between the two arms of the interferometer matters, β is set to zero and the phase difference is expressed in the value of α. The following graphs show the behavior of the detector pairings as a function of the phase difference α.

$\alpha = 0\text{deg}, 1\text{deg}..360\text{deg}$



When there is no phase difference in the two branches of the interferometer there is a strong correlation in the detector responses. Fifty percent of the time the photons arrive at the up-detectors and 50% of the time at the down-detectors. There are no coincidences between an up and a down detector. This might be called bosonic behavior - bosons like to do the same thing.

For convenience results will also be presented in numeric format. See the Appendix for a graphical display.

$\alpha = 0\ \text{deg}$

$$\begin{pmatrix} P_{u1u2}(\alpha,0) & P_{u1d2}(\alpha,0) \\ P_{d1u2}(\alpha,0) & P_{d1d2}(\alpha,0) \end{pmatrix} = \begin{pmatrix} 0.5 & 0 \\ 0 & 0.5 \end{pmatrix}$$

A 90 degree phase difference results in no correlation. The four detector pairs fire with equal frequency.

$\alpha = 90\ \text{deg}$

$$\begin{pmatrix} P_{u1u2}(\alpha,0) & P_{u1d2}(\alpha,0) \\ P_{d1u2}(\alpha,0) & P_{d1d2}(\alpha,0) \end{pmatrix} = \begin{pmatrix} 0.25 & 0.25 \\ 0.25 & 0.25 \end{pmatrix}$$

A 180 degree phase difference results in what might be called fermionic behavior. If one photon is detected at an up-detector, the other is registered at a down detector. They never both arrive at the same type of detector. Fermions don't like to do the same thing at the same time.

$\alpha = 180\ \text{deg}$

$$\begin{pmatrix} P_{u1u2}(\alpha,0) & P_{u1d2}(\alpha,0) \\ P_{d1u2}(\alpha,0) & P_{d1d2}(\alpha,0) \end{pmatrix} = \begin{pmatrix} 0 & 0.5 \\ 0.5 & 0 \end{pmatrix}$$

Intermediate correlation is achieved with a 60 degree phase difference.

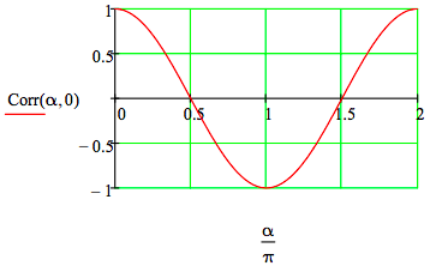
$\alpha = 60\ \text{deg}$

$$\begin{pmatrix} P_{u1u2}(\alpha,0) & P_{u1d2}(\alpha,0) \\ P_{d1u2}(\alpha,0) & P_{d1d2}(\alpha,0) \end{pmatrix} = \begin{pmatrix} 0.375 & 0.125 \\ 0.125 & 0.375 \end{pmatrix}$$

These tabular results can be summarized by displaying the correlation function. Perfect correlation +1; perfect anti-correlation -1; no correlation 0. Another graphical display can be found in the Appendix.

$\alpha = 0, .02..2\pi$

$$\text{Corr}(\alpha,\beta) = P_{u1u2}(\alpha,\beta) - P_{u1d2}(\alpha,\beta) - P_{d1u2}(\alpha,\beta) + P_{d1d2}(\alpha,\beta)$$



Note that the sums of the rows and the sums of the columns in the tables above always equal 1/2.

$$P_{1u} = P_{2u} = P_{1d} = P_{2d} = \frac{1}{2}$$

An individual detector fires 50% of the time in spite of the correlations that may occur between two detectors. Looking at individual detectors locally reveals totally random behavior. It is only when coincidences between pairs of detectors on the left and right are examined that correlations are observed.

The random behavior at each of the detectors can be directly shown by calculations in which only one detector is being monitored. This requires the projection operators for up and down motion given below. The calculations are shown for the arbitrary phases shown below. However, all phase relationships give the same results.

Projection operators:

$$uu^T = \begin{pmatrix} 1 & 0 \\ 0 & 0 \end{pmatrix} \quad dd^T = \begin{pmatrix} 0 & 0 \\ 0 & 1 \end{pmatrix}$$

Phases:

$$\alpha = 11 \text{ deg} \quad \beta = 58 \text{ deg}$$

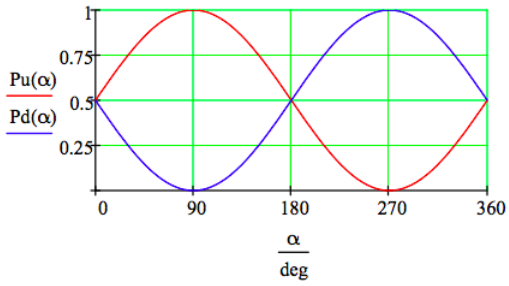
$Detector$	$ProbabilityofFiring$
$U1$	$\left(\left\|(uu^T,\ I)\,\text{kronecker}(BS,\ BS)\text{kronecker}(A(\alpha), A(\beta))\text{kronecker}(M,\ M)\Psi\right\|\right)^2 = 0.5$
$D1$	$\left(\left\|(dd^T,\ I)\,\text{kronecker}(BS,\ BS)\text{kronecker}(A(\alpha), A(\beta))\text{kronecker}(M,\ M)\Psi\right\|\right)^2 = 0.5$
$U2$	$\left(\left\|(I,\ uu^T)\,\text{kronecker}(BS,\ BS)\text{kronecker}(A(\alpha), A(\beta))\text{kronecker}(M,\ M)\Psi\right\|\right)^2 = 0.5$
$D2$	$\left(\left\|(I,\ dd^T)\,\text{kronecker}(BS,\ BS)\text{kronecker}(A(\alpha), A(\beta))\text{kronecker}(M,\ M)\Psi\right\|\right)^2 = 0.5$

At this point it is important to recall that interference at the individual detectors would be observed if the photons were not entangled. Looking at either half of the interferometer shown above and assuming an unentangled photon in the superposition, $\frac{1}{\sqrt{2}}\begin{pmatrix}1\\1\end{pmatrix}$, of being in the upper and lower arms of the truncated interferometer results in interference effects as a function of α at the detectors as is illustrated in the following graph.

$\alpha = 0 \text{ deg}, 1 \text{ deg}..360 \text{ deg}$

$$Pu(\alpha) = \left[\left|uu^T BSA(\alpha) M \frac{1}{\sqrt{2}}\begin{pmatrix}1\\1\end{pmatrix}\right|\right]^2$$

$$Pd(\alpha) = \left[\left|dd^T BSA(\alpha) M \frac{1}{\sqrt{2}}\begin{pmatrix}1\\1\end{pmatrix}\right|\right]^2$$



Recently, Art Hobson posted "Implications of bipartite interferometry for the measurement problem" at **arXiv:1301.1673**. In this manuscript he deals in depth with the results presented above. Therefore, in concluding this tutorial I will take relevant commentary from his manuscript without further comment. However, some excerpts have been slightly modified, but not in such a way as to change their original meanings.

- When two photons are entangled, the state actually detected by an observer of either photon is the local or reduced state of that photon. The reduced state operator of photon 2 is obtained by averaging (tracing) the total density operator over photon 1 as is shown below. This procedure shows that photon 2's reduced or local state operator is diagonal indicating a classical mixed state - it has been stripped of its off-diagonal interference terms. This result is consistent with the random behavior noted earlier for the measurements on individual photons.

$$\hat{\rho}_{12} = |\Psi\rangle\langle\Psi| = \frac{1}{2}[|u_1\rangle|d_2\rangle\langle d_2|\langle u_1| + |u_1\rangle|d_2\rangle\langle u_2|\langle d_1| + |d_1\rangle|u_2\rangle\langle d_2|\langle u_1| + |d_1\rangle|u_2\rangle\langle u_2|\rangle d_1|]$$

$$\hat{\rho}_2 = \frac{1}{2}[\langle u_1|\Psi\rangle\langle\Psi|u_1\rangle + \langle d_1|\Psi\rangle\langle\Psi|d_1\rangle] = \frac{1}{2}[|d_2\rangle\langle d_2| + |u_2\rangle\langle u_2|]$$

- Therefore, when a bipartite system is in an entangled superposition, its subsystems are not in superpositions but are instead mixed states with each subsystem in a definite, but unknown state.
- The detectors (U1, D1, U2, D2) show no local signs of interference of the type that would occur if the photons were not entangled, because each photon is a "which path" detector for the other photon, decohering the other photon and creating incoherent local mixtures.
- To summarize, an entangled photon is always "in" its local state, the state described by its reduced density operator (see above), because this is the state actually detected by an observer of the photon. The entangled state Ψ is a global superposition of photon correlations, not a superposition of local photon states.

Appendix

The tensor product of two vectors is shown below.

$$\begin{pmatrix} a \\ b \end{pmatrix} \otimes \begin{pmatrix} c \\ d \end{pmatrix} = \begin{pmatrix} ac \\ ad \\ bc \\ bd \end{pmatrix}$$

Mathcad does not have a command for the vector tensor product, so it is necessary to develop a way of implementing it using ***kronecker***, which requires square matrices. For this reason the spin vector is stored in the left column of a 2x2 matrix by augmenting the spin vector with the null vector. After the matrix tensor products have been carried out using ***kronecker*** the final spin vector resides in the left column of the final square matrix. Next the ***submatrix*** command is used to save this column, discarding the rest of the matrix.

The Mathcad syntax for the tensor multiplication of two vectors is as follows.

$$\Psi(a,\ b) = \text{submatrix}\left[\text{kronecker}\left[\text{augment}\left[a,\ \begin{pmatrix}0\\0\end{pmatrix}\right], \text{augment}\left[b,\ \begin{pmatrix}0\\0\end{pmatrix}\right]\right],\ 1,\ 4,\ 1,\ 1\right]$$

The initial photon state:

$$\frac{1}{\sqrt{2}}(\Psi(u,\ d)+\Psi(d,\ u))=\begin{pmatrix}0\\0.707\\0.707\\0\end{pmatrix}$$

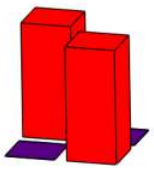
Tensor matrix multiplication is also known as Kronecker multiplication. Here it is shown that the Mathcad result using the ***kronecker*** command is identical to the hand calculation.

$$\text{kronecker}(BS,\ BS)=\begin{pmatrix}0.5 & 0.5i & 0.5i & -0.5i\\ 0.5i & 0.5 & -0.5 & 0.5i\\ 0.5i & -0.5 & 0.5 & 0.5i\\ -0.5 & 0.5i & 0.5i & 0.5\end{pmatrix}$$

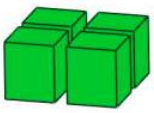
$$\widehat{BS}\otimes\widehat{BS}=\frac{1}{\sqrt{2}}\begin{pmatrix}1 & i\\ i & 1\end{pmatrix}\otimes\frac{1}{\sqrt{2}}\begin{pmatrix}1 & i\\ i & 1\end{pmatrix}$$
$$=\frac{1}{2}\begin{pmatrix}1\begin{pmatrix}1 & i\\ i & 1\end{pmatrix} & i\begin{pmatrix}1 & i\\ i & 1\end{pmatrix}\\ i\begin{pmatrix}1 & i\\ i & 1\end{pmatrix} & 1\begin{pmatrix}1 & i\\ i & 1\end{pmatrix}\end{pmatrix}=\frac{1}{2}\begin{pmatrix}1 & i & i & -1\\ i & 1 & -1 & i\\ i & -1 & 1 & i\\ -1 & i & i & 1\end{pmatrix}$$

A graphical display of tabular results presented earlier:

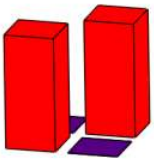
$$P(\alpha,\beta)=\begin{pmatrix}P_{u1u2}(\alpha,\beta) & P_{u1d2}(\alpha,\beta)\\ P_{d1u2}(\alpha,\beta) & P_{d1d2}(\alpha,\beta)\end{pmatrix}$$



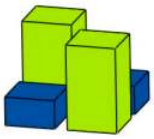
P(0·deg, 0·deg)



P(90·deg, 0·deg)



P(180·deg, 0·deg)



P(60·deg, 0·deg)

The following algebraic analysis of the experiment shows the evolution of the original entangled state. Consistent with the matrix mechanics analysis, it shows that when the phase diference is zero both photons arrive at either the U- or the D-detectors, and when the phase difference is π one photon arrives at U-detector and the other at the D-detector.

$\alpha=0\quad\beta=0$

$$\frac{1}{\sqrt{2}}(u_1d_2+d_1u_2)\left|\begin{array}{l}\text{substitute},\ u1=\frac{e^{i\alpha}}{\sqrt{2}}(iU1+D1)\\ \text{substitute},\ d2=\frac{1}{\sqrt{2}}(U2+iD2)\\ \text{substitute},\ u1=\frac{1}{\sqrt{2}}(U1+D1)\\ \text{substitute},\ d2=\frac{e^{i\beta}}{\sqrt{2}}(iU2+D2)\end{array}\right.\rightarrow\sqrt{2}\left(\frac{U1U2i}{2}+\frac{D1D2i}{2}\right)$$

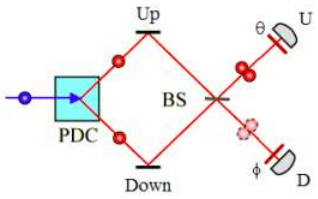
$\alpha=\pi\quad\beta=0$

$$\frac{1}{\sqrt{2}}(u_1 d_2 + d_1 u_2) \left| \begin{array}{l} \text{substitute, } u1 = \frac{e^{i\alpha}}{\sqrt{2}}(iU1 + D1) \\ \text{substitute, } d2 = \frac{1}{\sqrt{2}}(U2 + iD2) \\ \text{substitute, } u1 = \frac{1}{\sqrt{2}}(U1 + D1) \\ \text{substitute, } d2 = \frac{e^{i\beta}}{\sqrt{2}}(iU2 + D2) \end{array} \right. \rightarrow \sqrt{2}\left(\frac{D1U2}{2} - \frac{D2U2}{2}\right)$$

This page titled 7.38: Analyzing Two-photon Interferometry Using Mathcad and Tensor Algebra is shared under a CC BY 4.0 license and was authored, remixed, and/or curated by Frank Rioux via source content that was edited to the style and standards of the LibreTexts platform.

7.39: Analysis of a Two-photon Quantum Eraser

Greenberger, Horne and Zeilinger (GHZ) surveyed the then relatively new field of multiparticle interferometry in an August 1993 *Physics Today* article, "Multiparticle Interferometry and the Superposition Principle." This tutorial will use Mathcad and tensor algebra to analyze the results associated with Figure 5, which dealt with a two-photon quantum eraser. A parametric down converter (PDC) produces two horizontally polarized, entangled photons, one taking the upper path and the other the lower path. The beams are combined at a beam splitter as shown below. Polarizing films oriented at angles of θ and ϕ relative to the horizontal are placed in front of detectors.



As the figure shows both photons, as bosons, arrive at either the U detector or the D detector. This result will now be confirmed using tensor algebra.

The photons emerging from the PDC are entangled and can be moving up or down and be in a particular polarization state. We use the following vectors to represent the motional and polarization states of the photons.

$$u = \begin{pmatrix} 1 \\ 0 \end{pmatrix}$$

$$d = \begin{pmatrix} 0 \\ 1 \end{pmatrix}$$

$$\theta = \begin{pmatrix} \cos\theta \\ \sin\theta \end{pmatrix}$$

$$\phi = \begin{pmatrix} \cos\phi \\ \sin\phi \end{pmatrix}$$

The motional and polarization photon states are combined using vector tensor multiplication. The up motional state is tagged with θ polarization, and the down state with ϕ polarization. The photon polarization states can be the same or different.

$$u\theta = \begin{pmatrix} 1 \\ 0 \end{pmatrix} \begin{pmatrix} \cos\theta \\ \sin\theta \end{pmatrix} = \begin{pmatrix} \cos\theta \\ \sin\theta \\ 0 \\ 0 \end{pmatrix}$$

$$d\phi = \begin{pmatrix} 0 \\ 1 \end{pmatrix} \begin{pmatrix} \cos\phi \\ \sin\phi \end{pmatrix} = \begin{pmatrix} 0 \\ 0 \\ \cos\phi \\ \sin\phi \end{pmatrix}$$

There are four two-photon output states at the detectors. These are also represented using tensor algebra. The first two letters refer to photon 1, the second two refer to photon 2. The uθdϕ ($|u\theta>_1 |d\phi>_2$) state is constructed as an example.

$$u\theta d\phi = \begin{pmatrix} \cos\theta \\ \sin\theta \\ 0 \\ 0 \end{pmatrix} \begin{pmatrix} 0 \\ 0 \\ \cos\phi \\ \sin\phi \end{pmatrix}$$

$$u\theta d\phi = ud(\theta,\ \phi)$$

$$= (0 \quad 0 \quad \cos\theta\cos\phi \quad \cos\theta\sin\phi \quad 0 \quad 0 \quad \sin\theta\cos\phi \quad \sin\theta\sin\phi \quad 0 \quad 0 \quad 0 \quad 0 \quad 0 \quad 0 \quad 0 \quad 0)^T$$

The four output states are:

$$uu(\theta) = (\cos\theta^2 \quad cos\theta\sin\theta \quad 0 \quad 0 \quad \sin\theta\cos\theta \quad \sin\theta^2 \quad 0 \quad 0 \quad 0 \quad 0 \quad 0 \quad 0 \quad 0 \quad 0 \quad 0 \quad 0)^T$$

$$ud(\theta,\ \phi)$$
$$= (0 \quad 0 \quad \cos\theta\cos\phi \quad \cos\theta\sin\phi \quad 0 \quad 0 \quad \sin\theta\cos\phi \quad \sin\theta\sin\phi \quad 0 \quad 0 \quad 0 \quad 0 \quad 0 \quad 0 \quad 0 \quad 0)^T$$

$$du(\phi,\ \theta) =$$
$$(0 \quad 0 \quad 0 \quad 0 \quad 0 \quad 0 \quad 0 \quad 0 \quad \cos\phi\cos\theta \quad \cos\phi\sin\theta \quad 0 \quad 0 \quad \sin\phi\cos\theta \quad \sin\phi\cos\theta \quad \sin\phi\sin\theta \quad 0 \quad 0)^T$$

$$dd(\phi) = (0 \quad 0 \quad 0 \quad 0 \quad 0 \quad 0 \quad 0 \quad 0 \quad 0 \quad 0 \quad \cos\phi^2 \quad \cos\phi\sin\phi \quad 0 \quad 0 \quad \sin\phi\cos\phi \quad \sin\phi^2)^T$$

The matrix operators required for this analysis are,

Identity:

$$I = \begin{pmatrix} 1 & 0 \\ 0 & 1 \end{pmatrix}$$

Mirror:

$$M = \begin{pmatrix} 0 & 1 \\ 1 & 0 \end{pmatrix}$$

Beam splitter:

$$BS = \begin{pmatrix} \frac{1}{\sqrt{2}} & \frac{1}{\sqrt{2}} \\ \frac{1}{\sqrt{2}} & \frac{1}{\sqrt{2}} \end{pmatrix}$$

The mirrors and the beam splitter operate on the motional degree of freedom. Their operators as configured in the apparatus are constructed using matrix tensor multiplication, implemented with Mathcad′s kronecker command.

$$MI = \text{kronecker}(M,\ \text{kronecker}(I,\ \text{kronecker}(M,\ I)))$$

$$BSI = \text{kronecker}(BS,\ \text{kronecker}(I,\ \text{kronecker}(BS,\ I)))$$

As mentioned earlier, the PDC produces the following entangled state of horizontally polarized photons:

$$\Psi = \frac{1}{\sqrt{2}}(ud(0,\ 0) + du(0,\ 0))$$

The output state after the photons interact with the mirrors and the beam splitter is:

$$\Psi_{out} = BSI(MI)\Psi$$

Initially the films in front of the detectors are horizontally polarized and we see that both photons always arrive at the same detector, as is shown graphically in the figure. Fifty percent of the time it is U and fifty percent of the time it is D. No U-D coincidences are observed (off-diagonal elements are zero).

$\theta = 0$

$\phi = 0$

$$\begin{bmatrix} (|uu(\theta)\Psi_{out}|)^2 & (|ud(\theta,\phi)\Psi_{out}|)^2 \\ (|du(\phi,\theta)\Psi_{out}|)^2 & (|dd(\phi)\Psi_{out}|)^2 \end{bmatrix} = \begin{pmatrix} \frac{1}{2} & 0 \\ 0 & \frac{1}{2} \end{pmatrix}$$

Now assume that a 90 degree polarization rotator is placed in the lower arm which rotates the horizontal state to the vertical polarization orientation. This provides path information and even though polarization is not measured in this experiment it has a significant affect on the measurement results.

The entangled state is now:

$$\Psi = \frac{1}{\sqrt{2}}\left(ud\left(0,\ \frac{\pi}{2}\right) + du\left(\frac{\pi}{2},\ 0\right)\right)$$

$$\Psi_{out} = BSI(MI)\Psi$$

No photons are detected if the polarizers remain horizontally oriented or if they are both rotated to the vertical orientation.

$\theta = 0$

$\phi = 0$

$$\begin{bmatrix} (|uu(\theta)\Psi_{out}|)^2 & (|ud(\theta,\phi)\Psi_{out}|)^2 \\ (|du(\phi,\theta)\Psi_{out}|)^2 & (|dd(\phi)\Psi_{out}|)^2 \end{bmatrix} = \begin{pmatrix} 0 & 0 \\ 0 & 0 \end{pmatrix}$$

$\theta = \frac{\pi}{2}$

$\phi = \pi 2$

$$\begin{bmatrix} (|uu(\theta)\Psi_{out}|)^2 & (|ud(\theta,\phi)\Psi_{out}|)^2 \\ (|du(\phi,\theta)\Psi_{out}|)^2 & (|dd(\phi)\Psi_{out}|)^2 \end{bmatrix} = \begin{pmatrix} 0 & 0 \\ 0 & 0 \end{pmatrix}$$

However, if one of the polarizers is horizontal and the other vertical, U-D coincidences are observed (non-zero off-diagonal elements).

$\theta = 0$

$\phi = \frac{\pi}{2}$

$$\begin{bmatrix} (|uu(\theta)\Psi_{out}|)^2 & (|ud(\theta,\phi)\Psi_{out}|)^2 \\ (|du(\phi,\theta)\Psi_{out}|)^2 & (|dd(\phi)\Psi_{out}|)^2 \end{bmatrix} = \begin{pmatrix} 0 & \frac{1}{8} \\ \frac{1}{8} & 0 \end{pmatrix}$$

$\theta = \frac{\pi}{2}$

$\phi = 0$

$$\begin{bmatrix} (|uu(\theta)\Psi_{out}|)^2 & (|ud(\theta,\phi)\Psi_{out}|)^2 \\ (|du(\phi,\theta)\Psi_{out}|)^2 & (|dd(\phi)\Psi_{out}|)^2 \end{bmatrix} = \begin{pmatrix} 0 & \frac{1}{8} \\ \frac{1}{8} & 0 \end{pmatrix}$$

The photon path information can be erased by a diagonal orientation of the polarizers. Now the coincidences of the previous cases disappears and the original bosonic behavior is restored.

$\theta = \frac{\pi}{4}$

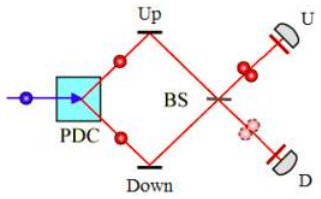
$\phi = \frac{\pi}{4}$

$$\begin{bmatrix} (|uu(\theta)\Psi_{out}|)^2 & (|ud(\theta,\phi)\Psi_{out}|)^2 \\ (|du(\phi,\theta)\Psi_{out}|)^2 & (|dd(\phi)\Psi_{out}|)^2 \end{bmatrix} = \begin{pmatrix} \frac{1}{8} & 0 \\ 0 & \frac{1}{8} \end{pmatrix}$$

This page titled 7.39: Analysis of a Two-photon Quantum Eraser is shared under a CC BY 4.0 license and was authored, remixed, and/or curated by Frank Rioux via source content that was edited to the style and standards of the LibreTexts platform.

7.40: Another Example of a Two-photon Quantum Eraser

Greenberger, Horne and Zeilinger (GHZ) surveyed the then relatively new field of multiparticle interferometry in an August 1993 Physics Today article, "Multiparticle Interferometry and the Superposition Principle." This tutorial will use Mathcad and tensor algebra to analyze the results associated with Figure 5, which dealt with a two-photon quantum eraser. A parametric down converter (PDC) produces two horizontally polarized, entangled photons, one taking the upper path and the other the lower path. The beams are combined at a beam splitter as shown below.



As the figure shows both photons arrive at either the U detector or the D detector. This result will now be confirmed using tensor algebra.

The photons emerging from the PDC are entangled and can be moving up or down with horizontal polarization. Later we will consider rotating the polarization in the lower arm to the vertical orientation in order to explore the consequences of providing path information. We use the following vectors to represent the motional and polarization states of the photons.

$$u = \begin{pmatrix} 1 \\ 0 \end{pmatrix} \quad d = \begin{pmatrix} 0 \\ 1 \end{pmatrix} \quad h = \begin{pmatrix} 1 \\ 0 \end{pmatrix} \quad v = \begin{pmatrix} 0 \\ 1 \end{pmatrix}$$

The four possible photon states are expressed using vector tensor multiplication.

$$uh = \begin{pmatrix} 1 \\ 0 \end{pmatrix} \begin{pmatrix} 1 \\ 0 \end{pmatrix}$$

$$uh = \begin{pmatrix} 1 \\ 0 \\ 0 \\ 0 \end{pmatrix}$$

$$uh = \begin{pmatrix} 1 \\ 0 \end{pmatrix} \begin{pmatrix} 0 \\ 1 \end{pmatrix}$$

$$uh = \begin{pmatrix} 0 \\ 1 \\ 0 \\ 0 \end{pmatrix}$$

$$uh = \begin{pmatrix} 0 \\ 1 \end{pmatrix} \begin{pmatrix} 1 \\ 0 \end{pmatrix}$$

$$uh = \begin{pmatrix} 0 \\ 0 \\ 1 \\ 0 \end{pmatrix}$$

$$uh = \begin{pmatrix} 0 \\ 1 \end{pmatrix} \begin{pmatrix} 0 \\ 1 \end{pmatrix}$$

$$uh = \begin{pmatrix} 0 \\ 0 \\ 0 \\ 1 \end{pmatrix}$$

There are sixteen photon measurement (output) states at the detectors. These are also represented using tensor algebra. The first two letters refer to photon 1, the second two refer to photon 2. The uhdv (|uh>1|dv>2) state is constructed as an example.

$$uhdv = \begin{pmatrix}1\\0\end{pmatrix}\begin{pmatrix}1\\0\end{pmatrix}\begin{pmatrix}0\\1\end{pmatrix}\begin{pmatrix}0\\1\end{pmatrix} = (0 \quad 0 \quad 0 \quad 1 \quad 0 \quad 0 \quad 0 \quad 0 \quad 0 \quad 0 \quad 0 \quad 0 \quad 0)^T$$

$$uhuh = (1 \quad 0 \quad 0 \quad 0 \quad 0 \quad 0 \quad 0 \quad 0 \quad 0 \quad 0 \quad 0 \quad 0 \quad 0 \quad 0 \quad 0 \quad 0)^T$$

$$uhuv = (0 \quad 1 \quad 0 \quad 0 \quad 0 \quad 0 \quad 0 \quad 0 \quad 0 \quad 0 \quad 0 \quad 0 \quad 0 \quad 0 \quad 0 \quad 0)^T$$

$$uhdh = (0 \quad 0 \quad 1 \quad 0 \quad 0 \quad 0 \quad 0 \quad 0 \quad 0 \quad 0 \quad 0 \quad 0 \quad 0 \quad 0)^T$$

$$uhdv = (= 0 \quad 0 \quad 0 \quad 1 \quad 0 \quad 0 \quad 0 \quad 0 \quad 0 \quad 0 \quad 0 \quad 0 \quad 0 \quad 0 \quad 0 \quad 0)^T$$

$$uvuh = (0 \quad 0 \quad 0 \quad 0 \quad 1 \quad 0 \quad 0 \quad 0 \quad 0 \quad 0 \quad 0 \quad 0 \quad 0 \quad 0 \quad 0 \quad 0)^T$$

$$uvuv = (0 \quad 0 \quad 0 \quad 0 \quad 0 \quad 1 \quad 0 \quad 0 \quad 0 \quad 0 \quad 0 \quad 0 \quad 0 \quad 0 \quad 0 \quad 0)^T$$

$$uvdh = (0 \quad 0 \quad 0 \quad 0 \quad 0 \quad 0 \quad 1 \quad 0 \quad 0 \quad 0 \quad 0 \quad 0 \quad 0 \quad 0 \quad 0 \quad 0)^T$$

$$uvdv = (0 \quad 0 \quad 0 \quad 0 \quad 0 \quad 0 \quad 0 \quad 1 \quad 0 \quad 0 \quad 0 \quad 0 \quad 0 \quad 0 \quad 0 \quad 0)^T$$

$$dhuh = (0 \quad 0 \quad 0 \quad 0 \quad 0 \quad 0 \quad 0 \quad 0 \quad 1 \quad 0 \quad 0 \quad 0 \quad 0 \quad 0 \quad 0 \quad 0)^T$$

$$dhuv = (0 \quad 0 \quad 0 \quad 0 \quad 0 \quad 0 \quad 0 \quad 0 \quad 0 \quad 1 \quad 0 \quad 0 \quad 0 \quad 0 \quad 0 \quad 0)^T$$

$$dhdh = (0 \quad 0 \quad 0 \quad 0 \quad 0 \quad 0 \quad 0 \quad 0 \quad 0 \quad 0 \quad 1 \quad 0 \quad 0 \quad 0 \quad 0 \quad 0)^T$$

$$dhdv = (0 \quad 0 \quad 0 \quad 0 \quad 0 \quad 0 \quad 0 \quad 0 \quad 0 \quad 0 \quad 0 \quad 1 \quad 0 \quad 0 \quad 0 \quad 0)^T$$

$$dvuh = (0 \quad 0 \quad 0 \quad 0 \quad 0 \quad 0 \quad 0 \quad 0 \quad 0 \quad 0 \quad 0 \quad 0 \quad 1 \quad 0 \quad 0 \quad 0)^T$$

$$dvuv = (0 \quad 0 \quad 0 \quad 0 \quad 0 \quad 0 \quad 0 \quad 0 \quad 0 \quad 0 \quad 0 \quad 0 \quad 0 \quad 1 \quad 0 \quad 0)^T$$

$$dvdh = (0 \quad 0 \quad 0 \quad 0 \quad 0 \quad 0 \quad 0 \quad 0 \quad 0 \quad 0 \quad 0 \quad 0 \quad 0 \quad 0 \quad 1 \quad 0)^T$$

$$dvdv = (0 \quad 0 \quad 0 \quad 0 \quad 0 \quad 0 \quad 0 \quad 0 \quad 0 \quad 0 \quad 0 \quad 0 \quad 0 \quad 0 \quad 0 \quad 1)^T$$

Matrix operators:

Identity:

$$I = \begin{pmatrix}1 & 0\\0 & 1\end{pmatrix}$$

Mirror:

$$M = \begin{pmatrix}0 & 1\\1 & 0\end{pmatrix}$$

Beam splitter:

$$BS = \frac{1}{\sqrt{2}}\begin{pmatrix}1 & i\\i & 1\end{pmatrix}$$

The mirrors and the beam splitter operate on the motional degree of freedom. Their operators as configured in the apparatus are constructed using matrix tensor multiplication, implemented with Mathcad's ***kronecker*** command.

$$MI = \text{kronecker}(M,\ \text{kronecker}(I,\ \text{kronecker}(M,\ I)))$$

$$BSI = \text{kronecker}(BS,\ \text{kronecker}(I,\ \text{kronecker}(BS,\ I)))$$

The entangled state produced by the PDC is:

$$\Psi_{boson} = \frac{1}{\sqrt{2}}(uhdh + dhuh)$$

The output state after the photons interact with the mirrors and the beam splitter is:

$$\Psi_{out} = BSI(MI)\Psi_{boson}$$

An equivalent algebraic analysis clearly shows the constructive and destructive interference between the probability amplitudes for the measurement states.

$$\Psi_{out} = \frac{1}{2\sqrt{2}}(i(uh)uh - uh(dh) + dh(uh) + i(dh)dh + i(uh)uh + uh(dh) - dh(uh) + i(dh)dh$$
$$= \frac{i}{\sqrt{2}}(uh(uh) - dh(dh))$$

We now calculate a matrix of all possible experimental outcomes, recognizing at this point that because the photons are horizontally polarized we could have just calculated a 2x2 matrix, eliminating columns 2 and 4, and rows 2 and 4.

$$P_{boson} = \begin{bmatrix} \left|(\overline{uhuh})^T\Psi_{out}\right|^2 & \left|(\overline{uhuv})^T\Psi_{out}\right|^2 & \left|(\overline{uhdh})^T\Psi_{out}\right|^2 & \left|(\overline{uhdv})^T\Psi_{out}\right|^2 \\ \left|(\overline{uvuh})^T\Psi_{out}\right|^2 & \left|(\overline{uvuv})^T\Psi_{out}\right|^2 & \left|(\overline{uvdh})^T\Psi_{out}\right|^2 & \left|(\overline{uvdv})^T\Psi_{out}\right|^2 \\ \left|(\overline{dhuh})^T\Psi_{out}\right|^2 & \left|(\overline{dhuv})^T\Psi_{out}\right|^2 & \left|(\overline{dhdh})^T\Psi_{out}\right|^2 & \left|(\overline{dhdv})^T\Psi_{out}\right|^2 \\ \left|(\overline{dvuh})^T\Psi_{out}\right|^2 & \left|(\overline{dvuv})^T\Psi_{out}\right|^2 & \left|(\overline{dvdh})^T\Psi_{out}\right|^2 & \left|(\overline{dvdv})^T\Psi_{out}\right|^2 \end{bmatrix}$$
$$= \begin{pmatrix} \frac{1}{2} & 0 & 0 & 0 \\ 0 & 0 & 0 & 0 \\ 0 & 0 & \frac{1}{2} & 0 \\ 0 & 0 & 0 & 0 \end{pmatrix}$$

$$P_{boson} = P_{uhuh} = P_{dhdh} = \frac{1}{2}$$

We see that this calculation is in agreement with the experimental results represented in the figure above: both photons always arrive at the same detector. 50 % of the time it is U and 50% of the time it is D.

Now assume that a 90 degree polarization rotator is placed in the lower arm which rotates the horizontal state to the vertical polarization orientation. This provides path information and even though polarization is not measured in this experiment it has a significant affect on the measurement results.

The entangled photon state after the PDC now is:

$$\Psi_{boson} = \frac{1}{\sqrt{2}}(uhdv + dvuh)$$

This leads to the following output state after interaction with the mirrors and the beam splitter:

$$\Psi_{out} = BSI(MI)\Psi_{boson}$$

The measurement outcome matrix now shows that the photons arrive at different detectors 50% of the time and the same detector 50% of the time. Remember that polarization is not being measured in this experiment. But the fact that polarization information exists changes the experimental results. The following algebraic expression for the output states shows that the interence effects that were seen previous do not occur because of the h/v polarization markers on the motional states.

$$\Psi_{out} = \frac{1}{\sqrt{2}}(i(uh)uv - uh(dv) + dh(uv) + i(dh)dv + i(uv)uh - uv(dh) - dv(uh) + i(dv)dh)$$

$$P_{boson} = P_{uhuv} = P_{uhdv} = P_{dhdv} = P_{uvuh} = P_{uvdh} = P_{dvuh} = P_{dvdh} = \frac{1}{8}$$

$$P_{boson} = \begin{bmatrix} \left[\left|(\overline{uhuh})^T\Psi_{out}\right|\right]^2 & \left[\left|(\overline{uhuv})^T\Psi_{out}\right|\right]^2 & \left[\left|(\overline{uhdh})^T\Psi_{out}\right|\right]^2 & \left[\left|(\overline{uhdv})^T\Psi_{out}\right|\right]^2 \\ \left[\left|(\overline{uvuh})^T\Psi_{out}\right|\right]^2 & \left[\left|(\overline{uvuv})^T\Psi_{out}\right|\right]^2 & \left[\left|(\overline{uvdh})^T\Psi_{out}\right|\right]^2 & \left[\left|(\overline{uvdv})^T\Psi_{out}\right|\right]^2 \\ \left[\left|(\overline{dhuh})^T\Psi_{out}\right|\right]^2 & \left[\left|(\overline{dhuv})^T\Psi_{out}\right|\right]^2 & \left[\left|(\overline{dhdh})^T\Psi_{out}\right|\right]^2 & \left[\left|(\overline{dhdv})^T\Psi_{out}\right|\right]^2 \\ \left[\left|(\overline{dvuh})^T\Psi_{out}\right|\right]^2 & \left[\left|(\overline{dvuv})^T\Psi_{out}\right|\right]^2 & \left[\left|(\overline{dvdh})^T\Psi_{out}\right|\right]^2 & \left[\left|(\overline{dvdv})^T\Psi_{out}\right|\right]^2 \end{bmatrix}$$
$$= \begin{pmatrix} 0 & \frac{1}{8} & 0 & \frac{1}{8} \\ \frac{1}{8} & 0 & \frac{1}{8} & 0 \\ 0 & \frac{1}{8} & 0 & \frac{1}{8} \\ \frac{1}{8} & 0 & \frac{1}{8} & 0 \end{pmatrix}$$

The path information provided by the h/v polarization states of the photons can be "erased" by placing diagonally (45 degrees to the veritcal and labelled s for slant) oriented polarizers after the beam splitter and before the detectors. Polarizers are projection operators, consequently only diagonally polarized photons reach the detectors. There are only four possible final measurement states,

$$usus = \frac{1}{2}(1 \quad 1 \quad 0 \quad 0 \quad 1 \quad 1 \quad 0 \quad 0 \quad 0 \quad 0 \quad 0 \quad 0 \quad 0 \quad 0 \quad 0 \quad 0)$$

$$usds = \frac{1}{2}(0 \quad 0 \quad 1 \quad 1 \quad 0 \quad 0 \quad 1 \quad 1 \quad 0 \quad 0 \quad 0 \quad 0 \quad 0 \quad 0 \quad 0 \quad 0)$$

$$dsus = \frac{1}{2}(0 \quad 0 \quad 0 \quad 0 \quad 0 \quad 0 \quad 0 \quad 0 \quad 1 \quad 1 \quad 0 \quad 0 \quad 1 \quad 1 \quad 0 \quad 0)$$

$$dsds = \frac{1}{2}(0 \quad 0 \quad 0 \quad 0 \quad 0 \quad 0 \quad 0 \quad 0 \quad 0 \quad 0 \quad 0 \quad 1 \quad 1 \quad 0)$$

where for example dsus is calculated as follows. Tensor multiplication is implied between the vector states.

$$dsus = \left[\begin{pmatrix}0\\1\end{pmatrix}\frac{1}{\sqrt{2}}\begin{pmatrix}1\\1\end{pmatrix}\begin{pmatrix}1\\0\end{pmatrix}\frac{1}{\sqrt{2}}\begin{pmatrix}1\\1\end{pmatrix}\right]^T$$

where

$$s = \frac{1}{\sqrt{2}}\begin{pmatrix}1\\1\end{pmatrix}$$

The recalculated experimental outcome matrix shows that the photons again always arrive at the same detector. The accompanying algebraic analysis reveals the revived interference effects that lead to the final result.

$$\begin{bmatrix} (|usus\Psi_{out}|)^2 & (|usds\Psi_{out}|)^2 \\ (|dsus\Psi_{out}|)^2 & (|dsds\Psi_{out}|)^2 \end{bmatrix} = \begin{pmatrix} \frac{1}{8} & 0 \\ 0 & \frac{1}{8} \end{pmatrix}$$

$$\Psi_s = \frac{1}{4\sqrt{2}} = (i(us)us - us(ds) + ds(us) + i(ds)ds + i(us)us + us(ds) - ds(us) + i(ds)ds)$$
$$= \frac{1}{2\sqrt{2}}(us(us) + ds(ds))$$

Photons are bosons and therefore have symmetric wave functions. This is why in the initial experiment they always arrive at the same detector. We will now assume that they are fermions, which have anti-symmetric wave functions, and repeat the calculations and observe the consequences.

The fermionic entangled photon wave function:

$$\Psi_{fermion} = \frac{1}{\sqrt{2}}(uhuh - dhdh)$$

The output state after the photons interact with the mirrors and the beam splitter is:

$$\Psi_{out} = BMI(MI)\Psi_{fermion}$$

The measurement outcome matrix shows that the fermions, as expected, always arrive at different detectors:

$$P_{fermion} = \begin{bmatrix} \left[\left|(\overline{uhuh})^T\Psi_{out}\right|\right]^2 & \left[\left|(\overline{uhuv})^T\Psi_{out}\right|\right]^2 & \left[\left|(\overline{uhdh})^T\Psi_{out}\right|\right]^2 & \left[\left|(\overline{uhdv})^T\Psi_{out}\right|\right]^2 \\ \left[\left|(\overline{uvuh})^T\Psi_{out}\right|\right]^2 & \left[\left|(\overline{uvuv})^T\Psi_{out}\right|\right]^2 & \left[\left|(\overline{uvdh})^T\Psi_{out}\right|\right]^2 & \left[\left|(\overline{uvdv})^T\Psi_{out}\right|\right]^2 \\ \left[\left|(\overline{dhuh})^T\Psi_{out}\right|\right]^2 & \left[\left|(\overline{dhuv})^T\Psi_{out}\right|\right]^2 & \left[\left|(\overline{dhdh})^T\Psi_{out}\right|\right]^2 & \left[\left|(\overline{dhdv})^T\Psi_{out}\right|\right]^2 \\ \left[\left|(\overline{dvuh})^T\Psi_{out}\right|\right]^2 & \left[\left|(\overline{dvuv})^T\Psi_{out}\right|\right]^2 & \left[\left|(\overline{dvdh})^T\Psi_{out}\right|\right]^2 & \left[\left|(\overline{dvdv})^T\Psi_{out}\right|\right]^2 \end{bmatrix}$$
$$= \begin{pmatrix} 0 & 0 & \frac{1}{2} & 0 \\ 0 & 0 & 0 & 0 \\ \frac{1}{2} & 0 & 0 & 0 \\ 0 & 0 & 0 & 0 \end{pmatrix}$$

Naturally an algebraic analysis yields the same result.

$$\Psi_{out} = \frac{1}{2\sqrt{2}}(i(uh)uh - uh(dh) + dh(uh) + i(dh)dh - i(uh)uh - uh(dh) + dh(uh) - i(dh)dh)$$
$$= \frac{1}{sqrt2}(dh(uh) - uh(dh))$$

$$P_{fermion} = P_{uhdh} = P_{dhuh} = \frac{1}{2}$$

As algebraic and matrix calculations show, introduction of path information for fermions yields the same result as for bosons, the photons sometimes arrive at the same detector and sometimes at different detectors.

$$\Psi_{fermion} = \frac{1}{\sqrt{2}} = \frac{1}{sqrt2}(uhdv = dvuh)$$

$$\Psi_{out} = BSI(MI)\Psi_{fermion}$$

$$\Psi_{out} = \frac{1}{2\sqrt{2}}(i(uh)uv - uh(dv) + dh(uv) + i(dh)dv - i(uv)uh - uv(dh) + dv(uh) - i(dv)dh)$$

$$P_{fermion} = P_{uhuv} = P_{uhdv} = P_{dhuv} = P_{dhdv} = P_{uvuh} = P_{uvdh} = P_{dvuh} = P_{dvdh} = \frac{1}{8}$$

$$P_{fermion} = \begin{bmatrix} \left[\left|(\overline{uhuh})^T\Psi_{out}\right|\right]^2 & \left[\left|(\overline{uhuv})^T\Psi_{out}\right|\right]^2 & \left[\left|(\overline{uhdh})^T\Psi_{out}\right|\right]^2 & \left[\left|(\overline{uhdv})^T\Psi_{out}\right|\right]^2 \\ \left[\left|(\overline{uvuh})^T\Psi_{out}\right|\right]^2 & \left[\left|(\overline{uvuv})^T\Psi_{out}\right|\right]^2 & \left[\left|(\overline{uvdh})^T\Psi_{out}\right|\right]^2 & \left[\left|(\overline{uvdv})^T\Psi_{out}\right|\right]^2 \\ \left[\left|(\overline{dhuh})^T\Psi_{out}\right|\right]^2 & \left[\left|(\overline{dhuv})^T\Psi_{out}\right|\right]^2 & \left[\left|(\overline{dhdh})^T\Psi_{out}\right|\right]^2 & \left[\left|(\overline{dhdv})^T\Psi_{out}\right|\right]^2 \\ \left[\left|(\overline{dvuh})^T\Psi_{out}\right|\right]^2 & \left[\left|(\overline{dvuv})^T\Psi_{out}\right|\right]^2 & \left[\left|(\overline{dvdh})^T\Psi_{out}\right|\right]^2 & \left[\left|(\overline{dvdv})^T\Psi_{out}\right|\right]^2 \end{bmatrix}$$
$$= \begin{pmatrix} 0 & \frac{1}{8} & 0 & \frac{1}{8} \\ \frac{1}{8} & 0 & \frac{1}{8} & 0 \\ 0 & \frac{1}{8} & 0 & \frac{1}{8} \\ \frac{1}{8} & 0 & \frac{1}{8} & 0 \end{pmatrix}$$

With erasure of path information the fermionic photons again always arrive at different detectors.

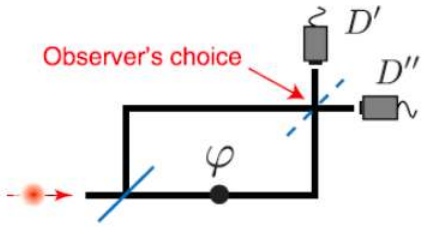
$$\begin{bmatrix} (|usus\Psi_{out}|)^2 & (|usds\Psi_{out}|)^2 \\ (|dsus\Psi_{out}|)^2 & (|dsds\Psi_{out}|)^2 \end{bmatrix} = \begin{pmatrix} 0 & \frac{1}{8} \\ \frac{1}{8} & 0 \end{pmatrix}$$

$$\Psi_s = \frac{1}{4\sqrt{2}}(i(us)us - us(ds) + ds(us) + i(ds)ds - i(us)us - us(ds) + ds(us) - i(ds)ds$$
$$= \frac{1}{2\sqrt{2}}(ds(us) - us(ds))$$

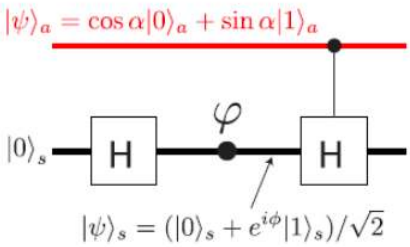
This page titled 7.40: Another Example of a Two-photon Quantum Eraser is shared under a CC BY 4.0 license and was authored, remixed, and/or curated by Frank Rioux via source content that was edited to the style and standards of the LibreTexts platform.

7.41: A Quantum Delayed-Choice Experiment

This tutorial works through the first half of the Science report (Nov. 2, 2012, pp . 634-637) by Peruzzo et al. with the title given above. The Wheeler-type delayed-choice experiment dealt with in this paper is shown schematically in the figure below. An observer has the option of inserting or removing a second beam splitter (BS) in a Mach-Zehnder interferometer (MZI) after a photon has passed the first BS.



This apparatus is implemented using Hadamard and controlled-Hadamard gates as shown below. A phase shift is also possible in the lower arm of the interferometer. The operation of the second Hadamard gate is controlled by an ancillary photon which can be prepared as a superposition. For this reason the second beam splitter is called a quantum beam splitter (QBS).



The Hadamard gate is a single-photon gate as is the phase shifter, while the controlled-Hadamard gate is a two-photon gate. Their matrix representations are as follows.

$$H = \frac{1}{\sqrt{2}}\begin{pmatrix}1 & 1\\ 1 & -1\end{pmatrix}$$

$$A(\phi) = \begin{pmatrix}1 & 0\\ 0 & e^{i\phi}\end{pmatrix}$$

$$A(\phi)H\begin{pmatrix}1\\0\end{pmatrix} \rightarrow \begin{pmatrix}\frac{\sqrt{2}}{2}\\ \frac{\sqrt{2}e^{\phi i}}{2}\end{pmatrix}$$

$$CH = \begin{pmatrix}1 & 0 & & 0 & 0\\ 0 & 1 & 0 & 0 & \\ 0 & 0 & \frac{1}{\sqrt{2}} & \frac{1}{\sqrt{2}} & \\ 0 & 0 & \frac{1}{\sqrt{2}} & \frac{-1}{\sqrt{2}} & \end{pmatrix}$$

The H gate and the phase-shifter create the superposition at the point of the arrow (see highlighted area above), just before the CH gate. This is the point at which this analysis begins. Using vector tensor multiplication, the composite state (a = ancilla; s = system) is shown below.

$$\begin{pmatrix}\cos\alpha\\ \sin\alpha\end{pmatrix}_a \otimes \frac{1}{\sqrt{2}}\begin{pmatrix}1\\ e^{i\phi}\end{pmatrix} = \frac{1}{\sqrt{2}}\begin{pmatrix}\cos\alpha\\ \cos\alpha e^{i\phi}\\ \sin\alpha\\ \sin\alpha e^{i\phi}\end{pmatrix}$$

The four output states expressed in the |0 > - |1 > basis are as follows.

$$|0\rangle_a|0\rangle_s = \begin{pmatrix}1\\0\end{pmatrix}_a \otimes \begin{pmatrix}1\\0\end{pmatrix}_s = \begin{pmatrix}1\\0\\0\\0\end{pmatrix}$$

$$|1\rangle_a|0\rangle_s = \begin{pmatrix}0\\1\end{pmatrix}_a \otimes \begin{pmatrix}1\\0\end{pmatrix}_s = \begin{pmatrix}0\\0\\1\\0\end{pmatrix}$$

$$|0\rangle_a|1\rangle_s = \begin{pmatrix}1\\0\end{pmatrix}_a \otimes \begin{pmatrix}0\\1\end{pmatrix}_s = \begin{pmatrix}0\\1\\0\\0\end{pmatrix}$$

$$|1\rangle_a|1\rangle_s = \begin{pmatrix}0\\1\end{pmatrix}_a \otimes \begin{pmatrix}0\\1\end{pmatrix}_s = \begin{pmatrix}0\\0\\0\\1\end{pmatrix}$$

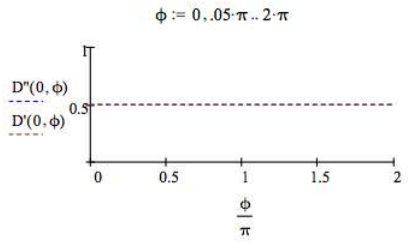
The probability that the photon is detected at D'' (|0 >s) is:

$$D''(\alpha,\phi) = \left[\left|\begin{pmatrix}1\\0\\0\\0\end{pmatrix}^T CH\frac{1}{\sqrt{2}}\begin{pmatrix}\cos\alpha\\\cos\alpha e^{i\phi}\\\sin\alpha\\\sin\alpha e^{i\phi}\end{pmatrix}\right|\right]^2 + \left[\left|\begin{pmatrix}0\\0\\1\\0\end{pmatrix}^T CH\frac{1}{\sqrt{2}}\begin{pmatrix}\cos\alpha\\\cos\alpha e^{i\phi}\\\sin\alpha\\\sin\alpha e^{i\phi}\end{pmatrix}\right|\right]^2$$

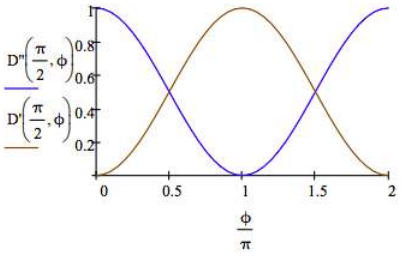
The probability that the photon is detected at D' (|1 >s) is:

$$D'(\alpha,\phi) = \left[\left|\begin{pmatrix}0\\1\\0\\0\end{pmatrix}^T CH\frac{1}{\sqrt{2}}\begin{pmatrix}\cos\alpha\\\cos\alpha e^{i\phi}\\\sin\alpha\\\sin\alpha e^{i\phi}\end{pmatrix}\right|\right]^2 + \left[\left|\begin{pmatrix}0\\0\\0\\1\end{pmatrix}^T CH\frac{1}{\sqrt{2}}\begin{pmatrix}\cos\alpha\\\cos\alpha e^{i\phi}\\\sin\alpha\\\sin\alpha e^{i\phi}\end{pmatrix}\right|\right]^2$$

The following graph shows that if α = 0 (the ancillary photon is in the |0 > state), the interferometer is open and the detectors each fire 50% of the time no matter what phase relationship exists between the arms of the interferometer.



However, if α = π/2 (the ancillary photon is in the |1 > state) the interferometer is closed and interference is observed. The firing of the detectors depends upon the phase relation between the two arms of the interferometer. If ϕ = 0 only D'' fires, while if ϕ = π only D' fires. As shown below, at other ϕ values both detectors fire.



If α = π/4 (the ancilla photon is in a 50-50 superposition of |0 > and |1 >), both detectors fire at all ϕ values.

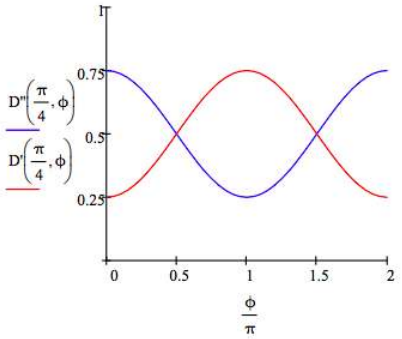
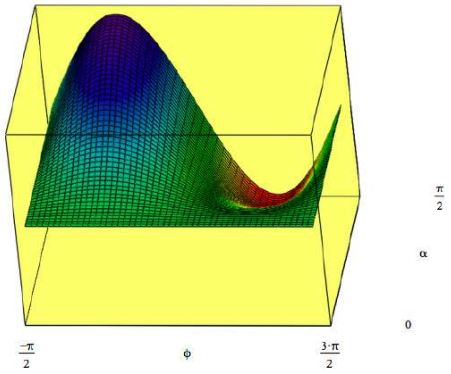


Figure 3B are reproduced.

$N = 50 \quad i = 0..N \quad j = 0..N \quad \alpha_1 = \frac{\frac{\pi}{2} i}{N} \quad \phi_j = \frac{-\pi}{2} + \frac{2\pi j}{N} \quad I_{i,\,j} = D'(\alpha_i, \phi_j)$



In summary, according to Peruzzo et al. this is a delayed-choice experiment for 0 < α < π/2 because the system photon is in the interferometer before it becomes entangled with the ancillary photon.

While this work represents an exquisite experimental tour de force, in my opinion it doesn′t reveal anything more about wave-particle duality than any other quantum optics experiment. We always measure particles (detectors click, photographic film is darkened, etc.), but we interpret what happened or predict what will happen by assuming wavelike behavior. In other words, quantum particles exhibit both wave and particle properties in every experiment. To paraphrase Nick Herbert (*Quantum Reality*), particles are always detected, but the experimental results observed are the result of wavelike behavior. Richard Feynman put it this way (*The Character of Physical Law*), ″I will summarize, then, by saying that electrons arrive in lumps, like particles, but the probability of arrival of these lumps is determined as the intensity of waves would be. It is in this sense that the electron behaves sometimes like a particle and sometimes like a wave. It behaves in two different ways at the same time.″ Bragg said, ″Everything in the future is a wave, everything in the past is a particle.″

In 1951 in his treatise *Quantum Theory*, David Bohm described wave-particle duality as follows: ″One of the most characteristic features of the quantum theory is the wave-particle duality, i.e. the ability of matter or light quanta to demonstrate the wave-like

property of interference, and yet to appear subsequently in the form of localiziable particles, even after such interference has taken place." In other words, to explain interference phenomena wave properties must be assigned to matter and light quanta prior to detection as particles.

Equation (1) in this paper is not a "particle" wave function, it is a superposition of the photon being in both arms of the interferometer. It is a wave function (period) and it accurately predicts the future detection results in both the absence and presence of the second beam splitter. See the Appendix for further comment. John Wheeler, designer of several delayed-choice experiments (both terrestrial and cosmological), had the following to say about the interpretation of such experiments.

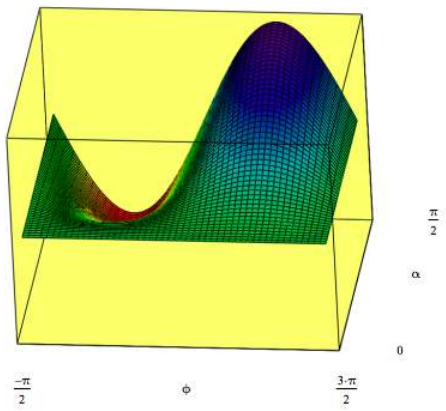
> ... in a loose way of speaking, we decide what the photon shall have done after it has already done it. In actuality it is wrong to talk of the 'route' of the photon. For a proper way of speaking we recall once more that it makes no sense to talk of a phenomenon until it has been brought to a close by an irreversible act of amplification. 'No elementary phenomenon is a phenomenon until it is a registered (observed) phenomenon.'

This statement was given a convincing and amusing graphical representation by Field Gilbert's sketch of Wheeler's 'Great Smokey Dragon' which can be found on page 154 of Jim Baggot's *The Meaning of Quantum Theory*.

Heisenberg said pretty much the same thing as Wheeler when he wrote in 1958: "If we want to describe what happens in an atomic event, we have to realize that the word 'happens' can only apply to the observation, not to the state of affairs between two observations."

I would also like to point out that equation (4) is mislabeled. The authors claim it is the detection probability at D' as a function of α and ϕ. However, the plot below shows that designation is not consistent with Figure 3B. Equation (4) is actually the detection probability at detector D''.

$$\ln(\alpha,\phi) = \frac{1}{2}\cos\alpha^2 + \cos\left(\frac{\phi}{2}\right)^2 \sin\alpha^2 \quad I_{i,\,j} = \ln(\alpha_i,\phi_j)$$



Appendix

Removing the phase shifter makes it easier to follow the evolution of the photons through the interferometer and to evaluate the authors' claim that they have demonstrated wave-particle duality as indicated in their equations 1, 2 and 3. We begin with the composite state prior to the controlled Hadamard gate.

$$\begin{pmatrix}\cos\alpha\\ \sin\alpha\end{pmatrix}_a \otimes \frac{1}{\sqrt{2}}\begin{pmatrix}1\\1\end{pmatrix}_s = \frac{\cos\alpha|0\rangle_a(0|\rangle_s+|1\rangle_s) + \sin\alpha|1\rangle_a(|0\rangle_s+|1\rangle_s)}{\sqrt{2}}$$

The operation of the controlled Hadamard (CH) gate is written algebraically.

$$CH|0\rangle_a|0\rangle_s = |0\rangle_a|0\rangle_s$$

$$CH|0\rangle_a|1\rangle_s = |0\rangle_a|1\rangle_s$$

$$CH|1\rangle_a|0\rangle_s = |1\rangle_a\frac{1}{\sqrt{2}}(|0\rangle_s+|1\rangle_s)$$

$$CH|1\rangle_a|1\rangle_s = |1\rangle_a \frac{1}{\sqrt{2}}(|0\rangle_s - |1\rangle_s)$$

The action of the controlled Hadamard gate leads to the following state which shows a superposition in blue and interference in red, depending on the state of the control qubit.

$$\frac{\cos\alpha|)\rangle_a(|0\rangle_s + |1\rangle_s) + \sin\alpha|1\rangle_a\left(\frac{|0\rangle_s+|1\rangle_s}{\sqrt{2}} + \frac{|0\rangle_s-|1\rangle_s}{\sqrt{2}}\right)}{\sqrt{2}} = \cos\alpha|0\rangle_a\frac{|0\rangle_s+|1\rangle_s}{\sqrt{2}} + \sin\alpha|1\rangle_a|0\rangle_s$$

According to Peruzzo *et al*. this leads to the following interpretive equation expressing their view of wave-particle duality.

$$\cos\alpha|0\rangle_a\Psi(\text{particle})\rangle_s + \sin\alpha|1\rangle_a|\Psi(\text{wave})\rangle_s$$

My objection is that a superposition, even if it dosen′t lead to interference, is an example of wavelike (delocalized) behavior. The fact that the superposition doesn′t lead to interference doesn′t mean the photon took a particular path to a particular detector, it simply means on observation the superposition collapsed with appropriate probability at that detector.

Quantum mechanical entities (quons) do not, as Peruzzo *et al*. assert, exhibit particle- or wavelike behavior depending on the design of the experimental apparatus they encounter. As Bohm, Feynman and Herbert have said quons exhibit wave and particle characteristics in every experiment.

This page titled 7.41: A Quantum Delayed-Choice Experiment is shared under a CC BY 4.0 license and was authored, remixed, and/or curated by Frank Rioux via source content that was edited to the style and standards of the LibreTexts platform.

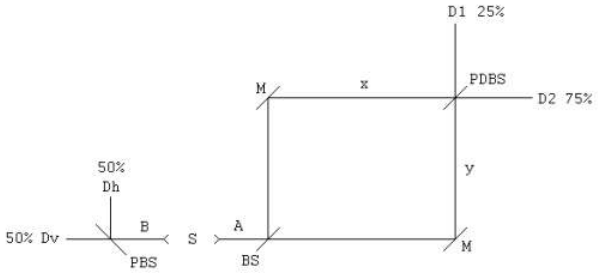
7.42: A Quantum Delayed-Choice Experiment

This note presents a critique of "Entanglement-Enabled Delayed-Choice Experiment," F. Kaiser, et al. Science **338**, 637 (2012). This experiment was also summarized in section 6.3 of *Quantum Weirdness*, by William Mullin, Oxford University Press, 2017.

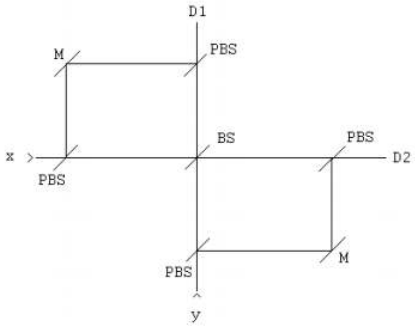
A source, S, emits two photons in opposite directions on the x-axis in the following polarization state, where v and h represent vertical and horizontal polarization, respectively.

$$|\Psi\rangle_{AB}\frac{1}{\sqrt{2}}\left[|xv\rangle_A|xv\rangle_B+|xh\rangle_A|xh\rangle_B\right]$$

Photon B travels to the left to a polarizing beam splitter, PBS. Photon A travels to the right entering an interferometer whose elements are a beam splitter (BS), two mirrors (M), and a polarization-dependent beam splitter (PDBS).



The implementation of the PDBS is shown here.



The operation of the optical elements are as follows. A mirror simply reflects the photon's direction of motion.

$$M = |y\rangle\langle x| + |x\rangle\langle y|$$

A 50-50 BS splits the photon beam into a superposition of motion in the x- and y-directions. By convention the reflected beam collects a pi/2 (i) phase shift relative to the transmitted beam.

$$BS = \frac{|x\rangle + i|y\rangle}{\sqrt{2}}\langle x| + \frac{i|x\rangle+|y\rangle}{\sqrt{2}}\langle y| = \frac{1}{\sqrt{2}}(|x\rangle\langle x| + i|y\rangle\langle x| + i|x\rangle\langle y| + |y\rangle\langle y|)$$

A PBS transmits vertically polarized photons and reflects horizontally polarized photons.

$$M = |y\rangle\langle x| + |x\rangle\langle y|$$

A 50-50 BS splits the photon beam into a superposition of motion in the x- and y-directions. By convention the reflected beam collects a pi/2 (i) phase shift relative to the transmitted beam.

$$BS = \frac{|x\rangle + i|y\rangle}{\sqrt{2}}\rangle x| + \frac{i|x\rangle+|y\rangle}{\sqrt{2}}\langle y| = \frac{1}{\sqrt{2}}(|x\rangle\langle x| + i|y\rangle\langle x| + i|x\rangle\langle y| + |y\rangle\langle y|)$$

A PBS transmits vertically polarized photons and reflects horizontally polarized photons.

$$PBS = |xv\rangle\langle xv| + |yh\rangle\langle xh| + |yv\rangle\langle yv| + |xh\rangle\langle yh|$$

The PDBS uses an initial PBS to reflect horizontally polarized photons to a second PBS which reflects them to the detectors. Vertically polarized photons are transmitted by the first PBS to a BS which has the action shown above, after which they are transmitted to the detectors by the second PBS. PBS/PDBS blue/red color coding highlights the action of the central BS.

$$PDPS = \frac{|xv\rangle + i|yv\rangle}{\sqrt{2}}\langle xv| + |yh\rangle\langle xh + \frac{i|xv\rangle + |yv\rangle}{\sqrt{2}}\langle yv| + |xh\rangle\langle yh|$$

Given the state produced by the source, half the time a horizontal photon will enter the interferometer and half the time a vertical photon will enter. The following algebraic analysis shows the progress of the h- and v-polarized photons entering the interferometer. It is clear from this analysis that D1 will fire 25% of the time and D2 75% of the time.

$$\begin{array}{cc} |xh\rangle & |xv\rangle \\ BS & BS \\ \frac{|xh\rangle+i|yh\rangle}{\sqrt{2}} & \frac{|xv\rangle+i|yv\rangle}{\sqrt{2}} \\ M & M \\ \frac{|yh\rangle+i|xh\rangle}{\sqrt{2}} & \frac{|yv\rangle+i|xv\rangle}{\sqrt{2}} \\ PDBS & PDBS \\ \frac{|D2\rangle|h\rangle+i|D1\rangle|h\rangle}{\sqrt{2}} & \frac{1}{\sqrt{2}}\left[\frac{|D1\rangle|v\rangle+i|D2\rangle|v\rangle}{\sqrt{2}} + \frac{i(i|D1\rangle|v\rangle+D2\rangle|v\rangle}{\sqrt{2}}\right] \\ & \downarrow \\ & i|D2\rangle|v\rangle \end{array}$$

This analysis suggests to some that inside the interferometer h-photons behave like particles and v-photons behave like waves. The argument for this view is that interference occurs at the PDBS for v-photons, but not for h-photons. However, in both cases the state illuminating the PDBS, highlighted in blue, is a superposition of the photon being in both arms of the interferometer. In my opinion this superposition implies delocalization which implies wavelike behavior. At the PDBS the h-photon superposition is reflected away from the central BS to D1 and D2, leading to the final superposition in the left-hand column above, which collapses on observation to either D1 or D2. The v-photon superposition is transmitted at the PDBS to the central BS allowing for destructive interference at D1 and constructive interference at D2 as is shown at the bottom of the right-hand column.

Those who interpret this experiment in terms of particle or wave behavior also invoke the concept of delayed-choice, claiming that if D2 fires we don't know for sure which behavior has occurred because both h and v photons can arrive there. They argue that until photon B has been observed at Dv or Dh, which by design can be long after photon A has exited the interferometer, the polarization of the photon detected at D2 is unknown and therefore so is whether particle or wave behavior has occurred. These analysts write the final two photon wavefunction as the following entangled superposition, where particle behavior is highlighted in red and wave behavior in blue.

$$|\Psi\rangle_{final} = \frac{1}{\sqrt{2}}\left(\left(\frac{|D2,h\rangle + i|D1,h\rangle}{\sqrt{2}}\right)_A |Dh\rangle_B + i|D2,v\rangle_A|Dv\rangle_B\right) = \frac{1}{\sqrt{2}}(|Particle\rangle_A|Dh\rangle_B + |Wave\rangle_A|Dv\rangle_B)$$

For the reasons expressed above I do not find this interpretation convincing. We always observe particles (detectors click, photographic film is darkened, etc.), but we interpret what happened or predict what will happen by assuming wavelike behavior. In other words, objects governed by quantum mechanical principles (quons) exhibit both wave and particle properties in every experiment. To paraphrase Nick Herbert (*Quantum Reality*), particles are always detected, but the experimental results observed are the result of wavelike behavior. Bragg summarized wave-particle duality saying, "Everything in the future is a wave, everything in the past is a particle."

This page titled 7.42: A Quantum Delayed-Choice Experiment is shared under a CC BY 4.0 license and was authored, remixed, and/or curated by Frank Rioux via source content that was edited to the style and standards of the LibreTexts platform.

CHAPTER OVERVIEW

Back Matter

Index

Index

A

Airy pattern
- 1.14: Quantum Mechanics and the Fourier Transform

alpha decay
- 10.4: A Rudimentary Model for Alpha Particle Decay

atomic properties
- 11.3: Commentary on “Probing the Orbital Energy of an Electron in an Atom”

Atomic volume
- 2.46: Calculating the Atomic Radius of Polonium

B

Bell states
- 1.7: Quantum Computation- A Short Course
- 8.53: Bell State Exercises

Bell Theorem
- 8.45: Yet Another Assault on Local Realism - A Matrix/Tensor Algebra Approach
- 8.46: Jim Baggott's Bell Theorem Analysis
- 8.48: Another Bell Theorem Analysis - Shorter Version

Bell’s theorem
- 1.5: Quantum Computation - A Short Course

C

Circularly polarized light
- 7.14: Matrix Mechanics Approach to Polarized Light
- 7.15: Matrix Mechanics Approach to Polarized Light - Version 2
- 7.24: Optical Activity - A Quantum Perspective

confinement energy
- 1.3: Atomic and Molecular Stability

cosmic microwave background radiation
- 11.19: Age of the Elements

Cosmic Radiation
- 11.18: Cosmic Background Radiation

cyanine dyes
- 4.3: Cyanine Dyes as Two-State Electronic Systems

D

Degenerate Perturbation Theory
- 10.35: First Order Degenerate Perturbation Theory - the Stark Effect of the Hydrogen Atom

density operator
- 7.9: Pure States, Mixtures and the Density Operator

Deutsch-Jozsa Algorithm
- 1.8: Quantum Computation- A Short Course

Deutsch's Problem
- 8.68: A Simple Solution to Deutsch's Problem

diffraction pattern
- 1.14: Quantum Mechanics and the Fourier Transform
- 5.9: Calculating Diffraction Patterns

Dirac delta function
- 1.25: The Dirac Delta Function

Dirac equation
- 1.36: Aspects of Dirac's Relativistic Matrix Mechanics

Dirac Notation
- 1.26: Elements of Dirac Notation

dodecahedrane
- 6.2: Dodecahedrane

down converter
- 7.39: Analysis of a Two-photon Quantum Eraser

downconversion
- 7.26: Two Photon Interference - The Creation of an Entangled Superposition

E

effective potential energy
- 1.3: Atomic and Molecular Stability

Electrons within a Ring
- 1.86: Quantum Corrals - Electrons within a Ring

Entangled Bipartate Superposition
- 8.64: Examining the Local States of an Entangled Bipartate Superposition

entanglement
- 1.7: Quantum Computation- A Short Course
- 8.59: An Entanglement Swapping Protocol

expectation value
- 7.10: Using the Trace Function to Calculate Expectation Values

F

Feshbach Potential
- 10.33: Variational Method for the Feshbach Potential
- 10.42: Variation Method Using the Wigner Function - The Feshbach Potential

G

GHZ Entanglement
- 8.16: GHZ Entanglement - A Tensor Algebra Analysis

Grover Search Algorithm
- 1.10: Quantum Computation- A Short Course

H

Hadamard gate
- 8.53: Bell State Exercises

Hardy's Paradox
- 8.52: Hardy's Paradox

L

ladder operators
- 1.28: Raising and Lowering; Creating and Annihilating
- 7.4: Single Photon Interference - Fourth Version

linearly polarized light
- 7.24: Optical Activity - A Quantum Perspective

locality
- 8.14: Greenaberger-Hrne-Zeilinger (GHZ) Entanglement and Local Realism

M

Mach-Zehnder interferometer
- 7.22: A Quantum Circuit for a Michelson Interferometer

maser
- 4.4: The Ammonia Inversion and the Maser

Matrix Mechanics
- 1.33: Basic Matrix Mechanics
- 1.35: Matrix Mechanics
- 7.16: Matrix Mechanics Exercises Using Polarized Light

methane
- 6.8: CH_4

Michelson Interferometer
- 7.21: Two Analyses of the Michelson Interferometer

Mixed states
- 7.9: Pure States, Mixtures and the Density Operator

Morse potential
- 4.8: Visualizing the Formally Forbidden Overtone Vibrational Transitions in HCl
- 9.12: Numerical Solutions for Morse Oscillator

N

Neutron Interferometry
- 7.18: Neutron Interferometry with Polarized Spin States

Numerical Solutions
- 9: Numerical Solutions for Schrödinger's Equation

O

optical activity
- 7.24: Optical Activity - A Quantum Perspective

Overlap integral
- 1.26: Elements of Dirac Notation

overtones
- 4.8: Visualizing the Formally Forbidden Overtone Vibrational Transitions in HCl

P

parametric down converter
- 1.7: Quantum Computation- A Short Course
- 7.27: Two-particle Interference for Bosons and Fermions

path integrals
- 1.9: Quantum Computation- A Short Course

Planck Distribution
- 11.18: Cosmic Background Radiation

Polarizability
- 10.36: Variational Calculation for the Polarizability of the Hydrogen Atom

Polarizing Beam Splitter
- 7.6: The Polarizing Beam Splitter and the Superposition Principle

polonium
- 2.46: Calculating the Atomic Radius of Polonium

Positronium
- 1.4: Atomic and Molecular Stability
- 2.4: A de Broglie-Bohr Model for Positronium

Positronium Annihilation
- 8.34: Positronium Annihilation

Pure state
- 7.9: Pure States, Mixtures and the Density Operator

Q

Quantum Beats
- 4.11: Quantum Beats

Quantum centrifugal potential
1.3: Atomic and Molecular Stability
quantum chemistry
11.3: Commentary on “Probing the Orbital Energy of an Electron in an Atom”
quantum cloning
1.6: Quantum Computation- A Short Course
Quantum Computation
1.5: Quantum Computation - A Short Course
1.6: Quantum Computation- A Short Course
1.7: Quantum Computation- A Short Course
1.8: Quantum Computation- A Short Course
quantum error correction
1.10: Quantum Computation- A Short Course
quantum pressure
1.98: Quantum Mechanical Pressure
Quantum Teleportation
1.6: Quantum Computation- A Short Course
8: Quantum Teleportation
8.2: Quantum Teleportation - A Brief Introduction
Quartic Oscillator
9.11: Numerical Solutions for the Quartic Oscillator
10.8: Variation Method for the Quartic Oscillator
10.41: Variation Method Using the Wigner Function - The Quartic Oscillator
qubits
8.65: A Brief Introduction to the Quantum Computer
quon
1.9: Quantum Computation- A Short Course

R

radioactive dating
11.19: Age of the Elements
Ramsey Atomic Interferometer
7.23: The Ramsey Atomic Interferometer
realism
8.14: Greenaberger-Hrne-Zeilinger (GHZ) Entanglement and Local Realism
Rotational Spectroscopy of Diatomic Molecules
4.6: Analyses of the Pure Rotational Spectrum of HCl
Rydberg Potential
10.7: Variation Method for the Rydberg Potential

S

Schrödinger equation
1.18: Exploring the Origin of Schrödinger’s Equations
Shor’s algorithm
1.7: Quantum Computation- A Short Course
Simon’s algorithm
1.10: Quantum Computation- A Short Course
Single Photon Interference
7.4: Single Photon Interference - Fourth Version
Slanted Well Potential
9.7: Particle in a Slanted Well Potential
10.11: Linear Variational Method for a Particle in a Slanted 1D Box
Stark Effect
10.35: First Order Degenerate Perturbation Theory - the Stark Effect of the Hydrogen Atom
superposition principle
1.24: Getting Accustomed to the Superposition Principle
7.6: The Polarizing Beam Splitter and the Superposition Principle

T

theoretical chemistry
11.3: Commentary on “Probing the Orbital Energy of an Electron in an Atom”
three polarizer paradox
7.14: Matrix Mechanics Approach to Polarized Light
7.15: Matrix Mechanics Approach to Polarized Light - Version 2
trace (matrix)
7.10: Using the Trace Function to Calculate Expectation Values
tunneling
4.5: A Symmetric Double Well Potential Illustrating Tunneling
Two Photon Interference
7.26: Two Photon Interference - The Creation of an Entangled Superposition

V

Variational Method
10.5: Variational Method for a Particle in a Finite Potential Well
Variational Theorem
10.3: The Variation Theorem in Dirac Notation
virial theorem
1.3: Atomic and Molecular Stability

W

Wheeler-type delayed-choice experiment
7.41: A Quantum Delayed-Choice Experiment
Wigner Function
10.38: Variation Method Using the Wigner Function- Finite Potential Well
10.39: 455. Variation Method Using the Wigner Function- V(x) = |x|

X

Xenon Tetrafluoride
6.3: Xenon Tetrafluoride

CHAPTER OVERVIEW

8: Quantum Teleportation

8.1: A Single Page Summary of Quantum Teleportation
8.2: Quantum Teleportation - A Brief Introduction
8.3: Quantum Teleportation at a Glance
8.4: Another Look at Quantum Teleportation
8.5: Teleportation Using Quantum Gates
8.6: Another Example of Teleportation Using Quantum Gates
8.7: Yet Another Quantum Teleportation Circuit
8.8: Quantum Teleportation - Another Look
8.9: A Quantum Teleportation Experiment for Undergraduates
8.10: A Simple Teleportation Exercise
8.11: Teleportation as a Quantum Computation
8.12: Quantum Teleportation - Four Perspectives
8.13: Teleportation of Two Qubits
8.14: Greenaberger-Hrne-Zeilinger (GHZ) Entanglement and Local Realism
8.15: GHZ Math Appendix
8.16: GHZ Entanglement - A Tensor Algebra Analysis
8.17: Simulation of a GHZ Gedanken Experiment
8.18: Another Simulation of a GHZ Gedanken Experiment
8.19: A Surgical Refutation of the Local Realism Heresy
8.20: GHZ Four-Photon Entanglement Analyzed Using Tensor Algebra
8.21: Quantum v. Realism
8.22: Elements of Reality- Another GHZ Gedanken Experiment Analyzed
8.23: Brief Elements of Reality
8.24: A Brief Analysis of Mermin's GHZ Thought Experiment
8.25: Lucien Hardy's Paradox as Presented by N. David Mermin
8.26: Hardy's Paradox - An Algebraic Analysis
8.27: Quantum Entanglement Leads to Nonclassical Correlations
8.28: Nonclassial Correlations Revealed with Mermin's Pentagram
8.29: Spooky Action at a Distance- The EPR Experiment with Photons
8.30: David Bohm's EPR Gedanken Experiment
8.31: An Extension of Bohm's EPR Experiment
8.32: A Surgical Adjudication of the Conflict Between Quantum Theory and Local Realism
8.33: A Thought Experiment Reveals the Conflict Between Quantum Theory and Local Realism
8.34: Positronium Annihilation
8.35: Mermin's Version of Bohm's EPR Gedanken Experiment
8.36: A Concise Version of Mermin's EPR Gedanken Experiment
8.37: Another Look at Mermin's EPR Gedanken Experiment
8.38: Mermin's Version of Bohm's EPR Gedanken Experiment Using Tensor Algebra
8.39: A GHZ Gedanken Experiment Using Spatial Degrees of Freedom and Tensor Algebra
8.40: Another GHZ Example Using Spin-1/2 Particles

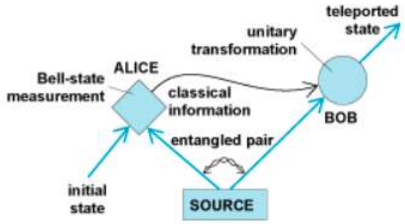
8.41: Entanglement Reveals a Conflict Between Local Realism and Quantum Theory
8.42: A Summary of Feynman's "Simulating Physics with Computers"
8.43: Another Summary of Fenyman's "Stimulating Physics with Computers"
8.44: Yet Another Assault on Local Realism
8.45: Yet Another Assault on Local Realism - A Matrix/Tensor Algebra Approach
8.46: Jim Baggott's Bell Theorem Analysis
8.47: Another Bell Theorem Analysis
8.48: Another Bell Theorem Analysis - Shorter Version
8.49: EPR Analysis for a Composite Singlet Spin System
8.50: EPR Analysis for a Composite Singlet Spin System - Short Version
8.51: Analysis of the Stern-Gerlach Experiment
8.52: Hardy's Paradox
8.53: Bell State Exercises
8.54: Expressing Bell and GHZ States in Vector Format Using Mathcad
8.55: Quantum Circuit for the Generation of GHZ States
8.56: A Brief Description of Aspect's Experiment
8.57: The Kochen-Specker Theorem Illustrated Using a Three-Qubit GHZ System
8.58: A Brief Introduction to Entanglement Swapping
8.59: An Entanglement Swapping Protocol
8.60: Quantum Correlations Simplified
8.61: Simulating Quantum Correlations with a Quantum Computer
8.62: Quantum Computer Simulation of Photon Correlations
8.63: Quantum Correlations Illustrated with Photons
8.64: Examining the Local States of an Entangled Bipartate Superposition
8.65: A Brief Introduction to the Quantum Computer
8.66: A Very Simple Example of Parallel Quantum Computation
8.67: Another Simple Example of Parallel Quantum Computation
8.68: A Simple Solution to Deutsch's Problem
8.69: Another Example of Deutsch's Algorithm
8.70: Evaluating a Function Using a Quantum Circuit and a Demonstration of Parallel Computation
8.71: A Simple Quantum Circuit for Parallel Computation
8.72: An Illustration of the Deutsch-Jozsa Algorithm
8.73: Another Illustration of the Deutsch-Jozsa Algorithm
8.74: Aspects of Simon's Algorithm
8.75: Qubit Quantum Mechanics
8.76: Implementation of Deutsch's Algorithm Using Mathcad
8.77: Using Quantum Gates to Create Superpositions and Entangled States
8.78: A Simple Quantum Computer
8.79: Solving Equations Using a Quantum Circuit
8.80: Introduction to Superdense Coding
8.81: A Brief Introduction to Quantum Dense Coding
8.82: The Discrete or Quantum Fourier Transform
8.83: Factoring Using Shor's Quantum Algorithm
8.84: Shor's Quantum Algorithm - A Summary
8.85: Simulating the Deutsch-Jozsa Algorithm with a Double-Slit Apparatus

8.86: Simulating a Quantum Computer with a Mach-Zehnder Interferometer
8.87: Quantum Restrictions on Cloning
8.88: Quantum Error Correction
8.89: Matrix Mechanics Analysis of the BB84 Key Distribution
8.90: 388. The Quantum Math Behind Ekert's Key Distribution Scheme
8.91: A Shorter Version of the Quantum Math Behind Ekert's Key Distribution Scheme
8.92: Quantum Key Distribution Using a Mach-Zehnder Interferometer
8.93: Coding and Decoding Venus
8.94: Grover's Quantum Search Algorithm
8.95: Grover's Search Algorithm- Implementation for Two Items
8.96: Grover's Search Algorithm- Four-Card Monte

This page titled 8: Quantum Teleportation is shared under a CC BY 4.0 license and was authored, remixed, and/or curated by Frank Rioux via source content that was edited to the style and standards of the LibreTexts platform.

8.1: A Single Page Summary of Quantum Teleportation

As shown in the graphic below (Nature, December 11, 1997, page 576), quantum teleportation is a form of information transfer that requires pre-existing entanglement and a classical communication channel to send information from one location to another. Alice has the photon to be teleported and a photon of an entangled pair (β00) that she shares with Bob. She performs a measurement on her photons that projects them into one of the four Bell states and Bob's photon, via the entangled quantum channel, into a state that has a unique relationship to the state of the teleportee. Bob carries out one of four unitary operations on his photon depending on the results of Alice's measurement, which she sends him through a classical communication channel.



The teleportee and the Bell states indexed in binary notation:

Teleportee:

$$\begin{pmatrix} \sqrt{\frac{1}{3}} \\ \sqrt{\frac{2}{3}} \end{pmatrix}$$

Bell states:

$$\beta_{00} = \frac{1}{\sqrt{2}} \begin{pmatrix} 1 \\ 0 \\ 0 \\ 1 \end{pmatrix} \quad \beta_{01} = \frac{1}{\sqrt{2}} \begin{pmatrix} 0 \\ 1 \\ 1 \\ 0 \end{pmatrix} \quad \beta_{10} = \frac{1}{\sqrt{2}} \begin{pmatrix} 1 \\ 0 \\ 0 \\ -1 \end{pmatrix} \quad \beta_{11} = \frac{1}{\sqrt{2}} \begin{pmatrix} 0 \\ 1 \\ -1 \\ 0 \end{pmatrix}$$

The three-cubit initial state is rewritten as a linear superposition of the four possible Bell states that Alice can find on measurement.

$$|\Psi\rangle = \begin{pmatrix} \sqrt{\frac{1}{3}} \\ \sqrt{\frac{2}{3}} \end{pmatrix} \otimes \beta_{00} = \frac{1}{2} \left[\beta_{00} \otimes \begin{pmatrix} \sqrt{\frac{1}{3}} \\ \sqrt{\frac{2}{3}} \end{pmatrix} + \beta_{01} \otimes \begin{pmatrix} \sqrt{\frac{2}{3}} \\ \sqrt{\frac{1}{3}} \end{pmatrix} + \beta_{10} \otimes \begin{pmatrix} \sqrt{\frac{1}{3}} \\ -\sqrt{\frac{2}{3}} \end{pmatrix} + \beta_{11} \otimes \begin{pmatrix} -\sqrt{\frac{2}{3}} \\ \sqrt{\frac{1}{3}} \end{pmatrix} \right]$$

Alice's Bell state measurement result (β_{00}, β_{01}, β_{10} or β_{11}) determines the operation (I, X, Z or ZX) that Bob performs on his photon. The matrices for these operations are as follows.

$$I = \begin{pmatrix} 1 & 0 \\ 0 & 1 \end{pmatrix} \quad X = \begin{pmatrix} 0 & 1 \\ 1 & 0 \end{pmatrix} \quad Z = \begin{pmatrix} 1 & 0 \\ 0 & -1 \end{pmatrix} \quad ZX = \begin{pmatrix} 0 & 1 \\ -1 & 0 \end{pmatrix}$$

Tabular summary of teleportation experiment:

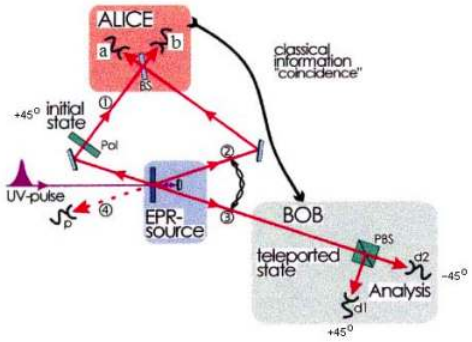
$$\begin{pmatrix} \text{Alice Measurement Result} & \beta_{00} & \beta_{01} & \beta_{10} & \beta_{11} \\ \text{Bob's Action} & I & X & Z & XZ \end{pmatrix}$$

Summary of the quantum teleportation protocol: "Quantum teleportation provides a 'disembodied' way to transfer quantum states from one object to another at a distant location, assisted by previously shared entangled states and a classical communication channel." Nature **518**, 516 (2015)

This page titled 8.1: A Single Page Summary of Quantum Teleportation is shared under a CC BY 4.0 license and was authored, remixed, and/or curated by Frank Rioux via source content that was edited to the style and standards of the LibreTexts platform.

8.2: Quantum Teleportation - A Brief Introduction

Alice wishes to teleport a photon in the polarization state, $\alpha h_1 + \beta v_1$, to Bob, where α and β are complex coefficients such that the sum of the square of their absolute magnitudes is unity. The letters *h* and *v* refer to the vertical and horizontal polarization states. In preparation for the teleportation event, Alice and Bob first prepare an entangled state involving photons 2 and 3, $\frac{h_2 v_3 - v_2 h_3}{\sqrt{2}}$, as shown in the figure below [*Nature* **390**, 576 (1997)].



Alice has photon 2 and Bob photon 3, but because they are in an entangled state the photons do not have well-defined individual polarization states.

Alice arranges for photons 1 and 2 to arrive at opposite sides of a beam splitter at the same time. This gives rise to the following state,

$$(\alpha h_1 \beta v_1)\frac{h_2 v_3 - v_2 h_3}{\sqrt{2}}$$

which upon expansion yields,

$$\frac{1}{2}\sqrt{2}\alpha h_1 h_2 v_3 - \frac{1}{2}\alpha h_1 v_2 h_3 + \frac{1}{2}\beta v_1 h_2 v_3 - \frac{1}{2}\beta v_1 v_2 h_3$$

Alice now makes a Bell-state measurement (vide infra) at the detectors (a and b) to the left and right of her beam splitter. Bell states are the four maximally entangled h-v polarization states of photons 1 and 2. They are as follows:

$$\Phi_p = \frac{h_1 h_2 + v_1 v_2}{\sqrt{2}} \quad \Phi_m = \frac{h_1 h_2 - v_1 v_2}{\sqrt{2}} \quad \Psi_p = \frac{h_1 v_2 + v_1 h_2}{\sqrt{2}} \quad \Psi_m = \frac{h_1 v_2 - v_1 h_2}{\sqrt{2}}$$

The products of the polarization states of photons 1 and 2 in equation (3) can be expressed as linear superpositions of the Bell states.

$$h_1 h_2 = \frac{\sqrt{2}}{2}(\Phi_p + \Phi_m) \quad h_1 v_2 = \frac{\sqrt{2}}{2}(\Psi_p + \Psi_m) \quad v_1 h_2 = \frac{\sqrt{2}}{2}(\Psi_p - \Psi_m) \quad v_1 v_2 = \frac{\sqrt{2}}{2}(\Phi_p - \Phi_m)$$

We can let Mathcad do the heavy lifting by having it expand (1), substitute equations (4) and collect on the Bell states.

$$(\alpha h_1 \beta v_1)\frac{h_2 v_3 - v_2 h_3}{\sqrt{2}}$$

expand

substitute, $h_1 h_2 = \frac{\sqrt{2}}{2}(\Phi_p + \Phi_m)$

substitute, $h_1 v_2 = \frac{\sqrt{2}}{2}(\Psi_p + \Psi_m)$

$\rightarrow \left(\frac{\beta h_3}{2} + \frac{\alpha v_3}{2}\right)\Phi_m + \left(\frac{\alpha v_3}{2} - \frac{\beta h_3}{2}\right)\Phi_p + \left(-\frac{\alpha h_3}{2} - \frac{\beta v_3}{2}\right)\Psi_m + \left(\frac{\beta v_3}{2} - \frac{\alpha h_3}{2}\right)\Psi_p$

substitute, $v_1 h_2 = \frac{\sqrt{2}}{2}(\Psi_p - \Psi_m)$

substitute, $v_1 v_2 = \frac{\sqrt{2}}{2}(\Phi_p - \Phi_m)$

collect, $\Phi_m,\ \Phi_p,\ \Psi_m,\ \Psi_p$

Thus Alice′s Bell-state measurement has four equally likely ($0.5^2 = 0.25$) outcomes. We will restrict our attention to the third term which says that if Alice measures Ψ_m, then Bob receives photon 1′s polarization state without further action by him.

$$-(\alpha h_3 + \beta v_3)\Psi_m$$

This will occur 25% of the time. The other three possible measurement outcomes are more complicated to analyze and will not be discussed further here. So we assume Alice measures Ψ_m and communicates this to Bob by classical means so that he knows that his photon (#3) now has the polarization state of the original photon 1. But, how does Alice know that the results she observes at detectors a and b mean that photons 1 and 2 are in Bell state Ψ_m?

First the short, qualitative answer. Of the four Bell states, Ψ_m is the only one that is antisymmetric with respect to the interchange of the labels of the photons. Thus, in spite of the fact that photons individually are bosons, this entangled state is fermionic - collectively the photons are behaving as fermions. This means that they can′t be in the same (measurement) state at the same time. If photon 1 is detected at *a*, then photon 2 will be detected at *b*. Therefore, if Alice observes *a*-*b* coincidences it means that photons 1 and 2 are in the Ψ_m Bell state and photon 1′s polarization state has been teleported to Bob′s photon (#3).

Bob confirms that he has received the polarization state of photon 1 using a polarizing beam splitter as shown in the figure above. Suppose Alice encodes photon 1 with a 45o polarization, then Bob sets his polarizing beam splitter to detect $+45^o$/-45^o polarized photons. A three-fold coincidence between detectors *a*, *b* and Bob′s $+45^o$ detector confirms teleportation. This was procedure employed in the original experiment published in Nature on December 11, 1997.

It should be pointed out that the initial entangled state used by Alice and Bob involving photons 2 and 3 is the Bell state Ψ_m. As was just seen, if Alice observes Ψ_m in her Bell-state measurement Bob receives photon 1′s polarization state without further action by him. As is shown below the analogous thing occurs if the initial entangled state is Ψ_p, Φ_p or Φ_m.

$$\Psi_p > \left(\frac{\alpha h_3}{2} + \frac{\beta v_3}{2}\right)\Psi_p$$

$$(\alpha h_1 \beta v_1)\frac{h_2 v_3 + v_2 h_3}{\sqrt{2}}$$

expand

substitute, $h_1 h_2 = \frac{\sqrt{2}}{2}(\Phi_p + \Phi_m)$

substitute, $h_1 v_2 = \frac{\sqrt{2}}{2}(\Psi_p + \Psi_m)$

$\rightarrow \left(\frac{\alpha v_3}{2} - \frac{\beta h_3}{2}\right)\Phi_m + \left(\frac{\beta h_3}{2} + \frac{\alpha v_3}{2}\right)\Phi_p + \left(\frac{\alpha h_3}{2} - \frac{\beta v_3}{2}\right)\Psi_m + \left(\frac{\alpha h_3}{2} + \frac{\beta v_3}{2}\right)\Psi_p$

substitute, $v_1 h_2 = \frac{\sqrt{2}}{2}(\Psi_p - \Psi_m)$

substitute, $v_1 v_2 = \frac{\sqrt{2}}{2}(\Phi_p - \Phi_m)$

collect, $\Phi_m,\ \Phi_p,\ \Psi_m,\ \Psi_p$

$$\Phi_p > \left(\frac{\alpha h_3}{2} + \frac{\beta v_3}{2}\right) \Phi_p$$

$$(\alpha h_1 \beta v_1) \frac{h_2 h_3 + v_2 v_3}{\sqrt{2}}$$

expand

substitute, $h_1 h_2 = \frac{\sqrt{2}}{2}(\Phi_p + \Phi_m)$

substitute, $h_1 v_2 = \frac{\sqrt{2}}{2}(\Psi_p + \Psi_m)$

$\rightarrow \left(\frac{\alpha h_3}{2} - \frac{\beta v_3}{2}\right) \Phi_m + \left(\frac{\alpha h_3}{2} + \frac{\beta v_3}{2}\right) \Phi_p + \left(\frac{\alpha v_3}{2} - \frac{\beta h_3}{2}\right) \Psi_m + \left(\frac{\beta h_3}{2} + \frac{\alpha v_3}{2}\right) \Psi_p$

substitute, $v_1 h_2 = \frac{\sqrt{2}}{2}(\Psi_p - \Psi_m)$

substitute, $v_1 v_2 = \frac{\sqrt{2}}{2}(\Phi_p - \Phi_m)$

collect, $\Phi_m,\ \Phi_p,\ \Psi_m,\ \Psi_p$

$$\Phi_m > \left(\frac{\alpha h_3}{2} + \frac{\beta v_3}{2}\right) \Phi_m$$

$$(\alpha h_1 \beta v_1) \frac{h_2 h_3 + v_2 v_3}{\sqrt{2}}$$

expand

substitute, $h_1 h_2 = \frac{\sqrt{2}}{2}(\Phi_p + \Phi_m)$

substitute, $h_1 v_2 = \frac{\sqrt{2}}{2}(\Psi_p + \Psi_m)$

$\rightarrow \left(\frac{\alpha h_3}{2} + \frac{\beta v_3}{2}\right) \Phi_m + \left(\frac{\alpha h_3}{2} - \frac{\beta v_3}{2}\right) \Phi_p + \left(-\frac{\beta h_3}{2} - \frac{\alpha v_3}{2}\right) \Psi_m + \left(\frac{\beta h_3}{2} - \frac{\alpha v_3}{2}\right) \Psi_p$

substitute, $v_1 h_2 = \frac{\sqrt{2}}{2}(\Psi_p - \Psi_m)$

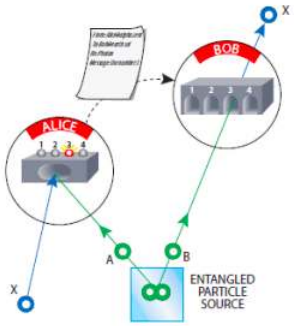
substitute, $v_1 v_2 = \frac{\sqrt{2}}{2}(\Phi_p - \Phi_m)$

collect, $\Phi_m,\ \Phi_p,\ \Psi_m,\ \Psi_p$

This page titled 8.2: Quantum Teleportation - A Brief Introduction is shared under a CC BY 4.0 license and was authored, remixed, and/or curated by Frank Rioux via source content that was edited to the style and standards of the LibreTexts platform.

8.3: Quantum Teleportation at a Glance

The purpose of this tutorial is to provide a brief mathematical outline of the basic elements of quantum teleportation, as illustrated in the figure below, using matrix and tensor algebra.



Alice wishes to teleport the following state (X in the figure) to Bob,

$$|\Phi\rangle = a|0\rangle + b|1\rangle = \begin{pmatrix} a \\ b \end{pmatrix} \quad |a|^2 + |b|^2 = 1$$

where,

$$|0\rangle = \begin{pmatrix} 1 \\ 0 \end{pmatrix} \quad |1\rangle = \begin{pmatrix} 0 \\ 1 \end{pmatrix}$$

They prepare the following entangled two-particle state, involving A and B, in which Alice has particle A and Bob has B.

$$|\Psi_{ab} = \frac{1}{\sqrt{2}}[|00\rangle + |11\rangle] = \frac{1}{\sqrt{2}}\left[\begin{pmatrix} 1 \\ 0 \end{pmatrix} \otimes \begin{pmatrix} 1 \\ 0 \end{pmatrix} + \begin{pmatrix} 0 \\ 1 \end{pmatrix} \otimes \begin{pmatrix} 0 \\ 1 \end{pmatrix}\right] = \frac{1}{\sqrt{2}} \begin{pmatrix} 1 \\ 0 \\ 0 \\ 1 \end{pmatrix}$$

Alice arranges for the particle to be teleported, |Φ >, and her entangled particle to meet simultaneously on opposite sides of a beam splitter, creating the following the three-particle state.

$$|\Phi\rangle|\Psi_{AB}\rangle = \begin{pmatrix} a \\ b \end{pmatrix} \otimes \frac{1}{\sqrt{2}} \begin{pmatrix} 1 \\ 0 \\ 0 \\ 1 \end{pmatrix} = \frac{1}{\sqrt{2}} \begin{pmatrix} a \\ 0 \\ 0 \\ a \\ b \\ 0 \\ 0 \\ b \end{pmatrix}$$

This state can be written as a superposition of the following 4-vectors, which are the well-known Bell states. Please see the Appendix for definitions of the Bell states.

$$\frac{1}{\sqrt{2}} \begin{pmatrix} a \\ 0 \\ 0 \\ a \\ b \\ 0 \\ 0 \\ b \end{pmatrix} = \frac{1}{2\sqrt{2}} \left[\begin{pmatrix} 1 \\ 0 \\ 0 \\ 1 \end{pmatrix} \otimes \begin{pmatrix} a \\ b \end{pmatrix} + \begin{pmatrix} 1 \\ 0 \\ 0 \\ -1 \end{pmatrix} \otimes \begin{pmatrix} a \\ -b \end{pmatrix} + \begin{pmatrix} 0 \\ 1 \\ 1 \\ 0 \end{pmatrix} \otimes \begin{pmatrix} b \\ a \end{pmatrix} + \begin{pmatrix} 0 \\ 1 \\ -1 \\ 0 \end{pmatrix} \otimes \begin{pmatrix} -b \\ a \end{pmatrix} \right]$$

We now write this three-particle state in terms of the Bell basis labels.

$$|\Phi\rangle|\Psi_{AB}\rangle = \frac{1}{2}\left[|\Phi^+\begin{pmatrix}a\\b\end{pmatrix} + |\Phi^-\rangle\begin{pmatrix}a\\-b\end{pmatrix} + |\Psi^+\begin{pmatrix}b\\a\end{pmatrix} + |\Psi^-\begin{pmatrix}-b\\a\end{pmatrix}\right]$$

Next, Alice makes a Bell-state measurement on her two particles, getting any of the four possible outcomes (Φ+ , Φ- , Ψ+ , or Ψ-) with equal probability, 25%. Her measurement collapses the state of Bob's particle into the companion of the result of her Bell-state measurement. Alice then sends the result of her measurement through a classical channel to Bob. Depending on her report, he carries out one of the following operations on his particle to complete the teleportation process.

$$|\Phi^+\rangle = \hat{I}\begin{pmatrix}a\\b\end{pmatrix} = \begin{pmatrix}1 & 0\\0 & 1\end{pmatrix}\begin{pmatrix}a\\b\end{pmatrix} = \begin{pmatrix}a\\b\end{pmatrix}$$

$$|\Phi^-\rangle = \widehat{\sigma_z}\begin{pmatrix}a\\-b\end{pmatrix} = \begin{pmatrix}1 & 0\\0 & -1\end{pmatrix}\begin{pmatrix}a\\-b\end{pmatrix} = \begin{pmatrix}a\\b\end{pmatrix}$$

$$|\Psi^+\rangle = \widehat{\sigma_x}\begin{pmatrix}b\\a\end{pmatrix} = \begin{pmatrix}0 & 1\\1 & 0\end{pmatrix}\begin{pmatrix}b\\a\end{pmatrix} = \begin{pmatrix}a\\b\end{pmatrix}$$

$$|\Psi^-\rangle = \widehat{\sigma_z}\widehat{\sigma_x}\begin{pmatrix}-b\\a\end{pmatrix} = \begin{pmatrix}1 & 0\\0 & -1\end{pmatrix}\begin{pmatrix}0 & 1\\1 & 0\end{pmatrix}\begin{pmatrix}-b\\a\end{pmatrix} = \begin{pmatrix}a\\b\end{pmatrix}$$

Appendix

The Bell basis is the following collection of maximally entangled two-qubit states.

$$|\Phi^+\rangle = \frac{1}{\sqrt{2}}[|00\rangle + |11\rangle] = \frac{1}{\sqrt{2}}\left[\begin{pmatrix}1\\0\end{pmatrix}\otimes\begin{pmatrix}1\\0\end{pmatrix} + \begin{pmatrix}0\\1\end{pmatrix}\otimes\begin{pmatrix}0\\1\end{pmatrix}\right] = \frac{1}{\sqrt{2}}\left[\begin{pmatrix}1\\0\\0\\0\end{pmatrix} + \begin{pmatrix}0\\0\\0\\1\end{pmatrix}\right] = \frac{1}{\sqrt{2}}\begin{pmatrix}1\\0\\0\\1\end{pmatrix}$$

$$|\Phi^-\rangle = \frac{1}{\sqrt{2}}[|00\rangle - |11\rangle] = \frac{1}{\sqrt{2}}\left[\begin{pmatrix}1\\0\end{pmatrix}\otimes\begin{pmatrix}1\\0\end{pmatrix} - \begin{pmatrix}0\\1\end{pmatrix}\otimes\begin{pmatrix}0\\1\end{pmatrix}\right] = \frac{1}{\sqrt{2}}\left[\begin{pmatrix}1\\0\\0\\0\end{pmatrix} - \begin{pmatrix}0\\0\\0\\1\end{pmatrix}\right] = \frac{1}{\sqrt{2}}\begin{pmatrix}1\\0\\0\\-1\end{pmatrix}$$

$$|\Psi^+\rangle = \frac{1}{\sqrt{2}}[|01\rangle + |10\rangle] = \frac{1}{\sqrt{2}}\left[\begin{pmatrix}1\\0\end{pmatrix}\otimes\begin{pmatrix}0\\1\end{pmatrix} + \begin{pmatrix}0\\1\end{pmatrix}\otimes\begin{pmatrix}1\\0\end{pmatrix}\right] = \frac{1}{\sqrt{2}}\left[\begin{pmatrix}0\\1\\0\\0\end{pmatrix} + \begin{pmatrix}0\\0\\1\\0\end{pmatrix}\right] = \frac{1}{\sqrt{2}}\begin{pmatrix}0\\1\\1\\0\end{pmatrix}$$

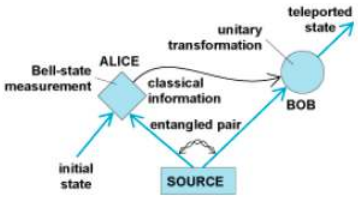
$$|\Psi^-\rangle = \frac{1}{\sqrt{2}}[|01\rangle - |10\rangle] = \frac{1}{\sqrt{2}}\left[\begin{pmatrix}1\\0\end{pmatrix}\otimes\begin{pmatrix}0\\1\end{pmatrix} - \begin{pmatrix}0\\1\end{pmatrix}\otimes\begin{pmatrix}1\\0\end{pmatrix}\right] = \frac{1}{\sqrt{2}}\left[\begin{pmatrix}0\\1\\0\\0\end{pmatrix} - \begin{pmatrix}0\\0\\1\\0\end{pmatrix}\right] = \frac{1}{\sqrt{2}}\begin{pmatrix}0\\1\\-1\\0\end{pmatrix}$$

The initial entangled state Alice and Bob prepare is the Bell state |Φ+ >.

This page titled 8.3: Quantum Teleportation at a Glance is shared under a CC BY 4.0 license and was authored, remixed, and/or curated by Frank Rioux via source content that was edited to the style and standards of the LibreTexts platform.

8.4: Another Look at Quantum Teleportation

The purpose of this tutorial is to provide a brief outline of the basic elements of quantum teleportation, as illustrated in the figure below, using matrix and tensor algebra in the Mathcad programming environment. The methods used here are closely related to those presented in the preceding tutorial on teleportation.



As is generally the case, the analysis requires the use of the maximally entangled two-quibit Bell states, the identity matrix and two of the unitary Pauli matrices.

Bell states:

$$\Phi_p = \frac{1}{\sqrt{2}} \begin{pmatrix} 1 \\ 0 \\ 0 \\ 1 \end{pmatrix}$$

$$\Phi_m = \frac{1}{\sqrt{2}} \begin{pmatrix} 1 \\ 0 \\ 0 \\ -1 \end{pmatrix}$$

$$\Psi_p = \frac{1}{\sqrt{2}} \begin{pmatrix} 0 \\ 1 \\ 1 \\ 0 \end{pmatrix}$$

$$\Psi_m = \frac{1}{\sqrt{2}} \begin{pmatrix} 0 \\ 1 \\ -1 \\ 0 \end{pmatrix}$$

Identity and x- and z-Pauli matrices:

$$I = \begin{pmatrix} 1 & 0 \\ 0 & 1 \end{pmatrix}$$

$$\sigma_x = \begin{pmatrix} 0 & 1 \\ 1 & 0 \end{pmatrix}$$

$$\sigma_z = \begin{pmatrix} 1 & 0 \\ 0 & -1 \end{pmatrix}$$

Alice wishes to teleport this state to Bob.

$$\begin{pmatrix} \sqrt{\frac{1}{3}} \\ \sqrt{\frac{2}{3}} \end{pmatrix} = \begin{pmatrix} 0.577 \\ 0.816 \end{pmatrix}$$

$$\left[\left\| \begin{pmatrix} \sqrt{\frac{1}{3}} \\ \sqrt{\frac{2}{3}} \end{pmatrix} \right\| \right]^2 = 1$$

They prepare the first Bell state (Φ_p) in which Alice has the first qubit and Bob the second. Alice arranges for the state to be teleported and her entangled qubit to meet creating the following three qubit state.

$$\begin{pmatrix} 0.577 \\ 0.816 \end{pmatrix} \frac{1}{\sqrt{2}} \begin{pmatrix} 1 \\ 0 \\ 0 \\ 1 \end{pmatrix}$$

$$\Psi = \frac{1}{\sqrt{2}} \begin{pmatrix} 0.577 \\ 0 \\ 0 \\ 0.577 \\ 0.816 \\ 0 \\ 0 \\ 0.816 \end{pmatrix}$$

$$\Psi^T \Psi = 1$$

Next Alice performs a Bell-state measurement, in other words she projects Ψ onto the Bell-state basis given above. The four equally likely outcomes are calculated below. But first let's use Φ_p as an example. Its projector is $|\Phi_p><\Phi_p|$.

$$\Phi_p \Phi_p^T = \begin{pmatrix} 0.5 & 0 & 0 & 0.5 \\ 0 & 0 & 0 & 0 \\ 0 & 0 & 0 & 0 \\ 0.5 & 0 & 0 & 0.5 \end{pmatrix}$$

However, Ψ is a three-qubit state in which Alice has the first two qubits and Bob the third. In other words, the projector does not operate directly on Bob's qubit. Thus the appropriate matrix for this operation uses the identity matrix to leave Bob's qubit alone. Kronecker is Mathcad's command for tensor multiplication of matrices.

$$\text{kronecker}(\Phi_p, \Phi_p,^T, I) = \begin{pmatrix} 0.5 & 0 & 0 & 0 & 0 & 0 & 0.5 & 0 \\ 0 & 0.5 & 0 & 0 & 0 & 0 & 0 & 0.5 \\ 0 & 0 & 0 & 0 & 0 & 0 & 0 & 0 \\ 0 & 0 & 0 & 0 & 0 & 0 & 0 & 0 \\ 0 & 0 & 0 & 0 & 0 & 0 & 0 & 0 \\ 0 & 0 & 0 & 0 & 0 & 0 & 0 & 0 \\ 0.5 & 0 & 0 & 0 & 0 & 0 & 0.5 & 0 \\ 0 & 0.5 & 0 & 0 & 0 & 0 & 0 & 0.5 \end{pmatrix}$$

Next we show that indeed there are four equally likely outcomes for the Bell-state measurement.

$$\left(\left|\text{kronecker}\left(\Phi_p, \Phi_p^T, I\right) \Psi\right|\right)^2 = 0.25$$

$$\left(\left|\text{kronecker}\left(\Phi_m, \Phi_m^T, I\right) \Psi\right|\right)^2 = 0.25$$

$$\left(\left|\text{kronecker}\left(\Psi_p, \Psi_p^T, I\right) \Psi\right|\right)^2 = 0.25$$

$$\left(\left|\text{kronecker}\left(\Psi_m, \Psi_m^T, I\right) \Psi\right|\right)^2 = 0.25$$

Alice's Bell-state measurement yields one of these results, which she communicates to Bob through a classical channel. As shown below, depending on Alice's report Bob carries out the following unitary operations on his qubit to receive the teleported state: I, σ_z, σ_x, and $\sigma_z\sigma_x$. The multiplicative factor of 2 normalizes the result of the Bell state measurement.

$$2\text{kronecker}(\Phi_p, \Phi_p^T, I)\Psi = \begin{pmatrix} 0.408 \\ 0.577 \\ 0 \\ 0 \\ 0 \\ 0 \\ 0.408 \\ 0.577 \end{pmatrix}$$

Factors to:

$$\frac{1}{\sqrt{2}} \begin{pmatrix} 1 \\ 0 \\ 0 \\ 1 \end{pmatrix} \begin{pmatrix} 0.577 \\ 0.816 \end{pmatrix}$$

So Bob does nothing:

$$I \begin{pmatrix} 0.577 \\ 0.816 \end{pmatrix} = \begin{pmatrix} 0.577 \\ 0.816 \end{pmatrix}$$

$$2\text{kronecker}(\Phi_m, \Phi_m^T, I)\Psi = \begin{pmatrix} 0.408 \\ -0.577 \\ 0 \\ 0 \\ 0 \\ 0 \\ -0.408 \\ 0.577 \end{pmatrix}$$

Factors to:

$$\frac{1}{\sqrt{2}} \begin{pmatrix} 1 \\ 0 \\ 0 \\ -1 \end{pmatrix} \begin{pmatrix} 0.577 \\ -0.816 \end{pmatrix}$$

So Bob does this:

$$\sigma_z \begin{pmatrix} 0.577 \\ -0.816 \end{pmatrix} = \begin{pmatrix} 0.577 \\ 0.816 \end{pmatrix}$$

$$2\text{kronecker}(\Psi_p, \Psi_p^T, I)\Psi = \begin{pmatrix} 0 \\ 0 \\ 0.577 \\ 0.408 \\ 0.577 \\ 0.408 \\ 0 \\ 0 \end{pmatrix}$$

Factors to:

$$\frac{1}{\sqrt{2}} \begin{pmatrix} 0 \\ 1 \\ 1 \\ 0 \end{pmatrix} \begin{pmatrix} 0.816 \\ 0.577 \end{pmatrix}$$

So Bob does this:

$$\sigma_x \begin{pmatrix} 0.816 \\ 0.577 \end{pmatrix} = \begin{pmatrix} 0.577 \\ 0.816 \end{pmatrix}$$

$$2\text{kronecker}(\Psi_m, \Psi_m^T, I)\Psi = \begin{pmatrix} 0 \\ 0 \\ -0.577 \\ 0.408 \\ 0.577 \\ 0.408 \\ 0 \\ 0 \end{pmatrix}$$

Factors to:

$$\frac{1}{\sqrt{2}} \begin{pmatrix} 0 \\ 1 \\ 1 \\ 0 \end{pmatrix} \begin{pmatrix} 0.816 \\ 0.577 \end{pmatrix}$$

So Bob does this:

$$\sigma_x \begin{pmatrix} 0.816 \\ 0.577 \end{pmatrix} = \begin{pmatrix} 0.577 \\ 0.816 \end{pmatrix}$$

Of course, only 25% of the time is the state of Alice′s photon teleported to Bob without further action on his part. Note that we began with Alice and Bob sharing the p Bell state. Consequently when Alice′s Bell state measurement yields Φ_p, Bob has Alice′s photon. We now show that teleportation can be presented quite simply using the density matrix formulation under this circumstance.

Bell state measurement result (normalized):

$$2\text{kronecker}(\Phi_p, \Phi_p^T, I)\Psi = \begin{pmatrix} 0.408 \\ 0.577 \\ 0 \\ 0 \\ 0 \\ 0 \\ 0.408 \\ 0.577 \end{pmatrix}$$

Density matrix of measurement state:

$$\begin{pmatrix} 0.408 \\ 0.577 \\ 0 \\ 0 \\ 0 \\ 0 \\ 0.408 \\ 0.577 \end{pmatrix} \begin{pmatrix} 0.408 \\ 0.577 \\ 0 \\ 0 \\ 0 \\ 0 \\ 0.408 \\ 0.577 \end{pmatrix}^T = \begin{pmatrix} 0.166 & 0.235 & 0 & 0 & 0 & 0 & 0.166 & 0.235 \\ 0.235 & 0.333 & 0 & 0 & 0 & 0 & 0.235 & 0.333 \\ 0 & 0 & 0 & 0 & 0 & 0 & 0 & 0 \\ 0 & 0 & 0 & 0 & 0 & 0 & 0 & 0 \\ 0 & 0 & 0 & 0 & 0 & 0 & 0 & 0 \\ 0 & 0 & 0 & 0 & 0 & 0 & 0 & 0 \\ 0.166 & 0.235 & 0 & 0 & 0 & 0 & 0.166 & 0.235 \\ 0.235 & 0.333 & 0 & 0 & 0 & 0 & 0.235 & 0.333 \end{pmatrix}$$

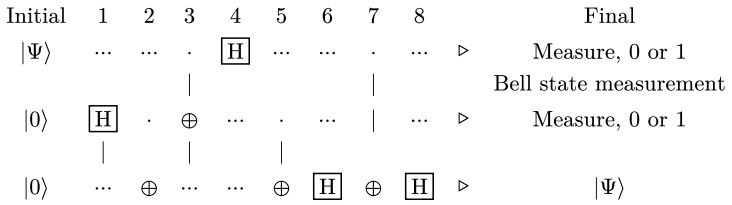
Next the density matrix is calculated assuming Bob has the teleported state. The density matrices are identical confirming that Alice′s initial state has been successfully teleported to Bob.

$$\text{kronecker}\left[\Phi_p, \Phi_p^T, \begin{pmatrix} 0.577 \\ 0.816 \end{pmatrix} \begin{pmatrix} 0.577 \\ 0.816 \end{pmatrix}^T\right] \begin{pmatrix} 0.166 & 0.235 & 0 & 0 & 0 & 0 & 0.166 & 0.235 \\ 0.235 & 0.333 & 0 & 0 & 0 & 0 & 0.235 & 0.333 \\ 0 & 0 & 0 & 0 & 0 & 0 & 0 & 0 \\ 0 & 0 & 0 & 0 & 0 & 0 & 0 & 0 \\ 0 & 0 & 0 & 0 & 0 & 0 & 0 & 0 \\ 0 & 0 & 0 & 0 & 0 & 0 & 0 & 0 \\ 0.166 & 0.235 & 0 & 0 & 0 & 0 & 0.166 & 0.235 \\ 0.235 & 0.333 & 0 & 0 & 0 & 0 & 0.235 & 0.333 \end{pmatrix}$$

This page titled 8.4: Another Look at Quantum Teleportation is shared under a CC BY 4.0 license and was authored, remixed, and/or curated by Frank Rioux via source content that was edited to the style and standards of the LibreTexts platform.

8.5: Teleportation Using Quantum Gates

Implementation of the following 8-step circuit using quantum gates teleports cubit |Ψ > from the top wire to the bottom wire. The circuit can be found on page 226 of Julian Brown's The Quest for the Quantum Computer. A final Bell state measurement on the top wires teleports |Ψ > to the bottom wire.



In the matrix version of quantum mechanics, vectors represent states and matrices represent operators or, in this application, quantum gates. Quantum gates are required to be unitary matrices.

The necessary quantum bits or qubit states are:

Base states:

$$0 = \begin{pmatrix} 1 \\ 0 \end{pmatrix}$$

$$1 = \begin{pmatrix} 0 \\ 1 \end{pmatrix}$$

A superposition of base states:

$$\begin{pmatrix} \alpha \\ \beta \end{pmatrix} = \alpha \begin{pmatrix} 1 \\ 0 \end{pmatrix} + \beta \begin{pmatrix} 0 \\ 1 \end{pmatrix}$$

where

$$(|a|)^2 + (|b|)^2 = 1$$

The identity operator and the following quantum gates are required to calculate the result of the teleportation circuit displayed above.

Identity:

$$I = \begin{pmatrix} 1 & 0 \\ 0 & 1 \end{pmatrix}$$

Hadamard gate:

$$H = \frac{1}{\sqrt{2}} \begin{pmatrix} 1 & 1 \\ 1 & -1 \end{pmatrix}$$

Controlled-NOT gate:

$$CNOT = \begin{pmatrix} 1 & 0 & 0 & 0 \\ 0 & 1 & 0 & 0 \\ 0 & 0 & 0 & 1 \\ 0 & 0 & 1 & 0 \end{pmatrix}$$

Step-7 Controlled-NOT gate:

$$\text{CnNOT} = \begin{pmatrix} 1 & 0 & 0 & 0 & 0 & 0 & 0 & 0 \\ 0 & 1 & 0 & 0 & 0 & 0 & 0 & 0 \\ 0 & 0 & 1 & 0 & 0 & 0 & 0 & 0 \\ 0 & 0 & 0 & 1 & 0 & 0 & 0 & 0 \\ 0 & 0 & 0 & 0 & 0 & 1 & 0 & 0 \\ 0 & 0 & 0 & 0 & 1 & 0 & 0 & 0 \\ 0 & 0 & 0 & 0 & 0 & 0 & 0 & 1 \\ 0 & 0 & 0 & 0 & 0 & 0 & 1 & 0 \end{pmatrix}$$

Using $\begin{pmatrix} \sqrt{\frac{2}{3}} \\ \sqrt{\frac{1}{3}} \end{pmatrix} = \begin{pmatrix} 0.816 \\ 0.577 \end{pmatrix}$ as the input qubit, the three-qubit initial state is,

$$\begin{pmatrix} \sqrt{\frac{2}{3}} \\ \sqrt{\frac{1}{3}} \end{pmatrix} \otimes \begin{pmatrix} 1 \\ 0 \end{pmatrix} \otimes \begin{pmatrix} 1 \\ 0 \end{pmatrix} = \begin{pmatrix} \sqrt{\frac{2}{3}} \\ 0 \\ 0 \\ 0 \\ \sqrt{\frac{1}{3}} \\ 0 \\ 0 \\ 0 \end{pmatrix}$$

$$\Psi = \begin{pmatrix} \sqrt{\frac{2}{3}} \\ 0 \\ 0 \\ 0 \\ \sqrt{\frac{1}{3}} \\ 0 \\ 0 \\ 0 \end{pmatrix}$$

The matrix operators required for the steps of the teleportation circuit are now constructed. In the Mathcad programming environment, *kronecker* is the command for matrix tensor multiplication.

$$\text{Step1} = \text{kronecker}(I, \text{kronecker}(H,\ I))$$

$$\text{Step2} = \text{kronecker}(I, CNOT)$$

$$\text{Step3} = \text{kronecker}(CNOT, I)$$

$$\text{Step4} = \text{kronecker}(H, \text{kronecker}(I,\ I))$$

$$\text{Step5} = \text{kronecker}(I, CNOT)$$

$$\text{Step6} = \text{kronecker}(I, \text{kronecker}(I,\ H))$$

$$\text{Step7} = CnNOT$$

$$\text{Step1} = \text{kronecker}(I, \text{kronecker}(I,\ H))$$

$$\text{QuantumCircuit} = \text{Step8Step7Step6Step5Step4Step3Step2Step1}$$

$$\Psi = \text{QuantumCircuit}\Psi$$

$$\Psi^T = (0.408 \quad 0.289 \quad 0.408 \quad 0.289 \quad 0.408 \quad 0.289 \quad 0.408 \quad 0.289)$$

A Bell state measurement on the top wires in the computational basis collapses the wave function and achieves the desired teleportation no matter what the actual measurement results are. There are, of course, four possibilites |0>|0>, |0>|1>, |1>|0> and |1>|1>. All result in |Ψ > on the bottom wire without further action as is now shown. (The calculations are multiplied by a factor 2 to normalize the result.)

Measurement operator for |0 >:

$$\begin{pmatrix}1\\0\end{pmatrix}\begin{pmatrix}1 & 0\end{pmatrix} = \begin{pmatrix}1 & 0\\0 & 0\end{pmatrix}$$

Measurement operator for |1 >:

$$\begin{pmatrix}0\\1\end{pmatrix}\begin{pmatrix}0 & 1\end{pmatrix} = \begin{pmatrix})0 & 0\\0 & 1\end{pmatrix}$$

$$\begin{bmatrix} a' & b' & c' \\ \begin{pmatrix}1\\0\end{pmatrix} & \begin{pmatrix}1\\0\end{pmatrix} & \begin{pmatrix}0.816\\0.577\end{pmatrix} \end{bmatrix}$$

$$\text{2kronecker}\left[\begin{pmatrix}1 & 0\\0 & 0\end{pmatrix}, \text{kronecker}\left[\begin{pmatrix}1 & 0\\0 & 0\end{pmatrix}, I\right]\right]\Psi' = \begin{pmatrix}0.816\\0.577\\0\\0\\0\\0\\0\\0\end{pmatrix}$$

$$\begin{bmatrix} a' & b' & c' \\ \begin{pmatrix}1\\0\end{pmatrix} & \begin{pmatrix}0\\1\end{pmatrix} & \begin{pmatrix}0.816\\0.577\end{pmatrix} \end{bmatrix}$$

$$\text{2kronecker}\left[\begin{pmatrix}1 & 0\\0 & 0\end{pmatrix}, \text{kronecker}\left[\begin{pmatrix}0 & 0\\0 & 1\end{pmatrix}, I\right]\right]\Psi' = \begin{pmatrix}0\\0\\0.816\\0.577\\0\\0\\0\\0\end{pmatrix}$$

$$\begin{bmatrix} a' & b' & c' \\ \begin{pmatrix}0\\1\end{pmatrix} & \begin{pmatrix}1\\0\end{pmatrix} & \begin{pmatrix}0.816\\0.577\end{pmatrix} \end{bmatrix}$$

$$\text{2kronecker}\left[\begin{pmatrix}0 & 0\\0 & 1\end{pmatrix}, \text{kronecker}\left[\begin{pmatrix}1 & 0\\0 & 0\end{pmatrix}, I\right]\right]\Psi' = \begin{pmatrix}0\\0\\0\\0\\0.816\\0.577\\0\\0\end{pmatrix}$$

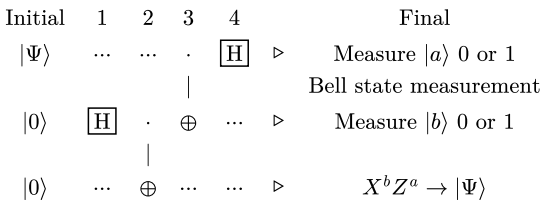
$$\begin{bmatrix} a' & b' & c' \\ \begin{pmatrix}0\\1\end{pmatrix} & \begin{pmatrix}0\\1\end{pmatrix} & \begin{pmatrix}0.816\\0.577\end{pmatrix} \end{bmatrix}$$

$$2\text{kronecker}\left[\begin{pmatrix}0 & 0\\ 0 & 1\end{pmatrix}, \text{kronecker}\left[\begin{pmatrix}0 & 0\\ 0 & 1\end{pmatrix}, I\right]\right]\Psi' = \begin{pmatrix}0\\ 0\\ 0\\ 0\\ 0\\ 0\\ 0.816\\ 0.577\end{pmatrix}$$

This page titled 8.5: Teleportation Using Quantum Gates is shared under a CC BY 4.0 license and was authored, remixed, and/or curated by Frank Rioux via source content that was edited to the style and standards of the LibreTexts platform.

8.6: Another Example of Teleportation Using Quantum Gates

In this example of teleportation using quantum gates we will dispense with Alice, Bob and Carol, and talk instead about transferring the cubit |Ψ > in the quantum circuit below from the first wire to the third wire.



The quantum teleportation circuit is adapted from the one shown on page 226 of *The Quest for the Quantum Computer* by Julian Brown. This tutorial also draws on Brad Rubin's "Quantum Teleportation" at the Wolfram Demonstration Project: http:demonstrations.wolfram.com/QuantumTeleportation/.

In the matrix version of quantum mechanics, vectors represent states and matrices represent operators or, in this application, quantum gates. Quantum gates are required to be unitary matrices.

The necessary quantum bits or qubit states are:

Base states:

$$0 = \begin{pmatrix} 1 \\ 0 \end{pmatrix}$$

$$1 = \begin{pmatrix} 0 \\ 1 \end{pmatrix}$$

A superposition of base states:

$$\begin{pmatrix} \alpha \\ \beta \end{pmatrix} = \alpha \begin{pmatrix} 1 \\ 0 \end{pmatrix} + \beta \begin{pmatrix} 0 \\ 1 \end{pmatrix}$$

where

$$(|a|)^2 + (|b|)^2 = 1$$

The identity operator and the following quantum gates are required to calculate the result of the teleportation circuit displayed above up to the point of the measurements on qubits 1 and 2.

Identity:

$$I = \begin{pmatrix} 1 & 0 \\ 0 & 1 \end{pmatrix}$$

Hadamard gate:

$$H = \frac{1}{\sqrt{2}} \begin{pmatrix} 1 & 1 \\ 1 & -1 \end{pmatrix}$$

Controlled-NOT gate:

$$\text{CNOT} = \begin{pmatrix} 1 & 0 & 0 & 0 \\ 0 & 1 & 0 & 0 \\ 0 & 0 & 0 & 1 \\ 0 & 0 & 1 & 0 \end{pmatrix}$$

We begin by using $\begin{pmatrix} \sqrt{\frac{2}{3}} \\ \sqrt{\frac{1}{3}} \end{pmatrix} = \begin{pmatrix} 0.816 \\ 0.577 \end{pmatrix}$ as the input qubit on wire 1. This choice means that the three-qubit initial state is,

$$\begin{pmatrix}\sqrt{\frac{2}{3}}\\ \sqrt{\frac{1}{3}}\end{pmatrix}\otimes\begin{pmatrix}1\\0\end{pmatrix}\otimes\begin{pmatrix}1\\0\end{pmatrix}=\begin{pmatrix}\sqrt{\frac{2}{3}}\\0\\0\\0\\\sqrt{\frac{1}{3}}\\0\\0\\0\end{pmatrix}$$

$$\Psi=\begin{pmatrix}\sqrt{\frac{2}{3}}\\0\\0\\0\\\sqrt{\frac{1}{3}}\\0\\0\\0\end{pmatrix}$$

The following operations on the initial state yield the state (Ψ') prior to the measurements on qubits 1 and 2. In the Mathcad programming environment, kronecker is the command for matrix tensor multiplication.

$$\text{Step1}=\text{kronecker}(I,\ \text{kronecker}(H,\ I))$$

$$\text{Step2}=\text{kronecker}(I,\ CNOT)$$

$$\text{Step13}=\text{kronecker}(CNOT,\ I)$$

$$\text{Step1}=\text{kronecker}(H,\ \text{kronecker}(I,\ I))$$

$$\Psi=\text{Step4Step3Step2Step1}$$

$$(0.408\quad 0.289\quad 0.289\quad 0.408\quad 0.408\quad -0.289\quad -0.289\quad 0.408)$$

There are four possible measurement outcomes on qubits 1 and 2 in the z-basis: |00>, |01>, |10 > and |11 >. The projection operators for |0 > and |1 > are given below.

Projection operator for I0>:

$$\begin{pmatrix}1\\0\end{pmatrix}(1\quad 0)=\begin{pmatrix}1&0\\0&0\end{pmatrix}$$

Projection operator for I1>:

$$\begin{pmatrix}0\\1\end{pmatrix}(0\quad 1)=\begin{pmatrix}0&0\\0&1\end{pmatrix}$$

As shown below, depending on the measurement results the following unitary operations are required to complete the transfer of $\begin{pmatrix}0.816\\0.577\end{pmatrix}$ to the third wire: I, σ_x, σ_z, and $\sigma_z\sigma_x$. The needed Pauli operators are:

$$\sigma_x=\begin{pmatrix}0&1\\1&0\end{pmatrix}$$

$$\sigma_z=\begin{pmatrix}1&0\\0&-1\end{pmatrix}$$

https://chem.libretexts.org/@go/page/142878

Measurement result for qubits 1 and 2	Final 3-qubit state	Required operation
$\text{kronecker}\left[\begin{pmatrix}1 & 0\\ 0 & 0\end{pmatrix}, \text{kronecker}\left[\begin{pmatrix}1 & 0\\ 0 & 0\end{pmatrix}, I\right]^{2}\right]$ $\Psi' = \begin{pmatrix}0.816\\ 0.577\\ 0\\ 0\\ 0\\ 0\\ 0\\ 0\end{pmatrix}$	$\begin{pmatrix}1\\ 0\end{pmatrix}\begin{pmatrix}1\\ 0\end{pmatrix}\begin{pmatrix}0.816\\ 0.577\end{pmatrix}$	$I\begin{pmatrix}0.816\\ 0.577\end{pmatrix} = \begin{pmatrix}0.816\\ 0.577\end{pmatrix}$
$\text{kronecker}\left[\begin{pmatrix}1 & 0\\ 0 & 0\end{pmatrix}, \text{kronecker}\left[\begin{pmatrix}0 & 0\\ 0 & 1\end{pmatrix}, I\right]^{2}\right]$ $\Psi' = \begin{pmatrix}0\\ 0\\ 0.577\\ 0.816\\ 0\\ 0\\ 0\\ 0\end{pmatrix}$	$\begin{pmatrix}1\\ 0\end{pmatrix}\begin{pmatrix}0\\ 1\end{pmatrix}\begin{pmatrix}0.577\\ 0.816\end{pmatrix}$	$\sigma_x\begin{pmatrix}0.577\\ 0.816\end{pmatrix} = \begin{pmatrix}0.816\\ 0.577\end{pmatrix}$
$\text{kronecker}\left[\begin{pmatrix}0 & 0\\ 0 & 1\end{pmatrix}, \text{kronecker}\left[\begin{pmatrix}1 & 0\\ 0 & 0\end{pmatrix}, I\right]^{2}\right]$ $\Psi' = \begin{pmatrix}0\\ 0\\ 0\\ 0\\ 0.816\\ -0.577\\ 0\\ 0\end{pmatrix}$	$\begin{pmatrix}0\\ 1\end{pmatrix}\begin{pmatrix}1\\ 0\end{pmatrix}\begin{pmatrix}0.816\\ -0.577\end{pmatrix}$	$\sigma_z\begin{pmatrix}0.816\\ -0.577\end{pmatrix} = \begin{pmatrix}0.816\\ 0.577\end{pmatrix}$
$\text{kronecker}\left[\begin{pmatrix}0 & 0\\ 0 & 1\end{pmatrix}, \text{kronecker}\left[\begin{pmatrix}0 & 0\\ 0 & 1\end{pmatrix}, I\right]^{2}\right]$ $\Psi' = \begin{pmatrix}0\\ 0\\ 0\\ 0\\ 0\\ 0\\ 0\\ -0.577\end{pmatrix}$	$\begin{pmatrix}0\\ 1\end{pmatrix}\begin{pmatrix}0\\ 1\end{pmatrix}\begin{pmatrix}-0.577\\ 0.816\end{pmatrix}$	$\sigma_z\sigma_x\begin{pmatrix}-0.577\\ 0.816\end{pmatrix} = \begin{pmatrix}0.816\\ 0.577\end{pmatrix}$

$$\begin{pmatrix} 0.816 \end{pmatrix}$$

In the interest of relating this example to other examples of quantum teleportation, it is pointed out that the first two steps in the diagram above create an entangled Bell state involving qubits 2 and 3.

$$\text{CNOT kronecker}(H,\ I) \begin{pmatrix} 1 \\ 0 \\ 0 \\ 0 \end{pmatrix} = \begin{pmatrix} 0.707 \\ 0 \\ 0 \\ 0.707 \end{pmatrix}$$

This page titled 8.6: Another Example of Teleportation Using Quantum Gates is shared under a CC BY 4.0 license and was authored, remixed, and/or curated by Frank Rioux via source content that was edited to the style and standards of the LibreTexts platform.

8.7: Yet Another Quantum Teleportation Circuit

This quantum teleportation circuit transfers Ψ from the top wire on the left to the lower wire on the right without the requirement of measurements on the top two wires, which are occupied by identical superposition states.

Initial	1	2	3	4	5	6	7	8	9	Final
$\|\Psi\rangle$	···	···	·	H	···	···	x	···	···	$\frac{1}{\sqrt{2}}(\|0\rangle+\|1\rangle)$
			|			|			
$\|0\rangle$	H	·	⊕	···	·	···	x	·	·	$\frac{1}{\sqrt{2}}(\|0\rangle+\|1\rangle)$
		|			|			|	
$\|0\rangle$	···	⊕	···	···	⊕	H	···	⊕	H	$\|\Psi\rangle$

The required matrix operators:

$$I = \begin{pmatrix} 1 & 0 \\ 0 & 1 \end{pmatrix}$$

$$H = \frac{1}{\sqrt{2}} \begin{pmatrix} 1 & 1 \\ 1 & -1 \end{pmatrix}$$

$$\text{CNOT} = \begin{pmatrix} 1 & 0 & 0 & 0 \\ 0 & 1 & 0 & 0 \\ 0 & 0 & 0 & 1 \\ 0 & 0 & 1 & 0 \end{pmatrix}$$

$$\text{Swap} = \begin{pmatrix} 1 & 0 & 0 & 0 \\ 0 & 0 & 1 & 0 \\ 0 & 1 & 0 & 0 \\ 0 & 0 & 0 & 1 \end{pmatrix}$$

The initial state:

$$\Psi = \begin{pmatrix} \sqrt{\frac{1}{3}} \\ \sqrt{\frac{2}{3}} \end{pmatrix} \begin{pmatrix} 1 \\ 0 \end{pmatrix} \begin{pmatrix} 1 \\ 0 \end{pmatrix}$$

$$\Psi = \begin{pmatrix} \sqrt{\frac{1}{3}} & 0 & 0 & 0 & \sqrt{\frac{2}{3}} & 0 & 0 & 0 \end{pmatrix}^T$$

Because of its length, the quantum circuit is written in steps.

$$\text{Step1} = \text{kronecker}(I, \text{kronecker}(\text{H, I}))$$

$$\text{Step2} = \text{kronecker}(\text{I, CNOT})$$

$$\text{Step3} = \text{kronecker}(\text{CNOT, I})$$

$$\text{Step4} = \text{kronecker}(H, \text{kronecker}(\text{I, I}))$$

$$\text{Step5} = \text{kronecker}(\text{I, CNOT})$$

$$\text{Step6} = \text{kronecker}(I, \text{kronecker}(\text{I, H}))$$

$$\text{Step7} = \text{kronecker}(\text{Swap, I})$$

$$\text{Step8} = \text{kronecker}(\text{I, CNOT})$$

$$\text{Step9} = \text{kronecker}(I, \text{kronecker}(\text{I, H}))$$

$$QC = \text{Step9Step8Step7Step6Step5Step4Step3Step2Step1}$$

The quantum circuit operates on the initial state, transfering Ψ from the top wire to the bottom wire.

$$QC\Psi = \begin{pmatrix} 0.289 \\ 0.408 \\ 0.289 \\ 0.408 \\ 0.289 \\ 0.408 \\ 0.289 \\ 0.408 \end{pmatrix}$$

$$\frac{1}{\sqrt{2}}\begin{pmatrix}1\\1\end{pmatrix}\frac{1}{\sqrt{2}}\begin{pmatrix}1\\1\end{pmatrix}\begin{pmatrix}\sqrt{\frac{1}{3}}\\\sqrt{\frac{2}{3}}\end{pmatrix} = \frac{1}{2}\begin{pmatrix}1\\1\\1\\1\end{pmatrix}\begin{pmatrix}\sqrt{\frac{1}{3}}\\\sqrt{\frac{2}{3}}\end{pmatrix} = \begin{pmatrix} 0.289 \\ 0.408 \\ 0.289 \\ 0.408 \\ 0.289 \\ 0.408 \\ 0.289 \\ 0.408 \end{pmatrix}$$

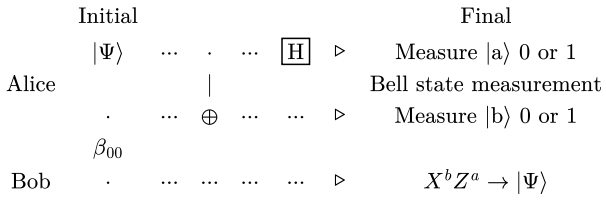
$$\frac{1}{2}\sqrt{\frac{1}{3}} = 0.289$$

$$\frac{1}{2}\sqrt{\frac{2}{3}} = 0.408$$

This page titled 8.7: Yet Another Quantum Teleportation Circuit is shared under a CC BY 4.0 license and was authored, remixed, and/or curated by Frank Rioux via source content that was edited to the style and standards of the LibreTexts platform.

8.8: Quantum Teleportation - Another Look

A graphic representation of the teleportation procedure is accompanied by a quantum circuit for its implementation.



Alice has the photon to be teleported (teleportee) and another photon belonging to an entangled pair that she shares with Bob.

Teleportee photon state:

$$\Psi = \begin{pmatrix} \sqrt{\frac{1}{3}} \\ \sqrt{\frac{2}{3}} \end{pmatrix}$$

Entangled Bell state photon pair:

$$\beta_{00} = \frac{1}{\sqrt{2}} \begin{pmatrix} 1 \\ 0 \\ 0 \\ 1 \end{pmatrix}$$

The shared Bell state and the remaining Bell states shown below are indexed in binary notation. The Appendix contains an explanation of the indexing scheme.

$$\beta_{01} = \frac{1}{\sqrt{2}} \begin{pmatrix} 0 \\ 1 \\ 1 \\ 0 \end{pmatrix}$$

$$\beta_{10} = \frac{1}{\sqrt{2}} \begin{pmatrix} 1 \\ 0 \\ 0 \\ -1 \end{pmatrix}$$

$$\beta_{11} = \frac{1}{\sqrt{2}} \begin{pmatrix} 0 \\ 1 \\ -1 \\ 0 \end{pmatrix}$$

In the teleportation circuit, the teleportee is initially on the top wire and the Bell state photons are on the two lower wires. Alice controls the top two wires, while Bob has the bottom wire. The initial product state is formed by vector tensor multiplication.

$$\Psi_{in} = \Psi\beta_{00}$$

$$\Psi_{in} = \frac{1}{\sqrt{2}}\left(\sqrt{\tfrac{1}{3}} \quad 0 \quad 0 \quad \sqrt{\tfrac{1}{3}} \quad \sqrt{\tfrac{2}{3}} \quad 0 \quad 0 \quad \sqrt{\tfrac{2}{3}}\right)^T$$

The matrix operators required to run the circuit and carry out the subsequent measurements and transformations are now identified.

$$I = \begin{pmatrix} 1 & 0 \\ 0 & 1 \end{pmatrix} \quad H = \tfrac{1}{\sqrt{2}} \begin{pmatrix} 1 & 1 \\ 1 & -1 \end{pmatrix} \quad X = \begin{pmatrix} 0 & 1 \\ 1 & 0 \end{pmatrix} \quad Z = \begin{pmatrix} 1 & 0 \\ 0 & -1 \end{pmatrix} \quad \text{CNOT} = \begin{pmatrix} 1 & 0 & 0 & 0 \\ 0 & 1 & 0 & 0 \\ 0 & 0 & 0 & 1 \\ 0 & 0 & 1 & 0 \end{pmatrix}$$

Measurement operator for |0 >:

$$\begin{pmatrix}1\\0\end{pmatrix}(1 \quad 0) = \begin{pmatrix}1 & 0\\0 & 0\end{pmatrix}$$

Measurement operator for |1 >:

$$\begin{pmatrix}0\\1\end{pmatrix}(0 \quad 1) = \begin{pmatrix}0 & 0\\0 & 1\end{pmatrix}$$

The foward slashes shown on the top two wires of the circuit represent measurements done by Alice. The matrix operator representing the quantum circuit prior to Alice's measurements is formed using tensor multiplication.

$$QC = \text{kronecker(H, kronecker (I, I)) kronecker(CNOT, I)}$$

After the controlled-not and Hadamard gates, but before measurement by Alice, the system is in a superposition state involving the Bell state indices on the top two registers. The third register contains a state that can be easily transformed into the teleportee once Alice tells Bob which Bell state she observed.

$$QC\Psi_{in} = \begin{pmatrix}0.289\\0.408\\0.408\\0.289\\0.289\\-0.408\\-0.408\\0.289\end{pmatrix}$$

which can be written

$$\frac{1}{2}\begin{pmatrix}1\\0\\0\\0\end{pmatrix}\begin{pmatrix}\sqrt{\frac{1}{3}}\\\sqrt{\frac{2}{3}}\end{pmatrix} + \frac{1}{2}\begin{pmatrix}0\\1\\0\\0\end{pmatrix}\begin{pmatrix}\sqrt{\frac{2}{3}}\\\sqrt{\frac{1}{3}}\end{pmatrix} + \frac{1}{2}\begin{pmatrix}0\\0\\1\\0\end{pmatrix}\begin{pmatrix}\sqrt{\frac{1}{3}}\\-\sqrt{\frac{2}{3}}\end{pmatrix} + \frac{1}{2}\begin{pmatrix}0\\0\\0\\1\end{pmatrix}\begin{pmatrix}-\sqrt{\frac{2}{3}}\\\sqrt{\frac{1}{3}}\end{pmatrix}$$

If Alice observes β_{00} Bob does nothing (the identity operation) because he has Ψ on his register. If Alice observes β_{01} Bob applies the X operator, if she finds β_{10} he uses the Z operator, and finally if Alice observes β_{11} Bob applies the X operator followed by the Z operator. Further mathematical detail is provided by showing explicitly the four equally probable measurement outcomes that Alice observes, and Bob's subsequent action on his register.

https://chem.libretexts.org/@go/page/142890

$$\text{kronecker}\left[\begin{pmatrix}1 & 0\\ 0 & 0\end{pmatrix}, \text{kronecker}\left[\begin{pmatrix}1 & 0\\ 0 & 0\end{pmatrix}, I\right]\right]^{2} \quad (1 \quad 0)\begin{pmatrix}1\\ 0\end{pmatrix}\begin{pmatrix}\sqrt{\frac{1}{3}}\\ \sqrt{\frac{2}{3}}\end{pmatrix} \quad I\begin{pmatrix}\sqrt{\frac{1}{3}}\\ \sqrt{\frac{2}{3}}\end{pmatrix} = \begin{pmatrix}0.577\\ 0.816\end{pmatrix}$$

$$QC\Psi_{in} = \begin{pmatrix}0.577\\ 0.816\\ 0\\ 0\\ 0\\ 0\\ 0\\ 0\end{pmatrix}$$

$$\text{kronecker}\left[\begin{pmatrix}1 & 0\\ 0 & 0\end{pmatrix}, \text{kronecker}\left[\begin{pmatrix}0 & 0\\ 0 & 1\end{pmatrix}, I\right]\right]^{2} \quad (1 \quad 0)\begin{pmatrix}0\\ 1\end{pmatrix}\begin{pmatrix}\sqrt{\frac{2}{3}}\\ \sqrt{\frac{1}{3}}\end{pmatrix} \quad X\begin{pmatrix}\sqrt{\frac{2}{3}}\\ \sqrt{\frac{1}{3}}\end{pmatrix} = \begin{pmatrix}0.577\\ 0.816\end{pmatrix}$$

$$QC\Psi_{in} = \begin{pmatrix}0\\ 0\\ 0.816\\ 0.577\\ 0\\ 0\\ 0\\ 0\end{pmatrix}$$

$$\text{kronecker}\left[\begin{pmatrix}0 & 0\\ 0 & 1\end{pmatrix}, \text{kronecker}\left[\begin{pmatrix}0 & 0\\ 0 & 1\end{pmatrix}, I\right]\right]^{2} \quad (0 \quad 1)\begin{pmatrix}1\\ 0\end{pmatrix}\begin{pmatrix}\sqrt{\frac{1}{3}}\\ -\sqrt{\frac{2}{3}}\end{pmatrix} \quad Z\begin{pmatrix}\sqrt{\frac{1}{3}}\\ -\sqrt{\frac{2}{3}}\end{pmatrix} = \begin{pmatrix}0.577\\ 0.816\end{pmatrix}$$

$$QC\Psi_{in} = \begin{pmatrix}0\\ 0\\ 0\\ 0\\ 0\\ 0\\ -0.816\\ 0.577\end{pmatrix}$$

$$\text{kronecker}\left[\begin{pmatrix}0 & 0\\ 0 & 1\end{pmatrix}, \text{kronecker}\left[\begin{pmatrix}0 & 0\\ 0 & 1\end{pmatrix}, I\right]\right]^{2} \quad (0 \quad 1)\begin{pmatrix}0\\ 1\end{pmatrix}\begin{pmatrix}-\sqrt{\frac{2}{3}}\\ \sqrt{\frac{1}{3}}\end{pmatrix} \quad ZX\begin{pmatrix}-\sqrt{\frac{2}{3}}\\ \sqrt{\frac{1}{3}}\end{pmatrix} = \begin{pmatrix}0.577\\ 0.816\end{pmatrix}$$

$$QC\Psi_{in} = \begin{pmatrix}0\\ 0\\ 0\\ 0\\ 0\\ 0\\ -0.816\\ 0.577\end{pmatrix}$$

The teleportation circuit can also be analyzed algebraically.

$$\left(\sqrt{\frac{1}{3}}\left|0\right\rangle+\sqrt{\frac{2}{3}}\left|1\right\rangle\right)\frac{1}{\sqrt{2}}\left(|00\rangle+|11\rangle\right)=\frac{1}{\sqrt{2}}\left[\sqrt{\frac{1}{3}}\left(|000\rangle+|011\rangle\right)+\sqrt{\frac{2}{3}}\left(|100\rangle+|111\rangle\right)\right]$$

$$\text{CNOT}\otimes\text{I}$$

$$\frac{1}{\sqrt{2}}\left[\sqrt{\frac{1}{3}}|0\rangle\left(|00\rangle+|11\rangle\right)+\sqrt{\frac{2}{3}}|1\rangle\left(|10\rangle+|01\rangle\right)\right]$$

$$\text{H}\otimes\text{I}\otimes\text{I}$$

$$\frac{1}{\sqrt{2}}\left[(\sqrt{\frac{1}{3}}|0\rangle(|1\rangle)+(|00\rangle+|11\rangle)+\sqrt{\frac{2}{3}}(0\rangle-|1\rangle)(|10\rangle+|01\rangle)\right]$$

$$\downarrow$$

$$\frac{1}{\sqrt{2}}\left[|00\rangle\left(\sqrt{\frac{1}{3}}|0\rangle+\sqrt{\frac{2}{3}}|1\rangle\right)+|01\rangle\left(\sqrt{\frac{2}{3}}|0\rangle+\sqrt{\frac{1}{3}}|1\rangle\right)+|10\rangle\left(\sqrt{\frac{1}{3}}|0\rangle-\sqrt{\frac{2}{3}}|1\rangle\right)+|11\rangle\left(-\sqrt{\frac{2}{3}}|0\rangle+\sqrt{\frac{1}{3}}|1\rangle\right)\right]$$

$$\downarrow$$

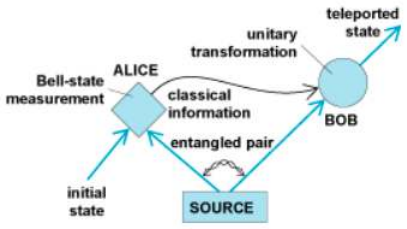
$$\frac{1}{2}\left[|00\rangle\begin{pmatrix}\sqrt{\frac{1}{3}}\\ \sqrt{\frac{2}{3}}\end{pmatrix}+|01\rangle\begin{pmatrix}\sqrt{\frac{2}{3}}\\ \sqrt{\frac{1}{3}}\end{pmatrix}+|10\rangle\begin{pmatrix}\sqrt{\frac{1}{3}}\\ -\sqrt{\frac{2}{3}}\end{pmatrix}+|11\rangle\begin{pmatrix}-\sqrt{\frac{2}{3}}\\ \sqrt{\frac{1}{3}}\end{pmatrix}\right]$$

$$\overset{Action}{\rightarrow}\frac{1}{2}\left[I\begin{pmatrix}\sqrt{\frac{1}{3}}\\ \sqrt{\frac{2}{3}}\end{pmatrix}+X\begin{pmatrix}\sqrt{\frac{2}{3}}\\ \sqrt{\frac{1}{3}}\end{pmatrix}+Z\begin{pmatrix}\sqrt{\frac{1}{3}}\\ -\sqrt{\frac{2}{3}}\end{pmatrix}+ZX\begin{pmatrix}-\sqrt{\frac{2}{3}}\\ \sqrt{\frac{1}{3}}\end{pmatrix}\right]$$

This page titled 8.8: Quantum Teleportation - Another Look is shared under a CC BY 4.0 license and was authored, remixed, and/or curated by Frank Rioux via source content that was edited to the style and standards of the LibreTexts platform.

8.9: A Quantum Teleportation Experiment for Undergraduates

This Mathcad document examines the math involved in a teleportation experiment for undergraduates using IBM's 5-qubit quantum processor (IBM Quantum Experience) posted by S. Fedortchenko at arXiv:1607.02398v1. Except for state preparation it is identical to the following teleportation circuit, which can be found in my "Teleportation: Another Look."



	Initial						Final
	$\lvert\Psi\rangle$	$\cdots$	$\cdot$	$\cdots$	$\boxed{\text{H}}$	$\triangleright$	Measure $\lvert a\rangle$ 0 or 1
Alice			$\lvert$				Bell state measurement
	$\cdot$	$\cdots$	$\oplus$	$\cdots$	$\cdots$	$\triangleright$	Measure $\lvert b\rangle$ 0 or 1
	β_{00}						
Bob	$\cdot$	$\cdots$	$\cdots$	$\cdots$	$\cdots$	$\triangleright$	$X^b Z^a \rightarrow \lvert\Psi\rangle$

Fedortchenko's teleportation circuit is shown below.

Initial		1	2	3	4	6	Final		
$\lvert 0\rangle$	$\triangleright$	$\boxed{\text{H}}$	$\boxed{\text{T}}$	$\boxed{\text{H}}$	$\boxed{\text{S}}$	$\cdot$	$\boxed{\text{H}}$	$\triangleright$	Measure $\lvert a\rangle$ 0 or 1
						$\lvert$			Bell state measurement
$\lvert 0\rangle$	$\triangleright$	$\cdots$	$\cdots$	$\cdots$	$\oplus$	$\oplus$	$\cdots$	$\triangleright$	Measure $\lvert b\rangle$ 0 or 1
					$\lvert$				
$\lvert 0\rangle$	$\triangleright$	$\cdots$	$\cdots$	$\boxed{\text{H}}$	$\cdot$	$\cdots$	$\cdots$	$\triangleright$	$X^b Z^a \rightarrow \lvert\Psi\rangle$

Single qubit operators:

$$I = \begin{pmatrix} 1 & 0 \\ 0 & 1 \end{pmatrix} \quad H = \frac{1}{\sqrt{2}} \begin{pmatrix} 1 & 1 \\ 1 & -1 \end{pmatrix} \quad S = \begin{pmatrix} 1 & 0 \\ 0 & i \end{pmatrix}$$

$$T = \begin{pmatrix} 1 & 0 \\ 0 & e^{i\frac{\pi}{4}} \end{pmatrix} \quad X = \begin{pmatrix} 0 & 1 \\ 1 & 0 \end{pmatrix} \quad Z = \begin{pmatrix} 1 & 0 \\ 0 & -1 \end{pmatrix}$$

Two qubit operators:

$$\text{CNOT} = \begin{pmatrix} 1 & 0 & 0 & 0 \\ 0 & 1 & 0 & 0 \\ 0 & 0 & 0 & 1 \\ 0 & 0 & 1 & 0 \end{pmatrix} \quad \text{ICNOT} = \begin{pmatrix} 1 & 0 & 0 & 0 \\ 0 & 0 & 0 & 1 \\ 0 & 0 & 1 & 0 \\ 0 & 1 & 0 & 0 \end{pmatrix}$$

Demonstrate the generation of the teleportee state held by Alice:

$$\text{SHTH} \begin{pmatrix} 1 \\ 0 \end{pmatrix} = \begin{pmatrix} 0.854 + 0.354i \\ 0.354 + 0.146i \end{pmatrix}$$

$$e^{i\frac{\pi}{8}} \left[\cos\left(\frac{\pi}{8}\right) \begin{pmatrix} 1 \\ 0 \end{pmatrix} + \sin\left(\frac{\pi}{8}\right) \begin{pmatrix} 0 \\ 1 \end{pmatrix} \right] = \begin{pmatrix} 0.854 + 0.354i \\ 0.354 + 0.146i \end{pmatrix}$$

Demonstrate the creation of the entangled Bell state shared by Alice and Bob:

$$\text{ICNOT } (\text{kronecker}(\text{I, H})) \begin{pmatrix} 1 \\ 0 \\ 0 \\ 0 \end{pmatrix} = \begin{pmatrix} 0.707 \\ 0 \\ 0 \\ 0.707 \end{pmatrix} \quad \frac{1}{\sqrt{2}} \left[\begin{pmatrix} 1 \\ 0 \end{pmatrix} \begin{pmatrix} 1 \\ 0 \end{pmatrix} + \begin{pmatrix} 0 \\ 1 \end{pmatrix} \begin{pmatrix} 0 \\ 1 \end{pmatrix} \right]$$

Creation of the teleportee state and the entangled Bell state occurs in the first four steps.

$$\text{StatePrep} = \text{kronecker (S, ICNOT) kronecker (H, kronecker(I, H)) kronecker (T, kronecker(I, I)) kronecker (H kronecker (I, I))}$$

Teleportation occurs in steps 5 and 6.

$$textTC = kronecker(H, kronecker(I, I))kronecker(CNOT, I)$$

$$\text{TC StatePrep} \begin{pmatrix} 1 \\ 0 \\ 0 \\ 0 \\ 0 \\ 0 \\ 0 \\ 0 \end{pmatrix} = \begin{pmatrix} 0.427 + 0.177i \\ 0.177 + 0.073i \\ 0.177 + 0.073i \\ 0.427 + 0.177i \\ 0.427 + 0.177i \\ -0.177 - 0.073i \\ -0.177 - 0.073i \\ 0.427 + 0.177i \end{pmatrix}$$

Measurement occurs in the final step on the top two wires with possible outcomes |00>, |01>, |10> and |11>. In other words, Alice makes a Bell state measurement (see first figure above) on the two qubits in her possession and informs Bob of the result through a classical channel. He then performs an operation on his qubit to recover the teleported state.

If Alice observes |00> Bob does nothing (the identity operation) because he has the teleportee on his register. If Alice observes |01> Bob applies the X operator, if she finds |10> he uses the Z operator, and finally if Alice observes |11> Bob applies the X operator followed by the Z operator. Further mathematical detail is provided by showing explicitly the four equally probable measurement outcomes that Alice observes, and Bob's subsequent action on his register.

Computational Details

Measurement operator for |0>:

$$\begin{pmatrix} 1 \\ 0 \end{pmatrix} \begin{pmatrix} 1 & 0 \end{pmatrix} = \begin{pmatrix} 1 & 0 \\ 0 & 0 \end{pmatrix}$$

Measurement operator for |1>:

$$\begin{pmatrix} 0 \\ 1 \end{pmatrix} \begin{pmatrix} 0 & 1 \end{pmatrix} = \begin{pmatrix} 0 & 0 \\ 0 & 1 \end{pmatrix}$$

Alice measures |00>:

$$\begin{pmatrix} 1 \\ 0 \end{pmatrix} \begin{pmatrix} 1 \\ 0 \end{pmatrix} = \begin{pmatrix} 0.854 + 0.354i \\ 0.354 + 0.146i \end{pmatrix}$$

Bob's action:

$$I \begin{pmatrix} 0.854 + 0.354i \\ 0.354 + 0.146i \end{pmatrix} = \begin{pmatrix} 0.854 + 0.354i \\ 0.354 + 0.146i \end{pmatrix}$$

$$2\text{kronecker} \left[\begin{pmatrix} 1 & 0 \\ 0 & 0 \end{pmatrix}, \text{kronecker} \left[\begin{pmatrix} 1 & 0 \\ 0 & 0 \end{pmatrix}, \text{I} \right] \right] \text{TC StatePrep} \begin{pmatrix} 1 \\ 0 \\ 0 \\ 0 \\ 0 \\ 0 \\ 0 \\ 0 \end{pmatrix} = \begin{pmatrix} 0.854 + 0.354i \\ 0.354 + 0.146i \\ 0 \\ 0 \\ 0 \\ 0 \\ 0 \\ 0 \end{pmatrix}$$

Alice measures |01>:

$$\begin{pmatrix} 1 \\ 0 \end{pmatrix} \begin{pmatrix} 0 \\ 1 \end{pmatrix} = \begin{pmatrix} 0.354 + 0.146i \\ 0.854 + 0.354i \end{pmatrix}$$

Bob's action:

$$X \begin{pmatrix} 0.354 + 0.146i \\ 0.854 + 0.354i \end{pmatrix} = \begin{pmatrix} 0.854 + 0.354i \\ 0.354 + 0.146i \end{pmatrix}$$

$$2\text{kronecker}\left[\begin{pmatrix} 1 & 0 \\ 0 & 0 \end{pmatrix}, \text{kronecker}\left[\begin{pmatrix} 0 & 0 \\ 0 & 1 \end{pmatrix}, \text{I}\right]\right] \text{TC StatePrep} \begin{pmatrix} 1 \\ 0 \\ 0 \\ 0 \\ 0 \\ 0 \\ 0 \\ 0 \end{pmatrix} = \begin{pmatrix} 0 \\ 0 \\ 0.354 + 0.146i \\ 0.854 + 0.354i \\ 0 \\ 0 \\ 0 \\ 0 \end{pmatrix}$$

Alice measures |10>:

$$\begin{pmatrix} 0 \\ 1 \end{pmatrix} \begin{pmatrix} 1 \\ 0 \end{pmatrix} = \begin{pmatrix} 0.854 + 0.354i \\ -0.354 - 0.146i \end{pmatrix}$$

Bob's action:

$$Z \begin{pmatrix} 0.854 + 0.354i \\ -0.354 - 0.146i \end{pmatrix} = \begin{pmatrix} 0.854 + 0.354i \\ 0.354 + 0.146i \end{pmatrix}$$

$$2\text{kronecker}\left[\begin{pmatrix} 0 & 0 \\ 0 & 1 \end{pmatrix}, \text{kronecker}\left[\begin{pmatrix} 1 & 0 \\ 0 & 0 \end{pmatrix}, \text{I}\right]\right] \text{TC StatePrep} \begin{pmatrix} 1 \\ 0 \\ 0 \\ 0 \\ 0 \\ 0 \\ 0 \\ 0 \end{pmatrix} = \begin{pmatrix} 0 \\ 0 \\ 0 \\ 0 \\ 0.854 + 0.354i \\ -0.354 - 0.146i \\ 0 \\ 0 \end{pmatrix}$$

Alice measures |11>:

$$\begin{pmatrix} 0 \\ 1 \end{pmatrix} \begin{pmatrix} 0 \\ 1 \end{pmatrix} = \begin{pmatrix} -0.354 - 0.146i \\ 0.854 + 0.354i \end{pmatrix}$$

Bob's action:

$$ZX \begin{pmatrix} 0.854 + 0.354i \\ -0.354 - 0.146i \end{pmatrix} = \begin{pmatrix} 0.854 + 0.354i \\ 0.354 + 0.146i \end{pmatrix}$$

$$2\text{kronecker}\left[\begin{pmatrix} 0 & 0 \\ 0 & 1 \end{pmatrix}, \text{kronecker}\left[\begin{pmatrix} 0 & 0 \\ 0 & 1 \end{pmatrix}, \text{I}\right]\right] \text{TC StatePrep} \begin{pmatrix} 1 \\ 0 \\ 0 \\ 0 \\ 0 \\ 0 \\ 0 \\ 0 \end{pmatrix} = \begin{pmatrix} 0 \\ 0 \\ 0 \\ 0 \\ 0 \\ 0 \\ -0.354 - 0.146i \\ 0.854 + 0.354i \end{pmatrix}$$

This page titled 8.9: A Quantum Teleportation Experiment for Undergraduates is shared under a CC BY 4.0 license and was authored, remixed, and/or curated by Frank Rioux via source content that was edited to the style and standards of the LibreTexts platform.

8.10: A Simple Teleportation Exercise

This circuit teleports |Ψ> from the top wire to the bottom wire. Measurement on the top wire yields |0> or |1>, the power to which the Z matrix on the bottom wire is raised. As shown below Z^0 is the identity matrix, in other words do nothing because |Ψ> is already on the bottom wire.

$$\begin{array}{lcccc} |\Psi\rangle & \triangleright & \cdot & H \triangleright & \text{Measure m} = 0 \text{ or } 1 \\ |0\rangle & \triangleright & \oplus & \triangleright & Z^m \rightarrow |\Psi\rangle \end{array}$$

$$|0\rangle = \begin{pmatrix} 1 \\ 0 \end{pmatrix} \quad |1\rangle = \begin{pmatrix} 0 \\ 1 \end{pmatrix} \quad |\Psi\rangle = \begin{pmatrix} \sqrt{\frac{1}{3}} \\ \sqrt{\frac{2}{3}} \end{pmatrix}$$

The required quantum gates in matrix format:

$$I = \begin{pmatrix} 1 & 0 \\ 0 & 1 \end{pmatrix} \quad H = \frac{1}{\sqrt{2}} \begin{pmatrix} 1 & 1 \\ 1 & -1 \end{pmatrix} \quad Z = \begin{pmatrix} 1 & 0 \\ 0 & -1 \end{pmatrix} \quad Z^0 = \begin{pmatrix} 1 & 0 \\ 0 & 1 \end{pmatrix} \quad \text{CNOT} = \begin{pmatrix} 1 & 0 & 0 & 0 \\ 0 & 1 & 0 & 0 \\ 0 & 0 & 0 & 1 \\ 0 & 0 & 1 & 0 \end{pmatrix}$$

Form the quantum circuit for teleportation:

$$\text{QC} = \text{kronecker(H, I) CNOT)} \qquad \text{QC} = \begin{pmatrix} 0.707 & 0 & 0 & 0.707 \\ 0 & 0.707 & 0.707 & 0 \\ 0.707 & 0 & 0 & -0.707 \\ 0 & 0.707 & -0.707 & 0 \end{pmatrix} \qquad \text{QC} = \frac{1}{\sqrt{2}} \begin{pmatrix} 1 & 0 & 0 & 1 \\ 0 & 1 & 1 & 0 \\ 1 & 0 & 0 & -1 \\ 0 & 1 & -1 & 0 \end{pmatrix}$$

Write the initial state as a 4-vector using tensor multiplication.

$$\begin{pmatrix} \sqrt{\frac{1}{3}} \\ \sqrt{\frac{2}{3}} \end{pmatrix} \begin{pmatrix} 1 \\ 0 \end{pmatrix} = \begin{pmatrix} \sqrt{\frac{1}{3}} \\ 0 \\ \sqrt{\frac{2}{3}} \\ 0 \end{pmatrix}$$

Calculate the output state of the circuit and write it as a superposition of |0> and |1> on the top wire.

$$\frac{1}{\sqrt{2}} \begin{pmatrix} 1 & 0 & 0 & 1 \\ 0 & 1 & 1 & 0 \\ 1 & 0 & 0 & -1 \\ 0 & 1 & -1 & 0 \end{pmatrix} \begin{pmatrix} \sqrt{\frac{1}{3}} \\ 0 \\ \sqrt{\frac{2}{3}} \\ 0 \end{pmatrix} = \frac{1}{\sqrt{2}} \begin{pmatrix} \sqrt{\frac{1}{3}} \\ \sqrt{\frac{2}{3}} \\ \sqrt{\frac{2}{3}} \\ -\sqrt{\frac{2}{3}} \end{pmatrix}$$

$$\frac{1}{\sqrt{2}} \begin{pmatrix} \sqrt{\frac{1}{3}} \\ \sqrt{\frac{2}{3}} \\ \sqrt{\frac{2}{3}} \\ -\sqrt{\frac{2}{3}} \end{pmatrix} = \frac{1}{\sqrt{2}} \left[\begin{pmatrix} 1 \\ 0 \end{pmatrix} \begin{pmatrix} \sqrt{\frac{1}{3}} \\ \sqrt{\frac{2}{3}} \end{pmatrix} + \begin{pmatrix} 0 \\ 1 \end{pmatrix} \begin{pmatrix} \sqrt{\frac{1}{3}} \\ -\sqrt{\frac{2}{3}} \end{pmatrix} \right]$$

It is clear that if |0> is measured on the top wire, |Ψ> is on the bottom wire without further action. If |1> is measured on the top wire the qubit on the bottom wire is converted to |Ψ> by multiplication by Z.

$$\begin{pmatrix}1\\0\end{pmatrix}\begin{pmatrix}\sqrt{\frac{1}{3}}\\\sqrt{\frac{2}{3}}\end{pmatrix} \qquad \begin{pmatrix}0\\1\end{pmatrix}\begin{pmatrix}1 & 0\\0 & -1\end{pmatrix}\begin{pmatrix}\sqrt{\frac{1}{3}}\\-\sqrt{\frac{2}{3}}\end{pmatrix} = \begin{pmatrix}0\\1\end{pmatrix}\begin{pmatrix}\sqrt{\frac{1}{3}}\\\sqrt{\frac{2}{3}}\end{pmatrix}$$

Matrix summary:

$$\frac{1}{\sqrt{2}}\begin{pmatrix}1 & 0 & 0 & 1\\0 & 1 & 1 & 0\\1 & 0 & 0 & -1\\0 & 1 & -1 & 0\end{pmatrix}\begin{pmatrix}\sqrt{\frac{1}{3}}\\0\\\sqrt{\frac{2}{3}}\\0\end{pmatrix} = \frac{1}{\sqrt{2}}\begin{pmatrix}\sqrt{\frac{1}{3}}\\\sqrt{\frac{2}{3}}\\\sqrt{\frac{1}{3}}\\-\sqrt{\frac{2}{3}}\end{pmatrix} = \frac{1}{\sqrt{2}}\left[\begin{pmatrix}1\\0\end{pmatrix}\otimes\begin{pmatrix}\sqrt{\frac{1}{3}}\\\sqrt{\frac{2}{3}}\end{pmatrix} + \begin{pmatrix}0\\1\end{pmatrix}\otimes\begin{pmatrix}\sqrt{\frac{1}{3}}\\-\sqrt{\frac{2}{3}}\end{pmatrix}\right]$$

Algebraic summary:

$$Z = \begin{pmatrix}0 & \text{to} & 0\\1 & \text{to} & -1\end{pmatrix} \quad H = \begin{bmatrix}0 & \text{to} & \frac{(0+1)}{\sqrt{2}}\\1 & \text{to} & \frac{(0-1)}{\sqrt{2}}\end{bmatrix} \quad \text{CNOT} = \begin{pmatrix}00 & \text{to} & 00\\01 & \text{to} & 01\\10 & \text{to} & 11\\11 & \text{to} & 10\end{pmatrix}$$

$$\left(\sqrt{\frac{1}{3}}\left|0\right\rangle + \sqrt{\frac{2}{3}}\left|1\right\rangle\right)|0\rangle = \sqrt{\frac{1}{3}}|00\rangle + \sqrt{\frac{2}{3}}|10\rangle$$

$$\text{CNOT}$$

$$\sqrt{\frac{1}{3}}|00\rangle + \sqrt{\frac{2}{3}}|11\rangle$$

$$\text{H}\otimes\text{I}$$

$$\frac{1}{\sqrt{2}}\left[\sqrt{\frac{1}{3}}\left(|0\rangle+|1\rangle\right)|0\rangle + \sqrt{\frac{2}{3}}\left(|0\rangle-|1\rangle\right)|1\rangle\right]$$

$$= \frac{1}{\sqrt{2}}\left[|0\rangle\left(\sqrt{\frac{1}{3}}|0\rangle + \sqrt{\frac{2}{3}}|1\rangle\right)|1\rangle + \left(\sqrt{\frac{1}{3}}|0\rangle - \sqrt{\frac{2}{3}}|1\rangle\right)\right]$$

$$\downarrow$$

$$\frac{1}{\sqrt{2}}\left[|0\rangle\begin{pmatrix}\sqrt{\frac{1}{3}}\\\sqrt{\frac{2}{3}}\end{pmatrix} + |1\rangle\begin{pmatrix}\sqrt{\frac{1}{3}}\\-\sqrt{\frac{2}{3}}\end{pmatrix}\right] \xrightarrow{Action} \frac{1}{\sqrt{2}}\left[I\begin{pmatrix}\sqrt{\frac{1}{3}}\\-\sqrt{\frac{2}{3}}\end{pmatrix} + Z\begin{pmatrix}\sqrt{\frac{1}{3}}\\-\sqrt{\frac{2}{3}}\end{pmatrix}\right]$$

Total matrix operator approach:

m = 0

$$\text{kronecker}(I,\ Z^0)\text{kronecker}\left[\begin{pmatrix}1 & 0\\0 & 0\end{pmatrix},\ I\right]\text{kronecker}(H,\ I)CNOT\begin{pmatrix}\sqrt{\frac{1}{3}}\\0\\\sqrt{\frac{2}{3}}\\0\end{pmatrix}$$

$$= \begin{pmatrix}0.408\\0.577\\0\\0\end{pmatrix} = \frac{1}{\sqrt{2}}\begin{pmatrix}1\\0\end{pmatrix}\begin{pmatrix}\sqrt{\frac{1}{3}}\\\sqrt{\frac{2}{3}}\end{pmatrix}$$

m = 1

$$\text{kronecker}(I,\ Z^1)\text{kronecker}\left[\begin{pmatrix}0 & 0\\ 0 & 1\end{pmatrix},\ I\right]\text{kronecker}(H,\ I)CNOT\begin{pmatrix}\sqrt{\frac{1}{3}}\\ 0\\ \sqrt{\frac{2}{3}}\\ 0\end{pmatrix}$$

$$= \begin{pmatrix}0\\ 0\\ 0.408\\ 0.577\end{pmatrix} = \frac{1}{\sqrt{2}}\begin{pmatrix}0\\ 1\end{pmatrix}\begin{pmatrix}\sqrt{\frac{1}{3}}\\ \sqrt{\frac{2}{3}}\end{pmatrix}$$

The measurement projection operators used above in the next to the last step are:

m = 0

$$\begin{pmatrix}1\\ 0\end{pmatrix}(1 \quad 0) = \begin{pmatrix}1 & 0\\ 0 & 0\end{pmatrix}$$

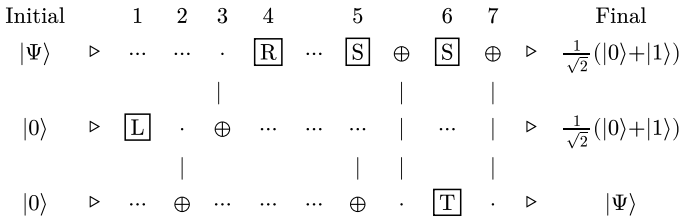
m = 1

$$\begin{pmatrix}0\\ 1\end{pmatrix}(0 \quad 1) = \begin{pmatrix}0 & 0\\ 0 & 1\end{pmatrix}$$

This page titled 8.10: A Simple Teleportation Exercise is shared under a CC BY 4.0 license and was authored, remixed, and/or curated by Frank Rioux via source content that was edited to the style and standards of the LibreTexts platform.

8.11: Teleportation as a Quantum Computation

This tutorial works through the following teleportation circuit provided by Gilles Brassard in "Teleportation as a Quantum Computation" (arXiv:quant-ph/9605035v1). The computational methodology employed here is similar to that used in the other teleportation examples given in this series of tutorials.



The necessary quantum bits or qubit states are:

Base states:

$$0 = \begin{pmatrix} 1 \\ 0 \end{pmatrix} \qquad 1 = \begin{pmatrix} 0 \\ 1 \end{pmatrix}$$

Superposition of base states:

$$\begin{pmatrix} \alpha \\ \beta \end{pmatrix} = \alpha \begin{pmatrix} 1 \\ 0 \end{pmatrix} + \beta \begin{pmatrix} 0 \\ 1 \end{pmatrix}$$

where

$$(|\alpha|)^2 + (|\beta|)^2 = 1$$

Using $\begin{pmatrix} \sqrt{\frac{2}{3}} \\ \sqrt{\frac{1}{3}} \end{pmatrix} = \begin{pmatrix} 0.816 \\ 0.577 \end{pmatrix}$ as the teleportee (|Ψ>), Brassard's circuit yields the final states shown in the circuit above. In other words |Ψ > is teleported from the first wire on the left to the third wire on the right.

Initial state:

$$\begin{pmatrix} \sqrt{\frac{2}{3}} \\ \sqrt{\frac{1}{3}} \end{pmatrix} \otimes \begin{pmatrix} 1 \\ 0 \end{pmatrix} \otimes \begin{pmatrix} 1 \\ 0 \end{pmatrix} = \begin{pmatrix} \sqrt{\frac{2}{3}} \\ 0 \\ 0 \\ 0 \\ \sqrt{\frac{1}{3}} \\ 0 \\ 0 \\ 0 \end{pmatrix}$$

Final state:

$$\frac{1}{\sqrt{2}}\begin{pmatrix}1\\1\end{pmatrix}\otimes\frac{1}{\sqrt{2}}\begin{pmatrix}1\\1\end{pmatrix}\otimes\begin{pmatrix}\sqrt{\frac{2}{3}}\\\sqrt{\frac{1}{3}}\end{pmatrix}=\begin{pmatrix}\sqrt{\frac{1}{6}}\\\sqrt{\frac{1}{12}}\\\sqrt{\frac{1}{6}}\\\sqrt{\frac{1}{12}}\\\sqrt{\frac{1}{6}}\\\sqrt{\frac{1}{12}}\\\sqrt{\frac{1}{6}}\\\sqrt{\frac{1}{12}}\end{pmatrix}$$

The identity operator and the following quantum gates are required to calculate the result of the teleportation circuit. L and R are single qubit rotations, S and T are single qubit phase shifts. The other gates (CNOT, CnNOT, and ICnNOT) are well-known in quantum circuitry.

$$I=\begin{pmatrix}1&0\\0&1\end{pmatrix}\quad L=\begin{pmatrix}1&-1\\1&1\end{pmatrix}\quad R=\frac{1}{\sqrt{2}}\begin{pmatrix}1&1\\-1&1\end{pmatrix}\quad S=\begin{pmatrix}i&0\\0&1\end{pmatrix}\quad T=\begin{pmatrix}-1&0\\0&-i\end{pmatrix}$$

$$\text{CNOT}=\begin{pmatrix}1&0&0&0\\0&1&0&0\\0&0&0&1\\0&0&1&0\end{pmatrix}\quad \text{CnNOT}=\begin{pmatrix}1&0&0&0&0&0&0&0\\0&1&0&0&0&0&0&0\\0&0&1&0&0&0&0&0\\0&0&0&1&0&0&0&0\\0&0&0&0&0&1&0&0\\0&0&0&0&1&0&0&0\\0&0&0&0&0&0&0&1\\0&0&0&0&0&0&1&0\end{pmatrix}$$

$$\text{ICnNOT}=\begin{pmatrix}1&0&0&0&0&0&0&0\\0&0&0&0&0&1&0&0\\0&0&1&0&0&0&0&0\\0&0&0&0&0&0&0&1\\0&0&0&0&1&0&0&0\\0&1&0&0&0&0&0&0\\0&0&0&0&0&0&1&0\\0&0&0&1&0&0&0&0\end{pmatrix}$$

$\text{Step1} = \text{kronecker(I, kronecker(L, I))}$ $\text{Step2} = \text{kronecker(I, CNOT)}$ $\text{Step3} = \text{kronecker(CNOT, I)}$

$\text{Step4} = \text{kronecker(R, kronecker(I, I))}$ $\text{Step5} = \text{kronecker(S, CNOT)}$ $\text{Step6} = \text{ICnNOT}$

$\text{Step7} = \text{kronecker(S, kronecker(I, T))}$ $\text{Step8} = \text{ICnNOT}$

According to this result |Ψ > has indeed been teleported to the bottom wire on the right, so the goal has been achieved. However, Brassard suggests that measurements on the top wires in the |0 >-|1 > basis are also instructive. There are four possible measurement outcomes: |00>, |01>, |10 > and |11 >. The projection operators for |0 > and |1 > are as follows.

Projection operator for |0>:

$$\begin{pmatrix}1\\0\end{pmatrix}\begin{pmatrix}1&0\end{pmatrix}=\begin{pmatrix}1&0\\0&0\end{pmatrix}$$

Projection operator for |1>:

$$\begin{pmatrix}0\\1\end{pmatrix}\begin{pmatrix}0&1\end{pmatrix}=\begin{pmatrix}0&0\\0&1\end{pmatrix}$$

These calculations also show successful teleportation.

Measurement result for qubits x and y		Final 3-qubit state
$2\text{kronecker}\left[\begin{pmatrix}1&0\\0&0\end{pmatrix}, \text{kronecker}\left[\begin{pmatrix}1&0\\0&0\end{pmatrix}, I\right]\right]\Psi_{final} =$	$\begin{pmatrix}0.816\\0.577\\0\\0\\0\\0\\0\\0\end{pmatrix}$	$\begin{bmatrix} x & y & z \\ \begin{pmatrix}1\\0\end{pmatrix} & \begin{pmatrix}1\\0\end{pmatrix} & \begin{pmatrix}0.816\\0.577\end{pmatrix}\end{bmatrix}$
$2\text{kronecker}\left[\begin{pmatrix}1&0\\0&0\end{pmatrix}, \text{kronecker}\left[\begin{pmatrix}0&0\\0&1\end{pmatrix}, I\right]\right]\Psi_{final} =$	$\begin{pmatrix}0\\0\\0.816\\0.577\\0\\0\\0\\0\end{pmatrix}$	$\begin{bmatrix} x & y & z \\ \begin{pmatrix}1\\0\end{pmatrix} & \begin{pmatrix}0\\1\end{pmatrix} & \begin{pmatrix}0.816\\0.577\end{pmatrix}\end{bmatrix}$
$2\text{kronecker}\left[\begin{pmatrix}0&0\\0&1\end{pmatrix}, \text{kronecker}\left[\begin{pmatrix}1&0\\0&0\end{pmatrix}, I\right]\right]\Psi_{final} =$	$\begin{pmatrix}0\\0\\0\\0\\0.816\\0.577\\0\\0\end{pmatrix}$	$\begin{bmatrix} x & y & z \\ \begin{pmatrix}0\\1\end{pmatrix} & \begin{pmatrix}1\\0\end{pmatrix} & \begin{pmatrix}0.816\\0.577\end{pmatrix}\end{bmatrix}$
$2\text{kronecker}\left[\begin{pmatrix}0&0\\0&1\end{pmatrix}, \text{kronecker}\left[\begin{pmatrix}0&0\\0&1\end{pmatrix}, I\right]\right]\Psi_{final} =$	$\begin{pmatrix}0\\0\\0\\0\\0\\0\\0.816\\0.577\end{pmatrix}$	$\begin{bmatrix} x & y & z \\ \begin{pmatrix}0\\1\end{pmatrix} & \begin{pmatrix}0\\1\end{pmatrix} & \begin{pmatrix}0.816\\0.577\end{pmatrix}\end{bmatrix}$

Appendix

In the inverse controlled-NOT gate of steps 6 and 8 of Brassard's teleportation circuit, c is the control, a is the target and b is unchanged.

$$\begin{pmatrix} a & b & c & ' & a' & b' & c' \\ 0&0&0&'&0&0&0 \\ 0&0&1&'&1&0&1 \\ 0&1&0&'&0&1&0 \\ 0&1&1&'&1&1&1 \\ 1&0&0&'&1&0&0 \\ 1&0&1&'&0&0&1 \\ 1&1&0&'&1&1&0 \\ 1&1&1&'&0&1&1 \end{pmatrix}$$

This page titled 8.11: Teleportation as a Quantum Computation is shared under a CC BY 4.0 license and was authored, remixed, and/or curated by Frank Rioux via source content that was edited to the style and standards of the LibreTexts platform.

8.12: Quantum Teleportation - Four Perspectives

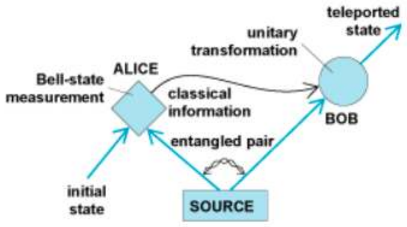
The science fiction dream of "beaming" objects from place to place is now a reality - at least for particles of light. Anton Zeilinger, Scientific American, April 2000, page 50.

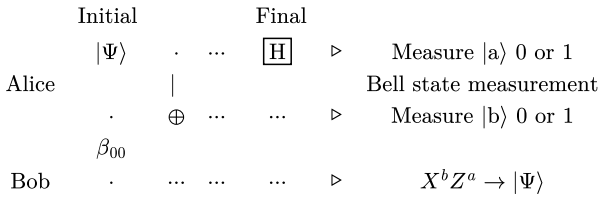
Quantum teleportation is a way of transferring the state of one particle to a second, effectively teleporting the initial particle. (Tony Sudbery, Nature, December 11, 1997, page 551.)

As shown in the graphic below, quantum teleportation is a form of information transfer that requires pre-existing entanglement and a classical communication channel to send information from one location to another.

Alice has the photon to be teleported and a photon of an entangled pair that she shares with Bob. She performs a measurement on her photons that projects them into one of the four Bell states and Bob's photon, via the entangled quantum channel, into a state that has a unique relationship to the state of the teleportee. Bob carries out one of four unitary operations on his photon depending on the results of Alice's measurement, which she sends him through a classical communication channel.

The figure (Nature, December 11, 1997, page 576) on the left provides a graphic summary of the first successful teleportation experiment. The quantum circuit on the right shows a method of implementation.





The teleportee and the Bell states indexed in binary notation:

Teleportee:

$$\begin{pmatrix} \sqrt{\frac{1}{3}} \\ \sqrt{\frac{2}{3}} \end{pmatrix}$$

Bell states:

$$\beta_{00} = \frac{1}{\sqrt{2}} \begin{pmatrix} 1 \\ 0 \\ 0 \\ 1 \end{pmatrix} \quad \beta_{01} = \frac{1}{\sqrt{2}} \begin{pmatrix} 0 \\ 1 \\ 1 \\ 0 \end{pmatrix} \quad \beta_{10} = \frac{1}{\sqrt{2}} \begin{pmatrix} 1 \\ 0 \\ 0 \\ -1 \end{pmatrix} \quad \beta_{11} = \frac{1}{\sqrt{2}} \begin{pmatrix} 0 \\ 1 \\ -1 \\ 0 \end{pmatrix}$$

Truth tables and matrices representing the various teleportation circuit operations:

$$|0\rangle = \begin{pmatrix} 1 \\ 0 \end{pmatrix} \quad |1\rangle = \begin{pmatrix} 0 \\ 1 \end{pmatrix} \quad X = \begin{pmatrix} 0 \text{ to } 1 \\ 1 \text{ to } -1 \end{pmatrix} \quad H = \begin{bmatrix} 0 \text{ to } \frac{(0+1)}{\sqrt{2}} \\ 1 \text{ to } \frac{(0-1)}{\sqrt{2}} \end{bmatrix} \quad \text{CNOT} = \begin{pmatrix} 00 \text{ to } 00 \\ 01 \text{ to } 01 \\ 10 \text{ to } 11 \\ 11 \text{ to } 10 \end{pmatrix}$$

$$I = \begin{pmatrix} 1 & 0 \\ 0 & 1 \end{pmatrix} \quad X = \begin{pmatrix} 0 & 1 \\ 1 & 0 \end{pmatrix} \quad Z = \begin{pmatrix} 1 & 0 \\ 0 & -1 \end{pmatrix} \quad H = \frac{1}{\sqrt{2}} \begin{pmatrix} 1 & 1 \\ 1 & -1 \end{pmatrix} \quad \text{CNOT} = \begin{pmatrix} 1 & 0 & 0 & 0 \\ 0 & 1 & 0 & 0 \\ 0 & 0 & 0 & 1 \\ 0 & 0 & 1 & 0 \end{pmatrix}$$

Perspective I. Using the truth tables, the operation of the teleportation circuit is expressed in Dirac notation.

$$\left(\sqrt{\frac{1}{3}}|0\rangle + \sqrt{\frac{2}{3}}|1\rangle\right) \frac{1}{\sqrt{2}} \left(|00\rangle + |11\rangle\right) = \frac{1}{\sqrt{2}} \left[\sqrt{\frac{1}{3}} \left(|00\rangle|0\rangle + |01\rangle|1\rangle\right) + \sqrt{\frac{2}{3}} \left(|10\rangle|0\rangle + |11\rangle|1\rangle\right)\right]$$

$$\text{CNOT} \otimes I$$

$$\frac{1}{\sqrt{2}} \left[\sqrt{\frac{1}{3}}(|00\rangle|0\rangle + |01\rangle|1\rangle) + \sqrt{\frac{2}{3}}(|11\rangle|0\rangle + |10\rangle|1\rangle)\right]$$
$$= \frac{1}{\sqrt{2}} \left[\sqrt{\frac{1}{3}}|0\rangle(|00\rangle + |11\rangle) + \sqrt{\frac{2}{3}}|1\rangle(|10\rangle + |01\rangle)\right]$$

$$H \otimes I \otimes I$$

$$\frac{1}{2} \left[\sqrt{\frac{1}{3}}(|0\rangle + |1\rangle)(|00\rangle + |11\rangle) + \sqrt{\frac{2}{3}}(|0\rangle - |1\rangle)(|10\rangle + |01\rangle)\right]$$

$$\downarrow$$

$$\frac{1}{2} \left[|00\rangle \begin{pmatrix} \sqrt{\frac{1}{3}} \\ \sqrt{\frac{2}{3}} \end{pmatrix} + |01\rangle \begin{pmatrix} \sqrt{\frac{2}{3}} \\ \sqrt{\frac{1}{3}} \end{pmatrix} + |10\rangle \begin{pmatrix} \sqrt{\frac{1}{3}} \\ -\sqrt{\frac{2}{3}} \end{pmatrix} + |11\rangle \begin{pmatrix} -\sqrt{\frac{2}{3}} \\ \sqrt{\frac{1}{3}} \end{pmatrix}\right] \xrightarrow{Action} \frac{1}{2}$$
$$\left[I \begin{pmatrix} \sqrt{\frac{1}{3}} \\ \sqrt{\frac{2}{3}} \end{pmatrix} + X \begin{pmatrix} \sqrt{\frac{2}{3}} \\ \sqrt{\frac{1}{3}} \end{pmatrix} + Z \begin{pmatrix} \sqrt{\frac{1}{3}} \\ -\sqrt{\frac{2}{3}} \end{pmatrix} + ZX \begin{pmatrix} -\sqrt{\frac{2}{3}} \\ \sqrt{\frac{1}{3}} \end{pmatrix}\right]$$

Alice's Bell state measurement result (|00>, |01>. |10> or |11>, see indexed Bell states above) determines the operation (I, X, Z or ZX) that Bob performs on his photon.

Perspective II. The three-cubit initial state is re-written as a linear superposition of the four possible Bell states that Alice can find on measurement. Note that this is a equivalent to the expression on the left side of the equation immediately above if the Bell states are replaced by their binary indices, as they would be after the Bell state measurement.

$$\Psi\rangle = \begin{pmatrix} \sqrt{\frac{1}{3}} \\ \sqrt{\frac{2}{3}} \end{pmatrix} \otimes \sqrt{\frac{1}{2}} \begin{pmatrix} 1 \\ 0 \\ 0 \\ 1 \end{pmatrix} = \sqrt{\frac{1}{2}} \begin{pmatrix} \sqrt{\frac{1}{3}} \\ 0 \\ 0 \\ \sqrt{\frac{1}{3}} \\ \sqrt{\frac{2}{3}} \\ 0 \\ 0 \\ \sqrt{\frac{2}{3}} \end{pmatrix}$$

$$= \frac{1}{2} \left[\sqrt{\frac{1}{2}} \begin{pmatrix} 1 \\ 0 \\ 0 \\ 1 \end{pmatrix} \otimes \begin{pmatrix} \sqrt{\frac{1}{3}} \\ \sqrt{\frac{2}{3}} \end{pmatrix} + \sqrt{\frac{1}{2}} \begin{pmatrix} 0 \\ 1 \\ 1 \\ 0 \end{pmatrix} \otimes \begin{pmatrix} \sqrt{\frac{2}{3}} \\ \sqrt{\frac{1}{3}} \end{pmatrix}\right.$$
$$\left. + \sqrt{\frac{1}{2}} \begin{pmatrix} 1 \\ 0 \\ 0 \\ -1 \end{pmatrix} \otimes \begin{pmatrix} \sqrt{\frac{1}{3}} \\ -\sqrt{\frac{2}{3}} \end{pmatrix} + \sqrt{\frac{1}{2}} \begin{pmatrix} 0 \\ 1 \\ -1 \\ 0 \end{pmatrix} \otimes \begin{pmatrix} -\sqrt{\frac{2}{3}} \\ \sqrt{\frac{1}{3}} \end{pmatrix}\right]$$

Condensed version of the equation:

$$|\Psi\rangle = \begin{pmatrix} \sqrt{\frac{1}{3}} \\ \sqrt{\frac{2}{3}} \end{pmatrix} \otimes \beta_{00} = \frac{1}{2}\left[\beta_{00} \otimes \begin{pmatrix} \sqrt{\frac{1}{3}} \\ \sqrt{\frac{2}{3}} \end{pmatrix} + \beta_{01} \otimes \begin{pmatrix} \sqrt{\frac{2}{3}} \\ \sqrt{\frac{1}{3}} \end{pmatrix} + \beta_{10} \otimes \begin{pmatrix} \sqrt{\frac{1}{3}} \\ -\sqrt{\frac{2}{3}} \end{pmatrix} + \beta_{11} \otimes \begin{pmatrix} -\sqrt{\frac{2}{3}} \\ \sqrt{\frac{1}{3}} \end{pmatrix}\right]$$

Another way to write the equation:

$$|\Psi\rangle = \begin{pmatrix} \sqrt{\frac{1}{3}} \\ \sqrt{\frac{2}{3}} \end{pmatrix} \otimes \beta_{00}$$
$$= \frac{1}{2}\left[\beta_{00} \otimes I \begin{pmatrix} \sqrt{\frac{1}{3}} \\ \sqrt{\frac{2}{3}} \end{pmatrix} + \beta_{01} \otimes X \begin{pmatrix} \sqrt{\frac{1}{3}} \\ \sqrt{\frac{2}{3}} \end{pmatrix} + \beta_{10} \otimes Z \begin{pmatrix} \sqrt{\frac{1}{3}} \\ \sqrt{\frac{2}{3}} \end{pmatrix} + \beta_{11} \otimes XZ \begin{pmatrix} \sqrt{\frac{1}{3}} \\ \sqrt{\frac{2}{3}} \end{pmatrix}\right]$$

Perspective III. The teleportation circuit (TC) is written as a composite matrix operator which then operates on the initial three-qubit state.

$$\Psi = \tfrac{1}{\sqrt{2}}\begin{pmatrix} \sqrt{\frac{1}{3}} & 0 & 0 & \sqrt{\frac{1}{3}}\sqrt{\frac{2}{3}} & 0 & 0 & \sqrt{\frac{2}{3}} \end{pmatrix}^2 \qquad \begin{array}{l} \mathrm{TC} = \mathrm{kronecker(H,\ kronecker(I,\ I))} \\ \mathrm{kronecker(CNOT,\ I)} \end{array}$$

After operation of the circuit the system is in a superposition state involving the Bell state indices on the top two registers. The third register contains a state that can easily be transformed into the teleportee once Alice tells Bob which Bell state she observed.

$$\mathrm{TC}\Psi = \begin{pmatrix} 0.289 \\ 0.408 \\ 0.408 \\ 0.289 \\ 0.289 \\ -0.408 \\ -0.408 \\ 0.289 \end{pmatrix}$$
$$= \tfrac{1}{2}\left[\begin{pmatrix} 1 \\ 0 \end{pmatrix} \otimes \begin{pmatrix} 1 \\ 0 \end{pmatrix} \otimes \begin{pmatrix} \sqrt{\frac{1}{3}} \\ \sqrt{\frac{2}{3}} \end{pmatrix} + \begin{pmatrix} 1 \\ 0 \end{pmatrix} \otimes \begin{pmatrix} 0 \\ 1 \end{pmatrix} \otimes \begin{pmatrix} \sqrt{\frac{2}{3}} \\ \sqrt{\frac{1}{3}} \end{pmatrix}\right.$$
$$\left. + \begin{pmatrix} 0 \\ 1 \end{pmatrix} \otimes \begin{pmatrix} 1 \\ 0 \end{pmatrix} \otimes \begin{pmatrix} \sqrt{\frac{1}{3}} \\ -\sqrt{\frac{2}{3}} \end{pmatrix} + \begin{pmatrix} 0 \\ 1 \end{pmatrix} \otimes \begin{pmatrix} 0 \\ 1 \end{pmatrix} \otimes \begin{pmatrix} -\sqrt{\frac{2}{3}} \\ \sqrt{\frac{1}{3}} \end{pmatrix}\right]$$
$$= \tfrac{1}{2}\left[\begin{pmatrix} 1 \\ 0 \\ 0 \\ 0 \end{pmatrix} \otimes \begin{pmatrix} \sqrt{\frac{1}{3}} \\ \sqrt{\frac{2}{3}} \end{pmatrix} + \begin{pmatrix} 0 \\ 1 \\ 0 \\ 0 \end{pmatrix} \otimes \begin{pmatrix} \sqrt{\frac{2}{3}} \\ \sqrt{\frac{1}{3}} \end{pmatrix} + \begin{pmatrix} 0 \\ 0 \\ 1 \\ 0 \end{pmatrix} \otimes \begin{pmatrix} \sqrt{\frac{1}{3}} \\ -\sqrt{\frac{2}{3}} \end{pmatrix} + \begin{pmatrix} 0 \\ 0 \\ 0 \\ 1 \end{pmatrix} \otimes \begin{pmatrix} -\sqrt{\frac{2}{3}} \\ \sqrt{\frac{1}{3}} \end{pmatrix}\right]$$

Tabular summary of teleportation experiment:

$$\begin{pmatrix} \text{Alice Measurement Result} & \beta_{00} & \beta_{01} & \beta 10 & \beta_{11} \\ \text{Bob's Action} & I & X & Z & ZX \end{pmatrix}$$

Bell state indices:

$$\text{kronecker (H, I) CNOT}\beta_{00} = \begin{pmatrix} 1 \\ 0 \\ 0 \\ 0 \end{pmatrix} \quad \text{kronecker (H, I) CNOT}\beta_{01} = \begin{pmatrix} 0 \\ 1 \\ 0 \\ 0 \end{pmatrix}$$
$$\text{kronecker (H, I) CNOT}\beta_{10} = \begin{pmatrix} 0 \\ 0 \\ 1 \\ 0 \end{pmatrix} \quad \text{kronecker (H, I) CNOT}\beta_{11} = \begin{pmatrix} 0 \\ 0 \\ 0 \\ 1 \end{pmatrix}$$

A similar approach is to use projection operators on the top two qubits to simulate the four measurement outcomes. See the Appendix for more on this method.

Bob's Action

$$\text{Measure}|00\rangle \quad \text{2kronecker}\left[\begin{pmatrix}1\\0\end{pmatrix}\begin{pmatrix}1\\0\end{pmatrix}^T, \text{kronecker}\left[\begin{pmatrix}1\\0\end{pmatrix}\begin{pmatrix}1\\0\end{pmatrix}^T, I\right]\right] \text{TC}\Psi \quad \text{No action required}$$

$$= \begin{pmatrix}0.577\\0.816\\0\\0\\0\\0\\0\\0\end{pmatrix}$$

$$\text{Measure}|01\rangle \quad \text{2kronecker}\left[\begin{pmatrix}1\\0\end{pmatrix}\begin{pmatrix}1\\0\end{pmatrix}^T, \text{kronecker}\left[\begin{pmatrix}0\\1\end{pmatrix}\begin{pmatrix}0\\1\end{pmatrix}^T, I\right]\right] \text{TC}\Psi \quad \text{Operate with X}$$

$$= \begin{pmatrix}0\\0\\0.816\\0.577\\0\\0\\0\\0\end{pmatrix}$$

$$\text{Measure}|10\rangle \quad \text{2kronecker}\left[\begin{pmatrix}0\\1\end{pmatrix}\begin{pmatrix}0\\1\end{pmatrix}^T, \text{kronecker}\left[\begin{pmatrix}1\\0\end{pmatrix}\begin{pmatrix}1\\0\end{pmatrix}^T, I\right]\right] \text{TC}\Psi \quad \text{Operate with Z}$$

$$= \begin{pmatrix}0\\0\\0\\0\\0.577\\-0.816\\0\\0\end{pmatrix}$$

$$\text{Measure}|11\rangle \quad \text{2kronecker}\left[\begin{pmatrix}0\\1\end{pmatrix}\begin{pmatrix}0\\1\end{pmatrix}^T, \text{kronecker}\left[\begin{pmatrix}0\\1\end{pmatrix}\begin{pmatrix}0\\1\end{pmatrix}^T, I\right]\right] \text{TC}\Psi \quad \text{Operate with ZX}$$

$$= \begin{pmatrix}0\\0\\0\\0\\0\\0\\-0.816\\0.577\end{pmatrix}$$

Perspective IV. Projecting the teleportee photon 1 (green) onto the result of Alice's Bell state measurement (blue) yields the state of photon 2 which was initially entangled with Bob's photon 3. Projection of this state onto the original 2-3 entangled state (red) transforms Bob's photon to the teleportee state 25% of the time. As is now shown this happens when Alice's Bell state measurment yields β_{00}.

$$ {}_{12}\langle\beta_{00}|\Psi\rangle_1|\beta_{00}\rangle_{23} = \frac{1}{\sqrt{2}}\left[\begin{pmatrix}1\\0\end{pmatrix}_1^T \otimes \begin{pmatrix}1\\0\end{pmatrix}_2^T + \begin{pmatrix}0\\1\end{pmatrix}_1^T \otimes \begin{pmatrix}0\\1\end{pmatrix}_2^T\right]\begin{pmatrix}\sqrt{\frac{1}{3}}\\ \sqrt{\frac{2}{3}}\end{pmatrix}_1 \frac{1}{\sqrt{2}} $$

$$ \left[\begin{pmatrix}1\\0\end{pmatrix}_2 \otimes \begin{pmatrix}1\\0\end{pmatrix}_3 + \begin{pmatrix}0\\1\end{pmatrix}_2 \otimes \begin{pmatrix}0\\1\end{pmatrix}_3\right] = \frac{1}{2}\begin{pmatrix}\sqrt{\frac{1}{3}}\\ \sqrt{\frac{2}{3}}\end{pmatrix}_3 $$

An algebraic analysis of this example is as follows.

Teleportee

$$ \frac{1}{\sqrt{2}}\left[{}_1\langle 0|_2\langle 0| + {}_1\langle 1|_2\langle 1|\right]\left[\alpha|0\rangle_1 + \beta|1\rangle_1\right]\frac{1}{\sqrt{2}}\left[|0\rangle_2|0\rangle_3 + |1\rangle_2|1\rangle_3\right] $$

$$ \downarrow $$

$$ \frac{1}{\sqrt{2}}\left[\alpha_2\langle 0| + \beta_2\langle 1|\right]\frac{1}{\sqrt{2}}\left[|0\rangle_2|0\rangle_3 + |1\rangle_2|1\rangle_3\right] $$

$$ \downarrow $$

$$ \frac{1}{2}\left[\alpha|0\rangle_3 + \beta|1\rangle_3\right] $$

Naturally this approach yields the same results as the previous perspectives when Alice's Bell state measurement is β_{01}, β_{10} and β_{11}. As demonstrated previously for these results Bob's action is X, Z and ZX, respectively.

$$ {}_{12}\langle\beta_{01}|\Psi\rangle_1|\beta_{00}\rangle_{23} = \frac{1}{\sqrt{2}}\left[\begin{pmatrix}1\\0\end{pmatrix}_1^T \otimes \begin{pmatrix}0\\1\end{pmatrix}_2^T + \begin{pmatrix}0\\1\end{pmatrix}_1^T \otimes \begin{pmatrix}1\\0\end{pmatrix}_2^T\right]\begin{pmatrix}\sqrt{\frac{1}{3}}\\ \sqrt{\frac{2}{3}}\end{pmatrix}_1 \frac{1}{\sqrt{2}} $$

$$ \left[\begin{pmatrix}1\\0\end{pmatrix}_2 \otimes \begin{pmatrix}1\\0\end{pmatrix}_3 + \begin{pmatrix}0\\1\end{pmatrix}_2 \otimes \begin{pmatrix}0\\1\end{pmatrix}_3\right] = \frac{1}{2}\begin{pmatrix}\sqrt{\frac{2}{3}}\\ \sqrt{\frac{1}{3}}\end{pmatrix}_3 $$

$$ {}_{12}\langle\beta_{10}|\Psi\rangle_1|\beta_{00}\rangle_{23} = \frac{1}{\sqrt{2}}\left[\begin{pmatrix}1\\0\end{pmatrix}_1^T \otimes \begin{pmatrix}1\\0\end{pmatrix}_2^T - \begin{pmatrix}0\\1\end{pmatrix}_1^T \otimes \begin{pmatrix}0\\1\end{pmatrix}_2^T\right]\begin{pmatrix}\sqrt{\frac{1}{3}}\\ \sqrt{\frac{2}{3}}\end{pmatrix}_1 \frac{1}{\sqrt{2}} $$

$$ \left[\begin{pmatrix}1\\0\end{pmatrix}_2 \otimes \begin{pmatrix}1\\0\end{pmatrix}_3 + \begin{pmatrix}0\\1\end{pmatrix}_2 \otimes \begin{pmatrix}0\\1\end{pmatrix}_3\right] = \frac{1}{2}\begin{pmatrix}\sqrt{\frac{1}{3}}\\ -\sqrt{\frac{2}{3}}\end{pmatrix}_3 $$

$$ {}_{12}\langle\beta_{11}|\Psi\rangle_1|\beta_{00}\rangle_{23} = \frac{1}{\sqrt{2}}\left[\begin{pmatrix}1\\0\end{pmatrix}_1^T \otimes \begin{pmatrix}0\\1\end{pmatrix}_2^T - \begin{pmatrix}0\\1\end{pmatrix}_1^T \otimes \begin{pmatrix}1\\0\end{pmatrix}_2^T\right]\begin{pmatrix}\sqrt{\frac{1}{3}}\\ \sqrt{\frac{2}{3}}\end{pmatrix}_1 \frac{1}{\sqrt{2}} $$

$$ \left[\begin{pmatrix}1\\0\end{pmatrix}_2 \otimes \begin{pmatrix}1\\0\end{pmatrix}_3 + \begin{pmatrix}0\\1\end{pmatrix}_2 \otimes \begin{pmatrix}0\\1\end{pmatrix}_3\right] = \frac{1}{2}\begin{pmatrix}-\sqrt{\frac{2}{3}}\\ \sqrt{\frac{1}{3}}\end{pmatrix}_3 $$

Summary of the quantum teleportation protocol: "Quantum teleportation provides a 'disembodied' way to tranfer quantum states from one object to another at a distant location, assisted by previously shared entangled states and a classical communication channel." Nature **518**, 516 (2015)

The paper cited above reported the first successful teleportation of two degrees of freedom of a single photon. The analysis is somewhat more complicated than that provided in this tutorial, but the general principle is the same. The quantum channel is a hyper-entangled state shared by Alice and Bob, rather than one of the simple entangled Bell states.

Appendix

Addendum to Perspective III. In these calculations the required operations by Bob are actually carried out on the third qubit.

Measure$|00\rangle$ do nothing

kronecker(I, kronecker(I, I)) 2

$$\text{kronecker}\left[\begin{pmatrix}1\\0\end{pmatrix}\begin{pmatrix}1\\0\end{pmatrix}^T, \text{kronecker}\left[\begin{pmatrix}1\\0\end{pmatrix}\begin{pmatrix}1\\0\end{pmatrix}^T, I\right]\right] \text{TC}\Psi = \begin{pmatrix}0.577\\0.816\\0\\0\\0\\0\\0\\0\end{pmatrix}$$

Measure$|01\rangle$ operate with X

kronecker(I, kronecker(I, X)) 2

$$\text{kronecker}\left[\begin{pmatrix}1\\0\end{pmatrix}\begin{pmatrix}1\\0\end{pmatrix}^T, \text{kronecker}\left[\begin{pmatrix}0\\1\end{pmatrix}\begin{pmatrix}0\\1\end{pmatrix}^T, I\right]\right] \text{TC}\Psi = \begin{pmatrix}0\\0\\0.577\\0.816\\0\\0\\0\\0\end{pmatrix}$$

Measure$|10\rangle$ operate with Z

kronecker(I, kronecker(I, Z)) 2

$$\text{kronecker}\left[\begin{pmatrix}0\\1\end{pmatrix}\begin{pmatrix}0\\1\end{pmatrix}^T, \text{kronecker}\left[\begin{pmatrix}1\\0\end{pmatrix}\begin{pmatrix}1\\0\end{pmatrix}^T, I\right]\right] \text{TC}\Psi = \begin{pmatrix}0\\0\\0\\0\\0.577\\0.816\\0\\0\end{pmatrix}$$

Measure$|11\rangle$ operate with Z

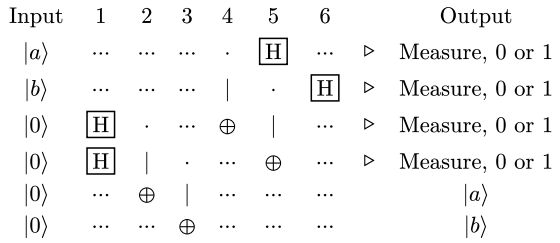
kronecker(I, kronecker(I, Z, X)) 2

$$\text{kronecker}\left[\begin{pmatrix}0\\1\end{pmatrix}\begin{pmatrix}0\\1\end{pmatrix}^T, \text{kronecker}\left[\begin{pmatrix}0\\1\end{pmatrix}\begin{pmatrix}0\\1\end{pmatrix}^T, I\right]\right] \text{TC}\Psi = \begin{pmatrix}0\\0\\0\\0\\0\\0\\0.577\\0.816\end{pmatrix}$$

This page titled 8.12: Quantum Teleportation - Four Perspectives is shared under a CC BY 4.0 license and was authored, remixed, and/or curated by Frank Rioux via source content that was edited to the style and standards of the LibreTexts platform.

8.13: Teleportation of Two Qubits

The following quantum circuit teleports |a>|b> from the top two wires on the left to the bottom two wires on the right.



There are 16 possible measurement results on the top four wires on the right ranging from |0> to |15> (|000000> to |111111> in binary notation), and these results determine the action required to transform the bottom two wires to |a>|b>.

As an initial example, if the teleportee in decimal notation is |3> the total input state is |48>.

Teleportee:

$$\begin{pmatrix}0\\1\end{pmatrix}\begin{pmatrix}0\\1\end{pmatrix}=\begin{pmatrix}0\\0\\0\\1\end{pmatrix}=|3\rangle$$

Total input state:

$$\Psi=\begin{pmatrix}0\\1\end{pmatrix}\begin{pmatrix}0\\1\end{pmatrix}\begin{pmatrix}1\\0\end{pmatrix}\begin{pmatrix}1\\0\end{pmatrix}\begin{pmatrix}1\\0\end{pmatrix}\begin{pmatrix}1\\0\end{pmatrix}=|48\rangle$$

Ψ_{48} is the only non-zero element in the input state vector.

$$i=0..63 \quad \Psi_i=0 \quad \Psi_48=1$$

	44	45	46	47	48	49	50	51	52	53
0	0	0	0	0	1	0	0	0	0	⋯

With the assistance of truth tables provided in the Appendix and a bit of tedious algebra the operation of the teleportation circuit on this input state can be summarized as follows.

Given $|\Psi\rangle_{input}=|1\rangle|1\rangle|0\rangle|0\rangle|0\rangle|0\rangle=|48\rangle$ the teleportation circuit yields

$$|\Psi\rangle_{output}=\frac{1}{4}\begin{bmatrix}(|3\rangle-|7\rangle-|11\rangle+|15\rangle)|00\rangle+(|2\rangle-|6\rangle-|10\rangle+|14\rangle)|01\rangle\\+(|1\rangle-|5\rangle-|9\rangle+|13\rangle)|10\rangle+(|0\rangle-|4\rangle-|8\rangle+|12\rangle)|11\rangle\end{bmatrix}$$

The output state shows that if the measurement result is 3, 7, 11 or 15, the NOT operator (|0> to |1> and |1> to |0>) should be applied to wires **5** and **6**. If the result is 2, 6, 10 or 14, the NOT operator is applied to wire **5**; if the result 1, 5, 9 or 13, the NOT operator is applied to wire **6**; if the result is 0, 4, 8 or 12, no action is required.

Now an example teleportation calculation will be carried out on the teleportee state given above. The following matrix operators are required for the teleportation circuit. They are the identity, the Hadamard gate, the measurement operators for |0> and |1>, and the CnNOT gate.

$$I = \begin{pmatrix} 1 & 0 \\ 0 & 1 \end{pmatrix} \quad H = \frac{1}{\sqrt{2}} \begin{pmatrix} 1 & 1 \\ 1 & -1 \end{pmatrix} \quad M_0 = \begin{pmatrix} 1 & 0 \\ 0 & 0 \end{pmatrix} \quad M_1 = \begin{pmatrix} 0 & 0 \\ 0 & 1 \end{pmatrix}$$

$$\text{CnNOT} = \begin{pmatrix} 1 & 0 & 0 & 0 & 0 & 0 & 0 & 0 \\ 0 & 1 & 0 & 0 & 0 & 0 & 0 & 0 \\ 0 & 0 & 1 & 0 & 0 & 0 & 0 & 0 \\ 0 & 0 & 0 & 1 & 0 & 0 & 0 & 0 \\ 0 & 0 & 0 & 0 & 0 & 1 & 0 & 0 \\ 0 & 0 & 0 & 0 & 1 & 0 & 0 & 0 \\ 0 & 0 & 0 & 0 & 0 & 0 & 0 & 1 \\ 0 & 0 & 0 & 0 & 0 & 0 & 1 & 0 \end{pmatrix}$$

The matrix operators for the six steps in the circuit are formed using tensor (Kronecker) multiplication.

$$\text{Step1} = \text{kronecker(I, kronecker(I, kronecker(H, kronecker(H, kronecker(I, I))))}$$

$$\text{Step2} = \text{kronecker(I, kronecker(I, kronecker(CnNOT, I)))}$$

$$\text{Step3} = \text{kronecker(I, kronecker(I, kronecker(I, CnNOT)))}$$

$$\text{Step4} = \text{kronecker(CnNOT, kronecker(I, kronecker(I, I)))}$$

$$\text{Step5} = \text{kronecker(H, kronecker(CnNOT, kronecker(I, I)))}$$

$$\text{Step6} = \text{kronecker(I, kronecker(H, kronecker(I, kronecker(I, kronecker(I, I)))))}$$

$$\text{Step7} = \text{kronecker}(M_0, \text{kronecker}(M_0, \text{kronecker}(M_0, \text{kronecker}(M_0, \text{kronecker}(I,\ I)))))$$

The output vector is calculated for the simple case of measuring |0>|0>|0>|0> on the top four wires. The factor of 4 takes into account that measuring |0>|0>|0>|0> has a probability amplitude of 1/4. It therefore normalizes the calculation.

$$\Psi_{out} = 4\text{Step7 Step6 Step 5 Step4 Step3 Step2 Step1}\Psi$$

$$\Psi_{out}^{T} = \left| \begin{array}{c|c|c|c|c|c|c|c|c|c|c} & 0 & 1 & 2 & 3 & 4 & 5 & 6 & 7 & 8 & 9 \\ \hline 0 & 0 & 0 & 0 & 1 & 0 & 0 & 0 & 0 & 0 & \cdots \end{array} \right|$$

$$\Psi_{out} = \begin{pmatrix} 1 \\ 0 \end{pmatrix} \begin{pmatrix} 1 \\ 0 \end{pmatrix} \begin{pmatrix} 1 \\ 0 \end{pmatrix} \begin{pmatrix} 1 \\ 0 \end{pmatrix} \begin{pmatrix} 0 \\ 1 \end{pmatrix} \begin{pmatrix} 0 \\ 1 \end{pmatrix} = |3\rangle$$

In a second example a superposition of |0 > + |1 > + |2 > + |3> is teleported.

Teleportee:

$$\frac{1}{\sqrt{2}} \begin{pmatrix} 1 \\ 1 \end{pmatrix} \frac{1}{\sqrt{2}} \begin{pmatrix} 1 \\ 1 \end{pmatrix} = \frac{1}{2} \begin{pmatrix} 1 \\ 1 \\ 1 \\ 1 \end{pmatrix} = \frac{|0\rangle + |1\rangle + |2\rangle + 3\rangle}{2}$$

Total input vector:

$$\Psi = \frac{1}{\sqrt{2}} \begin{pmatrix} 1 \\ 1 \end{pmatrix} \frac{1}{\sqrt{2}} \begin{pmatrix} 1 \\ 1 \end{pmatrix} \begin{pmatrix} 1 \\ 0 \end{pmatrix} \begin{pmatrix} 1 \\ 0 \end{pmatrix} \begin{pmatrix} 1 \\ 0 \end{pmatrix} \begin{pmatrix} 1 \\ 0 \end{pmatrix}$$

Non-zero vector elements:

$$\Psi_0 = \tfrac{1}{2} \quad \Psi_{16} = \tfrac{1}{2} \quad \Psi_{32} = \tfrac{1}{2} \quad \Psi_{48} = \tfrac{1}{2}$$

The output vector is calculated for the case of measuring |0>|0>|0>|0> on the top four wires.

$$\Psi_{out} = 4\text{Step7 Step6 Step 5 Step4 Step3 Step2 Step1}\Psi$$

$$\Psi_{out}^{T} = \begin{array}{|c|c|c|c|c|c|c|c|c|c|} \hline & 0 & 1 & 2 & 3 & 4 & 5 & 6 & 7 & 8 & 9 \\ \hline 0 & 0.5 & 0.5 & 0.5 & 1 & 0.5 & 0 & 0 & 0 & 0 & \cdots \\ \hline \end{array}$$

$$\Psi_{out} = \begin{pmatrix}1\\0\end{pmatrix}\begin{pmatrix}1\\0\end{pmatrix}\begin{pmatrix}1\\0\end{pmatrix}\begin{pmatrix}1\\0\end{pmatrix}\frac{1}{\sqrt{2}}\begin{pmatrix}1\\1\end{pmatrix}\frac{1}{\sqrt{2}}\begin{pmatrix}1\\1\end{pmatrix} = \begin{pmatrix}1\\0\end{pmatrix}\begin{pmatrix}1\\0\end{pmatrix}\begin{pmatrix}1\\0\end{pmatrix}\begin{pmatrix}1\\0\end{pmatrix}\frac{1}{2}\begin{pmatrix}1\\1\\1\\1\end{pmatrix} = \frac{|0\rangle+|1\rangle+|2\rangle+3\rangle}{2}$$

A final example:

Teleportee:

$$\frac{1}{\sqrt{2}}\begin{pmatrix}1\\1\end{pmatrix}\begin{pmatrix}\sqrt{\frac{1}{3}}\\\sqrt{\frac{2}{3}}\end{pmatrix}$$

Total input vector:

$$\frac{1}{\sqrt{2}}\begin{pmatrix}1\\1\end{pmatrix}\begin{pmatrix}\sqrt{\frac{1}{3}}\\\sqrt{\frac{2}{3}}\end{pmatrix}\begin{pmatrix}1\\0\end{pmatrix}\begin{pmatrix}1\\0\end{pmatrix}\begin{pmatrix}1\\0\end{pmatrix}\begin{pmatrix}1\\0\end{pmatrix}$$

Non-zero vector elements:

$$\Psi_0 = \sqrt{\tfrac{1}{6}} \quad \Psi_{16} = \sqrt{\tfrac{1}{3}} \quad \Psi_{32} = \sqrt{\tfrac{1}{6}} \quad \Psi_{48} = \sqrt{\tfrac{1}{3}}$$

$$\Psi_{out} = 4\text{Step7Step6Step5Step4Step3Step2Step1}\Psi$$

$$\Psi_{out}^{T} = \begin{array}{|c|c|c|c|c|c|c|c|c|c|} \hline & 0 & 1 & 2 & 3 & 4 & 5 & 6 & 7 & 8 \\ \hline 0 & 0.408 & 0.577 & 0.408 & 0.577 & 0 & 0 & 0 & 0 & \cdots \\ \hline \end{array}$$

$$\Psi_{out} = \begin{pmatrix}1\\0\end{pmatrix}\begin{pmatrix}1\\0\end{pmatrix}\begin{pmatrix}1\\0\end{pmatrix}\begin{pmatrix}1\\0\end{pmatrix}\frac{1}{\sqrt{2}}\begin{pmatrix}\sqrt{\frac{1}{3}}\\\sqrt{\frac{2}{3}}\end{pmatrix} = \begin{pmatrix}1\\0\end{pmatrix}\begin{pmatrix}1\\0\end{pmatrix}\begin{pmatrix}1\\0\end{pmatrix}\begin{pmatrix}1\\0\end{pmatrix}\begin{pmatrix}0.408\\0.577\\0.408\\0.577\end{pmatrix}$$

Appendix

$$\text{NOT} = \begin{pmatrix}0 \text{ to } 1\\1 \text{ to } 0\end{pmatrix} \quad H = \begin{bmatrix}0 \text{ to } \frac{1}{\sqrt{2}}(0+1)\\1 \text{ to } \frac{1}{\sqrt{2}}(0-1)\end{bmatrix}$$

$$= \begin{pmatrix} & \text{CnNOT} & \\ \text{Decimal} & \text{Binary to Binary} & \text{Decimal} \\ 0 & 000 \text{ to } 000 & 0 \\ 1 & 001 \text{ to } 001 & 1 \\ 2 & 010 \text{ to } 010 & 2 \\ 3 & 011 \text{ to } 011 & 3 \\ 4 & 011 \text{ to } 011 & 5 \\ 5 & 101 \text{ to } 100 & 4 \\ 6 & 110 \text{ to } 111 & 7 \\ 7 & 111 \text{ to } 110 & 6 \end{pmatrix}$$

This page titled 8.13: Teleportation of Two Qubits is shared under a CC BY 4.0 license and was authored, remixed, and/or curated by Frank Rioux via source content that was edited to the style and standards of the LibreTexts platform.

8.14: Greenaberger-Hrne-Zeilinger (GHZ) Entanglement and Local Realism

This tutorial summarizes experimental results on GHZ entanglement reported by Anton Zeilinger and collaborators in the 3 February 2000 issue of Nature (pp. 515-519). The GHZ experiment employs three-photon entanglement to provide a stunning attack on local realism.

Definitions

First some definitions:

- **Realism** - experiments yield values for properties that exist independent of experimental observation
- **Locality** - the experimental results obtained at location A at time t, do not depend on the results at some other location *B* at time *t*.
- **H/V** = horizontal/vertical linear polarization. **R/L** = right/left circular polarization. **H′/V′** rotated by 45° with respect to **H/V**.

Next some relationships between the various photon polarization states: See the appendix for vector definitions of |H>, |V>, |H′>, |V′>, |R> and |L>.

$$H' = \tfrac{1}{\sqrt{2}}(H+V) \quad V' = \tfrac{1}{\sqrt{2}}(H-V) \quad R = \tfrac{1}{\sqrt{2}}(H+iV) \quad L = \tfrac{1}{\sqrt{2}}(H-iV)$$

$$H = \tfrac{1}{\sqrt{2}}(H'+V') \quad V = \tfrac{1}{\sqrt{2}}(H'-V') \quad H = \tfrac{1}{\sqrt{2}}(R+L) \quad V = \tfrac{i}{\sqrt{2}}(L-R)$$

The initial GHZ three-photon entangled state:

$$\Psi = \frac{1}{\sqrt{2}}(H_1H_2H_3 + V_1V_2V_3)$$

After preparation of the initial GHZ state (see figure 1 in the reference cited above), polarization measurements are performed on the three photons. Zeilinger and collaborators use y to stand for a circular polarization measurement and x for a linear polarization measurement. Initially they perform circular polarization measurements on two of the photons and a linear polarization measurement on the other photon. The quantum mechanically predicted results and actual experimental measurements are given below. The quantum predictions are obtained by substituting equations (2) into equation (3).

yyx - experiment

$$\Psi_{yyx} = \frac{1}{\sqrt{2}}\left[\frac{R_1+L_1}{\sqrt{2}}\frac{R_2+L_2}{\sqrt{2}}\frac{H_3'+V_3'}{\sqrt{2}} + \frac{i(L_1-R_1)}{\sqrt{2}}\frac{i(L_2-R_2)}{\sqrt{2}}\frac{H_3'-V_3'}{\sqrt{2}}\right]$$

on expansion yields

$$\Psi_{yyx} = \frac{1}{2}R_1R_2V_3' + \frac{1}{2}R_1L_2H_3' + \frac{1}{2}L_1R_2H_3' + \frac{1}{2}L_1L_2V_3'$$

Each measurement (R/L or H′/V′) has two possible outcomes so, in principle, there could be 8 possible results. However, quantum mechanics predicts that only four equally probable, $(\frac{1}{2})^2 = 0.25$, outcomes are possible. The quantum mechanical prediction is in agreement with the experimental results shown in Figure 1 to within experimental error.

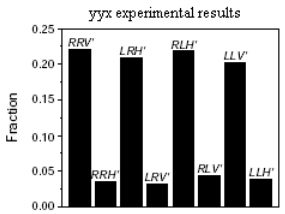


Figure 1.

For the two remaining experiments in this class (yxy and xyy), the agreement between theoretical prediction and experimental results is basically the same. While these agreements between quantum mechanics and experiment are impressive they do not directly challenge the local realist position. As will be shown later that will be accomplished by a fourth experiment involving the measurement of the linear polarization on all three photons - the xxx experiment.

yxy - experiment

$$\Psi_{yxy} = \frac{1}{\sqrt{2}}\left[\frac{R_1 + L_1}{\sqrt{2}}\frac{H_2' + V_2'}{\sqrt{2}}\frac{R_3 + L_3}{\sqrt{2}} + \frac{i(L_1 - R_1)}{\sqrt{2}}\frac{i(H_2' - V_2')}{\sqrt{2}}\frac{L_3 - R_3}{\sqrt{2}}\right]$$

on expansion yields

$$\Psi_{yxy} = \frac{1}{2}R_1H_2'L_3 + \frac{1}{2}R_1V_2'R_3 + \frac{1}{2}L_1H_2'R_3 + \frac{1}{2}L_1V_2'L_3$$

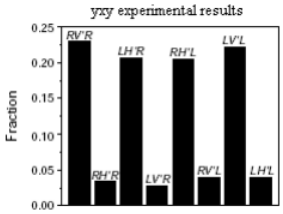


Figure 2.

xyy - experiment

$$\Psi_{xyy} = \frac{1}{\sqrt{2}}\left[\frac{H_1' + V_1'}{\sqrt{2}}\frac{R_2 + L_2}{\sqrt{2}}\frac{R_3 + L_3}{\sqrt{2}} + \frac{H_1' - V_1')}{\sqrt{2}}\frac{i(L_2 - R_2)}{\sqrt{2}}\frac{i(L_3 - R_3)}{\sqrt{2}}\right]$$

on expansion yields

$$\Psi_{xyy} = \frac{1}{2}H_1'R_2L_3 + \frac{1}{2}H_1'L_2R_3 + \frac{1}{2}V_1'R_2R_3 + \frac{1}{2}V_1'L_2L_3$$

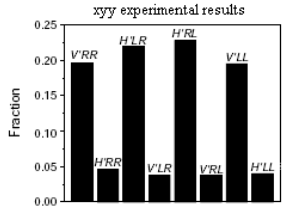


Figure 3.

Now for the critical experiment.

xxx - experiment

$$\Psi_{xyx} = \frac{1}{\sqrt{2}}\left[\frac{H_1' + V_1'}{\sqrt{2}}\frac{H_2' + V_2'}{\sqrt{2}}\frac{H_3' + V_3'}{\sqrt{2}} + \frac{H_1' - V_1')}{\sqrt{2}}\frac{i(H_2' - V_2')}{\sqrt{2}}\frac{H_3' - V_3')}{\sqrt{2}}\right]$$

on expansion yields

$$\Psi_{xxx} = \frac{1}{2}H_1'H_2'H_3' + \frac{1}{2}H_1'V_2'V_3' + \frac{1}{2}V_1'H_2'V_3' + \frac{1}{2}V_1'V_2'H_3'$$

This quantum mechanical prediction is displayed graphically in Figure 4.

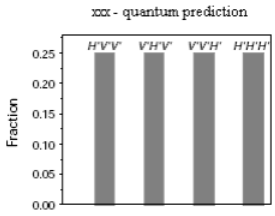


Figure 4.

According to local realism the experimental outcome should be as shown in Figure 5. The origin of this prediction will be outlined shortley.

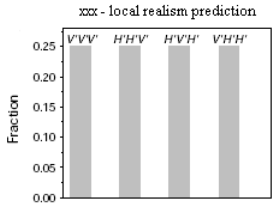


Figure 5.

The quantum mechanical prediction for the xxx experiment agrees with experiment, the local realist prediction doesn't.

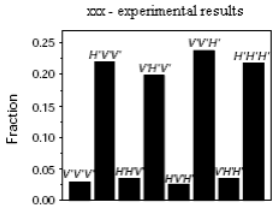


Figure 6.

To explain how the local realist prediction shown in Figure 5 is derived, we recall that this position assumes that physical properties exist independent of measurement. We associate with polarization measurements the following eigenvalues: H′ = +1, V′ = -1, R = +1 and L = -1. Substituting these measurement eigenvalues into the first three experimental results (yyx, yxy, xyy) yields,

$$Y_1Y_2Y_3 = Y_1X_2Y_3 = X_1Y_2Y_3 = -1$$

Therefore,

$$(Y_1Y_2Y_3)(Y_1X_2Y_3)(X_1Y_2Y_3) = -1$$

However, this means that $X_1X_2X_3 = -1$ because $Y_1Y_1 = Y_2Y_2 = Y_3Y_3 = 1$. According to the local realist view there are four ways to achieve this result V1V2V3, H1H2V3, H1V2H3 and V1H2H3, none of which are observed at a statistically meaningful level in the GHZ experiment.

For the xxx experiment, the mathematical predictions of quantum mechanics (Figure 4) and the local realist view (Figure 5) when compared with the actual experimental results (Figure 6) present a convincing refutation of local realism.

Appendix

$$H = \begin{pmatrix}1\\0\end{pmatrix} \quad V = \begin{pmatrix}0\\1\end{pmatrix} \quad H' = \tfrac{1}{\sqrt{2}}\begin{pmatrix}1\\1\end{pmatrix} \quad V' = \tfrac{1}{\sqrt{2}}\begin{pmatrix}1\\-1\end{pmatrix} \quad L = \tfrac{1}{\sqrt{2}}\begin{pmatrix}1\\-i\end{pmatrix} \quad R = \tfrac{1}{\sqrt{2}}\begin{pmatrix}1\\i\end{pmatrix}$$

This page titled 8.14: Greenaberger-Hrne-Zeilinger (GHZ) Entanglement and Local Realism is shared under a CC BY 4.0 license and was authored, remixed, and/or curated by Frank Rioux via source content that was edited to the style and standards of the LibreTexts platform.

8.15: GHZ Math Appendix

This appendix shows another way of "doing the math" in the GHZ experiment.

$$\Psi_{yyx} = \frac{1}{\sqrt{2}}(H_1H_2H_3 + V_1V_2V_3) \left| \begin{array}{l} \text{substitute, } H_1 = \frac{1}{\sqrt{2}}(R_1 + L_1) \\ \text{substitute, } H_2 = \frac{1}{\sqrt{2}}(R_2 + L_2) \\ \text{substitute, } H_3 = \frac{1}{\sqrt{2}}(H_3' + V_3') \\ \text{substitute, } V_1 = \frac{i}{\sqrt{2}}(L_1 - R_1) \\ \text{substitute, } V_2 = \frac{i}{\sqrt{2}}(L_2 - R_2) \\ \text{substitute, } V_3 = \frac{1}{\sqrt{2}}(H_3' - V_3') \\ \text{simplify} \end{array} \right. \rightarrow \Psi_{yyx}$$

$$= \frac{1}{2}R_1R_2V_3' + \frac{1}{2}R_1L_2H_3' + \frac{1}{2}L_1R_2H_3' + \frac{1}{2}L_1L_2V_3'$$

$$\Psi_{yxy} = \frac{1}{\sqrt{2}}(H_1H_2H_3 + V_1V_2V_3) \left| \begin{array}{l} \text{substitute, } H_1 = \frac{R_1+L_1}{\sqrt{2}} \\ \text{substitute, } H_2 = \frac{(H_2'+V_2')}{\sqrt{2}} \\ \text{substitute, } H_3 = \frac{R_3+L_3}{\sqrt{2}} \\ \text{substitute, } V_1 = \frac{i}{\sqrt{2}}(L_1 - R_1) \\ \text{substitute, } V_2 = \frac{H_2'-V_2'}{\sqrt{2}} \\ \text{substitute, } V_3 = \frac{i(L_3-R_3)}{\sqrt{2}} \\ \text{simplify} \end{array} \right. \rightarrow \Psi_{yxy}$$

$$= \frac{1}{2}R_1H_2'L_3 + \frac{1}{2}R_1V_2'R_3 + \frac{1}{2}L_1H_2'R_3 + \frac{1}{2}L_1V_2'L_3$$

$$\Psi_{xyy} = \frac{1}{\sqrt{2}}(H_1H_2H_3 + V_1V_2V_3) \left| \begin{array}{l} \text{substitute, } H_1 = \frac{H_1'+V_1'}{\sqrt{2}} \\ \text{substitute, } H_2 = \frac{R_2+L_2}{\sqrt{2}} \\ \text{substitute, } H_3 = \frac{R_3+L_3}{\sqrt{2}} \\ \text{substitute, } V_1 = \frac{H_1'-V_1'}{\sqrt{2}} \\ \text{substitute, } V_2 = \frac{i(L_2-R_2)}{\sqrt{2}} \\ \text{substitute, } V_3 = \frac{i(L_3-R_3}{\sqrt{2}} \\ \text{simplify} \end{array} \right. \rightarrow \Psi_{xyy}$$

$$= \frac{1}{2}H_1'R_2L_3 + \frac{1}{2}H_1'L_2R_3 + \frac{1}{2}V_1'R_2R_3 + \frac{1}{2}V_1'L_2L_3$$

$$\Psi_{xxx} = \frac{1}{\sqrt{2}}(H_1H_2H_3 + V_1V_2V_3) \left| \begin{array}{l} \text{substitute, } H_1 = \frac{H_1'+V_1'}{\sqrt{2}} \\ \text{substitute, } H_2 = \frac{H_2'+V_2'}{\sqrt{2}} \\ \text{substitute, } H_3 = \frac{H_3'+V_3'}{\sqrt{2}} \\ \text{substitute, } V_1 = \frac{H_1'-V_1'}{\sqrt{2}} \\ \text{substitute, } V_2 = \frac{H_2'-V_2')}{\sqrt{2}} \\ \text{substitute, } V_3 = \frac{H_3'-V_3'}{\sqrt{2}} \\ \text{simplify} \end{array} \right. \rightarrow \Psi_{xxx}$$

$$= \frac{1}{2}H_1'H_2'H_3' + \frac{1}{2}H_1'V_2'V_3' + \frac{1}{2}V_1'H_2'V_3' + \frac{1}{2}V_1'V_2'H_3'$$

This page titled 8.15: GHZ Math Appendix is shared under a CC BY 4.0 license and was authored, remixed, and/or curated by Frank Rioux via source content that was edited to the style and standards of the LibreTexts platform.

8.16: GHZ Entanglement - A Tensor Algebra Analysis

This tutorial analyses experimental results on a GHZ entanglement reported by Anton Zeilinger and collaborators in the 3 February 2000 issue of Nature (pp. 515-519) using tensor algebra. The GHZ experiment employs three-photon entanglement to provide a stunning attack on local realism.

First some definitions:

- Realism - experiments yield values for properties that exist independent of experimental observation
- Locality - the experimental results obtained at location A at time t, do not depend on the results at some other location B at time t.
- H/V = horizontal/vertical linear polarization.
- R/L = right/left circular polarization. H′/V′ rotated by 45° with respect to H/V.

Next the vector representations of the various photon polarization states:

$$H = \begin{pmatrix}1\\0\end{pmatrix} \quad V = \begin{pmatrix}0\\1\end{pmatrix} \quad H' = \frac{1}{\sqrt{2}}\begin{pmatrix}1\\1\end{pmatrix} \quad V' = \frac{1}{\sqrt{2}}\begin{pmatrix}1\\-1\end{pmatrix} \quad L = \frac{1}{\sqrt{2}}\begin{pmatrix}1\\-i\end{pmatrix} \quad R = \frac{1}{\sqrt{2}}\begin{pmatrix}1\\i\end{pmatrix} \quad N = \begin{pmatrix}0\\0\end{pmatrix}$$

Some additional matrices needed to form state vectors in Mathcad:

$$\text{HN} = \text{augment (H, N)} \quad \text{VN} = \text{augment (V, N)} \quad \text{RN} = \text{augment (R, N)}$$
$$\text{LN} = \text{augment (L, N)} \quad \text{H'N} = \text{augment (H', N)} \quad \text{V'N} = \text{augment (V', N)}$$

The operators associated with linear and cicular polarization:

$$H'V = \begin{pmatrix}0 & 1\\1 & 0\end{pmatrix} \quad RL = \begin{pmatrix}0 & -1\\i & 0\end{pmatrix}$$

The initial GHZ three-phon entangled state:

$$\Psi = \frac{1}{\sqrt{2}}(H_1H_2H_3 + V_1V_2V_3)$$

Initial state expressed in tensor format:

$$|\Psi\rangle = \frac{1}{\sqrt{2}}\left[\begin{pmatrix}1\\0\end{pmatrix}\otimes\begin{pmatrix}1\\0\end{pmatrix}\otimes\begin{pmatrix}1\\0\end{pmatrix} + \begin{pmatrix}0\\1\end{pmatrix}\otimes\begin{pmatrix}0\\1\end{pmatrix}\otimes\begin{pmatrix}0\\1\end{pmatrix}\right] = \frac{1}{\sqrt{2}}\begin{pmatrix}1\\0\\0\\0\\0\\0\\0\\1\end{pmatrix}$$

Constructing the initial state using Mathcad:

$$\Psi = \frac{1}{\sqrt{2}}\text{submatrix}(\text{kronecker (HN, HN)}) + \text{kronecker(VN, kronecker (VN, VN))}, 1,\ 8,\ 1,\ 1)$$

$$\Psi^T = (0 \quad 0 \quad 0 \quad 0 \quad 0 \quad 0 \quad 0.707)$$

After preparation of the initial GHZ state (see figure 1 in the reference cited above), polarization measurements are performed on the three photons. Zeilinger and collaborators use y to stand for a circular polarization measurement and x for a linear polarization measurement. Initially they perform circular polarization measurements on two of the photons and a linear polarization measurement on the other photon. The quantum mechanically predicted results and actual experimental measurements are given below.

yyx - experiment

The yyx operator is calculated and it is shown that Ψ is an eigenstate of the operator with eigenvalue -1.

$$\text{yyx} = \text{kronecker(RL, kronecker(RL, H'V'))} \quad \Psi^T \text{yyx} \Psi = -1$$

Each measurement (R/L or H′/V′) has two possible outcomes so, in principle, there could be 8 possible results. However, quantum mechanics predicts that only four equally probable outcomes are possible. This is because the eigenvalues of the individual results must be consistent with the eigenvalue the total operator. As shown below, the eigenvalues for H′ and R are +1, and for V′ and L they are -1.

$$H'V'H' = \begin{pmatrix} 0.707 \\ 0.707 \end{pmatrix} \quad H'V'V' = \begin{pmatrix} -0.707 \\ 0.707 \end{pmatrix} \quad RLR = \begin{pmatrix} 0.707 \\ 0.707i \end{pmatrix} \quad RLL = \begin{pmatrix} -0.707 \\ 0.707i \end{pmatrix}$$

Thus quantum mechanics predicts that RRV′ (++-), LRH′ (-++), RLH′ (+-+), and LLV′ (---) should be observed, but RRH′ (+++), LRV′ (-+-), RLV′ (+--) and LLH′ (--+) should not be observed. This prediction is in agreement with the experimental results shown in Figure 1 to within experimental error.

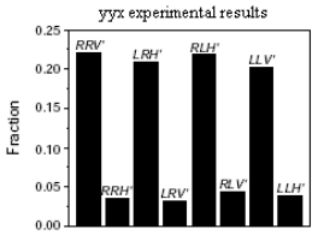


Figure 1.

Confirm the first two results in figure 1.

$$RRV' = \text{submatrix(kronecker(RN, kronecker(RN, V'N)), 1, 8, 1, 1)}(|RRV'\Psi|)^2 = 0.25$$
$$RRH' = \text{submatrix(kronecker(RN, kronecker(RN, H'N)), 1, 8, 1, 1)}(|RRH'\Psi|)^2 = 0$$

For the two remaining experiments in this class (yxy and xyy), the agreement between theoretical prediction and experimental results is basically the same.

While these agreements between quantum mechanics and experiment are impressive they do not directly challenge the local realist position. As will be shown later that will be accomplished by a fourth experiment involving the measurement of the linear polarization on all three photons - the xxx experiment.

yxy - experiment

The yxy operator is calculated and it is shown that Ψ is an eigenstate of the operator with eigenvalue -1.

$$\text{yxy} = \text{kronecker(RL, kronecker(H'V', RL))} \quad \Psi^T yxy \Psi = -1$$

Using reasoning identical to the yyx experiment, quantum mechanics predicts that RV′R (+-+), LH′R (-++), RH′L (++-), and LV′L (---) should be observed, but RH′R (+++), LV′R (--+), RV′L (+--) and LH′L (-+-) should not be observed. This prediction is in agreement with the experimental results shown in Figure 2 to within experimental error.

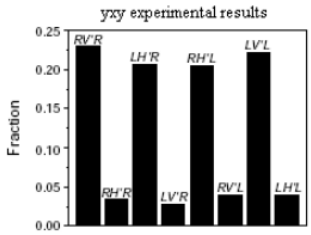


Figure 2.

Confirm the first two results in Figure 2.

$$RV'R = \text{submatrix(kronecker(RN, kronecker(V'N, RN)), 1, 8, 1, 1)}$$
$$(|RV'R\Psi|)^2 = 0.25$$
$$RH'R = \text{submatrix(kronecker(RN, kronecker(H'N, RN)), 1, 8, 1, 1)}$$
$$(|RH'R\Psi|)^2 = 0$$

xyy - experiment

The xyy operator is calculated and it is shown that Ψ is an eigenstate of the operator with eigenvalue -1.

$$\text{xyy} = \text{kronecker(H'V', kronecker(RL, RL))} \quad \Psi^T \text{xyy} \Psi = -1$$

Using reasoning identical to the previous experiments, quantum mechanics predicts that V′RR (-++), H′LR (+-+), H′RL (++-), and V′LL (---) should be observed, but H′RR (+++), V′LR (--+), V′RL (-+-) and H′LL (+--) should not be observed. This prediction is in agreement with the experimental results shown in Figure 3 to within experimental error.

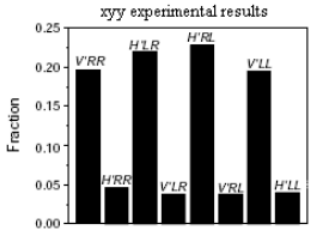


Figure 3.

Confirm the first two results in Figure 3.

$$\text{V'RR} = \text{submatrix(kronecker(V'N, kronecker(RN RN)), 1, 8, 1, 1)}(|V'RR\Psi|)^2 = 0.25$$
$$\text{H'RR} = \text{submatrix(kronecker(H'N, kronecker(RN, RN)), 1, 8, 1, 1)}(|H'RR\Psi|)^2 = 0$$

Now for the critical experiment.

xxx - experiment

The xxx operator is calculated and it is shown that Ψ is an eigenstate of the operator with eigenvalue +1.

$$\text{xxx} = \text{kronecker(H'V', kronecker(H'V', H'V'))} \quad \Psi^T \text{xxx} \Psi = 1$$

Using reasoning identical to the previous experiments, quantum mechanics predicts that only H′V′V′ (+--), V′H′V′ (-+-), V′V′H′ (--+), and H′H′H′ (+++) should be observed. This prediction is displayed graphically in Figure 4.

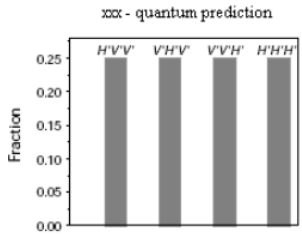


Figure 4.

QM calculation for xxx experiment.

$$V'V'V' = \text{submatrix(kronecker(V'N, kronecker(V'N, V'N)), 1, 8, 1, 1)}(|V'V'V'\Psi|)^2 = 0$$
$$H'V'V' = \text{submatrix(kronecker(H'N, kronecker(V'N, V'N)), 1, 8, 1, 1)}(|H'V'V'\Psi|)^2 = 0.25$$

According to local realism the experimental outcome should be as shown in Figure 5. To explain how the local realist prediction is derived, we recall that this position assumes that physical properties exist independent of measurement. Previously it has been shown that eigenvalues of the three-photon operators according to quantum mechanics are,

$$y_1y_2y_3 = y_1x_2y_3 = x_1y_2y_3 = -1 \quad x_1x_2x_3 = 1$$

It follows that,

$$(y_1y_2x_3)(y_1x_2y_3)(x_1y_2y_3) = -1$$

However, this means that $x_1x_2x_3$ = -1, because $y_1y_1 = y_2y_2 = y_3y_3 = 1$. (All of the three-photon operators commute, and therefore can have simultaneous eigenvalues. The commutation relations are shown in the Appendix.) According to the local realist view there are four ways to achieve this result ($x_1x_2x_3$ = -1) V'V'V', H'H'V', H'V'H' and V'H'H'.

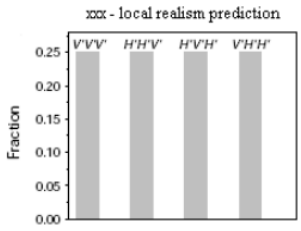


Figure 5.

LR results are contradicted by QM calculation.

$$V'V'V' = \text{submatrix}(\text{kronecker}(\text{V'N, kronecker}(\text{V'N, V'N})),\ 1,\ 8,\ 1,\ 1)(|V'V'V'\Psi|)^2 = 0$$
$$H'H'V' = \text{submatrix}(\text{kronecker}(\text{H'N, kronecker}(\text{H'N, V'N})),\ 1,\ 8,\ 1,\ 1)(|H'H'V'\Psi|)^2 = 0$$

Figure 6 shows that none local realistic predictions are observed at a statistically meaningful level in th GHZ experiment. The quantum mechanical prediction for the xxx experiment agrees with experiment, the local realist prediction doesn′t.

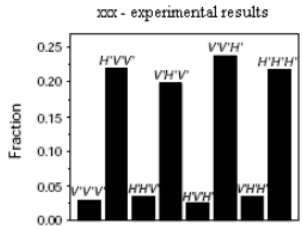


Figure 6.

QM calculations confirmed by experimental results.

$$V'V'V' = \text{submatrix}(\text{kronecker}(\text{V'N, kronecker}(\text{V'N, V'N})),\ 1,\ 8,\ 1,\ 1)(|V'V'V'\Psi|)^2 = 0$$
$$H'V'V' = \text{submatrix}(\text{kronecker}(\text{H'N, kronecker}(\text{V'N, V'N})),\ 1,\ 8,\ 1,\ 1)(|H'V'V'\Psi|)^2 = 0.25$$

For the xxx experiment, the mathematical predictions of quantum mechanics (Figure 4) and the local realist view (Figure 5) when compared with the actual experimental results (Figure 6) present a convincing refutation of local realism.

Appendix

Demonstration that the three-photon operators commute, allowing for simultaneous eigenvalues.

$$\text{xyyyxy} - \text{yxyxyy} \to 0 \quad \text{xyyyyx} - \text{yyxxyy} \to 0 \quad \text{xyyxxx} - \text{xxxxyy} \to 0$$
$$\text{yxyyyx} - \text{yyxyxy} \to 0 \quad \text{yxyxxx} - \text{xxxyxy} \to 0 \quad \text{yyxxxx} - \text{xxxyyx} \to 0$$

This page titled 8.16: GHZ Entanglement - A Tensor Algebra Analysis is shared under a CC BY 4.0 license and was authored, remixed, and/or curated by Frank Rioux via source content that was edited to the style and standards of the LibreTexts platform.

8.17: Simulation of a GHZ Gedanken Experiment

This tutorial analyzes a GHZ (Greenberger-Horne-Zeilinger) thought experiment involving three spin-1/2 particles that illustrates the clash between local realism and the quantum view of reality. The analysis consists of three parts: a traditional theoretical analysis, a quantum computer simulation, and an analysis based local realism. In the 1990s N. David Mermin published two articles in the general physics literature (Physics Today, June 1990; American Journal of Physics, August 1990) on the GHZ gedanken experiment. I drew heavily on these articles in developing this tutorial.

Theoretical Analysis

We begin with a quantum mechanical analysis of a version of the GHZ thought experiment suggested by Mermin. The initial state, Ψ, and Mermin's operator are as follows.

$$\Psi = \frac{1}{\sqrt{2}}(1 \quad 0 \quad 0 \quad 0 \quad 0 \quad 0 \quad 0 \quad i)^T$$

$$\hat{M} = \sigma_y\sigma_x\sigma_x + \sigma_x\sigma_y\sigma_x + \sigma_x\sigma_x\sigma_y - \sigma_y\sigma_y\sigma_y$$

The Pauli σ_x and σ_y individual spin operators and their composites required for Mermin's operator:

$$\sigma_x = \begin{pmatrix} 0 & 1 \\ 1 & 0 \end{pmatrix} \qquad \sigma_y = \begin{pmatrix} 0 & -i \\ i & 0 \end{pmatrix}$$

$$\sigma_{xxy} = \text{kronecker}(\sigma_x,\ \text{kronecker}(\sigma_x, \sigma_y)) \qquad \sigma_{xyx} = \text{kronecker}(\sigma_x,\ \text{kronecker}(\sigma_y, \sigma_x))$$

$$\sigma_{yxx} = \text{kronecker}(\sigma_y,\ \text{kronecker}(\sigma_x, \sigma_s)) \qquad \sigma_{yyy} = \text{kronecker}(\sigma_y,\ \text{kronecker}(\sigma_y, \sigma_y))$$

The composite operators commute (σ_x and σ_y don't) and therefore can have simultaneous eigenvalues.

$$\sigma_{xxy}\sigma_{xyx} - \sigma_{xyx}\sigma_{xxy} \to 0 \quad \sigma_{xxy}\sigma_{yxx} - \sigma_{yxx}\sigma_{xxy} \to 0 \quad \sigma_{xxy}\sigma_{yyy} - \sigma_{yyy}\sigma_{xxy} \to 0$$

$$\sigma_{xyx}\sigma_{yxx} - \sigma_{yxx}\sigma_{xyx} \to 0 \quad \sigma_{xyx}\sigma_{yyy} - \sigma_{yyy}\sigma_{xyx} \to 0 \quad \sigma_{yxx}\sigma_{yyy} - \sigma_{yyy}\sigma_{yxx} \to 0$$

The calculations of various expectation values bases on the proposed initial state and operator:

$$M = \sigma_{yxx} + \sigma_{xyx} + \sigma_{xxy} - \sigma_{yyy}$$

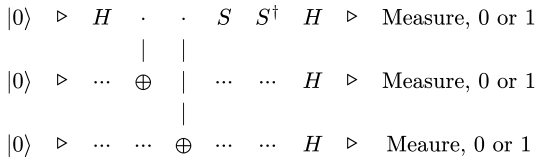
$$(\overline{\Psi})^T\sigma_{yxx}\Psi = 1 \quad (\overline{\Psi})^T\sigma_{xyx}\Psi = 1 \quad (\overline{\Psi})^T\sigma_{xxy}\Psi = 1 \quad (\overline{\Psi})^T\sigma_{yyy}\Psi = -1 \quad (\overline{\Psi})^T M\Psi = 4$$

The key result is that the expectation value for M is 4. Subsequently it will be shown that a quantum simulator circuit is in agreement with this result but that local realism is not.

Quantum Computer Simulation

"Quantum simulation is a process in which a quantum computer simulates another quantum system. Because of the various types of quantum weirdness, classical computers can simulate quantum systems only in a clunky, inefficient way. But because a quantum computer is itself a quantum system, capable of exhibiting the full repertoire of quantum weirdness, it can efficiently simulate other quantum systems. **The resulting simulation can be so accurate that the behavior the computer will be indistinguishable from the behavior of the simulated system itself.**" (Seth Lloyd, Programming the Universe, page 149.)

This is the most important part of the tutorial - a demonstration that the thought experiment can be simulated using the quantum circuit shown below which can be found at: arXiv:1712.06542v2; "Five Experimental Tests on the 5-qubit IBM Quantum Computer," Diego Garcia-Martin and German Sierra.



The required matrix operators and the build-up of the quantum circuit:

$$I = \begin{pmatrix} 1 & 0 \\ 0 & 1 \end{pmatrix} \quad H = \frac{1}{\sqrt{2}} \begin{pmatrix} 1 & 1 \\ 1 & -1 \end{pmatrix} \quad S = \begin{pmatrix} 1 & 0 \\ 0 & i \end{pmatrix} \quad S' = \begin{pmatrix} 1 & 0 \\ 0 & -i \end{pmatrix}$$

$$\text{CNOT} = \begin{pmatrix} 1 & 0 & 0 & 0 \\ 0 & 1 & 0 & 0 \\ 0 & 0 & 0 & 1 \\ 0 & 0 & 1 & 0 \end{pmatrix} \quad \text{CnNOT} = \begin{pmatrix} 1 & 0 & 0 & 0 & 0 & 0 & 0 & 0 \\ 0 & 1 & 0 & 0 & 0 & 0 & 0 & 0 \\ 0 & 0 & 1 & 0 & 0 & 0 & 0 & 0 \\ 0 & 0 & 0 & 1 & 0 & 0 & 0 & 0 \\ 0 & 0 & 0 & 0 & 0 & 1 & 0 & 0 \\ 0 & 0 & 0 & 0 & 1 & 0 & 0 & 0 \\ 0 & 0 & 0 & 0 & 0 & 0 & 0 & 1 \\ 0 & 0 & 0 & 0 & 0 & 0 & 1 & 0 \end{pmatrix}$$

$$\text{HII} = \text{kronecker(H, kronecker(I, i))} \quad \text{CNOTI} = \text{kronecker(CNOT, I)} \quad \text{SII} = \text{kronecker(S, kronecker,(I, I))}$$

$$\text{S'S'S'} = \text{kronecker(S', kronecker(S', S'))} \quad \text{HHH} = \text{kronecker(H, kronecker(H, H))} \quad \text{S'II} = \text{kronecker(S', kronecker(I, I))}$$

$$\text{IS'I} = \text{kronecker(I, kronecker(S', I))} \quad \text{IIS'} = \text{kronecker(I, kronecker(I, S'))}$$

First it is demonstrated that the first four steps of the circuit create the initial state.

$$[\text{SII (CnNOT) CNOT (HII)} (1 \quad 0 \quad 0 \quad 0 \quad 0 \quad 0 \quad 0 \quad 0)^T]^T = (0.707 \quad 0 \quad 0 \quad 0 \quad 0 \quad 0 \quad 0 \quad 0.707i)$$

The complete circuit shows the simulation for the expectation value of $\sigma_y\sigma_x\sigma_x$. The presence of S' on a line before the final H gates indicates the measurement of the σy. The subsequent simulations show the presence of S' on the middle and last line, and finally on all three lines for the simulation of the expectation value for $\sigma_y\sigma_y\sigma_y$.

Eigenvalue of |0> = +1; eigenvalue of |1> = -1

$$\langle \sigma_y \sigma_x \sigma_x \rangle = 1 \quad \text{HHH S'II SII CnNOT CNOTI}$$

$$\text{HII} \begin{pmatrix} 1 \\ 0 \\ 0 \\ 0 \\ 0 \\ 0 \\ 0 \\ 0 \end{pmatrix} = \begin{pmatrix} 0.5 \\ 0 \\ 0 \\ 0.5 \\ 0 \\ 0.5 \\ 0.5 \\ 0 \end{pmatrix} = \frac{1}{2} [|000\rangle + |011\rangle + |101\rangle + |110\rangle]$$

Given the eigenvalue assignments above the expectation value associated with this outcome is 1/4[(1)(1)(1)+(1)(-1)(-1)+(-1)(1)(-1)+(-1)(-1)(1)] = 1. Note that 1/2 is the probability amplitude for the product state. Therefore the probability of each member of the superposition being observed is 1/4. Similar reasoning is used for the remaining simulations.

$$\langle \sigma_x \sigma_y \sigma_x \rangle = 1 \quad \text{HHH IS'I SII CnNOT CNOTI}$$

$$\text{HII} \begin{pmatrix} 1 \\ 0 \\ 0 \\ 0 \\ 0 \\ 0 \\ 0 \\ 0 \end{pmatrix} = \begin{pmatrix} 0.5 \\ 0 \\ 0 \\ 0.5 \\ 0 \\ 0.5 \\ 0.5 \\ 0 \end{pmatrix} = \tfrac{1}{2} \left[|000\rangle + |011\rangle + |101\rangle + |110\rangle \right]$$

$$\langle \sigma_x \sigma_x \sigma_y \rangle = 1 \quad \text{HHH IIS' SII CnNOT CNOTI}$$

$$\text{HII} \begin{pmatrix} 1 \\ 0 \\ 0 \\ 0 \\ 0 \\ 0 \\ 0 \\ 0 \end{pmatrix} = \begin{pmatrix} 0.5 \\ 0 \\ 0 \\ 0.5 \\ 0 \\ 0.5 \\ 0.5 \\ 0 \end{pmatrix} = \tfrac{1}{2} \left[|000\rangle + |011\rangle + |101\rangle + |110\rangle \right]$$

$$\langle \sigma_y \sigma_y \sigma_y \rangle = 1 \quad \text{HHH S'S'S' SII CnNOT CNOTI}$$

$$\text{HII} \begin{pmatrix} 1 \\ 0 \\ 0 \\ 0 \\ 0 \\ 0 \\ 0 \\ 0 \end{pmatrix} = \begin{pmatrix} 0 \\ 0.5 \\ 0.5 \\ 0 \\ 0.5 \\ 0 \\ 0 \\ 0.5 \end{pmatrix} = \tfrac{1}{2} \left[|001\rangle + |010\rangle + |100\rangle + |111\rangle \right]$$

$$\langle M \rangle = \langle \sigma_y \sigma_x \sigma_x \rangle + \langle \sigma_x \sigma_y \sigma_x \rangle + \langle \sigma_x \sigma_x \sigma_y \rangle - \langle \sigma_y \sigma_y \sigma_y \rangle = 4$$

The simulation is in exact agreement with the initial theoretical analysis.

EPR Local Realistic Analysis

Local realism asserts that objects have definite properties independent of measurement. In this experiment it assumes that the x- and y-components of spin have definite values prior to measurement. This position leads to a contradiction with the quantum mechanical calculation and the simulation. There is no way to assign consistent eigenvalues (+/-1) to the results of the individual spin measurements that is consistent with the quantum mechanical result. Using a variety of possible x- and y-spin values shows that local realism predicts that $M \leq 2$, in sharp disagreement with the quantum mechanical result of M = 4.

$$\text{Sx1} = 1 \quad \text{Sx2} = 1 \quad \text{Sx3} = 1 \quad \text{Sy1} = 1 \quad \text{Sy2} = 1 \quad \text{Sy3} = 1$$

$$\text{M} = \text{Sy1 Sx2 Sx3} + \text{Sx1 Sy2 Sx3} + \text{Sx1 Sx2 Sy3} - \text{Sy1 Sy2 Sy3} = 2$$

$$\text{Sx1} = -1 \quad \text{Sx2} = 1 \quad \text{Sx3} = 1 \quad \text{Sy1} = 1 \quad \text{Sy2} = -1 \quad \text{Sy3} = -1$$

$$\text{M} = \text{Sy1 Sx2 Sx3} + \text{Sx1 Sy2 Sx3} + \text{Sx1 Sx2 Sy3} - \text{Sy1 Sy2 Sy3} = 2$$

$$\mathrm{Sx1}=1 \quad \mathrm{Sx2}=-1 \quad \mathrm{Sx3}=1 \quad \mathrm{Sy1}=-1 \quad \mathrm{Sy2}=1 \quad \mathrm{Sy3}=-1$$

$$\mathrm{M}=\mathrm{Sy1}\ \mathrm{Sx2}\ \mathrm{Sx3}+\mathrm{Sx1}\ \mathrm{Sy2}\ \mathrm{Sx3}+\mathrm{Sx1}\ \mathrm{Sx2}\ \mathrm{Sy3}-\mathrm{Sy1}\ \mathrm{Sy2}\ \mathrm{Sy3}=2$$

$$\mathrm{Sx1}=-1 \quad \mathrm{Sx2}=1 \quad \mathrm{Sx3}=-1 \quad \mathrm{Sy1}=-1 \quad \mathrm{Sy2}=1 \quad \mathrm{Sy3}=-1$$

$$\mathrm{M}=\mathrm{Sy1}\ \mathrm{Sx2}\ \mathrm{Sx3}+\mathrm{Sx1}\ \mathrm{Sy2}\ \mathrm{Sx3}+\mathrm{Sx1}\ \mathrm{Sx2}\ \mathrm{Sy3}-\mathrm{Sy1}\ \mathrm{Sy2}\ \mathrm{Sy3}=2$$

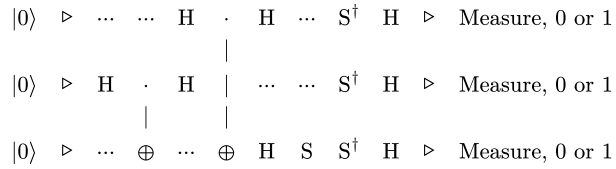
$$\mathrm{Sx1}=-1 \quad \mathrm{Sx2}=-1 \quad \mathrm{Sx3}=-1 \quad \mathrm{Sy1}=-1 \quad \mathrm{Sy2}=1 \quad \mathrm{Sy3}=-1$$

$$\mathrm{M}=\mathrm{Sy1}\ \mathrm{Sx2}\ \mathrm{Sx3}+\mathrm{Sx1}\ \mathrm{Sy2}\ \mathrm{Sx3}+\mathrm{Sx1}\ \mathrm{Sx2}\ \mathrm{Sy3}-\mathrm{Sy1}\ \mathrm{Sy2}\ \mathrm{Sy3}=-2$$

$$\mathrm{Sx1}=1 \quad \mathrm{Sx2}=1 \quad \mathrm{Sx3}=1 \quad \mathrm{Sy1}=-1 \quad \mathrm{Sy2}=-1 \quad \mathrm{Sy3}=-1$$

$$\mathrm{M}=\mathrm{Sy1}\ \mathrm{Sx2}\ \mathrm{Sx3}+\mathrm{Sx1}\ \mathrm{Sy2}\ \mathrm{Sx3}+\mathrm{Sx1}\ \mathrm{Sx2}\ \mathrm{Sy3}-\mathrm{Sy1}\ \mathrm{Sy2}\ \mathrm{Sy3}=-2$$

Alsina and Latorre ("Experimental test of Mermin inequalities on a five qubit quantum computer" available at arXiv:1605.04220V2) used the following alternative quantum circuit for the GHZ simulation. Here it is shown that it provides the same results for the $\sigma_y\sigma_y\sigma_y$ simulation.



$$\mathrm{IIS}=\mathrm{kronecker(I,\ kronecker(I,\ S))} \qquad \mathrm{HIH}=\mathrm{kronecker(H,\ kronecker(I,\ H))} \qquad \mathrm{HHI}=\mathrm{kronecker(H,\ kronecker(H,\ I))}$$

$$\mathrm{IHI}=\mathrm{kronecker(I,\ kronecker(H,\ I))} \qquad \mathrm{ICNOT}=\mathrm{kronecker(I,\ CNOT)}$$

$$\mathrm{HHH\ S'S'S'\ IIS\ HIH\ CnNOT\ HHI\ ICNOT\ IHI}=\begin{pmatrix}1\\0\\0\\0\\0\\0\\0\\0\end{pmatrix}$$

$$=\begin{pmatrix}0\\0.5\\0.5\\0\\0.5\\0\\0\\0.5\end{pmatrix}=\frac{1}{2}\left[|001\rangle+|010\rangle+|100\rangle+|111\rangle\right]$$

$$\langle\sigma_y\sigma_y\sigma_y\rangle=-1$$

The first six steps of this circuit generate the initial state.

$$\left[\mathrm{IIS\ HIH\ CnNOT\ HHI\ ICNOT\ IHI}\,(1\quad 0\quad 0\quad 0\quad 0\quad 0\quad 0\quad 0)^T\right]^T$$
$$=(0.707\quad 0\quad 0\quad 0\quad 0\quad 0\quad 0\quad 0.707i)$$

This page titled 8.17: Simulation of a GHZ Gedanken Experiment is shared under a CC BY 4.0 license and was authored, remixed, and/or curated by Frank Rioux via source content that was edited to the style and standards of the LibreTexts platform.

8.18: Another Simulation of a GHZ Gedanken Experiment

Many years ago N. David Mermin published two articles (Physics Today, June 1990; American Journal of Physics, August 1990) in the general physics literature on a Greenberger-Horne-Zeilinger (American Journal of Physics, December 1990; Nature, 3 February 2000) thought experiment involving spins that sharply revealed the clash between local realism and the quantum view of reality.

Three spin-1/2 particles are created in a single event and move apart in the horizontal y-z plane. Subsequent spin measurements will be carried out in units of h/4π with spin operators in the x- and y-directions. The z-basis eigenfunctions are:

$$Sz_{up} = \begin{pmatrix} 1 \\ 0 \end{pmatrix} \quad Sz_{down} = \begin{pmatrix} 0 \\ 1 \end{pmatrix}$$

The x- and y-direction spin operators:

\[

$$\sigma_x = \begin{pmatrix} 0 & 1 \\ 1 & 0 \end{pmatrix} \quad \text{eigenvals}(\sigma_x) = \begin{pmatrix} 1 \\ -1 \end{pmatrix} \quad \sigma_y = \begin{pmatrix} 0 & -i \\ i & 0 \end{pmatrix} \quad \text{eigenvals}(\sigma_y) = \begin{pmatrix} 1 \\ -1 \end{pmatrix} \tag{8.18.1}$$

\

The initial entangeld spin state for the three spin-1/2 particles in tensor notation is:

$$|\Psi\rangle = \frac{1}{\sqrt{2}} \left[\begin{pmatrix} 1 \\ 0 \end{pmatrix} \otimes \begin{pmatrix} 1 \\ 0 \end{pmatrix} \otimes \begin{pmatrix} 1 \\ 0 \end{pmatrix} - \begin{pmatrix} 0 \\ 1 \end{pmatrix} \otimes \begin{pmatrix} 0 \\ 1 \end{pmatrix} \otimes \begin{pmatrix} 0 \\ 1 \end{pmatrix} \right] = \frac{1}{\sqrt{2}} \begin{pmatrix} 1 \\ 0 \\ 0 \\ 0 \\ 0 \\ 0 \\ 0 \\ -1 \end{pmatrix} \quad \Psi = \frac{1}{\sqrt{2}} \begin{pmatrix} 1 \\ 0 \\ 0 \\ 0 \\ 0 \\ 0 \\ 0 \\ -1 \end{pmatrix}$$

The following operators represent the measurements to be carried out on spins 1, 2 and 3, in that order.

$$\sigma_x^1 \otimes \sigma_y^2 \otimes \sigma_y^3 \quad \sigma_y^1 \otimes \sigma_x^2 \otimes \sigma_y^3 \quad \sigma_y^1 \otimes \sigma_y^2 \otimes \sigma_x^3 \quad \sigma_x^1 \otimes \sigma_x^2 \otimes \sigma_x^3$$

The matrix tensor product is also known as the Kronecker product, which is available in Mathcad. The four operators in tensor format are formed as follows.

$$\sigma_{xyy} = \text{kronecker}(\sigma_x,\ \text{kronecker}(\sigma_y,\ \sigma_y)) \quad \sigma_{yxy} = \text{kronecker}(\sigma_y,\ \text{kronecker}(\sigma_x,\ \sigma_y))$$
$$\sigma_{yyx} = \text{kronecker}(\sigma_y,\ \text{kronecker}(\sigma_y,\ \sigma_x)) \quad \sigma_{xxx} = \text{kronecker}(\sigma_x,\ \text{kronecker}(\sigma_x,\ \sigma_x))$$

These composite operators are Hermitian and mutually commute which means they can have simultaneous eigenvalues.

$$\sigma_{xyy}\sigma_{yxy} - \sigma_{yxy}\sigma_{xyy} \to 0 \quad \sigma_{xyy}\sigma_{yyx} - \sigma_{yyx}\sigma_{xyy} \to 0 \quad \sigma_{xyy}\sigma_{xxx} - \sigma_{xxx}\sigma_{xyy} \to 0$$
$$\sigma_{yxy}\sigma_{yyx} - \sigma_{yyx}\sigma_{yxy} \to 0 \quad \sigma_{yxy}\sigma_{xxx} - \sigma_{xxx}\sigma_{yxy} \to 0 \quad \sigma_{yyx}\sigma_{xxx} - \sigma_{xxx}\sigma_{yyx} \to 0$$

The expectation values of the operators are now calculated.

$$\Psi^T\sigma_{xyy}\Psi = 1 \quad \Psi^T\sigma_{yxy}\Psi = 1 \quad \Psi^T\sigma_{yyx}\Psi = 1 \quad \Psi^T\sigma_{xxx}\Psi = 1$$

Consequently the product of the four operators has the expectation value of -1.

$$\Psi^T\sigma_{xyy}\sigma_{yxy}\sigma_{yyx}\sigma_{xxx}\Psi = -1$$

Local realism assumes that objects have definite properties independent of measurement. In this example it assumes that the x- and y-components of the spin have definite values prior to measurement. This position leads to a contradiction with the above result as demonstrated by Mermin (Physics Today, June 1990). Looking again at the measurement operators, notice that there is a σx measurement on the first spin in the first and fourth experiment. If the spin state is well-defined before measurement those results have to be the same, either both +1 or both -1, so that the product of the two measurements is +1.

$$\left(\sigma_x^1 \otimes \sigma_y^2 \otimes \sigma_y^3\right)\left(\sigma_y^1 \otimes \sigma_x^2 \otimes \sigma_y^3\right)\left(\sigma_y^1 \otimes \sigma_y^2 \otimes \sigma_x^3\right)\left(\sigma_x^1 \otimes \sigma_x^2 \otimes \sigma_x^3\right)$$

Likewise there is a σ_y measurement on the second spin in experiments one and three. By similar arguments those results will lead to a product of +1 also. Continuing with all pairs in the total operator using local realistic reasoning unambiguously shows that its expectation value should be +1, in sharp disagreement with the quantum mechanical result of -1. This result should cause all mathematically literate local realists to renounce and recant their heresy. However, they may resist saying this is just a thought experiment. It hasn't actually been performed. However, if you believe in quantum simulation it has been performed.

Quantum Simulation

"Quantum simulation is a process in which a quantum computer simulates another quantum system. Because of the various types of quantum weirdness, classical computers can simulate quantum systems only in a clunky, inefficient way. But because a quantum computer is itself a quantum system, capable of exhibiting the full repertoire of quantum weirdness, it can efficiently simulate other quantum systems. **The resulting simulation can be so accurate that the behavior the computer will be indistinguishable from the behavior of the simulated system itself.**" (Seth Lloyd, Programming the Universe, page 149.) The thought experiment can be simulated using the quantum circuit shown below which is an adaptation of one that can be found at: arXiv:1712.06542v2.

$$
\begin{array}{lccccccccc}
|1\rangle & \triangleright & \mathrm{H} & \cdot & \cdots & \cdots & \mathrm{H} & \triangleright & \text{Measure, 0 or 1} \\
 & & & | & & & & & \\
|0\rangle & \triangleright & \cdots & \oplus & \cdot & \mathrm{S} & \mathrm{H} & \triangleright & \text{Measure, 0 or 1} \\
 & & & & | & & & & \\
|0\rangle & \triangleright & \cdots & \cdots & \oplus & \mathrm{S} & \mathrm{H} & \triangleright & \text{Measure, 0 or 1}
\end{array}
$$

The matrix operators required for the implementation of the quantum circuit:

$$
I = \begin{pmatrix} 1 & 0 \\ 0 & 1 \end{pmatrix} \quad H = \frac{1}{\sqrt{2}} \begin{pmatrix} 1 & 1 \\ 1 & -1 \end{pmatrix} \quad S = \begin{pmatrix} 1 & 0 \\ 0 & -i \end{pmatrix} \quad \mathrm{CNOT} = \begin{pmatrix} 1 & 0 & 0 & 0 \\ 0 & 1 & 0 & 0 \\ 0 & 0 & 0 & 1 \\ 0 & 0 & 1 & 0 \end{pmatrix}
$$

$$
\begin{array}{ccc}
\mathrm{HII} = \mathrm{kronecker}(\mathrm{H}, \mathrm{kronecker}(\mathrm{I}, \mathrm{I})) & \mathrm{CNOTI} = \mathrm{kronecker}(\mathrm{CNOT}, \mathrm{I}) & \mathrm{ICNOT} = \mathrm{kronecker}(\mathrm{I}, \mathrm{CNOT}) \\
\mathrm{ISS} = \mathrm{kronecker}(\mathrm{I}, \mathrm{kronecker}(\mathrm{S}, \mathrm{S})) & \mathrm{SIS} = \mathrm{kronecker}(\mathrm{S}, \mathrm{kronecker}(\mathrm{I}, \mathrm{S})) & \mathrm{SSI} = \mathrm{kronecker}(\mathrm{S}, \mathrm{kronecker}(\mathrm{S}, \mathrm{I})) \\
\mathrm{HHH} = \mathrm{kronecker}(\mathrm{H}, \mathrm{kronecker}(\mathrm{H}, \mathrm{H})) & &
\end{array}
$$

First it is demonstrated that the first three steps of the circuit create the initial state

$$
[\mathrm{ICNOT\ CNOTI\ HII}\,(0 \quad 0 \quad 0 \quad 0 \quad 1 \quad 0 \quad 0 \quad 0)^T]^T = (0.707 \quad 0 \quad 0 \quad 0 \quad 0 \quad 0 \quad 0 \quad -0.707)
$$

The complete circuit shown above simulates the expectation value of the $\sigma_x\sigma_y\sigma_y$ operator. The presence of S on a line before the final H gates indicates the measurement of the σy, its absence a measurement of σ_x. The subsequent simulations show the absence of S on the middle and last line, and finally on all three lines for the simulation of the expectation value for $\sigma_x\sigma_x\sigma_x$.

Eigenvalue |0 > = +1; eigenvalue |1 > = -1

$$
\begin{gathered}
[\ \mathrm{HHH\ ISS\ ICNOT\ CNOT\ HII}\,(0 \quad 0 \quad 0 \quad 0 \quad 1 \quad 0 \quad 0 \quad 0)^T]^T \\
= (0.5 \quad 0 \quad 0 \quad 0.5 \quad 0 \quad 0.5 \quad 0.5 \quad 0)
\end{gathered}
$$

$$
\frac{1}{2}\left(|000\rangle + |011\rangle + |101\rangle + |110\rangle\right) \Rightarrow \langle \sigma_x\sigma_y\sigma_y \rangle = 1
$$

Given the eigenvalue assignments above the expectation value associated with this measurement outcome is 1/4[(1)(1)(1)+(1)(-1)(-1)+(-1)(1)(-1)+(-1)(-1)(1)] = 1. Note that 1/2 is the probability amplitude for the product state. Therefore the probability of each member of the superposition being observed is 1/4. The same reasoning is used for the remaining simulations.

$$
\begin{gathered}
[\ \mathrm{HHH\ ISS\ ICNOT\ CNOT\ HII}\,(0 \quad 0 \quad 0 \quad 0 \quad 1 \quad 0 \quad 0 \quad 0)^T]^T \\
= (0.5 \quad 0 \quad 0 \quad 0.5 \quad 0 \quad 0.5 \quad 0.5 \quad 0)
\end{gathered}
$$

$$
\frac{1}{2}\left(|000\rangle + |011\rangle + |101\rangle + |110\rangle\right) \Rightarrow \langle \sigma_y\sigma_x\sigma_y \rangle = 1
$$

$$\left[\text{ HHH ISS ICNOT CNOT HII}\,(0\quad 0\quad 0\quad 0\quad 1\quad 0\quad 0\quad 0)^T\right]^T$$
$$= (0.5\quad 0\quad 0\quad 0.5\quad 0\quad 0.5\quad 0.5\quad 0)$$

$$\frac{1}{2}\left(|000\rangle + |011\rangle + |101\rangle + |110\rangle\right) \Rightarrow \langle\sigma_y\sigma_y\sigma_x\rangle = 1$$

$$\left[\text{ HHH ISS ICNOT CNOT HII}\,(0\quad 0\quad 0\quad 0\quad 1\quad 0\quad 0\quad 0)^T\right]^T$$
$$= (0\quad 0.5\quad 0.5\quad 0\quad 0.5\quad 0\quad 0\quad 0.5)$$

$$\frac{1}{2}\left(|001\rangle + |010\rangle + |100\rangle + |111\rangle\right) \Rightarrow \langle\sigma_x\sigma_x\sigma_x\rangle = -1$$

Individually and in product form the simulated results are in agreement with the previous quantum mechanical calculations.

$$\langle\sigma_x\sigma_x\sigma_x\rangle\langle\sigma_x\sigma_y\sigma_y\rangle\langle\sigma_y\sigma_x\sigma_y\rangle\langle\sigma_y\sigma_y\sigma_x\rangle = -1$$

The appendix provides algebraic calculations of $\langle\sigma_x\sigma_y\sigma_y\rangle$ and $\langle\sigma_x\sigma_x\sigma_x\rangle$.

Appendix

Truth tables for the operation of the circuit elements:

$$I = \begin{pmatrix} 0 \text{ to } 0 \\ 1 \text{ to } 1 \end{pmatrix} \quad H = \begin{bmatrix} 0 \text{ to } \frac{(0+1)}{\sqrt{2}} \\ 1 \text{ to } \frac{(0-1)}{\sqrt{2}} \end{bmatrix} \quad \text{CNOT} = \begin{pmatrix} 00 \text{ to } 00 \\ 01 \text{ to } 01 \\ 10 \text{ to } 11 \\ 11 \text{ to } 10 \end{pmatrix} \quad S = \begin{pmatrix} 0 \text{ to } 0 \\ 1 \text{ to } \text{-i} \end{pmatrix}$$

$$|100\rangle$$
$$H \otimes I \otimes I$$
$$\tfrac{1}{\sqrt{2}}\left[|000\rangle - |100\rangle\right]$$
$$CNOT \otimes I$$
$$\tfrac{1}{\sqrt{2}}\left[|000\rangle - |110\rangle\right]$$
$$I \otimes CNOT$$
$$\tfrac{1}{\sqrt{2}}\left[|000\rangle - |111\rangle\right]$$
$$I \otimes S \otimes S$$
$$\tfrac{1}{\sqrt{2}}\left[|000\rangle - |1 - i - i\rangle\right]$$
$$H \otimes H \otimes H$$
$$\tfrac{1}{2}\left[|000\rangle + |011\rangle + |101\rangle + |110\rangle\right]$$
$$\langle\sigma_x\sigma_y\sigma_y\rangle = 1$$

$$|100\rangle$$
$$H \otimes I \otimes I$$
$$\tfrac{1}{\sqrt{2}}\left[|000\rangle - |100\rangle\right]$$
$$CNOT \otimes I$$
$$\tfrac{1}{\sqrt{2}}\left[|000\rangle - |110\rangle\right]$$
$$I \otimes CNOT$$
$$\tfrac{1}{\sqrt{2}}\left[|000\rangle - |111\rangle\right]$$
$$H \otimes H \otimes H$$
$$\tfrac{1}{\sqrt{2}}\left[|001\rangle + |010\rangle + |100\rangle + |111\rangle\right]$$
$$\langle\sigma_x\sigma_x\sigma_x\rangle = -1$$

This page titled 8.18: Another Simulation of a GHZ Gedanken Experiment is shared under a CC BY 4.0 license and was authored, remixed, and/or curated by Frank Rioux via source content that was edited to the style and standards of the LibreTexts platform.

8.19: A Surgical Refutation of the Local Realism Heresy

Three photons are created in a single event (***Nature***, February 3, 2000 pp. 515-519) and move apart in the horizontal y-z plane. The goal of this exercise is to demonstrate that an analysis of measurements in the diagonal and circular polarization basis reveals the impossibility of assigning definite values to the polarization states of the photons prior to and independent of measurement.

First some definitions:

Realism - experiments yield values for properties that exist independent of experimental observation

Locality - the experimental results obtained at location A at time t, do not depend on the results at some other remote location B at time t. The diagonal and circular polarization matrix operators:

$$D = \begin{pmatrix} 0 & 1 \\ 1 & 0 \end{pmatrix} \; C = \begin{pmatrix} 0 & -i \\ i & 0 \end{pmatrix}$$

The eigenvalues of the matrices are +/- 1:

$$\text{eigenvals(D)} = \begin{pmatrix} 1 \\ -1 \end{pmatrix} \quad \text{eigenvals(C)} = \begin{pmatrix} 1 \\ -1 \end{pmatrix}$$

The eigenvectors of the operators:

$$\text{eigenvecs(D)} = \begin{pmatrix} 0.707 & -0.707 \\ 0.707 & 0.707 \end{pmatrix} \quad \text{eigenvecs(C)} = \begin{pmatrix} -0.707i & 0.707 \\ 0.707 & -0.707i \end{pmatrix}$$

The following operators represent the measurement protocols for spins 1, 2 and 3. For example, the first operator designates that diagonal polarization is measured on the first photon and circular polarization on the second and third photons.

$$D_1C_2C_3 \quad C_1D_2C_3 \quad C_1C_2D_3 \quad D_1D_2D_3$$

The four operators are constructed in matrix format using tensor multiplication.

$$\text{DCC} = \text{kronecker(D, kronecker(C, C))} \quad \text{CDC} = \text{kronecker(C, kronecker(D, C))}$$
$$\text{CCD} = \text{kronecker(C, kronecker(C, D))} \quad \text{DDD} = \text{kronecker(D, kronecker(D, D))}$$

1. The operators are unitary. Demonstrate this for DDC and DDD.

$$\text{DCC}^2 = \begin{pmatrix} 1 & 0 & 0 & 0 & 0 & 0 & 0 & 0 \\ 0 & 1 & 0 & 0 & 0 & 0 & 0 & 0 \\ 0 & 0 & 1 & 0 & 0 & 0 & 0 & 0 \\ 0 & 0 & 0 & 1 & 0 & 0 & 0 & 0 \\ 0 & 0 & 0 & 0 & 1 & 0 & 0 & 0 \\ 0 & 0 & 0 & 0 & 0 & 1 & 0 & 0 \\ 0 & 0 & 0 & 0 & 0 & 0 & 1 & 0 \\ 0 & 0 & 0 & 0 & 0 & 0 & 0 & 1 \end{pmatrix} \quad \text{DDD}^2 = \begin{pmatrix} 1 & 0 & 0 & 0 & 0 & 0 & 0 & 0 \\ 0 & 1 & 0 & 0 & 0 & 0 & 0 & 0 \\ 0 & 0 & 1 & 0 & 0 & 0 & 0 & 0 \\ 0 & 0 & 0 & 1 & 0 & 0 & 0 & 0 \\ 0 & 0 & 0 & 0 & 1 & 0 & 0 & 0 \\ 0 & 0 & 0 & 0 & 0 & 1 & 0 & 0 \\ 0 & 0 & 0 & 0 & 0 & 0 & 1 & 0 \\ 0 & 0 & 0 & 0 & 0 & 0 & 0 & 1 \end{pmatrix}$$

2. The operators are also Hermitian. Demonstrate this for CDC. What is the significance of being Hermitian?

$$\text{CDC} = \begin{pmatrix} 0 & 0 & 0 & 0 & 0 & 0 & 0 & -1 \\ 0 & 0 & 0 & 0 & 0 & 0 & 1 & 0 \\ 0 & 0 & 0 & 0 & 0 & -1 & 0 & 0 \\ 0 & 0 & 0 & 0 & 1 & 0 & 0 & 0 \\ 0 & 0 & 0 & 1 & 0 & 0 & 0 & 0 \\ 0 & 0 & -1 & 0 & 0 & 0 & 0 & 0 \\ 0 & 1 & 0 & 0 & 0 & 0 & 0 & 0 \\ -1 & 0 & 0 & 0 & 0 & 0 & 0 & 0 \end{pmatrix} \quad \text{CDC}^T = \begin{pmatrix} 0 & 0 & 0 & 0 & 0 & 0 & 0 & -1 \\ 0 & 0 & 0 & 0 & 0 & 0 & 1 & 0 \\ 0 & 0 & 0 & 0 & 0 & -1 & 0 & 0 \\ 0 & 0 & 0 & 0 & 1 & 0 & 0 & 0 \\ 0 & 0 & 0 & 1 & 0 & 0 & 0 & 0 \\ 0 & 0 & -1 & 0 & 0 & 0 & 0 & 0 \\ 0 & 1 & 0 & 0 & 0 & 0 & 0 & 0 \\ -1 & 0 & 0 & 0 & 0 & 0 & 0 & 0 \end{pmatrix}$$

Hermitian operators have real eigenvalues.

3. The operators have eigenvalues +/- 1 and the same set of eigenvectors. Demonstrate this for DCC and CCD.

$$\text{eigenvals(CDC)} = \begin{pmatrix} 1 \\ -1 \\ 1 \\ -1 \\ 1 \\ -1 \\ 1 \\ -1 \end{pmatrix} \quad \text{eigenvecs(DCC)} = \begin{pmatrix} 0.707 & 0.707 & 0 & 0 & 0 & 0 & 0 & 0 \\ 0 & 0 & 0 & 0 & 0 & 0 & 0.707 & 0.707 \\ 0 & 0 & 0.707 & 0.707 & 0 & 0 & 0 & 0 \\ 0 & 0 & 0 & 0 & -0.707 & -0.707 & 0 & 0 \\ 0 & 0 & 0 & 0 & 0.707 & -0.707 & 0 & 0 \\ 0 & 0 & 0.707 & -0.707 & 0 & 0 & 0 & 0 \\ 0 & 0 & 0 & 0 & 0 & 0 & 0.707 & -0.707 \\ -0.707 & 0.707 & 0 & 0 & 0 & 0 & 0 & 0 \end{pmatrix}$$

$$\text{eigenvals(CDC)} = \begin{pmatrix} 1 \\ -1 \\ 1 \\ -1 \\ 1 \\ -1 \\ 1 \\ -1 \end{pmatrix} \quad \text{eigenvecs(DCC)} = \begin{pmatrix} 0.707 & 0.707 & 0 & 0 & 0 & 0 & 0 & 0 \\ 0 & 0 & 0 & 0 & 0 & 0 & -0.707 & 0.707 \\ 0 & 0 & 0.707 & 0.707 & 0 & 0 & 0 & 0 \\ 0 & 0 & 0 & 0 & 0.707 & -0.707 & 0 & 0 \\ 0 & 0 & 0 & 0 & 0.707 & 0.707 & 0 & 0 \\ 0 & 0 & 0.707 & -0.707 & 0 & 0 & 0 & 0 \\ 0 & 0 & 0 & 0 & 0 & 0 & 0.707 & 0.707 \\ -0.707 & 0.707 & 0 & 0 & 0 & 0 & 0 & 0 \end{pmatrix}$$

4. One of the eigenvectors is Ψ. Calculate its expectation values for the four operators.

$$\Psi = (0 \quad 0 \quad 0 \quad 1 \quad -1 \quad 0 \quad 0 \quad 0)$$

$$\Psi^T = \text{DCC}\Psi = 1 \qquad \Psi^T\text{CDC}\Psi = -1 \quad \Psi^T\text{CCD}\Psi = -1 \quad \Psi^T\text{DDD}\Psi = -1$$
$$\Psi^T\text{DCC CDC CCD}\Psi = 1$$

5. Demonstrate that Ψ is a maximally entangle three-photon state. These are called GHZ states.

In decimal notation:

$$\Psi = \frac{1}{\sqrt{2}}\left[\begin{pmatrix}1\\0\end{pmatrix}\begin{pmatrix}0\\1\end{pmatrix}\begin{pmatrix}0\\1\end{pmatrix} - \begin{pmatrix}0\\1\end{pmatrix}\begin{pmatrix}1\\0\end{pmatrix}\begin{pmatrix}1\\0\end{pmatrix}\right] = \frac{1}{\sqrt{2}}(3-4)$$

6. Demonstrate that these operators mutually commute (use the symbolic processor -->). What is the physical significance of this fact?

$$\text{DCC CDC} - \text{CDC DCC} \to 0 \quad \text{DCC CCD} - \text{CCD DCC} \to 0 \quad \text{DCC DDD} - \text{DDD DCC} \to 0$$
$$\text{CDC CCD} - \text{CCD CDC} \to 0 \quad \text{CDC DDD} - \text{DDD CDC} \to 0 \quad \text{CCD DDD} - \text{DDD CCD} \to 0$$

That these operators mutually commute means that they can have simultaneous eigenstates with simultaneous eigenvalues. In other words, they can be in well-defined states at the same time.

7. Display \(\text{DCC CDC CCD\) and DDD in matrix format (use the traditional =).

$$\begin{matrix} & & & & & & & \text{DCC CDC CCD} \\ = & \begin{pmatrix} 0 & 0 & 0 & 0 & 0 & 0 & 0 & -1 \\ 0 & 0 & 0 & 0 & 0 & 0 & -1 & 0 \\ 0 & 0 & 0 & 0 & 0 & -1 & 0 & 0 \\ 0 & 0 & 0 & 0 & -1 & 0 & 0 & 0 \\ 0 & 0 & 0 & -1 & 0 & 0 & 0 & 0 \\ 0 & 0 & -1 & 0 & 0 & 0 & 0 & 0 \\ 0 & -1 & 0 & 0 & 0 & 0 & 0 & 0 \\ -1 & 0 & 0 & 0 & 0 & 0 & 0 & 0 \end{pmatrix} \end{matrix} \quad \text{DDD} = \begin{pmatrix} 0 & 0 & 0 & 0 & 0 & 0 & 0 & 1 \\ 0 & 0 & 0 & 0 & 0 & 0 & 1 & 0 \\ 0 & 0 & 0 & 0 & 0 & 1 & 0 & 0 \\ 0 & 0 & 0 & 0 & 1 & 0 & 0 & 0 \\ 0 & 0 & 0 & 1 & 0 & 0 & 0 & 0 \\ 0 & 0 & 1 & 0 & 0 & 0 & 0 & 0 \\ 0 & 1 & 0 & 0 & 0 & 0 & 0 & 0 \\ 1 & 0 & 0 & 0 & 0 & 0 & 0 & 0 \end{pmatrix}$$

8. Write this result in simple algebraic format.

$$\text{DCC CDC CCD} = -\text{DDD}$$

9. Using arguments based on local realism demonstrate that this result leads to the following contradiction.

$$\text{DDD} = -\text{DDD}$$

Local realism assumes that objects have definite properties independent of measurement. In this example it assumes the diagonal and circular polarization states have definite values prior to measurement. This position leads to a contradiction with the above result. There is no way to assign eigenvalues (+/-1) to the operators that is consistent with the above result.

$$\text{DCC CDC CCD} = -\text{DDD}$$

Concentrating on the composite operator on the left side, we notice that there is a C measurement on the first photon in the second and third operators (green). If the photon state is well-defined before measurement those results have to be the same, either both +1 or both -1, so that the product of the two measurements is +1. There is a C measurement on the second photon in operators one and three (blue). By similar arguments those results will lead to a product of +1 also. Finally there is a C measurement on the third photon in operators one and two (red). By similar arguments those results will lead to a product of +1 also. Incorporating these observations into the expression above leads to the following contradiction.

$$\text{DDD} = -\text{DDD}$$

This result should cause all mathematically literate local realists to renounce and recant their heresy.

This page titled 8.19: A Surgical Refutation of the Local Realism Heresy is shared under a CC BY 4.0 license and was authored, remixed, and/or curated by Frank Rioux via source content that was edited to the style and standards of the LibreTexts platform.

8.20: GHZ Four-Photon Entanglement Analyzed Using Tensor Algebra

This tutorial analyzes the results reported in "Experimental Violation of Local Realism by Four-Photon GHZ Entanglement" by Zhao, et al. and published in ***Physical Review Letters*** on October 31, 2003.

The null vector and required photon polarization states:

$$N = \begin{pmatrix}0\\0\end{pmatrix} \quad H = \begin{pmatrix}1\\0\end{pmatrix} \quad V = \begin{pmatrix}0\\1\end{pmatrix} \quad H = \frac{1}{\sqrt{2}}\begin{pmatrix}1\\1\end{pmatrix} V = \frac{1}{\sqrt{2}}\begin{pmatrix}1\\-1\end{pmatrix} \quad L = \frac{1}{\sqrt{2}}\begin{pmatrix}1\\-i\end{pmatrix} \quad R = \frac{1}{\sqrt{2}}\begin{pmatrix}1\\i\end{pmatrix}$$

To facilitate tensor vector multiplication the polarization states are stored in the left column of a 2x2 matrix using the null vector

$$H = \text{augment(H, N)} \quad V = \text{augment(V, N)} \quad H' = \text{augment(H', N)} \quad V'N = \text{augment(V', N)} \quad R = \text{augment(R, N)} \quad L = \text{augment(L, N)}$$

$$H = \begin{pmatrix}1 & 0\\0 & 0\end{pmatrix} \quad V = \begin{pmatrix}0 & 0\\1 & 0\end{pmatrix} \quad H' = \begin{pmatrix}0.707 & 0\\0.707 & 0\end{pmatrix} \quad V' = \begin{pmatrix}0.707 & 0\\-0.707 & 0\end{pmatrix} \quad R = \begin{pmatrix}0.707 & 0\\0.707i & 0\end{pmatrix} \quad L = \begin{pmatrix}0.707 & 0\\-0.707i & 0\end{pmatrix}$$

Operators:

$$H'V' = \begin{pmatrix}0 & 1\\1 & 0\end{pmatrix} \quad RL = \begin{pmatrix}0 & -i\\i & 0\end{pmatrix}$$

Eigenvaues of various polarization states:

$$\text{H'V' H'} = \begin{pmatrix}0.707 & 0\\0.707 & 0\end{pmatrix} \quad \text{H'V' V'} = \begin{pmatrix}-0.707 & 0\\0.707 & 0\end{pmatrix} \quad \text{RL R} = \begin{pmatrix}0.707 & 0\\0.707i & 0\end{pmatrix} \quad \text{RL L} = \begin{pmatrix}-0.707 & 0\\0.707i & 0\end{pmatrix}$$

The initial GHZ four-photon entangled state:

$$\Psi = \frac{1}{\sqrt{2}}(H_1V_2V_3H_4 + V_1H_2H_3V_4)$$

$$|\Psi\rangle = \frac{1}{\sqrt{2}}\left[\begin{pmatrix}1\\0\end{pmatrix}\otimes\begin{pmatrix}0\\1\end{pmatrix}\otimes\begin{pmatrix}0\\1\end{pmatrix}\otimes\begin{pmatrix}1\\0\end{pmatrix} + \begin{pmatrix}0\\1\end{pmatrix}\otimes\begin{pmatrix}1\\0\end{pmatrix}\otimes\begin{pmatrix}1\\0\end{pmatrix}\otimes\begin{pmatrix}0\\1\end{pmatrix}\right]$$

Initial state set up in tensor format.

$$\Psi_i = \frac{1}{\sqrt{2}}(\text{submatrix(kronecker(H, kronecker(V, kronecker(V, H}))) + \text{kronecker(V, kronecker(H, kronecker(H, V}))),\ 1,\ 16,\ 1,\ 1))$$

$$\Psi^T = (0 \quad 0 \quad 0 \quad 0 \quad 0 \quad 0 \quad 0.707 \quad 0 \quad 0 \quad 0.707 \quad 0 \quad 0 \quad 0 \quad 0 \quad 0 \quad 0)$$

The authors initially consider three measurements which are summarized below. It is shown that the inital photon state is an eigenstate of each of the operators with eigenvalue +1. In the operators x refers to a linear polarization measurement (H'V') and y refers to a circular polarization measurement (RL). The experimental results are reported in Figure 3 of the paper. Below quantum mechanical (QM) calculations (predictions) are compared with experimental outcomes. QM agrees with experiment.

The following calculations are facilitated by the following general expression for the measurement eigenstates.

$$\Psi(\text{a, b, c, d}) = \text{submatrix(kronecker(a, kronecker(b, kronecker(c, d}))),\ 1,\ 16,\ 1,\ 1)$$

σ_{xxxx} experiment:

Operator:

$$\sigma_{xxxx} = \text{kronecker(H'V', kronecker(H'V', kronecker(H'V', H'V')))}$$

Eigenvalue/Expectation Value:

$$\Psi_i^T \sigma_{xxxx} \Psi_i = 1$$

Observed: H'H'H'H', H'H'V'V', H'V'H'V', H'V'V'H', V'H'H'V', V'H'V'H', V'V'H'H' and V'V'V'V'.

$$\begin{array}{cccc} (|\Psi(\text{H'}, \text{H'}, \text{H'}, \text{H'})^T & (|\Psi(\text{H'}, \text{H'}, \text{V'}, \text{V'})^T & (|\Psi(\text{H'}, \text{V'}, \text{V'}, \text{H'})^T & (|\Psi(\text{H'}, \text{V'}, \text{V'}, \text{H'})^T \\ \Psi_i|)^2 = 0.125 & \Psi_i|)^2 = 0.125 & \Psi_i|)^2 = 0.125 & \Psi_i|)^2 = 0.125 \\ (|\Psi(\text{V'}, \text{H'}, \text{H'}, \text{V'})^T & (|\Psi(\text{V'}, \text{H'}, \text{V'}, \text{H'})^T & (|\Psi(\text{V'}, \text{V'}, \text{H'}, \text{H'})^T & (|\Psi(\text{V'}, \text{V'}, \text{V'}, \text{V'})^T \\ \Psi_i|)^2 = 0.125 & \Psi_i|)^2 = 0.125 & \Psi_i|)^2 = 0.125 & \Psi_i|)^2 = 0.125 \end{array}$$

σ_{xyxy} experiment:

Operator:

$$\sigma_{xyxy} = \text{kronecker(H'V', kronecker(RL, kronecker(H'V', RL)))}$$

Eigenvalue/Expectation Value:

$$\Psi_i^T \sigma_{xyxy} \Psi_i = 1$$

Observed: H'RH'R, H'RV'L, H'LH'L, H'LV'R, V'RH'L, V'R'V'R, V'LH'R and V'LV'L.

$$\begin{array}{cccc} (|\Psi(\text{H'}, \text{R}, \text{H'}, \text{R})^T\Psi_i| & (|\Psi(\text{H'}, \text{R}, \text{V'}, \text{L})^T\Psi_i| & (|\Psi(\text{H'}, \text{L}, \text{H'}, \text{L})^T\Psi_i| & (|\Psi(\text{H'}, \text{L}, \text{V'}, \text{R})^T\Psi_i| \\ )^2 = 0.125 &)^2 = 0.125 &)^2 = 0.125 &)^2 = 0.125 \\ (|\Psi(\text{V'}, \text{R}, \text{H'}, \text{L})^T\Psi_i| & (|\Psi(\text{V'}, \text{R}, \text{V'}, \text{R})^T\Psi_i| & (|\Psi(\text{V'}, \text{L}, \text{H'}, \text{R})^T\Psi_i| & (|\Psi(\text{V'}, \text{L}, \text{V'}, \text{L})^T\Psi_i| \\ )^2 = 0.125 &)^2 = 0.125 &)^2 = 0.125 &)^2 = 0.125 \end{array}$$

σ_{xxyy} experiment:

Operator:

$$\sigma_{xxyy} = \text{kronecker(H'V', kronecker(H'V', kronecker(RL, RL)))}$$

Eigenvalue/Expectation Value:

$$\Psi_i^T \sigma_{xxyy} \Psi_i = 1$$

Observed: H'H'RR, H'H'LL, H'V'RL, H'V'LR, H'V'RL, V'H'LR, V'V'RR and V'V'LL.

$$\begin{array}{cccc} (|\Psi(\text{H'}, \text{H'}, \text{R}, \text{R})^T\Psi_i| & (|\Psi(\text{H'}, \text{H'}, \text{L}, \text{L})^T\Psi_i| & (|\Psi(\text{H'}, \text{V'}, \text{R}, \text{L})^T\Psi_i| & (|\Psi(\text{H'}, \text{V'}, \text{L}, \text{R})^T\Psi_i| \\ )^2 = 0.125 &)^2 = 0.125 &)^2 = 0.125 &)^2 = 0.125 \\ (|\Psi(\text{V'}, \text{H'}, \text{R}, \text{L})^T\Psi_i| & (|\Psi(\text{V'}, \text{H'}, \text{L}, \text{R})^T\Psi_i| & (|\Psi(\text{V'}, \text{V'}, \text{R}, \text{R})^T\Psi_i| & (|\Psi(\text{V'}, \text{V'}, \text{L}, \text{L})^T\Psi_i| \\ )^2 = 0.125 &)^2 = 0.125 &)^2 = 0.125 &)^2 = 0.125 \end{array}$$

This analysis shows that quantum mechanics (QM) is in agreement with experimental results. The next step is to perform an experiment that shows that local realism (LR) is not in agreement with experimental results.

The fact that the eigenvalues of the individual operators examined above is +1, guarantees that the same is true for their product.

$$(x_1x_2x_3x_4)\,(x_1y_2x_3y_4)\,(x_1x_2y_3y_4) = 1$$

Local realism assumes that physical properties exist independent of measurement. Because commuting operators have simultaneous eigenvalues $x_1x_1 = x_2x_2 = x_3x_3 = y_4y_4$. It follows that,

$$(x_1y_2y_3x_4) = 1$$

The following results are consistent with this local realism analysis: H'RRH', H'RLV', H'LRV', H'LLH', V'RRV', V'RLH', V'LRH' and V'LLV'. As shown below, this is in complete disagreement with quantum mechanics and the experimental data. QM shows that the eigenvalue of the operator is actually -1, and, furthermore none of LR predicted results are observed. QM, however, is in agreement with the experimental results.

σ_{xyyx} experiment:

Operator:

$$\sigma_{xyyx} = \text{kronecker(H'V', kronecker(RL, kronecker(RL, H'V')))}$$

Eigenvalue/Expectation Value:

$$\Psi_i^T \sigma_{xyyx} \Psi_i = 1$$

Observed: H'H'RR, H'H'LL, H'V'RL, H'V'LR, H'V'RL, V'H'LR, V'V'RR and V'V'LL.

$$\begin{array}{cccc} \left(\left|\Psi(\text{H', R, R, V'})^T \Psi_i\right|\right)^2 = 0.125 & \left(\left|\Psi(\text{H', R, L, H'})^T \Psi_i\right|\right)^2 = 0.125 & \left(\left|\Psi(\text{H', L, R, H'})^T \Psi_i\right|\right)^2 = 0.125 & \left(\left|\Psi(\text{H', L, L, V'})^T \Psi_i\right|\right)^2 = 0.125 \\ \left(\left|\Psi(\text{V', R, R, H'})^T \Psi_i\right|\right)^2 = 0.125 & \left(\left|\Psi(\text{V', R, L, V'})^T \Psi_i\right|\right)^2 = 0.125 & \left(\left|\Psi(\text{V', L, R, V'})^T \Psi_i\right|\right)^2 = 0.125 & \left(\left|\Psi(\text{V', L, L, H'})^T \Psi_i\right|\right)^2 = 0.125 \end{array}$$

Appendix

All four operators commute with each other allowing them to have simultaneous eigenvalues.

$$\begin{array}{ccc} \sigma_{xxxx}\sigma_{xyxy} - \sigma_{xyxy}\sigma_{xxxx} \to 0 & \sigma_{xxxx}\sigma_{xyyx} - \sigma_{xyyx}\sigma_{xxxx} \to 0 & \sigma_{xxxx}\sigma_{xxyy} - \sigma_{xxyy}\sigma_{xxxx} \to 0 \\ \sigma_{xxyy}\sigma_{xyxy} - \sigma_{xyxy}\sigma_{xxyy} \to 0 & \sigma_{xxyy}\sigma_{xyyx} - \sigma_{xyyx}\sigma_{xxyy} \to 0 & \sigma_{xyxy}\sigma_{xyyx} - \sigma_{xyyx}\sigma_{xyxy} \to 0 \end{array}$$

This page titled 8.20: GHZ Four-Photon Entanglement Analyzed Using Tensor Algebra is shared under a CC BY 4.0 license and was authored, remixed, and/or curated by Frank Rioux via source content that was edited to the style and standards of the LibreTexts platform.

8.21: Quantum v. Realism

This tutorial demonstrates the conflict between quantum theory and realism in an experiment described in *Physical Review Letters* on October 31, 2003 by Zhao, *et al*. titled "Experimental Violation of Local Realism by Four-Photon GHZ Entanglement." It draws on the methodology outlined by N. David Mermin in two articles in the general physics literature: *Physics Today*, June 1990; *American Journal of Physics*, August 1990.

The experiment involves the measurement of the diagonal and circular polarization states of a four-photon entangled state using the following measurement protocols.

$$\sigma_d^1 \otimes \sigma_d^2 \otimes \sigma_d^3 \otimes \sigma_d^4 \quad \sigma_d^1 \otimes \sigma_c^2 \otimes \sigma_d^3 \otimes \sigma_c^4 \quad \sigma_d^1 \otimes \sigma_d^2 \otimes \sigma_c^3 \otimes \sigma_c^4 \quad \sigma_d^1 \otimes \sigma_c^2 \otimes \sigma_c^3 \otimes \sigma_d^4$$

The individual polarization operators and their eigenvalues are:

$$D = \begin{pmatrix} 0 & 1 \\ 1 & 0 \end{pmatrix} \quad \text{eigenvals}(D) = \begin{pmatrix} 1 \\ -1 \end{pmatrix} \quad C = \begin{pmatrix} 0 & -i \\ i & 0 \end{pmatrix} \quad \text{eigenvals}(C) = \begin{pmatrix} 1 \\ -1 \end{pmatrix}$$

The composite operators are formed by tensor matrix multiplication, where kronecker is Mathcad′s command for tensor multiplication.

$\sigma_{dddd} = \text{kronecker(D, kronecker(D, kronecker(D, D)))}$ $\quad \sigma_{dcdc} = \text{kronecker(D, kronecker(C, kronecker(D, C)))}$

$\sigma_{ddcc} = \text{kronecker(D, kronecker(D, kronecker(C, C)))}$ $\quad \sigma_{dccd} = \text{kronecker(D, kronecker(C, kronecker(C, D)))}$

These operators commute with each other allowing them to have simultaneous eigenvalues.

$$\sigma_{dddd}\sigma_{dcdc} - \sigma_{dcdc}\sigma_{dddd} \to 0 \quad \sigma_{dddd}\sigma_{dccd} - \sigma_{dccd}\sigma_{dddd} \to 0 \quad \sigma_{dddd}\sigma_{ddcc} - \sigma_{ddcc}\sigma_{dddd} \to 0$$
$$\sigma_{ddcc}\sigma_{dcdc} - \sigma_{dcdc}\sigma_{ddcc} \to 0 \quad \sigma_{ddcc}\sigma_{dccd} - \sigma_{dccd}\sigma_{ddcc} \to 0 \quad \sigma_{dcdc}\sigma_{dccd} - \sigma_{dccd}\sigma_{dcdc} \to 0$$

Next we show that the null matrix results when the fourth operator is added to the product of the first three.

$$\sigma_{dddd}\sigma_{dcdc}\sigma_{ddcc} + \sigma_{dccd} = \begin{pmatrix} 0 & 0 & 0 & 0 & 0 & 0 & 0 & 0 & 0 & 0 & 0 & 0 & 0 & 0 & 0 & 0 \\ 0 & 0 & 0 & 0 & 0 & 0 & 0 & 0 & 0 & 0 & 0 & 0 & 0 & 0 & 0 & 0 \\ 0 & 0 & 0 & 0 & 0 & 0 & 0 & 0 & 0 & 0 & 0 & 0 & 0 & 0 & 0 & 0 \\ 0 & 0 & 0 & 0 & 0 & 0 & 0 & 0 & 0 & 0 & 0 & 0 & 0 & 0 & 0 & 0 \\ 0 & 0 & 0 & 0 & 0 & 0 & 0 & 0 & 0 & 0 & 0 & 0 & 0 & 0 & 0 & 0 \\ 0 & 0 & 0 & 0 & 0 & 0 & 0 & 0 & 0 & 0 & 0 & 0 & 0 & 0 & 0 & 0 \\ 0 & 0 & 0 & 0 & 0 & 0 & 0 & 0 & 0 & 0 & 0 & 0 & 0 & 0 & 0 & 0 \\ 0 & 0 & 0 & 0 & 0 & 0 & 0 & 0 & 0 & 0 & 0 & 0 & 0 & 0 & 0 & 0 \\ 0 & 0 & 0 & 0 & 0 & 0 & 0 & 0 & 0 & 0 & 0 & 0 & 0 & 0 & 0 & 0 \\ 0 & 0 & 0 & 0 & 0 & 0 & 0 & 0 & 0 & 0 & 0 & 0 & 0 & 0 & 0 & 0 \\ 0 & 0 & 0 & 0 & 0 & 0 & 0 & 0 & 0 & 0 & 0 & 0 & 0 & 0 & 0 & 0 \\ 0 & 0 & 0 & 0 & 0 & 0 & 0 & 0 & 0 & 0 & 0 & 0 & 0 & 0 & 0 & 0 \\ 0 & 0 & 0 & 0 & 0 & 0 & 0 & 0 & 0 & 0 & 0 & 0 & 0 & 0 & 0 & 0 \\ 0 & 0 & 0 & 0 & 0 & 0 & 0 & 0 & 0 & 0 & 0 & 0 & 0 & 0 & 0 & 0 \\ 0 & 0 & 0 & 0 & 0 & 0 & 0 & 0 & 0 & 0 & 0 & 0 & 0 & 0 & 0 & 0 \\ 0 & 0 & 0 & 0 & 0 & 0 & 0 & 0 & 0 & 0 & 0 & 0 & 0 & 0 & 0 & 0 \end{pmatrix}$$

To facilitate further analysis, the null result is written as follows.

$$\sigma_{dddd}\sigma_{dcdc}\sigma_{ddcc} = -\sigma_{dccd}$$

Realism maintains that objects have values for observable properties that exist prior to measurement and independent of the choice of measurement (noncontextual). If this assumption is valid, then the operators highlighted with the same color must have the same eigenvalues (+1 or -1) and therefore the product of their eigenvalues must be unity.

$$\left(\sigma_d^1 \otimes \sigma_d^2 \otimes \sigma_d^3 \otimes \sigma_d^4\right)\left(\sigma_d^1 \otimes \sigma_d^2 \otimes \sigma_d^3 \otimes \sigma_d^4\right)\left(\sigma_d^1 \otimes \sigma_d^2 \otimes \sigma_d^3 \otimes \sigma_d^4\right) = -\left(\sigma_d^1 \sigma_c^2 \sigma_c^3 \sigma_d^4\right)$$

Thus, applying a classical concept (noncontextual realism) to the above quantum mechanical equation leads to the following contradiction.

$$\sigma_d^1 \otimes \sigma_c^2 \otimes \sigma_c^3 \otimes \sigma_d^4 = -\sigma_d^1 \otimes \sigma_c^2 \otimes \sigma_c^3 \otimes \sigma_d^4$$

The experimental results reported by Zhao, *et al.* validate the quantum mechanical analysis, and contradict the realistic interpretation. See the preceding tutorial for a summary of their experimental results.

This page titled 8.21: Quantum v. Realism is shared under a CC BY 4.0 license and was authored, remixed, and/or curated by Frank Rioux via source content that was edited to the style and standards of the LibreTexts platform.

8.22: Elements of Reality- Another GHZ Gedanken Experiment Analyzed

Twenty years ago N. David Mermin published two articles (***Physics Today***, June 1990; ***American Journal of Physics***, August 1990) in the general physics literature on a Greenberger-Horne-Zeilinger (***American Journal of Physics***, December 1990; ***Nature***, 3 February 2000) gedanken experiment involving spins that sharply revealed the clash between local realism and the quantum view of reality. In what follows I present Mermin's gedanken experiment using tensor algebra.

Three spin-1/2 particles are created in a single event and move apart in the horizontal y-z plane. Subsequent spin measurements will be carried out in units of h/4Ψ with spin operators in the x- and y-directions.

The z-basis eigenfunctions are:

$$Sz_{up} = \begin{pmatrix} 1 \\ 0 \end{pmatrix} \quad Sz_{down} = \begin{pmatrix} 0 \\ 1 \end{pmatrix}$$

The x- and y-direction spin operators and eigenvalues:

$$\sigma_x = \begin{pmatrix} 0 & 1 \\ 1 & 0 \end{pmatrix} \quad \text{eigenvals}(\sigma_x) = \begin{pmatrix} 1 \\ -1 \end{pmatrix} \quad \sigma_y = \begin{pmatrix} 0 & -i \\ i & 0 \end{pmatrix} \quad \text{eigenvals}(\sigma_y) = \begin{pmatrix} 1 \\ -1 \end{pmatrix}$$

The initial spin state for the three spin-1/2 particles in tensor notation is:

$$|\Psi\rangle = \frac{1}{\sqrt{2}} \left[\begin{pmatrix} 1 \\ 0 \end{pmatrix} \otimes \begin{pmatrix} 1 \\ 0 \end{pmatrix} \otimes \begin{pmatrix} 1 \\ 0 \end{pmatrix} - \begin{pmatrix} 0 \\ 1 \end{pmatrix} \otimes \begin{pmatrix} 0 \\ 1 \end{pmatrix} \otimes \begin{pmatrix} 0 \\ 1 \end{pmatrix} \right] = \frac{1}{\sqrt{2}} \begin{pmatrix} 1 \\ 0 \\ 0 \\ 0 \\ 0 \\ 0 \\ 0 \\ -1 \end{pmatrix} \quad \Psi = \frac{1}{\sqrt{2}} \begin{pmatrix} 1 \\ 0 \\ 0 \\ 0 \\ 0 \\ 0 \\ 0 \\ -1 \end{pmatrix}$$

The Appendix shows how to carry out vector tensor products in Mathcad.

The following operators represent the actual measurements to be carried out on spins 1, 2 and 3, in that order.

$$\sigma_x^1 \otimes \sigma_y^2 \otimes \sigma_y^3 \quad \sigma_y^1 \otimes \sigma_x^2 \otimes \sigma_y^3 \quad \sigma_y^1 \otimes \sigma_y^2 \otimes \sigma_x^3$$

The matrix tensor product is also known as the Kronecker product, which is available in Mathcad. The three operators in tensor format are formed as follows.

$$\sigma_{xyy} = \text{kronecker}(\sigma_x, \text{kronecker}(\sigma_y, \sigma_y)) \quad \sigma_{xyy} = \begin{pmatrix} 0 & 0 & 0 & 0 & 0 & 0 & 0 & -1 \\ 0 & 0 & 0 & 0 & 0 & 0 & 1 & 0 \\ 0 & 0 & 0 & 0 & 0 & 1 & 0 & 0 \\ 0 & 0 & 0 & 0 & -1 & 0 & 0 & 0 \\ 0 & 0 & 0 & -1 & 0 & 0 & 0 & 0 \\ 0 & 0 & 1 & 0 & 0 & 0 & 0 & 0 \\ 0 & 1 & 0 & 0 & 0 & 0 & 0 & 0 \\ -1 & 0 & 0 & 0 & 0 & 0 & 0 & 0 \end{pmatrix}$$

$$\sigma_{yxy} = \text{kronecker}(\sigma_y, \text{kronecker}(\sigma_x, \sigma_y)) \quad \sigma_{yxy} = \begin{pmatrix} 0 & 0 & 0 & 0 & 0 & 0 & 0 & -1 \\ 0 & 0 & 0 & 0 & 0 & 0 & 1 & 0 \\ 0 & 0 & 0 & 0 & 0 & -1 & 0 & 0 \\ 0 & 0 & 0 & 0 & 1 & 0 & 0 & 0 \\ 0 & 0 & 0 & 1 & 0 & 0 & 0 & 0 \\ 0 & 0 & -1 & 0 & 0 & 0 & 0 & 0 \\ 0 & 1 & 0 & 0 & 0 & 0 & 0 & 0 \\ -1 & 0 & 0 & 0 & 0 & 0 & 0 & 0 \end{pmatrix}$$

$$\sigma_{yyx} = \text{kronecker}(\sigma_y, \text{kronecker}(\sigma_y, \sigma_x)) \quad \sigma_{yyx} = \begin{pmatrix} 0 & 0 & 0 & 0 & 0 & 0 & 0 & -1 \\ 0 & 0 & 0 & 0 & 0 & 0 & -1 & 0 \\ 0 & 0 & 0 & 0 & 0 & 1 & 0 & 0 \\ 0 & 0 & 0 & 0 & 1 & 0 & 0 & 0 \\ 0 & 0 & 0 & 1 & 0 & 0 & 0 & 0 \\ 0 & 0 & 1 & 0 & 0 & 0 & 0 & 0 \\ 0 & -1 & 0 & 0 & 0 & 0 & 0 & 0 \\ -1 & 0 & 0 & 0 & 0 & 0 & 0 & 0 \end{pmatrix}$$

That the initial state is an eigenfunction of these operators with eigenvalue +1 is now demonstrated.

$$\Psi^T \sigma_{xyy} \Psi = 1 \quad \Psi^T \sigma_{yxy} \Psi = 1 \quad \Psi^T \sigma_{yyx} \Psi = 1$$

The fact that the operators commute means that they can have simultaneous eigenvalues.

$$\sigma_{xyy}\sigma_{yxy} - \sigma_{yxy}\sigma_{xyy} \to 0 \quad \sigma_{xyy}\sigma_{yyx} - \sigma_{yyx}\sigma_{xyy} \to 0 \quad \sigma_{yxy}\sigma_{yyx} - \sigma_{yyx}\sigma_{yxy} \to 0$$

The significance of this is evident when we consider the eigenvalue of the product of the three operators which obviously must be +1.

$$\left(\sigma_x^1 \sigma_y^2 \sigma_y^3\right)\left(\sigma_y^1 \sigma_x^2 \sigma_y^3\right)\left(\sigma_y^1 \sigma_y^2 \sigma_x^3\right) = 1 \quad \Psi^T \sigma_{xyy}\sigma_{yxy}\sigma_{yyx} \Psi = 1$$

If it is assumed that this result occurs because the particles are in well-defined spin states (s_x, s_y) prior to measurement the following must be accepted,

$$\left(s_x^1 s_y^2 s_y^3\right)\left(s_y^1 s_x^2 s_y^3\right)\left(s_y^1 s_y^2 s_x^3\right) = 1$$

Given that the spin measurement values can be +/- 1 and that the individual operators can have simultaneous eigenvalues, the following must be true,

$$s_y^1 s_y^1 = s_y^2 s_y^2 = s_y^3 s_y^3 = 1$$

This reduces the previous equation involving the three operators to the following local realistic prediction.

$$\left(s_x^1 s_x^2 s_x^3\right) = \left(\sigma_x^1 \sigma_x^2 \sigma_x^3\right) = 1$$

The disagreement between quantum mechanics and the local realistic view becomes starkly apparent when the $\sigma_x^1\sigma_x^2\sigma_x^3$ measurement outcome is calculated.

$$\sigma_{xxx} = \text{kronecker}(\sigma_x, \text{kronecker}(\sigma_x, \sigma_x)) \quad \Psi^T \sigma_{xxx} \Psi = -1$$

Thus we see absolute disagreement between local realism and quantum mechanics. Local realism predicts an eigenvalue of +1 and quantum mechanics an eigenvalue of -1.

The validity of the reasoning above requires that $\sigma_x^1\sigma_x^2\sigma_x^3$ commutes with the other operators, which we now demonstrate.

$$\sigma_{xyy}\sigma_{xxx} - \sigma_{xxx}\sigma_{xyy} \to 0 \quad \sigma_{yxy}\sigma_{xxx} - \sigma_{xxx}\sigma_{yxy} \to 0 \quad \sigma_{yyx}\sigma_{xxx} - \sigma_{xxx}\sigma_{yyx} \to 0$$

Appendix

The tensor product of three vectors is shown below.

$$\begin{pmatrix} a \\ b \end{pmatrix} \otimes \begin{pmatrix} c \\ d \end{pmatrix} \otimes \begin{pmatrix} e \\ f \end{pmatrix} = \begin{pmatrix} a \\ b \end{pmatrix} \otimes \begin{pmatrix} ce \\ cf \\ de \\ df \end{pmatrix} = \begin{pmatrix} ace \\ acf \\ ade \\ adf \\ bce \\ bcf \\ bde \\ bdf \end{pmatrix}$$

Mathcad does not have a command for the vector tensor product, so it is necessary to develop a way of implementing it using kronecker, which requires square matrices. For this reason the spin vector is stored in the left column of a 2x2 matrix by augmenting the spin vector with the null vector. After all the matrix tensor products have been carried out using kronecker the final spin vector resides in the left column of the final square matrix. Next the submatrix cammand is used to save this column, discarding the rest of the matrix.

The Mathcad syntax for the tensor multiplication of three vectors is as follows.

$$\Psi(a,\ b,\ c) = \text{submatrix}\left[\text{kronecker}\left[\text{augment}\left[a,\ \begin{pmatrix}0\\0\end{pmatrix}\right],\right.\right.$$
$$\left.\left.\text{kronecker}\left[\text{augment}\left[b,\ \begin{pmatrix}0\\0\end{pmatrix}\right],\ \text{augment}\left[c,\ \begin{pmatrix}0\\0\end{pmatrix}\right]\right]\right], 1,\ 8,\ 1,\ 1\right]$$

The initial spin state:

$$\frac{1}{\sqrt{2}}\left(\Psi\left(Sz_{up},\ Sz_{up},\ Sz_{up}\right) - \Psi\left(Sz_{down},\ Sz_{down},\ Sz_{down}\right)\right) = \begin{pmatrix} 0.707 \\ 0 \\ 0 \\ 0 \\ 0 \\ 0 \\ 0 \\ -0.707 \end{pmatrix}$$

This page titled 8.22: Elements of Reality- Another GHZ Gedanken Experiment Analyzed is shared under a CC BY 4.0 license and was authored, remixed, and/or curated by Frank Rioux via source content that was edited to the style and standards of the LibreTexts platform.

8.23: Brief Elements of Reality

In the '90s N. David Mermin published two articles in the general physics literature (Physics Today, June 1990; American Journal of Physics, August 1990) on the Greenberger-Horne-Zeilinger (GHZ) gedanken experiment (American Journal of Physics, December 1990; Nature, 3 February 2000) involving three spin-1/2 particles that illustrated the clash between local realism and the quantum view of reality for the quantum nonspecialist.

The three spin-1/2 particles are created in a single event and move apart in the horizontal y-z plane. It will be shown that a consideration of spin measurements (in units of h/4π in the x- and y-directions reveals the impossibility of assigning values to the spin observables independent of measurement.

The x- and y-direction spin operators are the Pauli matrices:

$$\sigma_x = \begin{pmatrix} 0 & 1 \\ 1 & 0 \end{pmatrix} \quad \sigma_y = \begin{pmatrix} 0 & -i \\ i & 0 \end{pmatrix}$$

The eigenvalues of the Pauli matrices are +/- 1:

$$\text{eigenvals}(\sigma_x) = \begin{pmatrix} 1 \\ -1 \end{pmatrix} \quad \text{eigenvals}(\sigma_y) = \begin{pmatrix} 1 \\ -1 \end{pmatrix}$$

The following operators represent the measurement protocols for spins 1, 2 and 3.

$$\sigma_x^1 \otimes \sigma_y^2 \otimes \sigma_y^3 \quad \sigma_y^1 \otimes \sigma_x^2 \otimes \sigma_y^3 \quad \sigma_y^1 \otimes \sigma_y^2 \otimes \sigma_x^3 \quad \sigma_x^1 \otimes \sigma_x^2 \otimes \sigma_x^3$$

The tensor matrix product, also known as the Kronecker product, is available in Mathcad. The four operators in tensor format are formed as follows.

$$\sigma_{xyy} = \text{kronecker}(\sigma_x,\ \text{kronecker}(\sigma_y,\ \sigma_y)) \quad \sigma_{yxy} = \text{kronecker}(\sigma_y,\ \text{kronecker}(\sigma_x,\ \sigma_y))$$
$$\sigma_{yyx} = \text{kronecker}(\sigma_y,\ \text{kronecker}(\sigma_y,\ \sigma_x)) \quad \sigma_{xxx} = \text{kronecker}(\sigma_x,\ \text{kronecker}(\sigma_x,\ \sigma_x))$$

These operators mutually commute, meaning that they can be assigned simultaneous eigenstates with simultaneous eigenvalues.

$$\sigma_{xyy}\sigma_{yxy} - \sigma_{yxy}\sigma_{xyy} \to 0 \quad \sigma_{xyy}\sigma_{yyx} - \sigma_{yyx}\sigma_{xyy} \to 0 \quad \sigma_{xyy}\sigma_{xxx} - \sigma_{xxx}\sigma_{xyy} \to 0$$
$$\sigma_{yxy}\sigma_{yyx} - \sigma_{yyx}\sigma_{yxy} \to 0 \quad \sigma_{yxy}\sigma_{xxx} - \sigma_{xxx}\sigma_{yxy} \to 0 \quad \sigma_{yyx}\sigma_{xxx} - \sigma_{xxx}\sigma_{yyx} \to 0$$

The next step is to compare the matrix for the product of the first three operators (σ_{xyy} $\sigma_{yxy}\sigma_{yyx}$) with that of the fourth (σ_{xxx}).

$$\sigma_{xyy}\sigma_{yxy}\sigma_{yyx} = \begin{pmatrix} 0 & 0 & 0 & 0 & 0 & 0 & 0 & -1 \\ 0 & 0 & 0 & 0 & 0 & 0 & -1 & 0 \\ 0 & 0 & 0 & 0 & 0 & -1 & 0 & 0 \\ 0 & 0 & 0 & 0 & -1 & 0 & 0 & 0 \\ 0 & 0 & 0 & -1 & 0 & 0 & 0 & 0 \\ 0 & 0 & -1 & 0 & 0 & 0 & 0 & 0 \\ 0 & -1 & 0 & 0 & 0 & 0 & 0 & 0 \\ -1 & 0 & 0 & 0 & 0 & 0 & 0 & 0 \end{pmatrix} \quad \sigma_{xxx} = \begin{pmatrix} 0 & 0 & 0 & 0 & 0 & 0 & 0 & 1 \\ 0 & 0 & 0 & 0 & 0 & 0 & 1 & 0 \\ 0 & 0 & 0 & 0 & 0 & 1 & 0 & 0 \\ 0 & 0 & 0 & 0 & 1 & 0 & 0 & 0 \\ 0 & 0 & 0 & 1 & 0 & 0 & 0 & 0 \\ 0 & 0 & 1 & 0 & 0 & 0 & 0 & 0 \\ 0 & 1 & 0 & 0 & 0 & 0 & 0 & 0 \\ 1 & 0 & 0 & 0 & 0 & 0 & 0 & 0 \end{pmatrix}$$

This indicates the following relationship between the four operators and leads quickly to a refutation of the concept of noncontextual, hidden values for quantum mechanical observables.

$$\left(\sigma_x^1 \otimes \sigma_y^2 \otimes \sigma_y^3\right)\left(\sigma_y^1 \otimes \sigma_x^2 \otimes \sigma_y^3\right)\left(\sigma_y^1 \otimes \sigma_y^2 \otimes \sigma_x^3\right) = -\left(\sigma_x^1 \otimes \sigma_x^2 \otimes \sigma_x^3\right)$$

Local realism assumes that objects have definite properties independent of measurement. In this example it assumes that the x- and y-components of the spin have definite values prior to measurement. This position leads to a contradiction with the above result. There is no way to assign eigenvalues (+/-1) to the operators that is consistent with the above result.

Concentrating on the operator on the left side, we notice that there is a σ_y measurement on the first spin in the second and third term (blue). If the spin state is well-defined before measurement those results have to be the same, either both +1 or both -1, so that the product of the two measurements is +1. There is a σ_y measurement on the second spin in terms one and three (red). By similar arguments those results will lead to a product of +1 also. Finally there is a σ_y measurement on the third spin in terms one and two

(green). By similar arguments those results will lead to a product of +1 also. Incorporating these observations into the expression above leads to the following contradiction.

$$\sigma_x^1 \otimes \sigma_x^2 \otimes \sigma_x^3 = -\sigma_x^1 \otimes \sigma_x^2 \otimes \sigma_x^3$$

This result should cause all mathematically literate local realists to renounce and recant their heresy.

This page titled 8.23: Brief Elements of Reality is shared under a CC BY 4.0 license and was authored, remixed, and/or curated by Frank Rioux via source content that was edited to the style and standards of the LibreTexts platform.

8.24: A Brief Analysis of Mermin's GHZ Thought Experiment

Twenty years ago N. David Mermin published two articles (Physics Today, June 1990; American Journal of Physics, August 1990) in the general physics literature on a Greenberger-Horne-Zeilinger (American Journal of Physics, December 1990; Nature, 3 February 2000) gedanken experiment involving spins that sharply revealed the clash between local realism and the quantum view of reality.

Three spin-1/2 particles are created in a single event and move apart in the horizontal y-z plane. Subsequent spin measurements will be carried out in units of h/4π in the z-basis with spin operators in the x- and y-directions.

The z-basis eigenfunctions are:

$$Sz_{up} = \begin{pmatrix} 1 \\ 0 \end{pmatrix} \quad Sz_{down} = \begin{pmatrix} 0 \\ 1 \end{pmatrix}$$

The x- and y-direction spin operators in the z-basis are the Pauli matrices:

$$\sigma_x = \begin{pmatrix} 0 & 1 \\ 1 & 0 \end{pmatrix} \quad \sigma_y = \begin{pmatrix} 0 & -i \\ i & 0 \end{pmatrix}$$

The initial entangled spin state for the three spin-1/2 particles in tensor notation is:

$$|\Psi\rangle = \frac{1}{\sqrt{2}} \left[\begin{pmatrix} 1 \\ 0 \end{pmatrix} \otimes \begin{pmatrix} 1 \\ 0 \end{pmatrix} \otimes \begin{pmatrix} 1 \\ 0 \end{pmatrix} - \begin{pmatrix} 0 \\ 1 \end{pmatrix} \otimes \begin{pmatrix} 0 \\ 1 \end{pmatrix} \otimes \begin{pmatrix} 0 \\ 1 \end{pmatrix} \right] = \frac{1}{\sqrt{2}} \begin{pmatrix} 1 \\ 0 \\ 0 \\ 0 \\ 0 \\ 0 \\ 0 \\ -1 \end{pmatrix} \quad \Psi = \frac{1}{\sqrt{2}} \begin{pmatrix} 1 \\ 0 \\ 0 \\ 0 \\ 0 \\ 0 \\ 0 \\ -1 \end{pmatrix}$$

The following operators represent the measurements to be carried out on spins 1, 2 and 3, in that order.

$$\sigma_x^1 \otimes \sigma_y^2 \otimes \sigma_y^3 \quad \sigma_y^1 \otimes \sigma_x^2 \otimes \sigma_y^3 \quad \sigma_y^1 \otimes \sigma_y^2 \otimes \sigma_x^3 \quad \sigma_x^1 \otimes \sigma_x^2 \otimes \sigma_x^3$$

The matrix tensor product is also known as the Kronecker product, which is available in Mathcad. The four operators in tensor format are formed as follows.

$$\sigma_{xyy} = \text{kronecker}(\sigma_x,\ \text{kronecker}(\sigma_y,\ \sigma_y)) \quad \sigma_{yxy} = \text{kronecker}(\sigma_y,\ \text{kronecker}(\sigma_x,\ \sigma_y))$$
$$\sigma_{yyx} = \text{kronecker}(\sigma_y,\ \text{kronecker}(\sigma_y,\ \sigma_x)) \quad \sigma_{xxx} = \text{kronecker}(\sigma_x,\ \text{kronecker}(\sigma_x,\ \sigma_x))$$

The expectation values of the operators are now calculated.

$$\Psi^T \sigma_{xyy} \Psi = 1 \quad \Psi^T \sigma_{yxy} \Psi = 1 \quad \Psi^T \sigma_{yyx} \Psi = 1 \quad \Psi^T \sigma_{xxx} \Psi = -1$$

Consequently the product of the four operators has the expectation value of -1.

$$\Psi^T \sigma_{xyy} \sigma_{yxy} \sigma_{yyx} \sigma_{xxx} \Psi = -1$$

Local realism assumes that objects have definite properties independent of measurement. In this example it assumes that the x- and y-components of the spin have definite values prior to measurement. This position leads to a contradiction with the above result. The following analysis is taken from "Quantum Information Science" by Seth Lloyd.

Looking again at the measurement operators, notice that there is a σ_x measurement on the first spin in the first and fourth experiment. If the spin state is well-defined before measurement those results have to be the same, either both +1 or both -1, so that the product of the two measurements is +1.

$$\sigma_x^1 \otimes \sigma_y^2 \otimes \sigma_y^3 \quad \sigma_y^1 \otimes \sigma_x^2 \otimes \sigma_y^3 \quad \sigma_y^1 \otimes \sigma_y^2 \otimes \sigma_x^3 \quad \sigma_x^1 \otimes \sigma_x^2 \otimes \sigma_x^3$$

Likewise there is a σ_y measurement on the second spin in experiments one and three. By similar arguments those results will lead to a product of +1 also. Continuing with all the pairs in the total operator using local realistic reasoning unambiguously shows that

its expectation value should be +1, in sharp disagreement with the quantum mechanical result of -1.

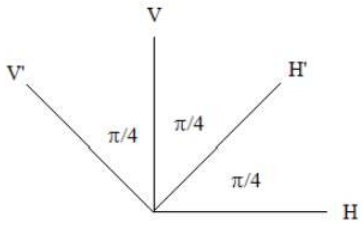
This page titled 8.24: A Brief Analysis of Mermin's GHZ Thought Experiment is shared under a CC BY 4.0 license and was authored, remixed, and/or curated by Frank Rioux via source content that was edited to the style and standards of the LibreTexts platform.

8.25: Lucien Hardy's Paradox as Presented by N. David Mermin

Hardy created a two-photon thought experiment for which a local hidden-variable (EPR) model for the photon states is not consistent with all the predictions of quantum theory.

A source emits two photons in the following entangled state, $\Psi = \frac{2}{\sqrt{3}}\left(H_A H_B - \frac{1}{2} H'_A H'_B\right)$, with the first photon traveling to Alice at a detector to the left of the source and the second to Bob at a detector on the right.

The following diagram shows the directions that linear polarization measurements will be made on the entangled two-photon system. The detectors can be set to measure in either the H-V or H'-V' basis.



Definition of polarization eigenstates:

$$H = \begin{pmatrix} 1 \\ 0 \end{pmatrix} \quad V = \begin{pmatrix} 0 \\ 1 \end{pmatrix} \quad H' = \frac{1}{\sqrt{2}} \begin{pmatrix} 1 \\ 1 \end{pmatrix} \quad V' = \frac{1}{\sqrt{2}} \begin{pmatrix} -1 \\ 1 \end{pmatrix}$$

Ψ is expressed in tensor format:

$$\Psi = \frac{2}{\sqrt{3}} \left[\begin{pmatrix} 1 \\ 0 \\ 0 \\ 0 \end{pmatrix} - \frac{1}{4} \begin{pmatrix} 1 \\ 1 \\ 1 \\ 1 \end{pmatrix} \right] \quad \Psi = \begin{pmatrix} 0.866 \\ -0.289 \\ -0.289 \\ -0.289 \end{pmatrix} \quad \Psi^T \Psi = 1$$

The first photon goes to Alice, the second to Bob. They record the results of a large number of independent, random polarization measurements on their photon pairs. They could for example enter their results in the following table which identifies all possible measurement outcomes.

$$\begin{pmatrix} \text{V'V'} & \text{V'V} & \text{V'H'} & \text{V'H} \\ \text{VV'} & \text{VV} & \text{VH'} & \text{VH} \\ \text{H'V'} & \text{H'V} & \text{H'H'} & \text{H'H} \\ \text{HV'} & \text{HV} & \text{HH'} & \text{HH} \end{pmatrix}$$

The next step is to calculate the probability that these observations will be made given Ψ as the initial state. To this end we form the product state vectors in tensor format using the definitions of H, V, H' and V' provided earlier.

$$\text{V'V'} = \tfrac{1}{2}\begin{pmatrix}1\\-1\\-1\\1\end{pmatrix} \quad \text{V'V} = \tfrac{1}{\sqrt{2}}\begin{pmatrix}0\\-1\\0\\1\end{pmatrix} \quad \text{V'H'} = \tfrac{1}{2}\begin{pmatrix}-1\\-1\\1\\1\end{pmatrix} \quad \text{V'H} = \tfrac{1}{\sqrt{2}}\begin{pmatrix}-1\\0\\1\\0\end{pmatrix}$$

$$\text{VV'} = \tfrac{1}{\sqrt{2}}\begin{pmatrix}0\\0\\-1\\1\end{pmatrix} \quad \text{VV} = \begin{pmatrix}0\\0\\0\\1\end{pmatrix} \quad \text{VH'} = \tfrac{1}{\sqrt{2}}\begin{pmatrix}0\\0\\1\\1\end{pmatrix} \quad \text{VH} = \begin{pmatrix}0\\0\\1\\0\end{pmatrix}$$

$$\text{H'V'} = \tfrac{1}{2}\begin{pmatrix}-1\\1\\-1\\1\end{pmatrix} \quad \text{H'V} = \tfrac{1}{\sqrt{2}}\begin{pmatrix}0\\1\\0\\1\end{pmatrix} \quad \text{H'H'} = \tfrac{1}{2}\begin{pmatrix}1\\1\\1\\1\end{pmatrix} \quad \text{H'H} = \tfrac{1}{\sqrt{2}}\begin{pmatrix}1\\0\\1\\0\end{pmatrix}$$

$$\text{HV'} = \tfrac{1}{\sqrt{2}}\begin{pmatrix}-1\\1\\0\\0\end{pmatrix} \quad \text{HV} = \begin{pmatrix}0\\1\\0\\0\end{pmatrix} \quad \text{HH'} = \tfrac{1}{\sqrt{2}}\begin{pmatrix}1\\1\\0\\0\end{pmatrix} \quad \text{HH} = \begin{pmatrix}1\\0\\0\\0\end{pmatrix}$$

Using these two-photon state functions we now calculate the probability of occurrence for each possible measurement outcome, as displayed in the following matrix.

$$\begin{bmatrix} \left(\left|V'V'^{T}\Psi\right|\right)^2 & \left(\left|V'V^{T}\Psi\right|\right)^2 & \left(\left|V'H'^{T}\Psi\right|\right)^2 & \left(\left|V'H^{T}\Psi\right|\right)^2 \\ \left(\left|VV'^{T}\Psi\right|\right)^2 & \left(\left|VV^{T}\Psi\right|\right)^2 & \left(\left|VH'^{T}\Psi\right|\right)^2 & \left(\left|VH^{T}\Psi\right|\right)^2 \\ \left(\left|H'V'^{T}\Psi\right|\right)^2 & \left(\left|H'V^{T}\Psi\right|\right)^2 & \left(\left|H'H'^{T}\Psi\right|\right)^2 & \left(\left|H'H^{T}\Psi\right|\right)^2 \\ \left(\left|HV'^{T}\Psi\right|\right)^2 & \left(\left|HV^{T}\Psi\right|\right)^2 & \left(\left|HH'^{T}\Psi\right|\right)^2 & \left(\left|HH^{T}\Psi\right|\right)^2 \end{bmatrix} = \begin{pmatrix} 0.333 & 0 & 0.333 & 0.667 \\ 0 & 0.083 & 0.167 & 0.083 \\ 0.333 & 0.167 & 0 & 0.167 \\ 0.667 & 0.083 & 0.167 & 0.75 \end{pmatrix}$$

So, where's the paradox, where's the problem? The paradox/problem is revealed by concentrating on four entries in the matrix above.

Alice	Bob	Result
V	V'	Never
V'	V	Never
V	V	Sometimes
H'	H'	Never

In any run the detectors might be set to measure [H'-V']/[H-V] or [H-V]/[H'-V']. So if one photon triggers a [H-V] detector to register V, its partner must require a [H'-V'] detector to register H' according to the first two rows of the matrix above. According to the local hidden-variable model (EPR) this means H' is an element of reality.

It follows that any [H-V]/[H-V] run in which both detectors register V (probability 0.083) each photon must require a [H'-V'] detector to register H'. Therefore, if a [H'-V']/[H'-V'] run had been selected both detectors would have registered H'.

However, given the initial photon state function the result H'H' should never be observed. In other words it is impossible to assign specific polarization states (instruction sets) to the photons prior to measurement that are in agreement with all quantum mechanical predictions for this thought experiment.

An algebraic analysis shows that destructive interference eliminates the H'H' term. It also gives the correct probabilities for V'V', V'H' and H'V' measurements. Algebraic analysis could be used to produce the entire measurement outcome matrix calculated above.

$$\tfrac{2}{\sqrt{3}}\left[|H\rangle_A|H\rangle_B - \tfrac{1}{2}H'\rangle_A|H'\rangle_B\right]$$

Substitute

$$|H\rangle = \tfrac{1}{\sqrt{2}}\left(|H'\rangle - |V'\rangle\right)$$

$$\downarrow$$

$$\tfrac{2}{\sqrt{3}}\left[\tfrac{1}{\sqrt{2}}\left(|H'\rangle_A - |V'\rangle_B\right)\tfrac{1}{\sqrt{2}}\left(|H'\rangle_A - |V'\rangle_B\right) - \tfrac{1}{2}|H'\rangle_A|H'\rangle_B\right]$$

$$\downarrow$$

$$\tfrac{1}{\sqrt{3}}\left[|V'\rangle_A|V'\rangle_B - |V'\rangle_A|H'\rangle_B - |H'\rangle_A|V'\rangle_B\right]$$

Sources:

Lucien Hardy, "Spooky Action at a Distance in Quantum Mechanics," ***Contemporary Physics*** **39**, 419-429 (1998).

N. David Mermin, "Quantum Mysteries Refined," ***American Journal of Physics*** **62**, 880-887 (1994). C. C. Gerry and K. M. Bruno, ***The Quantum Divide***, Oxford U. P., 2013, pp. 124-29.

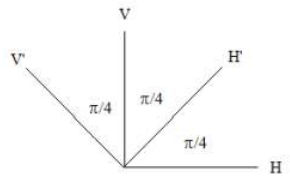
This page titled 8.25: Lucien Hardy's Paradox as Presented by N. David Mermin is shared under a CC BY 4.0 license and was authored, remixed, and/or curated by Frank Rioux via source content that was edited to the style and standards of the LibreTexts platform.

8.26: Hardy's Paradox - An Algebraic Analysis

Hardy created a two-photon thought experiment for which a local hidden-variable (EPR) model for the photon states is not consistent with all the predictions of quantum theory.

A source emits two photons in the following entangled state, $\Psi = \frac{2}{\sqrt{3}}\left(H_A H_B - \frac{1}{2} H'_A H'_B\right)$, with the first photon traveling to Alice at a detector to the left of the source and the second to Bob at a detector on the right.

The following diagram shows the directions that linear polarization measurements will be made on the entangled two-photon system. The detectors can be set to measure in either the H-V or H'-V' basis.



Alice and Bob record the results of a large number of independent, random polarization measurements on their photon pairs. The following table identifies all possible measurement outcomes. The probabilites of these outcomes are determined algebraically below.

$$\begin{pmatrix} \text{V'V'} & \text{V'V} & \text{V'H'} & \text{V'H} \\ \text{VV'} & \text{VV} & \text{VH'} & \text{VH} \\ \text{H'V'} & \text{H'V} & \text{H'H'} & \text{H'H} \\ \text{HV'} & \text{HV} & \text{HH'} & \text{HH} \end{pmatrix}$$

Alice and Bob both make H-V measurements:

$$\Psi = \frac{2}{\sqrt{3}}\left(H_A H_B - \frac{1}{2} H'_A H'_B\right)\left|\begin{array}{l}\text{substitute, } H'_A = \frac{1}{\sqrt{2}}(H'_A - V'_A) \\ \text{substitute, } H'_B = \frac{1}{\sqrt{2}}(H'_B - V'_B) \\ \text{simplify}\end{array}\right. \rightarrow \Psi$$
$$= \frac{\sqrt{3} V'_A V'_B}{3} - \frac{\sqrt{3} H'_B V'_A}{3} - \frac{\sqrt{3} H'_A V'_B}{3}$$

Measurement probabilities: V'V' = V'H' = H'V' = 0.333

Alice and Bob both make H'-V' measurements:

$$\Psi = \frac{2}{\sqrt{3}}\left(H_A H_B - \frac{1}{2} H'_A H'_B\right)\left|\begin{array}{l}\text{substitute, } H'_A = \frac{1}{\sqrt{2}}(H_A + V_A) \\ \text{substitute, } H_B = \frac{1}{\sqrt{2}}(H_B - V_B) \\ \text{simplify}\end{array}\right. \rightarrow \Psi$$
$$= \frac{\sqrt{3}\left(H_A V_B - 3 H_A H_B + H_B V_A + V_A V_B\right)}{6}$$

Measurement probabilities: HV = VH = VV = 0.083 HH = 0.75

Alice makes H-V measurements and Bob makes H'-V' measurements:

$$\Psi = \frac{2}{\sqrt{3}}\left(H_A H_B - \frac{1}{2} H'_A H'_B\right)\left|\begin{array}{l}\text{substitute, } H'_A = \frac{1}{\sqrt{2}}(H_A + V_A) \\ \text{substitute, } H_B = \frac{1}{\sqrt{2}}(H'_B - V'_B) \\ \text{simplify}\end{array}\right. \rightarrow \Psi$$
$$= \frac{\sqrt{6} H_A H'_B}{6} - \frac{\sqrt{6} H'_B V_A}{6} - \frac{\sqrt{6} H_A V'_B}{6}$$

Measurement probabilities: HH' = VH' = 0.167 HV' = 0.667

Alice makes H'-V' measurements and Bob makes H-V measurements:

$$\Psi = \frac{2}{\sqrt{3}}\left(H_A H_B - \frac{1}{2}H'_A H'_B\right)\Bigg|\begin{array}{l}\text{substitute, } H_A = \frac{1}{\sqrt{2}}(H'_A + V'_A)\\ \text{substitute, } H'_B = \frac{1}{\sqrt{2}}(H_B + V_B)\\ \text{simplify}\end{array} \rightarrow \Psi$$

$$= \frac{\sqrt{6}H_B H'_A}{6} - \frac{\sqrt{6}H'_A V_B}{6} - \frac{\sqrt{6}H_B V'_A}{3}$$

Measurement probabilities: H'H = H'V = 0.167 V'H = 0.667

The following measurement outcomes never occur: VV' = V'V = H'H' = 0

The results are collected in the following table.

$$\begin{bmatrix} \left(\left|V'V'^T\Psi\right|\right)^2 & \left(\left|V'V^T\Psi\right|\right)^2 & \left(\left|V'H'^T\Psi\right|\right)^2 & \left(\left|V'H^T\Psi\right|\right)^2 \\ \left(\left|VV'^T\Psi\right|\right)^2 & \left(\left|VV^T\Psi\right|\right)^2 & \left(\left|VH'^T\Psi\right|\right)^2 & \left(\left|VH^T\Psi\right|\right)^2 \\ \left(\left|H'V'^T\Psi\right|\right)^2 & \left(\left|H'V^T\Psi\right|\right)^2 & \left(\left|H'H'^T\Psi\right|\right)^2 & \left(\left|H'H^T\Psi\right|\right)^2 \\ \left(\left|HV'^T\Psi\right|\right)^2 & \left(\left|HV^T\Psi\right|\right)^2 & \left(\left|HH'^T\Psi\right|\right)^2 & \left(\left|HH^T\Psi\right|\right)^2 \end{bmatrix} = \begin{pmatrix} 0.333 & 0 & 0.333 & 0.667 \\ 0 & 0.083 & 0.167 & 0.083 \\ 0.333 & 0.167 & 0 & 0.167 \\ 0.667 & 0.083 & 0.167 & 0.75 \end{pmatrix}$$

Hardy's paradox is revealed by concentrating on four entries in the table.

$$\begin{pmatrix} \text{Alice} & \text{Bob} & \text{Result} \\ V & V' & \text{Never} \\ V' & V & \text{Never} \\ V & V & \text{Sometimes} \\ H' & H' & \text{Never} \end{pmatrix}$$

In any run the detectors might be set to measure [H'-V']/[H-V] or [H-V]/[H'-V']. So if one photon triggers a [H-V] detector to register V, its partner must require a [H'-V'] detector to register H' according to the first two rows of the table above. According to the local hidden-variable model (EPR) this means H' is an element of reality.

It follows that any [H-V]/[H-V] run in which both detectors register V (probability 0.083) each photon must require a [H'-V'] detector to register H'. Therefore, if a [H'-V']/[H'-V'] run had been selected both detectors would have registered H'. However, given the initial photon state function the result H'H' should never be observed. In other words it is impossible to assign specific polarization states (instruction sets) to the photons prior to measurement that are in agreement with all quantum mechanical predictions for this thought experiment.

C. C. Gerry and K. M. Bruno, ***The Quantum Divide***, Oxford U. P., 2013, pp. 124-29.

This page titled 8.26: Hardy's Paradox - An Algebraic Analysis is shared under a CC BY 4.0 license and was authored, remixed, and/or curated by Frank Rioux via source content that was edited to the style and standards of the LibreTexts platform.

8.27: Quantum Entanglement Leads to Nonclassical Correlations

This tutorial employs a tensor algebra approach to a gedanken experiment published by P. K. Aravind in the 2004 October issue of the ***American Journal of Physics***. Aravind's thought experiment demonstrates how quantum entanglement leads directly to bizarre nonclassical correlations.

A source emits the following four-particle entangled state, with particles 1 and 3 going to Alice and particles 2 and 4 going to Bob. α and β are the eigenstates of the Pauli σ_z operator.

$$\alpha = \begin{pmatrix} 1 \\ 0 \end{pmatrix} \quad \beta = \begin{pmatrix} 0 \\ 1 \end{pmatrix}$$

$$|\Psi\rangle = \tfrac{1}{\sqrt{2}}\left(|\alpha\rangle_1|\alpha\rangle_2 + |\beta\rangle_1|\beta\rangle_2\right) \otimes \tfrac{1}{\sqrt{2}}\left(|\alpha\rangle_3|\alpha\rangle_4 + |\beta\rangle_3|\beta\rangle_4\right)$$
$$= \tfrac{1}{2}\left(|\alpha\rangle_1|\alpha\rangle_2|\alpha\rangle_3|\alpha_4 + |\alpha\rangle_1|\alpha\rangle_2|\beta\rangle_3|\beta\rangle_4 + |\beta\rangle_1|\beta\rangle_2|\alpha\rangle_3|\alpha\rangle_4 + |\beta\rangle_1|\beta\rangle_2|\beta\rangle_3|\beta\rangle_4\right)$$
$$= \tfrac{1}{2}(1 \quad 0 \quad 0 \quad 1 \quad 0 \quad 0 \quad 0 \quad 0 \quad 0 \quad 0 \quad 0 \quad 0 \quad 1 \quad 0 \quad 0 \quad 1)^T$$
$$\Psi = \tfrac{1}{2}(1 \quad 0 \quad 0 \quad 1 \quad 0 \quad 0 \quad 0 \quad 0 \quad 0 \quad 0 \quad 0 \quad 0 \quad 1 \quad 0 \quad 0 \quad 1)^T$$

Alice and Bob each have six measurement choices: R1, R2, R3, C1, C2, and C3. Each choice consists of a sequence of three measurements on the entangled spin pair they receive. These are shown in the table below. A sequence of measurements is possible because the operators in each row and each column mutually commute, as will be shown later.

	$C1$	$C2$	$C3$
$R1$	$I \otimes \sigma_z$	$\sigma_z \otimes I$	$\sigma_z \otimes \sigma_z$
$R2$	$\sigma_x \otimes I$	$I \otimes \sigma_x$	$\sigma_x \otimes \sigma_x$
$R3$	$\sigma_x \otimes \sigma_z$	$\sigma_z \otimes \sigma_x$	$\sigma_y \otimes \sigma_y$

Alice and Bob independently and randomly set their detectors to one of the six possible settings each time the source emits the entangled particles, and record the result (+1 or -1) for each panel. After a statistically meaningful number of events they compare their results.

The operators required for this exercise are as follows:

$$I = \begin{pmatrix} 1 & 0 \\ 0 & 1 \end{pmatrix} \quad \sigma_x = \begin{pmatrix} 0 & 1 \\ 1 & 0 \end{pmatrix} \quad \sigma_y = \begin{pmatrix} 0 & -i \\ i & 0 \end{pmatrix} \quad \sigma_z = \begin{pmatrix} 1 & 0 \\ 0 & -1 \end{pmatrix}$$

Alice and Bob's measurement operators are constructed in tensor format:

$A(a,\ b,\ c,\ d) = \text{kronecker(a, kronecker(b, kronecker(c, d)))}$

$B(a,\ b,\ c,\ d) = \text{kronecker(a, kronecker(b, kronecker(c, d)))}$

Because Alice gets particles 1 and 3, and Bob particles 2 and 4, their measurement operators in tensor notation are as shown below.

Alice

$$\begin{pmatrix} A(I,\ I,\ \sigma_z,\ I) & A(\sigma_z,\ I,\ I,\ I) & A(\sigma_z,\ I,\ \sigma_z,\ I) \\ A(\sigma_x,\ I,\ I,\ I) & A(I,\ I,\ \sigma_x,\ I) & A(\sigma_x,\ I,\ \sigma_x,\ I) \\ A(\sigma_x,\ I,\ \sigma_z,\ I) & A(\sigma_z,\ I,\ \sigma_x,\ I) & A(\sigma_y,\ I,\ \sigma_y,\ I) \end{pmatrix}$$

Bob

$$\begin{pmatrix} B(I,\ I,\ I,\ \sigma_z) & B(I,\ \sigma_z,\ I,I) & B(I,\ \sigma_z,\ I,\ \sigma_z) \\ B(I,\ \sigma_x,\ I,\ I) & B(I,\ I,\ I,\ \sigma_x) & B(I,\ \sigma_x,\ I,\ \sigma_x) \\ B(I,\ \sigma_x,\ I,\ \sigma_z) & B(I,\ \sigma_z,\ I,\ \sigma_z) & B(I,\sigma_y,\ I,\ \sigma_y) \end{pmatrix}$$

Where $A(I,\ I,\ \sigma_z,\ I)$ stands for $I \otimes I \otimes \sigma_z \otimes I$ and means Alice's operator for her particle is $I \otimes \sigma_z$. Using a representative row and column, we show that the measurement operators in the rows and columns of the measurement grid commute.

First row:

$$\begin{pmatrix} A(I,\ I,\ \sigma_z,\ I)A(\sigma_z,\ I,\ I\ ,I) - A(\sigma_z,\ I,\ I\ ,I)A(I,\ I,\ \sigma_z,\ I) \\ A(I,\ I,\ \sigma_z,\ I)A(\sigma_z,\ I,\ \sigma_z\ ,I) - A(\sigma_z,\ I,\ \sigma_z\ ,I)A(I,\ I,\ \sigma_z,\ I) \\ A(\sigma_z,\ I,\ I,\ I)A(\sigma_z,\ I,\ \sigma_z\ ,I) - A(\sigma_z,\ I,\ \sigma_z\ ,I)A(\sigma_z,\ I,\ I,\ I) \end{pmatrix} \rightarrow \begin{pmatrix} 0 \\ 0 \\ 0 \end{pmatrix}$$

Third column:

$$\begin{pmatrix} A(\sigma_z,\ I,\ \sigma_z,\ I)A(\sigma_x,\ I,\ \sigma_x\ ,I) - A(\sigma_x,\ I,\ \sigma_x\ ,I)A(\sigma_z,\ I,\ \sigma_z,\ I) \\ A(\sigma_z,\ I,\ \sigma_z,\ I)A(\sigma_y,\ I,\ \sigma_y\ ,I) - A(\sigma_y,\ I,\ \sigma_y\ ,I)A(\sigma_z,\ I,\ \sigma_z,\ I) \\ A(\sigma_x,\ I,\ \sigma_x,\ I)A(\sigma_y,\ I,\ \sigma_y\ ,I) - A(\sigma_y,\ I,\ \sigma_y\ ,I)A(\sigma_x,\ I,\ \sigma_x,\ I) \end{pmatrix} \rightarrow \begin{pmatrix} 0 \\ 0 \\ 0 \end{pmatrix}$$

These results establish the validity of doing sequential measurements in any row or column.

The eigenvalues of the individual operators in each panel are +/-1, and for Ψ the expectation values for the operators of the individual panels making up the rows and columns are zero. This is demonstrated for both Alice and Bob.

Alice

$$\begin{pmatrix} \Psi^T A(I,\ I,\ \sigma_z,\ I)\Psi & \Psi^T A(\sigma_z,\ I,\ I,\ I)\Psi & \Psi^T A(\sigma_z,\ I,\ \sigma_z,\ I)\Psi \\ \Psi^T A(\sigma_x,\ I,\ I,\ I)\Psi & \Psi^T A(I,\ I,\ \sigma_x,\ I)\Psi & \Psi^T A(\sigma_x,\ I,\ \sigma_x,\ I)\Psi \\ \Psi^T A(\sigma_x,\ I,\ \sigma_z,\ I)\Psi & \Psi^T A(\sigma_z,\ I,\ \sigma_x,\ I)\Psi & \Psi^T A(\sigma_y,\ I,\ \sigma_y,\ I)\Psi \end{pmatrix} = \begin{pmatrix} 0 & 0 & 0 \\ 0 & 0 & 0 \\ 0 & 0 & 0 \end{pmatrix}$$

Bob

$$\begin{pmatrix} \Psi^T B(I,\ I,\ I,\ \sigma_z)\Psi & \Psi^T B(I,\ \sigma_z,\ I,\ I)\Psi & \Psi^T B(I,\ \sigma_z,\ I,\ \sigma_z)\Psi \\ \Psi^T B(I,\ \sigma_x,\ I,\ I)\Psi & \Psi^T B(I,\ I,\ I,\ \sigma_x)\Psi & \Psi^T B(I,\ \sigma_x,\ I,\ \sigma_x)\Psi \\ \Psi^T B(I,\ \sigma_x,\ I,\ \sigma_z)\Psi & \Psi^T B(I,\ \sigma_z,\ I,\ \sigma_x)\Psi & \Psi^T B(I,\ \sigma_y,\ I,\ \sigma_y)\Psi \end{pmatrix} = \begin{pmatrix} 0 & 0 & 0 \\ 0 & 0 & 0 \\ 0 & 0 & 0 \end{pmatrix}$$

These calculations indicate that the individual panels on the measurement grids will flash +1 and -1 with equal frequency. However, if Alice and Bob measure the same observable pair, they always obtain the same eigenvalue, suggesting at this point a classical correlation between their individual results.

$$\begin{pmatrix} \Psi^T A(I,\ I,\ \sigma_z,\ I) & \Psi^T A(\sigma_z,\ I,\ I,\ I)B(I,\ \sigma_z,\ I,\ I)\Psi & \Psi^T A(\sigma_z,\ I,\ \sigma_z,\ I) \\ B(I,\ I,\ I,\ \sigma_z)\Psi & & B(I,\ \sigma_z,\ I,\ \sigma_z)\Psi \\ \Psi^T A(\sigma_x,\ I,\ I,\ I) & \Psi^T A(I,\ I,\ \sigma_x,\ I)B(I,\ I,\ I,\ \sigma_x)\Psi & \Psi^T A(\sigma_x,\ I,\ \sigma_x,\ I) \\ B(I,\ \sigma_x,\ I,\ I)\Psi & & B(I,\ \sigma_x,\ I,\ \sigma_x)\Psi \\ \Psi^T A(\sigma_x,\ I,\ \sigma_z,\ I) & \Psi^T A(\sigma_z,\ I,\ \sigma_x,\ I)B(I,\ \sigma_z,\ I,\ \sigma_x)\Psi & \Psi^T A(\sigma_y,\ I,\ \sigma_y,\ I) \\ B(I,\ \sigma_x,\ I,\ \sigma_z)\Psi & & B(I,\ \sigma_y,\ I,\ \sigma_y)\Psi \end{pmatrix}$$
$$= \begin{pmatrix} 0 & 0 & 0 \\ 0 & 0 & 0 \\ 0 & 0 & 0 \end{pmatrix}$$

This striking result appears to require that Alice and Bob's observables are "elements of reality" and therefore represent preexisting properties of their spin-1/2 particles. In other words, the particles carry instruction sets to their detectors which determine how the nine measurement panels respond. Not only that, it requires that the instruction sets for both detectors be identical.

However, the calculations below show that the expectation values for the sequence of measurements for rows 1, 2, 3, and columns 1 and 2 are +1. For column 3 the expectation value is -1.

Alice

$$\begin{pmatrix} \Psi^T A(I,\ I,\ \sigma_z,\ I)A(\sigma_z,\ I,\ I,\ I) & \Psi^T A(I,\ I,\ \sigma_z,\ I)A(\sigma_x,\ I,\ I,\ I)A(\sigma_x,\ I,\ \sigma_z,\ I)\Psi \\ A(\sigma_z,\ I,\ \sigma_z,\ I)\Psi & \\ \Psi^T A(\sigma_x,\ I,\ I,\ I)A(I,\ I,\ \sigma_x,\ I) & \Psi^T A(\sigma_z,\ I,\ I,\ I)A(I,\ I,\ \sigma_x,\ I)A(\sigma_z,\ I,\ \sigma_x,\ I)\Psi \\ A(\sigma_x,\ I,\ \sigma_x,\ I)\Psi & \\ \Psi^T A(\sigma_x,\ I,\ \sigma_z,\ I)A(\sigma_z,\ I,\ \sigma_x,\ I) & \Psi^T A(\sigma_z,\ I,\ \sigma_z,\ I)A(\sigma_x,\ I,\ \sigma_x,\ I)A(\sigma_y,\ I,\ \sigma_y,\ I)\Psi \\ A(\sigma_y,\ I,\ \sigma_y,\ I)\Psi & \end{pmatrix}$$
$$= \begin{pmatrix} 1 & 1 \\ 1 & 1 \\ 1 & -1 \end{pmatrix}$$

Bob

$$\begin{pmatrix} \Psi^T B(I,\ I,\ I,\ \sigma_z) B(I,\ \sigma_z,\ I,\ I) B(I,\ \sigma_z,\ I,\ \sigma_z)\Psi & \Psi^T B(I,\ I,\ I,\ \sigma_z) B(I,\ \sigma_x,\ I,\ I) B(I,\ \sigma_x,\ I,\ \sigma_z)\Psi \\ \Psi^T B(I,\ \sigma_x,\ I,\ I) B(I,\ I,\ I,\ \sigma_x) B(I,\ \sigma_x,\ I,\ \sigma_x)\Psi & \Psi^T B(I,\ \sigma_z,\ I,\ I) B(I,\ I,\ I,\ \sigma_x) B(I,\ \sigma_z,\ I,\ \sigma_x)\Psi \\ \Psi^T B(I,\ \sigma_x,\ I,\ \sigma_z) B(I,\ \sigma_z,\ I,\ \sigma_x) B(I,\ \sigma_y,\ I,\ \sigma_y)\Psi & \Psi^T B(I,\ \sigma_z,\ I,\ \sigma_z) B(I,\ \sigma_x,\ I,\ \sigma_x) B(I,\ \sigma_y,\ I,\ \sigma_y)\Psi \end{pmatrix}$$

$$= \begin{pmatrix} 1 & 1 \\ 1 & 1 \\ 1 & -1 \end{pmatrix}$$

In order to validate a classical correlation between Alice and Bob's results based on the concept of "elements of reality", it is necessary to determine a set of instructions for the detectors that is in agreement with the highlighted results shown above. Unfortunately this is impossible; there is no way to assign definite eigenvalues (+1 or -1) to each of the nine panels of the measurement grid that satisfy these results.

> This contradiction shows that there is no solution to our puzzle based on instruction sets. A willingness to accept the notion of instruction sets (or "elements of reality") to begin with, followed by the recognition that they cannot provide a solution to our puzzle, amounts to an informal appreciation of the central point of Bell's theorem. P. K. Aravind, AJP 72, 1305 (2004).

On the basis of this gedanken experiment we must reject the position that quantum entities, quons (thank you Nick Herbert), have well-defined properties independent of measurement; in other words, that measurement simply reveals a preexisting state. Quantum entanglement is, as Schrödinger noted in 1935, "...the essential trait of the new theory, the one which forces a complete departure from all classical concepts."

This page titled 8.27: Quantum Entanglement Leads to Nonclassical Correlations is shared under a CC BY 4.0 license and was authored, remixed, and/or curated by Frank Rioux via source content that was edited to the style and standards of the LibreTexts platform.

8.28: Nonclassial Correlations Revealed with Mermin's Pentagram

A source emits the following six cubit state (|0> and |1> are orthogonal states), with cubits 1,3 and 5 going to Alice, and cubits 2, 4 and 6 going to Bob. This example is due to P. K. Aravind and available at arXiv:quant-ph/0701031v1.

$$|\Psi\rangle = \frac{1}{\sqrt{2}}(|0\rangle_1|0\rangle_2 + |1\rangle_1|1\rangle_2) \otimes \frac{1}{\sqrt{2}}(|0\rangle_3|0\rangle_4 + |1\rangle_3|1\rangle_4) \otimes \frac{1}{\sqrt{2}}(|0\rangle_5|0\rangle_6 + |1\rangle_5|1\rangle_6) = \frac{1}{2\sqrt{2}}$$
$$\left[\begin{matrix} |0\rangle_1|0\rangle_2|0\rangle_3|0\rangle_4|0\rangle_5|0\rangle_6 + |0\rangle_1|0\rangle_2|1\rangle_3|1\rangle_4|0\rangle_5|0\rangle_6 + |1\rangle_1|1\rangle_2|0\rangle_3|0\rangle_4|0\rangle_5|0\rangle_6 + |1\rangle_1|1\rangle_2|1\rangle_3|1\rangle_4|0\rangle_5|0\rangle_6 \\ |0\rangle_1|0\rangle_2|0\rangle_3|0\rangle_4|1\rangle_5|1\rangle_6 + |0\rangle_1|0\rangle_2|1\rangle_3|1\rangle_4|1\rangle_5|1\rangle_6 + |1\rangle_1|1\rangle_2|0\rangle_3|0\rangle_4|1\rangle_5|1\rangle_6 + |1\rangle_1|1\rangle_2|1\rangle_3|1\rangle_4|1\rangle_5|1\rangle_6 \end{matrix}\right]$$

Ψ can be written in condensed binary format as,

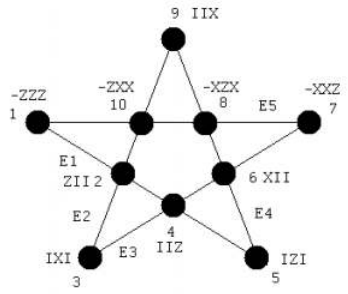
$$|\Psi\rangle = \frac{1}{2\sqrt{2}}\left[|000000\rangle + |001100\rangle + |110000\rangle + |111100\rangle + |000011\rangle + |001111\rangle + |110011\rangle + |111111\rangle\right]$$

In decimal notation the kets contain 0, 12, 48, 60, 3, 15, 51, and 63. All other vector elements are zero.

$$i = 0...63 \quad \Psi_i = 0$$

$$\Psi_0 = \frac{1}{2\sqrt{2}} \quad \Psi_3 = \frac{1}{2\sqrt{2}} \quad \Psi_{12} = \frac{1}{2\sqrt{2}} \quad \Psi_{15} = \frac{1}{2\sqrt{2}}$$
$$\Psi_{48} = \frac{1}{2\sqrt{2}} \quad \Psi_{51} = \frac{1}{2\sqrt{2}} \quad \Psi_{60} = \frac{1}{2\sqrt{2}} \quad \Psi_{63} = \frac{1}{2\sqrt{2}}$$

The following pentagram describes the measurement protocols followed by Alice and Bob.



Alice and Bob independently and randomly select one of five measurement protocols (E1, E2, E3, E4 and E5) shown on the edges of the pentagram above each time the source emits the entangled particles, and record the result (+1 or -1) for each vertex. After a statistically meaningful number of events they compare their results.

Each vertex represents a three qubit measurement sequence shown above and given in the following table. Note that Alice's sequence uses the identity operator for photons 2, 4 and 6 because she receives photons 1, 3 and 5, while Bob uses the identity operator for photons 1, 3 and 5 because he receives photons 2, 4 and 6.

Operator	Alice	Bob
1	$A(-\sigma_z,\ I,\ \sigma_z,\ I,\ \sigma_z,\ I)$	$B(I,\ -\sigma_z,\ I,\ \sigma_z,\ I,\ \sigma_z)$
2	$A(\sigma_z,\ I,\ I,\ I,\ I,\ I)$	$B(I,\ \sigma_z,\ I,\ I,\ I,\ I)$
3	$A(I,\ I,\ \sigma_x,\ I,\ I,\ I)$	$B(I,\ I,\ I,\ \sigma_x,\ I,\ I)$
4	$A(I,\ I,\ I,\ I,\ \sigma_z,\ I)$	$B(I,\ I,\ I,\ I,\ I,\ \sigma_z)$
5	$A(I,\ I,\ \sigma_z,\ I,\ I,\ I)$	$B(I,\ I,\ I,\ \sigma_z,\ I,\ I)$
6	$A(\sigma_x,\ I,\ I,\ I,\ I,\ I)$	$B(I,\ \sigma_x,\ I,\ I,\ I,\ I)$
7	$A(-\sigma_x,\ I,\ \sigma_x,\ I,\ \sigma_x,\ I)$	$B(I,\ -\sigma_x,\ I,\ \sigma_x,\ I,\ \sigma_z)$
8	$A(-\sigma_x,\ I,\ \sigma_z,\ I,\ \sigma_x,\ I)$	$B(I,\ -\sigma_x,\ I,\ \sigma_z,\ I,\ \sigma_x)$
9	$A(I,\ I,\ I,\ I,\ \sigma_x,\ I)$	$B(I,\ I,\ I,\ I,\ I,\ \sigma_x)$
10	$A(-\sigma_z,\ I,\ \sigma_x,\ I,\ \sigma_x,\ I)$	$B(I,\ -\sigma_z,\ I,\ \sigma_x,\ I,\ \sigma_x)$

The measurement operators required are:

$$I = \begin{pmatrix} 1 & 0 \\ 0 & 1 \end{pmatrix} \quad \sigma_x = \begin{pmatrix} 0 & 1 \\ 1 & 0 \end{pmatrix} \quad \sigma_z = \begin{pmatrix} 1 & 0 \\ 0 & -1 \end{pmatrix} \quad \text{eigenvals}(\sigma_x) = \begin{pmatrix} 1 \\ -1 \end{pmatrix} \quad \text{eigenvals}(\sigma_z) = \begin{pmatrix} 1 \\ -1 \end{pmatrix}$$

$$\mathrm{A(a,\ b,\ c,\ d,\ e,\ f) = kronecker(a,\ kronecker(b,\ kronecker(c,\ kronecker(d,\ kronecker(e,\ f)))))}$$
$$\mathrm{B(a,\ b,\ c,\ d,\ e,\ f) = kronecker(a,\ kronecker(b,\ kronecker(c,\ kronecker(d,\ kronecker(e,\ f)))))}$$

The eigenvalues of the Pauli operators are +/- 1. The first thing to note is that the individual vertices (measurement sites) flash +1 and -1 one randomly giving expectation values of zero at each vertex.

$$\begin{pmatrix} \Psi^T A(-\sigma_z,\ I,\ \sigma_z,\ I,\ \sigma_z,\ I)\Psi & \Psi^T B(I,\ -\sigma_z,\ I,\ \sigma_z,\ I,\ \sigma_z)\Psi \\ \Psi^T A(\sigma_z,\ I,\ I,\ I,\ I,\ I)\Psi & \Psi^T B(I,\ \sigma_z,\ I,\ I,\ I,\ I)\Psi \\ \Psi^T A(I,\ I,\ \sigma_x,\ I,\ I,\ I)\Psi & \Psi^T B(I,\ I,\ I,\ \sigma_x,\ I,\ I)\Psi \\ \Psi^T A(I,\ I,\ I,\ I,\ \sigma_z,\ I)\Psi & \Psi^T B(I,\ I,\ I,\ I,\ I,\ \sigma_z)\Psi \\ \Psi^T A(I,\ I,\ \sigma_z,\ I,\ I,\ I)\Psi & \Psi^T B(I,\ I,\ I,\ \sigma_z,\ I,\ I)\Psi \\ \Psi^T A(\sigma_x,\ I,\ I,\ I,\ I,\ I)\Psi & \Psi^T B(I,\ \sigma_x,\ I,\ I,\ I,\ I)\Psi \\ \Psi^T A(-\sigma_x,\ I,\ \sigma_x,\ I,\ \sigma_x,\ I)\Psi & \Psi^T B(I,\ -\sigma_x,\ I,\ \sigma_x,\ I,\ \sigma_z)\Psi \\ \Psi^T A(-\sigma_x,\ I,\ \sigma_z,\ I,\ \sigma_x,\ I)\Psi & \Psi^T B(I,\ -\sigma_x,\ I,\ \sigma_z,\ I,\ \sigma_x)\Psi \\ \Psi^T A(I,\ I,\ I,\ I,\ \sigma_x,\ I)\Psi & \Psi^T B(I,\ I,\ I,\ I,\ I,\ \sigma_x)\Psi \\ \Psi^T A(-\sigma_z,\ I,\ \sigma_x,\ I,\ \sigma_x,\ I)\Psi & \Psi^T B(I,\ -\sigma_z,\ I,\ \sigma_x,\ I,\ \sigma_x)\Psi \end{pmatrix} = \begin{pmatrix} 0 & 0 \\ 0 & 0 \\ 0 & 0 \\ 0 & 0 \\ 0 & 0 \\ 0 & 0 \\ 0 & 0 \\ 0 & 0 \\ 0 & 0 \\ 0 & 0 \end{pmatrix}$$

However, if Alice and Bob chose the same measurement protocol they always get the same eigenvalue, as is shown by the calculations below.

$$\begin{pmatrix} \Psi^T A(-\sigma_z,\ I,\ \sigma_z,\ I,\ \sigma_z,\ I)\Psi & \Psi^T B(I,\ -\sigma_z,\ I,\ \sigma_z,\ I,\ \sigma_z)\Psi \\ \Psi^T A(\sigma_z,\ I,\ I,\ I,\ I,\ I)\Psi & \Psi^T B(I,\ \sigma_z,\ I,\ I,\ I,\ I)\Psi \\ \Psi^T A(I,\ I,\ \sigma_x,\ I,\ I,\ I)\Psi & \Psi^T B(I,\ I,\ I,\ \sigma_x,\ I,\ I)\Psi \\ \Psi^T A(I,\ I,\ I,\ I,\ \sigma_z,\ I)\Psi & \Psi^T B(I,\ I,\ I,\ I,\ I,\ \sigma_z)\Psi \\ \Psi^T A(I,\ I,\ \sigma_z,\ I,\ I,\ I)\Psi & \Psi^T B(I,\ I,\ I,\ \sigma_z,\ I,\ I)\Psi \\ \Psi^T A(\sigma_x,\ I,\ I,\ I,\ I,\ I)\Psi & \Psi^T B(I,\ \sigma_x,\ I,\ I,\ I,\ I)\Psi \\ \Psi^T A(-\sigma_x,\ I,\ \sigma_x,\ I,\ \sigma_x,\ I)\Psi & \Psi^T B(I,\ -\sigma_x,\ I,\ \sigma_x,\ I,\ \sigma_z)\Psi \\ \Psi^T A(-\sigma_x,\ I,\ \sigma_z,\ I,\ \sigma_x,\ I)\Psi & \Psi^T B(I,\ -\sigma_x,\ I,\ \sigma_z,\ I,\ \sigma_x)\Psi \\ \Psi^T A(I,\ I,\ I,\ I,\ \sigma_x,\ I)\Psi & \Psi^T B(I,\ I,\ I,\ I,\ I,\ \sigma_x)\Psi \\ \Psi^T A(-\sigma_z,\ I,\ \sigma_x,\ I,\ \sigma_x,\ I)\Psi & \Psi^T B(I,\ -\sigma_z,\ I,\ \sigma_x,\ I,\ \sigma_x)\Psi \end{pmatrix} = \begin{pmatrix} 1 \\ 1 \\ 1 \\ 1 \\ 1 \\ 1 \\ 1 \\ 1 \\ 1 \\ 1 \end{pmatrix}$$

This result is somewhat surprising given the result immediately above. It suggests (at this point) that the particles involved in this experiment carry instruction sets telling the detectors how to operate, and that Alice and Bob's detectors receive the same sets of instructions.

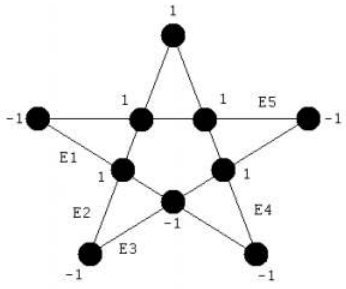
The edges (E1 through E5) shown on the pentagram identify a sequence of four mutually commuting operators (see Appendix). The net eigenvalues for these sequences of measurements for Alice and Bob are now calculated.

$$\begin{pmatrix} \Psi^T A(-\sigma_z,\ I,\ \sigma_z,\ I,\ \sigma_z,\ I)A(\sigma_z,\ I,\ I,\ I,\ I,\ I)A(I,\ I,\ I,\ I,\ \sigma_z,\ I)A(I,\ I,\ \sigma_z,\ I,\ I,\ I)\Psi \\ \Psi^T A(I,\ I,\ \sigma_x,\ I,\ I,\ I)A(I,\ I,\ I,\ I,\ \sigma_z,\ I)A(\sigma_x,\ I,\ I,\ I,\ I,\ I)A(-\sigma_x,\ I,\ \sigma_x,\ I,\ \sigma_z,\ I)\Psi \\ \Psi^T A(I,\ I,\ \sigma_x,\ I,\ I,\ I)A(\sigma_x,\ I,\ I,\ I,\ I,\ I)A(-\sigma_x,\ I,\ \sigma_x,\ I,\ \sigma_x,\ I)A(I,\ I,\ I,\ I,\ \sigma_x,\ I)\Psi \\ \Psi^T A(I,\ I,\ \sigma_z,\ I,\ I,\ I)A(\sigma_x,\ I,\ I,\ I,\ I,\ I)A(-\sigma_x,\ I,\ \sigma_z,\ I,\ \sigma_x,\ I)A(I,\ I,\ I,\ I,\ \sigma_x,\ I)\Psi \\ \Psi^T A(-\sigma_z,\ I,\ \sigma_z,\ I,\ \sigma_z,\ I)A(\sigma_z,\ I,\ \sigma_x,\ I,\ \sigma_x,\ I) \\ A(-\sigma_x,\ I,\ \sigma_z,\ I,\ \sigma_x,\ I)A(-\sigma_x,\ I,\ \sigma_x,\ I,\ \sigma_z,\ I)\Psi \end{pmatrix}$$
$$= \begin{pmatrix} -1 \\ -1 \\ -1 \\ -1 \\ -1 \end{pmatrix}$$

$$\begin{pmatrix} \Psi^T & B(I,\ \sigma_z,\ I,\ I, & B(I,\ I,\ I,\ I,\ I,\ \sigma_z) & B(I,\ I,\ I,\ \sigma_z,\ I,\ I) \\ B(I,\ -\sigma_z,\ I,\ \sigma_z, & I,\ I) & & \\ I,\ \sigma_z) & & & \\ \Psi^T & B(I,\ I,\ I,\ I, & B(I,\ \sigma_x,\ I,\ I,\ I,\ I) & B(I,\ -\sigma_x,\ I,\ \sigma_x,\ I,\ \sigma_z) \\ B(I,\ I,\ I,\ \sigma_x,\ I,\ I) & I,\ \sigma_z) & & \\ \Psi^T & B(I,\ \sigma_z,\ I,\ I, & B(I,\ -\sigma_z,\ I,\ \sigma_z,\ I,\ \sigma_x) & B(I,\ I,\ I,\ I,\ I,\ \sigma_x) \\ B(I,\ I,\ I,\ \sigma_x,\ I,\ I) & I,\ I) & & \\ \Psi^T & B(I,\ \sigma_x,\ I,\ I, & B(I,\ -\sigma_x,\ I,\ \sigma_z,\ I,\ \sigma_x) & B(I,\ I,\ I,\ I,\ I,\ \sigma_x) \\ B(I,\ I,\ I,\ \sigma_z,\ I,\ I) & I,\ I) & & \\ \Psi^T & B(I,\ -\sigma_z,\ I,\ \sigma_x, & B(I,\ -\sigma_x,\ I,\ \sigma_z,\ I,\ \sigma_x) & B(I,\ -\sigma_x,\ I,\ \sigma_x,\ I,\ \sigma_z) \\ B(I,\ -\sigma_z,\ I,\ \sigma_z, & I,\ \sigma_x) & & \\ I,\ \sigma_z) & & & \end{pmatrix}$$

$$\begin{pmatrix} -1 \\ -1 \\ -1 \\ -1 \\ -1 \end{pmatrix}$$

We now have the problem of reconciling these results with those immediately prior. How is it possible to assign +1s and -1s to the measurement vertices such that they satisfy the results immediately above. The answer is that it is not possible. The ideas of instruction sets and elements of reality are not capable of explaining these results.



For this assignment of vertex eigenvalues we see that the composite eigenvalue (-1) is satisfied for E1, E2, E3 and E4, but is violated for E5. All attempts to assign +/-1 values to the vertices fail to satisfy the composite eigenvalue for one of the measurement protocols.

Appendix

The four operators comprising the five measurement protocols mutually commute. This is demonstrated below for the E1 protocol.

$$(-\sigma_z\sigma_z\sigma_z)(\sigma_z\mathrm{I}\ \mathrm{I}) - (\sigma_z\mathrm{I}\ \mathrm{I})(-\sigma_z\sigma_z\sigma_z) = \begin{pmatrix} 0 & 0 \\ 0 & 0 \end{pmatrix} \quad (-\sigma_z\sigma_z\sigma_z)(\mathrm{I}\ \mathrm{I}\sigma_z) - (\mathrm{I}\ \mathrm{I}\sigma_z)(-\sigma_z\sigma_z\sigma_z) = \begin{pmatrix} 0 & 0 \\ 0 & 0 \end{pmatrix}$$

$$(-\sigma_z\sigma_z\sigma_z)(\mathrm{I}\sigma_z\mathrm{I}) - (\mathrm{I}\sigma_z\mathrm{I})(-\sigma_z\sigma_z\sigma_z) = \begin{pmatrix} 0 & 0 \\ 0 & 0 \end{pmatrix} \quad (\sigma_z\mathrm{I}\ \mathrm{I})(\mathrm{I}\ \mathrm{I}\sigma_z) - (\mathrm{I}\ \mathrm{I}\sigma_z)(\sigma_z\mathrm{I}\ \mathrm{I}) = \begin{pmatrix} 0 & 0 \\ 0 & 0 \end{pmatrix}$$

$$(\sigma_z\mathrm{I}\ \mathrm{I})(\mathrm{I}\sigma_z\mathrm{I}) - (\mathrm{I}\sigma_z\mathrm{I})(\sigma_z\mathrm{I}\ \mathrm{I}) = \begin{pmatrix} 0 & 0 \\ 0 & 0 \end{pmatrix} \quad (\mathrm{I}\ \mathrm{I}\sigma_z)(\mathrm{I}\sigma_z\mathrm{I}) - (\mathrm{I}\sigma_z\mathrm{I})(\mathrm{I}\ \mathrm{I}\sigma_z) = \begin{pmatrix} 0 & 0 \\ 0 & 0 \end{pmatrix}$$

It is also the case that the measurement protocols commute. This is demonstrated for E1 and E5.

$$[(-\sigma_z\sigma_z\sigma_z)(\sigma_z\mathrm{I}\ \mathrm{I}(\mathrm{I}\ \mathrm{I}\sigma_z)(\mathrm{I}\sigma_z\mathrm{I})]\,[(-\sigma_z\sigma_z\sigma_z)(-\sigma_z\sigma_x\sigma_x)(-\sigma_x\sigma_z\sigma_x)(-\sigma_x\sigma_x\sigma_z)]\,..$$
$$.+-[(-\sigma_z\sigma_z\sigma_z)(-\sigma_z\sigma_x\sigma_x)(-\sigma_x\sigma_z\sigma_x)(-\sigma_x\sigma_x\sigma_z)]\,[(-\sigma_z\sigma_z\sigma_z)(\sigma_z\mathrm{I}\ \mathrm{I})(\mathrm{I}\ \mathrm{I}\sigma_z)(\mathrm{I}\sigma_z\mathrm{I})] = \begin{pmatrix} 0 & 0 \\ 0 & 0 \end{pmatrix}$$

This page titled 8.28: Nonclassial Correlations Revealed with Mermin's Pentagram is shared under a CC BY 4.0 license and was authored, remixed, and/or curated by Frank Rioux via source content that was edited to the style and standards of the LibreTexts platform.

8.29: Spooky Action at a Distance- The EPR Experiment with Photons

Quantum theory is a very successful mathematical description of the structure of the atomic and molecular world. But unlike other scientific theories of wide applicability, its interpretation and meaning have been vigorously debated since its inception over seventy years ago. To clarify the unusual stature of quantum theory it might be helpful first to make a list of some of the characteristics we associate with a successful scientific theory.

- Experimental confirmation; predictive success
- Explanatory power; intelligibility
- Internal coherence; aesthetic appeal
- Breadth of applicability; philosophic implications

Scientists agree that quantum theory has received ample experimental confirmation, and that it is a coherent and mathematically appealing theory. In fact quantum mechanics has provided the computational methods and conceptual infra-structure that have catalyzed the impressive progress the physical sciences have experienced in the 20th century. However, in spite of its experimental validation, many would argue that quantum mechanics does not explain in the traditional sense, that it is not really intelligible, and that it merely offers a mathematical algorithm for making experimental predictions. And, if it has broad philosophic implications they are strange and unsettling to most people.

Basic Postulates of Quantum Mechanics

Before proceeding to the main issue, which is the analysis of an important experiment, it might be helpful to review some of the basic postulates of quantum theory.

1. The wave function, Y, provides a complete description of the physical properties of the system it represents.
2. Systems with the same wave function are identical and indistinguishable.
3. For every observable quantity there is an associated operator.
4. If the wave function is an eigenfunction of an operator the observable quantity represented by the operator has a definite value. Every time a measurement for the observable quantity is made the same value is obtained.

$$\hat{O}|\Psi\rangle = o|\Psi\rangle$$

5. If the wave function is not an eigenfunction of a particular operator the system is in a state which does not possess a definite value for the observable quantity associated with that operator. In this case quantum mechanics does not predict with certainty the results of a measurement, but only allows one to calculate (a) the "average value" when many determinations are made, or (b) predict the probability that a particular result will occur. For example, the two equations that follow show how to calculate the average position for a particle in state |Y> and the probability that the particle will be found in the spatial interval from x to x + dx.

$$\begin{aligned} a) \quad & \langle x \rangle = \langle \Psi | \hat{X} | \Psi \rangle \\ b) \quad & \Psi(x)^2 dx \end{aligned}$$

   Richard Feynman captured the significance of this postulate in the following quotation. "A philosopher once said, 'It is necessary for the very existence of science that the same conditions always produce the same results.' Well, they don't!"
6. After a measurement the wave function of the system is an eigenfunction of the measurement operator.
   - As Pascal Jordan has remarked, "Observations not only disturb what has to be measured, they produce it ... We compel the electron to assume a definite position ... We ourselves produce the result of the experiment."
7. Quantum mechanics does not provide a description of what actually happens between two consecutive observations.
   - As Heisenberg has succinctly put it, "If we want to describe what happens in an atomic event, we have to realize that the word 'happens' can apply only to the observation, not to the state of affairs between two observations."

The indeterministic nature of quantum mechanics is inherent in the basic principles listed above. Quantum theory says that a system can be in a well-defined state described by its wave function and yet the results of subsequent experiments are not

necessarily uniquely determined. For example, if the wave function of a system prior to a measurement is not an eigenfunction of the measurement operator, then a certain prediction of the measurement outcome cannot be made.

This is fundamentally different from the classical view in which an experimental result is always uniquely determined by the state of the system and the forces acting on it. According to classical physics, prior to measurement, every property of a system possesses a definite but unknown value, and experiment or observation merely reveals the value of that previously unknown property. By comparison, quantum mechanics denies the existence of certain physical properties independent of measurement. However, it does not deny, as is frequently erroneously claimed, the existence of the physical object itself in the absence of observation.

What is the reaction to such quantum weirdness? Here are some quotations from those who contributed to the foundation of quantum theory.

- Any one who is not shocked by quantum mechanics has not fully understood it. - Bohr
- I think it is safe to say that no one understands quantum mechanics. Do not keep saying to yourself, if you can possibly avoid it, 'But how can it possibly be like that?' because you will go down the drain into a blind alley from which nobody has yet escaped. Nobody know show it can be like that. - Feynman
- We have always had a great deal of difficulty understanding the world view that quantum mechanics represents. At least I do, because I'm an old enough man that I haven't got to the point that this stuff is obvious to me. Okay, I still get nervous with it... You know how it always is, every new idea, it takes a generation or two until it becomes obvious that there's no real problem. I cannot define the real problem, therefore I suspect that there is no real problem, but I'm not sure there's no real problem. - Feynman
- Quantum mechanics is certainly imposing. But an inner voice tells me that it is not yet the real thing. The theory says a lot, but does not really bring us any closer to the secret of the "old one." I, at any rate, am convinced that He is not playing at dice. - Einstein
- It seems hard to look at God's cards. But I cannot for a moment believe that he plays dice and makes use of 'telepathic' means as the current quantum theory alleges He does. - Einstein
- The mathematical predictions of quantum mechanics yield results that are in agreement with experimental findings. That is the reason we use quantum theory. That quantum theory fits experiment is what validates the theory, *but why experiment should give such peculiar results is a mystery.* This is the shock to which Bohr referred. - Marvin Chester

However strange it may seem, quantum theory has survived all the experimental tests it has been subjected to. Therefore, if quantum theory is strange, it is because the nano-world of electrons, atoms, and molecules is strange. Quantum mechanics is an accurate mathematical account of the behavior of the physical world at the nano scale.

In what follows an important experiment, stimulated by a thought experiment designed originally by Einstein, Podolsky, and Rosen in 1935, is described. Classical and quantum mechanical interpretations of the results and are offered. The classical interpretation fails to account fully for the experimental results, while the quantum mechanical analysis is in complete agreement with the experiment.

Apparatus

A schematic representation of an apparatus is shown in the figure below in which laser radiation is used to raise calcium atoms to an excited state. On returning to the ground state the calcium atoms emit two photons in opposite directions. The polarization of the photons is determined with a combination of polarizing film and a detector as illustrated in the figure. The polarizing films are oriented randomly in three directions as shown. The relative orientation of the polarizers is 60^{o}.

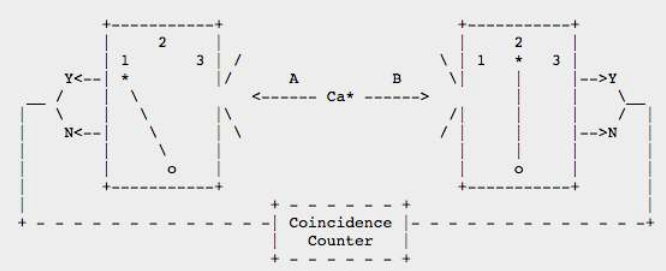


Figure 1.

The polarizers 1, 2, and 3 are oriented at angles of -60º, 0º, and 60º, and selected randomly. Thus the angle between any two polarizers is 60º.

Experiment

As the calcium atoms are excited by the laser radiation the polarizing films are oriented in a random way, and the detectors record whether or not a photon has arrived. The coincidence counter shown in the figure records whether or not both photons passed through the polarizing films. Note that there are nine possible orientations of the polarizing films: 11, 22, 33, 12, 21, 23, 32, 13, 31.

Results

Case 1. In runs for which the polarizing films are oriented at the same angle (11, 22, 33) the photons behave the same: they both either pass through the polarizers or they are both stopped by the polarizers. In other words, if the left detector registers a photon, so does the right detector, and vice versa.

Case 2. In runs for which the polarizing films are oriented at different angles (12, 21, 23, 32, 13, 31) the photons behave in the same way only 25% of the time. That is they both pass the films 25% of the time, while the other 75% of the time one passes and the other doesn't.

Overall. Because in 1/3 of the runs the photons behave the same and in 2/3 of the runs they behave the same way only 25% of the time, in a large number of runs it is found that the photons behave the same way 50% of the time.

Classical Interpretation

Belief in the doctrine of realism is considered by most scientists to be a necessary pre-condition for scientific inquiry. Realism, for the present purposes, might be described briefly as the philosophical belief that an experimental result is determined by a physical property of the system under study whose existence is independent of the experiment or the experimenter.

Thus, the results reported in **Case 1** indicate that the photons have the same polarization. In all cases in which the film orientations are the same both photons either pass or do not pass through the polarizing films.

This can lead one to assume that an intrinsic property of a photon is its ability to pass the polarizing film at the three angles chosen. If this assumption is correct, and it convincingly and simply accounts for the **Case 1** data, then eight states are required to account for the behavior of the photons. Each photon can come in eight varieties: YYY, YYN, YNY, NYY, YNN, NYN, NNY, NNN. Here Y (yes) and N (no) specify whether or not the photon will pass through the polarizing film when it is oriented at angles 1, 2, or 3. This view that photons or other systems under study have intrinsic properties which are independent of their measurement, but determine the result of a measurement, is one of the cornerstones of science.

The belief that photons carry information on their polarization along the three orientations of the films would yield the results shown in the table below. There are eight photon states and nine film orientations. Thus there are 72 types of encounters between the photons and the polarizing films as recorded by the detectors and the coincidence counter. The realist position (the one adopted by Einstein, for example) demands that the photons behave the same way 67% of the time (48/72), as is shown in the table. This is clearly not in agreement with the experimental result that overall the photons behave the same way only 50% of the time.

	11	22	33	12	21	13	31	23	32
YYY	Same	Same	Same	Same	Same	Same	Same	Same	Same
YYN	Same	Same	Same	Same	Same	Different	Different	Different	Different
YNY	Same	Same	Same	Different	Different	Same	Same	Different	Different
NNY	Same	Same	Same	Different	Different	Different	Different	Same	Same
YNN	Same	Same	Same	Different	Different	Different	Different	Same	Same
NYN	Same	Same	Same	Different	Different	Same	Same	Different	Different
NNY	Same	Same	Same	Same	Same	Different	Different	Different	Different
NNN	Same	Same	Same	Same	Same	Same	Same	Same	Same

Note that the realist position is in agreement with **Case 1** results, but in serious disagreement with **Case 2** results. For **Case 2** it predicts that 50% of the time the behavior of the photons is the same, when the experimental result is that the photons behave the same only 25% of the time.

Quantum Interpretation

According to quantum theory a photon polarized at some angle q to the vertical direction can be written as a linear combination of a vertically and horizontally polarized photon.

$$|\Theta\rangle = |v\rangle\langle v|\Theta\rangle + |h\rangle\langle h|\Theta\rangle = |v\rangle \cos\theta + |h\rangle \sin\Theta$$

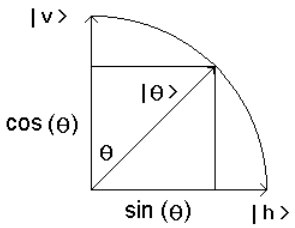


Figure 2.

$$|\langle v|\theta\rangle|^2 = \cos^2\theta$$

Thus the probability that a photon polarized at an angle q will pass a film with vertical polarization is $\cos^2$q. In general we can state that the probability that a photon will pass a polarizer is given by the square of the cosine of the angle its plane of polarization makes with the direction of the polarization of the film.

Now to a quantum mechanical explanation for the results of the experiment. For **Case 1**results, the fact that the photons behave in the same way when the detector settings are the same (11, 22, 33) indicates that the photons have the same polarization and, therefore, the same wave function. They are in the same state. This is basically the same as the classical interpretation.

However, for the **Case 2** results where the detector settings are different (12, 21, 23, 32, 13, 31) quantum mechanics gives a different explanation. Let's take a specific example. First of all, as Figure 1 shows, the three polarizing films have relative angles of 60^o. Now suppose for the 12 detector orientation that photon A moving to the left passes through its film indicating that it is polarized in that direction. Photon moving to the right has the same polarization and, therefore, the same wave function. It is approaching a film that is polarized at an angle of $60^o$to the one that A just passed. Thus, the probability that B will pass its film is $\cos^2 60$ or 25% in agreement with the **Case 2** experimental results described earlier.

Let's take a look at another example. Photon A is absorbed by a vertical polarizer indicating that it is horizontally polarized. Since the photons are in the same polarization state, B is also horizontally polarized. The probability it will pass a polarizer oriented 60^o relative to vertical is,

$$|\langle\theta = 60^o|h\rangle|^2 = \sin^2 60^o = 0.75$$

Thus, the probability that photons A and B behave differently (one is absorbed by its polarizer, the other passes its polarizer) is 0.75, again in agreement with **Case 2** results.

Of course this also means that the quantum interpretation is in agreement with the overall result that the photons behave the same way 50% of the time. The films have the same setting 1/3 of time and different settings 2/3 of the time. When the films are set the

same the photons behave the same way 100% of the time (either they both pass or they both don't pass). When the film settings are different the photons behave the same way only 25% of the time [(1/3) 100% + (2/3) 25% = 50%].

References:

- N. D. Mermin, "Spooky Actions at a Distance: Mysteries of the Quantum Theory," *The Great Ideas of Today*, Encyclopedia Britannica, Chicago, **1988**, pp 2-53.
- N. D. Mermin, "Bringing home the atomic world: Quantum mysteries for anybody," *American Journal of Physics*, **49**, 940-943, (1981).
- N. D. Mermin, "Is the moon there when nobody looks," *Physics Today* , **38(4)**, 38-47, (1985).
- N. D. Mermin, "Quantum mysteries revisited," *American Journal of Physics*, **58**, 731-734, (1990).
- J. C. Polkinghorne, *The Quantum World*, Princeton Science Library, Princeton, N.J.,1984.
- A. I. M Rae, *Quantum Mechanics*, 3rd Ed., Institute of Physics Publishing, Bristol, UK, 1992.

This page titled 8.29: Spooky Action at a Distance- The EPR Experiment with Photons is shared under a CC BY 4.0 license and was authored, remixed, and/or curated by Frank Rioux via source content that was edited to the style and standards of the LibreTexts platform.

8.30: David Bohm's EPR Gedanken Experiment

Quantum theory is both stupendously successful as an account of the small-scale structure of the world and it is also the subject of an unresolved debate and dispute about its interpretation. J. C. Polkinghorne, *The Quantum World*, p. 1.

In 1951 David Bohm proposed a gedanken experiment that further illuminated the conflict between local realism and quantum mechanics first articulated by Einstein, Podolsky and Rosen (EPR) in 1935. In this thought experiment a spin-1/2 pair is prepared in a singlet state and the individual particles travel in opposite directions on the y-axis to a pair of observers set up to measure spin in either the x- or z-direction.

In this summary tensor algebra will be used to analyze Bohm′s thought experiment. The vector states and matrix operators required are provided below.

Spin eigenvectors:

$$S_{zu} = \begin{pmatrix} 1 \\ 0 \end{pmatrix} \quad S_{zd} = \begin{pmatrix} 0 \\ 1 \end{pmatrix} \quad S_{xu} = \frac{1}{\sqrt{2}} \begin{pmatrix} 1 \\ 1 \end{pmatrix} \quad S_{xd} = \frac{1}{\sqrt{2}} \begin{pmatrix} 1 \\ -1 \end{pmatrix}$$

Spin operators in units of h/4π:

$$S_z = \begin{pmatrix} 1 & 0 \\ 0 & -1 \end{pmatrix} \quad S_x = \begin{pmatrix} 0 & 1 \\ 1 & 0 \end{pmatrix}$$

Identity:

$$I = \begin{pmatrix} 1 & 0 \\ 0 & 1 \end{pmatrix}$$

According to established quantum principles the singlet state for fermions is an entangled superposition written as follows in tensor format in the z-direction spin axis.

$$|\Psi\rangle = \frac{1}{\sqrt{2}} \left[|\uparrow\rangle_1 |\downarrow\rangle_2 - |\downarrow\rangle_1 |\uparrow\rangle_2 \right] = \frac{1}{\sqrt{2}} \left[\begin{pmatrix} 1 \\ 0 \end{pmatrix} \otimes \begin{pmatrix} 0 \\ 1 \end{pmatrix} - \begin{pmatrix} 0 \\ 1 \end{pmatrix} \otimes \begin{pmatrix} 1 \\ 0 \end{pmatrix} \right] = \frac{1}{\sqrt{2}} \begin{pmatrix} 0 \\ 1 \\ -1 \\ 0 \end{pmatrix}$$

$$\Psi = \frac{1}{\sqrt{2}} \begin{pmatrix} 0 \\ 1 \\ -1 \\ 0 \end{pmatrix}$$

First we calculate the expectation values for spin measurements in the z- and x-directions using the eigenvectors of the respective spin operators. We see that spin-up yields +1 and spin-down -1.

$$S_{zu}^T S_z S_{zu} = 1 \quad S_{zd}^T S_z S_{zd} = -1 \quad S_{xu}^T S_x S_{xu} = 1 \quad S_{xd}^T S_x S_{xd} = -1$$

Consequently the expectation value observed when both observers jointly measure the same spin direction is -1, because in the singlet state the spins have opposite orientations (kronecker performs the tensor multiplication of two matrices, as illustrated in the Appendix).

$$\Psi^T \text{kronecker}(S_z,\ S_z)\Psi = -1 \quad \Psi^T \text{kronecker}(S_x,\ S_x)\Psi = -1$$

Note that while the entangled singlet spin state shown above is written in the z-basis, it is the same to an over-all phase using the x-direction eigenvectors as is demonstrated in the Appendix. Next we show that in spite of the strong correlation shown above, individual spin measurements are totally random yielding expectation values of zero in both the z- and x-directions.

$$\Psi^T \text{kronecker}(S_z,\ I)\Psi = 0 \quad \Psi^T \text{kronecker}(I,\ S_z)\Psi = 0$$
$$\Psi^T \text{kronecker}(S_x,\ I)\Psi = 0 \quad \Psi^T \text{kronecker}(I,\ S_x)\Psi = 0$$

Quantum mechanics predicts the following results when the observers make different spin measurements on the particles.

$$\Psi^T \text{kronecker}(S_z,\ S_x)\Psi = 0 \quad \Psi^T \text{kronecker}(S_x,\ S_z)\Psi = 0$$

From a classical realist position the results for all the previous quantum calculations can be explained by assigning specific x- and z-spin states to the particles, as shown in the table below on the left (see Townsend′s *A Modern Approach to Quantum Mechanics*, page 135). Each particle can be in any one of four equally probable spin states, and taken together the particles form four equally probable joint spin states. In other words, the particles are in well-defined, although unknown, spin states prior to measurement. Measurement, according to a realist, simply reveals a pre-existing state. The right-hand part of the table gives the joint measurement results expected given the spin states specified on the left. The bottom row gives the expectation (average) values under the assumptions stated above.

$$\begin{pmatrix} \text{Particle 1} & \text{Particle 2} & ' & S_z(1)S_z(2) & S_x(1)S_x(2) & S_z(1)S_x(2) & S_x(1)S_z(2) \\ S_{zu}S_{xu} & S_{zd}S_{xd} & ' & -1 & -1 & -1 & -1 \\ S_{zu}S_{xd} & S_{zd}S_{xu} & ' & -1 & -1 & 1 & 1 \\ S_{zd}S_{xu} & S_{zu}S_{xd} & ' & -1 & -1 & 1 & 1 \\ S_{zd}S_{xd} & S_{zu}S_{xu} & ' & -1 & -1 & -1 & -1 \\ \text{Expectation} & \text{Value} & ' & -1 & -1 & 0 & 0 \end{pmatrix}$$

At this point one may ask, ″Where′s the problem? The quantum and classical pictures are in agreement on the prediction of experimental results.″ The difficulty is that quantum mechanics does not accept the legitimacy of the states shown in the table on the left. One way to state the problem is to note that Sx and Sz are noncommuting operators. This means that according to quantum mechanics spin in the x- and z-directions cannot simultaneously have well-defined values (like position and momentum, they are conjugate observables).

The S_x-S_z commutator:

$$S_zS_x - S_xS_z = \begin{pmatrix} 0 & 2 \\ -2 & 0 \end{pmatrix}$$

For example, if measurement reveals that particle 1 has S_{zu} then particle 2 is definitely S_{zd}. But that means it cannot have a well-defined value for the x-direction spin. In fact S_{zd} is a superposition of S_{xu} and S_{xd}, as shown below, with $\langle S_x \rangle = 0$.

$$S_{zd} = \begin{pmatrix} 0 \\ 1 \end{pmatrix} \quad \frac{1}{\sqrt{2}}(S_{xu} - S_{xd}) = \begin{pmatrix} 0 \\ 1 \end{pmatrix} \quad S_{sd}^T S_x S_{zd} = 0$$

Or, suppose particle 1 is found to have S_{xd}, then particle 2 is S_{xu} which is a superposition of spin up and down in the z-direction and therefore $\langle S_x \rangle = 0$.

$$S_{xu} = \begin{pmatrix} 0.707 \\ 0.707 \end{pmatrix} \quad \frac{1}{\sqrt{2}}(S_{zu} + S_{zd}) = \begin{pmatrix} 0.707 \\ 0.707 \end{pmatrix} \quad S_{xu}^T S_z S_{xu} = 0$$

To summarize, the states in the table are not valid, in spite of their agreement with the predictions of quantum mechanics, because they give well-defined values to incompatible (according to quantum theory) observables. The quantum objection to the classical spin states can also be expressed using the Uncertainty Principle. For a particle known to have spin-up in the z-direction, quantum theory requires that its x-direction spin be uncertain, as shown by the following calculation.

$$\Delta S_x = \sqrt{S_{zu}^T S_x^2 S_{zu} - (S_{zu}^T S_x S_{zu})^2} \quad \Delta S_x = 1 \text{ in units of } \frac{h}{4\pi}$$

Of course, the realist says that these arguments simply indicate that quantum mechanics is not a complete theory because it cannot assign definite values to all elements of reality independent of measurement.

While Bohm′s 1951 gedanken experiment clarified the conflict between quantum theory and classical realism, it did not provide for a direct experimental adjudication of the disagreement. That changed in 1964 with the theoretical analysis of John Bell who recognized the potential of Bohm′s thought experiment to decide the issue one way or the other empirically. As is well known, the subsequent experimental work based on Bell′s theorem decided the conflict between the two views in favor of quantum theory. See the other entries in this section for examples of the impact of Bell′s work and the experimentalist who verified the implications of his theorem.

Appendix

Tensor multiplication of several of the spin operators using Mathcad′s kronecker command:

$$\text{kronecker}(S_z,\ S_z) = \begin{pmatrix} 1 & 0 & 0 & 0 \\ 0 & -1 & 0 & 0 \\ 0 & 0 & -1 & 0 \\ 0 & 0 & 0 & 1 \end{pmatrix} \quad \text{kronecker}(S_x,\ S_x) = \begin{pmatrix} 0 & 0 & 0 & 1 \\ 0 & 0 & 1 & 0 \\ 0 & 1 & 0 & 0 \\ 1 & 0 & 0 & 0 \end{pmatrix}$$

$$\text{kronecker}(S_z,\ S_x) = \begin{pmatrix} 0 & 1 & 0 & 0 \\ 1 & 0 & 0 & 0 \\ 0 & 0 & 0 & -1 \\ 0 & 0 & -1 & 0 \end{pmatrix} \quad \text{kronecker}(S_z,\ I) = \begin{pmatrix} 1 & 0 & 0 & 0 \\ 0 & 1 & 0 & 0 \\ 0 & 0 & 1 & 0 \\ 0 & 0 & 0 & -1 \end{pmatrix}$$

The following shows that the singlet state used in this summary can be expressed in terms of either the z- or x-direction eigenvectors.

Mathcad′s kronecker command is only useful for matrix tensor multiplication, but can be adapted to carry out vector tensor multiplication in the manner shown below. Two matrices are created using the null vector, tensor multiplied and everything but the first column of the product matrix is discarded.

Null vector:

$$N = \begin{pmatrix} 0 \\ 0 \end{pmatrix} \quad \Psi(a,\ b) = \text{submatrix}(\text{kronecker}(\text{augment}(\text{a, N}),\ \text{augment}(\text{b, N})),\ 1,\ 4,\ 1,\ 1)$$

$$\frac{\Psi(S_{zu},\ S_{zd}) - \Psi(S_{zd},\ S_{zu})}{\sqrt{2}} = \begin{pmatrix} 0 \\ 0.707 \\ -0.707 \\ 0 \end{pmatrix} \quad \frac{\Psi(S_{xd},\ S_{xu}) - \Psi(S_{xu},\ S_{xd})}{\sqrt{2}} = \begin{pmatrix} 0 \\ 0.707 \\ -0.707 \\ 0 \end{pmatrix}$$

This page titled 8.30: David Bohm's EPR Gedanken Experiment is shared under a CC BY 4.0 license and was authored, remixed, and/or curated by Frank Rioux via source content that was edited to the style and standards of the LibreTexts platform.

8.31: An Extension of Bohm's EPR Experiment

Quantum theory is both stupendously successful as an account of the small-scale structure of the world and it is also the subject of an unresolved debate and dispute about its interpretation. J. C. Polkinghorne, *The Quantum World*, p. 1.

In 1951 David Bohm proposed a gedanken experiment that further illuminated the conflict between local realism and quantum mechanics first articulated by Einstein, Podolsky and Rosen (EPR) in 1935. In this thought experiment a spin-1/2 pair is prepared in a singlet state and the individual particles travel in opposite directions on the y-axis to a pair of observers set up to measure spin in either the x- or z-direction.

In this summary tensor algebra will be used to analyze Bohm′s thought experiment. The vector states and matrix operators required are provided below.

Spin eigenvectors:

$$S_{zu} = \begin{pmatrix} 1 \\ 0 \end{pmatrix} \quad S_{zd} = \begin{pmatrix} 0 \\ 1 \end{pmatrix} \quad S_{xu} = \frac{1}{\sqrt{2}} \begin{pmatrix} 1 \\ 1 \end{pmatrix} \quad S_{xd} = \frac{1}{\sqrt{2}} \begin{pmatrix} 1 \\ -1 \end{pmatrix}$$

Spin operators in units of h/4π:

$$S_z = \begin{pmatrix} 1 & 0 \\ 0 & -1 \end{pmatrix} \quad S_x = \begin{pmatrix} 0 & 1 \\ 1 & 0 \end{pmatrix}$$

Identity:

$$I = \begin{pmatrix} 1 & 0 \\ 0 & 1 \end{pmatrix}$$

According to established quantum principles the singlet state for fermions is an entangled superposition written as follows in tensor format in the z-direction spin axis.

$$|\Psi\rangle = \frac{1}{\sqrt{2}} \left[|S_{zu}\rangle_1 |\, S_{zd}\rangle_2 - |S_{zd}\rangle_1 |\, S_{zu}\rangle_2 \right] = \frac{1}{\sqrt{2}} \left[\begin{pmatrix} 1 \\ 0 \end{pmatrix} \otimes \begin{pmatrix} 0 \\ 1 \end{pmatrix} - \begin{pmatrix} 0 \\ 1 \end{pmatrix} \otimes \begin{pmatrix} 1 \\ 0 \end{pmatrix} \right] = \frac{1}{\sqrt{2}} \begin{pmatrix} 0 \\ 1 \\ -1 \\ 0 \end{pmatrix}$$

$$\Psi = \frac{1}{\sqrt{2}} \begin{pmatrix} 0 \\ 1 \\ -1 \\ 0 \end{pmatrix}$$

First we calculate the expectation values for spin measurements in the z- and x-directions using the eigenvectors of the respective spin operators. We see that spin-up yields +1 and spin-down -1.

$$S_{zu}^T S_z S_{zu} = 1 \quad S_{zd}^T S_z S_{zd} = -1 \quad S_{xu}^T S_x S_{xu} = 1 \quad S_{xd}^T S_x S_{xd} = -1$$

Consequently the expectation value observed when both observers jointly measure the same spin direction is -1, because in the singlet state the spins have opposite orientations (kronecker performs the tensor multiplication of two matrices, as illustrated in the Appendix).

$$\Psi^T \text{kronecker}(S_z,\ S_z) \Psi = -1 \quad \Psi^T \text{kronecker}(S_x,\ S_x) \Psi = -1$$

Note that while the entangled singlet spin state shown above is written in the z-basis, it is the same to an over-all phase using the x-direction eigenvectors.

$$\Psi = \frac{1}{\sqrt{2}}\left[|S_{xd}\rangle_1|\,S_{xu}\rangle_2 - |S_{xu}\rangle_1|\,S_{xd}\rangle_2\right]$$

$$= \frac{1}{\sqrt{2}}\left[\frac{1}{\sqrt{2}}\begin{pmatrix}1\\-1\end{pmatrix}\otimes\frac{1}{\sqrt{2}}\begin{pmatrix}1\\1\end{pmatrix} - \frac{1}{\sqrt{2}}\begin{pmatrix}1\\1\end{pmatrix}\otimes\frac{1}{\sqrt{2}}\begin{pmatrix}1\\-1\end{pmatrix}\right] = \frac{1}{\sqrt{2}}\begin{pmatrix}0\\1\\-1\\0\end{pmatrix}$$

Next we show that in spite of the strong correlation shown above, individual spin measurements are totally random yielding expectation values of zero in both the z- and x-directions.

$$\Psi^T\text{kronecker}(S_z,\ I)\Psi = 0 \quad \Psi^T\text{kronecker}(I,\ S_z)\Psi = 0$$
$$\Psi^T\text{kronecker}(S_x,\ I)\Psi = 0 \quad \Psi^T\text{kronecker}(I,\ S_x)\Psi = 0$$

Quantum mechanics predicts the following results when the observers make different spin measurements on the particles.

$$\Psi^T\text{kronecker}(S_z,\ S_x)\Psi = 0 \quad \Psi^T\text{kronecker}(S_x,\ S_z)\Psi = 0$$

From a classical realist position the results for all the previous quantum calculations can be explained by assigning specific x- and z-spin states to the particles, as shown in the table below on the left (see Townsend′s *A Modern Approach to Quantum Mechanics*, page 135). Each particle can be in any one of four equally probable spin states, and taken together the particles form four equally probable joint spin states. In other words, the particles are in well-defined, although unknown, spin states prior to measurement. Measurement, according to a realist, simply reveals a pre-existing state. The right-hand part of the table gives the joint measurement results expected given the spin states specified on the left. The bottom row gives the expectation (average) values under the assumptions stated above.

$$\begin{pmatrix} \text{Particle 1} & \text{Particle 2} & ' & S_z(1)S_z(2) & S_x(1)S_x(2) & S_z(1)S_x(2) & S_x(1)S_z(2) \\ S_{zu}S_{xu} & S_{zd}S_{xd} & ' & -1 & -1 & -1 & -1 \\ S_{zu}S_{xd} & S_{zd}S_{xu} & ' & -1 & -1 & 1 & 1 \\ S_{zd}S_{xu} & S_{zu}S_{xd} & ' & -1 & -1 & 1 & 1 \\ S_{zd}S_{xd} & S_{zu}S_{xu} & ' & -1 & -1 & -1 & -1 \\ \text{Expectation} & \text{Value} & ' & -1 & -1 & 0 & 0 \end{pmatrix}$$

At this point one may ask, "Where′s the problem? The quantum and classical pictures are in agreement on the prediction of experimental results." The difficulty is that quantum mechanics does not accept the legitimacy of the states shown in the table on the left. One way to state the problem is to note that Sx and Sz are noncommuting operators. This means that according to quantum mechanics spin in the x- and z-directions cannot simultaneously have well-defined values (like position and momentum, they are conjugate observables).

The S_x-S_z commutator:

$$S_zS_x - S_xS_z = \begin{pmatrix}0 & 2\\-2 & 0\end{pmatrix}$$

For example, if measurement reveals that particle 1 has S_{zu} then particle 2 is definitely S_{zd}. But that means it cannot have a well-defined value for the x-direction spin. In fact S_{zd} is a superposition of S_{xu} and S_{xd}, as shown below, with $\langle S_x \rangle = 0$.

$$S_{zd} = \begin{pmatrix}0\\1\end{pmatrix} \quad \tfrac{1}{\sqrt{2}}(S_{xu} - S_{xd}) = \begin{pmatrix}0\\1\end{pmatrix} \quad S_{sd}^T S_x S_{zd} = 0$$

Or, suppose particle 1 is found to have S_{xd}, then particle 2 is S_{xu} which is a superposition of spin up and down in the z-direction and therefore $\langle S_x \rangle = 0$.

$$S_{xu} = \begin{pmatrix}0.707\\0.707\end{pmatrix} \quad \tfrac{1}{\sqrt{2}}(S_{zu} + S_{zd}) = \begin{pmatrix}0.707\\0.707\end{pmatrix} \quad S_{xu}^T S_z S_{xu} = 0$$

To summarize, the states in the table are not valid, in spite of their agreement with the predictions of quantum mechanics, because they give well-defined values to incompatible (according to quantum theory) observables. The quantum objection to the classical

spin states can also be expressed using the Uncertainty Principle. For a particle known to have spin-up in the z-direction, quantum theory requires that its x-direction spin be uncertain, as shown by the following calculation.

While Bohm′s 1951 gedanken experiment clarified the conflict between quantum theory and classical realism, it did not provide for a direct experimental adjudication of the disagreement. That changed in 1964 with the theoretical analysis of John Bell who recognized the potential of Bohm′s thought experiment to decide the issue one way or the other empirically. As is well known, the subsequent experimental work based on Bell′s theorem decided the conflict between the two views in favor of quantum theory. See the other entries in this section for examples of the impact of Bell′s work and the experimentalist who verified the implications of his theorem.

A modified version of the thought experiment shows that there are experiments involving entangled spin systems for which a local hidden-variable theory gives predictions which are incompatible with those of quantum theory. Instead of measuring the spins in the z- and x-directions, measure one in the z-direction and the other at some non-orthogonal angle to the z-axis, say 45 degrees (π/4). The appropriate spin operator for this diagonal direction (an even superposition of Sx and Sz) and its eigenvalues and eigenvectors are given below, and the singlet spin state is written in the diagonal spin basis.

$$S_d = \frac{1}{\sqrt{2}}\begin{pmatrix}1 & 1\\ 1 & -1\end{pmatrix} \quad \text{eigenvals}(S_d) = \begin{pmatrix}1\\ -1\end{pmatrix} \quad \text{eigenvecs}(S_d) = \begin{pmatrix}0.924 & -0.383\\ 0.383 & 0.924\end{pmatrix}$$

$$\Psi = \frac{1}{\sqrt{2}}\left[|S_{du}\rangle_A |S_{dd}\rangle_B - |S_{dd}\rangle_A |S_{du}\rangle_B\right]$$

$$= \frac{1}{\sqrt{2}}\left[\begin{pmatrix}0.924\\ 0.383\end{pmatrix} \otimes \begin{pmatrix}-0.383\\ 0.924\end{pmatrix} - \begin{pmatrix}-0.383\\ 0.924\end{pmatrix} \otimes \begin{pmatrix}0.924\\ 0.383\end{pmatrix}\right] = \frac{1}{\sqrt{2}}\begin{pmatrix}0\\ 1\\ -1\\ 0\end{pmatrix}$$

As expected, perfect anti-correlation is observed if both spins are measured in the diagonal direction while the individual spin measurements are totally random with an expectation value of zero.

$$\Psi^T \text{kronecker}(S_d,\ S_d)\Psi = -1 \quad \Psi^T \text{kronecker}(S_d,\ I)\Psi = 0 \quad \Psi^T \text{kronecker}(I,\ S_d)\Psi = 0$$

Up to this point the calculations are consistent with those for the x- and z-directions, and would appear to justify the local realist in providing the following hidden-variable interpretation of the results.

$$\begin{pmatrix} \text{Particle 1} & \text{Particle 2} & ' & S_z(1)S_z(2) & S_d(1)S_d(2) & S_z(1)S_d(2) & S_d(1)S_z(2)\\ S_{zu}S_{du} & S_{zd}S_{dd} & ' & -1 & -1 & -1 & -1\\ S_{zu}S_{dd} & S_{zd}S_{du} & ' & -1 & -1 & 1 & 1\\ S_{zd}S_{du} & S_{zu}S_{dd} & ' & -1 & -1 & 1 & 1\\ S_{zd}S_{dd} & S_{zu}S_{du} & ' & -1 & -1 & -1 & -1\\ \text{Expectation} & \text{Value} & ' & -1 & -1 & 0 & 0 \end{pmatrix}$$

However when the spins are measured in different directions (the z- and d-directions) quantum mechanics predicts that the expectation values are not zero as predicted by the hidden-variable model. According to quantum theory there is significant anti-correlation in the joint spin measurements.

$$\Psi^T \text{kronecker}(S_z,\ S_d)\Psi = -0.707 \quad \Psi^T \text{kronecker}(S_d,\ S_z)\Psi = -0.707$$

This disagreement has been examined experimentally and the experimental evidence supports quantum theory.

Appendix: Vector and Matrix Math

This addendum reviews basic vector and matrix operations. At the end it illustrates how vector and matrix tensor multiplication are implemented in Mathcad.

Tensor multiplication of several of the spin operators using Mathcad′s kronecker command:

$$\text{kronecker}(S_z,\ S_z) = \begin{pmatrix} 1 & 0 & 0 & 0 \\ 0 & -1 & 0 & 0 \\ 0 & 0 & -1 & 0 \\ 0 & 0 & 0 & 1 \end{pmatrix} \qquad \text{kronecker}(S_x,\ S_x) = \begin{pmatrix} 0 & 0 & 0 & 1 \\ 0 & 0 & 1 & 0 \\ 0 & 1 & 0 & 0 \\ 1 & 0 & 0 & 0 \end{pmatrix}$$

$$\text{kronecker}(S_d,\ S_d) = \begin{pmatrix} 0.5 & 0.5 & 0.5 & 0.5 \\ 0.5 & -0.5 & 0.5 & -0.5 \\ 0.5 & 0.5 & -0.5 & -0.5 \\ 0.5 & -0.5 & -0.5 & 0.5 \end{pmatrix} \qquad \text{kronecker}(S_z,\ S_x) = \begin{pmatrix} 0 & 1 & 0 & 0 \\ 1 & 0 & 0 & 0 \\ 0 & 0 & 0 & -1 \\ 0 & 0 & -1 & 0 \end{pmatrix}$$

$$\text{kronecker}(S_z,\ S_d) = \begin{pmatrix} 0.707 & 0.707 & 0 & 0 \\ 0.707 & -0.707 & 0 & 0 \\ 0 & 0 & -0.707 & -0.707 \\ 0 & 0 & -0.707 & 0.707 \end{pmatrix} \qquad \text{kronecker}(S_z,\ I) = \begin{pmatrix} 1 & 0 & 0 & 0 \\ 0 & 1 & 0 & 0 \\ 0 & 0 & -1 & 0 \\ 0 & 0 & 0 & -1 \end{pmatrix}$$

$$\text{kronecker}(S_x,\ I) = \begin{pmatrix} 0 & 0 & 1 & 0 \\ 0 & 0 & 0 & 1 \\ 1 & 0 & 0 & 0 \\ 0 & 1 & 0 & 0 \end{pmatrix} \qquad \text{kronecker}(S_d,\ I) = \begin{pmatrix} 0.707 & 0 & 0.707 & 0 \\ 0 & 0.707 & 0 & 0.707 \\ 0.707 & 0 & -0.707 & 0 \\ 0 & 0.707 & 0 & -0.707 \end{pmatrix}$$

Mathcad′s kronecker command is only useful for matrix tensor multiplication, but can be adapted to carry out vector tensor multiplication in the manner shown below. Two matrices are created using the null vector, tensor multiplied and everything but the first column of the product matrix is discarded.

Null vector:

$$N = \begin{pmatrix} 0 \\ 0 \end{pmatrix} \qquad \Psi(a,\ b) = \text{submatrix}(\text{kronecker}(\text{augment}(\text{a, N}),\ \text{augment}(\text{b, N})),\ 1,\ 4,\ 1,\ 1)$$

$$\frac{\Psi(S_{zu},\ S_{zd}) - \Psi(S_{zd},\ S_{zu})}{\sqrt{2}} = \begin{pmatrix} 0 \\ 0.707 \\ -0.707 \\ 0 \end{pmatrix} \qquad \frac{\Psi(S_{xd},\ S_{xu}) - \Psi(S_{xu},\ S_{xd})}{\sqrt{2}} = \begin{pmatrix} 0 \\ 0.707 \\ -0.707 \\ 0 \end{pmatrix}$$

$$S_{du} = \begin{pmatrix} 0.924 \\ 0.383 \end{pmatrix} \qquad S_{dd} = \begin{pmatrix} -0.383 \\ 0.924 \end{pmatrix} \qquad \frac{\Psi(S_{du},\ S_{dd}) - \Psi(S_{dd},\ S_{du})}{\sqrt{2}} = \begin{pmatrix} 0 \\ 0.707 \\ -0.707 \\ 0 \end{pmatrix}$$

This page titled 8.31: An Extension of Bohm's EPR Experiment is shared under a CC BY 4.0 license and was authored, remixed, and/or curated by Frank Rioux via source content that was edited to the style and standards of the LibreTexts platform.

8.32: A Surgical Adjudication of the Conflict Between Quantum Theory and Local Realism

In 1951 David Bohm (*Quantum Theory*, pp. 614-623) proposed a gedanken experiment that further illuminated the conflict between local realism and quantum mechanics first articulated by Einstein, Podolsky and Rosen (EPR) in 1935. In his thought experiment a spin-1/2 pair is prepared in a singlet state and the individual particles travel in opposite directions on the y-axis to a pair of observers set up to measure spin in either the x- or z-direction. While Bohm's thought experiment clarified the conflict between quantum theory and classical realism, it did not provide for a direct experimental adjudication of the disagreement.

However, a slightly modified version of Bohm's thought experiment shows that there are experiments involving entangled spin systems for which a local hidden-variable theory makes predictions which are incompatible with those of quantum mechanics. For example, instead of measuring the spins in the xand z-directions, use the z-direction and another direction at some non-orthogonal angle to the z-axis, say 45 degrees, the diagonal or d-direction. My goal in the following analysis is to bring the conflict between quantum theory and local realism into sharp focus as quickly as possible.

The z-direction spin operator and its eigenvalues and eigenvectors:

$$S_z = \begin{pmatrix} 1 & 0 \\ 0 & -1 \end{pmatrix} \quad \text{eigenvals}(S_z) = \begin{pmatrix} 1 \\ -1 \end{pmatrix} \quad \text{eigenvecs}(S_z) = \begin{pmatrix} 1 & 0 \\ 0 & 1 \end{pmatrix}$$

The singlet spin state written using the z-direction eigenstates:

$$|\Psi\rangle = \frac{1}{\sqrt{2}}\left[|\uparrow\rangle_1|\downarrow\rangle_2 - |\downarrow\rangle_1|\uparrow\rangle_2\right] = \frac{1}{\sqrt{2}}\left[\begin{pmatrix}1\\0\end{pmatrix}\otimes\begin{pmatrix}0\\1\end{pmatrix} - \begin{pmatrix}0\\1\end{pmatrix}\otimes\begin{pmatrix}1\\0\end{pmatrix}\right] = \frac{1}{\sqrt{2}}\begin{pmatrix}0\\1\\-1\\0\end{pmatrix}$$

$$\Psi = \begin{pmatrix}0\\1\\-1\\0\end{pmatrix}$$

The d-direction spin operator and its eigenvalues and eigenvectors:

$$S_d = \tfrac{1}{\sqrt{2}}\begin{pmatrix} 1 & 1 \\ 1 & -1 \end{pmatrix} \quad \text{eigenvals}(S_d) = \begin{pmatrix} 1 \\ -1 \end{pmatrix} \quad \text{eigenvecs}(S_d) = \begin{pmatrix} 0.924 & -0.383 \\ 0.383 & 0.924 \end{pmatrix}$$

The singlet spin state written using the d-direction eigenstates:

$$|\Psi\rangle = \frac{1}{\sqrt{2}}\left[|\nearrow\rangle_1|\swarrow\rangle_2 - |\swarrow\rangle_1|\nearrow\rangle_2\right]$$

$$= \frac{1}{\sqrt{2}}\left[\begin{pmatrix}0.924\\0.383\end{pmatrix}\otimes\begin{pmatrix}-0.383\\0.924\end{pmatrix} - \begin{pmatrix}-0.383\\0.924\end{pmatrix}\otimes\begin{pmatrix}0.924\\0.383\end{pmatrix}\right] = \frac{1}{\sqrt{2}}\begin{pmatrix}0\\1\\-1\\0\end{pmatrix}$$

The calculations below show that the individual spin measurements are totally random yielding expectation values of zero in both the z- and d-directions. The identity operator, do nothing, is required for these calculations. However, the expectation value observed when both observers jointly measure the same spin direction is -1, because in the singlet state the spins have opposite orientations in both spin bases.

$$I = \begin{pmatrix} 1 & 0 \\ 0 & 1 \end{pmatrix}$$

$$\Psi^T \text{kronecker}(S_z,\ I)\Psi = 0 \quad \Psi^T \text{kronecker}(I,\ S_z)\Psi = 0 \quad \Psi^T \text{kronecker}(S_z,\ S_z)\Psi = -1$$
$$\Psi^T \text{kronecker}(S_d,\ I)\Psi = 0 \quad \Psi^T \text{kronecker}(I,\ S_d)\Psi = 0 \quad \Psi^T \text{kronecker}(S_d,\ S_d)\Psi = -1$$

The first four columns of the following table provide a local realist's explanation of these calculations. Specific z- and d-spin states are assigned to the particles in the first two columns, with each particle in one of four equally probable spin orientations consistent with the composite singlet state. The next two columns show that these assignments agree with the quantum calculations.

$$\begin{pmatrix} \text{Particle 1} & \text{Particle 2} & \hat{S}_z(1)\hat{S}_z(2) & \hat{S}_d(1)\hat{S}_d(2) & \hat{S}_z(1)\hat{S}_d(2) & \hat{S}_d(1)\hat{S}_z(2) \\ |\uparrow\rangle|\nearrow\rangle & |\downarrow\rangle|\swarrow\rangle & -1 & -1 & -1 & -1 \\ |\uparrow\rangle|\swarrow\rangle & |\downarrow\rangle|\nearrow\rangle & -1 & -1 & 1 & 1 \\ |\downarrow\rangle|\nearrow\rangle & |\uparrow\rangle|\swarrow\rangle & -1 & -1 & 1 & 1 \\ |\downarrow\rangle|\swarrow\rangle & |\uparrow\rangle|\nearrow\rangle & -1 & -1 & -1 & -1 \\ \text{Expectation} & \text{Value} & -1 & -1 & 0 & 0 \end{pmatrix}$$

At this point one may ask, "Where's the problem? The quantum and classical pictures are in agreement on the prediction of experimental results." The difficulty is that quantum mechanics does not accept the legitimacy of the states shown in the table on the left. One way to state the problem is to note that S_d and S_z are non-commuting operators. This means that spin in the d- and z-directions cannot simultaneously have well-defined values because like position and momentum they are conjugate observables.

The S_z-S_d commutator:

$$S_z S_d - S_d S_z = \begin{pmatrix} 0 & 1.414 \\ -1.414 & 0 \end{pmatrix}$$

In other words, the z-eigenstates are superpositions of d-eigenstates and vice versa.

$$.924\begin{pmatrix} .924 \\ .383 \end{pmatrix} - .383\begin{pmatrix} -.383 \\ .924 \end{pmatrix} = \begin{pmatrix} 1 \\ 0 \end{pmatrix} \quad .383\begin{pmatrix} .924 \\ .383 \end{pmatrix} + .924\begin{pmatrix} -.383 \\ .924 \end{pmatrix} = \begin{pmatrix} 0 \\ 1 \end{pmatrix}$$

$$.924\begin{pmatrix} 1 \\ 0 \end{pmatrix} + .383\begin{pmatrix} 0 \\ 1 \end{pmatrix} = \begin{pmatrix} 0.924 \\ 0.383 \end{pmatrix} \quad .924\begin{pmatrix} 0 \\ 1 \end{pmatrix} - .383\begin{pmatrix} 1 \\ 0 \end{pmatrix} = \begin{pmatrix} -0.383 \\ 0.924 \end{pmatrix}$$

Of course, the realist says this argument simply reveals that quantum mechanics does not provide a complete representation of reality because it is unable to assign definite values to all observables prior to and independent of measurement.

Fortunately another set of measurements can settle the dispute. If one spin is measured in the z-direction and the other in the d-direction, local realism predicts an expectation value of zero as shown in the last two columns of the table above. Quantum theory, however, predicts -0.707.

$$\Psi^T \text{kronecker}(S_z,\ S_d)\Psi = -0.707 \quad \Psi^T \text{kronecker}(S_d,\ S_z)\Psi = -0.707$$

This brief analysis demonstrates that there are conceptually simple, Stern-Gerlach like, experiments on spin-1/2 systems for which the predictions of quantum mechanics and local realism are in disagreement.

This page titled 8.32: A Surgical Adjudication of the Conflict Between Quantum Theory and Local Realism is shared under a CC BY 4.0 license and was authored, remixed, and/or curated by Frank Rioux via source content that was edited to the style and standards of the LibreTexts platform.

8.33: A Thought Experiment Reveals the Conflict Between Quantum Theory and Local Realism

In order to explore the conflict between quantum mechanics and local realism a spin-1/2 pair is prepared in a singlet state and the individual particles travel in opposite directions on the y-axis to a pair of observers set up to measure spin with Stern-Gerlach magnets oriented in either the d- or z-direction, where d (diagonal) refers to a 45 degree rotation clockwise from the vertical z-axis. The entangled singlet spin state can be written using either the z- or d-direction spin eigenstates.

$$|\Psi\rangle = \frac{1}{\sqrt{2}}\left[|\uparrow\rangle_1|\downarrow\rangle_2 - |\downarrow\rangle_1|\uparrow\rangle_2\right] = \frac{1}{\sqrt{2}}\left[|\nearrow\rangle_1|\swarrow\rangle_2 - |\swarrow\rangle_1|\nearrow\rangle_2\right] = \frac{1}{\sqrt{2}}(0 \quad 1 \quad -1 \quad 0)^T$$

The spin-up and spin-down eigenstates in the x-z plane are shown below in general and explicity for the z- and d-directions.

Spin-up Eigenvalue +1

$$\varphi_u(\varphi) = \begin{pmatrix} \cos\left(\frac{\varphi}{2}\right) \\ \sin\left(\frac{\varphi}{2}\right) \end{pmatrix}$$

Spin-down Eigenvalue -1

$$\varphi_d(\varphi) = \begin{pmatrix} -\sin\left(\frac{\varphi}{2}\right) \\ \cos\left(\frac{\varphi}{2}\right) \end{pmatrix}$$

$$z = 0\text{deg} \quad d = 45\text{deg} \quad \varphi_u(z) = \begin{pmatrix} 0 \\ 1 \end{pmatrix} \quad \varphi_d(z) = \begin{pmatrix} 0 \\ 1 \end{pmatrix} \quad \varphi_u(d) = \begin{pmatrix} 0.924 \\ 0.383 \end{pmatrix} \quad \varphi_d(d) = \begin{pmatrix} -0.383 \\ 0.924 \end{pmatrix}$$

If the observers measure their spins in the same direction quantum mechanics predicts they will get opposite values due to the singlet nature of the spin state. In other words, the combined expectation value is -1 for these measurements.

A realist believes that objects have well-defined properties prior to and independent of observation. The first four columns of the following table provide a local realist's explanation of this result. Specific z- and d-spin states are assigned to the particles in the first two columns, with each particle in one of four equally probable spin orientations consistent with the composite singlet state. The next two columns show that these assignments agree with the quantum prediction. Unfortunately quantum mechanics does not accept the legitimacy of the local realist's spin states because S_z and S_d are noncommuting spin operators and therefore cannot have simultaneous eigenvalues.

$$\begin{pmatrix} \text{Particle 1} & \text{Particle 2} & \hat{S}_z(1)\hat{S}_z(2) & \hat{S}_d(1)\hat{S}_d(2) & \hat{S}_z(1)\hat{S}_d(2) & \hat{S}_d(1)\hat{S}_z(2) \\ |\uparrow\rangle|\nearrow\rangle & |\downarrow\rangle|\swarrow\rangle & -1 & -1 & -1 & -1 \\ |\uparrow\rangle|\swarrow\rangle & |\downarrow\rangle|\nearrow\rangle & -1 & -1 & 1 & 1 \\ |\downarrow\rangle|\nearrow\rangle & |\uparrow\rangle|\swarrow\rangle & -1 & -1 & 1 & 1 \\ |\downarrow\rangle|\swarrow\rangle & |\uparrow\rangle|\nearrow\rangle & -1 & -1 & -1 & -1 \\ \text{Realist} & \text{Value} & -1 & -1 & 0 & 0 \\ \text{Quantum} & \text{Value} & -1 & -1 & -0.707 & -0.707 \end{pmatrix}$$

Putting this issue aside momentarily, if one spin is measured in the z-direction and the other in the d-direction, a realist predicts an expectation value of zero as shown in the last two columns of the table. However, quantum theory predicts an expectation value of -0.707. If one of the particles is observed to be spin-up in the z-direction (eigenvalue +1), the other is spin-down in the z-direction. The probability it will be found on measurement to be spin-up in the d-direction yielding a composite eigenvalue of +1 is 0.146. The probability it will be found to be spin-down in the d-direction yielding a composite eigenvalue of -1 is 0.854.

$$\begin{pmatrix} \left(\left|\varphi_u(d)^T\varphi_d(z)\right|\right)^2 = 0.146 & \left(\left|\varphi_d(d)^T\varphi_d(z)\right|\right)^2 = 0.854 & \left(\left|\varphi_u(d)^T\varphi_d(z)\right|\right)^2 - \left(\left|\varphi_d(d)^T\varphi_d(z)\right|\right)^2 \\ & & = -0.707 \end{pmatrix}$$

This brief analysis demonstrates that there are conceptually simple, Stern-Gerlach like, experiments on spin-1/2 systems which can adjudicate the conflict between local realism and quantum mechanics.

A Quantum Simulation

This thought experiment is simulated using the following quantum circuit. As shown below the results are in agreement with the previous theoretical quantum calculations. The initial Hadamard and CNOT gates create the singlet state from the |11> input. $R_z(\theta)$ rotates spin B. The final Hadamard gates prepare the system for measurement. See arXiv:1712.05642v2 for further detail.

$$\begin{array}{llllllll} \text{Spin A} & |1\rangle & \triangleright & \text{H} & \cdot & \cdots & \text{H} & \triangleright \quad \text{Measure 0 or 1: Eigenvalue } +1 \text{ or -1} \\ & & & & | & & & \\ \text{Spin B} & |1\rangle & \triangleright & \cdots & \oplus & \text{R}_z(\theta) & \text{H} & \triangleright \quad \text{Measure 0 or 1: Eigenvalue } +1 \text{ or -1} \end{array}$$

The quantum gates required to execute this circuit:

$$\begin{array}{cccc} \text{Identity} & \text{Hadamard gate} & \text{R}_z \text{ Rotation} & \text{Controlled NOT} \\ I = \begin{pmatrix} 1 & 0 \\ 0 & 1 \end{pmatrix} & H = \frac{1}{\sqrt{2}} \begin{pmatrix} 1 & 1 \\ 1 & -1 \end{pmatrix} & R_z(\theta) = \begin{pmatrix} 1 & 0 \\ 0 & e^{i\theta} \end{pmatrix} & \text{CNOT} = \begin{pmatrix} 1 & 0 & 0 & 0 \\ 0 & 1 & 0 & 0 \\ 0 & 0 & 0 & 1 \\ 0 & 0 & 1 & 0 \end{pmatrix} \end{array}$$

The operator representing the circuit is constructed from the matrix operators provided above.

$$\text{Op}(\theta) = \text{kronecker(H, H) kronecker(I, R)}_z(\theta))\text{CNOT kronecker(H, I)}$$

There are four equally likely measurement outcomes with the eigenvalues and overal expectation values shown below.

Illegal pream-token (&)

This page titled 8.33: A Thought Experiment Reveals the Conflict Between Quantum Theory and Local Realism is shared under a CC BY 4.0 license and was authored, remixed, and/or curated by Frank Rioux via source content that was edited to the style and standards of the LibreTexts platform.

8.34: Positronium Annihilation

The following provides an alternative mathematical analysis of the annihilation of positronium as presented in section 18-3 in Volume III of *The Feynman Lectures on Physics*.

Positronium is an analog of the hydrogen atom in which the proton is replaced by a positron, the electron's anti-particle. The electron-positron pair undergoes annihilation in 10^{-10} seconds producing two γ-ray photons. Positronium's effective mass is 1/2, yielding a ground state energy (excluding the magnetic interactions between the spin 1/2 anti-particles)

$$E = -0.5\mu Eh = -0.25Eh.$$

Considering spin the ground state is four-fold degenerate, but this degeneracy is split by the magnetic spin-spin hyperfine interaction shown below. See "The Hyperfine Splitting in the Hydrogen Atom" for further detail.

$$\hat{H}_{SpinSpin} = A\sigma^e\sigma^p \tag{8.34.1}$$

$$= A\left(\sigma_x^e\sigma_x^p + \sigma_y^e\sigma_y^p + \sigma_z^e\sigma_z^p\right) \tag{8.34.2}$$

The spin-spin Hamiltonian has the following eigenvalues (top row) and eigenvectors (columns beneath the eigenvalues), showing a singlet ground state and triplet excited state. The electron-positron spin states are to the right of the table with their m quantum numbers, showing that the singlet (j = 0, m = 0) is a superposition state as is one of the triplet states (j = 1, m = 0). The parameter A is much larger for positronium than for the hydrogen atom because the positron has a much larger magnetic moment than the proton.

$$\begin{pmatrix} -3A & A & A & A \\ 0 & 0 & 0 & 1 \\ \frac{1}{\sqrt{2}} & \frac{1}{\sqrt{2}} & 0 & 0 \\ -\frac{1}{\sqrt{2}} & \frac{1}{\sqrt{2}} & 0 & 0 \\ 0 & 0 & 1 & 0 \end{pmatrix} \begin{matrix} |++\rangle & m=1 \\ |+-\rangle & m=0 \\ |-+\rangle & m=0 \\ |--\rangle & m=-1 \end{matrix}$$

Feynman shows that when the singlet ground state (J = 0, m = 0) annihilates, conservation of momentum requires that the photons emitted in opposite directions (A and B) must have the same circular polarization state, either both in the right or both in left circular state in their direction of motion. This leads to the following entangled superposition. The negative sign is required by parity conservation. The positronium ground state has negative parity (see above), therefore the final photon state must have negative parity.

$$|\Psi\rangle = \frac{1}{\sqrt{2}}\left[|R\rangle_A|R\rangle_B - |L\rangle_A|L\rangle_B\right] \tag{8.34.3}$$

$$= \frac{1}{\sqrt{2}}\left[\begin{pmatrix}1\\i\end{pmatrix}_A \otimes \begin{pmatrix}1\\i\end{pmatrix}_B - \begin{pmatrix}1\\-i\end{pmatrix}_A \otimes \begin{pmatrix}1\\-i\end{pmatrix}_B\right] \tag{8.34.4}$$

$$= \frac{1}{2\sqrt{2}}\left[\begin{pmatrix}1\\i\\i\\-1\end{pmatrix} - \begin{pmatrix}1\\-i\\-i\\-1\end{pmatrix}\right] = \frac{i}{\sqrt{2}}\begin{pmatrix}0\\1\\1\\0\end{pmatrix} \tag{8.34.5}$$

The circular polarization states are:

$$R = \tfrac{1}{\sqrt{2}}\begin{pmatrix}1\\i\end{pmatrix} \quad L = \tfrac{1}{\sqrt{2}}\begin{pmatrix}1\\-i\end{pmatrix}$$

The appropriate operators are formed below:

$$RC = R(\overline{R})^T \rightarrow \begin{pmatrix}\frac{1}{2} & -\frac{1}{2}i\\ \frac{1}{2}i & \frac{1}{2}\end{pmatrix} \quad LC = L(\overline{L})^T \rightarrow \begin{pmatrix}\frac{1}{2} & -\frac{1}{2}i\\ \frac{1}{2}i & \frac{1}{2}\end{pmatrix} \quad RLC = R(\overline{R})^T - L(\overline{L})^T \rightarrow \begin{pmatrix}0 & -i\\ i & 0\end{pmatrix}$$

RLC is the angular momentum operator for photons. Below it is shown that $|R\rangle$ and $|L\rangle$ are eigenstates with eigenvalues of +1 and -1, respectively.

$$\text{eigenvals(RLC)} = \begin{pmatrix} 1 \\ -1 \end{pmatrix} \quad \text{RLC R} \rightarrow \begin{pmatrix} \frac{\sqrt{2}}{2} \\ \frac{\sqrt{2}i}{2} \end{pmatrix} \quad \text{RLC L} \rightarrow \begin{pmatrix} -\frac{\sqrt{2}}{2} \\ \frac{\sqrt{2}i}{2} \end{pmatrix}$$

Now we can consider some of the measurements that Feynman discusses in his analysis of positronium annihilation. Because the photons in state Ψ are entangled the measurements of observers A and B are correlated. For example, if observers A and B both measure the circular polarization of their photons and compare their results they always agree that they have measured the same polarization state. Their composite expectation value is 1.

$$\Psi = \frac{i}{\sqrt{2}} \begin{pmatrix} 0 \\ 1 \\ 1 \\ 0 \end{pmatrix} \quad (\overline{\Psi})^T \text{kronecker(RLC, RLC)} \Psi = 1$$

The identity operation, do nothing, is now needed:

$$I = \begin{pmatrix} 1 & 0 \\ 0 & 1 \end{pmatrix}$$

But their individual results are a random sequence of +1 and -1 outcomes averaging to an expectation value of zero.

$$(\overline{\Psi})^T \text{kronecker(I, RLC)} \Psi = 0 \quad (\overline{\Psi})^T \text{kronecker(RLC, I)} \Psi = 0$$

The probability that both observers will measure $|R\rangle$ or both measure $|L\rangle$ is 0.5. The probability that one will measure $|R\rangle$ and the other $|L\rangle$, or vice versa is zero.

$$(\overline{\Psi})^T \text{kronecker(RC, RC)} \Psi = 0.5 \quad (\overline{\Psi})^T \text{kronecker(LC, LC)} \Psi = 0.5 \quad (\overline{\Psi})^T \text{kronecker(LC, RC)} \Psi = 0$$

Because $|R\rangle$ and $|L\rangle$ are superpositions of |V> and |H>, the photon wave function can also be written in the V-H plane polarization basis as is shown below. See the Appendix for an alternative justification.

$$|\Psi\rangle = \frac{i}{\sqrt{2}} \left[|V\rangle_A |H\rangle_B - |H\rangle_A |V\rangle_B \right] \tag{8.34.6}$$

$$= \frac{1}{\sqrt{2}} \left[\begin{pmatrix} 1 \\ 0 \end{pmatrix}_A \otimes \begin{pmatrix} 0 \\ 1 \end{pmatrix}_B - \begin{pmatrix} 0 \\ 1 \end{pmatrix}_A \otimes \begin{pmatrix} 1 \\ 0 \end{pmatrix}_B \right] \tag{8.34.7}$$

$$= \frac{i}{\sqrt{2}} \left[\begin{pmatrix} 0 \\ 1 \\ 0 \\ 0 \end{pmatrix} - \begin{pmatrix} 0 \\ 0 \\ 1 \\ 0 \end{pmatrix} \right] = \frac{i}{\sqrt{2}} \begin{pmatrix} 0 \\ 1 \\ 1 \\ 0 \end{pmatrix} \tag{8.34.8}$$

The eigenstates for plane polarization are:

$$V = \begin{pmatrix} 1 \\ 0 \end{pmatrix} \quad H = \begin{pmatrix} 0 \\ 1 \end{pmatrix}$$

The appropriate measurement operators are:

$$V_{op} = \begin{pmatrix} 1 & 0 \\ 0 & 0 \end{pmatrix} \quad H_{op} = \begin{pmatrix} 0 & 0 \\ 0 & 1 \end{pmatrix} \quad VH = \begin{pmatrix} 1 & 0 \\ 0 & -1 \end{pmatrix}$$

As VH is diagonal it is obvious that its eigenvalues are +1 and -1, and that V is the eigenstate with eigenvalue +1 and H is the eigenstate with eigenvalue -1.

$$\text{VH V} = \begin{pmatrix} 1 \\ 0 \end{pmatrix} \quad \text{VH H} = \begin{pmatrix} 0 \\ -1 \end{pmatrix}$$

Just as for the circular polarization measurements, the observers individual plane polarization measurements are totally random, but when they compare their results they find perfect anti-correlation, always observing the opposite polarization state.

$(\overline{\Psi})^T \text{kronecker}(\text{VH}, \text{I})\Psi = 0$ $(\overline{\Psi})^T \text{kronecker}(\text{I}, \text{VH})\Psi = 0$ $(\overline{\Psi})^T \text{kronecker}(\text{VH}, \text{VH})\Psi = -1$

$(\overline{\Psi})^T \text{kronecker}(\text{Vop}, \text{Hop})\Psi = 0.5$ $(\overline{\Psi})^T \text{kronecker}(\text{Hop}, \text{Vop})\Psi = 0.5$

$(\overline{\Psi})^T \text{kronecker}(\text{Vop}, \text{Vop})\Psi = 0$ $(\overline{\Psi})^T \text{kronecker}(\text{Hop}, \text{Hop})\Psi = 0$

If one observer measures circular polarization and the other measures plane polarization the expectation value is 0. In other words there is no correlation between the measurements.

$$(\overline{\Psi})^T \text{kronecker}(\text{RLC}, \text{VH})\Psi = 0 \quad (\overline{\Psi})^T \text{kronecker}(\text{VH}, \text{RLC})\Psi = 0$$

Classical reasoning (according to Feynman) is in disagreement with the highlighted result. Earlier it was demonstrated that the photons are either $|L\rangle$ or $|R\rangle$ polarized. However, suppose photon A is measured in the V-H basis and found to be |V>, and given that B is either $|L\rangle$ or $|R\rangle$, which are superpositions of |V> and |H> (see Appendix), measurement of B in the V-H basis should yield |V> 50% of the time and |H> 50% of the time. There should be no correlation between the A and B measurements. The expectation value should be zero.

Feynman put it this way (parenthetical material added):

> Surely you (A) cannot alter the physical state of his (B) photons by changing the kind of observation you make on your photons. No matter what measurements you make on yours, his must still be either RHC ($|R\rangle$) or LHC ($|L\rangle$).

But according to quantum mechanics the photons are entangled in the R-L and V-H bases as shown above, and therefore measurement of |V> at A collapses the wave function to |H> at B.

The highlighted prediction is confirmed experimentally leading to the conclusion that reasoning classically in this manner about the photons created in positronium annihilation is not valid.

While this analysis of positronium annihilation clarifies the conflict between quantum theory and classical realism, it does not lead to an experimental adjudication of the disagreement. In 1964 John Bell demonstrated that entangled systems, like the positronium decay products, could be used to decide the conflict one way or the other empirically. As is well known the subsequent experimental work based on Bell's theorem decided the conflict between the two views in favor of quantum theory.

Appendix

The relationships between plane and circularly polarized light.

$$\begin{array}{cccc} |R\rangle & |L\rangle & |V\rangle & |H\rangle \\ \frac{1}{\sqrt{2}}(V+iH) \rightarrow \begin{pmatrix} \frac{\sqrt{2}}{2} \\ \frac{\sqrt{2}i}{2} \end{pmatrix} & \frac{1}{\sqrt{2}}(V-iH) \rightarrow \begin{pmatrix} \frac{\sqrt{2}}{2} \\ -\frac{\sqrt{2}i}{2} \end{pmatrix} & \frac{1}{\sqrt{2}}(L+R) \rightarrow \begin{pmatrix} 1 \\ 0 \end{pmatrix} & \frac{i}{\sqrt{2}}(L-R) \rightarrow \begin{pmatrix} 0 \\ 1 \end{pmatrix} \end{array}$$

Transforming Ψ from the R-L basis to the V-H basis using the superpositions above.

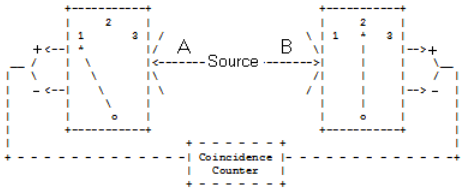
$$\psi = \frac{1}{\sqrt{2}}(R_A R_B - L_A L_B) \left| \begin{array}{l} \text{substitute, } R_A = \frac{1}{\sqrt{2}}(V_A + iH_A) \\ \text{substitute, } R_B = \frac{1}{\sqrt{2}}(V_B + iH_B) \\ \text{substitute, } L_A = \frac{1}{\sqrt{2}}(V_A + iH_A) \\ \text{substitute, } R_A = \frac{1}{\sqrt{2}}(V_B - iH_B) \\ \text{simplify} \end{array} \right. \rightarrow \psi = \sqrt{2}\left(\frac{H_A V_B}{2} + \frac{H_B V_A}{2}\right) i$$

This page titled 8.34: Positronium Annihilation is shared under a CC BY 4.0 license and was authored, remixed, and/or curated by Frank Rioux via source content that was edited to the style and standards of the LibreTexts platform.

8.35: Mermin's Version of Bohm's EPR Gedanken Experiment

The purpose of this tutorial is to summarize a gedanken experiment that reveals a conflict between the predictions of local realism and quantum mechanics. The thought experiment was presented by N. David Mermin in the American Journal of Physics (October 1981, pp 941-943) and Physics Today (April 1985, pp 38-47).

A spin-1/2 pair is prepared in a singlet state and the individual particles travel in opposite directions to a pair of detectors which are set up to measure spin in three directions in x-z plane: along the z-axis, and angles of 120 and 240 degrees with respect to the z-axis. The detector settings are labeled 1, 2 and 3, respectively.



The switches on the detectors are set randomly so that all nine possible settings of the two detectors occur with equal frequency.

Local realism holds that objects have properties independent of measurement and that measurements at one location on a particle cannot influence measurements of another particle at another distant location even if the particles were created in the same event. Local realism maintains that the spin-1/2 particles carry instruction sets which dictate the results of subsequent measurements. That is, prior to measurement the particles are in an unknown but well-defined state.

The following table presents the experimental results expected on the basis of local realism. Singlet spin states have opposite spin values for each of the three measurement directions. For example, if A's spin state is (+-+), then B's spin state is (-+-). If A's detector is set to spin direction "1" and B's detector is set to spin direction "3" the measured result will be recorded as +-.

Spin States	Detector Settings								
	12	13	21	23	31	32	11	22	33
+++/---	+-	+-	+-	+-	+-	+-	+-	+-	+-
++-/--+	+-	++	+-	++	--	--	+-	+-	-+
+-+/-+-	++	+-	--	--	+-	++	+-	-+	+-
-++/+--	--	--	++	+-	++	+-	-+	+-	+-
+--/-++	++	++	--	-+	--	-+	+-	-+	-+
-+-/+-+	--	-+	++	++	-+	--	-+	+-	-+
--+/++-	-+	--	-+	--	++	++	-+	-+	+-
---/+++	-+	-+	-+	-+	-+	-+	-+	-+	-+

Note that there are eight spin states and nine possible detector settings, giving 72 possible measurement outcomes all of which are equally probable.

The table shows that the assumption that the singlet-state particles have well-defined spin states prior to measurement requires that the probability the detectors will register opposite spin values is 0.67 (48/72). If the detectors are set to the same direction, they always register different spin values (24/24), and if they are set to different directions the probability they will register different spin values is 0.50 (24/48).

We now show that quantum mechanics disagrees with the local realistic view just presented. The analysis that follows is based on material in chapters 6 and 11 of A. I. M. Rae's Quantum Mechanics.

The singlet state produced by the source is the following entangled superposition, where the arrows indicate the spin orientation for any direction in the x-z plane. As noted above the directions used here are 0, 120 and 240 degrees, relative to the z-axis.

$$|\Psi\rangle = \frac{1}{\sqrt{2}}\left[|\uparrow\rangle_1 |\downarrow\rangle_2 - |\downarrow\rangle_1 |\uparrow\rangle_2\right]$$

The spin operator in the x-z plane is constructed from the Pauli spin operators in the x- and z-directions. φ is the angle of orientation of the measurement magnet with the z-axis. Note that the Pauli operators measure spin in units of h/4π. This provides for some mathematical clarity in the forthcoming analysis.

$$\sigma_z = \begin{pmatrix} 1 & 0 \\ 0 & -1 \end{pmatrix} \quad \sigma_x \begin{pmatrix} 0 & 1 \\ 1 & 0 \end{pmatrix} \quad S(\varphi) = \cos(\varphi)\sigma_z + \sin(\varphi)\sigma_x \rightarrow \begin{pmatrix} \cos\varphi & \sin\varphi \\ \sin\varphi & -\cos\varphi \end{pmatrix}$$

The spin-up and spin-down eigenvectors for this operator are as follow:

$$\text{Eigenvalue } +1 \quad \varphi_u(\varphi) = \begin{pmatrix} \cos\left(\frac{\varphi}{2}\right) \\ \sin\left(\frac{\varphi}{2}\right) \end{pmatrix} \quad S(\varphi)\varphi_u(\varphi)\text{simplify} \rightarrow \begin{pmatrix} \cos\left(\frac{\varphi}{2}\right) \\ \sin\left(\frac{\varphi}{2}\right) \end{pmatrix}$$

$$\text{Eigenvalue -1} \quad \varphi_d(\varphi) = \begin{pmatrix} -\sin\left(\frac{\varphi}{2}\right) \\ \cos\left(\frac{\varphi}{2}\right) \end{pmatrix} \quad S(\varphi)\varphi_d(\varphi)\text{simplify} \rightarrow \begin{pmatrix} \sin\left(\frac{\varphi}{2}\right) \\ -\cos\left(\frac{\varphi}{2}\right) \end{pmatrix}$$

Note that we get the expected eigenvectors for the z- and x-directions for angles of 0 and 90 degrees, respectively.

$$\varphi_u(0) = \begin{pmatrix} 1 \\ 0 \end{pmatrix} \quad \varphi_d(0) = \begin{pmatrix} 0 \\ 1 \end{pmatrix} \quad \varphi_u\left(\tfrac{\pi}{2}\right) = \begin{pmatrix} 0.707 \\ 0.707 \end{pmatrix} \quad \varphi_d\left(\tfrac{\pi}{2}\right) = \begin{pmatrix} -0.707 \\ 0.707 \end{pmatrix}$$

For spin measurements in which the detectors are set at the same angle quantum mechanics agrees with local realism that the detectors will register opposite spins. To illustrate what quantum mechanics predicts when the detectors are set at different angles we will consider a specific example. Suppose the particle at detector A is found to be spin-up in the z-direction, $\begin{pmatrix} 1 \\ 0 \end{pmatrix}$. It follows from the singlet spin state that the particle at B is spin-down in the z-direction, $\begin{pmatrix} 0 \\ 1 \end{pmatrix}$. But as shown below this state can be written as a superposition of φ_u and φ_d.

$$\sin\left(\frac{\varphi}{2}\right)\varphi_u(\varphi) + \cos\left(\frac{\varphi}{2}\right)\varphi_d(\varphi)\text{simplify} \rightarrow \begin{pmatrix} 0 \\ 1 \end{pmatrix}$$

The quantum mechanical prediction of the spin measurement at an angle φ on particle B is given by the squares of the coefficients of φ_u and φ_d. Therefore the probability that the measurement on particle B will be opposite of that on particle A is cos2(φ/2), which is 0.25 for angles of 120 and 240 degrees.

Thus over-all quantum mechanics predicts that opposite spins will be recorded [(1/3)100% + (2/3)25%] 50% of the time, in sharp disagreement with the 67% calculated on the basis on local realism.

Next it is shown that the result of 25% is general for detector angle differences of 120 degrees (2π/3). First the 0-120 degree result is calculated using a different but equivalent method. The particle at detector A was found to be spin-up in the z-direction (φ = 0 deg) requiring that particle B is spin-down in the z-direction. The probability that particle B will be found spin-down when its detector is set to 120 deg is the square of the projection of $\varphi_d(0)$ onto $\varphi_d(2\pi/3)$. The state vectors are real so it is not necessary to square the absolute magnitude.

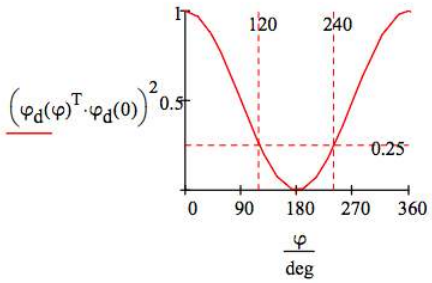
$$\left(\varphi_d(120\text{ deg})^T\varphi_d(0)\right)^2 = 0.25$$

This calculation is now repeated for the 30-150, 60-180, 90-210 and 120-240 detector orientations.

$$\left(\varphi_d(150\text{ deg})^T\varphi_d(30\text{ deg})\right)^2 = 0.25 \quad \left(\varphi_d(180\text{ deg})^T\varphi_d(60\text{ deg})\right)^2 = 0.25$$

$$\left(\varphi_d(210\text{ deg})^T\varphi_d(90\text{ deg})\right)^2 = 0.25 \quad \left(\varphi_d(120\text{ deg})^T\varphi_d(120\text{ deg})\right)^2 = 0.25$$

This graphic shows the probability calculation for all detector orientations.



Summary

Local realism maintains that objects have well-defined properties independent of observation, and that the acquisition of a definite value for a property by an object at B due to a measurement carried out on a distant object at A is "spooky action at a distance" and physically unintelligible and therefore impossible.

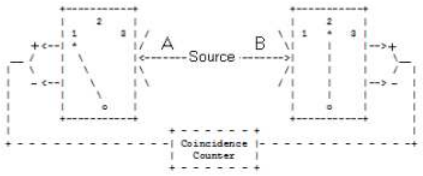
By contrast quantum theory teaches that quantum particles do not in general have well-defined properties independent of measurement, and that particles with a common origin are in an entangled state and therefore are not independent, no matter how far apart they may be. Together they are in a well-defined correlated state, but their individual properties are uncertain. When measurement determines the state of the particle at A, the correlated property of its distant partner at B becomes known instantaneously.

This page titled 8.35: Mermin's Version of Bohm's EPR Gedanken Experiment is shared under a CC BY 4.0 license and was authored, remixed, and/or curated by Frank Rioux via source content that was edited to the style and standards of the LibreTexts platform.

8.36: A Concise Version of Mermin's EPR Gedanken Experiment

In Bohm's EPR thought experiment (*Quantum Theory*, 1951, pp. 614-619), both local realism and quantum mechanics were shown to be consistent with the experimental data. However, the local realistic explanation used composite spin states that were invalid according to quantum theory. The local realist countered that this was an indication that quantum mechanics was incomplete, because it couldn't assign well-defined values to all observable properties. In this example a thought experiment is presented in which the predictions of local realism and quantum mechanics differ. The thought experiment was presented by N. David Mermin in the *American Journal of Physics* (October 1981, pp 941-943) and *Physics Today* (April 1985, pp 38-47).

A spin-1/2 pair is prepared in a singlet state and the individual particles travel in opposite directions to a pair of detectors which are set up to measure spin in three directions in x-z plane: along the z-axis, and angles of 120 and 240 degrees with respect to the z-axis. The detector settings are labeled 1, 2 and 3, respectively.



The switches on the detectors are set randomly so that all nine possible settings of the two detectors occur with equal frequency.

Local realism holds that objects have properties independent of measurement and that measurements at one location on a particle cannot influence measurements of another particle at another distant location even if the particles were created in the same event. Local realism maintains that the spin-1/2 particles carry instruction sets (hidden variables) which dictate the results of subsequent measurements. Prior to measurement the particles are in an unknown but well-defined state.

The following table presents the experimental results expected on the basis of local realism. Singlet spin states have opposite spin values for each of the three measurement directions. For example, if A's spin state is (+-+), then B's spin state is (-+-). If A's detector is set to spin direction "1" and B's detector is set to spin direction "3" the measured result will be recorded as +-.

Spin States	Detector Settings								
	12	13	21	23	31	32	11	22	33
+++/---	+-	+-	+-	+-	+-	+-	+-	+-	+-
++-/--+	+-	++	+-	++	--	--	+-	+-	-+
+-+/-+-	++	+-	--	--	+-	++	+-	-+	+-
-++/+--	--	--	++	+-	++	+-	-+	+-	+-
+--/-++	++	++	--	-+	--	-+	+-	-+	-+
-+-/+-+	--	-+	++	++	-+	--	-+	+-	-+
--+/++-	-+	--	-+	--	++	++	-+	-+	+-
---/+++	-+	-+	-+	-+	-+	-+	-+	-+	-+

Note that there are eight spin states and nine possible detector settings, giving 72 possible measurement outcomes all of which are equally probable.

The table shows that the assumption that the singlet-state particles have well-defined spin states prior to measurement requires that the probability the detectors will register opposite spin values is 0.67 (48/72). If the detectors are set to the same direction, they always register different spin values (24/24), and if they are set to different directions the probability they will register different spin values is 0.50 (24/48). Quantum mechanics disagrees with this local realistic analysis.

The singlet state produced by the source is the following entangled superposition, where the arrows indicate the spin orientation for any direction in the x-z plane. See the Appendix for a proof of this assertion. As noted above the directions used here are 0, 120 and 240 degrees, relative to the z-axis.

$$|\Psi\rangle = \frac{1}{\sqrt{2}}\left[|\uparrow\rangle_1|\downarrow\rangle_2 - |\downarrow\rangle_1|\uparrow\rangle_2\right] = \frac{1}{\sqrt{2}}\begin{pmatrix}0\\1\\-1\\0\end{pmatrix}$$

The orthonormal spin-up and spin-down vectors in the x-z plane are:

$$\varphi_u(\varphi) = \begin{pmatrix} \cos\left(\frac{\varphi}{2}\right) \\ \sin\left(\frac{\varphi}{2}\right) \end{pmatrix} \quad \varphi_d(\varphi) = \begin{pmatrix} -\sin\left(\frac{\varphi}{2}\right) \\ \cos\left(\frac{\varphi}{2}\right) \end{pmatrix}$$

$$\varphi_u(\varphi)^T \varphi_u(\varphi)\text{simplify} \rightarrow 1 \quad \varphi_d(\varphi)^T \varphi_d(\varphi)\text{simplify} \rightarrow 1 \quad \varphi_d(\varphi)^T \varphi_u(\varphi)\text{simplify} \rightarrow 0$$

For spin measurements in which the detectors are set at the same angle, quantum mechanics and local realism agree that the detectors will register opposite spins. Therefore we will concentrate on what quantum mechanics predicts when the detectors are set at different angles. Recall that local realism predicts that the detectors will behave differently 50% of the time.

If the particle at detector A is found to be spin-up in the z-direction, it follows from the singlet spin state that the particle at B is spin-down in the z-direction, φd(0). The probability that it will be detected spin down if detector B is rotated clockwise or counter-clockwise by 120 degrees is,

$$\left(\varphi_d(120\ \text{deg})^T \varphi_d(0\ \text{deg})\right)^2 = 0.25 \quad \left(\varphi_d(240\ \text{deg})^T \varphi_d(0\ \text{deg})\right)^2 = 0.25$$

Thus for those cases for which the detectors are set at different angles there is a sharp disagreement between local realism (50%) and quantum mechanics (25%) as to the percentage of the time the detectors behave differently. For all detector settings quantum mechanics predicts that opposite spins will be recorded [(1/3)100% + (2/3)25%] 50% of the time, compared with the 67% calculated on the basis of local realism.

Quantum theory maintains that the discrepancy in the predictions is due to the fact that the local realistic spin states in the left column of the table above are invalid because they assign definite values to incompatible observables. For example, if the z-axis spin value of the first particle is known to be +, then the state of the composite system is not +++/--- or ++-/--+ or +-+/-+- or +--/-++, but +??/-??. The Appendix demonstrates that the spin operators for 0, 120 and 240 degrees do not commute, which means that the observables associated with these operators cannot simultaneously be well defined.

Summary

Local realism maintains that objects have well-defined properties independent of observation, and that the acquisition of a definite value for a property by an object at B due to a measurement carried out on a distant object at A is "spooky action at a distance" and physically unintelligible and therefore impossible.

By contrast quantum theory teaches that quantum particles do not in general have well-defined properties independent of measurement, and that particles with a common origin are in an entangled state and therefore are not independent, no matter how far apart they may be. Together they are in a well-defined correlated state, but their individual properties are uncertain. When measurement determines the state of the particle at A, the correlated property of its distant partner at B becomes known instantaneously.

Appendix

The spin operator in the x-z plane is constructed from the Pauli spin operators in the x- and z-directions. ϕ is the angle of orientation of the measurement magnet with the z-axis. Note that the Pauli operators measure spin in units of h/4π.

$$\sigma_z = \begin{pmatrix} 1 & 0 \\ 0 & -1 \end{pmatrix} \quad \sigma_x = \begin{pmatrix} 0 & 1 \\ 1 & 0 \end{pmatrix} \quad S(\varphi) = \cos(\varphi)\sigma_z + \sin(\varphi)\sigma_x \rightarrow \begin{pmatrix} \cos(\varphi) & \sin(\varphi) \\ \sin(\varphi) & -\cos(\varphi) \end{pmatrix}$$

The following calculations demonstrate that the spin operators do not commute and therefore represent incompatible observables. In other words, they are observables that cannot simultaneously be in well-defined states.

$$S(0\ \text{deg})\ S(120\ \text{deg}) - S(120\ \text{deg})\ S(0\ \text{deg}) = \begin{pmatrix} 0 & 1.732 \\ -1.732 & 0 \end{pmatrix}$$

$$S(0\ \text{deg})\ S(240\ \text{deg}) - S(240\ \text{deg})\ S(0\ \text{deg}) = \begin{pmatrix} 0 & -1.732 \\ 1.732 & 0 \end{pmatrix}$$

$$S(1200\ \text{deg})\ S(240\ \text{deg}) - S(240\ \text{deg})\ S(120\ \text{deg}) = \begin{pmatrix} 0 & 1.732 \\ -1.732 & 0 \end{pmatrix}$$

For the singlet state produced by the source the arrows indicate the spin orientation for any direction in the x-z plane.

$$|\Psi\rangle = \frac{1}{\sqrt{2}}\left[|\uparrow\rangle_1|\downarrow\rangle_2 - |\uparrow\rangle_1|\downarrow\rangle_2\right]$$

$$= \frac{1}{\sqrt{2}}\left[\begin{pmatrix}\cos\left(\frac{\varphi}{2}\right)\\ \sin\left(\frac{\varphi}{2}\right)\end{pmatrix} \otimes \begin{pmatrix}-\sin\left(\frac{\varphi}{2}\right)\\ \cos\left(\frac{\varphi}{2}\right)\end{pmatrix} - \begin{pmatrix}-\sin\left(\frac{\varphi}{2}\right)\\ \cos\left(\frac{\varphi}{2}\right)\end{pmatrix} \otimes \begin{pmatrix}\cos\left(\frac{\varphi}{2}\right)\\ \sin\left(\frac{\varphi}{2}\right)\end{pmatrix}\right] = \frac{1}{\sqrt{2}}\begin{pmatrix}0\\ 1\\ -1\\ 0\end{pmatrix}$$

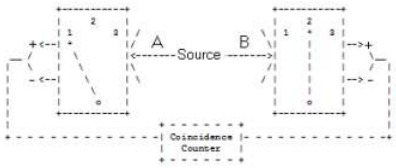
This page titled 8.36: A Concise Version of Mermin's EPR Gedanken Experiment is shared under a CC BY 4.0 license and was authored, remixed, and/or curated by Frank Rioux via source content that was edited to the style and standards of the LibreTexts platform.

8.37: Another Look at Mermin's EPR Gedanken Experiment

> Quantum theory is both stupendously successful as an account of the small-scale structure of the world and it is also the subject of an unresolved debate and dispute about its interpretation. J. C. Polkinghorne, *The Quantum World*, p. 1.

In Bohm's EPR thought experiment (*Quantum Theory*, 1951, pp. 611-623), both local realism and quantum mechanics were shown to be consistent with the experimental data. However, the local realistic explanation used composite spin states that were invalid according to quantum theory. The local realists countered that this was an indication that quantum mechanics was incomplete because it couldn't assign well-defined values to all observable properties prior to or independent of observation. In the 1980s N. David Mermin presented a related thought experiment [*American Journal of Physics* (October 1981, pp 941-943) and *Physics Today* (April 1985, pp 38-47)] in which the predictions of local realism and quantum mechanics disagree. As such Mermin's thought experiment represents a specific illustration of Bell's theorem.

A spin-1/2 pair is prepared in a singlet state and the individual particles travel in opposite directions to detectors which are set up to measure spin in three directions in x-z plane: along the z-axis, and angles of 120 and 240 degrees with respect to the z-axis. The detector settings are labeled 1, 2 and 3, respectively.



The switches on the detectors are set randomly so that all nine possible settings of the two detectors occur with equal frequency.

Local realism holds that objects have properties independent of measurement and that measurements at one location on a particle cannot influence measurements of another particle at a distant location even if the particles were created in the same event. Local realism maintains that the spin-1/2 particles carry instruction sets (hidden variables) which dictate the results of subsequent measurements. Prior to measurement the particles are in an unknown but well-defined state.

The following table presents the experimental results expected on the basis of local realism. Singlet spin states have opposite spin values for each of the three measurement directions. If A's spin state is (+-+), then B's spin state is (-+-). A '+' indicates spin-up and a measurement eigenvalue of +1. A '-' indicates spin-down and a measurement eigenvalue of -1. If A's detector is set to spin direction "1" and B's detector is set to spin direction "3" the measured result will be recorded as +-,with an eigenvalue of -1.

There are eight spin states and nine possible detector settings, giving 72 possible measurement outcomes all of which are equally probable. The next to bottom line of the table shows the average (expectation) value for the nine possible detector settings given the local realist spin states. When the detector settings are the same there is perfect anti-correlation between the detectors at A and B. When the detectors are set at different spin directions there is no correlation.

Spin States	Detector Settings								
	12	13	21	23	31	32	11	22	33
+++/---	+-	+-	+-	+-	+-	+-	+-	+-	+-
++-/--+	+-	++	+-	++	--	--	+-	+-	-+
+-+/-+-	++	+-	--	--	+-	++	+-	-+	+-
-++/+--	--	--	++	+-	++	+-	-+	+-	+-
+--/-++	++	++	--	-+	--	-+	+-	-+	-+
-+-/+-+	--	-+	++	++	-+	--	-+	+-	-+
--+/++-	-+	--	-+	--	++	++	-+	-+	+-
---/+++	-+	-+	-+	-+	-+	-+	-+	-+	-+
Average Value	0	0	0	0	0	0	-1	-1	-1
Quantum Value	.5	.5	.5	.5	.5	.5	-1	-1	-1

As will now be shown quantum mechanics (bottom line of the table) disagrees with this local realistic analysis. The singlet state produced by the source is the following entangled superposition, where the arrows indicate the spin orientation for any direction in the x-z plane. As noted above the directions used are 0, 120 and 240 degrees, relative to the z-axis.

$$|\Psi\rangle = \frac{1}{\sqrt{2}}\left[|\uparrow\rangle_1|\downarrow\rangle_2 - |\uparrow\rangle_1|\downarrow\rangle_2\right] \qquad \Psi = \frac{1}{\sqrt{2}}\begin{pmatrix}0\\1\\-1\\0\end{pmatrix}$$

$$= \frac{1}{\sqrt{2}}\left[\begin{pmatrix}\cos\left(\frac{\varphi}{2}\right)\\ \sin\left(\frac{\varphi}{2}\right)\end{pmatrix}\otimes\begin{pmatrix}-\sin\left(\frac{\varphi}{2}\right)\\ \cos\left(\frac{\varphi}{2}\right)\end{pmatrix} - \begin{pmatrix}-\sin\left(\frac{\varphi}{2}\right)\\ \cos\left(\frac{\varphi}{2}\right)\end{pmatrix}\otimes\begin{pmatrix}\cos\left(\frac{\varphi}{2}\right)\\ \sin\left(\frac{\varphi}{2}\right)\end{pmatrix}\right]$$

$$= \frac{1}{\sqrt{2}}\begin{pmatrix}0\\1\\-1\\0\end{pmatrix}$$

The single particle spin operator in the x-z plane is constructed from the Pauli spin operators in the x and z-directions. ϕ is the angle of orientation of the measurement magnet with the z-axis. Note that the Pauli operators measure spin in units of h/4π. This provides for some mathematical clarity in the forthcoming analysis.

$$\sigma_z = \begin{pmatrix}1 & 0\\ 0 & -1\end{pmatrix} \quad \sigma_x = \begin{pmatrix}0 & 1\\ 1 & 0\end{pmatrix} \quad S(\varphi) = \cos(\varphi)\sigma_z + \sin(\varphi)\sigma_x \rightarrow \begin{pmatrix}\cos(\varphi) & \sin(\varphi)\\ \sin(\varphi) & -\cos(\varphi)\end{pmatrix}$$

The joint spin operator for the two-spin system in tensor format is,

$$\begin{pmatrix}\cos\varphi_A & \sin\varphi_A\\ \sin\varphi_A & -\cos\varphi_A\end{pmatrix}\otimes\begin{pmatrix}\cos\varphi_B & \sin\varphi_B\\ \sin\varphi_B & -\cos\varphi_B\end{pmatrix}$$

$$= \begin{pmatrix}\cos\varphi_A\begin{pmatrix}\cos\varphi_B & \sin\varphi_B\\ \sin\varphi_B & -\cos\varphi_B\end{pmatrix} & \sin\varphi_A\begin{pmatrix}\cos\varphi_B & \sin\varphi_B\\ \sin\varphi_B & -\cos\varphi_B\end{pmatrix}\\ \sin\varphi_A\begin{pmatrix}\cos\varphi_B & \sin\varphi_B\\ \sin\varphi_B & -\cos\varphi_B\end{pmatrix} & -\cos\varphi_A\begin{pmatrix}\cos\varphi_B & \sin\varphi_B\\ \sin\varphi_B & -\cos\varphi_B\end{pmatrix}\end{pmatrix}$$

In Mathcad syntax this operator is:

$$\text{kronecker}(S(\varphi_A),\ S(\varphi_B))$$

When the detector settings are the same quantum theory predicts an expectation value of -1, in agreement with the analysis based on local realism.

Ψ^Tkronecker(S, (0 deg), S(0 deg)$\Psi = -1$	Ψ^Tkronecker(S, (120 deg), S(120 deg)$\Psi = -1$	Ψ^Tkronecker(S, (240 deg), S(240 deg)$\Psi = -1$

However, when the detector settings are different quantum theory predicts an expectation value of 0.5, in disagreement with the local realistic value of 0.

Ψ^Tkronecker(S, (0 deg), S(120 deg)$\Psi = 0.5$	Ψ^Tkronecker(S, (0 deg), S(240 deg)$\Psi = 0.5$	Ψ^Tkronecker(S, (120 deg), S(240 deg)$\Psi = 0.5$

Considering all detector settings local realism predicts an expectation value of -1/3 [2/3(0) + 1/3(-1)], while quantum theory predicts an expectation value of 0 [2/3(1/2) + 1/3(-1)]. (See the two bottom rows in the table above.)

Furthermore, the following calculations demonstrate that the various spin operators do not commute and therefore represent incompatible observables. In other words, they are observables that cannot simultaneously be in well-defined states. Thus, quantum theory also rejects the realist's spin states used in the table.

$$S(0\text{ deg})\ S(120\text{ deg}) - S(120\text{ deg})\ S(0\text{ deg}) = \begin{pmatrix}0 & 1.732\\ -1.732 & 0\end{pmatrix}$$

$$S(0\text{ deg})\ S(240\text{ deg}) - S(240\text{ deg})\ S(0\text{ deg}) = \begin{pmatrix}0 & -1.732\\ 1.732 & 0\end{pmatrix}$$

$$S(1200\text{ deg})\ S(240\text{ deg}) - S(240\text{ deg})\ S(120\text{ deg}) = \begin{pmatrix}0 & 1.732\\ -1.732 & 0\end{pmatrix}$$

The local realist is undeterred by this argument and the disagreement with the quantum mechanical predictions, asserting that the fact that quantum theory cannot assign well-defined states to all elements of reality independent of observation is an indication that it provides an incomplete description of reality.

However, results available for experiments of this type with photons support the quantum mechanical predictions and contradict the local realists analysis shown in the table above. Thus, there appears to be a non-local interaction between the two spins at their measurement sites. Nick Herbert provides a memorable and succinct description of such non-local influences on page 214 of *Quantum Reality*.

> A non-local interaction links up one location with another without crossing space, without decay, and without delay. A non-local interaction is, in short, unmediated, unmitigated, and immediate.

Jim Baggott puts it this way (*The Meaning of Quantum Theory*, page 135):

> The predictions of quantum theory (in this experiment) are based on the properties of a two-particle state vector which ... is 'delocalized' over the whole experimental arrangement. The two particles are, in effect, always in 'contact' prior to measurement and can therefore exhibit a degree of correlation that is impossible for two Einstein separable particles.

"...if [a hidden-variable theory] is local it will not agree with quantum mechanics, and if it agrees with quantum mechanics it will not be local. This is what the theorem says." John S. Bell

Further Information

The eigenvectors of the single particle spin operator, S(φ), in the x-z plane are given below along with their eigenvalues.

$$\varphi_u(\varphi) = \begin{pmatrix} \cos\left(\frac{\varphi}{2}\right) \\ \sin\left(\frac{\varphi}{2}\right) \\ \cos\left(\frac{\varphi}{2}\right) \end{pmatrix} \qquad \varphi_d(\varphi) = \begin{pmatrix} -\sin\left(\frac{\varphi}{2}\right) \end{pmatrix}$$

$$\varphi_u(\varphi)^T\varphi_u(\varphi)\text{simplify} \rightarrow 1 \quad \varphi_d(\varphi)^T\varphi_d(\varphi)\text{simplify} \rightarrow 1 \quad \varphi_d(\varphi)^T\varphi_u(\varphi)\text{simplify} \rightarrow 0$$

$$\begin{matrix} \text{Eigenvalue } +1 & \text{Eigenvalue -1} \\ S(\varphi)\varphi_u(\varphi)\text{simplify} \rightarrow \begin{pmatrix} \cos\left(\frac{\varphi}{2}\right) \\ \sin\left(\frac{\varphi}{2}\right) \\ \cos\left(\frac{\varphi}{2}\right) \end{pmatrix} & \\ S(\varphi)\varphi_d(\varphi)\text{simplify} \rightarrow \begin{pmatrix} \sin\left(\frac{\varphi}{2}\right) \end{pmatrix} & \end{matrix}$$

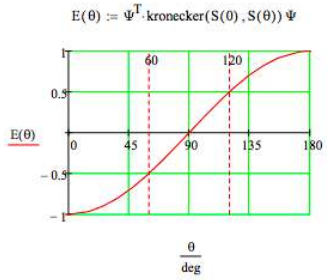
A summary of the quantum mechanical calculations:

$$\begin{pmatrix} \Psi^T\text{kronecker(S, (0 deg), S(120 deg)}\Psi \\ \Psi^T\text{kronecker(S, (0 deg), S(240 deg)}\Psi \\ \Psi^T\text{kronecker(S, (120 deg), S(0 deg)}\Psi \\ \Psi^T\text{kronecker(S, (120 deg), S(240 deg)}\Psi \\ \Psi^T\text{kronecker(S, (240 deg), S(0 deg)}\Psi \\ \Psi^T\text{kronecker(S, (240 deg), S(120 deg)}\Psi \\ \Psi^T\text{kronecker(S, (0 deg), S(0 deg)}\Psi \\ \Psi^T\text{kronecker(S, (120 deg), S(120 deg)}\Psi \\ \Psi^T\text{kronecker(S, (240 deg), S(240 deg)}\Psi \end{pmatrix}^T = \begin{pmatrix} 0.5 & 0.5 & 0.5 & 0.5 & 0.5 & 0.5 & -1 & -1 & -1 \end{pmatrix}$$

Calculation of the overall spin expectation value:

$$\sum_{i=0}^{2}\sum_{j=0}^{2}\left[\Psi^T\text{kronecker[S [i (120 deg)], S[j (120 deg)]]}\Psi\right] = 0$$

The expectation value as a function of the relative orientation of the detectors reveals the level of correlation between the two spin measurements. For θ = 0^0 there is perfect anti-correlation; for θ = 180^0 perfect correlation; for θ = 90^0 no correlation; for θ = 60^0 intermediate anti-correlation (-0.5) and for θ = 120^0 intermediate correlation (0.5).



A Quantum Simulation: This thought experiment is simulated using the following quantum circuit. As shown below the results are in agreement with the previous theoretical quantum calculations. The initial Hadamard and CNOT gates create the singlet state from the |11> input. Rz(θ) rotates spin B. The final Hadamard gates prepare the system for measurement. See arXiv:1712.05642v2 for further detail.

$$\begin{array}{llllllll} \text{Spin A} & |1\rangle & \triangleright & H & \cdot & \cdots & H & \triangleright \text{ Measure 0 or 1: Eigenvalue } +1 \text{ or -1} \\ & & & & | & & & \\ \text{Spin B} & |1\rangle & \triangleright & \cdots & \oplus & R_z(\theta) & H & \triangleright \text{ Measure 0 or 1: Eigenvalue } +1 \text{ or -1} \end{array}$$

The quantum gates required to execute this circuit:

$$\begin{array}{cccc} \text{Identity} & \text{Hadamard gate} & \text{R}_z \text{ Rotation} & \text{Controlled NOT} \\ I = \begin{pmatrix} 1 & 0 \\ 0 & 1 \end{pmatrix} & H = \frac{1}{\sqrt{2}} \begin{pmatrix} 1 & 1 \\ 1 & -1 \end{pmatrix} & R_z(\theta) = \begin{pmatrix} 1 & 0 \\ 0 & e^{i\theta} \end{pmatrix} & \text{CNOT} = \begin{pmatrix} 1 & 0 & 0 & 0 \\ 0 & 1 & 0 & 0 \\ 0 & 0 & 0 & 1 \\ 0 & 0 & 1 & 0 \end{pmatrix} \end{array}$$

The operator representing the circuit is constructed from the matrix operators provided above.

$$\text{Op}(\theta) = \text{kronecker(H, H) kronecker(I, R}_z(\theta))\text{CNOT kronecker(H, I)}$$

There are four equally likely measurement outcomes with the eigenvalues and overall expectation values shown below for relative measurement angles 0 and 120 deg (2π/3).

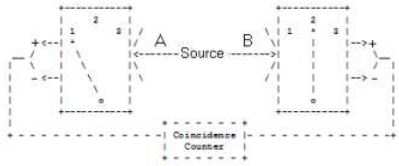
Illegal pream-token (&)

This page titled 8.37: Another Look at Mermin's EPR Gedanken Experiment is shared under a CC BY 4.0 license and was authored, remixed, and/or curated by Frank Rioux via source content that was edited to the style and standards of the LibreTexts platform.

8.38: Mermin's Version of Bohm's EPR Gedanken Experiment Using Tensor Algebra

The purpose of this tutorial is to summarize a gedanken experiment that reveals a conflict between the predictions of local realism and quantum mechanics. The thought experiment was presented by N. David Mermin in the *American Journal of Physics* (October 1981, pp 941-943) and *Physics Today* (April 1985, pp 38-47). In this summary the quantum mechanical analysis employs tensor algebra.

A spin-1/2 pair is prepared in a singlet state and the individual particles travel in opposite directions to a pair of detectors which are set up to measure spin in three directions in x-z plane: along the z-axis, and angles of 120 and 240 degrees with respect to the z-axis. The detector settings are labeled 1, 2 and 3, respectively.



The switches on the detectors are set randomly so that all nine possible settings of the two detectors occur with equal frequency.

Local realism holds that objects have properties independent of measurement and that measurements at one location on a particle cannot influence measurements of another particle at another distant location even if the particles were created in the same event. Local realism maintains that the spin-1/2 particles carry instruction sets which dictate the results of subsequent measurements. That is, prior to measurement the particles are in a well-defined state.

The following table presents the experimental results expected on the basis of local realism. Singlet spin states have opposite spin values for each of the three measurement directions. For example, if A's spin state is (+-+), then B's spin state is (-+-). If A's detector is set to spin direction "1" and B's detector is set to spin direction "3" the measured result will be recorded as +-.

Spin States	Detector Settings								
	12	13	21	23	31	32	11	22	33
+++/---	+-	+-	+-	+-	+-	+-	+-	+-	+-
++-/--+	+-	++	+-	++	--	--	+-	+-	-+
+-+/-+-	++	+-	--	--	+-	++	+-	-+	+-
-++/+--	--	--	++	+-	++	+-	-+	+-	+-
+--/-++	++	++	--	-+	--	-+	+-	-+	-+
-+-/+-+	--	-+	++	++	-+	--	-+	+-	-+
--+/++-	-+	--	-+	--	++	++	-+	-+	+-
---/+++	-+	-+	-+	-+	-+	-+	-+	-+	-+

Note that there are eight spin states and nine possible detector settings, giving 72 possible measurement outcomes all of which are equally probable.

The table shows that the assumption that the singlet-state particles have well-defined spin states prior to measurement requires that the probability the detectors will register opposite spin values is 0.67 (48/72). If the detectors are set to the same direction, they always register different spin values (24/24), and if they are set to different directions the probability they will register different spin values is 0.50 (24/48).

Now we show that a quantum mechanical analysis is in sharp disagreement with the local realistic view just presented.

The natural base states for this quantum analysis are spin-up and spin-down in the z-direction.

$$S_{zu} = \begin{pmatrix} 1 \\ 0 \end{pmatrix} \quad S_{zd} = \begin{pmatrix} 0 \\ 1 \end{pmatrix}$$

The singlet state produced by the source (fermions have anti-symmetric wave functions and are indistinguishable) in tensor format is,

$$|\Psi\rangle = \frac{1}{\sqrt{2}} \left[|\uparrow\rangle_1 |\downarrow\rangle_2 - |\downarrow\rangle_1 |\uparrow\rangle_2 \right] = \frac{1}{\sqrt{2}} \left[\begin{pmatrix} 1 \\ 0 \end{pmatrix} \otimes \begin{pmatrix} 0 \\ 1 \end{pmatrix} - \begin{pmatrix} 0 \\ 1 \end{pmatrix} \otimes \begin{pmatrix} 1 \\ 0 \end{pmatrix} \right] = \frac{1}{\sqrt{2}} \begin{pmatrix} 0 \\ 1 \\ -1 \\ 0 \end{pmatrix} \quad \Psi = \frac{1}{\sqrt{2}} \begin{pmatrix} 0 \\ 1 \\ -1 \\ 0 \end{pmatrix}$$

The single particle spin operator in the x-z plane is constructed from the Pauli spin operators in the xand z-directions. ϕ is the angle of orientation of the measurement magnet with the z-axis. Note that the Pauli operators measure spin in units of h/4π. This provides for some mathematical clarity in the forthcoming analysis.

$$\sigma_z = \begin{pmatrix} 1 & 0 \\ 0 & -1 \end{pmatrix} \quad \sigma_x = \begin{pmatrix} 0 & 1 \\ 1 & 0 \end{pmatrix} \quad S(\varphi) = \cos(\varphi)\sigma_z + \sin(\varphi)\sigma_x \rightarrow \begin{pmatrix} \cos(\varphi) & \sin(\varphi) \\ \sin(\varphi) & -\cos(\varphi) \end{pmatrix}$$

Obviously if ϕ or π/2 we recover σ_z and σ_x.

$$S(0) = \begin{pmatrix} 1 & 0 \\ 0 & -1 \end{pmatrix} \quad S\left(\tfrac{\pi}{2}\right) = \begin{pmatrix} 0 & 1 \\ 1 & 0 \end{pmatrix}$$

The spin operator for the two-particle system in tensor format is,

$$\begin{pmatrix} \cos\varphi_A & \sin\varphi_A \\ \sin\varphi_A & -\cos\varphi_A \end{pmatrix} \otimes \begin{pmatrix} \cos\varphi_B & \sin\varphi_B \\ \sin\varphi_B & -\cos\varphi_B \end{pmatrix}$$
$$= \begin{pmatrix} \cos\varphi_A \begin{pmatrix} \cos\varphi_B & \sin\varphi_B \\ \sin\varphi_B & -\cos\varphi_B \end{pmatrix} & \sin\varphi_A \begin{pmatrix} \cos\varphi_B & \sin\varphi_B \\ \sin\varphi_B & -\cos\varphi_B \end{pmatrix} \\ \sin\varphi_A \begin{pmatrix} \cos\varphi_B & \sin\varphi_B \\ \sin\varphi_B & -\cos\varphi_B \end{pmatrix} & -\cos\varphi_A \begin{pmatrix} \cos\varphi_B & \sin\varphi_B \\ \sin\varphi_B & -\cos\varphi_B \end{pmatrix} \end{pmatrix}$$

In Mathcad the two-spin operator is written as,

$$\text{kronecker}(S(\varphi_A),\ S(\varphi_B))$$

In the z-basis the eigenvalues for spin-up and spin-down are +1 and -1 respectively.

$$S_{zu}^T \sigma_z S_{zu} \rightarrow 1 \quad S_{zd}^T \sigma_z S_{zd} \rightarrow -1$$

The combined measurement of both spins when the detectors have the same x-z orientation yields an expectation value of -1, because Ψ is a singlet state and the individual spins have opposite orientations.

Ψ^Tkronecker(S, (0 deg), S(0 deg)$\Psi = -1$	Ψ^Tkronecker(S, (120 deg), S(120 deg)$\Psi = -1$	Ψ^Tkronecker(S, (240 deg), S(240 deg)$\Psi = -1$

These results are in agreement with the local realist predictions in the right third of the table above. When the detectors are oriented at the same angle in the x-z plane they always register opposite spin values for their respective particles. At this point, quantum mechanics appears to support the realistic position.

However, overall (considering all nine detector settings) quantum mechanics predicts that opposite spins are recorded only 50% of the time, as opposed to 67% predicted by local realism. In other words, the overall expectation value for the joint spin measurements is 0. Quantum mechanics strongly disagrees with local realism in the experiments in which the detector settings differ. In these cases, quantum theory predicts the detectors register opposite spin values 25% of the time and the same value 75% of the time: 0.25(-1) + 0.75(+1) = 0.5 as shown by the off-diagonal vlaues in the results matrix below.

$$i = 0.2 \quad j = 0.2 \quad R_{i,\,j} = \Psi^T \text{kronecker[S[i (120 deg)], (120 deg)]]}\Psi \quad R = \begin{pmatrix} -1 & 0.5 & 0.5 \\ 0.5 & -1 & 0.5 \\ 0.5 & 0.5 & -1 \end{pmatrix}$$

Calculation of the overall spin value:

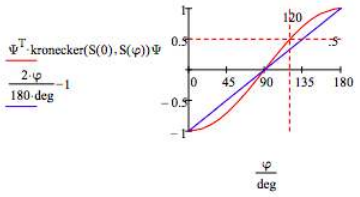
$$\sum_i \sum_j \left[\Psi^T \text{kronecker[S [i (120 deg)], S[j (120 deg)]]}\Psi\right] = 0$$

By comparison the spin expectation value based on local realism as represented by the table above is:

$$\frac{48}{72}(-1) + \frac{24}{72}(1) = -0.333$$

The fact that local realism and quantum mechanics can lead to different predictions that might be adjudicated by experimental measurement was first pointed out by John S. Bell [*Physics* 1, 195 (1964)].

Sections 6.2, 6.3 and 11.3 of A. I. M. Rae's *Quantum Mechanics*, 3rd Ed. contain,in a clear and succinct fashion, the necessary mathematical background for this thought experiment. The key quantum spin correlation function of Rae's analysis (Fig 11.3) is calculated as follows in tensor format. The linear function in blue is the hidden-variable correlation function.



One more comment can be made about local realism and quantum mechanics in this particular example. If we look at the results for the first spin in the table above, its over-all expectation value is 0. There are as many +s as -s. Quantum mechanics agrees with local realism with this result in addition to the case in which the detectors have the same setting.

We can calculate the expectation values for the first spin independent of the second spin by replacing the spin operator of the second spin with the identity operator.

$$I = \begin{pmatrix} 1 & 0 \\ 0 & 1 \end{pmatrix}$$

We see that the expectation values for the three detector orientations of the first spin are 0. In other words, the measurement results on the first spin are perfectly random.

$$\Psi^T\text{kronecker(S, (0 deg), I}\Psi = 0 \quad \Psi^T\text{kronecker(S, (120 deg), I}\Psi = 0 \quad \Psi^T\text{kronecker(S, (240 deg), I}\Psi = 0$$

The same holds for the second spin.

$$\Psi^T\text{kronecker(I, S(0 deg)}\Psi = 0 \quad \Psi^T\text{kronecker(I, S(120 deg)}\Psi = 0 \quad \Psi^T\text{kronecker(I, S(240 deg)}\Psi = 0$$

And yet when the angles are the same the measurement results (as shown above) are correlated.

$$\Psi^T\text{kronecker(S, (0 deg), S(0 deg)}\Psi = -1 \quad \Psi^T\text{kronecker(S, (120 deg), S(120 deg)}\Psi = -1 \quad \Psi^T\text{kronecker(S, (240 deg), S(240 deg)}\Psi = -1$$

"How is it possible that two events, each one objectively random, are always perfectly correlated." Anton Zeilinger, *Nature*, 8 December 2005.

All the calculations carried out above can also be done having the trace function operate on the product of the density matrix for Ψ and the matrices representing the measurement operators. Several examples are provided below.

Form the density matrix for Ψ.

$$\rho\Psi = \Psi\Psi^T$$

$$tr\left(\rho\Psi\text{kronecker(S (120 deg), S(120 deg))}\right) = -1 \quad tr\left(\rho\Psi\text{kronecker(S (0 deg), S(120 deg))}\right) = 0.5$$

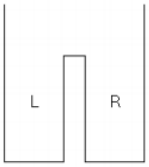
$$tr\left[\sum_i \sum_j \left[\rho\Psi\text{kronecker[S [i (120 deg)], S[j (120 deg)]]}\right]\right] = 0$$

This page titled 8.38: Mermin's Version of Bohm's EPR Gedanken Experiment Using Tensor Algebra is shared under a CC BY 4.0 license and was authored, remixed, and/or curated by Frank Rioux via source content that was edited to the style and standards of the LibreTexts platform.

8.39: A GHZ Gedanken Experiment Using Spatial Degrees of Freedom and Tensor Algebra

Tensor algebra is used to simplify the mathematical analysis of a gedanken experiment presented by John D. Norton in the February 2011 issue of the American Journal of Physics (pp 182-188). Norton's construction using spatial degrees of freedom is in my opinion highly contrived and actually not as simple as the original GHZ experiment involving polarized light [*Nature* 404, 515-519 (2000)] or Mermin's gedanken rendition involving spin-1/2 particles [*Physics Today* 43(6), 9-11 (1990)]. Besides using tensor algebra to avoid tedious algebraic manipulations, I adopt a more plausible model for the two-chambered Einstein boxes employed in Norton's approach.

The thought experiment involves three widely separated two-chamber boxes which I prefer to model as infinite potential wells with a finite internal barrier, as shown below. What I have in mind here is a simplified model for the ammonia molecule. See the Appendix for a more realistic double-well potential.



The orthonormal vectors |L> and |R> given below represent occupancy in the two chambers. Norton initially considers the consequences of placing the particle in two states, |P> and |M>, which are also orthonormal. I have no idea how these states would be created, and this is the main reason I find Norton's approach artificial.

$$L = \begin{pmatrix} 1 \\ 0 \end{pmatrix} \qquad R = \begin{pmatrix} 0 \\ 1 \end{pmatrix} \qquad L^T L = 1 \qquad R^T R = 1 \qquad L^T = 0$$

$$P = \tfrac{1}{\sqrt{2}}(L + iR) \quad M = \tfrac{1}{\sqrt{2}}(L - iR) \quad \overline{(P^T)}P = 1 \quad \overline{(M^T)}M = 1 \quad \overline{(P^T)}M = 0$$

In the second part of my analysis I use the following symmetric and anti-symmetric states. These represent the ground and first excited superposition states of the ammonia molecule regarding the position of the nitrogen atom to the left or right of the plane created by the three hydrogen atoms.

$$S = \tfrac{1}{\sqrt{2}}(L + R) \quad A = \tfrac{1}{\sqrt{2}}(L - R) \quad S^T S = 1 \quad A^T A = 1 \quad A^T S = 0$$

Construction of the initial three-box state highlighted below is facilitated by the use of three Mathcad commands: submatrix, kronecker, and augment. It is not difficult to do this by hand, however having a general expression for the wavefunction simplifies subsequent analysis.

$$\Psi\mathrm{a},\ \mathrm{b},\ \mathrm{c} = \mathrm{submatrix}\left[\mathrm{kronecker}\left[\mathrm{augment}\left[a, \begin{pmatrix} 0 \\ 0 \end{pmatrix}\right],\ \mathrm{kronecker}\left[\mathrm{augment}\left[b, \begin{pmatrix} 0 \\ 0 \end{pmatrix}\right],\ \mathrm{augment}\left[c, \begin{pmatrix} 0 \\ 0 \end{pmatrix}\right]\right]\right],\ 1,\ 8,\ 1,\ 1\right]$$

Initial state:

$$\Psi_{ABC} = \tfrac{1}{\sqrt{2}}(\Psi\ (\mathrm{P},\ \mathrm{P},\ \mathrm{P}) - \Psi\mathrm{M},\ \mathrm{M},\ \mathrm{M})) \quad \Psi_{ABC}^T = (0 \quad 0.5i \quad 0.5i \quad 0 \quad 0.5i \quad 0 \quad 0 \quad -0.5i)$$

For a three-box system this initial entangled states has eight possible position measurement outcomes, four of which are observed as shown in the probability calculations below.

$$\left(\left|\Psi(\mathrm{L},\ \mathrm{L},\ \mathrm{L})^T \Psi_{ABC}\right|\right)^2 = 0 \qquad \left(\left|\Psi(\mathrm{L},\ \mathrm{L},\ \mathrm{R})^T \Psi_{ABC}\right|\right)^2 = 0.25 \qquad \left(\left|\Psi(\mathrm{L},\ \mathrm{R},\ \mathrm{L})^T \Psi_{ABC}\right|\right)^2 = 0.25$$

$$\left(\left|\Psi(\mathrm{R},\ \mathrm{L},\ \mathrm{L})^T \Psi_{ABC}\right|\right)^2 = 0.25 \qquad \left(\left|\Psi(\mathrm{L},\ \mathrm{R},\ \mathrm{R})^T \Psi_{ABC}\right|\right)^2 = 0 \qquad \left(\left|\Psi(\mathrm{R},\ \mathrm{L},\ \mathrm{R})^T \Psi_{ABC}\right|\right)^2 = 0$$

$$\left(\left|\Psi(\mathrm{R},\ \mathrm{R},\ \mathrm{L})^T \Psi_{ABC}\right|\right)^2 = 0 \qquad \left(\left|\Psi(\mathrm{R},\ \mathrm{R},\ \mathrm{R})^T \Psi_{ABC}\right|\right)^2 = 0.25$$

These results show that position measurements on any two of the boxes enables one to determine which chamber the particle occupies in the third box without further measurement. If the measured particles are found to be on the same side (either both L or both R) the third particle is in the right chamber R. If they are different, the third particle is in the left chamber, L. Because we can predict with certainty the position of the particle in the third box, we say its position is an "element of reality." This leads to the conclusion that the permissible position eigenstates are: LLR, LRL, RLL, and RRR.

In a second set of experiments we shine light on two of the boxes with a frequency that just matches the energy difference between the ground state |S> and excited state |A>. If the light is absorbed the box is in the |S> state; if the box is in the |A> state stimulated emission occurs and a photon is released. This set of experiments measures the spectroscopic states of the boxes.

As the following probability calculations show, if the two boxes irradiated are found to be in the same spectroscopic state (SS or AA) a subsequent measurement of the position of the particle in the third box will yield L. Conversely, if they are in different spectroscopic state the position measurement on the third box will yield R. Thus, this set of measurements also indicate that position is an "element of reality."

$$\left(\left|\Psi(\mathrm{S,\ S,\ L})^T\Psi_{ABC}\right|\right)^2 = 0 \qquad \left(\left|\Psi(\mathrm{S,\ S,\ R})^T\Psi_{ABC}\right|\right)^2 = 0.25 \qquad \left(\left|\Psi(\mathrm{S,\ A,\ L})^T\Psi_{ABC}\right|\right)^2 = 0.25$$
$$\left(\left|\Psi(\mathrm{S,\ A,\ R})^T\Psi_{ABC}\right|\right)^2 = 0.25 \qquad \left(\left|\Psi(\mathrm{A,\ S,\ L})^T\Psi_{ABC}\right|\right)^2 = 0 \qquad \left(\left|\Psi(\mathrm{A,\ S,\ R})^T\Psi_{ABC}\right|\right)^2 = 0$$
$$\left(\left|\Psi(\mathrm{A,\ A,\ R})^T\Psi_{ABC}\right|\right)^2 = 0 \qquad \left(\left|\Psi(\mathrm{A,\ A,\ L})^T\Psi_{ABC}\right|\right)^2 = 0.25$$
$$\left(\left|\Psi(\mathrm{S,\ L,\ S})^T\Psi_{ABC}\right|\right)^2 = 0 \qquad \left(\left|\Psi(\mathrm{S,\ R,\ S})^T\Psi_{ABC}\right|\right)^2 = 0.25 \qquad \left(\left|\Psi(\mathrm{S,\ L,\ A})^T\Psi_{ABC}\right|\right)^2 = 0.25$$
$$\left(\left|\Psi(\mathrm{S,\ R,\ A})^T\Psi_{ABC}\right|\right)^2 = 0.25 \qquad \left(\left|\Psi(\mathrm{A,\ L,\ S})^T\Psi_{ABC}\right|\right)^2 = 0 \qquad \left(\left|\Psi(\mathrm{A,\ R,\ S})^T\Psi_{ABC}\right|\right)^2 = 0$$
$$\left(\left|\Psi(\mathrm{A,\ R,\ A})^T\Psi_{ABC}\right|\right)^2 = 0 \qquad \left(\left|\Psi(\mathrm{A,\ L,\ A})^T\Psi_{ABC}\right|\right)^2 = 0.25$$
$$\left(\left|\Psi(\mathrm{L,\ S,\ S})^T\Psi_{ABC}\right|\right)^2 = 0 \qquad \left(\left|\Psi(\mathrm{R,\ S,\ S})^T\Psi_{ABC}\right|\right)^2 = 0.25 \qquad \left(\left|\Psi(\mathrm{L,\ S,\ A})^T\Psi_{ABC}\right|\right)^2 = 0.25$$
$$\left(\left|\Psi(\mathrm{R,\ S,\ A})^T\Psi_{ABC}\right|\right)^2 = 0.25 \qquad \left(\left|\Psi(\mathrm{L,\ A,\ S})^T\Psi_{ABC}\right|\right)^2 = 0 \qquad \left(\left|\Psi(\mathrm{R,\ A,\ S})^T\Psi_{ABC}\right|\right)^2 = 0$$
$$\left(\left|\Psi(\mathrm{R,\ A,\ A})^T\Psi_{ABC}\right|\right)^2 = 0 \qquad \left(\left|\Psi(\mathrm{L,\ A,\ A})^T\Psi_{ABC}\right|\right)^2 = 0.25$$

The allowed states for these measurements are listed in the following table. The top row showing that SS or AA implies L and that SA or AS implies R.

$$\begin{pmatrix} \mathrm{SSL} & \mathrm{AAL} & \mathrm{SLS} & \mathrm{ALA} & \mathrm{LSS} & \mathrm{LAA} \\ \mathrm{SAR} & \mathrm{ASR} & \mathrm{SRA} & \mathrm{ARS} & \mathrm{RSA} & \mathrm{RAS} \end{pmatrix}$$

The measurement outcomes can also be grouped in two different ways: (a) measurements in which three pairs have the same spectroscopic state and (b) measurements in which one pair has the same spectroscopic state and the remaining pairs have different spectroscopic states. The following table organizes the experimental results grouped in these categories. The first two rows satisfy criterion (a) and the remaining six rows satisfy criterion (b). The left column shows the implied total spectroscopic state, the middle three columns how it is achieved, and the right column the position state consistent with the spectroscopic results.

$$\begin{pmatrix} \mathrm{SSS} & ' & \mathrm{SSL} & \mathrm{LSS} & \mathrm{SLS} & ' & \mathrm{LLL} \\ \mathrm{AAA} & ' & \mathrm{AAL} & \mathrm{ALA} & \mathrm{LAA} & ' & \mathrm{LLL} \\ \mathrm{SSA} & ' & \mathrm{SSL} & \mathrm{SRA} & \mathrm{RSA} & ' & \mathrm{RRL} \\ \mathrm{AAS} & ' & \mathrm{AAL} & \mathrm{ARS} & \mathrm{RAS} & ' & \mathrm{RRL} \\ \mathrm{SAS} & ' & \mathrm{SLS} & \mathrm{SAR} & \mathrm{RAS} & ' & \mathrm{RLR} \\ \mathrm{ASA} & ' & \mathrm{ALA} & \mathrm{ASR} & \mathrm{RSA} & ' & \mathrm{RLR} \\ \mathrm{ASS} & ' & \mathrm{LSS} & \mathrm{ARS} & \mathrm{ASR} & ' & \mathrm{LRR} \\ \mathrm{SAA} & ' & \mathrm{LAA} & \mathrm{SRA} & \mathrm{SAR} & ' & \mathrm{LRR} \end{pmatrix}$$

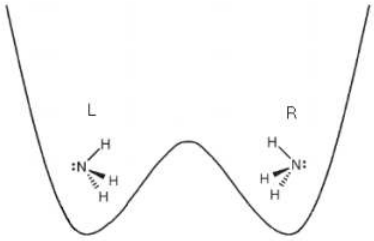
As this table demonstrates, according to the spectroscopic measurements the permissible position states are RRL, RLR, LRR and LLL. This is in direct contradiction to the earlier position measurements which gave the result LLR, LRL, RLL, and RRR. In other words two measurement protocols lead to the notion that position is an element of reality, but they dramatically disagree on the actual values of the allowed positions. Norton concludes his paper with the following assessment.

> Two principal assumptions were made in the arguments that generated this contradiction. One was that the empirical predictions of quantum theory are reliable. The other was that the EPR reality criterion, which in turn, depends on the

assumptions of separability and locality. One of these assumptions must be given up. The continuing empirical success of quantum theory has led to a consensus that it is the second assumption, the EPR reality criterion, which is to be discarded.

Appendix

A more realistic potential well for this problem is shown below.



This page titled 8.39: A GHZ Gedanken Experiment Using Spatial Degrees of Freedom and Tensor Algebra is shared under a CC BY 4.0 license and was authored, remixed, and/or curated by Frank Rioux via source content that was edited to the style and standards of the LibreTexts platform.

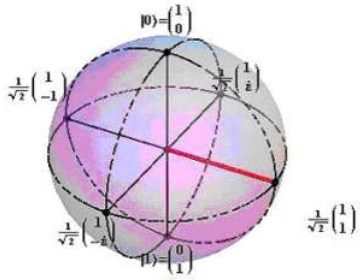
8.40: Another GHZ Example Using Spin-1/2 Particles

This exercise explores the outcomes of measurements on the three spin-1/2 entangled state, Ψ_{ABC}, highlighted below. It represents a lean GHZ protocol developed by H. J. Bernstein. Because much has been published on the GHZ protocol, I'm going to get right to the point without a lot of commentary.

The eigenstates for spin-up and spin-down in the z-, x- and y-directions in vector format are as follows.

$$Z_u = \begin{pmatrix}1\\0\end{pmatrix} \quad Z_d = \begin{pmatrix}0\\1\end{pmatrix} \quad X_u = \frac{1}{\sqrt{2}}\begin{pmatrix}1\\1\end{pmatrix} \quad X_d = \frac{1}{\sqrt{2}}\begin{pmatrix}1\\-1\end{pmatrix} \quad Y_u = \frac{1}{\sqrt{2}}\begin{pmatrix}1\\i\end{pmatrix} \quad Y_d = \frac{1}{\sqrt{2}}\begin{pmatrix}1\\-i\end{pmatrix}$$

These spin states are also shown on a Bloch sphere.



Tensor multiplication using Mathcad commands will be used to form the initial entangled spin state and subsequent measurement states. These results can be easily verified by hand calculation.

$$\Psi(\mathrm{a},\ \mathrm{b},\ \mathrm{c}) = \mathrm{submatrix}\left[\mathrm{kronecker}\left[\mathrm{augment}\left[\mathrm{a},\ \begin{pmatrix}0\\0\end{pmatrix}\right],\right.\right.$$
$$\left.\left.\mathrm{kronecker}\left[\mathrm{augment}\left[\mathrm{b},\ \begin{pmatrix}0\\0\end{pmatrix}\right],\ \mathrm{augment}\left[\mathrm{c},\ \begin{pmatrix}0\\0\end{pmatrix}\right]\right]\right],1,\ 8,\ 1,\ 1\right]$$

Initial state:

$$\Psi_{ABC} = \frac{1}{\sqrt{2}}\left(\Psi\left(Y_u,\ Y_u,\ Y_u\right) - \Psi\left(Y_d,\ Y_d,\ Y_d\right)\right) \quad \Psi_{ABC}^T = \begin{pmatrix}0 & 0.5i & 0.5i & 0 & 0.5i0 & 0 & -0.5i\end{pmatrix}$$

Given this initial state the probabilities for the various measurement outcomes for spin in the z-direction are calculated.

$$\left(\left|\Psi\left(Z_u,\ Z_u,\ Z_u\right)^T\Psi_{ABC}\right|\right)^2 = 0 \quad \left(\left|\Psi\left(Z_u,\ Z_u,\ Z_d\right)^T\Psi_{ABC}\right|\right)^2 = 0.25 \quad \left(\left|\Psi\left(Z_u,\ Z_d,\ Z_u\right)^T\Psi_{ABC}\right|\right)^2 = 0.25$$
$$\left(\left|\Psi\left(Z_d,\ Z_u,\ Z_u\right)^T\Psi_{ABC}\right|\right)^2 = 0.25 \quad \left(\left|\Psi\left(Z_u,\ Z_d,\ Z_d\right)^T\Psi_{ABC}\right|\right)^2 = 0 \quad \left(\left|\Psi\left(Z_d,\ Z_u,\ Z_d\right)^T\Psi_{ABC}\right|\right)^2 = 0$$
$$\left(\left|\Psi\left(Z_d,\ Z_d,\ Z_u\right)^T\Psi_{ABC}\right|\right)^2 = 0 \quad \left(\left|\Psi\left(Z_d,\ Z_d,\ Z_d\right)^T\Psi_{ABC}\right|\right)^2 = 0.25$$

These calculations predict that the following spin states are observed: $Z_uZ_uZ_d$, $Z_uZ_dZ_u$, $Z_dZ_uZ_u$ and $Z_dZ_dZ_d$. It is easily seen that the measurement of any two spin-states allows the prediction of the third without the need for a measurement. If two spins have the same value (uu or dd) then the third is d. If two spin states have different values (ud or du) then the third is u. Einstein, Podolsky and Rosen (EPR) wrote in their famous 1935 *Physical Review* paper,

> "If, without in any way disturbing a system, we can predict with certainty (i.e. with probability equal to unity) the value of a physical quantity, then there exists an element of reality corresponding to this physical quantity."

According to this definition spin in the z-direction is an "element of reality." In other words, it has a definite value independent of measurement.

Next we calculate the quantum mechanical predictions for the measurement of spin in the x-direction on two of the spins and in the z-direction for the third.

$$\left(\left|\Psi(Z_u,\ X_u\ Z_u)^T\Psi_{ABC}\right|\right)^2=0 \qquad \left(\left|\Psi(X_u,\ X_u,\ Z_d)^T\Psi_{ABC}\right|\right)^2=0.25 \qquad \left(\left|\Psi(X_u,X_d,\ X_u)^T\Psi_{ABC}\right|\right)^2=0.25$$

$$\left(\left|\Psi(X_u,\ X_d,\ Z_d)^T\Psi_{ABC}\right|\right)^2=0.25 \qquad \left(\left|\Psi(X_d,\ X_u,\ Z_u)^T\Psi_{ABC}\right|\right)^2=0 \qquad \left(\left|\Psi(X_d,\ X_u,\ Z_d)^T\Psi_{ABC}\right|\right)^2=0$$

$$\left(\left|\Psi(X_d,\ X_d,\ Z_d)^T\Psi_{ABC}\right|\right)^2=0 \qquad \left(\left|\Psi(X_d,\ X_d,\ Z_u)^T\Psi_{ABC}\right|\right)^2=0.25$$

$$\left(\left|\Psi(X_u,\ Z_u,\ X_u)^T\Psi_{ABC}\right|\right)^2=0 \qquad \left(\left|\Psi(X_u,\ Z_d,X_u)^T\Psi_{ABC}\right|\right)^2=0.25 \qquad \left(\left|\Psi(X_u,\ Z_u,\ X_d)^T\Psi_{ABC}\right|\right)^2=0.25$$

$$\left(\left|\Psi(X_u,\ Z_d,\ X_d)^T\Psi_{ABC}\right|\right)^2=0.25 \qquad \left(\left|\Psi(X_d,\ Z_u,\ X_u)^T\Psi_{ABC}\right|\right)^2=0 \qquad \left(\left|\Psi(X_d,\ Z_d,\ X_u)^T\Psi_{ABC}\right|\right)^2=0$$

$$\left(\left|\Psi(X_u,\ Z_d,\ X_d)^T\Psi_{ABC}\right|\right)^2=0 \qquad \left(\left|\Psi(X_d,\ Z_u,\ X_d)^T\Psi_{ABC}\right|\right)^2=0.25$$

$$\left(\left|\Psi(Z_u,\ X_u,\ X_u)^T\Psi_{ABC}\right|\right)^2=0 \qquad \left(\left|\Psi(Z_d,\ X_u,\ X_u)^T\Psi_{ABC}\right|\right)^2=0.25 \qquad \left(\left|\Psi(Z_u,X_u,X_d)^T\Psi_{ABC}\right|\right)^2=0.25$$

$$\left(\left|\Psi(Z_d,\ X_u,\ X_d)^T\Psi_{ABC}\right|\right)^2=0.25 \qquad \left(\left|\Psi(Z_u,X_d,X_u)^T\Psi_{ABC}\right|\right)^2=0 \qquad \left(\left|\Psi(Z_d,\ X_d,\ X_u)^T\Psi_{ABC}\right|\right)^2=0$$

$$\left(\left|\Psi(Z_d,\ X_d,\ X_d)^T\Psi_{ABC}\right|\right)^2=0 \qquad \left(\left|\Psi(Z_u,\ X_d,\ X_d)^T\Psi_{ABC}\right|\right)^2=0.25$$

The twelve possible outcomes are listed in two rows.

$$\begin{pmatrix} X_uX_uZ_u & X_dX_dZ_u & X_uZ_uX_u & X_dZ_uX_d & Z_uX_uX_u & Z_uX_dX_d \\ X_dX_dZ_d & X_dX_uZ_d & X_uZ_dX_d & X_dZ_dX_u & Z_dX_uX_d & Z_dX_dX_u \end{pmatrix}$$

These results are summarized as follows: if two spins have the same x-spin state then the z-spin state is u, but if they are different the z-spin state is d. Again according to the EPR criterion spin in the z-direction is an element of reality.

However, the calculations can be described in another way: (a) measurements in which three pairs have the same x spin state and (b) measurements in which one pair has the same x-spin state and the remaining pairs have different x-spin states. The following table organizes the experimental results grouped in these categories. The first two rows satisfy criterion (a) and the remaining six rows satisfy criterion (b). The left column shows the implied total x-spin state, the middle three columns how it is achieved, and the right column the z-spin state consistent with the x-spin measurement results.

$$\begin{pmatrix} X_uX_uX_u & ' & X_uX_uZ_d & Z_uX_uX_u & X_uZ_uX_u & ' & Z_uZ_uZ_u \\ X_dX_dX_d & ' & X_dX_dZ_u & X_dZ_uX_d & Z_uX_dX_d & ' & Z_uZ_uZ_u \\ X_uX_uX_d & ' & X_uX_uZ_u & X_uZ_dX_d & Z_dX_uX_d & ' & Z_dZ_dZ_u \\ X_dX_dX_u & ' & X_dX_dZ_u & X_dZ_dX_u & Z_dX_dX_u & ' & Z_dZ_dZ_u \\ X_uX_dX_u & ' & X_uZ_uX_u & X_uX_dZ_d & Z_dX_dX_u & ' & Z_dZ_uZ_d \\ X_dX_uX_d & ' & X_dZ_uX_d & X_dX_uZ_d & Z_dX_uX_d & ' & Z_dZ_uZ_d \\ X_dX_uX_u & ' & Z_uX_uX_u & X_dZ_dX_u & X_dX_uZ_d & ' & Z_uZ_dZ_d \\ X_uX_dX_d & ' & Z_uX_dX_d & X_uZ_dX_d & X_uX_dZ_d & ' & Z_uZ_dZ_d \end{pmatrix}$$

As this table demonstrates, according to the x-direction spin measurements the permissible z-direction states are $Z_uZ_uZ_u$, $Z_dZ_dZ_u$, $Z_dZ_uZ_d$ and $Z_uZ_dZ_d$. This is in direct contradiction to the earlier z-direction measurements which gave the result $Z_dZ_dZ_d$, $Z_uZ_uZ_d$, $Z_uZ_dZ_u$ and $Z_dZ_dZ_u$, using the same initial wavefunction Ψ_{ABC}. In other words two measurement protocols lead to the notion that z-direction spin is an element of reality according to the EPR definition, but they dramatically disagree on the actual z-direction spin values allowed.

In the February 2001 issue of the *American Journal of Physics* on page 187, John D. Norton summarizes the situation as follows:

> Two principal assumptions were made in the arguments that generated this contradiction. One was that the empirical predictions of quantum theory are reliable. The other was the EPR reality criterion, which in turn, depends on the assumptions of separability and locality. One of these assumptions must be given up. The continuing empirical success of quantum theory has led to a consensus that it is the second assumption, the EPR reality criterion, which is to be discarded.

This page titled 8.40: Another GHZ Example Using Spin-1/2 Particles is shared under a CC BY 4.0 license and was authored, remixed, and/or curated by Frank Rioux via source content that was edited to the style and standards of the LibreTexts platform.

8.41: Entanglement Reveals a Conflict Between Local Realism and Quantum Theory

A tensor algebra approach is used to demonstrate the challenge to the local realistic position of reality that quantum mechanical entanglement creates. The example is drawn from Chapter 3 of David Z Albert's text, *Quantum Mechanics and Experience*.

A quon (any entity that exhibits both wave and particle aspects in the peculiar quantum manner - Nick Herbert, *Quantum Reality*, page 64) has a variety of properties each of which can take on two values. For example, it has the property of *hardness* and can be either *hard* or *soft*. It also has the property of *color* and can be either *black* or *white*.

In the matrix formulation of quantum mechanics these states are represented by the following vectors.

$$\text{Hard} = \begin{pmatrix} 1 \\ 0 \end{pmatrix} \quad \text{Soft} = \begin{pmatrix} 0 \\ 1 \end{pmatrix} \quad \text{Black} = \begin{pmatrix} \frac{1}{\sqrt{2}} \\ \frac{1}{\sqrt{2}} \end{pmatrix} \quad \text{White} = \begin{pmatrix} \frac{1}{\sqrt{2}} \\ \frac{-1}{\sqrt{2}} \end{pmatrix}$$

Hard and *Soft* represent an orthonormal basis in the two-dimensional *Hardness* vector space.

$$\text{Hard}^T\text{Hard} = 1 \quad \text{Soft}^T\text{Soft} = 1 \quad \text{Hard}^T\text{Hard} = 0$$

Likewise *Black* and *White* are an orthonormal in the two-dimensional *Color* vector space.

$$\text{Black}^T\text{Black} = 1 \quad \text{White}^T\text{White} = 1 \quad \text{Black}^T\text{White} = 0$$

The relationship between the two bases is reflected in the following projection calculations.

$$\text{Hard}^T\text{Black} = 0.707 \quad \text{Hard}^T\text{White} = 0.707 \quad \text{Soft}^T\text{Black} = 0.707 \quad \text{Soft}^T\text{White} = -0.707 \quad \tfrac{1}{\sqrt{2}} = 0.707$$

Clearly *Black* and *White* can be written as superpositions of *Hard* and *Soft*, and vice versa.

$$\tfrac{1}{\sqrt{2}}(\text{Hard + Soft}) = \begin{pmatrix} 0.707 \\ 0.707 \end{pmatrix} \quad \tfrac{1}{\sqrt{2}}(\text{Hard - Soft}) = \begin{pmatrix} 0.707 \\ -0.707 \end{pmatrix}$$

$$\tfrac{1}{\sqrt{2}}(\text{Black + White}) = \begin{pmatrix} 1 \\ 0 \end{pmatrix} \quad \tfrac{1}{\sqrt{2}}(\text{Black - White}) = \begin{pmatrix} 0 \\ 1 \end{pmatrix}$$

Hard, *Soft*, *Black* and *White* are measurable properties and the vectors representing them are eigenstates of the *Hardness* and *Color* operators with eigenvalues +/- 1.

Operators

$$\text{Hardness} = \begin{pmatrix} 1 & 0 \\ 0 & -1 \end{pmatrix} \quad \text{Color} = \begin{pmatrix} 0 & 1 \\ 1 & 0 \end{pmatrix} \quad I = \begin{pmatrix} 1 & 0 \\ 0 & 1 \end{pmatrix}$$

Eigenvalue +1	Eigenvalue -1
$\text{Hardness Hard} = \begin{pmatrix} 1 \\ 0 \end{pmatrix}$	$\text{Hardness Soft} = \begin{pmatrix} 0 \\ -1 \end{pmatrix}$
$\text{Color Black} = \begin{pmatrix} 0.707 \\ 0.707 \end{pmatrix}$	$\text{Color White} = \begin{pmatrix} -0.707 \\ 0.707 \end{pmatrix}$

Hard and *Soft* are not eigenfunctions of the *Color* operator, and *Black* and *White* are not eigenfunctions of the *Hardness* operator.

$$\text{Hardness Black} = \begin{pmatrix} 0.707 \\ -0.707 \end{pmatrix} \quad \text{Hardness White} = \begin{pmatrix} 0.707 \\ 0.707 \end{pmatrix}$$

$$\text{Color Hard} = \begin{pmatrix} 0 \\ 1 \end{pmatrix} \quad \text{Color Soft} = \begin{pmatrix} 1 \\ 0 \end{pmatrix}$$

As the *Hardness-Color* commutator shows, the *Hardness* and *Color* operators do not commute. They represent incompatible observables; observables that cannot simultaneously have well-defined values.

$$\text{Hardness Color} - \text{Color Hardness} = \begin{pmatrix} 0 & 2 \\ -2 & 0 \end{pmatrix}$$

We now proceed with an analysis of the implications of the following two-quon entangled state, expressed in tensor format. A pair of quons is prepared in the following "singlet" state; one is hard and one is soft. (The Appendix shows how to set this state up using Mathcad.)

$$|\Psi\rangle = \frac{1}{\sqrt{2}}\left[|\text{Hard}\rangle_1|\text{Soft}\rangle_2 - |\text{Soft}\rangle_1|\text{Hard}\rangle_2\right] = \frac{1}{\sqrt{2}}\left[\begin{pmatrix}1\\0\end{pmatrix}\otimes\begin{pmatrix}0\\1\end{pmatrix} - \begin{pmatrix}0\\1\end{pmatrix}\otimes\begin{pmatrix}1\\0\end{pmatrix}\right]$$

$$\Psi = \frac{1}{\sqrt{2}}\begin{pmatrix}0\\1\\-1\\0\end{pmatrix}$$

Given |Ψ> the expectation value for measuring *Hardness* on the first quon is 0. The same is true for the second quon. In other words, it is equally likely for either quon to be *Hard* or *Soft*. (*Kronecker* is Mathcad's command for tensor multiplication of matrices. See the Appendix for more detail.)

$$\Psi^T\text{kronecker}(\text{Hardness, I})\Psi = 0 \quad \Psi^T\text{kronecker}(\text{I, Hardness})\Psi = 0$$

However, if one quon is found to be *Hard* by measurement, the second will be measured *Soft*, and vice versa. In other words, there is perfect anti-correlation between the joint measurement of this property on the two quons.

$$\Psi^T\text{kronecker}(\text{Hardness, Hardness})\Psi = -1$$

Given |Ψ> the expectation value for measuring *Color* on the first quon is 0. The same is true for the second quon. In other words, it is equally likely for either quon to be *Black* or *White*.

$$\Psi^T\text{kronecker}(\text{Color, I})\Psi = 0 \quad \Psi^T\text{kronecker}(\text{I, Color})\Psi = 0$$

However, if one quon is found to be Black by measurement, the second will be measured White and vice versa. In other words, there is perfect anti-correlation between the joint measurement of this property on the two quons.

$$\Psi^T\text{kronecker}(\text{Color, Color})\Psi = -1$$

Furthermore, as the following calculations show, there is no correlation between the measurement outcomes on *Color* and *Hardness*.

$$\Psi^T\text{kronecker}(\text{Hardness, Color})\Psi = 0 \quad \Psi^T\text{kronecker}(\text{Color, Hardness})\Psi = 0$$

As the foundation for their belief in local realism, Einstein, Podolsky and Rosen (EPR) defined the concept of element of reality in their famous 1935 *Physical Review* paper,

> "If, without in any way disturbing a system, we can predict with certainty (i.e. with probability equal to unity) the value of a physical quantity, then there exists an element of reality corresponding to this physical quantity."

It would seem from the above results, namely these,

$$\Psi^T\text{kronecker}(\text{Color, Color})\Psi = -1 \quad \Psi^T\text{kronecker}(\text{Hardness, Hardness})\Psi = -1$$

that according to *EPR* both hardness and color are *elements of reality*. If the hardness of quon 1 is measured and found to be soft, we know without measurement (given the reliability of quantum mechanical predictions) that quon 2 is hard. Likewise, if the color of quon 2 is measured and found to be white, we know without measurement that quon 1 is black. On the basis of these calculations, the realist constructs the following table which assigns well-defined hardness and color states to both quons and is consistent with all the quantum calculations.

Quon 1	Quon 2	HardnessHardness	ColorColor	HardnessColor
HB	SW	−1	−1	−1
HW	SB	−1	−1	1
SB	HW	−1	−1	1
SW	HB	−1	−1	−1
Realist	AverageValue	−1	−1	0
Quantum	AverageValue	−1	−1	0

The problem with this interpretation is that it has previously been shown that the *Hardness* and *Color* operators do not commute, meaning that they represent incompatible observables. Incompatible observables cannot be known (determined) simultaneously. A contradiction between the EPR reality criterion and quantum mechanics has thus been shown to exist.

Appendix

Tensor multiplication is used to construct the initial states using Mathcad commands *submatrix*, *kronecker*, and *augment*.

$$\Psi = \frac{1}{\sqrt{2}}$$

$$\begin{bmatrix} \text{submatrix}\left[\text{kronecker}\left[\text{augment}\left[\begin{pmatrix}1\\0\end{pmatrix}, \begin{pmatrix}0\\0\end{pmatrix}\right], \text{augment}\left[\begin{pmatrix}0\\1\end{pmatrix}, \begin{pmatrix}0\\0\end{pmatrix}\right]\right], 1, 4, 1, 1\right] \ \ldots \\ + - \text{submatrix}\left[\text{kronecker}\left[\text{augment}\left[\begin{pmatrix}0\\1\end{pmatrix}, \begin{pmatrix}0\\0\end{pmatrix}\right], \text{augment}\left[\begin{pmatrix}1\\0\end{pmatrix}, \begin{pmatrix}0\\0\end{pmatrix}\right]\right], 1, 4, 1, 1\right] \end{bmatrix}$$

Kronecker is the Mathcad command that carries out the tensor multiplication of matrices. For example, consider the tensor multiplication of the *Hardness* and *Color* matrix operators.

$$Hardness \otimes Color = \begin{pmatrix}1 & 0\\0 & -1\end{pmatrix} \otimes \begin{pmatrix}0 & 1\\1 & 0\end{pmatrix}$$

$$= \begin{pmatrix} 1\begin{pmatrix}0 & 1\\1 & 0\end{pmatrix} & 0\begin{pmatrix}0 & 1\\1 & 0\end{pmatrix} \\ 0 & \begin{pmatrix}0 & 1\\1 & 0\end{pmatrix} & -1\begin{pmatrix}0 & 1\\1 & 0\end{pmatrix} \end{pmatrix} = \begin{pmatrix}0 & 1 & 0 & 0\\1 & 0 & 0 & 0\\0 & 0 & 0 & -1\\0 & 0 & -1 & 0\end{pmatrix}$$

$$\text{kronecker}(\text{Hardness}, \text{Color}) = \begin{pmatrix}0 & 1 & 0 & 0\\1 & 0 & 0 & 0\\0 & 0 & 0 & -1\\0 & 0 & -1 & 0\end{pmatrix} \quad \text{kronecker}\left[\begin{pmatrix}1 & 0\\0 & -1\end{pmatrix}, \begin{pmatrix}0 & 1\\1 & 0\end{pmatrix}\right]$$

$$= \begin{pmatrix}0 & 1 & 0 & 0\\1 & 0 & 0 & 0\\0 & 0 & 0 & -1\\0 & 0 & -1 & 0\end{pmatrix}$$

This page titled 8.41: Entanglement Reveals a Conflict Between Local Realism and Quantum Theory is shared under a CC BY 4.0 license and was authored, remixed, and/or curated by Frank Rioux via source content that was edited to the style and standards of the LibreTexts platform.

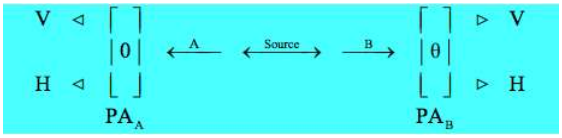
8.42: A Summary of Feynman's "Simulating Physics with Computers"

This tutorial is based on "Simulating Physics with Computers" by Richard Feynman, published in the *International Journal of Theoretical Physics* (volume 21, pages 481-485), and Julian Brown's *Quest for the Quantum Computer* (pages 91-100). Feynman used the experiment outlined below to establish that a local classical computer could not simulate quantum physics.

A two-stage atomic cascade emits entangled photons (A and B) in opposite directions with the same circular polarization according to observers in their path.

\[| \Psi \rangle = \frac{1}{ \sqrt{2}} \left[| L \rangle_A |L \rangle_B + |R \rangle_A | R \rangle_B \right] \nonumber \]

The experiment involves the measurement of photon polarization states in the vertical/horizontal measurement basis, and allows for the rotation of the right-hand detector through an angle of θ, in order to explore the consequences of quantum mechanical entanglement. PA stands for polarization analyzer and could simply be a calcite crystal.



In vector notation the left- and right-circular polarization states are expressed as follows:

Left circular polarization:

\[\text{L} = \frac{1}{ \sqrt{2}} \begin{pmatrix} 1 \\ i \end{pmatrix} \nonumber \]

Right circular polarization:

\[\text{R} = \frac{1}{ \sqrt{2}} \begin{pmatrix} 1 \\ -i \end{pmatrix} \nonumber \]

In tensor notation the initial photon state is,

\[| \Psi \rangle = \frac{1}{ \sqrt{2}} \left[| L \rangle_A | L \rangle_B + |R \rangle_A | R \rangle_B \right] = \frac{1}{ 2 \sqrt{2}} \left[\begin{pmatrix} 1 \\ i \end{pmatrix}_A \otimes \begin{pmatrix} 1 \\ i \end{pmatrix}_B + \begin{pmatrix} 1 \\ -i \end{pmatrix}_A \otimes \begin{pmatrix} 1 \\ -i \end{pmatrix}_B \right] = \frac{1}{2 \sqrt{2}} \left[\begin{pmatrix} 1 \\ i \\ i \\ -1 \end{pmatrix} + \begin{pmatrix} 1 \\ -i \\ -i \\ -1 \end{pmatrix} \right] = \frac{1}{ \sqrt{2}} \begin{pmatrix} 1 \\ 0 \\ 0 \\ -1 \end{pmatrix} \nonumber \]

However, as mentioned above, the photon polarization measurements will actually be made in the vertical/horizontal basis. These polarization states in vector representation are:

Vertical polarization:

\[V = \begin{pmatrix} 1 \\ 0 \end{pmatrix} \nonumber \]

Horizontal polarization:

\[H = \begin{pmatrix} 0 \\ 1 \end{pmatrix} \nonumber \]

It is easy to show that the equivalent vertical/horizontal polarization state is,

\[| \Psi \rangle = \frac{1}{ \sqrt{2}} \left[| V \rangle_A | V \rangle_B + |V \rangle_A | V \rangle_B \right] = \frac{1}{ 2 \sqrt{2}} \left[\begin{pmatrix} 1 \\ 0 \end{pmatrix}_A \otimes \begin{pmatrix} 1 \\ 0 \end{pmatrix}_B + \begin{pmatrix} 0 \\ 1 \end{pmatrix}_A \otimes \begin{pmatrix} 0 \\ 1 \end{pmatrix}_B \right] = \frac{1}{2 \sqrt{2}} \left[\begin{pmatrix} 1 \\ 0 \\ 0 \\ 0 \end{pmatrix} - \begin{pmatrix} 0 \\ 0 \\ 0 \\ 1 \end{pmatrix} \right] = \frac{1}{ \sqrt{2}} \begin{pmatrix} 1 \\ 0 \\ 0 \\ -1 \end{pmatrix} \nonumber \]

There are four measurement outcomes: both photons are vertically polarized, both are horizontally polarized, one is vertical and the other horizontal, and vice versa. The tensor representation of these measurement states are provided below.

\[\begin{matrix} | VV \rangle = \begin{pmatrix} 1 \\ 0 \end{pmatrix} \otimes \begin{pmatrix} 1 \\ 0 \end{pmatrix} = \begin{pmatrix} 1 \\ 0 \\ 0 \\ 0 \end{pmatrix} & | VH \rangle = \begin{pmatrix} 1 \\ 0

\end{pmatrix} \otimes \begin{pmatrix} 0 \\ 1 \end{pmatrix} = \begin{pmatrix} 0 \\ 1 \\ 0 \\ 0 \end{pmatrix} & | HV \rangle = \begin{pmatrix} \begin{pmatrix} 0 \\ 1 \end{pmatrix} \otimes \begin{pmatrix} 1 \\ 0 \end{pmatrix} = \begin{pmatrix} 0 \\ 0 \\ 1 \\ 0 \end{pmatrix} & | HH \rangle = \begin{pmatrix} \begin{pmatrix} 0 \\ 1 \end{pmatrix} \otimes \begin{pmatrix} 0 \\ 1 \end{pmatrix} = \begin{pmatrix} 0 \\ 0 \\ 0 \\ 1 \end{pmatrix} \\ \Psi = \frac{1}{ \sqrt{2}} \begin{pmatrix} 1 \\ 0 \\ 0 \\ -1 \end{pmatrix} & VV = \begin{pmatrix} 1 \\ 0 \\ 0 \\ 0 \end{pmatrix} & VH = \begin{pmatrix} 0 \\ 1 \\ 0 \\ 0 \end{pmatrix} & HV = \begin{pmatrix} \begin{pmatrix} 0 \\ 0 \\ 1 \\ 0 \end{pmatrix} & HH = \begin{pmatrix} 0 \\ 0 \\ 0 \\ 1 \end{pmatrix} \end{matrix} \nonumber \]

Next, the operator representing the rotation of PA_B by an angle θ relative to PA_A is constructed using matrix tensor multiplication. Kronecker is Mathcad's command for tensor matrix multiplication.

\[\text{RotOP}(\theta) = \text{kronecker} \left[\begin{pmatrix} 1 & 0 \\ 0 & 1 \end{pmatrix},~ \begin{pmatrix} \cos \theta & \sin \theta \\ - \sin \theta & \cos \theta \end{pmatrix} \right] \nonumber \]

Now we can get on with some actual calculations. If the relative angle between PAA and PAB is zero degrees we observe perfect correlation. In other words, 50% of the time the analyzers agree that both photons are vertically polarized, and 50% of the time they agree that they are horizontally polarized.

Perfect correlation:

\[\begin{matrix} \theta = 0 \text{deg} & \begin{bmatrix} \left(VV^T \text{RotOP}(\theta) \Psi \right)^2 & \left(VH^T \text{RotOP}(\theta) \Psi \right)^2 \\ \left(HV^T \text{RotOP}(\theta) \Psi \right)^2 & \left(HH^T \text{RotOP}(\theta) \Psi \right)^2 \end{bmatrix} = \begin{pmatrix} 50 & 0 \\ 0 & 50 \end{pmatrix}% \end{matrix} \nonumber \]

However, if the relative angle between the two polarization analyzers is 90 degrees, perfect anti-correlation is observed - the photons are always detected with the opposite polarizations.

Perfect anti-correlation:

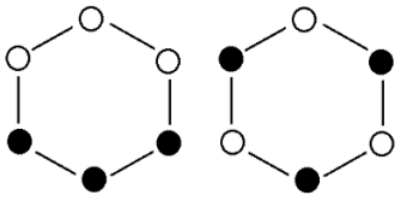
\[\begin{matrix} \theta = 90 \text{deg} & \begin{bmatrix} \left(VV^T \text{RotOP}(\theta) \Psi \right)^2 & \left(VH^T \text{RotOp}(\theta) \Psi \right)^2 \\ \left(HV^T \text{RotOP}(\theta) \Psi \right)^2 & \left(HH^T \text{RotOp}(\theta) \Psi \right)^2 \end{bmatrix} = \begin{pmatrix} 0 & 50 \\ 50 & 0 \end{pmatrix} \% \end{matrix} \nonumber \]

By comparison, if the relative angle between the analyzers is 30 degrees, the analysers behave the same way 75% of the time.

\[\begin{matrix} \theta = 30 \text{deg} & \begin{bmatrix} \left(VV^T \text{RotOp}(\theta) \Psi \right)^2 & \left(VH^T \text{RotOp}(\theta) \Psi \right)^2 \\ \left(HV^T \text{RotOp}(\theta) \Psi \right)^2 & \left(HH^T \text{RotOp}(\theta) \Psi \right)^2 \end{bmatrix} = \begin{pmatrix} 37.5 & 12.5 \\ 12.5 & 37.5 \end{pmatrix} \% \end{matrix} \nonumber \]

These quantum calculations are in agreement with experimental results. As we shall see they cannot be explained by a local realistic hidden-variable model of reality.

If you subscribe to the principle of local realism and believe that objects have well-defined properties independent of measurement or observation, the first two results (θ = 0 degrees, θ = 90 degrees) require that the photons carry the following instruction sets, where the hexagonal vertices refer to values of θ = 0, 30, 60, 90, 120, and 150 degrees. There are eight possible instruction sets, six of the type on the left and two of the type on the right. The white circles represent vertical polarization and the black circles represent horizontal polarization. In any given measurement, according to local realism, both photons (A and B) carry identical instruction sets, in other words the same one of the eight possible sets.



The problem is that while these instruction sets are in agreement with the 0 and 90 degree results, they can't explain the 30 degree data. The figure on the left shows that the same result should be obtained 2/3 of the time (4/6) and the figure on the right never.

Thus, local realism predicts that the same result should be obtained 50% of the time, as opposed to the actual result of 75% of the time.

\[\frac{6 \frac{2}{3} + 2 \times 0}{8} = 50 \% \nonumber \]

When Feynman gets to this point in "Simulating Physics with Computers" he writes,

> That's all. That's the difficulty. That's why quantum mechanics can't seem to be imitable by a local classical computer.

A local classical computer manipulates bits which are in well-defined states, 0s and 1s, shown above graphically in white and black. However, these classical states are incompatible with the quantum mechanical analysis which is consistent with experimental results. This two-photon experiment demonstrates that simulation of quantum physics requires a computer that can manipulate 0s and 1s, superpositions of 0 and 1, and entangled superpositions of 0s and 1s. Simulation of quantum physics requires a quantum computer!

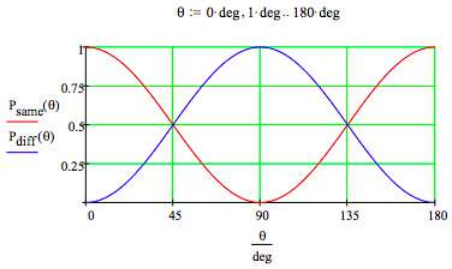
Earlier in his paper Feynman sharpened the focus of his analysis by saying "But the physical world is quantum mechanical, and therefore the proper problem is the simulation of quantum physics ..."

He ends his presentation with the following remark.

> And I'm not happy with all the analyses that go with just the classical theory, because nature isn't classical, dammit, and if you want to make a simulation of nature, you'd better make it quantum mechanical, ...

In conclusion, the quantum mechanical calculations are presented graphically for all θ values between 0 and 180 degrees.

\[\begin{matrix} P_{same} (\theta) = \left(VV^T \text{RotOp} (\theta) \Psi \right)^2 + \left(HH^T \text{RotOp} (\theta) \Psi \right)^2 \\ P_{diff} (\theta) = \left(VH^T \text{RotOp} (\theta) \Psi \right)^2 + \left(HV^T \text{RotOp} (\theta) \Psi \right)^2 \end{matrix} \nonumber \]



This page titled 8.42: A Summary of Feynman's "Simulating Physics with Computers" is shared under a CC BY 4.0 license and was authored, remixed, and/or curated by Frank Rioux via source content that was edited to the style and standards of the LibreTexts platform.

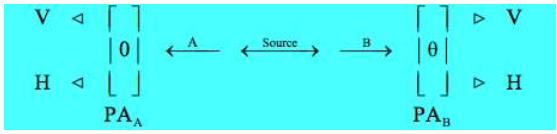
8.43: Another Summary of Fenyman's "Stimulating Physics with Computers"

This tutorial is based on "Simulating Physics with Computers" by Richard Feynman, published in the *International Journal of Theoretical Physics* (volume 21, pages 481-485), and Julian Brown's *Quest for the Quantum Computer* (pages 91-100). Feynman used the experiment outlined below to establish that a local classical computer could not simulate quantum physics.

A two-stage atomic cascade emits entangled photons (A and B) in opposite directions with the same circular polarization according to observers in their path.

\[| \Psi \rangle = \frac{1}{ \sqrt{2}} \left[|L \rangle_A |L \rangle_B + |R \rangle_A | \rangle_B \right] \nonumber \]

The experiment involves the measurement of photon polarization states in the vertical/horizontal measurement basis, and allows for the rotation of the right-hand detector through an angle θ, in order to explore the consequences of quantum mechanical entanglement. PA stands for polarization analyzer and could simply be a calcite crystal.



As mentioned above the photon polarization measurements are made in the V-H basis. The L and R polarization states are superpositions of the V and H polarization states, enabling the original state to be written in the measurement basis.

\[\begin{matrix} | L \rangle = \frac{1}{ \sqrt{2}} \left[| V \rangle + i | H \rangle \right] & | R \rangle = \frac{1}{ \sqrt{2}} \left[| V \rangle - i | H \rangle \right] & | \Psi \rangle = \frac{1}{ \sqrt{2}} \left[| V \rangle_A | V \rangle_B - | H \rangle_A |H \rangle_B \right] \end{matrix} \nonumber \]

Rotating the right-hand polarizer counter-clockwise by θ yields the following polarization states for B.

\[\begin{matrix} | V\ \rangle_B = \cos \theta | V \rangle_B - \sin \theta |H \rangle_B & | H' \rangle_B = \sin \theta | V \rangle_B + \cos \theta | H \rangle_B \end{matrix} \nonumber \]

After rotation of B's analyzer the four measurement outcomes, both photons vertically polarized, both horizontally polarized, one vertical and the other horizontal, are expressed mathematically below.

\[\begin{matrix} | \Psi_{VV'} \rangle = | V \rangle_A |V' \rangle_B & | \Psi_{VH'} \rangle = |V \rangle_A | H' \rangle_B & | \Psi_{HV'} \rangle = |H \rangle_A | V' \rangle_B & | \Psi_{HH'} \rangle = |H \rangle_A | H' \rangle_B \end{matrix} \nonumber \]

Using the equations provided the probability the photons will behave the same way, both vertically polarized or both horizontally polarized is $\cos^2(\theta)$.

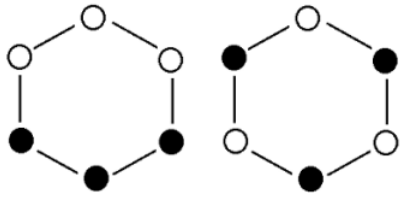
\[\left| \left\langle \Psi_{VV'} | \Psi \right\rangle \right|^2 + \left| \right|^2 = \cos^2 \theta \nonumber \]

Next the probability the photons will behave the same is calculated for three values of θ.

\[P_{same} \theta = \cos (\theta)^2 & P_{same} (0 \text{ deg}) = 1 & P_{same} (90 \text{ deg} = 0 & P_{same} (30 \text{ deg}) = 0.75 \nonumber \]

These quantum calculations are in agreement with experimental results, but cannot be explained by a local realistic hidden-variable model of reality.

If objects have well-defined properties independent of measurement or observation, the first two results (θ = 0 degrees, θ = 90 degrees) require that the photons carry the following instruction sets, where the hexagonal vertices refer to θ values of 0, 30, 60, 90, 120, and 150 degrees. There are eight possible instruction sets, six of the type on the left and two of the type on the right. The white circles represent vertical polarization and the black circles represent horizontal polarization. In any given measurement, according to local realism, both photons (A and B) carry identical instruction sets, in other words the same one of the eight possible sets.



The problem is that while these instruction sets are in agreement with the 0 and 90 degree results, they can't explain the 30 degree data. The figure on the left shows that the same result should be obtained 2/3 of the time (4/6) and the figure on the right never. Thus, local realism predicts that the same result should be obtained 50% of the time, as opposed to the actual result of 75% agreement.

\[\left(6 \frac{2}{3} + 2(0) \right) \div 8 = 50 \% \nonumber \]

When Feynman gets to this point in "Simulating Physics with Computers" he writes,

> That's all. That's the difficulty. That's why quantum mechanics can't seem to be imitable by a local classical computer.

A local classical computer manipulates bits which are in well-defined states, 0s and 1s, shown above graphically in white and black. However, these classical states are incompatible with the quantum mechanical analysis which is in agreement with experimental results. This two-photon experiment demonstrates that simulation of quantum physics requires a computer that can manipulate 0s and 1s, superpositions of 0 and 1, and entangled superpositions of 0s and 1s. Simulation of quantum physics requires a quantum computer!

Earlier in his paper Feynman sharpened the focus of his analysis by saying "But the physical world is quantum mechanical, and therefore the proper problem is the simulation of quantum physics ..."

He ends his presentation with the following remark.

> And I'm not happy with all the analyses that go with just the classical theory, because nature isn't classical, dammit, and if you want to make a simulation of nature, you'd better make it quantum mechanical, ...

This page titled 8.43: Another Summary of Fenyman's "Stimulating Physics with Computers" is shared under a CC BY 4.0 license and was authored, remixed, and/or curated by Frank Rioux via source content that was edited to the style and standards of the LibreTexts platform.

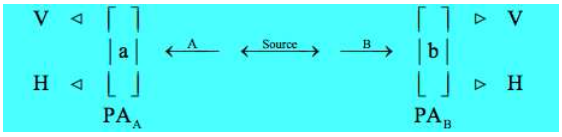
8.44: Yet Another Assault on Local Realism

The purpose of this tutorial is to review Nick Herbert's "simple proof of Bell's theorem" as presented in Chapter 12 of *Quantum Reality*.

A two-stage atomic cascade emits entangled photons (A and B) in opposite directions with the same circular polarization according to the observers in their path.

$$|\Psi\rangle = \frac{1}{\sqrt{2}}\left[|L\rangle_A|L\rangle_B + |R\rangle_A|R\rangle_B\right]$$

The experiment involves the measurement of photon polarization states in the vertical/horizontal measurement basis, and allows that the polarization analyzers (PAs) can be oriented at different angles a and b. (The figure below is similar to the one on page 125 of Jim Baggott's *The Meaning of Quantum Theory*, which provides a thorough analysis of correlated two-photon experiments.)



The dramatize the quantum weirdness of this EPR experiment, Herbert places P_A on Earth and PA_B on Betelgeuse, 540 light years away. The source is a space ship midway between the PAs.

In the vertical/horizontal measurement basis the initial polarization state is (see the Appendix for a justification),

$$|\Psi\rangle = \frac{1}{\sqrt{2}}\left[|V\rangle_A|V\rangle_B - |H\rangle_A|H\rangle_B\right]$$

There are four measurement outcomes: both photons are vertically polarized, both are horizontally polarized, one is vertical and the other horizontal, and vice versa. In other words, the PAs behave the same or differently. The probabilities for these events are given below (see "Simulating Physics with Computers" by Richard Feynman, published in the *International Journal of Theoretical Physics*, volume 21, pages 481-485, or *The Meaning of Quantum Theory*, by Jim Baggott, pages 125-127).

$$P_{same} = P_{vv} + P_{hh} \quad P_{same}(a,\ b) = \cos(a-b)^2 \quad P_{diff} = P_{vh} + P_{hv} \quad P_{diff}(a,\ b) = \sin(a-b)^2$$

The following calculations show that if the PAs are oriented at the same angle they behave the same way 100% of the time. This is called perfect correlation.

$$P_{same}(0\text{ deg},\ 0\text{ deg}) = 100\% \quad P_{same}(30\text{ deg},\ 30\text{ deg}) = 100\% \quad P_{same}(90\text{ deg},\ 90\text{ deg}) = 100\%$$
$$P_{diff}(0\text{ deg},\ 0\text{ deg}) = 0\% \quad P_{diff}(30\text{ deg},\ 30\text{ deg}) = 0\% \quad P_{diff}(90\text{ deg},\ 90\text{ deg}) = 0\%$$

These results appear to support the notion that the linear polarization states of the photons are "elements of reality." In other words, they are photon properties that exist independent of observation. This position is not supported by further calculation and experimentation.

Perfect anti-correlation occurs when the relative angle between the PAs is 90 degrees.

$$P_{same}(0\text{ deg},\ 90\text{ deg}) = 0\% \quad P_{diff}(0\text{ deg},\ 90\text{ deg}) = 100\%$$

At 45 degrees there is not correlation between the detectors.

$$P_{same}(0\text{ deg},\ 45\text{ deg}) = 50\% \quad P_{diff}(0\text{ deg},\ 45\text{ deg}) = 50\%$$

Using 0 degrees for both PAs at the benchmark, Herbert's analysis proceeds by moving PA_B to 30 degrees and noting that this leads to a 25% (1 in 4) discrepancy between the analyzers.

$$P_{same}(0\text{ deg},\ 30\text{ deg}) = 75\% \quad P_{diff}(0\text{ deg},\ 30\text{ deg}) = 25\%$$

If instead PA_A had been moved to -30 degrees the result is the same, the PAs disagree 25% of the time.

$$P_{same}(\text{-}30\text{ deg},\ 0\text{ deg}) = 75\% \quad P_{diff}(\text{-}30\text{ deg},\ 0\text{ deg}) = 25\%$$

Now the locality principal is invoked. The PAs are spatially separated so that according to conventional intuition, the change in the orientation of PA_B has no effect on the results at PA_A, and vice versa.

Now Herbert moves PA_B back to 30 degrees with the following result.

$$P_{same}(\text{-30 deg, 30 deg}) = 25\% \quad P_{diff}(\text{-30 deg, 30 deg}) = 75\%$$

The angular difference is now 60 degrees, and the PAs disagree 75% of the time. On the basis of local realism one would expect a discrepancy of no more than 50% . If the measurements at the PAs are independent of each other, we should simply be able to add 25% and 25%.

The experiment was performed by John Clauser and Stuart Freedman at Berkeley in 1972 and confirmed the quantum predictions. The agreement between quantum theory and experiment requires that some element of local realism must be abandoned. The consensus is that nature allows non-local interactions for entangled systems such as the photons in this example. The results at PA_A and PA_2 (light years apart) are connected by a non-local interaction. This type of interaction is, in the words of Herbert, "unmediated, unmitigated and immediate."

Many other experiments besides those of Clauser and Freedman (most notably by Aspect and co-workers) have confirmed quantum mechanical predictions and refuted local realism. Anton Zeilinger described the current situation as follows:

> By now, a number of experiments have confirmed quantum predictions to such an extent that a local-realistic world view can no longer be maintained.
>
> It appears that, certainly at least for entangled quantum systems, it is wrong to assume that the features of the world which we observe, the measurement results, exist prior to and independently of our observation.

Appendix

In vector notation the left- and right-circular polarization states are expressed as follows:

Left circular polarization:

$$L = \frac{1}{\sqrt{2}} \begin{pmatrix} 1 \\ i \end{pmatrix}$$

Right circular polarization:

$$R = \frac{1}{\sqrt{2}} \begin{pmatrix} 1 \\ -i \end{pmatrix}$$

In tensor notation the initial photon state is,

$$|\Psi\rangle = \frac{1}{\sqrt{2}} \left[|L\rangle_A |L\rangle_B + |R\rangle_A |R\rangle_B \right] = \frac{1}{2\sqrt{2}} \left[\begin{pmatrix} 1 \\ i \end{pmatrix}_A \otimes \begin{pmatrix} 1 \\ i \end{pmatrix}_B + \begin{pmatrix} 1 \\ -i \end{pmatrix}_A \otimes \begin{pmatrix} 1 \\ -i \end{pmatrix}_B \right]$$
$$= \frac{1}{2\sqrt{2}} \left[\begin{pmatrix} 1 \\ i \\ i \\ -1 \end{pmatrix} + \begin{pmatrix} 1 \\ -i \\ -i \\ -1 \end{pmatrix} \right] = \frac{1}{\sqrt{2}} \begin{pmatrix} 1 \\ 0 \\ 0 \\ -1 \end{pmatrix}$$

Vertical polarization:

$$V = \begin{pmatrix} 1 \\ 0 \end{pmatrix}$$

Horizontal polarization:

$$H = \begin{pmatrix} 0 \\ 1 \end{pmatrix}$$

It is easy to show that the equivalent vertical/horizontal polarization state is,

$$|\Psi\rangle = \frac{1}{\sqrt{2}}\left[|L\rangle_A|L\rangle_B + |R\rangle_A|R\rangle_B\right] = \frac{1}{2\sqrt{2}}\left[\begin{pmatrix}1\\0\end{pmatrix}_A \otimes \begin{pmatrix}1\\0\end{pmatrix}_B + \begin{pmatrix}0\\1\end{pmatrix}_A \otimes \begin{pmatrix}0\\1\end{pmatrix}_B\right]$$
$$= \frac{1}{2\sqrt{2}}\left[\begin{pmatrix}1\\0\\0\\0\end{pmatrix} + \begin{pmatrix}0\\0\\0\\1\end{pmatrix}\right] = \frac{1}{\sqrt{2}}\begin{pmatrix}1\\0\\0\\-1\end{pmatrix}$$

Naturally there are other ways to do this. The most direct would be to write |L> and |R> as superpositions of |V> and |H>, and substitute them into the initial state involving the circular polarization states.

$$\Psi = \frac{1}{\sqrt{2}}\left(L_A L_B + R_A R_B\right) \left| \begin{array}{l} \text{substitute, } L_A = \frac{1}{\sqrt{2}}(V_A + iH_A) \\ \text{substitute, } L_B = \frac{1}{\sqrt{2}}(V_B + iH_B) \\ \text{substitute, } R_A = \frac{1}{\sqrt{2}}(V_A - iH_A) \\ \text{substitute, } R_B = \frac{1}{\sqrt{2}}(V_B - iH_B) \\ \text{simplify} \end{array} \right. \rightarrow \Psi = \frac{\sqrt{2}V_A V_B}{2} - \frac{\sqrt{2}H_A H_B}{2}$$

This page titled 8.44: Yet Another Assault on Local Realism is shared under a CC BY 4.0 license and was authored, remixed, and/or curated by Frank Rioux via source content that was edited to the style and standards of the LibreTexts platform.

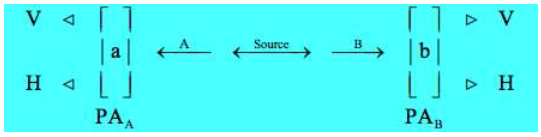
8.45: Yet Another Assault on Local Realism - A Matrix/Tensor Algebra Approach

The purpose of this tutorial is to review Nick Herbert's "simple proof of Bell's theorem" as presented in Chapter 12 of *Quantum Reality* using matrix and tensor algebra.

A two-stage atomic cascade emits entangled photons (A and B) in opposite directions with the same circular polarization according to the observers in their path.

$$|\Psi\rangle = \frac{1}{\sqrt{2}}\left[|L\rangle_A|L\rangle_B + |R\rangle_A|R\rangle_B\right]$$

The experiment involves the measurement of photon polarization states in the vertical/horizontal measurement basis, and allows that the polarization analyzers (PAs) can be oriented at different angles a and b. (The figure below is similar to the one on page 125 of Jim Baggott's *The Meaning of Quantum Theory*, which provides a thorough analysis of correlated two-photon experiments.)



To dramatize the quantum weirdness of this EPR experiment, Herbert places PAA on earth and PAB on Betelgeuse, 540 light years away. The source is a space ship midway between the PAs.

In the vertical/horizontal measurement basis the initial polarization state is (see Appendix A for a justification),

$$|VV\rangle = \begin{pmatrix}1\\0\end{pmatrix} \otimes \begin{pmatrix}1\\0\end{pmatrix} = \begin{pmatrix}1\\0\\0\\0\end{pmatrix} \quad |VH\rangle = \begin{pmatrix}1\\0\end{pmatrix} \otimes \begin{pmatrix}0\\1\end{pmatrix} = \begin{pmatrix}0\\1\\0\\0\end{pmatrix} \quad |HV\rangle = \begin{pmatrix}0\\1\end{pmatrix} \otimes \begin{pmatrix}1\\0\end{pmatrix} = \begin{pmatrix}0\\0\\1\\0\end{pmatrix} \quad |HH\rangle = \begin{pmatrix}0\\1\end{pmatrix} \otimes \begin{pmatrix}0\\1\end{pmatrix} = \begin{pmatrix}0\\0\\0\\1\end{pmatrix}$$

We now write all states, Ψ and the measurement states, in Mathcad's vector format.

$$\Psi = \frac{1}{\sqrt{2}}\begin{pmatrix}1\\0\\0\\-1\end{pmatrix} \quad |VV\rangle = \begin{pmatrix}1\\0\\0\\0\end{pmatrix} \quad |VH\rangle = \begin{pmatrix}0\\1\\0\\0\end{pmatrix} \quad |HV\rangle = \begin{pmatrix}0\\0\\1\\0\end{pmatrix} \quad |HH\rangle = \begin{pmatrix}0\\0\\0\\1\end{pmatrix}$$

Next, the operator representing the rotation of PA_A by angle a clockwise and PA_B by angle b counter-clockwise (so that the PAs turn in the same direction) is constructed using matrix tensor multiplication. Kronecker is Mathcad's command for tensor matrix multiplication.

$$\mathrm{RotOp}(a,\ b) = \mathrm{kronecker}\left[\begin{pmatrix}\cos a & -\sin a\\ \sin a & \cos a\end{pmatrix},\ \begin{pmatrix}\cos b & \sin b\\ -\sin b & \cos b\end{pmatrix}\right]$$

The probability that the detectors will behave the same or differently is calculated as follows.

$$\begin{pmatrix}P_{same}(a,\ b) = \left(VV^T\mathrm{RotOp}(a,\ b)\Psi\right)^2 + \left(HH^T\mathrm{RotOp}(a,\ b)\Psi\right)^2\\ P_{diff}(a,\ b) = \left(VH^T\mathrm{RotOp}(a,\ b)\Psi\right)^2 + \left(HV^T\mathrm{RotOp}(a,\ b)\Psi\right)^2\end{pmatrix}$$

Now we can get on with some actual calculations. The following calculations show that if the PAs are oriented at the same angle they behave the same way 100% of the time. This is called perfect correlation.

$$\begin{array}{lll} P_{same}(0\text{ deg},\ 0\text{ deg}) = 100\% & P_{same}(30\text{ deg},\ 30\text{ deg}) = 100\% & P_{same}(90\text{ deg},\ 90\text{ deg}) = 100\% \\ P_{diff}(0\text{ deg},\ 0\text{ deg}) = 0\% & P_{diff}(30\text{ deg},\ 30\text{ deg}) = 0\% & P_{diff}(90\text{ deg},\ 90\text{ deg}) = 0\% \end{array}$$

These results appear to support the notion that the linear polarization states of the photons are "elements of reality." In other words, they are photon properties that exist independent of observation. However, this position is not supported by further calculation and

experimentation.

Perfect anti-correlation occurs when the relative angle between the PAs is 90 degrees.

$$P_{same}(0 \text{ deg}, 0 \text{ deg}) = 100\% \quad P_{diff}(0 \text{ deg}, 0 \text{ deg}) = 0\%$$

At 45 degrees there is no correlation between the detectors.

$$P_{same}(0 \text{ deg}, 45 \text{ deg}) = 50\% \quad P_{diff}(0 \text{ deg}, 45 \text{ deg}) = 50\%$$

Using 0 degrees for both PAs as the bench mark, Herbert′s analysis proceeds by moving PAB to 30 degrees and noting that this leads to a 25% (1 in 4) discrepancy between the analyzers.

$$P_{same}(0 \text{ deg}, 30 \text{ deg}) = 75\% \quad P_{diff}(0 \text{ deg}, 30 \text{ deg}) = 25\%$$

If instead PA_A had been moved to -30 degrees the result is the same, the PAs disagree 25% of the time.

$$P_{same}(\text{-}30 \text{ deg}, 0 \text{ deg}) = 75\% \quad P_{diff}(\text{-}30 \text{ deg}, 0 \text{ deg}) = 25\%$$

Now the locality principal is invoked. The PAs are spatially separated so that according to conventional intuition, the change in the orientation of PA_B has no effect on the results at PA_A, and vice versa.

Now Herbert moves PA_B back to 30 degrees with the following result.

$$P_{same}(\text{-}30 \text{ deg}, 30 \text{ deg}) = 25\% \quad P_{diff}(\text{-}30 \text{ deg}, 30 \text{ deg}) = 75\%$$

The angular difference is now 60 degrees, and the PAs disagree 75% of the time. On the basis of local realism one would expect a discrepancy of no more than 50% . If the measurements at the PAs are independent of each other, we should simply be able to add 25% and 25%. A more general version this approach to Bell′s theorem can be found in the Appendix B.

The experiment was performed by John Clauser and Stuart Freedman at Berkeley in 1972 and confirmed the quantum predictions. The agreement between quantum theory and experiment requires that some element of local realism must be abandoned. The consensus is that nature allows non-local interactions for entangled systems such as the photons in this example. The results at PAA and PAB (light years apart) are connected by a non-local interaction. This type of interaction is, in the words of Herbert, ″unmediated, unmitigated and immediate.″

Many other experiments besides those of Clauser and Freedman (most notably by Aspect and co-workers) have confirmed quantum mechanical predictions and refuted local realism. Anton Zeilinger described the current situation as follows:

> By now, a number of experiments have confirmed quantum predictions to such an extent that a local-realistic world view can no longer be maintained.
>
> It appears that, certainly at least for entangled quantum systems, it is wrong to assume that the features of the world which we observe, the measurement results, exist prior to and independently of our observation.

Appendix A

In vector notation the left- and right-circular polarization states are expressed as follows:

Left circular polarization:

$$L = \frac{1}{\sqrt{2}} \begin{pmatrix} 1 \\ i \end{pmatrix}$$

Right circular polarization:

$$R = \frac{1}{\sqrt{2}} \begin{pmatrix} 1 \\ -i \end{pmatrix}$$

In tensor notation the initial photon state is,

$$|\Psi\rangle = \frac{1}{\sqrt{2}}\left[|L\rangle_A|L\rangle_B + |R\rangle_A|R\rangle_B\right] = \frac{1}{2\sqrt{2}}\left[\begin{pmatrix}1\\ i\end{pmatrix}_A \otimes \begin{pmatrix}1\\ i\end{pmatrix}_B + \begin{pmatrix}1\\ -i\end{pmatrix}_A \otimes \begin{pmatrix}1\\ -i\end{pmatrix}_B\right]$$
$$= \frac{1}{2\sqrt{2}}\left[\begin{pmatrix}1\\ i\\ i\\ -1\end{pmatrix} + \begin{pmatrix}1\\ -i\\ -i\\ -1\end{pmatrix}\right] = \frac{1}{\sqrt{2}}\begin{pmatrix}1\\ 0\\ 0\\ -1\end{pmatrix}$$

Vertical polarization:

$$V = \begin{pmatrix}1\\ 0\end{pmatrix}$$

Horizontal polarization:

$$H = \begin{pmatrix}0\\ 1\end{pmatrix}$$

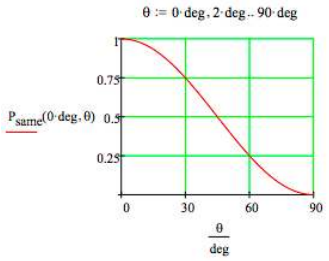
It is easy to show that the equivalent vertical/horizontal polarization state is,

$$|\Psi\rangle = \frac{1}{\sqrt{2}}\left[|V\rangle_A|V\rangle_B + |H\rangle_A|H\rangle_B\right] = \frac{1}{2\sqrt{2}}\left[\begin{pmatrix}1\\ 0\end{pmatrix}_A \otimes \begin{pmatrix}1\\ 0\end{pmatrix}_B + \begin{pmatrix}0\\ 1\end{pmatrix}_A \otimes \begin{pmatrix}0\\ 1\end{pmatrix}_B\right]$$
$$= \frac{1}{2\sqrt{2}}\left[\begin{pmatrix}1\\ 0\\ 0\\ 0\end{pmatrix} - \begin{pmatrix}0\\ 0\\ 0\\ 1\end{pmatrix}\right] = \frac{1}{\sqrt{2}}\begin{pmatrix}1\\ 0\\ 0\\ -1\end{pmatrix}$$

Naturally there are other ways to do this. The most direct would be to write |L> and |R> as superpositions of |V> and |H>, and substitute them into the initial state involving the circular polarization states.

$$\psi = \frac{1}{\sqrt{2}}(L_A L_B + R_A R_B) \left|\begin{array}{l}\text{substitute, } L_A = \frac{1}{\sqrt{2}}(V_A + iH_A)\\ \text{substitute, } L_B = \frac{1}{\sqrt{2}}(V_B + iH_B)\\ \text{substitute, } L_A = \frac{1}{\sqrt{2}}(V_A + iH_A)\\ \text{substitute, } L_A = \frac{1}{\sqrt{2}}(V_A + iH_A)\\ \text{simplify}\end{array}\right. \rightarrow \psi = \frac{\sqrt{2}V_A V_B}{2} - \frac{\sqrt{2}H_A H_B}{2}$$

Figure 12.4 on page 223 in Herbert's *Quantum Reality* is reproduced.



Appendix B

It is not difficult to derive the following Bell inequality based on local realism involving three sets of polarization measurement angles for the experiment described above. See *The Meaning of Quantum Theory* by Jim Baggott, pages 133-135.

$$P_{diff}(a,\ b) + P_{diff}(a,\ b) \geq P_{diff}(a,\ c)$$

Below it is shown that the inequality is violated for 0, 22.5 and 45 degrees, as well as for 0, 30 and 60 degrees.

$$P_{diff}(0\text{ deg},\ 22.5\text{ deg}) + P_{diff}(22.5\text{ deg},\ 45\text{ deg}) = 0.293 \qquad P_{diff}(0\text{ deg},\ 45\text{ deg}) = 0.5$$
$$P_{diff}(0\text{ deg},\ 30\text{ deg}) + P_{diff}(30\text{ deg},\ 60\text{ deg}) = 0.5 \qquad P_{diff}(0\text{ deg},\ 60\text{ deg}) = 0.75$$

The Bell inequality is also violated for other sets of angles. However, it is not violated for 0, 45 and 90 degrees.

$$P_{diff}(0 \text{ deg}, 45 \text{ deg}) + P_{diff}(45 \text{ deg}, 90 \text{ deg}) = 1 \quad P_{diff}(0 \text{ deg}, 90 \text{ deg}) = 1$$

On page 135 Baggott summarizes the significance of Bell′s inequality.

> The most important assumption ... made in the reasoning which led to this inequality was that of ... the local reality of the photons. It is therefore an inequality that is quite independent of the nature of any local hidden variable theory that we could possibly devise. The conclusion is inescapable, quantum theory is incompatible with any local hidden variable theory and hence local reality.

On page 131 he writes that after Bell′s work,

> Questions about local hidden variables immediately changed character. From being rather academic questions about philosophy they became questions of profound importance for quantum theory. The choice between quantum theory and local hidden variable theories was no longer a question of taste, it was a matter of correctness.

This obviously suggests that clever experimentalist might be able to decide which view of reality is correct. To date experimental results have been consistent with the quantum mechanical predictions.

This page titled 8.45: Yet Another Assault on Local Realism - A Matrix/Tensor Algebra Approach is shared under a CC BY 4.0 license and was authored, remixed, and/or curated by Frank Rioux via source content that was edited to the style and standards of the LibreTexts platform.

8.46: Jim Baggott's Bell Theorem Analysis

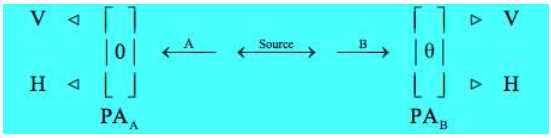
The purpose of this tutorial is to review Jim Baggott's analysis of Bell's theorem as presented in Chapter 4 of *The Meaning of Quantum Theory* using matrix and tensor algebra.

A two-stage atomic cascade emits entangled photons (A and B) in opposite directions with the same circular polarization according to the observers in their path.

$$|\Psi\rangle = \frac{1}{\sqrt{2}}\left[|L\rangle_A|L\rangle_B + |R\rangle_A|R\rangle_B\right] \qquad \Psi = \frac{1}{\sqrt{2}}\begin{pmatrix}1\\0\\0\\-1\end{pmatrix}$$

$$= \frac{1}{2\sqrt{2}}\left[\begin{pmatrix}1\\i\end{pmatrix}_A \otimes \begin{pmatrix}1\\i\end{pmatrix}_B + \begin{pmatrix}1\\-i\end{pmatrix}_A \otimes \begin{pmatrix}1\\-i\end{pmatrix}_B\right] = \frac{1}{\sqrt{2}}\begin{pmatrix}1\\0\\0\\-1\end{pmatrix}$$

The experiment involves the measurement of photon polarization states in the vertical/horizontal measurement basis using calcite crystals, and allows that the polarization analyzers (PAs) can be oriented at different angles a and b. The figure below is taken from Chapter 4 of Jim Baggott's *The Meaning of Quantum Theory*.



The equivalent wave function in the vertical/horizontal basis is:

$$|\Psi\rangle = \frac{1}{\sqrt{2}}\left[|V\rangle_A|V\rangle_B - |H\rangle_A|H\rangle_B\right] = \frac{1}{2\sqrt{2}}\left[\begin{pmatrix}1\\0\end{pmatrix}_A \otimes \begin{pmatrix}1\\0\end{pmatrix}_B + \begin{pmatrix}0\\1\end{pmatrix}_A \otimes \begin{pmatrix}0\\1\end{pmatrix}_B\right] = \frac{1}{\sqrt{2}}\begin{pmatrix}1\\0\\0\\-1\end{pmatrix}$$

The matrix operator representing the calcite crystal, where θ is the angle of rotation of the crystal relative to the vertical is:

$$\text{Calcite}(\theta) = \begin{pmatrix}\cos(2\theta) & \sin(2\theta)\\ \sin(2\theta) & -\cos(2\theta)\end{pmatrix} \qquad \text{Calcite}(0) = \begin{pmatrix}1 & 0\\0 & -1\end{pmatrix} \qquad \text{Calcite}\left(\tfrac{\pi}{4}\right) = \begin{pmatrix}0 & 1\\1 & 0\end{pmatrix} \qquad \text{Calcite}\left(\tfrac{\pi}{2}\right) = \begin{pmatrix}-1 & 0\\0 & 1\end{pmatrix}$$

The eigenvalues of the calcite operator for any orientation angle are +/- 1. Several examples are shown below.

$$\text{eigenvals}(\text{Calcite}(0)) = \begin{pmatrix}1\\-1\end{pmatrix} \qquad \text{eigenvals}\left(\text{Calcite}\left(\tfrac{\pi}{4}\right)\right) = \begin{pmatrix}1\\-1\end{pmatrix} \qquad \text{eigenvals}\left(\text{Calcite}\left(\tfrac{\pi}{6}\right)\right) = \begin{pmatrix}1\\-1\end{pmatrix}$$

The eigenvalue +1 is assigned to the vertical transmission channel and the -1 eigenvalue to the horizontal transmission channel.

Since only the relative angle between the two PAs is important, PA_1 is held at the vertical orientation (θ = 0) and PA_2 is rotated. The operator for this experimental set-up is as follows.

$$Rot(\theta)\begin{pmatrix}1 & 0\\0 & -1\end{pmatrix} \otimes \begin{pmatrix}\cos(2\theta) & \sin(2\theta)\\ \sin(2\theta) & -\cos(2\theta)\end{pmatrix} = \begin{pmatrix}\cos(2\theta) & \sin(2\theta) & 0 & 0\\ \sin(2\theta) & -\cos(2\theta) & 0 & 0\\ 0 & 0 & -\cos(2\theta) & -\sin(2\theta)\\ 0 & 0 & -\sin(2\theta) & \cos(2\theta)\end{pmatrix}$$

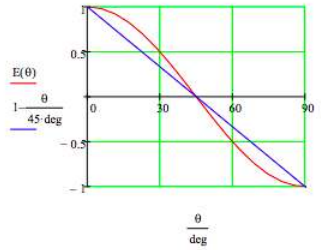
The expectation value of the Rot(θ) operator is a measure of the correlation between the joint measurements.

$$E(\theta) := \frac{1}{\sqrt{2}}\begin{pmatrix}1 & 0 & 0 & -1\end{pmatrix}\begin{pmatrix}\cos(2\theta) & \sin(2\theta) & 0 & 0\\ \sin(2\theta) & -\cos(2\theta) & 0 & 0\\ 0 & 0 & -\cos(2\theta) & -\sin(2\theta)\\ 0 & 0 & -\sin(2\theta) & \cos(2\theta)\end{pmatrix}\begin{pmatrix}1\\0\\0\\-1\end{pmatrix}\frac{1}{\sqrt{2}}\ \text{simplify}\ \rightarrow \cos(2\theta)$$

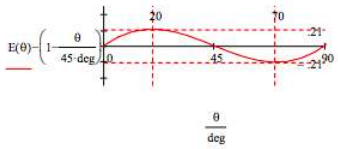
As shown above evaluation of E(θ) yields cos(2θ). For θ = 0^0 there is perfect correlation; for θ = 90^0 perfect anti-correlation; for θ = 45^0 no correlation.

$$E(0\ \text{deg}) = 1 \quad E(90\ \text{deg}) = -1 \quad E(45\ \text{deg}) = 0$$

Baggott derived a correlation function for this experiment based on a local hidden variable model of reality (pp. 110-113, 127-131). It (linear blue line) and the quantum mechanical correlation function, E(θ), are compared on the graph below. Quantum theory and local realism disagree at all angles except 0, 45 and 90 degrees.



Maximum disagreement between quantum theory and the local hidden variable model occurs at 20 and 70 degrees.



This page titled 8.46: Jim Baggott's Bell Theorem Analysis is shared under a CC BY 4.0 license and was authored, remixed, and/or curated by Frank Rioux via source content that was edited to the style and standards of the LibreTexts platform.

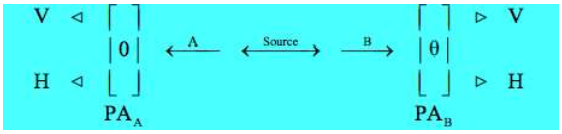
8.47: Another Bell Theorem Analysis

The purpose of this tutorial is to review Jim Baggott's analysis of Bell's theorem as presented in Chapter 4 of *The Meaning of Quantum Theory* using matrix and tensor algebra.

A two-stage atomic cascade emits entangled photons (A and B) in opposite directions with the same circular polarization according to observers in their path.

$$|\Psi\rangle = \frac{1}{\sqrt{2}}\left[|L\rangle_A|L\rangle_B + |R\rangle_A|R\rangle_B\right]$$

The experiment involves the measurement of photon polarization states in the vertical/horizontal measurement basis, and allows for the rotation of the right-hand detector through an angle of θ, in order to explore the consequences of quantum mechanical entanglement. PA stands for polarization analyzer and could simply be a calcite crystal.



In vector notation the left- and right-circular polarization states are expressed as follows:

Left circular polarization:

$$L = \frac{1}{\sqrt{2}}\begin{pmatrix}1\\ i\end{pmatrix}$$

Right circular polarization:

$$R = \frac{1}{\sqrt{2}}\begin{pmatrix}1\\ -i\end{pmatrix}$$

In tensor notation the initial state is the following entangled superposition,

$$|\Psi\rangle = \frac{1}{\sqrt{2}}\left[|L\rangle_A|L\rangle_B + |R\rangle_A|R\rangle_B\right] = \frac{1}{2\sqrt{2}}\left[\begin{pmatrix}1\\ i\end{pmatrix}_A \otimes \begin{pmatrix}1\\ i\end{pmatrix}_B + \begin{pmatrix}1\\ -i\end{pmatrix}_A \otimes \begin{pmatrix}1\\ -i\end{pmatrix}_B\right]$$
$$= \frac{1}{2\sqrt{2}}\left[\begin{pmatrix}1\\ i\\ i\\ -1\end{pmatrix} + \begin{pmatrix}1\\ -i\\ -i\\ -1\end{pmatrix}\right] = \frac{1}{\sqrt{2}}\begin{pmatrix}1\\ 0\\ 0\\ -1\end{pmatrix}$$

However, as mentioned above, the photon polarization measurements will actually be made in the vertical/horizontal basis. These polarization measurement states for photons A and B in vector representation are given below. Θ is the angle through which the PA_2 has been rotated.

Vertical polarization:

$$V_A = \begin{pmatrix}1\\ 0\end{pmatrix} \quad V_B = \begin{pmatrix}\cos\theta\\ -\sin\theta\end{pmatrix}$$

Horizontal polarization:

$$V_A = \begin{pmatrix}0\\ 1\end{pmatrix} \quad V_B = \begin{pmatrix}\sin\theta\\ \cos\theta\end{pmatrix}$$

It is easy to show that |Ψ> in the vertical/horizontal basis is,

$$|\Psi\rangle = \frac{1}{\sqrt{2}}\left[|V\rangle_A|V\rangle_B + |H\rangle_A|H\rangle_B\right] = \frac{1}{2\sqrt{2}}\left[\begin{pmatrix}1\\0\end{pmatrix}_A \otimes \begin{pmatrix}1\\0\end{pmatrix}_B + \begin{pmatrix}0\\1\end{pmatrix}_A \otimes \begin{pmatrix}0\\1\end{pmatrix}_B\right]$$
$$= \frac{1}{2\sqrt{2}}\left[\begin{pmatrix}1\\0\\0\\0\end{pmatrix} + \begin{pmatrix}0\\0\\0\\1\end{pmatrix}\right] = \frac{1}{\sqrt{2}}\begin{pmatrix}1\\0\\0\\-1\end{pmatrix}$$

There are four possible measurement outcomes: both photons are vertically polarized, both are horizontally polarized, one is vertical and the other horizontal, and vice versa. The vector representations of the measurement states are obtained by tensor multiplication of the individual photon states.

$$|V_A V_B\rangle = \begin{pmatrix}1\\0\end{pmatrix} \otimes \begin{pmatrix}\cos\theta\\-\sin\theta\end{pmatrix} = \begin{pmatrix}\cos\theta\\-\sin\theta\\0\\0\end{pmatrix} \quad |V_A H_B\rangle = \begin{pmatrix}1\\0\end{pmatrix} \otimes \begin{pmatrix}\sin\theta\\\cos\theta\end{pmatrix} = \begin{pmatrix}\sin\theta\\\cos\theta\\0\\0\end{pmatrix}$$
$$|H_A V_B\rangle = \begin{pmatrix}0\\1\end{pmatrix} \otimes \begin{pmatrix}\cos\theta\\-\sin\theta\end{pmatrix} = \begin{pmatrix}0\\0\\\cos\theta\\-\sin\theta\end{pmatrix} \quad |H_A H_B\rangle = \begin{pmatrix}0\\1\end{pmatrix} \otimes \begin{pmatrix}\sin\theta\\\cos\theta\end{pmatrix} = \begin{pmatrix}0\\0\\\sin\theta\\\cos\theta\end{pmatrix}$$

The initial state and the measurement eigenstates are written in Mathcad syntax.

$$\Psi = \frac{1}{\sqrt{2}}\begin{pmatrix}1\\0\\0\\-1\end{pmatrix} \quad V_a V_b(\theta) = \begin{pmatrix}\cos\theta\\-\sin\theta\\0\\0\end{pmatrix} \quad V_a H_b(\theta) = \begin{pmatrix}\sin\theta\\\cos\theta\\0\\0\end{pmatrix}$$
$$H_a V_b(\theta) = \begin{pmatrix}0\\0\\\cos(\theta)\\-\sin(\theta)\end{pmatrix} \quad H_a H_b(\theta) = \begin{pmatrix}0\\0\\\sin(\theta)\\\cos(\theta)\end{pmatrix}$$

The projections of the initial state onto the four measurement states are,

Probability amplitude:

$$\begin{pmatrix}V_a V_b(\theta)^T\Psi\\V_a H_b(\theta)^T\Psi\\H_a V_b(\theta)^T\Psi\\H_a H_b(\theta)^T\Psi\end{pmatrix} \rightarrow \begin{pmatrix}\frac{\sqrt{2}\cos(\theta)}{2}\\\frac{\sqrt{2}\sin(\theta)}{2}\\\frac{\sqrt{2}\sin(\theta)}{2}\\\frac{\sqrt{2}\cos(\theta)}{2}\end{pmatrix}$$

Probability:

$$\begin{bmatrix}(V_a V_b(\theta)^T\Psi)^2\\(V_a H_b(\theta)^T\Psi)^2\\(H_a V_b(\theta)^T\Psi)^2\\(H_a H_b(\theta)^T\Psi)^2\end{bmatrix} \rightarrow \begin{pmatrix}\frac{\cos(\theta)^2}{2}\\\frac{\sin(\theta)^2}{2}\\\frac{\sin(\theta)^2}{2}\\\frac{\cos(\theta)^2}{2}\end{pmatrix}$$

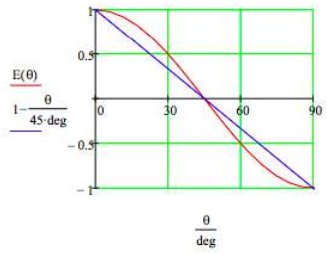
Assigning an eigenvalue of +1 to a vertical polarization measurement and -1 to a horizontal polarization measurement allows the calculation of the expectation value for the joint polarization measurements, a function which quantifies the correlation between the joint measurements. The eigenvalues for the four joint measurement outcomes are: V_aV_b = 1; V_aH_b = -1; H_aV_b = -1; H_aH_b = 1. Weighting these by the probability of their occurence gives the expectation value or correlation function.

$$E(\theta) = (V_a V_b(\theta)^T\Psi)^2 - (V_a H_b(\theta)^T\Psi)^2 - (H_a V_b(\theta)^T\Psi)^2 + (H_a H_b(\theta)^T\Psi)^2 \text{ simplify} \rightarrow \cos(2\theta)$$

As shown above the evaluation of E(θ) yields cos(2θ). For θ = 0^0 there is perfect correlation; for θ = 90^0 perfect anti-correlation; for θ = 45^0 no correlation.

$$E(0\ \text{deg}) = 1 \quad E(90\ \text{deg}) = -1 \quad E(45\ \text{deg}) = 0$$

Baggott presented a correlation function for this experiment based on a local hidden variable model of reality (pp. 110-113, 127-131). It (linear blue line) and the quantum mechanical correlation function, E(θ), are compared on the graph below. Quantum theory and local realism disagree at all angles except 0, 45 and 90 degrees.



This example illustrates Bell's theorem: no local hidden-variable theory can reproduce all the predictions of quantum mechanics for entangled composite systems. As the quantum predictions are confirmed experimentally, the local hidden-variable approach to reality must be abandoned.

Appendix

An equivalent computational approach creates a joint measurement operator from the A and B photon measurement eigenstates. This operator is then used to calculate the expectation value or correlation function.

$$\left(V_A V_A^T - H_A H_A^T\right) \otimes \left(V_B V_B^T - H_B H_B^T\right) = \begin{pmatrix} 1 & 0 \\ 0 & -1 \end{pmatrix} \otimes \begin{pmatrix} \cos(2\theta) & -\sin(2\theta) \\ -\sin(2\theta) & 2\sin(\theta)^2 - 1 \end{pmatrix}$$

Recalling that the vertical and horizontal measurement eigenvalues are +1 and -1, the mathematical structures of the A and B operators shown above are confirmed.

$$V_A V_A^T - H_A H_A^T \rightarrow \begin{pmatrix} 1 & 0 \\ 0 & -1 \end{pmatrix} \quad V_B V_B^T - H_B H_B^T \text{ simplify} \rightarrow \begin{pmatrix} \cos(2\theta) & -\sin(2\theta) \\ -\sin(2\theta) & 2\sin(\theta)^2 - 1 \end{pmatrix}$$

Tensor multiplication of the individual operators creates the joint measurement operator used in the calculation below.

$$E(\theta) = \Psi^T \begin{pmatrix} \cos(2\theta) & -\sin(2\theta) & 0 & 0 \\ -\sin(2\theta) & 2\sin(\theta)^2 - 1 & 0 & 0 \\ 0 & 0 & -\cos(2\theta) & \sin(2\theta) \\ 0 & 0 & \sin(2\theta) & 1 - 2\sin(\theta)^2 \end{pmatrix} \text{ simplify } \rightarrow \cos(2\theta)$$

The expectation value calculations can also be performed using the trace function as shown below.

$$\langle\Psi|\hat{O}|i\rangle\langle i|\Psi\rangle = \sum_i \langle\Psi|\hat{O}|i\rangle\langle i|\Psi\rangle = \sum_i \langle i|\Psi\rangle\langle\Psi|\hat{O}|i\rangle = Trace\left(|\Psi\rangle\langle\Psi|\hat{O}\right) \text{ where } \sum_i |i\rangle\langle i| = \text{Identity}$$

$$tr\left[\Psi\Psi^T \begin{pmatrix} \cos(2\theta) & -\sin(2\theta) & 0 & 0 \\ -\sin(2\theta) & 2\sin(\theta)^2 - 1 & 0 & 0 \\ 0 & 0 & -\cos(2\theta) & \sin(2\theta) \\ 0 & 0 & \sin(2\theta) & 1 - 2\sin(\theta)^2 \end{pmatrix}\right] \text{ simplify } \rightarrow \cos(2\theta)$$

This page titled 8.47: Another Bell Theorem Analysis is shared under a CC BY 4.0 license and was authored, remixed, and/or curated by Frank Rioux via source content that was edited to the style and standards of the LibreTexts platform.

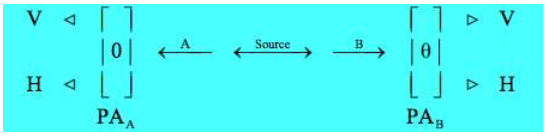
8.48: Another Bell Theorem Analysis - Shorter Version

The purpose of this tutorial is to review Jim Baggott's analysis of Bell's theorem as presented in Chapter 4 of *The Meaning of Quantum Theory* using matrix and tensor algebra.

A two-stage atomic cascade emits entangled photons (A and B) in opposite directions with the same circular polarization according to observers in their path.

$$|\Psi\rangle = \frac{1}{\sqrt{2}}\left[|L\rangle_A|L\rangle_B + |R\rangle_A|R\rangle_B\right]$$

The experiment involves the measurement of photon polarization states in the vertical/horizontal measurement basis, and allows for the rotation of the right-hand detector through an angle of θ, in order to explore the consequences of quantum mechanical entanglement. PA stands for polarization analyzer and could simply be a calcite crystal.



In vector notation the left- and right- circular polarization states are expressed as follows:

Left circular polarization:

$$L = \frac{1}{\sqrt{2}}\begin{pmatrix}1\\ i\end{pmatrix}$$

Right circular polarization:

$$R = \frac{1}{\sqrt{2}}\begin{pmatrix}1\\ -i\end{pmatrix}$$

In tensor notation the initial state is the following entangled superposition,

$$|\Psi\rangle = \frac{1}{\sqrt{2}}\left[|L\rangle_A|L\rangle_B + |R\rangle_A|R\rangle_B\right] = \frac{1}{2\sqrt{2}}\left[\begin{pmatrix}1\\ i\end{pmatrix}_A \otimes \begin{pmatrix}1\\ i\end{pmatrix}_B + \begin{pmatrix}1\\ -i\end{pmatrix}_A \otimes \begin{pmatrix}1\\ -i\end{pmatrix}_B\right]$$
$$= \frac{1}{2\sqrt{2}}\left[\begin{pmatrix}1\\ i\\ i\\ -1\end{pmatrix} + \begin{pmatrix}1\\ -i\\ -i\\ -1\end{pmatrix}\right] = \frac{1}{\sqrt{2}}\begin{pmatrix}1\\ 0\\ 0\\ -1\end{pmatrix}$$

However, as mentioned above, the photon polarization measurements will actually be made in the vertical/horizontal basis. These polarization measurement states for photons A and B in vector representation are given below. Θ is the angle through which the PA2 has been rotated.

Vertical polarization:

$$V_A = \begin{pmatrix}1\\ 0\end{pmatrix} \quad V_B = \begin{pmatrix}\cos\theta\\ \sin\theta\end{pmatrix}$$

Horizontal polarization:

$$V_A = \begin{pmatrix}0\\ 1\end{pmatrix} \quad V_B = \begin{pmatrix}\sin\theta\\ \cos\theta\end{pmatrix}$$

It is easy to show that |Ψ> in the vertical/horizontal basis is,

$$|\Psi\rangle = \frac{1}{\sqrt{2}}\left[|V\rangle_A|V\rangle_B + |H\rangle_A|H\rangle_B\right] = \frac{1}{2\sqrt{2}}\left[\begin{pmatrix}1\\0\end{pmatrix}_A \otimes \begin{pmatrix}1\\0\end{pmatrix}_B + \begin{pmatrix}0\\1\end{pmatrix}_A \otimes \begin{pmatrix}0\\1\end{pmatrix}_B\right]$$
$$= \frac{1}{2\sqrt{2}}\left[\begin{pmatrix}1\\0\\0\\0\end{pmatrix} + \begin{pmatrix}0\\0\\0\\1\end{pmatrix}\right] = \frac{1}{\sqrt{2}}\begin{pmatrix}1\\0\\0\\-1\end{pmatrix}$$

A joint measurement operator is created using the A and B photon measurement eigenstates, with vertical polarization assigned an eigenvalue of +1 and horizontal polarization an eigenvalue of -1. This operator is then used to calculate the expectation value or correlation function.

$$V_A V_A^T - H_A H_A^T \rightarrow \begin{pmatrix}1 & 0\\0 & -1\end{pmatrix} \quad V_B V_B^T - H_B H_B^T \text{simplify} \rightarrow \begin{pmatrix}\cos(2\theta) & -\sin(2\theta)\\-\sin(2\theta) & 2\sin(\theta)^2 - 1\end{pmatrix}$$

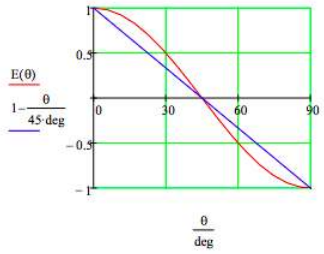
$$\begin{pmatrix}1 & 0\\0 & -1\end{pmatrix} \otimes \begin{pmatrix}\cos(2\theta) & -\sin(2\theta)\\-\sin(2\theta) & 2\sin^2(\theta) - 1\end{pmatrix} = \begin{pmatrix}\cos(2\theta) & -\sin(2\theta) & 0 & 0\\-\sin(2\theta) & 2\sin^2(\theta) - 1 & 0 & 0\\0 & 0 & -\cos(2\theta) & \sin(2\theta)\\0 & 0 & \sin(2\theta) & 2\sin^2(\theta) - 1\end{pmatrix}$$

$$\Psi = \frac{1}{\sqrt{2}}\begin{pmatrix}1\\0\\0\\-1\end{pmatrix} \qquad E(\theta)$$
$$= \Psi \begin{pmatrix}\cos(2\theta) & -\sin(2\theta) & 0 & 0\\-\sin(2\theta) & 2\sin^2(\theta) - 1 & 0 & 0\\0 & 0 & -\cos(2\theta) & \sin(2\theta)\\0 & 0 & \sin(2\theta) & 2\sin^2(\theta) - 1\end{pmatrix} \Psi\text{simplify} \rightarrow \cos(2\theta)$$

As shown above the evaluation of E(θ) yields cos(2θ). For θ = 0^0 there is perfect correlation; for θ = 90^0 perfect anti-correlation; for θ = 45^0 no correlation.

$$E(0 \text{ deg}) = 1 \quad E(90 \text{ deg}) = -1 \quad E(45 \text{ deg}) = 0$$

Baggott presented a correlation function for this experiment based on a local hidden variable model of reality (pp. 110-113, 127-131). It (linear blue line) and the quantum mechanical correlation function, E(θ), are compared on the graph below. Quantum theory and local realism disagree at all angles except 0, 45 and 90 degrees.



This example illustrates Bell's theorem: no local hidden-variable theory can reproduce all the predictions of quantum mechanics for entangled composite systems. As the quantum predictions are confirmed experimentally, the local hidden-variable approach to reality must be abandoned.

In spite of the correlation shown in the joint polarization measurements, the individual measurements on photons 1 and 2 are totally random for all values of θ, i.e. E(θ) = 0. For example, the following operator is used to calculate the expectation value for measurements on photon 2 as a function of its analyzer's angle θ. The identity operator represents no measurement on spin 1.

$$\begin{pmatrix}1 & 0\\0 & -1\end{pmatrix} \otimes \begin{pmatrix}\cos(2\theta) & -\sin(2\theta)\\-\sin(2\theta) & 2\sin^2(\theta) - 1\end{pmatrix} = \begin{pmatrix}\cos(2\theta) & -\sin(2\theta) & 0 & 0\\-\sin(2\theta) & 2\sin^2(\theta) - 1 & 0 & 0\\0 & 0 & -\cos(2\theta) & \sin(2\theta)\\0 & 0 & \sin(2\theta) & 2\sin^2(\theta) - 1\end{pmatrix}$$

$$E(\theta) = \Psi^T \begin{pmatrix} \cos(2\theta) & -\sin(2\theta) \\ -\sin(2\theta) & 2\sin^2(\theta) - 1 \end{pmatrix} = \begin{pmatrix} \cos(2\theta) & -\sin(2\theta) & 0 & 0 \\ -\sin(2\theta) & 2\sin^2(\theta) - 1 & 0 & 0 \\ 0 & 0 & -\cos(2\theta) & \sin(2\theta) \\ 0 & 0 & \sin(2\theta) & 2\sin^2(\theta) - 1 \end{pmatrix}$$

Naturally the same is true for photon 1.

$$\begin{pmatrix} \cos(2\theta) & -\sin(2\theta) \\ -\sin(2\theta) & 2\sin^2(\theta) - 1 \end{pmatrix} \otimes \begin{pmatrix} 1 & 0 \\ 0 & 1 \end{pmatrix}$$

$$= \begin{pmatrix} \cos(2\theta) & 0 & -\sin(2\theta) & 0 \\ 0 & \cos(2\theta) & 0 & -\sin(2\theta) \\ -\sin(2\theta) & 0 & 2\sin^2(\theta) - 1 & \\ 0 & -\sin(2\theta) & 0 & 2\sin^2(\theta) - 1 \end{pmatrix} \Psi \text{ simplify} \rightarrow 0$$

The expectation value calculations can also be performed using the trace function as shown below.

$$\langle \Psi | \hat{O} | \Psi \rangle = \sum_i \langle \Psi | \hat{O} | i \rangle \langle i | \Psi \rangle = \sum_i \langle i | \Psi \rangle \langle \Psi | \hat{O} | i \rangle = Trace\left(| \Psi \rangle \langle \Psi | \hat{O} \right) \text{ where } \sum_i | i \rangle \langle i | = \text{Identity}$$

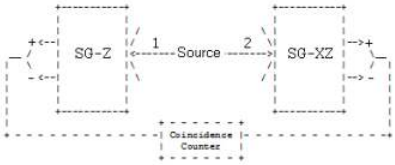
$$tr \left[\Psi \Psi^T \begin{pmatrix} \cos(2\theta) & -\sin(2\theta) & 0 & 0 \\ -\sin(2\theta) & 2\sin(\theta)^2 - 1 & 0 & 0 \\ 0 & 0 & -\cos(2\theta) & \sin(2\theta) \\ 0 & 0 & \sin(2\theta) & 1 - 2\sin(\theta)^2 \end{pmatrix} \right] \text{ simplify} \rightarrow \cos(2\theta)$$

$$tr \left[\Psi \ \Psi^T \begin{pmatrix} \cos(2\theta) & -\sin(2\theta) & 0 & 0 \\ -\sin(2\theta) & 2\sin(\theta)^2 - 1 & 0 & 0 \\ 0 & 0 & -\cos(2\theta) & \sin(2\theta) \\ 0 & 0 & \sin(2\theta) & 1 - 2\sin(\theta)^2 \end{pmatrix} \right] \text{ simplify} \rightarrow \cos(2\theta)$$

This page titled 8.48: Another Bell Theorem Analysis - Shorter Version is shared under a CC BY 4.0 license and was authored, remixed, and/or curated by Frank Rioux via source content that was edited to the style and standards of the LibreTexts platform.

8.49: EPR Analysis for a Composite Singlet Spin System

A spin-1/2 pair is prepared in an entangled singlet state and the individual particles travel in opposite directions on the y-axis to a pair of Stern-Gerlach detectors which are set up to measure spin in the x-z plane. Particle 1's spin is measured along the z-axis, and particle 2's spin is measured at an angle θ with respect to the z-axis.



For the singlet state the arrows below indicate the spin orientation for any direction in the x-z plane.

$$|\Psi\rangle = \frac{1}{\sqrt{2}}\left[|\uparrow\rangle_1|\downarrow\rangle_2 - |\downarrow\rangle_1|\uparrow\rangle_2\right]$$

$$= \frac{1}{\sqrt{2}}\left[\begin{pmatrix}\cos\left(\frac{\theta}{2}\right)\\ \sin\left(\frac{\theta}{2}\right)\end{pmatrix}_1 \otimes \begin{pmatrix}-\sin\left(\frac{\theta}{2}\right)\\ \cos\left(\frac{\theta}{2}\right)\end{pmatrix}_2 - \begin{pmatrix}-\sin\left(\frac{\theta}{2}\right)\\ \cos\left(\frac{\theta}{2}\right)\end{pmatrix}_1 \otimes \begin{pmatrix}\cos\left(\frac{\theta}{2}\right)\\ \sin\left(\frac{\theta}{2}\right)\end{pmatrix}_2\right] = \frac{1}{\sqrt{2}}\begin{pmatrix}0\\1\\-1\\0\end{pmatrix}$$

The single particle spin operator in the x-z plane is constructed from the Pauli spin operators in the xand z-directions. θ is the angle of orientation of the measurement magnet with the z-axis.

$$\sigma_z = \begin{pmatrix}1 & 0\\ 0 & -1\end{pmatrix} \quad \sigma_x = \begin{pmatrix}0 & 1\\ 1 & 0\end{pmatrix} \quad \sigma(\theta) = \cos(\theta)\sigma_z + \sin(\theta)\sigma_x \rightarrow \begin{pmatrix}\cos(\theta) & \sin(\theta)\\ \sin(\theta) & -\cos(\theta)\end{pmatrix}$$

Tensor multiplication of σ_z and σ(θ) creates a joint spin measurement operator.

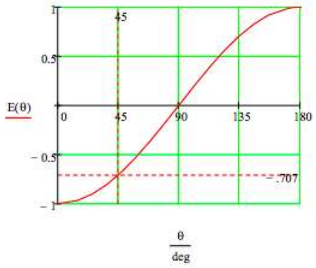
$$\begin{pmatrix}1 & 0\\ 0 & -1\end{pmatrix} \otimes \begin{pmatrix}\cos\theta & \sin\theta\\ \sin\theta & -\cos\theta\end{pmatrix} = \begin{pmatrix}\cos\theta & \sin\theta & 0 & 0\\ \sin\theta & -\cos\theta & 0 & 0\\ 0 & 0 & -\cos\theta & -\sin\theta\\ 0 & 0 & -\sin\theta & \cos\theta\end{pmatrix}$$

The expectation value as a function of the measurement angle of particle 2 is calculated and the result is displayed graphically.

$$E(\theta) = \frac{1}{\sqrt{2}}\begin{pmatrix}0 & 1 & -1 & 0\end{pmatrix}\begin{pmatrix}\cos\theta & \sin\theta & 0 & 0\\ \sin\theta & -\cos\theta & 0 & 0\\ 0 & 0 & -\cos\theta & -\sin\theta\\ 0 & 0 & -\sin\theta & \cos\theta\end{pmatrix}\frac{1}{\sqrt{2}}\begin{pmatrix}0\\1\\-1\\0\end{pmatrix} \rightarrow -\cos\theta$$

The expectation value measures correlation. For θ = 0^0 there is perfect anti-correlation; for θ = 180^0 perfect correlation (see the Appendix for a discussion of this case); for θ = 900 no correlation; for θ = 45^0 intermediate anti-correlation (-0.707). Calculations provided in the Appendix show that the individual spin measurements on particles 1 and 2 are totally random for all values of θ, i.e. E(θ) = 0.

$$E(0\text{ deg}) = -1 \quad E(180\text{ deg}) = 1 \quad E(90\text{ deg}) = 0 \quad E(45\text{ deg}) = -0.707$$



If both observers measure their spins in the z-direction quantum mechanics predicts they will get opposite values due to the singlet nature of the spin state. In other words, the combined expectation value is -1 for these measurements. If spin 2 is measured in the x-direction ($\theta = 90^o$) quantum mechanics predicts, as noted above, an expectation value of 0.

A realist believes that objects have well-defined properties prior to and independent of observation. The following table provide a local realist's explanation of these results. Specific z- and x-spin states are assigned to the particles in the first two columns, with each particle in one of four equally probable spin orientations consistent with the composite singlet state.

$$\begin{bmatrix} \text{Particle 1} & \text{Particle 2} & \hat{\sigma}_z(1)\hat{\sigma}_z(2) & \hat{\sigma}_z(1)\hat{\sigma}_x(2) \\ |\uparrow_z\rangle|\uparrow_x\rangle & |\downarrow_z\rangle|\downarrow_x\rangle & -1 & -1 \\ |\uparrow_z\rangle|\downarrow_x\rangle & |\downarrow_z\rangle|\uparrow_x\rangle & -1 & 1 \\ |\downarrow_z\rangle|\uparrow_x\rangle & |\uparrow_z\rangle|\downarrow_x\rangle & -1 & 1 \\ |\downarrow_z\rangle|\downarrow_x\rangle & |\uparrow_z\rangle|\uparrow_x\rangle & -1 & -1 \\ \text{Expectation} & \text{Value} & -1 & 0 \end{bmatrix}$$

The quantum and classical pictures agree on the prediction of experimental results. The difficulty is that quantum mechanics does not accept the legitimacy of the states shown in the table on the left. One way to state the problem is to note that σ_x and σ_z are noncommuting operators.

$$\sigma_z\sigma_x - \sigma_x\sigma_z \rightarrow \begin{pmatrix} 0 & 2 \\ -2 & 0 \end{pmatrix}$$

According to quantum mechanics spin in the z- and x-directions cannot simultaneously have well-defined values. The states in the table are not valid, in spite of their agreement with experimental results, because they give well-defined values to incompatible observables. Of course, the realist counters that these arguments simply indicate that quantum mechanics is not a complete theory because it cannot assign definite values to all elements of reality prior to and independent of measurement.

If the second spin is measured in the diagonal direction, $\theta = 45^o$, the realist again predicts an expectation value of 0, as shown in the following table.

$$\begin{bmatrix} \text{Particle 1} & \text{Particle 2} & \hat{\sigma}_z(1)\hat{\sigma}_d(2) \\ |\uparrow_z\rangle|\uparrow_d\rangle & |\downarrow_z\rangle|\downarrow_d\rangle & -1 \\ |\uparrow_z\rangle|\downarrow_d\rangle & |\downarrow_z\rangle|\uparrow_d\rangle & 1 \\ |\downarrow_z\rangle|\uparrow_d\rangle & |\uparrow_z\rangle|\downarrow_d\rangle & 1 \\ |\downarrow_z\rangle|\downarrow_d\rangle & |\uparrow_z\rangle|\uparrow_d\rangle & -1 \\ \text{Expectation} & \text{Value} & 0 \end{bmatrix}$$

The spin states in this table are also invalid according to quantum theory.

$$\sigma_z\sigma\left(\frac{\pi}{4}\right) - \sigma\left(\frac{\pi}{4}\right)\sigma_z \rightarrow \begin{pmatrix} 0 & \sqrt{2} \\ -\sqrt{2} & 0 \end{pmatrix}$$

However, as calculated earlier quantum mechanics predicts an expectation value of -0.707. This example illustrates Bell's theorem: no local realist hidden-variable theory can reproduce all the predictions of quantum mechanics for entangled composite systems. As the quantum predictions are confirmed experimentally, the local hidden-variable approach to reality must be abandoned. Appendix If particle 2's detector is rotated by 180 degrees, spin-up in the z-direction (blue in the table below) has eigenvalue -1 and spin-down (red in the table below) has eigenvalue +1.

$$\sigma(180 \text{ deg}) = \begin{pmatrix} -1 & 0 \\ 0 & 1 \end{pmatrix} \quad \text{eigenvec}(\sigma(180 \text{ deg}), \text{-1}) = \begin{pmatrix} 1 \\ 0 \end{pmatrix} \quad \text{eigenvec}(\sigma(180 \text{ deg}), 1) = \begin{pmatrix} 0 \\ 1 \end{pmatrix}$$

This leads to the local realist predictions in the right-hand column, which are in agreement with quantum mechanics.

$$\begin{bmatrix} \text{Particle 1} & \text{Particle 2} & \hat{\sigma}_z(1)\hat{\sigma}_z^{\pi}(2) \\ |\uparrow_z\rangle|\uparrow_x\rangle & |\downarrow_z\rangle|\downarrow_x\rangle & 1 \\ |\uparrow_z\rangle|\downarrow_x\rangle & |\downarrow_z\rangle|\uparrow_x\rangle & 1 \\ |\downarrow_z\rangle|\uparrow_x\rangle & |\uparrow_z\rangle|\downarrow_x\rangle & 1 \\ |\downarrow_z\rangle|\downarrow_x\rangle & |\uparrow_z\rangle|\uparrow_x\rangle & 1 \\ \text{Expectation} & \text{Value} & 1 \end{bmatrix}$$

The following operator is used to calculate the expectation value for measurements on spin 2 as a function of the detector angle θ. The identity operator represents no measurement on spin 1.

$$\begin{pmatrix} 1 & 0 \\ 0 & 1 \end{pmatrix} \otimes \begin{pmatrix} \cos\theta & \sin\theta \\ \sin\theta & -\cos\theta \end{pmatrix} = \begin{pmatrix} \cos\theta & \sin\theta & 0 & 0 \\ \sin\theta & -\cos\theta & 0 & 0 \\ 0 & 0 & \cos\theta & \sin\theta \\ 0 & 0 & \sin\theta & -\cos\theta \end{pmatrix}$$

The following calculation shows that the measurement results are totally random, yielding and an expectation value of 0 for all values of θ.

$$E(\theta) = \frac{1}{\sqrt{2}} \begin{pmatrix} 0 & 1 & -1 & 0 \end{pmatrix} \begin{pmatrix} \cos\theta & \sin\theta & 0 & 0 \\ \sin\theta & -\cos\theta & 0 & 0 \\ 0 & 0 & \cos\theta & \sin\theta \\ 0 & 0 & \sin\theta & -\cos\theta \end{pmatrix} \frac{1}{\sqrt{2}} \begin{pmatrix} 0 \\ 1 \\ -1 \\ 0 \end{pmatrix} \rightarrow 0$$

The same, of course, is true for the measurements on spin 1.

$$\begin{pmatrix} \cos\theta & \sin\theta \\ \sin\theta & -\cos\theta \end{pmatrix} \otimes \begin{pmatrix} 1 & 0 \\ 0 & 1 \end{pmatrix} = \begin{pmatrix} \cos\theta & 0 & \sin\theta & 0 \\ 0 & \cos\theta & 0 & \sin\theta \\ \sin\theta & 0 & -\cos\theta & 0 \\ 0 & \sin\theta & 0 & -\cos\theta \end{pmatrix}$$

$$E(\theta) = \frac{1}{\sqrt{2}} \begin{pmatrix} 0 & 1 & -1 & 0 \end{pmatrix} \begin{pmatrix} \cos\theta & 0 & \sin\theta & 0 \\ 0 & \cos\theta & 0 & \sin\theta \\ \sin\theta & 0 & -\cos\theta & 0 \\ 0 & \sin\theta & 0 & -\cos\theta \end{pmatrix} \frac{1}{\sqrt{2}} \begin{pmatrix} 0 \\ 1 \\ -1 \\ 0 \end{pmatrix} \rightarrow 0$$

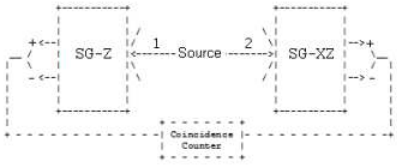
The expectation value calculations can also be performed using the trace function as shown below.

$$\langle\Psi|\hat{O}|\Psi\rangle = \sum_i \langle\Psi|\hat{O}|i\rangle\langle i|\Psi\rangle = \sum_i \langle i|\Psi\rangle\langle\Psi|\hat{O}|i\rangle = Trace\left(|\Psi\rangle\langle\Psi|\hat{O}\right) \text{ where } \sum_i |i\rangle\langle i| = \text{Identity}$$

This page titled 8.49: EPR Analysis for a Composite Singlet Spin System is shared under a CC BY 4.0 license and was authored, remixed, and/or curated by Frank Rioux via source content that was edited to the style and standards of the LibreTexts platform.

8.50: EPR Analysis for a Composite Singlet Spin System - Short Version

A spin-1/2 pair is prepared in an entangled singlet state and the individual particles travel in opposite directions on the y-axis to a pair of Stern-Gerlach detectors which are set up to measure spin in the x-z plane. Particle 1's spin is measured along the z-axis, and particle 2's spin is measured at an angle θ with respect to the z-axis.



For the singlet state the arrows below indicate the spin orientation for any direction in the x-z plane.

$$|\Psi\rangle = \frac{1}{\sqrt{2}}\left[|\uparrow\rangle_1|\downarrow\rangle_2 - |\downarrow\rangle_1|\uparrow\rangle_2\right]$$

$$= \frac{1}{\sqrt{2}}\left[\begin{pmatrix}\cos\left(\frac{\theta}{2}\right)\\ \sin\left(\frac{\theta}{2}\right)\end{pmatrix}_1 \otimes \begin{pmatrix}-\sin\left(\frac{\theta}{2}\right)\\ \cos\left(\frac{\theta}{2}\right)\end{pmatrix}_2 - \begin{pmatrix}-\sin\left(\frac{\theta}{2}\right)\\ \cos\left(\frac{\theta}{2}\right)\end{pmatrix}_1 \otimes \begin{pmatrix}\cos\left(\frac{\theta}{2}\right)\\ \sin\left(\frac{\theta}{2}\right)\end{pmatrix}_2\right] = \frac{1}{\sqrt{2}}\begin{pmatrix}0\\1\\-1\\0\end{pmatrix}$$

The single particle spin operator in the x-z plane is constructed from the Pauli spin operators in the x- and z-directions. φ is the angle of orientation of the measurement magnet with the z-axis.

$$\sigma_z = \begin{pmatrix}1 & 0\\ 0 & -1\end{pmatrix} \quad \sigma_x = \begin{pmatrix}0 & 1\\ 1 & 0\end{pmatrix} \quad S(\theta) = \cos(\theta)\sigma_z + \sin(\theta)\sigma_x \rightarrow \begin{pmatrix}\cos(\theta) & \sin(\theta)\\ \sin(\theta) & -\cos(\theta)\end{pmatrix} \quad S(0) = \begin{pmatrix}1 & 0\\ 0 & -1\end{pmatrix}$$

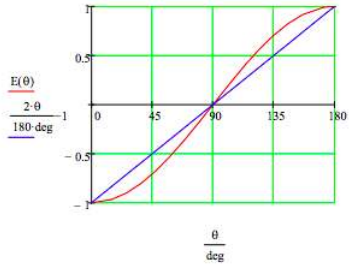
Tensor multiplication of S(0) and S(φ) creates a joint spin measurement operator.

$$\begin{pmatrix}1 & 0\\ 0 & -1\end{pmatrix} \otimes \begin{pmatrix}\cos\theta & \sin\theta\\ \sin\theta & -\cos\theta\end{pmatrix} = \begin{pmatrix}\cos\theta & \sin\theta & 0 & 0\\ \sin\theta & -\cos\theta & 0 & 0\\ 0 & 0 & -\cos\theta & -\sin\theta\\ 0 & 0-\sin\theta & \cos\theta & \end{pmatrix} \frac{1}{\sqrt{2}}\begin{pmatrix}0\\1\\-1\\0\end{pmatrix}$$

The expectation value as a function of the measurement angle of particle 2 is calculated and the result displayed graphically.

$$E(\theta) = \frac{1}{\sqrt{2}}\begin{pmatrix}0 & 1 & -1 & 0\end{pmatrix}\begin{pmatrix}\cos\theta & \sin\theta & 0 & 0\\ \sin\theta & -\cos\theta & 0 & 0\\ 0 & 0 & -\cos\theta & -\sin\theta\\ 0 & 0-\sin\theta & \cos\theta & \end{pmatrix}\frac{1}{\sqrt{2}}\begin{pmatrix}0\\1\\-1\\0\end{pmatrix} \rightarrow -\cos\theta$$

For θ = 0^0 there is perfect anti-correlation; for θ = 180^0 perfect correlation; for θ = 90^0 no correlation. A correlation function based on a local-realistic, hidden-variable model (see Fig. 11.2 and related text in A. I. M. Rae's Quantum Mechanics, 2nd Ed.) and the quantum mechanical correlation function, E(θ), are compared on the graph below. Quantum theory and local realism disagree at all angles except 0, 90 and 180 degrees.

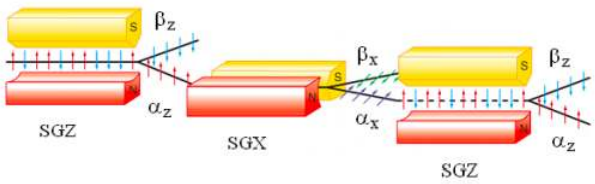


This example illustrates Bell's theorem: no local hidden-variable theory can reproduce all the predictions of quantum mechanics for entangled composite systems. As the quantum predictions are confirmed experimentally, the local hidden-variable approach to reality must be abandoned.

This page titled 8.50: EPR Analysis for a Composite Singlet Spin System - Short Version is shared under a CC BY 4.0 license and was authored, remixed, and/or curated by Frank Rioux via source content that was edited to the style and standards of the LibreTexts platform.

8.51: Analysis of the Stern-Gerlach Experiment

As will be demonstrated in this tutorial, the Stern-Gerlach experiment illustrates several key quantum concepts. The figure shown below is taken from Thomas Engel's text, Quantum Chemistry & Spectroscopy. The figure depicts the behavior of a beam of Na atoms as it interacts with a sequence of three Stern-Gerlach magnets.



We begin with a review of the quantum mechanics of electron spin.

Spin Eigenstates

Spin-up in the z-direction:

$$\sigma_z = \begin{pmatrix} 1 \\ 0 \end{pmatrix}$$

Spin-down in the z-direction:

$$\beta_z = \begin{pmatrix} 0 \\ 1 \end{pmatrix}$$

Spin-up in the x-direction:

$$\sigma_x = \frac{1}{\sqrt{2}} \begin{pmatrix} 1 \\ 1 \end{pmatrix}$$

Spin-down in the x-direction:

$$\beta_x = \frac{1}{\sqrt{2}} \begin{pmatrix} 1 \\ -1 \end{pmatrix}$$

Operators

The matrix operators associated with the two Stern-Gerlach magnets are shown below.

SGZ operator:

$$\mathrm{SGZ} = \begin{pmatrix} 1 & 0 \\ 0 & -1 \end{pmatrix}$$

SGX operator:

$$\mathrm{SGX} = \begin{pmatrix} 0 & 1 \\ 1 & 0 \end{pmatrix}$$

The α_z and β_z spin states are eigenfunctions of the SGZ operator with eigenvalues +1 and -1, respectively:

$$\mathrm{SGZ}\sigma_z = \begin{pmatrix} 1 \\ 0 \end{pmatrix} \quad \sigma_z^T \mathrm{SGZ} \alpha_z^T = 1 \quad \mathrm{SGZ}\beta_z = \begin{pmatrix} 0 \\ -1 \end{pmatrix} \quad \beta_z^T \mathrm{SGZ} \beta_z = -1$$

The α_x and β_x spin states are eigenfunctions of the SGX operator with eigenvalues +1 and -1, respectively:

$$\mathrm{SGX}\sigma_x = \begin{pmatrix} 0.707 \\ 0.707 \end{pmatrix} \quad \sigma_x^T \mathrm{SGX} \alpha_x^T = 1 \quad \mathrm{SGZ}\beta_x = \begin{pmatrix} -0.707 \\ 0.707 \end{pmatrix} \quad \beta_z^T \mathrm{SGX} \beta_x = -1$$

Analysis

Silver atoms are deflected by an inhomogeneous magnetic field because of the two-valued magnetic moment associated with their unpaired 5s electron ([Kr]$5s^1 4d^{10}$). The beam of silver atoms entering the Stern-Gerlach magnet oriented in the z-direction (SGZ) on the left is unpolarized. This means it is a mixture of randomly spin-polarized Ag atoms. As such, it is impossible to write a quantum mechanical wave function for this initial state. The density operator (or matrix), which is a more general quantum mechanical construct, can be used to represent both pure states and mixtures, as shown below.

$$\hat{\rho} = |\Psi\rangle\langle\Psi| \quad \hat{\rho} = \sum p)i|\Psi_i\rangle\langle\Psi_i|$$

In the equation on the right, pi is the fraction of the mixture in the state Ψ_i. The expectation value for a measurement on a pure or mixed state is written as follows in terms of the appropriate density operator.

$$\langle A\rangle = Trace(\hat{\rho}\hat{A})$$

An unpolarized beam can be written as a 50-50 mixture of any of the orthogonal spin eigenstates - α_z and β_z, or α_x and β_x, or α_y and β_y. The density operator for the unpolarized spin beam entering the first SGZ is calculated using α_z and β_z.

$$\rho_{mix} = \frac{1}{2}\begin{pmatrix}1\\0\end{pmatrix}(1 \quad 0) + \frac{1}{2}\begin{pmatrix}0\\1\end{pmatrix}(0 \quad 1) = \begin{pmatrix}0.5 & 0\\0 & 0.5\end{pmatrix}$$

The expectation value for passage through the SGZ magnet is 0, indicating equal amounts of Ag atoms in the spin-up and spin-down exit channels.

$$\mathrm{tr}(\rho_{mix}\mathrm{SGZ}) = 0$$

The α_z beam emerging from SGZ is directed to the SGX magnet and the αx beam emerging from it is directed to another SGZ magnet. Before the second SGZ it might be assumed that the Ag atoms in the beam are in the electronic spin state $|\alpha_z\rangle|\alpha_x\rangle$, in other words after the SGZ and SGX magnets the Ag 5s electrons have well-defined values for spin in both the z- and x-directions. The vector representing this state is written in tensor format.

$$I = \begin{pmatrix}1 & 0\\0 & 1\end{pmatrix} \quad \Psi^T\mathrm{kronecker(SGZ,\ I)}\Psi = 1 \quad \mathrm{kronecker(SGZ,\ I)}\Psi = \begin{pmatrix}0.707\\0.707\\0\\0\end{pmatrix}$$

However, the actual experiment illustrated above shows that the expectation value is 0, with equal numbers of silver atoms emerging in α_z and β_z channels.

The correct quantum mechanical interpretation is that the SGZ and SGX operators do not commute, meaning that they cannot have simultaneous eigenstates.

$$\mathrm{SGX\ SGZ} - \mathrm{SGZ\ SGX} = \begin{pmatrix}0 & -2\\2 & 0\end{pmatrix}$$

The Ag spin state entering the second SGZ magnet is α_x, an eigenstate of the SGX operator, not simultaneously an eigenstate of SGZ and SGX. It can be written as a superposition of α_z and β_z.

$$\alpha_x = \tfrac{1}{\sqrt{2}}(\alpha_z + \beta_z) \quad \tfrac{1}{\sqrt{2}}\left[\begin{pmatrix}1\\0\end{pmatrix} + \begin{pmatrix}0\\1\end{pmatrix}\right] = \begin{pmatrix}0.707\\0.707\end{pmatrix}$$

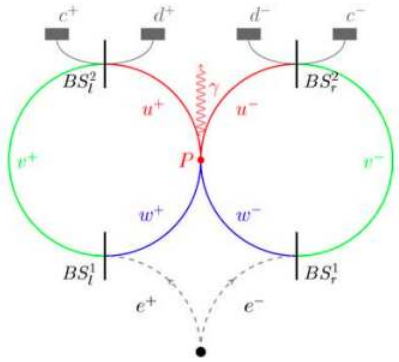
Quantu theory predicts that the exit channels of the second SGZ magnet will be equally populated with Ag atoms.

This page titled 8.51: Analysis of the Stern-Gerlach Experiment is shared under a CC BY 4.0 license and was authored, remixed, and/or curated by Frank Rioux via source content that was edited to the style and standards of the LibreTexts platform.

8.52: Hardy's Paradox

Hardy's paradox is based on analysis of the double Mach-Zehnder interferometer shown below. A positron enters one interferometer and an electron the other. One arm of each interferometer intersect allowing for electron-positron interaction.

In the subsequent quantum mechanical analysis it will be shown that the paradox in Hardy's thought experiment is that it shows that the electron and positron have some probability of interacting without annihilation occurring.



There are two 50-50 beam splitters in each interferometer. The probability amplitude for transmission is $\frac{1}{\sqrt{2}}$ and for reflection it is $\frac{i}{\sqrt{2}}$. By convention a 90 degree phase shift is assigned to reflection at the beam splitters.

Initially we ignore interaction at the intersection between the two interferometers. The initial state is |p>|e> represented by pe in Mathcad syntax - p represents the positron and e the electron. The rest of the terms are self-explanatory.

The evolution of the initial state is calculated below and we see that in the absence of interaction in the intersecting arms of the interferometers the electron and positron will be registered at their c-detectors. Recall that we calculate a probability amplitude and its absolute square gives the probability ($|-1|^2 = 1$).

$$p\ e \left| \begin{array}{l} \text{substitute, e} = \frac{1}{\sqrt{2}}(v_e + iw_e) \\ \text{substitute, p} = \frac{1}{\sqrt{2}}(v_p + iw_p) \\ \text{substitute, } v_p = \frac{1}{\sqrt{2}}(ic_p + d_p) \\ \text{substitute, } w_p = \frac{1}{\sqrt{2}}(c_p + id_p) \\ \text{substitute, } w_e = \frac{1}{\sqrt{2}}(c_e + id_e) \\ \text{substitute, } v_e = \frac{1}{\sqrt{2}}(ic_e + d_e) \end{array} \right.$$

Now we look at the situation immediately after the first set of beam splitters and explore the implication of interaction, or in this case electron-positron annihilation.

$$p\ e \left| \begin{array}{l} \text{substitute, e} = \frac{1}{\sqrt{2}}(v_e + iw_e) \\ \text{substitute, p} = \frac{1}{\sqrt{2}}(v_p + iw_p) \end{array} \right. \rightarrow \frac{v_e v_p}{2} + \frac{v_p w_e i}{2} - \frac{w_e w_p}{2} + \frac{v_e w_p i}{2}$$

The term $w_e w_p$ gives the probability (25%) that the electron and positron will be in the intersecting arms of the interferometers and annihilate each other. Annihilation removes that amplitude term from further evolution. Replacing it with the symbol γ and calculating what happens at the second set of beam splitters yields the following result.

$$p\ e \left| \begin{array}{l} \text{substitute, } v_p = \frac{1}{\sqrt{2}}(ic_p + d_p) \\ \text{substitute, } w_p = \frac{1}{\sqrt{2}}(c_p + id_p) \\ \text{substitute, } w_e = \frac{1}{\sqrt{2}}(c_e + id_e) \\ \text{substitute, } v_e = \frac{1}{\sqrt{2}}(ic_e + d_e) \end{array} \right. \rightarrow -\frac{\gamma}{2} - \frac{3c_e c_p}{4} + \frac{c_p d_e i}{4} - \frac{d_e d_p}{4} + \frac{c_e d_p i}{4}$$

This calculation reveals the paradox. Earlier it was shown that in the absence of interaction ce and cp should fire simultaneously 100% of the time. Now, with interaction/annihilation, that drops to a probability of 9/16 and a photon detected 25% of the time.

The bizarre part of the quantum mechanical calculation is in the next to the last term ($d_e d_p/4$) above. For both d detectors to fire requires the amplitude before the second set of beam splitters to be $w_e w_p$, as shown by the next to the last term on the right below.

$$\frac{1}{2} w_e w_p \left| \begin{array}{l} \text{substitute, } w_e = \frac{1}{\sqrt{2}}(c_e + i d_e) \\ \text{substitute, } w_p = \frac{1}{\sqrt{2}}(c_p + i d_p) \end{array} \right. \rightarrow -\frac{c_e c_p}{4} + \frac{c_p d_e i}{4} - \frac{d_e d_p}{4} + \frac{c_e d_p i}{4}$$

But this amplitude should lead to annihilation. So quantum theory appears to permit a positron/electron interaction that does not lead to annihilation with a probability of 1/16.

The Appendix shows how to carry out the analysis using tensor algebra.

Appendix

The motion of the positron and electron to the left and right is represented by the following orthonormal vectors.

$$L = \begin{pmatrix} 1 \\ 0 \end{pmatrix} \quad R = \begin{pmatrix} 0 \\ 1 \end{pmatrix}$$

Initially the positron moves to the left and the electron to the right, giving the following initial state in tensor format.

$$\mathrm{p\ e} = \begin{pmatrix} 1 \\ 0 \end{pmatrix} \begin{pmatrix} 0 \\ 1 \end{pmatrix} = \begin{pmatrix} 0 \\ 1 \\ 0 \\ 0 \end{pmatrix}$$

The beam splitters and mirrors are represented by 2x2 matrices. The mirrors are implied in the above figure by the change in direction between the two beam splitters.

Beam splitter:

$$\mathrm{BS} = \frac{1}{\sqrt{2}} \begin{pmatrix} 1 & i \\ i & 1 \end{pmatrix}$$

Mirror:

$$\mathrm{M} = \begin{pmatrix} 0 & 1 \\ 1 & 0 \end{pmatrix}$$

The four output states are calculated in tensor format using motional basis vectors, |L> and |R>.

$$c_p d_e = \begin{pmatrix} 1 \\ 0 \end{pmatrix} \begin{pmatrix} 1 \\ 0 \end{pmatrix} = \begin{pmatrix} 1 \\ 0 \\ 0 \\ 0 \end{pmatrix} \quad c_p c_e = \begin{pmatrix} 1 \\ 0 \end{pmatrix} \begin{pmatrix} 0 \\ 1 \end{pmatrix} = \begin{pmatrix} 0 \\ 1 \\ 0 \\ 0 \end{pmatrix} \quad d_p d_e = \begin{pmatrix} 0 \\ 1 \end{pmatrix} \begin{pmatrix} 1 \\ 0 \end{pmatrix} = \begin{pmatrix} 0 \\ 0 \\ 1 \\ 0 \end{pmatrix} \quad d_p c_e = \begin{pmatrix} 0 \\ 1 \end{pmatrix} \begin{pmatrix} 0 \\ 1 \end{pmatrix} = \begin{pmatrix} 0 \\ 0 \\ 0 \\ 1 \end{pmatrix}$$

The operator representing the dual Mach-Zehnder interferometers is constructed by tensor multiplication of BS and M matrix operators.

$$\mathrm{DMZ} = \mathrm{kronecker(BS,\ BS)\ kronecker(M,\ M)\ kronecker(BS,\ BS)}$$

The following calculations show that, in the absence of positron-electron interaction only the c-detectors fire simultaneously.

$$\left[\left|(1 \quad 0 \quad 0 \quad 0)\,\mathrm{DMZ}\begin{pmatrix}0\\1\\0\\0\end{pmatrix}\right|\right]^2 = 0 \qquad \left[\left|(0 \quad 1 \quad 0 \quad 0)\,\mathrm{DMZ}\begin{pmatrix}0\\1\\0\\0\end{pmatrix}\right|\right]^2 = 1$$

$$\left[\left|(0 \quad 0 \quad 1 \quad 0)\,\mathrm{DMZ}\begin{pmatrix}0\\1\\0\\0\end{pmatrix}\right|\right]^2 = 0 \qquad \left[\left|(0 \quad 0 \quad 0 \quad 1)\,\mathrm{DMZ}\begin{pmatrix}0\\1\\0\\0\end{pmatrix}\right|\right]^2 = 0$$

To complete the analysis in tensor format we look at the p-e state immediately after the first set of beam splitters.

$$\mathrm{kronecker(BS,\ BS)}\begin{pmatrix}0\\1\\0\\0\end{pmatrix} = \begin{pmatrix}0.5i\\0.5\\-0.5\\0.5i\end{pmatrix}$$

$$\frac{1}{2}\left[\begin{pmatrix}1\\0\end{pmatrix}\begin{pmatrix}i\\0\end{pmatrix} + \begin{pmatrix}1\\0\end{pmatrix}\begin{pmatrix}0\\1\end{pmatrix} + \begin{pmatrix}0\\i\end{pmatrix}\begin{pmatrix}i\\0\end{pmatrix} + \begin{pmatrix}0\\i\end{pmatrix}\begin{pmatrix}0\\1\end{pmatrix}\right]$$
$$= \frac{1}{2}\left[\begin{pmatrix}i\\0\\0\\0\end{pmatrix} + \begin{pmatrix}0\\1\\0\\0\end{pmatrix} - \begin{pmatrix}0\\0\\1\\0\end{pmatrix} + \begin{pmatrix}0\\0\\0\\i\end{pmatrix}\right] = \frac{1}{2}\begin{pmatrix}i\\1\\-1\\i\end{pmatrix}$$

The third position on the product vector is the probability amplitude that the positron is in the right arm of its interferometer and that the electron is in the left arm of its interferometer - the w arms in the figure above. If the positron-electron pair interact annihilation occurs and a photon is produced. That term, therefore, is set to zero and the state used for the remaining evolution is,

$$\frac{1}{2}\begin{pmatrix}i\\1\\0\\i\end{pmatrix}$$

This state interacts with the remaining mirrors and beam splitters.

$$\mathrm{BSM} = \mathrm{kronecker(BS,\ BS)\ kronecker(M,\ M)}$$

The following output probability calculations are in exact agreement with the earlier calculations.

$$\left[\left|(1 \quad 0 \quad 0 \quad 0)\,\mathrm{BSM}\tfrac{1}{2}\begin{pmatrix}i\\1\\0\\i\end{pmatrix}\right|\right]^2 = 0.0625 \qquad \left[\left|(0 \quad 1 \quad 0 \quad 0)\,\mathrm{BSM}\tfrac{1}{2}\begin{pmatrix}i\\1\\0\\i\end{pmatrix}\right|\right]^2 = 0.5625$$

$$\left[\left|(0 \quad 0 \quad 1 \quad 0)\,\mathrm{BSM}\tfrac{1}{2}\begin{pmatrix}i\\1\\0\\i\end{pmatrix}\right|\right]^2 = 0.0625 \qquad \left[\left|(0 \quad 0 \quad 0 \quad 1)\,\mathrm{BSM}\tfrac{1}{2}\begin{pmatrix}i\\1\\0\\i\end{pmatrix}\right|\right]^2 = 0.0625$$

This page titled 8.52: Hardy's Paradox is shared under a CC BY 4.0 license and was authored, remixed, and/or curated by Frank Rioux via source content that was edited to the style and standards of the LibreTexts platform.

8.53: Bell State Exercises

The Bell states are maximally entangled superpositions of two-particle states. Consider two spin-1/2 particles created in the same event. There are four maximally entangled wave functions representing their collective spin states. Each particle has two possible spin orientations and therefore the composite state is represented by a 4-vector in a four-dimensional Hilbert space.

$$|\Phi_p\rangle = \tfrac{1}{\sqrt{2}}\left[|\uparrow_1\rangle|\uparrow_2\rangle + |\downarrow_1\rangle|\downarrow_2\rangle\right] = \tfrac{1}{\sqrt{2}}\left[\begin{pmatrix}1\\0\end{pmatrix}\otimes\begin{pmatrix}1\\0\end{pmatrix} + \begin{pmatrix}0\\1\end{pmatrix}\otimes\begin{pmatrix}0\\1\end{pmatrix}\right] = \tfrac{1}{\sqrt{2}}\begin{pmatrix}1\\0\\0\\1\end{pmatrix} \qquad \Phi_p = \tfrac{1}{\sqrt{2}}\begin{pmatrix}1\\0\\0\\1\end{pmatrix}$$

$$|\Phi_m\rangle = \tfrac{1}{\sqrt{2}}\left[|\uparrow_1\rangle|\uparrow_2\rangle - |\downarrow_1\rangle|\downarrow_2\rangle\right] \qquad \Phi_p = \tfrac{1}{\sqrt{2}}\begin{pmatrix}1\\0\\0\\-1\end{pmatrix}$$

$$= \tfrac{1}{\sqrt{2}}\left[\begin{pmatrix}1\\0\end{pmatrix}\otimes\begin{pmatrix}1\\0\end{pmatrix} - \begin{pmatrix}0\\1\end{pmatrix}\otimes\begin{pmatrix}0\\1\end{pmatrix}\right] = \tfrac{1}{\sqrt{2}}\begin{pmatrix}1\\0\\0\\-1\end{pmatrix}$$

$$|\Psi_p\rangle = \tfrac{1}{\sqrt{2}}\left[|\uparrow_1\rangle|\downarrow_2\rangle + |\downarrow_1\rangle|\uparrow_2\rangle\right] = \tfrac{1}{\sqrt{2}}\left[\begin{pmatrix}1\\0\end{pmatrix}\otimes\begin{pmatrix}0\\1\end{pmatrix} + \begin{pmatrix}0\\1\end{pmatrix}\otimes\begin{pmatrix}1\\0\end{pmatrix}\right] = \tfrac{1}{\sqrt{2}}\begin{pmatrix}0\\1\\1\\0\end{pmatrix} \qquad \Phi_p = \tfrac{1}{\sqrt{2}}\begin{pmatrix}0\\1\\1\\0\end{pmatrix}$$

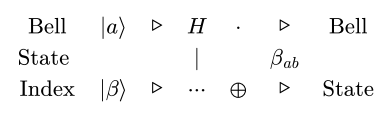
$$|\Psi_m\rangle = \tfrac{1}{\sqrt{2}}\left[|\uparrow_1\rangle|\downarrow_2\rangle - |\downarrow_1\rangle|\uparrow_2\rangle\right] \qquad \Phi_p = \tfrac{1}{\sqrt{2}}\begin{pmatrix}0\\1\\-1\\0\end{pmatrix}$$

$$= \tfrac{1}{\sqrt{2}}\left[\begin{pmatrix}1\\0\end{pmatrix}\otimes\begin{pmatrix}0\\1\end{pmatrix} - \begin{pmatrix}0\\1\end{pmatrix}\otimes\begin{pmatrix}1\\0\end{pmatrix}\right] = \tfrac{1}{\sqrt{2}}\begin{pmatrix}0\\1\\-1\\0\end{pmatrix}$$

The wave functions are not separable and consequently the entangled particles represented by these wave functions do not have separate identities or individual properties, they behave like a single entity. Individually the spins don't have a definite polarization, yet there is a definite spin orientation relationship between them. For example, if the spin orientation of particle 1 is learned through measurement, the spin orientation of particle 2 is also immediately known no matter how far away it may be. (The Appendix shows how such measurements destroy entanglement, forcing both particles into well-defined spin states.) Entanglement implies nonlocal phenomena which in the words of Nick Herbert are "unmediated, unmitigated and immediate."

The Bell states can be generated from two classical bits with the use of a quantum circuit involving a **Hadamard (H) gate**, the identity (I) and a controlled-not gate (CNOT) as shown below. The H gate operates on the top bit creating a superposition which controls the operation of the CNOT gate. The classical state on the left also serves as an index for the Bell state created from it: 0, 1, 2, 3. Kronecker, as discussed below, is Mathcad's command for matrix tensor multiplication.

$$H = \tfrac{1}{\sqrt{2}}\begin{pmatrix}1 & 1\\1 & -1\end{pmatrix} \qquad I = \begin{pmatrix}1 & 0\\0 & 1\end{pmatrix} \qquad \text{CNOT} = \begin{pmatrix}1 & 0 & 0 & 0\\0 & 1 & 0 & 0\\0 & 0 & 0 & 1\\0 & 0 & 1 & 0\end{pmatrix}$$



Bell state generator:

$$\text{BSG} = \text{CNOT kronecker(H, I)}$$

$$\text{Index} = 0 \qquad \text{Index} = 1$$

$$\begin{pmatrix}1\\0\end{pmatrix}\begin{pmatrix}1\\0\end{pmatrix} = \begin{pmatrix}1\\0\\0\\0\end{pmatrix} \quad \text{BSG}\begin{pmatrix}1\\0\\0\\0\end{pmatrix} = \begin{pmatrix}0.707\\0\\0\\0.707\end{pmatrix} \qquad \begin{pmatrix}1\\0\end{pmatrix}\begin{pmatrix}0\\1\end{pmatrix} = \begin{pmatrix}0\\1\\0\\0\end{pmatrix} \quad \text{BSG}\begin{pmatrix}0\\1\\0\\0\end{pmatrix} = \begin{pmatrix}0\\0.707\\0.707\\0\end{pmatrix}$$

$$\text{Index} = 2 \qquad \text{Index} = 3$$

$$\begin{pmatrix}0\\1\end{pmatrix}\begin{pmatrix}1\\0\end{pmatrix} = \begin{pmatrix}0\\0\\1\\0\end{pmatrix} \quad \text{BSG}\begin{pmatrix}0\\0\\1\\0\end{pmatrix} = \begin{pmatrix}0.707\\0\\0\\-0.707\end{pmatrix} \qquad \begin{pmatrix}1\\0\end{pmatrix}\begin{pmatrix}0\\1\end{pmatrix} = \begin{pmatrix}0\\1\\0\\0\end{pmatrix} \quad \text{BSG}\begin{pmatrix}0\\0\\0\\1\end{pmatrix} = \begin{pmatrix}0\\0.707\\-0.707\\0\end{pmatrix}$$

It is not surprising that a Bell state measurement (BSM) is just the reverse of this process.

$$\begin{array}{ccccccc} \text{Bell} & \triangleright & \cdot & H & \triangleright & |a\rangle & \text{Bell} \\ \beta_{ab} & & | & & & & \text{State} \\ \text{State} & \triangleright & \oplus & \cdots & \triangleright & |b\rangle & \text{Index} \end{array}$$

$$\text{BSM} = \text{BSG}^{-1}$$

$$\text{BSM}\begin{pmatrix}0.707\\0\\0\\0.707\end{pmatrix} = \begin{pmatrix}1\\0\\0\\0\end{pmatrix} \quad \text{BSM}\begin{pmatrix}0\\0.707\\0.707\\0\end{pmatrix} = \begin{pmatrix}0\\1\\0\\0\end{pmatrix} \quad \text{BSM}\begin{pmatrix}0.707\\0\\0\\-0.707\end{pmatrix} \quad \text{BSM}\begin{pmatrix}0\\0.707\\-0.707\\0\end{pmatrix} = \begin{pmatrix}0\\0\\0\\1\end{pmatrix}$$

$$= \begin{pmatrix}0\\0\\1\\0\end{pmatrix}$$

We will now explore some of the characteristics of the Bell states through a variety of calculations. First we list the spin eigenfunctions in the Cartesian directions.

$$\text{Szu} = \begin{pmatrix}1\\0\end{pmatrix} \quad \text{Szd} = \begin{pmatrix}0\\1\end{pmatrix} \quad \text{Sxu} = \frac{1}{\sqrt{2}}\begin{pmatrix}1\\1\end{pmatrix} \quad \text{Sxd} = \frac{1}{\sqrt{2}}\begin{pmatrix}-1\\1\end{pmatrix} \quad \text{Syu} = \frac{1}{\sqrt{2}}\begin{pmatrix}1\\i\end{pmatrix} \quad \text{Syd} = \frac{1}{\sqrt{2}}\begin{pmatrix}1\\-i\end{pmatrix}$$

Working in units of h/4π we can use the Pauli matrices to represent the spin operators in the Cartesian directions. We will also need the identity operator from above.

$$\sigma_x = \begin{pmatrix}0 & 1\\1 & 0\end{pmatrix} \quad \sigma_y = \begin{pmatrix}0 & -i\\i & 0\end{pmatrix} \quad \sigma_z = \begin{pmatrix}1 & 0\\0 & -1\end{pmatrix}$$

Composite two-particle operators are constructed using matrix tensor multiplication implemented with Mathcad's kronecker command.

$$\text{SxSx} = \text{kroncker}(\sigma_x,\ \sigma_x) \quad \text{SySy} = \text{kronecker}(\sigma_y,\ \sigma_y) \quad \text{SzSz} = \text{kroncker}(\sigma_z,\ \sigma_z)$$

The following matrix demonstrates that the Bell states are an orthonormal basis set.

$$\begin{pmatrix}\Phi_p^T\Phi_p & \Phi_p^T\Phi_m & \Phi_p^T\Psi_p & \Phi_p^T\Psi_m\\ \Phi_m^T\Phi_p & \Phi_m^T\Phi_m & \Phi_m^T\Psi_p & \Phi_m^T\Psi_m\\ \Psi_p^T\Phi_p & \Psi_p^T\Phi_m & \Psi_p^T\Psi_p & \Psi_p^T\Psi_m\\ \Psi_m^T\Phi_p & \Psi_m^T\Phi_m & \Psi_m^T\Psi_p & \Psi_m^T\Psi_m\end{pmatrix} = \begin{pmatrix}1 & 0 & 0 & 0\\0 & 1 & 0 & 0\\0 & 0 & 1 & 0\\0 & 0 & 0 & 1\end{pmatrix}$$

In the interest of brevity, the main quantum properties of the Bell states will be illustrated using the spin operator in the z-direction. Calculations involving the x- and y-spin operators can be found in the appendix.

The Bell states are eigenfunctions of the $\sigma_z\sigma_z$, $\sigma_x\sigma_x$ and $\sigma_y\sigma_y$ spin operators.

Illegal pream-token (&)

Calculations of the expectation values yield consistent results.

$$\Phi_p^T SzSz\Phi_p = 1 \quad \Phi_m^T SzSz\Phi_m = 1 \quad \Psi_p^T SzSz\Psi_p = -1 \quad \Psi_m^T SzSz\Psi_m = 1$$
$$\Phi_p^T SxSx\Phi_p = 1 \quad \Phi_m^T SxSx\Phi_m = -1 \quad \Psi_p^T SxSx\Psi_p = 1 \quad \Psi_m^T SxSx\Psi_m = -1$$
$$\Phi_p^T SySy\Phi_p = -1 \quad \Phi_m^T SySy\Phi_m = 1 \quad \Psi_p^T SySy\Psi_p = -1 \quad \Psi_m^T SySy\Psi_m = 1$$

We see that for the composite measurements in the z-basis the Φ Bell states exhibit perfect correlation, while the Ψ states show perfect anti-correlation. In the x-basis, the p states show perfect correlation and the m states show perfect anti-correlation.

This correlation is striking when you consider that the individual spin measurements on particles 1 and 2 are completely random giving expectation values of zero, as the following calculations show.

$$\Phi_p^T \text{kronecker}(\sigma_z,\ I)\Phi_p = 0 \quad \Phi_p^T \text{kronecker}(I,\ \sigma_z)\Phi_p = 0$$
$$\Phi_m^T \text{kronecker}(\sigma_z,\ I)\Phi_m = 0 \quad \Phi_m^T \text{kronecker}(I,\ \sigma_z)\Phi_m = 0$$
$$\Psi_p^T \text{kronecker}(\sigma_z,\ I)\Phi_p = 0 \quad \Psi_p^T \text{kronecker}(I,\ \sigma_z)\Psi_p = 0$$
$$\Psi_m^T \text{kronecker}(\sigma_z,\ I)\Psi_m = 0 \quad \Psi_m^T \text{kronecker}(I,\ \sigma_z)\Psi_m = 0$$

Individually the particles appear to behave like classical mixtures, but collectively they exhibit quantum correlations. We will now look at this issue from another perspective. First the density operators (|Ψ><Ψ|) are calculated for each of the Bell states. (See the Appendix for a graphical representation of the density matrices.

$$\Phi_p\Phi_p^T = \begin{pmatrix} 0.5 & 0 & 0 & 0.5 \\ 0 & 0 & 0 & 0 \\ 0 & 0 & 0 & 0 \\ 0.5 & 0 & 0 & 0.5 \end{pmatrix} \quad \Phi_m\Phi_m^T = \begin{pmatrix} 0.5 & 0 & 0 & -0.5 \\ 0 & 0 & 0 & 0 \\ 0 & 0 & 0 & 0 \\ -0.5 & 0 & 0 & 0.5 \end{pmatrix}$$
$$\Psi_p\Psi_p^T = \begin{pmatrix} 0 & 0 & 0 & 0 \\ 0 & 0.5 & 0.5 & 0 \\ 0 & 0.5 & 0.5 & 0 \\ 0 & 0 & 0 & 0 \end{pmatrix} \quad \Psi_m\Psi_m^T = \begin{pmatrix} 0 & 0 & 0 & 0 \\ 0 & 0.5 & -0.5 & 0 \\ 0 & -0.5 & 0.5 & 0 \\ 0 & 0 & 0 & 0 \end{pmatrix}$$

We also demonstrate that the Bell states are pure states by showing that (|Ψ><Ψ|)^2 = |Ψ><Ψ|.

$$\left(\Phi_p\Phi_p^T\right)^2 = \begin{pmatrix} 0.5 & 0 & 0 & 0.5 \\ 0 & 0 & 0 & 0 \\ 0 & 0 & 0 & 0 \\ 0.5 & 0 & 0 & 0.5 \end{pmatrix} \quad \left(\Phi_m\Phi_m^T\right)^2 = \begin{pmatrix} 0.5 & 0 & 0 & -0.5 \\ 0 & 0 & 0 & 0 \\ 0 & 0 & 0 & 0 \\ -0.5 & 0 & 0 & 0.5 \end{pmatrix}$$
$$\left(\Psi_p\Psi_p^T\right)^2 = \begin{pmatrix} 0 & 0 & 0 & 0 \\ 0 & 0.5 & 0.5 & 0 \\ 0 & 0.5 & 0.5 & 0 \\ 0 & 0 & 0 & 0 \end{pmatrix} \quad \left(\Psi_m\Psi_m^T\right)^2 = \begin{pmatrix} 0 & 0 & 0 & 0 \\ 0 & 0.5 & -0.5 & 0 \\ 0 & -0.5 & 0.5 & 0 \\ 0 & 0 & 0 & 0 \end{pmatrix}$$

The existence of off-diagonal elements in these matrix operators is the quantum signature of an entangled superposition. We concentrate on the |Φ$_m$><Φ$_m$| density operator which is shown below. The following analysis is adapted from AJP 77, 244-252 (2009).

$$|\Phi_m\rangle\langle\Phi_m| = \frac{1}{2}\left[|\uparrow_1\rangle \otimes |\uparrow_2\rangle - |\downarrow_1\rangle \otimes |\downarrow_2\rangle\right]\left[\langle\uparrow_2| \otimes \langle\uparrow_1| - \langle\downarrow_2| \otimes \langle\downarrow_1|\right]$$

In expanding this expression we will make use of identities like the following, which rearranges 1221 terms as 1122 terms.

$$|\uparrow_1\rangle\otimes|\uparrow_2\rangle\langle\downarrow_2| \otimes \langle\downarrow_1| = |\uparrow_1\rangle\langle\downarrow_1| \otimes |\uparrow_2\rangle\langle\downarrow_2|$$

$$|\Phi_m\rangle\langle\Phi_m|$$
$$= \frac{1}{2}\left[|\uparrow_1\rangle\langle\uparrow_1| \otimes |\uparrow_2\rangle\langle\uparrow_2| - |\uparrow_1\langle\downarrow_1| \otimes |\uparrow_2\rangle\langle\downarrow_2| - |\downarrow_1\rangle\langle\uparrow_1| \otimes |\downarrow_2\rangle\langle\uparrow_2| + |\downarrow_1\rangle\langle\downarrow_1| \otimes |\downarrow_2\rangle\langle\downarrow_2|\right]$$

To establish the validity of this arrangement we can recalculate |Φ$_m$><Φ$_m$|.

$$\frac{1}{2}\begin{bmatrix} \text{kronecker}\left[\begin{pmatrix}1\\0\end{pmatrix}(1\quad 0),\begin{pmatrix}1\\0\end{pmatrix}(1\quad 0)\right]-\text{kronecker}\left[\begin{pmatrix}1\\0\end{pmatrix}(0\quad 1),\begin{pmatrix}1\\0\end{pmatrix}(0\quad 1)\right]\cdots \\ +\text{-kronecker}\left[\begin{pmatrix}0\\1\end{pmatrix}(1\quad 0),\begin{pmatrix}0\\1\end{pmatrix}(1\quad 0)\right]+\text{kronecker}\left[\begin{pmatrix}0\\1\end{pmatrix}(0\quad 1),\begin{pmatrix}0\\1\end{pmatrix}(0\quad 1)\right] \end{bmatrix}$$
$$=\begin{pmatrix} 0.5 & 0 & 0 & -0.5 \\ 0 & 0 & 0 & 0 \\ 0 & 0 & 0 & 0 \\ -0.5 & 0 & 0 & 0.5 \end{pmatrix}$$

The reason for writing $|\Phi_m><\Phi_m|$ in this form is that it facilitates the calculation of the reduced density operator for particle 1 by "tracing" over the contribution of particle 2, or vice versa. (See the Appendix for a more transparent and thorough presentation of the partial trace.) Here we do the former and see that particle 1's "reduced or local" state operator is diagonal indicating a classical mixed state. This result is consistent with the random behavior observed earlier for the expectation values for the individual particles.

$$\frac{1}{2}\begin{bmatrix} \begin{pmatrix}1\\0\end{pmatrix}(1\quad 0)\,\text{tr}\left[\begin{pmatrix}1\\0\end{pmatrix}(1\quad 0)\right]-\begin{pmatrix}1\\0\end{pmatrix}(0\quad 1)\,\text{tr}\left[\begin{pmatrix}1\\0\end{pmatrix}(0\quad 1)\right]\cdots \\ +-\left[\begin{pmatrix}0\\1\end{pmatrix}(1\quad 0)\right]\text{tr}\left[\begin{pmatrix}0\\1\end{pmatrix}(1\quad 0)\right]+\begin{pmatrix}0\\1\end{pmatrix}(0\quad 1)\,\text{tr}\left[\begin{pmatrix}0\\1\end{pmatrix}(0\quad 1)\right] \end{bmatrix}=\begin{pmatrix}0.5 & 0\\ 0 & 0.5\end{pmatrix}$$

Naturally the same is true if we trace over the contribution of particle 1 to obtain the local state operator of particle 2.

$$\frac{1}{2}\begin{bmatrix} \text{tr}\left[\begin{pmatrix}1\\0\end{pmatrix}(1\quad 0)\right]\left[\begin{pmatrix}1\\0\end{pmatrix}(1\quad 0)\right]-\text{tr}\left[\begin{pmatrix}1\\0\end{pmatrix}(0\quad 1)\right]\left[\begin{pmatrix}1\\0\end{pmatrix}(0\quad 1)\right]\cdots \\ +-\text{tr}\left[\begin{pmatrix}0\\1\end{pmatrix}(1\quad 0)\right]\left[\begin{pmatrix}0\\1\end{pmatrix}(1\quad 0)\right]+\text{tr}\left[\begin{pmatrix}0\\1\end{pmatrix}(0\quad 1)\right]\left[\begin{pmatrix}0\\1\end{pmatrix}(0\quad 1)\right] \end{bmatrix}=\begin{pmatrix}0.5 & 0\\ 0 & 0.5\end{pmatrix}$$

That these local density operators represent mixed states is further demonstrated by showing that for each the trace of the square of density operator is less than 1. The Bell states are pure (see above) because for them the trace of the square of the density operator equals 1.

$$\text{tr}\left[\begin{pmatrix}0.5 & 0\\ 0 & 0.5\end{pmatrix}^2\right]=0.5\quad\begin{pmatrix}\text{tr}\left(\Phi_p\Phi_p^T\right)^2 & \text{tr}\left(\Phi_m\Phi_m^T\right)^2 & \text{tr}\left(\Psi_p\Psi_p^T\right)^2 & \text{tr}\left(\Phi_m\Psi_m^T\right)^2\end{pmatrix}=(1\quad 1\quad 1\quad 1)$$

These calculations, like the previous ones, also establish that while the composite system is a coherent quantum superposition and pure state, the subsystems of the Bell state, spins 1 and 2, exhibit the classical statistical behavior of mixtures. The quantum correlations of the entangled superposition are only apparent when the measurement results on the individual spins are compared side by side.

Appendix

The following table summarizes the expectation value calculations for all three spin operators.

$$\begin{pmatrix} \Phi_p^T SxSx\Phi_p & \Phi_p^T SySy\Phi_p & \Phi_p^T SzSz\Phi_p \\ \Phi_m^T SxSx\Phi_m & \Phi_m^T SySy\Phi_m & \Phi_m^T SzSz\Phi_m \\ \Psi_p^T SxSx\Psi_p & \Psi_p^T SySy\Psi_p & \Psi_p^T SzSz\Psi_p \\ \Psi_m^T SxSx\Psi_m & \Psi_m^T SySy\Psi_m & \Psi_m^T SzSz\Psi_m \end{pmatrix}=\begin{pmatrix} 1 & -1 & 1 \\ -1 & 1 & 1 \\ 1 & 1 & -1 \\ -1 & -1 & -1 \end{pmatrix}$$

This calculation can also be performed by tracing over the product of the density operator and the appropriate spin operator.

$$\langle\Psi|\hat{A}|\Psi\rangle=\sum_a\langle\Psi|\hat{A}|a\rangle\langle a|\Psi\rangle=\sum_a\langle a|\Psi\rangle\langle\Psi|\hat{A}|a\rangle=Tr\left(|\Psi\rangle\langle\Psi|\hat{A}\right)$$

$$\begin{pmatrix} \text{tr}\left(\Phi_p\Phi_p^T SxSx\right) & \text{tr}\left(\Phi_p\Phi_p^T SySy\right) & \text{tr}\left(\Phi_p\Phi_p^T SzSz\right) \\ \text{tr}\left(\Phi_m\Phi_m^T SxSx\right) & \text{tr}\left(\Phi_m\Phi_m^T SySy\right) & \text{tr}\left(\Phi_m\Phi_m^T SzSz\right) \\ \text{tr}\left(\Psi_p\Psi_p^T SxSx\right) & \text{tr}\left(\Psi_p\Psi_p^T SySy\right) & \text{tr}\left(\Psi_p\Psi_p^T SzSz\right) \\ \text{tr}\left(\Psi_m\Psi_m^T SxSx\right) & \text{tr}\left(\Psi_m\Psi_m^T SySy\right) & \text{tr}\left(\Psi_m\Psi_m^T SzSz\right) \end{pmatrix}=\begin{pmatrix} 1 & -1 & 1 \\ -1 & 1 & 1 \\ 1 & 1 & -1 \\ -1 & -1 & -1 \end{pmatrix}$$

It is clear from these results that the Bell states are eigenvectors of the total spin-spin operator.

$$H = \text{kronecker}\left(\sigma_x,\ \sigma_x\right) + \text{kronecker}\left(\sigma_y,\ \sigma_y\right) + \text{kronecker}\left(\sigma_z,\ \sigma_z\right) \quad H = \begin{pmatrix} 1 & 0 & 0 & 0 \\ 0 & -1 & 2 & 0 \\ 0 & 2 & -1 & 0 \\ 0 & 0 & 0 & 1 \end{pmatrix}$$

$$\Psi_m^T H \Psi_m = -3 \quad \Psi_p^T H \Psi_p = 1 \quad \Phi_p^T H \Phi_p = 1 \quad \Phi_m^T H \Phi_m = 1$$

$$-3\Psi_m \Psi_m^T + \Psi_p \Psi_p^T + \Phi_p \Phi_p^T + \Phi_m \Phi_m^T = \begin{pmatrix} 1 & 0 & 0 & 0 \\ 0 & -1 & 2 & 0 \\ 0 & 2 & -1 & 0 \\ 0 & 0 & 0 & 1 \end{pmatrix}$$

More about the partial trace:

The partial trace as given above is not particularly transparent in its matrix implementation. Here the partial trace over spin 1 is presented using conventional Dirac notation. First $|\Phi_m><\Phi_m|$ is expanded.

$$|\Phi_m\rangle\langle\Phi_m| = \frac{1}{2}\left[|\uparrow_1\rangle|\uparrow_2\rangle\langle\uparrow_2|\langle\uparrow_1| - |\uparrow_1\rangle|\uparrow_2\rangle\langle\downarrow_2|\langle\downarrow_1| - |\downarrow_1\rangle|\downarrow_2\rangle\langle\uparrow_2|\langle\uparrow_1| + |\downarrow_1\rangle|\downarrow_2\rangle\langle\downarrow_2|\langle\downarrow_1|\right]$$

Now the trace of spin 1 (bue) is generated showing that the cross terms in the middle of the above expression (red) vanish leaving the following result.

$$\frac{1}{2}\left[\langle\uparrow_1|\Phi_m\rangle\langle\Phi_m|\uparrow_1\rangle + \langle\downarrow_1|\Phi_m\rangle\langle\Phi_m|\downarrow_1\rangle\right] = \frac{1}{2}\left[|\uparrow_2\rangle\langle\uparrow_2| + |\downarrow_2\rangle\langle\downarrow_2|\right]$$

Wave function collapse:

Previously it was noted that if the spin orientation of particle 1 is learned through measurement, the spin orientation of particle 2 is also immediately known no matter how far away it may be. To show this we first create projection (measurement) operators for spin up and down in the z- and x-directions.

$$P_{zu} = \begin{pmatrix} 1 \\ 0 \end{pmatrix}\begin{pmatrix} 1 & 0 \end{pmatrix} \rightarrow \begin{pmatrix} 1 & 0 \\ 0 & 0 \end{pmatrix} \qquad P_{zd} = \begin{pmatrix} 0 \\ 1 \end{pmatrix}\begin{pmatrix} 0 & 1 \end{pmatrix} \rightarrow \begin{pmatrix} 0 & 0 \\ 0 & 1 \end{pmatrix}$$

$$P_{zu} = \begin{pmatrix} \frac{1}{\sqrt{2}} \\ \frac{1}{\sqrt{2}} \end{pmatrix}\begin{pmatrix} \frac{1}{\sqrt{2}} & \frac{1}{\sqrt{2}} \end{pmatrix} \rightarrow \begin{pmatrix} \frac{1}{2} & \frac{1}{2} \\ \frac{1}{2} & \frac{1}{2} \end{pmatrix} \quad P_{zd} = \begin{pmatrix} \frac{1}{\sqrt{2}} \\ -\frac{1}{\sqrt{2}} \end{pmatrix}\begin{pmatrix} \frac{1}{\sqrt{2}} & -\frac{1}{\sqrt{2}} \end{pmatrix} \rightarrow \begin{pmatrix} \frac{1}{2} & -\frac{1}{2} \\ -\frac{1}{2} & \frac{1}{2} \end{pmatrix}$$

For the Bell state Ψ_p, measurement of the z-direction spin of the first particle has two equally likely (probability 1/2) outcomes - spin-up or spin-down. These measurement outcomes cause the second particle to have the opposite spin. This result can, of course, be easily predicted by inspection of Ψ_p.

$$\Psi_p = \frac{1}{\sqrt{2}}\left[\begin{pmatrix} 1 \\ 0 \end{pmatrix}\begin{pmatrix} 0 \\ 1 \end{pmatrix} + \begin{pmatrix} 0 \\ 1 \end{pmatrix}\begin{pmatrix} 1 \\ 0 \end{pmatrix}\right]$$

$$\text{kronecker}(P_{zu},\ I)\Psi_p = \begin{pmatrix} 0 \\ 0.707 \\ 0 \\ 0 \end{pmatrix} \quad \frac{1}{\sqrt{2}}\begin{pmatrix} 1 \\ 0 \end{pmatrix}\begin{pmatrix} 0 \\ 1 \end{pmatrix}$$

$$\text{kronecker}(P_{zd},\ I)\Psi_p = \begin{pmatrix} 0 \\ 0 \\ 0.707 \\ 0 \end{pmatrix} \quad \frac{1}{\sqrt{2}}\begin{pmatrix} 0 \\ 1 \end{pmatrix}\begin{pmatrix} 1 \\ 0 \end{pmatrix}$$

Measurement of the x-direction spin of the first particle has two equally likely (probability 1/2) outcomes - spin-up or spin-down. However, for Ψ_p the measurements cause the second particle to have the same spin. This result is not obtained by inspection because the Bell states have been written in the z-basis.

$$\text{kronecker}(P_{xu},\ I)\Psi_p = \begin{pmatrix} 0.354 & 0.354 & 0.354 & 0.354 \end{pmatrix} \quad \frac{1}{\sqrt{2}}\frac{1}{\sqrt{2}}\begin{pmatrix} 1 \\ 1 \end{pmatrix}\frac{1}{\sqrt{2}}\begin{pmatrix} 1 \\ 1 \end{pmatrix}$$

$$\text{kronecker}(P_{xd},\ I)\Psi_p = \begin{pmatrix} -0.354 & 0.354 & 0.354 & -0.354 \end{pmatrix} \quad \frac{-1}{\sqrt{2}}\frac{1}{\sqrt{2}}\begin{pmatrix} 1 \\ -1 \end{pmatrix}\frac{1}{\sqrt{2}}\begin{pmatrix} 1 \\ -1 \end{pmatrix}$$

This seemingly peculiar result occurs because in the x-basis Ψ_p has the following form.

$$\Psi_p = \frac{1}{\sqrt{2}}\left[\frac{1}{\sqrt{2}}\begin{pmatrix}1\\1\end{pmatrix}\frac{1}{\sqrt{2}}\begin{pmatrix}1\\1\end{pmatrix} - \frac{1}{\sqrt{2}}\begin{pmatrix}1\\-1\end{pmatrix}\frac{1}{\sqrt{2}}\begin{pmatrix}1\\-1\end{pmatrix}\right] = \frac{1}{\sqrt{2}}\begin{pmatrix}0\\1\\1\\0\end{pmatrix}$$

Naturally, these results are consistent with the following expectation values.

$$\Psi_p^T SzSz\Psi_p = -1 \quad \Psi_p^T SxSx\Psi_p = 1$$

If we repeat these calculations using Φ_m the following results are obtained.

$$\Psi_p = \frac{1}{\sqrt{2}}\left[\begin{pmatrix}1\\0\end{pmatrix}\begin{pmatrix}1\\0\end{pmatrix} - \begin{pmatrix}0\\1\end{pmatrix}\begin{pmatrix}0\\1\end{pmatrix}\right]$$

$$\text{kronecker}(P_{zu},\ I)\Phi_m = \begin{pmatrix}0.707\\0\\0\\0\end{pmatrix} \quad \frac{1}{\sqrt{2}}\begin{pmatrix}1\\0\end{pmatrix}\begin{pmatrix}1\\0\end{pmatrix}$$

$$\text{kronecker}(P_{zd},\ I)\Phi_m = \begin{pmatrix}0\\0\\0\\-0.707\end{pmatrix} \quad \frac{-1}{\sqrt{2}}\begin{pmatrix}0\\1\end{pmatrix}\begin{pmatrix}0\\1\end{pmatrix}$$

The z-direction measurements can again be predicted by simple inspection of the entangled wave function.

$$\text{kronecker}(P_{xu},\ I)\Phi_m = \begin{pmatrix}0.354 & -0.354 & 0.354 & -0.354\end{pmatrix} \quad \frac{1}{\sqrt{2}}\frac{1}{\sqrt{2}}\begin{pmatrix}1\\1\end{pmatrix}\frac{1}{\sqrt{2}}\begin{pmatrix}1\\-1\end{pmatrix}$$

$$\text{kronecker}(P_{xd},\ I)\Phi_m = \begin{pmatrix}0.354 & 0.354 & -0.354 & -0.354\end{pmatrix} \quad \frac{-1}{\sqrt{2}}\frac{1}{\sqrt{2}}\begin{pmatrix}1\\-1\end{pmatrix}\frac{1}{\sqrt{2}}\begin{pmatrix}1\\1\end{pmatrix}$$

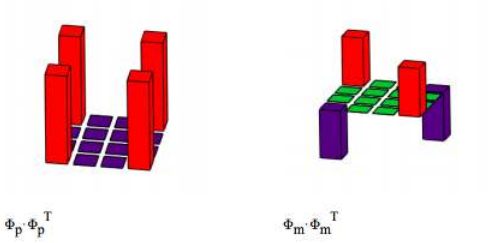
The x-direction results are obvious if we write Φ_m in the x-basis.

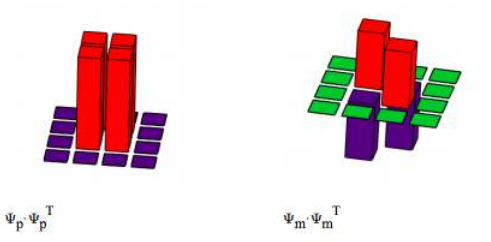
$$\Phi_m = \frac{1}{\sqrt{2}}\left[\frac{1}{\sqrt{2}}\begin{pmatrix}1\\1\end{pmatrix}\frac{1}{\sqrt{2}}\begin{pmatrix}1\\-1\end{pmatrix} + \frac{1}{\sqrt{2}}\begin{pmatrix}1\\-1\end{pmatrix}\frac{1}{\sqrt{2}}\begin{pmatrix}1\\1\end{pmatrix}\right] = \frac{1}{\sqrt{2}}\begin{pmatrix}1\\0\\0\\-1\end{pmatrix}$$

The results are also consisten with the appropriate expectation values.

$$\Phi_m^T SzSz\Phi_m = 1 \quad \Phi_m^T SxSx\Phi_m = -1$$

Graphical representations of the Bell state density matrices:





Algebraic analysis of Bell state generation (read left to right) and Bell state measurement (read right to left).

$$\begin{pmatrix}1\\0\\0\\0\end{pmatrix} = |0\rangle|0\rangle \underset{\longleftrightarrow}{H \otimes I} \frac{1}{\sqrt{2}}(|0\rangle + |1\rangle)|0\rangle = \frac{1}{\sqrt{2}}(|00\rangle + |10\rangle) \underset{\longleftrightarrow}{CNOT} \frac{1}{\sqrt{2}}(|00\rangle + |11\rangle) = \frac{1}{\sqrt{2}}\begin{pmatrix}1\\0\\0\\1\end{pmatrix}$$

$$\begin{pmatrix}0\\1\\0\\0\end{pmatrix} = |0\rangle|1\rangle \underset{\longleftrightarrow}{H \otimes I} \frac{1}{\sqrt{2}}(|0\rangle + |1\rangle)|1\rangle = \frac{1}{\sqrt{2}}(|01\rangle + |11\rangle) \underset{\longleftrightarrow}{CNOT} \frac{1}{\sqrt{2}}(|01\rangle + |10\rangle) = \frac{1}{\sqrt{2}}\begin{pmatrix}0\\1\\1\\0\end{pmatrix}$$

$$\begin{pmatrix}0\\0\\1\\0\end{pmatrix} = |1\rangle|0\rangle \underset{\longleftrightarrow}{H \otimes I} \frac{1}{\sqrt{2}}(|0\rangle - |1\rangle)|0\rangle = \frac{1}{\sqrt{2}}(|00\rangle - |10\rangle) \underset{\longleftrightarrow}{CNOT} \frac{1}{\sqrt{2}}(|00\rangle - |11\rangle) = \frac{1}{\sqrt{2}}\begin{pmatrix}1\\0\\0\\-1\end{pmatrix}$$

$$\begin{pmatrix}0\\0\\0\\1\end{pmatrix} = |1\rangle|01\rangle \underset{\longleftrightarrow}{H \otimes I} \frac{1}{\sqrt{2}}(|0\rangle - |1\rangle)|1\rangle = \frac{1}{\sqrt{2}}(|01\rangle - |11\rangle) \underset{\longleftrightarrow}{CNOT} \frac{1}{\sqrt{2}}(|00\rangle + |11\rangle) = \frac{1}{\sqrt{2}}\begin{pmatrix}0\\1\\-1\\0\end{pmatrix}$$

This page titled 8.53: Bell State Exercises is shared under a CC BY 4.0 license and was authored, remixed, and/or curated by Frank Rioux via source content that was edited to the style and standards of the LibreTexts platform.

8.54: Expressing Bell and GHZ States in Vector Format Using Mathcad

Mathcad provides the kronecker command for matrix tensor multiplication. It requires square matrices for its arguments and therefore cannot be used directly for vector tensor multiplication. However, if a vector is augmented with a null vector (or matrix) to produce a square matrix, vector tensor multiplication can be carried out using kronecker and a submatrix command that discards everything except the first column of the product matrix. This technique is illustrated by putting the Bell and GHZ states in vector format.

The z- and x-direction spin eigenfunctions and the appropriate null vector are required.

$$z_u = \begin{pmatrix}1\\0\end{pmatrix} \quad z_d = \begin{pmatrix}0\\1\end{pmatrix} \quad x_u = \frac{1}{\sqrt{2}}\begin{pmatrix}1\\1\end{pmatrix} \quad x_d = \frac{1}{\sqrt{2}}\begin{pmatrix}1\\-1\end{pmatrix} \quad n = \begin{pmatrix}0\\0\end{pmatrix}$$

The Mathcad syntax for tensor multiplication of two 2-dimensional vectors.

$$\psi(\mathrm{a},\ \mathrm{b}) = \mathrm{submatrix}(\mathrm{kronecker}(\mathrm{augment}(\mathrm{a},\ \mathrm{n}),\ \mathrm{augment}(\mathrm{b},\ \mathrm{n})),\ 1,\ 4,\ 1,\ 1)$$

The four maximally entangled Bell states will be expressed in both the z- and x-basis.

$$|\Phi_p\rangle = \frac{1}{\sqrt{2}}\left[|\uparrow_1\rangle|\uparrow_2\rangle + |\downarrow_1\rangle|\downarrow_2\rangle\right] = \frac{1}{\sqrt{2}}\left[\begin{pmatrix}1\\0\end{pmatrix}\otimes\begin{pmatrix}1\\0\end{pmatrix} + \begin{pmatrix}0\\1\end{pmatrix}\otimes\begin{pmatrix}0\\1\end{pmatrix}\right] = \frac{1}{\sqrt{2}}\begin{pmatrix}1\\0\\0\\1\end{pmatrix}$$

$$\Phi_p = \tfrac{1}{\sqrt{2}}\left(\psi(z_u,\ z_u) + \psi(z_d,\ z_d)\right) \quad \Phi_p = \begin{pmatrix}0.707\\0\\0\\0.707\end{pmatrix} \quad \Phi_p = \tfrac{1}{\sqrt{2}}\left(\psi(x_u,\ x_u)\right) + \left(\psi(x_d,\ x_d)\right) \quad \Phi_p = \begin{pmatrix}0.707\\0\\0\\0.707\end{pmatrix}$$

$$|\Phi_m\rangle = \frac{1}{\sqrt{2}}\left[|\uparrow_1\rangle|\uparrow_2\rangle - |\downarrow_1\rangle|\downarrow_2\rangle\right] = \frac{1}{\sqrt{2}}\left[\begin{pmatrix}1\\0\end{pmatrix}\otimes\begin{pmatrix}1\\0\end{pmatrix} - \begin{pmatrix}0\\1\end{pmatrix}\otimes\begin{pmatrix}0\\1\end{pmatrix}\right] = \frac{1}{\sqrt{2}}\begin{pmatrix}1\\0\\0\\-1\end{pmatrix}$$

$$\Phi_m = \tfrac{1}{\sqrt{2}}\left(\psi(z_u,\ z_u) - \psi(z_d,\ z_d)\right) \quad \Phi_m = \begin{pmatrix}0.707\\0\\0\\-0.707\end{pmatrix} \quad \Phi_m = \tfrac{1}{\sqrt{2}}\left(\psi(x_u,\ x_u)\right) + \left(\psi(x_d,\ x_d)\right) \quad \Phi_m = \begin{pmatrix}0.707\\0\\0\\-0.707\end{pmatrix}$$

$$|\Psi_p\rangle = \frac{1}{\sqrt{2}}\left[|\uparrow_1\rangle|\uparrow_2\rangle + |\downarrow_1\rangle|\downarrow_2\rangle\right] = \frac{1}{\sqrt{2}}\left[\begin{pmatrix}1\\0\end{pmatrix}\otimes\begin{pmatrix}0\\1\end{pmatrix} + \begin{pmatrix}0\\1\end{pmatrix}\otimes\begin{pmatrix}1\\0\end{pmatrix}\right] = \frac{1}{\sqrt{2}}\begin{pmatrix}0\\1\\1\\0\end{pmatrix}$$

$$\Psi_p = \tfrac{1}{\sqrt{2}}\left(\psi(z_u,\ z_u) + \psi(z_d,\ z_d)\right) \quad \Phi_p = \begin{pmatrix}0\\0.707\\0.707\\0\end{pmatrix} \quad \Psi_p = \tfrac{1}{\sqrt{2}}\left(\psi(x_u,\ x_u)\right) - \left(\psi(x_d,\ x_d)\right) \quad \Psi_p = \begin{pmatrix}0\\0.707\\0.707\\0\end{pmatrix}$$

$$|\Psi_m\rangle = \frac{1}{\sqrt{2}}\left[|\uparrow_1\rangle|\uparrow_2\rangle - |\downarrow_1\rangle|\downarrow_2\rangle\right] = \frac{1}{\sqrt{2}}\left[\begin{pmatrix}1\\0\end{pmatrix}\otimes\begin{pmatrix}0\\1\end{pmatrix} - \begin{pmatrix}0\\1\end{pmatrix}\otimes\begin{pmatrix}1\\0\end{pmatrix}\right] = \frac{1}{\sqrt{2}}\begin{pmatrix}0\\1\\-1\\0\end{pmatrix}$$

$$\Psi_m = \tfrac{1}{\sqrt{2}}\left(\psi(z_u,\ z_u) - \psi(z_d,\ z_d)\right) \quad \Psi_m = \begin{pmatrix}0\\0.707\\-0.707\\0\end{pmatrix} \quad \Psi_m = \tfrac{1}{\sqrt{2}}\left(\psi(x_u,\ x_u)\right) - \left(\psi(x_d,\ x_d)\right) \quad \Psi_m = \begin{pmatrix}0\\0.707\\-0.707\\0\end{pmatrix}$$

The Mathcad syntax for tensor multiplication of three 2-dimensional vectors.

$$\Psi(a,\ b,\ c) = \text{submatrix}(\text{kronecker}(\text{augment}(a,\ n),\ \text{kronecker}(\text{augment}(b,\ n),\ \text{augment}(c,\ n))),\ 1,\ 8,\ 1,\ 1)$$

$$|\Psi\rangle = \frac{1}{\sqrt{2}}\left[\begin{pmatrix}1\\0\end{pmatrix}\otimes\begin{pmatrix}1\\0\end{pmatrix}\otimes\begin{pmatrix}1\\0\end{pmatrix} \pm \begin{pmatrix}0\\1\end{pmatrix}\otimes\begin{pmatrix}0\\1\end{pmatrix}\otimes\begin{pmatrix}0\\1\end{pmatrix}\right] = \frac{1}{\sqrt{2}}(1\quad 0\quad 0\quad 0\quad 0\quad 0\quad 0\quad \pm 1)^T$$

$$\Psi_1 = \tfrac{1}{\sqrt{2}}\left(\psi(z_u,\ z_u,\ z_u) + \psi(z_d,\ z_d,\ z_d)\right) \qquad \Psi_1^T = (0.707\quad 0\quad 0\quad 0\quad 0\quad 0\quad 0\quad 0.707)$$

$$\Psi_2 = \tfrac{1}{\sqrt{2}}\left(\psi(z_u,\ z_u,\ z_u) - \psi(z_d,\ z_d,\ z_d)\right) \qquad \Psi_2^T = (0.707\quad 0\quad 0\quad 0\quad 0\quad 0\quad 0\quad -0.707)$$

$$|\Psi\rangle = \frac{1}{\sqrt{2}}\left[\begin{pmatrix}1\\0\end{pmatrix}\otimes\begin{pmatrix}1\\0\end{pmatrix}\otimes\begin{pmatrix}0\\1\end{pmatrix} \pm \begin{pmatrix}0\\1\end{pmatrix}\otimes\begin{pmatrix}0\\1\end{pmatrix}\otimes\begin{pmatrix}1\\0\end{pmatrix}\right] = \frac{1}{\sqrt{2}}(0\quad 1\quad 0\quad 0\quad 0\quad 0\quad \pm 1\quad 0)^T$$

$$\Psi_3 = \tfrac{1}{\sqrt{2}}\left(\psi(z_u,\ z_u,\ z_d) + \psi(z_d,\ z_d,\ z_u)\right) \qquad \Psi_3^T = (0\quad 0.707\quad 0\quad 0\quad 0\quad 0\quad 0.707\quad 0)$$

$$\Psi_4 = \tfrac{1}{\sqrt{2}}\left(\psi(z_u,\ z_u,\ z_d) - \psi(z_d,\ z_d,\ z_u)\right) \qquad \Psi_4^T = (0\quad 0.707\quad 0\quad 0\quad 0\quad 0\quad -0.707\quad 0)$$

$$|\Psi\rangle = \frac{1}{\sqrt{2}}\left[\begin{pmatrix}1\\0\end{pmatrix}\otimes\begin{pmatrix}0\\1\end{pmatrix}\otimes\begin{pmatrix}1\\0\end{pmatrix} \pm \begin{pmatrix}0\\1\end{pmatrix}\otimes\begin{pmatrix}1\\0\end{pmatrix}\otimes\begin{pmatrix}0\\1\end{pmatrix}\right] = \frac{1}{\sqrt{2}}(0\quad 0\quad 1\quad 0\quad 0\quad \pm 1\quad 0\quad 0)^T$$

$$\Psi_5 = \tfrac{1}{\sqrt{2}}\left(\psi(z_u,\ z_d,\ z_u) + \psi(z_d,\ z_u,\ z_d)\right) \qquad \Psi_5^T = (0\quad 0\quad 0.707\quad 0\quad 0\quad 0.707\quad 0\quad 0)$$

$$\Psi_6 = \tfrac{1}{\sqrt{2}}\left(\psi(z_u,\ z_d,\ z_u) - \psi(z_d,\ z_u,\ z_d)\right) \qquad \Psi_6^T = (0\quad 0\quad 0.707\quad 0\quad 0\quad -0.707\quad 0\quad 0)$$

$$|\Psi\rangle = \frac{1}{\sqrt{2}}\left[\begin{pmatrix}1\\0\end{pmatrix}\otimes\begin{pmatrix}0\\1\end{pmatrix}\otimes\begin{pmatrix}0\\1\end{pmatrix} \pm \begin{pmatrix}1\\0\end{pmatrix}\otimes\begin{pmatrix}1\\0\end{pmatrix}\otimes\begin{pmatrix}0\\1\end{pmatrix}\right] = \frac{1}{\sqrt{2}}(0\quad 0\quad 0\quad 1\quad \pm 1\quad 0\quad 0\quad 0)^T$$

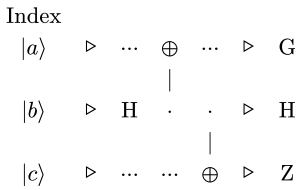
$$\Psi_7 = \tfrac{1}{\sqrt{2}}\left(\psi(z_u,\ z_d,\ z_d) + \psi(z_d,\ z_u,\ z_u)\right) \qquad \Psi_7^T = (0\quad 0\quad 0\quad 0.707\quad 0.707\quad 0\quad 0\quad 0)$$

$$\Psi_8 = \tfrac{1}{\sqrt{2}}\left(\psi(z_u,\ z_d,\ z_d) - \psi(z_d,\ z_u,\ z_u)\right) \qquad \Psi_8^T = (0\quad 0\quad 0\quad 0.707\quad -0.707\quad 0\quad 0\quad 0)$$

This page titled 8.54: Expressing Bell and GHZ States in Vector Format Using Mathcad is shared under a CC BY 4.0 license and was authored, remixed, and/or curated by Frank Rioux via source content that was edited to the style and standards of the LibreTexts platform.

8.55: Quantum Circuit for the Generation of GHZ States

The following circuit generates the eight GHZ maximally entangled states. A similar NMR circuit can be found on page 287 of *The Quest for the Quantum Computer* by Julian Brown.



Given the quantum gates in matrix form the quantum circuit is formed using Kronecker multiplication.

$$\mathrm{I} = \begin{pmatrix} 1 & 0 \\ 0 & 1 \end{pmatrix} \quad \mathrm{H} = \frac{1}{\sqrt{2}} \begin{pmatrix} 1 & 1 \\ 1 & -1 \end{pmatrix} \quad \mathrm{CNOT} = \begin{pmatrix} 1 & 0 & 0 & 0 \\ 0 & 1 & 0 & 0 \\ 0 & 0 & 0 & 1 \\ 0 & 0 & 1 & 0 \end{pmatrix} \quad \mathrm{ICNOT} = \begin{pmatrix} 1 & 0 & 0 & 0 \\ 0 & 0 & 0 & 1 \\ 0 & 0 & 1 & 0 \\ 0 & 1 & 0 & 0 \end{pmatrix}$$

$$\mathrm{GHZ} = \mathrm{kronecker}(\mathrm{I},\ \mathrm{CNOT})\ \mathrm{kronecker}(\mathrm{ICNOT},\ \mathrm{I})\ \mathrm{kronecker}(\mathrm{I},\ \mathrm{kronecker}(\mathrm{H},\ \mathrm{I}))$$

Using the index as input the quantum circuit generates the corresponding GHZ state.

https://chem.libretexts.org/@go/page/148206

$$G_0 = \mathrm{GHZ}\begin{pmatrix}1\\0\\0\\0\\0\\0\\0\\0\end{pmatrix} = \begin{pmatrix}0.707\\0\\0\\0\\0\\0\\0\\0.707\end{pmatrix} \qquad \begin{pmatrix}1\\0\end{pmatrix}\begin{pmatrix}1\\0\end{pmatrix}\begin{pmatrix}1\\0\end{pmatrix} = \frac{1}{\sqrt{2}}\left[\begin{pmatrix}1\\0\end{pmatrix}\begin{pmatrix}1\\0\end{pmatrix}\begin{pmatrix}1\\0\end{pmatrix} + \begin{pmatrix}0\\1\end{pmatrix}\begin{pmatrix}0\\1\end{pmatrix}\begin{pmatrix}0\\1\end{pmatrix}\right]$$

$$G_1 = \mathrm{GHZ}\begin{pmatrix}0\\1\\0\\0\\0\\0\\0\\0\end{pmatrix} = \begin{pmatrix}0\\0.707\\0\\0\\0\\0\\0.707\\0\end{pmatrix} \qquad \begin{pmatrix}1\\0\end{pmatrix}\begin{pmatrix}1\\0\end{pmatrix}\begin{pmatrix}0\\1\end{pmatrix} = \frac{1}{\sqrt{2}}\left[\begin{pmatrix}1\\0\end{pmatrix}\begin{pmatrix}1\\0\end{pmatrix}\begin{pmatrix}0\\1\end{pmatrix} + \begin{pmatrix}0\\1\end{pmatrix}\begin{pmatrix}0\\1\end{pmatrix}\begin{pmatrix}1\\0\end{pmatrix}\right]$$

$$G_2 = \mathrm{GHZ}\begin{pmatrix}0\\0\\1\\0\\0\\0\\0\\0\end{pmatrix} = \begin{pmatrix}0.707\\0\\0\\0\\0\\0\\0\\-0.707\end{pmatrix} \qquad \begin{pmatrix}1\\0\end{pmatrix}\begin{pmatrix}0\\1\end{pmatrix}\begin{pmatrix}1\\0\end{pmatrix} = \frac{1}{\sqrt{2}}\left[\begin{pmatrix}1\\0\end{pmatrix}\begin{pmatrix}1\\0\end{pmatrix}\begin{pmatrix}1\\0\end{pmatrix} - \begin{pmatrix}0\\1\end{pmatrix}\begin{pmatrix}0\\1\end{pmatrix}\begin{pmatrix}0\\1\end{pmatrix}\right]$$

$$G_3 = \mathrm{GHZ}\begin{pmatrix}0\\0\\0\\1\\0\\0\\0\\0\end{pmatrix} = \begin{pmatrix}0\\0.707\\0\\0\\0\\0\\-0.707\\0\end{pmatrix} \qquad \begin{pmatrix}1\\0\end{pmatrix}\begin{pmatrix}0\\1\end{pmatrix}\begin{pmatrix}0\\1\end{pmatrix} = \frac{1}{\sqrt{2}}\left[\begin{pmatrix}1\\0\end{pmatrix}\begin{pmatrix}1\\0\end{pmatrix}\begin{pmatrix}0\\1\end{pmatrix} - \begin{pmatrix}0\\1\end{pmatrix}\begin{pmatrix}0\\1\end{pmatrix}\begin{pmatrix}1\\0\end{pmatrix}\right]$$

$$G_4 = \mathrm{GHZ}\begin{pmatrix}0\\0\\0\\0\\1\\0\\0\\0\end{pmatrix} = \begin{pmatrix}0\\0\\0\\0.707\\0.707\\0\\0\\0\end{pmatrix} \qquad \begin{pmatrix}0\\1\end{pmatrix}\begin{pmatrix}1\\0\end{pmatrix}\begin{pmatrix}1\\0\end{pmatrix} = \frac{1}{\sqrt{2}}\left[\begin{pmatrix}1\\0\end{pmatrix}\begin{pmatrix}0\\1\end{pmatrix}\begin{pmatrix}0\\1\end{pmatrix} + \begin{pmatrix}0\\1\end{pmatrix}\begin{pmatrix}1\\0\end{pmatrix}\begin{pmatrix}1\\0\end{pmatrix}\right]$$

$$G_5 = \mathrm{GHZ}\begin{pmatrix}0\\0\\0\\0\\0\\1\\0\\0\end{pmatrix} = \begin{pmatrix}0\\0\\0.707\\0\\0\\0.707\\0\\0\end{pmatrix} \qquad \begin{pmatrix}0\\1\end{pmatrix}\begin{pmatrix}1\\0\end{pmatrix}\begin{pmatrix}0\\1\end{pmatrix} = \frac{1}{\sqrt{2}}\left[\begin{pmatrix}1\\0\end{pmatrix}\begin{pmatrix}0\\1\end{pmatrix}\begin{pmatrix}1\\0\end{pmatrix} + \begin{pmatrix}0\\1\end{pmatrix}\begin{pmatrix}1\\0\end{pmatrix}\begin{pmatrix}0\\1\end{pmatrix}\right]$$

$$G_6 = \mathrm{GHZ}\begin{pmatrix}0\\0\\0\\0\\0\\0\\0\\0\end{pmatrix} = \begin{pmatrix}0\\0\\0\\-0.707\\0.707\\0\end{pmatrix} \qquad \begin{pmatrix}0\\1\end{pmatrix}\begin{pmatrix}0\\1\end{pmatrix}\begin{pmatrix}1\\0\end{pmatrix} = \frac{1}{\sqrt{2}}\left[\begin{pmatrix}0\\1\end{pmatrix}\begin{pmatrix}1\\0\end{pmatrix}\begin{pmatrix}1\\0\end{pmatrix} - \begin{pmatrix}1\\0\end{pmatrix}\begin{pmatrix}0\\1\end{pmatrix}\begin{pmatrix}0\\1\end{pmatrix}\right]$$

Given the following truth tables the operation of the circuit is followed algebraically for G_2 and G_4.

$$\text{Identity} \quad \begin{pmatrix} 1 \\ 0 \end{pmatrix} \begin{pmatrix} 0 \\ 0 \end{pmatrix} \qquad \begin{pmatrix} 0 \\ 0 \end{pmatrix} \begin{pmatrix} 0 \\ 0 \end{pmatrix}$$

$$\text{Hadamard} \quad \mathrm{H} = \begin{bmatrix} 0 \text{ to } \frac{(0+1)}{\sqrt{2}} \text{ to } 0 \\ 1 \text{ to } \frac{(0-1)}{\sqrt{2}} \text{ to } 1 \end{bmatrix}$$

$$\begin{pmatrix} 0 \\ 0 \\ 0 \\ 0 \end{pmatrix} \begin{pmatrix} 0 \text{ to } 0 \\ 1 \text{ to } 1 \end{pmatrix} \begin{pmatrix} 0 \\ 0 \\ 0.707 \\ 0.707 \end{pmatrix}$$

$$G_7 = \mathrm{GHZ} = \begin{pmatrix} \text{Decimal} & \text{Binary} & \text{to} & \text{Binary} & \text{Decimal} \\ 0 & 00 & \text{to} & 00 & 0 \\ 1 & 01 & \text{to} & 11 & 3 \\ 2 & 10 & \text{to} & 10 & 2 \\ 3 & 11 & \text{to} & 01 & 1 \end{pmatrix}$$

$$\text{ICNOT} \quad \begin{pmatrix} 0 \\ 1 \end{pmatrix} \begin{pmatrix} 0 \\ 1 \end{pmatrix} = \frac{1}{\sqrt{2}} \left[\begin{pmatrix} 0 \\ 1 \end{pmatrix} \begin{pmatrix} 0 \\ 1 \end{pmatrix} - \begin{pmatrix} 1 \\ 0 \end{pmatrix} \begin{pmatrix} 0 \\ 1 \end{pmatrix} \right]$$

$$\text{CNOT} \quad \begin{pmatrix} \text{Decimal} & \text{Binary} & \text{to} & \text{Binary} & \text{Decimal} \\ 0 & 00 & \text{to} & 00 & 0 \\ 1 & 01 & \text{to} & 01 & 1 \\ 2 & 10 & \text{to} & 11 & 3 \\ 3 & 11 & \text{to} & 10 & 2 \end{pmatrix}$$

$$|010\rangle \qquad |100\rangle$$

$$\mathrm{I} \otimes \mathrm{H} \otimes \mathrm{I} \qquad \mathrm{I} \otimes \mathrm{H} \otimes \mathrm{I}$$

$$|0\rangle \left(\frac{|0\rangle - |1\rangle}{\sqrt{2}} \right) |0\rangle = \frac{1}{\sqrt{2}} [|000\rangle - |010\rangle] \qquad |1\rangle \left(\frac{|0\rangle + |1\rangle}{\sqrt{2}} \right) |0\rangle = \frac{1}{\sqrt{2}} [|100\rangle + |110\rangle]$$

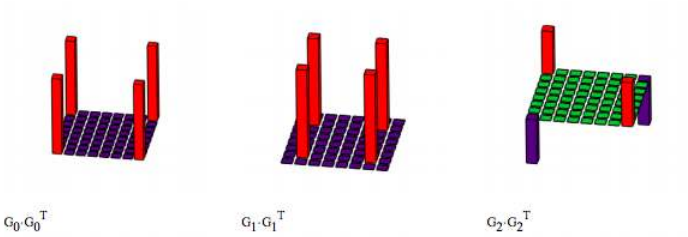
$$\mathrm{ICNOT} \otimes \mathrm{I} \qquad \mathrm{ICNOT} \otimes \mathrm{I}$$

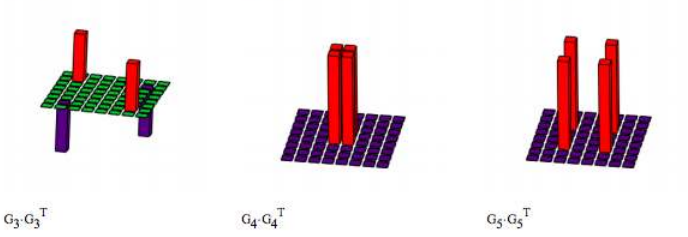
$$\frac{1}{\sqrt{2}} [|000\rangle - |110\rangle] \qquad \frac{1}{\sqrt{2}} [|100\rangle + |010\rangle]$$

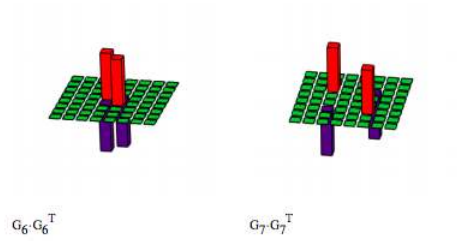
$$\mathrm{I} \otimes \mathrm{CNOT} \qquad \mathrm{I} \otimes \mathrm{CNOT}$$

$$\frac{1}{\sqrt{2}} [|000\rangle - |111\rangle] \qquad \frac{1}{\sqrt{2}} [|100\rangle + |011\rangle]$$

Next the GHZ density matrices are presented graphically.







Using the GHZ states as input and running the circuit in reverse yields the indices.

$$\mathrm{IGHZ} = \mathrm{GHZ}^{-}1$$

$$\text{IGHZ } G_0 = \begin{pmatrix} 1 \\ 0 \\ 0 \\ 0 \\ 0 \\ 0 \\ 0 \\ 0 \end{pmatrix} \quad \text{IGHZ } G_1 = \begin{pmatrix} 0 \\ 1 \\ 0 \\ 0 \\ 0 \\ 0 \\ 0 \\ 0 \end{pmatrix} \quad \text{IGHZ } G_2 = \begin{pmatrix} 0 \\ 0 \\ 1 \\ 0 \\ 0 \\ 0 \\ 0 \\ 0 \end{pmatrix} \quad \text{IGHZ } G_3 = \begin{pmatrix} 0 \\ 0 \\ 0 \\ 1 \\ 0 \\ 0 \\ 0 \\ 0 \end{pmatrix}$$

$$\text{IGHZ } G_4 = \begin{pmatrix} 0 \\ 0 \\ 0 \\ 0 \\ 1 \\ 0 \\ 0 \\ 0 \end{pmatrix} \quad \text{IGHZ } G_5 = \begin{pmatrix} 0 \\ 0 \\ 0 \\ 0 \\ 0 \\ 1 \\ 0 \\ 0 \end{pmatrix} \quad \text{IGHZ } G_6 = \begin{pmatrix} 0 \\ 0 \\ 0 \\ 0 \\ 0 \\ 0 \\ 1 \\ 0 \end{pmatrix} \quad \text{IGHZ } G_7 = \begin{pmatrix} 0 \\ 0 \\ 0 \\ 0 \\ 0 \\ 0 \\ 0 \\ 1 \end{pmatrix}$$

This page titled 8.55: Quantum Circuit for the Generation of GHZ States is shared under a CC BY 4.0 license and was authored, remixed, and/or curated by Frank Rioux via source content that was edited to the style and standards of the LibreTexts platform.

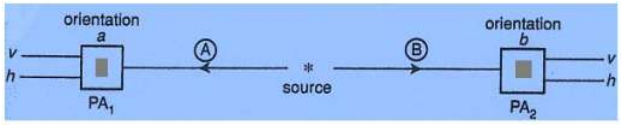
8.56: A Brief Description of Aspect's Experiment

The purpose of this tutorial is restricted to a brief computational summary of the EPR experiment reported by Aspect, Grangier and Roger, "Experimental Realization of Einstein-Podolsky-Rosen-Bohm Gedanken Experiment: A New Violation of Bell's Inequalities," in *Phys. Rev. Lett.* 49, 91 (1982). See Chapter 6 of *The Quantum Challenge* by Greenstein and Zajonc, Chapter 4 of Jim Baggott's *The Meaning of Quantum Theory*, and Chapter 12 of *Quantum Reality* by Nick Herbert for complete analyses of this historically important experiment.

A two-stage atomic cascade emits entangled photons (A and B) in opposite directions with the same circular polarization according to the observers in their path.

$$|\Psi\rangle = \frac{1}{\sqrt{2}}\left[|L\rangle_A|L\rangle_B + |R\rangle_A|R\rangle_B\right]$$

The experiment involves the measurement of photon polarization states in the vertical/horizontal measurement basis, and allows that the polarization analyzers (PAs) can be oriented at different angles a and b. (The figure below is taken from Chapter 4 of Baggott's book.)



Naturally the bipartate photon wave function is identical in both the circular or linear polarization bases.

Left circular polarization:

$$L = \frac{1}{\sqrt{2}}\begin{pmatrix}1\\ i\end{pmatrix}$$

Right circular polarization:

$$R = \frac{1}{\sqrt{2}}\begin{pmatrix}1\\ -i\end{pmatrix}$$

Vertical polarization:

$$V = \begin{pmatrix}1\\ 0\end{pmatrix}$$

Horizontal polarization:

$$H = \begin{pmatrix}0\\ 1\end{pmatrix}$$

$$|\Psi\rangle = \frac{1}{2\sqrt{2}}\left[|L\rangle_A|L\rangle_B + |R\rangle_A|R\rangle_B\right] = \frac{1}{\sqrt{2}}\left[\begin{pmatrix}1\\ i\end{pmatrix}_A \otimes \begin{pmatrix}1\\ i\end{pmatrix}_B + \begin{pmatrix}1\\ -i\end{pmatrix}_A \otimes \begin{pmatrix}1\\ -i\end{pmatrix}_B\right]$$
$$= \frac{1}{2\sqrt{2}}\left[\begin{pmatrix}1\\ i\\ i\\ -1\end{pmatrix} + \begin{pmatrix}1\\ -i\\ -i\\ -1\end{pmatrix}\right] = \frac{1}{\sqrt{2}}\begin{pmatrix}1\\ 0\\ 0\\ -1\end{pmatrix}$$

$$|\Psi\rangle = \frac{1}{2\sqrt{2}}\left[|V\rangle_A|V\rangle_B + |H\rangle_A|H\rangle_B\right] = \frac{1}{\sqrt{2}}\left[\begin{pmatrix}1\\ 0\end{pmatrix}_A \otimes \begin{pmatrix}1\\ 0\end{pmatrix}_B - \begin{pmatrix}0\\ 1\end{pmatrix}_A \otimes \begin{pmatrix}0\\ 1\end{pmatrix}_B\right]$$
$$= \frac{1}{2\sqrt{2}}\left[\begin{pmatrix}1\\ 0\\ 0\\ 0\end{pmatrix} - \begin{pmatrix}0\\ 0\\ 0\\ 1\end{pmatrix}\right] = \frac{1}{\sqrt{2}}\begin{pmatrix}1\\ 0\\ 0\\ -1\end{pmatrix}$$

There are four measurement outcomes: both photons are vertically polarized, both are horizontally polarized, one is vertical and the other horizontal, and vice versa. The tensor representation of these measurement states are provided below.

$$|VV\rangle = \begin{pmatrix}1\\0\end{pmatrix} \otimes \begin{pmatrix}1\\0\end{pmatrix} = \begin{pmatrix}1\\0\\0\\0\end{pmatrix} \quad |VH\rangle = \begin{pmatrix}1\\0\end{pmatrix} \otimes \begin{pmatrix}0\\1\end{pmatrix} = \begin{pmatrix}0\\1\\0\\0\end{pmatrix} \quad |HV\rangle = \begin{pmatrix}0\\1\end{pmatrix} \otimes \begin{pmatrix}1\\0\end{pmatrix} = \begin{pmatrix}0\\0\\1\\0\end{pmatrix} \quad |HH\rangle = \begin{pmatrix}0\\1\end{pmatrix} \otimes \begin{pmatrix}0\\1\end{pmatrix} = \begin{pmatrix}0\\0\\0\\1\end{pmatrix}$$

We now write all states, Ψ and the measurement states, in Mathcad's vector format.

$$\Psi = \frac{1}{\sqrt{2}}\begin{pmatrix}1\\0\\0\\-1\end{pmatrix} \quad \mathrm{VV} = \begin{pmatrix}1\\0\\0\\0\end{pmatrix} \quad \mathrm{VH} = \begin{pmatrix}0\\1\\0\\0\end{pmatrix} \quad \mathrm{HV} = \begin{pmatrix}0\\0\\1\\0\end{pmatrix} \quad \mathrm{HH} = \begin{pmatrix}0\\0\\0\\1\end{pmatrix}$$

Next, the operator representing the rotation of PA1 by angle a clockwise and PA_2 by angle b counter-clockwise (so that the PAs turn in the same direction) is constructed using matrix tensor multiplication. Kronecker is Mathcad′s command for tensor matrix multiplication.

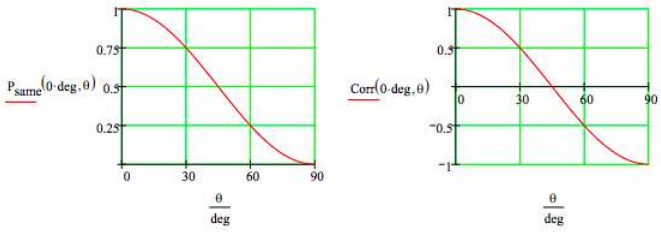
$$\mathrm{RotOp(a,\ b)} = \mathrm{kronecker}\left[\begin{pmatrix}\cos a & \sin a\\ -\sin a & \cos a\end{pmatrix}, \begin{pmatrix}\cos b & -\sin b\\ \sin b & \cos b\end{pmatrix}\right]$$

The probability that the detectors will behave the same or differently is calculated as follows.

$$P_{\mathrm{same}}(a,\ b) = \left(VV^T\mathrm{RotOp(a,\ b)}\Psi\right)^2 + \left(HH^T\mathrm{RotOp(a,\ b)}\Psi\right)^2$$
$$P_{\mathrm{diff}}(a,\ b) = \left(VH^T\mathrm{RotOp(a,\ b)}\Psi\right)^2 + \left(HV^T\mathrm{RotOp(a,\ b)}\Psi\right)^2$$

The expectation value as a function of the relative orientation of the polarization detectors is the difference between these two expressions. This is generally called the correlation function. In other words, the composite eigenvalues are: ++ = -- = +1 (same) and +- = -+ = -1 (diff).

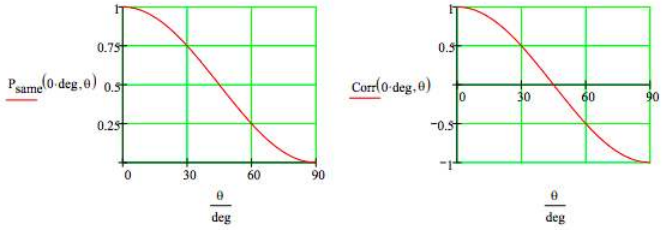
$$\mathrm{Corr(a,\ b)} = P_{same}(\mathrm{a,\ b}) - P_{diff}(\mathrm{a,\ b}) \quad \Theta = 0\mathrm{deg},\ 2\mathrm{deg}..90\mathrm{deg}$$



These graphical representations of the Aspect experiment are in agreement with those presented in Aspect's paper and also in *The Quantum Challenge*, *The Meaning of Quantum Theory*, and *Quantum Reality.*

These calculations are now repeated for the three other Bell states.

$$\Psi = \frac{1}{\sqrt{2}}(1 \quad 0 \quad 0 \quad 1)^T$$
$$P_{same}(\mathrm{a,\ b}) = \left(VV^T\mathrm{RotOp(a,\ b)}\Psi\right)^2 + \left(HH^T\mathrm{RotOp(a,\ b)}\Psi\right)^2$$
$$P_{diff}(\mathrm{a,\ b}) = \left(VH^T\mathrm{RotOp(a,\ b)}\Psi\right)^2 + \left(HV^T\mathrm{RotOp(a,\ b)}\Psi\right)^2$$
$$\mathrm{Corr(a,\ b)} = P_{same}(\mathrm{a,\ b}) - P_{diff}(\mathrm{a,\ b})$$

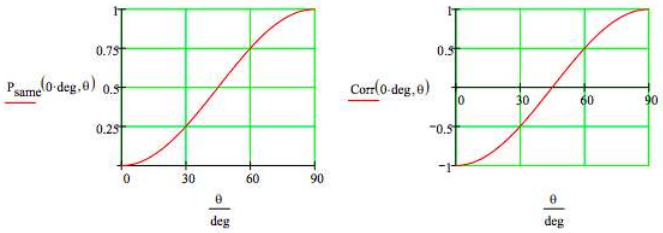


$$\Psi = \frac{1}{\sqrt{2}}(0 \quad 1 \quad 1 \quad 0)^T$$

$$P_{same}(\mathrm{a},\ \mathrm{b}) = \left(VV^T\mathrm{RotOp}(\mathrm{a},\ \mathrm{b})\Psi\right)^2 + \left(HH^T\mathrm{RotOp}(\mathrm{a},\ \mathrm{b})\Psi\right)^2$$

$$P_{diff}(\mathrm{a},\ \mathrm{b}) = \left(VH^T\mathrm{RotOp}(\mathrm{a},\ \mathrm{b})\Psi\right)^2 + \left(HV^T\mathrm{RotOp}(\mathrm{a},\ \mathrm{b})\Psi\right)^2$$

$$\mathrm{Corr}(\mathrm{a},\ \mathrm{b}) = P_{same}(\mathrm{a},\ \mathrm{b}) - P_{diff}(\mathrm{a},\ \mathrm{b})$$

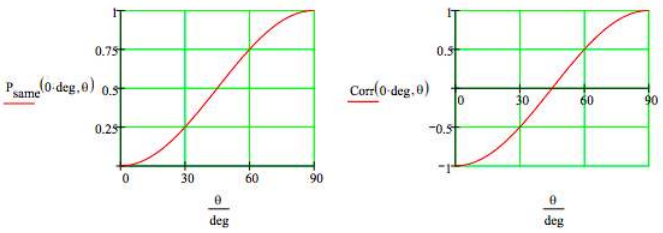


$$\Psi = \frac{1}{\sqrt{2}}(0 \quad 1 \quad -1 \quad 0)^T$$

$$P_{same}(\mathrm{a},\ \mathrm{b}) = \left(VV^T\mathrm{RotOp}(\mathrm{a},\ \mathrm{b})\Psi\right)^2 + \left(HH^T\mathrm{RotOp}(\mathrm{a},\ \mathrm{b})\Psi\right)^2$$

$$P_{diff}(\mathrm{a},\ \mathrm{b}) = \left(VH^T\mathrm{RotOp}(\mathrm{a},\ \mathrm{b})\Psi\right)^2 + \left(HV^T\mathrm{RotOp}(\mathrm{a},\ \mathrm{b})\Psi\right)^2$$

$$\mathrm{Corr}(\mathrm{a},\ \mathrm{b}) = P_{same}(\mathrm{a},\ \mathrm{b}) - P_{diff}(\mathrm{a},\ \mathrm{b})$$



This page titled 8.56: A Brief Description of Aspect's Experiment is shared under a CC BY 4.0 license and was authored, remixed, and/or curated by Frank Rioux via source content that was edited to the style and standards of the LibreTexts platform.

8.57: The Kochen-Specker Theorem Illustrated Using a Three-Qubit GHZ System

In the '90s N. David Mermin published two articles in the general physics literature (Physics Today, June 1990; American Journal of Physics, August 1990) on the Greenberger-Horne-Zeilinger (GHZ) gedanken experiment (American Journal of Physics, December 1990; Nature, 3 February 2000) involving three spin-1/2 particles that illustrated the clash between local realism and the quantum view of reality for the quantum nonspecialist. The purpose of this tutorial is to use the GHZ example to illustrate the Kochen-Specker (KS) theorem by stripping away the use of the three-spin wave function in the analysis of the thought experiment.

The KS theorem asserts that no noncontextual (NC) hidden variable (HV) model (NCHV) can agree with the measurement predictions of quantum theory for Hilbert space dimensions greater than 2. The problem dealt with here is, of course, three-dimensional.

The three spin-1/2 particles are created in a single event and move apart in the horizontal y-z plane. It will be shown that a consideration of spin measurements (in units of h/4π in the x- and y-directions reveals the impossibility of assigning values to the spin observables independent of measurement.

The x- and y-direction spin operators are the Pauli matrices:

$$\sigma_x = \begin{pmatrix} 0 & 1 \\ 1 & 0 \end{pmatrix} \quad \sigma_y = \begin{pmatrix} 0 & -i \\ i & 0 \end{pmatrix}$$

The eigenvalues of the Pauli matrices are +/- 1:

$$\text{eigenvals}(\sigma_x) = \begin{pmatrix} 1 \\ -1 \end{pmatrix} \quad \text{eigenvals}(\sigma_y) = \begin{pmatrix} 1 \\ -1 \end{pmatrix}$$

The following operators represent the measurement protocols for spins 1, 2, and 3.

$$\sigma_x^1 \otimes \sigma_y^2 \otimes \sigma_y^3 \quad \sigma_y^1 \otimes \sigma_y^2 \otimes \sigma_x^3 \quad \sigma_x^1 \otimes \sigma_x^2 \otimes \sigma_x^3$$

The tensor matrix product, also known as the Kronecker product, is available in Mathcad. The operators in tensor format are formed as follows.

$$\sigma_{xyy}\sigma_{yxy} - \sigma_{yxy}\sigma_{xyy} \to 0 \quad \sigma_{xyy}\sigma_{yyx} - \sigma_{yyx}\sigma_{xyy} \to 0 \quad \sigma_{xyy}\sigma_{xxx} - \sigma_{xxx}\sigma_{xyy} \to 0$$
$$\sigma_{yxy}\sigma_{yyx} - \sigma_{yyx}\sigma_{yxy} \to 0 \quad \sigma_{yxy}\sigma_{xxx} - \sigma_{xxx}\sigma_{yxy} \to 0 \quad \sigma_{yyx}\sigma_{xxx} - \sigma_{xxx}\sigma_{yyx} \to 0$$

The next step is to compare the matrix for the product of the first three operators $(\sigma_{xyy}\sigma_{yxy}\sigma_{yyx})$ with that of the fourth (σ_{xxx}).

$$\sigma_{xyy}\sigma_{yxy}\sigma_{yyx} = \begin{pmatrix} 0 & 0 & 0 & 0 & 0 & 0 & 0 & -1 \\ 0 & 0 & 0 & 0 & 0 & 0 & -1 & 0 \\ 0 & 0 & 0 & 0 & 0 & -1 & 0 & 0 \\ 0 & 0 & 0 & 0 & -1 & 0 & 0 & 0 \\ 0 & 0 & 0 & -1 & 0 & 0 & 0 & 0 \\ 0 & 0 & -1 & 0 & 0 & 0 & 0 & 0 \\ 0 & -1 & 0 & 0 & 0 & 0 & 0 & 0 \\ -1 & 0 & 0 & 0 & 0 & 0 & 0 & 0 \end{pmatrix} \quad \sigma_{xxx} = \begin{pmatrix} 0 & 0 & 0 & 0 & 0 & 0 & 0 & 1 \\ 0 & 0 & 0 & 0 & 0 & 0 & 1 & 0 \\ 0 & 0 & 0 & 0 & 0 & 1 & 0 & 0 \\ 0 & 0 & 0 & 0 & 1 & 0 & 0 & 0 \\ 0 & 0 & 0 & 1 & 0 & 0 & 0 & 0 \\ 0 & 0 & 1 & 0 & 0 & 0 & 0 & 0 \\ 0 & 1 & 0 & 0 & 0 & 0 & 0 & 0 \\ 1 & 0 & 0 & 0 & 0 & 0 & 0 & 0 \end{pmatrix}$$

This indicates the following relationship between the four operators and leads quickly to a refutation of the concept of noncontextual, hidden values for quantum mechanical observables.

$$\left(\sigma_x^1 \otimes \sigma_y^2 \otimes \sigma_y^3\right)\left(\sigma_y^1 \otimes \sigma_x^2 \otimes \sigma_y^3\right)\left(\sigma_y^1 \otimes \sigma_y^2 \otimes \sigma_x^3\right) = -\left(\sigma_x^1 \otimes \sigma_x^2 \otimes \sigma_x^3\right)$$

Local realism assumes that objects have definite properties independent of measurement. In this example it assumes that the x- and y-components of the spin have definite values prior to measurement. This position leads to a contradiction with the above result. There is no way to assign eigenvalues (+/-1) to the operators that is consistent with the above result.

Concentrating on the operator on the left side, we notice that there is a σ_y measurement on the first spin in the second and third term. If the spin state is well-defined before measurement those results have to be the same, either both +1 or both -1, so that the product of the two measurements is +1. There is a σ_y measurement on the second spin in terms one and three. By similar arguments those results will lead to a product of +1 also. Finally there is a σ_y measurement on the third spin in terms one and two. By similar

arguments those results will lead to a product of +1 also. Incorporating these observations into the expression above leads to the following contradiction.

$$\sigma_x^1 \otimes \sigma_x^2 \otimes \sigma_x^3 = -\sigma_x^1 \otimes \sigma_x^2 \otimes \sigma_x^3$$

A brute force method can be used to confirm this result by showing that the left and right sides of the equation are not equal for any legitimate set of values for the individual spins. This is shown for several such sets below.

$$x1 = 1 \quad x2 = 1 \quad x3 = 1 \quad y1 = 1 \quad y2 = 1 \quad y3 = 1$$

$$(\mathrm{x1\ y2\ y3})\ (\mathrm{y1\ x2\ y3})\ (\mathrm{y1\ y2\ x3}) = 1 \quad -(\mathrm{x1\ x2\ x3}) = -1$$

$$x1 = -1 \quad x2 = 1 \quad x3 = 1 \quad y1 = 1 \quad y2 = -1 \quad y3 = -1$$

$$(\mathrm{x1\ y2\ y3})\ (\mathrm{y1\ x2\ y3})\ (\mathrm{y1\ y2\ x3}) = \text{-1} \quad -(\mathrm{x1\ x2\ x3}) = 1$$

$$x1 = -1 \quad x2 = -1 \quad x3 = -1 \quad y1 = -1 \quad y2 = -1 \quad y3 = -1$$

$$(\mathrm{x1\ y2\ y3})\ (\mathrm{y1\ x2\ y3})\ (\mathrm{y1\ y2\ x3}) = -1 \quad -(\mathrm{x1\ x2\ x3}) = 1$$

The Kochen-Specker theorem demonstrates that it is, in general, impossible to ascribe to an individual quantum system a definite value for each of a set of observables not all of which necessarily commute. N. David Mermin, *Physical Review Letters*, 65, 3373 (1990).

This page titled 8.57: The Kochen-Specker Theorem Illustrated Using a Three-Qubit GHZ System is shared under a CC BY 4.0 license and was authored, remixed, and/or curated by Frank Rioux via source content that was edited to the style and standards of the LibreTexts platform.

8.58: A Brief Introduction to Entanglement Swapping

In the field of quantum information interference, superpositions and entangled states are essential resources. Entanglement, a non-factorable superposition, is routinely achieved when two photons are emitted from the same source, say a parametric down converter (PDC). Entanglement swapping involves the transfer of entanglement to two photons that were produced independently and never previously interacted. The Bell states are the four maximally entangled two-qubit entangled basis for a four-dimensional Hilbert space and play an essential role in quantum information theory and technology, including teleportation and entanglement swapping. The Bell states are shown below.

$$\Phi_p = \frac{1}{\sqrt{2}}\left[\begin{pmatrix}1\\0\end{pmatrix}\begin{pmatrix}1\\0\end{pmatrix} + \begin{pmatrix}0\\1\end{pmatrix}\begin{pmatrix}0\\1\end{pmatrix}\right] \quad \Phi_p = \frac{1}{\sqrt{2}}\begin{pmatrix}1\\0\\0\\1\end{pmatrix} \qquad \Phi_m = \frac{1}{\sqrt{2}}\left[\begin{pmatrix}1\\0\end{pmatrix}\begin{pmatrix}1\\0\end{pmatrix} - \begin{pmatrix}0\\1\end{pmatrix}\begin{pmatrix}0\\1\end{pmatrix}\right] \quad \Phi_m = \frac{1}{\sqrt{2}}\begin{pmatrix}1\\0\\0\\-1\end{pmatrix}$$

$$\Psi_p = \frac{1}{\sqrt{2}}\left[\begin{pmatrix}1\\0\end{pmatrix}\begin{pmatrix}0\\1\end{pmatrix} + \begin{pmatrix}1\\0\end{pmatrix}\begin{pmatrix}0\\1\end{pmatrix}\right] \quad \Psi_p = \frac{1}{\sqrt{2}}\begin{pmatrix}0\\1\\1\\0\end{pmatrix} \qquad \Psi_m = \frac{1}{\sqrt{2}}\left[\begin{pmatrix}1\\0\end{pmatrix}\begin{pmatrix}0\\1\end{pmatrix} - \begin{pmatrix}0\\1\end{pmatrix}\begin{pmatrix}1\\0\end{pmatrix}\right] \quad \Psi_m = \frac{1}{\sqrt{2}}\begin{pmatrix}0\\1\\-1\\0\end{pmatrix}$$

A four-qubit state is prepared in which photons 1 and 2 are entangled in Bell state Φ_p, and photons 3 and 4 are entangled in Bell state Ψ_m. The state multiplication below is understood to be tensor vector multiplication.

$$\Psi = \Phi_p\Psi_m = \frac{1}{\sqrt{2}}\begin{pmatrix}1\\0\\0\\1\end{pmatrix}\frac{1}{\sqrt{2}}\begin{pmatrix}0\\1\\-1\\0\end{pmatrix} \qquad \Psi = \frac{1}{2}\begin{pmatrix}0 & 1 & -1 & 0 & 0 & 0 & 0 & 0 & 0 & 0 & 0 & 0 & 0 & 1 & -1 & 0\end{pmatrix}^T \qquad I = \begin{pmatrix}1 & 0\\0 & 1\end{pmatrix}$$

$$=$$

Four Bell state measurements are now made on photons 2 and 3 which entangles photons 1 and 4. Projection of photons 2 and 3 onto Φ_p projects photons 1 and 4 onto Ψ_m.

$$\left(\text{kronecker}\left(\text{I},\ \text{kronecker}\left(\Phi_p,\ \Phi_p^T,\ \text{I}\right)\right)\Psi\right)^T$$

$$= \begin{pmatrix}0 & 0.25 & 0 & 0 & 0 & 0 & 0 & 0.25 & -0.25 & 0 & 0 & 0 & 0 & -0.25 & 0\end{pmatrix}$$

$$\frac{1}{2\sqrt{2}}\left[\begin{pmatrix}1\\0\end{pmatrix}\frac{1}{\sqrt{2}}\begin{pmatrix}1\\0\\0\\1\end{pmatrix}\begin{pmatrix}0\\1\end{pmatrix} - \begin{pmatrix}0\\1\end{pmatrix}\frac{1}{\sqrt{2}}\begin{pmatrix}1\\0\\0\\1\end{pmatrix}\begin{pmatrix}1\\0\end{pmatrix}\right]^T$$

$$= \frac{1}{4}\begin{pmatrix}0 & 1 & 0 & 0 & 0 & 0 & 0 & 1 & -1 & 0 & 0 & 0 & 0 & 0 & -1 & 0\end{pmatrix}$$

Projection of photons 2 and 3 onto Φ_m projects photons 1 and 4 onto Ψ_p.

$$\left(\text{kronecker}\left(\text{I},\ \text{kronecker}\left(\Phi_m,\ \Phi_m^T,\ \text{I}\right)\right)\Psi\right)^T$$

$$= \begin{pmatrix}0 & 0.25 & 0 & 0 & 0 & 0 & 0 & 0.25 & -0.25 & 0 & 0 & 0 & 0 & -0.25 & 0\end{pmatrix}$$

$$\frac{1}{2\sqrt{2}}\left[\begin{pmatrix}1\\0\end{pmatrix}\frac{1}{\sqrt{2}}\begin{pmatrix}1\\0\\0\\-1\end{pmatrix}\begin{pmatrix}0\\1\end{pmatrix} + \begin{pmatrix}0\\1\end{pmatrix}\frac{1}{\sqrt{2}}\begin{pmatrix}1\\0\\0\\-1\end{pmatrix}\begin{pmatrix}1\\0\end{pmatrix}\right]^T$$

$$= \frac{1}{4}\begin{pmatrix}0 & 1 & 0 & 0 & 0 & 0 & 0 & -1 & 1 & 0 & 0 & 0 & 0 & 0 & -1 & 0\end{pmatrix}$$

Projection of photons 2 and 3 onto Ψ_p projects photons 1 and 4 onto Φ_m.

$$\left(\text{kronecker}\left(\text{I},\ \text{kronecker}\left(\Psi_p,\ \Psi_p^T,\ \text{I}\right)\right)\Psi\right)^T$$

$$= \begin{pmatrix}0 & 0 & -0.25 & 0 & -0.25 & 0 & 0 & 0 & 0 & 0 & 0 & 0.25 & 0 & 0.25 & 0 & 0\end{pmatrix}$$

$$\frac{1}{2\sqrt{2}}\left[\begin{pmatrix}0\\1\end{pmatrix}\frac{1}{\sqrt{2}}\begin{pmatrix}0\\1\\1\\0\end{pmatrix}\begin{pmatrix}0\\1\end{pmatrix} - \begin{pmatrix}1\\0\end{pmatrix}\frac{1}{\sqrt{2}}\begin{pmatrix}0\\1\\1\\0\end{pmatrix}\begin{pmatrix}1\\0\end{pmatrix}\right]^T$$

$$= \frac{1}{4}\begin{pmatrix}0 & 0 & -1 & 0 & -1 & 0 & 0 & 0 & 0 & 0 & 0 & 1 & 0 & 1 & 0 & 0\end{pmatrix}$$

Finally, projection of photons 2 and 3 onto Ψ_m projects photons 1 and 4 onto Φ_p.

$$\begin{gathered}
\left(\text{kronecker}\left(\mathrm{I},\ \text{kronecker}\left(\Psi_m,\ \Psi_m^T,\ \mathrm{I}\right)\right)\Psi\right)^T \\
= \begin{pmatrix} 0 & 0 & -0.25 & 0 & 0.25 & 0 & 0 & 0 & 0 & 0 & -0.25 & 0 & 0.25 & 0 & 0 \end{pmatrix} \\
\frac{-1}{2\sqrt{2}}\left[\begin{pmatrix}1\\0\end{pmatrix}\frac{1}{\sqrt{2}}\begin{pmatrix}0\\1\\-1\\0\end{pmatrix}\begin{pmatrix}1\\0\end{pmatrix}+\begin{pmatrix}0\\1\end{pmatrix}\frac{1}{\sqrt{2}}\begin{pmatrix}0\\1\\-1\\0\end{pmatrix}\begin{pmatrix}0\\1\end{pmatrix}\right]^T \\
= \frac{1}{4}\begin{pmatrix} 0 & 0 & -1 & 0 & 1 & 0 & 0 & 0 & 0 & 0 & -1 & 0 & 1 & 0 & 0 \end{pmatrix}
\end{gathered}$$

This page titled 8.58: A Brief Introduction to Entanglement Swapping is shared under a CC BY 4.0 license and was authored, remixed, and/or curated by Frank Rioux via source content that was edited to the style and standards of the LibreTexts platform.

8.59: An Entanglement Swapping Protocol

In the field of quantum information, interference, superpositions and entangled states are essential resources. Entanglement, a non-factorable superposition, is routinely achieved when two photons are emitted from the same source, perhaps a parametric down converter (PDC). Entanglement swapping involves the transfer (teleportation) of entanglement to two photons that were produced independently and never previously interacted. The Bell states are the four maximally entangled two-qubit entangled basis for a four-dimensional Hilbert space and play an essential role in quantum information theory and technology, including teleportation and entanglement swapping. This analysis attempts to provide the essential matrix math needed to understand parts of "Entangled delayed-choice entanglement swapping" (arXiv1203.4834) and "Delayed-choice gedanken experiments and their realizations" (arXiv1407.2930). The following analysis deals exclusively with entanglement swapping and does not consider the delayed-choice aspect of the research presented in these papers.

Bell states and the identity operator:

$$\Phi_p = \frac{1}{\sqrt{2}}\begin{pmatrix}1\\0\\0\\1\end{pmatrix} \quad \Phi_m = \frac{1}{\sqrt{2}}\begin{pmatrix}1\\0\\0\\-1\end{pmatrix} \quad \Psi_p = \frac{1}{\sqrt{2}}\begin{pmatrix}0\\1\\1\\0\end{pmatrix} \quad \Psi_m = \frac{1}{\sqrt{2}}\begin{pmatrix}0\\1\\-1\\0\end{pmatrix} \quad I = \begin{pmatrix}1&0\\0&1\end{pmatrix}$$

A four-qubit state is prepared in which photons 1 and 2 are entangled in Bell state Ψ_m, and photons 3 and 4 are also entangled in Bell state Ψ_m. The state multiplication below is understood to be tensor vector multiplication.

$$\Psi_{1234} = \Psi_{m12}\Psi_{m34} = \frac{1}{\sqrt{2}}\begin{pmatrix}0\\1\\-1\\0\end{pmatrix}\frac{1}{\sqrt{2}}\begin{pmatrix}0\\1\\-1\\0\end{pmatrix} \qquad \Psi = \frac{1}{2}$$
$$(0 \quad 0 \quad 0 \quad 0 \quad 0 \quad 1 \quad -1 \quad 0 \quad 0 \quad -1 \quad 1 \quad 0 \quad 0 \quad 0 \quad 0 \quad 0)^T$$

The authors write this state as a superposition of Bell state products to suggest a way to transfer entanglement from 1&2-3&4 to 1&4-2&3: perform a Bell state measurement on photons 2 and 3.

$$|\Psi\rangle_{1234} = \frac{1}{2}\left[|\Psi_p\rangle_{14} \otimes |\Psi_P\rangle_{23} - |\Psi_m\rangle_{14} \otimes \Psi_m\rangle_{23} - |\Psi_m\rangle_{23} - |\Phi_p\rangle_{14} \otimes \Phi_p\rangle_{23} + |\Phi_m\rangle_{14} \otimes \Phi_m\rangle_{23}\right]$$

The following calculations agree with this product of entangled photon pairs 1&4 and 2&3. Projection of photons 2 and 3 onto Ψ_p projects photons 1 and 4 onto Ψ_p.

Projection of photons 2 and 3 onto Φ_p projects photons 1 and 4 onto Ψ_m.

$$\left(\text{kronecker}\left(\text{I},\ \text{kronecker}\left(\Psi_p,\ \Psi_p^T,\ \text{I}\right)\right)\Psi\right)^T$$
$$= (0 \quad 0 \quad 0 \quad 0.25 \quad 0 \quad 0.25 \quad 0 \quad 0 \quad 0 \quad 0 \quad 0.25 \quad 0 \quad 0.25 \quad 0 \quad 0 \quad 0)$$
$$\frac{1}{2\sqrt{2}}\left[\begin{pmatrix}1\\0\end{pmatrix}\frac{1}{\sqrt{2}}\begin{pmatrix}0\\1\\1\\0\end{pmatrix}\begin{pmatrix}0\\1\end{pmatrix} + \begin{pmatrix}0\\1\end{pmatrix}\frac{1}{\sqrt{2}}\begin{pmatrix}0\\1\\1\\0\end{pmatrix}\begin{pmatrix}1\\0\end{pmatrix}\right]^T$$
$$= \frac{1}{4}(0 \quad 0 \quad 0 \quad 1 \quad 0 \quad 1 \quad 0 \quad 1 \quad 0 \quad 0 \quad 0 \quad 0 \quad 1 \quad 0 \quad 1 \quad 0 \quad 0 \quad 0)$$

Projection of photons 2 and 3 onto Ψ_m projects photons 1 and 4 onto -Ψ_m.

$$\left(\text{kronecker}\left(\text{I},\ \text{kronecker}\left(\Psi_m,\ \Psi_m^T,\ \text{I}\right)\right)\Psi\right)^T$$
$$= (0 \quad 0 \quad 0 \quad -0.25 \quad 0 \quad 0.25 \quad 0 \quad 0 \quad 0 \quad 0 \quad 0.25 \quad 0 \quad -0.25 \quad 0 \quad 0 \quad 0)$$
$$\frac{-1}{2\sqrt{2}}\left[\begin{pmatrix}1\\0\end{pmatrix}\frac{1}{\sqrt{2}}\begin{pmatrix}0\\1\\-1\\0\end{pmatrix}\begin{pmatrix}0\\1\end{pmatrix} - \begin{pmatrix}0\\1\end{pmatrix}\frac{1}{\sqrt{2}}\begin{pmatrix}0\\1\\-1\\0\end{pmatrix}\begin{pmatrix}1\\0\end{pmatrix}\right]^T$$
$$= \frac{1}{4}(0 \quad 0 \quad 0 \quad -1 \quad 0 \quad 1 \quad 0 \quad 1 \quad 0 \quad 0 \quad 0 \quad 0 \quad 1 \quad 0 \quad -1 \quad 0 \quad 0 \quad 0)$$

Projection of photons 2 and 3 onto Φ_p projects photons 1 and 4 onto -Φ_p.

$$\left(\text{kronecker}\left(\mathrm{I},\ \text{kronecker}\left(\Phi_p,\ \Phi_p^T,\ \mathrm{I}\right)\right)\Psi\right)^T$$
$$= \begin{pmatrix} -0.25 & 0 & 0 & 0 & 0 & 0 & -0.25 & 0 & 0 & 0 & 0 & 0 & -0.25 \end{pmatrix}$$
$$\frac{-1}{2\sqrt{2}}\left[\begin{pmatrix}1\\0\end{pmatrix}\frac{-1}{\sqrt{2}}\begin{pmatrix}1\\0\\0\\1\end{pmatrix}\begin{pmatrix}0\\1\end{pmatrix}+\begin{pmatrix}0\\1\end{pmatrix}\frac{1}{\sqrt{2}}\begin{pmatrix}1\\0\\0\\1\end{pmatrix}\begin{pmatrix}0\\1\end{pmatrix}\right]^T$$
$$= \frac{1}{4}\begin{pmatrix} -1 & 0 & 0 & 0 & 0 & 0 & -1 & 0 & 0 & -1 & 0 & 0 & 0 & 0 & 0 & -1 \end{pmatrix}$$

Projection of photons 2 and 3 onto Φ_m projects photons 1 and 4 onto Φ_m.

$$\left(\text{kronecker}\left(\mathrm{I},\ \text{kronecker}\left(\Phi_m,\ \Phi_m^T,\ \mathrm{I}\right)\right)\Psi\right)^T$$
$$= \begin{pmatrix} 0.25 & 0 & 0 & 0 & 0 & 0 & -0.25 & 0 & 0 & -0.25 & 0 & 0 & 0 & 0 & 0 & 0.25 \end{pmatrix}$$
$$\frac{1}{2\sqrt{2}}\left[\begin{pmatrix}1\\0\end{pmatrix}\frac{1}{\sqrt{2}}\begin{pmatrix}1\\0\\0\\-1\end{pmatrix}\begin{pmatrix}1\\0\end{pmatrix}-\begin{pmatrix}0\\1\end{pmatrix}\frac{1}{\sqrt{2}}\begin{pmatrix}1\\0\\0\\-1\end{pmatrix}\begin{pmatrix}0\\1\end{pmatrix}\right]^T$$
$$= \frac{1}{4}\begin{pmatrix} 1 & 0 & 0 & 0 & 0 & 0 & -1 & 0 & 0 & -1 & 0 & 0 & 0 & 0 & 0 & 1 \end{pmatrix}$$

The initial four-particle state can be written in the H/V, A/D and R/L polarization bases. See the Appendix for details.

$$\Psi_{1234} = \tfrac{1}{2}(H_1V_2 - V_1H_2) = (H_3V_4 - V_3H_4)$$
$$= \tfrac{1}{2}(H_1V_2V_3V_4 - H_1V_2V_3H_4 - V_1H_2H_3V_4 + V_1H_2V_3H_4 + V_1H_2V_3H_4)$$
$$\Psi_{1234} = \tfrac{1}{2}(A_1D_2 - D_1A_2) = (A_3D_4 - D_3A_4)$$
$$= \tfrac{1}{2}(A_1D_2A_3D_4 - A_1D_2A_3D_4 - A_1D_2D_3A_4 + D_1A_2A_3D_4 + D_1A_2D_3A_4)$$
$$\Psi_{1234} = \tfrac{1}{2}(L_1R_2 - R_1L_2) = (L_3R_4 - R_3L_4)$$
$$= \tfrac{1}{2}(L_1R_2R_3R_4 - L_1R_2R_3L_4 - R_1L_2L_3R_4 + R_1L_2R_3L_4)$$

Where,

$$H = \begin{pmatrix}1\\0\end{pmatrix}\quad V = \begin{pmatrix}0\\1\end{pmatrix}\quad R = \frac{1}{\sqrt{2}}\begin{pmatrix}1\\i\end{pmatrix}\quad L = \frac{1}{\sqrt{2}}\begin{pmatrix}1\\1\end{pmatrix}\quad A = \frac{1}{\sqrt{2}}\begin{pmatrix}1\\-1\end{pmatrix}$$

$$H = \tfrac{1}{\sqrt{2}}(R+L)\quad V = \tfrac{i}{\sqrt{2}}(L-R)\quad H = \tfrac{1}{\sqrt{2}}(D+A)\quad V = \tfrac{1}{\sqrt{2}}(D-A)$$

$$R = \tfrac{1}{\sqrt{2}}(H+iV)\quad L = \tfrac{1}{\sqrt{2}}(H-iV)\quad R = \tfrac{1}{\sqrt{2}}(D+A)$$

After production, photon 1 is sent to Alice and photon 4 is sent to Bob. Photons 2 and 3 are sent to Victor. Alice and Bob can measure their photons in either the H/V, R/L or A/D bases. Victor can measure his photons separately in the H/V basis or he can carry out one of the four Bell state measurements on his photon pairs. This later choice as shown earlier projects photons 1 and 4 into the corresponding entangled Bell state.

The following table shows the possible measurement results that Alice and Bob will obtain, depending on the type of measurement Victor makes on his photons. In experiments 1-4 Victor measures his photons separately in the H/V basis and Alice and Bob do the same. In the remaining experiments Victor does a Bell state measurement on his photons and Alice and Bob measure in any of the three bases.

Experiment	1	2	3	4	′	5	6	7	8	′	9	10	11	12	′	13	14	15	16
Alice1	H	H	V	V'	H	V	H	V	′	L	R	L	R	′	D	A	A	D	
Bob4	V	H	V	H	′	V	H	H	V	′	L	L	R	R	′	D	D	A	A
Victor23	V	V	HH	HV	′	Ψ_p	Ψ_m	Φ_p	Φ_m	′	Ψ_p	Ψ_m	Φ_p	Φ'_m	Ψ_p	Ψ_m	Φ_p	Φ_m	
	H	V																	

Results 1-4 are consistent with the original state expressed in the H/V basis.

$$\Psi_{1234} = \frac{1}{2}(H_1V_2H_3V_4 - H_1V_2V_3H_4 - V_1H_2H_3V_4 + V_1H_2V_3H_4)$$

In the remaining experiments Victor makes a Bell state measurement on photons 2 and 3, and projects photons 1 and 4 into the following Bell states. The table shows measurement results that Alice and Bob could make on their photons given these states. See

the Appendix for more detail.

$$\Psi_{p14} = \frac{1}{\sqrt{2}}(H_1V_4 + V_1H_4) = \frac{i}{\sqrt{2}}(L_1L_4 - R_1R_4) = \frac{1}{\sqrt{2}}(D_1D_4 - A_1A_4)$$
$$\Psi_{m14} = \frac{1}{\sqrt{2}}(H_1V_4 - V_1H_4) = \frac{i}{\sqrt{2}}(L_1L_4 - R_1R_4) = \frac{1}{\sqrt{2}}(A_1D_4 - D_1A_4)$$
$$\Phi_{p14} = \frac{1}{\sqrt{2}}(H_1H_4 + V_1V_4) = \frac{i}{\sqrt{2}}(L_1R_4 + R_1L_4) = \frac{1}{\sqrt{2}}(A_1A_4 - D_1D_4)$$
$$\Phi_{m14} = \frac{1}{\sqrt{2}}(H_1H_4 - V_1V_4) = \frac{i}{\sqrt{2}}(L_1L_4 + R_1R_4) = \frac{1}{\sqrt{2}}(A_1D_4 + D_1A_4)$$

Appendix

The Bell states are written in the H/V, R/L, and A/D bases.

$$\Psi_p = \begin{pmatrix} 0 \\ 1 \\ 1 \\ 0 \end{pmatrix} \quad \frac{1}{\sqrt{2}}(H_iV_j + V_iH_j) \left| \begin{array}{l} \text{substitute, } H_i = \frac{1}{\sqrt{2}}(R_i + L_i) \\ \text{substitute, } V_j = \frac{i}{\sqrt{2}}(R_j - L_j) \\ \text{substitute, } V_i = \frac{i}{\sqrt{2}}(L_i - R_i) \\ \text{substitute, } H_j = \frac{1}{\sqrt{2}}(R_j + L_j) \end{array} \right. \rightarrow \sqrt{2}\left(-\frac{R_iR_ji}{2} + \frac{L_iL_ji}{2}\right)$$

$$\frac{1}{\sqrt{2}}(H_iV_j + V_iH_j) \left| \begin{array}{l} \text{substitute, } H_i = \frac{1}{\sqrt{2}}(D_i + A_i) \\ \text{substitute, } V_j = \frac{i}{\sqrt{2}}(D_j - A_j) \\ \text{substitute, } V_i = \frac{i}{\sqrt{2}}(D_i - A_i) \\ \text{substitute, } H_j = \frac{1}{\sqrt{2}}(D_j + A_j) \end{array} \right. \rightarrow \sqrt{2}\left(\frac{A_iA_ji}{2} - \frac{D_iD_ji}{2}\right)$$

$$\Psi_m = \begin{pmatrix} 0 \\ 1 \\ -1 \\ 0 \end{pmatrix} \quad \frac{1}{\sqrt{2}}(H_iV_j - V_iH_j) \left| \begin{array}{l} \text{substitute, } H_i = \frac{1}{\sqrt{2}}(R_i + L_i) \\ \text{substitute, } V_j = \frac{i}{\sqrt{2}}(L_j - R_j) \\ \text{substitute, } V_i = \frac{i}{\sqrt{2}}(L_i - R_i) \\ \text{substitute, } H_j = \frac{1}{\sqrt{2}}(R_j + L_j) \end{array} \right. \rightarrow \sqrt{2}\left(-\frac{L_iR_ji}{2} + \frac{L_iR_ji}{2}\right)$$

$$\frac{1}{\sqrt{2}}(H_iV_j - V_iH_j) \left| \begin{array}{l} \text{substitute, } H_i = \frac{1}{\sqrt{2}}(D_i + A_i) \\ \text{substitute, } V_j = \frac{i}{\sqrt{2}}(D_j - A_j) \\ \text{substitute, } V_i = \frac{i}{\sqrt{2}}(D_i - A_i) \\ \text{substitute, } H_j = \frac{1}{\sqrt{2}}(D_j + A_j) \end{array} \right. \rightarrow \sqrt{2}\left(\frac{A_iD_ji}{2} - \frac{A_iD_ji}{2}\right)$$

$$\Phi_p = \begin{pmatrix} 1 \\ 0 \\ 0 \\ 1 \end{pmatrix} \quad \frac{1}{\sqrt{2}}(H_iH_j + V_iV_j) \left| \begin{array}{l} \text{substitute, } H_i = \frac{1}{\sqrt{2}}(R_i + L_i) \\ \text{substitute, } V_j = \frac{i}{\sqrt{2}}(L_j - R_j) \\ \text{substitute, } V_i = \frac{i}{\sqrt{2}}(L_i - R_i) \\ \text{substitute, } H_j = \frac{1}{\sqrt{2}}(R_j + L_j) \end{array} \right. \rightarrow \sqrt{2}\left(\frac{L_iR_ji}{2} + \frac{L_iR_ji}{2}\right)$$

$$\frac{1}{\sqrt{2}}(H_iV_j + V_iH_j) \left| \begin{array}{l} \text{substitute, } H_i = \frac{1}{\sqrt{2}}(D_i + A_i) \\ \text{substitute, } V_j = \frac{i}{\sqrt{2}}(D_j - A_j) \\ \text{substitute, } V_i = \frac{i}{\sqrt{2}}(D_i - A_i) \\ \text{substitute, } H_j = \frac{1}{\sqrt{2}}(D_j + A_j) \end{array} \right. \rightarrow \sqrt{2}\left(\frac{A_iA_ji}{2} - \frac{D_iD_ji}{2}\right)$$

$$\Phi_m = \begin{pmatrix} 1 \\ 0 \\ 0 \\ -1 \end{pmatrix} \quad \frac{1}{\sqrt{2}}(H_iH_j - V_iV_j) \left| \begin{array}{l} \text{substitute, } H_i = \frac{1}{\sqrt{2}}(R_i + L_i) \\ \text{substitute, } V_j = \frac{i}{\sqrt{2}}(L_j - R_j) \\ \text{substitute, } V_i = \frac{i}{\sqrt{2}}(L_i - R_i) \\ \text{substitute, } H_j = \frac{1}{\sqrt{2}}(R_j + L_j) \end{array} \right. \rightarrow \sqrt{2}\left(\frac{L_iL_ji}{2} + \frac{R_iR_ji}{2}\right)$$

$$\frac{1}{\sqrt{2}}(H_iV_j - V_iH_j) \left| \begin{array}{l} \text{substitute, } H_i = \frac{1}{\sqrt{2}}(D_i + A_i) \\ \text{substitute, } V_j = \frac{i}{\sqrt{2}}(D_j - A_j) \\ \text{substitute, } V_i = \frac{i}{\sqrt{2}}(D_i - A_i) \\ \text{substitute, } H_j = \frac{1}{\sqrt{2}}(D_j + A_j) \end{array} \right. \rightarrow \sqrt{2}\left(\frac{A_iD_ji}{2} - \frac{A_jD_ii}{2}\right)$$

The initial state is written in the H/V, R/L, and A/D bases.

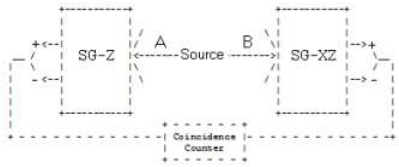
$$\frac{1}{2}(H_1V_2 - V_1H_2)(H_3V_4 - V_3H_4) \left| \begin{array}{l} \text{substitute, } \mathrm{H}_1 = \frac{1}{\sqrt{2}}(D_1 + A_1) \\ \text{substitute, } \mathrm{V}_2 = \frac{1}{\sqrt{2}}(D_2 - A_2) \\ \text{substitute, } \mathrm{V}_1 = \frac{1}{\sqrt{2}}(D_1 - A_1) \\ \text{substitute, } \mathrm{H}_2 = \frac{1}{\sqrt{2}}(D_2 + A_2) \\ \text{substitute, } \mathrm{H}_3 = \frac{1}{\sqrt{2}}(D_3 + A_3) \\ \text{substitute, } \mathrm{V}_3 = \frac{1}{\sqrt{2}}(D_3 - A_3) \\ \text{substitute, } \mathrm{H}_4 = \frac{1}{\sqrt{2}}(D_4 + A_4) \\ \text{substitute, } \mathrm{V}_4 = \frac{1}{\sqrt{2}}(D_4 - A_4) \end{array} \right. \rightarrow \frac{A_1D_2 - A_2D_1)(A_3D_4 - A_4D_3)}{2}$$

$$\frac{1}{2}(H_1V_2 - V_1H_2)(H_3V_4 - V_3H_4) \left| \begin{array}{l} \text{substitute, } \mathrm{H}_1 = \frac{1}{\sqrt{2}}(R_1 + L_1) \\ \text{substitute, } \mathrm{V}_2 = \frac{i}{\sqrt{2}}(L_2 - R_2) \\ \text{substitute, } \mathrm{V}_1 = \frac{i}{\sqrt{2}}(L_1 - R_1) \\ \text{substitute, } \mathrm{H}_2 = \frac{1}{\sqrt{2}}(R_2 + L_2) \\ \text{substitute, } \mathrm{H}_3 = \frac{1}{\sqrt{2}}(R_3 + L_3) \\ \text{substitute, } \mathrm{V}_3 = \frac{i}{\sqrt{2}}(L_3 - R_3) \\ \text{substitute, } \mathrm{H}_4 = \frac{1}{\sqrt{2}}(R_4 + L_4) \\ \text{substitute, } \mathrm{V}_4 = \frac{1}{\sqrt{2}}(L_4 - R_4) \end{array} \right. \rightarrow \frac{L_1R_2 - L_2R_1)(L_3R_4 - L_4R_3)}{2}$$

This page titled 8.59: An Entanglement Swapping Protocol is shared under a CC BY 4.0 license and was authored, remixed, and/or curated by Frank Rioux via source content that was edited to the style and standards of the LibreTexts platform.

8.60: Quantum Correlations Simplified

In order to explore the conflict between quantum mechanics and local realism a spin-1/2 pair is prepared in an entangled singlet state and the individual particles travel in opposite directions on the y-axis to a pair of Stern-Gerlach detectors which are set up to measure spin in the x-z plane. Particle A's spin is measured along the z-axis, and particle B's spin is measured at any angle θ with respect to the z-axis. The experimental setup is shown below.



The entangled singlet spin state is written in both the z- and θ-direction spin eigenstates.

$$|\Psi\rangle = \frac{1}{\sqrt{2}}\left[|\uparrow\rangle_A|\downarrow\rangle_B - |\downarrow\rangle_A|\uparrow\rangle_B\right]$$

$$= \frac{1}{\sqrt{2}}\left[\begin{pmatrix}\cos\left(\frac{\theta}{2}\right)\\ \sin\left(\frac{\theta}{2}\right)\end{pmatrix}_A \otimes \begin{pmatrix}-\sin\left(\frac{\theta}{2}\right)\\ \cos\left(\frac{\theta}{2}\right)\end{pmatrix}_B - \begin{pmatrix}-\sin\left(\frac{\theta}{2}\right)\\ \cos\left(\frac{\theta}{2}\right)\end{pmatrix}_A \otimes \begin{pmatrix}\cos\left(\frac{\theta}{2}\right)\\ \sin\left(\frac{\theta}{2}\right)\end{pmatrix}_B\right] = \frac{1}{\sqrt{2}}\begin{pmatrix}0\\1\\-1\\0\end{pmatrix}$$

$$\text{Spin-up Eigenvalue } +1 \quad \varphi_u(\theta) = \begin{pmatrix}\cos\left(\frac{\theta}{2}\right)\\ \sin\left(\frac{\theta}{2}\right)\end{pmatrix} \quad \text{Spin-down Eigenvalue -1} \quad \varphi_d(\theta) = \begin{pmatrix}-\sin\left(\frac{\theta}{2}\right)\\ \cos\left(\frac{\theta}{2}\right)\end{pmatrix}$$

If particle A is observed to be spin-up in the z-direction (eigenvalue +1), particle B is spin-down in the z-direction due to the singlet nature of the entangled state.

The probability B will be found on measurement to be spin-up in the θ-direction yielding a composite eigenvalue of +1 is:

$$\left(\varphi_u(\theta)^T\varphi_d(0)\right)^2 \text{ simplify } \rightarrow \frac{1}{2} - \frac{\cos\theta}{2}$$

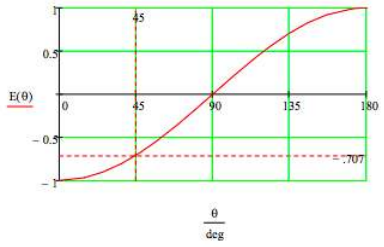
The probability B will be found on measurement to be spin-down in the θ-direction yielding a composite eigenvalue of -1 is:

$$\left(\varphi_d(\theta)^T\varphi_d(0)\right)^2 \text{ simplify } \rightarrow \frac{\cos\theta}{2} + \frac{1}{2}$$

Therefore the overall quantum correlation or expectation value is:

$$E(\theta) = \left(\varphi_u(\theta)^T\varphi_d(0)\right)^2 - \left(\varphi_d(\theta)^T\varphi_d(0)\right)^2 \text{ simplify } \rightarrow -\cos\theta$$

The expectation value as a function of the measurement angle difference is displayed below. In what follows we will concentrate on the data for only 0 degrees and 45 degrees, and show that a local realistic model is consistent with the 0-degree result but not the 45-degree result.



If the observers measure their spins in the same direction (both θ = 0 deg or both θ = 45 deg) quantum mechanics predicts they will get opposite values due to the singlet nature of the spin state. In other words, the combined expectation value is -1 for these

measurements as shown in the figure above. However, if they measure their spins at 0 and 45 degrees, the expectation value is -0.707.

Realists believe that objects have well-defined properties prior to and independent of observation. Specific 0- and 45-deg spin states are assigned to the particles in the first two columns, with each particle in one of four equally probable spin orientations consistent with the composite singlet state. The next two columns show that these assignments agree with the quantum predictions when both spins are measured at the same angle. The last column shows that these spin assignments disagree with the quantum prediction when one spin is measured at 0 degrees and the other at 45 degrees.

$$\begin{bmatrix} \text{Particle A} & \text{Particle B} & \hat{S}_0(\text{A})\hat{S}_0(\text{B}) & \hat{S}_{45}(\text{A})\hat{S}_{45}(\text{B}) & \hat{S}_0(\text{A})\hat{S}_{45}(\text{B}) \\ |\uparrow\rangle|\nearrow\rangle & |\downarrow\rangle|\swarrow\rangle & -1 & -1 & -1 \\ |\uparrow\rangle|\swarrow\rangle & |\downarrow\rangle|\nearrow\rangle & -1 & -1 & 1 \\ |\downarrow\rangle|\nearrow\rangle & |\uparrow\rangle|\swarrow\rangle & -1 & -1 & 1 \\ |\downarrow\rangle|\swarrow\rangle & |\uparrow\rangle|\nearrow\rangle & -1 & -1 & -1 \\ \text{Realist} & \text{Value} & -1 & -1 & 0 \\ \text{Quantum} & \text{Value} & -1 & -1 & -0.707 \end{bmatrix}$$

This brief analysis demonstrates that there are conceptually simple, Stern-Gerlach like, experiments on spin-1/2 systems which can adjudicate the conflict between local realism and quantum mechanics.

In addition to the disagreement shown in the last column of the table, quantum theory asserts that the realist's spin states are invalid. The spin operator at an angel θ to the vertical in the xz-plane is

$$\text{Op}(\theta) = \varphi_u(\theta)^T\varphi_d(\theta) - \varphi_d(\theta)\varphi_d(\theta)^T \text{ simplify } \rightarrow \begin{pmatrix} \cos(\theta) & \sin(\theta) \\ \sin(\theta) & -\cos(\theta) \end{pmatrix}$$

The operators for spin measurements at 0 and 45 degrees in the xz-plane do not commute.

$$\text{Op (0 deg) Op(45 deg)} - \text{Op(45 deg) Op(0 deg)} = \begin{pmatrix} 0 & 1.414 \\ -1.414 & 0 \end{pmatrix}$$

Therefore, according to quantum theory a particle's spin cannot be simultaneously well-defined for both 0 and 45 degrees.

Addendum

According to Richard Feynman it takes a quantum computer to simulate quantum pheonomenon. The following quantum circuit produces results that are in agreement with experiment as summarized in the graph above. The Hadamard and CNOT gates create the singlet state from the |11> input. $R_z(\theta)$ is the rotation of the measuring device of the second spin. The final Hadamard gates prepare the system for measurement in the x-basis. See arXiv:1712.05642v2 for further detail.

$$\begin{array}{lllllll} |1\rangle & \triangleright & \text{H} & \cdot & \cdots & \text{H} & \triangleright \text{ Measure 0 or 1} \\ & & & | & & & \\ |1\rangle & \triangleright & \cdots & \oplus & \text{R}_z(\theta) & \text{H} & \triangleright \text{ Measure 0 or 1} \end{array}$$

The quantum operators required to execute this circuit are:

$$\text{I} = \begin{pmatrix} 1 & 0 \\ 0 & 1 \end{pmatrix} \quad \text{H} = \frac{1}{\sqrt{2}}\begin{pmatrix} 1 & 1 \\ 1 & -1 \end{pmatrix} \quad \text{R}_z(\theta) = \begin{pmatrix} 1 & 0 \\ 0 & e^{i\theta} \end{pmatrix} \quad \text{CNOT} = \begin{pmatrix} 1 & 0 & 0 & 0 \\ 0 & 1 & 0 & 0 \\ 0 & 0 & 0 & 1 \\ 0 & 0 & 1 & 0 \end{pmatrix}$$

$$\text{BellCircuit}(\theta) = \text{kronecker(H, H) kronecker}\left((\text{I, R})_z(\theta)\right) \text{CNOT kronecker(H, I)}$$

The circuit is run for θ = π/4 to demonstrate that it produces the result highlighted in the graph above. In addition, by varying θ it can be shown that the circuit reproduces the entire plot of E(θ). There are four output states shown below. If the spins are measured in the same state, |00> or |11>, the eigenvalue is +1, if they are different, |01> or |10>, the eigenvalue is -1. The probability for each output state is calculated on the right.

Output state	Eigenvalue	Probability
$\lvert 00\rangle = \begin{pmatrix}1\\0\end{pmatrix} \otimes \begin{pmatrix}1\\0\end{pmatrix} = \begin{pmatrix}1\\0\\0\\0\end{pmatrix}$	1	$\left[\begin{pmatrix}1\\0\\0\\0\end{pmatrix}^T \text{BellCircuit}\left(\frac{\pi}{4}\right) \begin{pmatrix}0\\0\\0\\1\end{pmatrix}\right]^2 = 0.0732$
$\lvert 01\rangle = \begin{pmatrix}1\\0\end{pmatrix} \otimes \begin{pmatrix}0\\1\end{pmatrix} = \begin{pmatrix}0\\1\\0\\0\end{pmatrix}$	-1	$\left[\begin{pmatrix}0\\1\\0\\0\end{pmatrix}^T \text{BellCircuit}\left(\frac{\pi}{4}\right) \begin{pmatrix}0\\0\\0\\1\end{pmatrix}\right]^2 = 0.4268$
$\lvert 10\rangle = \begin{pmatrix}0\\1\end{pmatrix} \otimes \begin{pmatrix}1\\0\end{pmatrix} = \begin{pmatrix}0\\0\\1\\0\end{pmatrix}$	-1	$\left[\begin{pmatrix}0\\0\\1\\0\end{pmatrix}^T \text{BellCircuit}\left(\frac{\pi}{4}\right) \begin{pmatrix}0\\0\\0\\1\end{pmatrix}\right]^2 = 0.4268$
$\lvert 11\rangle = \begin{pmatrix}0\\1\end{pmatrix} \otimes \begin{pmatrix}0\\1\end{pmatrix} = \begin{pmatrix}0\\0\\0\\1\end{pmatrix}$	1	$\left[\begin{pmatrix}0\\0\\0\\1\end{pmatrix}^T \text{BellCircuit}\left(\frac{\pi}{4}\right) \begin{pmatrix}0\\0\\0\\1\end{pmatrix}\right]^2 = 0.0732$

Expectation value or correlation coeficient:

$$0.0732 - 0.4268 - 0.4268 + 0.0732 = -0.707$$

A classical computer manipulates bits which are in well-defined states consisting of 0s and 1s.This entangled two-spin experiment demonstrates that simulation of quantum physics requires a computer that can manipulate 0s and 1s, superpositions of 0 and 1, and entangled superpositions of 0s and 1s. Simulation of quantum physics requires a quantum computer, and the circuit shown above is a quantum computer.

An alternative computational method using projection operators:

Output state	Eigenvalue	Probability
$\lvert 00\rangle = \begin{pmatrix}1\\0\end{pmatrix} \otimes \begin{pmatrix}1\\0\end{pmatrix} = \begin{pmatrix}1\\0\\0\\0\end{pmatrix}$	1	$\left[\left\lvert \text{kronecker}\left[\begin{pmatrix}1&0\\0&0\end{pmatrix}, \begin{pmatrix}1&0\\0&0\end{pmatrix}\right] \text{BellCircuit}\left(\frac{\pi}{4}\right)\begin{pmatrix}0\\0\\0\\1\end{pmatrix}\right\rvert^2\right] = 0.0732$
$\lvert 01\rangle = \begin{pmatrix}1\\0\end{pmatrix} \otimes \begin{pmatrix}0\\1\end{pmatrix} = \begin{pmatrix}0\\1\\0\\0\end{pmatrix}$	−1	$\left[\left\lvert \text{kronecker}\left[\begin{pmatrix}1&0\\0&0\end{pmatrix}, \begin{pmatrix}0&0\\0&1\end{pmatrix}\right] \text{BellCircuit}\left(\frac{\pi}{4}\right)\begin{pmatrix}0\\0\\0\\1\end{pmatrix}\right\rvert^2\right] = 0.4268$
$\lvert 10\rangle = \begin{pmatrix}0\\1\end{pmatrix} \otimes \begin{pmatrix}1\\0\end{pmatrix} = \begin{pmatrix}0\\0\\1\\0\end{pmatrix}$	−1	$\left[\left\lvert \text{kronecker}\left[\begin{pmatrix}0&0\\0&1\end{pmatrix}, \begin{pmatrix}1&0\\0&0\end{pmatrix}\right] \text{BellCircuit}\left(\frac{\pi}{4}\right)\begin{pmatrix}0\\0\\0\\1\end{pmatrix}\right\rvert^2\right] = 0.4268$
$\lvert 11\rangle = \begin{pmatrix}0\\1\end{pmatrix} \otimes \begin{pmatrix}0\\1\end{pmatrix} = \begin{pmatrix}0\\0\\0\\1\end{pmatrix}$	1	$\left[\left\lvert \text{kronecker}\left[\begin{pmatrix}0&0\\0&1\end{pmatrix}, \begin{pmatrix}0&0\\0&1\end{pmatrix}\right] \text{BellCircuit}\left(\frac{\pi}{4}\right)\begin{pmatrix}0\\0\\0\\1\end{pmatrix}\right\rvert^2\right] = 0.0732$

Measuring only one spin using a projection operator and the identity:

$$\left[\left\lvert \text{kronecker}\left[\begin{pmatrix}1&0\\0&0\end{pmatrix}, \begin{pmatrix}1&0\\0&1\end{pmatrix}\right] \text{BellCircuit}\left(\frac{\pi}{4}\right)\begin{pmatrix}0\\0\\0\\1\end{pmatrix}\right\rvert^2\right] = 0.5 \qquad \left[\left\lvert \text{kronecker}\left[\begin{pmatrix}0&0\\0&1\end{pmatrix}, \begin{pmatrix}1&0\\0&1\end{pmatrix}\right] \text{BellCircuit}\left(\frac{\pi}{4}\right)\begin{pmatrix}0\\0\\0\\1\end{pmatrix}\right\rvert^2\right] = 0.5$$

$$\left[\left\lvert \text{kronecker}\left[\begin{pmatrix}1&0\\0&1\end{pmatrix}, \begin{pmatrix}1&0\\0&0\end{pmatrix}\right] \text{BellCircuit}\left(\frac{\pi}{4}\right)\begin{pmatrix}0\\0\\0\\1\end{pmatrix}\right\rvert^2\right] = 0.5 \qquad \left[\left\lvert \text{kronecker}\left[\begin{pmatrix}1&0\\0&1\end{pmatrix}, \begin{pmatrix}0&0\\0&1\end{pmatrix}\right] \text{BellCircuit}\left(\frac{\pi}{4}\right)\begin{pmatrix}0\\0\\0\\1\end{pmatrix}\right\rvert^2\right] = 0.5$$

This page titled 8.60: Quantum Correlations Simplified is shared under a CC BY 4.0 license and was authored, remixed, and/or curated by Frank Rioux via source content that was edited to the style and standards of the LibreTexts platform.

8.61: Simulating Quantum Correlations with a Quantum Computer

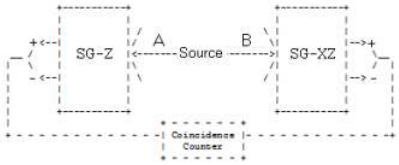
According to Richard Feynman it takes a quantum computer to simulate quantum phenomena. In this tutorial we begin with a traditional quantum analysis of a well-know thought experiment involving correlated spin-1/2 particles. After that the operation of a quantum circuit designed to simulate the thought experiment is analyzed. It will be shown that the quantum analysis and the simulation lead to the same result for the expectation value for the experiment.

The Thought Experiment

A spin-1/2 pair is prepared in an entangled singlet state and the individual particles travel in opposite directions on the y-axis to a pair of Stern-Gerlach (SG) detectors which are set up to measure spin in the x-z plane.

$$|\Psi_m\rangle = \frac{1}{\sqrt{2}}\left[|\uparrow_1\rangle|\downarrow_2\rangle - |\downarrow_1\rangle|\uparrow_2\rangle\right] = \frac{1}{\sqrt{2}}[] = \frac{1}{\sqrt{2}}\begin{pmatrix}0\\1\\-1\\0\end{pmatrix}$$

Particle A's spin is measured along with z-axis, and particle B's spin is measured at any angle θ with respect to the z-axis in the x-z plane. The experimental apparatus is shown below.



The single particle spin operator in the x-z plane is constructed from the Pauli spin operators in the x- and z-directions. θ is the angle of orientation of the measurement magnet with the z-axis.

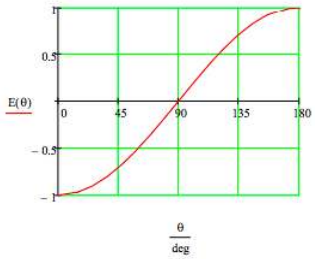
$$\sigma_z = \begin{pmatrix}1 & 0\\0 & -1\end{pmatrix} \quad \sigma_x = \begin{pmatrix}0 & 1\\1 & 0\end{pmatrix} \quad S(\theta) = \cos(\theta)\sigma_z + \sin(\theta)\sigma_x \rightarrow \begin{pmatrix}\cos\theta & \sin\theta\\ \sin\theta & -\cos\theta\end{pmatrix}$$

Tensor multiplication of $S_A(0)$ and $S_B(\theta)$ creates a joint measurement operator for spins A and B.

$$S_A(0)\otimes S_B(\theta) = \begin{pmatrix}1 & 0\\0 & -1\end{pmatrix}\otimes\begin{pmatrix}\cos\theta & \sin\theta\\ \sin\theta & -\cos\theta\end{pmatrix} = \begin{pmatrix}\cos\theta & \sin\theta & 0 & 0\\ \sin\theta & -\cos\theta & 0 & 0\\ 0 & 0 & -\cos\theta & -\sin\theta\\ 0 & 0 & -\sin\theta & \cos\theta\end{pmatrix}$$

The expectation value as a function of the measurement angle of spin B is calculated and the result displayed graphically.

$$\Psi_m = \frac{1}{\sqrt{2}}\begin{pmatrix}0\\1\\-1\\0\end{pmatrix} \quad E(\theta) = \Psi_m^T\begin{pmatrix}\cos\theta & \sin\theta & 0 & 0\\ \sin\theta & -\cos\theta & 0 & 0\\ 0 & 0 & -\cos\theta & -\sin\theta\\ 0 & 0 & -\sin\theta & \cos\theta\end{pmatrix}\Psi_m \rightarrow -\cos(\theta)$$



The Quantum Simulation

A classical computer can't simulate this thought experiment because it manipulates bits which are in well-defined states, 0s and 1s. These classical states are incompatible with the quantum mechanical state above which involves an entangled superposition. This two-spin thought experiment demonstrates that simulation of quantum physics requires a computer that can manipulate 0s and 1s, superpositions of 0 and 1, and entangled superpositions of 0s and 1s. As Feynman asserted, the simulation of quantum physics requires a quantum computer!

The following quantum circuit produces results that are in agreement with the thought experiment as summarized in the graph above. The initial Hadamard and CNOT gates create the singlet state from the |11> input. R z(θ) rotates the spin of B. The final Hadamard gates prepare the system for measurement. See arXiv:1712.05642v2 for further detail.

$$\begin{array}{lccccccc} |1\rangle & \triangleright & \mathrm{H} & \cdot & \cdots & \mathrm{H} & \triangleright & \text{Measure 0 or 1} \\ & & & | & & & & \\ |1\rangle & \triangleright & \cdots & \oplus & \mathrm{R}_z(\theta) & \mathrm{H} & \triangleright & \text{Measure 0 or 1} \end{array}$$

The quantum gates required to execute this circuit and their corresponding truth tables:

Identity	Hadamard gate	R_z rotation	Controlled NOT
$\mathrm{I} = \begin{pmatrix} 1 & 0 \\ 0 & 1 \end{pmatrix}$	$\mathrm{H} = \frac{1}{\sqrt{2}} \begin{pmatrix} 1 & 1 \\ 1 & -1 \end{pmatrix}$	$\mathrm{R}_z(\theta) = \begin{pmatrix} 1 & 0 \\ 0 & e^{i\theta} \end{pmatrix}$	$\mathrm{CNOT} = \begin{pmatrix} 1 & 0 & 0 & 0 \\ 0 & 1 & 0 & 0 \\ 0 & 0 & 0 & 1 \\ 0 & 0 & 1 & 0 \end{pmatrix}$
$\begin{pmatrix} 0 \text{ to } 0 \\ 1 \text{ to } 1 \end{pmatrix}$	$\begin{bmatrix} 0 \text{ to } \frac{1}{\sqrt{2}}(0+1) \\ 1 \text{ to } \frac{1}{\sqrt{2}}(0-1) \end{bmatrix}$	$\begin{pmatrix} 0 \text{ to } 0 \\ 1 \text{ to } \mathrm{e}^{i\theta} \end{pmatrix}$	$\begin{pmatrix} 00 \text{ to } 00 \\ 01 \text{ to } 01 \\ 10 \text{ to } 11 \\ 11 \text{ to } 10 \end{pmatrix}$

A flow diagram for the operation of the simulation circuit is prepared using the truth tables above. It clearly shows the formation of superpositions and an entangled superposition, the singlet spin state highlighted in red below, as the operation of the circuit proceeds.

$$|0\rangle = |\uparrow\rangle \text{ eigenvalue } +1 \; |1\rangle = |\downarrow\rangle \text{ eigenvalue -1}$$
$$|1\rangle|1\rangle = |11\rangle$$
$$\tfrac{1}{\sqrt{2}}\left[|0\rangle - |1\rangle\right]|1\rangle = \tfrac{1}{\sqrt{2}}\left[|01\rangle - |11\rangle\right]$$
$$\mathrm{CNOT}$$
$$\tfrac{1}{\sqrt{2}}\left[|01\rangle - |10\rangle\right]$$
$$\mathrm{I} \otimes \mathrm{R}_z(\theta)$$
$$\tfrac{1}{\sqrt{2}}\left[|0\rangle|e^{i\theta}\rangle - |1\rangle|0\rangle\right] = \tfrac{1}{\sqrt{2}}\left[|0\rangle e^{i\theta}|1\rangle - |1\rangle|0\rangle\right]$$
$$\mathrm{H} \otimes \mathrm{H}$$
$$\tfrac{1}{\sqrt{2}}\left[\tfrac{1}{\sqrt{2}}(|0\rangle+|1\rangle)e^{i\theta}\tfrac{1}{\sqrt{2}}(|0\rangle - |1\rangle) - \tfrac{1}{\sqrt{2}}(|0\rangle - |1\rangle)\tfrac{1}{\sqrt{2}}(|0\rangle+|1\rangle)\right]$$
$$\Downarrow$$
$$\tfrac{1}{2\sqrt{2}}\left[|00\rangle(e^{i\theta}-1) - |01\rangle(e^{i\theta}+1) + |10\rangle(e^{i\theta}+1) - |11\rangle(e^{i\theta}-1)\right]$$

There are four output states highlighted in blue above. If the spins are measured in the same state, |00> or |11>, the eigenvalue is +1, if they are different, |01> or |10>, the eigenvalue is -1. The probabilities for each of the two types of output states are now calculated.

$$|00\rangle \text{ or } |11\rangle \rightarrow \left|\pm\tfrac{1}{2\sqrt{2}}(e^{i\theta}-1)\right|^2 = \tfrac{1-\cos\theta}{4} \quad |01\rangle \text{ or } \rightarrow \left|\pm\tfrac{1}{2\sqrt{2}}(e^{i\theta}+1)\right|^2 = \tfrac{\cos\theta+1}{4}$$

Thus we see that the expectation value (or correlation coefficient) generated experimentally by the operation of this circuit is identical to the one calculated by the initial quantum mechanical analysis of the two-spin thought experiment. A quantum circuit has simulated an unperformed quantum experiment.

$$E(\theta) = 2\left(\frac{1-\cos\theta}{4}\right) - 2\left(\frac{\cos\theta+1}{4}\right) \rightarrow -\cos\theta$$

Another Look at the Simulation

As a companion to this algebraic analysis, the same result will now be demonstrated numerically. The probabilities of observing the four output states (|00>, |01>, |10> and |11>) are calculated for 0, 45, 60 and 90 degrees and shown to be in agreement with the following expectation values.

$$\mathrm{E}(0\ \mathrm{deg}) = \text{-}1 \quad \mathrm{E}(45\ \mathrm{deg}) = \text{-}0.707 \quad \mathrm{E}(60\ \mathrm{deg}) = \text{-}0.5 \quad \mathrm{E}(90\ \mathrm{deg}) = 0$$

The operator representing the circuit is constructed from the matrix operators provided alone.

$$\mathrm{Op}(\theta) = \mathrm{kronecker(H,\ H)}\ \mathrm{kronecker(I,\ R}_z(\theta))\mathrm{CNOT}\ \mathrm{kronecker(H,\ I)}$$

$$|00\rangle \text{ eigenvalue } +1 \left[\left|\begin{pmatrix}1\\0\\0\\0\end{pmatrix}^T \mathrm{Op}(0\ \mathrm{deg}) \begin{pmatrix}0\\0\\0\\1\end{pmatrix}\right|\right]^2 = 0 \qquad |01\rangle \text{ eigenvalue -1} \left[\left|\begin{pmatrix}0\\1\\0\\0\end{pmatrix}^T \mathrm{Op}(0\ \mathrm{deg}) \begin{pmatrix}0\\0\\0\\1\end{pmatrix}\right|\right]^2 = 0.5$$

$$|10\rangle \text{ eigenvalue -1} \left[\left|\begin{pmatrix}0\\0\\1\\0\end{pmatrix}^T \mathrm{Op}(0\ \mathrm{deg}) \begin{pmatrix}0\\0\\0\\1\end{pmatrix}\right|\right]^2 = 0.5 \qquad |11\rangle \text{ eigenvalue -1} \left[\left|\begin{pmatrix}0\\0\\0\\1\end{pmatrix}^T \mathrm{Op}(0\ \mathrm{deg}) \begin{pmatrix}0\\0\\0\\1\end{pmatrix}\right|\right]^2 = 0$$

Expectation value: $0 - 0.5 - 0.5 + 0 = -1$

$$|00\rangle \text{ eigenvalue } +1 \left[\left|\begin{pmatrix}1\\0\\0\\0\end{pmatrix}^T \mathrm{Op}(45\ \mathrm{deg}) \begin{pmatrix}0\\0\\0\\1\end{pmatrix}\right|\right]^2 = 0.073 \qquad |01\rangle \text{ eigenvalue -1} \left[\left|\begin{pmatrix}0\\1\\0\\0\end{pmatrix}^T \mathrm{Op}(45\ \mathrm{deg}) \begin{pmatrix}0\\0\\0\\1\end{pmatrix}\right|\right]^2 = 0.427$$

$$|10\rangle \text{ eigenvalue -1} \left[\left|\begin{pmatrix}0\\0\\1\\0\end{pmatrix}^T \mathrm{Op}(45\ \mathrm{deg}) \begin{pmatrix}0\\0\\0\\1\end{pmatrix}\right|\right]^2 = 0.427 \qquad |11\rangle \text{ eigenvalue -1} \left[\left|\begin{pmatrix}0\\0\\0\\1\end{pmatrix}^T \mathrm{Op}(45\ \mathrm{deg}) \begin{pmatrix}0\\0\\0\\1\end{pmatrix}\right|\right]^2 = 0.073$$

Expectation value: $0.073 - 0.427 - 0.427 + 0.073 = -0.708$

$$|00\rangle \text{ eigenvalue } +1 \left[\left|\begin{pmatrix}1\\0\\0\\0\end{pmatrix}^T \text{Op(60 deg)} \begin{pmatrix}0\\0\\0\\1\end{pmatrix}\right|\right]^2 = 0.125$$

$$|01\rangle \text{ eigenvalue -1} \left[\left|\begin{pmatrix}0\\1\\0\\0\end{pmatrix}^T \text{Op(60 deg)} \begin{pmatrix}0\\0\\0\\1\end{pmatrix}\right|\right]^2 = 0.375$$

$$|10\rangle \text{ eigenvalue -1} \left[\left|\begin{pmatrix}0\\0\\1\\0\end{pmatrix}^T \text{Op(60 deg)} \begin{pmatrix}0\\0\\0\\1\end{pmatrix}\right|\right]^2 = 0.375$$

$$|11\rangle \text{ eigenvalue -1} \left[\left|\begin{pmatrix}0\\0\\0\\1\end{pmatrix}^T \text{Op(60 deg)} \begin{pmatrix}0\\0\\0\\1\end{pmatrix}\right|\right]^2 = 0.125$$

Expectation value: $0.125 - 0.375 - 0.375 + 0.125 = -0.5$

$$|00\rangle \text{ eigenvalue } +1 \left[\left|\begin{pmatrix}1\\0\\0\\0\end{pmatrix}^T \text{Op(90 deg)} \begin{pmatrix}0\\0\\0\\1\end{pmatrix}\right|\right]^2 = 0.25$$

$$|01\rangle \text{ eigenvalue -1} \left[\left|\begin{pmatrix}0\\1\\0\\0\end{pmatrix}^T \text{Op(90 deg)} \begin{pmatrix}0\\0\\0\\1\end{pmatrix}\right|\right]^2 = 0.25$$

$$|10\rangle \text{ eigenvalue -1} \left[\left|\begin{pmatrix}0\\0\\1\\0\end{pmatrix}^T \text{Op(90 deg)} \begin{pmatrix}0\\0\\0\\1\end{pmatrix}\right|\right]^2 = 0.25$$

$$|11\rangle \text{ eigenvalue -1} \left[\left|\begin{pmatrix}0\\0\\0\\1\end{pmatrix}^T \text{Op(90 deg)} \begin{pmatrix}0\\0\\0\\1\end{pmatrix}\right|\right]^2 = 0.25$$

Expectation value: $0.25 - 0.25 - 0.25 + 0.25 = 0.5$

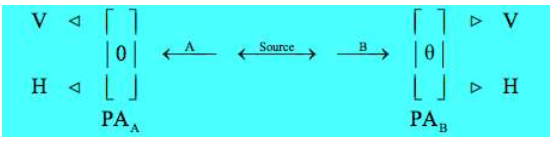
Conclusion

"Quantum simulation is a process in which a quantum computer simulates another quantum system. Because of the various types of quantum weirdness, classical computers can simulate quantum systems only in a clunky, inefficient way. But because a quantum computer is itself a quantum system, capable of exhibiting the full repertoire of quantum weirdness, it can efficiently simulate other quantum systems. The resulting simulation can be so accurate that the behavior the computer will be indistinguishable from the behavior of the simulated system itself ." (Seth Lloyd, Programming the Universe, page 149.)

This page titled 8.61: Simulating Quantum Correlations with a Quantum Computer is shared under a CC BY 4.0 license and was authored, remixed, and/or curated by Frank Rioux via source content that was edited to the style and standards of the LibreTexts platform.

8.62: Quantum Computer Simulation of Photon Correlations

A two-stage atomic cascade emits entangled photons (A and B) in opposite directions with the same circular polarization according to observers in their path. The experiment involves the measurement of photon polarization states in the vertical/horizontal measurement basis, and allows for the rotation of the right-hand detector through an angle θ, in order to explore the consequences of quantum mechanical entanglement. PA stands for polarization analyzer and could simply be a calcite crystal.



The entangled two-photon polarization state is written in the circular and linear polarization states,

$$\Psi\rangle = \frac{1}{\sqrt{2}}\left[|L\rangle_A|L\rangle_B + |R\rangle_A|R\rangle_B\right] = \frac{1}{\sqrt{2}}\left[|V\rangle_A|V\rangle_B - |H\rangle_A|H\rangle_B\right]$$

using

$$|L\rangle = \tfrac{1}{\sqrt{2}}\left[|V\rangle + i|H\rangle\right] \quad |R\rangle = \tfrac{1}{\sqrt{2}}\left[|V\rangle - i|H\rangle\right]$$

The vertical (eigenvalue +1) and horizontal (eigenvalue -1) polarization states for the photons in the measurement plane are given below. Θ is the angle of PA_B.

$$V(\theta) = \begin{pmatrix}\cos\theta \\ \sin\theta\end{pmatrix} \quad H(\theta) = \begin{pmatrix}-\sin\theta \\ \cos\theta\end{pmatrix} \quad V(0) = \begin{pmatrix}1 \\ 0\end{pmatrix} \quad H(0) = \begin{pmatrix}0 \\ 1\end{pmatrix}$$

If photon A has vertical polarization photon B also has vertical polarization, the probability that photon B has vertical polarization when measured at an angle θ giving a composite eigenvalue of +1 is,

$$\left(V(\theta)^T V(0)\right)^2 \rightarrow \cos(\theta)^2$$

If photon A has vertical polarization photon B also has vertical polarization, the probability that photon B has horizontal polarization when measured at an angle θ giving a composite eigenvalue of -1 is,

$$\left(H(\theta)^T V(0)\right)^2 \rightarrow \sin(\theta)^2$$

Therefore the overall quantum correlation coefficient or expectation value is:

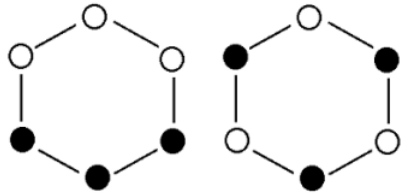
$$E(\theta) = \left(V(\theta)^T V(0)\right)^2 - \left(H(\theta)^T V(0)\right)^2 \text{ simplify } \rightarrow \cos(2\theta)$$

Now it will be shown that a local-realistic, hidden-variable model can be constructed which is in agreement with the quantum calculations for 0 and 90 degrees, but not for 30 and 60 degrees (highlighted).

$$\text{E}(0 \text{ deg}) = 1 \quad \text{E}(30 \text{ deg}) = 0.5 \quad \text{E}(60 \text{ deg}) = -0.5 \quad \text{E}(90 \text{ deg}) = -1$$

If objects have well-defined properties independent of measurement, the results for θ = 0 degrees and θ = 90 degrees require that the photons carry the following instruction sets, where the hexagonal vertices refer to θ values of 0, 30, 60, 90, 120, and 150 degrees.

There are eight possible instruction sets, six of the type on the left and two of the type on the right. The white circles represent vertical polarization with eigenvalue +1 and the black circles represent horizontal polarization with eigenvalue -1. In any given measurement, according to local realism, both photons (A and B) carry identical instruction sets, in other words the same one of the eight possible sets.



The problem is that while these instruction sets are in agreement with the 0 and 90 degree quantum calculations, with expectation values of +1 and -1 respectively, they can't explain the 30 degree predictions of quantum mechanics. The figure on the left shows that the same result should be obtained 4 times with joint eigenvalue +1, and the opposite result twice with joint eigenvalue of -1. For the figure on the right the opposite polarization is always observed giving a joint eigenvalue of -1. Thus, local realism predicts an expectation value of 0 in disagreement with the quantum result of 0.5.

$$\frac{6(1-1+1+1-1+1)+2(-1-1-1-1-1-1)}{8}=0$$

This exercise illustrates Bell's theorem: no local hidden-variable theory can reproduce all the predictions of quantum mechanics for entangled composite systems . As the quantum predictions are confirmed experimentally, the local hidden-variable approach to reality must be abandoned.

This analysis is based on "Simulating Physics with Computers" by Richard Feynman, published in the International Journal of Theoretical Physics (volume 21, pages 481-485), and Julian Brown's Quest for the Quantum Computer (pages 91-100). Feynman used the experiment outlined above to establish that a local classical computer could not simulate quantum physics.

A local classical computer manipulates bits which are in well-defined states, 0s and 1s, shown above graphically in white and black. However, these classical states are incompatible with the quantum mechanical analysis which is consistent with experimental results. This two-photon experiment demonstrates that simulation of quantum physics requires a computer that can manipulate 0s and 1s, superpositions of 0 and 1, and entangled superpositions of 0s and 1s.

Simulation of quantum physics requires a quantum computer. The following quantum circuit simulates this experiment exactly. The Hadamard and CNOT gates transform the input, |10>, into the required entangled Bell state. R(θ) rotates the polarization of photon B clockwise through an angle θ. Finally measurement yields one of the four possible output states: |00>, |01>, |10> or |11>.

$$\begin{array}{lllllll} |1\rangle & \triangleright & \mathrm{H} & \cdot & \cdots & \triangleright & \text{Measure 0 or 1} \\ & & & | & & & \\ |0\rangle & \triangleright & \cdots & \oplus & \mathrm{R}(\theta) & \triangleright & \text{Measure 0 or 1} \end{array}$$

The matrix operators required to build this circuit are as follows:

$$\mathrm{I}=\begin{pmatrix}1 & 0\\ 0 & 1\end{pmatrix}\quad \mathrm{H}=\frac{1}{\sqrt{2}}\begin{pmatrix}1 & 1\\ 1 & -1\end{pmatrix}\quad \mathrm{R}(\theta)=\begin{pmatrix}\cos\theta & -\sin\theta\\ \sin\theta & \cos\theta\end{pmatrix}\quad \mathrm{CNOT}=\begin{pmatrix}1 & 0 & 0 & 0\\ 0 & 1 & 0 & 0\\ 0 & 0 & 0 & 1\\ 0 & 0 & 1 & 0\end{pmatrix}$$

$$\mathrm{BellCircuit}(\theta)=\mathrm{kronecker}(\mathrm{I},\,\mathrm{R}(\theta))\mathrm{CNOT}\ \mathrm{kronecker}(\mathrm{H},\,\mathrm{I})$$

Calculating the probability of observing the four output states (|00>, |01>, |10> and |11>) shows that the quantum circuit correctly simulates the experiment for the 30 and 60 degree rotations.

$$|00\rangle = |VV\rangle \text{ eigenvalue} = +1 \qquad |01\rangle = |VH\rangle \text{ eigenvalue} = \text{-1}$$

$$\left[\left|\begin{pmatrix}1\\0\\0\\0\end{pmatrix}^T \text{BellCircuit}\left(\tfrac{\pi}{6}\right)\begin{pmatrix}0\\0\\1\\0\end{pmatrix}\right|\right]^2 = 0.375 \qquad \left[\left|\begin{pmatrix}0\\1\\0\\0\end{pmatrix}^T \text{BellCircuit}\left(\tfrac{\pi}{6}\right)\begin{pmatrix}0\\0\\1\\0\end{pmatrix}\right|\right]^2 = 0.125$$

$$|10\rangle = |HV\rangle \text{ eigenvalue} = \text{-1} \qquad |11\rangle = |HH\rangle \text{ eigenvalue} = +1$$

$$\left[\left|\begin{pmatrix}0\\0\\1\\0\end{pmatrix}^T \text{BellCircuit}\left(\tfrac{\pi}{6}\right)\begin{pmatrix}0\\0\\1\\0\end{pmatrix}\right|\right]^2 = 0.125 \qquad \left[\left|\begin{pmatrix}0\\0\\0\\1\end{pmatrix}^T \text{BellCircuit}\left(\tfrac{\pi}{6}\right)\begin{pmatrix}0\\0\\1\\0\end{pmatrix}\right|\right]^2 = 0.375$$

Expectation value: $0.375 - 0.125 + 0.375 - 0.125 = 0.5$

$$|00\rangle = |VV\rangle \text{ eigenvalue} = +1 \qquad |01\rangle = |VH\rangle \text{ eigenvalue} = \text{-1}$$

$$\left[\left|\begin{pmatrix}1\\0\\0\\0\end{pmatrix}^T \text{BellCircuit}\left(\tfrac{\pi}{3}\right)\begin{pmatrix}0\\0\\1\\0\end{pmatrix}\right|\right]^2 = 0.125 \qquad \left[\left|\begin{pmatrix}0\\1\\0\\0\end{pmatrix}^T \text{BellCircuit}\left(\tfrac{\pi}{3}\right)\begin{pmatrix}0\\0\\1\\0\end{pmatrix}\right|\right]^2 = 0.375$$

$$|10\rangle = |HV\rangle \text{ eigenvalue} = \text{-1} \qquad |11\rangle = |HH\rangle \text{ eigenvalue} = +1$$

$$\left[\left|\begin{pmatrix}0\\0\\1\\0\end{pmatrix}^T \text{BellCircuit}\left(\tfrac{\pi}{3}\right)\begin{pmatrix}0\\0\\1\\0\end{pmatrix}\right|\right]^2 = 0.375 \qquad \left[\left|\begin{pmatrix}0\\0\\0\\1\end{pmatrix}^T \text{BellCircuit}\left(\tfrac{\pi}{3}\right)\begin{pmatrix}0\\0\\1\\0\end{pmatrix}\right|\right]^2 = 0.125$$

Expectation value: $0.125 - 0.375 - 0.375 + 0.125 = -0.5$

Next an algebraic analysis of the quantum circuit shows that it yields the correct expectation value for all values of θ. This analysis requires the truth tables for the matrix operators.

Identity	Hadamard gate	R(θ) rotation	Controlled NOT
$\begin{pmatrix}0 \text{ to } 0\\1 \text{ to } 1\end{pmatrix}$	$\begin{bmatrix}0 \text{ to } \frac{1}{\sqrt{2}}(0+1)\\1 \text{ to } \frac{1}{\sqrt{2}}(0-1)\end{bmatrix}$	$\begin{pmatrix}1\\0\end{pmatrix} \xrightarrow{R(\theta)} \begin{pmatrix}\cos\theta\\\sin\theta\end{pmatrix}$ $\begin{pmatrix}0\\1\end{pmatrix} \xrightarrow{R(\theta)} \begin{pmatrix}-\sin\theta\\\cos\theta\end{pmatrix}$	$\begin{pmatrix}00 \text{ to } 00\\01 \text{ to } 01\\10 \text{ to } 11\\11 \text{ to } 10\end{pmatrix}$

$$|0\rangle = |V\rangle \text{ eigenvalue } +1 \quad |1\rangle = |H\rangle \text{ eigenvalue -1}$$

$$|1\rangle|0\rangle = |10\rangle$$

$$\text{H} \otimes \text{I}$$

$$\tfrac{1}{\sqrt{2}}\left[|0\rangle - |1\rangle\right]|0\rangle = \tfrac{1}{\sqrt{2}}\left[|00\rangle - |10\rangle\right]$$

$$\text{CNOT}$$

$$\tfrac{1}{\sqrt{2}}\left[|00\rangle - |11\rangle\right]$$

$$\text{I} \otimes \text{R}(\theta)$$

$$\tfrac{1}{\sqrt{2}}\left[|0\rangle(\cos\theta|0\rangle + \sin\theta|1\rangle) - |1\rangle(-\sin\theta|0\rangle + \cos\theta|1\rangle)\right]$$

$$\Downarrow \tfrac{1}{\sqrt{2}}\left[\cos\theta|00\rangle + \sin\theta|01\rangle + \sin\theta|10\rangle - \cos\theta|11\rangle\right]$$

$$\text{Probabilities}$$

$$\Downarrow$$

$$\tfrac{\cos^2\theta}{2}|00\rangle + \tfrac{\sin^2\theta}{2}|01\rangle + \tfrac{\sin^2\theta}{2}|10\rangle + \tfrac{\cos^2\theta}{2}|11\rangle$$

|00> = |VV> and |11> = |HH> have composite eigenvalues of +1. |01> = |VH> and |10> = |HV> have composites eigenvalue of -1. Therefore,

$$\text{E}(\theta) = \cos\theta^2 - \sin\theta^2 \text{ simplify } \rightarrow \cos(2\theta)$$

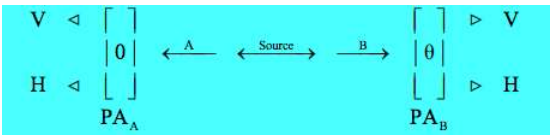
Summary

"Quantum simulation is a process in which a quantum computer simulates another quantum system. Because of the various types of quantum weirdness, classical computers can simulate quantum systems only in a clunky, inefficient way. But because a quantum computer is itself a quantum system, capable of exhibiting the full repertoire of quantum weirdness, it can efficiently simulate other quantum systems. The resulting simulation can be so accurate that the behavior the computer will be indistinguishable from the behavior of the simulated system itself. " (Seth Lloyd, Programming the Universe, page 149.)

This page titled 8.62: Quantum Computer Simulation of Photon Correlations is shared under a CC BY 4.0 license and was authored, remixed, and/or curated by Frank Rioux via source content that was edited to the style and standards of the LibreTexts platform.

8.63: Quantum Correlations Illustrated with Photons

A two-stage atomic cascade emits entangled photons (A and B) in opposite directions with the same circular polarization according to observers in their path. The experiment involves the measurement of photon polarization states in the vertical/horizontal measurement basis, and allows for the rotation of the right-hand detector through an angle θ, in order to explore the consequences of quantum mechanical entanglement. PA stands for polarization analyzer and could simply be a calcite crystal.



The entangled two-photon polarization state is written in the circular and linear polarization bases,

$$|\Psi\rangle = \frac{1}{\sqrt{2}}\left[|L\rangle_A|L\rangle_B + |R\rangle_A|R\rangle_B\right] = \frac{1}{\sqrt{2}}\left[|V\rangle_A|V\rangle_B - |H\rangle_A|H\rangle_B\right]$$

The vertical (eigenvalue +1) and horizontal (eigenvalue -1) polarization states for the photons in the measurement plane are given below. Θ is the angle of the measuring PA.

$$V(\theta) = \begin{pmatrix}\cos\theta \\ \sin\theta\end{pmatrix} \quad H(\theta) = \begin{pmatrix}-\sin\theta \\ \cos\theta\end{pmatrix} \quad V(0) = \begin{pmatrix}1 \\ 0\end{pmatrix} \quad H(0) = \begin{pmatrix}0 \\ 1\end{pmatrix}$$

If photon A has vertical polarization photon B also has vertical polarization, the probability that photon B has vertical polarization when measured at an angle θ giving a composite eigenvalue of +1 is,

$$\left(V(\theta)^T V(0)\right)^2 \rightarrow \cos(\theta)^2$$

If photon A has vertical polarization photon B also has vertical polarization, the probability that photon B has horizontal polarization when measured at an angle θ giving a composite eigenvalue of -1 is,

$$\left(H(\theta)^T V(0)\right)^2 \rightarrow \sin(\theta)^2$$

Therefore the overall quantum correlation coefficient or expectation value is:

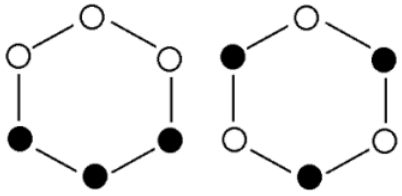
$$E(\theta) = \left(V(\theta)^T V(0)\right)^2 - \left(H(\theta)^T V(0)\right)^2 \text{ simplify } \rightarrow \cos(2\theta)$$

Now it will be shown that a local-realistic, hidden-variable model can be constructed which is in agreement with the quantum calculations for 0, 45 and 90 degrees, but not for 30 and 60 degrees (highlighted).

$$\text{E}(0 \text{ deg}) = 1 \quad \text{E}(30 \text{ deg}) = 0.5 \quad \text{E}(45 \text{ deg}) = 0 \quad \text{E}(60 \text{ deg}) = \text{-}0.5 \quad \text{E}(90 \text{ deg}) = \text{-}1$$

If objects have well-defined properties independent of measurement, the results for θ = 0 degrees and θ = 90 degrees require that the photons carry the following instruction sets, where the hexagonal vertices refer to θ values of 0, 30, 60, 90, 120, and 150 degrees.

There are eight possible instruction sets, six of the type on the left and two of the type on the right. The white circles represent vertical polarization with eigenvalue +1 and the black circles represent horizontal polarization with eigenvalue -1. In any given measurement, according to local realism, both photons (A and B) carry identical instruction sets, in other words the same one of the eight possible sets.



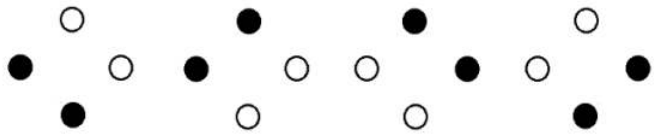
The problem is that while these instruction sets are in agreement with the 0 and 90 degree quantum calculations, with expectation values of +1 and -1 respectively, they can't explain the 30 degree predictions of quantum mechanics. The figure on the left shows that the same result should be obtained 4 times with joint eigenvalue +1, and the opposite result twice with joint eigenvalue of -1. For the figure on the right the opposite polarization is always observed giving a joint eigenvalue of -1. Thus, local realism predicts an expectation value of 0 in disagreement with the quantum result of 0.5.

$$\frac{6(1-1+1+1-1+1)+2(-1-1-1-1-1-1)}{8}=0$$

If we look at 60 degrees, E(60 deg) = 0,we reach the same conclusion: local realism disagrees with quantum result of -0.5.

$$\frac{(-1-1+1-1-1+1)+2(1+1+1+1+1+1)}{8}=0$$

Instruction sets for 45 degrees, E(45 deg) = 0, are shown below. The vertices are 0, 45, 90 and 135 degrees. The instruction sets are constructed so that they satisfy the 0 and 90 degree quantum expectation values of 1 and -1, respectively. It is clear that they also satisfy the 45 degree result yielding an expectation value of zero: (1-1+1-1) = (-1+1-1+1) = (1-1+1-1) = (-1+1-1+1) = 0.



This exercise illustrates Bell's theorem: no local hidden-variable theory can reproduce all the predictions of quantum mechanics for entangled composite systems . As the quantum predictions are confirmed experimentally, the local hidden-variable approach to reality must be abandoned.

This analysis is based on "Simulating Physics with Computers" by Richard Feynman, published in the I*nternational Journal of Theoretical Physics* (volume 21, pages 481-485), and Julian Brown's *Quest for the Quantum Computer* (pages 91-100). Feynman used the experiment outlined above to establish that a local classical computer could not simulate quantum physics.

A local classical computer manipulates bits which are in well-defined states, 0s and 1s, shown above graphically in white and black. However, these classical states are incompatible with the quantum mechanical analysis which is consistent with experimental results. This two-photon experiment demonstrates that simulation of quantum physics requires a computer that can manipulate 0s and 1s, superpositions of 0 and 1, and entangled superpositions of 0s and 1s. Simulation of quantum physics requires a quantum computer!

This page titled 8.63: Quantum Correlations Illustrated with Photons is shared under a CC BY 4.0 license and was authored, remixed, and/or curated by Frank Rioux via source content that was edited to the style and standards of the LibreTexts platform.

8.64: Examining the Local States of an Entangled Bipartate Superposition

Art Hobson recently posted "Implications of bipartite interferometry for the measurement problem" at arXiv:1301.1673. In this post he provides the following interpretation (modified slightly by F. Rioux) of entangled bipartite spin systems. The mathematics below is provided in support of Hobson's analysis.

> When a bipartite system is in an entangled superposition, its subsystems are not in superpositions but are instead mixed states with each subsystem in a definite, but unknown state. An entangled spin is always in its local state, the state described by its reduced density operator, because this is the state actually detected by an observer of the spin. The entangled state is a global superposition of spin correlations, not a superposition of local spin states.
>
> The reduced density operator of an entangled spin is obtained by tracing (averaging) the total density operator over the other spin. This procedure shows that a spin's reduced density operator is diagonal indicating a classical mixed state - it has been stripped of its off-diagonal interference terms.

An entangled bipartite superposition:

$$|\Psi\rangle = \frac{1}{\sqrt{2}}\left[|\uparrow_1\rangle|\downarrow_2\rangle - |\downarrow_1\rangle|\uparrow_2\rangle\right]$$

where

$$|\uparrow\rangle = \begin{pmatrix}1\\0\end{pmatrix} \quad |\downarrow\rangle = \begin{pmatrix}0\\1\end{pmatrix}$$

Its total density operator:

$$\hat{\rho_{12}} = |\Psi\rangle\langle\Psi| = \frac{1}{2}\left[|\uparrow_1\rangle|\downarrow_2\rangle - |\downarrow_1\rangle|\uparrow_2\rangle\right]\left[\langle\downarrow_2|\langle\uparrow_1| - \langle\uparrow_2|\langle\downarrow_1|\right] = \frac{1}{2}\begin{pmatrix}0&0&0&0\\0&1&-1&0\\0&-1&1&0\\0&0&0&0\end{pmatrix}$$

The total density operator written in two equivalent forms:

$$\hat{\rho_{12}} = |\Psi\rangle\langle\Psi| = \tfrac{1}{2}$$
$$\left[|\uparrow_1\rangle\otimes\langle\downarrow_2|\langle\downarrow_2|\otimes\langle\uparrow_1| - |\uparrow_1\rangle\otimes|\downarrow_2\rangle\langle\uparrow_2\otimes\langle\downarrow_1| - |\uparrow_1\rangle\otimes|\uparrow_2\rangle\langle\downarrow_2|\otimes\langle\uparrow_1| + |\downarrow_1\rangle\otimes|\uparrow_2\rangle\langle\uparrow_2|\otimes\langle\downarrow_1|\right]$$

$$\rho_{12} = \tfrac{1}{2}\left[\begin{pmatrix}0\\1\\0\\0\end{pmatrix}\begin{pmatrix}0&1&0&0\end{pmatrix} - \begin{pmatrix}0\\1\\0\\0\end{pmatrix}\begin{pmatrix}0&0&1&0\end{pmatrix} - \begin{pmatrix}0\\0\\1\\0\end{pmatrix}\begin{pmatrix}0&1&0&0\end{pmatrix} + \begin{pmatrix}0\\0\\1\\0\end{pmatrix}\begin{pmatrix}0&0&1&0\end{pmatrix}\right]$$
$$= \begin{pmatrix}0&0&0&0\\0&0.5&-0.5&0\\0&-0.5&0.5&0\\0&0&0&0\end{pmatrix}$$

$$\hat{\rho_{12}} = |\Psi\rangle\langle\Psi| = \tfrac{1}{2}$$
$$\left[|\uparrow_1\rangle\langle\uparrow_1|\otimes|\downarrow_2\rangle\langle\downarrow_2| - |\uparrow_1\rangle\langle\downarrow_1|\otimes|\downarrow_2\rangle\langle\uparrow_2| - |\downarrow_1\rangle\langle\uparrow_1|\otimes|\uparrow_2\rangle\langle\downarrow_2| + |\downarrow_1\rangle\langle\downarrow_1|\otimes|\uparrow_2\rangle\langle\uparrow_2|\right]$$

$$\rho_{12} = \tfrac{1}{2}\left[\begin{array}{l}\text{kronecker}\left[\begin{pmatrix}1\\0\end{pmatrix}\begin{pmatrix}0&1\end{pmatrix},\begin{pmatrix}0\\1\end{pmatrix}\begin{pmatrix}0&1\end{pmatrix}\right] - \text{kronecker}\left[\begin{pmatrix}1\\0\end{pmatrix}\begin{pmatrix}0&1\end{pmatrix},\begin{pmatrix}0\\1\end{pmatrix}\begin{pmatrix}1&0\end{pmatrix}\right]\ldots\\ +-\text{kronecker}\left[\begin{pmatrix}0\\1\end{pmatrix}\begin{pmatrix}1&0\end{pmatrix},\begin{pmatrix}1\\0\end{pmatrix}\begin{pmatrix}0&1\end{pmatrix}\right] + \text{kronecker}\left[\begin{pmatrix}0\\1\end{pmatrix}\begin{pmatrix}0&1\end{pmatrix},\begin{pmatrix}1\\0\end{pmatrix}\begin{pmatrix}1&0\end{pmatrix}\right]\end{array}\right]$$
$$= \begin{pmatrix}0&0&0&0\\0&0.5&-0.5&0\\0&-0.5&0.5&0\\0&0&0&0\end{pmatrix}$$

Calculation of the reduced density operator of spin 1 by tracing the total density operator over spin 2:

$$\hat{\rho_1} = \frac{1}{2}\left[\langle\uparrow_2|\Psi\rangle\langle\Psi|\uparrow_2\rangle + \langle\downarrow_2|\Psi\rangle\langle\Psi|\downarrow_2\rangle\right] = \frac{1}{2}\left[|\downarrow_1\rangle\langle\downarrow_1| + |\uparrow_1\rangle\langle\uparrow_1|\right]$$
$$= \frac{1}{2}\left[\begin{pmatrix}0\\1\end{pmatrix}\begin{pmatrix}0 & 1\end{pmatrix} + \begin{pmatrix}1\\0\end{pmatrix}\begin{pmatrix}1 & 0\end{pmatrix}\right] = \frac{1}{2}\begin{pmatrix}1 & 0\\0 & 1\end{pmatrix}$$

$$rho_1 = \frac{1}{2}\begin{bmatrix}\begin{pmatrix}1\\0\end{pmatrix}\begin{pmatrix}1 & 0\end{pmatrix}\ \mathrm{tr}\left[\begin{pmatrix}0\\1\end{pmatrix}\begin{pmatrix}0 & 1\end{pmatrix}\right] - \begin{pmatrix}1\\0\end{pmatrix}\begin{pmatrix}1 & 0\end{pmatrix}\ \mathrm{tr}\left[\begin{pmatrix}0\\1\end{pmatrix}\begin{pmatrix}1 & 0\end{pmatrix}\right]\ldots \\ +-\begin{pmatrix}0\\1\end{pmatrix}\begin{pmatrix}1 & 0\end{pmatrix}\ \mathrm{tr}\left[\begin{pmatrix}1\\0\end{pmatrix}\begin{pmatrix}0 & 1\end{pmatrix}\right] + \begin{pmatrix}0\\1\end{pmatrix}\begin{pmatrix}0 & 1\end{pmatrix}\ \mathrm{tr}\left[\begin{pmatrix}1\\0\end{pmatrix}\begin{pmatrix}1 & 0\end{pmatrix}\right]\end{bmatrix} \rightarrow \begin{pmatrix}\frac{1}{2} & 0\\0 & \frac{1}{2}\end{pmatrix}$$

Calculation of the reduced density operator of spin 2 by tracing the total density operator over spin 1:

$$\hat{\rho_2} = \frac{1}{2}\left[\langle\uparrow_1|\Psi\rangle\langle\Psi|\uparrow_1\rangle + \langle\downarrow_1|\Psi\rangle\langle\Psi|\downarrow_1\rangle\right] = \frac{1}{2}\left[|\downarrow_2\rangle\langle\downarrow_2| + |\uparrow_2\rangle\langle\uparrow_2|\right]$$
$$= \frac{1}{2}\left[\begin{pmatrix}0\\1\end{pmatrix}\begin{pmatrix}0 & 1\end{pmatrix} + \begin{pmatrix}1\\0\end{pmatrix}\begin{pmatrix}1 & 0\end{pmatrix}\right] = \frac{1}{2}\begin{pmatrix}1 & 0\\0 & 1\end{pmatrix}$$

$$rho_2 = \frac{1}{2}\begin{bmatrix}\mathrm{tr}\left[\begin{pmatrix}1\\0\end{pmatrix}\begin{pmatrix}1 & 0\end{pmatrix}\right]\begin{pmatrix}0\\1\end{pmatrix}\begin{pmatrix}0 & 1\end{pmatrix} - \mathrm{tr}\left[\begin{pmatrix}1\\0\end{pmatrix}\begin{pmatrix}1 & 0\end{pmatrix}\right]\begin{pmatrix}0\\1\end{pmatrix}\begin{pmatrix}1 & 0\end{pmatrix}\ldots \\ +-\mathrm{tr}\left[\begin{pmatrix}0\\1\end{pmatrix}\begin{pmatrix}1 & 0\end{pmatrix}\right]\begin{pmatrix}1\\0\end{pmatrix}\begin{pmatrix}0 & 1\end{pmatrix} + \mathrm{tr}\left[\begin{pmatrix}0\\1\end{pmatrix}\begin{pmatrix}0 & 1\end{pmatrix}\right]\begin{pmatrix}1\\0\end{pmatrix}\begin{pmatrix}1 & 0\end{pmatrix}\end{bmatrix} \rightarrow \begin{pmatrix}\frac{1}{2} & 0\\0 & \frac{1}{2}\end{pmatrix}$$

Now let's flesh this out with specific calculations. Below we have the entangled singlet spin state, its total density operator, and the reduced density operators for the individual spins.

$$\Psi = \frac{1}{\sqrt{2}}\begin{pmatrix}0\\1\\-1\\0\end{pmatrix} \quad \rho_{12} = \Psi\Psi^T = \begin{pmatrix}0 & 0 & 0 & 0\\0 & 0.5 & -0.5 & 0\\0 & 0 & 0 & 0\end{pmatrix} \quad \rho_1 = \frac{1}{2}\begin{pmatrix}1 & 0\\0 & 1\end{pmatrix} \quad \rho_2 = \frac{1}{2}\begin{pmatrix}1 & 0\\0 & 1\end{pmatrix}$$

Next we need the operator required for spin measurements in the z-direction and the identity operator, do nothing.

$$\sigma_z = \begin{pmatrix}1 & 0\\0 & -1\end{pmatrix} \quad I = \begin{pmatrix}1 & 0\\0 & 1\end{pmatrix}$$

Now we calculate expectation values for some spin measurements in the z-direction. As shown below this can be accomplished in two ways, the latter on the right, uses the trace function.

$$\langle\Psi|\hat{O}|\Psi\rangle = \sum_i\langle i|\Psi\rangle\langle\Psi|\hat{O}|i\rangle = Trace\left(|\Psi\rangle\langle\Psi|\hat{O}\right) \text{ where } \sum_i|i\rangle\langle i| = Identity$$

If we measure the z-component of both spins we find perfect anti-correlation which is expected for an entangled singlet state.

$$\Psi^T\mathrm{kronecker}\left(\sigma_z,\ \sigma_z\right)\Psi = -1 \quad \mathrm{tr}\left(\Psi\Psi^T\mathrm{kronecker}\left(\sigma_z,\ \sigma_z\right)\right) = 1$$

However, if only one spin is measured the expectation value is 0.

$$\Psi^T\mathrm{kronecker}\left(\sigma_z,\ \mathrm{I}\right)\Psi = 0 \qquad \mathrm{tr}\left(\Psi\Psi^T\ \mathrm{kronecker}\left(\sigma_z,\ \mathrm{I}\right)\right) = 0 \qquad \Psi^T\mathrm{kronecker}\left(\mathrm{I},\ \sigma_z\right)\Psi = 0 \qquad \mathrm{tr}\left(\Psi\Psi^T\ \mathrm{kronecker}\left(\mathrm{I},\ \sigma_z\right)\right) = 0$$

These results are consistent with the following calculations, which use the reduced density operators for the individual spins. In other words it assumes the spins are in local mixed states, as was asserted previously. The trace function is required for the calculation of expectation values of mixed states.

$$\mathrm{tr}\left(\rho_1,\ \sigma_z\right) = 0 \quad \mathrm{tr}\left(\rho_2,\ \sigma_z\right) = 0$$

To repeat, the entangled state Ψ is a global superposition of spin correlations, not a superposition of local spin states.

This page titled 8.64: Examining the Local States of an Entangled Bipartate Superposition is shared under a CC BY 4.0 license and was authored, remixed, and/or curated by Frank Rioux via source content that was edited to the style and standards of the LibreTexts platform.

8.65: A Brief Introduction to the Quantum Computer

A quantum computer exploits quantum mechanical effects such as superpositions, entanglement and interference to perform new types of calculations that are impossible on a classical computer. Quantum computation is therefore nothing less than a distinctly new way of harnessing nature. (Adapted from David Deutsch, The Fabric of Reality, page 195.)

Whereas classical computers perform operations on classical bits, which can be in one of two discrete states, 0 or 1, quantum computers perform operations on quantum bits, or qubits, which can be put into any superposition of two quantum states, |0> and |1>. Peter Pfeifer, McGraw-Hill Encyclopedia of Science and Industry.

The following example demonstrates how a quantum circuit can function as an algorithm for the evaluation of a mathematical function f(x), and how the same algorithm is capable of parallel evaluations of that function.

$$\begin{pmatrix} \mathrm{x} & \mathrm{f(x)} \\ 0 & 1 \\ 1 & 0 \end{pmatrix} \quad \begin{array}{ccccccc} |x\rangle & \cdots & \cdot & \cdots & \cdots & |x\rangle & \\ & & | & & & & \\ |0\rangle & \cdots & \oplus & \boxed{\mathrm{NOT}} & \cdots & |f(x)\rangle & \end{array} \quad \hat{U}_f|x\rangle|0\rangle = |x\rangle f(x)\rangle$$

As shown below, when |x> is |0> or |1> the circuit behaves like a classical computer yielding the value of f(x). When |x> is a superposition of |0> and |1> the circuit is a quantum computer, operating on both input values simultaneously in a single pass through the circuit, yielding both values of f(x). Note that in the latter case, the intermediate and final states are entangled Bell superpositions. The Bell states are an essential resource in many quantum information applications.

$$\begin{array}{ccccccc} \text{Input} & & \text{Operation} & & \text{Intermediate} & \text{Operation} & \text{Output} \\ |0\rangle|0\rangle & & & & |0\rangle|0\rangle & & |0\rangle|1\rangle \\ |1\rangle|0\rangle & & \xrightarrow{\text{CNOT}} & & |1\rangle|1\rangle & \xrightarrow{\text{I}\otimes\text{NOT}} & |1\rangle|0\rangle \\ \frac{1}{\sqrt{2}}\left[|0\rangle+|1\rangle\right] = \frac{1}{\sqrt{2}}\left[|0\rangle|0\rangle+|1\rangle|0\rangle\right] & & & & \frac{1}{\sqrt{2}}\left[|0\rangle|0\rangle+|1\rangle|1\rangle\right] & & \frac{1}{\sqrt{2}}\left[|0\rangle|1\rangle+|1\rangle|0\rangle\right] \end{array}$$

Haroche and Raimond (pages 94-95 of Exploring the Quantum) describe the latter process as follows: "By superposing the inputs of a computation, one operates the machine 'in parallel', making it compute simultaneously all the values of a function and keeping its state, before any final bit detection is performed, suspended in a coherent superposition of all the possible outcomes." However, as Haroche and Raimond note, on a practical level only one result can be realized for each operation of the circuit because on measurement the superposition created by the circuit collapses to one of the states forming the superposition. Therefore, the exploitation of quantum parallelism for practical purposes such as searches and factorization requires more elaborate quantum circuits than the one presented here.

Truth tables for the quantum circuit:

$$\text{NOT} \quad \begin{pmatrix} 0 \text{ to } 1 \\ 1 \text{ to } 0 \end{pmatrix} \quad \text{CNOT} \quad \begin{pmatrix} \text{Decimal} & \text{Binary} & \text{to} & \text{Binary} & \text{Decimal} \\ 0 & 00 & \text{to} & 00 & 0 \\ 1 & 01 & \text{to} & 01 & 1 \\ 2 & 10 & \text{to} & 11 & 3 \\ 3 & 11 & \text{to} & 10 & 2 \end{pmatrix}$$

This page titled 8.65: A Brief Introduction to the Quantum Computer is shared under a CC BY 4.0 license and was authored, remixed, and/or curated by Frank Rioux via source content that was edited to the style and standards of the LibreTexts platform.

8.66: A Very Simple Example of Parallel Quantum Computation

This tutorial deals with quantum function evaluation and parallel computation. The example is taken from pages 94-95 of Exploring the Quantum by Haroche and Raimond. A certain function of x yields the following table of results.

$$\begin{pmatrix} \text{x} & 0 & 1 \\ \text{f(x)} & 1 & 0 \end{pmatrix}$$

First we establish that the circuit shown below yields the results given in the table, and then demonstrate that it also carries out a parallel calculation in one step using both input values of x.

$$\begin{array}{ccccccc} |x\rangle & \cdots & \cdot & \cdots & \cdots & |x\rangle \\ & & | & & & \\ |0\rangle & \cdots & \oplus & \boxed{\text{NOT}} & \cdots & |f(x)\rangle \end{array} \quad \text{where, for example} \quad |0\rangle = \begin{pmatrix} 1 \\ 0 \end{pmatrix} \quad |1\rangle = \begin{pmatrix} 0 \\ 1 \end{pmatrix}$$

The top wire carries the value of x and the bottom wire is initially set to |0 >. After operation of the controlled-NOT and NOT gates, x remains on the top wire while the bottom wire carries the value of the function, f(x). In other words,

$$\hat{U}_f|x\rangle|0\rangle = |x\rangle|f(x)\rangle$$

The quantum gates in matrix form are:

$$\text{I} = \begin{pmatrix} 1 & 0 \\ 0 & 1 \end{pmatrix} \quad \text{NOT} = \begin{pmatrix} 0 & 1 \\ 1 & 0 \end{pmatrix} \quad \text{CNOT} = \begin{pmatrix} 1 & 0 & 0 & 0 \\ 0 & 1 & 0 & 0 \\ 0 & 0 & 0 & 1 \\ 0 & 0 & 1 & 0 \end{pmatrix}$$

U_f (controlled-NOT, followed by a NOT operation on the lower wire) is a reversible operator. Doing it twice in succession on the initial two-qubit state is equivalent to the identity operation.

Kronecker is Mathcad's command for carrying out matrix tensor multiplication. Note that the identity operator is required when a wire is not involved in an operation. In what follows the quantum circuit is constructed, displayed and its reversibility demonstrated. In other words, repeating the circuit is equivalent to the identity operation. Reversibility is a crucial property in quantum computer circuitry.

$$\text{QuantumCircuit} = \text{kronecker(I, NOT) CNOT}$$

$$\text{QuantumCircuit} = \begin{pmatrix} 0 & 1 & 0 & 0 \\ 1 & 0 & 0 & 0 \\ 0 & 0 & 1 & 0 \\ 0 & 0 & 0 & 1 \end{pmatrix} \quad \text{QuantumCircuit}^2 = \begin{pmatrix} 1 & 0 & 0 & 0 \\ 0 & 1 & 0 & 0 \\ 0 & 0 & 1 & 0 \\ 0 & 0 & 0 & 1 \end{pmatrix}$$

Given the simplicity of the matrix representing the circuit, the following calculations can easily be done by hand.

$$\begin{array}{lccc} & \text{Input} & \text{Calculation} & \text{Output} \\ \text{f(0)} = 1 & \begin{pmatrix} 1 \\ 0 \end{pmatrix} \otimes \begin{pmatrix} 1 \\ 0 \end{pmatrix} = \begin{pmatrix} 1 \\ 0 \\ 0 \\ 0 \end{pmatrix} & \text{QuantumCircuit} \begin{pmatrix} 1 \\ 0 \\ 0 \\ 0 \end{pmatrix} = \begin{pmatrix} 0 \\ 1 \\ 0 \\ 0 \end{pmatrix} & \begin{pmatrix} 0 \\ 1 \\ 0 \\ 0 \end{pmatrix} = \begin{pmatrix} 1 \\ 0 \end{pmatrix} \otimes \begin{pmatrix} 0 \\ 1 \end{pmatrix} \\ \text{f(1)} = 0 & \begin{pmatrix} 0 \\ 1 \end{pmatrix} \otimes \begin{pmatrix} 1 \\ 0 \end{pmatrix} = \begin{pmatrix} 0 \\ 0 \\ 1 \\ 0 \end{pmatrix} & \text{QuantumCircuit} \begin{pmatrix} 0 \\ 0 \\ 1 \\ 0 \end{pmatrix} = \begin{pmatrix} 0 \\ 0 \\ 1 \\ 0 \end{pmatrix} & \begin{pmatrix} 0 \\ 0 \\ 1 \\ 0 \end{pmatrix} = \begin{pmatrix} 0 \\ 1 \end{pmatrix} \otimes \begin{pmatrix} 1 \\ 0 \end{pmatrix} \end{array}$$

These calculations demonstrate that the quantum circuit is a valid algorithm for the calculation of f(x). We now demonstrate parallel computation by putting |x> in a balanced superposition of |0> and |1>. As shown below, the operation of the circuit yields a superposition of the previous results. The function has been evaluated for both values of x in a single pass through the circuit.

$$\frac{1}{\sqrt{2}}\begin{pmatrix}1\\1\end{pmatrix}\otimes\begin{pmatrix}1\\0\end{pmatrix}=\frac{1}{\sqrt{2}}\begin{pmatrix}1\\0\\1\\0\end{pmatrix}\quad \text{QuantumCircuit}\frac{1}{\sqrt{2}}\begin{pmatrix}1\\0\\1\\0\end{pmatrix}=\begin{pmatrix}0\\0.707\\0.707\\0\end{pmatrix}$$

$$\frac{1}{\sqrt{2}}\begin{pmatrix}0\\1\\1\\0\end{pmatrix}=\frac{1}{\sqrt{2}}\left[\begin{pmatrix}0\\1\\0\\0\end{pmatrix}+\begin{pmatrix}0\\0\\1\\0\end{pmatrix}\right]=\frac{1}{\sqrt{2}}\left[\begin{pmatrix}1\\0\end{pmatrix}\begin{pmatrix}0\\1\end{pmatrix}\begin{pmatrix}1\\0\end{pmatrix}\right]$$

Haroche and Raimond describe this process as follows: "By superposing the inputs of a computation, one operates the machine 'in parallel', making it compute simultaneously all the values of a function and keeping its state, before any final bit detection is performed, suspended in a coherent superposition of all the possible outcomes."

In summary, simple calculations have demonstrated how a quantum circuit can function as an algorithm for the evaluation of a mathematical function, and how the same circuit is capable of parallel evaluations of that function.

Input	Operation	Intermediate	Operation	Output
$\lvert 00\rangle$		$\lvert 00\rangle$		$\lvert 01\rangle$
$\lvert 10\rangle$	$\xrightarrow{\text{CNOT}}$	$\lvert 11\rangle$	$\xrightarrow{\text{I}\otimes\text{NOT}}$	$\lvert 10\rangle$
$\frac{1}{\sqrt{2}}[\lvert 0\rangle+\lvert 1\rangle]\lvert 0\rangle=\frac{1}{\sqrt{2}}[\lvert 00\rangle+\lvert 10\rangle]$		$\frac{1}{\sqrt{2}}[\lvert 00\rangle+\lvert 11\rangle]$		$\frac{1}{\sqrt{2}}[\lvert 01\rangle+\lvert 10\rangle]$

However, as Haroche and Raimond note, on a practical level only one result can be realized for each operation of the circuit because on measurement the superposition created by the circuit collapses to one of the states forming the superposition. This is simulated with projection operators (|0><1|) on both registers for the four possible measurement outcomes for each value of x.

$$\text{f}(0)=0\quad\left[\left|\text{kronecker}\left[\begin{pmatrix}1\\0\end{pmatrix}\begin{pmatrix}1\\0\end{pmatrix}^{T},\ \begin{pmatrix}1\\0\end{pmatrix}\begin{pmatrix}1\\0\end{pmatrix}^{T}\right]\ \text{QuantumCircuit}\frac{1}{\sqrt{2}}\begin{pmatrix}1\\0\\1\\0\end{pmatrix}\right|\right]^{2}=0$$

$$\text{f}(0)=1\quad\left[\left|\text{kronecker}\left[\begin{pmatrix}1\\0\end{pmatrix}\begin{pmatrix}1\\0\end{pmatrix}^{T},\ \begin{pmatrix}0\\1\end{pmatrix}\begin{pmatrix}0\\1\end{pmatrix}^{T}\right]\ \text{QuantumCircuit}\frac{1}{\sqrt{2}}\begin{pmatrix}1\\0\\1\\0\end{pmatrix}\right|\right]^{2}=0.5$$

$$\text{f}(1)=0\quad\left[\left|\text{kronecker}\left[\begin{pmatrix}0\\1\end{pmatrix}\begin{pmatrix}0\\1\end{pmatrix}^{T},\ \begin{pmatrix}1\\0\end{pmatrix}\begin{pmatrix}1\\0\end{pmatrix}^{T}\right]\ \text{QuantumCircuit}\frac{1}{\sqrt{2}}\begin{pmatrix}1\\0\\1\\0\end{pmatrix}\right|\right]^{2}=0.5$$

$$\text{f}(1)=1\quad\left[\left|\text{kronecker}\left[\begin{pmatrix}0\\1\end{pmatrix}\begin{pmatrix}0\\1\end{pmatrix}^{T},\ \begin{pmatrix}0\\1\end{pmatrix}\begin{pmatrix}0\\1\end{pmatrix}^{T}\right]\ \text{QuantumCircuit}\frac{1}{\sqrt{2}}\begin{pmatrix}1\\0\\1\\0\end{pmatrix}\right|\right]^{2}=0$$

As Haroche and Raimond write, "It is, however, one thing to compute potentially at once all the values of f(x) and quite another to be able to exploit this quantum parallelism and extract from it more information than from a mundane classical computation. The final stage of information acquisition must always be a measurement." Therefore, the exploitation of quantum parallelism for practical purposes such as searches and factorization requires more elaborate quantum circuits than the one presented here.

Truth tables for quantum circuit elements:

$$\text{Identity}\quad\begin{pmatrix}0\text{ to }0\\1\text{ to }1\end{pmatrix}\quad\text{NOT}\quad\begin{pmatrix}0\text{ to }1\\1\text{ to }0\end{pmatrix}\quad\text{CNOT}\quad\begin{pmatrix}\text{Decimal}&\text{Binary}&\text{to}&\text{Binary}&\text{Decimal}\\0&00&\text{to}&00&0\\1&01&\text{to}&01&1\\2&10&\text{to}&11&3\\3&11&\text{to}&10&2\end{pmatrix}$$

This page titled 8.66: A Very Simple Example of Parallel Quantum Computation is shared under a CC BY 4.0 license and was authored, remixed, and/or curated by Frank Rioux via source content that was edited to the style and standards of the LibreTexts platform.

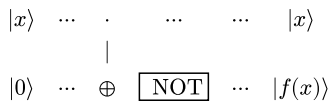
https://chem.libretexts.org/@go/page/148436

8.67: Another Simple Example of Parallel Quantum Computation

This tutorial deals with quantum function evaluation and parallel computation. A certain function of x yields the following table of results.

$$\begin{pmatrix} \text{x} & 0 & 1 \\ \text{f(x)} & 1 & 0 \end{pmatrix}$$

First we establish that the circuit shown below yields the results given in the table, and then demonstrate that it also carries out a parallel calculation in one step using both input values of x.



where, for example $|0\rangle = \begin{pmatrix} 1 \\ 0 \end{pmatrix}$ $|1\rangle = \begin{pmatrix} 0 \\ 1 \end{pmatrix}$

The top wire carries the value of x and the bottom wire is initially set to |0 >. After operation of the controlled-NOT and NOT gates, x remains on the top wire while the bottom wire carries the value of the function, f(x). In other words,

$$\hat{U}_f|x\rangle|0\rangle = |x\rangle|f(x)\rangle$$

The quantum gates in matrix form are:

$$\text{I} = \begin{pmatrix} 1 & 0 \\ 0 & 1 \end{pmatrix} \quad \text{NOT} = \begin{pmatrix} 0 & 1 \\ 1 & 0 \end{pmatrix} \quad \text{ICNOT} = \begin{pmatrix} 1 & 0 & 0 & 0 \\ 0 & 0 & 0 & 1 \\ 0 & 0 & 1 & 0 \\ 0 & 1 & 0 & 0 \end{pmatrix}$$

$$\text{QuantumCircuit} = \text{kronecker(I, NOT) ICNOT} \quad \text{QuantumCircuit} = \begin{pmatrix} 0 & 0 & 0 & 1 \\ 1 & 0 & 0 & 0 \\ 0 & 1 & 0 & 0 \\ 0 & 0 & 1 & 0 \end{pmatrix}$$

Given the simplicity of the matrix representing the circuit, the following calculations can easily be done by hand.

	Input	Calculation	Output
f(0) = 1	$\begin{pmatrix} 1 \\ 0 \end{pmatrix} \otimes \begin{pmatrix} 1 \\ 0 \end{pmatrix} = \begin{pmatrix} 1 \\ 0 \\ 0 \\ 0 \end{pmatrix}$	$\text{QuantumCircuit} \begin{pmatrix} 1 \\ 0 \\ 0 \\ 0 \end{pmatrix} = \begin{pmatrix} 0 \\ 1 \\ 0 \\ 0 \end{pmatrix}$	$\begin{pmatrix} 0 \\ 1 \\ 0 \\ 0 \end{pmatrix} = \begin{pmatrix} 1 \\ 0 \end{pmatrix} \otimes \begin{pmatrix} 0 \\ 1 \end{pmatrix}$
f(1) = 0	$\begin{pmatrix} 0 \\ 1 \end{pmatrix} \otimes \begin{pmatrix} 1 \\ 0 \end{pmatrix} = \begin{pmatrix} 0 \\ 0 \\ 1 \\ 0 \end{pmatrix}$	$\text{QuantumCircuit} \begin{pmatrix} 0 \\ 0 \\ 1 \\ 0 \end{pmatrix} = \begin{pmatrix} 0 \\ 0 \\ 1 \\ 0 \end{pmatrix}$	$\begin{pmatrix} 0 \\ 0 \\ 1 \\ 0 \end{pmatrix} = \begin{pmatrix} 0 \\ 1 \end{pmatrix} \otimes \begin{pmatrix} 1 \\ 0 \end{pmatrix}$

These calculations demonstrate that the quantum circuit is a valid algorithm for the calculation of f(x). We now demonstrate parallel computation by putting |x> in a balanced superposition of |0> and |1>. As shown below, the operation of the circuit yields a superposition of the previous results. The function has been evaluated for both values of x in a single pass through the circuit.

$$\tfrac{1}{\sqrt{2}} \begin{pmatrix} 1 \\ 1 \end{pmatrix} \otimes \begin{pmatrix} 1 \\ 0 \end{pmatrix} = \tfrac{1}{\sqrt{2}} \begin{pmatrix} 1 \\ 0 \\ 1 \\ 0 \end{pmatrix} \quad \text{QuantumCircuit} \tfrac{1}{\sqrt{2}} \begin{pmatrix} 1 \\ 0 \\ 1 \\ 0 \end{pmatrix} = \begin{pmatrix} 0 \\ 0.707 \\ 0 \\ 0.707 \end{pmatrix}$$

$$\frac{1}{\sqrt{2}} \begin{pmatrix} 0 \\ 1 \\ 0 \\ 1 \end{pmatrix} = \frac{1}{\sqrt{2}} \left[\begin{pmatrix} 0 \\ 1 \\ 0 \\ 0 \end{pmatrix} + \begin{pmatrix} 0 \\ 0 \\ 0 \\ 1 \end{pmatrix} \right] = \frac{1}{\sqrt{2}} \left[\begin{pmatrix} 1 \\ 0 \end{pmatrix} \begin{pmatrix} 0 \\ 1 \end{pmatrix} + \begin{pmatrix} 0 \\ 1 \end{pmatrix} \begin{pmatrix} 0 \\ 1 \end{pmatrix} \right]$$

In summary, simple calculations have demonstrated how a quantum circuit can function as an algorithm for the evaluation of a mathematical function, and how the same circuit is capable of parallel evaluations of that function.

Input	Operation	Intermediate	Operation	Output
$\|00\rangle$		$\|00\rangle$		$\|01\rangle$
$\|10\rangle$	$\xrightarrow{\text{ICNOT}}$	$\|11\rangle$	$\xrightarrow{\text{I}\otimes\text{NOT}}$	$\|10\rangle$
$\frac{1}{\sqrt{2}}\left[\|0\rangle+\|1\rangle\right]\|0\rangle = \frac{1}{\sqrt{2}}\left[\|00\rangle+\|10\rangle\right]$		$\frac{1}{\sqrt{2}}\left[\|00\rangle+\|10\rangle\right]$		$\frac{1}{\sqrt{2}}\left[\|01\rangle+\|11\rangle\right]$

However, on a practical level only one result can be realized for each operation of the circuit because on measurement the superposition created by the circuit collapses to one of the states forming the superposition.

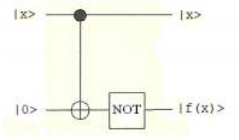
This page titled 8.67: Another Simple Example of Parallel Quantum Computation is shared under a CC BY 4.0 license and was authored, remixed, and/or curated by Frank Rioux via source content that was edited to the style and standards of the LibreTexts platform.

8.68: A Simple Solution to Deutsch's Problem

This tutorial is closely related to the preceding one. A certain function of x maps {0,1} to {0,1}. The four possible outcomes of the evaluation of f(x) are given in tabular form.

$$\begin{pmatrix} \text{x} & ' & 0 & 1 & ' & 0 & 1 & ' & 0 & 1 & ' & 0 & 1 \\ \text{f(x)} & ' & 0 & 0 & ' & 1 & 1 & ' & 0 & 1 & ' & 1 & 0 \end{pmatrix}$$

In the previous tutorial we established that the circuit shown below yields the result given in the right most section of the table. In other words, f(x) is a balanced function, because $f(0) \neq f(1)$, as is the result immediately to its left. The results in the first two sections are labelled constant because $f(0) = f(1)$.



where, for example

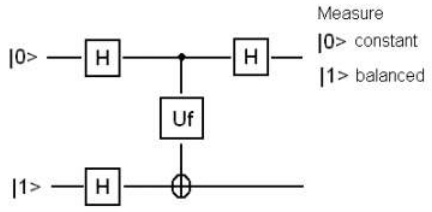
$$|0\rangle = \begin{pmatrix} 1 \\ 0 \end{pmatrix} \quad |1\rangle = \begin{pmatrix} 0 \\ 1 \end{pmatrix}$$

This circuit carries out,

$$\hat{U}_f|x\rangle|0\rangle = |x\rangle|f(x)\rangle$$

where Uf (controlled-NOT, followed by a NOT operation on the lower wire) is a unitary operator that accepts input |x> on the top wire and places f(x) on the bottom wire.

From the classical perspective, if the question (as asked by Deutsch) is whether f(x) is constant or balanced then one must calculate both f(0) and f(1) to answer the question. Deutsch pointed out that quantum superpositions and the interference effects between them allow the answer to be given with one pass through a modified version of the circuit as shown here.



The input |0>|1> is followed by a Hadamard gate on each wire. As is well known the Hadamard operation creates the following superposition states.

$$\text{H}\begin{pmatrix} 1 \\ 0 \end{pmatrix} = \tfrac{1}{\sqrt{2}}\begin{pmatrix} 1 \\ 1 \end{pmatrix} \quad \text{H}\begin{pmatrix} 0 \\ 1 \end{pmatrix} = \tfrac{1}{\sqrt{2}}\begin{pmatrix} 1 \\ -1 \end{pmatrix}$$

Therefore the Hadamard operations transform the input state to the following two-qubit state which is fed to U_f.

$$|x\rangle|y\rangle = \frac{1}{\sqrt{2}}\begin{pmatrix} 1 \\ 1 \end{pmatrix} \otimes \frac{1}{\sqrt{2}}\begin{pmatrix} 1 \\ -1 \end{pmatrix} = \frac{1}{2}\begin{pmatrix} 1 \\ -1 \\ 1 \\ -1 \end{pmatrix}$$

U_f processes its input to generate the following output.

$$\hat{U}_f|x\rangle|y\rangle = |x\rangle|\text{mod}_2(y + f(x))\rangle = |x\rangle|y \oplus f(x)\rangle$$

To facilitate an algebraic analysis of the circuit operation the input state is written as,

$$|x\rangle|y\rangle = \frac{1}{\sqrt{2}}\left[|0\rangle+|1\rangle\right]\frac{1}{\sqrt{2}}\left[|0\rangle-|1\rangle\right] = \frac{1}{2}\left[|0\rangle|0\rangle-|0\rangle|1\rangle+|1\rangle|0\rangle-|1\rangle|1\rangle\right]$$

In this format U_f creates the following output state.

$$\Psi_{out} = \frac{1}{2}\left[|0\rangle|f(0)\rangle-|0\rangle|1\oplus f(0)\rangle+|1\rangle|f(1)\rangle-|1\rangle|1\oplus f(1)\rangle\right]$$

As the table shows there are four possible outcomes depending on whether the function is constant (the first two) or balanced (the second two).

$$\Psi_{out} \xrightarrow[f(0)=0]{f(0)=f(1)} \tfrac{1}{2}\left[|0\rangle|0\rangle-|0\rangle|1\rangle+|1\rangle|0\rangle-|1\rangle|1\rangle\right] = \tfrac{1}{2}\left(|0\rangle+|1\rangle\right)\left(|0\rangle-|1\rangle\right)$$
$$\Psi_{out} \xrightarrow[f(0)=1]{f(0)=f(1)} \tfrac{1}{2}\left[|0\rangle|1\rangle-|0\rangle|0\rangle+|1\rangle|1\rangle-|1\rangle|0\rangle\right] = -\tfrac{1}{2}\left(|0\rangle+|1\rangle\right)\left(|0\rangle-|1\rangle\right)$$
$$\Psi_{out} \xrightarrow[f(0)=0]{f(0)\neq f(1)} \tfrac{1}{2}\left[|0\rangle|0\rangle-|0\rangle|1\rangle+|1\rangle|1\rangle-|1\rangle|0\rangle\right] = \tfrac{1}{2}\left(|0\rangle+|1\rangle\right)\left(|0\rangle-|1\rangle\right)$$
$$\Psi_{out} \xrightarrow[f(0)=1]{f(0)\neq f(1)} \tfrac{1}{2}\left[|0\rangle|1\rangle-|0\rangle|0\rangle+|1\rangle|0\rangle-|1\rangle|1\rangle\right] = -\tfrac{1}{2}\left(|0\rangle-|1\rangle\right)\left(|0\rangle-|1\rangle\right)$$

The Hadamard operation (see matrix below) on the first qubit brings about the following transformations.

$$H\tfrac{1}{2}\left(|0\rangle+|1\rangle\right) = \tfrac{1}{\sqrt{2}}|0\rangle \quad H\tfrac{1}{2}\left(|0\rangle-|1\rangle\right) = \tfrac{1}{\sqrt{2}}|1\rangle$$

The four possible output states are now,

$$\Psi_{out} \xrightarrow[f(0)=0]{f(0)=f(1)} \tfrac{1}{\sqrt{2}}|0\rangle\left(|0\rangle-|1\rangle\right) = \tfrac{1}{\sqrt{2}}\begin{pmatrix}1\\-1\\0\\0\end{pmatrix} \quad \Psi_{out} \xrightarrow[f(0)=1]{f(0)=f(1)} -\tfrac{1}{\sqrt{2}}|0\rangle\left(|0\rangle-|1\rangle\right) = \tfrac{1}{\sqrt{2}}\begin{pmatrix}-1\\1\\0\\0\end{pmatrix}$$
$$\Psi_{out} \xrightarrow[f(0)=0]{f(0)\neq f(1)} \tfrac{1}{\sqrt{2}}|1\rangle\left(|0\rangle-|1\rangle\right) = \tfrac{1}{\sqrt{2}}\begin{pmatrix}0\\0\\1\\-1\end{pmatrix} \quad \Psi_{out} \xrightarrow[f(0)=1]{f(0)\neq f(1)} -\tfrac{1}{\sqrt{2}}|1\rangle\left(|0\rangle-|1\rangle\right) = \tfrac{1}{\sqrt{2}}\begin{pmatrix}0\\0\\-1\\1\end{pmatrix}$$

Quantum mechanics answers Deutsch's question with a single measurement. A measurement on the first qubit reveals whether the function is constant (|0>) or balanced (|1>).

We now look at the same calculation using matrix algebra. The required quantum operators in matrix form are:

$$\mathrm{I} = \begin{pmatrix}1&0\\0&1\end{pmatrix} \quad \mathrm{NOT} = \begin{pmatrix}0&1\\1&0\end{pmatrix} \quad \mathrm{H} = \tfrac{1}{\sqrt{2}}\begin{pmatrix}1&1\\1&-1\end{pmatrix} \quad \mathrm{CNOT} = \begin{pmatrix}1&0&0&0\\0&1&0&0\\0&0&0&1\\0&0&1&0\end{pmatrix}$$

Kronecker is Mathcad's command for carrying out matrix tensor multiplication. Note that the identity operator is required when a wire is not involved in an operation.

$$\mathrm{U}_f = \mathrm{kronecker}(\mathrm{I},\ \mathrm{NOT})\ \mathrm{CNOT} \quad \mathrm{QuantumCircuit} = \mathrm{kronecker}(\mathrm{H},\ \mathrm{I})\ \mathrm{U}_f\ \mathrm{kronecker}(\mathrm{H},\ \mathrm{H})$$

Input state:

$$|0\rangle|1\rangle = \begin{pmatrix}1\\0\end{pmatrix}\otimes\begin{pmatrix}0\\1\end{pmatrix} = \begin{pmatrix}0\\1\\0\\0\end{pmatrix} \quad \mathrm{QuantumCircuit}\begin{pmatrix}0\\1\\0\\0\end{pmatrix} = \begin{pmatrix}0\\0\\-0.707\\0.707\end{pmatrix}$$

Comparing this with the previous algebraic analysis, we see that the quantum circuit produces the result $f(0) \neq f(1)$ with f(0) = 1, which we already knew from previous work.

The measurement on the first qubit is implemented with projection operators |0><1|, and confirms that the function is not constant but belongs to the balanced category.

$$\text{kronecker}\left[\begin{pmatrix}1\\0\end{pmatrix}\begin{pmatrix}1\\0\end{pmatrix}^{T},\ \mathrm{I}\right]\ \text{QuantumCircuit}\begin{pmatrix}0\\.\\0\\0\end{pmatrix}=\begin{pmatrix}0\\0\\0\\0\end{pmatrix}\qquad\text{Top qubit is not } |0>.$$

$$\text{kronecker}\left[\begin{pmatrix}0\\1\end{pmatrix}\begin{pmatrix}0\\1\end{pmatrix}^{T},\ \mathrm{I}\right]\ \text{QuantumCircuit}\begin{pmatrix}0\\1\\0\\0\end{pmatrix}=\begin{pmatrix}0\\0\\-0.707\\0.707\end{pmatrix}\qquad\text{Top qubit is } |1>.$$

This could have also been easily determined by inspection:

$$\frac{1}{\sqrt{2}}\begin{pmatrix}0\\0\\-1\\1\end{pmatrix}=\begin{pmatrix}0\\1\end{pmatrix}\frac{1}{\sqrt{2}}\left[\begin{pmatrix}0\\1\end{pmatrix}-\begin{pmatrix}1\\0\end{pmatrix}\right]$$

The following provides an algebraic analysis of the Deutsch algorithm.

$$\begin{array}{ccccccccc}|0\rangle & \triangleright & \boxed{\mathrm{H}} & \cdots & \cdot & \cdots & \boxed{\mathrm{H}} & \triangleright & \text{measure}\frac{|0\rangle\ \text{constant}}{|1\rangle\ \text{balance}}\\ & & & & | & & & & \\ |1\rangle & \triangleright & \boxed{\mathrm{H}} & \cdots & \oplus & \boxed{\mathrm{NOT}} & \cdots & & \end{array}$$

Hadamard operation:

$$\mathrm{H}|0\rangle\rightarrow\tfrac{1}{\sqrt{2}}\left[|0\rangle+|1\rangle\right]\quad\mathrm{H}|1\rangle\rightarrow\tfrac{1}{\sqrt{2}}\left[|0\rangle-|1\rangle\right]$$

$$\text{NOT}\quad\begin{pmatrix}0\text{ to }1\\1\text{ to }0\end{pmatrix}\quad\text{CNOT}\quad\begin{pmatrix}\text{Decimal} & \text{Binary} & \text{to} & \text{Binary} & \text{Decimal}\\ 0 & 00 & \text{to} & 00 & 0\\ 1 & 01 & \text{to} & 01 & 1\\ 2 & 10 & \text{to} & 11 & 3\\ 3 & 11 & \text{to} & 10 & 2\end{pmatrix}$$

$$|01\rangle$$
$$\mathrm{H}\otimes\mathrm{H}$$
$$\tfrac{1}{\sqrt{2}}\left[|0\rangle+|1\rangle\right]\tfrac{1}{\sqrt{2}}\left[|0\rangle-|1\rangle\right]=\tfrac{1}{2}\left[|00\rangle-|01\rangle+|10\rangle-|11\rangle\right]$$
$$\text{CNOT}$$
$$\tfrac{1}{2}\left[|00\rangle-|01\rangle+11\rangle-|10\rangle\right]=\tfrac{1}{2}\left(|0\rangle-|1\rangle\right)\left(|0\rangle-|1\rangle\right)$$
$$\mathrm{I}\otimes\mathrm{NOT}$$
$$\tfrac{1}{2}\left[\left(|0\rangle-|1\rangle\right)\left(|1\rangle-|1\rangle\right)\right]$$
$$\mathrm{H}\otimes\mathrm{I}$$
$$|1\rangle\tfrac{1}{\sqrt{2}}\left(|1\rangle-|0\rangle\right)$$

The top wire contains |1 > indicating the function is balanced.

The Hadamard operation is actually a simple example of a Fourier transform. In other words, the final step of Deutsch's algorithm is to carry out a Fourier transform on the input wire. This also occurs on the input wires in Grover's search algorithm, Simon's query algorithm and Shor's factorization algorithm.

This page titled 8.68: A Simple Solution to Deutsch's Problem is shared under a CC BY 4.0 license and was authored, remixed, and/or curated by Frank Rioux via source content that was edited to the style and standards of the LibreTexts platform.

8.69: Another Example of Deutsch's Algorithm

See the previous tutorial "A Simple Solution to Deutsch's Problem" in this section for further detail on Deutsch's algorithm. This tutorial presents a similar example, so only a brief outline will be provided.

A certain function of x maps {0,1} to {0,1}. The four possible outcomes of the evaluation of f(x) are given in tabular form.

$$\begin{pmatrix} \text{x} & \prime & 0 & 1 & \prime & 0 & 1 & \prime & 0 & 1 & \prime & 0 & 1 \\ \text{f(x)} & \prime & 0 & 0 & \prime & 1 & 1 & \prime & 0 & 1 & \prime & 1 & 0 \end{pmatrix}$$

From the classical perspective, if the question (as asked by Deutsch) is whether f(x) is constant $(f(0) = f(1))$ or balanced $(f(0) \neq f(1))$ then one must calculate both f(0) and f(1) to answer the question as shown below.

The following circuit carries out,

$$\hat{U}_f|x\rangle|0\rangle = |x\rangle|f(x)\rangle$$

where U_f (inverse controlled-NOT, followed by a NOT operation on the lower wire) is a unitary operator that accepts input |x> on the top wire and places f(x) on the bottom wire.

$$\begin{array}{ccccccc} |x\rangle & \cdots & \oplus & & \cdots & \cdots & |x\rangle \\ & & | & & & & \\ |0\rangle & \cdots & \cdot & \boxed{\text{NOT}} & \cdots & \cdots & |f(x)\rangle \end{array}$$

The required circuit elements in matrix format are:

$$\text{I} = \begin{pmatrix} 1 & 0 \\ 0 & 1 \end{pmatrix} \quad \text{H} = \frac{1}{\sqrt{2}} \begin{pmatrix} 1 & 1 \\ 1 & -1 \end{pmatrix} \quad \text{NOT} = \begin{pmatrix} 0 & 1 \\ 1 & 0 \end{pmatrix} \quad \text{ICNOT} = \begin{pmatrix} 1 & 0 & 0 & 0 \\ 0 & 0 & 0 & 1 \\ 0 & 0 & 1 & 0 \\ 0 & 1 & 0 & 0 \end{pmatrix}$$

$$\text{QuantumCircuit} = \text{kronecker(I, NOT) ICNOT} \quad \text{QuantumCircuit} = \begin{pmatrix} 0 & 0 & 0 & 1 \\ 1 & 0 & 0 & 0 \\ 0 & 1 & 0 & 0 \\ 0 & 0 & 1 & 0 \end{pmatrix}$$

	Input	Calculation	Output
$f(0) = 1$	$\begin{pmatrix} 1 \\ 0 \end{pmatrix} \otimes \begin{pmatrix} 1 \\ 0 \end{pmatrix} = \begin{pmatrix} 1 \\ 0 \\ 0 \\ 0 \end{pmatrix}$	$\text{QuantumCircuit} \begin{pmatrix} 1 \\ 0 \\ 0 \\ 0 \end{pmatrix} = \begin{pmatrix} 0 \\ 1 \\ 0 \\ 0 \end{pmatrix}$	$\begin{pmatrix} 0 \\ 1 \\ 0 \\ 0 \end{pmatrix} = \begin{pmatrix} 1 \\ 0 \end{pmatrix} \otimes \begin{pmatrix} 0 \\ 1 \end{pmatrix}$
$f(1) = 1$	$\begin{pmatrix} 0 \\ 1 \end{pmatrix} \otimes \begin{pmatrix} 1 \\ 0 \end{pmatrix} = \begin{pmatrix} 0 \\ 0 \\ 1 \\ 0 \end{pmatrix}$	$\text{QuantumCircuit} \begin{pmatrix} 0 \\ 0 \\ 1 \\ 0 \end{pmatrix} = \begin{pmatrix} 0 \\ 0 \\ 0 \\ 1 \end{pmatrix}$	$\begin{pmatrix} 0 \\ 0 \\ 0 \\ 1 \end{pmatrix} = \begin{pmatrix} 0 \\ 1 \end{pmatrix} \otimes \begin{pmatrix} 0 \\ 1 \end{pmatrix}$

We see by these operations of the circuit that f(x) is constant:

$$\begin{pmatrix} \text{x} & 0 & 1 \\ \text{f(x)} & 1 & 1 \end{pmatrix}$$

A quantum computer can also process a superposition of inputs, in this case a superposition of 0 and 1. The circuit produces a superposition of the outputs calculated above.

$$\text{Input state :} \quad \frac{1}{\sqrt{2}}\begin{pmatrix}1\\1\end{pmatrix}\otimes\begin{pmatrix}1\\0\end{pmatrix}=\frac{1}{\sqrt{2}}\begin{pmatrix}1\\0\\1\\0\end{pmatrix} \quad \text{QuantumCircuit}\frac{1}{\sqrt{2}}\begin{pmatrix}1\\0\\1\\0\end{pmatrix}=\begin{pmatrix}0\\0.707\\0\\0.707\end{pmatrix}$$

$$\text{Output state:} \quad \frac{1}{\sqrt{2}}\begin{pmatrix}0\\1\\0\\1\end{pmatrix}=\frac{1}{\sqrt{2}}\left[\begin{pmatrix}0\\1\\0\\0\end{pmatrix}+\begin{pmatrix}0\\0\\0\\1\end{pmatrix}\right]=\frac{1}{\sqrt{2}}\left[\begin{pmatrix}1\\0\end{pmatrix}\begin{pmatrix}0\\1\end{pmatrix}+\begin{pmatrix}0\\1\end{pmatrix}\begin{pmatrix}0\\1\end{pmatrix}\right]$$

However, this does not answer the balanced/constant question because observation of the output causes it to collapse to one value of the other, either |0>|1> or |1>|1>. Running the circuit just once will not answer the question.

Deutsch pointed out that quantum superpositions and the interference effects between them allow the answer to be given with one pass through a modified version of the circuit shown here.

$$|0\rangle \quad \triangleright \quad \boxed{\text{H}} \quad \cdots \quad \oplus \quad \cdots \quad \boxed{\text{H}} \quad \triangleright \quad \text{measure}\frac{|0\rangle \text{ constant}}{|1\rangle \text{ balanced}}$$

$$\text{QuantumCircuit} = \text{kronecker(H, I) kronecker(I, NOT) ICNOT kronecker(H, H)}$$

$$\text{QuantumCircuit} = \begin{pmatrix}0.707 & -0.707 & 0 & 0\\ 0.707 & 0.707 & 0 & 0\\ 0 & 0 & -0.707 & 0.707\\ 0 & 0 & 0.707 & 0.707\end{pmatrix}$$

$$\text{QuantumCircuit}\begin{pmatrix}0\\1\\0\\0\end{pmatrix}=\begin{pmatrix}-0.707\\0.707\\0\\0\end{pmatrix} \quad \frac{1}{\sqrt{2}}\begin{pmatrix}-1\\1\\0\\0\end{pmatrix}=\begin{pmatrix}1\\0\end{pmatrix}\frac{1}{\sqrt{2}}\begin{pmatrix}-1\\1\end{pmatrix}=\begin{pmatrix}1\\0\end{pmatrix}\frac{1}{\sqrt{2}}\left[\begin{pmatrix}0\\1\end{pmatrix}-\begin{pmatrix}1\\0\end{pmatrix}\right]$$

The appearance of |0 > on the top wire confirms that the function is constant with one pass through the circuit.

It is also possible using the following truth tables to trace the evolution of the input quibits through the quantum circuit.

Hadamard operation:

$$\begin{bmatrix}0 & ' & \text{H} & ' & \frac{1}{\sqrt{2}}(0+1) & ' & \text{H} & ' & 0\\ 1 & ' & \text{H} & ' & \frac{1}{\sqrt{2}}(0-1) & ' & \text{H} & ' & 1\end{bmatrix}$$

$$\text{Identity} \quad \begin{pmatrix}0 & \text{to} & 1\\ 1 & \text{to} & 0\end{pmatrix} \quad \text{ICNOT} \quad \begin{pmatrix}\text{Decimal} & \text{Binary} & \text{to} & \text{Binary} & \text{Decimal}\\ 0 & 00 & \text{to} & 00 & 0\\ 1 & 01 & \text{to} & 11 & 3\\ 2 & 10 & 10 & 10 & 2\\ 3 & 11 & \text{to} & 01 & 1\end{pmatrix}$$

$$|01\rangle$$
$$\text{H}\otimes\text{H}$$
$$\frac{1}{\sqrt{2}}\left[|0\rangle+|1\rangle\right]\frac{1}{\sqrt{2}}\left[|0\rangle-|1\rangle\right]=\frac{1}{2}\left[|00\rangle-|01\rangle+|10\rangle-|11\rangle\right]$$
$$\text{ICNOT}$$
$$\frac{1}{2}\left[|00\rangle-|11\rangle+|10\rangle-|01\rangle\right]=\frac{1}{2}\left(|0\rangle+|1\rangle\right)\left(|0\rangle-|1\rangle\right)$$
$$\text{I}\otimes\text{NOT}$$
$$\frac{1}{2}\left[\left(|0\rangle+|1\rangle\right)\left(|1\rangle-|0\rangle\right)\right]$$
$$\text{H}\otimes\text{I}$$
$$|0\rangle\frac{1}{\sqrt{2}}\left(|1\rangle-|0\rangle\right)$$

This page titled 8.69: Another Example of Deutsch's Algorithm is shared under a CC BY 4.0 license and was authored, remixed, and/or curated by Frank Rioux via source content that was edited to the style and standards of the LibreTexts platform.

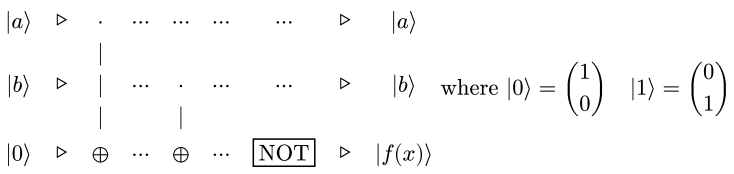
8.70: Evaluating a Function Using a Quantum Circuit and a Demonstration of Parallel Computation

This tutorial deals with quantum function evaluation and parallel computation. The example is taken from pages 94-95 of *Exploring the Quantum* by Haroche and Raimond. A certain function of x yields the following table of results.

$$\begin{pmatrix} \text{x} & 0 & 1 & 2 & 3 \\ \text{f(x)} & 1 & 0 & 0 & 1 \end{pmatrix}$$

First we establish that the circuit given below yields the results shown in the table, and then demonstrate that it also carries out a parallel calculation in one step using all four input values of x.

In Figure 2.22(b) Haroche and Raimond show a three wire quantum circuit which evaluates f(x). The top two wires are coded for the values of x (2 bits, 4 values) and the third wire is initially set to |0 >. After operation of the circuit on the initial state, the value of the function appears on the third wire. The qubits on the top wires are not changed by the circuit. The circuit consists of a CnNOT (controlled-controlled NOT) gate employing all three wires, followed by a CNOT gate involving the second and third wires, and finally a NOT gate operating on the third wire. A sketch is provided below.



The required quantum gates in matrix operator form are as follows:

$$\text{I} = \begin{pmatrix} 1 & 0 \\ 0 & 1 \end{pmatrix} \quad \text{NOT} = \begin{pmatrix} 0 & 1 \\ 1 & 0 \end{pmatrix} \quad \text{CNOT} = \begin{pmatrix} 1 & 0 & 0 & 0 \\ 0 & 1 & 0 & 0 \\ 0 & 0 & 0 & 1 \\ 0 & 0 & 1 & 0 \end{pmatrix}$$

$$\overset{\text{CnNOT}}{=} \begin{pmatrix} 1 & 0 & 0 & 0 & 0 & 0 & 0 & 0 \\ 0 & 1 & 0 & 0 & 0 & 0 & 0 & 0 \\ 0 & 0 & 1 & 0 & 0 & 0 & 0 & 0 \\ 0 & 0 & 0 & 1 & 0 & 0 & 0 & 0 \\ 0 & 0 & 0 & 0 & 0 & 1 & 0 & 0 \\ 0 & 0 & 0 & 0 & 1 & 0 & 0 & 0 \\ 0 & 0 & 0 & 0 & 0 & 0 & 0 & 1 \\ 0 & 0 & 0 & 0 & 0 & 0 & 1 & 0 \end{pmatrix}$$

Kronecker is Mathcad's command for carrying out the tensor multiplication of matrices. Note that the identity operator is required when a wire is not involved in an operation. In the Appendix the matrix form of the circuit is displayed and its reversibility is demonstrated.

$$\text{QuantumCircuit} = \text{kronecker(I, kronecker(I, NOT))}\ \text{kronecker(I, CNOT)}\ \text{CnNOT}$$

The operation of the quantum circuit is now illustrated.

$$\begin{array}{lcccccc} & \text{Input} & & \text{Calculation} & & \text{Output} & \\ \mathrm{f}(0)=1 & \begin{pmatrix}1\\0\\0\\0\end{pmatrix}\otimes\begin{pmatrix}1\\0\end{pmatrix}=\begin{pmatrix}1\\0\\0\\0\\0\\0\\0\\0\end{pmatrix} & \text{QuantumCircuit} & \begin{pmatrix}1\\0\\0\\0\\0\\0\\0\\0\end{pmatrix}=\begin{pmatrix}0\\1\\0\\0\\0\\0\\0\\0\end{pmatrix} & \begin{pmatrix}0\\1\\0\\0\\0\\0\\0\\0\end{pmatrix}=\begin{pmatrix}1\\0\\0\\0\end{pmatrix}\otimes\begin{pmatrix}0\\1\end{pmatrix} \\ \mathrm{f}(1)=0 & \begin{pmatrix}0\\1\\0\\0\end{pmatrix}\otimes\begin{pmatrix}1\\0\end{pmatrix}=\begin{pmatrix}0\\0\\1\\0\\0\\0\\0\\0\end{pmatrix} & \text{QuantumCircuit} & \begin{pmatrix}0\\0\\1\\0\\0\\0\\0\\0\end{pmatrix}=\begin{pmatrix}0\\0\\1\\0\\0\\0\\0\\0\end{pmatrix} & \begin{pmatrix}0\\0\\1\\0\\0\\0\\0\\0\end{pmatrix}=\begin{pmatrix}0\\1\\0\\0\end{pmatrix}\otimes\begin{pmatrix}1\\0\end{pmatrix} \\ \mathrm{f}(2)=0 & \begin{pmatrix}0\\0\\1\\0\end{pmatrix}\otimes\begin{pmatrix}1\\0\end{pmatrix}=\begin{pmatrix}0\\0\\0\\0\\1\\0\\0\\0\end{pmatrix} & \text{QuantumCircuit} & \begin{pmatrix}0\\0\\1\\0\\0\\0\\0\\0\end{pmatrix}=\begin{pmatrix}0\\0\\0\\0\\1\\0\\0\\0\end{pmatrix} & \begin{pmatrix}0\\0\\0\\0\\1\\0\\0\\0\end{pmatrix}=\begin{pmatrix}0\\0\\1\\0\end{pmatrix}\otimes\begin{pmatrix}1\\0\end{pmatrix} \\ \mathrm{f}(3)=0 & \begin{pmatrix}0\\0\\0\\1\end{pmatrix}\otimes\begin{pmatrix}1\\0\end{pmatrix}=\begin{pmatrix}0\\0\\0\\0\\0\\0\\1\\0\end{pmatrix} & \text{QuantumCircuit} & \begin{pmatrix}0\\0\\0\\0\\0\\0\\1\\0\end{pmatrix}=\begin{pmatrix}0\\0\\0\\0\\0\\0\\0\\1\end{pmatrix} & \begin{pmatrix}0\\0\\0\\0\\0\\0\\0\\1\end{pmatrix}=\begin{pmatrix}0\\0\\0\\1\end{pmatrix}\otimes\begin{pmatrix}0\\1\end{pmatrix} \end{array}$$

Now we come to the demonstration of parallel calculation that is possible in a quantum gate circuit such as the one shown above. If all the values of x (0, 1, 2, 3) are present simultaneously as a superposition, the |a>|b> part of the input register is (1/2 is the normalization constant),

$$\tfrac{1}{2}\begin{pmatrix}1\\1\\1\\1\end{pmatrix}\quad\text{which leads to this total input register}\quad\tfrac{1}{2}\begin{pmatrix}1\\1\\1\\1\end{pmatrix}\otimes\begin{pmatrix}1\\0\end{pmatrix}=\tfrac{1}{2}\begin{pmatrix}1\\0\\1\\0\\1\\0\\1\\0\end{pmatrix}$$

Operating on this register with the quantum circuit yields the following result, which by inspection is clearly a balanced superposition of the earlier results. The function has been evaluated for all values of x in one pass through the circuit.

$$\text{QuantumCircuit}\frac{1}{2}\begin{pmatrix}1\\0\\1\\0\\1\\0\\1\\0\end{pmatrix}=\begin{pmatrix}0\\0.5\\0.5\\0\\0.5\\0\\0\\0.5\end{pmatrix}\quad\frac{1}{2}\overset{f(0)=1}{\begin{pmatrix}0\\1\\0\\0\\0\\0\\0\\0\end{pmatrix}}+\frac{1}{2}\overset{f(1)=0}{\begin{pmatrix}0\\0\\1\\0\\0\\0\\0\\0\end{pmatrix}}+\frac{1}{2}\overset{f(2)=0}{\begin{pmatrix}0\\0\\0\\0\\1\\0\\0\\0\end{pmatrix}}+\frac{1}{2}\overset{f(3)=1}{\begin{pmatrix}0\\0\\0\\0\\0\\0\\0\\1\end{pmatrix}}=\begin{pmatrix}0\\0.5\\0.5\\0\\0.5\\0\\0\\0.5\end{pmatrix}$$

The amplitude of each contribution to the superposition is 1/2, so the probability of being observed on measurement is 0.25. The contributions to the superposition are rewritten to emphasize that the top two wires carry the input value of x, while the bottom wire has the value of f(x).

$$\overset{f(0)=1}{\begin{pmatrix}0\\10\\0\\0\\0\\0\\0\end{pmatrix}=\begin{pmatrix}1\\0\\0\\0\end{pmatrix}\otimes\begin{pmatrix}0\\1\end{pmatrix}}\quad\overset{f(1)=0}{\begin{pmatrix}0\\0\\1\\0\\0\\0\\0\\0\end{pmatrix}=\begin{pmatrix}0\\1\\0\\0\end{pmatrix}\otimes\begin{pmatrix}1\\0\end{pmatrix}}\quad\overset{f(2)=0}{\begin{pmatrix}0\\0\\0\\1\\0\\0\\0\end{pmatrix}=\begin{pmatrix}0\\0\\1\\0\end{pmatrix}\otimes\begin{pmatrix}1\\0\end{pmatrix}}\quad\overset{f(3)=1}{\begin{pmatrix}0\\0\\0\\0\\0\\0\\0\\1\end{pmatrix}=\begin{pmatrix}0\\0\\0\\1\end{pmatrix}\otimes\begin{pmatrix}0\\1\end{pmatrix}}$$

Haroche and Raimond describe this process as follows: "By superposing the inputs of a computation, one operates the machine 'in parallel', making it compute simultaneously all the values of a function and keeping its state, before any final bit detection is performed, suspended in a coherent superposition of all the possible outcomes."

This seems absolutely marvelous, four calculations in a single operation of the circuit. However, there's a catch, and that is that an inquiry (measurement) into the results of the calculation can yield only one of the results. On measurement the quantum superposition collapses, as it always does, to one value and the others are irretrievably lost. You can only learn one thing from a quantum state measurement. This is illustrated with projection operators on the top two wires to learn the value of x by measurment. The identity operator leaves the lower wire alone which now carriers the value of f(x).

$$f(0) = 1$$

$$\text{kronecker}\left[\begin{pmatrix}1\\0\end{pmatrix}\begin{pmatrix}1\\0\end{pmatrix}^T,\ \text{kronecker}\left[\begin{pmatrix}1\\0\end{pmatrix}\begin{pmatrix}1\\0\end{pmatrix}^T,\ \text{I}\right]\right] \quad \tfrac{1}{2}\begin{pmatrix}1\\0\end{pmatrix}\begin{pmatrix}1\\0\end{pmatrix}\begin{pmatrix}0\\1\end{pmatrix}$$

$$\text{QuantumCircuit}\tfrac{1}{2}\begin{pmatrix}1\\0\\1\\0\\1\\0\\1\\0\end{pmatrix} = \begin{pmatrix}0\\0.5\\0\\0\\0\\0\\0\\0\end{pmatrix}$$

$$f(1) = 0$$

$$\text{kronecker}\left[\begin{pmatrix}1\\0\end{pmatrix}\begin{pmatrix}1\\0\end{pmatrix}^T,\ \text{kronecker}\left[\begin{pmatrix}0\\1\end{pmatrix}\begin{pmatrix}0\\1\end{pmatrix}^T,\ \text{I}\right]\right] \quad \tfrac{1}{2}\begin{pmatrix}1\\0\end{pmatrix}\begin{pmatrix}0\\1\end{pmatrix}\begin{pmatrix}1\\0\end{pmatrix}$$

$$\text{QuantumCircuit}\tfrac{1}{2}\begin{pmatrix}1\\0\\1\\0\\1\\0\\1\\0\end{pmatrix} = \begin{pmatrix}0\\0\\0.5\\0\\0\\0\\0\\0\end{pmatrix}$$

$$f(2) = 0$$

$$\text{kronecker}\left[\begin{pmatrix}0\\1\end{pmatrix}\begin{pmatrix}0\\1\end{pmatrix}^T,\ \text{kronecker}\left[\begin{pmatrix}1\\0\end{pmatrix}\begin{pmatrix}1\\0\end{pmatrix}^T,\ \text{I}\right]\right] \quad \tfrac{1}{2}\begin{pmatrix}0\\1\end{pmatrix}\begin{pmatrix}1\\0\end{pmatrix}\begin{pmatrix}1\\0\end{pmatrix}$$

$$\text{QuantumCircuit}\tfrac{1}{2}\begin{pmatrix}1\\0\\1\\0\\1\\0\\1\\0\end{pmatrix} = \begin{pmatrix}0\\0\\0\\0\\0.5\\0\\0\\0\end{pmatrix}$$

$$f(2) = 0$$

$$\text{kronecker}\left[\begin{pmatrix}0\\1\end{pmatrix}\begin{pmatrix}0\\1\end{pmatrix}^T,\ \text{kronecker}\left[\begin{pmatrix}0\\1\end{pmatrix}\begin{pmatrix}0\\1\end{pmatrix}^T,\ \text{I}\right]\right] \quad \tfrac{1}{2}\begin{pmatrix}0\\1\end{pmatrix}\begin{pmatrix}0\\1\end{pmatrix}\begin{pmatrix}1\\0\end{pmatrix}$$

$$\text{QuantumCircuit}\tfrac{1}{2}\begin{pmatrix}1\\0\\1\\0\\1\\0\\1\\0\end{pmatrix} = \begin{pmatrix}0\\0\\0\\0\\0\\0\\0\\0.5\end{pmatrix}$$

As Haroche and Raimond write, "It is, however, one thing to compute potentially at once all the values of f and quite another to be able to exploit this quantum parallelism and extract from it more information than from a mundane classical computation. The final stage of information acquisition must always be a measurement."

In summary, this tutorial has demonstrated how a quantum circuit can function as an algorithm for the evaluation of a mathematical function, and how the same algorithm is capable of parallel evaluations of that function. The exploitation of quantum parallelism for practical outcomes such as factorization requires more elaborate quantum circuits than the one presented here.

Appendix

As promised earlier the matrix form of the quantum circuit is displayed here. As can be seen it is sparse!

$$\text{QuantumCircuit} = \begin{pmatrix} 0 & 1 & 0 & 0 & 0 & 0 & 0 & 0 \\ 1 & 0 & 0 & 0 & 0 & 0 & 0 & 0 \\ 0 & 0 & 1 & 0 & 0 & 0 & 0 & 0 \\ 0 & 0 & 0 & 1 & 0 & 0 & 0 & 0 \\ 0 & 0 & 0 & 0 & 1 & 0 & 0 & 0 \\ 0 & 0 & 0 & 0 & 0 & 1 & 0 & 0 \\ 0 & 0 & 0 & 0 & 0 & 0 & 0 & 1 \\ 0 & 0 & 0 & 0 & 0 & 0 & 1 & 0 \end{pmatrix}$$

An important property of circuits in quantum computation is reversibility. The reversibility of the quantum circuit is demonstrated by showing that using it twice is equivalent to the identity operator.

$$\text{QuantumCircuit}^2 = \begin{pmatrix} 1 & 0 & 0 & 0 & 0 & 0 & 0 & 0 \\ 0 & 1 & 0 & 0 & 0 & 0 & 0 & 0 \\ 0 & 0 & 1 & 0 & 0 & 0 & 0 & 0 \\ 0 & 0 & 0 & 1 & 0 & 0 & 0 & 0 \\ 0 & 0 & 0 & 0 & 1 & 0 & 0 & 0 \\ 0 & 0 & 0 & 0 & 0 & 1 & 0 & 0 \\ 0 & 0 & 0 & 0 & 0 & 0 & 1 & 0 \\ 0 & 0 & 0 & 0 & 0 & 0 & 0 & 1 \end{pmatrix}$$

An alternative summary of the calculation uses the truth tables for the NOT, CNOT and CnNOT directly.

NOT

$$\begin{pmatrix} 0 & \prime & 1 \\ 1 & \prime & 0 \end{pmatrix}$$

CNOT

$$\begin{pmatrix} \text{Decimal} & \text{Binary} & \prime & \text{Binary} & \text{Decimal} \\ 0 & 00 & \prime & 00 & 0 \\ 1 & 01 & \prime & 01 & 1 \\ 2 & 10 & \prime & 11 & 3 \\ 3 & 11 & \prime & 10 & 2 \end{pmatrix}$$

CnNOT

$$\begin{pmatrix} \text{Decimal} & \text{Binary} & \prime & \text{Binary} & \text{Decimal} \\ 0 & 000 & \prime & 000 & 0 \\ 1 & 001 & \prime & 001 & 1 \\ 2 & 010 & \prime & 010 & 2 \\ 3 & 011 & \prime & 011 & 3 \\ 4 & 100 & \prime & 101 & 5 \\ 5 & 101 & \prime & 100 & 4 \\ 6 & 110 & \prime & 111 & 7 \\ 7 & 111 & \prime & 110 & 6 \end{pmatrix}$$

The calculations are summarized in table format as follows. The CnNOT is a three-qubit gate, but only the four input states in which the third qubit is |0> are needed. The CNOT operates on the second and third qubits, while the NOT gate operates only on the third qubit.

$$\begin{array}{lllll} |000\rangle & \xrightarrow{CnNOT} & |0\rangle|00\rangle & \xrightarrow{I\otimes CNOT} & |00\rangle|0\rangle & \xrightarrow{I\otimes I\otimes NOT} & |00\rangle|1\rangle & f(0)=1 \\ |010\rangle & & |0\rangle|10\rangle & & |01\rangle|1\rangle & & |01\rangle|1\rangle & f(1)=0 \\ |100\rangle & & |1\rangle|01\rangle & & |10\rangle|1\rangle & & |10\rangle|0\rangle & f(2)=0 \\ |110\rangle & & |1\rangle|11\rangle & & |11\rangle|0\rangle & & |11\rangle|1\rangle & f(3)=1 \end{array}$$

A superposition of all four input states would behave as follows under the operation of the quantum circuit.

$$\frac{1}{2}\begin{pmatrix}|00\rangle|0\rangle\\+\\|01\rangle|0\rangle\\+\\|10\rangle|0\rangle\\+\\|11\rangle|0\rangle\end{pmatrix}\xrightarrow{CnNOT}\frac{1}{2}\begin{pmatrix}|0\rangle|00\rangle\\+\\|0\rangle|10\rangle\\+\\|1\rangle|01\rangle\\+\\|1\rangle|11\rangle\end{pmatrix}\xrightarrow{I\otimes CNOT}\frac{1}{2}\begin{pmatrix}|0\rangle|00\rangle\\+\\|0\rangle|11\rangle\\+\\|1\rangle|01\rangle\\+\\|1\rangle|10\rangle\end{pmatrix}$$

$$\xrightarrow{I\otimes I\otimes NOT}\frac{1}{2}\begin{pmatrix}|00\rangle|1\rangle\\+\\|01\rangle|0\rangle\\+\\|10\rangle|0\rangle\\+\\|11\rangle|1\rangle\end{pmatrix}\xrightarrow{Decimal}\frac{1}{2}\begin{pmatrix}|0\rangle|1\rangle\\+\\|1\rangle|0\rangle\\+\\|2\rangle|0\rangle\\+\\|3\rangle|1\rangle\end{pmatrix}$$

Another feature of this circuit is that if the bottom wire is measured, it projects the top two wires into a superposition of inputs that give the bottom wire result.

$$\text{QuantumCircuit}\frac{1}{2}\begin{pmatrix}1\\0\\1\\0\\1\\0\\1\\0\end{pmatrix}=\frac{1}{2}\begin{pmatrix}0\\1\\1\\0\\1\\0\\0\\1\end{pmatrix}=\frac{1}{2}\left[\begin{pmatrix}0\\1\\0\\0\end{pmatrix}+\begin{pmatrix}0\\0\\1\\0\end{pmatrix}\right]\begin{pmatrix}1\\0\end{pmatrix}+\frac{1}{2}\left[\begin{pmatrix}1\\0\\0\\0\end{pmatrix}+\begin{pmatrix}0\\0\\0\\1\end{pmatrix}\right]\begin{pmatrix}0\\1\end{pmatrix}$$

https://chem.libretexts.org/@go/page/148691

$$\text{f(1) = f(2) = 0}$$

$$\text{kronecker}\left[\text{I, kronecker}\left[\text{I, }\begin{pmatrix}1 & 0\\ 0 & 0\end{pmatrix}\right]\right]\text{QuantumCircuit}\frac{1}{2}\begin{pmatrix}1\\0\\1\\0\\1\\0\\1\\0\end{pmatrix}\quad\frac{1}{2}\left[\begin{pmatrix}1\\0\end{pmatrix}\begin{pmatrix}1\\0\end{pmatrix}+\begin{pmatrix}0\\1\end{pmatrix}\begin{pmatrix}1\\0\end{pmatrix}\right]\begin{pmatrix}1\\0\end{pmatrix}$$

$$=\begin{pmatrix}0\\0\\0.5\\0\\0.5\\0\\0\\0\end{pmatrix}$$

$$\text{f(0) = f(3) = 1}$$

$$\text{kronecker}\left[\text{I, kronecker}\left[\text{I, }\begin{pmatrix}0 & 0\\ 0 & 1\end{pmatrix}\right]\right]\text{QuantumCircuit}\frac{1}{2}\begin{pmatrix}1\\0\\1\\0\\1\\0\\1\\0\end{pmatrix}\quad\frac{1}{2}\left[\begin{pmatrix}1\\0\end{pmatrix}\begin{pmatrix}1\\0\end{pmatrix}+\begin{pmatrix}0\\1\end{pmatrix}\begin{pmatrix}0\\1\end{pmatrix}\right]\begin{pmatrix}0\\1\end{pmatrix}$$

$$=\begin{pmatrix}0\\0.5\\0\\0\\0\\0\\0\\0.5\end{pmatrix}$$

Here's an alternative analysis of the circuit operation.

$$\frac{1}{2}\left[|00\rangle+|01\rangle+|10\rangle+|11\rangle\right]|0\rangle=\frac{1}{2}\left[|000\rangle+|010\rangle+|100\rangle+|110\rangle\right]$$

$$\text{CnNOT}$$

$$\frac{1}{2}\left[|000\rangle+|010\rangle+|101\rangle+|111\rangle\right]=\frac{1}{2}\left[|0\rangle|00\rangle+|0\rangle|10\rangle+|1\rangle|01\rangle+|1\rangle|11\rangle\right]$$

$$\text{I}\otimes\text{CNOT}$$

$$\frac{1}{2}\left[|0\rangle|00\rangle+|0\rangle|11\rangle+|1\rangle|01\rangle+|1\rangle|10\rangle\right]=\frac{1}{2}\left[|00\rangle|0\rangle+|01\rangle|1\rangle+|10\rangle|1\rangle+|11\rangle|0\rangle\right]$$

$$\text{I}\otimes\text{I}\otimes\text{NOT}$$

$$\frac{1}{2}\left[|00\rangle|1\rangle+|01\rangle|0\rangle+|10\rangle|0\rangle+|11\rangle|1\rangle\right]\xrightarrow{\text{Decimal}}\frac{1}{2}\left[|0\rangle|1\rangle+|1\rangle|0\rangle+|2\rangle|0\rangle+|3\rangle|1\rangle\right]$$

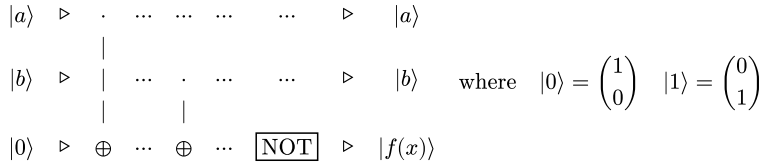
This page titled 8.70: Evaluating a Function Using a Quantum Circuit and a Demonstration of Parallel Computation is shared under a CC BY 4.0 license and was authored, remixed, and/or curated by Frank Rioux via source content that was edited to the style and standards of the LibreTexts platform.

8.71: A Simple Quantum Circuit for Parallel Computation

This tutorial deals with quantum function evaluation and parallel computation. The example is taken from pages 94-95 of Exploring the Quantum by Haroche and Raimond. A certain function of x yields the following table of results.

$$\begin{pmatrix} \text{x} & 0 & 1 & 2 & 3 \\ \text{f(x)} & 1 & 0 & 0 & 1 \end{pmatrix}$$

In the quantum circuit provided by Haroche and Raimond the top two wires carry the values of x in binary code (2 bits, 4 values) and the third wire is initially set to |0 >. After operation of the circuit on the initial state, the value of the function appears on the third wire. The qubits on the top wires are unchanged by the circuit. The circuit consists of a CnNOT gate employing all three wires, followed by a CNOT gate involving the second and third wires, and finally a NOT gate operating on the third wire.



First we establish that this circuit yields the results shown in the table, and then demonstrate that it also carries out a parallel calculation in one step using all four input values of x. The truth tables for the various quantum gates are provided in the Appendix.

$$\begin{array}{llllll} |000\rangle & \xrightarrow{CnNOT} & |0\rangle|00\rangle & \xrightarrow{I\otimes CNOT} & |00\rangle|0\rangle & \xrightarrow{I\otimes I\otimes NOT} & |00\rangle|1\rangle & f(0)=1 \\ |010\rangle & & |0\rangle|10\rangle & & |01\rangle|1\rangle & & |01\rangle|0\rangle & f(1)=0 \\ |100\rangle & & |1\rangle|01\rangle & & |10\rangle|1\rangle & & |10\rangle|0\rangle & f(2)=0 \\ |110\rangle & & |1\rangle|11\rangle & & |11\rangle|0\rangle & & |11\rangle|1\rangle & f(3)=1 \end{array}$$

A superposition of all four input states behaves as follows under the operation of the quantum circuit.

$$\frac{1}{2}\begin{pmatrix} |00\rangle|0\rangle \\ + \\ |01\rangle|0\rangle \\ + \\ |10\rangle|0\rangle \\ + \\ |11\rangle|0\rangle \end{pmatrix} \xrightarrow{CnNOT} \frac{1}{2}\begin{pmatrix} |0\rangle|00\rangle \\ + \\ |0\rangle|10\rangle \\ + \\ |1\rangle|01\rangle \\ + \\ |1\rangle|11\rangle \end{pmatrix} \xrightarrow{I\otimes CNOT} \frac{1}{2}\begin{pmatrix} |00\rangle|0\rangle \\ + \\ |01\rangle|1\rangle \\ + \\ |10\rangle|1\rangle \\ + \\ |11\rangle|0\rangle \end{pmatrix}$$

$$\xrightarrow{I\otimes I\otimes NOT} \frac{1}{2}\begin{pmatrix} |00\rangle|1\rangle \\ + \\ |01\rangle|0\rangle \\ + \\ |10\rangle|0\rangle \\ + \\ |11\rangle|1\rangle \end{pmatrix} \xrightarrow{Decimal} \frac{1}{2}\begin{pmatrix} |0\rangle|1\rangle \\ + \\ |1\rangle|0\rangle \\ + \\ |2\rangle|0\rangle \\ + \\ |3\rangle|1\rangle \end{pmatrix}$$

Haroche and Raimond describe this process as follows: "By superposing the inputs of a computation, one operates the machine 'in parallel', making it compute simultaneously all the values of a function and keeping its state, before any final bit detection is performed, suspended in a coherent superposition of all the possible outcomes."

It appears that we get four calculations in a single operation of the circuit. However, there's a catch, and that is that any inquiry into the results of the calculation can yield only one of the results. On measurement the quantum superposition collapses, as it always does, to one value and the others are irretrievably lost. As Haroche and Raimond write, "It is, however, one thing to compute potentially at once all the values of f and quite another to be able to exploit this quantum parallelism and extract from it more information than from a mundane classical computation. The final stage of information acquisition must always be a measurement."

In summary, this tutorial has demonstrated how a quantum circuit can function as an algorithm for the evaluation of a mathematical function, and how the same algorithm is capable of parallel evaluations of that function. The exploitation of quantum parallelism for practical outcomes such as factorization requires more elaborate quantum circuits than the one presented here.

Appendix

NOT

$$\begin{pmatrix} 0 & ' & 1 \\ 1 & ' & 0 \end{pmatrix}$$

CNOT

$$\begin{pmatrix} \text{Decimal} & \text{Binary} & ' & \text{Binary} & \text{Decimal} \\ 0 & 00 & ' & 00 & 0 \\ 1 & 01 & ' & 01 & 1 \\ 2 & 10 & ' & 11 & 3 \\ 3 & 11 & ' & 10 & 2 \end{pmatrix}$$

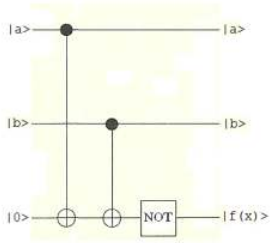
CnNOT

$$\begin{pmatrix} \text{Decimal} & \text{Binary} & ' & \text{Binary} & \text{Decimal} \\ 0 & 000 & ' & 000 & 0 \\ 1 & 001 & ' & 001 & 1 \\ 2 & 010 & ' & 010 & 2 \\ 3 & 011 & ' & 011 & 3 \\ 4 & 100 & ' & 101 & 5 \\ 5 & 101 & ' & 100 & 4 \\ 6 & 110 & ' & 111 & 7 \\ 7 & 111 & ' & 110 & 6 \end{pmatrix}$$

This page titled 8.71: A Simple Quantum Circuit for Parallel Computation is shared under a CC BY 4.0 license and was authored, remixed, and/or curated by Frank Rioux via source content that was edited to the style and standards of the LibreTexts platform.

8.72: An Illustration of the Deutsch-Jozsa Algorithm

The following circuit produces the table of results to its right. The top wires carry the value of x and the circuit places f(x) on the bottom wire. As is shown in the previous tutorial this circuit can also operate in parallel accepting as input all x-values and returning on the bottom wire a superposition of all values of f(x).



$$\begin{pmatrix} \text{x} & 0 & 1 & 2 & 3 \\ \text{f(x)} & 1 & 0 & 0 & 1 \end{pmatrix} \quad \text{where} \quad \begin{aligned} |0\rangle &= |0\rangle|0\rangle \\ |1\rangle &= |0\rangle|1\rangle \\ |2\rangle &= |1\rangle|0\rangle \\ |3\rangle &= |1\rangle|1\rangle \end{aligned}$$

The function belongs to the balanced category because it produces 0 and 1 with equal frequency. A modification of this circuit (Deutsch-Jozsa algoritm, p. 298 in *The Quest for the Quantum Computer*, by Julian Brown) answers the question of whether the function is constant or balanced. Naturally we already know the answer, so this is a simple demonstration that the circuit works.

The input is |0>|0>|1> followed by a Hadamard gate on each wire, as shown in the circuit on page 3. As is well known the Hadamard operation creates the following superposition states.

$$\text{H}\begin{pmatrix}1\\0\end{pmatrix} = \tfrac{1}{\sqrt{2}}\begin{pmatrix}1\\1\end{pmatrix} \quad \text{H}\begin{pmatrix}0\\1\end{pmatrix} = \tfrac{1}{\sqrt{2}}\begin{pmatrix}1\\-1\end{pmatrix}$$

Therefore the Hadamard operation transforms the input state to the following three-qubit state which is fed to the quantum circuit.

$$\frac{1}{\sqrt{2}}\begin{pmatrix}1\\1\end{pmatrix}\frac{1}{\sqrt{2}}\begin{pmatrix}1\\1\end{pmatrix}\frac{1}{\sqrt{2}}\begin{pmatrix}1\\-1\end{pmatrix} = \frac{1}{2\sqrt{2}}\begin{pmatrix}1\\-1\\1\\-1\\1\\-1\\1\\-1\end{pmatrix}$$

The following matrices are required to execute the circuit.

$$\text{I} = \begin{pmatrix}1&0\\0&1\end{pmatrix} \quad \text{NOT} = \begin{pmatrix}0&1\\1&0\end{pmatrix} \quad \text{H} = \tfrac{1}{\sqrt{2}}\begin{pmatrix}1&1\\1&-1\end{pmatrix}$$

$$\text{CNOT} = \begin{pmatrix}1&0&0&0\\0&1&0&0\\0&0&0&1\\0&0&1&0\end{pmatrix} \quad \text{CnNOT} = \begin{pmatrix}1&0&0&0&0&0&0&0\\0&1&0&0&0&0&0&0\\0&0&1&0&0&0&0&0\\0&0&0&1&0&0&0&0\\0&0&0&0&0&1&0&0\\0&0&0&0&1&0&0&0\\0&0&0&0&0&0&0&1\\0&0&0&0&0&0&1&0\end{pmatrix}$$

After the portion of the quantum circuit shown above, Hadamard gates are added to the top two wires, as shown in the circuit on page 3. The matrix representing the circuit is assembled using tensor matrix multiplication and then allowed to operate on the wave function. The full circuit is shown below.

$$\text{QuantumCircuit} = \text{kronecker(H, kronecker(H, I))}\ \text{kronecker(I, kronecker(I, NOT))}\ \text{kronecker(I, CNOT)}\ \text{CnNOT}$$

$$\text{QuantumCircuit} = \frac{1}{2}\begin{pmatrix} 0 & 1 & 1 & 0 & 1 & 0 & 0 & 1 \\ 1 & 0 & 0 & 1 & 0 & 1 & 1 & 0 \\ 0 & 1 & -1 & 0 & 1 & 0 & 0 & -1 \\ 1 & 0 & 0 & -1 & 0 & 1 & -1 & 0 \\ 0 & 1 & 1 & 0 & -1 & 0 & 0 & -1 \\ 1 & 0 & 0 & 1 & 0 & -1 & -1 & 0 \\ 0 & 1 & -1 & 0 & -1 & 0 & 0 & 1 \\ 1 & 0 & 0 & -1 & 0 & -1 & 1 & 0 \end{pmatrix} \qquad \text{QuantumCircuit}\frac{1}{2\sqrt{2}}\begin{pmatrix} 1 \\ -1 \\ 1 \\ -1 \\ 1 \\ -1 \\ 1 \\ -1 \end{pmatrix} \quad \begin{pmatrix} 0 \\ 1 \end{pmatrix}\begin{pmatrix} 0 \\ 1 \end{pmatrix}\frac{1}{\sqrt{2}}\begin{pmatrix} -1 \\ 1 \end{pmatrix}$$

$$= \begin{pmatrix} 0 \\ 0 \\ 0 \\ 0 \\ 0 \\ 0 \\ -0.707 \\ 0.707 \end{pmatrix}$$

Next the qubits on the top two wires are measured. If both are |0> the function is constant, but if at least one is |1> the function is balanced. The measurement on the top wires is implemented with projection operators |0><1|, and confirms that the function is not constant but belongs to the balanced category.

The first qubit is not $|0\rangle$. $\text{kronecker}\left[\begin{pmatrix}1\\0\end{pmatrix}\begin{pmatrix}1\\0\end{pmatrix}^T \text{kronecker(I, I)}\right]\text{QuantumCircuit}\frac{1}{2\sqrt{2}}$

$$\begin{pmatrix}1\\-1\\1\\-1\\1\\-1\\1\\-1\end{pmatrix} = \begin{pmatrix}0\\0\\0\\0\\0\\0\\0\\0\end{pmatrix}$$

The second qubit is not $|0\rangle$. $\text{kronecker}\left[\text{I, kronecker}\left[\begin{pmatrix}1\\0\end{pmatrix}\begin{pmatrix}1\\0\end{pmatrix}^T\text{, I}\right]\right]\text{QuantumCircuit}\frac{1}{2\sqrt{2}}$

$$\begin{pmatrix}1\\-1\\1\\-1\\1\\-1\\1\\-1\end{pmatrix} = \begin{pmatrix}0\\0\\0\\0\\0\\0\\0\\0\end{pmatrix}$$

The first qubit is $|1\rangle$. $\text{kronecker}\left[\begin{pmatrix}0\\1\end{pmatrix}\begin{pmatrix}0\\1\end{pmatrix}^T \text{kronecker(I, I)}\right]\text{QuantumCircuit}\frac{1}{2\sqrt{2}}\begin{pmatrix}1\\-1\\1\\-1\\1\\-1\\1\\-1\end{pmatrix}$

$$= \begin{pmatrix}0\\0\\0\\0\\0\\0\\-0.707\\0.707\end{pmatrix}$$

The second qubit is $|1\rangle$. $\text{kronecker}\left[\text{I, kronecker}\left[\begin{pmatrix}0\\1\end{pmatrix}\begin{pmatrix}0\\1\end{pmatrix}^T\text{, I}\right]\right]\text{QuantumCircuit}\frac{1}{2\sqrt{2}}$

$$\begin{pmatrix}1\\-1\\1\\-1\\1\\-1\\1\\-1\end{pmatrix} = \begin{pmatrix}0\\0\\0\\0\\0\\0\\-0.707\\0.707\end{pmatrix}$$

The following illustarted an algebraic analysis of the Deutsch-Jozsa algorithm.

$$\begin{array}{lccccccccccc}
\text{Initial} & & 1 & & 2 & & 3 & & 4 & & 5 & \text{Final} \\
|0\rangle & \triangleright & \boxed{\text{H}} & \cdots & \cdot & \cdots & \cdots & \cdots & \cdots & \cdots & \boxed{\text{H}} & \triangleright \text{ Measure, 0 or 1} \\
 & & & & | & & & & & & & \\
|0\rangle & \triangleright & \boxed{\text{H}} & \cdots & | & \cdots & \cdot & \cdots & \cdots & \cdots & \boxed{\text{H}} & \triangleright \text{ Measure, 0 or 1} \\
 & & & & | & & & & & & & \\
|1\rangle & \triangleright & \boxed{\text{H}} & \cdots & \oplus & \cdots & \oplus & \cdots & \boxed{\text{NOT}} & \cdots & \cdots &
\end{array}$$

$$\text{H}|0\rangle \rightarrow \tfrac{1}{\sqrt{2}}\left[|0\rangle+|1\rangle\right] \quad \text{H}|1\rangle \rightarrow \tfrac{1}{\sqrt{2}}\left[|0\rangle-|1\rangle\right]$$

NOT

$$\begin{pmatrix} 0 & \prime & 1 \\ 1 & \prime & 0 \end{pmatrix}$$

CNOT

$$\begin{pmatrix} \text{Decimal} & \text{Binary} & \prime & \text{Binary} & \text{Decimal} \\ 0 & 00 & \prime & 00 & 0 \\ 1 & 01 & \prime & 01 & 1 \\ 2 & 10 & \prime & 11 & 3 \\ 3 & 11 & \prime & 10 & 2 \end{pmatrix}$$

CnNOT

$$\begin{pmatrix} \text{Decimal} & \text{Binary} & \prime & \text{Binary} & \text{Decimal} \\ 0 & 000 & \prime & 000 & 0 \\ 1 & 001 & \prime & 001 & 1 \\ 2 & 010 & \prime & 010 & 2 \\ 3 & 011 & \prime & 011 & 3 \\ 4 & 100 & \prime & 101 & 5 \\ 5 & 101 & \prime & 100 & 4 \\ 6 & 110 & \prime & 111 & 7 \\ 7 & 111 & \prime & 110 & 6 \end{pmatrix}$$

$$\begin{gathered}
|000\rangle \\
\text{H}\otimes\text{H}\otimes\text{H} \\
\tfrac{1}{\sqrt{2}}\left[|0\rangle+|1\rangle\right]\tfrac{1}{\sqrt{2}}\left[|0\rangle+|1\rangle\right]\tfrac{1}{\sqrt{2}}\left[|0\rangle-|1\rangle\right] \\
= \tfrac{1}{2\sqrt{2}}\left[|000\rangle-|001\rangle+|010\rangle-|011\rangle+|100\rangle-|101\rangle+|110\rangle-|111\rangle\right] \\
\text{CnNOT} \\
\tfrac{1}{2\sqrt{2}}\left[|000\rangle-|001\rangle+|010\rangle-|011\rangle+|101\rangle-|100\rangle+|111\rangle-|110\rangle\right] \\
\text{I}\otimes\text{CNOT} \\
\tfrac{1}{2\sqrt{2}}\left[|000\rangle-|001\rangle+|011\rangle-|010\rangle+|101\rangle-|100\rangle+|110\rangle-|111\rangle\right] \\
\text{I}\otimes\text{I}\otimes\text{NOT} \\
\tfrac{1}{\sqrt{2}}\left[|0\rangle-|1\rangle\right]\tfrac{1}{\sqrt{2}}\left[|0\rangle-|1\rangle\right]\tfrac{1}{\sqrt{2}}\left[|1\rangle-|0\rangle\right] \\
\text{H}\otimes\text{H}\otimes\text{H}\otimes\text{I} \\
|1\rangle|1\rangle\tfrac{1}{\sqrt{2}}\left(|1\rangle-|0\rangle\right)
\end{gathered}$$

Since the top wires contain |1 > the function is balanced. This algorithm illustrates the roles of superposition, entanglement and interference in quantum computation. Regarding the latter, it is destructive interference in the last step that eliminates unwanted outcomes yielding the final result on the last line. One pass through the quantum circuit answers the question (is the function balanced or constrant) that would take four calculations on a classical computer.

The interference that occurs in the last step is illustrated by letting |a> = |0> and |b> = |1> and carrying out Hadamard transforms on the first two qubits.

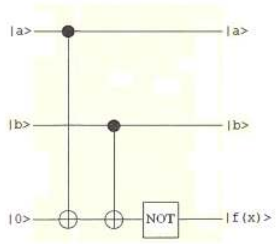
$$\frac{1}{4\sqrt{2}}\begin{bmatrix} (a_1+b_1)(a_2+b_2)b_3-(a_1+b_1)(a_2+b_2)a_3\cdots \\ +(a_1+b_1)(a_2-b_2)b_3-(a_1+b_1)(a_2-b_2)a_3\cdots \\ +(a_1-b_1)(a_2+b_2)b_3-(a_1-b_1)(a_2+b_2)a_3\cdots \\ +(a_1-b_1)(a_2-b_2)b_3-(a_1-b_1)(a_2-b_2)a_3 \end{bmatrix} \text{ simplify } \rightarrow -\frac{\sqrt{2}a_1a_2(a_3-b_3)}{2}$$

This page titled 8.72: An Illustration of the Deutsch-Jozsa Algorithm is shared under a CC BY 4.0 license and was authored, remixed, and/or curated by Frank Rioux via source content that was edited to the style and standards of the LibreTexts platform.

8.73: Another Illustration of the Deutsch-Jozsa Algorithm

The following circuit, U_f, produces the table of results to its right. The top wires carry the value of x and the circuit places f(x) on the bottom wire. As is shown in the previous tutorial this circuit can also operate in parallel accepting as input all x-values and returning on the bottom wire a superposition of all values of f(x).

U_f =



$$\begin{pmatrix} \text{x} & 0 & 1 & 2 & 3 \\ \text{f(x)} & 1 & 0 & 0 & 1 \end{pmatrix} \quad \text{where} \quad \begin{aligned} |0\rangle &= |0\rangle|0\rangle \\ |1\rangle &= |0\rangle|1\rangle \\ |2\rangle &= |1\rangle|0\rangle \\ |3\rangle &= |1\rangle|1\rangle \end{aligned}$$

The function belongs to the balanced category because it produces 0 and 1 with equal frequency. The modification of this circuit (Deutsch-Jozsa algoritm) highlighted below answers the question of whether the function is constant or balanced (see Julian Brown, *The Quest for the Quantum Computer*, page 298). Naturally we already know the answer, so this is a simple demonstration that the circuit works.

$$\begin{array}{lccccccccccc} |0\rangle & \cdots & \boxed{\text{H}} & \cdots & \cdot & \cdots & \cdots & \cdots & \cdots & \cdots & \boxed{\text{H}} & \triangleright \text{ Measure, 0 or 1} \\ & & & & | & & & & & & & \\ |0\rangle & \cdots & \boxed{\text{H}} & \cdots & | & \cdots & \cdot & \cdots & \cdots & \cdots & \boxed{\text{H}} & \triangleright \text{ Measure, 0 or 1} \\ & & & & | & & | & & & & & \\ |1\rangle & \cdots & \boxed{\text{H}} & \cdots & \oplus & \cdots & \oplus & \cdots & \boxed{\text{NOT}} & \cdots & \cdots & \end{array}$$

The input is $|0\rangle|0\rangle|1\rangle$: $\Psi_{in} = (0 \quad 1 \quad 0 \quad 0 \quad 0 \quad 0 \quad 0 \quad 0)^T$

The following matrices are required to execute the circuit.

$$\text{I} = \begin{pmatrix} 1 & 0 \\ 0 & 1 \end{pmatrix} \quad \text{NOT} = (0 \quad 1\ 1 \quad 0) \quad \text{H} = \frac{1}{\sqrt{2}} \begin{pmatrix} 1 & 1 \\ 1 & -1 \end{pmatrix}$$

$$\text{CNOT} = \begin{pmatrix} 1 & 0 & 0 & 0 \\ 0 & 1 & 0 & 0 \\ 0 & 0 & 0 & 1 \\ 0 & 0 & 1 & 0 \end{pmatrix} \quad \text{CnNOT} = \begin{pmatrix} 1 & 0 & 0 & 0 & 0 & 0 & 0 & 0 \\ 0 & 1 & 0 & 0 & 0 & 0 & 0 & 0 \\ 0 & 0 & 1 & 0 & 0 & 0 & 0 & 0 \\ 0 & 0 & 0 & 1 & 0 & 0 & 0 & 0 \\ 0 & 0 & 0 & 0 & 0 & 1 & 0 & 0 \\ 0 & 0 & 0 & 0 & 1 & 0 & 0 & 0 \\ 0 & 0 & 0 & 0 & 0 & 0 & 0 & 1 \\ 0 & 0 & 0 & 0 & 0 & 0 & 1 & 0 \end{pmatrix}$$

The quantum circuit is assembled out of these matrices using tensor (kronecker) multiplication.

$$U_f = \text{kronecker(I, kronecker(I, NOT))}\ \text{kronecker(I, CNOT)}\ \text{CnNOT}$$
$$\text{QuantumCircuit} = \text{kronecker(H, kronecker(H, I))}\ U_f \text{kronecker(H, kronecker(H, H))}$$

Operation of the quantum circuit on the input vector yields the following result which is written as a product of three qubits on the right.

$$\text{QuantumCircuit}\Psi_{\text{in}} = \begin{pmatrix} 0 \\ 0 \\ 0 \\ 0 \\ 0 \\ 0 \\ -0.707 \\ 0.707 \end{pmatrix} \quad \begin{pmatrix} 0 \\ 1 \end{pmatrix} \begin{pmatrix} 0 \\ 1 \end{pmatrix} \frac{1}{\sqrt{2}} \begin{pmatrix} -1 \\ 1 \end{pmatrix}$$

According to the Deutsch-Jozsa scheme, if both wires are |0> the function is constant, but if at least one wire is |1> the function is balanced. We see by inspection that both wires are |1> indicating that the function is balanced.

The measurements on the top wires can be simulated with projection operators |0><1|, and confirm that the function is not constant but belongs to the balanced category.

$$\text{The first qubit is not } |0\rangle \qquad \left[\text{kronecker}\left[\begin{pmatrix} 1 \\ 0 \end{pmatrix}\begin{pmatrix} 1 \\ 0 \end{pmatrix}^T, \text{kronecker(I, I)}\right]\text{QuantumCircuit}\Psi_{\text{in}}\right]^T$$
$$= (0 \quad 0 \quad 0 \quad 0 \quad 0 \quad 0 \quad 0 \quad 0)$$

$$\text{The second qubit is not } |0\rangle \qquad \left[\text{kronecker}\left[\text{I, kronecker}\left[\begin{pmatrix} 1 \\ 0 \end{pmatrix}\begin{pmatrix} 1 \\ 0 \end{pmatrix}^T, \text{I}\right]\right]\text{QuantumCircuit}\Psi_{\text{in}}\right]^T$$
$$= (0 \quad 0 \quad 0 \quad 0 \quad 0 \quad 0 \quad 0 \quad 0)$$

$$\text{The first qubit is } |1\rangle \qquad \left[\text{kronecker}\left[\begin{pmatrix} 0 \\ 1 \end{pmatrix}\begin{pmatrix} 0 \\ 1 \end{pmatrix}^T, \text{kronecker(I, I)}\right]\text{QuantumCircuit}\Psi_{\text{in}}\right]^T$$
$$= (0 \quad 0 \quad 0 \quad 0 \quad 0 \quad 0 \quad -0.707 \quad 0.707)$$

$$\text{The second qubit is } |1\rangle \qquad \left[\text{kronecker}\left[\text{I, kronecker}\left[\begin{pmatrix} 0 \\ 1 \end{pmatrix}\begin{pmatrix} 0 \\ 1 \end{pmatrix}^T, \text{I}\right]\right]\text{QuantumCircuit}\Psi_{\text{in}}\right]^T$$
$$= (0 \quad 0 \quad 0 \quad 0 \quad 0 \quad 0 \quad -0.707 \quad 0.707)$$

This page titled 8.73: Another Illustration of the Deutsch-Jozsa Algorithm is shared under a CC BY 4.0 license and was authored, remixed, and/or curated by Frank Rioux via source content that was edited to the style and standards of the LibreTexts platform.

8.74: Aspects of Simon's Algorithm

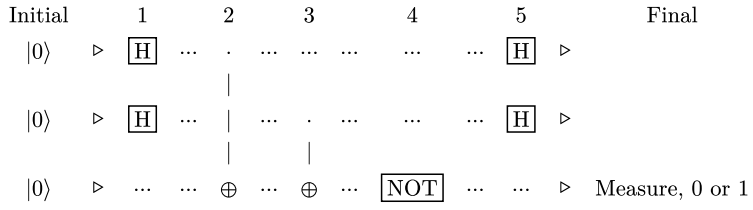
A concealed quantum algorithm calculates f(x) from an input register containing a superposition of all x-values. Pairs of x-values (x, x') generate the same output. Simon's algorithm is an efficient method for finding the relationship between the pairs: $f(x) = f(x') = f(x \oplus s)$, where s is a secret string and the addition on the right is bitwise modulo 2 . In a classical calculation one could compute f(x) until some pattern emerged and find the pairs by inspection. This approach is illustrated below.

Decimal	Binary		Binary	Decimal
$\|0\rangle$	$\|000\rangle$	$\xrightarrow{f(0)}$	$\|011\rangle$	$\|3\rangle$
$\|1\rangle$	$\|001\rangle$	$\xrightarrow{f(1)}$	$\|001\rangle$	$\|1\rangle$
$\|2\rangle$	$\|010\rangle$	$\xrightarrow{f(2)}$	$\|010\rangle$	$\|2\rangle$
$\|3\rangle$	$\|011\rangle$	$\xrightarrow{f(3)}$	$\|000\rangle$	$\|0\rangle$
$\|4\rangle$	$\|100\rangle$	$\xrightarrow{f(4)}$	$\|001\rangle$	$\|1\rangle$
$\|5\rangle$	$\|101\rangle$	$\xrightarrow{f(5)}$	$\|011\rangle$	$\|3\rangle$
$\|6\rangle$	$\|110\rangle$	$\xrightarrow{f(6)}$	$\|010\rangle$	$\|2\rangle$

The table of results reveals the pairs {(0,5), (1,4), (2,7), (3,6)} and that |s> = |101>. Adding |s> bitwise modulo 2 to any |x> reveals its partner |x'>.

The following quantum circuit is a rudimentary implementation of Simon's algorithm. The section in blue is the concealed algorithm. It has been discussed in two other tutorials: *Quantum Parallel Calculation* and *An Illustration of the Deutsch-Jozsa Algorithm*. Its operation yields the results shown in the following table.

$$\begin{pmatrix} x & 0 & 1 & 2 & 3 \\ f(x) & 1 & 0 & 0 & 1 \end{pmatrix}$$



Next we prepare a table showing the results of a classical calculation. It is clear that the pairs are (0,3) and (1,2), and that |s> = |11>.

Decimal	Binary		Binary	Decimal
$\|0\rangle$	$\|00\rangle$	$\xrightarrow{f(0)}$	$\|01\rangle$	$\|1\rangle$
$\|1\rangle$	$\|01\rangle$	$\xrightarrow{f(1)}$	$\|00\rangle$	$\|0\rangle$
$\|2\rangle$	$\|10\rangle$	$\xrightarrow{f(2)}$	$\|00\rangle$	$\|0\rangle$
$\|3\rangle$	$\|11\rangle$	$\xrightarrow{f(3)}$	$\|01\rangle$	$\|1\rangle$

Now we examine the operation of the quantum circuit that implements Simon's algoritm by two different, but equivalent methods. The matrices representing the quantum gates in the circuit are:

$$I = \begin{pmatrix} 1 & 0 \\ 0 & 1 \end{pmatrix} \quad NOT = \begin{pmatrix} 0 & 1 & 1 & 0 \end{pmatrix} \quad H = \frac{1}{\sqrt{2}} \begin{pmatrix} 1 & 1 \\ 1 & -1 \end{pmatrix}$$

$$\text{CNOT} = \begin{pmatrix} 1 & 0 & 0 & 0 \\ 0 & 1 & 0 & 0 \\ 0 & 0 & 0 & 1 \\ 0 & 0 & 1 & 0 \end{pmatrix} \quad \text{CnNOT} = \begin{pmatrix} 1 & 0 & 0 & 0 & 0 & 0 & 0 & 0 \\ 0 & 1 & 0 & 0 & 0 & 0 & 0 & 0 \\ 0 & 0 & 1 & 0 & 0 & 0 & 0 & 0 \\ 0 & 0 & 0 & 1 & 0 & 0 & 0 & 0 \\ 0 & 0 & 0 & 0 & 0 & 1 & 0 & 0 \\ 0 & 0 & 0 & 0 & 1 & 0 & 0 & 0 \\ 0 & 0 & 0 & 0 & 0 & 0 & 0 & 1 \\ 0 & 0 & 0 & 0 & 0 & 0 & 1 & 0 \end{pmatrix}$$

The three qubit input state is: $\Psi_{in} = (1 \quad 0 \quad 0 \quad 0 \quad 0 \quad 0 \quad 0 \quad 0)^T$

The concealed algorithm: $\text{U}_\text{f} = \text{kronecker(I, kronecker(I, NOT))}\ \text{kronecker(I, CNOT)}\ \text{CnNOT}$

The complete quantum circuit: $\text{QuantumCircuit} = \text{kronecker(H, kronecker(H, kronecker(H, I))}\ \text{U}_\text{f}\ \text{kronecker(H, kronecker(H, I))}$

The operation of the quantum circuit on the input state yields the following result:

$$\text{QuantumCircuit}\Psi_{in}$$

$$= \begin{pmatrix} 0.5 \\ 0.5 \\ 0 \\ 0 \\ 0 \\ 0 \\ -0.5 \\ 0.5 \end{pmatrix} = \tfrac{1}{2}\left[\begin{pmatrix}1\\0\end{pmatrix}\otimes\begin{pmatrix}1\\0\end{pmatrix} - \begin{pmatrix}0\\1\end{pmatrix}\otimes\begin{pmatrix}0\\1\end{pmatrix}\right]\begin{pmatrix}1\\0\end{pmatrix} + \tfrac{1}{2}\left[\begin{pmatrix}1\\0\end{pmatrix}\otimes\begin{pmatrix}1\\0\end{pmatrix}\begin{pmatrix}1\\0\end{pmatrix} + \begin{pmatrix}0\\1\end{pmatrix}\otimes\begin{pmatrix}0\\1\end{pmatrix}\right]\begin{pmatrix}0\\1\end{pmatrix}$$

$$= \tfrac{1}{2}\left[|00\rangle - |11\rangle\right]|0\rangle + \tfrac{1}{2}\left[|00\rangle + |11\rangle\right]|1\rangle$$

The terms in brackets are superpositions of the x-values which are related by $x' x = \oplus s$. Thus we see by inspection that |s> = |11>. The actual implementation of Simon's algorithm involves multiple measurements in order to determine the secret string. The Appendix modifies the quantum circuit to include the effect of measurement on the bottom wire.

The second method of analysis uses the following truth tables for the quantum gates and the operation of the Hadamard gate to trace the evolution of the input quibits through the quantum circuit.

NOT

0	′	1
1	′	0

CNOT

Decimal	Binary	′	Binary	Decimal
0	00	′	00	0
1	01	′	01	1
2	10	′	11	3
3	11	′	10	2

CnNOT

Decimal	Binary	′	Binary	Decimal
0	000	′	000	0
1	001	′	001	1
2	010	′	010	2
3	011	′	011	3
4	100	′	101	5
5	101	′	100	4
6	110	′	111	7
7	111	′	110	6

Hadamard operation:

0	′	H	′	$\frac{1}{\sqrt{2}}(0+1)$	′	H	′	0
1	′	H	′	$\frac{1}{\sqrt{2}}(0-1)$	′	H	′	1

$$|000\rangle$$
$$\mathrm{H}\otimes\mathrm{H}\otimes\mathrm{I}$$
$$\frac{1}{\sqrt{2}}\left[|0\rangle+|1\rangle\right]\frac{1}{\sqrt{2}}\left[|0\rangle+|1\rangle\right]|0\rangle=\frac{1}{2}\left[|000\rangle+|010\rangle+|100\rangle+|110\rangle\right]$$
$$\mathrm{CnNOT}$$
$$\frac{1}{2}\left[|000\rangle+|010\rangle+|101\rangle+|111\rangle\right]$$
$$\mathrm{I}\otimes\mathrm{CNOT}$$
$$\frac{1}{2}\left[|000\rangle+|011\rangle+|101\rangle+|110\rangle\right]$$
$$\mathrm{I}\otimes\mathrm{I}\otimes\mathrm{NOT}$$
$$\frac{1}{2}\left[|001\rangle+|010\rangle+|100\rangle+|111\rangle\right]$$
$$\mathrm{H}\otimes\mathrm{H}\otimes\mathrm{I}$$
$$\frac{1}{2}\left[\left(|00\rangle-|11\rangle\right)|0\rangle+\left(|00\rangle+|11\rangle\right)|1\rangle\right]$$

Appendix

The circuit modification shown below includes the effect of measurement on the bottom wire.

Measure |0> on the bottom wire:

$$\mathrm{QuantumCircuit}=\mathrm{kronecker}\left[\mathrm{H},\ \mathrm{kronecker}\left[\mathrm{H},\ \begin{pmatrix}1\\0\end{pmatrix}\begin{pmatrix}1\\0\end{pmatrix}^{T}\right]\right]\mathrm{U}_f\mathrm{kronecker}(\mathrm{H},\ \mathrm{kronecker}(\mathrm{H},\ \mathrm{I}))$$

$$\mathrm{QuantumCircuit}\Psi_{in}=\begin{pmatrix}0.5\\0\\0\\0\\0\\0\\-0.5\\0\end{pmatrix}\begin{pmatrix}0.5\\0\\0\\0\\0\\0\\-0.5\\0\end{pmatrix}=\frac{1}{2}\left[\begin{pmatrix}1\\0\end{pmatrix}\begin{pmatrix}1\\0\end{pmatrix}-\begin{pmatrix}0\\1\end{pmatrix}\begin{pmatrix}0\\1\end{pmatrix}\right]\begin{pmatrix}1\\0\end{pmatrix}$$

Measure |1> on the bottom wire:

$$\mathrm{QuantumCircuit}=\mathrm{kronecker}\left[\mathrm{H},\ \mathrm{kronecker}\left[\mathrm{H},\ \begin{pmatrix}0\\1\end{pmatrix}\begin{pmatrix}0\\1\end{pmatrix}^{T}\right]\right]\mathrm{U}_f\mathrm{kronecker}(\mathrm{H},\ \mathrm{kronecker}(\mathrm{H},\ \mathrm{I}))$$

$$\mathrm{QuantumCircuit}\Psi_{in}=\begin{pmatrix}0\\0.5\\0\\0\\0\\0\\0\\0.5\end{pmatrix}\begin{pmatrix}0\\0.5\\0\\0\\0\\0\\0\\0.5\end{pmatrix}=\frac{1}{2}\left[\begin{pmatrix}1\\0\end{pmatrix}\begin{pmatrix}1\\0\end{pmatrix}+\begin{pmatrix}0\\1\end{pmatrix}\begin{pmatrix}0\\1\end{pmatrix}\right]\begin{pmatrix}0\\1\end{pmatrix}$$

This page titled 8.74: Aspects of Simon's Algorithm is shared under a CC BY 4.0 license and was authored, remixed, and/or curated by Frank Rioux via source content that was edited to the style and standards of the LibreTexts platform.

8.75: Qubit Quantum Mechanics

In this document I reproduce most of the results presented in Professor Galvez's paper using the Mathcad programming environment.

State Vector

$$\text{Photon moving horizontally: } x = \begin{pmatrix}1\\0\end{pmatrix} \quad \text{Photon moving vertically: } y = \begin{pmatrix}0\\1\end{pmatrix} \quad \text{Null vector: } n = \begin{pmatrix}0\\0\end{pmatrix}$$

$$\text{Horizontal polarization: } h = \begin{pmatrix}1\\0\end{pmatrix} \quad \text{Vertical polarization: } v = \begin{pmatrix}0\\1\end{pmatrix} \quad \text{Diagonal polarization: } d = \begin{pmatrix}\frac{1}{\sqrt{2}}\\\frac{1}{\sqrt{2}}\end{pmatrix}$$

Single mode operators:

Projection operators for motion in the x- and y-directions:

$$X = \begin{pmatrix}1 & 0\\0 & 0\end{pmatrix} \quad Y = \begin{pmatrix}0 & 0\\0 & 1\end{pmatrix}$$

Operator for polarizing film oriented at an angle of θ to the horizontal.

$$\Theta_{op}(\theta) = \begin{pmatrix}\cos\theta\\\sin\theta\end{pmatrix}(\cos\theta \quad \sin\theta) \rightarrow \begin{pmatrix}\cos\theta^2 & \cos\theta\sin\theta\\\cos\theta\sin\theta & \sin\theta^2\end{pmatrix}$$

Beam splitter:

$$BS = \begin{pmatrix}\frac{1}{\sqrt{2}} & \frac{i}{\sqrt{2}}\\\frac{i}{\sqrt{2}} & \frac{1}{\sqrt{2}}\end{pmatrix}$$

Mirror:

$$M = \begin{pmatrix}0 & 1\\1 & 0\end{pmatrix}$$

Phase shift:

$$A(\delta) = \begin{pmatrix}e^{i\delta} & 0\\0 & 1\end{pmatrix}$$

Half and quarter wave plate:

$$W_2 = \begin{pmatrix}1 & 0\\0 & -1\end{pmatrix} \quad W_4 = \begin{pmatrix}1 & 0\\0 & -i\end{pmatrix}$$

Identity:

$$I = \begin{pmatrix}1 & 0\\0 & 1\end{pmatrix}$$

Rotated half wave plate:

$$W_2(\theta) = \begin{pmatrix}\cos(2\theta) & \sin(2\theta)\\\sin(2\theta) & -\cos(2\theta)\end{pmatrix} \quad W(\theta) = \begin{pmatrix}\cos(2\theta) & \sin(2\theta) & 0 & 0\\\sin(2\theta) & -\cos(2\theta) & 0 & 0\\0 & 0 & 0 & 0\\0 & 0 & 0 & -1\end{pmatrix}$$

Mach-Zehnder interferometer:

$$MZ(\delta) = BS\ A(\delta) M\ BS$$

Two mode states and operators:

Single-photon direction of propagation and polarization states:

$$\text{xh} = \begin{pmatrix}1\\0\\0\\0\end{pmatrix} \quad \text{xv} = \begin{pmatrix}0\\1\\0\\0\end{pmatrix} \quad \text{yh} = \begin{pmatrix}0\\0\\1\\0\end{pmatrix} \quad \text{yv} = \begin{pmatrix}0\\0\\0\\1\end{pmatrix}$$

Two-photon direction of propagation states.

$$\text{xx} = \begin{pmatrix}1\\0\\0\\0\end{pmatrix} \quad \text{xy} = \begin{pmatrix}0\\1\\0\\0\end{pmatrix} \quad \text{yx} = \begin{pmatrix}0\\0\\1\\0\end{pmatrix} \quad \text{yy} = \begin{pmatrix}0\\0\\0\\1\end{pmatrix}$$

Two-photon polarization states:

$$\text{hh} = \begin{pmatrix}1\\0\\0\\0\end{pmatrix} \quad \text{hv} = \begin{pmatrix}0\\1\\0\\0\end{pmatrix} \quad \text{vh} = \begin{pmatrix}0\\0\\1\\0\end{pmatrix} \quad \text{vv} = \begin{pmatrix}0\\0\\0\\1\end{pmatrix}$$

Polarizing beam splitter which transmits horizontally polarized photons and reflects vertically polarized photons.

$$\text{PBS} = \text{xh xh}^T + \text{yv xv}^T + \text{yh yh}^T + \text{xv yv}^T \quad \text{PBS} = \begin{pmatrix}1&0&0&0\\0&0&0&1\\0&0&1&0\\0&1&0&0\end{pmatrix}$$

Polarization M-Z interferometer:

$$\text{MZp}(\delta) = \text{PBS kronecker}(\text{A}(\delta),\ \text{I})\text{kronecker}(\text{M, I})\ \text{PBS}$$

Kronecker is Mathcad′s command for tensor multiplication of square matrices.

Mach-Zehnder interferometer for direction of propagation and polarization, which places a rotatable half-wave plate in the upper path.

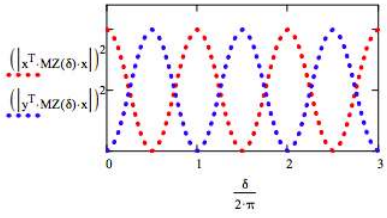
$$\text{MZ}_{\text{dp}}(\theta, \delta) = \text{kronecker (BS, I) kronecker(A }(\delta)\text{ ,I) W }(\theta)\text{ kronecker (M, I) kronecker (BS, I)}$$

Mach-Zehnder two-photon direction-of-propagation interferometer.

$$\text{BSBS} = \text{kronecker(BS, BS)} \quad \text{MM} = \text{kronecker(M, M)} \quad \text{AA}(\delta) = \text{kronecker(A}(\delta), \text{A}(\delta))$$
$$\text{MZ}_{\text{dd}}(\delta) = \text{BSBS AA}(\delta)\text{MM BSBS}$$

Confirm the results in Figure 2 for the Mach-Zehnder interferometer:

$$\delta = 0, .125\pi ... 6\pi$$

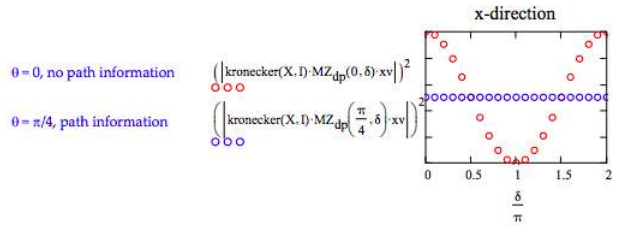


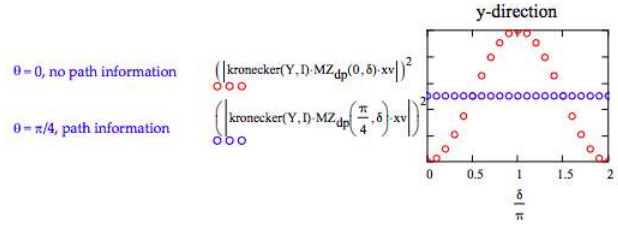
Demonstrate that a superposition is formed after the first beam splitter.

$$\text{BS x} = \begin{pmatrix}0.707\\0.707i\end{pmatrix} \quad \tfrac{1}{\sqrt{2}}(\text{x} + \text{iy}) = \begin{pmatrix}0.707\\0.707i\end{pmatrix}$$

Confirmation that path information destroys interference.

$$\delta = 0, .1\pi .. 2\pi$$



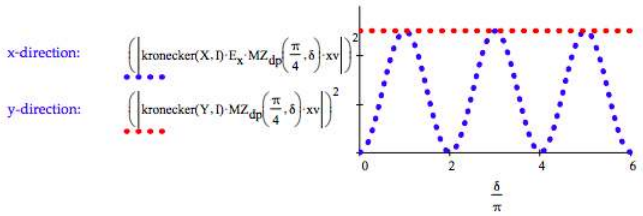


Erasure of path information restores interference. Erasers for the x- and y-directions place diagonal polarizers in those directions after the interferometer.

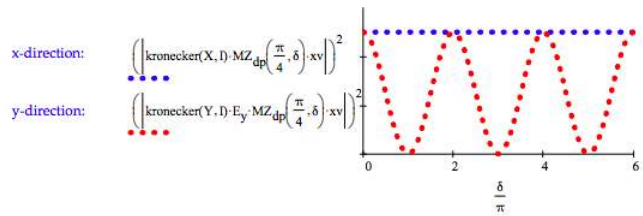
$$E_x = \begin{pmatrix} \frac{1}{2} & \frac{1}{2} & 0 & 0 \\ \frac{1}{2} & \frac{1}{2} & 0 & 0 \\ 0 & 0 & 1 & 0 \\ 0 & 0 & 0 & 1 \end{pmatrix} \quad E_y = \begin{pmatrix} 1 & 0 & 0 & 0 \\ 0 & 1 & 0 & 0 \\ 0 & 0 & \frac{1}{2} & \frac{1}{2} \\ 0 & 0 & \frac{1}{2} & \frac{1}{2} \end{pmatrix}$$

The x-direction has an erase and the y-direction does not.

$$\delta = 0, .1\pi..6\pi$$



The y-direction has an eraser and the x-direction does not.



For the MZ polarization interferometer diagonally polarized light enters in the x-direction, |xd>. Tensor vector multiplication is awkward in Mathcad as shown below.

$$\Psi_{in} = \frac{1}{\sqrt{2}} \begin{pmatrix} 1 \\ 1 \\ 0 \\ 0 \end{pmatrix} \quad \text{submatrix}(\text{kronecker}(\text{augment}(x, n), \text{augment}(d, n)), 1, 4, 1, 1) = \begin{pmatrix} 0.707 \\ 0.707 \\ 0 \\ 0 \end{pmatrix}$$

No light, however, exits in the x-direction. It exits in the y-direction showing no interference effects.

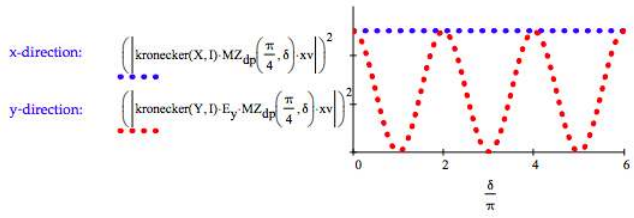
$$\delta = 0, .2\pi...\pi$$

x-direction: y-direction:

$$\left(\left|\text{kronecker}(X,\ I)\ MZ_p(\delta)\Psi_{in}\right|\right)^2 = \begin{pmatrix}0\\0\\0\\0\\0\\0\end{pmatrix} \quad \left(\left|\text{kronecker}(Y,\ I)\ MZ)_p(\delta)\Psi_{in}\right|\right)^2 = \begin{pmatrix}1\\1\\1\\1\\1\\1\end{pmatrix}$$

Placement of a D polarizer in the y-direction output erases distinguishing information and interference appears.

$$\delta = 0, .1\pi..6\pi$$

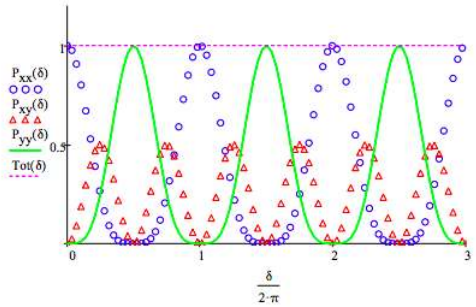


Calculation of exit probabilities for two photons in direction-of-propagation modes:

$$P_{xx}(\delta) = \left(\left|xx^T MZ_{dd}(\delta) xx\right|\right)^2 \quad P_{xy}(\delta) = \left[\left|\tfrac{1}{\sqrt{2}}(xy + yx)^T MZ_{dd}(\delta) xx\right|\right]$$
$$P_{yy}(\delta) = \left(\left|yy^T MZ_{dd}(\delta) xx\right|\right)^2 \quad Tot(\delta) = P_{xx}(\delta) + P_{xy}(\delta) + P_{yy}(\delta)$$

Reproduction of Figure 5b with the addition of P_{yy}.

$$\delta = 0, .07\pi..6\pi$$



"The striking result is that the (P_{xy}) interference pattern has twice the frequency of the single-photon interference pattern. Nonclassical interference shows new quantum aspects: two photons acting as a single quantum object (a biphoton)."

Hong-Ou-Mandel interference (right column, page 516):

$$BSBS\tfrac{1}{\sqrt{2}}(xy + yx) = \begin{pmatrix}0.707i\\0\\0\\0.707i\end{pmatrix} \quad \tfrac{i}{\sqrt{2}}(xx + yy) = \begin{pmatrix}0.707i\\0\\0\\0.707i\end{pmatrix}$$

Section III.D deals with distinguishing between pure and mixed states experimentally. The pure state and it density matrix are given below.

$$\Psi_{\text{pure}} = \frac{1}{\sqrt{2}}(\text{hh} + \text{vv}) \quad \Psi_{\text{pure}} = \begin{pmatrix} 0.707 \\ 0 \\ 0 \\ 0.707 \end{pmatrix} \quad \Psi_{\text{pure}} \Psi_{\text{pure}}^T = \begin{pmatrix} 0.5 & 0 & 0 & 0.5 \\ 0 & 0 & 0 & 0 \\ 0 & 0 & 0 & 0 \\ 0.5 & 0 & 0 & 0.5 \end{pmatrix}$$

The density matrix for the mixed state is calculated as follows.

$$\frac{1}{2}\text{hh hh}^T + \frac{1}{2}\text{vv vv}^T = \begin{pmatrix} 0.5 & 0 & 0 & 0 \\ 0 & 0 & 0 & 0 \\ 0 & 0 & 0 & 0 \\ 0 & 0 & 0 & 0.5 \end{pmatrix}$$

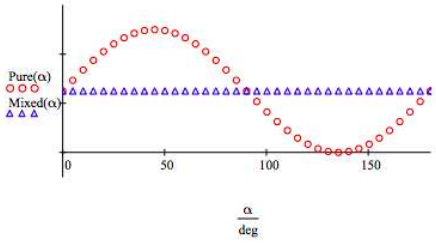
The following calculations and their graphical representation are in complete agreement with section III.D

$$\text{Pure}(\alpha) = \text{tr}\left[\frac{1}{2} \begin{pmatrix} 1 & 0 & 0 & 1 \\ 0 & 0 & 0 & 0 \\ 0 & 0 & 0 & 0 \\ 1 & 0 & 0 & 1 \end{pmatrix} \frac{1}{2} \left[\begin{pmatrix} \cos\alpha \\ \cos\alpha \\ \sin\alpha \\ \sin\alpha \end{pmatrix} \begin{pmatrix} \cos\alpha \\ \cos\alpha \\ \sin\alpha \\ sin\alpha \end{pmatrix}^T \right] \right] \text{simplify} \rightarrow \frac{\sin(2\alpha)}{4} + \frac{1}{4}$$

$$\text{Mixed}(\alpha) = \text{tr}\left[\frac{1}{2} \begin{pmatrix} 1 & 0 & 0 & 1 \\ 0 & 0 & 0 & 0 \\ 0 & 0 & 0 & 0 \\ 1 & 0 & 0 & 1 \end{pmatrix} \frac{1}{2} \left[\begin{pmatrix} \cos\alpha \\ \cos\alpha \\ \sin\alpha \\ \sin\alpha \end{pmatrix} \begin{pmatrix} \cos\alpha \\ \cos\alpha \\ \sin\alpha \\ sin\alpha \end{pmatrix}^T \right] \right] \text{simplify} \rightarrow \frac{1}{4}$$

Reproduce Figure 6 results.

$$\alpha = 0\text{deg},\ 5\text{deg}..180\text{deg}$$



The following calculation are in agreement with the math in the final paragraph of the section IV.D.

$$\text{kronecker}\left(\text{W}_2(0),\ \text{I}\right) \Psi_{\text{pure}} = \begin{pmatrix} 0.707 \\ 0 \\ 0 \\ -0.707 \end{pmatrix} \begin{pmatrix} 0.707 \\ 0 \\ 0 \\ -0.707 \end{pmatrix} \begin{pmatrix} 0.707 \\ 0 \\ 0 \\ -0.707 \end{pmatrix}^T = \begin{pmatrix} 0.5 & 0 & 0 & -0.5 \\ 0 & 0 & 0 & 0 \\ 0 & 0 & 0 & 0 \\ -0.5 & 0 & 0 & 0.5 \end{pmatrix}$$

Extra close brace or missing open brace

The paper shows this as $\frac{[1-\sin\alpha}{4}$ which I am confident is a typographical error.

This page titled 8.75: Qubit Quantum Mechanics is shared under a CC BY 4.0 license and was authored, remixed, and/or curated by Frank Rioux via source content that was edited to the style and standards of the LibreTexts platform.

8.76: Implementation of Deutsch's Algorithm Using Mathcad

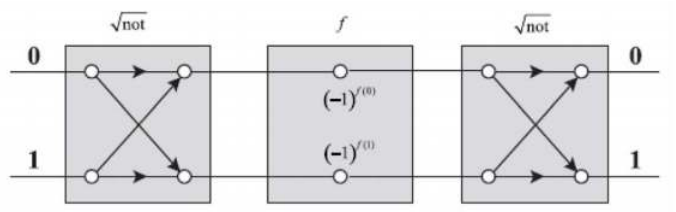
The following is a Mathcad implementation of David Deutsch's quantum computer prototype as presented on pages 10-11 in "Machines, Logic and Quantum Physics" by David Deutsch, Artur Ekert, and Rossella Lupacchini, which can be found at arXiv:math.HO/9911150v1.

A function f maps {0, 1} to {0, 1}. There are four possible outcomes: f(0) = 0; f(0) = 1; f(1) = 0; f(1) = 1. The task Deutsch tackled was to develop an implementable quantum algorithm which could determine whether f(0) and f(1) were the same or different in a single calculation. By comparison classical computers require two calculations for such a task - calculating both f(0) and f(1) to see if they are the same or different.

The proposed quantum computer consists of three one-qubit gates in the arrangement shown below. The $\sqrt{NOT}$ gates are 50-50 beam splitters that assign a π/2 (i, 90 degree) phase change to reflection relative to transmission. For example, the first gate creates the following superpositions of the inputs |0> and |1>.

$$|0\rangle \rightarrow [|0\rangle + i|1\rangle] \quad |1\rangle \rightarrow [i|0\rangle + |1\rangle]$$

The middle gate carries out phase shifts on the superposition created by the first gate. Depending on the f-values, the operation of the second $\sqrt{NOT}$ converts the superposition to either |0> or |1> multiplied by a phase factor or unity. The Deutsch circuit is essentially a two-port Mach-Zehnder interferometer with the possibility for unequal phase changes in its upper and lower arms.



The matrix representations for the gates are as follows:

$$0 = \begin{pmatrix} 1 \\ 0 \end{pmatrix} \qquad\qquad 0 = \begin{pmatrix} 1 \\ 0 \end{pmatrix}$$

$$\frac{1}{\sqrt{2}}\begin{pmatrix} 1 & i \\ i & 1 \end{pmatrix} \quad \begin{bmatrix} (-1)^{f(0)} & 0 \\ 0 & (-1)^{f(1)} \end{bmatrix} \quad \frac{1}{\sqrt{2}}\begin{pmatrix} 1 & i \\ i & 1 \end{pmatrix}$$

$$1 = \begin{pmatrix} 0 \\ 1 \end{pmatrix} \qquad\qquad 1 = \begin{pmatrix} 0 \\ 1 \end{pmatrix}$$

We begin with a matrix mechanics approach to Deutsch's algorithm using the definitions provided immediately above. There are two input ports and two output ports, but only one input port is used in any given computational run. First it is shown how the output result depends on the input port chosen in terms of the values of f(0) and f(1).

$$\begin{pmatrix} 1 \\ 0 \end{pmatrix} \text{ Input } \left[\frac{1}{\sqrt{2}}\begin{pmatrix} 1 & i \\ i & 1 \end{pmatrix}\right]\begin{bmatrix} (-1)^{f_0} & 0 \\ 0 & (-1)^{f_1} \end{bmatrix}\left[\frac{1}{\sqrt{2}}\begin{pmatrix} 1 & i \\ i & 1 \end{pmatrix}\right]\begin{pmatrix} 1 \\ 0 \end{pmatrix} \rightarrow \begin{bmatrix} \frac{(-1)^{f_0}}{2} - \frac{(-1)^{f_1}}{2} \\ \frac{(-1)_0^f}{2} + \frac{(-1)^{f_1} i}{2} \end{bmatrix}$$

$$\begin{pmatrix} 0 \\ 1 \end{pmatrix} \text{ Input } \left[\frac{1}{\sqrt{2}}\begin{pmatrix} 1 & i \\ i & 1 \end{pmatrix}\right]\begin{bmatrix} (-1)^{f_0} & 0 \\ 0 & (-1)^{f_1} \end{bmatrix}\left[\frac{1}{\sqrt{2}}\begin{pmatrix} 1 & i \\ i & 1 \end{pmatrix}\right]\begin{pmatrix} 0 \\ 1 \end{pmatrix} \rightarrow \begin{bmatrix} \frac{(-1)_0^f}{2} + \frac{(-1)^{f_1} i}{2} \\ \frac{(-1)^{f_0}}{2} - \frac{(-1)^{f_1}}{2} \end{bmatrix}$$

These calculations and the circuit diagram show that there are two paths to each output port from each input port. As will now be shown these paths interfere constructively or destructively depending on the phase changes brought about by the middle circuit element's values of f(0) and f(1).

The following calculations show that the probability that |0 > input leads to |0 > output is zero if f(0) and f(1) are the same (both 0 or both 1), and unity if they are different (one 0, the other 1). Thus the task has been successfully accomplished. The highlighted central region calculates the output state for input state |0> given the values of f(0) and f(1) to the left. On the right the probability that |0> is the output state is calculated.

$$f_0 = 0 \quad f_1 = 0 \qquad \left[\tfrac{1}{\sqrt{2}}\begin{pmatrix}1 & i\\ i & 1\end{pmatrix}\right]\begin{bmatrix}(-1)^{f_0} & 0\\ 0 & (-1)^{f_1}\end{bmatrix}\left[\tfrac{1}{\sqrt{2}}\begin{pmatrix}1 & i\\ i & 1\end{pmatrix}\right]\begin{pmatrix}1\\0\end{pmatrix} = \begin{pmatrix}0\\ i\end{pmatrix} \qquad \left|\begin{pmatrix}1 & 0\end{pmatrix}\begin{pmatrix}0\\ i\end{pmatrix}\right|^2 = 0$$

$$f_0 = 1 \quad f_1 = 1 \qquad \left[\tfrac{1}{\sqrt{2}}\begin{pmatrix}1 & i\\ i & 1\end{pmatrix}\right]\begin{bmatrix}(-1)^{f_0} & 0\\ 0 & (-1)^{f_1}\end{bmatrix}\left[\tfrac{1}{\sqrt{2}}\begin{pmatrix}1 & i\\ i & 1\end{pmatrix}\right]\begin{pmatrix}1\\0\end{pmatrix} = \begin{pmatrix}0\\ -i\end{pmatrix} \qquad \left|\begin{pmatrix}1 & 0\end{pmatrix}\begin{pmatrix}0\\ -i\end{pmatrix}\right|^2 = 0$$

$$f_0 = 1 \quad f_1 = 0 \qquad \left[\tfrac{1}{\sqrt{2}}\begin{pmatrix}1 & i\\ i & 1\end{pmatrix}\right]\begin{bmatrix}(-1)^{f_0} & 0\\ 0 & (-1)^{f_1}\end{bmatrix}\left[\tfrac{1}{\sqrt{2}}\begin{pmatrix}1 & i\\ i & 1\end{pmatrix}\right]\begin{pmatrix}1\\0\end{pmatrix} = \begin{pmatrix}-1\\ 0\end{pmatrix} \qquad \left|\begin{pmatrix}1 & 0\end{pmatrix}\begin{pmatrix}-1\\ 0\end{pmatrix}\right|^2 = 1$$

$$f_0 = 0 \quad f_1 = 1 \qquad \left[\tfrac{1}{\sqrt{2}}\begin{pmatrix}1 & i\\ i & 1\end{pmatrix}\right]\begin{bmatrix}(-1)^{f_0} & 0\\ 0 & (-1)^{f_1}\end{bmatrix}\left[\tfrac{1}{\sqrt{2}}\begin{pmatrix}1 & i\\ i & 1\end{pmatrix}\right]\begin{pmatrix}1\\0\end{pmatrix} = \begin{pmatrix}1\\ 0\end{pmatrix} \qquad \left|\begin{pmatrix}1 & 0\end{pmatrix}\begin{pmatrix}1\\0\end{pmatrix}\right|^2 = 1$$

As might be expected, similar calculations show that the probability that |1> input leads to |1> output is zero if f(0) and f(1) are the same, and unity if they are different.

$$f_0 = 0 \quad f_1 = 0 \qquad \left[\tfrac{1}{\sqrt{2}}\begin{pmatrix}1 & i\\ i & 1\end{pmatrix}\right]\begin{bmatrix}(-1)^{f_0} & 0\\ 0 & (-1)^{f_1}\end{bmatrix}\left[\tfrac{1}{\sqrt{2}}\begin{pmatrix}1 & i\\ i & 1\end{pmatrix}\right]\begin{pmatrix}0\\1\end{pmatrix} = \begin{pmatrix}i\\ 0\end{pmatrix} \qquad \left|\begin{pmatrix}0 & 1\end{pmatrix}\begin{pmatrix}i\\ 0\end{pmatrix}\right|^2 = 0$$

$$f_0 = 1 \quad f_1 = 1 \qquad \left[\tfrac{1}{\sqrt{2}}\begin{pmatrix}1 & i\\ i & 1\end{pmatrix}\right]\begin{bmatrix}(-1)^{f_0} & 0\\ 0 & (-1)^{f_1}\end{bmatrix}\left[\tfrac{1}{\sqrt{2}}\begin{pmatrix}1 & i\\ i & 1\end{pmatrix}\right]\begin{pmatrix}0\\1\end{pmatrix} = \begin{pmatrix}-i\\ 0\end{pmatrix} \qquad \left|\begin{pmatrix}0 & 1\end{pmatrix}\begin{pmatrix}-i\\ 0\end{pmatrix}\right|^2 = 0$$

$$f_0 = 1 \quad f_1 = 0 \qquad \left[\tfrac{1}{\sqrt{2}}\begin{pmatrix}1 & i\\ i & 1\end{pmatrix}\right]\begin{bmatrix}(-1)^{f_0} & 0\\ 0 & (-1)^{f_1}\end{bmatrix}\left[\tfrac{1}{\sqrt{2}}\begin{pmatrix}1 & i\\ i & 1\end{pmatrix}\right]\begin{pmatrix}0\\1\end{pmatrix} = \begin{pmatrix}0\\ 1\end{pmatrix} \qquad \left|\begin{pmatrix}0 & 1\end{pmatrix}\begin{pmatrix}0\\ 1\end{pmatrix}\right|^2 = 1$$

$$f_0 = 0 \quad f_1 = 1 \qquad \left[\tfrac{1}{\sqrt{2}}\begin{pmatrix}1 & i\\ i & 1\end{pmatrix}\right]\begin{bmatrix}(-1)^{f_0} & 0\\ 0 & (-1)^{f_1}\end{bmatrix}\left[\tfrac{1}{\sqrt{2}}\begin{pmatrix}1 & i\\ i & 1\end{pmatrix}\right]\begin{pmatrix}0\\1\end{pmatrix} = \begin{pmatrix}0\\ -1\end{pmatrix} \qquad \left|\begin{pmatrix}0 & 1\end{pmatrix}\begin{pmatrix}0\\ -1\end{pmatrix}\right|^2 = 1$$

Examination of the Deutsch circuit reveals certain similarities with the double-slit experiment. For example, there are two paths for input |0> to output |0> and input |1> to output |1> (and also for |0> --> |1> and |1> --> |0>, but they are not of interest here). As Deutsch and his co-authors state, this is the secret of the quantum computer - the possibility of constructive and destructive interference of the probability amplitudes for the various computational paths.

> Addition of probability amplitudes, rather than probabilities, is one of the fundamental rules for prediction in quantum mechanics and applies to all physical objects, in particular quantum computing machines. If a computing machine starts in a specific initial configuration (input) then the probability that after its evolution via a sequence of intermediate configurations it ends up in a specific final configuration (output) is the squared modulus of the sum of all the probability amplitudes of the computational paths that connect the input with the output. The amplitudes are complex numbers and may cancel each other, which is referred to as destructive interference, or enhance each other, referred to as constructive interference. The basic idea of quantum computation is to use quantum interference to amplify the correct outcomes and to suppress the incorrect outcomes of computations.

Recall from above (see the matrix representing the $\sqrt{NOT}$ beam splitters) that the probability amplitude for transmission at the beam splitters is $\frac{1}{\sqrt{2}}$, and the probability amplitude for reflection is $\frac{i}{\sqrt{2}}$. The middle element of the circuit causes phase shifts on its input wires that depend on the values of f(0) and f(1). From the circuit diagram we see that |0> output from |0> input can be achieved by two transmissions and a phase shift on the upper wire or reflection to the lower wire, phase shift, followed by

reflection to the upper wire. The absolute magnitude squared of the sum of these probability amplitudes is calculated for the four possible values for f(0) and f(1).

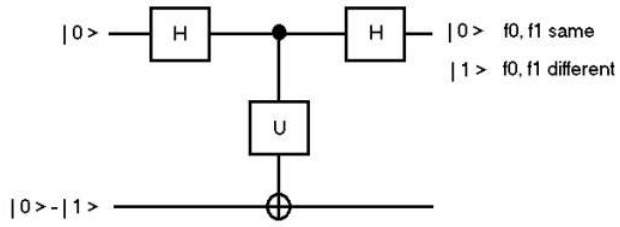
$$\begin{array}{llll} f_0 = 0 & f_1 = 0 & \left[\left|\frac{1}{\sqrt{2}}(-1)^{f_0}\frac{1}{\sqrt{2}} + \frac{1}{\sqrt{2}}(-1)^{f_1}\frac{i}{\sqrt{2}}\right|\right]^2 = 0 \\ f_0 = 1 & f_1 = 1 & \left[\left|\frac{1}{\sqrt{2}}(-1)^{f_0}\frac{1}{\sqrt{2}} + \frac{1}{\sqrt{2}}(-1)^{f_1}\frac{i}{\sqrt{2}}\right|\right]^2 = 0 \\ f_0 = 1 & f_1 = 0 & \left[\left|\frac{1}{\sqrt{2}}(-1)^{f_0}\frac{1}{\sqrt{2}} + \frac{1}{\sqrt{2}}(-1)^{f_1}\frac{i}{\sqrt{2}}\right|\right]^2 = 1 \\ f_0 = 0 & f_1 = 1 & \left[\left|\frac{1}{\sqrt{2}}(-1)^{f_0}\frac{1}{\sqrt{2}} + \frac{1}{\sqrt{2}}(-1)^{f_1}\frac{i}{\sqrt{2}}\right|\right]^2 = 1 \end{array}$$

As expected we see consistency with the previous calculations. However, this method has the advantage of more directly revealing what is happening from the quantum mechanical perspective. When f(0) and f(1) are the same the two path amplitudes interfere destructively; when they are different there is constructive interference between the path amplitudes.

As can be seen from above, in the absence of the middle element of the quantum circuit, the two paths from |0> to |0> are 180 degrees out of phase and therefore destructively interfere. In the presence of the middle element the paths are still 180 degrees out of phase unless the f-values are different, and then they are brought into phase and constructively interfere.

As Feynman emphasized in his eponymous lecture series on physics, the creation of superpositions and the interference of probability amplitudes are the essence of quantum mechanics.

Another implementation of Deutsch's algorithm is due to Artur Ekert and co-workers (see Julian Brown's *The Quest for the Quantum Computer*, pages 353-355).



The following table provides a summary of the results. If qubit 1 is |0> f(0) and f(1) are the same, but if it is |1> they are different.

$$\begin{bmatrix} f_0 & 0 & 1 & 1 & 0 \\ f_1 & 0 & 1 & 0 & 1 \\ \text{qubit1} & \begin{pmatrix}1\\0\end{pmatrix} & \begin{pmatrix}1\\0\end{pmatrix} & \begin{pmatrix}0\\1\end{pmatrix} & \begin{pmatrix}0\\1\end{pmatrix} \\ \text{qubit2} & \begin{pmatrix}-0.707\\0.707\end{pmatrix} & \begin{pmatrix}0.707\\-0.707\end{pmatrix} & \begin{pmatrix}0.707\\-0.707\end{pmatrix} & \begin{pmatrix}-0.707\\0.707\end{pmatrix} \\ \text{OutputState} & \begin{pmatrix}-0.707\\0.707\\0\\0\end{pmatrix} & \begin{pmatrix}0.707\\-0.707\\0\\0\end{pmatrix} & \begin{pmatrix}0\\0\\0.707\\-0.707\end{pmatrix} & \begin{pmatrix}0\\0\\-0.707\\0.707\end{pmatrix} \end{bmatrix}$$

The algorithm is implemented below.

$$\text{Identity} \quad \mathrm{I} = \begin{pmatrix}1 & 0\\0 & 1\end{pmatrix} \quad \text{Not gate:} \quad \mathrm{NOT} = \begin{pmatrix}0 & 1\\1 & 0\end{pmatrix} \quad \text{Hadamard gate:} \quad \mathrm{H} = \frac{1}{\sqrt{2}}\begin{pmatrix}1 & 1\\1 & -1\end{pmatrix}$$

$$f_0 = 0 \quad f_1 = 0 \quad \text{kronecker(H, I) kronecker} \left[\begin{bmatrix} (-1)^{f_0} & 0 \\ 0 & (-1)^{f_1} \end{bmatrix}, \text{NOT} \right] \text{kronecker(H, I)} \frac{1}{\sqrt{2}} \begin{pmatrix} 1 \\ -1 \\ 0 \\ 0 \end{pmatrix} = \begin{pmatrix} -0.707 \\ 0.707 \\ 0 \\ 0 \end{pmatrix}$$

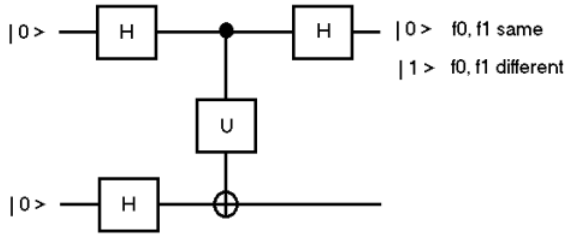
$$f_0 = 1 \quad f_1 = 1 \quad \text{kronecker(H, I) kronecker} \left[\begin{bmatrix} (-1)^{f_0} & 0 \\ 0 & (-1)^{f_1} \end{bmatrix}, \text{NOT} \right] \text{kronecker(H, I)} \frac{1}{\sqrt{2}} \begin{pmatrix} 1 \\ -1 \\ 0 \\ 0 \end{pmatrix} = \begin{pmatrix} 0.707 \\ -0.707 \\ 0 \\ 0 \end{pmatrix}$$

$$f_0 = 1 \quad f_1 = 0 \quad \text{kronecker(H, I) kronecker} \left[\begin{bmatrix} (-1)^{f_0} & 0 \\ 0 & (-1)^{f_1} \end{bmatrix}, \text{NOT} \right] \text{kronecker(H, I)} \frac{1}{\sqrt{2}} \begin{pmatrix} 1 \\ -1 \\ 0 \\ 0 \end{pmatrix} = \begin{pmatrix} 0 \\ 0 \\ 0.707 \\ -0.707 \end{pmatrix}$$

$$f_0 = 0 \quad f_1 = 1 \quad \text{kronecker(H, I) kronecker} \left[\begin{bmatrix} (-1)^{f_0} & 0 \\ 0 & (-1)^{f_1} \end{bmatrix}, \text{NOT} \right] \text{kronecker(H, I)} \frac{1}{\sqrt{2}} \begin{pmatrix} 1 \\ -1 \\ 0 \\ 0 \end{pmatrix} = \begin{pmatrix} 0 \\ 0 \\ -0.707 \\ 0.707 \end{pmatrix}$$

It is easy to show that the output of each of these calculations is the tensor product of qubits 1 and 2 in the summary table provided above.

Perhaps a better way to set up this circuit is to begin with |00> and have Hadamard gates operate on both wires.



$$f_0 = 0 \quad f_1 = 0 \quad \text{kronecker}(\text{H, I})\ \text{kronecker}\left[\begin{bmatrix}(-1)^{f_0} & 0\\ 0 & (-1)^{f_1}\end{bmatrix}, \text{NOT}\right]\text{kronecker}(\text{H, H})\frac{1}{\sqrt{2}}\begin{pmatrix}1\\0\\0\\0\end{pmatrix} = \begin{pmatrix}0.707\\0.707\\0\\0\end{pmatrix}$$

$$f_0 = 1 \quad f_1 = 1 \quad \text{kronecker}(\text{H, I})\ \text{kronecker}\left[\begin{bmatrix}(-1)^{f_0} & 0\\ 0 & (-1)^{f_1}\end{bmatrix}, \text{NOT}\right]\text{kronecker}(\text{H, H})\frac{1}{\sqrt{2}}\begin{pmatrix}1\\0\\0\\0\end{pmatrix} = \begin{pmatrix}-0.707\\-0.707\\0\\0\end{pmatrix}$$

$$f_0 = 1 \quad f_1 = 0 \quad \text{kronecker}(\text{H, I})\ \text{kronecker}\left[\begin{bmatrix}(-1)^{f_0} & 0\\ 0 & (-1)^{f_1}\end{bmatrix}, \text{NOT}\right]\text{kronecker}(\text{H, H})\frac{1}{\sqrt{2}}\begin{pmatrix}1\\0\\0\\0\end{pmatrix} = \begin{pmatrix}0\\0\\-0.707\\-0.707\end{pmatrix}$$

$$f_0 = 0 \quad f_1 = 1 \quad \text{kronecker}(\text{H, I})\ \text{kronecker}\left[\begin{bmatrix}(-1)^{f_0} & 0\\ 0 & (-1)^{f_1}\end{bmatrix}, \text{NOT}\right]\text{kronecker}(\text{H, H})\frac{1}{\sqrt{2}}\begin{pmatrix}1\\0\\0\\0\end{pmatrix} = \begin{pmatrix}0\\0\\0.707\\0.707\end{pmatrix}$$

As the following table shows, the same result is achieved in the previous circuit.

$$\begin{bmatrix} f_0 & 0 & 1 & 1 & 0 & & & & \\ f_1 & 0 & 1 & 1 & 0 & & & & \\ \text{qubit1} & \begin{pmatrix}1\\0\end{pmatrix} & \begin{pmatrix}1\\0\end{pmatrix} & \begin{pmatrix}0\\1\end{pmatrix} & \begin{pmatrix}0\\1\end{pmatrix} & & & & & \\ \text{qubit2} & \begin{pmatrix}0.707\\0.707\end{pmatrix} & \begin{pmatrix}-0.707\\-0.707\end{pmatrix} & \begin{pmatrix}-0.707\\-0.707\end{pmatrix} & \begin{pmatrix}0.707\\0.707\end{pmatrix} & \text{OutputState} & \begin{pmatrix}0.707\\0.707\\0\\0\end{pmatrix} & \begin{pmatrix}-0.707\\-0.707\\0\\0\end{pmatrix} & \begin{pmatrix}0\\0\\-0.707\\-0.707\end{pmatrix} & \begin{pmatrix}0\\0\\0.707\\0.707\end{pmatrix} \end{bmatrix}$$

This page titled 8.76: Implementation of Deutsch's Algorithm Using Mathcad is shared under a CC BY 4.0 license and was authored, remixed, and/or curated by Frank Rioux via source content that was edited to the style and standards of the LibreTexts platform.

8.77: Using Quantum Gates to Create Superpositions and Entangled States

In the matrix version of quantum mechanics, vectors represent states and matrices represent operators.

Quantum bits or qubit states:

$$\underset{0 = \begin{pmatrix}1\\0\end{pmatrix}\quad 1 = \begin{pmatrix}0\\1\end{pmatrix}}{\text{Base states:}} \qquad \underset{\begin{pmatrix}\alpha\\\beta\end{pmatrix} = \alpha\begin{pmatrix}1\\0\end{pmatrix} + \beta\begin{pmatrix}0\\1\end{pmatrix} \quad \text{where } (|\alpha|)^2 + (|\beta|)^2 = 1}{\text{A superposition of base states:}}$$

The identity operator and the two quantum gates that will be used to create quantum superpositions and entangled are provided below.

$$\underset{\mathrm{I} = \begin{pmatrix}1 & 0\\0 & 1\end{pmatrix}}{\text{Identity:}} \qquad \underset{\mathrm{H} = \frac{1}{\sqrt{2}}\begin{pmatrix}1 & 1\\1 & -1\end{pmatrix}}{\text{Hadamard gate:}} \qquad \underset{\mathrm{CNOT} = \begin{pmatrix}1 & 0 & 0 & 0\\0 & 1 & 0 & 0\\0 & 0 & 0 & 1\\0 & 0 & 1 & 0\end{pmatrix}}{\text{Controlled-NOT gate:}}$$

The Hadamard gate operates on the base states to create superpositions:

$$\frac{1}{\sqrt{2}}\begin{pmatrix}1 & 1\\1 & -1\end{pmatrix}\begin{pmatrix}1\\0\end{pmatrix} \rightarrow \begin{pmatrix}\frac{\sqrt{2}}{2}\\\frac{\sqrt{2}}{2}\end{pmatrix} \quad \frac{1}{\sqrt{2}}\begin{pmatrix}1 & 1\\1 & -1\end{pmatrix}\begin{pmatrix}0\\1\end{pmatrix} \rightarrow \begin{pmatrix}\frac{\sqrt{2}}{2}\\-\frac{\sqrt{2}}{2}\end{pmatrix}$$

When it operates on the superpositions it returns the base states, demonstrating that the Hadamard gate is reversible.

$$\frac{1}{\sqrt{2}}\begin{pmatrix}1 & 1\\1 & -1\end{pmatrix}\begin{pmatrix}\frac{\sqrt{2}}{2}\\\frac{\sqrt{2}}{2}\end{pmatrix} \rightarrow \begin{pmatrix}1\\0\end{pmatrix} \quad \frac{1}{\sqrt{2}}\begin{pmatrix}1 & 1\\1 & -1\end{pmatrix}\begin{pmatrix}\frac{\sqrt{2}}{2}\\-\frac{\sqrt{2}}{2}\end{pmatrix} \rightarrow \begin{pmatrix}0\\1\end{pmatrix}$$

Two-qubit states are created by tensor multiplication of single-qubit states. These binary tensor products correspond to the decimal numbers 0, 1, 2 and 3.

$$00 = \begin{pmatrix}1\\0\end{pmatrix}\begin{pmatrix}1\\0\end{pmatrix} = \begin{pmatrix}1\\0\\0\\0\end{pmatrix} \quad 01 = \begin{pmatrix}1\\0\end{pmatrix}\begin{pmatrix}0\\1\end{pmatrix} = \begin{pmatrix}0\\1\\0\\0\end{pmatrix} \quad 10 = \begin{pmatrix}0\\1\end{pmatrix}\begin{pmatrix}1\\0\end{pmatrix} = \begin{pmatrix}0\\0\\1\\0\end{pmatrix} \quad 11 = \begin{pmatrix}0\\1\end{pmatrix}\begin{pmatrix}0\\1\end{pmatrix} = \begin{pmatrix}0\\0\\0\\1\end{pmatrix}$$

The controlled-NOT gate operates on these states yielding the following results.

$$\mathrm{CNOT}\begin{pmatrix}1\\0\\0\\0\end{pmatrix} = \begin{pmatrix}1\\0\\0\\0\end{pmatrix} \quad \mathrm{CNOT}\begin{pmatrix}0\\1\\0\\0\end{pmatrix} = \begin{pmatrix}0\\1\\0\\0\end{pmatrix} \quad \mathrm{CNOT}\begin{pmatrix}0\\0\\1\\0\end{pmatrix} = \begin{pmatrix}0\\0\\0\\1\end{pmatrix} \quad \mathrm{CNOT}\begin{pmatrix}0\\0\\0\\1\end{pmatrix} = \begin{pmatrix}0\\0\\1\\0\end{pmatrix}$$

The results are summarized in the following table. The first qubit is the control. If it is 0, nothing happens to the second qubit. If it is 1, the second cubit is flipped using the NOT gate embedded in the lower right quadrant of the CNOT matrix. Thus the name controlled-NOT.

$$\begin{pmatrix}\mathrm{CNOT}\\00 > 00\\01 > 01\\10 > 11\\11 > 10\end{pmatrix} \quad \mathrm{CNOT} = \begin{pmatrix}1 & 0 & 0 & 0\\0 & 1 & 0 & 0\\0 & 0 & 0 & 1\\0 & 0 & 1 & 0\end{pmatrix}$$

Something altogether different happens when the CNOT gate operates on the following two-qubit states in which the first qubit is one of the superpositions from above and the second is one of the base states. There are four possible calculations and they yield the well known Bell states.

The Bell states are entangled superpositions and are of great importance in quantum information theory. They cannot be factored and therefore express quantum correlation in a most simple and striking way.

$$\frac{1}{\sqrt{2}}\begin{pmatrix}1\\1\end{pmatrix}\begin{pmatrix}1\\0\end{pmatrix}=\frac{1}{\sqrt{2}}\begin{pmatrix}1\\0\\1\\0\end{pmatrix}\quad \text{CNOT}\quad \frac{1}{\sqrt{1}}\begin{pmatrix}1\\0\\1\\0\end{pmatrix}=\begin{pmatrix}0.707\\0\\0\\0.707\end{pmatrix}\quad \frac{1}{\sqrt{2}}\left[\begin{pmatrix}1\\0\end{pmatrix}\begin{pmatrix}1\\0\end{pmatrix}+\begin{pmatrix}0\\1\end{pmatrix}\begin{pmatrix}0\\1\end{pmatrix}\right]$$

$$\frac{1}{\sqrt{2}}\begin{pmatrix}1\\-1\end{pmatrix}\begin{pmatrix}1\\0\end{pmatrix}=\frac{1}{\sqrt{2}}\begin{pmatrix}1\\0\\-1\\0\end{pmatrix}\quad \text{CNOT}\quad \frac{1}{\sqrt{1}}\begin{pmatrix}1\\0\\-1\\0\end{pmatrix}=\begin{pmatrix}0.707\\0\\0\\-0.707\end{pmatrix}\quad \frac{1}{\sqrt{2}}\left[\begin{pmatrix}1\\0\end{pmatrix}\begin{pmatrix}1\\0\end{pmatrix}-\begin{pmatrix}0\\1\end{pmatrix}\begin{pmatrix}0\\1\end{pmatrix}\right]$$

$$\frac{1}{\sqrt{2}}\begin{pmatrix}1\\1\end{pmatrix}\begin{pmatrix}0\\1\end{pmatrix}=\frac{1}{\sqrt{2}}\begin{pmatrix}0\\1\\0\\1\end{pmatrix}\quad \text{CNOT}\quad \frac{1}{\sqrt{1}}\begin{pmatrix}0\\1\\0\\1\end{pmatrix}=\begin{pmatrix}0\\0.707\\0.707\\0\end{pmatrix}\quad \frac{1}{\sqrt{2}}\left[\begin{pmatrix}1\\0\end{pmatrix}\begin{pmatrix}0\\1\end{pmatrix}+\begin{pmatrix}0\\1\end{pmatrix}\begin{pmatrix}1\\0\end{pmatrix}\right]$$

$$\frac{1}{\sqrt{2}}\begin{pmatrix}1\\-1\end{pmatrix}\begin{pmatrix}0\\1\end{pmatrix}=\frac{1}{\sqrt{2}}\begin{pmatrix}0\\1\\0\\-1\end{pmatrix}\quad \text{CNOT}\quad \frac{1}{\sqrt{1}}\begin{pmatrix}0\\1\\0\\-1\end{pmatrix}=\begin{pmatrix}0\\0.707\\-0.707\\0\end{pmatrix}\quad \frac{1}{\sqrt{2}}\left[\begin{pmatrix}1\\0\end{pmatrix}\begin{pmatrix}0\\1\end{pmatrix}-\begin{pmatrix}0\\1\end{pmatrix}\begin{pmatrix}1\\0\end{pmatrix}\right]$$

Bell states:

$$\Theta_p=\frac{1}{\sqrt{2}}\begin{pmatrix}1\\0\\0\\1\end{pmatrix}\quad \Theta_m=\frac{1}{\sqrt{2}}\begin{pmatrix}1\\0\\0\\-1\end{pmatrix}\quad \Psi_p=\frac{1}{\sqrt{2}}\begin{pmatrix}0\\1\\1\\0\end{pmatrix}\quad \Psi_m=\frac{1}{\sqrt{2}}\begin{pmatrix}0\\1\\-1\\0\end{pmatrix}$$

The same results can be obtained with |00>, |01>, |10> and |11> by operating on the first qubit with a Hadamard gate (creating a superposition) followed by a CNOT operation.

$$\text{CNOT kronecker(H, I)}=\begin{pmatrix}1\\0\\0\\0\end{pmatrix}=\begin{pmatrix}0.707\\0\\0\\0.707\end{pmatrix}\quad \text{CNOT kronecker(H, I)}\begin{pmatrix}0\\1\\0\\0\end{pmatrix}=\begin{pmatrix}0\\0.707\\0.707\\0\end{pmatrix}$$

$$\text{CNOT kronecker(H, I)}\begin{pmatrix}0\\0\\1\\0\end{pmatrix}=\begin{pmatrix}0.707\\0\\0\\-0.707\end{pmatrix}\quad \text{CNOT kronecker(H, I)}\begin{pmatrix}0\\0\\0\\1\end{pmatrix}=\begin{pmatrix}0\\0.707\\-0.707\\0\end{pmatrix}$$

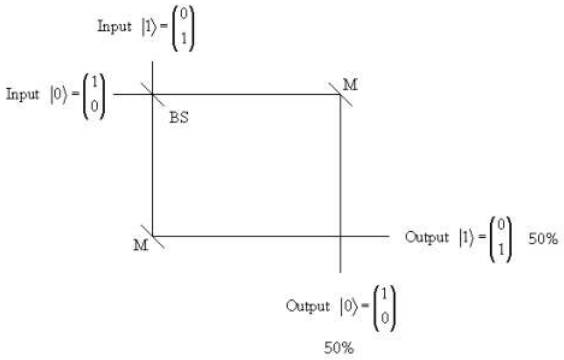
This page titled 8.77: Using Quantum Gates to Create Superpositions and Entangled States is shared under a CC BY 4.0 license and was authored, remixed, and/or curated by Frank Rioux via source content that was edited to the style and standards of the LibreTexts platform.

8.78: A Simple Quantum Computer

Giving a friend directions to his house, Yogi Berra said “When you come to a fork in the road, take it.” I will attempt to demonstrate that this well-known “yogi-ism” describes an essential feature of quantum phenomena and the parallelism that is exploited by a quantum computer.

A Mach-Zehnder interferometer (MZI) is a simple example of a quantum computer. Its main components are two optical beam splitters (think half-silvered mirrors). The first, the fork in the road, creates a superposition of two computational paths. The second beam splitter recombines the paths giving rise to the constructive and destructive interference that is essential to quantum computation.

The MZI quantum computer will be assembled in three steps. The first step shows a 50-50 beam splitter that can be illuminated by two input ports and their vector designations, |0> and |1>. Since we are dealing with computation it will eventually be shown that a 50-50 beam splitter is a square root of NOT gate - √NOT. The quantum aspects of computation are already appearing because there is no classical analog for a √NOT gate, and yet it exists physically as a simple 50-50 beam splitter.



The experimental results for illuminating ports |0> and |1> are reported in the table below. From a classical respective there is nothing unusual here. A 50-50 beam splitter transmits 50% of the radiation and reflects 50% of the radiation illuminating it. Even if we adopt the photon concept and consider many single photon events, there is still nothing worthy of comment. Statistically half the photons are transmitted and half reflected, no matter which input port is used. And the results are totally random. We cannot predict with certainty the results of individual events. We only know that if we record a statistically meaningful number of results this is what we get.

$\|0\rangle$ Input	$\|0\rangle$	Transmitted	$\|0\rangle$	50%
$\|0\rangle$ Input	$\|0\rangle$	Reflected	$\|1\rangle$	50%
$\|1\rangle$ Input	$\|1\rangle$	Reflected	$\|0\rangle$	50%
$\|1\rangle$ Input	$\|1\rangle$	Transmitted	$\|1\rangle$	50%

At this point we could interpret these results as saying that the source emits photons and the detector registers photons, and that the events at the beam splitter are random; we cannot predict with certainty the outcome of any single encounter of a photon with the beam splitter, only the statistical results given in the table.

Quantum mechanically, the beam splitter is Yogi’s fork in the road, and the photon as a quantum mechanical object (quon) takes both paths. The photon paths, |0> and |1>, are represented by the vectors in the figure. The beam splitter’s interaction with a photon is given by the following matrix. By convention the probability amplitude for transmission is 1/√2 and for reflection it is i/√2. In other words, a 90 degree phase change is assigned to reflection at the beam splitter.

$$\widehat{BS} = \sqrt{\widehat{NOT}} = \frac{1}{\sqrt{2}}\begin{pmatrix}1 & i\\ i & 1\end{pmatrix}$$

Thus, according to simple matrix algebra the consequence of a photon's interaction with a 50-50 beam splitter is the creation of a quantum mechanical superposition of the photon being present simultaneously in both paths.

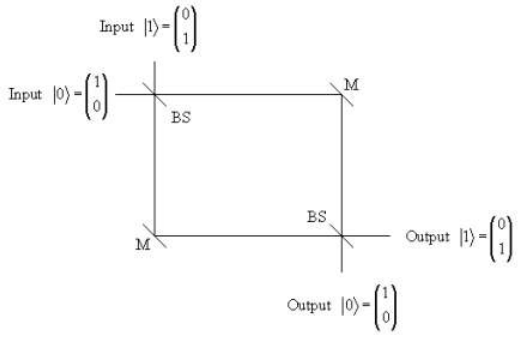
$$\widehat{BS}|0\rangle = \frac{1}{\sqrt{2}}\begin{pmatrix}1 & i\\ i & 1\end{pmatrix}\begin{pmatrix}1\\0\end{pmatrix} = \frac{1}{\sqrt{2}}\begin{pmatrix}1\\i\end{pmatrix} = \frac{1}{\sqrt{2}}\left[\begin{pmatrix}1\\0\end{pmatrix} + i\begin{pmatrix}0\\1\end{pmatrix}\right] = \frac{1}{\sqrt{2}}\left[|0\rangle + i|1\rangle\right]$$

$$\widehat{BS}|1\rangle = \frac{1}{\sqrt{2}}\begin{pmatrix}1 & i\\ i & 1\end{pmatrix}\begin{pmatrix}0\\1\end{pmatrix} = \frac{1}{\sqrt{2}}\begin{pmatrix}i\\1\end{pmatrix} = \frac{1}{\sqrt{2}}\left[i\begin{pmatrix}1\\0\end{pmatrix} + \begin{pmatrix}0\\1\end{pmatrix}\right] = \frac{1}{\sqrt{2}}\left[|0\rangle + i|1\rangle\right]$$

According to quantum mechanics, the photon is in an even superposition of being transmitted and reflected after the beam splitter. The probability of being detected in either output channel is the absolute square of the probability amplitudes, as calculated below.

$$\left|\frac{1}{\sqrt{2}}\right|^2 = \left|\frac{i}{\sqrt{2}}\right|^2 = \frac{1}{2}$$

From the quantum mechanical perspective, we say that upon observation or detection the superposition collapses into one of its classical possibilities. This interpretation of a simple experiment might seem a bit extravagant, until we proceed to the next step which involves the insertion of a second beam splitter at the intersection of the two output channels.



Now there are two paths to each output channel. The first beam splitter creates two paths, one to each detector (output channel), the second beam splitter recombines those paths giving two ways to reach each detector. This is a simple example of Feynman's "sum over histories" approach to quantum mechanics. We now have the possibility that the probability amplitudes for these "histories" or paths will interfere constructively or destructively, and of course they do.

Input	History	Output	Probability
$\|0\rangle$	TT + RR	$\|0\rangle$	0%
$\|1\rangle$	TR + RT	$\|0\rangle$	100%
$\|1\rangle$	TT + RR	$\|1\rangle$	0%

Note the strikingly different results from that with a single beam splitter. Now |0> input never yields |0> output, and |1> input never yields |1> output. That's why a beam splitter is called a √NOT gate - √NOT√NOT = NOT.

$$\widehat{NOT} = \sqrt{\widehat{NOT}}\sqrt{\widehat{NOT}} = \frac{1}{\sqrt{2}}\begin{pmatrix}1 & i\\ i & 1\end{pmatrix}\frac{1}{\sqrt{2}}\begin{pmatrix}1 & i\\ i & 1\end{pmatrix} = i\begin{pmatrix}0 & 1\\ 1 & 0\end{pmatrix}$$

The operation of the NOT gate on the two possible input states is as follows: the probability that input |0> will yield output |1> is |i|2 = 1, and, of course the probability that input |1> will yield output |0> is the same.

$$\widehat{NOT}|0\rangle = i\begin{pmatrix}0 & 1\\ 1 & 0\end{pmatrix}\begin{pmatrix}1\\0\end{pmatrix} = i\begin{pmatrix}0\\1\end{pmatrix} = i|1\rangle$$

$$\widehat{NOT}|1\rangle = i\begin{pmatrix}0 & 1\\ 1 & 0\end{pmatrix}\begin{pmatrix}0\\1\end{pmatrix} = i\begin{pmatrix}1\\0\end{pmatrix} = i|0\rangle$$

This is a matrix mechanics calculation. It is also instructive to use Feynman's "sum over histories" approach explicitly. There we sum the probability amplitudes for each history or path and take the square of the absolute magnitude. Recall that the probability amplitudes are 1/√2 and i/√2 for transmission and reflection, respectively.

$$|0\rangle \xrightarrow{TT+RR} |0\rangle \left|\frac{1}{\sqrt{2}}\frac{1}{\sqrt{2}} + \frac{i}{\sqrt{2}}\frac{i}{\sqrt{2}}\right|^2 = 0 \quad |0\rangle \xrightarrow{TR+RT} |1\rangle \left|\frac{i}{\sqrt{2}}\frac{1}{\sqrt{2}} + \frac{i}{\sqrt{2}}\frac{1}{\sqrt{2}}\right|^2 = 1$$

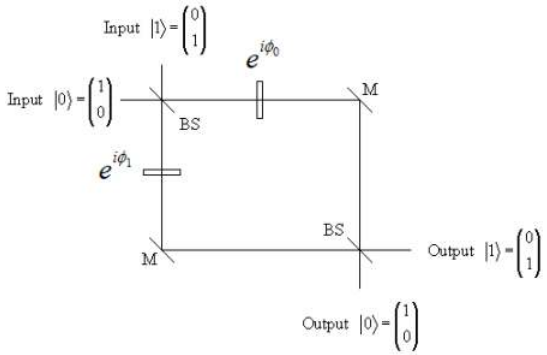
$$|1\rangle \xrightarrow{TT+RR} |1\rangle \left|\frac{1}{\sqrt{2}}\frac{1}{\sqrt{2}} + \frac{i}{\sqrt{2}}\frac{i}{\sqrt{2}}\right|^2 = 0 \quad |1\rangle \xrightarrow{TR+RT} |0\rangle \left|\frac{1}{\sqrt{2}}\frac{i}{\sqrt{2}} + \frac{i}{\sqrt{2}}\frac{1}{\sqrt{2}}\right|^2 = 1$$

For $|0\rangle \rightarrow |0\rangle$ and $|1\rangle \rightarrow |1\rangle$ the probability amplitudes for the paths (histories) interfere destructively, while for $|0\rangle \rightarrow |1\rangle$ and $|1\rangle \rightarrow |0\rangle$ they interfere constructively.

Now we are ready to see how a modified Mach-Zehnder interferometer can function as a quantum computer. But first a simple non-mathematical example will be examined.

Suppose you are asked whether two pieces of glass are the same thickness. Most likely you would use a caliper to measure the individual pieces and then compare the measurements. This is a bit of overkill because you were only asked if pieces of glass are the same thickness, not what the individual thicknesses are.

The question can be answered with a single measurement by placing the pieces of glass in opposite arms of the MZI as shown in the figure.



The speed of light in glass differs from that in air. Therefore the pieces of glass will cause phase shifts that depend on their thickness. This is the origin of the exponential terms in the figure. For example,

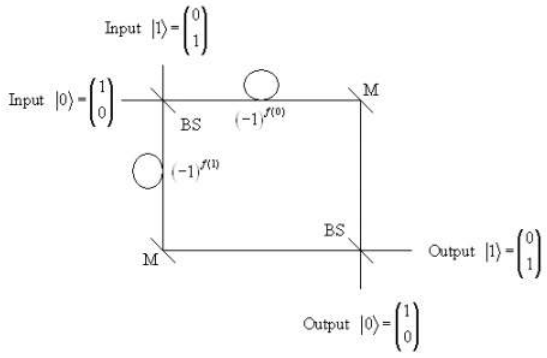
$$\phi_0 = 2\pi\frac{\delta_0}{\lambda}$$

is the phase shift (in radians) in the |0> arm of the interferometer. Here δ0 is the glass thickness and λ is the wavelength of the light. Recall that in the absence of the glass, the probability for |0> input to |0> output is zero. In the presence of the glass, using Feynman's sum over histories to calculate the probability yields the following expression.

$$\left|\frac{1}{\sqrt{2}}e^{i\phi_0}\frac{1}{\sqrt{2}} + \frac{i}{\sqrt{2}}e^{i\phi_1}\frac{i}{\sqrt{2}}\right|^2$$

We see that only if the phase changes are the same (glass thickness the same) in both arms of the interferometer is the $|0\rangle \rightarrow |0\rangle$ probability zero. If light emerges from the |0> output channel we know that the pieces of glass are not the same thickness, and have answered the thickness question with a single measurement.

This is a precursor to the proof of principle example David Deutsch provided for the quantum computer (see primary reference cited below). In his example, Deutsch proposed a binary function f that maps {0,1} to {0,1} for which there are four possibilities: f(0) = 0, f(0) = 1, f(1) = 0, and f(1) = 1. The question is (analogous to the glass thickness question) are f(0) and f(1) the same or different? Classically two calculations of f are required, one with input 0 and one with input 1. The modified MZI shown below illustrates how the answer can be achieved with a single parallel calculation. In other words, a photon transverses both arms of the interferometer and its output destination answers the question.



The delay loops replace the pieces of glass and cause a 1800 phase shift if taken ($180^0 = \pi$; $\exp(i\pi) = -1$). Whether they are taken is controlled by the value of f. If its value is 0 the loop is bypassed, if its value is 1 the loop is taken bringing about a 180^0 phase change in that arm of the interferometer.

Feynman's method provides the following results. The probability for $|0\rangle \rightarrow |0\rangle$ is 0 if f(0) = f(1) and 1 if f(0) ≠ f(1).

$$\left|\frac{1}{\sqrt{2}}(-1)^{f(0)}\frac{1}{\sqrt{2}} + \frac{i}{\sqrt{2}}(-1)^{f(1)}\frac{i}{\sqrt{2}}\right|^2 = \left|\frac{1}{2}\left[(-1)^{f(0)} - (-1)^{f(1)}\right]\right|^2 = \begin{Bmatrix}0 = & \text{if} f(0) = f(1)\\ 1 = & \text{if} f(0) \neq f(1)\end{Bmatrix}$$

Consequently the probability for $|0\rangle \rightarrow |1\rangle$ is 1 if f(0) = f(1) and 0 if f(0) ≠ f(1).

$$\left|\frac{1}{\sqrt{2}}(-1)^{f(0)}\frac{i}{\sqrt{2}} + \frac{i}{\sqrt{2}}(-1)^{f(1)}\frac{1}{\sqrt{2}}\right|^2 = \left|\frac{1}{2}\left[(-1)^{f(0)} - (-1)^{f(1)}\right]\right|^2 = \begin{Bmatrix}1 = & \text{if} f(0) = f(1)\\ 0 = & \text{if} f(0) \neq f(1)\end{Bmatrix}$$

In summary, a single output measurement answers the initial question. We might think of this as an example of mathematical multitasking. A Mach-Zehnder interferometer creates a superposition of two computational paths providing the opportunity for the constructive and destructive interference that is the essential characteristic of quantum computation.

Primary reference:

Machines, Logic and Quantum Physics

David Deutsch, Artur Ekert, and Rossella Lupacchini

arXiv:math.HO/9911150 v1; 19 November 1999

Other sources:

The Quest for the Quantum Computer

Julian Brown

Simon & Schuster, 2000

Quantum Mechanical Computers

Richard P. Feynman

Foundations of Physics 16, 507-531 (1985)

Quantum Information and Computation

Charles H. Bennett

Physics Today, October 1995, pp 24-30

Quantum Computers

T. D. Ladd, et al.

Nature, 4 March 2010, pp 45-53

This page titled 8.78: A Simple Quantum Computer is shared under a CC BY 4.0 license and was authored, remixed, and/or curated by Frank Rioux via source content that was edited to the style and standards of the LibreTexts platform.

8.79: Solving Equations Using a Quantum Circuit

This tutorial demonstrates the solution of two linear simultaneous equation using a quantum circuit. The circuit is taken from arXiv:1302.1210. See this reference for details on the experimental implementation of the circuit and also for a discussion of the potential of quantum solutions for systems of equations. Two other sources (arXiv:1302.1946 and 1302.4310) provide alternative quantum circuits and methods of implementation.

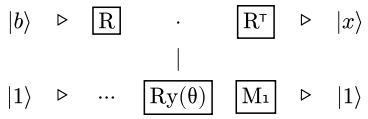
First we consider the conventional method of solving systems of linear equation for a particular matrix A and three different |b> vectors.

$$A|x\rangle = b\rangle \quad |x\rangle = A^{-1}|b\rangle$$

$$A = \begin{pmatrix} 1.5 & 0.5 \\ 0.5 & 1.5 \end{pmatrix} \qquad b_1 = \frac{1}{\sqrt{2}}\begin{pmatrix} 1 \\ 1 \end{pmatrix} \qquad b_2 = \frac{1}{\sqrt{2}}\begin{pmatrix} 1 \\ -1 \end{pmatrix} \qquad b_3 = \begin{pmatrix} 1 \\ 0 \end{pmatrix}$$

$$A^{-1}b_1 = \begin{pmatrix} 0.354 \\ 0.354 \end{pmatrix} \quad A^{-1}b_2 = \begin{pmatrix} 0.707 \\ -0.707 \end{pmatrix} \quad A^{-1}b_3 = \begin{pmatrix} 0.75 \\ -0.25 \end{pmatrix}$$

Next we show the quantum circuit (arXiv:1302.1210) that generates the same solutions. The Appendix considers two other equivalent circuits from this reference.



In this circuit, R is the matrix of eigenvectors of matrix A and R^T its transpose. The last step on the bottom wire is the measurement of |1>, which is represented by the projection operator M_1. The identity operator is required for cases in which a quantum gate operation is occurring on one wire and no operation is occurring on the other wire.

$$\mathrm{R} = \backslash\mathrm{eigenvecs}(\mathrm{A}) \quad \mathrm{R} = \begin{pmatrix} 0.707 & -0.707 \\ 0.707 & 0.707 \end{pmatrix} \quad \mathrm{R}^T = \begin{pmatrix} 0.707 & 0.707 \\ -0.707 & 0.707 \end{pmatrix} \quad \mathrm{M}_1 = \begin{pmatrix} 0 & 0 \\ 0 & 1 \end{pmatrix} \quad \mathrm{I} = \begin{pmatrix} 1 & 0 \\ 0 & 1 \end{pmatrix}$$

$$\leftarrow \begin{pmatrix} 0 \\ 1 \end{pmatrix}(0 \quad 1)$$

The controlled rotation, CR(θ), is the only two-qubit gate in the circuit. The rotation angle required is determined by the ratio of the eigenvalues of A as shown below.

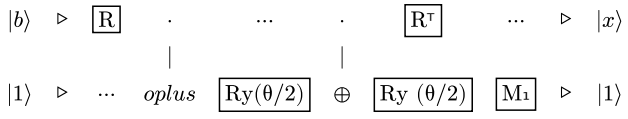
$$\mathrm{CR}(\theta) = \begin{pmatrix} 1 & 0 & 0 & 0 \\ 0 & 1 & 0 & 0 \\ 0 & 0 & \cos\left(\frac{\theta}{2}\right) & -\sin\left(\frac{\theta}{2}\right) \\ 0 & 0 & \sin\left(\frac{\theta}{2}\right) & \cos\left(\frac{\theta}{2}\right) \end{pmatrix} \quad \mathrm{eigenvals}(\mathrm{A}) = \begin{pmatrix} 2 \\ 1 \end{pmatrix} \quad \theta = -2\mathrm{acos}\left(\frac{1}{2}\right)$$

The input (|b>|1>) and output (|x>|1>) states are expressed in tensor format. Kronecker is Mathcad's command for the tensor product of matrices.

Input $\lvert b\rangle\lvert 1\rangle$	Quantum Circuit	Output $\lvert x\rangle\lvert 1\rangle$
$\frac{1}{\sqrt{2}}\begin{pmatrix}1\\1\end{pmatrix}\begin{pmatrix}0\\1\end{pmatrix}=\frac{1}{\sqrt{2}}\begin{pmatrix}0\\1\\0\\1\end{pmatrix}$	$\text{kronecker}(R^T,\ M_1)\text{CR}(\theta)\text{kronecker}(\text{R, I})\frac{1}{\sqrt{2}}\begin{pmatrix}0\\1\\0\\1\end{pmatrix}=\begin{pmatrix}0\\0.354\\0\\0.354\end{pmatrix}$	$\begin{pmatrix}0.354\\0.354\end{pmatrix}\begin{pmatrix}0\\1\end{pmatrix}$
$\frac{1}{\sqrt{2}}\begin{pmatrix}1\\-1\end{pmatrix}\begin{pmatrix}0\\1\end{pmatrix}=\frac{1}{\sqrt{2}}\begin{pmatrix}0\\1\\0\\-1\end{pmatrix}$	$\text{kronecker}(R^T,\ M_1)\text{CR}(\theta)\text{kronecker}(\text{R, I})\frac{1}{\sqrt{2}}\begin{pmatrix}0\\1\\0\\-1\end{pmatrix}=\begin{pmatrix}0\\0.707\\0\\-0.707\end{pmatrix}$	$\begin{pmatrix}0.707\\-0.707\end{pmatrix}\begin{pmatrix}0\\1\end{pmatrix}$
$\begin{pmatrix}1\\0\end{pmatrix}\begin{pmatrix}0\\1\end{pmatrix}=\begin{pmatrix}0\\1\\0\\0\end{pmatrix}$	$\text{kronecker}(R^T,\ M_1)\text{CR}(\theta)\text{kronecker}(\text{R, I})\begin{pmatrix}0\\1\\0\\0\end{pmatrix}=\begin{pmatrix}0\\0.75\\0\\-0.25\end{pmatrix}$	$\begin{pmatrix}0.75\\-0.25\end{pmatrix}\begin{pmatrix}0\\1\end{pmatrix}$

Appendix

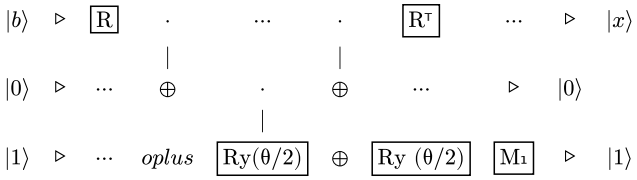
The alternative two-wire circuit shown in Fig. 1C requires CNOT and Ry rotation matrices.



The quantum circuit is set up as follows. The input and output states are the same as the previous circuit.

$$\text{QuantumCircuit} = \text{kronecker(I, M}_1\text{)kronecker}\left(\text{R}^T,\ \text{Ry}\left(\frac{\theta}{2}\right)\right)\text{CNOT}$$
$$\text{kronecker}\left(\text{I, Ry}\left(\frac{-\theta}{2}\right)\right)\text{CNOT kronecker(R, I)}$$

The three-wire circuit Fig. 1B produces the following transformation: $\lvert b\rangle\lvert 0\rangle\lvert 1\rangle \rightarrow \lvert x\rangle\lvert 0\rangle\lvert 1\rangle$.



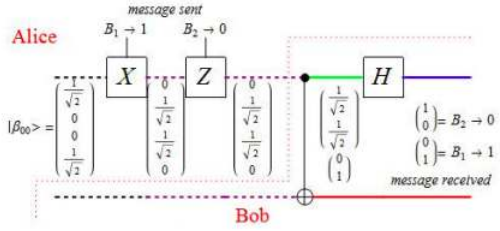
Input $\lvert b\rangle\lvert 0\rangle\lvert 1\rangle$	Quantum Circuit	Output $\lvert x\rangle\lvert 0\rangle\lvert 1\rangle$
$\frac{1}{\sqrt{2}}\begin{pmatrix}1\\1\end{pmatrix}\begin{pmatrix}1\\0\end{pmatrix}\begin{pmatrix}0\\1\end{pmatrix} = \frac{1}{\sqrt{2}}\begin{pmatrix}0\\1\\0\\0\\0\\0\\1\\0\\0\end{pmatrix}$	$\mathrm{QC}\frac{1}{\sqrt{2}}\begin{pmatrix}0\\1\\0\\0\\0\\0\\1\\0\\0\end{pmatrix} = \begin{pmatrix}0\\0.354\\0\\0\\0\\0.354\\0\\0\\0\end{pmatrix}$	$\begin{pmatrix}0.354\\0.354\end{pmatrix}\begin{pmatrix}1\\0\end{pmatrix}\begin{pmatrix}0\\1\end{pmatrix}$
$\frac{1}{\sqrt{2}}\begin{pmatrix}1\\-1\end{pmatrix}\begin{pmatrix}1\\0\end{pmatrix}\begin{pmatrix}0\\1\end{pmatrix} = \frac{1}{\sqrt{2}}\begin{pmatrix}0\\1\\0\\0\\0\\0\\-1\\0\\0\end{pmatrix}$	$\mathrm{QC}\frac{1}{\sqrt{2}}\begin{pmatrix}0\\1\\0\\0\\0\\0\\-1\\0\\0\end{pmatrix} = \begin{pmatrix}0\\0.707\\0\\0\\0\\0.707\\0\\0\\0\end{pmatrix}$	$\begin{pmatrix}0.707\\-0.707\end{pmatrix}\begin{pmatrix}1\\0\end{pmatrix}\begin{pmatrix}0\\1\end{pmatrix}$
$\frac{1}{\sqrt{2}}\begin{pmatrix}1\\0\end{pmatrix}\begin{pmatrix}1\\0\end{pmatrix}\begin{pmatrix}0\\1\end{pmatrix} = \frac{1}{\sqrt{2}}\begin{pmatrix}0\\1\\0\\0\\0\\0\\0\\0\\0\end{pmatrix}$	$\mathrm{QC}\frac{1}{\sqrt{2}}\begin{pmatrix}0\\1\\0\\0\\0\\0\\0\\0\\0\end{pmatrix} = \begin{pmatrix}0\\0.75\\0\\0\\0\\-0.25\\0\\0\\0\end{pmatrix}$	$\begin{pmatrix}0.75\\-0.25\end{pmatrix}\begin{pmatrix}1\\0\end{pmatrix}\begin{pmatrix}0\\1\end{pmatrix}$

This page titled 8.79: Solving Equations Using a Quantum Circuit is shared under a CC BY 4.0 license and was authored, remixed, and/or curated by Frank Rioux via source content that was edited to the style and standards of the LibreTexts platform.

8.80: Introduction to Superdense Coding

> Quantum superdense coding reliably transmits two classical bits through an entangled pair of particles, even though only one member of the pair is handled by the sender. Charles Bennett, *Physics Today*, October 1995, p. 27

This tutorial is based on Brad Rubin's "Superdense Coding" at the Wolfram Demonstration Project: http:demonstrations.wolfram.com/SuperdenseCoding/. The quantum gate circuit shown below illustrates superdense coding, with Alice in control above the dotted line and Bob controlling the bottom part. Alice and Bob share the entangled pair of photons in the Bell basis shown at the left. Alice encodes two classical bits of information (four possible messages) on her photon, and Bob subsequently reads her message by performing a Bell state measurement on the modified entangled photon pair. In other words, although Alice encodes two bits on her photon Bob's readout requires a measurement involving both photons.



As shown above Alice and Bob share the following maximally entangled two-qubit state. It is easily recognized as one of four two-quibit Bell states.

$$|\Phi_p\rangle = \frac{1}{\sqrt{2}}\left[|0\rangle_A|0\rangle_B + |1\rangle_A + |1\rangle_B\right] = \frac{1}{\sqrt{2}}\left[\begin{pmatrix}1\\0\end{pmatrix}\otimes\begin{pmatrix}1\\0\end{pmatrix} + \begin{pmatrix}0\\1\end{pmatrix}\otimes\begin{pmatrix}0\\1\end{pmatrix}\right] = \frac{1}{\sqrt{2}}\begin{pmatrix}1\\0\\0\\1\end{pmatrix}$$

Before proceeding let's supplement the figure by showing how Alice and Bob might generate this state from an initial state in which they both possess |0> qubits.

$$\begin{pmatrix}1\\0\end{pmatrix}\otimes\begin{pmatrix}1\\0\end{pmatrix} = \begin{pmatrix}1\\0\\0\\0\end{pmatrix}$$

This requires a Hadamard gate on the top wire followed by a two-qubit CNOT gate.

$$I = \begin{pmatrix}1 & 0\\0 & 1\end{pmatrix} \quad H = \frac{1}{\sqrt{2}}\begin{pmatrix}1 & 1\\1 & -1\end{pmatrix} \quad \text{CNOT} = \begin{pmatrix}1 & 0 & 0 & 0\\0 & 1 & 0 & 0\\0 & 0 & 0 & 1\\0 & 0 & 1 & 0\end{pmatrix} \quad \text{CNOT kronecker(H, I)}\begin{pmatrix}1\\0\\0\\0\end{pmatrix} = \begin{pmatrix}0.707\\0\\0\\0.707\end{pmatrix}$$

Now the circuit in the figure is implemented using the Pauli gates (X and Z) on the top wire and controlled by Alice. Note on the right below that X^0 and Z^0 are the identity matrix (do nothing).

$$\text{X} = \begin{pmatrix}0 & 1\\1 & 0\end{pmatrix} \quad \text{Z} = \begin{pmatrix}1 & 0\\0 & -1\end{pmatrix} \quad \text{X}^0 = \begin{pmatrix}1 & 0\\0 & 1\end{pmatrix} \quad \text{Z}^0 = \begin{pmatrix}1 & 0\\0 & 1\end{pmatrix}$$

Input

$$\text{B2= 0 B1 = 1 kronecker(H, I) CNOT}$$

$$\text{kronecker}\left(Z^{B2},\ \text{I}\right)\text{kronecker}\left(X^{B1},\ I\right)\frac{1}{\sqrt{2}}\begin{pmatrix}1\\0\\0\\1\end{pmatrix} = \begin{pmatrix}0\\1\\0\\0\end{pmatrix}$$

Output

$$\text{B2 B1} = \begin{pmatrix}1\\0\end{pmatrix}\begin{pmatrix}0\\1\end{pmatrix} = \begin{pmatrix}0\\1\\0\\0\end{pmatrix}$$

Next we do the same for the other classical two-bit states.

$$\text{B2= 0 B1 = 0 kronecker(H, I) CNOT} \qquad \text{B2 B1} = \begin{pmatrix}1\\0\end{pmatrix}\begin{pmatrix}0\\1\end{pmatrix} = \begin{pmatrix}1\\0\\0\\0\end{pmatrix}$$

$$\text{kronecker}\left(Z^{B2},\ \text{I}\right)\text{kronecker}(X^{B1},\ I)\tfrac{1}{\sqrt{2}}\begin{pmatrix}1\\0\\0\\1\end{pmatrix} = \begin{pmatrix}1\\0\\0\\0\end{pmatrix}$$

$$\text{B2= 0 B1 = 0 kronecker(H, I) CNOT} \qquad \text{B2 B1} = \begin{pmatrix}1\\0\end{pmatrix}\begin{pmatrix}0\\1\end{pmatrix} = \begin{pmatrix}0\\0\\1\\0\end{pmatrix}$$

$$\text{kronecker}\left(Z^{B2},\ \text{I}\right)\text{kronecker}(X^{B1},\ I)\tfrac{1}{\sqrt{2}}\begin{pmatrix}1\\0\\0\\1\end{pmatrix} = \begin{pmatrix}0\\0\\1\\0\end{pmatrix}$$

$$\text{B2= 1 B1 = 0 kronecker(H, I) CNOT} \qquad \text{B2 B1} = \begin{pmatrix}1\\0\end{pmatrix}\begin{pmatrix}0\\1\end{pmatrix} = \begin{pmatrix}0\\0\\0\\1\end{pmatrix}$$

$$\text{kronecker}\left(Z^{B2},\ \text{I}\right)\text{kronecker}(X^{B1},\ I)\tfrac{1}{\sqrt{2}}\begin{pmatrix}1\\0\\0\\1\end{pmatrix} = \begin{pmatrix}0\\0\\0\\1\end{pmatrix}$$

Of course we could have done all this starting with the |0>A|0>B state as is shown below using B2 and B1 from the last example. Note the mirror symmetry involving the beginning and end of this quantum gate circuit. It begins by creating a Bell state and ends by making a Bell state measurement. In between, depending on the values of B1 and B2, the initial Bell state is transformed by X and Z in steps into a final Bell state which is measured. This will be demonstrated below.

$$\text{kronecker(H, I) CNOT kronecker}\left(Z^{B2},\ I\right)\text{kronecker}\left(X^{B1},\ I\right)\text{CNOT}$$

$$\text{kronecker(H, I)}\begin{pmatrix}1\\0\\0\\0\end{pmatrix} = \begin{pmatrix}0\\0\\0\\1\end{pmatrix}$$

Bell states:

$$\Phi_p = \tfrac{1}{\sqrt{2}}\begin{pmatrix}1\\0\\0\\1\end{pmatrix} \quad \Phi_m = \tfrac{1}{\sqrt{2}}\begin{pmatrix}1\\0\\0\\-1\end{pmatrix} \quad \Psi_p = \tfrac{1}{\sqrt{2}}\begin{pmatrix}0\\1\\1\\0\end{pmatrix} \quad \Psi_m = \tfrac{1}{\sqrt{2}}\begin{pmatrix}0\\1\\-1\\0\end{pmatrix}$$

	Step1		Step 2		Measure
B2 = 0 B1 = 0	Φ_p	Φ_p	Φ_p	Φ_p	Φ_p

$$\text{kronecker}\left(X^{B1},\ \text{I}\right)\tfrac{1}{\sqrt{2}}\begin{pmatrix}1\\0\\0\\1\end{pmatrix} = \begin{pmatrix}0.707\\0\\0\\0.707\end{pmatrix} \quad \text{kronecker}\left(Z^{B2},\ I\right)\begin{pmatrix}0.707\\0\\0\\0.707\end{pmatrix} = \begin{pmatrix}0.707\\0\\0\\0.707\end{pmatrix} \quad \text{kronecker(H, I) CNOT}\begin{pmatrix}0.707\\0\\0\\0.707\end{pmatrix} = \begin{pmatrix}1\\0\\0\\0\end{pmatrix}$$

$$\begin{pmatrix}\frac{1}{\sqrt{2}}\\0\\0\\\frac{1}{\sqrt{2}}\end{pmatrix} \xrightarrow{\boxed{\text{X}}^0} \begin{pmatrix}\frac{1}{\sqrt{2}}\\0\\0\\\frac{1}{\sqrt{2}}\end{pmatrix} \xrightarrow{\boxed{\text{Z}}^0} \begin{pmatrix}\frac{1}{\sqrt{2}}\\0\\0\\\frac{1}{\sqrt{2}}\end{pmatrix} \xrightarrow{\boxed{\text{H}}} \begin{pmatrix}1\\0\\0\\0\end{pmatrix} = \begin{pmatrix}1\\0\end{pmatrix}\begin{pmatrix}1\\0\end{pmatrix} = |0\rangle$$

$$\frac{|00\rangle+|11\rangle}{\sqrt{2}} \xrightarrow{X^0\oplus I} \frac{|00\rangle+|11\rangle}{\sqrt{2}} \xrightarrow{Z^0\otimes I} \frac{|00\rangle+|11\rangle}{\sqrt{2}} \xrightarrow{\text{CNOT}} \frac{|00\rangle+|10\rangle}{\sqrt{2}}$$
$$\xrightarrow{H\otimes I} \frac{(|0\rangle+|1\rangle)|0\rangle+(|0\rangle-|1\rangle)|0\rangle}{\sqrt{2}} = |00\rangle = |0\rangle$$

B2 = 0 Φ_p Ψ_p Ψ_p Ψ_p Ψ_p
B1 = 1

kronecker $(X^{B1},\ \mathrm{I})\ \frac{1}{\sqrt{2}}$ $\begin{pmatrix}1\\0\\0\\1\end{pmatrix}$ $\begin{pmatrix}0\\0.707\\0.707\\0\end{pmatrix}$ kronecker $(Z^{B2},\ I)$ $\begin{pmatrix}0\\0.707\\0.707\\0\end{pmatrix}$ $\begin{pmatrix}0\\0.707\\0.707\\0\end{pmatrix}$ kronecker(H, I) CNOT $\begin{pmatrix}0\\0.707\\0.707\\0\end{pmatrix}$ $\begin{pmatrix}0\\1\\0\\0\end{pmatrix}$
= = =

$$\begin{pmatrix}\frac{1}{\sqrt{2}}\\0\\0\\\frac{1}{\sqrt{2}}\end{pmatrix} \boxed{\mathrm{X}}^1 \begin{pmatrix}\frac{1}{\sqrt{2}}\\\frac{1}{\sqrt{2}}\\0\\0\end{pmatrix} \boxed{\mathrm{Z}}^0 \begin{pmatrix}\frac{1}{\sqrt{2}}\\\frac{1}{\sqrt{2}}\\0\\0\end{pmatrix} \oplus \boxed{\mathrm{H}} \begin{pmatrix}0\\1\\0\\0\end{pmatrix} = \begin{pmatrix}1\\0\end{pmatrix}\begin{pmatrix}0\\1\end{pmatrix} = |1\rangle$$

$$\frac{|00\rangle+|11\rangle}{\sqrt{2}} \xrightarrow{X\oplus I} \frac{|10\rangle+|01\rangle}{\sqrt{2}} \xrightarrow{Z^0\otimes I} \frac{|10\rangle+|01\rangle}{\sqrt{2}} \xrightarrow{\text{CNOT}} \frac{|11\rangle+|01\rangle}{\sqrt{2}}$$
$$\xrightarrow{H\otimes I} \frac{(|0\rangle-|1\rangle)|1\rangle+(|0\rangle+|1\rangle)|1\rangle}{\sqrt{2}} = |01\rangle = |1\rangle$$

B2 = 1 Φ_p Φ_p Φ_p Φ_m Φ_m
B1 = 0

kronecker $(X^{B1},\ \mathrm{I})\ \frac{1}{\sqrt{2}}$ $\begin{pmatrix}1\\0\\0\\1\end{pmatrix}$ $\begin{pmatrix}0.707\\0\\0\\0.707\end{pmatrix}$ kronecker $(Z^{B2},\ I)$ $\begin{pmatrix}0.707\\0\\0\\0.707\end{pmatrix}$ $\begin{pmatrix}0.707\\0\\0\\-0.707\end{pmatrix}$ kronecker(H, I) CNOT $\begin{pmatrix}0.707\\0\\0\\-0.707\end{pmatrix}$ $\begin{pmatrix}0\\0\\1\\0\end{pmatrix}$
= = =

$$\begin{pmatrix}\frac{1}{\sqrt{2}}\\0\\0\\\frac{1}{\sqrt{2}}\end{pmatrix} \boxed{\mathrm{X}}^0 \begin{pmatrix}\frac{1}{\sqrt{2}}\\0\\0\\\frac{1}{\sqrt{2}}\end{pmatrix} \boxed{\mathrm{Z}}^1 \begin{pmatrix}\frac{1}{\sqrt{2}}\\0\\0\\-\frac{1}{\sqrt{2}}\end{pmatrix} \oplus \boxed{\mathrm{H}} \begin{pmatrix}0\\0\\1\\0\end{pmatrix} = \begin{pmatrix}0\\1\end{pmatrix}\begin{pmatrix}1\\0\end{pmatrix} = |2\rangle$$

$$\frac{|00\rangle+|11\rangle}{\sqrt{2}} \xrightarrow{X^0\oplus I} \frac{|00\rangle+|11\rangle}{\sqrt{2}} \xrightarrow{Z^0\otimes I} \frac{|00\rangle-|11\rangle}{\sqrt{2}} \xrightarrow{\text{CNOT}} \frac{|00\rangle-|10\rangle}{\sqrt{2}}$$
$$\xrightarrow{H\otimes I} \frac{(|0\rangle+|1\rangle)|0\rangle+(|0\rangle-|1\rangle)|0\rangle}{\sqrt{2}} = |10\rangle = |2\rangle$$

B2 = 1 Φ_p Φ_p Ψ_p Ψ_m Ψ_m
B1 = 1

kronecker $(X^{B1},\ \mathrm{I})\ \frac{1}{\sqrt{2}}$ $\begin{pmatrix}1\\0\\0\\1\end{pmatrix}$ $\begin{pmatrix}0\\0.707\\0.707\\0\end{pmatrix}$ kronecker $(Z^{B2},\ I)$ $\begin{pmatrix}0\\0.707\\0.707\\0\end{pmatrix}$ $\begin{pmatrix}0\\0.707\\-0.707\\0\end{pmatrix}$ kronecker(H, I) CNOT $\begin{pmatrix}0\\0.707\\-0.707\\0\end{pmatrix}$ $\begin{pmatrix}0\\0\\0\\1\end{pmatrix}$
= = =

$$\begin{array}{ccccccc} \cdot & \boxed{\text{X}}^1 & \cdot & \boxed{\text{Z}}^1 & \cdot & \cdot \boxed{\text{H}} & \cdot \\ \begin{pmatrix} \frac{1}{\sqrt{2}} \\ 0 \\ 0 \\ \frac{1}{\sqrt{2}} \end{pmatrix} & & \begin{pmatrix} \frac{1}{\sqrt{2}} \\ \frac{1}{\sqrt{2}} \\ 0 \end{pmatrix} & & \begin{pmatrix} \frac{1}{\sqrt{2}} \\ -\frac{1}{\sqrt{2}} \\ 0 \end{pmatrix} & \begin{matrix} | \\ | \\ | \\ | \end{matrix} & \begin{pmatrix} 0 \\ 0 \\ 0 \\ 1 \end{pmatrix} = \begin{pmatrix} 0 \\ 1 \end{pmatrix} \begin{pmatrix} 0 \\ 1 \end{pmatrix} = |3\rangle \\ \cdot & \cdots & \cdot & \cdots & \cdot & \oplus \cdots & \cdot \end{array}$$

$$\frac{|00\rangle+|11\rangle}{\sqrt{2}} \xrightarrow{X^0 \oplus I} \frac{|10\rangle+|01\rangle}{\sqrt{2}} \xrightarrow{Z^0 \otimes I} \frac{-|10\rangle+|01\rangle}{\sqrt{2}} \xrightarrow{\text{CNOT}} \frac{-|11\rangle+|01\rangle}{\sqrt{2}}$$
$$\xrightarrow{H \otimes I} \frac{-(|0\rangle-|1\rangle)|1\rangle+(|0\rangle+|1\rangle)|1\rangle}{\sqrt{2}} = |11\rangle = |3\rangle$$

It is now shown that steps 1 and 2 in the original calculation can be condensed into one step.

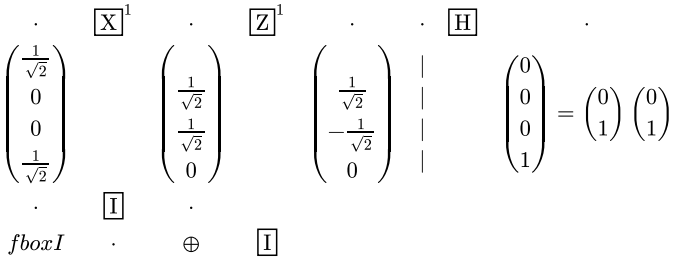
Binary Input		Binary Bell State Index	Decimal Bell State Intex
B2 = 0 B1 = 0	kronecker(H, I) CNOT $\text{kronecker}\left(Z^{B2}X^{B1},\ \text{I}\right)\Psi_p = \begin{pmatrix} 1 \\ 0 \\ 0 \\ 0 \end{pmatrix}$	$\|00\rangle$	$\|0\rangle$
B2 = 0 B1 = 1	kronecker(H, I) CNOT $\text{kronecker}\left(Z^{B2}X^{B1},\ \text{I}\right)\Psi_p = \begin{pmatrix} 0 \\ 1 \\ 0 \\ 0 \end{pmatrix}$	$\|01\rangle$	$\|1\rangle$
B2 = 1 B1 = 0	kronecker(H, I) CNOT $\text{kronecker}\left(Z^{B2}X^{B1},\ \text{I}\right)\Psi_p = \begin{pmatrix} 0 \\ 0 \\ 1 \\ 0 \end{pmatrix}$	$\|10\rangle$	$\|2\rangle$
B2 = 1 B1 = 1	kronecker(H, I) CNOT $\text{kronecker}\left(Z^{B2}X^{B1},\ \text{I}\right)\Psi_p = \begin{pmatrix} 0 \\ 0 \\ 0 \\ 1 \end{pmatrix}$	$\|11\rangle$	$\|3\rangle$

This page titled 8.80: Introduction to Superdense Coding is shared under a CC BY 4.0 license and was authored, remixed, and/or curated by Frank Rioux via source content that was edited to the style and standards of the LibreTexts platform.

8.81: A Brief Introduction to Quantum Dense Coding

> Quantum superdense coding reliably transmits two classical bits through an entangled pair of particles, even though only one member of the pair is handled by the sender. Charles Bennett, *Physics Today*, October 1995, p. 27

This tutorial is based on Brad Rubin's "Superdense Coding" at the Wolfram Demonstration Project: http:demonstrations.wolfram.com/SuperdenseCoding/. The quantum circuit shown below impliments quantum dense coding. Alice and Bob share the entangled pair of photons in the Bell basis shown at the left. Alice encodes two classical bits of information (four possible messages) on her photon, and Bob subsequently reads her message by performing a Bell state measurement on the modified entangled photon pair. In other words, although Alice encodes two bits on her photon Bob's readout requires a measurement involving both photons. In this example Alice sends |11> to Bob.



The operation of the circuit is outlined in both matrix and algebraic format. The necessary truth tables and matrix operators are provided in the Appendix.

Matrix Method

$$\mathrm{H}\otimes\mathrm{I}\ \mathrm{CNOT}\ \mathrm{Z}\otimes\mathrm{I}\ \mathrm{X}\otimes\mathrm{I}\frac{1}{\sqrt{2}}\begin{pmatrix}1\\0\\0\\1\end{pmatrix}=\begin{pmatrix}0\\0\\0\\1\end{pmatrix}=\begin{pmatrix}0\\1\end{pmatrix}\otimes\begin{pmatrix}0\\1\end{pmatrix}=|11\rangle$$

Algebraic Method

$$\frac{|00\rangle+|11\rangle}{\sqrt{2}}\xrightarrow{X^1\otimes I}\frac{|10\rangle+|01\rangle}{\sqrt{2}}\xrightarrow{Z^1\otimes 1}\frac{-|10\rangle+|01\rangle}{\sqrt{2}}\xrightarrow{CNOT}\frac{-|11\rangle+|01\rangle}{\sqrt{2}}$$

$$\xrightarrow{H\otimes I}\frac{-(|0\rangle-|1\rangle)|1\rangle+(|0\rangle+|1\rangle)|1\rangle}{2}=|11\rangle=\begin{pmatrix}0\\1\end{pmatrix}\otimes\begin{pmatrix}0\\1\end{pmatrix}=\begin{pmatrix}0\\0\\0\\1\end{pmatrix}$$

Appendix

Truth tables for the quantum circuit:

$$\mathrm{X}=\mathrm{NOT}\begin{pmatrix}0\text{ to }0\\1\text{ to }0\end{pmatrix}\quad\mathrm{Z}\begin{pmatrix}0\text{ to }0\\1\text{ to -1}\end{pmatrix}\quad\mathrm{H}=\mathrm{Hadamard}\begin{bmatrix}0\text{ to }\frac{1}{\sqrt{2}}(0+1)\\1\text{ to }\frac{1}{\sqrt{2}}(0-1)\end{bmatrix}\quad\mathrm{CNOT}\begin{pmatrix}00\text{ to }00\\01\text{ to }01\\10\text{ to }11\\11\text{ to }10\end{pmatrix}$$

Circuit elements in matrix formats:

$$I=\begin{pmatrix}1&0\\0&1\end{pmatrix}\quad X=\begin{pmatrix}0&1\\1&0\end{pmatrix}\quad Z=\begin{pmatrix}1&0\\0&-1\end{pmatrix}\quad H=\frac{1}{\sqrt{2}}\begin{pmatrix}1&1\\1&-1\end{pmatrix}\quad\mathrm{CNOT}=\begin{pmatrix}1&0&0&0\\0&1&0&0\\0&0&0&1\\0&0&1&0\end{pmatrix}$$

This page titled 8.81: A Brief Introduction to Quantum Dense Coding is shared under a CC BY 4.0 license and was authored, remixed, and/or curated by Frank Rioux via source content that was edited to the style and standards of the LibreTexts platform.

https://chem.libretexts.org/@go/page/149084

8.82: The Discrete or Quantum Fourier Transform

The continuous-variable Fourier transforms involving position and momentum are well known. In Dirac notation (see chapter 6 in *A Modern Approach to Quantum Mechanics* by John S. Townsend) they are,

$$\langle\ |\Psi\rangle = \int \langle\ |x\rangle\langle x|\Psi\rangle dx \quad \text{and} \quad \langle x|\Psi\rangle = \int \langle x|p\rangle\langle\ |\Psi\rangle dp$$

where

$$\langle x|p\rangle = \langle p|x\rangle * = \frac{1}{\sqrt{2\pi\hbar}} \exp\left(i\frac{2\pi px}{h}\right) = \frac{1}{\sqrt{2\pi\hbar}} \exp\left(i\frac{px}{\hbar}\right)$$

Using the coordinate and momentum completeness relations

$$\int |x\rangle\langle x|dx = 1 \quad \text{and} \quad \int |p\rangle\langle p|dp = 1$$

we can write the following generic Fourier transforms.

$$\langle p| = \int \langle p|x\rangle\langle x|dx \quad \text{and} \quad \langle x| = \int \langle x|p\langle p|dp$$

By analogy a discrete Fourier transform between the k and j indices can be created.

$$\langle k| = \sum_{j-0}^{N-1} \langle k|j\rangle\langle j|$$

were, again, by analogy

$$\langle k|j\rangle = \frac{1}{\sqrt{N}} \exp\left(i\frac{2\pi}{N}kj\right)$$

so that

$$\langle k| = \frac{1}{\sqrt{N}} \sum_{j=0}^{N-1} \exp\left(i\frac{2\pi}{N}kj\right) \langle j|$$

Summing over the k index and projecting on to |Ψ> yields a system of linear equations.

$$\sum_{k=0}^{N-1} \langle k|\Psi\rangle = \frac{1}{\sqrt{N}} \sum_{k=0}^{N-1} \sum_{j=0}^{N-1} \exp\left(i\frac{2\pi}{N}kj\right) \langle j|\Psi\rangle$$

Like all systems it is expressible in matrix form. For example, with N=2 and $\begin{pmatrix}1\\0\end{pmatrix}$ as the operand we have,

$$\frac{1}{\sqrt{2}}\begin{pmatrix}1\\1\end{pmatrix} = \frac{1}{\sqrt{2}}\begin{pmatrix}1 & 1\\1 & -1\end{pmatrix}\begin{pmatrix}1\\0\end{pmatrix}$$

Here the matrix operator is the well-known Hadamard transform. In this case it transforms spin-up in the z-direction to spin-up in the x-direction, or horizontal polarization to diagonal polarization, etc. Naturally it transforms spin-up in the x-direction to spin-up in the z-direction.

$$\begin{pmatrix}1\\0\end{pmatrix} = \frac{1}{\sqrt{2}}\begin{pmatrix}1 & 1\\1 & -1\end{pmatrix}\frac{1}{\sqrt{2}}\begin{pmatrix}1\\1\end{pmatrix}$$

This, of course, also occurs with the continuous-variable Fourier transform.

$$\langle x|\Psi\rangle \xrightarrow{FT} \langle p|\Psi\rangle \xrightarrow{\backslash} x|\Psi\rangle$$

The Mathcad implementation of the discrete or quantum Fourier transform (QFT) is now demonstrated.

$$N = 2 \quad m = 0..N-1 \quad n = 0..N-1 \quad QFT_{m,\,n} = \frac{1}{\sqrt{N}} \exp\left(i\frac{2\pi mn}{N}\right)$$

$$QFT = \begin{pmatrix}0.707 & 0.707\\0.707 & -0.707\end{pmatrix}$$

$$QFT \begin{pmatrix} 1 \\ 0 \end{pmatrix} = \begin{pmatrix} 0.707 \\ 0.707 \end{pmatrix} \quad QFT \frac{1}{\sqrt{2}} \begin{pmatrix} 1 \\ 1 \end{pmatrix} = \begin{pmatrix} 1 \\ 0 \end{pmatrix}$$
$$QFT \begin{pmatrix} 0 \\ 1 \end{pmatrix} = \begin{pmatrix} 0.707 \\ -0.707 \end{pmatrix} \quad QFT \frac{1}{\sqrt{2}} \begin{pmatrix} 1 \\ -1 \end{pmatrix} = \begin{pmatrix} 0 \\ 1 \end{pmatrix}$$

These calculations demonstrate that the QFT is a unitary operator:

$$\text{QFT QFT} = \begin{pmatrix} 1 & 0 \\ 0 & 1 \end{pmatrix}$$

This page titled 8.82: The Discrete or Quantum Fourier Transform is shared under a CC BY 4.0 license and was authored, remixed, and/or curated by Frank Rioux via source content that was edited to the style and standards of the LibreTexts platform.

8.83: Factoring Using Shor's Quantum Algorithm

This tutorial presents a toy calculation dealing with quantum factorization using Shor's algorithm. Before beginning that task, traditional classical factorization is reviewed with the example of finding the prime factors of 15. As shown below the key is to find the period of a^x modulo 15, where a is chosen randomly.

$$a = 4 \quad N = 5 \qquad f(x) = mod\,(a^x,\ N) \quad Q = 8 \quad x = 0..Q-1$$

$$x = \begin{bmatrix} 0 \\ 1 \\ 2 \\ 3 \\ 4 \\ 5 \\ 6 \\ 7 \end{bmatrix} \quad f(x) = \begin{bmatrix} 1 \\ 4 \\ 1 \\ 4 \\ 1 \\ 4 \\ 1 \\ 4 \end{bmatrix}$$

Seeing that the period of f(x) is two, the next step is to use the Euclidian algorithm by calculating the greatest common denominator of two functions involving the period and a, and the number to be factored, N.

$$\text{period} = 2 \quad \text{ged}\left(a^{\frac{\text{period}}{2}} - 1,\ N\right) = 3 \quad \text{ged}\left(a^{\frac{\text{period}}{2}} + 1,\ N\right) = 3$$

Factoring 15 by this method is trivial because it is the product of two small prime numbers. However, if N is the product of two large primes this method is impractical because finding the periodicity of f(x) would not be possible by inspection as it is above. If f(x) were plotted it would appear to be random noise with no recognizable periodic structure. Shor recognized that the discrete Fourier transform (or, quantum Fourier transform) provided an efficient method for finding the period of f(x) when N is the product of two extremely large prime numbers. So the contribution that quantum mechanics may eventually make to code breaking is efficiently finding the periodicity of f(x).

We proceed by ignoring the fact that we already know that the period of f(x) is 2 and demonstrate how it is determined using a quantum (discrete) Fourier transform. After the registers are loaded with x and f(x) using a quantum computer, they exist in the following superposition.

$$\frac{1}{\sqrt{Q}} \sum_{x=0}^{Q-1} |x\rangle|f(x)\rangle = \frac{1}{2}\left[|0\rangle|1\rangle + |1\rangle|4\rangle + |2\rangle|1\rangle + |3\rangle|4\rangle + \cdots\right] = \frac{1}{2}\left[\left(|0\rangle + |2\rangle\right)|1\rangle + \left(|1\rangle + |3\rangle\right)|4\rangle + \cdots\right]$$

The rearrangement on the right collects terms on the f(x) values. Now the x values appear in pairs with their f(x) partners. Note that the period of 2 is discernable in each pair of x values. After (|0 > + |2 >) the next pair is offset by 1. The Fourier transform on the x-register removes the offset, clearly revealing the period of 2.

In preparation for the Fourier transform the superposition is written as a sum of vector tensor products.

$$\frac{1}{2}\left[\begin{pmatrix}1\\0\\0\\0\end{pmatrix}\begin{pmatrix}0\\1\\0\\0\end{pmatrix} + \begin{pmatrix}0\\1\\0\\0\end{pmatrix}\begin{pmatrix}0\\0\\0\\1\end{pmatrix} + \begin{pmatrix}0\\0\\1\\0\end{pmatrix}\begin{pmatrix}0\\1\\0\\0\\0\end{pmatrix} + \begin{pmatrix}0\\0\\1\\0\end{pmatrix}\begin{pmatrix}0\\0\\0\\0\\1\end{pmatrix}\right] = \frac{1}{2}\left[\begin{pmatrix}1\\0\\1\\0\end{pmatrix}\begin{pmatrix}0\\1\\0\\0\\0\end{pmatrix} + \begin{pmatrix}0\\1\\0\\1\end{pmatrix}\begin{pmatrix}0\\0\\0\\0\\1\end{pmatrix}\right]$$

$$\frac{1}{2}(0 \quad 1 \quad 0 \quad 0 \quad 0 \quad 0 \quad 0 \quad 0 \quad 0 \quad 1 \quad 0 \quad 1 \quad 0 \quad 0 \quad 0 \quad 0 \quad 0 \quad 0 \quad 0 \quad 1)^T$$

The next step is to find the period of f(x) by performing a quantum Fourier transform (QFT) on the input register, |x>. The identity operation (do nothing) acts on the second register.

$$Q = 4 \quad m = 0..Q-1 \quad n = 0..Q-1 \quad QFT_{m,\,n} = \frac{1}{\sqrt{Q}} \exp\left(i\frac{2\pi mn}{Q}\right) \quad I = \text{identity}(5)$$

The result of the QFT is:

$$\text{kronecker}(\text{QFT}, \text{I})\frac{1}{2}\begin{pmatrix}0\\1\\0\\0\\0\\0\\0\\0\\0\\1\\0\\0\\1\\0\\0\\0\end{pmatrix} = \begin{pmatrix}0\\0.5\\0\\0\\0.5\\0\\0\\0\\0\\0.5\\0\\0\\-0.5\\0\\0\\0\\0\end{pmatrix} \quad \text{expressed in tensor format} \quad \frac{1}{2}\begin{pmatrix}0\\1\\0\\0\\1\\0\\0\\0\\0\\0\\1\\0\\0\\-1\\0\\0\\0\end{pmatrix} = \frac{1}{2}\left[\begin{pmatrix}1\\0\\0\\0\end{pmatrix}\begin{pmatrix}0\\1\\0\\0\\1\end{pmatrix} + \begin{pmatrix}0\\0\\1\\0\end{pmatrix}\begin{pmatrix}0\\1\\0\\0\\-1\end{pmatrix}\right]$$

The calculation at this point is summarized as follows:

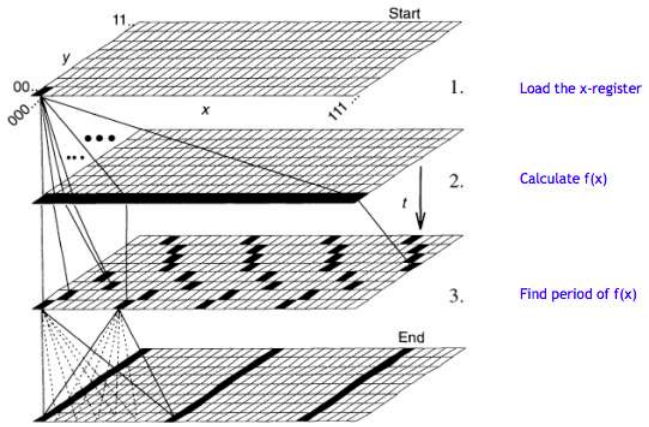
$$QFT\frac{1}{\sqrt{2}}\sum_{x=0}^{Q-1}|x\rangle|f(x)\rangle = \frac{1}{2}\left[|0\rangle\left(|1\rangle|\!|4\rangle\right) + |2\rangle\left(|1\rangle - |4\rangle\right)\right]$$

Recalling that x-register originally was a superposition involving 0, 1, 2, and 3, we see that the QFT brought about constructive and destructive interference because now the x-register (blue) contains only 0 and 2. This gives us a period of 2 and we can now proceed to the classical calculation that was demonstrated earlier. The details of how the QFTon the x-register gives rise to interference is given in the summary below.

Recommended reading: Two insightful analyses of quantum mechanics' role in factoring by David Mermin appear in the April and October 2007 issues of *Physics Today*. The first is titled "What has quantum mechanics to do with factoring?" and the second "Some curious facts about quantum factoring." Chapter 5 in Julian Brown's *The Quest for the Quantum Computer* deals in depth with code breaking and Shor's algorithm.

Summary

Figure 5 in "Quantum Computation," by David P. DiVincenzo, *Science* 270, 258 (1995) provides a graphical illustration of the steps of Shor's factorization algorithm.



This tutorial deals with steps 2 and 3 of the algorithm, summarized mathematically below. The negative sign in the far right column vector is an accumulated phase due to the quantum Fourier transform.

$$\frac{1}{\sqrt{Q}}\sum_{x=0}^{Q-1}|x\rangle|f(x)\rangle = \frac{1}{2}\,[\,] \xrightarrow{QFT} \frac{1}{2}\left[\begin{pmatrix}1\\0\\0\\0\end{pmatrix}\otimes\begin{pmatrix}0\\1\\0\\0\\1\end{pmatrix}+\begin{pmatrix}0\\0\\1\\0\end{pmatrix}\otimes\begin{pmatrix}0\\1\\0\\0\\-1\end{pmatrix}\right]$$

How a Fourier transform on the x-register can yield the periodicity of f(x) which is on the y-register is revealed by carrying out the Fourier transform on the individual members of the x-register in the middle superposition term above.

$$\frac{1}{2}\left[\text{QFT}\begin{pmatrix}1\\0\\0\\0\end{pmatrix}\begin{pmatrix}0\\1\\0\\0\\0\end{pmatrix}+\text{QFT}\begin{pmatrix}0\\1\\0\\0\end{pmatrix}\begin{pmatrix}0\\0\\0\\0\\1\end{pmatrix}+\text{QFT}\begin{pmatrix}0\\0\\1\\0\end{pmatrix}\begin{pmatrix}0\\1\\0\\0\\0\end{pmatrix}+\text{QFT}\begin{pmatrix}0\\0\\0\\1\end{pmatrix}\begin{pmatrix}0\\0\\0\\0\\1\end{pmatrix}\right]$$

$$\text{QFT}\begin{pmatrix}1\\0\\0\\0\end{pmatrix}=\begin{pmatrix}0.5\\0.5\\0.5\\0.5\end{pmatrix}\quad\text{QFT}\begin{pmatrix}0\\1\\0\\0\end{pmatrix}=\begin{pmatrix}0.5\\0.5i\\-0.5\\-0.5i\end{pmatrix}\quad\text{QFT}\begin{pmatrix}0\\0\\1\\0\end{pmatrix}=\begin{pmatrix}0.5\\-0.5\\0.5\\-0.5\end{pmatrix}\quad\text{QFT}\begin{pmatrix}0\\0\\0\\1\end{pmatrix}=\begin{pmatrix}0.5\\-0.5i\\-0.5\\0.5i\end{pmatrix}$$

Using the results from (B) the QFT on the x-register in (A) yields the following superposition.

$$\frac{1}{2}\left[\frac{1}{2}\begin{pmatrix}1\\1\\1\\1\end{pmatrix}\begin{pmatrix}0\\1\\0\\0\\0\end{pmatrix}+\frac{1}{2}\begin{pmatrix}1\\i\\-1\\-i\end{pmatrix}\begin{pmatrix}0\\0\\0\\0\\1\end{pmatrix}+\frac{1}{2}\begin{pmatrix}1\\-1\\1\\-1\end{pmatrix}\begin{pmatrix}0\\1\\0\\0\\0\end{pmatrix}+\frac{1}{2}\begin{pmatrix}1\\-i\\-1\\i\end{pmatrix}\begin{pmatrix}0\\0\\0\\0\\1\end{pmatrix}\right]$$

Constructive and destructive interference between the terms of this superposition leads to the final state.

$$\frac{1}{2}\left[\begin{pmatrix}1\\0\\0\\0\end{pmatrix}\begin{pmatrix}0\\1\\0\\0\\1\end{pmatrix}+\begin{pmatrix}0\\0\\1\\0\end{pmatrix}\begin{pmatrix}0\\1\\0\\0\\-1\end{pmatrix}\right]$$

The details of the interference between the terms in (C) can be seen by expanding them using vector tensor multiplication.

$$\frac{1}{4}\left[\begin{pmatrix}0\\1\\0\\0\\0\\0\\1\\0\\0\\0\\0\\1\\0\\0\\0\\1\\0\\0\\0\\0\\0\\0\\0\\0\\0\\0\\0\\0\\0\\0\end{pmatrix}+\begin{pmatrix}0\\0\\0\\0\\1\\0\\0\\0\\0\\0\\i\\0\\0\\0\\0\\0\\0\\0\\-1\\0\\0\\0\\-i\end{pmatrix}+\begin{pmatrix}0\\1\\0\\0\\0\\0\\-1\\0\\0\\0\\0\\1\\0\\0\\0\\0\\0\\0\\0\\-1\\0\\0\\0\\0\end{pmatrix}+\begin{pmatrix}0\\0\\0\\0\\1\\0\\0\\0\\0\\0\\-i\\0\\0\\0\\0\\0\\-1\\0\\0\\0\\0\\0\\i\end{pmatrix}\right]=\frac{1}{2}\begin{pmatrix}0\\1\\0\\0\\1\\0\\0\\0\\0\\0\\0\\1\\0\\0\\0\\-1\\0\\0\\0\\0\\0\\0\end{pmatrix}=\frac{1}{2}\left[\begin{pmatrix}1\\0\\0\\0\end{pmatrix}\begin{pmatrix}0\\1\\0\\0\\1\end{pmatrix}+\begin{pmatrix}0\\0\\1\\0\end{pmatrix}\begin{pmatrix}0\\1\\0\\0\\-1\end{pmatrix}\right]$$

An algebraic view of (C) also reveals the x-register interference. Destructive interference occurs with the terms highlighted in red (|1>) and within the terms highlighted in blue (|3>).

$$\begin{array}{l}\frac{1}{4}\left[|0\rangle+|1\rangle+|2\rangle+|3\rangle\right]|1\rangle\\+\\\frac{1}{4}\left[|0\rangle+i|1\rangle-|2\rangle-i|3\rangle\right]|4\rangle\\+\\\frac{1}{4}\left[|0\rangle-|1\rangle+|2\rangle-|3\rangle\right]|1\rangle\\+\\\frac{1}{4}\left[|0\rangle-i|1\rangle-|2\rangle+i|3\rangle\right]|4\rangle\end{array}\quad=\frac{1}{2}\left[|0\rangle\left(|1\rangle+|4\rangle\right)+|2\rangle\left(|1\rangle-|4\rangle\right)\right]$$

This page titled 8.83: Factoring Using Shor's Quantum Algorithm is shared under a CC BY 4.0 license and was authored, remixed, and/or curated by Frank Rioux via source content that was edited to the style and standards of the LibreTexts platform.

8.84: Shor's Quantum Algorithm - A Summary

This tutorial presents a toy calculation dealing with quantum factorization using Shor's algorithm. Before beginning that task, traditional classical factorization is reviewed with the example of finding the prime factors of 15. As shown below the key is to find the period of a^x modulo 15, where a is chosen randomly.

$$a = 4 \quad N = 15 \qquad f(x) = mod\,(a^x,\ N) \quad Q = 8 \quad x = 0..Q-1$$

$$x = \begin{bmatrix} 0 \\ 1 \\ 2 \\ 3 \\ 4 \\ 5 \\ 6 \\ 7 \end{bmatrix} \quad f(x) = \begin{bmatrix} 1 \\ 4 \\ 1 \\ 4 \\ 1 \\ 4 \\ 1 \\ 4 \end{bmatrix}$$

Seeing that the period of f(x) is two, the next step is to use the Euclidian algorithm by calculating the greatest common denominator of two functions involving the period and a, and the number to be factored, N.

$$\text{period} = 2 \quad \text{ged}\left(a^{\frac{\text{period}}{2}} - 1,\ N\right) = 3 \quad \text{ged}\left(a^{\frac{\text{period}}{2}} + 1,\ N\right) = 5$$

We proceed by ignoring the fact that we already know that the period of f(x) is 2 and demonstrate how it is determined using a quantum (discrete) Fourier transform. After the registers are loaded with x and f(x) using a quantum computer, they exist in the following superposition.

$$\frac{1}{\sqrt{Q}} \sum_{x=0}^{Q-1} |x\rangle|f(x)\rangle = \frac{1}{2}\left[|0\rangle|1\rangle + |1\rangle|4\rangle + |2\rangle|1\rangle + |3\rangle|4\rangle + \cdots\right]$$

The next step is to find the period of f(x) by performing a quantum Fourier transform (QFT) on the input register |x>.

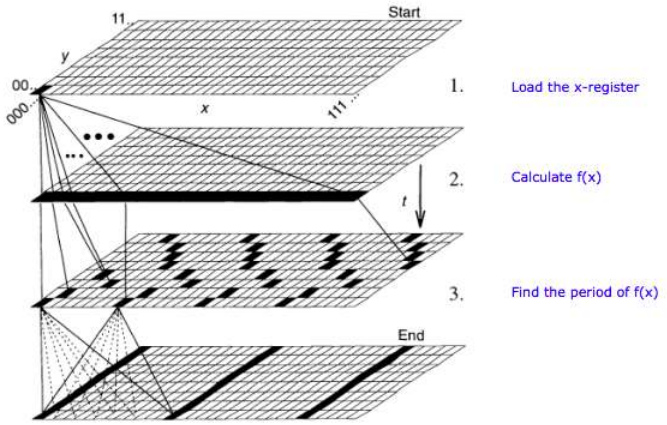
$$Q = 4 \quad m = 0..Q-1 \quad n = 0..Q-1 \quad QFT_{m,\,n} = \frac{1}{\sqrt{Q}} \exp\left(\frac{2\pi mn}{Q}\right) \qquad QFT = \frac{1}{2}\begin{pmatrix} 1 & 1 & 1 & 1 \\ 1 & i & -1 & -i \\ 1 & -1 & 1 & -1 \\ 1 & -i & -1 & i \end{pmatrix}$$

$$\begin{matrix} x \\ = 0 \end{matrix} \quad QFT \begin{pmatrix} 1 \\ 0 \\ 0 \\ 0 \end{pmatrix} = \begin{pmatrix} 0.5 \\ 0.5 \\ 0.5 \\ 0.5 \end{pmatrix} \qquad x = 1 \quad QFT \begin{pmatrix} 0 \\ 1 \\ 0 \\ 0 \end{pmatrix} = \begin{pmatrix} 0.5 \\ 0.5i \\ -0.5 \\ -0.5i \end{pmatrix} \qquad x = 2 \quad QFT \begin{pmatrix} 0 \\ 0 \\ 1 \\ 0 \end{pmatrix} = \begin{pmatrix} 0.5 \\ -0.5 \\ 0.5 \\ -0.5 \end{pmatrix} \qquad x = 3 \quad QFT \begin{pmatrix} 0 \\ 0 \\ 0 \\ 1 \end{pmatrix} = \begin{pmatrix} 0.5 \\ -0.5i \\ -0.5 \\ 0.5i \end{pmatrix}$$

The operation of the QFT on the x-register is expressed algebraically in the middle term below. Quantum interference in this term yields the result on the right which shows a period of 2 on the x-register.

$$QFT(x)\frac{1}{2}\left[|0\rangle|1\rangle+|1\rangle|4\rangle+|2\rangle|1\rangle+|3\rangle|4\rangle\right] = \begin{array}{c}\frac{1}{4}\left[|0\rangle+|1\rangle+|2\rangle+|3\rangle\right]|1\rangle \\ + \\ \frac{1}{4}\left[|0\rangle+i|1\rangle-|2\rangle-i|3\rangle\right]|4\rangle \\ + \\ \frac{1}{4}\left[|0\rangle-|1\rangle+|2\rangle-|3\rangle\right]|1\rangle \\ + \\ \frac{1}{4}\left[|0\rangle-i|1\rangle-|2\rangle+i|3\rangle\right]|4\rangle\end{array} = \frac{1}{2}\left[|0\rangle\left(|1\rangle+|4\rangle\right)+|2\rangle\left(|1\rangle-|4\rangle\right)\right]$$

Figure 5 in "Quantum Computation," by David P. DiVincenzo, *Science* 270, 258 (1995) provides a graphical illustration of the steps of Shor's factorization algorithm.



This page titled 8.84: Shor's Quantum Algorithm - A Summary is shared under a CC BY 4.0 license and was authored, remixed, and/or curated by Frank Rioux via source content that was edited to the style and standards of the LibreTexts platform.

8.85: Simulating the Deutsch-Jozsa Algorithm with a Double-Slit Apparatus

> The Deutsch-Jozsa algorithm determines if either [1] 2N numbers are either all 0 or all 1 (a constant function), or [2] half are 0 and half are 1 (a balanced function) in one step instead of up to 2N-1 + 1 steps. For N = 1, the Deutsch-Jozsa algorithm can be visualized as putting two pieces of glass, which may be thin (0) or thick (1), behind the apertures of a double-slit apparatus and measuring the interference pattern of a light source illuminating the slits. If the pattern is unchanged compared to the empty apparatus, the glass pieces have the same thickness (constant function); otherwise they have different thickness (balanced function). Peter Pfeifer, "Quantum Computation," *Access Science*, Vol. 17, p. 678, slightly modified by F. R.

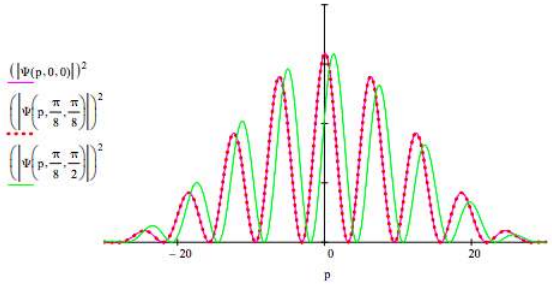
This is demonstrated by calculating the diffraction pattern without glass present, and with glass present of the same thickness and different thickness. The diffraction pattern is the momentum distribution, which is the Fourier transform of the slit geometry.

$$\text{Slit positions:}\quad x_L = 1 \quad x_R = 2 \quad \text{Slit width:}\quad \delta = 2$$

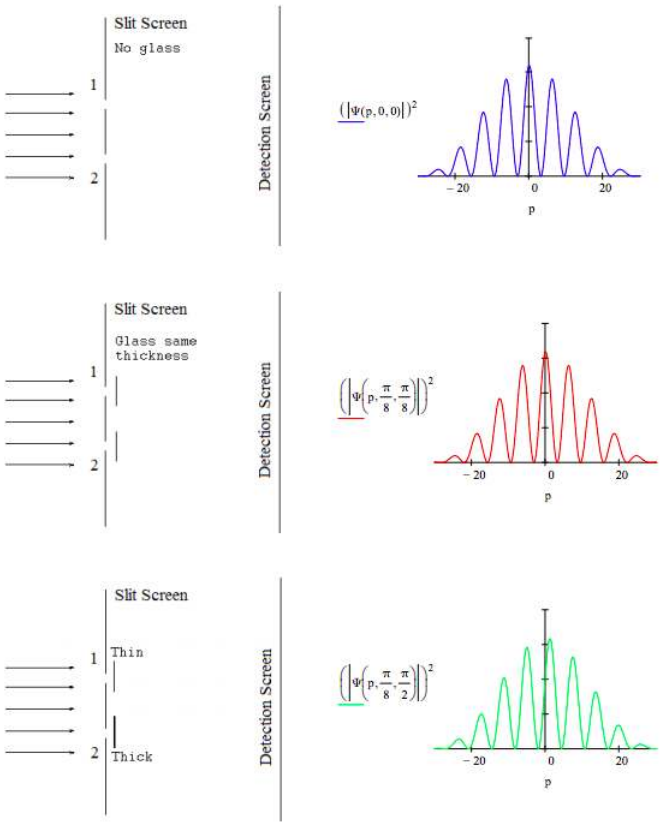
The momentum wave function with possible phase shifts θ and φ at the two slits is represented by the following superposition. The phase shifts are directly proportional to the thickness of the glass.

$$\Psi(p,\theta,\varphi) = \frac{\int_{x_L-\frac{\delta}{2}}^{x_L+\frac{\delta}{2}} \frac{1}{\sqrt{2\pi}}\exp(\text{-i p x})\frac{1}{\sqrt{\delta}}\text{dx}\ \exp(i\theta) + \int_{x_R-\frac{\delta}{2}}^{x_R+\frac{\delta}{2}} \frac{1}{\sqrt{2\pi}}\exp(\text{-i p x})\frac{1}{\sqrt{\delta}}\text{dx}\ \exp(i\varphi)}{\sqrt{2}}$$

The diffraction patterns (momentum distributions) for the empty apparatus (θ = φ = 0), for an apparatus with glass pieces of the same thickness (θ = φ = π/8) and for one that has glass of different thickness (θ = π/8 ϕ = π/2) behind the slits are displayed below.



Another look at the calculations with graphical support on the left is provided below.



This page titled 8.85: Simulating the Deutsch-Jozsa Algorithm with a Double-Slit Apparatus is shared under a CC BY 4.0 license and was authored, remixed, and/or curated by Frank Rioux via source content that was edited to the style and standards of the LibreTexts platform.

8.86: Simulating a Quantum Computer with a Mach-Zehnder Interferometer

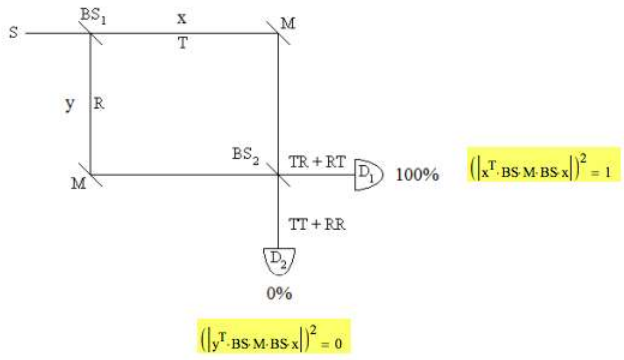
Suppose you are asked if two pieces of glass are the same thickness. The convential thing to do is to measure the thickness of each piece of glass and then compare the results. As David Deutsch pointed out this is overkill. You were asked only if they were the same thickness, but you made two measurements to answer that question, when in fact it can be done with one.

Quantum mechanics provides two ways to answer the question; using a double-slit apparatus or a Mach-Zehnder interferometer. They both operate on the same quantum principles. Using the double-slit apparatus you put a piece of glass behind each of the slits and shine light on the slits. If the resulting diffraction pattern is symmetrical about the center of the slits, the glasses are the same thickness. See the previous tutorial: Simulating the Deutsch-Jozsa Algorithm with a Double-Slit Apparatus.

Alternatively you could put a piece of glass in each arm of an equal-arm Mach-Zehnder interferometer (MZI). How this approach works is the subject of this tutorial. First we need to get acquainted with a MZI.

As shown in the following figure a MZI consists of a photon source, two 50-50 beam splitters, two mirrors and two detectors. The Appendix contains the mathematical information necessary to carry out a matrix mechanics analysis of the operation of the interferometer. The motional states of the photon are represented by vectors, while the beam splitters and mirrors are represented by matrices and operate on the vectors.

Yogi Berra has famously said "When you come to a fork in the road, take it." This is exactly what the photon does at a beam splitter. After the first beam splitter the photon, which was moving in the x-direction being emitted by the source, is now in a superposition of moving in both the x- and y-directions. It has been transmitted and reflected at the beam splitter. By convention a 90 degree (π/2, i) phase shift is assigned to reflection.



The following calculations illustrate the formation of the superposition state created by the photon's interaction with the first beam splitter.

$$\text{BS x} \rightarrow \begin{pmatrix} \frac{\sqrt{2}}{2} \\ \frac{\sqrt{2}i}{2} \end{pmatrix} \quad S = \frac{1}{\sqrt{2}}(T + iR) \quad \frac{1}{\sqrt{2}}x + \frac{i}{\sqrt{2}}y \rightarrow \begin{pmatrix} \frac{\sqrt{2}}{2} \\ \frac{\sqrt{2}i}{2} \end{pmatrix}$$

After the initial beam splitter, the mirrors direct the transmitted and reflected photon states to a second beam splitter where they are recombined. The consequence of this in an equal arm MZI is that the photon is alway registered at D_1. There are two paths (histories) to each detector and the amplitudes for these paths interfere. To reach D_1 both paths experience one reflection and so arrive in phase with each other with their phases shifted by 90 degrees. The paths to D_2, however, are 180 degrees out of phase and destructively interfere. The photon is never detected at D_2.

A photon entering the MZI in the x-direction exits in the x-direction phase-shifted by 90 degrees:

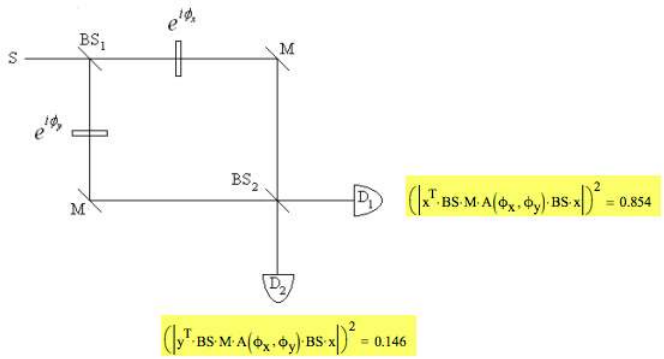
$$\text{BS M BS x} \rightarrow \begin{pmatrix} i \\ 0 \end{pmatrix} \quad \text{i x} \rightarrow \begin{pmatrix} i \\ 0 \end{pmatrix}$$

The highlighted areas above next to the detectors show the matrix mechanics calculations for the probability of the photon being registered at D_1 and D_2. The equations are read from the right. A photon moving in the x-direction interacts with a beam splitter, a

mirror and another beam splitter. This state is then projected onto x- and y-direction motion to calculate which detector will register the photon. The absolute square of this calculation (the probability amplitude) is the probability.

Now we place the pieces of glass in the arms of the interferometer as shown below. The speed of light in glass is different from that in air. Therefore glass causes a phase shift depending on its thickness as is shown below. If the pieces of glass are the same thickness, δ, they will cause the same phase shift and the photon will be detected at D_1. However, if they have different thicknesses, the phase shifts will be different in the two arms of the interferometer. For example, if ϕx is π/2 and ϕy is π/4 then D_2 will fire almost 15% of the time indicating that the glasses are not the same thickness.

$$\phi_x = 2\pi\frac{\delta_x}{\lambda} \quad \phi_x = \frac{\pi}{2} \quad \phi_y 2\pi\frac{\delta_y}{\lambda} \quad \phi_y = \frac{\pi}{4}$$



Appendix

State Vectors

$$\text{Photon moving horizontally:} \quad x = \begin{pmatrix} 1 \\ 0 \end{pmatrix} \quad \text{Photon moving vertically:} \quad y = \begin{pmatrix} 0 \\ 1 \end{pmatrix}$$

Operators

$$\text{Operator representing a beam splitter:} \quad \text{BS} = \frac{1}{\sqrt{2}} \begin{pmatrix} 1 & i \\ i & 1 \end{pmatrix}$$

$$\text{Operator representing interaction with glass:} \quad \text{A}\left(\phi_x,\ \phi_y\right) = \begin{pmatrix} e^{i\phi_x} & 0 \\ 0 & e^{i\phi_y} \end{pmatrix}$$

$$\text{Operator representing a mirror:} \quad \text{M} = \begin{pmatrix} 0 & 1 \\ 1 & 0 \end{pmatrix}$$

This page titled 8.86: Simulating a Quantum Computer with a Mach-Zehnder Interferometer is shared under a CC BY 4.0 license and was authored, remixed, and/or curated by Frank Rioux via source content that was edited to the style and standards of the LibreTexts platform.

8.87: Quantum Restrictions on Cloning

Suppose a quantum copier exists which is able to carry out the following cloning operation.

$$\begin{pmatrix}0\\1\end{pmatrix} \xrightarrow{Clone} \begin{pmatrix}0\\1\end{pmatrix} \otimes \begin{pmatrix}0\\1\end{pmatrix} = \begin{pmatrix}0\\0\\0\\1\end{pmatrix}$$

Next the cloning operation (using the same copier) is carried out on the general qubit shown below.

$$\begin{pmatrix}\cos\theta\\\sin\theta\end{pmatrix} \xrightarrow{Clone} \begin{pmatrix}\cos\theta\\\sin\theta\end{pmatrix} \otimes \begin{pmatrix}\cos\theta\\\sin\theta\end{pmatrix} = \begin{pmatrix}\cos^2\theta\\\cos\theta\sin\theta\\\sin\theta\cos\theta\\\sin^2\theta\end{pmatrix}$$

Quantum transformations are unitary, meaning probability is preserved. This requires that the scalar products of the initial and final states must be the same.

$$\text{Initial state:} \qquad (\cos\theta \quad \sin\theta)\begin{pmatrix}0\\1\end{pmatrix} = \sin\theta$$

$$\text{Final state:} \quad (\cos^2\theta \quad \cos\theta\sin\theta \quad \sin\theta\cos\theta \quad \sin^2\theta)\begin{pmatrix}0\\0\\0\\1\end{pmatrix} = \sin^2\theta$$

It is clear from this analysis that quantum theory puts a significant restriction on copying. Only states for which sin(θ) = 0 or 1 (0 and 90 degrees) can be copied by the original cloner.

In conclusion, two quotes from Wootters and Zurek, Physics Today, February 2009, page 76.

> Perfect copying can be achieved only when the two states are orthogonal, and even then one can copy those two states (...) only with a copier specifically built for that set of states.
>
> In sum, one cannot make a perfect copy of an unknown quantum state, since, without prior knowledge, it is impossible to select the right copier for the job. That formulation is one common way of stating the no-cloning theorem.

An equivalent way to look at this (see arXiv:1701.00989v1) is to assume that a cloner exists for the V-H polarization states.

$$\hat{C}|V\rangle|X\rangle = |V\rangle V\rangle \quad \hat{C}|H\rangle|X\rangle = |H\rangle|H\rangle$$

A diagonally polarized photon is a superposition of the V-H polarization states.

$$|D\rangle = \frac{1}{\sqrt{2}}\left(|V\rangle + |H\rangle\right)$$

However, due to the linearity of quantum mechanics the V-H cloner cannot clone a diagonally polarized photon.

$$\hat{C}|D\rangle|X\rangle = \hat{C}\tfrac{1}{\sqrt{2}}\left(|V\rangle+|H\rangle\right)|X\rangle = \tfrac{1}{\sqrt{2}}\left(|V\rangle|X\rangle+|H\rangle|X\rangle\right) = \tfrac{1}{\sqrt{2}}\left(|V\rangle|V\rangle+|H\rangle|H\rangle\right)$$

$$\hat{C}|D\rangle|X\rangle \neq |D\rangle|D\rangle = \tfrac{1}{2}\left(|V\rangle|V\rangle+|V\rangle|H\rangle+|H\rangle|V\rangle+|H\rangle|H\rangle\right)$$

This page titled 8.87: Quantum Restrictions on Cloning is shared under a CC BY 4.0 license and was authored, remixed, and/or curated by Frank Rioux via source content that was edited to the style and standards of the LibreTexts platform.

8.88: Quantum Error Correction

This tutorial deals with quantum error correction as presented by Julian Brown on pages 274-278 in *The Quest for the Quantum Computer*. Brown's three-qubit example includes an input qubit and two ancillary qubits in the initial state |Ψ00>. This state is encoded and subsequently decoded, with the possibility that in between it acquires an error. The quantum circuit demonstrates how correction occurs if a qubit is flipped due to decoherence at the intermediate state.

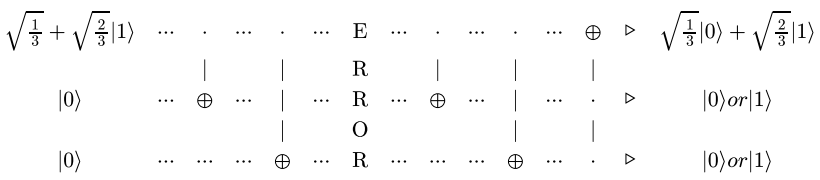
The quantum gates required for the error correction algorithm are:

$$\mathrm{I} = \begin{pmatrix} 1 & 0 \\ 0 & 1 \end{pmatrix} \quad \mathrm{CNOT} = \begin{pmatrix} 1 & 0 & 0 & 0 \\ 0 & 1 & 0 & 0 \\ 0 & 0 & 0 & 1 \\ 0 & 0 & 1 & 0 \end{pmatrix}$$

$$\mathrm{CnNOT} = \begin{pmatrix} 1 & 0 & 0 & 0 & 0 & 0 & 0 & 0 \\ 0 & 1 & 0 & 0 & 0 & 0 & 0 & 0 \\ 0 & 0 & 1 & 0 & 0 & 0 & 0 & 0 \\ 0 & 0 & 0 & 1 & 0 & 0 & 0 & 0 \\ 0 & 0 & 0 & 0 & 0 & 1 & 0 & 0 \\ 0 & 0 & 0 & 0 & 1 & 0 & 0 & 0 \\ 0 & 0 & 0 & 0 & 0 & 0 & 0 & 1 \\ 0 & 0 & 0 & 0 & 0 & 0 & 1 & 0 \end{pmatrix} \quad \mathrm{IToffoli} = \begin{pmatrix} 1 & 0 & 0 & 0 & 0 & 0 & 0 & 0 \\ 0 & 1 & 0 & 0 & 0 & 0 & 0 & 0 \\ 0 & 0 & 1 & 0 & 0 & 0 & 0 & 0 \\ 0 & 0 & 0 & 0 & 0 & 0 & 0 & 1 \\ 0 & 0 & 0 & 0 & 1 & 0 & 0 & 0 \\ 0 & 0 & 0 & 0 & 0 & 1 & 0 & 0 \\ 0 & 0 & 0 & 0 & 0 & 0 & 1 & 0 \\ 0 & 0 & 0 & 1 & 0 & 0 & 0 & 0 \end{pmatrix}$$

The encoding and decoding elements of the circuit in terms of these gates are shown in the appropriate place above the circuit diagram.

$$\mathrm{Encode} = \mathrm{CnNOT}\ \mathrm{kronecker}(\mathrm{CNOT}, \mathrm{I}) \quad \mathrm{Decode} = \mathrm{IToffoli}\ \mathrm{Encode})$$



Given an initial state, the encodng step creates an entangled Bell state as demonstrated below.

Initial State

$$\begin{pmatrix} \sqrt{\frac{1}{3}} \\ \sqrt{\frac{2}{3}} \end{pmatrix} \begin{pmatrix} 1 \\ 0 \end{pmatrix} \begin{pmatrix} 1 \\ 0 \end{pmatrix} = \begin{pmatrix} \sqrt{\frac{1}{3}} \\ 0 \\ 0 \\ 0 \\ \frac{\sqrt{2}}{3} \\ 0 \\ 0 \\ 0 \end{pmatrix}$$

Encode

$$\mathrm{Encode} \begin{pmatrix} \sqrt{\frac{1}{3}} \\ 0 \\ 0 \\ 0 \\ \sqrt{\frac{2}{3}} \\ 0 \\ 0 \\ 0 \end{pmatrix} = \begin{pmatrix} 0.577 \\ 0 \\ 0 \\ 0 \\ 0 \\ 0 \\ 0 \\ 0.816 \end{pmatrix}$$

Encoded state

$$\begin{pmatrix} \sqrt{\frac{1}{3}} \\ 0 \end{pmatrix} \begin{pmatrix} 1 \\ 0 \end{pmatrix} \begin{pmatrix} 1 \\ 0 \end{pmatrix}$$

$$+ \begin{pmatrix} 0 \\ \sqrt{\frac{2}{3}} \end{pmatrix} \begin{pmatrix} 0 \\ 1 \end{pmatrix} \begin{pmatrix} 0 \\ 1 \end{pmatrix} = \begin{pmatrix} \sqrt{\frac{1}{3}} \\ 0 \\ 0 \\ 0 \\ 0 \\ 0 \\ 0 \\ \sqrt{\frac{2}{3}} \end{pmatrix}$$

As an initial example, it is assumed that between encoding and decoding no errors are introduced to the encoded state. This case demonstrates that decoding simply returns the initial state. Susbsequent to this the operation of the circuit when errors occur on each of the wires are examined. These cases demonstrate that the original state appears on the top wire at the completion of the error correction circuit.

$$\text{No errors:} \quad \begin{pmatrix}\sqrt{\frac{1}{3}}\\0\end{pmatrix}\begin{pmatrix}1\\0\end{pmatrix}\begin{pmatrix}1\\0\end{pmatrix} + \begin{pmatrix}0\\sqrt\frac{2}{3}\end{pmatrix}\begin{pmatrix}0\\1\end{pmatrix}\begin{pmatrix}0\\1\end{pmatrix} = \begin{pmatrix}\sqrt{\frac{1}{3}}\\0\\0\\0\\0\\0\sqrt{\frac{2}{3}}\end{pmatrix} \quad \text{Decode} \begin{pmatrix}0.577\\0\\0\\0\\0\\0\\0\\0.816\end{pmatrix} = \begin{pmatrix}0.577\\0\\0\\0\\0.816\\0\\0\\0\end{pmatrix} \quad \begin{pmatrix}\sqrt{\frac{1}{3}}\\\sqrt{\frac{2}{3}}\end{pmatrix}\begin{pmatrix}1\\0\end{pmatrix}\begin{pmatrix}1\\0\end{pmatrix} = \begin{pmatrix}\sqrt{\frac{1}{3}}\\0\\0\\0\\\sqrt{\frac{2}{3}}\\0\\0\\0\end{pmatrix}$$

Next it is shown that if the input state, |Ψ>, is corrupted that the decoder corrects the error and returns the original |Ψ> to the top wire of the circuit. In the example shown below the top qubit is flipped.

$$\text{Top qubit flipped:} \quad \begin{pmatrix}0\\\sqrt{\frac{1}{3}}\end{pmatrix}\begin{pmatrix}1\\0\end{pmatrix}\begin{pmatrix}1\\0\end{pmatrix} + \begin{pmatrix}\sqrt{\frac{2}{3}}\\0\end{pmatrix}\begin{pmatrix}0\\1\end{pmatrix}\begin{pmatrix}0\\1\end{pmatrix} = \begin{pmatrix}0\\0\\0\\\sqrt{\frac{2}{3}}\\\sqrt{\frac{1}{3}}\\0\\0\\0\end{pmatrix} \quad \text{Decode} \begin{pmatrix}0\\0\\0\\\sqrt{\frac{2}{3}}\\\sqrt{\frac{1}{3}}\\0\\0\\0\end{pmatrix} = \begin{pmatrix}0\\0\\0\\0.577\\0\\0\\0\\0.816\end{pmatrix} \quad \begin{pmatrix}\sqrt{\frac{1}{3}}\\\sqrt{\frac{2}{3}}\end{pmatrix}\begin{pmatrix}1\\0\end{pmatrix}\begin{pmatrix}1\\0\end{pmatrix} = \begin{pmatrix}0\\0\\0\\\sqrt{\frac{1}{3}}\\0\\0\\0\\\sqrt{\frac{2}{3}}\end{pmatrix}$$

The circuit can also be expressed using Dirac notation. Truth tables for the gates are provided in the Appendix.

$$\left(\sqrt{\tfrac{1}{3}}|0\rangle + \sqrt{\tfrac{2}{3}}|1\rangle\right)|00\rangle \xrightarrow{encode} \sqrt{\tfrac{1}{3}}|000\rangle + \sqrt{\tfrac{2}{3}}|111\rangle \xrightarrow{flip\ top} [qubit]\sqrt{\tfrac{1}{3}}|100\rangle + \sqrt{\tfrac{2}{3}}|011\rangle$$
$$\xrightarrow{CNOT,\ I} \sqrt{\tfrac{1}{3}}|110\rangle + \sqrt{\tfrac{2}{3}}|011\rangle \xrightarrow{CnNOT} \sqrt{\tfrac{1}{3}}|111\rangle + \sqrt{\tfrac{2}{3}}|011\rangle$$
$$\xrightarrow{InToffoli} \sqrt{\tfrac{1}{3}}|011\rangle + \sqrt{\tfrac{2}{3}}|111\rangle = \left(\sqrt{\tfrac{1}{3}}|0\rangle + \sqrt{\tfrac{2}{3}}|1\rangle\right)|11\rangle$$

Naturally the ancillary qubits are also susceptible to errors. The following examples show that if a qubit flip occurs on the middle or bottom wire, the circuit still functions properly.

Middle qubit flipped:

$$\begin{pmatrix}\sqrt{\frac{1}{3}}\\0\end{pmatrix}\begin{pmatrix}0\\1\end{pmatrix}\begin{pmatrix}1\\0\end{pmatrix} \quad \text{Decode} \begin{pmatrix}0\\0\\\sqrt{\frac{1}{3}}\\0\\0\\\sqrt{\frac{2}{3}}\\0\\0\end{pmatrix} \quad \begin{pmatrix}\sqrt{\frac{1}{3}}\\\sqrt{\frac{2}{3}}\end{pmatrix}\begin{pmatrix}0\\1\end{pmatrix}\begin{pmatrix}1\\0\end{pmatrix}$$

$$+\begin{pmatrix}0\\\sqrt{\frac{2}{3}}\end{pmatrix}\begin{pmatrix}1\\0\end{pmatrix}\begin{pmatrix}0\\1\end{pmatrix} = \begin{pmatrix}0\\0\\\sqrt{\frac{2}{3}}\\0\\0\\\sqrt{\frac{1}{3}}\\0\\0\end{pmatrix} = \begin{pmatrix}0\\0\\0.577\\0\\0\\0\\0.816\\0\end{pmatrix} = \begin{pmatrix}0\\0\\\sqrt{\frac{1}{3}}\\0\\0\\0\\\sqrt{\frac{2}{3}}\\0\end{pmatrix}$$

$$\left(\sqrt{\tfrac{1}{3}}|0\rangle+\sqrt{\tfrac{2}{3}}|1\rangle\right)|00\rangle \xrightarrow{encode} \sqrt{\tfrac{1}{3}}|000\rangle+\sqrt{\tfrac{2}{3}}|111\rangle \xrightarrow{flip\ top} [qubit]\sqrt{\tfrac{1}{3}}|010\rangle+\sqrt{\tfrac{2}{3}}|101\rangle$$
$$\xrightarrow{CNOT,\ I} \sqrt{\tfrac{1}{3}}|010\rangle+\sqrt{\tfrac{2}{3}}|111\rangle \xrightarrow{CnNOT} \sqrt{\tfrac{1}{3}}|010\rangle+\sqrt{\tfrac{2}{3}}|110\rangle$$
$$\xrightarrow{InToffoli} \sqrt{\tfrac{1}{3}}|010\rangle+\sqrt{\tfrac{2}{3}}|110\rangle = \left(\sqrt{\tfrac{1}{3}}|0\rangle+\sqrt{\tfrac{2}{3}}|1\rangle\right)|10\rangle$$

Bottom qubit flipped:

$$\begin{pmatrix}\sqrt{\frac{1}{3}}\\0\end{pmatrix}\begin{pmatrix}1\\0\end{pmatrix}\begin{pmatrix}0\\1\end{pmatrix} \quad \text{Decode} \begin{pmatrix}0\\\sqrt{\frac{1}{3}}\\0\\0\\0\\\sqrt{\frac{2}{3}}\\0\end{pmatrix} \quad \begin{pmatrix}\sqrt{\frac{1}{3}}\\\sqrt{\frac{2}{3}}\end{pmatrix}\begin{pmatrix}1\\0\end{pmatrix}\begin{pmatrix}0\\1\end{pmatrix}$$

$$+\begin{pmatrix}0\\\sqrt{\frac{2}{3}}\end{pmatrix}\begin{pmatrix}0\\1\end{pmatrix}\begin{pmatrix}1\\0\end{pmatrix} = \begin{pmatrix}0\\\sqrt{\frac{1}{3}}\\0\\0\\0\\\sqrt{\frac{2}{3}}\\0\end{pmatrix} = \begin{pmatrix}0\\0.577\\0\\0\\0\\0.816\\0\\0\end{pmatrix} = \begin{pmatrix}0\\\sqrt{\frac{1}{3}}\\0\\0\\0\\\sqrt{\frac{2}{3}}\\0\\0\end{pmatrix}$$

$$\left(\sqrt{\tfrac{1}{3}}|0\rangle+\sqrt{\tfrac{2}{3}}|1\rangle\right)|00\rangle \xrightarrow{encode} \sqrt{\tfrac{1}{3}}|000\rangle+\sqrt{\tfrac{2}{3}}|111\rangle \xrightarrow{flip\ top} [qubit]\sqrt{\tfrac{1}{3}}|001\rangle+\sqrt{\tfrac{2}{3}}|110\rangle$$
$$\xrightarrow{CNOT,\ I} \sqrt{\tfrac{1}{3}}|001\rangle+\sqrt{\tfrac{2}{3}}|100\rangle \xrightarrow{CnNOT} \sqrt{\tfrac{1}{3}}|001\rangle+\sqrt{\tfrac{2}{3}}|101\rangle$$
$$\xrightarrow{InToffoli} \sqrt{\tfrac{1}{3}}|001\rangle+\sqrt{\tfrac{2}{3}}|101\rangle = \left(\sqrt{\tfrac{1}{3}}|0\rangle+\sqrt{\tfrac{2}{3}}|1\rangle\right)|01\rangle$$

Appendix

CNOT

Decimal	Binary	to	Binary	Decimal
0	00	to	00	0
1	01	to	01	1
2	10	to	11	3
3	11	to	10	2

CnNOT

Decimal	Binary	to	Binary	Decimal
0	000	to	000	0
1	001	to	001	1
2	010	to	010	2
3	011	to	011	3
4	100	to	101	5
5	101	to	100	4
6	110	to	111	7
7	111	to	110	6

IToffoli

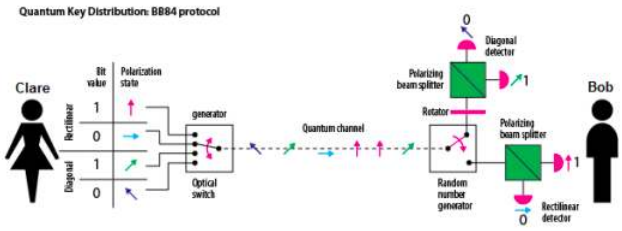
Decimal	Binary	to	Binary	Decimal
0	000	to	000	0
1	001	to	001	1
2	010	to	010	2
3	011	to	111	7
4	100	to	100	4
5	101	to	101	5
6	110	to	110	6
7	111	to	011	3

This page titled 8.88: Quantum Error Correction is shared under a CC BY 4.0 license and was authored, remixed, and/or curated by Frank Rioux via source content that was edited to the style and standards of the LibreTexts platform.

8.89: Matrix Mechanics Analysis of the BB84 Key Distribution

The figure below (www.nsa.gov/research/tnw/tnw201/article6.shtml) illustrates an implementation of the BB84 public key distribution protocol. Clare randomly sends Bob single photons in either the rectilinear or diagonal basis. Bob randomly chooses to measure the photons he receives in either the rectilinear or diagonal basis. The table below the figure displays typical results and how Clare and Bob use them to create a secret key.

While the key distribution protocol is clear enough from the graphic alone, the purpose of this tutorial is to show the details of its operation using the methods of matrix mechanics.



Quantum transmission & detection	Clare's photons	↖	↗	→	↑	↑	↗	↖	↑
	Clare's random bits	0	1	0	1	1	1	0	1
	Bob's detection events	↑	↗	↖	↑	↗	↗	↖	↖
	Bob's detected bit values	1	1	0	1	1	1	0	0
Public discussion (i.e., sifting)	Bob's measurement basis	Rect	Diag	Diag	Rect	Diag	Diag	Diag	Diag
	Clare tells Bob which bits to keep	✔		✔		✔	✔		
	Shared secret key	–	1	–	1	–	1	0	–

Direction of motion and polarization states are represented by the following vectors. The x-direction is horizontal in the figure above.

$$\text{Direction of propagation states:} x = \begin{pmatrix}1\\0\end{pmatrix} \quad y = \begin{pmatrix}0\\1\end{pmatrix}$$

$$\text{Photon polarization states:} \quad v = \begin{pmatrix}1\\0\end{pmatrix} \quad h = \begin{pmatrix}0\\1\end{pmatrix} \quad d = \frac{1}{\sqrt{2}}\begin{pmatrix}1\\1\end{pmatrix} \quad s = \frac{1}{\sqrt{2}}\begin{pmatrix}1\\-1\end{pmatrix}$$

There are eight propagation-polarization states which are created by tensor multiplication of the appropriate vectors.

$$xv = \begin{pmatrix}1\\0\end{pmatrix}\begin{pmatrix}1\\0\end{pmatrix} \quad xv = \begin{pmatrix}1\\0\\0\\0\end{pmatrix} \quad xh = \begin{pmatrix}1\\0\end{pmatrix}\begin{pmatrix}0\\1\end{pmatrix} \quad xh = \begin{pmatrix}0\\1\\0\\0\end{pmatrix} \quad yv = \begin{pmatrix}0\\1\end{pmatrix}\begin{pmatrix}1\\0\end{pmatrix} \quad yv = \begin{pmatrix}0\\0\\1\\0\end{pmatrix} \quad yh = \begin{pmatrix}0\\1\end{pmatrix}\begin{pmatrix}0\\1\end{pmatrix} \quad yh = \begin{pmatrix}0\\0\\0\\1\end{pmatrix}$$

$$xd = \begin{pmatrix}1\\0\end{pmatrix}\frac{1}{\sqrt{2}}\begin{pmatrix}1\\1\end{pmatrix} \quad xd = \frac{1}{\sqrt{2}}\begin{pmatrix}1\\1\\0\\0\end{pmatrix} \quad xs = \begin{pmatrix}1\\0\end{pmatrix}\frac{1}{\sqrt{2}}\begin{pmatrix}1\\-1\end{pmatrix} \quad xs = \frac{1}{\sqrt{2}}\begin{pmatrix}1\\-1\\0\\0\end{pmatrix}$$

$$yd = \begin{pmatrix}0\\1\end{pmatrix}\frac{1}{\sqrt{2}}\begin{pmatrix}1\\1\end{pmatrix} \quad yd = \frac{1}{\sqrt{2}}\begin{pmatrix}0\\0\\1\\1\end{pmatrix} \quad ys = \begin{pmatrix}0\\1\end{pmatrix}\frac{1}{\sqrt{2}}\begin{pmatrix}1\\-1\end{pmatrix} \quad ys = \frac{1}{\sqrt{2}}\begin{pmatrix}0\\0\\1\\-1\end{pmatrix}$$

The operators required for the BB84 implementation shown above are matrices representing the identity, mirror, rotator and polarization beam splitter, PBS.

$$\mathrm{I} = \begin{pmatrix}1&0\\0&1\end{pmatrix} \quad \mathrm{M} = \begin{pmatrix}0&1\\1&0\end{pmatrix} \quad \text{Rotator} = \frac{1}{\sqrt{2}}\begin{pmatrix}1&-1\\1&1\end{pmatrix} \quad \mathrm{PBS} = \begin{pmatrix}1&0&0&0\\0&0&0&1\\0&0&1&0\\0&1&0&0\end{pmatrix}$$

The rotator, which prepares photons for measurement in the diagonal basis, rotates the photon polarization state clockwise by 45 degrees.

$$\text{Rotator v} = \begin{pmatrix} 0.707 \\ 0.707 \end{pmatrix} = |d\rangle \qquad \text{Rotator h} = \begin{pmatrix} -0.707 \\ 0.707 \end{pmatrix} = -|s\rangle \qquad \text{Rotator d} = \begin{pmatrix} 0 \\ 1 \end{pmatrix} = |h\rangle \qquad \text{Rotator s} = \begin{pmatrix} 1 \\ 0 \end{pmatrix} = |v\rangle$$

The PBS transmits vertical and reflects horizontal photons. For example,

$$\text{PBS xv} = \begin{pmatrix} 1 \\ 0 \\ 0 \\ 0 \end{pmatrix} = |xv\rangle \qquad \text{PBS xh} = \begin{pmatrix} 0 \\ 0 \\ 0 \\ 1 \end{pmatrix} = yh\rangle \qquad \text{PBS yv} = \begin{pmatrix} 0 \\ 0 \\ 1 \\ 0 \end{pmatrix} = |yv\rangle \qquad \text{PBS yh} = \begin{pmatrix} 0 \\ 1 \\ 0 \\ 0 \end{pmatrix} = |xh\rangle$$

Interpreting Measurement Results

Suppose Bob measures Clare's photons (|v>, |h>, |d> and |s>) in the rectilinear basis. Note that the rectilinear detector is in the same direction as the photons are propagating. For |v> and |h> he correctly measures the polarization of Clare's photons. However, |d> and |s> are not eigenstates of the PBS, but superpositions of |v> and |h>, so for these photons half the time Bob will observe |v> and half the time |h>. According to quantum principles he always observes one of the eigenstates of the measurement operator. When Clare and Bob publicly discuss the result she will tell him for which events he chose the correct measurement basis.

$$\text{PBS xv} = \begin{pmatrix} 1 \\ 0 \\ 0 \\ 0 \end{pmatrix} = xv \qquad \text{PBS xh} = \begin{pmatrix} 0 \\ 0 \\ 0 \\ 1 \end{pmatrix} = yh \qquad \text{PBS xd} = \begin{pmatrix} 0.707 \\ 0 \\ 0 \\ 0.707 \end{pmatrix} \qquad \tfrac{1}{\sqrt{2}}\text{(xv + yh)} = \begin{pmatrix} 0.707 \\ 0 \\ 0 \\ 0.707 \end{pmatrix}$$

$$\text{PBS xs} = \begin{pmatrix} 0.707 \\ 0 \\ 0 \\ -0.707 \end{pmatrix} \qquad \tfrac{1}{\sqrt{2}}\text{(xv - yh)} = \begin{pmatrix} 0.707 \\ 0 \\ 0 \\ -0.707 \end{pmatrix}$$

Suppose Bob measures Clare's photons in the diagonal basis. The diagonal detector is reached in the vertical direction via a mirror. The rotator causes a basis change so that the |d> and |s> photons become eigenvectors of the PBS. Thus for |d> or |s> Bob always gets the correct result because they have been transformed to |h> or |v>. The states |v> and |h> are transformed by the rotator into superpositions of |v> and |h>, indicating that half the time he will observe |d> and half the time |s>. When Clare and Bob publicly discuss the result she will tell him which events he chose the correct measurement basis.

$$\text{PBS kronecker(M, Rotator) xd} = \begin{pmatrix} 0 \\ 1 \\ 0 \\ 0 \end{pmatrix} = xh \qquad \text{PBS kronecker(M, Rotator) xs} = \begin{pmatrix} 0 \\ 0 \\ 1 \\ 0 \end{pmatrix} = yv$$

$$\text{PBS kronecker(M, Rotator) xv} = \begin{pmatrix} 0 \\ 0.707 \\ 0.707 \\ 0 \end{pmatrix} \qquad \tfrac{1}{\sqrt{2}}\text{(xh + yv)} = \begin{pmatrix} 0 \\ 0.707 \\ 0.707 \\ 0 \end{pmatrix} \qquad \text{PBS kronecker(M, Rotator) xh} = \begin{pmatrix} 0 \\ 0.707 \\ -0.707 \\ 0 \end{pmatrix} \qquad \tfrac{1}{\sqrt{2}}\text{(xh - yv)} = \begin{pmatrix} 0 \\ 0.707 \\ -0.707 \\ 0 \end{pmatrix}$$

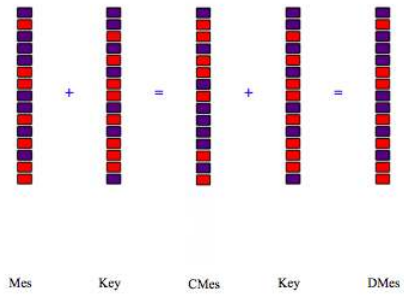
The following demonstrates how a binary message is coded and subsequently decoded using a binary key and modulo 2 arithmetic.

$$\underset{\text{Message}}{\text{Mes} = \begin{pmatrix} 0 \\ 1 \\ 0 \\ 0 \\ 0 \\ 1 \\ 1 \\ 0 \\ 0 \\ 1 \\ 0 \\ 1 \\ 0 \\ 1 \\ 1 \end{pmatrix}} \quad \underset{\text{Key}}{\text{Key} = \begin{pmatrix} 0 \\ 0 \\ 1 \\ 0 \\ 0 \\ 1 \\ 0 \\ 1 \\ 1 \\ 0 \\ 1 \\ 0 \\ 1 \\ 1 \\ 1 \\ 0 \end{pmatrix}} \quad \underset{\text{Coded Message}}{\text{CMes} = \text{mod}(\text{Mes} + \text{Key}, 2) = \begin{pmatrix} 0 \\ 1 \\ 1 \\ 0 \\ 1 \\ 1 \\ 0 \\ 1 \\ 0 \\ 0 \\ 0 \\ 0 \\ 1 \\ 0 \\ 1 \end{pmatrix}} \quad \underset{\text{Decoded Message}}{\text{DMes} = \text{mod}(\text{CMes} + \text{Key}, 2) = \begin{pmatrix} 0 \\ 1 \\ 0 \\ 0 \\ 0 \\ 1 \\ 1 \\ 0 \\ 0 \\ 1 \\ 0 \\ 1 \\ 0 \\ 1 \\ 1 \end{pmatrix}}$$

It is clear by inspection that the message has been accurately decoded. This is confirmed by calculating the difference between the message and the decoded message.

$$(\text{Mes} - \text{DMes})^T = (0 \quad 0 \quad 0 \quad 0 \quad 0 \quad 0 \quad 0 \quad 0 \quad 0 \quad 0 \quad 0 \quad 0 \quad 0 \quad 0 \quad 0)$$

Here's a graphical representation of the coding and decoding mechanism.



This page titled 8.89: Matrix Mechanics Analysis of the BB84 Key Distribution is shared under a CC BY 4.0 license and was authored, remixed, and/or curated by Frank Rioux via source content that was edited to the style and standards of the LibreTexts platform.

8.90: 388. The Quantum Math Behind Ekert's Key Distribution Scheme

Alice and Bob share an entangled photon (EPR) pair in the following state.

$$|\Psi\rangle = \frac{1}{\sqrt{2}}\left[|R\rangle_A|R\rangle_B + |L\rangle_A|L\rangle_B\right] = \frac{1}{2\sqrt{2}}\left[\begin{pmatrix}1\\ i\end{pmatrix}_A \otimes \begin{pmatrix}1\\ i\end{pmatrix}_B + \begin{pmatrix}1\\ -i\end{pmatrix}_A \otimes \begin{pmatrix}1\\ -i\end{pmatrix}_B\right]$$
$$= \frac{1}{\sqrt{2}}\begin{pmatrix}1\\ 0\\ 0\\ -1\end{pmatrix} = \frac{1}{\sqrt{2}}\left[|V\rangle_A|V\rangle_B - |H\rangle_A|H\rangle_B\right]$$

They agree to make random polarization measurements in the rectilinear and circular polarization bases. When a measurement is made on a quantum system the result is always an eigenstate of the measurement operator. The operators and eigenstates in the rectilinear and circular basis are:

$$I = \begin{pmatrix}1 & 0\\ 0 & 1\end{pmatrix} \quad V_{op} = \begin{pmatrix}1 & 0\\ 0 & 0\end{pmatrix} \quad V = \begin{pmatrix}1\\ 0\end{pmatrix} V_{op} \rightarrow \begin{pmatrix}1\\ 0\end{pmatrix} \quad H = \begin{pmatrix}0\\ 1\end{pmatrix} \quad H_{op} = \begin{pmatrix}0 & 0\\ 0 & 1\end{pmatrix} \quad H_{op}H \rightarrow \begin{pmatrix}0\\ 1\end{pmatrix}$$

$$R_{op} = \tfrac{1}{2}\begin{pmatrix}1 & -i\\ i & 1\end{pmatrix} \quad R = \tfrac{1}{\sqrt{2}}\begin{pmatrix}1\\ i\end{pmatrix} \quad R_{op}R \rightarrow \begin{pmatrix}\frac{\sqrt{2}}{2}\\ \frac{\sqrt{2}i}{2}\end{pmatrix} \quad L_{op} = \tfrac{1}{2}\begin{pmatrix}1 & i\\ -i & 1\end{pmatrix} \quad L = \tfrac{1}{\sqrt{2}}\begin{pmatrix}1\\ -i\end{pmatrix} \quad L_{op}L \rightarrow \begin{pmatrix}\frac{\sqrt{2}}{2}\\ -\frac{\sqrt{2}i}{2}\end{pmatrix}$$

Pertinent superpositions:

$$V = \tfrac{1}{\sqrt{2}}(\mathrm{R} + \mathrm{L}) \quad H = \tfrac{i}{\sqrt{2}}(\mathrm{L} - \mathrm{R}) \quad R = \tfrac{1}{\sqrt{2}}(\mathrm{V} + \mathrm{iH}) \quad L = \tfrac{1}{\sqrt{2}}(\mathrm{V} - \mathrm{iH})$$

Alice's random measurement effectively sends a random photon to Bob due to the correlations built into the entangled state of their shared photon pair. Alice's four measurement possibilities and their consequences for Bob are now examined.

Alice's photon is found to be right circularly polarized, |R>. If Bob measures circular polarization he is certain to find his photon to be |R>. But if he chooses to measure in the rectilinear basis the probability he will observe |V> is 0.5 and the probability he will observe |H> is 0.5.

$$\mathrm{kronecker}(R_{op},\ I)\tfrac{1}{\sqrt{2}}\begin{pmatrix}1\\ 0\\ 0\\ -1\end{pmatrix} = \begin{pmatrix}0.354\\ 0.354i\\ 0.354i\\ -0.354\end{pmatrix} \quad \tfrac{1}{\sqrt{2}}\left[\tfrac{1}{\sqrt{2}}\begin{pmatrix}1\\ i\end{pmatrix}\tfrac{1}{\sqrt{2}}\begin{pmatrix}1\\ i\end{pmatrix}\right] = \tfrac{1}{\sqrt{2}}RR = \tfrac{1}{\sqrt{2}}R\left[\tfrac{1}{\sqrt{2}}(\mathrm{V} + \mathrm{iH})\right]$$

If Alice observes |L>, Bob will also if he measures circular polarization. But if he measures in the rectilinear basis the probability he will observe |V> is 0.5 and the probability he will observe |H> is 0.5.

$$\mathrm{kronecker}(L_{op},\ I)\tfrac{1}{\sqrt{2}}\begin{pmatrix}1\\ 0\\ 0\\ -1\end{pmatrix} = \begin{pmatrix}0.354\\ -0.354i\\ -0.354i\\ -0.354\end{pmatrix} \quad \tfrac{1}{\sqrt{2}}\left[\tfrac{1}{\sqrt{2}}\begin{pmatrix}1\\ -i\end{pmatrix}\tfrac{1}{\sqrt{2}}\begin{pmatrix}1\\ -i\end{pmatrix}\right] = \tfrac{1}{\sqrt{2}}LL = \tfrac{1}{\sqrt{2}}L\left[\tfrac{1}{\sqrt{2}}(\mathrm{V} - \mathrm{iH})\right]$$

The same kind of reasoning applies to measurements Alice makes in the rectilinear basis.

$$\mathrm{kronecker}(V_{op},\ I)\tfrac{1}{\sqrt{2}}\begin{pmatrix}1\\ 0\\ 0\\ -1\end{pmatrix} = \begin{pmatrix}0.707\\ 0\\ 0\\ 0\end{pmatrix} \quad \tfrac{1}{\sqrt{2}}\begin{pmatrix}1\\ 0\end{pmatrix}\begin{pmatrix}1\\ 0\end{pmatrix} = \tfrac{1}{\sqrt{2}}VV = \tfrac{1}{\sqrt{2}}V\left[\tfrac{1}{\sqrt{2}}(\mathrm{R} + \mathrm{L})\right]$$

$$\text{kronecker}(H_{op},\ I)\frac{1}{\sqrt{2}}\begin{pmatrix}1\\0\\0\\-1\end{pmatrix}=\begin{pmatrix}0\\0\\0\\-0.707\end{pmatrix}\quad -\frac{1}{\sqrt{2}}\begin{pmatrix}0\\1\end{pmatrix}\begin{pmatrix}0\\1\end{pmatrix}=-\frac{1}{\sqrt{2}}HH=\frac{1}{\sqrt{2}}H\left[\frac{1}{\sqrt{2}}(\text{L - R})\right]$$

Alice and Bob keep the results for the experiments for which they measured in the same basis, and make the following bit value assignments: |V> = |R> = 0 and |H> = |L> = 1. This leads to the secret key on the bottom line.

Alice	*R*	V	*V*	*L*	H	L	*H*	*R*	*V*	L	*H*
Bob	*R*	L	*V*	*L*	R	H	*H*	*R*	*V*	V	*H*
Key	0		0	1		1	0	0		1	

This page titled 8.90: 388. The Quantum Math Behind Ekert's Key Distribution Scheme is shared under a CC BY 4.0 license and was authored, remixed, and/or curated by Frank Rioux via source content that was edited to the style and standards of the LibreTexts platform.

8.91: A Shorter Version of the Quantum Math Behind Ekert's Key Distribution Scheme

Alice and Bob share an entangled photon (EPR) pair in the following state.

$$|\Psi = \frac{1}{\sqrt{2}}\left[|R\rangle_A|R\rangle_B + |L\rangle_A|L\rangle_B\right] = \frac{1}{2\sqrt{2}}\left[\begin{pmatrix}1\\ i\end{pmatrix}_A \otimes \begin{pmatrix}1\\ i\end{pmatrix}_B + \begin{pmatrix}1\\ -i\end{pmatrix}_A \otimes \begin{pmatrix}1\\ -i\end{pmatrix}_B\right]$$
$$= \frac{1}{\sqrt{2}}\begin{pmatrix}1\\ 0\\ 0\\ -1\end{pmatrix} = \frac{1}{\sqrt{2}}\left[|V\rangle_A|V\rangle_B - |H\rangle_A|H\rangle_B\right]$$

They agree to make random polarization measurements in the rectilinear and circular polarization bases. When a measurement is made on a quantum system the result is always an eigenstate of the measurement operator. The eigenstates in the circular and rectilinear bases are:

$$R = \tfrac{1}{\sqrt{2}}\begin{pmatrix}1\\ i\end{pmatrix} \quad L = \tfrac{1}{\sqrt{2}}\begin{pmatrix}1\\ -i\end{pmatrix} \quad V = \begin{pmatrix}1\\ 0\end{pmatrix} \quad H = \begin{pmatrix}0\\ 1\end{pmatrix}$$

Pertinent superpositions:

$$V = \tfrac{1}{\sqrt{2}}(R+L) \quad H = \tfrac{i}{\sqrt{2}}(L-R) \quad R = \tfrac{1}{\sqrt{2}}(V+iH) \quad L = \tfrac{1}{\sqrt{2}}(V-iH)$$

Alice's random measurement effectively sends a random photon to Bob due to the correlations built into the entangled state of their shared photon pair. Alice's four measurement possibilities and their consequences for Bob are now examined.

Alice's photon is found to be right circularly polarized, |R>. If Bob measures circular polarization he is certain to find his photon to be |R>. But if he chooses to measure in the rectilinear basis the probability he will observe |V> is 0.5 and the probability he will observe |H> is 0.5.

$$\frac{1}{\sqrt{2}}RR = \frac{1}{\sqrt{2}}R\left[\frac{1}{\sqrt{2}}(V+iH)\right]$$

If Alice observes |L>, Bob will also if he measures circular polarization. But if he measures in the rectilinear basis the probability he will observe |V> is 0.5 and the probability he will observe |H> is 0.5.

$$\frac{1}{\sqrt{2}}LL = \frac{1}{\sqrt{2}}L\left[\frac{1}{\sqrt{2}}(V-iH)\right]$$

The same kind of reasoning applies to measurements Alice makes in the rectilinear basis.

$$\tfrac{1}{\sqrt{2}}VV = \tfrac{1}{\sqrt{2}}V\left[\tfrac{1}{\sqrt{2}}(R+L)\right] \quad \tfrac{1}{\sqrt{2}}HH = \tfrac{1}{\sqrt{2}}H\left[\tfrac{1}{\sqrt{2}}(L-R)\right]$$

Alice and Bob keep the results for the experiments for which they measured in the same basis (blue in the table below), and make the following bit value assignments: |V> = |R> = 0 and |H> = |L> = 1. This leads to the secret key on the bottom line.

Alice	*R*	V	*V*	*L*	H	L	*H*	*R*	*V*	L	*H*
Bob	*R*	L	*V*	*L*	R	H	*H*	*R*	*V*	V	*H*
Key	0		0	1		1	0	0		1	

The following demonstrates how a binary message is coded and subsequently decoded using a shared binary secret key and modulo 2 arithmetic.

$$\underset{\text{Message}}{\text{Mes} = \begin{pmatrix} 0 \\ 1 \\ 0 \\ 0 \\ 0 \\ 1 \\ 1 \\ 0 \\ 0 \\ 1 \\ 0 \\ 1 \end{pmatrix}} \quad \underset{\text{Key}}{\text{Key} = \begin{pmatrix} 0 \\ 0 \\ 1 \\ 1 \\ 0 \\ 0 \\ 1 \\ 0 \\ 0 \\ 1 \\ 1 \\ 0 \\ 0 \\ 1 \end{pmatrix}} \quad \underset{\text{Coded Message}}{\text{CMes} = \text{mod}(\text{Mes} + \text{Key}, 2) = \begin{pmatrix} 0 \\ 1 \\ 1 \\ 1 \\ 0 \\ 1 \\ 0 \\ 0 \\ 0 \\ 0 \\ 1 \\ 1 \\ 0 \\ 0 \end{pmatrix}} \quad \underset{\text{Decoded Message}}{\text{DMes} = \text{mod}(\text{CMes} + \text{Key}, 2) = \begin{pmatrix} 0 \\ 1 \\ 0 \\ 0 \\ 0 \\ 1 \\ 1 \\ 0 \\ 0 \\ 1 \\ 0 \\ 1 \\ 0 \\ 1 \end{pmatrix}}$$

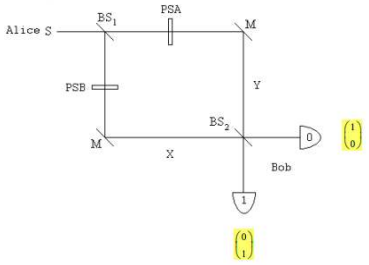
It is clear by inspection that the message has been accurately decoded. This is confirmed by calculating the difference between the message and the decoded message.

$$(\text{Mes} - \text{DMes})^T = (0 \quad 0 \quad 0 \quad 0 \quad 0 \quad 0 \quad 0 \quad 0 \quad 0 \quad 0 \quad 0 \quad 0 \quad 0 \quad 0)$$

This page titled 8.91: A Shorter Version of the Quantum Math Behind Ekert's Key Distribution Scheme is shared under a CC BY 4.0 license and was authored, remixed, and/or curated by Frank Rioux via source content that was edited to the style and standards of the LibreTexts platform.

8.92: Quantum Key Distribution Using a Mach-Zehnder Interferometer

Charles H. Bennett proposed the following Mach-Zehnder interferometer for quantum key distribution (*Physical Review Letters* 68, 3121 (1992)).



Alice's source at the left supplies single-photon states, which are split by a symmetric beam splitter BS_1 into a superposition being present in both arms of a Mach-Zehnder interferometer (MZI). Alice (PSA) applies a random 0-, 90-, 180-, or 270-degree phase shift in one arm and Bob (PSB) applies a random 0- or 90-degree phase shift in the other arm. Mirrors direct the photon to a second beam splitter creating two photon paths to each detector and thereby allowing for interference between the paths. After photon detection by Bob, Alice and Bob agree publicly to keep only those results for which their phase shifts differ by 0 or 180 degrees, settings for which the photons behave deterministically at the second beam splitter.

Direction of propagation vectors:

$$x = \begin{pmatrix}1\\0\end{pmatrix} \quad y = \begin{pmatrix}0\\1\end{pmatrix}$$

Matrix operators for the interferometer components:

$$\text{Beam splitter:}\quad \text{BS:} = \frac{1}{\sqrt{2}}\begin{pmatrix}1 & i\\ i & 1\end{pmatrix} \quad \text{Mirror:}\quad \text{M:} = \begin{pmatrix}0 & 1\\ 1 & 0\end{pmatrix} \quad \text{Phase shift:}\begin{pmatrix}e & i\,PSA & 0\\ 0 & e & i\,PSB\end{pmatrix}$$

Construct a Mach-Zehnder interferometer using these components.

$$\text{MZI(PSA, PSB)} = \text{BS M}\begin{pmatrix}e^{i\,PSA} & 0\\ 0 & e^{i\,PSB}\end{pmatrix}\text{BS}$$

'_' allowed only in math mode

For each of eight possible phase shift settings calculate the probability that detectors |0> and |1> will register the arrival of a photon.

The PSA/PSB settings for which a photon behaves deterministically are highlighted.

'_' allowed only in math mode

Demonstrate that the detection results at each detector are completely random. In other words, that if someone was monitoring Bob's detectors he or she would see no pattern in the results.

The settings of phase shifters PSA and PSB are changed randomly by Alice and Bob. So given a large number of runs, each pair of settings shown above will occur with probability 1/8 or 12.5%. Overall each detector will register a photon in half the runs.

$$Detector = \begin{pmatrix}1\\0\end{pmatrix} \quad \frac{1+\frac{1}{2}+\frac{1}{2}+1+0+\frac{1}{2}+\frac{1}{2}+0}{8} \to \frac{1}{2} \qquad Detector = \begin{pmatrix}0\\1\end{pmatrix} \quad \frac{0+\frac{1}{2}+\frac{1}{2}+0+1+\frac{1}{2}+\frac{1}{2}+1}{8} \to \frac{1}{2}$$

Demonstrate the use of a secret key to exchange a secure message between a sender and a receiver.

Coding and Decoding a Message

$j = 1..25$

$\text{Key}_j = \text{trunc}(\text{rnd}(2))$

$\text{Mes}_j = \text{trunc}(\text{rnd}(2))$

$\text{Key}^T =$
$(0\ 0\ 1\ 0\ 1\ 0\ 1\ 0\ 0\ 0\ 1\ 0\ 0\ 1\ 1\ 0\ 0\ 0\ 1\ 1\ 1\ 1\ 1\ 0\ 1)$

$\text{Mes}^T =$
$(1\ 1\ 1\ 0\ 1\ 0\ 1\ 0\ 0\ 1\ 1\ 0\ 1\ 0\ 1\ 1\ 1\ 1\ 0\ 0\ 1\ 1\ 0\ 0\ 1)$

$\text{CMes}_j = \text{Mes}_j \oplus \text{Key}_j$

$\text{CMes}^T =$
$(1\ 1\ 0\ 0\ 0\ 0\ 0\ 0\ 0\ 1\ 0\ 0\ 1\ 1\ 0\ 1\ 1\ 1\ 1\ 1\ 0\ 0\ 1\ 0\ 0)$

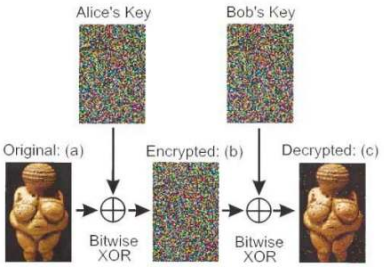
$\text{DMes}_j = \text{CMes}_j \oplus \text{Key}_j$

$\text{Mes}^T =$
$(1\ 1\ 1\ 0\ 1\ 0\ 1\ 0\ 0\ 1\ 1\ 0\ 1\ 0\ 1\ 1\ 1\ 1\ 0\ 0\ 1\ 1\ 0\ 0\ 1)$

It is clear by inspection that the message has been accurately decoded. This is confirmed by calculating the difference between the message and the decoded message.

$$(\text{DMes} - \text{Mes})^T = (0\ 0\ 0\ 0\ 0\ 0\ 0\ 0\ 0\ 0\ 0\ 0\ 0\ 0\ 0\ 0\ 0\ 0\ 0\ 0\ 0\ 0\ 0\ 0\ 0)$$

In 2000 Anton Zeilinger and his research team sent an encrypted photo of the fertility goddess Venus of Willendorf from Alice to Bob, two computers in two buildings about 400 meters apart. The figure summarizing this achievement first appeared in *Physical Review Letters* and later in a review article in *Nature*.



By extending the previous example to two dimensions, it easy to produce a rudimentary simulation of the experiment. Bitwise XOR is nothing more than addition modulo 2. (XOR = CNOT)

The original Venus and the shared key are represented by the following matrices, where the matrix elements are pixels that are either off (0) or on (1).

$$\text{Venus} = \begin{pmatrix} 1 & 1 & 1 & 1 & 1 & 1 \\ 0 & 1 & 1 & 1 & 1 & 0 \\ 0 & 0 & 1 & 1 & 0 & 0 \\ 0 & 0 & 1 & 1 & 0 & 0 \\ 0 & 0 & 1 & 1 & 0 & 0 \\ 0 & 1 & 1 & 1 & 1 & 0 \\ 1 & 1 & 1 & 1 & 1 & 1 \end{pmatrix} \quad \text{Key} = \begin{pmatrix} 1 & 0 & 0 & 1 & 1 & 0 \\ 1 & 1 & 0 & 1 & 0 & 1 \\ 0 & 0 & 1 & 0 & 0 & 1 \\ 0 & 1 & 0 & 1 & 1 & 0 \\ 1 & 0 & 1 & 0 & 1 & 1 \\ 1 & 0 & 1 & 1 & 0 & 1 \\ 0 & 1 & 0 & 0 & 1 & 0 \end{pmatrix}$$

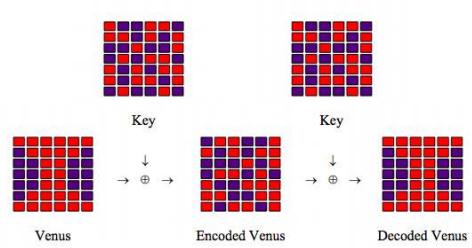
A coded version of Venus is prepared by adding Venus and the Key modulo 2 and sent to Bob.

$$i = 1..7 \quad j = 1..6 \quad \text{CVenus}_{i,\,j} = \text{Venus}_{i,\,j} \oplus \text{Key}_{i,\,j} \quad \text{CVenus} = \begin{pmatrix} 0 & 1 & 1 & 0 & 0 & 1 \\ 1 & 0 & 1 & 0 & 1 & 1 \\ 0 & 0 & 0 & 1 & 0 & 1 \\ 0 & 1 & 1 & 0 & 1 & 0 \\ 1 & 0 & 0 & 1 & 1 & 1 \\ 1 & 1 & 0 & 0 & 1 & 1 \\ 1 & 0 & 1 & 1 & 0 & 1 \end{pmatrix}$$

Bob adds the key to CVenus modulo 2 and sends the result to his printer.

$$\text{DVenus}_{i,\,j} = \text{CVenus}_{i,\,j} \oplus \text{Key}_{i,\,j} \quad \text{DVenus} = \begin{pmatrix} 1 & 1 & 1 & 1 & 1 & 1 \\ 0 & 1 & 1 & 1 & 1 & 0 \\ 0 & 0 & 1 & 1 & 0 & 0 \\ 0 & 0 & 1 & 1 & 0 & 0 \\ 0 & 0 & 1 & 1 & 0 & 0 \\ 0 & 1 & 1 & 1 & 1 & 0 \\ 1 & 1 & 1 & 1 & 1 & 1 \end{pmatrix}$$

A graphic summary of the simulation:



Random key production can be implemented as follows:

$$j = 1..20 \quad \text{PSA}_j = \text{trunc}(\text{rnd}(4))\ 90\ \text{deg} \quad \text{PSB}_j = \text{trunc}(\text{rnd}(2))\ 90\ \text{deg}$$

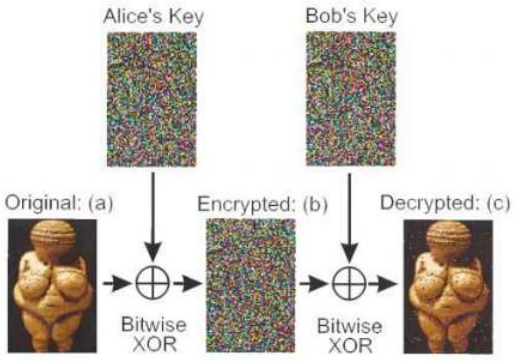
$$\text{Det0}_j = \left[\left| x^T \text{BS M} \begin{pmatrix} e^{i\ PSA_j} & 0 \\ 0 & e^{i\ PSB_j} \end{pmatrix} \text{BS x} \right| \right]^2 \quad \text{Det1}_j = \left[\left| y^T \text{BS M} \begin{pmatrix} e^{i\ PSA_j} & 0 \\ 0 & e^{i\ PSB_j} \end{pmatrix} \text{BS x} \right| \right]^2$$

$\frac{PSA_j}{deg} =$	$\frac{PSB_j}{deg} =$	$\mathrm{Det0}_j =$	$\mathrm{Det1}_j =$
0	0	1	0
0	90	0.5	0.5
180	0	0	1
90	90	1	0
270	90	0	1
0	0	1	0
270	90	0	1
0	90	0.5	0.5
270	0	0.5	0.5
0	90	0.5	0.5
180	90	0.5	0.5
90	90	1	0
180	90	0.5	0.5
180	90	0.5	0.5
0	0	1	0
...	...	...	...

This page titled 8.92: Quantum Key Distribution Using a Mach-Zehnder Interferometer is shared under a CC BY 4.0 license and was authored, remixed, and/or curated by Frank Rioux via source content that was edited to the style and standards of the LibreTexts platform.

8.93: Coding and Decoding Venus

In 2000 Anton Zeilinger and his research team sent an encrypted photo of the fertility goddess Venus of Willendorf from Alice to Bob, two computers in two buildings about 400 meters apart. The figure summarizing this achievement first appeared in *Physical Review Letters* and later in a review article in *Nature*.



It is easy to produce a rudimentary simulation of the experiment. Bitwise XOR is nothing more than addition modulo 2. The original Venus and the shared key are represented by the following matrices, where the matrix elements are pixels that are either off (0) or on (1).

$$i = 1..7 \quad j = 1..6 \quad \mathrm{Key}_{i,\,j} = \mathrm{trunc}(\mathrm{rnd}(2)) \quad \mathrm{Key} = \begin{pmatrix} 0 & 0 & 1 & 0 & 1 & 0 \\ 1 & 0 & 0 & 0 & 1 & 0 \\ 0 & 1 & 1 & 0 & 0 & 0 \\ 1 & 1 & 1 & 1 & 1 & 0 \\ 1 & 1 & 1 & 1 & 0 & 1 \\ 0 & 1 & 0 & 0 & 1 & 1 \\ 0 & 1 & 0 & 1 & 1 & 1 \end{pmatrix} \quad \mathrm{Venus} = \begin{pmatrix} 1 & 1 & 1 & 1 & 1 & 1 \\ 0 & 1 & 1 & 1 & 1 & 0 \\ 0 & 0 & 1 & 1 & 0 & 0 \\ 0 & 0 & 1 & 1 & 0 & 0 \\ 0 & 0 & 1 & 1 & 0 & 0 \\ 0 & 1 & 1 & 1 & 1 & 0 \\ 1 & 1 & 1 & 1 & 1 & 1 \end{pmatrix}$$

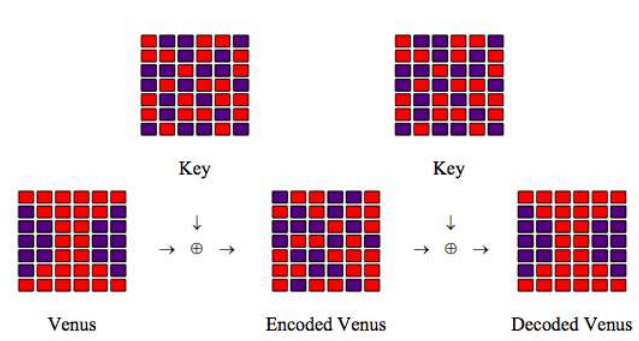
A coded version of Venus is prepared by adding Venus and the Key modulo 2 and sent to Bob.

$$\mathrm{CVenus}_{i,\,j} = \mathrm{Venus}_{i,\,j} \oplus \mathrm{Key}_{i,\,j} \quad \mathrm{CVenus} = \begin{pmatrix} 1 & 1 & 0 & 1 & 0 & 1 \\ 1 & 1 & 1 & 1 & 0 & 0 \\ 0 & 1 & 0 & 1 & 0 & 0 \\ 0 & 1 & 1 & 0 & 1 & 0 \\ 1 & 0 & 0 & 1 & 1 & 1 \\ 1 & 1 & 0 & 0 & 1 & 1 \\ 1 & 0 & 1 & 1 & 0 & 1 \end{pmatrix}$$

Bob adds the key to CVenus modulo 2 and sends the result to his printer.

$$\mathrm{DVenus}_{i,\,j} = \mathrm{CVenus}_{i,\,j} \oplus \mathrm{Key}_{i,\,j} \quad \mathrm{DVenus} = \begin{pmatrix} 1 & 1 & 1 & 1 & 1 & 1 \\ 0 & 1 & 1 & 1 & 1 & 0 \\ 0 & 0 & 1 & 1 & 0 & 0 \\ 0 & 0 & 1 & 1 & 0 & 0 \\ 0 & 0 & 1 & 1 & 0 & 0 \\ 0 & 1 & 1 & 1 & 1 & 0 \\ 1 & 1 & 1 & 1 & 1 & 1 \end{pmatrix}$$

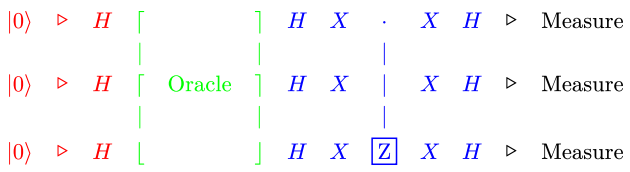
A graphic summary of the simulation:



This page titled 8.93: Coding and Decoding Venus is shared under a CC BY 4.0 license and was authored, remixed, and/or curated by Frank Rioux via source content that was edited to the style and standards of the LibreTexts platform.

8.94: Grover's Quantum Search Algorithm

D. Candela described a Grover search algorithm in the August (2015) issue of the American Journal of Physics. Chris Monroe's group recently published an experimental implementation of the same algorithm in Nature Communications 8, 1918 (2017). The Grover search is implemented for N = 3 using the three qubit quantum circuit shown below. The search algorithm (blue) runs an integer number of times closest to $\frac{\pi}{4}\sqrt{2^N}$. The closest integer for N = 3 is 2. The Appendix provides a demonstration of the implementation of the J operator shown at the far right below.



There are 8 items in the data base and the oracle, O, identifies the correct query with a minus sign. In other words, a search of the data base should return the result |110>. The J and Hadamard matrices required are shown below.

$$H = \frac{1}{\sqrt{2}}\begin{pmatrix} 1 & 1 \\ 1 & -1 \end{pmatrix} \qquad O = \begin{pmatrix} 1 & 0 & 0 & 0 & 0 & 0 & 0 & 0 \\ 0 & 1 & 0 & 0 & 0 & 0 & 0 & 0 \\ 0 & 0 & 1 & 0 & 0 & 0 & 0 & 0 \\ 0 & 0 & 0 & 1 & 0 & 0 & 0 & 0 \\ 0 & 0 & 0 & 0 & 1 & 0 & 0 & 0 \\ 0 & 0 & 0 & 0 & 0 & 1 & 0 & 0 \\ 0 & 0 & 0 & 0 & 0 & 0 & -1 & 0 \\ 0 & 0 & 0 & 0 & 0 & 0 & 0 & 1 \end{pmatrix} \qquad J = \begin{pmatrix} -1 & 0 & 0 & 0 & 0 & 0 & 0 & 0 \\ 0 & 1 & 0 & 0 & 0 & 0 & 0 & 0 \\ 0 & 0 & 1 & 0 & 0 & 0 & 0 & 0 \\ 0 & 0 & 0 & 1 & 0 & 0 & 0 & 0 \\ 0 & 0 & 0 & 0 & 1 & 0 & 0 & 0 \\ 0 & 0 & 0 & 0 & 0 & 1 & 0 & 0 \\ 0 & 0 & 0 & 0 & 0 & 0 & 1 & 0 \\ 0 & 0 & 0 & 0 & 0 & 0 & 0 & 1 \end{pmatrix}$$

HHH = kronecker(H, kronecker(H, H))

GroverSearch = HHH J HHH O

Initial Hadamard gates on the circuit wires feed the Grover search algorithm a superposition of all possible queries yielding a superposition of answers, but with the correct answer highly weighted as shown below.

$$\Psi = \frac{1}{4}\begin{pmatrix} 1 \\ 1 \\ 1 \\ 1 \\ 1 \\ 1 \\ 1 \\ 1 \end{pmatrix} \qquad \text{GroverSearch}^3\Psi = \begin{pmatrix} -0.088 \\ -0.088 \\ -0.088 \\ -0.088 \\ -0.088 \\ -0.088 \\ 0.972 \\ -0.088 \end{pmatrix}$$

This state is close to the correct result: $\begin{pmatrix} 0 \\ 1 \end{pmatrix}\begin{pmatrix} 0 \\ 1 \end{pmatrix}\begin{pmatrix} 1 \\ 0 \end{pmatrix}$

The probability of a successful search after two cycles of the circuit is $0.972^2 = 94.5\%$. For a classical search it would require on average 4 (8/2) queries.

It is easy to extend the algorithm to N = 4 by adding a row to the circuit above. In this example the search of the data base should return the result |1010>.

$$O = \begin{pmatrix} 1 & 0 & 0 & 0 & 0 & 0 & 0 & 0 & 0 & 0 & 0 & 0 & 0 & 0 & 0 & 0 \\ 0 & 1 & 0 & 0 & 0 & 0 & 0 & 0 & 0 & 0 & 0 & 0 & 0 & 0 & 0 & 0 \\ 0 & 0 & 1 & 0 & 0 & 0 & 0 & 0 & 0 & 0 & 0 & 0 & 0 & 0 & 0 & 0 \\ 0 & 0 & 0 & 1 & 0 & 0 & 0 & 0 & 0 & 0 & 0 & 0 & 0 & 0 & 0 & 0 \\ 0 & 0 & 0 & 0 & 1 & 0 & 0 & 0 & 0 & 0 & 0 & 0 & 0 & 0 & 0 & 0 \\ 0 & 0 & 0 & 0 & 0 & 1 & 0 & 0 & 0 & 0 & 0 & 0 & 0 & 0 & 0 & 0 \\ 0 & 0 & 0 & 0 & 0 & 0 & 1 & 0 & 0 & 0 & 0 & 0 & 0 & 0 & 0 & 0 \\ 0 & 0 & 0 & 0 & 0 & 0 & 0 & 1 & 0 & 0 & 0 & 0 & 0 & 0 & 0 & 0 \\ 0 & 0 & 0 & 0 & 0 & 0 & 0 & 0 & 1 & 0 & 0 & 0 & 0 & 0 & 0 & 0 \\ 0 & 0 & 0 & 0 & 0 & 0 & 0 & 0 & 0 & 1 & 0 & 0 & 0 & 0 & 0 & 0 \\ 0 & 0 & 0 & 0 & 0 & 0 & 0 & 0 & 0 & 0 & -1 & 0 & 0 & 0 & 0 & 0 \\ 0 & 0 & 0 & 0 & 0 & 0 & 0 & 0 & 0 & 0 & 0 & 1 & 0 & 0 & 0 & 0 \\ 0 & 0 & 0 & 0 & 0 & 0 & 0 & 0 & 0 & 0 & 0 & 0 & 1 & 0 & 0 & 0 \\ 0 & 0 & 0 & 0 & 0 & 0 & 0 & 0 & 0 & 0 & 0 & 0 & 0 & 1 & 0 & 0 \\ 0 & 0 & 0 & 0 & 0 & 0 & 0 & 0 & 0 & 0 & 0 & 0 & 0 & 0 & 1 & 0 \\ 0 & 0 & 0 & 0 & 0 & 0 & 0 & 0 & 0 & 0 & 0 & 0 & 0 & 0 & 0 & 1 \end{pmatrix}$$

$$J' = \begin{pmatrix} -1 & 0 & 0 & 0 & 0 & 0 & 0 & 0 & 0 & 0 & 0 & 0 & 0 & 0 & 0 & 0 \\ 0 & 1 & 0 & 0 & 0 & 0 & 0 & 0 & 0 & 0 & 0 & 0 & 0 & 0 & 0 & 0 \\ 0 & 0 & 1 & 0 & 0 & 0 & 0 & 0 & 0 & 0 & 0 & 0 & 0 & 0 & 0 & 0 \\ 0 & 0 & 0 & 1 & 0 & 0 & 0 & 0 & 0 & 0 & 0 & 0 & 0 & 0 & 0 & 0 \\ 0 & 0 & 0 & 0 & 1 & 0 & 0 & 0 & 0 & 0 & 0 & 0 & 0 & 0 & 0 & 0 \\ 0 & 0 & 0 & 0 & 0 & 1 & 0 & 0 & 0 & 0 & 0 & 0 & 0 & 0 & 0 & 0 \\ 0 & 0 & 0 & 0 & 0 & 0 & 1 & 0 & 0 & 0 & 0 & 0 & 0 & 0 & 0 & 0 \\ 0 & 0 & 0 & 0 & 0 & 0 & 0 & 1 & 0 & 0 & 0 & 0 & 0 & 0 & 0 & 0 \\ 0 & 0 & 0 & 0 & 0 & 0 & 0 & 0 & 1 & 0 & 0 & 0 & 0 & 0 & 0 & 0 \\ 0 & 0 & 0 & 0 & 0 & 0 & 0 & 0 & 0 & 1 & 0 & 0 & 0 & 0 & 0 & 0 \\ 0 & 0 & 0 & 0 & 0 & 0 & 0 & 0 & 0 & 0 & 1 & 0 & 0 & 0 & 0 & 0 \\ 0 & 0 & 0 & 0 & 0 & 0 & 0 & 0 & 0 & 0 & 0 & 1 & 0 & 0 & 0 & 0 \\ 0 & 0 & 0 & 0 & 0 & 0 & 0 & 0 & 0 & 0 & 0 & 0 & 1 & 0 & 0 & 0 \\ 0 & 0 & 0 & 0 & 0 & 0 & 0 & 0 & 0 & 0 & 0 & 0 & 0 & 1 & 0 & 0 \\ 0 & 0 & 0 & 0 & 0 & 0 & 0 & 0 & 0 & 0 & 0 & 0 & 0 & 0 & 1 & 0 \\ 0 & 0 & 0 & 0 & 0 & 0 & 0 & 0 & 0 & 0 & 0 & 0 & 0 & 0 & 0 & 1 \end{pmatrix}$$

HHHH = kronecker(H, kronecker(H, kronecker(H, H)))

GroverSearch = HHHH J' HHHH

O $\frac{\pi}{4}\sqrt{2^4} = 3.142$

$$\Psi = \frac{1}{4}\begin{pmatrix} 1 \\ 1 \\ 1 \\ 1 \\ 1 \\ 1 \\ 1 \\ 1 \\ 1 \\ 1 \\ 1 \\ 1 \\ 1 \\ 1 \\ 1 \\ 1 \end{pmatrix} \quad \text{GroverSearch}^3\Psi = \begin{pmatrix} 0.051 \\ 0.051 \\ 0.051 \\ 0.051 \\ 0.051 \\ 0.051 \\ 0.051 \\ 0.051 \\ 0.051 \\ 0.051 \\ -0.98 \\ 0.051 \\ 0.051 \\ 0.051 \\ 0.051 \\ 0.051 \end{pmatrix}$$

This state is close to the correct result: $\begin{pmatrix} 0 \\ 1 \end{pmatrix}\begin{pmatrix} 1 \\ 0 \end{pmatrix}\begin{pmatrix} 0 \\ 1 \end{pmatrix}\begin{pmatrix} 1 \\ 0 \end{pmatrix}$

The probability of a successful search after two cycles of the circuit is $(-0.98)^2 = 96.0\%$. For a classical search it would require on average 8 (16/2) queries.

Appendix

The following calculation demonstrates the identity on the right side of Grover search circuit. X is the NOT operator and CCZ is the controlled-controlled Z gate.

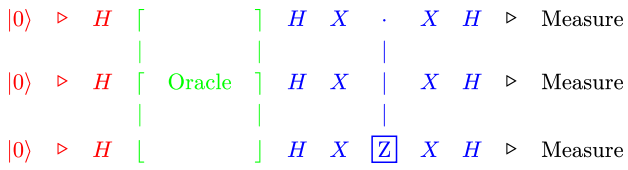
$$\begin{pmatrix} 0 & 1 \\ 1 & 0 \end{pmatrix} \quad \text{XXX} = \text{kronecker(X, kronecker(X, X))} \quad \text{CCZ} = \begin{pmatrix} 1 & 0 & 0 & 0 & 0 & 0 & 0 & 0 \\ 0 & 1 & 0 & 0 & 0 & 0 & 0 & 0 \\ 0 & 0 & 1 & 0 & 0 & 0 & 0 & 0 \\ 0 & 0 & 0 & 1 & 0 & 0 & 0 & 0 \\ 0 & 0 & 0 & 0 & 1 & 0 & 0 & 0 \\ 0 & 0 & 0 & 0 & 0 & 1 & 0 & 0 \\ 0 & 0 & 0 & 0 & 0 & 0 & 1 & 0 \\ 0 & 0 & 0 & 0 & 0 & 0 & 0 & -1 \end{pmatrix}$$

$$\text{XXX CCZ XXX} = \begin{pmatrix} -1 & 0 & 0 & 0 & 0 & 0 & 0 & 0 \\ 0 & 1 & 0 & 0 & 0 & 0 & 0 & 0 \\ 0 & 0 & 1 & 0 & 0 & 0 & 0 & 0 \\ 0 & 0 & 0 & 1 & 0 & 0 & 0 & 0 \\ 0 & 0 & 0 & 0 & 1 & 0 & 0 & 0 \\ 0 & 0 & 0 & 0 & 0 & 1 & 0 & 0 \\ 0 & 0 & 0 & 0 & 0 & 0 & 1 & 0 \\ 0 & 0 & 0 & 0 & 0 & 0 & 0 & 1 \end{pmatrix} \quad \text{J} = \begin{pmatrix} -1 & 0 & 0 & 0 & 0 & 0 & 0 & 0 \\ 0 & 1 & 0 & 0 & 0 & 0 & 0 & 0 \\ 0 & 0 & 1 & 0 & 0 & 0 & 0 & 0 \\ 0 & 0 & 0 & 1 & 0 & 0 & 0 & 0 \\ 0 & 0 & 0 & 0 & 1 & 0 & 0 & 0 \\ 0 & 0 & 0 & 0 & 0 & 1 & 0 & 0 \\ 0 & 0 & 0 & 0 & 0 & 0 & 1 & 0 \\ 0 & 0 & 0 & 0 & 0 & 0 & 0 & 1 \end{pmatrix}$$

This page titled 8.94: Grover's Quantum Search Algorithm is shared under a CC BY 4.0 license and was authored, remixed, and/or curated by Frank Rioux via source content that was edited to the style and standards of the LibreTexts platform.

8.95: Grover's Search Algorithm- Implementation for Two Items

Chris Monroe's research group recently published an experimental implementation of the Grover search algorithm in Nature Communications 8, 1918 (2017). In this report the Grover search is implemented for N = 3 using the three qubit quantum circuit shown below. In this particular example it is demonstrated that the search algorithm successfully searches for two items in one operation of the circuit. The lead sentence in the paper states "The Grover search algorithm has four stages: initialization (red), oracle (green), amplification (blue) and measurement (black)."



The oracle, highlighted below, contains 3(|011>) and 5(|101>).

$$H = \frac{1}{\sqrt{2}}\begin{pmatrix} 1 & 1 \\ 1 & -1 \end{pmatrix} \qquad X = \begin{pmatrix} 0 & 1 \\ 1 & 0 \end{pmatrix}$$

$$O = \begin{pmatrix} 1 & 0 & 0 & 0 & 0 & 0 & 0 & 0 \\ 0 & 1 & 0 & 0 & 0 & 0 & 0 & 0 \\ 0 & 0 & 1 & 0 & 0 & 0 & 0 & 0 \\ 0 & 0 & 0 & -1 & 0 & 0 & 0 & 0 \\ 0 & 0 & 0 & 0 & 1 & 0 & 0 & 0 \\ 0 & 0 & 0 & 0 & 0 & -1 & 0 & 0 \\ 0 & 0 & 0 & 0 & 0 & 0 & -1 & 0 \\ 0 & 0 & 0 & 0 & 0 & 0 & 0 & 1 \end{pmatrix} \qquad J = \begin{pmatrix} -1 & 0 & 0 & 0 & 0 & 0 & 0 & 0 \\ 0 & 1 & 0 & 0 & 0 & 0 & 0 & 0 \\ 0 & 0 & 1 & 0 & 0 & 0 & 0 & 0 \\ 0 & 0 & 0 & 1 & 0 & 0 & 0 & 0 \\ 0 & 0 & 0 & 0 & 1 & 0 & 0 & 0 \\ 0 & 0 & 0 & 0 & 0 & 1 & 0 & 0 \\ 0 & 0 & 0 & 0 & 0 & 0 & 1 & 0 \\ 0 & 0 & 0 & 0 & 0 & 0 & 0 & -1 \end{pmatrix}$$

$\mathrm{HHH} = \mathrm{kronecker}(\mathrm{H}, \mathrm{kronecker}(\mathrm{H}, \mathrm{H}))$ $\mathrm{XXX} = \mathrm{kronecker}(\mathrm{X}, \mathrm{kronecker}(\mathrm{X}, \mathrm{X}))$

The initial Hadamard gates on the three circuit wires feed the Grover search algorithm (in blue) a superposition of all possible queries yielding a superposition of the correct answers.

$$\mathrm{GroverSearch} = \mathrm{HHH\ XXX\ CCZ\ XXX\ HHH\ Oracle\ HHH} \qquad \mathrm{GroverSearch}\begin{pmatrix} 1 \\ 0 \\ 0 \\ 0 \\ 0 \\ 0 \\ 0 \\ 0 \end{pmatrix} = \begin{pmatrix} 0 \\ 0 \\ 0 \\ -0.707 \\ 0 \\ -0.707 \\ 0 \\ 0 \end{pmatrix} = -\frac{1}{\sqrt{2}}\left[|011\rangle + |101\rangle\right]$$

This page titled 8.95: Grover's Search Algorithm- Implementation for Two Items is shared under a CC BY 4.0 license and was authored, remixed, and/or curated by Frank Rioux via source content that was edited to the style and standards of the LibreTexts platform.

8.96: Grover's Search Algorithm- Four-Card Monte

Grover's search algorithm is great at playing four-card monte. As the following quantum circuit shows it can determine which card is the queen in one pass.

$$\begin{array}{llllllllllllllll} |0\rangle & H & \triangleright & \lceil & & \rceil & H & \lceil & & \rceil & H & \triangleright & \text{Measure} & & \lceil & & \rceil & & X & \cdot & X \\ & & & \mid & \text{Oracle} & \mid & & \mid & J & \mid & & & & \text{where} & \mid & J & \mid & = & & \mid & \\ |0\rangle & H & \triangleright & \lfloor & & \rfloor & H & \lfloor & & \rfloor & H & \triangleright & \text{Measure} & & \lfloor & & \rfloor & & X & \boxed{\text{Z}} & X \end{array}$$

The following matrix operators are required to construct the circuit. Giving |10> a negative phase in the Oracle designates it as the queen. The Appendix shows the calculation of J as shown on the right side above.

$$H = \frac{1}{\sqrt{2}}\begin{pmatrix} 1 & 1 \\ 1 & -1 \end{pmatrix} \quad \text{HH} = \text{kronecker(H, H)} \quad \text{Oracle} = \begin{pmatrix} 1 & 0 & 0 & 0 \\ 0 & 1 & 0 & 0 \\ 0 & 0 & -1 & 0 \\ 0 & 0 & 0 & 1 \end{pmatrix} \quad J = \begin{pmatrix} -1 & 0 & 0 & 0 \\ 0 & 1 & 0 & 0 \\ 0 & 0 & 1 & 0 \\ 0 & 0 & 0 & 1 \end{pmatrix}$$

Operating on the input state, which creates a superposition of all queries, enables the algorithm to identify which card is the queen in one operation of the circuit.

$$\text{GroverSearch} = \text{HH J HH Oracle HH} \quad \text{GroverSearch}\begin{pmatrix} 1 \\ 0 \\ 0 \\ 0 \end{pmatrix} = \begin{pmatrix} 0 \\ 0 \\ -1 \\ 0 \end{pmatrix} = -|10\rangle$$

Now the operation of the algorithm is carried out in stages to show the importance of constructive and destructive interference in quantum computers.

$$\text{Step 1} \qquad \text{HH}\begin{pmatrix} 1 \\ 0 \\ 0 \\ 0 \end{pmatrix} = \begin{pmatrix} 0.5 \\ 0.5 \\ 0.5 \\ 0.5 \end{pmatrix} = \frac{1}{2}\left[|00\rangle + |01\rangle + |10\rangle + |11\rangle\right]$$

$$\text{Step 2} \quad \text{Oracle}\begin{pmatrix} 0.5 \\ 0.5 \\ 0.5 \\ 0.5 \end{pmatrix} = \begin{pmatrix} 0.5 \\ 0.5 \\ -0.5 \\ 0.5 \end{pmatrix} = \frac{1}{2}\left[|00\rangle + |01\rangle - |10\rangle + |11\rangle\right]$$

$$\text{Step 3} \quad \text{HH}\begin{pmatrix} 0.5 \\ 0.5 \\ -0.5 \\ 0.5 \end{pmatrix} = \begin{pmatrix} 0.5 \\ -0.5 \\ 0.5 \\ 0.5 \end{pmatrix} = \frac{1}{2}\left[|00\rangle - |01\rangle + |10\rangle + |11\rangle\right]$$

$$\text{Step 4} \quad \text{J}\begin{pmatrix} 0.5 \\ -0.5 \\ 0.5 \\ 0.5 \end{pmatrix} = \begin{pmatrix} -0.5 \\ -0.5 \\ 0.5 \\ 0.5 \end{pmatrix} = \frac{1}{2}\left[-|00\rangle - |01\rangle + |10\rangle + |11\rangle\right]$$

$$\text{Step 5} \qquad \text{HH}\begin{pmatrix} -0.5 \\ -0.5 \\ 0.5 \\ 0.5 \end{pmatrix} = \begin{pmatrix} 0 \\ 0 \\ -1 \\ 0 \end{pmatrix} = -|10\rangle$$

Appendix

$$\begin{array}{lllll} \lceil & & \rceil & X & \cdot & X \\ \mid & J & \mid & = & & \mid \\ \lfloor & & \rfloor & X & \boxed{\text{Z}} & X \end{array}$$

$$J = \begin{pmatrix} -1 & 0 & 0 & 0 \\ 0 & 1 & 0 & 0 \\ 0 & 0 & 1 & 0 \\ 0 & 0 & 0 & 1 \end{pmatrix} \quad X = \begin{pmatrix} 0 & 1 \\ 1 & 0 \end{pmatrix} \quad \text{CZ} = \begin{pmatrix} 1 & 0 & 0 & 0 \\ 0 & 1 & 0 & 0 \\ 0 & 0 & 1 & 0 \\ 0 & 0 & 0 & -1 \end{pmatrix}$$

$$\text{kronecker(X, X) CZ kronecker(X, X)} = \begin{pmatrix} -1 & 0 & 0 & 0 \\ 0 & 1 & 0 & 0 \\ 0 & 0 & 1 & 0 \\ 0 & 0 & 0 & 1 \end{pmatrix}$$

This page titled 8.96: Grover's Search Algorithm- Four-Card Monte is shared under a CC BY 4.0 license and was authored, remixed, and/or curated by Frank Rioux via source content that was edited to the style and standards of the LibreTexts platform.

CHAPTER OVERVIEW

9: Numerical Solutions for Schrödinger's Equation

Numerically solving the Schrödinger equation is a complex problem that stems from the large number of points needed on a grid and the requirement to satisfy boundary conditions.

9.1: Introduction to Numerical Solutions of Schödinger's Equation
9.2: Particle in an Infinite Potential Well
9.3: Particle in a Gravitational Field
9.4: Particle in a One-dimensional Egg Carton
9.5: Particle in a Finite Potential Well
9.6: Particle in a Semi-infinite Potential Well
9.7: Particle in a Slanted Well Potential
9.8: Numerical Solutions for a Particle in a V-Shaped Potential Well
9.9: Numerical Solutions for the Harmonic Oscillator
9.10: Numerical Solutions for a Double-Minimum Potential Well
9.11: Numerical Solutions for the Quartic Oscillator
9.12: Numerical Solutions for Morse Oscillator
9.13: Numerical Solutions for the Lennard-Jones Potential
9.14: Numerical Solutions for the Double Morse Potential
9.15: Particle in a Box with an Internal Barrier
9.16: Another Look at the in a Box with an Internal Barrier
9.17: Particle in a Box with Multiple Internal Barriers
9.18: Particle in an Infinite Spherical Potential Well
9.19: Numerical Solutions for the Two-Dimensional Harmonic Oscillator
9.20: Numerical Solutions for the Three-Dimensional Harmonic Oscillator
9.21: Numerical Solutions for the Hydrogen Atom Radial Equation
9.22: Numerical Solutions for a Modified Harmonic Potential

This page titled 9: Numerical Solutions for Schrödinger's Equation is shared under a CC BY 4.0 license and was authored, remixed, and/or curated by Frank Rioux via source content that was edited to the style and standards of the LibreTexts platform.

9.1: Introduction to Numerical Solutions of Schödinger's Equation

Solving Schrödinger's equation is the primary task of chemists in the field of quantum chemistry. However, exact solutions for Schrödinger's equation are available only for a small number of simple systems. Therefore the purpose of this tutorial is to illustrate one of the computational methods used to obtain approximate solutions.

Mathcad offers the user a variety of numerical differential equation solvers. We will use Mathcad's ordinary differential equation solver, Odesolve, because it allows one to type Schrödinger's equation just as it appears on paper or on the blackboard; in other words it is pedagogically friendly. In what follows the use of Odesolve will be demonstrated for the one-dimensional harmonic oscillator. All applications of Odesolve naturally require the input of certain parameters: integration limits, mass, force constant, etc. Therefore the first part of the Mathcad worksheet will be reserved for this purpose.

- Integration limit: x_{max} := 5
- Effective mass: μ := 1
- Force constant: k := 1

The most important thing distinguishing one quantum mechanical problem from another is the potential energy term, $V(x)$. It is entered below.

Potential energy:

$$V(x) = \frac{1}{2}kx^2$$

Entering the potential energy separately, as done above, allows one to write a generic form for the Schrödinger equation applicable to any one-dimensional problem. This creates a template that is easily edited when moving from one quantum mechanical problem to another. All that is necessary is to type in the appropriate potential energy expression and edit the input parameters. This is the most valuable feature of the numerical approach - you don't need a new mathematical tool or trick for each new problem, a single template works for all one-dimensional problems after minor editing.

Mathcad's syntax for solving the Schrödinger equation is given below. As it may be necessary to do subsequent calculations, the wavefunction is normalized. Note that seed values for an initial value for the wavefunction and its first derivative are required. It is also important to note that the numerical integration is carried out in atomic units:

$$h/2\pi = me = e = 1.$$

Given

$$\frac{-1}{2\mu}\frac{d^2}{dx^2}\psi(x) + V(x)\psi(x) = E\psi(x)$$

with $\psi(-x_{max}) = 0$ and $\psi'(-x_{max}) = 0.1$.

$$\psi = Odesolve(x, x_{max})$$

Normalize wavefunction:

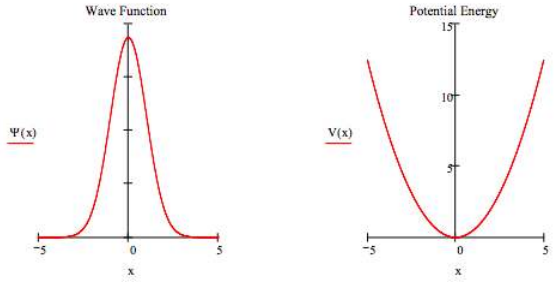
$$\psi(x) = \frac{\psi(x)}{\sqrt{\int_{-x_{max}}^{x_{max}} \psi(x)^2 dx}}$$

Numerical solutions also require an energy guess. If the correct energy is entered the integration algorithm will generate a wavefunction that satisfies the right-hand boundary condition. If the right boundary condition is not satisfied another energy guess is made. In other words it is advisable to sit on the energy input place holder, type a value and press F9 to recalculate.

Energy guesses that are too small yield wavefunctions that miss the right boundary condition on the high side, while high energy guesses miss the right boundary condition on the low side. Therefore it is generally quite easy to bracket the correct energy after a few guesses.

Enter energy guess: E ≡ .5

Of course the solution has to be displayed graphically to determine whether a solution (an eigenstate) has been found. The graphical display is shown below. It is frequently instructive to also display the potential energy function.




```
%matplotlib inline

from scipy.integrate import odeint
import matplotlib.pyplot as plt
import numpy as np


mu=1
k=1
E=.5
xmax=-5

def psi(y,x):
    psi1, psi2_dx2 = y
    return [psi2_dx2, ((2*mu)/(-1))*(E*psi1 - (1/2)*x**2*psi1)]

x0 = [0.0, 0.1]
val = np.linspace(-5,5,101)
sol = odeint(psi, x0, val)
#plot, legends, and titles
plt.plot(val,sol[:,0],color = "red",label = " ")
plt.title("Wave Function")
leg = plt.legend(title = "(x)  ", loc = "center", bbox_to_anchor=[-.11,.5],frameon=False)

```

run | run all | restart | restart & run all

```
%matplotlib inline

import matplotlib.pyplot as plt
import numpy as np
import math

# initialize constants k and create x array
k = 1
x = np.linspace(-5,5,100)

# set boundaries
plt.xticks([-5,5])
plt.yticks([0,5,10,15])

# plot
plt.plot(x,(.5)*k*(x**2), color = "red",label = " ")

# add titles and legend
plt.title("Potential Energy")
leg = plt.legend(title = "\u03A8  ", loc = "center", bbox_to_anchor=[-.11,.5],frameon=False)

plt.show()

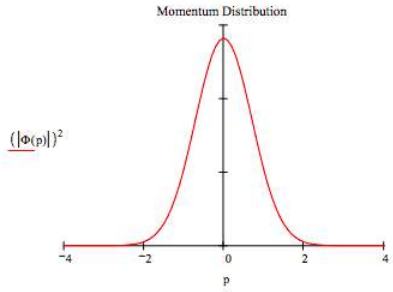
```

run | run all | restart | restart & run all

It is quite easy, as shown below, to generate the momentum-space wavefunction by a Fourier transform of its coordinate-space counterpart.

$$p := -4, -3.9..5$$

$$\Phi(p) = \frac{1}{\sqrt{2\pi}} \int_{-x_{max}}^{x_{max}} e^{-ipx} \psi(x) dx$$




```
%matplotlib inline

import numpy as np
import matplotlib.pyplot as plt
from scipy.integrate import odeint
import scipy.integrate as integrate
import math

#set constants
mu=1
k=1
E=.5
xmax=5

#create ode
def psi(y,x):
    psi1, psi2_dx2 = y
    return [psi2_dx2, ((2*mu)/(-1))*(E*psi1 - (1/2)*x**2*psi1)]

#create space
x0 = [0.0, 0.001]
val = np.linspace(-xmax,xmax,101)

#solve ode using odeint
```

run | run all | restart | restart & run all

This page titled 9.1: Introduction to Numerical Solutions of Schödinger's Equation is shared under a CC BY 4.0 license and was authored, remixed, and/or curated by Frank Rioux via source content that was edited to the style and standards of the LibreTexts platform.

9.2: Particle in an Infinite Potential Well

Numerical Solutions for Schrödinger's Equation

Integration limit: $x_{max} := 1$ Effective mass: $\mu := 1$

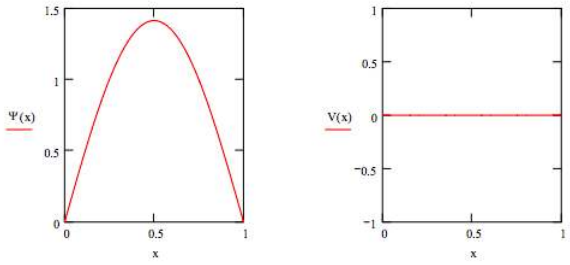
Potential energy: V(x) := 0

Numerical integration of Schrödinger's equation:

Given: $\frac{1}{2\mu}\frac{d^2}{dx^2}\Psi(x) + V(x)\Psi(x) = E\Psi(x)\ \Psi(0) = 0\ \Psi'(0) = 0.1$

$\Psi := Odesolve(x, x_{max})$ Normalize wave function: $\Psi(x) := \frac{\Psi(x)}{\sqrt{\int_0^{x_{max}} \Psi(x)^2 dx}}$

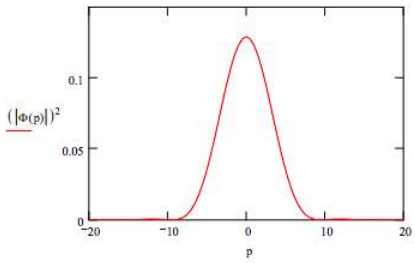
Enter energy guess: E = 4.934



Fourier transform coordinate wave function into momentum space:

p := -20, -19.5 .. 20

$\Phi(p) := \frac{1}{2\mu}\int_0^{x_{max}} exp(-i \cdot p \cdot x) \cdot \Psi(x) dx$



This page titled 9.2: Particle in an Infinite Potential Well is shared under a CC BY 4.0 license and was authored, remixed, and/or curated by Frank Rioux via source content that was edited to the style and standards of the LibreTexts platform.

9.3: Particle in a Gravitational Field

The Unhindered Quantized Bouncing Particle

- Integration limit: $z_{max} = 3$
- Mass: $m = 2$
- Acceleration due to gravity: $g = 1$

The first 10 roots of the Airy function are as follows:

a_1 = 2.33810	a_2 = 4.08794	a_3 = 5.52055	a_4 = 6.78670	a_5 = 7.94413
a_6 = 8.02265	a_7 = 10.04017	a_8 = 11.00852	a_9 = 11.93601	a_{10} = 12.82877

Calculate energy analytically by selecting the appropriate Airy function root:

$$\text{i} = 1 \quad E = \left(\frac{mg^2}{2}\right)^{\frac{1}{3}} a_1 \quad E = 2.338$$

Generate the associated wavefunction numerically: Potential energy: $V(z) = mgz$

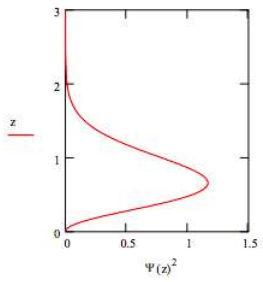
Given $\frac{-1}{2 \cdot m} \frac{d^2}{dz^2} \psi(z) + V(z)\psi(z) \equiv E\psi(z)$

$$\psi(0.0) = 0.0$$

$$\psi'(0.0) = 0.1$$

Given, $\psi = Odesolve(z, z_{max})$

Normalize wavefunction: $\psi(z) = \frac{\psi(z)}{\sqrt{\int_0^{z_{max}} \psi(z)^2 dz}}$



This page titled 9.3: Particle in a Gravitational Field is shared under a CC BY 4.0 license and was authored, remixed, and/or curated by Frank Rioux via source content that was edited to the style and standards of the LibreTexts platform.

9.4: Particle in a One-dimensional Egg Carton

Numerical Solutions for Schrödinger's Equation

Integration limit: x_{max} = 10 Effective mass: μ = 1

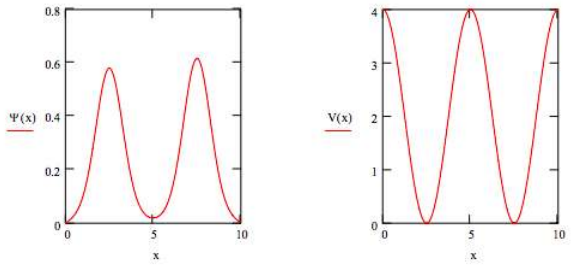
Potential energy: V_o = 2 atoms = 2 $V(x) = V_o(\cos(atoms 2\pi \frac{x}{x_{max}}) + 1)$

Numerical integration of Schrödinger's equation:

Given $\frac{-1}{2\mu}\psi(x) + V(x)\psi(x) = E\psi(x)$ $\psi(0) = 0$ $\psi' = 0.1$

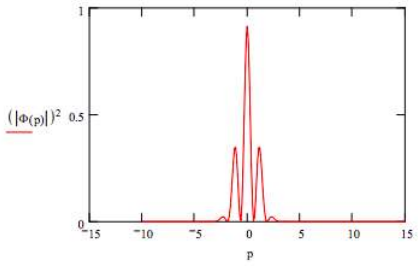
$\psi = Odesolve(x, x_{max})$ Normalize wave function: $\psi(x) = \frac{\psi(x)}{\sqrt{\int_0^{x_{max}} \psi(x)^2 dx}}$

Enter energy guess: E = 0.83583



Fourier transform coordinate wave function into momentum space.

p = -10, -9.9 .. 10 $\Phi(p) = \frac{1}{\sqrt{2\pi}} \int_0^{x_{max}} exp(-ipx)\psi(x)\, dx$



This page titled 9.4: Particle in a One-dimensional Egg Carton is shared under a CC BY 4.0 license and was authored, remixed, and/or curated by Frank Rioux via source content that was edited to the style and standards of the LibreTexts platform.

9.5: Particle in a Finite Potential Well

Numerical Solutions for the Finite Potential Well

Schrödinger's equation is integrated numerically for the first three energy states for a finite potential well. The integration algorithm is taken from J. C. Hansen, J. Chem. Educ. Software, 8C2, 1996.

Set parameters:

n = 100	xmin = -3	xmax = 3	$\Delta = \frac{xmax - xmin}{n-1}$
μ = 1	lb = -1	rb = 1	V_0 = 4

Calculate position vector, the potential energy matrix, and the kinetic energy matrix. Then combine them into a total energy matrix.

i = 1 .. n	j = 1 .. n	x_i = xmin + (i - 1) Δ

$$V_{i,i} = if[(x_i \geq lb)(x_i \leq rb), 0, V_0] \; T_{i,j} = if[i = j, \frac{\pi^2}{6\mu\Delta^2}, \frac{(-1)^{i-j}}{(i-j)^2\mu\Delta^2}]$$

Form Hamiltonian energy matrix: H = TV

Find eigenvalues: E = sort(eigenvals(H))

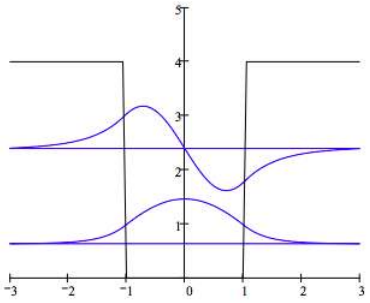
Display three eigenvalues: m = 1 .. 3

E_m =

0.63423174
2.39691438
4.4105828

Calculate associated eigenfunctions: k = 1 .. 2 ψ(k) = eigenvec(H, E_k)

Plot the potential energy and bound state eigenfunctions: $V_{pot1} := V_{i,i}$



This page titled 9.5: Particle in a Finite Potential Well is shared under a CC BY 4.0 license and was authored, remixed, and/or curated by Frank Rioux via source content that was edited to the style and standards of the LibreTexts platform.

9.6: Particle in a Semi-infinite Potential Well

Numerical Solutions to Schrödinger's Equation for the Particle in the Semi-infinite Box

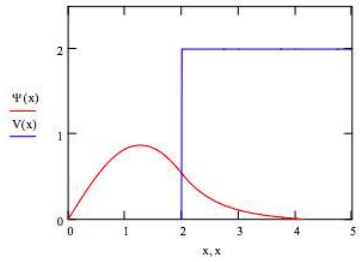
Parameters go here: $x_{min} = 0\ x_{max} = 5\ m = 1\ lb = 2$

Potential energy $V(x) = if[(x \geq lb), V_0, 0]$

Given $\frac{d^2}{dx^2}\psi(x) = 2m(V(x) - E)\psi(x)\ \psi(x_{min}) = 0\ \psi'(0) = 0.1$

$\psi := Odesolve(x, x_{max})\ \psi = \frac{\psi(x)}{\sqrt{\int_{x_{min}}^{x_{max}} \psi(x)^2 dx}}$

Enter energy guess: E = 0.766

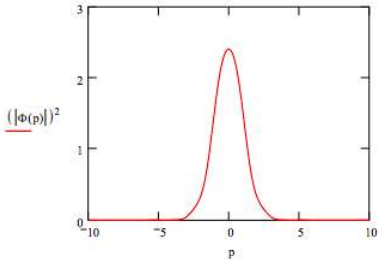


Calculate the probability that the particle is in the barrier: $\int_2^5 \psi(x)^2 dx = 0.092$

Calculate the probability that the particle is not in the barrier: $\int_0^2 \psi(x)^2 dx = 0.908$

Calculate and display the momentum distribution:

Fourier transform: p = -10,-9.9 .. 10 $\Phi(p) = \int_{-x_{min}}^{x_{max}} exp(-1px)\psi(x)\ dx$



This page titled 9.6: Particle in a Semi-infinite Potential Well is shared under a CC BY 4.0 license and was authored, remixed, and/or curated by Frank Rioux via source content that was edited to the style and standards of the LibreTexts platform.

9.7: Particle in a Slanted Well Potential

Numerical Solutions for Schrödinger's Equation for the Particle in the Slanted Box

Parameters go here: $x_{max} = 1$ $\mu = 1$ $V_0 = 2$

Potential energy $V(x) = V_0 x$

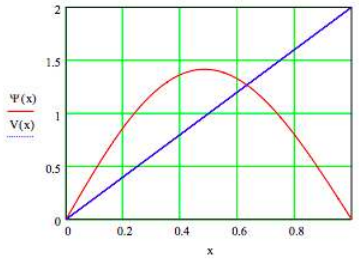
Given

$$\frac{-1}{2\mu}\frac{d^2}{dx^2}\psi(x) + V(x)\psi(x) = E\psi(x)$$

with these boundary conditions: $\psi(0) = 0$ and $\psi'(0) = 0.1$

$\psi = Odesolve(x, x_{max})$ Normalize wavefunction: $\psi(x) = \frac{\psi(x)}{\sqrt{\int_0^{x_{max}} \psi(x)^2 dx}}$

Enter energy guess: E = 5.925



Calculate most probably position: x = 0.5 Given $\frac{d}{dx}\psi(x) = 0$ Find (x) = 0.485

Calculate average position: $X_{avg} = \int_0^1 \psi(x)(x)\psi(x)dx$ $X_{avg} = 0.491$

Calculate potential and kinetic energy:

$V_{avg} = V_0 X_{avg}$ $V_{avg} = 0.983$

$T_{avg} = E - V_{avg}$ $T_{avg} = 4.942$

This page titled 9.7: Particle in a Slanted Well Potential is shared under a CC BY 4.0 license and was authored, remixed, and/or curated by Frank Rioux via source content that was edited to the style and standards of the LibreTexts platform.

9.8: Numerical Solutions for a Particle in a V-Shaped Potential Well

Schrödinger's equation is integrated numerically for a particle in a V-shaped potential well. The integration algorithm is taken from J. C. Hansen, ***J. Chem. Educ. Software,* 8C2**, 1996.

Set parameters:

$$n = 100 \quad xmin = -4 \quad xmax = 4 \quad \Delta = \frac{xmax - xmin}{n-1} \quad \mu = 1 \quad Vo = 2$$

Calculate position vector, the potential energy matrix, and the kinetic energy matrix. Then combine them into a total energy matrix.

$$i = 1 .. n \quad j = 1 .. n \quad x_i = xmin + (i - 1)\,\Delta$$

$$V_{i,\,i} = V_o\,|x_i| \quad T_{i,j} = \text{if}\left[i = j,\ \frac{\pi^2}{6\mu\Delta^2},\ \frac{(-1)^{i-j}}{(i-j)^2\mu\Delta^2}\right]$$

Hamiltonian matrix: H = T + V

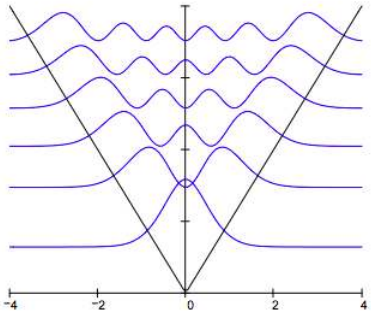
Calculate eigenvalues: E = sort(eigenvals(H))

Selected eigenvalues: m = 1 .. 6

E_m =

1.284
2.946
4.093
5.153
6.089
7.030

Display solution:



For $V = ax^n$ the virial theorem requires the following relationship between the expectation values for kinetic and potential energy: <T> = 0.5n<V>. The calculations below show the virial theorem is satisfied for this potential for which n = 1.

$$\begin{pmatrix} "Kinetic\ Energy" & "Potential\ Energy" & "Total\ Energy" \\ \psi(1)^T T \psi(1) & \psi(1)^T V \psi(1) & E_1 \\ \psi(2)^T T \psi(2) & \psi(2)^T V \psi(2) & E_2 \\ \psi(3)^T T \psi(3) & \psi(3)^T V \psi(3) & E_3 \end{pmatrix} = \begin{pmatrix} "Kinetic\ Energy" & "Potential\ Energy" & "Total\ Energy" \\ 0.428 & 0.857 & 1.284 \\ 0.982 & 1.964 & 2.946 \\ 1.365 & 2.728 & 4.093 \end{pmatrix}$$

This page titled 9.8: Numerical Solutions for a Particle in a V-Shaped Potential Well is shared under a CC BY 4.0 license and was authored, remixed, and/or curated by Frank Rioux via source content that was edited to the style and standards of the LibreTexts platform.

9.9: Numerical Solutions for the Harmonic Oscillator

Schrödinger's equation is integrated numerically for the first three energy states for the harmonic oscillator. The integration algorithm is taken from J. C. Hansen, ***J. Chem. Educ. Software,* 8C2**, 1996.

Set parameters:

Increments: n = 100

Integration limits: xmin = -5

xmax = 5

$$\Delta = \frac{xmax - xmin}{n - 1}$$

Effective mass: μ = 1

Force constant: k = 1

Calculate position vector, the potential energy matrix, and the kinetic energy matrix. Then combine them into a total energy matrix.

$$i = 1 .. n \quad j = 1 .. n \quad x_i = xmin + (i - 1)\,\Delta$$

$$V_{i,\,j} = if\left[i = j,\ \frac{1}{2}k(x)^2,\ 0\right]$$

$$T_{i,\,j} = if\left[i = j,\ \frac{\pi^2}{6\mu\Delta^2},\ \frac{(-1)^{i-j}}{(i-j)^2\mu\Delta^2}\right]$$

Hamiltonian matrix: H = T + V

Find eigenvalues: E = sort(eigenvals(H))

Display three eigenvalues: m = 1 .. 3

E_m =

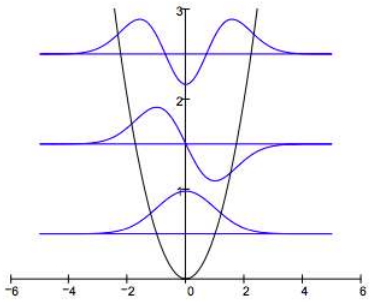
0.5000
1.5000
2.5000

Calculate associated eigenfunctions:

k = 1 .. 3

$$\psi(k) = eigenvec(H, E_k)$$

Plot the potential energy and selected eigenfunctions:



For $V = ax^n$ the virial theorem requires the following relationship between the expectation values for kinetic and potential energy: $\langle T \rangle = 0.5n\langle V \rangle$. The calculations below show the virial theorem is satisfied for the harmonic oscillator for which n = 2.

$$\begin{pmatrix} "Kinetic\ Energy" & "Potential\ Energy" & "Total\ Energy" \\ \psi(1)^T T \Psi(1) & \psi(1)^T V \psi(1) & E_1 \\ \psi(2)^T T \Psi(2) & \psi(2)^T V \psi(2) & E_2 \\ \psi(3)^T T \Psi(3) & \psi(3)^T V \psi(3) & E_3 \end{pmatrix} = \begin{pmatrix} "Kinetic\ Energy" & "Potential\ Energy" & "Total\ Energy" \\ 0.2500 & 0.2500 & 0.5000 \\ 0.7500 & 0.7500 & 1.5000 \\ 1.2500 & 1.2500 & 2.5000 \end{pmatrix}$$

This page titled 9.9: Numerical Solutions for the Harmonic Oscillator is shared under a CC BY 4.0 license and was authored, remixed, and/or curated by Frank Rioux via source content that was edited to the style and standards of the LibreTexts platform.

9.10: Numerical Solutions for a Double-Minimum Potential Well

Schrödinger's equation is integrated numerically for a double minimum potential well: $V = bx^4 - cx^2$. The integration algorithm is taken from J. C. Hansen, ***J. Chem. Educ. Software,* 8C2**, 1996.

Set parameters:

Increments: n = 100

Integration limits: xmin = -4

xmax = 4

$$\Delta = \frac{xmax - xmin}{n - 1}$$

Effective mass: μ = 1

Constants: b = 1 c = 6

Calculate position vector, the potential energy matrix, and the kinetic energy matrix. Then combine them into a total energy matrix.

$$i = 1 .. n \quad j = 1 .. n \quad x_i = xmin + (i - 1)\,\Delta$$

$$V_{i,\,j} = if\left[i = j,\ b(x_i)^4 - c(x_i)^2,\ 0\right]$$

$$T_{i,\,j} = if\left[i = j,\ \frac{\pi^2}{6\mu\Delta^2},\ \frac{(-1)^{i-j}}{(i-j)^2\mu\Delta^2}\right]$$

Hamiltonian matrix:

$$H = T + V$$

Calculate eigenvalues: E = sort(eigenvals(H))

Display three eigenvalues: m = 1 .. 5

E_m =

-6.64272702
-6.64062824
-2.45118605
-2.3155705
0.41561275

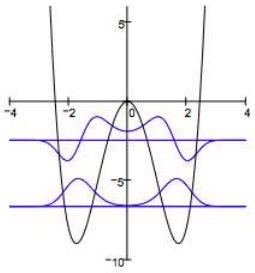
Calculate selected eigenvectors:

k = 1 .. 4

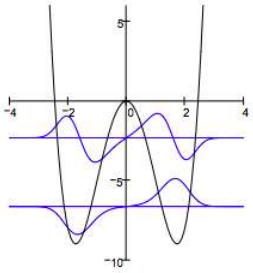
$$\psi(k) = eigenvec(H, E_k)$$

Display results:

First two even solutions:



First two odd solutions:



This page titled 9.10: Numerical Solutions for a Double-Minimum Potential Well is shared under a CC BY 4.0 license and was authored, remixed, and/or curated by Frank Rioux via source content that was edited to the style and standards of the LibreTexts platform.

9.11: Numerical Solutions for the Quartic Oscillator

Schrödinger's equation is integrated numerically for the first three energy states for the quartic oscillator. The integration algorithm is taken from J. C. Hansen, ***J. Chem. Educ. Software,* 8C2**, 1996.

Set parameters:

Increments: n = 100

Integration limits: xmin = -3

xmax = 3

$$\Delta = \frac{xmax - xmin}{n - 1}$$

Effective mass: μ = 1

Force constant: k = 1

Calculate position vector, the potential energy matrix, and the kinetic energy matrix. Then combine them into a total energy matrix.

$$i = 1 \,..\, n \quad j = 1 \,..\, n \quad x_i = xmin + (i - 1)\,\Delta$$

$$V_{i,\,j} = if\left[i = j,\ k(x_i)^4,\ 0\right]$$

$$T_{i,\,j} = if\left[i = j, \frac{\pi^2}{6\mu\Delta^2}, \frac{(-1)^{i-j}}{(i-j)^2\mu\Delta^2}\right]$$

Hamiltonian matrix: H = T + V

Find eigenvalues: E = sort(eigenvals(H))

Display three eigenvalues: m = 1 .. 3

E_m =

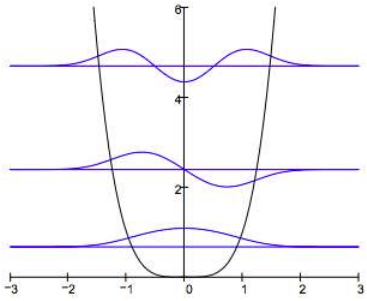
0.6680
2.3936
4.6968

Calculate associated eigenfunctions:

k = 1 .. 3

$$\psi(k) = eigenvec(H, E_k)$$

Plot the potential energy and selected eigenfunctions:



For $V = ax^n$ the virial theorem requires the following relationship between the expectation values for kinetic and potential energy: $\langle T \rangle = 0.5n\langle V \rangle$. The calculations below show the virial theorem is satisfied for the harmonic oscillator for which n = 4.

$$\begin{pmatrix} "Kinetic\ Energy" & "Potential\ Energy" & "Total\ Energy" \\ \psi(1)^T T \psi(1) & \psi(1)^T V \psi(1) & E_1 \\ \psi(2)^T T \psi(2) & \psi(2)^T V \psi(2) & E_2 \\ \psi(3)^T T \psi(3) & \psi(3)^T V \psi(3) & E_3 \end{pmatrix} = \begin{pmatrix} "Kinetic\ Energy" & "Potential\ Energy" & "Total\ Energy" \\ 0.4453 & 0.2227 & 0.6680 \\ 1.5958 & 0.7979 & 2.3936 \\ 3.1312 & 1.5656 & 4.6968 \end{pmatrix}$$

This page titled 9.11: Numerical Solutions for the Quartic Oscillator is shared under a CC BY 4.0 license and was authored, remixed, and/or curated by Frank Rioux via source content that was edited to the style and standards of the LibreTexts platform.

9.12: Numerical Solutions for Morse Oscillator

Schrödinger's equation is integrated numerically for the first three energy states for the Morse oscillator. The integration algorithm is taken from J. C. Hansen, ***J. Chem. Educ. Software,* 8C2**, 1996.

Set parameters:

n = 300

xmin = -2

xmax = 12

$$\Delta = \frac{xmax - xmin}{n - 1}$$

μ = 1

D = 2

β = 2

x_e = 0

Calculate position vector, the potential energy matrix, and the kinetic energy matrix. Then combine them into a total energy matrix.

$$i = 1 \,..\, n \quad j = 1 \,..\, n \quad x_i = xmin + (i - 1)\,\Delta$$

$$V_{i,\,j} = if\left[i = j,\ D[1 - exp[\beta(x_i - x_e)]]^2,\ 0\right]$$

$$T_{i,\,j} = if\left[i = j, \frac{\pi^2}{6\mu\Delta^2}, \frac{(-1)^{i-j}}{(i-j)^2\mu\Delta^2}\right]$$

Hamiltonian matrix: H = T + V

Find eigenvalues: E = sort(eigenvals(H))

Display three eigenvalues: m = 1 .. 3

E_m =

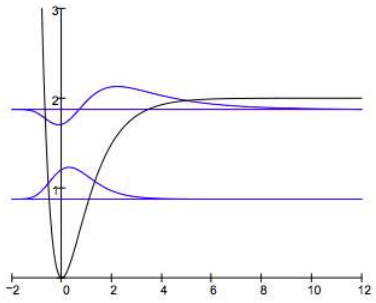
0.8750
1.8750
2.0596

Calculate associated eigenfunctions:

k = 1 .. 3

$$\psi(k) = eigenvec(H, E_k)$$

Plot the potential energy and selected eigenfunctions:



For $V = ax^n$, the virial theorem requires the following relationship between the expectation values for kinetic and potential energy:

$$< T >= 0.5n < V > .$$

The calculations below show that virial theorem is not satisfied for the Morse oscillator. The reason is revealed in the following series expansion in x. The expansion contains cubic, quartic and higher order terms in x, so the virial theorem **does not** apply to the quartic oscillator.

$D(1 - exp(-\beta x))^2$ converts to the series $D\beta^2x^2 + (-D)\beta^3x^3 + \frac{7}{12}D\beta^4x^4 + O(x^5)$

$$\begin{pmatrix} "Kinetic\ Energy" & "Potential\ Energy" & "Total\ Energy" \\ \psi(1)^T T \psi(1) & \psi(1)^T V \psi(1) & E_1 \\ \psi(2)^T T \psi(2) & \psi(2)^T V \psi(2) & E_2 \end{pmatrix} = \begin{pmatrix} "Kinetic\ Energy" & "Potential\ Energy" & "Total\ Energy" \\ 0.3750 & 0.5000 & 0.8750 \\ 0.3754 & 1.4996 & 1.8750 \end{pmatrix}$$

This page titled 9.12: Numerical Solutions for Morse Oscillator is shared under a CC BY 4.0 license and was authored, remixed, and/or curated by Frank Rioux via source content that was edited to the style and standards of the LibreTexts platform.

9.13: Numerical Solutions for the Lennard-Jones Potential

Merrill (Am. J. Phys. **1972**, *40*, 138) showed that a Lennard-Jones 6-12 potential with these parameters had three bound states. This is verified by numerical integration of Schrödinger's equation. The integration algorithm is taken from J. C. Hansen, ***J. Chem. Educ. Software,*** **8C2**, 1996.

Set parameters:

- n = 200
- $x_{min} = 0.75$
- $x_{max} = 3.5$
- $\Delta = \frac{xmax - xmin}{n-1}$
- μ = 1
- σ = 1
- ε = 100

Numerical integration algorithm:

$$i = 1 \,..\, n \quad j = 1 \,..\, n \quad x_i = xmin + (i - 1)\,\Delta$$

$$V_{i,\,j} = if\left[i = j,\ 4\varepsilon\left[\left(\frac{\sigma}{x_i}\right)^1 2 - \left(\frac{\sigma}{x_i}\right)^6\right], 0\right]$$

$$T_{i,\,j} = if\left[i = j, \frac{\pi^2}{6\mu\Delta^2}, \frac{(-1)^{i-j}}{(i-j)^2\mu\Delta^2}\right]$$

Hamiltonian matrix: H = T + V

Find eigenvalues: E = sort(eigenvals(H))

Display three eigenvalues: m = 1 .. 4

E_m =

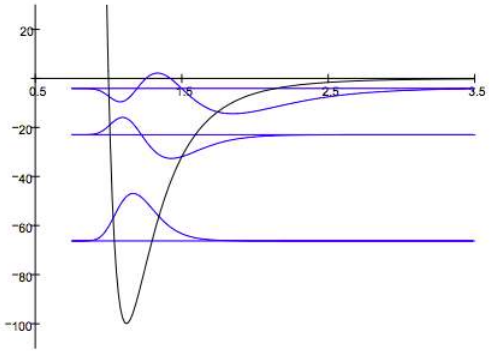
−66.269
−22.981
−4.132
1.096

Calculate eigenvectors:

k = 1 .. 3

$$\psi(k) = eigenvec(H, E_k)$$

Display results:



This page titled 9.13: Numerical Solutions for the Lennard-Jones Potential is shared under a CC BY 4.0 license and was authored, remixed, and/or curated by Frank Rioux via source content that was edited to the style and standards of the LibreTexts platform.

9.14: Numerical Solutions for the Double Morse Potential

Schrödinger's equation is integrated numerically for the first four energy states for the double Morse oscillator. The integration algorithm is taken from J. C. Hansen, ***J. Chem. Educ. Software,* 8C2**, 1996.

Set parameters:

n = 200

xmin = -10

xmax = 10

$$\Delta = \frac{xmax - xmin}{n - 1}$$

μ = 1

D = 2

β = 1

x_0 = 1

Calculate position vector, the potential energy matrix, and the kinetic energy matrix. Then combine them into a total energy matrix.

$$i = 1 \,..\, n \quad j = 1 \,..\, n \quad x_i = xmin + (i - 1)\,\Delta$$

$$V_{i,\,j} = if\left[i = j,\ D\left[1 - exp\left[-\beta(|x_i| - x_0)\right]\right]^2,\ 0\right]$$

$$T_{i,\,j} = if\left[i = j, \frac{\pi^2}{6\mu\Delta^2}, \frac{(-1)^{i-j}}{(i-j)^2\mu\Delta^2}\right]$$

Hamiltonian matrix: H = T + V

Find eigenvalues: E = sort(eigenvals(H))

Display four eigenvalues: m = 1 .. 4

E_m =

0.8092
0.9127
1.8284
1.8975

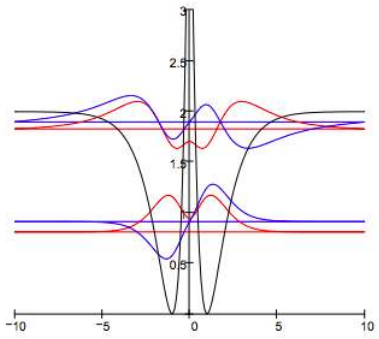
Calculate associated eigenfunctions:

k = 1 .. 4

$$\psi(k) = eigenvec(H, E_k)$$

Plot the potential energy and bound state eigenfunctions:

$$Vpot_i = V_{i,\,i}$$



This page titled 9.14: Numerical Solutions for the Double Morse Potential is shared under a CC BY 4.0 license and was authored, remixed, and/or curated by Frank Rioux via source content that was edited to the style and standards of the LibreTexts platform.

9.15: Particle in a Box with an Internal Barrier

Numerical integration of Schrödinger's equation:

Potential energy:

$$V(x) = \begin{cases} V_0 \text{ if } (x \geq lb)(x \leq rb) \\ 0 \text{ otherwise} \end{cases}$$

Given:

$$\frac{-1}{2\mu}\frac{d^2}{dx^2}\psi(x) + V(x)\psi(x) = E\psi(x)$$

$$\psi(0) = 0$$

$$\psi'(0) = 0.1$$

ψ = Odesolve(x, x_{max})

Normalize wave function:

$$\psi(x) = \frac{\psi(x)}{\sqrt{\int_0^x \psi(x)^2 dx}}$$

Integration limit: x_{max} = 1

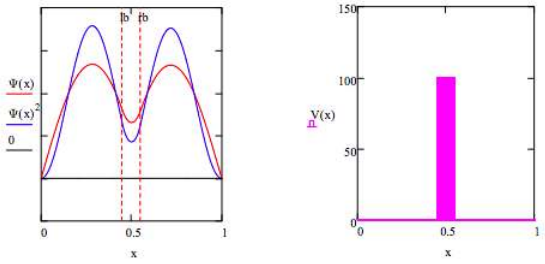
Effective mass: μ = 1

Barrier height: V_0 = 100

Barrier boundaries: lb = 0.45

rb = 0.55

Enter energy guess: E = 15.45



Calculate potential energy: $PE = \int_0^1 V(x)\psi(x)^2 dx$ PE = 4.932 $\int_0^1 \psi(x)^2 dx = 1.00$

Calculate kinetic energy: $KE = E - PE$ E = 10.518

Ratio of potential energy to total energy: $\frac{PE}{E} = 0.319$

Calculate probability in barrier: $\frac{PE}{V_0} = 0.049$

$$P = \int_{lb}^{rb} \psi(x)^2 dx = 0.049$$

1. Find the first four energy levels, sketch ψ^2 for each state, and fill in the table below. KE, PE and the probability in the electron is in the barrier are calculated above.

E	KE	PE	P
15.45	10.518	4.932	0.049
20.30	19.827	0.473	0.0047
62.20	47.745	14.455	0.145
80.80	78.968	1.832	0.018

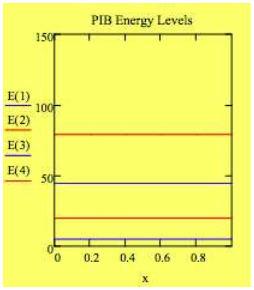
2. Interpret the results for energy in light of the fact that a 100 E_h (2720 eV) potential barrier of finite thickness exists in the center of the box.

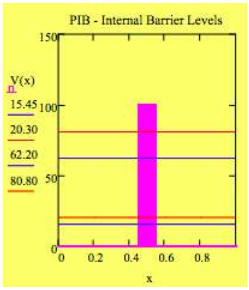
This is an excellent example of quantum mechanical tunneling. For the first four energy states the particle has probability of being found in the tunnel in spite of the fact that its energy is less than the barrier energy.

3. Explain the obvious bunching of energy states in pair in terms of the impact of the internal barrier. In other words why is the probability of being in the potential barrier larger for the n = 1 and 3 states than it is for the n = 2 and 4 states.

The PIB energy levels without an internal barrier are: $E(n) = \frac{\pi^2}{2}n^2$

The bunching can be seen by comparing the two energy manifolds. The n = 2 and 4 states have nodes at the middle of the box where the internal barrier is situated. Thus their potential energy does not increase as much as the n = 1 and 3 states which do not have nodes in the barrier.





4. Find the ground state energy for particle masses of 0.5 and 1.5. Record your results in the table below and interpret them.

$Mass$	E	T	V	P
0.5	23.95	14.411	9.539	0.095
1.0	15.45	10.518	4.932	0.049
1.5	11.55	8.684	2.866	0.029

The higher the mass the lower the energy because in quantum mechanics in $E \sim \frac{1}{mass}$. The greater the mass the lower the probability that tunneling will occur. This is due to the fact that the deBroglie wavelength is inversely proportional to mass.

5. Find the ground state energy for a m = 1 particle for barrier heights 50 and 150 Eh. Record your results in the table below and interpret them.

V_0	E	T	V	P
50	11.97	7.203	4.767	0.095
100	15.45	10.518	4.932	0.049
150	17.32	13.024	4.296	0.029

The higher the barrier energy the higher the ground-state energy and the lower the tunneling probability.

6. On the basis of your calculations in this exercise describe quantum mechanical tunneling. In your answer you should consider the importance of particle mass, barrier height and barrier width. Perform calculations for widths of 0.05 and 0.15 in atomic units.

Tunneling is inversely proportional to mass, barrier height and barrier width.

$Width$	E	T	V	P	$\frac{P}{Width}$
0.05	11.65	7.326	4.324	0.043	0.860
0.10	15.45	10.518	4.932	0.049	0.490
0.15	18.35	13.317	5.033	0.050	0.333

This page titled 9.15: Particle in a Box with an Internal Barrier is shared under a CC BY 4.0 license and was authored, remixed, and/or curated by Frank Rioux via source content that was edited to the style and standards of the LibreTexts platform.

9.16: Another Look at the in a Box with an Internal Barrier

The purpose of this tutorial is to explore the impact of the presence of a large (100 E_h) thin (0.10 a_0) internal barrier on the solutions to the particle-in-a-box (PIB) problem. Schrödinger's equation is integrated numerically for the first five energy states. (Integration algorithm taken form J. C. Hansen, *J. Chem. Educ. Software*, **8C2**, 1996.)

For the one-bohr PIB the energy eigenvalues are:

m = 1 .. 5

$E_m = \frac{m^2\pi^2}{2}$

E^T = (4.935 19.739 44.413 78.957 123.37)

Set parameters:

n = 100

xmin = 0

xmax = 1

$\Delta = \frac{xmax - xmin}{n-1}$

μ = 1

Vo = 100

lb = .45

rb = .55

Calculate position vector, the potential energy matrix, and the kinetic energy matrix. Then combine them into a total energy matrix.

$$i = 1 .. n \quad j = 1 .. n \quad x_i = xmin + (i - 1)\,\Delta$$

Potential energy:

$$V_{i\,j} = if[(x_i \geq lb)(x_i \leq rb), Vo,\ 0]$$

Kinetic energy:

$$T_{i,\,j} = if\left[i = j, \frac{\pi^2}{6\mu\Delta^2}, \frac{(-1)^{i-j}}{(i-j)^2\mu\Delta^2}\right]$$

$$V_{i,\,j} = if\left[i = j,\ D\left[1 - exp\left[-\beta(|x_i| - x_0)\right]\right]^2,\ 0\right]$$

$$T_{i,\,j} = if\left[i = j, \frac{\pi^2}{6\mu\Delta^2}, \frac{(-1)^{i-j}}{(i-j)^2\mu\Delta^2}\right]$$

Hamiltonian matrix: H = T + V

Find eigenvalues: E = sort(eigenvals(H))

Display selected eigenvalues: m = 1 .. 5

E_m =

15.011
19.589
60.453
78.268
137.903

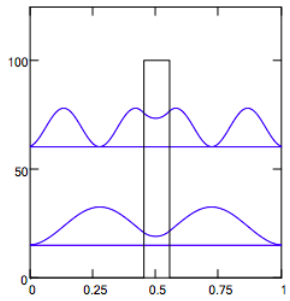
Calculate selected eigenvectors:

k = 1 .. 4

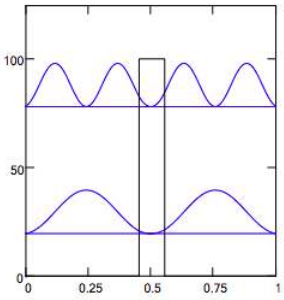
$$\psi(k) = eigenvec(H, E_k)$$

Display probability distributions and energy level manifold in the presence of the internal potential barrier:

n = 1 and n = 3 states:



n = 2 and n = 4 states:



It is clear from the numeric and graphic display of the energy manifold that the presence of the internal barrier causes a bunching of the energy eigenstates for the four lowest levels. This is frequently called "inversion doubling" because of an identical effect that appears in the analysis of the ammonia umbrella inversion. This gives the impression that a second set of quantized energy levels is created by the internal barrier. However, the correct explanation for this bunching is evident in the display of the four lowest wave functions. The presence of the barrier raises all energy levels relative to the simple PIB, but the n = 2 and n = 4 states have nodes in the barrier, thus reducing the barrier's effect on raising the energy. Thus the odd states are raised in energy more than the even states, causing the bunching.

This page titled 9.16: Another Look at the in a Box with an Internal Barrier is shared under a CC BY 4.0 license and was authored, remixed, and/or curated by Frank Rioux via source content that was edited to the style and standards of the LibreTexts platform.

9.17: Particle in a Box with Multiple Internal Barriers

Integration limit: x_{max} = 1

Effective mass: μ = 1

Barrier height: V_0 = 100

Potential energy:

$$V(x) = \begin{vmatrix} V_0 \ if \ (x \geq .185)(x \leq .215) + (x \geq .385)(x \leq .415) + (x \geq .585)(x \leq .615) + (x \geq .785)(x \leq .815) \\ 0 \ otherwise \end{vmatrix}$$

Numerical integration of Schrödinger's equation:

Given

$$\frac{-1}{2\mu}\frac{d^2}{dx^2}\psi(x) + V(x)\psi(x) = E\psi(x)$$

$$\psi(0) = 0$$

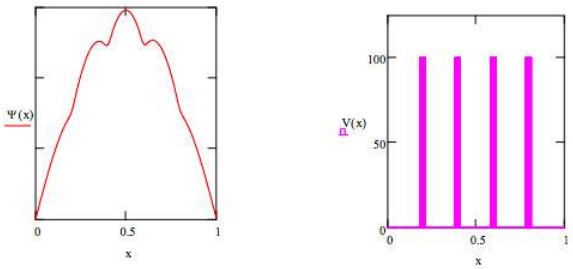
$$\psi'(0) = 0.1$$

$$\psi = Odesolve(x, x_{max})$$

Normalize wave function:

$$\psi(x) = \frac{\psi(x)}{\sqrt{\int_0^{x_{max}} \psi(x)^2 dx}}$$

Enter energy guess: E = 18.85



Calculate kinetic energy:

$$T = \int_0^1 \psi(x)\frac{-1}{2}\frac{d^2}{dx^2}\psi(x)dx = 5.926$$

Calculate potential energy:

$$V = E - T = 12.924$$

Tunneling probability:

$$\frac{V}{V_0} \times 100 = 12.924$$

This page titled 9.17: Particle in a Box with Multiple Internal Barriers is shared under a CC BY 4.0 license and was authored, remixed, and/or curated by Frank Rioux via source content that was edited to the style and standards of the LibreTexts platform.

9.18: Particle in an Infinite Spherical Potential Well

Reduced mass: $\mu = 1$

Angular momentum: L = 2

Integration limit: $r_{max} = 1$

Solve Schrödinger's equation numerically. Use Mathcad's ODE solve block:

Given

$$\frac{-1}{2\mu}\frac{d^2}{dr^2}\psi(r) - \frac{1}{r\mu}\frac{d}{dr}\psi(r) + \left[\frac{L(L+1)}{2\mu r^2}\right]\psi(r) = E\psi(r) \quad \psi(.0001) = .1 \quad \psi'(.0001) = 0$$

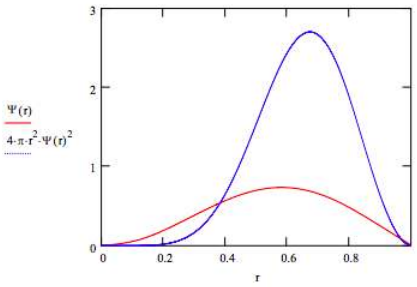
$$\psi = Odesolve(r, r_{max})$$

Normalize the wavefunction:

$$\psi(r) = \left(\int_0^{r_{max}} \psi(r)^2 4\pi r^2 dr\right)^{\frac{-1}{2}} \psi(r)$$

Energy guess: E = 16.51

r = 0, .001 .. r_{max}



This page titled 9.18: Particle in an Infinite Spherical Potential Well is shared under a CC BY 4.0 license and was authored, remixed, and/or curated by Frank Rioux via source content that was edited to the style and standards of the LibreTexts platform.

9.19: Numerical Solutions for the Two-Dimensional Harmonic Oscillator

Reduced mass: $\mu = 1$

Angular momentum: L = 2

Integration limit: $r_{max} = 5$

Force constant: k = 1

Energy guess: E = 3

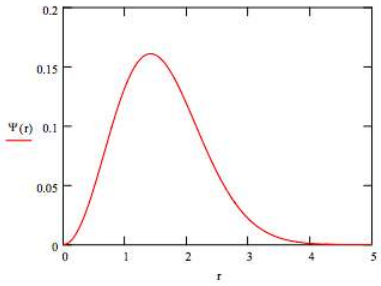
Solve Schrödinger's equation numerically. Use Mathcad's ODE solve block:

Given

$$\frac{-1}{2\mu}\frac{d^2}{dr^2}\psi(r) - \frac{1}{2\mu}\frac{d}{dr}\psi(r) + \left(\frac{L^2}{2\mu r^2} + \frac{1}{2}kr^2\right)\psi(r) = E\psi(r) \quad \psi(.001) = 1 \quad \psi'(.001) = 0.1$$

$$\psi = Odesolve(r, r_{max}, .001)$$

$$\psi(r) = \left(\int_0^{r_{max}} \psi(r)^2 4\pi r^2 dr\right)^{\frac{-1}{2}} \psi(r)$$



This page titled 9.19: Numerical Solutions for the Two-Dimensional Harmonic Oscillator is shared under a CC BY 4.0 license and was authored, remixed, and/or curated by Frank Rioux via source content that was edited to the style and standards of the LibreTexts platform.

9.20: Numerical Solutions for the Three-Dimensional Harmonic Oscillator

Reduced mass: $\mu = 1$

Angular momentum: L = 0

Integration limit: $r_{max} = 6$

Force constant: k = 1

Solve Schrödinger's equation numerically. Use Mathcad's ODE solve block:

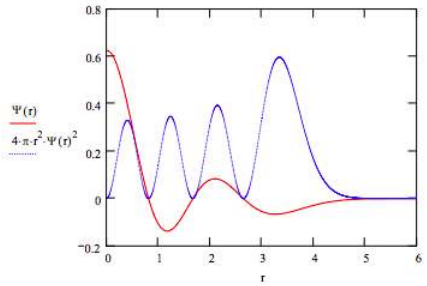
Given

$$\frac{-1}{2\mu}\frac{d^2}{dr^2}\psi(r) - \frac{1}{r\mu}\frac{d}{dr}\psi(r) + \left[\frac{L(L+1)}{2\mu r^2} + \frac{1}{2}kr^2\right]\psi(r) = E\psi(r) \quad \psi(.001) = 1 \quad \psi'(.001) = 0.1$$

$$\psi = Odesolve(r, r_{max})$$

$$\psi(r) = \left(\int_0^{r_{max}} \psi(r)^2 4\pi r^2 dr\right)^{\frac{-1}{2}} \psi(r)$$

Energy guess: E = 7.5



This page titled 9.20: Numerical Solutions for the Three-Dimensional Harmonic Oscillator is shared under a CC BY 4.0 license and was authored, remixed, and/or curated by Frank Rioux via source content that was edited to the style and standards of the LibreTexts platform.

9.21: Numerical Solutions for the Hydrogen Atom Radial Equation

Reduced mass: $\mu = 1$

Angular momentum: L = 0

Integration limit: $r_{max} = 18$

Nuclear charge: Z = 1

Solve Schrödinger's equation numerically. Use Mathcad's ODE solve block:

Given

$$\frac{-1}{2\mu}\frac{d^2}{dr^2}\psi(r) - \frac{1}{r\mu}\frac{d}{dr}\psi(r) + \left[\frac{L(L+1)}{2\mu r^2} + \frac{1}{2}kr^2\right]\psi(r) = E\psi(r) \quad \psi(.0001) = .1 \quad \psi'(.0001) = 0.1$$

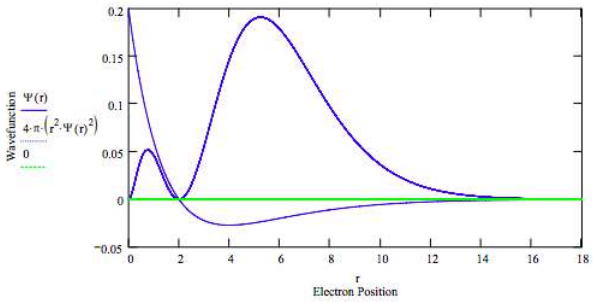
$$\psi = Odesolve(r, r_{max})$$

Normalize wave function:

$$\psi(r) = \left(\int_0^{r_{max}} \psi(r)^2 4\pi r^2 dr\right)^{\frac{-1}{2}} \psi(r)$$

Energy guess:

E = -.125 r = 0, .001 .. r_{max}



Calculate average position:

$$\int_0^{r_{max}} \psi(r) r \psi(r) 4\pi r^2 dr = 5.997$$

Calculate kinetic energy:

$$\int_0^{r_{max}} \psi(r)\left[\frac{-1}{2\mu}\frac{d^2}{dr^2}\psi(r) - \frac{1}{r\mu}\frac{d}{dr}\psi(r) + \left[\frac{L(L+1)}{2\mu r^2}\right]\psi(r)\right] 4\pi r^2 dr = 0.125$$

Calculate potential energy:

$$\int_0^{r_{max}} \psi(r)\frac{-Z}{r}\psi(r) 4\pi r^2 dr = -0.25$$

This page titled 9.21: Numerical Solutions for the Hydrogen Atom Radial Equation is shared under a CC BY 4.0 license and was authored, remixed, and/or curated by Frank Rioux via source content that was edited to the style and standards of the LibreTexts platform.

9.22: Numerical Solutions for a Modified Harmonic Potential

This tutorial deals with the following potential function:

$$V(x,d) = \begin{cases} \frac{1}{2}k(x-d)^2 \ if \ x \geq 0 + d \leq 0 \\ \infty \ otherwise \end{cases}$$

If d = 0 we have the harmonic oscillator on the half-line with eigenvalues 1.5, 3.5, 5.5, ... for k = μ = 1. For large values of d we have the full harmonic oscillator problem displaced in the x-direction by d with eigenvalues 0.5, 1.5, 2.5, ... for k = μ = 1. For small to intermediate values of d the potential can be used to model the interaction of an atom or molecule with a surface.

Integration limit: x_{max} = 10

Effective mass: μ = 1

Force constant: k = 1

Potential energy minimum: d = 5

Potential energy:

$$V(x,d) = \frac{k}{2}(x-d)^2$$

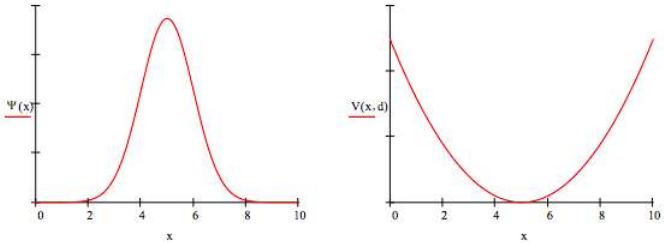
Integration algorithm:

Given

Normalize wavefunction:

$$\psi(x) = \frac{\psi(x)}{\sqrt{\int_0^{x_{max}} \psi(x)^2 dx}}$$

Energy guess: E = 0.5



Calculate average position:

$$X_{avg} = \int_0^{x_{max}} \psi(x) x \psi(x) dx = 5$$

Calculate potential and kinetic energy:

$$V_{avg} = \int_0^{x_{max}} \psi(x) V(x,d) \psi(x) dx = 0.25$$

$$T_{avg} = E - V_{avg} = 0.25$$

Exercises:

- For d = 0, k = μ = 1 confirm that the first three energy eigenvalues are 1.5, 3.5 and 5.5 E_h. Start with x_{max} = 5, but be prepared to adjust to larger values if necessary. xmax is effectively infinity.

- For d = 5, k = μ = 1 confirm that the first three energy eigenvalues are 0.5, 1.5 and 2.5 Eh. Start with x_{max} = 10, but be prepared to adjust to larger values if necessary.
- Determine and compare the virial theorem for the exercises above.
- Calculate the probability that tunneling is occurring for the ground state for the first two exercises. (Answers: 0.112, 0.157)

This page titled 9.22: Numerical Solutions for a Modified Harmonic Potential is shared under a CC BY 4.0 license and was authored, remixed, and/or curated by Frank Rioux via source content that was edited to the style and standards of the LibreTexts platform.

CHAPTER OVERVIEW

10: Approximate Quantum Mechanical Methods

10.1: Trial Wavefunctions for Various Potentials
10.2: Energy Minimization - Four Methods Using Mathcad
10.3: The Variation Theorem in Dirac Notation
10.4: A Rudimentary Model for Alpha Particle Decay
10.5: Variational Method for a Particle in a Finite Potential Well
10.6: Variation Method for a Particle in a Symmetric 1D Potential Well
10.7: Variation Method for the Rydberg Potential
10.8: Variation Method for the Quartic Oscillator
10.9: Momentum-Space Variation Method for the Quartic Oscillator
10.10: Variation Method for a Particle in a Gravitational Field
10.11: Linear Variational Method for a Particle in a Slanted 1D Box
10.12: Variation Method for a Particle in a Semi-Infinite Potential Well
10.13: Variation Method for a Particle in a Box with an Internal Barrier
10.14: Variation Method for a Particle in a 1D Ice Cream Cone
10.15: Variation Method for a Particle in an Ice Cream Cone
10.16: Variation Method for a Particle in a Finite 3D Spherical Potential Well
10.17: Variation Method for the Harmonic Oscillator
10.18: Trigonometric Trial Wave Function for the Harmonic Potential Well
10.19: Trigonometric Trial Wave Function for the 3D Harmonic Potential Well
10.20: Gaussian Trial Wavefunction for the Hydrogen Atom
10.21: Variation Calculation on the 1D Hydrogen Atom Using a Trigonometric Trial Wave Function
10.22: Variation Calculation on the 1D Hydrogen Atom Using a Gaussian Trial Wavefunction
10.23: Variational Calculation on the Two-dimensional Hydrogen Atom
10.24: Variational Calculation on Helium Using a Hydrogenic Wavefunction
10.25: Gaussian Trial Wave Function for the Helium Atom
10.26: Trigonometric Trial Wavefunction for the Helium Atom
10.27: Trigonometric Trial Wavefunction for the Hydrogen Atom
10.28: Hydrogen Atom Calculation Assuming the Electron is a Particle in a Sphere of Radius R
10.29: Electronic Structure - Variational Calculations on the Lithium Atom
10.30: The Variation Method in Momentum Space
10.31: Momentum-Space Variation Method for Particle in a Gravitational Field
10.32: Momentum-Space Variation Method for the Abs(x) Potential
10.33: Variational Method for the Feshbach Potential
10.34: Numerical Solution for the Feshbach Potential
10.35: First Order Degenerate Perturbation Theory - the Stark Effect of the Hydrogen Atom
10.36: Variational Calculation for the Polarizability of the Hydrogen Atom
10.37: Hybrid Variational Calculation for the 1D Hydrogen Atom with Delta Function Potential
10.38: Variation Method Using the Wigner Function- Finite Potential Well
10.39: 455. Variation Method Using the Wigner Function- V(x) = |x|
10.40: Variation Method Using the Wigner Function- The Harmonic Oscillator

10.41: Variation Method Using the Wigner Function - The Quartic Oscillator
10.42: Variation Method Using the Wigner Function - The Feshbach Potential

---

This page titled 10: Approximate Quantum Mechanical Methods is shared under a CC BY 4.0 license and was authored, remixed, and/or curated by Frank Rioux via source content that was edited to the style and standards of the LibreTexts platform.

10.1: Trial Wavefunctions for Various Potentials

This is list of functions and the potentials for which they would be suitable trial wave functions in a variation method calculation.

$$\psi(x,\alpha) = 2 \cdot \alpha^{\frac{3}{2}} \cdot x \cdot exp(-\alpha \cdot x)$$

$$\psi(x,\alpha) = (\tfrac{128 \cdot \alpha^3}{\pi})^{\frac{1}{4}} \cdot exp(-\alpha \cdot x^2)$$

- Particle in a gravitational field V(z) = mgz (z = 0 to ∞)
- Particle confined by a linear potential V(x) = ax (x = 0 to ∞)
- One-dimensional atoms and ions V(x) = -Z/x (x = 0 to ∞)
- Particle in semi-infinite potential well V(x) = if[x $\leq a, 0, b$] (x = 0 to ∞)
- Particle in semi-harmonic potential well V(x) = kx^2 (x = 0 to ∞)

$$\psi(x,\alpha) = (\tfrac{2 \cdot \alpha}{\pi})^{\frac{1}{4}} \cdot exp(-\alpha \cdot x^2)$$

- Quartic oscillator V(x) = bx^4 (x = -∞ to ∞)
- Particle in the finite one-dimensional potential well V(x) = if[(x ≥ -1 · (x \leq 1), 0, 2] (x = -∞ to ∞)
- 1D Hydrogen atom ground state
- Harmonic oscillator ground state
- Particle in V(x) = | x | potential well

$$\psi(x,\alpha) = \sqrt{\alpha} \cdot exp(-\alpha \cdot |x|)$$

- This wavefunction is discontinuous at x = 0, so the following calculations must be made in momentum space
- Dirac hydrogen atom V(x) = - Δ (x)
- Harmonic oscillator ground state
- Particle in V(x) = | x | potential well
- Quartic oscillator V(x) = bx^4 (x = -∞ to ∞)

$$\psi(x) = \sqrt{30} \cdot x \cdot (1-x)$$

$$\Gamma(x) = \sqrt{105} \cdot x \cdot (1-x)^2$$

$$\Theta(x) = \sqrt{105} \cdot x^2 \cdot (1-x)$$

- Particle in a one-dimensional, one-bohr box
- Particle in a slanted one-dimensional box
- Particle in a semi-infinite potential well (change 1 to variational parameter)
- Particle in a gravitational field (change 1 to variational parameter)

$$\Phi(r,a) = (a-r)$$

$$\Phi(r,a) = (a-r)^2$$

$$\Phi(r,a) = \tfrac{1}{\sqrt{2 \cdot \pi \cdot a}} \cdot \tfrac{\sin \frac{\pi \cdot r}{a}}{r}$$

- Particle in a infinite spherical potential well of radius a
- Particle in a finite spherical potential well (treat a as a variational parameter)

$$\psi(r,\beta) = (\tfrac{2 \cdot \beta}{\pi})^{\frac{3}{4}} \cdot exp(-\beta \cdot r^2)$$

- Particle in a finite spherical potential well
- Hydrogen atom ground state
- Helium atom ground state

$$\psi(r,\beta) = \sqrt{\tfrac{3 \cdot \beta^3}{\pi^3}} \cdot sech(\beta \cdot r)$$

- Particle in a finite potential well
- Hydrogen atom ground state
- Helium atom ground state

$$\psi(x,\beta) = \sqrt{\frac{\beta}{2}} \cdot sech(\beta \cdot x)$$

- Harmonic oscillator
- Quartic oscillator
- Particle in a gravitational field
- Particle in a finite potential well

$$\psi(\alpha,\beta) = \sqrt{\frac{12\alpha^3}{\pi}} \cdot x \cdot sech(\alpha \cdot x)$$

- Particle in a semi-infinite potential well
- Particle in a gravitational field
- Particle in a linear potential well (same as above) V(x) = ax (x = 0 to ∞)
- 1D hydrogen atom or one-electron ion

Some finite potential energy wells.

V(x) = if[(x ≥ -1 · (x ≤ 1), 0, V_0]

V(x) = if[(x ≥ -1 · (x ≤ 1), 0, |x| - 1]

V(x) = if[(x ≥ -1 · (x ≤ 1), 0, $\sqrt{|x|-1}$]

Some semi-infinite potential energy well.

V(x) = if (x ≤ a, 0, b)

V(x) = if[(x ≤ 2), 0, $\frac{5}{x}$]

V(x) = if[(x ≥ 2), 0, (x - 2)]

V(x) = if[(x ≤ 2), 0, $\sqrt{x-2}$]

This page titled 10.1: Trial Wavefunctions for Various Potentials is shared under a CC BY 4.0 license and was authored, remixed, and/or curated by Frank Rioux via source content that was edited to the style and standards of the LibreTexts platform.

10.2: Energy Minimization - Four Methods Using Mathcad

Using $\psi(\alpha, r) = \frac{\alpha^3}{\pi} exp(-\alpha r)$ as a trial wave function for the helium atom electrons leads to the following energy expression in terms of the variational parameter, α.

$$E(\alpha) = \alpha^2 - 4\alpha + \frac{5}{8}\alpha$$

The first term is electron kinetic energy, the second electron-nucleus potential energy and the final term electron-electron potential energy.

Mathcad provides four methods for energy minimization with respect to α. The second and third methods require a seed value for α.

First method

$$\alpha = \frac{d}{d\alpha} E(\alpha) = 0 \Big|_{float,5}^{solve,\alpha} \rightarrow 1.6875$$

$E(\alpha) = -2.8477$

Second method

α = 1. Given $\frac{d}{d\alpha} E(\alpha) = 0$ $\alpha = Find(\alpha)$ α = 1.685 $E(\alpha) = -2.8477$

Third method

α = 1. α : = Minimize(E, α) α = 1.685 $E(\alpha) = -2.8477$

Fourth method

Clear memory of α and X: α = α Z = Z

$$En(\alpha,\ Z) = \alpha^2 - 2Z\alpha + \frac{5}{8}\alpha\ \frac{d}{d\alpha} En(\alpha,\ Z) = 0\ solve, \alpha \rightarrow Z - \frac{5}{16}$$

$$En(\alpha,\ Z) = \alpha^2 - 2Z\alpha + \frac{5}{8}\ substitute, \alpha = Z - \frac{5}{16} \rightarrow -\frac{(16Z-5)^2}{256}$$

$$En(\alpha,\ 2) = -2.8477\ En\alpha,\ 3) = -7.2227\ En(\alpha,\ 4) = -13.5977$$

Two variables: a molecular orbital calculation yields the following result for the energy of the hydrogen molecule ion as a function of the internuclear separation and the orbital decay constant.

$$1s_a = \frac{\alpha^3}{\pi} exp(-\alpha r_a)$$

$$1s_b = \frac{\alpha^3}{\pi} exp(-\alpha r_b)$$

$$S_{ab} = \int 1s_a 1s_b d\tau$$

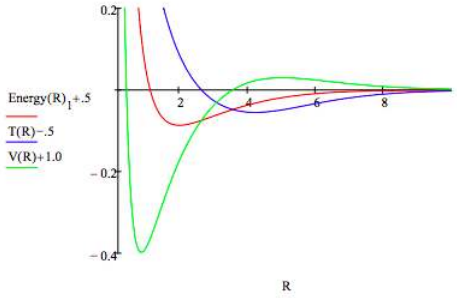
$$\psi_{mo} = \frac{1s_a + 1s_b}{\sqrt{2+2S_{ab}}}$$

$$E(\alpha, R) = \frac{-\alpha^2}{2} + \frac{[\alpha^2 - \alpha - \frac{1}{R} + \frac{1+\alpha R}{R} exp(-2\alpha R) + \alpha(\alpha - 2)(1 + \alpha R) exp(-\alpha R)]}{[1 + exp(-\alpha R)(1 + \alpha R + \frac{\alpha^2 R^3}{3})]} + \frac{1}{R}$$

α = 1 R = 1 $\begin{pmatrix} \alpha \\ R \end{pmatrix}$ = Minimize(E, α, R) $\begin{pmatrix} \alpha \\ R \end{pmatrix} = \begin{pmatrix} 1.2380 \\ 2.0033 \end{pmatrix}$ E(α, R) = -0.5865

α = 1 Energy = -2 Given Energy = E(α, R) $\frac{d}{d\alpha}$ E(α, R) = 0 Energy(R) = Find(α, Energy)

R = .2, .25 .. 10 T(R) = -Energy(R)$_1$ - R $\frac{d}{dR}$ Energy(R)$_1$ V(R) = 2 Energy(R)$_1$ + R $\frac{d}{dR}$ Energy(R)$_1$



This page titled 10.2: Energy Minimization - Four Methods Using Mathcad is shared under a CC BY 4.0 license and was authored, remixed, and/or curated by Frank Rioux via source content that was edited to the style and standards of the LibreTexts platform.

10.3: The Variation Theorem in Dirac Notation

The recipe for calculating the expectation value for energy using a trial wave function is,

$$\langle E\rangle = \langle\psi|\hat{H}|\psi\rangle \tag{10.3.1}$$

Now suppose the eigenvalues of $\hat{H}$ are denoted by $|i\rangle$. Then,

$$\hat{H}|i\rangle = \varepsilon_i|i\rangle = |i\rangle\varepsilon_i \tag{10.3.2}$$

Next we write $|\psi\rangle$ as a superposition of the eigenfunctions $|i\rangle$,

$$|\psi\rangle = \sum_i |i\rangle\langle I|\psi\rangle$$

and substitute it into Equation 10.3.1.

$$\langle E\rangle = \sum_i \langle\psi|\hat{H}|i\rangle\langle i|\psi\rangle$$

Making use of Equation 10.3.2 yields,

$$\langle E\rangle = \sum_i \langle\psi|i\rangle\varepsilon_i\langle i|\psi\rangle$$

After rearrangement we have,

$$\langle E\rangle = \sum_i \varepsilon_i|\langle i|\psi\rangle|^2$$

However, $|\langle i|\psi\rangle|^2$ is the probability that ε_i will be observed, p_i.

$$\langle E\rangle = \sum_i \varepsilon_i p_i \geq \varepsilon_0$$

Thus, the expectation value obtained using the trial wave function is an upper bound to the true energy. In other words, in valid quantum mechanical calculations you can't get a lower energy than the true energy.

This page titled 10.3: The Variation Theorem in Dirac Notation is shared under a CC BY 4.0 license and was authored, remixed, and/or curated by Frank Rioux via source content that was edited to the style and standards of the LibreTexts platform.

10.4: A Rudimentary Model for Alpha Particle Decay

Simple models for the potential energy experienced by an alpha particle in a nucleus have the form shown below. In the interest of mathematical simplicity we will not attempt to model any particular alpha emitter, but just try to capture the essentials of the quantum mechanical tunneling mechanism for alpha decay that was formulated by Gamov, Gurney and Condon in 1928.

$$V(x) := if[(x \geq 2), 0, \frac{5}{x}]$$



The attractive nuclear interaction (strong nuclear force) is represented by a well of depth 2.5 and range 2 in atomic units. The repulsive Coulomb interaction becomes dominant as the strong nuclear force fades for x values greater than 2. The trapped particle is assumed to have unit mass. A variational calculation will be carried out using the trial wavefunction given below. It is also possible to solve Schrödinger's equation for alpha decay by numerical integration.

Normalized trial wavefunction with variational parameter α, a decay constant:

$$\psi(x, \alpha) := 2\alpha^{\frac{3}{2}} x e^{-\alpha x}$$

$$\int_0^\infty \psi(x, \alpha)^2 dx |_{simplify}^{assume,\ \alpha>0} \rightarrow 1$$

Set up the variational energy integral:

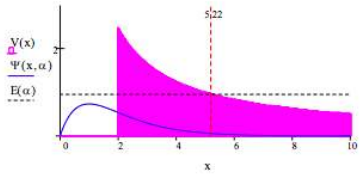
$$E(\alpha) := \int_0^\infty \psi(x, \alpha) \frac{1}{2} \frac{d^2}{dx^2} \psi(x, \alpha) dx + \int_0^\infty V(x) \psi(x, \alpha)^2 dx$$

Next the energy is minimized with respect to α numerically. This method requires a seed value for α.

α := 3 α := Minimize(E, α) α:= 1.003 E(α) = 0.958

In what follows the results of the variational calculation will be displayed graphically and interpreted.

Display the results of the variational calculation:



Calculate the probability that the particle is in the classically forbidden region. This is the region where the particle's total energy is less than the potential energy.

Because the energy of the particle is 0.958, the classical forbidden region extends from $x = 2$ to $x = 5.22$.

$$\frac{5}{x} = 0.958 |_{solve,\ x}^{float,\ 3} \rightarrow 5.22$$

Probability in classically forbidden region:

$$\int_2^{5.22} \psi(x, \alpha)^2 dx = 0.234$$

Calculate the probability that the particle has tunneled beyond the classically forbidden region.

$$\int_{5.22}^{\infty} \psi(x,\alpha)^2 dx \approx 1.879 \times 10^{-3}$$

Calculate the probability that the particle is still in the nucleus.

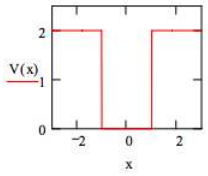
$$\int_{0}^{2} \psi(x,\alpha)^2 dx \approx 0.764$$

This page titled 10.4: A Rudimentary Model for Alpha Particle Decay is shared under a CC BY 4.0 license and was authored, remixed, and/or curated by Frank Rioux via source content that was edited to the style and standards of the LibreTexts platform.

10.5: Variational Method for a Particle in a Finite Potential Well

Definite potential energy: $V(x) := if[(x \geq -1) \cdot (x \leq 1), 0, 2]$

Display potential energy:



Choose trial wavefunction: $\psi(x, \beta) := (\frac{2 \cdot \beta}{\pi})^{\frac{1}{4}} \cdot (-\beta \cdot x^2)$

Demonstrate that the trial wavefunction is normalized.

$$\int_{-\infty}^{\infty} \psi(x, \beta)^2 dx \text{ assume, } \beta > 0 \rightarrow 1$$

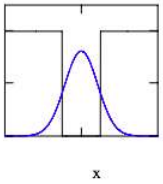
Evaluate the variational integral:

$$E(\beta) := \int_{-\infty}^{\infty} \psi(x, \beta) \cdot -\frac{1}{2} \cdot \frac{d^2}{dx^2} \psi(x, \beta) dx ... \Big|_{simplify}^{assume,\ \beta>0} \rightarrow \frac{1}{2} \cdot \beta + 2 - 2 \cdot erf(2^{\frac{1}{2}} \cdot \beta^{\frac{1}{2}})$$

Minimize the energy integral with respect to the variational parameter, β.

β := 1 β := Minimize(E, β) β = 0.678 E(β) = 0.538

Display wavefunction in the potential well and compare result with the exact energy, 0.530 E_h.



$$\frac{E(\beta) - 0.530}{0.530} = 1.546\%$$

Calculate the fraction of time tunneling is occurring.

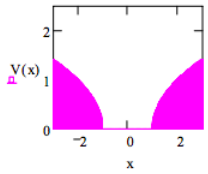
$$2 \cdot \int_{1}^{\infty} \psi(x, \beta)^2 dx = 0.1$$

This page titled 10.5: Variational Method for a Particle in a Finite Potential Well is shared under a CC BY 4.0 license and was authored, remixed, and/or curated by Frank Rioux via source content that was edited to the style and standards of the LibreTexts platform.

10.6: Variation Method for a Particle in a Symmetric 1D Potential Well

Definite potential energy: $V(x) := if[(x \geq -1) \cdot (x \leq 1), 0, \sqrt{|x| - 1}]$

Display potential energy:



Choose trial wave function: $\Psi(x, \beta) := (\frac{2 \cdot \beta}{\pi})^{\frac{1}{4}} \cdot exp(-\beta \cdot x^2)$

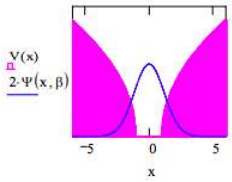
Evaluate the variational integral:

$$E(\beta) := \int_{-\infty}^{\infty} \Psi(x, \beta) \cdot -\frac{1}{2} \cdot \frac{d^2}{dx^2} \Psi(x, \beta) dx + \int_{-\infty}^{\infty} V(x) \cdot \Psi(x, \beta)^2 dx$$

Minimize the energy integral with respect to the variational parameter, β.

β := .2 β := Minimize(E, β) β := 0.363 E(β) = 0.313

Display wave function in the potential well.



Calculate the probability that the particle is in the potential barrier.

$$2 \cdot \int_{1}^{\infty} \Psi(x, \beta)^2 dx = 0.228$$

Define quantum mechanical tunneling.

> Tunneling occurs when a quon (a quantum mchanical particle) has probability of being in a nonclassical region. In other words, a region in which the total energy is less than the potential energy.

Calculate the probability that tunneling is occurring.

$$|x| - 1 = 0.313^2 \Big|_{solve,\, x}^{float,\, 4} \rightarrow \begin{pmatrix} 1.098 \\ -1.098 \end{pmatrix}$$

$$2 \cdot \int_{1.098}^{\infty} \Psi(x, \beta)^2 dx = 0.186$$

Calculate the kinetic and potential energy contributions to the total energy.

Kinetic energy:

$$\int_{-\infty}^{\infty} \Psi(x, \beta) \cdot -\frac{1}{2} \cdot \frac{d^2}{dx^2} \Psi(x, \beta) dx = 0.182$$

Potential energy:

$$\int_{-\infty}^{\infty} V(x) \cdot \Psi(x, \beta)^2 dx = 0.131$$

This page titled 10.6: Variation Method for a Particle in a Symmetric 1D Potential Well is shared under a CC BY 4.0 license and was authored, remixed, and/or curated by Frank Rioux via source content that was edited to the style and standards of the LibreTexts platform.

10.7: Variation Method for the Rydberg Potential

Approximate Methods: The Rydberg Potential

For unit mass the Rydberg potential function has the following energy operator in atomic units.

- Kinetic energy operator:

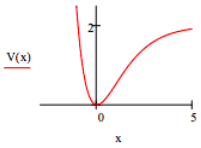
$$-\frac{1}{2}\frac{d^2}{dx^2}\blacksquare$$

- Potential energy operator:

$$V(x) = 2 - 2(1+x)exp(-x)$$

Limits of integration: x_{min} := -3 x_{max} := 5 $\int_{x_{min}}^{x_{max}} \blacksquare \, dx$

Display potential energy:



Suggested trial wave function:

$$\psi(x,\beta) = (\frac{2\beta}{\pi})^{\frac{1}{4}} exp(-\beta x^2)$$

$$\int_{-\infty}^{\infty} \psi(x,\beta)^2 dx \ assume, \ \beta > 0 \rightarrow 1$$

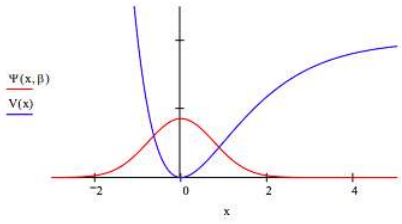
Evaluate the variational energy integral.

$$E(\beta) := \int_{x_{min}}^{x_{max}} \psi(x,\beta) - \frac{1}{2}\frac{d^2}{dx^2}\psi(x,\beta)dx + \int_{x_{min}}^{x_{max}} \psi(x,\beta)V(x)\psi(x,\beta)dx$$

Minimize the energy with respect to the variational parameter β and report its optimum value and the ground-state energy.

β := 1 β := Minimize(E, β) β := 0.86327 E(β) = 0.789456

Plot the optimum wave function and the potential energy on the same graph.



Numerical Solution for the Rydberg Potential

Compare the variational result to energy obtained by numerically integrating Schrödinger's equation for the Rydberg potential. For all practical purposes the numerical solution can be considered to be exact.

Numerical integration of Schrödinger's equation:

Given:

$$\frac{-1}{2}\frac{d^2}{dx^2}\Phi(x) + V(x)\Phi(x) = Energy\Phi(x)$$

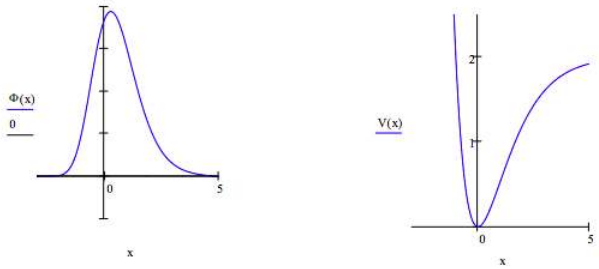
with $\Phi(x_{min} = 0)$ and $\Phi'(x_{min} = 0.1$

Φ = Odesolve(x, x_{max}) \nonumber \]

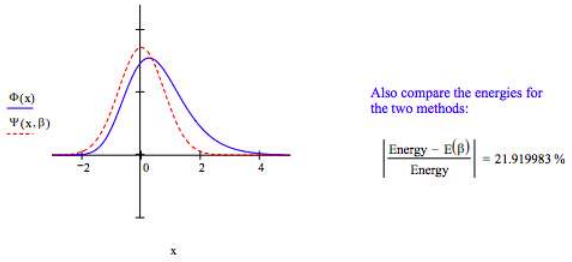
Normalize wave function:

$$\Phi(x) := \frac{\Phi(x)}{\sqrt{\int_{x_{min}}^{x_{max}} \Phi(x)^2 dx}}$$

Enter energy guess: Energy = 0.64752



Compare the variational and numerical solutions for the Morse oscillator by putting them on the same graph.



This page titled 10.7: Variation Method for the Rydberg Potential is shared under a CC BY 4.0 license and was authored, remixed, and/or curated by Frank Rioux via source content that was edited to the style and standards of the LibreTexts platform.

10.8: Variation Method for the Quartic Oscillator

Approximate Methods: The Quartic Oscillator

For unit mass the quartic oscillator has the following energy operator in atomic units.

$$H = -\frac{1}{2}\frac{d^2}{dx^2}\blacksquare + kx^4\blacksquare \int_{-\infty}^{\infty}\blacksquare dx$$

Suggested trial wavefunction: $\psi(x;\beta) := (\frac{2\beta}{\pi})^{\frac{1}{4}} exp(-\beta x^2)$

Demonstrate that the wavefunction is normalized.

$$\int_{-\infty}^{\infty} \psi(x;\beta)^2 dx \ assume,\ \beta > 0 \rightarrow 1$$

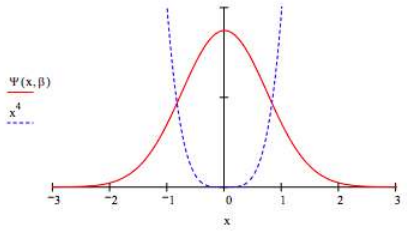
Evaluate the variational energy integral.

$$E(\beta) := \int_{-\infty}^{\infty} \psi(x,\beta) - \frac{1}{2}\frac{d^2}{dx^2}\psi(x,\beta)dx + \int_{-\infty}^{\infty} \psi(x,\beta)x^4\psi(x,\beta)dx \Big|_{simplify}^{assume,\ \beta>0} \rightarrow \frac{1}{16}\frac{8\beta^3}{\beta^2}$$

Minimize the energy with respect to the variational parameter β and report its optimum value and the ground-state energy.

β := 1 β := Minimize(E, β) β = 0.90856 E(β) = 0.68142

Plot the optimum wavefunction and the potential energy on the same graph.



Calculate the classical turning point and the probability that tunneling is occurring.

$$x_{ctp} = 0.68142^{\frac{1}{4}} \tag{10.8.1}$$

$$= 0.90856 \tag{10.8.2}$$

$$2\int_{x_{ctp}}^{\infty} \psi(x,\beta)^2 dx \approx 0.083265$$

Compare the variational result to energy obtained by numerically integrating Schrödinger's equation for the quartic oscillator using the numerical integration algorithm provided below.

Numerical Solutions for Schrödinger's Equation

Integration limit: x_{max} := 3 Effective mass: μ := 1 Force constant: k := 1

Potential energy: $V(x) := kx^4$

Numerical integration of Schrödinger's equation:

Given

$\frac{-1}{2\mu}\frac{d^2}{dx^2}\Phi(x) + V(x)\Phi(x) = energy\Phi(x)$

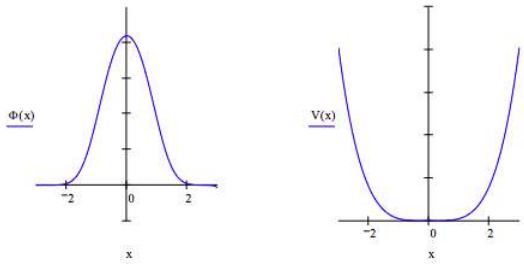
$\Phi(-x_{max} = 0$

$\Phi'(-x_{max} = 0.1$

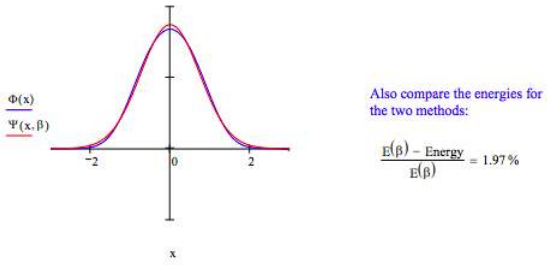
$\Phi := Odesolve(x, x_{max}$

Normalize wavefunction: $\Phi(x) := \frac{\Phi(x)}{\sqrt{\int_{-x_{max}}^{x_{max}} \Phi(x)^2 dx}}$

Enter energy guess: Energy = 0.6679864



Compare the variational and numerical solutions for the quartic oscillator by putting them on the same graph.



This page titled 10.8: Variation Method for the Quartic Oscillator is shared under a CC BY 4.0 license and was authored, remixed, and/or curated by Frank Rioux via source content that was edited to the style and standards of the LibreTexts platform.

10.9: Momentum-Space Variation Method for the Quartic Oscillator

For unit mass the quartic oscillator has the following energy operator in atomic units in coordinate space.

$$H = -\frac{1}{2}\frac{d^2}{dx^2}$$

Suggested trial wavefunction:

$$\psi(x,\beta) = (\frac{2\beta}{\pi})^{\frac{1}{4}} exp(-\beta x^2)$$

Demonstrate that the wavefunction is normalized.

$$\int_{-\infty}^{\infty} \psi(x,\beta)^2 dx \ assume, \beta > 0 \rightarrow 1$$

Fourier transform the coordinate wavefunction into the momentum representation.

$$\Phi(p,\beta) = \frac{1}{\sqrt{2\pi}} \int_{-\infty}^{\infty} exp(-ipx)\psi(x,\beta)dx|_{simplify}^{assume,\ \beta>1} \rightarrow \frac{1}{2}\frac{2^{\frac{3}{4}}}{\pi^{\frac{1}{4}}}\frac{e^{\frac{-1}{4}\frac{p^2}{\beta}}}{\beta^{\frac{1}{4}}}$$

Demonstrate that the momentum wavefunction is normalized.

$$\int_{-\infty}^{\infty} \overline{\Phi(p,\beta)}\Phi(p,\beta)dp assume,\ \beta > 0 \rightarrow 1$$

The quartic oscillator energy operator in momentum space:

$$H = \frac{p^2}{2}\blacksquare + \frac{d^4}{dp^4}\blacksquare$$

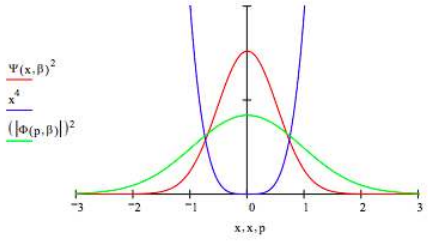
Evaluate the variational energy integral.

$$E(\beta) = \int_{-\infty}^{\infty} \overline{\Phi(p,\beta)}\frac{p^2}{2}\Phi(p,\beta)dp + \int_{-\infty}^{\infty} \overline{\Phi(p,\beta)}\frac{d^4}{dp^4}\Phi(p,\beta)dp|_{simplify}^{assume,\ \beta>0} \rightarrow \frac{1}{16}\frac{8\beta^3+3}{\beta^2}$$

Minimize the energy with respect to the variational parameter β and report its optimum value and the ground-state energy.

$$\beta = 1\ \beta = Minimize(E,\beta)\ \beta = 0.90856\ E(\beta) = 0.688142$$

Plot the coordinate and momentum wavefunctions and the potential energy on the same graph.



These results demonstrate the uncertainty principle. For the harmonic potential, $x^2/2$, the coordinate and momentum wavefunctions are identical. Compared to the harmonic potential the quartic potential, x^4, constrains the spatial wavefunction leading to less uncertainty in position. The uncertainty principle, therefore, requires an increase in the momentum uncertainty. This is clearly revealed in graph above.

This page titled 10.9: Momentum-Space Variation Method for the Quartic Oscillator is shared under a CC BY 4.0 license and was authored, remixed, and/or curated by Frank Rioux via source content that was edited to the style and standards of the LibreTexts platform.

10.10: Variation Method for a Particle in a Gravitational Field

The particle of unit mass in a gravitational field for which g = 1 has the energy operator shown below.

$$-\frac{1}{2}\frac{d^2}{dz^2}\blacksquare + z\blacksquare$$

$$\int_0^\infty \blacksquare dz$$

The following trial wave function for this problem is:

$$\Phi(\alpha, z) := 2\left(\frac{2\alpha}{\pi^{\frac{1}{3}}}\right)^{\frac{3}{4}} z\ exp(-\alpha z^2)$$

Determine whether or not the wave function is normalized.

$$\int_0^\infty \Psi(\alpha, z)^2 dz \Big|_{simplify}^{assume,\ \alpha>0} \rightarrow 1$$

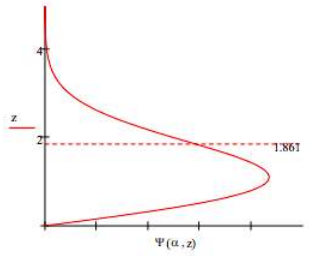
Evaluate the variational energy integral.

$$E(\alpha) := \int_0^\infty \Psi(\alpha, z) - \frac{1}{2}\frac{d^2}{dz^2}\Phi(\alpha, z) dz... \Big|_{simplify}^{assume,\ \alpha>0} \rightarrow \frac{1}{2\pi^{\frac{1}{2}}}\frac{3\pi^{\frac{1}{2}}\alpha^2 + 2(2)^{\frac{1}{2}}\alpha^{\frac{1}{2}}}{\alpha} + \int_0^\infty z\Psi(\alpha, z)^2 dz$$

Minimize the energy with respect to the variational parameter α and report its optimum value and the ground-state energy.

$$\alpha := 1\ \alpha := Minimize(E, \alpha)\ \alpha = 0.4136\ E(\alpha) = 1.8611\ E_{exact} := 1.8558$$

Plot the wave function with the distance of the particle from the surface on the vertical axis.



Tunneling threshold.

$$E(0.4136) = z \Big|_{float, 4}^{solve, z} \rightarrow 1.861$$

Find that distance below which there is a 90% probability of finding the particle.

$$\alpha := 1$$

Given $\int_0^a \Psi(\alpha, z)^2 dz = .90$

Find (a) = 1.9440

Find the most probable value of the position of the particle from the surface.

$$\frac{d}{dz}\Psi(0.4136, z) = 0 \Big|_{float,\ 3}^{solve,\ z} \rightarrow \begin{pmatrix} -1.10 \\ 1.10 \end{pmatrix}$$

Calculate the probability that the particle will be found below the most probable distance from the surface.

$$\int_0^{1.10} \Psi(\alpha, z)^2 dz = 0.4279$$

Calculate the probability that tunneling is occurring: $\int_{1.861}^\infty \Psi(\alpha, z)^2 dz = 0.1256$

Kinetic energy: $\int_0^\infty \Psi(\alpha, z) - \frac{1}{2}\frac{d^2}{dz^2}\Psi(\alpha, z) dz = 0.6204$

Potential energy: $\int_0^\infty z\Psi(\alpha, z)^2 dz = 1.2407$

What is the apparent virial theorem for this system: $E = 3T = \frac{3}{2}V$

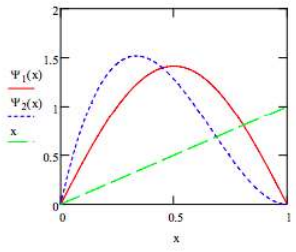
This page titled 10.10: Variation Method for a Particle in a Gravitational Field is shared under a CC BY 4.0 license and was authored, remixed, and/or curated by Frank Rioux via source content that was edited to the style and standards of the LibreTexts platform.

10.11: Linear Variational Method for a Particle in a Slanted 1D Box

Trial wavefunctions:

- $\psi_1(x) = \sqrt{2}\sin(\pi x)$
- $\psi_2(x) = \sqrt{105}x(1-x)^2$

Plot trial wavefunctions and potential energy. x = 0, .005 ... 1



Evaluate matrix elements:

$$S_{11} = \int_0^1 \psi_1(x)^2 dx \tag{10.11.1}$$

$$= 1 \tag{10.11.2}$$

$$S_{12} = \int_0^1 \psi_1(x)\psi_2(x) dx \tag{10.11.3}$$

$$= 0.9347 \tag{10.11.4}$$

$$S_{22} = \int_0^1 \psi_2(x)^2 dx \tag{10.11.5}$$

$$= 1 \tag{10.11.6}$$

$$H_{11} = \int_0^1 \psi_1(x)(-\tfrac{1}{2})\tfrac{d^2}{dx^2}\psi_1(x)dx + \int_0^1 \psi_1(x)\ x\ \psi_1(x)dx\ H_{11} = 5.4348$$

$$H_{12} = \int_0^1 \psi_1(x)(-\tfrac{1}{2})\tfrac{d^2}{dx^2}\psi_2(x)dx + \int_0^1 \psi_1(x)\ x\ \psi_2(x)dx\ H_{12} = 5.0163$$

$$H_{22} = \int_0^1 \psi_2(x)(-\tfrac{1}{2})\tfrac{d^2}{dx^2}\psi_2(x)dx + \int_0^1 \psi_2(x)\ x\ \psi_2(x)dx\ H_{22} = 7.375$$

Solve the secular equations and normalization constraint for the energy and coefficients.

Seed values for energy and coefficients: E = 5 c_1 = .5 c_2 = .5

Given

$$(H_{11} - ES_{11})c_1 + (H_{12} - ES_{12})c_2 = 0$$

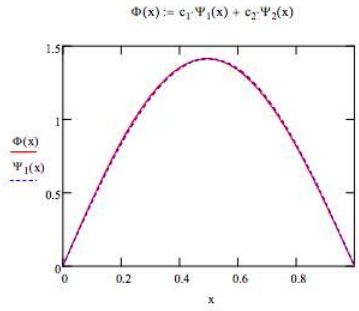
$$(H_{12} - ES_{12})c_1 + (H_{22} - ES_{22})c_2 = 0$$

$$c_1^2 S_{11} + 2c_1c_2S_{12} + c_2^2 S_{22} = 1$$

$$\begin{pmatrix} E \\ c_1 \\ c_2 \end{pmatrix} = Find(E, c_1, c_2)$$

$$\begin{pmatrix} E \\ c_1 \\ c_2 \end{pmatrix} = \begin{pmatrix} 5.4328 \\ 0.971 \\ 0.031 \end{pmatrix}$$

Compare variational ground state to PIB ground state:



Calculate average position of the particle in the box:

$$\int_0^1 x\Phi(x)^2 dx = 0.496$$

Calculate the probability that the particle is in the left half of the box:

$$\int_0^{0.5} \Phi(x)^2 dx = 0.5088$$

This page titled 10.11: Linear Variational Method for a Particle in a Slanted 1D Box is shared under a CC BY 4.0 license and was authored, remixed, and/or curated by Frank Rioux via source content that was edited to the style and standards of the LibreTexts platform.

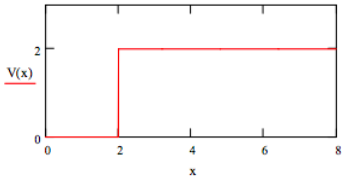
10.12: Variation Method for a Particle in a Semi-Infinite Potential Well

This problem deals with the variational approach to the particle in the semi-infinite potential well.

Kinetic energy operator: $-\frac{1}{2}\frac{d^2}{dx^2}\blacksquare$

Integral: $\int_0^\infty \blacksquare dx$

Potential energy: $V(x) := if[(x \le 2), 0, 2]$



Trial wave function: $\Phi(x,\beta) := 2\beta^{\frac{3}{2}}\ x\ exp(-\beta x)$

If the trial wave function is not normalized, normalize it.

$$\int_0^\infty \Phi(x,\beta)^2 dx\ assume,\ \beta > 0 \rightarrow 1$$

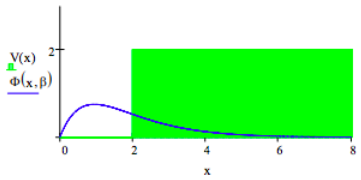
Evaluate the variational energy integral.

$$E(\beta) := \int_0^\infty \Phi(x,\beta)(-\tfrac{1}{2})\tfrac{d^2}{dx^2}\Phi(x,\beta)dx...|^{assume,\ \beta>0}_{simplify} \rightarrow \tfrac{1}{2}\beta^2 + 16\beta^2 e^{-4\beta} + 8\beta e^{-4\beta} + 2e^{-4\beta} + \int_2^\infty 2\Phi(x,\beta)^2 dx$$

Minimize the energy with respect to β:

$$\beta := .3\ \beta := \text{Minimize}\ (E,\beta)\ \beta = 1.053\ E(\beta) = 0.972$$

Display optimized trial wave function and potential energy:



Calculate average position and most probable position of the particle:

$$\int_0^\infty x\Phi(x,\beta)^2 dx = 1.425$$

$$\frac{d}{dx}\Phi(x,\beta) = 0|^{float,\ 3}_{solve,\ x} \rightarrow \frac{1}{\beta} = 0.95$$

Calculate the probability of the particle in the barrier.

$$\int_2^\infty \Phi(x,\beta)^2 dx = 20.891$$

Calculate the potential energy, and the kinetic energy.

$$V := \int_2^\infty 2\Phi(x,\beta)^2 dx\ V = 0.418$$

$$T := E(\beta) - V\ T = 0.554$$

This page titled 10.12: Variation Method for a Particle in a Semi-Infinite Potential Well is shared under a CC BY 4.0 license and was authored, remixed, and/or curated by Frank Rioux via source content that was edited to the style and standards of the LibreTexts platform.

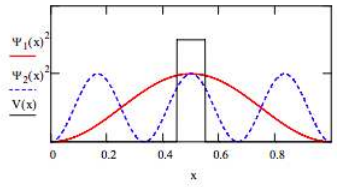
10.13: Variation Method for a Particle in a Box with an Internal Barrier

$$\psi_1(x) = \sqrt{2}\sin \pi x$$

$$\psi_2(x) = \sqrt{2}\sin 3\pi x$$

$$V(x) = if[(x \geq .45)(x \leq .55), 3, 0]$$

Plot trial wavefunctions and potential energy.



Evaluate matrix elements for $100E_h$ internal barrier:

$$S_{11} = \int_0^1 \psi_1(x)^2 dx \; S_{11} = 1$$

$$S_{12} = \int_0^1 \psi_1(x)\psi_2(x) dx \; S_{12} = 0$$

$$S_{22} = \int_0^1 \psi_2(x)^2 dx \; S_{22} = 1$$

$$H_{11} = \int_0^1 \psi_1(x)(-\frac{1}{2})\frac{d^2}{dx^2}\psi_1(x)dx + \int_{.45}^{.55} \psi_1(x)\ 100\ \psi_1(x)dx \tag{10.13.1}$$

$$\approx 24.7711 \tag{10.13.2}$$

$$H_{12} = \int_0^1 \psi_1(x)(-\frac{1}{2})\frac{d^2}{dx^2}\psi_2(x)dx + \int_{.45}^{.55} \psi_1(x)\ 100\ \psi_2(x)dx \tag{10.13.3}$$

$$\approx -19.1912 \tag{10.13.4}$$

$$H_{22} = \int_0^1 \psi_2(x)(-\frac{1}{2})\frac{d^2}{dx^2}\psi_2(x)dx + \int_{.45}^{.55} \psi_2(x)\ 100\ \psi_2(x)dx \tag{10.13.5}$$

$$\approx 62.9972 \tag{10.13.6}$$

Solve the secular equations and normalization constraint for the energy and coefficients.

Seed values for energy and coefficient: E = 5 c_1 = .5 c_2 = .5

Given

$$(H_{11} - ES_{11})c_1 + (H_{12} - ES_{12})c_2 = 0$$

$$(H_{12} - ES_{12})c_1 + (H_{22} - ES_{22})c_2 = 0$$

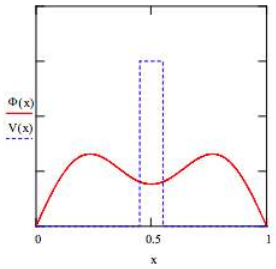
$$c_1^2 S_{11} + 2c_1 c_2 S_{12} + c_2^2 S_{22} = 1$$

$$\begin{pmatrix} E \\ c_1 \\ c_2 \end{pmatrix} = Find(E, c_1, c_2)$$

$$\begin{pmatrix} E \\ c_1 \\ c_2 \end{pmatrix} = \begin{pmatrix} 16.7989 \\ 0.9235 \\ 0.3836 \end{pmatrix}$$

Plot variational results:

$$\Phi(x) = c_1\Phi_1(x) + c_2\psi_2(x)$$



Calculate the probability the particle is in the barrier:

$$\int_{0.45}^{0.55} \Phi(x)^2 dx = 0.0605$$

Calculate potential and kinetic energy:

$$V = 100 \int_{0.45}^{0.55} \Phi(x)^2 dx \; V = 6.0541$$

$$T = E - V$$

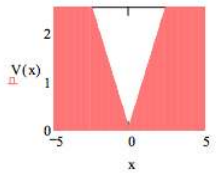
$$T = 10.7448$$

This page titled 10.13: Variation Method for a Particle in a Box with an Internal Barrier is shared under a CC BY 4.0 license and was authored, remixed, and/or curated by Frank Rioux via source content that was edited to the style and standards of the LibreTexts platform.

10.14: Variation Method for a Particle in a 1D Ice Cream Cone

Define potential energy: V(x) := |x|

Display potential energy:



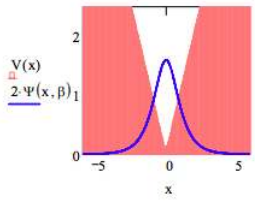
Choose trial wave function: $\Psi(x,\beta) := \sqrt{\frac{\beta}{2}}sech(\beta x)$

$$E(\beta) := \int_{-\infty}^{\infty} \Psi(x,\beta)\frac{1}{2}\frac{d^2}{dx^2}\Psi(x,\beta)dx + \int_{-\infty}^{\infty} V(x)\Psi(x,\beta)^2 dx$$

Minimize the energy integral with respect to the variational parameter, β.

$$\beta := 2\ \beta := \text{Minimize(E, } \beta)\ \beta = 1.276\ \text{E(} \beta) = 0.815$$

Display wave function in the potential well.



Calculate the probability that the particle is in the potential barrier.

$$2\int_{0}^{\infty} \Psi(x,\beta)^2 dx = 1$$

Define quantum mechanical tunneling.

> Tunneling occurs when a quon (a quantum mechanical particle) has probability of being in a nonclassical region. In other words, a region in which the total energy is less than the potential energy.

Calculate the probability that tunneling is occurring.

$$|x| = 0.815 \Big|^{solve,\ x}_{float,\ 4} \rightarrow \begin{pmatrix} 0.8150 \\ -0.8150 \end{pmatrix}$$

$$2\int_{0.815}^{\infty} \Psi(x,\beta)^2 dx = 0.222$$

Calculate the kinetic and potential energy contributions to the total energy.

Kinetic energy:

$$\int_{-\infty}^{\infty} \Psi(x,\beta) - (\frac{1}{2})\frac{d^2}{dx^2}\Psi(x,\beta)dx = 0.272$$

Potential energy:

$$\int_{-\infty}^{\infty} V(x)\Psi(x,\beta)^2 dx = 0.543$$

This page titled 10.14: Variation Method for a Particle in a 1D Ice Cream Cone is shared under a CC BY 4.0 license and was authored, remixed, and/or curated by Frank Rioux via source content that was edited to the style and standards of the LibreTexts platform.

https://chem.libretexts.org/@go/page/136251

10.15: Variation Method for a Particle in an Ice Cream Cone

A Gaussian function is proposed as a trial wavefunction in a variational calculation for a particle experiencing a linear radial potential energy. Determine the optimum value of the parameter β and the optimum ground state energy. Use atomic units: h = 2π, m_e = 1, e = -1.

$$\psi(r,\beta) := (\frac{2\beta}{\pi})^{\frac{3}{4}} exp(-\beta r^2)$$

$$T = \frac{1}{2r}\frac{d^2}{dr^2}(r\blacksquare)$$

$$V = r$$

$$\int_0^\infty \blacksquare 4\pi r^2 dr$$

a. Demonstrate the wave function is normalized.

$$\int_0^\infty \psi(r,\beta)^2 4\pi r^2 dr|_{simplify}^{assume,\ \beta>0} \rightarrow 1$$

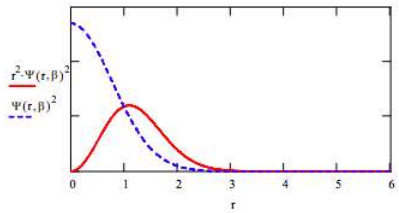
b. Evaluate the variational integral.

$$E(\beta) := \int_0^\infty \psi(r,\beta[(-\frac{1}{2r})\frac{d^2}{dr^2}(r\psi(r,\beta))]4\pi r^2 dr...|_{simplify}^{assume,\ \beta>0} \rightarrow \frac{1}{2}\frac{3\pi^{\frac{1}{2}}\beta^2 + (2)2^{\frac{1}{2}}\beta^{\frac{1}{2}}}{\pi^{\frac{1}{2}}\beta}$$

c. Minimize the energy with respect to the variational parameter β.

β := 1 β := Minimize(E, \beta) β = 0.414 E(β) = 1.861

d. Plot the optimized trial wave function.



This page titled 10.15: Variation Method for a Particle in an Ice Cream Cone is shared under a CC BY 4.0 license and was authored, remixed, and/or curated by Frank Rioux via source content that was edited to the style and standards of the LibreTexts platform.

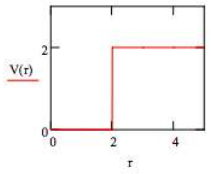
10.16: Variation Method for a Particle in a Finite 3D Spherical Potential Well

This problem deals with a particle of unit mass in a finite spherical potential well of radius 2 a_o and well height 2 E_h. The trial wave function is given below.

$$\psi(r,\beta) := (\frac{2\beta}{\pi})^{\frac{3}{4}} exp(-\beta r^2)$$

$$T = -\frac{1}{2r}\frac{d^2}{dr^2}(r\blacksquare)$$

$$V(r) := if[(r \le 2), 0, 2]$$



a. Demonstrate that the wave function is normalized.

$$\int_0^\infty \psi(r,\beta)^2 4\pi r^2 dr|_{simplify}^{assume,\ \beta>0} \rightarrow 1$$

b. Evaluate the variational integral.

$$E(\beta) := \int_0^\infty \psi(r,\beta)[-\frac{1}{2r}\frac{d^2}{dr^2}(r\psi(r,\beta))]4\pi r^2 dr...|_{simplify}^{assume,\ \beta>0} + \int_2^\infty 2\psi(r,\beta)^2 4\pi r^2 dr$$

$$E(\beta) := \frac{1}{2}\frac{3\pi^{\frac{1}{2}}\beta + 4\pi^{\frac{1}{2}} + 16exp(-8\beta)2^{\frac{1}{2}}\beta^{\frac{1}{2}} - 4\pi^{\frac{1}{2}}erf((2)2^{\frac{1}{2}}\beta^{\frac{1}{2}})}{\pi^{\frac{1}{2}}}$$

c. Minimize the energy with respect to the variational parameter β.

β := 5 β := Minimize (E, \beta) β = 0.381 $E(\beta) = 0.786$

d. Calculate the average value of r.

$$\int_0^\infty r\psi(r,\beta)^2 4\pi r^2 dr = 1.293$$

e. Calculate the kinetic and potential energy.

Potential energy:

$$\int_2^\infty r\psi(r,\beta)^2 4\pi r^2 dr = 0.215$$

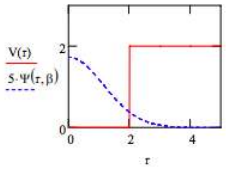
Kinetic energy:

$$E(\beta) - 0.215 = 0.571$$

f. Calculate the probability that the particle is in the barrier.

$$1 - \int_0^2 \psi(r,\beta)^2 4\pi r^2 dr = 0.107$$

g. Plot the wavefunction on the same graph as the potential energy.



This page titled 10.16: Variation Method for a Particle in a Finite 3D Spherical Potential Well is shared under a CC BY 4.0 license and was authored, remixed, and/or curated by Frank Rioux via source content that was edited to the style and standards of the LibreTexts platform.

10.17: Variation Method for the Harmonic Oscillator

This exercise deals with a variational treatment for the ground state of the simple harmonic oscillator which is, of course, an exactly soluble quantum mechanical problem.

The energy operator for a harmonic oscillator with unit effective mass and force constant is:

$$H = \frac{-1}{2}\frac{d^2}{dx^2}\blacksquare + \frac{x^2}{2}\blacksquare$$

The following trial wavefunction is selected:

$$\psi(x,\beta) = \frac{1}{1+\beta x^2}$$

The variational energy integral is evaluated (because of the symmetry of the problem it is only necessary to integrate from 0 to ∞, rather than from -∞ to ∞:

$$E(\beta) = \frac{\int_0^\infty \psi(x,\beta)\frac{-1}{2}\frac{d^2}{dx^2}\psi(x,\beta)dx + \int_0^\infty \psi(x,\beta)\frac{x^2}{2}\psi(x,\beta)dx}{\int_0^\infty \psi(x,\beta)^2 dx}\Big|^{assume,\ \beta>0}_{simplify} \rightarrow \frac{1}{4}\frac{\beta^2+2}{\beta}$$

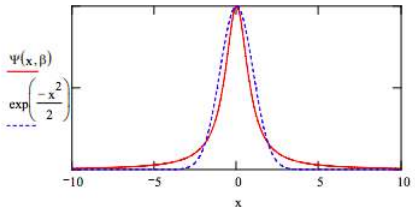
The energy integral is minimized with respect to the variational parameter:

β := 1 β := Minimize (E, β) β = 1.414 E(β) = 0.707

The % error is calculated given that the exact result is $0.50 E_h$.

$$\frac{E(\beta)-0.5}{0.5} = 41.421\%$$

The optimized trial wavefunction is compared with the SHO ground-state eigenfunction.



Now a second trial function is chosen:

$$\psi(x,\beta) := \frac{1}{(1+\beta x^2)^2}$$

Evaluate the variational energy integral:

$$E(\beta) := \frac{\int_0^\infty \psi(x,\beta)\frac{-1}{2}\frac{d^2}{dx^2}\psi(x,\beta)dx + \int_0^\infty \psi(x,\beta)\frac{x^2}{2}\psi(x,\beta)dx}{\int_0^\infty \psi(x,\beta)^2 dx}\Big|^{assume,\ \beta>0}_{simplify} \rightarrow \frac{1}{10}\frac{7\beta^2+1}{\beta}$$

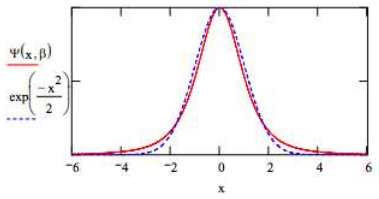
Minimize the energy integral with respect to the variational parameter:

β := 1 β := Minimize (E, β) β = 0.378 E(β) = 0.529

Calculate the % error given that the exact result is 0.50 E_h.

$$\frac{E(\beta)-0.5}{0.5} = 5.83\%$$

The optimized trial wavefunction is compared with the SHO ground-state eigenfunction.



Suggestion: Continue this exercise with the following trial wavefunction and interpret the improved agreement with the exact solution.

$$\psi(x, \beta) - \frac{1}{(1+\beta x^2)^n}$$

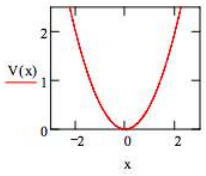
where n is an integer greater than 2.

This page titled 10.17: Variation Method for the Harmonic Oscillator is shared under a CC BY 4.0 license and was authored, remixed, and/or curated by Frank Rioux via source content that was edited to the style and standards of the LibreTexts platform.

10.18: Trigonometric Trial Wave Function for the Harmonic Potential Well

Definte potential energy: V(x) := $\frac{s^2}{2}$

Display potential energy:



Choose trial wave function: $\Psi(x,\beta) := \sqrt{\frac{\beta}{2}}sech(\beta x)$

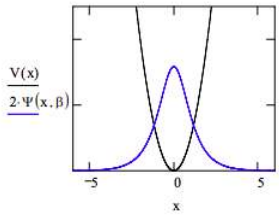
Set up variational energy integral:

$$E(\beta) := \frac{\int_{-\infty}^{\infty} \Psi(x,\beta)\frac{-1}{2}\frac{d^2}{dx^2}\Psi(x,\beta)dx + \int_{-\infty}^{\infty} \Psi(x,\beta)\frac{x^2}{2}\Psi(x,\beta)dx}{\int_0^{\infty} \Psi(x,\beta)^2 dx}\Big|_{simplify}^{assume,\ \beta>0} \rightarrow \frac{1}{24}\frac{4\beta^2+\pi^2}{\beta^2}$$

Minimize the energy integral with respect to the variational parameter, β.

β := 0.2 β := Minimize (E, β) β = 1.253 E(β) = 0.524

Display wave function in the potential well.



Calculate the probability that the particle is in the potential barrier.

$$2\int_0^{\infty} \Psi(x,\beta)^2 dx = 1$$

Define quantum mechanical tunneling.

> Tunneling occurs when a quon (a quantum mechanical particle) has probability of being in a nonclassical region. In other words, a region in which the total energy is less than the potential energy.

Calculate the probability that tunneling is occurring.

> Calculate the classical turning point.
>
> $$\frac{x^2}{2} = 0.524\Big|_{float,\ 4}^{solve,\ x} \rightarrow \begin{pmatrix} -1.024 \\ 1.024 \end{pmatrix}$$
>
> $$2\int_{1.024}^{\infty} \Psi(x,\beta)^2 dx = 0.143$$

Calculate the kinetic and potential energy contributions to the total energy.

> Kinetic energy:
>
> $$\int_{-infty}^{\infty} \Psi(x,\beta)\frac{-1}{2}\frac{d^2}{dx^2}\Psi(x,\beta)dx = 0.262$$
>
> Potential energy:
>
> $$\int_{-\infty}^{\infty} V(x)\Psi(x,\beta)^2 dx = 0.262$$

Is the virial theorem satisfied?

Yes, for the harmonic potential the virial theorem is T = V = E/2.

This page titled 10.18: Trigonometric Trial Wave Function for the Harmonic Potential Well is shared under a CC BY 4.0 license and was authored, remixed, and/or curated by Frank Rioux via source content that was edited to the style and standards of the LibreTexts platform.

10.19: Trigonometric Trial Wave Function for the 3D Harmonic Potential Well

Trial wave function: $\Psi(r,\beta) := \sqrt{\frac{3\beta^3}{\pi^3}}sech(\beta r)$

Integral: $\int_0^\infty \blacksquare 4\pi r^2 dr$

Kinetic energy operator: $T = \frac{-1}{2r}\frac{d^2}{dr^2}(r\blacksquare)$

Potential energy operatory: $V = \frac{1}{2}kr^2$

a. Demonstrate the wave function is normalized.

$$\int_0^\infty \Psi(r,\beta)^2 4\pi r^2 dr \Big|_{simplify}^{assume,\ \beta>0} \rightarrow 1$$

b. Evaluate the variational integral.

$$E(\beta) := \int_0^\infty \Psi(r,\beta)[\frac{-1}{2r}\frac{d^2}{dr^2}(r\Psi(r,\beta))]4\pi r^2 dr + \int_0^\infty \Psi(r,\beta)\frac{1}{2}r^2\Psi(r,\beta)4\pi r^2 dr$$

c. Minimize the energy with respect to the variational parameter β.

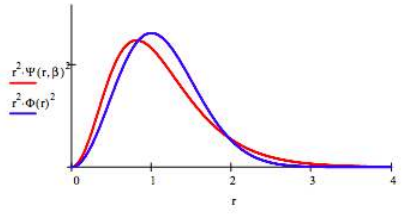
β := 1 β := Minimize (E, β) β = 1.471 E(β) = 1.597

d. The exact ground state energy for the 3D harmonic oscillator is 1.5 E_h. Calculate the percent error.

$$\frac{E(\beta)-1.5}{1.5} = 6.488\%$$

e. Compare the optimized trial wave function with the exact solution by plotting the radial distribution functions.

$$\Phi(r) := (\frac{1}{\pi})^{\frac{3}{4}} exp(\frac{r^2}{2})$$



h. Calculate the overlap integral between the trial wave function and the exact wave function.

$$\int_0^\infty \Psi(r,\beta)\Phi(r)4\pi r^2 dr = 0.989$$

i. Calculate the probability that tunneling is occurring.

Classical turning point:

$$1.597 = \frac{1}{2}r^2\Big|_{float,\ 3}^{solve,\ r} \rightarrow \begin{pmatrix} -1.79 \\ 1.79 \end{pmatrix}$$

Tunneling probability:

$$\int_{1.79}^\infty \Psi(r,\beta)^2 4\pi r^2 dr = 12.598\%$$

This page titled 10.19: Trigonometric Trial Wave Function for the 3D Harmonic Potential Well is shared under a CC BY 4.0 license and was authored, remixed, and/or curated by Frank Rioux via source content that was edited to the style and standards of the LibreTexts platform.

10.20: Gaussian Trial Wavefunction for the Hydrogen Atom

A Gaussian function, $\exp(-\alpha r^2)$, is proposed as a trial wavefunction in a variational calculation on the hydrogen atom. Determine the optimum value of the parameter α and the ground state energy of the hydrogen atom. Use atomic units: h = 2π, m_e = 1, e = -1.

$$\Phi(r,\beta) := \left(\frac{2\beta}{\pi}\right)^{\frac{3}{4}} exp(-\beta r^2)$$

$$T = \frac{-1}{2r}\frac{d^2}{dr^2}(r\blacksquare)$$

$$V = \frac{1}{r}$$

$$\int_0^\infty \blacksquare 4\pi r^2 dr$$

a. Demonstrate the wave function is normalized.

$$\int_0^\infty \Psi(r,\beta)^2 4\pi r^2 dr\Big|_{simplify}^{assume,\ \beta>0} \rightarrow 1$$

b. Evaluate the variational integral.

$$E(\beta) := \int_0^\infty \Psi(r,\beta)\left[\frac{-1}{2r}\frac{d^2}{dr^2}(r\Psi(r,\beta))\right]4\pi r^2 dr...$$

$$\Big|_{simplify}^{assume,\ \beta>0} \rightarrow \frac{1}{2}\frac{3\pi^{\frac{1}{2}}\beta - (4)2^{\frac{1}{2}}\beta^{\frac{1}{2}}}{\pi^{\frac{1}{2}}} + \int_0^\infty \Psi(r,\beta)\frac{-1}{r}\Psi(r,\beta)4\pi r^2 dr$$

c. Minimize the energy with respect to the variational parameter β.

β := 1 β := Minimize (E, β) β = 0.283 E(β) = -0.424

d. The exact ground state energy for the hydrogen atom is -.5 E_h. Calculate the percent error.

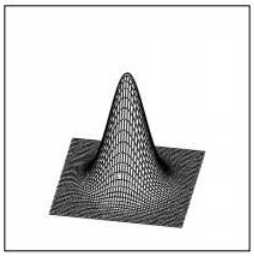
$$\frac{-.5 - E(\beta)}{-.5} = 15.117$$

e. The differences between the Gaussian and Slate type wavefunctions are illustrated with the surface plots shown below.

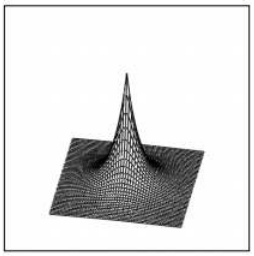
N := 50 b := 5 i := 0..N j := 0..N $y_i := -b + \frac{2bi}{N}$ $x_j := -b + \frac{2bj}{N}$

$$Gauss_{i,\,j} := \left(\frac{2\beta}{\pi}\right)^{\frac{3}{4}} exp[-\beta[(x_i)^2 + (y_j)^2]]$$

$$Slater_{i,\,j} := \frac{1}{\sqrt{\pi}} exp[-\sqrt{(x_i)^2 + (y_j)^2}]$$



Gauss



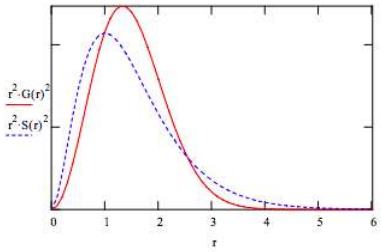
Slater

f. These wavefunctions can also be compared to their radial distribution functions:

r := 0, .1 .. 6

$$G(r) := \left(\frac{2\beta}{\pi}\right)^{\frac{3}{4}} exp(-\beta r^2)$$

$$S(r) := \frac{1}{\sqrt{\pi}} exp(-r)$$



This page titled 10.20: Gaussian Trial Wavefunction for the Hydrogen Atom is shared under a CC BY 4.0 license and was authored, remixed, and/or curated by Frank Rioux via source content that was edited to the style and standards of the LibreTexts platform.

10.21: Variation Calculation on the 1D Hydrogen Atom Using a Trigonometric Trial Wave Function

The energy operator for this problem is:

$$\frac{-1}{2}\frac{d^2}{dx^2}\blacksquare - \frac{1}{x}\blacksquare$$

The trial wave function:

$$\Psi(\alpha, x) := \frac{\sqrt{12\alpha^3}}{\pi}(x)sech(\alpha, x)$$

Evaluate the variational energy integral.

$$E(\alpha) := \int_0^\infty \Psi(\alpha, x) - \frac{1}{2}\frac{d^2}{dx^2}\Psi(\alpha, x)dx + \int_0^\infty \frac{-1}{x}\Psi(\alpha, x)^2 dx$$

$$\left|^{assume,\ \alpha>0}_{simplify}\right. \rightarrow \frac{1}{6}\alpha\frac{12\alpha_\alpha\pi^2 - 72ln(2)}{\pi^2}$$

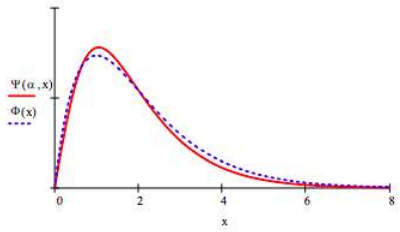
Minimize the energy with respect to the variational parameter α and report its optimum value and the ground-state energy.

α := 1 α := Minimize (E, α) α = 1.1410 E(α) = -0.4808

The exact ground-state energy for the hydrogen atom is -.5 E_h. Calculate the percent error.

$$\left|\frac{-.5 - E(\alpha)}{-.5}\right| = 3.8401$$

Plot the optimized trial wave function and the exact solution, $\Phi(x) := 2(x)exp(-x)$.



Find the distance from the nucleus within which there is a 95% probability of finding the electron.

α := 1. Given:

$$\int_0^a \Psi(\alpha, x)^2 dx = 0.95$$

Find (a) = 2.8754

Find the most probable value of the position of the electron from the nucleus.

$$\alpha := 1.1410 \quad \frac{d}{dx}\left|\frac{\sqrt{12\alpha^3}}{\pi}(x)sech(\alpha, x)\right| = 0 \left|^{solve,\ x}_{float,\ 3}\right. \rightarrow 1.05$$

Calculate the probability that the electron will be found between the nucleus and the most probable distance from the nucleus.

$$\int_0^{1.05} \Psi(\alpha, x)^2 dx = 0.3464$$

Break the energy down into kinetic and potential energy contributions. Is the virial theorem obeyed?

$$T := \int_0^\infty \Psi(\alpha, x)\frac{-1}{2}\frac{d^2}{dx^2}\Psi(\alpha, x)dx \quad T = 0.4808$$

$$V := \int_0^{\infty} \frac{-1}{x} \Psi(\alpha, x)^2 dx \quad V = -0.9616$$

$$\left|\frac{V}{T}\right| = 2.0000$$

Use the exact result to discuss the weakness of this trial function.

E_{exact} := -0.5

Using the virial theorem we know: T_{exact} := 0.500 V_{exact} := -1.00

Calculate the difference between the variational results and the exact calculation:

E(α) - E_{exact} = 0.0192

T - T_{exact} = -0.0192

V - V_{exact} = 0.0384

The variational wave function yields a lower kinetic energy, but at the expense of a potential energy that is twice as unfavorable as the kinetic energy result is favorable.

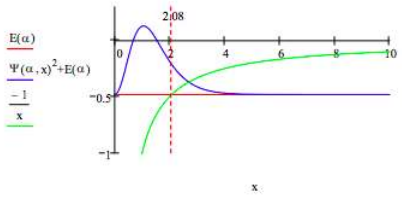
Calculate the probability that tunneling is occurring.

Classical turning point:

$$E(\alpha) = \frac{-1}{x} \Big|^{solve,\ x}_{float,\ 3}$$

Tunneling probability:

$$\int_{2.08}^{\infty} \Psi(\alpha, x)^2 dx = 0.1783$$



This page titled 10.21: Variation Calculation on the 1D Hydrogen Atom Using a Trigonometric Trial Wave Function is shared under a CC BY 4.0 license and was authored, remixed, and/or curated by Frank Rioux via source content that was edited to the style and standards of the LibreTexts platform.

10.22: Variation Calculation on the 1D Hydrogen Atom Using a Gaussian Trial Wavefunction

The energy operator for this problem is:

$$\frac{-1}{2}\frac{d^2}{dx^2}\blacksquare - \frac{1}{x}\blacksquare$$

The trial wave function is:

$$\psi(x,\alpha) = 2(\frac{2\alpha}{\pi^{\frac{1}{3}}})(x)exp(-\alpha x^2)$$

Evaluate the energy integral.

$$E(\alpha) = \int_x^{\alpha} -\frac{1}{2}\frac{d^2}{dx^2}\psi(x,\alpha)dx + \int_0^{\infty}\frac{-1}{x}\psi(x,\alpha)^2 dx\Big|_{simplify}^{assume,\ \alpha>0} \rightarrow \frac{-1}{2\pi^{\frac{1}{2}}}[(-3)\pi^{\frac{1}{2}}\alpha + (4)2^{\frac{1}{2}}\alpha^{\frac{1}{2}}]$$

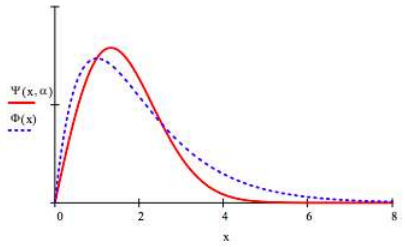
Minimize the energy with respect to the variational parameter α and report its optimum value and the ground-state energy.

α = 1 α = Minimize (E, α) α = 0.2829 E (α) = -0.4244

The exact ground state energy for the hydrogen atom is -0.5 E_h. Calculate the percent error.

$$\left|\frac{-0.5 - E(\alpha)}{-0.5}\right| = 15.1174$$

Plot the optimized trial wave function and the exact solution, $\Phi(x) = 2(x)exp(-x)$.



Find the distance from the nucleus within which there is a 95% probability of finding the electron.

α = 1. Given:

$$\int_0^a \psi(x,\alpha)^2 dx = .95$$

Find (a) = 2.6277

Find the most probable value of the position of the electron from the nucleus.

$$\alpha = 0.2829\frac{d}{dx}|\psi(x,\alpha)| = 0\Big|_{float,\ 3}^{solve,\ x} \rightarrow \begin{pmatrix}-1.33\\1.33\end{pmatrix}$$

Calculate the probability that the electron will be found between the nucleus and the most probable distance from the nucleus.

$$\int_0^{1.33} \psi(\alpha,x)^2 dx = 0.3584$$

Break the energy down into kinetic and potential energy contributions. Is the *virial theorem* obeyed?

$$T = \int_0^{\infty}\psi(x,\alpha)\frac{1}{2}\frac{d^2}{dx^2}\psi(x,\alpha)dx$$
$$= 0.4244$$

$$V = \int_0^{\infty} \frac{-1}{x} \psi(x,\alpha)^2 dx$$
$$= -0.8488$$

$$|\frac{V}{T}| = 2.00$$

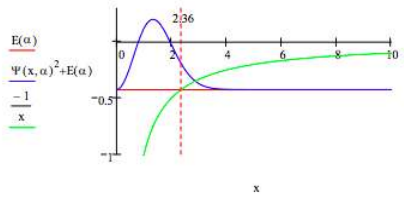
Calculate the probability that tunneling is occurring.

Classical turning point:

$$E(\alpha) = \frac{-1}{x} |^{solve,\ x}_{float,\ 3} \rightarrow 2.36$$

Tunneling probability:

$$\int_{2.36}^{\infty} \psi(x,\alpha)^2 dx = 0.0978$$



This page titled 10.22: Variation Calculation on the 1D Hydrogen Atom Using a Gaussian Trial Wavefunction is shared under a CC BY 4.0 license and was authored, remixed, and/or curated by Frank Rioux via source content that was edited to the style and standards of the LibreTexts platform.

10.23: Variational Calculation on the Two-dimensional Hydrogen Atom

Normalized trial wave function:

$$\psi(\alpha, r) = \sqrt{\frac{2}{\pi}}\alpha e^{-\alpha r}$$

$$\int_0^\infty \psi(\alpha, r)^2 2\pi r dr \;\; assume, \;\; \alpha > 0 \rightarrow 1$$

Calculate electron kinetic energy:

$$T(\alpha) = \int_0^\infty \psi(\alpha, r)\frac{-1}{2r}\frac{d}{dr}(r\frac{d}{dr}\psi(\alpha, r))2\pi r dr \;\; assume, \;\; \alpha > 0 \rightarrow (-2)\alpha Z$$

Calculate electron-nucleus potential energy:

$$V_{NE}(\alpha, Z) = \int_0^\infty \psi(\alpha, r)\frac{-Z}{r}\psi(\alpha, r)2\pi r dr \; assume, \;\; \alpha > 0 \rightarrow (-2)\alpha Z$$

Calculate total electronic energy for the 2D H atom:

α = 1 α = Minimize (E, α) α = 2 E(α) = -2

Demonstrate that the virial theorem is satisfied:

$$\frac{T(\alpha)}{E(\alpha)} = -1 \quad \frac{T(\alpha)}{V_{NE}(\alpha, 1)} = -0.5 \quad \frac{V_{NE}(\alpha, 1)}{E(\alpha)} = 2$$

This page titled 10.23: Variational Calculation on the Two-dimensional Hydrogen Atom is shared under a CC BY 4.0 license and was authored, remixed, and/or curated by Frank Rioux via source content that was edited to the style and standards of the LibreTexts platform.

10.24: Variational Calculation on Helium Using a Hydrogenic Wavefunction

Gaussian trial wavefunction:

$$\psi(r,\beta) := \sqrt{\frac{\beta^3}{\pi}} exp(-\beta r)$$

Demonstrate the wavefunction is normalized.

$$\int_0^\infty \psi(r,\beta)^2 4\pi r^2 dr \Big|_{simplify}^{assume,\ \beta>0} \rightarrow 1$$

The terms contributing to the total electronic energy of the helium atom are the kinetic energy of each electron, each electron's interaction with the nucleus, and the interaction of electrons with each other.

Calculate kinetic energy:

$$2\int_0^\infty \psi(x,\beta)^2 \left[\frac{-1}{2}\frac{d^2}{dx^2}(r\psi(r,\beta))\right] 4\pi r^2 dr \Big|_{simplify}^{assume,\ \beta>0} \rightarrow \beta^2$$

Calculate electron-nucleus potential energy:

a. a. Calculate the electric potential of one of the electrons in the presence of the other:

$$\frac{1}{r}\int_0^r \psi(x,\beta)^2 4\pi x^2 dx + \int_r^\infty \frac{\psi(x,\beta)^2 4\pi x^2}{x} dx \Big|_{simplify}^{assume,\ \beta>0} \rightarrow \frac{-[r\beta e^{(-2)r\beta} + e^{(-2)r\beta} - 1]}{r}$$

b. b. Calculate the electron-electron potential energy using result of part a:

$$\int_\infty^r \psi(x,\beta)^2 \frac{-[r\beta e^{(-2)r\beta} + e^{(-2)r\beta} - 1]}{r} 4\pi r^2 dr \Big|_{simplify}^{assume,\ \beta>0\rightarrow\frac{5}{8}\beta}$$

Write the equation for the total electronic energy in terms of the variational parameter β and minimize the energy with respect to β:

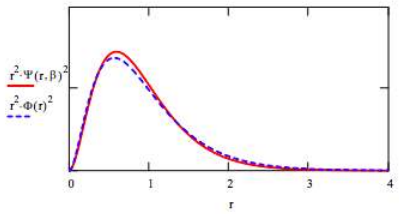
$$E(\beta) := \beta^2 - 4\beta + \frac{5}{8}\beta \quad \beta := \frac{d}{d\beta}E(\beta) = 0\ solve,\ \beta \rightarrow \frac{27}{16} \quad E(\beta) = -2.848$$

Compare the variational calculation to the Hartree-Fock limit: ($E_{HF} \approx -2.8617$)

$$\frac{E_{HF} - E(\beta)}{E_{HF}} = 0.491\%$$

Compare optimized trial wavefunction with the Hartree-Fock wavefunction by plotting the radial distribution functions.

$$\Phi(r) = 0.75738\exp(-1.430r) + 0.43658\exp(-2.4415r) + 0.17295\exp(-4.0996r)$$
$$- 0.02730\exp(-6.4843r) + 0.06675\exp(-7.978r)$$



This page titled 10.24: Variational Calculation on Helium Using a Hydrogenic Wavefunction is shared under a CC BY 4.0 license and was authored, remixed, and/or curated by Frank Rioux via source content that was edited to the style and standards of the LibreTexts platform.

10.25: Gaussian Trial Wave Function for the Helium Atom

Gaussian trial wave function:

$$\Psi(r,\beta) := (\frac{2\beta}{\pi})^{\frac{3}{4}} exp(-\beta r^2)$$

Demonstrate the wave function is normalized.

$$\int_0^\infty \Psi(r,\beta)^2 4\pi r^2 dr|_{simplify}^{assume,\ \beta>0} \rightarrow 1$$

The terms contributing to the total electronic energy of the helium atom are the kinetic energy of each electron, each electron′s interaction with the nucleus, and the interaction of the electrons with each other.

Calculate kinetic energy:

$$2\int_0^\infty \Psi(r,\beta)[\frac{-1}{2r}\frac{d^2}{dr^2}(r\Psi(r,\beta))]4\pi r^2 dr|_{simplify}^{assume,\ \beta>0} \rightarrow 3\beta]$$

Calculate electron-nucleus potential energy:

$$2\int_0^\infty \Psi(r,\beta)\frac{-2}{r}\Psi(r,\beta)4\pi r^2 dr|_{simplify}^{assume,\ \beta>0} \rightarrow (-8)\frac{2^{\frac{1}{2}}}{\pi}(\beta\pi)^{\frac{1}{2}}$$

Calculation of electron-electron potential energy:

a. Calculate the electric potential of one of the electrons in the presence of the other:

$$\frac{1}{r}\int_0^r \Psi(x,\beta)^2 4\pi x^2 dx + \int_r^\infty \frac{\Psi(x,\beta)^2 4\pi x^2}{x} dx|_{simplify}^{assume,\ \beta>0} \rightarrow \frac{erf(r2^{\frac{1}{2}}\beta^{\frac{1}{2}})}{r}$$

b. Calculate the electron-electron potential energy using result of part a:

$$\int_0^\infty \Psi(r,\beta)^2(\frac{erf(r2^{\frac{1}{2}}\beta^{\frac{1}{2}})}{r})4\pi r^2 dr|_{simplify}^{assume,\ \beta>0} /rightarrow \frac{2}{\pi}(\beta\pi)^{\frac{1}{2}}$$

Write the equation for the total electronic energy in terms of the variational parameter β:

$$E(\beta) := 3\beta + (-8)\frac{2^{\frac{1}{2}}}{\pi}(\beta\pi)^{\frac{1}{2}} + \frac{2}{\pi}(\beta\pi)^{\frac{1}{2}} simplify \rightarrow \frac{-[(-3)\beta\pi + (8)2^{\frac{1}{2}}(\beta\pi)^{\frac{1}{2}-2(\beta\pi)^{\frac{1}{2}}}]}{\pi}$$

Minimize the energy with respect to the variational parameter β.

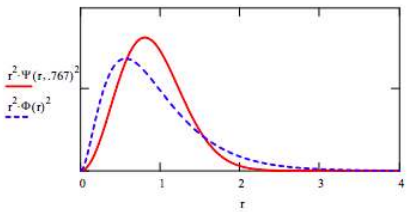
$$\frac{d}{d\beta}E(\beta) = 0 \quad solve,\ \beta \rightarrow \frac{-1}{9}\frac{(-33)+8(2)^{\frac{1}{2}}}{\pi} = 0.767 \quad E(.767) = -2.301$$

Compare the variational calculation to the Hartree-Fock limit: E_{HF} := -2.8617

$$\frac{E_{HF} - E(.767)}{E_{HF}} = 19.594$$

Compare optimized trial wave function with the Hartree-Fock wave function (see McQuarrie and Simon, page 283) by plotting the radial distribution functions.

$$\Phi(r) := .75738exp(-1.430r) + .43658exp(-2.4415r) + .17295exp(-4.0996r)$$
$$- .02730exp(-6.4843r) + .06675exp(-7.978)$$



This page titled 10.25: Gaussian Trial Wave Function for the Helium Atom is shared under a CC BY 4.0 license and was authored, remixed, and/or curated by Frank Rioux via source content that was edited to the style and standards of the LibreTexts platform.

10.26: Trigonometric Trial Wavefunction for the Helium Atom

Trigonometric trial wavefunction:

$$\psi(r,\beta) = \sqrt{\frac{3\beta^3}{\pi^3}}\operatorname{sech}(\beta r)$$

Demonstrate the wavefunction is normalized.

$$\int_0^\infty \psi(r,\beta)^2 4\pi r^2 dr \Big|_{simplify}^{assume,\ \beta>0}$$

The terms contributing to the total electronic energy of the helium atom are the kinetic energy of each electron, each electron′s interaction with the nucleus, and the interaction of the electrons with each other.

Calculate kinetic energy:

$$2\int_0^\infty \psi(r,\beta)\left[\frac{-1}{2r}\frac{d^2}{dr^2}(r\psi(r,\beta))\right]4\pi r^2 dr \Big|_{simplify}^{assume,\ \beta>0} \rightarrow \frac{1}{3}\beta^2\frac{12+\pi^2}{\pi^2}$$

Calculate electron-nucleus potential energy:

$$2\int_0^\infty \psi(r,\beta)\frac{-2}{r}\psi(r,\beta)4\pi r^2 dr \Big|_{simplify}^{assume,\ \beta>0} \rightarrow (-48)\beta\frac{\ln(2)}{\pi^2}$$

Calculate electron-electron potential energy:

$$\int_0^\infty \psi(r,\beta)^2\left(\frac{1}{r}\int_0^r \psi(x,\beta)^2 4\pi x^2 dx + \int_r^\infty \frac{\psi(x,\beta)^2 4\pi x^2}{x}dx\right)4\pi r^2 dr$$

Write the equation for the total electronic energy in terms of the variational parameter β:

$$E(\beta) = \frac{1}{3}\beta^2\frac{12+\pi^2}{\pi^2} + (-48)\beta\frac{\ln(2)}{\pi^2}$$
$$+\int_0^\infty \psi(r,\beta)^2\left(\frac{1}{r}\int_0^r \psi(x,\beta)^2 4\pi x^2 dx + \int_r^\infty \frac{\psi(x,\beta)^2 4\pi x^2}{x}\right)4\pi r^2 dr$$

Minimize the energy with respect to the variational parameter β.

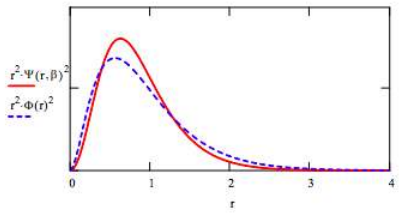
β = 1 β = Minimize(E, β β = 1.902 E(β = -2.672

Compare the variational calculation to the **Hartree-Fock limit**: $E_{HF} = -2.8617$

$$\frac{E_{HF} - E(\beta)}{E_{HF}} = 6.614$$

Compare optimized trial wavefunction with the Hartree-Fock wavefunction (see McQuarrie and Simon, page 283) by plotting the radial distribution functions.

$$\Phi(r)$$
$$= 0.75738\exp(1.430r) + 0.43658\exp(-2.4415r) + 0.17295\exp(-4.0996r) - 0.02730\exp(-6.4843r)$$
$$+ 0.06675\exp(7.97)$$



This page titled 10.26: Trigonometric Trial Wavefunction for the Helium Atom is shared under a CC BY 4.0 license and was authored, remixed, and/or curated by Frank Rioux via source content that was edited to the style and standards of the LibreTexts platform.

10.27: Trigonometric Trial Wavefunction for the Hydrogen Atom

Trial wave function:

$$\Psi(r,\beta) := \sqrt{\frac{3\beta^3}{\pi^3}} sech(\beta r)$$

Integral:

$$\int_0^\infty \blacksquare 4\pi r^2 dr$$

Kinetic energy operator:

$$T = \frac{-1}{2r}\frac{d^2}{dr^2}(r\blacksquare)$$

Potential energy operator:

$$V = \frac{1}{r}$$

a. Demonstrate the wave function is normalized.

$$\int_0^\infty \Psi(r,\beta)^2 4\pi r^2 dr|_{simplify}^{assume,\ \beta>0} \rightarrow 1$$

b. Evaluate the variational integral.

$$E(\beta) := \Psi(r,\beta)[\frac{-1}{2r}\frac{d^2}{dr^2}(r\Psi(r,\beta))]4\pi r^2 dr...$$

$$|_{simplify}^{assume,\ \beta>0} \rightarrow \frac{1}{6}\beta\frac{12\beta+\beta\pi^2-72ln(2)}{\pi^2} + \int_0^\infty \Psi(r,\beta)\frac{-1}{r}\Psi(r,\beta)4\pi r^2 dr$$

c. Minimize the energy with respect to the variational parameter β.

β := 1 β := Minimize (E, β β = 1.141 E(β) = -0.481

d. The exact ground state energy for the hydrogen atom is -.5E_h. Calculate the percent error.

$$\frac{-.5-E(\beta)}{-.5}(100) = -0.481$$

e. Compare optimized trial wave function with the exact solution by plotting the radial distribution functions.

$$S(r) := \frac{1}{\sqrt{\pi}} exp(-r)$$

f. Calculate the kinetic and potential energy contributions for the trial wave function. Is the virial theorem satisfied?

Kinetic energy:

$$\int_0^\infty \Psi(r,\beta)[\frac{1}{2r}\frac{d^2}{dr^2}(r\Psi(r,\beta))]4\pi r^2 dr = 0.481$$

Potential energy:

$$\int_0^\infty \Psi(r,\beta)\frac{-1}{r}\Psi(r,\beta)4\pi r^2 dr = -0.962$$

Yes, the virial theorem is satisfied: T = -E = \(\frac{-V}{2}.

g. Given that the virial theorem is (of course) satisfied for the exact solution, explain the deficiency of the trigonometric trial wave function.

For the exact solution T = 0.500 and V = -1.00. Thus, while the kinetic energy is lower by 0.019 for the trial wave function, its potential energy is higher by twice that amount. As can be seen in the graph above, an electron in the trial wave function spends less time close to the nucleus.

This page titled 10.27: Trigonometric Trial Wavefunction for the Hydrogen Atom is shared under a CC BY 4.0 license and was authored, remixed, and/or curated by Frank Rioux via source content that was edited to the style and standards of the LibreTexts platform.

10.28: Hydrogen Atom Calculation Assuming the Electron is a Particle in a Sphere of Radius R

Trial wave function:

$$\Phi(r, R) := \frac{1}{\sqrt{2\pi R}} \frac{\sin(\frac{\pi r}{R})}{r}$$

Integral:

$$\int_0^{\infty} \blacksquare 4\pi r^2 dr$$

Kinetic energy operator:

$$T = \frac{1}{2r} \frac{d^2}{dr^2}(r\blacksquare)$$

Potential energy operator:

$$V = \frac{1}{r}$$

Demonstrate the wave function is normalized.

Set up the variational energy integral.

$$E(R) := \int_0^R \Phi(r, R)[\frac{-1}{2r} \frac{d^2}{dr^2}(r\Phi(r, R))]4\pi r^2 dr + \int_0^R \Phi(r, R) \frac{-1}{r} \Phi(r, R) 4\pi r^2 dr]$$

Minimize the energy with respect to the variational parameter R.

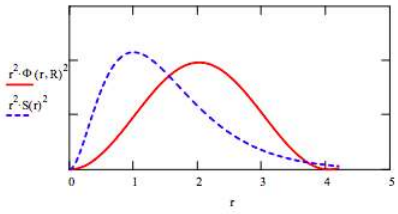
R := 1 R := Minimize(E, R) R = 4.049 E(R) = -0.301

The exact ground state energy for the hydrogen atom is -.5 E_h. Calculate the percent error.

$$\frac{-.5 - E(R)}{-.5} = 39.793$$

Compare optimized trial wave function with the exact solution by plotting the radial distribution functions.

$$S(r) := \frac{1}{\sqrt{\pi}} exp(-r) \quad r := 0, .02..4.2$$



This page titled 10.28: Hydrogen Atom Calculation Assuming the Electron is a Particle in a Sphere of Radius R is shared under a CC BY 4.0 license and was authored, remixed, and/or curated by Frank Rioux via source content that was edited to the style and standards of the LibreTexts platform.

10.29: Electronic Structure - Variational Calculations on the Lithium Atom

The electronic structure of lithium is $1s^2 2s^1$.

One Parameter Estimation

The trial hydrogenic 1s and 2s orbitals are as follows:

$$\psi(1s) = \sqrt{\frac{\alpha^3}{\pi}} e^{-\alpha r} \tag{10.29.1}$$

$$\psi(2s) = \sqrt{\frac{\alpha^3}{32\pi}} (2 - \alpha r) e^{\frac{-\alpha r}{2}} \tag{10.29.2}$$

If these orbitals are used, the variational expression for the lithium atom energy $E(\alpha)$ is given below.

$$E(\alpha) = \alpha^2 - 2Z\alpha + \frac{5}{8}\alpha + \frac{\alpha^2}{8} - \frac{Z\alpha}{4} + \frac{34\alpha}{81} \tag{10.29.3}$$

Minimize energy with respect to the variational parameter, α.

$$\frac{d}{d\alpha} E(\alpha) = 0 \tag{10.29.4}$$

with

- Nuclear charge: $Z = 3$
- Seed value for $\alpha = Z$ for minimization

results in a minimum at $\alpha = 2.5357$ with $E(\alpha) = -7.2333\ E_h$.

This simple one-parameter variational calculation is in error by 3.27% from the experimental value measured by energy necessary to fully ionize the atom (i.e., the sum of the ionization energies in Table A6).

$$E_{exp} = \frac{-5.392\ E_h - 75.638\ E_h - 122.451\ E_h}{27.2114\ E_h} \tag{10.29.5}$$

$$= -7.4778\ E_h \tag{10.29.6}$$

$$\left| \frac{E(\alpha) - E_{exp}}{E_{exp}} \right| = 3.2695\% \tag{10.29.7}$$

As expected the Variational Method estimated energy **always** overestimates the ground state energy (unless the extract wavefunction is describable by the trial wavefunction and then the exact energy is determined).

Two Parameter Estimation

It is possible to improve the results by using a two-parameter calculation in which the 2s electron has a different scale factor that the 1s electrons. In other words the electronic structure would be $1s(\alpha)^2 2s(\beta)^1$.

$$\psi(1s) = \sqrt{\frac{\alpha^3}{\pi}} e^{-\alpha r} \tag{10.29.8}$$

$$\psi(2s) = \sqrt{\frac{\beta^3}{32\pi}} (2 - \beta r) e^{\frac{-\beta r}{2}} \tag{10.29.9}$$

This calculation was first published by E. Bright Wilson (J. Chem. Phys 1, 210 (1933)) in 1933.

- Nuclear charge: $Z = 3$
- Seed values
  - $\alpha = Z$
  - $\beta = Z - 1$ (lower to add a little bit of screening by the 1s electrons)

When the wave function for the $1s(\alpha)^2 2s(\beta)$ electron configuration is written as a Slater determinant, the following variational integrals arise.

$$T_{1s} = \frac{\alpha^2}{2} \tag{10.29.10}$$

$$T_{1s} = \frac{\beta^2}{8} \tag{10.29.11}$$

$$V_{N1a} = -Z\alpha \tag{10.29.12}$$

$$V_{N2s}(\beta) = \frac{-Z\beta}{4} \tag{10.29.13}$$

$$V_{1a1a}(\alpha) = \frac{5}{8}\alpha \tag{10.29.14}$$

$$V_{1s2s}(\alpha,\beta) = \alpha\beta\frac{\beta^4 + 10\alpha\beta^3 + 8\alpha^4 + 20\alpha^3\beta + 12\alpha^2\beta^2}{(2\alpha+\beta)^5} \tag{10.29.15}$$

$$T_{1s2s}(\alpha,\beta) = -4\sqrt{2}\alpha^{\frac{5}{2}}\beta^{\frac{5}{2}}\frac{\beta - 4\alpha}{(2\alpha+\beta)^4} \tag{10.29.16}$$

$$V_{N1a2s}(\alpha,\beta) = \tag{10.29.17}$$

$$V_{1112}(\alpha,\beta) = 32\sqrt{2}\alpha^{\frac{3}{2}}\beta^{\frac{3}{2}}\frac{-28\alpha^3\beta + 264\alpha^4 - 21\alpha\beta^3 - \beta^4 - 86\alpha^2\beta^2}{(2\alpha+\beta)^3(\beta+6\alpha)^4} \tag{10.29.18}$$

$$V_{1212}(\alpha,\beta) = 16\alpha^3\beta^3\frac{13\beta^2 + 20\alpha^2 - 30\beta\alpha}{(\beta+2\alpha)^7} \tag{10.29.19}$$

$$V_{1s2s}(\alpha,\beta) = 32\sqrt{2}\alpha^{\frac{3}{2}}\beta^{\frac{3}{2}}\frac{\alpha-\beta}{(2\alpha+\beta)^4} \tag{10.29.20}$$

The next step in this calculation is to collect these terms in an expression for the total energy of the lithium atom and then minimize it with respect to the variational parameters, α and β. The results of this minimization procedure are shown below

$$\begin{aligned} E'(\alpha,\beta) &= 2T_{1s}(\alpha) + T_{2s}(\beta) - T_{1s}(\alpha)2S_{1s2s}(\alpha\beta)^2 - 2T_{1s2s}(\alpha,\beta)S_{1s2s}(\alpha,\beta) \\ &+2V_{N1s}(\alpha) + V_{N2s}(\beta) - V_{N1s}(\alpha)S_{1s2s}(\alpha,\beta)^2 - 2V_{N1s2s}(\alpha,\beta)S_{1s2s}(\alpha,\beta) \\ &+2V_{1s2s}(\alpha,\beta) + V_{1s1s}(\alpha) - 2V_{1112}(\alpha,\beta)S_{1s2s}(\alpha,\beta) - V_{1212}(\alpha,\beta) \end{aligned} \tag{10.29.21}$$

$$E''(\alpha,\beta) = 1 - S_{1s2s}\alpha\beta)^2 \tag{10.29.22}$$

$$E(\alpha,\beta) = \frac{E'(\alpha,\beta)}{E''(\alpha,\beta)} \tag{10.29.23}$$

Minimization of $E(\alpha,\beta)$ simultaneously with respect to α and β.

$$\frac{d}{d\alpha}E(\alpha) = \frac{d}{d\alpha}E(\beta) = 0 \tag{10.29.24}$$

results in

- α: 2.6797
- β: 1.8683
- $E(\alpha,\beta)$: $-7.3936\ E_h$

Comparison with experiment value of $-7.4778\ E_h$ in Equation 5:

$$\left|\frac{E(\alpha,\beta) - E_{exp}}{E_{exp}}\right| = 1.1258\% \tag{10.29.25}$$

This result is slightly different from that reported by Wilson in 1933.

- α: 2.686
- β: 1.776
- $E(\alpha, \beta)$: -7.3922

These parameters result in a slight higher energy than those above so it is likely that they did not quite find the energy minimum.

Reference

1. E. Bright Wilson (J. Chem. Phys 1, 210 (1933))

Contributors and Attributions

- Prof. Emeritus Frank Rioux (St. John's University and College of St. Benedict)

This page titled 10.29: Electronic Structure - Variational Calculations on the Lithium Atom is shared under a CC BY 4.0 license and was authored, remixed, and/or curated by Frank Rioux via source content that was edited to the style and standards of the LibreTexts platform.

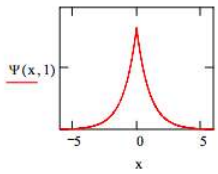
10.30: The Variation Method in Momentum Space

The following normalized trial wavefunction is proposed for a variational calculation on the harmonic oscillator.

$$\psi(x,a) := \sqrt{\frac{1}{a}}exp(\frac{-|x|}{a})$$

$$\int_{-\infty}^{\infty} \psi(x,a)^2 dx \quad assume,\ a > 0 \rightarrow 1$$

However, the graph below shows a cusp at x = 0, indicating that the wavefunction is not well-behaved and therefore cannot be used for quantum mechanical calculations.

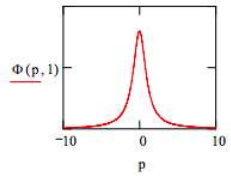


Therefore, the wavefunction is Fourier transformed into the momentum representation.

$$\Phi(p,a) := \int_{-\infty}^{\infty} \frac{exp(-ipx)}{\sqrt{2\pi}} \sqrt{\frac{1}{a}}exp(\frac{-|x|}{a})dx \ |^{assume,\ a>0}_{simplify} \rightarrow (-a^{\frac{1}{2}})\frac{2^{\frac{1}{2}}}{(ipa-1)\pi^{\frac{1}{2}}(ipa+1)}$$

Normalization is checked and the function is graphed.

$$\int_{-\infty}^{\infty} \Phi(p,a)^2 dp \quad assume,\ a > 0 \rightarrow 1$$



The momentum wavefunction appears to be well-behaved, so a variational calculation will be carried out in momentum space.

Assuming a m = k =1 and h = 2π, we have for the harmonic oscillator in momentum space.

- Momentum space integral: $\int_{-\infty}^{\infty} \blacksquare dp$
- Momentum operator: $p\blacksquare$
- Kinetic energy operator: $\frac{p^2}{2}$
- Position operator: $i\frac{d}{dp}\blacksquare$
- Potential energy operator: $\frac{-1}{2}\frac{d^2}{dp^2}\blacksquare$

Evaluate the energy integral in the momentum representation:

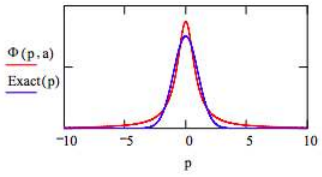
$$E(a) := \int_{-\infty}^{\infty} \Phi(p,a)\frac{p^2}{2}\Phi(p,a)dp... + \int_{-\infty}^{\infty} \Phi(p,a)\frac{-1}{2}\frac{d^2}{dp^2}\Phi(p,a)dp \ |^{simplify}_{assume,\ a>0} \rightarrow \frac{1}{4}\frac{2+a^4}{a^2}$$

Minimize energy with respect to the variational parameter:

a := 1 a := Minimize (E, a) a = 1.189 E(a) = 0.707

Display optimum wavefunction along with exact wavefunction:

$$Exact(p) := \frac{1}{\pi^{\frac{1}{4}}} e^{\frac{-1}{2}p^2}$$



Naturally the agreement with the exact solution is not favorable because of the poor quality of the original coordinate space wavefunction.

$$\frac{E(a) - 0.5}{0.5} = 41.421$$

This page titled 10.30: The Variation Method in Momentum Space is shared under a CC BY 4.0 license and was authored, remixed, and/or curated by Frank Rioux via source content that was edited to the style and standards of the LibreTexts platform.

10.31: Momentum-Space Variation Method for Particle in a Gravitational Field

The following problem deals with a particle of unit mass in a gravitational field with acceleration due to gravity equal to 1.

Energy operator for particles near Earth's surface:

$$\frac{-1}{2\mu}\frac{d^2}{dz^2}\blacksquare + z\blacksquare$$

Trial wave function:

$$\Psi(\alpha, z) := 2\alpha^{\frac{3}{2}} z exp(-\alpha z)$$

Fourier the position wave function into momentum space:

$$\Phi(\alpha, p) := \frac{1}{\sqrt{2\pi}}\int_0^\infty exp(-1pz)\Psi(\alpha, z)dz\Big|_{simplify}^{assume,\ \alpha>0} \rightarrow \frac{2^{\frac{1}{2}}}{\pi^{\frac{1}{2}}}\frac{\alpha^{\frac{3}{2}}}{(ip+a)^2}$$

Demonstrate that the momentum wave function is normalized.

$$\int_{-\infty}^{\infty}\overline{\Phi(\alpha, p)}\Phi(\alpha, p)dp \quad assume,\ \alpha > 0 \rightarrow 1$$

Energy operator in momentum space:

$$\frac{p^2}{2}\blacksquare + i\frac{d}{dp}\blacksquare$$

Evaluate the variational expression for the energy:

$$E(\alpha) := \int_{-\infty}^{\infty}\overline{\Phi(\alpha, p)}\frac{p^2}{2}\Phi(\alpha, p)dp... + \int_{-\infty}^{\infty}\overline{\Phi(\alpha, p)}i(\frac{d}{dp}\Phi(\alpha, p))dp$$

Minimize energy with respect to variational parameter α:

$\alpha := 1$ $\alpha :=$ Minimize (E, α α = 1.145 E(α) = 1.966

This momentum space result is in exact agreement with the coordinate-space result. The exact value for the energy is 1.856.

$$\frac{E(\alpha) - 1.856}{1.856} = 5.9$$

This page titled 10.31: Momentum-Space Variation Method for Particle in a Gravitational Field is shared under a CC BY 4.0 license and was authored, remixed, and/or curated by Frank Rioux via source content that was edited to the style and standards of the LibreTexts platform.

10.32: Momentum-Space Variation Method for the Abs(x) Potential

The energy operator in atomic units in coordinate space for a unit mass particle with potential energy V = |x| is given below.

$$H = \frac{-1}{2}\frac{d^2}{dx^2}\blacksquare + |x|\blacksquare$$

Suggested trial wave function:

$$\Psi(x,\beta) := (\frac{2\beta}{\pi})^{\frac{1}{4}} exp(-\beta x^2)$$

Demonstrate that the wave function is normalized.

$$\int_{-\infty}^{\infty} \Psi(x,\beta)^2 dx \quad assume,\ \beta > 0 \rightarrow 1$$

Carry out Fourier transform to get momentum wave function:

$$\Phi(p,\beta) := \frac{1}{\sqrt{2\pi}} \int_{-\infty}^{\infty} exp(-ipx)\Psi(x,\beta)dx|_{simplify}^{assume,\ \beta>1} \rightarrow \frac{1}{2}\frac{2^{\frac{3}{4}}}{\pi^{\frac{1}{4}}}\frac{e^{\frac{-1}{4}\frac{p^2}{\beta}}}{\beta^{\frac{1}{4}}}$$

Demonstrate that the momentum wave function is normalized.

$$\int_{-\infty}^{\infty} \overline{\Phi(p,\beta)}\Phi(p,\beta)dp \quad assume,\ \beta > 0 \rightarrow 1$$

The energy operator in momentum space is:

$$H = \frac{p^2}{2}\blacksquare + |i + \frac{d}{dp}\blacksquare|$$

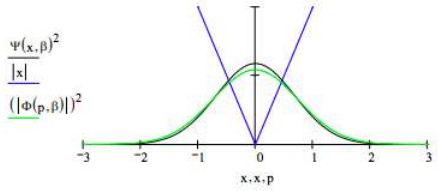
Evaluate the variational energy integral:

$$E(\beta) := \int_{-\infty}^{\infty} \overline{\Phi(p,\beta)}\frac{p^2}{2}\Phi(p,\beta)dp + \int_{-\infty}^{\infty} \overline{\Phi(p,\beta)}|i\frac{d}{dp}\Phi(p,\beta)|dp|_{simplify}^{assume,\ \beta>0} \frac{1}{2}\frac{\pi^{\frac{1}{2}}\beta^{\frac{3}{2}} + 2^{\frac{1}{2}}}{\beta^{\frac{1}{2}}\pi^{\frac{1}{2}}}$$

Minimize the energy with respect to the variational parameter β and report its optimum value and the ground-state energy.

$\beta := 1$ $\beta :=$ Minimize (E, β) $\beta = 0.542$ E(β) = 0.813

Plot the coordinate and momentum wave functions and the potential energy on the same graph.

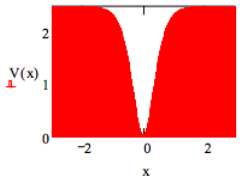


This page titled 10.32: Momentum-Space Variation Method for the Abs(x) Potential is shared under a CC BY 4.0 license and was authored, remixed, and/or curated by Frank Rioux via source content that was edited to the style and standards of the LibreTexts platform.

10.33: Variational Method for the Feshbach Potential

Define potential energy: V_0 = 2.5 d = 0.5 $V(x) = V_o \tanh\left(\frac{x}{d}\right)^2$

Display potential energy:



Choose Gaussian trial wavefunction:

$$\psi(x,\beta) = \left(\frac{2\beta}{\pi}\right)^{\frac{1}{4}} exp(-\beta x^2)$$

Demonstrate that the trial wavefunction is normalized.

$$\int_{-\infty}^{\infty} \psi(x,\beta)^2 dx \quad assume,\ \beta > 0 \rightarrow 1$$

Evaluate the variational integral.

$$E(\beta) = \int_{-\infty}^{\infty} \psi(x,\beta)\frac{-1}{2}\frac{d^2}{dx^2}\psi(x,\beta)dx + \int_{-\infty}^{\infty} V(x)\psi(x,\beta)^2 dx$$

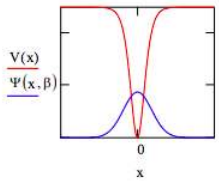
Minimize the energy integral with respect to the variational parameter, β.

β = 1 β = Minimize (E, β) β = 0.913 E(β) = 1.484

Calculate the % error given that numerical integration of Schrödinger's equation (see next tutorial) yields E = 1.44949 E_h.

$$\frac{E(\beta) - 1.44949}{1.44949} \times 100 = 2.36$$

Display wavefunction in the potential well.



Calculate the probability that tunneling is occurring.

$$V(x) = 1.484 \Big|^{solve,\ x}_{float,\ 3} \rightarrow \begin{pmatrix} -1.511 \\ 0.511 \end{pmatrix}$$

$$2\int_{0.511}^{\infty} \psi(x,\beta)^2 dx = 0.329$$

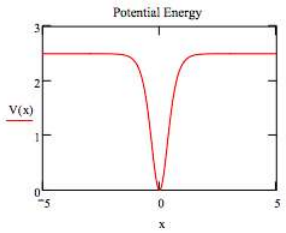
This page titled 10.33: Variational Method for the Feshbach Potential is shared under a CC BY 4.0 license and was authored, remixed, and/or curated by Frank Rioux via source content that was edited to the style and standards of the LibreTexts platform.

10.34: Numerical Solution for the Feshbach Potential

Parameters go here: x_{max} = 5 m = 1 V_0 = 2.5 μ = 0 d = .5

Potential energy:

$$V(x) = V_0 tanh\left(\frac{x}{d}\right)^2$$



Given:

$$\frac{-1}{2m}\left(\frac{d^2}{dx^2}\psi(x)\right) + V(x)\psi(x) = E\psi(x)$$

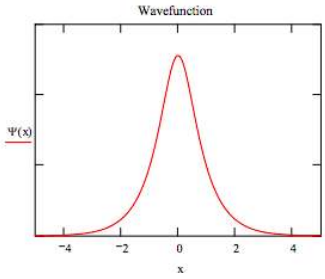
$$\psi(-x_{max} = 0 \quad \psi(-x_{max}) = 0.1$$

$$\psi = Odesolve(x, x_{max})$$

Normalize wavefunction:

$$\psi(x) = \frac{\psi(x)}{\sqrt{\int_0^{x_{max}} \psi(x)^2 dx}}$$

Enter energy guess: E = 1.44949

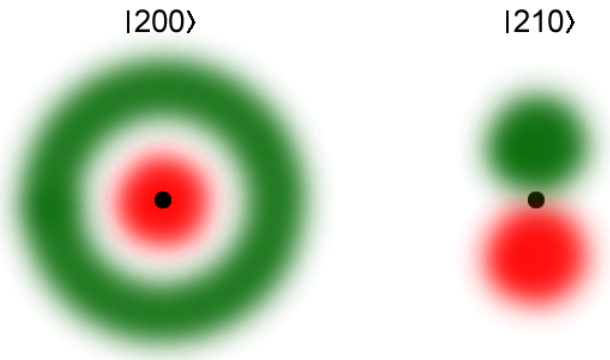


This page titled 10.34: Numerical Solution for the Feshbach Potential is shared under a CC BY 4.0 license and was authored, remixed, and/or curated by Frank Rioux via source content that was edited to the style and standards of the LibreTexts platform.

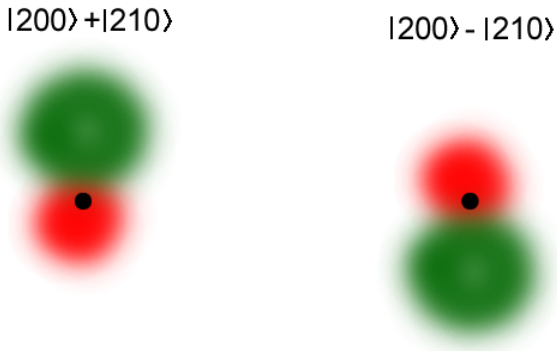
10.35: First Order Degenerate Perturbation Theory - the Stark Effect of the Hydrogen Atom

The n = 2 level of the hydrogen atom is 4-fold degenerate with energy -0.125 E_h. In terms of the $|nlm\rangle$ quantum numbers these states are $|2,0,0\rangle$, $|2,1,0\rangle$, $|2,1,1\rangle$, and $|2,2,-1\rangle$. An electric field in the z-direction splits the degeneracy because it mixes the $2s$ and the $2p_z$ orbitals creating one linear combination polarized in the direction of the field and an other polarized against the field.

What happens is that the s and p wavefunctions "mixed" to produce eigenstates that have shifted centers. This means the atom gets an induced electric dipole moment, whose interaction with the external field either lowers or raises the eigenenergy.



The $|2,0,0\rangle$ wavfunction is spherically symmetric (left), while the $|2,2,0\rangle$ wavefunction has two lobes where the wavefunction has different signs. If the applied field is strong, then the eigenstates will be even mixtures of these, but with different phases.



Note in particular that the electronic center of charge has moved from the origin, which means the states have nonzero dipole moments. With the electric field pointing downwards, the state to the left has a lower energy and the one to the right is raised.

Degenerate Perturbation Theory

The Hamiltonian for this perturbation in atomic units is:

$$H' = \varepsilon z,$$

which in spherical polar coordinates is:

$$H' = \varepsilon r \cos(\theta),$$

where ε is the electric field strength.

In this perturbation method treatment the hydrogen atom eigenfunctions are used to evaluate the matrix elements associated with the total Hamiltonian,

$$H = H^o + H'$$

Since the results for H^o are known (-0.125 E_h) only the matrix elements for H' need to be evaluated and most of these are zero. Below we show that = = -3ε and that the other matrix elements involving the $n = 2$ orbitals are equal to zero.

$$\psi_{2s}(r) = \frac{1}{\sqrt{32\pi}}(2-r)\exp\left(\frac{-r}{2}\right)$$

$$\psi_{2p_z}(r,\theta) = \frac{1}{\sqrt{32\pi}}(r)\ exp\left(\frac{-r}{2}\right)\cos(\theta)$$

$$\psi_{2p_z}(r,\theta,\phi) = \frac{1}{\sqrt{32\pi}}(r)\exp\left(\frac{-r}{2}\right)\sin(\theta)\cos(\phi)$$

$$\psi_{2p_z}(r,\theta,\phi) = \frac{1}{\sqrt{32\pi}}(r)\exp\left(\frac{-r}{2}\right)\sin(\theta)\sin(\phi)$$

$\langle 2s|H'|2s\rangle = 0$

$$\int_0^\infty\int_0^\pi\int_0^{2\pi}\psi_{2s}(r)\varepsilon r\cos(\theta)\psi_{2s}(r)r^2\sin(\theta)d\pi d\theta dr \rightarrow 0$$

$\langle 2p_z|H'|2p_z\rangle = \langle 2p_y|H'|2p_y\rangle = \langle 2p_x|H'|2p_x\rangle = 0$

$$\int_0^\infty\int_0^\pi\int_0^{2\pi}\psi_{2pz}(r,\theta)\varepsilon r\cos(\theta)\psi_{2pz}(r,\theta)r^2\sin(\theta)d\phi\, d\theta\, dr \rightarrow 0$$

$$\int_0^\infty\int_0^\pi\int_0^{2\pi}\psi_{2py}(r,\theta,\phi)\varepsilon r\cos(\theta)\psi_{2py}(r,\theta,\phi)r^2\sin(\theta)d\phi\, d\theta\, dr \rightarrow 0$$

$$\int_0^\infty\int_0^\pi\int_0^{2\pi}\psi_{2px}(r,\theta,\phi)\varepsilon r\cos(\theta)\psi_{2px}(r,\theta,\phi)r^2\sin(\theta)d\phi\, d\theta\, dr \rightarrow 0$$

$\langle 2s|H'|2p_z\rangle = -3\varepsilon$

$$\int_0^\infty\int_0^\pi\int_0^{2\pi}\psi_{2s}(r)\varepsilon r\cos(\theta)\psi_{2pz}(r,\theta)r^2\sin(\theta)d\phi\, d\theta\, dr \rightarrow -3\varepsilon$$

$\langle 2s|H'|2p_x\rangle = \langle 2s|H'|2p_y\rangle = 0$

$$\int_0^\infty\int_0^\pi\int_0^{2\pi}\psi_{2s}(r)\varepsilon r\cos(\theta)\psi_{2px}(r,\theta,\phi)r^2\sin(\theta)d\phi\, d\theta\, dr \rightarrow 0$$

$$\int_0^\infty\int_0^\pi\int_0^{2\pi}\psi_{2s}(r)\varepsilon r\cos(\theta)\psi_{2py}(r,\theta,\phi)r^2\sin(\theta)d\phi\, d\theta\, dr \rightarrow 0$$

$\langle 2p_x|H'|2p_y\rangle = \langle 2p_x|H'|2p_z\rangle = \langle 2p_y|H'|2p_z\rangle = 0$

$$\int_0^\infty\int_0^\pi\int_0^{2\pi}\psi_{2px}(r,\theta,\phi)\varepsilon r\cos(\theta)\psi_{2py}(r,\theta,\phi)r^2\sin(\theta)d\phi\, d\theta\, dr \rightarrow 0$$

$$\int_0^\infty\int_0^\pi\int_0^{2\pi}\psi_{2px}(r,\theta,\phi)\varepsilon r\cos(\theta)\psi_{2pz}(r,\theta)r^2\sin(\theta)d\phi\, d\theta\, dr \rightarrow 0$$

$$\int_0^\infty\int_0^\pi\int_0^{2\pi}\psi_{2py}(r,\theta,\phi)\varepsilon r\cos(\theta)\psi_{2pz}(r,\theta)r^2\sin(\theta)d\phi\, d\theta\, dr \rightarrow 0$$

The matrix elements of the 4x4 perturbation matrix are

$$\langle\psi_i|H^o + H'|\psi_j\rangle,$$

where the ψ′s are the 2s, $2p_z$, $2p_x$, and $2p_y$ hydrogen atomic orbitals. Using the values of the integrals evaluated above the perturbation matrix is formed and its eigenvalues and eigenvectors found.

$$\begin{pmatrix} -0.125-E & -3\varepsilon & 0 & 0 \\ -3\varepsilon & -0.125-E & 0 & 0 \\ 0 & 0 & -0.125-E & 0 \\ 0 & 0 & 0 & -0.125-E \end{pmatrix} \begin{pmatrix} c_1 \\ c_2 \\ c_3 \\ c_4 \end{pmatrix} = 0$$

This 4x4 energy matrix is clearly one 2x2 and two 1x1 energy matrices. In other words, as we learned from evaluating the matrix elements, the $2p_x$ and $2p_y$ are not perturbed by the electric field to first order and have energy -0.125 E_h.

The eigenvectors and eigenvalues of the 2x2 are found as follows.

$$\begin{bmatrix} (-0.125-E)c_1 - 3\varepsilon c_2 = 0) \\ -3\varepsilon c_1 + (-0.125-E)c_2 = 0) \\ c_1^2 + c_2^2 = 1 \end{bmatrix} \Big|_{float,\,3}^{solve,\,\begin{pmatrix} c_1 \\ c_2 \\ E \end{pmatrix}} \rightarrow \begin{pmatrix} -0.707 & 0.707 & 3.0\varepsilon - 0.125 \\ 0.707 & -0.707 & 3.0\varepsilon - 0.125 \\ 0.707 & 0.707 & -3.0\varepsilon - 0.125 \\ -0.707 & -0.707 & -3.0\varepsilon - 0.125 \end{pmatrix}$$

The wavefunctions of the perturbed 2s and $2p_z$ orbitals are sp_z hybrid states as shown below.

$$\frac{1}{\sqrt{2}}(2s + 2p_z) \quad E = (-0.125 - 3\varepsilon)E_h$$

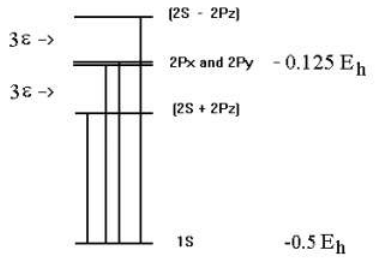
$$\frac{1}{\sqrt{2}}(2s - 2p_z) \quad E = (-0.125 + 3\varepsilon)E_h$$

Because the energy of the symmetric 1s state is unaffected by the electric field, the effect of this perturbation on the electronic spectrum of hydrogen is to split the n = 1 to n = 2 transition into three lines of relative intensity 1:2:1.

< 2s | H′ | 2s > = 0

$$\psi_{1s}(r) = \frac{1}{\sqrt{\pi}} exp(-r)$$

$$\int_0^{\infty}\int_0^{\pi}\int_0^{2\pi} \psi_{1s}(r)\varepsilon r\cos(\theta)\psi_{1s}(r)r^2\sin(\theta)d\phi\, d\theta\, dr \rightarrow 0$$



Contributors and Attributions

- Prof. Emeritus Frank Rioux (St. John's University and College of St. Benedict)
- Emilio Pisanty via StackExchange (Physics)

This page titled 10.35: First Order Degenerate Perturbation Theory - the Stark Effect of the Hydrogen Atom is shared under a CC BY 4.0 license and was authored, remixed, and/or curated by Frank Rioux via source content that was edited to the style and standards of the LibreTexts platform.

10.36: Variational Calculation for the Polarizability of the Hydrogen Atom

In this exercise the polarizability of the hydrogen atom is calculated according to the procedure outlined in Problem 8-31 in the second edition of McQuarrie's Quantum Chemistry. In the interest of clarity of mathematical expression atomic units are used:

$$e = me = h/2\pi = 4\pi\varepsilon_o = 1.$$

Polarizability, α, is a measure of the distortion of the electron density in the presence of an electric field. The interaction (perturbation) energy due to a field of strength ε with the hydrogen atom electron is easily shown to be:

$$E = \frac{-\alpha\varepsilon^2}{2}$$

Given that the ground state energy of the hydrogen atom is -0.5, in the presence of the electric field we would expect the electronic energy of the perturbed hydrogen atom to be,

$$E_{H\ atom} = \frac{-1}{2} - \frac{\alpha\varepsilon^2}{2}$$

It is assumed that the field direction is along the z axis. In this case the operator for the interaction of the external field with the electron density is, in spherical coordinates,

$$H' = \varepsilon r\cos(\theta)$$

Thus the total energy operator for the hydrogen atom in the presence of an electric field is this term plus the kinetic and electron-nucleus operator.

$$H = \frac{-1}{2r}\frac{d^2}{dr^2}(r\blacksquare) - \frac{1}{2r^2\sin(\theta)}\frac{d}{d\theta}\left(\sin(\theta)\frac{d}{d\theta}\blacksquare\right) - \frac{1}{2r^2\sin(\theta)^2}\frac{d^2}{d\phi^2}\blacksquare - \frac{1}{r}\blacksquare + \varepsilon r\cos(\theta)\blacksquare$$

The empty place holders indicate the location of the wave function to be operated on.

In the absence of the electric field the hydrogen atom is in the 1s electronic state. The field distorts (polarizes) the electron density and this can be modeled by assuming that in the presence of the external field the electron is in a state which is a superposition of the 1s and $2p_z$ electronic states.

$$\Phi(r) = c_1\psi_{1s}(r) + c_2\psi_{2pz}(r,\theta)$$

$$\psi_{1s}(r) = \frac{1}{\sqrt{\pi}}exp(-r) \quad \psi_{2pz}(r,\theta) = \frac{1}{\sqrt{32\pi}}(r)exp\left(-\frac{r}{2}\right)\cos(\theta)$$

Within the variational method, using such a trial wave function requires solving the following secular determinant.

$$\begin{vmatrix} H_{11} - ES_{11} & H_{12} - ES_{12} \\ H_{21} - ES_{21} & H_{22} - ES_{22} \end{vmatrix} = 0$$

Due to normalization, orthogonality and symmetry we know that: $H_{12} = H_{21}$; $S_{11} = S_{22} = 1$; $S_{12} = S_{21} = 0$. We now evaluate H_{11}, H_{12} and H_{22} and solve the secular determinant.

$$H_{11} = \int_0^\infty\int_0^\pi\int_0^{2\pi}\psi_{1s}(r)\begin{bmatrix} -\frac{1}{2r}\frac{d^2}{dr^2}(r\psi_{1s}(r))\ldots \\ +\frac{-1}{2r^2\sin(\theta)}\left[\frac{d}{d\theta}\sin(\theta)\frac{d}{d\theta}\psi_{1s}(r)\right] \\ +\frac{-1}{2r^2sin(\theta)^2}\frac{d^2}{d\phi^2}\psi_{1s}(r)\end{bmatrix} r^2sin(\theta)d\ phid\theta dr\ldots$$

$$\rightarrow \frac{-1}{2} + \int_0^\infty\int_0^\pi\int_0^{2\pi}\psi_{1s}(r)\left(-\frac{1}{r} + \varepsilon r\cos(\theta)\right)\psi_{1s}(r)r^2\sin(\theta)d\phi d\theta dr$$

$$H_{12} = \int_0^\infty\int_0^\pi\int_0^{2\pi}\psi_{1s}(r)\begin{bmatrix} -\frac{1}{2r}\frac{d^2}{dr^2}(r\psi_{2pz}(r,\theta))\ldots \\ +\frac{-1}{2r^2\sin(\theta)}\left[\frac{d}{d\theta}\sin(\theta)\frac{d}{d\theta}\psi_{2pz}(r,\theta)\right] \\ +\frac{-1}{2r^2sin(\theta)^2}\frac{d^2}{d\phi^2}\psi_{2pz}(r,\theta)\end{bmatrix} r^2sin(\theta)d\ phid\theta dr\ldots$$

$$\rightarrow \frac{128}{243}2^{\frac{1}{2}}\varepsilon + \int_0^\infty\int_0^\pi\int_0^{2\pi}\psi_{1s}(r)\left(-\frac{1}{r} + \varepsilon r\cos(\theta)\right)\psi_{2pz}(r,\theta)r^2\sin(\theta)d\phi d\theta dr$$

$$H_{22} = \int_0^{\infty} \int_0^{\pi} \int_0^{2\pi} \psi_{2pz}(r,\theta) \begin{bmatrix} -\frac{1}{2r}\frac{d^2}{dr^2}(r\psi_{2pz}(r,\theta))... \\ +\frac{-1}{2r^2\sin(\theta)}\left[\frac{d}{d\theta}\sin(\theta)\frac{d}{d\theta}\psi_{2pz}(r,\theta)\right] \\ +\frac{-1}{2r^2 sin(\theta)^2}\frac{d^2}{d\phi^2}\psi_{2pz}(r,\theta) \end{bmatrix} r^2 sin(\theta) d\ phid\theta dr...$$

$$\rightarrow \frac{-1}{8} + \int_0^{\infty} \int_0^{\pi} \int_0^{2\pi} \psi_{2pz}(r,\theta)\left(-\frac{1}{r} + \varepsilon r\cos(\theta)\right)\psi_{2pz}(r,\theta) r^2\sin(\theta) d\phi d\theta dr$$

Solving the secular determinant for the energy eigenvalues:

$$\left|\begin{pmatrix} H_{11}-E & H_{12} \\ H_{12} & H_{22}-E \end{pmatrix}\right| = 0 \Big|_{float,\ 4}^{solve,\ E} \begin{bmatrix} (-.3125) + .2572e(-3)(.5314e6 + .8389e7\varepsilon^2)^{\frac{1}{2}} \\ (-.3125) - .2572e(-3)(.5314e6 + .8389e7\varepsilon^2)^{\frac{1}{2}} \end{bmatrix}$$

The lowest energy eigenvalue is expanded in ε in order to compare the variational calculation with equation 2.

$$(-.3125 - .2572e - 3\left(.5314e6 + .8389e7\varepsilon^2\right)^{\frac{1}{2}}$$

This comparison shows that, in atomic units, α has the value of 2.96. This value is in error by 35% when compared to the experimental result of 4.0. Although it is not apparent when atomic units are used, this calculation does reveal that atomic polarizability is proportional to atomic volume.

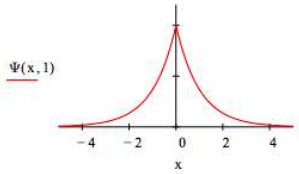
This page titled 10.36: Variational Calculation for the Polarizability of the Hydrogen Atom is shared under a CC BY 4.0 license and was authored, remixed, and/or curated by Frank Rioux via source content that was edited to the style and standards of the LibreTexts platform.

10.37: Hybrid Variational Calculation for the 1D Hydrogen Atom with Delta Function Potential

The following normalized trial wave function is used in a variational calculation for the energy of a one-dimensional model of the hydrogen atom that postulates a delta-function potential energy interaction between the electron and the proton. The variational parameter, α, is a decay constant which controls the spatial extent of the wave function.

$$\Psi(x,\alpha) = \sqrt{\alpha} exp(-\alpha|x|)$$

$$\int_{-\infty}^{\infty} \Psi(x,\alpha)^2 dx \ assume,\ \alpha > 0 \rightarrow 1$$



The Hamiltonian energy operator in coordinate space in atomic units ($h/2\pi = m_e = e = 1$) is:

$$H = \frac{-1}{2}\frac{d^2}{dx^2}\blacksquare - \Delta(x)\blacksquare$$

The problem this tutorial seeks to solve is that it is obvious that the coordinate wave function is unsuitable for the calculation of the expectation value for kinetic energy because it is not well-behaved at x = 0. The wave function and its first and second derivatives are discontinuous at x = 0. In spite of this defect, calculation of the expectation value for potential energy presents no problem in coordinate space.

Therefore the plan is to calculate the potential energy in coordinate space and Fourier transform the coordinate wave function into momentum space, where the wave function is well behaved, for the calculation of kinetic energy. Then the energy will be minimized with respect to α, yielding the following results: α = 1, E = -0.5.

Using several values for x and the optimum value of α it is shown that solving Schrödinger's equation in the coordinate representation for the energy gives the correct value except at the discontinuity, x = 0.

$$x = 0 \quad \frac{-1}{2}\frac{d^2}{dx^2}\Psi(x,1) - \Delta(x)\Psi(x,1) = E\Psi(x,1)\ solve,\ E \rightarrow 0$$

$$x = 2 \quad \frac{-1}{2}\frac{d^2}{dx^2}\Psi(x,1) - \Delta(x)\Psi(x,1) = E\Psi(x,1)\ solve,\ E \rightarrow \frac{-1}{2}$$

$$x = -1 \quad \frac{-1}{2}\frac{d^2}{dx^2}\Psi(x,1) - \Delta(x)\Psi(x,1) = E\Psi(x,1)\ solve,\ E \rightarrow \frac{-1}{2}$$

Calculation of Potential Energy in Coordinate Space

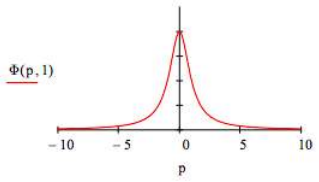
$$V(\alpha) = \int_{-\infty}^{\infty} \Psi(x,\alpha) - \Delta(x)\Psi(x,]alpha)dx \ \rightarrow -\alpha$$

Fourier Transform of the Coordinate Space Wave Function into Momentum Space

$$\Phi(p,\alpha) = \int_{-\infty}^{\infty} \frac{exp(-pix)}{\sqrt{2\pi}}\Psi(x,\alpha)dx \ \Big|_{simplify}^{assume,\ \alpha>0} \rightarrow \frac{\sqrt{2}\alpha^{\frac{3}{2}}}{\sqrt{\pi}(\alpha^2+p^2)}$$

Before proceeding, we demonstrate that the momentum space wavefunction is normalized and well behaved.

$$\int_{\infty}^{-\infty} \Phi(p,\alpha)^2 dp \ assume,\ \alpha > 0 \rightarrow 1$$



The kinetic energy operator in momentum space for an electron is: $\frac{p^2}{2}$■

Therefore, the kinetic energy is:

$$T(\alpha) := \int_{-\infty}^{\infty} \Phi(p,\alpha)\frac{p^2}{2}\Phi(p,\alpha)dp \ asssume,\ \alpha > 0 \rightarrow \frac{\alpha^2}{2}$$

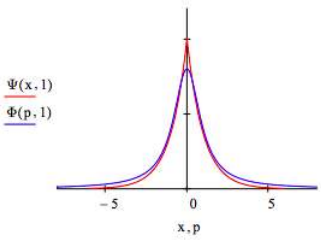
Now the coordinate and momentum space calculations are combined and the total energy is minimized with respect to the variational parameter, α.

$$E(\alpha) := T(\alpha) + V(\alpha)$$

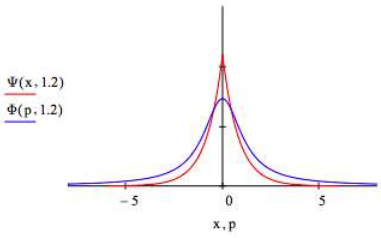
$$\alpha := \frac{d}{d\alpha}E(\alpha) = 0 \ solve,\ \alpha \rightarrow 1$$

$$E(\alpha) \rightarrow \frac{-1}{2}$$

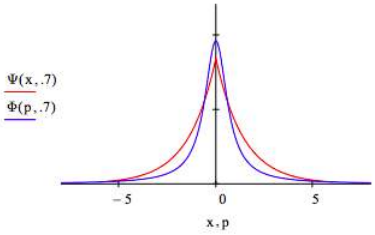
The optimum coordinate and momentum wavefunctions are compared below: x = -6, -5.99 .. 6



The uncertainty principle is illustrated by displaying the coordinate and momentum wave functions for different values of the decay constant, α. For α = 1.2 the spatial distribution contracts and the momentum distribution expands relative to the optimum value α =1. In other words, less uncertainty in position requires greater uncertainty in momentum.



For α = 0.7 the spatial distribution expands and the momentum distribution contracts. More uncertainty in position leads to less uncertainty in momentum.



Numerically the Heisenberg uncertainty principle states that the product of the uncertainties in position and momentum must be greater than or equal to 0.5 in atomic units.

$$\Delta x = \sqrt{\langle x^2 \rangle - \langle x \rangle^2}$$

$$\Delta p = \sqrt{\langle x^2 \rangle - \langle x \rangle^2}$$

$$\Delta x \Delta p \geq \frac{h}{2}$$

The momentum wave function is now used to verify that the uncertainty principle is satisfied.

$$\begin{pmatrix} Operator & Coordinate\ Space & Momentum\ Space \\ position & x\blacksquare & i\frac{d}{dp}\blacksquare \\ momentum & \frac{1}{i}\frac{d}{dx}\blacksquare & p\blacksquare \end{pmatrix}$$

$$x_{ave} = \int_{-\infty}^{\infty} \Phi(p,1) i \frac{d}{dp} \Phi(p,1) dp \rightarrow 0$$

$$x2_{ave} = \int_{-\infty}^{\infty} \Phi(p,1) - \frac{d}{dp} \Phi(p,1) dp \rightarrow \frac{1}{2}$$

$$p_{ave} = \int_{-\infty}^{\infty} \Phi(p,1)^2 dp \rightarrow 0$$

$$p2_{ave} = \int_{-\infty}^{\infty} p^2 \Phi(p,1)^2 dp \rightarrow 1$$

$$\sqrt{x2_{ave} - x_{ave}^2} \sqrt{p2_{ave} - p_{ave}^2} = 0.707$$

Concluding Remarks

This hybrid variational calculation on a one-dimensional model of the hydrogen atom using a delta function potential interaction between the proton and electron yields the correct ground state energy. The model is composed of two peculiar elements: a trial wave function that has discontinuity at x = 0 and a potential energy interaction that is zero everywhere except at x = 0.

In *Molecular Quantum Mechanics*, 3rd ed., p. 43 Atkins and Friedman list the following criteria for an acceptable wave function.

1. It must be single valued (strictly Ψ*Ψ must be single valued).
2. It must not be infinite over a finite range.
3. It must be continuous everywhere.
4. It must have a continuous first derivative, except at ill-behaved regions of the potential.

Ψ(x,α) does not satisfy criterion 3, making it impossible to calculate kinetic energy in the coordinate representation. However, it does satisfy criterion 4, so it is possible to calculate potential energy in the coordinate representation. Φ(p,α) is well-behaved for all values of p. It is used to calculate kinetic energy, but it is not suitable for the calculation of potential energy. That's why a hybrid variational calculation was used.

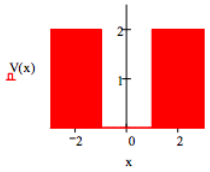
This page titled 10.37: Hybrid Variational Calculation for the 1D Hydrogen Atom with Delta Function Potential is shared under a CC BY 4.0 license and was authored, remixed, and/or curated by Frank Rioux via source content that was edited to the style and standards of the LibreTexts platform.

10.38: Variation Method Using the Wigner Function- Finite Potential Well

Define potential energy:

$$V(x) = if[(x \geq -1)(x \leq 1), 0, 20$$

Display potential energy:



Choose trial wave function:

$$\psi(x, \beta) = \left(\frac{2\beta}{\pi}\right)^2 exp(-\beta x^2)$$

Calculate the Wigner distribution function:

$$W(x, p, \beta) = \frac{1}{2\pi}\int_{-\infty}^{\infty} \psi\left(x + \frac{s}{2}, \beta\right) ds \Big|_{assume,\ \beta>0}^{simplify} \rightarrow \frac{1}{\pi} e^{\frac{-1}{2}\frac{4\beta^2 x^2 + p^2}{\beta}}$$

Evaluate the variational integral:

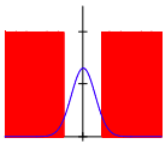
$$E(\beta) = \int_{-\infty}^{\infty}\int_{-\infty}^{\infty} (W, x, p, \beta)\left(\frac{p^2}{2} V(x)\right) dx\ dp$$

Minimize the energy integral with respect to the variational parameter, β.

β = 1 β = Minimize (E, β) β = 0.678 E(β) = 0.538

Calculate and display the coordinate distribution function:

$$P(x, \beta) = \int_{-\infty}^{\infty} W(x, p, \beta) dp$$

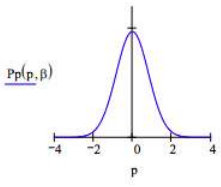


Probability that tunneling is occuring:

$$2\int_{1}^{\infty} P(x, \beta) dx = 0.1$$

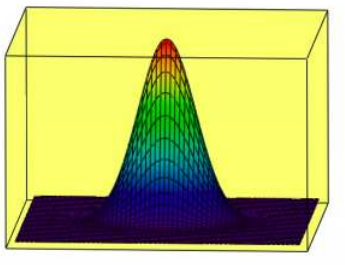
Calculate and display the momentum distribution function:

$$Pp(p, \beta) = \int_{-\infty}^{\infty} W(x, p, \beta) dx$$



Display the Wigner distribution function:

$N = 60$ i = 0 .. N $x_i = -3 + \frac{6j}{N}$ j =) .. N $p_j = -5 + \frac{10j}{N}$ $Wigner_{i,j} = W(x_i, p_j, \beta$



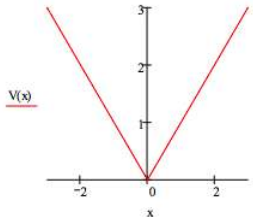
This page titled 10.38: Variation Method Using the Wigner Function- Finite Potential Well is shared under a CC BY 4.0 license and was authored, remixed, and/or curated by Frank Rioux via source content that was edited to the style and standards of the LibreTexts platform.

10.39: 455. Variation Method Using the Wigner Function- V(x) = |x|

Define potential energy:

$$V(x) = |x|$$

Display potential energy:



Choose trial wave function:

$$\psi(x, \beta = \left(\frac{2\beta}{\pi}\right)^{\frac{1}{4}} exp(-\beta x^2)$$

Calculate the Wigner distribution function:

$$W(x,p,\beta) = \frac{1}{2\pi}\int_{-\infty}^{\infty} \psi\left(x + \frac{s}{2}, \beta\right) exp(isp)\psi(\left(x - \frac{s}{2}, \beta\right)\, ds \,\Big|_{assume,\ \beta>0}^{simplify} \rightarrow \frac{1}{\pi} e^{\frac{-1}{2}\frac{4\beta^2x^2+p^2}{\beta}}$$

Evaluate the variational integral:

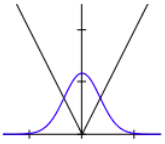
$$E(\beta) = \int_{-\infty}^{\infty}\int_{-\infty}^{\infty} W(x,p,\beta)\left(\frac{p^2}{2} + V(x)\right) dx\ dp \,\Big|_{simplify}^{assume,\ \beta>0} \rightarrow \frac{1}{2}\frac{\beta^{\frac{3}{2}}\pi^{\frac{1}{2}} + 2^{\frac{1}{2}}}{\pi^{\frac{1}{2}}\beta^{\frac{1}{2}}}$$

Minimize the energy integral with respect to the variational parameter, β.

β = 1 β = Minimize (E, β) β = 0.542 E(β) = 0.813

Calculate and display the coordinate distribution function:

$$Px(x,\beta) = \int_{-\infty}^{\infty} W(x,p,\beta)dp$$



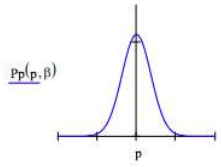
Classical turning points: +/- 0.813

Probability that tunneling is occurring:

$$2\int_{0.813}^{\infty} Px(x,\beta)dx = 0.231$$

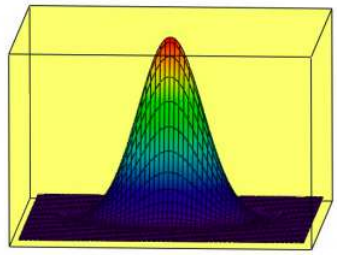
Calculate and display the momentum distribution function:

$$Pp(p,\beta) = \int_{-\infty}^{\infty} W(x,p,\beta)dx$$



Display the Wigner distribution function:

$$N = 60 \quad i = 0 .. N \quad x_i = -3 + \frac{6i}{N} \quad j = 0 .. N \quad p_j = -5 + \frac{10j}{N} \quad Wigner_{i,j} = W(x_i, p_j, \beta)$$



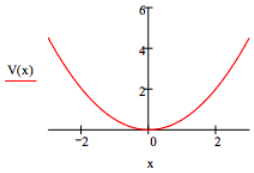
This page titled 10.39: 455. Variation Method Using the Wigner Function- V(x) = |x| is shared under a CC BY 4.0 license and was authored, remixed, and/or curated by Frank Rioux via source content that was edited to the style and standards of the LibreTexts platform.

10.40: Variation Method Using the Wigner Function- The Harmonic Oscillator

Define potential energy:

$$V(x) = \frac{x^2}{2}$$

Display potential energy:



Choose trial wave function:

$$\psi(x, \beta = \left(\frac{2\beta}{\pi}\right)^{\frac{1}{4}} exp(-\beta x^2)$$

Calculate the Wigner distribution function:

$$W(x, p, \beta) = \frac{1}{2\pi} \int_{-\infty}^{\infty} \psi\left(x + \frac{s}{2}, \beta\right) exp(isp) \psi(\left(x - \frac{s}{2}, \beta\right) ds \Big|_{assume,\ \beta>0}^{simplify} \rightarrow \frac{1}{\pi} e^{\frac{-1}{2} \frac{4\beta^2 x^2 + p^2}{\beta}}$$

Evaluate the variational integral:

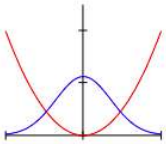
$$E(\beta) = \int_{-\infty}^{\infty} \int_{-\infty}^{\infty} W(x, p, \beta) \left(\frac{p^2}{2} + V(x)\right) dx\ dp$$

Minimize the energy integral with respect to the variational parameter, β.

β = 1 β = Minimize (E, β) β = 0.5 E(β) = 0.5

Calculate and display the coordinate distribution function:

$$Px(x, \beta) = \int_{-\infty}^{\infty} W(x, p, \beta) dp$$



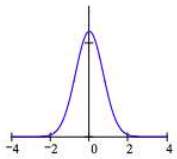
Classical turning point: $x_{cl} = 0.5^{\frac{1}{2}} \quad x_{cl} = 0.707$

Probability that tunneling is occurring:

$$2 \int_{0.707}^{\infty} Px(x, \beta) dx = 0.317$$

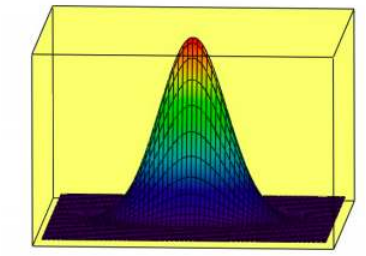
Calculate and display the momentum distribution function:

$$Pp(p, \beta) = \int_{-\infty}^{\infty} W(x, p, \beta) dx$$



Display the Wigner distribution function:

$$N = 60 \quad i = 0 .. N \quad x_i = -3 + \frac{6i}{N} \quad j = 0 .. N \quad p_j = -5 + \frac{10j}{N} \quad Wigner_{i,j} = W(x_i, p_j, \beta)$$



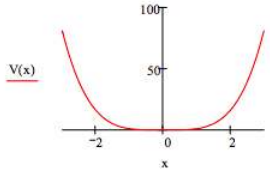
This page titled 10.40: Variation Method Using the Wigner Function- The Harmonic Oscillator is shared under a CC BY 4.0 license and was authored, remixed, and/or curated by Frank Rioux via source content that was edited to the style and standards of the LibreTexts platform.

10.41: Variation Method Using the Wigner Function - The Quartic Oscillator

Define potential energy:

$$V(x) = x^4$$

Display potential energy:



Choose trial wave function:

$$\psi(x, \beta = \left(\frac{2\beta}{\pi}\right)^{\frac{1}{4}} exp(-\beta x^2)$$

Calculate the Wigner distribution function:

$$W(x,p,\beta) = \frac{1}{2\pi}\int_{-\infty}^{\infty} \psi\left(x + \frac{s}{2}, \beta\right) exp(isp)\psi(\left(x - \frac{s}{2}, \beta\right) ds \left|_{assume,\ \beta>0}^{simplify} \rightarrow \frac{1}{\pi} e^{\frac{-1}{2}\frac{4\beta^2x^2+p^2}{\beta}}\right.$$

Evaluate the variational integral:

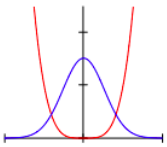
$$E(\beta) = \int_{-\infty}^{\infty}\int_{-\infty}^{\infty} W(x,p,\beta)\left(\frac{p^2}{2} + V(x)\right) dx\ dp$$

Minimize the energy integral with respect to the variational parameter, β.

β = 1 β = Minimize (E, β) β = 0.90856 E(β) = 0.68142

Calculate and display the coordinate distribution function:

$$Px(x,\beta) = \int_{-\infty}^{\infty} W(x,p,\beta)dp$$



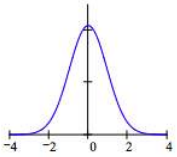
Classical turning points: $x_{cl} = 0.681^{\frac{1}{4}} \quad x_{cl} = 0.90842$

Probability that tunneling is occurring:

$$2\int_{0.908}^{\infty} Px(x,\beta)dx = 0.08345$$

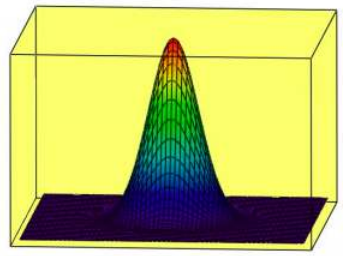
Calculate and display the momentum distribution function:

$$Pp(p,\beta) = \int_{-\infty}^{\infty} W(x,p,\beta)dx$$



Display the Wigner distribution function:

$$N = 60 \quad i = 0 .. N \quad x_i = -3 + \frac{6i}{N} \quad j = 0 .. N \quad p_j = -5 + \frac{10j}{N} \quad Wigner_{i,j} = W(x_i, p_j, \beta)$$



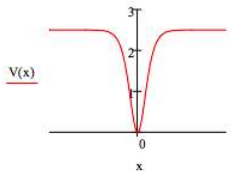
This page titled 10.41: Variation Method Using the Wigner Function - The Quartic Oscillator is shared under a CC BY 4.0 license and was authored, remixed, and/or curated by Frank Rioux via source content that was edited to the style and standards of the LibreTexts platform.

10.42: Variation Method Using the Wigner Function - The Feshbach Potential

Define potential energy:

$$V_0 = 2.5 \quad d = 0.5 \quad V(x) = V_0 tanh\left(\frac{x}{2}\right)^2$$

Display potential energy:



Choose trial wave function:

$$\psi(x,\beta) = \left(\frac{2\beta}{\pi}\right)^{\frac{1}{4}} exp(-\beta x^2)$$

Calculate the Wigner distribution function:

$$W(x,p,\beta) = \frac{1}{2\pi}\int_{-\infty}^{\infty} \psi\left(x+\frac{s}{2},\beta\right) exp(isp)\psi\left(\left(x-\frac{s}{2},\beta\right)\right) ds \Big|^{simplify}_{assume,\ \beta>0} \rightarrow \frac{1}{\pi} e^{\frac{-1}{2}\frac{4\beta^2x^2+p^2}{\beta}}$$

Evaluate the variational integral:

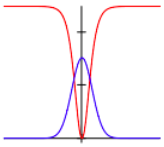
$$E(\beta) = \int_{-\infty}^{\infty}\int_{-\infty}^{\infty} W(x,p,\beta)\left(\frac{p^2}{2}+V(x)\right) dx\ dp$$

Minimize the energy integral with respect to the variational parameter, β.

$\beta = 1$ β = Minimize (E, β) $\beta = 0.913$ E(β) = 1.484

Calculate and display the coordinate distribution function:

$$Px(x,\beta) = \int_{-\infty}^{\infty} W(x,p,\beta)dp$$



Classical turning point:

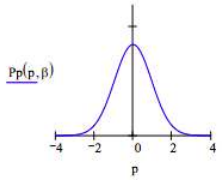
$$V_0 tanh\left(\frac{x}{2}\right)^2 = 1.484 \Big|^{solve,\ x}_{float,\ 3} \rightarrow \begin{pmatrix} -.511 \\ .511 \end{pmatrix}$$

Probability that tunneling is occurring:

$$2\int_{0.511}^{\infty} Px(x,\beta)dx = 0.329$$

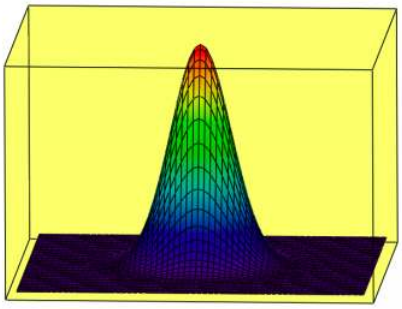
Calculate and display the momentum distribution function:

$$Pp(p,\beta) = \int_{-\infty}^{\infty} W(x,p,\beta)dx$$



Display the Wigner distribution function:

$$N = 60 \quad i = 0 .. N \quad x_i = -3 + \frac{6i}{N} \quad j = 0 .. N \quad p_j = -5 + \frac{10j}{N} \quad Wigner_{i,j} = W(x_i, p_j, \beta)$$



This page titled 10.42: Variation Method Using the Wigner Function - The Feshbach Potential is shared under a CC BY 4.0 license and was authored, remixed, and/or curated by Frank Rioux via source content that was edited to the style and standards of the LibreTexts platform.

CHAPTER OVERVIEW

11: Miscellaneous

11.1: The Art of Science
11.2: Mass-Energy Equivalence
11.3: Commentary on “Probing the Orbital Energy of an Electron in an Atom”
11.4: The Use of Models in Introductory Chemistry
11.5: Reaction to Gillespie's Six Great Ideas in Chemistry - Another Great Idea
11.6: An Alternative Derivation of Gas Pressure Using the Kinetic Theory
11.7: Examining Fourier Synthesis with Dirac Notation
11.8: Finding Roots of Transcendental Equations
11.9: Calculation of the Composition of a Weak Polyprotic Acid Using Mathcad
11.10: Solving Linear Equations Using Mathcad
11.11: Let's Teach High School Students Computer Algebra Methods
11.12: Thermodynamics and Kinetics
11.13: Simple Kinetic Derivations of Thermodynamic Relations
11.14: The Global Approach to Thermodynamics
11.15: Global Thermodynamic Analyses of Heat Engines
11.16: Using Charles' Law to Determine Absolute Zero
11.17: The Origin of KE = 3/2 RT
11.18: Cosmic Background Radiation
11.19: Age of the Elements

This page titled 11: Miscellaneous is shared under a CC BY 4.0 license and was authored, remixed, and/or curated by Frank Rioux via source content that was edited to the style and standards of the LibreTexts platform.

11.1: The Art of Science

> Science is valued for its practical advantages, it is valued because it gratifies disinterested curiosity, and it is valued because it provides the contemplative imagination with objects of great aesthetic charm. *J. W. N. Sullivan*

> The popular notion that the sciences are bodies of established fact is entirely mistaken. Nothing in science is permanently established, nothing unalterable, and indeed science is quite clearly changing all the time, and not through the accretion of new certainties. *Karl Popper*

> The progress of science is strewn, like an ancient desert trail, with the bleached skeletons of discarded theories which once seemed to possess eternal life. *Arthur Koestler*

Popular views of science imply that there exists a mechanical and logically certain relationship between scientific facts and their explanations. According to these views scientific knowledge possesses a certainty which is not to be found in other disciplines such as the humanities or the social sciences. The quotations by Sullivan, Popper and Koestler suggest that there might be more to it than this.

The purpose of this paper is to present an outline of one view of the structure of scientific knowledge and to argue that aesthetics plays an important role in the evolution and progress of scientific thought. The ideas presented here represent a distillation of the thinking of several important scientists — at least those who took the time to explain to others what it was they thought they were doing.

T. H. Huxley, the 19th-century English evolutionist, speaking to a British trade union, described science in the following way:

> The aim of science is the discovery of the rational order which pervades the universe. The method of science consists of observation and experimentation for the determination of the facts of Nature. Science uses inductive and deductive reasoning for the discovery of the mutual relations and connections between the facts of nature. In other words, scientists use inductive and deductive reasoning to generate hypotheses and theories which order the facts of nature. Science rests on verified, or more correctly, on uncontradicted hypotheses, and, therefore, an important condition of its progress has been the invention or creation of verifiable hypotheses.

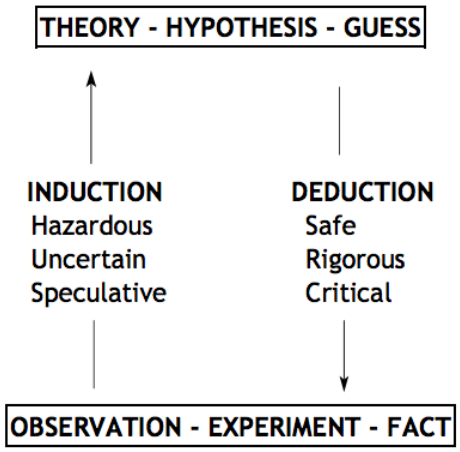
Albert Einstein, a 20th-century physicist, concerned with scientific problems a world apart from Huxley, described science in much the same way.

> The supreme task of the scientist is to arrive at those universal elementary laws from which the physical cosmos can be built up by pure deduction. His work thus falls into two parts. He must first discover the laws and then draw the conclusions which follow from them. For the second of these tasks he receives an admirable training at school. However, the first, namely that of establishing the starting point of his deductions, is of an entirely different nature. Here there is no method capable of being learned and systematically applied so that it leads to the goal. There is no logical path to these principles; only intuition, resting on a sympathetic understanding of experience can reach them.

Carl Hempel, a contemporary philosopher of science, said much the same thing.

> There are no generally applicable "rules of induction" by which hypotheses or theories can be mechanically derived or inferred directly from empirical data. The transition from data to theory requires creative imagination. Theories are not derived from the data, but invented in order to account for them.

In the diagram below I have attempted to provide a graphical representation of these statements on the structure of scientific knowledge.



The essential point is that induction is not a logically rigorous process; it is incapable of leading us with certainty to the truth. As Max Jammer has said, "The fact that all past futures have resembled past pasts does not guarantee that all future futures will resemble future pasts."

Another way to put this is to say that scientific hypotheses go beyond the facts, always claiming more than is justified. In a certain sense they are works of fiction. Thus, Peter Medawar has described scientific reasoning as "an exploratory dialogue that can always be resolved into two voices or episodes of thought, imaginative and critical, which alternate and interact." Scientific thinking is a dialogue between what might be and what actually is.

The objectivity of scientific knowledge is preserved by its critical voice, by the requirement that scientific creations must ultimately face reality. In this critical episode, a scientific theory cannot really be confirmed or proven true, it can only survive; survive at least until the next confrontation with reality. According to Karl Popper, observation and experiment in science serve as critical tests of hypotheses rather than inductive bases for them. "The logic of science and an essential criterion for its progress is the falsification of conjectures."

In the light of the above considerations, Einstein posed the following question.

> If, then, it is true that the axiomatic basis of science cannot be extracted from experience but must be freely invented, can we ever hope to find the right way?

This was, of course, a rhetorical question. Einstein demanded two things of a scientific theory: external confirmation and internal perfection. A theory must not only be consistent with experiment, it must also be pleasing to the mind. Simplicity and beauty, he argued, can guide the scientific thinker toward the truth. Einstein was not being immodest when he said of his own General Theory of Relativity, "No one who fully understands this theory can escape its magic."

Later, when asked if he was troubled by the early lack of experimental confirmation of his General Theory, he replied,

> Such questions did not lie in my path. The result could not be otherwise than correct. I was only concerned with putting the theory into a lucid form. I did not for one second doubt that it would agree with observation. The sense of the thing was too evident.

More recently, Paul Dirac, a successor to Newton as Lucasian Professor of Mathematics at Cambridge (some great physicists are apparently really mathematicians) and co-winner of the 1933 Nobel prize in physics with Erwin Schrödinger, described Schrödinger's seminal achievement in the following way.

> Schrödinger got his equation by pure thought, looking for some beautiful generalization of De Broglie's idea, and not by keeping close to the experimental development of the subject... It seems that if one is working from the point of view getting beauty in one's equations, and if one has really sound insight, one is on a sure line of progress.

We have come to call Schrödinger's work "wave mechanics" and it does for the nano-world of atoms and molecules what Newton's Laws of Motion do for the macro-world of solar systems, pendulums and billiard balls. At about the same time as Schrödinger's work came out, Werner Heisenberg, a brilliant, young (full professor at Leipzig at the age of 25; Nobel prize at 31) physicist

created an alternative approach to the nano-world called "matrix mechanics." Schrödinger found Heisenberg's approach "repulsive and distasteful" and threatened to quit physics if "matrix mechanics" held sway. Subsequently it was shown (by Schrödinger!) that the two theories were formally equivalent, suggesting that in science beauty is also in the eye of the beholder.

Immediately after this period, Niels Bohr, Max Born and Dirac added to the contributions of Schrödinger and Heisenberg to create a more comprehensive theory called "quantum mechanics." It is widely regarded as the most successful scientific theory ever. Like any good scientific theory, it has been found to be very helpful in interpreting experimental results and in serving as a guide for further inquiry. But, it wasn't good enough for Einstein. Recall that in his opinion external confirmation was only one aspect of a healthy scientific theory. Quantum mechanics failed his other criterion. He expressed his dissatisfaction frequently, but perhaps never more poignantly as in the following comment he made to Max Born.

> Quantum mechanics is certainly imposing. But an inner voice tells me that it is not yet the real thing. The theory says a lot, but does not really bring us any closer to the secret of the 'old one.' I, at any rate, am convinced that He is not playing at dice.

Quantum mechanics challenges our traditional ideas of objectivity and causality, and Einstein claimed these as the fundamental principles of all science. He did not believe that God would make a world based on quantum mechanical principles. For almost forty years Einstein remained quantum mechanics' foremost critic, isolating himself in his mature years from the rest of the creative scientific community. The best experimental evidence we have today indicates that Einstein's intuition led him astray this time. Several of quantum mechanics' most bizarre predictions with regard to the principle of cause and effect at the nanoscopic level have been confirmed experimentally. Long before this evidence was available Bohr became exasperated by Einstein's continual criticisms and retorted, "Einstein, stop telling God what to do!"

A final example recounts the peculiar role that aesthetics and creative imagination played in the birth of modern astronomy. Johann Kepler, a contemporary of Galileo and Shakespeare, was driven by two Pythagorean convictions in his attempts to explain celestial dynamics. These were that the structure of the solar system could be modeled using the five perfect solids and that the planetary motions could be interpreted in terms of the musical harmonies. Guided by these obsessions, Kepler ultimately discovered the three laws of planetary motion for which he is famous today. But these early examples of modern scientific laws, which eventually had such a profound impact on the evolution of physical science, were so deeply embedded in his semi-mystical writings that few of his contemporaries found them. And Kepler himself considered them to be of secondary importance to the grandiose models he built on the basis of the perfect solids and the musical harmonies. Newton and his generation did find them, recognized their significance and used them to build a new and powerful science.

The following quotations, the first by Jacob Bronowski and the second by Einstein, summarize the position presented in this paper.

> Science is basically an artistic endeavor. It has all the freedom of any other imaginative endeavor. The artist and the scientist both live at the edge of mystery, surrounded by it. Both struggle to make order out of the chaos.
>
> Science as an existing, finished product is the most objective, most un-personal thing human beings know. But science as something coming into being, as aim, is just as subjective and psychologically conditioned as any other of man's efforts.

Published in St. John's Magazine, Winter 1986. Revised January 2006.

This page titled 11.1: The Art of Science is shared under a CC BY 4.0 license and was authored, remixed, and/or curated by Frank Rioux via source content that was edited to the style and standards of the LibreTexts platform.

11.2: Mass-Energy Equivalence

This derivation of the mass-energy equivalence equation is based on the analyses of an elementary photon emission event by two sets of inertial observers as shown in the figures below.

A block which is stationary with respect to observers A^o and B^o emits photons of equal frequency in opposite directions.

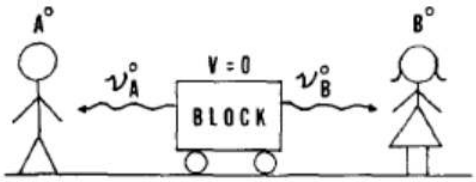


Fig. 1. Photon emission as viewed by two observers at rest relative to the block.

According to these observers the energy and momentum changes of the block are as follows:

$$\Delta E^o = -2 \cdot h\nu \; \Delta p^o = -\Delta p\gamma^o = -(\nu_B^o - \nu_A^o) \cdot \tfrac{h}{c} = 0 \; \nu_A^o = \nu_B^o = \nu$$

The block is moving with velocity v with respect to observers A and B.

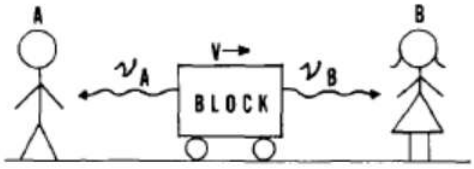


Fig. 2. Photon emission as viewed by viewed two observers relative to which the block has velocity v.

A and B observe photon frequencies shifted by 1/k and k respectively, where k is the optical Doppler shift factor. Their determinations of ΔE and Δp are given below. As there was no block recoil for A^o and B^o, the relativity principle requires the same for A and B. This means that the momentum change for these observers is due to a change in mass of the block, Δp = vΔm.

$$\Delta E = -h\nu_A - h\nu_B = -(k + \tfrac{1}{k}) \cdot h\nu$$

$$\Delta p = v\Delta m = -(\nu_B - \nu_A) \cdot \tfrac{h}{c} = -(k - \tfrac{1}{k}) \cdot \tfrac{h\nu}{c}$$

These equations and the optical Doppler shift factor k yield the mass-energy equivalence relation.

$$k = \sqrt{\tfrac{1+\frac{v}{c}}{1-\frac{v}{c}}}$$

$$\Delta E = -(k + \tfrac{1}{k}) \cdot h\nu$$

substitute, $h\nu = \tfrac{-c \cdot \nu \cdot \Delta m}{k - \frac{1}{k}}$ | substitute, $k = \sqrt{\tfrac{1+\frac{v}{c}}{1-\frac{v}{c}}}$

simplify: $\Delta E = \Delta m \cdot c^2$

The differences in the energy and momentum changes determined by the two sets of observers are restated below (recall that k > 0).

$$\Delta E^o = -2 \cdot h\nu \; \Delta p^o = 0 \; \Delta E = -(\tfrac{k^2+1}{k}) \cdot h\nu \; \Delta p = -(\tfrac{k^2-1}{k})) \cdot \tfrac{h\nu}{c}$$

These results bring the principles of energy and momentum conservation into question. However, they are the foundation of modern science, so they are preserved by recognizing that energy and mass are equivalent to two currencies with an exchange rate of c^2, $E = mc^2$. In releasing energy (photons) the block is also releasing mass ($\Delta m = \Delta E/c^2$). Therefore the kinetic energy of the moving block decreases. This is the cause of the extra energy loss in the reference frame in which the block is moving. It is also the explanation for the negative change in momentum in that reference frame.

This presentation is based on the following paper: Daniel J. Steck and Frank Rioux, "An elementary development of mass-energy equivalence," Am. J. Phys. 51(5), 461 (1983).

This page titled 11.2: Mass-Energy Equivalence is shared under a CC BY 4.0 license and was authored, remixed, and/or curated by Frank Rioux via source content that was edited to the style and standards of the LibreTexts platform.

11.3: Commentary on “Probing the Orbital Energy of an Electron in an Atom”

We wish to comment on a recent article by Bills, “Probing the Orbital Energy of an Electron in an Atom” (1). Bills’ thesis is that the behavior of electrons in atoms can be successfully analyzed using classical concepts. For example, he writes

- A theoretical snapshot of an atom, showing the screened nuclear charge and the electron to be ionized at its radius of zero kinetic energy, enables anyone to approximate its ionization energy.
- Each eigenvalue is the constant sum of classical values of potential and kinetic energy.
- The classical potential energy, $V(R)$, is independent of n, but the classical kinetic energy, $T_n(R)$, depends on n.
- When the electron i reaches r_0, much of the charge of electron j is distributed within r_0.

From these statements we infer that the electron is executing a classical trajectory; that it has well-defined classical values for position, momentum, and kinetic and potential energy. Unfortunately, this classical picture violates accepted and validated quantum mechanical principles.

To support his model Bills draws on the authority of John C. Slater by referencing Slater’s classic monograph on the quantum theory of atomic structure (2). We acknowledge that Slater strove to provide an intuitive meaning to quantum theory by exploiting classical ideas. He was one of the early users of quantum theory in the search for an understanding of atomic and molecular structure, and so we should not be surprised that he attempted to use the classical concepts of kinetic and potential energy as guides for interpretive purposes. However, today we know that this program is not viable; classical concepts cannot provide an acceptable model for the stability and structure of atoms and molecules, nor their interaction with electromagnetic radiation.

We live in a macroscopic, classical world and are therefore challenged by the nonclassical model of the nanoscopic world of atoms and molecules that quantum mechanics requires. Peter Atkins said it well recently in his forward to Jim Baggott’s most recent book. (3)

> *No other theory of the physical world has caused such consternation as quantum theory, for no other theory has so completely overthrown the previously cherished concepts of classical physics and our everyday interpretation of reality.*

Along the same lines Niels Bohr once said that if you are not shocked by quantum mechanics, you do not understand what it is saying.

We now articulate in detail our objections to the classical model that Bills proposes.

By assigning classical meaning to $T(r)$ and $V(r)$, and identifying a special electron position, r_0, where its kinetic energy is zero, Bills contradicts accepted quantum mechanical ideas regarding the behavior of electrons in atoms. The wavefunctions of atomic electrons are not eigenfunctions of the position, momentum, kinetic energy or potential energy operators. Consequently, according to quantum mechanics, the physical properties represented by these operators do not have well-defined values. Therefore, it is impossible to attach any physical significance to the values of $T(r)$ or $V(r)$ shown in Figure 1 of Bills’ paper because they are neither eigenvalues nor expectation values of their respective operators.

The only physically meaningful entries in Table 1 of Bills’ paper are the calculated orbital energies and the experimental ionization energies. As Figure 1 shows a good Hartree-Fock wavefunction gives a constant orbital energy and therefore a reliable estimate, according to Koopmans’ theorem, for the ionization energy. What is the real meaning of r_0?

It is simply the inflection point of the wavefunction, nothing more and nothing less. Initially defining r_0 as the electron’s radius of zero kinetic energy, Bills goes on to identify r_0 with atomic size in two places – one explicitly and one implicitly.

- Each r_0 measures the orbital size of the weakest-held electron.
- This r_0 is analogous to the classical turning point of the harmonic oscillator.

The latter statement implies that the electron has reached its apogee and is turning back in the direction of the nucleus, again suggesting a classical trajectory. However, a serious difficulty emerges if one associates the calculated r_0 values with atomic size. The r_0 values in Table 1 of Bills’ paper are significantly larger than the literature values for the atomic radii for the chemically active elements, while for the inert gases they are significantly smaller than the literature values for the atomic radii. (4) This doesn’t make physical sense.

Bills' r_0 is physically meaningless because his model violates the basic quantum mechanical principles that govern the nanoscopic world of atoms and molecules. This is easily seen by looking at the ionization process in terms of two fundamental physical principles which hold both classically and quantum mechanically: They are energy conservation

$$\Delta E = \Delta T + \Delta V$$

and the virial theorem

$$\Delta E = \frac{\Delta V}{2} = -\Delta T.$$

Under Bills' model with $\Delta T = 0$ the first equation says that $\Delta E = \Delta V$, while the second equation says $\Delta E = \frac{\Delta V}{2} = -\Delta T = 0$!

Bills' model also violates the uncertainty principle. If the position of the electron is precisely known, the uncertainty in momentum and therefore kinetic energy must be infinitely large. In other words, an electron cannot have a well-defined position (r_0) at the same time it has a precise value for kinetic energy (zero). In addition, since he takes a classical view of electronic behavior in the atom Bills is left with the challenging problem of assigning meaning to the negative kinetic energies that result for values of r greater than r0 (see Bills' Figure 1).

A quantum mechanically correct description of the behavior of electrons in atoms and molecules has been provided by Harris (5):

> *Electrons are characterized by their entire distributions (called wavefunctions or orbitals) rather than by instantaneous positions and velocities: an electron may be considered always to be (with appropriate probability) at all points of its distribution (which does not vary with time).*

"There is no space-time inside the atom," is Heisenberg's succinct summary of the electron's behavior in the atom. Pascal Jordan provided further insight by stating that we measure the position of the electron, not to find out where it is, but to cause it to be somewhere.

In exploring the message of quantum theory Anton Zeilinger recently wrote (6):

> *It is not just that we are unable to measure two complementary quantities of a particle, such as position and momentum, at the same time. Rather the assumption that a particle possesses both position and momentum, before the measurement is made, is wrong.*

Thus it is impossible, within the quantum mechanical view, to assign a classical trajectory to an electron confined in an atom or molecule. In fact, assigning such a trajectory to an electron calls into question the stability of matter because an orbiting electron would continuously radiate energy and (according to classical physics) collapse into the nucleus. Bohr famously remarked that the stability of matter is "a pure miracle when considered from the standpoint of classical physics."

In summary, classical concepts fail at the atomic and molecular level because they cannot account for the stability and internal electronic structure of atoms and molecules, nor the interaction of matter with electromagnetic radiation. This has been known for more than a century. It is well beyond time to abandon classical models of the nano-world and teach our students atomic and molecular structure from the quantum mechanical perspective. Richard Feynman made this point forcibly in his inimitable colloquial style when he said, (7)

> And I'm not happy with all the analyses that go with just the classical theory, because nature isn't classical, dammit, and if you want to make a simulation of nature, you'd better make it quantum mechanical…

Literature Cited

1. Bills, J. J. Chem. Educ. 2006, 83, 473-476.
2. Slater, J. C. Quantum Theory of Atomic Structure; McGraw-Hill: New York, 1960; Vol. 1.
3. Baggott, J. E. Beyond Measure: Modern Physics, Philosophy, and the Meaning of Quantum Theory; Oxford University Press: New York, 2004.
4. Emsley, J. The Elements, 3rd ed.; Clarendon Press: Oxford, 1998.
5. Harris, F. E. "Molecules," Encyclopedia of Physics, 2nd ed.; Lerner, R. G.; Trigg, G. L. Ed.; VCH Publishers, Inc.: New York, 1990; p 763.
6. Zeilinger, A. Nature, 2005, 438, 743.

7. Feynman, R. P. International Journal of Physics, 1982, 21, 486.

This page titled 11.3: Commentary on “Probing the Orbital Energy of an Electron in an Atom” is shared under a CC BY 4.0 license and was authored, remixed, and/or curated by Frank Rioux via source content that was edited to the style and standards of the LibreTexts platform.

11.4: The Use of Models in Introductory Chemistry

The *Journal of Chemical Education* has published three responses (*1*,*2*,*3*) to a paper Roger DeKock and I published stressing the importance of kinetic energy in interpreting trends in atomic ionization energies (*4*). We have previously responded to Carlton (*5*, *6*), and I would now like to respond to Gillespie, Moog, and Spencer. We have jointly submitted a response to John P. Lowe, a copy of which can be found on this page.

For the most part Gillespie, Moog, and Spencer (*1*) defend themselves against criticisms we do not make and ignore the major argument we do make. For example, we do not criticize the use of the shell model to teach the most basic elements of atomic structure in introductory chemistry courses. However, we do challenge the use of the shell model for purposes that extend beyond its range of validity.

Among these would be the use of the shell model to explain the trend of ionization energies within a given shell and the more fundamental issue of atomic stability. With regard to the former, one asks why is the ionization energy for He less than twice that for H? With regard to the latter, one asks why doesn't the electron collapse into the nucleus under the electrostatic force of attraction between the electron and the nucleus? The shell model has much to offer as a pedagogical tool to answer some rudimentary questions about atomic and molecular structure, but it cannot answer these question. Quantum mechanics is required to answer questions of this type as we demonstrated in our critique.

Gillespie, Moog, and Spencer concede that our criticism is valid within the context of quantum mechanics, implying that quantum mechanics is just another model on the menu of models that could be used to explain atomic and molecular phenomena. For example, they say,

At the general chemistry level it is probably sufficient to state simply that the high IE of He with respect to H is due to the greater attraction of the nucleus for electrons, offset by the repulsion between electrons.

Unfortunately this is not a valid explanation as we demonstrated in our critique. In attempting to reach and educate all of the constituencies of general chemistry, we should not over-simplify the concepts because it makes them easier to teach. Teaching simple models that students can easily digest is tempting, but these easily digestible models are frequently fundamentally incorrect. Perhaps these incorrect models do no great harm at the introductory level simply because general chemistry is a terminal course for most of those who take it, and the retention half-life for the good or the bad content is relatively short. However, over-simplifications must eventually must be un-taught, or retracted, at some later time in the education of the chemistry major or others who study chemistry beyond the general chemistry sequence. The explanation by Gillespie *et al.* for the H/He ionization ratio falls into this category. It has to be retracted eventually, so why teach it at all?

Why not simply state that the answer to the question of the trend in ionization energies within the shells (or the explanation of atomic stability) is too complicated for general chemistry students. Valid explanations require quantum mechanics which, for chemistry majors, will be encountered in the junior or senior year. Furthermore, quantum mechanics is not just another mouse click on the model menu, it is the benchmark theory, the one against which all other approximate models are judged. For example, in their seminal treatise on molecular mechanics Burkert and Allinger wrote (*8*),

Calculations that do not use the Schrödinger equation are acceptable only to the extent that they reproduce the results of high level quantum mechanical calculations.

Literature cited:

1. Gillespie, R. J.; Moog, R. S.; Spencer, J. N. *J. Chem. Educ*. **1998**, *75*, 539-540.
2. Carlton, T. S. *J. Chem. Educ*. **1999**, *76*, 605.
3. Lowe, J. P. *J. Chem. Educ*. **2000**, *77*, 155-156.
4. Rioux, F.; DeKock, R. L. *J. Chem. Educ*. **1998**, *75*, 537-539.
5. Rioux, F. *J. Chem. Educ*. **1999**, *76*, 605.
6. DeKock, R. L. *J. Chem. Educ*. **1999**, *76*, 605-606.
7. *CRC Handbook of Chemistry and Physics*, 80th ed.; CRC: Boca Raton, FL, 1999; p. 12-15.
8. Burkert, U.; Allinger, N. L. *Molecular Mechanics*, American Chemical Society, Washington, D. C., 1982; p. 10.

This page titled 11.4: The Use of Models in Introductory Chemistry is shared under a CC BY 4.0 license and was authored, remixed, and/or curated by Frank Rioux via source content that was edited to the style and standards of the LibreTexts platform.

11.5: Reaction to Gillespie's Six Great Ideas in Chemistry - Another Great Idea

I wish to respond to an article by Ronald J. Gillespie published in The Journal on the content of the general chemistry sequence (1). While I agree with his major premise, I strongly disagree with a number of his specific recommendations. Operating under the assumption that the teaching of chemistry is enriched by lively debate and critical analysis, I would like to share my observations with the readership of The Journal. In what follows, text in italic font is taken directly from Professor Gillespie's paper. I will follow the italicized text with my comments and observations.

Critique

We must remember that the general chemistry course is not (or should not be) designed as a first step in the training of future professional chemists.

I agree with this sentiment, but I have reservations about its implementation. In attempting to reach and educate all of the constituencies of general chemistry in a single course, we should not oversimplify the course simply for the benefit of the non-major, and thereby teach things which must be retracted at some later point in the education of the chemistry major. Teaching simple models that students can easily digest is tempting, but these easily digestible models are frequently scientifically incorrect. In my opinion Gillespie presents several models of this kind of simplicity that are incorrect and, if taught, would have to be un-taught, or retracted, at some later time in the education of the chemistry major or others who study chemistry beyond the general chemistry sequence. We should follow Einstein's advice in our teaching and "make things as simple as possible, but no simpler."

Elements are a kind of matter that consists of atoms of only one kind.

Besides being casual in tone, the definition is not correct. It is clear from reading this paper and its footnote, that it is a transcription of a talk given at a national ACS meeting. However, The Journal is a peer reviewed scientific journal and by not correcting this statement it appears to be sanctioning this rather informal and inaccurate definition.

All chemical bonds are formed by electrostatic attractions between positively charged cores and negatively charged valence electrons. Electrostatic forces are the only important force (sic) in chemistry.

At this point I will simply observe that there is only one electrostatic force - Coulomb's Law. There are, however, many types of electrostatic interactions: ion-ion, ion-dipole, dipole-dipole, etc. In other words, there are a large number of ways charge is distributed in matter, and therefore a large number of ways these charge distributions can interact with one another. However, whatever its form, the electrostatic interaction is ultimately calculated using one equation - Coulomb's Law. If this fact was more widely appreciated the grammatical error in the second sentence wouldn't have occurred.

(Overlap of atomic orbitals) *distracts attention from the real reason for bond formation: the electrostatic attraction between electrons and nuclei.*

Unfortunately this simple idea is simply false, but it is easy to teach (see earlier remark). To put it bluntly, if the electrostatic force was all that was important, the electrons would reside inside the nuclei and never in the region between them or anywhere else. A simple electrostatic calculation will show that placing an electron exactly between two positive charges is not the most energetically favorable configuration of charges (see appendix). Solely on the basis of Coulomb's law the electron would be drawn toward one nucleus or the other; unless like Buridan's mule the electron is immobilized by its inability to distinguish between two identically attractive alternatives.

Orbitals and the LCAO-MO method are indeed only models, but at least they give a scientifically respectable picture of the covalent bond. Using the orbital model it can be shown that constructive interference due to overlap of atomic orbitals leads to charge build up in the internuclear region. This build up of charge, which is frequently described as the glue that holds atoms together, is funded by a decrease in kinetic energy due to the delocalization of electron density as Ruedenberg's insightful analysis of the chemical bond showed more than forty years ago (2). The potential energy actually increases during this process, as the exercise outlined in the appendix shows.

I am not recommending that we teach general chemistry students full-blown quantum mechanics, I am simply saying that Gillespie's simplistic electrostatic model is incorrect, and therefore shouldn't be taught to anyone, especially general chemistry students who are most vulnerable to specious arguments. We are accustomed to making simplifying approximations in chemistry,

but Gillespie's model is not acceptable because it neglects a fundamental physical property, electron kinetic energy, which is essential to the understanding of atomic and molecular phenomena.

Moreover, the orbital model gives students the incorrect impression that chemistry is a difficult, abstract, mathematical subject based on a mysterious concept that is not and cannot be satisfactorily explained at the introductory level.

As a matter of fact chemistry is difficult and abstract, and students find this out long before they get to orbitals and quantum numbers. Furthermore, if quantum theory and the orbital concept are mysterious it is because the nano-scale world of electrons, nuclei, atoms, and molecules is mysterious. The fact that nano-world of atoms and molecules is not simply a miniature of the macro-world is one of the most important discoveries in the history of science. The classical principles that work in the macro-world are inadequate in the nano-world and need to be supplemented by the de Broglie hypothesis (see later, 7th great idea). In other words, the need for quantum theory is 'data driven,' to use a slogan currently in vogue within the community of chemical educators. Marvin Chester (3) put this most cogently when he wrote, "The mathematical predictions of quantum mechanics yield results that are in agreement with experimental findings. That is the reason we use quantum theory. That quantum theory fits experiment is what validates the theory, **but why experiment should give such peculiar results is a mystery** (emphasis added)."

This aspect of chemistry (molecular geometry) *receives too little emphasis in the introductory course, although it is one that can stimulate and excite students by showing that chemistry is practical, useful, and challenging, not dull, theoretical, mathematical, and abstract.*

I agree that structural and synthetic chemistry deserve more attention and are exciting and interesting areas of contemporary chemistry, but the last part of this sentence is simply a cheap shot. Theory is also exciting, useful, and challenging, especially when taught by those who understand its significance. Theory is an essential part of 20th Century chemistry and should be taught in a positive manner to students at all levels. In addition, it should be noted that theory has always been an essential part of chemistry. To describe chemistry simply as an experimental science, is to use a halftruth to describe a discipline that is much richer than a single-sentence definition can capture. I will return to the role of theory in science teaching in my conclusion.

Molecular modeling programs now make it even easier for students to understand and become familiar with the shapes of molecules.

This is indeed true, but molecular modeling programs (except for molecular mechanics calculations) are built on quantum mechanics and mainly exploit the orbital approximation, which Professor Gillespie has previously criticized as a "mysterious concept that is not and cannot be satisfactorily explained at the introductory level." Is he proposing we hide this fact from the students and treat the molecular modeling programs as black boxes? If so this is not a valid or honest pedagogy.

By kinetic theory I do not mean the derivation of $PV = \frac{1}{3}nmc^2 = nRT$...

This equation cannot be derived from kinetic theory as Dewy Carpenter showed some thirty-five years ago in this Journal (4). Temperature is not a mechanical concept; it lies outside the kinetic molecular theory. The kinetic theory yields $PV = \frac{1}{3}nmc^2$, which when compared to the empirically based ideal gas law, $PV = nRT$, leads to the conclusion that the average molecular kinetic energy is proportional to the absolute temperature: $< KE >= \frac{1}{2}Mc^2 = \frac{3}{2}RT$.

Everyone can understand the concept of disorder and that is really all there is to entropy.

While this erroneous belief is uncritically accepted by many, there is no scientific justification for its widespread use in teaching, as McGlashan showed so many years ago on these very pages (5a). More recently, Lambert has incisively exposed the error in equating entropy with disorder (5b). On Ludwig Boltzmann's tombstone in Vienna is inscribed his famous formula, S = k logW. With this simple, but powerful equation, Boltzmann connected the macro-world with the nano-world. S is entropy and W stands for the German word, wahrscheinlichkite, which in English means likelihood or more formally probability. Probability is not an overly difficult concept so why not use it here. In addition it is so much more accurate and powerful than the more comfortable and casual, but scientifically vague, concept of disorder.

A Seventh Great Idea

The fact that atomic and molecular structure and stability, and the physical nature of the chemical bond cannot be understood with the six great ideas Gillespie promotes is evidence to me that another great idea is essential in the general chemistry curriculum. This seventh great idea, the corner stone of quantum mechanics, is de Broglie's hypothesis that matter has wave-like properties and

is, therefore, subject to interference phenomena (constructive and destructive) normally associated with wave-like phenomena. This is especially important for the light-weight electron and is the idea that is necessary to explain the chemical bond, and atomic and molecular stability, and atomic and molecular structure, and atomic and molecular spectroscopy.

From de Broglie's wave equation, $\lambda = \frac{h}{mv}$, it follows that in the nano-world kinetic energy is $\frac{h^2}{2m\lambda^2}$, which means that if the space an electron occupies is restricted, its kinetic energy is quantized and increased significantly. Thus, kinetic energy behaves like an outward force that counter balances the inward electrostatic force and prevents the electron from collapsing into the nucleus under the electrostatic attraction that Gillespie says is all that is needed to explain chemical phenomena. As Ruedenberg has pointed out there are no ground states or quantized energy levels in the classical, macroscopic world. We need de Broglie's hypothesis to explain chemical phenomena at the atomic and molecular level.

We have just left the century which began with the quantum revolution of Planck, Einstein, and Bohr. We have also recently celebrated the 100th anniversary of the discovery of the electron, that fundamental particle whose behavior dictates chemistry. Today, as far as we can tell, the behavior of the electron is accurately described by the principles of quantum mechanics. At some rudimentary level we should be teaching this important theory to all of our students.

Here is what I try to do. In my general chemistry course I teach de Broglie's wave equation and its implications. I concentrate on the consequences of confinement and delocalization at the atomic and molecular level. I outline the origin of quantized energy levels and quantum numbers from de Broglie's fundamental idea. I regard it as one of the most astonishing, provocative, and creative ideas of the 20th Century, and I want my students, majors and non-majors, to be aware of its existence and importance.

A survey of the current general chemistry texts will reveal that all of them present deBroglie's hypothesis. My point is that it should be elevated to an essential part of the introductory chemistry curriculum. If we are going to select a small number of essential ideas or principles, deBroglie's wave-particle duality for matter should be among them.

Conclusion

Chemistry is a great intellectual adventure and we must present the spirit of that adventure to all of our students, no matter what their academic major or their particular career objectives. If we are going to teach an honest first course in chemistry we have to describe both its experimental and theoretical features. I am offended and disturbed by Gillespie's gratuitous attack on mathematics and theory in the general chemistry sequence. He misrepresents chemistry because chemistry is not simply an experimental science, nor has it ever been so. I believe every scientific discipline involves a lively exchange between theory and experiment, and this is what we should tell our students. There is no hierarchy here, both theory and experiment are essential, on a day to day basis, for all practitioners of the art and science of chemistry. More than 20 years ago Roald Hoffmann wrote eloquently and incisively about the "symbiosis of theory and experiment." He spoke then of "... a vital interweaving of experiment inspired by theory, theory motivated by experiment, binding in a truly interdisciplinary way chemistry, physics, and engineering (5)."

According to Peter Medawar we can think of science as an on-going dialogue between what might be and what is actually so.

> Scientific reasoning is an explanatory dialogue that can always be resolved into two voices or episodes of thought, imaginative (theoretical) and critical (experimental), which alternate and interact (6).

Hoffmann and Medawar, both Nobel Laureates, offer a much richer and more accurate description of science than the negative dichotomous view (experiment/theory, good/bad) that permeates Gillespie's paper.

Appendix

When asked what motivated the creation of his model of the atom Bohr replied "the stability of matter, a pure miracle when considered from the standpoint of classical physics." The following simple calculation will demonstrate what Bohr meant by this statement. This calculation will be carried out in atomic units where the charge on the electron is -1, the charge on the nucleus +1, and distances are measured in bohr, a_o.

Two nuclei (Z = 1) are placed at x = 0.0 and 2.0, respectively. An electron is located exactly between them at x = 1.0, where we instinctively, but incorrectly, think it would want to be on the basis of electrostatic considerations. The potential energy consists of three interactions (nuclear-nuclear repulsion and two electron-nuclear attractions) and is calculated to be:

$$V = \frac{(+1)(+1)}{2} + \frac{(-1)(+1)}{1} + \frac{(-1)(+1)}{1} = 1.5$$

Now move the electron 0.5 bohr closer to one of the nuclei.

$$V = \frac{(+1)(+1)}{2} + \frac{(-1)(+1)}{0.5} + \frac{(-1)(+1)}{1.5} = -2.17$$

And so it goes, on the basis of electrostatic considerations, until the electron is inside one nucleus or the other. While the electron was treated as a point charge in this calculation, a rigorous quantum mechanical calculation tells the same story - moving charge to the internuclear region increases electrostatic potential energy.

The failure of classical physics to explain the stability and structure of matter and its interaction with electromagnetic radiation must be emphasized in the undergraduate curriculum at all levels. Again, the need for quantum mechanics is data driven, and it should be taught at an elementary level initially (see above) and at more sophisticated levels as science students progress through the undergraduate curriculum. Perhaps by the time they graduate chemistry and physics majors might be able to appreciate what Peter Atkins is saying here (8).

> In a sense, the difference between classical and quantum mechanics can be seen to be due to the fact that classical mechanics took too superficial a view of the world: it dealt with appearances. However, quantum mechanics accepts that appearances are the manifestation of a deeper structure (the wavefunction, the amplitude of the state, not the state itself), and that all calculations must be carried out on this substructure.

Literature Cited

1. Gillespie, R. J. J. Chem. Educ. 1997, 74, 862.

2. Ruedenberg, K. Rev. Mod. Phys. 1962, 34, 326.

3. Chester, M. Primer of Quantum Mechanics, Krieger Publishing Co, Malabar, Florida, 1992.

4. Carpenter, D. K. J. Chem. Educ. 1966, 43, 333.

5. a) McGlashan, M. L. J. Chem. Educ. 1966, 43, 226. b) Lambert, F. L. J. Chem. Educ. 1999, 76, 1385.

6. Hoffmann, R. Chem. Eng. News, July 29, 1974, p 32.

7. Medawar, P. B. Induction and Intuition in Scientific Thought; Methuen: London, 1969, p. 46.

8. Atkins, P. W. Quanta, Oxford University Press: Oxford, 2nd Ed., 1991, p. 348.

This page titled 11.5: Reaction to Gillespie's Six Great Ideas in Chemistry - Another Great Idea is shared under a CC BY 4.0 license and was authored, remixed, and/or curated by Frank Rioux via source content that was edited to the style and standards of the LibreTexts platform.

11.6: An Alternative Derivation of Gas Pressure Using the Kinetic Theory

General chemistry and physical chemistry texts that use the kinetic theory to derive the pressure of an ideal gas do so by studying a gas in a cubic or rectangular container (1). The purpose of this note is to outline this derivation for a gas in a spherical container. A visual representation of this approach in coordinate and momentum space is provided in the accompanying figure.

A sphere of diameter D contains gas molecules moving randomly, executing elastic collisions with each other and the surface of the container as postulated by the kinetic theory. Consider a molecule labeled i of mass m and velocity vi making a collision with the surface at an angle 2 relative to the perpendicular to the surface. The momentum transferred to the container in the direction perpendicular to the surface by the collision is

$$\Delta(m\nu)_{surf} = 2m\nu_i \cos(\Theta)$$

Because the molecule travels a distance between $Dcos(\Theta)$ collisions with the surface, the time interval between collisions is

$$\Delta t = \frac{D\cos(\Theta)}{v_i}$$

The force (F) exerted on the surface is the rate of momentum transfer,

$$F_i = \frac{\Delta(m\nu)_{surf}}{\Delta t} = \frac{2mv_i^2}{D}$$

Pressure (P) is force divided by area (A) and the surface area of a sphere is πD^2. The volume of a sphere (V) is $\frac{1}{6}\pi D^3$, therefore

$$P_i = \frac{F_i}{A} = \frac{2mv_i^2}{\pi D^3} = \frac{mv_i^2}{3V}$$

For a mole of gas molecules the total pressure is

$$P = \sum_i^{N_A} P_i = \frac{m}{3V}\sum_i^{N_A} v_i^2 = \frac{M\langle v^2\rangle}{3V} = \frac{3\langle KE\rangle}{3V}$$

where $\langle v^2\rangle = \frac{1}{N_A}\sum_i^{N_A} v_i^2$ and $M = N_A m$.

As Dewey Carpenter pointed out many years ago (2), it is through a comparison of equation (5) with the ideal gas law that we conclude that the average molar kinetic energy of a gas is proportional to its absolute temperature.

$$\langle KE\rangle = \frac{1}{2}M\langle v^2\rangle = \frac{3}{2}RT$$

Unfortunately most introductory texts incorrectly include this result as a postulate of the kinetic theory (3). With regard to the formal assumptions of the kinetic theory Carpenter noted (2), “No reference is made in these postulates to the property of temperature. This is because the kinetic theory is a purely mechanical theory, whereas the concept of temperature belongs to the discipline of thermodynamics.”

References

1. See for example: Zumdahl, S. S.; Zumdahl, S. A. Chemistry, 5th ed.; Houghton Mifflin Co.: Boston, 2000; pp A14-A16. Atkins, P. W. Physical Chemistry, 6th ed., W. H. Freeman and Co., New York, 1998, pp 23-25.
2. Carpenter, D. K. J. Chem. Educ. 1966, 43, 332.
3. A survey of 15 currently available general chemistry textbooks revealed that ten included equation (6), or some form of it, as an assumption of the kinetic theory.

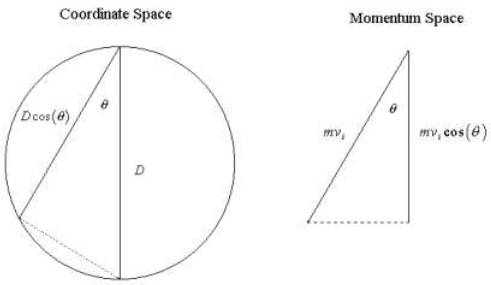


Figure caption: Coordinate and momentum space representations of a gas molecule in a spherical container colliding with the surface at an angle 2 relative to the perpendicular to the surface.

This page titled 11.6: An Alternative Derivation of Gas Pressure Using the Kinetic Theory is shared under a CC BY 4.0 license and was authored, remixed, and/or curated by Frank Rioux via source content that was edited to the style and standards of the LibreTexts platform.

11.7: Examining Fourier Synthesis with Dirac Notation

The purpose of this tutorial is to use Dirac notation to examine Fourier synthesis. The first step is to write the function symbolically in Dirac notation.

$$f(x) = \langle x|f\rangle$$

Select an orthonormal basis set, |n>, for which the completeness relation holds

$$\sum_n |n\rangle\langle n| = 1$$

Expand |f> in terms of |n> by inserting equation (2) into the right side of equation (1). In other words write f(x) as a weighted () superposition using the basis set (the |n> basis set expressed in the coordinate representation).

$$f(x) = \sum_n \langle x|n\rangle\langle n|f\rangle$$

Evaluate the Fourier coefficient, , using the continuous completeness relation in coordinate space.

$$\int |x'\rangle\langle x'|dx' = 1$$

Equation (3) becomes,

$$f(x) = \sum_n \langle x|n\rangle \int \langle n|x'\rangle\langle x'|f\rangle dx'$$

Now select a function

$$\langle x'|f\rangle = x'^3(1-x')$$

over the interval (0,1). Choose the following orthonormal basis set over the same interval.

$$\langle x|n\rangle = \sqrt{2}sin(n\pi x)$$

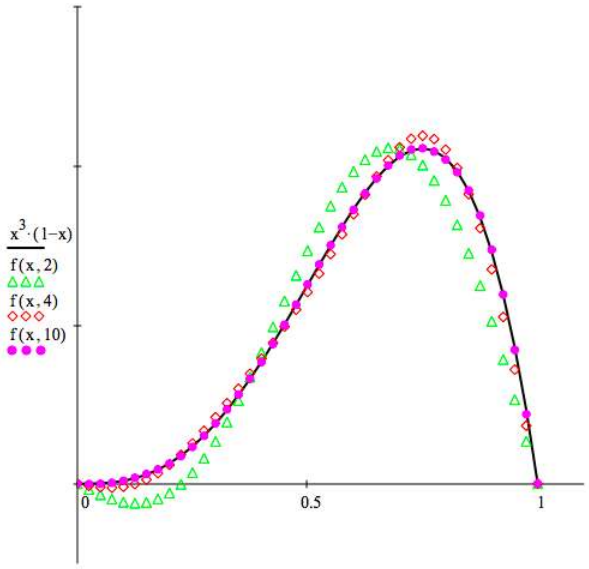
Substitution of equations (6) and (7) into (5) yields

$$f(x) = \sum_n \sqrt{2}sin(n\pi x)\int_0^1 \sqrt{2}(n\pi x')x'^3(1-x')dx'$$

The Fourier synthesis and the original function are shown for n = 2, 4, and 10 in the figure below.

$$x := 0, .025..1.0$$

$$f(x,n) := \sum_{i=1}^{n}[\sqrt{2}\cdot sin(i\cdot\pi\cdot x)\cdot\int_0^1 \sqrt{2}\cdot sin(i\cdot\pi\cdot x')\cdot x'^3\cdot(1-x')dx')]$$



This page titled 11.7: Examining Fourier Synthesis with Dirac Notation is shared under a CC BY 4.0 license and was authored, remixed, and/or curated by Frank Rioux via source content that was edited to the style and standards of the LibreTexts platform.

11.8: Finding Roots of Transcendental Equations

The attempt to find analytical solutions to Schrödinger′s equation for some problems yields transcendental equations which must be solved by a combination of graphical and numerical techniques. Mathcad is particularly well-suited for such applications.

Solving Schrödinger′s equation for the particle in the box with an internal barrier yields the trancendental equation $f(E)$ shown below. This equation is solved by plotting f(E) vs E to find the approximate values of the bound energy states.

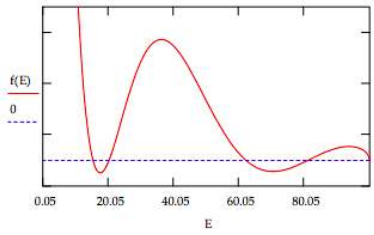
The box is 1 bohr wide and the barrier is 0.1 bohr thick and located in the center of the box.

- Vo is the barrier height in hartrees. Vo := 100
- The barrier thickness in bohrs. BT := .1
- Left barrier boundary in bohrs. LB := .45

E := 0.05, .1 .. 100

$$f(E) := tanh[BT \cdot \sqrt{2 \cdot (V_o - E)}] \cdot (\tfrac{V_o - E}{E} \cdot \sin(LB \cdot \sqrt{2 \cdot E})^2 + \cos(LB \cdot \sqrt{2 \cdot E})^2) \cdots + 2 \cdot \sqrt{\tfrac{V_o - E}{E}} \cdot \sin(LB \cdot \sqrt{2 \cdot E}) \cdot \cos(LB \cdot \sqrt{2 \cdot E})$$

For a derivation of this formula see: Johnson and Williams, Amer. J. Phys. 1982, 50, 239-244.



By inspection of the graph one can see that there are roots at approximately 15, 20, 62, and 80. The exact energy is found with Mathcad′s root function using the approximate energy as a seed value as illustrated below.

E := 15 root(f(E), E) = 15.43

E := 20 root(f(E), E) = 20.29

E := 62 root(f(E), E) = 62.24

E := 80 root(f(E), E) = 81.07

This exercise can be extended by noting that this problem can also be solved by numerical integration of Schrödinger′s equation. Comparisions of this sort help are helpful in strengthening the students understanding of the computational techniques available to the quantum chemist. Below the problem is solved by numerical integration of Schroedinger′s equation.

Integration limit: x_{max} := 1 Effective mass: μ := 1 Barrier height: V_0 := 100

Barrier boundaries: lb := .45 rb := .55 Potential energy: $V(x) := if[(x \geq lb) \cdot (x \leq rb), V_0, 0]$

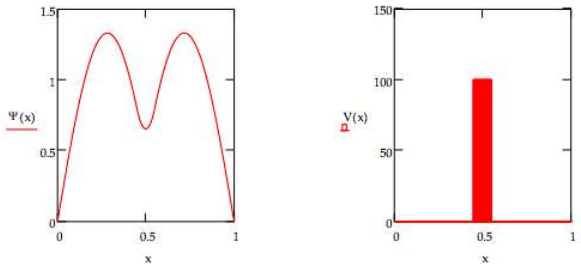
Numerical integration of Schrödinger′s equation: $\frac{-1}{2 \cdot \mu} \cdot \frac{d^2}{dx^2}\psi(x) + V(x) \cdot \psi(x) = E \cdot \psi(x)$

$$\psi(0) = 0.\ \psi'(0) = 0.1$$

Enter energy guess: E := 15.43

ψ := Odesolve(x, x_{max})

Normalize wave function: $\psi(x) := \frac{\psi(x)}{\sqrt{\int_0^{x_{max}} \psi(x)^2 dx}}$



This page titled 11.8: Finding Roots of Transcendental Equations is shared under a CC BY 4.0 license and was authored, remixed, and/or curated by Frank Rioux via source content that was edited to the style and standards of the LibreTexts platform.

11.9: Calculation of the Composition of a Weak Polyprotic Acid Using Mathcad

Polyprotic Acids - Calculating the composition of 0.1M H_3AsO_4

Excluding water there are six species in this solution of arsenic acid. Therefore six constraints are required to calculate the composition of the solution. Four of them are the following equilibria, and the other two are the charge and mass balance equations given below.

Equilibria:

$$H_3AsO_4 \rightleftharpoons H^+ + H_2AsO_4^-$$

$$H_2AsO_4^- \rightleftharpoons H^+ + HAsO_4^{2-}$$

$$HAsO_4^{2-} \rightleftharpoons H^+ + AsO_4^{3-}$$

$$H_2O \rightleftharpoons H^+ + OH^-$$

Charge balance:

$$[H^+] = [H_2AsO_4^-] + 2[HAsO_4^{2-}] + 3[AsO_4^{3-}] + [OH^-]$$

Mass balance:

$$H_3AsO_4 + H_2AsO_4^- + HAsO_4^{2-} + AsO_4^{3-} = 0.1$$

Relevant equilibrium constants:

$$Ka1 := 4.5 \times 10^{-4}\ Ka2 := 5.6 \times 10^{-8}\ Ka3 := 3.0 \times 10^{-13}\ Kw := 10^{-14}$$

Mathcad's live symbolic solver is used to calculate the concentrations of the species in solution by creating two 6x1 vectors. In one vector the six constraints are entered, and in the other the symbols for the species being calculated. The results of the calculation are given below.

$$\begin{pmatrix} \frac{H \cdot H_2AsO_4}{H_3AsO_4} = Ka1 \\ \frac{H \cdot HAsO_4}{H_2AsO_4} = Ka2 \\ \frac{H \cdot AsO_4}{HAsO_4} = Ka3 \\ H \cdot OH = Kw \\ H = H_2AsO_4 + 2 \cdot HAsO_4 + 3 \cdot AsO_4 + OH \\ H_3AsO_4 + H_2AsO_4 + HAsO_4 + AsO_4 = 0.1 \end{pmatrix}^{solve,} \begin{pmatrix} H \\ H_3AsO_4 \\ H_2AsO_4 \\ HAsO_4 \\ AsO_4 \\ OH \end{pmatrix}$$

$$\rightarrow \begin{pmatrix} -6.94 \cdot 10^{-3} & .107 & -6.94 \cdot 10^{-3} & -2.42 \cdot 10^{-18} & -1.44 \cdot 10^{-12} & \\ -1.12 \cdot 10^{-7} & -4.98 \cdot 10^{-5} & 0.200 & -.100 & 2.68 \cdot 10^{-7} & -8.93 \cdot 10^{-8} \\ -4.68 \cdot 10^{-13} & 2.42 \cdot 10^{-15} & -2.33 \cdot 10^{-6} & .279 & -.179 & -2.14 \cdot 10^{-2} \\ -3.21 \cdot 10^{-14} & -4.88 \cdot 10^{-}19 & 6.85 \cdot 10^{-9} & -1.20 \cdot 10^{-2} & .112 & -.312 \\ 6.49 \cdot 10^{-3} & 9.35 \cdot 10^{-}2 & 6.49 \cdot 10^{-3} & 5.60 \cdot 10^{-8} & 2.59 \cdot 10^{-18} & 1.54 \cdot 10^{-12} \end{pmatrix}^{float,3}$$

The last row contains the physically meaningful solution to the fifth order polynomial that is solved. The pH of this solution is calculated below.

$$pH := -\log(6.49 \times 10^{-3})\ pH = 2.188$$

This page titled 11.9: Calculation of the Composition of a Weak Polyprotic Acid Using Mathcad is shared under a CC BY 4.0 license and was authored, remixed, and/or curated by Frank Rioux via source content that was edited to the style and standards of the LibreTexts platform.

11.10: Solving Linear Equations Using Mathcad

Numeric Methods: A system of equations is solved numerically using a Given/Find solve block. Mathcad requires seed values for each of the variables in the numeric method.

Seed values: x :=1 y :=1 z :=1

Given: $5 \cdot x + 2 \cdot y + z = 36$ $x + 7 \cdot y + 3 \cdot z = 63$ $2 \cdot x + 3 \cdot y + 8 \cdot z = 81$

$$\text{Find (x, y, z)} = \begin{pmatrix} 3.6 \\ 5.4 \\ 7.2 \end{pmatrix}$$

Other Given/Find solve blocks can be used.

$$\text{Given} \begin{pmatrix} 5 \cdot x + 2 \cdot y + z = 36 \\ x + 7 \cdot y + 3 \cdot z = 63 \\ 2 \cdot x + 3 \cdot y + 8 \cdot z = 81 \end{pmatrix} = \begin{pmatrix} 36 \\ 63 \\ 81 \end{pmatrix} \text{Find(x, y, z)} = \begin{pmatrix} 3.6 \\ 5.4 \\ 7.2 \end{pmatrix}$$

$$\text{Given} \begin{pmatrix} 5 & 2 & 1 \\ 1 & 7 & 3 \\ 2 & 3 & 8 \end{pmatrix} \cdot \begin{pmatrix} x \\ y \\ z \end{pmatrix} = \begin{pmatrix} 36 \\ 63 \\ 81 \end{pmatrix} \text{Find(x, y, z)} = \begin{pmatrix} 3.6 \\ 5.4 \\ 7.2 \end{pmatrix}$$

Matrix methods: The equations can also be solved using matrix algebra as shown below. In matrix form, the equations are written as MX = C. The solution vector is found by matrix mutiplication of by the inverse of M.

$$\text{M:=} \begin{pmatrix} 5 & 2 & 1 \\ 1 & 7 & 3 \\ 2 & 3 & 8 \end{pmatrix} \text{C:=} \begin{pmatrix} 36 \\ 63 \\ 81 \end{pmatrix} \text{X := } M^{-1} \cdot C \text{ X} = \begin{pmatrix} 3.6 \\ 5.4 \\ 7.2 \end{pmatrix}$$

Confirm that a solution has been found:

$$\text{M} \cdot \text{X} = \begin{pmatrix} 36 \\ 63 \\ 81 \end{pmatrix}$$

Alternative matrix solution using the lsolve command.

$$\text{X := lsolve(M,C) X} = \begin{pmatrix} 3.6 \\ 5.4 \\ 7.2 \end{pmatrix} \text{M} \cdot \text{X} = \begin{pmatrix} 36 \\ 63 \\ 81 \end{pmatrix}$$

Live symbolic method: To use the live symbolic method within this Mathcad document recursive definitions are required clear previous values of x, y and z. This would not be necessary if x, y and z had not been previous defined.

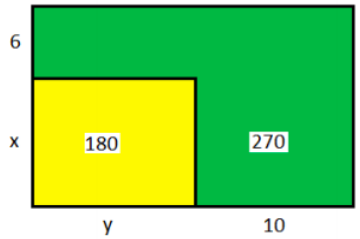
x := x y := y z := z

$$\begin{pmatrix} 5 \cdot x + 2 \cdot y + z = 36 \\ x + 7 \cdot y + 3 \cdot z = 63 \\ 2 \cdot x + 3 \cdot y + 8 \cdot z = 81 \end{pmatrix} solve, \begin{pmatrix} x \\ y \\ z \end{pmatrix} \rightarrow \left(\frac{18}{5} \quad \frac{27}{5} \quad \frac{36}{5}\right) = (3.6 \quad 5.4 \quad 7.2)$$

This page titled 11.10: Solving Linear Equations Using Mathcad is shared under a CC BY 4.0 license and was authored, remixed, and/or curated by Frank Rioux via source content that was edited to the style and standards of the LibreTexts platform.

11.11: Let's Teach High School Students Computer Algebra Methods

The algebra problem shown below appears in my grandson's 9th grade math text. He is asked to solve for x and y using the "guess and check" method. It is early in the semester so I do not object, figuring he will be taught more reliable standard methods soon. The method I strongly recommend is to stress that if you have two unknowns, you need two equations, and that those equations should be stated explicitly up front. After that some standard method should be used to find the solution or solutions, by hand or using a calculator or a computer. In this case there are two solutions.



In what follows two computer algebra methods using Mathcad are presented. The total area (yellow plus green) is 450, so my two equations are given below. This is the most important part in solving the problem - setting it up and it is what should be stressed in math education. Let the computer or calculator do the tedious stuff. The Mathcad syntax for the first method is as follows:

$$\begin{bmatrix} (x+6)\cdot(y+10)=450 \\ x\cdot y=180 \end{bmatrix} \text{ solve, (x, y)} \rightarrow \begin{pmatrix} 12 & 15 \\ 9 & 20 \end{pmatrix}$$

The second method involves eliminating y in the first equation by substitution using the second equation, solving for x and then using the second equation to get the appropriate values for y.

$$\text{x} := (\text{x} + 6)\cdot(\text{y} + 10) = 450 \text{ substitute, y} = \tfrac{180}{x} \rightarrow \tfrac{10\cdot(x+6)\cdot(x+18)}{x} = 450 \text{ solve, x} \rightarrow \begin{pmatrix} 9 \\ 12 \end{pmatrix}$$

$$\text{Write } y \text{ in terms of } x\text{: y} := \tfrac{180}{x} \text{ Display } y \text{ values: y} = \begin{pmatrix} 20 \\ 15 \end{pmatrix}$$

High school students are facile in using the computer for word processing, and the internet for resourcing term papers and social networking purposes. It's time they were taught how to use the computer to solve math and science problems.

Solution templates can be provided to the students so that they can concentrate on setting up the problem, rather than the programming syntax.

Template for first method: $\begin{pmatrix} \square = \blacksquare \\ \blacksquare = \blacksquare \end{pmatrix}$ solve, (■ ■) →

Template for second method: ■ := ■ = ■ substitute, ■ = ■ → solve, ■ →

This page titled 11.11: Let's Teach High School Students Computer Algebra Methods is shared under a CC BY 4.0 license and was authored, remixed, and/or curated by Frank Rioux via source content that was edited to the style and standards of the LibreTexts platform.

11.12: Thermodynamics and Kinetics

Most thermodynamics expression in textbooks are "intramural" relations. They tell us how to determine numerical values for unfamiliar quantities, such as ΔS and ΔG (Equation 11.12.1-11.12.4) for example), or how one such quantity depends on another such quantity (Equation 11.12.3-11.12.4).

$$\Delta S = \frac{Q_{rev}}{T} \tag{11.12.1}$$

$$\Delta G^{\circ} = -RT \ln K_{eq} \tag{11.12.2}$$

$$\Delta G = \Delta H - T\Delta S \tag{11.12.3}$$

$$\left[\frac{\delta(\Delta G)}{\delta T}\right]_P = -\Delta S \tag{11.12.4}$$

Only a few thermodynamic expressions are "extramural" relations--ones that tell us immediately something about "directly measurable" or familiar quantities: how, for example, an equilibrium pressure P, or concentration N_2, or quotient of concentrations K or cell voltage ξ varies with temperature (Equations 11.12.1-11.12.4).

$$\frac{dP}{dT} = \frac{Q}{T\Delta V} \tag{11.12.5}$$

$$\frac{dN_2}{dT_{fp}} = \frac{-Q}{RT_{nfp}^2} \tag{11.12.6}$$

$$\ln \frac{K_2}{K_1} = \frac{Q_{irrev}}{R}\left(\frac{1}{T_1} - \frac{1}{T_2}\right) \tag{11.12.7}$$

$$nF\frac{d\xi}{dT} = \frac{Q_{rev}}{T} \tag{11.12.8}$$

These extramural relations (Equation 11.12.5-11.12.8) show how equilibrium parameters (P, N_2, K, ξ) must change with temperature if perpetual motion of the second kind is impossible. Perpetual motion of the second kind is production of work (an increase in energy of a mechanical system) solely at the expense of the energy of a thermal reservoir. In its net effect upon the environment, it is, with respect to energy transformations, precisely the opposite of friction.

The most general statement of the Second-Law like behavior of Nature states that any process whose net effect is precisely the opposite of friction -- or heat flow, or any natural event -- is impossible. From that statement can be developed by relatively long and mathematically demanding arguments, as shown in many physical chemistry texts, the extramural relations (Equation 11.12.5-11.12.8).

It is the chief purpose of this paper to show that the Clapeyron equation (11.12.5), the colligative property relations (such as Equation 11.12.6), van 't Hoff's relation (Equation 11.12.7), Gibbs-Helmholtz-type equations (such as Equation 11.12.8) and, also (discussed later), the osmotic pressure law (Equation 19), Boltzmann's factor (equation 25), and Carnot's theorem (equation 35) can be obtained directly from the laws of chemical kinetics, without the use of calculus.

Our kinetic derivations of the extramural relations of the thermodynamics are based on Arrhenius's rate-constant expression

$$k = A^{-\Delta H^*/RT}.$$

It will be shown that the derivations depend ultimately, therefore, on van 't Hoff's thermodynamic equilibrium-constant expression

$$K = C^{-\Delta H/RT}. \tag{11.12.9}$$

Thus, the kinetic derivations are not, in a logical sense, a substitute for the usual thermodynamics arguments. It is often illuminating, however, to see abstract expressions (such as those of thermodynamics) emerge seemingly unexpectedly from more concrete equations (those of chemical kinetics).

The mathematical procedures in this paper can be used, also, in purely thermodynamic arguments. With no change in the algebraic steps given below, one can derive the extramural relations of thermodynamics directly from the thermodynamic expression in Equation 11.12.9. Thus one can move rigorously and easily from one extramural relation to another without employing calculus and

the entropy function (or the chemical potential), or Carnot cycles. This simplification of the syntax of thermodynamics serves to emphasize an essential point: there is essentially only one physically independent extramural thermodynamic relation. There is only one Second Law. Expressions (Equations 11.12.5-11.12.8), the osmotic pressure rule (19), and Boltzmann's factor (25) are all special instances of Carnot's theorem (35).

In summary the present discussion is, simultaneously: a set of novel applications to thermodynamics of Arrhenius's rate-constant expression; a non-calculus review from several new points of view of the central expressions of classical (and, briefly, statistical) thermodynamics; and, in close, a brief account of the origins in kinetics and thermodynamics of activated complex theory.

Henry's Law and Raoult's Law

Many texts give this kinetic interpretation of Henry and Raoult laws. Consider the change

$$x\ (solution) \underset{k_b}{\overset{k_f}{\rightleftharpoons}} x\ (gas)$$

Let $R_{f(b)}$ represent the rate of the forward (backward) reaction, specific rate constant $k_{f(b)}$. Let C_x be the concentration (in any units) of X in the condensed phase, N_x its mole fraction therein, P_x its partial pressure in the gas phase, P_x^o the vapor pressure of pure X. On the assumption that one has

$$R_f = k_f C_x \tag{11.12.10}$$

$$R_c = k_b P_{x'} \tag{11.12.11}$$

that at equilibrium ($R_f = R_b$)

$$P_x = \frac{k_f}{k_b} c_x = K_{eq} C_x$$

$$\underbrace{K_{eq} = \frac{P_x}{C_x} = 1}_{\text{Henry's Law}} \tag{11.12.12}$$

$$= \underbrace{\frac{P_x}{C_x} = N_x = 1}_{\text{Raoult's Law}} \tag{11.12.13}$$

$$\equiv P^\circ_{X'}$$

Similar derivations of mathematical expressions for other colligative properties can be achieved by introducing Arrhenius's expression for the dependence upon temperature (and pressure) of the specific rate constants k_f and k_b.

Arrhenius's Rate-Constant Law

According to Arrhenius (in modern notation), for forward and backward reactions

$$k = Ae^{-\Delta H^*/RT} \tag{11.12.14}$$

where, over small temperature intervals, A and ΔH^* may be treated as constants, and where, Fig. 1,

$$\Delta_f H^* - \Delta_b H^* = \Delta H \tag{11.12.15}$$

$$= H_{products} - H_{reactions} \tag{11.12.16}$$

$$= \Delta E + \Delta(PV). \tag{11.12.17}$$

The Ideal Solubility Equation and Freezing Point Depression

To illustrate the use of the Arrhenius Rate-Constant Law to obtain by a kinetic analysis expressions normally obtained through reasoning based on thermodynamic principles, consider the solution, or melting, of a pure solid.

$$x\ (pure\ solid) \underset{k_b}{\overset{k_f}{\rightleftharpoons}} x\ (solution)$$

On the assumption that $R_f = k_f$ and $R_b = k_b N_X$, one has that, at equilibrium, $k_f = k_b N_X$ or, on using the Arrhenius expression, (Equation 11.12.14), that

$A_f^{(-\Delta_f H^*/RT)} = N_X A_b^{(-\Delta_b H^*/RT)}$.

Rearrangement and use of Equation 11.12.15 yields

$$\frac{A_f}{A_b} = N_x e^{\frac{\Delta H}{RT}}$$

ΔH is the enthalpy of solution, or melting, of X. Taking the natural logarithm of both sides of Equation ???, one obtains

$$(a)\frac{\Delta H}{RT} + \ln(N_x) = \ln(\frac{A_f}{A_b})$$

$\ln(\frac{A_f}{A_b})$ *is a constant*

$$\text{(b) } \frac{\Delta H}{RT}|_{N_x=1}$$

$$\text{(c) } \frac{\Delta H}{RT_{nfp}}$$

From (9c),

$$\ln(\frac{N_x}{1}) = \frac{\Delta H}{R}\left(\frac{1}{T_{nfp}} - \frac{1}{T}\right)$$

For $N_X \approx 1$, $\ln N_X \approx -(1-N_X) \equiv -N_2$, $T \approx T_{nfp}$, and equation 10 reduces to

$$N_2 = \frac{-\Delta H}{RT^2 nfp}(T - T_{nfp})$$

Equation 10, the ideal solubility equation, is a special case of equation 2c. Equation 11, the thermodynamic expression for freezing point depressions, is an integrated form of equation 2b.

Clapeyron's Equation

If a pure solid dissolves (melts) in its *pure* liquid,

$$x\ (pure\ solid) \underset{k_b}{\overset{k_f}{\rightleftharpoons}} x\ (pure\ liquid)$$

$N_X = 1$ and, in place of Equation 9, one that has, at equilibrium, $\frac{A_f}{A_b} = 1 \cdot \frac{\Delta H}{RT}$. Taking the natural logarithm of both sides, one obtains in place of Equation 9a

$$\frac{\Delta H}{RT} = \ln\frac{A_f}{A_b}, \qquad \text{(a constant)}$$

$$= \frac{\Delta E + P\Delta V}{RT} \qquad (11.12.18)$$

Equation 11.12.18 is obtained through equation 7b.

If the pressure and temperature change from values P and T that satisfy equation to new values $P + dP$ and $T + dT$, for equilibrium to be maintained, dP and dT must be such that

$$\frac{\Delta E + (P + dP)\Delta V}{R(T + dT)} = \frac{\Delta E + P\Delta V}{RT} \qquad (11.12.19)$$

In writing Equation 11.12.19, it has been assumed that, like $\frac{A_f}{A_b}$, ΔE and ΔV are temperature- and pressure-independent. Simplification of Equation 11.12.19 yields, on solving for the ration of dP to dT in Equation 11.12.5 with

$$Q = \Delta E + P\Delta V = \Delta H.$$

A kinetic analysis of the similar but slightly more complicated case of the vaporization of a liquid (or solid) is given in Appendix 1, together with a kinetic analysis of the effect on a vapor pressure of squeezing a liquid (the *Gibbs-Poynting effect*), with an application to osmosis.

Osmotic Equilibrium

Consider, next, diffusion of a pure solvent at pressure P through a rigid, semi-permeable membrane into a solution at pressure P + π,

$$x\ (pure\ solvent) \underset{k_b}{\overset{k_f}{\rightleftharpoons}} x\ (solution)$$

	Pure Solvent	Solution
Pressure	P	P + π
Mole Fraction	$N_X = 1$	$N_X < 1$

The kinetic analysis $R_f = k_f = R_b = k_b N_X$ yields with Arrhenius's relation, (6), expressions identical to (9) and (9a). In this instance, at least approximately, ΔE = ΔV = 0. Thus for (15)

$$\Delta H = \Delta(PV)\ (P+\pi)\bar{V}_x - P\bar{V}_x = \pi\bar{V}_x$$

Substitution from (16) into (9a) yields

$$\frac{\pi\bar{V}_x}{RT} + \ln(N_x) = \ln\frac{A_f}{A_b}$$

where $\ln(\frac{A_f}{A_b})$ *is a constant.*

For $N_X = 1$, π = 0 (at equilibrium). In this instance, therefore,

$$\ln(\frac{A_f}{A_b}) = 0$$

Substitution from (18) into (17) yields for dilute solutions ($\ln N_X \approx -N_2$) the usual thermodynamic expression for a solution's osmotic pressure π:

$$\pi \approx \frac{RTN_2}{barV_x} \approx RTC_2$$

in moles/liter.

Chemical Equilibrium

By the *Principle of Microscopic Reversibility*, one has that for chemical change

$$aA + bB \underset{k_b}{\overset{k_f}{\rightleftharpoons}} dD + eE$$

the rate at which A and B disappear by the (perhaps unlikely) *mechanism* aA + bB, rate law $R_f = k_f c_A{}^a c_B{}^b$, is *at equilibrium* equal to the rate at which A and B appear by the mechanism dD + eE, rate law $R_b = k_b c_D{}^d c_E{}^e$.[1] Thus, from $R_b = R_f$ one obtains the familiar Law of Mass Action, equation 21 below, which with equations 6 and 7 yields equation 22, from which can be obtained directly equation 2c ($Q_{irrev} = \Delta H$).

$$\frac{C_D^d C_E^e}{C_A^a C_B^b}\Big|_{equil.} = \frac{k_f}{k_b} = K_{eq}$$

$$= \frac{A_f}{A_b} e^{\frac{-\Delta H}{RT}}$$

For later reference, we note that, from equations 21 and 22,

$$K_{eq} = \frac{A_f}{A_b} e^{\frac{-\Delta H}{RT}}$$

(b) $e^{\frac{-[\Delta H - RT\ln\frac{A_f}{A_b}]}{RT}}$

[1]For a further discussion of this point see: Frost, A. A., and Pearson, R. G., "Kinetics and Mechanism," John Wiley and Sons, Inc., 1953, Ch. 8; or Frost, A. A., J. Chem. Educ., 18, 272 (1941).

Boltzmann's Factor

A particularly simple "chemical" change is the transition of a molecule X in a quantum energy state i, energy ε_i, to a quantum energy state j, energy ε_j.

$$x\ (state\ i) \underset{k_b}{\overset{k_f}{\rightleftharpoons}} x\ (state\ j)$$

By arguments identical to those given in the preceding section, one obtains expressions of the form of equations 21 and 22. In this simple instance $K_{eq} = \frac{C_j}{C_i}$ [$C_{j(i)}$ = concentrations of molecules in state j (i)], $\Delta H = N_o\ (\varepsilon_j - \varepsilon_i)$ [$\Delta(PV) = 0$\, and $A_f = A_b$. Thus, for a system that is at equilibrium with respect to the change indicated in equation 24,

$$\frac{C_j}{C_i} = e^{\frac{-(\varepsilon_j - \varepsilon_i)}{kT}}$$

where $k \equiv \frac{R}{N_o}$

From the Boltzmann factor expression, equation 25 can be obtained directly by summation partition functions and thence, by differentiation and the taking of logarithms, the other standard expressions of statistical thermodynamics.

Electrochemical Equilibrium

For the flow of electrons from a potential V_1 to a potential V_2,

$$e\ (potential\ V_1) \underset{k_b}{\overset{k_f}{\rightleftharpoons}} e\ (potential\ V_2)$$

in an *electrochemical* circuit, cell voltage $\xi = V_2 - V_1$, one has that at equilibrium (a "balanced circuit"), $R_f = k_f = R_b = k_b$. Thus, by the Arrhenius relation, equation 6, *at equilibrium*

$$\frac{A_f}{A_b} = e^{\frac{\Delta_f H^* - \Delta_b H^*}{RT}}$$

The activation enthalpies of ΔH^{*} contain, in this instance, two contributions: one from the enthalpy of activation of the *chemical* change to which the electron flow is coupled in an electrochemical cell; the other from the enthalpy of activation for the *physical* transfer of electrons across a potential difference ξ. Thus, in this instance,

$$(a)\frac{\Delta_f H^* - \Delta_b H^*}{RT} = \frac{\Delta_{rx} H + nF\xi}{RT}$$

$$= \ln \frac{A_f}{A_b}, \text{ a constant (b)}$$

At equilibrium the right-hand-side of (28) is equal to $\ln \frac{A_f}{A_b}$, a constant, equation 28b. If the temperature and voltage change from values T and ξ that satisfy equations 28 to new values T + dT and ξ + dξ, for equilibrium to be maintained, dT and dξ must be such that

$$\frac{\Delta_{rx} H + nF(\xi + d\xi)}{R(T + dT)} = \frac{\Delta_{rx} H + nF\xi}{RT}$$

In writing equation 29 it has been assumed (again) that, like $\frac{A_f}{A_b}$, $\Delta_{rx}H$ is temperature independent: simplification of equation 29 yields on solving for the ratio of dξ to dT

$$nf\frac{d\xi}{dT} = \frac{\Delta_{rx} H + nF\xi}{T}$$

Equation 30 is, in disguise, equation 2d. For consider this universe (or isolated system): a chemical system σ, an atmosphere atm, mechanical surroundings wt, and thermal surroundings θ [for example, as here, a chemical cell σ at constant temperature (owing to thermal contact with θ) and constant pressure (owing to mechanical contact with atm) performing useful work nFξ]. Application of

the First Law (the conservation of energy) to the universe σ + atm + wt + θ yields, on introducing the definitions of P, $\Delta_{rx}H$, and Q, the expression in equation 31.

$$\Delta E_{total} = \Delta E_{\sigma} + \Delta E_{atm} + \Delta E_{wt} + \Delta E_{\theta} = 0$$

where $\Delta E_{atm} = P\Delta V_{\sigma}$; $\Delta E_{\sigma} + \Delta E_{atm} = \Delta H_{\sigma} = \Delta_{rx}H$; $\Delta E_{wt} = nF\xi$; $\Delta E_{\theta} = -Q$.

Thus, for a universe σ (a chemical cell) + atm + wt + θ, $\Delta_{rx}H + nF\xi = Q$. When the universe is in internal equilibrium (the change in equation 26 is reversible), one may write

$$\Delta_{rx}H + nF\xi_{rev} = Q_{rev}$$

Substitution from equation 32 into equation 30 yields equation 2d.

Carnot's Theorem

The previous results can be generalized. The work obtained from a spontaneous chemical change need not appear as electrical energy. Replacing nFξ in equation 28a by W, any useful work, one has for reversible changes that

$$\frac{\Delta H + W_2}{T_2} = \frac{\Delta H + W_1}{T_1} \lable33$$

In writing Equation ???, it has been assumed (again) that ΔH is *independent* of temperature, i.e., that

$$C_p(products) = C_p(reactants)$$

W_2 and W_1 represent the work obtained at, respectively, temperatures T_1 and T_2.

Consider now this partial cycle (a cycle for a composite chemical system $\sigma_1 + \sigma_2$, not, however, for its thermal and mechanical surroundings): A chemical reaction for which the change in enthalpy is ΔH advances *forward* reversibly at temperature T_2 in a system σ_2 in contact with a thermal reservoir θ_2 performing useful work W_2 with $Q_{rev} \equiv Q_2 = \Delta H + W_2$ (by Equation ???). Next the reaction is run *backward* reversibly at a lower temperature T_1 in a system σ_1 (except for its temperature, identical with σ_2) in contact with thermal reservoir θ_1 consuming useful work W_1. Finally with a graded series of external thermal reservoirs the products in σ_1 (chemically identical to the reactants in σ_2) are *warmed* reversibly from T_1 to T_2 and, using the same set of thermal reservoirs, but in the opposite order, the products in σ_2 (chemically identical to the reactants in σ_1) are *cooled* from T_2 to T_1. By Equation ???, the individual external reservoirs suffer no net change. The net work obtained from the overall, reversible process (cyclic for $\sigma_1 + \sigma_2$) is $W_1 - W_2$. By Equation ???,

$W_1 = \frac{T_1}{T_2}(\Delta H + W_2 - \Delta H$.

Thus

$$W_2 - W_1 = (W_2 + \Delta H)(1 - \tfrac{T_1}{T_2})$$

where $W_2 + \Delta H = Q_2$.

Division of both sides by Q_2, the energy absorbed from the warmer thermal reservoir, yields Carnot's theorem.

$$\frac{W}{Q_2}|_{rev} = 1 - \frac{T_1}{T_2} \tag{11.12.20}$$

Our discussion of the kinetic derivation of the *extramural* relations of chemical thermodynamics concludes with Equation 11.12.20 and its companion

$$\frac{dW_{rev}}{dT} = \frac{Q_{rev}}{T} \tag{11.12.21}$$

obtained, after replacing nFξ by W, from Equations ??? and ???. All the second-law based relations of thermodynamics are essentially special instances of Equations 11.12.20 or 11.12.21.

ΔS and ΔG - Clausius-Gibbs Thermodynamics

The major *intramural* relations of chemical thermodynamics are obtained by introducing the abbreviation

$$R \ln \frac{A_f}{A_b} = \Delta S \tag{11.12.22}$$

From the present viewpoint Equation 11.12.22 may be considered a definition of ΔS.

Use of Equation 11.12.22 in Equation 11.12.18 yields for the melting-freezing equilibrium.

$$\Delta S = \frac{\Delta H}{T}$$

Use of Equation 11.12.22 in Equation ??? yields

$$K_{eq} = e^{\frac{-(\Delta H - T\Delta S^\circ)}{RT}}$$

The superscript ° on S in Equation ??? is added to indicate that in this instance the numerical value of ΔS calculated from equation 37 will depend on the units used to express the concentrations of, for example, A and B, since the latter will determine, in part, the numerical value assigned to the kinetic parameter A_f in the rate law $R_f = A_f^{\frac{-\Delta_f H^*}{RT}} C_A^a C_B^b$.

Use of Equation 11.12.22 in Equations ??? and ??? yields (with nFξ = W)

$$\frac{\Delta H + W_{rev}}{T} = \Delta S$$

or,

$$\text{(b) } W_{rev} = -(\Delta H - T\Delta S)$$

Taken with equation 32, equation 40a yields equation 1a, which, with equation 36, yields

$$\frac{dW_{rev}}{dT} = \Delta S$$

Together, equations 40a and 41 yield $\frac{dW_{rev}}{dT} = \frac{\Delta H + W_{rev}}{T}$ or

$$\frac{d\frac{W_{rev}}{T}}{dT} = \frac{\Delta H}{T^2}$$

This last relation is an extramural relation. The symbols S and/or G do not appear in it. It can be obtained directly from equation 36 and equation 32, with $nF\xi_{rev} = W_{rev}$).

Introduction of the abbreviation of equation 1c, a definition of ΔG, yields with equation 39 (an th ideal-solution theory approximation that ΔH is concentration independent) equation 1b. Use of equation 1c in equation 40b yields $W_{rev} = -\Delta G$. The latter with equation 41 yields equation 1d and, with equation 42, the Gibbs-Helmholtz equation:

$$\frac{d\frac{\Delta G}{T}}{dT} = -\frac{\Delta H}{T^2}$$

Equivalence of the Inter- and Extra-Mural Relations of Thermodynamics

Introduction of the symbols ΔS and ΔG with the assigned properties

$$\text{(1a)} \Delta S = \frac{Q_{rev}}{T}$$

$$\text{(1c) } \Delta G = \Delta H - T\Delta S$$

$$\text{(1d) } \left[\frac{\delta(\Delta G)}{\delta T}\right]_P = -\Delta S$$

does not increase the physical content of thermodynamics, namely that:

$$\text{(32) } Q = \Delta H + W \textit{ The First Law}^2$$

$$\text{(36) } \frac{dW_{rev}}{dT} = \frac{Q_{rev}}{T} \textit{ The Second Law}$$

[2]For a universe σ + θ + atm + wt

With definitions of Equations 11.12.3 and 11.12.1, Equations ??? and 11.12.21 imply Equation 11.12.4:

$$\Delta G = \Delta H - T\Delta S = \Delta H - Q_{rev} = -W_{rev} \Rightarrow \frac{\delta \Delta G}{\delta T} = \Delta S$$

Conversely, with Definitions 11.12.3 and 11.12.1, Equations ??? and 11.12.4 imply Equation 11.12.21. *The intramural and extramural relations of thermodynamics are logically equivalent to each other.* To write equation 1b

$$-RT \ln K_{eq} = \Delta G^{\circ}$$

is, with Equations 11.12.4 and 11.12.3, equivalent mathematically, to writing the van 't Hoff relation (Equation 11.12.7) in its differential form

$$\frac{d \ln K_{eq}}{dT} = \frac{\Delta H}{RT^2}$$

The position in the above, hierarchical arrangement of ideas of the expression $\Delta S_{total} \geq 0$ is described in Appendix 2.

Summary and Conclusions

Equations of classical (and statistical) thermodynamics based on the Second Law can be divided into two classes: those that contain the symbols S and/or G (or A) (the intramural relations) and those that do not (the extramural relations). The latter relations, those of immediate practical use, can be obtained quickly and easily, without calculus, from simple kinetic arguments based on Arrhenius's Rate-Constant Law and the assumptions of ideal solution theory (ΔH independent of concentration; activities of solvents equal to mole fractions, those of gases to partial pressures); the assumption, or approximation, that $\Delta C_p = 0$; and, in some instances, the Principle of Microscopic Reversibility. The kinetic treatment is, thus, a complement to, not a complete substitute for, the usual thermodynamic derivations of, for example, Clapeyron's equation and Carnot's theorem, which are valid relations even for non-ideal systems and for systems in which $\Delta C_p = 0$.

Arrhenius's Law is the non-thermodynamically inclined chemist's friend. While not encompassing the full content of the Second Law, and probably precisely because of that fact, Arrhenius's Rate-Constant Law embodies in a form immediately and easily applicable to many problems (both classical and statistical) those implications of the Second Law of particular interest to chemists. One may wonder how Arrhenius was led to an expression that captures so simply yet effectively the chemically significant features of the Second Law of thermodynamics.

Origin of Arrhenius's Rate-Constant Law

"In his notable book *Studies in Chemical Dynamics* van 't Hoff gives a theoretically-based formulation of the influence of temperature on the rate of reaction," wrote Arrhenius in 1889 in a paper (his chief contribution to chemical kinetics) On the Reaction Velocity of the Inversion of Cane Sugar by Acids *(1)*.

"It may be proved, by means of thermodynamics," van 't Hoff had written *(2)*, "that the values of k_1 and k_2 [our k_f and k_b] must satisfy the following equation: -

$$\frac{d \log k_1}{dT} - \frac{d \log k_2}{dT} = \frac{q}{2T^2}''$$

[Today we usually write ln for log, ΔH for q, R for 2.]

"Although this equation does not directly give the relationship between the constants k and the temperature," continued van 't Hoff, "it shows that this relationship must be of the form

$$\frac{d \log k}{dT} = \frac{A}{T^2} + B$$

where A and B are constants" *(2)*.

Implicit in van 't Hoff's remarks is the understanding that $A_1 - A_2 = q$ (cf. equation 7a) and that $B_1 = B_2$.[3]

"It is, however, easily seen," notes Arrhenius, "that B can be any function, F(T), of the temperature... [provided only that] the F(T) belonging to two reciprocal reactions are the same" *(1)*.

"Since F(T) can be anything at all," continues Arrhenius, "it is not possible to proceed further without introducing *a new hypothesis*, which is in a certain sense *a paraphrase of the observed facts*" [emphasis added].

Noting that the influence of temperature on specific reaction rate is very large, much larger than increasing gas-phase collision frequencies or decreasing liquid-phase viscicities, Arrhenius suggests by analogy with the "similar extraordinary large change in specific reaction velocity (k)... brought about by weak basis and acids" [an effect arising from the catalytic effect of often an *infinitesimal amount* of H^+ or OH^-] that in, for example, the inversion of cane sugar, the rate of which is sharply temperature-dependent, the "actual reacting substance is not [ordinary] sugar, since its amount does not change with temperature, but is another hypothetical substance... which we call 'active cane sugar' [today, 'activated cane sugar']... that is generated [in small amounts, by activation] from [ordinary, inactive] cane sugar... and must [be supposed to] increase rapidly in quantity with increasing temperature."

Continuing with his paraphrase of the observed facts, Arrhenius writes that "since the reaction velocity is approximately proportional to the amount [concentration] of [ordinary] cane sugar... the amount [concentration] of 'active can sugar', M_a, must be take to be approximately proportional to the amount of inactive cane sugar, M_i. The *equilibrium condition* [emphasis added] is thus:

$$M_a = kM_i$$

"The form of this equation shows us that a molecule of 'active cane sugar' is formed from a molecule of inactive cane sugar either by a displacement of the atom or by addition of water", whose amount is constant; its concentration, therefore, does not appear in equation 46.

The constant k in equation 46 wears two hats. It is simultaneously a thermodynamic parameter and a rate parameter. It is the thermodynamic equilibrium constant for the postulated equilibrium between active and inactive cane sugar molecules (it would be written today as K* or $K^{\ddagger}$). And, if the rate of inversion is, as postulated, proportional to M_a, k is proportional to the kinetic rate constant for the inversion of cane sugar.

Carrying over in this way to kinetics a thermodynamic relation, Arrhenius applies van 't Hoff's *thermodynamic* expression, equation 44, for the temperature variation of an equilibrium constant K ($= frack_1k_2$ to the thermodynamic-*kinetic* constant k of equation 46. In the spirit of modern absolute rate theory, he write that "Thus for the constant k (or what is the same thing $\frac{M_a}{M_i}$ we have the equation

$$\frac{d\log_{nat} k}{dT} = \frac{q}{2T^2}\text{''}$$

which on integration yields, with $q = \Delta H^{\ddagger}$ (and 2 = R), equation 6.

That Arrhenius's Rate-Constant Law captures for chemistry the essential features of the Second Law of thermodynamics is, thus, no mystery. It is a plausible application, based on a selective if brief axiomatization of nearly universal features of chemical reaction rates, of van 't Hoff's thermodynamic relation (equation 44), which is a special instance - THE CHEMICAL INSTANCE - of the Gibbs-Helmholtz equation (equation 43), which in turn is a general instance, if not quite the complete embodiment of Carnot's theorem (equations 35 and 36), itself THE most general mathematical statement of the Second-Law-like behavior of nature. As we have shown, however, in many chemical problems Arrhenius's Law (equation 6) is a more quickly an easily-used expression of the Second Law than is Carnot's more widely applicable and, though mathematically simpler, chemically more remote theorem (equation 35).

[3]In absolute rate theory $k = \frac{RT}{h} e^{\frac{\Delta S^{\ddagger}}{R}} e^{\frac{\Delta H^{\ddagger}}{RT}}$. Hence, for $\Delta C_p^{\ddagger} = 0$, $d\ln\frac{k}{dT} = \frac{\Delta H^{\ddagger}}{RT} + \frac{1}{T}$ and $B = \frac{1}{T}$. More generally, if, empirically, one has $k = aT^n e^{\frac{A}{T}}$, a, A, constants, then, by equation 45, $B = \frac{n}{T}$.

Appendix 1

Derivation of Clapeyron's Equation for the Phase Change

$$x_{(pure\ liquid)} \underset{k_b}{\overset{k_f}{\rightleftharpoons}} x_{(gas)}$$

With a Note on the Gibbs-Poynting Effect and Osmotic Pressure

At equilibrium ($R_f = R_b$), $k_f = k_bP$. Using equations 6 and 7a, one obtains on taking logarithms.

$$\frac{\Delta H}{RT} + \ln(P) = \ln\frac{A_f}{A_b}, \text{ a constant}$$

Thus, on going from an equilibrium point T,P to another equilibrium point T + dT, P + dP, one has that if ΔH is (in this instance) independent of T and P, dT must be such that

$$\frac{\Delta H}{R(T+dT)} + \ln(P+dP) = \frac{\Delta H}{RT} + \ln(P).$$

Multiplying through by R(T + dT)T, simplifying, noting that $\ln(P+dP) - \ln(P) = \ln(l + \frac{dP}{P} = \frac{dP}{P}$ and that $\frac{RT^2}{P} = TV^{-g}$ and dropping the term containing dP x dT, one obtains

$$\frac{dP}{dT} = \frac{\Delta H}{T\overline{V}^g} \approx \frac{\Delta H}{T\Delta V}.$$

If the partial pressure on the gas, P^g, is not the same as the pressure on the liquid phase, P^1, (the liquid, for example, might be squeezed -- as in an osmotic experiment--behind a rigid, x-permeable barrier), the first equation above should be written

$$\frac{\Delta E + P^g\overline{V}^g - P^1\overline{V}^1}{RT} + \ln(P^g) = \ln(\frac{A_f}{A_b}), \text{ a constant.}$$

For vapors behaving as ideal gases, one has $P^g\overline{V}^g = RT$. If, now, *at constant temperature*, the two pressures change from values P^1 and P^g that satisfy the above relation to new values $P^1 + dP^1$ and $P^g + dP^g$, for equilibrium to be maintained, dP^1 and dP^g must be such that

$$\frac{\Delta E + RT - (P^1 + dP^1}{RT} - \ln(P^g + dP^g) = \frac{\Delta E + RT - P^1\overline{V}^1}{RT} + \ln(P^g).$$

Simplifying, one obtains the Gibbs-Poynting equation

$$dP^g = \frac{\overline{V}^1}{\overline{V}^g} dP^1.$$

Consider, now, a *squeezed*, *impure* liquid X in equilibrium with the pure, unsqueezed liquid, equation 15, equilibration occurring (in one's mind) via a common vapor phase. A finite squeeze $\Delta P^1 = \pi$ *increases* the vapor pressure (the pressure of the gas that maintains equilibrium with the liquid) by an amount (see above) $\frac{\overline{V}^1}{\overline{V}^g}\pi$. The presence, however, of a second component, 2, *decreases* the vapor pressure from that of the pure liquid, P_x^o, by an amount, (see equation 5b) $P_x^\circ - P_x^\circ N_x = P_x^\circ(1 - N_x) \equiv P_x^\circ N_2$. Equating those two terms, one finds that the amount π an *impure* liquid must be squeezed to maintain equilibrium with the *pure* liquid is given by the expression

$$\pi = \frac{P_x^\circ \overline{V}^g N_2}{\overline{V}^1} = \frac{RTN_2}{\overline{V}^1}$$

(in agreement with equation 19).

Appendix 2

$$\Delta S_\sigma,\ \Delta S_\theta,\ \Delta S_{atm},\ \Delta S_{wt} \text{ and } \Delta S_{total}$$

The primary implications for classical thermodynamics of the Second-Law-type behavior of nature are embodied in expression 36: $\frac{dW_{rev}}{dT} = \frac{Q_{rev}}{T}$. The variation with temperature of W_{rev} is a property jointly of the initial *and* final states of a system σ. It is, so to speak, a "double state function". *Define*, in the spirit with which equation 36 was introduced,

$$\Delta S \equiv \frac{dW_{rev}}{dT} \text{ For convenience}^4$$

$$= \frac{Q_{rev}}{T} \text{ By Carnot's Theorem}$$

$$= \frac{-\Delta_{rev}E_\theta}{T} \text{ By definition: } Q \equiv -\Delta E_\theta$$

$$\frac{\Delta H_{sigma} + W_{rev}}{T} \text{ By the First Law}$$

Define, also, purely for bookkeeping purposes,

$$\Delta S_\theta \equiv \frac{\Delta E\theta}{T}$$

$$\Delta S_{atm} \equiv 0$$

$$\Delta S_{wt} \equiv 0$$

$$\Delta S_{wt} \equiv \Delta S_\sigma + \Delta S_{theta} + \Delta S_{atom} + \Delta S_{wt}$$

Clearly, for a reversible process, $\Delta S_{total} = 0$. For irreversible processes, one has that

$$W_{irrev} = \Delta H_\sigma + Q_{irrev} < W_{rev} = \Delta H_\sigma + Q_{rev}$$

$$\Rightarrow Q_{irrev} < Q_{rev} or (Q \equiv -\Delta E_\theta$$

$$\Delta_{irrev} E_\theta > \Delta_{rev} E_\theta$$

$$\Rightarrow \Delta_{irrev} S_\theta > \Delta_{rev} S_\theta$$

$$\Rightarrow \Delta_{irrev} S_{total} > 0.$$

[4]It's easier to write "ΔS" than "$\frac{dW_{rev}}{dT}$".

Literature Cited

1. Arrhenius, S., *Z. Physik. Chem.*, 4, 226 (1889); excerpted and translated by Back, M. H. and Laidler, K. J., "Selected Readings in Chemical Kinetics," Pergamon Press, New York 1967, pp31-35.

2. van 't Hoff, J.H., "Studies in Chemical Dynamics," translated by Thomas Ewan, Chemical Publishing Co., Easton, Pa., 1896, pp122-3.

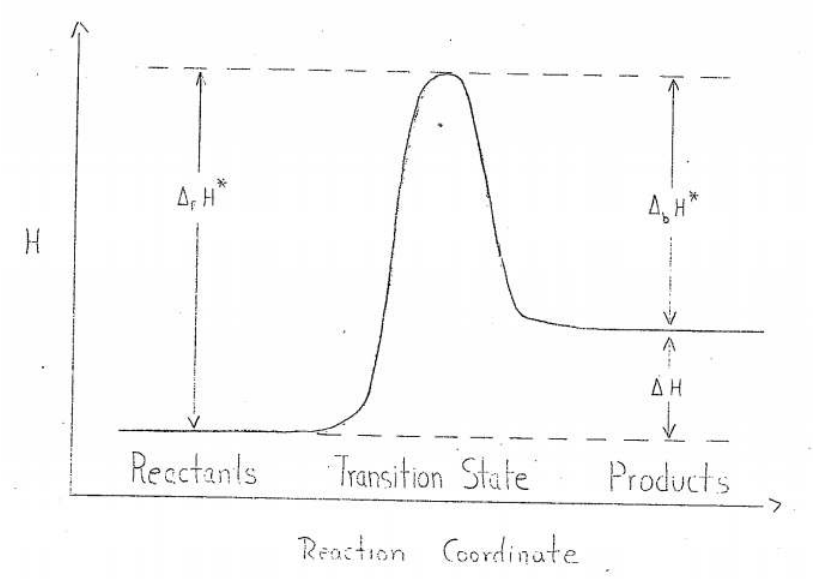


Figure 1. The Arrhenius-van 't Hoff relation between the kinetic parameters $\Delta_{f,b} H^*$ and the thermodynamic parameter ΔH:

$$\Delta H = \Delta_f H^* = \Delta_b H^*$$

This page titled 11.12: Thermodynamics and Kinetics is shared under a CC BY 4.0 license and was authored, remixed, and/or curated by Frank Rioux via source content that was edited to the style and standards of the LibreTexts platform.

11.13: Simple Kinetic Derivations of Thermodynamic Relations

Introduction

Kinetics and thermodynamics seem like very different disciplines. They emphasize different phenomena (change; equilibrium) and introduce different concepts (rate constants; energy/entropy). It is not widely known that a useful connection between those disparate fields was suggested late in the 19th century by Svante Arrhenius when he introduced the concept of the activated molecule to account for the exponential dependence on temperature of kinetic rate constants (1,2). Textbook accounts of Arrhenius's rate-constant law fail to reveal the creative use Arrhenius made of thermodynamic principles in his analysis of the temperature dependence of chemical reaction rates, and, thus, fail to exploit Arrhenius's insights into the teaching of thermodynamics.

After a brief review of Arrhenius's work, we will show that the relations of classical thermodynamics of chief interest to chemists can be obtained by simple algebra from elementary rate laws and Arrhenius's rate constant expression

$$k = Ae^{\frac{\Delta H^*}{RT}}$$

The Origin of Arrhenius's Rate Constant Expression (1)

Facts: Reaction rate have significant temperature dependencies (typically on the order of +8 percent per degree), which cannot be accounted for by increase gas-phase collision frequencies or decreased liquid-phase viscocities.

For all practical purposes, the concentration of reactant molecules are not temperature dependent.

Hypothesis: Since the concentration of a reactant (M) does not vary with temperature, the actual reactant species (in a unimolecular reaction) might be an activated form of the molecule M^*, with

$$Rate = \mathcal{K}(M^*)$$

where the constant $\mathcal{K}$ is independent of temperature and (M^*) is directly proportional to (M) and is sharply dependent on temperature.

$$(M^*) = k(T)\ (M)$$

Implications: Relationship 471.3 can be substituted into 471.2

$$Rate = \mathcal{K}k(T)\ (M)$$

which emphasizes that k(T) is a kinetic rate parameter. Relationship 471.3 can be rewritten as

$$k(T) = \frac{(M^*)}{(M)}$$

which emphasizes that k(T) is, also, a thermodynamic parameter: an equilibrium constant. As such it satisfies van 't Hoff's expression[1]

$$\frac{d\ln(k(T))}{dT} = \frac{\Delta H^*}{RT^2}$$

where ΔH^* is the enthalpy change accompanying the formation of M^* from M - the enthalpy of activation. If over small intervals ΔH^* may be treated as a constant, the integrated form of Equation 471.6 is essentially expression 471.1: $k(T) = Ae^{-\Delta H^*\ RT}$, where A is a constant independent of T. As indicated in Figure 1 (f = forward, b = backward),

$$\Delta_f H^* = \Delta_b H^* = \Delta H \Delta E + \Delta(PV)$$

Discussion: Thermodynamics played a large role in Arrhenius's elucidation of the temperature dependence of rate constants. It is not surprising, then, that the relations of classical thermodynamics can be obtained from elementary rate laws and Arrhenius's rate-constant expression. Below are eight illustrative examples of simple kinetic derivations of thermodynamic relations.

[1]Arrhenius employed van 't Hoff's equation in the form $\frac{d(\ln(k)}{dT} = \frac{q}{RT^2}$. Under the usual conditions of constant pressure $q = \Delta H$. This accounts for our use of ΔH^* rather than E_a in equation 471.1.

Clapeyron's Equation for Condensed Phases

In this analysis and those that follow, the simplest mechanism consistent with overall stoichiometry is employed. It is not difficult to show that more complicated mechanisms would yield the same result (see paper cited by Frost in footnote 2).

For equilibrium with respect to the change:

$$x_{(solution)} \underset{k_b}{\overset{k_f}{\rightleftharpoons}} x_{(pure\ liquid)}$$

R_f (melting rate) = k_f = R_b (freezing rate) = k_b. The concentrations of pure substances are constant and therefore absorbed in the rate constants. Thus, by equation 471.1, at equilibrium

$$A_f e^{\frac{-\Delta_f H^*}{RT}} = A_b e^{\frac{-\Delta_b H^*}{RT}}$$

Hence, by equation 471.7, on taking logarithms,

$$\frac{\Delta E + P\Delta V}{RT} = \ln(\frac{A_f}{A_b}) = constant$$

For equilibrium to be maintained when T and P change from values satisfying the above expression to new values T + dT and P + dP, dT and dP must be such that

$$\frac{\Delta E + (P+dP)\,\Delta V}{R(T+dT)} = \frac{\Delta E + P\Delta V}{RT}$$

Simplification yields Clapeyron's equation

$$\frac{dP}{dT} = \frac{\Delta H}{T\Delta V}$$

Ideal Solubility and Freezing Point Depression

For equilibrium with respect to the change

$$x_{(solid)} \underset{k_b}{\overset{k_f}{\rightleftharpoons}} x_{(ideal\ solution)}$$

R_f (melting or solution rate) = k_f = R_b (freezing or precipitation rate) = $k_b N_x$. Thus, by equations 471.1 and 471.7, for all mole fractions N_x,

$$\ln(\frac{A_f}{A_b} = \frac{\Delta H}{RT} + \ln(N_x) = \frac{\Delta H}{RT}|_{N_x=1} = \frac{\Delta H}{RT_{nfp}}.$$

Hence,

$$\ln(N_x) = \frac{\Delta H}{R}(\frac{1}{T_{nfp} - \frac{1}{T}}) = \frac{\Delta H(T - T_{nfp})}{RTT_{nfp}}$$

For $N_x \cong 1$, $T \cong T_{nfp}$ (of x), $\ln(N_x \cong N_x - 1 \cong N_2$ and

$$-(T - T_{nfp}) \cong \frac{RT_{nfp}^2}{\Delta H} N_2$$

Osmotic Equilibrium

For equilibrium with respect to the change

$$x_{(pure\ liquid)} \underset{k_b}{\overset{k_f}{\rightleftharpoons}} x_{(ideal\ solution)}$$

	Pure Liquid	Ideal Solution
Pressure	P	P + π
Mole Fraction	N_x = 1	N_x < 1

R_f = k_f = R_b = $k_b N_x$. Thus, by equations 471.1 and 471.7,

$$ln\frac{A_f}{A_b} = \frac{\Delta E + \Delta(PV)}{RT} + \ln(N_x)$$

In this instance:

$$\Delta E = \Delta V = 0$$

$$\Delta(PV) = (P+\pi)\overline{V}_x - P\overline{V}_x = \pi\overline{V}_x.$$

Hence,

$$\frac{A_f}{A_b} = \frac{\pi\overline{V}_x}{RT} + \ln(N_x).$$

For $N_x = 1$, $\pi = 0$. Thus $\ln(\frac{A_f}{A_b}) = 0$.

Hence,

$$\pi = -\frac{RT}{\overline{V}_x}\ln(N_x) \cong \frac{RTN_2}{\overline{V}_x} \cong RTC_2$$

where $N_2 << 1$.

Chemical Equilibrium

For equilibrium with respect to the change

$$aA + bB = cC + dD$$

the *Principle of Microscopic Reversibility* states that the rate at which A and B disappear by the (perhaps unlikely) mechanism aA + bB, rate law $R_f = k_f c_A{}^a c_B{}^b$, is equal to the rate at which A and B appear by the mechanism cC + dD, rate law $R_b = k_b c_C{}^c c_D{}^d$.[2] Thus, with equations 471.1 and 471.7, one obtains

$$K \equiv \frac{c_C^c}{C_D^d}|_{equilibrium} = \frac{k_f}{k_b} = \frac{A_f}{A_b}e^{\frac{-\Delta H}{RT}}$$

or,

$$\ln(K) + \frac{\Delta H}{RT} = \ln(\frac{A_f}{A_b}) = constant$$

If T changes from T_1 to T_2, the change in K, from K_1 to K_2, must be such that, by equation 471.12,

$$\ln(\frac{K_2}{K_1}) = \frac{\Delta H}{R}(\frac{1}{T_1} - \frac{1}{T_2})$$

[2]For a further discussion of this point, see Frost, A. A. and Pearson, R. G., "Kinetics and Mechanism," John Wiley and Sons, Inc., 1953, Ch. 8; or Frost, A. A., *J. Chem. Educ.*, 18, 272 (1941).

Boltzmann's Factor

For equilibrium with respect to the simple "chemical" change

$$x\ (quantum\ state\ i) \underset{b}{\overset{f}{\rightleftharpoons}} x\ (quantum\ state\ j)$$

one has by 471.11,

$$K = \frac{C_j}{C_i} = \frac{A_f}{A_b}e^{\frac{-\Delta H}{RT}}$$

In this instance:

$$A_f = A_b$$

$$\Delta H = \Delta E\ +\ P\Delta V = \Delta E \equiv N_A(\varepsilon_j - \varepsilon_i).$$

$$\frac{C_j}{C_i} = \frac{N_j}{N_i}$$

Hence,

$$\frac{N_j}{N_i} = e^{\frac{-(\varepsilon_j - \varepsilon_i)}{kT}}$$

Electrochemical Equilibrium

For equilibrium with respect to the flow of electrons in an electrochemical circuit

$$e\ (potential\ V_1) \underset{k_b}{\overset{k_f}{\rightleftharpoons}} e\ (potential\ V_2)$$

$R_f = k_f = R_b = k_b$. Thus, by equation 471.1,

$$\ln \frac{A_f}{A_b} = \frac{\Delta_f H^* - \Delta_b H^*}{RT}$$

The activation enthalpies contain in this instance two contributions: one from the enthalpy of activation of the *chemical* change to which the electron flow is coupled in an electrochemical cell; the other from the enthalpy of activation for the *physical* transfer of electrons across a potential difference $E = V_1 - V_2$. In this instance, $\Delta_f H^* - \Delta_b H^* = \Delta H + nFE$.

Hence,

$$\ln \frac{A_f}{A_b} = \frac{\Delta H + nFE}{RT}.$$

For equilibrium to be maintained when T and E change from values satisfying the above expression to new values T + dT and E + dE, dT and dE must be such that

$$\frac{\Delta H + nF(E + dE)}{R(T + dT)} = \frac{\Delta H + nFE}{RT}$$

Simplification yields

$$nF\frac{dE}{dT} = \frac{\Delta H + nFE}{T}$$

By the First Law, $\Delta H + nFE = Q_{rev}$.

Hence,

$$nF\frac{dE}{dT} = \frac{Q_{rev}}{T}$$

Equation 471.16 is a special instance of the general thermodynamic relation

$$\frac{dW_{rev}}{dT} = \frac{Q_{rev}}{T}$$

Alternatively:

$$\frac{dW_{rev}}{Q_{rev}} = \frac{dT}{T}$$

[In Gibbs-Clausius notation: $\frac{\delta(\Delta G)}{\delta T} = -\Delta S$]

Equation 471.18 is, in turn, a special instance of the Kelvin-formula for the efficiency of a reversible heat engine.

$$\varepsilon_{rev} = \frac{T_2 - T_1}{T_2}$$

Mechanical Equilibrium

For equilibrium with respect to a change, in the energy E of a purely mechanical system say a change in altitude, h, of a weight, wt,

$$wt(E_i = Mgh_i) \underset{b}{\overset{f}{\rightleftharpoons}} wt(E_j = Mgh_j),$$

$R_f = k_f = R_b = k_b$. Hence, by equations 471.1, 471.7 with, again, $A_f = A_b$,

$$\frac{R_f}{R_b} = \frac{k_f}{k_b} = e^{\frac{-(E_j - E_i)}{kT}} = e^{-\Delta E_{wt} kT}$$

For, for example, Δh = +0.1m, M = 0.05 kg, and g = 9.8 $\frac{m}{s^2}$, ΔE_{wt} = +0.0049 J. Thus, at T = 300K (k = 1.38 x 10^{-23} J),

$$\frac{R_f}{R_b} = 10^{-(10^{18.7})}$$

Boltzmann's Relation

For change 471.20 let the number of macroscopically indistinguishable, microscopically distinct quantum states accessible jointly to the mechanical system wt and its thermal surroundings θ in (wt + θ)'s initial state i, its transition state *, and its final state j be denoted, respectively, $(\Omega_{total})_i$, (Ω^*_{total}), and $(\Omega_{total})_j$. If all quantum states are, *a priori*, equally probably, $R_f = k\frac{(\Omega_{total})^*}{(\Omega_{total})_i}$ and $R_b = k\frac{(\Omega_{total})^*}{(\Omega_{total})_j}$. Thus, for equilibrium with respect to change 471.20, by 471.21,

$$\frac{(\Omega_{total})_j}{(\Omega_{total})_i} = e^{\frac{\Delta E_{wt}}{kT}}$$

By the First Law, for a universe wt + θ, $-\Delta_{wt} = \Delta E_\theta$. By the Second Law, $\frac{\Delta E_\theta}{T} = \Delta S_\theta$. By the law of statistical independence, $\Omega_{total} = \Omega_\theta \Omega_{wt}$. And by the law of the reversibility of purely mechanical changes, Ω_{wt} = constant. Thus, by equation 471.22,

$$\frac{(\Omega_\theta)_{final}}{(\Omega_\theta)_{initial}} = e^{\frac{\Delta S_\theta}{k}}$$

By the Third Law, S = 0 when $\Omega = 1$ (for example, a perfect crystal at T = 0K). Thus, by equation 471.23, for systems in internal equilibrium,

$$S = k \ln \Omega$$

Summary and Concluding Comments

Arrhenius's expression (equation 471.1) embodies in a form immediately applicable to chemical problems those implications of the Second-Law-like behavior of Nature of particular interest to chemists. It is, from a chemical point of view, a more quickly and easily used expression of the Second Law than is the more widely applicable but, though mathematically simpler, chemically more remote expression 471.19.

Expression 1 is in a certain sense, said Arrhenius, "a paraphrase of the observed facts" (1). It is an axiomatization of a nearly universal feature of chemical reactions. If chemical (and physical) changes had no enthalpies of activation, it would be impossible to store energy - as, for example, fat or fuel plus oxygen. Everything would slide quickly to equilibrium, including the sun. Without energy *barriers* there would be no life - and energy *crises*.

Arrhenius's expression 1 is based on van 't Hoff's thermodynamic expression $K = Ce^{\frac{-\Delta H}{RT}}$ (1, 2). Thus, the kinetic derivations above are not, in a logical sense, substitutes for thermodynamic arguments. It is often instructive, however, to see abstract expressions emerge unexpectedly from concrete, special instances.

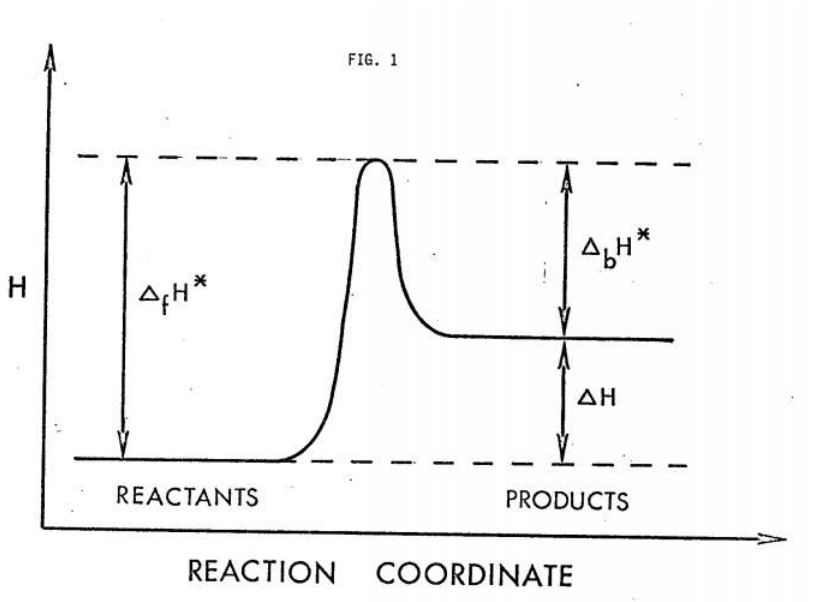
The present mathematical procedures can be used without change in purely thermodynamic arguments. From the expression $K = Ce^{\frac{-\Delta H}{RT}}$ one can obtain quickly, as above, expressions 471.8-471.16 without using calculus, the entropy function, the chemical potential, or Carnot's cycle.

Conventional expressions that involve the entropy function can be obtained from the present discussion by introducing the abbreviation $\Delta S \equiv R \ln \frac{A_f}{A_b}$.

Literature Cited

1. Arrhenius, S., Z. *Physik Chem.*, 4, 226 (1889); excerpted and translated by Back, M. H. and Laidler, K. J., "Selected Readings in Chemical Kinetics," Pergamon Press, New York, 1967, pp. 31-35.

2. van 't Hoff, J. H., "Studies in Chemical Dynamics," translated by Thomas Ewan, Chemical Publishing Co., Easton, Pennsylvania, 1896, pp. 122-123.



This page titled 11.13: Simple Kinetic Derivations of Thermodynamic Relations is shared under a CC BY 4.0 license and was authored, remixed, and/or curated by Frank Rioux via source content that was edited to the style and standards of the LibreTexts platform.

11.14: The Global Approach to Thermodynamics

Thermodynamics: Energy conservation with an entropy-based limitation on energy utilization. Nick Herbert

Cochran and Heron recently published an assessment of student ability to apply the laws of thermodynamics to heat engines and refrigerators with special emphasis on the second law.[1] They reported exam question results for three levels of instruction: (a) standard; (b) standard plus a tutorial on Carnot's theorem; (c) standard plus a tutorial on the use of the entropy inequality. The performance of students exposed to instruction levels (b) and (c) was significantly better than that for students who had only the standard level of instruction.

The three levels of instruction all use the system-centered approach to thermodynamics. I would like to propose that a future study include another option – the global approach to thermodynamics.2 In the global approach, after a sketch of the phenomenon under study is made, the sums of the energy and entropy changes are calculated.

$$\Delta E_{tot} = \sum_i \Delta E_i \; \Delta S_{tot} = \sum_i \Delta S_i$$

Thermodynamics requires that $\Delta E_{tot} = 0$ and $\Delta S \geq 0$ for all phenomena.

The global method will be illustrated by applying it to the heat engine shown in the figure, which is the same heat engine as shown in Figure 2 of reference 1. As shown in the appended figure, work is represented by a weight which can rise or fall in the gravitational field.

The global statement of the first law is

$$\Delta E_{tot} = \Delta E_{800} + \Delta E_{sys} + \Delta E_{400} + \Delta E_{wt}$$

Because the working substance of the system completes a thermodynamic cycle, $\Delta E_{sys} = 0$. Using the energy values in the figure we find that the first law is satisfied; energy is conserved.

$$\Delta E_{tot} = -900J + 0J + 400J + 500J = 0$$

In the global statement for the second law is

$$\Delta S_{tot} = \Delta S_{800} + \Delta S_{sys} + \Delta S_{400} + \Delta S_{wt}$$

For thermal reservoirs $\Delta S = \frac{\Delta E_T}{T}$, where ΔE_T is the thermal energy change of a reservoir at temperature T. Again, because the working substance undergoes a thermodynamic cycle, $\Delta S_{sys} = 0$. The movement of a weight in a gravitational field does not change its entropy, therefore, $\Delta S_{wt} = 0$.

Using the information from the figure we calculate a negative value for the total entropy change, indicating that a heat engine operating under these conditions is not possible.

$$\Delta S_{tot} = \frac{-900J}{800K} + 0\frac{J}{K} + \frac{400J}{400K} + 0\frac{J}{K} = -0.125\frac{J}{K}$$

By comparison with this global analysis, Cochran and Heron use an auxiliary thermodynamic function, the entropy inequality, to arrive at the same conclusion.

$$\Delta S_{sys} \geq \sum \frac{Q_{to\ sys}}{T_{env}} = \frac{900J}{800K} - \frac{400J}{400K} = 0.125\frac{J}{K}$$

This result contradicts the fact that a cyclic process for the system's working substance requires that $\Delta S_{sys} = 0$. Therefore, the proposed heat engine will not function. However, this method is less direct because the entropy inequality is an auxiliary thermodynamic function which is derived from the second law of thermodynamics.

Employing a global thermodynamic analysis of the other figures shown in reference 1, as well as other types of physical and chemical phenomena is straightforward.[2]

It is, of course, important to explore the limits thermodynamics places on the performance of heat engines and refrigerators. These limits can be obtained from the global statements of the first and second laws of thermodynamics by elementary mathematical methods. For traditional heat engines and refrigerators (two thermal reservoirs) the first and second laws are,

$$\Delta E_{hot} + \Delta E_{cold} + \Delta E_{wt} = 0$$

$$\frac{\Delta E_{hot}}{T_{hot}} + \frac{\Delta E_{cold}}{T_{cold}} \geq 0$$

Using the first law to eliminate ΔEcold in the equation for the second law yields the efficiency relation for heat engines.

$$\varepsilon = \frac{\Delta E_{wt}}{-\Delta E_{hot}} \leq 1 - \frac{T_{cold}}{T_{hot}}$$

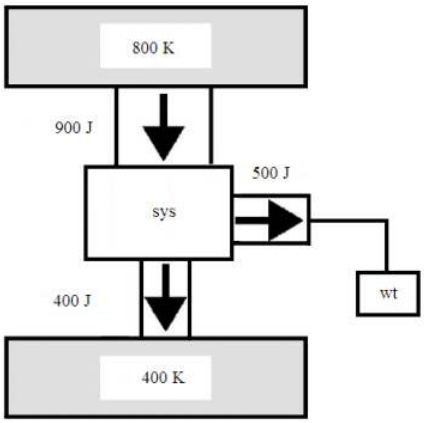
Using the first law to eliminate ΔE_{hot} in the equation for the second law yields the coefficient of performance for refrigerators.

$$\kappa = \frac{-\Delta E_{cold}}{\Delta E_{wt}} \leq \frac{T_{cold}}{T_{hot} - T_{cold}}$$

The most appealing feature of the non-system centered, global approach to thermodynamics is that the first and second laws are front and center, starring you in the face, and not represented by surrogates. Another important feature is not to have to subscript terms involving thermal energy and work with “to sys” and “on sys”. Each part of the phenomenon under study carries its own label; the system is just another part, neither more nor less important than any other part.

[1]M. J. Cochran and P. R. L. Heron, “Development and assessment of research-based tutorials on heat engines and the second law of thermodynamics,” Am. J. Phys. 74, 734- 741 (2006).

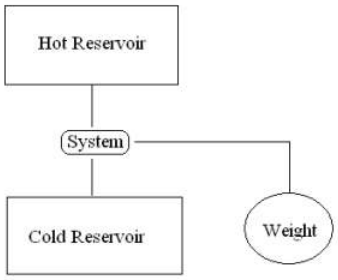
[2]H. A. Bent, *The Second Law: An Introduction to Classical and Statistical Thermodynamics* (Oxford University Press, New York, 1965).



This page titled 11.14: The Global Approach to Thermodynamics is shared under a CC BY 4.0 license and was authored, remixed, and/or curated by Frank Rioux via source content that was edited to the style and standards of the LibreTexts platform.

11.15: Global Thermodynamic Analyses of Heat Engines

The purpose of this tutorial is to demonstrate the clarity that the global method of doing thermodynamics brings to the analysis of heat engines, which under other names are power plants, heat pumps and refrigerators. The analyses provided are based on the schematic diagram shown below. The "system" is a working substance that undergoes a thermodynamic cycle ($\Delta E_{sys} = \Delta S_{sys} = 0$, under reversible conditions), so it does not appear in the mathematical analyses that follows.



Under the circumstances regarding the role of the system outlined above, the first and second laws of thermodynamics are:

$$\Delta E_{tot} = \Delta E_{hot} + \Delta E_{cold} + \Delta E_{wt} = 0$$

$$\Delta S_{tot} = \Delta S_{hot} + \Delta S_{cold} = \frac{\Delta E_{hot}}{T_{hot}} + \frac{\Delta E_{cold}}{T_{cold}} \geq 0$$

Since we will be interested in the best case scenario, we will use the equal sign for the entropy change, $\Delta S_{tot} = 0$, in our calculations.

Power Plant

A power plant harnesses the natural flow of thermal energy from a hot object to a cold object in order to generate useful energy, most likely in the form of electricity. Suppose a power plant operates with a high temperature thermal reservoir at 500K and the ambient temperature is taken to be 300K. How much electricity can, ideally ($\Delta S_{tot} = 0$), be generated per 100 J of thermal energy flowing from the high temperature reservoir to the low (ambient) temperature reservoir?

Input parameters: ΔE_{hot} := -100 J T_{hot} := 500 K T_{cold} := 300 K

$$\begin{pmatrix} \Delta E_{hot} + \Delta E_{cold} + \Delta E_{wt} = 0 \\ \frac{\Delta E_{hot}}{T_{hot}} + \frac{\Delta E_{cold}}{T_{cold}} = 0 \end{pmatrix} \Big|_{float,3}^{solve,\begin{pmatrix} \Delta E_{wt} \\ \Delta E_{cold} \end{pmatrix}} \rightarrow (40.0J \ 60.0J)$$

It is clear from this analysis that the power plant is theoretically 40% efficient: $|\frac{40.0J}{-100J}| = 40\%$.

Heat Pump

Non-spontaneous processes occur when they are driven by some other spontaneous process, such as described in the previous example.

Heat pumps are in the news again today, as they were in the late 70s and early 80s. Here we ask the question of how much energy we can pump from the ambient thermal environment into a house by buying 100 J of energy from the local utility. We assume that the ambient thermal source temperature is 270K and the house is being maintained at 300K.

Clear ΔE_{hot} memory: $\Delta E_{hot} := \Delta E_{hot}$

Input parameters: ΔE_{wt} := -100 J T_{hot} := 300 K T_{cold} := 270 K

$$\begin{pmatrix} \Delta E_{hot} + \Delta E_{cold} + \Delta E_{wt} = 0 \\ \frac{\Delta E_{hot}}{T_{hot}} + \frac{\Delta E_{cold}}{T_{cold}} = 0 \end{pmatrix} \Big|_{float,4}^{solve,\begin{pmatrix} \Delta E_{hot} \\ \Delta E_{cold} \end{pmatrix}} \rightarrow (1000.0J \ -900.0J)$$

This remarkable result shows that by buying 100 J from the local utility one can pump 1,000 J of thermal energy from the ambient source into the house. Again this is assuming the ideal, theoretical limit, $\Delta S_{tot} = 0$.

Refrigerator

A refrigerator is also a heat pump. However, with a refrigerator we are interested in how much energy we can pump out of the low temperature reservoir (the contents of the refrigerator) at a certain cost, rather than how much we can deliver to the high temperature reservoir. Here we ask how much energy we must purchase to pump 100 J out of the refrigerator.

Clear ΔE_{wt} memory: $\Delta E_{wt} := \Delta E_{wt}$

Input parameters: $\Delta E_{cold} :=$ -100 J $T_{hot} :=$ 300 K $T_{cold} :=$ 280 K

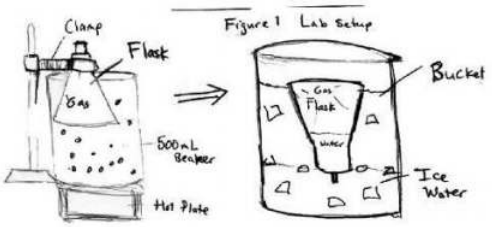
$$\begin{pmatrix} \Delta E_{hot} + \Delta E_{cold} + \Delta E_{wt} = 0 \\ \frac{\Delta E_{hot}}{T_{hot}} + \frac{\Delta E_{cold}}{T_{cold}} = 0 \end{pmatrix} \Big|^{solve,}_{float,4} \begin{pmatrix} \Delta E_{hot} \\ \Delta E_{wt} \end{pmatrix} \rightarrow (107.1J \ -7.143J)$$

This result tells us something we already know, but doesn′t obtrude on our senses: **operating a refrigerator is not particularly expensive**. One hundred joules can be pumped out of the refrigerator for a cost of just over 7 joules, under ideal circumstances.

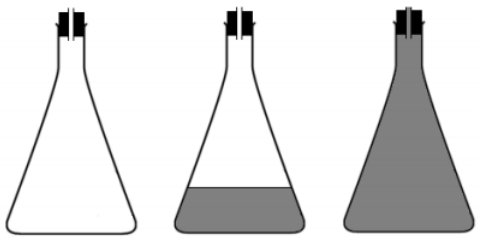
This page titled 11.15: Global Thermodynamic Analyses of Heat Engines is shared under a CC BY 4.0 license and was authored, remixed, and/or curated by Frank Rioux via source content that was edited to the style and standards of the LibreTexts platform.

11.16: Using Charles' Law to Determine Absolute Zero

A simple experiment to determine absolute zero using Charles' Law is illustrated below. An Erlenmeyer flask is weighed and placed in a boiling water bath and allowed to come to thermal equilibrium. The temperature is measured and found to be 99.0 ^{o}C. The flask is then submerged, inverted, in an ice bath (0.20 ^{o}C) and allowed to come to thermal equilibrium. The contraction of the air in the flask at the lower temperature draws water into the flask. The flask is carefully removed, the outside dried and it is weighed. Finally, the flask is filled with water (as shown below on the right) and weighed. The mass measurements are converted to high and low temperature gas volumes and Charles's Law, V = a· T+ b, is used to calculate absolute zero.



Sketch by Matt Zimmer



83.0 gm 120.8 gm 224.4 gm

Convert mass measurements to high and low temperature gas volumes:

High temperature: $V_h := \frac{224.4gm-83.0gm}{1\frac{gm}{mL}}$ = 0.141 L; T_h := 99.0 Celsius

Low temperature: $V_l := \frac{224.4gm-120.8gm}{1\frac{gm}{mL}}$ = 0.104 L; T_l := 0.20 Celsius

An algebraic method is used to calculate absolute zero. Three equations are required because there are three unknowns: a, b, and T_0. Absolute zero is interpreted as the temperature at which the gas volume goes to zero. This is the last equation in the set of equations used to calculate a, b and T_0.

$$\begin{pmatrix} V_h = aT_h + b \\ V_1 = aT_l + b \\ 0 = aT_0 + b \end{pmatrix} \Big|^{solve,\begin{pmatrix} a \\ b \\ T_o \end{pmatrix}}_{float,4} \rightarrow [0.3826\frac{mL}{Celsius}\ 103.5mL\ (-270.6)Celsius]$$

The correct value for absolute zero is -273.2 ^{o}C. So this result is in error by approximately 1%.

This page titled 11.16: Using Charles' Law to Determine Absolute Zero is shared under a CC BY 4.0 license and was authored, remixed, and/or curated by Frank Rioux via source content that was edited to the style and standards of the LibreTexts platform.

11.17: The Origin of KE = 3/2 RT

The Kinetic Molecular Theory of Gases

A gas consists of a collection of molecules in continuous random motion with varying speed.

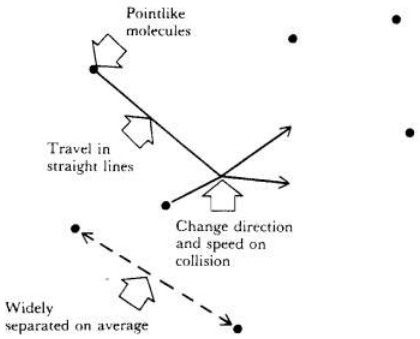
The individual gas molecules are extremely small when compared with the volume of the container they occupy.

The molecules move in straight lines until they collide with each other or the walls of the container.

The molecules do not interact with each other or the walls of the container except during these collisions.

The laws of classical physics can be used to analyze the motion of the gas molecules and to calculate the bulk properties of the gas.

The basic features of the kinetic molecular theory (KMT) are illustrated in the figure below.



When the KMT is used to calculate the pressure of a gas the following expression results

$$P = \frac{\frac{1}{3}nMV^2}{V}$$

where n is the number of moles of gas, M is the molar mass of the gas, v2 is the average of the velocity squared, and V is the volume of the container.

The ideal gas law summarizes the behavior of gases with respect to the macroscopic variables of temperature, pressure, volume and moles of gas.

$$P = \frac{nRT}{V}$$

A comparison of equations (1) and (2), that is, a comparison between the results of a theoretical analysis using the KMT and the actual experimental behavior of gases reveals that

$$\frac{1}{2}Mv^2 = \frac{3}{2}RT$$

Thus, the proportionality of the average molecular kinetic energy to the absolute temperature is a conclusion drawn by comparing a theoretical expression with an empirical equation which summarizes macroscopic gas facts.

The resulting equation, (3), provides an interpretation of temperature in terms of molecular motion.

This page titled 11.17: The Origin of KE = 3/2 RT is shared under a CC BY 4.0 license and was authored, remixed, and/or curated by Frank Rioux via source content that was edited to the style and standards of the LibreTexts platform.

11.18: Cosmic Background Radiation

The cosmic background radiation fills all space and is a relic from the "big bang" that created the universe approximately 18 billion years ago. The data[1] shown below, spectral brightness[2] as a function of wave number, was recorded (1989) by the Cosmic Background Explorer satellite (COBE). Below the data is fit with the Planck blackbody radiation equation to determine the cosmic background temperature.

Define the fundamental constants h, k, and c.

$$h := 6.62608 \cdot 10^{-34} \quad k := 1.380622 \cdot 10^{-23} \quad c := 2.99792458 \cdot 10^{8}$$

$$\nu_i := 100 \cdot \nu_i \quad B_i := 10^{-18} \cdot B_i$$

Provide a seed value for the background temperature: T := 10

Define spectral brightness equation:

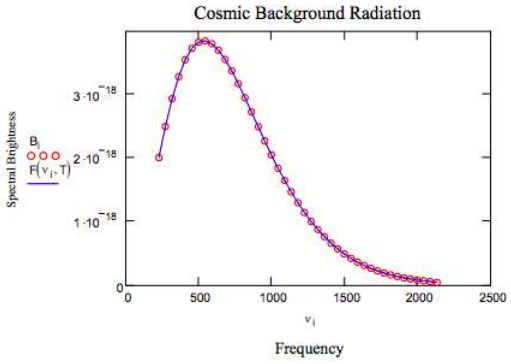
$$F(\nu, T) := 2 \cdot h \cdot \nu^3 \cdot c \cdot \frac{1}{(exp(\frac{h \cdot \nu}{k \cdot T}) - 1)}$$

SSD stands for sum of the square of the deviations between data and the equation that is being fit to the data.

$$SSD(T) = \sum_i (B_i - F(\nu_i, T))^2$$

Given SSD(T) := 0 T := Minerr(T) T := 2.728

Thus the best fit to the data is obtained with a cosmic background temperature of 2.728 K.



Notes:

1. Data taken from: S. Bluestone, JCE 78, 215-218 (2001).

2. The relationship between spectral brightness and Planck's radiation density function is:

$$B(\nu, T) = \frac{c}{4 \cdot \pi} \cdot \rho(\nu, T)$$

n := 43 i := 1 .. n

ν_i :=

2.27
2.72
3.18
3.63
4.08
4.54
4.99
5.45
5.90
6.35
6.81
7.26
7.71
8.17
8.62
9.08
9.53
9.98
10.44
10.89
10.89
11.34
11.80
12.25
12.71
13.16
13.61
14.07

https://chem.libretexts.org/@go/page/135893

$B_1 := 14.07$
14.52
14.97
15.43
15.88
16.34
16.79
17.24
17.70
18.15
18.61
19.06
19.51
19.97
20.42
20.87
21.33

2.0110
2.5003
2.9369
3.2858
3.5503
3.7316
3.8269
3.8477
3.8027
3.7025
3.5551
3.3773
3.1752
2.9535
2.7281
2.4957
2.2721
2.0552
1.8483
1.6488
1.4672
1.2973
1.1438
1.0019
0.8771
0.7648
0.6631
0.5749

0.5749
0.4965
0.4265
0.3669
0.3136
0.2684
0.2287
0.1945
0.1657
0.1396
0.1185
0.1003
0.0846
0.0717
0.0587
0.0459

This page titled 11.18: Cosmic Background Radiation is shared under a CC BY 4.0 license and was authored, remixed, and/or curated by Frank Rioux via source content that was edited to the style and standards of the LibreTexts platform.

11.19: Age of the Elements

Analysis of cosmic microwave background radiation (CMBR) obtained by the Planck satellite telescope has added 80 million years to the age of the universe, making the best estimate of the current age 13.8 billion years. This tutorial deals with the more modest task of estimating the age of the elements found in the earth's crust.

As is well-known from examples such as carbon-14 dating, radioactivity can be used to tell time. Radioactive isotopes decay exponentially according to the following equation.

$$A_t = A_0(\tfrac{1}{2})^{\frac{1}{t_{1/2}}}$$

The amount of a radioactive isotope remaining at time t is equal to the original amount times 1/2 raised to the number of half-lives ($t/t_{1/2}$) that have occurred. Using this equation plus plausible assumptions, some information about uranium isotopes and rudimentary math, the time elapsed since the isotopes were produced is calculated.

Assume that ^{238}U and ^{235}U were produced in equal amounts originally. Today the $^{238}U/^{235}U$ ratio is 140/1. The half-lives of ^{238}U and ^{235}U are 4.5 billion years and 800 million years, respectively. How long ago where these isotopes synthesized?

$$\begin{bmatrix} U_{238} = \frac{1}{2}^{\frac{t}{4.5 \cdot 10^9 year}} \\ U_{235} = \frac{1}{2}^{\frac{t}{0.8 \cdot 10^9 year}} \\ U_{238} = 140 \cdot U_{235} \end{bmatrix} \Big|_{float,3}^{\begin{pmatrix} t \\ U_{238} \\ U_{235} \end{pmatrix}} \rightarrow (0.694e10\ year\ 0.344\ 0.245e-2)$$

According to this rudimentary model, the uranium in the earth's crust is about half the age of the universe.

This page titled 11.19: Age of the Elements is shared under a CC BY 4.0 license and was authored, remixed, and/or curated by Frank Rioux via source content that was edited to the style and standards of the LibreTexts platform.

Index

A

Airy pattern
- 1.14: Quantum Mechanics and the Fourier Transform

alpha decay
- 10.4: A Rudimentary Model for Alpha Particle Decay

atomic properties
- 11.3: Commentary on “Probing the Orbital Energy of an Electron in an Atom”

Atomic volume
- 2.46: Calculating the Atomic Radius of Polonium

B

Bell states
- 1.7: Quantum Computation- A Short Course
- 8.53: Bell State Exercises

Bell Theorem
- 8.45: Yet Another Assault on Local Realism - A Matrix/Tensor Algebra Approach
- 8.46: Jim Baggott's Bell Theorem Analysis
- 8.48: Another Bell Theorem Analysis - Shorter Version

Bell’s theorem
- 1.5: Quantum Computation - A Short Course

C

Circularly polarized light
- 7.14: Matrix Mechanics Approach to Polarized Light
- 7.15: Matrix Mechanics Approach to Polarized Light - Version 2
- 7.24: Optical Activity - A Quantum Perspective

confinement energy
- 1.3: Atomic and Molecular Stability

cosmic microwave background radiation
- 11.19: Age of the Elements

Cosmic Radiation
- 11.18: Cosmic Background Radiation

cyanine dyes
- 4.3: Cyanine Dyes as Two-State Electronic Systems

D

Degenerate Perturbation Theory
- 10.35: First Order Degenerate Perturbation Theory - the Stark Effect of the Hydrogen Atom

density operator
- 7.9: Pure States, Mixtures and the Density Operator

Deutsch-Jozsa Algorithm
- 1.8: Quantum Computation- A Short Course

Deutsch's Problem
- 8.68: A Simple Solution to Deutsch's Problem

diffraction pattern
- 1.14: Quantum Mechanics and the Fourier Transform
- 5.9: Calculating Diffraction Patterns

Dirac delta function
- 1.25: The Dirac Delta Function

Dirac equation
- 1.36: Aspects of Dirac′s Relativistic Matrix Mechanics

Dirac Notation
- 1.26: Elements of Dirac Notation

dodecahedrane
- 6.2: Dodecahedrane

down converter
- 7.39: Analysis of a Two-photon Quantum Eraser

downconversion
- 7.26: Two Photon Interference - The Creation of an Entangled Superposition

E

effective potential energy
- 1.3: Atomic and Molecular Stability

Electrons within a Ring
- 1.86: Quantum Corrals - Electrons within a Ring

Entangled Bipartate Superposition
- 8.64: Examining the Local States of an Entangled Bipartate Superposition

entanglement
- 1.7: Quantum Computation- A Short Course
- 8.59: An Entanglement Swapping Protocol

expectation value
- 7.10: Using the Trace Function to Calculate Expectation Values

F

Feshbach Potential
- 10.33: Variational Method for the Feshbach Potential
- 10.42: Variation Method Using the Wigner Function - The Feshbach Potential

G

GHZ Entanglement
- 8.16: GHZ Entanglement - A Tensor Algebra Analysis

Grover Search Algorithm
- 1.10: Quantum Computation- A Short Course

H

Hadamard gate
- 8.53: Bell State Exercises

Hardy's Paradox
- 8.52: Hardy's Paradox

L

ladder operators
- 1.28: Raising and Lowering; Creating and Annihilating
- 7.4: Single Photon Interference - Fourth Version

linearly polarized light
- 7.24: Optical Activity - A Quantum Perspective

locality
- 8.14: Greenaberger-Hrne-Zeilinger (GHZ) Entanglement and Local Realism

M

Mach-Zehnder interferometer
- 7.22: A Quantum Circuit for a Michelson Interferometer

maser
- 4.4: The Ammonia Inversion and the Maser

Matrix Mechanics
- 1.33: Basic Matrix Mechanics
- 1.35: Matrix Mechanics
- 7.16: Matrix Mechanics Exercises Using Polarized Light

methane
- 6.8: CH_4

Michelson Interferometer
- 7.21: Two Analyses of the Michelson Interferometer

Mixed states
- 7.9: Pure States, Mixtures and the Density Operator

Morse potential
- 4.8: Visualizing the Formally Forbidden Overtone Vibrational Transitions in HCl
- 9.12: Numerical Solutions for Morse Oscillator

N

Neutron Interferometry
- 7.18: Neutron Interferometry with Polarized Spin States

Numerical Solutions
- 9: Numerical Solutions for Schrödinger's Equation

O

optical activity
- 7.24: Optical Activity - A Quantum Perspective

Overlap integral
- 1.26: Elements of Dirac Notation

overtones
- 4.8: Visualizing the Formally Forbidden Overtone Vibrational Transitions in HCl

P

parametric down converter
- 1.7: Quantum Computation- A Short Course
- 7.27: Two-particle Interference for Bosons and Fermions

path integrals
- 1.9: Quantum Computation- A Short Course

Planck Distribution
- 11.18: Cosmic Background Radiation

Polarizability
- 10.36: Variational Calculation for the Polarizability of the Hydrogen Atom

Polarizing Beam Splitter
- 7.6: The Polarizing Beam Splitter and the Superposition Principle

polonium
- 2.46: Calculating the Atomic Radius of Polonium

Positronium
- 1.4: Atomic and Molecular Stability
- 2.4: A de Broglie-Bohr Model for Positronium

Positronium Annihilation
- 8.34: Positronium Annihilation

Pure state
- 7.9: Pure States, Mixtures and the Density Operator

Q

Quantum Beats
- 4.11: Quantum Beats

Quantum centrifugal potential
- 1.3: Atomic and Molecular Stability

quantum chemistry
- 11.3: Commentary on “Probing the Orbital Energy of an Electron in an Atom”

quantum cloning
- 1.6: Quantum Computation- A Short Course

Quantum Computation
1.5: Quantum Computation - A Short Course
1.6: Quantum Computation- A Short Course
1.7: Quantum Computation- A Short Course
1.8: Quantum Computation- A Short Course
quantum error correction
1.10: Quantum Computation- A Short Course
quantum pressure
1.98: Quantum Mechanical Pressure
Quantum Teleportation
1.6: Quantum Computation- A Short Course
8: Quantum Teleportation
8.2: Quantum Teleportation - A Brief Introduction
Quartic Oscillator
9.11: Numerical Solutions for the Quartic Oscillator
10.8: Variation Method for the Quartic Oscillator
10.41: Variation Method Using the Wigner Function - The Quartic Oscillator
qubits
8.65: A Brief Introduction to the Quantum Computer
quon
1.9: Quantum Computation- A Short Course

R

radioactive dating
11.19: Age of the Elements
Ramsey Atomic Interferometer
7.23: The Ramsey Atomic Interferometer
realism
8.14: Greenaberger-Hrne-Zeilinger (GHZ) Entanglement and Local Realism
Rotational Spectroscopy of Diatomic Molecules
4.6: Analyses of the Pure Rotational Spectrum of HCl
Rydberg Potential
10.7: Variation Method for the Rydberg Potential

S

Schrödinger equation
1.18: Exploring the Origin of Schrödinger's Equations
Shor's algorithm
1.7: Quantum Computation- A Short Course
Simon's algorithm
1.10: Quantum Computation- A Short Course
Single Photon Interference
7.4: Single Photon Interference - Fourth Version
Slanted Well Potential
9.7: Particle in a Slanted Well Potential
10.11: Linear Variational Method for a Particle in a Slanted 1D Box
Stark Effect
10.35: First Order Degenerate Perturbation Theory - the Stark Effect of the Hydrogen Atom
superposition principle
1.24: Getting Accustomed to the Superposition Principle
7.6: The Polarizing Beam Splitter and the Superposition Principle

T

theoretical chemistry
11.3: Commentary on "Probing the Orbital Energy of an Electron in an Atom"
three polarizer paradox
7.14: Matrix Mechanics Approach to Polarized Light
7.15: Matrix Mechanics Approach to Polarized Light - Version 2
trace (matrix)
7.10: Using the Trace Function to Calculate Expectation Values
tunneling
4.5: A Symmetric Double Well Potential Illustrating Tunneling
Two Photon Interference
7.26: Two Photon Interference - The Creation of an Entangled Superposition

V

Variational Method
10.5: Variational Method for a Particle in a Finite Potential Well
Variational Theorem
10.3: The Variation Theorem in Dirac Notation
virial theorem
1.3: Atomic and Molecular Stability

W

Wheeler-type delayed-choice experiment
7.41: A Quantum Delayed-Choice Experiment
Wigner Function
10.38: Variation Method Using the Wigner Function- Finite Potential Well
10.39: 455. Variation Method Using the Wigner Function- V(x) = |x|

X

Xenon Tetrafluoride
6.3: Xenon Tetrafluoride

Detailed Licensing

Overview

Title: Quantum Tutorials (Rioux)

Webpages: 535

All licenses found:

- CC BY 4.0: 95% (508 pages)
- Undeclared: 5% (27 pages)

By Page

- Quantum Tutorials (Rioux) - *CC BY 4.0*
  - Front Matter - *Undeclared*
    - TitlePage - *Undeclared*
    - InfoPage - *Undeclared*
    - Table of Contents - *Undeclared*
    - Licensing - *Undeclared*
  - 1: Quantum Fundamentals - *CC BY 4.0*
    - 1.1: An Approach to Quantum Mechanics - *CC BY 4.0*
    - 1.2: Atomic and Molecular Stability - *CC BY 4.0*
    - 1.3: Atomic and Molecular Stability - *CC BY 4.0*
    - 1.4: Atomic and Molecular Stability - *CC BY 4.0*
    - 1.5: Quantum Computation - A Short Course - *CC BY 4.0*
    - 1.6: Quantum Computation- A Short Course - *CC BY 4.0*
    - 1.7: Quantum Computation- A Short Course - *CC BY 4.0*
    - 1.8: Quantum Computation- A Short Course - *CC BY 4.0*
    - 1.9: Quantum Computation- A Short Course - *CC BY 4.0*
    - 1.10: Quantum Computation- A Short Course - *CC BY 4.0*
    - 1.11: Quantum Computation- A Short Course - *CC BY 4.0*
    - 1.12: Quantum Computation- A Short Course - *CC BY 4.0*
    - 1.13: Quantum Mechanics and the Fourier Transform - *CC BY 4.0*
    - 1.14: Quantum Mechanics and the Fourier Transform - *CC BY 4.0*
    - 1.15: Quantum Mechanics and the Fourier Transform - *CC BY 4.0*
    - 1.16: Quantum Mechanics and the Fourier Transform - *CC BY 4.0*
    - 1.17: Quantum Mechanics and the Fourier Transform - *CC BY 4.0*
    - 1.18: Exploring the Origin of Schrödinger's Equations - *CC BY 4.0*
    - 1.19: Basic Quantum Mechanics in Coordinate, Momentum and Phase Space - *CC BY 4.0*
    - 1.20: The Repackaging of Quantum Weirdness - *CC BY 4.0*
    - 1.21: Quantum Principles Illuminated with Polarized Light - *CC BY 4.0*
    - 1.22: Relationship Between the Coordinate and Momentum Representations - *CC BY 4.0*
    - 1.23: Very Brief Relationship Between the Coordinate and Momentum Representations - *CC BY 4.0*
    - 1.24: Getting Accustomed to the Superposition Principle - *CC BY 4.0*
    - 1.25: The Dirac Delta Function - *CC BY 4.0*
    - 1.26: Elements of Dirac Notation - *CC BY 4.0*
    - 1.27: The Dirac Notation Applied to Variational Calculations - *CC BY 4.0*
    - 1.28: Raising and Lowering; Creating and Annihilating - *CC BY 4.0*
    - 1.29: Single Slit Diffraction and the Fourier Transform - *CC BY 4.0*
    - 1.30: From Coordinate Space to Momentum Space and Back - *CC BY 4.0*
    - 1.31: The Position and Momentum Commutation Relation in Coordinate and Momentum Space - *CC BY 4.0*
    - 1.32: Simulating the Aharonov-Bohm Effect - *CC BY 4.0*
    - 1.33: Basic Matrix Mechanics - *CC BY 4.0*
    - 1.34: Rudimentary Matrix Mechanics - *CC BY 4.0*
    - 1.35: Matrix Mechanics - *CC BY 4.0*
    - 1.36: Aspects of Dirac′s Relativistic Matrix Mechanics - *CC BY 4.0*
    - 1.37: The Double-Slit Experiment - *CC BY 4.0*

- 1.38: Double-Slit Experiment with Polarized Light - *CC BY 4.0*
- 1.39: The Consequences of Path Information in a Mach-Zehnder Interferometer - *CC BY 4.0*
- 1.40: Another look at the Consequences of Path Information in a Mach-Zehnder Interferometer - *CC BY 4.0*
- 1.41: The Double-Slit Experiment with Polarized Light - *CC BY 4.0*
- 1.42: The Quantum Eraser - *CC BY 4.0*
- 1.43: Which Way Did It Go? - The Quantum Eraser - *CC BY 4.0*
- 1.44: Which Path Information and the Quantum Eraser - *CC BY 4.0*
- 1.45: Terse Analysis of Triple-slit Diffraction with a Quantum Eraser - *CC BY 4.0*
- 1.46: Which Path Information and the Quantum Eraser (Brief) - *CC BY 4.0*
- 1.47: Terse Analysis of Triple-slit Diffraction with a Quantum Eraser - *CC BY 4.0*
- 1.48: Which-way Markers and Post-selection in the Double-slit Experiment - *CC BY 4.0*
- 1.49: A Stern-Gerlach Quantum "Eraser" - *CC BY 4.0*
- 1.50: Using the Mach-Zehnder Interferometer to Illustrate the Impact of Which-way Information - *CC BY 4.0*
- 1.51: Quantum Theory, Wave-Particle Duality and the Mach-Zehnder Interferometer - *CC BY 4.0*
- 1.52: Analysis of a Temporal Double-slit Experiment - *CC BY 4.0*
- 1.53: An Analysis of Three-Path Interference - *CC BY 4.0*
- 1.54: An Analysis of Three-Slit Interference - *Undeclared*
- 1.55: Using a Mach-Zehnder Interferometer to Illustrate Feynman's Sum Over Histories Approach to Quantum Mechanics - *CC BY 4.0*
- 1.56: The Paradox of Recombined Beams - *CC BY 4.0*
- 1.57: Evidence for Quantized Gravitational States of the Neutron - *CC BY 4.0*
- 1.58: Quantized Gravitational States A Variational Approach - *CC BY 4.0*
- 1.59: The Quantum Bouncer Doesn't Bounce, Unless... - *CC BY 4.0*
- 1.60: Kinetic Energy Is Important in the Nanoscale World - *CC BY 4.0*
- 1.61: Energy Expectation Values and the Origin of the Variation Principle - *CC BY 4.0*
- 1.62: Examining the Wigner Distribution Using Dirac Notation - *CC BY 4.0*
- 1.63: The Wigner Function for the Single Slit Diffraction Problem - *CC BY 4.0*
- 1.64: Wigner Distribution for the Double Slit Experiment - *CC BY 4.0*
- 1.65: Wigner Distribution for the Triple Slit Experiment - *CC BY 4.0*
- 1.66: Wigner Distribution for the Quadruple Slit Experiment - *CC BY 4.0*
- 1.67: Quantum Tunneling in Coordinate, Momentum and Phase Space - *CC BY 4.0*
- 1.68: Another Look at the Wigner Function - *CC BY 4.0*
- 1.69: The Wigner Distribution Function for the Harmonic Oscillator - *CC BY 4.0*
- 1.70: Wigner Distribution for the Particle in a Box - *CC BY 4.0*
- 1.71: The Wigner Distribution for a Particle in a One-dimensional Box - *CC BY 4.0*
- 1.72: Superposition vs. Mixture - *CC BY 4.0*
- 1.73: Time-dependent Wigner Function for Harmonic Oscillator Transitions - *CC BY 4.0*
- 1.74: Momentum Operator in Coordinate Space - *CC BY 4.0*
- 1.75: Momentum Wave Functions for the Particle in a Box - *CC BY 4.0*
- 1.76: A Graphical Illustration of the Heisenberg Uncertainty Relationship - *CC BY 4.0*
- 1.77: The Quantum Harmonic Oscillator - *CC BY 4.0*
- 1.78: Coherent Superpositions for the Harmonic Oscillator - *CC BY 4.0*
- 1.79: The Harmonic Oscillator and the Uncertainty Principle - *CC BY 4.0*
- 1.80: Another view of the Harmonic Oscillator and the Uncertainty Principle - *CC BY 4.0*
- 1.81: Hydrogen Atom and Helium Ion Spatial and Momentum Distribution Functions Illustrate the Uncertainty Principle - *CC BY 4.0*
- 1.82: The Position-Momentum Uncertainty Relation in the Hydrogen Atom - *CC BY 4.0*
- 1.83: Demonstrating the Uncertainty Priniciple for Angular Momentum and Angular Position - *CC BY 4.0*
- 1.84: A Brief Tutorial on Wavepackets - *CC BY 4.0*
- 1.85: The Difference Between Fermions and Bosons - *CC BY 4.0*
- 1.86: Quantum Corrals - Electrons within a Ring - *CC BY 4.0*

- 1.87: Planck's Radiation Equation Fit to Experimental Data - *CC BY 4.0*
- 1.88: Planck's Radiation Equation Fit to Experimental Data - Another Algorithm - *CC BY 4.0*
- 1.89: Fitting Einstein's Heat Capacity Equation to Experimental Data for Silver - *CC BY 4.0*
- 1.90: Einstein's Heat Capacity Equation Fit to Experimental Data - Another Algorithm - *CC BY 4.0*
- 1.91: Fitting Debye's Heat Capacity Equation to Experimental Data for Silver - *CC BY 4.0*
- 1.92: Debye's Heat Capacity Equation Fit to Experimental Data - Another Algorithm - *CC BY 4.0*
- 1.93: Wave-particle Duality and the Uncertainty Principle - *CC BY 4.0*
- 1.94: Wave-Particle Duality for Matter and Light - *CC BY 4.0*
- 1.95: What Part of the Quantum Theory Don't You Understand? - *CC BY 4.0*
- 1.96: Quantum Potpourri - An Attempt to Demonstrate Two Fundamental Quantum Concepts- Wave-particle Duality and The Superposition Principle - *CC BY 4.0*
- 1.97: Quantum Dynamics- One Step at a Time - *CC BY 4.0*
- 1.98: Quantum Mechanical Pressure - *CC BY 4.0*
- 1.99: Visualizing the Difference Between a Superposition and a Mixture - *CC BY 4.0*
- 1.100: Analysis of the Stern-Gerlach Experiment - *CC BY 4.0*
- 1.101: Related Analysis of the Stern-Gerlach Experiment - *CC BY 4.0*
- 1.103: Bloch Sphere - *CC BY 4.0*
- 1.104: 88. Related Analysis of the Stern-Gerlach Experiment - *Undeclared*
- 1.105: Bill the Cat and the Superposition Principle - *Undeclared*
- 1.106: Schroedinger's Dog - *Undeclared*
- 1.107: The Bloch Sphere - *Undeclared*
- 1.108: Density Matrix, Bloch Vector and Entropy - *Undeclared*
- 1.109: State Vectors and State Operators- Superpositions, Mixed States, and Entanglement - *Undeclared*
- 1.110: The Gram-Schmidt Procedure - *Undeclared*

- 2: Atomic Structure - *CC BY 4.0*
  - 2.1: The de Broglie-Bohr Model for the Hydrogen Atom - *CC BY 4.0*
  - 2.2: The de Broglie-Bohr Model for the Hydrogen Atom - Version 3 - *CC BY 4.0*
  - 2.3: The de Broglie-Bohr Model for the Hydrogen Atom - Version 3 - *CC BY 4.0*
  - 2.4: A de Broglie-Bohr Model for Positronium - *CC BY 4.0*
  - 2.5: The de Broglie-Bohr Model for the Hydrogen Atom - Version 4 - *CC BY 4.0*
  - 2.6: The de Broglie-Bohr Model for a Hydrogen Atom Held Together by a Gravitational Interaction - *CC BY 4.0*
  - 2.7: The de Broglie-Bohr Model for Positronium - *CC BY 4.0*
  - 2.8: The Bohr Model for the Earth-Sun System - *CC BY 4.0*
  - 2.9: Extracting Atomic and Molecular Parameters from the deBroglie-Bohn Model for the Atom - *CC BY 4.0*
  - 2.10: Electronic Structure and the Superposition Principle - *CC BY 4.0*
  - 2.11: Atomic Spectroscopy and the Correspondence Principle - *CC BY 4.0*
  - 2.12: Hydrogen-Like Calculations with Variable Lepton Mass - *CC BY 4.0*
  - 2.13: Atomic Stability - *CC BY 4.0*
  - 2.14: Quantum Mechanical Calculations for the One-Dimensional Hydrogen Atom - *CC BY 4.0*
  - 2.15: Quantum Mechanical Calculations for the Hydrogen Atom - *CC BY 4.0*
  - 2.16: Atomic Stability - *CC BY 4.0*
  - 2.17: Atomic Stability - Mathcad Version - *CC BY 4.0*
  - 2.18: 110. Critique of the Centrifugal Effect in the Hydrogen Atom - *CC BY 4.0*
  - 2.19: A Shorter Critique of the Centrifugal Effect in the Hydrogen Atom - *CC BY 4.0*
  - 2.20: Exploring the Role of Lepton Mass in the Hydrogen Atom - *CC BY 4.0*
  - 2.21: The Effect of Lepton Mass on the Energy and Bond Length of the Hydrogen Molecule Ion - *CC BY 4.0*
  - 2.22: The Hydrogen Atom with Finite Sized Nucleus - *CC BY 4.0*
  - 2.23: The Hyperfine Interaction in the Hydrogen Atom - *CC BY 4.0*
  - 2.24: Positronium Annihilation - *CC BY 4.0*
  - 2.25: Positronium Annihilation- Another View - *CC BY 4.0*
  - 2.26: Positronium Annihilation- Yet Another View - *CC BY 4.0*
  - 2.27: The Hyperfine Interaction in the Deutrium Atom - *CC BY 4.0*

- 2.28: A Tensor Algebra Approach to Spin-Orbit Coupling - *CC BY 4.0*
- 2.29: A Bohr Model for Multi-electron Atoms and Ions - *CC BY 4.0*
- 2.30: Atomic Variational Calculations- Hydrogen to Boron - *CC BY 4.0*
- 2.31: Some Calculations on the Lithium Atom Ground State - *CC BY 4.0*
- 2.32: E. B. Wilson's Calculation on the Lithium Atom Ground State - *CC BY 4.0*
- 2.33: The Importance of the Pauli Principle - *CC BY 4.0*
- 2.34: Splitting the 2s-2p Degeneracy in the Lithium Atom - *CC BY 4.0*
- 2.35: Addition of Spin Angular Momentum- A Tensor Algebra Approach - *CC BY 4.0*
- 2.36: Hund's Rule - *CC BY 4.0*
- 2.37: Hund's Rule - Singlet-Triplet Calculations with Mathcad - *CC BY 4.0*
- 2.38: Electron Correlation in Two-electron Systems - *CC BY 4.0*
- 2.39: First Trial Wave Function - *CC BY 4.0*
- 2.40: Second Trial Wavefunction - *CC BY 4.0*
- 2.41: Third Trial Wavefunction - *CC BY 4.0*
- 2.42: 129.4 Fourth Trial Wavefunction - *CC BY 4.0*
- 2.43: Fifth Trial Wavefunction and Summary - *CC BY 4.0*
- 2.44: The Crucial Role of Kinetic Energy in Interpreting Ionization Energies - *CC BY 4.0*
- 2.45: Quantum Dots Are Artificial Atoms - *CC BY 4.0*
- 2.46: Calculating the Atomic Radius of Polonium - *CC BY 4.0*
- 2.47: Calculating the Atomic Radius of Gold - *CC BY 4.0*
- 2.48: How Many Bibles Can Fit on the Head of a Pin - *CC BY 4.0*
- 2.49: Momentum Wavefunctions and Distributions for the Hydrogen Atom - *CC BY 4.0*
- 2.50: The SCF Method for Two Electrons - *CC BY 4.0*
- 2.51: Outline of the SCF Method for Two Electrons - *CC BY 4.0*
- 2.52: The SCF Method for Two Electrons Using a Gaussian Wave Function - *CC BY 4.0*
- 2.53: An Interactive SCF Calculation for the Helium Atom - *CC BY 4.0*
- 2.54: Quantum Calculations on the Hydrogen Atom in Coordinate, Momentum and Phase Space - *CC BY 4.0*
- 2.55: The Wigner Distribution for the 1s State of the 1D Hydrogen Atom - *CC BY 4.0*
- 2.56: The Wigner Distribution for the 2s State of the 1D Hydrogen Atom - *CC BY 4.0*
- 2.57: The Wigner Distribution for the 2p State of the 1D Hydrogen Atom - *CC BY 4.0*
- 2.58: The Wigner Distribution for the 3s State of the 1D Hydrogen Atom - *CC BY 4.0*
- 2.59: The Wigner Distribution for the 3p State of the 1D Hydrogen Atom - *CC BY 4.0*
- 2.60: The Wigner Distribution for the 4s State of the 1D Hydrogen Atom - *CC BY 4.0*
- 2.61: One-dimensional H-atom with Delta Function Potential - *CC BY 4.0*
- 2.62: The Atomic Structure Factor in Coordinate and Momentum Space - *CC BY 4.0*

3: Chemical Bonding - *CC BY 4.0*

- 3.1: The Covalent Bond and Quantum Mechanics - *CC BY 4.0*
- 3.2: The Covalent Bond in the Hydrogen Molecule - *CC BY 4.0*
- 3.3: The Covalent Bond Clarified Through the Use of the Virial Theorem - *CC BY 4.0*
- 3.4: Brief Version of the Covalent Bond Clarified Through the Use of the Virial Theorem - *CC BY 4.0*
- 3.5: The H2 Covalent Bond and the Virial Theorem - *CC BY 4.0*
- 3.6: The Covalent Bond According to Slater and Ruedenberg - *CC BY 4.0*
- 3.7: Slater's Analysis of the Covalent Bond using the Virial Theorem - *CC BY 4.0*
- 3.8: Two Analyses of the Covalent Bond using the Virial Theorem - *CC BY 4.0*
- 3.9: A Simple Charge Cloud Model for Molecular Hydrogen- Or, Is It a DFT Model? - *CC BY 4.0*
- 3.10: Three Mechanisms for Bond Formation in the Hydrogen Molecule Ion - *CC BY 4.0*
- 3.11: A Mechanistic Approach to Bond Formation in the Hydrogen Molecule Ion - *CC BY 4.0*
- 3.12: A Lite Version of Ruedenberg's Analysis of the Covalent Bond in the Hydrogen Molecule Ion - *CC BY 4.0*
- 3.13: Molecular Orbital Analysis for the Hydrogen Molecule Ion Bond - *CC BY 4.0*
- 3.14: A One-dimensional Model for the Covalent Bond in the Hydrogen Molecule Ion - *CC BY 4.0*
- 3.15: Localized and Delocalized Molecular Orbitals - *CC BY 4.0*

- 3.16: Two Perspectives on the Bonding in Water - *CC BY 4.0*
- 3.17: Covalent Bonding in Ammonia from Several Perspectives - *CC BY 4.0*
- 3.18: A Molecular Orbital Approach to Bonding in Methane - *CC BY 4.0*
- 3.19: A Simple Calculation of the Lattice Energy of LiH - *CC BY 4.0*
- 3.20: An Even Simpler LiH Lattice Energy Calculation - *CC BY 4.0*
- 3.21: Charge Cloud Models for Some Simple Atomic, Molecular and Solid Systems - *CC BY 4.0*
- 3.22: A Critique of the Valence Shell Electron Pair Repulsion Model - *CC BY 4.0*
- 3.23: A Simple Electrostatic Critique of VSEPR - *CC BY 4.0*
- 3.24: Another Critique of VSEPR - *CC BY 4.0*
- 3.25: Why Nonbonding Electrons Occupy the Equatorial Position in Trigonal Bipyramidal Geometry - *CC BY 4.0*
- 3.26: A Modified Tangent Spheres Model Analysis of Trigonal Bipyramidal Geometry - *CC BY 4.0*
- 3.27: A Symbolic Huckel MO Calculation Using Mathcad - *CC BY 4.0*
- 3.28: A Numeric Huckel MO Calculation Using Mathcad - *CC BY 4.0*
- 3.29: A Numerical Huckel MO Calculation on C60 - *CC BY 4.0*
- 3.30: Chemical Bonding and Electronic Structure of Buckminsterfullerene - *CC BY 4.0*
- 3.31: Quantum Mechanics, Group Theory and C60 - *CC BY 4.0*
- 3.32: A Numerical Huckel Calculation on Anthracene and Phenanthrene - *CC BY 4.0*
- 3.33: A Numerical Huckel Calculation on C10H8 Isomers - *CC BY 4.0*
- 3.34: Semi-empirical Molecular Orbital Calculation on HF - *CC BY 4.0*
- 3.35: Semi-empirical Molecular Orbital Calculation on XeF2 - *CC BY 4.0*
- 3.36: Posch-Teller Potential Model for Metals - *CC BY 4.0*

- 4: Spectroscopy - *CC BY 4.0*
  - 4.1: Rudiments of Atomic Spectroscopy Using Mathcad - *CC BY 4.0*
  - 4.2: A Particle-in-a-Box Model for Color Centers - *CC BY 4.0*
  - 4.3: Cyanine Dyes as Two-State Electronic Systems - *CC BY 4.0*
  - 4.4: The Ammonia Inversion and the Maser - *CC BY 4.0*
  - 4.5: A Symmetric Double Well Potential Illustrating Tunneling - *CC BY 4.0*
  - 4.6: Analyses of the Pure Rotational Spectrum of HCl - *CC BY 4.0*
  - 4.7: A Rudimentary Analysis of the Vibrational-Rotational HCl Spectrum - *CC BY 4.0*
  - 4.8: Visualizing the Formally Forbidden Overtone Vibrational Transitions in HCl - *CC BY 4.0*
  - 4.9: The Quantum Jump - *CC BY 4.0*
  - 4.10: Another Look at the Quantum Jump - *CC BY 4.0*
  - 4.11: Quantum Beats - *CC BY 4.0*
  - 4.12: The 1s-2s Electronic Transition in the 1D Hydrogen Atom - *CC BY 4.0*
  - 4.13: The Quantum Jump in Momentum Space - *CC BY 4.0*
  - 4.14: The Harmonic Oscillator Quantum Jump - *CC BY 4.0*
  - 4.15: Coherent States of the Harmonic Oscillator - *CC BY 4.0*
  - 4.16: Analysis of the Electronic Spectrum of Ti(H2O)3+ - *CC BY 4.0*
  - 4.17: Quantum Jumps for an Electron on a Ring - *CC BY 4.0*
  - 4.18: Analysis of the Vibrational and Electronic Spectrum of Benzene - *CC BY 4.0*
  - 4.19: NMR - Quantum Mechanics of a Three Proton System - *CC BY 4.0*
  - 4.20: AB Proton NMR Using Tensor Algebra - *CC BY 4.0*
  - 4.21: Calculating the AB Proton NMR Using Tensor Algebra - *CC BY 4.0*
  - 4.22: AB Proton NMR Analysis for 2,3-dibromothiophene - *CC BY 4.0*
  - 4.23: ABC Proton NMR Using Tensor Algebra - *CC BY 4.0*
  - 4.24: AB2 Proton NMR Using Tensor Algebra - *CC BY 4.0*
  - 4.25: AB3 Proton NMR Using Tensor Algebra - *CC BY 4.0*
  - 4.26: HD-Like NMR Spectrum Calculated Using Tensor Algebra - *CC BY 4.0*
  - 4.27: The Michelson Interferometer and Fourier Transform Spectroscopy - *CC BY 4.0*
  - 4.28: A Sum Over Histories Approach to Fourier Transform Infrared Spectroscopy - *CC BY 4.0*
  - 4.29: Modeling the Pi-electrons of Benzene as Particles on a Ring - *CC BY 4.0*

- 4.30: Modeling the Pi-electrons of Benzene as Particles on a Ring - Version 2 - *CC BY 4.0*
- 4.31: Calculating the Pi-electron HOMO-LUMO Electronic Transition for Benzene - *CC BY 4.0*
- 4.32: Modeling the Pi-electrons of Benzene as Particles in a Ring - *CC BY 4.0*
- 4.33: Modeling the Pi-electrons of Corannulene as Particles in a Ring - *CC BY 4.0*
- 4.34: The Vibrational and Electronic States of C60 - *CC BY 4.0*

- 5: Diffraction Phenomena - *CC BY 4.0*
  - 5.1: Using Optical Transforms to Teach Quantum Mechanics - *CC BY 4.0*
  - 5.2: Single-slit Diffraction and the Uncertainty Principle - *CC BY 4.0*
  - 5.3: Single-slit Diffraction and the Uncertainty Principle (Mathcad Version) - *CC BY 4.0*
  - 5.4: Simulating DNA's Diffraction Pattern - *CC BY 4.0*
  - 5.5: Simulating DNA's Diffraction Pattern with a More Realistic Model - *CC BY 4.0*
  - 5.6: Simulating DNA's Diffraction Pattern - Short Version - *CC BY 4.0*
  - 5.7: A Model Graphene Diffraction Pattern - *CC BY 4.0*
  - 5.8: Is a Two-dimensional Fibonacci Array a Quasilattice? - *CC BY 4.0*
  - 5.9: Calculating Diffraction Patterns - *CC BY 4.0*
  - 5.10: Modeling the C60 Diffraction Pattern - *CC BY 4.0*
  - 5.11: Diffraction Pattern for Pentagonal Point Scatterers - *CC BY 4.0*
  - 5.12: Diffraction Pattern for Pentagonal Finite Point Scatterers - *CC BY 4.0*
  - 5.13: Pentagram Diffraction Pattern - *CC BY 4.0*
  - 5.14: Model Diffraction Pattern for Napthalene - *CC BY 4.0*
  - 5.15: Calculating the Airy Diffraction Pattern - *CC BY 4.0*
  - 5.16: Diffraction Pattern for Two Concentric Rings - *CC BY 4.0*
  - 5.17: Density Operator Approach to the Double-Slit Experiment - *CC BY 4.0*
  - 5.18: Another Look at the Double-Slit Experiment - *CC BY 4.0*
  - 5.19: A Quantum Mechanical Interpretation of Diffraction - *CC BY 4.0*
  - 5.20: Electron Diffraction at Multiple Slits - *CC BY 4.0*
  - 5.21: Multiple Slit Diffraction and the Fourier Transform - *CC BY 4.0*
  - 5.22: The Double-Slit Experiment with C60 Molecules - *CC BY 4.0*
  - 5.23: Crystal Structure, Rotational Symmetry, and Quasicrystals - *CC BY 4.0*
  - 5.24: X-ray Crystallography from a Quantum Mechanical Perspective - *CC BY 4.0*
  - 5.25: Holography Involves Single Photon Interference - *CC BY 4.0*
  - 5.26: X-ray Diffraction - *CC BY 4.0*
  - 5.27: Holography Involves Single Photon Interference - *CC BY 4.0*
- 6: Group Theory with Mathcad - *CC BY 4.0*
  - Front Matter - *Undeclared*
    - TitlePage - *Undeclared*
    - InfoPage - *Undeclared*
  - 6.1: Group Theory Principles Applied to H2O - *CC BY 4.0*
  - 6.2: Dodecahedrane - *CC BY 4.0*
  - 6.3: Xenon Tetrafluoride - *CC BY 4.0*
  - 6.4: Diborane - *CC BY 4.0*
  - 6.5: Cubane - *CC BY 4.0*
    - 6.5.1: Buckminsterfulerene - *CC BY 4.0*
  - 6.6: BCl3 - *CC BY 4.0*
  - 6.7: Ti(H2O)6 3+ - *CC BY 4.0*
  - 6.8: CH_4 - *CC BY 4.0*
  - 6.9: P_4 - *CC BY 4.0*
  - 6.10: Tetrahedrane - *CC BY 4.0*
  - 6.11: PH3 - *CC BY 4.0*
  - 6.12: Cyclopropane - *CC BY 4.0*
  - 6.13: An Extensive Set of Group Theory Problems for Chemists - *CC BY 4.0*
  - Back Matter - *Undeclared*
    - Index - *Undeclared*
- 7: Quantum Optics - *CC BY 4.0*
  - Front Matter - *Undeclared*
    - TitlePage - *Undeclared*
    - InfoPage - *Undeclared*
  - 7.1: Single-Photon Interference - First Version - *CC BY 4.0*
  - 7.2: Single-Photon Interference - Second Version - *CC BY 4.0*
  - 7.3: Single-photon Interference - Third Version - *CC BY 4.0*
  - 7.4: Single Photon Interference - Fourth Version - *CC BY 4.0*

- 7.5: Single Photon Interference - Mathcad version - *CC BY 4.0*
- 7.6: The Polarizing Beam Splitter and the Superposition Principle - *CC BY 4.0*
- 7.7: Mach-Zehner Polarization Interferometer Analyzed Using Tensor Algebra - *CC BY 4.0*
- 7.8: Illustrating the Superposition Principle with Single Photon Interference - *CC BY 4.0*
- 7.9: Pure States, Mixtures and the Density Operator - *CC BY 4.0*
- 7.10: Using the Trace Function to Calculate Expectation Values - *CC BY 4.0*
- 7.11: Polarized Light and Quantum Superposition - *CC BY 4.0*
- 7.12: Polarized Light and Quantum Mechanics - *CC BY 4.0*
- 7.13: The Three-Polarizer Paradox - *CC BY 4.0*
- 7.14: Matrix Mechanics Approach to Polarized Light - *CC BY 4.0*
- 7.15: Matrix Mechanics Approach to Polarized Light - Version 2 - *CC BY 4.0*
- 7.16: Matrix Mechanics Exercises Using Polarized Light - *CC BY 4.0*
- 7.17: Polarized Light and Quantum Mechanics - *CC BY 4.0*
- 7.18: Neutron Interferometry with Polarized Spin States - *CC BY 4.0*
- 7.19: Interaction Free Measurement - Seeing in the Dark - *CC BY 4.0*
- 7.20: Quantum Seeing in the Dark - A Matrix-Tensor Analysis - *CC BY 4.0*
- 7.21: Two Analyses of the Michelson Interferometer - *CC BY 4.0*
- 7.22: A Quantum Circuit for a Michelson Interferometer - *CC BY 4.0*
- 7.23: The Ramsey Atomic Interferometer - *CC BY 4.0*
- 7.24: Optical Activity - A Quantum Perspective - *CC BY 4.0*
- 7.25: A Quantum Optical Cheshire Cat - *CC BY 4.0*
- 7.26: Two Photon Interference - The Creation of an Entangled Superposition - *CC BY 4.0*
- 7.27: Two-particle Interference for Bosons and Fermions - *CC BY 4.0*
- 7.28: Analysis of a Two-photon Interferometer - *CC BY 4.0*
- 7.29: Two-photon Interferometry - *CC BY 4.0*
  - 7.29.1: Another Two Photon Interference Experiment - *CC BY 4.0*
- 7.30: Another Two Photon Interference Experiment - *CC BY 4.0*
- 7.31: Quantum Correlations Illuminated with Tensor Algebra - *CC BY 4.0*
- 7.32: Two Photon Entanglement - A Tensor Algebra Analysis - *CC BY 4.0*
- 7.33: Two Photon Interference - Matrix Mechanics Approach - *CC BY 4.0*
- 7.34: Two-electron Interference - *CC BY 4.0*
- 7.35: Bosonic and Fermionic Photon Behavior at Beam Splitters - *CC BY 4.0*
- 7.36: Bosonic and Fermionic Photon Behavior at Beam Splitters- A Tensor Algebra Analysis - *CC BY 4.0*
- 7.37: Entangled Photons Can Behave Like Fermions - *CC BY 4.0*
- 7.38: Analyzing Two-photon Interferometry Using Mathcad and Tensor Algebra - *CC BY 4.0*
- 7.39: Analysis of a Two-photon Quantum Eraser - *CC BY 4.0*
- 7.40: Another Example of a Two-photon Quantum Eraser - *CC BY 4.0*
- 7.41: A Quantum Delayed-Choice Experiment - *CC BY 4.0*
- 7.42: A Quantum Delayed-Choice Experiment - *CC BY 4.0*
- Back Matter - *Undeclared*
  - Index - *Undeclared*

8: Quantum Teleportation - *CC BY 4.0*

- 8.1: A Single Page Summary of Quantum Teleportation - *CC BY 4.0*
- 8.2: Quantum Teleportation - A Brief Introduction - *CC BY 4.0*
- 8.3: Quantum Teleportation at a Glance - *CC BY 4.0*
- 8.4: Another Look at Quantum Teleportation - *CC BY 4.0*
- 8.5: Teleportation Using Quantum Gates - *CC BY 4.0*
- 8.6: Another Example of Teleportation Using Quantum Gates - *CC BY 4.0*
- 8.7: Yet Another Quantum Teleportation Circuit - *CC BY 4.0*
- 8.8: Quantum Teleportation - Another Look - *CC BY 4.0*
- 8.9: A Quantum Teleportation Experiment for Undergraduates - *CC BY 4.0*
- 8.10: A Simple Teleportation Exercise - *CC BY 4.0*
- 8.11: Teleportation as a Quantum Computation - *CC BY 4.0*

- 8.12: Quantum Teleportation - Four Perspectives - *CC BY 4.0*
- 8.13: Teleportation of Two Qubits - *CC BY 4.0*
- 8.14: Greenaberger-Hrne-Zeilinger (GHZ) Entanglement and Local Realism - *CC BY 4.0*
- 8.15: GHZ Math Appendix - *CC BY 4.0*
- 8.16: GHZ Entanglement - A Tensor Algebra Analysis - *CC BY 4.0*
- 8.17: Simulation of a GHZ Gedanken Experiment - *CC BY 4.0*
- 8.18: Another Simulation of a GHZ Gedanken Experiment - *CC BY 4.0*
- 8.19: A Surgical Refutation of the Local Realism Heresy - *CC BY 4.0*
- 8.20: GHZ Four-Photon Entanglement Analyzed Using Tensor Algebra - *CC BY 4.0*
- 8.21: Quantum v. Realism - *CC BY 4.0*
- 8.22: Elements of Reality- Another GHZ Gedanken Experiment Analyzed - *CC BY 4.0*
- 8.23: Brief Elements of Reality - *CC BY 4.0*
- 8.24: A Brief Analysis of Mermin's GHZ Thought Experiment - *CC BY 4.0*
- 8.25: Lucien Hardy's Paradox as Presented by N. David Mermin - *CC BY 4.0*
- 8.26: Hardy's Paradox - An Algebraic Analysis - *CC BY 4.0*
- 8.27: Quantum Entanglement Leads to Nonclassical Correlations - *CC BY 4.0*
- 8.28: Nonclassial Correlations Revealed with Mermin's Pentagram - *CC BY 4.0*
- 8.29: Spooky Action at a Distance- The EPR Experiment with Photons - *CC BY 4.0*
- 8.30: David Bohm's EPR Gedanken Experiment - *CC BY 4.0*
- 8.31: An Extension of Bohm's EPR Experiment - *CC BY 4.0*
- 8.32: A Surgical Adjudication of the Conflict Between Quantum Theory and Local Realism - *CC BY 4.0*
- 8.33: A Thought Experiment Reveals the Conflict Between Quantum Theory and Local Realism - *CC BY 4.0*
- 8.34: Positronium Annihilation - *CC BY 4.0*
- 8.35: Mermin's Version of Bohm's EPR Gedanken Experiment - *CC BY 4.0*
- 8.36: A Concise Version of Mermin's EPR Gedanken Experiment - *CC BY 4.0*
- 8.37: Another Look at Mermin's EPR Gedanken Experiment - *CC BY 4.0*
- 8.38: Mermin's Version of Bohm's EPR Gedanken Experiment Using Tensor Algebra - *CC BY 4.0*
- 8.39: A GHZ Gedanken Experiment Using Spatial Degrees of Freedom and Tensor Algebra - *CC BY 4.0*
- 8.40: Another GHZ Example Using Spin-1/2 Particles - *CC BY 4.0*
- 8.41: Entanglement Reveals a Conflict Between Local Realism and Quantum Theory - *CC BY 4.0*
- 8.42: A Summary of Feynman's "Simulating Physics with Computers" - *CC BY 4.0*
- 8.43: Another Summary of Fenyman's "Stimulating Physics with Computers" - *CC BY 4.0*
- 8.44: Yet Another Assault on Local Realism - *CC BY 4.0*
- 8.45: Yet Another Assault on Local Realism - A Matrix/Tensor Algebra Approach - *CC BY 4.0*
- 8.46: Jim Baggott's Bell Theorem Analysis - *CC BY 4.0*
- 8.47: Another Bell Theorem Analysis - *CC BY 4.0*
- 8.48: Another Bell Theorem Analysis - Shorter Version - *CC BY 4.0*
- 8.49: EPR Analysis for a Composite Singlet Spin System - *CC BY 4.0*
- 8.50: EPR Analysis for a Composite Singlet Spin System - Short Version - *CC BY 4.0*
- 8.51: Analysis of the Stern-Gerlach Experiment - *CC BY 4.0*
- 8.52: Hardy's Paradox - *CC BY 4.0*
- 8.53: Bell State Exercises - *CC BY 4.0*
- 8.54: Expressing Bell and GHZ States in Vector Format Using Mathcad - *CC BY 4.0*
- 8.55: Quantum Circuit for the Generation of GHZ States - *CC BY 4.0*
- 8.56: A Brief Description of Aspect's Experiment - *CC BY 4.0*
- 8.57: The Kochen-Specker Theorem Illustrated Using a Three-Qubit GHZ System - *CC BY 4.0*
- 8.58: A Brief Introduction to Entanglement Swapping - *CC BY 4.0*
- 8.59: An Entanglement Swapping Protocol - *CC BY 4.0*
- 8.60: Quantum Correlations Simplified - *CC BY 4.0*
- 8.61: Simulating Quantum Correlations with a Quantum Computer - *CC BY 4.0*
- 8.62: Quantum Computer Simulation of Photon Correlations - *CC BY 4.0*
- 8.63: Quantum Correlations Illustrated with Photons - *CC BY 4.0*
- 8.64: Examining the Local States of an Entangled Bipartate Superposition - *CC BY 4.0*

- 8.65: A Brief Introduction to the Quantum Computer - *CC BY 4.0*
- 8.66: A Very Simple Example of Parallel Quantum Computation - *CC BY 4.0*
- 8.67: Another Simple Example of Parallel Quantum Computation - *CC BY 4.0*
- 8.68: A Simple Solution to Deutsch's Problem - *CC BY 4.0*
- 8.69: Another Example of Deutsch's Algorithm - *CC BY 4.0*
- 8.70: Evaluating a Function Using a Quantum Circuit and a Demonstration of Parallel Computation - *CC BY 4.0*
- 8.71: A Simple Quantum Circuit for Parallel Computation - *CC BY 4.0*
- 8.72: An Illustration of the Deutsch-Jozsa Algorithm - *CC BY 4.0*
- 8.73: Another Illustration of the Deutsch-Jozsa Algorithm - *CC BY 4.0*
- 8.74: Aspects of Simon's Algorithm - *CC BY 4.0*
- 8.75: Qubit Quantum Mechanics - *CC BY 4.0*
- 8.76: Implementation of Deutsch's Algorithm Using Mathcad - *CC BY 4.0*
- 8.77: Using Quantum Gates to Create Superpositions and Entangled States - *CC BY 4.0*
- 8.78: A Simple Quantum Computer - *CC BY 4.0*
- 8.79: Solving Equations Using a Quantum Circuit - *CC BY 4.0*
- 8.80: Introduction to Superdense Coding - *CC BY 4.0*
- 8.81: A Brief Introduction to Quantum Dense Coding - *CC BY 4.0*
- 8.82: The Discrete or Quantum Fourier Transform - *CC BY 4.0*
- 8.83: Factoring Using Shor's Quantum Algorithm - *CC BY 4.0*
- 8.84: Shor's Quantum Algorithm - A Summary - *CC BY 4.0*
- 8.85: Simulating the Deutsch-Jozsa Algorithm with a Double-Slit Apparatus - *CC BY 4.0*
- 8.86: Simulating a Quantum Computer with a Mach-Zehnder Interferometer - *CC BY 4.0*
- 8.87: Quantum Restrictions on Cloning - *CC BY 4.0*
- 8.88: Quantum Error Correction - *CC BY 4.0*
- 8.89: Matrix Mechanics Analysis of the BB84 Key Distribution - *CC BY 4.0*
- 8.90: 388. The Quantum Math Behind Ekert's Key Distribution Scheme - *CC BY 4.0*
- 8.91: A Shorter Version of the Quantum Math Behind Ekert's Key Distribution Scheme - *CC BY 4.0*
- 8.92: Quantum Key Distribution Using a Mach-Zehnder Interferometer - *CC BY 4.0*
- 8.93: Coding and Decoding Venus - *CC BY 4.0*
- 8.94: Grover's Quantum Search Algorithm - *CC BY 4.0*
- 8.95: Grover's Search Algorithm- Implementation for Two Items - *CC BY 4.0*
- 8.96: Grover's Search Algorithm- Four-Card Monte - *CC BY 4.0*

9: Numerical Solutions for Schrödinger's Equation - *CC BY 4.0*

- 9.1: Introduction to Numerical Solutions of Schödinger's Equation - *CC BY 4.0*
- 9.2: Particle in an Infinite Potential Well - *CC BY 4.0*
- 9.3: Particle in a Gravitational Field - *CC BY 4.0*
- 9.4: Particle in a One-dimensional Egg Carton - *CC BY 4.0*
- 9.5: Particle in a Finite Potential Well - *CC BY 4.0*
- 9.6: Particle in a Semi-infinite Potential Well - *CC BY 4.0*
- 9.7: Particle in a Slanted Well Potential - *CC BY 4.0*
- 9.8: Numerical Solutions for a Particle in a V-Shaped Potential Well - *CC BY 4.0*
- 9.9: Numerical Solutions for the Harmonic Oscillator - *CC BY 4.0*
- 9.10: Numerical Solutions for a Double-Minimum Potential Well - *CC BY 4.0*
- 9.11: Numerical Solutions for the Quartic Oscillator - *CC BY 4.0*
- 9.12: Numerical Solutions for Morse Oscillator - *CC BY 4.0*
- 9.13: Numerical Solutions for the Lennard-Jones Potential - *CC BY 4.0*
- 9.14: Numerical Solutions for the Double Morse Potential - *CC BY 4.0*
- 9.15: Particle in a Box with an Internal Barrier - *CC BY 4.0*
- 9.16: Another Look at the in a Box with an Internal Barrier - *CC BY 4.0*
- 9.17: Particle in a Box with Multiple Internal Barriers - *CC BY 4.0*
- 9.18: Particle in an Infinite Spherical Potential Well - *CC BY 4.0*
- 9.19: Numerical Solutions for the Two-Dimensional Harmonic Oscillator - *CC BY 4.0*
- 9.20: Numerical Solutions for the Three-Dimensional Harmonic Oscillator - *CC BY 4.0*
- 9.21: Numerical Solutions for the Hydrogen Atom Radial Equation - *CC BY 4.0*

- 9.22: Numerical Solutions for a Modified Harmonic Potential - *CC BY 4.0*

- 10: Approximate Quantum Mechanical Methods - *CC BY 4.0*
  - 10.1: Trial Wavefunctions for Various Potentials - *CC BY 4.0*
  - 10.2: Energy Minimization - Four Methods Using Mathcad - *CC BY 4.0*
  - 10.3: The Variation Theorem in Dirac Notation - *CC BY 4.0*
  - 10.4: A Rudimentary Model for Alpha Particle Decay - *CC BY 4.0*
  - 10.5: Variational Method for a Particle in a Finite Potential Well - *CC BY 4.0*
  - 10.6: Variation Method for a Particle in a Symmetric 1D Potential Well - *CC BY 4.0*
  - 10.7: Variation Method for the Rydberg Potential - *CC BY 4.0*
  - 10.8: Variation Method for the Quartic Oscillator - *CC BY 4.0*
  - 10.9: Momentum-Space Variation Method for the Quartic Oscillator - *CC BY 4.0*
  - 10.10: Variation Method for a Particle in a Gravitational Field - *CC BY 4.0*
  - 10.11: Linear Variational Method for a Particle in a Slanted 1D Box - *CC BY 4.0*
  - 10.12: Variation Method for a Particle in a Semi-Infinite Potential Well - *CC BY 4.0*
  - 10.13: Variation Method for a Particle in a Box with an Internal Barrier - *CC BY 4.0*
  - 10.14: Variation Method for a Particle in a 1D Ice Cream Cone - *CC BY 4.0*
  - 10.15: Variation Method for a Particle in an Ice Cream Cone - *CC BY 4.0*
  - 10.16: Variation Method for a Particle in a Finite 3D Spherical Potential Well - *CC BY 4.0*
  - 10.17: Variation Method for the Harmonic Oscillator - *CC BY 4.0*
  - 10.18: Trigonometric Trial Wave Function for the Harmonic Potential Well - *CC BY 4.0*
  - 10.19: Trigonometric Trial Wave Function for the 3D Harmonic Potential Well - *CC BY 4.0*
  - 10.20: Gaussian Trial Wavefunction for the Hydrogen Atom - *CC BY 4.0*
  - 10.21: Variation Calculation on the 1D Hydrogen Atom Using a Trigonometric Trial Wave Function - *CC BY 4.0*
  - 10.22: Variation Calculation on the 1D Hydrogen Atom Using a Gaussian Trial Wavefunction - *CC BY 4.0*
  - 10.23: Variational Calculation on the Two-dimensional Hydrogen Atom - *CC BY 4.0*
  - 10.24: Variational Calculation on Helium Using a Hydrogenic Wavefunction - *CC BY 4.0*
  - 10.25: Gaussian Trial Wave Function for the Helium Atom - *CC BY 4.0*
  - 10.26: Trigonometric Trial Wavefunction for the Helium Atom - *CC BY 4.0*
  - 10.27: Trigonometric Trial Wavefunction for the Hydrogen Atom - *CC BY 4.0*
  - 10.28: Hydrogen Atom Calculation Assuming the Electron is a Particle in a Sphere of Radius R - *CC BY 4.0*
  - 10.29: Electronic Structure - Variational Calculations on the Lithium Atom - *CC BY 4.0*
  - 10.30: The Variation Method in Momentum Space - *CC BY 4.0*
  - 10.31: Momentum-Space Variation Method for Particle in a Gravitational Field - *CC BY 4.0*
  - 10.32: Momentum-Space Variation Method for the Abs(x) Potential - *CC BY 4.0*
  - 10.33: Variational Method for the Feshbach Potential - *CC BY 4.0*
  - 10.34: Numerical Solution for the Feshbach Potential - *CC BY 4.0*
  - 10.35: First Order Degenerate Perturbation Theory - the Stark Effect of the Hydrogen Atom - *CC BY 4.0*
  - 10.36: Variational Calculation for the Polarizability of the Hydrogen Atom - *CC BY 4.0*
  - 10.37: Hybrid Variational Calculation for the 1D Hydrogen Atom with Delta Function Potential - *CC BY 4.0*
  - 10.38: Variation Method Using the Wigner Function-Finite Potential Well - *CC BY 4.0*
  - 10.39: 455. Variation Method Using the Wigner Function- V(x) = |x| - *CC BY 4.0*
  - 10.40: Variation Method Using the Wigner Function-The Harmonic Oscillator - *CC BY 4.0*
  - 10.41: Variation Method Using the Wigner Function - The Quartic Oscillator - *CC BY 4.0*
  - 10.42: Variation Method Using the Wigner Function - The Feshbach Potential - *CC BY 4.0*
- 11: Miscellaneous - *CC BY 4.0*
  - 11.1: The Art of Science - *CC BY 4.0*
  - 11.2: Mass-Energy Equivalence - *CC BY 4.0*
  - 11.3: Commentary on “Probing the Orbital Energy of an Electron in an Atom” - *CC BY 4.0*

- 11.4: The Use of Models in Introductory Chemistry - *CC BY 4.0*
- 11.5: Reaction to Gillespie's Six Great Ideas in Chemistry - Another Great Idea - *CC BY 4.0*
- 11.6: An Alternative Derivation of Gas Pressure Using the Kinetic Theory - *CC BY 4.0*
- 11.7: Examining Fourier Synthesis with Dirac Notation - *CC BY 4.0*
- 11.8: Finding Roots of Transcendental Equations - *CC BY 4.0*
- 11.9: Calculation of the Composition of a Weak Polyprotic Acid Using Mathcad - *CC BY 4.0*
- 11.10: Solving Linear Equations Using Mathcad - *CC BY 4.0*
- 11.11: Let's Teach High School Students Computer Algebra Methods - *CC BY 4.0*
- 11.12: Thermodynamics and Kinetics - *CC BY 4.0*
- 11.13: Simple Kinetic Derivations of Thermodynamic Relations - *CC BY 4.0*
- 11.14: The Global Approach to Thermodynamics - *CC BY 4.0*
- 11.15: Global Thermodynamic Analyses of Heat Engines - *CC BY 4.0*
- 11.16: Using Charles' Law to Determine Absolute Zero - *CC BY 4.0*
- 11.17: The Origin of KE = 3/2 RT - *CC BY 4.0*
- 11.18: Cosmic Background Radiation - *CC BY 4.0*
- 11.19: Age of the Elements - *CC BY 4.0*

Back Matter - *Undeclared*

- Index - *Undeclared*
- Glossary - *Undeclared*
- Detailed Licensing - *Undeclared*